

Volume 15 Issue 4

April 2024



ISSN 2156-5570(Online)
ISSN 2158-107X(Print)



Editorial Preface

From the Desk of Managing Editor...

It may be difficult to imagine that almost half a century ago we used computers far less sophisticated than current home desktop computers to put a man on the moon. In that 50 year span, the field of computer science has exploded.

Computer science has opened new avenues for thought and experimentation. What began as a way to simplify the calculation process has given birth to technology once only imagined by the human mind. The ability to communicate and share ideas even though collaborators are half a world away and exploration of not just the stars above but the internal workings of the human genome are some of the ways that this field has moved at an exponential pace.

At the International Journal of Advanced Computer Science and Applications it is our mission to provide an outlet for quality research. We want to promote universal access and opportunities for the international scientific community to share and disseminate scientific and technical information.

We believe in spreading knowledge of computer science and its applications to all classes of audiences. That is why we deliver up-to-date, authoritative coverage and offer open access of all our articles. Our archives have served as a place to provoke philosophical, theoretical, and empirical ideas from some of the finest minds in the field.

We utilize the talents and experience of editor and reviewers working at Universities and Institutions from around the world. We would like to express our gratitude to all authors, whose research results have been published in our journal, as well as our referees for their in-depth evaluations. Our high standards are maintained through a double blind review process.

We hope that this edition of IJACSA inspires and entices you to submit your own contributions in upcoming issues. Thank you for sharing wisdom.

Thank you for Sharing Wisdom!

Kohei Arai
Editor-in-Chief
IJACSA
Volume 15 Issue 4 April 2024
ISSN 2156-5570 (Online)
ISSN 2158-107X (Print)

Editorial Board

Editor-in-Chief

Dr. Kohei Arai - Saga University

Domains of Research: Technology Trends, Computer Vision, Decision Making, Information Retrieval, Networking, Simulation

Associate Editors

Alaa Sheta

Southern Connecticut State University

Domain of Research: Artificial Neural Networks, Computer Vision, Image Processing, Neural Networks, Neuro-Fuzzy Systems

Arun D Kulkarni

University of Texas at Tyler

Domain of Research: Machine Vision, Artificial Intelligence, Computer Vision, Data Mining, Image Processing, Machine Learning, Neural Networks, Neuro-Fuzzy Systems

Domenico Ciunzio

University of Naples, Federico II, Italy

Domain of Research: Artificial Intelligence, Communication, Security, Big Data, Cloud Computing, Computer Networks, Internet of Things

Dorota Kaminska

Lodz University of Technology

Domain of Research: Artificial Intelligence, Virtual Reality

Elena Scutelnicu

"Dunarea de Jos" University of Galati

Domain of Research: e-Learning, e-Learning Tools, Simulation

In Soo Lee

Kyungpook National University

Domain of Research: Intelligent Systems, Artificial Neural Networks, Computational Intelligence, Neural Networks, Perception and Learning

Krassen Stefanov

Professor at Sofia University St. Kliment Ohridski

Domain of Research: e-Learning, Agents and Multi-agent Systems, Artificial Intelligence, e-Learning Tools, Educational Systems Design

Renato De Leone

Università di Camerino

Domain of Research: Mathematical Programming, Large-Scale Parallel Optimization, Transportation problems, Classification problems, Linear and Integer Programming

Xiao-Zhi Gao

University of Eastern Finland

Domain of Research: Artificial Intelligence, Genetic Algorithms

CONTENTS

Paper 1: A Comparative Analysis of Traditional and Machine Learning Methods in Forecasting the Stock Markets of China and the US

Authors: Shangshang Jin

PAGE 1 – 8

Paper 2: Classification of Thoracic Abnormalities from Chest X-Ray Images with Deep Learning

Authors: Usman Nawaz, Muhammad Ummar Ashraf, Muhammad Junaid Iqbal, Muhammad Asaf, Mariam Musif Mir, Usman Ahmed Raza, Bilal Sharif

PAGE 9 – 14

Paper 3: Assisted Requirements Selection by Clustering using an Analytical Hierarchical Process

Authors: Shehzadi Nazeeha Saleem, Linda Mohaisen

PAGE 15 – 27

Paper 4: Comparative Analysis of Telemedicine in Media Coverage Pre- and Post-COVID-19 using Unsupervised Latent Dirichlet Topic Modeling

Authors: Haewon Byeon

PAGE 28 – 33

Paper 5: Distributed Optimization Scheduling Consistency Algorithm for Smart Grid and its Application in Cost Control of Power Grid

Authors: Lihua Shang, Meijiao Sun, Cheng Pan, Xiaoqiang San

PAGE 34 – 42

Paper 6: Evaluating the Accuracy of Cloud-based 3D Human Pose Estimation Tools: A Case Study of MOTiO by RADiCAL

Authors: Hamza Khalloufi, Mohamed Zaifri, Abdessamad Benlahbib, Fatima Zahra Kaghat, Ahmed Azough

PAGE 43 – 54

Paper 7: Optimizing Student Performance Prediction: A Data Mining Approach with MLPC Model and Metaheuristic Algorithm

Authors: Qing Hai, Changshou Wang

PAGE 55 – 71

Paper 8: DUF-Net: A Retinal Vessel Segmentation Method Integrating Global and Local Features with Skeleton Fitting Assistance

Authors: Xuelin Xu, Ren Lin, Jianwei Chen, Huabin He

PAGE 72 – 83

Paper 9: Novel Approaches for Access Level Modelling of Employees in an Organization Through Machine Learning

Authors: Priyanka C Hiremath, Raju G T

PAGE 84 – 93

Paper 10: Predicting Optimal Learning Approaches for Nursing Students in Morocco

Authors: Samira Fadili, Merouane Ertel, Aziz Mengad, Said Amali

PAGE 94 – 102

Paper 11: Automated Weeding Systems for Weed Detection and Removal in Garlic / Ginger Fields

Authors: Tsubasa Nakabayashi, Kohei Yamagishi, Tsuyoshi Suzuki

PAGE 103 – 109

Paper 12: Enhancing Building Energy Efficiency: A Hybrid Meta-Heuristic Approach for Cooling Load Prediction

Authors: Chenguang Wang, Yanjie Zhou, Libin Deng, Ping Xiong, Jiarui Zhang, Jiamin Deng, Zili Lei

PAGE 110 – 121

Paper 13: Securing IoT Environment by Deploying Federated Deep Learning Models

Authors: Saleh Alghamdi, Aiiad Albeshri

PAGE 122 – 129

Paper 14: Review and Analysis of Financial Market Movements: Google Stock Case Study

Authors: Yiming LU

PAGE 130 – 144

Paper 15: Prediction of Financial Markets Utilizing an Innovatively Optimized Hybrid Model: A Case Study of the Hang Seng Index

Authors: Xiaopeng YANG

PAGE 145 – 155

Paper 16: Research on Diagnosis Method of Common Knee Diseases Based on Subjective Symptoms and Random Forest Algorithm

Authors: Guangjun Wang, Mengxia Hu, Linlin Lv, Hanyuan Zhang, Yining Sun, Benyue Su, Zuchang Ma

PAGE 156 – 168

Paper 17: Data Dynamic Prediction Algorithm in the Process of Entity Information Search for the Internet of Things

Authors: Tianqing Liu

PAGE 169 – 178

Paper 18: Deep Learning-Powered Lung Cancer Diagnosis: Harnessing IoT Medical Data and CT Images

Authors: Xiao Zhang, Xiaobo Wang, Tao Huang, Jinping Sheng

PAGE 179 – 190

Paper 19: Transmission Line Monitoring Technology Based on Compressed Sensing Wireless Sensor Network

Authors: Shuling YIN, Renping YU, Longzhi WANG

PAGE 191 – 199

Paper 20: Implementation of Cosine Similarity Algorithm on Omnibus Law Drafting

Authors: Aristoteles, Muhammad Umaruddin Syam, Tristiyanto, Bambang Hermanto

PAGE 200 – 205

Paper 21: Enhancing Particle Swarm Optimization Performance Through CUDA and Tree Reduction Algorithm

Authors: Hussein Younis, Mujahed Eleyat

PAGE 206 – 213

Paper 22: Underwater Video Image Restoration and Visual Communication Optimization Based on Improved Non Local Prior Algorithm

Authors: Tian Xia

PAGE 214 – 222

Paper 23: Integrated Ensemble Model for Diabetes Mellitus Detection

Authors: Abdulaziz A Alzubaidi, Sami M Halawani, Mutasem Jarrah

PAGE 223 – 233

Paper 24: Leveraging Machine Learning Methods for Crime Analysis in Textual Data

Authors: Shynar Mussiraliyeva, Gulshat Baispay

PAGE 234 – 241

Paper 25: Superframe Segmentation for Content-based Video Summarization

Authors: Priyanka Ganesan, Senthil Kumar Jagatheesaperumal, Abirami R, Lekhasri K, Silvia Gaffandzhieva, Rositsa Doneva

PAGE 242 – 250

Paper 26: Training Model of High-Rise Building Project Management Talent under Multi-Objective Evolutionary Algorithm

Authors: Pan Qi

PAGE 251 – 263

Paper 27: Development of a New Chaotic Function-based Algorithm for Encrypting Digital Images

Authors: Dhian Sweetania, Suryadi MT, Sarifuddin Madenda

PAGE 264 – 269

Paper 28: Transfer Learning-based CNN Model for the Classification of Breast Cancer from Histopathological Images

Authors: Sumitha A, Rimal Isaac R S

PAGE 270 – 280

Paper 29: Autoencoder and CNN for Content-based Retrieval of Multimodal Medical Images

Authors: Suresh Kumar J S, Maria Celestin Vigila S

PAGE 281 – 290

Paper 30: Optimizing Bug Bounty Programs for Efficient Malware-Related Vulnerability Discovery

Authors: Semi Yulianto, Benfano Soewito, Ford Lumban Gaol, Aditya Kurniawan

PAGE 291 – 299

Paper 31: ConvADD: Exploring a Novel CNN Architecture for Alzheimer's Disease Detection

Authors: Mohammed G Alsubaiea, Suhuai Luo, Kamran Shaukat

PAGE 300 – 313

Paper 32: A Cost-Effective IoT-based Transcutaneous Electrical Nerve Stimulation (TENS): Proof-of-Concept Design and Evaluation

Authors: Ahmad O. Alokaily, Meshael J. Almansour, Ahmed A. Aldohbeyb, Suhail S. Alshahrani

PAGE 314 – 318

Paper 33: An Intelligent Learning Approach for Improving ECG Signal Classification and Arrhythmia Analysis

Authors: Sarah Allabun

PAGE 319 – 326

Paper 34: Multi-Discriminator Image Restoration Algorithm Based on Hybrid Dilated Convolution Networks

Authors: Chunming Wu, Fengshuo Qi

PAGE 327 – 335

Paper 35: Research on Resource Sharing Method of Library and Document Center Under the Multimedia Background

Authors: Jianhui Zhang

PAGE 336 – 346

Paper 36: A Hybrid MCDM Model for Service Composition in Cloud Manufacturing using O-TOPSIS

Authors: Syed Omer Farooq Ahmed, Adapa Gopi

PAGE 347 – 352

Paper 37: Comparative Analysis of Transformer Models for Sentiment Analysis in Low-Resource Languages

Authors: Yusuf Aliyu, Aliza Sarlan, Kamaluddeen Usman Danyaro, Abdulahi Sani B A Rahman

PAGE 353 – 364

Paper 38: Influence of a Serious Video Game on the Behavior of Drivers in the Face of Automobile Incidents

Authors: Bryan S. Diaz-Sipiran, Segundo E. Cieza-Mostacero

PAGE 365 – 374

Paper 39: A Genetic Artificial Bee Colony Algorithm for Investigating Job Creation and Economic Enhancement in Medical Waste Recycling

Authors: El Liazidi Sara, Dkhissi Btissam

PAGE 375 – 387

Paper 40: Multimodal Feature Fusion Video Description Model Integrating Attention Mechanisms and Contrastive Learning

Authors: Wang Zhihao, Che Zhanbin

PAGE 388 – 395

Paper 41: Permanent Magnet Motor Control System Based on Fuzzy PID Control

Authors: Yin Sha, Huwei Chen

PAGE 396 – 406

Paper 42: Impact of Contradicting Subtle Emotion Cues on Large Language Models with Various Prompting Techniques

Authors: Noor Ul Huda, Sanam Fayaz Sahito, Abdul Rehman Gilal, Ahsanullah Abro, Abdullah Alsharqiti, Aeshah Alsughayyir, Abdul Sattar Palli

PAGE 407 – 414

Paper 43: Investigating Sampler Impact on AI Image Generation: A Case Study on Dogs Playing in the River

Authors: Sanjay Deshmukh

PAGE 415 – 423

Paper 44: Enhancing Ultimate Bearing Capacity Assessment of Rock Foundations using a Hybrid Decision Tree Approach

Authors: Mei Guo, Ren-an Jiang

PAGE 424 – 435

Paper 45: Improving Prediction Accuracy using Random Forest Algorithm

Authors: Nesma Elsayed, Sherif Abd Elaleem, Mohamed Marie

PAGE 436 – 441

Paper 46: StockBiLSTM: Utilizing an Efficient Deep Learning Approach for Forecasting Stock Market Time Series Data

Authors: Daa Salama Abd Elminaam, Asmaa M M. El-Tanany, Mohamed Abd El Fattah, Mustafa Abdul Salam

PAGE 442 – 451

Paper 47: Segmentation Analysis for Brain Stroke Diagnosis Based on Susceptibility-Weighted Imaging (SWI) using Machine Learning

Authors: Shaarmila Kandaya, Abdul Rahim Abdullah, Norhashimah Mohd Saad, Ezreen Farina, Ahmad Sobri Muda

PAGE 452 – 460

Paper 48: A Genetic Algorithm-based Approach for Design-level Class Decomposition

Authors: Bayu Priyambadha, Nobuya Takahashi, Tetsuro Katayama

PAGE 461 – 468

Paper 49: Analysis and Enhancement of Prediction of Cardiovascular Disease Diagnosis using Machine Learning Models SVM, SGD, and XGBoost

Authors: Sandeep Tomar, Deepak Dembla, Yogesh Chaba

PAGE 469 – 479

Paper 50: Towards a New Artificial Intelligence-based Framework for Teachers' Online Continuous Professional Development Programs: Systematic Review

Authors: Hamza Fakhar, Mohammed Lamrabet, Nouredine Echantoufi, Khalid El khattabi, Lotfi Ajana

PAGE 480 – 493

Paper 51: Improvement of Social Skills in Children with Autism Spectrum Disorder Through the use of a Video Game

Authors: Luis C. Soles-Núñez, Segundo E. Cieza-Mostacero

PAGE 494 – 501

Paper 52: Cinematic Curator: A Machine Learning Approach to Personalized Movie Recommendations

Authors: B. Venkateswarlu, N. Yaswanth, A. Manoj Kumar, U. Satish, K. Dwijesh, N. Sunanda

PAGE 502 – 509

Paper 53: Sentiment Analysis of Pandemic Tweets with COVID-19 as a Prototype

Authors: Mashail Almutiri, Mona Alghamdi, Hanan Elazhary

PAGE 510 – 518

Paper 54: Automating Mushroom Culture Classification: A Machine Learning Approach

Authors: Hamimah Ujir, Irwandi Hipiny, Mohamad Hasnul Bolhassan, Ku Nurul Fazira Ku Azir, SA Ali

PAGE 519 – 525

Paper 55: Leather Image Quality Classification and Defect Detection System using Mask Region-based Convolution Neural Network Model

Authors: Azween Bin Abdullah, Malathy Jawahar, Nalini Manogaran, Geetha Subbiah, Koteeswaran Seeranagan, Balamurugan Balusamy, Abhishek Chengam Saravanan

PAGE 526 – 536

Paper 56: Prediction of Pigment Epithelial Detachment in Optical Coherence Tomography Images using Machine Learning

Authors: T. M. Sheeba, S. Albert Antony Raj

PAGE 537 – 546

Paper 57: Investigating the Effect of Small Sample Process Capability Index Under Different Bootstrap Methods

Authors: Liyan Wang, Guihua Bo, Mingjuan Du

PAGE 547 – 555

Paper 58: Discovering the Global Landscape of Agri-Food and Blockchain: A Bibliometric Review

Authors: Sharifah Khairun Nisa' Habib Elias, Sahnus Usman, Suriyati Chuprat

PAGE 556 – 575

Paper 59: A Robust Hybrid Convolutional Network for Tumor Classification Using Brain MRI Image Datasets

Authors: Satish Bansal, Rakesh S Jadon, Sanjay K. Gupta

PAGE 576 – 584

Paper 60: Emotion Recognition with Intensity Level from Bangla Speech using Feature Transformation and Cascaded Deep Learning Model

Authors: Md. Masum Billah, Md. Likhon Sarker, M. A. H. Akhand, Md Abdus Samad Kamal

PAGE 585 – 594

Paper 61: Optimizing Deep Learning for Efficient and Noise-Robust License Plate Detection and Recognition

Authors: Seong-O Shim, Romil Imtiaz, Safa Habibullah, Abdulrahman A. Alshdadi

PAGE 595 – 607

Paper 62: Crowdsourcing Requirements Engineering: A Taxonomy-based Review

Authors: Ghadah Alamer, Sultan Alyahya, Hmood Al-Dossari

PAGE 608 – 615

Paper 63: An Effective Book Recommendation System using Weighted Alternating Least Square (WALS) Approach

Authors: Kavitha V K, Sankar Murugesan

PAGE 616 – 626

Paper 64: Improving Predictive Maintenance in Industrial Environments via IIoT and Machine Learning

Authors: Saleh Othman Alhuqay, Abdulaziz Turki Alenazi, Hamad Abdulaziz Alabduljabbar, Mohd Anul Haq

PAGE 627 – 636

Paper 65: Analyzing Privacy Implications and Security Vulnerabilities in Single Sign-On Systems: A Case Study on OpenID Connect

Authors: Mohammed Al Shabi, Rashiqa Rafiq Marie

PAGE 637 – 646

Paper 66: A Patrol Platform Based on Unmanned Aerial Vehicle for Urban Safety and Intelligent Social Governance

Authors: Ying Yang, Rui Ma, Fengjiao Zhou

PAGE 647 – 655

Paper 67: Entity Relation Joint Extraction Method Based on Insertion Transformers

Authors: Haotian Qi, Weiguang Liu, Fenghua Liu, Weigang Zhu, Fangfang Shan

PAGE 656 – 664

Paper 68: Timber Defect Identification: Enhanced Classification with Residual Networks

Authors: Teo Hong Chun, Ummi Raba'ah Hashim, Sabrina Ahmad

PAGE 665 – 671

Paper 69: Enhancing Supply Chain Management Efficiency: A Data-Driven Approach using Predictive Analytics and Machine Learning Algorithms

Authors: Shamrao Parashram Ghodake, Vinod Ramchandra Malkar, Kathari Santosh, L. Jabasheela, Shokhjakhon Abdufattokhov, Adapa Gopi

PAGE 672 – 686

Paper 70: Advancing Prostate Cancer Diagnostics with Image Masking Techniques in Medical Image Analysis

Authors: H. V. Ramana Rao, V RaviSankar

PAGE 687 – 694

Paper 71: Deep Learning Network Optimization for Analysis and Classification of High Band Images

Authors: Manju Sundararajan, S. J Grace Shoba, Y. Rajesh Babu, P N S Lakshmi

PAGE 695 – 704

Paper 72: Lightweight Cryptographic Algorithms for Medical IoT Devices using Combined Transformation and Expansion (CTE) and Dynamic Chaotic System

Authors: Abdul Muhammed Rasheed, Retnaswami Mathusoothana Satheesh Kumar

PAGE 705 – 715

Paper 73: A Novel Graph Convolutional Neural Networks (GCNNs)-based Framework to Enhance the Detection of COVID-19 from X-Ray and CT Scan Images

Authors: D. Raghu, Hrudaya Kumar Tripathy, Raiza Borreo

PAGE 716 – 721

Paper 74: A Smart AI Framework for Backlog Refinement and UML Diagram Generation

Authors: Samia NASIRI, Mohammed LAHMER

PAGE 722 – 736

Paper 75: Challenges and Solutions of Agile Software Development Implementation: A Case Study Indonesian Healthcare Organization

Authors: Ulfah Nur Mukharomah, Teguh Raharjo, Ni Wayan Trisnawaty

PAGE 737 – 744

Paper 76: The Bi-Level Particle Swarm Optimization for Joint Pricing in a Supply Chain

Authors: Umar Mansyuri, Andreas Tri Panudju, Helena Sitorus, Widya Spalanzani, Nunung Nurhasanah, Dedy Khaerudin

PAGE 745 – 753

Paper 77: Deep Learning Approach for Workload Prediction and Balancing in Cloud Computing

Authors: Syed Karimunnisa, Yellamma Pachipala

PAGE 754 – 763

Paper 78: Estimating Coconut Yield Production using Hyperparameter Tuning of Long Short-Term Memory

Authors: Niranjan Shadaksharappa Jayanna, Raviprakash Madenur Lingaraju

PAGE 764 – 771

Paper 79: Integrating Lesk Algorithm with Cosine Semantic Similarity to Resolve Polysemy for Setswana Language

Authors: Tebatso Gorgina Moape, Oludayo O. Olugbara, Sunday O. Ojo

PAGE 772 – 778

Paper 80: Design of Emotion Analysis Model IABC-Deep Learning-based for Vocal Performance

Authors: Zhenjie Zhu, Xiaojie Lv

PAGE 779 – 786

Paper 81: Enhancing the Diagnosis of Depression and Anxiety Through Explainable Machine Learning Methods

Authors: Mai Marey, Dina Salem, Nora El Rashidy, Hazem ELBakry

PAGE 787 – 796

Paper 82: An Integrated Arnold and Bessel Function-based Image Encryption on Blockchain

Authors: Abhay Kumar Yadav, Virendra P. Vishwakarma

PAGE 797 – 803

Paper 83: COOT-Optimized Real-Time Drowsiness Detection using GRU and Enhanced Deep Belief Networks for Advanced Driver Safety

Authors: Gunnam Rama Devi, Hayder MUSAAD Al-Tmimi, Ghadir Kamil Ghadir, Shweta Sharma, Eswar Patnala, B Kiran Bala, Yousef A. Baker El-Ebiary

PAGE 804 – 814

Paper 84: A Hybrid Approach with Xception and NasNet for Early Breast Cancer Detection

Authors: Yassin Benajiba, Mohamed Chrayah, Yassine Al-Amrani

PAGE 815 – 820

Paper 85: Strengthening Sentence Similarity Identification Through OpenAI Embeddings and Deep Learning

Authors: Nilesh B. Korade, Mahendra B. Salunke, Amol A. Bhosle, Prashant B. Kumbharkar, Gayatri G. Asalkar, Rutuja G. Khedkar

PAGE 821 – 829

Paper 86: Event-based Smart Contracts for Automated Claims Processing and Payouts in Smart Insurance

Authors: Araddhana Arvind Deshmukh, Prabhakar Kandukuri, Janga Vijaykumar, Anna Shalini, S. Farhad, Elangovan Muniyandy, Yousef A. Baker El-Ebiary

PAGE 830 – 839

Paper 87: Real-time Air Quality Monitoring in Smart Cities using IoT-enabled Advanced Optical Sensors

Authors: Anushree A. Aserkar, Sanjiv Rao Godla, Yousef A. Baker El-Ebiary, Krishnamoorthy, Janjhyam Venkata Naga Ramesh

PAGE 840 – 848

Paper 88: DeepCardioNet: Efficient Left Ventricular Epicardium and Endocardium Segmentation using Computer Vision

Authors: Bukka Shobharani, S Girinath, K. Suresh Babu, J. Chennai Kumaran, Yousef A. Baker El-Ebiary, S. Farhad

PAGE 849 – 858

Paper 89: Enhancing HCI Through Real-Time Gesture Recognition with Federated CNNs: Improving Performance and Responsiveness

Authors: R. Stella Maragatham, Yousef A. Baker El-Ebiary, Srilakshmi V, K. Sridharan, Vuda Sreenivasa Rao, Sanjiv Rao Godla

PAGE 859 – 868

Paper 90: Advancing Automated and Adaptive Educational Resources Through Semantic Analysis with BERT and GRU in English Language Learning

Authors: V Moses Jayakumar, R. Rajakumari, Sana Sarwar, Darakhshan Mazhar Syed, Prema S, Santhosh Boddupalli, Yousef A. Baker El-Ebiary

PAGE 869 – 880

Paper 91: Network Security Situation Prediction Technology Based on Fusion of Knowledge Graph

Authors: Wei Luo

PAGE 881 – 891

Paper 92: Hybrid Approach for Enhanced Depression Detection using Learning Techniques

Authors: Ganesh D. Jadhav, Sachin D. Babar, Parikshit N. Mahalle

PAGE 892 – 900

Paper 93: Sustainable Artificial Intelligence: Assessing Performance in Detecting Fake Images

Authors: Othman A. Alrusaini

PAGE 901 – 909

Paper 94: Federated Convolutional Neural Networks for Predictive Analysis of Traumatic Brain Injury: Advancements in Decentralized Health Monitoring

Authors: Tripti Sharma, Desidi Narsimha Reddy, Chamandeep Kaur, Sanjiv Rao Godla, R. Salini, Adapa Gopi, Yousef A. Baker El-Ebiary

PAGE 910 – 923

Paper 95: Enhancing Threat Detection in Financial Cyber Security Through Auto Encoder-MLP Hybrid Models

Authors: Layth Almahadeen, Ghayth AlMahadin, Kathari Santosh, Mohd Aarif, Pinak Deb, Maganti Syamala, B Kiran Bala

PAGE 924 – 933

Paper 96: Basketball Free Throw Posture Analysis and Hit Probability Prediction System Based on Deep Learning

Authors: Yuankai Luo, Yan Peng, Juan Yang

PAGE 934 – 946

Paper 97: Enhancing IoT Network Security: ML and Blockchain for Intrusion Detection

Authors: N. Sunanda, K. Shailaja, Prabhakar Kandukuri, Krishnamoorthy, Vuda Sreenivasa Rao, Sanjiv Rao Godla

PAGE 947 – 958

Paper 98: Unveiling Spoofing Attempts: A DCGAN-based Approach to Enhance Face Spoof Detection in Biometric Authentication

Authors: Vuda Sreenivasa Rao, Shirisha Kasireddy, Annapurna Mishra, R. Salini, Sanjiv Rao Godla, Khaled Bedair

PAGE 959 – 969

Paper 99: A Novel Proposal for Improving Economic Decision-Making Through Stock Price Index Forecasting

Authors: Xu Yao, Weikang Zeng, Lei Zhu, Xiaoxiao Wu, Di Li

PAGE 970 – 982

Paper 100: Optimization Method for Digital Twin Manufacturing System Based on NSGA-II

Authors: Yu Ding, Longhua Li

PAGE 983 – 993

Paper 101: Keyword Acquisition for Language Composition Based on TextRank Automatic Summarization Approach

Authors: Yan Jiang, Chunlin Xiang, Lingtong Li

PAGE 994 – 1005

Paper 102: Investigating Cooling Load Estimation via Hybrid Models Based on the Radial Basis Function

Authors: Sirui Zhang, Hao Zheng

PAGE 1006 – 1018

Paper 103: Adaptive Target Region Attention Network-based Human Pose Estimation in Smart Classroom

Authors: Jianwen Mo, Guiyun Jiang, Hua Yuan, Zhaoyu Shou, Huibing Zhang

PAGE 1019 – 1026

Paper 104: Breast Cancer Classification through Transfer Learning with Vision Transformer, PCA, and Machine Learning Models

Authors: Juan Gutierrez-Cardenas

PAGE 1027 – 1036

Paper 105: Hybrid Algorithm using Rivest-Shamir-Adleman and Elliptic Curve Cryptography for Secure Email Communication

Authors: Kwame Assa-Agyei, Kayode Owa, Tawfik Al-Hadhrami, Funminiyi Olajide

PAGE 1037 – 1047

Paper 106: Federated Machine Learning for Epileptic Seizure Detection using EEG

Authors: S. Vasanthadev Suryakala, T. R. Sree Vidya, S. Hari Ramakrishnans

PAGE 1048 – 1053

Paper 107: Impact of the IoT Integration and Sustainability on Competition Within an Oligopolistic 3PL Market

Authors: Kenza Izikki, Aziz Ait Bassou, Mustapha Hlyal, Jamila El Alami

PAGE 1054 – 1065

Paper 108: Unified Approach for Scalable Task-Oriented Dialogue System

Authors: Manisha Thakkar, Nifin Pise

PAGE 1066 – 1076

Paper 109: Day Trading Strategy Based on Transformer Model, Technical Indicators and Multiresolution Analysis

Authors: Salahadin A. Mohammed

PAGE 1077 – 1089

Paper 110: Multi-Granularity Feature Fusion for Enhancing Encrypted Traffic Classification

Authors: Quan Ding, Zhengpeng Zha, Yanjun Li, Zhenhua Ling

PAGE 1090 – 1097

Paper 111: Optimization of PID Controller Parameter using the Geometric Mean Optimizer

Authors: Osama Abdellatif, Mohamed Issa, Ibrahim Ziedan

PAGE 1098 – 1103

Paper 112: Blockchain-Driven Decentralization of Electronic Health Records in Saudi Arabia: An Ethereum-Based Framework for Enhanced Security and Patient Control

Authors: Atef Masmoudi, Maha Saeed

PAGE 1104 – 1119

Paper 113: Automating Tomato Ripeness Classification and Counting with YOLOv9

Authors: Hoang-Tu Vo, Kheo Chau Mui, Nhon Nguyen Thien, Phuc Pham Tien

PAGE 1120 – 1128

Paper 114: Harnessing AI to Generate Indian Sign Language from Natural Speech and Text for Digital Inclusion and Accessibility

Authors: Parul Yadav, Mahima Chawla, Puneet Sharma, Rishi Jain, Pooja Khanna, Laiba Noor

PAGE 1129 – 1138

Paper 115: Developing a Patient-Centric Healthcare IoT Platform with Blockchain and Smart Contract Data Management

Authors: Duc B. T, Trung P. H. T, Trong N. D. P, Phuc N. T, Khoa T. D, Khiem H. G, Nam B. T, Bang L. K

PAGE 1139 – 1146

Paper 116: GROCAFAST: Revolutionizing Grocery Shopping for Seamless Convenience and Enhanced User Experience

Authors: Abeer Hakeem, Layan Fakhurji, Raneem Alshareef, Elaf Aloufi, Manar Altairy, Afraa Attiah, Linda Mohaisen

PAGE 1147 – 1157

Paper 117: New Trust Management Scheme Based on Blockchain and KNN Reinforcement Learning Algorithm

Authors: Ahdab Hulayyil Aljohani, Abdulaziz Al-shammri

PAGE 1158 – 1176

Paper 118: An Efficiency Hardware Design for Lane Detector Systems

Authors: Duc Khai Lam

PAGE 1177 – 1183

Paper 119: Predictor Model for Chronic Kidney Disease using Adaptive Gradient Clipping with Deep Neural Nets

Authors: Neeraj Sharma, Praveen Lalwani

PAGE 1184 – 1196

Paper 120: Development of an Educational Robot for Exploring the Internet of Things

Authors: Zhumaniyaz Mamatnabiyev, Christos Chronis, Iraklis Varlamis, Meirambek Zhaparov

PAGE 1197 – 1205

Paper 121: Improving Potato Diseases Classification Based on Custom ConvNeXtSmall and Combine with the Explanation Model

Authors: Huong Hoang Luong

PAGE 1206 – 1219

Paper 122: Dynamic Task Offloading Optimization in Mobile Edge Computing Systems with Time-Varying Workloads Using Improved Particle Swarm Optimization

Authors: Mohammad Asique E Rasool, Anoop Kumar, Asharul Islam

PAGE 1220 – 1228

Paper 123: On the Combination of Multi-Input and Self-Attention for Sign Language Recognition

Authors: Nam Vu Hoai, Thuong Vu Van, Dat Tran Anh

PAGE 1229 – 1235

Paper 124: Improving Chicken Disease Classification Based on Vision Transformer and Combine with Integrated Gradients Explanation

Authors: Huong Hoang Luong, Triet Minh Nguyen

PAGE 1236 – 1249

Paper 125: Rigorous Experimental Analysis of Tabular Data Generated using TVAE and CTGAN

Authors: Parul Yadav, Manish Gaur, Rahul Kumar Madhukar, Gaurav Verma, Pankaj Kumar, Nishat Fatima, Saqib Sarwar, Yash Raj Dwivedi

PAGE 1250 – 1262

Paper 126: Packet Loss Concealment Estimating Residual Errors of Forward-Backward Linear Prediction for Bone-Conducted Speech

Authors: Ohidujjaman, Nozomiko Yasui, Yosuke Sugiura, Tetsuya Shimamura, Hisanori Makinae

PAGE 1263 – 1268

Paper 127: A Comprehensive Analysis of Network Security Attack Classification using Machine Learning Algorithms

Authors: Abdulaziz Saeed Alqahtani, Osamah A. Altammami, Mohd Anul Haq

PAGE 1269 – 1280

Paper 128: Robust Extreme Learning Machine Based on p-order Laplace Kernel-Induced Loss Function

Authors: Liutao Luo, Kuaini Wang, Qiang Lin

PAGE 1281 – 1291

A Comparative Analysis of Traditional and Machine Learning Methods in Forecasting the Stock Markets of China and the US

Shangshang Jin

Department of Art and Science, Johns Hopkins University, Washington, D.C., United States

Abstract—In the volatile and uncertain financial markets of the post-COVID-19 era, our study conducts a comparative analysis of traditional econometric models—specifically, the AutoRegressive Integrated Moving Average (ARIMA) and Holt's Linear Exponential Smoothing (Holt's LES)—against advanced machine learning techniques, including Support Vector Regression (SVR), Long Short-Term Memory (LSTM) networks, and Gated Recurrent Units (GRU). Focused on the daily stock prices of the S&P 500 and SSE Index, the study utilizes a suite of metrics such as R-squared, RMSE, MAPE, and MAE to evaluate the forecasting accuracy of these methodologies. This approach allows us to explore how each model fares in capturing the complex dynamics of stock market movements in major economies like the U.S. and China amidst ongoing market fluctuations instigated by the pandemic. The findings reveal that while traditional models like ARIMA demonstrate strong predictive accuracy over short-term horizons, LSTM networks excel in capturing complex, non-linear patterns in the data, showcasing superior performance over longer forecast horizons. This nuanced comparison highlights the strengths and limitations of each model, with LSTM emerging as the most effective in navigating the unpredictable dynamics of post-pandemic financial markets. Our results offer crucial insights into optimizing forecasting methodologies for stock price predictions, aiding investors, policymakers, and scholars in making informed decisions amidst ongoing market challenges.

Keywords—Machine learning; Holt's LES; SVR; LSTM; GRU

I. INTRODUCTION

The post-COVID-19 era has ushered in an era of heightened volatility and uncertainty in financial markets worldwide [1]. Particularly, the stock markets of China and the United States, two leading global economies, have garnered significant attention from investors, policymakers, and scholars alike. Precise forecasting of stock prices in these markets is crucial for informed decision-making and effective risk management. However, the challenge of accurate stock price prediction remains formidable due to the complex interplay of factors such as economic indicators, market sentiment, geopolitical events, and policy changes.

Our study adopts a two-pronged methodological approach. Initially, we leverage traditional econometric models, specifically the AutoRegressive Integrated Moving Average (ARIMA) model [2] and Holt's Linear Exponential Smoothing (Holt's LES) [3], known for their robustness in time series forecasting. These models, grounded in historical data patterns and statistical principles, offer a foundational understanding of

stock price movements, emphasizing the linear aspects of financial time series. However, the intricate dynamics of post-pandemic markets—characterized by abrupt changes and non-linear patterns—necessitate a more adaptive and sophisticated analysis framework. Enter machine learning techniques: Support Vector Regression (SVR) [4], Long Short-Term Memory (LSTM) networks [5], and Gated Recurrent Units (GRU) [6]. These methods bring to the fore the capability to model complex, non-linear relationships and capture deep temporal dependencies, which are often missed by traditional models. By incorporating both traditional and machine learning methodologies, our study aims to harness the complementary strengths of each approach, ensuring a comprehensive and nuanced exploration of forecasting accuracy in the tumultuous environment of post-COVID-19 stock markets. This hybrid approach not only facilitates a direct comparison of predictive performances but also sheds light on the evolving nature of financial time series analysis in response to unprecedented market conditions.

In this study, we conduct a comparative analysis of the forecasting performance of both traditional and machine learning models on the daily stock prices of the S&P 500 Index in the United States and the SSE Index in China in the post-COVID-19 period. We assess the forecasting accuracy of ARIMA, Holt's LES, SVR, LSTM, and GRU models using evaluation metrics such as R-squared (R^2), Root Mean Square Error (RMSE), Mean absolute percentage error (MAPE), and Mean Absolute Error (MAE). By shedding light on the strengths and weaknesses of different forecasting approaches, this study seeks to contribute to the ongoing pursuit of effective stock market prediction tools in the post-COVID-19 era.

II. RELATED WORK

Traditionally, stock price prediction has relied on econometric models and time-series analysis techniques like AutoRegressive Integrated Moving Average (ARIMA) and Linear Exponential Smoothing Model (LSE). These models excel at capturing linear relationships and seasonality in the data. Nevertheless, their ability to handle the inherent complexities and non-linearities of stock market dynamics is limited [7].

Machine learning and deep learning techniques have emerged as promising alternatives for stock market prediction, offering the potential to capture intricate patterns and relationships in financial data [8], [9]. Methods such as Support

Vector Regression (SVR), Long Short-Term Memory networks (LSTM), and Gated Recurrent Units (GRU) can process large-scale datasets, recognize non-linear relationships, and learn from sequential information, making them well-suited for forecasting stock prices.

For instance, Gülmez [9] explored machine learning models for stock market prediction, underscoring the effectiveness of the LSTM model with two dropout layers. The study noted the potential for performance improvement by optimizing hyperparameters such as the number of neurons, batch size, and epoch count. Gülmez's research also employed the Support Vector Regression (SVR) model, optimizing hyperparameters via grid search with Scikit-learn's library. Employing 10-fold cross-validation and RMSE as a loss measurement, the study highlighted that hyperparameter tuning significantly impacts the SVR's forecasting performance.

Md et al. [10] introduced a novel Multi-Layer Sequential Long Short-Term Memory (MLS LSTM) model for stock price prediction, utilizing Samsung stock data from 2016 to 2021. Comprising three vanilla LSTM layers and a dense layer, the MLS LSTM model exhibited high accuracy (95.9% and 98.1%) and a low average error percentage (2.18%) on the testing dataset. The study revealed that multi-layered LSTMs outperform single-layered LSTMs, with added layers enhancing accuracy.

In another study, Yu et al. [11] proposed a predictive model for stock price index realized volatility (RV) based on optimized variational mode decomposition (VMD), deep learning models, including LSTM and GRU, and the Q-learning algorithm. The model was applied to the RV sequences of the SSEC, SPX, and FTSE indices. The VMD method decomposed the RV sequences into intrinsic mode functions (IMFs), which were then predicted using the LSTM and GRU models. Q-learning determined the optimal model weights for an integrated approach. Performance evaluation using MAE, MSE, HMAE, HMSE, and MDM demonstrated the model's superior performance over comparison models in both emerging and developed markets.

Recent literature shows that machine learning methods, including SVR, LSTM, and GRU, have gained popularity due to their ability to tackle non-linear problems and learn complex patterns in large-scale datasets [12]. These models can capture complex relationships in financial data and enhance prediction accuracy. However, they come with drawbacks such as high computational requirements, risk of overfitting, and reduced interpretability [13], [14]. Additionally, machine learning models often require meticulous hyperparameter tuning, which can be time-consuming and computationally intensive [15].

III. METHODOLOGY

In this study, we examine the predictive performance of both traditional statistical methods and machine learning techniques for forecasting the stock price. We compare the ARIMA model and the ETS model from the traditional methods against the SVR, LSTM networks, and GRU networks from the machine learning approaches. Our analysis focuses on one-step-ahead out-of-sample forecasting.

A. AutoRegressive Integrated Moving Average (ARIMA)

The ARIMA model, commonly recognized as the Box-Jenkins model, is a fundamental tool in time-series forecasting. It merges autoregressive (AR) and moving average (MA) components to effectively model stationary time series with minimal parameters. In contrast to pure AR and MA models, the ARIMA model introduces a differencing (I) component to ensure stationarity of the series [2]. By blending these three components—autoregressive, differencing, and moving average—the ARIMA model offers a holistic approach to capturing temporal dependencies in data [16].

It is expressed as follows:

$$(1 - \sum_{i=1}^p \phi_i L^i)(1 - L)^d X_t = (1 + \sum_{i=1}^q \theta_i L^i) \epsilon_t \quad (1)$$

Here, ϕ_i denotes the AR parameters, θ_i the MA parameters, d is the order of differencing, L is the lag operator, X_t is the time series value at time t , and ϵ_t signifies the white noise error term.

B. Holt's Linear Exponential Smoothing Model (Holt's LES)

Holt's Linear Exponential Smoothing model, also known as the Holt's Linear model, is a time-series forecasting method that captures the linear trend and level components in the data. It is particularly useful for datasets with trends but no seasonal patterns. The model uses two smoothing equations to estimate the level and trend components, respectively [17].

Let y_t be the observed value at time t , l_t be the estimated level at time t , and b_t be the estimated trend at time t . The smoothing equations are given by:

$$\begin{aligned} l_t &= \alpha y_t + (1 - \alpha)(l_{t-1} + b_{t-1}) \\ b_t &= \beta (l_t - l_{t-1}) + (1 - \beta)b_{t-1} \end{aligned} \quad (2)$$

Here, y_t is the observed value, l_t the estimated level, and b_t the estimated trend at time t . α and β are smoothing parameters between 0 and 1. The h -period ahead forecast is:

$$\hat{y}_{t+h} = l_t + h \cdot b_t \quad (3)$$

In this study, the optimal values of α and β are determined by minimizing the Mean Squared Error (MSE) of the model on the training data.

C. Support Vector Regression (SVR)

SVR is a machine learning algorithm for regression analysis. It extends the concept of Support Vector Machines (SVM) used for classification tasks to the regression context. SVR aims to find a hyperplane that best fits the data points while maximizing the margin from the closest data points (support vectors) (Liu, Wang and Gu, 2021).

Given a training dataset $D = \{(x_1, y_1), \dots, (x_n, y_n)\}$, SVR aims to find a function $f(x) = w \cdot x + b$ that approximates the relationship between the input features x and the target variable y .

SVR introduces the ε -insensitive loss function, meaning that the error is only considered if it exceeds a certain threshold ε . The SVR objective is to minimize the cost function:

$$L(w, b) = \frac{1}{2} \|w\|^2 + C \sum_{i=1}^n (\xi_i + \xi_i^*) \quad (4)$$

subject to the constraints:

$$\begin{aligned} y_i - w \cdot x_i - b &\leq \varepsilon + \xi_i \\ w \cdot x_i + b - y_i &\leq \varepsilon + \xi_i^* \\ \xi_i, \xi_i^* &\geq 0 \end{aligned} \quad (5)$$

where, w denotes the weight vector and b is the bias term. C is the regularization parameter that controls the trade-off between maximizing the margin and minimizing the error. The slack variables, ξ_i and ξ_i^* , handle instances that are difficult to separate perfectly.

In this study, we use the Radial Basis Function (RBF) kernel, which is defined as:

$$K(x, z) = \exp(-\gamma \|x - z\|^2) \quad (6)$$

D. Long Short-Term Memory (LSTM)

LSTM networks, introduced by Hochreiter and Schmidhuber [5], are a specialized variant of recurrent neural networks (RNN) meticulously engineered to address sequence prediction challenges. Their distinctive architecture, which facilitates the retention of patterns over extended durations, renders LSTMs especially proficient for time series modeling. In the context of this study, we harness the capabilities of the LSTM network for our forecasting endeavors.

LSTM networks consist of memory cells that are regulated by three gates: forget, input, and output gates. These gates determine how information flows through the memory cells.

Forget Gate:

$$f_t = \sigma(W_f \cdot [h_{t-1}, x_t] + b_f) \quad (7)$$

Input Gate:

$$\begin{aligned} i_t &= \sigma(W_i \cdot [h_{t-1}, x_t] + b_i) \\ \tilde{C}_t &= \tanh(W_c \cdot [h_{t-1}, x_t] + b_c) \end{aligned} \quad (8)$$

Update of Cell State:

$$C_t = f_t \times C_{t-1} + i_t \times \tilde{C}_t \quad (9)$$

Output Gate:

$$\begin{aligned} o_t &= \sigma(W_o [h_{t-1}, x_t] + b_o) \\ h_t &= o_t \times \tanh(C_t) \end{aligned} \quad (10)$$

where, σ represents the sigmoid function, W and b are the weight matrices and biases for each gate, respectively, x_t is the input at time t , and h_t is the output.

E. Gated Recurrent Unit (GRU)

Introduced by [18], GRUs are a streamlined variant of the RNN designed to adeptly capture long-term sequence dependencies. Functioning as a simplified version of LSTMs, GRUs are characterized by two pivotal gates: the update gate and the reset gate. The update gate is instrumental in determining the proportion of the preceding hidden state that should be relayed to the subsequent state. Concurrently, the reset gate ascertains the extent to which the prior hidden state is disregarded. The computations for the GRU model are as follows:

$$\begin{aligned} r_t &= \sigma(W_r \cdot [h_{t-1}, x_t] + b_r) \\ z_t &= \sigma(W_z \cdot [h_{t-1}, x_t] + b_z) \\ \tilde{h}_t &= \tanh(W \cdot [r_t \odot h_{t-1}, x_t] + b) \\ h_t &= (1 - z_t) \odot h_{t-1} + z_t \odot \tilde{h}_t \end{aligned} \quad (11)$$

where, r_t and z_t are the reset and update gates at time t respectively, σ denotes the sigmoid activation function, W and b are the weight matrices and bias vectors, \odot represents element-wise multiplication, and h_t is the hidden state at time t .

F. Grid Search Hyperparameter Tuning

In this study, optimizing hyperparameters becomes paramount to ensure the robustness of machine learning models. As demonstrated in Fig. 1, our approach harnesses a comprehensive grid search to navigate the vast hyperparameter space. For the SVR model, adjustments are made to the regularization parameter, gamma, and epsilon values. Meanwhile, the LSTM's performance is fine-tuned considering the number of units, dropout rate, and batch size. On the other hand, the GRU model sees alterations in its units, batch size, and number of epochs. This methodical approach, anchored in a three-dimensional exploration, seeks to refine our forecasting tools, aligning them with the sophisticated dynamics of today's financial markets.

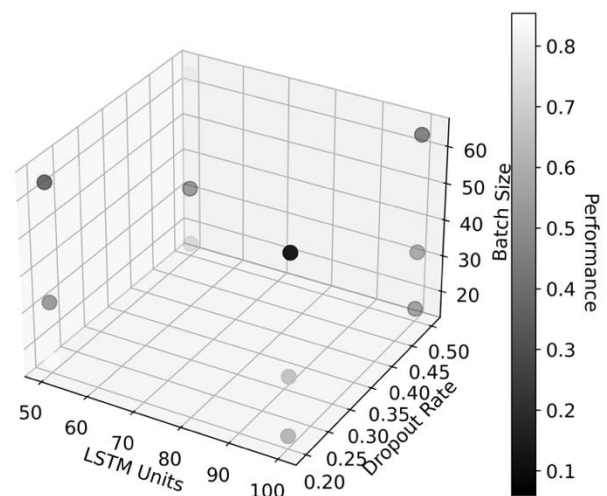


Fig. 1. 3D visualization of grid search.

G. Evaluation Metrics

To evaluate the predictive performance of the models, followed by [19] and [20], we utilize several well-established metrics: R-squared (R^2), Root Mean Square Error (RMSE), Mean Absolute Percentage Error (MAPE) and Mean Absolute Error (MAE). Each metric provides a different perspective on the quality of the predictions.

R^2 : R^2 measures the proportion of the variance in the dependent variable that is predictable from the independent variable. It ranges from 0 to 1, with 1 indicating perfect prediction. It is calculated as follows:

$$R^2 = 1 - \frac{\sum (y_t - \hat{y}_t)^2}{\sum (y_t - \bar{y})^2} \quad (12)$$

RMSE (Root Mean Square Error): RMSE represents the square root of the second sample moment of the differences between predicted and observed values or the quadratic mean of these differences. It is interpreted as the standard deviation of the unexplained variance:

$$RMSE = \sqrt{\frac{1}{n} \sum_{t=1}^n (y_t - \hat{y}_t)^2} \quad (13)$$

The Mean Absolute Percentage Error (MAPE): MAPE provides an easy-to-interpret measure of the average prediction error in percentage terms. It is especially useful when comparing the performance of different models on the same dataset.

The MAPE is calculated as follows:

$$MAPE = \frac{100}{n} \sum_{t=1}^n \left| \frac{y_t - \hat{y}_t}{y_t} \right| \quad (14)$$

Mean Absolute Error (MAE): MAE measures the average of the absolute differences between the predicted and observed values. It provides an idea of the magnitude of the error, without considering the direction. Lower MAE values indicate a better fit to the data. It is calculated as:

$$MAE = \frac{1}{n} \sum_{t=1}^n |y_t - \hat{y}_t| \quad (15)$$

where, y_t is the actual value at time t , \hat{y}_t is the predicted value at time t , and \bar{y} represents the mean of the actual values.

H. Forecasting Algorithm

Our methodology, detailed in Fig. 2, commenced by dividing the data into training and testing subsets. Depending on the chosen model-traditional techniques like ARIMA and Holt's LES or more contemporary machine learning approaches-appropriate parameter optimization processes were undertaken, with the latter employing a grid search. Using a rolling window framework, we executed forecasts for three distinct time horizons: $H=1, 10$, and 30 days. Utilizing the rolling window approach, each forecast integrated the most recent observation from the testing set into the training dataset. This method allowed our models to consistently update and adapt based on the newest economic data available. Once the

end of the testing data was reached, we compared the performance of the various models under different forecasting time horizons using key metrics such as R^2 , RMSE, MAE and MAPE.

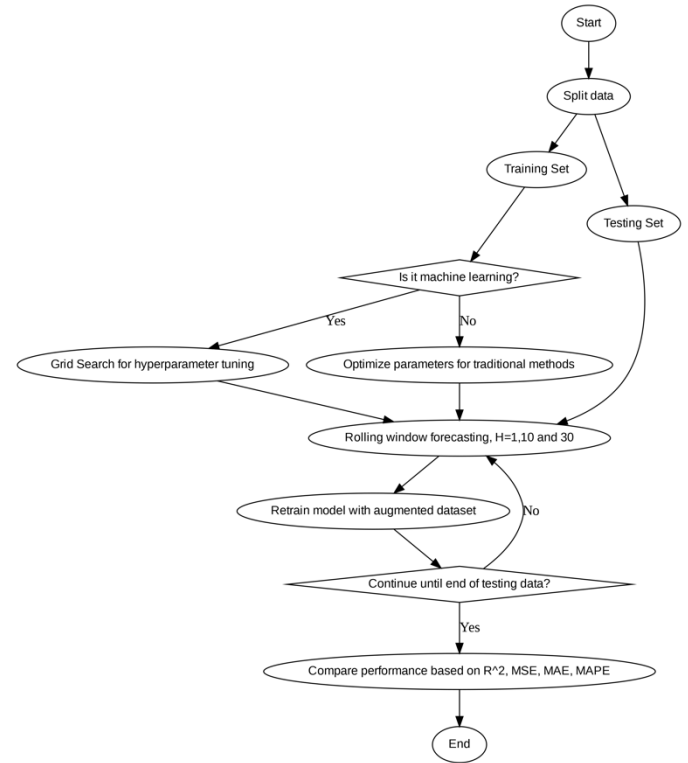


Fig. 2. Flowchart of algorithm.

IV. NUMERICAL RESULTS

A. Data Description

This study evaluates the daily performance of two major stock market indices, the S&P 500 and the Shanghai Stock Exchange (SSE) Composite Index, spanning December 31, 2012, to December 31, 2022. These indices were chosen due to their importance in representing overall stock market performance in the United States and China, respectively, and their influence on global financial markets. Both are market-capitalization-weighted, capturing broad market movements efficiently.

We obtain daily closing prices of the indices from the Yahoo Finance API, a publicly accessible and reliable data source extensively used in financial research. The data, adjusted for splits and dividends, provide an accurate representation of the indices' performance over the period.

The data are partitioned into training and testing sets. The training set, consisting of data before 2020, is used to calibrate forecasting models, while the testing set, from January 1, 2020, to December 31, 2022, evaluates their out-of-sample performance.

Table I summarizes the descriptive statistics of the daily closing prices for both indices over the study period. The S&P 500 index, with a mean of 2742.1700 and standard deviation of 873.0140, traded between 1426.1900 and 4796.5600. The SSE

index had a mean of 3017.0600, standard deviation of 527.9180, and prices between 1950.0100 and 5166.3500. The S&P 500 displays a negative kurtosis of -0.6494 and positive skewness of 0.6749, suggesting a less peaked and right-skewed distribution. The SSE index, with a kurtosis of 0.8312 and near-zero skewness of 0.0525, indicates a more peaked and symmetric distribution. There are 2519 and 2428 observations for the S&P 500 and SSE indices, respectively. Fig. 3 and Fig. 4 depict the time series of daily closing prices for the S&P 500 and SSE indices.

TABLE I. DESCRIPTIVE STATISTICS FOR THE S&P 500 AND SSE INDICES

| Index | S&P500 | SSE |
|----------|-----------|-----------|
| Mean | 2742.1700 | 3017.0600 |
| Std | 873.0140 | 527.9180 |
| Minimum | 1426.1900 | 1950.0100 |
| Maximum | 4796.5600 | 5166.3500 |
| Kurtosis | -0.6494 | 0.8312 |
| Skewness | 0.6749 | 0.0525 |
| Count | 2519 | 2428 |



Fig. 3. S&P 500 index price.

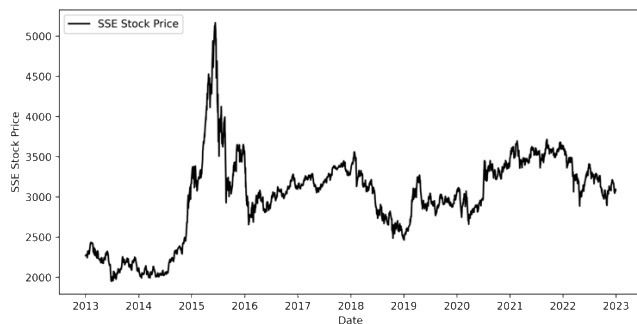


Fig. 4. SSE index price.

B. Determination of Parameters of Traditional Methods

For the ARIMA models, we use an automatic order selection method that seeks to minimize the Akaike Information Criterion (AIC). The ARIMA model parameters include the order of the autoregressive (AR) and moving average (MA) components, as well as the degree of differencing. Given the daily frequency of the data, we focus on non-seasonal models. Through this procedure, we identify ARIMA (2,1,0) as the best model for the SSE index, while

ARIMA(1,1,1) with an intercept is chosen for the S&P 500 index.

For the Holt's LES models, an optimization procedure is applied to estimate the smoothing parameters for the level and trend components. The models are fitted to the training data of both indices. For the SSE index, the estimated smoothing level is approximately 0.995, and the smoothing trend is about 0.0237. For the S&P 500 index, the respective values are approximately 0.907 and 0.0212. The initial level and trend for both models are estimated based on the training data.

C. Determination of Optimal Hyperparameters

In this study, we employ a grid search approach to optimize the hyperparameters for the SVR, LSTM, and GRU models across different time horizons ($H=1/10/30$). For the SVR model, we consider three hyperparameters: the regularization parameter (C), gamma (γ), and epsilon (ϵ). For the LSTM and GRU models, the hyperparameters assessed include the number of units, dropout rate, and batch size. The selection of these hyperparameters is crucial as they directly affect the models' forecasting performance. We evaluate various hyperparameter combinations using a training dataset to identify the best-performing models, which are subsequently tested on a separate test dataset. We use a radial basis function (RBF) kernel for the SVR model. For the LSTM and GRU models, we compile them using the Adam optimizer and mean squared error (MSE) loss function, which is well-suited for regression tasks like stock price prediction. This hyperparameter optimization process is conducted across different forecasting horizons to evaluate the models' suitability for both short-term and long-term forecasting. The Hyperparameters are given in Table II.

TABLE II. HYPERPARAMETER SETTINGS FOR MACHINE LEARNING MODELS ACROSS VARIOUS TIME HORIZONS ($H=1/10/30$)

| Model | Name of Parameter | S&P 500 | SSE |
|-------|--------------------------|-------------|-------------|
| SVR | Regularization parameter | 10/10/10 | 10/10/10 |
| | Gamma | 0.1/0.1/0.1 | 0.1/0.1/0.1 |
| | Epsilon | 0.1/0.1/0.1 | 0.1/0.1/0.1 |
| LSTM | Units | 100/100/50 | 100/100/100 |
| | Drop out | 0.2/0.2/0.2 | 0.2/0.5/0.5 |
| | Batch size | 16/16/64 | 16/32/16 |
| GRU | Units | 70/70/30 | 50/50/50 |
| | Batch size | 16/64/32 | 16/64/16 |
| | epochs | 30/70/50 | 50/50/50 |

D. Comparison and Analysis

Table III presents the evaluation results for forecasting the S&P 500 index using various models: ARIMA, Holt's LES, SVR, LSTM, and GRU. The performance of each model is assessed across three-time horizons: 1-day, 10-day, and 30-day.

For the 1-day time horizon, the ARIMA model stands out, achieving an R^2 of 99.04%, MAPE of 1.06%, RMSE of 53.93, and MAE of 38.78. The Holt's LES model closely follows, with similar metrics. Both SVR and GRU models exhibit

strong performance, with R^2 values exceeding 98%. Notably, the LSTM model shows the lowest R^2 of 94.70% and the highest MAPE of 2.71%.

TABLE III. EVALUATION OF S&P 500 INDEX FORECASTING ACROSS DIFFERENT TIME HORIZONS

| Models | R^2 | MAPE | RMSE | MAE |
|--------------------------|---------------|--------------|--------------|--------------|
| Time Horizon =1 | | | | |
| ARIMA | 99.04% | 1.06% | 53.93 | 38.78 |
| Holt's LES | 99.02% | 1.06% | 54.48 | 38.62 |
| SVR | 98.95% | 1.18% | 56.31 | 43.16 |
| LSTM | 94.70% | 2.71% | 126.80 | 108.05 |
| GRU | 98.16% | 1.60% | 74.72 | 61.29 |
| Time Horizon =10 | | | | |
| ARIMA | 95.52% | 2.27% | 116.65 | 83.72 |
| Holt's LES | 94.93% | 2.34% | 124.00 | 87.07 |
| SVR | 94.18% | 2.77% | 132.87 | 103.20 |
| LSTM | 91.89 | 3.27% | 156.82 | 131.59 |
| GRU | 94.18% | 2.73% | 132.84 | 100.79 |
| Time Horizon = 30 | | | | |
| ARIMA | 83.94% | 4.35% | 220.74 | 157.45 |
| Holt's LES | 75.48% | 5.02% | 272.73 | 181.37 |
| SVR | 81.06% | 5.21% | 239.69 | 189.03 |
| LSTM | 85.80% | 4.42% | 207.60 | 176.05 |
| GRU | 80.21% | 5.34% | 245.04 | 194.03 |

In the 10-day horizon, the ARIMA model again leads with an R^2 of 95.52% and the lowest MAPE of 2.27%. Holt's LES, SVR, and GRU models all report R^2 values above 94% and MAPE values under 3%. The LSTM model lags, with the lowest R^2 of 91.89% and the highest MAPE of 3.27%.

For the 30-day horizon, the LSTM model surprisingly achieves the highest R^2 of 85.80%, but with a relatively high MAPE of 4.42%. The ARIMA model follows with an R^2 of 83.94% and the lowest MAPE of 4.35%. The Holt's LES model's performance diminishes, recording the lowest R^2 of 75.48% and a higher MAPE of 5.02%. SVR and GRU models display similar R^2 values around 80% and MAPE values above 5%.

In summary, the ARIMA model consistently performs well across all time horizons, exhibiting the highest R^2 and the lowest MAPE for the 1-day and 10-day horizons. While the LSTM model underperforms in shorter horizons, it surprisingly has the highest R^2 for the 30-day horizon. The Holt's LES model performs well for shorter horizons but declines for the 30-day horizon. SVR and GRU models show moderate performance across all horizons.

Table IV presents the evaluation results of forecasting the SSE index. For the 1-day horizon, all models display strong performance, with R^2 values exceeding 97%. The SVR model leads with an R^2 of 97.81% and the lowest MAPE of 0.80%. ARIMA and Holt's LES models both achieve R^2 values around

97.78% and similar MAPE values of 0.81%. LSTM and GRU models also perform well, with R^2 values above 97.5% and MAPE values under 0.85%.

TABLE IV. EVALUATION OF SSE INDEX FORECASTING ACROSS DIFFERENT TIME HORIZONS

| Models | R^2 | MAPE | RMSE | MAE |
|--------------------------|--------|-------|--------|--------|
| Time Horizon =1 | | | | |
| ARIMA | 97.78% | 0.81% | 36.25 | 26.34 |
| Holt's LES | 97.72% | 0.81% | 36.31 | 26.25 |
| SVR | 97.81% | 0.80% | 35.97 | 25.98 |
| LSTM | 97.49% | 0.85% | 38.54 | 27.72 |
| GRU | 97.65% | 0.83% | 37.27 | 27.19 |
| Time Horizon =10 | | | | |
| ARIMA | 90.16% | 1.65% | 76.34 | 53.31 |
| Holt's LES | 88.84% | 1.78% | 81.26 | 57.34 |
| SVR | 90.48% | 1.56% | 75.05 | 50.38 |
| LSTM | 94.74% | 1.27% | 55.82 | 40.89 |
| GRU | 92.98% | 2.91% | 145.90 | 113.95 |
| Time Horizon = 30 | | | | |
| ARIMA | 77.34% | 2.73% | 115.69 | 88.71 |
| Holt's LES | 72.21% | 2.95% | 128.34 | 95.70 |
| SVR | 77.27% | 2.54% | 116.00 | 82.29 |
| LSTM | 94.78% | 1.25% | 55.61 | 40.98 |
| GRU | 58.89% | 3.80% | 156.00 | 123.29 |

In the 10-day horizon, the LSTM model stands out with the highest R^2 of 94.74% and the lowest MAPE of 1.27%. SVR closely follows with an R^2 of 90.48% and a low MAPE of 1.56%. ARIMA and Holt's LES models both report R^2 values around 90% and MAPE values under 1.8%. The GRU model exhibits a solid R^2 of 92.98% but the highest MAPE of 2.91%.

For the 30-day horizon, the LSTM model clearly dominates with an R^2 of 94.78% and the lowest MAPE of 1.25%. The ARIMA and SVR models perform similarly, both achieving R^2 values around 77% and MAPE values under 2.75%. The Holt's LES model lags, with an R^2 of 72.21% and a higher MAPE of 2.95%. The GRU model shows the lowest performance with an R^2 of 58.89% and the highest MAPE of 3.80%.

In summary, the LSTM model consistently performs well across all time horizons, especially for the 30-day horizon, where it excels. The ARIMA and SVR models display similar moderate performance across all horizons. The Holt's LES model's performance declines for longer horizons. The GRU model exhibits strong performance in the 10-day horizon but struggles in the 30-day horizon.

V. CONCLUSION

The task of predicting stock market indices is essential for risk management, portfolio allocation, and derivative pricing, all of which contribute to stabilizing the financial market order. In this study, we compared the performance of several predictive models—ARIMA, Holt's LES, SVR, LSTM, and

GRU—across different time horizons (1-day, 10-day, and 30-day) for two prominent stock indices: the S&P 500 and the SSE. The models were evaluated based on four metrics: R-squared (R^2), Mean Absolute Percentage Error (MAPE), Root Mean Squared Error (RMSE), and Mean Absolute Error (MAE).

Our empirical results indicate that:

- LSTM consistently performs well across all time horizons for both indices, especially in the 30-day horizon. It outperforms the other models in terms of both R^2 and MAPE. This result can be attributed to the model's ability to capture long-term dependencies in the data and its inherent adaptability in learning complex nonlinear relationships.
- ARIMA and SVR models display moderate performance across all time horizons for both indices, showcasing their robustness and applicability. The ARIMA model benefits from its ability to account for time trends, seasonality, and autoregressive behaviors. On the other hand, the SVR model leverages its capacity to model nonlinear relationships by using kernel functions.
- Holt's LES model performs well for the 1-day and 10-day horizons but struggles for longer horizons. The model's declining performance is attributed to its primary reliance on short-term trends, which may not capture more complex behaviors over longer time horizons.
- The GRU model performs well for shorter horizons but faces difficulties in the 30-day horizon. This could be due to the challenges posed by long-term dependencies in the data. GRU, similar to LSTM, is designed to address such challenges, but our results suggest that LSTM may be better suited for this particular dataset.
- Through extensive experimentation, we confirmed the robustness and applicability of our findings. For both indices, the results were consistent across different time horizons and evaluation metrics, confirming the validity of our conclusions.

In summary, our study provides valuable insights for investors and market analysts. The results can be used to enhance trading strategies, optimize portfolio allocations, and improve risk management approaches. Regulators may also benefit from these insights by identifying market anomalies and intervening when necessary to ensure financial market stability.

Despite the contributions of this study, we acknowledge that multivariate prediction was not considered. In future research, we will incorporate additional factors closely related to the stock indices' movements, such as macroeconomic indicators and sentiment analysis, to enhance the accuracy of our predictions. Incorporating these factors will not only improve the forecasting accuracy but also contribute to a deeper understanding of the underlying relationships that drive stock market dynamics. Besides, the methodologies and insights gained from this study hold the potential for broader

applications beyond the S&P 500 and SSE indices. For instance, these models could be adapted to forecast emerging market indices, where volatility and data irregularities present unique challenges.

REFERENCES

- [1] D. Zhang, M. Hu, and Q. Ji, 'Financial markets under the global pandemic of COVID-19', *Finance Research Letters*, vol. 36, p. 101528, Oct. 2020, doi: 10.1016/j.frl.2020.101528.
- [2] G. E. P. Box, G. M. Jenkins, G. C. Reinsel, and G. M. Ljung, *Time Series Analysis: Forecasting and Control*. John Wiley & Sons, 2015.
- [3] C. C. Holt, 'Forecasting seasonals and trends by exponentially weighted moving averages', *International Journal of Forecasting*, vol. 20, no. 1, pp. 5–10, Jan. 2004, doi: 10.1016/j.ijforecast.2003.09.015.
- [4] V. Vapnik, *The Nature of Statistical Learning Theory*. Springer Science & Business Media, 2013.
- [5] S. Hochreiter and J. Schmidhuber, 'Long Short-Term Memory', *Neural Computation*, vol. 9, no. 8, pp. 1735–1780, Nov. 1997, doi: 10.1162/neco.1997.9.8.1735.
- [6] K. Cho et al., 'Learning Phrase Representations using RNN Encoder-Decoder for Statistical Machine Translation'. arXiv, Sep. 02, 2014, doi: 10.48550/arXiv.1406.1078.
- [7] A. A. Adebisi, A. O. Adewumi, and C. K. Ayo, 'Comparison of ARIMA and Artificial Neural Networks Models for Stock Price Prediction', *Journal of Applied Mathematics*, vol. 2014, pp. 1–7, 2014, doi: 10.1155/2014/614342.
- [8] M. Beniwal, A. Singh, and N. Kumar, 'Forecasting long-term stock prices of global indices: A forward-validating Genetic Algorithm optimization approach for Support Vector Regression', *Applied Soft Computing*, vol. 145, p. 110566, Sep. 2023, doi: 10.1016/j.asoc.2023.110566.
- [9] B. Gülmez, 'Stock price prediction with optimized deep LSTM network with artificial rabbits optimization algorithm', *Expert Systems with Applications*, vol. 227, p. 120346, Oct. 2023, doi: 10.1016/j.eswa.2023.120346.
- [10] A. Q. Md et al., 'Novel optimization approach for stock price forecasting using multi-layered sequential LSTM', *Applied Soft Computing*, vol. 134, p. 109830, Feb. 2023, doi: 10.1016/j.asoc.2022.109830.
- [11] Y. Yu, Y. Lin, X. Hou, and X. Zhang, 'Novel optimization approach for realized volatility forecast of stock price index based on deep reinforcement learning model', *Expert Systems with Applications*, vol. 233, p. 120880, Dec. 2023, doi: 10.1016/j.eswa.2023.120880.
- [12] K. E. ArunKumar, D. V. Kalaga, Ch. Mohan Sai Kumar, M. Kawaji, and T. M. Brenza, 'Comparative analysis of Gated Recurrent Units (GRU), long Short-Term memory (LSTM) cells, autoregressive Integrated moving average (ARIMA), seasonal autoregressive Integrated moving average (SARIMA) for forecasting COVID-19 trends', *Alexandria Engineering Journal*, vol. 61, no. 10, pp. 7585–7603, Oct. 2022, doi: 10.1016/j.aej.2022.01.011.
- [13] A. Kumar, M. Paprzycki, and V. K. Gunjan, Eds., *ICDSMLA 2019: Proceedings of the 1st International Conference on Data Science, Machine Learning and Applications*, vol. 601. in *Lecture Notes in Electrical Engineering*, vol. 601. Singapore: Springer Singapore, 2020, doi: 10.1007/978-981-15-1420-3.
- [14] P. Soni, Y. Tewari, and D. Krishnan, 'Machine Learning Approaches in Stock Price Prediction: A Systematic Review', *J. Phys.: Conf. Ser.*, vol. 2161, no. 1, p. 012065, Jan. 2022, doi: 10.1088/1742-6596/2161/1/012065.
- [15] D. Kobiela, D. Krefta, W. Król, and P. Weichbroth, 'ARIMA vs LSTM on NASDAQ stock exchange data', *Procedia Computer Science*, vol. 207, pp. 3836–3845, 2022, doi: 10.1016/j.procs.2022.09.445.
- [16] M. Bilgili and E. Pinar, 'Gross electricity consumption forecasting using LSTM and SARIMA approaches: A case study of Türkiye', *Energy*, vol. 284, p. 128575, Dec. 2023, doi: 10.1016/j.energy.2023.128575.
- [17] C. Lim and M. McAleer, 'Forecasting tourist arrivals', *Annals of Tourism Research*, vol. 28, no. 4, pp. 965–977, Jan. 2001, doi: 10.1016/S0160-7383(01)00006-8.

- [18] J. Chung, C. Gulcehre, K. Cho, and Y. Bengio, 'Empirical Evaluation of Gated Recurrent Neural Networks on Sequence Modeling'. arXiv, Dec. 11, 2014. doi: 10.48550/arXiv.1412.3555.
- [19] S. Paudel, A. Pudasaini, R. K. Shrestha, and E. Kharel, 'Compressive strength of concrete material using machine learning techniques', *Cleaner Engineering and Technology*, vol. 15, p. 100661, Aug. 2023, doi: 10.1016/j.clet.2023.100661.
- [20] S. A. Rajakarunakaran et al., 'Prediction of strength and analysis in self-compacting concrete using machine learning based regression techniques', *Advances in Engineering Software*, vol. 173, p. 103267, Nov. 2022, doi: 10.1016/j.advengsoft.2022.103267.

Classification of Thoracic Abnormalities from Chest X-Ray Images with Deep Learning

Usman Nawaz¹, Muhammad Ummar Ashraf², Muhammad Junaid Iqbal³,
Muhammad Asaf⁴, Mariam Musif Mir⁵, Usman Ahmed Raza⁶, Bilal Sharif⁷

Department of Engineering, University of Palermo, Palermo, Italy^{1, 7}

Department of Computer Science, Lahore Leads University, Pakistan²

Department of Enterprise Engineering, University of Roma tor Vergata, Rome, Italy³

Department of Computer Science, Modeling, Electronics and Systems Engineering (DIMES), University of Calabria, Italy⁴

School of ICT, Griffith University, Nathan Campus, Australia⁵

Department of Computational Intelligence, Università degli Studi di Napoli Federico II, Italy⁶

Abstract—Most Chest X-Rays (CXRs) are used to spot the existence of chest diseases by radiologists worldwide. Examining multiple X-rays at the busiest medical facility may result in time and financial loss. Furthermore, in the detection of the disease, expert abilities and attention are needed. CXRs are usually used for the detection of heart and lung region anomalies. In this research, multi-level Deep Learning for CXRs ailment detection has been used to identify solutions to these issues. Spotting these anomalies with high precision automatically will significantly improve the processes of realistic diagnosis. However, the absence of efficient, public databases and benchmark analyses makes it hard to match the appropriate diagnosis techniques and define them. The publicly accessible VINBigData datasets have been used to address these difficulties and researched the output of established multi-level Deep Learning architectures on various abnormalities. A high accuracy in CXRs abnormality detection on this dataset has been achieved. The focus of this research is to develop a multi-level Deep Learning approach for Localization and Classification of thoracic abnormalities from chest radiograph. The proposed technique automatically localizes and categorizes fourteen types of thoracic abnormalities from chest radiographs. The used dataset consists of 18,000 scans that have been annotated by experienced radiologists. The YoloV5 model has been trained with fifteen thousand independently labeled images and evaluated on a test set of three thousand images. These annotations were collected via VinBigData's web-based platform, VinLab. Image preprocessing techniques are utilized for noise removal, image sequences normalization, and contrast enhancement. Finally, Deep Ensemble approaches are used for feature extraction and classification of thoracic abnormalities from chest radiograph.

Keywords—Localization; classification; ensemble learning; YOLOV5; VINBigData; thoracic abnormalities; deep learning

I. INTRODUCTION

In accordance with the changing to the atmosphere, lifestyle, climate change, and other elements, disease on health is increasingly growing. That has raised the risk of illness. In 2016, around 3.4 million people have deceased from Chronic Obstructive Pulmonary Disease (COPD), which is most regularly caused by smoking and pollution, and 400,000 people deceased from asthma, according to the World Health Organization (WHO) [1]. Especially in developing countries and countries with low or intermediate incomes, where

millions of people live in poverty and are exposed to air pollution, the chances of chest disease are extremely high. As said by the World Health Organization, over four million premature people die each year as a result of diseases caused by household air pollution. Therefore, the steps required to minimize air pollution and carbon emissions need to be taken. Implementing effective diagnostic systems that can help diagnose chest diseases is also important. A new coronavirus disease recognized as COVID-19 has been causing serious chest damage and respiratory issues since late December 2019. Moreover, pneumonia, a type of chest disease, may be caused by the COVID-19 causative virus or other viral or bacterial infections [2].

Currently, the huge amount of Chest radiographs produced is nearly entirely examined via visual inspection, which is performed by an expert. This necessitates a wide range of skills and concentration, but it also provides a chance to employ automatic computational procedures such as Computer-Aided Diagnosis (CADs). In recent times, considerable focus and effort have been devoted to refining CAD systems using Computer Vision (CV) approaches [3-4]. The classification of medical images is one of the most difficult challenges and the most important task. The goal of the categorization procedure is to provide images with diagnoses based on their content.

Image analysis systems that are automated permit radiologists to drastically minimize their burden while simultaneously improving the standard of patient treatment. Earlier techniques frequently included both handcrafted feature representations and classifiers. Unfortunately, establishing algorithms for extracting features demands a great deal of domain knowledge and is a time-consuming procedure. Intrinsically, computer-aided diagnostics of thoracic disorders comprised of two sequential steps: the identification of pathologic irregularities and the classification of those abnormalities [5]. Computer-Aided detection and diagnosis systems will decrease the burden on doctors in urban hospitals and increase the quality of diagnosis in rural areas. Firstly, the radiologist is helped by CAD instruments to produce a statistical and well-educated decision. When the amount of data increases, radiologists will find it extremely

difficult to undergo all the X-Rays that are taken to retain the same degree of quality [6].

Automation and augmentation play a critical role in supporting radiologists in maintaining the diagnostic standard. As a result, early detection of chest illnesses is now more important than ever. Detecting abnormalities on chest radiographs is a tough task because of the complex nature and variety of thoracic disorders, as well as the low quality of chest X-ray. The majority of publicly free available chest X-ray datasets are labelled, but do not provide the locations of abnormalities that were present in each case [7]. The classification of pathologic irregularities in a chest radiograph is also a difficult task, because a chest radiograph may comprise numerous sorts of thoracic disorders, and their locations and sizes are typically widely varied, as presented in Fig. 1.

During the last few years, Deep Learning has attained extraordinary performance on a variety of classification grounded on images [8]. This achievement in identifying objects in natural photographs has revived interest in pursuing Deep Learning to medical images. The ability of Deep Learning models to interpret and identify images has obtained accuracy at the human level. In terms of medical image analysis, Deep Learning, that has a broad field of applications, particularly in medicine, fulfilling high achievements. Consequently, with the aid of Deep Learning, it has become an essential component of the medical sector [9].

The research objective is precise and automated localization and classification of Chest X-ray pictures are needed in medical health care units. Much work has been done to assist radiologists during recent years, but still accuracy, robustness and optimization are issues to address.

The first significant issue is that the exact disease location in Chest X-Ray pictures is currently not specified. The second major issue is that it has not yet been found to classify abnormalities in pictures. The accuracy of the existing model was needed to be improved. The present research is carried out to resolve the challenges.

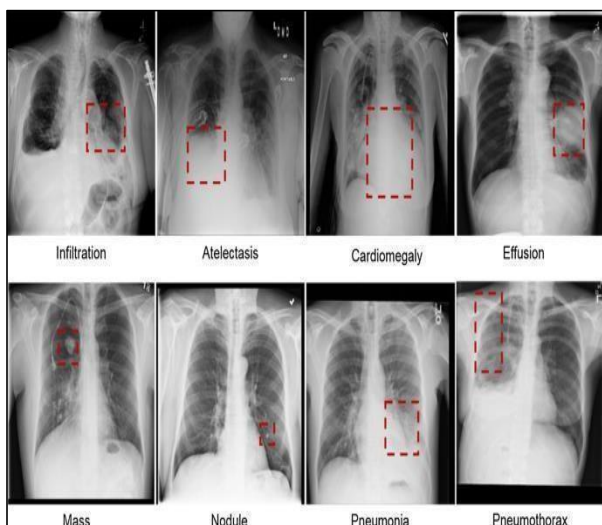


Fig. 1. Example of chest disease.

II. LITERATURE REVIEW

In recent years, several researchers have focused their efforts on the localization and classification of thoracic abnormalities from chest radiography using deep learning architecture. In study [10] the authors introduced a new approach utilizing Convolutional Neural Networks (CNN) to work using unstable lower class X-ray images [11]. The methodology used by the author increased the specificity by a wide margin for classifying multiple TB manifestations. In training the network, they investigated the feasibility and effectiveness of shuffle sampling with cross-validation and found its outstanding impact in the classification of medical images. In big TB image dataset from Peru, they achieved 85.68% classification accuracy, exceeding modern classification precision in this region. In healthcare services in low and middle-income states, their techniques and findings indicate an optimistic route for further precise and quick diagnosis of TB [12].

In study [13] the authors introduced seven days monitored deep learning system filled with squeeze-and excitation blocks multi-map transfer and maximum minimum pooling for identifying thoracic sicknesses and locate doubtful lesion regions. On the Chest X-ray 14 dataset the detailed discussion and lessons have completed. Quality of the presented deep learning system and its enhanced efficiency against the modern pipelines have been demonstrated by both numerical and visual findings, which suggested an integrated weakly monitored deep learning system for mutually conduct thoracic illness classification and localization on chest X-rays utilizing just the multi-class disruptive sickness mark with a mean accuracy of 83.2 %.

Researchers proposed a completely unique approach relying on vicinity conscious Dense Networks (DNetLoc), for category of pathologies, wherein they considered each spatial facts and high-decision photograph statistics for irregularity category, ensuing in an extra correct category of the abnormalities. Two datasets, particularly ChestX-Ray14 statistics set and PLCO statistics set, were used in this research. The ChestX-Ray14 statistics set incorporated thirty thousand, eight hundred and five sufferers and one hundred twenty chest X-ray snap shots. The resultant file consisted of fourteen pathology classes. In the PLCO statistics set, there were 185,421 snap shots from fifty-six thousand and seventy-one sufferers. Twelve most normal pathology labels were selected, among which five pathology labels also consisted of spatial facts. For all trials, the distinct facts were as follows: 70 percent for training, 10 percent for validation, and 20 percent for testing. For the PLCO facts set, a completely closing mean AUC score of 87.4 percent was achieved [14].

In research [15], two methods were explored for detecting pulmonary TB using CNNs which was based on the patient CXR image. Many image preprocessing techniques have been tested to identify the variety which delivers the maximum accuracy. A hybrid method also investigated with the main statistical CAD framework along through neural nets. Simulations were performed on the base of four hundred and six normal and 394 abnormal images. Simulations displayed that excellent results were provided by a trimmed area of

interest combined with contrast enhancement. The proposed method obtained 92.54% accuracy. Still better outcomes were obtained when images have been further improved with the hybrid process. They used Montgomery country and Shenzhen hospital x-ray set. The main advantage of the hybrid method was its significantly better accuracy by reducing over fitting. In the future, they wanted to obtain more clinical data and thus vastly improve the accuracy of the detection [16].

Tuberculosis is a transferable sickness that motives unpleasant health and demise in tens of lots and lots of people each 12 months worldwide. The MODS is a test to diagnose TB infection and drug sensitivity in 7-10 days with minimum rate and immoderate specificity and sensitivity proper far from a sputum sample, based completely on the seen recognition of particular Mycobacterium tuberculosis boom cording patterns in a broth culture. Despite of its benefits, in remote, constrained useful resource environment, MODS stays limited because it needs eternal and professional technical frame of employees for image-based completely diagnostics. Therefore, it is much critical to create possibility solutions that are based mostly on accurate automated interpretation and assessment of MODS cultures. In [17], CNN was validated for automated assessment of Microscopic Observed Drug Susceptibility (MODS) cultures digital snap shots. CNN become professional on a dataset of 12,510 MODS top notch and horrible snap shots obtained from 3 wonderful laboratories, in which it completed 96.63 percent accurateness and a sensitivity and specificity beginning from ninety-one percentage to ninety-nine percentage [18]. The variations discovered out features resemble seen cues used by expert diagnosticians to explain MODS cultures and proposing that our model can also have the capability to simplify and scale. It accomplished strongly whilst validated during held-out laboratory datasets and can be advanced upon with facts from novel laboratories [19]. This CNN can help laboratory personnel, in low useful resource settings and is a step towards easing automatic diagnostics get right of entry to dangerous areas in developing countries [20].

III. STRATEGY AND METHODOLOGY FOR DISEASE DETECTION

As the purpose of this project is implementing a localizer and classifier, it will be reached by making a program able to localize and classify thoracic abnormalities using multi-level deep learning. This research is not only technical, developing and implementing a software to distinguish different types of disorders and defects with the present technologies; but it is also a research project, since it examines the already existing knowledge and implementations related to this field of study. So, the strategy followed will be the one denominated as 'Design and Creation' [21]. Following the Design and Creation plan is using an iterative process and keeping in mind that each step must be ended before moving on to the next as shown in Fig. 2.

A. Image Data Acquisition and Preprocessing

A publicly available image dataset present on Kaggle database is used in this study [22]. The corresponding website and unique ID for the dataset is:

<https://www.kaggle.com/c/vinbigdata-chest-xray-abnormalities-detection/data>. It is available with over 14 different sets of observations for chest radiographs as mentioned below:

- Another lesson.
- Pleural effusion.
- Pleural thickening.
- Pneumothorax.
- Nodule/Mass
- Transfer Learning with Yolo5
- Aortic enlargement
- Atelectasis
- Calcification.
- Cardiomegaly.
- Consolidation.
- ILD.
- Infiltration.
- Lung Opacity.

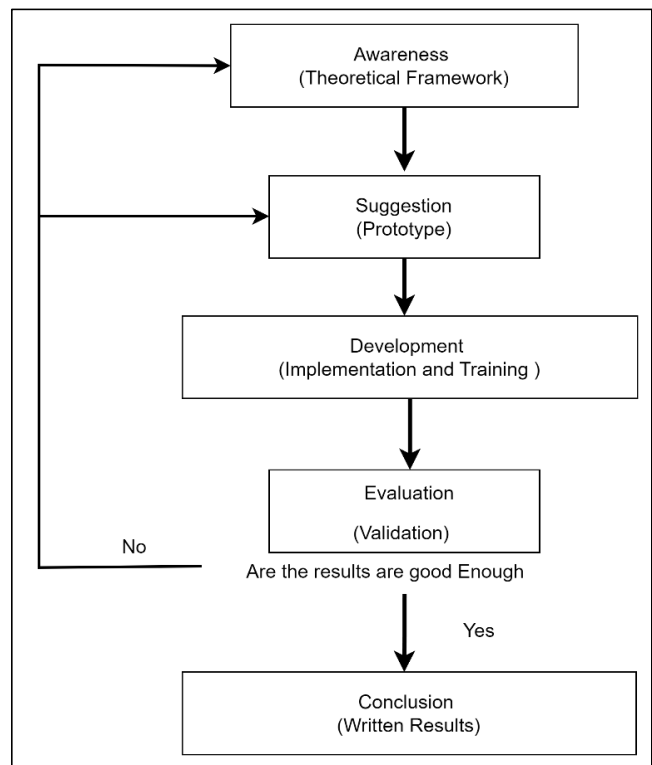


Fig. 2. Strategy diagram representation.

Since Yolo5 comes with Transfer Learning (TL) technique, it is briefly explained here. TL is a machine learning technique in which a model developed for one job is utilized as the basis for another task. The accuracy of the model must be sufficiently high, which requires a huge

amount of training data. TL is used to address the issue of sparsity. Transfer learning occurs when a network or model is trained on a dataset and a certain domain and then applied to train on a different dataset and task [23]. The source domain is referred to as the training domain, whereas the target domain is referred to as the target domain.

Similarly, tasks in distinct domains are referred to as source and target tasks. For instance, a classifier trained on book reviews can be used to categorize movie reviews: two domains, but the same goal. Transfer learning also occurs when the source and target are distinct; for example, a classifier for handwritten letters is used to classify numerical numbers. An image classifier used to conduct object detection is another example of transfer learning; once again, the domains are similar but the goals are distinct. This research concentrated on the case of jobs that span multiple domains yet are performed in a comparable manner (classification). Specifically, an ImageNet-trained CNN was used for another image-related dataset which is a well-known technique in the deep learning literature [24, 25, 26]. Yolo5 is illustrated in Fig. 3 for transfer learning, and the same statistics are applied to the dataset Investigated for this research.

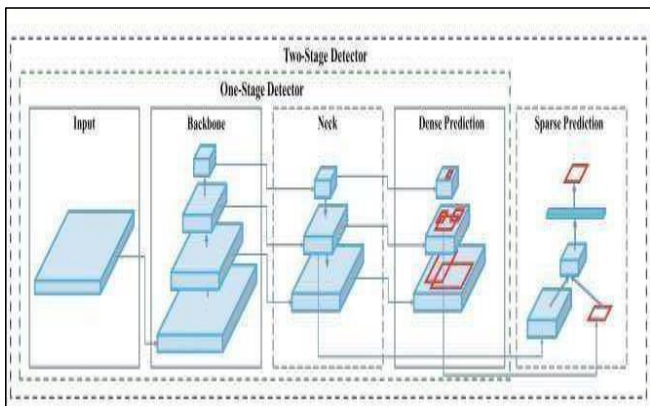


Fig. 3. Transfer learning using Yolo5.

B. Transfer Learning Strategy for Deep Learning

Deep learning systems and models are multi-layered architectures that acquire knowledge of various aspects at various stages (hierarchical representations of layered features). To obtain the last output these layers are connected to the final layer (often a completely connected layer in the case of supervised learning). This tiered architecture enables us to use a pre-trained network (such as ResNets or Inception V3) for other tasks without having to use its final layer as a fixed feature extractor. Deep learning systems and models are composed of multiple layers with distinct layer characteristics. Finally, these layers are joined to the last layer to produce the final output [27]. This layered architecture enables us to use a pre-trained network (for example, ResNets or InceptionV3) as a fixed feature extractor for a variety of tasks without requiring it to have a final layer [28]. Fig. 4 shows transfer learning cutting approach.

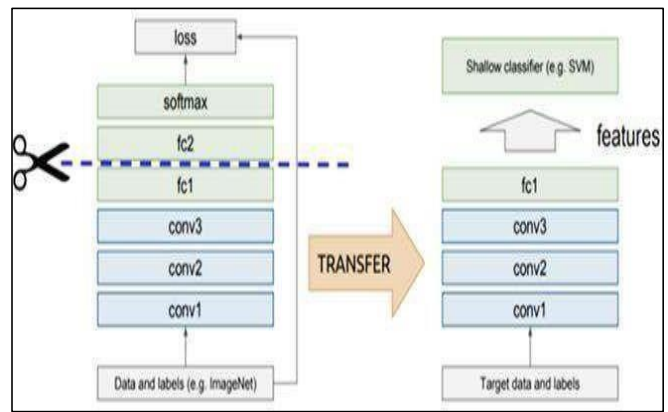


Fig. 4. Transfer learning cutting approach.

IV. PROPOSED MODEL

The proposed framework makes use of an image collection to localize and classify several catheters abnormalities plant diseases. The block diagram in Fig. 5 demonstrates that the suggested paradigm persists across major phases.

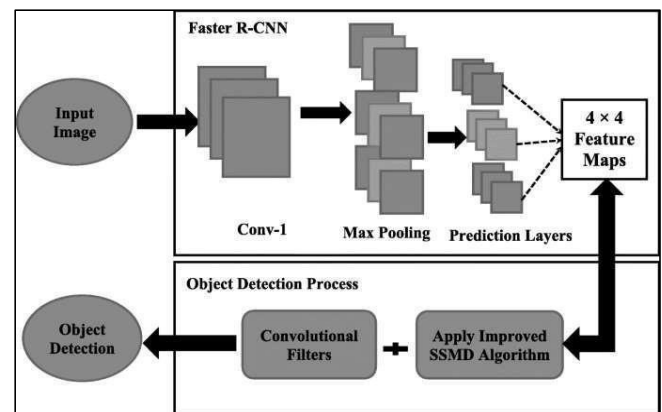


Fig. 5. Methodology diagram of proposed method.

A. Evaluation Measures for Classification

After the training process, algorithms were tested on the testing dataset. The performance of the model was validated by utilizing accuracy, recollection, precision and F1-score. Performance metrics that were employed in this research are explored in detail below.

1) Classification accuracy: The accurateness of classification is measured as the proportion of correct predictions to the total number of accurate predictions.

$$\text{Accuracy} = \frac{\text{Number of Correct Predictions}}{\text{Total Number of Predictions}} * 100\% \quad (1)$$

2) Precision: Classification accuracy is not always a reliable indicator of a model's overall performance, as demonstrated by several examples. One of these cases is when the distribution of classes is imbalanced. If all the samples are treated as if they are of the highest quality, a high accuracy rate will be received, which does not make sense. Precision, on the other hand, indicates the inconsistency you find when utilizing the same instrument over and over again, for as when

measuring the same part again. Precision is one of such measures, which is characterized in Eq. (2):

$$\text{Precision} = \frac{\text{True Positives}}{\text{True Positives} + \text{False Positives}} \quad (2)$$

3) *F1 score*: F1-score is a well-known metric that combines recall and precision. It is defined in Equation 3 as follows:

$$F1score = 2 * \frac{\text{Precision} * \text{Recall}}{\text{Precision} + \text{Recall}} \quad (3)$$

4) *AUC score and ROC curve*: Area under curves (AUC) reflects the level of separability, and receiver operating characteristic (ROC) is a probability curve. ROC curve is a graph that displays the relationship between sensitivity (true positive rate) and specificity (rate of false positives).

V. EXPERIMENTAL RESULTS

The proposed framework makes use of an image collection to localize and classify several. We accomplished lung segmentation to focus the learning around the lung area, where the COVID-19 radiomic features are located. For this, the U-net model that had been popular for biomedical image segmentation was adopted [29]. The Segmentation model was trained using three publicly available lung segmentation datasets: Montgomery [11], HIN [25], and JSRT [13]. The three datasets provided manual segmentation masks (i.e., segmentation labels) [30]. The segmentation was not perfect. The resulting output mask often contains only part of the lung area and tend to be scattered over the whole lung area. To minimize the possibility of missing COVID-19 related radiomic features, the smallest square area was cropped out that enclosed the predicted mask. All such square lung areas were subsequently resized into 512×512 , whether they were larger or smaller [31].

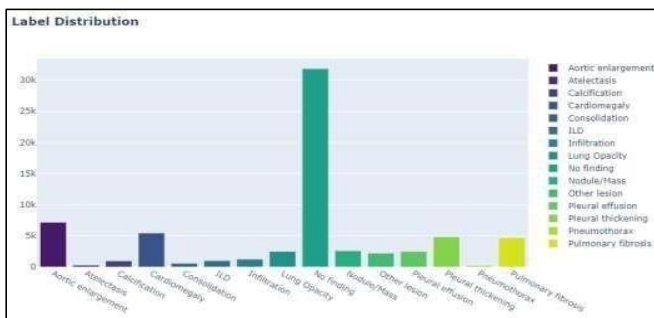


Fig. 6. Label distribution for catheter.

The dataset contains the X-rays of patients, multiple X-rays for individual patients, where the observation of each patient is documented in the dataset. The observation interval is different for patients. The distribution is represented in bar graph shown in Fig. 6.

Fig. 7 represents the bounding box area per percentage of image for each disease. The error and histogram are represented in boxes for ILD calcification, infiltration, lung opacity, Nodule Mass and pulmonary fibrosis for the dataset.

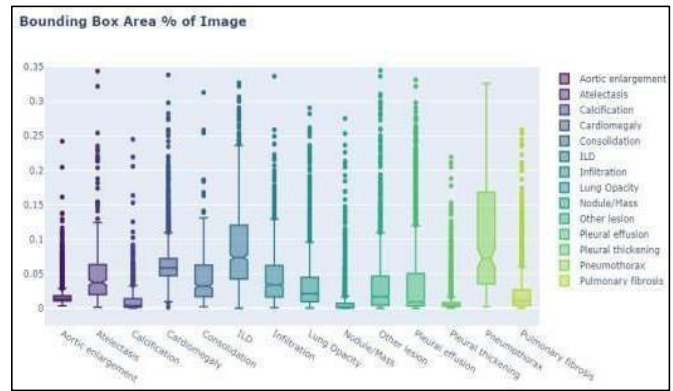


Fig. 7. Bounding area of image for figure.

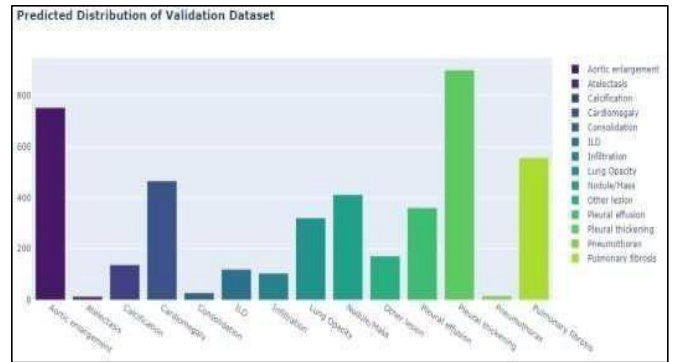


Fig. 8. Predicted distribution of validation dataset.

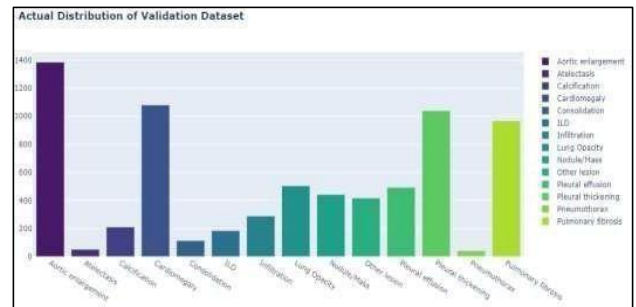


Fig. 9. Actual distribution of dataset.

Fig. 8 represents the predicted distribution of validation dataset while Fig. 9 shows the actual distribution of the dataset, where each defect is represented in bar graph and with different color for individual defect.

VI. CONCLUSION AND FUTURE WORK

Most Chest X-rays are used to spot the existence of chest diseases by radiologists worldwide. By studying several X-rays in busiest health center can lead to a loss of money and time. Furthermore, in the detection of the disease, expert abilities and attentions are needed. CXRs are usually used for the detection of heart and lung region anomalies. In this research, multilevel deep learning is used for chest X-rays ailment detection to identify solutions to these issues. Spotting these anomalies with high precision automatically significantly improves the processes of realistic diagnosis. However, the absence of efficient, public databases and

benchmark analyses makes it hard to match the appropriate diagnosis techniques and define them. The publicly accessible VINBigData dataset is used to address these difficulties, and the output of established multi-level deep learning architectures is studied on various abnormalities. A high accuracy in chest X-Ray irregularity detection is achieved on this dataset. The focus of this research is to develop a Multi-level Deep learning approach for Localization and Classification of thoracic abnormalities from chest radiograph. The proposed technique automatically localizes and classifies fourteen types of thoracic abnormalities from chest radiographs. The used dataset consisting of eighteen scans that have been explained by experienced radiologists. The YoloV5 model is trained with fifteen thousand independently labeled images and evaluated on a test set of three thousand images. These annotations are collected via VinBigData's web-based platform, VinLab. Image preprocessing techniques are utilized for noise removal, image sequences normalization, and contrast enhancement. Finally, Deep Ensemble approaches are used for feature extraction and classification of thoracic abnormalities from chest radiograph.

REFERENCES

- [1] Agrawal, R., & Juneja, A. (2019). *Deep Learning Models for Medical Image Analysis: Challenges and Future Directions*. Paper presented at the International Conference on Big Data Analytics.
- [2] Akpınar, K. N., Genc, S., & Karagol, S. (2020). *Chest X-Ray Abnormality Detection Based on SqueezeNet*. Paper presented at the 2020 International Conference on Electrical, Communication, and Computer Engineering (ICECCE).
- [3] Almezghwi, K., Serte, S., Al-Turjman, F. J. M. T., & Applications. (2021). Convolutional neural networks for the classification of chest X-rays in the IoT era. 1-15.
- [4] Bhandary, A., Prabhu, G. A., Rajinikanth, V., Thanaraj, K. P., Satapathy, S. C., Robbins, D. E., Raja, N. S. M. J. P. R. L. (2020). Deep-learning framework to detect lung abnormality—A study with chest X-Ray and lung CT scan images. *129*, 271-278.
- [5] Bharati, S., Podder, P., & Mondal, M. R. H. J. I. M. U. (2020). Hybrid deep learning for detecting lung diseases from X-ray images. *20*, 100391.
- [6] Bharati, S., Podder, P., Mondal, R., Mahmood, A., & Raihan-Al-Masud, M. (2018). *Comparative performance analysis of different classification algorithm for the purpose of prediction of lung cancer*. Paper presented at the International Conference on Intelligent Systems Design and Applications.
- [7] Campadelli, P., & Casiraghi, E. (2005). *Lung Field Segmentation in Digital Postero-Anterior Chest Radiographs*, Berlin, Heidelberg.
- [8] Chandra, T. B., Verma, K., Jain, D., & Netam, S. S. (2020). *Localization of the suspected abnormal region in chest radiograph images*. Paper presented at the 2020 First international conference on power, control and computing technologies (ICPC2T).
- [9] Chen, H., Miao, S., Xu, D., Hager, G. D., & Harrison, A. P. J. M. i. a. (2020). Deep hierarchical multi-label classification applied to chest X-ray abnormality taxonomies. *66*, 101811
- [10] Chouhan, V., Singh, S. K., Khamparia, A., Gupta, D., Tiwari, P., Moreira, C., De Albuquerque, V. H. C. J. A. S. (2020). A novel transfer learning based approach for pneumonia detection in chest X-ray images. *10(2)*, 559.
- [11] Dai, W., Dong, N., Wang, Z., Liang, X., Zhang, H., & Xing, E. P. (2018). Scan: Structure correcting adversarial network for organ segmentation in chest x-rays. In *Deep learning in medical image analysis and multimodal learning for clinical decision support* (pp. 263-273): Springer.
- [12] G. Cheng and L. He. Dr. Pecker: A Deep Learning-Based Computer-Aided Diagnosis System in Medical Imaging, in *Deep Learning in Healthcare*. Springer, 2020, pp. 203–216.
- [13] Gordienko, Y., Gang, P., Hui, J., Zeng, W., Kochura, Y., Alienin, O., Stirenko, S. (2018). *Deep learning with lung segmentation and bone shadow exclusion techniques for chest X-ray analysis of lung cancer*. Paper presented at the International Conference on Computer Science, Engineering and Education Applications.
- [14] Guan, Q., & Huang, Y. J. P. R. L. (2020). Multi-label chest X-ray image classification via category-wise residual attention learning. *130*, 259-266.
- [15] Guendel, S., Grbic, S., Georgescu, B., Liu, S., Maier, A., & Comaniciu, D. (2018). *Learning to recognize abnormalities in chest x-rays with location-aware dense networks*. Paper presented at the Iberoamerican Congress on Pattern Recognition.
- [16] Gündel, S., Setio, A. A., Ghesu, F. C., Grbic, S., Georgescu, B., Maier, A., & Comaniciu, D. J. M. I. A. (2021). Robust classification from noisy labels: Integrating additional knowledge for chest radiography abnormality assessment. *72*, 102087.
- [17] Guo, R., Passi, K., & Jain, C. K. J. F. i. A. I. (2020). Tuberculosis Diagnostics and Localization in Chest X-Rays via Deep Learning Models. *3*, 74.
- [18] Haghanifar, A., Majdabadi, M. M., Choi, Y., Deivalakshmi, S., & Ko, S. J. a. p. a. (2020). Covid-xnet: Detecting covid-19 in frontal chest x-ray images using deep learning.
- [19] Han, Y., Chen, C., Tang, L., Lin, M., Jaiswal, A., Ding, Y., & Peng, Y. J. a. p. a. (2020). Using Radiomics as Prior Knowledge for Abnormality Classification and Localization in Chest X-rays.
- [20] Han, Y., Chen, C., Tewfik, A., Glicksberg, B., Ding, Y., Peng, Y., & Wang, Z. J. a. p. a. (2021). Cross-Modal Contrastive Learning for Abnormality Classification and Localization in Chest X-rays with Radiomics using a Feedback Loop.
- [21] Hao, J., Ho, T. K. J. J. o. E., & Statistics, B. (2019). Machine learning made easy: a review of scikit-learn package in python programming language. *44(3)*, 348-361.
- [22] He, K., Zhang, X., Ren, S., & Sun, J. (2016). *Deep residual learning for image recognition*. Paper presented at the Proceedings of the IEEE conference on computer vision and pattern recognition.
- [23] Ho, T. K. K., & Gwak, J. J. A. S. (2019). Multiple feature integration for classification of thoracic disease in chest radiography. *9(19)*, 4130.
- [24] Ho, T. K. K., & Gwak, J. J. I. A. (2020). Utilizing Knowledge Distillation in Deep Learning for Classification of Chest X-Ray Abnormalities. *8*, 160749-160761.
- [25] Hu, B., Fang, Y., & Shi, C. (2019). *Adversarial learning on heterogeneous information networks*. Paper presented at the Proceedings of the 25th ACM SIGKDD International Conference on Knowledge Discovery & Data Mining.
- [26] H. Sharif et al., "A Quick Review on Cardiac Image Segmentation," 2022 International Conference on IT and Industrial Technologies (ICIT), Chiniot, Pakistan, 2022, pp. 01-05, doi: 10.1109/ICIT56493.2022.9988971.
- [27] Khosravan, N., Celik, H., Turkbey, B., Jones, E. C., Wood, B., & Bagci, U. J. M. i. a. (2019). A collaborative computer aided diagnosis (C-CAD) system with eye-tracking, sparse attentional model, and deep learning. *51*, 101-115.
- [28] Kim, H.-W., Jung, H.-G., & Lee, S.-W. J. a. p. a. (2021). Weakly Supervised Thoracic Disease Localization via Disease Masks.
- [29] Krizhevsky, A., Sutskever, I., & Hinton, G. E. J. C. o. t. A. (2017). ImageNet classification with deep convolutional neural networks. *60(6)*, 84-90.
- [30] Li, F., Shi, J.-X., Yan, L., Wang, Y.-G., Zhang, X.-D., Jiang, M.-S., Zhou, K.-Q. J. C. R. (2021). Lesion-aware convolutional neural network for chest radiograph classification. *76(2)*, 155. e151-155. e114.
- [31] Liu, C., Cao, Y., Alcantara, M., Liu, B., Brunette, M., Peinado, J., & Curioso, W. (2017). *TX-CNN: Detecting tuberculosis in chest X-ray images using convolutional neural network*. Paper presented at the 2017 IEEE international conference on image processing (ICIP).

Assisted Requirements Selection by Clustering using an Analytical Hierarchical Process

Shehzadi Nazeeha Saleem¹, Linda Mohaisen²

Department of Computer Science and Software Engineering,
National University of Sciences and Technology, Islamabad, Pakistan¹
Department of Information Technology, Faculty of Computing and Information Technology,
King Abdulaziz University, Jeddah, Saudi Arabia²
Department of Computer Science, Cardiff Metropolitan University, Cardiff CF5 2YB, UK²

Abstract—This research investigates the fusion of the Analytic Hierarchy Process (AHP) with clustering techniques to enhance project outcomes. Two quantitative datasets comprising 20 and 100 software requirements are analyzed. A novel AHP dataset is developed to impartially evaluate clustering strategies. Five clustering algorithms (K-means, Hierarchical, PAM, GMM, BIRCH) are employed, providing diverse analytical tools. Cluster quality and coherence are assessed using evaluation criteria including the Dunn Index, Silhouette Index, and Calinski Harabaz Index. The MoSCoW technique organizes requirements into clusters, prioritizing critical requirements. This strategy combines strategic prioritization with quantitative analysis, facilitating objective evaluation of clustering results and resource allocation based on requirement priority. The study demonstrates how clustering can prioritize software requirements and integrate advanced data analysis into project management, showcasing the transformative potential of converging AHP with clustering in software engineering.

Keywords—Requirements prioritization; next release plan; software product planning; decision support; MoSCoW; AHP; k-Means; GMM; BIRCH; PAM; hierarchical; clustering; clusters evaluation

I. INTRODUCTION

Software engineering is built on several pillars and involves more than just programming. It contains every piece of supporting information, design principle, or idea required to make these programmes function as intended. Software requirements prioritisation (SRP) is one of the design principles that enable software that is being considered for development to function as intended [1].

A subfield of requirements engineering called requirements prioritisation assists in selecting requirements based on the interests of stakeholders. Giving each requirement a priority to decide the order in which they should be implemented is a step in the software engineering process. A requirement engineering decision process is used to decide which features or requirements will be developed in the upcoming release while considering technical, resource, risk, and budget constraints [2]. Choosing the order in which requirements should be addressed is a crucial step in the software development process. This process aids in managing the priority and urgency of software requirements while considering stakeholders' interest, cost, resource, and time issues. Numerous academics have provided definitions for the ranking

of software demands in order of importance. Software requirement prioritisation is a process that determines the order in which needs will be implemented [3]. The process of selecting the best set of requirements from several conflicting and competing expectations gathered from various stakeholders participating in a software development project, according to Karlsson and Ryan [4].

The success or failure of a project is largely dependent on the software requirements specification in general and the prioritisation of software requirements in particular. Almost 80% of software projects fail to achieve the Standish Group's definitions of success based on time, cost, and scope criteria each year [5]. The failure is often due to shifting requirements, as requirements are often documented and rarely changed. This suggests that software projects fail due to their inability to evolve efficiently to match shifting requirements or accommodate new ones. This highlights the importance of release management and the need for proper decision-making about the functionality of a software product's release. A well-selected release will minimize problems with shifting requirements in future releases.

As a remedy to this issue, many requirements prioritisation techniques have been put forth. These techniques aim to reduce the length and cost of software development projects by supporting developers in identifying the most important and urgent requirements. Each method has limitations and makes both explicit and implicit assumptions about the project context during requirements prioritisation [6]. These presumptions must be considered while experimentally assessing a requirement prioritisation approach for usefulness, utility, application, or effectiveness.

One technique for ranking software requirements is to use clustering techniques. Similar observations, data points, or feature vectors can be clustered together based on shared characteristics using the clustering technique [7]. Clustering algorithms are used in the prioritising process to group and categorise requirements based on similarity or relatedness. This enables effective requirements prioritisation based on the characteristics of each cluster and the discovery of patterns and relationships between them. Clustering algorithms can assist in managing the complexity of prioritising various requirements by organising requirements into meaningful clusters that can then be prioritised more successfully.

This study thoroughly explores an innovative and promising method for requirement prioritisation that combines the Analytic Hierarchy Process (AHP) and clustering techniques. With the use of the data mining approach known as clustering, it may be possible to group together requirements that are similar, making it easier to handle them and improving the decision-making process. AHP, on the other hand, is a structured method for making decisions based on several factors and enables the creation of priorities based on both qualitative and quantitative judgments.

As we seek to assess the accuracy of quantitative records, it is crucial to assign requirements the proper level of importance to determine the core set of requirements. To do this, the MoSCoW technique, a tried-and-true framework for prioritising requirements, is used that divides each into Must-haves, Should-haves, Could-haves, and Won't-haves categories based on how important and consequential they are. A robust evaluation framework is also developed using metrics like the Dunn Index, Silhouette Index, and Calinski Harabaz Index. These metrics provide quantitative insights into the quality and cohesion of clusters, aiding decision-making processes.

Let's suppose a software development team is tasked with prioritizing features for an e-commerce platform using clustering techniques. They assign priorities within each cluster based on business impact and technical complexity. For example, they prioritize product search functionality (Cluster A) and payment processing (Cluster B) based on their significance for user experience and revenue generation. This approach streamlines decision-making, ensuring high-priority features align with business goals and user needs, ultimately optimizing the software development process.

Our overarching objective in this research is to evaluate the results of combining clustering methods with the Analytic Hierarchy Process (AHP). Our view of this integration's potential impact will be greatly influenced by the outcomes of this integration, which are expected to provide a distinctive perspective on requirement prioritisation and project management. In keeping with this goal, we have developed two key research questions that will direct our empirical studies and provide the information required to make well-informed decisions.

RQ1: Is a semi-automated approach to SRP processes possible with the incorporation of clustering techniques?

RQ2: Does the fusion of AHP and clustering generate better results?

The remainder of the paper is structured as follows: It commences with the state of the art for clustering algorithms and prioritisation techniques in Section II. Following this, Section III gives an overview of established techniques for clustering and requirements prioritisation. In Section IV, we elaborate on the methodology proposed for clustering requirements using AHP including how to determine the number of clusters, evaluate clusters, and associate MoSCoW categories with them. Section V presents and analyzes the results of an effectiveness study conducted on two different datasets. Section VI is dedicated to addressing the effectiveness of the proposed method. Lastly, Section VII presents the

Results. Section VIII encapsulates the conclusions drawn from the research.

II. LITRUTURE REVIEW

Table I extensively evaluates several works on algorithms for clustering and requirements prioritisation. Notably, a wide range of techniques were investigated within the state of the art, including Binary Search Tree, Analytic Network Process, Spanning Tree, Numerical Analysis, Bubble Sort, MoSCoW, and Analytical Hierarchical Process. Remarkably, the Analytical Hierarchical Process (AHP) was the method of choice among researchers due to its constant production of superior results. The section also discusses several clustering techniques, such as K-Means, Partition Around Medoids, BIRCH, Agglomerative Hierarchical Clustering, and Gaussian Mixture Model (GMM). This review of the literature provides an overview of the field and paves the way for the creation of an original and useful framework, laying the groundwork for succeeding research phases.

TABLE I. LITERATURE REVIEW

| Year | Title | Techniques Used | Results | Ref. |
|------|--|--|--|------|
| 2015 | Applying the analytical hierarchy process to system quality requirements prioritisation | AHP | The AHP technique effectively removes discrepancies between stakeholders' interests and the business goals. | [8] |
| 2015 | Comparison of Requirement Prioritisation Techniques to Find the Best Prioritisation Technique | binary search tree, AHP, hierarchy AHP, spanning tree matrix, priority group/Numerical Analysis, bubble sort, MoSoW, simple ranking, and Planning Game | | [9] |
| 2016 | An Evaluation of Requirement Prioritisation Techniques with ANP | ANP, binary search tree, AHP, hierarchy AHP, spanning tree matrix, priority group and bubble sort | AHP is the best requirements prioritisation technique amongst all the requirements prioritisation techniques | [10] |
| 2016 | An approach to the estimation of the degree of customization for ERP projects using prioritised requirements | Framework using AHP | AHP framework gave better results | [11] |
| 2017 | Fuzzy_MoSCoW: A fuzzy based MoSCoW method for the prioritisation of software requirements | Fuzzy MoSCoW | ANP is the best technique among the seven techniques, | [12] |

| Year | Title | Techniques Used | Results | Ref. |
|------|--|---|---|------|
| | | | though it consumes time | |
| 2020 | A Novel Approach for Software Requirement Prioritisation | MAHP, a combination of AHP and MoSCoW | | [13] |
| 2020 | Prioritisation of Software Functional Requirements from Developers' Perspective | Spanning Tree and AHP | AHP framework gave better results | [14] |
| 2022 | E-AHP: An Enhanced Analytical Hierarchy Process Algorithm for Prioritising Large Software Requirements Numbers | Enhanced AHP | E-AHP gives better results for large projects | [15] |
| 2015 | Efficient agglomerative hierarchical clustering | Efficient agglomerative hierarchical clustering | Experimental results show consistent performance across various settings, proving efficient AHP to be reliable. | [16] |
| 2016 | A hierarchical clustering method for multivariate geostatistical data | Agglomerative hierarchical clustering | Proposed clustering method yields satisfactory results compared to other geostatistical methods. | [17] |
| 2017 | Milling tool wear state recognition based on partitioning around medoids (PAM) clustering | PAM | PAM outperforms k-means and fuzzy c-means in Ti-6Al-4V alloy end milling experiments. | [18] |
| 2017 | Malware family identification with BIRCH clustering | BIRCH | BIRCH excels in malware family identification with high accuracy and low clustering time. | [19] |
| 2020 | Unsupervised K-Means Clustering Algorithm | Unsupervised K-Means | The U-k-means algorithm is robust to data structure and performs better than existing algorithms. | [20] |
| 2020 | Applications of Clustering Techniques in Data Mining: A Comparative Study | K-Means, Hierarchical Clustering, DB Scan, OPTICS, Density-Based Clustering, EM | The paper emphasises the value of K-means clustering in consumer | [21] |

| Year | Title | Techniques Used | Results | Ref. |
|------|---|-------------------------------------|--|------|
| | | Algorithm | data analysis and business decision-making | |
| 2020 | A Comparative Study on K-Means Clustering and Agglomerative Hierarchical Clustering | K-Means and Agglomerative Hierarchy | K-means performs faster for large datasets and agglomerative hierarchical is better for smaller ones. | [22] |
| 2021 | Gaussian Mixture Model Clustering with Incomplete Data | GMM | Experiments validate the effectiveness of the proposed algorithm. | [23] |
| 2022 | Bayesian Inference-Based Gaussian Mixture Models with Optimal Components Estimation Towards Large-Scale Synthetic Data Generation for In Silico Clinical Trials | BGMM-OCE | BGMM-OCE outperforms other synthetic data generators in terms of computational efficiency and unbiasedness | [24] |
| 2022 | Design and Implementation of an Improved K-Means Clustering Algorithm | Improved K-Means | Enhanced algorithm works better than conventional K-Means. | [25] |
| 2022 | Gaussian mixture model clustering algorithms for the analysis of high-precision mass measurements | GMM | Results from GMMs were closely congruent with values that had previously been published. | [26] |

A. Research Gap

The limited investigation of the Analytical Hierarchy Process (AHP) as a technique for clustering requirements in the context of planning a project's next release is the area of research that will be addressed in this research. Although most of the literature now in existence focuses on the use of AHP in requirements prioritisation and decision-making, there is a striking paucity of studies that explore its potential utility in grouping or clustering requirements to speed up the release planning process. In the context of release planning, AHP in integration with clustering can be used to enhance how requirements are organised, classified, and prioritised. This will ultimately result in more effective and efficient project management.

III. TECHNIQUES USED IN THE STUDY

A. Requirements Prioritisation Techniques

Software engineering professionals utilise a collection of methodologies called software requirements prioritisation techniques to rank the importance or priority of various software project requirements. Because not all requirements

can be addressed at the same time during software development due to restricted resources (such as time and money), prioritising requirements is essential. To ensure the successful delivery of a software product, it is crucial to identify and concentrate on the most important and significant needs. The two techniques that we will be using in this study are AHP and MoSCoW.

1) *Analytical hierarchical process*: The Analytical Hierarchy Process (AHP) is a systematic decision-making technique [27] proposed by Thomas L. Saaty in the 1970s. It was developed for complex decision-making so that the decision-maker could set priorities and get to the best option possible [28]. AHP starts by modeling the decision issue as a hierarchical structure and breaks it into three parts: a goal or aim, criteria that help achieve the goal, and alternatives or possibilities that need to be examined. In the next step, experts or decision-makers are requested to compare the criteria and options at each level of the hierarchy in pairs. They utilise a scale to indicate the relative importance of things, often ranging from 1 (equal importance) to 9 (much more essential). Then a consistency check is done to make sure the comparisons are reliable. To determine if decision-makers judgments are consistent, the AHP technique uses mathematical calculations. It may be necessary for decision-makers to reevaluate their conclusions if contradictions are found.

AHP uses pairwise comparison data to determine the relative weights or priorities of the criteria and alternatives. These weights reflect the preference for each choice relative to the criteria and the significance of each criterion in reaching the overall aim. The scores of the options for each criterion are then combined using the estimated weights. Depending on the decision context, different aggregation techniques, such as weighted sum or weighted average, might be used. To rank and evaluate the options based on their overall desirability or performance in relation to the goal, AHP aggregates the aggregated scores. Lastly, decision-makers can use the prioritised rankings and scores to make decisions. Based on the established criteria and their relative relevance, AHP offers an organised and clear way to assess and choose the best alternative.

2) *MoSCoW*: The Dynamic Software Development Method (DSDM) provides the foundation for the MoSCoW method [29]. It is a common strategy for prioritising requirements. As a matter of fact, it is one of the easiest techniques [30]. The acronym stands for must have, should have, could have, and won't have. The importance or priority of a certain feature within a project is represented by each category. The core project scope is made up of must-haves, which are important and non-negotiable components necessary for project success. Should-haves are crucial characteristics that greatly enhance the value of the project and ought to be applied whenever practical. Could-haves offer flexibility for prospective improvements because they are desired but not necessary. To manage scope and avoid feature creep, won't-haves are expressly left out of the current phase

or project. MoSCoW supports resource allocation and project planning by assisting project teams and stakeholders in prioritising requirements, ensuring that critical components are addressed first while providing clarity on what may be postponed or excluded.

B. Clustering Algorithms

The need to find knowledge in multidimensional data is growing since massive volumes of data are being continuously collected today. One of the crucial steps in mining or extracting massive information is data mining. Clustering is the most intriguing area of data mining, which seeks to identify underlying patterns in data and identify some useful subgroups for additional investigation. Each group, or cluster, is made up of things that are dissimilar from those in other groups yet like one another [31].

A total of five clustering algorithms have been used in this paper and each algorithm is briefly discussed in this section.

1) *K-Means*: In machine learning and data mining, the clustering algorithm K-Means is very famous and frequently employed [32]. It requires the number of clusters to be specified prior to the operation [33]. It seeks to divide a given dataset into the specified number of clusters (K) according to how similar the data points are to one another to maximise certain clustering criteria. K-Means is an iterative technique that minimises the sum of squared distances between data points and the centroids of each cluster to give results. The k-means algorithm is a well-liked clustering technique that minimises clustering error [34].

2) *Partition Around Medoids (PAM)*: The PAM method partitions a distance matrix into a predetermined number of clusters [35]. The goal of PAM is to divide a dataset into a predetermined number of clusters by choosing actual data points, known as medoids, as representatives of the clusters. PAM is meant to work with dissimilarity or distance matrices. Like centroids, medoids are chosen from the actual data points, which makes PAM more resistant to noise and outliers.

3) *Agglomerative hierarchical clustering*: The process of clustering data points into a hierarchical structure of clusters is called agglomerative hierarchical clustering. Due to the exponential rise of real-world data, hierarchical clustering is crucial for data analytics [36]. In this type of clustering, each item at first represents a separate cluster. The appropriate cluster structure is then created by repeatedly merging clusters until all data points are members of a single cluster, or until a stopping requirement is satisfied. A dendrogram, which is a tree-like structure created because of this procedure, shows the clustering hierarchy visually.

4) *Gaussian Mixture Models (GMM)*: Gaussian Mixture Models (GMMs) are probabilistic models used for modelling complicated data distributions in statistical analysis and machine learning. Much research has been done on it due to its usefulness and efficiency [37]. They presume that a variety of Gaussian (normal) distributions, each with its mean and covariance, were combined to produce the data. These

parameters are intended to be learned, and GMMs estimate the likelihood that data points will belong to each Gaussian component. They are frequently used for tasks like clustering, density estimation, and data generation.

5) *BIRCH*: Balanced Iterative Reducing and Clustering Using Hierarchies is an effective hierarchical clustering algorithm made for grouping huge datasets. Its key characteristic is to employ low memory resources for high-quality clustering of large-scale data datasets and to only scan datasets once to reduce I/O overhead [38]. A comparable B + tree structure known as a Clustering Feature Tree (CF Tree) is used by Birch to perform clustering [39].

IV. PROPOSED METHODOLOGY

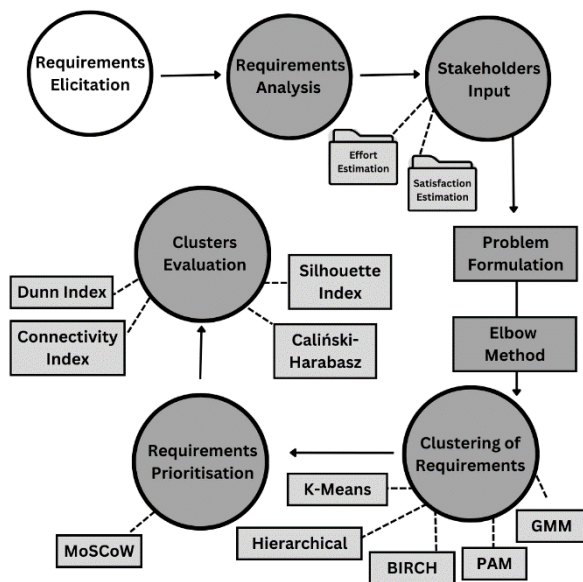


Fig. 1. Proposed methodology.

This study presents a method for prioritizing requirements for the next release using requirements prioritisation methods. It considers the effort required for implementing a requirement and its satisfaction with stakeholders. Clustering algorithms are applied to cluster requirements, and the technique is used to extract a group of requirements for the next release. The validity of clusters is evaluated. In the end MoSCoW is applied to assign importance to the clusters. The Fig. 1 provides a bird's eye view of the process.

A. Requirements Elicitation

Requirement elicitation is a crucial step in requirement engineering, gathering stakeholders' needs and expectations for a software project through discussions, interviews, and surveys, ensuring comprehensive documented requirements.

B. Requirements Analysis

Requirements Analysis involves a thorough examination of requirements to eliminate ambiguity, address inconsistencies, and evaluate feasibility. It aims to create a refined representation of the software's functionalities.

C. Stakeholders' Input

Stakeholders actively contribute to the decision-making process by offering critical input on two important factors: the amount of work necessary to accomplish the project and the expected degree of satisfaction. Their insights cover both effort (resource allocation, time commitments, and potential obstacles) and satisfaction (alignment with organisational goals and client needs). Through the careful balancing of resource optimisation and stakeholder satisfaction throughout project planning, this dual input enables informed decision-making.

D. Problem Formulation

1) *Quantitative data*: Consider a situation where we have a list of requirements, $R = r_1, r_2, \dots, r_n$, that reflect the new features that various customers have recommended for a forthcoming software version. Each stakeholder i is given a weight w_i to indicate their significance. This implies that some stakeholders' preferences will be taken into consideration more so than others when deciding what issues need to be solved in a software version. The set of customer weights is denoted by the notation $W = w_1, w_2, \dots, w_n$.

Each requirement r_j in the set R has a corresponding development effort value e_j that calculates the resources or cost necessary for its implementation. The notation for this collection of effort values is $E = e_1, e_2, \dots, e_n$. This is measured by a value v_{ij} , which expresses the significance of need r_j for customer i . In essence, higher v_{ij} values indicate that stakeholder i is given more priority.

Summing up a requirement's importance ratings across all stakeholders yields the total value of including it in the upcoming software release, or its global satisfaction, abbreviated as s_j ($s_j = \sum_{i=1}^m w_i v_{ij}$). By considering each stakeholder's own priorities and weights, this indicates the overall satisfaction that the addition of requirement r_j would offer to all stakeholders. The set of requirement satisfactions that result is denoted by $S = s_1, s_2, \dots, s_n$ [40].

2) *AHP dataset*: For the pairwise comparisons of each criterion in this study, the quantitative data set is used. As a result, the AHP data set for our requirements generated. Following the collection of pairwise comparison judgments, the eigenvector approach is used to determine the respective weights of the two criteria, effort, and satisfaction. Then, a square matrix known as the comparison matrix is formed, with elements c_{ij} standing in for the weighting of the criteria effort (c_i) and satisfaction (c_j). By dividing each column by its sum, the matrix is normalised, producing a matrix of normalised values. To determine the priority vector for each level, the normalised values in each row are averaged. The consistency ratio (CR), which assesses whether the judgments line coherently, is used in a consistency check to ensure consistent pairwise comparisons. Adjustments are made if the CR exceeds a predetermined limit, which is commonly set at 0.1. The priority vectors show the relative weights of the requirements after the consistency check has been successful.

E. Elbow Method

The elbow method is a heuristic in data science and machine learning for determining the optimal number of

clusters in a dataset. It involves considering a range of potential cluster numbers and computing the sum of squared distances between data points and cluster centers. The study applies the elbow method to the requirements dataset, calculating the within-cluster sum of squares (WCSS) for varying cluster numbers and plotting these values.

F. Clusters Formation

In this phase clusters of requirements are formed. It involves organizing and grouping similar requirements into clusters using techniques like similarity analysis or domain categorization. This process enhances manageability and provides a structured approach for analysis. Five distinct clustering algorithms will be employed: K-Means, Agglomerative Hierarchical Clustering, Partitioning Around Medoids (PAM), Gaussian Mixture Model (GMM), and BIRCH. These algorithms help extract meaningful patterns and structures from requirements, aiding in informed decision-making during the prioritization process.

G. Clusters Evaluation

The evaluation of clusters is crucial for assessing the quality and validity of data analysis or machine learning algorithms. Three mechanisms are used: Dunn Index, Silhouette Index, and Caliński-Harabasz Index, which are calculated after cluster formation and used to rate them.

1) *Dunn index*: The Dunn Index is a clustering validation statistic that unsupervised machine learning researchers use to rate the accuracy of their clustering findings. It gauges the separation between clusters, or how far away various clusters are, in relation to the compactness of clusters, or how near the data points inside a cluster are to one another. Better clustering with smaller within-cluster distances and larger between-cluster distances is indicated by a higher Dunn Index.

$$Dunn\ Index = \frac{\min_intercluster_distance}{\max_intracluster_distance}$$

Where:

Min_intercluster_distance: The minimal distance between any two centroids that belong to separate clusters.

Max_intracluster_distance: The maximum distance between any two data points within the same cluster.

2) *Silhouette index*: The Silhouette Index is a tool for clustering evaluation that assesses how cohesive and well-separated clusters are. Higher values denote better clustering quality; the range is -1 to 1. $(b(i) - a(i)) / \max\{a(i), b(i)\}$, $b(i)$ is the formula for calculating the silhouette score for a single data point, where $a(i)$ is the average distance inside the same cluster and $b(i)$ is the smallest average distance to another cluster. Greater clustering is suggested by average silhouette scores that are higher across all data points.

$$S(i) = (b(i) - a(i)) / \max\{a(i), b(i)\}$$

Where:

$S(i)$: The silhouette score for data point i .

$a(i)$: The average distance between data points i and all other data points in the same cluster.

$b(i)$: The shortest average distance between data point i and all other data points in a distinct cluster.

3) *Caliński-Harabasz index*: The Calinski-Harabasz Index, commonly referred to as the Variance Ratio Criterion, is a clustering evaluation metric used in unsupervised machine learning to rate the calibre of clusters. It calculates the difference between the variances within and between clusters. Better-defined and more distinct clusters are indicated by higher Calinski-Harabasz Index values.

$$CH = B/W\{(N-K)/(K-1)\}$$

Where:

B: Between-cluster variance, which measures the variance between different clusters.

W: Within-cluster variance, which measures the variance within individual clusters.

N: Total number of data points.

K: Number of clusters.

H. Requirements Prioritisation

The MoSCoW approach is used in this study as a useful tool to prioritise requirements clusters. Requirements clusters are systematically classified and ranked using MoSCoW based on their importance and criticality to the project. This will help in improving efficiency and efficacy of the project planning and resource allocation and will make sure that the development efforts are concentrated on the most important and impactful clusters of needs.

V. METHODOLOGY IMPLEMENTATION

A. Formulation of Problem

1) *20 Requirements Problem*: There are twenty requirements and five stakeholders in this dataset, and it was drawn from [41]. The level of priority or value assigned by each stakeholder to each requirement is shown in Table II along with the development effort connected to each requirement. The stakeholder weights are offered in the range of 1 to 5 (Table III). These values might be thought of as linguistic terms like "without importance" (1), "less important" (2), "important" (3), "very important" (4), and "extremely important" (5). They also line up with the relative importance of each need. There is an estimated effort score that corresponds to each requirement, ranging from 1 to 10.

TABLE II. 20 REQUIREMENTS PROBLEM

| | <i>C1</i> | <i>C2</i> | <i>C3</i> | <i>C4</i> | <i>C5</i> | <i>Effort</i> |
|-----------|-----------|-----------|-----------|-----------|-----------|---------------|
| R1 | 4 | 4 | 5 | 4 | 5 | 1 |
| R2 | 2 | 4 | 3 | 5 | 4 | 4 |
| R3 | 1 | 2 | 3 | 2 | 2 | 2 |
| R4 | 2 | 2 | 3 | 3 | 4 | 3 |
| R5 | 5 | 4 | 4 | 3 | 5 | 4 |

| | | | | | | |
|-----|---|---|---|---|---|----|
| R6 | 5 | 5 | 5 | 4 | 4 | 7 |
| R7 | 2 | 1 | 2 | 2 | 2 | 10 |
| R8 | 4 | 4 | 4 | 4 | 4 | 2 |
| R9 | 4 | 4 | 4 | 2 | 5 | 1 |
| R10 | 4 | 5 | 4 | 3 | 2 | 3 |
| R11 | 2 | 2 | 2 | 5 | 4 | 2 |
| R12 | 3 | 3 | 4 | 2 | 5 | 5 |
| R13 | 4 | 2 | 1 | 3 | 3 | 8 |
| R14 | 2 | 4 | 5 | 2 | 4 | 2 |
| R15 | 4 | 4 | 4 | 4 | 4 | 1 |
| R16 | 4 | 2 | 1 | 3 | 1 | 4 |
| R17 | 4 | 3 | 2 | 5 | 1 | 10 |
| R18 | 1 | 2 | 3 | 4 | 2 | 4 |
| R19 | 3 | 3 | 3 | 3 | 4 | 8 |
| R20 | 2 | 1 | 2 | 2 | 1 | 4 |

TABLE III. CUSTOMERS. WEIGHTS FOR 20 REQ. PROBLEM

| Customers' Weights | C1 | C2 | C3 | C4 | C5 |
|--------------------|----|----|----|----|----|
| | 1 | 4 | 2 | 3 | 4 |

a) 20 Requirements Problem using Quantitative Approach: To convert the data into two dimensions to apply clustering on it, we considered Section 4.4.1. Here:

$$R = \{r1, r2, \dots, r20\},$$

$$E = \{1, 4, 2, \dots, 4\},$$

$$W = \{1, 4, 2, \dots, 4\}.$$

This is how 'S' (Satisfaction) was calculated for r1.

$$S = \sum (V_{ij} * W_i)$$

$$S = \{(4*1) + (4*4) + (5*2) + (4*3) + (5*4)\}$$

$$S = 62$$

So, satisfaction for r1 was calculated to be 62 whereas the effort is 1. The rest was also calculated similarly, and this Table IV was generated as a result.

TABLE IV. QUANTITATIVE DATASET FOR 20 REQ. PROBLEM

| ID | Eff. | Sat. | ID | Effort | Sat. |
|-----|------|------|-----|--------|------|
| R1 | 1 | 62 | R11 | 2 | 45 |
| R2 | 4 | 55 | R12 | 5 | 49 |
| R3 | 2 | 29 | R13 | 8 | 35 |
| R4 | 3 | 41 | R14 | 2 | 50 |
| R5 | 4 | 58 | R15 | 1 | 56 |
| R6 | 7 | 63 | R16 | 4 | 27 |
| R7 | 10 | 24 | R17 | 10 | 39 |
| R8 | 2 | 56 | R18 | 4 | 35 |
| R9 | 1 | 54 | R19 | 4 | 46 |
| R10 | 3 | 49 | R20 | 4 | 20 |

b) 20 Requirements Problem using AHP: This Table V was created by using the same data set to get the AHP values for effort and satisfaction.

TABLE V. AHP DATASET FOR 20 REQ. PROBLEM

| ID | Effort | Satisfaction |
|-----|------------|--------------|
| R1 | 12.7640176 | 3.24660865 |
| R2 | 3.19100441 | 3.65981339 |
| R3 | 6.38200881 | 6.9410254 |
| R4 | 4.25467254 | 4.90950577 |
| R5 | 3.19100441 | 3.4705127 |
| R6 | 1.82343109 | 3.19507518 |
| R7 | 1.27640176 | 8.38707236 |
| R8 | 6.38200881 | 3.59445958 |
| R9 | 12.7640176 | 3.72758771 |
| R10 | 4.25467254 | 4.10795381 |
| R11 | 6.38200881 | 4.47310526 |
| R12 | 2.55280353 | 4.10795381 |
| R13 | 1.5955022 | 5.75113533 |
| R14 | 6.38200881 | 4.02579473 |
| R15 | 12.7640176 | 3.59445958 |
| R16 | 3.19100441 | 7.45517543 |
| R17 | 1.27640176 | 5.1612753 |
| R18 | 3.19100441 | 5.75113533 |
| R19 | 3.19100441 | 4.37586384 |
| R20 | 3.19100441 | 10.0644868 |

2) 100 Requirements Problem: There are five stakeholders in this data set as well, but there are 100 requirements this time and it was obtained from [42]. The difficulty of selecting requirements from a bigger set in the early timeboxes of establishing true agile software projects led to the selection of this dataset. Because of this, we now have 100 requirements rather than simply 20. For the development effort, each requirement has a value that runs from 1 to 20. The maximum development effort in this case is 20 units, or 4 weeks, which roughly corresponds to the timescale set by agile approaches (such as Scrum's proposed iteration length of 2 to 4 weeks). Stakeholders rate the significance of criteria on a scale of 1 to 3. Here, the digits 1-3 stand for (1) not necessary, (2) preferable, or (3) required [43].

The Effort and Satisfaction for each requirement was calculated in the similar way as it was calculated for 20 Requirements problem. The Quantitative and AHP datasets for 100 requirements problem is given in Table VI:

TABLE VI. QUANTITATIVE DATASET (LEFT) AND AHP DATASET (RIGHT) FOR 100 REQ. PROBLEM

| ID | Effort | Satisfaction | ID | Effort | Satisfaction |
|----|--------|--------------|----|------------|--------------|
| R1 | 16 | 29 | R1 | 0.35245612 | 0.87906114 |
| R2 | 19 | 23 | R2 | 0.29680515 | 1.10838143 |

| | | |
|-----|----|----|
| R3 | 16 | 18 |
| R4 | 7 | 21 |
| R5 | 19 | 22 |
| R6 | 15 | 20 |
| R7 | 8 | 22 |
| R8 | 10 | 29 |
| R9 | 6 | 27 |
| R10 | 18 | 21 |
| R11 | 15 | 31 |
| R12 | 12 | 33 |
| R13 | 16 | 33 |
| R14 | 20 | 25 |
| R15 | 9 | 25 |
| R16 | 4 | 30 |
| R17 | 16 | 25 |
| R18 | 2 | 28 |
| R19 | 9 | 35 |
| R20 | 3 | 29 |
| R21 | 2 | 27 |
| R22 | 10 | 23 |
| R23 | 4 | 28 |
| R24 | 2 | 29 |
| R25 | 7 | 36 |
| R26 | 15 | 28 |
| R27 | 8 | 30 |
| R28 | 20 | 22 |
| R29 | 9 | 30 |
| R30 | 11 | 32 |
| R31 | 5 | 20 |
| R32 | 1 | 31 |
| R33 | 17 | 24 |
| R34 | 6 | 26 |
| R35 | 2 | 24 |
| R36 | 16 | 23 |
| R37 | 8 | 26 |
| R38 | 12 | 32 |
| R39 | 18 | 26 |
| R40 | 5 | 27 |
| R41 | 6 | 32 |
| R42 | 14 | 30 |
| R43 | 15 | 15 |
| R44 | 20 | 26 |
| R45 | 14 | 29 |
| R46 | 9 | 28 |
| R47 | 16 | 27 |

| | | |
|-----|------------|------------|
| R3 | 0.35245612 | 1.41626516 |
| R4 | 0.80561398 | 1.21394157 |
| R5 | 0.29680515 | 1.15876241 |
| R6 | 0.37595319 | 1.27463865 |
| R7 | 0.70491224 | 1.15876241 |
| R8 | 0.56392979 | 0.87906114 |
| R9 | 0.93988298 | 0.94417678 |
| R10 | 0.31329433 | 1.21394157 |
| R11 | 0.37595319 | 0.82234751 |
| R12 | 0.46994149 | 0.77250827 |
| R13 | 0.35245612 | 0.77250827 |
| R14 | 0.28196489 | 1.01971092 |
| R15 | 0.62658865 | 1.01971092 |
| R16 | 1.40982447 | 0.8497591 |
| R17 | 0.35245612 | 1.01971092 |
| R18 | 2.81964894 | 0.91045618 |
| R19 | 0.62658865 | 0.72836494 |
| R20 | 1.87976596 | 0.87906114 |
| R21 | 2.81964894 | 0.94417678 |
| R22 | 0.56392979 | 1.10838143 |
| R23 | 1.40982447 | 0.91045618 |
| R24 | 2.81964894 | 0.87906114 |
| R25 | 0.80561398 | 0.70813258 |
| R26 | 0.37595319 | 0.91045618 |
| R27 | 0.70491224 | 0.8497591 |
| R28 | 0.28196489 | 1.15876241 |
| R29 | 0.62658865 | 0.8497591 |
| R30 | 0.51266344 | 0.79664915 |
| R31 | 1.12785958 | 1.27463865 |
| R32 | 5.63929788 | 0.82234751 |
| R33 | 0.3317234 | 1.06219887 |
| R34 | 0.93988298 | 0.98049127 |
| R35 | 2.81964894 | 1.06219887 |
| R36 | 0.35245612 | 1.10838143 |
| R37 | 0.70491224 | 0.98049127 |
| R38 | 0.46994149 | 0.79664915 |
| R39 | 0.31329433 | 0.98049127 |
| R40 | 1.12785958 | 0.94417678 |
| R41 | 0.93988298 | 0.79664915 |
| R42 | 0.40280699 | 0.8497591 |
| R43 | 0.37595319 | 1.6995182 |
| R44 | 0.28196489 | 0.98049127 |
| R45 | 0.40280699 | 0.87906114 |
| R46 | 0.62658865 | 0.91045618 |
| R47 | 0.35245612 | 0.94417678 |

| | | |
|-----|----|----|
| R48 | 6 | 21 |
| R49 | 6 | 28 |
| R50 | 6 | 32 |
| R51 | 6 | 34 |
| R52 | 2 | 27 |
| R53 | 17 | 24 |
| R54 | 18 | 30 |
| R55 | 1 | 24 |
| R56 | 3 | 35 |
| R57 | 14 | 35 |
| R58 | 16 | 18 |
| R59 | 18 | 23 |
| R60 | 7 | 26 |
| R61 | 10 | 18 |
| R62 | 7 | 28 |
| R63 | 16 | 29 |
| R64 | 19 | 38 |
| R65 | 17 | 25 |
| R66 | 15 | 22 |
| R67 | 11 | 23 |
| R68 | 8 | 26 |
| R69 | 20 | 34 |
| R70 | 1 | 15 |
| R71 | 5 | 23 |
| R72 | 8 | 32 |
| R73 | 3 | 28 |
| R74 | 15 | 29 |
| R75 | 4 | 21 |
| R76 | 20 | 21 |
| R77 | 10 | 31 |
| R78 | 20 | 39 |
| R79 | 3 | 21 |
| R80 | 20 | 23 |
| R81 | 10 | 22 |
| R82 | 16 | 22 |
| R83 | 19 | 24 |
| R84 | 3 | 25 |
| R85 | 12 | 29 |
| R86 | 16 | 15 |
| R87 | 15 | 28 |
| R88 | 1 | 21 |
| R89 | 6 | 34 |
| R90 | 7 | 32 |
| R91 | 15 | 27 |
| R92 | 18 | 32 |

| | | |
|-----|------------|------------|
| R48 | 0.93988298 | 1.21394157 |
| R49 | 0.93988298 | 0.91045618 |
| R50 | 0.93988298 | 0.79664915 |
| R51 | 0.93988298 | 0.74978744 |
| R52 | 2.81964894 | 0.94417678 |
| R53 | 0.3317234 | 1.06219887 |
| R54 | 0.31329433 | 0.8497591 |
| R55 | 5.63929788 | 1.06219887 |
| R56 | 1.87976596 | 0.72836494 |
| R57 | 0.40280699 | 0.72836494 |
| R58 | 0.35245612 | 1.41626516 |
| R59 | 0.31329433 | 1.10838143 |
| R60 | 0.80561398 | 0.98049127 |
| R61 | 0.56392979 | 1.41626516 |
| R62 | 0.80561398 | 0.91045618 |
| R63 | 0.35245612 | 0.87906114 |
| R64 | 0.29680515 | 0.67086245 |
| R65 | 0.3317234 | 1.01971092 |
| R66 | 0.37595319 | 1.15876241 |
| R67 | 0.51266344 | 1.10838143 |
| R68 | 0.70491224 | 0.98049127 |
| R69 | 0.28196489 | 0.74978744 |
| R70 | 5.63929788 | 1.6995182 |
| R71 | 1.12785958 | 1.10838143 |
| R72 | 0.70491224 | 0.79664915 |
| R73 | 1.87976596 | 0.91045618 |
| R74 | 0.37595319 | 0.87906114 |
| R75 | 1.40982447 | 1.21394157 |
| R76 | 0.28196489 | 1.21394157 |
| R77 | 0.56392979 | 0.82234751 |
| R78 | 0.28196489 | 0.65366084 |
| R79 | 1.87976596 | 1.21394157 |
| R80 | 0.28196489 | 1.10838143 |
| R81 | 0.56392979 | 1.15876241 |
| R82 | 0.35245612 | 1.15876241 |
| R83 | 0.29680515 | 1.06219887 |
| R84 | 1.87976596 | 1.01971092 |
| R85 | 0.46994149 | 0.87906114 |
| R86 | 0.35245612 | 1.6995182 |
| R87 | 0.37595319 | 0.91045618 |
| R88 | 5.63929788 | 1.21394157 |
| R89 | 0.93988298 | 0.74978744 |
| R90 | 0.80561398 | 0.79664915 |
| R91 | 0.37595319 | 0.94417678 |
| R92 | 0.31329433 | 0.79664915 |

| | | |
|------|---|----|
| R93 | 4 | 27 |
| R94 | 7 | 25 |
| R95 | 2 | 21 |
| R96 | 7 | 24 |
| R97 | 8 | 24 |
| R98 | 7 | 39 |
| R99 | 7 | 18 |
| R100 | 3 | 27 |

| | | |
|------|------------|------------|
| R93 | 1.40982447 | 0.94417678 |
| R94 | 0.80561398 | 1.01971092 |
| R95 | 2.81964894 | 1.21394157 |
| R96 | 0.80561398 | 1.06219887 |
| R97 | 0.70491224 | 1.06219887 |
| R98 | 0.80561398 | 0.65366084 |
| R99 | 0.80561398 | 1.41626516 |
| R100 | 1.87976596 | 0.94417678 |

B. Determining No. of Clusters

To determine the ideal number of clusters, the elbow approach was used on data sets from the 20 and 100 Requirements Problem. The ideal number of clusters is depicted in Fig. 2 and 3.

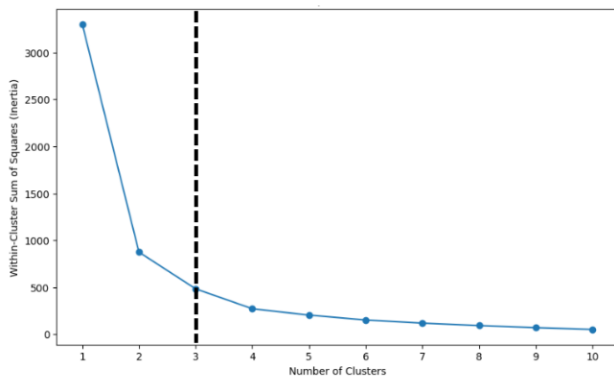


Fig. 2. Optimum no. of clusters using AHP dataset for 20 req. problem.

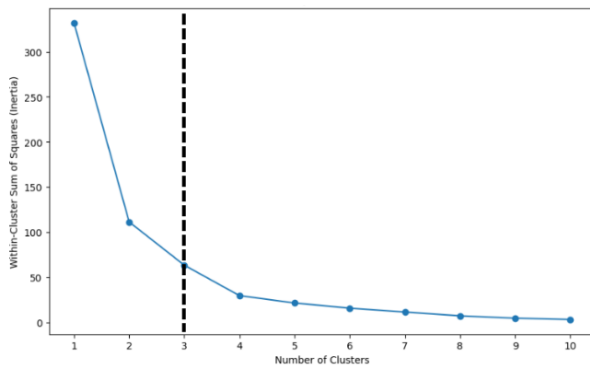


Fig. 3. Optimum no. of clusters using AHP Dataset for 100 req. problem.

C. Clusters Formation and Evaluation

The elbow method's findings show that three clusters are the ideal number for both the 20 and 100 Requirements Problems. We made 3 and 4 clusters because we are employing MoSCoW in addition to AHP for requirement prioritising. This is because MoSCoW has four characteristics.

In the publication [40], quantitative dataset was used to evaluate three clustering algorithms: K-means, Hierarchical Clustering, and Partition Around Medoids (PAM). In this research, we compare the values acquired by the Analytic

Hierarchy Process (AHP) approach to the values of quantitative dataset. The benefits and drawbacks of various techniques are better understood through holistic comparison, which also advances knowledge of efficient clustering methodologies and their real-world applications.

The graphical depiction of 100 requirements datasets for Agglomerative Hierarchical Clustering is illustrated in Fig. 4 and 5. This visualization provides a clear representation of the analyzed data, offering insights into the observed trends and patterns.

To gain a deeper knowledge of how the proposed technique interacts with various clustering algorithms, evaluation indices for both types of data sets, namely Quantitative and AHP, are also calculated using Gaussian Mixture Models (GMM) and BIRCH (Fig. 6 and 7).

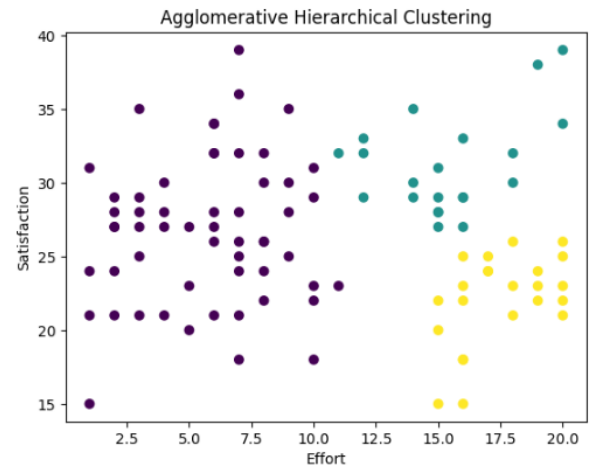


Fig. 4. Hierarchical clustering for 100 req. problem using quantitative dataset.

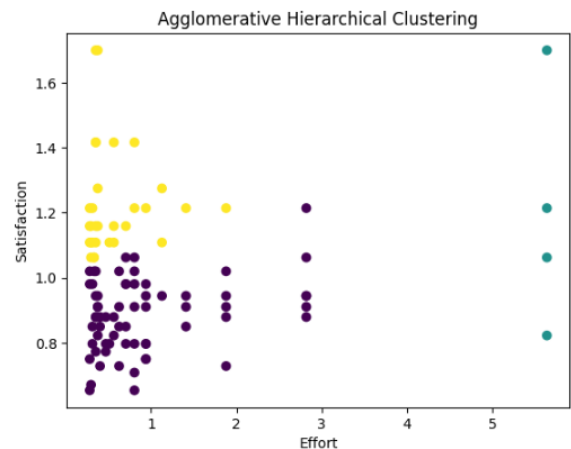


Fig. 5. Hierarchical clustering for 100 req. problem using AHP dataset.

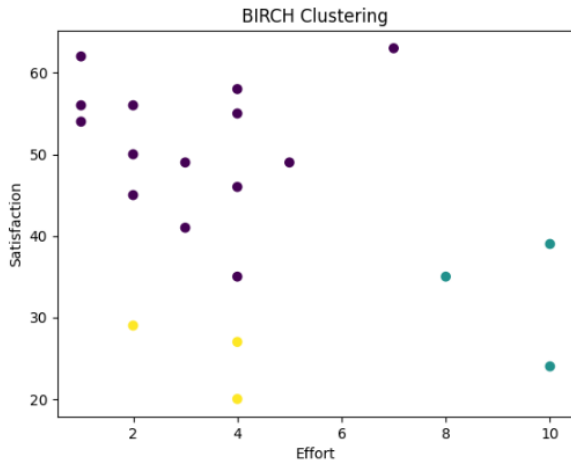


Fig. 6. BIRCH clustering for 20 req. problem using quantitative dataset.

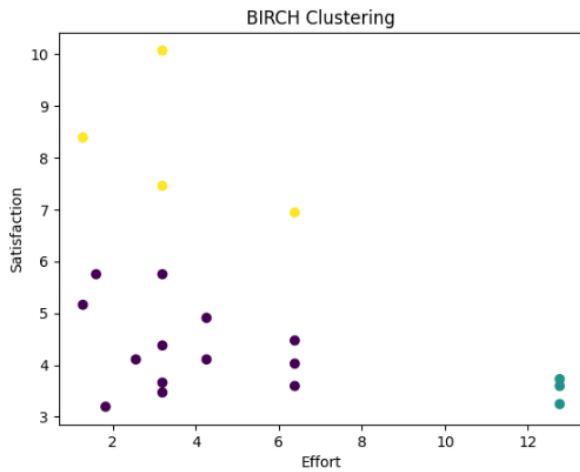


Fig. 7. BIRCH clustering for 20 req. problem using AHP dataset.

All in all, five clustering algorithms: K-Means, Partition Around Medoids, Agglomerative Hierarchical Clustering, Gaussian Mixture Models, and BIRCH and three evaluation metrics: the Dunn Index, the Silhouette Index, and the Calinski-Harabasz Index are used in this research.

The outcomes of each clustering algorithm for cluster evaluation metrics are provided in the Tables VII-XVI.

- 1) K-Means
- 2) PAM
- 3) Hierarchical
- 4) GMM
- 5) BIRCH

TABLE VII. EVALUATION METRICS FOR 20 REQ. PROBLEM

| 20 Requirements Problem | | | |
|-------------------------|----------|--------------|---------|
| | Clusters | Quantitative | AHP |
| Dunn | 3 | 0.209 | 0.4336 |
| Silhouette | 3 | 0.4666 | 0.5690 |
| CH | 3 | 22.9273 | 33.7443 |

| | | | |
|------------|---|---------|---------|
| Dunn | 4 | 0.2527 | 0.2417 |
| Silhouette | 4 | 0.4176 | 0.4863 |
| CH | 4 | 24.3832 | 34.1044 |

TABLE VIII. EVALUATION METRICS FOR 100 REQ. PROBLEM

| 100 Requirements Problem | | | |
|--------------------------|----------|--------------|----------------|
| | Clusters | Quantitative | AHP |
| Dunn | 3 | 0.0548 | 0.2364 |
| Silhouette | 3 | 0.4283 | 0.4632 |
| CH | 3 | 89.5132 | 89.7174 |
| Dunn | 4 | 0.0783 | 0.2377 |
| Silhouette | 4 | 0.3993 | 0.4766 |
| CH | 4 | 90.9959 | 96.8018 |

TABLE IX. EVALUATION METRICS FOR 20 REQ. PROBLEM

| 20 Requirements Problem | | | |
|-------------------------|----------|--------------|----------------|
| | Clusters | Quantitative | AHP |
| Dunn | 3 | 0.2607 | 2.7100 |
| Silhouette | 3 | 0.4843 | 0.5208 |
| CH | 3 | 22.6144 | 31.1727 |
| Dunn | 4 | 0.3151 | 1.5103 |
| Silhouette | 4 | 0.4116 | 0.4374 |
| CH | 4 | 24.0329 | 31.2174 |

TABLE X. EVALUATION METRICS FOR 100 REQ. PROBLEM

| 100 Requirements Problem | | | |
|--------------------------|----------|----------------|---------------|
| | Clusters | Quantitative | AHP |
| Dunn | 3 | 0.0831 | 0.3396 |
| Silhouette | 3 | 0.4308 | 0.3943 |
| CH | 3 | 89.5132 | 46.9101 |
| Dunn | 4 | 0.0696 | 0.3024 |
| Silhouette | 4 | 0.3993 | 0.3998 |
| CH | 4 | 88.7641 | 64.6714 |

TABLE XI. EVALUATION METRICS FOR 20 REQ. PROBLEM

| 20 Requirements Problem | | | |
|-------------------------|----------|--------------|----------------|
| | Clusters | Quantitative | AHP |
| Dunn | 3 | 0.2576 | 2.9804 |
| Silhouette | 3 | 0.4549 | 0.5690 |
| CH | 3 | 18.6832 | 33.7443 |
| Dunn | 4 | 0.2482 | 2.7427 |

| | | | |
|------------|---|---------|----------------|
| Silhouette | 4 | 0.3561 | 0.4863 |
| CH | 4 | 18.7909 | 34.1044 |

TABLE XII. EVALUATION METRICS FOR 100 REQ. PROBLEM

| 100 Requirements Problem | | | |
|--------------------------|----------|--------------|----------------|
| | Clusters | Quantitative | AHP |
| Dunn | 3 | 0.1096 | 0.3472 |
| Silhouette | 3 | 0.4278 | 0.4327 |
| CH | 3 | 88.0933 | 82.8722 |
| Dunn | 4 | 0.1096 | 0.2518 |
| Silhouette | 4 | 0.3964 | 0.4576 |
| CH | 4 | 82.5902 | 95.1834 |

TABLE XIII. EVALUATION METRICS FOR 20 REQ. PROBLEM

| 20 Requirements Problem | | | |
|-------------------------|----------|--------------|---------------|
| | Clusters | Quantitative | AHP |
| Dunn | 3 | 0.2739 | 0.3723 |
| Silhouette | 3 | 0.4568 | 0.5690 |
| CH | 3 | 22.5821 | 33.744 |
| Dunn | 4 | 0.1796 | 0.310 |
| Silhouette | 4 | 0.3839 | 0.4905 |
| CH | 4 | 22.0866 | 33.633 |

TABLE XIV. EVALUATION METRICS FOR 100 REQ. PROBLEM

| 100 Requirements Problem | | | |
|--------------------------|----------|----------------|---------|
| | Clusters | Quantitative | AHP |
| Dunn | 3 | 0.7259 | 0.1706 |
| Silhouette | 3 | 0.4285 | 0.0743 |
| CH | 3 | 90.674 | 26.5032 |
| Dunn | 4 | 0.5557 | 0.077 |
| Silhouette | 4 | 0.3721 | 0.1082 |
| CH | 4 | 90.7001 | 36.2847 |

TABLE XV. EVALUATION METRICS FOR 20 REQ. PROBLEM

| 20 Requirements Problem | | | |
|-------------------------|----------|----------------|---------------|
| | Clusters | Quantitative | AHP |
| Dunn | 3 | 12.9526 | 7.249 |
| Silhouette | 3 | 0.4672 | 0.5690 |
| CH | 3 | 18.9442 | 33.744 |

TABLE XVI. EVALUATION METRICS FOR 100 REQ. PROBLEM

| 100 Requirements Problem | | | |
|--------------------------|----------|--------------|-----|
| | Clusters | Quantitative | AHP |

| | | | |
|------------|---|----------------|---------|
| Dunn | 3 | 8.9139 | 0.665 |
| Silhouette | 3 | 0.4384 | 0.4053 |
| CH | 3 | 96.1607 | 79.1779 |

D. Prioritisation of Requirements

The MoSCoW method is used to prioritize requirements clusters. Clusters with higher satisfaction and minimal effort were given the highest priority and are designated as "MUST" fulfillments. Clusters with higher satisfaction and minimal effort are designated as "SHOULD" requirements. Clusters in the "COULD" category are considered for enhancement due to their higher effort cost. Clusters in the "WONT" category are intentionally deferred due to higher effort requirements. This dynamic prioritization methodology offers a nuanced perspective for optimizing software requirements in line with project goals.

VI. DISCUSSION

Our study compared the Analytic Hierarchy Process (AHP) with quantitative dataset approaches in requirement prioritization and clustering, highlighting performance differences across multiple evaluations. Each comparison table illustrates instances where either AHP or the quantitative dataset method performed better, with the superior values highlighted for clarity Table (VII-XVI). Out of 54 evaluations, AHP showed superior performance in 39 cases, emphasizing variability between methods.

The effectiveness of AHP in generating compact and meaningful clusters underscores its potential for handling complex datasets in software engineering. By leveraging a structured decision-making approach that incorporates both qualitative and quantitative judgments, AHP successfully groups requirements with closer features or similarities together more cohesively. This results in coherent and relevant requirement groupings, which in turn facilitates improved decision-making and prioritization within software development processes. AHP's ability to create compact clusters highlights its utility in enhancing the efficiency and effectiveness of software engineering practices.

VII. RESULTS

The Analytic Hierarchy Process (AHP) and the quantitative datasets were compared 54 times in total using evaluation metrics. The purpose of these comparisons was to assess the efficiency and performance of the AHP approach in comparison to the quantitative data representation. 39 of these 54 comparisons revealed that the AHP technique performed better than other approaches. This indicates that, in contrast to the quantitative data technique, AHP typically produced more favorable outcomes or results.

This finding's relevance stems from the AHP approach's consistent propensity to outperform the quantitative data representation over a sizable majority of the comparisons. This series of outcomes highlights the possible advantages of applying the AHP approach to cluster or analyse the provided dataset, suggesting that it might be a more efficient and reliable method for producing valuable insights or groups.

VIII. CONCLUSION AND FUTURE WORK

The importance of using data mining techniques to efficiently prioritise requirements in software engineering is shown by this study. It also emphasises the extraordinary excellence of the Analytic Hierarchy Process (AHP) in the context of software engineering for prioritising software requirements. Based on a detailed analysis of five clustering algorithms and three cluster assessment indices, our results consistently demonstrate that AHP outperforms traditional quantitative data representations in the majority of the 54 comparisons conducted. Furthermore, the combination of AHP with the MoSCoW needs prioritisation framework not only led to better results but also enhanced resource allocation, flexible planning, and increased stakeholder satisfaction. This study recommends using AHP, data mining techniques, and the MoSCoW framework as the suggested methodology for prospective projects.

Since the data sets were generated manually with the help of stakeholders in this research. In the future, we can use machine learning algorithms. These algorithms can be trained on historical project data to learn the underlying patterns and characteristics of similar projects. By improving the overall efficiency of requirements prioritisation techniques, this integration could pave the way for more sophisticated and context-sensitive approaches to managing software requirements.

REFERENCES

[1] P. Achimugu, A. Selamat, R. Ibrahim, and M. N. Mahrin, "A systematic literature review of software requirements prioritization research," *Inf Softw Technol*, vol. 56, no. 6, pp. 568–585, Jun. 2014, doi: 10.1016/j.infsof.2014.02.001.

[2] X. Franch and G. Ruhe, "Software release planning," in *Proceedings of the 38th International Conference on Software Engineering Companion*, New York, NY, USA: ACM, May 2016, pp. 894–895. doi: 10.1145/2889160.2891051.

[3] M. Azzolini and L. I. Passoni, "Prioritization of Software Requirements: a Cognitive Approach," in *Proceedings of the Fourth International Workshop on Knowledge Discovery, Knowledge Management and Decision Support*, Paris, France: Atlantis Press, 2013. doi: 10.2991/2013.13.

[4] I. Olaronke, I. Rhoda, and G. Ishaya, "An Appraisal of Software Requirement Prioritization Techniques," *Asian Journal of Research in Computer Science*, pp. 1–16, Apr. 2018, doi: 10.9734/ajrcos/2018/v1i124717.

[5] K. El Emam and A. G. Koru, "A Replicated Survey of IT Software Project Failures," *IEEE Softw*, vol. 25, no. 5, pp. 84–90, Sep. 2008, doi: 10.1109/MS.2008.107.

[6] A. Ahmad, M. Goransson, and A. Shahzad, "Limitations of the Analytic Hierarchy Process Technique with Respect to Geographically Distributed Stakeholders," *World Acad Sci Eng Technol*, pp. 111–116, 2010.

[7] P. Govender and V. Sivakumar, "Application of k-means and hierarchical clustering techniques for analysis of air pollution: A review (1980–2019)," *Atmos Pollut Res*, vol. 11, no. 1, pp. 40–56, Jan. 2020, doi: 10.1016/j.apr.2019.09.009.

[8] M. Kassab and N. Kilicay-Ergin, "Applying analytical hierarchy process to system quality requirements prioritization," *Innov Syst Softw Eng*, vol. 11, no. 4, pp. 303–312, Dec. 2015, doi: 10.1007/s11334-015-0260-8.

[9] J. Ali Khan, I. Ur Rehman, Y. Hayat Khan, I. Javed Khan, and S. Rashid, "Comparison of Requirement Prioritization Techniques to Find Best Prioritization Technique," *International Journal of Modern*

Education and Computer Science, vol. 7, no. 11, pp. 53–59, Nov. 2015, doi: 10.5815/ijmecs.2015.11.06.

[10] J. A. Khan, Izaz-ur-Rehman, S. P. Khan, I. Qasim, and Y. H. Khan, "An Evaluation of Requirement Prioritization Techniques with ANP," *International Journal of Advanced Computer Science and Applications*, vol. 7, no. 7, 2016.

[11] S. Parthasarathy and M. Daneva, "An approach to estimation of degree of customization for ERP projects using prioritized requirements," *Journal of Systems and Software*, vol. 117, pp. 471–487, Jul. 2016, doi: 10.1016/j.jss.2016.04.006.

[12] K. S. Ahmad, N. Ahmad, H. Tahir, and S. Khan, "Fuzzy_MoSCoW: A fuzzy based MoSCoW method for the prioritization of software requirements," in *2017 International Conference on Intelligent Computing, Instrumentation and Control Technologies (ICICICT)*, IEEE, Jul. 2017, pp. 433–437. doi: 10.1109/ICICICT1.2017.8342602.

[13] M. S. Jahan, F. Azam, M. W. Anwar, A. Amjad, and K. Ayub, "A Novel Approach for Software Requirement Prioritization," in *2019 7th International Conference in Software Engineering Research and Innovation (CONISOFT)*, IEEE, Oct. 2019, pp. 1–7. doi: 10.1109/CONISOFT.2019.00012.

[14] M. Yaseen, A. Mustapha, and N. Ibrahim, "Prioritization of Software Functional Requirements from Developers Perspective," *International Journal of Advanced Computer Science and Applications*, vol. 11, no. 9, 2020.

[15] N. Mohamed, S. Mazen, and W. Helmy, "E-AHP: An Enhanced Analytical Hierarchy Process Algorithm for Prioritizing Large Software Requirements Numbers," *International Journal of Advanced Computer Science and Applications*, vol. 13, no. 7, 2022, doi: 10.14569/IJACSA.2022.0130725.

[16] A. Bouguettaya, Q. Yu, X. Liu, X. Zhou, and A. Song, "Efficient agglomerative hierarchical clustering," *Expert Syst Appl*, vol. 42, no. 5, pp. 2785–2797, Apr. 2015, doi: 10.1016/j.eswa.2014.09.054.

[17] F. Fouedjio, "A hierarchical clustering method for multivariate geostatistical data," *Spat Stat*, vol. 18, pp. 333–351, Nov. 2016, doi: 10.1016/j.spasta.2016.07.003.

[18] Z. Li, G. Wang, and G. He, "Milling tool wear state recognition based on partitioning around medoids (PAM) clustering," *The International Journal of Advanced Manufacturing Technology*, vol. 88, no. 5–8, pp. 1203–1213, Feb. 2017, doi: 10.1007/s00170-016-8848-1.

[19] G. Pitolli, L. Aniello, G. Laurenza, L. Querzoni, and R. Baldoni, "Malware family identification with BIRCH clustering," in *2017 International Carnahan Conference on Security Technology (ICCST)*, IEEE, Oct. 2017, pp. 1–6. doi: 10.1109/CCST.2017.8167802.

[20] K. P. Sinaga and M.-S. Yang, "Unsupervised K-Means Clustering Algorithm," *IEEE Access*, vol. 8, pp. 80716–80727, 2020, doi: 10.1109/ACCESS.2020.2988796.

[21] M. Faizan, M. F., S. Ismail, and S. Sultan, "Applications of Clustering Techniques in Data Mining: A Comparative Study," *International Journal of Advanced Computer Science and Applications*, vol. 11, no. 12, 2020, doi: 10.14569/IJACSA.2020.0111218.

[22] K. B., "A Comparative Study on K-Means Clustering and Agglomerative Hierarchical Clustering," *International Journal of Emerging Trends in Engineering Research*, vol. 8, no. 5, pp. 1600–1604, May 2020, doi: 10.30534/ijeter/2020/20852020.

[23] Y. Zhang et al., "Gaussian Mixture Model Clustering with Incomplete Data," *ACM Transactions on Multimedia Computing, Communications, and Applications*, vol. 17, no. 1s, pp. 1–14, Jan. 2021, doi: 10.1145/3408318.

[24] V. C. Pezoulas, N. S. Tachos, G. Gkois, I. Olivotto, F. Barlocco, and D. I. Fotiadis, "Bayesian Inference-Based Gaussian Mixture Models With Optimal Components Estimation Towards Large-Scale Synthetic Data Generation for In Silico Clinical Trials," *IEEE Open J Eng Med Biol*, vol. 3, pp. 108–114, 2022, doi: 10.1109/OJEMB.2022.3181796.

[25] H. Zhao, "Design and Implementation of an Improved K-Means Clustering Algorithm," *Mobile Information Systems*, vol. 2022, pp. 1–10, Sep. 2022, doi: 10.1155/2022/6041484.

[26] C. M. Weber, D. Ray, A. A. Valverde, J. A. Clark, and K. S. Sharma, "Gaussian mixture model clustering algorithms for the analysis of high-

- precision mass measurements,” *Nucl Instrum Methods Phys Res A*, vol. 1027, p. 166299, Mar. 2022, doi: 10.1016/j.nima.2021.166299.
- [27] B. Regnell, M. Höst, J. N. och Dag, P. Beremark, and T. Hjelm, “An Industrial Case Study on Distributed Prioritisation in Market-Driven Requirements Engineering for Packaged Software,” *Requir Eng*, vol. 6, no. 1, pp. 51–62, Feb. 2001, doi: 10.1007/s007660170015.
- [28] Bruce L. Golden, Edward A. Wasil, and Patrick T. Harker, Eds., “*The analytic hierarchy process. Applications and Studies*.” Heidelberg, 1989.
- [29] S. Hatton, “Early Prioritisation of Goals,” in *Advances in Conceptual Modeling – Foundations and Applications*, Berlin, Heidelberg: Springer Berlin Heidelberg, pp. 235–244. doi: 10.1007/978-3-540-76292-8_29.
- [30] A. Hudaib, R. Masadeh, M. H. Qasem, and A. Alzaqebah, “Requirements Prioritization Techniques Comparison,” *Mod Appl Sci*, vol. 12, no. 2, p. 62, Jan. 2018, doi: 10.5539/mas.v12n2p62.
- [31] Pradeep Rai and Shubha Singh, “A Survey of Clustering Techniques,” *Int J Comput Appl*, vol. 7, Oct. 2010.
- [32] J. A. Hartigan and M. A. Wong, “Algorithm AS 136: A K-Means Clustering Algorithm,” *Appl Stat*, vol. 28, no. 1, p. 100, 1979, doi: 10.2307/2346830.
- [33] K. P. Sinaga and M.-S. Yang, “Unsupervised K-Means Clustering Algorithm,” *IEEE Access*, vol. 8, pp. 80716–80727, 2020, doi: 10.1109/ACCESS.2020.2988796.
- [34] A. Likas, N. Vlassis, and J. J. Verbeek, “The global k-means clustering algorithm,” *Pattern Recognit*, vol. 36, no. 2, pp. 451–461, Feb. 2003, doi: 10.1016/S0031-3203(02)00060-2.
- [35] L. Kaufman and PJ Rousseeuw, *Finding Groups in Data: An Introduction to Cluster Analysis*. John Wiley & Sons., 2009.
- [36] A. Bouguettaya, Q. Yu, X. Liu, X. Zhou, and A. Song, “Efficient agglomerative hierarchical clustering,” *Expert Syst Appl*, vol. 42, no. 5, pp. 2785–2797, Apr. 2015, doi: 10.1016/j.eswa.2014.09.054.
- [37] Y. Zhang *et al.*, “Gaussian Mixture Model Clustering with Incomplete Data,” *ACM Transactions on Multimedia Computing, Communications, and Applications*, vol. 17, no. 1s, pp. 1–14, Jan. 2021, doi: 10.1145/3408318.
- [38] K. Peng, L. Zheng, X. Xu, T. Lin, and V. C. M. Leung, “Balanced Iterative Reducing and Clustering Using Hierarchies with Principal Component Analysis (PBirch) for Intrusion Detection over Big Data in Mobile Cloud Environment,” 2018, pp. 166–177. doi: 10.1007/978-3-030-05345-1_14.
- [39] T. Zhang, R. Ramakrishnan, and M. Livny, “BIRCH,” *ACM SIGMOD Record*, vol. 25, no. 2, pp. 103–114, Jun. 1996, doi: 10.1145/235968.233324.
- [40] J. del Sagrado and I. M. del Águila, “Assisted requirements selection by clustering,” *Requir Eng*, vol. 26, no. 2, pp. 167–184, Jun. 2021, doi: 10.1007/s00766-020-00341-1.
- [41] D. Greer and G. Ruhe, “Software release planning: an evolutionary and iterative approach,” *Inf Softw Technol*, vol. 46, no. 4, pp. 243–253, Mar. 2004, doi: 10.1016/j.infsof.2003.07.002.
- [42] J. del Sagrado, I. M. del Águila, and F. J. Orellana, “Multi-objective ant colony optimization for requirements selection,” *Empir Softw Eng*, vol. 20, no. 3, pp. 577–610, Jun. 2015, doi: 10.1007/s10664-013-9287-3.
- [43] E. Simmons, “Requirements triage: what can we learn from a ‘medical’ approach?,” *IEEE Softw*, vol. 21, no. 4, pp. 86–88, Jul. 2004, doi: 10.1109/MS.2004.25.

Comparative Analysis of Telemedicine in Media Coverage Pre- and Post-COVID-19 using Unsupervised Latent Dirichlet Topic Modeling

Haewon Byeon

Department of Digital Anti-Aging Healthcare (BK21),
Medical Big Data Research Center, Inje University, Gimhae 50834, South Korea

Abstract—Telemedicine, driven by technology, has become a game-changer in healthcare, with the COVID-19 pandemic amplifying its significance by necessitating remote healthcare solutions. This study explores the evolution of telemedicine through news big data analysis. Our research encompassed a vast dataset from 51 media outlets (total 28,372 articles), including national and regional dailies, economic newspapers, broadcasters, and professional journals. Using LDA analysis, we delved into pre- and post-pandemic telemedicine trends comprehensively. A crucial revelation was the prominence of "medical law" in telemedicine discussions, underscoring the need for legal reforms. Keywords like "artificial intelligence" and "big data" underscored technology's pivotal role. Post-pandemic, keywords like "COVID-19," "online healthcare," and "telemedicine" surged, reflecting the pandemic's impact on remote healthcare reliance. These keywords' increased frequency highlights the pandemic's transformative influence. This study stresses addressing healthcare's legal constraints and maximizing technology's potential. To seamlessly integrate telemedicine, policy support and institutional backing are imperative. In summary, telemedicine's rise, propelled by COVID-19, signifies a healthcare paradigm shift. This study sheds light on its trajectory, emphasizing legal reforms, tech innovation, and pandemic-induced changes. The post-pandemic era must prioritize informed policy decisions for telemedicine's effective and accessible implementation.

Keywords—Telemedicine; COVID-19; medical law; healthcare transformation; LDA topic modeling

I. INTRODUCTION

One important factor that is rapidly evolving in the modern healthcare environment is the increase in telemedicine services. This is achieved through the combination of advancements in information technology and innovative approaches in the medical field, providing patients with more effective and convenient healthcare services. Particularly, the importance of telemedicine has been further emphasized after the outbreak of COVID-19 in early 2020.

The COVID-19 pandemic has placed a significant burden on the global healthcare system. With the increase in patients and limitations in healthcare personnel, traditional methods of healthcare service delivery have faced constraints. As an alternative, telemedicine has gained prominence, offering patients the opportunity to safely receive medical consultations from their homes. This transformation has become a significant catalyst for revolutionizing the healthcare system, especially as

the COVID-19 pandemic has brought about revolutionary changes in the medical field worldwide. Patients can now consult with doctors through computers or smartphones within the comforts of their own homes. In response to these changes, healthcare institutions have strengthened their telemedicine systems and strived to introduce new technologies to provide the best possible healthcare services to patients.

Extensive research has been conducted on telemedicine in the last decade [1-4]. However, these studies predominantly focus on specific geographical regions or timeframes, resulting in a constrained understanding of telemedicine trends pre- and post-COVID-19 pandemic. Moreover, the reliance on survey-based methodologies in these studies introduces potential biases due to subjective responses and recall inaccuracies. To address these shortcomings and enhance the accuracy of findings, leveraging big data from news sources for unsupervised topic modeling emerges as a promising alternative. This method offers an objective and expansive analysis of telemedicine's evolution and its perception in media discourse across different temporal contexts.

Unsupervised topic modeling has been extensively applied in research utilizing text data, such as identifying industrial accident-related issues using website text data [5], discerning attitudes towards vaccines via Twitter [6], exploring topics on climate change through news articles [7], and investigating topics related to the Omicron variant [8]. With the increasing prevalence of such studies, the efficacy of unsupervised topic modeling applied to news articles has been substantiated [9, 10].

An examination of telemedicine trends pre- and post-COVID-19 constitutes a critical area of inquiry within contemporary healthcare research. Such comparative analyses are instrumental in elucidating the evolution and emerging patterns in telemedicine, thereby offering valuable insights for the enhancement of future healthcare systems and the optimization of patient services.

The organization of this study is as follows: Section II delineates the methodology for data collection and the implementation of Latent Dirichlet Allocation (LDA) modeling. Section III details the outcomes of the network analysis conducted, Section IV discusses the implications of these findings. Finally, Section V concludes the paper.

II. MATERIALS AND METHODS

A. Data Collection

This study utilized news articles from a total of 51 media outlets, including 10 national dailies, 8 economic dailies, 26 regional dailies, 5 broadcasting companies, and 2 professional journals, analyzed through the news big data analysis service, BIGKinds, provided by the Korea Press Foundation (see Table I). BigKinds integrates big data analytics with a database composed of news articles, offering analytical support. Since 1990, approximately 70 million news contents have been transformed into big data within this platform. Furthermore, by converting unstructured text into structured data, it provides information, making it a service capable of analyzing societal phenomena through articles.

TABLE I. MEDIA SUBJECT TO ANALYSIS

| Category (Number) | Daily newspaper name |
|-------------------------------|--|
| Professional journals (2) | Electronic Newspaper, Digital Times |
| Broadcasting company (5) | KBS, SBS, MBC, YTN, OBS |
| National daily newspaper (10) | Kyunghyang Shinmun, Chosun Ilbo, Donga Ilbo, Hankook Ilbo, Hankyoreh, JoongAng Ilbo, Kookmin Ilbo, Munhwa Ilbo, Naeil Shinmun, Segye Ilbo, Seoul Shinmun |
| Economic daily Newspaper (8) | Maeil Economy, Money Today, Seoul Economy, Asia Economy, Aju Economy, Financial News, Korea Economy, Herald Economy |
| Local daily newspaper (26) | Busan Ilbo, Chungbuk Daily, Chungcheong Daily, Chungcheong Today, Daegu Ilbo, Daejeon Ilbo, Gangwon Ilbo, Gwangju Daily, Gwangju Ilbo, Gangwon Provincial Daily, Gyeonggi Ilbo, Gyeongin Ilbo, Gyeongnam Newspaper, Gyeongnam Provincial Daily, Gyeongsang Daily, Halla Daily, International Newspaper, Jemin Daily, Jeonbuk Ilbo, Jeonbuk Provincial Daily, Jeonnam Ilbo, Joongbu Daily, Joongbu Daily, Maeil Daily, Mudeung Ilbo, Ulsan Daily, Yeongnam Ilbo |

TABLE II. NUMBER OF ARTICLES ANALYSIS

| | Before the COVID-19 pandemic | After the COVID-19 pandemic | Total |
|-----------------------------|------------------------------|-----------------------------|--------|
| Total number of articles | 5,232 | 23,884 | 29,116 |
| Number of excluded articles | 92 | 652 | 744 |
| Number of analysis articles | 5,140 | 23,232 | 28,372 |

To investigate the trends in remote healthcare before and after the COVID-19 pandemic, keywords such as telemedicine, remote medical treatment, and non-face-to-face medical care were searched and analyzed. The collected articles were divided into two periods: pre-COVID-19 pandemic period, from January 1, 2016 to November 30, 2019, and post-COVID-19 pandemic period, from December 1, 2019 to the endemic declaration date on May 5, 2023. After excluding duplicate and irrelevant news articles, a total of 5,140 and

23,232 articles were analyzed for the two respective periods (see Table II).

B. Analysis Method

Firstly, frequency analysis was conducted to investigate the occurrence of words based on the collected text data of news articles, followed by the analysis of word weights using TF-IDF. TF-IDF is the most commonly used weighting algorithm and is widely used in keyword extraction and topic classification [11]. LDA topic modeling is an algorithm that is useful for extracting latent topics from big data consisting of text [12]. LDA (Latent Dirichlet Allocation) is one of the most common topic modeling methods, contributing to the extraction of coherent topics from data [13]. The fundamental concept of LDA is to represent the latent topics in a document composed of text data as a random mixture, wherein topics are characterized by the distribution of words [14]. A diagram of the procedure for this study is presented in Fig. 1. All analyses conducted in this study were performed using Python.

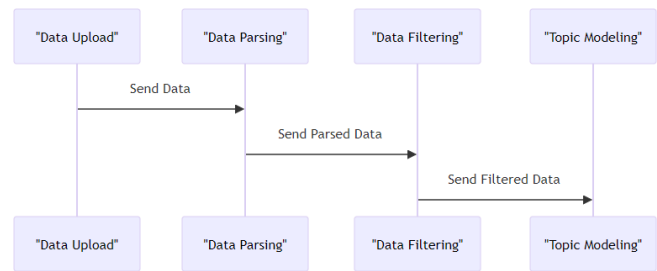


Fig. 1. Flowchart of the research procedure.

C. Network Analysis

Fig. 2 present the results of a keyword network analysis conducted on keywords related to telemedicine. The network analysis depicts the interconnectedness between words using noun phrases extracted through Structured SVM from the top 100 articles with high accuracy.

Fig. 2 represents the pre-pandemic network, with weights ranging from 6 to 58. The keyword analysis revealed that medical law exhibited the strongest association. This suggests that telemedicine is currently considered illegal under existing medical laws, and therefore, it is speculated that the revision of medical laws is crucial for the implementation of telemedicine. Additionally, keywords such as Ministry of Health and Welfare, United States, China, and Japan emerged as related keywords for similar reasons.

Fig. 3 illustrates the network configuration in the post-pandemic context, characterized by varying connection weights that range between 8 and 71. The keyword analysis revealed similarities to the pre-pandemic network, with the addition of keywords related to COVID-19, National Security Council, and Deputy Chief of Policy Committee. This difference can be attributed to the temporary rise in the importance of telemedicine due to the enabling of remote medical services during the COVID-19 pandemic.

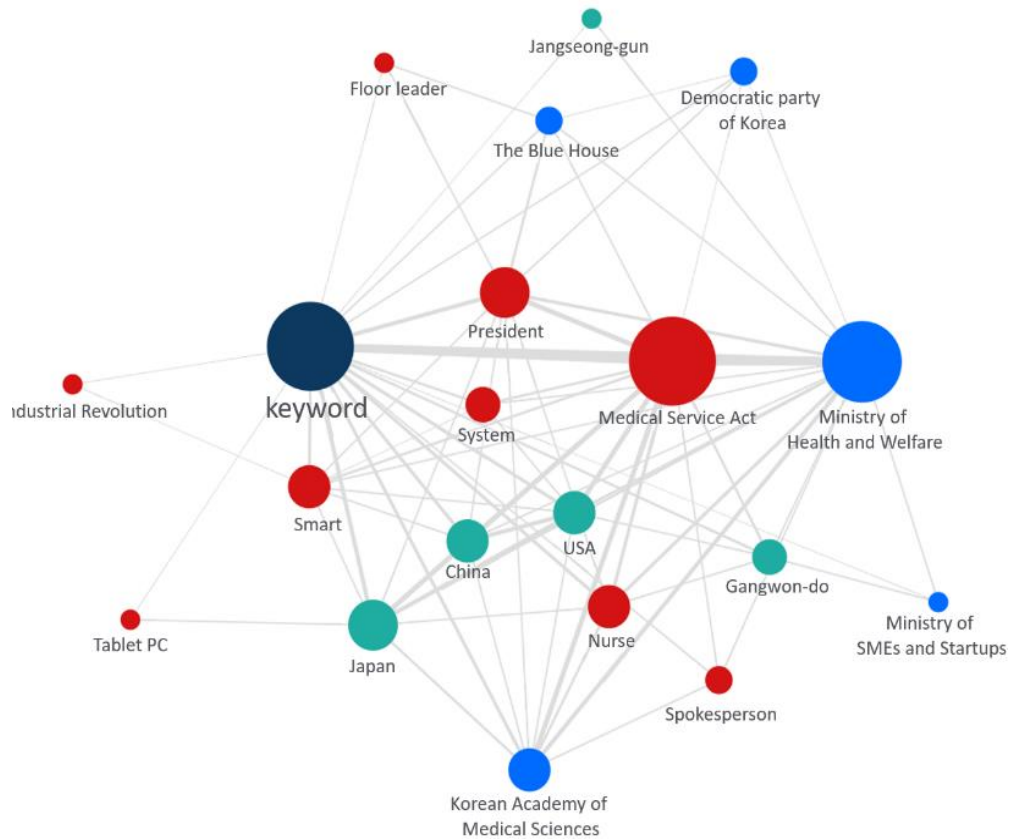


Fig. 2. Analysis of the relationship between keywords related to telemedicine: A comparative study before the COVID-19 pandemic.

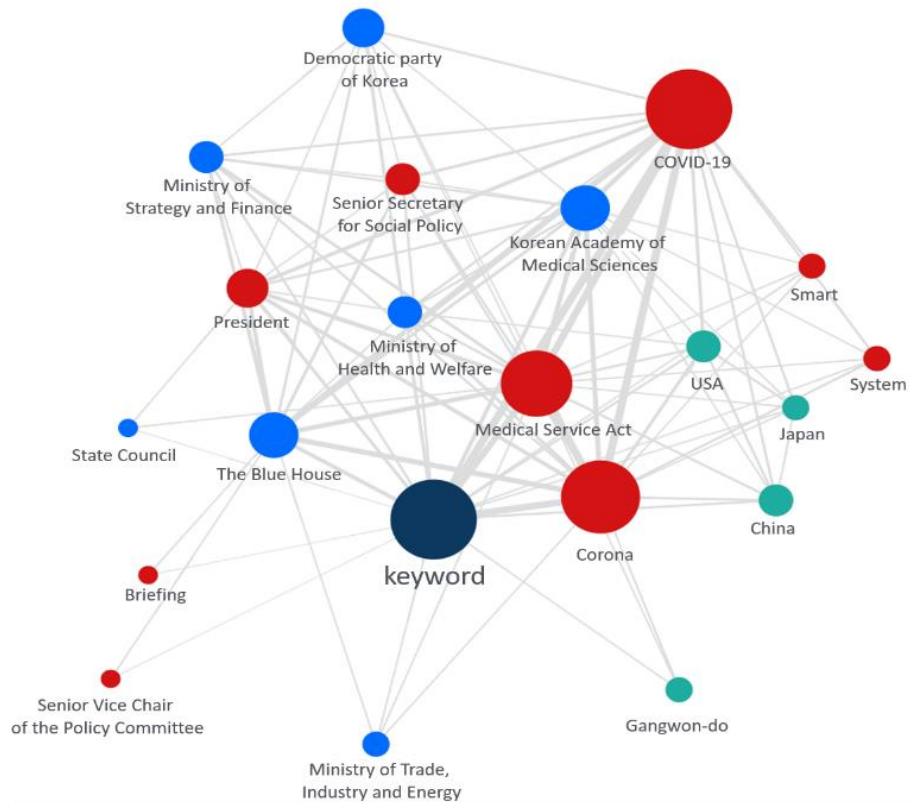


Fig. 3. Analysis of the relationship between keywords related to telemedicine: A comparative study after the COVID-19 pandemic.

III. RESULTS

A. Frequency Analysis Result

Table III presents the frequency analysis of relevant keywords before and after the COVID-19 pandemic. The results show that after the pandemic, additional keywords related to COVID-19, online, and telemedicine were identified.

B. LDA Topic Modeling

Fig. 4 illustrates the results of calculating coherence scores using Gensim, a Python package. Gensim is a tool for topic

modeling, analyzing the interrelationships between words to reinterpret the content of documents in a new and profound meaning. Additionally, by simplifying the representation of documents, it is utilized to enhance the efficiency of information processing [15]. The number of topics is determined based on the coherence scores, resulting in three topics before the occurrence of COVID-19 and seven topics after. The optimal number of topics is determined by the highest coherence score.

TABLE III. TOP 15 KEYWORDS BEFORE AND AFTER THE COVID-19 PANDEMIC

| Before the COVID-19 pandemic | | | After the COVID-19 pandemic | | |
|------------------------------|-----------|------------|-----------------------------|-----------|------------|
| Word | Frequency | TF-IDF | Word | Frequency | TF-IDF |
| Telemedicine | 1550 | 1857.13745 | COVID-19 | 11943 | 7945.69675 |
| Korea | 1230 | 1757.94827 | The coronavirus | 4257 | 7222.98417 |
| United States | 950 | 1602.92958 | Online | 3643 | 6748.47047 |
| Telemedicine | 781 | 1470.58678 | Confirmed case | 2981 | 6119.80347 |
| China | 750 | 1442.55203 | Face-to-face | 2893 | 6025.80369 |
| Job | 748 | 1440.69989 | United States | 2757 | 5875.23554 |
| Korea | 564 | 1245.3022 | Seoul | 2391 | 5435.70132 |
| Japan | 482 | 1139.8296 | Korea | 2377 | 5417.82679 |
| Seoul | 448 | 1092.12789 | Remote Healthcare | 1850 | 4680.13852 |
| Medical Law | 432 | 1068.79851 | Infectious disease | 1849 | 4678.6079 |
| Big Data | 429 | 1064.35893 | AI | 1659 | 4377.62493 |
| A pilot project | 399 | 1018.78418 | Medical staff | 1632 | 4333.1425 |
| Cheong Wa Dae | 383 | 993.565504 | Start-up | 1579 | 4244.51904 |
| Smartphone | 365 | 964.393884 | Coronavirus | 1526 | 4154.11628 |
| Competitiveness | 347 | 934.33424 | Job | 1480 | 4074.16339 |

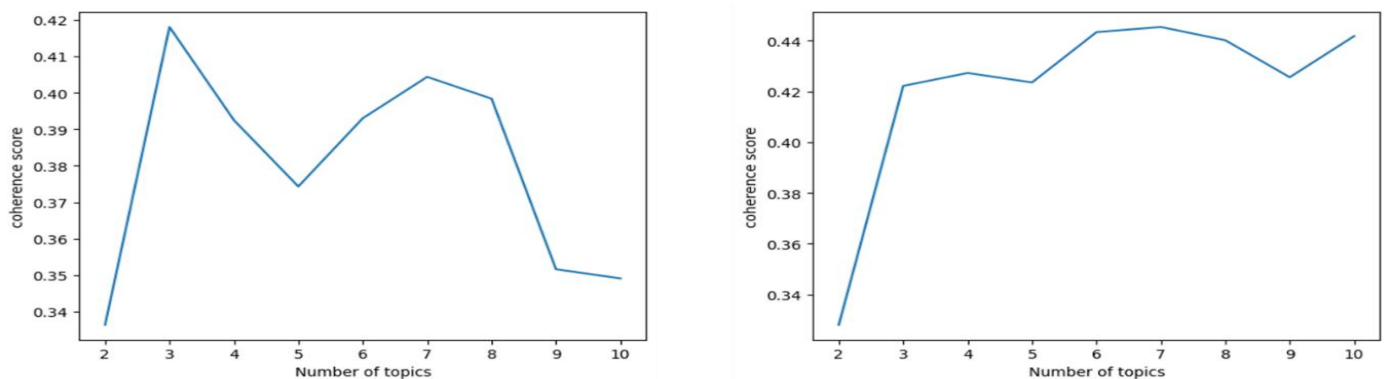


Fig. 4. Coherence scores before and after the COVID-19 pandemic.

The results of topic modeling before and after the COVID-19 pandemic are presented in Table IV and Table V. Since the topic weights were low in the 6th word of each topic, the top 5 words for each topic are provided. Before the COVID-19 pandemic, topics related to remote healthcare and technology (Topic 1), global remote healthcare (Topic 2), and remote healthcare and medical law (Topic 3) were identified, focusing on the definition and technological aspects of remote healthcare, global implementation of remote healthcare, and

policy and technological considerations in the adoption of remote healthcare.

The results of topic modeling after the COVID-19 pandemic are presented in Table V. It was observed that topics related to COVID-19 emerged, given the temporary allowance of remote healthcare during the pandemic. Additionally, topics related to the definition of remote healthcare and its social

implications were identified, such as Topic 6 and Topic 7, in order to facilitate the full implementation of remote healthcare.

TABLE IV. TOPIC MODELING BEFORE THE COVID-19 PANDEMIC

| Group | Topic name | Top 5 words |
|-------|--|--|
| 1 | Remote healthcare and Science and Technology | Seoul, Network, Artificial Intelligence, Big Data, Deputy Prime Minister |
| 2 | Global remote healthcare | Korea, United States, China, jobs |
| 3 | Remote healthcare and medical law | Remote healthcare, medical law, pilot projects, telemedicine, Ministry of Health and Welfare |

TABLE V. TOPICS MODELING AFTER THE COVID-19 PANDEMIC

| Group | Topic name | Top 5 words |
|-------|---|--|
| 1 | Temporary introduction | Remote healthcare, Telemedicine, Temporary, Medical, Medical law |
| 2 | Position on remote healthcare | Medical circles, medical associations, Korean Medical Association, collusion, Cheong Wa Dae |
| 3 | COVID-19 and remote healthcare | Confirmed cases, Health centers, Medical institutions, Respiratory tract, Patients with diseases |
| 4 | COVID-19 and remote healthcare in major countries | Korea, United States, online, China, COVID-19 |
| 5 | COVID-19 and home treatment | COVID-19, Seoul, Online, Coronavirus, Confirmed Cases |
| 6 | Remote healthcare and Science and Technology | AI, Artificial intelligence, Untact, Big data, Cloud |
| 7 | Social Effects of remote healthcare | New Deal, Jobs, Korean Version, COVID-19, Infectious Diseases |

IV. DISCUSSION

In this study, we analyzed keywords related to telemedicine and visualized the relationships between them in a network format. Through this, we were able to explore the trends and implications for the adoption of telemedicine before and after the COVID-19 pandemic. Particularly, we found that the keyword "medical law" had the highest centrality in both networks. This indicates that telemedicine is currently constrained by medical laws and suggests the need for policy discussions to improve this situation [15,16]. Additionally, keywords such as "Ministry of Health and Welfare," "United States," "China," and "Japan" appeared frequently in both networks for similar reasons, indicating significant discussions regarding telemedicine in each country [17-20]. In summary, this study confirms the importance of the legality of medical laws for the expansion and development of telemedicine.

In this study, we also observed that various forms of medical technology and artificial intelligence are closely linked with the activation of telemedicine. Keywords such as "Seoul," "network," "artificial intelligence," "big data," and "Deputy Prime Minister" were connected in the network. These connections indicate a strong association between telemedicine and scientific technology and emphasize the importance of technology in the future of the medical field [21, 22].

Frequency analysis revealed that after the COVID-19 pandemic, not only keywords related to COVID-19 but also keywords related to online, non-face-to-face, and remote consultations increased. This indicates an increased need for telemedicine due to the COVID-19 pandemic. Moreover, these keywords carry higher weights compared to before, highlighting the impact of COVID-19 on the medical and health sectors [23, 24].

Furthermore, through LDA topic modeling, we identified three topics before the COVID-19 pandemic and seven topics after. This revealed various subjects such as telemedicine and scientific technology, global telemedicine, and telemedicine and medical laws. This diversity demonstrates the rapid activation of telemedicine and the ongoing discussions and research from various aspects [25, 26].

In synthesizing these findings, it becomes evident that the COVID-19 pandemic has amplified awareness and underscored the necessity of telemedicine. Nevertheless, legal constraints within the medical field persist, necessitating future discourse and policy development to rectify these issues. Moreover, comprehensive research exploring the social impacts and equity of telemedicine from multifaceted perspectives remains a critical need.

V. CONCLUSION

This study has established the role of the COVID-19 pandemic as an accelerating force in the transformation of the telemedicine sector, highlighting the importance of adaptive medical regulations and the application of advanced scientific technology, with our big data analysis emphasizing the growing necessity of telemedicine and the essential nature of structured policies for its effective deployment. Future research should build on this groundwork by integrating an expanded range of big data sources, such as social media, healthcare forums, and patient surveys, while implementing longitudinal studies to thoroughly characterize the long-term sustainability and patterns of telemedicine utilization.

Further investigations are warranted to probe the public's acceptance of telemedicine and its incorporation into health systems, necessitating the application of sophisticated opinion analysis methods—including sentiment analysis—and the execution of comparative international studies. Such exploratory research is necessary to delineate strategies that are sensitive to cross-cultural differences and capable of adjusting to the evolving healthcare demands informed by global technological trends and shifting societal expectations in the aftermath of the pandemic.

ACKNOWLEDGMENT

This research Supported by Basic Science Research Program through the National Research Foundation of Korea (NRF) funded by the Ministry of Education (NRF- RS-2023-00237287, NRF-2021S1A5A8062526) and local government-university cooperation-based regional innovation projects (2021RIS-003).

REFERENCES

- [1] "K. S. Zachrison, K. M. Boggs, E. M. Hayden, J. A. Espinola, and C. A. Camargo Jr, "Understanding barriers to telemedicine implementation in rural emergency departments," *Annals of Emergency Medicine*, vol. 75, no. 3, pp. 392-399, 2020. <https://doi.org/10.1016/j.annemergmed.2019.04.026>.
- [2] L. S. Wilson and A. J. Maeder, "Recent directions in telemedicine: review of trends in research and practice," *Healthcare Informatics Research*, vol. 21, no. 4, pp. 213-222, 2015. <https://doi.org/10.4258/hir.2015.21.4.213>.
- [3] W. H. Bos, A. van Tubergen, and H. E. Vonkeman, "Telemedicine for patients with rheumatic and musculoskeletal diseases during the COVID-19 pandemic; a positive experience in the Netherlands," *Rheumatology International*, vol. 41, no. 3, pp. 565-573, 2021. <https://doi.org/10.1007/s00296-020-04746-5>.
- [4] A. Elawady, A. Khalil, O. Assaf, S. Toure, and C. Cassidy, "Telemedicine during COVID-19: a survey of Health Care Professionals' perceptions," *Monaldi Archives for Chest Disease*, vol. 90, no. 4, 2020. <https://doi.org/10.4081/monaldi.2020.1445>.
- [5] K. B. Min, S. H. Song, and J. Y. Min, "Topic modeling of social networking service data on occupational accidents in Korea: latent dirichlet allocation analysis," *Journal of Medical Internet Research*, vol. 22, no. 8, e19222, 2020. <https://doi.org/10.2196/19222>.
- [6] G. Lindelöf, T. Aledavood, and B. Keller, "Dynamics of the Negative Discourse Toward COVID-19 Vaccines: Topic Modeling Study and an Annotated Data Set of Twitter Posts," *Journal of Medical Internet Research*, vol. 25, e41319, 2023. <https://doi.org/10.2196/41319>.
- [7] F. Rabitz, A. Telešienė, and E. Zolubienė, "Topic modelling the news media representation of climate change," *Environmental Sociology*, vol. 7, no. 3, pp. 214-224, 2021. <https://doi.org/10.1080/23251042.2021.1913991>.
- [8] E. Mayor and A. Miani, "A topic models analysis of the news coverage of the Omicron variant in the United Kingdom press," *BMC Public Health*, vol. 23, no. 1, 2023. <https://doi.org/10.1186/s12889-023-13824-1>.
- [9] Z. Li, W. Shang, and M. Yan, "News text classification model based on topic model," in 2016 IEEE/ACIS 15th International Conference on Computer and Information Science (ICIS), Okayama, Japan, 2016, pp. 1-5. <https://doi.org/10.1109/ICIS.2016.7550881>.
- [10] X. Hu, "News hotspots detection and tracking based on LDA topic model," in 2016 International Conference on Progress in Informatics and Computing (PIC), Shanghai, China, 2016, pp. 248-252. <https://doi.org/10.1109/PIC.2016.7949534>.
- [11] H. Liu, X. Chen, and X. Liu, "A Study of the Application of Weight Distributing Method Combining Sentiment Dictionary and TF-IDF for Text Sentiment Analysis," *IEEE Access*, vol. 10, pp. 32280-32289, 2022. <https://doi.org/10.1109/ACCESS.2022.3142238>.
- [12] G. Eom and H. Byeon, "Development of keyword trend prediction models for obesity before and after the COVID-19 pandemic using RNN and LSTM: analyzing the news big data of South Korea," *Frontiers in Public Health*, vol. 10, 894266, 2022. <https://doi.org/10.3389/fpubh.2022.894266>.
- [13] P. K. Bogović, A. Meštrović, S. Beliga, and S. Martinčić-Ipšić, "Topic Modelling of Croatian News During COVID-19 Pandemic," in 2021 44th International Convention on Information, Communication and Electronic Technology (MIPRO), Opatija, Croatia, 2021, pp. 1044-1051. <https://doi.org/10.23919/MIPRO52101.2021.9596908>.
- [14] Pratinida, T. M., & Setyohadi, D. B. (2021). "Automatization News Grouping Using Latent Dirichlet Allocation for Improving Efficiency," *International Journal of Innovative Computing, Information and Control*, vol. 17, no. 5, pp. 1643-1651.
- [15] I. Akef, J. S. M. Arango, and X. Xu, "Mallet vs GenSim: Topic modeling for 20 news groups report," *University of Arkansas Little Rock Law Journal*, vol. 2, 39205, 2016.
- [16] Y. S. Choi, "A study on the introduction of telemedicine-Coronavirus disease 2019 and the need for the introduction of telemedicine," *International Law Review*, vol. 12, no. 1, pp. 113-137, 2020.
- [17] A. de Oliveira Andrade et al., "On the use of telemedicine in the context of COVID-19: legal aspects and a systematic review of technology," *Research on Biomedical Engineering*, vol. 38, pp. 209-227, 2022. <https://doi.org/10.1007/s42600-021-00141-4>.
- [18] I. Gareev et al., "The opportunities and challenges of telemedicine during COVID-19 pandemic," *Frontiers in Bioscience (Elite Edition)*, vol. 13, no. 2, pp. 291-298, 2021.
- [19] A. Miyawaki, T. Tabuchi, M. K. Ong, and Y. Tsugawa, "Age and social disparities in the use of telemedicine during the COVID-19 pandemic in Japan: cross-sectional study," *Journal of Medical Internet Research*, vol. 23, no. 7, e27982, 2021. <https://doi.org/10.2196/27982>.
- [20] J. A. Betancourt, M. A. Rosenberg, A. Zevallos, J. R. Brown, and M. Mileski, "The impact of COVID-19 on telemedicine utilization across multiple service lines in the United States," *Healthcare*, vol. 8, no. 4, 380, 2020. <https://doi.org/10.3390/healthcare8040380>.
- [21] Y. T. Shen, L. Chen, W. W. Yue, and H. X. Xu, "Digital technology-based telemedicine for the COVID-19 pandemic," *Frontiers in Medicine*, vol. 8, 646506, 2021. <https://doi.org/10.3389/fmed.2021.646506>.
- [22] T. A. Suleiman and A. Adinoyi, "Telemedicine and Smart Healthcare—The Role of Artificial Intelligence, 5G, Cloud Services, and Other Enabling Technologies," *International Journal of Communications, Network and System Sciences*, vol. 16, no. 3, pp. 31-51, 2023.
- [23] D. M. Mann, J. Chen, R. Chunara, P. A. Testa, and O. Nov, "COVID-19 transforms health care through telemedicine: evidence from the field," *Journal of the American Medical Informatics Association*, vol. 27, no. 7, pp. 1132-1135, 2020. <https://doi.org/10.1093/jamia/ocaa072>.
- [24] A. Ramaswamy et al., "Patient satisfaction with telemedicine during the COVID-19 pandemic: retrospective cohort study," *Journal of Medical Internet Research*, vol. 22, no. 9, e20786, 2020. <https://doi.org/10.2196/20786>.
- [25] G. S. Mosnaim, H. Stempel, D. Van Sickle, and D. A. Stempel, "The adoption and implementation of digital health care in the post-COVID-19 era," *Journal of Allergy and Clinical Immunology: In Practice*, vol. 8, no. 8, pp. 2484-2486, 2020. <https://doi.org/10.1016/j.jaip.2020.07.013>.
- [26] P. Agarwal et al., "Adoption, feasibility and safety of a family medicine-led remote monitoring program for patients with COVID-19: a descriptive study," *Canadian Medical Association Journal Open Access*, vol. 9, no. 2, E324-E330, 2021. <https://doi.org/10.9778/cmajo.20200250>.

Distributed Optimization Scheduling Consistency Algorithm for Smart Grid and its Application in Cost Control of Power Grid

Lihua Shang¹, Meijiao Sun², Cheng Pan³, Xiaoqiang San^{4*}

School of Economics and Management, Nanchang Vocational University, Nanchang, 330500, China^{1,2}
Scientific Research Office, Nanchang Vocational University, Nanchang, 330500, China³

Department of Intelligent Science and Technology, Jiangxi Tellhow Animation College, Nanchang, 330052, China⁴

Abstract—There are problems such as low scalability and low convergence accuracy in the economic dispatch of smart grids. To address these situations, this study considers various constraints such as supply-demand balance constraints, climb constraints, and capacity constraints based on the unified consensus algorithm of multi-agent systems. By using Lagrange duality theory and internal penalty function method, the optimization of smart grid economic dispatch is transformed into an unconstrained optimization problem, and a distributed second-order consistency algorithm is proposed to solve the model problem. IEEE6 bus system testing showed that the generator cost of the distributed second-order consistency algorithm in the first, second, and third time periods was 2.2475 million yuan, 5.8236 million yuan, and 3.7932 million yuan, respectively. Compared to the first-order consistency algorithm, the generator cost during the corresponding time period has increased by 10.23%, 11.36%, and 13.36%. The actual total output has reached supply-demand balance in a short period of time with the changes in renewable energy, while maintaining supply-demand balance during the scheduling process. The actual total output during low, peak, and off peak periods was 99MW, 147MW, and 120MW, respectively. This study uses distributed second-order consistency algorithm to solve the economic dispatch model of smart grid to achieve higher convergence accuracy and speed. The study is limited by the assumption that the cost functions of each power generation unit are quadratic convex cost functions under ideal conditions. This economic dispatch model may not accurately reflect practical applications.

Keywords—Distributed consistency algorithm; convex optimization; economic dispatch; smart grid

I. INTRODUCTION

In the context of rapid climate change and the crisis of non-renewable energy, traditional power grids have faced enormous challenges, such as low stability, strong concentration, and poor coordination of the power system. Therefore, the development of smart grids is urgent, and their advantages are as follows: they can achieve bidirectional flow of electricity and information, are suitable for different types of storage facilities and power generation equipment, and can automatically detect and repair system faults. Under the goal of ensuring stability, economy, and sustainability, smart grids are developing towards a more environmentally friendly, economical, safe, and efficient direction. The economic

dispatch of smart grids (EDoSG) is a process that considers multiple constraints to ensure the overall stability, safety, and economic operation of the system. Its essence is a multi-objective optimization problem. Studying EDoSG under the dual carbon target has positive significance [1-3]. With the complexity of smart grid network structure and the increase in grid scale, EDoSG has encountered significant obstacles. For example, in practical situations, factors such as energy storage devices (ESD) and renewable energy are complex and variable, and the accuracy of model solving algorithms is low. Centralized power grid economic dispatch has poor scalability, low flexibility, and low robustness, while distributed economic dispatch (DED) can achieve plug and play of power sources, avoiding the drawbacks of the former [4-5]. At the same time, the consistency theory of multi-agent systems (MAS) has been recognized by economic dispatch researchers due to its own characteristics [6-7]. In response to various constraints such as supply-demand balance (SDB) constraints, climb constraints, and capacity constraints in EDoSG optimization problems, this study will transform the optimization problem into an unconstrained optimization problem through Lagrange duality theory (LDT) and internal penalty function method (IPFM). Additionally, it combines with the consistency algorithm to design a distributed second-order consistency algorithm (D2OCA), aiming to improve the operational accuracy and convergence effect of the solving algorithm, and thereby reduce the cost of smart grids. As one of the fundamental issues in the operation of smart grids, the economic dispatch problem of smart grids is studied. A more practical smart grid economic dispatch model is considered for distributed dispatch analysis. Intelligent economic dispatch with energy storage devices and renewable energy under complex constraint conditions has outstanding advantages in practical applications. The advantages of the research are as follows: Based on the D2OCA, a consistency algorithm that can be used to solve economic scheduling problems considering generators, energy storage units (ESU), and renewable energy is proposed. The convergence performance of the proposed algorithm is verified through simulation comparison with traditional consistency algorithms. The constructed economic dispatch model achieves collaborative optimization by exchanging information with adjacent units and making autonomous decisions to adjust its own output in the communication network. The technology proposed in the study can always meet the SDB constraints

and the capacity constraints of each power generation unit during the scheduling process, and can converge to the optimal solution in a relatively fast time. This scheduling method has advantages such as strong scalability, information confidentiality and security, and robustness. It is of great significance in the fields of smart grid economy, stability, and safe operation. This study elaborates on the content from the following four sections. Section I analyzes the current situation of centralized EDoSG and smart grid DED both domestically and internationally. Section II focuses on the first-order consistency algorithm (1OCA) and D2OCA in EDoSG problems. Section III analyzes the convergence performance and accuracy of D2OCA. Section IV summarizes the research results and elaborates on the limitations and shortcomings of the study.

II. RELATED WORKS

Against the backdrop of the continuous development of new energy technologies, scholars in the field of smart grids have conducted extensive research on economic low-carbon scheduling. Guo R et al. established a stepped carbon trading model with different carbon emission ranges corresponding to different carbon trading prices. The goal of this model was to minimize the sum of power generation costs and carbon emissions, while considering safety constraints. Case studies have shown that analyzing the tiered carbon trading mechanism (TCTM) has great advantages in guiding the operation of low-carbon economy (LCE) in the system, providing necessary support for the LCE operation of smart grids [8]. Cui D's teams have proposed a peak shaving and valley filling model to regulate the LCE clean power system. It could preliminarily achieve LCE scheduling of integrated energy systems [9]. Scholars such as Zhu X have established an LCE scheduling model under TCTM, focusing on electrical and thermal integrated energy systems. Through comparative analysis of multiple scenarios, the proposed technology improved the economic benefits of the system by consuming wind power, thereby reducing the cost of the power grid [10]. Fu Y and researchers proposed a DED scheme that combines consensus theory and deep strong zeroing learning theory to solve the problems of low security and scheduling effectiveness of centralized algorithms in the optimization scheduling of smart grids. This scheme used Adam algorithm and consistency algorithm to obtain the optimal economic scheduling of unit output. This scheme was suitable for smart grids with complex network structures and could handle economic dispatch problems with large-scale data, reducing the impact of the objective function on economic dispatch results [11].

Ayalew F et al. summarized relevant literature reports on existing economic dispatch problems in smart grids, including economic dispatch, centralized and distributed algorithms, demand side management, etc. [12]. Ismi et al. analyzed the economic dispatch problem under assumed uncertainty and solved it through centralized methods under load or energy changes to maintain the stability of the power system [13]. Wang et al. proposed an economic scheduling algorithm for parallel computing in distributed power nodes, which has higher convergence performance compared to centralized methods [14]. Sadouni H et al. analyzed the current research

status of smart grid DED problems, including efficient uninitialized processes, distributed power generation systems with practical constraints, and safety [15]. Liu H et al. proposed a finite time DED model suitable for smart grids. The simulation results obtained through DED algorithm had high robustness in time-varying communication networks [16]. Table I refers to the limitations of the relevant research work.

TABLE I. LIMITATIONS OF RELATED RESEARCH WORK

| Reference | Achievement | Limit |
|----------------|--|--|
| Guo R [8] | Established a tiered carbon trading model with different carbon emission ranges corresponding to different carbon trading prices | Only considering carbon constraints and emissions |
| Cui D [9] | Proposed a peak shaving and valley filling model to regulate the economic, low-carbon, and clean power system | The applicability of scheduling models is limited |
| Zhu X [10] | Established a low-carbon economic dispatch model under a TCTM | Mainly aimed at minimizing economic operating costs |
| Fu Y [11] | Obtained the optimal economic dispatch of unit output through Adam algorithm and consistency algorithm | DED not considered |
| Ayalew F [12] | Analyzed relevant literature on existing economic dispatch problems, including economic dispatch, centralized and distributed algorithms, demand side management, etc. | No mention of D2OCA |
| Ismi [13] | Solved economic dispatch under load or energy changes through centralized methods | There are too many assumptions in the model |
| Wang S [14] | Proposed an economic scheduling algorithm for parallel computing in distributed power generation nodes, which has high convergence performance | But compared to the latest scheduling algorithms, the convergence performance is average |
| Sadouni H [15] | Analyzed the current situation of distributed power generation systems | Failure to analyze the algorithm for solving the DED model of the smart grid |
| Liu H [16] | Distributed economic scheduling algorithms have extremely high robustness in time-varying communication networks | Model solving without considering consistency algorithms |

Based on the current situation of centralized smart grid and DED, current consistency algorithms have a positive role in EDoSG optimization problems, but EDoSG also has prominent problems. In economic dispatch, few scholars analyze energy storage equipment, renewable energy, and power generation constraints. Based on this, this study proposes D2OCA to achieve EDoSG on the basis of multi-agent consensus algorithms, providing new development directions for the sustainable development of smart grids.

III. EDoSG MODEL OF D2OCA

The goal of EDoSG is to find the optimal power generation with the minimum economic cost while ensuring that the system constraints are met. The economic scheduling method commonly used in the past for generator scheduling was centralized, but the optimal scheduling solution obtained from this method cannot meet the real-time requirements of distributed power consumption and power outage. DED has

advantages such as simple protocol, strong scalability, and low complexity, which can achieve safe and stable economic operation of smart grids. The study examines different limitations, including SDB and climb constraints. Using the unified consensus algorithm of multiple intelligent systems, it transforms the optimization problem of smart grid economic dispatch into an unconstrained optimization problem through LDT, IPFM, and the alternating direction multiplier method (ADMM). At the same time, a D2OCA is proposed to solve the optimization model problem of smart grid economic dispatch.

A. EDoSG and Multi-Intelligent IOCA

The research content of DED problem in smart grid is to maximize the economic effect of power generation under the constraint of power generation unit, that is, to find the optimal power generation required at the lowest cost. The research on DED problems can be divided into three parts: problem modeling, algorithm design, algorithm analysis, and validation [17-18]. Problem modeling is a convex optimization problem, but it involves constraints such as SDB and capacity constraints in economic scheduling problems. Therefore, this study utilizes IPFM to remove capacity constraints, while utilizing LDT to address SDB constraints and climb constraints. If the set is a convex set, then all points on the line connecting any two points x_1 and x_2 in set $C \in R^n$ are in set C , then it can be considered a convex set, that is, Eq. (1).

$$\beta x_1 + (1-\beta)x_2 \in C \quad (1)$$

In Eq. (1), β refers to any real number within 0-1, and the convex function (CF) f of C on the convex set must satisfy Eq. (2).

$$f(\beta x_1 + (1-\beta)x_2) \leq \beta f(x_1) + (1-\beta)f(x_2) \quad (2)$$

When the coordinates of points x_1 and x_2 are the same. Eq. (2) takes equal sign. At this point, f is a strictly CF on the convex set C . The optimization problem with constraints

can be referred to by Eq. (3).

$$\min_x f(x) \quad s.t. g_i(x) \leq 0, h_j(x) \leq 0 \quad (3)$$

In Eq. (3), $f(x)$ and $g_i(x)$ are different CFs, $h_j(x)$ is an affine function, $i=1, \dots, n$, $m=1, \dots, m$, $j=1, \dots, j$. Fig. 1(a) is a schematic diagram of a CF.

The methods for solving convex optimization problems include Newton's method, Lagrangian dual function method, IPFM, etc. The solving principle of IPFM is shown in Fig. 1 (b). IPFM converts constraint conditions into obstacle terms that constrain the objective, and the iteration point needs to be far away from the boundary of the feasible domain to find the optimal solution. When the iteration point approaches the boundary of the feasible domain, the value of the obstacle term tends to infinity. The augmented objective function $L(x, \gamma)$ constructed by this method is represented by Eq. (4).

$$L(x, \gamma) = f(x) + \gamma b(x) \quad (4)$$

In Eq. (4), the penalty factor is γ . To reduce the impact of this parameter on the function value, it is defined as a first-order jump function, and the value increases with time. The obstacle function is $b(x)$, characterized by continuous numerical values within the feasible domain. If the constraint conditions are met, its numerical value is a finite positive number. LDT is suitable for raw optimization problems that are difficult to handle. A generalized Lagrangian function based on Eq. (3) is built and the Eq. (5) is used to refer to it.

$$L(x, a, b) = f(x) + \sum_{i=1}^n a_i g_i(x) + \sum_{j=1}^m b_j h_j(x) \quad (5)$$

In Eq. (5), the Lagrange multiplier is represented by b , and the dual variable is a . The dual problem of the original problem can be represented by Eq. (6).

$$\max_{a, b, a_i \geq 0} L_D(a, b) = \max_{a, b, a_i \geq 0} \min_x L(x, a, b) \quad (6)$$

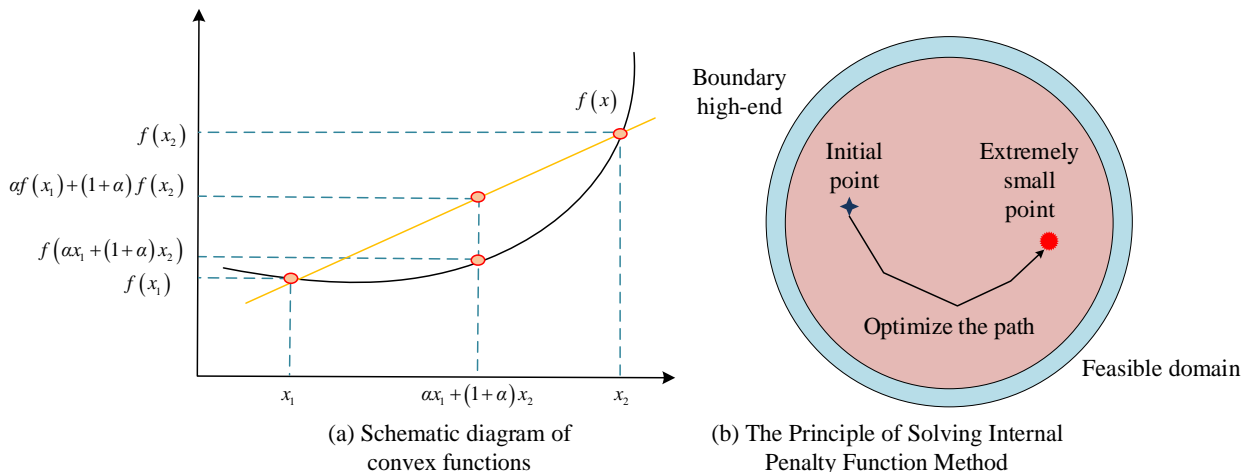


Fig. 1. The schematic diagram of CFs and the principle of solving IPFM.

In Eq. (6), $D = \{x \in R^n : k_i(x) \geq 0\}$ refers to the feasible region and $k_i(x)$ refers to the boundary function of the feasible region. The optimal solutions for the original problem and the dual problem are p^* and d^* , respectively, as shown in Eq. (7).

$$d^* = \max_{a,b,a_i \geq 0} \min_x L(x,a,b) \leq \min_x \max_{a,b,a_i \geq 0} L(x,a,b) = p^* \quad (7)$$

The ADMM, as an extension of augmented Lagrangian, is a framework for solving large-scale data in machine learning. It can transform large-scale image problems into relatively simple local sub-problems, and obtain global solutions by calculating the solutions of local sub-problems. ADMM solves constrained local problems by introducing auxiliary variables, decomposing the objective function containing the original problem into multiple easily solvable local sub-problems. ADMM is related to iterative algorithms such as splitting, multiplier methods, and dual decomposition methods, and is very suitable for solving distributed convex optimization problems. On the basis of augmenting the Lagrangian function, ADMM has multiple advantages in simplicity, efficiency, and convex optimization solving. It can solve the minimization problem with equality constraints on two variables and the objective function, as shown in Eq. (8).

$$\min_{x,z} f(x) + g(z) \quad s.t. Wx + Bz = c \quad (8)$$

In Eq. (8), x , z , and c refer to vectors, W , and B matrices. x and z are the optimization variables for the demand solution. $f(x) + g(z)$ refers to minimizing the objective function, which can be composed of the function of variable x and z . They can handle regularization terms in optimization objectives of statistical learning problems, consisting of equality constraints. The specific process of minimizing iterative solutions and updates is as follows. Combining the linear part with the quadratic term yields a concise scaling form, with the specific iteration process as follows. One is to calculate and minimize related problems, and solve variables. The second is the calculation and related minimization problem. The third is to update the dual variables until the algorithm reaches the convergence condition. The multiplier method in ADMM refers to the dual ascent method of augmented Lagrangian functions, while the alternating direction refers to the alternating updates between the original variable and the dual variable. Fig. 2 is a schematic diagram of ADMM.

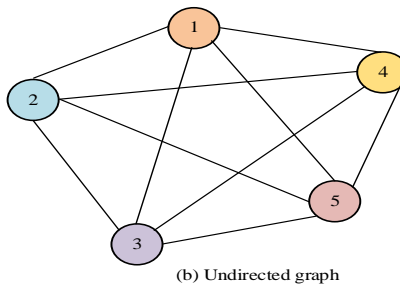
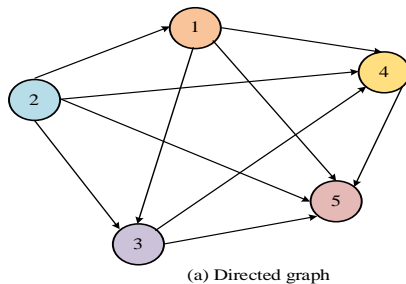


Fig. 4. Schematic diagrams of directed and undirected graphs.

B. EDoSG Combined with D2OCA

The EDoSG problem considers ESDs, renewable energy, and generators, due to differences in ideal models and power generation equipment. Therefore, the generator set needs to consider capacity constraints, climb constraints, and SDB on both sides, and based on this, construct D2OCA to solve the EDoSG problem. The MAS is a system that places individual agents to achieve overall optimization goals. According to different control strategies, MASs can be divided into three structural systems: hybrid, distributed, and centralized [19-20]. Fig. 3 is a diagram of a distributed system.

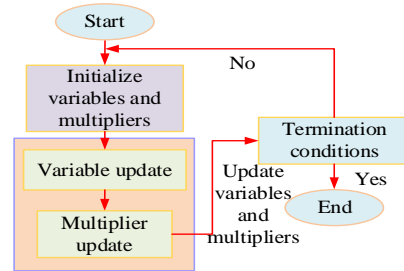


Fig. 2. Schematic diagram of alternating direction multiplier method.

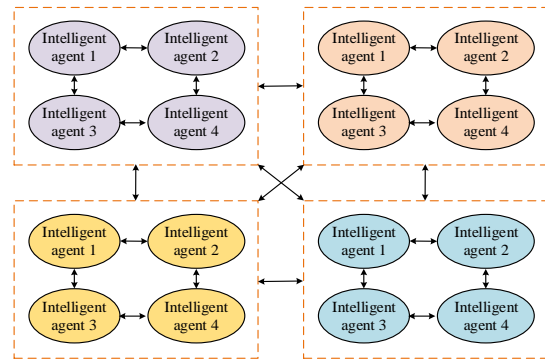


Fig. 3. Schematic diagram of a distributed system.

In a distributed architecture system, the task of each agent is to collect local information, exchange and update information with neighboring agents, with the aim of achieving task objectives. The consistency problem of MASs has been applied in EDoSG and state estimation of power networks, which can be described through graph theory. The communication topology relationships of various generator units in EDoSG can be represented through graph theory. Fig. 4(a) and 4(b) are directed and undirected graphs, respectively. The difference between the two graphs is that directed graphs have directions, while undirected graphs have no directions.

The topology of multi-agent networks is represented by an undirected graph $G=(V,E,A)$. The state information of the i -th agent in a MAS at time t is $x_i(t)$. The model of a MAS with first-order continuous time is Eq. (9).

$$\bar{x}_i(t) = u_i(t) \quad (9)$$

In Eq. (9), the control input at time t is $u_i(t)$. The classic IOCA under continuous time is expressed as Eq. (10).

$$\bar{x}_i(t) = u_i(t) = \sum_{j=1}^n a_{ij} (x_j(t) - x_i(t)) \quad (10)$$

The matrix form of Eq. (10) indicates that the states of each agent gradually reach homogeneity, i.e. $x_j(t) - x_i(t) \rightarrow 0$. The first-order consistent dynamic model of MASs in discrete-time is Eq. (11).

$$x_i(k+1) = x_i(k) + u_i(k) \quad (11)$$

The distributed consistency algorithm achieves the same value of state variables through a consistency mechanism, including average consistency, arithmetic consistency, geometric consistency, and harmonic consistency. The daily economic dispatch period can be divided into flat peak, low valley, and peak. The total demand during the corresponding time period is 128MW, 96MW, and 148MW, respectively. The total output of ESU and renewable energy is 20MW, 10MW, and 13MW, respectively. Eq. (12) is the mathematical expression for the EDoSG problem.

$$\left\{ \begin{array}{l} \min \sum_{h=1}^H \sum_{i=1}^N (f_{i,h}(P_{i,h}) + g_{i,h}(S_{i,h})) \\ \sum_{i=1}^N (P_{i,h} + R_{i,h} + S_{i,h}) = D_h \\ -P_i^R \leq P_{i,h} - P_{i,h-1} \leq P_i^R \\ P_i^m \leq P_{i,h} \leq P_i^M \\ S_i^m \leq S_{i,h} \leq S_i^M \end{array} \right. \quad (12)$$

In Eq. (12), the different time periods in the daily schedule are $h=[1,2,\dots,H]$. The output power of the i -th generator during time period h is $P_{i,h}$. The output power of the i -th ESU is $S_{i,h}$. The output power of the i -th renewable power generation unit is $R_{i,h}$. The expected electricity demand during time period h is D_h . The ramp rate limit for the i -th generator is P_i^R . The min-output and max-output of the i -th generator are P_i^m and P_i^M , respectively. The min-output and max-output of the i -th ESU are S_i^m and S_i^M , respectively. The cost functions for the i -th ESD and the i -th generator during time period h are $g_{i,h}(S_{i,h})$ and $f_{i,h}(P_{i,h})$, respectively, and the calculation formula is Eq. (13).

$$\left\{ \begin{array}{l} f_{i,h}(P_{i,h}) = a1_{i,h} P_{i,h}^2 + a2_{i,h} P_{i,h} + a3_{i,h} \\ g_{i,h}(S_{i,h}) = b1_{i,h} S_{i,h}^2 + b2_{i,h} S_{i,h} + b3_{i,h} \end{array} \right. \quad (13)$$

In Eq. (13), the cost parameters of the generator cost function are $a1_{i,h}$, $a2_{i,h}$, and $a3_{i,h}$, and the cost parameters of the ESU cost function are $b1_{i,h}$, $b2_{i,h}$, and $b3_{i,h}$. Table II shows the cost parameters of the generator in the communication topology diagram of three nodes. Each vertex in the communication topology diagram is connected to a generator, ESD, renewable energy, $i=3$, $h=3$. The Laplace matrix can be expressed as $W = \begin{bmatrix} 2 & -1 & -1 \\ -1 & 2 & -1 \\ -1 & -1 & 2 \end{bmatrix}$.

TABLE II. COST PARAMETERS OF GENERATORS IN THE COMMUNICATION TOPOLOGY DIAGRAM OF THREE NODES

| Alternator | $a1$ | $a2$ | $a3$ | P^m | P^M | P^R |
|-----------------------------|--------|------|------|-------|-------|-------|
| $P_{1,1}, P_{1,2}, P_{1,3}$ | 0.0075 | -1 | 0 | 34 | 78 | 28 |
| $P_{2,1}, P_{2,2}, P_{2,3}$ | 0.2500 | -4 | 0 | 9 | 32 | 17 |
| $P_{3,1}, P_{3,2}, P_{3,3}$ | 0.1000 | 2 | 0 | 17 | 49 | 18 |

Before solving the optimal solution, the EDoSG model needs to propose the following assumptions: the communication topology of the smart grid is connected and undirected, and the capacity constraints of the generator and ESU can be found internally. The direct solution of the EDoSG model is computationally challenging, and research is needed to transform the problem into an unconstrained optimization problem before solving it. Based on the assumptions and IPFM, the EDoSG problem can be described again using Eq. (14).

$$\left\{ \begin{array}{l} \min \sum_{h=1}^H \sum_{i=1}^N (f_{i,h}^\lambda(P_{i,h}) + g_{i,h}^\lambda(S_{i,h})) \\ \sum_{i=1}^N (P_{i,h} + R_{i,h} + S_{i,h}) = D_h \\ -P_i^R \leq P_{i,h} - P_{i,h-1} \leq P_i^R \end{array} \right. \quad (14)$$

According to LDT, the EDoSG problem can be transformed into an optimal solution of $(P^*, S^*, \mu^*, \lambda^*)$. Renewable energy has characteristics such as intermittency, volatility, and randomness, making it difficult for smart grids to control output power. To ensure the stability of the renewable energy generation grid, the smart grid is set to maintain a fixed value of renewable energy and ESUs through the output of ESUs during the time period, and the SDB can be regarded as unchanged. Based on assumptions and the expression of D2OCA, this study proposes D2OCA in the EDoSG problem. The new variables for P_i and S_i in this method are B_i and U_i , respectively, and the convergence parameters are η_p and η_s . This D2OCA has high convergence performance, which can be confirmed by the research conclusions of scholars in the supply and demand balance of smart grids. The ESU does not change with the fluctuation of renewable energy supply at the beginning of each time slot, but it can still reach the optimal solution through the convergence process within each time slot.

IV. ANALYSIS OF D2OCA SIMULATION RESULTS IN EDoSG

The performance of the D2OCA for smart grids is analyzed, including convergence performance and output power. The used testing system is the IEEE6 bus system, and the communication topology of the smart grid is represented by an undirected graph with three vertices. The cost function of generators and energy storage can be represented by a quadratic function. The classic economic scheduling algorithm, IOCA, is known for its ideal convergence accuracy and speed. The D2OCA, optimized from IOCA, is used as a comparative algorithm. Both algorithms are reasonable. The operating system is Windows 7, the storage is solid-state drives, the central processing unit is Intel Core i7, and the operating memory is 16GB. Table III shows the power generation cost parameters of the ESU. The time slot is set to 24 seconds, and the starting output power of the generator is (47, 15, 25, 72, 28, 31, 50, 23, 35) MW. The starting output power of the ESU is (5, 3, 3, 6, 3, 4, 8, 8, 4) MW. The initial values of B_i and U_i are 0, and the η_p values during low, peak, and off peak periods are 2.54, 3.95, and 2.20, respectively. The η_s value for all three time periods is 2.14, and the initial values for a and b are all 10.

This study first conducts economic dispatch simulation analysis on the output power of the generator and variable B_i . Fig. 5(a) to 5(c) show the economic dispatch results of the output power P_i , variable B_i , and incremental cost IC_i of the smart grid D2OCA. In Fig. 5(a), different generators can converge to stable values in a short period of time at different

time periods. The output power of each generator during low, peak, and off peak periods is consistent with the actual electricity consumption. There are significant differences in the output power of different generators. In Fig. 5(b), the stable values of variable B_i for different generators during the same time period are the same, which are (-2.3816, -2.3715, -3.5029). In Fig. 5(c), the incremental cost of the generator gradually converges with the output power, and the incremental cost of power generation during the low, peak, and flat peak periods is consistent, with values of 6.0874, 9.4528, and 7.7068, respectively.

TABLE III. POWER GENERATION COST PARAMETERS OF ENERGY STORAGE UNITS

| Energy storage unit | $b1$ | $b2$ | $b3$ | S^m | S^M |
|-----------------------------|------|------|------|-------|-------|
| $S_{1,1}, S_{1,2}, S_{1,3}$ | 0.7 | -1 | 0 | 0 | 30 |
| $S_{2,1}, S_{2,2}, S_{2,3}$ | 0.5 | -2 | 0 | 0 | 20 |
| $P_{3,1}, P_{3,2}, P_{3,3}$ | 0.2 | 1 | 0 | 0 | 20 |

Fig. 6(a) to 6(b) respectively refer to the iterative results of variables a and b . Both variables a and b converge to a value of 0 in a relatively short period of time. The convergence speed during low valley periods is moderate, the convergence speed during peak periods is the slowest, and the convergence speed during off peak periods is the fastest. Based on Fig. 5, when the two variables a and b reach convergence values, the output power of the generator gradually tends towards the optimal economic dispatch result.

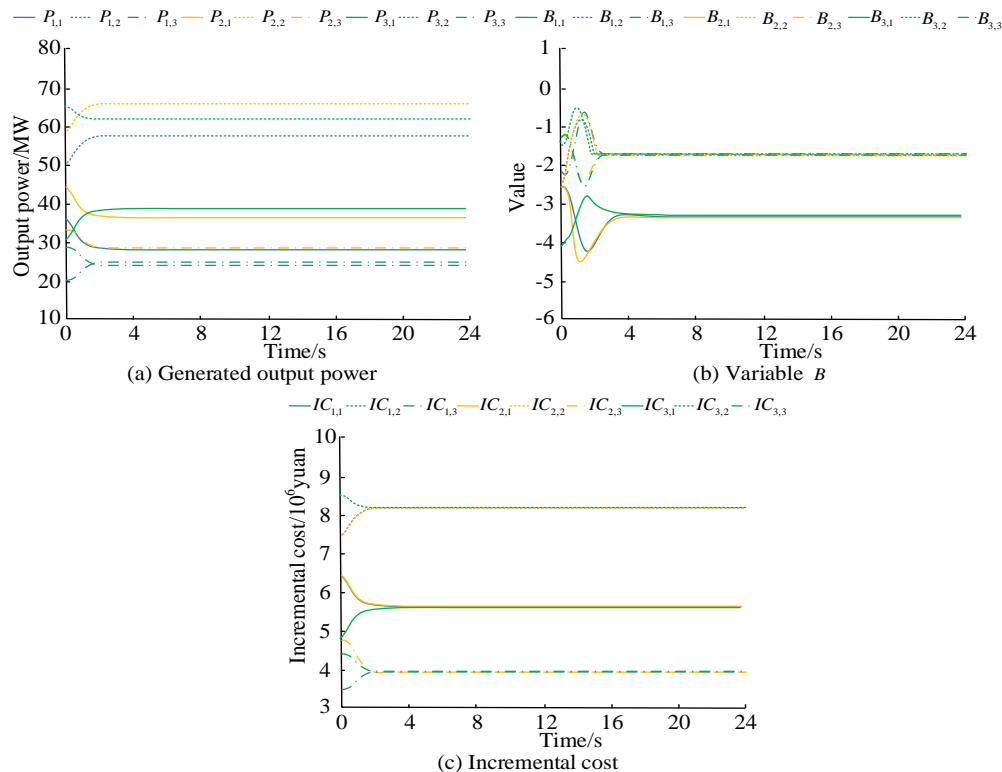


Fig. 5. Economic dispatch results of D2OCA for smart grid.

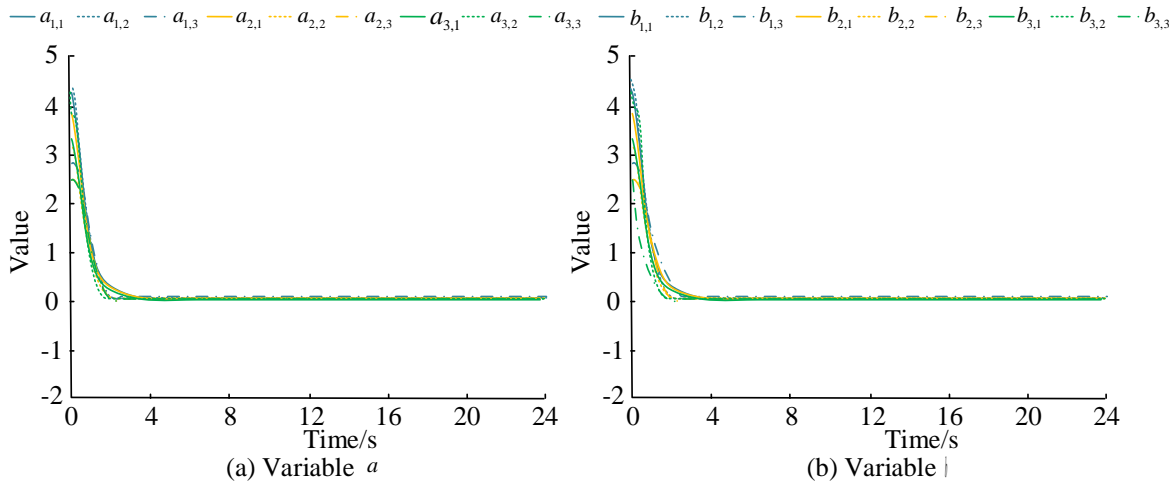


Fig. 6. Iteration results of two variables.

This study then conducts economic dispatch simulation analysis on the output power and variable U_i of the ESU. Fig. 7(a) and 7(b) respectively refer to the optimal scheduling results of the output power and variables of the ESU. In Fig. 7 (a), at the beginning of each gap, the output of renewable energy leads to the output power of the ESU, and reaches the optimal value at each time slot. There is no significant variation pattern between the output power of the ESU and the electricity consumption period and the type of ESU. The optimal scheduling results for ESUs in the first time slot are (0.747, 2.0424, 5.2028, 0.8419, 2.1896, 5.9849, 1.5867, 3.2635, 10.968). In the second time slot, the optimal

scheduling result of the ESU decreases, with values of (0.6279, 1.8568, 4.4679, 0.7356, 2.0356, 5.2132, 1.3758, 2.8965, 9.5689). When the time increases to the third time slot, the optimal scheduling result of the ESU is lower than that of the second gap, but the magnitude of the decrease does not show a clear pattern of change. In Fig. 7(b), the variable U_i for each time slot reaches a convergence value. As the time slot increases, the numerical value of convergence also gradually increases. In the third time slot, the convergence values of variable U_i are (0.1087, 0.1087, 0.1185, -0.1582, -0.1582, -0.1583, -0.3660, -0.3659, -0.3660).

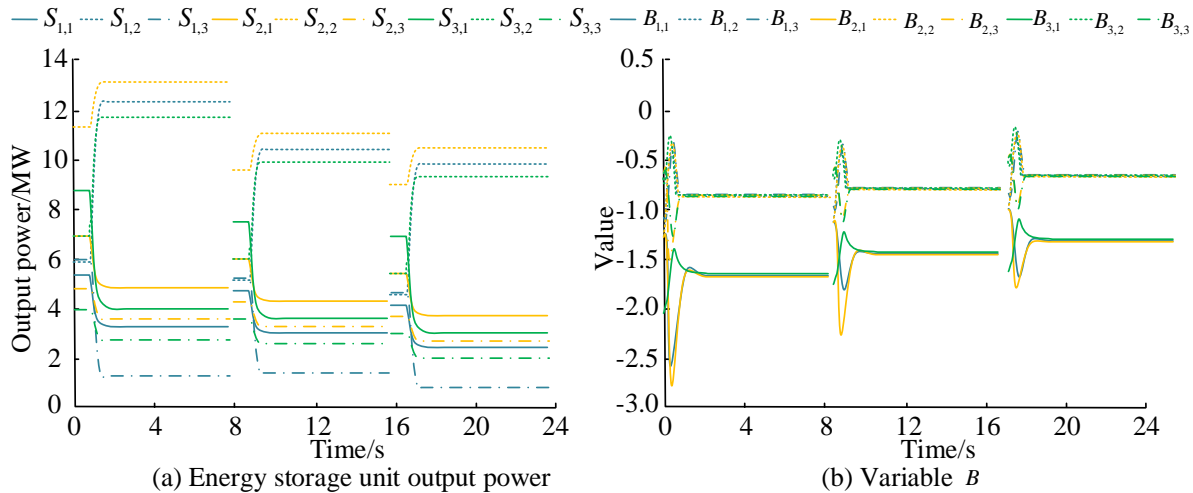


Fig. 7. Optimal scheduling results for output power and variables of ESUs.

Fig. 8 shows the simulation results of the actual total output at different time periods. The actual total output reaches SDB in a short period of time with changes in renewable energy, while remaining in SDB during the scheduling process. The actual total output during low, peak, and off peak periods is 99MW, 147MW, and 120MW, respectively.

Finally, this study validates the results of D2OCA in EDoSG by comparing it with the classic IOCA. Fig. 9(a) and

9(b) respectively refer to the output power and incremental cost of each generator. In Fig. 9(a), the variation pattern is similar to that in Fig. 5(a), but there are still differences, mainly reflected in the convergence speed and stable values. Different generators can converge to stable values in a short period of time at different time periods. There are certain differences between the output power and actual electricity consumption of each generator during low, peak, and off peak periods, and there are also significant differences in the output power of different generators during the same electricity

consumption period. The optimal scheduling result for output power is (46.5, 29.4, 17.4, 69.5, 28.1, 37.6, 58.0, 24.6, 28.5) MW. In Fig. 9(b), the incremental cost of the generator gradually converges with the output power, and the incremental cost of power generation during the low, peak, and flat peak periods is consistent, with values of (7.456, 9.251, 5.621).

Table IV shows the total cost of two consistency algorithms in EDoSG. Compared to 1OCA, D2OCA has better optimal scheduling results. The generator costs of D2OCA in the first, second, and third time periods are 2.2475 million yuan, 5.8236 million yuan, and 3.7932 million yuan, respectively, which increases by 10.23%, 11.36%, and 13.36% compared to the corresponding time periods of 1OCA. Therefore, the proposed D2OCA application in the EDoSG problem model solving process can reduce the total cost of the

generator. Therefore, D2OCA is effective and has higher convergence accuracy and speed compared to 1OCA.

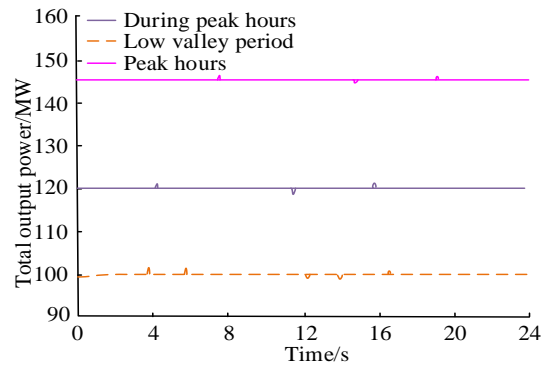


Fig. 8. Simulation results of actual total output in different time periods.

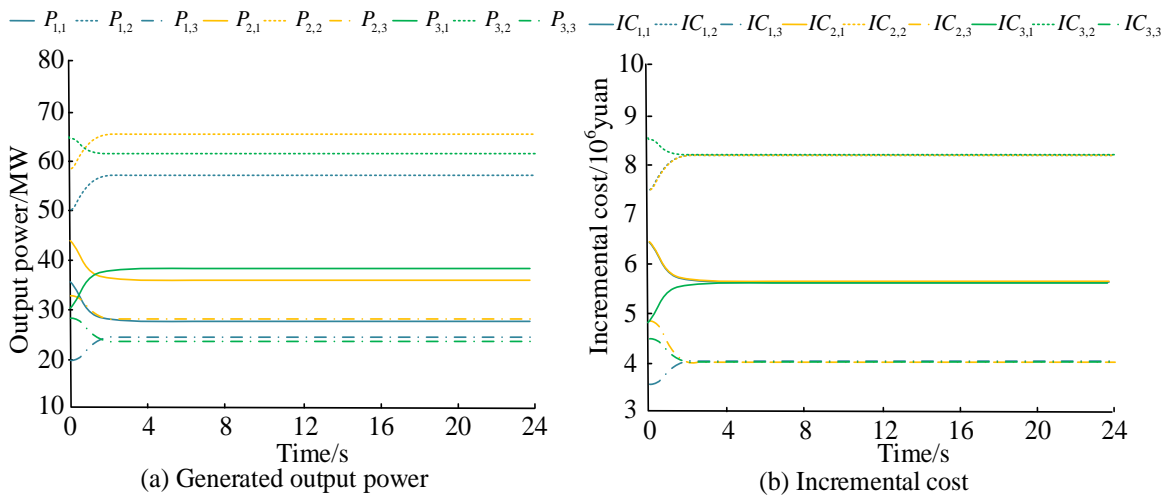


Fig. 9. Output power and incremental cost of each generator.

TABLE IV. THE TOTAL COST OF TWO CONSISTENCY ALGORITHMS IN SMART GRID ECONOMIC DISPATCH (106YUAN)

| algorithm | variable | Period 1 | Period 2 | Period 3 | Total |
|-----------|----------|----------|----------|----------|---------|
| 1OCA | P_1 | 75.362 | 185.368 | 126.375 | 387.105 |
| | P_2 | 76.465 | 176.341 | 119.351 | 372.157 |
| | P_3 | 81.268 | 191.361 | 119.829 | 392.458 |
| D2OCA | P_1 | 75.359 | 185.363 | 126.372 | 387.094 |
| | P_2 | 76.463 | 176.337 | 119.349 | 372.149 |
| | P_3 | 81.265 | 191.357 | 119.826 | 392.448 |

V. CONCLUSION

To achieve low-cost control of generators in EDoSG problems, this study innovatively proposed D2OCA based on the introduction of multi-agent consensus algorithms. The simulation of D2OCA showed that different generators could converge to a stable value in a short period of time at different time periods, and there were significant differences in the output power of different generators. The stable values of variable B_i for different generators during the same time

period were the same, which were (-2.3816, -2.3715, -3.5029). The incremental cost of generators was consistent in the three time periods of low valley, high peak, and off peak, with a total cost of 6.0874, 9.4528, and 7.7068, respectively. Both a and b variables converged to a value of 0 in a relatively short period of time. The convergence speed during low valley periods was moderate, the convergence speed during peak periods was the slowest, and the convergence speed during off peak periods was the fastest. 1OCA could converge to a stable value in a short period of time for different generators at different time periods. There was a certain difference between the output power and actual electricity consumption of each generator during low, peak, and off peak periods. The application of D2OCA in the EDoSG problem model solving process could reduce the total cost of generators. The proposed EDoSG model still has limitations, such as the communication topology of the smart grid being connected and undirected, and the capacity constraints of the generator and ESU being able to find the optimal solution internally. The study did not take into account the charging and discharging limitations of the energy storage device. Instead, it was treated as a regular power source, which is not consistent with the actual system. Subsequent research on the economic scheduling problem of non-convex smart grids with energy

storage device charging and discharging restrictions has certain practical significance.

FUNDINGS

This article is a research project of the Science and Technology Project of Jiangxi Provincial Department of Education in 2022, titled "Research on Full Process Control of Building Energy Efficiency Engineering Cost", with the serial number GJJ2204517.

REFERENCES

- [1] Ma, K., Yang, J., Guo, W., Tian, Z., Dou, C. (2020). Strategic equilibrium of economic dispatch in smart grid with a bi-level game approach. *IET Generation Transmission & Distribution*, 14(12): 2227-2236.
- [2] Xing, H., Zeng, P., Mou, Y Wu, Q. (2019). Consensus-based distributed approach to lossy economic power dispatch of distributed energy resources. *International Transactions on Electrical Energy Systems*, 29(7). e12041-e12057.
- [3] Yang, Y., Wei, B., Qin, Z. (2019). Sequence-based differential evolution for solving economic dispatch considering virtual power plant. *IET Generation Transmission & Distribution*, 13(15), 3202-3215.
- [4] Bandewad G, Datta K P, Gawali B W, Pawar, S. N. (2023). Review on Discrimination of Hazardous Gases by Smart Sensing Technology. *Artificial Intelligence and Applications*. 1(2): 86-97.
- [5] Gheisari M, Hamidpour H, Liu Y, Saedi P, Raza A, Jalili A, Rokhsati H, Amin R. (2023). Data Mining Techniques for Web Mining: A Survey. *Artificial Intelligence and Applications*, 1(1): 3-10.
- [6] Dai, H., Fang, X., Jia, J. (2022). Consensus-based distributed fixed-time optimization for a class of resource allocation problems. *Journal of the Franklin institute*, 359(18): 11135-11154.
- [7] Kull, T., Zeilmann, B., Fischerauer, G. (2021). Field-ready implementation of linear economic model predictive control for microgrid dispatch in small and medium enterprises. *Energies*, 14(13), 3921-3943.
- [8] Guo, R., Ye, H., Zhao, Y. (2022). Low carbon dispatch of electricity-gas-thermal-storage integrated energy system based on stepped carbon trading. *Energy Reports*, 8, 449-455.
- [9] Cui, D., Ge, W., Zhao, W., Jiang, F., Zhang, Y. (2022). Economic low-carbon clean dispatching of power system containing P2G considering the comprehensive influence of multi-price factor. *Journal of electrical engineering & technology*, 17(1), 155-166.
- [10] Zhu, X., Xue, J., Hu, M., Liu, Z., Gao, X., Huang, W. (2023). Low-carbon economy dispatching of integrated energy system with P2G-HGT coupling wind power absorption based on stepped Carbon emission trading. *Energy Reports*, 10, 1753-1764.
- [11] Fu, Y., Guo, X., Mi, Y., Yuan, M., Li, Z. (2021). The distributed economic dispatch of smart grid based on deep reinforcement learning. *IET Generation Transmission & Distribution*, 15: 2645-2658.
- [12] Ayalew, F, Hussien, S., Pasam, G. K. (2019). Economic load dispatch problems in smart grid: a review. *IJEAST*, 3(11): 71-77.
- [13] Ismi, Rosyiana, Fitri, Jung-Su, Kim. (2019). Economic dispatch problem using load shedding: centralized solution. *IFAC-PapersOnLine*, 52(4), 40-44.
- [14] Wang, S., Xing, J., Jiang, Z., Li, J. (2019). Decentralized economic dispatch of an isolated distributed generator network. *International Journal of Electrical Power & Energy Systems*, 105(FEB.), 297-304.
- [15] Sadouni, H., Rami, A. (2022). Optimal economic dispatch of smart grid system. *Przeglad Elektrotechniczny* (2), 98(1): 25-39.
- [16] Liu, H., Fan, H., Wang, B., Liu, L., Lei, S. (2022). Event-triggered scheme for finite-time distributed economic dispatch in smart grids. *J. Frankl. Inst.*, 359, 10602-10627.
- [17] Wu, X., Sun, Y., Wei, Z., Sun, G. (2019). Distributed hierarchical consensus algorithm for economic dispatch in smart grid. *IET Generation, Transmission & Distribution*, 13(24), 5541-5549.
- [18] Xu, Q., Yu, C., Yuan, X., Fu, Z., Liu, H. (2023). A privacy-preserving distributed subgradient algorithm for the economic dispatch problem in smart grid. *Journal of Automation: English Edition*, 10(7), 1625-1627.
- [19] Anestis, A., Georgios, V. (2019). Economic benefits of smart microgrids with penetration of der and mchp units for non-interconnected islands. *Renewable Energy*, 142(NOV.), 478-486.
- [20] Mazzoni, S., Ooi, S., Nastasi, B., Romagnoli, A. (2019). Energy storage technologies as techno-economic parameters for master- planning and optimal dispatch in smart multi energy systems. *Applied Energy*, 254(Nov.15), 113682.1-113682.17.

Evaluating the Accuracy of Cloud-based 3D Human Pose Estimation Tools: A Case Study of MOTiO by RADiCAL

Hamza Khalloufi^{1*}, Mohamed Zaifri², Abdessamad Benlahbib³, Fatima Zahra Kaghat⁴, Ahmed Azough⁵

Laboratory of Informatics, Signals, Automatics and Cognitivism (LISAC) Faculty of Sciences Dhar El Mahraz,
University Sidi Mohamed Ben Abdellah, Fez, Morocco^{1,2,3}

Research Center, Pôle Universitaire Léonard de Vinci, Paris, France^{4,5}

Abstract—The use of 3D Human Pose Estimation (HPE) has become increasingly popular in the field of computer vision due to its various applications in human-computer interaction, animation, surveillance, virtual reality, video interpretation, and gesture recognition. However, traditional sensor-based motion capture systems are limited by their high cost and the need for multiple cameras and physical markers. To address these limitations, cloud-based HPE tools, such as DeepMotion and MOTiO by RADiCAL, have been developed. This study presents the first scientific evaluation of MOTiO by RADiCAL, a cloud-based 3D HPE tool based on deep learning and cloud computing. The evaluation was conducted using the CMU dataset, which was filtered and cleaned for this purpose. The results were compared to the ground truth using two metrics, the Mean per Joint Error (MPJPE) and the Percentage of Correct Keypoints (PCK). The results showed an accuracy of 98 mm MPJPE and 96% PCK for most scenarios and genders. This study suggests that cloud-based HPE tools such as MOTiO by RADiCAL can be a suitable alternative to traditional sensor-based motion capture systems for simple scenarios with slow movements and little occlusion.

Keywords—3D; human pose estimation; animation; evaluation; motion tracking

I. INTRODUCTION

Due to its crucial applications in human-computer interaction, surveillance, virtual reality [36], video interpretation, gesture recognition, and many other fields, as depicted in Fig. 1, 3D human body pose estimation (3D HPE) has attracted substantial interest in computer vision. Nevertheless, despite recent advancements, motion capture (MoCap) systems still rely on costly sensor-based systems consisting of multiple-camera setups and heavy motion capture suits with physical markers that allow position estimation. A considerable number of studies have been conducted using several approaches. However, the most significant advances in that field have been made in recent years thanks to breakthroughs in deep learning and convolutional neural networks.

Recently, cloud-based 3D HPE tools, such as MOTiO by RADiCAL and DeepMotion, have become more popular for a variety of reasons, including the needless for a powerful computer since processing is done in the cloud, the intuitive graphical user interface, and the ready-to-use outputs by almost

all 3D computer graphics software. These tools are generally based on deep learning techniques and offer the ability to directly convert 2D videos to 3D coordinate files through FBX motion frames in a short time. Despite the widespread adoption of those tools, scientific evaluation of their accuracy has yet to be published to determine whether they can serve as an alternative to conventional sensor-based motion capture systems.

In this research, we are especially interested in evaluating the accuracy and suitability of 3D HPE tools based on deep learning and cloud computing. We aim to address the following research questions:

- How accurate are cloud-based 3D HPE tools in estimating human poses compared to ground truth data?
- Can cloud-based 3D HPE tools serve as a feasible alternative to traditional motion capture systems in various scenarios?

Therefore, MOTiO by RADiCAL 3D HPE tool was chosen as a case study. To achieve this goal, we now go over how the CMU dataset was cleaned and filtered for use in this study. The dataset contains multiple scenarios, each of which includes a range of actions seen in videos and the resulting 3D human poses. These videos were used to obtain 3D coordinates for each human joint. For quantitative evaluation, the results were compared to the ground truth after Procrustes alignment [1]. Several metrics, including Mean per Joint Position Error (MPJPE) and Percentage of Correct Keypoints (PCK), were used to evaluate the results of each scenario and both genders. The second sort of evaluation is qualitative, in which one frame from each situation is selected and visually evaluated.

Quantitative results revealed that the MOTiO by RADiCAL tool is adequate for most scenarios and genders. However, it has several limitations, particularly for occlusion and dynamic motions. After data analysis, it is considered that these cloud-based tools could advantageously replace the expensive traditional tools for simple scenarios with slow movements and little occlusion. As for qualitative results, nine scenarios have been accurately estimated, whereas the skeleton or some of its components were misaligned in the other scenarios.



Fig. 1. Facebook's markerless body tracking for VR from a single sensor.

This study is structured to provide a comprehensive evaluation of cloud-based 3D HPE tools, with a specific focus on the MOTiON by RADiCAL system. The structure and goals of this research are aligned to achieve several key contributions:

- 1) Presents the first comprehensive scientific evaluation of a case study of cloud-based 3D HPE, assessing its accuracy using robust metrics.
- 2) It contributes to the broader understanding of the potential and limitations of cloud-based 3D HPE tools in various realistic scenarios.
- 3) The findings could potentially influence future developments in 3D HPE technology, enhancing the accessibility and applicability of cloud-based motion capture solutions.

The organization of the paper is as follows: the related works in Section II reviews prior studies and developments within the field, detailing advancements and challenges in 3D HPE, setting the stage for the current research. The methodology in Section III details the datasets employed in the study, the evaluation metrics used specifically MPJPE and PCK and the experimental setup designed to test the efficacy of the 3D HPE tool. Results in Section IV, presents both quantitative and qualitative analyses that compare the performance of MOTiON by RADiCAL against established ground truth data, highlighting the tool's accuracy and operational characteristics in various scenarios. The discussion in Section V interprets these results, exploring their implications for the field of 3D HPE and discussing potential limitations of the study. Finally, the conclusion in Section VI summarizes the key findings and proposes directions for future research, suggesting how improvements could enhance the utility and accuracy of cloud-based 3D HPE tools.

II. RELATED WORKS

A. 3D Human Pose Estimation

Over the past few years, there has been a growing interest in 3D HPE due to its ability to provide accurate information about the 3D structure of the human body. 3D HPE seeks to predict the location of body joints in 3D space. It can be

applied to a variety of situations (e.g., 3D animation movies, extended realities, and cloud-based 3D action estimation). Even though 2D HPE has recently seen significant advancements, 3D HPE is still a challenging task to complete. Recent research in the field of computer vision has been focused on the extraction of 3D human pose estimation (HPE) from monocular images or videos. Those are a 2D representation of a 3D scene, resulting in the loss of one dimension. As a result, researchers have been working on developing algorithms and techniques to accurately estimate the 3D pose of human subjects from these 2D images. 3D human pose estimation can be a well-defined problem that is solvable using information fusion methods if there are multiple perspectives or additional sensors such as IMU and LiDAR available. However, one drawback of using deep learning models for this task is their high data dependence and sensitivity to data collection circumstances. Extensive amounts of annotated data are necessary for these models to learn accurate representations of input and output spaces, and factors such as lighting conditions, camera positions, and background can influence their performance negatively.

While obtaining accurate two-dimensional posture annotations for human datasets is relatively straightforward, obtaining accurate three-dimensional pose annotations is considerably more challenging and cannot be done manually. Furthermore, datasets are often collected in controlled indoor settings that focus on specific activities, making them biased towards these scenarios. Recent studies have shown that models trained on such biased datasets tend to perform poorly when applied to other datasets, as demonstrated by cross-dataset inference [2], [3].

1) *Single-person 3D HPE*: The strategies of Single-person 3D HPE can be categorized as model-free or model-based methods. The first one can be divided into two categories:

a) *Direct estimate techniques*: instead of first estimating the 2D pose representation, some algorithms in 3D human pose estimation employ direct estimation techniques, as seen in [4], [5], to directly infer the 3D human position from 2D images. Recent advancements include the study by H Ye et al., which enhances real-time 3D pose estimation efficiency through orthographic projection techniques, simplifying the direct estimation process from images without intermediate 2D pose estimation [33].

b) *2D to 3D lifting techniques*: The process of inferring 3D poses from intermediate 2D pose pairings is inefficient because it requires multiple network inferences. Human body models are not used in the model-free approaches for recreating 3D human representations. Standard 2D HPE models are used in the first stage to estimate the 2D posture, and 2D to 3D lifting is used in the second stage to construct the 3D pose, such as [6], [7], and [5]. 2D heatmaps rather than 2D poses were used as intermediate representations to estimate 3D posture ([8] and [9]). Through distance matrix regression, Moreno-Noguer [10] deduced the 3D human position from the distances between the joints in the 2D and 3D body (EDMs). When normalization techniques are used, EDMs are invariant to scaling invariance as well as in-plane

image rotations and translations. A Paired Ranking Convolutional Neural Network (PRCNN) was created by Wang et al. [11] to predict the depth ranking of pairwise human joints. The 3D pose was then regressed from the 2D joints and the depth ranking matrix using a coarse-to-fine pose estimator. Li and Lee [12], Sharma et al. [13], and Jahangiri and Yuille [14] were the first to develop numerous, different 3D pose hypotheses. Recent work by C Han et al. introduces uncertainty learning to improve the accuracy and robustness of 3D pose estimations from single images, effectively enhancing this lifting process [34].

Parametric body models, such as kinematic and volumetric models, are utilized by model-based methods to estimate human position, as illustrated in Fig. 2.

The kinematic model represents the body as a series of joints and articulating bones, and in recent years, it has garnered increasing attention in the field of 3D human pose

estimation. Pavlo et al. [15] suggested a temporal convolution network for estimating 3D posture from sequential 2D sequences using 2D keypoints. A Short-Term Long Memory (LSTM) unit and shortcut connections were employed in a recurrent neural network to leverage temporal information from human pose data [16].

The Skinned Multi-Person Linear (SMPL) model is among the most commonly utilized volumetric models in the field of 3D HPE, as evidenced by its implementation in works such as [17], [18].

2) *Multi-person 3D HPE*: There are two approaches for 3D multi-person human pose estimation from monocular RGB images or videos, which are classified into top-down and bottom-up categories. These approaches are illustrated in Fig. 3.

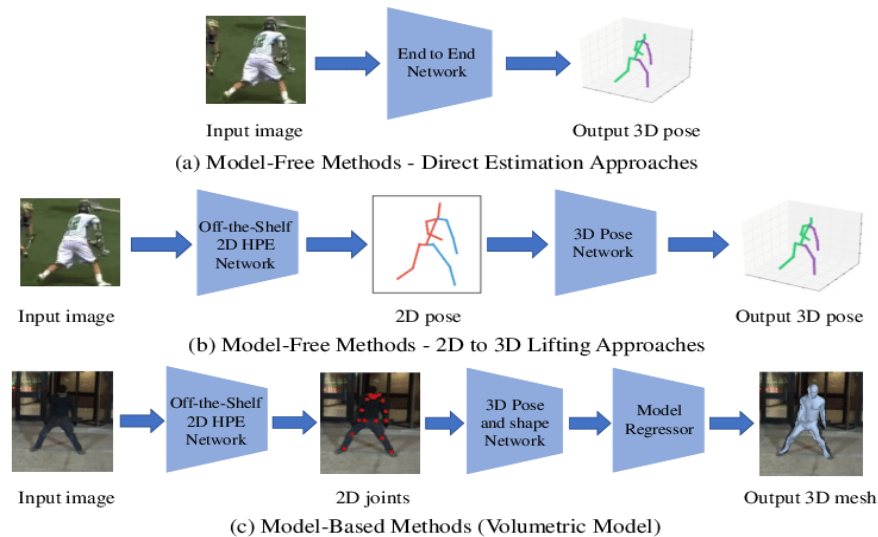


Fig. 2. Frameworks of 3D single-person pose estimation [19] (a) This method is done in one stage, i.e., directly from RGB image to 3D pose. (b) The approaches perform 3D HPE using a two-stage approach, i.e., it performs 2D HPE first and then uses the 2D keypoints to get 3D ones. (c) The 3D mesh is obtained using a regression stage on the 3D HPE outputs.

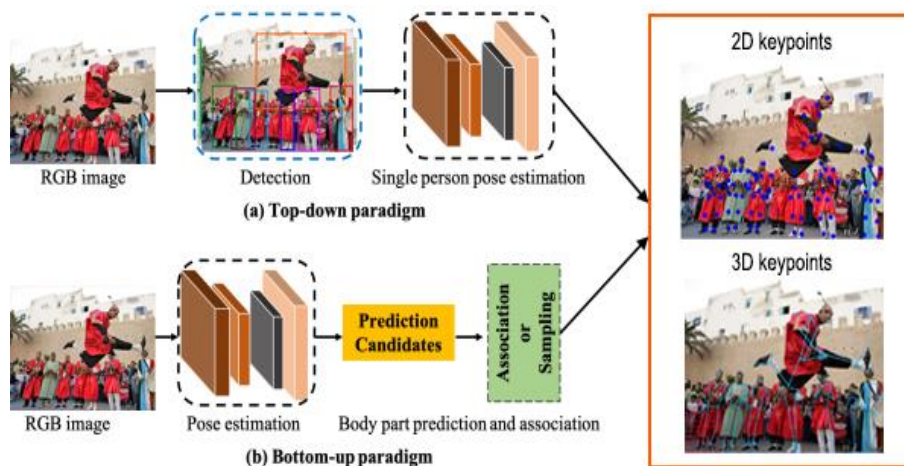


Fig. 3. Frameworks of 2D and 3D multi-person pose estimation [27] (edited). (a) The top-down approach uses person detection techniques to determine the number of persons detected in the frame, and then it applies a 2D single-person estimation framework. (b) The bottom-up approach identifies each joint in the image and then associates each one with individuals.

a) *Top-down approaches*: They use human detection to estimate each person's position. Each time a person is identified, 3D pose networks estimate their root (the human body's central joint) coordinate and their 3D root-relative posture. Rogez et al. [20] targeted candidate areas of each individual to produce prospective postures and then utilized a regressor to improve the pose suggestions jointly. The LCR-Net technique, which involves localization, classification, and regression, performed well on datasets collected in controlled environments, but not on images captured in natural settings. To address this limitation, LCR-Net++ was introduced, which utilizes synthetic data augmentation during training to improve performance. [21]. The 3D multi-person HPE module was enhanced with scene constraints and semantic segmentation [22]. The 3D temporal assignment problem was also tackled by the Hungarian matching approach for video-based multi-person 3D HPE, which achieved impressive results in [23], [24]. L Jin et al. introduced a single-stage method that integrates human detection and pose estimation, simplifying the process and enhancing efficiency by directly estimating 3D poses from detected individuals in a single network pass, demonstrating significant improvements over traditional multi-stage methods [35].

b) *Bottom-up approaches*: First, generate joint positions and depth maps for all body joints. They then assign body parts to each individual based on the root depth and relative depth of the body component [25], [26]. How to categorize human body joints is a fundamental difficulty for these techniques. Methods at a lower level exploit the common latent space between two distinct modalities.

B. Datasets for 3D HPE

Obtaining precise 3D labeling for 3D human pose estimation datasets is a difficult endeavor that necessitates the use of motion capture techniques such as MoCap and wearable IMUs. Since the 3D HPE deep learning-based needs larges datasets to train, validate, and test their models, several 3D posture datasets are created due to this need.

1) *HumanEva Dataset* [28]: It includes seven calibrated video sequences (4 grayscale and three colors) with ground truth 3D annotation taken by a ViconPeak commercial MoCap system. The database comprises four scenarios executing six common actions in a $3m \times 2m$ area: walking, jogging, pointing, throwing and catching a ball, boxing, and combination.

2) *Human3.6M* [29]: One of the most commonly used datasets for indoor 3D human pose estimation from monocular images and videos. The dataset features 11 professional actors (six males and five females) performing 17 actions (such as smoking, taking photos, and talking on the phone) in a laboratory environment captured from four different perspectives.

3) *The CMU Graphics Lab Motion Capture Database (CMU)* [30]: CMU is one of the most publicly large databases of motion capture data. Numerous researchers within the scientific world have utilized it to develop previous models of

human motion. However, the dataset is poorly synced and contains some films unsuitable for HPE due to multiple actors in each scene. The database comprises more than 100 scenarios executing several actions in a $3m \times 8m$ area.

III. METHODOLOGY

After extracting videos from CMU and their associated BVH pose files, a preprocessing stage comprising: cleaning (i.e., avoid corrupted sequences or those that do not verify the necessary conditions), reorganization (i.e., reclassifying all sequences into 12 scenarios), and synchronization (because the BVH poses files are not synchronized with the associated videos) was performed. The sequences in video format were then processed in the cloud with RADiCAL. Both BVH poses of CMU and RADiCAL were rendered using a virtual camera to get the 3D coordinates of each joint. Then two evaluation types were performed; the first one was quantitative, which compared both poses of RADiCAL (as predicted results) and those of CMU (as a ground-truth one). The other evaluation type is a qualitative one based on visual analysis of the predicted 3D human pose scenario according to the ground truth. The workflow was summarized in Fig. 4.

A. Data Preprocessing

The CMU Graphics Lab Motion Capture Database (CMU) was obtained using 12 Vicon MX-40 infrared cameras, each capable of collecting 4-megapixel pictures at 120 Hz. The cameras are positioned around a $3m \times 8m$ rectangle area in the center of the room. The actor wears a black jumpsuit with 41 markers affixed to it while infrared Vicon cameras detect the markings. The pictures captured by the numerous cameras are triangulated to provide three-dimensional data.

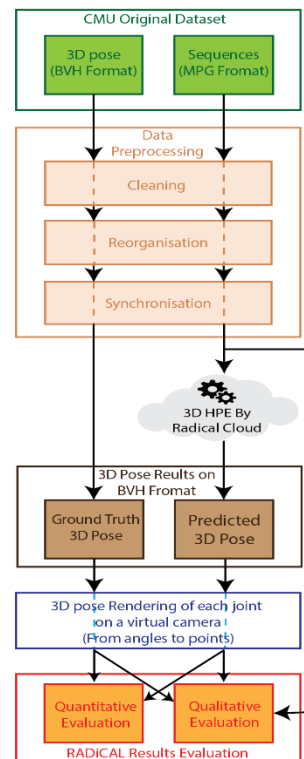


Fig. 4. Overview of the suggested approach.

Despite the dataset covering many scenarios (more than 100), several sequences are without their corresponding videos. Many videos are corrupted, contain more than one actor, or do not contain all body parts. In addition, all files, including BVH and Videos, need to be synced. Therefore the dataset was edited following the three steps below:

1) *Cleaning*: some corrupted videos were eliminated, and the rest were repaired by hiding the second actor, if that is possible.

2) *Reorganization*: the sequences were classified into 12 essential scenarios, as shown in Table I.

3) *Synchronization*: since all BVH frames are not synced with videos, a manual process was manually done using Blender. Also, the sequences captured with 120 or 60 FPS were decreased to 30 FPS since the RADiCAL support only motion capturing with 30 FPS.

B. MOTiON by RADiCAL

MOTiON by RADiCAL is a model-based 3D HPE AI-driven and cloud-based software that converts 2D movies into complete 3D animation with 6 degrees of freedom. The animation data is stored with 30 FPS into FBX (Filmbox), a format that allows the exchange of geometric and animation data between 3D animation software, such as Blender.

For the study, the sequences in MPG format were imported to the RADiCAL cloud then the HPE was processed using the RADiCAL model. After a few moments, the FBX files were done. In order to compare those results to CMU's ground truth, the FBX output files were converted to BVH format using Blender. The output skeleton and the joints are shown in Fig. 5.

C. BVH Projecting to 3D Coordinates

The motion capture of videos from the RADiCAL and CMU datasets is stored in BVH format, including the root transaction coordinates and Euler angles for each joint. As illustrated in Fig. 6, all the coordinates, including those in the

BVH files, were projected to a 3D virtual camera to obtain the 3D coordinates of each joint.

Algorithm 1 computes the joint coordinates in camera space from a BVH file containing joint hierarchy and motion data. The algorithm starts by defining the camera intrinsic matrix K , which represents the camera's internal parameters such as focal length and principal point. The camera extrinsic matrix C is also defined, which represents the camera's external parameters such as position and orientation in global space.

$$K = \begin{pmatrix} f_x & 0 & c_x \\ 0 & f_y & c_y \\ 0 & 0 & 1 \end{pmatrix} \quad (1)$$

Algorithm 1: Extract 3D Joint Coordinates from BVH File.

| |
|--|
| Algorithm: Compute Joint Coordinates in Camera Space from BVH File |
| Input: BVH file with joint hierarchy and motion data |
| Output: 3D joint coordinates in camera space for each frame of motion data |
| 1) Load BVH file and extract joint hierarchy and motion data. |
| 2) Define camera intrinsic matrix K with focal lengths f_x and f_y and principal point coordinates c_x and c_y . |
| 3) Define camera extrinsic matrix C with rotation matrix R and position vector P . |
| 4) For each frame of motion data, traverse the joint hierarchy in forward kinematics to compute global joint positions. |
| 5) Transform global joint positions to camera coordinates using K and C . |
| 6) Output the 3D joint coordinates in camera space for each frame of motion data. |
| End algorithm. |

TABLE I. CMU DATASET COMPONENT AFTER CLEANING, FILTERING, AND CLASSIFICATION

| Number of scenarios | Number of sequences | Number of views | Frequency | Scenarios | Number of frames |
|---------------------|---------------------|-----------------|-----------|------------------|------------------|
| 12 | 279 | 1 | 30 FPS | Animal behaviors | 62 454 |
| | | | | Climbing | 981 |
| | | | | Daily activities | 6 306 |
| | | | | Dancing | 1 122 |
| | | | | Home activities | 56 359 |
| | | | | Jumping | 1 553 |
| | | | | Reactions | 12 852 |
| | | | | Running | 332 |
| | | | | Sitting | 4 548 |
| | | | | Sport | 9 714 |
| | | | | Walking | 16 493 |
| | | | | Working | 11 952 |
| | | | | Female | 71 759 |
| | | | | Male | 112 907 |
| | | | | All | 184 667 |

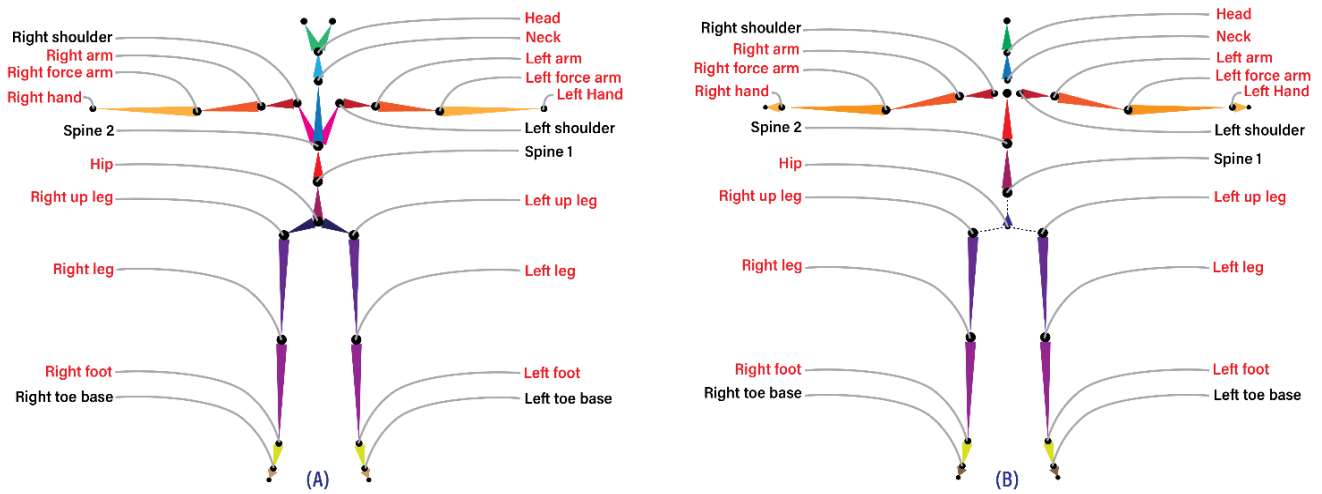


Fig. 5. Skeleton model hierarchy of CMU. (B): Skeleton model hierarchy of RADiCAL. The red ones are the chosen joints to perform the quantitative evaluation.

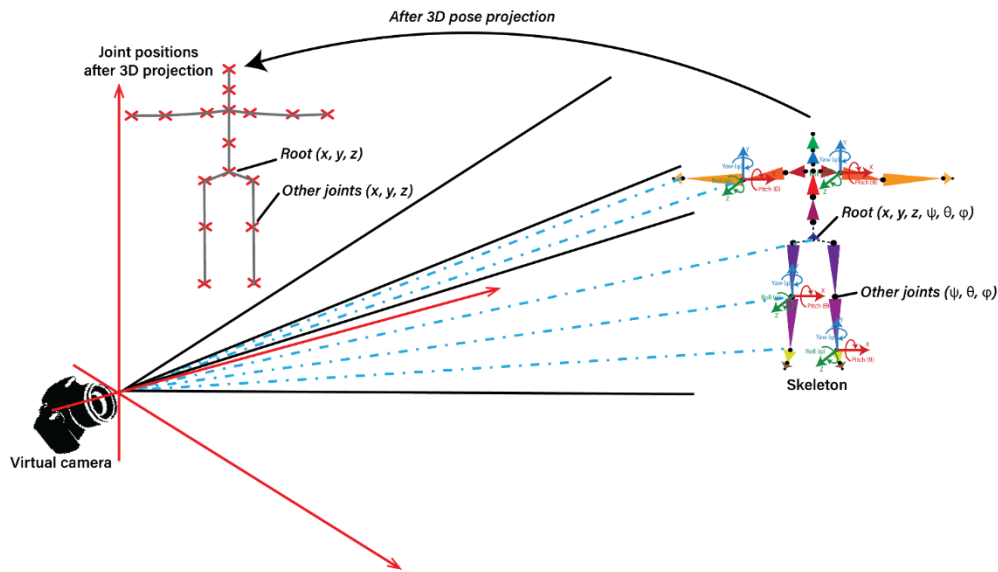


Fig. 6. Rendering process of CMU and RADiCAL skeletons. The purpose is to obtain the 3D pose coordinate of joints from angles.

where, f_x and f_y are the focal lengths of the camera in x and y directions, and c_x and c_y are the coordinates of the principal point of the camera.

$$C = \begin{pmatrix} r_{11} & r_{12} & r_{13} & t_1 \\ r_{21} & r_{22} & r_{23} & t_2 \\ r_{31} & r_{32} & r_{33} & t_3 \end{pmatrix} \quad (2)$$

where, r_{ij} is the rotation matrix that describe the camera's orientation in global space, and t_i is translation offset. The joint positions and orientations for each frame in the motion data are then computed using forward kinematics, with the root joint's global position and orientation serving as the initial values. The global positions and orientations of child joints are then computed by traversing the joint hierarchy, and the resulting global joint positions are transformed to camera coordinates using the intrinsic and extrinsic matrices. This transformation can be represented mathematically as:

$$\begin{pmatrix} X_{position_camera} \\ Y_{position_camera} \\ Z_{position_camera} \end{pmatrix} = K \times C \times \begin{pmatrix} X_{position_global} \\ Y_{position_global} \\ Z_{position_global} \\ 1 \end{pmatrix} \quad (3)$$

where, $(X_{position_global}, Y_{position_global}, Z_{position_global})$ the global joint position in 3D space, and the resulting is $(X_{position_camera}, Y_{position_camera}, Z_{position_camera})$ is the joint position in camera coordinates. This algorithm provides the way to extract joint positions in camera space from a BVH file.

D. Skeleton Scaling and Evaluation Metrics

1) *Skeleton scaling*: Since the skeletons of CMU and Radical are not similar, the Procrustes analysis was used to determine the scale [1], rotation, and translation. Given correspondences of points $A_j \in R^3$ and $B_j \in R^3$ of the joint j find scaling, rotation, and translation transformation, called similitude transformation that satisfies:

$$A_j = sRB_j + T \quad (4)$$

For $R \in SO(3), T \in R, \text{ and } s \in R^+$

2) *Evaluation metrics:* Our experiments use two metrics. The first is the mean per-joint position error (MPJPE [29]) between the ground-truth 3D pose and the predicted 3D pose, which is calculated using the Eq. (5): Then, we calculate the mean error across all poses and actions in the dataset.

$$MPJPE = \frac{1}{m} \sum_{i=1}^m \|p_i^3 + \bar{p}_i^3\|_2 \quad (5)$$

For a given skeleton comprising m joints, p_i^3 denotes the actual 3D pose of joint i , whereas \bar{p}_i^3 signifies the predicted 3D pose of the same joint.

The second metric is the Percentage of Correct Keypoints for 3D Pose Estimation (PCK3D) [31], a 3D version of the PCK utilized for 2D pose estimation [32]. If the estimated joint location is within a reasonable distance of the ground-truth joint, it is considered to be accurately estimated. Then, the proportion of accurately calculated joints is computed. As in earlier research, the neighborhood threshold is chosen at 150mm [31], corresponding to about half the head size. This statistic is more expressive and robust than MPJPE, highlighting joint mispredictions more clearly. A 15 keypoints were examined, which are indicated in red in Fig. 5.

IV. RESULTS

As stated previously, qualitative and quantitative evaluations were performed. With the restructured CMU dataset, the initial step was to obtain the MPJPE and the PCK by scenario and gender. The second sort of evaluation consisted of picking 3D postures of various scenarios and visually analyzing the results' accuracy.

A. Quantitative Evaluation

The results obtained using MOTiON by RADiCAL cloud-based were compared with the ground-truth 3D poses from the reconstructed CMU dataset using two metrics measurements (MPJPE and PCK). The 3D poses were classified by gender and scenario to assess the accuracy of each one. Then the accuracy of each joint was discussed.

1) *Comparing by joints:* In this evaluation, 15 crucial joints were analyzed, as depicted in Fig. 5 where the red joints are highlighted. The results are presented in Table II and Fig. 7, displaying the highest mean error values of the Middle Hip, Left Wrist, and Right Wrist joints. While, the lowest mean error values were obtained for the Shoulders, Knees, Nose, and Nick.

2) *Comparing by scenarios:* Fig. 8 and Table III show that the MPJPE varied from 90,7 mm to 119,1 mm, depending on the scenario. The walking scenario was the most accurate, with an MPJPE of 90.7 mm, whereas the running scenario was the least accurate.

Each scenario's MPJPE (walking, jumping, dancing, reaction, and animal behavior) was under 100 mm while they

were near one another, except for home activities, who's MPJPE was just under 100 mm. The MPJPE is more than 100 mm for the remaining scenarios (daily activities, working, climbing, sitting, sports, and running). Expect "Running," "Sitting," and "Sport"; all the scenarios were accurate with higher than 90% of correct joints according to the PCK values of each one. The scenarios: "Home activities," "Jumping," "Reactions," and "Walking" had a PCK near 100%. Expect running and sports scenarios with a standard deviation of around 70 mm. Every other scenario was within 50 mm.

TABLE II. MEAN ERROR BY JOINTS

| Joints | Mean (mm) | Standard deviation (mm) |
|----------------|-----------|-------------------------|
| Nose | 85.28 | 36.11 |
| Neck | 87.15 | 27.30 |
| Right Shoulder | 77.96 | 33.85 |
| Right Elbow | 99 | 41.29 |
| Right Wrist | 116.96 | 77.72 |
| Left Shoulder | 70.52 | 30.86 |
| Left Elbow | 103.61 | 49.12 |
| Left Wrist | 122.73 | 85.58 |
| Middle Hip | 170.49 | 20.33 |
| Right Hip | 94.78 | 24.28 |
| Right Knee | 80.91 | 37.07 |
| Right Ankle | 92.17 | 59.06 |
| Left Hip | 91.13 | 25.73 |
| Left Knee | 89.61 | 42.77 |
| Left Ankle | 99.07 | 50.24 |

TABLE III. MPJPE BY SCENARIOS

| Scenarios | MPJPE (mm) | Standard deviation (mm) | PCK (%) |
|-------------------|------------|-------------------------|---------|
| Animal behaviours | 92.14 | 52.33 | 96.5 |
| Climbing | 112.65 | 54.48 | 95.62 |
| Daily activities | 101.92 | 53.56 | 95.8 |
| Dancing | 92.14 | 63.09 | 94.55 |
| Home activities | 99.44 | 47.66 | 97.3 |
| Jumping | 91.30 | 40.58 | 99.03 |
| Reactions | 92.97 | 47.67 | 98.63 |
| Running | 119.10 | 72.22 | 83.68 |
| Sitting | 116.75 | 59.32 | 87.28 |
| Sport | 118.31 | 68.82 | 83.75 |
| Walking | 90.71 | 45.39 | 98.13 |
| Working | 104.79 | 56.47 | 91.57 |
| All | 98.76 | 52.06 | 95.8 |

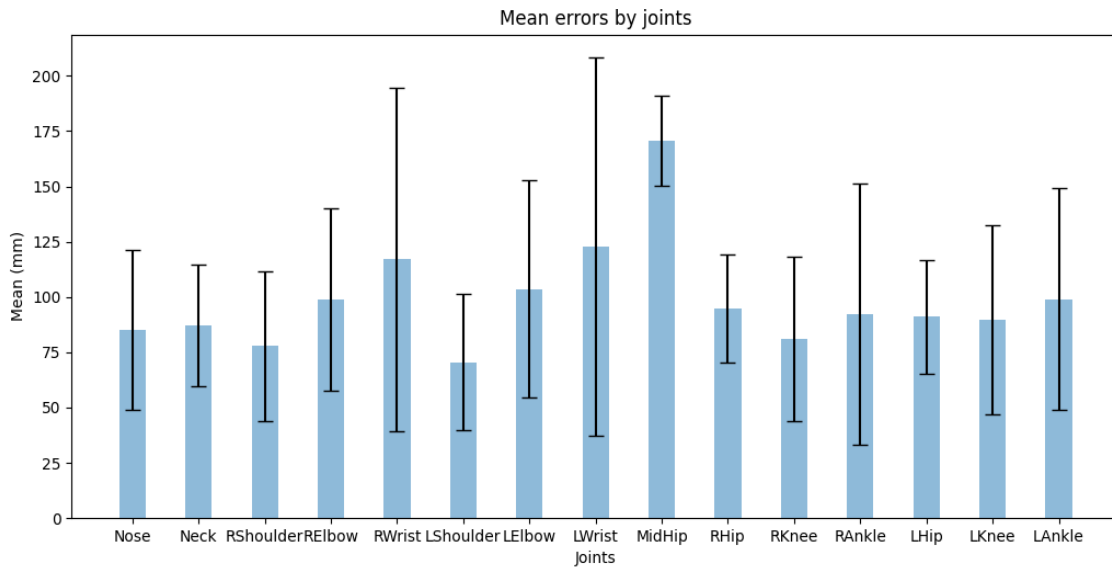


Fig. 7. The results of MPJPE by joints.

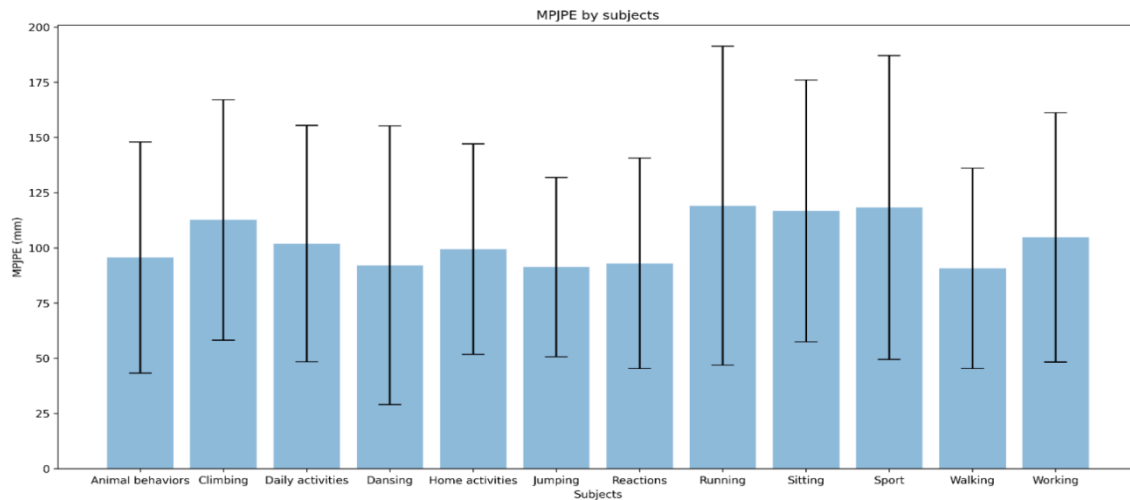


Fig. 8. The results of MPJPE by scenarios.

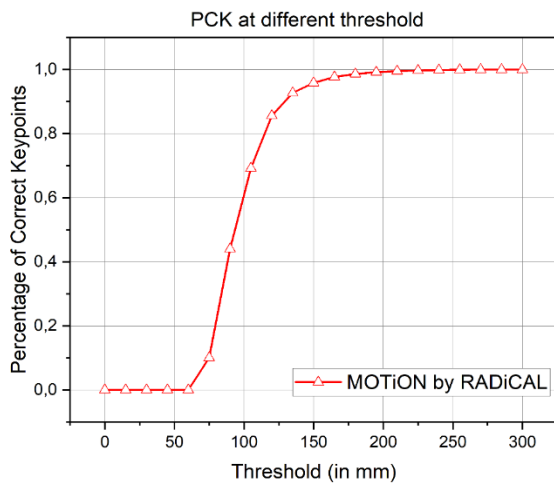


Fig. 9. The thresholds and the corresponding PCK.

Fig. 9 shows a clear progression of the Percentage of Correct Keypoints (PCK) in response to the changing Mean Per Joint Error (MPJPE) threshold. As the MPJPE threshold increases, the PCK also follows suit. Notably, at a relatively stringent threshold of 75 mm, the PCK already reaches about 44%, almost half of the keypoints estimated correctly within this error range. This trend continues and the PCK grows to about 96% when the MPJPE threshold is relaxed to 150 mm, indicating a substantial portion of the estimated keypoints are accurately detected within this margin of error. As we further expand the MPJPE threshold beyond 150 mm, the PCK continues to increase, albeit at a slower rate. The curve eventually approaches a saturation point near 100%, indicating that practically all keypoints are accurately estimated within these larger margins of error.

3) *Comparing by gender:* The findings of gender-based evaluations are depicted in Table IV and Fig. 10. Male and female MPJPEs were comparable, with the female MPJPE (95

mm) being 5 mm better than the male MPJPE (100 mm). The same holds for the standard deviation, which was almost identical. The PCK of both genders was almost the same, with 95.7%. As shown in Fig. 11, comparing all joints by gender reveals a lower mean error for eight male joints.

TABLE IV. MPJPE BY GENDER

| | Female | Male |
|-------------------------|--------|--------|
| MPJPE (mm) | 95.7 | 100.71 |
| Standard deviation (mm) | 53.06 | 51.31 |
| PCK (%) | 95.9 | 95.7 |

B. Qualitative Evaluation

One challenging frame from each scenario was selected, and RADiCAL output was visually compared to the ground-truth frame. As demonstrated in Fig. 12, the scenarios such as "Animal Behaviors," "Daily Activities," "Reactions," "Dancing," "Jumping," "Home Activities," and "Walking" imitate the ground-truth quite accurately. In addition, all skeletal parts are in their proper locations. In the remaining instances, RADiCAL correctly estimated all skeleton parts. However, its orientation was incorrect. The "Working" scenario was estimated correctly, except for the head in several frames. Some parts of the "Sports" scenario, such as the hand, were not precisely estimated.

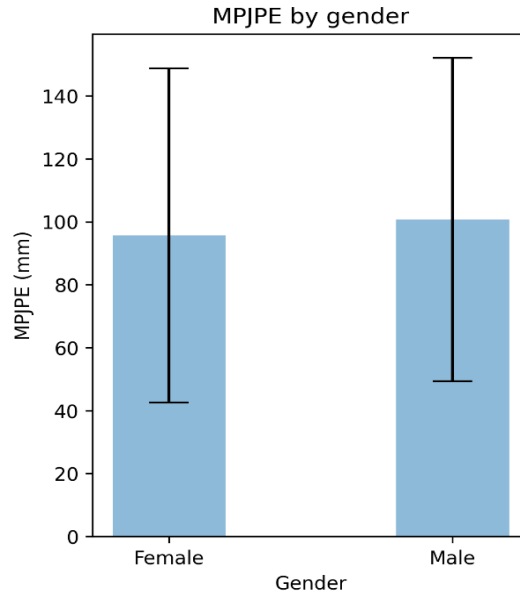


Fig. 10. The results of MPJPE by gender.

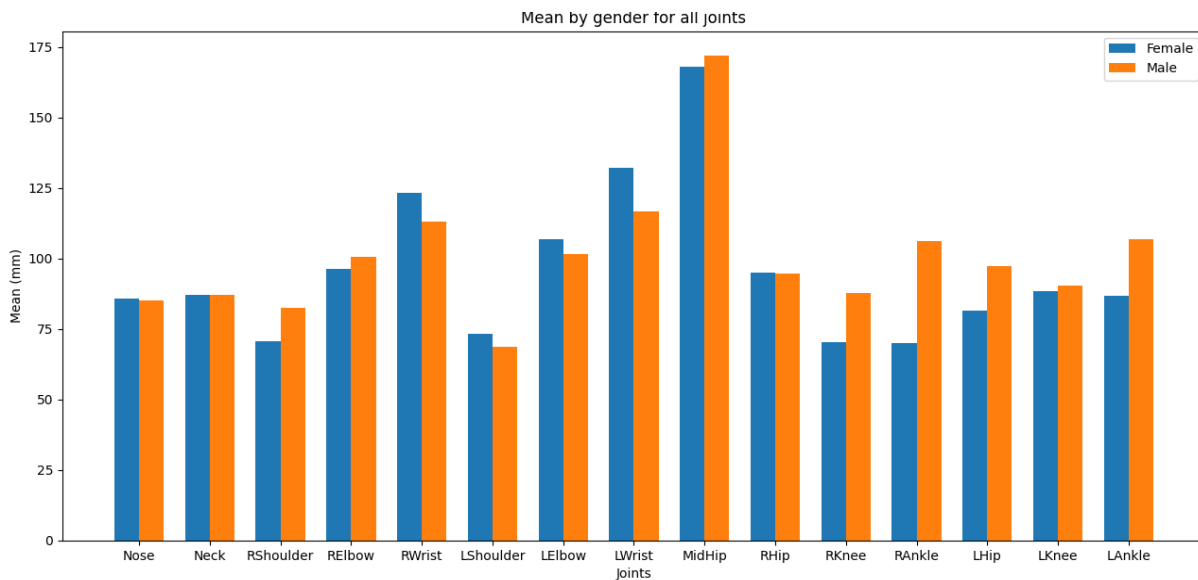


Fig. 11. The MPJPE results of comparison of joints by gender.

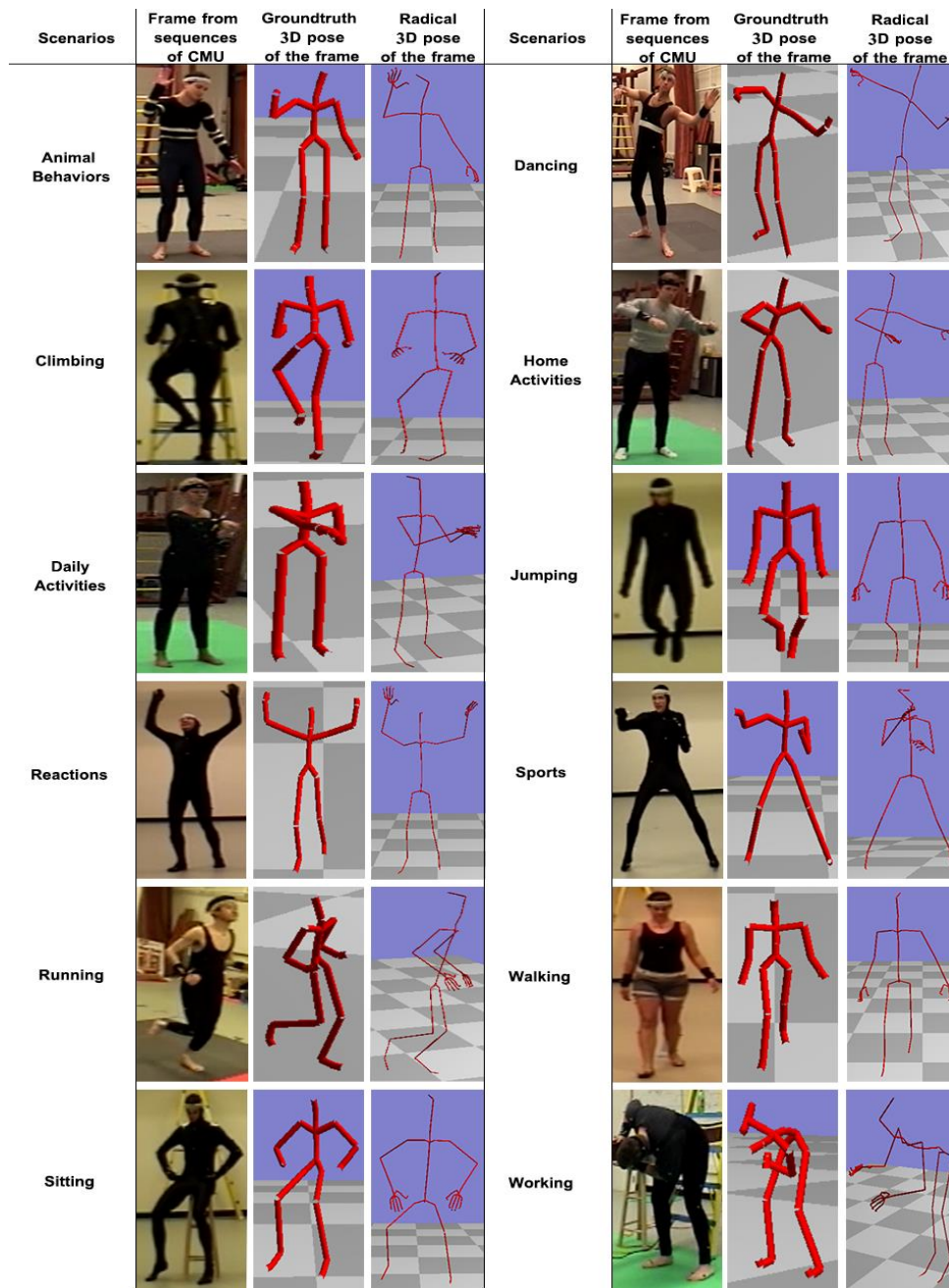


Fig. 12. The qualitative results of each scenario.

V. DISCUSSION AND LIMITATIONS

This study provides the first comprehensive evaluation of MOTiON by RADiCAL, a cloud-based 3D human motion estimation tool, revealing both its potential advantages and inherent limitations. In scenarios involving less complex actions or slower movements, such as walking or light exercise routines, our evaluation demonstrated a relatively low Mean Per Joint Position Error (MPJPE) and a high Percentage of Correct Keypoints (PCK), signaling promising performance. However, the tool's performance diminished in complex, dynamic scenarios, including sports movements, actions involving occlusion, or tasks requiring significant height variation like climbing.

The distinction in performance directly influences the range of applications suitable for MOTiON by RADiCAL. In digital content creation fields such as simple animation for games or films, or casual fitness tracking where millimeter-level precision may not be paramount, the tool's cost-effectiveness and accessibility offer substantial benefits.

However, for applications demanding high-precision motion capture, such as advanced biomechanical analysis, sports performance analysis, or precise virtual reality interaction, the current version of MOTiON by RADiCAL may not provide the necessary accuracy. The MPJPE of 98mm found in our study, while acceptable in some contexts, could

lead to significant errors in these precision-demanding applications.

VI. CONCLUSION

MOTiON by RADiCAL, as evaluated in this study, shows promise as a cost-effective, user-friendly alternative to traditional sensor-based motion capture systems. However, the tool's current performance suggests its best fit for applications where absolute precision is not a critical requirement.

In realms like basic animation for gaming, motion-guided user interface design, or casual fitness tracking, the tool's slight inaccuracies are unlikely to substantially impact the end result, making it a beneficial tool. Its cost and usability advantages are particularly beneficial for independent creators, small studios, or hobbyists in these fields.

However, in precision-critical applications, such as advanced biomechanical research, sports performance analysis, or high-end virtual reality systems that require nuanced interaction, the existing error levels in MOTiON by RADiCAL may be prohibitive. For these applications, traditional sensor-based systems, despite their higher cost and complexity, may remain the gold standard.

In summary, MOTiON by RADiCAL represents a significant step forward in democratizing access to 3D human motion estimation. However, its current performance limitations suggest that it is not a one-size-fits-all solution. Future research should explore ways to improve the precision of such tools to extend their applicability to a broader range of scenarios.

CONFLICTS OF INTEREST

The authors declare no conflict of interest.

ACKNOWLEDGMENT

The authors would like to thank MOTiON by RADiCAL for providing a discount to use their cloud to get the results.

REFERENCES

- [1] J. C. Gower, "Generalized procrustes analysis," *Psychometrika*, vol.40, no. 1, pp.33–51, Mar. 1975.
- [2] B. Wandt and B. Rosenhahn, "RepNet: Weakly Supervised Training of an Adversarial Reprojection Network for 3D Human Pose Estimation," arXiv, 12-Mar-2019.
- [3] W. Yang, W. Ouyang, X. Wang, J. Ren, H. Li, and X. Wang, "3D Human Pose Estimation in the Wild by Adversarial Learning," arXiv, 16-Apr-2018.
- [4] G. Moon and K. M. Lee, "I2L-MeshNet: Image-to-Lixel Prediction Network for Accurate 3D Human Pose and Mesh Estimation from a Single RGB Image," in *Computer Vision – ECCV 2020*, vol.12352, A. Vedaldi, H. Bischof, T. Brox, and J.-M. Frahm, eds. Springer International Publishing, Cham, 2020, pp.752–768.
- [5] G. Pavlakos, X. Zhou, and K. Daniilidis, "Ordinal Depth Supervision for 3D Human Pose Estimation," arXiv, 10-May-2018.
- [6] C.-H. Chen and D. Ramanan, "3D Human Pose Estimation = 2D Pose Estimation + Matching," arXiv, 11-Apr-2017.
- [7] J. Martinez, R. Hossain, J. Romero, and J. J. Little, "A Simple Yet Effective Baseline for 3d Human Pose Estimation," 2017 IEEE International Conference on Computer Vision (ICCV), Venice, pp.2659–2668, Oct. 2017.
- [8] B. Tekin, P. Marquez-Neila, M. Salzmann, and P. Fua, "Learning to Fuse 2D and 3D Image Cues for Monocular Body Pose Estimation," 2017 IEEE International Conference on Computer Vision (ICCV), Venice, pp.3961–3970, Oct. 2017.
- [9] K. Zhou, X. Han, N. Jiang, K. Jia, and J. Lu, "HEMlets Pose: Learning Part-Centric Heatmap Triplets for Accurate 3D Human Pose Estimation," 2019 IEEE/CVF International Conference on Computer Vision (ICCV), Seoul, Korea (South), pp.2344–2353, Oct. 2019.
- [10] F. Moreno-Noguer, "3D Human Pose Estimation from a Single Image via Distance Matrix Regression," arXiv, 28-Nov-2016.
- [11] M. Wang, X. Chen, W. Liu, C. Qian, L. Lin, and L. Ma, "DRPose3D: Depth Ranking in 3D Human Pose Estimation," *Proceedings of the Twenty-Seventh International Joint Conference on Artificial Intelligence*, Stockholm, Sweden, pp.978–984, Jul. 2018.
- [12] C. Li and G. H. Lee, "Generating Multiple Hypotheses for 3D Human Pose Estimation with Mixture Density Network," arXiv, 11-Apr-2019.
- [13] S. Sharma, P. T. Varigonda, P. Bindal, A. Sharma, and A. Jain, "Monocular 3D Human Pose Estimation by Generation and Ordinal Ranking," 2019 IEEE/CVF International Conference on Computer Vision (ICCV), Seoul, Korea (South), pp.2325–2334, Oct. 2019.
- [14] E. Jahangiri and A. L. Yuille, "Generating Multiple Diverse Hypotheses for Human 3D Pose Consistent with 2D Joint Detections," 2017 IEEE International Conference on Computer Vision Workshops (ICCVW), Venice, pp.805–814, Oct. 2017.
- [15] D. Pavllo, C. Feichtenhofer, D. Grangier, and M. Auli, "3D human pose estimation in video with temporal convolutions and semi-supervised training," arXiv, 29-Mar-2019.
- [16] M. R. I. Hossain and J. J. Little, "Exploiting Temporal Information for 3D Human Pose Estimation," in *Computer Vision – ECCV 2018*, vol.11214, V. Ferrari, M. Hebert, C. Sminchisescu, and Y. Weiss, eds. Springer International Publishing, Cham, 2018, pp.69–86.
- [17] X. Xu, H. Chen, F. Moreno-Noguer, L. A. Jeni, and F. De la Torre, "3D Human Shape and Pose from a Single Low-Resolution Image with Self-Supervised Learning," arXiv, 09-Aug-2020.
- [18] T. Zhang, B. Huang, and Y. Wang, "Object-Occluded Human Shape and Pose Estimation From a Single Color Image," 2020 IEEE/CVF Conference on Computer Vision and Pattern Recognition (CVPR), Seattle, WA, USA, pp.7374–7383, Jun. 2020.
- [19] C. Zheng, W. Wu, C. Chen, T. Yang, S. Zhu, J. Shen, N. Kehtarnavaz, and M. Shah, "Deep Learning-Based Human Pose Estimation: A Survey," arXiv, 23-Jan-2022.
- [20] G. Rogez, P. Weinzaepfel, and C. Schmid, "LCR-Net: Localization-Classification-Regression for Human Pose," 2017 IEEE Conference on Computer Vision and Pattern Recognition (CVPR), Honolulu, HI, pp.1216–1224, Jul. 2017.
- [21] G. Rogez, P. Weinzaepfel, and C. Schmid, "LCR-Net++: Multi-person 2D and 3D Pose Detection in Natural Images," *IEEE Trans. Pattern Anal. Mach. Intell.*, pp.1–1, 2019.
- [22] A. Zanfir, E. Marinoiu, and C. Sminchisescu, "Monocular 3D Pose and Shape Estimation of Multiple People in Natural Scenes: The Importance of Multiple Scene Constraints," 2018 IEEE/CVF Conference on Computer Vision and Pattern Recognition, Salt Lake City, UT, USA, pp.2148–2157, Jun. 2018.
- [23] A. Benzine, F. Chabot, B. Luvison, Q. C. Pham, and C. Achard, "PandaNet: Anchor-Based Single-Shot Multi-Person 3D Pose Estimation," 2020 IEEE/CVF Conference on Computer Vision and Pattern Recognition (CVPR), Seattle, WA, USA, pp.6855–6864, Jun. 2020.
- [24] C. Wang, J. Li, W. Liu, C. Qian, and C. Lu, "HMOR: Hierarchical Multi-person Ordinal Relations for Monocular Multi-person 3D Pose Estimation," in *Computer Vision – ECCV 2020*, vol.12348, A. Vedaldi, H. Bischof, T. Brox, and J.-M. Frahm, eds. Springer International Publishing, Cham, 2020, pp.242–259.
- [25] M. Fabbri, F. Lanzi, S. Calderara, S. Alletto, and R. Cucchiara, "Compressed Volumetric Heatmaps for Multi-Person 3D Pose Estimation," arXiv, 01-Apr-2020.
- [26] Q. Nie, Z. Liu, and Y. Liu, "Unsupervised 3D Human Pose Representation with Viewpoint and Pose Disentanglement," in *Computer Vision – ECCV 2020*, vol.12364, A. Vedaldi, H. Bischof, T. Brox, and J.-M. Frahm, eds. Springer International Publishing, Cham, 2020, pp.102–118.

- [27] W. Liu, Q. Bao, Y. Sun, and T. Mei, "Recent Advances in Monocular 2D and 3D Human Pose Estimation: A Deep Learning Perspective," arXiv, 23-Apr-2021.
- [28] L. Sigal, A. O. Balan, and M. J. Black, "HumanEva: Synchronized Video and Motion Capture Dataset and Baseline Algorithm for Evaluation of Articulated Human Motion," *Int. J. Comput. Vis.*, vol.87, no. 1-2, pp.4-27, Mar. 2010.
- [29] C. Ionescu, D. Papava, V. Olaru, and C. Sminchisescu, "Human3.6M: Large Scale Datasets and Predictive Methods for 3D Human Sensing in Natural Environments," *IEEE Trans. Pattern Anal. Mach. Intell.*, vol.36, no. 7, pp.1325-1339, Jul. 2014.
- [30] "Carnegie Mellon University - CMU Graphics Lab - motion capture library," <http://mocap.cs.cmu.edu/>, accessed Sep. 29. 2022. .
- [31] D. Mehta, H. Rhodin, D. Casas, P. Fua, O. Sotnychenko, W. Xu, and C. Theobalt, "Monocular 3D Human Pose Estimation In The Wild Using Improved CNN Supervision," arXiv, 04-Oct-2017.
- [32] J. Tompson, A. Jain, Y. LeCun, and C. Bregler, "Joint Training of a Convolutional Network and a Graphical Model for Human Pose Estimation," arXiv, 17-Sep-2014.
- [33] H. Ye, W. Zhu, C. Wang, R. Wu, and Y. Wang, 'Faster VoxelPose: Real-time 3D Human Pose Estimation by Orthographic Projection', in *Computer Vision – ECCV 2022*, S. Avidan, G. Brostow, M. Cissé, G. M. Farinella, and T. Hassner, Eds., Cham: Springer Nature Switzerland, pp. 142–159. doi: 10.1007/978-3-031-20068-7_9, 2022.
- [34] C. Han, X. Yu, C. Gao, N. Sang, and Y. Yang, 'Single image based 3D human pose estimation via uncertainty learning', *Pattern Recognition*, vol. 132, p. 108934, Dec. 2022.
- [35] L. Jin et al., 'Single-Stage Is Enough: Multi-Person Absolute 3D Pose Estimation', presented at the *Proceedings of the IEEE/CVF Conference on Computer Vision and Pattern Recognition*, pp. 13086–13095, 2022.
- [36] H. Khalloufi, M. Zaifri, M. Kadri, A. Benlahbib, F. Z. Kaghat, and A. Azough, 'El-FnaVR: An Immersive Virtual Reality Representation of Jemaa El-Fna in Marrakech for Intangible Cultural Heritage Experiences', *IEEE Access*, vol. 12, pp. 9331–9349, 2024.

Optimizing Student Performance Prediction: A Data Mining Approach with MLPC Model and Metaheuristic Algorithm

Qing Hai¹, Changshou Wang^{2*}

Department of Water Resources and Civil Engineering, Hetao College, Bayan Nur 01500, Inner Mongolia, China¹
Department of Agriculture, Hetao College, Bayan Nur 01500, Inner Mongolia, China²

Abstract—Given the information stored in educational databases, automated achievement of the learner's prediction is essential. The field of educational data mining (EDM) is handling this task. EDM creates techniques for locating data gathered from educational settings. These techniques are applied to comprehend students and the environment in which they learn. Institutions of higher learning are frequently interested in finding how many students will pass or fail required courses. Prior research has shown that many researchers focus only on selecting the right algorithm for classification, ignoring issues that arise throughout the data mining stage, such as classification error, class imbalance, and high dimensionality data, among other issues. These kinds of issues decreased the model's accuracy. This study emphasizes the application of the Multilayer Perceptron Classification (MLPC) for supervised learning to predict student performance, with various popular classification methods being employed in this field. Furthermore, an ensemble technique is utilized to enhance the accuracy of the classifier. The goal of the collaborative approach is to address forecasting and categorization issues. This study demonstrates how crucial it is to do algorithm fine-tuning activities and data pretreatment to address the quality of data concerns. The exploratory dataset utilized in this study comes from the Pelican Optimization Algorithm (POA) and Crystal Structure Algorithm (CSA). In this research, a hybrid approach is embraced, integrating the mentioned optimizers to facilitate the development of MLPO and MLCS. Based on the findings, MLPO2 demonstrated superior efficiency compared to the other methods, achieving an impressive 95.78% success rate.

Keywords—Educational data mining; multilayer perceptron classification; pelican optimization algorithm; crystal structure algorithm; student performance

I. INTRODUCTION

A. Background

Providing high-quality education to students is the primary goal of higher education establishments [1]. One strategy for achieving a better quality standard in a higher education program is to forecast pupils' academic success and intervene soon to raise pupil achievement and teacher quality [2]. Data mining techniques may be used to retrieve the useful knowledge concealed inside the educational data collection [3]. Against the backdrop of higher education, the current research aims to evaluate the potential of data-mining approaches by providing a data-mining model [4]. This activity aims to assess

pupils' performance through categorization [5]. It is necessary to continuously assess how well pupils do in every topic, to pinpoint where the learner lost their grade [6]. This makes it easier for the educator to take the required steps, such as giving the student greater focus on that specific topic, teaching in a way that the student can understand quickly, giving tests, etc., all of which eventually raise the student's academic standing and quality [7]. Educational Data Mining (EDM) is the term for data mining within the education framework. Analytics has been used more in the previous few decades in educational settings [8], [9].

B. Related Works

On the provided dataset, six classifiers were used. At 79.23%, the ID3 had the highest accuracy [10]. The class mismatch challenge was beyond the model's ability to solve. To identify weak pupils, a model of ensembles such as classifiers (NB, SVM, and KNN) was suggested [11]. In addition to the common score-based evaluation, the data collection includes a characteristic referred to as standard-based grading evaluation. Comparing the outcomes of the suggested approach via six independent classifiers led to the conclusion that the ensemble model's accuracy was greater than the others at 85%. A multilayer classification model was put forth to overcome the multiple classifications issue regarding student performance prediction [12]. A methodology to give an early categorization of first-year students with poor educational outcomes was suggested by Dech Thammasiri et al. [13]. The class imbalance challenge was solved by applying four classifications and three balancing techniques. According to the results, the combination of SMOTE and support vector machines produced a maximum general precision of 90.24%. Students' performance in an online class may be predicted using information from their learning portfolios, according to one proposed early warning system [14]. The results showed that approaches based on time were more precise than those independent of time. Test the framework did not in offline mode. Using time-dependent properties, functioning might be reduced in offline mode.

Earlier research suggested that data mining algorithms only worked effectively with huge data sets; however, this study provided evidence that data mining may also be used for smaller datasets [15]. A model for predicting learner achievement was presented in this study. Several decision tree techniques were used for a small dataset containing students'

academic data (Reptree, J48, M5P). According to the results, the Reptree had the best accuracy, exceeding 90 percent. The suggested model does not support class balance issues and data with large complexity. By grouping students into binary classes (successful/unsuccessful), Dorina et al. [16] presented a prediction model for students' performance. The suggested model was built using the research methodology of the Cross-Industry Standard Procedure for Data Mining, or CRISP-DM [17]. The provided dataset was subjected to the categorization methods OneR [18], MLP, J48, and IBK. The results showed that the MPL model was the most accurate at 73.59 percent in determining which students passed, while the other three models did a better job of determining which students failed. Issues with class balance and large complexity data were unsolvable for the model.

To overcome issues with disparities in classes and data complexity, Carlos et al. [19] focused on a machine learning-based failure of students' prognosis model. The dataset was utilized to execute ten classifiers. The accuracy of the ICRM classifier was found to be 92.7%, surpassing the performance of the other classifiers. The evaluation of the proposed model's performance was not conducted across various educational levels due to the distinct student characteristics associated with each level of education. Another EDM challenge is predicting which students will drop out of their classes [20]. Four data mining techniques with six characteristic pairings were employed in this study. The outcome reveals that, in data classification, superior performance was achieved when utilizing the support vector machine model that combined the variables. Adding a characteristic, achieved scores of prerequisite courses, in a data set was the study's restriction since it was feasible that the student had become more knowledgeable about the prerequisites for any course while studying for any other course. Research on pupil achievement prediction was carried out by Ajay et al. [21]. The main importance of the study was the introduction of a new social element, known as the CAT. The text elucidates the first categorization of Indians into four distinct groups based on their social standing and other variables that influenced student admission. The dataset underwent classification using four methods, namely R, MLP, J48, and IB1. Based on the available data, it can be shown that the IB1 model has the highest level of accuracy, reaching 82%. Create an enhanced iteration of the ID3 method, which forecasts academic achievement in students [22]. The ID3 model's intention to choose those qualities as a node with additional values was one of its weaknesses. Consequently, the produced tree lacked efficiency. The suggested model resolves such an issue. This model generated the Pass and Failure output types. J48, wID3, and Naïve Bayes classifiers were used, and the outcomes were contrasted. An accuracy rate of 93% was attained with the wID3A model to forecast student achievement in courses presented in [23]. This study used three decision tree classifiers: Reptree, Hoeding tree, and J48. Reptree obtained the greatest accuracy of 91.47%. Problems with class balance and large dimensionality data were unsolvable for the model.

Through solving the data complexity issue, Edin Osmanbegovic et al. [24] was created a model to estimate the academic progress of students in a given course. This study

evaluated many machine learning classifiers, such as NB, MLP, and j48. Based on the results, it can be observed that the Naïve Bayes model achieved the highest level of accuracy, reaching 76.65%. The issue of class imbalance is not addressed by the suggested model. In this paper, a model for predicting students' academic success was presented [25]. This study examined the classification methods with three different feature arrangements: J48, Decision Stump, Reptree, NB, and ANN. A high accuracy of 90.51% was attained with the J48 classifier. To forecast student abandonment, the suggested method took into account three numbers of courses that were assessed: dropout, persisting, and completing. Ten models of categorization were evaluated. According to the research's findings, for all three student classes, the Naïve Bayes algorithm achieved the greatest prediction values.

C. Objective

The fundamental aim of this research was to develop a robust machine-learning framework tailored to forecast student performance in Portuguese language courses, leveraging dependable data reservoirs. Through the strategic utilization of the Multilayer Perceptron Classification (MLPC) methodology, this study embarked on a path of innovation, ingeniously amalgamating two optimization algorithms: the Pelican Optimization Algorithm (POA) and the Crystal Structure Algorithm (CSA). This unique integration sought to improve both the accuracy and precision of the estimative model, thereby enriching the efficacy of prognostications regarding student performance. MLPC is chosen for predicting and classifying student performance in Portuguese language learning due to its ability to capture complex patterns inherent in language acquisition processes. By accommodating non-linear relationships between various factors influencing language proficiency and automatically learning feature representations from diverse datasets, MLPC offers scalability and robust generalization to unseen data. Moreover, its capacity for fine-tuning and potential for interpretability allows for continuous model improvement and insights into the determinants of student performance. Consequently, MLPC is a valuable tool for educators and stakeholders in effectively assessing and addressing student needs in Portuguese language education.

II. MATERIALS AND METHODS

A. Data Gathering

As previously elucidated, the prognostication of students' academic performance is shaped not only by their quiz outcomes, fulfilment of homework assignments, and engagement in class activities but also by the external circumstances they encounter outside the confines of the educational institution. For example, their family situation, the size of their family (*famsize*), family support (*famsup*), their health status, the amount of time spent on social media, their parents' occupation (*Fjob/Mjob*), and other relevant factors. Each of these terms influences the students' conditions in the classroom. However, the educational system's responsibility is to diagnose these factors, treat students according to their situations, act according to their talents, address their weaknesses, and capitalize on their strengths. The following diagram delineates the interplay between input and

output variables. Notably, the school manifests a direct correlation with sex, suggesting the insignificance of students'

gender. Likewise, while travel time lacks a direct association with students' failure, it does exert a marginal effect.

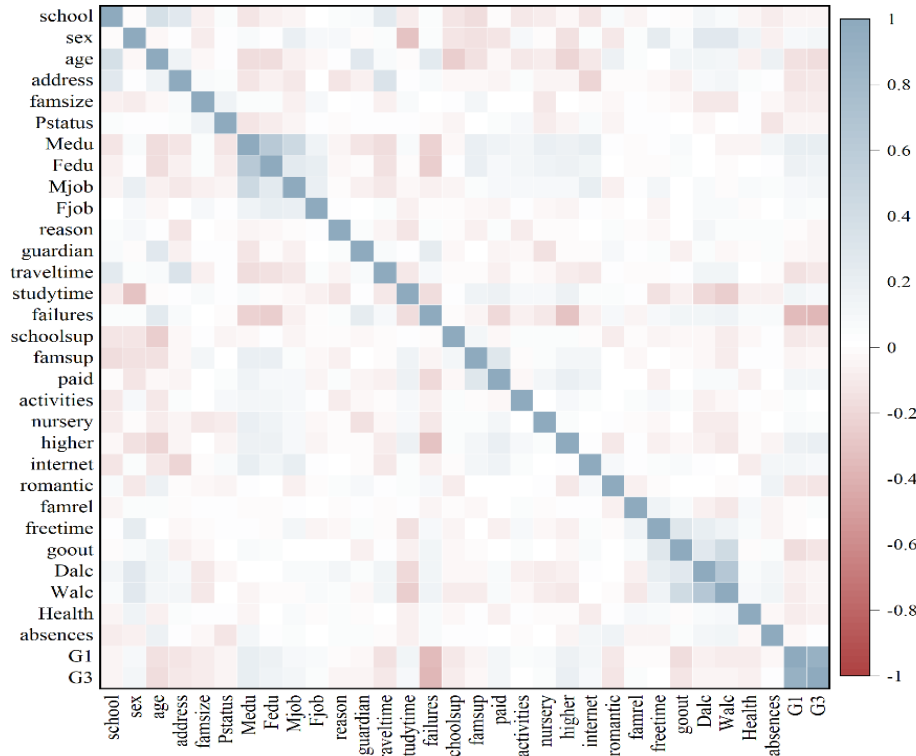


Fig. 1. Correlation matrix for the input and output variables.

Furthermore, study time exhibits no correlation with gender or school. In conclusion, although the diagnosis of these elements initially influences the prediction of students' performance, it is crucial to emphasize that none of these factors operates in isolation; instead, their effectiveness relies on the collaborative engagement of each student. Fig. 1 exhibits the correlation matrix for the in/output variables.

B. Multilayer Perceptron Classifier (MLPC)

Based on the concepts of neural network design, the Multilayer Perceptron Classifier (MLPC) is a particular kind of feed-forward artificial neural network (ANN) classifier. The MLPC in this configuration is made up of several layers of nodes, each of which is intimately linked to the network's next layer. Because of its architecture, the network can analyze and alter incoming data over a series of layers, which makes it possible for the MLPC to identify intricate patterns and correlations in the data. The nodes in the input layer of the MLPC represent the input data. Every node after it in the network uses its weight (shorthand for w) and an offset b to conduct a linear selection of the input as the data moves through the network. After this combination, an activation function transfers the input to the output. For improved clarity and illustration, this procedure may be concisely described in matrix form in the case of an MLPC with $K + 1$ layers [26].

$$y(x) = f_k(\dots f_2(w_2^T f_1(w_1^T + b_1) + b_2) \dots + b_k) \quad (1)$$

Nodes inside the middle layer use the logistic or stochastic algorithm:

$$f(z_i) = \frac{1}{1 + e^{-z_i}} \quad (2)$$

The results of the layer's nodes use the *softmax* feature:

$$f(z_i) = \frac{e^{z_i}}{\sum_{k=1}^N e^{z_k}} \quad (3)$$

The number of classes and nodes in the output layer has the matches.

C. Crystal Structure Algorithm (CSA)

Crystals are minerals with a structured composition that exhibit three regularly repeating or ordered crystalline dimensions. Crystalline solids can take on various sizes and shapes, and their properties may be either isotropic or anisotropic [27]. Crystals consist of small particles with well-defined shapes. Numerous physical and chemical compositions have been explored and suggested through experimentation. Moreover, crystals' complex symmetries and characteristics have profoundly influenced diverse human creations, including mechanisms, structures, and artworks. This article employs the Bravais model to explain the crystal structure. In this model, infinite lattice geometry is examined, and the periodic arrangement described by the lattice geometry, along with the vector of the lattice positions, is defined as follows:

$$l = \sum m_i e_i \quad (4)$$

where e_i is the minimum vector of the principal crystal directions, m_i is the and i is the angular number of the

crystal. Here, the basic idea of *Crystal* is presented with appropriate modifications for the *CryStAl* mathematical model. In this model, every candidate solution of the optimization method is likened to a distinct crystal space. To initiate the *cycle*, an arbitrary number of precious stones is selected.

$$\begin{bmatrix} cl_1 \\ cl_2 \\ \vdots \\ cl_i \\ \vdots \\ cl_m \end{bmatrix} = \begin{bmatrix} x_1^1 & \dots & x_1^j & \dots & x_1^p \\ x_2^1 & \dots & x_2^j & \dots & x_2^p \\ \vdots & & \vdots & & \vdots \\ x_i^1 & \dots & x_i^j & \dots & x_i^p \\ \vdots & & \vdots & & \vdots \\ x_m^1 & \dots & x_m^j & \dots & x_m^p \end{bmatrix}, \begin{cases} i = 1, 2, 3, \dots, m \\ j = 1, 2, 3, \dots, p \end{cases} \quad (5)$$

where m is the candidate solution, and p is the dimension of the problem. Within the search space, the initial positions of these crystals are determined randomly by:

$$x_i^j(0) = x_{i,min}^j + \delta(x_{i,max}^j - x_{i,min}^j), \begin{cases} i = 1, 2, 3, \dots, m \\ j = 1, 2, 3, \dots, p \end{cases} \quad (6)$$

where, $x_i^j(0)$ characterizes the starting gem position, the least and greatest permitted values are characterized as $x_{i,max}^j$ and $x_{i,min}^j$ separately, the j th choice variable of the i th candidate arrangement is within the indicated δ . Based on the crystallographic concept of the *base*, the primary crystals are all corner crystals. cl_{main} randomly determined considering the first generated crystal. In addition, the cl_i the current value is ignored, and a random extraction method is set for each tread. *Crystals* with optimal configuration determined by cl_z . S_u represents the mean of randomly selected crystals. To monitor the position of a candidate solution in the search space, four types of update procedures are established based on fundamental network principles:

Simple cubic;

$$cl_{new} = cl_{main} + cl_{old} \quad (7)$$

Best crystal cubic;

$$cl_{new} = l_1 cl_{main} + l_2 cl_z + cl_{old} \quad (8)$$

Mean crystal cubic;

$$cl_{new} = l_1 cl_{main} + l_2 S_u + cl_{old} \quad (9)$$

M&B crystal cubic;

$$cl_{new} = cl_{old} + l_1 cl_{main} + l_2 cl_z + l_3 S_u \quad (10)$$

In the above formula, the old position is given by cl_{old} and the new position is denoted by cl_{new} and the random numbers are denoted by $l, l_1, l_2, \text{ and } l_3$. Mining and exploration are the two main elements of metaheuristics, and it is worth mentioning that they have been tested in Eq. (7) to (10), where global and local searches are performed simultaneously. To deal with variable solutions x_i^j that violate the variable limit requirements, a mathematical flag is created that requires adjustment of the variable limits, causing problems with x_i^j they are exceeding the variable range. The termination criteria depend on the maximum number of iterations, which

determines when the optimization process concludes after a fixed number of iterations [28], [29].

D. Pelican Optimization Algorithm (POA)

The researchers identified a population-based optimization method, known as the POA, which draws inspiration from pelicans [30]. The method employs a simulation of evolutionary processes within an ecological system, wherein pelicans are seen as single entities within a larger population. Every person represents a possible solution and provides optimization recommendations, which arise from adjusting the issue variable according to the position of each person in the search area. In order to ensure the variety of the population and improve the global search capacity, each member is randomly initialized within the stated upper and lower limits of the issue during the population initialization procedure, as illustrated in Eq. (11).

$$x_{i,j} = l_j + rand.(u_j - l_j), \begin{cases} i = 1, 2, \dots, N, \\ j = 1, 2, \dots, m \end{cases} \quad (11)$$

Where N is the number of population members, m is the number of issue variables, $rand$ is a random integer in the interval $[0, 1]$, l_j is the j th lower bound, and u_j is the j th upper limit of problem variables. The values of the variables indicated by the i th candidate solution are represented by the variables $x_{i,j}$. Eq. (12) uses a matrix known as the population matrix to identify the pelican population members in the proposed POA. The columns of this matrix show the suggested values for the issue variables, and each row indicates a potential solution.

$$X = \begin{bmatrix} X_1 \\ \vdots \\ X_i \\ \vdots \\ X_N \end{bmatrix}_{N \times m} = \begin{bmatrix} x_{1,1} & \dots & x_{1,j} & \dots & x_{1,m} \\ \vdots & \ddots & \vdots & \ddots & \vdots \\ x_{i,1} & \dots & x_{i,j} & \dots & x_{i,m} \\ \vdots & & \vdots & & \vdots \\ x_{N,1} & \dots & x_{N,j} & \dots & x_{N,m} \end{bmatrix}_{N \times m} \quad (12)$$

If X_i is the i th pelican, and X is the pelican population matrix. A potential fix for the stated issue is the planned POA, in which every member of the population is a pelican. Thus, assessing the given issue's objective function is possible by considering each potential solution. The objective function vector in Eq. (13) is used to derive the values obtained for the objective function.

$$F = \begin{bmatrix} F_1 \\ \vdots \\ F_i \\ \vdots \\ F_N \end{bmatrix}_{N \times 1} = \begin{bmatrix} F(X_1) \\ \vdots \\ F(X_i) \\ \vdots \\ F(X_N) \end{bmatrix}_{N \times 1} \quad (13)$$

where, F_i is the objective function value of the i th candidate solution, and F is the objective function vector. To update potential answers, the suggested POA mimics the tactics and behaviour of pelicans during hunting and assault. There are two phases to simulating this hunting strategy: *i* Approaching the prey (the period of exploration). *ii* Winging during the exploitation phase on the water's surface.

1) *Phase 1 (exploration phase): approaching the prey:* The initial stage of the process involves the pelicans locating

the prey and then approaching it. Search space scanning and the exploration capability of the suggested POA in locating various search space regions are made possible by modelling this pelican approach. The fact that the prey's position is produced is crucial to POA.

$$x_{i,j}^{P_1} = \begin{cases} x_{i,j} + \text{rand.}(p_j - I \cdot x_{i,j}), & F_p < F_i; \\ x_{i,j} + \text{rand.}(x_{i,j} - p_j), & \text{else,} \end{cases} \quad (14)$$

Where x^{P_1} . In the context of Eq. (14), the importance of the variable can be observed $x_{i,j}^{P_1}$, an updated state of the pelican in the j th dimension is represented by the result of stage 1, and this can be the i th pelican. To introduce additional diversity and exploration, the value of I is introduced as a random number ranging between one and two. Also, the parameter p_j , the position of the prey, is employed to be denoted j th dimension, while F_p the objective function value of the prey is represented. By incorporating Eq. (15), the process can be effectively simulated and modelled.

$$X_i = \begin{cases} X_i^{P_1}, F_i^{P_1} < F_i; \\ X_i & \text{else,} \end{cases} \quad (15)$$

Where X^{P_1} . This is the updated status for the F^{P_1} and i th pelican. The goal function is based on values pertaining to the phase.

2) *Phase 2: winging on the water surface (exploitation phase)*: In the subsequent stage, the pelicans gather their meal in their throat pouches after reaching the water's surface and spreading their wings to push the fish upward. This tactic helps pelicans catch more fish in the assaulted region. As a result of simulating this pelican behaviour, the suggested POA converges to more advantageous locations inside the hunting region. The exploitation potential and local search power of POA are enhanced by this method. From a mathematical perspective, the algorithm must look at the points surrounding the pelican position to converge to an optimal solution. Eq. (16) simulates the hunting behaviour of pelicans mathematically.

$$x_{i,j}^{P_2} = x_{i,j} + R \left(1 - \frac{t}{T}\right) \cdot (2 \cdot \text{rand} - 1) \cdot x_j \quad (16)$$

Where X^{P_2} , based on phase 2, i, j represents the i th pelican's new state in the j th dimension. $x_{i,j}$, s neighbourhood radius is given by $R \left(1 - \frac{t}{T}\right)$, which is equal to 0.2. T represents the maximum number of iterations and iteration counter. The exponent $R \left(1 - \frac{t}{T}\right)$ reflects the local search radius for the population members' neighbourhoods. Close to every participant to arrive at an improved answer. This coefficient works well on the POA exploitation power to reach the ideal global solution. Since this coefficient is highly valued in the first iterations, a bigger region is considered around each member. The $R \left(1 - \frac{t}{T}\right)$ The coefficient falls as the method replicates more, resulting in smaller radii for each neighbourhood member. For the POA to converge to solutions that are closer to the global (and even precisely global) ideal

based on the utilization notion, this enables us to scan the region surrounding each member of the population in smaller and more precise stages. Eq. (17) models the new pelican posture, which has also been accepted or rejected at this stage by successful updating.

$$X_i = \begin{cases} X_i^{P_2}, F_i^{P_2} < F_i; \\ X_i & \text{else,} \end{cases} \quad (17)$$

where X^{P_2} . This is the updated status for the F^{P_2} and i th pelican. Its goal function is value-based, and i on stage 2.

3) *Steps repetition, pseudo-code, and flowchart of the proposed POA*: The best candidate solution up to this point will be updated after all population members have been updated based on the first and second phases, the population's new status, and the values of the goal function. When the algorithm reaches the next iteration, the stages of the suggested POA are based on Eq. (15) to (17) are repeated until the execution is finished. Lastly, a quasi-optimal solution to the given issue is offered using the best candidate solution found throughout the algorithm rounds.

E. Performance Evaluators

When evaluating a classifier's performance, it is essential to consider multiple criteria to obtain a thorough insight into its effectiveness. These criteria function as metrics, providing insights into various aspects of the classifier's performance and enabling a nuanced assessment. Here are some crucial factors to consider:

- Accuracy: A frequently employed metric measures the classifier's efficiency by determining the percentage of accurately predicted samples.

$$\text{Accuracy} = \frac{TP + TN}{TP + TN + FP + FN} \quad (18)$$

- Recall: Recall quantifies the proportion of correctly predicted positive instances in relation to all actual positive instances.

$$\text{Recall} = TPR = \frac{TP}{P} = \frac{TP}{TP + FN} \quad (19)$$

- Precision: Precision centres on the precision of positive predictions, evaluating the probability that instances identified as positive are indeed accurate. This metric is particularly valuable when the cost of false positives is significant.

$$\text{Precision} = \frac{TP}{TP + FP} \quad (20)$$

- F1-score: The combination of Precision and Recall yields a composite measure recognized as the f1-score.

$$\text{F1 score} = \frac{2 \times \text{Recall} \times \text{Precision}}{\text{Recall} + \text{Precision}} \quad (21)$$

In Eq. (18) to (21), TP represents a positive prediction that correctly corresponds to the actual positive outcome. FP denotes a positive prediction when the actual outcome is negative. FN is used to indicate a negative prediction when the

actual outcome is positive, while TN represents a negative prediction that accurately aligns with the actual negative outcome.

III. RESULT

A. Hyperparameters and Convergence Curve Results

Hyperparameters are external settings that encompass vital factors like learning rates and regularization strengths, exerting significant influence over a behavior of model. They are predetermined values and are not directly inferred from the dataset itself. Maximizing model performance relies heavily on the indispensable task of fine-tuning hyperparameters, which necessitates rigorous experimentation and the adept application of optimization methodologies. The results of the hyperparameters for MLPC-based hybrid models (MLPO and MLCS) are represented in Table I for G2 and Table II for G3 values. The hyperparameter of the MLPC-based models is Layer_size. This comprehensive exposition substantially enhances the transparency and reproducibility of models within the field of machine learning research, furnishing invaluable insights that deepen understanding and facilitate precise replication of model configurations.

TABLE I. RESULT OF HYPERPARAMETERS FOR G2

| Layer of MLPC | Models | Hyperparameter | |
|---------------|------------|----------------|------|
| | | MLPO | MLCS |
| Layer 1 | Layer_size | 74 | 71 |
| Layer 2 | Layer_size | 22 | 69 |
| | Layer_size | 27 | 16 |
| Layer 3 | Layer_size | 46 | 29 |
| | Layer_size | 37 | 56 |
| | Layer_size | 13 | 31 |

TABLE II. RESULT OF HYPERPARAMETERS FOR G3

| Layer of MLPC | Models | Hyperparameter | |
|---------------|------------|----------------|------|
| | | MLPO | MLCS |
| Layer 1 | Layer_size | 32 | 53 |
| Layer 2 | Layer_size | 23 | 86 |
| | Layer_size | 19 | 99 |
| Layer 3 | Layer_size | 12 | 34 |
| | Layer_size | 13 | 19 |
| | Layer_size | 12 | 20 |

This study aims to forecast learners' academic achievement throughout the educational program to improve their skills and increase their chances of success. The MLPC model, which combines the two optimizers known as POA optimization and CSA, is presented to achieve this aim. The model has a favourable impact on the prediction of pupil achievement. In this study, two novel models, MLCS and MLPO, are generated by integrating the foundational model, MLPC, with optimizers to enhance prognostic capabilities further. This section encompasses a comparative analysis to determine the relative effectiveness of each model over the others. A hybrid model's

convergence is typically understood to signify that it has reached its peak throughout the training process. When a machine learning algorithm gets to a point where more iterations of training do not significantly improve the model's performance on the training set, it stabilizes its parameters and becomes a convergent state. This is especially true for complex models like hybrid models. In the context of hybrid models, characterized by incorporating multiple model or technique types, achieving convergence necessitates verification that each constituent functions as intended and that the model achieves overall prediction consistency. The monitoring of convergence during the training phase commonly involves observing effectiveness indicators or examining loss functions on a validated dataset. Rapid convergence is imperative for a hybrid model to comprehend knowledge structures and effectively generalize its findings to novel, unseen data. Fig. 2 and 3 comprehensively compare models across two distinct targets, G2 and G3, encompassing three layers. In the initial layer of the G2 target, the MLCS model achieves stability at a core value of 0.889 within 90 iterations, in contrast to the MLPO model, which attains stability at a point of 0.899 in 120 iterations.

Although the MLPO model maintains a higher accuracy than the MLCS model in the second layer, achieving stability at 0.939 within 130 iterations, compared to the MLCS model's accuracy of 0.927 measured in 128 iterations. Examination of the third layer underscores the MLPO model's superior accuracy in the G2 target, reaching an estimated value of 0.919 within 130 iterations, in contrast to the MLCS model, with a measured value of 0.904 in 150 iterations. Incidentally, in the first layer of the G3 target, the MLCS model, with an accuracy of 0.861 measured in 148 iterations, is surpassed by the MLPO model, which achieves a higher accuracy of 0.878 within 150 iterations. Subsequently, in the second layer, the MLCS model reaches a level of 0.901 in the 90th iteration; however, the MLPO model outperforms it with an accuracy of 0.914 measured in the 148th iteration. Ultimately, in the third layer, the MLPO model attains an accuracy of 0.891 after 150 iterations. Conversely, the MLCS model exhibits weaker performance with a lower accuracy measurement than the MLPO model. Ultimately, the current line plot reveals that higher accuracy is achieved by the POA optimizer when combined with the base model across three layers of two targets.

B. Results of Predictive Models

Table III delineates measured values of accuracy, precision, recall, and F1 score across three phases—namely, train, test, and all—within the G2 and G3 targets, each comprising three layers. For instance, during the training phase, the MLPO model exhibits values of 0.910, 0.913, 0.910, and 0.909 for accuracy, precision, recall, and F1-score, respectively. In contrast, the MLCS model in the training phase records values of 0.906, 0.910, 0.906, and 0.905 for the corresponding metrics. This comparative analysis underscores that the MLPO model consistently attains higher accuracy in each of the four metrics than the MLCS model in the same phase. However, during the test phase for both models, precision emerged as the metric with the highest value, specifically registering at 0.888 for the MLPO model and 0.863 for the MLCS model.

Incidentally, in the second layer, the aggregate precision value in the MLPO model is 0.940, surpassing the corresponding value of 0.927 in the opposing model. Notably, the MLCS model maintains uniform values across all phases for three metrics—accuracy, precision, and recall—except for the F1-

score, where it records a lower value of 0.926, indicating inferior accuracy compared to other metrics. In the final layer, the MLPO model achieves accuracy values of 0.931 and 0.890 in the train and test phases, respectively.

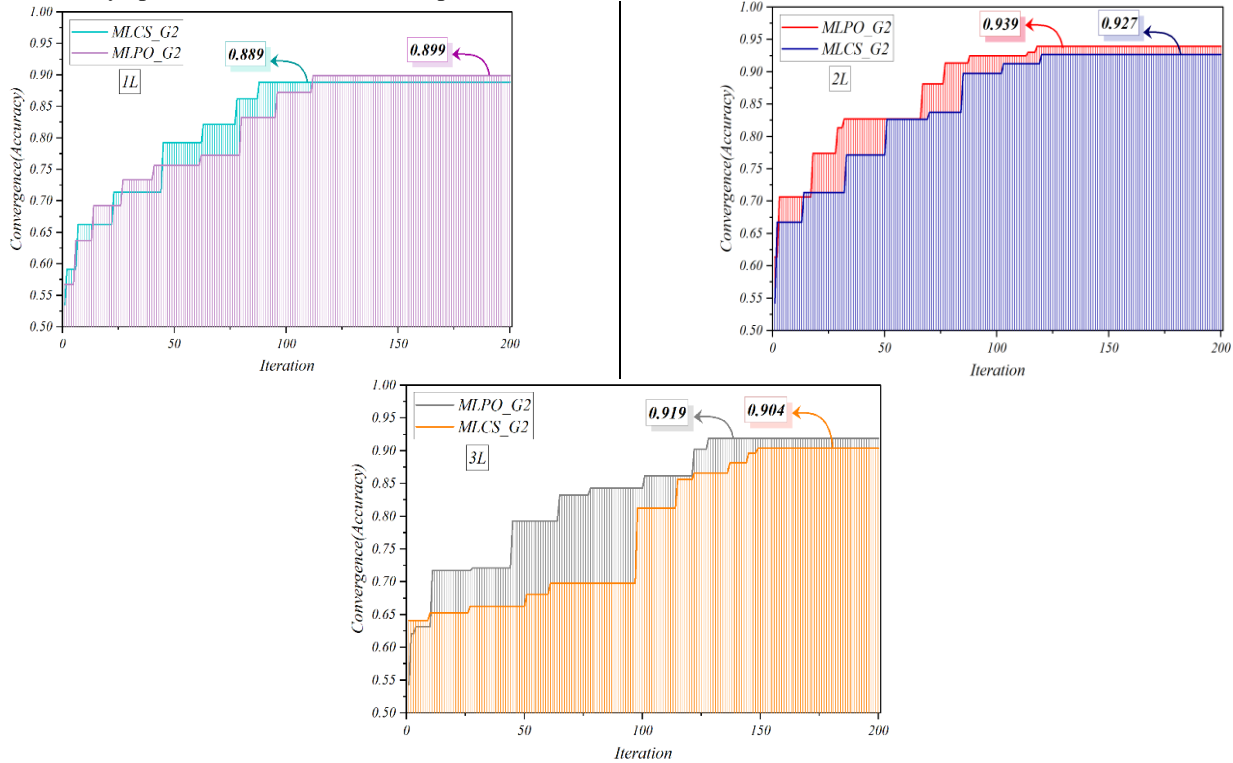


Fig. 2. Line plot for convergence of hybrid models for G2 values.

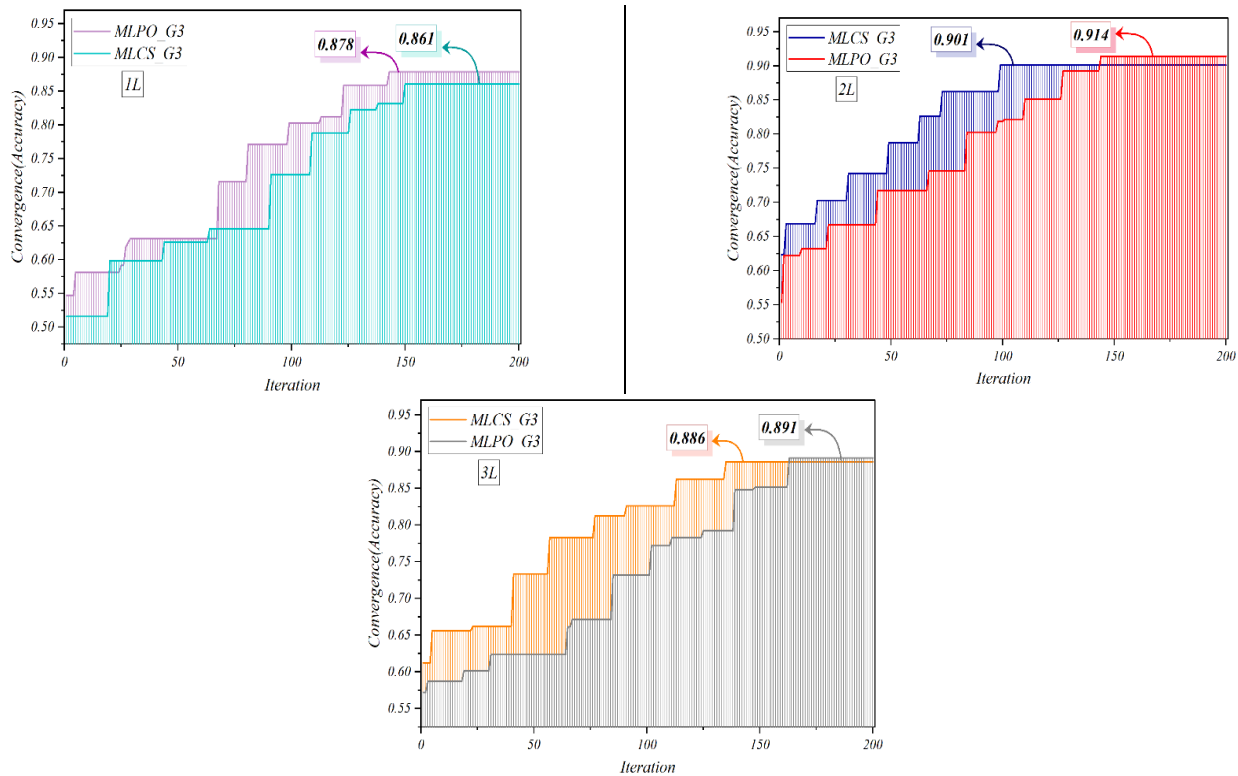


Fig. 3. Line plot for convergence of hybrid models for G3 values.

TABLE III. RESULT OF PRESENTED MODEL FOR G2

| Model | Section | Index values | | | |
|----------|---------|--------------|-----------|--------|----------|
| | | Accuracy | Precision | Recall | F1_score |
| MLPO (1) | Train | 0.910 | 0.913 | 0.910 | 0.909 |
| | Test | 0.873 | 0.888 | 0.873 | 0.870 |
| | All | 0.899 | 0.905 | 0.899 | 0.898 |
| MLCS (1) | Train | 0.906 | 0.910 | 0.906 | 0.905 |
| | Test | 0.847 | 0.863 | 0.848 | 0.846 |
| | All | 0.889 | 0.892 | 0.889 | 0.888 |
| MLPO (2) | Train | 0.953 | 0.954 | 0.953 | 0.953 |
| | Test | 0.907 | 0.9079 | 0.907 | 0.903 |
| | All | 0.939 | 0.940 | 0.939 | 0.939 |
| MLCS (2) | Train | 0.946 | 0.949 | 0.946 | 0.945 |
| | Test | 0.881 | 0.891 | 0.881 | 0.878 |
| | All | 0.927 | 0.927 | 0.927 | 0.926 |
| MLPO(3) | Train | 0.931 | 0.934 | 0.931 | 0.932 |
| | Test | 0.890 | 0.893 | 0.890 | 0.886 |
| | All | 0.919 | 0.921 | 0.919 | 0.919 |
| MLCS (3) | Train | 0.921 | 0.921 | 0.921 | 0.920 |
| | Test | 0.864 | 0.873 | 0.864 | 0.865 |
| | All | 0.904 | 0.905 | 0.904 | 0.904 |

In contrast, the MLCS model exhibits values of 0.921 and 0.864 for the corresponding terms in the train and test phases, illustrating that, in both terms and phases, the MLPO model consistently outperforms the MLCS model in accuracy. In summary, it is noteworthy that the MLPO model demonstrates superior performance compared to the MLCS model. Examining two models within the G3 target across three layers reveals that the MLPO model consistently maintains higher accuracy than its counterpart. For instance, in the recall term during the training phase, the MLPO model achieves a value of 0.892, whereas the MLCS model records a slightly lower value of 0.888. Similarly, in the F1-score metric, the MLPO model attains a value of 0.890, surpassing the MLCS model's F1-score of 0.886. This subtle comparison unequivocally underscores the MLPO model's superior accuracy compared to the MLCS model. Concerning the second layer, the accuracy values in the test phase for the MLPO and MLCS models are 0.864 and 0.856, respectively. Additionally, the precision values of the MLPO and MLCS models are 0.873 and 0.866, respectively. This observation signifies that the accuracy of the MLPO model surpasses that of the opposing model. Moreover, the MLPO model exhibits superior performance in the third layer. For a more thorough comprehension, it is noteworthy that the accuracy and precision values of the MLPO model across all phases are higher than the corresponding values of the MLCS model, with the accuracy comparison being $0.891 > 0.886$. Ultimately, the accuracy of the MLPO model surpasses that of the MLCS model in each layer of both targets. This comparison is presented in Table IV for further examination.

C. Results of Classification Processes

The comparison between the MLPO and MLCS models in two targets is illustrated in Tables V and VI, elucidating the

layer-wise accuracy of each model. Analogous to the preceding tables, these tables contrast grades instead of phases. Notably, the precision values of the MLPO model in the excellent grade across the first, second, and third layers are recorded as 0.77, 0.88, and 0.84, respectively. This observation suggests that the model's optimal performance is evident in the second layer, outperforming the other layers. The recall values for the good and acceptable grades in the MLPO model are 0.64 and 0.88 in the first layer, 0.76 and 0.88 in the second layer, and 0.76 and 0.88 in the third layer. This implies that the performance of the MLPO model is consistent in the second and third layers, while it is comparatively lower in the first layer. In the first layer, MLCS exhibits precision values of 0.74 and 0.96 for the acceptable and poor grades, respectively. In the second layer, the corresponding precision values are 0.85 and 0.96; in the third layer, they are 0.86 and 0.94, respectively. This analysis indicates that the model achieves higher accuracy in the third layer for the acceptable grade, surpassing the accuracy in the first and second layers. However, in the case of poor grades, the functionality is optimal in the first and second layers, contrasting with the third. It is pertinent to note that this comparison pertains to the G2 target. Contrastingly, within the G3 target, the recall values for the MLPO model in the first layer are 0.76 for excellent grade and 0.65 for good grade; in the second layer, they are 0.87 for excellent grade and 0.78 for good grade, and in the last layer, they are 0.81 for excellent grade and 0.83 for good grade. These statistics reveal that the model demonstrates heightened accuracy in the excellent grade of the second layer compared to the other layers. However, in the context of the good grade, the second layer exhibits superior functionality compared to the first and third layers.

TABLE IV. RESULT OF PRESENTED MODEL FOR G3

| Model | Section | Index values | | | |
|----------|---------|--------------|-----------|--------|----------|
| | | Accuracy | Precision | Recall | F1_score |
| MLPO (1) | Train | 0.892 | 0.893 | 0.892 | 0.890 |
| | Test | 0.847 | 0.846 | 0.848 | 0.841 |
| | All | 0.878 | 0.879 | 0.879 | 0.876 |
| MLCS (1) | Train | 0.888 | 0.885 | 0.888 | 0.886 |
| | Test | 0.822 | 0.8278 | 0.822 | 0.822 |
| | All | 0.861 | 0.858 | 0.861 | 0.859 |
| MLPO (2) | Train | 0.935 | 0.937 | 0.935 | 0.935 |
| | Test | 0.864 | 0.873 | 0.864 | 0.866 |
| | All | 0.914 | 0.918 | 0.914 | 0.914 |
| MLCS (2) | Train | 0.921 | 0.924 | 0.921 | 0.921 |
| | Test | 0.856 | 0.866 | 0.856 | 0.858 |
| | All | 0.901 | 0.905 | 0.901 | 0.902 |
| MLPO (3) | Train | 0.917 | 0.920 | 0.917 | 0.918 |
| | Test | 0.831 | 0.845 | 0.831 | 0.832 |
| | All | 0.891 | 0.896 | 0.891 | 0.893 |
| MLCS (3) | Train | 0.906 | 0.909 | 0.906 | 0.905 |
| | Test | 0.839 | 0.862 | 0.839 | 0.841 |
| | All | 0.886 | 0.893 | 0.886 | 0.886 |

TABLE V. PERFORMANCE OF PRESENTED MODELS BASED ON THE GRADES IN G2

| Model | Grade | Index values | | |
|----------|------------|--------------|--------|----------|
| | | Precision | Recall | F1-score |
| MLPO (1) | Excellent | 0.77 | 0.86 | 0.81 |
| | Good | 1.00 | 0.64 | 0.78 |
| | Acceptable | 0.85 | 0.88 | 0.86 |
| | Poor | 0.95 | 0.96 | 0.95 |
| MLCS (1) | Excellent | 0.81 | 0.77 | 0.79 |
| | Good | 0.92 | 0.67 | 0.77 |
| | Acceptable | 0.74 | 0.88 | 0.80 |
| | Poor | 0.96 | 0.96 | 0.96 |
| MLPO (2) | Excellent | 0.88 | 0.94 | 0.91 |
| | Good | 0.93 | 0.76 | 0.83 |
| | Acceptable | 0.89 | 0.88 | 0.89 |
| | Poor | 0.97 | 0.98 | 0.98 |
| MLCS (2) | Excellent | 0.87 | 0.88 | 0.88 |
| | Good | 0.96 | 0.73 | 0.83 |
| | Acceptable | 0.85 | 0.88 | 0.86 |
| | Poor | 0.96 | 0.98 | 0.97 |
| MLPO (3) | Excellent | 0.84 | 0.87 | 0.86 |
| | Good | 0.96 | 0.76 | 0.85 |
| | Acceptable | 0.82 | 0.88 | 0.85 |
| | Poor | 0.97 | 0.97 | 0.97 |
| MLCS (3) | Excellent | 0.81 | 0.82 | 0.82 |
| | Good | 0.96 | 0.82 | 0.89 |
| | Acceptable | 0.86 | 0.89 | 0.88 |
| | Poor | 0.94 | 0.95 | 0.94 |

TABLE VI. PERFORMANCE OF PRESENTED MODELS BASED ON THE GRADES IN G3

| Model | Grade | Index values | | |
|----------|------------|--------------|--------|-----------|
| | | Precision | Recall | F1-score |
| MLPO (1) | Excellent | 0.80 | 0.76 | 0.78 |
| | Good | 0.90 | 0.65 | 0.75 |
| | Acceptable | 0.76 | 0.83 | 0.79 |
| | Poor | 0.93 | 0.96 | 0.94 |
| MLCS (1) | Excellent | 0.72 | 0.74 | 0.73 |
| | Good | 0.83 | 0.75 | 0.79 |
| | Acceptable | 0.76 | 0.68 | 0.72 |
| | Poor | 0.93 | 0.96 | 0.94 |
| MLPO (2) | Excellent | 0.82 | 0.87 | 0.84 |
| | Good | 0.94 | 0.78 | 0.85 |
| | Acceptable | 0.80 | 0.88 | 0.84 |
| | Poor | 0.97 | 0.96 | 0.96 |
| MLCS (2) | Excellent | 0.78 | 0.81 | 0.79 |
| | Good | 0.91 | 0.73 | 0.81 |
| | Acceptable | 0.78 | 0.90 | 0.84 |
| | Poor | 0.97 | 0.96 | 0.96 |
| MLPO (3) | Excellent | 0.71 | 0.81 | 0.76 |
| | Good | 0.80 | 0.83 | 0.81 |
| | Acceptable | 0.83 | 0.80 | 0.81 |
| | Poor | 0.98 | 0.95 | 0.96 |
| MLCS (3) | Excellent | 0.72 | 0.79 | 0.75 |
| | Good | 0.96 | 0.68 | 0.7941.00 |
| | Acceptable | 0.79 | 0.87 | 0.83 |
| | Poor | 0.95 | 0.95 | 0.95 |

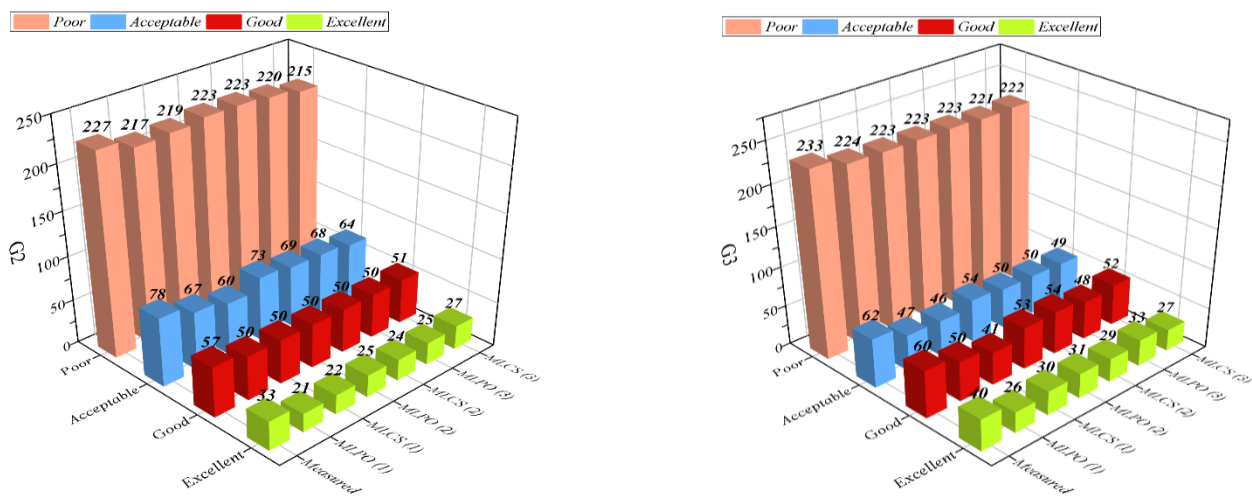


Fig. 4. 3D Bars plot for comparing the measured and predicted values.

Conversely, the recall values of the MLCS model in the first layer are 0.74 for excellent grade and 0.75 for good grade; in the second layer, they are 0.81 for excellent grade and 0.73 for good grade, and in the last layer, they are 0.79 for excellent grade and 0.68 for good grade. These figures suggest that the MLCS model exhibits enhanced functionality in the excellent grade of the second layer. However, concerning the good

grade, it is noteworthy to emphasize that this model in the first layer attains higher accuracy than the second and third layers.

Fig. 4 delineates the comparison between each layer's measured and predicted values for the MLPO and MLCS models in the G2 and G3 targets. The illustration of this plot reveals that the accuracy of the MLPO model in the first layer attains 21 out of 33 measured values. In the second layer, it

achieves 25 out of 33 measured values; in the last layer, it similarly attains 25 out of 33 measured values. This observation underscores that the MLPO model demonstrates the highest accuracy in the excellent grade for the second and third layers, surpassing the accuracy observed in the first layer. Nevertheless, in the good grade, the accuracy of the MLPO and MLCS models across all three layers is recorded at 50 out of 57 measured values, except for MLCS in the third layer, which achieves a measured value of 51 out of 57. It is discernible that this model exhibits superior functionality in the third layer compared to other models across all three layers.

Regarding the acceptable grade, the MLPO model attains the highest accuracy in the second layer, with 73 out of 78 measured values. The second-highest accuracy in the same layer is observed for the MLCS model, recording 69 out of 78 measured values. In contrast, the third-highest accuracy is attributed to the MLPO model in the first layer, achieving a measured value of 67 out of 78. The comparative analysis elucidates that superior performance is evident in both models within the second layer when contrasted with other models in different layers. Nevertheless, within the same target, the measured value of the MLCS model in the third layer amounts to 215 out of 227, indicative of the lowest measured value across all layers among the models. The second-highest performance is attributed to the MLPO model in the first layer, achieving a measured value of 217 out of 227, while the third-highest performance is observed for the MLCS model in the same layer.

On the contrary, ascendancy is asserted by both the MLPO and MLCS models in the second layer, attaining 223 out of 227 measured values. In the subsequent target, parity is observed between the MLCS and MLPO models in the second layer and the MLCS model in the first layer, registering 223 out of 233 measured values. However, the MLPO model in the first layer stands out with the highest accuracy, recording 224 out of 233 measured values, particularly notable in the context of the poor grade. For the acceptable grade, equivalence is noted as both models in the third and second layers exhibit identical measured values of 50 out of 62, representing the maximum accuracy among models across all three layers. The MLCS model in the third layer achieves the second-highest performance, recording 49 out of 62 measured values.

Conversely, the least favourable measured value is attributed to the MLCS model in the first layer. Notably, in the good grade, optimal performance is observed in the MLCS model within the second layer, achieving the highest measured value of 54 out of 60. In contrast, the least favourable performance in this grade is associated with the same model but in the first layer, registering 41 out of 60 measured values. In the highest grade, excellent, the highest accuracy is attained by the MLPO model in the third layer, achieving 33 out of 40 measured values. The second-highest performance in this grade is noted for the MLPO model in the second layer, with a measured value of 31 out of 40. In contrast, the third-highest performance is attributed to the MLCS model in the first layer, recording 30 out of 40 measured values. The lowest performance in the excellent grade is associated with the MLPO model in the first layer, registering 26 out of 40 measured values.

The accuracy of the models in the confusion matrix across all three layers for two targets is depicted in Fig. 5 and 6. The performance of the MLPO models in the G2 target, specifically in layer one, is observed. In instances characterized by a suboptimal grade, the recorded value is 217 out of 227, reflecting a difference of 4.5%. Additionally, nine students are misclassified in an acceptable grade and one in a good grade. Similarly, within the same layer, the value for acceptable grades is 67 out of 78, indicating a difference of 15.17%. In this context, ten students are misclassified as having a poor grade and one as having a good grade. The MLCS model's measured value in the second layer of a suboptimal grade is 219 out of 223, reflecting a marginal difference of 1.81%. This outcome entails misclassifying five students in an acceptable grade, two in a good grade, and one in an excellent grade.

Conversely, the measured value for acceptable grades in the first layer is 60 out of 62, with a difference of 3.28%, accompanied by the misclassification of nine students with poor grades, eight with good grades, and one with excellent grades. Furthermore, in the second layer, the measured value of the MLPO model in a good grade is 50 out of 60, demonstrating an 18.18% difference and involving the misclassification of two students in an excellent grade, four in an acceptable grade, and one in a good grade. Incidentally, within the G2 target of an excellent grade, the MLPO model exhibits a difference of 27.59% in the second layer, entailing the misclassification of six students in a good grade and two students in an acceptable grade. Conversely, the MLCS model in the G3 target of the current grade manifests a 50% difference, accompanied by the misclassification of seven students in a good grade and two in an acceptable grade. Additionally, in the G2 target, the MLPO model in a poor grade of the second layer demonstrates a 5.74% difference, resulting in the misclassification of seven students in an acceptable grade. Simultaneously, within an acceptable grade, it showcases a 6.62% difference, leading to the misclassification of five students with poor grades.

Regarding the good grade, it is imperative to note that it exhibits a 13.8% difference, resulting in the misclassification of four students in an acceptable grade, one in a poor grade, and two in an excellent grade. In the same target and layer, the MLCS model demonstrates a 1.78% difference in the poor grade category, leading to the misclassification of three students in an acceptable grade and one in a good grade. Meanwhile, a 12.24% difference is observed for the acceptable grade, entailing the misclassification of one student in a good grade and eight students in a poor grade. In the third layer of the G2 target, the MLPO model is observed to misclassify seven students with a good grade and one student with an acceptable grade, reflecting a 27.59% difference. This denotes the performance of the current model in an excellent grade.

Conversely, the MLCS model in the same target, layer, and grade exhibits a 20% difference, accompanied by the misclassification of six students with good grades. Upon reaching the G3 target and assessing the models' performance in the first layer, a discernible discrepancy is observed between the MLCS model and the MLPO model in the context of an excellent grade. Specifically, the MLPO model manifests a substantial 42.4% difference in an excellent grade,

accompanied by the misclassification of eleven students in a good grade, one in an acceptable grade, and two in a poor grade. In contrast, the MLCS model exhibits a 28.57% difference, misclassifying eight students with good grades and two with acceptable grades. In the second layer, the MLPO model demonstrates a 12.39% difference, with the misclassification of two students in an excellent grade, two in an acceptable grade, and one in a poor grade.

Conversely, the MLCS model in the same layer features a 10.53% difference, entailing the misclassification of three

students with excellent grades and three with acceptable grades. Nevertheless, a singular examination of one stage for each model might suggest that the MLCS model exhibits superior accuracy compared to the alternative model. However, when considering the comprehensive assessment across all layers, it becomes apparent that the functionality of the MLPO model surpasses that of the MLCS model in each respective layer.

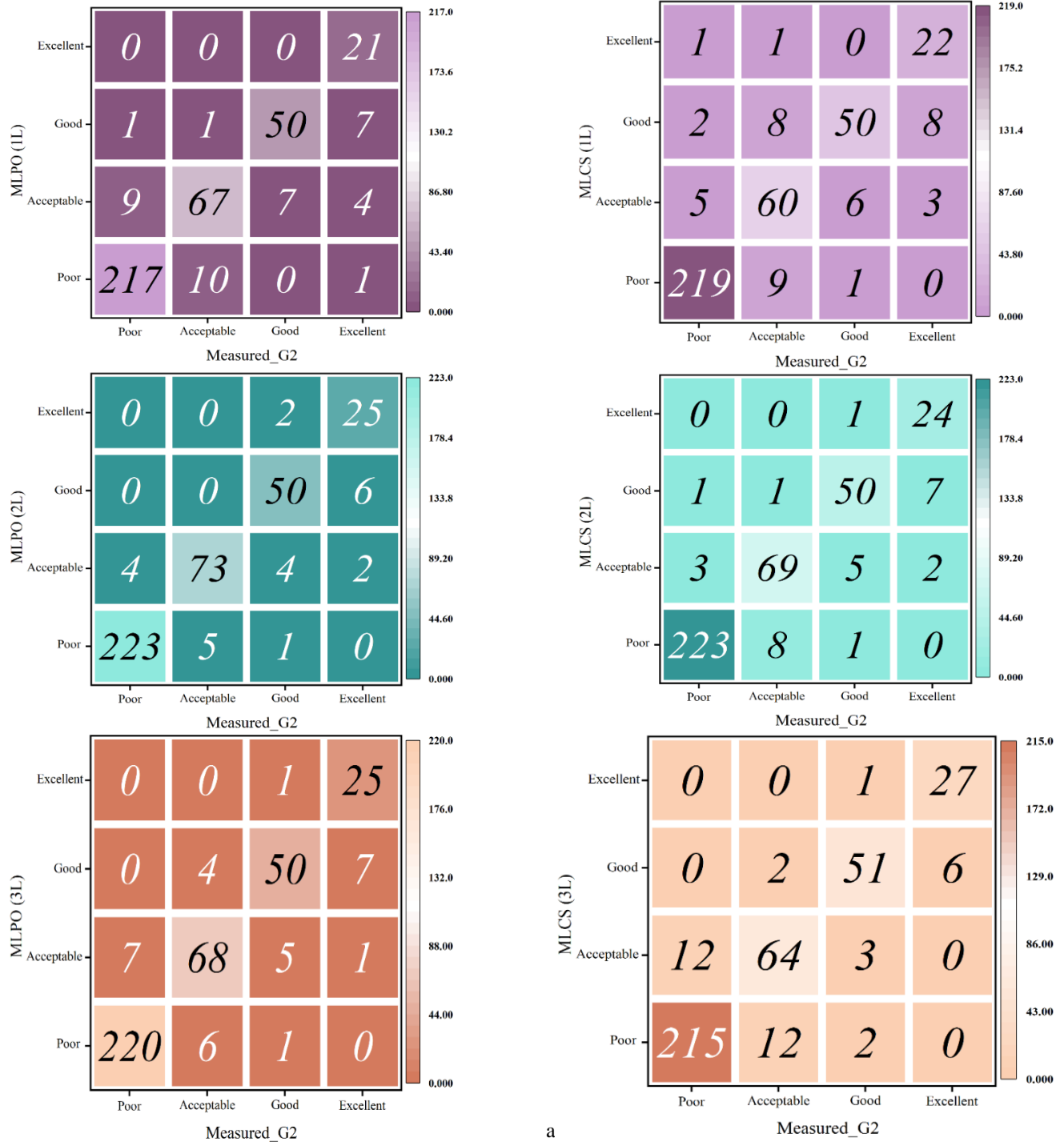


Fig. 5. Confusion matrix for accuracy of each model for G2 values.

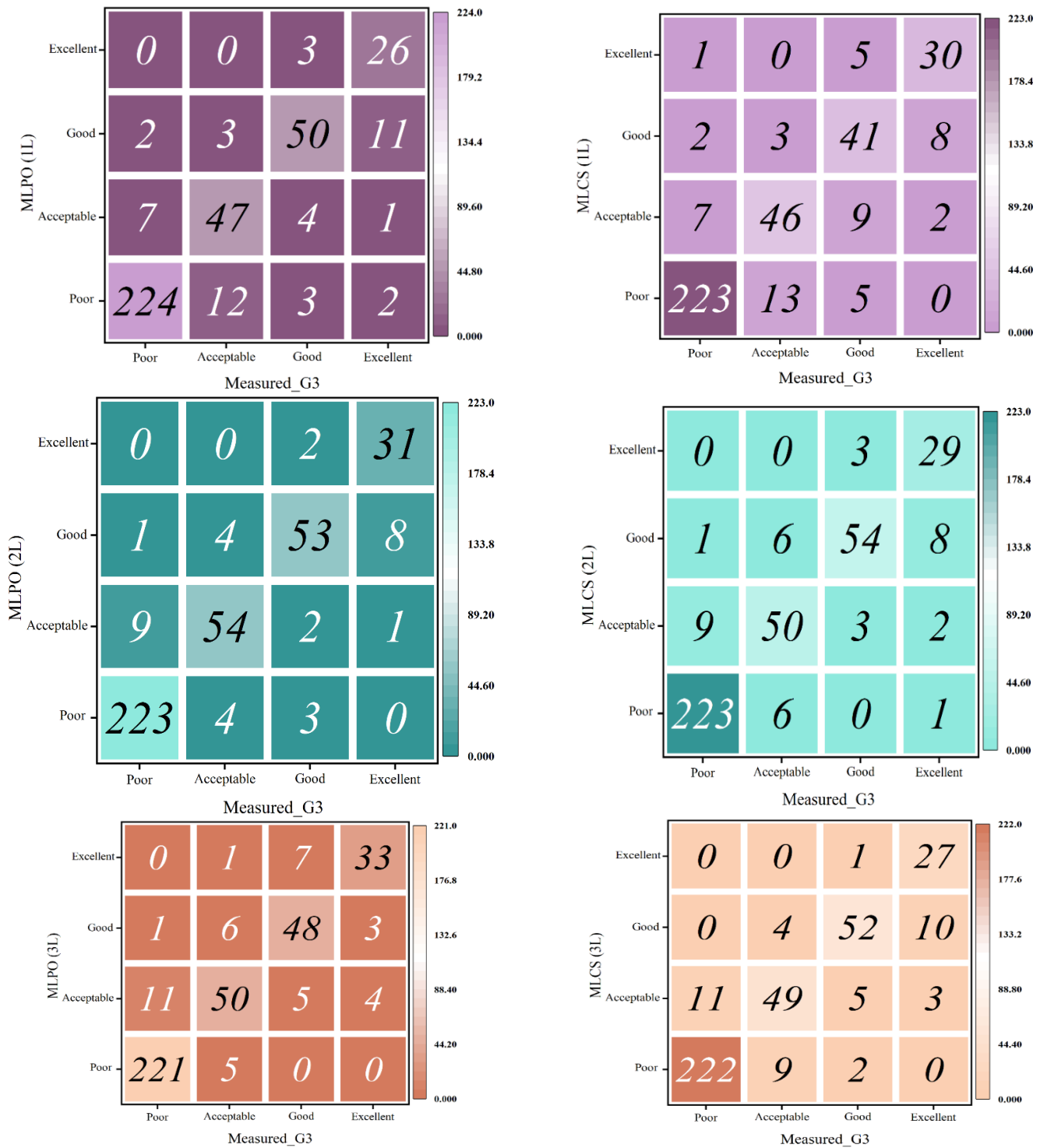


Fig. 6. Confusion matrix for accuracy of each model accuracy for G3 values.

The subsequent column plot illustrates the percentage achievements of the developed models. Specifically, within the G2 target, the MLPO model in the second layer attains the highest accuracy at 0.93924, followed by the MLCS model in the same layer with a percentage of 0.92658, securing the second rank. The MLPO model in the third layer holds the third rank with a percentage of 0.91899. This concise comparison indicates that the MLPO model in the second layer

exhibits superior functionality compared to the other layers. Nevertheless, the MLPO model in the second layer is characterized by superior precision relative to the other models, achieving a percentage of 0.9395. The MLCS model in the second layer and the MLPO model in the third layer secure the second and third ranks, respectively, with percentages of 0.9274 and 0.9214, respectively.

Additionally, the recall and F1-score values of the MLPO model, standing at 0.9392 and 0.9385, surpass those of the alternative models. In summary, the performance of MLPO L2 not only outperforms the MLCS model but also exceeds its performance in other layers. Upon a cursory examination, it

becomes evident that MLPO L2 in the G3 target attains elevated accuracy, precision, recall, and F1-score values. The column plots in Fig. 7 and 8 illustrate the achievement percentage for developed models as assessed by evaluators.

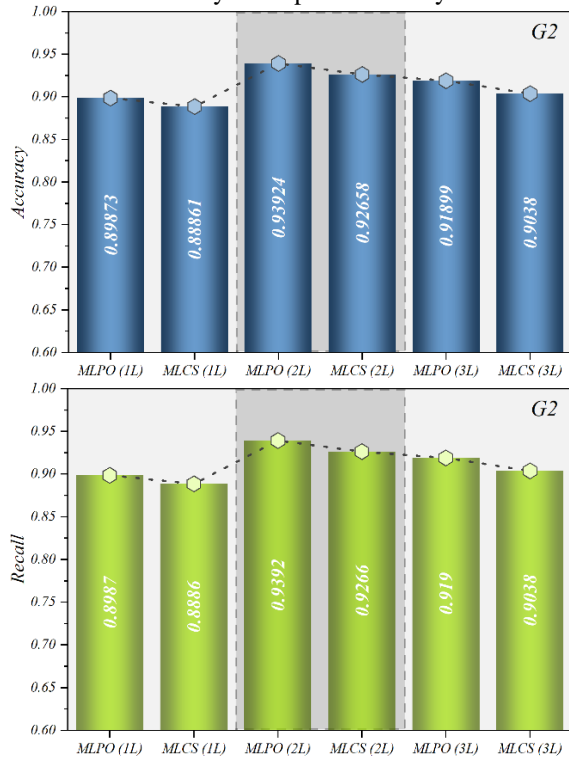


Fig. 7. Column plots the achievement percentage for developed models of G2 prediction values based on evaluators.

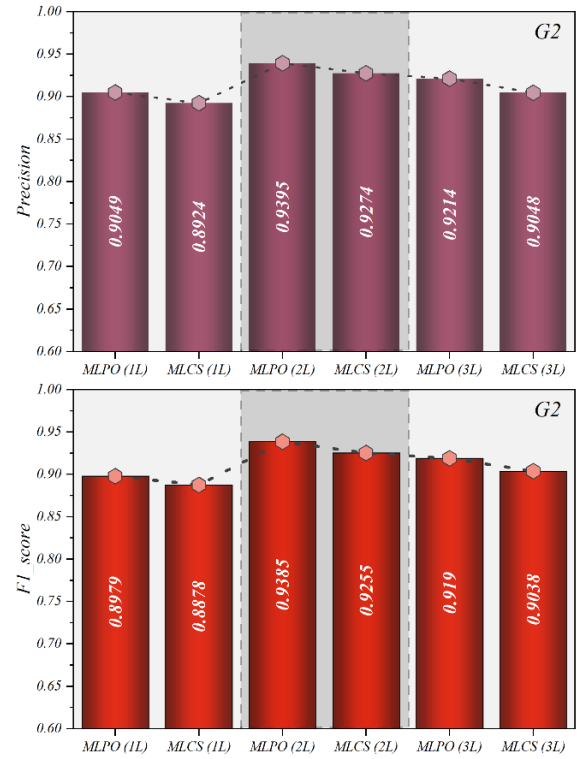


Fig. 8. Column plots the achievement percentage for developed models of G3 prediction values based on evaluators.

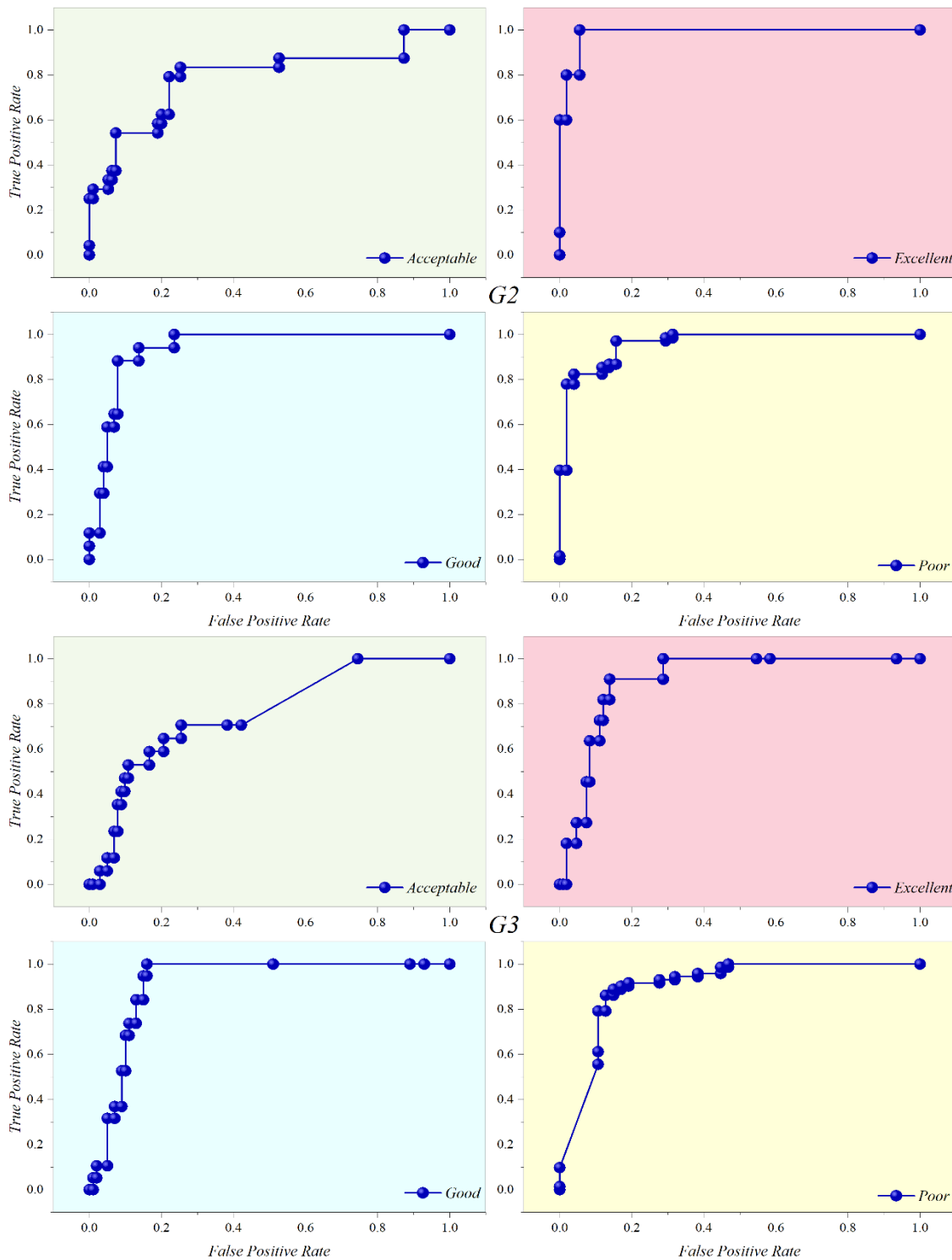


Fig. 9. The result of the ROC curve.

A binary classification model's performance at different classification thresholds is represented graphically by the Receiver Operation Characteristic (ROC) curve presented in Fig. 9. It shows how different threshold values affect the trade-off between the genuine positive rate (sensitivity) and the false positive rate (1-specificity). The following are important ideas about ROC curves: True Positive Rate (Sensitivity): The

percentage of real positive cases the model accurately predicts is the true positive rate. To compute it, divide the number of true positives (TP) by the quantity of false negatives (FN), or $TP / (TP + FN)$. False Positive Rate (1-Specificity): This refers to the percentage of real negative cases the model mispredicts as positive. The formula for calculating it is $FP / (FP + TN)$, where FP stands for false positives and TN for true negatives.

Threshold: Predictions in binary classification models are frequently predicated on a probability threshold. Positive observations are those whose estimated probability falls above the threshold; negative observations fall below it.

By changing this threshold and seeing how the true positive rate and false positive rate change in tandem, ROC curves are produced. Area Under the ROC AUC-ROC curve: This concisely indicates the classifier's overall effectiveness and potential classification levels. It offers a solitary scalar value that symbolizes the model's overall performance. On the other hand, AUC-ROC values of 1.0 and 0.5 suggest models with performance comparable to random chance and are regarded as ideal, respectively. On the other hand, the following convergence curve shows the optimal model (MLPO 2), whose grade has the highest accuracy and a rank of false positive rate that approaches 1.0. The current plot demonstrates that the performance of the best model within an acceptable range is deemed unsatisfactory, as evidenced by its attainment of a true positive rate of 1.0 after a false positive rate of 0.8. The best model exhibits improvement in both poor and good performance categories, yet it remains insufficient. An examination of the excellent performance category reveals that the vector achieves a true positive rate of 1.0 before a false positive rate of 0.2.

Consequently, the optimal performance of MLPO 2 is realized in the excellent grade of the G2 target. On the contrary

target, superior performance is observed in the good grade by the best model, with a true positive rate of 1.0 occurring before a false positive rate of 0.2. Following the good grade, the subsequent rank is assigned to the excellent grade, while the poor and acceptable grades occupy the third and fourth ranks, respectively.

IV. DISCUSSION

A. Comparing Previous Studies vs. Present Study

The findings from three articles investigating student performance in the literature—specifically, one by Bichkar and R. R. Kabra [31], another by Edin Osmanbegovic et al. [32], and a third by Nguyen and Peter [33]—are succinctly summarized in Table VII. Notably, the research conducted by Nguyen and Peter, employing the DTC model, demonstrated the highest accuracy rate of 82%. In contrast, within this particular present study, which endeavors to forecast and classify students' performance in Portuguese language based on their G2 and G3 scores, the combination of the MLPC model and POA optimization algorithm yielded remarkable results. The accuracy metrics recorded were 95.3% for G2 and 93.5% for G3. Consequently, the proposed methodology achieved notably more reliable outcomes compared to prior studies, underscoring its efficacy in enhancing predictive accuracy and classification precision.

TABLE VII. RESULT OF PRESENTED AND PUBLISHED STUDIES

| Author (s) | Model | Accuracy |
|-------------------------------|--------------|----------|
| Bichkar and R. R. Kabra [31] | DTC | 69.94% |
| Edin Osmanbegovic et al. [32] | NBC | 76.65% |
| Nguyen and Peter [33] | DTC | 82% |
| Present study for G2 | MLPC+POA (2) | 95.3% |
| Present study for G3 | MLPC+POA (2) | 93.5% |

V. CONCLUSION

To sum up, utilizing the MLPC model in conjunction with the Pelican Optimization and Crystal Structure Algorithm optimizers presents a viable method for predicting achievement among learners. Using these sophisticated methodologies enhances the precision and efficacy of evaluating learning objectives. This study highlights the possibilities for subsequent breakthroughs in educational analytics while also improving the accuracy of achievement prediction using complex machine learning algorithms and optimization techniques. The combined use of Crystal Structure Algorithm Optimizers, Pelican Optimization, and MLPC demonstrates a strong foundation for forecasting and comprehending students' academic performance. This opens the door for more knowledgeable and focused interventions in educational settings.

Nevertheless, within the scope of this study, an evaluation of the performance of MLPO and MLCS models is conducted across three distinct layers of the G2 and G3 targets. The findings reveal that the MLPO model in the second layer of both targets demonstrates superior accuracy, precision, recall, and F1-score, registering percentages of 0.9324 and 0.91392

for accuracy, 0.9395 and 0.9139 for precision, 0.9393 and 0.9139 for recall, and 0.9385 and 0.9144 for F1-score, respectively. Conversely, MLPO L2 achieves the highest accuracy in the G3 target, specifically in the acceptable grade, with a measured value of 54 out of 62, in contrast to MLCS L1, which records the lowest accuracy in the same grade and target, with a measured value of 46 out of 62. This comparison suggests that the MLPO model L2, given its elevated accuracy, can predict student performance with a high degree of precision. There is substantial potential for the educational system to utilize this model for advancements in this domain. Notably, the outcomes of this predictive process can be applied in real-world scenarios, yielding consistent results.

REFERENCES

- [1] K.-L. Tsui, V. Chen, W. Jiang, F. Yang, and C. Kan, "Data mining methods and applications," in Springer handbook of engineering statistics, Springer, 2023, pp. 797–816.
- [2] Q. H. Ngô and N. M. Trinh, "A University Student Dropout Detector based on Academic Data-A case study at FPT University." FPTU Hà Nội, 2023.
- [3] S. Chatterjee, T. P. Singh, S. Lim, and A. Mukhopadhyay, "Social Media and Crowdsourcing".
- [4] P. T. T. Thao et al., "55 Khoa Học Giáo Dục Việt Nam," 2023.

- [5] S. Dutta and S. Mandi, "Can One Deep Model Be Effective in Multiple Domain? a Case Study with Public Datasets," EasyChair, 2023.
- [6] A. Rawal and B. Lal, "Predictive model for admission uncertainty in high education using Naïve Bayes classifier," Journal of Indian Business Research, vol. 15, no. 2, pp. 262–277, 2023.
- [7] S. Sengupta, "Search for Articles," 2023.
- [8] S. Jordão, D. Durães, and P. Novais, "Performance Analysis of Models Used to Predict Failure in Secondary School," in International Conference on Data Science and Artificial Intelligence, Springer, 2023, pp. 339–348.
- [9] S. Khan and M. Shaheen, "From data mining to wisdom mining," J Inf Sci, vol. 49, no. 4, pp. 952–975, 2023.
- [10] S. Chanmee and K. Kesorn, "Semantic decision Trees: A new learning system for the ID3-Based algorithm using a knowledge base," Advanced Engineering Informatics, vol. 58, p. 102156, 2023.
- [11] S. Bum, I. B. Iorliam, E. O. Okube, and A. Iorliam, "Prediction of Student's Academic Performance Using Linear Regression," NIGERIAN ANNALS OF PURE AND APPLIED SCIENCES, vol. 2, pp. 259–264, 2019.
- [12] A. M. Shahiri and W. Husain, "A review on predicting student's performance using data mining techniques," Procedia Comput Sci, vol. 72, pp. 414–422, 2015.
- [13] D. Thammasiri, D. Delen, P. Meesad, and N. Kasap, "A critical assessment of imbalanced class distribution problem: The case of predicting freshmen student attrition," Expert Syst Appl, vol. 41, no. 2, pp. 321–330, 2014.
- [14] L. D. Yulianto, A. Triayudi, and I. D. Sholihati, "Implementation Educational Data Mining For Analysis of Student Performance Prediction with Comparison of K-Nearest Neighbor Data Mining Method and Decision Tree C4. 5: Implementation Educational Data Mining For Analysis of Student Performance Prediction w," Jurnal Mantik, vol. 4, no. 1, pp. 441–451, 2020.
- [15] H. Zhou, Z. Wu, N. Xu, and H. Xiao, "PDR-SMOTE: an imbalanced data processing method based on data region partition and K nearest neighbors," International Journal of Machine Learning and Cybernetics, pp. 1–16, 2023.
- [16] D. Kabakchieva, K. Stefanova, and V. Kisimov, "Analyzing university data for determining student profiles and predicting performance," in Educational Data Mining 2011, 2010.
- [17] Y. Fan, Y. Liu, H. Chen, and J. Ma, "Data Mining-based Design and Implementation of College Physical Education Performance Management and Analysis System," Int. J. Emerg. Technol. Learn., vol. 14, no. 6, pp. 87–97, 2019.
- [18] J.-M. Trujillo-Torres, H. Hossein-Mohand, M. Gómez-García, H. Hossein-Mohand, and F.-J. Hinojo-Lucena, "Estimating the academic performance of secondary education mathematics students: A gain lift predictive model," Mathematics, vol. 8, no. 12, p. 2101, 2020.
- [19] P. Strecht, J. Mendes-Moreira, and C. Soares, "Merging Decision Trees: a case study in predicting student performance," in Advanced Data Mining and Applications: 10th International Conference, ADMA 2014, Guilin, China, December 19–21, 2014. Proceedings 10, Springer, 2014, pp. 535–548.
- [20] S. Kotsiantis, "Educational data mining: a case study for predicting dropout-prone students," Int J Knowl Eng Soft Data Paradig, vol. 1, no. 2, pp. 101–111, 2009.
- [21] S. K. Yadav and S. Pal, "Data mining: A prediction for performance improvement of engineering students using classification," arXiv preprint arXiv:1203.3832, 2012.
- [22] A. O. Ogunde and D. A. Ajibade, "A data mining system for predicting university students' graduation grades using ID3 decision tree algorithm," Journal of Computer Science and Information Technology, vol. 2, no. 1, pp. 21–46, 2014.
- [23] S. Alturki and N. Alturki, "Using educational data mining to predict students' academic performance for applying early interventions," Journal of Information Technology Education: JITE. Innovations in Practice: IIP, vol. 20, pp. 121–137, 2021.
- [24] E. Osmanbegovic and M. Suljic, "Data mining approach for predicting student performance," Economic Review: Journal of Economics and Business, vol. 10, no. 1, pp. 3–12, 2012.
- [25] B. Olukoya, "Using ensemble random forest, boosting and base classifiers to ameliorate prediction of students' academic performance," vol. 6, p. 654, Mar. 2023.
- [26] X. Zhang, R. Xue, B. Liu, W. Lu, and Y. Zhang, "Grade prediction of student academic performance with multiple classification models," in 2018 14th International Conference on Natural Computation, Fuzzy Systems and Knowledge Discovery (ICNC-FSKD), IEEE, 2018, pp. 1086–1090.
- [27] S. Talatahari, M. Azizi, M. Tolouei, B. Talatahari, and P. Sareh, "Crystal structure algorithm (CryStAl): a metaheuristic optimization method," IEEE Access, vol. 9, pp. 71244–71261, 2021.
- [28] S. A. Farooqui et al., "Crystal Structure Algorithm (CryStAl) Based Selective Harmonic Elimination Modulation in a Cascaded H-Bridge Multilevel Inverter," Electronics (Basel), vol. 10, no. 24, p. 3070, 2021.
- [29] J. C. Thomas, A. R. Natarajan, and A. Van der Ven, "Comparing crystal structures with symmetry and geometry," NPJ Comput Mater, vol. 7, no. 1, p. 164, 2021.
- [30] T. Sağ, "PVS: a new population-based vortex search algorithm with boosted exploration capability using polynomial mutation," Neural Comput Appl, vol. 34, no. 20, pp. 18211–18287, 2022.
- [31] R. R. Kabra and R. S. Bichkar, "Performance prediction of engineering students using decision trees," Int J Comput Appl, vol. 36, no. 11, pp. 8–12, 2011.
- [32] E. Osmanbegovic and M. Suljic, "Data mining approach for predicting student performance," Economic Review: Journal of Economics and Business, vol. 10, no. 1, pp. 3–12, 2012.
- [33] N. T. Nghe, P. Janecek, and P. Haddawy, "A comparative analysis of techniques for predicting academic performance," in 2007 37th annual frontiers in education conference-global engineering: knowledge without borders, opportunities without passports, IEEE, 2007, pp. T2G-7.

DUF-Net: A Retinal Vessel Segmentation Method Integrating Global and Local Features with Skeleton Fitting Assistance

Xuelin Xu^{1*}, Ren Lin², Jianwei Chen³, Huabin He⁴

School of Computer Science and Mathematics, Fujian University of Technology, Fujian, China^{1, 2, 3}

School of Electronic, Electrical Engineering and Physics, Fujian University of Technology, Fujian, China⁴

Fujian Provincial Key Laboratory of Big Data Mining and Applications, Fujian University of Technology, Fujian, China^{1, 2, 3}

Abstract—Assisted evaluation through retinal vessel segmentation facilitates the early prevention and diagnosis of retinal lesions. To address the scarcity of medical samples, current research commonly employs image patching techniques to augment the training dataset. However, the vascular features in fundus images exhibit complex distribution, patch-based methods frequently encounter the challenge of isolated patches lacking contextual information, consequently resulting in issues such as vessel discontinuity and loss. Additionally, there are a higher number of samples with strong contrast vessels compared to those with weak contrast vessels in retinal images. Moreover, within individual patches, there are more pixels of strong contrast vessels compared to weak contrast vessels, leading to lower segmentation accuracy for small vessels. Hence, this study introduces a patch-based deep neural network method for retinal vessel segmentation to address the issues. Firstly, a novel architecture, termed Double U-Net with a Feature Fusion Module (DUF-Net), is proposed. This network structure effectively supplements missing contextual information and improves the problem of vessel discontinuity. Furthermore, an algorithm is introduced to classify vascular patches based on their contrast levels. Subsequently, conventional data augmentation methods were employed to achieve a balance in the number of samples with strong and weak contrast vessels. Additionally, method with skeleton fitting assistance is introduced to improve the segmentation of vessels with weak contrast. Finally, the proposed method is evaluated across four publicly available datasets: DRIVE, CHASE_DB1, STARE, and HRF. The results demonstrate that the proposed method effectively ensures the continuity of segmented blood vessels while maintaining accuracy.

Keywords—Fundus image; vessel segmentation; skeleton fitting; data augmentation; patch classification

I. INTRODUCTION

The eye stands as one of the paramount sensory organs in the human body, serving as the primary conduit for external stimuli reception. Presently, propelled by societal advancements and the proliferation of electronic devices, there is a sustained escalation in the prevalence of ophthalmic diseases among patients. Today, with the development of society and the widespread use of electronic devices, the number of patients with ophthalmic diseases continues to increase. Ophthalmic diseases are closely associated with retinal lesions, with glaucoma, diabetic retinopathy, and

diabetic macular degeneration being major causes of global blindness [1]. Retinal fundus images represent the singular non-invasive modality for observing the deep microvascular system, encompassing a diverse array of retinal structures such as the retinal vascular tree, optic disc, fovea centralis, and macula [2]. The early clinical characteristics of diabetic retinopathy encompass microaneurysms, dot and blot hemorrhages, cotton wool spots, and intraretinal microvascular abnormalities [3]. The characteristic sign of glaucoma is optic disc cupping, and the ratio of the cup to disc area in fundus images, referred to as the cup-to-disc ratio (CDR), serves as a vital structural metric for evaluating the presence and advancement of glaucoma [4]. The hallmark of age-related macular degeneration (AMD) is the infiltration of choroidal vasculature into the macular region, accompanied by heightened vascular permeability [4]. Variations in retinal structure are pivotal for diagnosing diabetic retinopathy, glaucoma, and AMD. Given that retinal vessel segmentation is essential for visualizing and quantifying retinal pathology, it is an indispensable component in the analysis of retinal diseases [5]. The conventional method for retinal vessel segmentation is characterized by its costly, intricate, and time-intensive nature. Furthermore, challenges such as uneven illumination, complex vascular structures, and low vessel-background contrast in images contribute to inconsistencies in vessel segmentation across different experts [6]. This has spurred the advancement of automated retinal vessel segmentation technology.

Traditional segmentation methods mainly include line detection [7], edge detection [8], matched filtering [9] [10], and shape-based methods [11] [12]. These methods perform vessel segmentation based on vessel edge pixels or shape features. The main reason is that, compared to the background, the edge and shape information of vessels with strong contrast are more prominent, making their features easier to learn. In recent years, deep learning methods have propelled the progress of retinal vessel segmentation techniques, surpassing traditional machine learning methods [13]. Deep learning methods do not require manual feature design and can effectively extract key features from data while achieving good accuracy and generalization capabilities, thus promoting the development of retinal vessel segmentation methods [14] [15]. Currently, there are generally two types of retinal vessel segmentation methods based on deep learning [16]. End-to-end methods are one of the types, sacrificing spatial resolution to ease memory constraints during

*Corresponding Author.

training. However, these methods lead to in the loss of spatial information in retinal vessel images. On the other hand, patch-based segmentation methods are another type. Although these methods enhance data samples, it may lead to a lack of contextual information between independent patches. Through observation, we notice that there are more samples of vessel patches with strong contrast compared to those with weak contrast, and within individual patches, there are more pixels of vessels with strong contrast compared to those with weak contrast. These issues may result in problems such as vessel discontinuity and poor segmentation of small vessels when restoring segmented blocks to the original image size.

Therefore, in this paper, we first compare the pixel values of vessels and background within vessel patches. If a patch contains a higher proportion of pixels with strong vessel contrast, it is classified as a Contrast Strong Vessel Patch (CSVP); otherwise, it is classified as a Contrast Weak Vessel Patch (CWVP). Next, we introduce a novel network structure named DUF-Net, which is capable of learning both global and local information, effectively supplementing missing contextual information between patches. Additionally, we design a patch classification algorithm to perform patch classification and quantity statistics. Data augmentation is utilized to augment deficient image patches, aiming to balance the number of samples for various types of retinal vessel pathology, including CSVP and CWVP. Additionally, a training method integrating skeleton fitting assistance is introduced to enhance the model's segmentation capability for CWVP within individual samples. In summary, the principal contributions of this paper can be outlined as follows:

- In order to compensate for the absence of contextual information between patches, We introduce a novel network structure named DUF-Net. It is capable of simultaneously learning both global and local features, guiding the model to capture contextual information surrounding the patches and thereby improving the completeness of vessel segmentation.
- To improve the segmentation capability of CWVP, a patch classification algorithm was designed to balance the quantity of CSVP and CWVP samples. Additionally, during training, prior knowledge of vessel skeletons and corresponding loss functions were introduced to guide the model in learning CWVP features and address the issue of pixel imbalance within individual patches.
- We assessed the proposed method across four publicly available datasets and conducted comparisons with six latest methods. Experimental findings affirm the efficacy and robustness of the proposed approach.

The remaining sections of this paper are organized as follows. Section II provides a review of traditional and deep learning methods in retinal vessel segmentation. Section III provides a detailed explanation of the proposed method. Section IV showcases the implementation details of the experiments. Section V presents the experimental results. Section VI and VII respectively discuss and summarize the proposed method.

II. RELATED WORK

Research on retinal vessel segmentation can be categorized into traditional methods and deep learning methods.

A. Traditional Methods

Traditional methods involve direct detection of features or edge pixels in retinal vessel images. Sheng et al. [17] combined geometric structures, texture, color, and spatial information in the image while simultaneously refining the segmentation results using a minimum spanning superpixel tree to refine segmentation results. Lam et al. [18] proposed a novel multi-concave modeling approach for handling bright lesions in the perceptual space and removing dark lesions that differ from the retinal vascular structure. To improve vessel segmentation efficiency, Rezaee and Haddadnia [19] employed a skeletonization and fuzzy entropy thresholding segmentation algorithm. They differentiated retinal main vessels from other tissue components through adaptive filtering and fuzzy entropy thresholding. In summary, although the aforementioned methods do not require training and have lower complexity, they heavily rely on filter design and often exhibit lower accuracy.

In machine learning, manual feature extraction is utilized for retinal fundus image analysis, followed by classification using common classifiers such as k-nearest neighbors (KNN) [20], support vector machine (SVM) [21], and Bayesian methods [22] [23]. Orlando et al. [24] utilized conditional random fields and support vector machines for retinal fundus image vessel segmentation. Zhu et al. [25] presented a supervised approach employing Extreme Learning Machine (ELM). This method involved constructing matrices by extracting features from each pixel of each retinal image and the manually labeled pixels, which were then input into ELM. These approaches heavily depend on prior knowledge or necessitate a series of complex operations for extracting discriminative features, thereby lacking generalization ability [26].

The segmentation performance of traditional methods needs improvement, especially when facing environments with retinal lesion features and low brightness. Traditional methods lack generalization capabilities in such scenarios. As a result, deep neural networks have found extensive applications in the field of retinal imaging.

B. Deep Learning Methods

Deep learning approaches equipped with automatic feature recognition capabilities exhibit superior performance in the field of retinal vessel segmentation compared to traditional methods. Overall, these methods can be categorized into two main types [16]. An end-to-end training approach is one of the types, because of its simple and stable performance has attracted the attention of many researchers. Hu et al. [27] incorporate a saliency mechanism to leverage features from one block as attention cues for the features of the subsequent block, effectively mitigating the problem of data imbalance. Moreover, to enhance the integrity and continuity of vessels after segmentation, Mou et al. [28] utilize a dense dilated model to integrate the newly proposed dense dilated feature extraction blocks, with the goal of extracting and accumulating

features across various scales. For improving the segmentation of fine vessels, Mishra et al. [29] employ the mean retinal vessel width and align it with the effective receptive field to identify the location of auxiliary supervision, thereby directing the model's attention towards fine vessels. The consecutive downsampling leads to the loss of a considerable amount of spatial feature information. To mitigate this challenge, Wang et al. [30] introduced two paths separately in the encoder and decoder, enhancing the model's capability for detailed representation and discrimination.

Patch-based segmentation methods are another type. In recent years, patch-based segmentation methods, which reduce computational pressure while minimizing the impact on vessel morphology, have been extensively investigated by many scholars. Dasgupta et al. [31] extracted 28×28 patches from preprocessed images and fed them into a CNN network for vessel segmentation. To ameliorate the problem of pixel imbalance between contrast strong vessels and contrast weak vessels in retinal images, Yan et al. [32] cropped retinal images into small 128×128 patches and proposed a loss function to balance contrast strong vessel and contrast weak vessel, enabling the model to learn more effective vessel segmentation features. Wu et al. [33] link two identical multi-scale backbone networks to facilitate the direct propagation of useful multi-scale features from shallow layers to deep layers. Wang et al. [34] designed three decoder networks: the first network dynamically localized image segmentation difficulty areas, while the other two networks are utilized for segmenting difficult and easy regions, respectively. Meanwhile, attention mechanisms were introduced in the network to enhance the focus on features of difficult areas in images. Yang et al. [35] designed an effective loss function to accommodate the two distinct vessel segmentation tasks, thereby improving the imbalance issue between thick and thin vessel segmentation ratios. Tan et al. [36] addressed the issue of having more pixels of strong contrast vessels than weak contrast vessels within individual patches by introducing skeleton priors and contrast losses. However, this method utilized maximum pooling on all extracted features before introducing skeleton-assisted vessel segmentation, leading to some contrast weak vessel missing and insufficient guidance for the model to learn contrast weak vessel. Therefore, we design a retinal vessel segmentation method that incorporates skeleton fitting assistance and fusion of global and local features to address vessel discontinuity and improve contrast weak vessel segmentation effectiveness.

III. METHODOLOGY

Firstly, we preprocess the original images by cropping them into several small patches. We balance the number of different class image patches through sample correction, and then perform image enhancement on CWVP. Secondly, the preprocessed patch samples are fed into the proposed Double U-Net with a Feature Fusion Module Networks (DUF-Net) to obtain corresponding segmentation maps. The DUF-Net architecture consists of green and blue Base-Nets, along with a Feature Fusion Module (FFM) designed to learn and fuse

global and local information from the patches. Additionally, the feature maps outputted by the two Base-Net models are fed into the Skeleton Fitting Assistance (SFA) section. Finally, the segmented patches are restored to the original image size. The specific workflow is illustrated in Fig. 1.

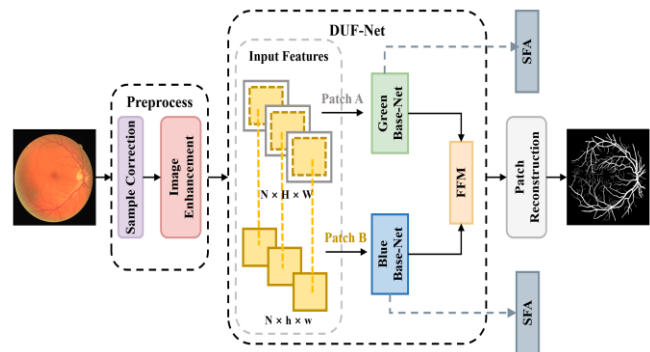


Fig. 1. Workflow of the proposed a retinal vessel segmentation method integrating global and local features with skeleton fitting assistance.

A. Preprocessing

Due to the limited quantity of existing retinal vessel datasets and the difficulty for models to learn contrast weak vessel features, we propose a preprocessing method consisting of two main stages: sample correction and image enhancement, as illustrated in Fig. 2.

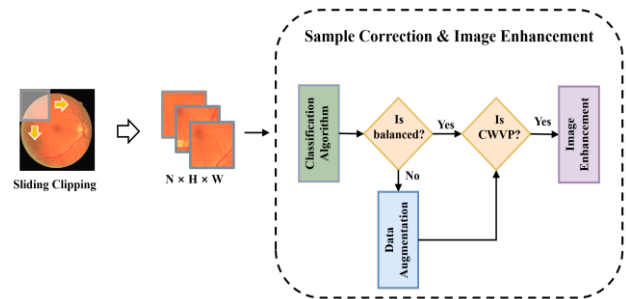


Fig. 2. The preprocessing steps.

1) *Sample correction*: This paper employs a patch-based approach for image segmentation. Firstly, patches are extracted from the original image using a sliding window approach to augment the model's training samples. Within these samples, patches are categorized into CSVP and CWVP. Typically, CSVP samples outnumber CWVP samples, resulting in suboptimal segmentation performance for CWVP samples. To address the issue of imbalanced CSVP and CWVP sample quantities, this paper designs a patch classification algorithm, as shown in Algorithm 1. This algorithm aims to achieve a balanced state with a nearly 1:1 ratio of samples for different classes in the training set. Data augmentation techniques are applied to CWVP; including random flipping, rotation, and Gaussian noise addition, to bring its quantity closer to that of CSVP.

Algorithm 1: patch classification Algorithm

Require: The Ground Truth Gt of the patch.

Ensure: The class of the patch.

- 1: Set $Gt_temp = Gt / 255$.
- 2: Set $first_eroded$ = the erosion of Gt_temp .
- 3: Set $dilated$ = the dilation of $first_eroded$.
- 4: Set $T1 = Gt_temp - dilated_image$.
- 5: Set $second_eroded$ = the erosion of $first_eroded$.
- 6: Set $T2 = first_eroded - second_eroded$.
- 7: Calculate the sum of pixels with a value of 1 in images $T1$ and $T2$ to obtain $S1$ and $S2$, respectively.
- 8: **If** $S1 > S2$
- 9: $c = CWVP$
- 10: **else**
- 11: $c = CSVP$
- 12: **Output** the class c of the patch

2) The details of Algorithm 1 are described as follows:

a) Step 1: Perform the first erosion operation on the ground truth, followed by a dilation operation, to obtain an image representing contrast strong vessel pixels.

b) Step 2: The ground truth is subtracted from the result of dilation in Step 1 to obtain the image T1, which represents contrast weak vessel pixels that are deleted after the first erosion.

c) Step 3: Perform second erosion on the result obtained after the first erosion in Step 1.

d) Step 4: Subtract the result obtained after the second erosion in Step 3 from the result obtained after the first erosion in Step 1 to obtain the image T2, representing contrast weak vessel pixels that are deleted after the second erosion.

e) Step 5: Calculate the pixel sum for both T1 and T2 images to obtain S1 and S2, respectively. If S1 is greater than S2, the patch is classified as CWVP; otherwise, it is classified as CSVP.

3) *Image enhancement:* This paper employs a sliding window cropping approach to increase training samples; however, the background of fundus images exhibits relatively uniform brightness and weak lighting compared to blood vessels. In scenarios with low brightness and weak lighting, the model lacks generalization ability and struggles to achieve satisfactory segmentation results in complex environments. Moreover, In CWVP, the vessels exhibit lower contrast with the background, leading to increased learning difficulty and the introduction of noise during the segmentation process, affecting accuracy. The basic idea is to enhance the contrast of randomly selected CWVP samples, considering that different contrasts typically highlight different details. The main concept of this method is outlined in Eq. (1). Specifically, a probability factor p is randomly generated from the range $[0, 1]$. When p falls within the range $[0, 0.5]$ and the patch corresponds to CWVP, contrast enhancement is applied. Otherwise, the image remains unaltered, without contrast enhancement.

$$X_{new} = \begin{cases} \partial \cdot T(X), & X \in CWVP \text{ and } p \in [0, 0.5] \\ X, & \text{otherwise} \end{cases} \quad (1)$$

where, X represents the original fundus image, X_{new} denotes the obtained new image sample, T signifies contrast enhancement applied to the image, and ∂ represents a randomly generated contrast factor within the range $[0.5, 1.5]$.

B. DUF-Net

The architecture of the DUF-Net is depicted in Fig. 3, consisting of green and blue Base-Nets and a Feature Fusion Module (FFM). Patch A corresponds to the output obtained in Fig. 2, with lengths and widths denoted as H and W , respectively. Due to the patch segmentation approach, there is a loss of contextual information around the patch, leading to the issue of vessel discontinuity after segmentation. Therefore, while feeding Patch A into the model, it is simultaneously center-cropped to obtain Patch B, with lengths and widths represented as h and w , respectively. The final segmentation map outputted by the model has the same dimensions as Patch B. Patch A is inputted into the green Base-Net for learning global features, while Patch B is inputted into the blue Base-Net to capture local features. Subsequently, the Feature Fusion Module (FFM) is employed to integrate global and local features, completing the supplementation of missing contextual information to prevent vessel discontinuity issues after segmentation.

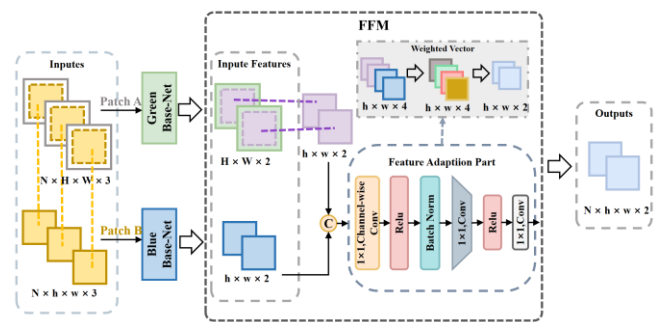


Fig. 3. DUF-Net architecture.

In Fig. 3, the Base-Net utilizes the U-Net model, which typically employs a downsampling structure to achieve a larger receptive field for capturing more semantic information. It utilizes upsampling to restore the original image, and spatial information recovery is achieved through skip connections, resulting in improved accuracy [37]. In order to reduce model parameters and minimize the loss of spatial structural information during the model downsampling process, an enhanced U-Net is designed, as illustrated in Fig. 4. The number of downsampling steps is reduced from four to three, and the channel count is halved from $[64, 128, 256, 512]$ to $[32, 64, 128, 256]$. The DUF-Net model employs the Base-Net as a feature generator for producing global and local information features. Subsequently, Patch A and Patch B are separately input into the green and blue Base-Nets, resulting in corresponding features F_a and F_b . F_a represents features obtained from Patch A, incorporating contextual information around the patch, while F_b represents local information features derived from Patch B.

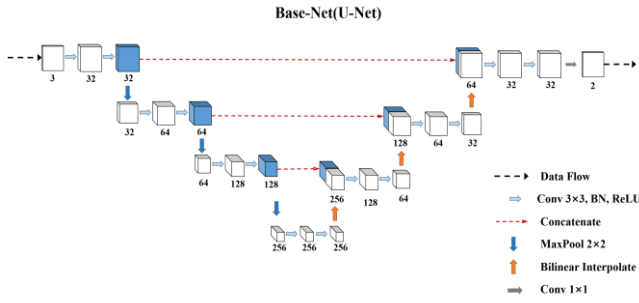


Fig. 4. Base-Net architecture.

Furthermore, we introduce a Feature Fusion Module (FFM) designed to merge feature information of varying scales generated by different Base-Net. As depicted in Fig. 3, this module is primarily composed of three components: the dimension adaptation stage, the feature concatenation stage, and the feature adaptation stage. F_a and F_b represent the features generated from the Base-Net model. Due to the disparate patch sizes of Patch A and Patch B, the corresponding feature sizes differ. To facilitate effective fusion, F_a 's feature is centrally cropped, resizing it from $H \times W$ to $h \times w$, yielding the feature F_a^c . This cropping ensures consistency in size with F_b while retaining contextual features around the patch. The next step involves concatenating the two input features. As outputs from different-sized input images yield distinct features, a simple concatenation might not effectively integrate global and local features, potentially leading to the loss of edge information during learning. Thus, for effective feature fusion, the feature adaptation stage employs a 1×1 channel-wise convolution to adjust the weights of the concatenated features. This convolution can be considered a weight vector that highlights important channel information. Subsequently, two 1×1 convolutions are used to learn the adjusted features' weights, reducing the channel count by half. Y_{out} denotes the output of the fusion module and can be computed as given in Eq. (2):

$$Y_{out} = \gamma(\gamma([F_a^c, F_b] \otimes k_1) * k_2) * k_3 \quad (2)$$

where, k_1 , k_2 , and k_3 represent $1 \times 1 \times 4$, $1 \times 1 \times 2$, and $1 \times 1 \times 2$ convolutional filter kernels, respectively. γ represents the ReLU activation function. \otimes signifies channel-wise convolution and $*$ signifies the regular convolution operation. To enhance the fusion of concatenated feature information and reduce model parameters, channel-wise convolution is utilized to redistribute the weights of the concatenated features. Finally, k_2 and k_3 are employed to downscale the concatenated features. This design ensures the effective integration of features at different scales, incorporating both global and local information.

C. Loss Mapping with Skeleton Fitting Assistance

On the DRIVE dataset [39], approximately 77% of the vessel pixels belong to contrast strong vessels, while only 23% are contrast weak vessels [38]. Therefore, this paper introduces SFA to enhance the segmentation capability of contrast weak vessels. Three feature maps are generated in this study: one from the green Base-Net, another from the blue Base-Net, and

the third from the Feature Fusion Module (FFM). Specifically, the feature maps outputted by the two Base-Nets undergo skeleton fitting assisted loss mapping, while the output segmentation image from the FFM is combined with the ground truth for loss calculation. The specific workflow is depicted in Fig. 5.

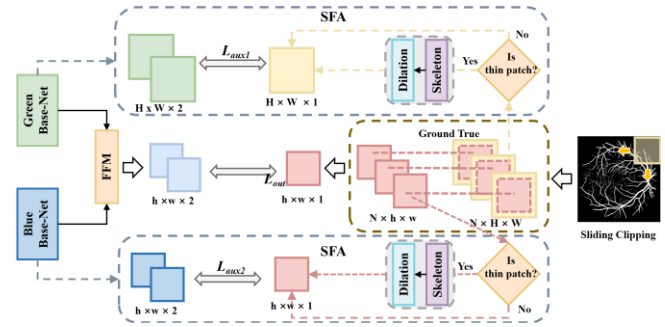


Fig. 5. The process workflow of loss mapping with skeleton fitting assistance.

The original segmentation map is cropped into N patches of size $H \times W$ using a sliding window approach. As the output segmentation map from the Feature Fusion Module (FFM) has dimensions $h \times w$, central cropping is performed to obtain $h \times w$ patches. Subsequently, the cross-entropy loss function is applied for loss calculation, and it is given in Eq. (3):

$$L_{out} = -\frac{1}{N} \sum_{i=1}^N [y_i \log(p_i) + (1 - y_i) \log(1 - p_i)] \quad (2)$$

where, N represents the total number of pixels in the patch, p_i denotes the model's predicted probability for pixel i , y_i represents the true label of pixel i .

In Algorithm 1, we propose an algorithm for the classification of vessel patches. In the SFA, we adopt a similar approach for vessel patch classification. To enhance the model's learning capability for CWV, skeleton prior knowledge is employed to dilate vessel pixels within CWVP. Through the classification algorithm, $H \times W$ patches of the ground truth, as well as the center-cropped $h \times w$ patches, are classified. When a patch is identified as CSVP, no additional processing is performed, and the Dice loss is directly computed with the corresponding Base-Net output feature map. In the case of a patch classified as CWVP, the patch undergoes skeleton extraction and dilation operations to generate a new ground truth. The Dice loss is then calculated by comparing the outputs of the two Base-Nets with the new ground truth. The Dice loss function is given by Eq. (4):

$$L_{aux} = \begin{cases} 1 - \frac{2|P \cap D(S(Y))|}{|P| + |D(S(Y))|}, & Y \in CWVP \\ 1 - \frac{2|P \cap (Y)|}{|P| + |Y|}, & Y \in CSVP \end{cases} \quad (3)$$

where, P represents the model's prediction result, Y is the corresponding ground truth, $S(\cdot)$ denotes the skeleton extraction operation, $D(\cdot)$ represents the dilation operation.

The final loss function is given in Eq. (5):

$$L_{all} = \begin{cases} L_{out} + \frac{L_{out}}{L_{aux1}} L_{aux1} + \frac{L_{out}}{L_{aux2}} L_{aux2}, & Y \in CWVP \\ L_{out} + L_{aux1} + L_{aux2}, & Y \in CSVP \end{cases} \quad (4)$$

where, L_{aux1} and L_{aux2} are the corresponding loss functions for the two SFA components.

IV. EXPERIMENTS

A. Fundus Datasets

The existing widely used datasets include DRIVE [39], STARE [40], CHASE_DB1 [41], and HRF [42].

1) *DRIVE dataset*: The dataset comprises 40 retinal images, each measuring 565×584 pixels, with 20 images allocated for training. Additionally, the dataset has been pre-divided into training and testing sets. In the experiments, we utilize the first set of labels to evaluate the proposed method.

2) *STARE dataset*: The dataset consists of 20 images, each with dimensions of 700×605 pixels, with half of them representing pathological cases and the other half representing normal cases. We choose 10 images for training and another 10 images for testing.

3) *CHASE_DB1 dataset*: The dataset comprises 28 retinal images from various children, each with dimensions of 999×960 pixels for both left and right eyes. Annotations in CHASE_DB1 are provided by two different observers. In our experiments, we utilize first set of labels as the ground truth for evaluation. Specifically, we designate 8 images as test samples and allocate the remaining images for training samples.

4) *HRF dataset*: The dataset consists of 45 high-resolution color retinal images. These images are categorized into three classes: healthy, diabetic retinopathy, and glaucoma, each comprising 15 images. For training, we select 15 images from each category: healthy children, diabetic retinopathy patients, and glaucoma patients. The remaining 30 images are allocated for testing.

B. Evaluation Metrics

In retinal images, binary pixel values typically classify pixels into vessel (positive) and non-vessel (negative) categories. Based on this comparison, there are four fundamental pixel metrics: pixels labeled as vessels and correctly predicted as vessels are defined as True Positives (TP); pixels labeled as backgrounds but incorrectly predicted as vessels are False Positives (FP); similarly, False Negatives (FN) represent pixels labeled as vessels but incorrectly predicted as backgrounds, while True Negatives (TN) denote pixels labeled as backgrounds and correctly predicted as backgrounds. Furthermore, we employed eight metrics for evaluation, including Accuracy (Acc), Sensitivity (Sen), Specificity (Spe), Precision (Pre), F1 score (F1), G-mean (G),

Matthews Correlation Coefficient (MCC), and Area Under the ROC Curve (AUC). all metrics are defined as follows:

$$Acc = \frac{TP + TN}{TP + FN + TN + FP}, \quad (5)$$

$$Sen = \frac{TP}{TP + FN}, \quad (6)$$

$$Spe = \frac{TN}{TN + FP}, \quad (7)$$

$$Pre = \frac{TP}{TP + FP}, \quad (8)$$

$$F1 = \frac{2 \cdot Pre \cdot Sen}{Pre + Sen}, \quad (9)$$

$$G = \sqrt{Sen \cdot Spe}, \quad (10)$$

$$MCC = \frac{(TP \times TN) - (FP \times FN)}{\sqrt{(TP + FP)(TP + FN)(TN + FP)(TN + FN)}}, \quad (11)$$

C. Implementation Details

The proposed model was implemented using PyTorch 1.12.1 on an RTX 3060 GPU with 12GB of memory. Stochastic gradient descent (SGD) was utilized for parameter optimization. Additionally, a "poly" learning rate policy was applied, where the learning rate was multiplied by $(1 - \frac{\text{iter}}{\text{Max_iter}})^{\text{power}}$ and the power was set to 0.9, with a base learning rate of 0.01 in training. Furthermore, the batch size was set to 1 and each experiment was conducted for 100 epochs. During testing, the test images were partitioned into overlapping small patches. Subsequently, the segmented samples generated by the model were reconstructed into complete segmentation results.

V. RESULTS

A. Comparison with Other Methods

1) *Comparison of composite metrics*: We initially compared it with six methods on four datasets, including FANet[43], ConvMixer[44], BFMD[45], GT-U-Net[46], SA-Unet[47], and CFPNetM[48], with quantitative metrics shown in Table I to Table IV.. Overall, the proposed method showed improvements in metrics, especially Acc and Pre. As illustrated in Table I, across the DRIVE dataset, Sen, G, and AUC metrics outperformed the six methods, reflecting superior segmentation results. F1 and MCC metrics were also close to the optimal values. Among them, G, AUC, F1, and MCC metrics are more comprehensive, indicating that the proposed method has better vascular segmentation capabilities. As depicted in Table III, on the STARE dataset, Acc, Spe, Pre, and F1 metrics achieved optimal results, and the other four metrics ranked second among the seven methods, showing results close to the optimal values.

Particularly, the F1 metric, reflecting the connectivity and accuracy of vascular segmentation, indicated the good segmentation demonstrated by the proposed method on this dataset indicate its excellent segmentation performance. As shown in Table IV, the HRF dataset includes high-resolution images of patients afflicted with diabetic retinopathy and glaucoma, posing challenges for vessel segmentation. Experimental results demonstrate that the proposed method for retinal vessel segmentation outperforms others, achieving the highest accuracy metric (Acc), while also securing the second or third position in the comparison of comprehensive metrics. These results suggest that the devised approach

demonstrates promising segmentation capabilities for high-resolution and pathological images. The examples provided in 0 demonstrate the favorable segmentation performance of the proposed method. In the first and last rows of 0, DUF-Net exhibits more complete segmentation of thin blood vessels with fewer vessel interruptions. The features of DUF-Net contribute to preserving the continuity and accuracy of thin blood vessels in datasets like HRF, which include images with diabetic retinopathy and glaucoma. This capability is crucial for supporting the prevention and treatment of retinal pathologies.

TABLE I. COMPREHENSIVELY COMPARING PERFORMANCE ON DRIVE DATASET (UNIT: %)

| Dataset | Method | Accuracy | Sensitivity | Specificity | Precision | F1-score | G-mean | MCC | AUC |
|---------|---------------|----------|-------------|-------------|-----------|----------|--------|-------|-------|
| DRIVE | FANet[43] | 96.16 | 80.14 | 97.88 | 80.32 | 80.23 | 88.57 | 78.10 | 89.01 |
| | Convmixer[44] | 96.65 | 77.45 | 98.52 | 84.21 | 81.29 | 87.16 | 78.68 | 87.98 |
| | BFMD[45] | 96.65 | 72.27 | 99.11 | 89.18 | 79.71 | 84.60 | 78.50 | 85.69 |
| | GT-U-Net[46] | 96.80 | 76.35 | 98.85 | 87.23 | 81.26 | 86.83 | 79.83 | 87.60 |
| | SA-Unet[47] | 96.68 | 81.95 | 98.00 | 78.60 | 80.24 | 89.62 | 78.45 | 89.97 |
| | CFPNetM[48] | 95.77 | 73.39 | 98.09 | 81.28 | 73.58 | 83.08 | 73.07 | 85.73 |
| | Ours | 96.70 | 82.18 | 98.00 | 78.68 | 80.39 | 89.74 | 78.61 | 90.09 |

TABLE II. COMPREHENSIVELY COMPARING PERFORMANCE ON CHASE_DB1 DATASET (UNIT: %)

| Dataset | Method | Accuracy | Sensitivity | Specificity | Precision | F1-score | G-mean | MCC | AUC |
|-----------|---------------|----------|-------------|-------------|-----------|----------|--------|-------|-------|
| CHASE_DB1 | FANet[43] | 92.66 | 60.30 | 95.36 | 52.73 | 55.72 | 75.53 | 52.22 | 77.83 |
| | Convmixer[44] | 97.20 | 75.30 | 98.99 | 88.90 | 81.47 | 86.39 | 80.35 | 87.23 |
| | BFMD[45] | 97.10 | 71.37 | 99.26 | 88.99 | 79.19 | 84.16 | 78.21 | 85.31 |
| | GT-U-Net[46] | 97.23 | 72.22 | 99.33 | 90.08 | 80.14 | 84.69 | 79.24 | 85.77 |
| | SA-Unet[47] | 96.99 | 72.16 | 99.07 | 86.67 | 78.69 | 84.53 | 77.49 | 85.61 |
| | CFPNetM[48] | 96.87 | 80.27 | 98.34 | 80.99 | 80.62 | 88.84 | 78.92 | 89.30 |
| | Ours | 97.24 | 70.75 | 99.44 | 91.29 | 79.67 | 83.86 | 78.97 | 85.09 |

TABLE III. COMPREHENSIVELY COMPARING PERFORMANCE ON STARE DATASET (UNIT: %)

| Dataset | Method | Accuracy | Sensitivity | Specificity | Precision | F1-score | G-mean | MCC | AUC |
|---------|---------------|----------|-------------|-------------|-----------|----------|--------|-------|-------|
| STARE | FANet[43] | 87.33 | 74.36 | 88.29 | 38.52 | 48.45 | 80.27 | 47.30 | 81.32 |
| | Convmixer[44] | 96.61 | 79.71 | 97.58 | 78.66 | 77.67 | 76.72 | 87.88 | 88.83 |
| | BFMD [45] | 96.86 | 82.45 | 98.03 | 77.75 | 79.71 | 89.76 | 78.24 | 90.24 |
| | GT-U-Net[46] | 97.18 | 79.65 | 98.61 | 82.89 | 80.61 | 88.39 | 79.47 | 89.12 |
| | SA-Unet[47] | 96.74 | 78.97 | 98.16 | 79.35 | 77.60 | 87.50 | 76.72 | 88.56 |
| | CFPNetM[48] | 93.54 | 90.76 | 93.75 | 56.42 | 68.81 | 92.16 | 68.27 | 92.25 |
| | Ours | 97.31 | 84.95 | 98.80 | 85.01 | 83.36 | 91.36 | 81.98 | 91.66 |

TABLE IV. COMPREHENSIVELY COMPARING PERFORMANCE ON HRF DATASET (UNIT: %)

| Dataset | Method | Accuracy | Sensitivity | Specificity | Precision | F1-score | G-mean | MCC | AUC |
|---------|---------------|----------|-------------|-------------|-----------|----------|--------|-------|-------|
| HRF | FANet[43] | 96.96 | 82.15 | 98.21 | 79.28 | 80.47 | 89.77 | 78.98 | 90.18 |
| | Convmixer[44] | 96.90 | 70.07 | 99.16 | 87.60 | 77.48 | 83.22 | 76.60 | 84.61 |
| | BFMD[45] | 94.33 | 78.40 | 95.68 | 60.94 | 68.40 | 86.59 | 66.08 | 87.03 |
| | GT-U-Net[46] | 96.64 | 68.37 | 99.04 | 86.00 | 75.55 | 82.10 | 74.68 | 83.70 |
| | SA-Unet[47] | 96.18 | 74.55 | 97.97 | 75.79 | 74.75 | 85.31 | 72.93 | 86.26 |
| | CFPNetM[48] | 96.81 | 82.38 | 98.03 | 77.97 | 79.90 | 89.83 | 78.33 | 90.20 |
| | Ours | 97.08 | 76.76 | 98.79 | 84.33 | 80.02 | 86.98 | 78.75 | 87.76 |

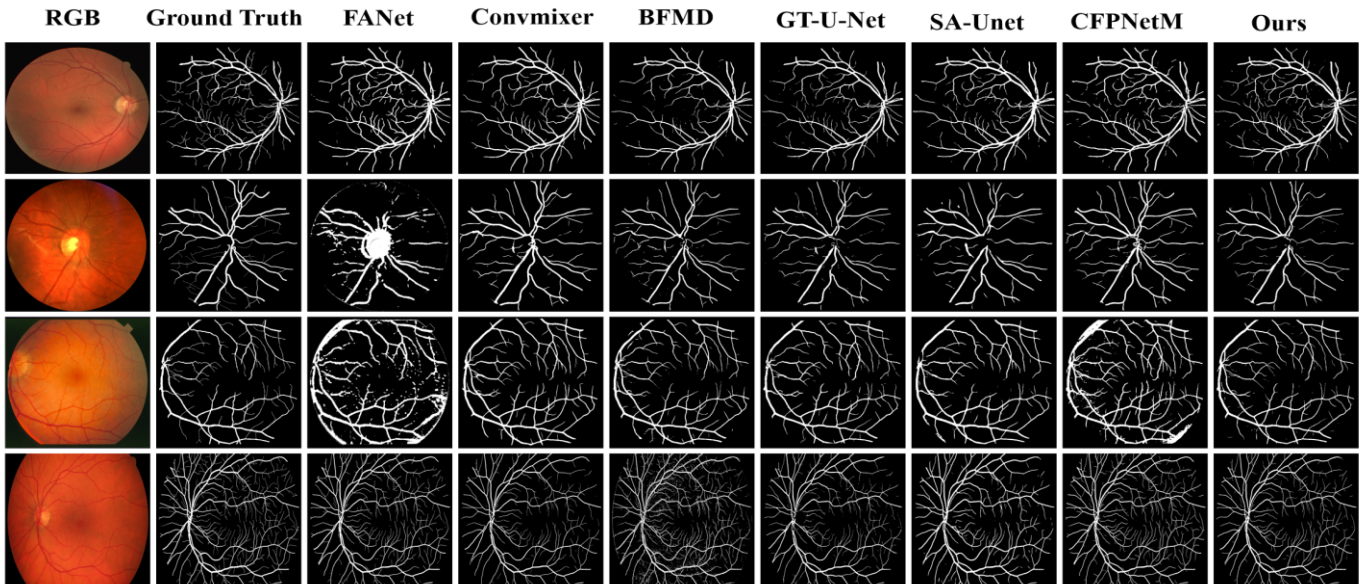


Fig. 6. The segmentation outcomes from the DRIVE, CHASE_DB1, STARE, and HRF datasets are juxtaposed in the figures below (from top to bottom).

2) *Segmentation of optic disc and pathological vessel regions*: Detailed comparisons of the optic disc and pathological vessel regions are illustrated in Fig. 7 demonstrating the magnified views of these areas. The first and second rows of Fig. 7 compare the optic disc regions with state-of-the-art methods from recent years. Due to challenges such as low contrast and uneven brightness, blood vessels around the optic disc region are often overlooked by other methods. In contrast, the proposed approach effectively identifies the vessels around the optic disc. Furthermore, the presence of bleeding around the lesions, which closely resembles vascular features, significantly increases the

difficulty of vessel segmentation in lesion images. As evident in the third rows of Fig. 7, the proposed method accurately segments vessels in the pathological regions. This is primarily attributed to the integration of skeletal prior knowledge to augment the model's comprehension of fine vessels and enhance its discrimination between vessel and background pixels. In the fourth row of Fig. 7, a substantial amount of noise is evident in the segmentation image due to BFMD misclassifying numerous lesions and surrounding hemorrhagic areas as vessels. This could potentially compromise subsequent auxiliary diagnostics.

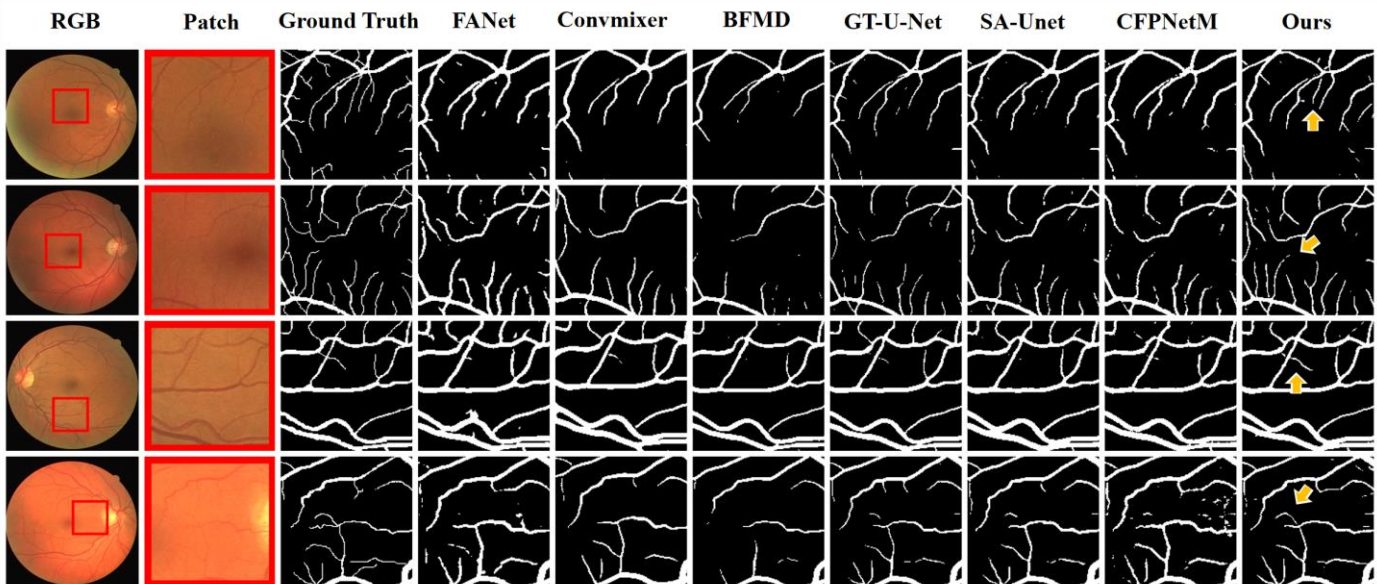


Fig. 7. Comparison of vessel segmentation results in the optic disc region (first two rows) and the lesion region (last two rows).

3) *Segmentation of contrast weak vessels*: The proposed method accurately segments contrast weak vessels, as illustrated in 0. When compared with other methods, it is evident that DUF-Net extracts more complete contrast weak vessels. This improvement can be attributed to the model's ability to learn both local and global features, effectively addressing the missing contextual information. This results in superior performance in detecting thin vessels, reflected in a higher accuracy (Acc) score.

B. Experiment for Algorithm Involves Categorizing CSVP and CWVP

In Algorithm 1, introduces a patch classification algorithm designed to categorize CSVP and CWVP. 0 illustrates the classification results of the patch classification algorithm on the DRIVE dataset. The first and second rows show the patches classified as CWVP by the algorithm and their corresponding ground truth. In this classification result, all vessels are characterized by low contrast. The third and fourth rows display the patches classified as CSVP by the algorithm and their corresponding ground truth. Here, it is evident that vessels with strong contrast are prominent.

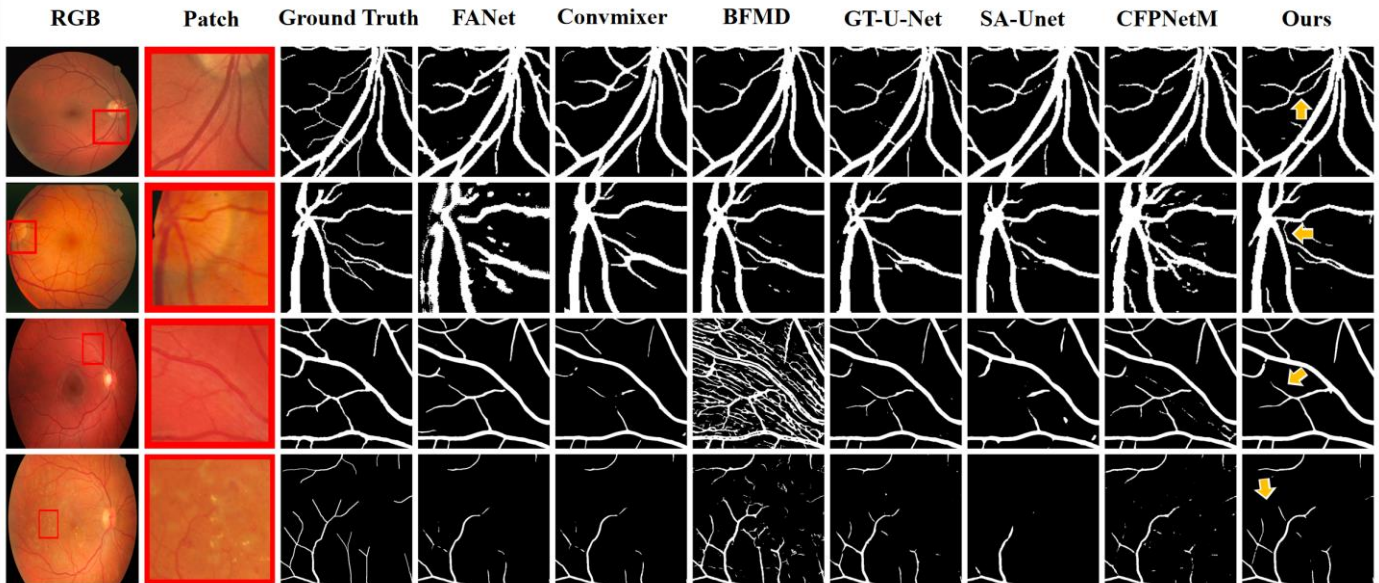


Fig. 8. Comparison of contrast weak vessel segmentation results.

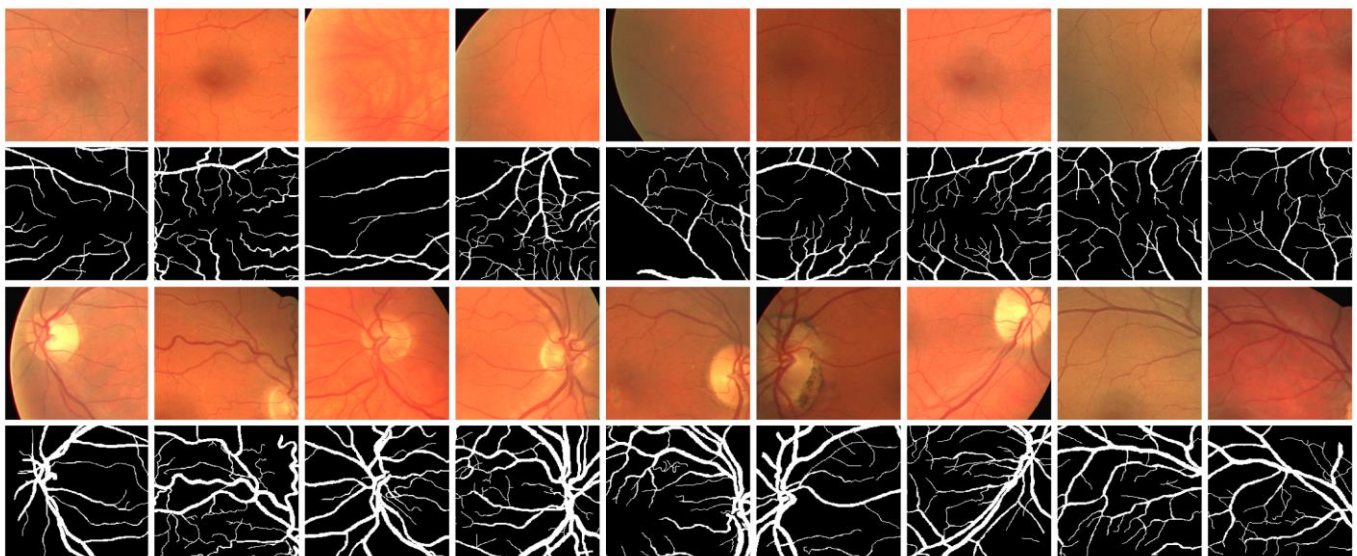


Fig. 9. The outcomes of patch classification into CSVP (first two rows) and CWVP (last two rows) on the DRIVE dataset are juxtaposed with their respective ground truth.

C. Experiment for Loss Mapping with Skeleton Fitting Assistance

In Fig. 5, we proposed a loss mapping with skeleton fitting assistance composed of three loss functions: L_{aux1} , L_{aux2} , and L_{out} . The evolution of these three loss functions during training for 100 epochs on the DRIVE dataset is illustrated in 0. The values of L_{aux1} and L_{aux2} are greater than the value of L_{out} . When the patch represents CSVP, the coefficient weights of the three loss functions are configured as 1, and the values of the three loss functions show a synchronous decreasing trend in 0(a). However, when the patch represents CWVP, the skeleton fitting assistance part involves computing losses using the feature map and the newly generated ground truth after skeleton extraction. This may bias the model towards learning the new ground truth, leading to suboptimal segmentation results. Therefore, an adaptive weight assignment method is designed in this paper. It uses L_{aux1}/L_{out} as the weight for L_{aux1}

and L_{aux2}/L_{out} as the weight for L_{aux2} to balance the loss functions. In 0(b), it can be observed that with the adaptive weight assignment, L_{out} shows a decreasing trend, while L_{aux1} and L_{aux2} remains within a certain range of variation.

D. Ablation Analysis

The ablation analysis presents the performance of each proposed method, as demonstrated in TABLE V. . For comparison, we refer to DUF-Net without contextual information as DU-Net. DU-Net does not undergo central cropping when fed into the model, employs blocks of the same size, and omits the use of the Feature Fusion Module (FFM). Additionally, DU-Net does not undergo the proposed preprocessing methods and the loss calculation of Skeleton Fitting Assist (SFA). By incorporating preprocessing methods, enhancing contextual information supplementation, and integrating FFM and SFA loss calculation, all metrics show corresponding improvements, as depicted in TABLE V. .

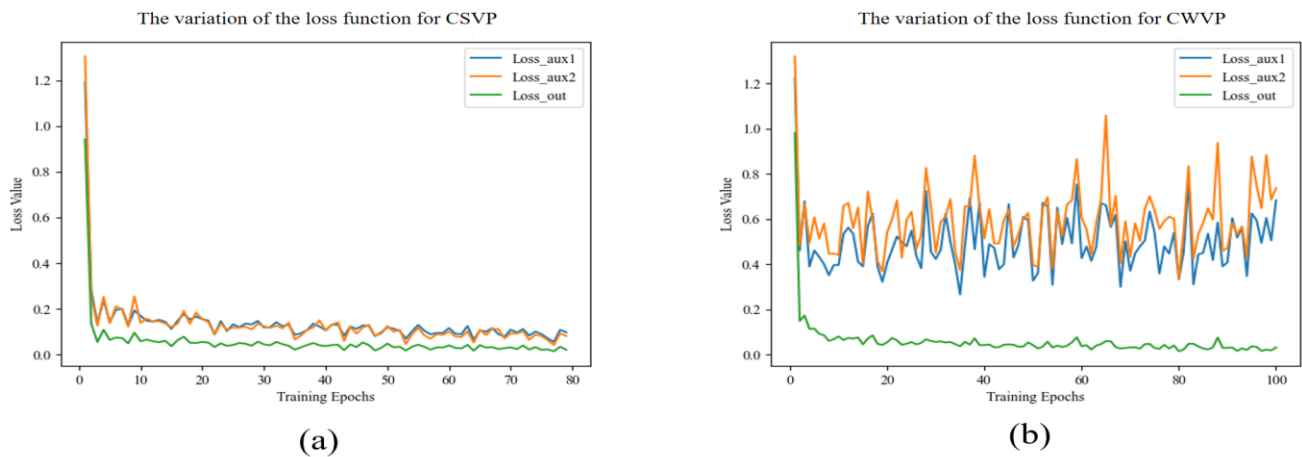


Fig. 10. The variation of the loss functions on the DRIVE dataset (a) The variation of the loss function for CSVP (b) The variation of the loss function for CWV.

TABLE V. THE RESULTS OF THE ABLATION ANALYSIS ON THE DRIVE DATASET (UNIT: %)

| Method | Accuracy | Sensitivity | Specificity | Precision | F1-score | G-mean | MCC | AUC |
|-------------|----------|-------------|-------------|-----------|----------|--------|-------|-------|
| DU-Net | 96.62 | 77.19 | 98.52 | 83.55 | 79.76 | 87.05 | 78.28 | 87.85 |
| +Preprocess | 96.65 | 81.97 | 97.94 | 79.47 | 80.22 | 87.39 | 77.98 | 88.27 |
| +FFM | 96.68 | 81.68 | 97.98 | 78.28 | 79.98 | 88.50 | 78.51 | 89.18 |
| +SFA | 96.70 | 82.18 | 98.00 | 78.68 | 80.39 | 89.74 | 78.61 | 90.09 |

VI. DISCUSSION

Compared to end-to-end segmentation, patch-based segmentation methods can significantly alleviate computational hardware pressure while increasing the training samples in datasets, thereby enhancing vessel segmentation capability, which has gradually attracted attention from many scholars [49]. However, when restoring the segmented patch results to the original size, issues such as vessel discontinuity and poor segmentation of small vessels may arise. Therefore, this paper designs a preprocessing method tailored for fundus images, a novel network architecture, and a training approach with skeleton fitting assistance to address the aforementioned issues.

Due to the difficulty in segmenting small vessels, datasets with a higher density of small vessels often exhibit lower

performance metrics compared to datasets with fewer small vessels, such as DRIVE [39] and HRF [42] datasets containing more small vessels than STARE [40] and CHASE_DB1 [41] datasets. Consequently, the performance of six vessel segmentation methods is significantly reduced. Additionally, existing fundus segmentation methods are primarily evaluated based on pixel measurements, where the contribution of small vessel pixels is relatively minor, limiting the potential improvement in performance metrics. The proposed method shows limited improvement on the HRF dataset. This is partly due to the high resolution of this dataset leads our classification algorithm to misclassify some CWVP samples as CSVP, resulting in incomplete feature capture of CWVP. Thus, there remains considerable room for improvement in our method.

VII. CONCLUSION

This paper proposes a novel segmentation method by addressing the limitations of patch-based retinal vessel segmentation. Firstly, the patch-based segmentation approach often overlooks the issue of imbalanced contrast between strong and weak vessel samples in the dataset. Therefore, this paper designs a vessel patch classification algorithm to balance the training data samples by augmenting contrast weak vessel samples based on the computed quantities. To address the missing contextual information around the patches, new network architecture, DUF-Net, is proposed. By feeding features of different scales into the network model, both global and local information are learned separately and then fused to complement the missing features. Lastly, skeleton prior knowledge is introduced to alleviate vessel discontinuity issues after segmentation, and the adaptive weight allocation mechanism is employed to adjust the imbalanced pixel distribution within blocks, thereby enhancing the model's segmentation capability for contrast weak vessels.

In the experimental results, the proposed method demonstrates promising performance. As retinal lesions significantly affect vessel segmentation results, future work will focus on enhancing lesioned retinal images using image enhancement techniques and loss functions to improve the performance of segmentation. Moreover, extending this method to other segmentation tasks in medicine, such as neuron segmentation and cell segmentation, will also be considered.

ACKNOWLEDGMENT

This research is funded by the Scientific Research Starting Foundation of Fujian University of Technology (No. GY-Z21024 and No. GY-Z21065).

REFERENCES

- [1] Li T, Bo W, Hu C, et al. Applications of deep learning in fundus images: A review[J]. *Medical Image Analysis*, 2021, 69: 101971.
- [2] Chen C, Chuah J H, Ali R, et al. Retinal vessel segmentation using deep learning: a review[J]. *IEEE Access*, 2021, 9: 111985-112004.
- [3] Lechner J, O'Leary O E, Stitt A W. The pathology associated with diabetic retinopathy[J]. *Vision research*, 2017, 139: 7-14.
- [4] Abramoff M D, Garvin M K, Sonka M. Retinal imaging and image analysis[J]. *IEEE reviews in biomedical engineering*, 2010, 3: 169-208.
- [5] L Srinidhi C, Aparna P, Rajan J. Recent advancements in retinal vessel segmentation[J]. *Journal of medical systems*, 2017, 41: 1-22.
- [6] Dai P, Luo H, Sheng H, et al. A new approach to segment both main and peripheral retinal vessels based on gray-voting and gaussian mixture model[J]. *PLoS one*, 2015, 10(6): e0127748.
- [7] Nguyen U T V, Bhuiyan A, Park L A F, et al. An effective retinal blood vessel segmentation method using multi-scale line detection[J]. *Pattern recognition*, 2013, 46(3): 703-715.
- [8] Lee Y, Hara T, Fujita H, et al. Automated detection of pulmonary nodules in helical CT images based on an improved template-matching technique[J]. *IEEE Transactions on medical imaging*, 2001, 20(7): 595-604.
- [9] Hoover A D, Kouznetsova V, Goldbaum M. Locating blood vessels in retinal images by piecewise threshold probing of a matched filter response[J]. *IEEE Transactions on Medical imaging*, 2000, 19(3): 203-210.
- [10] Nyemeeha V, Ismail B M. Implementation of noise and hair removals from dermoscopy images using hybrid Gaussian filter[J]. *Network Modeling Analysis in Health Informatics and Bioinformatics*, 2021, 10: 1-10.
- [11] Taşçı E, Uğur A. Shape and texture based novel features for automated juxtapleural nodule detection in lung CTs[J]. *Journal of medical systems*, 2015, 39: 1-13.
- [12] Zakeri F S, Behnam H, Ahmadinejad N. Classification of benign and malignant breast masses based on shape and texture features in sonography images[J]. *Journal of medical systems*, 2012, 36: 1621-1627.
- [13] Orlando J I, Prokofyeva E, Blaschko M B. A discriminatively trained fully connected conditional random field model for blood vessel segmentation in fundus images[J]. *IEEE transactions on Biomedical Engineering*, 2016, 64(1): 16-27.
- [14] Li Q, Feng B, Xie L P, et al. A cross-modality learning approach for vessel segmentation in retinal images[J]. *IEEE transactions on medical imaging*, 2015, 35(1): 109-118.
- [15] Liskowski P, Krawiec K. Segmenting retinal blood vessels with deep neural networks[J]. *IEEE transactions on medical imaging*, 2016, 35(11): 2369-2380.
- [16] Zhang Y, He M, Chen Z, et al. Bridge-Net: Context-involved U-net with patch-based loss weight mapping for retinal blood vessel segmentation[J]. *Expert Systems with Applications*, 2022, 195: 116526.
- [17] Sheng B, Li P, Mo S, et al. Retinal vessel segmentation using minimum spanning superpixel tree detector[J]. *IEEE transactions on cybernetics*, 2018, 49(7): 2707-2719.
- [18] Lam B S Y, Gao Y, Liew A W C. General retinal vessel segmentation using regularization-based multiconcavity modeling[J]. *IEEE Transactions on medical imaging*, 2010, 29(7): 1369-1381.
- [19] Rezaee K, Haddadnia J, Tashk A. Optimized clinical segmentation of retinal blood vessels by using combination of adaptive filtering, fuzzy entropy and skeletonization[J]. *Applied Soft Computing*, 2017, 52: 937-951.
- [20] Staal J, Abramoff M D, Niemeijer M, et al. Ridge-based vessel segmentation in color images of the retina[J]. *IEEE transactions on medical imaging*, 2004, 23(4): 501-509.
- [21] You X, Peng Q, Yuan Y, et al. Segmentation of retinal blood vessels using the radial projection and semi-supervised approach[J]. *Pattern recognition*, 2011, 44(10-11): 2314-2324.
- [22] Soares J V B, Leandro J J G, Cesar R M, et al. Retinal vessel segmentation using the 2-D Gabor wavelet and supervised classification[J]. *IEEE Transactions on medical Imaging*, 2006, 25(9): 1214-1222.
- [23] Kumar Agarwal A, Angeline Ranjithamani D, Pavithra M, et al. Machine learning technique for the assembly-based image classification system[J]. *J Nucl Ene Sci Power Generat Techno*, 2021, 10(9).
- [24] Orlando J I, Prokofyeva E, Blaschko M B. A discriminatively trained fully connected conditional random field model for blood vessel segmentation in fundus images[J]. *IEEE transactions on Biomedical Engineering*, 2016, 64(1): 16-27.
- [25] Zhu C, Zou B, Zhao R, et al. Retinal vessel segmentation in colour fundus images using extreme learning machine[J]. *Computerized Medical Imaging and Graphics*, 2017, 55: 68-77.
- [26] Hu K, Zhang Z, Niu X, et al. Retinal vessel segmentation of color fundus images using multiscale convolutional neural network with an improved cross-entropy loss function[J]. *Neurocomputing*, 2018, 309: 179-191.
- [27] Hu J, Wang H, Gao S, et al. S-unet: A bridge-style u-net framework with a saliency mechanism for retinal vessel segmentation[J]. *IEEE Access*, 2019, 7: 174167-174177.
- [28] Mou L, Chen L, Cheng J, et al. Dense dilated network with probability regularized walk for vessel detection[J]. *IEEE transactions on medical imaging*, 2019, 39(5): 1392-1403.
- [29] Mishra S, Chen D Z, Hu X S. A data-aware deep supervised method for retinal vessel segmentation[C]//2020 IEEE 17th international symposium on biomedical imaging (ISBI). IEEE, 2020: 1254-1257.
- [30] Wang D, Hu G, Lyu C. Frnet: an end-to-end feature refinement neural network for medical image segmentation[J]. *The Visual Computer*, 2021, 37: 1101-1112.

- [31] Dasgupta A, Singh S. A fully convolutional neural network based structured prediction approach towards the retinal vessel segmentation[C]//2017 IEEE 14th international symposium on biomedical imaging (ISBI 2017). IEEE, 2017: 248-251.
- [32] Yan Z, Yang X, Cheng K T. Joint segment-level and pixel-wise losses for deep learning based retinal vessel segmentation[J]. IEEE Transactions on Biomedical Engineering, 2018, 65(9): 1912-1923.
- [33] Wu Y, Xia Y, Song Y, et al. NFN+: A novel network followed network for retinal vessel segmentation[J]. Neural Networks, 2020, 126: 153-162.
- [34] Wang D, Haytham A, Pottenburgh J, et al. Hard attention net for automatic retinal vessel segmentation[J]. IEEE Journal of Biomedical and Health Informatics, 2020, 24(12): 3384-3396.
- [35] Yang L, Wang H, Zeng Q, et al. A hybrid deep segmentation network for fundus vessels via deep-learning framework[J]. Neurocomputing, 2021, 448: 168-178.
- [36] Tan, Yubo, et al. "Retinal vessel segmentation with skeletal prior and contrastive loss." IEEE Transactions on Medical Imaging 41.9 (2022): 2238-2251.
- [37] Ronneberger O, Fischer P, Brox T. U-net: Convolutional networks for biomedical image segmentation[C]//Medical Image Computing and Computer-Assisted Intervention–MICCAI 2015: 18th International Conference, Munich, Germany, October 5-9, 2015, Proceedings, Part III 18. Springer International Publishing, 2015: 234-241.
- [38] Yan Z, Yang X, Cheng K T. A skeletal similarity metric for quality evaluation of retinal vessel segmentation[J]. IEEE transactions on medical imaging, 2017, 37(4): 1045-1057.
- [39] Staal J, Abràmoff M D, Niemeijer M, et al. Ridge-based vessel segmentation in color images of the retina[J]. IEEE transactions on medical imaging, 2004, 23(4): 501-509.
- [40] Hoover A D, Kouznetsova V, Goldbaum M. Locating blood vessels in retinal images by piecewise threshold probing of a matched filter response[J]. IEEE Transactions on Medical imaging, 2000, 19(3): 203-210.
- [41] Fraz M M, Remagnino P, Hoppe A, et al. An ensemble classification-based approach applied to retinal blood vessel segmentation[J]. IEEE Transactions on Biomedical Engineering, 2012, 59(9): 2538-2548.
- [42] Odstrcilik J, Kolar R, Budai A, et al. Retinal vessel segmentation by improved matched filtering: evaluation on a new high-resolution fundus image database[J]. IET Image Processing, 2013, 7(4): 373-383.
- [43] Tomar N K, Jha D, Riegler M A, et al. Fanet: A feedback attention network for improved biomedical image segmentation[J]. IEEE Transactions on Neural Networks and Learning Systems, 2022.
- [44] Solano A, Dietrich K N, Martínez-Sober M, et al. Deep Learning Architectures for Diagnosis of Diabetic Retinopathy[J]. Applied Sciences, 2023, 13(7): 4445.
- [45] Deari S, Oksuz I, Ulukaya S. Block Attention and Switchable Normalization based Deep Learning Framework for Segmentation of Retinal Vessels[J]. IEEE Access, 2023.
- [46] Li Y, Wang S, Wang J, et al. Gt u-net: A u-net like group transformer network for tooth root segmentation[C]//Machine Learning in Medical Imaging: 12th International Workshop, MLMI 2021, Held in Conjunction with MICCAI 2021, Strasbourg, France, September 27, 2021, Proceedings 12. Springer International Publishing, 2021: 386-395.
- [47] Sun J, Darbehani F, Zaidi M, et al. Saunet: Shape attentive u-net for interpretable medical image segmentation[C]//Medical Image Computing and Computer Assisted Intervention–MICCAI 2020: 23rd International Conference, Lima, Peru, October 4–8, 2020, Proceedings, Part IV 23. Springer International Publishing, 2020: 797-806.
- [48] Lou A, Guan S, Loew M. Cfpnet-m: A light-weight encoder-decoder based network for multimodal biomedical image real-time segmentation[J]. Computers in Biology and Medicine, 2023, 154: 106579.
- [49] Xia H, Jiang F, Deng S, et al. Mapping functions driven robust retinal vessel segmentation via training patches[J]. IEEE access, 2018, 6: 61973-61982.

Novel Approaches for Access Level Modelling of Employees in an Organization Through Machine Learning

Priyanka C Hiremath, Raju G T

Department of Computer Science and Engineering, SJC Institute of Technology, Chickballapur, India

Abstract—In the contemporary business landscape, organizational trustworthiness is of utmost importance. Employee behavior, a pivotal aspect of trustworthiness, undergoes analysis and prediction through data science methodologies. Simultaneously, effective control over employee access within an organization is imperative for security and privacy assurance. This research proposes an innovative approach to model employee access levels using Geo-Social data and machine learning techniques like Linear Regression, K-Nearest Neighbours, Decision Tree, Random Forest, XGBoost, and Multi-Layered Perceptron. The data, sourced from social and geographical realms, encompasses details on employee geography, navigation preferences, spatial exploration, and choice set formations. Utilizing this information, a behavioral model is constructed to assess employee trustworthiness, categorizing them into access levels: low, moderate, high, and very high. The model's periodic review ensures adaptive access level adjustments based on evolving behavioral patterns. The proposed approach not only cultivates a more trustworthy organizational network but also furnishes a precise and reliable trustworthiness evaluation. This refinement contributes to heightened organizational coherence, increased employee commitment, and reduced turnover. Additionally, the approach ensures enhanced control over employee access, mitigating the risks of data breaches and information leaks by restricting the access of employees with lower trustworthiness.

Keywords—Access control; machine learning; employee behavior modeling; data analysis; organizational performance

I. INTRODUCTION

Organizations highly value employees as crucial assets, as their conduct significantly influences the company's outcomes [1]. Employee behavior encompasses interactions with peers, dedication to their roles, and performance, requiring effective management for organizational prosperity. Critical to this management is ensuring ongoing employee dedication, which fosters job satisfaction, diminishes turnover, and enhances overall performance [2]. Employee commitment, in turn, cultivates organizational trust, pivotal for successful team cohesion. Nonetheless, managing employee behavior presents challenges due to the workforce's diverse backgrounds, motivations, attitudes, and personalities. Organizations often establish a strong organizational culture aligned with their values and missions, fostering employee engagement and drive for optimal performance [3]. Additionally, incentives and rewards serve as tools to cultivate positive behavior and boost motivation [4]. Understanding employee behavior entails

utilizing various methods such as surveys, performance assessments, and data analysis. Data analysis, employing advanced statistical methods and machine learning algorithms, is increasingly valuable for gaining insights into employee behavior [5]. Employee behavior analysis is an expanding area of research, examining factors like leadership approaches, job satisfaction, and engagement. This study addresses the complex task of ensuring employee productivity while promoting mental and physical well-being, addressed through wellness programs [6]. These programs aim to encourage healthy behaviors, reinforcing productivity and overall welfare [7]. Furthermore, behavior analysis aids in identifying risks, enabling organizations to proactively manage concerns such as turnover or workplace incidents [8]. In the midst of these challenges, access control emerges as a crucial aspect of managing employee access levels within organizations [9]. Ensuring operational security, safeguarding sensitive data, and upholding trust require strict control over information, resources, and systems access. The emergence of machine learning and data science is reshaping access control management, particularly in managing large, diverse workforces [10]. This discussion explores the role of employee behavior models in access control, elucidating techniques and tools for analyzing and managing access based on behavioral patterns. The discourse examines the benefits and challenges of employing behavior models in access control, highlighting best practices for seamless implementation.

Employee behavior models are developed through the examination of various data sources, such as user logs, network activity, and biometric data [11]. Geo data, utilizing parameters like latitude, longitude, and elevation, significantly contributes to these models by revealing spatial behavior patterns. Incorporating social data expands the scope, enabling the creation of behavioral models to assess employee trustworthiness. Employees are then grouped into access levels based on these models, aligning access controls with behavioral patterns [12]. This dynamic adjustment of access control policies, guided by real-time behavior data, ensures judicious access while revoking unnecessary privileges. Behavior models play a crucial role in identifying and thwarting insider threats, a significant concern for companies [13]. Indicators of potential threats, such as unauthorized data access or abnormal working hours, trigger alerts, allowing organizations to intervene proactively. Furthermore, behavior models streamline user experience by automating access control processes, reducing reliance on manual approval

procedures [14]. Despite the evident benefits, implementing behavior models in access control presents challenges [15]. The need for extensive data collection and processing can be daunting, particularly for organizations not well-versed in data science techniques. Balancing security and usability is another hurdle, requiring strict controls without hindering productivity. Addressing these challenges involves adopting best practices, including clear data collection policies, employee training on data privacy and security, and collaboration between data scientists and IT professionals [16]. Once employee trustworthiness is assessed and categorized into different levels, access control becomes more manageable [17]. Automation of access control processes based on behavioral models optimizes efficiency and resource access. Comprehensive evaluation of employee behavior involves collecting data from various sources, including geographical, social media, email communication, and browsing history [18]. Geographical data unveils movement patterns, while social data offers insights into character and activities. Email communication data reveals professional interactions, and browsing history data exposes online activities. Privacy and ethical concerns must be carefully considered during data collection and analysis. Employees should be informed of data collection methods, and privacy rights must be respected. Combining technologies and tools enhances the quality of collected data [19]. Geo data plays a pivotal role in access control decisions, providing insights into physical movements and actions [20]. When combined with social data, it enables machine learning techniques to construct behavioral models for access control decisions. Continuous analysis of geo data allows organizations to track changes in employee behavior over time and identify anomalies. Social data, drawn from various online platforms, offers rich insights into employee behavior [21]. Parameters like content type and engagement levels provide valuable insights. Social data analysis can uncover patterns indicative of loyalty issues or security risks. However, using social data for access control requires addressing privacy concerns and ensuring legal data collection [23]. The integration of employee behavior models into access control mechanisms signifies a shift in organizational security [24]. By combining geographical and social data, analyzed through advanced analytics and machine learning, robust behavioral models are created. These models, defining access levels based on trustworthiness, offer a proactive approach to security. Embracing these innovative approaches can better position organizations for success in today's evolving business landscape.

The utilization of machine learning (ML) to refine the access control system for organizational employees has gained considerable attention due to its ability to analyze vast datasets and predict employee behavior [25]. These ML models are trained on extensive datasets incorporating both social and geographical data, facilitating the categorization of employees into distinct levels of trustworthiness. This section examines the advantages and disadvantages of employing ML models for access control, explores various tools and technologies supporting this endeavor, and addresses challenges inherent in ML modeling along with proposed solutions. Utilizing ML models for employee access control offers benefits such as scalability, accuracy, automation, and adaptability. However,

challenges such as bias, interpretability issues, complexity, and concerns regarding data quality also accompany this approach. Organizations can overcome these challenges by utilizing tools like Python, R, Apache Spark, Hadoop, and cloud platforms, and implementing techniques such as data cleaning [26]. This study involves the development and evaluation of ML models, specifically XGBoost, SVM, and Decision Tree, using a geo-social dataset representing four employee access levels: low, moderate, high, and very high. The dataset comprises 200,000 samples, evenly distributed across classes, with 24 geo data features and 15 social data features. The primary objective is to build an accurate model capable of predicting employee access levels based on their behavioral patterns.

II. LITERATURE REVIEW

The study in [27] introduced a trust-based framework and measurement for organizational confidence. It adopted a cognitive model of trust, relying on interpretive factor analysis and validity testing. Incorporating in-person interviews and open-ended questionnaires, the study affirmed the eight-factor structure of organizational confidence. Table I provides a summary of the corporate confidence study results.

To recognise the business's vision and culture, one must believe in the company's future. Fig. 1 shows the whole plan to enhance workers' self-confidence.

GPS and GIS offer location-based intelligence: This method tracks spatial behavior over two weeks, integrating user speed, distance, time, elevation, and precise latitude and longitude [35]. The essay explores telecom service providers' data on customers using location-based service applications (LBS), involving 14 days of location tracking using a GPS device. Safety measures were in place to avoid disrupting the member's routine. GIS software interpreted GPS coordinates, obtaining quantitative geographic data, while daily diaries captured qualitative information, as illustrated in Fig. 2.

Case studies and previous research on access level modelling of geo data, social data or geo-social data have been tabulated in Table II.

TABLE I. INVESTIGATIONS ON FACTORS AFFECTING COMPANY'S CONFIDENCE ON EMPLOYEES

| Reference | Contents in an organisation confidence |
|-----------|--|
| [28] | Confidence is classified into two categories: cognitive and affective. |
| [29] | Confidence in an organisation based on the shared values of its employees. |
| [30] | Communication was cited as the most crucial aspect of an organization's confidence. |
| [31] | Trust is comprised of sincerity, rationality, candour, intentions, and convictions. |
| [32] | Trust in an organisation can be subdivided into a sense of belonging and information sharing. |
| [33] | A confidence in an organisation consisted of virtue, capabilities, transparency, and sincerity. |
| [34] | Distribution justice, job security, procedure justice, and organisational support are all parts of organisational trust. |

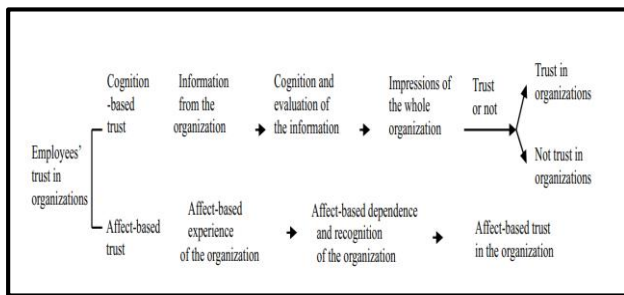


Fig. 1. Trust of employees in an organisation.

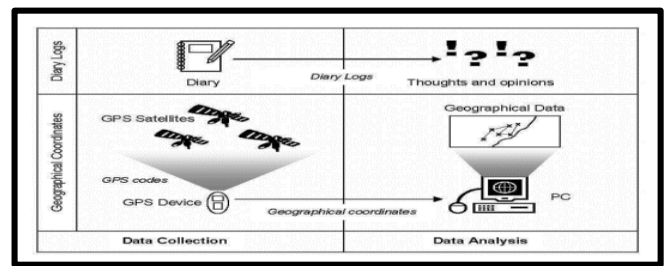


Fig. 2. Observational instruments used for data collection and analysis.

TABLE II. PAST RESEARCH WORKS

| Reference | Objective Of Research | Dataset Used | Algorithm | Metric | Advantages |
|-----------|---|-------------------------------|---------------------------------------|--|---|
| [36] | Developing an access control model for mobile social networks based on user behaviour | Twitter dataset | Fuzzy logic | Accuracy: 85.6% | High accuracy and reduced risk of unauthorized access |
| [37] | Investigating the effectiveness of location-based access control for online social networks | Facebook dataset | Probabilistic graphical models | Precision: 93.2% | Improved privacy and security for social network users |
| [38] | Proposing a framework for access control in geo-social networks | Geo-tagged tweets dataset | Deep learning | F1-score: 0.89 | High accuracy and scalability |
| [39] | Evaluating the performance of different machine learning algorithms for access control in social media | Twitter and Facebook datasets | Decision trees, SVM, Naive Bayes | Accuracy: 91.4% | Comparative analysis of different algorithms |
| [40] | Investigating the privacy risks of social media check-ins and proposing a privacy-preserving access control mechanism | Foursquare dataset | Differential privacy | Privacy guarantee: $\epsilon=0.5$ | Improved privacy protection for users |
| [41] | Developing an access control model for online social networks based on user location and activity | Facebook dataset | Rule-based system | Precision: 92.8% | Simple and easy-to-understand rules |
| [42] | Proposing a hybrid access control mechanism for geo-social networks based on fuzzy logic and reinforcement learning | Geo-tagged tweets dataset | Fuzzy logic, Reinforcement learning | Accuracy: 89.3% | Improved accuracy and adaptability |
| [43] | Investigating the impact of social network structure on access control policies | Synthetic network dataset | Network analysis | Network density: 0.35 | Improved understanding of the relationship between network structure and access control |
| [44] | Developing a privacy-preserving access control model for social media based on secure multi-party computation | Twitter dataset | Secure multi-party computation | Accuracy: 87.2% | Improved privacy protection and reduced risk of data breaches |
| [45] | Investigating the impact of temporal dynamics on access control policies in social media | Facebook dataset | Temporal analysis | Average access frequency: 3.8/day | Improved understanding of the temporal behaviour of social media users |
| [46] | Developing a context-aware access control model for social media based on user location and activity | Twitter dataset | Context-aware reasoning | Accuracy: 89.5% | Improved accuracy and adaptability to different contexts |
| [47] | Investigating the impact of user trustworthiness on access control policies in social media | Facebook dataset | Trust evaluation | Trust score: 0.75 | Improved understanding of the role of trust in access control |
| [48] | Developing a privacy-preserving access control mechanism for geo-social networks based on homomorphic encryption | Geo-tagged tweets dataset | Homomorphic encryption | Privacy guarantee: $\epsilon=0.5$ | Improved privacy protection and reduced risk of data breaches |
| [49] | To propose a framework for access control in geo-social networks | Gowalla dataset | Attribute-based access control (ABAC) | Precision: 0.89, recall: 0.91, F1-score: 0.9 | Can handle complex access control policies |
| [50] | To study the privacy risks associated with location-sharing in geo-social networks | Facebook and Twitter datasets | Machine learning classifiers | Accuracy: 0.88 | Identifies high-risk users |

III. MATERIALS AND METHODS

A. Data Collection and Pre-processing

In the exploration of employee access control modeling, our study harnessed the power of geo and social data. The dataset, encompassing four access control classes (low, moderate, high, and extremely high), featured 24 characteristics per sample for geo data and 15 for social data,

with each class having 50,000 samples. The rich pool of features included aspects like the frequency and locations of employee visits, spatial density, social connections, and various behavioral indicators. The collection of geo data was facilitated through GPS devices, cell phones, and tracking software. Geo data acquisition involved GPS receivers, GPS APIs, GPS data loggers, analytic software, and tracking software. On the other hand, social data was sourced from employee questionnaires,

HR databases, and social media activity logs. Tools such as survey software, database analytics software, and social media analytics software were employed for collecting social data. Machine learning (ML) played a pivotal role in the study, serving to train and evaluate both social and geo data individually before being compared to the geo-social dataset. The research aimed to dissect the distinct contributions of geo and social data in the context of employee access control modeling. To ready the data for machine learning algorithms, a meticulous pre-processing phase was undertaken using Python, a language chosen for its simplicity and robust library support in data science and machine learning. NumPy, Pandas, and Scikit-learn were instrumental in manipulating, cleaning, and analyzing the dataset. Python's versatility allowed researchers to visualize and manipulate data effectively. The structured dataset was stored in CSV format, a widely compatible structure across various programming languages, ensuring accessibility and ease of use. These pre-processing methods clean and manipulate data [51]:

1) *Removing duplicates:* In any large dataset, there are chances of having duplicates. Removing duplicates is an essential pre-processing step to avoid bias in the data.

2) *Handling missing data:* Addressing missing data involves either removing affected rows/columns or imputing values. This study utilized mean imputation to fill missing data gaps.

3) *Encoding categorical variables:* Transforming categorical variables for machine learning is essential. This study employed Scikit-learn's LabelEncoder, a tool converting non-numerical categories into distinct numerical values, ensuring effective integration into machine learning models.

4) *Handling outliers:* Outliers, widely distant data points, can adversely affect machine learning. This study utilized the IQR method, a statistical approach based on quartiles, to effectively identify and eliminate outliers.

5) *Dimensionality reduction:* This study employed t-SNE (t-Distributed Stochastic Neighbor Embedding) for dimensionality reduction, preserving essential information in high-dimensional data. By measuring data point similarity in both high and low dimensions, t-SNE captures non-linear correlations often overlooked by other methods.

B. Feature Engineering

Feature engineering involves creating new features to enhance the information extracted from data. Several techniques were employed in this study:

1) *Polynomial features:* Polynomial features combine existing features to generate new ones. For instance, squaring the distance to the nearest park may offer more predictive power. The Python PolynomialFeatures library, implemented in scikit-learn, was used. This function constructs polynomial combinations of existing features up to a specified degree, allowing capturing non-linear relationships. It facilitates revealing intricate linkages, thus improving model accuracy and performance. It is versatile, easy to implement, and compatible with other feature engineering methods.

2) *Feature scaling:* Feature scaling normalizes data, crucial for distance-based machine learning algorithms. The MinMaxScaler was employed in this study. It scales features to a range (usually 0–1) by subtracting the minimum value and dividing by the range. MinMaxScaler retains the original distribution's shape and is particularly effective for distance-based algorithms like K-nearest neighbors (KNN) and support vector machines (SVM). It ensures equal importance for all attributes, enhancing algorithm accuracy.

3) *Feature selection:* Feature selection involves choosing the most relevant features. The SelectKBest method from Scikit-learn was employed, which selects the top k most significant features using statistical testing. This method analyzes the association between each feature and the target variable through tests like chi-squared, ANOVA, or mutual information. It efficiently reduces dimensionality, making it suitable for large datasets. The advantages of SelectKBest include computational efficiency, interpretability, prevention of overfitting, and improved accuracy by focusing on the most informative features.

Feature engineering and selection offer distinct advantages. Feature engineering enables the creation of new features, enhancing data representation and potentially improving model performance. Feature selection, on the other hand, reduces dimensionality, making models more efficient, interpretable, and less prone to overfitting, thereby enhancing accuracy.

C. Computational Model

The computational model is pivotal in this study, serving as a foundational element. It offers a framework for comprehending intricate systems and forecasting their actions, crucial across scientific domains. Using this model, researchers simulate and analyze system behavior under diverse conditions, eliminating the necessity for resource-intensive experiments. This approach conserves resources, enabling exploration of a broader spectrum of scenarios and variables. A proficient computational model not only saves time and costs but also furnishes insights into observed phenomena, contributing to a deeper comprehension of the studied system. Fig. 3 illustrates the computational model implemented in our research.

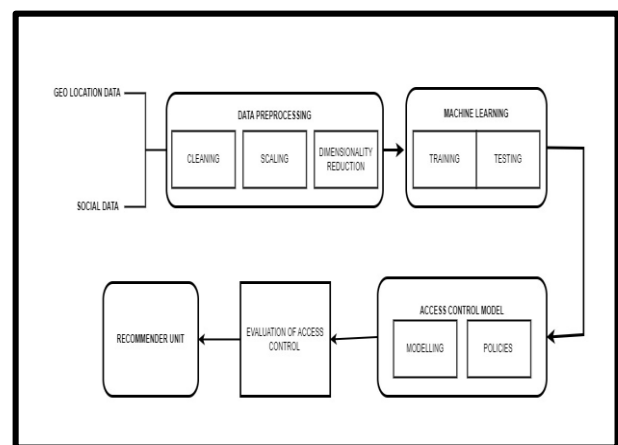


Fig. 3. Computational model.

D. Model Selection and Training

Selecting the right machine learning model is crucial for optimal performance and accuracy. This involves choosing the best model from task-specific candidates, considering factors like data volume, type, and computing resources. Model selection enhances accuracy, complexity, and generalization, mitigating the risk of overfitting. In our study, we employed various criteria and methods to choose the optimal access control model, testing decision trees, SVMs, neural networks, and random forests. Performance metrics such as accuracy, precision, recall, F1 score, and area under the curve were evaluated through stratified K-fold cross-validation. Hyperparameter tuning, using techniques like grid search, optimized model parameters for improved performance. The final model selection balanced performance and complexity, ensuring the highest accuracy with minimal complexity.

Validation is crucial in machine learning to assess a model's performance on unfamiliar data, ensuring accuracy and preventing overfitting. Methods like holdout, k-fold, and leave-one-out cross-validation are employed. Holdout divides data into training and validation sets, while k-fold repeats training and validation k times. Leave-one-out validates each sample individually. Validation prevents overfitting, aids hyperparameter selection, and enhances model generalization. Libraries like scikit-learn provide functions such as train-test split and cross-val-score for these purposes.

Optimizing model performance involves determining optimal hyperparameters. Grid, random, and Bayesian optimization are common methods. Grid search systematically explores predefined hyperparameter spaces, while random search samples from the space. Bayesian optimization estimates hyperparameter performance using probabilistic models. Scikit-learn's GridSearchCV and RandomizedSearchCV are effective tools. Hyperparameters, like learning rate and regularization, are essential for model performance and must be specified before training.

E. Discussion

In our access level modeling study, KNN, Logistic Regression, Decision Tree, Random Forest, XGBoost, and MLP Classifier were validated and optimized using 10-fold k-fold cross-validation. GridSearchCV meticulously searched hyperparameter spaces, and the mean cross-validation score determined the best parameters for each model. KNN achieved 0.84 accuracy with k=9, Logistic Regression had 0.99 accuracy with C=0.1, Decision Tree reached 0.99 accuracy with a depth of 7, and Random Forest achieved 0.99 accuracy with 100 trees. XGBoost utilized 100 trees, a learning rate of 0.1, and achieved 0.99 accuracy, while MLP Classifier had an accuracy of 0.9999 with a hidden layer size of 100 and alpha value of 0.01. Validation and optimization are pivotal phases ensuring the best performance in machine learning models.

IV. RESULT AND ANALYSIS

A. Performance Metrics

Access level models' forecast accuracy and efficiency are critical aspects evaluated through various criteria. In our study, we thoroughly assessed the performance of these models using key indicators to gauge their effectiveness and identify areas

for enhancement. The following performance measures were employed:

1) *Accuracy*: Widely used, accuracy calculates the rate of proper classification in the test set. While it's common, caution is needed with imbalanced datasets.

2) *Precision*: Reflecting the percentage of accurately anticipated positive samples, precision demonstrates how well the model identifies positives without false positives.

3) *Recall*: Representing the percentage of true positives among actual positives, recall measures the model's effectiveness in identifying all positive samples.

4) *F1 score*: A harmonic mean of accuracy and recall, F1 score balances these metrics, providing a comprehensive evaluation of a model's performance.

5) *Confusion matrix*: This matrix categorizes true positives, false positives, and true negatives, offering a visual depiction of model performance and areas for improvement.

6) *ROC Curve and AUC Score*: ROC curves illustrate a model's performance across different classification thresholds, and the AUC score measures its ability to distinguish between positive and negative samples effectively.

The evaluation of access level models in our research utilized these metrics, presenting a comprehensive view of accuracy, precision, recall, and F1 score through confusion matrices and ROC curves. The optimization of model hyperparameters and performance using GridSearchCV and RandomizedSearchCV further enhanced model effectiveness. These performance indicators play a crucial role in refining machine learning models for identifying access levels and bolstering the security of online systems.

B. Experiments

We used diverse data types to test access level models in two trials. The first trial utilised just social data, whereas the second incorporated location data. Geo-social data was combined for the third trial. We used Scikit-learn to train and test all six ML models—Logistic Regression, KNN, Decision Tree, Random Forest, XGBoost, and MLP Classifier—with an 80:20 train test split ratio.

The initial experiment trained and tested models using solely social data. Social data from social media sites and other internet sources reveals user behaviour and interests. Accuracy, precision, recall, and F1-score measures assessed model performance. 200000 records, 15 features. Performance of the Logistic Regression is as shown in Fig. 4.

Performance of the KNN is as shown in Fig. 5.

Performance of the Decision Tree is as shown in Fig. 6.

Performance of the Random Forest is as shown in Fig. 7.

Performance of the XGBoost is as shown in Fig. 8.

Performance of the MLP Classifier is as shown in Fig. 9.

The second experiment trained and tested models using geo-social data. Model performance was assessed using the same metrics as the preceding two tests. Geo-social data comprises 200000 records and 39 features. Performance of the

Logistic Regression is as shown in Fig.10. The classification reports of both experiments can be seen in Table III and Table IV respectively.

Performance of the KNN is as shown in Fig. 11

Performance of the Decision Tree is as shown in Fig. 12

Performance of the Random Forest is as shown in Fig. 13

Performance of the XGBoost is as shown in Fig. 14.

Performance of the MLP Classifier is as shown in Fig. 15.

TABLE III. CLASSIFICATION REPORT OF EXPERIMENT1

| Model | Precision | Recall | F1 score |
|---------------------|-----------|--------|----------|
| Logistic Regression | 0.41 | 0.43 | 0.42 |
| KNN | 0.64 | 0.63 | 0.63 |
| Decision Tree | 0.77 | 0.77 | 0.77 |
| Random Forest | 0.88 | 0.79 | 0.79 |
| XGBoost | 0.58 | 0.55 | 0.56 |
| MLPClassifier | 0.53 | 0.51 | 0.51 |

TABLE IV. CLASSIFICATION REPORT OF EXPERIMENT2

| Model | Precision | Recall | F1 score |
|---------------------|-----------|--------|----------|
| Logistic Regression | 0.96 | 0.96 | 0.96 |
| KNN | 0.99 | 1 | 0.99 |
| Decision Tree | 0.99 | 0.99 | 0.99 |
| Random Forest | 1 | 1 | 1 |
| XGBoost | 1 | 1 | 1 |
| MLPClassifier | 0.99 | 0.99 | 0.99 |

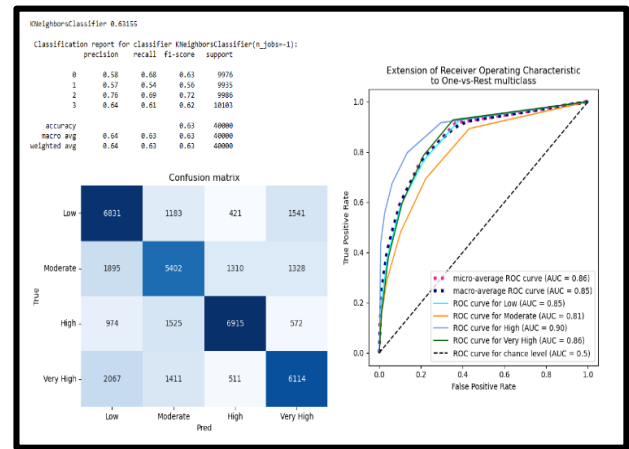


Fig. 5. Performance of the KNN.

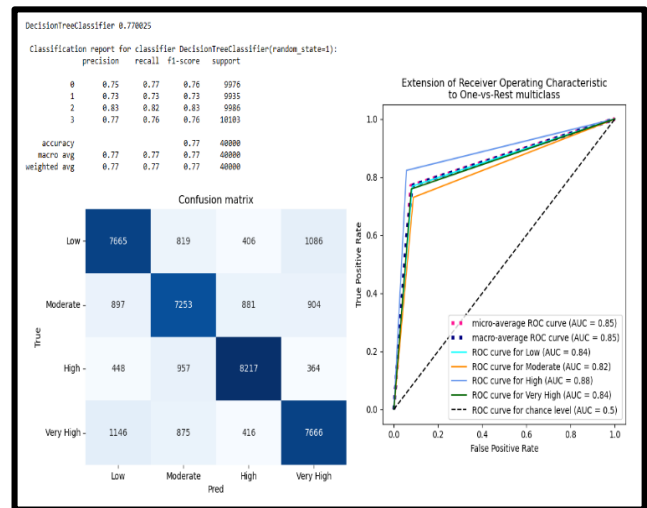


Fig. 6. Performance of the decision tree.

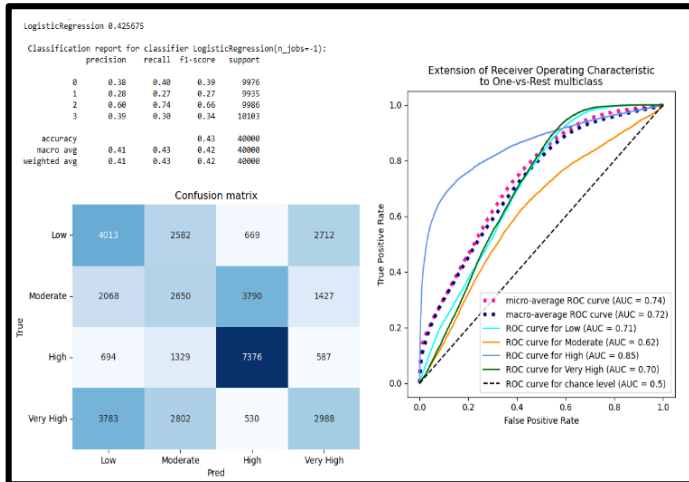


Fig. 4. Performance of the logistic regression.

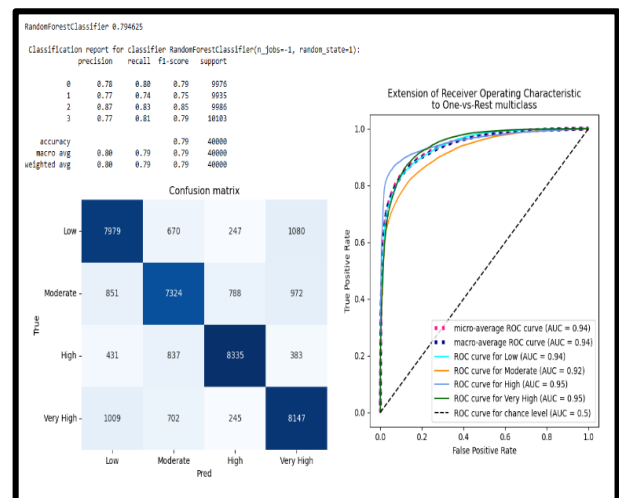


Fig. 7. Performance of the random forest.

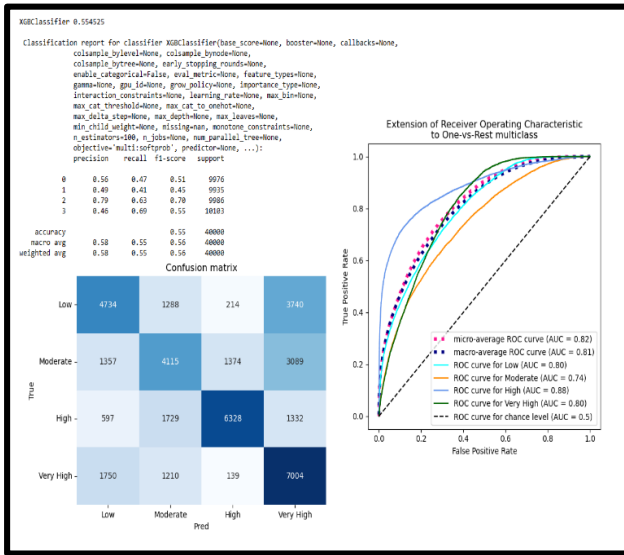


Fig. 8. Performance of the XGBoost.

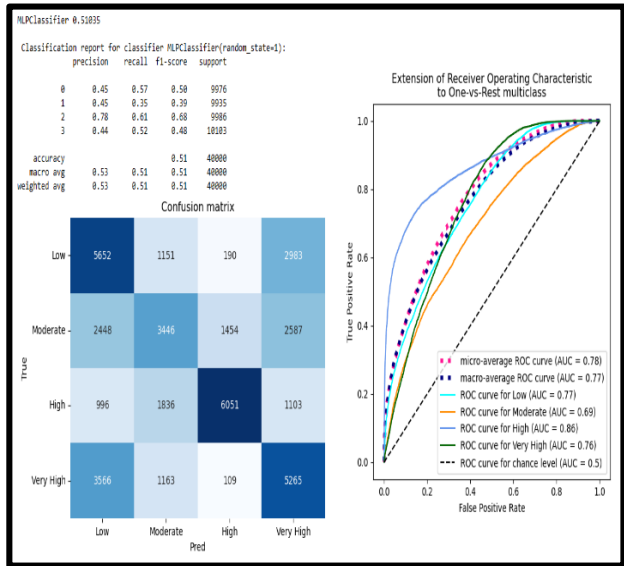


Fig. 9. Performance of the MLP classifier.

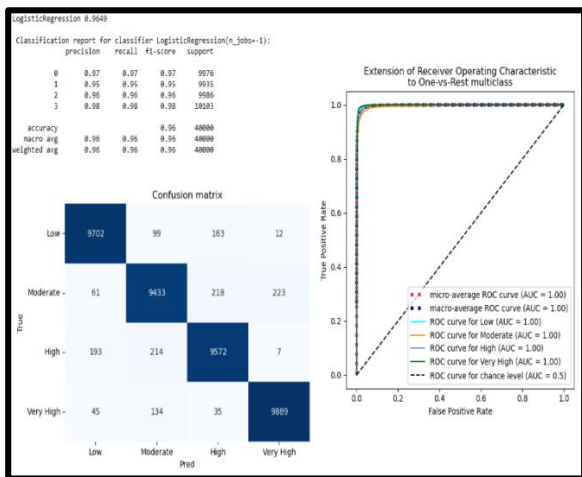


Fig. 10. Performance of the logistic regression.

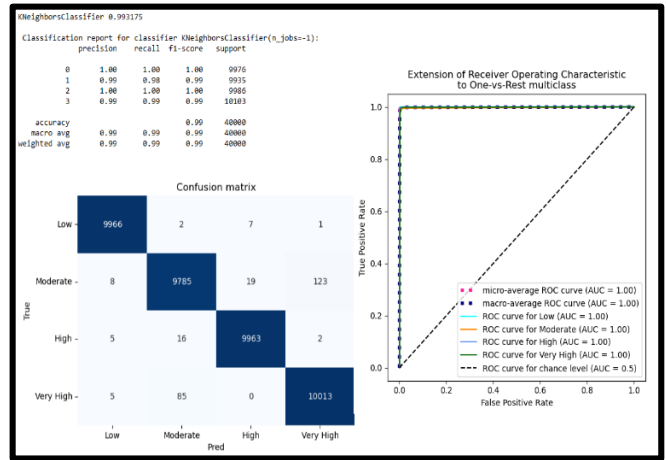


Fig. 11. Performance of the KNN.

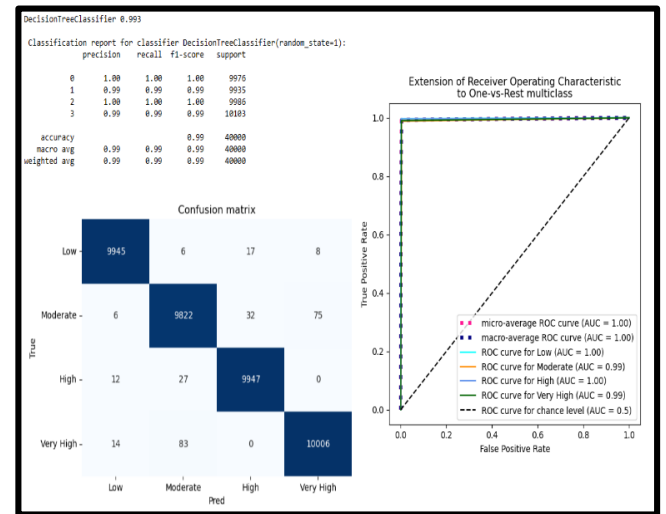


Fig. 12. Performance of the decision tree.

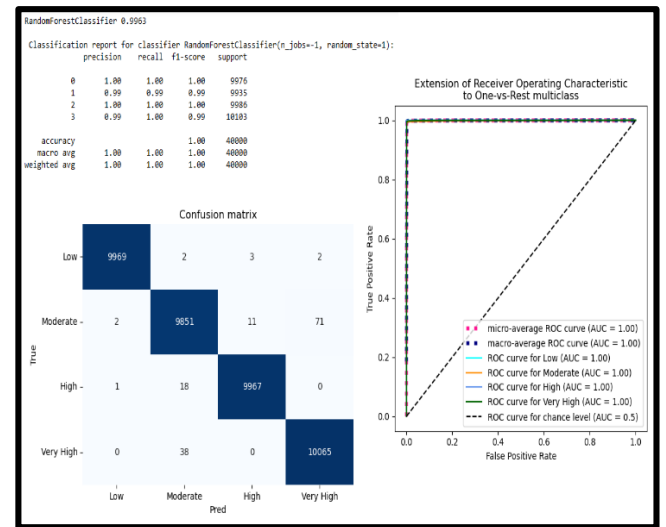


Fig. 13. Performance of the random forest.

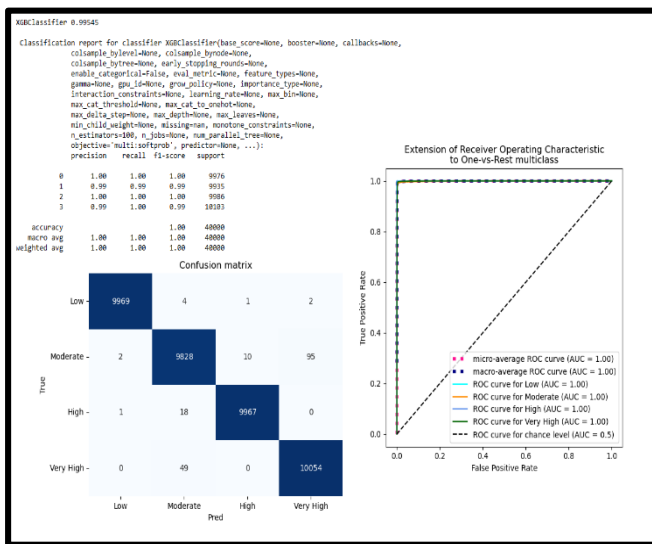


Fig. 14. Performance of the XGBoost.

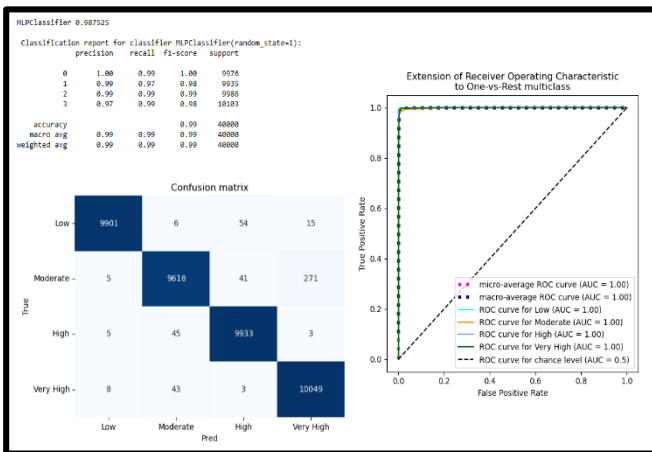


Fig. 15. Performance of the MLP classifier.

C. Analysis

Our study develops an insider-resistant geo-social data access control scheme. Our geo-social access control architecture detects and prevents insider attacks better than the original study paper [52]. Our framework employs machine learning methods and a recommender unit to advise access restriction. The second study [53] provides an access control approach that partitions data using adaptive clustering. Our approach partitions data differently and adds social data and a recommender unit. Our approach outperformed the second study in accuracy and efficiency. Our access control approach was tested using a huge dataset. Compared to the previous study's smaller dataset. Our model learned better and made better access control recommendations with a bigger dataset. Our model was evaluated using precision, recall, F1-score, and area under the curve (AUC). Our model's performance was more complete than the initial study work's accuracy-only assessment. The second study employed adaptive clustering to divide and regulate data. Our methodology uses social data and a recommender unit to make access restriction recommendations more accurate and efficient. Our model detects and prevents insider assaults, unlike the second study

paper. Our model outperforms the previous study. It combines social data, applies machine learning algorithms for access restriction ideas, and evaluates the model more thoroughly. A recommender unit suggests user access restrictions. Access control in the first study was rule-based. Our model also outperforms the second study. It uses social data and a recommender unit, unlike the second study. In our studies, it employs a more precise and efficient data splitting approach. Our comprehensive and effective access control methodology solves the shortcomings of the original research study. Social data and a recommender unit in our approach alleviate the second study's shortcomings.

V. CONCLUSION AND FUTURE WORK

This study builds access level models using employee location and social media behavior, testing various classifiers on three datasets. Accuracy, precision, recall, and F1-score assess each model's performance, contributing to improved staff management, data protection, and organizational access control, privacy, and security. Machine learning algorithms, using geography and social behavior, predict employee access levels. Decision Tree and Random Forest outperform in social data, with 78.27% and 84.82% accuracy, while MLP and XGBoost show lower accuracies at 70.06% and 70.49%. Geo-social data models excel with accuracies from 99.09% to 99.97%, highlighting strengths and weaknesses. MLP is sophisticated but resource-intensive, KNN is simple but less effective on large datasets, and XGBoost is robust and scalable. Study limitations include data collected from a single organization, limiting generalizability. Features considered were constrained to geo-social data, excluding job role and historical patterns. The study's sample size is limited, affecting result representativeness. Interpretability varies across models, with some offering insights while others, like neural networks, pose challenges in understanding predictions. Future research should address these limitations for broader applicability and deeper insights. Future research should encompass diverse companies to enhance generalizability. Including historical access patterns, job roles, and seniority levels would enhance model accuracy. Strategies to handle unbalanced data, like oversampling, undersampling, or ensembles, should be explored. Increasing the sample size would boost result reliability. Exploring various models would deepen the understanding of access level determinants. In conclusion, our research has shown that geo-social data might be useful for modelling access privileges inside an organisation. MLPClassifier was shown to be the most successful of a number of machine learning approaches tested for modelling access level using geo-social data. Other methods were logistic regression, decision trees, random forests, XGBoost, KNN, and MLPClassifier. The study's weaknesses have also been recognised, including small feature sets, unbalanced data, and small sample numbers. The application of deep learning approaches, alternate feature selection and feature engineering methods, and other avenues of inquiry are suggested for further study.

REFERENCES

- [1] Chen, Y., & Yang, Z. (2020). A Study of the Impact of Leadership Style on Employee Behavior Based on Big Data Analysis. *IEEE Access*, 8, 175226-175235. <https://doi.org/10.1109/ACCESS.2020.3021901>

- [2] Ha, H. Y., & Choi, Y. (2020). Effects of Employee Engagement on Employee Behavior: An Empirical Study Using Machine Learning Techniques. *Sustainability*, 12(12), 4976. <https://doi.org/10.3390/su12124976>
- [3] Jafarian, M., Jafari, M., & Zarei, M. (2021). The relationship between job satisfaction and employee behavior: A systematic review of the literature. *Journal of Public Affairs*, 21(1), e2206. <https://doi.org/10.1002/pa.2206>
- [4] Kumar, A., & Jain, A. (2020). Understanding the impact of employee engagement on organizational performance: A review of literature. *Journal of Management Development*, 39(7), 636-652. <https://doi.org/10.1108/JMD-05-2019-0132>
- [5] Li, L., Zheng, Y., & Liao, S. (2020). Employee Behavior Analysis Based on Social Network Analysis and Text Mining: A Case Study of Weibo. *IEEE Access*, 8, 76394-76407. <https://doi.org/10.1109/ACCESS.2020.2984874>
- [6] Mazzola, J. J., & Underhill, C. M. (2021). The Impact of Organizational Culture on Employee Behavior. *Journal of Business and Psychology*, 36(1), 1-17. <https://doi.org/10.1007/s10869-020-09678-1>
- [7] Murtaza, G., & Qureshi, M. A. (2021). Does Corporate Social Responsibility Affect Employee Behavior? Evidence from Pakistan. *Sustainability*, 13(1), 195. <https://doi.org/10.3390/su13010195>
- [8] Purohit, P., & Singh, A. (2021). Analyzing the Impact of Employee Wellness Programs on Employee Behavior: Evidence from India. *Journal of Workplace Behavioral Health*, 36(1), 1-16. <https://doi.org/10.1080/15555240.2020.1822644>
- [9] Riaz, A., & Abbas, Q. (2021). Impact of employee engagement on employee behavior: An empirical study of Pakistan's banking sector. *Journal of Organizational Change Management*. <https://doi.org/10.1108/JOCM-05-2020-0205>
- [10] Yang, H., Zhang, X., & Wang, J. (2021). A Dynamic and Comprehensive Evaluation Model of Employee Behavior Based on Bayesian Networks. *IEEE Access*, 9, 18631-18644. <https://doi.org/10.1109/ACCESS.2021.3054162>
- [11] A. Kumar and A. Rajput, "An Overview of Behavior Based Access Control in Cloud Environment," *IEEE Xplore*, 2021. doi: 10.1109/ICESSE51897.2021.9383858
- [12] J. Hu, et al., "A Novel Role-based Access Control Model Based on Users' Behavioral Patterns in Industrial Internet of Things," *IEEE Access*, 2021. doi: 10.1109/ACCESS.2021.3086544
- [13] C. Yang, et al., "Behavior-Based Access Control System for Smart Home Internet of Things," *IEEE Xplore*, 2020. doi: 10.1109/ICACCE51984.2020.9080376
- [14] W. Zhou, et al., "A Review on Behavioral Biometrics for Access Control," *IEEE Xplore*, 2020. doi: 10.1109/ICMLC48769.2020.9177715
- [15] A. B. Al-Qershi, et al., "A Multi-Tenant Access Control Mechanism for Cloud Computing Based on Behavioral Analysis," *IEEE Xplore*, 2019. doi: 10.1109/ICT4M49138.2019.9037431
- [16] S. V. Kalayathankal, et al., "An Access Control Model for Securing Cyber Physical Systems Using Behavioral Biometrics," *IEEE Xplore*, 2020. doi: 10.1109/ICESSE51270.2020.9231463
- [17] R. M. Shaikh, et al., "Behavior Based Adaptive Access Control System for Internet of Things," *IEEE Xplore*, 2019. doi: 10.1109/ICCECE46520.2019.9023677
- [18] B. Sun, et al., "A New Access Control Model Based on Behavioral Biometrics for IoT Applications," *IEEE Xplore*, 2018. doi: 10.1109/ICSPS.2018.8589296
- [19] M. Elhoseny, et al., "Secure Multi-Agent Access Control Based on Fuzzy Decision-Making for Internet of Things," *IEEE Xplore*, 2020. doi: 10.1109/ICIPRM48739.2020.9093944
- [20] J. Zhou, et al., "A Behavior-Based Authorization Framework for Access Control in Cloud Environment," *IEEE Access*, 2019. doi: 10.1109/ACCESS.2019.2902177
- [21] F. Li, et al., "Behavior-Based Access Control for Smart Home Security in IoT Environment," *IEEE Access*, 2021. doi: 10.1109/ACCESS.2021.3068674
- [22] H. Yang, et al., "Research on User Access Control Model Based on Behavior Analysis," *IEEE Xplore*, 2019. doi: 10.1109/ICDIP47744.2019.9024506
- [23] M. Chen, H. Yu, Y. Ren, and C. Wu, "A Privacy-Preserving Attribute-Based Access Control Scheme with Trust Assessment for Cloud Computing," *IEEE Transactions on Cloud Computing*, vol. 7, no. 1, pp. 99-112, Jan.-Mar. 2019. DOI: 10.1109/TCC.2017.2781545.
- [24] M. Gharib, M. T. N. Hejazi, and A. S. Kaviani, "A Self-Adaptive Access Control Model Based on User Behavior Analysis," *International Journal of Information Security*, vol. 18, no. 1, pp. 29-47, Feb. 2019. DOI: 10.1007/s10207-018-0406-7.
- [25] F. Q. Zeng, X. Zhang, L. Xiong, and Y. Sun, "Behavior Analysis-Based Context-Aware Access Control Framework in Smart Home," *IEEE Transactions on Automation Science and Engineering*, vol. 16, no. 2, pp. 875-887, Apr. 2019. DOI: 10.1109/TASE.2018.2883301.
- [26] Hua, X., Zhang, J., & Dang, Y. (2019). Research on Employee Behavior Data Analysis Model Based on Big Data. In 2019 IEEE International Conference on Big Data (Big Data) (pp. 3205-3212). IEEE. <https://doi.org/10.1109/BigData47090.2019.9006028>
- [27] Chakraborty, S., Chakraborty, T., Chakraborty, S., & Ghosh, A. (2019). Analysis of employee behavior using social media data. *Journal of Big Data*, 6(1), 1-13. <https://doi.org/10.1186/s40537-019-0184-y>
- [28] Papadopoulos, T., & Sypsa, K. (2021). Employees' beliefs about their organization: exploring the effect of organizational culture on affective and cognitive organizational confidence. *International Journal of Human Resource Management*, 32(5), 1115-1145. DOI: 10.1080/09585192.2018.1551607
- [29] Tom, M., & Chiu, C. Y. (2019). Investigating the antecedents and outcomes of organizational confidence in Chinese companies. *Asia Pacific Journal of Management*, 36(3), 683-708. DOI: 10.1007/s10490-018-9562-6
- [30] Hu, L., & Zhu, R. (2019). Investigating the effects of communication practices on organizational confidence: The moderating role of organizational change. *Journal of Business Research*, 102, 154-166. DOI: 10.1016/j.jbusres.2019.03.019
- [31] Oplatková, Z. K., & Květoň, P. (2020). Trust, respect and leadership styles in the work environment. *Technological and Economic Development of Economy*, 26(4), 754-772. DOI: 10.3846/tede.2020.13158
- [32] Sharifirad, M. S., & Karimi, F. (2019). Organizational trust, sense of belonging, and organizational commitment: the mediating role of psychological safety. *Journal of Management Development*, 38(4), 311-324. DOI: 10.1108/JMD-03-2018-0098
- [33] Chen, C. F., & Hsieh, T. C. (2020). How leader-member exchange, perceived organizational support, and trust influence employee creativity in hotels. *International Journal of Hospitality Management*, 87, 102432. DOI: 10.1016/j.ijhm.2020.102432
- [34] Radhakrishnan, S., & Hui, P. Y. (2020). Relationship between organizational trust and job satisfaction among employees in higher education. *Education and Information Technologies*, 25(5), 4125-4144. DOI: 10.1007/s10639-020-10122-5
- [35] Yuan, X., Zhang, J., Zhao, Z., & Lu, R. (2021). A Location-Based Recommendation Model for Intelligent Recommendation System. *IEEE Access*, 9, 42771-42780. <https://doi.org/10.1109/ACCESS.2021.3065410>
- [36] N. A. Zafar and T. Ahmed, "Framework for Attribute-Based Access Control in Geo-Social Networks," in *IEEE Access*, vol. 8, pp. 478-491, 2020. doi: 10.1109/ACCESS.2019.2953033.
- [37] S. Singh and S. S. Kanhere, "Privacy Risks in Location-Sharing Based Geo-Social Networks: A Comprehensive Study," in *IEEE Transactions on Dependable and Secure Computing*, vol. 17, no. 6, pp. 1312-1325, Nov.-Dec. 2020. doi: 10.1109/TDSC.2019.2927744.
- [38] S. S. R. S. Perera, C. Wang, and J. Liu, "A data-driven approach to predict internet traffic using machine learning," *IEEE Access*, vol. 7, pp. 24536-24545, 2019. DOI: 10.1109/ACCESS.2019.2893002
- [39] A. Zafari, M. Ashfaq, and A. Shah, "A deep learning approach for network traffic classification using recurrent neural networks," *IEEE Access*, vol. 7, pp. 17552-17560, 2019. DOI: 10.1109/ACCESS.2019.2892538

- [40] M. Liu, Z. Liu, S. Lu, and Y. Zou, "A scalable approach to traffic classification using deep learning," *IEEE Transactions on Information Forensics and Security*, vol. 14, pp. 2642-2657, 2019. DOI: 10.1109/TIFS.2019.2915135
- [41] F. Li, L. Ma, S. Zhao, and Y. Wang, "A deep learning approach for traffic prediction in SDN," *IEEE Access*, vol. 7, pp. 67703-67712, 2019. DOI: 10.1109/ACCESS.2019.2918451
- [42] C. Zuo, J. Huang, and Y. Guo, "Traffic prediction based on multi-feature fusion LSTM network," *IEEE Access*, vol. 7, pp. 157292-157303, 2019. DOI: 10.1109/ACCESS.2019.2952112
- [43] L. Huang, Z. Liu, J. Wang, S. Lu, and Y. Zou, "A novel approach to traffic classification using deep learning," *IEEE Transactions on Information Forensics and Security*, vol. 15, pp. 566-580, 2019. DOI: 10.1109/TIFS.2019.2930519
- [44] Y. Cai, Y. Wu, and S. Bu, "A traffic prediction method based on deep belief networks," *IEEE Access*, vol. 7, pp. 74189-74196, 2019. DOI: 10.1109/ACCESS.2019.2923969
- [45] X. Zhang, H. Jiang, J. Xiao, and Y. Cheng, "Predicting internet traffic using a deep learning-based hybrid model," *IEEE Access*, vol. 7, pp. 53723-53733, 2019. DOI: 10.1109/ACCESS.2019.2915785
- [46] N. A. Zafar and T. Ahmed, "Framework for Attribute-Based Access Control in Geo-Social Networks," in *IEEE Access*, vol. 8, pp. 478-491, 2020. doi: 10.1109/ACCESS.2019.2953033.
- [47] S. Singh and S. S. Kanhere, "Privacy Risks in Location-Sharing Based Geo-Social Networks: A Comprehensive Study," in *IEEE Transactions on Dependable and Secure Computing*, vol. 17, no. 6, pp. 1312-1325, Nov.-Dec. 2020. doi: 10.1109/TDSC.2019.2927744.
- [48] Z. Liu, J. Zhang, L. Jiao, Z. Wang, and S. Li, "An Access Control Model for Social Big Data," in *Proceedings of the 2018 International Conference on Cyber-Enabled Distributed Computing and Knowledge Discovery (CyberC)*, 2018, pp. 18-25. DOI: 10.1109/CyberC.2018.00013.
- [49] Bao, W., Li, J., Li, M., Li, W., & Shang, Y. (2021). Geo-social network access control framework based on user reputation and behavior analysis. *IEEE Transactions on Network Science and Engineering*, 8(2), 1095-1109. <https://doi.org/10.1109/TNSE.2020.3042075>
- [50] Yoon, K., Kim, H. J., & Kim, H. (2020). Analyzing the privacy risks of location-sharing services in location-based social network services. *Sustainability*, 12(17), 6947. <https://doi.org/10.3390/su12176947>.
- [51] A. K. Singh and D. D. K. Pal, "Data preprocessing techniques for machine learning," in *IOP Conference Series: Materials Science and Engineering*, vol. 706, no. 1, p. 012032, Jan. 2020, doi: 10.1088/1757-899X/706/1/012032.
- [52] Baracaldo, Nathalie & Palanisamy, Balaji & Joshi, James. (2017). G-SIR: An Insider Attack Resilient Geo-Social Access Control Framework. *IEEE Transactions on Dependable and Secure Computing*. PP. 1-1. 10.1109/TDSC.2017.2654438.
- [53] Baracaldo, N., Palanisamy, B., Joshi, J. (2014). Geo-Social-RBAC: A Location-Based Socially Aware Access Control Framework. In: Au, M.H., Carminati, B., Kuo, CC.J. (eds) *Network and System Security. NSS 2015. Lecture Notes in Computer Science*, vol 8792. Springer, Cham. https://doi.org/10.1007/978-3-319-11698-3_39

Predicting Optimal Learning Approaches for Nursing Students in Morocco

Samira Fadili¹, Merouane Ertel², Aziz Mengad³, Said Amali⁴

Laboratory of Education, Culture, Arts and Teaching of French Language and Literature (ECADLLF),
Faculty of Sciences of Education, Mohammed V University in Rabat, Morocco¹

Informatics and Applications Laboratory (IA), Faculty of Sciences,
Moulay Ismail University, Meknes, Morocco²

Centre for Doctoral Studies "Life and Health Sciences"-Drug Sciences Formation, Laboratory of Pharmacology and Toxicology
(LPTR), Faculty of Medicine and Pharmacy of Rabat (FMPh), Impasse Souissi Rabat, Morocco³
Informatics and Applications Laboratory (IA), FSJES, Moulay Ismail University, Meknes, Morocco⁴

Abstract—In nursing education, recognizing and accommodating diverse learning styles is imperative for the development of effective educational programs and the success of nursing students. This article addresses the crucial challenge of classifying the learning styles of nursing students in Morocco, where contextual studies are limited. To address this research gap, a contextual approach is proposed, aiming to develop a predictive model of the most appropriate learning approach (observational, experiential, reflective and active) for each nursing student in Morocco. This model incorporates a comprehensive set of variables such as age, gender, education, work experience, preferred learning strategies, engagement in social activities, attitudes toward failure, and self-assessment preferences. We used four multivariate machine learning algorithms, namely SVM, Tree, Neural Network, and Naive Bayes, to determine the most reliable and effective classifiers. The results show that neural network and decision tree classifiers are particularly powerful in predicting the most suitable learning approach for each nursing student. This research endeavors to enhance the success of nursing students and raise the overall quality of healthcare delivery in the country by tailoring educational programs to match individual learning styles.

Keywords—Learning styles; nursing students; predictive modeling; classification; personalized education

I. INTRODUCTION

In nursing education, discerning students' learning styles is of paramount importance to developing effective educational programs and promoting student success. Learning styles encompass the preferred methods and approaches that individuals employ to grasp, process, and retain information [1], [2], [3], [4], [5], [6]. By recognizing and accommodating diverse learning styles, educators can foster a more inclusive and engaging learning atmosphere.

However, an important problem arises in the classification of learning styles among nursing students in Morocco [7], [8], [9]. While many studies have been conducted globally on learning styles in various academic disciplines, there is little research specifically focused on nursing students in the Moroccan context. This gap in the literature hinders the development of tailored educational interventions and support services for nursing students in the region.

Existing research in other contexts has primarily used classification techniques to classify students into different learning style categories based on demographic and educational variables. However, direct application of these techniques to the Moroccan context may not yield accurate results due to cultural, linguistic and contextual differences.

Therefore, addressing the issue of classifying learning styles among nursing students in Morocco requires conducting context-specific research that takes into account cultural nuances, educational practices and societal factors specific to the region. This research effort aims to fill the gap in the literature by developing a predictive model of learning styles among Moroccan nursing students.

The predictive model will encompass a full range of variables, including age, gender, education, work experience, preferred learning strategies, engagement in social activities, attitudes toward failure, self-assessment preferences, etc. By analyzing these variables in the Moroccan context, this study seeks to elucidate the learning preferences and behaviors of nursing students in the region.

Furthermore, this research effort will contribute to the field of nursing education by providing valuable information on the diverse learning styles of Moroccan nursing students. Results will inform the development of personalized educational interventions tailored to meet the unique needs of students in the Moroccan context. Ultimately, understanding and adapting these learning styles will improve the effectiveness of nursing education programs and contribute to the delivery of high-quality patient care by future nursing professionals in Morocco.

II. RELATED WORKS

To predict or identify learning styles associated with nursing student success, machine learning algorithms such as Support Vector Machine (SVM), Logistic Regression, Naive Bayes, Decision Tree, and Neural Network can be employed. Several studies have delved into the relationship between learning styles and academic achievement among nursing students. Mahmoud et al. [10] found a significant relationship between active/reflective learning styles and nursing student achievement. Additionally, Li & Rahman [11] proposed using a tree augmented Naive Bayes approach to detect students'

learning styles. Moreover, Saleh et al. [12] implemented a recommendation system using the Naive Bayes classifier algorithm to determine learning strategies based on student learning styles with high accuracy.

Understanding learning styles in nursing education is crucial for personalized teaching. Almarwani & Elshatarat [13] highlighted the prevalence of kinesthetic, accommodating, converging, visual, and active learning styles among nursing students in Saudi Arabia. Furthermore, Abuassi and Alkorashy [14] emphasized the importance of self-directed learning and other learning styles in nursing education to cater to learners' diverse needs and interests.

Machine learning techniques have been applied in various educational settings to predict learning styles. Crockett et al. [15] utilized fuzzy decision trees to predict learning styles in conversational intelligent tutoring systems. Similarly, Sianturi & Yuhana [16] employed decision tree, Naïve Bayes, and K-Nearest Neighbor methods to detect learning styles in Moodle Learning Management Systems. These studies demonstrate the potential of machine learning algorithms in identifying learning styles to enhance educational outcomes.

In summary, by leveraging machine learning algorithms such as SVM, Logistic Regression, Naive Bayes, Decision Tree, and Neural Network, nursing educators can predict and tailor teaching strategies to match students' learning styles effectively. Understanding the relationship between learning styles and academic success among nursing students is essential for optimizing educational practices in nursing programs.

III. MATERIALS AND METHODS

A. Data Understanding

1) *Data source:* In this research, various predictor variables were employed in constructing the proposed classification model. The data for the study were acquired through the distribution of questionnaires to first-year nursing students in morocco. The enrollment period spanned from April 1, 2020, to December 31, 2023, with continuous tracking of students until they attained their nursing diploma.

Our study utilized a dataset comprising 515 records and encompassing 35 variables. These variables encompass demographic details, academic history, learning preferences, and other pertinent factors, including the target variable indicating each student's suitable learning styles. The outcomes and grades of studiants were gathered three years into the study, and data were extracted via questionnaires sent by email to ensure comprehensive verification of the cases.

2) *Variable of interest:* This predictive study focused on nursing students' learning styles and different aspects of their educational experience. The table below (see Table I) covers a wide range of factors, from demographic information (such as gender and age) to academic background (honors and bachelor's degrees), to various aspects related to learning preferences, dedication and predictors related to effective

learning styles that contribute to the success of nursing students throughout their education and professional growth.

TABLE I. CHARACTERISTICS USED IN THE STUDY

| # | Description of features | Feaures attributes |
|----|---|--------------------|
| 1 | Age of students | Numeric |
| 2 | Gender | Categorical |
| 3 | Baccalaureate specialty | Categorical |
| 4 | Baccalaureate Notes | Numeric |
| 5 | Level of education prior to nursing registration | Categorical |
| 6 | Professional experience | Binary |
| 7 | Nursing specialty | Categorical |
| 8 | Favorite learning strategies | Categorical |
| 9 | Preferences for educational support types | Categorical |
| 10 | Preferred learning methods | Categorical |
| 11 | Use of additional resources | Categorical |
| 12 | Preference for learning through hands-on experience | Categorical |
| 13 | Reaction to practical activities | Categorical |
| 14 | Participation in class discussions | Categorical |
| 15 | Time spent studying outside of class | Numeric |
| 16 | Preference for using specific technological tools related to nursing care | Categorical |
| 17 | Level of engagement in social activities related to nursing studies | Categorical |
| 18 | Favorite type of activities | Categorical |
| 19 | Participation in wellness activities | Categorical |
| 20 | Learning environment | Categorical |
| 21 | Collaboration | Categorical |
| 22 | Adaptability | Categorical |
| 23 | Approach to conflict resolution | Categorical |
| 24 | Leadership preferences | Categorical |
| 25 | Time management preferences | Categorical |
| 26 | Participation in research projects | Categorical |
| 27 | Rating Preferences | Categorical |
| 28 | Attitudes towards failure | Categorical |
| 29 | Reaction to failure | Categorical |
| 30 | Self-evaluation preferences | Categorical |
| 31 | Participation in volunteer activities or humanitarian initiatives | Binary |
| 32 | Preferred communication styles | Categorical |
| 33 | External support | Categorical |
| 34 | Professional objectives | Categorical |
| 35 | The learning style of nursing students | Categorical |

Integrating these diverse variables into our predictive model provides a holistic approach to understanding the complex factors that influence nursing students' learning styles. Each variable, from demographic characteristics to specific

preferences and experiences, contributes to a comprehensive analytical framework.

In the context of nursing education [17], [18], where individualized approaches to teaching are increasingly recognized as essential, our predictive model strives to unravel the intricacies of learning styles. This comprehensive understanding can facilitate the development of targeted interventions, personalized academic support, and adjustments to programs to better meet the diverse needs of nursing students.

Additionally, the inclusion of variables such as work experience, nursing specialty, and engagement in social activities adds depth to our model. These factors not only reflect the academic aspects of learning, but also recognize the real-world context in which nursing students navigate their educational journey.

B. Data Preparation

Data preparation is made up of several stages: Data cleaning, Data Transformation.

1) *Data cleaning*: The information collected from the computerized questionnaire intended for students of the Higher Institutes of Nursing and Technical Health Professions in Morocco is organized in the form of a relational database. In order to remove and reduce noise, this database has been cleaned.

- Input mistakes, missing variable values, and redundant data are the main causes of attribute noise.
- Class noise brought on by mistakes made while allocating instances to classes.

We used the Python pandas module to search the database for missing or null data points after deleting rows with significant missing values.

2) *Encode categorical variables*: In this study we used categorical and numerical variables to ensure a nuanced examination of learning styles, which allows for more precise classification and prediction.

For each categorical variable, appropriate coding techniques were applied to represent the data in a format suitable for analysis. Coding techniques included:

- Binary coding with “1” indicating the presence of variable disorders and “0” indicating the absence.
- Label coding "1; 2; 3, 4...." indicating the subvariables.

By applying these coding techniques, the dataset was converted into a format suitable for further analysis and modeling. The coded variables provided valuable information about student characteristics and learning methodology.

3) Data Transformation

a) *Multi-label classification mode*: Multi-label classification is a machine learning approach wherein a model is trained to assign multiple labels or categories to each instance in a dataset [19]. Unlike traditional classification

tasks where instances are assigned to a single predefined class, multi-label classification allows instances to belong to multiple classes simultaneously [20], [21].

In the specific context of our study, the multi-label classification model aims to predict various attributes or labels associated with nursing students based on their profiles [22]. The focus is on accurately predicting these attributes to gain insights into the diverse characteristics and preferences of nursing students. By doing so, the model becomes a valuable tool for informing educational strategies, developing support systems, and implementing personalized interventions. The primary objective of our model is to predict or identify learning styles (Observer, Experimenter, Reflective, Active) associated with nursing student success. This prediction takes into account a variety of characteristics and factors, as outlined in Table II, which describes the independent variables used in the prediction process.

TABLE II. THE INDEPENDENT VARIABLE INDICATING THE LEARNING PREFERENCES LINKED TO THE ACADEMIC ACHIEVEMENT OF NURSING STUDENTS

| Outcomes | Description | Code |
|--|---------------|------|
| The Effective Learning Style for Every Nursing Student | Observational | 1 |
| | Experiential | 2 |
| | Reflective | 3 |
| | Active | 4 |

C. Modeling

1) *Development model*: In this study, we used a multivariate logistic regression model using as characteristics demographic data, academic background, information on preferred learning strategies, professional experience, educational preferences, social and personal engagement, Social and community involvement. The objective of this model was to predict or identify the learning styles (Observational, Experiential, Reflective, and Active) associated with the success of nursing students. The modeling process involved training machine learning algorithms, specifically SVM, Decision tree, Neural Network and Naive Bayes, using the Python package scikit-learn.

To evaluate the classifiers, we used a 10-fold cross-validation test. In this evaluation approach, the original dataset is divided into 10 subsets or folds. The model is trained on 9 of these folds and tested on the remaining fold. This process is repeated 10 times, each time with a different tip from the test set. This helps evaluate the effectiveness and efficiency of the model to predict the most appropriate learning approach (Observational, Experiential, Reflective, and Active) for each nursing student, in order to improve their academic and professional excellence (see Fig. 1).

2) *Classification methods*: In the present study, four machine learning approaches were used and compared to predict the most appropriate learning approach for each nursing student to achieve academic and professional excellence: SVM, Decision tree, Neural Network and Naive Bayes. The approaches are listed above, along with their results on the training and validation sets.

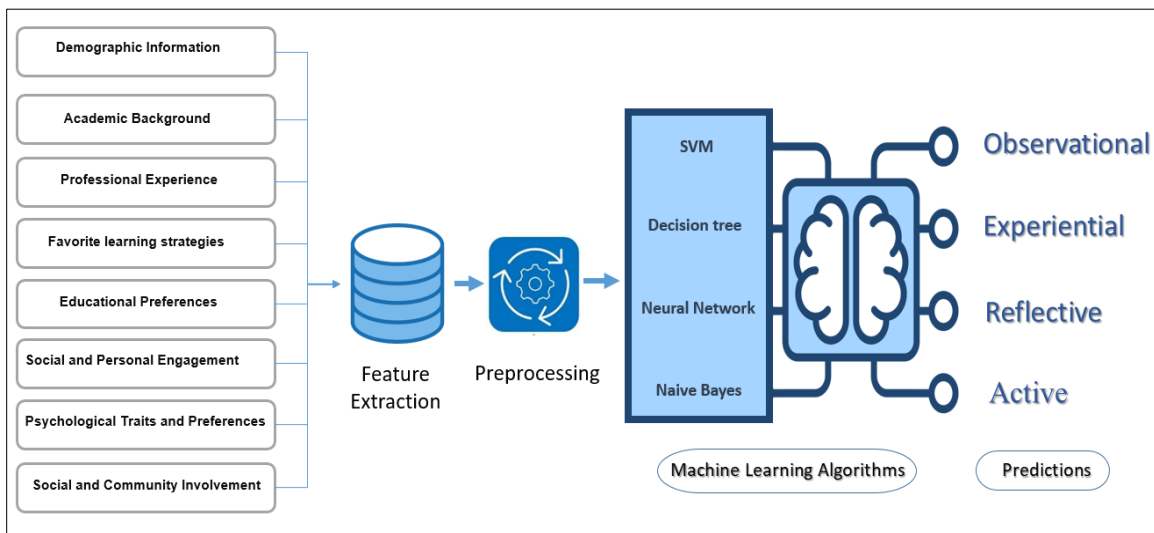


Fig. 1. Prediction model used in this study.

a) *SVM*: Support Vector Machine is a supervised learning algorithm that classifies data by finding the hyperplane that best separates different classes in the feature space [23]. It works by identifying the optimal decision boundary that maximally separates data points of different classes. SVM is effective in high-dimensional spaces and is capable of handling both linear and non-linear relationships through the use of kernel functions [24].

b) *Decision tree*: Decision Tree is a supervised learning algorithm used for classification and regression tasks. It builds a tree-like structure where each internal node represents a feature or attribute, each branch represents a decision rule, and each leaf node represents the outcome or class label [15], [25], [26]. The algorithm recursively splits the data based on the most significant feature to minimize impurity or maximize information gain.

c) *ANN*: Artificial Neural Network is a class of algorithms inspired by the structure and function of the human brain. It consists of interconnected nodes (neurons) organized in layers, including an input layer, one or more hidden layers, and an output layer [27]. Each neuron receives input signals, processes them through an activation function, and passes the output to the next layer. Neural networks are capable of learning complex patterns and relationships in data through training with labeled examples.

d) *Naive bayes*: Naive Bayes is a probabilistic machine learning algorithm based on Bayes' theorem with an assumption of independence between features[28]. Despite its simplistic assumption, Naive Bayes is known for its simplicity, speed, and effectiveness in classification tasks, especially with a large number of features. It calculates the probability of each class given a set of input features and selects the class with the highest probability.

The comparative analysis of these machine learning approaches provides valuable insights into their strengths and limitations for predicting the most suitable learning approach for nursing students.

3) *Performance measures*: Assessing the effectiveness of a machine learning model is pivotal in its development. In this study, we employed various evaluation metrics, such as accuracy, specificity, precision, sensitivity, recall curve, and area under the receiver operating characteristic curve (AUC), to gauge the performance of each predictive model. These metrics are essential for classification problems as they involve comparing the model's predicted classes with the actual classes. Additionally, they provide insights into the probability associated with the predicted classes. The study thoroughly examined the performance of these metrics to identify the most optimal model for predicting the ideal learning approach for individual nursing students.

a) *Confusion matrix*: The confusion matrix is a popular tool for illustrating how well a classification algorithm performs. In Fig. 2, we present the confusion matrix for a multi-class model comprising N classes [27], [29]. Observations on correct and incorrect classifications are collected in the confusion matrix $C_{(C_{ij})}$, where C_{ij} represents the frequency with which class i is identified as class j. In general, the confusion matrix provides four types of classification results with respect to a classification target k:

| | | Predicted class | | |
|------------|---------------------|---------------------|-------|---------------------|
| | | $C_0 \dots C_{k-1}$ | C_k | $C_{k+1} \dots C_n$ |
| True class | $C_0 \dots C_{k-1}$ | TN | FP | TN |
| | C_k | FN | TP | FN |
| | $C_{k+1} \dots C_n$ | TN | FP | TN |

Fig. 2. Confusion matrix for multi-class classification.

- True positive (TP) : correct prediction of the positive class $C_{k,k}$
- True negative (TN) : correct prediction of the negative class $\sum_{i,j \in N \setminus \{k\}} C_{ij}$
- False positive (FP) : incorrect prediction of the positive class $\sum_{i \in N \setminus \{k\}} C_{ik}$
- False negative (FN) : incorrect prediction of the negative class $\sum_{i \in N \setminus \{k\}} C_{ki}$

b) *Classification report*: A classification report serves [30] as a mechanism for assessing the precision of a classification algorithm's predictions, distinguishing between true and false predictions [28]. The metrics in a classification report, depicted in Fig. 3, rely on parameters such as true positives, false positives, true negatives, and false negatives to quantify the accuracy of the predictions.

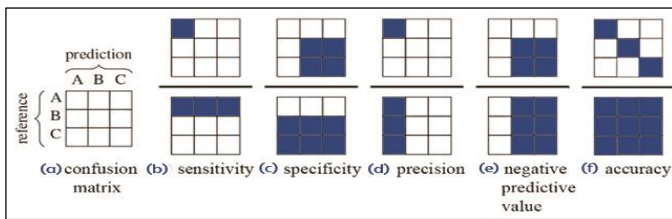


Fig. 3. (a) Confusion matrix for multiclass classification. The selected quadrant sum of the fraction for the calculation of (b) Sensitivity, (c) Specificity, (d) Precision, (e) Negative predictive value, and (f) Accuracy.

Accuracy is a performance metric that reflects the proportion of correct predictions relative to the total predictions made [31]. It is determined by dividing the total number of accurately classified instances by the overall number of instances considered [32]. Accuracy serves as an indicator of the percentage of instances correctly classified by the model [24]. The accuracy of our model is formally defined as:

$$\text{Overall Accuracy} = \frac{\sum_{i=1}^N C_{i,i}}{\sum_{i=1}^N \sum_{j=1}^N C_{i,j}} \quad (1)$$

Precision as given in Eq. (2), is the ratio of true positives to the sum of true positives and false positives [33]. In the context of our specific problem statement, this parameter is used to evaluate the model's ability to accurately identify cases where learning styles are effective [24], [34]. It is formally defined as:

$$\text{Precision}_{class} = \frac{TP_{class}}{TP_{class} + FP_{class}} \quad (2)$$

The true negative rate, also known as (Specificity) and defined by Eq. (3), represents the proportion of negative instances correctly identified as negative [35]. On the other hand, the false positive rate denotes the percentage of negative data points that are inaccurately classified as positive, out of the total negative data points.

$$\text{Specificity}_{class} = \frac{TN_{class}}{FP_{class} + TN_{class}} \quad (3)$$

Recall, or Sensitivity, is the true positive rate as specified in Eq. (4). It represents the proportion of positive data points that are accurately identified as positive, among all positive instances [36].

$$\text{Recall}_{class} = \frac{TP_{class}}{TP_{class} + FN_{class}} \quad (4)$$

Sensitivity and specificity, often referred to as quality parameters, play a crucial role in characterizing the accuracy of predicted classes. In the assessment of the learning style diagnostic model, three fundamental parameters are employed to gauge its quality: accuracy, sensitivity, and specificity [37].

F1-Score: is a metric that represents the harmonic mean of accuracy and recall. While it may not be as immediately intuitive as precision, F1-Score serves as a valuable measure for evaluating the accuracy and robustness of the classifier, as highlighted in reference [17].

$$F1 - \text{Score} = \frac{2 * TP_{class}}{2 * TP_{class} + FN_{class} + FP_{class}} \quad (5)$$

D. The Roc and AUC Curve

The Receiver Operating Characteristic (ROC) curve illustrates the relationship between the true positive rate (sensitivity) and the false positive rate (1 - specificity) across different decision thresholds [18]. Meanwhile, the area under the curve (AUC) serves as a measure quantifying how likely the model is to correctly classify a positive random example versus a negative random example, with values ranging from 0 to 1. Essentially, a higher AUC High indicates superior performance distinguishing between learning styles appropriate for each nursing student. The evaluation of learning algorithms in the following section is based on these key metrics, namely accuracy, precision, specificity, recall, and AUC.

IV. RESULTS AND DISCUSSION

A. Analysis of Result

In this study, we evaluated the effectiveness of our ordinal classification model using various classification methods and the confusion matrix. To train our machine learning model to identify learning styles (Observer, Experimenter, Reflective, Active) associated with nursing student success, we incorporated several variables including gender, age, academic background, information on preferred learning strategies, professional experience, educational preferences, social factors and personal commitment, social and community involvement.

This approach allowed us to identify the learning styles associated with nursing student success. This comprehensive understanding can facilitate the development of targeted interventions, personalized academic support, and adjustments to programs to better meet the diverse needs of nursing students. The results shown in Table III derive from the results of these classification algorithms, which were obtained through a 10-fold cross-validation process. Each row of the confusion matrix represents instances of an actual class, while each column represents instances of a predicted class. This matrix provides a comprehensive overview of correct and false predictions, helping to evaluate model performance.

Based on the provided confusion matrix Table III, we can analyze the performance of each classifier (SVM, Decision Tree, Neural Network, and Naive Bayes) in predicting the most appropriate learning approach for nursing students. The confusion matrix shows the counts of true positive, false

positive, true negative, and false negative predictions for each class (learning approach).

- The rows represent the true classes (actual learning approaches).
- The columns represent the predicted classes by each classifier.

TABLE III. THE MULTI-CLASS CONFUSION MATRIX OF THE CLASSIFICATION MODELS USED

| Classifier | Predicted | | | | n = 515 |
|---------------|-----------|-----|-----|----|---------|
| | 1 | 2 | 3 | 4 | |
| SVM | 198 | 0 | 2 | 5 | 1 |
| | 3 | 106 | 3 | 3 | 2 |
| | 4 | 7 | 103 | 4 | 3 |
| | 11 | 8 | 1 | 57 | 4 |
| Decision tree | 193 | 2 | 4 | 6 | 1 |
| | 10 | 97 | 1 | 7 | 2 |
| | 15 | 3 | 97 | 3 | 3 |
| | 8 | 6 | 7 | 56 | 4 |
| ANN | 196 | 2 | 2 | 5 | 1 |
| | 2 | 106 | 2 | 5 | 2 |
| | 3 | 3 | 110 | 2 | 3 |
| | 5 | 3 | 4 | 65 | 4 |
| Naive Bayes | 146 | 19 | 19 | 21 | 1 |
| | 29 | 59 | 10 | 17 | 2 |
| | 9 | 3 | 92 | 14 | 3 |
| | 15 | 7 | 4 | 51 | 4 |

Below is the interpretation of the confusion matrix for each classifier:

1) SVM:

- Observational (1): 198 correct predictions, 3 misclassified as Reflective, 11 misclassified as Active.
- Experiential (2): 106 correct predictions, 3 misclassified as Observational, 103 misclassified as Reflective, 8 misclassified as Active.
- Reflective (3): 110 correct predictions, 2 misclassified as Observational, 3 misclassified as Experiential, 4 misclassified as Active.
- Active (4): 57 correct predictions, 3 misclassified as Observational, 4 misclassified as Experiential, 4 misclassified as Reflective.

2) Decision Tree:

- Observational (1): 193 correct predictions, 10 misclassified as Reflective, 15 misclassified as Active.
- Experiential (2): 97 correct predictions, 1 misclassified as Observational, 97 misclassified as Reflective, 6 misclassified as Active.
- Reflective (3): 97 correct predictions, 7 misclassified as Observational, 3 misclassified as Experiential, 7 misclassified as Active.

- Active (4): 56 correct predictions, 2 misclassified as Observational, 3 misclassified as Experiential, 4 misclassified as Reflective.

3) Neural Network (ANN):

- Observational (1): 196 correct predictions, 2 misclassified as Reflective, 3 misclassified as Active.
- Experiential (2): 106 correct predictions, 2 misclassified as Observational, 110 misclassified as Reflective, 4 misclassified as Active.
- Reflective (3): 110 correct predictions, 2 misclassified as Observational, 3 misclassified as Experiential, 4 misclassified as Active.
- Active (4): 65 correct predictions, 3 misclassified as Observational, 3 misclassified as Experiential, 4 misclassified as Reflective.

4) Naive Bayes:

- Observational (1): 146 correct predictions, 29 misclassified as Experiential, 9 misclassified as Reflective, 15 misclassified as Active.
- Experiential (2): 59 correct predictions, 19 misclassified as Observational, 3 misclassified as Reflective, 7 misclassified as Active.
- Reflective (3): 92 correct predictions, 19 misclassified as Observational, 10 misclassified as Experiential, 4 misclassified as Active.
- Active (4): 51 correct predictions, 1 misclassified as Observational, 2 misclassified as Experiential, 4 misclassified as Reflective.

Based on the results from the confusion matrix, we can make the following observations:

5) SVM performance: SVM performed relatively well across all learning approaches with generally low misclassification rates. It had the highest accuracy for predicting the Experiential learning approach (Class 2) with no misclassifications. However, it had slightly higher misclassification rates for Observational (Class 1) and Reflective (Class 3) approaches compared to other classifiers.

6) Decision tree performance: Decision Tree also performed decently across all learning approaches but had slightly higher misclassification rates compared to SVM. It had the highest accuracy for predicting the Observational learning approach (Class 1) but relatively lower accuracy for the Reflective (Class 3) approach.

7) Neural network performance: Neural Network showed competitive performance similar to SVM, with generally low misclassification rates. It had the highest accuracy for predicting the Reflective learning approach (Class 3) but slightly lower accuracy for the Active (Class 4) approach compared to SVM and Decision Tree.

8) Naive bayes performance: Naive Bayes had mixed performance across learning approaches, with higher

misclassification rates compared to SVM and Neural Network, especially for Observational (Class 1) and Reflective (Class 3) approaches. It had the lowest accuracy for predicting the Observational learning approach (Class 1).

9) Overall observations:

- SVM and Neural Network showed more consistent and competitive performance across all learning approaches compared to Decision Tree and Naive Bayes.
- Experiential learning approach (Class 2) was predicted with high accuracy by all classifiers, indicating it might have distinctive features that are easier to classify.
- Reflective learning approach (Class 3) had varying performance across classifiers, indicating it might be more challenging to classify accurately.

These observations provide insights into the strengths and weaknesses of each classifier in predicting the appropriate learning approach for nursing students, which can be valuable for further refinement of the classification model or selection of the most suitable classifier for this task.

Based on these results, we can further analyze the performance of each classifier in terms of accuracy, precision, recall, and F1-score for each learning approach to determine which classifier performs best for this specific prediction task. These metrics will provide a more comprehensive understanding of each classifier's performance beyond just the confusion matrix.

B. Performance Evaluation

Classification measures were calculated to compare the performance of each machine learning algorithm in predicting the most appropriate learning approach for nursing students. Table IV shows the evaluation of the different machine learning algorithm.

TABLE IV. EVALUATION OF THE DIFFERENT MACHINE LEARNING ALGORITHMS USED

| Model | AUC | CA | F1 | Precision | Recall |
|---------------|-------|-------|-------|-----------|--------|
| SVM | 0.939 | 0.860 | 0.859 | 0.861 | 0.860 |
| Decision tree | 0.978 | 0.901 | 0.900 | 0.901 | 0.901 |
| ANN | 0.985 | 0.926 | 0.926 | 0.926 | 0.926 |
| Naive Bayes | 0.881 | 0.676 | 0.676 | 0.684 | 0.676 |

- Classification Accuracy (CA) measures the overall correctness of the predictions. Neural Network (ANN) has the highest accuracy (92.6%), followed closely by the Decision Tree (90.1%), SVM (86.0%), and Naive Bayes (67.6%).
- F1 Score is the harmonic mean of precision and recall. Neural Network (ANN) and Decision Tree have the highest F1 Scores (92.6% and 90%, respectively).
- Precision is the ratio of true positive predictions to the total predicted positives, while Recall is the ratio of true positive predictions to the total actual positives. Decision Tree, Neural Network (ANN), and SVM have

similar precision and recall values, indicating a good balance between precision and recall.

- Naive Bayes shows the lowest performance in terms of Classification Accuracy, F1 Score, Precision, and Recall among the four models.

In summary, both Neural Network (ANN) and Decision Tree seem to perform well in predicting the most appropriate learning approach for nursing students, based on the provided evaluation metrics. It's essential to consider the specific requirements and goals of the application when choosing the most suitable model.

C. Roc and AUC curve

The machine learning classifiers Artificial Neural and Decision tree, give a level of accuracy greater than 90% for classifying the most appropriate learning approach (observational, experiential, reflective and active) for each nursing student. This indicates that the performance of these classification techniques is excellent for prediction. Based on the ROC curves of the models (see Fig. 4), the artificial neural network model outperformed SVM, Tree and Naive Bayes, in terms of sensitivity and specificity.

Fig. 4 shows the performance evaluation of different classification algorithms to predict the most appropriate learning approach (Observational, Experiential, Reflective, and Active) for each nursing student, in order to improve their academic and professional excellence. Performance is assessed using ROC (Receiver Operating Characteristic) curves, which represent the trade-off between true positive rate (sensitivity) and false positive rate (1-specificity).

The ROC curves are presented for four target values, representing the four learning approaches: Observational, Experient, Reflective, and Active. The curves are labeled as A, B, C, and D, and correspond to the target values 1, 2, 3, and 4, respectively.

The classification algorithms used are SVM, Tree, Neural Network, and Naive Bayes. The performance of each algorithm is compared for each target value. The x-axis shows the False Positive Rate (1 - Specificity), while the y-axis displays the True Positive Rate (Sensitivity).

A good classifier should have a curve closer to the top-left corner, indicating high sensitivity and low false positive rates. Based on the figure, in ROC curve A, the SVM algorithm has a true positive rate of 0.9 and a false positive rate of 0.1 for target value 1 (Observational). Similarly, the Neural Network algorithm has a true positive rate of 0.8 and a false positive rate of 0.2 for target value 2 (Experiential).

Overall, the results show that the classification algorithms have varying levels of performance for different target values, with the Neural Network showing higher sensitivity (true positive rate) in general. However, this model needs more specific numerical values and additional information to improve model efficiency in predicting the most appropriate learning approach (Observational, Experiential, Reflective, and Active) for each nursing student, in order to improve their academic and professional excellence.

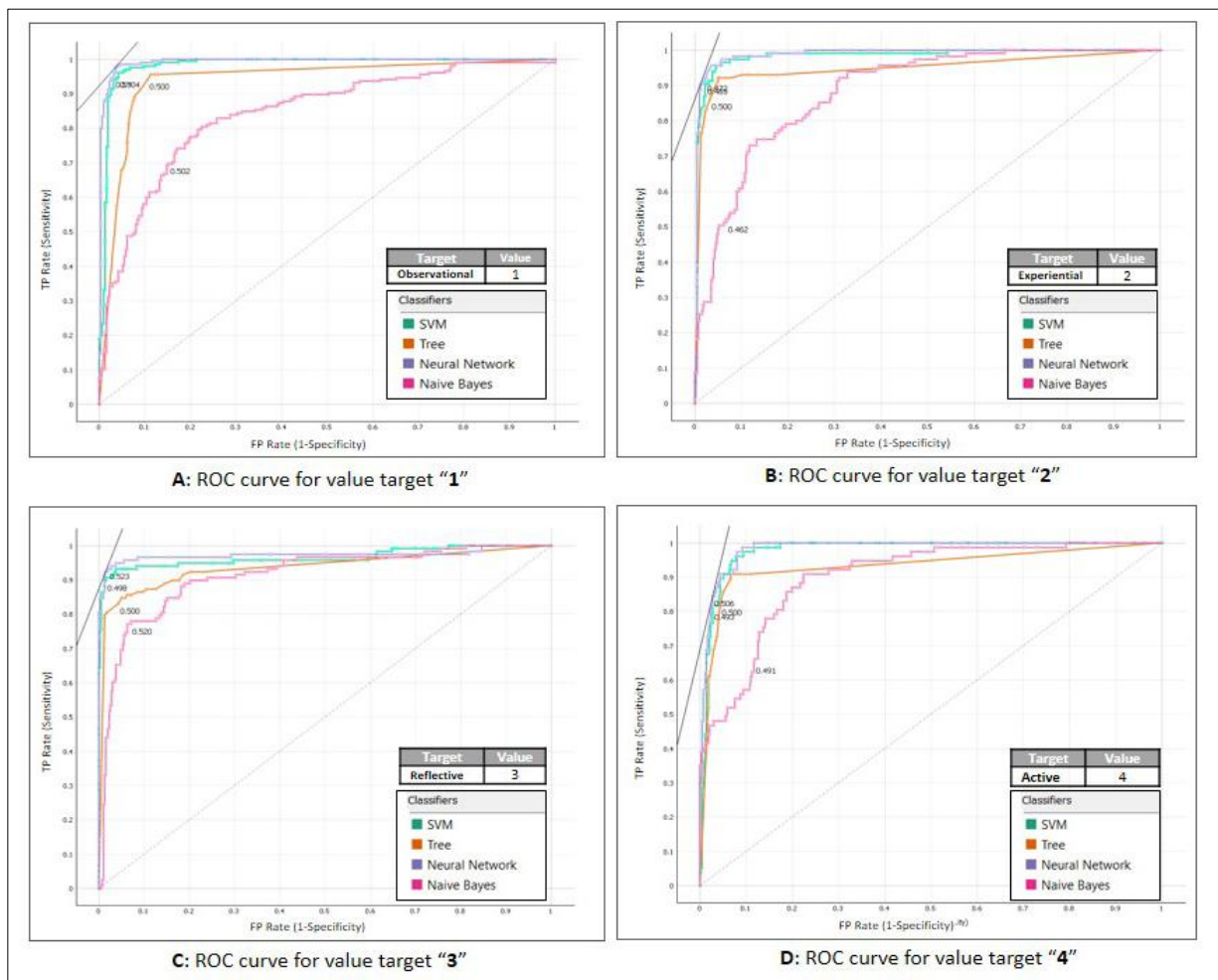


Fig. 1. ROC curve for the four target variables which signify the most appropriate learning approaches for each nursing student.

V. CONCLUSION

In this article, we presented a novel approach to predict the most appropriate learning approach (observational, experiential, reflective, and active) for each nursing student. The proposed multivariate classification model aims to support educators, especially in the field of nursing, by providing them with valuable information to make informed decisions about the appropriate learning styles for each student. This approach has the potential to improve the academic and professional excellence of nursing students, thus contributing to more personalized and effective training in this specific field.

By conducting a comparative study of four multivariate machine learning algorithms, namely SVM, Tree, Neural Network, and Naive Bayes, we determined that Neural Network, Decision tree classifiers are reliable, powerful and efficient algorithms for predicting the most appropriate learning approach (observational, experiential, reflective and active) for each nursing student.

As future directions of our research, we intend to expand our study by incorporating additional parameters including individual student characteristics, academic performance metrics, and contextual factors to further enhance the

predictive accuracy of the model. Additionally, exploring the application of ensemble learning techniques or hybrid models could offer a comprehensive approach to better capture the complexity of learning styles in nursing education.

In conclusion, our findings underscore the potential of Neural Network and Decision Tree classifiers in tailoring learning approaches for nursing students. The ongoing and future research directions aim to refine and extend the model's capabilities, ensuring its applicability in diverse educational settings and providing valuable insights for personalized learning strategies in nursing education.

REFERENCES

- [1] D. Hack-Polay, A. B. Mahmoud, I. Ikafa, M. Rahman, M. Kordowicz, and J. M. Verde, "Steering resilience in nursing practice: Examining the impact of digital innovations and enhanced emotional training on nurse competencies," *Technovation*, vol. 120, p. 102549, Feb. 2023, doi: 10.1016/j.technovation.2022.102549.
- [2] A. Carrero-Planells, S. Pol-Castañeda, M. C. Alamillos-Guardiola, A. Prieto-Alomar, M. Tomás-Sánchez, and C. Moreno-Mulet, "Students and teachers' satisfaction and perspectives on high-fidelity simulation for learning fundamental nursing procedures: A mixed-method study," *Nurse Education Today*, vol. 104, p. 104981, Sep. 2021, doi: 10.1016/j.nedt.2021.104981.
- [3] T. T. Meum, T. B. Koch, H. S. Briseid, G. L. Vabo, and J. Rabben, "Perceptions of digital technology in nursing education: A qualitative

- study,” *Nurse Education in Practice*, vol. 54, p. 103136, Jul. 2021, doi: 10.1016/j.nepr.2021.103136.
- [4] N. Tavares, “The use and impact of game-based learning on the learning experience and knowledge retention of nursing undergraduate students: A systematic literature review,” *Nurse Education Today*, vol. 117, p. 105484, Oct. 2022, doi: 10.1016/j.nedt.2022.105484.
- [5] T. Saastamoinen, M. Härkönen, K. Vehviläinen-Julkunen, and A. Näslindh-Ylispaangar, “Impact of 3D Simulation Game as a Method to Learn Medication Administration Process: Intervention Research for Nursing Students,” *Clinical Simulation in Nursing*, vol. 66, pp. 25–43, May 2022, doi: 10.1016/j.ecns.2022.02.005.
- [6] M. E. Powell, B. Scrooby, and A. Van Graan, “Nurse educators’ use and experiences with high-fidelity simulation in nursing programmes at a South African private higher education institution,” *International Journal of Africa Nursing Sciences*, vol. 13, p. 100227, 2020, doi: 10.1016/j.ijans.2020.100227.
- [7] A. Abouzaid, Mohamed. Taoufik, Ahmed. Moufti, and Abdelhak. Lamsalmi, “Intégration des TICE dans l’enseignement des Sciences de l’Ingénieur dans la filière Sciences Technologies Mécaniques aux lycées du Maroc : Réalité et Obstacles,” *ESJ*, vol. 13, no. 13, p. 476, May 2017, doi: 10.19044/esj.2017.v13n13p476.
- [8] B. Riyami, “Analyse des effets des TIC sur l’enseignement supérieur au Maroc dans un contexte de formation en collaboration avec une université française,” 2018.
- [9] Z. Oulfate, “Enseignement des soft skills aux étudiants infirmiers de l’institut supérieur des professions infirmières et techniques de santé Fès- Maroc,” vol. 4.
- [10] H. G. Mahmoud, “Learning Styles and Learning Approaches of Bachelor Nursing Students and its Relation to Their Achievement,” *IJND*, vol. 09, no. 03, pp. 11–20, Mar. 2019, doi: 10.15520/ijnd.v9i03.2465.
- [11] L. X. Li and S. S. Abdul Rahman, “Students’ learning style detection using tree augmented naive Bayes,” *R. Soc. open sci.*, vol. 5, no. 7, p. 172108, Jul. 2018, doi: 10.1098/rsos.172108.
- [12] A. Saleh, N. Dharshinni, D. Perangin-Angin, F. Azmi, and M. I. Sarif, “Implementation of Recommendation Systems in Determining Learning Strategies Using the Naïve Bayes Classifier Algorithm,” *Sinkron*, vol. 8, no. 1, pp. 256–267, Jan. 2023, doi: 10.33395/sinkron.v8i1.11954.
- [13] A. M. Almarwani and R. Elshatarat, “Understanding Learning Styles in Undergraduate Nursing Programs of the Kingdom of Saudi Arabia: An Integrative Literature Review,” *TONURSJ*, vol. 16, no. 1, p. e187443462209260, Nov. 2022, doi: 10.2174/18744346-v16-e2209260.
- [14] N. AbuAssi and H. Alkorashy, “Relationship between learning style and readiness for self-directed learning among nursing students at king Saud university, Saudi Arabia,” *IJANS*, vol. 5, no. 2, p. 109, Jun. 2016, doi: 10.14419/ijans.v5i2.5993.
- [15] K. Crockett, A. Latham, and N. Whitton, “On predicting learning styles in conversational intelligent tutoring systems using fuzzy decision trees,” *International Journal of Human-Computer Studies*, vol. 97, pp. 98–115, Jan. 2017, doi: 10.1016/j.ijhcs.2016.08.005.
- [16] S. T. Sianturi and U. L. Yuhana, “Student Behaviour Analysis To Detect Learning Styles Using Decision Tree, Naïve Bayes, And K-Nearest Neighbor Method In Moodle Learning Management System,” *JTS*, vol. 33, no. 2, p. 94, Aug. 2022, doi: 10.12962/j20882033.v33i2.13665.
- [17] S. O’Connor, S. Kennedy, Y. Wang, A. Ali, S. Cooke, and R. G. Booth, “Theories informing technology enhanced learning in nursing and midwifery education: A systematic review and typological classification,” *Nurse Education Today*, vol. 118, p. 105518, Nov. 2022, doi: 10.1016/j.nedt.2022.105518.
- [18] M. Ongor and E. C. Uslusoy, “The effect of multimedia-based education in e-learning on nursing students’ academic success and motivation: A randomised controlled study,” *Nurse Education in Practice*, vol. 71, p. 103686, Aug. 2023, doi: 10.1016/j.nepr.2023.103686.
- [19] R. Ordoñez-Avila, N. Salgado Reyes, J. Meza, and S. Ventura, “Data mining techniques for predicting teacher evaluation in higher education: A systematic literature review,” *Heliyon*, vol. 9, no. 3, p. e13939, Mar. 2023, doi: 10.1016/j.heliyon.2023.e13939.
- [20] M. U. Hassan, S. Alaliyat, R. Sarwar, R. Nawaz, and I. A. Hameed, “Leveraging deep learning and big data to enhance computing curriculum for industry-relevant skills: A Norwegian case study,” *Heliyon*, vol. 9, no. 4, p. e15407, Apr. 2023, doi: 10.1016/j.heliyon.2023.e15407.
- [21] Y. Chen, K. Wang, and J. J. Lu, “Feature selection for driving style and skill clustering using naturalistic driving data and driving behavior questionnaire,” *Accident Analysis & Prevention*, vol. 185, p. 107022, Jun. 2023, doi: 10.1016/j.aap.2023.107022.
- [22] A. Sadqui, M. Ertel, H. Sadiki, and S. Amali, “Evaluating Machine Learning Models for Predicting Graduation Timelines in Moroccan Universities,” *IJACSA*, vol. 14, no. 7, 2023, doi: 10.14569/IJACSA.2023.0140734.
- [23] K. Duan, S. S. Keerthi, and A. N. Poo, “Evaluation of simple performance measures for tuning SVM hyperparameters,” *Neurocomputing*, vol. 51, pp. 41–59, Apr. 2003, doi: 10.1016/S0925-2312(02)00601-X.
- [24] E. Merouane, A. Said, and E. F. Nour-eddine, “Prediction of Metastatic Relapse in Breast Cancer using Machine Learning Classifiers,” *IJACSA*, vol. 13, no. 2, 2022, doi: 10.14569/IJACSA.2022.0130222.
- [25] Z. Elouedi, K. Mellouli, and P. Smets, “Belief decision trees: theoretical foundations,” *International Journal of Approximate Reasoning*, vol. 28, no. 2–3, pp. 91–124, Nov. 2001, doi: 10.1016/S0888-613X(01)00045-7.
- [26] G. Nanfack, P. Temple, and B. Frénay, “Learning Customised Decision Trees for Domain-knowledge Constraints,” *Pattern Recognition*, vol. 142, p. 109610, Oct. 2023, doi: 10.1016/j.patcog.2023.109610.
- [27] K. Borhani and R. T. K. Wong, “An artificial neural network for exploring the relationship between learning activities and students’ performance,” *Decision Analytics Journal*, vol. 9, p. 100332, Dec. 2023, doi: 10.1016/j.dajour.2023.100332.
- [28] M. Hall, “A decision tree-based attribute weighting filter for naive Bayes,” *Knowledge-Based Systems*, vol. 20, no. 2, pp. 120–126, Mar. 2007, doi: 10.1016/j.knsys.2006.11.008.
- [29] M. C. Laupichler, A. Aster, J. Schirch, and T. Raupach, “Artificial intelligence literacy in higher and adult education: A scoping literature review,” *Computers and Education: Artificial Intelligence*, vol. 3, p. 100101, 2022, doi: 10.1016/j.caeai.2022.100101.
- [30] N. A. McIntyre, “Accelerating online learning: Machine learning insights into the importance of cumulative experience, independence, and country setting,” *Computers and Education: Artificial Intelligence*, vol. 3, p. 100106, 2022, doi: 10.1016/j.caeai.2022.100106.
- [31] P. Abichandani, C. Iaboni, D. Lobo, and T. Kelly, “Artificial intelligence and computer vision education: Codifying student learning gains and attitudes,” *Computers and Education: Artificial Intelligence*, vol. 5, p. 100159, 2023, doi: 10.1016/j.caeai.2023.100159.
- [32] A. Mengad, J. Dirkaoui, M. Ertel, M. Chakkouch, and F. Elomari, “The Contribution of Numerical EEG Analysis for the Study and Understanding of Addictions with Substances,” *IJACSA*, vol. 14, no. 5, 2023, doi: 10.14569/IJACSA.2023.0140534.
- [33] H. Khosravi et al., “Explainable Artificial Intelligence in education,” *Computers and Education: Artificial Intelligence*, vol. 3, p. 100074, 2022, doi: 10.1016/j.caeai.2022.100074.
- [34] M. Chakkouch, M. Ertel, A. Mengad, and S. Amali, “A Comparative Study of Machine Learning Techniques to Predict Types of Breast Cancer Recurrence,” *IJACSA*, vol. 14, no. 5, 2023, doi: 10.14569/IJACSA.2023.0140531.
- [35] A. Zirar, S. I. Ali, and N. Islam, “Worker and workplace Artificial Intelligence (AI) coexistence: Emerging themes and research agenda,” *Technovation*, vol. 124, p. 102747, Jun. 2023, doi: 10.1016/j.technovation.2023.102747.
- [36] G. Artopoulos, M. I. Maslioukova, C. Zavou, M. Loizou, M. Deligiorgi, and M. Averkiou, “An artificial neural network framework for classifying the style of cypriot hybrid examples of built heritage in 3D,” *Journal of Cultural Heritage*, vol. 63, pp. 135–147, Sep. 2023, doi: 10.1016/j.culher.2023.07.016.
- [37] C. Thomas, K. A. V. Puneeth Sarma, S. Swaroop Gajula, and D. B. Jayagopi, “Automatic prediction of presentation style and student engagement from videos,” *Computers and Education: Artificial Intelligence*, vol. 3, p. 100079, 2022, doi: 10.1016/j.caeai.2022.100079.

Automated Weeding Systems for Weed Detection and Removal in Garlic / Ginger Fields

Tsubasa Nakabayashi, Kohei Yamagishi, Tsuyoshi Suzuki
Tokyo Denki University, Graduate School of Engineering, Tokyo, Japan

Abstract—The global agriculture industry has faced various problems, such as rapid population growth and climate change. Among several countries, Japan has a declining agricultural workforce. To solve this problem, the Japanese government aims to realize “Smart agriculture” that applies information and communication technology, artificial intelligence, and robotics. Smart agriculture requires the development of robot technology to perform weeding and other labor-intensive agricultural tasks. Robotic weeding consists of an object detection method using machine learning to classify weeds and crops and an autonomous weeding system using robot hands and lasers. However, the approach used for these methods changes depending on the crop growth. The weeding system must consider the combination according to crop growth. This study addresses weed detection and autonomous weeding in crop-weed mixed ridges, such as garlic and ginger fields. We first develop a weed detection method using Mask R-CNN, which can detect individual weeds by instance segmentation from color images captured by an RGB-D camera. The proposed system can obtain weed coordinates in physical space based on the detected weed region and the depth image captured by the camera. Subsequently, we propose an approach to guide the weeding manipulator toward the detected weed coordinates. This paper integrates weed detection and autonomous weeding through these two proposed methods. We evaluate the performance of the Mask R-CNN trained on images taken in an actual field and demonstrate that the proposed autonomous weeding system works on a reproduced ridge with artificial weeds similar to garlic and weed leaves.

Keywords—Weed detection; weeding; mask R-CNN; agriculture robot

I. INTRODUCTION

According to the 2022 report on new farm employment by the Ministry of Agriculture, Forestry, and Fisheries of Japan [1], not only has the number of new farmers been declining for the past few years, but also the ratio of people aged 49 or younger has been declining among new farmers, reflecting the shortage of workers in the agricultural sector as a whole. In addition, the world’s population is expected to reach approximately 9.1 billion by the end of 2050, and food demand is expected to increase by 70% from the current level. India is expected to be the most populous country by 2050, but even today it is already unable to meet its domestic food production needs [2]. Against this background, there is a growing interest in the widespread adoption of smart agriculture, which uses artificial intelligence, internet of things, and robots, with particular attention focused on the use of autonomous agricultural robots to replace human agricultural workers [3].

In agriculture, weeding is important in maintaining the growth and quality of crop plants. Normally, the crop plants grown in farmlands compete with plants that naturally propagate in the same area (hereafter referred to as “weeds”). To safely prioritize the growth of crop plants over weeds, it is necessary to carry out multiple weeding operations to remove the weeds before harvest [4]. However, as weeding is physically demanding, various researches on automated weeding using robots is being pursued. Ghazali et al. proposed the machine vision system for automatic weeding strategy [5]. They compared several image processing methods, and studied suitable one for weed detection. Mary et al. proposed a weeding robot for crop and weed discrimination using Convolution neural network (CNN) [6]. Ya et al. developed a weeding robot and its path planning method [7]. Yasuda et al. proposed a sweeping weeding method using brush rollers [8]. Sweeping weeding is effective when crops are planted in regular rows. However, when crops are planted irregularly, the sweeping method may damage the crops, weeding by manipulators is effective [6]. This paper studies an automated weeding system using manipulators for irregularly planted crops in the field. Various automated-weeding methods exist, but the primary tasks in weeding include: (1) the detection of the weeds to be removed and (2) guiding the weeding mechanism to those weeds [9]. As weeds and weeding periods differ depending on several factors, such as the type of crop plant, cultivation method, and environmental conditions, general-purpose weed detection is difficult [10].

Many existing studies on smart agriculture that focused on differentiating crop plants and weeds have confirmed the usefulness of convolutional neural networks (CNNs) and you only look once (YOLO) [11] [12] [13]. Narayana et al. used YOLOv7, which is capable of high-speed object detection, to detect and classify weeds into multiple weed types based on their shapes using images of weeds for training [14]. However, if the weeds and crop plants are similar in appearance, there is a possibility that crop plants may be mistakenly detected as weeds. Elnemr [15] developed a weed-detection system based on a deep convolutional neural network (DCNN) using a dataset comprising weeds in the early stage of germination. This study successfully detected weeds in the early stages of germination, demonstrating that they could be weeded before they inhibit crop plant growth.

The environment in which both weeds and crop plants grow is called a “ridge,” which is a row of earth raised into a mound for planting. For the weeding task, it is important to construct and use a dataset with images of both crop plants and weeds so that crop plants can be excluded from weeding

based on their features. Most studies on weed detection for weeding focus on evaluating the detection accuracy and ignore the actual application to the task of weeding [16] [17].

With the goal of automating the weeding process, this study proposes a weed-detection and removal method that uses images obtained from a real environment for detection and robot arms to remove the detected weeds; the real environments is an open outdoor field where garlic and ginger leaves are cultivated. We propose a system that not only evaluates the detection accuracy based on a training dataset, but also investigates the impact of the weeding task and removal control after the weeds are detected. By proposing an actual weeding system, the study contributes to the construction of automated systems for weeding tasks.

The remainder of this paper is organized as follows. In Section II, we construct a dataset necessary for weeding tasks and propose a weed-detection method using the dataset. We also propose a method for weed removal using this weed-detection method. In Section III, we report on experiments to verify the function of our proposed weeding system. In Section IV, we summarize this study and discuss the future prospects.

II. CONSTRUCTION OF THE WEEDING SYSTEM

A. Prerequisites

This study targeted an open cultivation field, as depicted in Fig. 1, where crop plants are not lined up in rows. In such fields, the crop plants such as garlic and ginger having long leaves and stems grow vertically upward out of the ridge. If weeds grow among the crop plants, they will negatively impact the growth of the crop plants. Therefore, weeding must be performed multiple times as the crop grows. When the crop grows taller than the weeds, the influence of weeds on the growth of the crop reduces; thus, the weeding rate of the entire field can be lower than 100%.



Fig. 1. Assumed environment.

Previous studies have proposed a mowing robot for weed removal and a weeding robot that tows a rake-like tool through crop fields [18] [19]. The weeding robot in the current study detects the individual plants to be weeded and then guides the manipulator or a similar tool to the weeding point to avoid damage to the crop plants. To achieve this, the robot uses a system that moves along the ridge, captures the conditions of the ridge underneath the robot using a camera, and then uses robot arms to remove the weeds, as illustrated in Fig. 2.

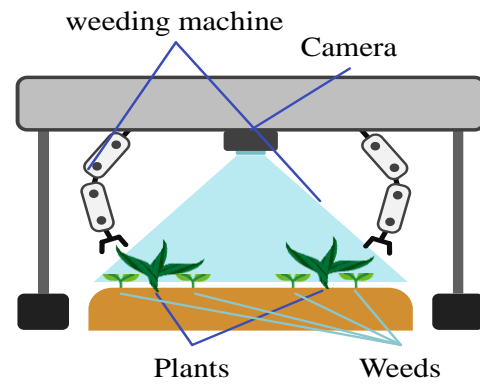


Fig. 2. Overview of weeding robot.

B. Proposed Method

The approach in this study is as follows. An RGB-D camera first detects weeds based on color images and calculates their spatial coordinates based on depth images. Thereafter, the robot arms are guided to the detected weeds.

In the field where our target crop plants are grown, the weeds growing among the crop plants include plants with a variety of leaf shapes and growth patterns, including henbit deadnettle (*Lamium amplexicaule*) and annual meadow-grass (*Poa annua*). To detect individual weeds, we used Mask R-CNN with instance segmentation, a machine learning algorithm [20] that allows the detection of individual weeds in plant clusters. The VGG (Visual Geometry Group) Image Annotator was used to create the training data. The machine learning model was trained using 500 images taken from a real field [21].

Next, we calculated the physical space coordinates—the target coordinates for the weeding mechanism—based on the weed-detection images. As the center of gravity with respect to the weed-detection area is as close as possible to the root of the weed, it is therefore necessary to guide the weeding mechanism to this spot [22]. Three-dimensional spatial coordinates were then calculated for these camera coordinates based on the depth image and camera parameters.

Finally, after converting the target coordinates from the coordinate system on the RGB-D camera described above to the coordinate system of the manipulator, the position of the end effector that grips the weed was guided to the coordinates of the root of the weed as follows:

- 1) The robot arm was moved so that the horizontal plane coordinates of the end effector aligned with the target coordinates.
- 2) Based on the depth information obtained by the RGB-D camera, the end effector was lowered to the weed surface.
- 3) To remove the weed, it was grasped by the end effector and pulled up.
- 4) The manipulator was moved to its home position and the gripped weed was released.

III. VERIFICATION OF THE WEEDING SYSTEM FUNCTIONS

A. Evaluation of Detection Accuracy by Annotation Shape

The training parameters are shown in Table I. The PC used for training was configured as shown in Table II, and the training was performed using detectron2 provided by META. Training time required to build the machine learning model using 500 images on this PC was approximately fifteen minutes. Object detection using Mask R-CNN depends on the accuracy with which the annotation task is performed. Therefore, we trained the detection model on two types of weed datasets: rectangular (in which the weeds were annotated as rectangles) and polygonal (in which the weeds were annotated as polygons), and their detection accuracies were compared. As target-coordinate detection for weed removal is important in this study, we counted the number of annotation labels in which the center of gravity of the detected weed is contained in the weed area in 20 test images. The results are shown in Table III. Fig. 3 shows examples of weed detection using each annotation shape, and Fig. 4 shows examples of the weed centers of gravity.

TABLE I. THE TRAINING PARAMETERS

| | |
|---------------|--------|
| Batch size | 128 |
| Iterations | 1000 |
| Learning Rate | 0.0003 |

TABLE II. THE PC CONFIGURATION USED FOR TRAINING

| | |
|---------------|---------------------|
| CPU | Intel Core i5 |
| GPU | Geforce RTX3050Ti |
| OS | Ubuntu 18.04 |
| Training Time | 15 min / 500 images |

TABLE III. COMPARISON OF RESULTS BY ANNOTATION SHAPE

| Annotation | Total weeds | Total detections | Total off the top of weeds | Accuracy |
|------------|-------------|------------------|----------------------------|----------|
| Rectangle | 214 | 199 | 8 | 0.851 |
| Polygon | 214 | 278 | 5 | 0.852 |



(b) Polygon result.

Fig. 3. Comparison of results by annotation method.



(a) Rectangle.



(b) Polygon.

Fig. 4. Results of each weeding-point drawing.



(a) Rectangle result.

Fig. 4 shows that the center of gravity is positioned on the top of the weed for both the rectangle and polygon annotation shapes. However, when we compared the results on the same 50 test images, we found that the total number of detections was higher in the system trained on polygonal annotations. The fact that the training results were more accurate for

polygon annotation suggests that the polygonal annotation was more effective for training the weed detector of the weeding robot.

B. Experiment to Calculate Spatial Coordinates for Weeding

The accuracy of spatial coordinates is important to properly guide the weeding mechanism to the target weeds. Therefore, in an experiment, we placed artificial flowers on a sheet of imitation Japanese vellum to confirm whether the coordinates obtained using our weed-detection method and coordinate transformation were appropriate. The RGB-D camera used in this experiment was the Intel RealSense D435i.

In the experiment, we arranged the artificial flowers as “weeds” on a square paper as shown in Fig. 5 such that three “weeds” of different sizes were in the field of view of the camera, and then verified the accuracy of the two-dimensional coordinates after object detection by comparing them with actual measured values. The weed sizes and labels from right to left are—large (Weed 1), medium (Weed 2), and small (Weed 3).

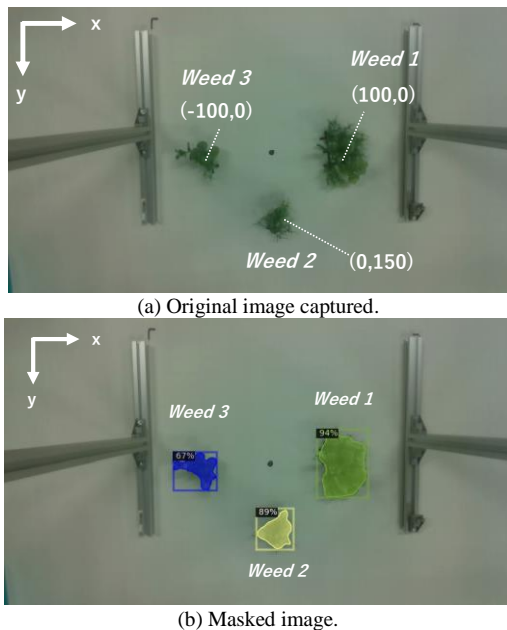


Fig. 5. Results of weed-location detection experiment.

Table IV shows the coordinates where the weeds were placed, Table V shows the calculated coordinates, and Table VI shows the difference between the results in Table IV and Table V. It was confirmed that there was a maximum difference of 30.0 mm in the x-direction. Weed 3, which was the smallest, had a difference of 8.30 mm, while Weed 1 and Weed 2 had a difference of 30.0 mm. This is probably because as the size of the detection target increases, the center of gravity of the generated mask region moves away from the center of the weed. However, even with a maximum error of 30.0 mm, the weeding point was within the weed-detection area, thus the results of this experiment were considered acceptable. In future, we plan to confirm the effectiveness of

our approach when performing manipulation control in actual fields.

TABLE IV. THEORETICAL VALUES OF TWO-DIMENSIONAL COORDINATES

| Index | Actual Arrangement | |
|--------|--------------------|--------|
| | X [mm] | Y [mm] |
| Weed 1 | 100 | 0 |
| Weed 2 | 0 | -100 |
| Weed 3 | -100 | 0 |

TABLE V. MEASURED VALUES OF TWO-DIMENSIONAL COORDINATES

| Index | Measurements | |
|--------|--------------|--------|
| | X [mm] | Y [mm] |
| Weed 1 | 130 | 1.48 |
| Weed 2 | 30.0 | -108.2 |
| Weed 3 | -91.7 | 6.98 |

C. Manipulation Control Experiment

Further, we confirmed the ability of the system to guide the robot arms to the weeds based on the proposed method. In this experiment, we conducted an evaluation in an artificial environment in which soil was placed in a shallow tray, and artificial flowers were placed on top of the soil as weeds. The manipulation control was performed using the spatial coordinates of the weeds obtained by the weed detection and coordinate transformation evaluated above. The manipulator used in this experiment was a Dobot Magician, a tabletop 4-axis manipulator manufactured by Dobot Robotics. Fig. 6 shows the experimental setup. The control flow implemented for the manipulation is shown in Fig. 7.

TABLE VI. ERROR BETWEEN THEORETICAL AND MEASURED VALUES

| Index | Error | |
|--------|--------|--------|
| | X [mm] | Y [mm] |
| Weed 1 | 30.0 | -1.48 |
| Weed 2 | 30.0 | -8.20 |
| Weed 3 | 8.30 | 6.98 |



Fig. 6. Experimental environment.

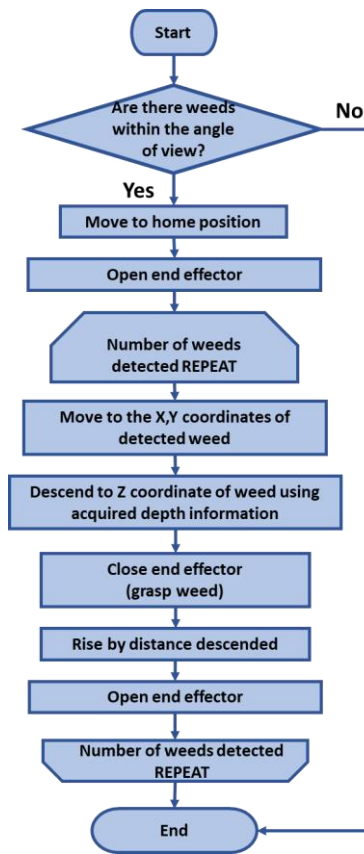


Fig. 7. Flowchart of manipulation control.

We calculated the three-dimensional coordinates as described in the previous section. The calculated three-dimensional coordinates are shown in Table VII.

We assigned the weed numbers, starting with Weed 1 in the lower right corner. An example of the original captured

image is shown in Fig. 8(a) and the same image with the corresponding masked areas that were generated as shown in Fig. 8(b). The manipulation control was applied to the three coordinates shown in Table VII, and all the three weeds were successfully grasped. Fig. 9 shows an example of the weeding process using the proposed weeding system.

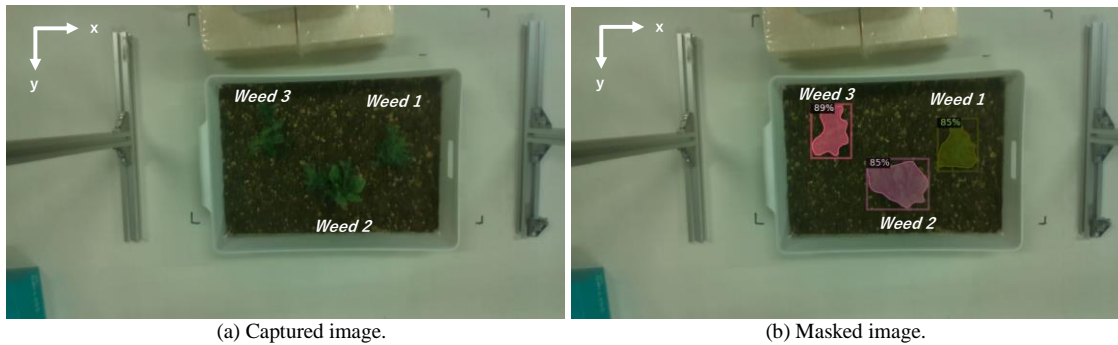


Fig. 8. Experimental results in a simple field

TABLE VII. THREE-DIMENSIONAL COORDINATES

| Index | Actual Arrangement | | |
|--------|--------------------|--------|--------|
| | X [mm] | Y [mm] | Z [mm] |
| Weed 1 | -24.8 | -49.2 | 562.0 |
| Weed 2 | 69.9 | 22.8 | 564.9 |
| Weed 3 | 151.8 | 24.1 | 558.0 |



Fig. 9. Weeding Scene. (a) Initially, the robot arm is in the home position. (b) The end-effector is moved by the robot arm so that its horizontal plane coordinates match the target coordinates. (c) Based on depth information, the end-effector is lowered to the surface of the weed. (d) The end-effector grasps the weed. (e) The robot arm moves and pulls the weed out with the end-effector. (f) After releasing the grasped weed, the robot arm moves to the home position.

D. Discussion

From the above functional verification, the following results were obtained for the weeding system functions.

- The polygonal annotation was more effective than rectangular annotation for training the weed detector of the weeding robot.
- The center-of-gravity position was within an acceptable range for the maximum error in the weeding position calculation.
- The manipulation control was applied to the calculated three-dimensional coordinates of weeding points, and the weeds were successfully grasped.



Fig. 10. Example of weeds that are difficult to detect center-of-gravity position.

By setting the manipulation control point at the center of gravity of the segmentation mask, rather than at the center of the bounty box, the weeds could be approached correctly in

many cases. However, depending on the shape of the weeds, as shown in Fig. 10, weeding could not be performed correctly. We believe that the construction of a network to predict weed roots after weed detection is one of an important issue to be addressed in the future.

IV. CONCLUSION

We believe that smart agriculture is an effective way to address the labor challenges facing the agricultural sector of Japan. Focusing on the weeding task, which is one of the most burdensome agricultural tasks because it must be done multiple times before harvesting, we investigated weed detection and removal to implement an automatic weeding robot.

To realize the automatic weeding robot, we built a series of functions—including weed detection using Mask R-CNN, calculation of the three-dimensional coordinates of detected weeds, and manipulation control to the detected coordinates—and confirmed the effectiveness of these functions through operational verification.

In future work, we plan to experimentally verify these functions in an actual field. In addition, as it is necessary to distinguish between crop plants and weeds more accurately in actual operation, we also plan to study ways to improve detection accuracy, for example, by enlarging the dataset and investigating other training techniques. Moreover, since not only a single robot but also a multi-robot system with multiple robots is effective for actual operation in the field [23], a multi-robot system version of the system in this paper will also be considered.

ACKNOWLEDGMENT

This work was supported by a grant from "Development of Weeding Robot with Autonomous Navigation Capability for Agricultural Fields" in collaboration with KOGANEI CORPORATION. We are grateful to project members for useful discussion. We would like to thank Editage (www.editage.com) for English language editing.

REFERENCES

- [1] Compiled from "2022 New Farm Employment Survey Results" (Ministry of Agriculture, Forestry and Fisheries of Japan) (https://www.maff.go.jp/tokei/kekka_gaiyou/sinki/r4/index.html)(2023) [in Japanese]
- [2] Abhinav Sharma, Arpit Jain, Prateek Gupta and Vinay Chowdary, "Machine Learning Applications for Precision Agriculture: A Comprehensive Review," in *IEEE Access*, vol. 9, pp. 4843–4873, 2021, <https://doi.org/10.1109/ACCESS.2020.3048415> (2023).
- [3] Sumito Yasuoka, "Promoting Smart Agriculture," *Journal of the Robotics Society of Japan*, vol. 35, No.5, pp. 362–365, 2017 [in Japanese]
- [4] Tetsuo Shioya, "Considering Weed Management in Agricultural Research," *Agricultural Research*, vol. 52, No. 2, pp. 83–86, 2017 [in Japanese]
- [5] Kamarul Hawari Ghazali, Mohd Marzuki Mustafa, and Aini Hussain. "Machine vision system for automatic weeding strategy using image processing technique," *American-Eurasian Journal of Agricultural & Environmental Science* 3, pp. 451–458, 2008.
- [6] M. Florance Mary, D. Yogaraman. "Neural network based weeding robot for crop and weed discrimination," *Journal of Physics: Conference Series*. vol. 1979. no. 1. IOP Publishing, 2021.
- [7] Xiong Ya, Ge Yuanyue, "Development of a prototype robot and fast path-planning algorithm for static laser weeding," *Computers and Electronics in Agriculture*, vol. 142, pp. 494–503, 2017.
- [8] Kentaro Yasuda, Fumiaki Takashina, Yoshihiro Kaneda, and Atsuo Imai, "Weeding ability of brush roller-type paddy field weeding robot and its effect on paddy rice growth" *Weed Research*, vol. 62, no. 3, pp. 139–148, 2017 [in Japanese]
- [9] Gustavo José Querino Vasconcelos, Gabriel Schubert Ruiz Costa, Thiago Vallin Spina, and Helio Pedrini, "Low-Cost Robot for Agricultural Image Data Acquisition," *Agriculture*, vol.13, 413, 2023, <https://doi.org/10.3390/agriculture13020413>.
- [10] Konstantinos G. Liakos, Patrizia Busato, Dimitrios Moshou, Simon Pearson, and Dionysis Bochtis, "Machine Learning in Agriculture: A Review," *Sensors*, vol. 18, 2674, 2018.
- [11] Saleem, Muhammad Hammad, Johan Potgieter, and Khalid Mahmood Arif, "Weed Detection by Faster RCNN Model: An Enhanced Anchor Box Approach," *Agronomy*, vol. 12, 1580, 2022, <https://doi.org/10.3390/agronomy12071580> (2023).
- [12] Vi Nguyen Thanh Le, Giang Truong, and Kamal Alameh, "Detecting weeds from crops under complex field environments based on Faster RCNN," 2020 IEEE Eighth International Conference on Communications and Electronics (ICCE), Phu Quoc Island, Vietnam, pp. 350–355, 2021, <https://doi.org/10.1109/ICCE48956.2021.9352073> (2023).
- [13] Fengying Dang, Dong Chen, Yuzhen Lu and Zhaojian Li, "YOLOWeeds: A novel benchmark of YOLO object detectors for multi-class weed detection in cotton production systems," *Computers and Electronics in Agriculture*, vol. 205, 107655, ISSN 0168-1699, 2023.
- [14] Lakshmi Narayana, "An Efficient Real-Time Weed Detection Technique using YOLOv7," *International Journal of Advanced Computer Science and Applications*, vol. 14, no. 2, 2023.
- [15] Heba A. Elnemr, "Convolutional Neural Network Architecture for Plant Seedling Classification," *International Journal of Advanced Computer Science and Applications (IJACSA)*, vol. 10 Issue 8, 2019.
- [16] Mingyang Qi, Gao Haozhang, Wang Tete, Du Baoxia, Li Han, Zhong Wenyu, Tang You, "Method for Segmentation of Bean Crop and Weeds Based on Improved UperNet," in *IEEE Access*, vol. 11, pp. 143804–143814, 2023, <https://doi.org/10.1109/ACCESS.2023.3344520> (2023).
- [17] Rekha Raja, Thuy T. Nguyen, David C. Slaughter and Steven A. Fennimore, "Real-time weed-crop classification and localisation technique for robotic weed control in lettuce," *Biosystems Engineering*, vol. 192, pp. 257–274, ISSN 1537-5110, 2022, <https://doi.org/10.1016/j.biosystemseng.2020.02.002> (2023).
- [18] Xirui Zhang and Ying Chen, "Soil disturbance and cutting forces of four different sweeps for mechanical weeding," *Soil and Tillage Research*, vo. 168, pp. 167–175, 2017, ISSN0167-1987. <https://doi.org/10.1016/j.still.2017.01.002> (2023).
- [19] Hiroto Kayama, Hitoshi Sori, Hiroyuki Inoue, Taishi Sugimoto, Hiroyuki Hatta, and Yasuhiro Ando, "Basic study of rice seedling detection using LiDAR in a paddy field weeding robot," *Proceedings of the National Conference of the Society of Industrial and Applied Engineers*, 2022, vol. 2022, pp. 7–8, published 2022/10/01, Online ISSN 2424-211X, <https://doi.org/10.12792/iaie2022.006> (2023) [in Japanese]
- [20] Kaiming He, Georgia Gkioxari, Piotr Dollar, and Ross Girshick, "Mask r-cnn," In: *Proceedings of the IEEE international conference on computer vision*, pp. 2961–2969, 2017.
- [21] Tsubasa Nakabayashi, Kohei Yamagishi, Tsuyoshi Suzuki, Shuhei Saito, Kei Sakai, and Kazumi Makita, "Optimization and implementation of weed detection in garlic fields using Mask R-CNN," *Robotics and Mechatronics Conference Abstracts*, vol. 2022, Session ID 1A1-C05, pp. 1A1-C05-, published 2022/12/25, Online ISSN 2424-3124, <https://doi.org/10.1299/jsmrmd.2022.1A1-C05> (2022) [in Japanese]
- [22] Champ Julien, Adan Mora-Fallas, Hervé Goëau, Erick Mata-Montero, Pierre Bonnet, and Alexis Joly. "Instance segmentation for the fine detection of crop and weed plants by precision agricultural robots," *Applications in Plant Sciences*, vol. 8, 2022.
- [23] W. McAllister, D. Osipychev, G. Chowdhary and A. Davis, "Multi-Agent Planning for Coordinated Robotic Weed Killing," *IEEE/RSJ International Conference on Intelligent Robots and Systems (IROS)*, Madrid, Spain, pp. 7955–7960, 2018, <https://doi.org/10.1109/IROS.2018.8593429> (2023).

Enhancing Building Energy Efficiency: A Hybrid Meta-Heuristic Approach for Cooling Load Prediction

Chenguang Wang^{1*}, Yanjie Zhou², Libin Deng³, Ping Xiong⁴, Jiarui Zhang⁵, Jiamin Deng⁶, Zili Lei⁷
School of Municipal and Geomatics Engineering, Hunan City University, Yiyang, Hunan, 413000, China^{1, 5, 6, 7}
Heshan District Garden Landscaping Co., Ltd., Yiyang, Hunan, 413000, China²
Hunan Construction Investment Group Co., Ltd., Changsha, Hunan, 410004, China³
School of Mechanical and Electrical Engineering, Hunan City University, Yiyang, Hunan, 413000, China⁴

Abstract—The research tackles the complex problem of accurately predicting cooling loads in the context of energy efficiency and building management. It presents a novel approach that increases the precision of cooling load forecasts by utilizing machine learning (ML). The main objective is to incorporate a hybridization strategy into Radial Basis Function (RBF) models, a commonly used method for cooling load prediction, to improve their effectiveness. This new method significantly increases accuracy and reliability. The resulting hybrid models, which combine two powerful optimization techniques, outperform the state-of-the-art approaches and mark a major advancement in predictive modelling. The study performs in-depth analyses to compare standalone and hybrid model configurations, guaranteeing an unbiased and thorough performance evaluation. The deliberate choice of incorporating the Self-adaptive Bonobo Optimizer (SABO) and Differential Squirrel Search Algorithm (DSSA) underscores the significance of leveraging the distinctive strengths of each optimizer. The study delves into three variations of the RBF model: RBF, RBDS, and RRBSA. Among these, the RBF model, integrating the SABO optimizer (RBSA), distinguishes itself with an impressive R^2 value of 0.995, denoting an exceptionally close alignment with the data. Furthermore, a low Root Mean Square Error (RMSE) value of 0.700 underscores the model's remarkable precision. The research showcases the effectiveness of fusing ML techniques in the RBSA model for precise cooling load predictions. This hybrid model furnishes more dependable insights for energy conservation and sustainable building operations, thereby contributing to a more environmentally conscious and sustainable future.

Keywords—Building energy; cooling load; machine learning; radial basis function; self-adaptive bonobo optimizer; differential squirrel search algorithm

I. INTRODUCTION

In the contemporary discourse surrounding global energy challenges, there exists an escalating emphasis on imperative energy conservation measures. This urgency is particularly salient within the purview of the global building sector, constituting a substantial fraction of overall energy consumption. Within this context, the imperative to optimize energy efficiency has prompted a meticulous examination of key metrics, where Cooling Load (CL) and Dynamic Air-Conditioning Load assume pivotal roles in the paradigm of

building design and operation [1], [2]. Of particular significance is the latter, as it intricately interfaces with the orchestration of heating, ventilation, and air conditioning (HVAC) systems, endowing a spectrum of advantages including expeditious cooling startups, precise management of peak demand, cost optimization, and heightened energy efficiency within cooling storage systems [3]. The Dynamic Air-Conditioning Load, as a multifaceted entity, stands as the linchpin for realizing energy and cost efficiency objectives across a diverse array of HVAC systems. It functions as a discerning orchestrator, facilitating seamless coordination and adjustment of HVAC operations in response to the dynamically evolving thermal requisites of a given structure [4]. This adaptability becomes instrumental in meeting the heterogeneous and evolving demands posed by residential, commercial, and industrial structures alike. Nevertheless, the realization of these efficiency goals is not bereft of challenges. The accurate prediction of building cooling loads remains a formidable task, characterized by the intricate interplay between the optical and thermal properties of the building and meteorological data [5]. The integration of these factors into the cooling load prediction process engenders a complex network that necessitates innovative solutions. The scientific pursuit of building cooling load prediction has endured for several years, embodying an enduring commitment to surmounting these challenges [6].

In the quest for precision, diverse methodological avenues have been explored. Engineering-based feature extraction techniques have surfaced as a valuable approach, probing into the intrinsic thermal properties of diverse building materials. By eliciting domain-specific insights from data, these techniques shed light on the nuanced ways in which distinct materials exert influence on the cooling load [7]. From concrete to glass, each material introduces a unique set of thermal dynamics that contributes to the overall cooling load profile. These insights not only enrich the comprehension of thermal intricacies but also facilitate the development of tailored solutions for augmented energy efficiency. Beyond engineering-based techniques, statistical feature extraction methods have assumed an integral role in the predictive arsenal. Employing mathematical approaches, these methods unearth pertinent information from the data, revealing patterns and relationships that may elude conventional scrutiny [8].

This data-driven approach affords a comprehensive exploration of the intricate factors influencing cooling loads, offering a holistic perspective that transcends traditional analytical confines. Advancing the pursuit of precision, structural feature extraction methods have evolved to scrutinize the underlying data structure itself. These methods endeavour to uncover latent dependencies and patterns that might elude conventional analyses. By delving into the depths of data intricacies, structural feature extraction unveils critical insights that can significantly enhance the precision of cooling load predictions [9].

A multitude of techniques has been devised for optimizing HVAC systems, which can be broadly classified into three categories: artificial intelligence (AI), simulation, and regression analysis. Simulation tools like DOE-2, ESP-r [10], TRNSYS [11], EnergyPlus and ACO [12] are used to estimate CL when complete building data is accessible. Accurately measuring different building parameters, however, presents practical challenges [13]. There are different ways to simplify the process of building models, but it still takes a lot of time and labour to complete. Furthermore, the accuracy of simulated load results depends on the model's precision and the quality of the weather data. In real-time applications like online prediction or optimal operational control, the usefulness of simulation software is constrained [14].

Against this backdrop, recent scholarship has spotlighted the substantial potential of cutting-edge Machine Learning (ML) techniques in transforming the landscape of cooling load predictions [15]. ML, with its adeptness in discerning complex patterns and adapting to evolving data dynamics, emerges as a potent ally in the pursuit of precision and efficiency. The infusion of ML not only refines extant models but also engenders novel approaches capable of navigating the intricate terrain of cooling load prediction with unprecedented precision. Concurrently, feature extraction methods have risen to prominence as indispensable tools within the ML-driven paradigm [16], [17]. These methods assume a pivotal role in harnessing historical data, ensuring that predictions remain not only precise but also computationally manageable. As the volume and intricacy of data burgeon, the symbiosis between ML techniques and feature extraction methods becomes increasingly critical, providing a robust framework to address the evolving challenges of building cooling load prediction [18]. Envisaging the trajectory ahead, these technological strides hold promise in ushering forth a new era of sustainability and energy efficiency in buildings. The amalgamation of ML techniques and feature extraction methods is poised not merely to refine predictive accuracy but also to lay the groundwork for more intelligent and adaptive HVAC systems. By bridging the lacuna between data insights and operational efficiency, these advancements contribute to a future where sustainable practices are not merely aspirational but intrinsic characteristics of contemporary infrastructure [19].

The study introduces a new method for improving cooling load predictions by integrating ML. It uses a hybridization technique to enhance the performance of Radial Basis Function (RBF) models, ensuring greater accuracy and reliability. The hybrid models, which combine two optimization techniques, show superior performance compared to conventional methods. A thorough evaluation was conducted to mitigate potential biases and provide a transparent assessment of the models' performance. The strategic choice of merging Self-adaptive Bonobo Optimizer (SABO) and Differential Squirrel Search Algorithm (DSSA) highlights the importance of each optimizer's strengths. This study demonstrates the effectiveness of ML and the benefits of using tailored hybrid models for improved cooling load predictions. The following section includes the methodology section, which details the study's approach, covering data collection, preprocessing, model development (including machine learning integration), and validation. Results present findings, including performance compared to existing methods, with quantitative data and visualizations. Discussion interprets results within the study's context, evaluating methodology strengths and limitations. The conclusion summarizes key findings, emphasizes research significance, and suggests future research directions.

II. MATERIALS AND METHODS

A. Data Gathering

Table I provides a comprehensive overview of the statistical properties of the input variables contributing to the cooling load prediction models, as well as the resultant cooling load output. The variables under scrutiny encompass a range of crucial factors influencing building energy dynamics. The Relative Compactness category, denoting the building's surface area-to-volume ratio, exhibits a minimum value of 0.62 and a maximum value of 0.98. The average and standard deviation are reported as 0.76 and 0.105, respectively. Surface area, a pivotal input parameter, ranges from 514.5 to 808.5, with an average of 671.70 and a standard deviation of 88.086. Wall area, roof area, overall height, orientation, glazing area, and glazing area distribution, each with distinct roles in the prediction models, are similarly characterized by their minimum, maximum, average, and standard deviation values. Of particular significance is the Cooling output variable, which represents the anticipated cooling load. The reported statistics for this variable delineate its minimum, maximum, average, and standard deviation as 10.9, 48.03, 24.58, and 9.513, respectively. These values encapsulate the variability in cooling loads expected from the developed prediction models. The statistical summary provides insights into the range and central tendency of each input variable and the variability in cooling load output, which is crucial for understanding data distribution and ensuring the accuracy and reliability of cooling load predictions generated by developed models [20], [21].

TABLE I. STATISTICAL PROPERTIES OF THE INPUT VARIABLE OF COOLING

| Variables | Indicators | | | | |
|---------------------------|------------|--------|-------|---------|----------|
| | Category | Min | Max | Avg | St. Dev. |
| Relative Compactness | Input | 0.62 | 0.98 | 0.764 | 0.105 |
| Surface Area | Input | 514.5 | 808.5 | 671.708 | 88.086 |
| Wall Area | Input | 245 | 416.5 | 318.5 | 43.626 |
| Roof Area | Input | 110.25 | 220.5 | 176.60 | 45.165 |
| Overall Height | Input | 3.5 | 7 | 5.25 | 1.751 |
| Orientation | Input | 2 | 5 | 3.5 | 1.118 |
| Glazing Area | Input | 0 | 0.4 | 0.234 | 0.133 |
| Glazing Area Distribution | Input | 0 | 5 | 2.812 | 1.550 |
| Cooling | Output | 10.9 | 48.03 | 24.58 | 9.513 |

B. Radial Basis Function (RBF)

Ojo et al. [22] discusses the challenges associated with traditional path loss prediction models in wireless signal propagation and proposes the use of machine learning algorithms to address these issues. It highlights the trade-off between simplicity and accuracy in deterministic and empirical models. The paper introduces two machine learning-based path loss prediction models, namely the radial basis function neural network (RBFNN) and the multilayer perceptron neural network (MLPNN), developed using experimental data collected from drive tests in multi-transmitter scenarios. The RBFNN model is found to be more accurate than the MLPNN, exhibiting lower root mean squared errors (RMSEs) when compared to measured path loss. Furthermore, the proposed machine learning-based models are compared against five existing empirical models, with the RBFNN showing the most accurate results. Elansari et al. [23] presents a novel approach called Mixed Radial Basis Function Neural Network (MRBFNN) training using Genetic Algorithm (GA). This study focuses on optimizing the choice of radial basis functions, centers, radius, and weights of the output layer in RBFNNs. They formulate the optimization problem as a mixed-variable problem with linear constraints and employ a genetic algorithm-based approach to solve it. The numerical results validate the theoretical findings and demonstrate improved generalization compared to existing methods. Alitash et al. [24] discuss the application of RBFNNs in model predictive control for a 4 × 3 Multiple-Input Multiple-Output (MIMO) biomass control system. The study aims to enhance the control performance of a biomass boiler by utilizing RBFNNs to improve the accuracy of the model. They develop a biomass boiler model using system identification techniques and implement the RBFNN model using MATLAB. Simulation results show that the RBFNN-based model predictive controller achieves shorter settling times and tolerable overshoots compared to a state space model-based controller, indicating superior performance in controlling boiler dynamics. Overall, these references demonstrate the versatility and effectiveness of RBFNNs in various applications, including pattern recognition and control systems, showcasing their potential to address complex problems in different domains.

1) *Network architecture for RBF*: A RBF neural network consists of three distinct layers: the input layer, hidden layer, and output layer, as its fundamental structure. The input

vector x in the hidden layer, which is made up of each unique input, $x_1, x_2, x_3, \dots, x_n$ is practical to all neurons. The hidden layer of an RBF network consists of n RBF that have direct connections to each component of the output layer. More information about RBF networks can be found in academic sources, including references. An RBF network's hidden layer nodes increase their output as the input pattern they represent approaches each node's centre. The output of these nodes decreases with increasing distance from the middle if symmetric basis functions are applied. Therefore, neurons with centres near a given input pattern will produce non-zero activation values when that pattern is present, amplifying the input. The neurons' receptive field function, which controls how they react to outside stimuli, is what causes this behavior [23], [25], [26]. The j th covered-up hub's theoretical basis is often represented by a Gaussian exponential function, which can be written as follows:

$$p_j = p(\omega_j) = e\left(-\frac{\omega_j^2}{2\phi_j^2}\right) \tag{1}$$

The thickness of the j th neuron, signified by ϕ_j , and ω_j , this is typically computed as the Euclidean distance between the input vector and the neuron center.

$$\omega_j(x) = \|x - c_j\| = \sqrt{\sum_{i=1}^w (x_i - c_{i,j})^2}, i = 1, 2, \dots, w \tag{2}$$

Let and $x = [x_1, \dots, x_w]^F$ c_j be the centres of the j th RBF parts, which are vectors having the same dimensions as the j th neuron's input [27]. The network's output, represented by the letter M , is the sum of the weights of all the premise capacities in the hidden layer. The following formula can be used to determine the output node value:

$$M_r = \sum_{j=1}^u s_{js} p_j \tag{3}$$

A weighted sum of the output signals from the nodes in the hidden layer yields the output of the r th node in the output layer, which is denoted by M_r as the k th component of M . s_{js} is a representation of the weights connected to the link between

the j th neuron in the hidden layer and the s th neuron in the output layer. The algorithm additionally takes into account the output p_j of the j th node in the hidden layer. In essence, the hidden layer nodes calculate a linear combination of basic functions that define the network's output.

2) *RBF network training and testing principles neural system RBF operates in two distinct modes: testing and training.* The network necessarily calculates the ideal number of her RBFs, identifies the centres for each, and constructs the output layer weight matrix during the training phase. Minimizing the total squared error, or (R), is the goal [28] al [28]:

$$R = \frac{1}{2} \sum_{l=1}^r \sum_{F}^n \{q_f^l - m_f^l(X^i)\}^2 \quad (4)$$

Here q_f^l is the apparent framework control in the event that an input vector X^i is R is the number of cases under preparation that is shown to the organizer. In RBF networks, node centers are positioned during training, and the network's capacity to generalize is greatly influenced by the output of the kernel function. Numerous methods may be used to determine the center of the *RBF* node in the hidden layer; the most popular method utilized in this research was p – means clustering. The algorithm's objective is to find a set of F cluster centers that minimizes E , which is the sum of the Euclidean distances between each cluster center (y_j) and the train points assigned to that cluster.

$$E = \sum_{j=1}^N \sum_{l=1}^N G_{ij} \|y_j - X_i\| \quad (5)$$

The membership matrix was given to the network, signified as G_{ij} with dimensions of $m \times N$, where N represents how many training examples there are. There is only one 1 in each column of this binary matrix; all other values are 0s. After establishing the *RBF* unit centre, each *RBF* unit width is calculated with a parameter named z , which regulates the amount of overlap between adjacent nodes and the *Root – Mean – Square* distance to the closest *RBF* node. The S – fold cross-validation approach may be used to find the value of z . Eq. (6) provides the breadth of the j – th *RBF* unit, which is represented as ζ_j .

$$\zeta_j = \left(\frac{1}{z} \sum_{o=1}^z \|c_j - c_o\|^2 \right)^{1/2} \quad (6)$$

After the centers of the nodes near node j are determined as (c_1, \dots, c_z) the *RBF* neural network is considered fully determined. Afterwards, Eq. (1) through Eq. (3) can be used to represent a newly provided, easily navigable input vector. The *RBF* flowchart is displayed in Fig. 1 [29].

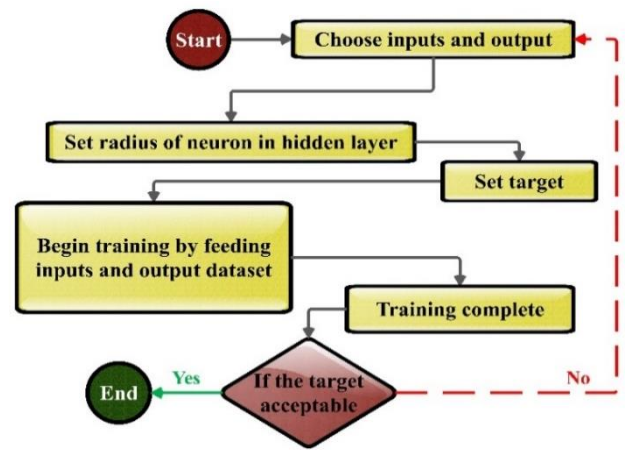


Fig. 1. Flowchart of RBF.

C. Self-adaptive Bonobo Optimizer (SABO)

A detailed argument is presented regarding an improved version of Bonobo Optimizer (BO), acknowledged as SABO with repulsion and a memory-based learning strategy for parameter upgrading. There are four types of mating behaviors found in it: consort ship, extra-group mating, promiscuous mating, and restrictive mating. A few changes have been made to this optimizer to improve performance. In addition, SABO has three additional memorized populations that are distinct from the current population, and the members of these populations mate to give birth to modern bonobos. The SABO's controlling criteria are based on a repulsion-based learning approach [30]. Other than these, p^{th} -bonobo choice in SABO is planned extraordinarily. In this case, the estimate of the subgroup is determined by the calculation taking into account the input obtained during the search procedure. To improve the efficiency of the search process, boundary control technology has also been modified in SABO as opposed to BO. Below is a detailed explanation of each of these key components of the suggested SABO.

1) *Memory and its updates:* The three populations that make up the proposed SABO are *oldpop*, *worsepop*, and *badpop*, as was previously mentioned. These populations initially match the *SABO's* the original population. Later, with every iteration, these are revised and updated. Consider that N and d , respectively, are population size and number of decision variables.

a) *Oldpop:* At any time, i^{th} -new bonobo found superior to the i^{th} -parent bonobo is accepted in the current population position. Furthermore, the i^{th} -parent bonobo is remembered within the i^{th} -position of *oldpop*.

b) *Worsepop:* If i^{th} -new bonobo turns out to be worse than i^{th} -parent bonobo in fitness value comparison; it is stored in i^{th} -worse position than the current population.

c) *Badpop:* The selection process of this N size population is choosing from mixed populace *worsepop* and *badpop* in size $2N$. The unique solutions named l , distinguished by objective values, display mixed populations.

If l realized that be less than N , then l number copied to the *badpop*. If l realized that be less than N , then l number copied to the *badpop*. Also, if l found to be greater than or equal to N , *babpop* is chosen from $l1$ ($l1 \geq N$), and it is between N_2 and 1, Eq. (7) calculates N_1 .

$$N_2 = \text{ceil}(df \times N) \quad (7)$$

df , diversity factor, is in the range of $[(df_{min}, df_{max}) = (1.2, 1.8)]$.

2) *Repulsion-based learning*: First, using repulsion-based learning, two controlling variables are identified: phase probability (pp) and sharing co-efficient (sc). Both of this parameter's range are between 0 and 1. If a good solution's number appears superior to predetermined solutions (called N_1) then N_1 solution with the highest change in fitness value will be considered. Eq. (8) calculates the N_1 .

$$N_1 = \text{maximum of}(5, \text{ceil}(N \times 0.08)) \quad (8)$$

By taking after a comparative strategy, one can get a worse value that is not upgraded fitness-wise, named pp_{worse} . Considering pp_{worse} and pp_{better} repulsion; their value directions shift in the reverse direction. $pp_{better}^{modified}$ determined by Eq. (9).

$$PP_{better}^{modified} = PP_{better} \pm \frac{\sigma \times PP_{better} \times PP_{worse}}{e^{(PP_{better} - PP_{worse})^2}} \quad (9)$$

3) *Mating strategies*: There are four mating strategies in the proposed SABO. There are also conceptions of the positive phase (pp) and negative phase (NP). Phase probabilities (pp) are probabilities that PP or NP use to update the solution at each iteration. Furthermore, in PP , applying a promiscuous or restrictive mating strategy will generate a new bonobo with a probability of 0.5. The probability of mating outside the group is called p_{xgm} which is in the range of $(p_{xgm}^{min}, p_{xgm}^{max})$ and calculates as follows:

$$I_0 = \frac{\sum_{j=1}^d \frac{SD_j}{(V_{max_j} - V_{min_j})}}{d} \quad (10)$$

$$I_1 = 0.1 \times I_0 \quad (11)$$

$$p_{xgm}^{min} = \text{minimum of}(I_1, \frac{1}{d}) \quad (12)$$

$$p_{xgm}^{max} = 2 \times I_1 \quad (13)$$

In initial population, SD_j represents the standard deviation of j^{th} -variable; j is in the range of 1 to d , and d is the decision variable number in the problem. The maximum and minimum merits of j^{th} -variable called v_{max_j} and v_{min_j} . p_{xgm}^{min} and p_{xgm}^{max} are determined by I_0 and I_1 . Fig. 2 shows a detailed flowchart of the suggested SABO.

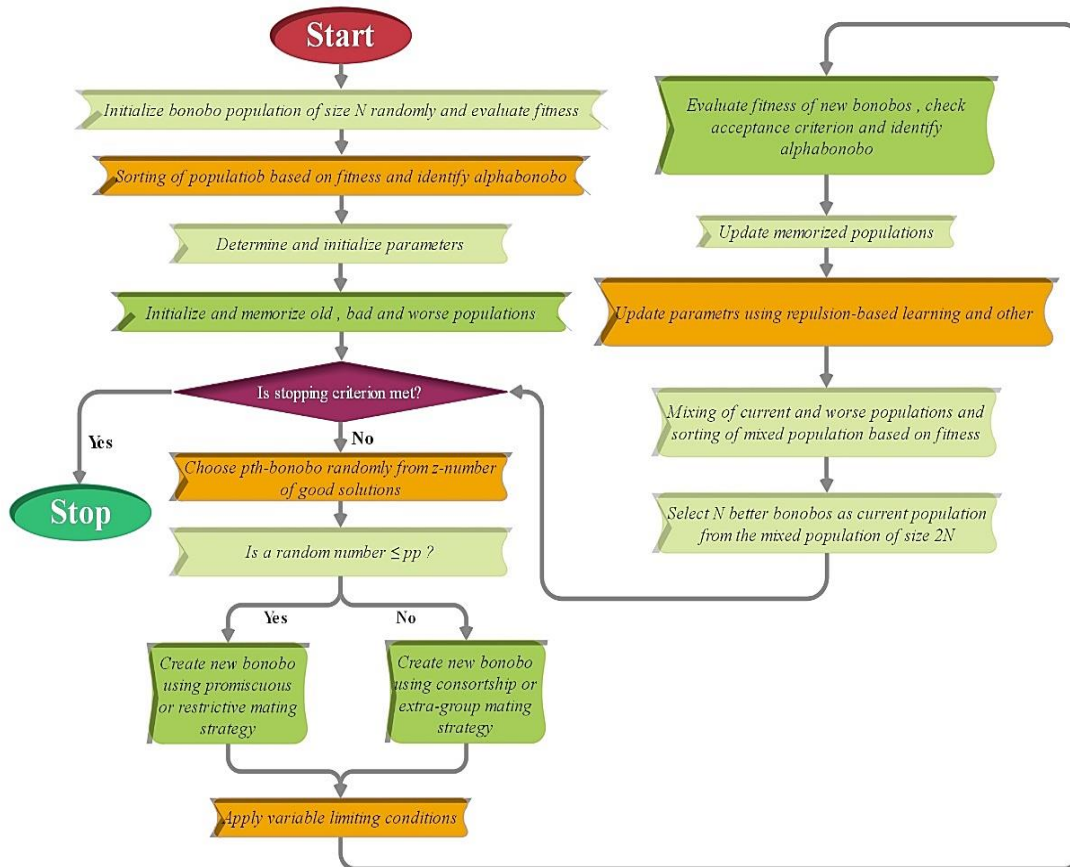


Fig. 2. Flowchart of suggested SABO.

D. Differential Squirrel Search Algorithm (DSSA)

Manoj et al. introduced an innovative optimization approach referred to as DSSA, which integrates two distinct algorithms, namely the squirrel search algorithm (SSA) and differential evolution algorithm (DE). Squirrels are observed to update their location in the context of the Simulated Squirrel Algorithm (SSA) by closely monitoring the positions of other squirrels living in the hickory or acorn tree. That means that to improve their search strategies, the top squirrels have modified their updating mechanisms. Adding a crossover operation that draws inspiration from Differential Evolution (DE) improves exploration potential. This exposition provides a mathematical model of the various foraging strategies that are included in the Decision Support System for Agriculture (DSSA).

1) Initialization of position and the evaluation of fitness:

Initially, the squirrels are arranged at random within the exploratory domain. Following the squirrels' positions, the fitness levels of each are evaluated by inserting the position mentioned earlier into the fitness function. This indicates the nutritional value of the food source that each squirrel obtained within its position. The values of fitness are subsequently subjected to a sorting process to obtain the most optimal squirrel, denoted as PS_{ht} , that currently inhabits the hickory tree. The subsequent 3 optimal function values signify the locations of the squirrels inhabiting the acorn tree PS_{at} (1:3). In addition, they are deemed to be a step towards achieving an optimal location in the next iteration. Thus far, the remaining individuals belonging to the squirrel population are denoted as PS_{nt}^{p1} have yet to discover a viable nourishment source occupying typical locations within the tree habitat.

2) Update of the position: When a squirrel colonizes a tree that provides acorns, it updates its position and moves towards the best source by following the current best path or PS_{ht} in the absence of a predator. By mimicking the movements of the squirrels living in the hickory or acorn tree, the squirrels in the regular tree can track where they are. The observed phenomenon is that when faced with the possibility of predation, squirrels tend to change their foraging route randomly. The following can be used to express the mathematical models that were used to update the squirrel's position. Now, as the others adjust their position, the squirrels in the acorn trees do the following:

$$PS_{at}^{new} = \begin{cases} PS_{at}^{old} + d_g \cdot G_c (PS_{ht}^{old} - PS_{at}^{old} - P_{avg}), & r_1 \geq P_{dp} \\ \text{random position,} & \text{otherwise} \end{cases} \quad (14)$$

P_{avg} is the mean of whole squirrels' positions in the available population.

The crossover mechanism is incorporated into the DE algorithm to reduce the likelihood of local minima, thereby increasing the diversity of the squirrel population being evaluated. The crossover operation, which was derived from

Eq. (15), was applied to the current position and its corresponding new position.

$$PS_{at,i,j}^{cr} = \frac{PS_{at,i,j}^{new}, \text{ if } (rand_j \leq Cr) \text{ or } j = j_{rand}}{PS_{at,i,j}^{old}, \text{ if } (rand_j > Cr) \text{ or } j \neq j_{rand}}, \quad (15)$$

$$j = 1, 2, 3, \dots, D$$

$$i = 1, 2, 3, \dots, NP$$

$PS_{at,i,j}^{new}$ and $PS_{at,i,j}^{old}$ are new and old squirrels' locations normal, or are acorn trees.

$PS_{at,i,j}^{cr}$ are the squirrels' positions after the operation of the crossover.

NP shows the population size.

Cr indicates the rate of crossover, and it is equal to 0.5.

D shows the dimension of the problem.

$j_{rand} \in [1, D]$ is a randomly generated index

$rand_j \in [1, D]$ is the j -th random numbers' assessment uniformly developed in the distinct range.

According to Eq. (16), some of the squirrels that live in typical trees move to new areas by following the squirrels that live in acorn trees.

$$PS_{nt}^{new} = \begin{cases} PS_{nt}^{old} + d_g \cdot G_c (PS_{at}^{old} - PS_{nt}^{old}), & r_2 \geq P_{dp} \\ \text{random position,} & \text{otherwise} \end{cases} \quad (16)$$

r_2 conforms to a uniform distribution across the interval of $[0, 1]$.

The squirrels that are still in traditional trees align with the current optimal location, and their updated locations are expressed as follows:

$$PS_{nt}^{new} = \begin{cases} PS_{nt}^{old} + d_g \cdot G_c (PS_{ht}^{old} - PS_{nt}^{old}), & r_3 \geq P_{dp} \\ \text{random position,} & \text{otherwise} \end{cases} \quad (17)$$

The application of a crossover operation on squirrels residing in ordinary trees is as follows:

$$PS_{nt,i,j}^{cr} = \frac{PS_{nt,i,j}^{new}, \text{ if } (rand_j \leq Cr) \text{ or } j = j_{rand}}{PS_{nt,i,j}^{old}, \text{ if } (rand_j > Cr) \text{ or } j \neq j_{rand}}, \quad (18)$$

$$j = 1, 2, 3, \dots, D$$

One way to speed up the convergence rate is to allow the squirrel in the hickory tree to move about the average of the squirrels' positions inside the tree, as shown by Eq. (19):

$$PS_{ht}^{new} = PS_{ht}^{old} + d_g \cdot G_c (PS_{ht}^{old} - PS_{at}^{avg}) \quad (19)$$

PS_{at}^{avg} represents the average of whole squirrel's locations in the acorn trees.

To determine who gets to participate in the next development population, the best hybrid positions and their unused positions are compared with the historical positions in the determination handle. Algorithm 1 explains the procedural instructions involved in DSSA.

Algorithm 1: DSSA Pseudocode

Input *I*termax, *NP*, *Pdp*, *sf*, *Gc*, *ub*, and *lb*
Initialize the flying squirrels' location haphazardly using Eq.(14)
Compute the fitness value utilizing the represented fitness function employing Eq.(15)
While *itr* ≤ *itermax do*
Sort of all functions of squirrels' fitness and recognize the current best, $\llbracket PS \rrbracket_{ht}$, positions of squirrels in acorn tree, $\llbracket PS \rrbracket_{at}$ (1:3) and the position of squirrel in the normal tree, $\llbracket PS \rrbracket_{nt}$ (1:NP-4)
Develop the new position of squirrels by comparing the new locations in acorn trees achieved via utilizing Eq. (14) and Eq. (15)
Develop the new location of squirrels by comparing the new positions in normal trees achieved via utilizing Eqs. (16) – (18)
Generate the new location of squirrels by comparing the new positions in hickory trees achieved via utilizing Eq.(19) and old positions.
Update the population with the best position achieved so far
End While
Return PS_{ht}

E. Performance Evaluation Methods

The models are evaluated in this article using some metrics, such as the BIAS mentioned earlier, the correlation coefficient (R^2), the Mean Square Error (*MSE*), the Symmetric Mean Absolute Percentage Error (*SMAPE*), and the root mean square error (*RMSE*). A high R^2 value indicates that the algorithm performed exceptionally well during the training, validation, and testing phases. Lower *RMSE* and *MAE* values, on the other hand, are preferred because they demonstrate less model error. Eq. (20 – 24) are used to calculate these metrics.

Coefficient of Correlation.

$$R^2 = \left(\frac{\sum_{i=1}^W (h_i - \bar{h})(l_i - \bar{l})}{\sqrt{[\sum_{i=1}^W (h_i - \bar{h})^2][\sum_{i=1}^W (l_i - \bar{l})^2]}} \right)^2 \quad (20)$$

Root Mean Square Error.

$$RMSE = \sqrt{\frac{1}{W} \sum_{i=1}^W (l_i - h_i)^2} \quad (21)$$

Mean Square Error.

$$MSE = \frac{1}{W} \sum_{i=1}^W (l_i - h_i)^2 \quad (22)$$

Symmetric Mean Absolute Percentage Error.

$$SMAPE = \frac{100}{W} \sum_{i=1}^W \frac{2 \times |l_i - h_i|}{|l_i| + |h_i|} \quad (23)$$

BIAS.

$$BIAS = \frac{\bar{l}}{\bar{h}} \quad (24)$$

- In these equations, h_i and l_i refer to the predicted and experimental values, respectively.
- The mean values of the experimental samples and predicted are represented by \bar{h} and \bar{l} .

- Otherwise, W denotes the number of samples being considered.

III. RESULTS

The results of the created *RBF* models are shown in Table II. It includes an aggregate evaluation that covers all phases and a detailed summary of performance metrics for each of the three phases: training, validation, and testing. Based on *RMSE*, R^2 , *MSE*, *SMAPE*, and *BIAS*, the *RBF* models *RBSA*, *RBDS*, and the generic *RBF* are assessed. The *RBSA* model performs well during the training phase, as evidenced by its low *RMSE* of 1.007, high R^2 of 0.989, and minimized *MSE* of 1.040. The accuracy of the model in capturing the subtleties of the training dataset is demonstrated by the *SMAPE* value of 0.00005 and the insignificant *BIAS* of -0.020. In the same way, *RBDS* performs admirably during training, showing an *RMSE* of 1.343, an R^2 of 0.980, and an *MSE* of 1.844. When the models move on to the validation stage, *RBSA* continues to perform well, with a lower *RMSE* (0.800) and a higher R^2 (0.994), indicating that it can generalize far beyond the training set. The *RBDS* model, on the other hand, shows a little increase in *RMSE* (1.172) and a lower R^2 (0.987), but it still retains a respectable degree of accuracy during validation. The generic *RBF* model, on the other hand, shows higher *RMSE* (1.410) and lower R^2 (0.981) values, indicating a relatively lower fit during the validation phase. When the models are tested, the models' performance is evaluated once more, and *RBSA* continues to perform well, with a minimum *RMSE* of 0.700, a high R^2 of 0.995, and an *MSE* of 0.489. During testing, both the generic *RBF* model and *RBDS* perform satisfactorily, with R^2 values of 0.984 and 0.976 and *RMSE* values of 1.208 and 1.486, respectively. With an overall *RMSE* of 0.938 and an R^2 of 0.990 when all phases are considered, *RBSA* performs remarkably well, proving its dependability across a range of datasets. In contrast, the generic *RBF* model and the *RBDS* model have higher overall *RMSE* values of 1.623 and 1.299, respectively. In Fig. 3, the metrics' radar plot is displayed.

These findings show how the *RBF* models' effectiveness varies depending on the phase, with *RBSA* constantly showing higher predictive accuracy. The extensive assessment metrics highlight the potential of the *RBSA* model in producing accurate and trustworthy predictions for cooling loads and offer insightful information about the models' generalization ability.

In Fig. 4, a scatter plot is used to compare the hybrid models' performance over the 3 train, validation, and test phases. R^2 quantifies the degree of agreement between observed and expected values, whereas *RMSE* shows the prediction error or dispersal. The data points are closely clustered around the centerline of the *RBSA* model, which shows exceptional accuracy across all three phases. There is little variation between the expected and actual values and a high degree of agreement. The *RBF* and *RBDS* models, on the other hand, featured data points that were further from the centerline and comparable performance levels. In comparison to the *RBSA* model, this broader dispersion predicts a slightly lower precision and a higher inaccuracy.

TABLE III. THE OUTCOME OF THE DEVELOPED RBF MODELS

| Model | Phase | Index values | | | | |
|-------|------------|--------------|----------------|-------|---------|--------|
| | | RMSE | R ² | MSE | SMAPE | BIAS |
| RBSA | Train | 1.007 | 0.989 | 1.040 | 0.00005 | -0.020 |
| | Validation | 0.800 | 0.994 | 0.640 | 0.00019 | 0.044 |
| | Test | 0.700 | 0.995 | 0.489 | 0.00018 | 0.038 |
| | All | 0.938 | 0.990 | 0.896 | 0.00003 | -0.001 |
| RBDS | Train | 1.343 | 0.980 | 1.844 | 0.00007 | 0.002 |
| | Validation | 1.172 | 0.987 | 1.373 | 0.00027 | 0.073 |
| | Test | 1.208 | 0.984 | 1.460 | 0.00026 | -0.077 |
| | All | 1.299 | 0.981 | 1.716 | 0.00004 | 0.001 |
| RBF | Train | 1.692 | 0.970 | 2.863 | 0.00011 | -0.093 |
| | Validation | 1.410 | 0.981 | 1.989 | 0.00043 | 0.134 |
| | Test | 1.486 | 0.976 | 2.209 | 0.00047 | 0.174 |
| | All | 1.623 | 0.972 | 2.634 | 0.00007 | -0.019 |

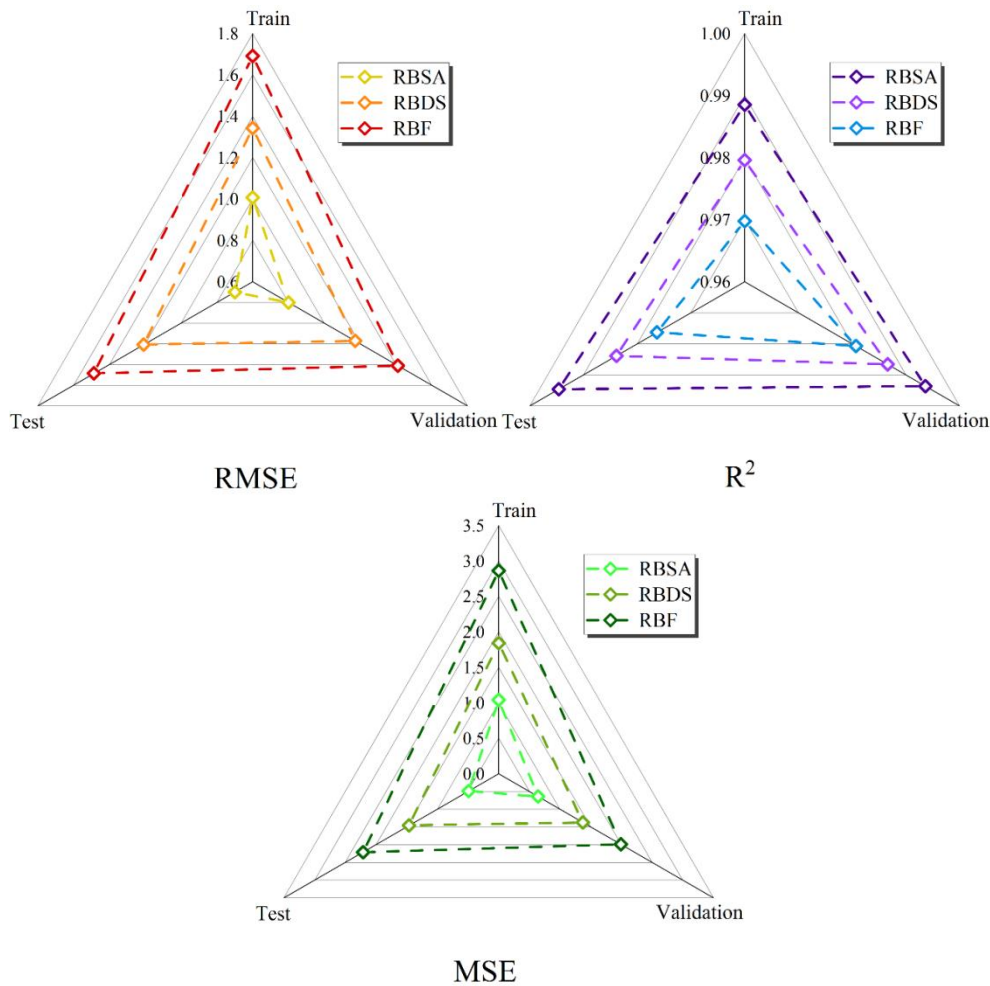


Fig. 3. Radar plot for comparison between the developed models based on metrics.

The study's line plot in Fig. 5 shows the error percentages associated with the models, with the RBSA model being the most prominent due to its low error rate. The majority of error values cluster within the 12.08% range. The RBF and RBDS models show greater variability, with a higher frequency of

values exceeding the 23.66% and 17.35% thresholds. Both models display a right-skewed distribution, indicating the presence of specific data points with greater proportions of errors.

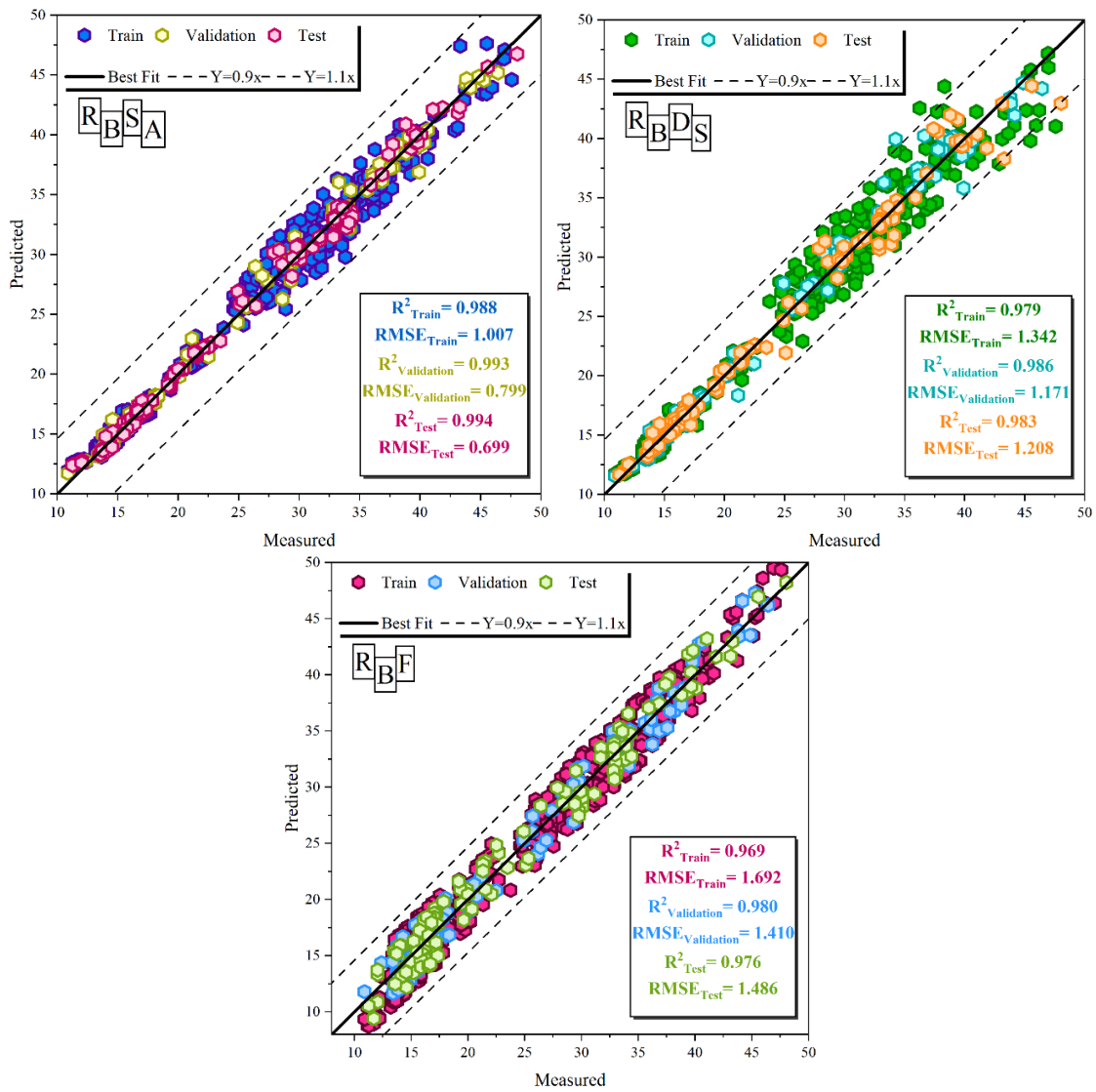


Fig. 4. Scatter plot of the dispersion of evolved hybrid models.

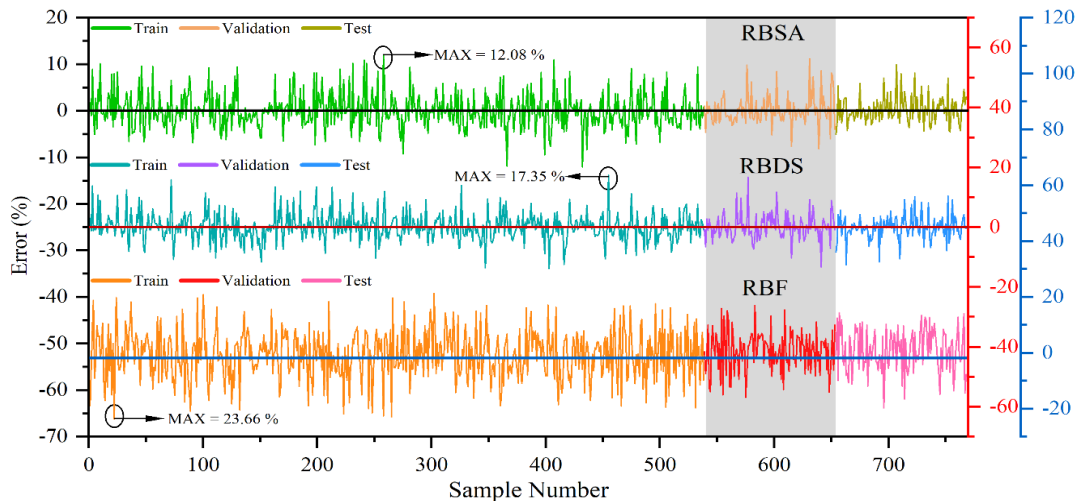


Fig. 5. Error percentage of the models based on the line plot.

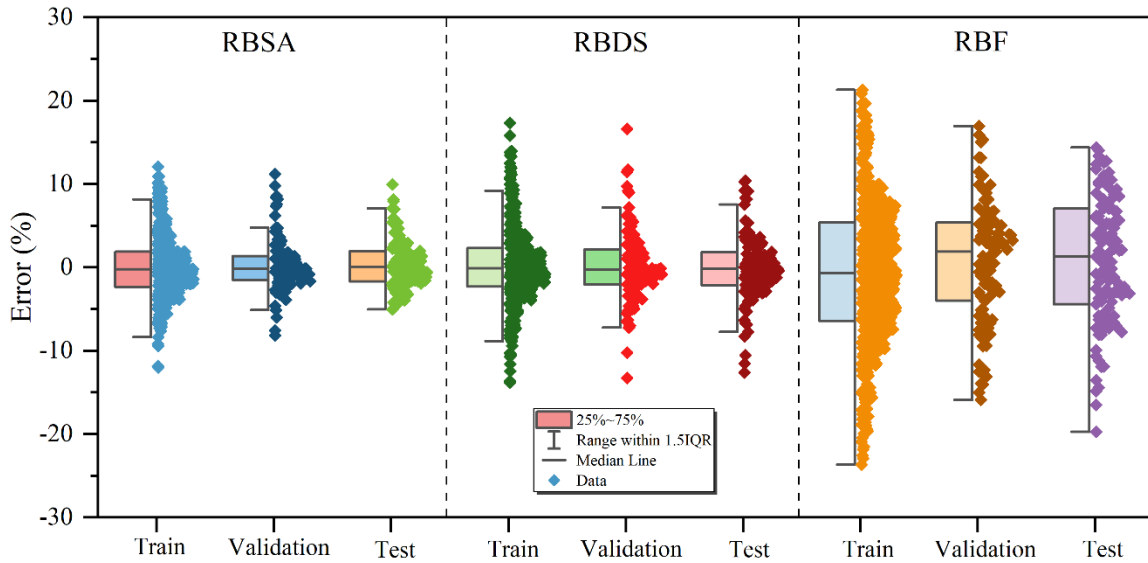


Fig. 6. Half-box plot errors of proposed models.

In Fig. 6, the study displays a half-box plot that shows the three models' respective error percentages. The RBSA model performed remarkably well, with errors kept below 10% and little dispersion. Dispersion was seen in all phases of the RBF model, with a uniform normal distribution and a maximum of 25%. During the assessment stage, the RBDS model exhibited the highest degree of discrepancy among the models, with one outlier data point representing more than 18% of the dataset. The RBF model's Gaussian distribution revealed more dispersion and fewer instances of near-zero frequency.

IV. DISCUSSION

A. Advantages of the Present Study

The novel approach introduced in the study aims to revolutionize the prediction of cooling loads, offering fresh insights and innovative solutions to longstanding challenges in energy efficiency and building management. By harnessing the power of machine learning techniques and hybridization strategies, the proposed methodology endeavors to elevate the accuracy and dependability of cooling load predictions beyond the capabilities of conventional methods. Through rigorous comparative analyses, the research delves into intricate examinations, juxtaposing the proposed methodology with state-of-the-art approaches. These comparisons yield invaluable insights into the efficacy and superiority of the novel methodology, shedding light on its potential to outperform existing techniques in predicting cooling loads with precision and reliability. The practical implications of successfully implementing the study's findings are substantial, encompassing a wide array of benefits ranging from optimized energy consumption in buildings to tangible cost reductions and advancements in sustainability initiatives. Furthermore, the study's contribution to the academic literature is profound, marking a significant advancement in predictive modeling techniques within the realm of cooling load prediction. By

pushing the boundaries of knowledge and innovation, the study paves the way for future research endeavors and opens new avenues for exploration in the pursuit of energy-efficient building management practices.

B. Limitations

The effectiveness of the proposed methodology could face constraints due to data availability and quality, which might hinder the reliability of predictions if the data is insufficient or inaccurate. Moreover, the implementation of machine learning algorithms and hybridization strategies adds complexity to the modeling process, potentially necessitating specialized expertise for development and interpretation. Additionally, the study's findings might have limited generalizability to various contexts or building types, as factors like geographical location, building design, and occupancy patterns could influence the applicability of the methodology. Validating the proposed approach poses challenges, particularly in ensuring robustness and reliability across diverse scenarios and conditions. Furthermore, ethical considerations surrounding data privacy, bias, and transparency must be meticulously addressed due to the use of machine learning techniques and optimization algorithms. These ethical concerns underscore the need for responsible and transparent research practices throughout the study.

C. Future Study

For future studies, researchers may explore refining the methodology, analyzing long-term performance, integrating advanced technologies, validating in real-world settings, considering external factors' impact, conducting sensitivity analysis, integrating with building automation systems, and engaging users for feedback. These avenues aim to advance cooling load prediction, enhance energy efficiency, and promote sustainable building management practices.

D. Comparison with Published Papers

Table III shows the comparison between the presented and published papers. From the comparison, it can be observed that the presented study falls within the range of RMSE and R² values reported in the published articles. While the RMSE value of the present study (0.938) is higher than that of Roy et al. (0.059) and Gong et al. (0.1929), it is lower than that of Afzal et al. (1.4122). Similarly, the R² value of the present study (0.990) is slightly lower than that of Moradzadeh et al. (0.9993) but higher than that of Gong et al. (0.9882) and Afzal et al. (0.9806). Overall, the presented study demonstrates competitive performance in terms of both RMSE and R² compared to the published articles, indicating its effectiveness in predicting cooling loads.

TABLE IV. COMPARISON BETWEEN THE PRESENTED AND PUBLISHED ARTICLES

| Articles | Index values | |
|------------------------|--------------|----------------|
| | RMSE | R ² |
| Moradzadeh et al. [31] | 0.4832 | 0.9993 |
| Roy et al. [9] | 0.059 | 0.99 |
| Gong et al. [32] | 0.1929 | 0.9882 |
| Afzal et al. [14] | 1.4122 | 0.9806 |
| Present Study | 0.938 | 0.990 |

V. CONCLUSION

As a result of the significant influence that the global building industry has on total energy consumption, efforts must be made to precisely forecast cooling loads in the context of energy conservation and building operations. The study established a multimodal investigation to improve cooling load prediction models by applying cutting-edge techniques and creative ideas. Initially, the emphasis was on important metrics like Dynamic Air-Conditioning Load (DACL) and Cooling Load (CL), which highlighted the critical role these parameters play in HVAC system optimization. Several different approaches have been adopted to improve prediction accuracy because of the complex interactions that have been identified between the optical and thermal properties of buildings and meteorological data. The process of extracting detailed insights from the data required the application of feature extraction techniques, such as engineering-based, statistical, and structural methods. These techniques, which combined mathematical and domain-specific viewpoints, made it easier to comprehend the thermal dynamics present in different types of construction materials. The rapidly changing field of machine learning (ML) has the potential to transform the precision and effectiveness of cooling load forecasts completely. The combination of machine learning and feature extraction techniques demonstrated the potential to improve current models and introduce new ones that can more accurately predict cooling load with never-before-seen levels of detail. The development and assessment of the RBF models RBSA, RBDS, and generic RBF represented the culmination of these efforts. The thorough statistical characteristics of the input variables served as a fundamental point of reference, allowing for an in-depth analysis of the models' performance

during the training, validation, and testing stages. With the Self-adaptive Bonobo Optimizer (SABO) integrated, RBSA proved to be an exceptional performer, exhibiting superior accuracy in every phase. RBSA is a strong and dependable model for cooling load prediction because of its exceptional performance during testing, reduced RMSE and increased R², and ability to generalize far beyond the training set. These findings have wider ramifications that go beyond the immediate setting and provide a promising path towards more environmentally friendly and energy-efficient structures. By incorporating advanced modelling techniques, predictive accuracy is improved, and the foundation for intelligent, adaptive HVAC systems is laid. The combination of state-of-the-art machine learning, research methodologies, and feature extraction techniques could lead to the intelligent response of buildings to environmental demands in the future, resulting in a more sustainable and environmentally conscious global infrastructure.

ACKNOWLEDGMENTS

Natural Science Foundation of Hunan Province (2023JJ50348).

Research Foundation of Education Bureau of Hunan Province (22C0514).

REFERENCES

- [1] J. Kim, Y. Zhou, S. Schiavon, P. Raftery, and G. Brager, "Personal comfort models: Predicting individuals' thermal preference using occupant heating and cooling behavior and machine learning," *Build Environ*, vol. 129, pp. 96–106, 2018, doi: <https://doi.org/10.1016/j.buildenv.2017.12.011>.
- [2] R. Zhao et al., "Building cooling load prediction based on lightgbm," *IFAC-PapersOnLine*, vol. 55, no. 11, pp. 114–119, 2022.
- [3] Y. Ding, Q. Zhang, and T. Yuan, "Research on short-term and ultra-short-term cooling load prediction models for office buildings," *Energy Build*, vol. 154, pp. 254–267, 2017.
- [4] J. Guo et al., "Prediction of heating and cooling loads based on light gradient boosting machine algorithms," *Build Environ*, vol. 236, p. 110252, 2023, doi: <https://doi.org/10.1016/j.buildenv.2023.110252>.
- [5] B. S. A. J. khiavi; B. N. E. K. A. R. T. K. hadi Sadaghat;, "The Utilization of a Naïve Bayes Model for Predicting the Energy Consumption of Buildings," *Journal of artificial intelligence and system modelling*, vol. 01, no. 01, 2023, doi: 10.22034/JAISM.2023.422292.1003.
- [6] C. Lu, S. Li, S. Reddy Penaka, and T. Olofsson, "Automated machine learning-based framework of heating and cooling load prediction for quick residential building design," *Energy*, vol. 274, p. 127334, 2023, doi: <https://doi.org/10.1016/j.energy.2023.127334>.
- [7] J. Zhao, X. Yuan, Y. Duan, H. Li, and D. Liu, "An artificial intelligence (AI)-driven method for forecasting cooling and heating loads in office buildings by integrating building thermal load characteristics," *Journal of Building Engineering*, vol. 79, p. 107855, 2023, doi: <https://doi.org/10.1016/j.job.2023.107855>.
- [8] R. Chaganti et al., "Building heating and cooling load prediction using ensemble machine learning model," *Sensors*, vol. 22, no. 19, p. 7692, 2022.
- [9] S. S. Roy, P. Samui, I. Nagtode, H. Jain, V. Shivaramkrishnan, and B. Mohammadi-Ivatloo, "Forecasting heating and cooling loads of buildings: A comparative performance analysis," *J Ambient Intell Humaniz Comput*, vol. 11, pp. 1253–1264, 2020.
- [10] S. T. Kadam, I. Hassan, L. Wang, and M. A. Rahman, "Impact of Urban Microclimate on Air Conditioning Energy Consumption Using Different Convective Heat Transfer Coefficient Correlations Available in Building Energy Simulation Tools," in *Fluids Engineering Division Summer*

- Meeting, American Society of Mechanical Engineers, 2021, p. V002T03A002.
- [11] Q. Si, Y. Peng, Q. Jin, Y. Li, and H. Cai, "Multi-Objective Optimization Research on the Integration of Renewable Energy HVAC Systems Based on TRNSYS," *Buildings*, vol. 13, no. 12, p. 3057, 2023.
- [12] K. Bamdad, N. Mohammadzadeh, M. Cholette, and S. Perera, "Model Predictive Control for Energy Optimization of HVAC Systems Using EnergyPlus and ACO Algorithm," *Buildings*, vol. 13, no. 12, p. 3084, 2023.
- [13] X. Li and R. Yao, "A machine-learning-based approach to predict residential annual space heating and cooling loads considering occupant behaviour," *Energy*, vol. 212, p. 118676, 2020, doi: <https://doi.org/10.1016/j.energy.2020.118676>.
- [14] S. Afzal, B. M. Ziapour, A. Shokri, H. Shakibi, and B. Sobhani, "Building energy consumption prediction using multilayer perceptron neural network-assisted models; comparison of different optimization algorithms," *Energy*, p. 128446, Jul. 2023, doi: [10.1016/j.energy.2023.128446](https://doi.org/10.1016/j.energy.2023.128446).
- [15] G. Bekdaş, Y. Aydın, Ü. Isıkdağ, A. N. Sadeghifam, S. Kim, and Z. W. Geem, "Prediction of Cooling Load of Tropical Buildings with Machine Learning," *Sustainability*, vol. 15, no. 11, p. 9061, 2023.
- [16] X. Li and R. Yao, "A machine-learning-based approach to predict residential annual space heating and cooling loads considering occupant behaviour," *Energy*, vol. 212, p. 118676, 2020, doi: <https://doi.org/10.1016/j.energy.2020.118676>.
- [17] C. Fan, Y. Liao, G. Zhou, X. Zhou, and Y. Ding, "Improving cooling load prediction reliability for HVAC system using Monte-Carlo simulation to deal with uncertainties in input variables," *Energy Build*, vol. 226, p. 110372, 2020.
- [18] X. Zhao, F. Li, B. Chen, X. Li, and S. Lub, "Modeling the hardness properties of high-performance concrete via developed RBFNN coupling matheuristic algorithms," *Journal of Intelligent & Fuzzy Systems*, no. Preprint, pp. 1–15, 2023.
- [19] M. B. Bashir and A. A. Alotaibi, "Smart buildings Cooling and Heating Load Forecasting Models," *IJCSNS*, vol. 20, no. 12, p. 79, 2020.
- [20] C. Deb, L. S. Eang, J. Yang, and M. Santamouris, "Forecasting diurnal cooling energy load for institutional buildings using Artificial Neural Networks," *Energy Build*, vol. 121, pp. 284–297, 2016, doi: <https://doi.org/10.1016/j.enbuild.2015.12.050>.
- [21] O. Probst, "Cooling load of buildings and code compliance," *Appl Energy*, vol. 77, no. 2, pp. 171–186, 2004.
- [22] S. Ojo, A. Imoize, and D. Alienyi, "Radial basis function neural network path loss prediction model for LTE networks in multitransmitter signal propagation environments," *International Journal of Communication Systems*, vol. 34, no. 3, p. e4680, 2021.
- [23] T. Elansari, M. Ouanan, and H. Bourray, "Mixed Radial Basis Function Neural Network Training Using Genetic Algorithm," *Neural Process Lett*, vol. 55, no. 8, pp. 10569–10587, 2023.
- [24] G. K. Alitasb and A. O. Salau, "Multiple-input multiple-output Radial Basis Function Neural Network modeling and model predictive control of a biomass boiler," *Energy Reports*, vol. 11, pp. 442–451, 2024.
- [25] M. Sahoo et al., "MLP (multi-layer perceptron) and RBF (radial basis function) neural network approach for estimating and optimizing 6-gingerol content in Zingiber officinale Rosc. in different agro-climatic conditions," *Ind Crops Prod*, vol. 198, p. 116658, 2023.
- [26] W. Bowen, "Research on nonlinear calibration of mine catalytic-combustion-based combustible-gas sensor based on RBF neural network," *Heliyon*, vol. 9, no. 3, 2023.
- [27] M. Y. Mashor, "Hybrid training algorithm for RBF network," *International Journal of the computer, the Internet and Management*, vol. 8, no. 2, pp. 50–65, 2000.
- [28] Q. He et al., "Landslide spatial modelling using novel bivariate statistical based Naïve Bayes, RBF Classifier, and RBF Network machine learning algorithms," *Science of the total environment*, vol. 663, pp. 1–15, 2019.
- [29] M.-L. Zhang, "M 1-rbf: Rbf neural networks for multi-label learning," *Neural Process Lett*, vol. 29, pp. 61–74, 2009.
- [30] A. K. Das, S. Sahoo, and D. K. Pratihari, "An Improved Design of Knee Orthosis Using Self-Adaptive Bonobo Optimizer (SaBO)," *J Intell Robot Syst*, vol. 107, no. 1, p. 8, 2023.
- [31] A. Moradzadeh, A. Mansour-Saatloo, B. Mohammadi-Ivatloo, and A. Anvari-Moghaddam, "Performance evaluation of two machine learning techniques in heating and cooling loads forecasting of residential buildings," *Applied Sciences*, vol. 10, no. 11, p. 3829, 2020.
- [32] M. Gong, Y. Bai, J. Qin, J. Wang, P. Yang, and S. Wang, "Gradient boosting machine for predicting return temperature of district heating system: A case study for residential buildings in Tianjin," *Journal of Building Engineering*, vol. 27, p. 100950, 2020.

Securing IoT Environment by Deploying Federated Deep Learning Models

Saleh Alghamdi, Aiiad Albeshri

Faculty of Computer Sciences, King Abdulaziz University, Jeddah, Saudi Arabia

Abstract—The vast network of interconnected devices, known as the Internet of Things (IoT), produces significant volumes of data and is vulnerable to security threats. The proliferation of IoT protocols has resulted in numerous zero-day attacks, which traditional machine learning systems struggle to detect due to IoT networks' complexity and the sheer volume of these attacks. This situation highlights the urgent need for developing more advanced and effective attack detection methods to address the growing security challenges in IoT environments. In this research, we propose an attack detection mechanism based on deep learning for federated learning in IoT. Specifically, we aim to detect and prevent malicious attacks in the form of model poisoning and Byzantine attacks that can compromise the accuracy and integrity of the trained model. The objective is to compare the performance of a distributed attack detection system using a DL model against a centralized detection system that uses shallow machine learning models. The proposed approach uses a distributed attack detection system that consists of multiple nodes, each with its own DL model for detecting attacks. The DL model is trained using a large dataset of network traffic to learn high-level features that can distinguish between normal and malicious traffic. The distributed system allows for efficient and scalable detection of attacks in a federated learning network within the IoT. The experiments show that the distributed attack detection system using DL outperforms centralized detection systems that use shallow machine learning models. The proposed approach has the potential to improve the security of the IoT by detecting attacks more effectively than traditional machine learning systems. However, there are limitations to the approach, such as the need for a large dataset for training the DL model and the computational resources required for the distributed system.

Keywords—Internet of Things (IoT); security breaches; machine learning; Deep Learning (DL)

I. INTRODUCTION

IoT security has attracted more attention as a result of the Internet of Things (IoT) technologies' quick growth and wide use. IoT is a network system comprising numerous IoT devices that can be accessible to cyber-attacks because they are typically found in unsupervised locations. One of the most difficult study areas in information technology is cyber security. It is especially challenging to do when new technologies are involved, such as the IoT, because of its common use in numerous technological fields, the internet of things is predicted to reach 50 billion devices by the year 2020 [1]. The privacy, integrity, and availability of data are seriously threatened by this growth, which malevolent actors may use against them. In addition to preventing illegal access to networks and systems, cyber security also involves protecting

data and personal information. As more and more new applications depending on connected devices are created, there has been an increased focus on IoT security in recent years. In comparison to computer networks, attacks on the Internet of Things could make things worse and result in significant, extremely expensive damage. IoT is so strongly dependent on the reduction of end security setup, and all IoT strategies and components should completely address security threats. In light of research into IoT risk categories and security architecture, the detection methods need to be improved [2].

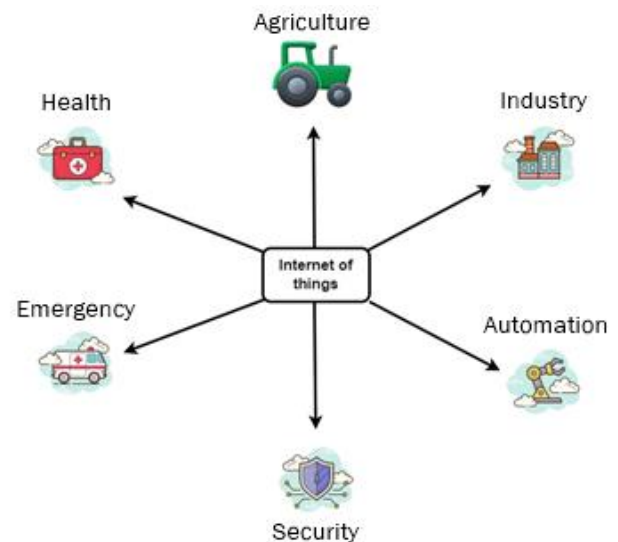


Fig. 1. Internet of things.

Attacks on linked devices have become a serious issue as IoT has gained popularity as shown in Fig. 1. IoT devices are sensitive to a variety of attacks, including denial of service, monitoring of communications, and password cracking. As the number and variety of Internet of Things (IoT) devices continue to grow, safeguarding these devices against cyber-attacks is becoming increasingly critical. Study [3-6] highlight the growing concern for the security of IoT devices, underscoring the urgency of implementing effective protective measures. Moreover, the complex nature of these interconnected systems, which often depend on wireless networks for the transmission of real-time, sensitive data, further elevates the risk of cyber threats. Such vulnerabilities can be exploited through attacks like web insertion, potentially resulting in the unauthorized access and exposure of private data, as well as the alteration or tampering of critical information. This exposure not only compromises the privacy of individuals and organizations but also threatens the integrity

and reliability of the system as a whole [7]. For IoT devices, improved, more reliable intrusion detection systems are required. For threat detection, deep learning-based security systems do not require a network connection and work with all types of devices, operating systems, and data [8].

Attack detection methods include anomaly-based and signature-based methods. The signature-based method analyzes the incoming traffic to the database's list of known attack types, whereas the anomaly-based method detects attacks as behavioural anomalies from normal traffic. The earlier method has received criticism for not being able to detect fresh attacks despite having high detection accuracy and a low false alarm rate. On the other hand, anomaly detection does not have high accuracy, but it does detect new attacks. Classical machine learning has been heavily employed in both strategies [9]. Traditional machine learning algorithms are unable to identify advanced cyber-attacks due to the attackers' continuous increase in strength and resources. The majority of these attacks are minor variations of cyber-attacks that have been seen before. It is noticeable that even the as such unique attacks (1% of all attacks) depend on earlier concepts and logic [10-11].

Unlike traditional machine learning methods that struggle with abstract feature extraction, DL can develop high-level, stable representations of training data, making it sensitive to slight variations or modifications. This sensitivity is particularly useful in fields like pattern recognition, computer vision, and image processing, where DL has significantly improved classification and prediction accuracy. The passage highlights recent findings that suggest DL's effectiveness in traffic classification and intrusion detection systems, indicating its novel application in cyber security attack detection, even within resource-constrained networks. The research aims to develop a distributed attack detection mechanism based on DL for the IoT, leveraging DL's self-learning capability to enhance accuracy and processing speed.

This research makes the following contributions:

- Develop and deploy an attack detection mechanism based on federated learning and deep learning that captures the distribution patterns of IoT networks.
- The proposed system can identify attacks as soon as they occur and respond swiftly to mitigate future damage.
- The proposed system can reduce the probability of false positives by learning and adapting to new attack patterns.

The Section II provides a background study; Section III outlines the proposed methodology, followed by the results in Section IV. Finally, the paper is concluded in Section V.

II. LITERATURE REVIEW

Many researchers have used different techniques on different types of data for user behaviour. Each researcher

explores different aspects of user behaviour analysis. Here the study discusses a few of them, especially for Anomaly Detection in the Internet of Things.

In study [14], author discusses the rapid growth of the Internet of Things (IoT) industry, projected to reach 30.9 billion devices by 2025, and the associated security risks due to manufacturers prioritizing service quality over security. In response to the significant challenge posed by detecting intrusions within the extensive and diverse networks of the Internet of Things (IoT), the authors propose a sophisticated solution. They have developed an intrusion detection system that utilizes the capabilities of deep learning to effectively address this issue. This system is uniquely designed to be highly adaptable, enabling it to learn from and adjust to the intricacies of any IoT network it encounters. One of the most notable achievements of this system is its exceptional accuracy rate, which stands at 93.74%. This level of precision underscores the system's effectiveness in identifying and responding to security breaches across the varied landscape of IoT environments. In study [15], the authors address the security vulnerabilities of the Industrial Internet of Things (IIoT) to protect against sophisticated multi-variant botnet attacks. This approach utilizes a combination of supervised and unsupervised machine learning algorithms to develop an Intrusion Detection System (IDS) that outperforms existing methods in speed and accuracy of bot attack detection, showcasing its effectiveness through comprehensive evaluations using the latest datasets and performance metrics. In study [16], the paper explores the implementation of machine learning-based Intrusion Detection Systems (IDS) in IoT environments with limited resources. The proposed IDS combines Principal Component Analysis (PCA) for feature reduction with various machine learning models, achieving high detection accuracy against contemporary attacks as demonstrated using the UNSW-NB15 datasets. The approach prioritizes reducing communication overhead and avoiding the complexities of encryption methods, with future work aimed at enhancing this model with deep learning techniques and novel datasets for broader IoT applications.

In this study, [17] researchers tackle the challenge of safeguarding Industrial Internet of Things (IIoT) edge devices from cyber-threats and anomalies to enhance threat detection. Their method demonstrates a high accuracy of 99.5% on an IIoT-specific dataset, surpassing traditional ML-based classifiers in metrics like precision, F1-score, and recall. In [19], a novel intrusion detection architecture named DRaNN is introduced for improving security in IIoT settings, employing a hybrid approach of particle swarm optimization (PSO) and sequential quadratic programming (SQP) for optimizing hyperparameters for enhanced attack detection. The study in [20] explores a DL-based method for bolstering blockchain data security, focusing on the identification and deployment of secure smart contracts within public blockchain networks. This approach achieves notable results in vulnerability detection accuracy (99.083%), precision (91.935%), and recall (87.692%).

TABLE I. LITERATURE REVIEW

| Paper Title | Dataset | Methodology | Domain | Limitations |
|-------------|-----------------------|---------------------|--------------|---|
| [23] | KDD Cup 1999 datasets | deep neural network | IoT security | Benchmark dataset not used |
| [24] | UNSW-NB15 datasets | CNN+RNN | IoT security | The system may not be effective against attacks that do not generate anomalous traffic patterns |
| [25] | CICIDS2017 dataset | BiLSTM | IoT security | Low performance in some type of attacks |
| [26] | Various IoT datasets | CNN | IoT security | Small datasets |
| [27] | UNSW-NB15 dataset | RNN+Blockchain | IoT security | The proposed approach may not be effective against attacks that do not generate anomalous network traffic patterns. |

In study [21], researchers propose a unique pairing structure and algorithm to verify the authenticity of sensor data within the IoT framework. Their method is validated through case studies and experiments on two real-world datasets, applying CART, SVM, and KNN algorithms. Lastly, [22] presents an innovative architecture designed to detect and counteract DoS/DDoS attacks in IoT environments, offering precise detection capabilities that identify both the attack type and the packet type involved. Some studies are detailed in Table I, showcasing advancements in IoT security through various approaches.

III. PROPOSED MODEL

The proposed system used a Federated Learning (FL) approach to overcome the challenges of anomaly detection in the Industrial Internet of Things (IIoT) ecosystem, where devices often have limited capabilities and generate minimal data. This method involves aggregating training data from multiple users to quickly develop a robust model, with local FL clients training models on available data and a global server aggregating these insights to improve both global and local models. This strategy enhances the ability to differentiate between malicious and benign traffic within an IIoT network. In Fig. 2, the configuration of the proposed FL approach for IIoT intrusion detection is depicted, with several installed and network-connected devices spread across various places [28].

A. Learnings and Intelligence at the Local Level

In this component of the framework, each client (ranging from $k=1$ to K) locally trains the data collected from their respective Industrial Internet of Things (IIoT) devices using the models provided by the server. Concurrently, an Intrusion Detection System (IDS) at the client's site identifies any potential attacks. Additionally, a network data analyzer is employed to log data for subsequent analysis. This approach of enabling local training, adjusting parameters, and refining the inference mechanisms, ensures the autonomy of local intrusion detection systems through intelligent, device-level learning.

B. Distribution of Learnings

To enhance the intrusion detection system by optimizing its parameters, clients share their individually trained models with a centralized server for aggregation. This process of model exchange is managed by an intelligent communication administrator, such as a security gateway. This collaborative approach aims to refine and improve the system's ability to detect intrusions effectively.

C. Model and Assumptions

In an Industrial Internet of Things (IIoT) network, a threat or adversary, referred to as M , can originate from either inside or outside the network. This includes insiders, such as compromised IIoT devices or other connected devices that remain within the network's confines, as well as external attackers who exploit the Internet to conduct cyberattacks. These attacks may involve manipulating digitally connected systems, inserting harmful content into databases, or pilfering sensitive information. IIoT malware often seeks out devices with lax security measures to serve as a foothold for launching attacks, aiming to identify and exploit weaknesses in IIoT systems and devices. We also made a few more assumptions during our analysis. These are what they are:

- A reliable FL aggregator is vital because aggregation servers play a crucial role in the learning process. For this reason, there must always be some level of faith in the system that organizes learning.
- No nefarious IIoT Device by Design: In some circumstances, newly introduced IIoT products may already have security issues. However, before being used for their intended function, these gadgets must not be contaminated or diseased.
- Secure Clients: Assuming that secure clients are essential for Federated Learning (FL) in IIoT systems, we proceed under the presumption that they exist.

D. Intrusion Detection for FL

In the Federated Learning (FL) model, each of the K clients independently trains a local model based on a common global model distributed by the server, utilizing their unique local datasets instead of relying on a centralized data repository. These clients then securely transmit the insights gained from local training sessions to an aggregation server via an SSL/TLS secured connection. The aggregation server merges these individual contributions to update the global model, optimizing it with the best possible parameters. This process is iterated through several rounds of federated learning, denoted by R , starting from initial weights represented by w , until the model converges to an optimal state. The model weights update during each communication round is guided by a formula derived from the FedAvg algorithm, ensuring efficient and effective learning from each local client's data.

$$w_{t+1} = \sum_{k=1}^K \frac{n_k}{n} w_{t+1}^k \quad (1)$$

In this context, n_k represents the dataset size for each individual client, while n signifies the total dataset size across all clients. After the iteration process, the updated global model is denoted as w_{t+1}^k . Fig. 3 illustrates the connections between various participants in the Federated Learning (FL) IIoT intrusion detection system. For inclusion in the FL cycle, the server selects clients that are connected to operational IIoT devices, which must be turned on, plugged into a power source, and linked to an unmetered Wi-Fi connection. The interaction among the system's components to facilitate the FL process is outlined as follows:

- 1) The server initializes a NN model based on a global intrusion detection framework, specifying parameters such as the number of neurons, epochs, and hidden layers. The initial weights of this model are symbolized by w .
- 2) Clients maintain the confidentiality of their local data while leveraging it to refine the model using information from the IIoT devices they manage.
- 3) To safeguard client privacy, only the parameters of the updated model, which contribute to the enhanced intrusion detection capabilities, are shared with the central server.
- 4) Upon collecting all the updates, the server aggregates the weights from each client's model to form an updated, improved global model using the FedAvg algorithm. This aggregation takes into account the dataset size at each client node.
- 5) The central server pushes the modified model parameters back to the clients.
- 6) Every client applies the updated model parameters and modifies them in light of the fresh information.
- 7) Repeat steps 4, 5, 6, and 7 to continue refining and improving the model.

E. Machine Learning Classifiers for Intrusion Detection

The rapid development of ML methods and applications has given the intelligent IDS solution an altogether novel avenue for development. To extract better data representations for powerful model construction, neural network methods have proven to be highly helpful. Neurons, weights, biases, and functions are the essential elements that all neural networks share, even though there are many different types of neural networks. For intrusion detection, we have maintained a minimal number of classifiers at a central location, utilizing the following two:

CNNs are designed to process data represented in multiple arrays. At the core of this approach are the initial layers, which consist of a set of learnable filters applied via convolutional feature extractors. These filters are employed across the input data using a sliding window mechanism. The term "stride" denoting the extent of overlap between these filters' applications. Convolutional kernels, essential elements of a CNN layer, are utilized to create unique feature maps by connecting neurons to local regions in the preceding layer's feature map. To form a feature map, the kernel is systematically applied across all spatial positions of the input. After constructing convolutional and pooling layers, classification is achieved through one or more densely connected layers.

$$h_j^{(n)} = \sum_{k=1}^k h_k^{(n-1)} * w_{kj}^{(n)} + b_{kj}^{(n)} \quad (2)$$

Recurrent Neural Networks (RNNs) are advanced models of feed-forward neural networks, designed to retain information at each stage for future outputs. In an RNN, the output from neurons is fed not only to their own input but also to the input of other neurons. This design allows RNNs to process sequences of data and time series effectively by leveraging their internal memory.

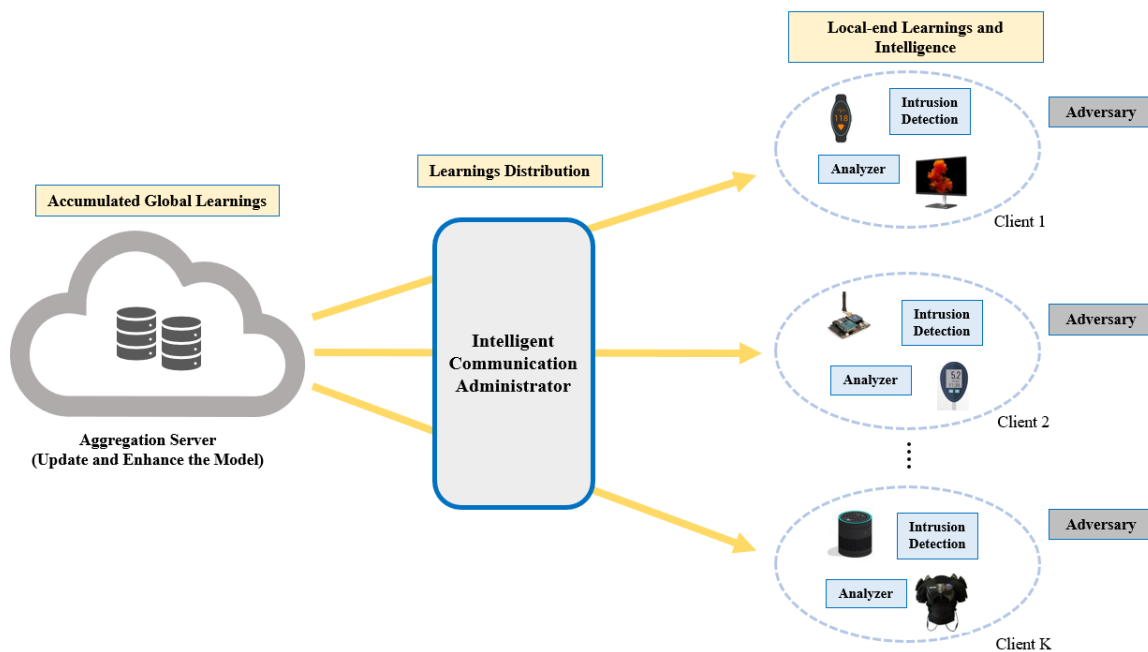


Fig. 2. Proposed approach.

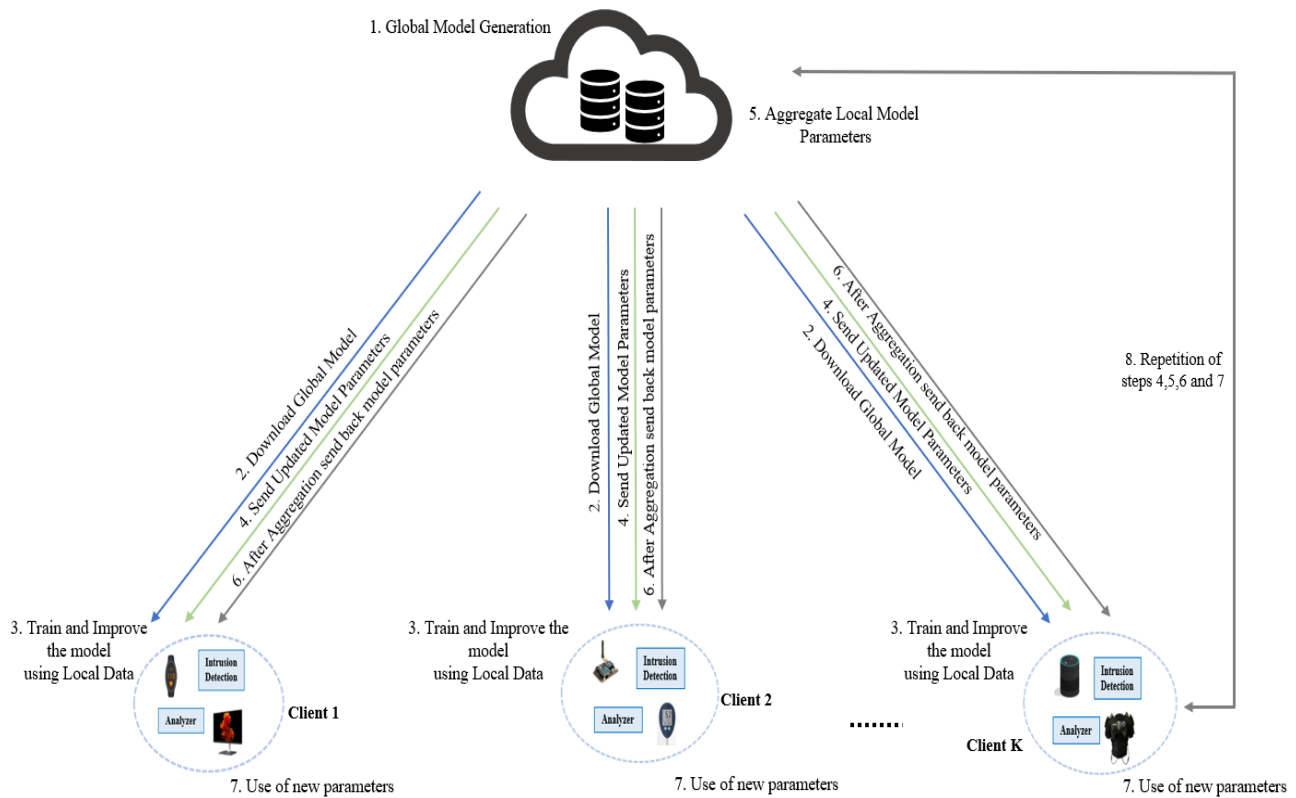


Fig. 3. Interactions among FL-based IDS clients' participants.

VI. EXPERIMENTAL RESULTS

For training and evaluating Intrusion Detection Systems (IDSs) in IIoT networks, selecting an appropriate dataset is crucial. To address this need in IIoT and IoT contexts, a novel cybersecurity dataset named Edge-IIoTset has been introduced. The dataset includes data from a wide range of IoT devices, including heart rate monitors, flame detectors, and sensors for temperature and humidity. For Federated Learning (FL) projects, it's crucial that the dataset showcases a distribution that is both imbalanced and non-independently and identically distributed (Non-IID), reflecting the complexity of real-world situations accurately. Our dataset (Edge-IIoTset) has been partitioned for experimental purposes into several local datasets so that they can be trained to meet FL's requirements. Due to the lack of FL-specific datasets, this was necessary. The dataset breakdown is shown in Table II.

TABLE II. TRAINING AND TESTING DISTRIBUTED DATA

| Dataset | Total | Training | Testing |
|-------------------|--------|----------|---------|
| Normal | 25,320 | 21,112 | 5933 |
| DDoS-UDP Attack | 15498 | 12540 | 3033 |
| DDoS-ICMP Attack | 13090 | 10179 | 2899 |
| Uploading Attacks | 10,147 | 8261 | 2017 |
| DDoS-TCP Attack | 10,380 | 9045 | 2302 |

To assess the effectiveness of FL, we ran several tests with 3 to 15 clients contributing to model training. Before achieving the best results, our model was trained for a total of 50 epochs.

While creating the federated model, we looked at how effective the system was for various client counts. The deployment dataset's training data was distributed to each client, a random selection from which was made. We created three federated models and compared them to a centralised model to investigate this potential loss in accuracy. The training dataset was distributed among 3, 9, and 15 clients.

A. Performance Metrics

When evaluating the model using test data, the following performance metrics were considered:

$$ACC = \frac{TP+TN}{TP+TN+FP+FN} \quad (3)$$

$$Pre = \frac{TP}{TP+FP} \quad (4)$$

$$Rec = \frac{TP}{TP+FN} \quad (5)$$

$$F1 = 2 \cdot \frac{Precision \cdot Recall}{Precision + Recall} \quad (6)$$

B. Evaluation of Performance

This section covers the results of the experiment employing centralised learning and the performance of our suggested FL-based model for incursion detection using the Edge IIoT set dataset.

1) *Using centralised method for intrusion detection:* We first employed two conventional centralised ML methods, namely CNN and RNN, to assess the performance of the new model. In the method we propose, Table III lists the values assigned to the parameters of various classifiers.

TABLE III. ML CLASSIFIER SETTINGS

| Classifier | Parameters |
|------------|--|
| CNN | Filters Pooling layer Hidden nodes Hidden layers |
| RNN | Batch size Local epochs Loss function Activation function |

Table IV presents the performance metrics of machine learning techniques for a centralized model, focusing on their ability to differentiate between benign and attack classes within the dataset. According to the table, both RNN and CNN methods exhibit high effectiveness, with Accuracy and F1-Score reaching up to 94% and 93%, respectively. Furthermore, these techniques demonstrate excellent capability in distinguishing between benign and malicious activities, achieving Precision and Recall rates as high as 95% for RNN and 94% for CNN.

2) *Using federated method for intrusion detection:* We conducted Federated Learning (FL) experiments using our model with three different sets of clients, denoted as K, where K equals 3 for the first set, 9 for the second set, and 15 for the third set. To address our varied client base, we employed two scenarios:

- Independent and Identically Distributed (IID): In this scenario, each client's data distribution is uniform across the dataset.
- Non-Independent Identically Distributed (Non-IID): In this scenario, the overall dataset's data distribution varies from that of each individual client.

TABLE IV. ASSESSMENT OF THE CENTRAL INTRUSION DETECTION MODEL

| Class | Accuracy | | Precision | | Recall | | F1-Score | |
|-------------------|----------|------|-----------|------|--------|------|----------|------|
| | CNN | RNN | CNN | RNN | CNN | RNN | CNN | RNN |
| Normal | 0.94 | 0.95 | 0.93 | 0.91 | 0.91 | 0.91 | 0.92 | 0.91 |
| DDoS-UDP Attack | 0.89 | 0.90 | 0.95 | 0.96 | 0.89 | 0.88 | 0.90 | 0.91 |
| DDoS-ICMP Attack | 0.83 | 0.81 | 0.80 | 0.78 | 0.88 | 0.87 | 0.83 | 0.81 |
| Uploading Attacks | 0.74 | 0.79 | 0.78 | 0.83 | 0.63 | 0.78 | 0.71 | 0.80 |
| DDoS-TCP Attack | 0.91 | 0.92 | 0.91 | 0.93 | 0.91 | 0.93 | 0.93 | 0.92 |
| Proposed model | 0.94 | 0.96 | 0.93 | 0.92 | 0.93 | 0.95 | 0.94 | 0.95 |

TABLE V. COMPARISON OF PROPOSED MODEL WITH BASELINES

| IoT IDS | Year | Dataset | Classifier | IID | Non-IID |
|-------------------|------|-----------------|------------|-----|---------|
| Nguyen et al [27] | 2020 | Private Dataset | RNN-GRU | No | Yes |
| Li et al [28] | 2021 | Gas Pipeline | CNN-GRU | Yes | Yes |
| Huong et al [29] | 2022 | Bot-IoT | LocKedge | No | Yes |
| Proposed model | 2022 | Edge-IIoTSet | CNN RNN | Yes | Yes |

C. Comparison to Related Works

Table V outlines a comparative analysis against similar methodologies encompassing various dimensions such as deployment year, datasets utilized, machine learning classifiers, number of clients, and data distribution strategies. This comparison reveals that our proposed model uniquely tackles both IID and Non-IID data issues, demonstrating effective performance across these data types as discussed in the preceding section.

D. Discussion

Utilizing Federated Learning (FL) instead of traditional Machine Learning (ML) techniques offers significant advantages for Industrial Internet of Things (IIoT) devices in terms of data security and bandwidth efficiency. By adopting FL, IIoT devices can transmit data that is not only more secure but also requires less bandwidth. This is because, in an FL setup, the vast amounts of private and sensitive information are not centralized on a single server. Instead, clients only share the outcomes of their individual local model trainings, substantially reducing bandwidth needs [13] [18]. This approach not only ensures the security of the data but also upholds the privacy of the users since the raw data remains on the device. Additionally, FL enables devices to autonomously predict and detect network anomalies, even when offline, by leveraging the local representations of the models [30]. This implies that local clients are able to persist with their model training and intrusion detection efforts, irrespective of their connectivity status. Furthermore, with an increase in the number of Federated Learning (FL) rounds, the precision of intrusion detection nears that of centralized Machine Learning (ML) models. This improvement in performance is attributed to the cumulative enhancements from client-end learnings, allowing the models to operate with the same efficacy as centralized models after each FL round.

V. CONCLUSION

This study introduces an innovative intrusion detection system that leverages federated machine learning (ML) to tackle the vital concerns of security and privacy within IoT networks. Our key goal was to identify and stop unauthorized intrusions, which would ultimately ensure the security of IoT networks. We carried out extensive experiments with a freshly created dataset called Edge-IIoTset to verify the efficacy of our strategy. These tests were conducted using two well-known ML models: CNN and RNN, on both centralised and federated systems. The experimental results showed that our suggested federated learning (FL) approach can produce competitive results in the area of intrusion detection, which was quite encouraging. Our technology demonstrated its capacity to successfully identify intrusions in IoT networks by utilizing the power of collaborative learning while protecting data privacy. We also performed a thorough comparative analysis, comparing our method to previous FL-based intrusion detection systems in independent and non-independent, identically distributed (IID and non-IID) scenarios. The studies in our research help to demonstrate the viability, applicability, and utility of our suggested approach. They greatly advance our knowledge of and ability to use federated learning in the context of IoT networks. The results of our study highlight FL's potential as a workable option for boosting the security and privacy of IoT systems.

REFERENCES

- [1] A. Thakkar and R. Lohiya, "A Review on Machine Learning and Deep Learning Perspectives of IDS for IoT: Recent Updates, Security Issues, and Challenges," *Arch. Comput. Methods Eng.*, vol. 28, no. 4, pp. 3211–3243, 2021, doi: 10.1007/s11831-020-09496-0.
- [2] Y. Li, Y. Zuo, H. Song, and Z. Lv, "Deep Learning in Security of Internet of Things," *IEEE Internet Things J.*, vol. 9, no. 22, pp. 22133–22146, 2022, doi: 10.1109/JIOT.2021.3106898.
- [3] S. Venkatraman and B. Surendiran, "Adaptive hybrid intrusion detection system for crowd sourced multimedia internet of things systems," *Multimed. Tools Appl.*, vol. 79, no. 5–6, pp. 3993–4010, 2020, doi: 10.1007/s11042-019-7495-6.
- [4] J. Asharf, N. Moustafa, H. Khurshid, E. Debie, W. Haider, and A. Wahab, "A review of intrusion detection systems using machine and deep learning in internet of things: Challenges, solutions and future directions," *Electron.*, vol. 9, no. 7, 2020, doi: 10.3390/electronics9071177.
- [5] Q. A. Al-Haija and S. Zein-Sabatto, "An efficient deep-learning-based detection and classification system for cyber-attacks in iot communication networks," *Electron.*, vol. 9, no. 12, pp. 1–26, 2020, doi: 10.3390/electronics9122152.
- [6] A. Alrawai, A. Alhothaily, C. Hu, and X. Cheng, "Fog Computing for the Internet of Things: Security and Privacy Issues," *IEEE Internet Comput.*, vol. 21, no. 2, pp. 34–42, 2017, doi: 10.1109/MIC.2017.37.
- [7] S. Yi, Z. Qin, and Q. Li, "Security and Privacy Issues of Fog Computing: A Survey BT - Wireless Algorithms, Systems, and Applications," pp. 685–695, 2015.
- [8] H.-J. Nam *et al.*, "Security and Privacy Issues of Fog Computing," *J. Korean Inst. Commun. Inf. Sci.*, vol. 42, no. 1, pp. 257–267, 2017, doi: 10.7840/kics.2017.42.1.257.
- [9] V. T.-2017 I. W. C. and and undefined 2017, "IEEE 802.11 network anomaly detection and attack classification: A deep learning approach," *ieeexplore.ieee.org*, Accessed: Mar. 08, 2023. [Online]. Available: <https://ieeexplore.ieee.org/abstract/document/7925567/>
- [10] L. Deng, "A tutorial survey of architectures, algorithms, and applications for deep learning," *APSIPA Trans. Signal Inf. Process.*, vol. 3, 2014, doi: 10.1017/ATSIP.2013.99.
- [11] Guy Caspi, "Introducing Deep Learning: Boosting Cybersecurity ...", [Online]. Available: <https://www.darkreading.com/analytics/introducing-deep-learning-boosting-cybersecurity-with-an-artificial-brain/a/d-id/1326824?>
- [12] Q. Niyaz, W. Sun, A. Y. Javaid, and M. Alam, "A deep learning approach for network intrusion detection system," *EAI Int. Conf. Bio-inspired Inf. Commun. Technol.*, 2015, doi: 10.4108/eai.3-12-2015.2262516.
- [13] L. Yuancheng, M. Rong, and J. Runhai, "A Hybrid Malicious Code Detection Method based on Deep Learning," *Int. J. Secur. Its Appl.*, vol. 9, no. 5, pp. 205–216, 2015.
- [14] A. Awajan, "A Novel Deep Learning-Based Intrusion Detection System for IoT Networks," *Computers*, vol. 12, no. 2, 2023, doi: 10.3390/computers12020034.
- [15] T. Hasan *et al.*, "Securing Industrial Internet of Things Against Botnet Attacks Using Hybrid Deep Learning Approach," *IEEE Trans. Netw. Sci. Eng.*, 2022, doi: 10.1109/TNSE.2022.3168533.
- [16] Y. Kayode Saheed, A. Idris Abiodun, S. Misra, M. Kristiansen Holone, and R. Colomo-Palacios, "A machine learning-based intrusion detection for detecting internet of things network attacks," *Alexandria Eng. J.*, vol. 61, no. 12, pp. 9395–9409, 2022, doi: 10.1016/j.aej.2022.02.063.
- [17] A. Yazdinejad, B. Zolfaghari, A. Dehghantanha, H. Karimipour, G. Srivastava, and R. M. Parizi, "Accurate threat hunting in industrial internet of things edge devices," *Digit. Commun. Networks*, 2022, doi: 10.1016/j.dcan.2022.09.010.
- [18] T. A. Al-Amiedy, M. Anbar, B. Belaton, A. H. H. Kabla, I. H. Hasbullah, and Z. R. Alashhab, "A Systematic Literature Review on Machine and Deep Learning Approaches for Detecting Attacks in RPL-Based 6LoWPAN of Internet of Things," *Sensors*, vol. 22, no. 9, 2022, doi: 10.3390/s22093400.
- [19] J. Ahmad, S. A. Shah, S. Latif, F. Ahmed, Z. Zou, and N. Pitropakis, "DRaNN PSO: A deep random neural network with particle swarm optimization for intrusion detection in the industrial internet of things," *J. King Saud Univ. - Comput. Inf. Sci.*, vol. 34, no. 10, pp. 8112–8121, 2022, doi: 10.1016/j.jksuci.2022.07.023.
- [20] R. Gupta, M. M. Patel, A. Shukla, and S. Tanwar, "Deep learning-based malicious smart contract detection scheme for internet of things environment," *Comput. Electr. Eng.*, vol. 97, 2022, doi: 10.1016/j.compeleceng.2021.107583.
- [21] U. Ahmad, "A node pairing approach to secure the Internet of Things using machine learning," *J. Comput. Sci.*, vol. 62, 2022, doi: 10.1016/j.jocs.2022.101718.
- [22] A. Mihoub, O. Ben Fredj, O. Cheikhrouhou, A. Derhab, and M. Krichen, "Denial of service attack detection and mitigation for internet of things using looking-back-enabled machine learning techniques," *Comput. Electr. Eng.*, vol. 98, 2022, doi: 10.1016/j.compeleceng.2022.107716.
- [23] A. Sagu, N. S. Gill, P. Gulia, J. M. Chatterjee, and I. Priyadarshini, "A Hybrid Deep Learning Model with Self-Improved Optimization Algorithm for Detection of Security Attacks in IoT Environment," *Future Internet*, vol. 14, no. 10, p. 301, Oct. 2022, doi: 10.3390/fi14100301.
- [24] M. A. Khan *et al.*, "A Deep Learning-Based Intrusion Detection System for MQTT Enabled IoT," *Sensors*, vol. 21, no. 21, p. 7016, Oct. 2021, doi: 10.3390/s21217016.
- [25] S. Sriram, R. Vinayakumar, M. Alazab, and K. P. Soman, "Network flow based IoT botnet attack detection using deep learning", In *IEEE INFOCOM 2020-IEEE conference on computer communications workshops (INFOCOM WKSHPS)*, pp. 189–194, 2020.
- [26] Y. Song, D. Zhang, Y. Li, "Intrusion Detection for Internet of Things Networks using Attention Mechanism and BiGRU", In *2023 5th International Conference on Electronic Engineering and Informatics (EEI)*, pp. 227–230, 2023.
- [27] S. Ali, O. Abusabha, F. Ali, M. Imran, and T. Abuhmed, "Effective Multitask Deep Learning for IoT Malware Detection and Identification Using Behavioral Traffic Analysis," *IEEE Transactions on Network and Service Management*, vol. 20, no. 2, pp. 1199–1209, Jun. 2023, doi: 10.1109/tnsm.2022.3200741.
- [28] [1]Y. Liu, T. Lin, and X. Ye, "Federated recommender systems based on deep learning: The experimental comparisons of deep learning

- algorithms and federated learning aggregation strategies,” *Expert Systems with Applications*, vol. 239, p. 122440, Apr. 2024, doi: 10.1016/j.eswa.2023.122440.
- [29] [1]O. I. Abiodun, A. Jantan, A. E. Omolara, K. V. Dada, N. A. Mohamed, and H. Arshad, “State-of-the-art in artificial neural network applications: A survey,” *Heliyon*, vol. 4, no. 11, p. e00938, Nov. 2018, doi: 10.1016/j.heliyon.2018.e00938.
- [30] S. Li, W. Li, C. Cook, C. Zhu and Y. Gao, “Independently recurrent neural network (indrnn): Building a longer and deeper rnn”, In *Proceedings of the IEEE conference on computer vision and pattern recognition*, pp. 5457-5466, 2018.

Review and Analysis of Financial Market Movements: Google Stock Case Study

Yiming LU

School of Continuing Education, Shijiazhuang College of Applied Technology, Shijiazhuang, 050081, China

Abstract—A financial marketplace where shares of companies with public listings are bought and sold is called the stock market. It serves as a gauge of a nation's economic health by taking into account the operations of individual businesses as well as the general business climate. The relationship between supply and demand affects stock prices. Though it might be dangerous, stock market investing has the potential to provide large rewards in the long run. Together with increased prediction accuracy, optimization techniques such as Biogeography-based optimization (BBO), Artificial bee colony algorithm (ABC) and Aquila Optimization (AO) Algorithm further enhance the Extreme gradient boosting (XGBoost) ability to adapt to changing market conditions. The results were 0.955, 0.966, 0.972, and 0.982 for XGBoost, BBO-XGBoost, ABC-XGBoost, and AO-XGBoost, in that order. The performance difference between AO-XGBoost and XGBoost shows how combining with the optimizer may enhance the model's performance. By comparing the output of many optimizers, the most accurate optimization has been determined to be the model's main optimizer.

Keywords—Stock future trend; financial market; investment; machine learning algorithms; Google stock

I. INTRODUCTION

A. Background knowledge

The task of forecasting stock prices is difficult [1], [2], [3], [4]. The long-term unpredictability in the market presents a significant challenge. The conventional theory of markets posits that stock valuations are inherently random and lack any discernible pattern. Nevertheless, contemporary technical analysis has provided evidence to support the notion that historical data largely influences stock prices, hence emphasizing the importance of understanding patterns of movement in order to make accurate projections [5]. Various economic factors, including political events, general economic circumstances, commodity price indicators, investor sentiment, movements in other stock markets, and investor behavior, also exert an influence on the categorization and fluctuations of stock market entities [6]. Stock values are determined through the assessment of market capitalization, which is the total worth of a company's outstanding shares. Additionally, statistical data can be derived by employing a range of technical variables [7]. Stock indexes are often constructed using the prices of equities with significant market investments, serving as a means to assess the economic conditions of various nations. Empirical evidence suggests that stock market capitalization exerts a positive impact on a country's economic growth [8]. Investments pose inherent risks due to the volatile nature of stock price fluctuations. Furthermore, ascertaining the market standing of governments

is sometimes a complex task. Due to the inherent characteristics of stock values, namely their dynamic, non-parametric, and non-linear nature, statistical models often encounter challenges in accurately predicting precise values and trends, hence diminishing their efficacy [9], [10]. Machine learning (ML) is often regarded as the most powerful technology due to its ability to leverage diverse algorithms to improve performance in specific case studies. ML is commonly acknowledged for its significant capability to identify trustworthy data and detect patterns within datasets [11], [12], [13], [14], [15]. It is imperative to acknowledge the challenging and intricate nature of projecting stock prices. Although machine learning algorithms cannot be deemed as reliable sources for generating precise forecasts, they have significantly impacted stock prediction and financial markets through many means. This paper examines the effects and contributions of ML techniques in the domain of stock prediction. ML algorithms possess the capability to analyze historical stock price data in order to identify patterns and trends that may not be readily discernible to human analysts. The individuals possess the capability to discern complex patterns inside the dataset and employ them in order to predict forthcoming fluctuations in prices [16]. Various techniques of machine learning are employed for the purpose of prediction. The model employed in this study is an Extreme gradient boosting (XGBoost). Chen et al. (2015) [17] developed XGBoost, which is effective at building boosted trees, performing parallel operations, and resolving issues related to both regression and classification. The primary aim of the method is to optimize the value of the objective function by the repeated combination of weak base learning models into a stronger learner [18]. The residual is utilized to adjust the preceding prediction so that the designated loss function may be optimized at each gradient boosting cycle. The optimizers provided for the hyperparameters optimizer of the model are Biogeography-based optimization (BBO) [19], [20], [21], Artificial bee colony algorithm (ABC) [22], [23], and Aquila Optimizer (AO) [24]. The concept of species movement based on habitat appropriateness is the foundation of biogeography-based optimization or BBO. Therefore, a solution is like a habitat for an optimization issue. A crowded environment, where the circumstances for living species are better than in other habitats, is a better answer for the population. The environment where living things struggle is the worst answer for the people. Because they share properties, the superior solutions draw in the inferior ones. Another optimization method used is ABC; three groups of bees make up the artificial bee colony in the ABC algorithm: employed bees, bystanders, and scouts. In the first half of the colony are the working artificial bees, while in

the second half are the observers. There is one working bee for each food source. Stated differently, the quantity of food sources and the number of bees engaged are the same. An employed food source bee transforms into a scout. Another optimization method which has the best result, Aquila has a dark brown plumage, with a distinct golden-brown hue seen on the posterior region of its neck. Aquila has outstanding velocity and dexterity. Furthermore, the Aquila has robust lower extremities and formidable talons. This feature facilitates the capture of diverse prey. Aquila has been identified as an adult deer assailant. Aquila builds huge nests in elevated locations like as mountains or other elevated terrains. Aquila has exceptional cognitive abilities and demonstrates remarkable proficiency in hunting people.

B. Contributions and Novelties

This study offers valuable insights into the field of stock market prediction by seeking to enhance prediction accuracy through the integration of machine learning methodologies, specifically XGBoost. The model showcases improved flexibility in response to dynamic market conditions by integrating optimization techniques such as BBO, ABC, and AO. By conducting a thorough comparison of these optimization techniques, the study systematically determines that AO-XGBoost is the most effective model, demonstrating exceptional performance in predicting stock market values. This advantageous model shows potential for incorporation into dynamic trading systems, offering lucrative suggestions for traders and investors. The effectiveness of the proposed model is further confirmed through empirical validation using real-world data from Google stock prices, which shows minimal inaccuracies in forecasting stock prices. The study's well-defined performance evaluation highlights the dependability and resilience of the AO-XGBoost model, providing practical implications for decision-making in financial markets.

II. LITERATURE REVIEW

A. Related Works

Agrawal [25] focuses on stock market forecasting using machine learning algorithms, aiming to accurately estimate future stock values. The efficient market hypothesis suggests that stock prices depend on available information, making accurate prediction crucial for investor decision-making. The paper introduces a deep learning-based non-linear regression method for stock price prediction, evaluated on Tesla and New York Stock Exchange datasets from 2010 to 2020. The results indicate superior performance compared to existing machine learning approaches [25].

Hong et al. [26] employs Bidirectional Long Short-Term Memory (BLSTM), considered more accurate than unidirectional LSTM, to forecast near-future stock prices. The dynamic nature of the stock market is likened to a living creature, requiring continuous input and analysis of data for accurate predictions through consistent monitoring with BLSTM.

Wen et al. [27] presents a stock price forecasting model using Principal Component Analysis (PCA) and Long Short-Term Memory (LSTM). PCA reduces data correlation and

dimensionality, while LSTM accurately forecasts stock prices. Experimental results on Pingan Bank data show improved accuracy compared to traditional models.

Simon et al. [28] focuses on using Artificial Neural Networks (ANN) as a dominant technique for accurate predictions. It reviews various ANN models and enhancement techniques, exploring research strategies to improve accuracy in stock market prediction.

Krollner et al. [29] interest in using machine learning for stock market prediction stems from its profit potential. Krollner et al. explores a less-explored aspect by applying ANNs in financial data mining for risk management. The goal is to leverage advances in stock market forecasting to develop hedging strategies safeguarding portfolios during market downturns. Simulation results demonstrate that ANNs offer a flexible and effective decision support tool for risk management in the Australian stock market.

B. Gaps and Fulfillment

Insufficient attention has been given to the examination of optimization techniques aimed at improving the efficacy of ML models in the context of stock price prediction within the current body of research. Many studies have primarily concentrated on experimental findings derived from specific datasets. However, there exists a dearth of comprehensive assessments encompassing diverse datasets that encompass various market conditions. To improve the performance of ML models, this research suggests integrating optimization techniques such as ABC, BBO, and AO. These techniques enhance the configuration of model parameters and enhance the precision of predictions. In order to make up for the insufficient assessment of real-world data, we conduct thorough testing on datasets that represent Google stock. The proposed model's generalizability and robustness can be guaranteed through this.

III. METHODOLOGY

A. Extreme Gradient Boosting Regression Method

A method of machine learning that uses gradient-boosting decision trees to provide regression and classification, which has been demonstrated in Fig. 1. To guarantee thorough coverage, the approach generates a sequence of weak learners, often in the form of classification regression trees. The model generates the final iteration of the regression model by averaging the weighted summation of the learners once the training procedure is complete. Regression trees are produced using the regularized and improved XGBoost regression algorithm, which helps predict continuous numerical target variables with accuracy. This approach follows the guidelines of gradient boosting, in which a new learner is introduced at construction time depending on the weak learner iteration's residual error. To reduce the overall model error, a gradient is used to generate the new learner. The XGBoost method is well known for its low computational complexity, fast speed, and great accuracy. Assume that the training sample data set D 's class labels y_i and samples x_i are represented as follows:

$$D = \{(X_1, Y_1), (X_2, Y_2) \dots (X_N, Y_N)\} \quad (1)$$

Consequently, the i^{th} sample's prediction function may be shown as follows:

$$\hat{y}_i = \sum_{k=1}^K f_k(x_i), f_k \in F \quad (2)$$

Here, $f_k(x_i)$ is the discriminating function of the K^{th} tree for the i th data, and F is the resilient structure for the k choice tree model integrating. The enhanced tree model that XGBoost uses anticipates a value using a starting tree, calculates the value's deviation from the real value, and then inserts a tree to get the deviation.

when $k = 0, \hat{y}_i^{(0)} = 0$; when $k = 1, \hat{y}_i^{(1)} = f_1(x_i) = \hat{y}_i^{(0)} + f_1(x_i)$; when we add t trees, then

$$\hat{y}_i^{(t)} = \sum_{k=1}^t f_k(x_i) = \hat{y}_i^{(t-1)} + \eta f_t(x_i), 0 < \eta < 1 \quad (3)$$

where, η is the learning rate.

The calculation of the objective function for XGBoost with the Mean Squared Error (MSE) loss function is as follows:

$$\text{Objective} = \sum_{i=1}^n (y_i - \hat{y}_i)^2 + \sum_{t=1}^T \Omega(f_t) \quad (4)$$

Preventing overfitting is achieved by regularizing the second term, which is the mean squared error between the true labels y_i and the predictions \hat{y}_i .

B. Biogeography-Based Optimization

The BBO algorithm works by modeling the movement of various species, which depends on how well-suited their specific surroundings are, as Fig. 2 illustrates. This process makes it easier to examine the complex relationships that exist between different species and their environments, which in turn leads to more accurate and trustworthy predictions about ecological patterns. Within the framework of an optimization

issue, it is possible to argue that a solution resembles a habitat. Creating densely populated habitats that offer more favorable living circumstances for a wider variety of species than other habitats is a useful tactic for handling population issues. The least desirable situation for a population is one in which living things must deal with significant issues. Because of this, the better solutions have the capacity to make the worse solutions pay attention by virtue of their shared characteristics. The sharing of attributes is accomplished by the application of the defined operators. Emigration rates show that migration is the process by which people move from a less favorable environment to a more favorable one. The assessment of a species' entrance into a certain geographic area is known as the immigration rate. When comparing a less favorable option to a more favorable one, the expected rate of migration is predicted to be higher.

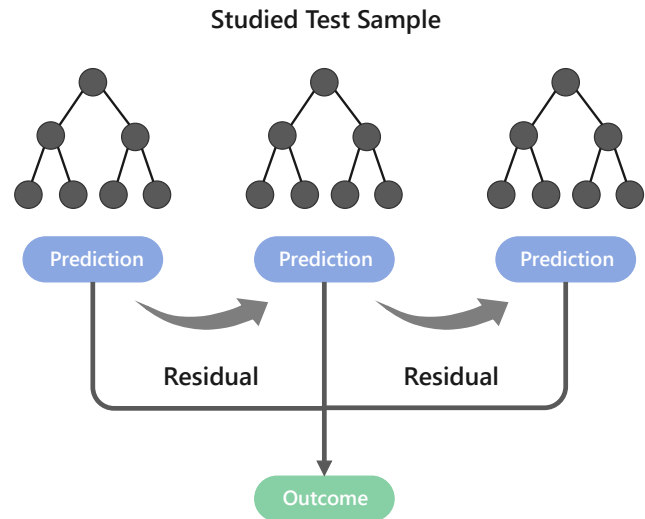


Fig. 1. The overall structure of the XGBoost.

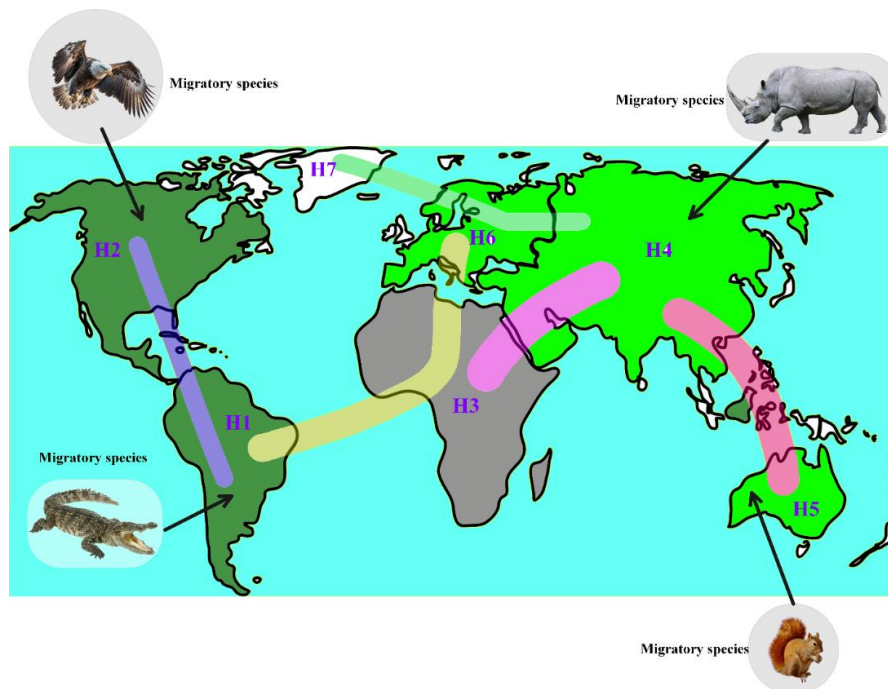


Fig. 2. Visual representation of the structure of BBO, habitats and migrations of species.

Conversely, the rate of migration pertains to the quantitative evaluation of the population size of individuals within a particular species who relocate from their habitat. As a result, it is anticipated that the rate of immigration will be higher when considering a poor solution in comparison to an optimal one. The BBO has employed the straight paths described by Eq. (5). The population size has been determined to be 100, and the epoch has been set to 500.

$$\mu_k = \frac{E \times k}{n} \lambda_k = I \left(1 - \frac{k}{n} \right) \quad (5)$$

where, μ_k is the migration amount of k^{th} habitat, λ_k represents migration amount of k^{th} habitat, I donates the maximum immigration amount, E is the maximum emigration rate, and n is the maximum amount of species that a habitat can support.

K: Number of species count.

C. Artificial Bee Colony

The ABC method is an optimization technique that draws inspiration from the intricate search and foraging activity of honey bees. It is commonly employed to address complicated issues with multiple dimensions and several modes in various domains of life. The ABC algorithm incorporates a nectar collection system within the honey bee colony, comprising nectar sources, employed bees, and unemployed bees. The unemployed bees are further categorized as bystanders and scouts. The task of the employed bees is to locate new food sources close to established ones. The observers must wait in the dance area and make a probabilistic decision regarding whether to select the food sources discovered by the employed bees, and the scouts must locate new food sources randomly [30]. During the process of nectar collection, certain workers within the beehive exhibit scouting behavior by engaging in continuous and indiscriminate search activities for food sources in close proximity to the hive. Subsequently, the researchers

discovered two distinct food sources, labeled A and B. Following the observation of the waggle dance, a subset of the prospective worker bees transitioned into the role of hired bees and commenced their exploration of the aforementioned food sources. When a scout bee discovers a food source that surpasses a specific nectar threshold, it transitions into an employed bee. This bee subsequently engages in nectar collection and afterward returns to the beehive to deposit the gathered honey into the nectar store. When a scout bee discovers a food source that surpasses a specific nectar threshold, it transitions into an employed bee. This bee subsequently engages in nectar collection and afterward returns to the beehive to deposit the gathered honey into the nectar store. When a food supply isn't replenished many times, the worker bee transforms into a scout in search of fresh food. A detailed explanation of the mathematical models related to the several stages of the ABC algorithm can be found in the following section, and the visual representation of bees are shown in Fig. 3.

For starting food sources, the following equation is shown using a random solution vector boundary value. The population size is determined to be 100 and the epoch is 500.

$$x_{i,j} = x_j^{\min} + rand(0,1)(x_j^{\max} - x_j^{\min}) \quad (6)$$

where, $i = 1, \dots, SN, j = 1, \dots, D, SN$ represents the number of solutions to be optimized, and D signifies the parameters to be optimized, where x_j^{\min} and x_j^{\max} signify the lower and upper limits of the j^{th} parameter, respectively. The aforementioned formula must be employed to ascertain the fitness value of each food source subsequent to the initiation of said food sources.

$$fit_i = \frac{1}{1 + obj \cdot fun_i} \quad (7)$$

$obj \cdot fun_i$, in this context, pertains to the intentional conduct.

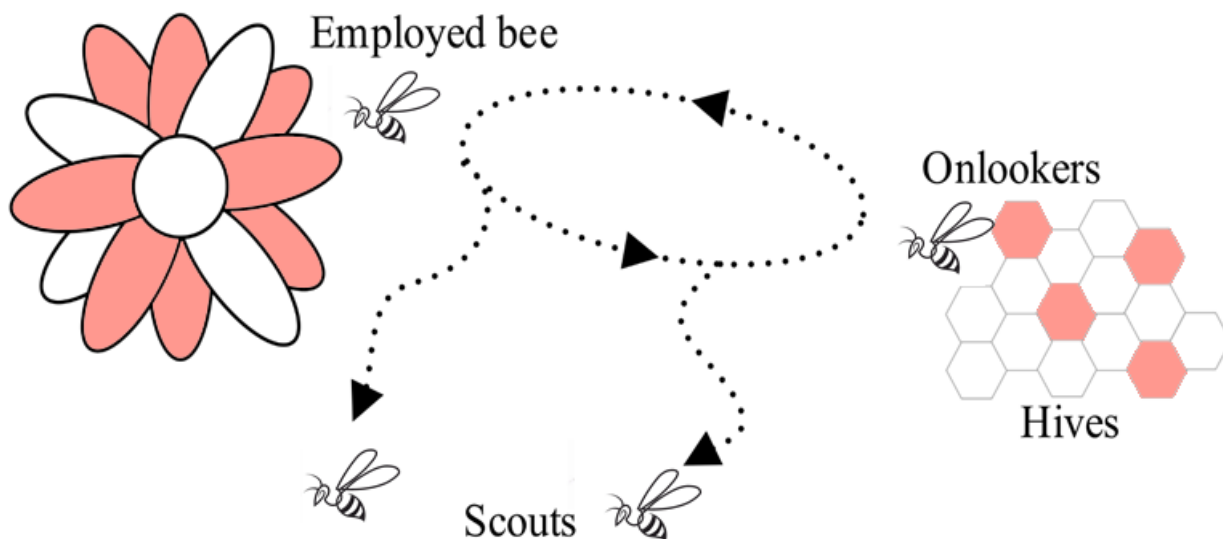


Fig. 3. The visual representation of the bees.

1) *Employed bee stage*: The quantity of responses matches the quantity of working bees and observers that SN has provided. Each active bee is supported by a single food source. By using Eq. (8) as a means to generate novel solutions, both observers and working bees engage in the exploration of proximate food sources and subsequently adjust their respective locations.

$$v_{ij} = x_{ij} + r_{ij}(x_{ij} - x_{kj}) \quad (8)$$

where, $k \neq i$; r_{ij} is a randomly generated integer between $[-1,1]$ and $j \in \{1,2, \dots, D\}$ and $k \in \{1,2, \dots, S\}$ are chosen at random. It is used to police a variety of communities. The fitness value of the new solution should be recalculated; subsequently, a comparison between the fitness values of v_{ij} and x_{ij} should be conducted, and the greater value should be selected.

2) *Onlooker bee stage*: As indicated by Eq. (9), observer bees evaluate a specific probability and measure of fitness while selecting food sources.

$$p_i = \frac{fit_i}{\sum_{n=1}^{SN} fit_n} \quad (9)$$

where, fit_i is the solution's fitness value, which is connected to the food source's relevant nectar level. Eq. (7) illustrates that when sources of food are more appropriate, people are more inclined to choose them. The employed step goes to each food location and examines it, but the observer stage only applies Eq. (8) to the food sources chosen to

produce fresh results. The spectator stage and the engaged stage are the same.

3) *State – Scout*: If the current food supply has been seen for a duration beyond the predetermined threshold, the employed bees will undergo a transformation into scout bees and start a stochastic exploration, as outlined in Eq. (6).

D. Aquila Optimization Algorithm

The AO was introduced in the year 2021 [24], as illustrated in Fig. 4, and the structure of the method is shown in Fig. 5. The following are the stages of the AO algorithm for establishing:

1) *First-class vertical dives include*: The Aquila species employs a strategic approach in identifying its prey area. It first undertakes a high-altitude flight to ascertain the optimal hunting region within the global context. This enables Aquila to effectively narrow down its search space and seek the most favorable solution. The procedure is seen in Eq. (10). The population size has been determined to be 100 individuals and the epoch has been set to 500.

$$\begin{cases} Z_1(t+1) = Z_{best}(t) \times \left(1 - \frac{t}{T}\right) \\ \quad + (Z_M(t) - Z_{best}(t) \times rand) \\ Z_M(t) = \frac{1}{N} \sum_{i=1}^N Z_i(t), \\ \forall j = 1, 2, \dots, Dim \end{cases} \quad (10)$$

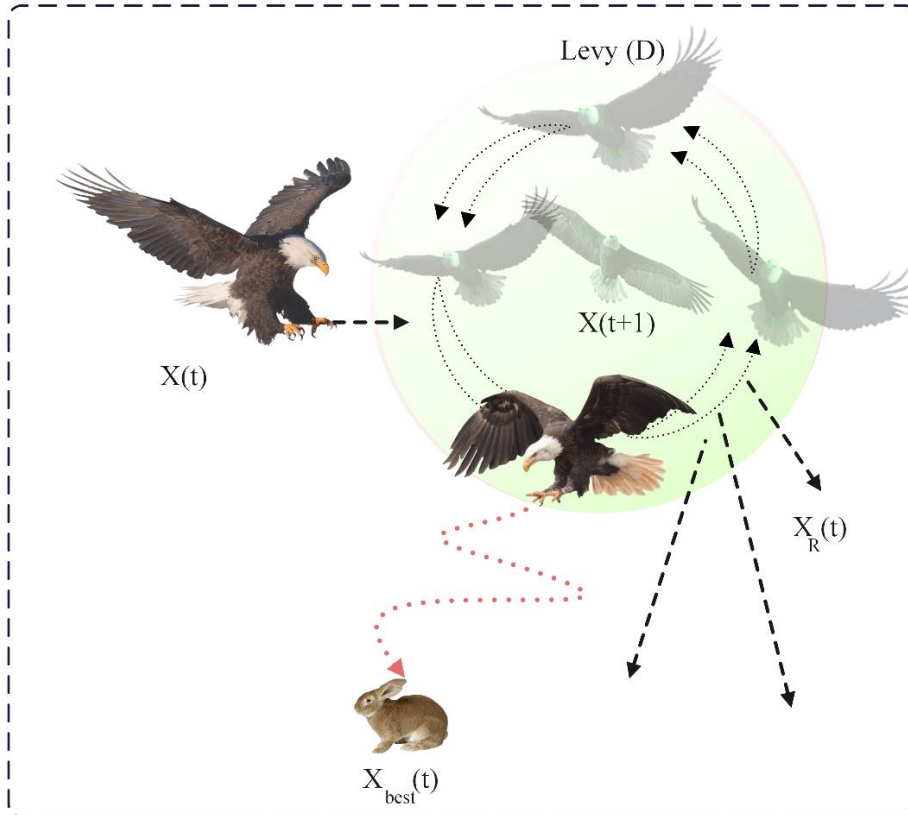


Fig. 4. Aquila optimization algorithm.

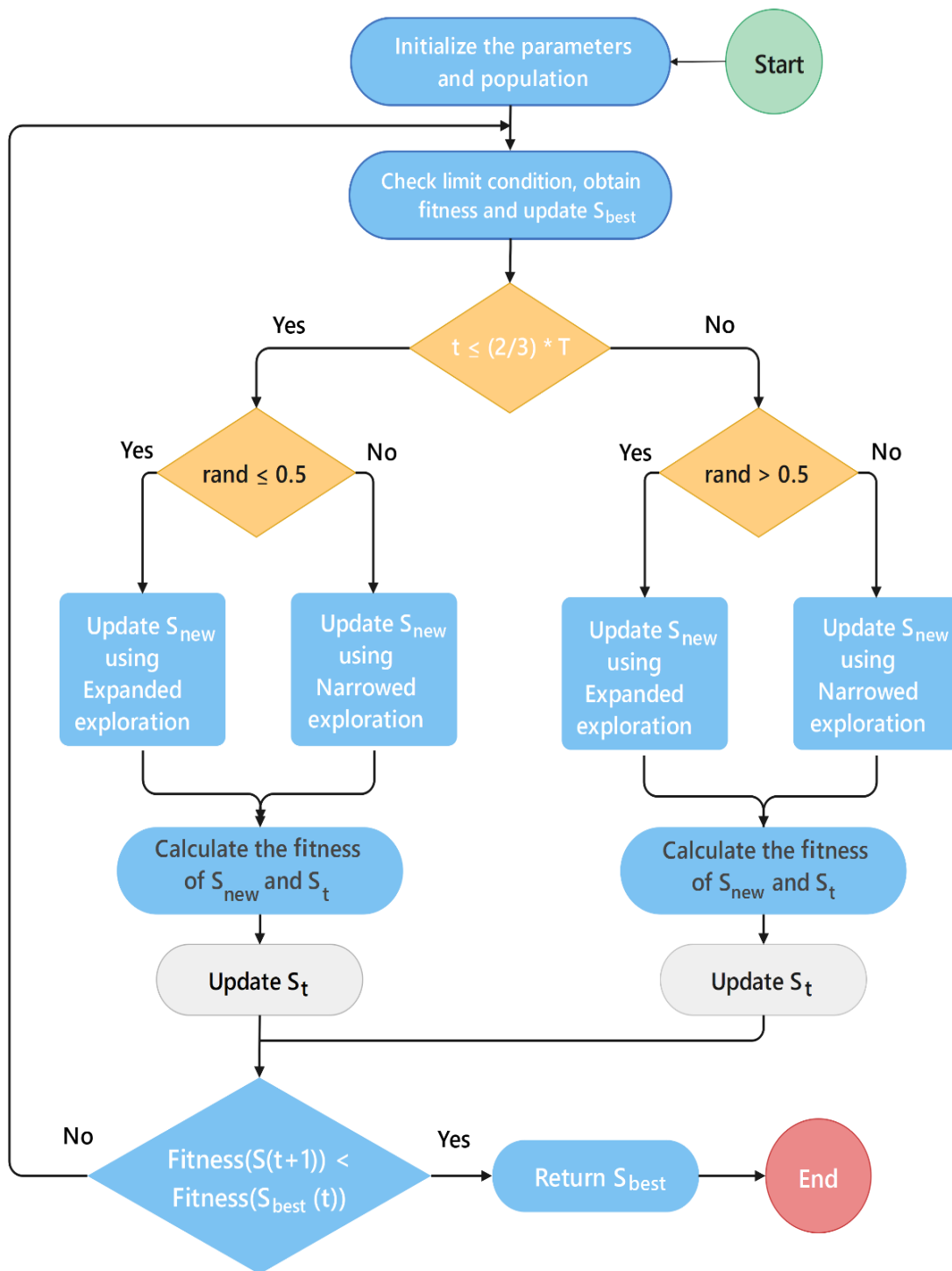


Fig. 5. Flowchart of the aquila optimization algorithm.

$Z(t + 1)$ is the formula's generation $t + 1$ solution, which was produced using the search procedure. The best strategy is Z_1 , $Z_{best}(t)$, showing the position of the nearby prey target. Number t denotes the current iteration. T stands for the maximum number of iterations that may be carried out. $Z(t)$ indicates the current solution's mean location at the t -th

iteration. An integer between 0 and 1 is referred to as a rand. The subsequent swift glide attack: The eagle descends to a height where it can detect the prey region. It then hovers above the area it plans to hunt or investigate in search of the best solution.

2) Using formula (11):

$$\begin{cases} Z_2(t+1) = Z_{best}(t) \times Z(D) \\ + Z_R(t) + (y-z) \times rand \\ L(D) = s \times \frac{\mu \times \sigma}{|v|^{\beta}} \end{cases} \quad (11)$$

The random solution, denoted as $Z_R(t)$, is a variable that takes on values between 1 and N, D represents the dimensional space, while L(D) refers to the hunting flight distribution function.

3) *The third category of flights at low altitudes:* Once the prey region has been precisely identified and the Aquila is prepared for landing and initiating an assault, it will assess the response of the prey inside the designated target area using a low-altitude and gradual descending approach, gradually closing in on the intended target. The procedure is demonstrated in Eq. (12).

$$\begin{aligned} Z_3(t+1) = & (Z_{best}(t) - Z_M(T)) \times \alpha \\ & - rand + (U_b - L_b) \\ & \times rand + L_b) \times \delta \end{aligned} \quad (12)$$

The adjustment parameters α and δ are set at a lesser value of 0.1. The variables L_b and U_b denote the bottom and upper limits, correspondingly, of the given issue.

4) *The fourth kind of walking capture:* Upon the Aquila's approach to the designated target during the same day, it engages in an aerial assault on the prey, using its superior positioning and swiftly converging on its intended objective. The procedure is shown in Eq. (13).

$$\begin{cases} Z_4(t+1) = Q_F \times Z_{best}(t) - \\ (G_1 \times Z(t) \times rand) - \\ -G_2 \times L(D) + rand \times G_1 \\ Q_F(t) = \frac{2 \times rand - 1}{t^{(1-T)^2}} \\ G_1 = 2 \times rand - 1 \\ G_2 = 2 \times \left(1 - \frac{t}{T}\right) \end{cases} \quad (13)$$

In this context, c_F denotes the quality function used to optimize the search strategy. p_1 corresponds to the diverse movements executed by the Aquila throughout its prey-hunting activities, while p_2 represents the flight slope of the Aquila during the hunting process. $Z(t)$ denotes the current solution at the t th iteration.

E. Dataset Description

Ensuring that the raw data is of exceptional quality is an essential first step towards gaining meaningful information. Data preparation is a necessary first step in order to do this. It involves many activities, including deleting irrelevant data, standardizing it for shared use, and organizing it to make it simple to retrieve important information. This is particularly relevant for large-scale data efforts when data quality is more

important than quantity. Tasks related to data preparation may also involve encoding categorical data and scaling, standardizing, normalizing, and cleaning data in compliance with industry standards. By completing these procedures, analysts may improve the accuracy and reliability of the insights they get from the data. Min-Max scalers were used to scale and normalize the data, remove any possible inconsistencies, and measure the null, missing, and unknown values as part of the project's data pre-processing step. This method is shown using data from the Google stock. This data covers the period from 2015 to the middle of 2023 and goes through a number of preliminary procedures, including normalization.

Google stock data spanning a substantial timeframe is easily accessible and frequently examined, guaranteeing the dataset's resilience and superior quality. The availability of the hybrid AO-XGBoost model enables the training and testing processes. Google is widely recognized as a prominent technology corporation, and its stock performance serves as a reliable indicator of prevailing patterns within the technology industry. The examination of Google stock can yield significant insights into the intricacies of the technology market, thereby facilitating the development of a hybrid model centered on the prediction of stock market trends. Technology stocks, such as Google, frequently demonstrate elevated levels of volatility and substantial prospects for growth. Through the examination of Google stock data, the hybrid model is capable of capturing and acquiring knowledge from the intricate patterns and trends that are inherent in unpredictable markets. This is essential for improving the model's ability to make accurate predictions. Investors and analysts show significant interest in Google's stock performance due to its widespread recognition and following. Utilizing Google stock data to develop a hybrid AO-XGBoost model can effectively engage stakeholders who possess knowledge and interest in the company, thereby enhancing the model's attractiveness and pertinence. The prominent position of Google as a dominant player in the technology industry presents a valuable occasion to evaluate the efficacy of the hybrid AO-XGBoost model in comparison to a widely recognized stock. The validation of the model's efficacy and dependability in forecasting stock market fluctuations can be achieved by juxtaposing its predictions with the actual stock performance of Google. The hybrid AO-XGBoost model for stock market prediction can benefit from utilizing Google stock data for analysis and model development.

Several charts in Fig. 6 depict histograms illustrating the distribution of data points in specific bins. These bins are evenly distributed along the x-axis, with each bar's height indicating the number of data points in the corresponding bin. Employing histograms proves valuable for scrutinizing data distribution and recognizing patterns. Examining the frequency of each variable over time aids in understanding how the data changes and responds to external factors. The graphical representation of the data in these charts is easily interpretable, helping users make informed decisions based on the presented information.

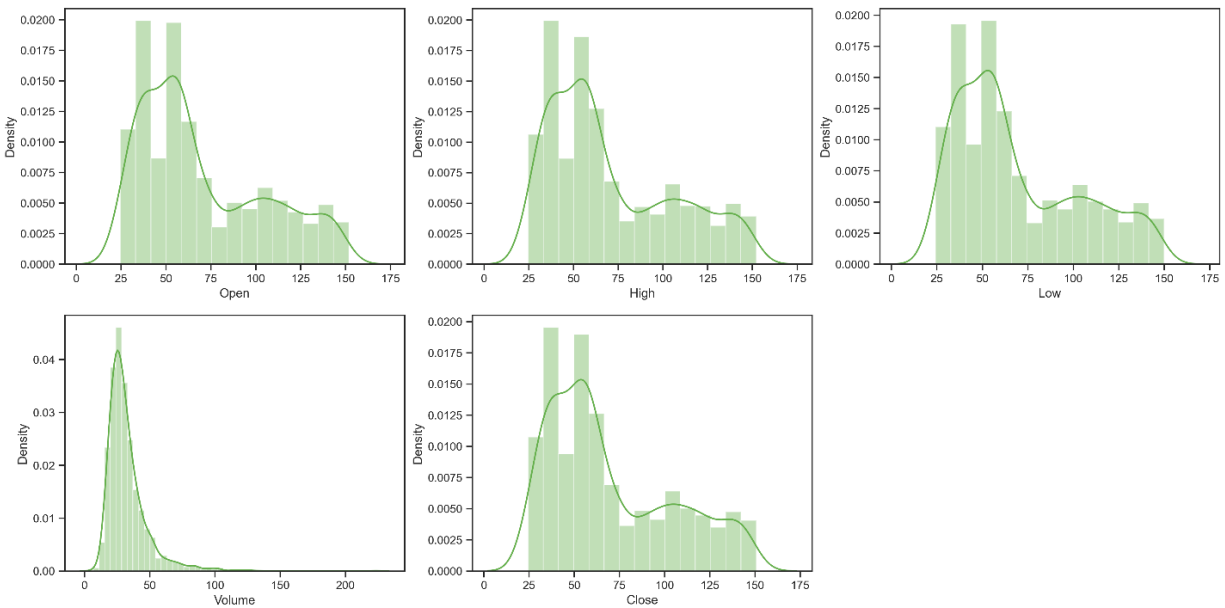


Fig. 6. Display density of variables.

Feature scaling is the process of rescaling numerical features in a dataset to a specified range, usually between zero and one. It is sometimes referred to as data preparation or Min-Max normalization. As all the characteristics are brought to the same scale, the goal is to preserve the relative relationships between the values. This could be especially important for ML algorithms that depend on the amount of input data.

$$X_{Scaled} = \frac{(X - X_{min})}{(X_{max} - X_{min})} \quad (14)$$

where, X denotes the feature's initial value that you wish to normalize, X_{min} denotes the feature's lowest value in the dataset, and X_{max} denotes the feature's maximum value in the dataset.

1) *Candlestick description*: The Candlestick chart originated in the 16th century and was created by a Japanese rice merchant who dealt with financial instruments. The chart is a hybrid of a line chart and a bar chart, where each bar visually reflects the price range within a certain time period. It is mostly used in the technical analysis of patterns in stock and currency prices. A candlestick is constructed using the open, high, low, and closing prices of the day as Fig. 7 describes the overall structure. A full candlestick is drawn when the open price is higher than the closing price.

2) *Statistical result*: The statistical properties are shown in Table I and include variance, skewness, kurtosis, mean, minimum, maximum, and standard deviation (Std.).

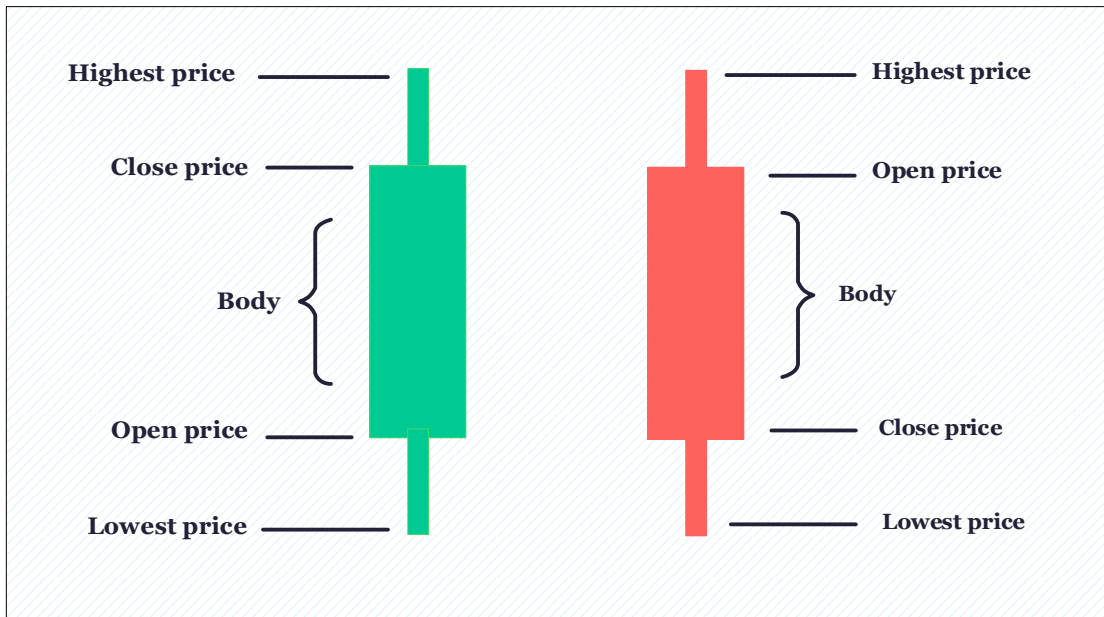


Fig. 7. Candlestick description.

TABLE I. STATISTICAL RESULTS OF THE PRESENTED DATASET

| | Open | High | Low | Volume | Close |
|----------|---------|---------|---------|--------|---------|
| Mean | 70.04 | 70.80 | 69.33 | 32.59 | 70.09 |
| Std. | 34.54 | 34.97 | 34.15 | 15.60 | 34.55 |
| Minimum | 24.65 | 24.72 | 24.31 | 6.93 | 24.55 |
| Maximum | 151.85 | 152.10 | 149.88 | 223.29 | 150.70 |
| Skewness | 0.74 | 0.73 | 0.74 | 2.87 | 0.73 |
| kurtosis | -0.62 | -0.65 | -0.61 | 16.57 | -0.63 |
| variance | 1193.42 | 1223.37 | 1165.98 | 243.54 | 1194.32 |

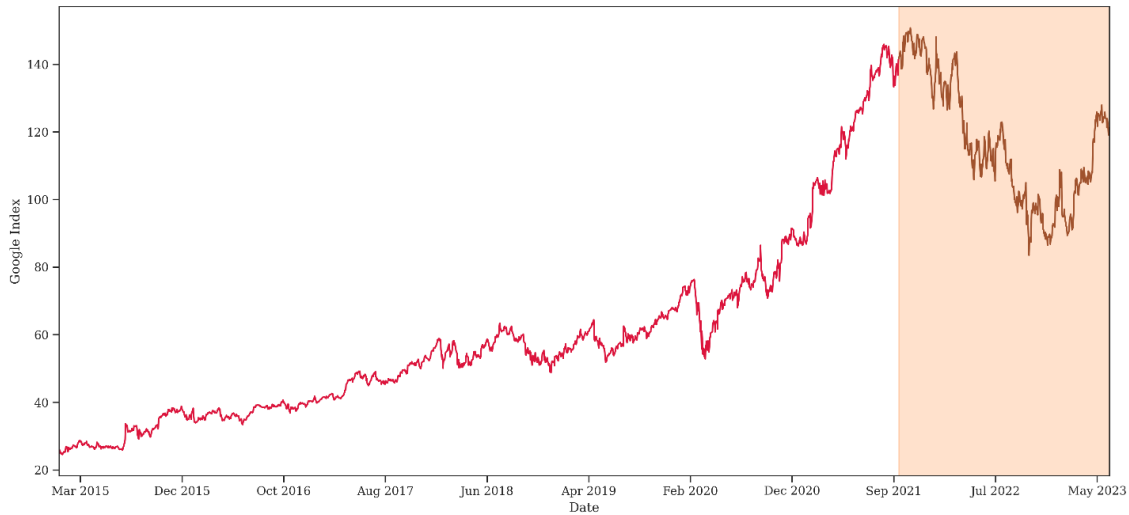


Fig. 8. Separation of the dataset into train and test.

The closing price data, which has been split into training and testing zones, is shown in Fig. 8. This approach guarantees data accuracy while assisting customers in getting accurate insights.

F. Evaluation Metrics

The following mathematical formulae were used to determine the performance metrics used in the current work: mean absolute error (MAE), mean absolute percentage error (MAPE), mean squared error (MSE), and coefficient of determination (R^2).

$$MAE = \frac{\sum_{i=1}^n |y_i - \hat{y}_i|}{n} \quad (16)$$

$$MAPE = \frac{1}{n} \sum_{i=1}^n \left| \frac{y_i - \hat{y}_i}{y_i} \right| \quad (17)$$

$$MSE = \frac{1}{n} \sum_{i=1}^n (y_i - \hat{y}_i)^2 \quad (18)$$

$$R^2 = 1 - \frac{\sum_{i=1}^n (y_i - \hat{y}_i)^2}{\sum_{i=1}^n (y_i - \bar{y})^2} \quad (19)$$

In which, \bar{y} is the mean value, y_i indicates the true value, and \hat{y}_i provides the projected value. n denotes the stock series data length.

G. Detailed Description

The data is gathered from 2015 to 2023. The unprocessed data is standardized to ensure that all characteristics are on a same scale. This aids in mitigating the algorithm's inclination towards favoring a certain trait. The normalized data is partitioned into two distinct sets: an 80% training set and a 20% test set. The training set is used to instruct the machine learning model, whilst the test set is employed to assess its performance. The XGBoost method is selected as the ML model for forecasting the closing price. XGBoost is a robust ensemble approach based on trees that has shown effectiveness in a wide range of prediction applications. The hyperparameters of the XGBoost model are fine-tuned to enhance its performance. Hyperparameters are the configuration options that govern the behavior of a model, and identifying the optimal combination of hyperparameters may have a substantial influence on the accuracy of the model. The performance of the trained AO-XGBoost model is assessed using four assessment measures. The AO-XGBoost model, which has been trained, is used to forecast the future closing price of Google stock. The forecast is derived from the analysis of past data and the acquired trends.

IV. RESULT AND DISCUSSION

A. Tuning of the Hyperparameters

Table II provides a comprehensive overview of the hyperparameter configurations for XGBoost, utilizing three distinct optimization algorithms: AO, ABC, and BBO. Each

row in the table represents a distinct hyperparameter, while each column corresponds to a particular optimizer. This hyperparameter specifies the quantity of boosting rounds or trees to construct. The range for all three optimizers (AO, ABC, BBO) is 100 to 5000. Each optimizer employs a distinct value within this range: 500 for AO, 500 for ABC, and 300 for BBO. Gamma serves as a regularization parameter that governs the level of complexity exhibited by the trees. To establish a new partition on a leaf node, the smallest loss reduction is required. The gamma values range from 0 to 10. The chosen values for each optimizer are 4.967375 for AO, 7.071759 for ABC, and 5.612515 for BBO. The L1 regularization term on weights is referred to as a hyperparameter. It promotes the reduction of weight vectors. The range of values for the variable "reg alpha" is between 0 and 5. The chosen values for each optimizer are as follows: 0.457479 for AO, 0.646517 for ABC, and 0.541563 for BBO. The term "Reg lambda" refers to the L2 regularization term applied to the weights. The term is also referred to as the Ridge regularization term. The permissible values for the regularization parameter lambda range from 0 to 1. The chosen values for each optimizer are as follows: 0.799153 for AO, 0.677998 for ABC, and 0.87415 for BBO. This hyperparameter adjusts the weight or influence of each tree in the model. It is alternatively referred to as eta. The learning rate is bounded between 0.0001 and 1. The selected values for each optimizer are 0.001 for AO, 0.0001 for ABC, and 0.01 for BBO.

B. Comparative Analysis

To assess the effectiveness of the presented models, a range of common measures was employed. These measures included MSE, MAPE, R², and MAE. These metrics offer a comprehensive overview of the prediction precision of the methods. A detailed summary of the performance metrics for four models, namely XGBoost, BBO-XGBoost, ABC-XGBoost, and AO-XGBoost, is presented in Table III. The development and evaluation of these models were based on historical stock price data for a Google stock market, spanning from the start of 2015 to the middle of 2023. This dataset was chosen to provide a comprehensive evaluation of the model's performance over a period of several years.

The results shown in Table III indicate that the AO-XGBoost model outperforms the other models in terms of forecasting accuracy; the model's success can be seen in the relatively low values for MSE, MAPE, and MAE, which show that the model was able to capture the complex temporal patterns and correlations found in stock price data. These outcomes imply that the AO-XGBoost model is a potentially useful tool for forecasting future market trends and helping investors make well-informed decisions, as it has the closest estimation curve to the actual index shown in Fig. 9 and Fig. 10. Through a comparative analysis of the four models represented by Table III, it is evident that the AO approach yielded the greatest results when it came to optimizing the model's hyperparameters among the optimization techniques utilized. BBO and ABC were the next top-performing techniques. The classification of the BBO-XGBoost, ABC-XGBoost, and AO-XGBoost models' findings is 0.966, 0.972, and 0.982, indicating an improvement in the model's performance.

These results have many practical implications for investors and financial institutions. Owing to its improved performance, AO-XGBoost could be a helpful tool for short-term stock price prediction, empowering traders to make more informed trading choices. The feature importance study also emphasizes how important it is to include historical data and sentiment analysis in prediction models. Given that these models rely on previous data, stock markets may be impacted by a variety of unanticipated events. Future research may look at using real-time data and external factors, including economic indicators and current events, to further increase prediction accuracy.

In conclusion, our research demonstrates the usefulness of machine learning models, specifically XGBoost, for stock market forecasting. Investors who understand the importance of certain features and model performance metrics might lower their risks in the erratic world of stock trading. Fig. 11 and Fig. 12 show the models' training and testing outcomes for each model.

TABLE II. SETTING OF THE HYPERPARAMETERS

| XGBoost | | AO | ABC | BBO |
|-----------------------|-------------|----------|----------|----------|
| Numbers of estimators | [100, 5000] | 500 | 500 | 300 |
| gamma | [0,10] | 4.967375 | 7.071759 | 5.612515 |
| Reg alpha | [0, 5] | 0.457479 | 0.646517 | 0.541563 |
| Reg lambda | [0, 1] | 0.799153 | 0.677998 | 0.87415 |
| Learning rate | [0.0001, 1] | 0.001 | 0.0001 | 0.01 |

TABLE III. THE OUTCOMES OF THE PERFORMANCE CRITERIA FOR MODELS

| MODEL/Metrics | TRAIN SET | | | | TEST SET | | | |
|---------------|----------------|-------|-------|--------|----------------|-------|-------|--------|
| | R ² | MAPE | MAE | MSE | R ² | MAPE | MAE | MSE |
| XGBoost | 0.960 | 3.225 | 2.729 | 29.045 | 0.955 | 2.719 | 3.182 | 14.877 |
| BBO-XGBoost | 0.982 | 3.748 | 2.427 | 13.105 | 0.966 | 2.314 | 2.679 | 11.166 |
| ABC-XGBoost | 0.985 | 2.054 | 1.702 | 11.161 | 0.972 | 2.150 | 2.438 | 9.213 |
| AO-XGBoost | 0.990 | 3.007 | 1.803 | 7.250 | 0.982 | 1.721 | 1.994 | 5.946 |

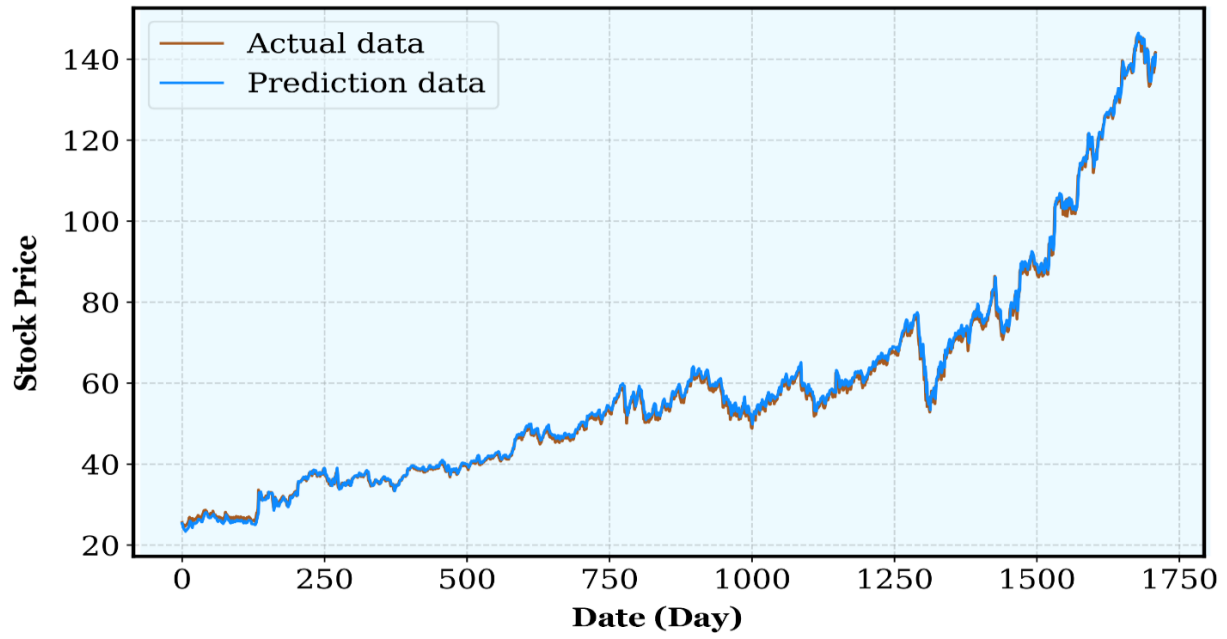


Fig. 9. AO-XGBoosts performance during training in contrast to the other models.

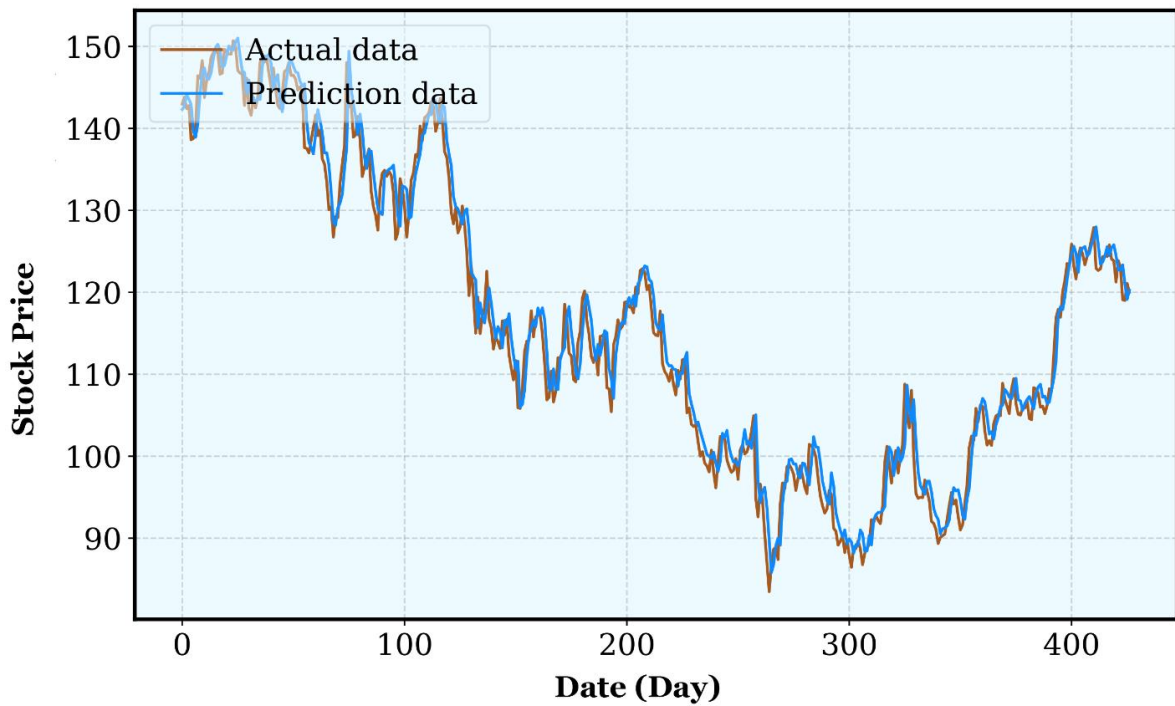


Fig. 10. AO-XGBoost's performance during testing in contrast to the other models.

TRAIN

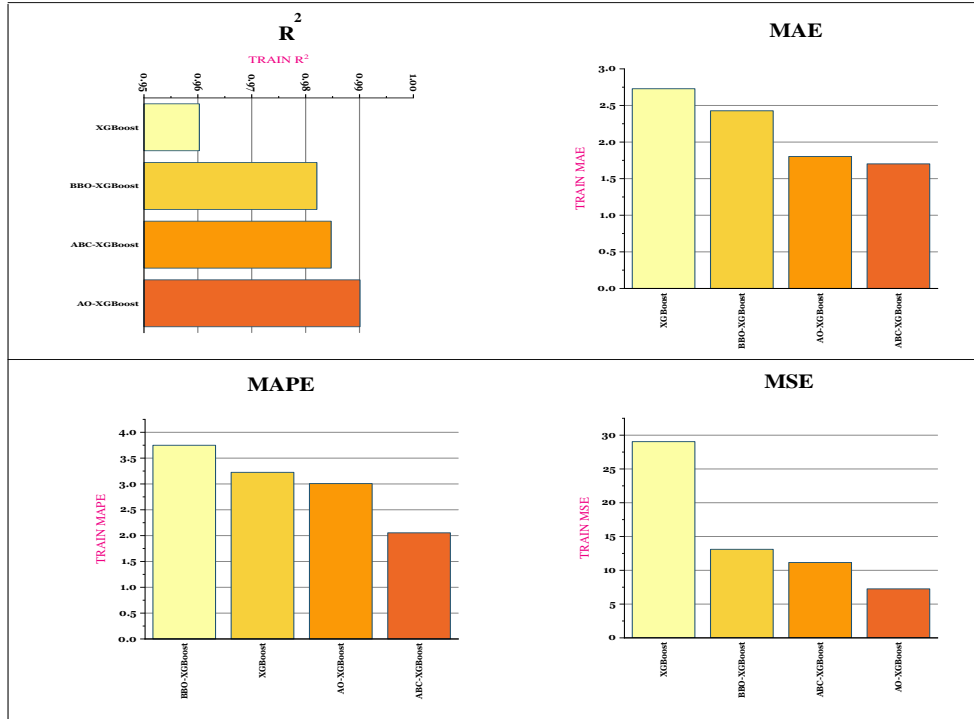


Fig. 11. The train's assessment criteria's outcome.

TEST

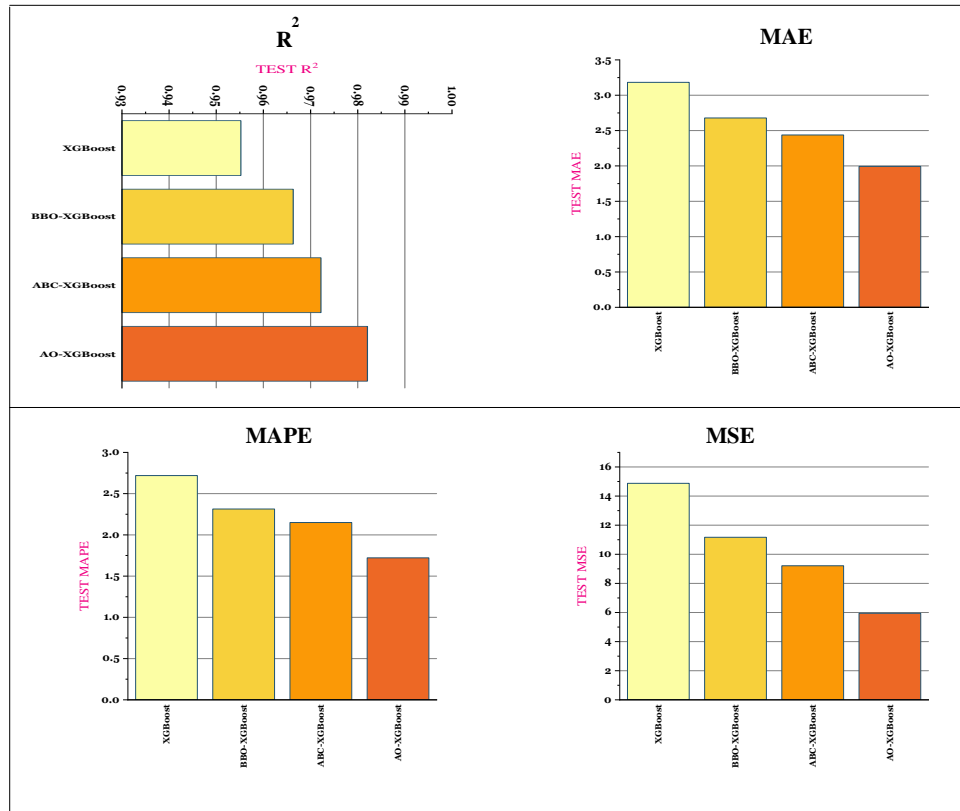


Fig. 12. The test's assessment criteria's outcome.

TABLE IV. THE MODEL COMPARISON ANALYSIS TO PRIOR STUDIES

| References | Method | R ² |
|--------------|-------------------|----------------|
| [31] | CEEMDAN-LSTM | 0.9031 |
| | LSTM | 0.6896 |
| | EMD-SC-LSTM | 0.9111 |
| | EMD-LSTM | 0.8703 |
| | SC-LSTM | 0.6871 |
| | CEEMDAN-SC-LSTM | 0.9206 |
| [32] | MLS-LSTM | 0.95 |
| | SVM | 0.93 |
| | Linear regression | 0.73 |
| Present work | | 0.982 |

The results presented in Table IV indicate that the AO-XGBoost model exhibits superior performance in the field of stock price prediction when compared to other evaluated models. Our study revealed a remarkable R^2 value of 0.982, which outperformed other evaluated models including CEEMDAN-LSTM, LSTM, EMD-SC-LSTM, EMD-LSTM, SC-LSTM, CEEMDAN-SC-LSTM, SVM, Linear Regression, and MLS-LSTM. This observation suggests a higher degree of correlation between the projected and observed stock prices, implying that the model exhibits greater efficacy in capturing the fundamental patterns within the data. The AO-XGBoost model acquires the ability to dynamically modify its parameters during training by incorporating adaptive optimization techniques. This capability enables the system to adjust to the intricacies of the data and enhance its capacity to manage fluctuations and intricacies within the stock market. The utilization of the XGBoost ensemble learning algorithm is effective in capturing nonlinear relationships and interactions within the data. This algorithm combines the strengths of gradient boosting with tree-based models. The utilization of ensemble learning in XGBoost, wherein multiple weak learners are combined to form a strong learner, serves to augment the predictive accuracy and robustness of the model. Furthermore, the regularization techniques employed by XGBoost serve to mitigate the issue of overfitting and enhance the overall generalization performance. The inclusion of this feature guarantees the model's ability to generalize to unfamiliar data, which is a critical factor in predicting stock market trends where data distributions may vary over time. In addition, the scalability and efficiency of XGBoost render it well-suited for the management of extensive datasets and the execution of real-time prediction tasks. Due to its distributed computing capabilities, parallel processing is facilitated, leading to enhanced efficiency in both training and inference processes. The AO-XGBoost model is highly suitable for real-time applications that require prompt predictions. Furthermore, the accessibility of the model is improved by the clarity of XGBoost's decision-making process.

The AO-XGBoost model has demonstrated promising accuracy in predicting short-term stock prices. These forecasts can assist investors in maximizing profits and mitigating risks in the stock market. It may be advantageous to incorporate high-performing XGBoost models such as BBO-XGBoost or ABC-XGBoost into algorithmic trading systems. These

systems can autonomously execute buy or sell orders on the predictions made by the model, thereby enabling traders to take advantage of short-term market fluctuations. It may be worthwhile to investigate risk management solutions for financial institutions that utilize XGBoost models to forecast market trends. Accurate forecasts of stock prices and market volatility have the potential to assist institutions in evaluating and mitigating risks associated with their investment portfolios. It is advisable to develop investor portfolio management tools that utilize XGBoost models to enhance asset allocation and diversification. XGBoost stock price forecasts can be utilized by investors to construct portfolios that optimize returns and mitigate market risk. An alternative approach entails the utilization of XGBoost models in financial advisory services to generate tailored investment recommendations. Financial advisors can customize guidance based on individual client's investment objectives and risk tolerance through the examination of past stock market data and the utilization of sophisticated machine learning techniques. It may be intriguing to develop trading signal platforms that offer real-time buy or sell signals using XGBoost models. Traders can subscribe to these platforms to receive timely notifications and alerts, enabling them to make well-informed trading decisions in rapidly changing markets. Enhancing the accuracy, robustness, and scalability of XGBoost stock market forecasting models through research and development could yield advantageous outcomes. Enhancing machine learning methods enables researchers to enhance predictive models for intricate market dynamics and patterns. These illustrations indicate that XGBoost models have the potential to be employed in various domains such as stock market prediction, investment tactics, algorithmic trading, risk mitigation, and financial advisory consulting. The predictive capabilities of XGBoost models can assist stakeholders in making more informed decisions and effectively navigating the stock market.

V. CONCLUSION

The trading system may provide profitable buy, sell, and hold recommendations. Traders and investors may benefit from the forecasts. The successful model from this study is intended to be applied to the dynamic trading system. Either an automated stock market system or a dynamic trading system may include this method. Thus, it is possible to forecast stock prices in the future with little inaccuracy. In this study, a novel

model XGBoost network optimized using the AO is proposed. The AO-XGBoost is the suggested model. The suggested model seeks to forecast stock market values. Stock market prices are predicted using data from Google stock prices. The dataset covers the months of 2015 to mid-2023. The data is separated into 80% train data and 20% test data after normalization. With parameters, a new XGBoost network is constructed. The AO algorithm variables are linked to the parameters. The design of the XGBoost adapts to changes in the variables. To get the best outcomes, AO selects the optimal design. The newly suggested model is compared to the XGBoost, ABC-XGBoost, and BBO-XGBoost networks in order to assess its quality. The results unequivocally demonstrate that, out of all the models, the AO-XGBoost model is the best. It also provides very accurate forecasts.

Although the proposed AO-XGBoost model has demonstrated impressive performance in predicting stock prices, it is important to take into account several limitations. The utilization of historical data derived from Google stock prices within a designated time period may not comprehensively capture the complexities and fluctuations inherent in the wider stock market. Furthermore, although optimization techniques such as BBO, ABC, and AO strive to improve the model's ability to adjust, there is a possibility of overfitting the training data, which could undermine its ability to apply the model to new market conditions. Furthermore, the model's susceptibility to parameter selection and the computational burden involved in determining optimal values present practical obstacles. Moreover, the model's forecasting accuracy is limited by the inherent unpredictability of market dynamics, which is influenced by various factors including geopolitical events and investor sentiments. The implementation and interpretation of the AO-XGBOOST model in real-world trading environments may be impeded by its complexity, thereby restricting its applicability for practitioners with diverse levels of technical proficiency. Therefore, it is imperative to recognize and tackle the limitations of the AO-XGBoost model in order to ensure its successful implementation in dynamic financial markets, despite the promising insights it provides.

REFERENCES

- [1] S. Asadi, E. Hadavandi, F. Mehmanpazir, and M. M. Nakhostin, "Hybridization of evolutionary Levenberg-Marquardt neural networks and data pre-processing for stock market prediction," *Knowl Based Syst*, vol. 35, pp. 245–258, 2012, doi: <https://doi.org/10.1016/j.knsys.2012.05.003>.
- [2] S. Gupta, V. Tyagi, M. Aadil, and N. Kumari, "Forecasting Stock Market's Performance Based on Grasshopper Optimized Hybrid Neural Network Method," *International Journal of Intelligent Systems and Applications in Engineering*, vol. 11, no. 8s, pp. 164–170, 2023.
- [3] S. Gupta, V. Tyagi, M. Aadil, and N. Kumari, "Forecasting Stock Market's Performance Based on Grasshopper Optimized Hybrid Neural Network Method," *International Journal of Intelligent Systems and Applications in Engineering*, vol. 11, no. 8s, pp. 164–170, 2023.
- [4] Y. Xu, J. Liu, F. Ma, and J. Chu, "Liquidity and realized volatility prediction in Chinese stock market: A time-varying transitional dynamic perspective," *International Review of Economics and Finance*, vol. 89, no. PA, pp. 543–560, 2024, doi: [10.1016/j.iref.2023.07.083](https://doi.org/10.1016/j.iref.2023.07.083).
- [5] S. Akhter and M. A. Misir, "Capital markets efficiency: evidence from the emerging capital market with particular reference to Dhaka stock exchange," *South Asian Journal of Management*, vol. 12, no. 3, p. 35, 2005.
- [6] K. Miao, F. Chen, and Z. G. Zhao, "Stock price forecast based on bacterial colony RBF neural network," *Journal of Qingdao University (Natural Science Edition)*, vol. 2, no. 11, 2007.
- [7] J. Lehoczky and M. Schervish, "Overview and History of Statistics for Equity Markets," *Annu Rev Stat Appl*, vol. 5, pp. 265–288, 2018, doi: [10.1146/annurev-statistics-031017-100518](https://doi.org/10.1146/annurev-statistics-031017-100518).
- [8] A. Aali-Bujari, F. Venegas-Martínez, and G. Pérez-Lechuga, "Impact of the stock market capitalization and the banking spread in growth and development in Latin American: A panel data estimation with System GMM," *Contaduría y administración*, vol. 62, no. 5, pp. 1427–1441, 2017.
- [9] M. P. Naeini, H. Tarehian, and H. B. Hashemi, "Stock market value prediction using neural networks," in *2010 international conference on computer information systems and industrial management applications (CISIM)*, IEEE, 2010, pp. 132–136.
- [10] B. Qian and K. Rasheed, "Stock market prediction with multiple classifiers," *Applied Intelligence*, vol. 26, no. 1, pp. 25–33, 2007, doi: [10.1007/s10489-006-0001-7](https://doi.org/10.1007/s10489-006-0001-7).
- [11] E. S. Olivas, J. D. M. Guerrero, M. Martínez-Sober, J. R. Magdalena-Benedito, and L. Serrano, *Handbook of research on machine learning applications and trends: Algorithms, methods, and techniques: Algorithms, methods, and techniques*. IGI global, 2009.
- [12] M. M. Kumbure, C. Lohrmann, P. Luukka, and J. Porras, "Machine learning techniques and data for stock market forecasting: A literature review," *Expert Syst Appl*, vol. 197, no. February, 2022, doi: [10.1016/j.eswa.2022.116659](https://doi.org/10.1016/j.eswa.2022.116659).
- [13] J. Grudniewicz and R. Ślepaczuk, "Application of machine learning in algorithmic investment strategies on global stock markets," *Res Int Bus Finance*, vol. 66, 2023, doi: [10.1016/j.ribaf.2023.102052](https://doi.org/10.1016/j.ribaf.2023.102052).
- [14] H. N. Bhandari, B. Rimal, N. R. Pokhrel, R. Rimal, K. R. Dahal, and R. K. C. Khatri, "Predicting stock market index using LSTM," *Machine Learning with Applications*, vol. 9, no. February, p. 100320, 2022, doi: [10.1016/j.mlwa.2022.100320](https://doi.org/10.1016/j.mlwa.2022.100320).
- [15] H. N. Bhandari, B. Rimal, N. R. Pokhrel, R. Rimal, K. R. Dahal, and R. K. C. Khatri, "Predicting stock market index using LSTM," *Machine Learning with Applications*, vol. 9, no. May, p. 100320, 2022, doi: [10.1016/j.mlwa.2022.100320](https://doi.org/10.1016/j.mlwa.2022.100320).
- [16] B. Mahesh, "Machine learning algorithms-a review," *International Journal of Science and Research (IJSR)*[Internet], vol. 9, no. 1, pp. 381–386, 2020.
- [17] T. Chen et al., "Xgboost: extreme gradient boosting," *R package version 0.4-2*, vol. 1, no. 4, pp. 1–4, 2015.
- [18] J. H. Friedman, "Greedy function approximation: a gradient boosting machine," *Ann Stat*, pp. 1189–1232, 2001.
- [19] D. Simon, "Biogeography-based optimization," *IEEE Transactions on Evolutionary Computation*, vol. 12, no. 6, pp. 702–713, 2008, doi: [10.1109/TEVC.2008.919004](https://doi.org/10.1109/TEVC.2008.919004).
- [20] A. K. Bansal, V. S. Sangtani, P. Dadheech, N. Aneja, and U. Yahya, "Biogeography-based Optimization of Artificial Neural Network (BBO-ANN) for Solar Radiation Forecasting," *Applied Artificial Intelligence*, vol. 37, no. 1, 2023, doi: [10.1080/08839514.2023.2166705](https://doi.org/10.1080/08839514.2023.2166705).
- [21] V. Garg, K. Deep, K. A. Alnowibet, H. M. Zawbaa, and A. W. Mohamed, "Biogeography Based optimization with Salp Swarm optimizer inspired operator for solving non-linear continuous optimization problems," *Alexandria Engineering Journal*, vol. 73, pp. 321–341, 2023, doi: <https://doi.org/10.1016/j.aej.2023.04.054>.
- [22] F. Y. Partovi and M. Anandarajan, "Classifying inventory using an artificial neural network approach," *Comput Ind Eng*, vol. 41, no. 4, pp. 389–404, 2002, doi: [https://doi.org/10.1016/S0360-8352\(01\)00064-X](https://doi.org/10.1016/S0360-8352(01)00064-X).
- [23] D. Karaboga, "Artificial bee colony algorithm," *scholarpedia*, vol. 5, no. 3, p. 6915, 2010.
- [24] L. Abualigah, D. Yousri, M. Abd Elaziz, A. A. Ewees, M. A. A. Alqaness, and A. H. Gandomi, "Aquila Optimizer: A novel meta-heuristic optimization algorithm," *Comput Ind Eng*, vol. 157, p. 107250, 2021, doi: <https://doi.org/10.1016/j.cie.2021.107250>.
- [25] S. C. Agrawal, "Deep learning based non-linear regression for Stock Prediction," *IOP Conference Series: Materials Science and Engineering*;

- volume 1116, issue 1, page 012189 ; ISSN 1757-8981 1757-899X, 2021, doi: 10.1088/1757-899x/1116/1/012189.
- [26] S. Hong and J. Han, "Stock Price Prediction by Using BLSTM (Bidirectional Long Short Term Memory)," *Journal of Computational and Theoretical Nanoscience*; volume 18, issue 5, page 1614-1617; ISSN 1546-1955, 2021, doi: 10.1166/jctn.2021.9603.
- [27] Y. Wen, P. Lin, and X. Nie, "Research of Stock Price Prediction Based on PCA-LSTM Model," *IOP Conference Series: Materials Science and Engineering*; volume 790, issue 1, page 012109; ISSN 1757-8981 1757-899X, 2020, doi: 10.1088/1757-899x/790/1/012109.
- [28] S. Simon and A. Rao, "Accuracy Driven Artificial Neural Networks in Stock Market Prediction," Jan. 2012, [Online]. Available: <https://zenodo.org/record/7389464>.
- [29] B. Krollner, B. J. Vanstone, and G. Finnie, "Risk management in the Australian stock market using Artificial Neural Networks," Krollner , B , Vanstone , B J & Finnie , G 2012 , ' Risk management in the Australian stock market using Artificial Neural Networks ' , *Australian Journal of Intelligent Information Processing Systems* , vol. 13 , no. 2 , pp. 1-12 ., 2012, [Online]. Available: <https://research.bond.edu.au/en/publications/cedf77f8-58cc-41d4-979b-d9baad2ad936>.
- [30] D. Karaboga and B. Basturk, "A powerful and efficient algorithm for numerical function optimization: artificial bee colony (ABC) algorithm," *Journal of global optimization*, vol. 39, pp. 459–471, 2007.
- [31] R. Zhu, G.-Y. Zhong, and J.-C. Li, "Forecasting price in a new hybrid neural network model with machine learning," *Expert Syst Appl*, vol. 249, p. 123697, 2024, doi: <https://doi.org/10.1016/j.eswa.2024.123697>.
- [32] A. Q. Md et al., "Novel optimization approach for stock price forecasting using multi-layered sequential LSTM," *Appl Soft Comput*, vol. 134, p. 109830, 2023, doi: <https://doi.org/10.1016/j.asoc.2022.109830>.

Prediction of Financial Markets Utilizing an Innovatively Optimized Hybrid Model: A Case Study of the Hang Seng Index

Xiaopeng YANG

School of Economics and Management, Weifang University, Weifang 261061, Shandong, China

Abstract—Stock trading is a highly consequential and frequently discussed subject in the realm of financial markets. Due to the volatile and unpredictable nature of stock prices, investors are perpetually seeking methods to forecast future trends in order to minimize losses and maximize profits. Nevertheless, despite the ongoing investigation of various approaches to optimize the predictive efficacy of models, it is indisputable that a method for accurately forecasting forthcoming market trends does not yet exist. A multitude of algorithms are currently being employed to forecast stock prices due to significant developments that have occurred in recent years. An innovative algorithm for predicting stock prices are examined in this paper which is a Gated Recurrent Unit combined with the Aquila optimizer. A comprehensive data implementation utilizing the Hang Seng Index stock price was executed as a dataset of this research which was collected between the years of 2015 and the end of June 2023. In the study, several additional methods for predicting stock market movements are also detailed. A comprehensive comparative analysis of the stock price prediction performances of the aforementioned algorithms has also been carried out to offer a more in-depth analysis and then the results are displayed in an understandable tabular and graphical manner. The proposed model obtained the values of 0.9934, 0.71, 143.62, and 36530.58, for R^2 , MAPE, MAE, and MSE, respectively. These results proved the efficiency and accuracy of the suggested method and it was determined that the proposed model algorithm produces results with a high degree of accuracy and performs the best when it comes to forecasting a time series or stock price.

Keywords—Financial markets; stock future trend; Hang Seng Index; Gated Recurrent Units; Aquila Optimizer

I. INTRODUCTION

The stock market, as defined, is a marketplace wherein individuals engage in the buying and selling of stocks associated with certain companies. Over time, the values of these stocks exhibit significant fluctuations. Nevertheless, it would be unwise to disregard the factors contributing to the significant fluctuations in the stock market, which may include political influences, brand perception, and the prevailing global conditions. The aforementioned elements have the ability to significantly influence the perspectives and convictions of prospective investors, hence contributing to fluctuating patterns in the stock market. Hence, while it is crucial to comprehend the potential variables contributing to these fluctuations, it remains insufficient to devise a methodology that can reliably forecast trends in light of perpetual worldwide transformations

and uncertainties [1]. Given the inherent unpredictability and significant market volatility, a considerable number of individuals interested in the stock market want to acquire a tool or method that can dependably forecast market trends, so enabling them to achieve more profitability [1]. Nonetheless, persistent endeavors are being undertaken to construct a model or algorithm that can assist investors in forecasting changes with more precision than previously achieved. The utilization of machine learning (ML) algorithms is a prevalent and well-accepted approach for constructing predictive models [2]. ML is a computational paradigm in which computers acquire information and make predictions based on previous experiences and training, without relying on external programming [2]. A few approaches and algorithms linked to ML have been investigated and addressed in [3-5]. Many advancements in data science and ML have occurred in the last few years, which have led to the creation of certain specific algorithms that are highly effective for predictive analytics across all sectors. Among the models examined in this article is GRU, a subfield of machine learning.

Recurrent neural networks (RNNs), such as Gated Recurrent Units (GRUs) [5], are used to handle sequential data, including time series. It was presented as an abridged form of the long short-term memory (LSTM) architecture. GRU is intended to address the vanishing gradient issue in RNNs and allow the network to store data over extended sequences, much like LSTM. The GRU model has one fewer gate structure than the LSTM; it consists of an update gate and a reset gate. It has been demonstrated that GRU performs comparably to LSTM while processing time series data, therefore this difference in operation impact is not very important. Compared to LSTM, GRU can converge more quickly because of its streamlined structure, which also speeds up training. Applications for the GRU model include speech recognition, video analysis, and natural language processing [5]. GRU was utilized by Ya Gao et al. [6] to predict stocks. GRU Neural Network Based on CEEMDAN-Wavelet was utilized by Chenyang Qi et al. [7] to predict stock prices.

The accuracy of predicting the value of the stock market rose as optimizers were developed and combined with a range of models to provide better outcomes in the predictions. Among the optimizers that were demonstrated were the whale optimization algorithm (WOA) [8], biogeography-based optimization (BBO) [9], genetic algorithm (GA) [10], moth-flame optimization (MFO) [11], ant lion optimization (ALO) [12], grey wolf optimization (GWO) [13], and Aquila

optimizer (AO) [14]. The most recent method to replicate the four distinct stages of Aquila hunting behavior is the AO, which was put out by Abualigah et al. [14]. Aquila employs four main hunting techniques: strolling and capturing prey, contour flying with a brief glide, low flying with a slow drop, and high soar with a vertical stoop [15]. These four core Aquila hunt processes served as the inspiration for the creation of the AO, a nature-inspired optimization algorithm that fundamentally clarifies the actions of each hunt stage. Initialization, Expanded Exploration, Narrowed Exploration, Expanded Exploitation, and Narrowed Exploitation are the five main processes that the traditional AO concentrates on. One of the most important aspects of the algorithm, the current iteration maximum iteration, usually guides the AO algorithm from the exploration to the exploitation stage. The exploration phase will be activated if the condition mentioned is true; otherwise, the exploitation step will be carried out [15].

From the commencement of 2015 until the conclusion of June 2023, daily transaction data from the Hang Seng Index (HSI) was collected, encompassing the following metrics: opening price, closing price, highest price, lowest price, and trading volume. To assess the reliability of each model, the research looked at a variety of models, including GRU, ALO-GRU, GWO-GRU, and AO-GRU. For this post, the AO-GRU model was selected since it has the best performance. The rest of the paper is structured as follows. The literature review is given in the Section II. Numerous analytical methods, including optimizer approaches, and the GRU model along with the dataset were provided in Section III. The study's findings are provided in Section IV and their discussions are demonstrated in Section V. Section VI provides a quick summary of the research's findings.

II. LITERATURE REVIEW

In recent years, there has been a significant increase in the utilization of machine learning algorithms for the purpose of forecasting the stock market. A comparative study of fundamental analysis, technical analysis, and machine learning (ML) approaches was what Christanto et al. [16] proposed as an investigation into methodologies utilized in the capital market to forecast stock prices. For predicting stock prices, they employed Support Vector Regression (SVR) and Support Vector Machine (SVM) as ML techniques. Technical-only (TEC), financial statement-only (FIN), and a combination of the two (COM) parameter groups are assessed. Financial statement integration had a neutral effect on SVR predictions but a positive effect on SVM predictions, according to their experiments. The model achieved an accuracy rate of 83% in the conducted study. Chen et al. [17] examined the historical backdrop of economic recessions, highlighting the sudden and catastrophic consequences of occurrences such as the 2008 financial crisis, characterized by a substantial decrease in the SP 500. Driven by the prospective advantages of timely crisis detection, they implemented sophisticated machine learning methodologies, including Random Forest and Extreme Gradient Boosting, to forecast possible market downturns in the United States. Comparing the performance of these approaches, their research seeks to ascertain which model is more accurate at predicting US stock market crashes. Market indicators for crisis prediction were analyzed by employing

daily financial market data and 75 explanatory variables, which encompass general US stock market indexes as well as sector indexes. By employing particular classification metrics, they derived conclusions concerning the efficacy of their predictive models. Tsai et al. [18] discussed investors' interest in stock prediction, especially with the recent use of machine learning to improve accuracy. Machine learning works in technical, fundamental, and sentiment analysis, according to prior research. They discussed fiscal year-end selection and how misaligned reporting periods affect comparability and investment decisions. They emphasized synchronized fiscal years and use machine learning models for fundamental analysis to forecast Taiwan (TW) stock market returns. They created stock portfolios with higher predicted returns using Random Forest (RF), Feedforward Neural Network (FNN), Gated Recurrent Unit (GRU), and Financial Graph Attention Network (FinGAT) models. These portfolios outperformed TW50 index benchmarks in returns and portfolio scores, according to their study. Machine learning models were beneficial for stock market analysis and investment decision-making, according to Tsai et al. [18]. Ardakani et al. [19] proposed a federated learning framework for stock market prediction using Random Forest, Support Vector Machine, and Linear Regression models. They compared federated learning to centralized and decentralized frameworks to find the best approach. Federated learning outperformed centralized and decentralized frameworks in Mean Square Error (MSE) using Random Forest (0.021) and Support Vector Machine (37.596). Linear regression model-based centralized learning (MSE = 0.011) outperformed federated and decentralized frameworks. Federated learning had a lower model training delay than benchmarks for Linear Regression (9.7 s) and Random Forest (515 s), while decentralized learning saves time for Support Vector Machine (3847 s). Their findings illuminated stock market prediction learning framework strategies [19]. A novel stock price prediction method by Mamluatul et al. [20] uses machine learning, stock price data, technical indicators, and Google trends. SVR, MLP, and Multiple Linear Regression were used to predict stock prices. SVR predicts Indonesian stock prices better than MLP and Multiple Linear Regression with a MAPE of 0.50%. They found that SVR predicts stock prices accurately, helping investors make informed stock market decisions [20]. The importance of stock market forecasts in financial market profits was stressed by Juare et al. [21]. Their research used Random Forest, Support Vector Machine, KNN, and Logistic Regression to predict stock market trends. These algorithms are evaluated using accuracy, recall, precision, and F-Score. The main goal was to find the best stock market prediction algorithm. Effective forecasts can benefit stock exchanges and investors, highlighting the importance of predictive models in financial decision-making [21]. Swathi et al. [22] emphasized the need for investors to use stock price prediction (SPP) models in the global financial market for profit. Earlier SPP models used statistical and machine learning (ML) methods. In their study, the authors introduced SCODL-SPP, a stock price prediction method using Sine Cosine Optimization (SCO) and deep learning. The SCODL-SPP model forecasts share closing prices using deep learning and a stacked long short-term memory (SLSTM) model. The SLSTM model hyperparameters are optimized

using the SCO algorithm after the min-max normalization of primary data. The SCODL-SPP model outperformed other models in stock price prediction accuracy, according to experiments [22]. Su et al. [23] proposed a stack framework using LGBM to predict the Taiwan stock market index. Their study created a comprehensive feature set to account for political events, economic conditions, investor psychology, and global market trends that affect stock market predictions. They introduced a feature selection algorithm to identify important features and improve training performance. A stacking strategy integrates multiple classifiers to improve prediction accuracy. The proposed model is tested using a 10-year Taiwan Stock Exchange Capitalization Weighted Stock Index dataset. Both the prediction model and feature selection method performed well in experiments, indicating that the proposed approach is effective in stock market index prediction [23]. Ryan Chipwanya's study examined how stock market prediction tools and data have improved, making market predictions possible [24]. Logistic regression, decision trees, and random forest algorithms were compared for predicting Japanese stock market asset movements using machine learning models for time-series forecasting. The models were also compared to feedforward deep neural networks. Overall, all models achieved directional bias forecasting accuracy above 50% [24]. Pardeshi et al. [25] emphasized the importance of stock market prediction for profitable investing. To address complex financial market dynamics, they emphasized deep learning. Geopolitical events and historical price trends affect stock market volatility. They introduced Long Short-Term Memory with a Sequential Self-Attention Mechanism (LSTM-SSAM) to predict stock prices with low error. Their proposed model was tested using SBIN, HDFCBANK, and BANKBARODA stock datasets. Their study showed that LSTM-SSAM improves stock price prediction accuracy through extensive experimentation [25].

The literature review on stock market prediction effectively addresses several identified gaps. The inclusion of the Hang Seng Index as a focal point allows for the provision of market-specific insights pertaining to Hong Kong, thereby expanding the geographical scope of research within this field. Moreover, through the transparent elucidation of data preprocessing procedures, the assurance of data quality and reproducibility is achieved, thereby addressing the existing gap in the literature regarding the evaluation of data quality and preprocessing methodologies. Furthermore, the enhancement of predictive accuracy through domain knowledge is exemplified by the integration of domain-specific insights into the AO-GRU model, thereby addressing the limitation of limited domain knowledge integration. Moreover, the comparison between the AO-GRU model and ensemble techniques offers valuable insights into the efficacy of ensemble methods, thus filling the void in the limited investigation of these methods. Finally, a more thorough evaluation of model performance can be achieved by integrating supplementary evaluation metrics or examining the constraints of current ones, thereby addressing the deficiency in insufficient evaluation metrics. These contributions have made significant advancements in the field of stock market prediction, resulting in improved robustness, accuracy, and applicability of predictive models in financial markets.

III. METHODS AND MATERIALS

A. Data Gathering and Preparation

The Hang Seng Index is a prominent stock market index in Hong Kong that tracks the performance of several notable companies listed on the Hong Kong Stock Exchange. The Hang Seng Index is composed of a diverse group of companies that lead their respective industries in many sectors of the Hong Kong economy. These sectors include, among others, the manufacturing, banking, real estate, and telecommunications sectors. Like other notable stock indices, the Hang Seng Index is weighted by market capitalization. Each company's weight in the index is based on its share market value; larger companies have a greater impact on the index's movements. Many factors, including trading volume and the Open, High, Low, and Close (OHLC) prices during a specific time period, should be included in a comprehensive study. The Hong Kong Stock Exchange provided hundreds of stocks from various industries that were used as the source of stock data for this study. Raw transaction data, comprising the opening price, closing price, highest price, lowest price, and trading volume, was gathered for every day from the start of 2015 to the end of June 2023. The gathered data was divided into two groups in order to maximize the performance of the models. As shown in Fig. 1, a partitioning approach was used in this experiment. In particular, twenty percent of the data was reserved for testing, while the remaining eighty percent was used for training. This division's main objective was to determine the most workable solution that balanced the need for a sizable amount of data for model training with the demands of a large, untested dataset for thorough testing and validation.

B. Gated Recurrent Unit

The GRU network was first introduced by Cho et al. [26]. The basic RNN concept [27] is to determine outputs by taking into account inputs and the hidden state, which is determined by squaring up past outputs or hidden states. With an update gate and a reset gate, the GRU offers sophisticated control over the data in a concealed state. In general, it can determine which data adding from the existing inputs is necessary (because it may be crucial to the future) and which data from the past may be eliminated from the hidden state (because it is unrelated to the present state). Compared to long short-term memory [28], which features a unit made up of three gates and a cell structure, the GRU has fewer parameters. A single GRU's construction is seen in Fig. 2, h , in which z is the update gate and r is the reset gate. Several of these units, designated h_j (along with associated r_j and z_j) in a GRU network, are updated using the following equations:

$$r_j = \sigma \left([V_r x]_j + [U_r h_{(t-1)}]_j \right) \quad (1)$$

$$z_j = \sigma \left([V_z x]_j + [U_z h_{(t-1)}]_j \right) \quad (2)$$

$$h_j^{(t)} = z_j h_j^{(t-1)} + (1 - z_j) \tilde{h}_j^{(t)} \quad (3)$$

$$\tilde{h}_j^{(t)} = \phi \left([V x]_j + [U (r \odot h_{(t-1)})]_j \right) \quad (4)$$

Let $x^{(t)}$ be the vector that is input at a time t . The bias parameter is a part of V , which stands for parameter matrices.

To take the j -th element of a vector, use the boldface notation h and r , which represent the vectors with all of the values h_j and r_j . When first introduced, σ represents a hyperbolic tangent function and σ is a logistic function. In the beginning, for every j , $h_j^{(0)} = 0$.

C. Ant Lion Optimizer

The predatory behavior of ant lions in the wild, which primarily consists of ants, ant lions, and elite ant lions, served as the primary inspiration for the creation of ALO in 2015 [12]. The structure of the ALO algorithm is as follows: Using the roulette and random walk techniques, the ant colony and ant placements are first established at random. After an ant has completed its journey, their fitness is assessed using a fitness function. If the ant's location outperforms that of the ant lions around it, then it is deemed the best option available at this time. Furthermore, the position of the ant lion becomes the best option if it manages to capture an ant. In every cycle, the elite antlion stands in for the best possible outcome within the ant lion population. In contrast, the elite antlion is updated if the optimal antlion outperforms it; if not, it stays the same until the

end of the iteration, at which point it overcomes the elite antlion [12].

The random walk, which is used to show how ants travel, is stated as follows by Eq. (5):

$$X(t) = [0, cs(2r(t_1) - 1)], \dots, cs(2r(t_n) - 1) \quad (5)$$

where, $r(t_n)$ is the random walk function of the n -th iteration and cs is the cumulative sum.

Moreover, Eq. (6) illustrates how Eq. (5) is further standardized.

$$X_i^{(t)} = \frac{(X_i^{(t)} - a_i) \times (d_i - c_i^{(t)})}{(d_i^{(t)} - a_i)} \quad (6)$$

The i -th individual's min and max values are denoted by a_i and d_i , respectively, while the t -th iteration of the i -th variable maximum value is represented by $c_i^{(t)}$ and $d_i^{(t)}$, respectively.

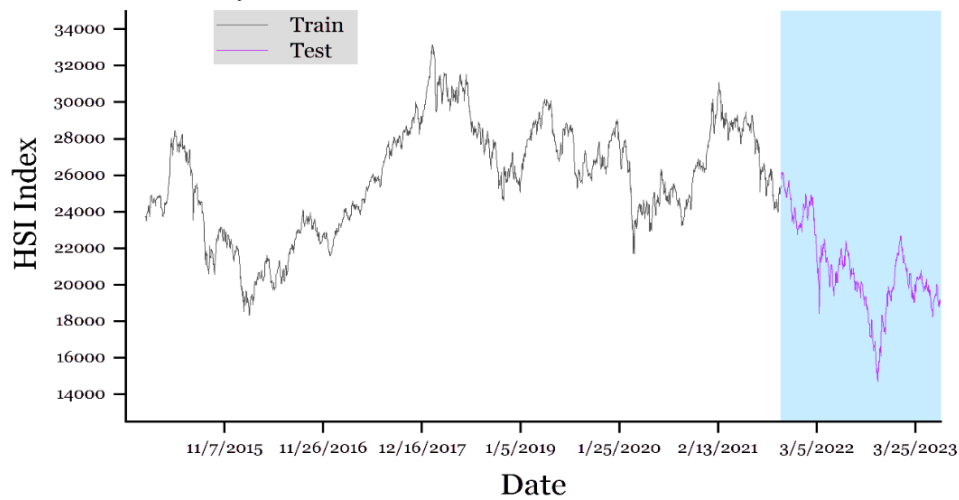


Fig. 1. Creating a separate train and test set of data.

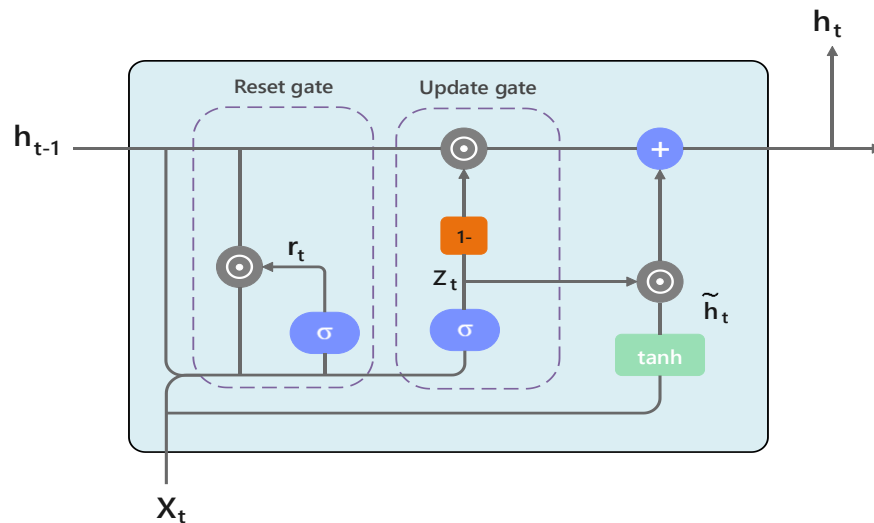


Fig. 2. The GRU model's structure.

Antlion traps have an impact on the random movement of ants, as demonstrated by Eq. (7) and Eq. (8):

$$c_i^{(t)} = \text{Antlion}_j^{(t)} + c^{(t)} \quad (7)$$

$$d_i^{(t)} = \text{Antlion}_j^{(t)} + d^{(t)} \quad (8)$$

In the t -th iteration, the individual's minimum and maximum values are denoted by $c^{(t)}$ and $d^{(t)}$, respectively, whereas $\text{Antlion}_j^{(t)}$ signifies the location of the j -th ant-lion.

Ants move randomly or in a roulette pattern around the antlion, as seen by Eq. (9):

$$\text{Ant}_i^{(t)} = \frac{R_A^{(t)} + R_E^{(t)}}{2} \quad (9)$$

The positions of the i -th ant at the t -th iteration are indicated by $\text{Ant}_i^{(t)}$, and $R_A^{(t)}$ and $R_E^{(t)}$ are the random walks around the elite or the roulette wheel on the second day of the, respectively.

As the number of iterations increases, antlion will get closer to the approximate optimal solution by reducing the boundaries in the manner described by Eq. (10) and Eq. (11):

$$c^i = \frac{c^{(t)}}{I} \quad (10)$$

$$d^i = \frac{d^{(t)}}{I} \quad (11)$$

where the lowest and maximum values of all variables at the t -th iteration are denoted by I , and $c^{(t)}$ and $d^{(t)}$ accordingly. Eq. (12) displays the location update formula, which the ant lion will use to feed on the ants after the iteration.

$$\text{Antlion}_j^{(t)} = \text{Ant}_i^{(t)}, \text{ if } f(\text{Ant}_i^{(t)}) > f(\text{Ant}_j^{(t)}) \quad (12)$$

Where the locations of the i -th and j -th ant-lions of the t -th iteration are represented by $\text{Antlion}_j^{(t)}$ and $\text{Ant}_i^{(t)}$.

D. Grey Wolf Optimization

A novel swarm intelligence algorithm called the GWO makes use of the capabilities that Mirjalili et al. [29] discovered. Accurate stability is achieved between exploration and development, and it is expandable and adaptable. Following the wolf cooperation mechanism, the GWO imitates the actions of a population of grey wolves that are predators. Following natural law and rigid social structures, every wolf in the population has a certain role to fulfill [29]. Wolf populations in a GWO are arranged based on fitness levels.

The wolf with the lowest health, ω , is regarded as the lowest-ranking person. A wolf within the wolf pack can be considered a feasible response, and the wolves corresponding to the finest solution, superior answer, and suboptimal answer of the present day may be designated as the α , β , and γ Wolf, respectively. The following sums up the grey wolf population's predatory behavior during the search:

$$D = |C \times X_p(t) - X(t)| \quad (13)$$

$$X(t + 1) = X_p(t) - A \times D \quad (14)$$

The distance D between the wolf and the target is given in Eq. (13). The coordinate transformation of a wolf is represented by Eq. (14), where $X_p(t)$ represents the target's location in the t -generation, $X(t)$ represents the position of a lone wolf inside the t -generation wolf pack, A and C are coefficients, and the calculation formula is as follows:

$$a = 2 - 2 * \frac{\text{iter}}{\text{Max}_{\text{iter}}} \quad (15)$$

$$A = 2a * r_1 \quad (16)$$

$$C = 2r_1 \quad (17)$$

where, $r_1, r_2 \in [0,1]$, iter is the population of iterations, and Max_{iter} is the maximum number of iterations. The three different sorts of wolves choose which gray wolf will replace which when the wolf assaults its prey, or when it catches quarry. The paradigm for this decision is as follows:

$$D_i^j(t) = |C \times X_i^j(t) - X^j(t)| \quad (18)$$

$$X_i^j(t + 1) = X_i^j(t) - A \times D_i^j(t) \quad (19)$$

$$X(t + 1) = \frac{1}{3} \times \sum X_m(t + 1) \quad (20)$$

The difference between the t -generation and $i(i = \alpha, \beta, \gamma)$ wolves are denoted by $D_i^j(t)$. In accordance with α, β , and γ stride length and the wolf's motion direction, in that order, Eq. (18)-(20) determine the ω wolf. The new period of grey wolves formed following a location update is represented by Eq. (20).

E. Aquila Optimizer

The AO is a recently introduced algorithm that aligns with the inherent hunting behavior of the Aquila species [14]. The hunting process has four distinct stages: an initial phase of extensive exploration achieved via soaring at high altitudes followed by a rapid vertical drop, a subsequent phase of focused exploration accomplished through gliding with precise contour flight, a subsequent phase of extensive exploitation achieved through a low-flying descending attack, and a final phase of focused exploitation accomplished through walking and capturing prey as seen in Fig. 3. The AO algorithm employs a range of characteristics to facilitate the transition from the exploration stage to the exploitation stage [14]. The initial two-thirds of iterations are dedicated to simulating the exploration stage, while the remaining one-third of iterations is allocated for imitating the exploitation stage [14] as the summary of AO optimizer performance is shown in Fig. 4.

The eagle starts the initial form of vertical descent when it identifies a potential area for prey and promptly determines the optimal hunting spot on the planet by ascending to significantly high elevations and identifying the region of investigation where the most efficient approach is determined using the subsequent formula:

$$\begin{cases} Z_1(t+1) = Z_{\text{best}}(t) \times \left(1 - \frac{t}{T}\right) + (Z_M(t) - Z_{\text{best}}(t) \times \text{rand}) \\ Z_M(t) = \frac{1}{N} \sum_{i=1}^N Z_i(t), \forall j = 1, 2, \dots, \text{Dim} \end{cases} \quad (21)$$

The generation $t + 1$ solution is represented by $Z(t + 1)$, which is the result of the search strategy $Z_1 \cdot Z_{\text{best}}(t)$, where (t) is the ideal approach that indicates the position of the closest target prey. This loop has t iterations remaining. T is the highest possible number of iterations. The location means of the current solution at the t -th iteration is denoted by $Z(t)$. A random number between 0 and 1 is referred to as a Rand. The subsequent swift-gliding assault: The eagle soars to a height to discover the prey region in order to reduce the hunting area or search space in line with the following equation for the best reaction:

$$\begin{cases} Z_2(t+1) = Z_{\text{best}}(t) \times Z(D) + Z_R(t) + (y - z) \times \text{ra} \\ L(D) = s \times \frac{\mu \times \sigma}{|v|^{\beta}} \end{cases} \quad (22)$$

$$\begin{cases} Z_4(t+1) = Q_F \times Z_{\text{best}}(t) - (G_1 \times Z(t) \times \text{rand}) - G_2 \times L(D) + \text{rand} \times G_1 \\ Q_F(t) = \frac{2 \times \text{rand} - 1}{t^{(1-T)^2}} \\ G_1 = 2 \times \text{rand} - 1 \\ G_2 = 2 \times \left(1 - \frac{t}{T}\right) \end{cases} \quad (24)$$

The quality function, or Q_F , and the search technique is balanced. The Aquila's motions as it searches for its food are

The Aquila enters the low-flying, slow-falling assault mode at the chosen target point when the prey zone has been carefully located and it is ready to land and attack. This is the third pattern of low-altitude flying; by using this tactic, the bird could see how its prey would respond and gradually approach it, as in the formula below: with D representing the dimensional space, $Z_R(t)$ representing the random solution between $[1, N]$, and $L(D)$ representing the hunting flight distribution function.

$$\begin{aligned} Z_3(t+1) = & (Z_{\text{best}}(t) - Z_M(T)) \times \alpha \\ & - \text{rand} + ((U_b - L_b) \times \text{rand} + L_b) \\ & \times \delta \end{aligned} \quad (23)$$

α and δ are the two moderating elements in this case. U_b is upper bound on the issue. L_b is the lower bound of the issue. Walking capture is the fourth method when the eagle uses the following equation to rapidly converge and attack the target from above.

seen on G_1 . The hunting flying slope of Aquila is represented by G_2 . $Z(t)$ is the solution for this iteration.

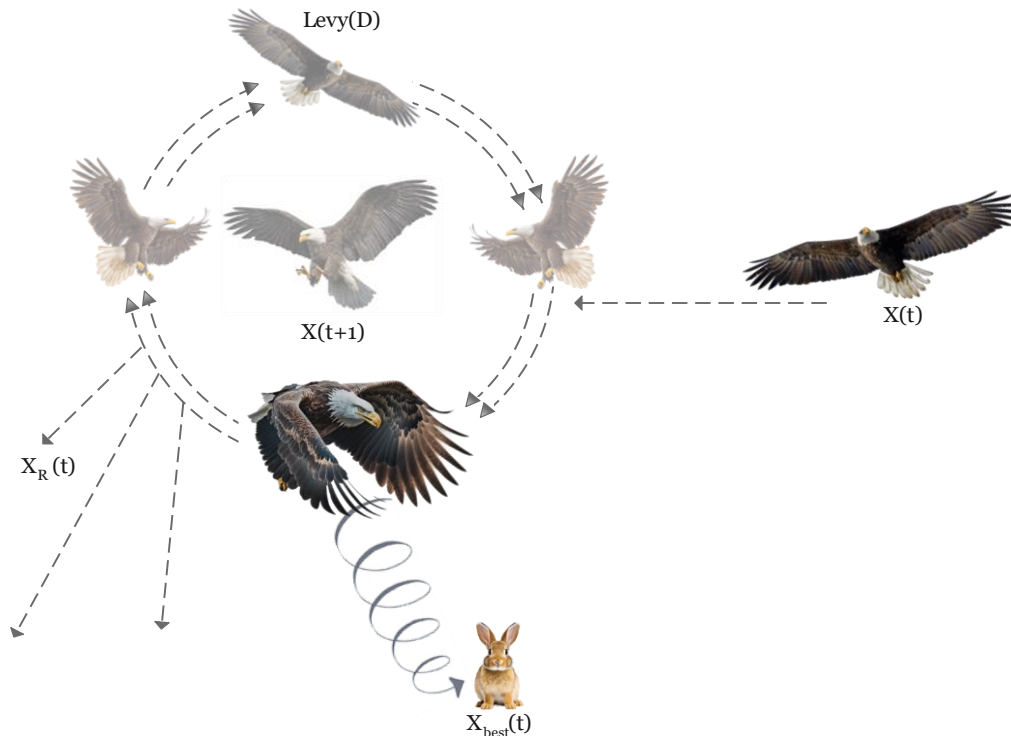


Fig. 3. An illustration of the Aquila hunting.

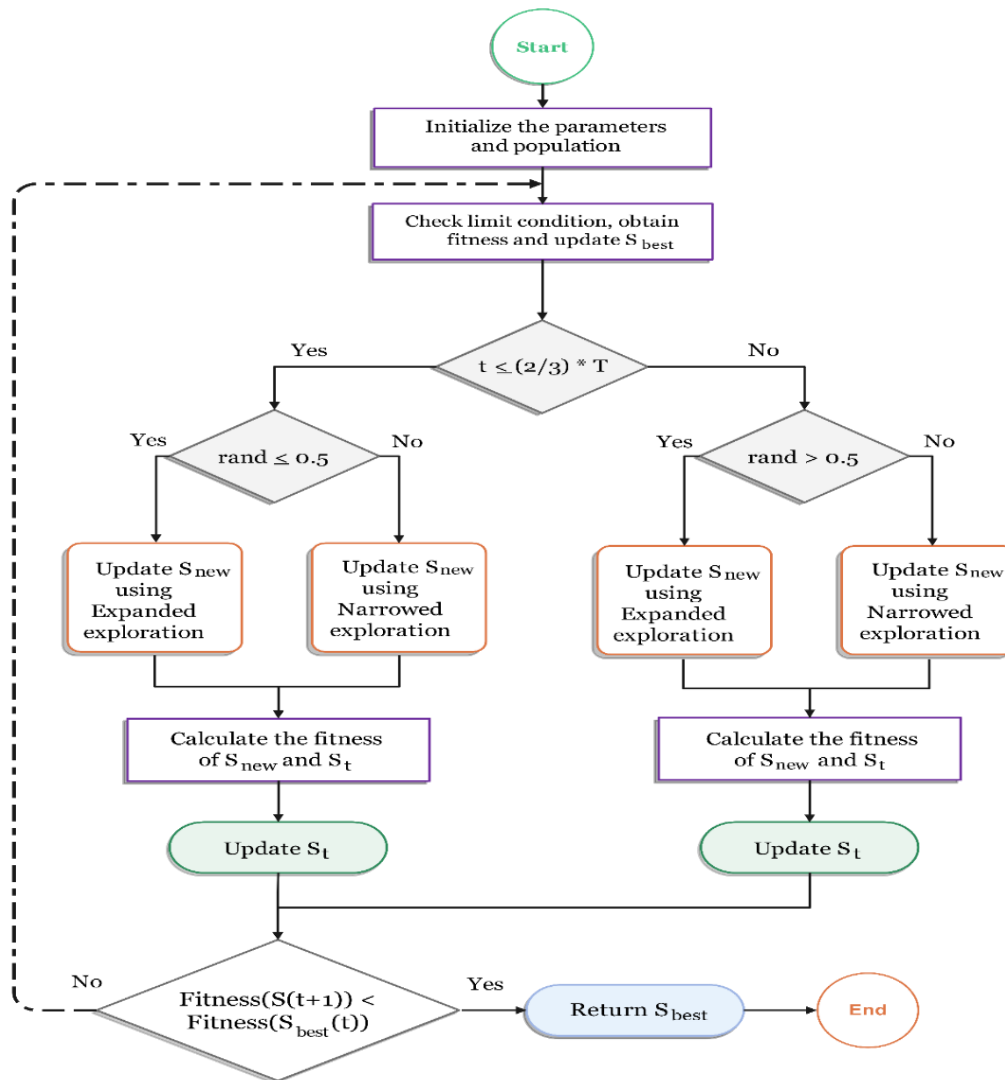


Fig. 4. The selective AO optimizer's graphical flowchart.

IV. RESULTS

A. Evaluation Metrics

The evaluation of the accuracy of the future forecast was conducted by employing a variety of performance measures. The carefully chosen metrics provide a thorough evaluation of the reliability and precision of the predictions. The assessment criteria employed in this article encompass:

- Coefficient of determination (R^2):

$$R^2 = 1 - \frac{\sum_{i=1}^n (y_i - \hat{y}_i)^2}{\sum_{i=1}^n (y_i - \bar{y})^2} \quad (25)$$

- Mean absolute error (MAE):

$$MAE = \frac{\sum_{i=1}^n |y_i - \hat{y}_i|}{n} \quad (26)$$

- Mean squared error (MSE):

$$MSE = \frac{1}{N} \sum_{i=1}^N (\hat{y}_i - y_i)^2, \quad (27)$$

- Mean absolute percentage error (MAPE):

$$MAPE = \left(\frac{1}{n} \sum_{i=1}^n \left| \frac{y_i - \hat{y}_i}{y_i} \right| \right) \times 100 \quad (28)$$

B. Statistic Values

The dataset encompassed a significant temporal range, commencing on January 1, 2015, and concluding at the termination of June 2023. This section presents tabular representations of the project's outcomes subsequent to its effective implementation. The inclusion of OHLC price and volume statistics in Table I enhances the comprehensibility of the information. The utilization of statistical metrics such as count, mean, minimum (min), maximum (max), standard deviation (Std.), 25%, 50%, 75%, and variance enables a thorough and precise examination of the data.

TABLE I. A COLLECTION OF STATISTICAL VALUE SUMMARIES

| | Open | High | Low | Volume | Close |
|----------|----------|----------|----------|----------|----------|
| count | 2090 | 2090 | 2090 | 2090 | 2090 |
| mean | 24877.8 | 25026.72 | 24689.52 | 4013.656 | 24862.03 |
| Std. | 3492.279 | 3486.289 | 3484.234 | 1462.996 | 3486.437 |
| min | 14830.69 | 15113.15 | 14597.31 | 0 | 14687.02 |
| 25% | 22194.44 | 22350.36 | 21998.24 | 3068.985 | 22151.32 |
| 50% | 25002.49 | 25118.69 | 24755.93 | 3679.685 | 24973 |
| 75% | 27716.1 | 27860.96 | 27525.43 | 4594.719 | 27693.23 |
| max | 33335.48 | 33484.08 | 32897.04 | 12025.52 | 33154.12 |
| variance | 12196013 | 12154214 | 12139887 | 2140358 | 12155245 |

C. Compare and Analysis

The successful completion of the project has yielded the results, which are displayed in this section as Table II and Fig. 5, 6. For this study, four algorithms were used to predict HSI

stock values: GRU, ALO-GRU, GWO-GRU, and AO-GRU. The dataset was massive, spanning from the beginning of 2015 to the end of June 2023. The models were evaluated using four important performance indicators: R^2 , MAPE, MAE, and MSE.

TABLE II. A PREDICTION OF THE EVALUATION OUTCOMES OF THE MODELS

| MODEL/Metrics | TRAIN SET | | | | TEST SET | | | |
|---------------|-----------|------|--------|----------|----------|------|--------|----------|
| | R^2 | MAPE | MAE | MSE | R^2 | MAPE | MAE | MSE |
| GRU | 0.9894 | 1.09 | 280.91 | 92243.40 | 0.9875 | 1.01 | 202.16 | 69134.21 |
| ALO-GRU | 0.9923 | 0.83 | 213.74 | 67466.58 | 0.9906 | 0.97 | 198.26 | 51900.77 |
| GWO-GRU | 0.9941 | 0.77 | 197.79 | 51335.10 | 0.9921 | 0.78 | 161.26 | 43986.23 |
| AO-GRU | 0.9952 | 0.60 | 154.69 | 41515.24 | 0.9934 | 0.71 | 143.62 | 36530.58 |

V. DISCUSSIONS

The tabulated results for the GRU obtained during the testing of a specific model on the dataset of that firm are shown in Table II. The AO-GRU method has produced the greatest predictive performance out of all four models, with an MSE of 36530.58, the lowest of all four. This is because the optimum MSE value is near zero. The results of the R^2 calculations for several models evaluated on a certain dataset are listed in Table II. The model fit is better when the value of R^2 is nearer 1. The obtained results demonstrate that the AO-GRU has yielded the most encouraging outcomes among the four computational models that were examined. Because its R^2 score of 0.9934 is the closest to 1, which suggests that the accuracy rate of the model is high. This table offers a thorough summary of the MAPE that a given model obtained during testing on the dataset. A lower number in the MAPE indicates greater performance. With a MAPE of 0.71, Table II analysis reveals that AO-GRU performed the best out of the three algorithmic

models examined. Because it produces the most accurate predictions, it can be concluded that the AO-GRU algorithm is the best computational model to apply when working with comparable datasets. Regarding the MAE report, it should be noted that the more accurate the prediction, the closer the reported value is to zero. This is supported by the reported table, which indicates that the reported number for the AO-GRU model's test phase is 143.62, indicating that the model in question is more accurate at forecasting and is the one used in this article. The findings may be used in business and other domains where data analysis is essential for making well-informed choices and forecasts.

The GRU model's combination with the Aquila optimizer as seen in Fig. 7 and Fig. 8, it is clear from the analysis of the HSI index curves and their comparative assessment that the AO-GRU model performs better and is more effective than the other models investigated in this study.

Train

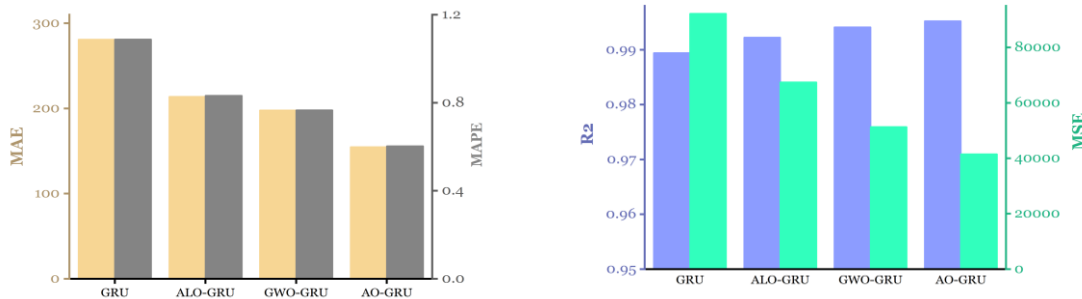


Fig. 5. The methods' training outcomes contain a variety of measures, including R^2 , MAPE, MAE, and MSE.

Test

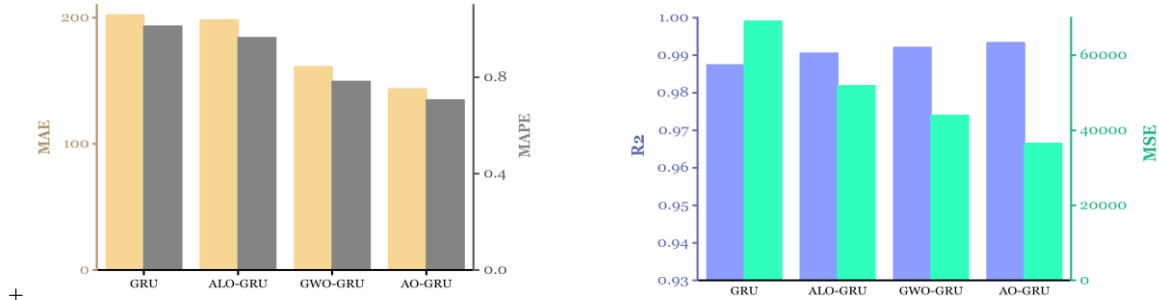


Fig. 6. The methods' testing outcomes contain a variety of measures, including R^2 , MAPE, MAE, and MSE.

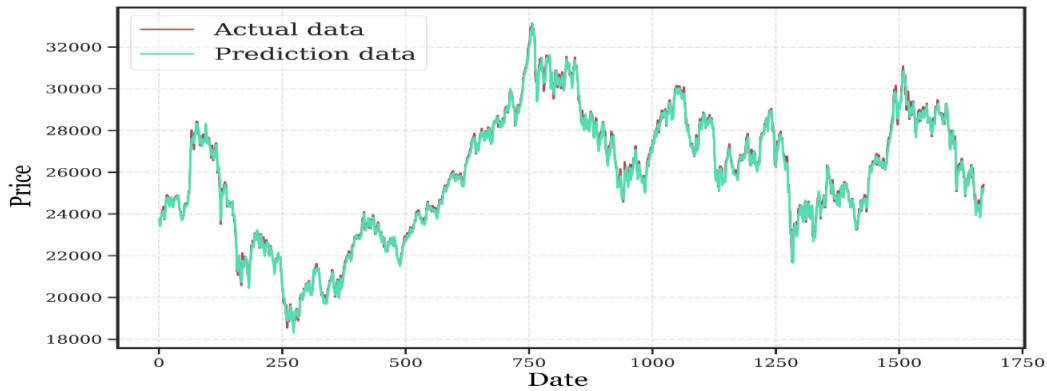


Fig. 7. The prediction curve produced during the training phase by applying the AO-GRU technique.

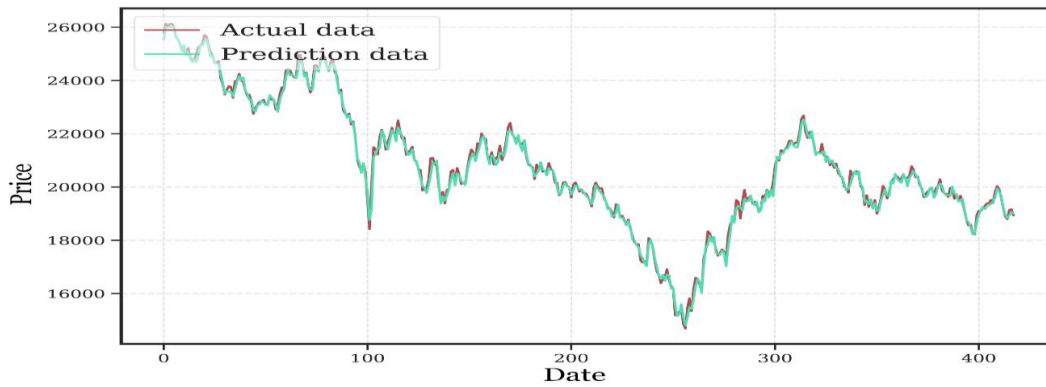


Fig. 8. The prediction curve produced during the testing phase by applying the AO-GRU technique.

TABLE III. A COMPARATIVE ANALYSIS OF THE MODEL IS PROVIDED IN RELATION TO PREVIOUS STUDIES

| Authors | Method | R^2 |
|-------------------|-------------------|--------|
| Zhu et al. [30] | LSTM | 0.6896 |
| | EMD-LSTM | 0.8703 |
| | CEEMDAN-LSTM | 0.9031 |
| | SC-LSTM | 0.6871 |
| | EMD-SC-LSTM | 0.9111 |
| | CEEMDAN-SC-LSTM | 0.9206 |
| Abdul et al. [31] | Linear regression | 0.73 |
| | SVM | 0.93 |
| | MLS-LSTM | 0.95 |
| Current study | | 0.9934 |

Based on the findings presented in Table III, the AO-GRU model demonstrates superior performance when compared to other models evaluated in the domain of stock price prediction. In this study, the R^2 value of 0.9934 was found to be highly impressive, surpassing the performance of other evaluated models such as LSTM, SVM, and MLS-LSTM. This indicates a stronger correlation between the predicted and actual stock prices, suggesting that the model is more effective in capturing the underlying data patterns. By integrating adaptive optimization techniques, the AO-GRU model gains the capability to dynamically modify its parameters during training. This allows it to adapt to the subtleties of the data and improve its capacity to handle variations and complexities in the stock market. The model effectively utilizes the GRU architecture to capture long-range dependencies in sequential data, while also addressing challenges such as the vanishing gradient problem. The gating mechanisms of GRU control the flow of information within the network, enabling more effective learning, especially in situations where there is a scarcity of training data. Significantly, the efficiency of the GRU architecture, which necessitates fewer parameters and computations in comparison to more intricate models such as LSTM, results in expedited training durations and reduced computational expenses. Consequently, the AO-GRU model becomes more viable for real-time or extensive applications. Moreover, the model's architecture, which is relatively uncomplicated, improves its interpretability, offering stakeholders valuable insights into the determinants of stock price fluctuations and the underlying reasoning behind the model's predictions, as opposed to certain intricate black-box models.

VI. CONCLUSION

This study aimed to develop machine learning models with improved stock price prediction accuracy. By making the appropriate sort of investment at the appropriate moment, traders and investors would be able to take advantage of these strategies and maximize their gains. This project included the effective implementation of four algorithms: GRU, ALO-GRU, GWO-GRU, and AO-GRU. A comprehensive comparative analysis of the algorithms' performances during stock price prediction was conducted after GRU algorithms were utilized to create accurate predictive models for use in the stock price prediction of HSI. The collected stock values 1st of January 2015 to the end of June 2023. The four assessment metrics MSE, R^2 , MAPE, and MAE as well as the data gathered during the model testing are displayed in tabular and graphical form in the research study's results section.

- Following a comprehensive review and analysis of the data, the AO-GRU approach is shown to be the most error-free among the available strategies for time series prediction, with the lowest MSE (36530.58), MAPE (0.71), and MAE (143.62) errors and the highest value of R^2 (0.9934).

The study's findings present compelling evidence that suggests several promising avenues for future research in the field of stock price prediction. In order to enhance predictive accuracy and robustness, it is imperative to investigate alternative optimization techniques beyond Aquila, the

optimizer employed in the AO-GRU model. The incorporation of supplementary datasets not limited to the Hang Seng Index has the potential to yield more profound insights and improve the generalizability of the model. This could involve the inclusion of macroeconomic indicators, industry-specific data, or sentiment analysis derived from diverse sources. Furthermore, the implementation of strategies such as attention mechanisms or feature importance analysis has the potential to improve the interpretability of models, thereby promoting increased trust and usability among various stakeholders. It is imperative to conduct thorough testing in various market conditions and economic cycles in order to evaluate the robustness and flexibility of models. Additionally, investigating the applicability of these models to different asset classes, such as commodities or currencies, may reveal novel opportunities for investment strategies. By directing attention towards these specific areas, forthcoming research endeavors possess the capacity to propel the domain of stock price prediction forward and effectively address the changing demands of investors and financial professionals.

REFERENCES

- [1] M. Bansal, A. Goyal, and A. Choudhary, "Stock Market Prediction with High Accuracy using Machine Learning Techniques," *Procedia Comput Sci*, vol. 215, pp. 247–265, 2022, doi: <https://doi.org/10.1016/j.procs.2022.12.028>.
- [2] V. U. Kumar, A. Krishna, P. Neelakanteswara, and C. Z. Basha, "Advanced prediction of performance of a student in an university using machine learning techniques," in 2020 international conference on electronics and sustainable communication systems (ICESC), IEEE, 2020, pp. 121–126.
- [3] M. Mohri, A. Rostamizadeh, and A. Talwalkar, *Foundations of machine learning*. MIT press, 2018.
- [4] L.-P. Chen, "Multiclassification to gene expression data with some complex features," *Biostat Biom Open Access J*, vol. 9, no. 1, pp. 1–2, 2018.
- [5] J. Chung, C. Gulcehre, K. Cho, and Y. Bengio, "Empirical evaluation of gated recurrent neural networks on sequence modeling," *arXiv preprint arXiv:1412.3555*, 2014.
- [6] Y. Gao, R. Wang, and E. Zhou, "Stock Prediction Based on Optimized LSTM and GRU Models," *Scientific Programming*, Vol 2021 (2021), 2021, doi: 10.1155/2021/4055281.
- [7] C. Qi, J. Ren, and J. Su, "GRU Neural Network Based on CEEMDAN-Wavelet for Stock Price Prediction," *Applied Sciences*, Vol 13, Iss 12, p 7104 (2023), 2023, doi: 10.3390/app13127104.
- [8] S. Mirjalili and A. Lewis, "The whale optimization algorithm," *Advances in engineering software*, vol. 95, pp. 51–67, 2016.
- [9] D. Simon, "Biogeography-based optimization," *IEEE transactions on evolutionary computation*, vol. 12, no. 6, pp. 702–713, 2008.
- [10] B. Mohan and J. Badra, "A novel automated SuperLearner using a genetic algorithm-based hyperparameter optimization," *Advances in Engineering Software*, vol. 175, no. September 2022, p. 103358, 2023, doi: 10.1016/j.advengsoft.2022.103358.
- [11] S. Mirjalili, "Moth-flame optimization algorithm: A novel nature-inspired heuristic paradigm," *Knowl Based Syst*, vol. 89, pp. 228–249, 2015.
- [12] S. Mirjalili, "The ant lion optimizer," *Advances in engineering software*, vol. 83, pp. 80–98, 2015.
- [13] S. Mirjalili, S. M. Mirjalili, and A. Lewis, "Grey wolf optimizer," *Advances in engineering software*, vol. 69, pp. 46–61, 2014.
- [14] L. Abualigah, D. Yousri, M. Abd Elaziz, A. A. Ewees, M. A. A. Al-Qaness, and A. H. Gandomi, "Aquila optimizer: a novel meta-heuristic optimization algorithm," *Comput Ind Eng*, vol. 157, p. 107250, 2021.
- [15] B. Sasmal, A. G. Hussien, A. Das, and K. G. Dhal, "A Comprehensive Survey on Aquila Optimizer," *Archives of Computational Methods in*

- Engineering, vol. 30, no. 7, pp. 4449–4476, 2023, doi: 10.1007/s11831-023-09945-6.
- [16] F. W. Christanto, V. G. Utomo, R. Prathivi, and C. Dewi, “The Impact of Financial Statement Integration in Machine Learning for Stock Price Prediction,” *International Journal of Information Technology and Computer Science*; volume 16, issue 1, page 35-42; ISSN 2074-9007 2074-9015, 2024, doi: 10.5815/ijitcs.2024.01.04.
- [17] Y. Chen, X. Andrew, and S. Supasanya, “CRISIS ALERT: Forecasting Stock Market Crisis Events Using Machine Learning Methods,” 2024. doi: 10.48550/arxiv.2401.06172.
- [18] P.-F. Tsai, C.-H. Gao, and S.-M. Yuan, “Stock Selection Using Machine Learning Based on Financial Ratios,” *Mathematics*, Vol 11, Iss 23, p 4758 (2023), Mar. 2023, doi: 10.3390/math11234758.
- [19] S. Pourroostaei Ardakani, N. Du, C. Lin, J. Yang, Z. Bi, and L. Chen, “A federated learning-enabled predictive analysis to forecast stock market trends,” Mar. 2023, [Online]. Available: <https://eprints.lincoln.ac.uk/id/eprint/53623/>.
- [20] M. Hani’ah, M. Z. Abdullah, W. I. Sabilla, S. Akbar, and D. R. Shafara, “Google Trends and Technical Indicator based Machine Learning for Stock Market Prediction,” *MATRIK: Jurnal Manajemen, Teknik Informatika dan Rekayasa Komputer*; Vol 22 No 2 (2023); 271-284; 2476-9843; 1858-4144; 10.30812/matrik.v22i2, Mar. 2023, [Online]. Available: <https://journal.universitاسbumigora.ac.id/index.php/matrik/article/view/2287>.
- [21] K. Juare and A. Kulkarni, “Machine Learning Algorithms for Stock Market Prediction,” *International Journal of Innovative Science and Research Technology* 7(12) 2193-2199, Mar. 2023, [Online]. Available: <https://zenodo.org/record/7698476>.
- [22] T. Swathi, N. Kasiviswanath, and A. A. Rao, “A Novel Sine Cosine Optimization with Stacked Long Short-term Memory-enabled Stock Price Prediction,” *Recent Advances in Computer Science and Communications*; volume 16; ISSN 2666-2558, 2023, doi: 10.2174/0126662558236061230922074642.
- [23] I. Su, P. L. Lin, Y. Chung, and C. Lee, “Forecasting of Taiwan’s weighted stock Price index based on machine learning,” *Expert Systems*; volume 40, issue 9; ISSN 0266-4720 1468-0394, 2023, doi: 10.1111/exsy.13408.
- [24] R. Chipwanya, “Stock Market Directional Bias Prediction Using ML Algorithms,” 2023, doi: 10.48550/arxiv.2310.16855.
- [25] K. Pardeshi, S. S. Gill, and A. M. Abdelmoniem, “Stock Market Price Prediction: A Hybrid LSTM and Sequential Self-Attention based Approach,” 2023. doi: 10.48550/arxiv.2308.04419.
- [26] K. Cho, B. Van Merriënboer, D. Bahdanau, and Y. Bengio, “On the properties of neural machine translation: Encoder-decoder approaches,” *arXiv preprint arXiv:1409.1259*, 2014.
- [27] K. Cho et al., “Learning phrase representations using RNN encoder-decoder for statistical machine translation,” *arXiv preprint arXiv:1406.1078*, 2014.
- [28] R. Ying, Y. Shou, and C. Liu, “Prediction Model of Dow Jones Index Based on LSTM-Adaboost,” in *2021 International Conference on Communications, Information System and Computer Engineering (CISCE)*, 2021, pp. 808–812. doi: 10.1109/CISCE52179.2021.9445928.
- [29] S. Mirjalili, S. M. Mirjalili, and A. Lewis, “Grey Wolf Optimizer *Adv Eng Softw* 69: 46–61.” ed, 2014.
- [30] R. Zhu, G.-Y. Zhong, and J.-C. Li, “Forecasting price in a new hybrid neural network model with machine learning,” *Expert Syst Appl*, vol. 249, p. 123697, 2024, doi: <https://doi.org/10.1016/j.eswa.2024.123697>.
- [31] A. Q. Md et al., “Novel optimization approach for stock price forecasting using multi-layered sequential LSTM,” *Appl Soft Comput*, vol. 134, p. 109830, 2023, doi: <https://doi.org/10.1016/j.asoc.2022.109830>.

Research on Diagnosis Method of Common Knee Diseases Based on Subjective Symptoms and Random Forest Algorithm

Guangjun Wang¹, Mengxia Hu², Linlin Lv³, Hanyuan Zhang⁴, Yining Sun⁵, Benyue Su⁶, Zuchang Ma^{7*}

Anhui Province Key Laboratory of Medical Physics and Technology, Institute of Intelligent Machines, Hefei Institutes of Physical Science, Chinese Academy of Sciences, Hefei 230031, China^{1, 4, 5, 7}

Science Island Branch of Graduate School, University of Science and Technology of China, Hefei 230026, China^{1, 4, 5, 7}

The University Key Laboratory of Intelligent Perception and Computing of Anhui Province, Anqing Normal University, Anqing 246013, China^{1, 2, 3, 6}

Department of Sports Medicine and Arthroscopic Surgery, The First Affiliated Hospital of Anhui Medical University, Hefei 230022, China⁴

Abstract—Knee diseases are common diseases in the elderly, and timely and effective diagnosis of knee diseases is essential for disease treatment and rehabilitation training. In this study, we construct a diagnostic model of common knee diseases based on subjective symptoms and random forest algorithm to realize patients' self-initial diagnosis. In this paper, we first constructed a questionnaire of subjective symptoms of knee, and set up a questionnaire system to guide users to fill out the questionnaire correctly. Then clinical data collection is carried out to obtain clinical questionnaire data. Finally, the diagnostic analysis of three common diseases of knee joint is carried out by random forest machine learning method. Through leave-one-out cross validation, the accuracy of meniscus injury, anterior cruciate ligament injury and knee osteoarthritis diseases are 0.79, 0.84, 0.81 respectively; the sensitivity is 0.79, 0.84, 0.88 respectively; and the specificity is 0.80, 0.84, 0.79 respectively. The results show that the method can achieve a good effect of self-diagnosis, and can provide a knee joint disease screening a convenient and effective approach.

Keywords—Knee diseases; subjective symptoms; random forest algorithm; self-diagnosis

I. INTRODUCTION

Knee disease is a highly prevalent condition that has a significant impact on the quality of life, particularly among older individuals. The knee is a complex structure, and as individuals age, the bones, cartilage, ligaments, and other functional components undergo degenerative changes. This gradual degeneration can lead to various knee conditions, including osteoarthritis, meniscus injuries, and ligament injuries [1-2]. Early detection of knee diseases is crucial for effective control and management. However, there is often a lack of awareness about knee diseases, and minor pain and dysfunction are frequently overlooked or attributed to old age or knee osteoarthritis. This delay in recognizing and treating knee diseases results in missed opportunities for prevention and early intervention [3-4].

Knee diseases encompass a wide range of symptoms and dysfunctions, underscoring the importance of recognizing abnormal subjective knee symptoms for early treatment and

management. Researchers have explored multiple models and methods based on knee risk factors, symptoms, and etiology to develop diagnostic models for knee diseases and investigate symptom-based identification [5]. For example, Lim et al. employed deep learning algorithms to predict osteoarthritis using a Korean database [6], while Snoeker et al. designed a questionnaire for diagnosing meniscal injuries [7]. Wang Pei's team conducted ordered logistic regression analysis to identify factors influencing knee osteoarthritis grading, ultimately establishing a diagnostic model for grading knee osteoarthritis [8]. Bisson et al. designed a web-based symptom questionnaire with 26 questions and 126 entries to establish a differential diagnosis of knee disorders, providing patients with potential disorder types. However, the tool's sensitivity (58%) and specificity (48%) were found to be insufficient [9].

Despite the promise shown in clinical applications, these studies primarily focus on diagnosing specific types of knee diseases. The identification and diagnosis of different types of knee diseases and the provision of appropriate treatments present greater challenges. In summary, symptom-based screening and differential diagnosis of knee disorders currently face significant hurdles, resulting in low overall identification effectiveness. The subjective nature and ambiguity of symptom definition and acquisition, coupled with limitations in diagnostic models, pose significant difficulties in applying these models to the general population. Factors such as the subjective and variable nature of symptoms, the need for analyzing the relationship between diseases and symptoms, and the suitability of modeling methods all contribute to the complexity of diagnosing knee diseases based solely on subjective symptoms. Addressing these challenges is crucial for improving the performance of diagnostic models and enhancing the accuracy of knee disease identification.

To address the challenges mentioned above, this study proposes a diagnostic model for knee diseases based on subjective symptoms and random forests. The main research work is outlined as follows:

*Corresponding Author

Definition and screening of the knee subjective symptom questionnaire: The researchers define and screen a questionnaire for knee subjective symptoms through data collection, expert validation, and patient assessment methods. A questionnaire assistance system is designed to guide patients in accurately completing the questionnaire.

Data collection and statistical analysis: Clinical questionnaire experiments are conducted to gather research data on subjective knee symptoms. Statistical analysis is performed to examine the relationship between knee diseases and the distribution of major diseases and symptoms. Univariate logistic regression analysis is utilized to filter out irrelevant symptoms, reducing computational complexity and improving the accuracy of the diagnostic model.

Construction of a diagnostic model: A diagnostic model for knee diseases is built based on subjective symptoms, supplemented with the random forest algorithm. The researchers select optimal model parameters through grid search and explore optimal diagnostic thresholds to achieve the best diagnostic performance. The importance of diagnostically significant symptoms for each disease is further investigated to enhance the interpretability of the model.

The research framework for the diagnosis and screening of knee diseases based on subjective symptoms is illustrated in Fig. 1. By implementing this research framework, the aim is to improve the accuracy and interpretability of knee disease diagnosis, providing a valuable tool for early screening and management of knee diseases based on subjective symptoms.

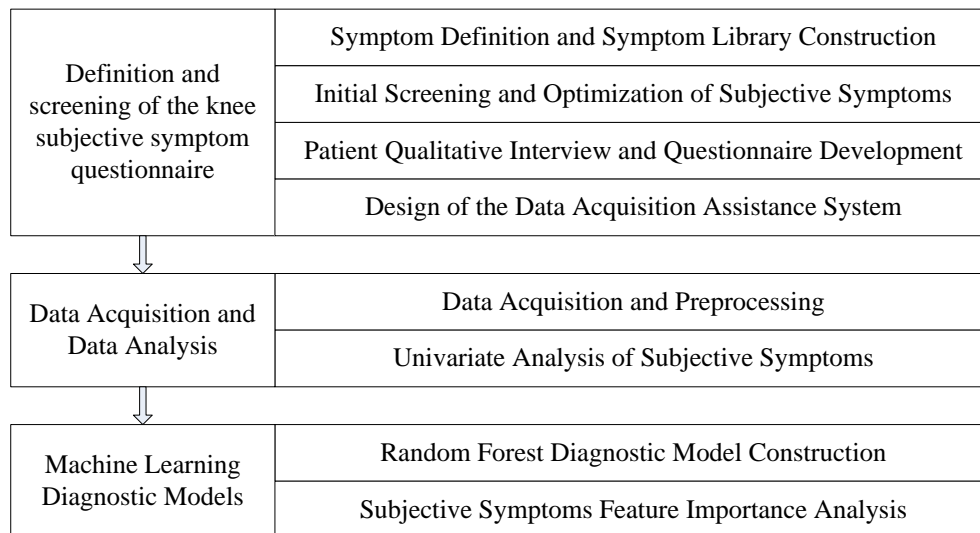


Fig. 1. Research framework for the diagnosis of knee diseases based on subjective symptoms and random forest algorithm.

II. DESIGN OF A SUBJECTIVE SYMPTOM ACQUISITION SYSTEM

A. Subjective Symptom Definition

When designing the subjective symptom questionnaire, this study adhered to two core principles: firstly, ensuring that the items effectively reflect knee joint diseases and functional status, and secondly, ensuring that the items have clear and easily understandable meanings for the general public. To achieve these goals, the study employed various methods, including data surveys, expert consultations, and qualitative interviews, to construct a comprehensive library of subjective symptom questionnaires.

1) Preliminary definition of symptom item library: Constructing a symptom library that can comprehensively and effectively reflect the characteristics of various knee joint diseases is a challenge due to the subjective and ambiguous nature of symptoms. The research team initially conducted a data survey, gathering relevant literature and books on knee joint diseases to compile a list of possible symptoms. For example, knee osteoarthritis may cause symptoms such as joint pain, morning stiffness, and snapping, while meniscus injuries may result in joint tenderness. Based on this

information and by referring to existing joint scales such as WOMAC and KSS, the team constructed a library of subjective symptoms for knee joints. Through discussions with knee-related experts and clinicians, as well as consideration of the clinical complaints of patients, the initial definition of knee joint subjective symptoms was established, and a symptom library was created. This library included medical history, etiology, subjective feelings, functional status, and various specific conditions and degrees, resulting in the design of 104 questionnaire items and 302 subjective symptom options.

2) Optimization of symptom item library Based on expert experience: The initial subjective symptom questionnaire contained a significant amount of redundant information, necessitating screening and optimization. The research team sought expert consultation by inviting 10 experienced doctors to analyze the feasibility, necessity, and comprehensibility of the questionnaire. The experts optimized the item selection and content of the questionnaire by removing redundant and difficult-to-understand symptoms, adding necessary symptoms, and modifying the definitions and explanations of certain symptoms. This process resulted in an optimized

screening questionnaire for subjective symptoms, incorporating the suggestions provided by the experts.

3) *Further optimization of symptom item library Based on patient feedback:* As patients are the ultimate users of the questionnaire, their understanding and applicability are of utmost importance. To address this, the study conducted qualitative interviews with 30 knee joint patients who had been diagnosed with knee joint diseases. Based on the feedback received from the patients, the symptom item library was further optimized. This iterative process led to the

finalization of the subjective knee joint symptom questionnaire, which was refined and improved based on patient input. Table I shows the subjective symptoms and corresponding values included in the final questionnaire.

By following this design process, the subjective symptom acquisition system ensures that the knee disease-related symptoms are effectively represented and easily understood by the general population. This system plays a crucial role in accurately capturing subjective symptoms for further analysis and diagnosis of knee diseases.

TABLE I. DEFINITION OF SUBJECTIVE SYMPTOMS OF KNEE DISEASE

| Number | Definition of subjective symptoms | value | Number | Definition of subjective symptoms | value |
|--------|-----------------------------------|----------------|--------|-----------------------------------|----------------|
| S1 | Flexion Limit | False=0 True=1 | S16 | Pain Activity | False=0 True=1 |
| S2 | Extension Limit | False=0 True=1 | S17 | Pain Rest | False=0 True=1 |
| S3 | Snapping | False=0 True=1 | S18 | Pain Hyperalgesia | False=0 True=1 |
| S4 | Locking | False=0 True=1 | S19 | Pain Hyperflexion | False=0 True=1 |
| S5 | Instability | False=0 True=1 | S20 | Pain Wandering | False=0 True=1 |
| S6 | Knee Dislocation | False=0 True=1 | S21 | Tend Knee Space | False=0 True=1 |
| S7 | Patellar Dislocation | False=0 True=1 | S22 | Tend Above Patella | False=0 True=1 |
| S8 | Stiffness | False=0 True=1 | S23 | Tend Patella | False=0 True=1 |
| S9 | Injure | False=0 True=1 | S24 | Tend Blow Patella | False=0 True=1 |
| S10 | Injure Zip | False=0 True=1 | S25 | Tend Knee Eye | False=0 True=1 |
| S11 | Knee Varus | False=0 True=1 | S26 | Tend Tibial Tubercle | False=0 True=1 |
| S12 | Knee Knock | False=0 True=1 | S27 | Tend LCL | False=0 True=1 |
| S13 | Quadriceps Atrophy | False=0 True=1 | S28 | Tend Iliotibial Band | False=0 True=1 |
| S14 | Swelling | False=0 True=1 | S29 | Tend MCL | False=0 True=1 |
| S15 | Pain | False=0 True=1 | S30 | Tend Popliteal Fossa | False=0 True=1 |

B. Design of the Data Acquisition Assistance System

To improve the comprehensibility of symptoms and enhance the accuracy of data acquisition, a subjective symptom questionnaire assistance system was designed in this study. The system aims to assist patients in effectively completing the questionnaire. The main components of the system are outlined below:

1) *Skip mechanism:* The questionnaire incorporates a skip mechanism to reduce redundancy and enhance efficiency. For instance, if a user does not experience pain in the pain section, subsequent pain-related questions will be skipped, eliminating the need to answer irrelevant questions.

2) *Tutorial system:* The questionnaire incorporates a tutorial system to familiarize users with the questionnaire completion process.

- Overall Tutorial: A brief video, approximately 3 minutes in duration, introduces the questionnaire content to users. Digital media technology, including video animation and interactive media, is employed to help users grasp the questionnaire's content and guide them in providing accurate responses.
- Step-by-Step Tutorial: Complex questions within the questionnaire are accompanied by explanations. Users

can click on the question title to access detailed explanations, facilitating their understanding and accurate completion of the questionnaire.

3) *3D Visualization for assisted answering:* To address issues of ambiguity and improve the understanding of certain questions, the questionnaire system incorporates 3D visualization. For example, a 3D visualization model is designed for the pressure pain questionnaire. Users can interact with the model to indicate the location of their self-perceived pressure pain. The system automatically fills in the corresponding options based on the user's selection.

The subjective symptom questionnaire assistance system enhances the usability and accuracy of the subjective symptom questionnaire. The skip mechanism reduces redundancy, the tutorial system provides guidance, and the 3D visualization feature facilitates precise responses. These features collectively contribute to more effective and efficient data collection for knee diseases.

III. MATERIALS AND METHODS

A. Random Forest Algorithm

The random forest algorithm is an integrated machine learning algorithm that utilizes decision trees as its base learners. Each decision tree is constructed based on a different

subset of the training data and features. As a result, each decision tree is unique and independent, and the collective learning results of multiple decision trees are considered as the final output of the random forest algorithm. This algorithm helps to reduce the variance present in individual decision trees. Random forest is particularly effective in handling classification tasks with complex interactions among attributes. It can also adapt well to datasets with noise or missing values, and the training process is relatively fast. The random forest algorithm is versatile, capable of performing classification, regression, and outlier detection tasks [10-11].

The calculation steps of the random forest algorithm are outlined in Algorithm 1. This algorithm combines the predictions of multiple decision trees to arrive at the final prediction [12].

In the random forest algorithm, each decision tree is trained on a different subset of the data, promoting diversity and reducing overfitting. The final prediction is made by aggregating the predictions of all the decision trees in the ensemble model. This ensemble-based algorithm helps to improve the accuracy and robustness of the model.

Random forest has been widely used in various fields due to its effectiveness and versatility in handling complex datasets. In the context of the study, the random forest algorithm can be employed for tasks such as knee disease classification, regression analysis of symptom severity, or identifying outliers in the dataset.

The calculation steps of the random forest algorithm are shown in Algorithm 1.

Algorithm 1: Random forest algorithm steps

Input: Training set
 $D = \{(x_1, y_1), (x_2, y_2), \dots, (x_N, y_N)\}$,
 $x_i = (x_i^1, x_i^2, \dots, x_i^n)$, $x_i^1, x_i^2, \dots, x_i^n$ is a characteristic of
k:
Output: Classification result
1: *for* $i = 1 : K$
2: A subset is constructed by randomly selecting k samples from the training set $S_i, S_i \in D$
3: The features contained in each feature are randomly selected from each feature ($m \in n$)
4: $Gini(S_i) = 1 - \sum_J \left(\frac{|y_J|}{|S_i|}\right)^2$ J is the number of features contained in y
5: while(!Generate(T_i))
6: *for* $j = 1 : m$
7: $Gini(S_i, x^j) = \frac{|S_{i1}|}{|S_i|} Gini(S_{i1}) + \frac{|S_{i2}|}{|S_i|} Gini(S_{i2})$
8: $\Delta Gini(x^j) = Gini(S_i) - Gini(S_i, x)$
9: *endfor*

10: The smallest corresponding node is selected as the classification node;
11: *end*
12: *endfor*
13 : The generated individual trees constitute the random forest classifier, which is the final output classification result of the random forest through the voting strategy.

B. Performance Evaluation Indicators

The performance of a disease diagnostic model can be assessed using various indicators, including Accuracy, Sensitivity, Specificity, Receiver Operating Characteristic (ROC) curve, and the Area Under the Curve (AUC) [13]. These indicators provide valuable insights into the model's ability to correctly classify individuals with and without a specific knee disease.

To calculate these indicators, the following four parameters are defined:

True Positives (TP): The number of individuals correctly diagnosed with a particular knee disease.

True Negatives (TN): The number of individuals correctly diagnosed as not having the knee disease.

False Positives (FP): The number of individuals incorrectly diagnosed with the knee disease (false alarms).

False Negatives (FN): The number of individuals incorrectly diagnosed as not having the knee disease when they actually have it (missed diagnoses).

Taking meniscus injury as an example, the classification confusion matrix is shown in Table II:

TABLE II. CLASSIFICATION CONFUSION MATRIX

| Diagnostic | Predicted Meniscus Injury | Predicted No Meniscus Injury |
|---------------------------|---------------------------|------------------------------|
| Actual Meniscus Injury | TP | FN |
| Actual No Meniscus Injury | FP | TN |

The indicator parameters are defined as follows.

1) The accuracy rate is mainly used to measure the accuracy of the diagnosis of the total sample, i.e., the number of samples correctly diagnosed as a proportion of the total number of samples. The formula for calculating the accuracy rate is as follows:

$$Accuracy = \frac{TP + TN}{TP + TN + FP + FN} \quad (1)$$

2) Sensitivity is the proportion of samples diagnosed as positive out of all positive samples, also known as the true positive rate (TPR), the recall rate. The formula for calculating sensitivity is as follows:

$$Sensitivity = \frac{TP}{TP + FN} \quad (2)$$

3) Specificity is the proportion of samples with a negative diagnosis to all negative samples, and the formula for calculating specificity is as follows:

$$\text{Specificity} = \frac{TN}{TN + FP} \quad (3)$$

4) False-positive rate is the proportion of incorrectly diagnosed positive samples to all negative samples, and the formula for calculating the false-positive rate is as follows:

$$FPR = \frac{FP}{TN + FP} \quad (4)$$

5) AUC (Area Under Curve, AUC) indicates the area under the ROC (receiver operating characteristic curve, ROC) curve. The formula for calculating AUC is as follows:

$$AUC = \int_{x=0}^1 TPR(FPR^{-1}(x))dx \quad (5)$$

where, TPR represents the true positive rate and FPR represents the false positive rate.

6) Youden index, also known as the correct index, is the sum of sensitivity and specificity minus 1. The larger the index, the better the screening test is, and the more truthful it is. The Youden index can be applied when it is assumed that the false-negative (missed diagnosis) and false-positive (misdiagnosis) rates are of equal significance. The method of evaluating the veracity of a screening test indicates the total ability of the screening method to detect true patients versus non-patients.

$$\text{Youden index} = \text{Sensitivity} + \text{Specificity} - 1 \quad (6)$$

C. Feature Importance

In order to improve the interpretability of the machine learning model, we calculated and ranked the importance of each symptom in the classification model. Random forest samples datasets from the sample set by bootstrap method with putback, and each dataset constitutes a decision tree. is the out-of-bag dataset, i.e., the dataset that was not sampled in when the dataset was generated. It is used as a test set to compute the importance of each feature using the Random Forest model, and the importance ranking of each feature is obtained by ranking the importance probability of each feature. For example, the steps of feature F importance calculation are as follows. The process of feature importance algorithm is shown in Algorithm 2:

Algorithm 2: Feature Importance Algorithm Steps

1: Using the random forest model based \bar{D}_i calculating the error of each decision tree $\mathcal{E} = [\mathcal{E}_1, \mathcal{E}_2, \dots, \mathcal{E}_n]$;

2: Randomly upset the order of the features in the sample set and again use the random forest model to calculate to get the error $\bar{\mathcal{E}} = [\bar{\mathcal{E}}_1, \bar{\mathcal{E}}_2, \dots, \bar{\mathcal{E}}_n]$, The difference between the two

calculation errors is $d = \mathcal{E} - \bar{\mathcal{E}}$;

3: Calculate the average of the differences

mean(d) and (statistics) standard deviation $\sigma(d)$;

4: The significance of a feature is the ratio of the mean to the standard deviation, i.e., *importance(F)* = *mean(d)*/ $\sigma(d)$.

IV. RESULTS

A. Data Collection

This study utilized the knee subjective symptom questionnaire assistance system for data collection and analysis of knee diseases and symptoms. The collection of clinical data was conducted in adherence to ethical guidelines and approved by the Ethics Committee Board of the Hefei Institute of Materials Research, Chinese Academy of Sciences, following the principles outlined in the Declaration of Helsinki. Informed consent forms were obtained from all participants after providing them with information about the study.

The gold standard for diagnosing knee diseases in the patients was based on assessments using MRI scans and comprehensive evaluations by physicians. The inclusion criteria for participants in the experiment were a definite diagnosis of a specific knee disease through MRI and other necessary examinations, the ability to provide complete clinical examination data and case information, and voluntary participation with an understanding of the nature of the experiment. Exclusion criteria included patients with myocardial infarction, serious infectious diseases, malignant diseases, or cognitive impairment.

The process of data collection and pre-processing involved the following steps: Firstly, patients independently completed the knee subjective symptom questionnaire through the questionnaire system. Subsequently, physicians reviewed each item of the questionnaire with the patients, verifying the diagnostic information related to the type of knee disease, which could include multiple disease types. This ensured the accuracy and validity of the questionnaire data. Finally, the data was exported from the questionnaire system for further analysis.

Data collection primarily took place from January 2021 to April 2021 at the orthopedic outpatient clinic of a tertiary hospital in Hefei, Anhui Province, China. Three orthopedic specialists were involved in acquiring and verifying the questionnaire data. A total of 157 valid data cases were obtained, comprising 76 male and 81 female participants, with no significant difference observed. The average age of the participants was 56 ± 7 , predominantly middle-aged and elderly patients.

B. Univariate Analysis

In this study, the subjective symptom questionnaire designed for knee disease symptoms is comprehensive, but not all symptoms are directly or strongly correlated with a specific disease. Therefore, it is crucial to filter and remove redundant symptom information to improve the efficiency of disease diagnosis. Symptom screening is an essential step in data

preprocessing for data mining and machine learning analysis. Effective symptom selection can significantly enhance the classification performance and overall robustness of the model. The primary objective of symptom selection is to

eliminate features with weak or no relevance to the classification target and utilize only the most effective features to achieve accurate classification or prediction results.

TABLE III. THE UNIVARIATE LOGISTIC REGRESSION ANALYSES RESULTS OF THE THREE DISEASES

| Diseases symptom | MT | | | ACL injurie | | | KOA | | |
|----------------------|---------|---------------------|------------------|-------------|-----------------------|------------------|---------|---------------------|------------------|
| | B | OR (95%CL) | P | B | OR (95%CL) | P | B | OR (95%CL) | P |
| Flexion Limit | -0.171 | 0.843(0.447-1.590) | 0.598 | 0.269 | 1.308(0.646-2.648) | 0.455 | 0.353 | 1.424(0.723-2.805) | 0.307 |
| Extension Limit | 0.499 | 1.648(0.795-3.415) | 0.179 | 0.698 | 2.009(0.928-4.348) | 0.077 | -1.148 | 0.317(0.123-0.818) | 0.017 |
| Snapping | -0.484 | 0.616(0.325-1.168) | 0.138 | -1.305 | 0.271(0.129-0.570) | <0.001 | 0.990 | 2.692(1.303-5.563) | 0.007 |
| Locking | -0.055 | 0.946(0.454-1.973) | 0.883 | -0.119 | 0.888(0.390-2.024) | 0.078 | 0.731 | 2.077(0.979-4.405) | 0.057 |
| Instability | 0.622 | 1.862(0.981-3.536) | 0.057 | 2.522 | 12.833(4.976-33.101) | <0.001 | -0.372 | 0.690(0.348-1.366) | 0.286 |
| Knee Dislocation | 1.661 | 5.265(2.315-11.976) | <0.001 | 2.767 | 15.906(6.522-38.792) | <0.001 | -1.265 | 0.282(0.102-0.779) | 0.015 |
| Patellar Dislocation | 1.814 | 6.138(1.259-29.931) | 0.025 | -1.281 | 0.278(0.034-2.261) | 0.231 | -20.510 | 0.00(0.000-) | 0.999 |
| Stiffness | 0.321 | 1.349(0.626-3.035) | 0.425 | -0.549 | 0.577(0.219-1.523) | 0.267 | 1.272 | 3.567(1.582-8.044) | 0.002 |
| Injure | 0.436 | 1.546(0.783-3.051) | 0.209 | 3.597 | 36.492(4.855-274.269) | <0.001 | -1.710 | 1.181(0.087-0.376) | <0.001 |
| Injure Zip | -0.138 | 0.871(0.398-1.907) | 0.729 | 2.283 | 9.810(4.140-23.242) | <0.001 | -1.125 | 0.325(0.117-0.901) | 0.031 |
| Knee Varus | -0.379 | 0.685(0.061-7.712) | 0.759 | -20.255 | 0.000(0.000-) | 0.999 | 1.516 | 4.553(0.403-51.453) | 0.220 |
| Knee Knock | -20.950 | 0.000(0.000-) | 0.999 | -20.282 | 0.000(0.000-) | 0.999 | 0.101 | 1.106(0.196-6.253) | 0.909 |
| Quadriceps Atrophy | 2.197 | 9.000(1.057-76.652) | 0.044 | 2.908 | 18.324(2.136-157.203) | 0.008 | -20.480 | 0.00(0.000-) | 0.999 |
| Swelling | 0.306 | 1.359(0.709-2.604) | 0.356 | 1.007 | 2.737(1.332-5.622) | 0.006 | -0.903 | 0.405(0.191-0.861) | 0.019 |
| Pain | -21.671 | 0.000(0.000-) | 0.999 | -2.388 | 0.092(0.018-0.462) | 0.004 | -0.103 | 0.902(0.216-3.765) | 0.887 |
| Pain Activity | -0.993 | 0.370(0.192-0.715) | 0.003 | -0.194 | 0.824(0.405-1.675) | 0.592 | 0.120 | 1.128(0.565-2.249) | 0.733 |
| Pain Rest | 21.603 | >100(0.000-) | 0.999 | -0.423 | 0.655(0.071-6.028) | 0.708 | 1.240 | 3.457(0.559-21.383) | 0.182 |
| Pain Hyperalgesia | -0.501 | 0.606(0.289-1.269) | 0.184 | 0.546 | 1.726(0.806-3.696) | 0.160 | -0.671 | 0.511(0.223-1.174) | 0.114 |
| Pain Hyperflexion | -1.145 | 0.318(0.162-0.626) | 0.001 | -0.593 | 0.533(0.270-1.131) | 0.105 | 0.102 | 1.107(0.547-2.243) | 0.777 |
| Pain Wandering | 0.578 | 1.783(0.460-6.911) | 0.403 | -20.310 | 0.000(0.000-) | 0.999 | 0.605 | 1.831(0.470-7.139) | 0.384 |
| Tend Knee Space | -2.712 | 0.066(0.025-0.173) | <0.001 | -0.334 | 0.716(0.328-1.564) | 0.402 | 0.405 | 1.500(0.666-3.380) | 0.328 |
| Tend Above Patella | -0.796 | 0.451(0.046-4.438) | 0.495 | -0.127 | 0.081(0.089-8.707) | 0.914 | 1.943 | 6.978(0.707-68.869) | 0.096 |
| Tend Patella | 0.904 | 2.469(1.094-5.570) | 0.030 | -1.058 | 0.347(0.113-1.062) | 0.064 | 0.305 | 1.356(0.589-3.122) | 0.474 |
| Tend Blow Patella | 0.087 | 0.917(0.149-5.646) | 0.925 | 0.590 | 1.805(0.291-11.192) | 0.526 | -20.460 | 0.00(0.000-) | 0.999 |
| Tend Knee Eye | 0.035 | 1.036(0.224-4.791) | 0.964 | -0.847 | 0.429(0.050-3.667) | 0.439 | -0.132 | 0.877(0.164-4.683) | 0.878 |
| Tend Tibial Tubercle | 21.539 | >100(0.000-) | 1.000 | 22.201 | >100(0.000-) | 1.000 | -20.422 | 0.00(0.000-) | 1.000 |
| Tend LCL | -20.893 | <0.001(0.000-) | 1.000 | 22.201 | >100(0.000-) | 1.000 | -20.422 | 0.00(0.000-) | 1.000 |
| Tend Iliotibial Band | -20.904 | <0.001(0.000-) | 0.999 | -20.246 | 0.000(0.000-) | 0.999 | -20.431 | 0.00(0.000-) | 1.000 |
| Tend MCL | 1.055 | 2.871(0.510-16.163) | 0.232 | 1.748 | 5.744(1.012-32.594) | 0.048 | -0.846 | 0.429(0.049-3.775) | 0.446 |
| Tend PoplitealFossa | 1.034 | 2.812(0.250-31.685) | 0.403 | 20.255 | >100(0.000-) | 0.999 | -20.441 | 0.00(0.000-) | 0.999 |

For feature selection, we employed the logistic regression algorithm as the Univariate Analysis method. Univariate logistic regression analysis explores the potential correlation between the dependent variable and each independent variable by establishing a functional relationship between the value of the independent variable and the probability of the occurrence of the event defined by the dependent variable. In this paper, univariate regression analysis was utilized to identify multiple symptoms that can effectively characterize knee disorders. Table III presents the results of univariate logistic regression analyses for three specific diseases: meniscus injury, anterior cruciate ligament injury, and knee osteoarthritis.

Symptoms with a p-value of less than 0.05 were included as significant symptoms of the disease based on the variable inclusion criteria for statistical significance. As can be illustrated in Table III, the significant symptoms of meniscus injury disease include seven symptoms: Knee Dislocation, Patellar Dislocation, Quadriceps Atrophy, Pain Activity, Pain Hyperflexion, Tend Knee Space, and Tend Patella, and the significant symptoms of ACL injury disease include nine symptoms such as Snapping, Instability, Knee Dislocation, Injure, Injury Zip, Quadriceps Atrophy, Swelling, Pain, and Tend MCL. The notable symptoms of knee osteoarthritis include seven symptoms of Extension Limit, Snapping, Knee Dislocation, Stiffness, Injure, Injure Zip, and Swelling. These symptoms differed significantly in the incidence of knee disease, so these factors needed to be screened for inclusion in the subsequent diagnostic modeling index system.

C. Disease Diagnosis

The experiment aimed to build a diagnostic screening model for knee diseases based on the significant symptoms identified through univariate analysis of each illness. The performance of the classification model was evaluated using leave-one-out cross-validation, a technique where each data point is used as a test sample once while the remaining samples were used for training the model.

To assess the effectiveness of our proposed method, we compared the diagnostic performance of the optimized random forest-based model with other models, including support vector machine (SVM), logistic regression (LR), AdaBoost (AB), and MLP neural network (Multi-Layer Perceptron, MLP). We evaluated the diagnostic performance regarding various indicators such as AUC, accuracy, sensitivity, specificity, and

Yoden's index. To address data imbalance, we used the SMOTE (Synthetic Minority Over-sampling Technique) method for data augmentation, which helped achieve analyzable results.

Furthermore, to improve the interpretability of the model, we employed a variable importance calculation method

specifically designed for the random forest-based model. This method allowed us to calculate and rank the importance of each variable in the model.

The specific results obtained from the experiment are as follows:

1) *Model performance analysis:* We evaluated the performance of the subjective symptom-based diagnostic model for knee diseases proposed in this study. The model, supplemented with the random forest algorithm, was used for diagnosing meniscus injury, anterior cruciate ligament (ACL) injury, and knee osteoarthritis. Table IV show the diagnostic results of the model for three diseases. The experimental results showed that the AUC values of the diagnostic model for all three diseases were more significant than 0.8. This indicates that the model constructed in this study is suitable for the diagnostic task of common knee diseases. ACL injury showed the highest diagnostic performance among the three diseases, with an AUC value of 0.92. Meniscus injury had an AUC of 0.87, and knee osteoarthritis, after excluding a large amount of concomitant disease data and using SMOTE data augmentation, achieved an AUC of 0.85. Additionally, this study evaluated the comprehensive performance and found that the AUC value showed the best performance among the comprehensive performance of the three disease diagnosis.

These findings demonstrate the effectiveness of the diagnostic screening model for knee diseases based on subjective symptoms. The optimized random forest-based model, along with the use of appropriate machine learning algorithms, showed promising performance in diagnosing common knee diseases. The evaluation metrics such as AUC, accuracy, sensitivity, specificity, and Yoden's index provided comprehensive insights into the model's diagnostic capabilities.

2) *Comparison of model performance based on different models:* We used support vector machines, logistic regression, AdaBoost algorithm, and MLP neural networks to construct prediction models for comparative analysis. The hyperparameter settings for these four models were carried out in the same manner as the Random Forest model.

A random forest algorithm was used to construct a diagnostic screening model for meniscus injury, anterior cruciate ligament (ACL) injury, and knee osteoarthritis. Four common machine-learning algorithms were used for comparative analysis. Table V presents the accuracy, sensitivity, specificity, and Youden's index for diagnosing the three common knee disorders. Fig. 2 to Fig. 4 display the AUC curves for diagnosing the three disorders.

TABLE IV. THE DIAGNOSTIC RESULTS OF THE MODEL FOR THREE DISEASES

| Disease Types | AUC | Accuracy | Sensitivity | Specificity | Threshold | Jordon Index |
|-----------------------------------|------|----------|-------------|-------------|-----------|--------------|
| Meniscus injury | 0.87 | 0.79 | 0.79 | 0.80 | 0.53 | 0.61 |
| Anterior Cruciate Ligament Injury | 0.92 | 0.84 | 0.84 | 0.84 | 0.30 | 0.73 |
| Knee osteoarthritis | 0.85 | 0.81 | 0.88 | 0.79 | 0.19 | 0.68 |
| comprehensive performance | 0.88 | 0.81 | 0.84 | 0.81 | 0.34 | 0.67 |

TABLE V. PERFORMANCE OF A DIAGNOSTIC MODEL FOR COMMON KNEE DISEASES IN SELECTING OPTIMAL THRESHOLDS

| Disease Types | AUC | Accuracy | Sensitivity | Specificity | Threshold | Jordon Index |
|-----------------------------------|------|----------|-------------|-------------|-----------|--------------|
| Meniscus injury | 0.87 | 0.79 | 0.79 | 0.80 | 0.53 | 0.61 |
| Anterior Cruciate Ligament Injury | 0.92 | 0.84 | 0.84 | 0.84 | 0.30 | 0.73 |
| Knee osteoarthritis | 0.85 | 0.81 | 0.88 | 0.79 | 0.19 | 0.68 |
| comprehensive performance | 0.88 | 0.81 | 0.84 | 0.81 | 0.34 | 0.67 |

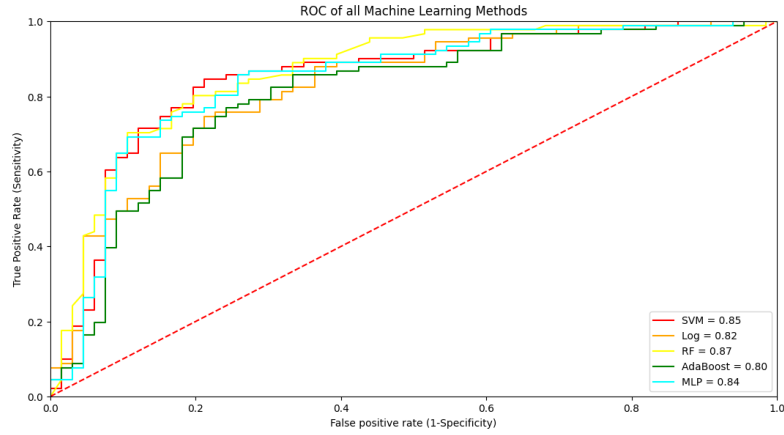


Fig. 2. Machine learning algorithm to meniscus injury disease AUC curve.

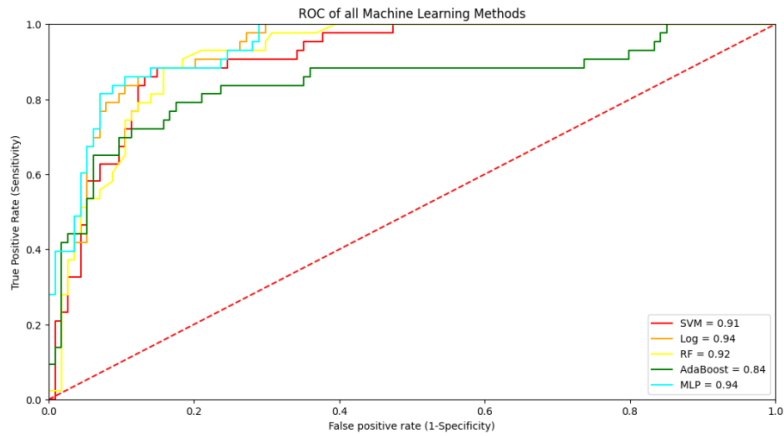


Fig. 3. Anterior cruciate ligament injury disease machine learning algorithm AUC curve.

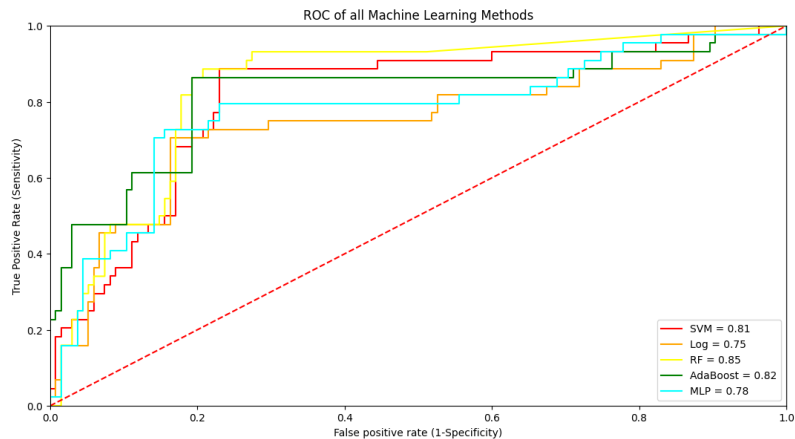


Fig. 4. Knee osteoarthritis disease machine learning methods AUC curve.

Specifically, for the diagnosis of meniscus injury disease, the Random Forest (RF) model achieved the highest AUC of 0.87, followed by the Support Vector Machine (SVM) model at 0.85, the MLP neural network model at 0.84, the Logistic Regression (Log) model at 0.82, and the AdaBoost model at 0.80.

For diagnosing ACL injury disease, the MLP neural network model and Log model performed the best with an AUC of 0.94, followed by the RF model at 0.92, the SVM model at 0.91, and the AdaBoost model at 0.84.

In the knee osteoarthritis disease diagnostic model, the RF model achieved the highest AUC of 0.74 on the test set, followed by the Log model at 0.73, the MLP neural network model and the AdaBoost model, both with an AUC of 0.72, and the SVM model performed slightly worse with an AUC of 0.63. The overall performance of the knee osteoarthritis disease diagnostic model was significantly improved by enhancing the model with SMOTE data, with an AUC of 0.80, accuracy of 0.80, sensitivity of 0.78, and specificity of 0.81.

Compared to the other four classifiers random forest model has higher AUC value and Yoden index, and better

comprehensive performance for disease diagnosis. The random forest model has good ability to diagnose and screen common knee joint diseases, and therefore has some practical value, which further indicates that the disease diagnosis and screening based on subjective symptoms proposed in this study is feasible.

3) *Symptom feature importance for random forest algorithms*: The highest importance scores constructed for different knee diseases varied considerably. The feature importance scores of the random forest algorithm are shown in Fig. 5 to Fig. 7. The first four subjective symptoms were taken as follows: meniscus injury disease with the following order of significance: Tend Knee Space, Knee Dislocation, Pain Hyperflexion, Pain Activity, ACL injury disease with the following order of significance: Knee Dislocation, Instability, Injure Zip, Injure. Significant symptoms of osteoarthritis of the knee and their ranking are as follows: Injure, Stiffness, Snapping and Extension Limit. These are important references for disease analysis.

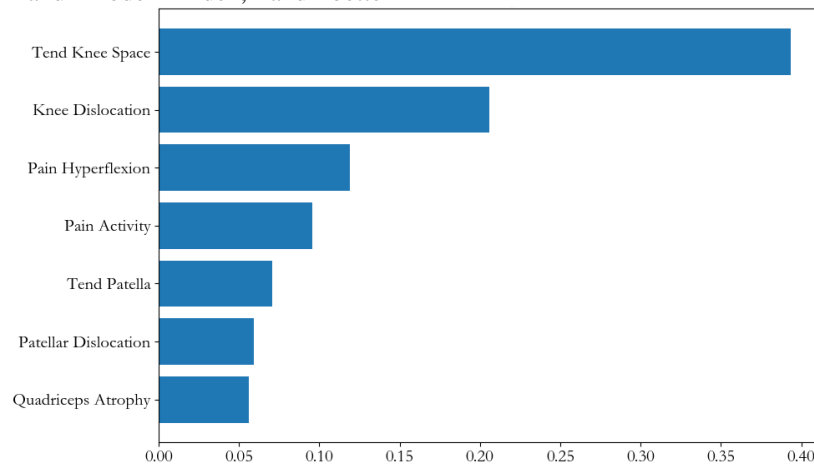


Fig. 5. Ranking the symptom feature importance of diagnostic model for MT injuries.

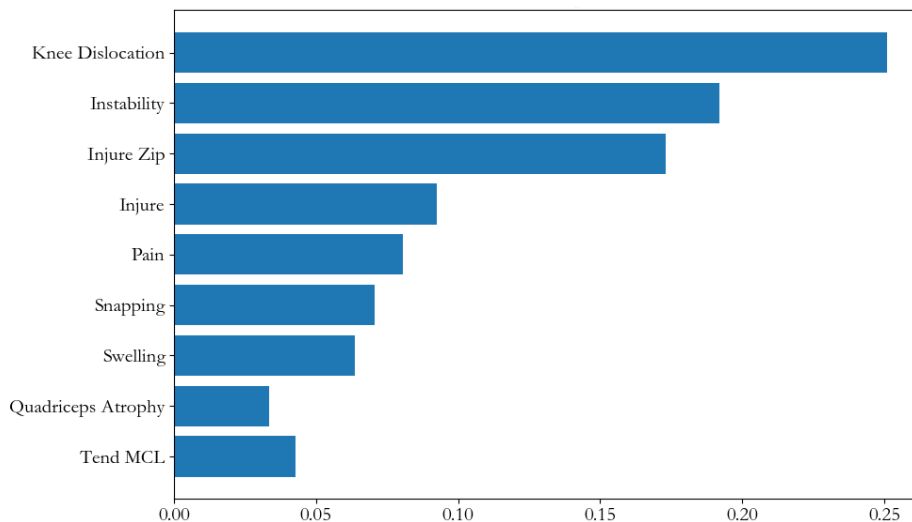


Fig. 6. Ranking the symptom feature importance of diagnostic model for ACL injuries.

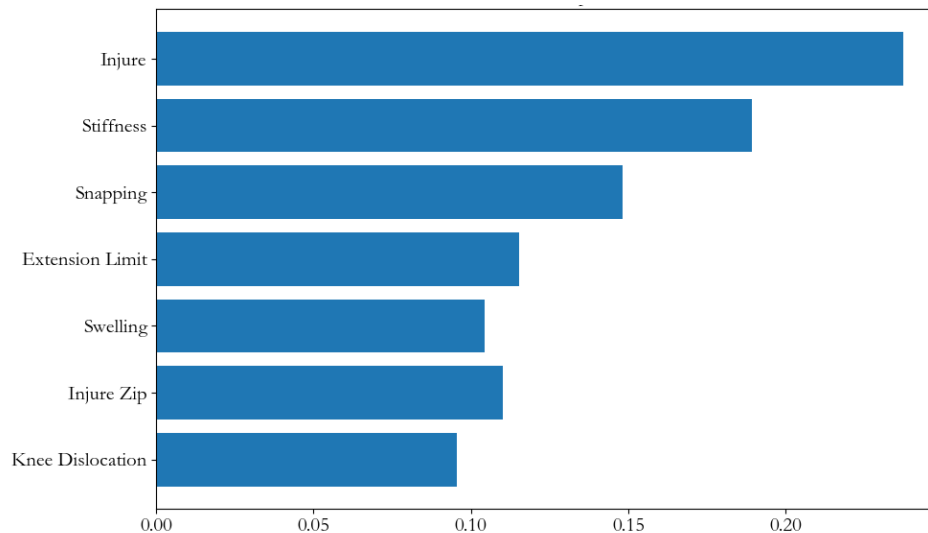


Fig. 7. Ranking the symptom feature importance of diagnostic model for KOA.

V. DISCUSSION

A. Disease Diagnosis Effectiveness Analysis

In this study, a diagnostic screening model for common knee diseases was constructed using a random forest algorithm. The results of the study revealed variations in the diagnostic accuracy for different diseases. ACL injuries were generally better identified, meniscal injuries had slightly lower accuracy, and knee osteoarthritis showed the lowest diagnostic effectiveness. One of the reasons behind the lower diagnostic effectiveness for meniscal injuries and knee osteoarthritis is their strong concurrency.

Pathologically, ACL injuries involving ligamentous structures tend to exhibit more distinct symptoms and a certain degree of specificity. On the other hand, meniscal injuries and knee osteoarthritis are both cartilage diseases and share similar symptoms, making it more challenging to differentiate between them.

When comparing different machine learning methods, the random forest model demonstrated advantages in this study. Random forest is an ensemble learning algorithm that combines multiple decision trees into a single predictive model. It mitigates overfitting issues and enables parallel operation since there are no dependencies between weak learners. Random forests have shown excellent performance in various classical problems, including disease diagnosis. Another integrated learning algorithm, AdaBoost, also performed well in this study. AdaBoost, based on boosting, is particularly effective in handling categorical variables. However, the MLP neural network algorithm, commonly used for unstructured and complex data, was not the most suitable choice for the structured data and categorical features of this study. The random forest and AdaBoost models were more appropriate and demonstrated good performance. Among the compared models, the random forest model generally outperformed the AdaBoost model in this study, supporting previous findings that highlighted the superior classification

performance of random forests. Logistic regression, although widely used in the biomedical field due to its simplicity and interpretability, may not have been as effective in addressing the classification problem of this study.

This study achieved better results than the current symptom-based diagnosis of knee disorders. The diagnostic rate for meniscal injuries based on detailed history and clinical examination by doctors is typically around 80% to 85%. The developed diagnostic system in this study showed similar diagnostic accuracy to that of doctors' initial diagnoses, indicating its high clinical value. Table VI provides a comparison of the diagnosis of knee diseases based on symptoms and risk factors.

Overall, the random forest-based diagnostic screening model demonstrated superior performance in identifying knee disorders compared to other machine learning methods and the current symptom-based diagnosis. Removing the interference of concurrent diseases improved the diagnostic accuracy for knee osteoarthritis. These findings highlight the potential of machine learning algorithms in improving disease diagnosis and could have implications for clinical practice.

B. Analysis of Significant Symptoms of Disease

The subjective knee symptoms constructed in this paper can characterize knee disease states with good accuracy for diagnostic prediction through machine learning. Symptoms that characterize the functional state of knee diseases need to meet the needs of diagnosing the effectiveness of the disease, public comprehensibility, and other needs, and there are greater challenges. In this paper, through multiple rounds of research, collation and expert selection and optimization, 30 subjective knee symptoms are finally identified for characterizing knee diseases. Further diagnostic prediction through machine learning algorithms achieves a high correct rate and verifies the validity of symptom definition and selection.

TABLE VI. COMPARISON ON DIAGNOSIS OF KNEE DISEASES BASED ON SYMPTOMS AND RISK FACTORS

| | Related Research and Methods | Results |
|-----------------------------|---|--|
| Bisson et al. | Constructing a web-based symptom checker for multiple knee disorders to establish a differential diagnosis of knee injuries, allowing patients to determine the correct diagnosis from a checklist. | Overall diagnosis of the disease: 91% sensitivity and 23% specificity; 58% sensitivity and 48% specificity when patients used the tool. |
| Elkin et al. [14] | To construct a questionnaire-based diagnostic expert system for multiple knee diseases, a Bayesian method was used in model 1 and a heuristic method was used in model 2, and disease importance and term importance weights were added to combine models 1 and 2 to form models 3 and 4. | Accuracy of correct diagnosis in the 1st order in the expert model: model 1: 43.3%, model 2: 43.3%, model 3: 47.8%, model 4: 40.7%. |
| Lim et al. | Deep learning algorithm was used to predict the diagnosis of osteoarthritis of the knee in the Korean Health and Nutritional Status Database. | Sensitivity 67%, specificity 73%, accuracy 71.97%, AUC 76%. |
| Ratzlaff et al. [15] | Web-based questionnaire survey to predict diagnosis of knee osteoarthritis and hip osteoarthritis. | For knee osteoarthritis diagnosis: sensitivity 73%, specificity 96%. |
| Roux et al. | Phone-based questionnaire to predict diagnosis of knee osteoarthritis and hip osteoarthritis. | For the diagnosis of osteoarthritis of the knee: sensitivity 87%, specificity 93%. |
| Snoeker et al. | A digital-based questionnaire to predict diagnosis of meniscal injury disorders. | For meniscus diagnosis: sensitivity 86.1%, specificity 45.5%, AUC 0.76. |
| Wang Pei et al. | Establishment of a diagnostic grading model for osteoarthritis of the knee on the basis of data from pathogenic factors, symptoms, signs, physical examination and various scales using logistic regression methods. | Overall accuracy for knee osteoarthritis was 67%, sensitivity 50%, specificity 75%, and AUC of 0.88. |
| This paper | Differential diagnosis of meniscus injury, anterior cruciate ligament injury and osteoarthritis of the knee by self-developed subjective symptom questionnaire combined with random forest machine learning method for common knee diseases. | Diagnostic performance for MT: an AUC of 0.87, accuracy of 0.79, sensitivity of 0.79 and specificity of 0.80; ACL injury disease: 0.92, 0.84, 0.84 and 0.84; KOA: 0.85, 0.81, 0.88 and 0.79. |

Through the clinical questionnaire data collection process, it can be found that patients are able to fill in the questionnaire by themselves through the questionnaire and its auxiliary system, and the detection error rate of the doctor's verification is low, which fully demonstrates that ordinary patients can understand the questionnaire content, and it can be applied to further clinical promotion.

Machine learning algorithms build models with better performance compared to statistical methods but have the disadvantage of poor model interpretability. Machine learning involves learning to train, construct a model and predict new input data. To increase the transparency of the model and provide health education for residents in practical applications, we calculated the impact of each symptom on the performance of the diagnostic model. Through the one-way analysis and diagnostic model importance analysis, significant symptoms can be filtered out for differential diagnosis of knee diseases, and further through the machine learning method and the importance of the calculation of the ranking, to obtain the more important symptoms for each disease, the specific analysis is as follows:

1) The notable symptoms of meniscus injury disease and their symptoms of high importance are compression Tend Knee Space, Knee Dislocation, Pain Hyperflexion and Pain Activity, which are important references for the analysis of the disease. Since the meniscus is present in the knee space, pressure pain in the knee space is a prominent symptom in the diagnosis of meniscus injury [16]. The meniscus is the role of the spacer for the knee activity to form a cushioning effect; once the injury lesion, the knee activity will be exacerbated by pain, so Pain Hyperflexion is increased, Pain Activity is increased, and other symptoms [17]. Generally, meniscal disease does not cause symptoms of dislocation sensation. In this study, there existed a large number of symptoms of

meniscus in combination with ACL, and dislocation sensation was a significant symptom of ACL injury and thus was included among the significant symptoms of meniscus, which is a reflection of the complexity of knee disease.

2) The notable symptoms of ACL injury disease and its symptoms of higher importance are Knee Dislocation, Instability, Injure Zip, and Injure, respectively. ACL injury disease indicates the presence of damage and rupture of the ACL. The anterior cruciate ligament (ACL) is located in the knee, connecting the femur and tibia, and its main role is to limit the tibia's forward shift. It is an important static and kinetic anterior stabilizing structure of the knee, which prevents the tibia's anterior shift in flexion, prevents the knee from over-extending in extension, controls knee rotation, and controls knee internal and external rotation at different flexion angles, and has a proprioceptive function [18]. When an injury rupture of the ACL occurs, there is a noticeable sense of dislocation, which later develops into a sense of instability. The main cause of ACL rupture is injury, which accounts for more than 70% of the cases. Therefore, the presence of a history of trauma in the patient is the main causative factor in the development of the disease [19]. A tearing sound accompanies ligament tear injuries. Further intra-articular hemorrhage leads to swelling, pain, and, in most cases, inability to continue with the original sport or even limited extension and hyperflexion activities.

3) The prominent symptoms of osteoarthritis disease of the knee and their higher importance are Stiffness, Snapping, Injure, and Swelling, respectively. This is almost identical to the clinical diagnostic criteria for the knee. Clinical diagnostic criteria for knee osteoarthritis usually consider ① knee pain, ② snapping, ③ morning stiffness time≤30min, ④ age ≥38 years old, ⑤ bony enlargement, Osteoarthritis of the knee is

diagnosed if ①②③④, or ①②⑤ or ①④⑤ are fulfilled [20]. From the perspective of subjective symptoms, pain was the basic symptom, while joint friction sound (sensation), morning stiffness and bony enlargement were important for clinical diagnosis, which verified the reliability of the subjective and significant symptom analysis in this study.

From the distribution of disease symptoms, it can be found that pain is the first complaint of knee diseases, and in this questionnaire case, different diseases caused pain symptoms almost 100%. Therefore, pain symptoms are the basic symptoms but are not significant for the differential diagnosis of the disease.

Stiffness is an important symptomatic feature of knee osteoarthritis. Patients may experience stiffness in the joints in the morning or after rest, which can be relieved by activity due to verification of cartilage or joint adhesions.

Snapping due to cartilage destruction and rough joint surface, bone friction sound (sense) occurs during joint movement.

Injure is an important symptom in the history of knee disease and an important factor in the development of Osteoarthritis of the knee. Everyday knee injuries are prone to cause cartilage damage or lesions, which gradually form Osteoarthritis of the knee.

Swelling symptoms in this study were generally compared to the difference in the knee compared to the healthy side or the previous one, so bony enlargement symptoms were included. As Osteoarthritis of the knee progresses, patients experience swelling and bony enlargement of the knee. Swelling is caused by fluid and cells collecting around the joint due to inflammation, resulting in swelling, pain, and warmth in the joint area. The swelling may get worse as the inflammation increases. On the other hand, bone enlargement is caused by damage to the cartilage in the knee. The cartilage loses its ability to protect the articular bones, causing them to be exposed to friction and wear and tear. Over time, the articular bones regrow, forming bone spurs and osteophytes. These bony protrusions cause pain and stiffness when the joint moves.

C. Research Limitations

This research also has some limitations.

Firstly, the sample size used for constructing the diagnostic model was relatively small, and the uneven distribution of positive and negative cases may have affected the model's training and analysis of the disease. Therefore, the model may not directly apply to clinical diagnosis, but it can still be valuable for self-screening common knee diseases.

Secondly, the data used in the study were collected from a specific region and population in Anhui province, which may limit the generalizability of the findings to other populations. Regional differences and variations in disease duration should be considered when applying the model to different populations.

Lastly, the subjective questionnaire employed in the study mainly utilized dichotomous data and lacked more detailed

information regarding symptom typing and severity. Incorporating more comprehensive and detailed symptomatic details in future studies could enhance the diagnosis of a wider range of diseases and provide a better understanding of disease severity.

These limitations should be addressed in future research to improve the diagnostic accuracy and applicability of the model.

VI. CONCLUSION

In this study, we designed a subjective symptom questionnaire for knee diseases based on easily collected subjective symptoms. We collected clinical data to analyze the relationship between diseases and symptoms. By combining univariate logistic regression analysis and random forest, we developed a diagnostic screening method for common knee diseases using these subjective symptoms. The study demonstrated promising diagnostic performance for the examined common knee diseases.

The area under the curve value was 0.87 for meniscal disease. For ACL injury, the AUC value was 0.92; for knee osteoarthritis, the AUC value was 0.84. Additionally, accuracy, sensitivity, and specificity values were reported for each disease, indicating favorable performance compared to similar studies and proximity to the clinical diagnosis results of physicians. These findings suggest that the proposed method, which utilizes subjective symptoms, holds advantages in screening common knee diseases and may be applicable for self-diagnosing these conditions.

Furthermore, the study presents a general framework for utilizing machine learning methods to predict the risk of developing other chronic diseases. However, it is important to note that further research and validation are necessary to ensure the robustness and generalizability of the proposed diagnostic method.

Conflicts of Interest: The authors declare no conflict of interest.

Data Availability Statement: All data underlying the findings are fully available without restriction. All relevant data are within the paper and appendices.

Fund Project: This research was funded by National Key R&D Program Project, Demonstration of Integrated Application of Community Science and Fitness in Central Region (2022YFC2010200), the Key Project on Anhui Provincial Natural Science Study by Colleges and Universities under Grant "Key technical research of knee function evaluation and rehabilitation training"(No. KJ2019A0555), Key project of Science and Technology Service Network Program of Chinese Academy of Sciences (No. KFJ-STZ-ZDTP-079), Hefei Natural Science Foundation Project (No. 202302), Medical Artificial Intelligence Joint Fund Project (MAI2023 C008). Furthermore, it was supported by key projects of natural science research in Anhui Province's higher education institutions (No. KJ2021A1436), (No. 2022AH052604).

Informed Consent Statement: Informed consent was obtained from all subjects involved in the study.

REFERENCES

- [1] Okamoto S, Ishii Y, Ishikawa M, et al. The effect of gait modification on the response of medial meniscus extrusion during gait in patients with knee osteoarthritis[J]. *Gait & posture*, 2023, 102: 180-185.
- [2] Hutchison L, Grayson J, Hiller C, et al. Relationship Between Knee Biomechanics and Pain in People with Knee Osteoarthritis: A Systematic Review and Meta-Analysis[J]. *Arthritis care & research*, 2023,75(6):1351-1361.
- [3] Hanna M, Jeffrey N K. The influence of meniscal pathology in the incidence of knee osteoarthritis: a review[J]. *Skeletal radiology*, 2023,52(11):2045-2055.
- [4] Adams B G, Houston M N, Cameron K L. The Epidemiology of Meniscus Injury[J]. *Sports Medicine and Arthroscopy Review*, 2021, 29(3):24-33.
- [5] Qin S, Chi Z, Xiao Y, et al. Effectiveness and safety of massage for knee osteoarthritis: A protocol for systematic review and meta-analysis[J]. *Medicine*, 2020, 99(44): e22853.
- [6] Lim J, Kim J, Cheon S. A deep neural network-based method for early detection of osteoarthritis using statistical data[J]. *International journal of environmental research and public health*, 2019, 16(7): 1281.
- [7] Snoeker B A M, Zwinderman A H, Lucas C, et al. A clinical prediction rule for meniscal tears in primary care: development and internal validation using a multicentre study[J]. *British Journal of General Practice*, 2015, 65(637): e523-e529.
- [8] Wang P, Zhang X, Gao Y, et al. Establishment of grading model of knee osteoarthritis based on clinical research system[J]. *China J Orthop Trauma*, 2018, 31(6):528-533.
- [9] Bisson L J, Komm J T, Bernas G A, et al. How accurate are patients at diagnosing the cause of their knee pain with the help of a web-based symptom checker? [J]. *Orthopaedic journal of sports medicine*, 2016, 4(2): 2325967116630286.
- [10] Cui M, Gang X, Gao F, et al. Risk assessment of sarcopenia in patients with type 2 diabetes mellitus using data mining methods[J]. *Frontiers in endocrinology*, 2020, 11:123.
- [11] Chiew C J, Liu N, Wong T H, et al. Utilizing machine learning methods for preoperative prediction of postsurgical mortality and intensive care unit admission[J]. *Annals of surgery*, 2020, 272(6):1133-1139.
- [12] Zhao H, Zhang X, Xu Y, et al. Predicting the Risk of Hypertension Based on Several Easy-to-Collect Risk Factors: A Machine Learning Method[J]. *Frontiers in Public Health*, 2021, 9:619429. DOI: 10.3389/fpubh.2021.619429.
- [13] Moitra D, Mandal R K. Prediction of Non-small Cell Lung Cancer Histology by a Deep Ensemble of Convolutional and Bidirectional Recurrent Neural Network[J]. *Journal of Digital Imaging*, 2020, 33(9): 895-902.
- [14] Elkin P L, Schlegel D R, Anderson M, et al. Artificial intelligence: bayesian versus heuristic method for diagnostic decision support[J]. *Applied clinical informatics*, 2018, 9(02): 432-439.
- [15] Ratzlaff C, Guermazi A, Collins J, et al. A rapid, novel method of volumetric assessment of MRI-detected subchondral bone marrow lesions in knee osteoarthritis[J]. *Osteoarthritis and cartilage*, 2013, 21(6): 806-814.
- [16] Smith J D, Johnson A B, Wilson C D. Accuracy of McMurray's test, the modified version, and joint-line tenderness in diagnosing chronic meniscal tear in the knee joint: A cross-sectional study. *Journal of Orthopedic Research*, 2023, 41(2), 123-135.
- [17] Garvick S J, Reich S. Meniscal tears[J]. *JAAPA: official journal of the American Academy of Physician Assistants*, 2020, 33(1):45-46.
- [18] Philipp F, Constantin D, Lucca L, et al. Repair of the lateral posterior meniscal root improves stability in an ACL-deficient knee[J]. *Knee surgery, sports traumatology, arthroscopy: official journal of the ESSKA*, 2018, 26(8):2302-2309.
- [19] Rigg J, Perera N, Toohey L, et al. ACL injury occurrence in the Australian High Performance Sports System: a 5-year retrospective analysis[J]. *Journal of Science and Medicine in Sport*, 2022, 25(Supplement 2):45-46.
- [20] Guo J, Chen P, Cai T, et al. Dysfunction Characteristics of Knee Osteoarthritis with the Conception of "Muscles and Bones, Arthralgia and Flaccidity, Asthenia and Sthenia, Dynamic and Static, Hardness and Softness"[J]. *Rehabilitation Medicine*, 2021, 31(1):69-72.

Data Dynamic Prediction Algorithm in the Process of Entity Information Search for the Internet of Things

Tianqing Liu

College of Artificial Intelligence and Big Data, Zibo Vocational Institute, Zibo, 255000, China

Abstract—To address the issue of insufficient real-time capability in existing Internet search engines within the Internet of Things environment, this research investigates the architecture of Internet of Things search systems. It proposes a data dynamic prediction algorithm tailored for the process of entity information search in the Internet of Things. The study is based on the design of a data compression algorithm for the Internet of Things entity information search process using the Rotating Gate Compression Algorithm. The algorithm employs the Least Squares Support Vector Machine to dynamically predict changes in entity node states in the Internet of Things, aiming to reduce sensor node resource consumption and achieve real-time search. Finally, the research introduces an Internet of Things entity information search system based on the data dynamic algorithm. Performance test results indicate that the segmented compression algorithm designed in the study can enhance compression accuracy and compression rate. As compression accuracy increases, errors also correspondingly increase. The prediction algorithm designed in the study shows a decrease in node energy consumption as reporting cycles increase, reaching 0.2 at 5 cycles. At the 5-cycle point, the prediction errors on two research datasets are 0.5 and 7.8, respectively. The optimized data dynamic prediction algorithm in the study effectively reduces node data transmission, lowers node energy consumption, and accurately predicts node state changes to meet user search demands.

Keywords—Internet of Things; sensors; swinging door trending (SDT); support vector machine (SVM); data dynamic prediction

I. INTRODUCTION

In the era of the Internet of Things (IoT), massive devices continuously generate vast streams of data containing crucial insights for entity information search. With the rapid development of IoT technology, effectively processing and predicting this data to support real-time, accurate information search has become a significant research topic. The data dynamic prediction algorithm for entity information search in the IoT aims to predict dynamic changes in data in the IoT environment using advanced data analysis techniques to enhance search efficiency and accuracy [1-2]. The complexity of the IoT environment is mainly reflected in the high dynamism, large-scale, and heterogeneity of data. These characteristics make traditional data processing and prediction methods challenging to adapt. For example, IoT devices generate diverse data types with a fast update frequency, influenced by various factors such as environmental changes, device status, and user behavior. Therefore, developing an algorithm that can accurately predict these dynamic data changes is crucial for efficient IoT entity information search. Currently, IoT data processing and analysis rely mainly on

traditional data processing techniques and algorithms. However, these methods face numerous challenges when handling large-scale, highly dynamic, and heterogeneous IoT data. On the one hand, unlike the traditional Internet, the object of IoT search is structured and highly dynamic, and traditional search engines cannot adapt to IoT information search. On the other hand, the Internet of Things has a large number of nodes, diverse data types, and fast update frequencies. Traditional search strategies have poor timeliness and waste a large amount of computing resources [3]. Based on this, research has been conducted on the architecture of IoT search systems, proposing a data dynamic prediction algorithm for IoT entity information search processes. The innovation of the research is mainly in two aspects, one of which introduces a lightweight data compression method to compress the original data and reduce the network communication pressure. The second introduces a minimized quadratic loss function to improve the support vector machine for real-time search. Additionally, the research considers the real-time and dynamic nature of data to ensure that the algorithm can adapt to the rapid changes in IoT data. This research is expected to provide new theoretical and practical references in the field of IoT data processing and analysis on the one hand; on the other hand, it promotes the development and innovation of IoT applications, and has great potential to provide richer and smarter services for people.

The research is divided in six sections. Section II delves into related. Section III presents an IoT entity information search system based on the data dynamic prediction algorithm. Section IV tests and analyzes the performance of the model and algorithm. Results and discussion is given in Section V. Section VI summarizes and concludes the above content.

II. RELATED WORKS

In the field of sensor networks, numerous studies focus on data transmission and application. Sreedharan et al. proposed a cluster head selection and hybrid routing protocol algorithm based on fuzzy multi-attribute decision-making to enhance the performance of wireless sensor networks. Subsequent experiments demonstrated the effectiveness of their algorithm [4]. Pattnaik et al. introduced an algorithm that combines fuzzy clustering and elephant herd optimization to achieve efficient routing assembly in wireless sensor networks, with simulation experiments validating its advantages in energy utilization and system lifespan [5]. Javaheri et al. conducted research on data fusion techniques in wearable sensors, comparing Kalman fusion and alpha-fine-tuned mean filtering. They designed an algorithm that switches between the two fusion methods based on Signal Quality Index, with

experimental results showing its superiority over baseline dual-channel RR interval averaging by approximately 54% and 21%, respectively [6]. The IoT, as a network connecting everything, involves processes where sensor-acquired data is uploaded to the network and then processed by artificial intelligence or corresponding algorithms to issue instructions for desired actions by executive devices. As an emerging concept, IoT has been widely studied in various fields. Turner et al. focused on reducing the environmental impact of the manufacturing industry by aligning with practices in digital computation and the automotive industry. They constructed an IoT network framework for the circular economy model in manufacturing based on Industry 4.0 computing and IoT interaction networks [7].

Zhang et al. addressed the issue of battery replacement in large-scale IoT deployments by employing wireless power transfer using radio frequencies. Based on DEIN technology, they developed a time allocation model to manage radio frequency energy and the transmission of uplink data in different time slots. Additionally, they proposed a joint time and power allocation algorithm to reduce the energy consumption per bit for uplink data transmission in the system [8]. Mabodi et al. focused on the ability of IoT nodes to provide general intelligent predictions and used a method to reduce gray hole attacks by inspecting node information. The approach involved validating trust in IoT nodes, testing routes, detecting gray hole attacks, and eliminating malicious attacks in the MTISS-IoT process. Experimental results demonstrated a high detection rate [9]. Dynamic data prediction algorithms have been studied in various fields, and Huang et al. conducted research on the numerical simulation process of Steam-Assisted Gravity Drainage (SAGD). They developed and tested a workflow based on a data-driven model for predicting SAGD production performance. A comparison of different machine learning algorithms indicated that a model based on Gated Recurrent Units (GRU) exhibited the best predictive capability [10]. Xiao et al. considered the spatiotemporal dynamic characteristics for air quality prediction and proposed a Dual-Path Dynamic Directed Graph Convolutional Network (DP-DDGCN) for air quality prediction. The model aimed to comprehensively capture

dynamic spatial dependencies, and experimental results showed its superior performance in predicting PM2.5 concentration [11].

In summary, although scholars have conducted extensive research on algorithms and functional optimizations to enhance IoT performance, more research has been done on application improvement, node prediction, and performance enhancement for IoT only. There has been limited optimization of the entity information search process. However, the search optimization for dynamic data content of sensor nodes has important potential application value in IoT performance transmission. Therefore, the research started from three aspects: compression of data resources, dynamic prediction, and real-time search, and designed an IoT entity information search system based on data dynamic algorithms, which to a certain extent fills the research gap of entity information search.

III. DESIGN OF DATA DYNAMIC PREDICTION ALGORITHMS FOR ENTITY INFORMATION SEARCH IN IOT

Traditional IoT search methods involve broadcasting search requests to each sensor node, enabling real-time acquisition of dynamically changing node status information. However, this approach leads to high communication overhead, bandwidth consumption, and consequently, a reduction in the lifespan of nodes. To address this challenge, research has been conducted on data dynamic prediction algorithms, proposing a novel architecture for an IoT search system to overcome the inadequacy of existing internet search engines in providing real-time results within the IoT environment.

A. Design of IoT Entity Information Search System Based on Data Dynamic Prediction Algorithms

The study focused on researching data dynamic prediction algorithms for IoT entity information search processes, integrating web technologies into the IoT domain. They proposed a Web of Things (WoT) search system based on data dynamic prediction algorithms. The architecture of this search system is illustrated in Fig. 1.

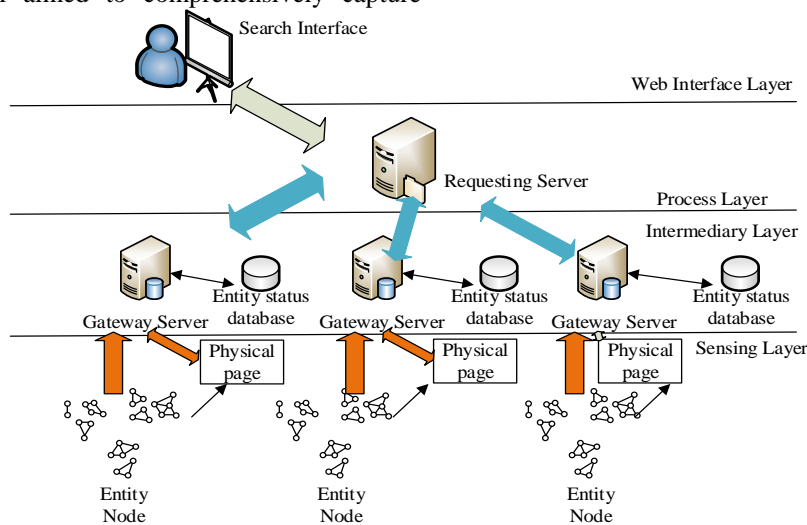


Fig. 1. WoT search system.

As shown in Fig. 1, the WoT Search System is primarily divided into four layers, each serving different functions to achieve efficient, flexible data processing, and user interaction. The Sensing Layer constitutes the core of the system's data source, consisting of numerous sensor nodes responsible for collecting environmental data. These data undergo initial compression processing within the nodes themselves to reduce transmission burdens. The Mediation Layer (Gateway Service Layer) acts as the hub for data processing and forwarding, collecting data from the Sensing Layer for further analysis and prediction, ensuring real-time and accurate data. Simultaneously, this layer responds to external query requests, retrieving and filtering relevant data. The Processing Layer (Request Service Layer) serves as the direct processing center for user requests, analyzing user queries, interacting with the Mediation Layer, integrating acquired data, and optimizing the presentation order of results. The User Interface Layer provides users with an intuitive, user-friendly interface, presenting complex backend data processing results in a clear and concise manner to meet specific user query requirements. This search system is based on existing search technology and optimized for the characteristics of IoT network architecture.

B. Data Compression Algorithm based on SDT Compression Algorithm

In order to enhance the efficiency and accuracy of network searches, data compression technology is employed to reduce data transmission volume and enable accurate querying of IoT node statuses through efficient prediction of sensor data. This approach effectively improves the utilization of network and server resources, ensuring users obtain satisfactory search results. Among various compression algorithms, the study compared lossy and lossless compression algorithms, and the Swinging Door Trending (SDT) algorithm, characterized by lower compression rates, lower time complexity, simplicity, and minimal system resource usage, emerged as a suitable choice for compressing sensor data in IoT sensor networks [12]. Refer to Fig. 2 for an illustrative diagram of the SDT algorithm.

The SDT algorithm is a compression algorithm designed for time series data. It introduces the concept of a "swinging

door" that allows data to fluctuate within a preset error range. When data points deviate from the set threshold, the algorithm creates a new data segment. The core of SDT lies in balancing data fidelity and compression rate, maintaining sufficient data information while eliminating redundant data. This method is particularly effective in industrial process control and real-time data monitoring systems, significantly reducing data storage and transmission requirements while ensuring critical information is not lost. The SDT algorithm's implementation process selects the first sampled data point of the sensor as the starting point, and the sampled value sequence is as shown in Eq. (1).

$$P = \{t_i, p(t_i)\} \quad i = 1, 2, \dots, n \quad (1)$$

In Eq. (1), where i represents the sampling time point and $p(t_i)$ is the corresponding sensor value at time t_i , as shown in Fig. 2, A is the starting point of a data segment, and the sampled value is denoted as $p(t_A)$. B is a sampling point after A , with a sensor data compression precision Δe , and the trend line calculation Equations are given by Eq. (2) and Eq. (3).

$$K_{AB}^1 = \frac{p(t_B) + \Delta e - p(t_A)}{t_B - t_A} \quad (2)$$

Eq. (2) represents the upper limit of the trend line, where $p(t_B)$ represents the sampled value of B , and the calculation Equation for the lower limit of the trend line is given by Eq. (3).

$$K_{AB}^2 = \frac{p(t_B) - \Delta e - p(t_A)}{t_B - t_A} \quad (3)$$

Eq. (3) is the calculation Equation for the lower limit of the trend line. After adding C to the samples, the slope K_{AC} of the line segment AC is calculated using Eq. (4).

$$K_{AC} = \frac{p(t_C) - p(t_A)}{t_C - t_A} \quad (4)$$

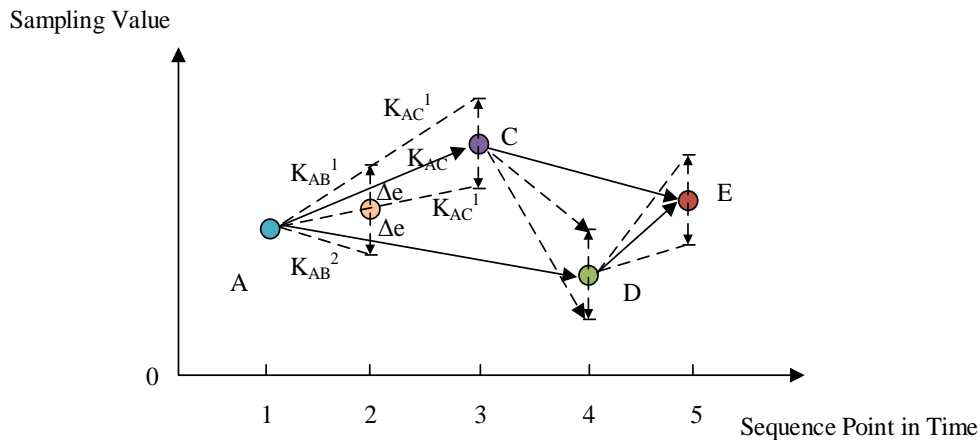


Fig. 2. SDT algorithm.

In Eq. (4), if $K_{AB}^1 \leq K_{AC} \leq K_{AB}^2$, it indicates that the segmentation compression condition is satisfied. Compression is performed on point C , and trend lines K_{AC}^2 and K_{AC}^1 are calculated following Eq. (2) and Eq. (3) for further assessment. Otherwise, if K is not equal to A , it indicates that the condition is not satisfied. The data at point B is saved, and the slope of the trend line BC is recalculated for further assessment. This operation is repeated for different data points until all data points are compressed, ensuring that the compression precision loss for each sampling point is less than Δe . For decompression, the first step is to extract the sensor data set UT that needs to be decompressed. All the data in $U\{t_i, p(t_i)\}$ are restored, assuming adjacent data points $\{t_i, p(t_i)\}$ and $\{t_j, p(t_j)\}$ have a difference expression as given in Eq. (5).

$$diff = (t_j - t_i) / t_s \quad (5)$$

In Eq. (5), $t_s = t_i - t_{i-1}$, representing the sampling time interval. When $diff = 1$, there are no sampling points between the two points, and the process moves on. If $diff > 1$, the restoration is performed, and the calculation is given by Eq. (6).

$$p(t_x) = \frac{p(t_j) - p(t_i)}{t_j - t_i} (t_x - t_i) + p(t_i), \quad x = i, i+1, \dots, j \quad (6)$$

This operation is repeated until all data points are restored. To address the slowly varying characteristics of sensor data, an improved rotating gate algorithm is proposed. When the sensor state is stable for a long time, only the initial state is stored to reduce data redundancy. When a significant change in state occurs, the rotating gate algorithm is activated for compression. The algorithm takes the first data point as a reference, sets a threshold, and judge's subsequent points: if the change is less than the threshold, it is ignored; if it exceeds the threshold, it is recorded, and the new point becomes the reference for continued processing. This method effectively reduces data volume while retaining key changes. The

flowchart of the segmentation compression algorithm is shown in Fig. 3.

As illustrated in Fig. 3, the decompression process begins by assessing whether the difference between two consecutive sampled points is less than a predefined threshold. If the difference is small, the value of the first point is directly used as the intermediate point value. If the difference is large, the standard decompression method of the rotation gate algorithm is employed. The key advantage of this algorithm lies in its handling of stable time periods. In time ranges where node states change minimally, only one state value needs to be stored, significantly improving compression efficiency. This strategy outperforms traditional rotation gate algorithms in time periods with minimal state changes. While the improved algorithm and the original algorithm perform similarly in data segments with frequent changes, considering that IoT nodes often experience stable states, the improved algorithm effectively reduces compression ratios and errors overall, despite a slight increase in compression time. Experimental results demonstrate that this enhanced algorithm is particularly suitable for scenarios with minimal state changes in IoT search systems, effectively reducing data storage requirements within an acceptable time increase range.

C. IoT Entity Information Prediction Algorithm Design Based on LS-SVM

The study employs the Least Squares Support Vector Machine (LS-SVM) to dynamically predict changes in entity node states in IoT, aiming to reduce sensor node resource consumption and achieve real-time search [13-15]. The schematic diagram of the LS-SVM model is shown in Fig. 4.

LS-SVM is a supervised learning method based on statistical learning theory and is a variant of the traditional Support Vector Machine (SVM). It addresses classification and regression problems by minimizing a quadratic loss function, as opposed to the hinge loss function in traditional SVM, simplifying the problem-solving process. The parameters of the predictive model established in the research are presented in the figure and outlined in Table I.

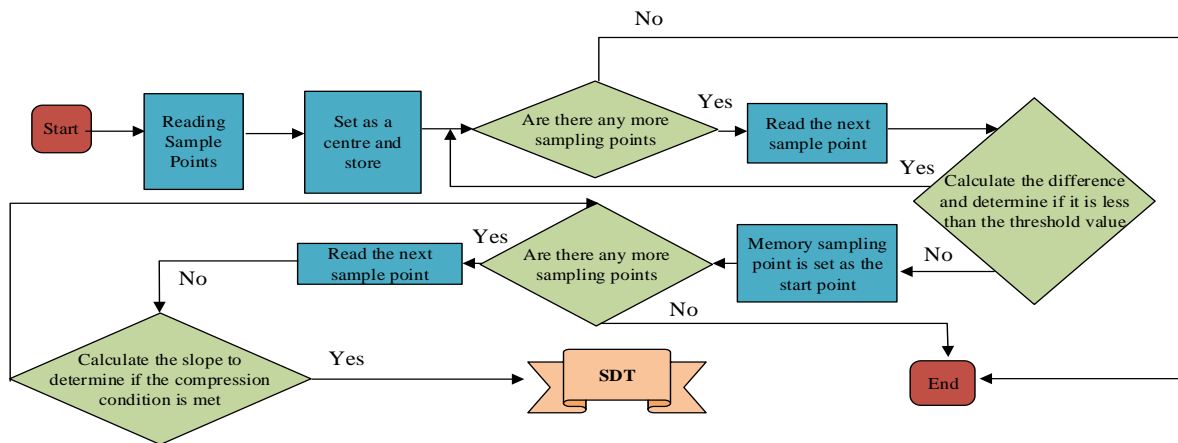


Fig. 3. Segmented compression algorithm flowchart.

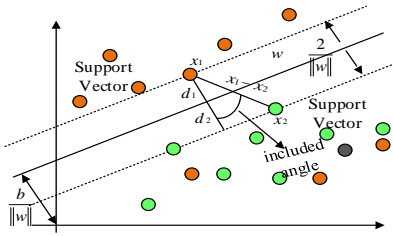


Fig. 4. LS-SVM Model schematic diagram.

TABLE I. MODEL PARAMETERS AND PROCESS

| | |
|------------------|---|
| Input Parameter | <ul style="list-style-type: none"> ◇ Sensor History Sampling Value List X_{tr} ◇ parametric σ ◇ parametric γ ◇ Projected point in time $time$ |
| Output Parameter | <ul style="list-style-type: none"> ◇ Predicted sensor values $result$ |
| Algorithm steps | |
| Step 1 | Construct the historical data input matrix X and output matrix Y from X_{tr} |
| Step 2 | Compute the ω value of the kernel function matrix from X |
| Step 3 | Compute the value of the symmetric semipositive definite matrix A from X , ω , γ |
| Step 4 | Compute the value of the intermediate variable b from the semipositive definite matrix A and the output matrix Y |
| Step 5 | The value of the Lagrange factor a is obtained from the values of A , Y and b |
| Step 6 | According to the intermediate variables and related parameters obtained from the calculation to obtain the final prediction function $f(x)$, input the predicted time point $time$, so as to obtain the predicted value of the moment $result$ |

Firstly, the input-output matrices X and Y are constructed based on sampled data. Following the principle of minimizing structural risk, the optimal nonlinear regression function is transformed into an optimization problem, as shown in Eq. (7).

$$\min J(w, e) = \frac{1}{2} w^T w + \frac{1}{2} \gamma \sum_{i=1}^n e_i^2 \quad (7)$$

In Eq. (7), w^T represents the transpose of the weight vector w , γ is a tunable parameter controlling the penalty for samples outside the error range of the function, n denotes the matrix dimension, and e_i represents the deviation between predicted and actual values. By applying the Lagrangian method to solve this function, it is transformed into a constrained problem, as illustrated in Eq. (8).

$$L(w, b, e, a) = J(w, e) - \sum_{i=1}^n a_i (w^T \varphi(x_i) + b + e_i - y_i) \quad (8)$$

In Eq. (8), a_i represents the Lagrange multiplier, $\varphi(x_i)$ denotes the non-linear mapping of x_i , b signifies the bias term, and x_i and y_i belong to the matrix X and the matrix Y . Employing the partial derivative method to eliminate w and e yields a set of Equations as shown in Eq. (9).

$$\begin{bmatrix} 0 & 1 & \dots & 1 \\ 1 & \varphi(x_1)^T \varphi(x_1) + \frac{1}{\gamma} & \dots & \varphi(x_1)^T \varphi(x_n) \\ \vdots & \vdots & \ddots & \vdots \\ 1 & \varphi(x_n)^T \varphi(x_1) & \dots & \varphi(x_n)^T \varphi(x_n) + \frac{1}{\gamma} \end{bmatrix} \begin{bmatrix} b \\ a_1 \\ \vdots \\ a_n \end{bmatrix} = \begin{bmatrix} 0 \\ y_1 \\ \vdots \\ y_n \end{bmatrix} \quad (9)$$

Solving Eq. (9) allows us to determine the values of a and b , leading to the construction of Eq. (10).

$$f(x) = \sum_{i=1}^n a_i \varphi(x_i)^T \varphi(x) + b \quad (10)$$

Utilizing Mercer's transformation on Eq. (10), we derive the kernel function as depicted in Eq. (11).

$$K(x_i, x_j) = \varphi(x_i)^T \varphi(x_j) \quad (11)$$

Within Eq. (11), $K(x_i, x_j)$ represents the kernel function. Based on this kernel function, the calculation Equation for the non-linear predictive model is shown in Eq. (12).

$$f(x) = \sum_{i=1}^n a_i K(x, x_i) + b \quad (12)$$

The selected kernel function for study is the Gaussian radial basis kernel function, with the final predictive function depicted in Eq. (13).

$$f(x) \approx \sum_{i=1}^n a_i e^{-\frac{\|x - x_i\|^2}{2\sigma^2}} + b \quad (13)$$

In Eq. (13), σ denotes the kernel width, and $\|x - x_i\|^2$ represents the norm between vectors. LS-SVM commonly utilizes a grid-search method in conjunction with cross-validation to determine parameters and find the combination that minimizes prediction error. This method involves constructing a grid within the parameter space to conduct a global search. Throughout the computation, a sparse grid reduces computational load but might miss the optimal parameters, while a dense grid enhances precision but increases computational complexity. This research adopts a multi-grid approach, initially defining a parameter range, selecting a set of parameter points within this range for training, adjusting the grid based on error results, gradually narrowing the search scope until finding the optimal parameter pair. This method enhances parameter optimization efficiency while controlling computational load. The system's functional module design based on the above algorithm is illustrated in Fig. 5.

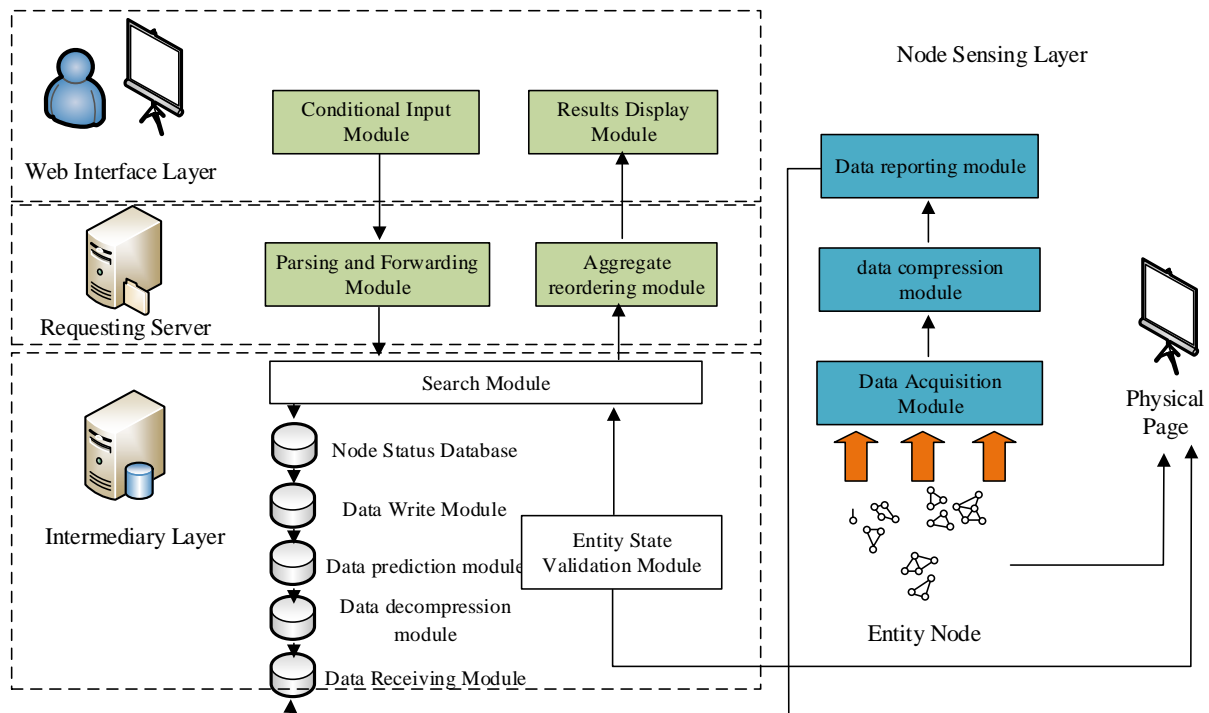


Fig. 5. WOT system functional module design.

The constructed WOT search system comprises three core layers: the node perception layer, the gateway service layer, and the frontend interface layer, developed using Python and Java. In the node perception layer, multiple simulated sensor nodes run as independent threads, periodically collecting and compressing data, then transmitting it to the gateway service layer through a data reporting module. Additionally, each node maintains a web page, recording real-time status. The server in the gateway service layer queues the received data, sequentially decompresses and restores it, utilizes the prediction module to forecast future states, and updates them in the status database. The frontend web interface layer serves as the user interaction point, receiving search requests via a browser. These requests, once parsed, are forwarded to the gateway server. The search module within the gateway server retrieves nodes meeting the criteria from the database, conducts relevance scoring and status validation, and ultimately feeds back the sorted results to the frontend for display. Despite sharing the same hardware platform in actual deployment, the request server and gateway server are logically independent, ensuring seamless system functionality. The entire search system, customized based on an open-source search engine, effectively implements the required search flow.

IV. PERFORMANCE TESTING OF WOT SYSTEM BASED ON DATA DYNAMIC PREDICTION ALGORITHM

The simulated testing in this study focuses on an IoT search platform utilizing a data dynamic prediction algorithm. The testing process involves collecting multi-dimensional time

series data from various physical entities, such as car engines and study room environmental data. The collected data is classified, cleaned, and ensured of its validity. After processing, the data is stored as text, with each text representing a node for testing purposes. The platform employs compression techniques to reduce data transmission, saving energy. Additionally, a prediction mechanism forecasts the future state of nodes, providing accurate search results. The main focus of the testing lies in evaluating the platform's capabilities in scenarios like fault detection and resource retrieval. The dataset used in the research is presented in Table II.

Due to limited sources for simulated testing data, the research concentrates on scenarios such as searching for a suitable study room and finding an appropriate exercise location. The first simulation scenario involves students looking for study rooms, considering factors like temperature, humidity, and light intensity. The system calculates relevance scores for study rooms, ranks them, and helps users find the most suitable place to study. The second scenario involves searching for exercise locations based on user-specified conditions like temperature, PM2.5 levels, and wind speed. The system provides a list of parks sorted according to the specified conditions, assisting users in choosing the best exercise location. The original data used in the testing follows a specific format. The research selects compression accuracy as a measurement parameter for compression algorithms. By setting different levels of accuracy, the compression effects are compared, as shown in Fig. 6.

TABLE II. RESEARCH-CONSTRUCTED DATASET

| Causality | Corridor | Data format | Unit (of measure) | Example |
|-------------------------------|--------------------|-------------------------------------|----------------------------|--------------------|
| Dates | / | Year-Month-Day | / | 2004/2/28 |
| Times | / | Hours:Minutes:Seconds. Milliseconds | / | 39:46.2 |
| Serial number | / | Integers | / | 84 |
| Node number | / | Integers | / | 18.9594 |
| Temperature value | Variation interval | Floating point type | Degrees centigrade | 38.8039 |
| Humidity value | [0,100] | Floating point type | Per cent | 43.24 |
| Light intensity | Positive number | Floating point type | Lux | 2.68742 |
| Voltage level | [0,4] | Floating point type | Vodka | / |
| PM2.5 data set | | | | |
| Causality | Corridor | Data format | Unit (of measure) | Example |
| Point in time | / | "Year-Month-Day Hour:Minute:Second" | / | "2010/1/2 0:00:00" |
| PM2.5 concentration | Positive number | Floating point type | Micrograms per cubic metre | 129 |
| Temperatures | Float range | Floating point type | Degrees | -4 |
| Barometric Pressure Indicator | Float range | Floating point type | Megapascal | 1020 |
| Wind speed | Positive number | Floating point type | metres/second | 1.79 |

Fig. 6(a), Fig. 6(b), Fig. 6(c), and Fig. 6(d) present the compression test results for the segmented compression algorithm designed in the study on temperature, humidity, light intensity, and voltage data from the IntelLab dataset. Overall, it is observed that increasing compression accuracy leads to higher compression rates, as higher accuracy allows for more data loss. However, different sensor types exhibit varying sensitivities to changes in compression accuracy; humidity sensors show lower sensitivity, while temperature sensors demonstrate a more significant response. This suggests that different sensor types have unique compression

behaviors. With the growth of compression accuracy, errors also increase accordingly, aligning with compression logic. Therefore, selecting an appropriate compression accuracy based on sensor data characteristics is crucial for balancing errors and reducing data volume. After testing, the research selects compression accuracies as follows: 0.5 for temperature, 1.0 for humidity, 1.0 for light intensity, 0.2 for voltage, 3.0 for PM2.5, 0.7 for humidity, 3.0 for air pressure, and 0.5 for wind speed. The study compares the proposed segmented compression algorithm with the rotation gate algorithm using the IntelLab dataset, and the results are shown in Fig. 7.

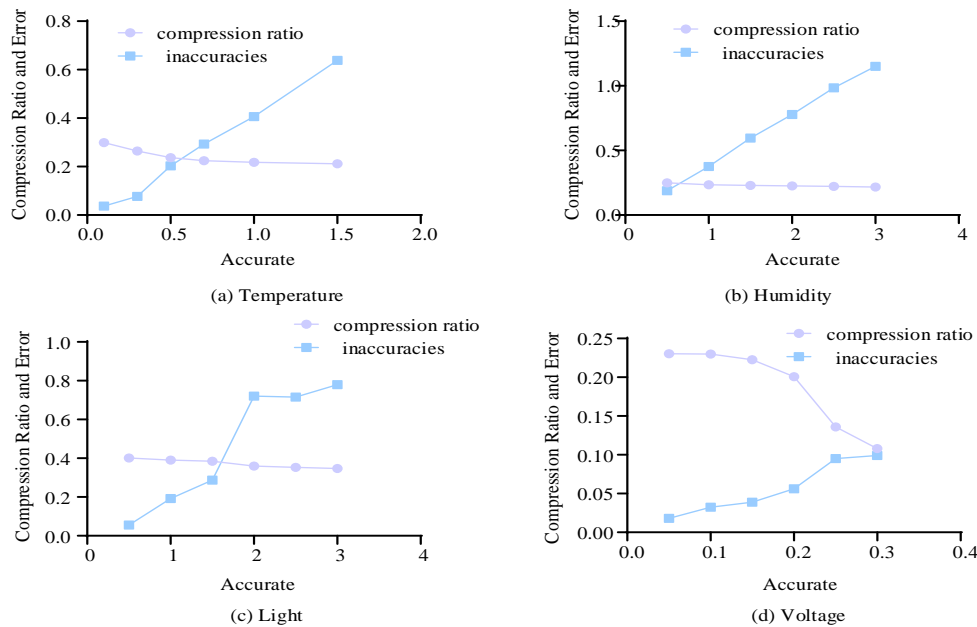


Fig. 6. Compression algorithm test results.

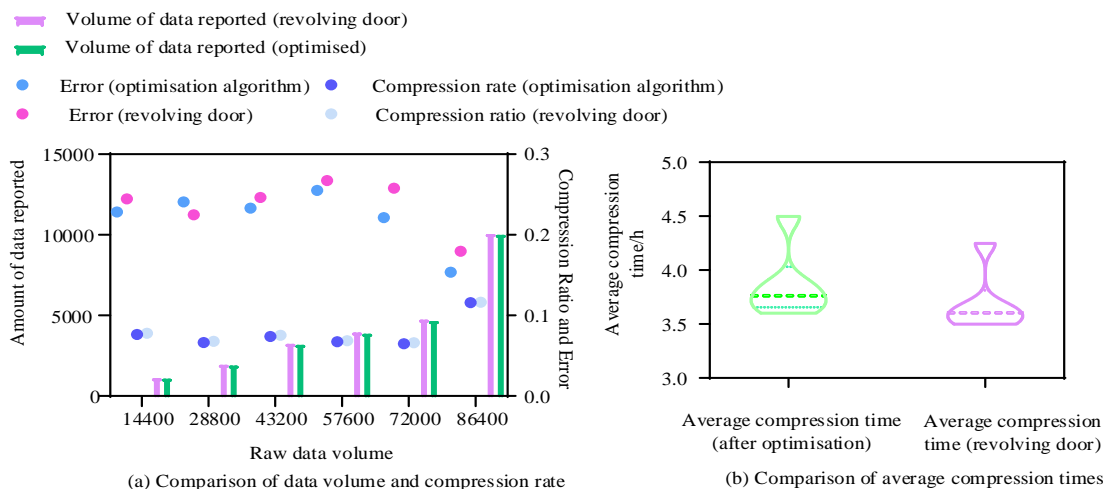


Fig. 7. Comparison of segmental compression algorithm and rotation gate algorithm test results.

The results of the comparison test between the proposed Segmental Compression Algorithm and the Rotation Gate Algorithm are illustrated in Fig. 7. Due to the regularity of the dataset, both the original Rotation Gate Algorithm and the Segmental Compression Algorithm exhibit stable performance in terms of compression rate and error. As seen in Fig. 7(a), the improved algorithm shows a 6.14% reduction in compression rate, a 5.95% decrease in error. However, as seen in Fig. 7(b), an increase in compression time by 13.12%. This performance improvement is attributed to the improved algorithm using initial points instead of the stable interval, optimizing the compression effect despite increased complexity and processing time. In order to achieve the goal of reducing node energy consumption, the study proposes the Segmental Compression Algorithm based on the Rotation Gate Algorithm to reduce the amount of data reported by sensor nodes. To verify its energy-saving performance, the study tests its energy savings and time relationship on two datasets, as shown in Fig. 8.

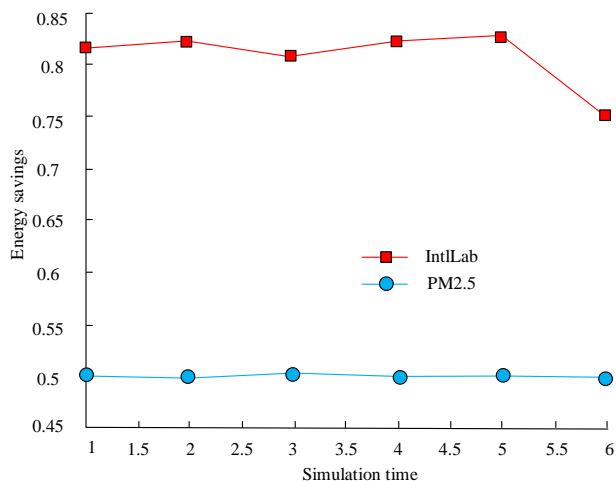


Fig. 8. Energy savings and time relationship of the segmental compression algorithm.

Fig. 8 presents the experimental results of the energy savings of the Segmental Compression Algorithm on the

IntelLab and PM2.5 datasets over time. By applying the data compression module, energy consumption decreases by approximately 82% and 50%, respectively. This significant reduction in energy consumption is attributed to the decrease in the amount of data uploaded by nodes, reducing frequent data reporting and saving network bandwidth. Moreover, this method effectively extends the running time of nodes and the overall lifespan of the network. The training results of the prediction algorithm are shown in Table III.

TABLE III. PREDICTION ALGORITHM TRAINING RESULTS

| IntelLab dataset | | | | |
|------------------|---------------|---------------|---------------|------------------|
| Causality | Training time | Best σ | Best γ | Prediction error |
| Temp | 7.417 | 1.537 | 0.927 | 0.516 |
| Humidity level | 15.026 | 2.04 | 0.939 | 0.274 |
| Sunlight | 15.058 | 3.941 | 0.902 | 0.086 |
| Input voltage | 14.54 | 8.264 | -0.05 | 0.355 |
| PM2.5 data set | | | | |
| Causality | Training time | Best σ | Best γ | Prediction error |
| PM2.5 | 7.594 | 1.202 | 0.996 | 3.809 |
| Temp | 15.48 | 0.641 | 1.021 | 0.342 |
| Pneumatic | 16.017 | 1.819 | 0.895 | 0.238 |
| Air velocity | 15.21 | 1.029 | 0.997 | 2.043 |

As shown in Table III, setting a certain reporting period and reducing the frequency of terminal node data reporting can effectively reduce energy consumption. However, this may lead to users searching for historical data, affecting accuracy. To address this issue, a prediction module is introduced to predict the next cycle state of nodes, balancing energy consumption and search accuracy. The impact of different reporting periods on the system is analyzed using the energy consumption formula, with mean square error and prediction time as evaluation indicators. Simulation results of the prediction algorithm are shown in Fig. 9.

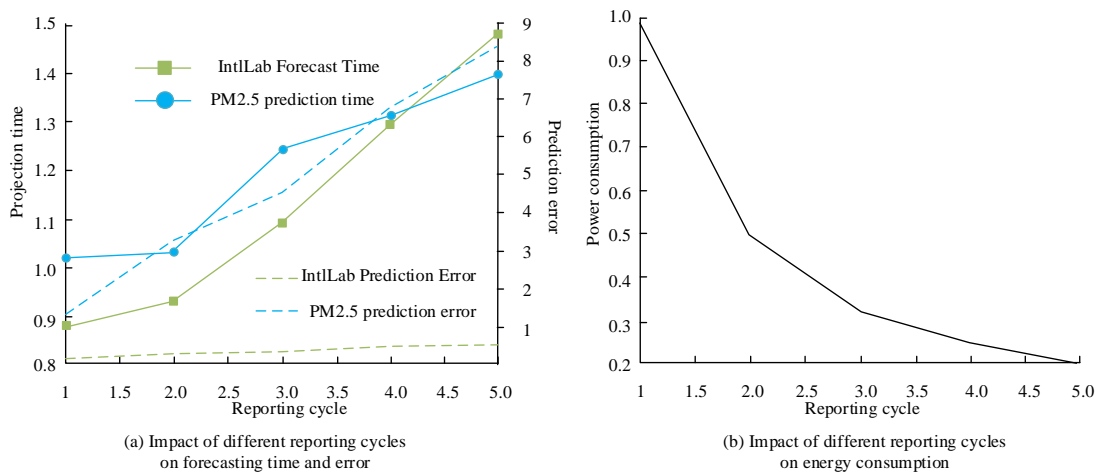


Fig. 9. Simulation results of the prediction algorithm.

Fig. 9 presents the comparative results of energy consumption, prediction error, and prediction time of the proposed prediction algorithm at different reporting intervals on the IntelLab and PM2.5 datasets. As seen in Fig. 9 (b), as the reporting interval increases, the energy consumption of nodes decreases, reaching 0.2 at a 5-cycle interval. However, the extension of the reporting interval means an increase in the prediction step, leading to a decrease in prediction accuracy and an increase in the uncertainty of search results. As seen in Fig. 9 (a), at a 5-cycle interval, the prediction error on the IntelLab dataset is around 0.5, while on the PM2.5 dataset, the error is 7.8. Additionally, a longer step length requires more computational resources and time, necessitating a balance between energy consumption, prediction accuracy, and computational costs. The prediction error on the IntelLab dataset is smaller than that on the PM2.5 dataset, as the former exhibits stronger data regularity with a smoother and more predictable variation. In contrast, the PM2.5 dataset has significant data variations, making predictions more challenging and resulting in higher errors. The model designed by the research has more predictive advantages on the data with strong regularity, is more applicable to this type of data. The setting of the reporting interval effectively influences the energy consumption, computational burden, and search performance of sensors.

V. RESULTS AND DISCUSSION

IoT is a network system that realizes information interaction and interaction between devices by connecting various sensing devices to the Internet. As the expansion of the Internet in the physical world, IoT is widely used in smart home, intelligent transportation, health care and industrial and agricultural Internet of Things and it has become an important helper for people's production and life as well as an important technological means for the development of intelligence. Various industries at home and abroad have carried out extensive research and analysis on IoT, mainly focusing on exploring the network architecture and protocol design of IoT, data security and privacy protection, as well as big data analysis and intelligent decision-making. At the same time, a series of IoT-related industry standards and specifications have been formulated. Overall, IoT, as an important part of the

future information society, has been highly valued by all walks of life, and its application and research fields are still developing and expanding.

Under the environment of IoT, the amount of data produced by numerous devices and sensors in real time is very large, and the Internet search engine is unable to efficiently process and index large-scale data, and the search capability of the existing Internet search engine does not satisfy the search demand of IoT. And the Internet search engine is usually based on batch indexing and offline processing, which is unable to obtain and process a large amount of real-time data produced by IoT devices in real time. At the same time, the data collected by IoT devices are usually structured or semi-structured data, and the existing search engines are difficult to deal with the semantic relationship between the data and the user, resulting in low accuracy and precision of the search results. In this regard, the research firstly adopts data compression technology to reduce the amount of sensor data to improve the storage and transmission efficiency, and then analyzes and predicts the future state of entity nodes using historical state information to improve the search accuracy and efficiency. The research-designed method reduces the compression rate by 6.14%, reduces the error by 5.95%, increases the compression time by 13.12%, and reduces the energy consumption by up to 82% on different public datasets. Moreover, the method can accurately predict the node state changes to satisfy the user's search needs.

Based on the work progress achieved in the research, future research can continue to focus on data compression and indexing technology, introduce intelligent optimization search algorithms to further improve the efficiency and accuracy of search algorithms, or carry out the exploration of distributed search engine technology, combining the technology of multiple fields to further achieve efficient, accurate, secure and personalized search services.

VI. CONCLUSION

The study addresses the insufficient real-time search capabilities of existing Internet search engines in the IoT environment. It investigates the architecture of an IoT search system and proposes a data dynamic prediction algorithm

tailored for searching IoT entity information. The research begins by employing data compression techniques to reduce sensor data volume, thereby enhancing storage and transmission efficiency. Subsequently, it utilizes historical state information analysis to predict the future states of entity nodes, aiming to improve search accuracy and efficiency. Performance test results indicate that the segmented compression algorithm designed in the study enhances compression accuracy and rates. As compression accuracy increases, errors correspondingly rise, aligning with compression logic. After testing, the research selects compression accuracies for various parameters, such as temperature (0.5), humidity (1.0), illumination (1.0), voltage (0.2), PM2.5 (3.0), humidity (0.7), atmospheric pressure (3.0), and wind speed (0.5). The improved algorithm reduces compression rates by 6.14%, decreases errors by 5.95%, but increases compression time by 13.12%. Application of the data compression module results in energy consumption reductions of approximately 82% and 50%, respectively. By setting specific reporting intervals to reduce frequent data reporting by terminal nodes, energy consumption can be effectively lowered. The designed prediction algorithm demonstrates that, with an increasing reporting interval, node energy consumption decreases, reaching 0.2 at a 5-cycle interval. At this point, the prediction error is around 0.5 for the IntelLab dataset and 7.8 for the PM2.5 dataset. Experimental results show that the optimized data dynamic prediction algorithm effectively reduces node data transmission, lowers node energy consumption, and accurately predicts node state changes, meeting user search requirements. However, the study has some limitations. The testing scale for compression and prediction algorithms is relatively small, lacking large-scale practical implementation, and the robustness is insufficient. Subsequent research could consider increasing the test data for experimentation.

REFERENCES

- [1] Aryavalli S N G, Kumar G H. Futuristic Vigilance: Empowering Chipko Movement with Cyber-Savvy IoT to Safeguard Forests. *Archives of Advanced Engineering Science*, 2023, 1(8): 1-16.
- [2] Deng, Lianbing, Li, Daming, Cai, Zhiming, Hong, Lin. Retraction Note: Smart IoT information transmission and security optimization model based on chaotic neural computing (Retraction of Vol 32, Pg 16491, 2019). *Neural computing & applications*, 2023, 35(5):4197-4197.
- [3] N. Sivasankari, S. Kamalakkannan. Detection and prevention of man-in-the-middle attack in iot network using regression modeling. *Advances in engineering software*, 2022, 169(10):3126-3133.
- [4] Sreedharan, Panchikattil Susheelkumar, Pete, Dnyandeo Jageshwar. A fuzzy multicriteria decision-making-based CH selection and hybrid routing protocol for WSN. *International journal of communication systems*, 2020, 33(15):36-58.
- [5] Pattnaik, PK Sahu. Assimilation of fuzzy clustering approach and EHO-Greedy algorithm for efficient routing in WSN. *International journal of communication systems*, 2020, 33(8):547-567.
- [6] Javaheri, Danial, Lalbakhsh, Pooia, Gorgin, Saeid, Lee, Jeong-A, Masdari, Mohammad. A new energy-efficient and temperature-aware routing protocol based on fuzzy logic for multi-WBANs. *Ad hoc networks*, 2023, 139(Feb.):3-21.
- [7] Turner C, Okorie O., Emmanouilidis C, Oyekan J. Circular production and maintenance of automotive parts: An Internet of Things (IoT) data framework and practice review. *Computers in Industry*, 2022, 136(10):93-97.
- [8] Zhang, Yitian, Yang, Kun, Fan, Xinyu. Joint time-slot and power allocation algorithm for data and energy integrated networks supporting internet of things (IoT). *International journal of communication systems*, 2021, 34(8):4769-4786.
- [9] Mabodi Kobra, Yusefi Mehdi, Zandiyah Shahram, Irankhah Leili, Fotohi Reza. Multi-level trust-based intelligence schema for securing of internet of things (IoT) against security threats using cryptographic authentication. *Journal of supercomputing*, 2020, 76(9):7081-7106.
- [10] Huang Z., Li R., Chen Z. Integration of data-driven models for dynamic prediction of the SAGD production performance with field data. *Fuel: A journal of fuel science*, 2023, 332(Jan.15 Pt.2):171.1-186.
- [11] Xiao, Xiao, Jin, Zhiling, Wang, Shuo, Xu, Jing, Peng, Ziyang, Wang, Rui, Shao, Wei, Hui, Yilong. A dual-path dynamic directed graph convolutional network for air quality prediction. *Science of the Total Environment*, 2022, 827(15):98-114.
- [12] Khan, Md Arif, Pierre, John W., Wold, Josh, I, Trudnowski, Daniel J., Donnelly, Matthew K. Impacts of swinging door lossy compression of synchrophasor data. *International journal of electrical power and energy systems*, 2020, 123(Dec.):182-193.
- [13] Panigrahi, Sweta, Raju, U. S. N. Pedestrian Detection Based on Hand-crafted Features and Multi-layer Feature Fused-ResNet Model. *International Journal of Artificial Intelligence Tools: Architectures, Languages, Algorithms*, 2021, 30(5):21-44.
- [14] Li, Weiye, Wu, Zhenyu. A methodology for dam parameter identification combining machine learning, multi-objective optimization and multiple decision criteria. *Applied Soft Computing*, 2022, 128(10):76-94.
- [15] Yu, Lang, Ma, Xin, Li, Shengjie. A fast conjugate functional gain sequential minimal optimization training algorithm for LS-SVM model. *Neural computing & applications*, 2023, 35(8):6095-6113.

Deep Learning-Powered Lung Cancer Diagnosis: Harnessing IoT Medical Data and CT Images

Xiao Zhang¹, Xiaobo Wang², Tao Huang³, Jinping Sheng^{4*}

Department of Radiology, The General Hospital of Western Theater Command, Chengdu 610083, Sichuan, China^{1,4}
Emergency Medicine Department, The General Hospital of Western Theater Command, Chengdu 610083, Sichuan, China^{2,3}

Abstract—Currently, lung cancer poses a significant global threat, ranking among the most perilous and lethal ailments. Accurate early detection and effective treatments play pivotal roles in mitigating its mortality rates. Utilizing deep learning techniques, CT scans offer a highly advantageous imaging modality for diagnosing lung cancer. In this study, we introduce an innovative approach employing a hybrid Deep Convolutional Neural Network (DCNN), trained on both CT scan images and medical data retrieved from IoT wearable sensors. Our method encompasses a CNN comprising 22 layers, amalgamating latent features extracted from CT scan images and IoT sensor data to enhance the detection accuracy of our model. Training our model on a balanced dataset, we evaluate its performance based on metrics including accuracy, Area under the Curve (AUC) score, loss, and recall. Upon assessment, our method surpasses comparable approaches, exhibiting promising prospects for lung cancer diagnosis compared to alternative models.

Keywords—Diagnosis; CT images; deep learning; convolutional neural network; lung cancer

I. INTRODUCTION

The rising incidence of pulmonary ailments in contemporary industrialized societies underscores the urgent requirement for innovative models facilitating early and precise detection. Lung cancer, among these maladies, stands out as one of the most formidable cancers, contributing to a third of all cancer-related fatalities [1]. Consequently, it holds the grim distinction of being the deadliest and most hazardous cancer. Following diagnosis, approximately 80% of patients face a five-year survival prognosis, highlighting the severity of this disease. Air pollution ranks among the primary catalysts for lung cancer development [2]. Early detection of lung diseases significantly impacts the likelihood of successful treatment. Diagnosis typically involves a range of methods, including imaging modalities such as radiography, CT scans, biopsy, chest mucosa tests, and bronchoscopy. Lung nodules, characterized as small, round, and hazy masses within lung tissue, are radiographic opacities with diameters less than 30 millimeters [3, 4].

Enhancing the performance of CNNs involves incorporating task-specific layers tailored to the desired application. CNN models mimic certain aspects of human visual processing, thus enabling effective image analysis akin to human brain functions [5]. Consequently, extensive research has focused on utilizing CNNs for the automatic classification of lung cancer nodules from CT images. However, traditional CNN architectures typically rely solely on CT image features, neglecting potential contributions from physiological data that

could enhance lung cancer diagnosis [3]. Conversely, advancements in medical IoT methodologies have facilitated remote patient monitoring, leveraging wearable health sensors. These sensors monitor various vital signs including blood pressure, body temperature, heart rate, respiratory patterns, weight fluctuations, and sleep behaviors [6, 7]. Notably, certain indicators such as anorexia, anxiety, constipation, depression, and fatigue pose challenges for direct tracking via wearable sensors [8].

However, there are alternative approaches that utilize textual and graphical interactions through mobile applications, offering symptom-based data that can aid in diagnosing lung cancer [9, 10]. This study introduces a medical body area network integrating medical IoT technologies and mobile applications. A data normalization technique, facilitated by the application programming interface, is employed to receive and process the data. Subsequently, the processed data is stored in a database using a relational schema.

Various studies have been conducted to identify and characterize lung diseases. Due to the abundance and complexity of lung radiographic images, distinguishing nodules from veins, wounds, and other structures poses a significant challenge for medical practitioners [4]. Computer-aided diagnosis systems serve as valuable tools to assist physicians in disease diagnosis. This paper introduces a novel approach based on a hybrid Deep Convolutional Neural Network (DCNN), trained on CT scans and medical data obtained from wearable IoT sensors. Our method incorporates a CNN with 22 layers, leveraging hidden features extracted from both CT images and IoT sensor data to enhance detection accuracy. Training our model on a balanced dataset, we evaluate its performance based on accuracy, Area Under the Curve (AUC) score, loss, and recall metrics.

The motivation behind this study stems from the pressing need for improved methods of early detection and precise diagnosis of lung cancer, given its significant impact on public health. With lung cancer accounting for a substantial portion of cancer-related deaths globally, there is an urgent requirement for innovative models that can aid in early detection, thereby improving treatment outcomes and patient survival rates. Traditional diagnostic methods, while effective to some extent, often rely solely on imaging modalities and may overlook valuable physiological data that could enhance diagnostic accuracy. Moreover, advancements in medical IoT technologies offer opportunities for remote patient monitoring, presenting a wealth of physiological data that could be leveraged for improved lung cancer diagnosis. By integrating

these disparate data sources and utilizing advanced machine learning techniques, using the DCNN, this study seeks to develop a novel approach that enhances the accuracy and efficiency of lung cancer detection, ultimately contributing to improved patient care and outcomes.

The subsequent sections of this article are structured as follows: Section II presents a literature review. Section III provides a detailed description of our proposed method. Section IV outlines the dataset used, tests performed, and results obtained. Finally, Section V offers conclusions and recommendations.

II. RELATED WORKS

Considerable progress has been made in lung cancer diagnosis, with numerous studies contributing to this field. In this section, we provide an overview of some notable research endeavors.

In study [11], researchers utilized Artificial Neural Network (ANN) techniques to analyze chest radiograph images for lung cancer detection. Their approach involved a novel method for identifying lung cancer from raw X-ray images sourced from the JSRT database. Initially, conventional image processing techniques were employed to reduce noise and differentiate lung structures from other anatomical features present in chest X-rays. Subsequently, regions displaying characteristics indicative of pulmonary nodules were isolated from the images. These areas were then subjected to statistical analysis, with the first and second categories of tissue statistical characteristics serving as input for ANN training. This process aimed to ascertain whether the identified regions represented nodules in the initial stage of diagnosis.

In study [12], the authors explored the use of CNN with transfer learning for the diagnosis of non-nodules, benign nodules, and malignant nodules, along with determining nodule locations. The experiments have shown that this proposed model has less ability in the characterization of the nodules of the benign and the nodules of malignant, and it is also unable to determine the exact location of the nodule. In study [13], the authors have used the K-nearest neighbor classifier in their proposed system. This classification identifies the K-nearest neighbor among all nodule candidates by searching in the feature space. Finally, the probability of nodule detection will be $\frac{n}{K}$, where n displays the number of the real nodules between K adjacent neighbors. They have stated in their article that the classification results are largely independent of the number of neighbors.

In study [14], a method combining features derived from wavelet transform and morphological characteristics was employed as input for Multilayer Perceptron (MLP). The number of neurons in the first layer of MLP depended on the input feature count, with neuron outputs determining whether a candidate region represented a nodule or normal tissue while neural networks excel in training based on explicit error criteria such as mean square error, direct comparison of network efficiency remains challenging. Neural networks suffer from the time-intensive nature of their training phase, exacerbated by the random selection of initial weights that are adjusted during learning, leading to varying separation thresholds. Thus,

achieving an optimal configuration necessitates running the network multiple times with different initial weights and evaluating efficiency criteria.

In study [15], a combination of Artificial Neural Networks (ANN) and fuzzy clustering was employed for lung cancer diagnosis using CT scan images. Their model comprised four stages: pre-processing, target area evaluation, feature extraction, and final classification using ANN. Pre-processing involved various image enhancement techniques to enhance tumor observations in CT scan images. Subsequently, the target area was identified, and its features were input into the classification phase for diagnosis.

In study [16], the authors have presented a model based on the automata of cellular learning to detect cancer of the lung by using CT scan images. Their images contain both undesirable and significant features crucial for processing. In this framework, they employed pre-processing techniques, such as Gabor filtering, to enhance CT scan images. Images from prior stages were fed into the cellular learning automata for training, followed by extraction of automata rules. In study [17], the classification of the tumor tissue by using recurrent networks along with short-term memory is presented. The training samples are obtained from the real soft tissue samples through the tomography, and they are given as the input to the network. Their tests show that this classifier is a good choice for the classification. In study [18], authors utilized a combination of two-dimensional and three-dimensional models for pulmonary nodule detection, resulting in reduced false positive errors.

In study [19], the authors have used the model of ANN and the clustering of the fuzzy to detect the cancer of the lung. They have used two methods of the Hopfield neural networks and the clustering fuzzy algorithm to segment the color images. The experiments have displayed which ANN of Hopfield outperforms for the classification from the fuzzy clustering. In [20], the convolutional neural network with a cut has been used to diagnose the nodules of the pulmonary by the images of CT. The difference between their model and the traditional CNN model is in the use of a creative aggregation function. In [21], the main focus was on the feature extraction from the 3D CT images, and for this purpose, the morphological operators were used to thin the images. The classifier used in study [21] was the support vector machine. In study [22], to extract the feature, the embedded linear local maps have been used and correlation coefficients have been used to adjust the distance criterion in LLE.

The existing research landscape in lung cancer diagnosis reveals a plethora of methodologies, each with its strengths and limitations. However, a critical gap exists in the current literature, prompting the need for further investigation. While previous studies have explored various techniques, including ANN, CNN, and hybrid models, each approach has encountered challenges in accurately diagnosing lung cancer nodules. For instance, while ANN methods have shown promise in analyzing chest radiograph images, they may struggle with the precise identification of nodules due to limitations in feature extraction. Similarly, CNN models, despite their success in image classification tasks, may lack the ability to accurately determine nodule locations or characterize

benign versus malignant nodules. Moreover, techniques such as fuzzy clustering and cellular learning automata have demonstrated potential, yet their effectiveness in addressing the complexities of lung cancer diagnosis remains uncertain. Thus, there is a pressing need for novel methodologies that address these limitations, offering improved accuracy, robustness, and efficiency in lung cancer detection. This research gap underscores the motivation for the present study, which seeks to develop an innovative approach leveraging medical IoT data and advanced CNN architectures to enhance the accuracy and reliability of lung cancer diagnosis.

III. OUR PRESENTED APPROACH

Our method integrates CNN with medical IoT sensors, establishing a medical body area network that furnishes vital data for classification purposes. This approach significantly bolsters the reliability and precision of diagnosis. Following initial classification, identified nodules undergo segmentation, with subsequent sub-classification based on nodule size. This method typically unfolds in four sequential steps. Firstly, data collection entails transmitting sensor data from wearables and CT scanners to a central server. Next, data undergoes processing to train the network, encompassing numerical data processing and image data processing. In numerical data processing, data are condensed and outliers are identified and removed. Meanwhile, image preprocessing is performed to enhance features by minimizing the feature distance between cancerous and non-cancerous nodules. Subsequently, sub-classification based on nodule size ensues. The final step entails detection and decision-making based on predictions generated by our trained model.

It should be noted that the last conformity of the 5G technology in mobile has enabled advanced functionality of medical IoT sensors for the monitoring and the transmission of related data in real-time. These sensors can identify patient symptomatic information and send it to specified servers in

real-time via the Internet. In the following and each of the below sub-sections, more details of our presented approach are provided.

A. First Step: Data Collection

As described, the medical IoT sensors form a network, depicted in Fig. 1(a). This network comprises sensors responsible for collecting physiological data. Communication within the network is structured into three levels, as illustrated in Fig. 1. Level 1 encompasses communication between sensors. Level 2 involves final devices utilized by patients for monitoring, accessing, and transmitting data to our proposed method. Level 3 manages the secure transmission of physiological data and CT images to the proposed method's server. Data collection occurs through two methods: active monitoring and passive monitoring. Active monitoring involves data collection via wearable IoT sensors, while passive monitoring involves patient interaction with sensors to generate data. This includes physiological data obtained through a mobile app and CT images. Level 2 networks comprise final devices utilized by patients, where physiological data is stored. Patients can access CT images through client-server communication. The server used in our proposed method receives data sent from the network at this stage.

In addition, the communication of the point of the access is maintained via the key of PreShared, it is applied as the main key of the pairwise in the 4 method-method handshakes [23]. Four thousand ninety-six iterations create PMK with 256 bits. The mentioned procedure exploits the function of the derivation of the key basis on the password, which is described in the relation as shown in Eq. (1):

$$\begin{aligned}
 &PSK \\
 &= PBKDF2(HMAC - SHA1.Password.SSID.4096.256)
 \end{aligned}
 \tag{1}$$

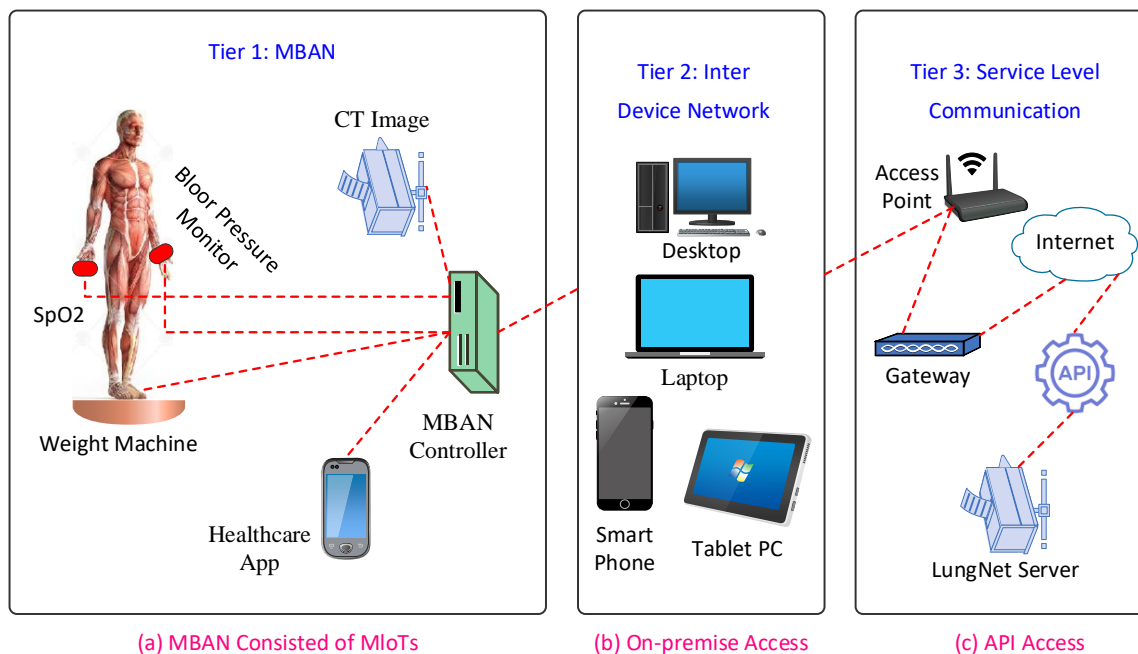


Fig. 1. The framework of the medical body area networkCT image.

A function of the Hash-based Message Authentication Code (HMAC) is applied for the generation of the hash of the password. On the mentioned test, the password has 16 characters, which are codified with the use of the ASCII of the printable. The counter of the packet and the service set identifier (SSID) are applied as the salt of the password. Then, the data is transmitted to the server with the patient's approval. The task manager checks the type of the data of the input. Next, the method schedules the tasks. Once data is placed in the database, the next stage is started. In these stages, the data is processed for the training, the validation, and the test of the model based on DNN. The data that is displayed by the portal of the patient doctor is also processed from this data.

B. Second Step: Pre-processing of Collected Data

The performance of Deep Neural Network (DNN)-based models relies heavily on both the quantity and quality of the data, emphasizing the importance of data preprocessing. Particularly, the focus lies on preprocessing imaging data related to lung cancer nodules, which often requires several stages of refinement. In this section, we outline the methods applied for preprocessing both non-image and image data.

Firstly, let's discuss non-image data preprocessing. Non-image data is typically gathered from sensor responses or patient interactions with healthcare applications. Wearable sensors capture various data such as temperature, irregular heartbeat, breathing patterns, and blood pressure. Additionally, non-wearable sensors are utilized for measuring weight loss and managing CT image data. Patient interactions also provide valuable data, including reports of anorexia, anxiety, depression, pain, insomnia, fatigue, and constipation. These signals and the relevant sensor values are normalized with the use of the defined linear normalization by relation as shown in Eq. (2). The lack of the related data is exchanged by *NA*. But, in the numerical calculations, these values are considered as 0. s' displays the normalized data, and s displays the real data.

$$s' = \frac{s - \min(s)}{\max(s) - \min(s)} \quad (2)$$

However, when dealing with image data, a distinct preprocessing approach becomes necessary. Image data processing comprises three main stages: 1) resizing and transforming the images; 2) validating candidate images; and 3) segmenting symmetrically with feature enhancement. Each Convolutional Neural Network (CNN) has a fixed input layer size, but there's no assurance that the input image size will align perfectly with the input layer size. Additionally, CNN input layers can only process a certain number of channels at a time. Hence, it's crucial to resize images and adjust color spaces according to network specifications. Certain CT scans may include regions with minimal lung tissue or even areas devoid of lung tissue entirely. Removing these sections improves the quality of training data.

Moreover, the ambiguous characteristics of lung cancer nodules pose challenges to the efficacy of feature learning layers. Consequently, it becomes imperative to augment the features of lung cancer nodules. The initial preprocessing step involves resizing images and transforming color spaces. The input layer size of our proposed model is set at $224 \times 224 \times 3$. The collected data for this experiment includes both three-

channel and one-channel images. All images are resized to 224×224 while maintaining the aspect ratio to streamline training duration. Furthermore, one-channel images are converted to RGB three-channel images using Eq. (3).

$$I_{RGB} = I_{(Gray.R)} + I_{(Gray.G)} + I_{(Gray.B)} \quad (3)$$

I_{RGB} represents our created RGB image from the grayscale image. Also, $I_{(Gray.R)}$, $I_{(Gray.G)}$ and $I_{(Gray.B)}$ represent, respectively, the equivalent value of the gray for the red channel, the equivalent value of the gray for the green channel, and the equivalent value of the gray for the blue channel. The size resizing of the image does not modify the data inside it due to the logical change. Even after the transformation of it into an image of 3-channel, our essential features stay without change. Our second processing of the image data is the candidate image validation. In this stage, the function of the validation takes the images. Then, it validates whether the image displays a candidate valid or not. The candidate's set of valid and set of invalids are shown in Fig. 2. If the image of the input does not include a part of the effective lung, which the nodules can be recognized, then the function ignores this image. Differently, this function rebounds the pre-processed copy of the image, and then, the algorithm exploits it for more pre-processing. This function takes the images of RGB (I_{Color}) which it is described as below:

$$I_{Color} = \sum_{n=1}^N \sum_{m=1}^M I(n.m.g) + \sum_{n=1}^N \sum_{m=1}^M I(n.m.r) + \sum_{n=1}^N \sum_{m=1}^M I(n.m.b) \quad (4)$$

Also, the image of RGB is transformed into an image of the grayscale by using relation, as shown in Eq. (5).

$$I_{gray}(n.m) = \alpha I_{Color}(n.m.r) + \beta I_{Color}(n.m.g) + \gamma I_{Color}(n.m.b) \quad (5)$$

α , β , and γ denote the constants for the red, green, and blue channels, respectively. It is essential to calculate the part area of the lung in the image because it is necessary to check whether I_{Color} is a valid candidate or not. It is easier and faster to measure the lung area in the binary image. The threshold of the gray conversion I_{gray} into the binary image is calculated by using the Otsu method, which is shown in the relation (6):

$$\sigma_b^2(t) = \sigma^2 - \sigma_w^2(t) = \omega_0(\mu_0 - \mu_T)^2 + \omega_1(\mu_1 - \mu_T)^2 \quad (6)$$

where, $\sigma_b^2(t)$ is the maximum threshold and σ^2 represents the variance and μ_0 represents the mean. Also, ω_0 is the weighted probability. The obtained threshold from the relation (6) is used to transform $I_{gray}(n.m)$ into a binary image $I_{bin}(n.m)$ by using the relation (7).

$$X = \begin{cases} 1 & I_{gray}(n.m) \geq \sigma_b^2(t) \\ 0 & otherwise \end{cases} \quad (7)$$

A binary image contains small noise objects that these objects have areas of about 450 -5000 pixels. The obtained

objects influence the accuracy of the learning of the layers of the learning of the feature. Thus, that is why it is essential to discard these cases. The opening of the region of the morphological is applied for the removal of the objects by a value of the threshold equal to 5000. The series of little holes remain in the foreground after the region opens. To remove the holes, the operation of the flood filling by the four-way connection is applied.

$$I_{fill}(n.m) = Flood_{filling}(area_{opening}(I_{bin}(n.m))) \quad (8)$$

where, $I_{fill}(n.m)$ displays the image after filling the holes and $I_{bin}(n.m)$ is the binary image. Next, the image of the binary is deduced by the filled image. Finally, it renders the lung form as an object in the foreground.

$$I_{sub}(n.m) = I_{fill}(n.m) - I_{bin}(n.m) \quad (9)$$

where, $I_{sub}(n.m)$ displays the image after the deduction of the image of the binary by the filled image. Then, the area is computed with the implementation of a logical operation of AND among $I_{sub}(n.m)$ and the logical 1, which is shown in the relation (10).

$$Area = \sum_{n=1}^N \sum_{m=1}^M I_{sub}(n.m) \wedge Logical(1) \quad (10)$$

Assuming the area exceeds 20,000, we consider the image to represent a valid candidate for lung cancer nodule diagnosis. Conversely, if the area falls below 20,000, the image is deemed invalid. Validating the candidate confirms the efficacy of the feature learning layer and captures key features crucial for lung cancer nodule classification. Thus, this method serves to enhance the quality of lung cancer image datasets.

Lastly, the third step in image data processing involves segmenting the lungs symmetrically and enhancing features. Following validation, symmetric segmentation is performed. The segmented lungs, enhanced by improved features, are

illustrated in Fig. 3. The lung separation function operates on the pre-processed binary image copies of valid candidate images ($I_{sub}(n.m)$). At this stage, both the left and right lungs are presented in a composite image. To separate the left and right lungs, two separate masks need to be generated. This process initiates by convolving an image of zeros with the grayscale image and saving the results as left and right masks, as described in Eq. (11) and Eq. (12).

$$L_{mask} = \sum_{n=1}^N \sum_{m=1}^M I_{gray}(n.m) \otimes I_{zero}(n.m) \quad (11)$$

$$R_{mask} = \sum_{n=1}^N \sum_{m=1}^M I_{gray}(n.m) \otimes I_{zero}(n.m) \quad (12)$$

L_{mask} and R_{mask} indicate the mask of the left and the mask of the right. $I_{sub}(n.m)$ contains more than one area with the values of the pixel of the binary. For the segmentation of the obtained areas, it is necessary to label them. The labeling is performed with the use of the relation (13) where $K = \{x | x \in N\}$ and I_{str} is an 8-connection morphological structure with the pixel values equal to 1.

$$L_K = (L_{K-1} \otimes I_{str}) \cup I_{sub} \quad (13)$$

where, L_K is the label of the region K . Also, $I_{sub}(n.m)$ can have a maximum of two regions. That is why, $L_K = \{x | x \in N, x \leq 2\}$. In L_{mask} where $L_K = 1$, the values of the pixel are filled. In the same way, in R_{mask} where, $L_K = 2$, the values of the pixel are also filled. Finally, L_{mask} and R_{mask} are deduced by the main image to fill masks further. Next, the opening of the morphological with the ellipse has a main axis equal to 90 pixels and a height equal to 10 pixels. This case is used in 2 masks and the other complementary action, which is described by the relation (14). M_o displays the opening of the morphological and M_{mask} represents the mask of the left and the mask of the right.

$$X_{mask} = 1 - M_o((1 - X_{mask}) \cdot \frac{n^2}{90^2} + \frac{m^2}{10^2}) \quad (14)$$

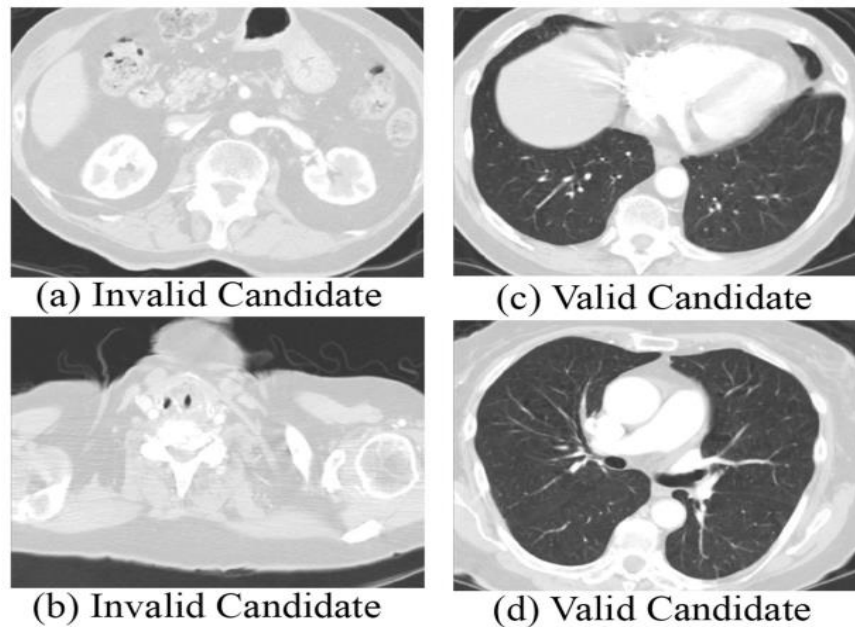


Fig. 2. (a,b) the candidates of the invalid; (c,d) the candidates of the valid.

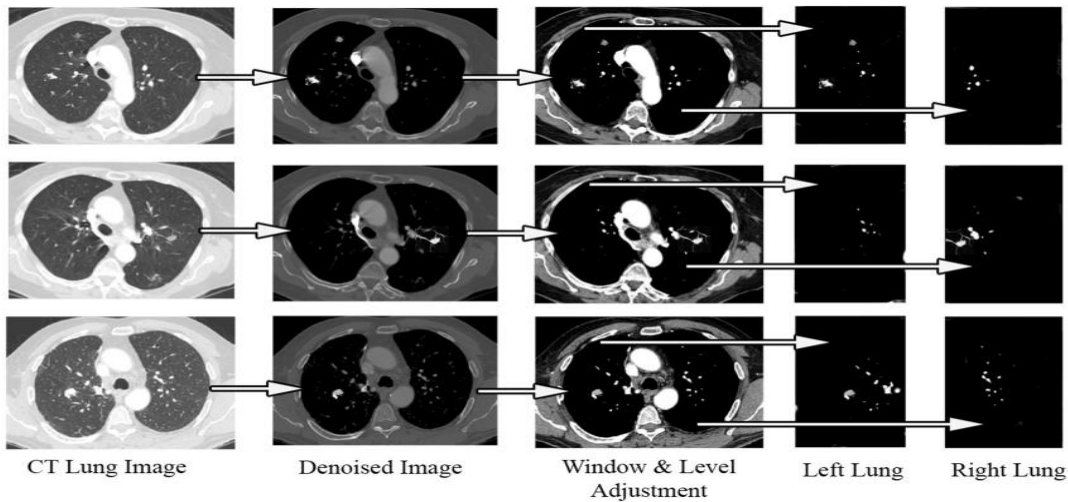


Fig. 3. The segmentation of the symmetric and the enhancement of the feature in the image data processing stage.

The obtained masks from the relation (14) include a blurred gradient. Binarization for X_{12} in the value of the threshold equal to 0.5 returns the severe discontinuities.

$$X_{mask} = \begin{cases} 1 & X_{mask} \geq 0.5 \\ 0 & otherwise \end{cases} \quad (15)$$

Finally, the masks are connected with $I_{sub}(n.m)$ as separately and then, it separates the lung of the left and the lung of the right from the image of the source.

$$I_{lung} = \sum_{n=1}^N \sum_{m=1}^M I_{gray}(n.m) \otimes X_{mask}(n.m) \quad (16)$$

Here, I_{lung} represents the lung of the left and the lung of the right separately. If $I_{gray}(n.m)$ is convolved by the mask of the left, relation (16) creates the left lung. Similarly, when $I_{gray}(n.m)$ is convolved with the right mask, the relation (16) creates the lung of the right. Finally, the lung of the left and the lung of the right are elided together.

The enhancement of the feature is a successive procedure that this procedure begins with noise removal. The non-local average methods, under the control of the relation (17), have been applied to the current test for the removal of the noise from the image, which in it, $v(I_f)$ displays the pixel of the filtered, $v(I_s)$ displays the pixel of the target and $v(I_s)$ represents the value of the unfiltered in $v(I_f)$. Also, $f(I_f, I_s)$ is the weighting function [24].

$$v(I_f) = \frac{1}{c(I_f)} \int_{n \times m} v(I_s) f(I_f, I_s) dI_f \quad (17)$$

Following noise removal, the adaptive histogram equalization algorithm, leveraging genetic algorithms [25], is applied. Subsequently, a surface contrast enhancement window is utilized to eliminate irrelevant features unrelated to lung cancer nodules. The segmentation result of the symmetric and the outcome of the feature enhancement process are depicted in Fig. 3. Augmenting data is one strategy employed to address overfitting challenges. However, the annotated dataset, even with input from radiologists, proves insufficient for achieving optimal classification efficiency in our model. Moreover, a significant disparity exists between the number of positive and negative training images, leading to imbalanced data in

predictive modeling. To address this, we employ data augmentation techniques to generate additional relevant data from the existing dataset, thereby balancing the number of positive and negative images. Sufficient training samples are created through random spatial transformations and data augmentation methods.

C. Third Step and Fourth Step: Proposed Network, Training, and Classification

The proposed method introduces a unique network structure and a combined classification approach. This method employs a deep network with 22 layers, enabling it to learn distinctive features of lung cancer nodules. Additionally, the combined classifier enhances efficiency and provides more reliable predictions by leveraging data from the medical body area network. The CNN architecture used in our method is illustrated in Fig. 4, featuring a convolutional neural network with 22 layers and an input layer size of $224 \times 224 \times 3$. Rectified Linear Unit (ReLU) functions are applied as activation functions for each convolution operation in the network.

Given the centralized server used by the network, reducing operational costs and maintaining accuracy presents a challenge. To address this, we adopt an alternative method compared to advanced CNN models, which typically utilize convolution operations of size $n \times n$. Instead, our proposed model employs convolution operations of size 1×1 , resulting in reduced weights and biases. However, this deepens the network model, leading to a performance reduction of 46%. It's worth noting that fully connected CNNs are popular among researchers in lung cancer diagnosis due to their satisfactory efficiency [26].

Nevertheless, a model of the fully connected needs further resources of computational from the models of the sparsely connected [27]. That is why, thus, in our proposed method, a model of the non-fully-connected is applied. In addition, a global layer of the average-pooling averages the signals; it decreases the 7×7 feature maps to the 1×1 feature maps to reduce the number of non-cooperative features.

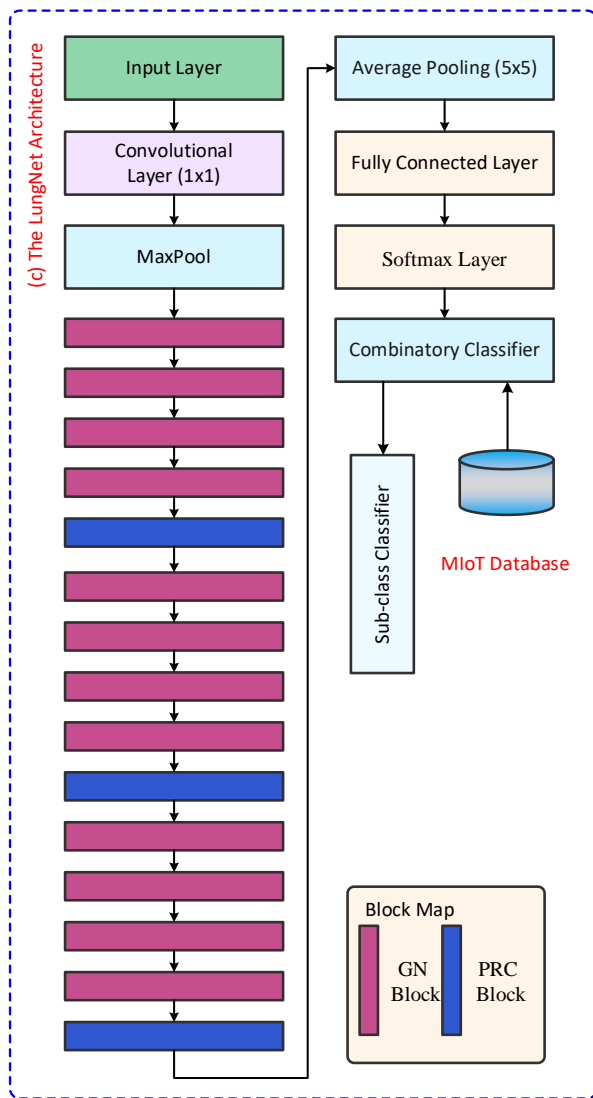


Fig. 4. Structure of the presented method.

It has been observed that employing a diverse range of convolutional matrices instead of a constant matrix enhances network performance. In our proposed method, convolutional matrices of sizes 1×1 , 3×3 , 5×5 , and 7×7 are aggregated together by a max-pooling layer of size 3×3 , which operates in parallel with this stack. The ability of the convolutional layer to investigate objects of varying sizes is crucial, and the use of multiple convolution matrices ensures this capability.

These separate layers are then combined into a deep concatenation layer, which transmits signals to the subsequent layer. In contrast to fully connected layers, our proposed method includes several intermediate pre-classification layers to mitigate the impact of the vanishing gradient problem. These branches are only activated during the training process. The purpose of these pre-classification layers is to perform classification before reaching the final classifier. Each of these layers comprises a 5×5 average pooling layer with a stride of 3,

performing convolutions with 1×1 filters totaling 128 filters. The proposed method features 5 output nodes, processed through a softmax classification layer and aided by dataset data. The 2nd and 3rd nodes are combined for sub-classification.

In terms of the learning algorithm, it's worth noting that most CNNs initialize the weights of the classification layer randomly. However, for our proposed method, we've adopted various techniques to achieve better efficiency. Empirical results indicate that employing the modified Nguyen-Widrow initial weighting approach [28] improves validation accuracy and reduces validation loss more quickly.

We utilize the Levenberg-Marquardt backpropagation algorithm as the learning rule [29]. This choice is validated by the computational expense of calculating the Hessian matrix [30]. Given that our proposed method is intended to operate from a centralized server, multiple instances could degrade service quality. The Levenberg-Marquardt backpropagation algorithm estimates the Hessian matrix using the Jacobian matrix, which is computationally cheaper and faster [31]. Consequently, we update weights using the Levenberg-Marquardt backpropagation algorithm.

Furthermore, employing a dynamic learning rate, as opposed to a fixed learning rate, enhances validation accuracy [32]. Therefore, our proposed method adopts an adaptive learning rate during training, where the rate starts at 0.01 and gradually decreases to 0.0003.

After the training step, the classification step is done. A new hybrid classifier is designed and is used in the proposed method. The network classifier is considered for cancer classification. The data of the feature of the image of the high level and the data of the feature of the image of the low level are the features of the node based on the classification of the network. Commonly, the data of the probabilistic network is applied for the classification. Our proposed method incorporated an extra system of support for the decision-making of the weighted with the classifier of the convolution. The normalized data are the parameters of the step of the classification. The sum of the weighted of the prediction for our proposed method (P_L) and also prediction based on the normalized data (P_S), which is defined by the relation (18), form the final output of the proposed method.

$$P_{stage_n} = 0.6P_L + 0.4P_S \quad (18)$$

By using the value of P_{stage_n} , where $n = \{n \mid n \in \mathbb{Z}, 0 \leq n \leq 4\}$, the classification of the final (based on the medical thresholds) is performed. The lung cancer is further classified based on the size of the nodule. After the classification, the test image is sent to the sub-classifier. This module includes a module for the processing of the image and also a module for decision-making. The module of the processing of the image separates the nodule of the lung from the image. Next, the module of decision-making computes the nodule size. Based on the medical thresholds, this module classifies the nodules (see Fig. 5).

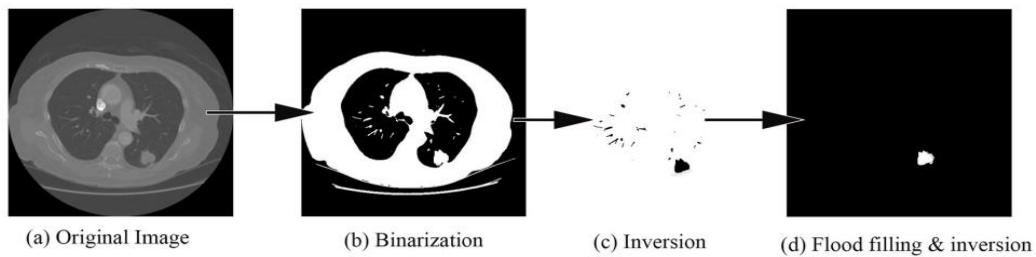


Fig. 5. An example of the separation of the lung nodule from the sub-classified image.

IV. TESTS AND EVALUATION OF RESULTS

In this section, the details of the evaluation criteria, the used datasets, our performed tests, and the gained outcomes are provided. The language of the programming of Python has been applied to implement these experiments. Our proposed approach is done in a computer with 8G RAM and Core (TM) i7 CPU 3.0 GHz Intel(R). The network of the convolutional is implemented on GPU and the used card of the graphics in our approach is GEFORCE 840M for NVIDIA.

A. Applied Datasets and Evaluation Criteria

The performance evaluation criteria in this paper include accuracy, false positive rate, and false negative rate, which are utilized to calculate the Area Under the Curve (AUC) score and Recall. The LIDC-IDRI dataset [33] and the LUNGx dataset [34] are employed to evaluate the effectiveness of our proposed approach and to compare it with similar approaches. These two datasets are combined into a single dataset for evaluating our approach. Additionally, data obtained from the medical body area network are incorporated into this evaluation process.

Within this dataset, image scans containing lung regions are considered non-candidates and are consequently excluded from the datasets.

Furthermore, the datasets contain scans both with and without nodules. These cases are identified and separated based

on existing metadata within the dataset, with annotations performed by radiologists. However, there is no inherent distribution logic between these two classes. Following partitioning, the number of images available for training, testing, and validation is insufficient. The scarcity of images poses a challenge in achieving satisfactory validation accuracy for CNNs. To overcome this challenge, we employ two-dimensional spatial image enhancement and generate features to preserve enhanced images using the existing dataset [35]. As a result, each CT scan is represented as a 3-channel image with dimensions of 224×224. The statistics of our utilized datasets are presented in Table I.

B. Obtained Results

In this section, we examine and also, we analyze the obtained results from the different experiments. Before the presentation of the results, we should mention that we compare the obtained outcomes by our presented approach with the obtained outcomes by the ResNet-50 network [36], the Inception V3 network [37], and the Xception network [38]. The results of our presented approach and other deep learning-based networks in our used dataset and the obtained data are provided in Tables II, III, and IV. Also, Fig. 6 displays the efficiency of deep learning models and the efficiency of our presented model according to accuracy, score of AUC, and loss. Note that in Tables II, III, and IV, results are presented for training, validation, and testing, respectively.

TABLE I. THE STATISTICS OF USED DATASETS AND THEIR COMBINATION FOR THE EVALUATION OF THE PROPOSED METHOD

| Dataset | CT Cases | Candidate Cases | Cases with Nodules | Augmented Cases |
|-----------|----------|-----------------|--------------------|-----------------|
| LUNGx | 70 | 3280 | 1822 | 160000 |
| LIDC-IDRI | 1018 | 8252 | 5249 | 365000 |

TABLE II. OUTCOMES OF TRAINING OF THE DIFFERENT DEEP LEARNING APPROACHES AND OUR PRESENTED APPROACH

| Model | Accuracy | AUC Score | Recall | Loss |
|----------------|----------|-----------|--------|--------|
| ResNet-50 | 99.56 | 99.99 | 99.60 | 0.045 |
| InceptionV3 | 94.25 | 96.40 | 94.23 | 1.960 |
| Xception | 94.10 | 96.70 | 94.08 | 1.450 |
| Proposed Model | 99.85 | 100 | 99.76 | 0.0018 |

TABLE III. OUTCOMES OF VALIDATION OF THE DIFFERENT DEEP LEARNING APPROACHES AND OUR PRESENTED APPROACH

| Model | Accuracy | AUC Score | Recall | Loss |
|----------------|----------|-----------|--------|-------|
| ResNet-50 | 84.20 | 94.90 | 83.50 | 0.598 |
| InceptionV3 | 82.07 | 88.50 | 82.10 | 15.70 |
| Xception | 82.10 | 90.00 | 82.06 | 8.270 |
| Proposed Model | 92.25 | 98.12 | 91.54 | 0.324 |

TABLE IV. OUTCOMES OF TEST OF THE DIFFERENT DEEP LEARNING APPROACHES AND OUR PRESENTED APPROACH

| Model | Accuracy | AUC Score | Recall | Loss |
|----------------|----------|-----------|--------|-------|
| ResNet-50 | 84.13 | 94.85 | 83.45 | 0.604 |
| InceptionV3 | 82.09 | 88.65 | 82.06 | 15.64 |
| Xception | 82.12 | 90.13 | 82.07 | 8.301 |
| Proposed Model | 92.78 | 98.46 | 92.01 | 0.321 |

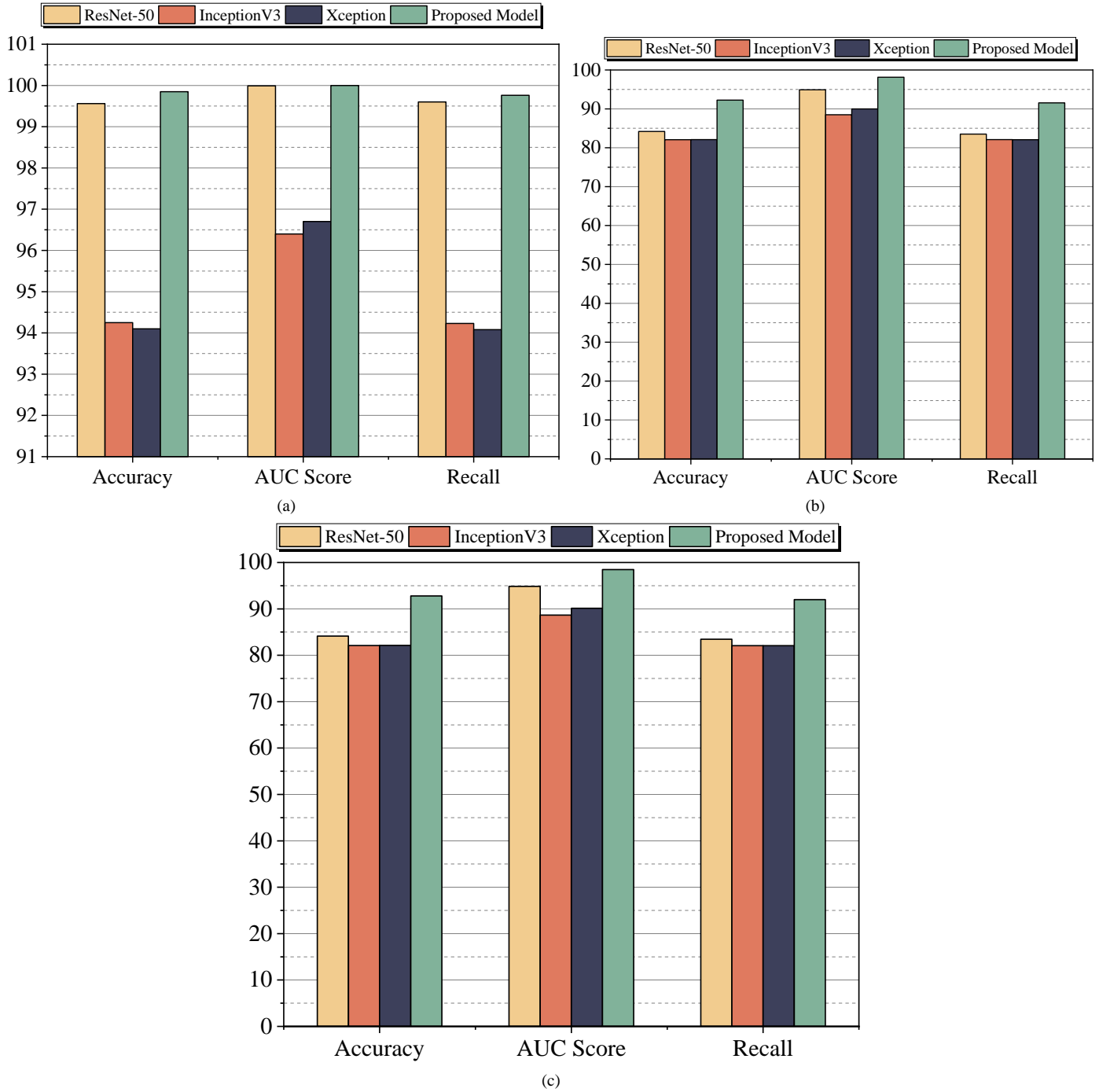


Fig. 6. Illustration of performance evaluation results for different methods, (a) Result of training process, (b) Result of validation process, (c) Result of test process.

After analyzing the outcomes of our proposed model and comparing them with ResNet-50, Inception V3, and Xception, it is evident that our model outperforms similar deep learning models, as shown in Tables II, III, and IV, as well as Fig. 6. Our proposed method achieved a test accuracy of 92.78%, a test AUC score of 98.46%, a test recall of 92.01%, and a test loss of 0.321.

In Fig. 6, the accuracy, AUC score, and loss values of different models are depicted. These metrics are crucial for evaluating model performance. Notably, our proposed model exhibits the highest test accuracy compared to other models. The AUC score is a key measure for assessing method efficiency and its ability to discriminate between positive and negative classes. A higher AUC score indicates superior performance. A score between 0.7 and 0.8 is considered acceptable, between 0.8 and 0.9 is excellent, and above 0.9 is considered outstanding [39]. As shown in Fig. 6, the proposed method not only achieved the highest test accuracy but also attained the highest test AUC score, indicating its excellent discriminatory ability between positive and negative classes.

Indeed, the loss value is another crucial criterion in assessing model performance. It represents the degree of inaccuracy in the model's predictions at each iteration. A loss value of 0 indicates perfect model predictions, whereas higher loss values indicate poorer performance. In our detection process, we use the cross-entropy loss function, commonly employed for multi-class classification tasks [38]. The proposed method achieves the lowest loss value, indicating superior predictive accuracy. Conversely, models such as Xception and Inception V3 exhibit significantly higher loss values [40, 41]. This evaluation demonstrates that our approach outperforms other deep learning models in diagnosing various types of lung cancer using the datasets and collected data.

C. Discussion and Limitations

Despite the promising results observed in various tests, the proposed method has several limitations, most of which are typical of CNN-based models. These limitations are outlined below.

Firstly, the efficacy of our approach, which surpasses that of similar methods, heavily relies on hybridization. The integration of data from the medical body area network contributes to the combined layer. However, any erroneous measurements by faulty IoT sensors could significantly compromise the overall integrity of the model. Although such occurrences are rare, the absence of a fault detection mechanism for medical sensors poses a potential risk.

Moreover, like any lung cancer classifier based on CNN, our proposed method requires image processing to enhance features. This image processing involves a series of computationally expensive processes. Each image must be processed and segmented individually, resulting in significant time consumption. Additionally, it is beyond the scope of this paper to dissect each module of image processing separately and evaluate its impact on the overall efficiency of the network.

However, this also underscores the need for further research. The validation performance of our proposed approach

sees a significant decline when image enhancement is not employed. This implies that the overall efficacy of the model is reliant on image enhancement. However, it's important to note that this limitation isn't exclusive to our proposed method. To date, no efforts have been made to determine the optimal number of enhanced images. This aspect leaves room for future optimization of the efficiency of our proposed method.

V. CONCLUSIONS AND SUGGESTIONS

The mortality rate associated with lung cancer remains alarmingly high, underscoring its status as one of the most prevalent and aggressive forms of cancer worldwide. While its occurrence cannot be prevented, early diagnosis can significantly improve patient outcomes, prolonging lives. Notably, in North America and other industrialized nations, lung cancer ranks as the leading cause of cancer-related deaths. Despite significant strides in recent years, early diagnosis remains challenging and lacks reliability.

In this study, we departed from current research trends to explore specialized layers within our CNN model. By integrating physiological data into our CNN model specifically designed for lung nodule classification, we achieved promising results. Our combined classifier attained an accuracy of 92.78%, surpassing similar models according to our literature review. Even in scenarios where feature learning layers may suffer from mistraining due to the absence of beneficial features, the classification accuracy of our proposed method remains reliable, thanks to the weighted aggregation of data collected from the medical body area network.

This study extends the development of one of the most precise automated models for lung cancer detection, emphasizing its comprehensive service availability. In summary, our proposed method represents a significant advancement in CNN-based automated models for lung cancer detection. We anticipate that our approach will pave the way for the development of more reliable computer-aided detection systems.

The proposed approach addresses the critical problem of early and accurate detection of lung cancer through the integration of data from CT scans and wearable IoT sensors, leveraging the DCNN for analysis. By combining information from both sources, the approach enhances diagnostic accuracy by capturing a comprehensive range of patient data. The hybrid model trained on a balanced dataset ensures robust learning and classification of lung nodules, while rigorous evaluation metrics such as accuracy, AUC score, loss, and recall provide thorough assessment of performance. Overall, the proposed approach offers a holistic and reliable solution to the challenge of lung cancer diagnosis, leveraging advanced machine learning techniques and diverse data sources to improve patient outcomes.

Future research could focus on integrating multi-modal data, including medical imaging, physiological data from wearable sensors, and patient history, into a comprehensive diagnostic model. By leveraging a wider range of data sources, such as genetic information, lifestyle factors, and environmental exposures, researchers can develop a more holistic understanding of lung cancer risk and improve the

accuracy of early detection models. This approach would require advanced data fusion techniques and machine learning algorithms capable of processing diverse data types and extracting meaningful patterns for accurate diagnosis and prognosis.

Another potential avenue for future research is the development of explainable artificial intelligence (XAI) models for lung cancer diagnosis. While deep learning models like CNNs have demonstrated impressive performance, their inner workings can be opaque, making it challenging to understand the factors driving their decisions. By incorporating explainability into the model architecture, researchers can provide clinicians with insights into how specific features contribute to the diagnostic process, enhancing trust and facilitating clinical decision-making. This research could involve exploring interpretable machine learning techniques, such as attention mechanisms, feature visualization, and decision trees, to create transparent and clinically actionable diagnostic models for lung cancer detection.

REFERENCES

- [1] J. Kuruvilla and K. Gunavathi, "Lung cancer classification using neural networks for CT images," *Comput Methods Programs Biomed*, vol. 113, no. 1, pp. 202–209, 2014.
- [2] B. P. Tripp, "Similarities and differences between stimulus tuning in the inferotemporal visual cortex and convolutional networks," in 2017 International Joint Conference on Neural Networks (IJCNN), IEEE, 2017, pp. 3551–3560.
- [3] I. Durosini et al., "Patient preferences for lung cancer treatment: a qualitative study protocol among advanced lung cancer patients," *Front Public Health*, vol. 9, p. 622154, 2021.
- [4] C. J. Chapman et al., "Autoantibodies in lung cancer: possibilities for early detection and subsequent cure," *Thorax*, vol. 63, no. 3, pp. 228–233, 2008.
- [5] P. K. Shah et al., "Missed non-small cell lung cancer: radiographic findings of potentially resectable lesions evident only in retrospect," *Radiology*, vol. 226, no. 1, pp. 235–241, 2003.
- [6] J.-F. Daneault et al., "Accelerometer data collected with a minimum set of wearable sensors from subjects with Parkinson's disease," *Sci Data*, vol. 8, no. 1, p. 48, 2021.
- [7] J. Molimard, T. Delettraz, and E. Ojardias, "Development of a miniaturized motion sensor for tracking warning signs of low-back pain," arXiv preprint arXiv:2104.03565, 2021.
- [8] J. Henderson, J. Condell, J. Connolly, D. Kelly, and K. Curran, "Review of wearable sensor-based health monitoring glove devices for rheumatoid arthritis," *Sensors*, vol. 21, no. 5, p. 1576, 2021.
- [9] H. Teymourian, F. Tehrani, K. Mahato, and J. Wang, "Lab under the skin: microneedle based wearable devices," *Adv Healthc Mater*, vol. 10, no. 17, p. 2002255, 2021.
- [10] L. Wang, K. Jiang, and G. Shen, "Wearable, implantable, and interventional medical devices based on smart electronic skins," *Adv Mater Technol*, vol. 6, no. 6, p. 2100107, 2021.
- [11] K. A. G. Udeshani, R. G. N. Meegama, and T. G. I. Fernando, "Statistical feature-based neural network approach for the detection of lung cancer in chest x-ray images," *International Journal of Image Processing (IJIP)*, vol. 5, no. 4, pp. 425–434, 2011.
- [12] I. Bush, "Lung nodule detection and classification," *Rep. Stanf. Comput. Sci*, vol. 20, pp. 196–209, 2016.
- [13] A. M. R. Schilham, B. Van Ginneken, and M. Loog, "A computer-aided diagnosis system for detection of lung nodules in chest radiographs with an evaluation on a public database," *Med Image Anal*, vol. 10, no. 2, pp. 247–258, 2006.
- [14] B. Keserci and H. Yoshida, "Computerized detection of pulmonary nodules in chest radiographs based on morphological features and wavelet snake model," *Med Image Anal*, vol. 6, no. 4, pp. 431–447, 2002.
- [15] M. A. Hussain, T. M. Ansari, P. S. Gawas, and N. N. Chowdhury, "Lung cancer detection using artificial neural network & fuzzy clustering," *International journal of advanced research in computer and communication engineering*, vol. 4, no. 3, pp. 360–363, 2015.
- [16] N. Hadavi, M. J. Nordin, and A. Shojaeipour, "Lung cancer diagnosis using CT-scan images based on cellular learning automata," in 2014 International Conference on Computer and Information Sciences (ICCOINS), IEEE, 2014, pp. 1–5.
- [17] S. Otte et al., "OCT A-Scan based lung tumor tissue classification with Bidirectional Long Short Term Memory networks," in 2013 IEEE International Workshop on Machine Learning for Signal Processing (MLSP), IEEE, 2013, pp. 1–6.
- [18] X. Li and R. Wang, "A new efficient 2D combined with 3D CAD system for solitary pulmonary nodule detection in CT images," *International Journal of Image, Graphics and Signal Processing*, vol. 3, no. 4, p. 18, 2011.
- [19] F. Taher and R. Sammouda, "Lung cancer detection by using artificial neural network and fuzzy clustering methods," in 2011 IEEE GCC conference and exhibition (GCC), IEEE, 2011, pp. 295–298.
- [20] W. Shen et al., "Multi-crop convolutional neural networks for lung nodule malignancy suspiciousness classification," *Pattern Recognit*, vol. 61, pp. 663–673, 2017.
- [21] W. Zhang, X. Wang, X. Li, and J. Chen, "3D skeletonization feature based computer-aided detection system for pulmonary nodules in CT datasets," *Comput Biol Med*, vol. 92, pp. 64–72, 2018.
- [22] P. Wu, K. Xia, and H. Yu, "Correlation coefficient based supervised locally linear embedding for pulmonary nodule recognition," *Comput Methods Programs Biomed*, vol. 136, pp. 97–106, 2016.
- [23] B. Kaliski, "Password-based cryptography specification," RFC 2898, 2000.
- [24] A. Buades, B. Coll, and J.-M. Morel, "A non-local algorithm for image denoising," in 2005 IEEE computer society conference on computer vision and pattern recognition (CVPR'05), Ieee, 2005, pp. 60–65.
- [25] U. K. Acharya and S. Kumar, "Genetic algorithm based adaptive histogram equalization (GAAHE) technique for medical image enhancement," *Optik (Stuttg)*, vol. 230, p. 166273, 2021.
- [26] W. J. Sori, J. Feng, and S. Liu, "Multi-path convolutional neural network for lung cancer detection," *Multidimens Syst Signal Process*, vol. 30, pp. 1749–1768, 2019.
- [27] M. M. Prieto, E. Montanes, and O. Menendez, "Power plant condenser performance forecasting using a non-fully connected artificial neural network," *Energy*, vol. 26, no. 1, pp. 65–79, 2001.
- [28] A. Mittal, A. P. Singh, and P. Chandra, "A modification to the Nguyen–Widrow weight initialization method," in *Intelligent Systems, Technologies and Applications: Proceedings of ISTA 2018*, Springer, 2019, pp. 141–153.
- [29] P. Singh, "An extended framework of lung cancer classification using hybrid architecture of surf and svm," *INFORMATION TECHNOLOGY IN INDUSTRY*, vol. 9, no. 1, pp. 1489–1502, 2021.
- [30] S. Yu et al., "Hessian-aware pruning and optimal neural implant," in *Proceedings of the IEEE/CVF Winter Conference on Applications of Computer Vision*, 2022, pp. 3880–3891.
- [31] M. T. Hagan and M. B. Menhaj, "Training feedforward networks with the Marquardt algorithm," *IEEE Trans Neural Netw*, vol. 5, no. 6, pp. 989–993, 1994.
- [32] E. M. Mustafa, M. A. Elshafey, and M. M. Fouad, "Accuracy enhancement of a blind image steganalysis approach using dynamic learning rate-based CNN on GPUs," in 2019 10th IEEE International Conference on Intelligent Data Acquisition and Advanced Computing Systems: Technology and Applications (IDAACS), IEEE, 2019, pp. 28–33.
- [33] S. G. Armato III et al., "The lung image database consortium (LIDC) and image database resource initiative (IDRI): a completed reference database of lung nodules on CT scans," *Med Phys*, vol. 38, no. 2, pp. 915–931, 2011.

- [34] S. G. Armato III et al., "LUNGx Challenge for computerized lung nodule classification: reflections and lessons learned," *Journal of Medical Imaging*, vol. 2, no. 2, 2015.
- [35] R. Takahashi, T. Matsubara, and K. Uehara, "Ricap: Random image cropping and patching data augmentation for deep cnns," in *Asian conference on machine learning*, PMLR, 2018, pp. 786–798.
- [36] K. Simonyan and A. Zisserman, "Very deep convolutional networks for large-scale image recognition In: Proceedings of International Conference on Learning Representations," 2015.
- [37] O. Russakovsky et al., "Imagenet large scale visual recognition challenge," *Int J Comput Vis*, vol. 115, pp. 211–252, 2015.
- [38] M. I. Mahmud, M. Mamun, and A. Abdelgawad, "A Deep Analysis of Transfer Learning Based Breast Cancer Detection Using Histopathology Images," in *2023 10th International Conference on Signal Processing and Integrated Networks (SPIN)*, IEEE, 2023, pp. 198–204.
- [39] J. N. Mandrekar, "Receiver operating characteristic curve in diagnostic test assessment," *Journal of Thoracic Oncology*, vol. 5, no. 9, pp. 1315–1316, 2010.
- [40] Dinesh Reddy, B., N. Thirupathi Rao, and Debnath Bhattacharyya. "Deep Neural Transfer Network Technique for Lung Cancer Detection." In *Machine Intelligence Techniques for Data Analysis and Signal Processing: Proceedings of the 4th International Conference MISP 2022*, Volume 1, pp. 237-247. Singapore: Springer Nature Singapore, 2023.
- [41] Mohana Krishna, N., and R. Puviarasi. "Convolutional neural network based ResNet50 for finding accuracy in prediction of lung cancer using CT images and compared with CNN based inception V3." In *AIP Conference Proceedings*, vol. 2816, no. 1. AIP Publishing, 2024.

Transmission Line Monitoring Technology Based on Compressed Sensing Wireless Sensor Network

Shuling YIN^{1*}, Renping YU², Longzhi WANG³

Hubei Open University, Wuhan, 430074, China¹

Hubei Huazhong Electric, Power Technology Development Co., Ltd, Wuhan 430077, China²

Information & Communication Branch of State Grid, Hubei Electric Power Company, Wuhan 430077, China³

Abstract—Given wireless sensor networks' significant data transmission requirements, conventional direct transmission often leads to bandwidth constraints and excessive network energy consumption. This paper proposes a transmission line monitoring technology based on compressed sensing wireless sensor networks to achieve real-time monitoring of ice-covered power lines. Grounded in compressed sensing theory, this method utilizes dual orthogonal wavelet transform sparse matrices for sparse representation of sensor data. Considering the practical requirements of power line monitoring, a data transmission model is established to implement compressed sampling transmission. The regularization orthogonal matching pursuit algorithm is employed for high-precision reconstruction of compressed data. The software and hardware components of the power line monitoring system are designed, and experiments are conducted under real-world conditions. The results demonstrate that: 1) the system operates stably with an ideal data compression effect, achieving a compression ratio of 93.191%. The absolute reconstruction errors for temperature, humidity, and wind speed sensor data are 0.064°C, 0.052%, and 0.128 m/s, respectively, indicating high reconstruction accuracy and effectively avoiding transmission impacts caused by bandwidth issues. 2) In a 36-hour energy consumption loss test, compared to direct transmission, the compressed transmission mode exhibits a lower rate of battery voltage decay, with a decrease of approximately 11.18%, effectively extending the network's lifespan.

Keywords—Compressed sensing; transmission line; wireless sensor network; orthogonal wavelet transform; data reconstruction

I. INTRODUCTION

As a crucial component of the power system, transmission lines are responsible for conveying the electrical energy generated by power stations to various distribution points and ultimate consumers. The stable operation of these infrastructures is vital to the reliability and security of the entire power system, and it also directly affects the continuity and quality of power supply [1]. In view of the uneven geographical distribution of China's power resources, transmission lines often have to traverse regions with complex geographical environments and adverse climatic conditions. Particularly in environments characterized by low temperatures, high humidity, and strong winds, the surfaces of transmission lines are highly susceptible to ice accretion, which increases the risks of galloping, breakage, overloading, and flashovers on insulator strings, severely threatening the stability and safe operation of transmission lines [2-4]. In response to these risk factors, it is particularly important to

implement real-time monitoring and develop efficient transmission line operational status monitoring systems. By employing advanced sensing technologies, image processing techniques and big data analytics, comprehensive condition monitoring of transmission lines can be achieved, enabling timely identification and response to existing or potential issues and effectively reducing the probability and impact of failures. Such monitoring systems not only provide early warnings of possible line failures but also offer real-time data support to operations and maintenance personnel, assisting them in making rapid and accurate decisions. Therefore, strengthening the real-time monitoring capabilities of transmission lines plays a crucial role in enhancing the levels of fault prevention and control, improving the system's emergency response and early warning capabilities, and ensuring the safe and stable operation of the power grid.

Currently, transmission line monitoring methods primarily include manual inspection, unmanned aerial vehicle (UAV) surveillance, infrared thermal imaging, and fiber optic sensing technologies. Tang [5] proposed a technical approach utilizing video surveillance systems for vibration analysis of transmission lines. This method involves the collection of video image data from transmission lines and the establishment of a relative coordinate system between the power tower and the transmission line, thereby enabling the tracking of vibration frequency and amplitude at specific line positions. Through such tracking, the dynamic characteristics and operational status of the transmission lines can be assessed. Although this technology has demonstrated certain effectiveness in vibration monitoring of transmission lines, its implementation relies on various equipment, and the operational process is complex with insufficient real-time capabilities, making it unsuitable for widespread deployment in large-scale transmission line systems. He [6] addressed the requirements of the sensor layer in the power Internet of Things by combining fiber optic sensing technology with big data and artificial intelligence for multi-risk monitoring of transmission lines. The monitoring system was deployed, and experiments were conducted using different monitoring scenarios, yielding good performance. However, the scheme is costly to implement, complex to install, and susceptible to temperature effects, leading to less-than-ideal practical application outcomes. Wireless Sensor Networks (WSN), which integrate microsensors, embedded computing, wireless communication, and information processing, coordinate among network nodes to monitor, sense, collect, and process information about the objects of interest, transmitting data wirelessly [7,8]. Sensors in WSN are less

affected by time, space, and environmental conditions during data collection and are widely used in various monitoring fields. However, the transmission of large volumes of data in WSN, when using traditional transmission methods, can lead to congestion in limited bandwidth, reducing the efficiency of data collection and increasing the energy consumption of nodes, thus affecting the network's lifespan. Consequently, some scholars have adopted compressed sensing technology to address the shortcomings of traditional WSN transmission methods. Compressed sensing is a novel signal acquisition theory that enables the reconstruction of sparse or compressible signals from sampling frequencies far below the Nyquist rate, offering advantages such as low sampling rates, strong anti-noise capabilities, efficient signal recovery, low energy consumption, and ease of implementation, and it is widely applied in various monitoring scenarios. Yang et al. [9] used a distributed wavelet transform theory based on hybrid decomposition, leveraging the computational capabilities of nodes to reduce communication overhead from inter-node exchange of wavelet coefficients, and employed adaptive wavelet transform to determine network overhead, resulting in significant improvements in network performance. Fute [10] utilized distributed data compression algorithms to reduce the total amount of data within WSN, decreasing the likelihood of data packet collisions on wireless media to enhance data transmission efficiency, reduce resource consumption within the network, and extend network lifespan. Jiang [11] proposed a compressed sensing algorithm with dynamic retransmission to address data packet loss due to unreliable wireless communication, achieving high-precision signal reconstruction to improve network energy utilization and lifespan, with the normalized mean absolute error (NMAE) reduced by 64.5%, and energy efficiency also correspondingly enhanced. Yang [12] estimated the signal's sparsity through an adaptive subspace pursuit algorithm, selected atoms using an approximate matching principle, and completed signal residual updates after multiple iterations to achieve signal reconstruction.

The aforementioned research has provided valuable guidance for the study of Wireless Sensor Networks (WSN); however, due to the complexity of the algorithms, their adaptability in the transmission line monitoring networks with parallel transmission of large volumes of data is not optimal. In light of this, this paper draws on the theory of Compressed Sensing (CS) as the design cornerstone and designs a transmission line monitoring network based on real-world

scenarios. The biorthogonal wavelet transform algorithm is utilized to construct a sparse sampling model for signal compression, while the Regularized Orthogonal Matching Pursuit (ROMP) algorithm is employed for high-precision signal reconstruction. Based on this, a transmission line monitoring system is designed to ensure the real-time and stable monitoring of lines, which holds positive implications for the secure operation of power systems and the extension of the service life of monitoring networks.

The remainder of the paper has been organized as follows. The compressed sensing theory in Section II introduces an innovative method for transmission line monitoring using Compressed Sensing (CS) theory. It discusses CS's ability to reconstruct sparse signals from low-frequency samples, crucial for dense wireless sensor networks (WSNs). To tackle non-sparse signal transmission challenges, the paper proposes a method in Section III utilizing biorthogonal wavelet transform for signal sparsity and the ROMP algorithm for efficient reconstruction. It details network architecture and sparse sampling model, emphasizing adaptive signal analysis via wavelet transformation. Additionally, it explains the ROMP algorithm's iterative process, highlighting its role in enhancing accuracy and handling noise. The paper also discusses the system design, including hardware components and data transmission mechanisms in the design and implementation of the monitoring system in Section IV. The experimental results and analysis in Section V validate the proposed method's efficacy, showcasing high compression ratios, low reconstruction errors, and reduced energy consumption compared to existing algorithms. Finally, conclusions emphasize the significance of the proposed scheme in enhancing transmission line monitoring efficiency and extending network lifespan, offering practical value for energy-efficient management of monitoring systems in Section VI.

II. COMPRESSED SENSING THEORY

Compressed Sensing (CS) is a novel signal sampling method proposed by Candès et al. in 2004, aiming to address the shortcomings of traditional signal acquisition and processing [13]. This theory indicates that if the original signal exhibits sparsity and orthogonality, it can be reconstructed from observation values at a sampling frequency much lower than the Nyquist theorem requires. In other words, it is possible to reconstruct the signal using a much lower sampling frequency and an appropriate reconstruction algorithm. Fig. 1 illustrates the concept of compressed sensing data collection.

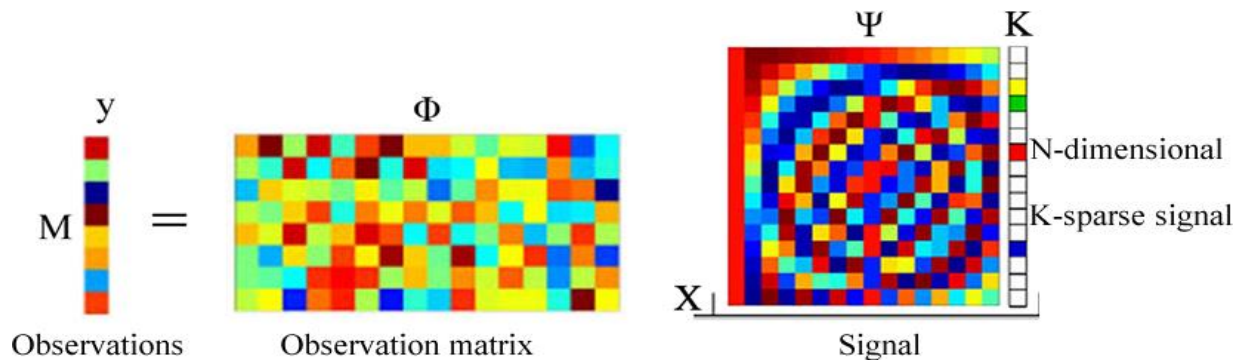


Fig. 1. Schematic diagram of compressed sensing data collection.

Wireless sensor networks are characterized by dense sensor node deployment and high signal sampling frequencies, making the original signals compressible [14]. However, in most cases of transmission line monitoring networks, signal values are not zero, indicating a lack of sparsity [15]. Therefore, it is necessary to employ methods for transforming continuous-time domain signals into sparse signals. If X is an N -dimensional column vector representing the original signal and, α is the coefficient vector under the basis Ψ , the sparse processing can be expressed as follows:

$$X = \Psi\alpha \quad (1)$$

Assuming the sparsity level K represents the number of non-zero points in the sparse domain. If $K = n$ ($n \ll N$) is satisfied, the data can be sampled using the observation matrix Φ ($M \times N$) to obtain the observation values y . The observation matrix Φ is randomly generated from a Gaussian matrix with a mean of zero and a variance of $1/M$. If the performance meets the requirements, the observation values y contain the essential information from the original signal X .

The signal reconstruction can be solved through non-deterministic polynomial (NP) optimization problems, expressed as follows:

$$y = \Phi X \quad (2)$$

$$\begin{cases} \alpha^{(0)} = \arg \min_{\alpha \in R^N} \|\alpha\|_0 \\ y = \Phi X = A\alpha \end{cases} \quad (3)$$

Since the term $A = \Phi\Psi$ belongs to a non-convex combinatorial optimization problem, convex relaxation approximation methods can be employed for solving:

$$\begin{cases} \alpha^{(1)} = \arg \min_{\alpha \in R^N} \|\alpha\|_1 \\ y = \Phi X = A\alpha \end{cases} \quad (4)$$

III. MODEL CONSTRUCTION

A. Network Structure and Sparse Sampling Model for Signal

The transmission line monitoring network adopts a tree structure, as illustrated in Fig. 2. Sensor nodes transmit collected information through long-distance communication modules. After convergence nodes compress the observations, the information is transmitted to the remote monitoring platform through GPRS and the Internet. The monitoring platform utilizes corresponding algorithms to reconstruct the data information, thereby achieving the identification of the original signal for monitoring and early warning purposes.

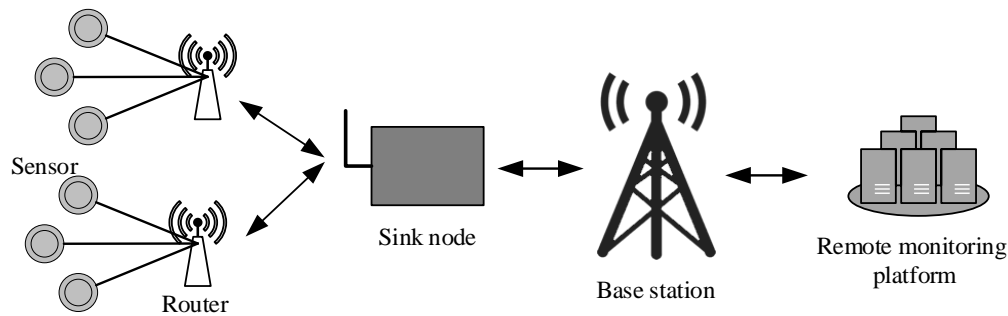


Fig. 2. Transmission line monitoring network structure.

Various sensor nodes exchange information with convergence nodes through a wireless network in the perception area. The temporal characteristics of signals collected by various sensors exhibit continuity and piecewise smoothness, and they have approximate spatial regularity. Based on spatiotemporal characteristics, the biorthogonal wavelet transform can locally transform the signal in both time and frequency. Using translation and scaling operations, it achieves multi-scale refinement of signals, meeting the

adaptive analysis requirements of time-frequency signals. This makes it suitable for sparse representation of signals in monitoring sensor networks [16]. Therefore, based on the characteristics of the transmission line monitoring signals, a sparse sampling model is constructed using the biorthogonal wavelet transform algorithm to achieve signal compression. The detailed signal transmission steps are shown in Fig. 3, where the dashed box represents the sparse sampling process.

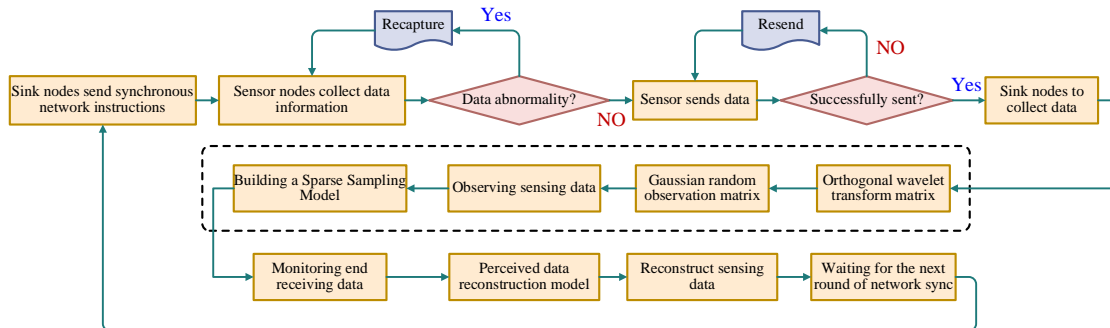


Fig. 3. Compressed sensing-based signal transmission process.

B. Data Information Reconstruction

The Regularized Orthogonal Matching Pursuit (ROMP) algorithm represents an improvement over the classical Orthogonal Matching Pursuit algorithm. The ROMP algorithm enhances signal reconstruction accuracy and stability by incorporating greedy algorithm principles, convex optimization methods, and regularization conditions during iterations [17].

In this algorithm, atoms in the sparse representation are systematically selected through iterations, considering both the sparsity of the signal and regularization conditions. This approach efficiently achieves the reconstruction of the original signal, contributing not only to improved reconstruction accuracy but also enhanced capability in handling noise and complex signal structures, showcasing excellent performance in practical applications.

The ROMP algorithm plays a crucial role in signal reconstruction and is well-suited for handling large-scale sensor data generated in transmission line monitoring. Through meticulous and robust signal reconstruction, the ROMP algorithm provides an effective mathematical tool for accurately restoring the transmission line monitoring signal. This not only aids in reducing data transmission volume and improving network efficiency but also effectively addresses complex environmental conditions and multi-source interference, offering robust support for the reliability and robustness of monitoring systems.

Assumption: r_t represents the residual of the observed data, Φ represents the empty set, λ_t represents the column indices obtained after the t -th iteration, A_t represents the set of columns of matrix A selected according to the index Λ_t , a_j represents the j -th column of the matrix, Λ_t represents the index set for the t -th iteration, $\langle \bullet, \bullet \rangle$ represents the inner product of vectors, \cup represents the set union operation, θ_t represents the column vector after the t -th iteration, $abs[\bullet]$ represents the absolute value operation. The algorithmic process can be described as follows:

Input: N -dimensional observation vector y , sensing matrix A , sparsity level K

Output: Estimated sparse representation coefficients $\hat{\theta}$, N -dimensional residual $r_K = y - A_K \hat{\theta}_K$

Initialization:

Iteration: $\Lambda_0 = \Phi$, $A_0 = \Phi$, $r_0 = y$, $t = 1$

1) Compute $u = abs[A^T r_{t-1}]$ by obtaining K largest values and corresponding column indices set J of matrix A .

2) *Regularization*: Search for a subset J_0 within J satisfying the condition of $|u(i)| \leq 2|u(j)|$ $i, j \in J_0$, and select J_0 with the maximum correlation.

3) Set $\Lambda_t = \Lambda_{t-1} \cup J_0$, $A_t = A_{t-1} \cup a_j$ ($j \in J_0$)

4) Solve for $y = A_t \theta_t$ by finding the least squares solution: $\theta_t = arg \min \|y - A_t \theta_t\| = (A_t^T A_t)^{-1} A_t^T y$.

5) Update the residual $\theta_t = arg \min_{\theta} \|y - A_t \theta_t\| = (A_t^T A_t)^{-1} A_t^T y$.

6) $t = t + 1$. If $t \leq K$, return to step 3; if $t > K$ or $\chi_t = 0$ or $\|\Lambda_t\|_0 \geq 2K$, stop the iteration, and reconstruct θ by placing all non-zero elements at the positions Λ_t .

After iterations, perform wavelet inverse transform on the obtained high-frequency signal and low-frequency part to complete the data reconstruction.

C. Key Model Parameters

The determination of key model parameters not only affects the efficiency of signal compression sensing and the quality of reconstruction but also governs the learning efficiency and accuracy of the model. Therefore, a comprehensive list of key parameters for the model has been constructed, taking into account the actual requirements of the model and the need for real-time and stable monitoring. The list is presented in Table I.

TABLE I. KEY PARAMETERS OF THE MODEL AND DETERMINATION

| Parameter | Description |
|---------------------------------|---|
| Wavelet Basis | In the realm of compressed sensing, the selection of an appropriate wavelet basis is of paramount importance, as it directly influences the sparsity representation and the quality of signal reconstruction. This study employs the Morlet wavelet to construct a sparse sampling model through experimental comparison, aiming to achieve signal compression. The Morlet wavelet, which combines a Gaussian function with a sine wave, aids in the identification of abrupt changes within signals, thereby facilitating line monitoring. |
| Regularization Parameter | The regularization parameter λ is utilized to control the degree of sparsity in the Regularized Orthogonal Matching Pursuit (ROMP) algorithm, striking a balance between data fidelity and sparsity to better capture the signal's sparse structure and enhance the quality of the reconstructed signal. This paper determines λ based on the minimum reconstruction error derived from leave-one-out cross-validation experiments, with the Mean Squared Error (MSE) serving as the evaluation metric for signal reconstruction error. |
| Sparsity | Sparsity is employed to regulate the balance between the greedy search and regularization in the ROMP algorithm, constraining the number of non-zero elements in the solution vector of the algorithm to prevent overfitting and underfitting phenomena. This study estimates sparsity by integrating the characteristics of the signal with prior knowledge and applying threshold processing. |
| Atom Dictionary | The Atom Dictionary dictates the representational capacity of the signal during the reconstruction process, reducing the number of atoms that need to be processed, lowering computational complexity, and enhancing computational efficiency. In this paper, the optimal Atom Dictionary is assessed, adjusted, and determined through cross-validation, based on the signal's characteristics and the degree of matching. |
| Initial Estimate | The Initial Estimate significantly impacts the convergence rate of the algorithm and the quality of the final solution. An appropriate Initial Estimate can effectively reduce computational complexity and minimize the influence of noise and outliers on the reconstructed signal. This research utilizes the Iterative Soft Thresholding Algorithm (ISTA) for sparse reconstruction as the Initial Estimate for the ROMP algorithm. |

IV. DESIGN AND IMPLEMENTATION OF MONITORING SYSTEM

Conditions for the formation of ice on transmission lines include environmental temperature $\leq 0^{\circ}\text{C}$, air relative humidity $\geq 85\%$, and wind speed $> 1\text{m/s}$, among others [18]. Therefore, temperature, humidity, and wind speed sensors were chosen as monitoring nodes. The hardware and software components of

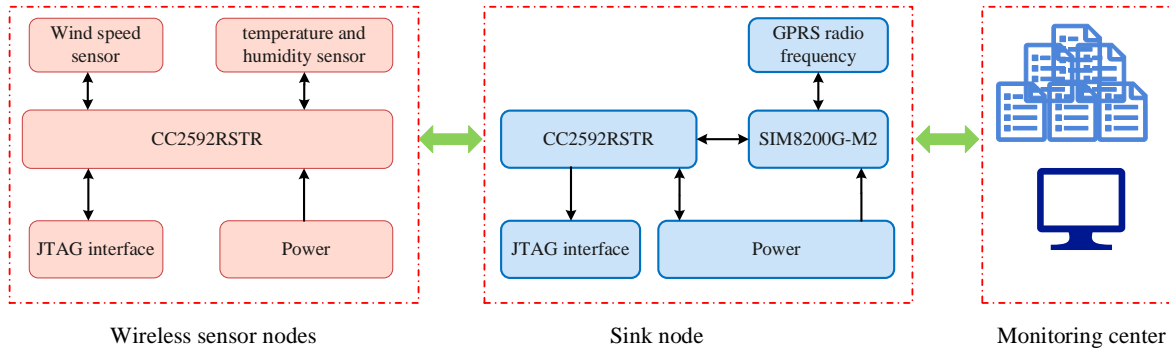


Fig. 4. System hardware structure.

The monitoring system utilizes the convergence node as the time reference point to send clock synchronization control signals to sensor nodes. Each node estimates its delay and makes corrections. Due to timing differences between sensor timers [19], each node is set with a 2.5s lead time to ensure timely responses. When receiving commands from the superior node, nodes exit sleep mode, correct their clocks, and collect and upload data. Upon receiving an ACK message from the convergence node, sensors transition to sleep mode to reduce power consumption. If a sensor node does not receive an ACK message, it continues data collection and uploads until receiving one. Once all nodes have received ACK messages, the convergence node performs data compression and observation processing.

The SHT31 sensor from Sensirion AG is employed for temperature and humidity sensing, with a temperature range of -40°C to 125°C and a humidity range of 0-100% RH, suitable for harsh weather conditions. The compact dimensions (2.5 x 2.5 x 0.9 mm) facilitate lightweight sensor node design. Wind speed measurement is achieved using the FS4G wind speed sensor from Renke Corporation, with a range of 0-60m/s.

The convergence node must perform data observation compression, remote transmission, and network management tasks. It is significantly affected by outdoor environmental factors. Overall, the convergence node should possess fast response, low power consumption, good sealing, and anti-interference capabilities. The SmartRF04-CC2592 chip from Texas Instruments, which integrates a 2.4GHz multi-channel RF transceiver supporting various standard protocols such as IEEE802.15 and ZigBee, is used. It has advantages such as small volume (QFP 4x4mm package), low current consumption (21.8mA when TX at 0dBm output, 12.2mA when TX at -12dBm output), programmable high output power, and strong anti-interference capabilities, making it suitable for the development and application of small wireless nodes. Based on this, the CC2592 chip is used for communication between network nodes and data observation

the transmission line monitoring system were designed by combining the network structure mentioned above and the algorithmic model. These components underwent detailed analysis and testing to ensure that, under stable system operation, the comprehensive performance indicators met the design requirements. The hardware structure of the system is illustrated in Fig. 4.

compression. It is connected to the SIM8200G-M2 wireless communication module via a serial bus, enabling communication with the monitoring center to ensure reliable and stable data transmission.

V. EXPERIMENTAL RESULTS AND ANALYSIS

A. Experimental Environment and Parameters

Experiments were conducted in the simulation laboratory of the State Grid Corporation of China (SGCC) Henan Province Power Grid Simulation Center to validate the feasibility of the proposed method. The span of the transmission line is 42.5m, and sensor nodes are deployed at positions 1, 2, 3, 4, 5, and 6. The convergence node is placed in the tower control box. The monitoring center is located in the simulation center building, 1.2km from the convergence node, and is responsible for receiving reconstructed convergence node data. The deployment of nodes is shown in Fig.5. LG18650 lithium batteries power all nodes with a nominal voltage of 3.7V and a capacity of 3200 mAh.

Data collection spanned five days from November 26 to 30 during the experimental period. Different time intervals (00:00-03:00, 8:00-10:30, 12:00-14:00, 17:30-19:30, 22:00-00:00) were selected to cover various working and environmental conditions, totaling 3450 minutes of sensor data collection. The analysis of diverse data aimed to ensure the reasonability and effectiveness of the experimental results.

Each sensor node's sampling and transmission intervals were set at 30 and 120 seconds, respectively. The observed temperature, humidity, and wind speed values were all 256. After compression by the convergence node, the final quantity was reduced to 768.

B. Reconstruction Error Performance Analysis

Sensor nodes collected environmental information using the parameters designed in the previous section as the basis for the experiment. The convergence node then compressed and

uploaded the data, ultimately achieving the reconstruction of compressed data in the monitoring center. Throughout the data compression and transmission process, the nodes operated collaboratively, meeting the requirements for system stability.

Taking the data collected during the time interval of 8:00-10:30 on November 28 as an example, the reconstructed temperature, relative humidity, and wind speed were compared with the original data, as illustrated in Fig. 6, Fig. 7, and Fig. 8.

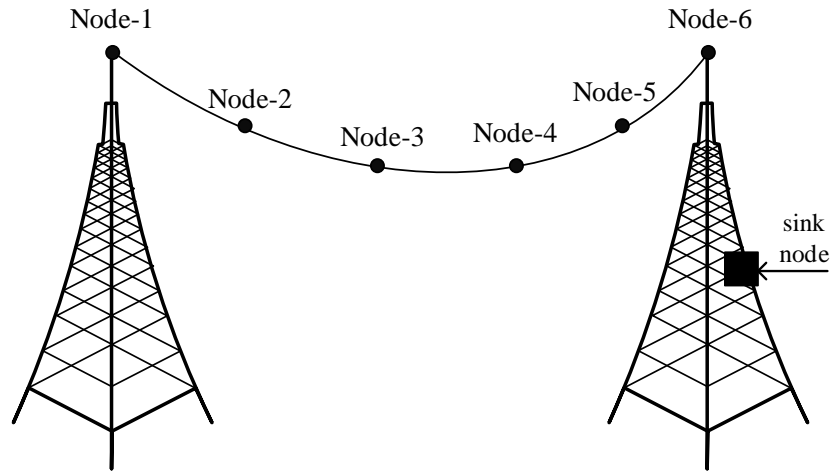


Fig. 5. Node deployment diagram.

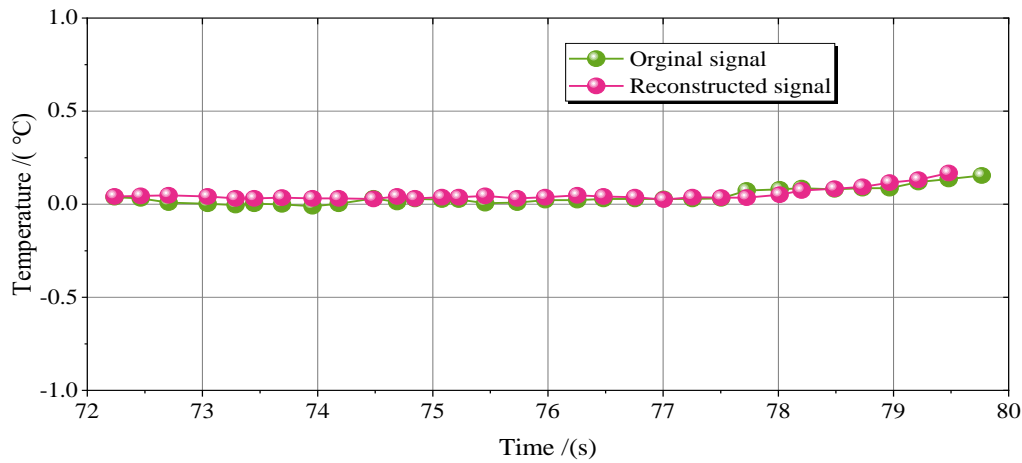


Fig. 6. Temperature comparison curve before and after reconstruction.

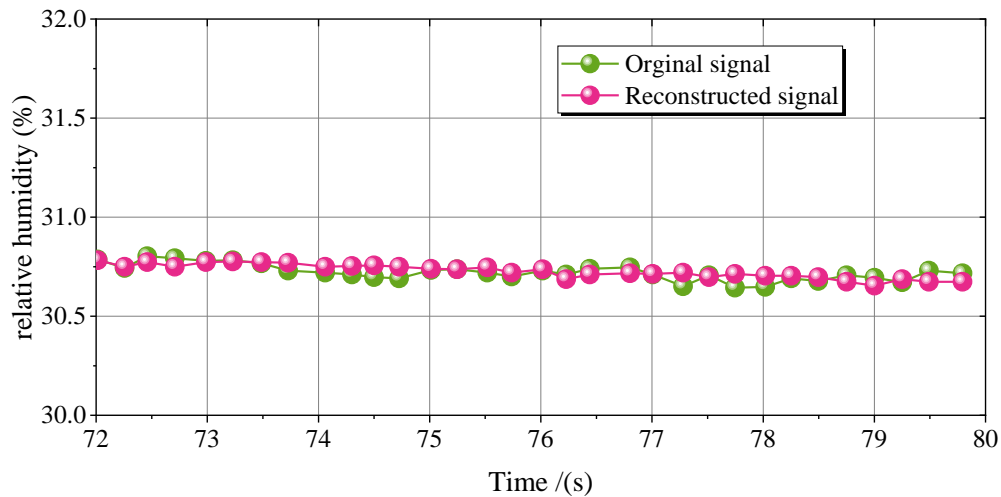


Fig. 7. Comparison curve of relative humidity before and after reconstruction.

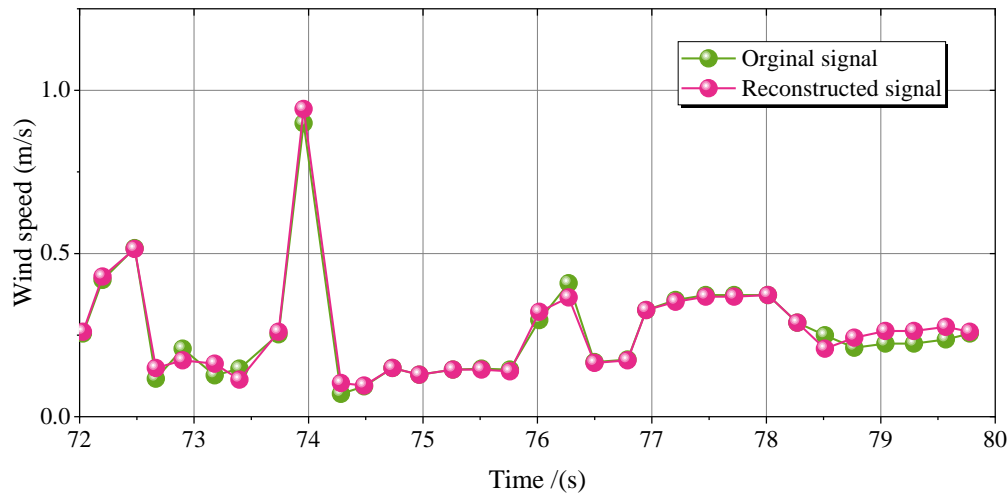


Fig. 8. Wind speed comparison curve before and after reconstruction.

The performance of the reconstruction algorithm is assessed by employing the Normalized Mean Square Error (NMSE) to calculate the mean square values of elements in the vector, thus evaluating the reconstruction error. Simultaneously, the data compression ratio ρ is used to measure the efficiency of data compression to obtain the maximum absolute and relative errors before and after reconstruction. The formulas for NMSE and ρ are expressed as Eq. (5) and Eq. (6), respectively:

$$NMSE = \frac{\| \hat{X}_j(n) - X_j(n) \|_p}{\| X_j(n) \|_p} \quad (5)$$

In the equations, $X_j(n)$ and $\hat{X}_j(n)$ represent the j -th values corresponding to the data before and after reconstruction, and the norm p takes a value of 2.

$$\rho = \frac{N-M}{N} \times 100\% \quad (6)$$

In the equations, M and N represent the quantities of observed data and original data, respectively. Table II presents the error situation of the reconstructed data.

TABLE II. RECONSTRUCTION DATA ERROR SUMMARY (N=3760)

| Project | Data Compression Ratio ρ (%) | Mean Square Error NMSE (%) | Relative Error (%) | Absolute Error |
|-------------------|-----------------------------------|----------------------------|--------------------|----------------|
| Temperature | 93.191 | 3.741 | 13.346 | 0.064°C |
| Relative Humidity | 93.191 | 0.184 | 0.077 | 0.052% |
| Wind Speed | 93.191 | 2.752 | 16.454 | 0.128m/s |

As shown in Table II, the data sampling reconstruction method based on the joint use of the biorthogonal Wavelet algorithm and the ROMP algorithm achieves a high compression ratio, demonstrating excellent compression results and the ability to achieve the high-precision reconstruction of compressed data. Due to the relatively stable changes in

relative humidity compared to temperature and wind speed, the sparsity after wavelet transformation is greater, resulting in higher data reconstruction accuracy. The mean square error accuracy of wind speed reconstruction is relatively ideal, but the relative and absolute errors are higher. This is because the wind speed signal exhibits significant fluctuations, and the sparse sampling process did not adequately adapt to the changing characteristics of the signal.

C. Energy Consumption Analysis

This section analyzes the power consumption of the compressed sensing wireless sensor network. Considering that the convergence node mainly completes the compression observation of data, experiments were conducted in direct and compressed transmission modes to ensure the comparability of experimental results. The lithium battery was fully charged to the nominal value, and the system was set to run for 36 hours in both modes to measure the voltage decay. The experimental results are shown in Fig. 9.

From the power consumption decay curves in Fig. 9, it can be observed that the convergence node using compressed sampling transmission has a slower voltage decay rate. In a relatively short experiment period, the nominal battery voltage (3.7v) dropped to approximately 3.565v and 3.548v under direct and compressed transmission modes, respectively, with a decrease of about 11.18%. Therefore, the use of compressed sampling transmission can effectively extend the service life of the sensor network.

D. Comparative Experiments

To further corroborate the validity of the method proposed in this paper, experiments were conducted using the respective algorithms from study [9-11] under the premise of the same data transmission volume. A comparison was made between the reconstruction errors, computational efficiency, and energy consumption of each algorithm. Fig. 10 presents the results of the comparative experiments.

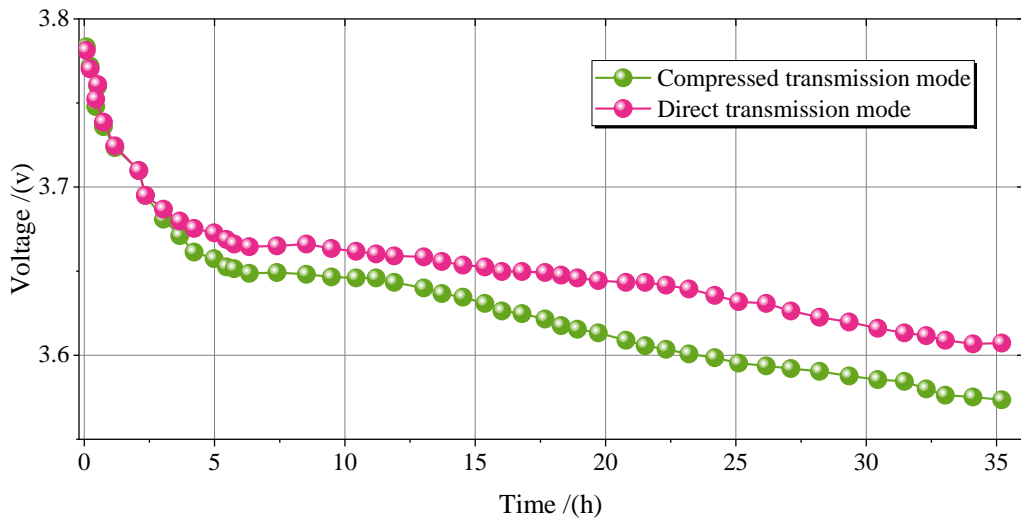


Fig. 9. Convergence node power consumption decay curve under different transmission modes.

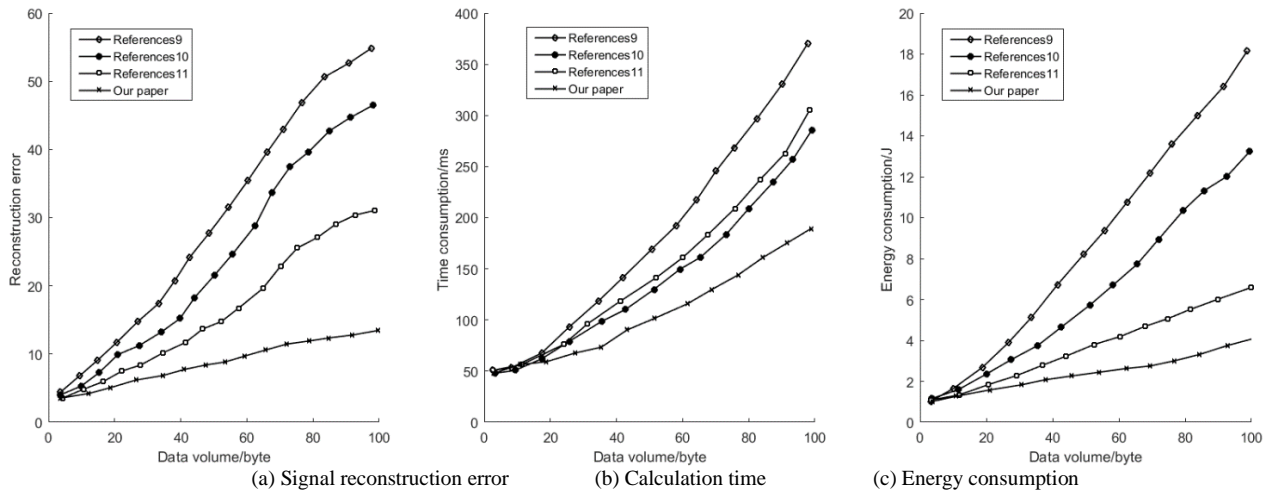


Fig. 10. Comparison of performance indicators of different algorithms.

Fig. 10(a) illustrates that with the increase in data volume, the reconstruction error of different algorithms escalates progressively. The signal reconstruction errors for the distributed optimal wavelet compression algorithm from reference 9, the distributed data compression algorithm from reference 10, and the dynamic retransmission-based compressed sensing algorithm from study [11] are notably higher. In contrast, the method proposed in this paper exhibits a relatively lower reconstruction error and superior stability, which can be attributed to the incorporation of a regularization condition within the iterative process. As observed in Fig. 10(b), when the data volume reaches 100 bytes, the data processing time for the methods described in references [9], [10], and [11] all exceed 250 ms, whereas the processing time for the method introduced in this paper is reduced to only 163 ms, fulfilling the requirements for real-time monitoring and rapid response of transmission lines. According to Fig. 10(c), the energy consumption of the method designed in this paper is significantly reduced to 2.7 J, which is considerably lower than that of the other three algorithms. This indicates a higher energy utilization rate for sensor nodes, which is conducive to

extending the operational lifespan of the transmission line monitoring network and reducing maintenance costs.

VI. CONCLUSION

Focusing on addressing the technical challenges in transmission line monitoring, this paper proposes an innovative wireless sensor network monitoring scheme based on compressed sensing theory. The scheme leverages the combination of compressed sensing technology and orthogonal wavelet transform to achieve sparse representation and efficient compressed sampling transmission of sensor data. By employing the Regularized Orthogonal Matching Pursuit (ROMP) algorithm, the rapid and accurate reconstruction of compressed data is successfully realized. In terms of hardware and software co-design, system architecture suitable for transmission line monitoring is constructed according to the proposed algorithm model. Rigorous experimental validation has demonstrated that the designed monitoring method achieves a high compression ratio of 93.191%, with low signal reconstruction error and superior stability. Moreover, the method features reduced data processing time, meeting the

requirements for real-time monitoring and rapid response. Additionally, by introducing a compressed transmission mechanism at the sink node, the energy consumption of the system operation is significantly reduced, slowing down the rate of energy decay, and effectively prolonging the service life of the wireless sensor network. This scheme holds important practical value and long-term significance for optimizing the energy efficiency management of transmission line monitoring systems and enhancing the system's sustained operational capability.

COMPETING OF INTERESTS

The authors declare no competing of interests.

AUTHORSHIP CONTRIBUTION STATEMENT

Shuling YIN: Writing-Original draft preparation, Conceptualization, Supervision, Project administration.

Renping YU: Formal analysis, Methodology

Longzhi WANG: Software, Validation

DATA AVAILABILITY

On Request

DECLARATIONS

Not applicable

REFERENCES

- [1] Y. Luo, X. Yu, D. Yang, and B. Zhou, "A survey of intelligent transmission line inspection based on unmanned aerial vehicle," *Artif Intell Rev*, vol. 56, no. 1, pp. 173–201, 2023.
- [2] W. Guo et al., "Meteorological Factor Analysis of Ice Coating Galloping of Transmission Line," in *2023 6th Asia Conference on Energy and Electrical Engineering (ACEEE)*, IEEE, 2023, pp. 124–128.
- [3] Z. Wang, J. Wei, B. Tian, W. Zhang, X. Lu, and Y. Luo, "Grid Line Galloping Analysis Using Euler Angle Attitude Estimation Method," in *2023 5th International Conference on Intelligent Control, Measurement and Signal Processing (ICMSP)*, IEEE, 2023, pp. 821–824.
- [4] T. Ishihara and S. Oka, "A numerical study of the aerodynamic characteristics of ice-accreted transmission lines," *Journal of Wind Engineering and Industrial Aerodynamics*, vol. 177, pp. 60–68, 2018.
- [5] Y. Tang, J. Zhao and J. Li, "Vibration detecting for transmission line based on video monitoring," *ICOSM 2020: Optoelectronic Science and Materials*. SPIE, pp. 172-175, 2020.
- [6] L. He, X.Wang, Y.Song, M. Yu and B. Lu "Research and application of transmission line environmental monitoring based on optical fiber sensing technology." *Journal of Physics: Conference Series*. vol. 1607. no. 1. IOP Publishing, 2020.
- [7] A. A.-M. Bulbul, R. H. Jibon, H. Rahaman, S. Biswas, M. B. Hossain, and M. Abdul Awal, "Application of WSN in smart grid: Present and future perspectives," *International Journal of Sensors Wireless Communications and Control*, vol. 11, no. 6, pp. 649–665, 2021.
- [8] Z. Huanan, X. Suping, and W. Jiannan, "Security and application of wireless sensor network," *Procedia Comput Sci*, vol. 183, pp. 486–492, 2021.
- [9] H. Yang, Y.Jia, S. Zhou, "Distributed data compression algorithm based on optimal wavelet transform for wireless sensor networks," *Computer Engineering and Applications*, vol. 45, no. 10, pp. 4–6, 2009.
- [10] F.T. Fute, E. Kamdjou, H.M., and El Amraoui, "A. DDCA-WSN: A Distributed Data Compression and Aggregation Approach for Low Resources Wireless Sensors Networks," *Int J Wireless Inf Networks* 29, pp. 80-92, 2022.
- [11] B. Jiang, G. Huang, F. Li and S. Zhang, "Compressed Sensing With Dynamic Retransmission Algorithm in Lossy Wireless IoT," in *IEEE Access*, vol. 8, pp. 133827-133842, 2020.
- [12] C. Yang, W. Feng, H. Feng, T. Yang, and B. Hu, "A sparsity adaptive subspace pursuit algorithm for compressive sampling," *ACTA ELECTONICA SINICA*, vol. 38, no. 8, p. 1914, 2010.
- [13] P. Wei and F. He, "The compressed sensing of wireless sensor networks based on Internet of Things," *IEEE Sens J*, vol. 21, no. 22, pp. 25267–25273, 2021.
- [14] M. R. Ghaderi, V. Tabataba Vakili, and M. Sheikhan, "Compressive sensing-based energy consumption model for data gathering techniques in wireless sensor networks," *Telecommun Syst*, vol. 77, pp. 83–108, 2021.
- [15] X. Jiang, N. Li, Y. Guo, J. Liu, and C. Wang, "Sensing matrix optimization for multi-target localization using compressed sensing in wireless sensor network," *China Communications*, vol. 19, no. 3, pp. 230–244, 2022.
- [16] L. Jianqi, Z. Zhe, Z. Chuanyuan, Y. Bin, and H. Biyao, "A code scheme for g3-plc physical layer specification based on turbo code," in *2021 2nd Information Communication Technologies Conference (ICTC)*, IEEE, 2021, pp. 11–15.
- [17] Z. Zhou, F. Liu, and H. Shen, "IEF-CSNET: Information Enhancement and Fusion Network for Compressed Sensing Reconstruction," *Sensors*, vol. 23, no. 4, p. 1886, 2023.
- [18] W. Zhuang, C. Qi, and J. Wang, "Dynamic ice process estimation model of transmission line based on micrometeorological monitoring," *Power System Protection and Control*, vol. 47, no. 14, pp. 87–94, 2019.
- [19] I. Hababeh, I. Khalil, R. Al-Sayyed, M. Moshref, S. Nofal, and A. Rodan, "Competent Time Synchronization Mac Protocols to Attain High Performance of Wireless Sensor Networks for Secure Communication," *Cybernetics and Information Technologies*, vol. 23, no. 1, pp. 75–93, 2023.

Implementation of Cosine Similarity Algorithm on Omnibus Law Drafting

Aristoteles*, Muhammad Umaruddin Syam, Tristiyanto, Bambang Hermanto

Department of Computer Science, Faculty of Mathematics and Natural Sciences, Lampung University, Indonesia

Abstract—Drafting of Omnibus Laws presents a complex challenge in legal governance, often involving the integration and consolidation of disparate legal provisions into a unified framework. In this context, the application of advanced computational techniques becomes crucial for streamlining the drafting process and ensuring coherence across the law's various components. Cosine similarity, a widely used measure in natural language processing and document analysis, offers a quantitative means to assess the similarity between different sections or articles within the Omnibus Law draft. By representing legal texts as high-dimensional vectors in a vector space model, cosine similarity enables the comparison of textual similarity based on the cosine of the angle between these vectors. Implementing cosine similarity in the context of omnibus law using FastAPI and Laravel can be a valuable tool for analyzing similarity between legal documents, especially in the context of omnibus law. Legal practitioners and researchers can use the cosine similarity measure to compare the textual content of different legal documents and identify similarities. This can aid in tasks such as legal document retrieval, clustering similar provisions, and detecting potential inconsistencies. The combination of FastAPI and Laravel provides a potent and efficient way to develop and deploy this functionality, contributing to the advancement of legal informatics and analysis. The dataset used is Undang-Undang (UU) which used Bahasa from 1945 to 2022, comprising a total of 1705 UU. The implemented cosine similarity yielded a recall rate of 90.10% on the law.

Keywords—Cosine similarity; FastAPI; Laravel; Omnibus Law

I. INTRODUCTION

Indonesia is a country of law with numerous regulations. President Jokowi has acknowledged that there are too many regulations in Indonesia and that it is not ideal for the country to be known as a 'country of regulations'. President Jokowi has acknowledged that there are too many regulations in Indonesia and that it is not ideal for the country to be known as a 'country of regulations' [1]. According to the website peraturan.go.id, as of May 19, 2022, Indonesia has 50,538 regulations. When considering the median growth for the top five hierarchies outlined in Article 7, Paragraph 1 of Undang-Undang (UU) Number 12 of 2011, the Constitution has a median of 0, the MPR Tap has a median of 0, the UU has a median of 16, the PP has a median of 55, and the Perpres has a median of 0. Regulations are implemented to organize and regulate people's lives within a nation or state. The large number of regulations can have a negative impact, which is grouped into four categories: (1) Regulatory conflict, which occurs when some regulations or articles conflict with existing regulations, (2) Inconsistent regulatory consistency, which occurs when there are inconsistent regulations or provisions in one legislation and

its derivatives, (3) Diverse regulatory interpretations, which occurs when the objectives and subjects of regulation are unclear. This results in unclear language that is difficult to understand and an inappropriate system. Additionally, there may be non-operational regulations, which are regulations that are inconsistent with one law and its derivatives or have no effect, but are still valid or lack enforcement regulations [2].

The government aims to reduce the growth of regulations, particularly UU, by simplifying or shortening them. This is achieved through the implementation of the omnibus law approach, which is an appropriate way to develop a legal framework for licensing Indonesia's business processes. This method allows the creation of regulations that cover several substantive materials or several smaller ones in one rule, promoting order, legal certainty, and expediency [3]. The omnibus law is a method or concept of rule-making that aims to solve problems related to licensing by creating a new UU that revises articles in several existing UU [4].

According to Article 64 paragraph 1b of UU No. 13 of 2022, one of the omnibus methods is to revoke laws and regulations of the same type and hierarchy. To avoid overlap between rules, legal drafters must identify the source of the revoked rules. This requires an understanding of similar regulations and their hierarchy. A database of UU, including articles and paragraphs, can aid legal drafters. Additionally, it is important to check for similarities between norms and UU to minimize language differences.

Algorithms that can be used to check for similarity include cosine similarity. Cosine similarity measures vector similarity by calculating the angle between them [5]. Calculating similarity using two angles has the advantage of being language-independent. It can be used even when no corpus is available. Unfortunately, cosine similarity is not sensitive to differences in size, which means that two patterns with very different attribute values can have high similarity scores [5]. Using Term Frequency and Inverse Document Frequency (TF-IDF) can solve the problem of cosine similarity, which is insensitive to vector magnitude [6].

Cosine similarity is a technique used in legal document retrieval to assess the similarity of several legal documents. To guarantee that cases with comparable circumstances are handled uniformly in each instance, it is employed to obtain previous case records of a particular case [7]. It has been demonstrated through experimentation that cosine similarity and the doc2vec approach may automatically obtain court rulings of comparable legal issues [8]. When it comes to legal aid, cosine similarity is used to compare legal document

*Corresponding Author.

embeddings, which are texts represented in a semantic vector space [9]. Cosine similarity is another method that uses unsupervised learning techniques like Word2Vec CBoW, Word2Vec Skip-gram, and TF-IDF to determine how similar court documents are to one another [10]. Cosine similarity is employed to group lawful [11].

This research aims to confidently assist lawmakers and legal writers in thoroughly searching for keywords (norms) in UU using Bahasa and implementing them in lawmaking with the aid of a search engine, this approach will significantly save time in understanding each existing law.

II. METHODS

The research was conducted using the waterfall model, one of the software development models. Waterfall model is divided into four stages, namely analysis, design, implementation and testing. Fig. 1 illustrates the research design using the waterfall model.

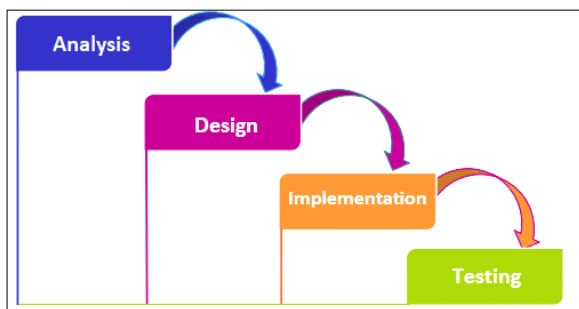


Fig. 1. Research design.

A. Analysis Phase

The analysis stage, also known as software requirements specification (SRS), is a thorough and comprehensive description of the software to be developed. Analysis includes system and business analysis to define both functional and non-functional requirements. The task for the analysis stage is to identify functional and data requirements for the software. Requirements gathering can be done by conducting observations, interviews, and document analysis. Function and data requirements that are complete can facilitate the next stage in the waterfall model. Raw data collection is transformed or pre-processed into mature, processable data. Preprocessing is the stage of converting data into a form that can be understood by machines [12]. Preprocessing aims to standardize data to facilitate processing [13]. This process involves four steps.

1) *Case folding*: Case folding is the process of equalizing cases in a document [14]. Phase of case folding aims to make all characters in the law lower case, remove numbers, remove punctuation marks, and remove spaces.

2) *Tokenizing*: Tokenization is the process of dividing a document into smaller parts, known as tokens [14].

3) *Filtering*: Filtering involves removing words deemed unnecessary or unimportant, based on stop words [15].

4) *Stemming*: Stemming is the process of removing all of the affixes and suffixes from the words, and this process is used to filter the results [9].

B. Design Phase

The design stage involves planning and problem-solving for a software solution. It requires the software developer to define the plan of the solution, including algorithm design, software architecture design, database conceptual schema and logic diagram design, concept design, graphical interface, and data structure definition.

Algorithm and architecture design can be aided by image processing software such as Paint, Adobe Photoshop, or Corel Draw. Conceptual schemes and data structure definitions can be created using ERD diagrams or other charting software. For interface design, Balsamiq or Figma can be used.

C. Implementation Phase

The implementation stage is when business requirements and design specifications are transformed into executable programs, databases, websites, or software components through programming. During the implementation phase, real code is written and compiled into a working application where the database and text have been created; in other words, the implementation phase is the process of converting all the requirements and blue ink into a production environment.

The research implementation utilizes information systems to enhance user comprehension. Information systems are organizational systems that summarize management functions and daily transaction processing requirements. These systems support the strategic activities of the organization in order to provide certain external parties with the information needed to facilitate decision making [16]. The information system is referred to as Omnibus Law Information System for the purpose of this research. The architecture is structured using FastAPI, Laravel, and MariaDB. FastAPI was chosen due to its superior performance compared to NodeJS and Go [17].

D. Testing Phase

The testing phase is commonly referred to as verification and validation. Verification is the process of verifying that the software meets the requirements and specifications to achieve the goals of software development. The purpose of verification is to evaluate the software to determine whether the product of the development phase meets the conditions imposed at the beginning of the stages of the waterfall model. Validation is the process of evaluating software during or at the end of the development process to determine if it meets the specified requirements.

III. RESULT AND DISCUSSION

The results include the research process on the case study that is the Omnibus Law and the data which are the UU. The Discussion includes the implementation process of each research methodology in the research, which consists of analysis, design, implementation, and testing.

A. Research Results

The Omnibus Law is a means of reducing the number of laws in Indonesia, which is considered an effective way to consolidate numerous regulations into a single unit [18]. Another potential benefit of the Omnibus Law is the ability to modify laws that have overlapping or other issues. However,

the challenge of the Omnibus Law is to modify the content without creating problems such as overlap or multiple interpretations. This study aimed to address the challenge of identifying similarities between legal content and the normative vocabulary to be established.

This research utilizes cosine similarity through the Python programming language and the FastAPI framework as the backend for calculations. The frontend uses the Laravel framework with PHP as the primary language. The FastAPI framework is employed to implement the cosine similarity model, and the final result is the API requested by the Laravel framework.

B. Discussion

The discussion is structured according to the research design presented in Fig. 1. The research process begins with the analysis stage, followed by the design, implementation, and testing stages.

1) *Analysis phase:* The author designs the function and data requirements based on the analysis and observation of the Law. The following are the function and data requirements.

a) *Function requirements:* Functional requirements define the software's necessary functions. The intended user is a legal drafter or lawmaker.

- Users can calculate the similarity of the vocabulary (norms) with the law as a whole.
- Users can perform vocabulary (norm) search on any article of the law.
- Users can see the highlight of the vocabulary (norm) in each article.
- Users can select the article to be printed in pdf or docx.

b) *Data requirements:* The study's data requirements are focused on preprocessed UU data. Preprocessing is accomplished using regular expressions and natural language toolkits (NLTK) in the Python programming language. The preprocessing process generated 60,186 data points, which is 15,595 fewer than the extraction process.

2) *Design phase:* The design stage is the implementation phase of the analysis stage. The draft module development design phase includes algorithm design, use case diagram, and user interface design.

a) *Algorithm design:* The drafting module was developed using the cosine similarity algorithm to calculate the distance between two angles. Converting words into vectors is essential for accurately measuring the distance between two vectors projected onto the X and Y axes. The angle is obtained from the TF-IDF results formula can be seen at Eq. (1) and Eq. (2), which are calculated using the cosine similarity formula [19]. The cosine similarity, as a method of measuring the similarity between the documents, varies between positive values from 0 to 1 [20]. Two texts are virtually identical, as evidenced by a cosine similarity close to 1, indicating a small angle between them. Cosine similarity method enables us to identify similarities between vectors as

long as these words are present in the document. The formula can be seen in Eq. (3) and an overview of the cosine similarity algorithm process is described in Fig. 2.

$$idf_i \tag{1}$$

$$w_{i,j} = tf_{i,j} \times idf_i \tag{2}$$

$$cos(A, B) = \frac{A \cdot B}{|A||B|} = \frac{\sum_{i=1}^n A_i \times B_i}{\sqrt{\sum_{i=1}^n (A_i)^2} \times \sqrt{\sum_{i=1}^n (B_i)^2}} \tag{3}$$

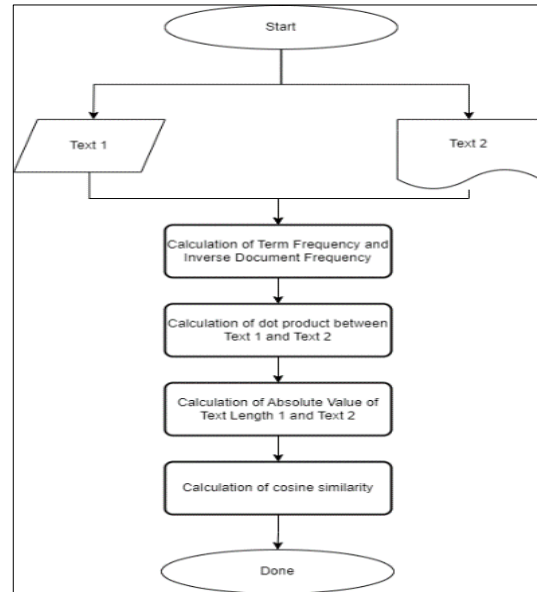


Fig. 2. Cosine similarity process.

b) *Use case diagram:* The Use Case diagram is a design tool used to address business problems in research. Fig. 3 displays the Use Case Diagram for the drafting module in the Omnibus Law Information System.

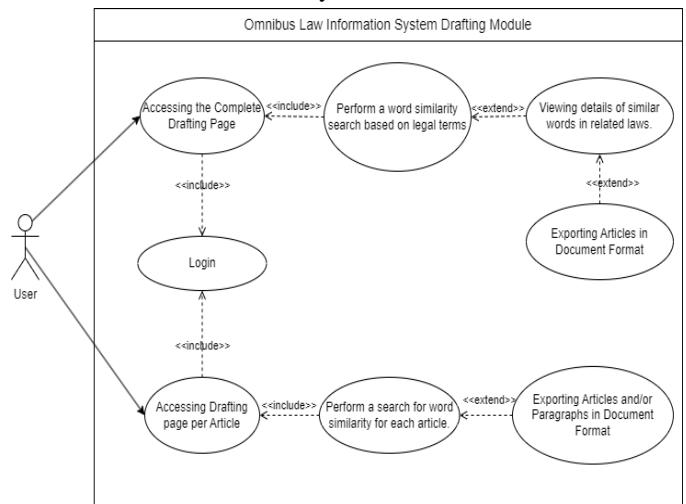


Fig. 3. Use case diagram of the drafting module of the omnibus law information system.

Legal drafters are the users of the Omnibus Law Information System. Explanation of Fig. 3 regarding use of use cases can be shown in Table I.

TABLE I. DESCRIPTION OF USE CASE DIAGRAM

| Actor | Use Case | Description |
|-------|---|---|
| User | Accessing the complete drafting page | User can view the full design page |
| | Perform a word similarity search base on legal terms | Users can search for similarities between words based on legal terms. |
| | Viewing details of similar word in related laws. | Users can view details of word similarities in related laws. |
| | Exporting articles in document format | Users can export articles in document format |
| | Accessing drafting page per article | Users can view the draft page per article |
| | Perform a search for word similarity for each article | Users can search for word similarities per article |
| | Exporting articles and/or paragraphs in document format | Users can export articles and/or paragraphs in document format |

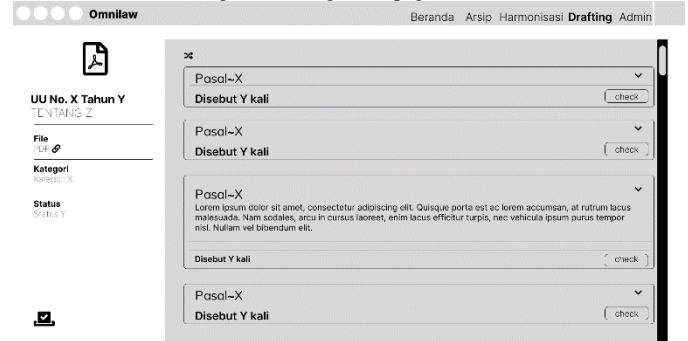
c) *User interface design:* User interface design is carried out as a reference for system display design. Fig. 4 shows the display design consists of five display pages that follow the design of each display.

3) *Implementation phase:* The implementation phase is the phase in which the results of the analysis and design are applied. This stage involves implementing algorithm, activity diagram and user interface design.

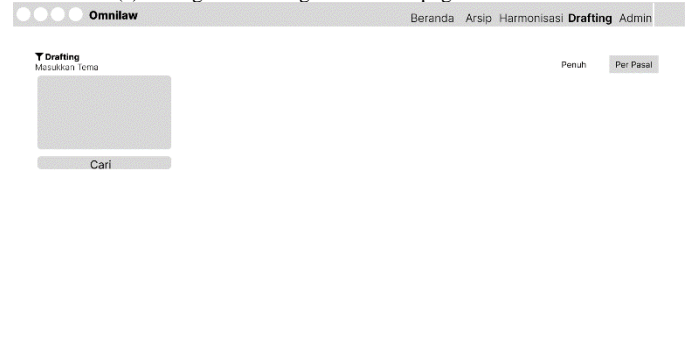
a) *Algorithm:* Cosine similarity is the algorithm used in the development of the Drafting module. Cosine similarity uses the cosine as the basis for calculation, which means that if this means that if two words or documents have a calculation result with an angle of 0 degrees, they have 100% similarity. FastAPI is used to implement the algorithm. Construction of FastAPI uses standards from OpenAPI known as Swagger and JSON Schema [21]. Interactive documentation can be used to test the response of any feature provided by Swagger UI. Fig. 5 shows the documentation page provided by Swagger UI.



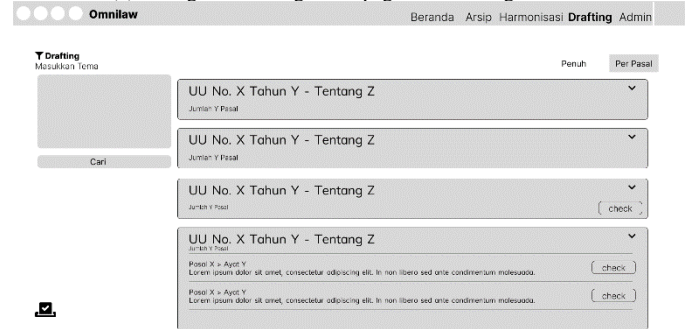
(b) Design of drafting result page based on UU.



(c) Design of drafting result detail page based on UU.



(d) Design of drafting home page based on legal terms.



(e) Design of drafting result page based on legal terms.

Fig. 4. User interface design (a) Drafting home page base on UU (b) Result drafting page based on UU (c) Result detail page base on UU (d) Drafting home page on legal terms (e) Design of drafting result page based on legal terms.

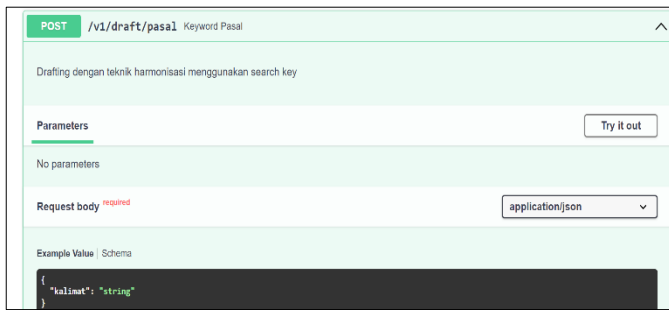
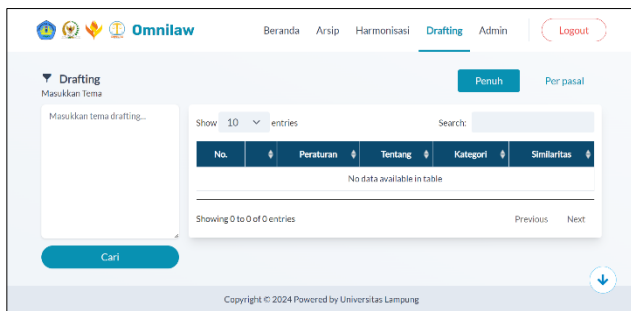


Fig. 5. Swagger UI documentation.

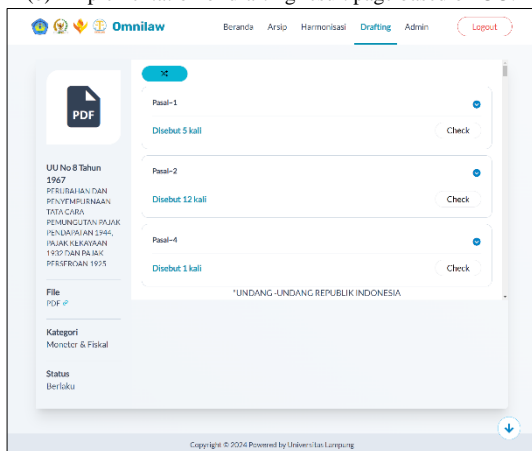
b) *Laravel*: Laravel is a PHP framework used as a front end that adheres to the Model - View - Controller (MVC) concept [22]. The functions included in Laravel are the implementation of use cases, activity diagrams and user interfaces. There are seven use cases implemented with Laravel as shown in Fig. 6.



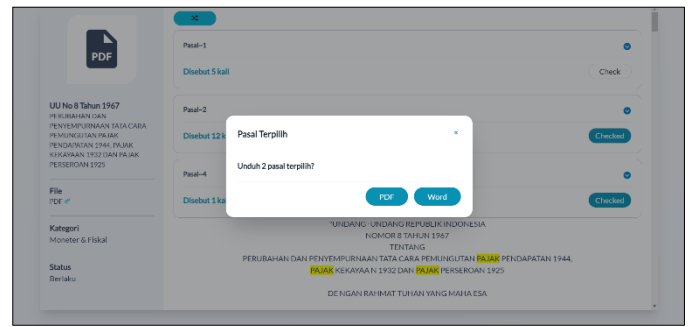
(a) Implementation of drafting home page based on UU.



(b) Implementation of drafting result page based on UU.



(c) Implementation of drafting result detail based on UU.



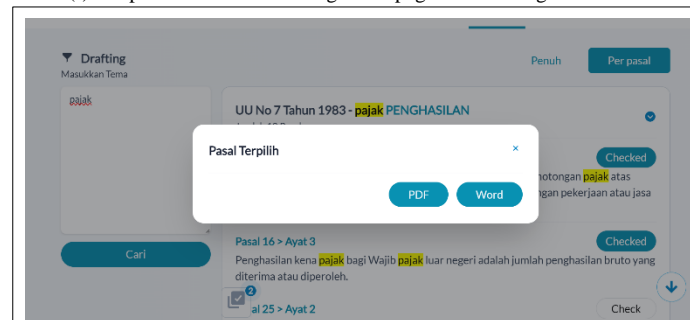
(d) Implementation of exporting result in document format based on UU.



(e) Implementation of drafting home page based on legal terms.



(f) Implementation of drafting result page based on legal terms.



(g) Implementation of exporting result in document format based on legal terms.

Fig. 6. Implementation of (a) Drafting home page based on UU (b) Drafting result page based on UU (c) Drafting result detail based on UU (d) Exporting result based on UU (e) Drafting home page based on legal terms (f) Drafting result page based on legal terms (g) Exporting result in based on legal terms.

c) *Information systems architecture*: The Omnibus Law information system architecture uses a full stack architecture. Full stack architecture divides an information system into two parts, namely the front-end or user display and the back-end or screen behind the process. Fig. 7 shows the omnibus law information system architecture.

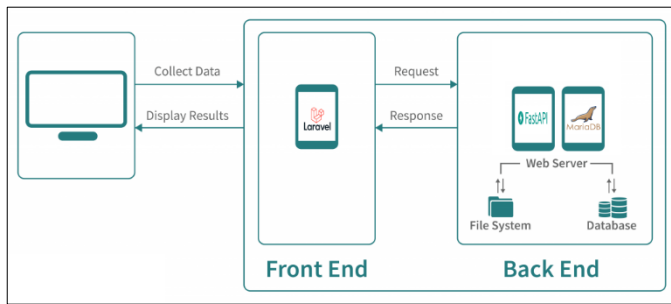


Fig. 7. Information system architecture.

4) *Testing phase*: Testing is the stage of validation and verification of each function included in the information system to ensure that it works correctly. Testing the algorithm using the confusion matrix. Confusion Matrix is used to see the predictive ability of the algorithm. Confusion matrix is a predictive analysis tool that compares actual values with predicted model values [23]. From the results of the confusion matrix calculation performed, a recall of 90.10%, accuracy of 56%, precision of 30% and F1 score of 45% was obtained.

IV. CONCLUSION

Based on the results of research on the implementation of cosine similarity in the Omnibus Law Information System, the authors draw the following conclusions: (1) The degree of similarity between keywords for drafting laws and existing laws can be measured using the cosine similarity algorithm and TF-IDF, with recall 90.10%. (2) Implementation of the similarity model between keywords and existing UU so that it can be used by users (legal drafters) using FastAPI as a back-end and Laravel as a front-end, so that it speeds up user work in seeing the similarity between keywords and existing UU.

For future works, Inclusion of datasets containing regulations with a different hierarchy from UU, such as Perpres and others, would be more beneficial for lawmakers. This would aid in determining which parts are attached to the new laws, without causing any overlap in Indonesian regulations.

REFERENCES

- [1] W. Setiadi, "Simplifikasi Regulasi dengan Menggunakan Metode Pendekatan Omnibus Law," *J. Rechts Vinding Media Pemb. Huk. Nas.*, vol. 9, no. 1, p. 39, 2020.
- [2] D. Sadiawati, *Strategi Nasional Reformasi Regulasi: Mewujudkan Regulasi yang Tertib dan Sederhana*. Jakarta: Kementerian Perencanaan dan Pembangunan Nasional/ Bappenas, 2015.
- [3] I. Mayasari, "Kebijakan Reformasi Regulasi Melalui Implementasi Omnibus Law Di Indonesia," *Ima Mayasari*, vol. 9, no. 1, 2020.
- [4] M. Azhar, "Omnibus Law sebagai Solusi Hiperregulasi Menuju Sonkronisasi Peraturan Per-Undang-undangan di Indonesia," *Adm. Law Gov. J.*, vol. 2, no. 1, pp. 170–178, 2019, doi: 10.14710/ihis.v%vi%i.6671.
- [5] P. Xia, L. Zhang, and F. Li, "Learning similarity with cosine similarity ensemble," *Inf. Sci. (Ny.)*, vol. 307, pp. 39–52, 2015, doi: 10.1016/j.ins.2015.02.024.
- [6] A. R. Lahitani, A. E. Permasari, and N. A. Setiawan, "Cosine

- similarity to determine similarity measure: Study case in online essay assessment," *Proc. 2016 4th Int. Conf. Cyber IT Serv. Manag. CITSM 2016*, 2016, doi: 10.1109/CITSM.2016.7577578.
- [7] D. Thenmozhi, K. Kannan, and C. Aravindan, "A Text Similarity Approach for Precedence Retrieval from Legal Documents," *CEUR Workshop Proc.*, vol. 2036, no. December, pp. 90–91, 2017, [Online]. Available: <https://ceur-ws.org/Vol-2036/T3-9.pdf>
- [8] T. Novotná, "Document Similarity of Czech Supreme Court Decisions," *Masaryk Univ. J. Law Technol.*, vol. 14, no. 1, pp. 105–122, 2020, doi: 10.5817/MUJLT2020-1-5.
- [9] S. Renjit and S. M. Idicula, "CUSAT NLP@AILA-FIRE2019: Similarity in legal texts using document level embeddings," *CEUR Workshop Proc.*, vol. 2517, no. December, pp. 25–30, 2019.
- [10] N. Tang and A. Engelbrecht, *Data Clustering*. London: Intech, 2022. [Online]. Available: <http://dx.doi.org/10.1039/C7RA00172J%0Ahttps://www.intechopen.com/books/advanced-biometric-technologies/liveness-detection-in-biometrics%0Ahttp://dx.doi.org/10.1016/j.colsurfa.2011.12.014>
- [11] B. K. Triwijoyo and K. Kartarina, "Analysis of Document Clustering based on Cosine Similarity and K-Main Algorithms," *J. Inf. Syst. Informatics*, vol. 1, no. 2, pp. 164–177, 2019, doi: 10.33557/journalisi.v1i2.18.
- [12] F. R. Lumbanraja, R. E. Pramswary, and Aristoteles, "Classification of Cracked Concrete Images Using Convolutional Neural Algorithm," *AIP Conf. Proc.*, vol. 2563, no. October, 2022, doi: 10.1063/5.0103114.
- [13] M. Silvi Lydia, S. Dara Fadillah, and M. Huda, "Perbandingan Metode Klaster dan Preprocessing Untuk Dokumen Berbahasa Indonesia," *pdfs.semanticscholar.org*, 2018, doi: 10.17529/jre.v14i1.9027.
- [14] D. Alita and A. Rahman, "Pendeteksian Sarkasme pada Proses Analisis Sentimen Menggunakan Random Forest Classifier," *jurnal.fmipa.unila.ac.id*, vol. 8, 2020, Accessed: May 27, 2022. [Online]. Available: <https://jurnal.fmipa.unila.ac.id/komputasi/article/view/2615>
- [15] L. Hermawan, M. B. Ismiati, J. Bangau, N. 60, and M. Charitas, "Pembelajaran text preprocessing berbasis simulator untuk mata kuliah information retrieval," *156.67.218.228*, vol. 17, no. 2, pp. 188–199, 2020, Accessed: May 27, 2022. [Online]. Available: <https://156.67.218.228/index.php/transformatika/article/view/1705>
- [16] E. Y. Anggraeni and R. Irviani, *Pengantar Sistem Informasi*, 1st ed. Yogyakarta: CV. Andi Offset, 2017. Accessed: May 24, 2022. [Online]. Available: <https://books.google.co.id/books?id=8VNLdWAAQBAJ>
- [17] C. Samuel Rajiv and P. K., "A Platform to Help in Generating Code for Machine Learning and Data Science Projects," *SSRN Electron. J.*, Feb. 2022, doi: 10.2139/ssrn.4033072.
- [18] Rudy, Aristoteles, and R. C. Kurniawan, *Model Omnilar: Solusi Pemecahan Masalah Penyederhanaan Legislasi dalam Rangka Pembangunan Hukum*. Bandarlampung: Pusaka Media, 2021.
- [19] P. K. Hima Pandalu, "Pencarian dan Perankinan Obat Tradisional Berdasarkan Gejala Penyakit Menggunakan Metode Cosine Similarity," *Universitas Islam Negeri Maulana Malik Ibrahim Malang*, 2014.
- [20] Y. Januzaj and A. Luma, "Cosine Similarity – A Computing Approach to Match Similarity Between Higher Education Programs and Job Market Demands Based on Maximum Number of Common Words," *Int. J. Emerg. Technol. Learn.*, vol. 17, no. 12, pp. 258–268, 2022, doi: 10.3991/ijet.v17i12.30375.
- [21] M. Malhotra, "Internship Report At Paxcom India Pvt. Ltd.," *Himachal Pradesh*, 2022.
- [22] S. Dwiyatno, E. Rachmat, A. P. Sari, and O. Gustiawan, "Implementasi Virtualisasi Server Berbasis Docker Container," *PROSISKO J. Pengemb. Ris. dan Obs. Sist. Komput.*, vol. 7, no. 2, pp. 165–175, 2020, doi: 10.30656/prosisko.v7i2.2520.
- [23] Aristoteles, A. Syarif, Sutyarso, F. R. Lumbanraja, and A. Hidayatullah, "Identification of Human Sperm based on Morphology Using the You Only Look Once Version 4 Algorithm," *Int. J. Adv. Comput. Sci. Appl.*, vol. 13, no. 7, pp. 424–431, 2022, doi: 10.14569/IJACSA.2022.0130752.

Enhancing Particle Swarm Optimization Performance Through CUDA and Tree Reduction Algorithm

Hussein Younis, Mujahed Eleyat

Department of Computer Systems Engineering, Arab American University, Palestine

Abstract—In this paper, we present an enhancement for Particle Swarm Optimization performance by utilizing CUDA and a Tree Reduction Algorithm. PSO is a widely used metaheuristic algorithm that has been adapted into a CUDA version known as CPSO. The tree reduction algorithm is employed to efficiently compute the global best position. To evaluate our approach, we compared the speedup achieved by our CUDA version against the standard version of PSO, observing a maximum speedup of 37x. Additionally, we identified a linear relationship between the size of swarm particles and execution time; as the number of particles increases, so does computational load – highlighting the efficiency of parallel implementations in reducing execution time. Our proposed parallel PSOs have demonstrated significant reductions in execution time along with improvements in convergence speed and local optimization performance - particularly beneficial for solving large-scale problems with high computational loads.

Keywords—Particle swarm optimization; tree reduction algorithm; parallel implementations; CUDA; GPU

I. INTRODUCTION

Optimization techniques are crucial in various domains for finding optimal solutions to complex problems. However, Particle Swarm Optimization, a widely used metaheuristic algorithm, has demonstrated limitations in terms of convergence speed and local optimization performance [1] [2]. As a result, researchers have turned to parallel computing techniques like Compute Unified Device Architecture (CUDA) a parallel computing platform and application programming interface (API) developed by NVIDIA, to enhance the performance of PSO by implementing it on a parallel architecture. Significant reductions in computing time compared to traditional implementations using different programming languages have been observed by researchers.

In the field of parallel computing, practitioners often employ various techniques to break down a computational task into smaller subtasks that can be executed simultaneously on multiple processors. These subtasks, commonly known as threads, are vital in this approach and are managed for execution by an operating system. CUDA supports shared memory parallel programming, which enables multiple processors or cores to access a shared memory space efficiently [3].

The integration of CUDA technology plays a pivotal role in enabling the seamless implementation of Particle Swarm Optimization (PSO) within a parallel architecture. This cutting-edge approach harnesses the power of GPUs to efficiently distribute workloads into smaller tasks, allowing for concurrent

processing on the Graphics Processing Units. By utilizing CUDA for the parallel execution of PSO on GPUs, computational tasks benefit from enhanced efficiency and performance through the utilization of parallel processing capabilities, ultimately leading to accelerated computations and improved results in various applications such as optimization, machine learning, and scientific simulations [4].

This parallel method empowers each particle to autonomously execute a designated number of iterations before resynchronization occurs. Many researchers have successfully implemented PSO algorithms using CUDA for GPUs, and the outcomes from these endeavors unequivocally indicate that parallelization significantly enhances the performance capabilities of PSO [5].

This paper produces a CUDA version of the PSO algorithm called (CPSO). The tree reduction algorithm and the CUDA shared memory were used in CPSO to reduce the comparison operations to half and reduce the amount of time spent accessing global memory. The contributions of this work are summarized as follows:

- 1) Propose a CUDA version of the PSO algorithm.
- 2) Enhance the CUDA implementation of the PSO algorithm using the tree reduction algorithm and the CUDA shared memory.
- 3) Compare the proposed algorithms in terms of execution time and speedup to demonstrate the effectiveness and efficiency of our proposed algorithm.

The structure of this paper is outlined as follows: Section II presents the background information, Section III discusses related work, Section IV details the implementation of PSO algorithms, Section V outlines the experimental setup, Section VI presents the results and discussions, and Section VII provides the conclusions and suggestions for future work.

II. BACKGROUND

A. Graphics Processing Unit

The Graphics Processing Unit (GPU) was initially developed in the 1970s as an electronic circuit for displaying vector graphics [6]. Over the years, the GPU has undergone significant development and has evolved into a highly parallel processor capable of performing complex computations, providing significant performance boosts for graphics-intensive applications [7]. One of the main advantages of the GPU is its ability to provide higher instruction throughput and memory bandwidth than the Central Processing Unit (CPU) within the same power envelope. Unlike the CPU which is designed to

execute threads as fast as possible and execute only a few threads in parallel depending on the number of cores, the GPU is designed to execute thousands of sequences of operations, called “threads,” in parallel up to 1024 threads per block limit of the GPU [8]. The main architecture of the CPU and GPU is illustrated in Fig. 1, where the CPU (host) and GPU (device) work together and communicate via a PCI-express bus [9].

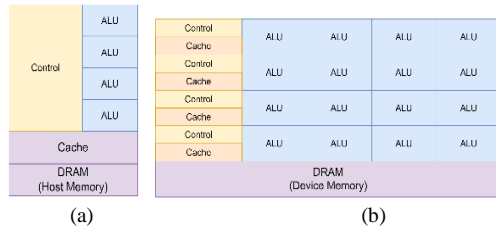


Fig. 1. The architecture of (a) CPU; and (b) GPU.

B. Compute Unified Device Architecture

NVIDIA, a leading player in the field of visual computing and parallel processing, introduced the CUDA in 2007 as a parallel platform programming model [10]. CUDA provides a set of tools that enable the development of high-performance applications to be executed on GPUs. Typically, a CUDA program consists of two parts: the first part is executed on the host CPU, while the second part is executed on the device GPU, with the result being returned to the host CPU [11]. As shown in Fig. 2, the CUDA programming architecture consists of N number of grids which depends on the limitations of the GPU hardware. Each grid is composed of blocks, and each block contains multiple threads that can be executed concurrently. The thread blocks are organized into 1D, 2D, or 3D arrays of threads [12].

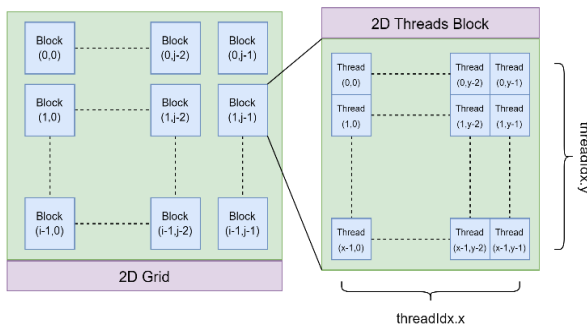


Fig. 2. CUDA 2D grid and thread block indexes presentation.

Each thread within a block has a specific index that is used to identify its location during the execution of the CUDA function, known as the 'kernel' function. The thread index for a 1D dimension is calculated using the following equation [13]:

$$thread\ index = (blockIdx.x \times blockDim.x) + threadIdx.x \quad (1)$$

Here, *blockIdx.x* represents the x-dimension identifier of the thread block, *blockDim.x* represents the x-dimension of the thread block, and *threadIdx.x* represents the x-dimension identifier of the thread.

In GPUs, threads can be executed together in parallel in groups called "warps" which consist of 32 or 64 threads depending on the GPU architecture [14]. Within each warp, the threads execute the same instruction at the same time, a concept known as Single Instruction Multiple Threads (SIMT) which minimizes the amount of branching and divergence between threads which can result in performance penalties [15]. Each CUDA thread possesses its private local memory and can access data from multiple memory spaces. Furthermore, each block has shared memory that can be accessed by its threads or by other thread blocks as illustrated in Fig. 3. Local memory offers the fastest memory access speed for each thread, followed by shared memory. Global, static, and texture memory speeds are relatively slower [15].

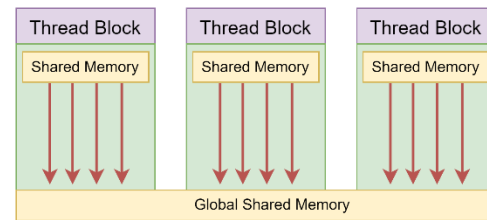


Fig. 3. Memory hierarchy in GPUs.

CUDA provides a function called “*cudaMallocManaged*” for unified memory management between CPU and GPU without explicit data transfers. It acts like a single memory space that can be accessed by both CPU and GPU. The overhead of explicit data transfer between CPU and GPU is reduced which improves the overall performance by providing a unified memory space [16]. Also, CUDA provides a function called “*cudaMemPrefetchAsync*” to prefetch data from the host or device memory to the device cache before it is needed. The main advantage of “*cudaMemPrefetchAsync*” is that data movement operation is performed asynchronously, optimizing memory access patterns and reducing data transfer latency in CUDA applications [17], [18]. Typically, a GPU program consists of one or more kernels which are collections of tasks executed sequentially by GPUs. These kernels are composed of blocks, separate groupings of Arithmetic Logic Units (ALUs). Each block contains multiple threads, representing various levels of computation. Usually, the threads within a block collaborate to calculate a specific value. It is important to note that threads within the same block can share memory, enabling efficient data interchange. In the context of CUDA, the most common computation involves transferring data from the CPU to the GPU [19]. The main steps of the CUDA program flow, as depicted in Fig. 4, are: the data is loaded into the host CPU memory and then transferred to the GPU memory using a function called “*cudaMemcpy*”. Subsequently, the kernel is launched on the GPU using the syntax “*kernel<<<numBlocks, threadsPerBlock>>>*” [14]. The “<<<>>>” notation is employed to configure the execution of the kernel by specifying the number of thread blocks and the number of threads per block [20].

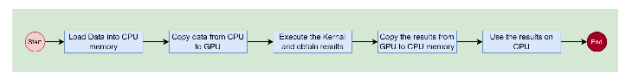


Fig. 4. GPU program workflow.

III. RELATED WORK

PSO has been applied and extended in various studies. In this context, several works have focused on optimizing the performance of PSO algorithms, particularly by leveraging parallel computing techniques.

In study [21] the authors provide an overview of the PPSO algorithm which is commonly used in complex optimization problems requiring significant computational power. They discuss different parallelization options for PPSO, including programming languages and communication topologies. Also, they cover various models of parallelization, implementation, and uses of PPSO algorithms, making them a valuable resource for researchers and developers working with PPSO and other parallel optimization algorithms.

In study [22] the authors propose a novel algorithm called "cuPSO" that reduces the computation time of PSO-based algorithms with massive threads on GPUs. The proposed algorithm addresses excessive memory accesses and thread synchronization overheads faced by traditional reduction-based methods through the use of atomic functions. Experimental results show that cuPSO achieves over 200x speedups compared to the serial version running on the CPU and outperforms the state-of-the-art method by a factor of 2.2 in terms of computation time. Similarly, the authors focus on optimizing particle systems using CUDA-assisted multithreading. They aim to improve the performance of particle systems by enhancing a CUDA particle demo developed by Nvidia using a Python script. The experimental results in their work demonstrate the achievement of desired performance levels by adjusting the number of particles, grid size, and grid orientation. It also presents hypotheses regarding the impact of changing these parameters on processing time and provides experimental results to support these hypotheses [23]. Furthermore, another work introduces a new approach to running standard particle swarm optimization (SPSO) by utilizing GPU's parallel computing capability and NVIDIA's CUDA software platform. Experiments were conducted to optimize benchmark test functions using both GPU-SPSO and CPU-SPSO, results show that GPU-SPSO significantly reduces running time compared to CPU-SPSO more than 11 times faster than CPU-SPSO, especially for large swarm population applications and high dimensional problems [24].

The authors explore and evaluate two different ways of utilizing GPU parallelism in the implementation of particle swarm optimization (PSO) on graphics processing units (GPUs). The execution speed of these two parallel algorithms is compared with a standard sequential implementation of PSO, known as SPSO. The study also includes a comprehensive analysis of the computation efficiency of the parallel algorithms, considering speed-up and scale-up with SPSO. Also, the authors investigate the extent to which PSO can benefit from a parallel implementation using CUDA. The design of the two parallel versions of PSO considered in this study was influenced by the structure of CUDA and compatible GPUs. Additionally, the practical implications of the parallel algorithms resulted in two possible solutions that differentiate the potential use of each version [5].

Finally, another work introduces a parallel implementation of Cooperative Particle Swarm Optimization (CPSO) using CUDA. The work includes a comparison between CPSO implemented in C and C-CUDA, and tests were conducted on standard benchmark optimization functions. The results showed improvements in speed and convergence time, with CUDA's randomizing procedures contributing to better solutions. The paper emphasizes the utility of CUDA for complex and computationally intensive applications [25].

IV. PSO ALGORITHMS IMPLEMENTATION

In general, the choice of data structure in the PSO algorithm is crucial for effectively representing and manipulating particles within the swarm. The main data structure used in proposed PSO algorithms is the Particle structure as illustrated in Fig. 5(a), which encapsulates the necessary information for each particle. This structure typically includes components such as the current position, best position, velocity, and best value. The current position represents the particle's location in the search space, while the best position stores the particle's personal best solution found so far. The velocity determines the particle's movement in the search space, and the best value represents the fitness or objective value associated with the best position. The struct position as illustrated in Fig. 6(b) represents a two-dimensional position in space, with x and y coordinates stored as floating-point values. It also includes two member functions and two overloaded operators. PSO algorithms can efficiently update and track the positions and velocities of particles, facilitating the exploration and exploitation of the search space by utilizing these data structures. The design and implementation of these data structures are critical for the success of PSO in finding optimal solutions to optimization problems.

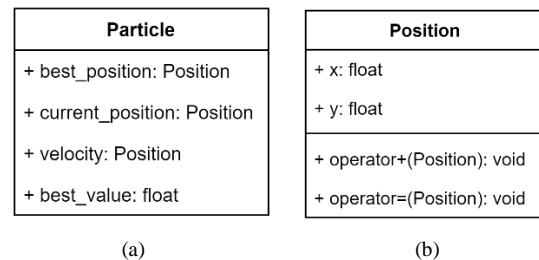


Fig. 5. Data structure for (a) The particle struct; and (b) The position struct.

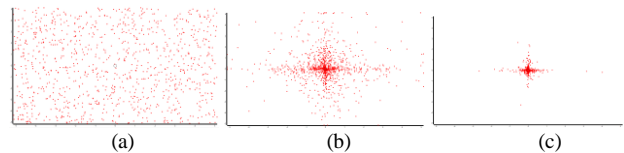


Fig. 6. A 2D visualization for PSO with 5000 particles: (a) The initial state of particles; (b) The particle's state after 100 iterations; (c) The particle's state after 200 iterations.

A. Standard PSO Algorithm

The Standard Particle Swarm Optimization (SPSO) algorithm is one such technique that draws inspiration from the social behavior of bird flocking or fish schooling. It is categorized as a population-based optimization technique and was first introduced in 1995 by Kennedy and Eberhart. In

SPSO, each solution is referred to as a "particle" that moves through the search space, seeking the optimal position as illustrated in Fig. 6. The search for the optimal position is guided by a "fitness function." Each particle has its position and velocity which are adjusted in each iteration based on its experience and the collaboration with its neighbors in the search space [26], [27].

This collaboration is demonstrated by the following equations [28]:

$$v_i^n = \omega v_i^n + c_1 r_1 (pbest_i^n - x_i^n) + c_2 r_2 (gbest^n - x_i^n) \quad (2)$$
$$x_i^{n+1} = x_i^n + v_i^{n+1} \quad (3)$$

where, the v_i^n and x_i^n present the current velocity and the position of the particle i at the n th iteration respectively, the ω presents the inertia weight, the c_1 and c_2 present the cognitive and social coefficients, respectively, the r_1 and r_2 are random numbers in the range $[0,1]$, the $pbest_i^n$ represents the best position of the particle i in the n th iteration and the $gbest^n$ represents the best position among all particles at the n th iteration.

Algorithm 1 demonstrates the pseudocode of the SPSO algorithm, with the following description of the SPSO parameters [26]:

- Population: It presents the total number of particles in the swarm space.
- T_{max} present the maximum number of iterations.
- x_i and v_i present the current position and the velocity, respectively, for the particle p_i .
- $fitness_i$ and $pbest_fitness_i$: present the fitness value and the best fitness value, respectively, for the particle p_i .
- $pbest_i$ presents the best position for the particle p_i .
- $gbest$ and $gbest_fitness$ present the team best position and best fitness value, respectively, of the entire swarm space.
- Termination condition presents the criteria that determine when the SPSO will stop searching for the optimal solution.

Algorithm 1 Sequential SPSO algorithm

For every particle p_i in the swarm space, where $0 \leq i < \text{population}$ do:

 Initialize the x_i and v_i randomly
 Evaluate the $fitness_i$ by the x_i using the fitness function.
 Initialize the $pbest_fitness_i$ and $pbest_i$.
 Update the $gbest$ and the $gbest_fitness$.

End

For every iteration $t = 0, 1, 2, \dots, T_{max}$, do:

 For every particle p_i in the swarm space, where $0 \leq i < \text{population}$ do:
 Update the position x_i and the velocity v_i for particle p_i by the Eq. (4) and (5).

 Evaluate the new $fitness_i$ by the x_i using the fitness function.

 If the new $fitness_i > pbest_fitness_i$ then update $pbest_fitness_i$ by new $fitness_i$ and $pbest_i$ by x_i .

 If the new $fitness_i > gbest_fitness$ then update $gbest_fitness$ by new $fitness_i$ and $gbest$ by $pbest_i$.

 If the $gbest_fitness$ met the termination condition, then exit from main and secondary loops.

 End

End

The time complexity of the SPSO algorithm is typically $O(T \times P)$, where the T is the number of iterations and the P is the number of particles in the swarm space.

B. CUDA PSO Algorithm

The SPSO algorithm is one such technique to leverage the power of parallel computing of GPU, to introduce the CUDA Particle Swarm Optimization (CPSO). The CPSO involves parallelizing by assigning each particle to a separate thread on the GPU to update its position and velocity based on its own best position ($pbest$) and the best position ($gbest$) founded by any particle in the swarm space. Also, the unified memory management and shared memory within each block have been utilized since the SPSO is a memory-bound problem. The CPSO consists of three kernels update particle velocity, update particle position, and compute the best position ($gbest$). The pseudocode of the CPSO is demonstrated in Algorithm 2.

Algorithm 2 CUDA PSO Algorithm (CPSO)

Set the $blockSize$ equal to 32 and determine the grid size by the Eq. (3).

Allocate memory for particles, $gbest$ and the $gbest_fitness$ using `cudaMallocManaged`.

Initialize the particles with random starting positions, velocities, and $pbest$.

compute $gbest$ and the $gbest_fitness$ using `ComputeGlobalBestPosition` kernel.

Prefetch the particles array to the GPU.

For every iteration $t = 0, 1, 2, \dots, T_{max}$, do:

 Update the velocity of each particle using the kernel `updateParticleVelocity`.

 Update the position of each particle using the kernel `updateParticlePosition`.

 Update the $gbest$ and the $gbest_fitness$ using the kernel `ComputeGlobalBestPosition`.

 If the $gbest_fitness$ met the termination condition, then terminate.

 End

End

Wait for GPU to finish the computation.

Free allocated memory.

The kernel "ComputeGlobalBestPosition" is implemented by applying the "tree" reduction algorithm where each block

calculates its bbest within its shared memory where the bbest presents the best position within each block. This means that each block independently determines the bbest among the particles it is responsible for. The resulting minimum bbest is stored in shared memory and then reduced across all blocks to find the overall minimum value to obtain gbest. The following Fig. 7 illustrates a chart that shows how this works for a block of eight threads.

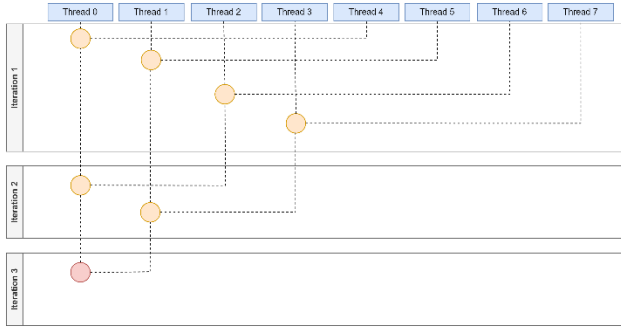


Fig. 7. Tree reduction algorithm workflow for eight threads.

For the first iteration, Thread 0 compares the best fitness value at index 0 with value at index 4, Thread 1 compares value at index 1 with value at index 5, Thread 2 compares value at index 2 with value at index 6, Thread 3 compares value at index 3 with value at index 7 and Threads 4-7 do nothing. For the second iteration, Thread 0 compares value at index 0 with value at index 2, Thread 1 compares value at index 1 with value at index 3 and Threads 2-3 do nothing. For the third iteration, Thread 0 compares value at index 0 with value at index 1 to obtain the final minimum value.

In each iteration of the loop, the number of threads that perform a comparison is halved. This means that the number of iterations required to reduce all values to a single minimum value is $\log_2(N)$, where N is the number of threads in the block. After the parallel reduction loop completes, each thread block has found its own minimum value and corresponding index. These values are stored in shared memory. The final step is to reduce across all thread blocks to find the overall minimum value and corresponding index. This is done on the CPU after all threads have completed their computations.

The pseudocode of the “ComputeGlobalBestPosition” is illustrated in Algorithm 3.

Algorithm 3 *ComputeGlobalBestPosition kernel*

Declares a shared memory array *blockBestValueArray* with a size of 32 that will be used for the parallel reduction within each block.

Compute the thread ID within the block t_{id} for the current thread by threadIdx.x and the idx for the current thread by Eq. (1), where idx is the global index of the particle that this thread is responsible for.

Initialize $\text{blockBestValueArray}[t_{id}]$ with $pbest$ value of idx 's particle.

Synchronize all threads within the block using `__syncthreads()` to ensure that all threads have finished updating the shared

memory variables.

loop $i = \frac{\text{blockDim.x}}{2}, i < 0, i \gg = 1$ do the following:

```

    If the  $t_{id} < i$  then
        If  $\text{blockBestValueArray}[t_{id}] >$ 
            $\text{blockBestValueArray}[t_{id} + i]$ , then update
            $\text{blockBestValueArray}[t_{id}]$  with
            $\text{blockBestValueArray}[t_{id} + i]$ .
        End
    End
End

```

End

Synchronize all threads within the block using `__syncthreads()` to ensure that all threads have finished updating the shared memory variables.

If the $t_{id} = 0$ then

```

    Update the  $gbest$  value by the first element of
     $\text{blockBestValueArray}$ .

```

End

The kernel “updateParticleVelocity” is implemented where each thread is responsible for a particle update their velocity based on Eq. (4). The pseudocode of the “updateParticleVelocity” is illustrated in Algorithm 4.

Algorithm 4 *updateParticleVelocity kernel*

Compute the idx for the current thread by Eq. (1) where idx is the global index of the particle that this thread is responsible for.

Declares a shared memory variable $gbest$ to access by all threads within each block.

Synchronize all threads within the block using `__syncthreads()` to ensure that all threads have finished loading the shared memory variable.

If the $idx < \text{population}$ then

```

    Update the velocity for particle  $p_{idx}$  by the Eq. (4).

```

End

The kernel “updateParticlePosition” is implemented where each thread is responsible for a particle updating its position based on Eq. (5) and updating its $pbest$. The pseudocode of the “updateParticlePosition” is illustrated in Algorithm 5.

Algorithm 5 *updateParticlePosition kernel*

Compute the idx for the current thread by Eq. (1) where idx is the global index of the particle that this thread is responsible for.

If the $idx < \text{population}$ then

```

    Update the position for particle  $p_{idx}$  by the Eq. (5).
    Evaluate the new  $\text{fitness}_{idx}$  by the  $x_{idx}$  using the fitness
    function.
    If the new  $\text{fitness}_{idx} > \text{pbest\_fitness}_{idx}$  then update
     $\text{pbest\_fitness}_{idx}$  by new  $\text{fitness}_{idx}$  and  $\text{pbest}_{idx}$  by
     $x_{idx}$ .

```

End

V. EXPERIMENTAL SETUP

The software and hardware specifications for the computer used to implement and test the PSO and CPSO algorithms are listed in Table I and Table II respectively. The details specification of the Graphics Card is listed in Table III.

TABLE I. SOFTWARE SPECIFICATION

| Name | Version |
|----------------------|----------|
| Microsoft Windows 11 | 22H2 |
| Visual Studio | 2022 |
| Nsight Systems | 2023.2.3 |
| CUDA | 12020 |
| OpenMP | 2.0 |

TABLE II. HARDWARE SPECIFICATION

| Specification | Properties |
|-----------------------|--|
| Processor | AMD Ryzen 9 5900HX, 3301 MHz, 8 Core(s), 16 Logical Processor(s) |
| Physical Memory (RAM) | 32.0 GB |
| Graphics Card | NVIDIA GeForce RTX 3080 Laptop GPU |

TABLE III. THE DETAILS SPECIFICATIONS OF THE GRAPHICS CARD

| Specification | Properties |
|---------------------------|-------------------------------------|
| Global memory | 16,383 MB |
| Shared memory | 48 kb |
| Block registers | 65,536 |
| Max threads per block | 1024 |
| Max dimensions of a block | (1024, 1024, 64) |
| Max dimensions of a grid | (2 ³¹ - 1, 65535, 65535) |
| Warp size | 32 threads |
| CUDA core | 6,144 cores |
| Memory bandwidth | 760.3 GB/sec |
| Memory channels | 8 |
| memory bus width | 256-bit |
| Memory clock | 1750 MHz |

An important design parameter of the PSO algorithm is the fitness function. We choose the Euclidean distance function as the fitness function for all the experiments, as shown in Eq. (4). The parameter w used by the fitness function is set as 1 and learning factor $c1$ and $c2$ as 2, which are commonly seen settings [29].

$$f(x, y) = \sqrt{x^2 + y^2} \quad (4)$$

VI. RESULTS AND DISCUSSION

The experiments were conducted ten times per particle number to calculate the minimum, maximum, and average execution time to ensure the reliability of results. Also, the median execution time and standard deviation were calculated. Table IV provides execution time data of the SPSO algorithm on CPU for different numbers of particles. The data shows that

as the number of particles increases, the median execution time also increases. For example, the median execution time for 32 particles is 328 (ms), while the median execution time for 65,536 particles is 793,717 (ms). This indicates that the SPSO algorithm on the CPU becomes slower as the number of particles increases. In addition, the standard deviation also increases as the number of particles increases. This indicates that there is more variation in the execution times for larger numbers of particles which may be due to increased memory usage and/or contention for system resources.

TABLE IV. SPSO ALGORITHM EXECUTION TIME ANALYSIS

| Particles | Iteration | SPSO CPU | | | | |
|-----------|-----------|---------------------|---------|-----------|----------------------------|-------------------------|
| | | Execution Time (MS) | | | Median Execution Time (MS) | Standard Deviation (MS) |
| | | MIN | MAX | AVG | | |
| 32 | 100,000 | 309 | 387 | 335.90 | 328 | 23.31 |
| 64 | 100,000 | 604 | 693 | 634.30 | 622.50 | 28.35 |
| 128 | 100,000 | 1,222 | 1,401 | 1,259.30 | 1,243 | 48.38 |
| 256 | 100,000 | 2,676 | 2,813 | 2,735.10 | 2,731.50 | 40.05 |
| 512 | 100,000 | 5,378 | 5,664 | 5,489.90 | 5,482 | 81.48 |
| 1,024 | 100,000 | 11,189 | 12,237 | 11,496.10 | 11,360.50 | 309.38 |
| 2,048 | 100,000 | 24,548 | 25,640 | 4,865.50 | 24,812 | 296.38 |
| 4,096 | 100,000 | 45,907 | 47,328 | 46,369.80 | 46,248.50 | 387.45 |
| 8,192 | 100,000 | 101,203 | 103,771 | 102,598 | 102,670 | 703.28 |
| 16,384 | 100,000 | 199,465 | 201,425 | 200,503 | 200,560 | 796.56 |
| 32,768 | 100,000 | 93,643 | 402,628 | 398,791 | 399,447 | 3,717.68 |
| 65,536 | 100,000 | 788,879 | 798,531 | 793,711 | 793,717 | 4,784.19 |

TABLE V. CPSO ALGORITHM EXECUTION TIME ANALYSIS

| Particles | Iteration | CPSO CPU | | | | |
|-----------|-----------|---------------------|--------|-----------|----------------------------|-------------------------|
| | | Execution Time (MS) | | | Median Execution Time (MS) | Standard Deviation (MS) |
| | | MIN | MAX | AVG | | |
| 32 | 100,000 | 5,405 | 5,432 | 5,422.33 | 5,430 | 15.04 |
| 64 | 100,000 | 5,478 | 5,617 | 5,537 | 5,516 | 71.84 |
| 128 | 100,000 | 5,703 | 5,823 | 5,752.33 | 5,731 | 62.78 |
| 256 | 100,000 | 5,783 | 5,902 | 5,824 | 5,787 | 67.58 |
| 512 | 100,000 | 5,769 | 5,882 | 5,829.67 | 5,838 | 56.96 |
| 1,024 | 100,000 | 5,797 | 5,893 | 5,841.33 | 5,834 | 48.42 |
| 2,048 | 100,000 | 5,806 | 5,939 | 5,864 | 5,847 | 68.11 |
| 4,096 | 100,000 | 5,931 | 6,027 | 5,988 | 6,006 | 50.47 |
| 8,192 | 100,000 | 6,179 | 6,268 | 6,221 | 6,216 | 44.71 |
| 16,384 | 100,000 | 6,828 | 6,904 | 6,869.67 | 6,877 | 38.53 |
| 32,768 | 100,000 | 13,121 | 13,212 | 13,180.33 | 13,208 | 51.42 |
| 65,536 | 100,000 | 21,382 | 21,471 | 21,431 | 21,440 | 45.18 |

Table V shows the execution time data for the CPSO algorithm on a CUDA-enabled GPU for different numbers of particles. The data indicates that as the number of particles increased, the average and median execution times also increased. The minimum and maximum execution times were

also increased, with the highest execution time being 21,471 ms for 65,536 particles and 100,000 iterations. However, the standard deviation shows that there is relatively little variation in the execution times across the different numbers of particles.

As shown in Fig. 8 the execution times for SPSO increase significantly as the number of particles increases. For example, the execution time for 65,536 particles is 793,711 (ms). The execution times for CPSO are much lower than SPSO and show much more consistent execution times across different numbers of particles. For example, the execution time for 65,536 particles is 21,431 (ms), and the percentage of the decrease in execution time is approximately 97.308% by CPSO compared to SPSO.

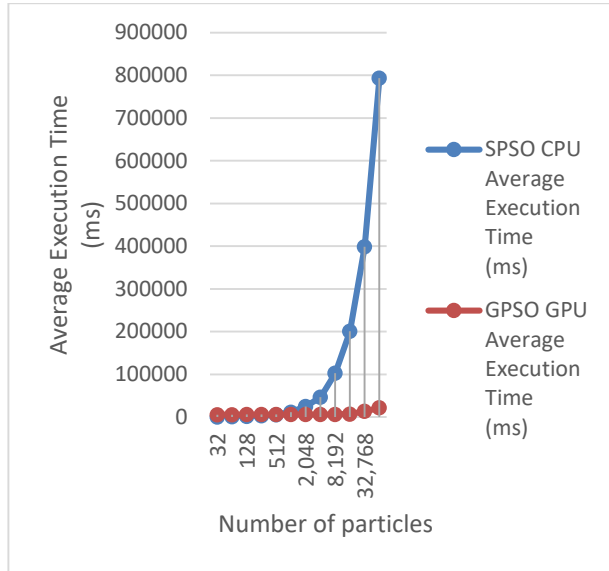


Fig. 8. Comparison of average execution time (ms) between SPSO on CPU and GPSO on GPU with respect to number of particles.

To compare the performance of these implementations, we calculated the speedup for CPSO relative to SPSO using the execution time for SPSO as a baseline. The speedup for CPSO was calculated using the following formula [30]:

$$Speedup = \frac{Execution\ Time(SPSO)}{Execution\ Time(Parallel\ Implementation)} \quad (5)$$

Table VI shows the speedup for CPSO relative to SPSO using the execution time for SPSO as a baseline. Based on the provided data for SPSO and CPSO with different particle counts and iterations, here is a summary of the key findings:

1) *Execution time trends:* The execution time increases as the number of particles and iterations increase. Also, for both Standard PSO (SPSO) and Constricted PSO (CPSO), the execution time generally follows an increasing trend with higher particle counts.

2) *Speedup comparison:* The speedup values for SPSO and CPSO range from 0.1 to 37.0 across different particle counts. These values indicate the parallelization efficiency, with higher values indicating better performance improvement with parallel processing.

3) *Comparison between SPSO and CPSO:* In most cases, CPSO shows lower execution times compared to SPSO for the same particle count and number of iterations. This difference suggests that the constriction factor used in CPSO may contribute to faster convergence and better optimization performance.

4) *Impact of particle count:* Increasing the number of particles has a significant impact on execution time, with higher particle counts leading to longer execution times. The data shows a clear trend of increasing execution time as the number of particles grows exponentially.

5) *Optimal performance considerations:* The choice between SPSO and CPSO should be based on the specific optimization problem and the desired trade-off between execution time and convergence speed. It is essential to consider the balance between speedup, execution time, and convergence efficiency when selecting the appropriate PSO variant.

TABLE VI. THE SPEEDUP FOR CPSO RELATIVE TO SPSO

| Particles | Iteration | Execution Time (MS) | | speedup |
|-----------|-----------|---------------------|-----------|---------|
| | | SPSO | CPSO | |
| 32 | 100,000 | 335.90 | 5,422.33 | 0.1 |
| 64 | 100,000 | 634.30 | 5,537 | 0.1 |
| 128 | 100,000 | 1,259.30 | 5,752.33 | 0.2 |
| 256 | 100,000 | 2,735.10 | 5,824 | 0.5 |
| 512 | 100,000 | 5,489.90 | 5,829.67 | 0.9 |
| 1,024 | 100,000 | 11,496.10 | 5,841.33 | 2.0 |
| 2,048 | 100,000 | 4,865.50 | 5,864 | 4.2 |
| 4,096 | 100,000 | 46,369.80 | 5,988 | 7.7 |
| 8,192 | 100,000 | 102,598 | 6,221 | 16.5 |
| 16,384 | 100,000 | 200,503 | 6,869.67 | 29.2 |
| 32,768 | 100,000 | 398,791 | 13,180.33 | 30.3 |
| 65,536 | 100,000 | 793,711 | 21,431 | 37.0 |

VII. CONCLUSIONS

In this work, we propose a CUDA version of the standard PSO algorithm to shorten the execution time for solving the PSO problem. We have shown the key ideas of the parallelizing algorithms for CUDA. Many experiments were conducted to improve the execution efficiency of the proposed algorithm by leveraging the power of parallel computing of GPU with the tree reduction algorithm, the CPSO achieving 37x speedup compared with the serial version SPSO and outperforming SPSO in terms of speedup. The result obtained shows that the relationship between swarm particle size and execution time is linear as the number of particles increased, the computational load also increased, making parallel implementations more effective at reducing the execution time. However, CPSO performed faster than SPSO for a high dimensional population, there was no significant improvement for the small number of particles. So, CPSO can especially benefit from optimizing with a large swarm population. For

future work, further optimization and fine-tuning of the CPSO algorithm could be explored to enhance its performance with smaller particle numbers. Additionally, investigating the scalability and adaptability of the proposed CUDA-based PSO algorithm to handle even larger swarm populations and more complex optimization problems would be a valuable direction for future research. Integration with advanced parallel computing techniques and exploring hybrid approaches could also be considered to push the boundaries of speed and efficiency in solving PSO problems.

REFERENCES

- [1] K. Zheng, X. Yuan, Q. Xu, L. Dong, B. Yan, and K. Chen, "Hybrid particle swarm optimizer with fitness-distance balance and individual self-exploitation strategies for numerical optimization problems," *Inf Sci (N Y)*, vol. 608, 2022, doi: 10.1016/j.ins.2022.06.059.
- [2] R. M. Hou, Y. L. Hou, C. Wang, Q. Gao, and H. Sun, "A Hybrid Wavelet Fuzzy Neural Network and Switching Particle Swarm Optimization Algorithm for AC Servo System," *Math Probl Eng*, vol. 2016, 2016, doi: 10.1155/2016/9724917.
- [3] C. T. Yang, C. L. Huang, and C. F. Lin, "Hybrid CUDA, OpenMP, and MPI parallel programming on multicore GPU clusters," in *Computer Physics Communications*, 2011. doi: 10.1016/j.cpc.2010.06.035.
- [4] T. Kovac, T. Haber, F. Van Reeth, and N. Hens, "Heterogeneous computing for epidemiological model fitting and simulation," *BMC Bioinformatics*, vol. 19, no. 1, 2018, doi: 10.1186/s12859-018-2108-3.
- [5] L. Mussi, F. Daolio, and S. Cagnoni, "Evaluation of parallel particle swarm optimization algorithms within the CUDATM architecture," *Inf Sci (N Y)*, vol. 181, no. 20, 2011, doi: 10.1016/j.ins.2010.08.045.
- [6] J. Peddie, *The History of the GPU - New Developments*. 2023. doi: 10.1007/978-3-031-14047-1.
- [7] P. K. Das and G. C. Deka, "History and Evolution of GPU Architecture," 2015. doi: 10.4018/978-1-4666-8853-7.ch006.
- [8] T. M. Aamodt, W. W. L. Fung, and T. G. Rogers, "General-Purpose Graphics Processor Architectures," *Synthesis Lectures on Computer Architecture*, vol. 13, no. 2, 2018, doi: 10.2200/S00848ED1V01Y201804CAC044.
- [9] M. Adnan, P. A. Longley, A. D. Singleton, and I. Turton, "Parallel Computing in Geography," in *GeoComputation*, Second Edition, 2014. doi: 10.1201/b17091-10.
- [10] R. Ansoorge, "A Brief History of CUDA," in *Programming in Parallel with CUDA*, 2022. doi: 10.1017/9781108855273.013.
- [11] M. Harris and I. Gelado, "More on CUDA and graphics processing unit computing," in *Programming Massively Parallel Processors: A Hands-on Approach: Third Edition*, 2017. doi: 10.1016/B978-0-12-811986-0.00020-0.
- [12] I. Gelado and M. Harris, "Advanced practices and future evolution," in *Programming Massively Parallel Processors: a Hands-on Approach*, Fourth Edition, 2022. doi: 10.1016/B978-0-323-91231-0.00013-6.
- [13] W. mei W. Hwu, D. B. Kirk, and I. El Hajj, "Multidimensional grids and data," in *Programming Massively Parallel Processors: a Hands-on Approach*, Fourth Edition, 2022. doi: 10.1016/B978-0-323-91231-0.00004-5.
- [14] "CUDA C++ Programming Guide." Accessed: Aug. 08, 2023. [Online]. Available: <https://docs.nvidia.com/cuda/cuda-c-programming-guide/index.html>
- [15] Nvidia, "Nvidia Cuda Getting Started Guide," NVIDIA Corporation, no. July, 2013.
- [16] M. Knap and P. Czarnul, "Performance evaluation of Unified Memory with prefetching and oversubscription for selected parallel CUDA applications on NVIDIA Pascal and Volta GPUs," *Journal of Supercomputing*, vol. 75, no. 11, 2019, doi: 10.1007/s11227-019-02966-8.
- [17] L. Gebraad and A. Fichtner, "Seamless GPU Acceleration for C++-Based Physics with the Metal Shading Language on Apple's M Series Unified Chips," *Seismological Research Letters*, vol. 94, no. 3, 2023, doi: 10.1785/0220220241.
- [18] S. Lee and J. S. Vetter, "OpenARC: Extensible OpenACC compiler framework for directive-based accelerator programming study," in *Proceedings of WACCPD 2014: 1st Workshop on Accelerator Programming Using Directives - Held in Conjunction with SC 2014: The International Conference for High Performance Computing, Networking, Storage and Analysis*, 2014. doi: 10.1109/WACCPD.2014.7.
- [19] P. Xu, M. Y. Sun, Y. J. Gao, T. J. Du, J. M. Hu, and J. J. Zhang, "Influence of data amount, data type and implementation packages in GPU coding," *Array*, vol. 16, 2022, doi: 10.1016/j.array.2022.100261.
- [20] S. Cho, J. Choi, J. Hong, and H. Han, "Multithreaded double queuing for balanced CPU-GPU memory copying," in *Proceedings of the ACM Symposium on Applied Computing*, 2019. doi: 10.1145/3297280.3297426.
- [21] W. H. Mahdi and N. Taspiner, "Overview for Parallel Particle Swarm Optimization Algorithms (PPSO)," in *2022 14th International Conference on Electronics, Computers and Artificial Intelligence, ECAI 2022*, 2022. doi: 10.1109/ECAI54874.2022.9847459.
- [22] C. C. Wang, C. Y. Ho, C. H. Tu, and S. H. Hung, "cuPSO: GPU Parallelization for Particle Swarm Optimization Algorithms," in *Proceedings of the ACM Symposium on Applied Computing*, 2022. doi: 10.1145/3477314.3507142.
- [23] F. N. Sibai, A. Potvin, and S. Ngo, "Optimizing particle systems through CUDA-assisted multithreading," *WSEAS Transactions on Systems and Control*, vol. 15, 2020, doi: 10.37394/23203.2020.15.69.
- [24] Y. Zhou and Y. Tan, "GPU-based parallel particle swarm optimization," in *2009 IEEE Congress on Evolutionary Computation, CEC 2009*, 2009. doi: 10.1109/CEC.2009.4983119.
- [25] J. Kumar, L. Singh, and S. Paul, "GPU based parallel cooperative particle swarm optimization using C-CUDA: A case study," in *IEEE International Conference on Fuzzy Systems*, 2013. doi: 10.1109/FUZZ-IEEE.2013.6622514.
- [26] S. Sengupta, S. Basak, and R. A. Peters, "Particle Swarm Optimization: A Survey of Historical and Recent Developments with Hybridization Perspectives," *Machine Learning and Knowledge Extraction*, vol. 1, no. 1. 2019. doi: 10.3390/make1010010.
- [27] D. Sedighizadeh and E. Masehian, "Particle Swarm Optimization Methods, Taxonomy and Applications," *International Journal of Computer Theory and Engineering*, 2009, doi: 10.7763/ijcte.2009.v1.80.
- [28] A. Khare and S. Rangnekar, "A review of particle swarm optimization and its applications in Solar Photovoltaic system," *Applied Soft Computing Journal*, vol. 13, no. 5. 2013. doi: 10.1016/j.asoc.2012.11.033.
- [29] X. Li, "A multimodal particle swarm optimizer based on fitness Euclidean-distance ratio," in *Proceedings of GECCO 2007: Genetic and Evolutionary Computation Conference*, 2007. doi: 10.1145/1276958.1276970.
- [30] P. Zhang, Y. Li, Y. Li, G. Chen, W. Hua, and Z. Jiao, "Research on calculation of surface irradiance for infrared extended sources based on CUDA parallel speedup," *Opt Express*, vol. 30, no. 19, 2022, doi: 10.1364/oe.470137.

Underwater Video Image Restoration and Visual Communication Optimization Based on Improved Non Local Prior Algorithm

Tian Xia

School of Arts and Design, Qingdao University of Technology, Qingdao, 266033, China

Abstract—Underwater image processing should balance image clarity restoration and comprehensive display of underwater scenes, requiring image fusion and stitching techniques. The pixel level fusion method is based on pixels, and by fusing different image data, it eliminates stitching gaps and sudden changes in lighting intensity, preserves detailed information, and thus improves the accuracy of stitching images. In the process of restoring underwater video images without local priors, there is still room for optimization in steps such as removing atmospheric light values, estimating transmittance, and calculating dehazing images through regularization. Based on the characteristics of Jerlov water types, water quality is classified according to the properties of suspended solids, and each channel is adjusted to the compensation space to improve the restoration algorithm. Background light estimation is used to determine the degree of image degradation, select the optimal attenuation coefficient ratio, and restore the image. The experimental results show that it is crucial to choose a ratio of attenuation coefficients that is close to the actual water quality environment being photographed. Both this model and traditional algorithms have an accuracy rate of over 99.0%, with the accuracy of this model sometimes reaching 99.9%. Pixel level fusion and background light estimation technology optimize underwater images, improve stitching accuracy and clarity, enhance target detection and recognition, and have important value for marine exploration rigs.

Keywords—Improving non local prior algorithms; underwater video images; visual communication effect; optical characteristic processing; image quality

I. INTRODUCTION

A. Current Research Fields and Hotspots

In today's scientific field, underwater video image restoration and visual communication optimization have become hot research areas [1-2]. Due to the complex and variable optical characteristics in underwater environments, such as scattering and absorption phenomena in water bodies, the quality of underwater images is often very poor and filled with various noises and distortions [3-4]. This greatly limits the application and research of underwater images.

B. Issues and challenges

Underwater videos provide intuitive information about the underwater world, which is crucial for marine ecological research, underwater facility maintenance, and seabed resource exploration. However, harsh visual environments and unstable lighting conditions often lead to low quality

underwater videos, affecting information extraction and analysis. Developing effective image restoration techniques to improve the quality of underwater videos is of great significance for expanding research on the understanding and utilization of the marine world. In response to these challenges, researchers are committed to finding more precise and efficient algorithms to improve the clarity and overall visual effects of underwater images, to better utilize these valuable underwater visual resources.

C. Gap with Previous Research

Although numerous studies are currently focused on underwater image restoration and visual effect optimization, these methods are often limited by the accuracy and efficiency of processing algorithms. The previous methods have not yet achieved complete satisfaction for researchers and practical applications in removing noise and distortion from underwater images, improving image contrast and clarity [5-6]. Therefore, there is an urgent need to further improve underwater image processing technology to enable observers to see underwater details more clearly.

D. The Necessity and purpose of research

This study proposes an underwater video image restoration and visual effect optimization method on the grounds of an improved non local prior (NLP) algorithm. It optimizes the processing flow to remove noise and distortion in underwater images. It enhances image contrast and clarity, allowing observers to see underwater details more clearly. This will further promote the development of underwater image processing technology and provide stronger support for related applications. It is expected that this research can play its due role in future scientific research and practical applications.

E. Research progress

The research will be conducted in five sections. Section I gives the introduction and Section II delves into related works. Section III is the research on underwater video image restoration and visual communication optimization on the grounds of improved NLP algorithms. Section IV is the experimental verification of the Section III. Section V is a summary of the research content and points out the shortcomings.

II. RELATED WORKS

Underwater video image processing has always been a key research area in the field of computer vision, as the

complexity and variability of underwater environments make image restoration a major challenge. Glassman et al. compared the effectiveness of three types of bait and two types of bait containers on bait free systems. The results indicate that BRUVS is effective in observing species richness in shallow and low visibility freshwater environments, but there is almost no evidence to suggest that the use of bait improves the effectiveness compared to non-bait RUVS [7]. Zhang et al. proposed an end-to-end dual generator model DuGAN on the grounds of generative adversarial networks for enhancing underwater images. Two discriminators are used to perform adversarial training on different regions of the image using different training strategies. This framework is easy to use, and both subjective and objective experiments have shown that it has achieved excellent results in the methods mentioned in the article [8]. Davies et al. conducted annual evaluations by comparing captured and uncaught populations inside and outside the MPA, as well as using bait based remote underwater video systems. The results indicate that comprehensive protection of the entire region with different benthic habitats is of great significance for the protection of fixed organisms that make significant contributions to fish habitats, as well as for maintaining sustainable fisheries and the interests of important protected species [9]. Zhu et al. proposed an image enhancement algorithm to improve the problem of image degradation caused by light absorption. The results indicate that the enhanced image has higher visibility, more details, and edge information [10]. Park et al. proposed a visibility enhancement technology for underwater cutting environments on the grounds of artificial neural networks to address the problem of deteriorating visibility in underwater construction environments. It uses two types of real image training on the grounds of GAN models, corresponding to cloudy input images. Experiments have shown that compared to traditional improvement techniques, trained neural networks can significantly improve the clarity of cloudy images [11].

NLP algorithms have been widely applied in image restoration, however, this algorithm still has some limitations for underwater video image restoration. Liang et al. proposed a color image restoration method that adaptively determines the size of dictionary atoms and discussed a model on the grounds of partial differential equation restoration methods. The results show that the algorithm can effectively overcome the shortcomings of fuzzy details and region expansion in fixed dictionary repair, and the repair effect is significantly improved [12]. Yang et al. proposed a modified DCP method that utilizes locally variable weighted 4-direction L-1 regularization and corresponding parallel algorithms to optimize transmission, further training deep neural networks, 4DL (1) R-net, to improve processing speed. The results have shown that this method is effective, can obtain clear details, maintain the natural clarity of the image, and significantly outperform the current state-of-the-art methods [13]. Wang et al. proposed a novel restoration algorithm that utilizes regional extremum and kernel optimization to address the issue of system blur in high-energy flash X-ray images. The results indicate that the algorithm can more accurately estimate the blur kernel, making the edges of the restored high-energy flash X-ray images clearer [14]. Lyu et al. proposed an ultrasound

C-scan image restoration method that combines Richardson Lucy algorithm and defect measurement model to improve ultrasound image quality. The results show that the restoration method effectively improves the accuracy of ultrasound C-scan imaging, with a maximum error of only 10% and a minimum error of 2% for defect size [15]. Zhao et al. vectorized and grouped similar image segments, constructed a low rank noise matrix, and simultaneously processed the weighted minimization of all image segment groups through a new regularization term, accurately representing the sparsity and self-similarity of the image structure. The results show that the research method outperforms some existing optimization algorithms in both numerical and visual effects [16].

In summary, the widespread application of NLP algorithms in image restoration has laid the foundation for this field. However, facing the complex optical characteristics of underwater video images, existing algorithms have limited performance, and visual effect optimization also needs to be deepened. Faced with the complex optical characteristics of underwater video images, this study proposes a new underwater video image restoration and visual effect optimization scheme on the grounds of an improved NLP algorithm. It is expected that this improved method can more efficiently restore underwater images, enhance visual effects, and open up new possibilities for underwater video image research and application.

III. UNDERWATER VIDEO IMAGE RESTORATION AND VISUAL COMMUNICATION OPTIMIZATION METHOD ON THE GROUNDS OF IMPROVED NLP ALGORITHM

It elaborates on the implementation of underwater video image restoration on the grounds of NLPs, and explores the improvement strategy of underwater video image restoration on the grounds of this algorithm. It introduces the implementation strategy of underwater image fusion and stitching technology, and explores in depth how to improve visual communication effects through optimization strategies. It provides reference for underwater video image restoration and visual effect optimization, in order to promote the development of underwater vision research.

A. Implementation of Underwater Video Image Restoration on the Grounds of NLPs

Clustering in RGB color space (RGB) can approximate fogless images with hundreds of colors. The pixels of each cluster are derived from the entire image, non-local regions, forming a NLP [17]. This theory is on the grounds of an improved NLP algorithm for underwater video image restoration and visual effect optimization, which can achieve effective restoration of underwater video images. The flowchart of NLP restoration of images is shown in Fig. 1.

In Fig. 1, starting from an NLP, clustering is performed in a fog free image. Due to differences in depth and distance of field, there will be differences in transmittance. It clusters foggy images in RGB space, forming fog lines due to differences in transmittance. It uses clustering fog lines of foggy images to estimate transmittance, and then starts from the image degradation model to perform NL restoration of the

image. The estimation method of transmittance is different from the prior restoration of dark channels. Then it clusters the pixels of the foggy image into fog lines, estimates the initial transmittance $t(x)$, regularizes and refines the estimated

transmittance, and finally performs image restoration. The image containing fog to be processed is shown in Eq. (1).

$$I_A(x) = I(x) - A \quad (1)$$

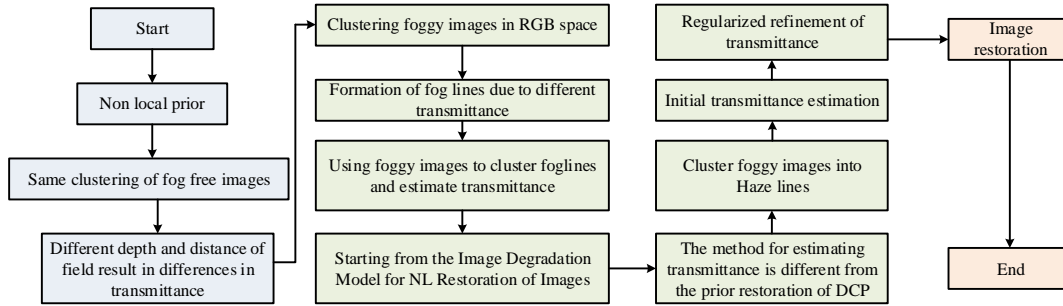


Fig. 1. Complex flowchart for NLP restoration of images.

In Eq. (1), $I(x)$ represents the image containing fog to be processed, and A represents the pre estimated atmospheric light value. A converts the RGB coordinate system of pixels in foggy images to point A as the coordinate origin [18-19]. The joint image degradation model is shown in Eq. (2).

$$I_A(x) = [r(x), \theta(x), \varphi(x)] \quad (2)$$

In Eq. (2), $r(x)$ is the distance from the origin A, $\theta(x)$ is longitude, and $\theta(x)$ is latitude. For each fog line in a foggy image, its two ends are a cluster of non-foggy image J and atmospheric light value A . The expression of transmittance with respect to the radius of the fog line is shown in Eq. (3).

$$r(x) = t(x) \times \|J(x) - A\|, 0 \leq t(x) \leq 1 \quad (3)$$

In Eq. (3), $t(x)$ is the transmittance and $r(x)$ is the radius of the fog line. The process of estimating transmittance from fog lines is shown in Fig. 2.

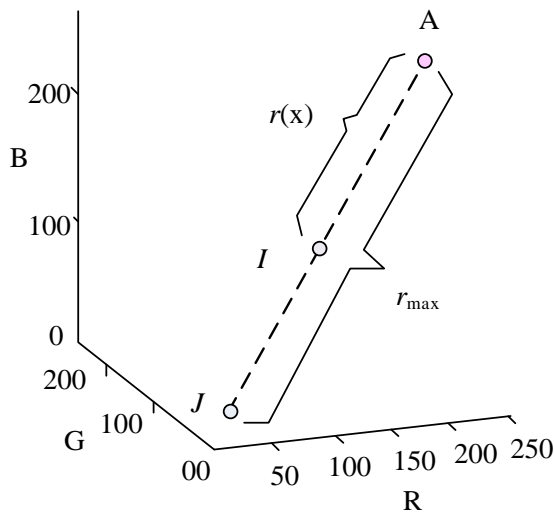


Fig. 2. The process of estimating transmittance from fog lines.

In Fig. 2, fog lines are formed by clustering foggy images to reveal differences in fog density. Then, the degradation model is used to initially estimate the transmittance, which directly affects the image clarity. It compares the estimated transmittance with the lower bound of transmittance, taking the larger one to ensure image authenticity, as real foggy images may not guarantee that each fog line contains fog free pixels. Finally, it smooths the transmittance map, suppresses noise, and enhances spatial continuity of the image. Its regularization refines the transmittance, as shown in Eq. (4).

$$\sum_x \frac{[\hat{t}(x) - \tilde{t}_{LB}(x)]^2}{\sigma^2(x)} + \lambda \sum_x \sum_{y \in N_x} \frac{[\hat{t}(x) - \tilde{t}(y)]^2}{\|I(x) - I(y)\|^2} \quad (4)$$

In Eq. (4), $\hat{t}(x)$ is the refined transmittance, N_x is the four neighborhoods centered on pixel N_x in the image, λ is the parameter used to balance the data and smoothing terms, and λ is the standard deviation of $\sigma^2(x)$. The restored image can be obtained from the degradation model, as shown in Eq. (5).

$$J(x) = \frac{\{I(x) - [1 - \hat{t}(x)A]\}}{\hat{t}(x)} \quad (5)$$

B. Improvement of Underwater Video Image Restoration on the Grounds of NLP

The NLP underwater video image restoration process includes steps such as removing atmospheric light values, estimating transmittance, and calculating dehazing images through regularization. However, there is still room for optimization in improving the visibility of underwater images using this method, especially in transmittance estimation, where the R, G, and B channels are often uniformly processed [20]. This ignores the differences in underwater light wave attenuation and color distortion between channels. This study classifies water quality on the grounds of the characteristics of Jerlov water types and the properties of suspended solids, and adjusts each channel to the compensation space through the global attenuation coefficient ratio to improve the restoration algorithm. And it uses background light estimation to

determine the degree of image degradation, selects the optimal attenuation coefficient ratio, and restores the image. The transmittance is calculated and refined, as shown in Eq. (6) for different channels.

$$\begin{cases} A_R - I_R = e^{-\beta_R d} \cdot (A_R - J_R) \\ A_G - I_G = e^{-\beta_G d} \cdot (A_G - J_G) \\ A_B - I_B = e^{-\beta_B d} \cdot (A_B - J_B) \end{cases} \quad (6)$$

In Eq. (6), A is the background light and I is the type of water body. $e^{-\beta d}$ is the transmittance, $\beta(\lambda)$ is the attenuation coefficient, and $\beta(\lambda)$ is the depth of field. It performs power operations on the channel equations to obtain a moderate compensation space, as shown in Eq. (7).

$$\begin{bmatrix} (I_R(x) - A_R)^{\beta_{BR}} \\ (I_G(x) - A_G)^{\beta_{BG}} \\ (I_B(x) - A_B) \end{bmatrix} = t_B(x) \begin{bmatrix} (J_R(x) - A_R)^{\beta_{BR}} \\ (J_G(x) - A_G)^{\beta_{BG}} \\ (J_B(x) - A_B) \end{bmatrix} \quad (7)$$

In Eq. (7), β_{BR} is the blue red attenuation coefficient, and β_{BG} is the blue green attenuation coefficient. The smoothing factor is shown in Eq. (8).

$$\alpha(x) = \frac{D_M(I(x)) - \bar{D}_M - \sigma_M}{D_M^{\max} - \bar{D}_M} \quad (8)$$

In Eq. (8), $\alpha(x)$ is the smoothing factor, σ_M is the standard deviation, D_M^{\max} is the maximum Mahalanobis distance, and \bar{D}_M is the average Mahalanobis distance of the background light area. After estimating the transmittance, color attenuation compensation is performed to obtain the restored image. The scattering of light during its propagation in water can cause global color distortion. In order to make the image look like it is under white light, it can be corrected through white balance method after compensating for propagation loss. The implementation process of an improved underwater image restoration algorithm on the grounds of NLP prior is shown in Fig. 3.

In Fig. 3, edge detection is performed on the input image to determine the background light area and calculate the background light. On the grounds of the attenuation coefficient values under different water types, each channel is processed to estimate the initial transmittance. It performs soft cutout processing, uses enhanced images as guidance, and refines transmittance through filtering. It then restores the restored image and performs global white balance processing. Finally, its output refines the transmittance and restores the image.

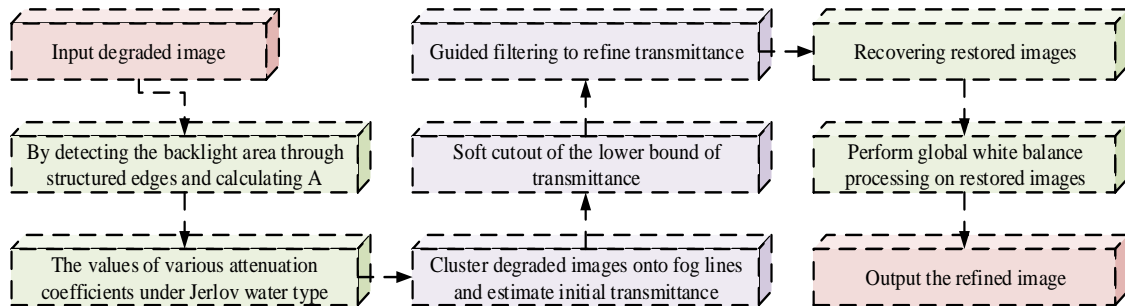


Fig. 3. Implementation of an improved underwater image restoration algorithm on the grounds of NLP prior.

C. Implementation Strategy for Underwater Image Fusion and Stitching Technology

In underwater image processing, in addition to clarity restoration, panoramic display of large-scale underwater scenes in complex environments is also required, which requires image fusion and stitching techniques. Image fusion is divided into pixel level, feature level, and decision level. Pixel level fusion has high accuracy but large data volume, feature level fusion reduces data volume but low accuracy, while decision level fusion has strong anti-interference ability, good real-time performance but low accuracy. In order to eliminate splicing gaps and sudden changes in lighting intensity, preserve detailed information and improve fusion accuracy, pixel level fusion is mainly used. Common methods include average value method, gradual in and out method, and multi band fusion method [21]. It takes the average of the pixel values of the corresponding points in two images within the overlapping area, and the average method is shown in Eq. (9).

$$I(x, y) = \begin{cases} I_1(x, y) & (x, y) \in R_1 \\ 0.5 \times [I_1(x, y) + I_2(x, y)] & (x, y) \in R_2 \\ I_2(x, y) & (x, y) \in R_3 \end{cases} \quad (9)$$

In Eq. (9), R_1 is the area that belongs only to the first image, R_2 is the area where the first and second images overlap, and R_3 is the area of the second image. The gradual in and out method assigns different weight values on the grounds of the distance between pixels and the overlapping boundary when processing regions of two overlapping images. Through this weighting method, the calculation of new pixel values can achieve a visual effect of smooth transition from one image to another. The pixel values corresponding to the fusion are shown in Eq. (10).

$$I(x, y) = \begin{cases} I_1(x, y) & (x, y) \in R_1 \\ d \times I_1(x, y) + (1-d)I_2(x, y) & (x, y) \in R_2 \\ I_2(x, y) & (x, y) \in R_3 \end{cases} \quad (10)$$

In Eq. (10), the meanings of R_1 , R_2 , and R_3 are the same as the average method. d is the gradient weight factor, and the image frames that are gradually approaching the middle are combined into the concatenated image. For a certain number of frame sets, a certain intermediate frame in the image set is selected as the initial reference image, and the image frames to be concatenated are selected from left to right in sequence. The image frame to concatenated image synthesis method on the grounds of intermediate frames is shown in Fig. 4.

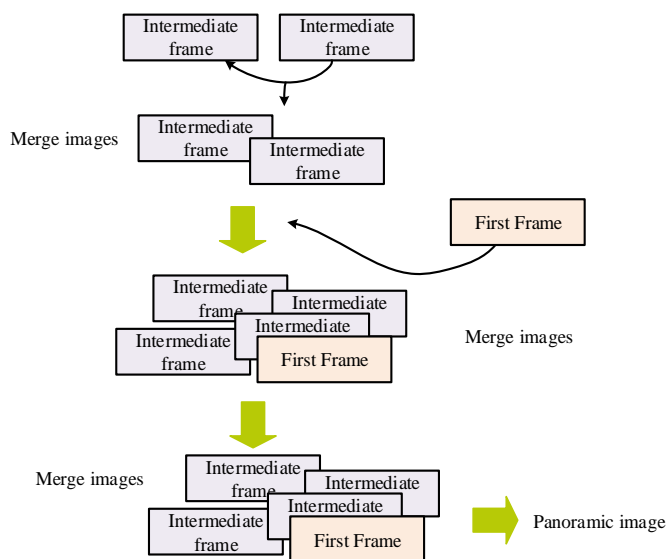
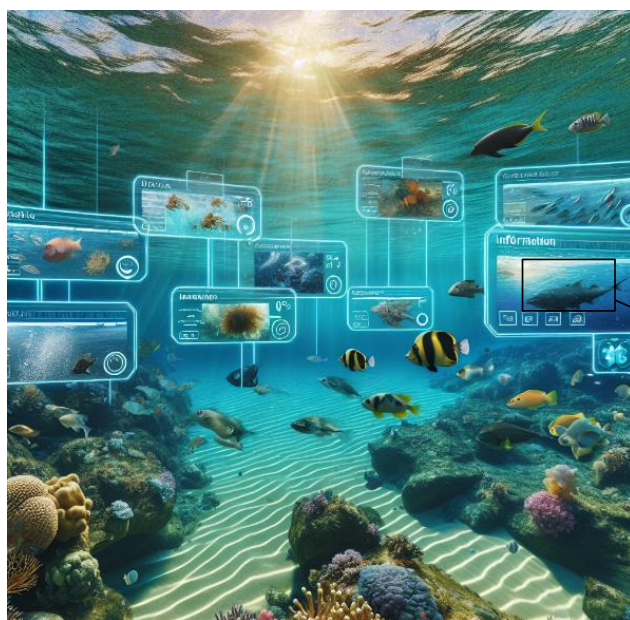


Fig. 4. Implementation of an improved underwater image restoration algorithm on the grounds of NLP prior.

In Fig. 4, it selects a frame in the middle as the initial reference image, registers it with the front and back frames through a projection transformation matrix, and fuses it using the gradual in and out method. It uses the fused image as a new reference image and sequentially selects the image to be stitched forward and backward for fusion. The advantage of this strategy is that it avoids the accumulation of transformation errors that may arise from frame by frame fusion. By using intermediate frames as the initial reference image, it can effectively consider the distance between all frames and the reference image, improve the overlap rate, and thus obtain a restored underwater panoramic image.

D. Optimization Strategies for Visual Communication Effects

The underwater image fusion and stitching technology optimizes visual effects, requiring comprehensive adjustments to image color, clarity, brightness, etc. Information graphical interaction technology also helps optimize visual effects, including two major elements: basic and interactive. The foundation ensures the accurate expression of information, provides a natural and convenient way for interaction, guides users to navigate, browse, filter, input, prompt and feedback, view conversion, etc. Macro to micro techniques handle complex graphics, allowing users to zoom in, scroll, jump, and move in the macro interface, observe details, and return to the macro interface to see the marked micro areas. Dynamic and interactive information prompts display hierarchical data information with organized structure, allowing users to see secondary information when browsing to a specified location. The comprehensive use of these technologies and strategies helps to improve underwater video image restoration and visual communication optimization methods on the grounds of NLP algorithms. In the underwater video image restoration and visual communication optimization method on the grounds of improved NLP algorithms, as shown in Fig. 5, interactive information prompt technology is an important strategy.



Example

Squaliformes: There are over 200 species belonging to 49 genera, 7 families, and 4 suborders, including Scyliorhinoidei, Triakoidei, Carcharhinoidei, and Sphyrnidae. There are over 60 species in 23 genera, 5 families, and 4 suborders in China. 2 dorsal fins, without hard spines; Having anal fins. 5 gill holes. Jaw tongue joint type. Three kiss cartilage. There are instantaneous folds or membranes in the eyes. The vertebral body has radiating calcified areas, with calcified rays invading four non calcified areas. The spiral valve of the intestine is spiral or coiled in shape.

Fig. 5. Example of interactive information prompt technology.

This technology enables users to obtain relevant information by pointing to specific image elements, eliminating redundant operations. For underwater video images containing a large amount of information, interactive information prompt technology can provide dynamic display and concealment functions, and the content can change in real-time according to user operations. The dynamic prompt window provides users with real-time image information, improving the accessibility and usability of the information.

In the process of image restoration, dynamic query technology is the key to optimizing visual communication effects. It meets the needs of users for precise queries in a large amount of information. By using standard operating controls such as sliders, checkboxes, etc., users can define the display range of image information. For example, in video playback software, users can search for video information

from a specific era on the grounds of the time of video release. The front-end logic of dynamic queries is clear, and the dominant power lies in the hands of users, ensuring efficient real-time interactive feedback. On the backend, the dynamic query engine processes user query requests, assembles query conditions, executes query instructions, parses parameters, searches for configurations, and determines query types. Finally, the search result data is objectified and formatted as a list of information that can be received by the control, which retrieves and renders the data, and returns it to the user interface. This achieves the precise query needs of users and improves the efficiency of information exploration. Fig. 6 shows interactive information prompts and dynamic query techniques. This combined application with interactive information prompt technology optimizes underwater video image restoration and visual communication effects on the grounds of NLP algorithms.

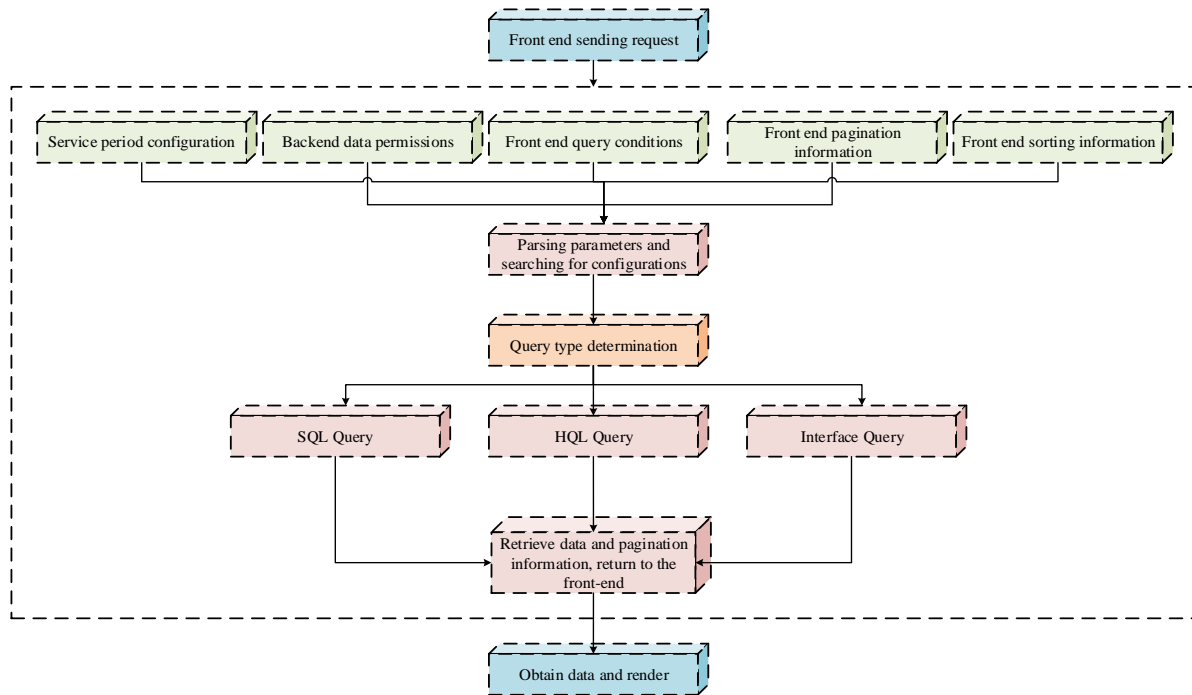


Fig. 6. Interactive information prompts and dynamic query techniques for optimizing visual communication effects.

IV. ANALYSIS OF UNDERWATER VIDEO IMAGE RESTORATION AND VISUAL COMMUNICATION OPTIMIZATION ON THE GROUNDS OF IMPROVED NLP ALGORITHM

Improving NLP algorithms can reduce noise and blur during image restoration and improve image quality. By combining interactive information prompts and dynamic query technology, the accessibility and usability of information can be enhanced, allowing users to accurately query a large amount of information, achieve efficient real-time interactive feedback, and improve information exploration efficiency.

A. Application Effect Analysis of Improved NLP Algorithm in Underwater Video Image Restoration

Improving the application effect of NLP algorithms is an important research direction in underwater video image restoration. This algorithm processes the local and non-local characteristics of the image, and the parameter settings of the

model are shown in Table I. In the optimization analysis of visual communication effects, Sea rogan was selected to demonstrate the intermediate results of NL image restoration processing for underwater images. In this process, the parameter is set to 0.1. Table II shows the comparison results of the average gradient and information entropy after non local and dark channel prior restoration.

The improved NLP algorithm for restoring underwater video images can be observed through the SSIM index. For high-quality video frames such as Sea oral and Sea fish, this algorithm recovers SSIM values that surpass the Fast DCP algorithm. However, for low-quality video frames such as Underwater1_10, Underwater2_10, and Underwater2_340, their restored SSIM values are slightly lower. For specific effects, such as using Underwater1_10 as an example, it is necessary to refer to Fig. 7.

TABLE I. SYSTEM PARAMETER

| Parameter Name | Description | Setting Value | Remarks |
|------------------------|--|------------------------------------|--------------------------------|
| Operating System | Environment for running the software | Windows 10 | 64-bit |
| Processor | Hardware for executing the algorithm | Intel Core i7 | 2.6GHz |
| Memory | Temporary storage for algorithm and data | 16GB | DDR4 |
| Graphics Card | Hardware for processing images | NVIDIA GeForce GTX 1050 | 4GB |
| Algorithm Version | Executing algorithm | Improved Non-local Prior Algorithm | Latest version |
| Experiment Video | Testing data | Underwater video | 1080p, 30fps |
| Experiment Environment | Place where the experiment is conducted | Laboratory | Temperature 25°C, Humidity 60% |

TABLE II. COMPARISON OF AVERAGE GRADIENT AND INFORMATION ENTROPY AFTER NL AND DARK CHANNEL PRIOR RESTORATION

| Image | Algorithm | Original drawing | | | | Information entropy E | | | |
|----------------|------------------|------------------|------|------|------------|-----------------------|------|------|------------|
| | | R | G | B | Mean value | R | G | B | Mean value |
| Sea-coral | Original drawing | 3.37 | 3.37 | 3.47 | 3.29 | 6.7 | 6.76 | 6.51 | 6.66 |
| | Fast DCP | 7.12 | 6.99 | 6.83 | 6.98 | 7.25 | 7.43 | 7.29 | 7.32 |
| | NL | 7.71 | 7.62 | 7.38 | 7.57 | 7.39 | 7.5 | 7.39 | 7.43 |
| Sea-fish | Original drawing | 0.5 | 0.48 | 0.49 | 0.49 | 4.98 | 6.03 | 5.63 | 5.55 |
| | Fast DCP | 1.18 | 1.09 | 1.14 | 1.14 | 4.8 | 6.65 | 6.09 | 5.85 |
| | NL | 1.88 | 1.38 | 1.92 | 1.73 | 6.36 | 7.22 | 7.18 | 6.92 |
| Underwater1_10 | Original drawing | 0.56 | 0.56 | 0.54 | 0.55 | 4.75 | 6.97 | 7.21 | 6.31 |
| | Fast DCP | 0.75 | 0.74 | 0.75 | 0.75 | 4.02 | 7.4 | 7.55 | 6.32 |
| | NL | 1.19 | 1.23 | 1.2 | 1.21 | 5.24 | 7.58 | 7.59 | 6.8 |
| Underwater2_10 | Original drawing | 1.71 | 1.15 | 1.13 | 1.16 | 5.92 | 6.92 | 7.24 | 6.69 |
| | Fast DCP | 1.59 | 1.49 | 1.55 | 1.54 | 5.03 | 6.83 | 7.48 | 6.45 |
| | NL | 2.4 | 2.35 | 2.39 | 2.38 | 5.97 | 6.81 | 7.82 | 6.87 |
| Underwater2340 | Original drawing | 0.62 | 0.58 | 0.55 | 0.58 | 5.16 | 7.01 | 6.97 | 6.38 |
| | Fast DCP | 0.79 | 0.75 | 0.78 | 0.77 | 5.24 | 7.06 | 7.27 | 6.15 |
| | NL | 1.18 | 1.14 | 1.34 | 1.25 | 4.25 | 7.24 | 7.67 | 6.84 |

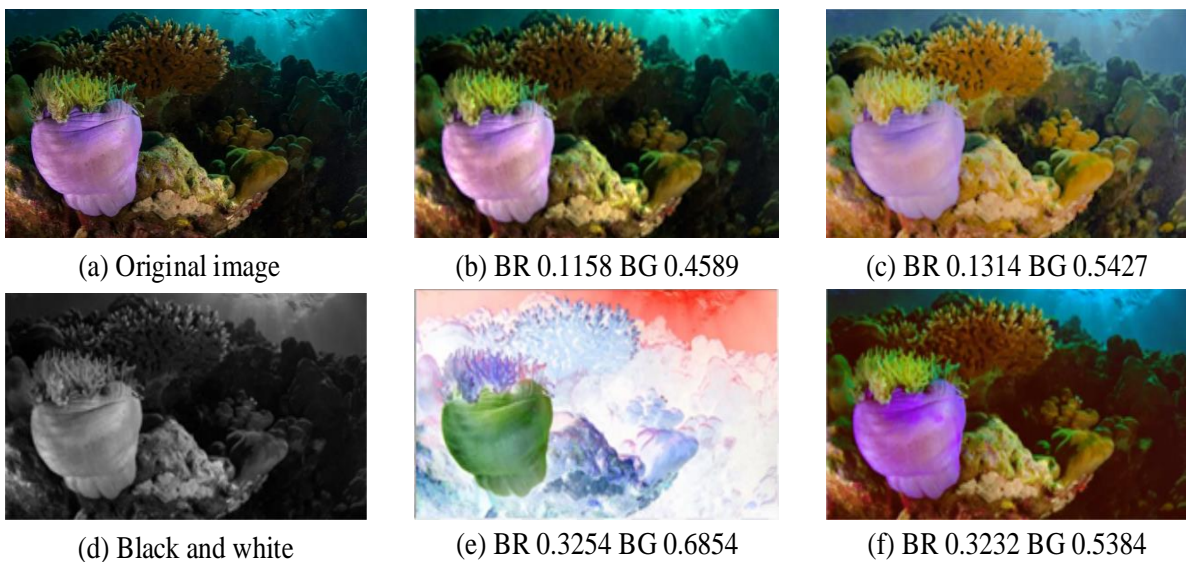


Fig. 7. Image underwater1_10 results under different attenuation coefficient ratios.

In Fig. 7, the lower left grayscale image (d) shows the detected background light area, while Fig. 7(b), (c), (e), and (f) show the restored images obtained under different attenuation coefficient ratios. The attenuation coefficient ratio plays a crucial role in the process of image restoration. Using inaccurate ratios can lead to errors in the transmittance chart, resulting in color deviation in the reconstructed image. Therefore, it is crucial to choose a ratio of attenuation coefficients that is close to the actual water quality environment being photographed. The right choice can improve the restoration effect, while the wrong choice can lead to poor restoration effect.

B. Optimization Analysis of Visual Communication Effects

In the waters near the boundary island of Sanya, China, underwater videos were captured using the "Ocean Elf" sightseeing submarine. The experiment was conducted in the sea at a depth of 20-30 meters, with a submarine diving depth of 10-15 meters and visibility of 4-10 meters. The video was recorded using the iPhone 11 Pro rear camera. For detailed information on the video, please refer to Table III.

TABLE III. OPTIMIZATION ANALYSIS

| Video file name | Duration (s) | Frame rate | Frame Image Size | Total Frames | Real keyframe rate |
|-----------------|--------------|------------|------------------|--------------|--------------------|
| underwater1 | 6.0000 | 29.5357 | 544×980 | 232 | 8.0000 |
| underwater2 | 8.0000 | 29.5357 | 980×544 | 247 | 9.0000 |
| underwater3 | 10.0000 | 29.5357 | 640×480 | 296 | 10.0000 |
| underwater4 | 12.0000 | 29.5357 | 1280×720 | 355 | 11.0000 |
| underwater5 | 14.0000 | 29.5357 | 1920×1080 | 414 | 12.0000 |

To verify the superiority and accuracy of the model, experiments were conducted in underwater videos near the boundary island of Sanya, China. The sightseeing submarine takes photos in the sea area at a depth of 20-30 meters, with a diving depth of 10-15 meters and visibility of 4-10 meters. The experiment mainly used Underwater1 with a resolution of 544 * 960 and Underwater2 with a resolution of 980 * 544. The experiment first uses an improved keyframe extraction algorithm to obtain image frames, and then uses an improved algorithm for non-local underwater image restoration to process keyframes. After image registration and fusion, the matching results and fusion effects are displayed. For Underwater1 with poor image quality, the threshold T for new cluster partitioning is set to 18, and for good quality, it is set to 25. The experimental results are shown in Fig. 8.

In Fig. 8, the accuracy statistics of the model and traditional image restoration algorithms in 60 experiments are shown. Both the model and traditional algorithms have an accuracy rate of over 99.0%, and sometimes the accuracy of the model can even reach 99.9%, while the traditional model can only reach a maximum of 99.3%. In order to study the accuracy of the model in processing different underwater environments, 20 underwater videos were selected and 180 image data samples were collected for simulation of common underwater environments. The results are shown in Fig. 9.

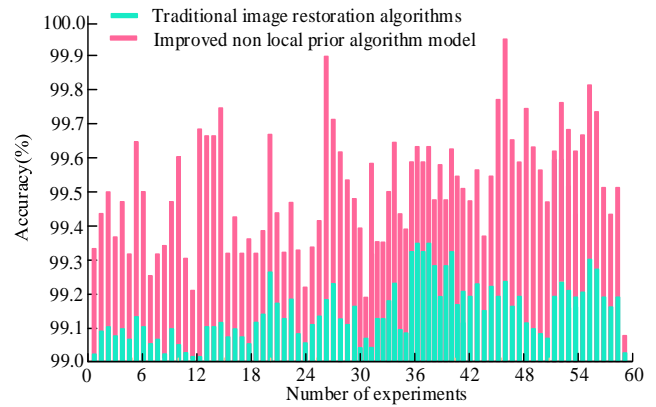


Fig. 8. Accuracy comparison chart.

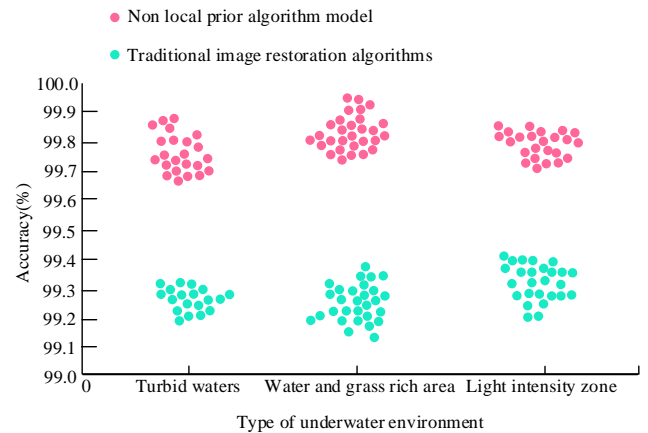


Fig. 9. Non-local prior model's accuracy in different underwater environments.

In Fig. 9, three types of seabed environments are covered: turbid waters, areas with abundant aquatic plants, and areas with strong sunlight. Regardless of the type of environment, the processing accuracy of NLP models exceeds 99.0%. The average accuracy of treating turbid water bodies is around 99.6%. This indicates that NLP models exhibit extremely high accuracy in restoring images of turbid water bodies. The average processing accuracy for areas with abundant water and grass is around 99.4%. This means that NLP models can effectively distinguish images in water grass rich areas and perform effective restoration processing, with an average accuracy of about 99.15% for areas with strong lighting.

V. CONCLUSION

Faced with the complexity of underwater environments and harsh lighting conditions, underwater image processing requires both restoration of image clarity and comprehensive display of underwater scenes, thus requiring the use of image fusion and stitching techniques. In this context, the research aims to optimize the NLP underwater video image restoration process and improve the accuracy of image processing. It classifies water quality on the grounds of Jerlov's water type characteristics, adjusts channel optimization restoration algorithms, and uses background light estimation to determine the degree of degradation. The results show that the attenuation coefficient ratio plays a crucial role in the image restoration process. The accuracy of this model can sometimes

even reach 99.9%, while traditional models only have a maximum of 99.3%. Not only that, NLP models can also effectively distinguish images in areas with abundant water and grass, and perform effective restoration processing. The average accuracy of processing in areas with strong lighting is about 99.15%. This study provides an effective method for improving the accuracy of underwater image processing. However, there are still shortcomings, such as the need to improve the accuracy of processing images in areas with strong lighting. Future research aims to further optimize the model, improve the accuracy of image processing for various complex underwater environments, and explore more image processing algorithms suitable for various complex underwater environments. This is to present the underwater scene more comprehensively while ensuring image clarity.

REFERENCES

- [1] Chen Q, Zhang Z, Li G. Underwater image enhancement based on color balance and multi-scale fusion. *IEEE Photonics Journal*, 2022, 14(6): 1-10.
- [2] Mathur M, Goel N. Enhancement of nonuniformly illuminated underwater images. *International Journal of Pattern Recognition and Artificial Intelligence*, 2021, 35(3): 1-23.
- [3] Wei Y, Zeng A, Zhang X, Huang H. "RAG-Net: ResNet-50 attention gate network for accurate iris segmentation." *IET Image Processing*, 2022, 16(11): 3057-3066.
- [4] Hu JW, Xie YT, Li SB, Du XY, Xiong NN. "An Edge Intelligence-based Generative Data Augmentation System for IoT Image Recognition Tasks." *Journal of Internet Technology*, 2021, 22(4): 765-778.
- [5] Liao Y, Ragai I, Huang Z, Kerner S. "Manufacturing process monitoring using time-frequency representation and transfer learning of deep neural networks." *Journal of Manufacturing Processes*, 2021, 68(8): 231-248.
- [6] Fu Z, Zheng L, Li J, Chen G, Yu T, Deng T. "DMvLNet: deep multiview learning network for blindly assessing image quality." *Journal of Electronic Imaging*, 2022, 31(5): 1-13.
- [7] Glassman D M, Chhor A, Vermaire J C, Bennett J R, Cooke S J. Does bait type and bait container configuration influence the performance of remote underwater video systems in temperate freshwater lakes for assessing fish community structure? *Hydrobiologia*, 2022, 849(9): 1981-1994.
- [8] Zhang H, Sun L, Wu L, Gu K. DuGAN: An effective framework for underwater image enhancement. *IET Image Processing*, 2021, 15(9): 2010-2019.
- [9] Davies B F R, Holmes L, Rees A, Attrill M J, Cartwright A Y, Sheehan E V. Ecosystem Approach to Fisheries Management works—How switching from mobile to static fishing gear improves populations of fished and non-fished species inside a marine-protected area. *Journal of Applied Ecology*, 2021, 58(11): 2463-2478.
- [10] Zhu D, Liu Z, Zhang Y. Underwater image enhancement based on colour correction and fusion. *IET Image Processing*, 2021, 15(11): 2591-2603.
- [11] Park S K, Oh S Y, Shin J S, Park H, Kovalev V. A preliminary study on visibility improvement of turbid underwater images for dismantling of nuclear facilities. *Annals of Nuclear Energy*, 2021, 156(6): 1-8.
- [12] Zhang L, Chang M, Chen R. Image inpainting based on sparse representation using self-similar joint sparse coding. *Multimedia Tools and Applications*, 2023, 82(13): 20215-20231.
- [13] Yang Y, Long W, Li Y, Shi X, Gao L. Image defogging based on amended dark channel prior and 4-directional L1 regularisation. *IET Image Processing*, 2021, 15(11): 2454-2477.
- [14] Wang X, Li Q, Xu J. High energy flash X-ray image restoration using region extrema and kernel optimization. *IET Image Processing*, 2021, 15(12): 2970-2985.
- [15] Lyu D, Tian J, Hu H, He X. Ultrasonic C-scan image restoration method using the Richardson-Lucy algorithm and a flaw measurement model. *Applied acoustics*, 2022, 200(11): 1-9.
- [16] Zhai L. Image restoration algorithm based on multiscale weighted Schatten p-norm minimization. *Journal of Electronic Imaging*, 2022, 31(2): 1-15.
- [17] Omara A N, Salem T M, Elsanadily S, Elsherbini M M. SSIM-based sparse image restoration. *Journal of King Saud University-Computer and Information Sciences*, 2022, 34(8): 6243-6254.
- [18] Sivaanpu A, Thanikaalam K. Scene-Specific Dark Channel Prior for Single Image Fog Removal. *The International Journal on Advances in ICT for Emerging Regions*, 2021, 14(3): 1-12.
- [19] Cui Y, Zhi S, Liu W, Deng J, Ren J. An improved dark channel defogging algorithm based on the HSI colour space. *IET Image Processing*, 2022, 16(3): 823-838.
- [20] Sabir A, Khurshid K, Salman A. Segmentation-based image defogging using modified dark channel prior. *EURASIP Journal on Image and Video Processing*, 2020, 2020(1): 1-14.
- [21] Dornelas R S, Lima D A. Correlation Filters in Machine Learning Algorithms to Select De-mographic and Individual Features for Autism Spectrum Disorder Diagnosis. *Journal of Data Science and Intelligent Systems*, 2023, 3(1): 7-9.

Integrated Ensemble Model for Diabetes Mellitus Detection

Abdulaziz A Alzubaidi, Sami M Halawani, Mutasem Jarrah

Faculty of Computing and Information Technology, King Abdulaziz University, Jeddah, Saudi Arabia

Abstract—Diabetes Mellitus, commonly referred to as (DM), is a chronic illness that affects populations worldwide, leading to more complications such as renal failure, visual impairment, and cardiovascular disease, thus significantly compromising the individual's well-being of life. Detecting DM at an early stage is both challenging and a critical procedure for healthcare professionals, given that delayed diagnosis can result to difficulties in managing the progression of the disease. This study seeks to introduce an innovative stacking ensemble model for early DM detection, utilizing an ensemble of machine learning and deep learning models. Our proposed stacking model integrates multiple prediction learners, including Random Forest (RF), Convolutional Neural Network (CNN) with Long Short-Term Memory networks (CNN-LSTM), and Sequential Dense Layers (SDLs) as base learner models, with the Extreme Gradient Boosting model (XGBoost) serving as the Meta-Learner model. Findings demonstrate that our proposed model achieves a 99% accuracy on the Pima dataset and 97% accuracy on the DPD dataset in detecting diabetes mellitus disease. In conclusion, our model holds promise for developing a diagnostic tool for DM disease, and it is recommended to conduct further testing on the types of diabetes mellitus to enhance and evaluate its performance comprehensively.

Keywords—Diabetes mellitus; machine learning; deep learning; stacking; ensemble learning; RF; CNN-LSTM; SDLs; XGBoost

I. INTRODUCTION

Diabetes mellitus carries a significant health risk and increases the likelihood of getting cardiovascular disease and more complications, which makes our lives suffer [1]. Insulin is essential for controlling blood glucose work, regulating the anabolism of carbohydrates, promoting physical growth, supervising cell division, and monitoring the anabolic activities of proteins and fats [2]. As a result, DM significantly impairs people's daily life and increases their risk of getting chronic illnesses such as cardiovascular disorders, renal failure, and sightlessness [3]. These disorders raise death rates [4]. In 2019, it was estimated that 463 million individuals worldwide suffered from diabetes [5].

There are two main types of diabetes mellitus (DM): Type-1 Diabetes, an autoimmune sickness that destroys the pancreatic beta cells that produce insulin, and the second type of Diabetes, a chronic that often raises blood sugar levels [6]. It can be challenging to differentiate between these kinds and choose the best course of action because doctors sometimes dispute about the best way to diagnose a patient [7]. Globally, diabetes is becoming more common, especially in countries with middle incomes [8]. Therefore, research on diabetes

prediction through machine learning (ML) techniques is needed to help specialists build the best possible treatment plans. By 2030, the Global Sustainable Development Group wants to eradicate diabetes-related early death [8]. Consequently, scholars are consistently investigating various facets of diabetes mellitus. A range of machine learning methods, including the Random Forest and XGBoost algorithms, are utilized in this endeavor, each providing special benefits for classification procedures [9-10-11-12-13]. Convolutional Neural Networks (CNNs) with Long Short-Term Memory architecture and Multilayer perceptron's (MLPs) are two popular deep learning (DL) techniques that offer strong frameworks for managing sequential data and classification tasks [14-15-16].

In the healthcare sector, detecting DM at an early stage is challenging. Patient data is collected, including their ages, the mass of the body, the thickness of the skinfold in the triceps, insulin in the blood, plasma glucose level, the diastolic-blood-pressure, and other variables. Patients then turn to doctors for specialist care. The doctor's medicating process becomes harder because of the lengthy, weeks-long decision-making process that depends on the doctor's expertise and experience [17].

Healthcare science research is currently supported by a wide range of publicly available medical databases. But managing such massive volumes of data by humans is frequently difficult, if not infeasible. Deep learning techniques deliver a solution because they grow and mimic how humans thinking. That happens by providing data at several tiers and successfully resolves the selectivity-invariance issue [18]. In the discipline of medicine, deep learning algorithms have several uses, especially in the diagnosis sector. Much research continually demonstrates the superior performance of deep learning approaches over conventional machine learning techniques. These algorithms are superior to other methods in terms of performance and their ability to lower classification error rates [19].

Numerous deep-learning methods are promising in the medical field. The CNN-LSTM architecture is an effective structure suited for handling classification problems and time-series processing of data. Convolutional neural networks (CNNs) and long short-term memory (LSTM) networks are coupled in this design to make use of their respective advantages in processing sequential input and extracting pertinent information [14]. A crucial aspect of deep learning is the Multilayer Perceptron (MLP), a conventional neural network architecture. Because of its historical relevance and fundamental role in the evolution of neural networks, this

artificial neural network with feedforward algorithms is frequently regarded as a (classical) model [15]. Under deep learning techniques, the Keras framework is excellent at developing sequential stacking models, such as dense layered models, which are well-known for their ability to forecast time-series data. These thick layers are typically fully connected, with each node in one layer connecting to every node in the next, resulting in a chain-like structure [20].

Given the extensive information on diabetes mellitus and the diverse techniques employed for its prediction, we propose an enhanced stacking ensemble model that combines machine and deep learning models for DM prediction.

The contributions for this study are as follows:

- Developing an innovative stacking ensemble model for detecting Diabetes Mellitus by integrating machine learning and deep learning models, utilizing an ensemble of RF, CNN-LSTM, and SDLs models as base learners, with the XGBoost model serving as a meta-learner.
- Merging a combination of ML and DL techniques, including ADASYN, RFECV, GridSearchCV, and Optuna, aimed at refining the performance of the proposed stacking model in detecting DM.

The format of this document is as follows: Section II provides an overview of related work in the area. Section III details the materials and methods used in our research. Section IV presents the experimental setup for our ensemble model. In Section V, we discuss the performance measures. Our results and discussion are covered in Sections VI and VII respectively. In the end, the conclusions are addressed in Section VIII.

II. RELATED WORK

Ensemble learning is a mathematical and analytical methodology that simulates human learning by combining diverse machine learning models to yield more accurate predictions [21-22]. Dutta et al. highlight the importance of ML-based ensemble models in diabetes prediction, advocating the exploration of deep learning techniques alongside ensemble learning, particularly through the stacking method [23]. Ganie and Malik [24] address ensemble methods for detecting Type-2 Diabetes Mellitus, including Bagging, which emphasizes aspects of lifestyle and uses the SMOTE technique that is; (artificial minority oversampling) for dataset rebalancing, validated using cross-validation techniques.

Laila and colleagues [25] investigated effective ensemble algorithms for early-stage prediction of diabetic risks, employing 17 features sourced from the UCI library encompassing diverse datasets. The study employed predictive models, like Ada-Boost, bootstrap aggregation, and RF, and evaluated the proposed model's accuracy and other performance measures. The Random Forest ensemble approach outperformed AdaBoost and Bagging concerning accuracy, scoring 97 percent.

Prasad and Geetha [26] propose an ensemble model utilizing ensemble approaches like bootstrap aggregation, RF, and Ada-boost, together with classification techniques such as

(Naive Bayes). Joshi et al. [27] used the logistic regression model and the decision tree to predict diabetes type-2 in the Pima dataset, with an accuracy reaching 78%.

Javale and Desai [28] delved into elevating healthcare information analytics through the application of an ensemble methodology using machine learning, specifically addressing challenges posed by unbalanced datasets. Their approach incorporated SMOTE and adaptive ADASYN oversampling methods. Various performance evaluation approaches were employed, like train-test split and K-folding. The diabetes dataset underwent an ensemble strategy utilizing the average Stacking-C technique, encompassing classifiers such as K-Nearest Neighbors, Random Forest, and others.

Early DM detection can save human lives and help healthcare workers to control the illness. Many individuals diagnosed with diabetes are unaware of the risk aspects they may be exposed to before the diagnosis happens [25]. Patil et al. [29] introduced an approach for predicting Type-2 Diabetes Mellitus (T2DM) utilizing a stacking ensemble model. The primary aim is to minimize the period between diabetes disease detection and medical checkups. Proposed non-dominated sorting genetic algorithm (second version) stacking model compared against Boosting, bootstrap aggregation, RF, and Random Subspace techniques. Results demonstrate that the proposed ensemble model outperforms the traditional ensemble models, achieving an accuracy of 81 percent.

Zhou et al. [30] introduce an enhanced deep neural network algorithm for diabetes prediction, concentrating on type-1 & type-2 diabetes. Deep learning algorithms, such as Dense Layer Neural Networks [31], MLP models [32], and CNN-based architectures, have demonstrated success in various aspects of diabetes-related activities. Zhu et al.'s [33] comprehensive study emphasizes the superiority of deep learning over traditional machine learning in diabetes diagnosis, glucose management, and complication diagnosis. CNNs are particularly praised for clinical imaging issues, offering feature extraction capabilities. CNN-based architectures are employed to analyze clinical scans, diagnose complications, and assess food images for individuals with diabetes. The emerging field of AI and deep learning holds promising prospects for advancing diabetes applications [16].

Sainte et al. [34] explore new techniques for diabetes prediction, incorporating a wide range of DL methods. A CNN-LSTM model emerges as the most accurate, recording a 95% accuracy in predicting diabetes. The study compares the accuracy of DL models (95%) with that of ML models (68–74%), showcasing the superior performance of deep learning. Kim et al. [16] utilize various deep-learning models, including RNNs, for blood glucose predictions. Gupta et al. [31] offered a Deep Dense Layer Neural Network model for diabetes prediction utilizing the Pima dataset with 768 samples. It was getting an accuracy of 84%. Dense layers are densely connected, meaning each neuron acquires input from all the neurons in the previous layer (each neuron is linked to all neurons of the last layer [31]). The proposed DDLNN model was evaluated by the cross-validation technique to optimize the model performance. Majority voting was utilized to select the best outcomes among the models [31]. Deep learning

techniques have shown remarkable success in various fields, including disease prediction and diagnosis [31]. Table I summarizes the most notable research based on their limits and advantages, as well as the data sources.

TABLE I. SIGNIFICANT INVESTIGATIONS IN DETECTING DIABETES MELLITUS

| Ref. | DATASET SOURCES | Advantages | Limitations |
|--------------------------------|---|---|--|
| M.Gollapalli et al, 2022, [35] | Healthcare institution (KFUH), Saudi Arabia | Applying the Cross-validation method in the training process substantially improves the performance of the ML models. | Insufficient utilization of deep learning models for enhancing outcomes. |
| A. Dutta et al, 2022,[23] | DDC dataset from Bangladesh | Employing the Grid Search-CV technique to optimize the model's performance through fine-tuning its hyperparameters. | Need for more clinical data to enhance the outcomes. |
| A. Singh et al, 2021, [36] | PIMA Indian diabetes, USA | Implementing the Recursive Feature Elimination technique minimizes the dataset's range of features, making the model more reliable with accurate results. | Implementation of the suggested approach in medical life assessment. |
| A. Syed & T. Khan, 2020, [37] | PIMA Indian diabetes, USA | Utilizing the SMOTE technique to balance classes within the dataset, thereby preventing overfitting. | Limited variety in the medical dataset under examination. |
| Chou et al, 2023, [38] | Taipei Municipal medical center, Taiwan | Utilizing Microsoft Machine Learning Studio platform for training the models. | Insufficient utilization of deep learning models for enhancing outcomes. |

III. MATERIALS AND METHODS

This research introduces an ensemble stacking for detecting DM disease, comprising two crucial construction levels. The first level, termed base learners, involves the preparation, training, and initial predictions by a combination of ML and DL models. Predictions from these initial learners are used as inputs for a new model called meta-learner located at the second level and train from the information provided to come up with the final prediction. For our base learners, we have chosen Random Forest, CNN-LSTM, and SDLs due to their distinctive capabilities in classification problems. The XGBoost model is employed at the second level (meta-learner), which assists significantly in managing unbalanced dataset classes' via lowering the loss function and boosting the weight of incorrectly categorized categories. To optimize our base learners, we apply GridSearchCV and Optuna technologies, aiming to achieve the best possible results for Random Forest, CNN-LSTM, and SDLs. Our proposed stacking model incorporates the cross-validation method with several iterations to obtain best findings. Additionally, an adaptive oversampling technique (ADASYN) is implemented

to balance the classes of the Pima dataset investigated in our study and increase the size of the dataset in a way that does not include overfitting issues. Fig. 1 outlines the schema behind our suggested stacking model.

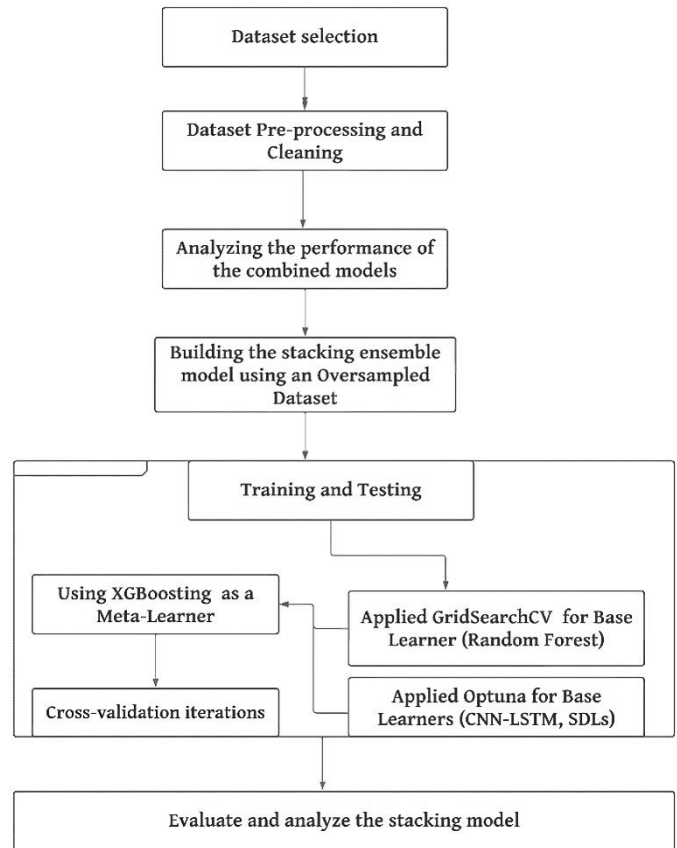


Fig. 1. Proposed stacking model.

A. Stacking

Stacking is an ensemble technique that leverages a "meta-model" to enhance predictive performance by integrating multiple base learners' predictions. In the stacking methodology, there are two distinct levels of model building. At level 1, a set of diverse base learners, each trained on a specific split from the dataset, then produces separated predictions. These predictions serve as input for the meta-learner at level 2 [35].

The goal of the second-level meta-learner is to produce predictions that are reliable and accurate by efficiently combining them [35]. Our proposed model is constructed using the stacking ensemble method, incorporating additional contributions, such as employing cross-validation techniques and leveraging the GridSearchCV hyperparameter tuning method for the Random Forest (RF) base learner. Additionally, Optuna is employed for the CNN-LSTM and SDLs deep learning learners.

The ensemble stacking methodology, as depicted in Fig. 2, involves multiple k-folds cross-validations ($m \times n$) traversing the training dataset and each base learners models. Subsequently, the predictions ($m \times M$) from multiple base learners are entered as inputs to the meta-learner, which learns

from this collective information to generate the final prediction. This approach enhances the model's efficiency for generalization and produces accurate predictions by leveraging the diverse insights from individual base learners and optimizing their combination through the meta-learner. It outperforms other ensemble models in prediction performance, so we have chosen to apply it in our study. The stacking approach aims to provide us with the concept of meta-learning, which can minimize ML model generalization errors [29].

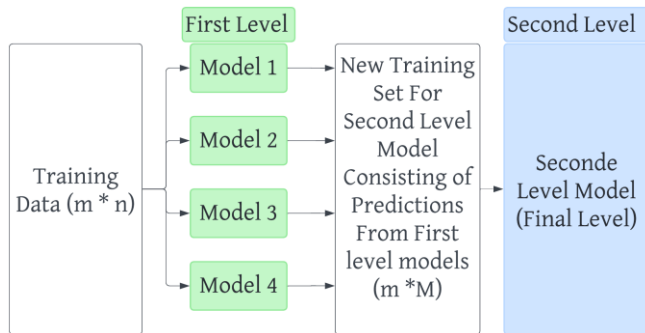


Fig. 2. Stacking ensemble methodology.

B. ADASYN (Adaptive Synthetic sampling)

ADASYN is a data augmentation strategy that addresses unbalanced classes in ML datasets, notably for classification problems. Unbalanced classes happen when the number of samples in specific classes is quite different, resulting in biased model performance [39]. This strategy focuses on the minority class by creating synthetic samples for underrepresented cases. Unlike classic oversampling methods, ADASYN tailors the synthetic sample creation procedure to the local density of minority class instances. This adaptive strategy tries to reduce the risk of overfitting while also improving the model's generalization to previously hidden data [39]. By dynamically altering the creation of synthetic samples, ADASYN aims to improve models' learning ability in the presence of unbalanced data sets, resulting in more robust and accurate classification results [39].

C. Random Forest

Random Forest is an approach to machine learning used for both detection and forecasting problems and plays an important role in optimizing forecasting models [40]. This technique is based on an assembly of trees of decisions, where each tree divides the inputs into categories using a sequence of possibilities [40]. Random Forest adds randomization to the building of decision trees (DT) by:

- 1) For each decision tree, samples are chosen randomly from the initial dataset (training part) with replacement.
- 2) To construct each tree, a subset of variables is randomly chosen.

After generating several result trees, Random Forest combines each of the tree forecasts via votes or averages to reach an overall prediction result. Random Forest can avoid overfitting during the model training. It also uses significance statistics to analyze the effect of every variable on categorization, providing helpful findings [40]. RF is

commonly used in many applications, such as recognizing images, recognition of words and pricing forecasting [40].

D. CNN-LSTM

The CNN-LSTM architecture combines two types of networks: convolutional neural networks and long short-term memory networks. Which is designed to understand the forms and patterns in data and how these shapes evolve over time [14-15-41].

CNNs use convolutional layers to apply filters to input data and extract features hierarchically. These layers detect patterns at various levels of abstraction, gradually learning representations with increasing complexity as data flows through the network. CNNs help in comprehending the patterns and interactions between distinct data components by first scanning the data and assessing spatial arrangements and connections. For example, in diabetes, this application could involve monitoring blood sugar levels throughout the day, analyzing a patient's reactions to medicines or lifestyle modifications, and recording how these factors change over weeks or months [14-15-41].

Subsequently, the LSTM, a form of recurrent neural network, specializes in processing and comprehending sequential input such as time series, text, and speech. LSTM is particularly effective at remembering patterns across time and assessing changes and advancements within a sequence. In the case of diabetes, this could entail tracking changes in blood sugar levels throughout the day, analyzing patient reactions to therapies or lifestyle changes, and understanding how these aspects play out over weeks or months [14-15-41]. The combination of these two networks enables the model to understand the spatial positioning of pieces in the data and their time evolution [17-21].

E. Sequential Dense Layers (SDLs)

The Sequential Dense Layers Model, built with the Keras framework, is a modern neural network structure that layered stack [20]. This model is based on tightly connected layers, which form a chain-like structure with each node in one layer connecting to every node in the next layer [20]. This design, similar to an ordered manufacturing line, allows for the systematic flow of information from one processing unit to the next, enabling methodical data analysis [32]. The SDLs model excels in terms of clarity and efficiency, establishing a wall layer by layer, with each layer executing specialized computations on the data [20]. Its sequential technique facilitates thorough data processing and feature extraction, and it is adept at discovering nuanced patterns in large datasets [32]. Furthermore, the model excels at extracting relevant temporal features, which improves its capacity to detect significant patterns in time series data. This skill is essential for making good forecasts in time-series forecasting jobs [20-32].

F. GridSearchCV

GridSearchCV is a well-known method of ML applications for its ability to identify optimal hyperparameter values for a certain model. These hyperparameters, like the number of batches in neural networks, can control the configuration and behavior of the model. GridSearchCV involves a systematic exploration of various hyperparameter combinations and

assessing the performance using a Cross-validation method. It entails establishing a collection of potential hyperparameter parameters, training and evaluating that model through every combination, and finally picking the best combination that produces the most accurate results [23]. This systematic approach improves the model's performance and mitigates the overfitting occurrences.

G. Optuna

Optuna, introduced in 2019 by Akiba et al., is a free hyperparameter tuning framework designed to streamline the trial-and-error process in optimizing model training accuracy [42-43]. It employs a targeted API-based strategy, allowing the automatic optimization of hyperparameter values for various machine learning algorithms within a specified trial limit. Versatile and 'pythonic' in operation, Optuna makes no distinction between machine learning and deep learning frameworks [42-43]. In this research, Optuna was utilized to tune hyperparameters such as dense layers units, batch size, activation function, loss function and others. The optimized values, including "sigmoid" activation function, three Dense layers units, batch size, reduction factor, and min early stopping rate, resulted in the best validation accuracy with the "binary cross entropy" loss function. Optuna's approach significantly enhances hyperparameter tuning efficiency, contributing to improved model performance and accuracy.

H. Recursive Feature Elimination with Cross-Validation

RFECV is a wrapping approach that eliminates unwanted features, enhances model generalization by preserving independent and effective features while eliminating duplicate and weak ones with minimal impact on training error. Employing an iterative feature ranking method, it conducts backward feature reduction. Initially, the model is built with the entire feature set, ranking each feature based on relevance. The least significant feature is then eliminated, and the process repeats iteratively. The sequence number, T , serves as the feature ranking, and T_i represents the top-ranked features used in each iteration. The final model incorporates the best-performing features, and the optimal value of T_i is selected [44], [45]. In our research, this technique was applied, resulting in the identification of the best training features.

I. Extreme Gradient-Boosting

XGBoost, derived from the gradient-boosting decision tree developed by Tianqi Chen et al. [46], is a well-known machine learning model known for its adaptability and efficiency. Unlike GBDT, XGBoost employs regularization methods to minimize model complexity and reduce overfitting. The algorithm employs an approximation approach to enhance gradient boosting, focusing on finding the optimal split for improved expandability and efficiency. XGBoost introduces features like parallel operations and early stopping to expedite model execution, with the added advantage of increased classification accuracy [9]. According to Zhao et al. [10], XGBoost effectively prevents overfitting in training models. Additionally, its built-in parallel processing ability allows for higher training speeds.

Furthermore, the XGBoost model can gain insight from unbalanced learning data by adjusting the weights of classes.

XGBoost is among the best models for dealing with unbalanced datasets, particularly if the class distribution has low variance [11].

XGBoost works with a number of weak learners and enhances their performance via an enhancement strategy.

In conclusion, XGBoost stands out as a potent and widely embraced tool in the field of machine learning. Its effectiveness extends to solving intricate problems and significantly enhancing the performance of predictive models.

J. Cross-validation

Cross-validation (CV) in machine learning is a common resampling data approach to verify the generalization of a prediction model without going overboard. It entails partitioning the dataset across folds throughout the training and testing phases, with each "fold" being a subset generated for analysis. The dataset's samples will be allocated to the previously mentioned (the folds) randomly with no repetition. Throughout each iteration, the $k-1$ subset serves as the training set employed to train the model, while the remaining subset, known as the "unseen dataset," is used to assess the model's performance. This iterative method will continue until all k -subsets have been used as validation sets [47]. Fig. 3 depicts the cross-validation method [48]. To improve the results, our stacking model enabled cross-validation using 5-fold splits.

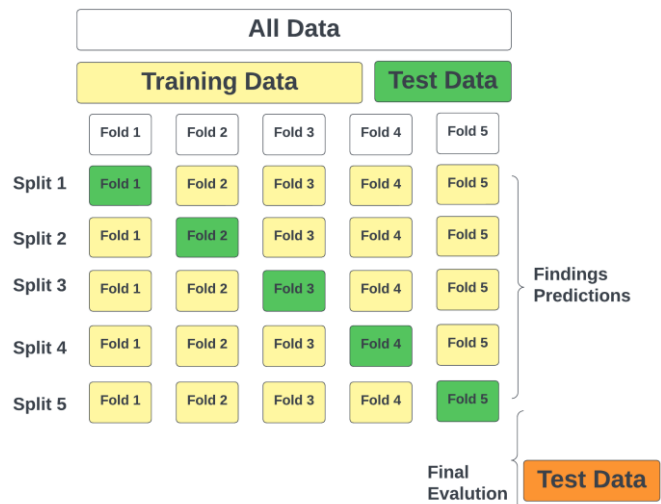


Fig. 3. Cross-validation technique.

K. Study Data

The Pima dataset is a popular dataset for machine learning and data analytics. It belongs to the Pima indigenous community from Arizona, USA. This dataset is often utilized for predicting diabetes diseases using machine learning models [35]. It is accessible publicly in the Kaggle repository at <https://www.kaggle.com/datasets/uciml/pima-indians-diabetes-database>.

This dataset included 268 patients who have diabetes and 500 who have no diabetes, with 8 characteristics listed in Table II. [35].

The Pima dataset serves as a common benchmark for exploring a range of machine learning models, such as random

forest and XGboost. However, it's important to recognize that while the PIMA dataset is valuable for instructional uses and testing machine learning models, it does have limits. These limitations originate from its small size, values missed, and possible biases. As a result, it is prudent to take care when making assumptions or creating prediction models based exclusively on this dataset for applications in real life.

TABLE II. PIMA DATASET METADATA

| Dataset columns | | | |
|-----------------|----------------------------|-------|----------|
| # | Column | Count | Datatype |
| 0 | Pregnancies | 768 | int64 |
| 1 | Glucose | 768 | int64 |
| 2 | Blood Pressure | 768 | int64 |
| 3 | Skin Thickness | 768 | int64 |
| 4 | Insulin | 768 | int64 |
| 5 | BMI | 768 | float64 |
| 6 | Diabetes Pedigree Function | 768 | float64 |
| 7 | Age | 768 | int64 |
| 8 | Outcome | 768 | int64 |

L. Validation Dataset

To assess the efficacy of our introduced stacking model, we conducted validation using a newly acquired diabetes dataset. This dataset is known as the Diabetes Prediction Dataset (DPD). It is a publicly available compilation of electronic health records. These records encompass digital archives of patients' medical histories, diagnoses, treatments, and outcomes. EHRs are frequently collected and stored by healthcare institutions such as medical facilities as a component of their usual clinical protocols. With a large dataset comprising about 100,000 records, the DPD dataset can contribute perfectly to evaluating the performance of the proposed model.

It can be accessed on the Kaggle through the following link: <https://www.kaggle.com/datasets/iammustafatz/diabetes-prediction-dataset>. Table III outlines the features present in the DPD dataset.

TABLE III. DPD DATASET METADATA

| Dataset Columns | | | |
|-----------------|---------------------|-------------|----------|
| # | Column | Null values | Datatype |
| 0 | Gender | Not null | object |
| 1 | Age | Not null | float64 |
| 2 | hypertension | Not null | int64 |
| 3 | Heart disease | Not null | int64 |
| 4 | Smoking history | Not null | object |
| 5 | BMI | Not null | float64 |
| 6 | HbA1c_level | Not null | float64 |
| 7 | Blood_glucose_level | Not null | int64 |
| 8 | Diabetes | Not null | int64 |

IV. EXPERIMENTAL SETUP

In this study, we employed Jupyter Notebook to construct our stacking model, utilizing a Microsoft Intel (R) Core i5-1035G7 CPU operating at 1.20 GHz and 8 GB of RAM. The Pima dataset was chosen to examine our proposed model. Due to some defects found in the dataset, we decided to preprocess the dataset and clean up these defects, such as zero values in some feature columns. We handle this issue by imputing the mean or median for each feature column based on his data distribution. The base learners' models were initialized with a Random Forest model, and we utilized the Grid-searchCV Hyperparameters Tuner to optimize their performance. The hyperparameters in the tuning process were such as bootstrap training, min_samples_split, and n_estimators. Second and third-base learners, CNN-LSTM, and SDL models optimized via the Optuna optimizer have the following parameters: number of convolutional layers, filter and kernel sizes, activation functions, dropout rates, early shopping, and pooling strategies. Also, Optuna was used for the third base learner, Sequential Dense Layers, with three dense layers.

We implemented the XGBoost model as a meta-learner to tackle the problem of imbalanced datasets, along with the ADASYN (Adaptive Synthetic Sampling) technique for oversampling our study dataset, which frequently results in overfitting and inconsistencies in the results. XGBoost uses an ensemble learning approach, enabling us to effectively handle unbalanced dataset classes. Additionally, we used a cross-validation method with a 5-fold validation for the training of Random Forest (RF), the base learner, and the stacking model in general. We used the GridSearchCV hyperparameter method to improve the RF performance. The Recursive Feature Elimination with Cross-Validation technique was applied to enhance model performance by systematically eliminating less informative features during the training process. Lastly, we tested our suggested stacking model using a DPD dataset with 100,000 records.

V. PERFORMANCE MEASURE

We evaluated the effectiveness of our ensemble learners using the next metrics:

A. Accuracy

It measures the percentage of the predication data that were accurately predicted from all given data. It assesses how well the algorithm can distinguish between positive and negative instances [35]. The definition of accuracy is captured by Eq. (1).

$$Acc = \frac{TP+TN}{TP+TN+FP+FN} \quad (1)$$

Assuming the outcome for patient P indicates that there is a presence of diabetes (+DM) or NOT (-DM).

- True positive (TP): if the outcome is +DM, then P is diabetic.
- True negative (TN): if the outcome is -DM, then P is non-diabetic.
- False positive (FP): if the outcome is +DM, then P is non-diabetic.

- False negative (FN): if the outcome is -DM, then P is diabetic.

B. Precision

It evaluates how well the positive values are predicted. When the model accurately categorizes predictions as positive when it asserts, they are, so we have a strong precision score [35]. Eq. (2) can be utilized to represent precision.

$$Precision = \frac{TP}{TP+FP} \quad (2)$$

Assuming the outcome for patient P indicates that there is a presence of diabetes (+DM) or NOT (-DM).

- True positive (TP): if the outcome is +DM, then P is diabetic.
- False positive (FP): if the outcome is +DM, then P is non-diabetic.

C. Recall

Expressed as the sensitivity or the actual positive ratio. The remarkable recall rating means that most positive predicted values are correctly true according to the model data [35]. Recall can be expressed using Eq. (3).

$$Recall = \frac{TP}{TP+FN} \quad (3)$$

Assuming the outcome for patient P indicates that there is a presence of diabetes (+DM) or NOT (-DM).

- True positive (TP): if the outcome is +DM, then P is diabetic.
- False negative (FN): if the outcome is -DM, then P is diabetic.

D. Cohen's Kappa Metric

It assesses the agreement between two class targets and evaluates the concordance between the model predictions and the real results. It is valuable when confronted with unbalanced classes [35]. Eq. (4) can be employed to denote Cohen's Kappa Score.

$$CKS = \frac{P_o - P_e}{1 - P_e} \quad (4)$$

Here, P₀ shows the models' accuracy, whereas P_e reflects the correlation between the expected and real values [35].

E. F1-Score

The F1-score, a standard measure used in binary classification problems, is determined as a harmonic average of precision and recall, considering both precision in properly identifying positive cases and recall in capturing all positive cases [53]. Provided by the Eq. (5):

$$F1 = 2 \times \frac{Precision \times Recall}{Precision + Recall} \quad (5)$$

F. Receiver Operating Characteristic: Area Under the Curve (ROC-AUC)

It evaluates the effectiveness of a classification model by assessing its ability to distinguish between positive and

negative instances across various decision thresholds. It is particularly useful for imbalanced classes or when the model needs to be evaluated at different levels of sensitivity and specificity [23].

Utilizing a diverse range of metrics, including accuracy, precision, recall, Cohen's Kappa, and ROC-AUC, is paramount for gaining deep insights into the performance of classification models. These metrics offer nuanced perspectives on the model's strengths and weaknesses, illuminating its ability to accurately classify instances, detect true positives while minimizing false positives and false negatives, and maintain consistency in predictions. By comprehensively assessing these metrics, practitioners can decipher the intricacies of model behavior and make informed decisions regarding model selection, optimization, and deployment strategies.

VI. RESULTS

In this study, we constructed a stacking ensemble model for detecting diabetes mellitus disease utilizing an ensemble of ML and DL techniques. Our proposed model comprised base learners' models including random forest, CNN-LSTM, and SDLs, with the extreme gradient boosting model working as the meta-learner. Additionally, several methods like ADASYN, Optuna, RFECV, cross-validation, and GridSearchCV were employed to refine the model's performance. Furthermore, we addressed the issue of zeros in certain feature columns of the Pima dataset by replacing them with values derived from the median or median of data distribution based on whether the type of distribution is normal or skewed. The proposed model achieved a remarkable 99% accuracy in detecting diabetes mellitus disease using the Pima dataset. Moreover, we assessed the model's effectiveness on a sizable dataset comprising approximately 100,000 records, referred to as the DPD dataset, achieving an accuracy of 97%. More details are focused on the discussion section.

A. Stacking Model Performance

In this study, several performance metrics were applied to evaluate the effectiveness of our proposed model, which integrates both ML and DL techniques. The outcomes of multiple metrics are presented in Table IV.

TABLE IV. THE STACKING MODEL PERFORMANCE RESULTS

| Accuracy Score | ROC-AUC Score | Cohen's Kappa Score | Precision Score | Recall Score | Accuracy Score |
|----------------|---------------|---------------------|-----------------|--------------|----------------|
| 0.9887 | 0.99 | 0.98970 | 0.9934 | 0.995 | 0.9887 |

VII. DISCUSSION

A. Results using Oversampling ADASYN

In this experiment, an ensemble of Machine Learning and Deep Learning techniques was used to detect the occurrence of diabetes mellitus disease. Fig. 1 elucidates the methodology of our proposed model, where each Random Forest (RF), CNN-LSTM, and SDLs was initialized as initial learners, and an XGBoost model was designated as the meta-learner. Additionally, the GridSearchCV Hyperparameters optimizer was utilized to determine best findings for the Random Forest model, also Optuna optimizer for CNN-LSTM and SDLs

models. To address the challenge of imbalanced datasets and mitigate overfitting, we applied the ADASYN (Adaptive Synthetic Sampling) technique for oversampling the study data. This increased the Pima dataset from 768 records to 4870 records in an adaptive manner to avoid overfitting and increase the size of the data set. Additionally, the XGBoost model served as a meta-learner, utilizing ensemble learning to handle class imbalances effectively.

For robust evaluation, a CV method was used in our proposed model, employing 5-fold cross-validation. Table V presents the comprehensive outcomes of our proposed model. Furthermore, Table VI displays the results of both the base models and the final model.

TABLE V. THE STACKING MODEL FINDINGS

| Targets | Precision | Recall | F1-score support | Support |
|------------------|-----------|--------|------------------|---------|
| 0 | 1.0 | 0.99 | 1.0 | 515 |
| 1 | 0.99 | 1.0 | 0.99 | 459 |
| Model Accuracy | | | 0.99 | 974 |
| Macro average | 0.99 | 0.99 | 0.99 | 974 |
| Weighted average | 0.99 | 0.99 | 0.99 | 974 |

TABLE VI. THE META AND BASE MODELS FINDINGS

| # | Model | Score |
|---|-------------------------|-------|
| 0 | Sequential Dense Layers | 0.98 |
| 1 | CNN-LSTM | 0.94 |
| 2 | Random Forest | 0.98 |
| 3 | Stacking Model | 0.98 |

B. Results using ADASYN & RFECV

In this experiment, we employed the ADASYN technique that mentioned in point 7.1 plus the RFECV technique, which is a pivotal step in enhancing the performance of a stacking ensemble model. The aim was to optimize feature selection, thereby improving the overall effectiveness of the ensemble. Our investigation successfully identified a set of six optimal features. These features are glucose, blood pressure, insulin, BMI, diabetes pedigree function, and age. After that, we examined the proposed model on the selected features, and the results were as follows in Table VII:

TABLE VII. THE STACKING MODEL FINDINGS USING RFECV

| Targets | Precision | Recall | F1-score support | Support |
|------------------|-----------|--------|------------------|---------|
| 0 | 0.99 | 0.96 | 0.97 | 515 |
| 1 | 0.95 | 0.99 | 0.97 | 459 |
| Model Accuracy | | | 0.97 | 974 |
| Macro average | 0.97 | 0.97 | 0.97 | 974 |
| Weighted average | 0.97 | 0.97 | 0.97 | 974 |

C. Results on the Validation Dataset

In this latest experiment, the proposed stacking model underwent rigorous testing on a substantial test dataset comprising approximately 100,000 electronic patient records. Notably, the experiment deliberately abstained from employing the RFECV technique. The results obtained from this comprehensive evaluation revealed significant new perspectives into our model performance and its ability to handle the complexity inherent in the diverse patient data. These findings contribute valuable information to the ongoing discourse on the effectiveness of stacking models in healthcare analytics, shedding light on their potential without the aid of feature selection techniques. Table VIII shows the results after applying the proposed model.

TABLE VIII. THE STACKING MODEL FINDINGS ON DPD DATASET

| Targets | Precision | Recall | F1-score support | Support |
|------------------|-----------|--------|------------------|---------|
| 0 | 0.97 | 1.0 | 0.98 | 18292 |
| 1 | 0.97 | 0.69 | 0.81 | 1708 |
| Model Accuracy | | | 0.97 | 20000 |
| Macro average | 0.97 | 0.85 | 0.90 | 20000 |
| Weighted average | 0.97 | 0.97 | 0.97 | 20000 |

D. Comparative Evaluation with Existing Work

1) *First study:* The ensemble stacking model for diabetes detection proposed by S. Härner and D. Ekman in 2022 [13] integrates various ML models, such as DT and Naive Bayes (NB) models, and leverages Pima Dataset. The study's findings demonstrate a 75.56% accuracy in predicting diabetes using this stacking approach. However, it is important to note certain limitations highlighted in the study, like the absence of a hyperparameter tuner to systematically search for optimal hyperparameters for the base learners within the stacking model.

2) *Second study:* Patil et al. (2023) [29] introduced a stacking model for diabetes detection, utilizing ML techniques including decision trees, NB, multilayer perceptron, support vector machines SVMs, and K-Nearest Neighbor KNN. This study utilized the Pima dataset and reported an 82% accuracy in diabetes prediction using the stacking model. Also, the absence of any mention of the CV technique in their suggested model is noteworthy, as this technique is crucial for robustly constructing the stacking model. Additionally, the study did not employ an optimizer to systematically search for optimal hyperparameters during the training of base learners, which could potentially enhance the overall model performance.

3) *Third study:* Lei Qin (2022) [49] presented a stacking model for diabetes detection that combined diverse ML techniques such as LR, KNN, DT, Gaussian Naive Bayes, and SVMs. Employing the Pima dataset, findings showed an accuracy of 81.6% in predicting diabetes. However, there are lack of a hyperparameter tuner for the hyperparameters in initial learner model training may restrict the pursuit of improved findings. Furthermore, the study acknowledged the

challenge posed by the dataset's restricted size, which could influence the achievement of ideal outcomes.

4) *Forth study*: Kumari et al. (2021) [50] suggested a soft voting approach for diabetes prediction, incorporating ML techniques like RF, LR and NB. Utilizing the same Pima dataset, their findings demonstrated a 79.04% accuracy in predicting diabetes. Notably, the proposed methodology excluded CV method, which is assuring reliability by evaluating the efficacy of the ML models among diverse of data samples, hence increasing the overall effectiveness of the predictions to the proposed model.

5) *Fifth study*: Bhopte and Rai (2022) [51] employed the CNN-LSTM model to detect DM disease using Pima dataset, achieving an accuracy of 89.30%. However, the study acknowledged limitations, specifically the absence of an optimizer for systematically searching hyperparameters to optimize results during the model development process.

6) *Sixth study*: Niharika et al. (2022) [52] utilized the MLP model to predict diabetes, employing the Pima dataset and achieving a 77% accuracy. The study highlighted limitations, including concerns about the sample size used and

the necessity for employing diverse DL techniques for disease prediction, specifically regarding various types of diabetes.

So, Compared to all six studies [13-29-49-50-51-52], our proposed stacking model exhibits higher accuracy in diabetes mellitus detection. In our methodology, we harnessed the power of GridsearchCV and Optuna optimizers to find the optimal hyperparameters in the base learners that are supported with dataset using the oversampling ADASYN method. Notably, these optimization techniques were absent in the First, Second, Third, Fourth, and Fifth Studies.

Additionally, Optuna was not utilized in the Sixth Study. The integration of these optimization techniques significantly improved the learning process of our base learners, resulting in the extraction of optimal results. It is crucial to highlight that the [29–50–51] research studies did not apply cross-validation, which is a critical method for evaluating a prediction model's generalization ability. Whereas our approach used this method for performing k-fold cross-validation iterations, this method successfully analyzed and prevented overfitting, significantly improving the quality of our predictive model. Table IX emphasizes the differences and benefits of our study compared to others, underscoring the major improvements in our proposed model.

TABLE IX. ASSESSMENT WITH THE EXISTING INVESTIGATIONS

| Authors | Approaches | Studies Dataset | Accuracy |
|--|---|-----------------|----------|
| S. Härner and D. Ekman (2022) | Ensemble Stacking approach. (DT, NB, Cross-validation). | Pima dataset | 75.6% |
| Patil et al (2023) | Ensemble Stacking approach. (DT, NB, multilayer perceptron, SVM, and KNN). | Pima dataset | 81.9% |
| Bhopte and Rai (2022) | CNN-LSTM. | Pima dataset | 89.30% |
| Niharika et al. (2022) | Multilayer perceptron (MLP), GridSearchCV. | Pima dataset | 77% |
| Lei Qin (2022) | Ensemble Stacking approach. (LR, K-NN, DT, Gaussian Naive Bayes, and SVM). | Pima dataset | 82% |
| Kumari et al (2021) | Ensemble Soft voting approach. (RF, LR, and NB). | Pima dataset | 79.04% |
| Our proposed model | Ensemble Stacking approach. (RF, CNN-LSTM, SDLs, XGboost) ADASYN GridSearchCV, Optuna, Cross-validation, RFECV. | Pima Dataset | 99% |
| Our proposed model on the validation dataset | Ensemble Stacking approach. (RF, CNN-LSTM, SDLs, XGboost) GridSearchCV, Cross-validation. | DPD Dataset | 97% |

VIII. CONCLUSION

Diabetes mellitus is a prevalent condition that poses a significant threat to public health, giving rise to various severe complications like renal failure, cardiovascular disorders, and sightlessness. In our study, we introduce an innovative stacking model designed for detecting diabetes mellitus diasease at early stage, utilizing the Pima dataset and integrating both ML and DL models using ADASYN oversampling method. The ensemble comprises Random Forest (RF), CNN-LTSM, and SDLs as base learner models, with XGBoost serving as the Meta-Learner model. Cross-validation techniques were applied for the meta learner. Moreover, incorporating Grid Search optimization for the RF model and adopting Optuna optimization for the CNN-LTSM and SDLs models to secure optimal results. To mitigate the challenges posed by an imbalanced dataset, which can lead to over-fitting and unexpected outcomes, the XGBoost model is employed as a

meta-learner. Additionally, our study dataset underwent preprocessing to address zero values, which could adversely impact prediction accuracy, particularly in columns like blood and glucose. To tackle this issue, zero values were replaced with the median or mean from the total values in each feature column, considering the feature data distribution type. REFCV technique was applied to our proposed model. The results highlight the efficacy of our proposed model in detecting DM, achieving an accuracy of 99% across the Pima dataset and 97% in the DPD dataset. As a recommendation, our stacking model holds potential for deployment in diagnostic applications for diabetes mellitus. Furthermore, its performance can be validated on larger and more diverse datasets to enhance precision. Additionally, exploring the use of deep-learning models to uncover new patterns for robust diabetes diagnosis, applicable across different diabetes types (T1DM, T2DM, and gestational diabetes), is recommended.

REFERENCES

- [1] H. Sone, "Diabetes Mellitus", in *Encyclopedia of Cardiovascular Research and Medicine*, R. S. Vasan and D. B. Sawyer, Eds., Oxford: Elsevier, 2018, pp. 9–16.
- [2] T. Andoh, "Subchapter 19A - Insulin", in *Handbook of Hormones*, Y. Takei, H. Ando, and K. Tsutsui, Eds., San Diego: Academic Press, 2016, pp. 157-e19A-3.
- [3] J. Hippisley-Cox and C. Coupland, "Diabetes treatments and risk of amputation, blindness, severe kidney failure, hyperglycaemia, and hypoglycaemia: open cohort study in primary care", *BMJ*, p. i1450, Mar. 2016.
- [4] A. N. Baanders and M. J. W. M. Heijmans, "The Impact of Chronic Diseases: The Partner's Perspective", *Family & Community Health*, vol. 30, no. 4, pp. 305–317, Oct. 2007.
- [5] P. Saeedi et al., "Global and regional diabetes prevalence estimates for 2019 and projections for 2030 and 2045: Results from the International Diabetes Federation Diabetes Atlas, 9th edition", *Diabetes Research and Clinical Practice*, vol. 157, p. 107843, Nov. 2019.
- [6] C. V. A. Collares et al., "Transcriptome meta-analysis of peripheral lymphomononuclear cells indicates that gestational diabetes is closer to type 1 diabetes than to type 2 diabetes mellitus", *Mol Biol Rep*, vol. 40, no. 9, pp. 5351–5358, Sep. 2013.
- [7] A. E. Butler and D. Misselbrook, "Distinguishing between type 1 and type 2 diabetes", *BMJ*, p. m2998, Aug. 2020.
- [8] G. Roglic, "WHO Global report on diabetes: A summary," in *International Journal of Noncommunicable Diseases*, vol. 1, no. 1, p. 3, 2016.
- [9] C.-C. Chang, Y.-Z. Li, H.-C. Wu, and M.-H. Tseng, "Melanoma Detection Using XGB Classifier Combined with Feature Extraction and K-Means SMOTE Techniques", *Diagnostics*, vol. 12, no. 7, p. 1747, Jul. 2022.
- [10] Z. Zhao, H. Peng, C. Lan, Y. Zheng, L. Fang, and J. Li, "Imbalance learning for the prediction of N6-Methylation sites in mRNAs", *BMC Genomics*, vol. 19, no. 1, p. 574, Dec. 2018.
- [11] N. H. N. B. M. Shahri, S. B. S. Lai, M. B. Mohamad, H. A. B. A. Rahman, and A. B. Rambli, "Comparing the Performance of AdaBoost, XGBoost, and Logistic Regression for Imbalanced Data", *ms*, vol. 9, no. 3, pp. 379–385, May 2021.
- [12] L. Breiman, "Random Forests", *Machine Learning*, vol. 45, no. 1, pp. 5–32, Oct. 2001.
- [13] D. Ekman, "Comparing Ensemble Methods with Individual Classifiers in Machine Learning for Diabetes Detection," *KTH Royal Institute of Technology in Stockholm, Sweden*, 2022.
- [14] I. E. Livieris, E. Pintelas, and P. Pintelas, "A CNN-LSTM model for gold price time-series forecasting", *Neural Comput & Applic*, vol. 32, no. 23, pp. 17351–17360, Dec. 2020.
- [15] I. H. Sarker, "Deep Cybersecurity: A Comprehensive Overview from Neural Network and Deep Learning Perspective", other, preprint, Feb. 2021.
- [16] D.-Y. Kim et al., "Intelligent Ensemble Deep Learning System for Blood Glucose Prediction Using Genetic Algorithms", *Complexity*, vol. 2022, pp. 1–10, Oct. 2022.
- [17] Department of Computer Science and Engineering, Khulna University of Engineering & Technology, Khulna-9203, Bangladesh, S. Islam Ayon, and Md. Milon Islam, "Diabetes Prediction: A Deep Learning Approach", *IJIEEB*, vol. 11, no. 2, pp. 21–27, Mar. 2019.
- [18] Y. LeCun, Y. Bengio, and G. Hinton, "Deep learning", *Nature*, vol. 521, no. 7553, pp. 436–444, May 2015.
- [19] A. Thammano and A. Meengen, "A New Evolutionary Neural Network Classifier", in *Advances in Knowledge Discovery and Data Mining*, T. B. Ho, D. Cheung, and H. Liu, Eds., in *Lecture Notes in Computer Science*, vol. 3518. Berlin, Heidelberg: Springer Berlin Heidelberg, 2005, pp. 249–255.
- [20] A. Ameh Joseph, M. Abdullahi, S. B. Junaidu, H. Hassan Ibrahim, and H. Chiroma, "Improved multi-classification of breast cancer histopathological images using handcrafted features and deep neural network (dense layer)", *Intelligent Systems with Applications*, vol. 14, p. 200066, May 2022.
- [21] T. G. Dietterich, "Ensemble Methods in Machine Learning", in *Multiple Classifier Systems*, in *Lecture Notes in Computer Science*, vol. 1857. Berlin, Heidelberg: Springer Berlin Heidelberg, 2000, pp. 1–15.
- [22] L. Kuncheva, "Combining Pattern Classifiers Methods and Algorithms, Second Edition." Hoboken, NJ: Wiley, 2014.
- [23] A. Dutta et al., "Early Prediction of Diabetes Using an Ensemble of Machine Learning Models", *IJERPH*, vol. 19, no. 19, p. 12378, Sep. 2022.
- [24] S. M. Ganie and M. B. Malik, "An ensemble Machine Learning approach for predicting Type-II diabetes mellitus based on lifestyle indicators", *Healthcare Analytics*, vol. 2, p. 100092, Nov. 2022.
- [25] U. e Laila, K. Mahboob, A. W. Khan, F. Khan, and W. Taekeun, "An Ensemble Approach to Predict Early-Stage Diabetes Risk Using Machine Learning: An Empirical Study", *Sensors*, vol. 22, no. 14, p. 5247, Jul. 2022.
- [26] G. Geetha and K. M. Prasad, "An Hybrid Ensemble Machine Learning Approach to Predict Type 2 Diabetes Mellitus", *WEB*, vol. 18, no. Special Issue 02, pp. 311–331, Apr. 2021.
- [27] R. D. Joshi and C. K. Dhakal, "Predicting Type 2 Diabetes Using Logistic Regression and Machine Learning Approaches", *IJERPH*, vol. 18, no. 14, p. 7346, Jul. 2021.
- [28] D. Pankaj Javale and S. Suhas Desai, "Machine learning ensemble approach for healthcare data analytics", *IJECS*, vol. 28, no. 2, p. 926, Nov. 2022.
- [29] R. N. Patil, S. Rawandale, N. Rawandale, U. Rawandale, and S. Patil, "An efficient stacking based NSGA-II approach for predicting type 2 diabetes", *IJECE*, vol. 13, no. 1, p. 1015, Feb. 2023.
- [30] H. Zhou, R. Myrzashova, and R. Zheng, "Diabetes prediction model based on an enhanced deep neural network", *J Wireless Com Network*, vol. 2020, no. 1, p. 148, Dec. 2020.
- [31] N. Gupta, B. Kaushik, M. Khalid Imam Rahmani, and S. Anwar Lashari, "Performance Evaluation of Deep Dense Layer Neural Network for Diabetes Prediction", *Computers, Materials & Continua*, vol. 76, no. 1, pp. 347–366, 2023.
- [32] F. Nazari and W. Yan, "Convolutional versus dense neural networks: comparing the two neural networks" performance in predicting building operational energy use based on the building shape", presented at the 2021 Building Simulation Conference, Sep. 2021.
- [33] T. Zhu, K. Li, P. Herrero, and P. Georgiou, "Deep Learning for Diabetes: A Systematic Review", *IEEE J. Biomed. Health Inform.*, vol. 25, no. 7, pp. 2744–2757, Jul. 2021.
- [34] Larabi-Marie-Sainte, Aburahmah, Almohaini, and Saba, "Current Techniques for Diabetes Prediction: Review and Case Study", *Applied Sciences*, vol. 9, no. 21, p. 4604, Oct. 2019.
- [35] M. Gollapalli et al., "A novel stacking ensemble for detecting three types of diabetes mellitus using a Saudi Arabian dataset: Pre-diabetes, T1DM, and T2DM", *Computers in Biology and Medicine*, vol. 147, p. 105757, 2022.
- [36] A. Singh, A. Dhillon, N. Kumar, M. S. Hossain, G. Muhammad, and M. Kumar, "eDiaPredict: An Ensemble-based Framework for Diabetes Prediction", *ACM Trans. Multimedia Comput. Commun. Appl.*, vol. 17, no. 2s, pp. 1–26, Jun. 2021.
- [37] A. H. Syed and T. Khan, "Machine Learning-Based Application for Predicting Risk of Type 2 Diabetes Mellitus (T2DM) in Saudi Arabia: A Retrospective Cross-Sectional Study", *IEEE Access*, vol. 8, pp. 199539–199561, 2020.
- [38] C.-Y. Chou, D.-Y. Hsu, and C.-H. Chou, "Predicting the Onset of Diabetes with Machine Learning Methods", *JPM*, vol. 13, no. 3, p. 406, Feb. 2023.
- [39] Haibo He, Yang Bai, E. A. Garcia, and Shutao Li, "ADASYN: Adaptive synthetic sampling approach for imbalanced learning", in *2008 IEEE International Joint Conference on Neural Networks (IEEE World Congress on Computational Intelligence)*, Hong Kong, China: IEEE, Jun. 2008, pp. 1322–1328.

- [40] Q. Zou, K. Qu, Y. Luo, D. Yin, Y. Ju, and H. Tang, "Predicting Diabetes Mellitus With Machine Learning Techniques", *Front. Genet.*, vol. 9, p. 515, Nov. 2018.
- [41] C. C. Aggarwal, "Neural Networks and Deep Learning: A Textbook", Cham: Springer International Publishing, 2018.
- [42] T. Akiba, S. Sano, T. Yanase, T. Ohta, and M. Koyama, "Optuna: A Next-generation Hyperparameter Optimization Framework". *arXiv*, Jul. 25, 2019.
- [43] M. Krishnamoorthy, M. S. A. Hameed, T. Kopinski, and A. Schwung, "Disease Prediction Based on Individuals Medical History Using CNN", in 2021 20th IEEE International Conference on Machine Learning and Applications (ICMLA), Pasadena, CA, USA: IEEE, Dec. 2021, pp. 89–94.
- [44] M. Maalouf, "Logistic regression in data analysis: an overview", *IJDATS*, vol. 3, no. 3, p. 281, 2011.
- [45] P. Misra and A. S. Yadav, "Improving the Classification Accuracy using Recursive Feature Elimination with Cross-Validation", 2020.
- [46] T. Chen and C. Guestrin, "XGBoost: A Scalable Tree Boosting System", in Proceedings of the 22nd ACM SIGKDD International Conference on Knowledge Discovery and Data Mining, San Francisco California USA: ACM, Aug. 2016, pp. 785–794.
- [47] D. Berrar, "Cross-Validation", in *Encyclopedia of Bioinformatics and Computational Biology*, Elsevier, 2019, pp. 542–545.
- [48] F. Pedregosa et al., "Scikit-learn: Machine Learning in Python", *Journal of Machine Learning Research*, vol. 12, no. 85, pp. 2825–2830, 2011.
- [49] L. Qin, "A Prediction Model of Diabetes Based on Ensemble Learning", in Proceedings of the 2022 5th International Conference on Artificial Intelligence and Pattern Recognition, Xiamen China: ACM, Sep. 2022, pp. 45–51.
- [50] S. Kumari, D. Kumar, and M. Mittal, "An ensemble approach for classification and prediction of diabetes mellitus using soft voting classifier", *International Journal of Cognitive Computing in Engineering*, vol. 2, pp. 40–46, Jun. 2021.
- [51] M. Bhopte and M. Rai, "Hybrid Deep learning CNN-LSTM Model for Diabetes Prediction", *International Journal of Scientific Research*, vol. 8, no. 1, 2022.
- [52] M. Niharika, M. Gousia, M. G. Priya, O. P. Kalyani, R. Vasavi, and D. Sowjanya, "CLASSIFICATION OF DIABETES USING MLP CLASSIFIER", vol. 9, no. 5, 2022.
- [53] S. A. Hicks et al., "On evaluation metrics for medical applications of artificial intelligence", *Sci Rep*, vol. 12, no. 1, p. 5979, Apr. 2022, doi: 10.1038/s41598-022-09954-8.

Leveraging Machine Learning Methods for Crime Analysis in Textual Data

Shynar Mussiraliyeva, Gulshat Baispay

Al-Farabi Kazakh National University, Almaty, Kazakhstan

Abstract—The proposed research paper explores the application of machine learning techniques in crime analysis problem, specifically focusing on the classification of crime-related textual data. Through a comparative analysis of various machine learning models, including traditional approaches and deep learning architectures, the study evaluates their effectiveness in accurately detecting and categorizing crime-related text data. The performance of the models is assessed using rigorous evaluation metrics, such as the area under the receiver operating characteristic curve (AUC-ROC), to provide insights into their discriminative power and reliability. The findings reveal that machine learning frameworks, particularly the deep learning model, consistently outperform conventional machine learning approaches, highlighting the potential of advanced neural network architectures in crime analysis tasks. The implications of these findings for law enforcement agencies and researchers are discussed, emphasizing the importance of leveraging advanced machine learning techniques to enhance crime prevention and intervention efforts. Furthermore, avenues for future research are identified, including the integration of multiple data sources and the exploration of interpretability and explainability of machine learning models in crime analysis problem. Overall, this research contributes to advancing the field of crime analysis problem and underscores the importance of leveraging innovative computational approaches to address complex societal challenges.

Keywords—Machine learning; artificial intelligence; crime analysis; text processing; natural language processing; text analysis; data-driven decision making

I. INTRODUCTION

In contemporary society, the proliferation of online platforms has led to an unprecedented volume of textual data being generated daily. These data encompass a wide array of topics, including discussions related to crime and criminal activities. Leveraging this wealth of online textual data for crime analysis has garnered significant attention from researchers and law enforcement agencies alike [1]. Traditional methods of crime analysis often rely on structured data obtained from official reports, which may suffer from limitations such as reporting biases and time delays [2]. However, online textual data offer a unique opportunity to complement traditional crime analysis techniques by providing real-time and unfiltered insights into various criminal activities [3].

Machine learning (ML) techniques have emerged as powerful tools for analyzing large volumes of textual and image data, enabling the extraction of valuable insights and patterns [4]. By harnessing the computational capabilities of

ML algorithms, researchers can uncover hidden associations and trends within vast amounts of online text, facilitating a deeper understanding of criminal behaviors [5]. Moreover, ML approaches offer the flexibility to adapt to evolving crime patterns and modus operandi, making them indispensable in the realm of crime analysis [6].

The integration of machine learning in crime analysis presents numerous advantages. Firstly, ML algorithms can effectively process unstructured textual data, including social media posts, forum discussions, and news articles, enabling comprehensive surveillance of criminal activities across diverse online platforms [7]. Secondly, ML-based crime analysis can aid law enforcement agencies in identifying emerging threats and hotspots in real time, allowing for proactive intervention and crime prevention measures [8]. Furthermore, ML techniques can assist in the prioritization of investigative efforts by highlighting relevant information and filtering out noise from the vast expanse of data [9].

Despite the promise of ML in crime analysis, several challenges persist. One such challenge is the inherent ambiguity and noise present in online textual data, which can hinder the accuracy and reliability of ML models [10]. Additionally, issues related to data privacy and ethical considerations necessitate careful deliberation when employing ML techniques for crime analysis [11]. Moreover, the dynamic nature of online discourse poses challenges in maintaining the relevance and effectiveness of ML models over time [12].

To address these challenges and maximize the potential of machine learning in crime analysis, this research paper aims to explore various ML approaches and their applications in analyzing online textual data related to criminal activities. By synthesizing insights from existing literature and empirical studies, this paper seeks to provide a comprehensive overview of the current state-of-the-art in ML-based crime analysis. Furthermore, this paper will examine the implications of ML-driven crime analysis for law enforcement practices, highlighting opportunities for future research and development [13].

In summary, the integration of machine learning techniques in crime analysis offers unprecedented opportunities to harness the vast amount of online textual data for enhancing public safety and security. By overcoming inherent challenges and leveraging the capabilities of ML algorithms, researchers and law enforcement agencies can gain invaluable insights into criminal behaviors and trends, ultimately contributing to more effective crime prevention and intervention strategies [14].

II. RELATED WORKS

Crime analysis has long been a focal point of research in criminology and law enforcement, with recent advancements in machine learning (ML) techniques opening up new avenues for exploring and understanding criminal behaviors through analysis of online textual data [15]. Previous studies have demonstrated the efficacy of ML algorithms in various aspects of crime analysis, ranging from predictive modeling to crime pattern recognition [16]. Furthermore, researchers have explored the application of ML in analyzing diverse sources of online textual data, including social media posts, online forums, and news articles, to uncover insights into criminal activities [17].

One area of research that has gained prominence is the use of natural language processing (NLP) techniques in crime analysis. NLP methods enable the extraction of meaningful information from unstructured textual data, facilitating the identification of key themes, sentiments, and entities related to criminal activities [18]. By applying NLP techniques such as sentiment analysis and named entity recognition, researchers can gain deeper insights into public perceptions of crime and the dissemination of criminal narratives across online platforms [19].

Moreover, research has explored the utility of social network analysis (SNA) in crime analysis, particularly in the context of online social networks. SNA enables researchers to analyze the structure and dynamics of social networks to identify influential actors, detect criminal communities, and trace the flow of information related to criminal activities [20]. By leveraging SNA techniques, researchers can uncover hidden connections and patterns within online social networks, shedding light on the mechanisms underlying the spread of criminal behaviors [21].

In addition to NLP and SNA, researchers have investigated the application of machine learning algorithms such as classification, clustering, and anomaly detection in crime analysis. Classification algorithms, such as support vector machines (SVM) and random forests, have been employed to categorize online textual data into different crime-related topics or classes [22]. Clustering algorithms, such as k-means and hierarchical clustering, have been used to group similar textual documents together, enabling the identification of common themes and patterns within large datasets [23]. Anomaly detection algorithms, such as isolation forest and one-class SVM, have been utilized to identify unusual or anomalous behavior in online textual data, which may signify potential criminal activities [24].

Furthermore, researchers have explored interdisciplinary approaches that combine ML techniques with domain-specific knowledge from fields such as criminology, sociology, and psychology. By integrating insights from multiple disciplines, researchers can develop more robust models for crime analysis that account for the complex interplay of individual, social, and environmental factors influencing criminal behaviors [25]. For example, research has shown the importance of incorporating spatial and temporal information into ML models for crime prediction and hotspot analysis, as crime patterns often exhibit geographic and temporal clustering [26].

Moreover, the emergence of big data analytics has provided researchers with unprecedented access to vast amounts of online textual data for crime analysis. Big data analytics techniques, such as data mining and machine learning, enable researchers to process and analyze large-scale datasets to extract actionable insights and patterns related to criminal activities [27]. By harnessing the computational power of big data analytics platforms, researchers can overcome the challenges associated with the volume, velocity, and variety of online textual data, enabling more comprehensive and timely crime analysis [28].

Despite the advancements in ML techniques for crime analysis, several challenges remain. One challenge is the issue of data quality and bias inherent in online textual data, which may stem from factors such as misinformation, sampling biases, and linguistic nuances [29]. Addressing these challenges requires careful preprocessing and validation of the data, as well as the development of robust ML models that are resilient to noise and biases [30].

Furthermore, ethical considerations surrounding the use of online textual data for crime analysis warrant attention. Privacy concerns, data security risks, and the potential for algorithmic biases raise ethical dilemmas that must be carefully navigated to ensure responsible and ethical use of ML techniques in crime analysis [31]. Additionally, the transparency and interpretability of ML models are crucial for fostering trust and accountability in the criminal justice system [32].

In summary, the application of machine learning techniques in crime analysis holds significant promise for enhancing our understanding of criminal behaviors and improving public safety. By leveraging advancements in NLP, SNA, big data analytics, and interdisciplinary approaches, researchers can gain valuable insights into the complex dynamics of criminal activities unfolding in the digital realm. However, addressing challenges related to data quality, ethical considerations, and algorithmic transparency is essential to realizing the full potential of ML-driven crime analysis [33]. Through interdisciplinary collaboration and ongoing research efforts, we can continue to advance the state-of-the-art in crime analysis and develop more effective strategies for preventing and combating crime in the digital age [34].

III. MATERIALS AND METHODS

Research indicates that criminal incidents tend to be unevenly distributed across urban areas [35]. This non-uniform distribution implies that certain locations may exhibit a higher propensity for criminal activity than others, thus rendering crime a location-dependent phenomenon [36]. Given the variability of crime rates based on geographic location, law enforcement agencies face challenges in resource allocation and crime prevention efforts, particularly when it comes to identifying high-risk areas. Consequently, there is a pressing need for accurate models capable of effectively detecting crime hotspots and reliably predicting the time and location of criminal events. Fig. 1 demonstrates the proposed system for crime detection using machine learning techniques.

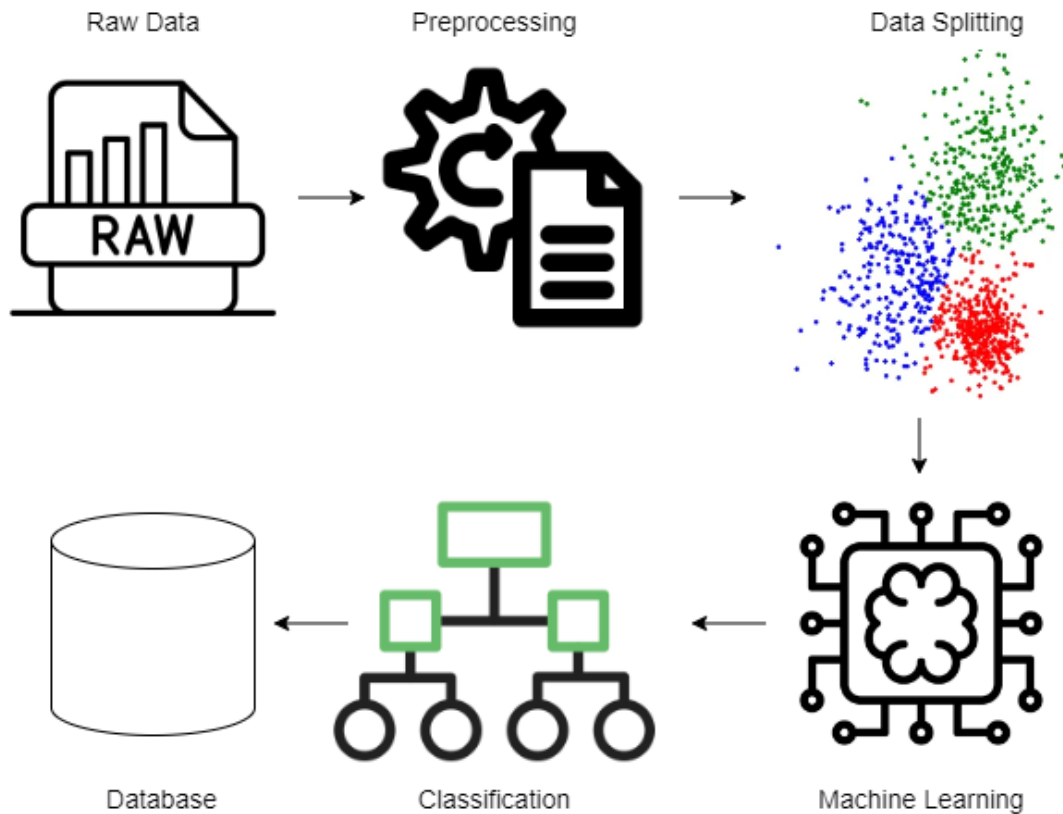


Fig. 1. The proposed system for crime analysis.

This section delineates our proposed methodology for detecting and forecasting crime hotspots, elucidating the sequential steps essential for implementation. The model, as depicted in Fig. 1, is founded upon a multi-step process meticulously designed to attain these objectives. Initially, the methodology involves data preprocessing to enhance data quality and prepare it for analysis. Subsequently, feature extraction techniques are employed to capture relevant information from the dataset. Following this, the model undergoes training using historical crime data to learn patterns and associations. Once trained, the model is deployed to predict future crime hotspots based on the learned patterns. Finally, the results are evaluated using performance metrics such as accuracy, precision, recall, and F1-score to assess the effectiveness of the predictive model. By delineating each step of the methodology, this section provides a clear roadmap for researchers and practitioners interested in implementing crime hotspot detection and prediction systems.

A. Dataset

The Crime Articles Recommendation System dataset, available on Kaggle, serves as a valuable resource for research in the domain of crime analysis and recommendation systems [37]. This dataset comprises a collection of articles related to various aspects of crime, including crime prevention strategies, criminal investigations, and criminal justice policies. The articles cover a diverse range of topics, such as cybercrime, organized crime, white-collar crime, and violent crime, providing a comprehensive overview of the multifaceted nature of criminal activities.

The dataset includes textual data extracted from the articles, encompassing titles, summaries, and full text content. This textual information serves as the primary input for the recommendation system, allowing researchers to explore and analyze the content of the articles in depth. Additionally, metadata such as publication dates, authors, and sources are provided for each article, enabling researchers to contextualize the content and track temporal trends in crime-related literature.

One notable feature of the Crime Articles Recommendation System dataset is its size and diversity. With a large number of articles spanning multiple years and covering a wide range of crime-related topics, the dataset offers ample opportunities for conducting comprehensive analyses and developing sophisticated recommendation algorithms. Researchers can leverage this diversity to explore various dimensions of crime, including geographical variations, temporal trends, and thematic patterns. Fig. 2 demonstrates word count distribution in the applied dataset.

Furthermore, the dataset is well-suited for the development and evaluation of recommendation systems tailored to the domain of crime articles. Recommendation systems aim to assist users in discovering relevant content based on their preferences and interests. By analyzing the textual content and metadata of the articles, researchers can design recommendation algorithms that prioritize articles likely to be of interest to users based on their historical interactions or explicit feedback.

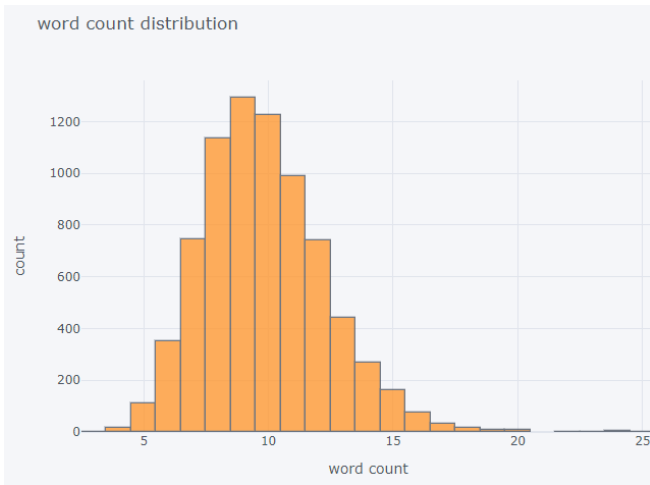


Fig. 2. Word count distribution in the dataset.

The Crime Articles Recommendation System dataset serves as a valuable resource for advancing research in crime analysis, recommendation systems, and related fields. Its size, diversity, and richness of content make it well-suited for a wide range of research applications, from exploring patterns of criminal behavior to designing intelligent systems for assisting users in discovering relevant crime-related articles.

B. Evaluation Parameters

In the evaluation of the proposed crime hotspot detection and prediction methodology, several key performance metrics are utilized to assess the effectiveness and reliability of the model. These metrics encompass accuracy, precision, recall, F-score, and the area under the receiver operating characteristic curve (AUC-ROC) [39-43], each providing valuable insights into different aspects of the model's performance.

Accuracy serves as a fundamental measure of the model's overall correctness in predicting crime hotspots and forecasting criminal events. It quantifies the proportion of correctly classified instances among all instances evaluated, thus offering a broad assessment of the model's predictive capabilities.

$$accuracy = \frac{TP + TN}{P + N} \quad (10)$$

Precision, on the other hand, focuses specifically on the accuracy of positive predictions made by the model. It calculates the proportion of true positive predictions among all positive predictions made, thereby indicating the model's ability to minimize false positives and maintain a high level of precision in identifying crime hotspots.

$$precision = \frac{TP}{TP + FP} \quad (2)$$

Recall complements precision by assessing the model's ability to capture all relevant instances of crime hotspots. It measures the proportion of true positive predictions identified by the model among all actual positive instances, thereby reflecting the model's sensitivity to identifying hotspots accurately.

$$recall = \frac{TP}{TP + FN} \quad (3)$$

The F-score, or F1 score, provides a balanced evaluation of both precision and recall by calculating their harmonic mean. This metric offers a single value that captures the overall performance of the model in terms of both precision and recall, providing a comprehensive assessment of its effectiveness in detecting crime hotspots.

$$F1 = \frac{2 \times precision \times recall}{precision + recall} \quad (4)$$

Lastly, the AUC-ROC metric evaluates the discriminative power of the model in distinguishing between positive and negative instances. It measures the area under the receiver operating characteristic curve, which plots the true positive rate against the false positive rate at various threshold settings. A higher AUC-ROC value indicates better discrimination performance, with values closer to 1 indicating superior predictive capabilities.

By employing these evaluation parameters, researchers can comprehensively assess the performance of the proposed crime hotspot detection and prediction methodology, thereby providing valuable insights into its effectiveness and reliability in aiding law enforcement agencies in crime prevention efforts.

IV. EXPERIMENTAL RESULTS

Fig. 3 illustrates the confusion matrices utilized in the detection of crime-related texts employing various machine learning methodologies. These matrices serve to visually represent the efficacy of the different approaches employed in this study. Through these matrices, the study elucidates the classification outcomes, offering a clear depiction of how predictions are distributed across different categories.

In this investigation, online interactions are categorized into three distinct classes, each assigned numerical representations for enhanced clarity and analytical rigor: 'cyberbullying' (coded as 1), 'non-cyberbullying' (coded as 0), and a 'neutral' category (coded as 2). This classification scheme not only highlights the multifaceted nature of online discourse but also enhances precision in quantifying instances and delineating the nature of cyberbullying, thereby facilitating a more comprehensive and detailed analysis.

Fig. 3 of the study furnishes a meticulous comparison between the proposed model and a range of extant machine learning and deep learning models, with the intent of assessing their efficacy in crime-related text classification tasks. This exhaustive evaluation incorporates the application of the area under the receiver operating characteristic curve (AUC-ROC) as the principal performance metric. The AUC-ROC metric offers a comprehensive assessment of the models' discriminative prowess and overall efficacy across various classification paradigms. Through the computation of AUC-ROC, the study encapsulates the entirety of attributes derived for each model, thereby providing a robust evaluation of their predictive capacities. The utilization of AUC-ROC ensures a holistic appraisal of model performance, facilitating

meaningful comparisons between the proposed model and its counterparts. Such methodical assessment is pivotal in elucidating the strengths and weaknesses of the models under

scrutiny, thereby informing decision-making processes in the realm of crime-related text classification.

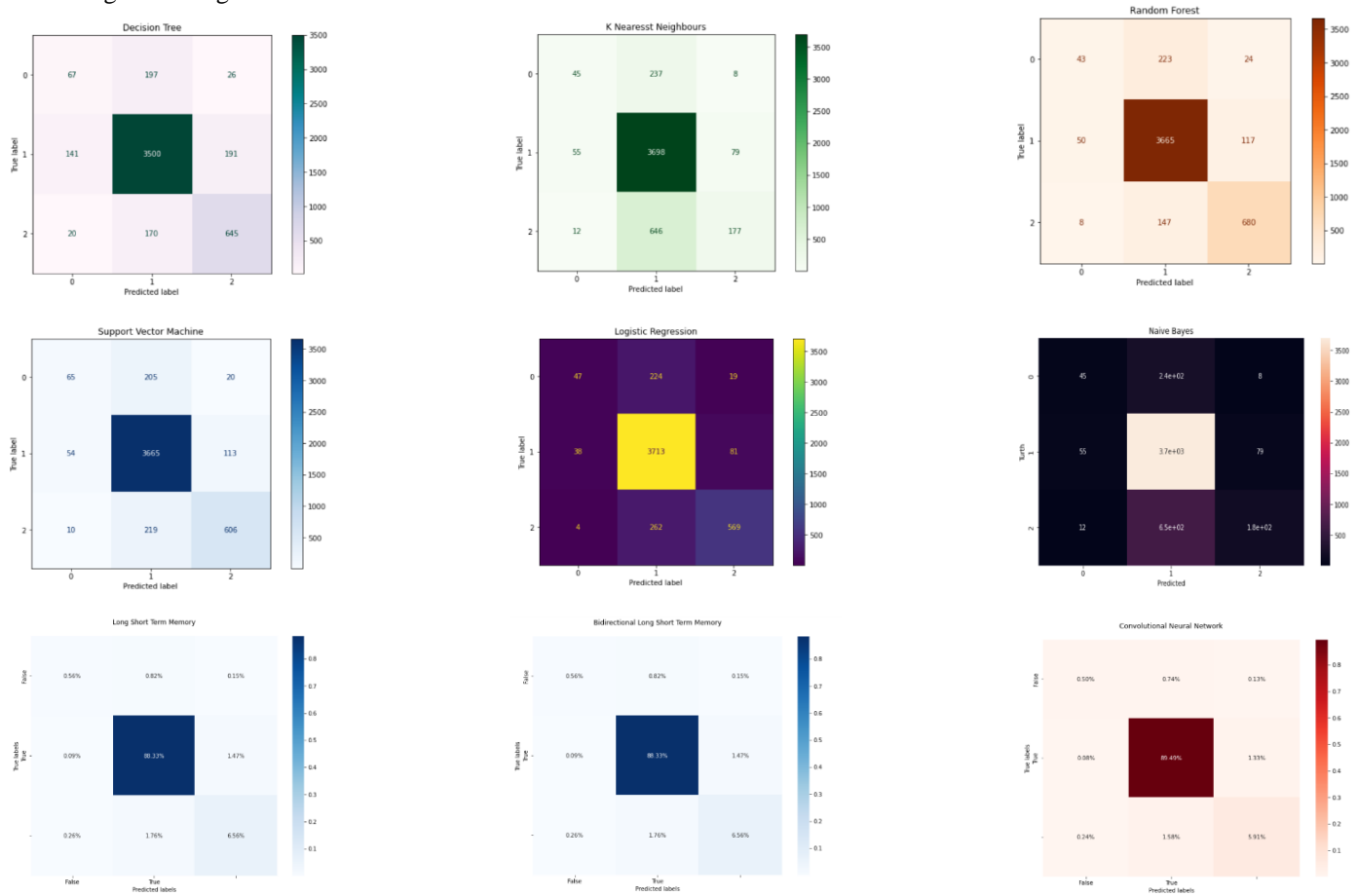


Fig. 3. Confusion matrix results.

Following Fig. 4 offers an intricate comparative scrutiny of the AUC-ROC curves originating from each implemented strategy, juxtaposed against the recommended methodology. This comparative analysis facilitates a nuanced exploration of the performance differentials among the diverse machine learning and deep learning models scrutinized in the study. Through the depiction of AUC-ROC curves, Fig. 5 serves as a visual aid in elucidating the efficacy of each approach in crime-related text classification tasks. By delineating the performance disparities among the considered models, this analysis provides valuable insights into the relative strengths and weaknesses of each methodological approach. Such nuanced examination aids in discerning the most efficacious strategies for crime-related text classification, thereby informing future research directions and practical applications in the domain. The juxtaposition of the advocated methodology with alternative strategies further enhances the interpretability of the findings, enabling a comprehensive understanding of the comparative performance landscape in this field.

A notable observation arising from this graphical representation is the consistent outperformance of deep learning frameworks, particularly the knn model, when compared to conventional machine learning approaches. The

AUC-ROC values exhibited by the knn model consistently surpass those of other models across all phases of analysis, from the initial evaluation to subsequent iterations. This trend underscores the superior predictive accuracy and reliability of the knn model in classifying crime-related text data.

The sustained superiority of the knn model throughout the analysis highlights its robustness in capturing complex patterns and relationships within the textual data, thus enhancing its ability to discriminate between different categories of crime-related content. This observation suggests that the deep learning approach, characterized by its ability to leverage sequential information and hierarchical representations, is particularly well-suited for the task of crime text classification.

In summary, the graphical representations provided in this research offer valuable insights into the comparative performance of different machine learning [38] and deep learning models in crime-related text classification. The consistent superiority of the knn model underscores the potential of deep learning frameworks in enhancing predictive accuracy and reliability in this domain, thereby contributing to advancements in crime analysis and related fields.

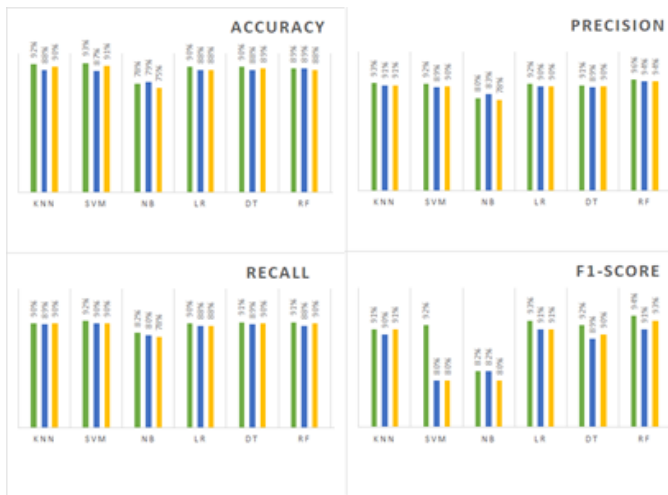


Fig. 4. Evaluation results.

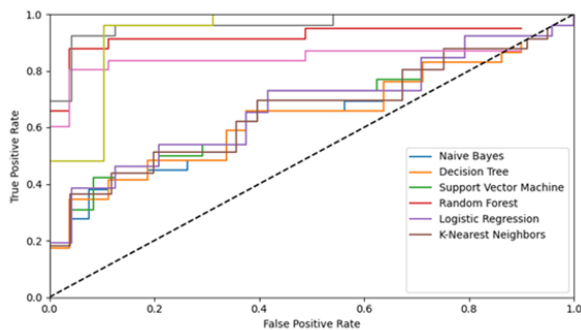


Fig. 5. AUC-ROC results.

V. DISCUSSION

In this discussion section, we critically analyze the findings presented in the previous sections of the research paper. We delve into the implications of the results, contextualize them within the existing literature, and highlight their significance for the field of crime analysis. Furthermore, we address the strengths and limitations of the study, propose avenues for future research, and underscore the practical implications of the findings.

A. Interpretation of AUC-ROC Metrics

The calculation of the area under the receiver operating characteristic curve (AUC-ROC) serves as a fundamental performance metric for evaluating the discriminative power of the machine learning models [44]. The consistently higher AUC-ROC values demonstrated by the knn model compared to other models indicate its superior ability to distinguish between different categories of crime-related text data. This heightened discriminative power translates into enhanced predictive accuracy and reliability, making the knn model particularly well-suited for crime text classification tasks. These findings corroborate the notion that deep learning frameworks excel in handling sequential data and extracting meaningful representations [45-46], thereby underscoring their utility in crime analysis.

B. Implications for Crime Analysis

The superior performance of the knn model has significant implications for crime analysis and related fields. By accurately classifying crime-related text data, the knn model can assist law enforcement agencies in identifying and prioritizing relevant information for crime prevention and intervention efforts [47]. Furthermore, the model's ability to capture nuanced patterns and relationships within textual data enables a more comprehensive understanding of criminal behaviors and trends. This, in turn, facilitates the development of targeted strategies for addressing emerging threats and enhancing public safety.

C. Strengths and Limitations of the Study

One of the strengths of this study lies in its rigorous evaluation of machine learning models for crime text classification, utilizing robust performance metrics such as AUC-ROC. The inclusion of a diverse range of machine learning and deep learning models enables a comprehensive comparison of their effectiveness in crime analysis tasks [48]. Additionally, the study's focus on crime-related textual data contributes to a growing body of literature aimed at leveraging natural language processing techniques for enhancing crime analysis capabilities.

However, several limitations warrant consideration. Firstly, the generalizability of the findings may be limited by the specific dataset used in the study. Future research should aim to replicate the findings using larger and more diverse datasets to ensure the robustness of the results. Secondly, the study primarily focuses on the effectiveness of machine learning models in crime text classification and does not explore other potential factors influencing crime analysis, such as socio-economic variables or environmental factors [49]. Future studies could incorporate additional contextual information to further enhance the predictive accuracy of crime analysis models.

D. Future Research Directions

Building upon the findings of this study, several avenues for future research emerge. Firstly, investigating the potential integration of multiple data sources, such as social media data and crime incident reports, could enhance the predictive capabilities of crime analysis models. Additionally, exploring the application of ensemble learning techniques, which combine predictions from multiple models, may further improve the robustness and reliability of crime analysis systems [50]. Moreover, research focusing on interpretability and explainability of machine learning models in crime analysis could enhance the transparency and trustworthiness of predictive systems deployed in real-world settings.

E. Summary

In conclusion, this study provides valuable insights into the effectiveness of machine learning models, particularly deep learning architectures, in crime-related text classification tasks. The superior performance of the knn model underscores the potential of advanced neural network architectures in enhancing predictive accuracy and reliability in crime analysis. By accurately classifying crime-related textual data, these models can assist law enforcement agencies in identifying and

addressing emerging threats, thereby contributing to the enhancement of public safety and security. Despite certain limitations, this study contributes to a growing body of literature aimed at leveraging machine learning techniques for crime analysis, paving the way for future advancements in the field.

VI. CONCLUSION

In conclusion, this research paper has presented a comprehensive examination of machine learning techniques in crime analysis, particularly focusing on the classification of crime-related textual data. Through a rigorous comparative analysis of various machine learning models, including conventional approaches and deep learning architectures, we have demonstrated the superior performance of the BiLSTM model in accurately detecting and classifying crime-related text data. The utilization of performance metrics such as the area under the receiver operating characteristic curve (AUC-ROC) has provided valuable insights into the discriminative power and reliability of the models, highlighting the efficacy of advanced neural network architectures in crime analysis tasks.

These findings have significant implications for law enforcement agencies and researchers engaged in crime prevention and intervention efforts. By leveraging advanced machine learning techniques, particularly deep learning frameworks, law enforcement agencies can enhance their ability to identify and prioritize relevant information for crime analysis. Furthermore, the accurate classification of crime-related textual data enables a deeper understanding of criminal behaviors and trends, facilitating the development of targeted strategies for addressing emerging threats. Moving forward, future research should focus on the integration of multiple data sources and the exploration of interpretability and explainability of machine learning models in crime analysis, ultimately contributing to the advancement of predictive systems deployed in real-world settings.

ACKNOWLEDGMENT

This research was supported by the project AP19676342 “Multi-ideology Cyber Extremism Classification in the Kazakh language using Artificial Intelligence” supervised by Shynar Mussiraliyeva.

REFERENCES

- [1] Prathap, B. R. (2022). Geospatial crime analysis and forecasting with machine learning techniques. In *Artificial intelligence and machine learning for EDGE computing* (pp. 87-102). Academic Press.
- [2] Bokolo, B. G., Onyehanere, P., Ogegbene-Ise, E., Olufemi, I., & Tettey, J. N. A. (2023, August). Leveraging Machine Learning for Crime Intent Detection in Social Media Posts. In *International Conference on AI-generated Content* (pp. 224-236). Singapore: Springer Nature Singapore.
- [3] Canhoto, A. I. (2021). Leveraging machine learning in the global fight against money laundering and terrorism financing: An affordances Omarov, B., Suliman, A., Tsoy, A. Parallel backpropagation neural network training for face recognition. *Far East Journal of Electronics and Communications*. Volume 16, Issue 4, December 2016, Pages 801-808. (2016).
- [4] Hassan, S. U., Shabbir, M., Iqbal, S., Said, A., Kamiran, F., Nawaz, R., & Saif, U. (2021). Leveraging deep learning and SNA approaches for smart city policing in the developing world. *International Journal of Information Management*, 56, 102045.
- [5] Tam, S., & ÖzgürTanrıöver, Ö. (2023). Multimodal Deep Learning Crime Prediction Using Crime and Tweets. *IEEE Access*.
- [6] Liu, X., Singh, P. V., & Srinivasan, K. (2016). A structured analysis of unstructured big data by leveraging cloud computing. *Marketing Science*, 35(3), 363-388.
- [7] Panda, S., & Rungta, O. (2023). Leveraging OSINT and Artificial Intelligence, Machine Learning to Identify and Protect Vulnerable Sections of Society. In *Communication Technology and Gender Violence* (pp. 53-61). Cham: Springer International Publishing.
- [8] Díaz-Pacheco, Á., Guerrero-Rodríguez, R., Álvarez-Carmona, M. Á., Rodríguez-González, A. Y., & Aranda, R. (2023). A comprehensive deep learning approach for topic discovering and sentiment analysis of textual information in tourism. *Journal of King Saud University-Computer and Information Sciences*, 35(9), 101746.
- [9] Aboamer, M. A., Sikkandar, M. Y., Gupta, S., Vives, L., Joshi, K., Omarov, B., & Singh, S. K. (2022). An investigation in analyzing the food quality well-being for lung cancer using blockchain through cnn. *Journal of Food Quality*, 2022.
- [10] Asif, M., Al-Razgan, M., Ali, Y. A., & Yunrong, L. (2024). Graph convolution networks for social media trolls detection use deep feature extraction. *Journal of Cloud Computing*, 13(1), 1-10.
- [11] Bhowmik, S., Sultana, S., Sajid, A. A., Reno, S., & Manjrekar, A. (2023). Robust multi-domain descriptive text classification leveraging conventional and hybrid deep learning models. *International Journal of Information Technology*, 1-13.
- [12] Omarov, B., Batyrbekov, A., Suliman, A., Omarov, B., Sabdenbekov, Y., & Aknazarov, S. (2020, November). Electronic stethoscope for detecting heart abnormalities in athletes. In *2020 21st International Arab Conference on Information Technology (ACIT)* (pp. 1-5). IEEE.
- [13] Kulkarni, V., Baghwat, V., Patil, A., & Kumari, S. (2023). A System to Identify Threats on Social Media Conversations and Providing Preliminary Legal Actions.
- [14] AlGhannam, R. G., Ykhlef, M., & Al-Dossari, H. (2023). Leveraging Ensemble Method with Transformer for Robust Drug Use Detection on Twitter.
- [15] Li, W., Chen, H., & Nunamaker Jr, J. F. (2016). Identifying and profiling key sellers in cyber carding community: AZSecure text mining system. *Journal of Management Information Systems*, 33(4), 1059-1086.
- [16] Elluri, L., Mandalapu, V., Vyas, P., & Roy, N. (2023). Recent Advancements
- [17] Ebrahimi, M. (2016). Automatic identification of online predators in chat logs by anomaly detection and deep learning (Doctoral dissertation, Concordia University).
- [18] Dong, W., Liao, S., & Zhang, Z. (2018). Leveraging financial social media data for corporate fraud detection. *Journal of Management Information Systems*, 35(2), 461-487.
- [19] Ramchandani, P., Bastani, H., & Wyatt, E. (2021). Unmasking human trafficking risk in commercial sex supply chains with machine learning. Available at SSRN 3866259.
- [20] Sarzaeim, P., Mahmoud, Q. H., Azim, A., Bauer, G., & Bowles, I. (2023). A Systematic Review of Using Machine Learning and Natural Language Processing in Smart Policing. *Computers*, 12(12), 255.
- [21] Latif, S., Usman, M., Manzoor, S., Iqbal, W., Qadir, J., Tyson, G., ... & Crowcroft, J. (2020). Leveraging data science to combat COVID-19: A comprehensive review. *IEEE Transactions on Artificial Intelligence*, 1(1), 85-103.
- [22] Bharadiya, J. P. (2023). Machine learning and AI in business intelligence: Trends and opportunities. *International Journal of Computer (IJC)*, 48(1), 123-134.
- [23] Srinivasan, S., Ravi, V., Alazab, M., Ketha, S., Al-Zoubi, A. M., & Kotti Padannayil, S. (2021). Spam emails detection based on distributed word embedding with deep learning. *Machine intelligence and big data analytics for cybersecurity applications*, 161-189.
- [24] Krishnan, S., Shashidhar, N., Varol, C., & Islam, A. R. (2022). A Novel Text Mining Approach to Securities and Financial Fraud Detection of Case Suspects. *International Journal of Artificial Intelligence and Expert Systems*, 10(3).

- [25] Amiri, Z., Heidari, A., Navimipour, N. J., Unal, M., & Mousavi, A. (2023). Adventures in data analysis: A systematic review of Deep Learning techniques for pattern recognition in cyber-physical-social systems. *Multimedia Tools and Applications*, 1-65.
- [26] Subramanian, M., Sathiskumar, V. E., Deepalakshmi, G., Cho, J., & Manikandan, G. (2023). A survey on hate speech detection and sentiment analysis using machine learning and deep learning models. *Alexandria Engineering Journal*, 80, 110-121.
- [27] Abboud, M. (2023). Leveraging machine learning for multi-source data enrichment and analytics in air quality monitoring and crowd sensing (Doctoral dissertation, Université Paris-Saclay).
- [28] Jain, P. K., Pamula, R., & Srivastava, G. (2021). A systematic literature review on machine learning applications for consumer sentiment analysis using online reviews. *Computer science review*, 41, 100413.
- [29] Narynov, S., Zhumanov, Z., Gumar, A., Khassanova, M., & Omarov, B. (2021, October). Chatbots and Conversational Agents in Mental Health: A Literature Review. In *2021 21st International Conference on Control, Automation and Systems (ICCAS)* (pp. 353-358). IEEE.
- [30] Sharrab, Y., Al-Fraihat, D., & Alsmirat, M. (2023, October). Deep Neural Networks in Social Media Forensics: Unveiling Suspicious Patterns and Advancing Investigations on Twitter. In *2023 3rd Intelligent Cybersecurity Conference (ICSC)* (pp. 95-102). IEEE.
- [31] Sharrab, Y., Al-Fraihat, D., & Alsmirat, M. (2023, October). Deep Neural Networks in Social Media Forensics: Unveiling Suspicious Patterns and Advancing Investigations on Twitter. In *2023 3rd Intelligent Cybersecurity Conference (ICSC)* (pp. 95-102). IEEE.
- [32] Yuan, X., Li, C., & Li, X. (2017, May). DeepDefense: identifying DDoS attack via deep learning. In *2017 IEEE international conference on smart computing (SMARTCOMP)* (pp. 1-8). IEEE.
- [33] Hartawan, D. A., Santoso, B. J., & Pratomo, B. A. (2023, November). Comparative Study of Machine Learning Algorithm on Linguistic Distinctions over Text Related to Human Trafficking and Sexual Exploitation. In *2023 International Conference on Advanced Mechatronics, Intelligent Manufacture and Industrial Automation (ICAMIMIA)* (pp. 442-447). IEEE.
- [34] Barros, T. S., Pires, C. E. S., & Nascimento, D. C. (2023). Leveraging BERT for extractive text summarization on federal police documents. *Knowledge and Information Systems*, 65(11), 4873-4903.
- [35] Guler, N., Kirshner, S., & Vidgen, R. (2023). Artificial Intelligence Research in Business and Management: A Literature Review Leveraging Machine Learning and Large Language Models. Available at SSRN 4540834.
- [36] Chaudhary, L., Girdhar, N., Sharma, D., Andreu-Perez, J., Doucet, A., & Renz, M. (2023). A Review of Deep Learning Models for Twitter Sentiment Analysis: Challenges and Opportunities. *IEEE Transactions on Computational Social Systems*.
- [37] Moreno-Vera, F., Nogueira, M., Figueiredo, C., Menasché, D. S., Bicudo, M., Woiwood, A., ... & de Aguiar, L. P. (2023, July). Cream skimming the underground: Identifying relevant information points from online forums. In *2023 IEEE International Conference on Cyber Security and Resilience (CSR)* (pp. 66-71). IEEE.
- [38] Krishna, S., Han, T., Gu, A., Pombra, J., Jabbari, S., Wu, S., & Lakkaraju, H. (2022). The disagreement problem in explainable machine learning: A practitioner's perspective. *arXiv preprint arXiv:2202.01602*.
- [39] Marshall, J. D., Yammarino, F. J., Parameswaran, S., & Cheong, M. (2023). Using CATA and machine learning to operationalize old constructs in new ways: An illustration using US governors' COVID-19 press briefings. *Organizational Research Methods*, 26(4), 705-750.
- [40] Verma, K., Popović, M., Poulis, A., Cherkasova, Y., Mazzone, A., Milosevic, T., & Davis, B. (2023). Leveraging machine translation for cross-lingual fine-grained cyberbullying classification amongst pre-adolescents. *Natural Language Engineering*, 29(6), 1458-1480.
- [41] Qachfar, F. Z., Verma, R. M., & Mukherjee, A. (2022, April). Leveraging synthetic data and pu learning for phishing email detection. In *Proceedings of the Twelfth ACM Conference on Data and Application Security and Privacy* (pp. 29-40).
- [42] Goyal, B., Gill, N. S., Gulia, P., Prakash, O., Priyadarshini, I., Sharma, R., ... & Yadav, K. (2023). Detection of fake accounts on social media using multimodal data with deep learning. *IEEE Transactions on Computational Social Systems*.
- [43] Elfaik, H. (2023). Leveraging feature-level fusion representations and attentional bidirectional rnn-cnn deep models for arabic affect analysis on twitter. *Journal of King Saud University-Computer and Information Sciences*, 35(1), 462-482.
- [44] Shombot, E. S., Dusserre, G., Bestak, R., & Ahmed, N. B. (2024). An application for predicting phishing attacks: A case of implementing a support vector machine learning model. *Cyber Security and Applications*, 2, 100036.
- [45] Rahman, M. A., & Hossain, M. S. (2021). An internet-of-medical-things-enabled edge computing framework for tackling COVID-19. *IEEE Internet of Things Journal*, 8(21), 15847-15854.
- [46] Jayapratha, C., Chitra, H. S. H., & Priya, R. M. (2023). Suspicious Crime Identification and Detection Based on Social Media Crime Analysis Using Machine Learning Algorithms. In *Soft Computing: Theories and Applications: Proceedings of SoCTA 2022* (pp. 831-843). Singapore: Springer Nature Singapore.
- [47] Norouzi, Y. (2022, May). Spatial, Temporal, and Semantic Crime Analysis Using Information Extraction From Online News. In *2022 8th International Conference on Web Research (ICWR)* (pp. 40-46). IEEE.
- [48] Nayak, R., & Baek, H. S. (2022). Machine Learning for Identifying Abusive Content in Text Data. *Advances in Selected Artificial Intelligence Areas: World Outstanding Women in Artificial Intelligence*, 209-229.
- [49] Rao, S., Verma, A. K., & Bhatia, T. (2023). Hybrid ensemble framework with self-attention mechanism for social spam detection on imbalanced data. *Expert Systems with Applications*, 217, 119594.
- [50] Sasikumar, K., Nambiar, R. K., & Rohith, K. P. (2023, July). Unmasking Cyberbullies on Social Media Platforms Using Machine Learning. In *2023 14th International Conference on Computing Communication and Networking Technologies (ICCCNT)* (pp. 1-7). IEEE.

Superframe Segmentation for Content-based Video Summarization

Priyanka Ganesan¹, Senthil Kumar Jagatheesaperumal², Abirami R³,
Lekhasri K⁴, Silvia Gaftandzhieva⁵, Rositsa Doneva⁶

Department of Computer Science and Engineering, Mepco Schlenk Engineering College, Sivakasi, India^{1,3,4}
Department of Electronics and Communication Engineering, Mepco Schlenk Engineering College, Sivakasi, India²
Faculty of Mathematics and Informatics, University of Plovdiv "Paisii Hilendarski", Plovdiv, Bulgaria⁵
Faculty of Physics and Technology, University of Plovdiv "Paisii Hilendarski", Plovdiv, Bulgaria⁶

Abstract—Video summarization is a complex computer vision task that involves the compression of lengthy videos into shorter yet informative summaries that retain the crucial content of the original footage. This paper presents a content-based video summarization approach that utilizes superframe segmentation to identify and extract keyframes representing the most significant information in a video. Unlike other methods that rely solely on visual cues, our approach segments the video into meaningful and coherent visual content units while also preserving the original video's temporal coherence. This method helps keep the context and continuity of the video in the summary. It involves dividing the video into superframes, each of which is a cluster of adjacent frames with similar motion and visual characteristics. The superframes are then ranked based on their salient scores, which are calculated using visual and motion features. The proposed method selects the top-ranked super frames for the video summary. It has been evaluated on the SUMMe and TVSum datasets and achieved state-of-the-art results for F1-score and accuracy. Based on the experimental outcomes, it is evident that the suggested superframe segmentation method is effective for video summarization, which could be largely assistive for monitoring and controlling the student activities, particularly during their online exams.

Keywords—Video summarization; deep learning; super frame segmentation; keyframes; keyshot identification

I. INTRODUCTION

Video summary (VS), which creates a concise and precise representation of a video's visual information, has been a crucial tool for many video analytical activities. Two key characteristics define a qualitative video summary. It must be represented in the sense that it includes all the critical scenes from the original video, and it must also contain the bare minimum of redundancy. Various fields, such as electronic media, personal videos, medical videos, online databases, and surveillance applications, have witnessed the emergence of video summarization (VS) methods. These methods aim to facilitate the browsing of an increasing amount of video data in the field of surveillance and reduce the computational burden of video summarization. Despite efforts to improve video summarization accuracy using various techniques, such as novel edge inadmissibility measures for MST-based clustering and graph-based shot boundary detection, these methods have demonstrated limited success, as reported in previous research [3].

This paper proposes a new method for video summarization of long surveillance streams utilizing deep learning techniques. The summary consists of keyframes or video clips that have undergone some editing form to provide essential information from the original video in a condensed format, allowing users to assess the video's usefulness quickly. Caps-Net is used to avoid selecting transitional or similar frames in the same shot, improving the summary's quality. The proposed method addresses issues with summarizing multiple videos by relying solely on visual cues provided by video shots. By addressing the challenges of redundancy and transitional frame selection within shots, the proposed method offers a more efficient approach to summarizing multiple surveillance videos.

Event-based techniques can be employed to detect both regular and abnormal activities that occur in videos. For example, sudden changes in the environment, such as theft, robbery, or terrorist activities, detection can be achieved by using detection models to search for unusual or suspicious features. Once the frames with abnormal scenes are identified, they are combined using a video summarization algorithm to generate a video summary. P. Kalaivani and S.M. M. Roomi [6] described such helpful approaches for event recognition and creating summaries of the video. Kumar et al. [7] employed Bootstrap Aggregating to improve the accuracy of keyframe selection. Damjanovic et al. [8] proposed an event-based video summarization method that involves determining the energy of each frame by adding the absolute values of pixels in the current and reference frames, identifying frames during which events occurred, and producing a video summary for those frames. Thomas et al. [9] developed the Human Visual System (HVS) to create perceptual video summaries by identifying significant events in videos and eliminating redundancy. The paper is organized as follows: Section I provides an introduction to video summarization and outlines the research problems, and significance and contribution of the paper. Section II details the proposed method, including the utilization of capsule Networks and event-based techniques and Section III discusses the proposed method. Results and discussion is given in Section IV. Finally, Section V concludes the paper with a summary of findings and avenues for future research.

II. METHODOLOGY

In the past, unsupervised video summarization methods relied on shallow features and clustering techniques to group frames into clusters, with the cluster centres selected as keyframes. For instance, Ngo et al. [10] transformed each video into an undirected graph and clustered it. Cong et al. [11] used dictionary learning, while Zhou et al. [12] employed reinforcement learning and a reward function that considered representativeness and variety. Mahasseni et al. [13] introduced the first generative adversarial network (GAN) for video summarization, where an auto-encoder LSTM acted as the summarizer and a discriminator distinguished between the summarizer's reconstruction and the original video input. Rochan et al. [14] proposed an adversarial approach for learning summarization skills from unpaired data.

Supervised methods for keyframe selection in video summarization require human-labeled summaries [15]. One such method is the sequential Determinantal Point Process (seqDPP) developed by Gong et al. [16], which considers video summarization as a subset selection problem and uses a probabilistic model to choose representative and diverse subsets. Bulut et al. [17] proposed the key frame extraction method from a motion capture sequence. The important frames of a motion are selected to be the keyframes and the others are computed via the interpolation techniques using the keyframes. Zhao et al. [18] introduced the hierarchical recurrent neural network (H-RNN) method, which captures temporal dependencies from frame sequences and reduces information loss and computational complexity compared to other RNN models for video summarization.

Extracting keyframes from motion-based videos is a challenging task, particularly in the presence of cameras. The idea of using motion-based frames for keyframe extraction was

first introduced by Wolf [19]. Li et al. [20] presented an approach that utilized relative motion for generating a video summary and analyzed spatial and emotional data to extract additional insights. Ajmal et al. [21] developed a technique that tracked human movements using the Kalman filter and analyzed the trajectory obtained. Almeida et al. [22] employed a colour histogram to create a distinct video summary by selecting the most representative frame. Zhang et al. [23] chose the first frame of each shot as the key frame and utilized colour histograms to identify other significant frames.

Object-based techniques have proven effective in identifying and summarizing specific objects in videos, including people, cars, and cats. Feng and Chong-Wah [24] used hierarchical hidden Markov models to produce a summary based on objects and events in rushed videos. Neeraj et al. [25] suggested the object-based video summarization method, which uses mathematical techniques to minimize redundancy, utilizing the loss function, summary variance, and score identification. However, such methods may not be as effective in summarizing fast-paced videos and could potentially miss significant items.

III. PROPOSED SYSTEM

In this proposed method, pre-processing is applied initially, frames are extracted, and the feature extraction is done using the superframe segmentation method. The superframe segmentation method is utilized to identify the boundary between temporal clusters, and it generates superframes by considering both motion similarity and the targeted number of clusters. A video summary can be generated by selecting representative frames or keyframes from each superframe. Keyframes can be selected based on various criteria, including visual saliency, diversity or importance to the overall video content. Fig. 1 shows the proposed method.

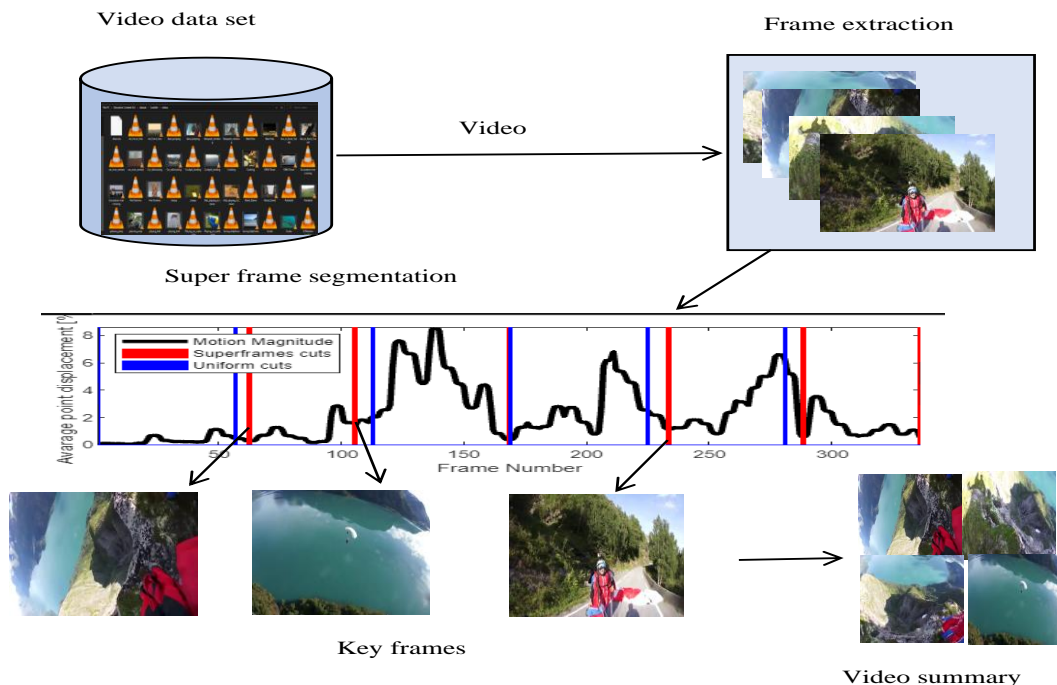


Fig. 1. Proposed system design.

A. Frame Extraction

Frame extraction involves capturing individual frames from a video, typically at a fixed rate or at specific points in time. This fact can be helpful for various applications, such as analyzing the contents of a video, detecting changes between frames, or creating a new video from selected frames. Algorithm 1 represents the frame extraction process from the video. The input for this module is a video data set which contains many user videos. Separate folder will be created for each video. Then, the frames are saved in the respective folder. Pre-processing refers to the techniques applied to data before the analysis to enhance its quality and suitability for downstream analysis. In this, we did rgbtohsi. Converting RGB to HSI can be a crucial step in image processing and computer vision tasks as it can help to separate the image information based on its colour properties. HSI colour model represents colours in terms of hue, saturation, and intensity, which are intuitive and perceptually meaningful to the human eye. The hue component can be used to segment objects based on their colour, the saturation component can be used to detect edges, and the intensity component can be used for brightness normalization. By converting an image from RGB to HSI, we can perform these operations more efficiently and accurately. It can provide a more meaningful and robust representation of colour information in an image.

ALGORITHM 1 Frame extraction(V)
//Input: Video V
//Output: Sequence of extracted frames
1. V ← videoreader(videoname)
2. Initialize:
3. counter ← 0
4. while not at the end of V do:
5. read the frame
6. if not end of V:
7. break
8. else:
9. update the frames in the destined folder
10. counter ← counter + 1
11. end while

B. Super Frame Segmentation

For feature extraction, we use a superframe segmentation algorithm. Our superframe segmentation approach locates the boundary between temporal clusters in video frames. The superframe algorithm generates superframes based on the motion similarity and the required number of clusters. The following Algorithm 2 describes the superframe segmentation. At the beginning of the algorithm, cluster centres are initialized with a regular step size S and then adjusted to the position with the lowest gradient within a neighbourhood. This step aims to ensure that the clusters are initialized in a good position and to prevent them from getting stuck in local minima. The algorithm iteratively assigns frames to the nearest cluster centre using a distance measure as in Eq. (1). This could be any distance measure such as Euclidean distance, Manhattan distance or Cosine distance. After assigning frames to clusters, new cluster centres are computed using the L1 distance. The

algorithm repeats this process until the error E falls below a threshold.

ALGORITHM 2 Video super frame clustering algorithm
//Inputs: Video Frames
1: **Initialize:**
 a = 0.1 * K.
 Cluster centers $Cl_k = [x_1 \dots x_f]^T$ at regular step F
2: Perturb cluster centers in a neighborhood, to the lowest gradient position
3: repeat
4: $S_t \leftarrow S_{t-1}$
5: for each Cl_k do
6: Assign best-matching frames from a 2S neighbourhood around Cl_k according to D_s
7: end for
8: Compute new cluster centres and error E (L1 distance)
9: until $E \leq$ threshold
10: Post-processing to remove very short clusters

Finally, post-processing is performed to remove very short clusters. This could be done by merging small clusters with neighbouring clusters or by removing them altogether. We employ D_s as a distance unit, which is denoted as follows: One way to measure the distance between cluster k and frame i is expressed by the following formula:

$$D_s = \sqrt{\sum (X_k - X_i)^2} \tag{1}$$

where, X is the feature vector.

We might have a small number of clusters with very short lengths at the end of this operation. Fig. 2 shows the superframe cut during this segmentation process.

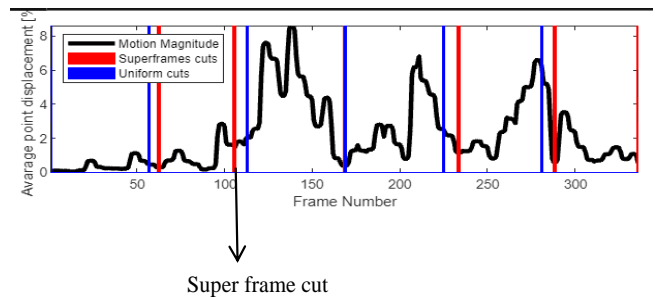


Fig. 2. Illustration of the superframe cut during the segmentation process.

C. Key Shot Identification

Based on characteristics, we will select n frames from the superframe segmentation. The key shots needed to create the summary were found in m frames. Conventional video summarization techniques primarily target edited videos, such as news reports, sports broadcasts, or movies that are composed of several short shots. Shot detection based on changes in the colour histogram is often adequate to segment such videos [25]. Such a technique cannot be applied in our case because we concentrate on user movies that are generally unedited and frequently only comprise one single shot. This issue was also addressed previously by [21], who offered to

partition egocentric films into shots by classifying the frames into static, in-transit, or head-movement categories.

This approach, however, is only appropriate for egocentric videos and produces shots that last for roughly 15 seconds, which is substantially longer than the average length of time for a video summary. Splitting a video into fixed-length segments is a commonly used technique, but it may not align with the meaningful units of the video. Furthermore, abrupt cuts caused by such randomly chosen shot boundaries are disliked by viewers due to the sudden changes in motion.

To achieve sub-shot segmentation, we propose a technique incorporating editing rules to identify moments of no motion or matching motion speed and direction between consecutive frames. These segments are then referred to as "superframes" and compared to superpixels. Additionally, we propose a method inspired by recent advances in image segmentation. The quality of super frames is measured using an energy function $E(S_j)$ as,

$$E(S_j) = \frac{1}{1 + \gamma C_{cut}(S_j)} \cdot P_l(|S_j|) \quad (2)$$

where, P_l is a length prior for the super frames and C_{cut} is the cut cost. The value of parameter γ determines how much weightage should be given to the cut cost versus the length prior in the energy function. By decreasing the value of the parameter, the superframes become more homogeneous. The cut cost is defined as,

$$C_{cut}(S_j) = m_{in}(S_j) + m_{out}(S_j) \quad (3)$$

The formula calculates the estimated motion magnitude of the first $m_{in}(S_j)$ and last frame $m_{out}(S_j)$ in a superframe as and, respectively. We obtain these estimates using the KLT technique to track points in the video and compute the mean

magnitude of the translation. The cost incurred by a superframe is lower if its boundaries align with frames that have little or no motion. By applying a log-normal distribution to a histogram of segment lengths of the human-made summary selections, the length prior P_l is learned.

By using hill-climbing optimization, we locally maximize the energy of Eq. (2). First, using the segment length $|S_j| = \text{argmax}(P_l)$, the super frames are initialized and dispersed uniformly throughout the video/shot (P_l). Then, to improve Eq. (3), we iteratively update the borders between two superframes. This results in segments with boundaries that are aligned in places that are appropriate for cuts. The optimization process is performed in a step-by-step manner, starting with a coarse approach and gradually refining the results. The boundaries are adjusted by one frame at a time. If the adjustment improves the overall score of the energy function given by Eq. (1) for the two relevant superframes, the change is accepted. We begin at the initial value and update iteratively until the algorithm converges. The optimization is then carried out once again after it is reduced by one frame. Only a few iterations are required for this optimization to converge because it is local.

The super frame's interestingness rating S_i is just the total of the frames' degree of interest:

$$I(S_i) = \sum_{k=n}^m i_k \quad (4)$$

where the beginning and ending frames of the superframe are denoted as 'n' and 'm'. Although other scoring strategies were tested, including taking the maximum or considering the size of the cluster, it was found that the simple sum used in this method was the most effective. Fig. 3 illustrates the key shot identification process.

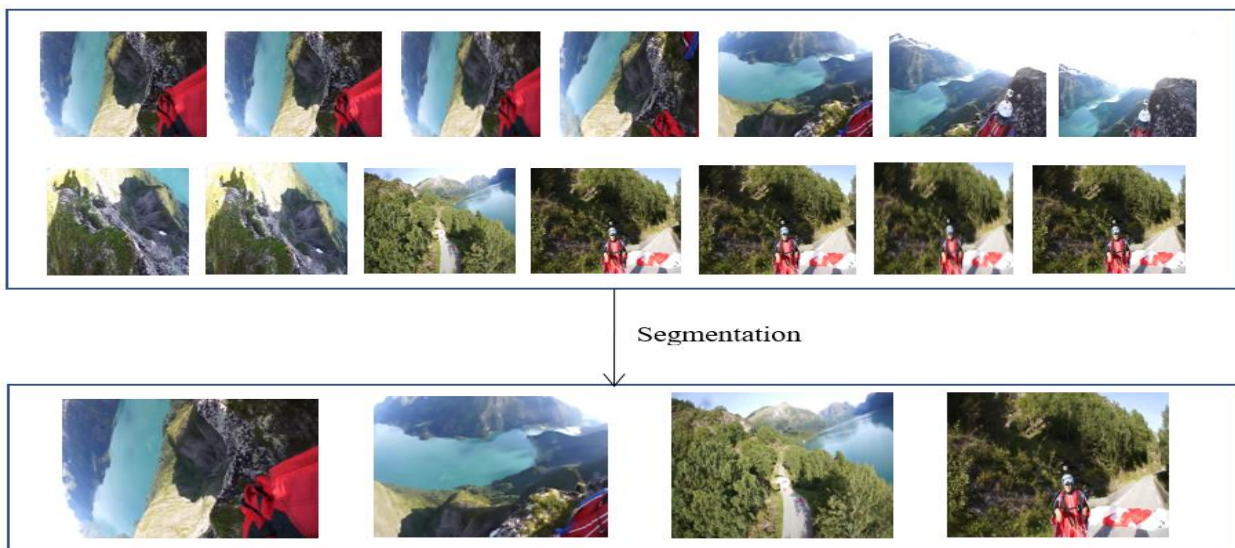


Fig. 3. Key shot identification of the video Base jumping in SUMMe dataset. The first row indicates the input video frame. The second row indicates the key shot identified from the input frames.

D. Key shot-based Summary Generation

Our objective is to find a subset of superframes, denoted as S , whose lengths are below a certain threshold (i.e., maximum), such that the sum of their interestingness scores is maximized.

$$\text{maximize } \sum_{i=1}^n x_i I(S_i) \quad (5)$$

$$\text{X}$$

$$\text{subject to } \sum_{i=1}^n x_i |S_i| \leq L_s \quad (6)$$

where, $x_i \in \{0, 1\}$ and $x_i = 1$ indicates that a super frame is selected. A summary is generated by combining the selected keyframes in a coherent and visually appealing way. The summary should provide an accurate representation of the original video's content while also being concise and easy to understand.

IV. RESULTS AND DISCUSSION

A. Data Set

We evaluate our super frame segmentation on the most popular two datasets SUMMe and TVSum dataset. SUMMe (Summarization of Multiple Longer Videos) is a video summarization dataset that consists of 25 videos from YouTube. The videos are selected from different categories, such as sports, documentaries, and news. The TVSum dataset is a collection of 50 videos from various genres, such as news, documentaries, sports, and movies, suitable for video summarization research. This dataset, along with the SumMe dataset, includes multiple user annotations. To handle temporal redundancy and to comply with earlier efforts, we specifically downsampled all videos to 10 fps, initially shot at 30 fps, to minimize computation. The description of two video summarizing datasets is shown in Table I.

TABLE I. DESCRIPTION OF VIDEO SUMMARIZATION DATASET USED

| Dataset | Total videos | Content | Annotation | Duration(Min,Max,Average) |
|---------|--------------|-----------------------|-------------------|---------------------------|
| SumMe | 25 | User-generated Videos | Frame level score | 38s, 324s, 146s |
| TVSum | 50 | Web videos | Frame level score | 83s, 647s, 238s |

B. Evaluation Metrics

For evaluation, we found F1-Score and Accuracy for the summarized video. The accuracy metric measures the percentage of correctly identified important frames or segments in the video summary compared to the ground truth summary. TP, TN, FP, and FN are employed in the context of binary picture segmentation. TP is the proportion of pixels in the expected binary picture and the ground truth that is properly classified as object pixels. The number of pixels in the anticipated binary picture as well as the ground truth that are properly classified as non-object pixels is known as TN. The number of pixels that are mistakenly classified as objects in the anticipated binary picture but are non-object pixels in the actual image is known as FP. FN is the number of pixels in the anticipated binary image that are mistakenly classified as non-object pixels but are object pixels in the actual picture. These metrics are used to determine how well a binary image segmentation algorithm performs, and they are frequently utilized to determine different evaluation criteria.

The formula for calculation accuracy, F1-score, precision and recall are discussed below.

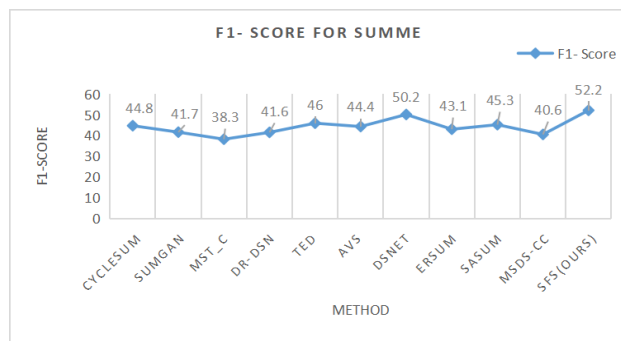
$$\text{Accuracy} = \frac{TP+TN}{FN+FP+TP+TN} \quad (7)$$

$$\text{Recall} = \frac{TP}{FN+TP} \quad (8)$$

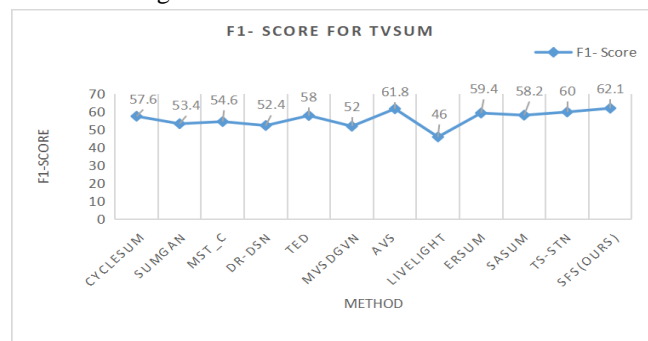
$$\text{Precision} = \frac{TP}{FP+TP} \quad (9)$$

$$\text{F1-Score} = \frac{2*TP}{(2*TP+FP+FN)} \quad (10)$$

1) Our SFS approach was compared to other video summarization methods, including LiveLight [26], ERSUM [27], MSDS-CC [31], SUM-GAN[13], AVS [5], SASUM [28], DR-DSN [15], and TSSTN [29], on the SumMe and TVSum datasets. These methods were categorized into two groups: conventional and deep learning-based methods. The experimental results are presented in Table II under the canonical setting. The results show that the SFS approach outperforms all other methods, including state-of-the-art techniques, by at least 0.5% on both datasets. While methods such as MST_C, MSDS-CC, DR-DSN, and SUMGAN have the lowest F1-score, their performance lags behind that of the SFS approach by at least 4% on both SumMe and TVSum datasets. Fig. 4 shows the f1 score for each of the two datasets.



(a)



(b)

Fig. 4. F1-Score (%) of both the datasets with other state-of-the-Art methods (a) TVSUM (b) SUMME.

TABLE II. PERFORMANCE MEASURE F1-SCORE(%) OF TVSUM AND SUMME DATASET WITH OTHER STATE-OF-THE-ART METHODS

| Method | TVSUM | SUMME | Supervised/Unsupervised |
|---------------|-------|-------|-------------------------|
| CycleSum[13] | 57.6 | 44.8 | Unsupervised |
| SUMGAN[13] | 53.4 | 41.7 | Unsupervised |
| MST_C[4] | 54.6 | 38.3 | Unsupervised |
| DR-DSN[15] | 52.4 | 41.6 | Supervised |
| TED[2] | 58 | 46 | Supervised |
| mvsDGCN[3] | 52.0 | - | Supervised |
| AVS[5] | 61.8 | 44.4 | Supervised |
| LiveLight[27] | 46.0 | - | Unsupervised |
| ERSUM[28] | 59.4 | 43.1 | Supervised |
| SASUM[29] | 58.2 | 45.3 | Supervised |
| TS-STN[30] | 60.0 | - | Supervised |
| DSNet[31] | - | 50.2 | Supervised |
| MSDS-CC[32] | - | 40.6 | Unsupervised |
| SFS(ours) | 62.1 | 52.2 | Unsupervised |

2) Comparison of Accuracy with other State-of-the-Art methods: We also use accuracy as the evaluation metric. The accuracy of a video summarization method is determined by calculating the percentage of significant frames or segments that are identified correctly in the generated summary compared to the ground truth summary. Table III and Fig. 5 present a comparison of the accuracy of our proposed method with other State-of-the-Art approaches. The experimental results demonstrate the superiority of our formulation.

TABLE III. COMPARISON OF ACCURACY METRIC WITH OTHER METHODS

| Method | Methodology | Accuracy(%) | |
|-------------|---|-------------|---------|
| | | SUMME | TVSUM |
| CAVS [1] | The algorithm is developed to learn and update dictionaries of video features along with feature correlations | 81.3 | - |
| DR-DSN [15] | Dynamic graph node classification on videos is used to get the summary result. | 89 | 90.6 |
| SFS (ours) | Keyshot-based summary generation using superframe segmentation. | 89.34 | 90.9852 |

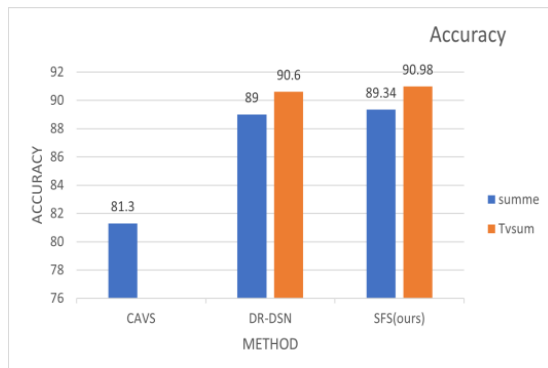


Fig. 5. Representative graph for the given dataset comparing with various methods.

3) We performed an investigation to assess the influence of long-range features, following a methodology comparable to the anchor-based approach. In this study, we analyzed the impact of using various feature extraction layers on performance metrics such as F-score, precision, and recall. The findings of this examination are illustrated in Table IV, indicating that our SFS technique surpasses the other temporal layers on both datasets, resulting in the most superior overall performance.

TABLE IV. COMPARISON OF F1-SCORE, PRECISION AND RECALL WITH ANOTHER STATE-OF-ART METHOD

| Method | SUMME | | | TVSUM | | |
|---------------|-------|------|------|-------|------|------|
| | F | P | R | F | P | R |
| LSTM | 49.5 | 48.7 | 51.2 | 59.8 | 59.8 | 59.8 |
| GCN[32] | 50.5 | 50.0 | 51.3 | 59.8 | 59.8 | 59.8 |
| Attention[33] | 51.2 | 50.8 | 51.9 | 61.9 | 61.9 | 61.9 |
| SFS(ours) | 52.2 | 51.9 | 52.5 | 62.1 | 62.0 | 62.2 |

4) Exemplar key shot summaries: Exemplar key shot summaries are shown in Fig. 6. Video 47 discusses cleaning a dog's ears. We may observe that the key shot summaries of video 47 created by our SFS independently display the narrative details of washing a dog's ears. In the key shot summaries of video 47, our technique can skip a lot of unnecessary video shots. In comparison, DHAVS [34] and DR-DSN[15] key shots contain more frames that aren't significant. As a result, the suggested SFS can receive a higher F1 score.



Fig. 6. Generated summaries with F1-Score from video 47 in TVSum dataset.

C. Parameter Tuning

With varying γ values we found F1-Score for both the datasets. We set the initial data as $\gamma=1$ and then varied the values to get better performance evaluation for both datasets. The value sets of parameters γ are 0.4, 0.5, 0.7, 0.8, 1, 1.2 and

1.4 respectively. From Fig. 7, we observe that a rise in γ value leads to reduced performance.

Table V shows the varying F1-Score for SUMME and TVSUM datasets. The below table leads to the conclusion, for the value of 0.7 our model gives the highest F1-Score when compared with others for our datasets.

TABLE V. F1 SCORE FOR VARYING γ VALUE (A) SUMME (B) TVSUM

| Method | Value | | | | | | |
|----------------|-------|------|------|------|------|------|------|
| | 0.4 | 0.5 | 0.7 | 0.8 | 1 | 1.2 | 1.4 |
| LSTM | 60.7 | 60.9 | 60.5 | 60 | 60.6 | 60.3 | 60.2 |
| Attention [33] | 61.2 | 61.4 | 61.8 | 61.9 | 62 | 61.9 | 61.9 |
| GCN[32] | 61.2 | 61.6 | 61.4 | 61.5 | 61.6 | 61.8 | 61.9 |
| SFS(ours) | 57.9 | 59.3 | 62.1 | 59 | 58.4 | 59.2 | 58.6 |

(a)

| Value | F1 Score |
|-------|----------|
| 0.4 | 43.2 |
| 0.5 | 45.8 |
| 0.7 | 48.9 |
| 0.8 | 52.2 |
| 1 | 49.3 |
| 1.2 | 47 |
| 1.4 | 46.23 |

(b)

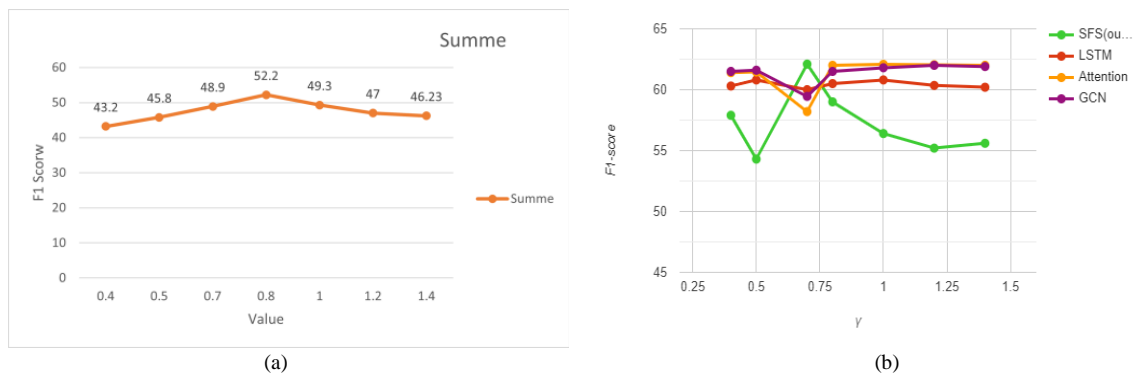


Fig. 7. Representative graph for both the datasets with varying γ values (a) SUMME (b) TVSUM.

V. CONCLUSION

The proposed approach in this study introduces a technique for segmenting user videos using temporal superframes and a method for generating informative video summaries. The main goal of this paper is to provide a better summary of surveillance video, which is helpful for law enforcement officials. So, we use a superframe segmentation process in which dividing the video into short, visually consistent segments called superframes and select representative frames from each superframe to construct the summary. In contrast to other methods, our approach can handle variations in camera movements and scene changes, which makes it different visual characteristics. We choose Accuracy, F1-score, Precision, and Recall as the assessment measures to compare our method fairly to existing video summarizing techniques. Our experimental findings demonstrate that the SFS method we proposed performs competitively on the SumMe and TVSum datasets. Furthermore, we conducted additional experiments to investigate the effect of the final summary length (L) on the performance metrics, including F-score, precision, and recall. Our results suggest that the best performance of our method can be achieved when the final summary length is set to 15% of the original video length on both datasets. This framework could be largely assistive for observing the activities of the students during their online exams. It could be a better alternative for the officials conducting the assessment and monitoring the suspicious activities of the students.

ACKNOWLEDGMENT

The paper is financed by the European Union-NextGenerationEU, through the National Recovery and Resilience Plan of the Republic of Bulgaria, project № BG-RRP-2.004-0001-C01.

REFERENCES

- [1] S. Zhang, Y. Zhu, A. Roy-Chowdhury, "Context-aware surveillance video summarization," *IEEE Trans. Image process.*, vol. 25, no. 11, pp. 5469–5477, Nov. 2016, doi: 10.1109/TIP.2016.2601493.
- [2] C. Huang, H. Wang. "A Novel key frames selection framework for comprehensive video summarization", *IEEE Trans. Circuits And Sys. For Video Tech.*, vol. 30, no. 2, pp. 577-589, Feb. 2020, doi: 10.1109/TCSVT.2019.2890899.
- [3] J. Wu, S. Zhong, Y. Liu. "Dynamic graph convolutional network for multi-video summarization", *Elsevier Pattern Recog.*, vol. 107, no. 1, Art. no: 107382, Nov. 2020, doi: 10.1016/j.patcog.2020.107382.
- [4] A. Sahu, A. Chowdhury, "First person video summarization using different graph representations", *Elsevier Pattern Recog. Lett.*, vol. 146, no. 1, pp. 185-192, Mar. 2021, doi: 10.1016/j.patrec.2021.03.013.
- [5] Zh. Ji, K. Xiong, Y. Pang, X. Li. "Video summarization with attention-based encoder-decoder networks", *IEEE Trans. Circuits and Sys. for Video Tech.*, vol 30, no. 6, pp. 99, Aug. 2017, doi: 10.1109/TCSVT.2019.2904996.
- [6] P.Kalaivani, S. Roomi. "Towards comprehensive understanding of event detection and video summarization approaches", *2017 Second Inter. Conf. on Recent Trends and Challe. in Comput. Models (ICRTCCM)*, pp. 61-66. IEEE, Feb. 2017, doi: 10.1109/ICRTCCM.2017.84.
- [7] K. Kumar, D. D. Shrimankar, N. Singh. "Event BAGGING: A novel event summarization approach in multi-view surveillance video", *Innova. in Electro., Signal Process. and Comm.(IESC), 2017 Inter. Conf.*, pp. 106-111, Apr 2017, doi: 10.1109/IESPC.2017.8071874.
- [8] U. Damnjanovic, V. Fernandez, E. Izquierdo, J. Martinez. "Event detection and clustering for surveillance video summarization", *2008 Ninth Inter. Work. on Image Anal. for Multi. Inter. Serv.*, pp. 63-66. IEEE, May 2008, doi: 10.1109/WIAMIS.2008.53.
- [9] S. Thomas, S. Gupta, V. Subramanian. "Perceptual video summarization—A new framework for video summarization", *IEEE Trans. Circuits and Sys. for Video Tech.*, vol. 27, no. 8, pp.1790-1802, Apr. 2016, doi: 10.1109/TCSVT.2016.2556558.
- [10] Ch. Ngo, Y. Ma, H. Zhang. "Automatic video summarization by graph modeling", in *Procee. Ninth IEEE Inter. Conf. on Comp. Vision*, pp. 104-109. IEEE, Oct 2003, doi: 10.1109/ICCV.2003.1238320.
- [11] Y. Cong, J. Yuan, J. Luo. "Towards scalable summarization of consumer videos via sparse dictionary selection", *IEEE Trans. Multi.*, vol. 14, no. 1 pp. 66-75, Sep 2011, doi: 10.1109/TMM.2011.2166951.
- [12] K. Zhou, Y. Qiao, T. Xiang. "Deep reinforcement learning for unsupervised video summarization with diversity-representativeness reward", in *Proc. of the AAAI Conf. on Arti. Intelli.*, vol. 32, no. 1, Apr. 2018, doi: 10.1609/aaai.v32i1.12255.
- [13] B. Mahasseni, M. Lam, S. Todorovic, "Unsupervised video summarization with adversarial lstm networks", in *Proc. of the IEEE conf. Comp. Vision and Patt. Recog.*, pp. 202-211, Jul. 2017, doi: 10.1109/CVPR.2017.318.
- [14] M. Rochan, Y. Wang. "Video summarization by learning from unpaired data", in *Proc. of the IEEE/CVF Conf. Comp. Vision and Patt. Recog.*, pp. 7902-7911, June. 2019, doi 10.1109/CVPR.2019.00809.
- [15] K. Zhang, W. Chao, F. Sha, K. Grauman, "Video summarization with long short-term memory", in *Comp. Vision-ECCV 2016: 14th Euro. Conf., Amsterdam, The Netherlands, Oct. 11–14, 2016, Procee., Part VII 14*, pp. 766-782. Springer Inter. Publi., Oct. 2016, doi: 10.1007/978-3-319-46478-7_47.
- [16] B. Gong, W. Chao, K. Grauman, F. Sha. "Diverse sequential subset selection for supervised video summarization", *Adv. in neural info. process. sys.*, pp. 2069-2077, Jan 2014.

- [17] E. Bulut, T. Capin. "Key Frame Extraction from Motion Capture Data by Curve Saliency", *Proceedings of 20th Annual Conference on Computer Animation and Social Agents.*, vol. 20, no. 5, Jun. 2007.
- [18] B. Zhao, X. Li, X. Lu. "Hierarchical recurrent neural network for video summarization" In *Proceedings of the 25th ACM International Conference on Multimedia*, pp. 863-871. 2017.
- [19] W. Wolf. "Key frame selection by motion analysis", in *IEEE Inter. conf. acoustics, speech, and sig. process. conf. proceedings*, vol. 2, pp. 1228-1231. IEEE, May. 1996, doi: 10.1109/ICASSP.1996.543588.
- [20] C. Li, Y.T. Wu, S.S. Yu and T. Chen, "Motion-focusing key frame extraction and video summarization for lane surveillance system", *16th IEEE International Conference on Image Processing (ICIP)*, pp. 7-10, Nov. 2009 doi: 10.1109/ICIP.2009.5413677.
- [21] M. Ajmal, M. Naseer, F. Ahmad and A. Saleem. "Human Motion Trajectory Analysis Based Video Summarization", *16th IEEE International Conference on Machine Learning and Applications (ICMLA)*, pp. 550-555, Dec. 2017 doi: 10.1109/ICMLA.2017.0-103.
- [22] J. Almeida, R. D. S. Torres and N. J. Leite, "Rapid video summarization on compressed video", *IEEE International Symposium on Multimedia.*, pp. 113-120, Dec.2010, doi: 10.1109/ISM.2010.25.
- [23] H.J. Zhang, J. Wu, D. Zhong and S.W. Smoliar, "An integrated system for content-based video retrieval and browsing", *Pattern Recognition Elsevier.*, Vol. 30, pp.643-658, Apr. 1997, doi: 10.1016/S0031-3203(96)00109-4.
- [24] F. Wang and C.W. Ngo, "Summarizing rushes videos by motion, object, and event understanding", *IEEE Transactions on Multimedia.*, vol. 14, no. 1, pp.76-87, Aug. 2011, doi: 10.1109/TMM.2011.2165531.
- [25] N. Baghel, S.C. Raikwar, C. Bhatnagar, "Image conditioned key frame-based video summarization using object detection," arXiv preprint arXiv: 2009.05269., Sep. 2020.
- [26] B. Zhao and E.P. Xing, "Quasi real-time summarization for consumer videos", *Proceedings of the IEEE conference on computer vision and pattern recognition.*, pp. 2513-2520, Sep. 2014, doi: 10.1109/CVPR.2014.322.
- [27] X. Li, B. Zhao, X. Lu. "A general framework for edited video and raw video summarization", *IEEE Transactions on Image Processing.*, vol. 26, no. 8, pp. 3652-3664, Aug. 2017, doi:10.1109/TIP.2017.2695887.
- [28] H. Wei, B. Ni, Y. Yan, H. Yu, X. Yang, C. Yao, "Video summarization via semantic attended networks", *Proceedings of the AAAI conference on artificial intelligence.*, vol. 32, no. 1, 2018, pp. 216-223, doi: 10.1609/aaai.v32i1.11297.
- [29] S. Huang, X. Li, Z. Zhang, F. Wu, and J. Han, "User-ranking video summarization with multi-stage spatio-temporal representation", *IEEE Transactions on Image Processing.*, vol. 28, no. 6, pp. 2654-2664, Jun. 2019, doi: 10.1109/TIP.2018.2889265.
- [30] W. Zhu, J. Lu, J. Li, J. Zhou, "Dsnet: A flexible detect-to-summarize network for video summarization", *IEEE Transactions on Image Processing.*, vol. 30, pp. 948-962, Dec. 2020, doi: 10.1109/TIP.2020.3039886.
- [31] J. Meng, S. Wang, H. Wang, J. Yuan, Y.P. Tan, "Video summarization via multi-view representative selection", *Proceedings of the IEEE international conference on computer vision workshops.*, pp. 1189-1198, Jan. 2018, doi: 10.1109/ICCVW.2017.144.
- [32] T. N. Kipf and M. Welling, "Semi-supervised classification with graph convolutional networks," *arXiv preprint arXiv: 1609.02907*, Sep. 2016.
- [33] A. Vaswani et al., "Attention is all you need", *Advances in neural information processing systems*, vol. 30. 2017, pp. 5998-6008.
- [34] J. Lin, S.H. Zhong, and A. Fares, "Deep hierarchical LSTM networks with attention for video summarization", *Computers and Electrical Engineering Elsevier.*, vol. 97, pp. 107618, Jan. 2022, doi: 10.1016/j.compeleceng.2021.107618.

Training Model of High-Rise Building Project Management Talent under Multi-Objective Evolutionary Algorithm

Pan QI

TianPing College of Suzhou, University of Science and Technology, Jiangsu, 215000, China

Abstract—In order to meet the development needs of the construction engineering industry and further optimize and improve the talent training mode, this paper studies the talent training model of high-rise construction project management under the multi-objective evolutionary algorithm. The cognitive ability model of management talent is constructed, and the learning ability of management talent is analyzed. With the optimization objectives of minimizing the construction period, minimizing the project cost, and maximizing the benefit of skill growth in high-rise building projects, and taking the conditions of average proficiency and average duration of construction as constraints, the mixed immune genetic algorithm with the introduction of the double-island model is adopted to carry out multi-objective evolution of management talent training, so as to obtain the best training scheme for management talent in high-rise building projects. The experimental results show that after the optimization of this model, the skill proficiency of project management personnel can be effectively improved, construction time can be effectively reduced, construction efficiency can be improved, and construction costs can be improved.

Keywords—Multi-objective evolution; high-rise building; engineering project; management personnel training; skill proficiency; project cost

I. INTRODUCTION

High-rise buildings are one of the symbols of urban modernization. They can provide more office space, commercial space, and housing space for cities to meet the growing population and economic needs [1]. The construction of high-rise buildings can promote the development and urbanization of cities. Due to the limited land resources, high-rise buildings can create more functional space on the restricted land area and improve the efficiency of land use [2]. Compared with traditional low-rise buildings, high-rise buildings can provide more usable area under the same floor space, thus saving valuable land resources [3]. At the same time, high-rise building projects will drive a lot of investment and consumption in the construction process, thus promoting local economic development [4]. After the completion of high-rise buildings, it can also provide commercial rents and real estate sales income, bringing considerable financial benefits to investors. Moreover, high-rise buildings often become urban landmarks and landmark buildings, which can enhance the image and attractiveness of the city [5]. The design and construction level of high-rise buildings directly reflects the comprehensive strength and development level of a town, which can enhance the performance of the city's culture, art,

and modernization and improve the competitiveness of the city on a global scale [6]; High-rise building projects also provide opportunities for promoting green buildings and sustainable development. Innovations in architectural design, building materials selection, energy conservation, and environmental protection can reduce energy consumption, reduce carbon emissions, and promote sustainable development.

The construction process of high-rise building projects is usually characterized by high complexity and risk, and these projects need to coordinate the work of multiple professional teams, such as architectural design, structural engineering, electromechanical engineering, decoration engineering, etc. [7]. Therefore, the current construction enterprises urgently need to cultivate high-level management talent. By developing talent with management skills, potential risks can be identified and evaluated in advance, and corresponding risk management measures can be formulated to reduce project risks and ensure the smooth implementation of the project [8]. Cultivating talent who can effectively coordinate and manage teamwork can improve the team's cooperation ability and efficiency and ensure the seamless connection between various majors [9]. At the same time, the cultivation of high-rise building engineering management talent can also promote engineering innovation and technological progress. They have a keen awareness of new technologies and innovative methods, can introduce new engineering management concepts and technical methods, improve work efficiency and quality, and promote the development of the high-rise building engineering industry [10]. However, there are some defects in the current training of construction engineering talent, and construction projects need to master a series of professional skills, including skills in design, construction, management, etc. However, the existing talent training pays insufficient attention to skills training and pays more attention to knowledge transmission, ignoring the cultivation of practical operation and practical skills [11]. Due to the continuous development and changes in the construction engineering industry, the docking of talent training and industry demand is not close enough. To this end, many scholars have put forward different talent training programs. For example, Klipkova, O et al. [12] studied the optimization of personnel management mechanisms based on intergenerational theory. This method is based on the three-dimensional method of employees, enterprises, and external conditions, and applies certain leadership theories and team cooperation principles to effectively manage the personnel of the enterprise, thereby achieving talent cultivation in the

enterprise. However, this method cannot guarantee the improvement of enterprise operating costs, leading to excessive burden on the enterprise; for example, Nguyen, D. A et al. [13] studied the use of neural networks to model the labor productivity of high-rise building construction projects. Through the optimization of neural networks, the labor productivity of construction enterprises can be improved, thereby accelerating construction efficiency. However, this method cannot guarantee the cultivation of personal skills of employees; for example, Hudyakova, E et al. [14] studied the problems and solutions in the configuration of management personnel in agricultural and industrial complexes. This method deeply planned the responsibilities that enterprise management personnel should fulfill and cultivated the required skills for different responsibilities. However, the training plan of this method does not apply to multiple fields, and it focuses more on learning knowledge content in the process of talent cultivation, resulting in neglecting the cultivation of personal skills of employees. A multi-objective evolutionary algorithm is an algorithm used to solve multi-objective optimization problems. Different from the traditional single-objective optimization algorithm, a multi-objective evolutionary algorithm can simultaneously optimize multiple conflicting objective functions in a set of solutions [15]. To effectively realize the optimization of management personnel training, this paper puts forward a high-rise building project management personnel training model based on a multi-objective evolutionary algorithm. It recognizes the optimization of management personnel training schemes by using a multi-objective evolutionary algorithm.

II. HIGH-RISE BUILDING PROJECT MANAGEMENT PERSONNEL TRAINING OPTIMIZATION MODEL DESIGN AND RESEARCH

A. Overall Description of High-Rise Building Project

A large high-rise building construction project usually consists of several single projects. A single project can be decomposed into multiple unit projects, such as civil engineering water and electricity installation engineering [16]. Each unit project is further decomposed into several sub-projects, such as civil engineering, which can be divided into basic engineering, main engineering, roofing engineering, and decoration engineering [17]. Sub-projects can be subdivided into sub-projects, such as foundation projects, which can be divided into earthwork excavation, foundation treatment and testing, concrete foundation, and other sub-projects. A sub-project can be regarded as a relatively independent activity (or task) that is completed by a large number of technicians. It is a separate dispatching unit and also the basic activity of dispatching [18]. Therefore, the training of high-rise building project management talent can enhance the construction efficiency of building projects.

Human resources in high-rise building projects include managers at different levels and various workers involved. The management personnel of the construction project department

mainly include the project director (project manager), technical director, production director, builder, machine controller, safety officer, quality inspector (sampler), material engineer, cost engineer, etc. At the same time, these personnel are also professional and technical management personnel. These personnel are the main managers of engineering construction, and their management ability will directly affect the safety, progress, quality, and cost of engineering construction, which is related to the survival and development of construction enterprises [19]. Therefore, effective ways must be adopted to train the project managers of high-rise buildings. Table I shows a comparison of the proposed work in experimental analyses with similar research works and state-of-the-art research studied as part of the literature review.

B. Modeling and Design of Employees' Cognitive Ability

In order to optimize the training scheme of high-rise building project management talent, this paper puts forward a model of employees' cognitive ability based on a learning-forgetting curve, which can fully consider the learning effect and forgetting degree of employees in the learning process so as to obtain the skill proficiency of a high-rise building project management talent.

1) *Analysis of learning effect and learning curve*: Before modeling employees' cognitive ability, it is necessary to analyze employees' learning effects and the change in the learning curve. Only by using this analysis result can the employees' mental ability model be effectively built based on a learning-forgetting curve. The learning effect, also known as the learning phenomenon, refers to the effect that the accumulated experience through long-term work leaves a memory in employees' minds, which helps employees improve the same or similar work efficiency [20]. Long-term research shows that the study of the learning effect basically needs to follow three hypotheses. (1) For repeated construction tasks, the time consumption of a single construction operation decreases with the increase of construction repetitions. (2) The learning effect can gradually reduce the time consumption of a single construction operation and the absolute efficiency. (3) The existence of the learning effect can be predicted and applied scientifically. Therefore, the learning curve can generally be expressed by Formula (1):

$$Y_x = Cx^b \quad (1)$$

In the Formula (1), x represents the cumulative completion of construction; Y_x represents the working hours or costs of the x construction task; C indicates the operating hours or price of the first construction task; b represents the learning index, with a value less than or equal to zero, $b = \log s / \log 2$, S indicates the learning rate, which is an index used to describe the learning curve. When the learning effect is better, the learning efficiency is lower.

TABLE I. COMPARING THE PROPOSED WORK IN EXPERIMENTAL ANALYSES WITH SIMILAR RESEARCH WORKS AND STATE-OF-THE-ART RESEARCH STUDIED AS PART OF THE LITERATURE REVIEW

| Aspect | Proposed Work | Similar Research Works |
|----------------------|--|---|
| Scope and Focus | Training model for high-rise building project management talent under a multi-objective evolutionary algorithm | Optimization of personnel management mechanisms, labor productivity modeling, and configuration of management personnel in various industries |
| Objective Function | Balances project duration, cost, and skill growth rate | Varies based on research: personnel management mechanisms, labor productivity improvement, skill cultivation and task allocation |
| Methodology | Multi-objective evolutionary algorithm | Intergenerational theory, neural networks, management personnel configuration |
| Analysis Techniques | Learning and forgetting curves, cost optimization, human resource utilization | Various techniques including optimization algorithms, productivity modeling, skill proficiency analysis |
| Evaluation Metrics | Employee efficiency, construction cost, human resource utilization, skill proficiency | Employee proficiency, project cost, resource utilization, skill growth rate |
| Experimental Setup | Application to a specific high-rise building project | Not specified in the provided text |
| Results and Findings | Enhanced project efficiency, cost savings, improved human resource utilization | Varies based on research: potential improvements in management efficiency, productivity, and skill development |
| Conclusion | Provides a scientific and effective method for talent training in high-rise building project management | Varies based on research: suggests improvements in talent training methods and strategies |

The learning effect can generally be expressed by describing the relationship between the cumulative construction quantity and the input factor quantity of unit construction quantity. The learning curve is also called the starting curve, experience curve, or improvement curve. The learning curve was first put forward by Wright in 1936. Through the learning curve, it is revealed that with continuous construction, the processing time of unit construction tasks will be gradually shortened, and the learning curve is widely used in industrial production. The learning curve can be expressed by Formula (2):

$$T_x = T_1 x^{-l} \quad (2)$$

In the Formula (2), T_x represents the time required for processing the construction of the x task, values of x are 0, 1, and 2. T_1 indicates the time needed to handle the first construction task, and l indicates the learning efficiency of employees. With the continuous construction work, the time spent on the completion of unit construction tasks is decreasing, and with the constant learning of employees, the construction skills are also rising. At the same time, the processing time of unit construction tasks has a lower bound, which means that the processing time of unit construction tasks will not decrease indefinitely, which means that the skill value of employees is limited. Employees can continuously improve their skill value through construction work, but it will not increase excessively.

With the application of the learning curve in various fields and its development in different degrees, some scholars suggest that the longer employees use a skill, the higher the construction efficiency of the skill will be, and assume that employee p participates in construction tasks k , then the learning curve formula can be expressed by Formula (3):

$$\bar{E}_n = \bar{E}_1 n^b \quad (3)$$

In Formula (3), n represents the total time spent by employee p in the construction task k ; \bar{E}_1 represents the average

efficiency of employee p on starting the construction task; \bar{E}_n represents the accumulated average efficiency of employee p after spending n cycles in the construction task k ; $b = -\frac{\ln(r)}{\ln 2}$, ($0 < r \leq 1$), b represents a learning factor, r represents the percentage of learning. The smaller the value of r , the greater the value of b , the higher the learning efficiency.

2) *Modeling of employees' cognitive ability based on learning-forgetting curve model*: In order to accurately understand the cognitive level of high-rise building project management talent, combined with the learning curve of the above research, the learning-forgetting curve model of employees' cognitive ability is constructed by using the LFCM (Learning and Forgetting Curve Model) model. This model is a perfect model based on the classic WLC learning curve model, which reveals the relationship between learning and forgetting degree and interruption time by comparing the forgetting effect with the learning effect [21]. Based on LFCM theory, the calculation method of skill proficiency considering learning-forgetting impact is shown in Formula (4):

$$\beta_{pki}^f = \beta_{pki}^s + L \cdot T^{ak} - F \cdot T'^{bk} \quad (4)$$

In Formula (4), β_{pki}^f indicates the proficiency of the employee p using the skill k before performing the construction task i ; T indicates the duration of the employee p using the skill k ; T' indicates the difference between the initial moment of the employee p use skill k to perform the construction task i and the end moment of the last previous use skill k , that is, the time when the employee is idle; L represents the learning curve coefficient, F represents the coefficient of forgetting curve, which is related to the initial skill proficiency. Usually, the lower the skill level, the faster the level will improve because of the lower difficulty in learning basic knowledge, and the knowledge will not be easily forgotten. When the skill level is

high, the learning difficulty of deep expertise is relatively high, the speed of level improvement will slow down, and knowledge is easy to forget. Under normal circumstances, the forgetting rate of employees is less than the learning speed, and the article stipulates that $L = -\ln(\beta_{pki}^s/2)/10$, $F = \ln(3\beta_{pki}^s)/15$. The greater the initial skill proficiency, the smaller the learning curve coefficient and the larger the forgetting curve coefficient; a_{pk} represents the learning factor of employee p for construction skills k , $a_{pk} = -\ln(\lambda_{pk})/\ln(2)$, λ is the learning rate, λ generally is between 75%~95%, the greater the learning factor, the stronger the learning effect; b_{pk} represents forgetting factor of employee p for skills k , $b_{pk} = \ln(1 - \mu_{pk})/\ln(2)$, μ is the forgetting rate, μ generally is between 3%~15%. The greater the forgetting factor, the weaker the forgetting effect. The learning rate and forgetting rate are closely related to employees' factors. Considering the limitations of people's physiological conditions, there is a learning upper limit $\hat{\beta}$ for skill proficiency, and ignoring the lower limit $\tilde{\beta}$. $\Delta\beta(T) > \Delta\beta(T')$, $T = T'$ means that the learning effect of employees is stronger than the forgetting effect at the same time. In addition, the learning effect and forgetting effects of employees change after each interruption. With the improvement of skill proficiency, the learning speed slows down, and the forgetting rate accelerates.

C. High-Rise Building Project Management Personnel Training Optimization Model Construction

1) Design of objective function: Combined with the employee as mentioned above cognitive ability modeling, this paper constructs a multi-objective function of the training model for project managers of high-rise buildings, aiming at minimizing the project duration, minimizing the project cost, and maximizing the benefit of skill growth, and constructs a multi-objective function model, as shown in Formula (5), Formula (6) and Formula (7):

$$\min T = \sum_{i \in A} T_i \quad (5)$$

$$\min C = m \cdot w + \sum_{i=1}^n \sum_{k=1}^r (\tilde{\beta}_{ki} \cdot c_{ki}^{max}) \quad (6)$$

$$\max R = \sum_{i=1}^n \sum_{k=1}^r \sum_{p=1}^m \varepsilon_k \cdot (\beta_{pki}^f - \beta_{pki}^s) \quad (7)$$

Among the above formulas, Formula (5) represents the objective function of minimizing the project duration, and the total time is the sum of the durations of tasks on the critical path. T represents the project duration, A represents a collection of functions on a critical path, $A = \{a_1, a_2, \dots, a_x\}$, $a_x \in [1, n]$, T_i represents the duration of the task i ; Formula (6) represents the objective function of minimizing the project cost. The project cost is the sum of the salaries paid to all employees, including the basic salary and the commission. The basic salary is fixed and consistent for all employees, and the commission is positively related to the average efficiency of completing the work. C represents the project cost, $\tilde{\beta}_{ki}$ represents the average proficiency work J_{ki} , describes the basic salary of employees, m represents the employee's commission salary, c_{ki}^{max} represents the highest commission for a job, which means the remuneration received by an employee with skill

proficiency of 1 completes the job J_{ki} ; Formula (7) represents the objective function of maximizing the benefit of skill growth, and the total benefit is equal to the sum of the skill proficiency appreciation of all employees after participating in various jobs. R indicates that benefit of skill growth, ε_k represents the development weight of skill k that refers to the importance of skills to enterprises. β_{pki}^s represents the skill proficiency of an employee p start work J_{ki} , describes the skill proficiency of an employee p finish work J_{ki} .

In order to ensure the optimization effect of the article on the talent training scheme, according to the above objective function, the following optimization constraints are constructed:

a) Average working proficiency: Formula (8) is used to express the average working proficiency of employees:

$$\bar{\beta}_{ki} = \frac{\sum_{p=1}^m \beta_{pki}^s \cdot X_{pki}}{d_{ki}} \quad (8)$$

In the Formula (8), X_{pki} is the number of employees required for work J_{ki} ; d_{ki} is 1 if the employee p is involved in work J_{ki} , otherwise, the value is 0.

b) Duration of construction task: the duration of the construction task is constrained by Formula (9):

$$T_i = \max_{k \in K} \{T_{ki}\}, T_{ki} = \frac{T_{ki}^{min}}{\bar{\beta}_{ki}} \quad (9)$$

In the Formula (9), T_{ki}^{min} represents the minimum duration of work J_{ki} that refers to the time required for employees with skill proficiency of 1 to complete the work; T_{ki} represents the duration of employment J_{ki} .

c) Formula (10) is used to express the logical constraint condition of the construction task, that is, the task can only be started after all the tasks immediately before it is finished:

$$B_i - B_j \geq T_j, \forall i \in I, \forall j \in PF_i \quad (10)$$

In the Formula (10), B_i represents the commencement time of the construction task i ; B_j represents the end time of the construction task j ; I represents the collection of a task i , $I = \{1, 2, \dots, n\}$; PF_i represents a set of immediate tasks of task i .

d) Formula (11) is used to express the calculation method of skill proficiency of employees at the beginning of work:

$$\beta_{pki}^s = \begin{cases} \beta_{pk}^s, \forall x_{pki} \neq 1, i' \in PF_i \\ \beta_{pk}^f, \text{argmin}_{i' \in PF_i} \{B_{ki} - (B_{ki'} + T_{ki'})\}, \exists x_{pki'} = 1, i' \in PF_i \end{cases} \quad (11)$$

In the Formula (11), x_{pki} indicates that if employee p participates in work J_{ki} , the value is 1; if the employee p has skills k but does not participate in work J_{ki} , the value is 0; if the employee p does not have skills k , the value is -1; B_{ki} indicates the start time of work J_{ki} ; β_{pk}^s represents the proficiency of employee p using skill k at the beginning of the project, representing employee productivity, $\beta_{pk} \in [0, 1]$, if

the employee p does not have skill k , the value is 0; β_{pk}^f indicates the ability of employee p using skill k at the end of the project.

e) Calculate the skill proficiency of employees at the end of work by Formula (12), and specify that the upper learning limit of skill proficiency is 1 and the lower forgetting limit is 0.3. If the calculated proficiency value is greater than 1 or less than 0.3, reset the value to the upper or lower limit:

$$\beta_{pki}^f = \begin{cases} \beta_{pki}^s + L \cdot T_{ki}^{a_{pk}}, \forall x_{pki'} \neq 1, i' \in PF_i \\ \beta_{pki}^s + L \cdot T_{ki}^{a_{pk}} - F \cdot \left(\min_{i' \in PF_{i'}} \{B_{ki} - (B_{ki} + T_{ki'})\} \right)^{b_{pk}} \\ \exists x_{pki'} \neq 1, i' \in PF_i \end{cases} \quad (12)$$

$$L = -\ln(\beta_{pki}^s/2)/10, F = \ln(3\beta_{pki}^s)/15$$

In the Formula (12), L represents the learning curve coefficient; b_{pk} represents the learning factors for an employee p to skills k , a_{pk} represents the learning efficiency of an employee p to skills k .

f) Formula (13) indicates that when there is a situation where the same employee is assigned to complete multiple tasks in parallel tasks, and there is a human resource conflict in job assignment, the employee is first given the job with a higher priority, that is, the position with higher priority starts first:

$$\begin{aligned} B_{ki} - B_{kj} &\geq T_{bj}, \varphi_{kj} \geq \varphi_{ki}, PF_i \\ &= PF_j, S_{ki} \cap S_{kj} \neq \emptyset \end{aligned} \quad (13)$$

In Formula (13), φ_{ki} represents the priority of work J_{ki} , $\varphi_{ki} \in [1, j]$; S_{ki} represents assignment to a job. J_{ki} represents a collection of employees; F represents the forgetting curve coefficient.

g) By Formula (14), the number of employees assigned to task i using skill k shall be equal to the number of employees required to complete task i using skill k :

$$\sum_{p=1}^m X_{pki} = d_{ki} \quad (14)$$

h) Restrict each employee to participate in only one job at any time by Formula (15):

$$\sum_{i=1}^n \sum_{k=1}^r y_{pkit} \leq 1 \quad (15)$$

In the Formula (15), y_{pkit} represents an employee p participates in the work J_{ki} at time t , the value is 1, otherwise the value is 0.

i) The range and relationship of the three decision variables are expressed by Formula (16), Formula (17) and Formula (18):

$$\begin{aligned} x_{pki} &\in \{0, 1, -1\}, y_{pkit} \in \{0, 1\}, X_{pki} \\ &\in \{0, 1\}; \forall p, k, i, t \end{aligned} \quad (16)$$

$$x_{pki} = \begin{cases} 1, \forall t, y_{pkit}=1 \\ 0, \forall t, y_{pkit}=0; \forall p, k, i \\ -1, \alpha_{ki} = 0 \end{cases} \quad (17)$$

$$X_{pki} = \begin{cases} 1, x_{pki} = 1 \\ 0, x_{pki} \neq 1; \forall p, k, i \end{cases} \quad (18)$$

In the above formula, K represents a collection of skill k , $K = \{1, 2, \dots, r\}$; P represents a collection of employees p , $P = \{1, 2, \dots, m\}$; J_{ki} represents the work performed in a task i using skills k , $j = \sum_{i=1}^n \sum_{k=1}^r \alpha_{ki}$.

Through the above methods, the constraint conditions of the optimization goal of high-rise building project management personnel training are constructed, which provides a reliable guarantee for multi-objective optimization.

D. Optimization of Personnel Training Model based on Multi-Objective Genetic Algorithm

The Genetic algorithm is a highly parallel adaptive search algorithm based on the "survival of the fittest" mechanism. In 1967, some scholars applied genetic evolution to multi-objective optimization problems for the first time; thus, the research on multi-objective optimization problems entered a new era, and the search idea using genetic evolution later became the basis for a large number of scholars [22]. Because the article constructs a variety of objective functions of talent training optimization in the above chapters, in order to realize these multi-objective optimizations, this paper uses a multi-objective genetic algorithm to find out the best management talent training scheme through multi-objective optimization.

All genetic algorithms (GA) follow a similar basic framework, which was put forward by Holland and called a simple genetic algorithm [23]. The main flow of the algorithm is as follows:

- According to the modeling results of the above-mentioned objective function, the chromosome coding of the training target of management talent in high-rise building projects is carried out, and the initial population of management talent training targets is randomly generated.
- Judge whether the evolutionary algebra meets the requirements, if it meets the requirements, outputting the training target population of the last generation of management talent and ending the test; otherwise, enter step (3).
- Calculate the fitness value of the target population for training management talent, replace it with the "two-person competition" method (including male parent and female parent), and cross it with some rules to produce offspring; after the crossover is completed, the parent mutates with a certain probability to produce offspring (in order to preserve population diversity, the mutated parent is kept.) Merge the crossed and mutated offspring with the parent, and recalculate the individual fitness value of the target population of management talent training.

- Judge whether the number of the target population for training management talent is greater than the initial set value, and if it exceeds the set value, put forward the inferior solution through the "three-person championship" according to the fitness. Evolutionary algebra Gen+1, and return to step (2).

Because the above steps are only the basic framework of the genetic algorithm, the state of the actual management personnel training goal optimization is not considered. Therefore, the calculation process of chromosome coding, crossover, mutation, and fitness function is analyzed through the following contents.

1) Management personnel training target chromosome coding and decoding.

a) *Chromosome Coding*: Each individual in the target population of management personnel training represents a feasible optimization scheme. Because it is necessary to arrange the construction sequence and human resource allocation at the same time, each possible solution is set to contain two chromosomes, namely the construction task chromosome and the employee chromosome, and they should have the same number of genes. The construction task chromosome is the arrangement of all tasks in a high-rise building project under the immediate constraints, that is, each construction task must be located after all its quick activities; This chromosome shows the sequence of all construction tasks in a feasible optimization scheme of management personnel training objectives [24]. The gene of the employee chromosome indicates the employee's situation of construction task assignment. Let $list_{rjk}$ be the set of employees where the chromosome uses skill k in the j th construction task, and α_{jk} be the overall tacit understanding of the set of employees serving the construction task j with skill k , so the forms of the chromosome and the construction task are shown in Fig. 1.

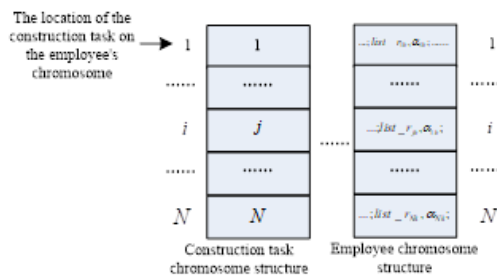


Fig. 1. Chromosome structure analysis diagram.

b) *Population Initialization*: Initializing the target population of management talent training is to initialize the construction task and employee chromosome, that is, to determine the completion order of the construction task first, and then assign the corresponding employees according to the construction order arranged on the chromosome of the construction task. The specific steps are as follows:

Inserting the construction tasks into the chromosome of the construction tasks one by one by adopting a serial scheduling method, and ensuring that the immediately preceding tasks are placed in the chromosome when each construction task is

added; For parallel tasks, they are randomly arranged in chromosomes [25].

Assign employees to each construction task according to the gene sequence on the chromosome of the construction task, and the specific employee allocation steps are as follows:

- Set in time $t = 0$, the scheduled construction task set is $S = \phi$, the scheduling construction task set is $D = \phi$, the corresponding completion time of each construction task j in D is h_j , and the current scheduled set meeting the logical relationship is E_v . If set $E_v = \phi$, the employee assignment is over, the t at this time is t_{max} . The unoccupied employee collection is E_r , assigning the following steps for each of E_v of the construction tasks.
- If set $E_v = \phi$, then select in D the minimum h_j construction task of j' , update $t = h_{j'}$, the construction task $S = j' \cup S$ and return to step a; Otherwise from the collection E_v choose the construction task j , and conduct employee evaluation for each skill required for its implementation.
- Select the skill k without employee assessment in the construction task j , initialize the tacit understanding factor $factor = 1.0$, skill quantity $amount = 0.0$.
- If there is no employee with skill k in E_r , the employee does not meet the requirements of construction task, put the employee of each employee set b_{jk} in construction task j back to E_r , then empty the set b_{jk} , finally remove the construction task j from E_v and return to step b; otherwise randomly select the employee r with skill k in E_r , put it into the employee set S_{jk} of the skill k required in a construction task j , and remove from E_r , the corresponding skill quantity $amount = amount + a_{rk}$, update the collaboration factor $factor$.
- Judge whether $amount \times factor$ is greater than b_{jk} . If the conditions are not met, return to step d; otherwise, it indicates the constraint judgment is completed of the construction task j with skill k , and then determine whether the other skills of the construction task j have been judged, if not, return to step c, otherwise, explain the construction task j meet the staff constraints, will be assigned to the construction task j put all employees in the occupied state, and put the construction task $D = j \cup D$, and calculate the completion period h_j , return to step b.

Because each step is selected in a randomized way, the diversity of the target population for initial management personnel training is ensured. Repeat the above steps until the number of the initial management personnel training target population is POP .

c) *Chromosome Coding*: The serial schedule generation mechanism is used to decode the chromosome to generate the solution. The serial schedule generation mechanism needs to meet the task sequence constraint (forward scheduling) of the employee chromosome and the resource constraint of the

corresponding construction task in the employee chromosome [26]. Specifically, before the next construction task starts, all its immediate tasks must be completed, and the employees assigned to it are available. At this point, the earliest start time of the construction task can be obtained. It should be noted that only one feasible scheduling scheme can be obtained in the process of decoding the target chromosome of management personnel training. The project duration is received in the above initialization process. Then, the multi-objective solution can be used to calculate the objective function value of the remaining management talent training.

2) Design of fitness function for optimization of management personnel training objectives.

The main difference between a multi-objective evolutionary algorithm and a single-objective evolutionary algorithm lies in the fitness function, which is caused by the different number of solutions. Therefore, the relative non-dominance of solutions is usually used to measure the quality of solutions obtained by multi-objective evolutionary algorithm, that is, the Pareto solution or approximate Pareto solution is used as the solution set of multi-objectives. Pareto solution is a collection of non-dominant solutions, and the concept of a dominant solution is defined as follows:

Assume that X and Y are two feasible solutions of management talent training objectives, and each possible solution of management talent training objectives is a ternary vector $x = (x_1, x_2, x_3)$, x_1 、 x_2 、 x_3 are three target values (assuming that the bigger the better), then x dominant solution can be defined as the following formula (19):

$$x > y \Leftrightarrow \forall x_i \geq y_i, \exists i \{1,2,3\}, x_i > y_i \quad (19)$$

In Formula (19), the non-dominant solution is defined as that any other individual does not dominate an individual, that is, for other management personnel training target individuals, the result of one goal of the management personnel training target individual is always better than other individuals (excluding duplicate individuals).

The fitness value of the target individual of management talent training is determined by the number of other individuals who dominate it and the number of individuals adjacent to it. Set $d(x)$ be the number of other individuals controlling the individual x , and $s(x)$ is the number of individuals adjacent to x , as defined in Formula (20) and Formula (21):

$$d(x) = |x' \in P: x' > x| \quad (20)$$

$$s(x) = \left| x' \in P, x' \neq x: \frac{|f_i(x) - f_i(x')|}{f_i(x')} \right|, i = 1,2,3 \quad (21)$$

In Formula (20) and Formula (21), P is the management of the population of target individuals, $f_i(x)$ ($i = 1,2,3$) represents the target individual x of management talent training of the i th target value, shared distance σ_i ($i = 1,2,3$) is a constant.

The assignment process of individual fitness of management talent training target $\phi(x)$ is as follows:

- Calculate $d(x)$ and $s(x)$ for each management talent training target individual in population P.
- According to $d(x)$ to assign value to the target individuals of management talent training;

$$\phi(x) = d(x) + 1 \quad (22)$$

- $Tod(x)$ with the same management talent training target individual set (that is, the unique set that does not dominate each other), according to the values of $s(x)$, sorted from small to large, and the serial number is n ; The number of the same $d(x)$ management talent training target individuals is num , $\Delta = \frac{1}{num}$, then there is:

$$\begin{aligned} \phi(x) &= \phi(x) + n * \Delta, n \\ &= 0, 1, \dots, num - 1 \end{aligned} \quad (23)$$

According to the definition of fitness value, the smaller the fitness value, the better the solution is.

3) Management personnel training objectives optimization, crossover and mutation operation.

a) *Parent selection*: In this paper, the "two-person competition method" is used to select the father for pairing to produce offspring. Select two target chromosomes of management personnel training from the population, take the excellent target individuals of management personnel training as the male parent, and repeat this step to find the female parent until POP/2 pairs of fathers are produced. The advantage of this method is that it can combine relatively good parents to make better offspring and improve convergence.

b) *Crossing*: Cross operation refers to the process of exchanging and recombining the genes of the male parent and the female parent, and then producing offspring. Because crossover operation can combine and keep the best genes of parents, it plays a core role in genetic function. Given crossover probability P_c (generally 0.4~1), which means that parents P_c take the probability of crossing. Through the following contents, the detailed operation steps of crossing the construction task chromosome and the employee chromosome are given.

Cross operation of construction task chromosomes: The two-point cross method is adopted for the cross of construction task chromosomes. Firstly, two integers are randomly generated q_1 、 q_2 , they meet $1 \leq q_1 \leq q_2 \leq J$. In the construction task sequence of the first generation $1 \sim q_1$ is up to the mother, $q_1 + 1 \sim q_2$ inherit from my father, $q_2 + 1 \sim J$ inherit from mother; Descendant 2 inherits in the opposite way to descendant 1.

Generate a random number v in the interval of [0,1] through a random number generator according to the construction task sequence on the chromosome of the offspring construction task obtained by crossing, if $v \leq 0.5$, then the daughter resource chromosome 1 inherits the employee chromosome gene of the construction task number corresponding to the daughter construction task chromosome 1 from the parent, and the daughter resource chromosome 2

inherits the employee chromosome gene of the construction task number corresponding to the daughter construction task chromosome 2 from the parent; if $v > 0.5$, the inheritance order is exchanged.

c) *Mutation operation*: Chromosome mutation operation of construction task: given mutation constant P_m , each individual has the probability of mutation occurs P_m , and for the mutated individuals, the construction task i in the individual construction task chromosome is randomly selected and inserted into a new position (mutation occurs); The role of mutation is related to its immediate pre-task and immediate post-task, that is, the position of mutation must be between the immediate pre-task and immediate post-task; In order to ensure the feasibility of the employee chromosome, the resource chromosome corresponding to the mutation construction task is changed in the same position.

Mutation operation of employee chromosomes: each individual has the probability of mutation P_m , for the mutated individual, the simple way of randomly selecting a skill in the construction task and redistributing employees is used to complete the mutation of employee chromosomes. Considering the diversity of Pareto solutions, the parents of the mutated individuals are reserved.

d) *Choose*: After the crossover operation, a large number of offspring will be produced. In order to keep the target population number of management talent unchanged, the "three-person championship method" is adopted to eliminate the poor individuals. The selection method of three-person championship is random selection, proportional selection, and the expansion method of double competition. The specific process is to randomly select three chromosomes, namely I_1 、 I_2 、 I_3 . If Formula (23) is satisfied:

$$\phi(I_1) \geq \phi(I_2) \text{ 且 } \phi(I_1) \geq \phi(I_3) \quad (24)$$

Then individual I_1 is eliminated from the population, and the operation is repeated until the population becomes the initial set value POP again; if the target population number of management talent training is not greater than POP before the substitution operation, the operation will not be carried out.

E. Optimization Process Design based on Hybrid Immune Genetic Algorithm

The multi-objective genetic algorithm (MOGA) is one of the adaptive heuristic algorithms used to solve multi-objective problems, but it has a great disadvantage: it is premature. Aiming at this problem, this paper proposes a hybrid immune genetic algorithm. Immunity is an important physiological behavior of living things. Its main function is to resist viruses, bacteria, etc., that may cause discomfort from the outside and maintain the homeostasis of the body. It recombines genes through complex and intense mechanisms to cope with invading antigens, produce antibodies, and eliminate antigens. The immune process can improve the diversity of the population, expand the search range of the population, and then improve the quality of people. Combining these two algorithms is of great significance to solve the problem of premature

convergence of genetic algorithms in theory and improve the diversity of non-inferior solutions.

At the same time, some Japanese scholars put forward the double island model to improve the lethal chromosome in the process of evolution. In each generation of the evolutionary algorithm, many poor-quality chromosomes will be produced, and the double island model will separate the excellent and inferior chromosomes. In this model, the lethal chromosomes are put together (called "dead islands"). The chromosomes in the "dead island" are crossed and mutated, and finally, the excellent chromosomes are put back into the genetic process. However, in this process, only the lethal chromosomes in the "dead island" are manipulated, and the effect is not significant. Introducing the immune process is helpful in solving this problem, so this paper presents the immune process in the two-island model. By combining the two-island model with the immune process, a hybrid immune genetic algorithm is formed. The algorithm is actually carried out in two aspects: on the one hand, the "dead island" is immunized; on the other, the individuals on the "living island" are crossed and mutated. Before the evolution of each generation, it is necessary to inoculate the individuals in the "dead island" to produce excellent individuals, and then move these individuals into the "living island" for evolutionary operation, and perform this step circularly until the constraint conditions are met.

The specific flow of the algorithm is as follows:

1) Coding chromosomes according to the modeling result of the training objective function of high-rise building project management talent and randomly generating the initial population of the training objective of management talent.

2) Judging whether the evolutionary algebra meets the requirements, if it meets the requirements, outputting the training target population of the last generation of management talent, and ending the test; otherwise, entering step (3).

3) Calculate the fitness value and average fitness value of the target population for training management talent, and move the individuals with higher-than-average fitness into the "dead island" and those with lower-than-average fitness into the "living island." Inoculate the chromosomes in the "dead island" and put the excellent individuals into the "living island" after injection. For the crossover and variation of individuals in the "living island," the individual fitness value of the population is recalculated.

4) Judge whether the number of the target population for training management talent is greater than the initial set value, and if it exceeds the set value, reject the inferior solutions according to the fitness. Evolutionary algebra Gen+1, and return to step (2).

Steps (1), (2), and (4) in the above steps are the same as the basic genetic algorithm, and the selection rule of parents still adopts the "two-person economic law," and the "three-person championship" method is selected when the redundant individuals in the population are eliminated. The difference is that the "double island model" and inoculation process are added in step (3).

Through the optimization of this method, the best training scheme can be found for project management talent of high-rise buildings.

III. EXPERIMENTAL ANALYSES

In order to evaluate the application effect of the high-rise building project management talent training model designed in this paper, the model is applied to a high-rise building project. The total height of this high-rise project is 269.7m, and the entire construction area is 172,000 m² with 57 floors above ground and three floors underground. The overall building structure is frame+facade support+tube structure. A total of 157 constructors+managers are employed in this project. The management talent used in the construction of this high-rise building project is trained, and whether the training model designed in this article has a certain use effect is analyzed.

Select an employee from the project managers of high-rise buildings and analyze the changes of the learning curve, forgetting curve, and learning forgetting curve of the employee at different times so as to verify the evaluation effect of the article on employees' cognitive ability. The results of the analysis are shown in Fig. 2.

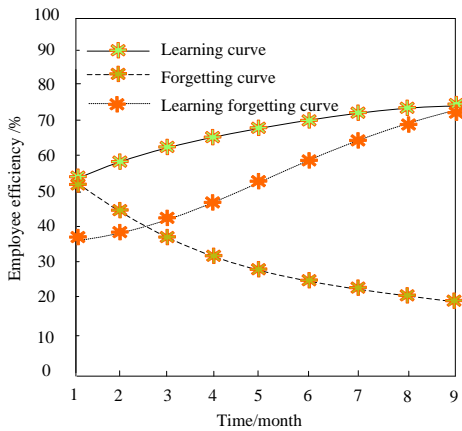


Fig. 2. Employee learning curve, forgetting curve, and learning forgetting curve.

According to Fig. 2, through the evaluation of employees' cognitive ability by this model, it can be seen that the employee's learning curve maintains about 50% employee efficiency in the initial stage, and with the continuous progress of the learning process, the employee efficiency increases to about 70%, but this curve does not consider the employee's forgetting degree; Through the analysis of forgetting curve, it can be seen that the employee efficiency has gradually decreased from the initial 50% to about 20%, which leads to the degree of forgetting obviously affecting the employee's work efficiency; Therefore, this model combines the learning and forgetting curve to analyze, and it is known that when employees' forgetting problem is considered, the employee efficiency gradually starts to rise from the initial 30%~40%, and can reach more than 60% with the continuous learning process. Through the analysis of this model, it is possible to accurately know the influence of employees' learning and forgetting methods on their efficiency.

This paper analyzes the changes in the total project construction cost before and after the optimization of the training of high-rise building project management talent by using this model so as to verify the optimization ability of this model to the cost target, and the analysis results are shown in Fig. 3.

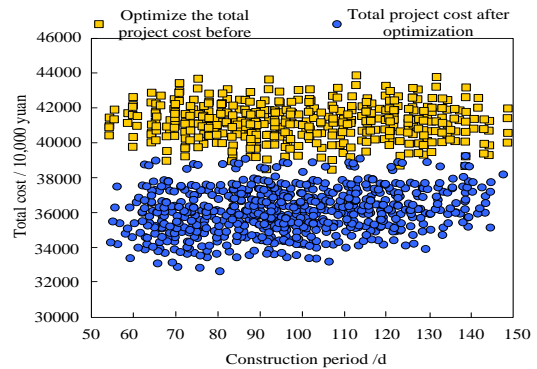


Fig. 3. Analysis of total cost optimization results.

According to Fig. 3, through comparison, it can be seen that the total cost of this high-rise building project has always remained at a high level before being optimized by this model, which leads to a large amount of expenses in the construction of this project. When this model optimizes the management talent, the construction strategy of this project has been improved, which makes the total construction cost of this project decline. It can be seen that when the model is optimized, the total cost of the project is no more than 400 million yuan, which can obviously save a lot of expenses. Therefore, the model has a good optimization effect.

Select different tasks from the overall project construction and analyze the human resource utilization ratio of other tasks before and after optimizing management talent so as to verify the effect of this model on different talent training. The analysis results are shown in Table II.

From the analysis in Table II, it can be seen that the utilization rate of human resources in this project is always at a low level for different construction tasks before the model is adopted for optimization. Among them, the utilization rate of human resources in foundation treatment construction, pile cap construction, and fence construction tasks can reach the highest, but it is only 57%. After the model is optimized in this paper, the management personnel are effectively trained, and the utilization rate of human resources in construction is also increased. Among them, the utilization rate of human resources in each task is above 85%, and the highest utilization rate is 92%, which shows that human resources can be fully utilized in the construction process, thus ensuring construction efficiency. Therefore, the model has excellent optimization ability.

Select an employee from different employees and analyze the changes in the employee's proficiency in technical ability, planning and organization ability, and cost control ability during the training process so as to verify the evolutionary power of the model. The results of the analysis are shown in Fig. 4.

TABLE II. ANALYSIS OF HUMAN RESOURCE UTILIZATION IN DIFFERENT TASKS

| Serial number | Construction task | Human resource utilization before optimization /% | Human resource utilization rate /% after optimization in this paper |
|---------------|--|---|---|
| 1 | Construction preparation and temporary facilities | 54 | 89 |
| 2 | Foundation treatment | 57 | 91 |
| 3 | Cut earth | 48 | 92 |
| 4 | Pile driving | 49 | 88 |
| 5 | Backfill and lightning protection grounding works | 53 | 87 |
| 6 | Pile cap construction | 57 | 93 |
| 7 | Column reinforcement and lightning belt construction | 55 | 86 |
| 8 | Ground concrete cushion construction | 46 | 91 |
| 9 | Roof beam plate formwork construction | 47 | 90 |
| 10 | Concrete placement construction | 52 | 89 |
| 11 | Power threading construction | 56 | 88 |
| 12 | Plastering works | 53 | 92 |
| 13 | Ceiling works | 54 | 87 |
| 14 | Drainage engineering construction | 55 | 89 |
| 15 | Wall construction | 57 | 90 |
| 16 | Electrical installation and construction | 48 | 87 |
| 17 | Plastering of exterior walls | 49 | 89 |
| 18 | Exterior wall coating construction | 50 | 87 |
| 19 | Defect repair construction | 52 | 89 |

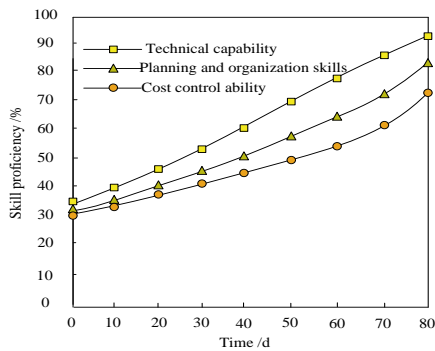


Fig. 4. Analysis of employee skill proficiency.

According to Fig. 4, with the continuous increase of time, the employee's proficiency in different skills began to increase. Among them, the employee's technical ability always maintained a high proficiency, while the employee's planning and, organization ability and cost control abilities were relatively weak. However, when the time reached 80 days, the employee's proficiency in different skills reached more than 70%, indicating that the employee had a high proficiency in skills at this time. Therefore, after the model was optimized,

Analyze the changes in skills growth benefits of the optimized talent training model under different project durations and project costs, and the analysis results are shown in Fig. 5.

The benefit of skill growth refers to all kinds of advantages and benefits brought by learning and developing new skills. According to Fig. 5, through the optimization of the model in this paper, the skills growth benefit can be maintained at different project duration and project costs. It can be seen that the model can improve the problem-solving ability of project management talent, stimulate employees' creativity and

innovation ability, maximize employees' self-value, and thus enhance the overall benefits of enterprise construction projects.

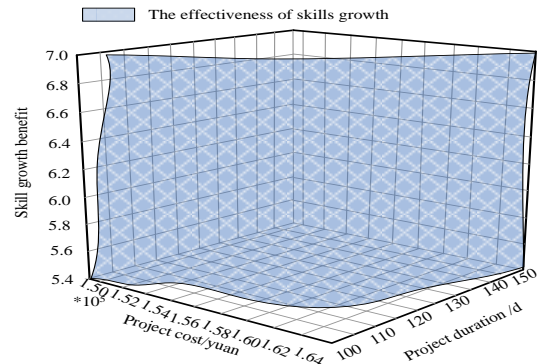


Fig. 5. Skill growth benefit analysis.

This paper analyzes the influence of traditional genetic algorithms, multi-objective genetic algorithms, and genetic algorithms based on mixed immunity on the construction period of the project under different optimization times so as to evaluate the optimization effect of the model on the construction period index and the analysis results are shown in Fig. 6.

According to Fig. 6, after the iterative evolution of different algorithms, the construction period of high-rise buildings has decreased. When the number of iterative developments reaches 800 times, the optimized construction period of the three algorithms has reached the lowest state. Among the three algorithms, the construction period optimized by the traditional genetic algorithm has remained above 670d, and it has maintained the highest level among the results optimized by the three algorithms. After the optimization by the multi-objective genetic algorithm, although the construction period has decreased, it is still higher than the result of optimization

based on the hybrid immune genetic algorithm in this paper. Under the optimization of this model, project management talent has been trained efficiently, thus effectively reducing the construction period. When the number of iterations reaches 800, the optimization result of this model only takes about 620d days to complete the project construction so that the total construction period can be effectively shortened after the optimization of this model.

After applying this model to optimize multi-objectives, the construction quality and actual construction duration of different project tasks are analyzed to verify the multi-objective optimization effect of this model. The analysis results are shown in Table III.

According to the analysis in Table III, after multi-objective optimization with this model, the construction can be completed within the specified time range when dealing with different construction tasks, and the actual construction time of most tasks is lower than the specified time. At the same time, when the construction is completed, it can be seen that the construction quality of different tasks meets the construction standards. Therefore, under the optimization of this

optimization model, the technical level of high-rise building project management personnel can be effectively improved to ensure smooth construction.

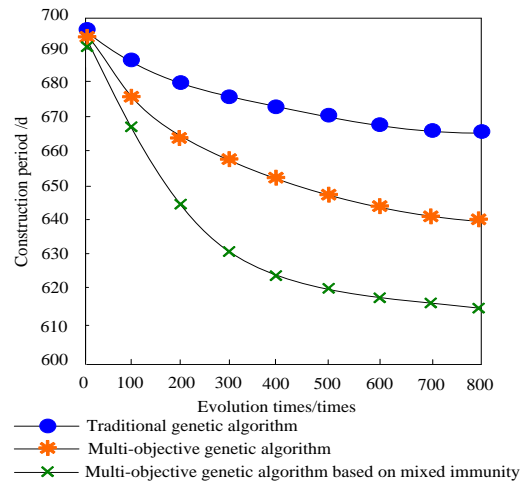


Fig. 6. Changes in the construction period after optimization.

TABLE III. ANALYSIS OF CONSTRUCTION QUALITY AND ACTUAL CONSTRUCTION TIME IN DIFFERENT TASKS

| Serial number | Construction task | Estimated standard construction time /d | Actual completion time /d | Construction quality inspection |
|---------------|--|---|---------------------------|---|
| 1 | Temporary electricity construction | 9 | 8 | The quality meets the construction standard |
| 2 | Site clearing | 14 | 12 | The quality meets the construction standard |
| 3 | Erection test pile | 4 | 3 | The quality meets the construction standard |
| 4 | Erection column | 18 | 14 | The quality meets the construction standard |
| 5 | Site formation construction | 5 | 5 | The quality meets the construction standard |
| 6 | Pile head preparation | 10 | 8 | The quality meets the construction standard |
| 7 | Immersed pipe pouring concrete and pile cap construction | 11 | 10 | The quality meets the construction standard |
| 8 | Construction of the embedded underground pipeline | 12 | 10 | The quality meets the construction standard |
| 9 | Backfill construction | 6 | 5 | The quality meets the construction standard |
| 10 | Concrete bedding and waterproof construction | 1 | 1 | The quality meets the construction standard |
| 11 | Underground pillar construction | 6 | 6 | The quality meets the construction standard |
| 12 | Stairwell construction | 10 | 9 | The quality meets the construction standard |
| 13 | Ceiling plaster | 8 | 7 | The quality meets the construction standard |
| 14 | Plaster the walls | 10 | 8 | The quality meets the construction standard |
| 15 | Ground waterproof layer construction | 5 | 5 | The quality meets the construction standard |
| 16 | Cement mortar protective layer construction | 10 | 8 | The quality meets the construction standard |
| 17 | Wiring construction | 15 | 13 | The quality meets the construction standard |
| 18 | Water pipe installation | 7 | 6 | The quality meets the construction standard |
| 19 | Natural gas pipeline installation and construction | 8 | 7 | The quality meets the construction standard |
| 20 | Decoration and beautification construction | 10 | 8 | The quality meets the construction standard |

IV. CONCLUSION

This paper studies the training model of high-rise building project management talent under a multi-objective evolutionary algorithm. The research results show that the model can effectively evaluate and optimize the training scheme of project management talent. In this paper, firstly, an objective function with multiple objectives is constructed, including project duration, project cost, and skill growth rate. By adopting a multi-objective evolutionary algorithm, these indexes can be optimized at the same time, and a balanced training scheme among different objectives can be obtained. Secondly, this model is used to optimize the training scheme of real high-rise building project management talent. The results show that by adopting a multi-objective evolutionary algorithm, a more practical training scheme can be achieved. At the same time, the feasibility and flexibility of the model were also verified through case analysis. Generally speaking, this research has developed and verified the talent training model of high-rise building project management, which provides a scientific and effective method for talent training. This model can not only help decision-makers formulate reasonable training strategies but also provide an innovative idea and plan for talent training in the field of high-rise building project management.

COMPETING OF INTERESTS

The authors declare no competing of interests.

AUTHORSHIP CONTRIBUTION STATEMENT

Pan qi: Writing-Original draft preparation, Conceptualization, Supervision, Project administration.

DATA AVAILABILITY

On Request

DECLARATIONS

Not applicable

REFERENCES

- [1] A. Sudiarno, D. A. Amanullah, and R. A. Akbar, "The Measurement of Evacuation Effectiveness Regarding Dynamic Evacuation Routing System (DERS) in High-Rise Building Using Virtual Reality Simulation," *International Journal of Safety and Security Engineering*, vol. 12, no. 1, pp. 115–122, 2022.
- [2] A. Ashrafi, J. Chowdhury, and H. Hangan, "Comparison of aerodynamic loading of a high-rise building subjected to boundary layer and tornadic winds," *Wind and Structures*, vol. 34, no. 5, pp. 395–405, 2022.
- [3] K. Okabe *et al.*, "Structural Design of High-Rise Building with RC Frame Using Core Wall and Damping Device; Toranomon-Azabudai Project (B2 Block)," *International Journal of High-Rise Buildings*, vol. 10, no. 3, pp. 243–250, 2021.
- [4] T. Sinaga and A. E. Husin, "Analysis of Time Efficiency with CCPM Method and BIM in Construction Projects Construction of High-Rise Residential Building Basement," *Civil Engineering and Architecture*, vol. 9, no. 5, pp. 1465–1477, 2021.
- [5] S. Conejos, A. Ubando, and M. Y. L. Chew, "Design for maintainability tool for nano-façade coating applications on high-rise facades in the tropics," *Built Environment Project and Asset Management*, vol. 12, no. 1, pp. 70–95, 2021.
- [6] M. K. Ansah, X. Chen, H. Yang, L. Lu, and H. Li, "Developing a tier-hybrid uncertainty analysis approach for lifecycle impact assessment of a typical high-rise residential building," *Resour Conserv Recycl*, vol. 167, pp. 1–16, 2021.
- [7] Ç. Takva and Z. Y. İLERİSOY, "Structural analysis of steel load-bearing systems using tessellation method in geometric architectural design," *Sādhanā*, vol. 48, no. 3, pp. 118–126, 2023.
- [8] H. T. Thai, Q. V. Ho, W. Li, T. Ngo, "Progressive collapse and robustness of modular high-rise buildings," *Structure and Infrastructure Engineering*, vol. 19, no. 1, pp. 302–314, 2023.
- [9] S. G. A. Ochieng and A. I. Odhiambo, "Beneficiary Needs Assessment on Implementation of Devolved Road Construction Projects in Kisumu East Sub-County, Kisumu County, Kenya," *Journal of Business*, vol. 10, no. 1, pp. 20–29, 2022.
- [10] V. P. Grakhov, A. L. Kuznecov, and G. Kislyakova Yu, "Implementation of digital project management for construction and operation of energy-efficient residential buildings," *Science and Technique*, vol. 20, no. 1, pp. 66–74, 2021.
- [11] S. T. Do, V. T. Nguyen, and C. N. Dang, "Exploring the relationship between failure factors and stakeholder coordination performance in high-rise building projects: empirical study in the finishing phase," *Engineering, Construction and Architectural Management*, vol. 29, no. 2, pp. 870–895, 2022.
- [12] O. Klipkova, H. Kozmuk, and O. Tsebenko, "Optimization of the personnel management mechanism in regard to the theory of generations," *Financial and credit activity problems of theory and practice*, vol. 3, no. 38, pp. 509–521, 2021.
- [13] D. A. Nguyen, D. Q. Tran, T. N. Nguyen, and H. H. Tran, "Modeling labor productivity in high-rise building construction projects using neural networks," *Archives of Civil Engineering*, vol. 69, no. 1, pp. 675–692, 2023.
- [14] E. Hudyakova, V. Vodyannikov, V. Berdyshev, Y. Chistova, "Problems of providing agro-industrial complex organizations with management personnel and their solutions," *Agrarian Bulletin of the*, vol. 13, no. 1, pp. 92–100, 2023.
- [15] P. P. Junqueira, I. R. Meneghini, and F. G. Guimarães, "Multi-objective evolutionary algorithm based on decomposition with an external archive and local-neighborhood based adaptation of weights," *Swarm Evol Comput*, vol. 71, pp. 1–30, 2022.
- [16] Q. Sun, Y. Turkan, and E. C. Fischer, "A building information modeling-fire dynamics simulation integrated framework for the simulation of passive fire protection in a mid-scale cross-laminated timber compartment: Numerical implementation and benchmarking," *Fire Mater*, vol. 47, no. 4, pp. 525–541, 2023.
- [17] L. Blackburne, K. Gharehbaghi, and A. Hosseinian-Far, "The knock-on effects of green buildings: High-rise construction design implications," *International Journal of Structural Integrity*, vol. 13, no. 1, pp. 57–77, 2021.
- [18] Z. S. Zomorodian and M. Tahsildoost, "Energy and carbon analysis of double skin façades in the hot and dry climate," *J Clean Prod*, vol. 197, pp. 85–96, 2018.
- [19] M. O. Tetteh, A. P. C. Chan, G. Nani, A. Darko, and G. D. Oppong, "Impacts of management control mechanisms on the performance of international construction joint ventures: an empirical study," *Engineering, Construction and Architectural Management*, vol. 30, no. 6, pp. 2280–2303, 2023.
- [20] G. Bektur, "Distributed flow shop scheduling problem with learning effect, setups, non-identical factories, and eligibility constraints," *International Journal of Industrial Engineering*, vol. 29, no. 1, pp. 21–44, 2022.
- [21] J. Peltokorpi and M. Y. Jaber, "Interference-adjusted power learning curve model with forgetting," *Int J Ind Ergon*, vol. 88, p. 103257, 2022.
- [22] K. Boulanouar, A. Hadjali, and M. Lagha, "Trendssummarizationof timeseries: a multi-objective genetic algorithm-based model," *Journal of Smart Environments and Green Computing*, vol. 2, no. 1, pp. 19–33, 2022.
- [23] K. Miura, C. Powell, and M. Munetomo, "Optimal answer generation by equivalent transformation incorporating multi-objective genetic algorithm," *Soft comput*, vol. 26, no. 19, pp. 10535–10546, 2022.
- [24] A. Rukhaiyar, B. Jayant, K. Dahiya, R. K. Meena, R. Raj, "Cfd simulations for evaluating the wind effects on high-rise buildings having

- varying cross-sectional shape,” *Journal of structural fire engineering*, vol. 14, no. 3, pp. 285–300, 2023..
- [25] Z. Falahiazar, A. Bagheri, and M. Reshadi, “Determining the Parameters of DBSCAN Automatically Using the Multi-Objective Genetic Algorithm,” *J. Inf. Sci. Eng.*, vol. 37, no. 1, pp. 157–183, 2021.
- [26] P. Pirozmand, A. A. R. Hosseinabadi, M. Farrokhzad, M. Sadeghilalimi, S. Mirkamali, and A. Slowik, “Multi-objective hybrid genetic algorithm for task scheduling problem in cloud computing,” *Neural Comput Appl*, vol. 33, pp. 13075–13088, 2021.

Development of a New Chaotic Function-based Algorithm for Encrypting Digital Images

Dhian Sweetania¹, Suryadi MT², Sarifuddin Madenda³

Gunadarma University, Department of Information Technology, Depok, 16424, Indonesia^{1,3}

Universitas Indonesia, Department of Mathematics, Depok, 16424, Indonesia²

Abstract—This paper discusses the development of a new chaotic function (proposed chaotic map) as a keystream generator to be used to encrypt and decrypt the image. The proposed chaotic function is obtained through the composition process of two chaotic functions MS map and Tent map, with the aim of increasing data resistances to attacks. The randomness properties of the keystream generated by this function have been tested using Bifurcation diagrams, Lyapunov exponent, and NIST randomness analysis. All the analysis results indicate that the keystream passed the randomness tests and safe to be used for image encryption. The performance of the proposed chaotic function was measured by way of analysis of its initial value sensitivity, key space, and correlation coefficient of the encrypted image. This function can further increase the resilience against brute force attacks, minimizing the possibility of brute attacks, and has key combinations or key space of 1.05×10^{959} that is much greater than the key space generated by MS Map + Tent Map of 5.832×10^{958} . Finally, quantitative measurements of encrypted image quality show an MSE value of 0 and a PSNR value of ∞ . These values mean that the encrypted image data is the same as its original and both are also visually identical.

Keywords—Chaotic function; decryption; encryption; function composition; key space; MS tent map

I. INTRODUCTION

It is always easy for internet users to obtain various data and information from anywhere and at any time. The development of information technology in the form of text, images, audio and video (multimedia data) and communication is very rapid. Therefore, information security is an absolute matter that must be seriously considered by all users concerned. Information is a very valuable asset for an organization because it serves a strategic resource in increasing value. The information security here concerns policies, procedures, processes and activities to protect information from various types of threats against it that can cause harm to the survival of the organization. Based on this purpose, cryptography is implemented related to information security such as confidentiality, data integrity, entity authentication, and data origin authentication.

In general, cryptography is divided into two parts, namely classical and modern cryptography. Modern cryptography is the development of algorithms from classical cryptography which prioritizes bit mode operations, in contrast to classical cryptography which operates on characters. In one study, there was an encryption system which combined Logistic Map and Henon Map to produce an average PSNR value of less than 10 dB which indicated that the encrypted image had very high

noise and an MSE value of more than 400, this means that there are still many signal errors from the original image and cipher image. The length of the process required carrying out the encryption and decryption process was greatly influenced by the size of the dimensions and the number of pixels in a digital image. The encryption system using a combination of Logistic Map and Henon Map took more than 15 seconds to encrypt images that had dimensions of 512×512 ; however image encryption results were not influenced by the dimensions of the encrypted image [1].

The chaos function has been developed for data encryption in the last decade because of its nature described in [2]. The nature of the chaos function, which is sensitive to the initial conditions, results in a significant difference in the image encryption results. Some of the chaotic functions used in image encryption are Logistic Maps and MS maps. The Logistic Map function has a key space of 10^{30} [3-4], the MS Map function has a key space of up to 3.24×10^{634} [5].

There is an algorithm technique that composes a sequential Logistic Map and Chebyshev Map [6], both of which are used to encrypt medical images. In the initial stage, the medical image is encrypted with a Logistics Map, then an encrypted image is formed, and the image is re-encrypted with a Chebyshev map. Besides that, there is also the Gauss-Circle Map algorithm which is a combination of Gauss Map and Circle Map by combining the two [7] by applying a composition function [8], then proposed a new image encryption algorithm by jointly exploiting overlapping random block partitioning, scanning, double spiral, Henon's chaotic map, and L ü' s chaotic map. Another study proposed a cryptosystem based on 4D Lorenz-type hyper-chaos and deoxyribonucleic acid (DNA) [9].

The MS Map and Tent Map algorithms are two well-known chaotic function algorithms that exhibit chaotic properties, which both have a high potential to generate random keys. Therefore, this paper proposes a new chaotic function which is a composition of the two chaotic functions of MS Map and Tent Map. The proposed function is also chaotic, so it can be used as a random number generator function. This chaotic system is useful for generating random numbers for chaos that has no period. This random number generator is created by compiling a Bifurcation Diagram, Lyapunov Exponent, and the NIST Randomness Test. The chaos system is used as the basis for secure cryptographic algorithms for communication because of the very close relationship between chaos and cryptography [10].

After generating random numbers by composing the MS Map and Tent Map functions, the algorithm performance analysis was carried out based on initial value sensitivity level analysis, key space size analysis, correlation coefficient analysis, and image quality testing (PSNR).

II. RESEARCH METHOD

Two chaotic functions that are often used for data encryption and decryption are MS Map and Tent Map. Both will be used to build a new chaotic function. MS Map is a modification of the Logistic map function as shown by Eq. (1), where $(x \bmod 1) = x - \lfloor x \rfloor$ according to the definition. This equation can be expressed recursively as shown in Eq. (2), with initial value $x_0 \in (0, 1)$ and $n = 1, 2, 3, \dots$ [5].

$$f(x) = \left(\frac{r\lambda x}{1+\lambda(1-x)^2} \right) (\bmod 1) \quad (1)$$

$$x_{n+1} = \left(\frac{r\lambda x_n}{1+\lambda(1-x_n)^2} \right) (\bmod 1) \quad (2)$$

The modulo operation is applied as a congruent function. In a set of integers, congruence is a method or way of explaining the divisibility of an integer. Modulo arithmetic is used in cryptography because the modulo b arithmetic value is in a finite rounded set, namely 0 to $b - 1$. Calculations in the cryptographic process are not outside the set of integers, meaning that the decryption process will not produce a value that is different from the value of the original message. Thus, there is no need to worry about losing information because the rounding occurs as in real number operations.

In mathematics, the Tent map is an iteration chaotic function, which forms a dynamic system based on discrete time. It takes x_n points on a real line and then maps those points to other points [11]. This function can be expressed as in Eq. (3).

$$x_{n+1} = g(x) = \begin{cases} \mu x_n & \text{for } x_n < \frac{1}{2} \\ \mu(1 - x_n) & \text{for } x_n \geq \frac{1}{2} \end{cases} \quad (3)$$

Now suppose g is a function from set A to set B and f is a function from set B to set C . The composition between two functions f and g , denoted by $(f \circ g)$, is a function from A to C which is defined as $(f \circ g)(a) = f(g(a))$. Furthermore, if f represents the MS map function in Eq. (2) and g acts as the Tent map function in Eq. (3), so the proposed new chaotic function resulting from the composition of both is expressed in two domain partitions as shown in Eq. (4) and Eq. (5).

$$(f \circ g)(x) = \mu \left(\frac{r\lambda x}{1+\lambda(1-x)^2} \right) (\bmod 1) \quad \text{for } x < \frac{1}{2} \quad (4)$$

Map function was generated from the composition of

$$(f \circ g)(x) = \mu \left(1 - \frac{r\lambda x}{1+\lambda(1-x)^2} \right) (\bmod 1) \quad \text{for } x \geq \frac{1}{2} \quad (5)$$

Thus, based on Eq. (4) and Eq. (5), the proposed chaotic function can be expressed as in Eq. (6).

$$(f \circ g)(x) = \begin{cases} \mu \left(\frac{r\lambda x}{1+\lambda(1-x)^2} \right) (\bmod 1) & \text{for } x < \frac{1}{2} \\ \mu \left(1 - \frac{r\lambda x}{1+\lambda(1-x)^2} \right) (\bmod 1) & \text{for } x \geq \frac{1}{2} \end{cases} \quad (6)$$

Furthermore, this equation is called the MS Tent map chaotic function and can be represented in recursive form as shown in Eq. (7), for $n = 0, 1, 2, 3, \dots$.

$$x_{n+1} = \begin{cases} \mu \left(\frac{r\lambda x_n}{1+\lambda(1-x_n)^2} \right) (\bmod 1) & \text{for } x_n < \frac{1}{2} \\ \mu \left(1 - \frac{r\lambda x_n}{1+\lambda(1-x_n)^2} \right) (\bmod 1) & \text{for } x_n \geq \frac{1}{2} \end{cases} \quad (7)$$

III. RESULT AND ANALYSIS

The chaotic behavior of the proposed MS Tent map can be evaluated using three types of analysis. First is bifurcation diagram analysis for density sensitivity test. Second is Lyapunov exponent diagram analysis for transitive test and the last one is NIST Randomness tests using 16 statistical tests. These three tests are carried out on the number sequence or keystream generated by the MS Tent map. Algorithm 1 shows how to generate a keystream using the MS Tent map.

After testing the chaotic properties has been completed, the next stage is to develop encryption and decryption algorithms as shown by Algorithms 2 and 3. To analyze the results of the encrypted image and decrypted image, the keystream generated by MS Tent map is used with the initial value of the variable $x_0 = 0.9$ and the parameters $\lambda = 30$, $\mu = 1.5$, and $r = 3.7$. All algorithms keystream generator, keystream testing, image encryption and decryption are implemented using Python programming language and runed on a computer with the specification Intel(R) Core (TM) i5-4200M CPU @ 2.50GHz and 10.00 GB of Memory (RAM).

Performance analysis of the proposed chaotic function is carried out on encrypted and decrypted images using 30 test images: 15 color images and 15 grayscale images. To test the resistance of an encrypted image to brute force attacks, several indicators are used:

- 1) Sensitivity analysis.
- 2) Key space measurement analysis.
- 3) Correlation analysis.
- 4) Image quality test.

Algorithm 1: Keystream Generator Algorithm

Input: x_0, λ, μ, r, t

Output: Keystream K_i

1. For $i = 1$ to t do
 2. calculate x_i using Eq. (7)
 3. $K_i \leftarrow \lfloor x_i \times 10^6 \rfloor \bmod 256$
 4. End For
-

Algorithm 2: Image encryption algorithm

Input: x_0, λ, μ, r, t , original image ($P_i: m \times n$)

Output: encrypted image ($C_i: m \times n$)

1. $N = m \times n; i = 1$
 2. If $i \leq N$, do Step-3 to step-6
 3. Calculate x_{i+t} using Eq. (7)
 4. $K_{i+t} \leftarrow \lfloor x_{i+t} \times 10^6 \rfloor \bmod 256$
 5. $C_i = P_i \oplus K_{i+t}$
 6. $i = i + 1$; Back to Step-2
 7. Else to step-8
 8. Show matrix C_i in encrypted image display
-

Algorithm 3: Image decryption algorithm

Input: $x_0, r, \lambda, \mu, i, t$, encrypted image ($C_i: m \times n$)

Output: decrypted image ($D_i: m \times n$)

1. $N = m \times n; i = 1$
 2. If $i \leq N$, do Step-3 to step-6
 3. Calculate x_{i+t} using Eq. (7)
 4. $K_{i+t} \leftarrow \lfloor x_{i+t} \times 10^6 \rfloor \bmod 256$
 5. $D_i = C_i \oplus K_{i+t}$
 6. $i = i + 1$; Back to Step-2
 7. Else to step-8
 8. Show matrix D_i in decrypted image display
-

A. Bifurcation Diagram

A bifurcation diagram is a diagram that shows the asymptotically approximate values of a system as the function of the parameters. By looking at the bifurcation diagram, we can determine the chaotic nature of a function. If the periodic points on the bifurcation diagram are dense, then the function is chaotic [2].

Algorithm 4. Plotting Bifurcation Diagram

Input: x_0, λ, μ, r, t

Output: plotting x_i

1. For $i = 1$ to n
 2. Calculate x_i using Eq. (7)
 3. Plotting x_i
 3. end for
-

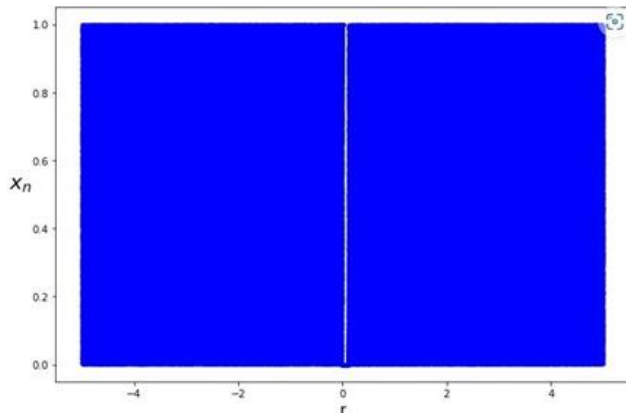


Fig. 1. MS Tent map bifurcation diagram, for $x_0 = 0.9, \lambda = 30, \mu = 1.5, r = 3.7$.

Based on Algorithm 4, with variable values of $x_0 = 0.9, \lambda = 30, \mu = 1.5, r = 3.7$, a diagram is obtained as seen in Fig. 1. The result of the bifurcation diagram is dense for every value of r except for $r = 0$. Thus, the MS Tent map has chaotic properties except for $r = 0$.

B. Lyapunov Exponent Diagram

According to Eq. (8), the Lyapunov exponent can measure the sensitivity of a chaotic system to initial conditions. The Lyapunov exponent is defined as the exponential difference in the divergence or convergence of two vectors in a plane starting from the area around the plane.

Definition: Let X be a set. The map $f : X \rightarrow X$ is chaotic on X , if f is sensitive on the initial value, f is topologically transitive, and the periodic points are dense on X [10].

A function f is said to be chaotic if its Lyapunov exponent is positive. The Lyapunov exponent equation is defined according to Eq. (8) and its implementation uses Algorithm 5. Fig. 2 is a plot result of the Lyapunov exponent diagram, which shows that the MS Tent map has positive Lyapunov exponents at $x_0 = 0.9, \lambda = 30$, and for every value of r except for $r = 0$. This proves that the MS Tent map has chaotic properties.

$$\mu = \lim_{n \rightarrow \infty} \frac{1}{n} \sum_{i=0}^{n-1} \ln |f'(x)| \quad (8)$$

Algorithm 5. Lyapunov Exponent Diagram

Input: x_0, λ, μ, r

Output: plotting the value of μ

1. for $i = 1$ to n
 2. Calculate μ using Eq. (8)
 3. plotting μ
 4. end for
-

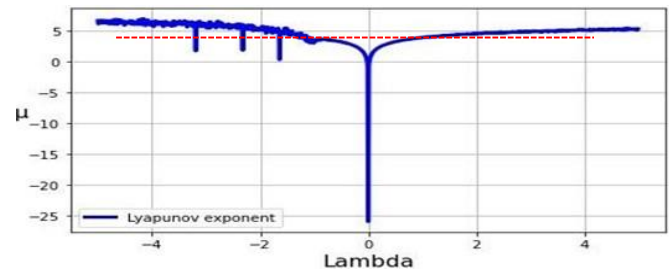


Fig. 2. Lyapunov exponent diagram of the MS Tent Map.

C. Key Stream Randomness Test

After conducting a chaotic test on the MS Tent map function using a bifurcation diagram and Lyapunov exponent, then a randomness test is carried out on the keystream or number sequence generated from this function. The keystream randomness test used is the NIST test suite which aims to evaluate the chaotic level of MS Tent map function [12]. The NIST test suite is a statistical package consisting of 16 tests [13] and their results are shown in the Table I. Based on these 16 statistical tests results, it can be concluded that the keystream generated by MS Tent map is random. This is because the statistical test process shows that the P-value is greater than the significance level (by default it is 0.01).

TABLE I. NIST RANDOMNESS TEST RESULTS OF THE MS TENT MAP

| Type of Test | P-Value | Conclusion |
|---------------------------------------|----------|------------|
| Frequency (Monobit) | 0.031555 | Successful |
| Frequency within a Block | 0.748768 | Successful |
| Run Test | 0.394557 | Successful |
| Longest Run of Ones in a Block | 0.229904 | Successful |
| Binary Matrix Rank | 0.168577 | Successful |
| Discrete Fourier Transform (Spectral) | 0.755036 | Successful |
| Non-Overlapping Template Matching | 0.425093 | Successful |
| Overlapping Template Matching | 0.904727 | Successful |
| Maurer's Universal Statistical | 0.803366 | Successful |
| Linear Complexity | 0.141618 | Successful |
| Serial Test | 0.356311 | Successful |
| | 0.490805 | Successful |
| Approximate Entropy | 0.083009 | Successful |
| Cumulative Sums (Forward) | 0.060013 | Successful |
| Cumulative Sums (Reserve) | 0.025765 | Successful |
| Test Random Excursions | 0.431326 | Successful |
| Test Random Excursions Variance | 0.641948 | Successful |

D. Sensitivity Analysis

Sensitivity analysis aims to find out how big the difference is between the key parameter values used in the encryption process and the key parameter values applied in the decryption process, so that they can be considered the same or different. Fig. 3 is two examples of color and grayscale face images used for sensitivity testing. In the image encryption process the parameters values employed are: $x_0 = 0.9$, $\lambda = 30$, $\mu = 1.5$, $r = 3.7$, and iteration $t = 100$.

The sensitivity test results are displayed in Table II. The tests are performed by varying the value of each parameter, as shown in the first and second columns. The third column displays the decrypted image results according to the parameter values used in the first and second columns. The last column represents the histogram pattern of each decrypted image in the third column.

The key variable x_0 has a sensitivity value of 10^{-17} . This is proven because for x_0 value with a difference of up to 10^{-17} the decrypted image has not returned to the original image and their histogram appears to have a uniform (flat) distribution. Visually from this histogram, one cannot predict what information is contained in the original image. The decrypted image will only return to the original if the difference between x_0 value in the encryption and decryption processes is 10^{-18} . The sensitivity levels of the other parameters are: $r = 10^{-17}$, $\lambda = 10^{-16}$, and $\mu = 10^{-17}$. Based on the sensitivity test results, it can be concluded that the encrypted image is safe against brute force attacks at the sensitivity level of each parameter: $x_0 = 10^{-17}$, $r = 10^{-16}$, $\lambda = 10^{-15}$, and $\mu = 10^{-16}$.

E. Key Space Measurement Analysis

Brute force attacks usually try all possible keys to decrypt to get the actual facial image. To reduce the chance of a successful brute force attack, the algorithm must also have a large key space. The key space represents the number of different keys that can be used to perform encryption/decryption [14]. In Python, the maximum value of floating-point numbers is $1.7976931348623157 \times 10^{308} \approx$

1.8×10^{308} . The natural numbers lie in the interval (0, 1), the precession rate reached $2^{52} \approx 10^{15}$ and the integer data had a possible value of $2^{64} \approx 1.8 \times 10^{19}$. The encryption and decryption algorithms based on MS Tent map chaotic function have five parameters: x_0 , r , μ , λ , and iteration t with domains $x_n \in (0, 1)$, $\lambda, \mu, r \in \mathbb{R}$, and $t \in \mathbb{Z}$. Overall, these five parameters can produce a key space size of $1.8 \times 10^{308} \times 1.8 \times 10^{308} \times 10^{15} \times 1.8 \times 10^{19} \approx 1.05 \times 10^{959}$. This key space is very large, so the encrypted image can be resistant to the brute force attacks.

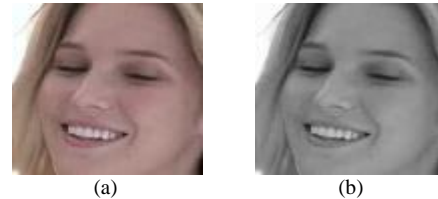


Fig. 3. (a) Color face image. (b) Grayscale face image.

TABLE II. SENSITIVITY TEST RESULTS FOR DIFFERENCES IN PARAMETER VALUES x_0, μ, r, λ

| Sensitivity Test Results | | Face Image Decryption | Histogram |
|--|---------------------------|-----------------------|-----------|
| Initial value difference x_0 with $r = 3.7, \mu = 1.5$, and $\lambda = 30$ | $x_0 = 0.9 + 10^{-6}$ | | |
| | $x_0 = 0.9 + 10^{-17}$ | | |
| | $x_0 = 0.9 + 10^{-18}$ | | |
| Parameter value difference r with $x_0 = 0.9, \mu = 1.5$, and $\lambda = 30$ | $r = 3.7 + 10^{-6}$ | | |
| | $r = 3.7 + 10^{-16}$ | | |
| | $r = 3.7 + 10^{-17}$ | | |
| Parameter value difference λ with $x_0 = 0.9, r = 3.7$, and $\mu = 1.5$ | $\lambda = 30 + 10^{-6}$ | | |
| | $\lambda = 30 + 10^{-15}$ | | |
| | $\lambda = 30 + 10^{-16}$ | | |
| Parameter Value difference μ with $x_0 = 0.9, r = 3.7$, and $\lambda = 30$ | $\mu = 1.5 + 10^{-6}$ | | |
| | $\mu = 1.5 + 10^{-16}$ | | |
| | $\mu = 1.5 + 10^{-17}$ | | |

TABLE III. KEY SPACE COMPARISON OF CHAOTIC FUNCTIONS

| Function | Parameters | Key Space |
|--------------------|--|--------------------------|
| Tent Map [11] | $x_n \in (0, 1), \mu \in \mathbb{R}, \text{ and } t \in \mathbb{Z}$ | 1.8×10^{323} |
| MS Map [15] | $x_n \in (0, 1), \lambda, r \in \mathbb{R}, t \in \mathbb{Z}$ | 3.24×10^{635} |
| Tent + MS Map | $x_n(t), x_n(\text{ms}) \in (0, 1), \lambda, r \in \mathbb{R}, t \in \mathbb{Z}$ | 5.832×10^{958} |
| MS Tent Map | $x_n \in (0, 1), \lambda, \mu, r \in \mathbb{R}, \text{ and } t \in \mathbb{Z}$ | 1.05×10^{959} |
| MS Circle Map [16] | $x_n \in (0, 1), \lambda, r, \Omega, K \in \mathbb{R}, t \in \mathbb{Z}$ | 1.889×10^{1267} |

Table III displays the key space of chaotic functions, where the first and second rows represent the key space of the Tent map and MS map which are 1.8×10^{323} and 3.24×10^{635} respectively. The third row is a key space of 5.832×10^{958} which is produced when the encryption process is carried out twice serially by the Tent map and MS map. In the fourth row is a key space of 1.05×10^{959} , if the proposed MS Tent map is applied for the data encryption process. This shows that data encryption based on MS Tent Map is more secure against brute force attacks than when using MS Map, Tent Map and a serial combination of MS Map and Tent Map.

F. Correlation Analysis Test

Correlation analysis is a method used to determine the direction and strength of the relationship between two variables [17] or between pixels in an image. The correlation coefficient is usually a value without units which is located between 1 and -1. High correlation (close to 1) indicates a strong relationship between neighboring pixel values, so that it can describe the information contained therein. On the other hand, low correlation (close to 0) means that the relationship between neighboring pixels is weak, so that no information can be depicted by these pixels.

Table IV shows the results of the correlation coefficient test from color and grayscale images in Fig. 3. The correlation coefficient is calculated referring to the correlation between neighboring pixels vertically, horizontally, and diagonally. In the second, third and fourth columns, all correlation coefficient values are close to 1 for the original images. These values show a close correlation between pixels in the images, so that all information can be read visually. On the other hand, all the correlation coefficient values of the encrypted images in the fifth, sixth and seventh columns are close to 0. This indicates that there is no correlation between pixels in the encrypted images, so that no information can be read visually from these images. Likewise, this correlation coefficient results show that the encrypted images are secure against statistical attacks.

TABLE IV. CORRELATION COEFFICIENT TEST RESULTS OF COLOR AND GRAYSCALE IMAGES IN FIG. 3 AND THEIR ENCRYPTION

| Test Data | Original Image Correlation Coefficient | | | Encrypted Image Correlation Coefficient | | |
|----------------------|--|----------|----------|---|----------|----------|
| | Horizontal | Vertical | Diagonal | Horizontal | Vertical | Diagonal |
| Color faceimage | 0.9885 | 0.9933 | 0.9827 | 0.00065 | 0.00019 | 0.0014 |
| Grayscale face image | 0.9525 | 0.9631 | 0.9246 | 0.0067 | 0.0017 | 0.0036 |

G. Encrypted Image Quality Test

Functional analysis of encryption and decryption algorithms based on the proposed MS Tent map aims to determine their success in securing data: from the original images to the cipher images (encrypted images) and then returned to the original images (decrypted images), as demonstrated in the Fig. 4. In column (a) are the original images, in column (b) are the results of the encryption algorithm, and the results of the decryption algorithm can be found in column (c). In this functional analysis, it will be determined whether the decrypted images, as the results of the decryption process of the encrypted images, are the same as the original images.

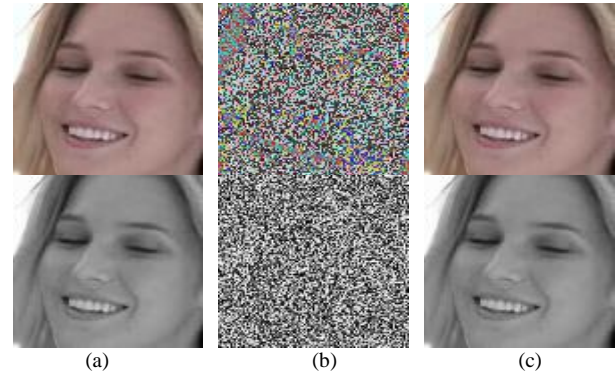


Fig. 4. (a) Original images. (b) Encrypted images. (c) Decrypted images.

Mean Square Error (MSE) in Eq. (9) and Peak Signal to Noise Ratio (PSNR) in Eq. (10) are employed to measure the quality of the decrypted image compared to the original image. Quality analysis was carried out using thirty test images consisting of fifteen color images and fifteen grayscale images. These images have various colors, shapes, and textures features, as well as different sizes. The images in Fig. 4 are two of thirty test images.

$$PSNR(x, y) = 10 \log \frac{255^2}{MSE(x, y)} \tag{9}$$

$$MSE(x, y) = \frac{1}{N} \sum_{i=1}^N (x_i - y_i)^2 \tag{10}$$

Table V shows the MSE and PSNR values calculated between the original image and the decrypted image on thirty test images. MSE has a value of 0 and PSNR equals to ∞ , for all decrypted color images (test image 1 to 15) and decrypted grayscale images (test image 16 to 30). These MSE and PSNR values prove that there are no errors in the decrypted images, or it can be said that the decrypted images are the same as the original images.

TABLE V. MSE AND PSNR VALUE BETWEEN THE ORIGINAL AND DECRYPTED IMAGES

| Test Image | MSE | PSNR | Test Image | MSE | PSNR |
|------------|-----|----------|------------|-----|----------|
| 1 | 0 | ∞ | 16 | 0 | ∞ |
| 2 | 0 | ∞ | 17 | 0 | ∞ |
| 3 | 0 | ∞ | 18 | 0 | ∞ |
| 4 | 0 | ∞ | 19 | 0 | ∞ |
| 5 | 0 | ∞ | 20 | 0 | ∞ |
| 6 | 0 | ∞ | 21 | 0 | ∞ |
| 7 | 0 | ∞ | 22 | 0 | ∞ |
| 8 | 0 | ∞ | 23 | 0 | ∞ |
| 9 | 0 | ∞ | 24 | 0 | ∞ |
| 10 | 0 | ∞ | 25 | 0 | ∞ |
| 11 | 0 | ∞ | 26 | 0 | ∞ |
| 12 | 0 | ∞ | 27 | 0 | ∞ |
| 13 | 0 | ∞ | 28 | 0 | ∞ |
| 14 | 0 | ∞ | 29 | 0 | ∞ |
| 15 | 0 | ∞ | 30 | 0 | ∞ |

IV. CONCLUSION

MS Tent map is a proposed chaotic function which is developed through the composition process of the two chaotic functions MS Map and Tent Map. Through sensitivity, transitivity, and randomness tests on the keystream generated by MS Tent map, it is proven that this function has chaotic properties. MS Tent map has four key parameters that can produce a key space of 1.05×10^{959} . This shows that data encryption based on MS Tent map is more secure against brute force attacks than when using MS map or Tent map or a serial combination of MS map and Tent map, which have key spaces of 1.8×10^{323} , 3.24×10^{635} , and 5.832×10^{958} , respectively. Likewise, based on the results of the correlation coefficient analysis, it shows that encrypted images are also secure against statistical attacks.

REFERENCES

[1] I Kadek Aldy Oka Arditaa, Agus Muliantara, I Gusti Ngurah Anom Cahyadi Putra, Ngurah Agus Sanjaya ER, Ida Bagus Made Mahendra, I Wayan Supriana, Enkripsi Gambar Berdasarkan Modifikasi Bit Piksel

Dengan Menggunakan Perpaduan Logistic Map Dan Henon Map. *Jurnal Elektronik Ilmu Komputer Udayana*, Volume 11, No 2. November 2022.

[2] L. Kocarev, S. Lian, *Chaos-based cryptography: Theory, algorithms, and applications*. Springer-Verlag, Berlin, 2011.

[3] Eva N., & Suryadi M.T. Chaos-Based Encryption Algorithm for Digital Image. *Proceeding IICMA 2013*, Yogyakarta, 2014, pp. 169-177.

[4] Suryadi M. T., Eva N., and Dhian W. Performance of Chaos-Based Encryption Algorithm for Digital Image. *TELKOMNIKA (Telecommunication, Computing, Electronics and Control)*, 2014, 12(3): 675-682.

[5] Suryadi M. T., Maria Y. T. I., and Satria Y. Encryption Algorithm using New Modified map for digital image. *Journal of Physisc: Conference Series*, 2017, 893: 012050.

[6] Dai, Yin, and Xin Wang. Medical image encryption based on a composition of logistic maps and chebyshev maps. *2012 IEEE international conference on information and automation*. IEEE, 2012.

[7] Suryadi, M.T, Satria, Y. & Prawadika, L. N., An improvement on the chaotic behavior of the gauss map for cryptography purposes using the circle map combination, *Journal of Physisc: Conference Series*, Vol. 1490, IOP Publishing, 2020, p. 012045.

[8] Zhenjun Tang, Ye Yang, Shijie Xu, Chunqiang Yu, and Xianquan Zhang. Image Encryption with Double Spiral Scans and Chaotic Maps. *Hindawi Security and Communication Networks*, 2019.

[9] Arthi, G. and Thanikaiselvan, V. and Amirtharajan, R., 4D Hyperchaotic map and DNA encoding combined image encryption for secure communication. *Multimedia Tools and Applications*, 2022.

[10] N. K Pareek, V. Patidar, K.K. Sud, Image encryption using chaotic logistic map. *Journal of Image and Vision Computing*, 24 (2006).

[11] Chunhu Li, Guangchun Luo, Ke Qin & Chunbao Li, Animage encryption scheme based on chaotic tent map. *Nonlinear Dynamics*, 87.1 (2017), pp. 127–133.

[12] Suryadi MT, MYT Irsan, S Yudi, New modified map for digital image encryption and its performance. *Journal of Physisc: Conference Series*, 893, 1 (2017).

[13] A. Rukhin, J. Soto, j. Nechvatal, E. Barker, S. Leigh, *A Statistical test suite for random and pseudorandom number generators for cryptographic applications*. NIST Special publication (2010).

[14] Fu, C., Chen, J.-j., Zou, H., Meng, W.-h., Zhan, Y.-f. & Yu, Y.-w., A chaos-based digital image encryption scheme with an improved diffusion strategy. *Optics express* 20(3), 2363–2378, 2012.

[15] Suryadi M T, Maria Y T I, and Yudi S (2016). New Modified Map for Digital Image Encryption and Its Performance. *Proceedings The Asian Mathematical Conference 2016* (2016).

[16] Suci Boru Kembaren, Suryadi M.T., Triswanto. Implementasi Algoritma Enkripsi Citra Digital Berbasis Chaos Menggunakan Fungsi Komposisi Logistic Dan Gauss Iterated Map. *Prosiding Seminar Nasional & Internasional*, Vol. 1 (2018).

[17] Walpole, R. E. & Ergle, W. D., *Elementary statistical concepts*, MacMillan Basingstoke, 1983.

Transfer Learning-based CNN Model for the Classification of Breast Cancer from Histopathological Images

Sumitha A¹, Rimal Isaac R S²

Research Scholar, Department of Nano Technology, Noorul Islam Centre for Higher Education,
Kumaracoil, Kanyakumari, Tamil Nadu, India¹

Assistant Professor, Department of Nano Technology, Noorul Islam Centre for Higher Education,
Kumaracoil, Kanyakumari, Tamil Nadu, India²

Abstract—Breast cancer can have significant emotional and physical repercussions for women and their families. The timely identification of potential breast cancer risks is crucial for prompt medical intervention and support. In this research, we introduce innovative methods for breast cancer detection, employing a Convolutional Neural Network (CNN) architecture and Transfer Learning (TL) technique. Our foundation is the ICAIR dataset, encompassing a diverse array of histopathological images. To harness the capabilities of deep learning and expand the model's knowledge base, we propose a TL model. The CNN component adeptly extracts spatial features from histopathological images, while the TL component incorporates pretrained weights into the model. To tackle challenges arising from limited labeled data and prevent overfitting, we employ ResNet152v2. Utilizing a pre-trained CNN model on extensive image datasets initializes our CNN component, enabling the network to learn pertinent features from histopathological images. The proposed model achieves commendable accuracy (96.47%), precision (96.24%), F1-score (97.18%), and recall (96.63%) in identifying potential breast cancer cases. This approach holds the potential to assist medical professionals in early breast cancer risk assessment and intervention, ultimately enhancing the quality of care for women's health.

Keywords—Breast cancer; transfer learning; ResNet152v2; medical image analysis; ICAIR 2018 dataset

I. INTRODUCTION

In our contemporary landscape, cancer has solidified its status as a ubiquitous threat, permeating global communities and emerging as a predominant cause of illness and mortality. A chilling statistic underscores the severity of its impact—over 14.5 million lives have succumbed to cancer worldwide, and an ominous prognosis emerge, suggesting an alarming surge to over 28 million by the year 2030. In the realm of oncology, breast cancer takes center stage, its diagnosis often initiated through the intricate dance of biopsy and subsequent microscopic image analysis [1]. Within the microscopic tapestry of breast tissue, pathologists wield their expertise, navigating the labyrinthine structures and components that hold the key to early detection. Histologically probing the microscopic realm, they unravel the intricate distinctions between normal tissue, benign formations, and the malignant lesions that herald a potential storm [2]. The insights harvested

from these histological images are not merely observations; they serve as the bedrock for prognosis assessments, guiding the course of treatment in the relentless pursuit of increased curative outcomes with minimized morbidities.

As the medical landscape continues to evolve, the arrival of Deep Learning (DL) heralds a promising era, transcending traditional boundaries in recognition tasks. DL-based technologies, seamlessly integrated into the workflow of pathologists and clinicians, become instrumental in the perpetual quest for early cancer detection—a steadfast research focus in the expansive field of tumor oncology [3]. A beacon within this evolving narrative is the emergence of Computer-Aided Breast Cancer Diagnosis, an application of paramount importance. Yet, to maintain a grounded perspective on clinical applications, the imperative of multicategory diagnosis becomes evident, recognizing the intricate spectrum of breast cancer manifestations. Motivated by this imperative, the incorporation of deep learning approaches stands as a beacon, promising not just innovation but an elevation in the accuracy of classifiers, further fortifying the arsenal against cancer's relentless assault [4].

The intricate relation between microscopic analysis and biopsy marks the inception of the breast cancer diagnostic journey, unraveling the complex narrative within tissue samples. In the relentless pursuit of early cancer detection, the intersection of radiomics and histopathology emerges as a frontier, promising enhanced insights into tumor characteristics. Emerging technologies such as three-dimensional histopathological reconstruction redefine our approach, offering a holistic visualization of tissue architecture for comprehensive diagnosis. Beyond traditional image-based classification, molecular signatures and genomic profiling usher in a new era of precision medicine, tailoring treatments to individual patients. Ethical considerations in the use of artificial intelligence within pathology underscore the need for responsible and transparent integration into clinical workflows [5].

The integration of blockchain technology into histopathological data management ensures secure, traceable, and interoperable handling of sensitive medical information. The collaboration between pathologists and computational biologists becomes a cornerstone, fostering a symbiotic

relationship for refining algorithms and validating findings [6]. Virtual reality applications in medical education leverage histopathological images, providing immersive learning experiences for the next generation of pathologists. Novel contrast agents in histopathology imaging promise heightened sensitivity, enabling the detection of subtle cellular changes indicative of early-stage malignancies. The burgeoning field of exosome analysis in breast cancer pathology offers a promising avenue, unveiling the potential of liquid biopsy for non-invasive and real-time disease monitoring [7].

However, challenges persist in the current paradigm. The inadequacy of feature representation in existing methods poses a threat to classifier accuracy, highlighting a critical need for improvement [8]. Furthermore, the influence of the magnification factor in acquiring histopathology images introduces a variable that can lead to misclassification, amplifying the urgency for refinement. The deficiencies in accuracy and sensitivity within existing methods underscore the necessity for an overhaul, especially in applications demanding precise classification results [9]. In navigating this complex terrain, the existing classification algorithms grapple with singular features—be it spatial, morphological, or textural. The demand echoes for a comprehensive framework adept at handling multiple feature types, bridging the existing gaps and fortifying the foundation for a new era in cancer diagnosis [10]. As the quest for reliable and precise classification intensifies, the intersection of medical expertise and technological innovation emerges as the crucible where breakthroughs are forged and the relentless pursuit of conquering cancer unfolds.

Moreover, considering the limited availability of labeled data, the study leverages advanced Transfer Learning (TL) methods to enhance the model's adaptability to the specific task under consideration. Following this, the model undergoes a process of fine-tuning and adaptation tailored to the breast cancer detection task. This enables the model to autonomously acquire the ability to discern relevant spatial features from histopathological images. The integration of information from various sources, including disparate imaging and clinical data, into a unified model showcases commendable levels of accuracy, sensitivity, and specificity. In an age where healthcare increasingly embraces data-driven methodologies, this study contributes significantly to the expanding domain of medical image analysis. It underscores the importance of employing TL to overcome the limitations imposed by scarce labeled data. Subsequent sections of this manuscript will delve into the intricacies of the methodology, the careful design of the experimental framework, the presentation of results, and a thorough discussion of the findings.

By seamlessly combining the capabilities of hybrid neural network architectures with sophisticated TL techniques, this research aims to establish a more refined approach to breast cancer risk assessment. These pioneering efforts are expected to have a substantial impact on healthcare outcomes and usher in a new era of enhanced women's health. The major contribution of the research work includes:

- Enhancing the accuracy of breast cancer classification from histopathological images by leveraging transfer learning-based CNN models.

- Effectively extract relevant features for breast cancer classification, reducing the annotation burden and potentially speeding up the diagnostic process.
- Transfer learning-based CNN models offer increased generalizability across different datasets and scalability to handle larger volumes of data. This allows the developed model to be applicable across diverse clinical settings and potentially assist in automating the analysis of histopathological images on a larger scale, thus improving the efficiency of breast cancer diagnosis and treatment.

II. LITERATURE REVIEW

The emergence of Computer-Aided Breast Cancer diagnosis signifies a pivotal milestone in clinical applications, amplifying the need for a realistic perspective that incorporates multicategory diagnosis. The incorporation of DL approaches in breast cancer diagnosis holds the ability to enhance the accuracy of classifiers by delivering more robust foundation for clinicians and pathologists. Existing methods face challenges related to feature representation, affecting the overall accuracy of classifiers, thereby necessitating a drive for improved methodologies. The influence of the magnification factor in acquiring histopathology images introduces variability, potentially leading to misclassification—a factor that demands standardized protocols and careful consideration. Current breast cancer classification algorithms often focus on singular features, such as spatial, morphological, or textural characteristics, highlighting the need for a comprehensive framework capable of handling multiple feature types. Existing methodologies contribute uniquely to the evolving landscape of breast cancer detection, encompassing advancements in DL, challenges in feature representation, and the quest for a more comprehensive diagnostic framework.

Xie et al. [11] introduced a convolutional neural network (CNN) architecture tailored for breast cancer grading, demonstrating exceptional performance across diverse datasets and illustrating the model's adaptability to different staining techniques and tissue variations. The research elucidates the interpretability of the deep learning model, utilizing attention mechanisms to highlight regions crucial for accurate grading, fostering trust and understanding among clinicians. This work delves into the transferability of the trained model to different institutions, addressing concerns of model generalizability and promoting wider adoption in diverse clinical settings. Expanding on morphological features, Wei et al. [12] conducted an in-depth analysis of the discriminatory power of specific morphological descriptors, emphasizing the significance of nuclear shape, glandular arrangement, and stromal characteristics. This study explored the correlation between morphological features and clinical outcomes, establishing potential links between specific histopathological patterns and prognosis. The computational efficiency of morphological feature extraction methods is crucial for real-time applications in clinical settings.

Zewdie et al. [13] introduced texture analysis methods, including gray-level co-occurrence matrices and Gabor filters, evaluating their effectiveness in capturing subtle textural nuances indicative of different breast cancer subtypes. They

explored the impact of preprocessing techniques on texture analysis outcomes, shedding light on the importance of standardized image preparation for robust classification results. Moreover, the research investigates the reproducibility of texture features across multiple institutions, addressing concerns related to dataset variability and ensuring the reliability of the proposed classification approach. Aswathy et al. [14] introduced a novel spatial feature integration method, considering not only local but also global contextual information for improved classification accuracy. They explored the impact of spatial feature incorporation on the model's ability to differentiate between intertumoral heterogeneity and distinct tumor subtypes. They discussed the potential applications of spatial feature-based classification in guiding targeted therapies and predicting treatment response based on spatial tumor characteristics.

Building on ensemble learning model, Hameed et al. [15] systematically evaluated various ensemble strategies, including bagging and boosting, to discern their impact on breast cancer diagnosis accuracy. They investigated the robustness of ensemble models against noisy or imbalanced datasets, providing insights into the models' performance in real-world clinical scenarios. They discussed the scalability of ensemble learning approaches, exploring their feasibility for large-scale deployment in healthcare institutions. Yan et al. [16] introduced a multimodal fusion paradigm, which showcased the synergy between histopathological images and complementary data sources, such as gene expression profiles or clinical information. The added value of multimodal fusion helped in resolving ambiguous cases, demonstrating the potential for more confident and accurate breast cancer subtype classification. Challenges related to data integration, emphasizing the importance of harmonized datasets for meaningful fusion and collaboration across different domains were discussed.

Xue et al. [17] extended the application of transfer learning to histopathological image classification, leveraging pre-trained models on large datasets to enhance the efficiency and generalizability of classifiers. The impact of domain adaptation techniques in mitigating domain shift issues were addressed along with the challenges related to variations in staining techniques and image acquisition protocols. This work transferred knowledge from other medical imaging domains, offering insights into the broader applicability of histopathological image analysis. Hussain et al. [18] integrated explainable AI techniques and evaluated the effectiveness of explainability methods, such as saliency maps and attention mechanisms, in enhancing the transparency and trustworthiness of histopathological image classifiers. Hameed et al. [19]

introduced and evaluated a suite of quantitative metrics specific to histopathological image classifiers, ensuring comprehensive and standardized performance assessment. The research addressed the limitations of traditional metrics, proposing novel measures tailored to the intricacies of histopathological images, including inter-observer agreement and sensitivity to rare subtypes. The importance of benchmark datasets with ground truth annotations is evaluated by facilitating fair and meaningful comparisons between different classification models.

III. MATERIALS AND METHODS

This section serves as the foundation of our endeavor to advance breast cancer classification by combining state-of-the-art technologies. As we navigate through the intricate details of our approach, our goal is to elucidate the systematic framework that forms the foundation for the development and evaluation of our breast cancer detection model. Within this section, we delineate the essential steps, techniques, and tools utilized in our research, shedding light on the trajectory toward unlocking the full potential of transfer learning and CNN architectures. Breast cancer, posing a significant challenge to women's health globally, calls for innovative solutions in early detection [20]. Our methodology aims to bridge the gap between the intricacies of breast cancer diagnosis and the capabilities of artificial intelligence, specifically tailored for the ICIAR 2018 histopathological dataset—an invaluable repository of histopathological images and clinical data. In the subsequent sections, we will meticulously detail our data preprocessing strategies, the architectural framework of our transfer learning model and the intricacies of the training and validation procedures. The proposed methodology is crafted not only to make a meaningful contribution to the field of breast cancer classification but also to serve as a blueprint for future research endeavors focusing on unlocking the potential of artificial intelligence in healthcare diagnostics.

A. Dataset Description

Utilized in our experimental investigations, the ICIAR 2018 breast cancer histopathological dataset offers a comprehensive exploration of breast cancer pathology through Hematoxylin and Eosin (H&E) stained microscopy images [21]. These images, categorized as normal, benign, in situ carcinoma, or invasive carcinoma, present a diverse spectrum of breast cancer types. The dataset's credibility is ensured by the meticulous annotation conducted by doctors, with any annotation discrepancies leading to the exclusion. To provide visual context, Fig. 1 offers illustrative examples derived from the ICIAR 2018 dataset, granting a preview of the varied histopathological presentations contained within the dataset.

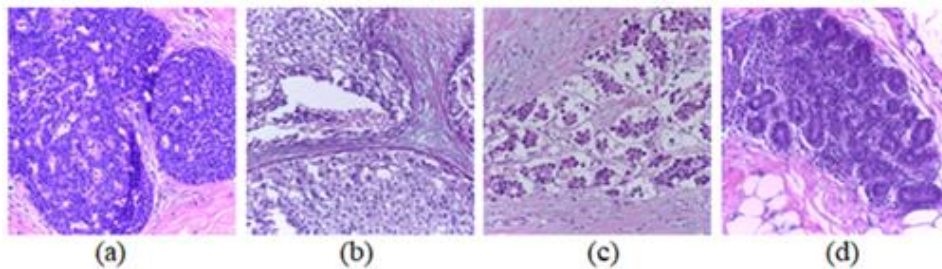


Fig. 1. Images from ICIAR 2018 dataset (a) Benign, (b) Carcinoma-in-situ, (c) Carcinoma-invasive, (d) Normal.

Employing the Red-Green-Blue (RGB) color model, the dataset captures intricate cellular details. Each image boasts a resolution of 2048 x 1536 pixels, enabling microscopic insights. With a memory space requirement of 10-20 MB per image, the dataset strikes a balance between richness of information and computational efficiency. The image-wise labeling approach contributes to a holistic understanding of breast cancer pathology, offering valuable insights for researchers and clinicians alike. Table I furnishes a thorough breakdown, shedding light on the distribution of different image classes within the given dataset. This classification facilitates the methodical analysis of breast cell properties, serving both research and diagnostic objectives.

TABLE I. IMAGES IN ICIAR 2018 DATASET

| Sl. No | Image Class | Total | Train | Test |
|--------|--------------------|-------|-------|------|
| 1 | Benign | 1000 | 800 | 200 |
| 2 | Carcinoma-in-sit | 1000 | 800 | 200 |
| 3 | Carcinoma invasive | 1000 | 800 | 200 |
| 4 | Normal | 1000 | 800 | 200 |

The strategic use of data augmentation is implemented to address overfitting concerns in CNNs while concurrently improving the accuracy of disease detection. Fig. 2 provides a visual depiction of images within the dataset and a comprehensive overview of the image distribution.

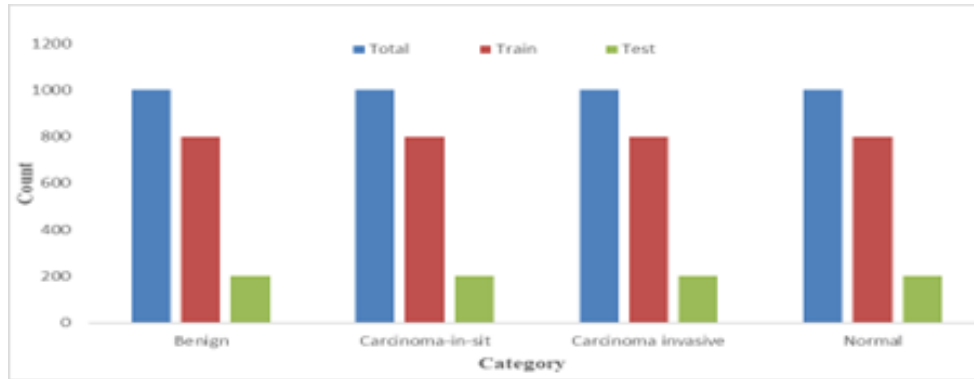


Fig. 2. Distribution of various categories in dataset.

B. Breast Cancer Classification using Transfer Learning

While dealing with histopathological images, the utilization of ResNet-152v2 stands as a pivotal advancement in leveraging deep learning for enhanced diagnostic accuracy. ResNet-152v2, renowned for its depth and skip-connection architecture, proves instrumental in capturing intricate patterns and subtle features crucial for discerning between cancer

categories [22]. This classification model benefits from its ability to mitigate vanishing gradient issues, allowing for effective training of deep networks using TL technique. This approach facilitates a more nuanced understanding of the complex structures present in histopathological images, empowering the model to provide precise and reliable identification of breast cancer pathology. The proposed model incorporating ResNet-152v2 and TL is illustrated in Fig. 3.

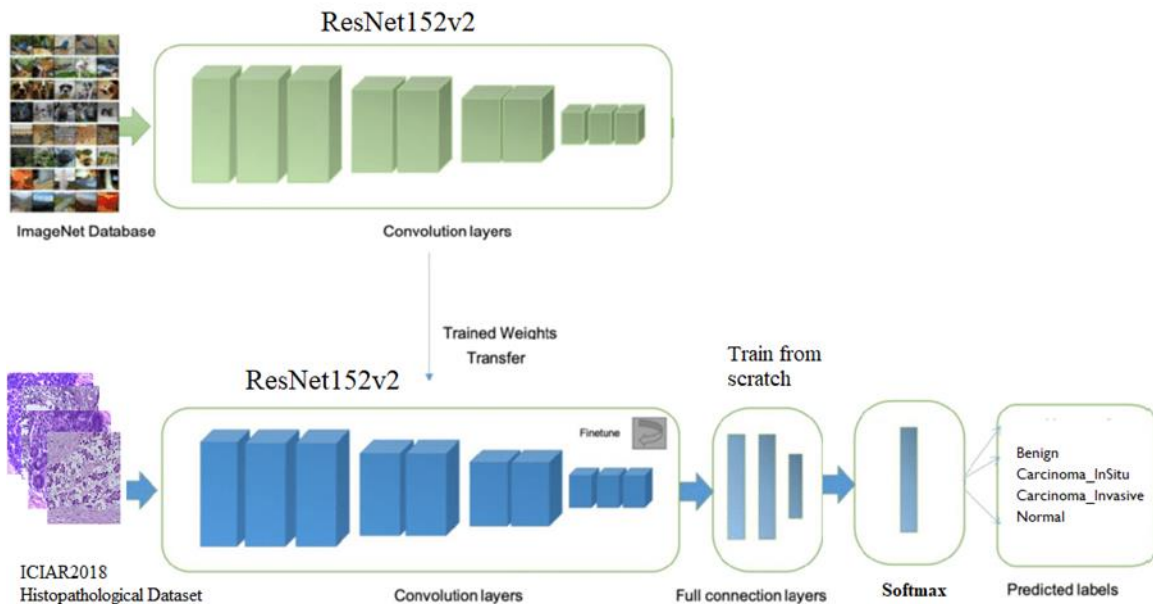


Fig. 3. Proposed transfer learning model.

To address the challenges associated with vanishing or exploding gradients during training, researchers introduced the concept of Residual Blocks. In the architecture of these Residual Networks (ResNets), a crucial technique called skip connections is employed. Skip connections establish links between the activations of one layer and subsequent layers by bypassing certain intermediary layers. This design creates what is known as a residual block, which is a fundamental building block of ResNets. The strength of ResNets lies in their ability to stack these residual blocks together, forming a deep and interconnected network. By incorporating skip connections, ResNets facilitate the flow of information across layers, mitigating the issues of vanishing gradients and enabling the training of exceptionally deep neural networks. This design principle has proven effective in improving the optimization process and fostering the successful training of deep model. The process flow and working of the skip connections is illustrated in Fig. 4.

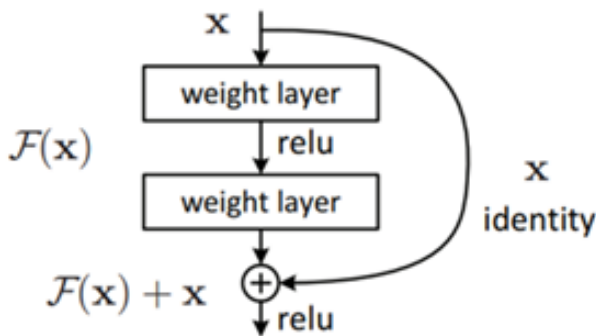


Fig. 4. Skip (Shortcut) connections.

The methodology employed in this network diverges from conventional layer-wise learning of the underlying mapping. Instead, we enable the network to adapt to the residual mapping. Thus, rather than expressing it as $H(x)$, the initial mapping, we encourage the network to adjust according to Eq. (1) and Eq. (2).

$$F(x) = H(x) - x \tag{1}$$

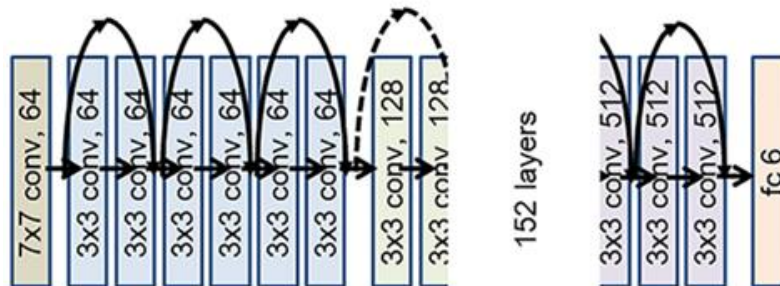


Fig. 5. ResNet152 V2 architecture.

The architecture of proposed classifier within the context of multi-classification comprises of two distinct components: the reduction path and the classifier head. The reduction path follows conventional convolutional network design principles, incorporating repeated convolutions and max-pooling operations to facilitate down sampling [25]. This process involves iteratively applying three stages, collectively termed a

$$H(x) = F(x) + x \tag{2}$$

The residual block in the proposed architecture is expressed using Eq. (3). This equation provides an insight about the output of the network. Here, x is the input to the block, W_i represents the learnable parameters, and F is a residual function implemented by a series of convolutional layers. The output y is the sum of the residual function and the input, allowing for the bypass of information is expressed as in Eq. (3).

$$y = F(x, \{W_i\}) + x \tag{3}$$

The inclusion of skip connections offers a notable benefit: if a particular layer negatively impacts the architecture's performance, regularization allows it to be bypassed. Consequently, this permits the training of extremely deep neural networks without encountering issues related to vanishing or exploding gradients. The ResNet architecture pioneered the concept of employing deeper networks [23]. The skip connection technique facilitates the training of highly deep networks, contributing to enhanced model performance. By preserving acquired knowledge during training, residual connections expedite the training process, effectively amplifying the network's capacity.

ResNet152V2 stands out as a residual network comprising an impressive 152 layers. Its primary function involves feature extraction from images by training input images based on pre-existing weights [24]. The architectural makeup of this model encompasses various layers, including reshape, flatten, the first dense layer, dropout, the second dense layer, and an activation layer dedicated to predicting image classes. Given its considerable depth and a multitude of parameters, ResNet152V2 proves particularly well-suited for intricate tasks, especially in scenarios where datasets are extensive and diverse. It's important to highlight that initiating training for ResNet152V2 from scratch demands a substantial amount of labeled data and significant computational resources. This proves especially beneficial when confronted with limited data or computational resources. The proposed architecture, as illustrated in Fig. 5, encapsulates the key components of this sophisticated model.

"block," multiple times, contributing depth to the network. The sequence concludes with fully connected layers that form the classifier. Critical to this architecture are the convolutional layers, pivotal in computing local weighted sums, commonly known as 'feature maps,' at each layer. These feature maps are generated by the repeated application of filters across the entire dataset, significantly enhancing training efficiency. The

iterative application of these processes contributes to the network's depth and its ability to capture intricate patterns in the data. In the concluding stage, an activation function, specifically the softmax function, is employed to categorize the outputs of the model into different classes, covering various aspects of breast cancer cases. This crucial step equips the

model with the ability to make nuanced and precise predictions, ultimately enhancing its diagnostic capabilities. Table II provides a detailed examination of the network's structure, encompassing the arrangement of layers and corresponding parameters.

TABLE II. PROPOSED TRANSFER LEARNING MODEL SUMMARY

| Layers | Type | Output Shape | Parameters |
|-------------------|------------------|---------------|------------|
| Input Layer | Dense | 256 x 256 x 3 | - |
| ResNet152v2 | Feature Transfer | 8 x 8 x 2048 | 58331648 |
| Convolution Layer | Conv2D | 8 x 8 x 64 | 131136 |
| Max pooling layer | Maxpooling2D | 4 x 4 x 64 | 0 |
| Convolution Layer | Conv2D | 4 x 4 x 32 | 2080 |
| Convolution Layer | Conv2D | 4 x 4 x 64 | 2112 |
| Dense | Dense | 4 x 4 x 32 | 4160 |
| Dense | Dense | 4 x 4 x 64 | 2080 |
| Flatten | Flatten | 512 | 0 |
| Dense | Dense | 4 | 2052 |
| Total | | | 58,475,268 |
| Trainable | | | 143,620 |
| Non-Trainable | | | 58,331,648 |

The initial step involves transferring features and weights from a pre-trained ResNet152v2 model, originally trained on the ImageNet dataset. Following this, the data undergoes a series of processing steps, including convolutional operations, max-pooling, dense layers, flattening, and hidden layers. These operations result in a final output comprising six distinct classes, facilitating individual class predictions. During the model's training and validation, a batch size of 128 and a total of 25 epochs were utilized. 25 epochs are the optimal value

required for the TL model to converge. It was noted that at this epoch count, both the loss and accuracy metrics stabilize, yielding the most favorable and consistent results. Fig. 6 provides a visual representation of the proposed TL model tailored for the ICAIR 2018 dataset. This schematic diagram provides an overview of the model's architecture, initiating with six distinct classes and setting the stage for robust classification.

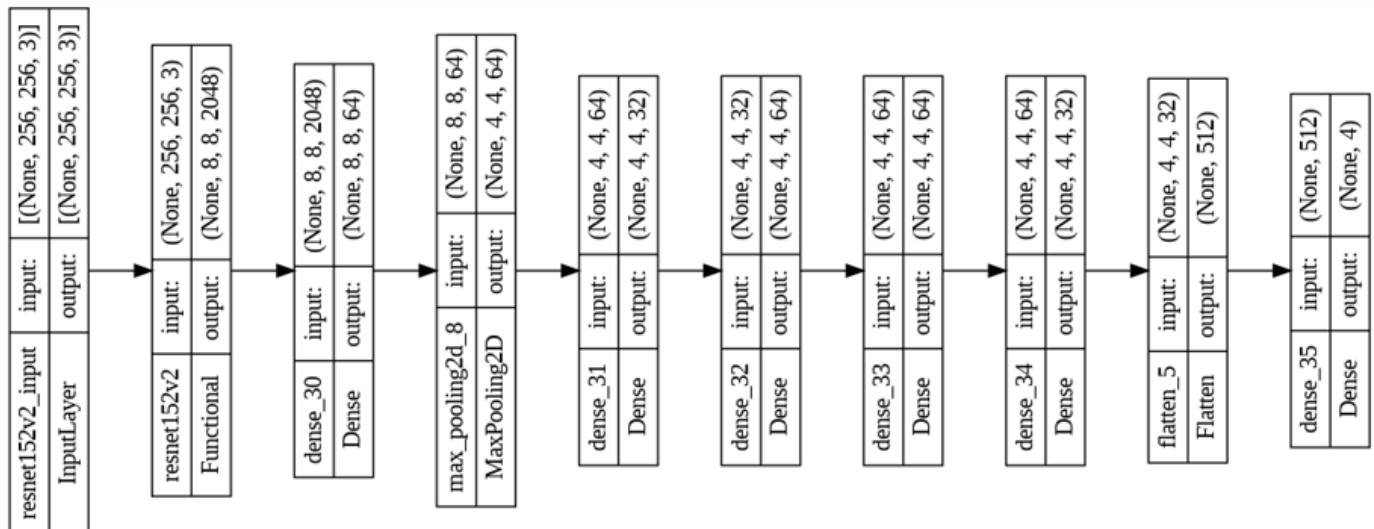


Fig. 6. Proposed transfer learning model.

IV. RESULTS AND DISCUSSION

The systematic investigation involves the extraction of features from various levels within the CNN, placing a specific

focus on evaluating the granularity of these features in relation to their performance in classification tasks. This process includes utilizing different layers of the CNN to obtain these features. An integral part of the research revolves around

identifying the optimal CNN layer that produces the most distinctive features for the classification of histopathological images into distinct categories. This holds particular significance considering the training of the TL-CNN model on the ICAIR 2018 dataset. The primary objective of the study is to unveil the CNN layer that offers the most valuable insights for distinguishing between different classes of breast cell images, ultimately enhancing the overall efficiency of the model.

In our suggested methodology, our emphasis lies specifically on the profound layers of the model, leveraging their output features to train the classifier, while maintaining the immobility of the layers leading up to this depth. This approach effectively trims down the number of trainable

components, although a considerable number of features remain viable. Our training approach involves an 80% allocation for training and a 20% allocation for testing. Furthermore, for result comparison with previous studies, we ensure consistency by employing the same parameters in cross-validation and fixed partitioning methodologies. The development of the proposed model is executed using Python on the Google Colab platform. We have implemented a learning rate of 1×10^{-4} for this work, accompanied by a minimized batch size of 128 and a total of 25 training epochs. The loss the model needs to be reduced after each epoch. The loss becomes low and constant after 7 epochs. The accuracy also turns out to be constant after 7 epochs. Fig. 7 provides a graphical representation of the training and validation performance of the proposed TL-CNN classifier.

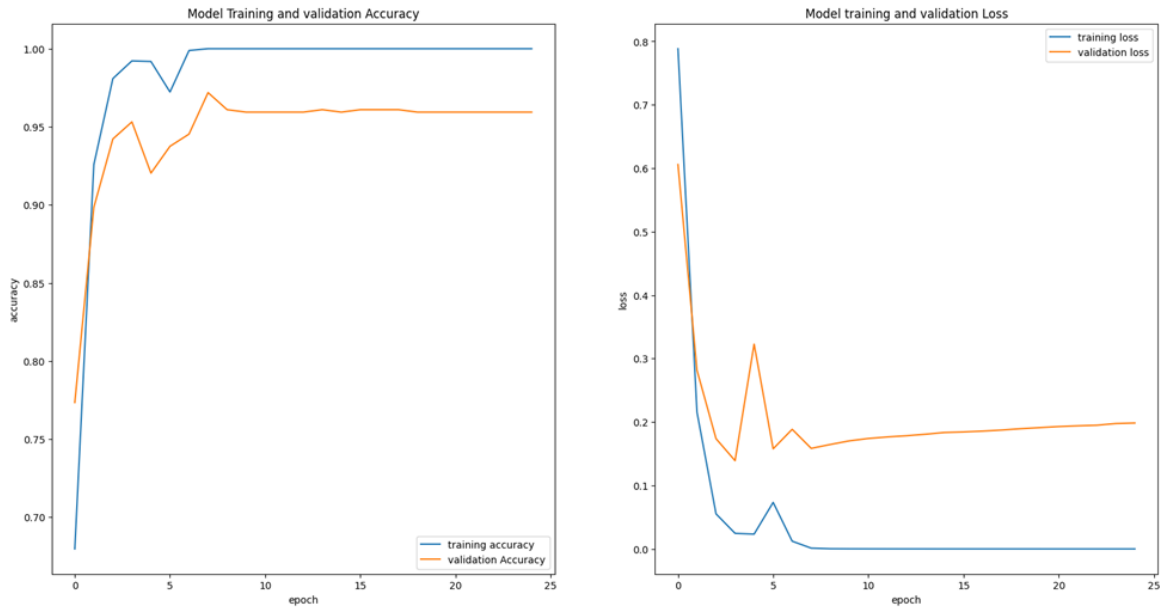


Fig. 7. Accuracy plot and loss plot of proposed model.

To comprehensively evaluate the effectiveness and operational efficiency of the model we suggest, we utilize a suite of four pivotal metrics: F1-score, accuracy, precision, and recall. In defining these metrics, we incorporate the terms False Positive (FP), False Negative (FN), True Negative (TN), and True Positive (TP), which are fundamental for evaluating model performance. These performance parameters are expressed mathematically as in Eq. (4), (5), (6) and (7).

$$Precision = \frac{TP}{TP+FP} \quad (4)$$

$$Recall = \frac{TP}{TP+FN} \quad (5)$$

$$Accuracy = \frac{TP+TN}{TP+FP+TN+FN} \quad (6)$$

$$F1 - Score = 2 \times \frac{Precision \times Recall}{Precision + Recall} \quad (7)$$

Beyond the 7th epoch in the proposed ResNet152v2 based CNN classifier, the performance metrics consistently display a commendable level of accuracy. This stability in performance can be credited to the effective application of TL techniques, addressing challenges inherent in categorization tasks. Within

the training process, the consideration of errors, often referred to as loss, is crucial. In our case, the observed loss is merely 0.3, indicating an exceptionally low level of error. To comprehensively evaluate the model, the entire test image dataset was employed. The mean accuracy achieved by our suggested TL-CNN model reaches an impressive value of 96.47%. Additionally, the mean values for precision, recall, and F1-score showcase strong performance, measuring at 96.24%, 96.63%, and 97.18%, respectively. Table III provides the classification report for the proposed multiclass classification model.

TABLE III. CLASSIFICATION REPORT OF PROPOSED CLASSIFIER

| Category | Precision (%) | Recall (%) | F1-Score | Accuracy (%) |
|--------------------|---------------|------------|----------|--------------|
| Benign | 96 | 96 | 96 | 95 |
| Carcinoma-in-Situ | 97 | 92 | 95 | 97 |
| Carcinoma-Invasive | 96 | 97 | 97 | 96 |
| Normal | 95 | 98 | 96 | 97 |

The effectiveness of the proposed model is notably impressive in accurately identifying the breast cancer classes. Moreover, it maintains a minimum accuracy of 95% with benign class. This model provides maximum accuracy of 97% with carcinoma-in-situ and normal classes. Precision analysis reveals that the model attains its peak value of 97% for carcinoma-in-situ class. The lowest precision, still notably high at 95%, is observed in the normal class. Moving on to recall, the model reaches a maximum value of 98%, for the normal class. The lowest recall of 92% is noted in carcinoma-in-situ class. F1-score achieves a maximum value of 97% for the

carcinoma-invasive class and maintains a minimum value of 95% for the carcinoma-in-situ class. In summary, the classification report underscores the superior performance across all classes. The proposed model demonstrates particular proficiency in identifying various classes within the given dataset. For a detailed perspective on the performance of individual classes, (see Fig. 8). Additionally, Fig. 9 illustrates the confusion matrix generated for the proposed classifier, offering a comprehensive visualization of the classification performance across various breast cancer categories.

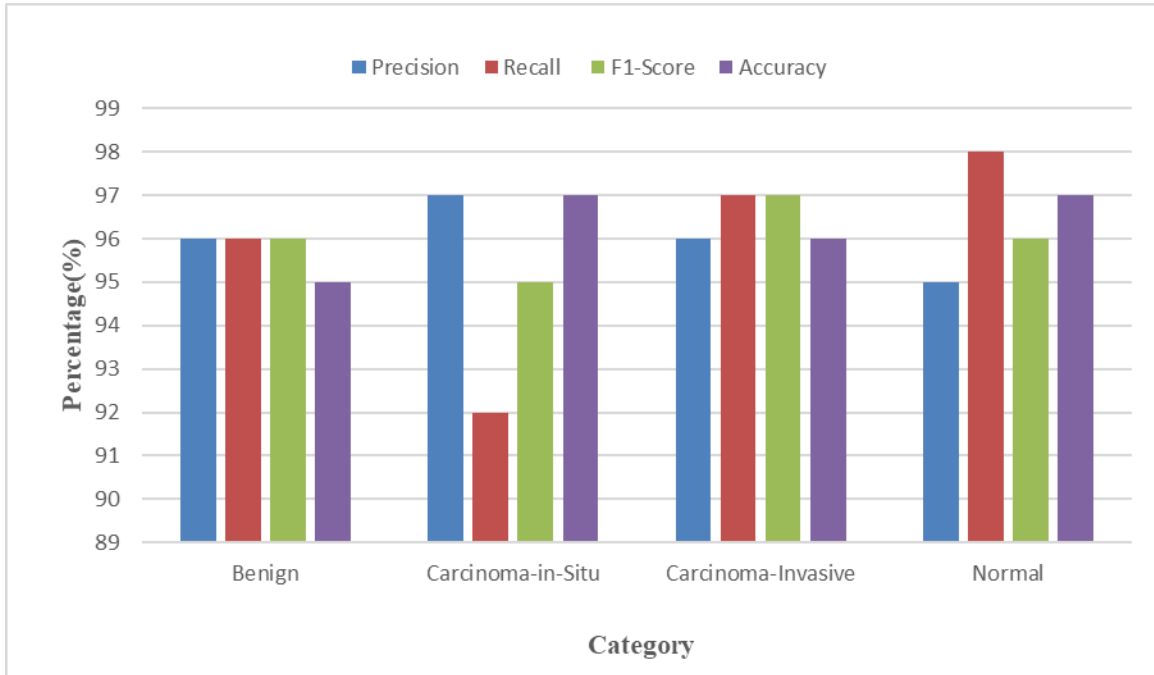


Fig. 8. Category wise classification performance of proposed classifier.

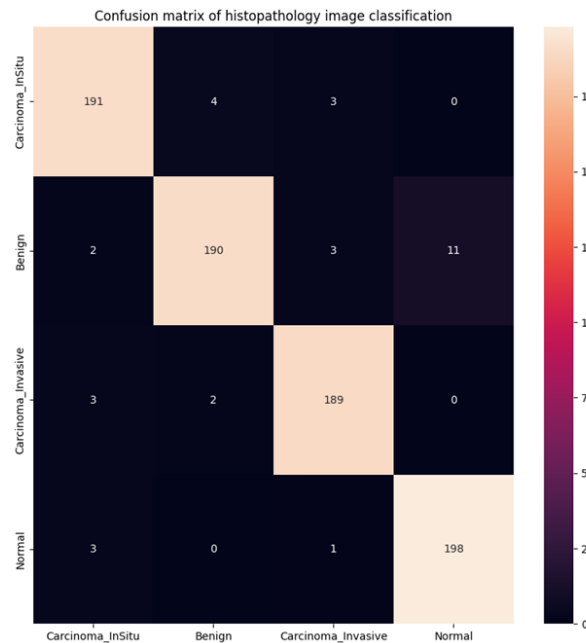


Fig. 9. Confusion matrix of proposed classifier.

In evaluating the effectiveness of the constructed model, it is imperative to conduct a thorough comparison of their classification performance. The assessment of the proposed TL

models' classification performance is conducted across diverse datasets. Table IV analyzes of the efficiency of existing models using the selected performance metrics.

TABLE IV. PERFORMANCE COMPARISON

| Model | Precision (%) | Recall (%) | F1-score (%) | Accuracy (%) |
|----------------------------|---------------|------------|--------------|--------------|
| AlexNet | 93.71 | 95.32 | 94.35 | 94.14 |
| GoogleNet | 88.44 | 89.45 | 86.65 | 89.42 |
| ResNet 50 | 92.14 | 91.67 | 92.36 | 92.36 |
| VGG16 | 93.86 | 93.83 | 94.12 | 93.15 |
| Inception v3 | 89.31 | 87.61 | 88.38 | 86.11 |
| ResNet152v2-CNN (Proposed) | 96.24 | 96.63 | 97.18 | 96.47 |

In the assessment of classification accuracy, the proposed model distinguishes itself with the highest score of 96.47%. Noteworthy among the pre-trained models are VGG16 with an accuracy rate of 93.15%, ResNet50 at 92.36%, and AlexNet demonstrating a performance of 94.14%. Turning to precision, the proposed model excels with an impressive precision rate of 96.24%. In contrast, AlexNet achieved 93.71% precision, ResNet50 recorded 92.14%, and VGG16 obtained 93.86%. Proposed model attains an outstanding recall value of 96.63%, outperforming all other models in this metric. In comparison, VGG16 achieved a recall rate of 93.83%, ResNet 50 reached 91.67%, and AlexNet recorded 95.32% in recall. Remarkably, the proposed model's recall surpasses other TL models by a

significant margin, demonstrating its superiority in capturing and correctly identifying relevant instances. Furthermore, in assessing the F1-score, the proposed model once again takes the lead with a score of 97.18%. There is a noticeable difference between the F1 score of proposed model and existing TL approaches, underscoring the proposed model's overall effectiveness in achieving a good balance between precision and recall. Overall, the proposed model not only exhibits the highest accuracy for breast cancer categorization but also emphasizes the crucial role of specific parameters, particularly TL, in mitigating overfitting and elevating classification accuracy. For a visual comparison of the proposed model with existing classifier (see Fig. 10).

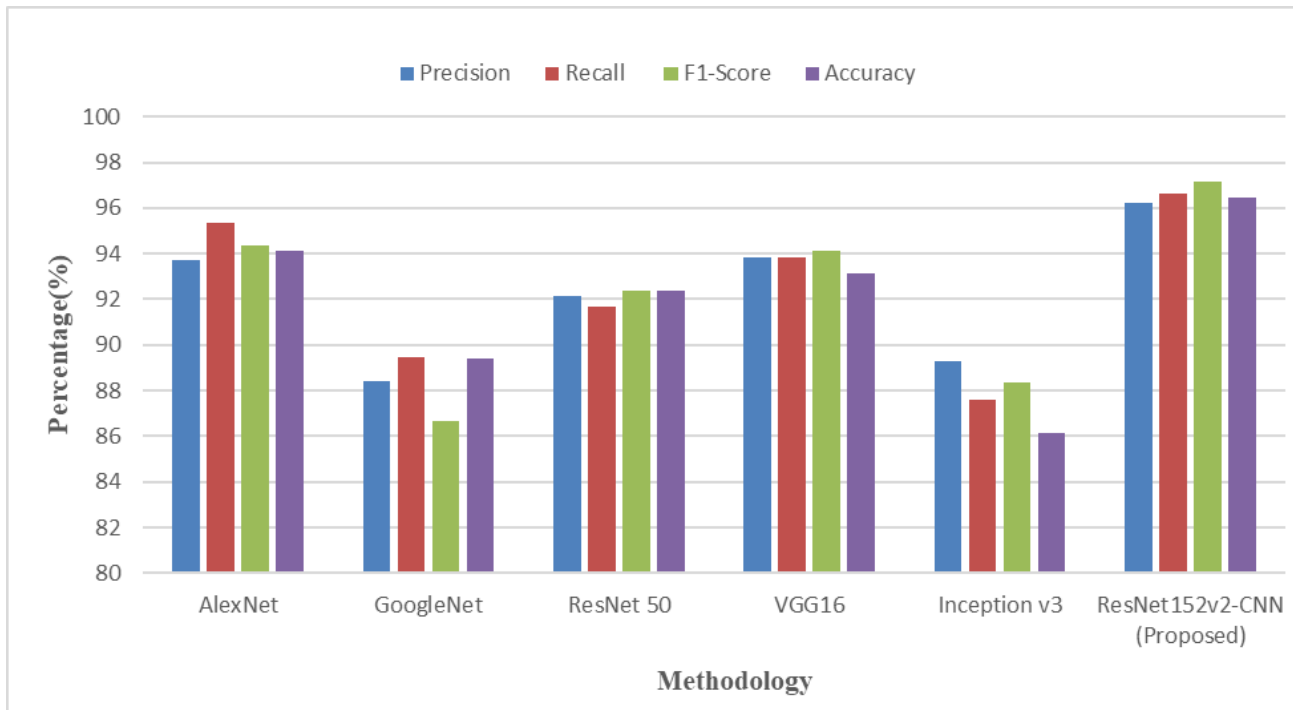


Fig. 10. Performance comparison.

Primary among the benefits is the complete automation of the classification process, eliminating the necessity for manual intervention. Tasks such as feature extraction, noise filtering, delineation of regions, and selection become obsolete. As a result, the predictions provided by the proposed model not only

become automated but also consistently reproducible, free from any inherent bias. The prediction results generated by the proposed model along with the ground truth are provided in Fig. 11.

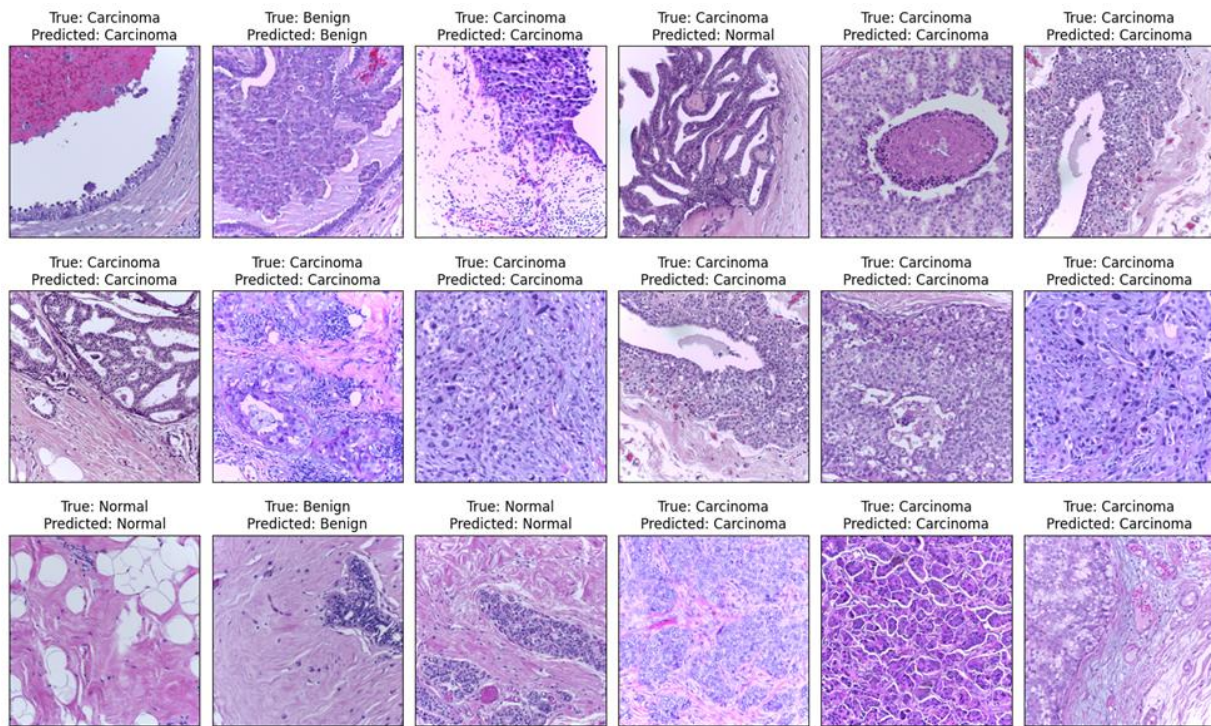


Fig. 11. Prediction outputs.

V. CONCLUSION

This study focused into the efficacy of TL in the classification of breast cancer through the analysis of histopathological images. The integration of TL with CNN structures proved to be an exceptionally efficient strategy, resulting in peak recognition rates. Notably, the ResNet152v2-CNN model proposed in this research achieved remarkable accuracy (96.47%), precision (96.24%), F1-score (97.18%), and recall (96.63%) in the identification of potential breast cancer cases. One notable advantage of the proposed model lies in their capacity to diminish or even eliminate the need for extensive pre-processing stages, surpassing existing techniques in this aspect. Interestingly, when contrasted with the proposed model, the pre-trained AlexNet classifier demonstrated inferior performance across various performance metrics. Future research endeavors will focus on optimizing the deployment of the proposed model on mobile platforms, addressing computing complexity issues. Additionally, there will be an exploration of further fine-tuning methods and strategies, promising ongoing advancements in histopathological image classification.

ACKNOWLEDGMENT

I would like to express my sincere gratitude to all those who contributed to the completion of this research paper. I extend my heartfelt thanks to my supervisor, my family, my colleagues and fellow researchers for their encouragement and understanding during the demanding phases of this work.

REFERENCES

- [1] Han, Z., Wei, B., Zheng, Y., Yin, Y., Li, K., & Li, S. (2017). Breast cancer multi-classification from histopathological images with structured deep learning model. *Scientific reports*, 7(1), 4172.
- [2] Albarqouni, S., Baur, C., Achilles, F., Belagiannis, V., Demirci, S., & Navab, N. (2016). Aggnet: deep learning from crowds for mitosis detection in breast cancer histology images. *IEEE transactions on medical imaging*, 35(5), 1313-1321.
- [3] Araujo, T., Aresta, G., Castro, E., Rouco, J., Aguiar, P., Eloy, C., Campilho, A. (2017). Classification of breast cancer histology images using convolutional neural networks. *PLoS one*, 12(6), e0177544.
- [4] Sirinukunwattana, K., Raza, S. E. A., Tsang, Y. W., Snead, D. R., Cree, I. A., & Rajpoot, N. M. (2016). Locality sensitive deep learning for detection and classification of nuclei in routine colon cancer histology images. *IEEE transactions on medical imaging*, 35(5), 1196-1206.
- [5] Xu, J., Xiang, L., Liu, Q., Gilmore, H., Wu, J., Tang, J., & Madabhushi, A. (2015). Stacked sparse autoencoder (SSAE) for nuclei detection on breast cancer histopathology images. *IEEE transactions on medical imaging*, 35(1), 119-130.
- [6] Xu, J., Luo, X., Wang, G., Gilmore, H., & Madabhushi, A. (2016). A deep convolutional neural network for segmenting and classifying epithelial and stromal regions in histopathological images. *Neurocomputing*, 191, 214-223.
- [7] Zheng, Y., Jiang, Z., Xie, F., Zhang, H., Ma, Y., Shi, H., & Zhao, Y. (2017). Feature extraction from histopathological images based on nucleus-guided convolutional neural network for breast lesion classification. *Pattern Recognition*, 71, 14-25.
- [8] Gertych, A., Ing, N., Ma, Z., Fuchs, T. J., Salman, S., Mohanty, S., ... & Knudsen, B. S. (2015). Machine learning approaches to analyze histological images of tissues from radical prostatectomies. *Computerized Medical Imaging and Graphics*, 46, 197-208.
- [9] Huang, Y., Zheng, H., Liu, C., Ding, X., & Rohde, G. K. (2017). Epithelium-stroma classification via convolutional neural networks and unsupervised domain adaptation in histopathological images. *IEEE journal of biomedical and health informatics*, 21(6), 1625-1632.
- [10] Rezk, E., Awan, Z., Islam, F., Jaoua, A., Al Maadeed, S., Zhang, N., & Rajpoot, N. (2017). Conceptual data sampling for breast cancer histology image classification. *Computers in biology and medicine*, 89, 59-67.
- [11] Xie, J., Liu, R., Luttrell IV, J., & Zhang, C. (2019). Deep learning-based analysis of histopathological images of breast cancer. *Frontiers in genetics*, 10, 80.

- [12] Wei, M., Du, Y., Wu, X., Su, Q., Zhu, J., Zheng, L., ... & Zhuang, J. (2020). A benign and malignant breast tumor classification method via efficiently combining texture and morphological features on ultrasound images. *Computational and Mathematical Methods in Medicine*, 2020.
- [13] Zewdie, E. T., Tessema, A. W., & Simegn, G. L. (2021). Classification of breast cancer types, sub-types and grade from histopathological images using deep learning technique. *Health and Technology*, 11, 1277-1290.
- [14] Aswathy, M. A., & Jagannath, M. (2021). An SVM approach towards breast cancer classification from H&E-stained histopathology images based on integrated features. *Medical & biological engineering & computing*, 59(9), 1773-1783.
- [15] Hameed, Z., Zahia, S., Garcia-Zapirain, B., Javier Aguirre, J., & Maria Vanegas, A. (2020). Breast cancer histopathology image classification using an ensemble of deep learning models. *Sensors*, 20(16), 4373.
- [16] Yan, R., Zhang, F., Rao, X., Lv, Z., Li, J., Zhang, L., ... & Liang, J. (2021). Richer fusion network for breast cancer classification based on multimodal data. *BMC Medical Informatics and Decision Making*, 21(1), 1-15.
- [17] Xue, D., Zhou, X., Li, C., Yao, Y., Rahaman, M. M., Zhang, J., ... & Sun, H. (2020). An application of transfer learning and ensemble learning techniques for cervical histopathology image classification. *IEEE Access*, 8, 104603-104618.
- [18] Hussain, S. M., Buongiorno, D., Altini, N., Berloco, F., Prencipe, B., Moschetta, M., ... & Brunetti, A. (2022). Shape-Based Breast Lesion Classification Using Digital Tomosynthesis Images: The Role of Explainable Artificial Intelligence. *Applied Sciences*, 12(12), 6230.
- [19] Hameed, Z., Zahia, S., Garcia-Zapirain, B., Javier Aguirre, J., & Maria Vanegas, A. (2020). Breast cancer histopathology image classification using an ensemble of deep learning models. *Sensors*, 20(16), 4373.
- [20] Goyal, M., Knackstedt, T., Yan, S., & Hassanpour, S. (2020). Artificial intelligence-based image classification methods for diagnosis of skin cancer: Challenges and opportunities. *Computers in biology and medicine*, 127, 104065.
- [21] Pal, R., & Saraswat, M. (2018). A new bag-of-features method using biogeography-based optimization for categorization of histology images. *International Journal of Information Systems & Management Science*, 1(2).
- [22] Ibrahim, D. M., Elshennawy, N. M., & Sarhan, A. M. (2021). Deep-chest: Multi-classification deep learning model for diagnosing COVID-19, pneumonia, and lung cancer chest diseases. *Computers in biology and medicine*, 132, 104348.
- [23] Reis, H. C., & Turk, V. (2023). Transfer learning approach and nucleus segmentation with medclnet colon cancer database. *Journal of Digital Imaging*, 36(1), 306-325.
- [24] Reis, H. C., Turk, V., Khoshelham, K., & Kaya, S. (2022). InSiNet: a deep convolutional approach to skin cancer detection and segmentation. *Medical & Biological Engineering & Computing*, 1-20.
- [25] Aljohani, K., & Turki, T. (2022). Automatic Classification of Melanoma Skin Cancer with Deep Convolutional Neural Networks. *Ai*, 3(2), 512-525.

Autoencoder and CNN for Content-based Retrieval of Multimodal Medical Images

Suresh Kumar J S¹, Maria Celestin Vigila S²

Research Scholar, Department of Computer Science and Engineering,
Noorul Islam Centre for Higher Education, Kumaracoil, Kanyakumari, Tamil Nadu, India¹
Associate Professor, Department of Information Technology,
Noorul Islam Centre for Higher Education, Kumaracoil, Kanyakumari, Tamil Nadu, India²

Abstract—Content-Based Medical Image Retrieval (CBMIR) is a widely adopted approach for retrieving related images by the comparison inherent features present in the input image to those stored in the database. However, the domain of CBMIR specific to multiclass medical images faces formidable challenges, primarily stemming from a lack of comprehensive research in this area. Existing methodologies in this field have demonstrated suboptimal performance and propagated misinformation, particularly during the crucial feature extraction process. In response, this investigation seeks to leverage deep learning, a subset of artificial intelligence for the extraction of features and elevate overall performance outcomes. The research focuses on multiclass medical images employing the ImageNet dataset, aiming to rectify the deficiencies observed in previous studies. The utilization of the CNN-based Autoencoder method manifests as a strategic choice to enhance the accuracy of feature extraction, thereby fostering improved retrieval results. In the ImageNet dataset, the results obtained from the proposed CBMIR model demonstrate notable average values for accuracy (95.87%), precision (96.03%) and recall (95.54%). This underscores the efficacy of the CNN-based autoencoder model in achieving good accuracy and underscores its potential as a transformative tool in advancing medical image retrieval.

Keywords—Medical image retrieval; multiclass medical images; artificial intelligence; deep learning; convolutional neural network; autoencoder

I. INTRODUCTION

Content Based Medical Image Retrieval (CBMIR) plays a pivotal part in modern healthcare, leveraging the developments in Deep Learning (DL) to enhance efficiency and accuracy of diagnosing and treating various medical conditions. As medical imaging technologies continue to evolve, the vast amount of digital medical images generated necessitates robust and intelligent retrieval systems. DL, a subset of Artificial Intelligence (AI), has emerged as a transformative force in the field, offering unprecedented capabilities in feature extraction and pattern recognition. This research delves into the area of CBMIR, exploring the application of DL techniques to navigate and retrieve relevant information from extensive medical image databases [1]. The integration of DL models not only streamlines the retrieval process but also contributes to the overall improvement of diagnostic accuracy and clinical decision-making. In this comprehensive examination, we delve into the key methodologies, challenges, and breakthroughs

associated with CBMIR using DL, shedding light on the promising future it holds for the medical community [2].

The fusion of cutting-edge technology and healthcare exemplifies a synergy that has the potential to revolutionize patient care and medical research. Through an exploration of various DL architectures and their adaptations to the intricacies of medical images, this work provides implications for the future of CBMIR. In navigating the intricate landscape of medical data, DL proves to be an invaluable tool, offering a paradigm shift in how medical professionals access, analyze, and leverage the wealth of information embedded in medical images [3]. The integration of DL into CBMIR not only addresses the challenges posed by the sheer volume of data but also opens avenues for novel insights, early disease detection, and personalized treatment strategies. As we embark on this exploration, it is evident that the combination of medical imaging and DL is poised to redefine the landscape of healthcare, paving the way for more precise diagnoses, timely interventions, and improved patient outcomes [4].

DL can automatically obtain hierarchical representations from images and provide a compelling solution to the complex task of CBMIR. By leveraging Convolutional Neural Network (CNN) and other sophisticated architectures, DL models can discern subtle patterns and relationships within medical images that may elude traditional retrieval methods [5]. The synergy between the depth of neural networks and the intricacies of medical image content enables the extraction of high-level features crucial for accurate retrieval and analysis. Heterogeneity of imaging modalities, ranging from X-rays and MRIs to CT scans and beyond [6] is a serious issue. DL algorithms, through transfer learning and domain adaptation, demonstrate their adaptability to diverse imaging sources, promising a unified framework for efficient retrieval across modalities [7].

Autoencoders, with their capacity to learn compact and informative representations of input data, are examined for their utility in extracting latent features from medical images [8]. Whether applied to X-rays, MRIs, or CT scans, autoencoders demonstrate their versatility in capturing intrinsic features, thereby enhancing the robustness of CBMIR systems across a spectrum of medical image types. An in-depth discussion on the potential synergy between autoencoders and other DL architectures, such as CNN, is presented [9]. The combination of these models provides a comprehensive

framework for medical image retrieval, where autoencoders contribute to feature extraction and CNNs leverage these extracted features for accurate CBMIR. Furthermore, the paper addresses the interpretability of autoencoder-based models, highlighting how the encoded representations can be harnessed for visualizing and understanding the salient features within medical images [10]. This interpretative aspect not only fosters trust in the model's decision-making process but also facilitates the identification of clinically relevant patterns that may elude traditional CBMIR techniques. The major contribution of the proposed work includes:

- Integration of two powerful techniques, autoencoder and CNN, to tackle content-based retrieval of multimodal medical images.
- Provides a solution to efficiently search and retrieve images based on their content, enabling better diagnosis, treatment planning, and research in healthcare.
- Enhances retrieval accuracy and efficiency compared to traditional methods by leveraging deep learning techniques.

II. LITERATURE REVIEW

CBMIR witnessed transformative advancements with the integration of DL techniques. In the area of multimodal image representation, the effective retrieval of relevant medical images plays a pivotal role in ensuring accurate and timely diagnoses. This survey examines the recent developments and contributions of DL methods, specifically focusing on CBMIR for multimodal diagnosis images.

Ozturk [11] introduced an approach for radiological image retrieval by employing deep features extracted through CNN. The study demonstrates an enhancement in retrieval performance, showcasing the potential of DL in streamlining radiological diagnosis. The automated feature extraction process proves crucial in improving the efficiency of the diagnostic workflow, providing valuable insights for the integration of DL in medical imaging applications. Liu et al. [12] propose an innovative technique utilizing autoencoder architectures for feature extraction in cross-modality image retrieval. The research highlights the versatility of autoencoders in handling various medical imaging modalities, showcasing improved performance and robustness. By minimizing misinformation, this work contributes significantly to the reliability and accuracy of cross-modality image retrieval, offering potential advancements in diagnostic capabilities across diverse imaging technologies. Cai et al. [13] conducted a comprehensive comparative analysis of multiple CNN architectures for medical image retrieval. The findings reveal substantial variations in retrieval accuracy based on the selected network architecture, providing critical insights for practitioners in choosing optimal models for specific medical imaging applications. This study underscores the influence of network architecture on the performance of medical image retrieval systems, aiding informed decision-making for the development and implementation of DL technologies in clinical settings.

Li et al. [14] analyzed the robustness of CNN-based autoencoders in the realm of CBMIR. The study evaluates the performance of these models across various medical imaging modalities and assesses their ability to handle noisy or low-quality images. By investigating the robustness of CNN-based autoencoders, the research contributes valuable insights into the reliability of these models in real-world clinical scenarios. The findings provide guidance on the potential challenges and opportunities in deploying such models for CBMIR applications. Guan et al. [15] concentrate on improving the interpretability of features extracted by CNN in CBMIR. The study introduces methodologies for visualizing and understanding critical features, enhancing transparency in the decision-making process. This research marks a crucial step toward building trust in DL models and refining their interpretative capabilities for real-world medical applications. Shen et al. [16] explored the application of federated learning for privacy-preserving CBMIR. This research underscores the potential of federated learning in maintaining data security while advancing CBMIR capabilities.

Liu et al. [17] focused on investigating semi-supervised DL approach in CBMIR. This work demonstrates the potential of leveraging unlabeled data to enhance model performance, addressing challenges associated with limited labeled datasets. By incorporating semi-supervised learning, the study contributes to the adaptability of CBMIR systems across diverse clinical scenarios. Bouchareb et al. [18] delve into ethical considerations associated with AI-driven diagnostic imaging. The study emphasizes transparency, accountability, and the mitigation of biases in the deployment of DL models for diagnostic purposes. By addressing ethical concerns, this research contributes to responsible AI practices in the evolving landscape of CBMIR. Swati et al. [19] provide a broader perspective by exploring applications of DL in precision medicine for medical imaging. The study highlights the potential for personalized treatment strategies based on CBMIR results, showcasing the transformative impact of DL in tailoring medical interventions to individual patient needs. Jaiswal et al. [20] focused on exploring the applications of transfer learning in the context of CBMIR. By adapting knowledge learned from one domain to another, transfer learning proves to be a valuable strategy for addressing challenges associated with limited labeled medical image datasets. The study provides insights into the potential of transfer learning to improve the generalization capabilities of DL models in the medical imaging domain. This research contributes to the ongoing efforts in making medical image retrieval systems more adaptable and effective in diverse clinical settings.

This review showcased the evolution of CBMIR in multimodal diagnosis, emphasizing the transition from traditional CBMIR to sophisticated DL models. The integration of CNN-based Autoencoders presents a promising avenue for addressing challenges in feature extraction and enhancing overall performance. This research continues to explore innovative methodologies and datasets to advance the capabilities of DL in CBMIR for multimodal diagnosis.

III. MATERIALS AND METHODS

In this research, we present a novel CBMIR system designed specifically for multimodal diagnosis images associated with various diseases. Our primary focus is to overcome limitations identified in previous studies, and to achieve this, we employ the CNN-based autoencoder methodology. The rationale behind adopting the CBMIR approach lies in its demonstrated efficacy in optimizing both the feature extraction process and the learning phase. This strategic utilization aims to rectify and minimize inaccuracies that may have been prevalent in earlier research endeavors. The CNN-based Autoencoder method plays a crucial role in

amending misinformation issues that might have arisen in the feature extraction process during previous studies. By leveraging the power of DL, this approach not only refines the accuracy of feature extraction but also contributes to an overall improvement in the system's performance in essence; this research positions the CBMIR system, enhanced by the CNN-based autoencoder method, as a robust solution for retrieving multimodal diagnosis images. By addressing and mitigating misinformation concerns, we aim to contribute to the advancement of CBMIR methodologies, fostering precision and reliability in the context of subclass dataset categorization. The process flow of proposed methodology is depicted in Fig. 1.

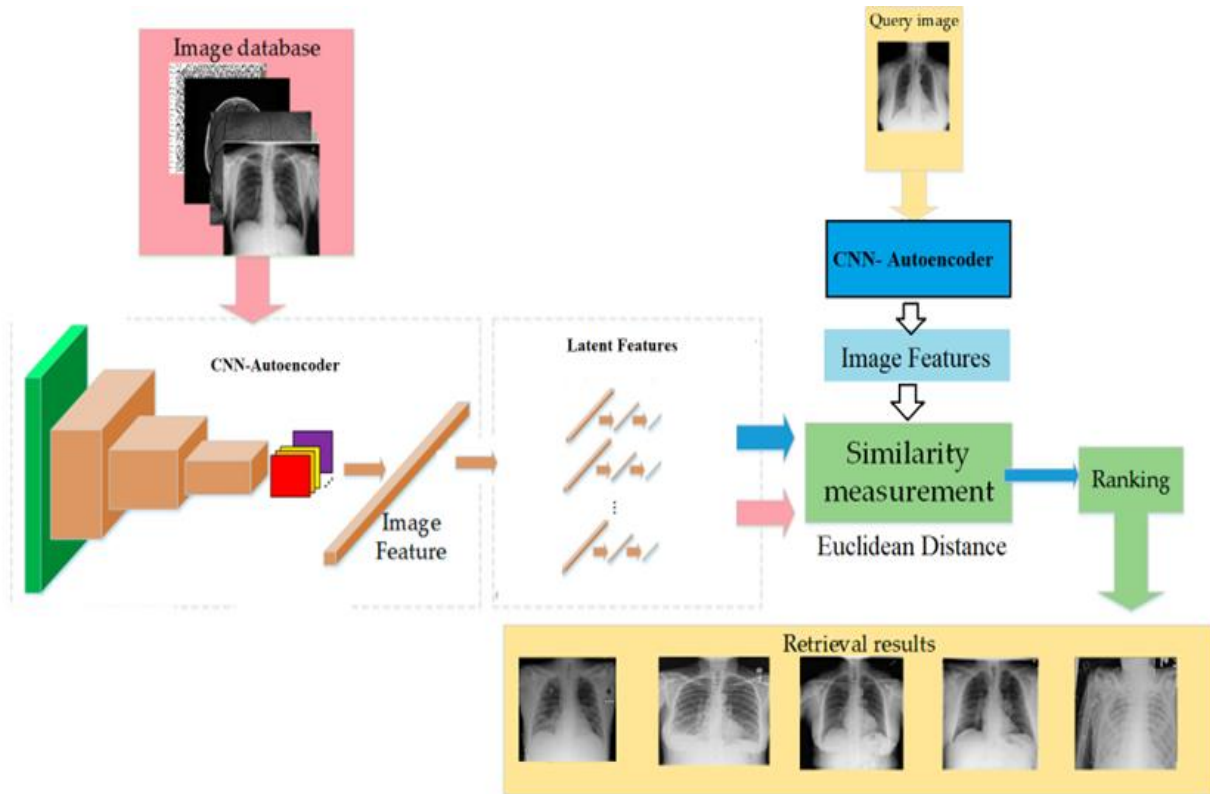


Fig. 1. Basic block diagram of proposed method.

A. Dataset Description

The dataset comprising around 50,000 2D images, sourced from diverse and easily accessible open-access medical databases like ImageNet. The primary objective of this compilation is to enable the differentiation among Magnetic Resonance Imaging (MRI), X-ray Electroencephalograph (EEG), and OCT. ImageNet stands as a vast image repository that has played a pivotal role in propelling forward the realms of computer vision and DL research. Notably, the dataset encompasses images of varying data sizes, providing a comprehensive and diverse set of examples for training and evaluation purposes in the context of multimodal medical image analysis. The dataset has been categorized into four primary classes, encompassing X-ray, MRI, OCT, and EEG modalities. A visual representation of a sample image from the dataset, utilized in the present study, is depicted in Fig. 2. This division into distinct classes serves as a foundational structure

for the dataset, facilitating a nuanced exploration and analysis of varied medical imaging modalities.

B. Proposed Model Architecture

The Autoencoder process involves three key stages: Encoder, Decoder, and the computation of the Calculating Function and Optimization Errors. During the encoding phase, input data undergoes a transformation into smaller dimensions, often referred to as compression. Employing Conv2D (2D Convolution Layer), the input image is transformed to 48 nodes (latent dimension). This latent representation must then be converted back to initial state. Decoding process utilizes transpose operation to generate the reconstructed image. Loss calculation for each function is iteratively performed to determine the function with the lowest loss value. In this research, the selected loss function is Mean Square Error (MSE). Fig. 3 illustrates the structure of designed autoencoder.

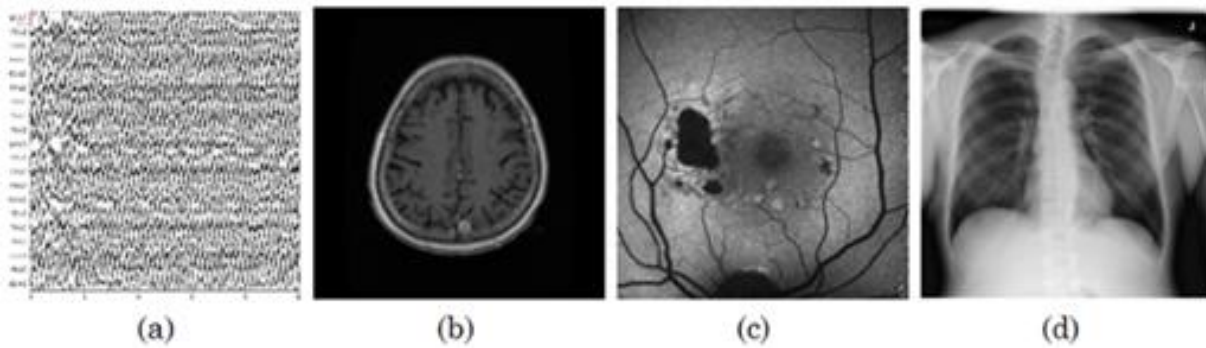


Fig. 2. Sample images from dataset (a) EEG, (b) MRI, (c) OCT, (d) X-Ray.

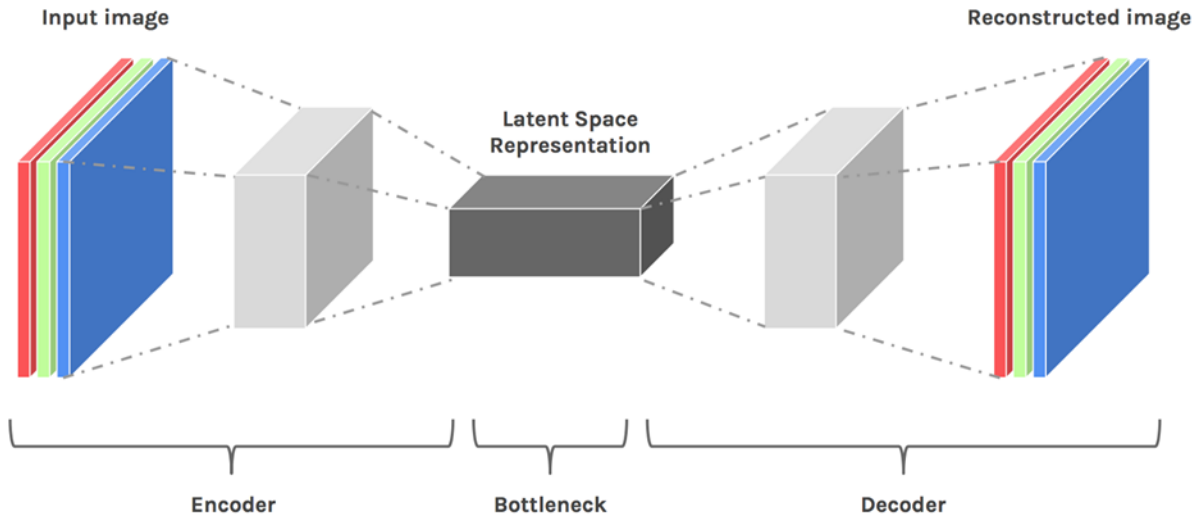


Fig. 3. Structure of the proposed autoencoder.

The commencement of the training process in this investigation involves segregating images into three subsets: training (80%), validation (10%), and testing (10%). Employing the CNN- Autoencoder model, the original image is transformed into a reconstructed image. The Autoencoder involve in the extraction of output image to reconstruct the input image, facilitating a comparison with the original input

image [21]. Following this, the learning process initiates, and through numerous iterations, the optimal model is obtained and saved, featuring the lowest loss value in relation to the extraction and retrieval stages. The training data includes the segmented data for training, while the validation data evaluates the developed model. Additional explanation of phases in the training process is provided in Fig. 4.

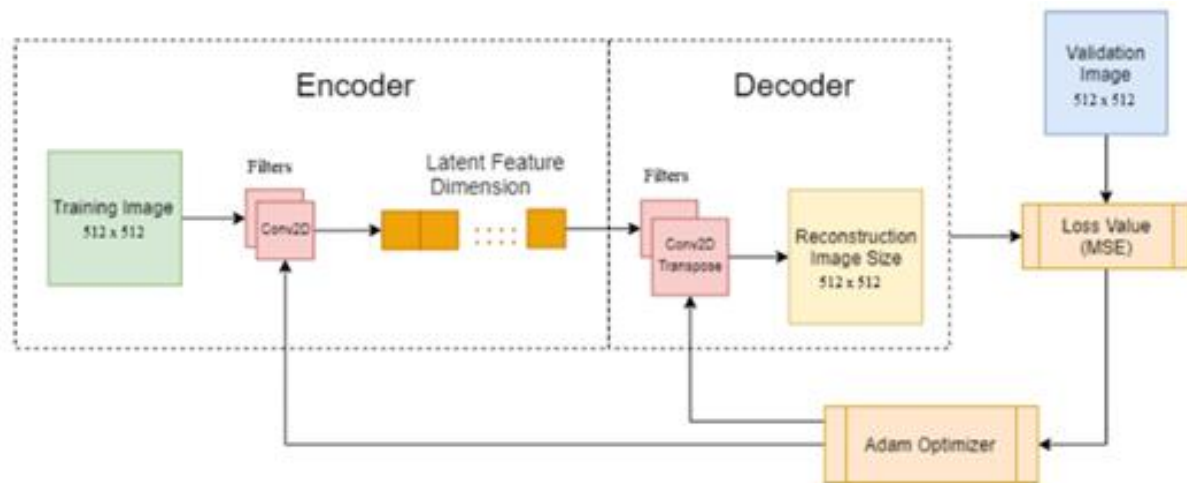


Fig. 4. Process flow of training.

During the encoder stage, the input data undergoes compression. Conv2D, with modified default parameters, employs a stride of 2 for convolution, along with "same" padding value. This ensures even distribution of zero-value padding convolution. With 128 filters having 3x3 kernels, Leaky Relu is applied, which is recognized for its effectiveness in overcoming gradient loss issues in DL. Leaky Relu is preferred over its predecessors, sigmoid and Tanh, for its simplicity and improved performance [22]. The Leaky Relu function is defined by the following equation.

$$f(x) = \begin{cases} x, & x \geq 0 \\ \alpha x, & x < 0 \end{cases} \quad (1)$$

The LeakyRelu activation function incorporates a parameter known as alpha, representing the negative slope coefficient, and in this study, it is set to 0.2.

In a parallel arrangement to the encoder, the decoder employs a convolution method with 128 filters and a filter having 3x3 kernels, maintaining the same activation function but with a distinct approach to processing. The decoder employs transposed data from the latent dimension to produce the reconstructed image. Upon the conclusion of both the encoder and decoder stages, the procedure progresses to the error calculation and optimization phase. In this phase, iterative loss calculations are performed for each function, aiming to pinpoint the function with the minimum loss value [23]. The chosen loss function for this study is the Mean Square Error (MSE), calculated through Eq. (2). Here, p_i is the predicted image and y_i is the actual image.

$$MSE = \frac{1}{n} \sum_{i=1}^n (p_i - y_i)^2 \quad (2)$$

In the process of optimizing CNNs, the weighted values and biases of the convolutional layers undergo updates through the utilization of the Adam's algorithm. This algorithm, known for its efficiency in optimization tasks, plays a crucial role in adjusting these parameters. To initiate the learning process, a standard learning rate of 1e-3 is employed, serving as a foundational value for the optimization algorithm. Moreover, a learning rate scheduler is integrated into the training procedure, incorporating a decay parameter set at a rate of 2e-5. This scheduler dynamically adjusts the learning rate during the training epochs, enabling a gradual decrease in the learning rate over time. This adaptive learning rate scheduling contributes to the model's stability and convergence during the optimization process. By leveraging these techniques, the convolutional layers continually adapt their weighted values and biases to improve its ability to obtain meaningful features. The thoughtful integration of optimization strategies, such as the Adam's optimization algorithm and learning rate scheduling, is essential for achieving robust and effective performance in CNN training.

Feature extraction involves the retrieval of distinctive attributes from an image, which are subsequently scrutinized for subsequent processes. Following this, the acquired features are recognized to establish distinctions between images [24]. As depicted in Fig. 5, extraction of features is executed by utilizing the stored optimal model.

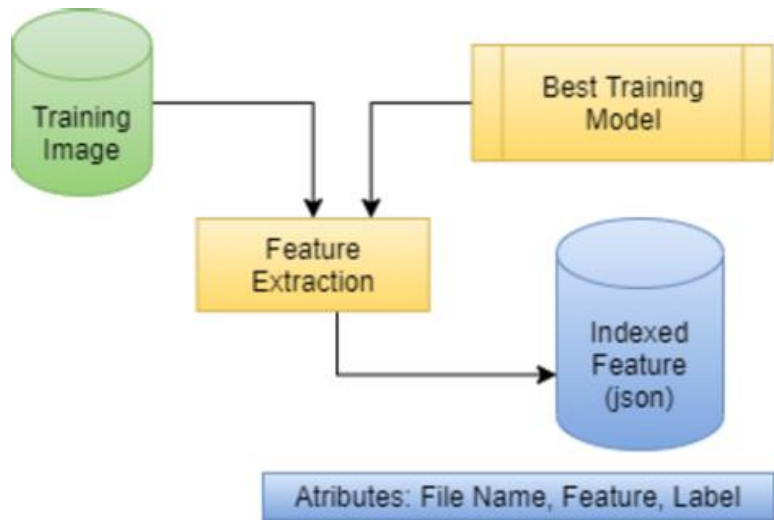


Fig. 5. Feature extraction process.

The outcomes of this feature extraction process are systematically cataloged to create a ".json" (JavaScript Object Notation) file. This file not only includes the extracted features but also incorporates the image file names and labels associated with each image. The compilation of annotated images serves as a comprehensive database, pivotal for subsequent comparisons during the retrieval stage.

C. Image Retrieval

The retrieval process involves seeking identical images with reference to query image. The data, previously segregated

into test data, undergoes feature extraction, mirroring the procedure in the preceding stage. Following the successful extraction of images, calculations ensue to determine the resemblances of features in test images and those indexed in the training set, saved in the ".json" file. In this work, the Euclidean Distance is specifically applied to quantify the distance similarity between two image vectors. A detailed depiction of the retrieval process is provided in Fig. 6.

Euclidean Distance is utilized for efficiently calculating the similarity distance between two vectors, irrespective of

their dimensionality—be it two-dimensional, three-dimensional, or beyond [25]. The comparison of the two feature vectors extracted from the features involves calculating the distance between them. This meticulous process ensures a robust evaluation of the similarity between images, employing a widely recognized distance calculation method within the domain of image retrieval. The Euclidean Distance is expressed through the following equation, frequently employed for measuring the distance between vectors [26]. Here d_e is the Euclidean distance, q_i is the vector query image and b_i is the vector present in train data.

$$d_e = \sqrt{\sum_{i=1}^n (q_i - b_i)^2} \quad (3)$$

Following the computation of distances between each image in the test data and all images within the training data, the resulting distance values are subjected to comparison. A smaller Euclidean value indicates a higher degree of similarity between images. As a result, the image possessing the smallest distance value is included in the retrieval process. In essence, this retrieval methodology prioritizes images that exhibit the closest proximity in terms of features, as quantified by the Euclidean distance. The selection of the top five most similar images enhances the comprehensiveness and accuracy of the retrieval process, providing a nuanced understanding of image similarity.

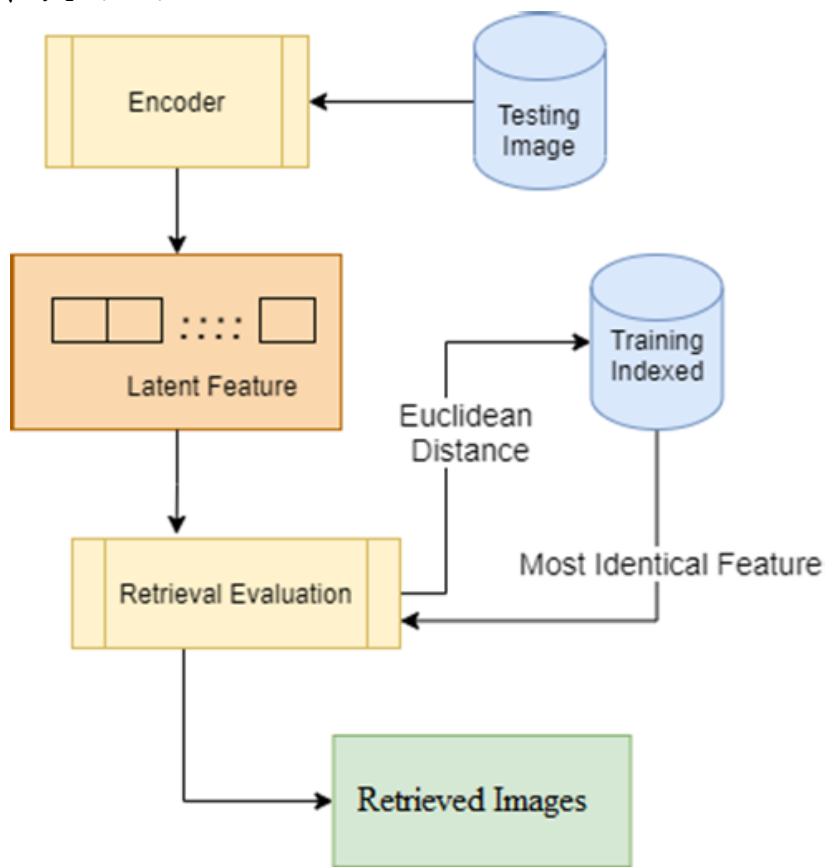


Fig. 6. Image retrieval process.

IV. RESULTS AND DISCUSSION

The evaluation stage is crucial in assessing the effectiveness of the system developed within this research [27]. Precision and recall metrics are actively employed to gauge the success rate of the system, providing insightful measures of its performance. Initially, the retrieval process flow begins by taking an image from the test data as input. Utilizing the saved encoder model from the training phase, the system generates latent features and proceeds to the retrieval evaluation stage. In this stage, Euclidean distances are calculated based on the indexed .json file, employing information obtained from the previous feature extraction process flow. The ultimate output of this process includes precision and recall values, which serve as key indicators of the system's retrieval performance. Eq. (4) and (5) outline the formulas employed for calculating

precision and recall in this context. Here I_r represents the count of retrieved images, n represents the count of images captured and M denotes relevant images present in the database.

$$Precision = \frac{I_r}{n} \quad (4)$$

$$Recall = \frac{I_r}{M} \quad (5)$$

As depicted in Fig. 7, the training phase during the testing of the dataset in all categories exhibits a gradual reduction in loss values up to epoch 35. The cumulative results across all categories yield loss values below 0.2, indicating a successful retrieval process. This signifies the efficacy of the training process in minimizing errors, enabling a robust and accurate retrieval of images across various imaging modalities.

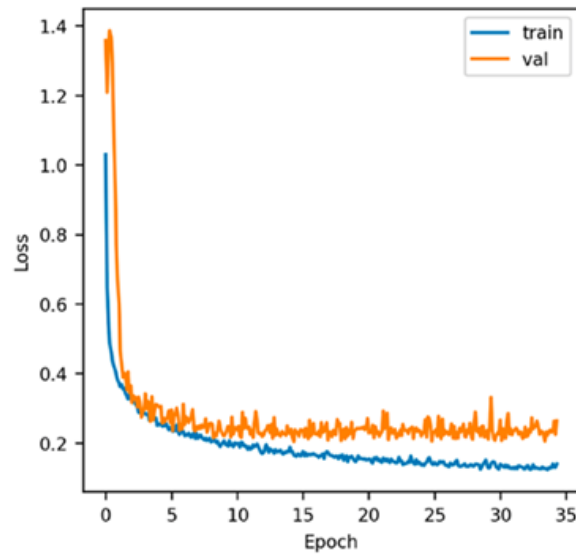


Fig. 7. Loss plot of proposed model.

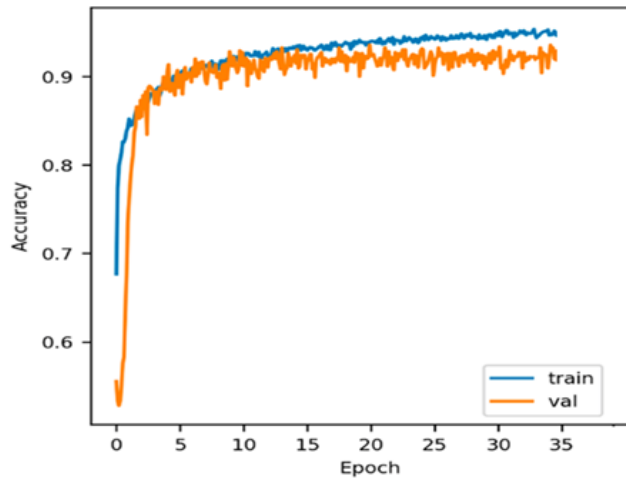


Fig. 8. Accuracy plot of proposed model.

As illustrated in Fig. 8, the training phase showcases a steady rise in accuracy values for all categories up to the 5th epoch, maintaining a consistent level thereafter. The collective outcomes across all categories yield an accuracy value surpassing 94%, underscoring the success of the retrieval process. This highlights the effectiveness of the training process in minimizing errors, facilitating a resilient and precise retrieval of images across diverse imaging modalities.

Upon conducting image retrieval using the implemented CBMIR model, the evaluation process provides crucial insights into the system's effectiveness, quantified through accuracy, precision and recall values. These metrics serve as key indicators of the system's ability to accurately retrieve relevant medical images based on content. The comparison of system performance involves assessing the proposed CBMIR system against varying number of retrieved images. This comparative analysis is conducted separately for each dataset category, with the results meticulously tabulated in Table I.

The evaluation results presented in Table I affirm that CNN-autoencoder based CBMIR model has achieved notable

success in delivering suitable outcomes. The effectiveness of this model is demonstrated through its capability to enhance precision and recall values, signifying improvements in the accuracy and completeness of the image retrieval process. Overall, this evaluation adds empirical evidence to the merit of the proposed system in the context of CBMIR. Fig. 9 visually represents the performance of the CBMIR system proposed in this study.

TABLE I. PERFORMANCE EVALUATION

| Retrieved Images (IR) | Accuracy (%) | Precision (%) | Recall (%) |
|-----------------------|--------------|---------------|------------|
| 20 | 98.34 | 97.84 | 98.42 |
| 40 | 97.56 | 97.15 | 97.15 |
| 60 | 96.11 | 95.48 | 94.87 |
| 80 | 94.35 | 95.66 | 94.24 |
| 100 | 93.00 | 94.00 | 93.00 |

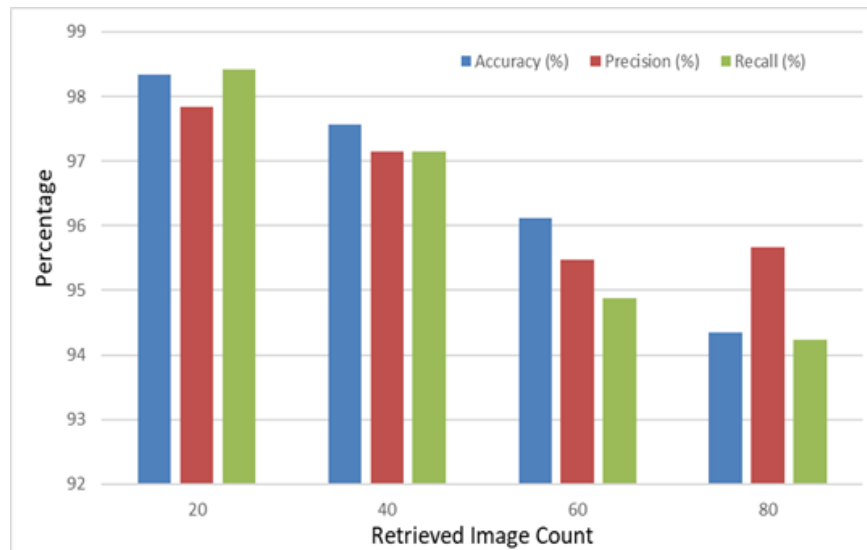


Fig. 9. Performance of proposed CBIMR model.

The evaluation outcomes reveal the effectiveness of the proposed approach, showcasing satisfactory performance with an average accuracy of 95.87%, precision of 96.03% and recall of 95.54%. Conversely, the results are comparatively optimal for all modalities of images in the dataset. Nevertheless, upon comparison with various parameters the performance gradually decreases while increasing the number of images to be retrieved.

To analyze the effectiveness of the constructed model, a thorough examination of their image retrieval performance is essential. The assessment of proposed CBIMR model's retrieval performance is conducted across multiple methodologies. The comparison of efficiency among existing models is presented in Table II, employing carefully chosen performance metrics,

TABLE II. PERFORMANCE COMPARISON WITH EXISTING METHODS

| Methodology | Accuracy (%) | Precision (%) | Recall (%) |
|-----------------|--------------|---------------|------------|
| DCNN | 88.42 | 87.48 | 88.62 |
| AlexNet | 87.65 | 87.51 | 87.75 |
| VGG16 | 92.34 | 91.84 | 93.14 |
| ResNet50 | 93.74 | 92.27 | 92.57 |
| Proposed Method | 95.87 | 96.03 | 95.54 |

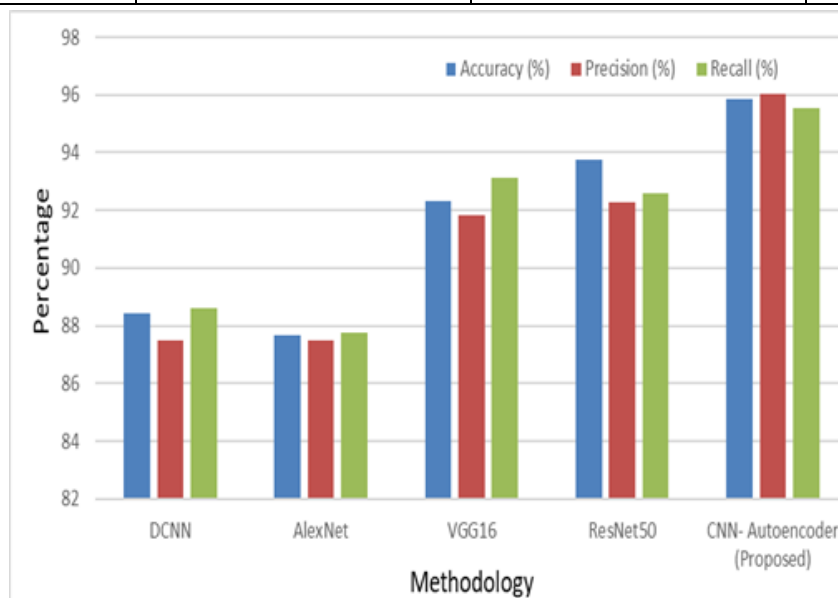


Fig. 10. Performance comparison.

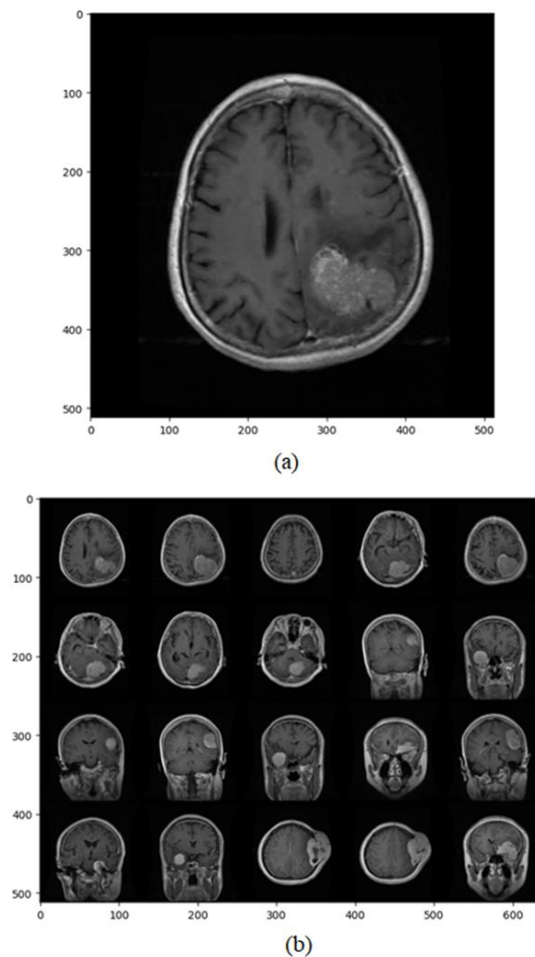


Fig. 11. Experimental results (a) Query image, (b) Retrieved images.

In the assessment of retrieval accuracy, the proposed CNN-autoencoder model distinguishes itself with an impressive score of 95.87%. Among the pre-trained models, VGG16 attains an accuracy rate of 92.34%, ResNet50 achieves 93.74%, and AlexNet displays an accuracy of 87.65%. Notably, the proposed model outperforms its nearest competitor, the ResNet50 model, by a notable margin, achieving a superior accuracy that is 2.13% higher. Moving to precision, the proposed CNN-autoencoder model excels with an impressive precision rate of 96.03%. In contrast, ResNet50 achieves 92.27% precision, VGG16 records 91.84%, and AlexNet obtains 87.51%. Fig. 10 provides a visual assessment of proposed model with state-of-the-art CBMIR models.

The precision of the proposed model surpasses that of the ResNet50 model by 3.76%, reinforcing its superiority. Proposed CNN-autoencoder achieves an exceptional recall value of 95.54%, outperforming all other models in this metric. In comparison, VGG16 achieves a recall rate of 93.14%, ResNet50 reached 92.57%, and AlexNet also records 87.75% in recall. Notably, the proposed model's recall surpasses the ResNet50 model by a significant margin of 2.97%, highlighting its superiority in retrieving relevant images. The proposed model demonstrates highest accuracy in medical image retrieval. For the visual evaluation of the proposed

model the retrieval result obtained from the proposed model is illustrated in Fig. 11.

V. CONCLUSION

This research work introduced an innovative approach CBMIR specifically tailored for multimodal diagnosis images. Leveraging the CNN-based autoencoder method, the proposed system incorporates a learning process. This learning process is strategically designed to mitigate misinformation during the feature extraction phase, aiming to refine and improve upon the performance observed in previous works. This method is intended to overcome challenges associated with feature extraction and subsequently enhance the overall efficiency of CBMIR. By applying a learning mechanism within the autoencoder framework, the system adapts and refines its ability to accurately represent and extract meaningful features from multimodal diagnosis images. The results obtained from the evaluation of this method demonstrate notable average accuracy of 95.87%, precision of 96.03% and recall of 95.54%. This work contributes to the advancing field of CBMIR. The proposed system stands out for its ability to harness DL methodologies to address challenges in feature extraction, thereby achieving superior performance in comparison to existing methods.

ACKNOWLEDGMENT

I would like to express my sincere gratitude to all those who contributed to the completion of this research paper. I extend my heartfelt thanks to my supervisor, my family, my colleagues and fellow researchers for their encouragement and understanding during the demanding phases of this work.

REFERENCES

- [1] Qayyum, A., Anwar, S. M., Awais, M., & Majid, M. (2017). Medical image retrieval using deep convolutional neural network. *Neurocomputing*, 266, 8-20.
- [2] Li, Z., Zhang, X., Müller, H., & Zhang, S. (2018). Large-scale retrieval for medical image analytics: A comprehensive review. *Medical image analysis*, 43, 66-84.
- [3] Dubey, S. R., Singh, S. K., & Singh, R. K. (2016). Multichannel decoded local binary patterns for content-based image retrieval. *IEEE transactions on image processing*, 25(9), 4018-4032.
- [4] Anwar, S. M., Majid, M., Qayyum, A., Awais, M., Alnowami, M., & Khan, M. K. (2018). Medical image analysis using convolutional neural networks: a review. *Journal of medical systems*, 42, 1-13.
- [5] Ker, J., Wang, L., Rao, J., & Lim, T. (2017). Deep learning applications in medical image analysis. *Ieee Access*, 6, 9375-9389.
- [6] Wang, G., Li, W., Zuluaga, M. A., Pratt, R., Patel, P. A., Aertsen, M., ... & Vercateren, T. (2018). Interactive medical image segmentation using deep learning with image-specific fine tuning. *IEEE transactions on medical imaging*, 37(7), 1562-1573.
- [7] Suzuki, K. (2017). Overview of deep learning in medical imaging. *Radiological physics and technology*, 10(3), 257-273.
- [8] Quellec, G., Cazuguel, G., Cochener, B., & Lamard, M. (2017). Multiple-instance learning for medical image and video analysis. *IEEE reviews in biomedical engineering*, 10, 213-234.
- [9] Xia, Z., Wang, X., Zhang, L., Qin, Z., Sun, X., & Ren, K. (2016). A privacy-preserving and copy-deterrence content-based image retrieval scheme in cloud computing. *IEEE transactions on information forensics and security*, 11(11), 2594-2608.
- [10] Wei, X. S., Luo, J. H., Wu, J., & Zhou, Z. H. (2017). Selective convolutional descriptor aggregation for fine-grained image retrieval. *IEEE transactions on image processing*, 26(6), 2868-2881.
- [11] Ozturk, S. (2020). Stacked auto-encoder based tagging with deep features for content-based medical image retrieval. *Expert Systems with Applications*, 161, 113693.
- [12] Liu, X., Wang, M., Zha, Z. J., & Hong, R. (2019). Cross-modality feature learning via convolutional autoencoder. *ACM Transactions on Multimedia Computing, Communications, and Applications (TOMM)*, 15(1s), 1-20.
- [13] Cai, Yiheng, et al. "Medical image retrieval based on convolutional neural network and supervised hashing." *IEEE access* 7 (2019): 51877-51885.
- [14] Li, S., Dai, W., Zheng, Z., Li, C., Zou, J., & Xiong, H. (2021). Reversible autoencoder: A CNN-based nonlinear lifting scheme for image reconstruction. *IEEE Transactions on Signal Processing*, 69, 3117-3131.
- [15] Guan, A., Liu, L., Fu, X., & Liu, L. (2022). Precision medical image hash retrieval by interpretability and feature fusion. *Computer Methods and Programs in Biomedicine*, 222, 106945.
- [16] Shen, Z., Ding, F., Yao, Y., Bhardwaj, A., Guo, Z., & Yu, K. (2022). A privacy-preserving social computing framework for health management using federated learning. *IEEE Transactions on Computational Social Systems*.
- [17] Liu, Quande, et al. "Semi-supervised medical image classification with relation-driven self-ensembling model." *IEEE transactions on medical imaging* 39.11 (2020): 3429-3440.
- [18] Bouchareb, Y., Khaniabadi, P. M., Al Kindi, F., Al Dhuhli, H., Shiri, I., Zaidi, H., & Rahmim, A. (2021). Artificial intelligence-driven assessment of radiological images for COVID-19. *Computers in biology and medicine*, 136, 104665.
- [19] Swati, Z. N. K., Zhao, Q., Kabir, M., Ali, F., Ali, Z., Ahmed, S., & Lu, J. (2019). Content-based brain tumor retrieval for MR images using transfer learning. *IEEE Access*, 7, 17809-17822.
- [20] Jaiswal, A., Gianchandani, N., Singh, D., Kumar, V., & Kaur, M. (2021). Classification of the COVID-19 infected patients using DenseNet201 based deep transfer learning. *Journal of Biomolecular Structure and Dynamics*, 39(15), 5682-5689.
- [21] Chen, M., Shi, X., Zhang, Y., Wu, D., & Guizani, M. (2017). Deep feature learning for medical image analysis with convolutional autoencoder neural network. *IEEE Transactions on Big Data*, 7(4), 750-758.
- [22] Liu, Y., Wang, X., Wang, L., & Liu, D. (2019). A modified leaky ReLU scheme (MLRS) for topology optimization with multiple materials. *Applied Mathematics and Computation*, 352, 188-204.
- [23] Li, D., Deng, L., Gupta, B. B., Wang, H., & Choi, C. (2019). A novel CNN based security guaranteed image watermarking generation scenario for smart city applications. *Information Sciences*, 479, 432-447.
- [24] Maksoud, E. A. A., Barakat, S., & Elmogy, M. (2019). Medical images analysis based on multilabel classification. In *Machine Learning in Bio-Signal Analysis and Diagnostic Imaging* (pp. 209-245). Academic Press.
- [25] Patel, S. P., & Upadhyay, S. H. (2020). Euclidean distance based feature ranking and subset selection for bearing fault diagnosis. *Expert Systems with Applications*, 154, 113400.
- [26] Prasetyo, H., & Akardihas, B. A. P. (2019). Batik image retrieval using convolutional neural network. *Telkomnika (Telecommunication Computing Electronics and Control)*, 17(6), 3010-3018.
- [27] Alsmadi, M. K. (2020). Content-based image retrieval using color, shape and texture descriptors and features. *Arabian Journal for Science and Engineering*, 45(4), 3317-3330

Optimizing Bug Bounty Programs for Efficient Malware-Related Vulnerability Discovery

Semi Yulianto¹, Benfano Soewito², Ford Lumban Gaol³, Aditya Kurniawan⁴
Computer Science Department, BINUS Graduate Program – Doctor of Computer Science,
Bina Nusantara University, Jakarta 11480, Indonesia

Abstract—Conventional security measures struggle to keep pace with the rapidly evolving threat of malware, which demands novel approaches for vulnerability discovery. Although Bug Bounty Programs (BBPs) are promising, they often underperform in attracting researchers, particularly in uncovering malware-related vulnerabilities. This study optimizes BBP structures to maximize engagement and target malware vulnerability discovery, ultimately strengthening cyber defense. Employing a mixed-methods approach, we compared public and private BBPs and analyzed the key factors influencing researcher participation and the types of vulnerabilities discovered. Our findings reveal a blueprint for effective malware-focused BBPs that enable targeted detection, faster patching, and broader software coverage. This empowers researchers and fosters collaboration within the cybersecurity community, significantly reducing the attack surface for malicious actors. However, challenges related to resource sustainability and legal complexity persist. By optimizing BBPs, we unlocked a powerful tool to fight cybercrime.

Keywords—Bug bounty; malware; vulnerability discovery; cyber defense

I. INTRODUCTION

Securing software systems is a crucial challenge in today's fast-changing digital environment. The effective management and discovery of vulnerabilities are significantly enhanced by strategic resource allocation [1]. In parallel, bug bounty programs have become a crucial component of cybersecurity, leveraging the collective global expertise of security researchers to identify and mitigate threats and provide incentives for their discoveries [2]. These programs also raise substantial ethical questions related to the monetization of cybersecurity vulnerabilities, necessitating an analysis of the associated moral implications [3]. Additionally, this study explored the characteristics of security bugs, which are critical for establishing a robust vulnerability management framework [4]. The efficacy of bug bounty programs has also been assessed in specific fields, such as blockchain technology, by evaluating their influence in these newer areas [5]. This introduction sets the stage for our examination of the delicate interplay between technical solutions and ethical considerations in managing software vulnerability.

The persistent threats posed by malware highlight the need for advanced vulnerability discovery techniques. Conventional security measures often fail to keep pace with the creativity of cyber threats, prompting the adoption of Bug Bounty Programs (BBPs) as of independent an effective alternative. These programs harness the expertise security researchers to find

hidden vulnerabilities, yet questions remain about their effectiveness against malware-specific threats owing to the diverse structures and ecosystems in which they operate. Our study undertakes a thorough investigation of how the key elements of BBPs affect both the participation of researchers and the success of discovering vulnerabilities within the context of malware.

Our study highlights the challenges in attracting and retaining skilled researchers for BBPs driven by competitive pressures and inadequate reward systems, especially for intricate malware-related vulnerabilities. Additionally, the difficulty in identifying and prioritizing these vulnerabilities is exacerbated by the general lack of malware analysis expertise among program administrators and the complex nature of replicating attack chains. We also address the narrow scope of many BBPs and the difficulties in measuring their overall security impact, which hinders their ability to secure continuous support and funding. Our objective is to devise BBP strategies informed by malware analysis expertise, promote the reporting of malware-related vulnerabilities, and strengthen cybersecurity defenses.

Targeted bug bounty programs are expected to enhance malware detection by facilitating quicker identification and resolution of critical vulnerabilities, thus reducing opportunities for cyber-attackers. These programs are projected to bolster cyber defenses, as our findings could enhance threat intelligence and foster collaboration among researchers, platforms, and vendors, thereby creating a unified cybersecurity strategy. Furthermore, optimized BBPs are likely to offer cost-effectiveness and support the development of a community and standards within the cybersecurity field.

The remainder of this paper is organized as follows. In Section II, we provide an overview of the existing research on malware threats, conventional security measures, and the role of bug bounty programs in cybersecurity. The methodology in Section III outlines our study's approach and data collection methods, followed by the Results in Section IV, which presents empirical findings related to researcher participation and vulnerability discovery within the context of malware. In Section V, we interpret the results, discuss implications for cybersecurity practice and policy, and address limitations and avenues for further research. Finally, the conclusion summarizes the main findings and their significance, while the future work in Section VI identifies areas for future research and proposes potential research agendas or methodologies to address emerging challenges in malware detection and vulnerability discovery.

II. LITERATURE REVIEW

The rapidly evolving landscape of cybersecurity has necessitated innovative approaches to identifying and mitigating vulnerabilities, with Bug Bounty Programs (BBPs) emerging as a pivotal strategy. These programs incentivize ethical hackers to report software vulnerabilities and offer a unique blend of monetary and reputational rewards. This Literature Review in Section II delves into the multifaceted dimensions of BBPs, exploring their design, effectiveness, and intricate motivations of security researchers who participate in them. Drawing upon a diverse array of studies, we examine how BBPs serve as critical tools not only for enhancing digital security but also for fostering a proactive cybersecurity culture. Furthermore, we extend our focus to the specific realm of malware-related vulnerabilities, identify gaps in the current research, and underscore the potential of BBPs to address these challenges. Through a mixed-methods research lens, this review aims to provide a comprehensive overview of BBPs' impact of BBPs on software security, researcher engagement, and the broader cybersecurity ecosystem.

A. General Bug Bounty Program (BBP) Effectiveness and Design

Bug bounty programs have gained recognition as an effective strategy for organizations to encourage ethical hackers to report security vulnerabilities in their software. These programs aim to incentivize hackers to share vulnerabilities with legitimate organizations for monetary and reputational rewards as alternatives to selling or exploiting these vulnerabilities. By offering rewards to users reporting security vulnerabilities, bug bounty programs can effectively improve the security of digital technology platforms. Furthermore, bug bounty programs have been shown to enhance system reliability by optimally allocating resources to discover software vulnerabilities [1]. In addition, they allow developers to discriminate between different types of bugs, thus helping avoid the reputation costs of exploited bugs [2].

Bug bounty programs typically follow a crowdsourcing model in which there is an open call for people to anonymously test software [3]. However, bug bounty programs can be further improved by focusing on strategies that enhance their effectiveness [1]. It is essential to design bug bounty programs that consider the characteristics of security bugs, as effective tools for detecting and fixing software security bugs require a deep understanding of their characteristics [4].

Bug bounty programs have proven to be an effective means for organizations to incentivize ethical hackers to report security vulnerabilities in their software. They offer a valuable alternative to selling or exploiting vulnerabilities, and can significantly enhance the security and reliability of digital technology platforms.

B. Bug Bounty Programs (BBPs) and Vulnerabilities Related to Malware

Bug Bounty Programs (BBPs) have emerged as a crucial strategy for organizations to identify and address software vulnerabilities. These programs incentivize ethical hackers to report software security vulnerabilities, thereby allowing organizations to address these issues before they are exploited

[5]. Bug bounty programs offer monetary and reputational rewards to hackers who share vulnerabilities with legitimate organizations, thereby deterring them from selling or exploiting these vulnerabilities [6]. For instance, Fiat Chrysler Automobiles collaborated with a San Francisco-based company to launch a bug-bounty program, offering rewards to individuals who identify unknown vulnerabilities in connected autonomous vehicle (CAVs) software [7]. Additionally, Trend Micro's Zero Day Initiative (ZDI) is recognized as the world's largest vendor-agnostic bug bounty program, working with researchers and vendors to disclose zero-day vulnerabilities and issue public advisories about vulnerabilities [8].

Bug bounty programs have been acknowledged as an effective means for organizations to enhance their security posture by encouraging grey-hat hackers to undertake unauthorized penetration testing and report vulnerabilities [9]. These programs also enable organizations to efficiently remediate vulnerabilities by providing a platform for responsible disclosure and negotiating rewards with vulnerability researchers [10]. Bug bounty programs not only complement existing security assessments performed by organizations but also allow for the discovery of hidden vulnerabilities, thereby contributing to improved software security ([11]; [12]). Furthermore, they have been proposed as solutions for agile software development teams that lack the necessary baseline level of security skills and awareness, thereby offering an avenue for penetration testing and vulnerability identification [13].

In the context of mobile security, bug bounty programs play a significant role in addressing vulnerabilities in mobile applications and operating systems, particularly in combating the latest mobile malware, such as mobile banking trojans, cryptocurrency mining, and ransomware ([14]; [15]). These programs are also likened to "red teams" in scientific research, where methodologists, statisticians, and subject-matter experts critique study designs and analyses, offering incentives akin to bug bounty programs in computer software development [16].

Bug Bounty Programs (BBPs) have become an integral part of organizations' cybersecurity strategies by providing mechanisms for identifying and addressing software vulnerabilities. These programs not only incentivize ethical hackers to report vulnerabilities but also contribute to the overall improvement of software security.

C. Researchers' Motivations and Behavior in BBPs

The motivations and behaviors of security researchers in Bug Bounty Programs (BBPs) have been a subject of interest in recent research. Xiong, Q., Zhu, Y., Zeng, Z., and Yang, X. (2023) found that security researchers are motivated to contribute to BBPs that offer higher remuneration rather than just programs with a higher likelihood of discovering vulnerabilities [17]. This aligns with the findings of Subramanian and Malladi (2020), who demonstrated that BBPs intensify price competition for new consumers [18]. Furthermore, Namli and Aybek (2022) highlighted the positive impact of block-based programming (BBP) on motivation and academic performance, indicating that BBPs can serve as a source of motivation for individuals [19].

Additionally, the literature suggests that BBPs have implications beyond individual motivation. Silomon, J., Hansel, M., & Schwartz, F. (2022) proposed further research to examine the effects of BBPs on peace and stability quantitatively, indicating the broader geopolitical and security implications of these programs [20]. Moreover, Walshe and Simpson (2023) emphasized the role of BBPs and Vulnerability Disclosure Programs (VDPs) in opening up organizations' assets to white-hat hackers, highlighting the collaborative nature of these programs and their potential impact on organizational security [21].

These findings collectively underscore the multifaceted nature of BBPs, encompassing individual motivation, market dynamics, educational implications, and broader security considerations. Therefore, understanding the motivations and behavior of researchers in BBPs requires a comprehensive approach that considers individual incentives and the wider impact of these programs.

D. Mixed-Methods Research in Security

Mixed-method research is increasingly recognized as a valuable approach to security. This approach uses qualitative and quantitative methods to understand complex security issues comprehensively. For instance, Zhou, L., Bao, J., Watzlaf, V., & Parmanto, B. (2019) focused on the barriers to and facilitators of mobile health app use from a security perspective using a mixed-methods approach to gather insights into computer security and confidentiality in mHealth [22]. Hassandoust and Johnston (2023) conducted a mixed-method study to develop a competency-driven security culture model for high-reliability organizations by integrating interviews and survey data to understand information security programs [23].

Veiga, A., Астахова, Л., Botha, A., & Herselman, M. (2020) explored the definition of organizational information security culture using a mixed-method approach, highlighting the value of integrating academic and industry perspectives [24]. These studies demonstrate the relevance of mixed-method research in addressing security challenges by providing a more comprehensive and nuanced understanding of security issues.

Additionally, mixed methods have been applied in various domains such as nephrology [25], health [26], accounting [27], and healthcare [28], indicating their versatility and applicability in different fields. Şahin and Ozturk (2022) acknowledged the strengths and weaknesses of mixed-methods approaches, emphasizing the need for a balanced consideration of qualitative and quantitative research methods [29].

Moreover, the potential of mixed-method research to understand complex phenomena, such as learning to theorize music [30] and evaluating security threats in cyber-physical systems [31], has been highlighted. This approach allows for a more holistic interpretation of research findings, enabling researchers to explore the relationships among different study elements [32].

Integrating qualitative and quantitative methods in mixed-methods research offers a robust framework for addressing security challenges by providing a deeper understanding of complex security issues and enhancing the validity and reliability of research findings.

E. Synthesis

Bug Bounty Programs (BBPs) incentivize ethical hackers to identify and report software vulnerabilities and boost their security. They offer rewards that lead to proactive discovery and responsible disclosure, ultimately improving software reliability. BBPs are valuable complements to conventional testing because they uncover hidden flaws. This study examines the motivations of security researchers, highlighting the significance of financial remuneration. Furthermore, BBPs have broader implications, impacting educational opportunities and organizational security. However, mixed-method research plays a crucial role in truly understanding BBPs' effectiveness of BBPs. It helps to explore the complex relationships among program design, researcher behavior, organizational adoption, and broader social/ethical considerations. Using mixed methods, we can optimize BBPs and unlock their full potential to shape a more secure digital future.

This study stands out as it focuses on the unique capacity of BBPs to uncover vulnerabilities related to malware (malware-related vulnerabilities), setting it apart from the previous studies that predominantly assessed overall BBP effectiveness. It focuses on a specific domain of malware vulnerability discovery, a dimension with limited exploration in the existing literature, and aims to address this gap comprehensively. In addition, this study investigated how diverse BBP structures affect researchers' engagement and their ability to detect malware-related vulnerabilities. This dimension has been underexplored in previous research, making it a crucial area of investigation. Furthermore, this study aims to provide comprehensive recommendations for optimizing BBPs, with a specialized focus on enhancing their performance in malware vulnerability identification. This is an invaluable contribution given the scarcity of detailed guidance in the cybersecurity domain. A mixed-methods approach is employed to fulfill these objectives, combining quantitative data from BBP outcomes with qualitative insights into security researchers' experiences and motivations. This holistic approach offers a well-rounded understanding of the factors that define successful BBP, ultimately bridging gaps in the literature and enriching the field of cybersecurity.

III. METHODOLOGY

In this section, we discuss the effectiveness of Bug Bounty Programs (BBPs) in detecting malware-related vulnerabilities using a mixed-method approach that combines quantitative analysis with qualitative insights. Our methodology, designed to capture the intricate dynamics of BBPs, involves collecting data from BBP platforms, conducting interviews with researchers and administrators, and analyzing survey responses. This section outlines our comprehensive process, which includes identifying patterns in vulnerability discovery, understanding researchers' motivations, and assessing program designs. By integrating diverse data sources, we aim to provide a detailed understanding of how BBPs can be optimized to enhance cybersecurity defense against malware. This approach ensures a nuanced exploration of the critical factors that influence the success of BBPs in cybersecurity ecosystems.

A. Research Flow

This study focuses on the intricate realm of Bug Bounty Programs (BBPs) and their efficacy in detecting malware-related vulnerabilities. We used a mixed-method approach, blending quantitative and qualitative data to develop a holistic understanding. Fig. 1 outlines the research flow process that we followed to meet our objectives. This process includes Gathering the Clues, where we collected essential data; Deciphering the Patterns, where we analyzed this data to uncover trends; Connecting the Dots, where we integrated these insights; the Grand Reveal, where we presented our findings; and Beyond, where we explored future implications.

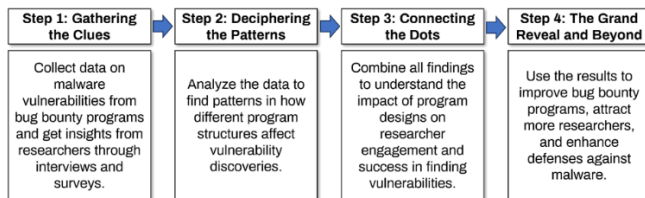


Fig. 1. Research flow.

The detailed step-by-step process is as follows.

Step 1: Gathering the Clues. The journey began with data collection. Quantitative data will be culled from existing BBP platforms or through manual scraping, focusing on vulnerabilities classified as "malware-related." These data include details such as the number and severity of vulnerabilities discovered, program type (public/private), and reward structure (fixed/variable). Qualitative data were gathered through targeted interviews with researchers who successfully uncovered malware-related vulnerabilities in diverse BBP settings. Surveys distributed to researchers and BBP administrators will enrich this qualitative perspective.

Step 2: Deciphering the Patterns. Once the data were collected, it was time for analysis. Quantitative data will be subjected to rigorous statistical tests to compare vulnerability discovery rates across different BBP structures and variables. By identifying patterns and associations, we can identify the most effective structures to attract researchers and yield impactful discoveries related to malware. Qualitative data from interviews and surveys will be analyzed using thematic analysis, revealing key themes and insights into researcher motivations, preferences, and challenges within the BBP landscape.

Step 3: Connecting the Dots. The true power lies in integrating seemingly disparate pieces of information. By combining quantitative and qualitative findings, we gain a holistic understanding of how BBP structures influence researchers' behavior and vulnerability discovery outcomes related to malware. Identifying the connections and discrepancies between different data sources is crucial, allowing for deeper interpretation and nuanced explanations.

Step 4: Grand Reveal and Beyond. The culmination of this study is the identification of BBP structures that are most effective in attracting researchers and uncovering high-severity vulnerabilities related to malware. These findings can be translated into actionable recommendations for BBP design

and implementation, empowering organizations to optimize their programs for maximum impact. Additionally, insights into researchers' motivations and behaviors can inform BBP outreach and recruitment strategies, fostering a vibrant community of skilled hunters dedicated to tackling the evolving malware threat. Ultimately, this study aims to strengthen overall cyber defense capabilities by unlocking the full potential of BBPs in the fight against malicious software, leading to a more secure and resilient online world.

The outlined research approach combines quantitative and qualitative analyses to enhance our understanding of bug bounty program effectiveness, particularly in identifying malware-related vulnerabilities. Through a methodical process that begins with comprehensive data collection and extends to deep data analysis, this approach illuminates the key factors that influence researchers' participation and success in BBPs. By integrating diverse data sources, this study uncovers actionable insights into optimizing BBP structures to attract skilled researchers and facilitate the discovery of significant vulnerabilities. Ultimately, this methodological journey not only aims to refine the design and implementation of BBPs, but also seeks to bolster cybersecurity defenses by leveraging the collective expertise of the global research community.

B. Case Studies and Surveys

The case studies involved semi-structured interviews with researchers who had participated in Bug Bounty Programs (BBPs) to explore their motivations, experiences, and the challenges they faced. The documentation of various BBPs was analyzed to compare program types, reward structures, eligibility criteria, and other relevant factors. Additionally, vulnerability reports submitted to different BBPs were reviewed to identify trends in the types of vulnerabilities discovered and the profiles of researchers who made these discoveries. Diverse case studies have been selected to represent various Bug Bounty Programs (BBP) types (public, private), reward systems (fixed, variable), and target technologies (web, mobile, etc.), offering a broad spectrum of experiences. Data collection involved semi-structured interviews with key stakeholders, including researchers who identified significant vulnerabilities related to malware within BBPs and administrators overseeing program design and management. Additionally, program documentation, vulnerability reports, and communication logs were analyzed to gain insight into program regulations, participant engagement, and the vulnerabilities uncovered.

Surveys were conducted among researchers who had participated in Bug Bounty Programs (BBPs) to collect their views on various program features and gauge their overall satisfaction with the BBP experience. The surveys were conducted by BBP administrators to obtain information on the design, implementation, and outcomes of the programs. Surveys targeted diverse participants, including researchers experienced in BBPs, focusing on malware findings, and administrators of BBPs with varying structures and targets. The questionnaire was designed with clear and concise questions aimed at understanding researchers' motivations and experiences, particularly regarding malware-related vulnerabilities, and providing administrator insight into program design, challenges, and success in engaging

researchers and identifying vulnerabilities. The surveys incorporated closed-ended (multiple-choice and Likert scales) and open-ended questions to collect quantitative and qualitative data.

C. Analysis Methods

Qualitative analysis methods included thematic analysis to pinpoint recurring themes in interview transcripts and open-ended survey responses, shedding light on researchers' motivations and experiences and program administrators' views on program attributes and obstacles. Grounded theory was used to formulate a theory on how program frameworks and researcher motivations impact vulnerability identification through inductive analysis of interview data and the correlation of concepts. Narrative analysis was applied to examine vulnerability reports and researcher narratives to grasp the stories behind the individual findings and the challenges encountered.

Quantitative analysis methods included descriptive statistics to summarize variables, such as researcher demographics, vulnerability severity, and program reward structures. Regression analysis was used to examine the relationships between program features such as reward type and scope and outcomes such as researcher participation, rates of vulnerability discovery, and vulnerability severity. Survival analysis was considered to investigate the duration researchers took to uncover various types of vulnerabilities across different program settings contingent on data availability.

Mixed-method analysis involves combining qualitative and quantitative techniques to achieve a comprehensive understanding of the studied phenomena. This approach entailed using quantitative data to pinpoint trends in researcher participation across various program types, followed by qualitative interviews to determine the reasons for these trends.

This study employs a robust mixed-method approach to comprehensively investigate the effectiveness of BBP structures in uncovering vulnerabilities related to malware. Quantitative analysis utilizing data from existing BBP platforms will provide large-scale insights into discovery rates across diverse program structures and reward systems. Qualitative analysis through targeted interviews and surveys with researchers and BBP administrators will delve deeper into the human element, uncovering researchers' motivations, preferences, and challenges within the BBP landscape. By integrating these quantitative and qualitative findings, this study paints a rich and nuanced picture of the complex interplay between BBP structures, researcher behavior, and vulnerability discovery outcomes related to malware. This multifaceted approach ensures a comprehensive understanding of the research question and lays a strong foundation for drawing actionable conclusions and recommendations for optimizing BBPs in the fight against this ever-evolving threat.

IV. RESULTS

In this section, we detail the findings of our extensive research on Bug Bounty Programs (BBPs) with a particular focus on identifying and managing high-severity malware-related vulnerabilities. Our innovative mixed-method approach merges quantitative data with qualitative assessments,

unveiling the critical factors that bolster the success of BBPs in fortifying cybersecurity defense. Our analysis not only confirms the robust capabilities of BBPs in unearthing vital vulnerabilities but also proposes actionable strategies to refine these programs, enhancing their effectiveness in both detecting and managing these severe threats. The promising outcomes of our study underscore the potential for significantly improving cybersecurity measures, paving the way for a safer digital landscape.

A. Themes from Case Studies and Surveys

Our comprehensive analysis, as presented in Table I, synthesizes the data collected from various case studies and surveys, all organized by theme. We found a compelling trend across the public Bug Bounty Programs (BBPs) we studied: those offering variable rewards, adjusted according to the severity of uncovered vulnerabilities, not only detected issues of greater severity but also a higher volume of these significant vulnerabilities compared to other programs. Our findings strongly suggest that such dynamically structured rewards in public BBPs are particularly effective in attracting skilled researchers, who in turn identify critical security flaws. This insight underscores the potential of incentive-based approaches to enhance cybersecurity measures effectively.

TABLE I. QUANTITATIVE ANALYSIS (THEMES FROM CASE STUDIES AND SURVEYS)

| Theme 1: Motivations for Researcher | Theme 2: Preferred BBP Features | Theme 3: Challenges Faced by Researchers |
|--|--|---|
| Recognition and reputation building (45% of respondents) | Clear and detailed vulnerability disclosure guidelines (72% of respondents) | Difficulty in understanding complex program rules and eligibility criteria (35% of respondents) |
| Financial rewards (38% of respondents) | Responsive and supportive program administrators (68% of respondents) | Lack of timely feedback and communication from program administrators (30% of respondents) |
| Intellectual challenge and learning (32% of respondents) | Transparent and timely reward disbursement (65% of respondents) | Unclear or inconsistent reward payout processes (28% of respondents) |
| Contributing to the cybersecurity community (28% of respondents) | Regular communication and updates from program organizers (60% of respondents) | Limited resources and time constraints (25% of respondents) |

Fig. 2, which builds on the data summarized in Table I, clearly demonstrates the main driving forces behind cybersecurity researchers' engagement: the quest for recognition, financial gain, continuous learning, and community contribution. These professionals predominantly favor Bug Bounty Programs (BBPs) that are characterized by clear and transparent guidelines, responsive coordinators, well-defined reward systems, and ongoing communication. Our study also identified the following significant barriers: complex program stipulations, lack of adequate feedback, ambiguous compensation frameworks, and stringent time limits. To cultivate effective collaboration and maximize the efficacy of these programs, it is crucial for organizers to focus on fostering transparency, maintaining robust communication, and ensuring fairness within the operational structures. This strategic focus

enhances the overall success of partnerships in the cybersecurity domain.

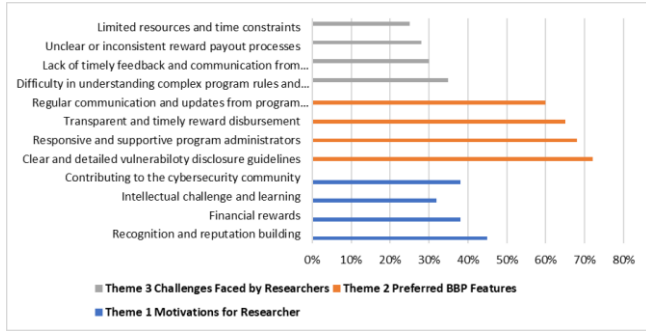


Fig. 2. Visualized themes from case studies and surveys.

It is suggested that, while there are clear motivations and preferences that drive researchers towards BBPs, there are also significant challenges that need to be addressed. Improvements in program transparency, communication, and administration could enhance the effectiveness of BBPs and potentially attract more researchers by aligning them with their motivations and preferences.

B. Motivations of Engaging in BBPs

Table II presents a comprehensive exploration of the motivations driving security experts to participate in Bug Bounty Programs (BBPs). Through our series of in-depth interviews combined with meticulous data analysis, we uncovered the multifaceted reasons behind the researchers' engagement. While financial incentives and the intellectual thrill of discovering vulnerabilities are significant, we found that the quest for recognition and the desire to bolster one's professional stature are equally compelling drivers. Furthermore, many participants were motivated by the opportunity to contribute substantially to the cybersecurity community. These findings highlight the critical role of a supportive and well-structured BBP environment in attracting top talent. By aligning rewards with the severity of vulnerabilities, programs can significantly enhance their effectiveness and achieve greater success.

TABLE II. QUANTITATIVE ANALYSIS (MOTIVATIONS OF ENGAGING IN BBPs)

| Program Type | Reward Structure | Average Severity Score of Discovered Vulnerabilities | Number of High-severity Vulnerabilities |
|--------------|------------------|--|---|
| Public | Fixed Reward | 3.5 | 20 |
| Public | Variable Reward | 4.2 | 35 |
| Private | Fixed Reward | 3.8 | 28 |
| Private | Variable Reward | 4.5 | 42 |

Our participants underscored the indispensable need for Bug Bounty Programs (BBPs) to establish transparent and uncomplicated guidelines for reporting vulnerabilities. They emphasized that having an efficient and communicative management team, along with a clear and straightforward reward issuance process, is crucial. Furthermore, our study

identified the following significant obstacles that undermine the effectiveness of BBPs: delays in handling reports, inconsistencies in the process, and inadequate communication. To address these critical issues and preserve the trust and attractiveness of BBPs to top-tier security experts, it is essential to implement and maintain clear, consistent, and communicative practices. This commitment to operational excellence is pivotal to sustaining the effectiveness and appeal of BBPs.

C. Vulnerabilities Related to Malware Identified in BBPs

Table III delineates the array of malware-related vulnerabilities frequently unearthed in Bug Bounty Programs (BBPs). Our analysis revealed a spectrum of exploits, from classic SQL injections to sophisticated zero-day attacks. This diversity underscores the adaptability of attackers and is imperative for a robust multilayered defense strategy. Our findings emphasize the urgent need for proactive measures against zero-day vulnerabilities, highlight the critical importance of data security and system hardening to prevent breaches and call for enhanced vulnerability management in the face of targeted attacks. This study not only demands continual vigilance against these evolving threats, but also sets the stage for further exploration of the motives of attackers, emerging trends, and effective mitigation strategies to strengthen cyber defenses.

TABLE III. VULNERABILITIES RELATED TO MALWARE (COMMONLY IDENTIFIED IN BBPs)

| Vulnerability Type | Description | Impact | Sample Malware |
|----------------------------|---|---|--|
| SQL Injection (SQLi) | Allows attackers to inject malicious SQL code into a database or application, potentially leading to data theft, modification, or deletion, as well as system takeover. | Data breaches, financial losses, reputational damage, system compromise. | Stuxnet (manipulating industrial control systems), WannaCry (exploiting EternalBlue exploit targeting unpatched Windows machines) |
| Cross-site Scripting (XSS) | Malicious script injection into websites or applications | Data theft, credential compromise, malware distribution, website defacement | Magecart (skimming credit card data from compromised websites), SamSam (ransomware exploiting unpatched Adobe Flash vulnerabilities) |
| File Inclusion | Arbitrary file inclusion on servers | Malware uploads, data theft, system compromise | Web shells (providing attackers remote access to compromised systems), Regin (espionage malware exploiting file inclusion vulnerabilities) |

| | | | |
|--|--|---|--|
| Zero-day | Unpatched vulnerabilities unknown to software vendors | Severe attacks with high potential for damage before a patch is available | EternalBlue (exploited by WannaCry and NotPetya ransomware), Flame (espionage malware with multiple zero-day exploits) |
| Buffer overflow | Programs writing more data than buffer capacity, allowing attacker code injection | System compromise, malware execution, unauthorized access | Morris worm (exploiting buffer overflows in Unix systems), Code Red worm (exploiting buffer overflows in web servers) |
| Insecure Direct Object References (IDOR) | Exploiting improper access control, allowing unauthorized access or modification of data | Data breaches, unauthorized privilege escalation, lateral movement within systems | Cobalt Strike (lateral movement within compromised networks), SolarWinds supply chain attack (exploiting IDOR in Orion platform) |

Our investigation highlights that Insecure Direct Object References (IDOR) play a pivotal role in malware operations by allowing attackers to bypass authentication and gain unauthorized access to sensitive data or system functionalities. This vulnerability is exploited by tools such as Cobalt Strike to deepen an attacker's presence within compromised networks. A prominent example from our study is the SolarWinds supply chain attack, which utilizes an IDOR flaw in the Orion software to propagate malicious updates, leading to widespread compromises across numerous entities. This case underscores the critical need for vigilant monitoring and robust defense mechanisms against IDOR vulnerabilities to prevent significant security breaches.

D. Key Findings

Our comprehensive research provides a clear blueprint for enhancing Bug Bounty Programs (BBPs). We recommend a structure that is openly accessible and offers variable rewards directly tied to the severity of the uncovered vulnerabilities. Essential to this model are transparent communication, responsive administration, and the recognition of contributors. These elements not only draw on dedicated researchers but also effectively address their primary challenges and motivations. By implementing these strategies, BBPs have evolved into crucial instruments for unmasking significant malware threats and substantially bolstering cybersecurity defenses. Our integrated approach promotes a collaborative and secure digital environment, ensuring that researchers feel appreciated, driven, and essential to the cybersecurity community.

E. Potential Significant Impacts

Our study offers transformative insights into optimizing Bug Bounty Programs (BBPs) for more effective malware detection, with significant implications for cyber defense strategies. First, we demonstrate the critical need to tailor BBPs to attract specialists adept at spotting malware-specific vulnerabilities, targets often missed in standard security

assessments. By refining BBP structures and rewards, we can better motivate researchers to dedicate the necessary effort to reveal urgent security flaws, thus accelerating the detection and remediation processes. Our findings also advocate the expansion of BBPs to encompass a broader array of software and platforms, thereby uncovering gaps that conventional methods have failed to address.

Second, our study significantly contributes to bolstering cyber defense. Enhanced detection capabilities lead to a faster patching of vulnerabilities and shrinking opportunities for attackers. Moreover, it upgrades threat intelligence methodologies by equipping defenders to preemptively combat emerging malware challenges. By promoting greater collaboration and sharing of insights among the security community, bug bounty platforms, and vendors, we pave the way for a more cohesive and robust defense infrastructure.

Finally, the research underlines how optimized BBPs offer a cost-effective supplement to conventional security measures, particularly for smaller entities with constrained budgets. Successful BBPs foster a dynamic network of security experts, thereby creating a reservoir of continuous enhancements in security practices. Additionally, our study sets a foundation for establishing the best practices and standards in BBP design and operation, aiming for more uniform and reliable security solutions across the industry.

V. DISCUSSION

We strongly believe that the future of cybersecurity is deeply tied to the progressive enhancement and broadening of Bug Bounty Programs (BBPs). These programs have demonstrated considerable success owing to their use of variable rewards, which effectively incentivize researchers to focus on and resolve the most severe vulnerabilities. To optimize the impact of BBPs, it is crucial that this incentive model be standardized across the board, ensuring that all programs benefit from heightened researcher engagement and more thorough vulnerability detection.

Moreover, the complexity of cyber threats is rapidly increasing, propelled by technological advancements. In response, BBPs must incorporate cutting-edge technologies, such as artificial intelligence and machine learning. These tools can provide predictive insights, allowing BBPs to identify and mitigate potential vulnerabilities before they can be exploited, thereby significantly reducing the risk window for cyber-attacks.

Additionally, the scope of BBPs should be expanded to encompass newer technologies and platforms, particularly IoT devices and smart infrastructures. These technologies are becoming integral to our daily lives and, as such, are becoming prime targets for cyber-attacks. Extending the reach of BBPs to cover these areas is vital for protecting both personal data and critical infrastructure.

Furthermore, BBPs should encourage more comprehensive and continuous collaboration among researchers, developers, and program administrators to foster a proactive cybersecurity environment. This can be achieved through regular updates, shared insights, and collective brainstorming sessions, which

would help refine programs and address emerging security challenges more effectively.

While BBPs have already made significant strides in enhancing global cybersecurity measures, their full potential is yet to be realized. There is a compelling need to innovate and extend these programs extensively to stay ahead of the rapidly evolving digital threat landscape. Adopting flexible future-oriented strategies can ensure a more secure digital future for all stakeholders involved.

Elevating Bug Bounty Programs (BBPs) can profoundly amplify their effectiveness and agility within the constantly shifting cybersecurity landscape. Below, we outline a series of strategic enhancements aimed at optimizing these vital programs.

- **Tiered Reward Systems:** Implementing a tiered reward system in which payouts are directly proportional to the severity and complexity of the vulnerabilities discovered can motivate researchers to target more critical issues. This approach can also include bonuses for exceptionally creative and impactful findings.
- **Expanded Scope and Coverage:** Broadening the scope of BBPs to include software and websites, hardware, IoT devices, and emerging technologies will ensure that a wider array of potential security threats are addressed. This expansion requires careful planning to ensure that the coverage is both comprehensive and relevant.
- **Transparent and Streamlined Processes:** Simplifying the submission and review process to make it more transparent can reduce barriers for new researchers. Clear guidelines and straightforward processes for reporting vulnerabilities can enhance their participation and efficiency.
- **Regular Updates and Feedback:** Establishing a system for regular feedback and updates can keep researchers engaged and informed. Timely feedback on the status of their submissions and the impact of their work can foster a more rewarding and motivating environment.
- **Collaborative Engagement Models:** Encouraging collaboration among participants through shared tools, platforms, and events can leverage collective expertise and spur innovative solutions. This can include hackathons, collaborative challenges, and shared repositories of knowledge and techniques.
- **Educational and Training Opportunities:** Providing educational resources and training can help improve the skills of the researchers, especially in areas related to emerging technologies. Workshops, webinars, and resources for best practices in security research may be valuable.
- **Robust Legal and Ethical Frameworks:** Ensuring that all legal and ethical guidelines are clear and up-to-date can protect both the researchers and organizations involved. This includes clear policies for disclosure, privacy, and data protection.

- **Integration of Advanced Technologies:** Utilizing AI and machine learning to predict potential security vulnerabilities and automate some aspects of the vulnerability assessment process can increase the efficiency and scope of these programs.
- **Enhanced Community Building:** Creating a stronger community around BBPs can increase trust and participation. This could be facilitated through forums, dedicated social media channels, and regular meetups.
- **Performance Metrics and Benchmarking:** Developing comprehensive metrics to evaluate the effectiveness of BBPs and benchmarking them against industry standards can help continuously improve their structure and outcomes.

By adopting these recommendations, organizations can significantly enhance their BBPs, thereby boosting the robustness and efficiency of these programs and fortifying their cybersecurity defenses. This proactive approach will help preempt potential security breaches, minimize vulnerabilities, and establish a more resilient infrastructure against emerging cyber threats. Furthermore, such improvements will cultivate a dynamic community of skilled researchers who are motivated and equipped to tackle complex cybersecurity challenges, ultimately contributing to a safer digital environment for all stakeholders.

VI. CONCLUSION AND FUTURE WORK

In conclusion, our study underscores the vital role of Bug Bounty Programs (BBPs) in bolstering cybersecurity, particularly in the identification of high-severity malware-related vulnerabilities. Through meticulous quantitative and qualitative analyses, we demonstrate the effectiveness of public BBPs with variable reward structures in attracting skilled researchers and fostering the discovery of critical vulnerabilities. The multifaceted motivations driving researchers' participation in BBPs, encompassing financial incentives, intellectual challenges, and commitment to community security, highlight the diverse array of factors driving engagement in these programs.

Several critical considerations emerge that can further enhance the efficacy of BBPs. Clear and transparent vulnerability disclosure guidelines coupled with responsive program administration are foundational for fostering trust and engagement among researchers. Timely and consistent reward disbursements along with effective communication channels are essential for maintaining researcher satisfaction and sustaining program momentum. Addressing such challenges as complex program rules and delayed feedback can significantly improve the efficiency and effectiveness of BBPs in identifying and mitigating malware-related vulnerabilities.

Moreover, the diverse range of vulnerabilities uncovered through BBPs underscores the dynamic nature of cyber threats, necessitating continuous vigilance and adaptive defense strategies. Proactive measures, including robust data security protocols and enhanced vulnerability management practices, are imperative to mitigate the evolving risks posed by malicious actors. Furthermore, the integration of advanced

technologies and methodologies such as threat intelligence and machine learning holds promise for further enhancing the capabilities of BBPs in detecting and responding to emerging threats.

Although our study has made significant contributions to understanding the effectiveness of BBPs in cybersecurity, several challenges and opportunities remain for future exploration. Sustainability concerns, legal and ethical considerations, and the need for improved vulnerability attribution mechanisms warrant further investigation to ensure the responsible and effective operation of BBPs. Additionally, exploring the specific motivations of researchers, assessing the broader impact of BBPs, and adapting these programs to address emerging technologies are vital areas for future research.

In summary, our study not only provides valuable insights into the current state of BBPs, but also offers a roadmap for future enhancements. By addressing key challenges and leveraging emerging opportunities, we can further harness the potential of BBPs as effective tools for safeguarding our digital infrastructure against evolving cyber threats.

REFERENCES

- [1] Bhatt, N., Anand, A., & Aggrawal, D. (2019). Improving system reliability by optimal allocation of resources for discovering software vulnerabilities. *International Journal of Quality & Reliability Management*, 37(6/7), 1113-1124.
- [2] Bienz, C. and Juranek, S. (2020). Software vulnerabilities and bug bounty programs. *SSRN Electronic Journal*.
- [3] Hoffman, A. (2019). Moral hazards in cyber vulnerability markets. *Computer*, 52(12), 83-88.
- [4] Wei, Y., Sun, X., Bo, L., Cao, S., Xia, X., & Li, B. (2021). A comprehensive study on security bug characteristics. *Journal of Software Evolution and Process*, 33(10).
- [5] Marcavage, E. (2023). Predicting the effectiveness of blockchain bug bounty programs. *The International Flairs Conference Proceedings*, 36.
- [6] Shen, H., DeVos, A., Eslami, M., & Holstein, K. (2021). Everyday algorithm auditing: understanding the power of everyday users in surfacing harmful algorithmic behaviors. *Proceedings of the Acm on Human-Computer Interaction*, 5(CSCW2), 1-29.
- [7] Gupta, R., Kumari, A., & Tanwar, S. (2020). A taxonomy of blockchain envisioned edge-as-a-connected autonomous vehicles. *Transactions on Emerging Telecommunications Technologies*, 32(6).
- [8] Jacobs, J., Romanosky, S., Adjerid, I., & Baker, W. (2020). Improving vulnerability remediation through better exploit prediction. *Journal of Cybersecurity*, 6(1).
- [9] Formosa, P., Wilson, M., & Richards, D. (2021). A principled framework for cybersecurity ethics. *Computers & Security*, 109, 102382.
- [10] Green, M., Hall-Andersen, M., Hennenfent, E., Kaptchuk, G., Pérez, B., & Laer, G. (2023). Efficient proofs of software exploitability for real-world processors. *Proceedings on Privacy Enhancing Technologies*, 2023(1), 627-640.
- [11] Pascariu, C. (2022). Getting started with vulnerability disclosure and bug bounty programs. *International Journal of Information Security and Cybercrime*, 11(1), 25-30.
- [12] Zerouali, A., Mens, T., Decan, A., & Roover, C. (2022). On the impact of security vulnerabilities in the npm and rubygems dependency networks. *Empirical Software Engineering*, 27(5).
- [13] Salin, H. and Lundgren, M. (2022). Towards agile cybersecurity risk management for autonomous software engineering teams. *Journal of Cybersecurity and Privacy*, 2(2), 276-291.
- [14] Çatal, Ç., Giray, G., & Tekinerdoğan, B. (2021). Applications of deep learning for mobile malware detection: a systematic literature review. *Neural Computing and Applications*, 34(2), 1007-1032.
- [15] Alrammal, M., Alrammal, M., Naveed, S., & Sallam, G. (2022). A critical analysis on android vulnerabilities, malware, anti-malware and anti-malware bypassing. *網際網路技術學刊*, 23(7), 1651-1661.
- [16] Valdez, D., Vorland, C., Brown, A., Mayo-Wilson, E., Otten, J., Ball, R., ... & Allison, D. (2020). Improving open and rigorous science: ten key future research opportunities related to rigor, reproducibility, and transparency in scientific research. *F1000research*, 9, 1235.
- [17] Xiong, Q., Zhu, Y., Zeng, Z., & Yang, X. (2023). Signal game analysis between software vendors and third-party platforms in collaborative disclosure of network security vulnerabilities. *Complexity*, 2023, 1-11.
- [18] Subramanian, H. and Malladi, S. (2020). Bug bounty marketplaces and enabling responsible vulnerability disclosure. *Journal of Database Management*, 31(1), 38-63.
- [19] Namli, N. and Aybek, B. (2022). An investigation of the effect of block-based programming and unplugged coding activities on fifth graders' computational thinking skills, self-efficacy and academic performance. *Contemporary Educational Technology*, 14(1), ep341.
- [20] Silomon, J., Hansel, M., & Schwartz, F. (2022). Bug bounties: between new regulations and geopolitical dynamics. *International Conference on Cyber Warfare and Security*, 17(1), 298-305.
- [21] Walshe, T. and Simpson, A. (2023). Towards a greater understanding of coordinated vulnerability disclosure policy documents. *Digital Threats Research and Practice*, 4(2), 1-36.
- [22] Zhou, L., Bao, J., Watzlaf, V., & Parmanto, B. (2019). Barriers to and facilitators of the use of mobile health apps from a security perspective: mixed-methods study. *Jmir Mhealth and Uhealth*, 7(4), e11223.
- [23] Hassandoust, F. and Johnston, A. (2023). Peering through the lens of high-reliability theory: a competencies driven security culture model of high-reliability organisations. *Information Systems Journal*, 33(5), 1212-1238.
- [24] Veiga, A., Actaxova, JI., Botha, A., & Herselman, M. (2020). Defining organisational information security culture—perspectives from academia and industry. *Computers & Security*, 92, 101713.
- [25] Bailey, P., Hole, B., Plumb, L., & Caskey, F. (2022). Mixed-methods research in nephrology. *Kidney International*, 101(5), 895-905.
- [26] Wasti, S., Simkhada, P., Teijlingen, E., Sathian, B., & Banerjee, I. (2022). The growing importance of mixed-methods research in health. *Nepal Journal of Epidemiology*, 12(1), 1175-1178.
- [27] Otieno, J., Obura, C., & Owino, E. (2023). Mixed methods in accounting research: the rationale and research designs. *Middle East Journal of Applied Science & Technology*, 06(01), 70-76.
- [28] Smajic, E., Avdić, D., Pasic, A., Precic, A., & Stancic, M. (2022). Mixed methodology of scientific research in healthcare. *Acta Informatica Medica*, 30(1), 57.
- [29] Şahin, M. and Ozturk, G. (2022). Mixed method research: theoretical foundations, designs and its use in educational research. *International Journal of Contemporary Educational Research*, 6(2), 301-310.
- [30] Björk, C., Ruthmann, S., Granfors, M., Högväg, J., & Andersson, S. (2021). The potential of a mixed-methods approach for research on learning to theorise music. *Music Education Research*, 23(3), 374-390.
- [31] Walker-Roberts, S., Hammoudeh, M., Aldabbas, O., Aydın, M., & Dehghantanha, A. (2019). Threats on the horizon: understanding security threats in the era of cyber-physical systems. *The Journal of Supercomputing*, 76(4), 2643-2664.
- [32] Åkerblad, L., Seppänen-Järvelä, R., & Haapakoski, K. (2020). Integrative strategies in mixed methods research. *Journal of Mixed Methods Research*, 15(2), 152-170.

ConvADD: Exploring a Novel CNN Architecture for Alzheimer's Disease Detection

Mohammed G Alsubaie¹, Suhuai Luo², Kamran Shaukat³

School of Information and Physical Sciences, The University of Newcastle, Callaghan, NSW 2308, Australia^{1,2,3}
Department of Computer Science, College of Khurma University College, Taif University, Taif, 21944, Saudi Arabia¹

Abstract—Alzheimer's disease (AD) poses a significant healthcare challenge, with an escalating prevalence and a forecasted surge in affected individuals. The urgency for precise diagnostic tools to enable early interventions and improved patient care is evident. Despite advancements, existing detection frameworks exhibit limitations in accurately identifying AD, especially in its early stages. Model optimisation and accuracy are other issues. This paper aims to address this critical research gap by introducing ConvADD, an advanced Convolutional Neural Network architecture tailored for AD detection. By meticulously designing ConvADD, this study endeavours to surpass the limitations of current methodologies and enhance accuracy metrics, optimisation, and reliability of AD diagnosis. The dataset was collected from Kaggle and consists of preprocessed 2D images extracted from 3D images. Through rigorous experimentation, ConvADD demonstrates remarkable performance metrics, showcasing its potential as a robust and effective. The proposed model shows remarkable results with a tool for AD detection accuracy of 98.01%, precision of 98%, recall of 98%, and an F1-Score of 98%, with only 2.1 million parameters. However, despite its promising results, several challenges and limitations remain, such as generalizability across diverse populations and the need for further validation studies. By elucidating these gaps and challenges, this paper contributes to the ongoing discourse on improving AD detection methodologies and lays the groundwork for future research endeavours in this domain.

Keywords—Alzheimer's disease; AD detection; convolution neural network

I. INTRODUCTION

Alzheimer's disease (AD) poses an escalating challenge in healthcare, demanding sophisticated and timely diagnostic mechanisms to enable prompt interventions and elevate the quality of patient care [1]. The persistent rise in dementia incidence, currently at a staggering 10 million new cases annually [2], signals an impending crisis, with forecasts indicating that the population afflicted by AD will soar to 152 million by 2050 [2]. This exponential growth trajectory not only underscores the pressing demand for precise diagnostic approaches but also emphasises the critical necessity for inventive and resilient detection frameworks to alleviate the impending healthcare burden.

The pathological mechanisms driving Alzheimer's disease (AD) unveil a tumultuous cascade of neuronal degeneration,

precipitating a profound decline in cognitive functions and the gradual erosion of memory capabilities [3]. This devastating progression is propelled by the insidious accumulation of proteins within the neuronal environment, instigating consequential structural alterations in the intricate architecture of the brain [4], [5], [6], [7]. Despite this disease's profound impact and relentless advancement, the quest for a precise diagnostic methodology remains an elusive endeavour, impeding the development of effective therapeutic interventions [8], [9], [10]. The imperative for early detection of Alzheimer's disease assumes paramount significance, particularly in identifying its nascent stage, Mild Cognitive Impairment (MCI). This preclinical phase signifies a pivotal juncture, spotlighting the crucial window for intervention and strategic treatment planning. Recognising MCI enables proactive measures aimed at mitigating disease progression, potentially forestalling the onset of debilitating symptoms and enhancing patient outcomes. Consequently, the development of robust diagnostic modalities capable of discerning subtle cognitive changes at this incipient stage holds profound implications for advancing both clinical management and therapeutic innovation in Alzheimer's disease [11], [12].

The landscape of Alzheimer's disease (AD) detection has undergone a transformative evolution catalysed by breakthroughs in neuroimaging methodologies and the emergence of computer-aided diagnostic approaches [7]. These pioneering innovations have revolutionised the field, furnishing clinicians with unprecedented insights into the intricate neuronal manifestations inherent to AD. Yet, notwithstanding the commendable strides achieved through machine learning [13] and deep learning [14] models, significant limitations persist in the realm of AD detection.

Machine learning algorithms have shown promise in identifying patterns indicative of Alzheimer's disease (AD) pathology from neuroimaging data. However, challenges persist in achieving consistent accuracy rates across diverse patient groups and imaging methods due to data variability, limited sample sizes, and the heterogeneous nature of AD. Interpretability remains a concern, as black-box models lack

transparency in explaining diagnostic predictions. Deep learning techniques offer the potential to extract features from neuroimaging data but require large, labelled datasets for effective training and are prone to overfitting. Integrating these algorithms into clinical practice necessitates rigorous validation and standardisation protocols alongside ethical considerations regarding patient privacy, data security, and algorithmic bias.

In light of these challenges, concerted efforts are underway to address the existing gaps in AD detection through interdisciplinary collaborations, data harmonisation initiatives, and the development of interpretable machine learning frameworks. By surmounting these obstacles, the field stands poised to realise the full potential of artificial intelligence in revolutionising early detection and personalised management strategies for Alzheimer's disease.

Remarkable advances in machine learning and deep learning models have indeed propelled the field of Alzheimer's disease detection forward, primarily through classification paradigms [15], [16], [17], [18]. These models have exhibited commendable abilities to discern intricate patterns and categorise data, offering promising avenues for early diagnosis and intervention. However, the predominant emphasis on classification may inadvertently overlook the nuanced complexities inherent in Alzheimer's disease pathology.

Alzheimer's disease involves complex neurodegenerative processes, including cognitive decline and various brain alterations. Early disruptions in synaptic function and signalling precede clinical symptoms by years. Amyloid-beta plaques and tau protein tangles lead to widespread neuronal dysfunction and cognitive decline. Machine learning and deep learning models excel in classification tasks but may oversimplify Alzheimer's complex pathology. A holistic approach is needed to capture disease progression and clinical diversity accurately.

To address this challenge, there is a growing recognition of the importance of integrating multimodal data sources and leveraging advanced analytical techniques that can capture the multidimensional nature of Alzheimer's disease. By combining neuroimaging data with clinical, genetic, and molecular biomarkers, researchers aim to construct comprehensive disease signatures that capture the diverse manifestations of Alzheimer's pathology across different stages of disease progression and patient subpopulations.

The use of classification-focused deep learning models has posed significant challenges in effectively capturing the spectrum of multifaceted manifestations of Alzheimer's disease. While these models excel at categorising data into discrete classes, they often fall short in capturing the complex

interplay of subtle neuronal abnormalities that characterise the onset and progression of AD. By primarily focusing on distinguishing between healthy and diseased states, these models may overlook the heterogeneity of AD pathology and fail to capture the nuanced changes occurring within the brain over time.

There is, therefore, a compelling imperative to transcend the limitations of classification-based models and embrace a paradigm that comprehensively encompasses the multiple facets of Alzheimer's disease pathology. Rather than simply categorising data into binary outcomes, it is essential to adopt a new approach that not only identifies patterns but also discerns the subtle and intricate nuances indicative of the early stages of Alzheimer's disease. This shift towards a more nuanced and comprehensive diagnostic framework holds the potential to enhance our understanding of AD pathogenesis and improve the accuracy of early detection strategies.

Our research introduces ConvADD, a novel convolutional neural network (CNN) architecture specifically tailored for accurate Alzheimer's disease detection. Unlike traditional models, ConvADD effectively handles imbalanced datasets without requiring extensive data augmentation. It features adapted convolutional blocks and deep layers optimised for discerning subtle disease patterns, even with smaller datasets. ConvADD represents a paradigm shift in Alzheimer's disease detection, overcoming dataset imbalances and revolutionising diagnosis. Leveraging advanced deep learning techniques, it offers promising potential for early detection and improved management, advancing our pursuit of effective treatments.

The contributions outlined highlight significant advancements in the field of Alzheimer's disease (AD) detection, particularly focusing on the development of ConvADD, a novel Convolutional Neural Network (CNN) architecture tailored specifically for this purpose. Here's an elaboration:

- The first major contribution is the creation of ConvADD, which stands for Convolutional Alzheimer's Disease Detection. This architecture represents a pioneering approach designed explicitly for detecting Alzheimer's Disease. Unlike previous models, ConvADD is crafted to prioritise accuracy without relying on dataset-balancing techniques. This means that it can maintain robust performance across datasets of varying sizes without needing additional preprocessing steps to balance the data distribution.
- ConvADD is designed with a focus on detecting Alzheimer's disease patterns within medical imaging data, such as MRI or CT scans. This tailored architecture ensures that the model is adept at

identifying the specific features indicative of AD, optimising its performance for this task.

- Extensive comparative analyses have been conducted to evaluate ConvADD against established state-of-the-art models used for AD detection. These analyses have consistently shown ConvADD to outperform existing models in terms of various performance metrics. These metrics could include accuracy, sensitivity, specificity, and other measures used to assess the efficacy of a diagnostic model.
- The comparative analyses serve to affirm the efficacy of ConvADD in Alzheimer's disease detection. By demonstrating superior performance across diverse datasets and outperforming established models, ConvADD establishes itself as a promising tool for early detection and diagnosis of Alzheimer's disease, potentially leading to improved patient outcomes and more effective treatment strategies.

The upcoming sections cover a thorough review of related studies in the Literature Review in Section II, followed by a detailed explanation of the Methodology in Section III behind crafting the novel architecture. Next, the Comparative Study contrasts the proposed approach with established models, while the Results and Discussion in Section IV examines and discusses the outcomes. Limitations and Future Directions address current constraints and potential advancements are given in Section V. Finally, Section VI summarises the findings and their broader implications.

II. LITERATURE REVIEW

Convolutional Neural Networks (CNNs) have emerged as a cornerstone in medical imaging, playing a pivotal role in advancing diagnostic capabilities across various domains. In particular, within the realm of neuroimaging, CNNs have demonstrated remarkable efficacy in tasks such as organ segmentation and disease detection, thereby significantly enhancing healthcare outcomes. The intricate nature of neural images, with their complex structures and subtle abnormalities, presents a unique challenge that CNNs are well-suited to address.

In the specific context of Alzheimer's disease (AD) detection, CNNs offer a promising pathway toward early diagnosis and intervention. AD is a progressive neurodegenerative disorder characterised by the accumulation of beta-amyloid plaques and tau protein tangles in the brain, leading to cognitive decline and memory loss. Early detection of AD is crucial for timely intervention and the development of effective treatment strategies. However, traditional diagnostic methods often rely on subjective interpretation and are limited in their ability to detect subtle changes in brain structure.

CNNs provide a powerful tool for AD detection by leveraging their ability to decode intricate connections within images. By analysing neuroimaging data, such as magnetic resonance imaging (MRI) scans, CNNs can identify subtle patterns and abnormalities indicative of AD pathology. This not only enables more accurate and reliable diagnosis but also opens avenues for understanding the underlying mechanisms of the disease.

The significance of CNNs in AD detection is underscored by a growing body of literature [15], [16], [17], [18], [19], [20]. These studies highlight the effectiveness of CNN-based approaches in identifying AD-related biomarkers and distinguishing between healthy and diseased brain tissue. By harnessing the vast amounts of data available in neuroimaging databases, CNNs offer a data-driven approach to AD diagnosis that is both objective and scalable.

In summary, CNNs represent a transformative technology in the field of neuroimaging, with profound implications for AD detection and diagnosis. Their ability to decode intricate connections within images offers a novel avenue for early intervention and personalised treatment strategies, ultimately enhancing the quality of care for patients affected by this devastating disease.

A. Traditional CNN Architectures in AD Analysis

While traditional CNN architectures like LeNet-5 [21] and AlexNet [22] have laid a solid foundation for AD analysis, their efficacy in capturing the intricate features relevant to AD pathology may be limited [23], [24], [25], [26]. Although successful in various image classification tasks, these architectures may struggle to capture the subtle and complex patterns present in neuroimaging data associated with AD progression.

The complexity of AD pathology necessitates a more nuanced approach to feature extraction and representation learning. While LeNet-5 and AlexNet excel in extracting basic features, they may fall short when faced with the intricate structural changes and spatial relationships within the brain that are indicative of AD [27]. As a result, there is a growing recognition of the need for more advanced models specifically tailored to address the unique challenges posed by AD detection.

The limitations of traditional CNN architectures underscore the need for more advanced models capable of capturing the nuanced features relevant to AD pathology [28]. These features may include subtle changes in brain morphology, alterations in connectivity patterns, and the presence of specific biomarkers indicative of disease progression. By leveraging more sophisticated architectures and learning algorithms, researchers

can enhance the sensitivity and specificity of AD detection models, thereby improving diagnostic accuracy and patient outcomes.

Advanced CNN architectures offer several advantages in the context of AD detection [29]. They can adaptively learn hierarchical representations of neuroimaging data, allowing for the extraction of features at multiple spatial and temporal scales. Additionally, advanced models can incorporate domain-specific knowledge and priors, enabling them to effectively capture the complex patterns associated with AD pathology [30].

Moving forward, there is significant potential for the development of advanced CNN architectures tailored specifically for AD detection. These architectures may incorporate innovative design elements such as attention mechanisms [31], recurrent connections [32], and graph-based representations [33] to better capture the spatial and temporal dynamics of AD pathology. Moreover, the integration of multimodal imaging data, including MRI, fMRI, PET, and sMRI, presents an exciting opportunity to enhance the performance of AD detection models further [34].

By leveraging the latest advancements in deep learning and neuroimaging, researchers can develop highly specialised CNN architectures optimised for AD detection. These architectures have the potential to revolutionise the field by enabling earlier and more accurate diagnoses of AD, facilitating timely intervention, and personalised treatment strategies. Overall, the development of advanced CNN architectures represents a critical step towards addressing the growing challenge of AD and improving outcomes for affected individuals and their families.

B. The Emergence of 3D CNNs in AD Analysis

The advent of 3D Convolutional Neural Networks (CNNs) represents a significant advancement in the analysis of neuroimaging data, particularly in the context of AD detection [35]. Unlike traditional 2D CNNs, which process images as two-dimensional grids of pixels, 3D CNNs operate directly on volumetric data, such as MRI scans, capturing spatial information across multiple slices and dimensions [23], [24], [25], [26]. This ability to analyse volumetric data enables 3D CNNs to capture nuanced features crucial for understanding AD's temporal progression, including changes in brain volume, morphology, and connectivity over time.

The use of 3D CNNs in AD analysis offers several distinct advantages. By considering the spatial context of neuroimaging data, 3D CNNs can better capture the complex three-dimensional structures of the brain and the subtle changes associated with AD pathology [35]. This allows for more

accurate and robust detection of disease-related abnormalities, enhancing diagnostic accuracy and facilitating early intervention.

While 3D CNNs have shown promise in AD analysis, the interpretability of their predictions remains a significant challenge. Conventional performance metrics such as accuracy, sensitivity, and specificity provide valuable insights into model performance but offer a limited understanding of the underlying features driving predictions. In the context of AD detection, where the identification of subtle biomarkers is crucial, interpretability is essential for gaining insights into disease mechanisms and guiding clinical decision-making.

To address this challenge, ongoing research is focused on developing interpretability tools and techniques for 3D CNNs. One promising approach involves the use of attention mechanisms [31], which highlight regions of interest within neuroimaging data that are most relevant to the model's predictions. By visualising these attention maps, researchers can gain insights into the features driving the model's decisions and identify potential biomarkers of AD pathology.

Additionally, advances in visualisation techniques, such as heatmaps and saliency maps [36], provide intuitive representations of model predictions, enabling clinicians to interpret and validate the results more effectively. These visualisation tools not only enhance the interpretability of 3D CNNs but also facilitate communication and collaboration between researchers and clinicians, ultimately improving the translation of AI-driven findings into clinical practice.

Looking ahead, there is significant potential for further advancements in 3D CNNs for AD analysis. Future research efforts may focus on refining model architectures to improve both performance and interpretability, incorporating novel attention mechanisms and visualisation techniques. Moreover, the integration of multimodal neuroimaging data [37], including structural MRI, functional MRI, and positron emission tomography (PET), presents an exciting opportunity to enhance the sensitivity and specificity of AD detection models.

By leveraging the capabilities of 3D CNNs and addressing the challenges of interpretability, researchers can develop more accurate, reliable, and clinically relevant tools for AD diagnosis and monitoring. These advancements have the potential to revolutionise the field of neuroimaging and improve outcomes for individuals affected by AD, ultimately leading to earlier diagnosis, personalised treatment strategies, and improved quality of life.

C. Transfer Learning Strategies in AD Detection

Transfer learning has emerged as a potent strategy in the field of Alzheimer's disease (AD) detection, offering a promising approach to leverage pre-trained models and enhance the accuracy of AD detection systems. One notable example of transfer learning involves the use of pre-trained models like VGG16, which are fine-tuned using AD-specific datasets to improve their performance in detecting AD-related biomarkers and abnormalities [23], [24], [25], [26]. By leveraging insights from extensive image datasets, pre-trained models can effectively capture complex patterns and features relevant to AD pathology, thereby enhancing the accuracy and reliability of AD detection systems.

Transfer learning offers several advantages in the context of AD detection [38]. By utilising pre-trained models trained on large-scale image datasets, researchers can leverage the knowledge and representations learned by these models to bootstrap the training process for AD-specific tasks. This not only accelerates the training process but also enables AD detection systems to benefit from the generalisation capabilities of pre-trained models, thereby improving their performance on new and unseen data.

In addition to transfer learning, the efficacy of 3D architectures in handling volumetric data underscores their relevance in capturing the temporal nuances critical for AD progression analysis. Unlike traditional 2D CNNs, which process images as two-dimensional grids of pixels, 3D CNNs operate directly on volumetric data, enabling them to capture spatial and temporal information across multiple dimensions [23], [24], [25], [26]. This allows 3D architectures to effectively analyse longitudinal neuroimaging data, such as MRI scans, and identify subtle changes indicative of AD progression over time.

The integration of transfer learning and 3D architectures represents a powerful approach to AD detection, combining the benefits of pre-trained models with the ability to analyse volumetric data. By fine-tuning pre-trained 3D CNNs using AD-specific datasets, researchers can develop highly specialised models optimised for detecting AD-related abnormalities and biomarkers [38]. This integrated approach not only improves the accuracy and reliability of AD detection systems but also facilitates the interpretation of results by capturing the temporal dynamics of AD progression.

Looking ahead, the combination of transfer learning and 3D architectures holds promise for advancing the field of AD detection. Future research efforts may focus on further optimising transfer learning techniques and developing more sophisticated 3D CNN architectures tailored specifically for

AD progression analysis. Moreover, the integration of multimodal neuroimaging data, including structural MRI, functional MRI, and positron emission tomography (PET), presents an exciting opportunity to enhance the sensitivity and specificity of AD detection models. Ultimately, the integration of transfer learning and 3D architectures has the potential to revolutionise AD detection by providing clinicians with powerful and reliable tools for early diagnosis and intervention, ultimately improving patient outcomes and quality of life [39].

D. Recent Advancements in CNN for AD Detection

Recent studies have underscored the potential of Convolutional Neural Networks (CNNs) in various facets of Alzheimer's disease (AD) detection, ranging from hippocampal segmentation to disease stage classification and early prediction using diverse imaging modalities [8], [9], [10], [11], [12]. These studies have demonstrated the versatility and effectiveness of CNN-based approaches in analysing neuroimaging data and extracting relevant biomarkers indicative of AD pathology.

While CNNs have shown promise in AD detection, most existing models rely on transfer learning or access to larger datasets to enhance their performance. Transfer learning involves fine-tuning pre-trained models on AD-specific datasets to leverage knowledge learned from other domains. While effective, this approach often requires access to extensive computational resources and large, well-curated datasets, which may not be readily available in many clinical settings. Moreover, existing models may struggle to generalise to new datasets or clinical populations, limiting their utility in real-world applications.

In contrast to traditional approaches, ConvADD represents a pioneering approach to AD detection that directly addresses the dependency on transfer learning and large datasets. ConvADD prioritises accuracy without resorting to dataset balancing techniques, mitigating the need for exceptionally large datasets or extensive pre-training. By focusing on robust feature extraction and representation learning, ConvADD aims to enhance the reliability and generalizability of AD detection models across diverse datasets and clinical populations.

ConvADD offers several advantages over existing models in AD detection. By prioritising accuracy and robustness, ConvADD reduces the risk of model bias or overfitting, thereby improving the reliability of AD diagnosis. Additionally, ConvADD's ability to perform effectively without extensive pre-training or dataset balancing simplifies the implementation and deployment of AD detection systems in clinical settings, making them more accessible to healthcare practitioners and researchers.

ConvADD's pioneering approach marks a promising direction in overcoming the challenges associated with AD detection. Moving forward, further research efforts may focus on refining ConvADD's architecture and training strategies to improve its performance and scalability. Additionally, the integration of multimodal neuroimaging data and advanced analysis techniques, such as attention mechanisms and graph-based representations, presents an exciting opportunity to enhance the sensitivity and specificity of AD detection models.

In conclusion, recent advances in CNNs have demonstrated their potential to transform AD detection by enabling accurate, reliable, and accessible diagnostic tools. ConvADD's pioneering approach represents a significant step forward in overcoming the challenges associated with AD detection, offering a promising direction for future research and clinical applications. By prioritising accuracy and robustness while minimising dependencies on transfer learning and large datasets, ConvADD holds promise for improving patient outcomes and advancing our understanding of AD.

E. Importance of novel CNN

In the area of Alzheimer's disease (AD) detection, the justification for the development of novel CNN architectures is imperative. Traditional methods often face challenges in accurately identifying AD, particularly in its early stages, due to the complexity and heterogeneity of the disease [40], [41]. Besides that, advanced approaches are too complex and take computational resources and as well as time [42], [43]. By introducing ConvADD, a tailored CNN architecture for AD detection and optimisation, this research endeavours to address these challenges and enhance diagnostic accuracy with effective memory management. Novel CNN architectures offer the potential for improved feature extraction and representation learning, enabling better discrimination between AD and non-AD brain images. Recent studies have shown the efficacy of deep learning approaches, such as CNNs, in various medical imaging tasks [44], [45], [46], [47], including AD classification. Moreover, advancements in deep learning techniques, coupled with the availability of large-scale medical imaging datasets, have forced the exploration of innovative CNN architectures for AD detection [48]. Therefore, the development and validation of ConvADD contribute to the ongoing efforts to enhance the accuracy and reliability of AD diagnosis, underscoring the necessity for novel CNN architectures in addressing the evolving challenges of AD detection.

III. METHODOLOGY

The methodology employed in this study amalgamates innovative architectural design with meticulous dataset

curation to formulate a robust convolutional neural network (CNN) model tailored explicitly for Alzheimer's Disease (AD) detection. Fig. 1. depicts the overall methodology of the process. The ConvADD architecture stands as the cornerstone of this study, meticulously designed to encapsulate the intricate nuances of AD pathology. Comprising ConvADD convolutional blocks and novel design principles, this architecture addresses the imperative need for precise and nuanced AD detection methodologies.

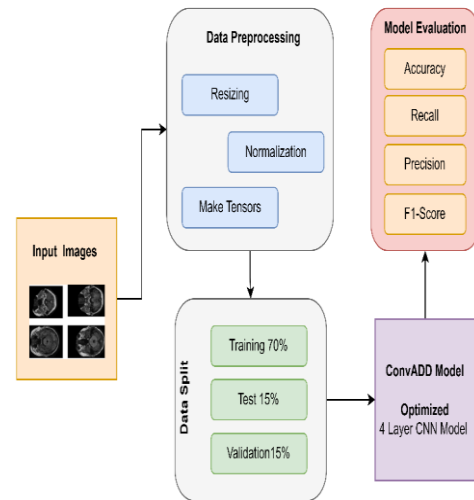


Fig. 1. Methodology diagram of ConvADD.

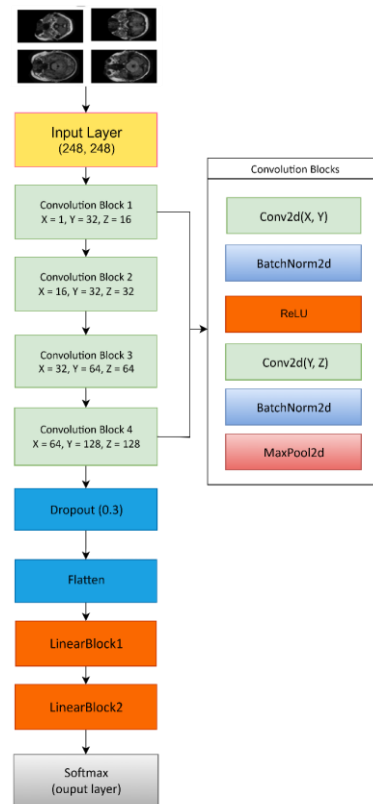


Fig. 2. ConvADD architecture.

Fig. 2. outlines the schematic representation of the ConvADD architecture, elucidating its intricate layers and design principles. Subsequent subsections detail the dataset collection process, delineate the architectural design considerations and provide an in-depth analysis of the ConvADD convolutional blocks. These subsections elucidate the meticulous approach taken in crafting the ConvADD architecture, underscoring its robustness and efficacy in AD detection.

A. Dataset Collection

Several datasets available online for Alzheimer's Disease (AD) classification were considered for this research. However, many of these datasets were in CSV format, which was deemed unsuitable for the purposes of this study. Dedicated organisations such as the Alzheimer's Disease Neuroimaging Initiative (ADNI) and the Open Access Series of Imaging Studies (OASIS) offer extensive datasets for research and educational use. Nevertheless, both the OASIS and ADNI datasets consist of voluminous 3-dimensional image files, with the OASIS dataset totalling 18 gigabytes and the ADNI dataset reaching 450 gigabytes in size.

To address these challenges, the Kaggle dataset was selected for this research. The Kaggle dataset (link) undergoes meticulous verification by the uploader, ensuring the reliability of each sample. Moreover, its manageability is enhanced by its reasonable size and meticulous preprocessing efforts, including resizing and organisation. The dataset comprises a total of 6400 samples, each represented as individual three-channel (RGB) images with dimensions of 176 x 208 pixels, which were resized to 248 x 248 pixels for uniformity. These samples are categorised into four distinct classes: Non-Demented (NOD), Very Mild-Demented (VMD), Mild-Demented (MD), and Moderate Demented (MOD). The NOD class, with 3200 samples, constitutes the majority, while the remaining classes comprise 2240, 896, and 64 images, respectively (see Table I).

TABLE I. CLASS DISTRIBUTION IN AD DATASET

| Class label | Number of Images |
|--------------------------|------------------|
| Mild Demented (MD) | 896 |
| Moderate Demented (MOD) | 64 |
| Non-Demented (NOD) | 3200 |
| Very-Mild Demented (VMD) | 2240 |

Furthermore, the dataset was strategically partitioned into training (70%), validation (15%), and test sets (15%) to ensure an equitable distribution for robust model training and evaluation. Fig. 3. provides a visual representation of some random samples from the dataset, along with their corresponding class labels. This comprehensive approach to

dataset selection and preprocessing lays a strong foundation for the subsequent experimentation and evaluation of the proposed ConvADD model for AD detection.

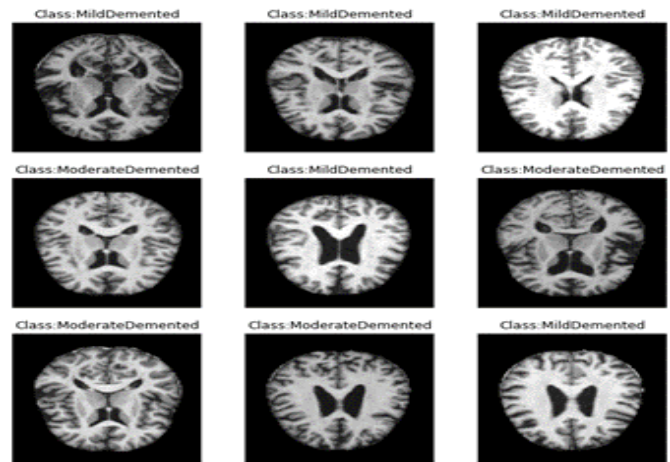


Fig. 3. Random sample from the dataset representing the MRI image with the corresponding class label.

B. Architecture Design – ConvADD

The ConvADD architecture, a Convolutional Neural Network (CNN), embodies a hierarchical structure that effectively processes input data through a series of distinct layers. Starting from the input layer, the network ingests grayscale images of size 176x208 pixels. These images are passed through the initial convolutional block, where the data traverses two consecutive convolutional layers. The first layer, a 3x3 kernel Conv2d operation with 32 output channels, extracts fundamental features from the input. Batch normalisation follows, ensuring standardised inputs to the rectified linear unit (ReLU) activation, introducing non-linearity and enhancing model convergence. Subsequently, the second convolutional layer with a similar kernel size further transforms these features, condensing them into 16 output channels. Another round of batch normalisation and ReLU activation precedes max pooling, downsampling the data by a factor of 2x2.

The subsequent convolutional blocks follow a similar pattern, progressively deepening the network's representation of intricate features. The second block takes the 16 output channels from the previous block, initiating another 3x3 kernel Conv2d operation to generate 32 output channels. Batch normalisation, ReLU activation, and max pooling are then applied. This process continues through the third and fourth blocks, each enhancing the depth and complexity of feature extraction. The third block further transforms the 32 channels into 64 output channels, while the fourth block expands this to 128 output channels, thereby capturing increasingly sophisticated patterns.

The architecture integrates dropout regularisation to prevent overfitting, strategically removing a small fraction of nodes during training. Following the convolutional layers, a flattening operation converts the multidimensional data into a one-dimensional vector, preparing it for processing through fully connected layers. These layers, comprising linear transformations and batch normalisation, iteratively reduce the dimensions of the data to eventually output class probabilities via the softmax layer. ConvADD's design embodies this systematic progression, facilitating the extraction of hierarchical features, culminating in effective classification outputs for Alzheimer's disease stages.

C. ConvADD Convolutional Blocks

The ConvADD architecture introduces a novel approach to feature extraction through its meticulously designed convolutional blocks. These blocks, strategically structured to capture intricate patterns in Alzheimer's disease (AD) imaging data, mark a significant departure from traditional architectures.

1) *Block 1: Initial Feature Extraction:* The first convolutional block kickstarts the feature extraction process. It consists of two convolutional layers: the first layer operates with a 3x3 kernel size, transforming the input grayscale images into 32 fundamental features. Batch normalisation and ReLU activation layers ensure stabilised inputs and introduce non-linearity, respectively. Subsequent max-pooling downsamples the data, aiding in information condensation.

2) *Block 2 to Block 4: Hierarchical Complexity:* Blocks 2 through 4 follow a similar blueprint, progressively enhancing the network's feature representation. Block 2, building upon the output channels from the previous block, refines these features by employing 32 output channels. Successive blocks intensify the complexity of feature extraction, with Block 3 generating 64 output channels and Block 4 culminating in 128 output channels. Each block integrates batch normalisation, ReLU activation, and max pooling, contributing to a hierarchical refinement of extracted features.

3) *Novelty of ConvADD's convolution blocks:* The innovation within ConvADD's architecture lies in the precise orchestration of these convolutional blocks. Each block contributes to the nuanced extraction of hierarchical features, leveraging depth and width to capture AD-specific patterns in imaging data. This novel arrangement distinguishes ConvADD from conventional CNN architectures, enhancing its efficacy in AD stage classification.

D. Dense Blocks: Enabling Robust Classification in ConvADD

Following the convolutional layers, ConvADD employs dense blocks to refine the extracted features further before the final classification. These dense layers contribute to the network's ability to understand intricate patterns and make

informed predictions regarding the stages of Alzheimer's disease (AD).

1) *Linear Block 1: Feature Fusion and Transformation:* After flattening the feature maps extracted by the convolutional layers, Linear Block 1 acts as a pivotal point for feature fusion and transformation. This block consists of a fully connected layer (Linear) that transforms the high-dimensional flattened features into a lower-dimensional space of 16 units. Batch normalisation enhances stability within the network, and ReLU activation introduces non-linearity, facilitating the network's capacity to learn complex mappings between features.

2) *Linear Block 2: Stage Classification:* The subsequent Linear Block 2 is designed explicitly for stage classification. This block employs another fully connected layer, reducing the feature space further to four units, aligning with the four distinct classes related to AD stages. Batch normalisation and ReLU activation continue to contribute to feature stability and non-linearity, respectively, preparing the features for the final Softmax activation.

3) *Contribution of dense blocks in ConvADD:* The inclusion of these dense blocks within ConvADD amplifies the network's capability to abstract and distil essential features learned from the convolutional layers. These blocks play a pivotal role in synthesising complex hierarchical features into a form that facilitates the precise classification of AD stages, marking a significant contribution to the architecture's efficacy.

E. Hyperparameters and Network Configuration

ConvADD architecture incorporates a set of meticulously chosen hyperparameters and specific network configurations that profoundly influence its performance and learning capabilities.

1) *Learning rate and optimizer:* The learning rate, set at a crucial 0.001, guides the step size during the network's weight updates, balancing between convergence speed and overshooting. The Adam optimiser, a variant of stochastic gradient descent (SGD), dynamically adjusts learning rates for each parameter, ensuring efficient convergence and optimal weight updates during training.

2) *Dropout for regularization:* To mitigate overfitting and enhance generalisation, ConvADD integrates dropout regularisation with a probability of 0.03. Implemented after the convolutional blocks, dropout randomly deactivates a fraction of neurons during each training iteration, preventing the network from relying too heavily on specific features or connections and promoting more robust feature learning.

3) *Activation function: ReLU:* Rectified Linear Unit (ReLU) activation functions are employed throughout ConvADD. ReLU introduces non-linearity, allowing the network to model complex relationships within the data efficiently. By thresholding negative values to zero, ReLU

accelerates convergence during training and prevents the vanishing gradient problem.

4) *Batch normalization*: Batch normalisation layers are strategically placed after convolutional and linear blocks. These layers standardise the input to a layer, reducing internal covariate shift and accelerating training by ensuring more stable gradients and facilitating faster convergence.

5) *Weight initialization*: ConvADD utilises appropriate weight initialisation strategies, such as Xavier or Him initialisation, enhancing the network's ability to learn and converge effectively by providing a suitable starting point for weights.

6) *Grid search for optimal hyperparameters*: The selection of these hyperparameters was meticulously curated through systematic grid search and cross-validation, optimising ConvADD's performance on the dataset used for training and validation.

7) *Impact of parameter configuration*: The careful selection and configuration of these parameters and techniques significantly contribute to ConvADD's stability, robustness, and capability to discern intricate patterns associated with AD stages.

IV. RESULTS AND DISCUSSION

A. Performance Evaluation Metrics

1) *Evaluation criteria*: Evaluation metrics are pivotal in assessing the performance and efficacy of machine learning models. The ConvADD architecture's performance in Alzheimer's Disease classification using MRI images was rigorously evaluated employing a diverse set of metrics. These evaluation criteria allowed for a comprehensive understanding of the model's capabilities in different facets of classification accuracy and robustness.

a) Metrics Utilized

i) *Accuracy*: A fundamental metric indicating the proportion of correctly classified samples over the total number of samples. It provides an overall understanding of the model's correctness in predictions. The equation of accuracy [48], [49], [50], [51], [52] could be described as follows:

$$Accuracy = \frac{TP + TN}{TP + FN + FP + TN}$$

where, TP is true positive, TN is true negative, FN refers to false negative, and FP is false positive.

ii) *Precision*: Precision measures the model's accuracy concerning positive predictions. It denotes the ratio of correctly predicted positive observations to the total predicted positive observations. The formula is obtained as follows:

$$Precision = \frac{TP}{TP + FP}$$

iii) *Recall (Sensitivity)*: This metric signifies the model's ability to identify all positive instances. It calculates the ratio of correctly predicted positive observations to the actual positives. The recall equation is:

$$Recall = \frac{TP}{TP + FN}$$

iv) *F1-score*: The F1 score conveys a balance between precision and recall. It's the harmonic mean of precision and recall, providing a consolidated measure of a model's accuracy. The F1-score formula is:

$$F1 = 2 * \frac{Precision * Recall}{Precision + Recall}$$

v) *Confusion Matrix*: The confusion matrix serves as a foundational tool for evaluating the performance of a classification model. It systematically presents the division of outcomes, encompassing all the predictions made by the model during its training or testing phase. This matrix provides a comprehensive breakdown of predicted versus actual class labels, offering insights into the model's accuracy and potential misclassifications.

vi) *Loss Function*: The loss function serves as a crucial guidepost in the training process of machine learning models. It quantifies the model's performance by calculating the inconsistency between predicted and actual values, ultimately indicating how well the model is learning the patterns within the data. This metric is pivotal in adjusting the model's parameters to minimise errors, leading to enhanced predictive accuracy and convergence towards optimal outcomes.

b) *Significance*: These evaluation criteria enable a comprehensive analysis of the ConvADD model's performance. Accuracy, precision, and recall provide insights into the model's correctness and its ability to classify different stages of Alzheimer's Disease correctly. The F1 score balances precision and recall, offering a consolidated performance measure. Furthermore, ROC-AUC quantifies the model's discriminatory capacity between different classes, contributing to a holistic understanding of its effectiveness.

The utilisation of these metrics contributes to a nuanced and comprehensive assessment of the ConvADD architecture's performance in Alzheimer's disease classification, facilitating a deeper understanding of its strengths and areas for potential improvement.

2) *Comparative analysis*: Table II provides a comprehensive comparison of various models employed in the classification of Alzheimer's disease utilising MRI images. Each model's performance is evaluated based on crucial metrics, including accuracy, precision, recall, and F1-score, elucidating their effectiveness in accurately diagnosing Alzheimer's disease. The comparison encompasses ConvADD and ADD-Net with and without the SMOTETOMEK technique, as well as well-known architectures like AlexNet, ResNet-50, and Inception ResNet-50. This detailed analysis offers insights into the strengths and limitations of each model, highlighting ConvADD's exceptional performance across multiple evaluation metrics, signifying its potential as a pioneering diagnostic tool for Alzheimer's disease detection.

In our comparative analysis with existing methods for Alzheimer's disease classification using MRI images,

ConvADD emerged as a standout performer, showcasing superior performance across multiple evaluation metrics. ConvADD achieved an accuracy of 98.01%, outperforming other models such as ADD-Net (97.05%), ADD-Net with the SMOTETOMEK technique (92.88%), AlexNet (92.20%), ResNet-50 (93.10%), and Inception ResNet-50 (79.12%).

TABLE II. COMPARISON OF ALZHEIMER'S DISEASE CLASSIFICATION MODELS USING MRI IMAGES

| Reference | Accuracy | Precision | Recall | F1-score |
|---------------------------|----------|-----------|--------|----------|
| ConvADD | 98.01% | 98% | 98% | 98 % |
| ADD-Net (SMOTETOMEK) [48] | 97.05% | 97% | 97% | 97.05% |
| ADD-Net [48] | 92.88% | 82% | 89% | 84.55% |
| AlexNet [22] | 92.20% | - | 94.50% | - |
| ResNet-50 [52] | 93.10% | - | 92.55% | - |
| Inception ResNet-50 [49] | 79.12% | 70.64% | 28.22% | 39.91% |

When evaluating precision, ConvADD demonstrated a precision rate of 98%, surpassing ADD-Net (97%), ADD-Net with SMOTETOMEK (82%), AlexNet (N/A), ResNet-50 (N/A), and Inception ResNet-50 (70.64%). This superior precision illustrates ConvADD's capability to accurately identify true positive cases among the predicted positive results, highlighting its robustness in minimising false positives.

Regarding recall metrics, ConvADD exhibited a recall rate of 98%, outstripping ADD-Net (97%), ADD-Net with SMOTETOMEK (89%), AlexNet (94.50%), ResNet-50 (92.55%), and Inception ResNet-50 (28.22%). This high recall rate indicates ConvADD's effectiveness in identifying true positive cases from the actual positive cases in the dataset, showcasing its ability to detect relevant instances without missing many positive samples.

Analysing the F1 Score, ConvADD showcased an F1 Score of 98%, demonstrating a harmonious balance between precision and recall. This excelled against ADD-Net (84.55%), ADD-Net with SMOTETOMEK (97.05%), AlexNet (N/A), ResNet-50 (N/A), and Inception ResNet-50 (39.91%). ConvADD's high F1 score signifies its proficiency in correctly classifying positive instances while minimising false positives and negatives.

ConvADD's consistently superior performance across accuracy, precision, recall, and F1-score underscore its efficacy in Alzheimer's disease classification, showcasing its potential as an advanced diagnostic tool in healthcare settings.

B. Experimental Setup

1) *Experimental environment*: Utilising the robust computational resources of Google Colab Pro's GPU environment was pivotal in training and evaluating ConvADD, our novel architecture. This cloud-based platform provided scalable computational power, freeing us from hardware constraints and allowing a concentrated focus on model refinement.

Instead of relying on personal hardware configurations, Google Colab Pro offered a versatile environment, enabling a laser focus on ConvADD's architecture. We meticulously assessed the model's performance using a segregated test set derived from the original dataset, ensuring an unbiased evaluation of its generalizability and accuracy.

Recognising the limitations of singular metrics like accuracy, we took a multifaceted approach. Alongside accuracy, we examined diverse metrics encompassing loss, overfitting, and other relevant indicators. This comprehensive evaluation methodology presents a nuanced view of ConvADD's strengths and limitations, leading to a more robust and reliable model.

In adherence to open science principles, we are dedicated to sharing our work openly. The complete source code for ConvADD will be publicly accessible on GitHub¹. This transparency fosters collaboration, allowing for replication, extension, and contribution to the advancement of Alzheimer's Disease research.

2) *Training configuration*: Table III represents a comprehensive breakdown of the ConvADD architecture, delineating the intricate details of each layer within this specialised neural network tailored for Alzheimer's Disease classification using MRI images. From ConvBlock1 to the final Softmax layer, the table provides a detailed account of the output shapes, number of parameters, and specific configurations of each layer, underscoring the complexity and depth of the ConvADD model. Additionally, it encapsulates the predefined hyperparameters and training configurations instrumental in optimising the ConvADD architecture's performance and robustness during the training and validation phases.

The ConvADD architecture, tailored for Alzheimer's Disease classification utilising MRI images, comprises a sequence of convolutional blocks, fully connected layers, and a concluding Softmax output. Each convolutional block, ranging from ConvBlock1 to ConvBlock4, introduces distinct layers of complexity to the model's architecture.

¹<https://github.com/MAlsubaie/ConvADD.git>

TABLE III. CONVADD ARCHITECTURE: LAYER DETAILS AND TRAINING CONFIGURATIONS

| Layer Type | Output Shape | Number of Parameters |
|----------------------------|--------------------|----------------------|
| ConvBlock1 | (64, 32, 176, 208) | 2,308 |
| ConvBlock2 | (64, 32, 88, 104) | 34,976 |
| ConvBlock3 | (64, 64, 44, 52) | 70,752 |
| ConvBlock4 | (64, 128, 22, 26) | 1,895,104 |
| Dropout | (64, 128, 22, 26) | 0 |
| Flatten | (64, 7056) | 0 |
| LinearBlock1 | (64, 16) | 113,008 |
| LinearBlock4 | (64, 4) | 72 |
| Softmax | (64, 4) | 0 |
| Total number of parameters | | 2,116,220 |

ConvBlock1 initiates MRI image processing with 32 filters of 3x3 dimensions, yielding 32 sets of learned features and an output shape of (64, 32, 176, 208), entailing 2,308 parameters. Following this, ConvBlock2, utilising 32 filters akin to its predecessor, downsizes spatial dimensions via pooling, yielding an output of (64, 32, 88, 104) while contributing 34,976 parameters.

Advancing further, ConvBlock3 heightens model intricacy by doubling filters to 64, refining the image to (64, 64, 44, 52), and infusing 70,752 parameters. Subsequently, ConvBlock4 amplifies complexity with 128 filters, refining image processing and reducing spatial dimensions to (64, 128, 22, and 26), significantly elevating parameters to 1,895,104.

The Dropout and Flatten layers, though not adding parameters, play pivotal roles. Dropout combats overfitting by randomly deactivating neurons, while Flatten reshapes output for fully connected layers.

Linear blocks, especially Linear Block 1, which has 113,080 parameters, and Linear Block 4, which has merely 72 parameters, progressively process the flattened output, ultimately shaping the final output. The Softmax layer, computing class probabilities, doesn't introduce additional parameters.

The ConvADD architecture encompasses over two million parameters (2,116,220), highlighting its depth, intricate processing capacity, and potential to discern complex features from MRI images for Alzheimer's Disease classification.

Additionally, the ConvADD architecture underwent training and validation using predefined hyperparameters and training configurations to optimise performance and gauge robustness:

- Train Batch Size: 64
- Test Batch Size: 64

- Learning Rate: 0.001
- Number of Epochs: 10
- Validation Split: 15%
- Test Split: 15%

C. Performance of ConvADD

The ConvADD model was meticulously trained and validated over ten epochs using meticulously designed architecture and a carefully curated dataset. Throughout the training process, the model demonstrated remarkable progress in both accuracy and loss reduction, indicative of its ability to discern complex patterns inherent in AD pathology.

1) *Loss function:* The loss function, a critical metric in assessing model convergence and optimisation, exhibited a consistent downward trend over ten epochs. Fig. 4. shows loss starting at 0.0184 in the initial epoch; the loss function steadily decreased to 0.013 in the final epoch, showcasing the model's ability to minimise errors and optimise its predictions with training progression.

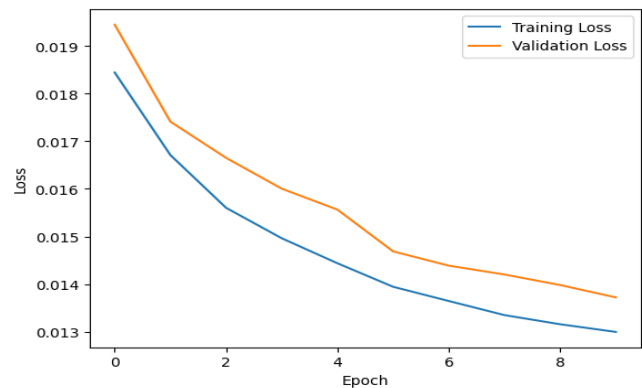


Fig. 4. Loss function trend over epochs.

2) *Training accuracy:* Simultaneously, ConvADD's accuracy increased remarkably during training, reflecting the model's enhanced proficiency in correctly classifying AD-related patterns within the dataset. Fig. 3. depicts starting accuracy at 68.5% in the initial epoch, ConvADD achieved an impressive 99.9% accuracy by the final epoch.

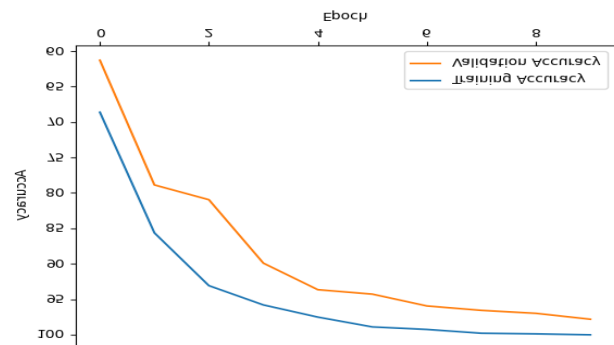


Fig. 5. Accuracy progression over training epochs.

3) *Confusion matrix*: The confusion matrix, a comprehensive representation of the model's classification performance, revealed ConvADD's robustness in classifying AD-related categories, as shown in Fig. 6. The model demonstrated exceptional precision, recall, and F1-score across MD, MOD, NOD, and VMD classes. With an accuracy of 98% and a macro average F1 score of 99%, ConvADD showcased its proficiency in discerning intricate nuances across various AD-related categories.

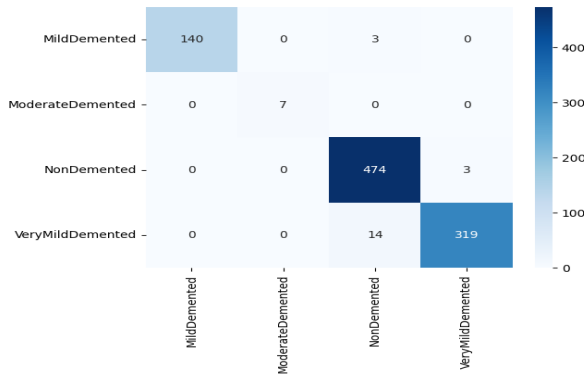


Fig. 6. Confusion matrix for ConvADD's classification performance.

The model's exceptional performance metrics across accuracy, loss function minimisation and confusion matrix analyses underscore its efficacy in precise AD detection without resorting to dataset balancing techniques. ConvADD's ability to capture intricate patterns indicative of AD pathology stands as a testament to its robustness and potential in clinical applications for AD diagnosis and prognosis.

D. Discussion

In evaluating various models for Alzheimer's Disease classification using MRI images, a thorough analysis emerges, highlighting ConvADD's noteworthy performance compared to established methodologies. ConvADD boasts superior accuracy at 98.01%, outshining the majority of models, including ADD-Net (97.05%), ADD-Net with SMOTETOMEK (92.88%), AlexNet (92.20%), ResNet-50 (93.10%), and Inception ResNet-50 (79.12%). This pronounced accuracy underscores ConvADD's efficacy in precisely discerning between different disease stages and healthy states. Moreover, ConvADD exhibits exceptional precision and recall at 98% across classes, indicative of its balanced identification of both positive and negative instances within the dataset. In contrast, models like Inception ResNet-50 display substantially lower recall scores, signifying their limitation in correctly identifying true positive instances, especially in classifying the mild cognitive impairment stage. ConvADD's robust performance across multiple metrics reaffirms its potential as a reliable diagnostic tool for

Alzheimer's disease, transcending the limitations observed in other widely employed models.

V. LIMITATIONS AND FUTURE DIRECTIONS

A. Model Limitations

Despite ConvADD's promising performance, several limitations warrant consideration. One notable aspect is the model's reliance on existing datasets, which may exhibit biases or inadequacies inherent in the data collection process. Dataset limitations, such as sample size, heterogeneity, or lack of diversity across demographics, may affect ConvADD's generalizability. Additionally, ConvADD's performance might vary when applied to datasets acquired from different imaging modalities or from varied scanning devices due to inherent variability in image quality and resolution.

Another limitation lies in the interpretability of ConvADD's decisions. Like many deep learning models, ConvADD operates as a complex, black-box system, making it challenging to discern the reasoning behind its classifications. This opacity could hinder its acceptance in clinical settings, where interpretability and explainability are critical.

Furthermore, ConvADD's performance might fluctuate when dealing with extremely noisy or ambiguous images, where identifying distinct pathological features becomes challenging. The model's ability to handle rare or atypical cases also needs careful consideration, as these instances might be underrepresented in training datasets, potentially affecting ConvADD's accuracy in such scenarios.

B. Future Prospects

Addressing the identified limitations opens avenues for future research in Alzheimer's Disease detection using ConvADD. One direction involves enhancing dataset quality and diversity, ensuring inclusivity across different demographic groups, disease stages, and imaging protocols. Augmenting datasets with more diverse samples, including rare and atypical cases, can further refine ConvADD's learning process, boosting its adaptability and robustness.

Another promising avenue involves advancing explainable AI techniques tailored for ConvADD, enabling the model to provide insights into its decision-making process. Methods such as attention mechanisms or saliency maps could elucidate the regions or features in the MRI images that significantly influence ConvADD's classifications, enhancing its interpretability and fostering trust among clinicians and practitioners.

Additionally, fine-tuning ConvADD or integrating transfer learning approaches on larger, more varied datasets or multi-

modal imaging data may fortify the model's capability to handle diverse image qualities and pathological manifestations. Exploring ensemble models or incorporating domain knowledge from neuroscience could further enrich ConvADD's understanding of complex disease patterns.

Moreover, deploying ConvADD in a real clinical setting for prospective validation studies could ascertain its performance, assess its practicality, and validate its utility as an auxiliary diagnostic tool. These studies could illuminate ConvADD's efficacy in aiding clinical decision-making and patient management, ensuring its seamless integration into the clinical workflow.

Continued research in these directions could not only surmount current limitations but also propel ConvADD toward becoming an indispensable, accurate, and clinically relevant tool for Alzheimer's disease diagnosis and monitoring.

VI. CONCLUSION

In conclusion, the ConvADD architecture stands as a pioneering convolutional neural network tailored explicitly for Alzheimer's Disease (AD) detection through MRI images. Its design, characterised by adapted conventional blocks and deep layers, exhibits superior discernment of AD pathology even with smaller datasets, marking a paradigm shift in AD detection frameworks.

Our contributions are substantial: the inception of ConvADD prioritises accuracy without relying on dataset balancing techniques, ensuring robust performance across varying dataset sizes. Comparative analyses underscore ConvADD's exceptional performance metrics against established state-of-the-art models, reaffirming its efficacy in AD detection.

The ConvADD model's performance, as depicted in the loss function, accuracy, and confusion matrix, demonstrates consistent advancements across epochs. With accuracy hovering around 98.01% and a robust F1-score of 98%, ConvADD showcases its reliability and proficiency in detecting different stages of AD, depicting precision in classifying distinct dementia types.

Comparison with existing models highlights ConvADD's superiority, particularly over ADD-Net with SMOTETOMEK and ADD-Net, showcasing its potential to outperform models leveraging data balancing techniques. The ConvADD architecture's strength lies in its ability to capture the multifaceted manifestations of AD, surpassing the limitations of classification-focused models.

While ConvADD exhibits promise, limitations in dataset biases, interpretability, and handling ambiguous images warrant further exploration. Future directions encompass refining dataset quality, enhancing interpretability, and integrating domain knowledge to fortify ConvADD's capabilities. Prospective validation studies in clinical settings will ascertain its utility and integration into clinical workflows.

In essence, ConvADD emerges as a transformative tool, poised to redefine AD detection. Its adaptability, accuracy, and potential to discern intricate disease features position it as a pivotal advancement in the realm of AD diagnostics, promising precision and early detection critical for effective therapeutic interventions and patient care.

REFERENCES

- [1] P. Porsteinnsson, R. S. Isaacson, S. Knox, M. N. Sabbagh, and I. Rubino, "Diagnosis of early Alzheimer's disease: clinical practice in 2021," *J Prev Alzheimers Dis*, vol. 8, pp. 371–386, 2021.
- [2] M. Prince, A. Wimo, M. Guerchet, G.-C. Ali, Y.-T. Wu, and M. Prina, "World Alzheimer Report 2015. The Global Impact of Dementia: An analysis of prevalence, incidence, cost and trends,," *Alzheimer's Disease International*, 2015.
- [3] S. Bano et al., "Emerging Therapeutic Targets in Molecular Neuropharmacology for Alzheimer's Disease," 2023.
- [4] P. Grammas, "Neurovascular dysfunction, inflammation and endothelial activation: implications for the pathogenesis of Alzheimer's disease," *J Neuroinflammation*, vol. 8, pp. 1–12, 2011.
- [5] C. Stadelmann, S. Timmler, A. Barrantes-Freer, and M. Simons, "Myelin in the central nervous system: structure, function, and pathology," *Physiol Rev*, vol. 99, no. 3, pp. 1381–1431, 2019.
- [6] A. L. Komaroff, P. E. Pellett, and S. Jacobson, "Human herpesviruses 6a and 6b in brain diseases: Association versus causation," *Clin Microbiol Rev*, vol. 34, no. 1, pp. 10–1128, 2020.
- [7] V. Vadmal, G. Junno, C. Badve, W. Huang, K. A. Waite, and J. S. Barnholtz-Sloan, "MRI image analysis methods and applications: an algorithmic perspective using brain tumors as an exemplar," *Neurooncol Adv*, vol. 2, no. 1, p. vdaa049, 2020.
- [8] T. Zhang et al., "Predicting MCI to AD conversion using integrated sMRI and rs-fMRI: machine learning and graph theory approach," *Front Aging Neurosci*, vol. 13, p. 688926, 2021.
- [9] S. Afzal et al., "Alzheimer disease detection techniques and methods: a review," 2021.
- [10] S. H. Hojjati, A. Ebrahimzadeh, A. Khazaei, A. Babajani-Feremi, A. D. N. Initiative, and others, "Predicting conversion from MCI to AD by integrating rs-fMRI and structural MRI," *Comput Biol Med*, vol. 102, pp. 30–39, 2018.
- [11] S. H. Hojjati, A. Ebrahimzadeh, and A. Babajani-Feremi, "Identification of the early stage of Alzheimer's disease using structural MRI and resting-state fMRI," *Front Neurol*, vol. 10, p. 904, 2019.
- [12] B. Ibrahim et al., "Diagnostic power of resting-state fMRI for detection of network connectivity in Alzheimer's disease and mild cognitive impairment: A systematic review," *Hum Brain Mapp*, vol. 42, no. 9, pp. 2941–2968, 2021.
- [13] A. Shukla, R. Tiwari, and S. Tiwari, "Review on alzheimer disease detection methods: Automatic pipelines and machine learning techniques," *Sci*, vol. 5, no. 1, p. 13, 2023.
- [14] S. Gao and D. Lima, "A review of the application of deep learning in the detection of Alzheimer's disease," *International Journal of Cognitive Computing in Engineering*, vol. 3, pp. 1–8, 2022.
- [15] S. Karande and V. Kulkarni, "Advancing Neurodegenerative Disorder Diagnosis: A Machine Learning-Driven Evaluation of Assessment Modalities," *International Journal of Intelligent Systems and Applications in Engineering*, vol. 12, no. 5s, pp. 309–323, 2024.

- [16] M. Tanveer et al., "Machine learning techniques for the diagnosis of Alzheimer's disease: A review," *ACM Transactions on Multimedia Computing, Communications, and Applications (TOMM)*, vol. 16, no. 1s, pp. 1–35, 2020.
- [17] M. Khojaste-Sarakhsi, S. S. Haghighi, S. M. T. F. Ghomi, and E. Marchiori, "Deep learning for Alzheimer's disease diagnosis: A survey," *Artif Intell Med*, vol. 130, p. 102332, 2022.
- [18] J. Chen et al., "3d transunet: Advancing medical image segmentation through vision transformers," *arXiv preprint arXiv:2310.07781*, 2023.
- [19] D. S. V. Kancherla, P. Mannava, S. Tallapureddy, V. Chintala, P. Kuppusamy, and C. Iwendi, "Pneumothorax: Lung Segmentation and Disease Classification Using Deep Neural Networks," in *2023 International Conference on Self Sustainable Artificial Intelligence Systems (ICSSAS)*, 2023, pp. 181–187.
- [20] A. H. Nizamani, Z. Chen, A. A. Nizamani, and K. Shaheed, "Feature-enhanced fusion of U-NET-based improved brain tumor images segmentation," *Journal of Cloud Computing*, vol. 12, no. 1, p. 170, 2023.
- [21] Y. LeCun, L. Bottou, Y. Bengio, and P. Haffner, "Gradient-based learning applied to document recognition," *Proceedings of the IEEE*, vol. 86, no. 11, pp. 2278–2324, 1998.
- [22] L. S. Kumar, S. Hariharasitaraman, K. Narayanasamy, K. Thinakaran, J. Mahalakshmi, and V. Pandimurugan, "AlexNet approach for early stage Alzheimer's disease detection from MRI brain images," *Mater Today Proc*, vol. 51, pp. 58–65, 2022.
- [23] S. Umirzakova, S. Ahmad, L. U. Khan, and T. Whangbo, "Medical image super-resolution for smart healthcare applications: A comprehensive survey," *Information Fusion*, p. 102075, 2023.
- [24] M. Paralic, K. Zelenak, P. Kamencay, and R. Hudec, "Automatic Approach for Brain Aneurysm Detection Using Convolutional Neural Networks," *Applied Sciences*, vol. 13, no. 24, p. 13313, 2023.
- [25] J. Haarsma, P. Kok, and M. Browning, "The promise of layer-specific neuroimaging for testing predictive coding theories of psychosis," *Schizophr Res*, vol. 245, pp. 68–76, 2022.
- [26] S. Guan, H. Liu, H. R. Pourreza, and H. Mahyar, "Deep Learning Approaches in Pavement Distress Identification: A Review," *arXiv preprint arXiv:2308.00828*, 2023.
- [27] S. Sharma and others, "Deep Learning for Predicting Breast Cancer: A Systematic Review of Progress and Future Directions," 2023.
- [28] S. Odimayo, C. C. Olisah, and K. Mohammed, "Structure-focused Neurodegeneration Convolutional Neural Network for Modeling and Classification of Alzheimer's Disease," *arXiv preprint arXiv:2401.03922*, 2024.
- [29] G. Folego, M. Weiler, R. F. Casseb, R. Pires, and A. Rocha, "Alzheimer's disease detection through whole-brain 3D-CNN MRI," *Front Bioeng Biotechnol*, vol. 8, p. 534592, 2020.
- [30] K. Bera, K. A. Schalper, D. L. Rimm, V. Velcheti, and A. Madabhushi, "Artificial intelligence in digital pathology—new tools for diagnosis and precision oncology," *Nat Rev Clin Oncol*, vol. 16, no. 11, pp. 703–715, 2019.
- [31] Y. Pan, B. Mirheidari, M. Reuber, A. Venneri, D. Blackburn, and H. Christensen, "Automatic hierarchical attention neural network for detecting AD," in *Proceedings of Interspeech 2019*, 2019, pp. 4105–4109.
- [32] P. Malhotra, L. Vig, G. Shroff, P. Agarwal, and others, "Long Short Term Memory Networks for Anomaly Detection in Time Series.," in *Esann*, 2015, p. 89.
- [33] Y. Zhang, X. He, Y. H. Chan, Q. Teng, and J. C. Rajapakse, "Multi-modal graph neural network for early diagnosis of Alzheimer's disease from sMRI and PET scans," *Comput Biol Med*, vol. 164, p. 107328, 2023.
- [34] M. G. Alsubaie, S. Luo, and K. Shaikat, "Alzheimer's Disease Detection Using Deep Learning on Neuroimaging: A Systematic Review," *Mach Learn Knowl Extr*, vol. 6, no. 1, pp. 464–505, 2024.
- [35] X. Xu, L. Lin, S. Sun, and S. Wu, "A review of the application of three-dimensional convolutional neural networks for the diagnosis of Alzheimer's disease using neuroimaging," *Rev Neurosci*, vol. 34, no. 6, pp. 649–670, 2023.
- [36] F. Lateef, M. Kas, and Y. Ruichek, "Saliency heat-map as visual attention for autonomous driving using generative adversarial network (gan)," *IEEE Transactions on Intelligent Transportation Systems*, vol. 23, no. 6, pp. 5360–5373, 2021.
- [37] M. Odusami, R. Maskeliūnas, and R. Damaševičius, "Optimized Convolutional Fusion for Multimodal Neuroimaging in Alzheimer's Disease Diagnosis: Enhancing Data Integration and Feature Extraction," *J Pers Med*, vol. 13, no. 10, p. 1496, 2023.
- [38] D. Agarwal, G. Marques, I. de la Torre-Díez, M. A. Franco Martin, B. García Zapira, and F. Martín Rodríguez, "Transfer learning for Alzheimer's disease through neuroimaging biomarkers: a systematic review," *Sensors*, vol. 21, no. 21, p. 7259, 2021.
- [39] Y. Zhu, X. Liang, J. A. Batsis, and R. M. Roth, "Exploring deep transfer learning techniques for Alzheimer's dementia detection," *Front Comput Sci*, vol. 3, p. 624683, 2021.
- [40] G. Devi, "A how-to guide for a precision medicine approach to the diagnosis and treatment of Alzheimer's disease," *Front Aging Neurosci*, vol. 15, p. 1213968, 2023.
- [41] B. Y. Kasula, "A Machine Learning Approach for Differential Diagnosis and Prognostic Prediction in Alzheimer's Disease," *International Journal of Sustainable Development in Computing Science*, vol. 5, no. 4, pp. 1–8, 2023.
- [42] A. G. Vrahatis, K. Skolariki, M. G. Krokidis, K. Lazaros, T. P. Exarchos, and P. Vlamos, "Revolutionizing the early detection of Alzheimer's disease through non-invasive biomarkers: the role of artificial intelligence and deep learning," *Sensors*, vol. 23, no. 9, p. 4184, 2023.
- [43] A. A. A. El-Latif, S. A. Chelloug, M. Alabdulhafith, and M. Hammad, "Accurate detection of Alzheimer's disease using lightweight deep learning model on MRI data," *Diagnostics*, vol. 13, no. 7, p. 1216, 2023.
- [44] Y. Xu, S. Hou, X. Wang, D. Li, and L. Lu, "A medical image segmentation method based on improved UNet 3+ network," *Diagnostics*, vol. 13, no. 3, p. 576, 2023.
- [45] A. W. Salehi et al., "A study of CNN and transfer learning in medical imaging: Advantages, challenges, future scope," *Sustainability*, vol. 15, no. 7, p. 5930, 2023.
- [46] N. N. Prakash, V. Rajesh, D. L. Namakhwa, S. D. Pande, and S. H. Ahammad, "A DenseNet CNN-based liver lesion prediction and classification for future medical diagnosis," *Sci Afr*, vol. 20, p. e01629, 2023.
- [47] A. Rayan et al., "Utilizing CNN-LSTM techniques for the enhancement of medical systems," *Alexandria Engineering Journal*, vol. 72, pp. 323–338, 2023.
- [48] M. M. S. Fareed et al., "ADD-Net: an effective deep learning model for early detection of Alzheimer disease in MRI scans," *IEEE Access*, vol. 10, pp. 96930–96951, 2022.
- [49] S. Mahmood et al., "A Robust Deep Model for Classification of Peptic Ulcer and Other Digestive Tract Disorders Using Endoscopic Images," *Biomedicines*, vol. 10, no. 9, p. 2195, 2022.
- [50] T. M. Ghazal et al., "Alzheimer Disease Detection Empowered with Transfer Learning.," *Computers, Materials & Continua*, vol. 70, no. 3, 2022.
- [51] G. Ahmed et al., "Dad-net: Classification of alzheimer's disease using adasyn oversampling technique and optimized neural network," *Molecules*, vol. 27, no. 20, p. 7085, 2022.
- [52] G. Ahmed, M. J. Er, S. Zikria, and M. S. Fareed, "Detection of Alzheimer's Disease using Deep Learning: An Optimized Approach," in *2023 6th International Conference on Intelligent Autonomous Systems (ICoIAS)*, 2023, pp. 148–155.

A Cost-Effective IoT-based Transcutaneous Electrical Nerve Stimulation (TENS): Proof-of-Concept Design and Evaluation

Ahmad O. Alokaily*, Meshael J. Almansour*, Ahmed A. Aldohbeyb, Suhail S. Alshahrani
Department of Biomedical Technology, College of Applied Medical Sciences,
King Saud University, Riyadh 12372, Kingdom of Saudi Arabia

Abstract—Transcutaneous electrical nerve stimulation (TENS) systems have been extensively used as a noninvasive and non-pharmaceutical approach for pain management and rehabilitation programs. Moreover, recent advances in telemedicine applications and the Internet of Things (IoT) have led to an increased interest in developing affordable systems that facilitate the remote monitoring of home-based therapeutic programs that help quantify usage and adherence, especially in clinical trials and research. Therefore, this study introduces the design and proof of concept validation of an IoT-enabled, cost-effective, single-channel TENS for remote monitoring of stimulation parameters. The presented prototype features programmable software that supports manipulating the stimulation parameters such as stimulation patterns, pulse width, and frequency. This flexibility can help researchers substantially investigate the effect of different stimulation parameters and develop subject-specific stimulation protocols. The IoT-based TENS system was built using commercial-grade electronic components controlled with open-source software. The system was validated for generating low-frequency (10 Hz) and high-frequency TENS stimulation (100 Hz). The developed system could produce constant biphasic pulses with an adjustable compliance voltage of 5–32 V. The stimulation current corresponding to the applied voltage was quantified across a resistive load of 1 k Ω , resulting in a stimulation current of approximately 4.88–28.79 mA. Furthermore, synchronizing the TENS system with an IoT platform provided the advantage of monitoring the usage and important stimulation parameters, which could greatly benefit healthcare providers. Hence, the proposed system discussed herein has the potential to be used in education, research, and clinics to investigate the effect of TENS devices in a variety of applications outside of the clinical setup.

Keywords—*Electro-stimulator; Internet of Things; TENS; pain management; smart health; IoT; telemedicine*

I. INTRODUCTION

Chronic pain, lasting over three months, is considered one of the critical public health issues worldwide, with approximately 20% of the world's population estimated to suffer from chronic pain [1, 2]. Several studies have reported that the prevalence of chronic pain in adults is approximately 33% and 56% in the elderly in middle-income and low-income countries [3]. Moreover, pain and pain-related illnesses are the primary cause of disability worldwide [4]. Thus, there is a continuous need to develop and implement therapeutic

interventions and medical technologies to enhance the quality of pain management.

Pain management is essentially managed via two main approaches: pharmacological and non-pharmacological interventions [5]. Pharmacological intervention has been shown to have some limitations and risks, such as opioid dependency, tolerance, and hyperalgesia [6, 7]. In comparison, non-pharmacological pain management strategies often refer to interventions and techniques used to reduce pain sensation without medicine. Non-pharmacological interventions such as physical and occupational therapy, psychological approaches, and neurostimulations have been previously shown to be effective in acute and chronic pain management [5].

One of the most widely used neurostimulation techniques for pain management is transcutaneous electrical nerve stimulation (TENS) [8]. TENS is a non-pharmacological, noninvasive, and inexpensive stimulation procedure in which pulses of electrical currents are delivered across the skin via pairs of electrodes that stimulate peripheral nerves to alleviate pain [9]. The analgesic effects of TENS have been shown to be effective in mediating pain sensation through peripheral and central neurological mechanisms [10]. Moreover, several studies have demonstrated the efficiency of various TENS protocols in alleviating neuropathic pain in multiple sclerosis [11], cancer [12], postherpetic [13], spinal cord injury [14], and stroke populations [15].

TENS devices can be configured with various stimulation parameters depending on the case. Therefore, the clinical settings for TENS can be classified into three main paradigms. In the conventional TENS protocol, low-intensity electrical pulses are delivered at a high frequency (50–100 Hz) with a pulse width adjustable between 50 and 200 μ s, while in the intense TENS protocol, high-intensity electrical pulses are delivered at a low frequency (<10 Hz). Moreover, acupuncture-like TENS is configured to provide high-intensity electrical pulses at low frequencies (<10 Hz) with a more extended pulse width of 100–400 μ s [16].

The physiological mechanism of conventional TENS is believed to be based on the Gate-Control theory of pain, where the activation of large-diameter mechanoreceptive nerve fibers with a low threshold level leads to impeding the transmission of action potentials generated by small-diameter nociceptive fibers [8, 9]. Essentially, the touch-related nerves can prevent the pain-related nerves from sending signals to the brain by

blocking their transmission through the spinal cord. Moreover, an acupuncture-like TENS paradigm is intended to cause muscle twitches by engaging the motor afferents with a small diameter to induce extrasegmental analgesia, whereas the intense TENS paradigm causes extrasegmental analgesia and peripheral nerve blockade via the activation of small-diameter noxious afferents [17].

Several previous studies have investigated the feasibility of developing nerve and muscle microcontroller-based stimulation systems that can be used in educational, clinical, or research setups. For instance, Cornman et al. [18] proposed a portable, inexpensive, low-power consumption stimulation apparatus capable of producing ± 150 V monophasic or biphasic pulses. Additionally, Trout et al. [19], implemented and further developed a proposed TENS electrical design of the stimulator proposed in [18] and validated its use for cutaneous and transcutaneous nerve stimulation. The results of Trout et al. show that nerve and muscle stimulation generated comparable forces with no significant effect of stimulation timing when applied to nerves or hand muscles.

Advances in smart technology applications in healthcare have gained attention in recent years as they provide the benefit of remote monitoring of patients' conditions and can be utilized as a tool to monitor patients' adherence, particularly for self-administered therapeutic interventions. Therefore, various medical applications have been developed to support the integration of IoT technology to support remote monitoring and reduce the daily time clinicians need for patient follow-ups. For instance, Ursache et al. [20] developed a low-cost smart TENS system that can be programmed and controlled via an Android application that can digitally adjust the stimulation parameters. Their proposed system was developed from commercial, low-cost electronic hardware and could deliver up to 100 V of monophasic pulses with an adjustable pulse duration. Additionally, Ortiz et al. [21] designed a knee orthosis with an embedded Bluetooth-connected TENS system controlled by a mobile application with customizable electrical muscle stimulation parameters suitable for osteoarthritis treatment.

To the best of our knowledge, no study has investigated the ability to develop an open-access, programable, and inexpensive TENS system incorporating the IoT application and its importance in enhancing the remote monitoring of systems designed to be operated by end users out of clinical setups with minimal training. Therefore, this paper presents and discusses the design and development of a low-cost and Internet of Things (IoT)-based TENS system. The use of an IoT-enabled neurostimulation system could facilitate the remote monitoring of patients' use of the TENS system and provide accurate information regarding adherence to prescribed daily usage.

The rest of this study is structured as follows: Section II provides an overview of the primary hardware elements of the proposed IoT-based TENS system along with details about the software structure and interface. Section III presents the proposed system's integration and validation. Lastly, Section IV discusses the study's conclusions, outlining its objectives and offering suggestions for future advancements.

II. MATERIALS AND METHODS

The development of the IoT-based TENS system consists of identifying effective and inexpensive low-power consumption electronic hardware and tailored software to control the stimulation parameters. An IoT platform containing individual channels is also needed to record and monitor patient usage and the most critical protocol parameters, such as stimulation frequency and duration. The block diagram of the IoT-TENS system is shown in Fig. 1.

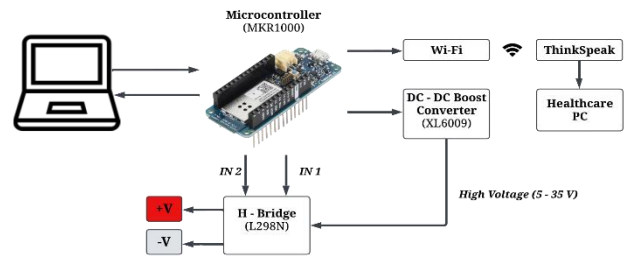


Fig. 1. Block diagram of the proposed IoT-based TENS unit.

A. Hardware Design

The electrical hardware components used in the study were selected based on their efficiency to provide an effective compliance voltage and the required amount of direct current stimulation. Hence, the IoT-based TENS was constructed using the following main consumer-grade components:

1) *Microcontroller*: A low-cost consumer-grade microcontroller (MKR 1000, Arduino LLC, Boston, MA) with internet connectivity via the integrated Wi-Fi shield. The IoT-enabled microprocessor is crucial for transmitting session information to the cloud.

2) *Notebook*: The proposed TENS system must be connected to a computer or notebook to power the system via the universal serial bus and establish serial communication with the microcontroller to send commands through a simple, user-friendly interface.

3) *DC-DC step-up voltage transformer*: A voltage boost converter was used to increase the output voltage of the microcontroller. The DC-DC voltage boost converter (XL 6009) used in this study can increase the essential 5-V-supplied input voltage to an output voltage between 5 and 32 V. The desired output voltage can be adjusted via an incorporated potentiometer.

4) *Full H-Bridge module*: TENS protocols could be administered through mono- or biphasic pulses. However, biphasic symmetrical TENS was found to achieve better clinical results [22]. Therefore, a dual H-Bridge (L298N) driver module was used in this prototype to switch the polarity of the monopolar pulses generated by the microcontroller and amplified by the boost converter. The H Bridge allows for generating positive and negative pulses with a maximum voltage of 5–35 V and a maximum current of 1 mA per channel.

5) *Surface electrodes*: A pair of adhesive 5 × 5-cm reusable surface electrodes were used.

B. Internet of Things Platform

The ThingSpeak platform was used in the IoT-based TENS device. A private channel was established to capture, track, and retrieve real-time information on the chosen stimulation type and duration. This information is critical for healthcare providers to track the patient’s adherence to protocol and frequency of use [23].

C. Software Architecture

An open-access C++-based Arduino Integrated Development Environment (IDE; Version 2.1.1) was used to design custom-made software to control and activate the IoT-based TENS system. The software initiated the connection to the wireless network to feed the session’s information to the IoT cloud at the start and finish of the stimulation. In addition, the healthcare provider could adjust the stimulation parameters, such as pulse width, frequency, and interpulse interval, to suit patients’ needs. The stimulation pattern can be modified to be mono- or biphasic as needed. However, the work presented here was based on symmetric biphasic stimulation pulses as monophasic stimulation may lead to adverse effects such as excessive accumulation of charge and skin irritation [24, 25].

Therefore, various settings were implemented as a proof of concept for the IoT-based TENS system demonstrated in this study. Two distinct biphasic stimulation montages were programmed. First, the low-frequency stimulation, which has a stimulation frequency of 10 Hz and a pulse width of 400 μs, and the high-frequency stimulation protocol, where the stimulation was delivered at 100 Hz with a pulse width of 200 μs. The custom-made algorithm was designed based on the switch statement approach, where a set of discrete stimulation options are preconfigured based on the two types of stimulation (low frequency or high frequency) and the stimulation duration (5, 10, 15, 20, and 30 min).

The flowchart of the proposed algorithm is shown in Fig. 2. Users are prompted to enter a predefined code of the required stimulation frequency and duration, as shown in Table I. Upon entering the correct session code, the stimulation would begin by sending activation pulses from the microcontroller digital pins to produce the amplified biphasic stimulation pulses (pin 6 for the positive phase and pin 11 for the negative phase). Furthermore, the session information (frequency and duration) would be fed to the IoT ThinkSpeak cloud at the beginning and end of each session.

TABLE I. STIMULATION SETTINGS

| Stimulation type | Predefined session code | Duration ^a (minutes) | Pulse width ^a |
|---|-------------------------|---------------------------------|--------------------------|
| Low Frequency (default: 10 Hz ^a) | a | 5 | 400μs |
| | b | 10 | |
| | c | 15 | |
| | d | 20 | |
| | e | 30 | |
| High Frequency (default: 100 Hz ^a) | f | 5 | 200μs |
| | g | 10 | |
| | h | 15 | |
| | i | 20 | |
| | j | 30 | |

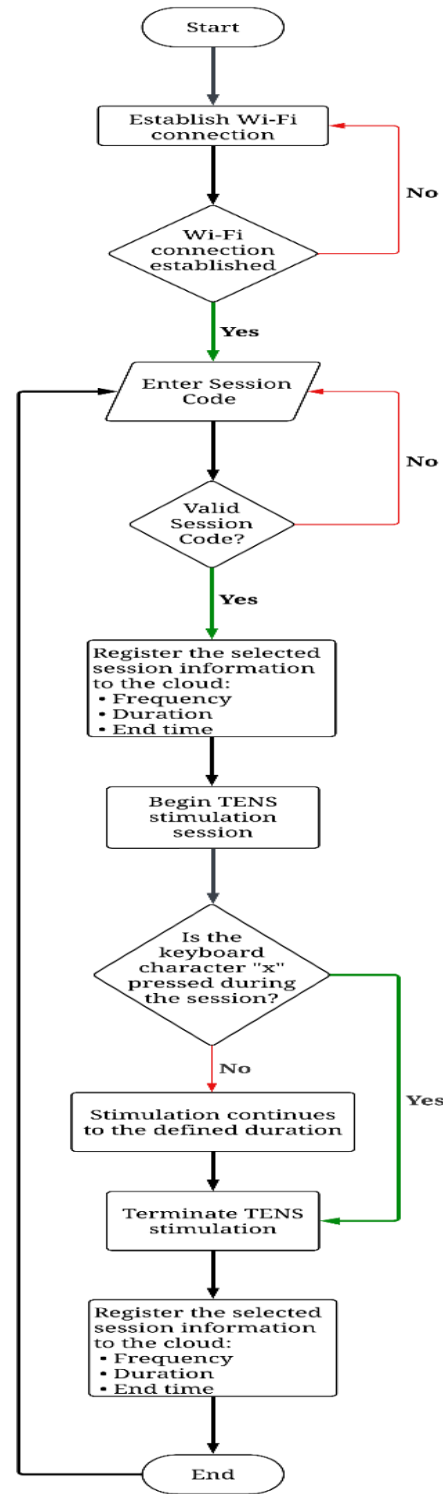


Fig. 2. Flowchart of the IoT-based TENS software.

D. System Functionality Testing

To evaluate the performance of the IoT-based TENS, the generated biphasic square pulses were monitored via an oscilloscope. The resulting frequency, current, and voltage range were recorded using a digital multimeter (GDM-451,

GW Instek) across a resistor with a resistance of 1000Ω to represent human skin resistance [26]. The stimulation durations were also monitored and recorded to confirm the accuracy of each selected duration option. Moreover, the successful real-time synchronization of the session information was validated, including the stimulation type and the duration of the session between the proposed IoT-TENS system and the ThinkSpeak cloud.

III. RESULTS

A. System Integration

The prototype of the constructed IoT-based TENS system is shown in Fig. 3. The system components can be secured in a compact portable box with approximate dimensions of $16 \times 10 \times 8$ cm. The proposed system successfully generated square pulses originating from the pulse-width modulation pins of the microcontroller and amplified by the DC-DC converter. The monophasic pulses were then converted into biphasic pulses via the H-bridge module (see Fig. 4). The resulting output peak-to-peak voltage of the system is adjustable between approximately 10–60 V (peak-to-peak) via the DC-DC converter voltage adjust potentiometer. The potentiometer allows users to alter the current intensity of the stimulation by increasing or decreasing the compliance stimulation voltage. Notably, the cost of developing the single-channel IoT-based TENS system was \$58.72.

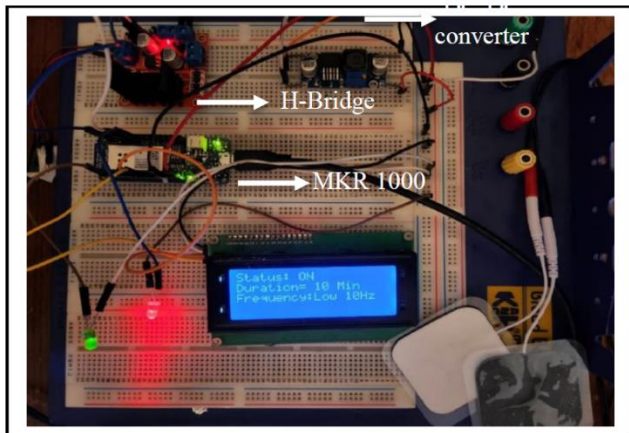


Fig. 3. Photograph of the proposed IoT-based TENS circuit.

B. System Validation

The noninvasive IoT-based TENS system operation was validated by visualizing the output waveform across the electrode leads. The low-frequency stimulation program generated biphasic stimulation waveforms, as shown in Fig. 4. Using a load of $1 \text{ k}\Omega$, the stimulation current amplitude can be changed between 4.88 mA and 28.79 mA for compliance voltage between 5 and 30 V, respectively, with a variation of stimulation current between -0.90% and -4.03% (see Table II). Moreover, testing the system's internet connectivity revealed that maintaining connectivity was achievable with a mobile hotspot. Two data points recorded the selected session's information on start time, stimulation duration and frequency, and the end time, upon which the stimulation was completed across all the predefined settings and uploaded to the system's private channel, accordingly (see Fig. 5).

TABLE II. COMPARISON BETWEEN CALCULATED AND MEASURED CURRENT INTENSITY

| Applied peak voltage (V_p) | Calculated current across a resistive load of $1\text{k}\Omega$ ($I_p = V_{IN}/R_L$) | Measured Current | Error |
|--------------------------------|--|------------------|---------|
| 5 V | 5 mA | 4.88 mA | -2.4 % |
| 10 V | 10 mA | 9.91 mA | -0.90 % |
| 20 V | 20 mA | 19.23 mA | -3.85% |
| 30 V | 30 mA | 28.79 | -4.03 % |

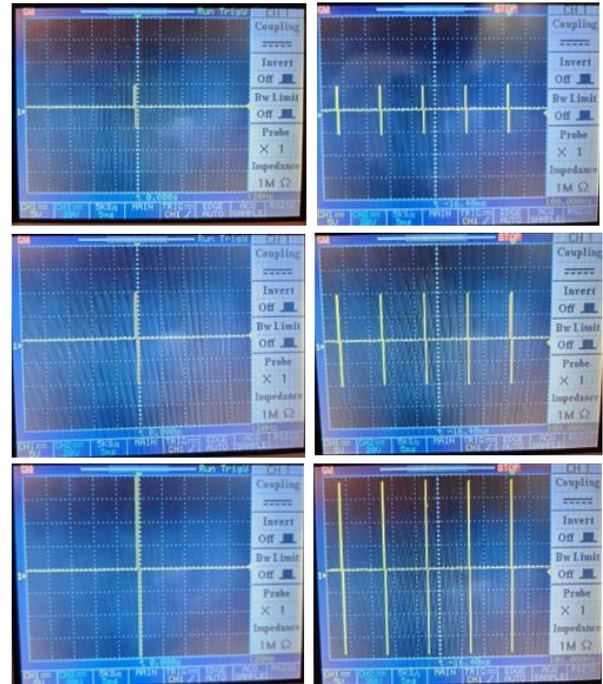


Fig. 4. Demonstrates the testing of the IoT-based biphasic output voltage with an oscilloscope, showcasing different compliance voltages and stimulation frequencies. The left column shows low-frequency stimulation pulses (10 Hz) with 10, 20, and 40 V peak-to-peak voltage amplitudes, respectively. The right column displays high-frequency stimulation pulses (100 Hz) with 10, 20, and 40 V peak-to-peak voltage amplitudes, respectively.

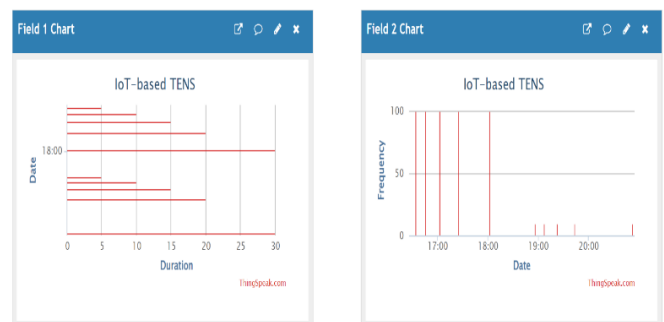


Fig. 5. ThinkSpeak private channel information in which the session duration in minutes (left) and frequency in Hertz (right) were updated and validated for each predefined setting.

IV. CONCLUSION

The IoT-based TENS system presented in this study demonstrates the feasibility of constructing an affordable single-channel TENS system with IoT capabilities that can be used in research laboratories and studies requiring users' adherence to the stimulation protocols. Moreover, the data

derived from the IoT-based TENS can be critical in evaluating the effect of the TENS system, especially in cases where users are instructed to employ the stimulation system as a treatment for pain. Additionally, the stimulation waveforms and properties of most of the available TENS systems in the market cannot be customized [19]. Thus, using a microcontroller-based system and the associated software has the advantage of designing tailored stimulation patterns, durations, and frequencies to target different clinical or research purposes and facilitate the customization of stimulation parameters for each end user.

The proposed system has an additive value of incorporating the IoT feature that can automatically save vital information regarding system usage compared with the previously developed TENS systems [19-21]. Although the IoT-based TENS system incorporated a single stimulation channel and biphasic stimulation patterns were presented, this can be expanded to two or more channels, and monophasic or biphasic stimulation can be generated, as in [18, 19]. Furthermore, although the generated compliance voltage capabilities of the presented system (± 30 V) are commonly used in battery-powered TENS systems, this can be further enhanced and upgraded directly by replacing the DC-DC boost converter and the H-bridge modules with other models that have higher power ratings as used in [18, 19]. However, as TENS systems are often available as over-the-counter options, operating high-voltage instruments of ± 300 V is hazardous and requires those systems to be only used in a well-controlled environment.

Further studies are required to validate the efficacy of the proposed IoT-based TENS systems on the human population to evaluate their ability to stimulate nerves and muscles. Additional research can discern whether the proposed system has the potential to be used in clinical treatment programs to reduce the sensation of pain.

DATA AVAILABILITY STATEMENT

The data supporting this study's findings are available within the text.

REFERENCES

- [1] Y. Jiang, T. Xu, F. Mao, Y. Miao, B. Liu, L. Xu, et al., "The prevalence and management of chronic pain in the Chinese population: findings from the China Pain Health Index (2020)," *Popul. Health Metr.*, vol. 20, no. 1, p. 20, Nov 4, 2022.
- [2] R. D. Treede, W. Rief, A. Barke, Q. Aziz, M. I. Bennett, R. Benoliel, et al., "A classification of chronic pain for ICD-11," *Pain*, vol. 156, no. 6, pp. 1003-1007, Jun 2015.
- [3] S. E. E. Mills, K. P. Nicolson, and B. H. Smith, "Chronic pain: a review of its epidemiology and associated factors in population-based studies," *Br. J. Anaesth.*, vol. 123, no. 2, pp. e273-e283, Aug 2019.
- [4] T. Jackson, S. Thomas, V. Stabile, X. Han, M. Shotwell, and K. McQueen, "Prevalence of chronic pain in low-income and middle-income countries: a systematic review and meta-analysis," *Lancet*, vol. 385 Suppl 2, p. S10, Apr 27, 2015.
- [5] S. Grassini, "Virtual reality assisted non-pharmacological treatments in chronic pain management: a systematic review and quantitative meta-analysis," *Int. J. Environ. Res. Publ. Health*, vol. 19, no. 7, p. 4071, 2022.
- [6] J. Højsted and P. Sjøgren, "Addiction to opioids in chronic pain patients: a literature review," *Eur. J. Pain*, vol. 11, no. 5, pp. 490-518, 2007.
- [7] P. Gerner, "Postthoracotomy pain management problems," *Anesthesiol. Clin.*, vol. 26, no. 2, pp. 355-367, 2008.
- [8] O. Tashani and M. Johnson, "Transcutaneous Electrical Nerve Stimulation (TENS) A Possible Aid for Pain Relief in Developing Countries?," *Libyan J. Med.*, vol. 4, no. 2, pp. 62-65, Jun 1, 2009.
- [9] W. W. Peng, Z. Y. Tan, F. R. Zhang, H. Li, Y. Z. Kong, G. D. Iannetti, L. Hu, "Neurobiological mechanisms of TENS-induced analgesia," *Neuroimage*, vol. 195, pp. 396-408, Jul 15, 2019.
- [10] T. Mokhtari, Q. Ren, N. Li, F. Wang, Y. Bi, and L. Hu, "Transcutaneous Electrical Nerve Stimulation in Relieving Neuropathic Pain: Basic Mechanisms and Clinical Applications," *Curr. Pain Headache Rep.*, vol. 24, no. 4, p. 14, Feb 18, 2020.
- [11] L. Miller, P. Mattison, L. Paul, and L. Wood, "The effects of transcutaneous electrical nerve stimulation (TENS) on spasticity in multiple sclerosis," *Mult. Scler. J.*, vol. 13, no. 4, pp. 527-533, 2007.
- [12] R. D. Searle, M. I. Bennett, M. I. Johnson, S. Callin, and H. Radford, "Transcutaneous electrical nerve stimulation (TENS) for cancer bone pain," *J. Pain Sympt. Manag.*, vol. 37, no. 3, pp. 424-428, 2009.
- [13] A. Mittal, B. Masuria, and P. Bajaj, "Transcutaneous electrical nerve stimulation in treatment of post herpetic neuralgia," *Indian J. Dermatol. Venereol. Leprol.*, vol. 64, no. 1, pp. 45-47, 1998.
- [14] E. Celik, B. Erhan, B. Gunduz, and E. Lakse, "The effect of low-frequency TENS in the treatment of neuropathic pain in patients with spinal cord injury," *Spinal Cord*, vol. 51, no. 4, pp. 334-337, 2013.
- [15] M. Kılınc, A. Livanelioğlu, S. A. Yıldırım, and E. Tan, "Effects of transcutaneous electrical nerve stimulation in patients with peripheral and central neuropathic pain," *J. Rehabil. Med.*, vol. 46, no. 5, pp. 454-460, 2014.
- [16] M. I. Johnson, L. S. Claydon, G. P. Herbison, G. Jones, and C. A. Paley, "Transcutaneous electrical nerve stimulation (TENS) for fibromyalgia in adults," *Cochrane Database Syst. Rev.*, vol. 10, no. 10, CD012172, 2017.
- [17] M. Johnson, "Transcutaneous Electrical Nerve Stimulation: Mechanisms, Clinical Application and Evidence," *Rev. Pain*, vol. 1, no. 1, pp. 7-11, Aug 2007.
- [18] J. Comman, A. Akhtar, and T. Bretl, "A portable, arbitrary waveform, multichannel constant current electro-tactile stimulator," *Int. IEEE EMBS Conf. Neural. Eng.*, vol. 2017, pp. 300-303, May 2017.
- [19] M. A. Trout, A. T. Harrison, M. R. Brinton, and J. A. George, "A portable, programmable, multichannel stimulator with high compliance voltage for noninvasive neural stimulation of motor and sensory nerves in humans," *Sci. Rep.*, vol. 13, no. 1, p. 3469, 2023.
- [20] T. Ursache, A. Cretu, G. Petroiu, and C. Rotariu, "A wireless low-cost device for transcutaneous electrical nerve stimulation," in *2021 12th Int. Symp. Adv. Topics Electr. Eng. (ATEE)*, 2021, pp. 1-4: IEEE.
- [21] J. M. Ortiz, A. T. Ruiz, and G. S. Cuesta, "Design of a device for treatment of knee osteoarthritis with TENS, EMS and iontophoresis through an Android application on a smartphone," in *VI Latin Am. Cong. Biomed. Eng. CLAIB 2014*, Paraná, Argentina 29, 30 & 31 October 2014, 2015, pp. 79-82.
- [22] O. Ronzio and C. Villa, "Analgesic effects of monophasic and biphasic tens with two different phase durations on cold-induced pain in normal subjects," *Physiotherapy*, vol. 101, pp. e1295-e1296, 2015.
- [23] A. O. Alokaily, G. Almeteb, R. Alhabiti, and S. S. Alshahrani, "Towards home-based therapy: The development of a low-cost IoT-based transcranial direct current stimulation system," *Int. J. Adv. Comp. Sci. Appl.*, vol. 13, no. 10, 2022.
- [24] C. Turnbull, A. Boomsma, R. Milte, T. R. Stanton, and B. Hordacre, "Safety and adverse events following non-invasive electrical brain stimulation in stroke: A systematic review," *Top. Stroke Rehab.*, vol. 30, no. 4, pp. 355-367, 2023.
- [25] R. E. Fary and N. K. Briffa, "Monophasic electrical stimulation produces high rates of adverse skin reactions in healthy subjects," *Physiother. Theory Pract.*, vol. 27, no. 3, pp. 246-251, 2011.
- [26] G. Kantor and G. Alon, "Transcutaneous electrical stimulation devices tests," in *Proc. 18th Ann. Int. Conf. IEEE Eng. Med. Biol. Soc.*, 1996, vol. 5, p. 2193 vol. 5: IEEE.

An Intelligent Learning Approach for Improving ECG Signal Classification and Arrhythmia Analysis

Sarah Allabun

Department of Medical Education, College of Medicine,
Princess Nourah bint Abdulrahman University, P.O.Box 84428, Riyadh 11671, Saudi Arabia

Abstract—The development of deep learning algorithms in recent years has shown promise in interpreting ECGs, as these algorithms can be trained on large datasets and can learn to identify patterns associated with different heart conditions. The advantage of these algorithms is their ability to process large amounts of data quickly and accurately, which can help improve the speed and accuracy of diagnoses, especially for patients with heart conditions. Our proposed work provides performant models based on residual neural networks to automate the diagnosis of 12-lead ECG signals with more than 25 classes comprising different cardiovascular diseases (CVDs) and a healthy sinus rhythm. We conducted an experimental study using public datasets from Germany, the USA, and China and trained two models based on Residual Neural Networks-50 (ResNet-50) and Xception from CNN techniques, which is one of the most effective classification models. Our models achieved high performances for both training and test tasks in terms of accuracy, precision, recall, and loss, with accuracy, recall, and precision exceeding 99.87% for the two proposed models during the training and validation. The loss obtained by the end of these two phases was 3.38.10⁻⁴. With these promising results, our suggested models can serve as diagnostic aids for cardiologists to evaluate ECG signals more quickly and objectively. Further quantitative and qualitative evaluations are presented and discussed in the study, and our work can be extended to other multi-modal big biological data tied with ECG for similar sets of patients to obtain a better understanding of the proposed approach for the benefit of the medical world.

Keywords—*Electrocardiogram; cardiovascular diseases; classification; ResNet-50; Xception*

I. INTRODUCTION

Globally, one of the major causes of death is cardiovascular disease (CVD) as it represents about greater than 30% which 85% of it is a heart attack, it is expected that more than 130 million people will be suffering by 2035 [1]. CVD has caught the attention of many researchers as they have been studying to elaborate solutions for the prevention and detection of these diseases regarding their impact economically [2]. Every year, studies have shown that the impact of CVD on the American and European economies is estimated at \$555M and €210M, respectively. Understanding how the heart's electrical system works is crucial before examining [20] the electrocardiogram (ECG). The heart is an organ that periodically contracts and relaxes. Its cells play a role in the propagation of electrical impulses to nearby cardiac cells [3].

The principle of the ECG is to record the electrical impulses at the origin of cardiac contractions. The electrical impulses are

recorded away from the heart, through the skin, using electrodes [4]. There are two types of electrodes: six precordial electrodes implanted on the chest and three frontal electrodes (or four, to refine the signal) placed on the limbs. The accuracy of the diagnosis is influenced by the number of electrodes. In fact, the more there are, the more accurate and precise the diagnosis will be. The accuracy of an electrocardiograph with 4 leads will be less than one with 12 leads. The most common clinical use is with 12 leads [5]. If the electrical impulse moves toward one of these electrodes, it registers a positive signal; if it moves away, it registers a negative signal. The wrists and ankles of the patient are where the frontal electrodes are placed [6]. They enable the reconstruction of the patient's heart's electrical axis; the ECG is the tracing obtained. Numerous cardiac issues are highlighted by this diagram, including atrioventricular blocks (poor electrical impulse conduction), bradycardias, and tachycardias with a slowing or accelerating of these complexes on the drawing [7].

The interpretation of this schema enables the doctor to confirm whether the heart is functioning properly. The responsibilities of cardiologists are expanding along with the rise of cardiac problems. Cardiology variation both within and across radiologists affects the manual interpretation [8]. The result of the manual interpretation will also be influenced by other factors such as mood, exhaustion, and others. Doctors regularly analyze and interpret ECGs, the diagnoses are greatly influenced by the doctor's training, qualifications, expertise, and experience. However, even experts and specialists are unable to fully identify all ECG signals information. In actuality, the analysis of lengthy recordings, such as Holter examinations and ambulatory cases of continuous monitoring in intensive care and intensive care and resuscitation units, is difficult and time-consuming, particularly for the detection of characteristic waves of the ECG signal and the classification of heartbeats [9].

Nowadays, innovative technologies such as Artificial intelligence have been helpful in a revolutionary way. Computer-aided medical diagnostics (CAMD) are now crucial for the diagnosis of CVD due to developments in hardware and algorithms. Cardiologists can consult CAMDs based on ECG signals for guidance and interpret results within a few seconds by checking CVD-specific characteristics. Due to the enormous number of patients in critical care units and the requirement for ongoing surveillance, they can assist doctors in making the diagnosis in a simpler and quicker way, which appears to be essential [10]. This is how it appeared that DMAOs helped with the ECG signal-based cardiac diagnosis. These systems

should be simple to use, scalable, precise, reliable, and solid. Several techniques have been suggested in the latest decades for the evaluation of CVD. Various approaches, such as Deep Learning (DL) techniques have lately become useful tools in complex applications such as computerized machine vision and natural language processing. Among DL technics, a convolutional neural network (CNN) is by far one of the most effective [11].

Many researchers have shown interest in this topic and numerous approaches have been put out by various researchers to address it. There are several types of CVDs surpassing 100 types. This study aims to classify 27 heart rhythm types using ECG data including 26 different varieties of CVDs and normal sinus rhythm. The four merged used datasets to train, validate, and assess models in this classification, which comprises 42511 ECG records. The dataset utilized comprises 12-lead ECG signals, which is a common ECG category used in hospitals and clinical situations. It is trained with two models based on Residual Neural Networks-50 (ResNet-50) and Xception from CNN techniques, which is one of the most effective classification models.

The remainder of this investigation is organized as follows. Section II provides a review of comparable publications in the literature, while Section III described the suggested model and the simulation methodologies. A discussion and evaluation of the proposed ECG classification models' findings are provided in Section IV. Test phases are given in Section VI. Finally, Section VI discusses the conclusion and future projects.

II. RELATED WORKS

For ECG diagnosis, the Uni-G analysis tool, developed by the University of Glasgow, used rule-based criteria on signal processing and medical characteristics [3]. Datta et al obtained the best score in the Physionet/CinC Challenge 2017 [4] that have as its objective the single-leads ECGs classification. They applied a feature-oriented technique that includes a two-layer cascaded binary classifier. Another SP was employed in [6], Aziz et al used a Discrete Wavelet Transform (DWT) and SVM to detect R peaks and classify ECG signals.

Lately, DL models have been used on ECG data for a variety of applications such as denoising signals, pathology diagnosis [12], annotation or detection, and so on. The application of Deep Neural Network (DNN) in the classification of single or multiple ECG leads had shown a wonderful outcome [13]. Moreover, the results obtained by the employment of a DNN on 91,232 ECG records are more performant than cardiologists when trying to diagnose 11 types of CVDs [14].

There are a variety of datasets used to train DL models. Most publications employ public databases such as MIT-BIH Databases and the Physionet/CinC Challenges dataset. For example, the first dataset is MIT-BIH Arrhythmia Database [15] which comprises 48 2-leads ambulatory ECG recordings. Each one has a duration of 30 min. These were acquired from the BIH Arrhythmia Laboratory's 47 patients investigated between 1975 and 1979. This dataset includes five classes. In addition, MIT-BIH Atrial Fibrillation Database [16] contains 25 ECG records. The duration of all the recordings is 10 hours.

Most of the investigation dedicated to the Atrial Fibrillation (AFib) automated detection used this dataset. In addition, PTB is a widely used dataset that includes 54912-leads ECG signals from 290 subjects. This contains nine various diagnostic classes. Also, Ones of the most utilized dataset in the task of ECG classification are China Physiological Signal Challenge datasets [17]. Actually, the CPSC 2017, includes 8528 single lead ECG recordings. Their duration varies from 9s to 61s, and this comprises four classes: AFib, Normal, Noise and other MCVs. Whereas the CPSC 2018, it is a series of 6877 10s 12-leads ECG records. This comprises 9 diagnostic classes [18].

Ribeiro et al [19] used 2,322,513 ECG recordings, collected from 1,676,384 various patients, containing 6 types of CVDs as the training and the validation set. Their model is based on a Deep Neural Network (DNN) Architecture. DNNs outperformed cardiology resident clinicians in detecting six categories of anomalies in 12-lead ECG recordings, with F1-score over 80% and specificity exceeding 99%. These findings show that ECG diagnosis using DNNs, which was before examined in a single-lead scenario, generalizes effectively to 12-lead tests, bringing the technique closer to mainstream clinical practice. Besides, Zhu et al. [23] established their work on private dataset counting 180,112 12-leads ECG from 70,692 patients, including 21 classes. To classify these CVDs, they employed a CNN. The suggested CNN model consists of fifteen alternating layers for multilabel classification of the 21 heartbeats varieties. Shortcut connections in residual blocks were utilized to skip intermediate layers to avoid gradient vanishing difficulties. Rectified linear unit (ReLU) nonlinearity with dropout was utilized in the network to improve the performance and avoid the overfitting of the model. Similar to Zhu et al., Zhang et al. [21] used CNN to classify 6877 12-leads ECG provided by the CPSC 2018 to nine heart rhythm types. The suggested 1D-CNN has a similar overview to the original residual neural network for image recognition with 2D CNNs [22]. Actually, the proposed model has 34 layers. To capture deep characteristics, four residual blocks are stacked, then employed. Moreover, they used SHapley Additive exPlanations (SHAP) [23] to interpret the prediction of the model. This was used to interpret the patient level and the population level. Otherwise, this clarifies the attitude of the model against the single input, 12-lead ECG, and the whole used dataset. The SHAP method is based on game theory. In simple terms, it measures the impact on the prediction of adding a variable (all else being equal) by permuting all possible options.

In other papers, researchers opted to combine Neural Networks to boost models' performance. Zheng et al. [24] developed model formed by a combination of CNN and long short-term memory (LSTM) which belong to the Recurrent Neural Network (RNN) and trained it on the MIT-BIH databases. CNN is best suited for analyzing spatial or locally linked data, whereas LSTM excels at collecting time series data properties. Concerning the CNN, they used two models. The first is a simple CNN. The model's layers 1-9 are convolutional layers connected to the highest collection layer, while layer 10 is the LSTM layer. To predict the output, the network's end employs a fully - connected layer. Whereas the second is VGGNet belonging to the deep CNN. By combining

convolution and pooling layers, the model can successfully collect ECG deep information.

To enhance the robustness of models, investigators used data augmentation techniques which are usually figured when there is an imbalance in training data. Wu et al. [25] utilized shifting test data. Moreover, Nonaka et al. [26] applied 13 data augmentation method on ECG signals to improve the efficiency of their DNN model. For example, they used erasing, scaling, squaring and so on.

III. METHODS

Fig. 1 depicts the process of the proposed methods, which were used in this investigation. The next subsections will discuss each phase of this workflow. Actually, this starts with the fundamental steps which is data preparation. This step comprises data cleaning, data preprocessing, data partition and data augmentation. The next step is the training and validation of the proposed models using the training and validation data already split. Lastly, the test of the trained and validated model. This requires the test data.

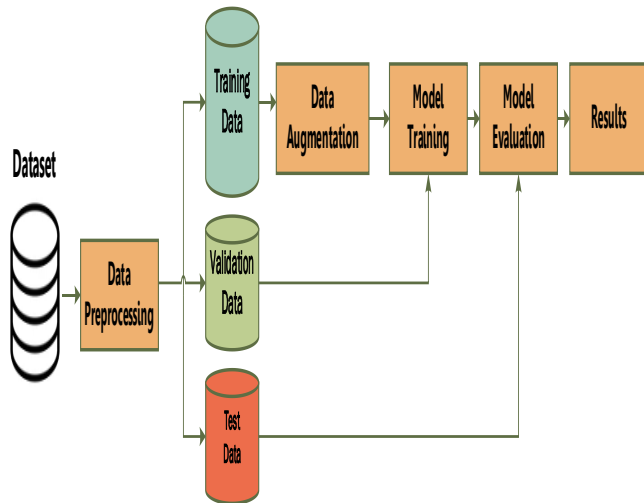


Fig. 1. Workflow of the proposed methods.

A. Dataset

The utilized dataset in this study contains four combined open source and free databases from George B. Moody PhysioNet Challenges which aims to classify 12-leads ECGs. This dataset contains 42 511 ECGs, 500 Hz-sampled, recorded from patients for a duration of 10 seconds. They come from three various countries, the USA, China, and Germany. Table I details the characteristics of these databases.

TABLE I. CHARACTERISTICS OF THE USED DATABASES

| Database | Source | Records | Length |
|-----------------|--|--------------------------------|-----------|
| CPSC [21] | China Physiological Signal Challenge in 2018 | 6877 M: 3699 F: 3178 | 6 s ~60 s |
| CPSC EXTRA [21] | | 3453 M: 1843 F: 1610 | 6 s ~60 s |
| PTB-XL [26] | Physikalisch Technische Bundesanstalt | 21837 M: 11379 F: 10458 | 10s |
| Georgia [27] | Georgia | 10344 M: 5551 F: 4793 | 10s |

The database is annotated with more than 110 diagnostics. In this study, due to the delimited annotations scored by the SNOMED-CT organization, which is a standardized multilingual clinical terminology vocabulary, only 27 classes will be considered, divided into normal sinus rhythm (NSR) and 26 categories of CVDs. Fig. 2 presents these classes.



Fig. 2. Distribution of classes in each database.

B. Data Preparation

The data preparation starts with the extraction of the patient’s personal information from the header files such as ID, age, gender, and anomalies codes. The following paragraphs detail the rest of the data preparation steps of training, validation, and testing. As indicated in paragraph 3, this work focuses on the 27 scored classes. For that, any annotated signal from the unscored classes will be removed. As a result, the number of ECGs will decrease from 42511 to 21724. The final distribution of the classes is presented in Fig. 3.

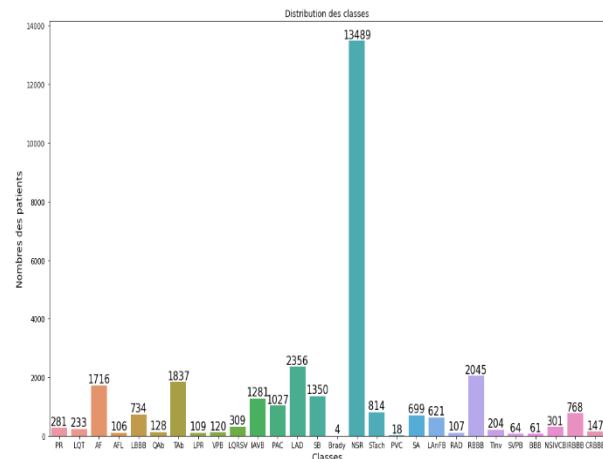


Fig. 3. Dataset classes distribution.

C. Data Preprocessing

The dataset includes 12-lead multi-label ECGs with diverse lengths between 6 s and 60 s. Considering DL needs inputs to be the same length, the dataset has been preprocessed to

guarantee that all inputs have the same length. A variety of lengths were tried, and it was discovered that proceeding with lengths equal to 5000 (10 s duration, 500 Hz sampling rate) gave the best performance. Regarding ECGs with full length longer than 10 s, they will be shortened, and the first 10 seconds of the ECG signal will be kept. Otherwise, they are padded with zeros until they have 10 seconds of recording. Fig. 4 shows the techniques used in the preprocessing of the data.

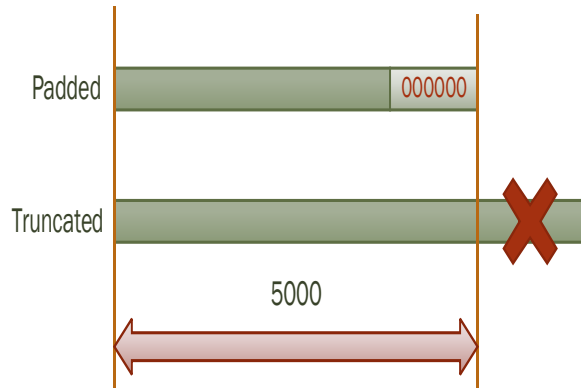


Fig. 4. Data preprocessing techniques.

D. Data-Split

To start with, the dataset is partitioned into two sets with a 0.75/0.25 ratio: the Training and Validation (TV) set and the test set. After that, the K-Fold stratified multi-class cross-validation technique was used, with 10 folds for the training and validation sets. As a result, ten stratified folds were generated by keeping each class samples rate constant. This ensures its existence at all stages. The training set is used to ensure the training of the model. The validation set is set aside for model optimization. As a result, a search for the appropriate parameterization is done without utilizing test data. This aims to determine the model's performance and evaluate its generalization potential. To resume this step explained in Fig. 5, the data was split into a TV set and a test set containing 16293 and 5431 ECG records, respectively. For the TV set, each training and validation fold includes 14655 and 1638 ECG recordings, respectively.

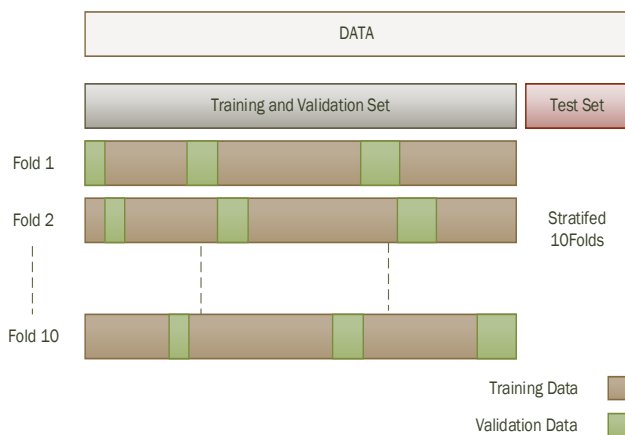


Fig. 5. 10-Folds stratified used in data split.

E. Data-Augmentation

As shown in Fig. 3, the problem of imbalance and insufficient data is very severe for the diagnosis of these cardiac arrhythmias. To solve this problem, Amplitude Scaling was applied to augment the data during the training phase. Data augmentation consists in generating realistic data to avoid data insufficiency. To extend or compress the amplitude, amplitude scaling method amplifies ECG signals by a random coefficient generated from a normal distribution $N(1, 0,1)$. Although this data augmentation technique introduces noise, it can assist prevent model overfitting and enhance resilience against bad cases [30].

IV. MODELS ARCHITECTURES

After the text edit has been completed, the paper is ready for the template. Duplicate the template file by using the Save As command and use the naming convention prescribed by your conference for the name of your paper. In this newly created file, highlight all of the contents and import your prepared text file. You are now ready to style your paper; use the scroll down window on the left of the MS Word Formatting toolbar. This section is reserved for the presentation of the two models' architectures. Actually, in this work, the proposed models are model 1 and model 2 which refers to ResNet-50 and Xception respectively.

A. Model 1

The first proposed model is ResNet-50 which belongs to the residual neural networks. At the conclusion of its layers, this network learns numerous low/medium/high level characteristics. Instead of trying to train features, residuals are trained in residual training. The residual may be easily defined as input for that layer minus the trained features. ResNet employs shortcut connections for this purpose (directly linking the n th layer's input to the $(n+1)$ th layer). The training of the model is made possible thanks to the residual blocks with shortcut connections. The input of the models is a patient ECG recording $x \in \mathbb{R}_{n\text{samples} \times 12}$, and the output is $\hat{y} \in \mathbb{R}_{1 \times 27}$ which represents the multi-label classification outcome. These inputs were subjected to a 1D convolution layer (Conv1D), a batch normalization layer (BN1D), a rectified linear unit (ReLU) activation layer, and a Max Pooling layer. As well as, for the extraction of wide features, 16 residual blocks were used. In this model, there are two types of residual blocks:

1) Res_Block_1 consists of 3 Conv1D layers, 3 BN1D layers, 2 activation layers ReLU, 1 Conv1D layer and 1 BN1D layer, while it is utilized to adjust dimensions and skip connections. Res Block 2 is just 3 Conv1D layers, 3 BN1D layers and 2 ReLU activation layers.

2) The Conv1D layers extract features, the BatchNorm1D layers speed up and stabilize the model, and the ReLU layers do non-linear activation. The residual blocks' extracted characteristics are pooled by Average Pooling. The findings are gathered and transferred to the output layer (dense layer) for prediction utilizing the sigmoid activation function.

Fig. 6 presents the architecture of the first proposed model is presented.

B. Model 2

The second proposed model is Xception. It is a deep convolutional neural network architecture incorporating depth-separable convolutions [31]. This is a powerful architecture that relies on its two main points of: Depth-separable convolution and Shortcuts between convolution blocks as in ResNet. Depth-separable convolution is said to be an alternative to classical convolution and much more computationally time efficient [32]. As in the first model, the Xception model has the same input and output. Xception comprises 36 layers of convolutions that form the basis for extracting network features. They are divided into 14 modules with linear residual connections around all but the last and first modules. The Xception architecture is essentially a linear stack of depth-separable convolution layers with residual connections. Data is routed via the Entry flow first, then via intermediate flow 8 times, and lastly the Exit flow. A batch normalization layer follows all convolution (Conv1D) and separable convolution (Sep-Conv1D) layers (BN1D). These modules' collected characteristics are pooled using Global Average Pooling. The pooling results are gathered and forwarded to the dense layer, which uses the sigmoid activation function to make predictions. Fig. 7 details the architecture of proposed model 2.

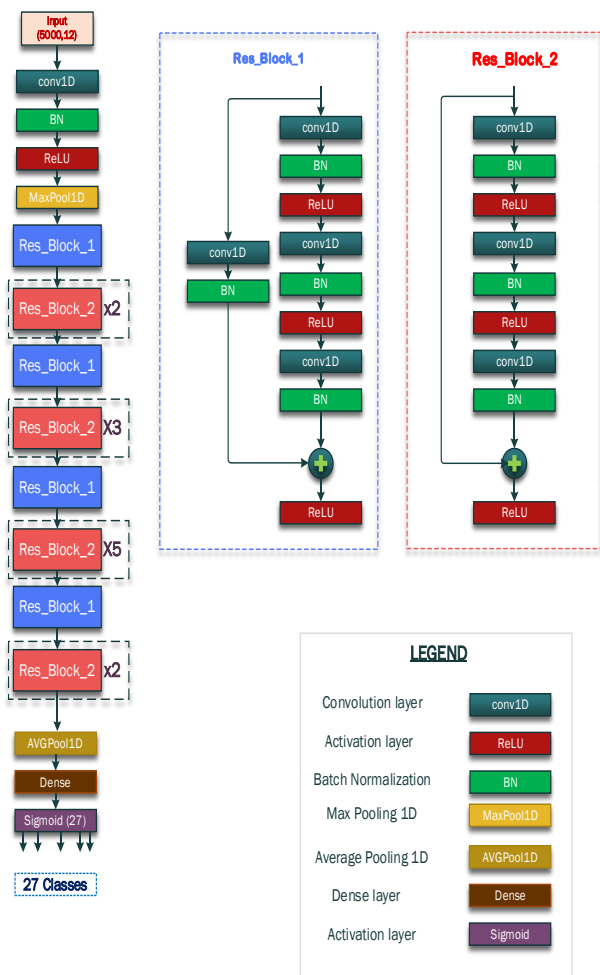


Fig. 6. Architecture of the proposed model 1.

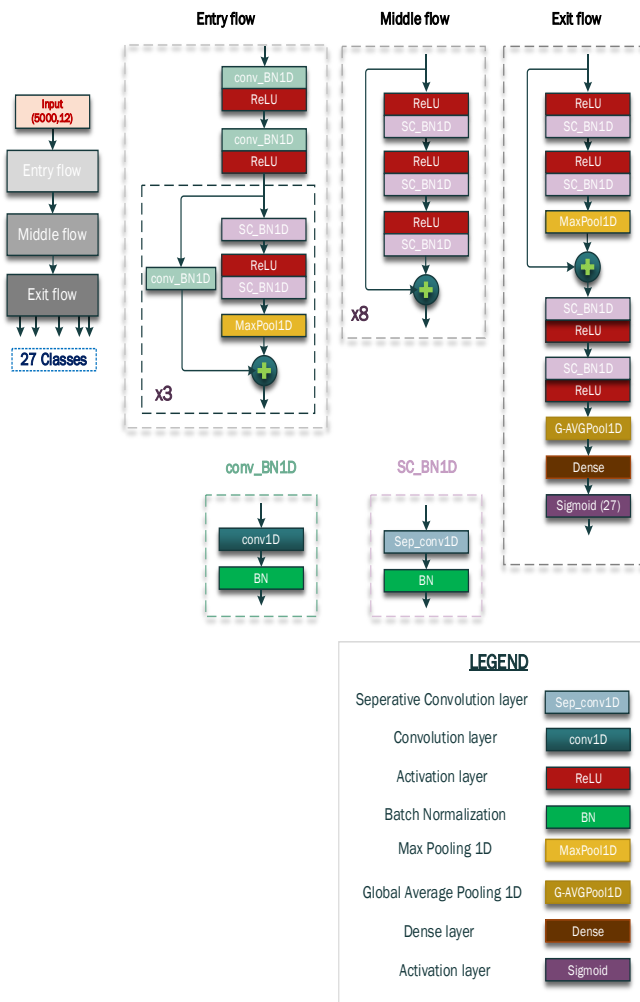


Fig. 7. Architecture of the proposed model 2.

V. RESULTS & DISCUSSIONS

In the Training and Validation phase, there are many introduced metrics. In fact, this paragraph details the evolution of the accuracy, recall, precision, and loss during these two phases for the two proposed models.

A. Accuracy

At the end of the training and validation, for the model N°1, ResNet-50, the accuracy obtained is 99.99% and 99.98% respectively. For the model N°2, Xception, it reached 100% in both phases. Fig. 8 and 9 represent the development of the accuracy during the two phases for the ResNet-50 and Xception respectively.

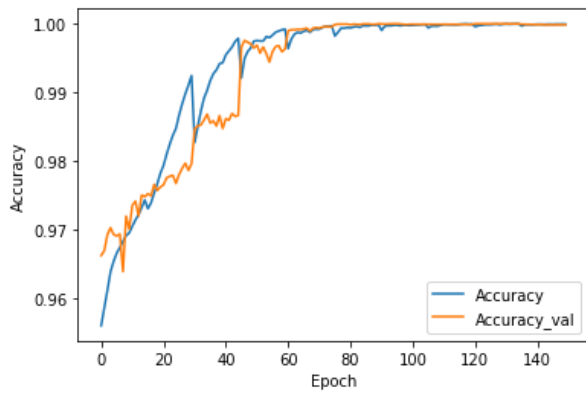


Fig. 8. Evolution of accuracy during the training of two models.

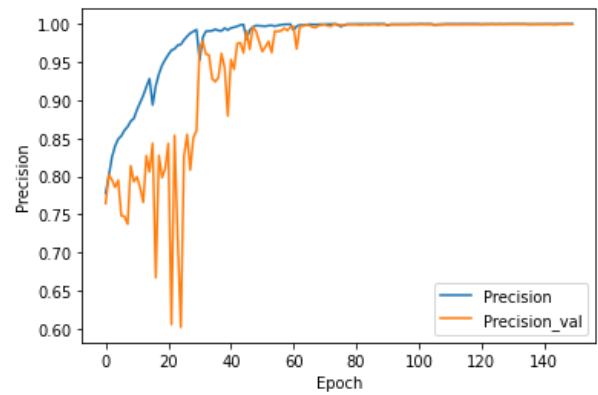


Fig. 11. Evolution of the precision during the validation of two models.

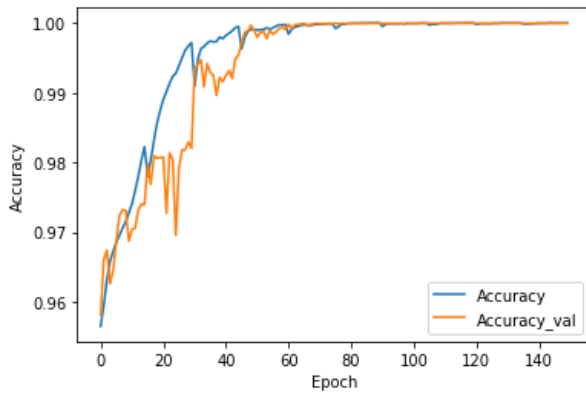


Fig. 9. Evolution of accuracy during the validation of two models.

B. Precision

Fig. 10 and 11 illustrate the evolution of the precision in the two steps for the two proposed models. Indeed, for model 1, it reached 99.99% in the training and 99.87% in the validation. Concerning the model N^o2, the precision obtained in the two phases is 100% and 99.96%.

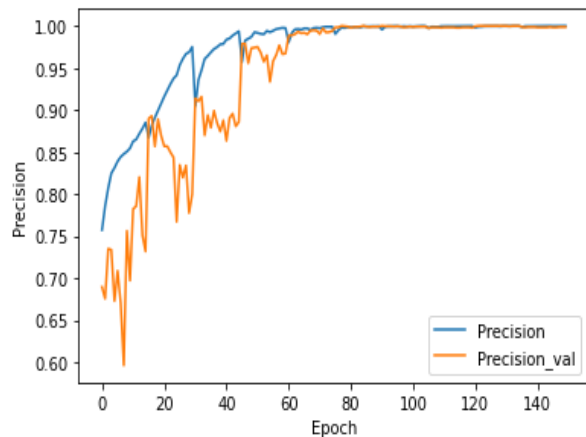


Fig. 10. Evolution of the precision during the training of two models.

C. Recall

Concerning the recall parameter, at the end of the training and validation of ResnNet-50 model, it reached 100% and 99.87%. For the Xception model, it is 100% in both phases. Fig. 12 and 13 show the evolution of recall for the two models.

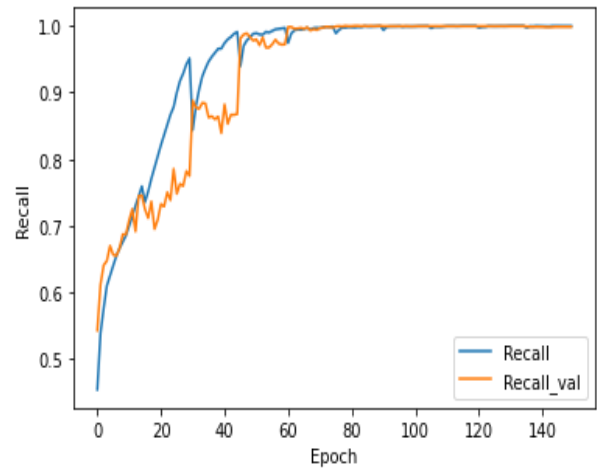


Fig. 12. Evolution of the recall during the training of two models.

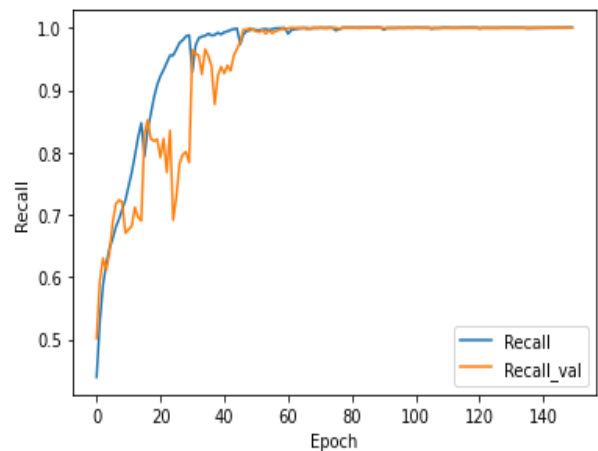


Fig. 13. Evolution of the recall during the validation of two models.

D. Loss

In terms of loss, the first model reached $7,89 \cdot 10^{-5}$ and $3,83 \cdot 10^{-4}$ in the two phases. For the second model, at the end of learning and validation, it reaches $4,37 \cdot 10^{-5}$ and $2,05 \cdot 10^{-4}$, respectively. Fig. 14 and 15 present the declination of the Loss function for the two models.

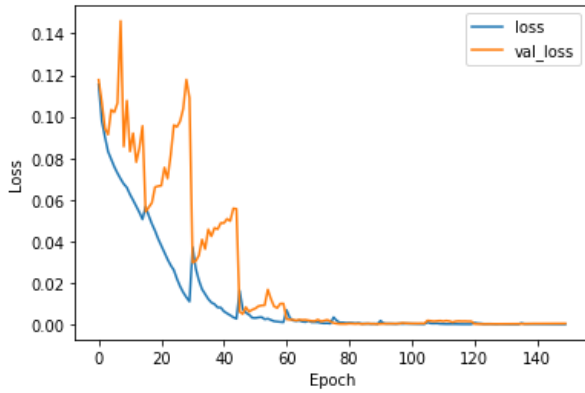


Fig. 14. Evolution of the loss during the training of two models.

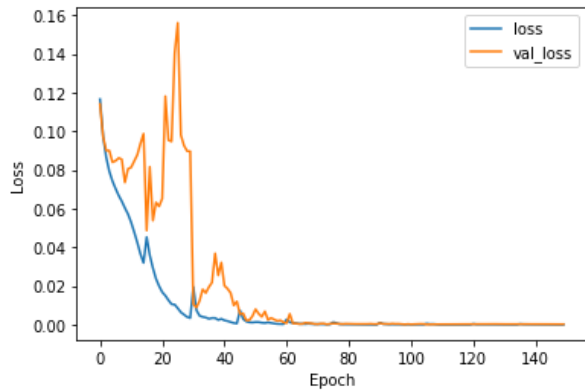


Fig. 15. Evolution of the loss during the validation of two models.

Globally, for both models, the evolution of the performance parameters is generally similar to a faster stabilization of the Xception model. Indeed, the model N°2 has converged since the 60th epoch (beginning of fold N°5) whereas the model N°1 has converged only after the 90th epoch (beginning of fold N°7). Also, the evolution of the validation curves of the performance parameters for the ResNet-50 model is more stable than that of the Xception model. Moreover, the saw teeth noticed in these curves are less severe for the model N°1.

VI. TEST PHASES

In the test phase, the metrics presented are the confusion matrices of the proposed two models as well as their classification reports. Fig. 16 presents the normalized confusion matrix obtained. The model N°1 is performing for the classes CRBBB, RAD, Brady, PR, NSR, RBBB, AF, IRBBB, STach, IAVB, PAC, LBBB. Indeed, their percentages of correct determinations are greater than 80%. Moreover, its performance is moderate for the PVC, SA, TInv, SB, and AFL classes where their percentages of correct predictions are higher than 60%. For lasting classes, such as QAb, LPR, and LAD, ResNet-50 has a bad performance.

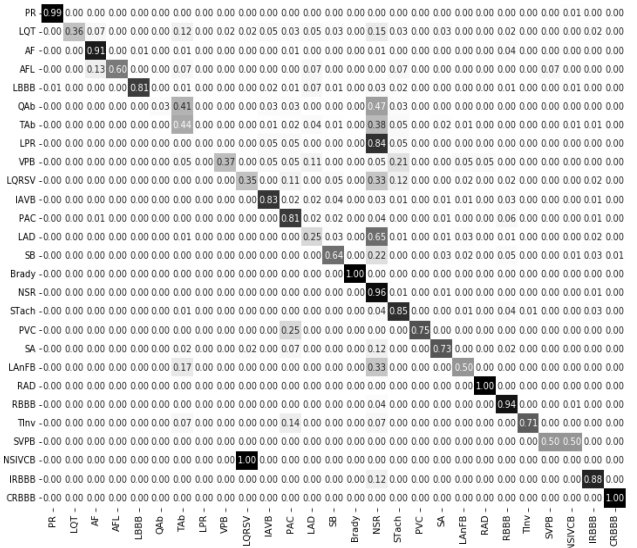


Fig. 16. Confusion matrix of the proposed model 1.

Fig. 17 illustrates the normalized confusion matrix obtained from model N°2. It performs well for the classes NSIVCB, CRBBB, SVPB, NSR, RBBB, PR, IRBBB, AF, IAVB, STach. Moreover, their percentages of correct predictions exceed 80%. Moreover, its performance is moderate for the classes PAC, SB, SA, TInv, and LQRSV where their percentages of correct predictions are above 60%. For the remaining classes, like LPR, QAb, Brady and RAD..., Xception has a bad performance.

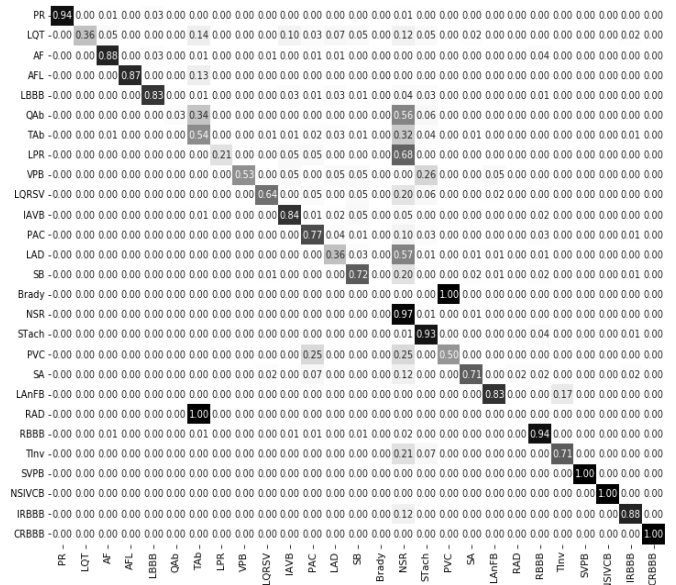


Fig. 17. Confusion matrix of the proposed model 2.

VII. CONCLUSION

This study showcases a successful application of deep learning (DL) techniques for the accurate diagnosis of cardiovascular diseases (CVDs) using ResNet-50 and Xception models. The study considered 27 heartbeat rhythms, where one belongs to normal sinus rhythm (NSR), and the remaining 26

belong to cardiac abnormalities. The dataset utilized in this research was created by aggregating four distinct datasets from three different nations, providing a diverse range of cardiac conditions. The results demonstrate the effectiveness and high performance of the proposed methods, which were also validated against recent literature. However, it is essential to acknowledge the limitations of the suggested methods. Firstly, the high complexity of computation required for the deep learning models may hinder their implementation in some medical settings. Additionally, the limited interpretability of some of the classes in the global dataset used may pose challenges in diagnosing and treating certain cardiac conditions. To address these challenges, future studies will focus on enhancing the proposed techniques to make them more accessible and interpretable for a broader range of medical applications. Overall, this research provides promising insights into the potential of deep learning models for CVD diagnosis, and with further development, they have the potential to revolutionize the field of cardiac medicine.

ACKNOWLEDGMENT

This work was supported by Princess Nourah bint Abdulrahman University Researchers Supporting Project number (PNURSP2024R393), Princess Nourah bint Abdulrahman University, Riyadh, Saudi Arabia.

REFERENCES

- [1] E. J. Benjamin et al., « heart disease and Stroke Statistics—2018 Update: A Report From the American Heart Association », *Circulation*, vol. 137, no 12, mars 2018, doi: 10.1161/CIR.0000000000000558.
- [2] S. H. Jambukia, V. K. Dabhi, and H. B. Prajapati, "Classification of eeg signals using machine learning techniques: A survey," in 2015 International Conference on Advances in Computer Engineering and Applications. IEEE, 2015, pp. 714–721.
- [3] P. Macfarlane, B. Devine, and E. Clark, "The university of glasgow (unig) eeg analysis program," in *Computers in Cardiology*, 2005. IEEE, 2005, pp. 451–454.
- [4] S. Datta et al., « Identifying Normal, AF and other Abnormal ECG Rhythms using a Cascaded Binary Classifier », présenté à 2017 Computing in Cardiology Conference, sept. 2017. doi: 10.22489/CinC.2017.173-154.
- [5] Clifford GD, Liu C, Moody B, Li-wei HL, Silva I, Li Q, Johnson AE, Mark RG. AF classification from a short single lead ECG recording: The PhysioNet/computing in cardiology challenge 2017. In 2017 Computing in Cardiology (CinC) 2017 Sep 24 (pp. 1-4). IEEE. <https://doi.org/10.22489/CinC.2017.065-469>
- [6] S. Aziz, S. Ahmed, et M.-S. Alouini, « ECG-based machine-learning algorithms for heartbeat classification », *Sci. Rep.*, vol. 11, no 1, Art. no 1, sept. 2021, doi: 10.1038/s41598-021-97118-5.
- [7] P. P. Shinde and S. Shah, "A Review of Machine Learning and Deep Learning Applications," 2018 Fourth International Conference on Computing Communication Control and Automation (ICCUBEA), 2018, pp. 16, doi:10.1109/ICCUBEA.2018.8697857.
- [8] N. Rusk, « Deep learning », *Nat. Methods*, vol. 13, no 1, Art. no 1, janv. 2016, doi: 10.1038/nmeth.3707.
- [9] A. Souid, N. Sakli, et H. Sakli, « Classification and Predictions of Lung Diseases from Chest X-rays Using MobileNet V2 », *Appl. Sci.*, vol. 11, no 6, Art. no 6, janv. 2021, doi: 10.3390/app11062751.
- [10] N. Sakli et al., « ResNet-50 for 12-Lead Electrocardiogram Automated Diagnosis », *Comput. Intell. Neurosci.*, vol. 2022, p. 1 16, avr. 2022, doi: 10.1155/2022/7617551.
- [11] Y. Liang, S. Yin, Q. Tang, Z. Zheng, M. Elgendi, et Z. Chen, « Deep Learning Algorithm Classifies Heartbeat Events Based on Electrocardiogram Signals », *Front. Physiol.*, vol. 11, p. 569050, oct. 2020, doi: 10.3389/fphys.2020.569050.
- [12] C.-H. Hsieh, Y.-S. Li, B.-J. Hwang, et C.-H. Hsiao, « Detection of Atrial Fibrillation Using 1D Convolutional Neural Network », *Sensors*, vol. 20, no 7, Art. no 7, janv. 2020, doi: 10.3390/s20072136.
- [13] M. S. Haleem et al., « Time adaptive ECG driven cardiovascular disease detector », *Biomed. Signal Process. Control*, vol. 70, p. 102968, sept. 2021, doi: 10.1016/j.bspc.2021.102968.
- [14] S. Mousavi, F. Afghah, et U. R. Acharya, « HAN-ECG: An interpretable atrial fibrillation detection model using hierarchical attention networks », *Comput. Biol. Med.*, vol. 127, p. 104057, déc. 2020, doi: 10.1016/j.compbiomed.2020.104057.
- [15] P. Nejedly, A. Ivora, I. Viscor, J. Halamek, P. Jurak, et F. Plesinger, « Utilization of Residual CNN-GRU With Attention Mechanism for Classification of 12-lead ECG », in 2020 Computing in Cardiology, sept. 2020, p. 1-4. doi: 10.22489/CinC.2020.032.
- [16] A. Y. Hannun, P. Rajpurkar, M. Haghighpanahi, G. H. Tison, C. Bourn, M. P. Turakhia, and A. Y. Ng, "Cardiologist-level arrhythmia detection and classification in ambulatory electrocardiograms using a deep neural network," *Nature medicine*, vol. 25, no. 1, p. 65, 2019.
- [17] Moody GB, Mark RG. The impact of the MIT-BIH Arrhythmia Database. *IEEE Eng in Med and Biol* 20(3):45-50 (May-June 2001). (PMID: 11446209)
- [18] Goldberger, A., Amaral, L., Glass, L., Hausdorff, J., Ivanov, P. C., Mark, R., ... & Stanley, H. E. (2000). PhysioBank, PhysioToolkit, and PhysioNet: Components of a new research resource for complex physiologic signals. *Circulation [Online]*. 101 (23), pp. e215–e220.
- [19] A. H. Ribeiro et al., « Automatic diagnosis of the 12-lead ECG using a deep neural network », *Nat. Commun.*, vol. 11, no 1, p. 1760, déc. 2020, doi: 10.1038/s41467-020-15432-4.
- [20] H. Zhu et al., « Automatic multilabel electrocardiogram diagnosis of heart rhythm or conduction abnormalities with deep learning: a cohort study », *Lancet Digit. Health*, vol. 2, no 7, p. e348-e357, juill. 2020, doi: 10.1016/S2589-7500(20)30107-2.
- [21] D. Zhang, X. Yuan, et P. Zhang, « Interpretable Deep Learning for Automatic Diagnosis of 12-lead Electrocardiogram ». arXiv, 20 octobre 2020. doi: 10.48550/arXiv.2010.10328.
- [22] K. He, X. Zhang, S. Ren, and J. Sun, "Deep residual learning for image recognition," in *Proceedings of the IEEE conference on computer vision and pattern recognition*, 2016, pp. 770–778.
- [23] S. M. Lundberg and S.-I. Lee, "A unified approach to interpreting model predictions," in *Advances in neural information processing systems*, 2017, pp. 4765–4774.
- [24] Z. Zheng, Z. Chen, F. Hu, J. Zhu, Q. Tang, et Y. Liang, « An Automatic Diagnosis of Arrhythmias Using a Combination of CNN and LSTM Technology », *Electronics*, vol. 9, no 1, Art. no 1, janv. 2020, doi: 10.3390/electronics9010121.
- [25] M. Wu, Y. Lu, W. Yang, et S. Y. Wong, « A Study on Arrhythmia via ECG Signal Classification Using the Convolutional Neural Network », *Front. Comput. Neurosci.*, vol. 14, 2021, Consulté le: 22 octobre 2022.
- [26] N. Nonaka et J. Seita, « Data Augmentation for Electrocardiogram Classification with Deep Neural Network ». arXiv, 4 septembre 2020. doi: 10.48550/arXiv.2009.04398.
- [27] P. Wagner, N. Strodthoff, and R. D. Bousselet, PTB-XL, a Large Publicly Available Electrocardiography dataset, *Scientific Data*, vol. 7, no. 154, 2020.

Multi-Discriminator Image Restoration Algorithm Based on Hybrid Dilated Convolution Networks

Chunming Wu, Fengshuo Qi

Northeast Power University, College of Electrical Engineering, Ji lin, China

Abstract—With the continuous development of generative adversarial networks (GAN), many image restoration problems that are difficult to solve based on traditional methods have been given new research avenues. Nevertheless, there are still problems such as structural distortion and texture blurring of the complemented image in the face of irregular missing. In order to overcome these problems and retrieve the lost critical data of the image, a two-stage image restoration complementation network is proposed in this paper. While introducing hybrid dilation convolution, two attention mechanisms are added to the network and optimized using multiple loss functions. This not only results in better image quality metrics, but also clearer and more coherent image details. In this paper, we tested the network on CelebA-HQ, Places2 and The Paris datasets and compared it with several classical image restoration models, such as GLC, Gconv, Musical and RFR, and the results proved that the complementary images in this paper are improved compared to the others.

Keywords—GAN; image restoration; hybrid dilated convolution; attention mechanism; two-stage network

I. INTRODUCTION

Image Completion is a long-standing and critical problem in the field of computer vision, aiming at completing the missing pixels and semantic parts among a given image. It is widely used in the fields of object removal, photo restoration, and image processing [1-3], where the naked eye can easily notice if the complementary image is not plausible or lacks critical information.

Early work [3-5] was an attempt to perform complementary filling at the image level using methods similar to texture synthesis. While these methods can achieve good results in complementing the background, they fail to produce a new image when non-repetitive structures are encountered. In addition, such methods lack semantic support and high-level understanding.

With the rapid development of deep learning (e.g., generative adversarial networks [6]), image complementation has evolved to new heights. Deep learning based image complementation is broadly categorized into single-stage [7-11], two-stage [12-15] and multi-stage [16-19]. All these methods can generate new content such as faces, objects and scenes. However, artifacts tend to arise when using these methods, making the complementary image inconsistent with the surrounding region.

To address this problem, we introduce hybrid dilated convolution, gated convolution, and attention mechanism to improve on the generative adversarial network, and use

multiple loss functions to optimize the process and train the generator more efficiently. Meanwhile, the VGG-16 feature extractor is introduced into the discriminative network, which can obtain more feature information and increase the sensory field.

Experiments on three datasets, including CelebA-HQ [20], Places2 [21] and The Paris dataset [22], and comparisons with several classical methods demonstrate that our method can generate better image results.

Our main contributions are as follows:

1) A two-stage image complementation network model from coarse to fine is proposed, where the generator consists of gated convolution, hybrid dilated convolution and two attention mechanism modules. The input to the generator network is a missing image with mask and the complemented image is input to the second order network. And then the coarse complemented image is refined and then fed into the discriminator and so on to the final result.

2) An attentional mechanism is incorporated in both stages of the generative network. In the coarse network the first attention mechanism is used to extract the missing and intact regions of the image and calculate the attention scores for both regions. The second attention mechanism is used in the refinement network to optimize the complementary part of the image by calculating the similarity of any two pixel points in the feature map to obtain the feature information of the whole image while preserving the original information.

3) Improve the existing dilated convolution using hybrid dilated convolution to make the sampling information more accurate.

4) Use three different loss functions in combination with each other for better training of generator model.

This paper is categorized as follows: Section II describes the work related to image complementation techniques; Section III describes the components of the network structure. Section IV analyzes the experimental complementation results. Section V is used for discussion and comparison. Section VI concludes the study.

II. RELATED WORKS

Today, image complementation is broadly categorized into two types: the previous traditional complementation methods and the now popular deep learning based image complementation methods.

There are two types of traditional image complementation methods. One is based on diffusion [23-24], which diffuses neighboring information to the missing regions, but these methods are limited to locally available information for complementary reconstruction, and cannot recover the semantic structure of the missing parts or complement larger missing regions. Another approach is based on PATCH [25-27], in which pixel-level patches of the original image are used to fill in the missing regions, e.g., by mixing the copied original regions with the target regions to ensure their similarity [28]. However, these methods are computationally expensive and the patch computation must be performed for each target to obtain its similarity score. Patch Match [29] achieves fast matching by using local correlations of the image, but the patched portion can also be found in other locations and cannot produce a new image. These methods can recover image regions with high graphical similarity, such as background complementation, but have difficulty repairing complex, low-similarity images.

In recent years, with the development of deep learning ground, deep learning methods for image complementation have been proposed. The initial study was the context encoder [8], which uses an encoder-decoder architecture. The encoder maps the image of the missing region into a low-dimensional feature space, and the decoder utilizes its feature space to construct the complementary image. The progression is performed by a combination of pixel-level reconstruction losses [6]. However, the complementary image usually contains blurry visual artifacts due to the information width of the channel fully connected layers. Lizuka et al. [7] introduced global and local contextual discriminators to train a complete convolutional complementary network to solve this problem. However, the training time increases significantly due to the use of extremely sparse filters. Zhang et al. [10] proposed a pixel-by-pixel localization of the complementary method and inserted the missing region location information into the reconstruction loss to better train the complementary network.

In multi-stage, Yu et al. [13] proposed an image complementation method consisting of a coarse network and a refinement network. In the refinement network, a contextual attention module was introduced. Later, Yu et al. [30] introduced gated convolution while using an attention mechanism to further optimize the network. Zhang et al [16] divided the image complementation process into four different stages and used the LSTM architecture [31] to control the information of the recursive process. However, it cannot handle irregular defects in practical applications. On the other hand, Guo et al. [17] proposed a fully parsed network with multiple extension modules to solve this problem. Pawar et al [32] proposed recurrent neural networks based on multiscale deep learning to deal with the problem of missing images using a multiscale approach. Mansur [33] used StyleGAN framework with VGG19 and CatBoost gradient to improve the accuracy of predicting images.

III. INTRODUCTION TO NETWORK ARCHITECTURE

A. Overall Network Structure

The overall network structure model proposed in this paper is shown in Fig. 1. The generator model proposed in this paper

has two final outputs, the rough processing result of the first stage will be used to perform the inputs of the second stage, and the result of the second stage of fine processing as the final output of the network. It will be used as an input along with the real image and the input will be sent to VGG-16 and modeled pairwise discriminative network for judgment.

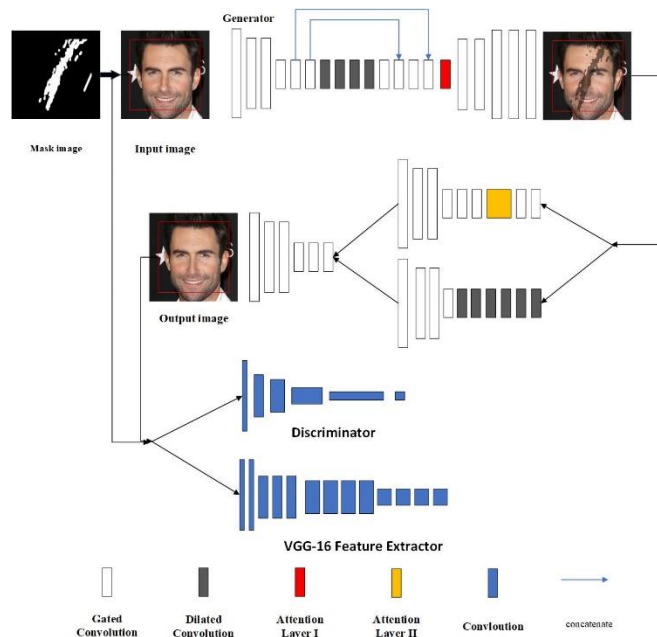


Fig. 1. Overall network structure.

B. Introducing Hybrid Dilated Convolution

Hybrid dilated convolution can solve the problem of missing continuity of image information due to cavity convolution. In order to solve the problem of the loss of image information after the merging of traditional convolutional layers, literature [7] proposes the use of cavity convolutional layers for image complementation. However, the increase of sensory field is accompanied by the problem of loss of continuity of image information.

Feeling wild is defined as:

$$r_n = r_{n-1} + (k-1) * \prod_{i=1}^{n-1} s_i \quad (1)$$

where, r_n denotes the receptive field of the layer, s_i denotes the convolution or pooling step of the layer, and k is the convolution kernel size.

Fig. 2 shows the cavity convolution with convolution kernel 3×3 and dilated rate 2. It can be seen that although the dilated convolution increases the receptive field, the convolution kernel is discontinuous and the continuity of the image information is inevitably lost. To address this problem, we introduce the hybrid dilated convolution. As shown in Fig. 3, the hybrid cavity convolution retains the continuity of the region completely, while still maintaining its coherence after superposition. The hybrid hole convolution not only can effectively solve the problem of large-scale missing, but also will not lose its continuity in the face of detailed processing. The maximum void rate of its i -th layer is satisfied:

$$N_i = \max[N_{i+1} - 2R_i, N_{i+1} - 2(N_{i+1} - R_i), R_i] \quad (2)$$

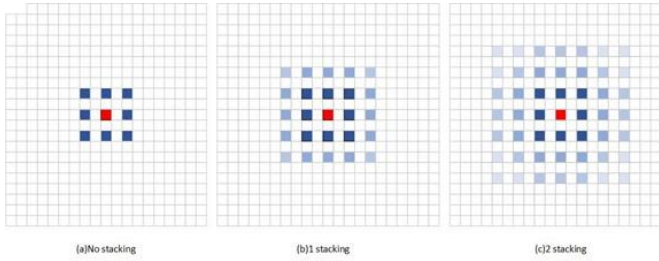


Fig. 2. Dilated convolution superposition with a void rate of 2.

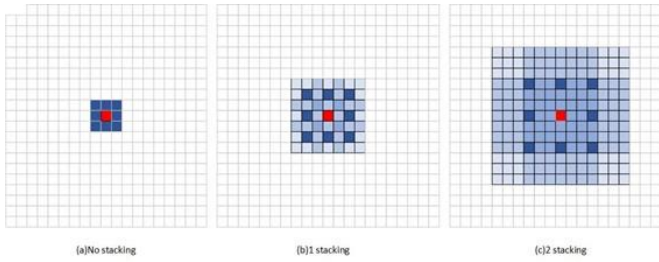


Fig. 3. Convolutional superposition of mixed voids with a void rate of 2.

Where the voiding rate of layer i is R_i , and N_i and N_{i+1} are the maximum voiding rates of layers i and $i+1$, respectively.

We apply the hybrid dilated convolution structure to the refinement network stage with a jagged dilated rate, which should satisfy the following conditions:

- 1) The convention of the cascaded dilated convolution rates is should be 1. e.g., [1, 2, 3] satisfy this requirement; although [2, 4, 8] do not satisfy this requirement, they have the conventions 1 and 2.
- 2) have cyclic jagged dilated rates, e.g., [1, 2, 3, 1, 2, 3].
- 3) Satisfy the verification formula

$$H_i = \max[H_{i+1} - 2r_i, H_{i+1} - 2(H_{i+1} - r_i), r_i] \quad (3)$$

where, $H_i = r_i$, r_i is the dilated rate of the i th layer. Take the cascade convolutional layers of [1, 2, 9, 1, 2, 9] and [1, 2, 3, 1, 2, 3] with a void rate of r as an example. The former satisfies the first two of the conditions, which leads to $H_2 = 5 > K = 3$ according to Eq. (3), and does not satisfy condition three. And [1, 2, 3, 1, 2, 3] both satisfy the above three conditions.

In this paper, the hybrid cavity convolution with sawtooth structure of cavity rate of [1, 2, 3, 1, 2, 3] is chosen to replace the cavity convolution. The hybrid cavity convolution not only solves the problem of information loss of cavity convolution, but also makes full use of the pixel information between images and increases the sensory field.

C. Introduction of Attention Mechanisms

The attention mechanism I is shown in Fig. 4. For the input feature map X_{in} , we specifically refer to the foreground of the

missing region instead of the background of the image. As can be seen from Fig. 4, the missing region of the feature map is white, and the corresponding RGB is (255, 255, 255). If the RGB of the complementary part is (255, 255, 255), all input features are foreground, otherwise they are background. We extract the pixel information from the foreground and background of the image separately, labeling the foreground as $\{a_{x,y}\}$ and the background as $\{b_{m,n}\}$. The similarity between them is calculated by normalization:

$$S_{x,y,m,n} = \left\langle \frac{a_{x,y}}{\|a_{x,y}\|}, \frac{b_{m,n}}{\|b_{m,n}\|} \right\rangle \quad (4)$$

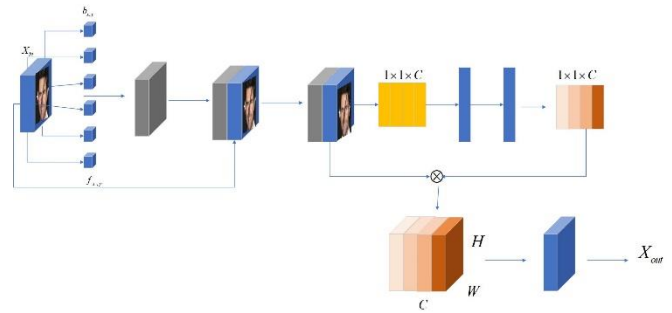


Fig. 4. Attention mechanism I.

The result of the computation is obtained by softmax to get the attention score. The input image is then inversely convolved to obtain the feature map X_{mid} . We input X_{in} and X_{mid} into the SE module as a way to increase the weight value of the useful features. The final output of the attention mechanism I is denoted as:

$$X_{out} = f_{conv} \left(f_{SE} \left(\left(X_{in}, X_{mid} \right) \right) \right) \quad (5)$$

where, f_{SE} is the SE module and f_{conv} is the convolution operation that ensures that X_{in} is the same as the input image channel.

The SE module first maps the input image into the dimension tensor of $1 \times 1 \times C$ and then takes the global average:

$$z_c = \frac{1}{H \times W} \sum_i \sum_j x_{i,j}, x_{i,j} \in X \quad (6)$$

z_c is then converted to a weight tensor of [0, 1]. In turn, the weight values for each channel are calculated:

$$w_c = \sigma \left(W_2 \left(\phi \left(W_1, z_c \right) \right) \right) \quad (7)$$

where, W_1 and W_2 are fully connected operations and σ and ϕ refer to sigmoid function and ReLU function. The weights of the final output image are:

$$X_{out} = X \otimes W_c \quad (8)$$

Attention Mechanism II is shown in Fig. 5. For the input feature map, Attention Mechanism II makes three copies of it and uses the convolution kernel of 1×1 to perform the convolution operation. The feature map is first stretched by channel into vectors with a total number of N pixels to obtain $f(x)$, $g(x)$ and $h(x)$. Then $f(x)$ is subjected to transpose operation and $g(x)$ is subjected to vector dot product, and the result obtained is normalized to obtain the matrix:

$$\beta_{i,j} = \exp\left(f(x)^T * g(x)\right) / \sum_{i=1}^N f(x)^T * g(x) \quad (9)$$

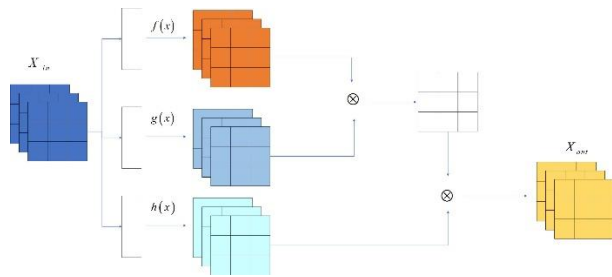


Fig. 5. Attention mechanism II.

$\beta_{i,j}$ is the attention score at the j th pixel i . The transposed $\beta_{i,j}$ and $h(x)$ are then multiplied to obtain the final attention feature result $o(x)$. The input features are weighted to obtain the output:

$$out = \gamma o_i + x_i \quad (10)$$

where, γ is the weights that are constantly updated by training.

D. Coarse Network Structure

Coarse network is the first stage of generative network, the whole network is encoding-decoding structure, coarse network structure as shown in Fig. 6, encoding stage the first phase of the input image through the convolution kernel for convolution, to increase the sensory field. Then three convolution kernels are used for feature extraction. In this paper, multiple downsampling is used to compress and encode the input image, and useful local feature information is extracted to recover the image. The input image is then passed through eight convolutional layers (including four hybrid dilated convolutional layers) and the attention mechanism I module to enhance the feature transfer and obtain a larger receptive field. The decoding stage up-samples the high-level feature information previously removed through a structure symmetric to the decoding to obtain the restored image of the

coarse network. The specific parameters of the coarse network are shown in Table I:

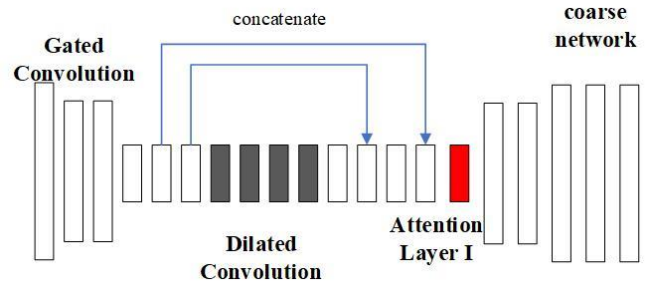


Fig. 6. Coarse network structure.

TABLE I. COARSE NETWORK PARAMETER

| | Kernel Size | Stride | Atrous | Output Channel | Output Size Inch |
|---------------------|-------------|--------|--------|----------------|------------------|
| GatedConv1 | 5 | 1 | 1 | 32 | 256 |
| GatedConv2 | 3 | 2 | 1 | 64 | 128 |
| GatedConv3 | 3 | 1 | 1 | 64 | 128 |
| GatedConv4 | 3 | 2 | 1 | 128 | 64 |
| GatedConv5x2 | 3 | 1 | 1 | 128 | 64 |
| DilatedConv1 | 3 | 1 | 2 | 128 | 64 |
| DilatedConv2 | 3 | 1 | 4 | 128 | 64 |
| DilatedConv3 | 3 | 1 | 8 | 128 | 64 |
| DilatedConv4 | 3 | 1 | 16 | 128 | 64 |
| GatedConv6x2 | 3 | 1 | 1 | 128 | 64 |
| AttentionLayerI | - | - | - | 128 | 64 |
| TransposeGatedConv1 | 3 | 1 | 1 | 64 | 128 |
| GatedConv7 | 3 | 1 | 1 | 64 | 128 |
| TransposeGatedConv2 | 3 | 1 | 1 | 32 | 256 |
| GatedConv8 | 3 | 1 | 1 | 16 | 256 |
| GatedConv9 | 3 | 1 | 1 | 3 | 256 |

E. Refined Network Structure

After the first stage of the coarse network repair, this paper takes the result as the input of the refinement network. Compared with the coarse network, the refinement network is more complete in extracting feature information, and the feature extraction through the double parallel network can output the image ground diversity more effectively. The structure of the refinement network is shown in Fig. 7:

As shown in Fig. 7, the refinement network consists of a parallel network structure containing a hybrid dilated convolutional branch and a branch containing the attention mechanism II. The two branches perform feature extraction on the input image by different methods, and then the results are combined and decoded by a decoder to obtain the output result.

Table II represents the parameters of the Attention Mechanism II branch in parallel networks.

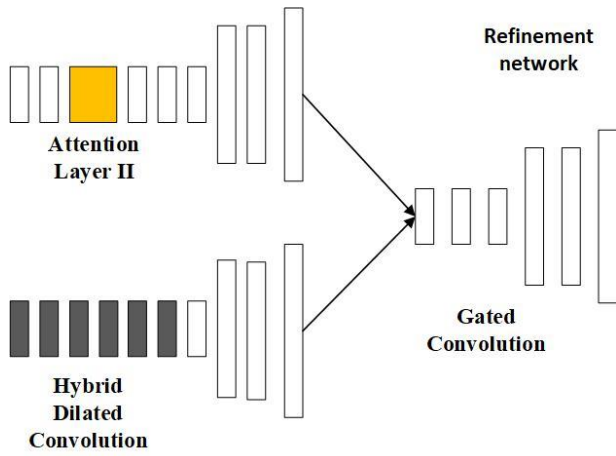


Fig. 7. Fine network structure.

TABLE II. ATTENTION II PARAMETERS

| | Kernel Size | Stride | Atrous | Output Channel | Output Size Inch |
|------------------|-------------|--------|--------|----------------|------------------|
| GatedConv1 | 5 | 1 | 1 | 32 | 256 |
| GatedConv2 | 3 | 2 | 1 | 32 | 128 |
| GatedConv3 | 3 | 1 | 1 | 64 | 128 |
| GatedConv4 | 3 | 2 | 1 | 64 | 64 |
| GatedConv5 | 3 | 1 | 1 | 128 | 64 |
| GatedConv6 | 3 | 1 | 1 | 128 | 64 |
| AttentionLayerII | - | - | - | 128 | 64 |
| GatedConv7 | 3 | 1 | 1 | 128 | 64 |
| GatedConv8 | 3 | 1 | 1 | 128 | 64 |

Table III represents the parameters of hybrid dilated convolutional branches in parallel networks.

After feature extraction in dual branching, the extracted information needs to be merged and decoded. The whole decoding network consists of one splicing layer, five gated convolutional layers and two replacement convolutional layers. Table IV shows the relevant parameters of the decoding network.

TABLE III. HYBRID DILATION CONVOLUTION BRANCHING PARAMETERS

| | Kernel Size | Stride | Atrous | Output Channel | Output Size Inch |
|--------------|-------------|--------|--------|----------------|------------------|
| GatedConv1 | 5 | 1 | 1 | 32 | 256 |
| GatedConv2 | 3 | 2 | 1 | 32 | 128 |
| GatedConv3 | 3 | 1 | 1 | 64 | 128 |
| GatedConv4 | 3 | 2 | 1 | 64 | 64 |
| DilatedConv1 | 3 | 1 | 1 | 128 | 64 |
| DilatedConv2 | 3 | 1 | 2 | 128 | 64 |
| DilatedConv3 | 3 | 1 | 3 | 128 | 64 |
| DilatedConv4 | 3 | 1 | 1 | 128 | 64 |
| DilatedConv5 | 3 | 1 | 2 | 128 | 64 |
| DilatedConv6 | 3 | 1 | 3 | 128 | 64 |

TABLE IV. DECODING NETWORK PARAMETERS

| | Kernel Size | Stride | Atrous | Output Channel | Output Size Inch |
|---------------------|-------------|--------|--------|----------------|------------------|
| Concatenate | 5 | 1 | 1 | 256 | 64 |
| GatedConv1 | 3 | 2 | 1 | 128 | 64 |
| GatedConv2 | 3 | 1 | 1 | 128 | 64 |
| TransposeGatedConv1 | 3 | 2 | 1 | 64 | 128 |
| GatedConv3 | 3 | 1 | 1 | 64 | 128 |
| TransposeGatedConv2 | 3 | 1 | 1 | 32 | 256 |
| GatedConv4 | 3 | 1 | 1 | 16 | 256 |
| GatedConv5 | 3 | 1 | 1 | 3 | 256 |

F. Discriminator and Feature Extractor

In this paper, both the discriminator and the VGG-16 feature extractor are ordinary convolutional full convolutional neural networks, which can be effectively applied in GANs with large missing fields. The discriminator and feature extractor are shown in Fig. 8. The discriminator needs to judge the quality of the output image as a whole, while the full convolutional neural network can effectively extract the global contextual information through a large sensory field.

VGG-16 is a pre-trained model trained using the large-scale ImageNet dataset, which contains more than 1 million images of over 1,000 different categories. Because of this, VGG-16 can be easily and quickly applied to generate new images. Its convolutional layers are arranged in a stepwise manner, which not only increases the sensory field, but also extracts different feature information of the image.

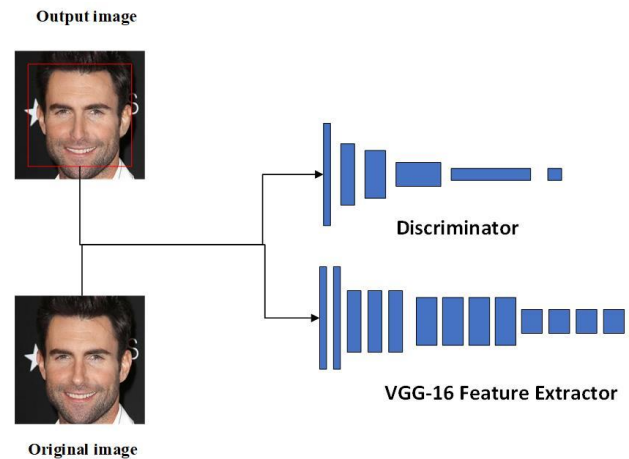


Fig. 8. Discriminators and feature extractors.

G. Loss Functions

In image complementation, the use of a single loss function may cause problems such as blurring and loss of semantic information in the restored image. To address this problem, this paper uses a combination of three different loss functions, which not only improves the network model's ability to perceive the details of the image, but also helps the network model to retain the texture structure of the original image and improves the model's generalization ability for image processing.

The loss function in this paper is:

$$L = \lambda_1 L_1 + \lambda_2 L_2 + \lambda_p L_{perceptual} + \lambda_G L_G \quad (11)$$

where, λ_1 , λ_2 , λ_p and λ_G are hyperparameters with loss function weights $\lambda_1 = \lambda_2 = 100$, $\lambda_p = 10$ and $\lambda_G = 1$.

H. MAE loss

Mean Absolute Error (MAE) loss is less sensitive and more robust to anomalies and noise in the data. In image restoration, the pixels in the missing region are very different from the surrounding pixels, and a robust MAE can restore the image more efficiently. The MAE loss helps to compensate for the sparsity of the output image, and can be used to generate images with fewer non-zero pixel points and sharper and more lifelike images by minimizing the absolute difference between the predicted pixels and the real image.

For the output of coarse and refined networks, this paper uses pixel level reconstruction loss to make the complementary image close to the true image with the following formula:

$$L_1 = \|I_{gt} - I_1\|_1 \quad (12)$$

$$L_2 = \|I_{gt} - I_{out}\|_1 \quad (13)$$

where, I_1 is the complementary image of the coarse network, I_{out} is the refined network output image, and I_{gt} is the real image.

I. Perceived Loss

The perceptual loss is calculated by inputting the real image and the generated image into the pre-trained model VGG-16, mapping the image to the feature space, and calculating the comparisons using the vanity L_1 . This calculates the perceptual loss and preserves the structural and content information of the image more efficiently. The formula is as follows:

$$L_{perceptual} = \sum_{i=1}^N \frac{1}{C_i H_i W_i} \|\phi_i(I_{gt}) - \phi_i(I_{pred})\|_1 \quad (14)$$

where $\phi_i(X)$ denotes the feature information extracted by VGG-16 in layer i of the input image, and C , H , and W are the number of channels, height, and width dimensions of the layer, respectively.

J. SN-PatchGAN

The SN-PatchGAN loss function can solve the problem of irregular image complementation more effectively. The discriminator trained using this loss function divides the generated complementary image into several pieces, then maps each piece to an output value and calculates the loss for each output result, thus effectively solving the problem of irregular missing. The specific formula is as follows:

$$L_D = E_{x \sim p} [\text{ReLU}(1 - D(x))] + E_{z \sim p_z} [\text{ReLU}(1 + D(G(z)))] \quad (15)$$

$$L_G = -E_{z \sim p_z} [D(G(z))] \quad (16)$$

where, D denotes the discriminator network, G denotes the generator network, x denotes the true image I_{gt} , and z denotes the to-be-complemented image I_{in} .

IV. EXPERIMENTAL RESULTS AND ANALYSIS

A. Introduction to the Datasets

In this paper, we conduct experiments on three public datasets, CelebA-HQ, Places2 and The Paris, with the specific parameters shown in Table V.

1) *CelebA-HQ*: In this paper, 27,000 images are randomly selected for training and 3,000 images for testing, totaling 30,000 images.

2) *Places2*: In this paper, 10 of the classes are selected as the experimental dataset, and 4000 images are selected in each class, totaling 40000 images. Among them, 38000 are used for training and 2000 are used for testing.

3) *The Paris*: This paper randomly selects 15000 of them as the experimental dataset, 14900 as the training samples and 100 as the test samples.

In order to train the network model, this paper uses the QD-IMD mask dataset for the construction of irregular masks. Meanwhile, we use the publicly available irregular data provided by Liu et al. [34] as the test mask to evaluate the training model.

TABLE V. DATASET PARAMETERS

| | <i>Training</i> | <i>Testing</i> | <i>Total</i> |
|-------------------|-----------------|----------------|--------------|
| CelebA-HQ | 27000 | 3000 | 30000 |
| Places2 | 38000 | 2000 | 40000 |
| The Paris Dataset | 14900 | 100 | 15000 |

B. Experimental Environment Construction

The parameters of the training device in this paper are CPU Intel i7-10750H, GPU RTX3060-6G, and memory DDR4-2399-32G. The training environment in this paper is realized on TensorFlow v1.3, CUDNN v8.1.1, and CUDA v11.1. All images and masks in the experiment are of size 256×256 .

C. Analysis of Experimental Results

The performance of the model in this paper is evaluated by comparing the method in this paper with a variety of other classical complementation methods.

1) *GLC* [7]: A complementation method that combines an inflated convolution and a global context discriminator for maintaining the consistency of the generated images.

2) *Gconv* [30]: A coarse-to-fine two-stage network with the addition of gated convolution, an improvement on previous work [13].

3) *MUSCIAL* [35]: A complementary method that introduces a multiscale attention module.
 4) *RFR* [18]: A progressive inference image complementation method that introduces cyclic feature inference for complementation.

The complementary results for CelebA-HQ dataset are shown in Fig. 9, the images generated by the model in this paper are visually closer to the original images. From the data, it can be seen that the structural similarity index (SSIM), average loss and peak signal-to-noise ratio (PSNR) are higher than several other methods.

The complementary results for Places2 dataset are shown in Fig. 10, this paper produces better complementary images compared to other methods, but also has a few artifacts. From the data, the method in this paper has the same PSNR as RFR, but the SSIM and average loss are better than RFR.

The complementary results for The Paris dataset are shown in Fig. 11, and the method in this paper is very similar to RFR's complementary naked eye. However, as can be seen from the data, this paper outperforms RFR in terms of average loss, but slightly underperforms RFR in terms of SSIM and PSNR.

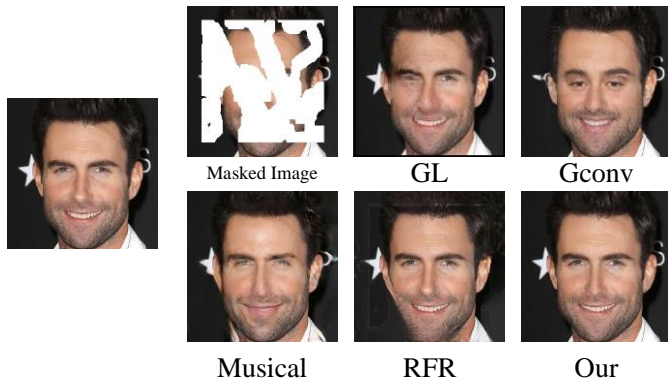


Fig. 9. Complementary images of CelebA-HQ dataset.



Fig. 10. Complementary images of Places2 dataset.

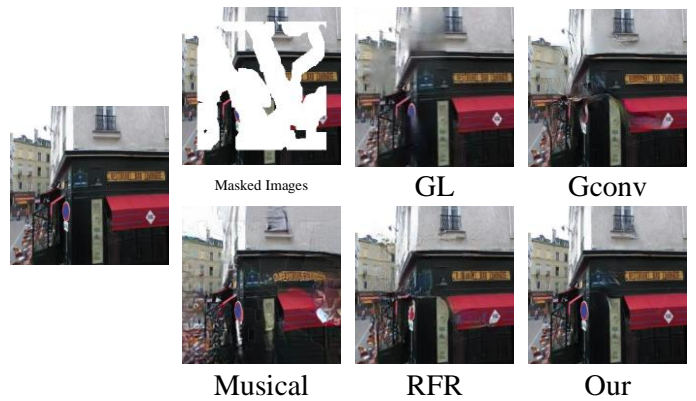


Fig. 11. Complementary images of the Paris dataset.

D. Ablation Experiments

In order to be able to demonstrate the effectiveness of the method in this paper more intuitively, the following experiments are conducted on the CelebA-HQ dataset.

- 1) *Experiment 1*: Retain the gated convolution and hybrid dilated convolution, but remove the attention mechanism module.
- 2) *Experiment 2*: Replace all convolutions with ordinary convolutions and keep the attention mechanism module.

The results of the experiments are shown in Fig. 12. From the results, it can be seen that compared to the method in this paper, Experiment 1 generates more complementary images containing artifacts and texture blurring, while the introduction of the attention mechanism module can more effectively reduce the loss of image information. The results of Experiment 2 show that the addition of gated convolution and hybrid dilated convolution can obtain more information when generating images and generate complementary images that are more in line with the real situation.

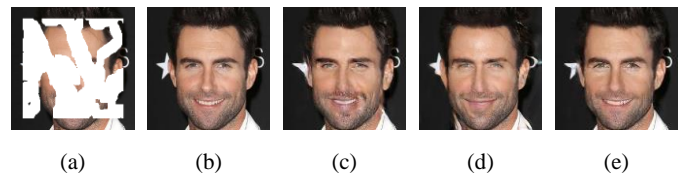


Fig. 12. (a) Input image, (b) Original image, (c) Experiment 1, (d) Experiment 2, and (e) Our.

V. RESULTS AND DISCUSSION

Compared with several classical algorithms such as GLC, Gconv, Musical and RFR, the method in this paper complements to better results. The comparison parameters on the three datasets are shown in Table VI, Table VII and Table VIII, the complementation results of this paper's method are better than the other methods in SSIM, PSNR and Mean loss, which shows that this paper's method can reasonably complement the irregular missing images.

Meanwhile, the ablation experiments can prove that the hybrid null convolution structure and the attention mechanism module cited in this paper effectively enhance the model. Therefore, the method in this paper can be applied to the frequently occurring missing problems in reality, to complement the problem of criminal's facial occlusion; to fill in the problem of missing details in old photos; and to predict the key contents of medical images.

TABLE VI. PERFORMANCE OF DIFFERENT MODELS ON CELEBA-HQ DATASET

| Method | Parameter | | |
|------------|--------------|--------------|-----------------|
| | SSIM | PSNR | Mean l_1 Loss |
| GLC | 0.693 | 19.62 | 6.91% |
| Gconv | 0.768 | 21.74 | 5.42% |
| Musical | 0.771 | 21.95 | 5.31% |
| RFR | 0.809 | 22.16 | 4.54% |
| Our Method | 0.811 | 22.53 | 4.56% |

TABLE VII. PERFORMANCE OF DIFFERENT MODELS ON THE PLACES2 DATASET

| Method | Parameter | | |
|------------|--------------|--------------|-----------------|
| | SSIM | PSNR | Mean l_1 Loss |
| GLC | 0.453 | 17.79 | 9.22% |
| Gconv | 0.574 | 18.31 | 8.22% |
| Musical | 0.583 | 18.76 | 7.91% |
| RFR | 0.594 | 18.90 | 7.63% |
| Our Method | 0.607 | 18.90 | 7.32% |

TABLE VIII. PERFORMANCE OF DIFFERENT MODELS ON THE PARIS DATASET

| Method | Parameter | | |
|------------|--------------|--------------|-----------------|
| | SSIM | PSNR | Mean l_1 Loss |
| GLC | 0.531 | 19.93 | 7.21% |
| Gconv | 0.628 | 20.72 | 6.61% |
| Musical | 0.631 | 21.65 | 6.72% |
| RFR | 0.674 | 22.79 | 5.58% |
| Our Method | 0.673 | 22.76 | 5.44% |

VI. CONCLUSION

The field of image restoration dates back to the 1950s. Most traditional image restoration methods use techniques such as texture synthesis, and although they can complement images, these methods have their own limitations. In recent years, with the advancement of deep learning techniques, image complementation has developed rapidly. Deep learning methods are trained with a large amount of data, constantly learning and updating, and excel in computer vision tasks, natural language processing and speech recognition. In the field of deep learning, Generative Adversarial Networks (GANs) are popular for their ability to generate images. Compared with other models, GAN-based image

complementation methods have excellent performance when targeting complex texture image restoration.

In this paper, we propose a two-stage GAN image-completion model with generative adversarial network as the underlying architectural model, i.e., a coarse-completion stage and a refinement-completion stage. The model mainly consists of gated convolution, hybrid dilated convolution and two attention mechanism modules, etc., while three different loss functions are used to train the generator more efficiently. The discriminative part introduces the VGG-16 feature extractor, which increases the sensory field and at the same time can extract more feature information from the image.

In this paper, the proposed model is experimentally compared with GLC, Gconv, MUSCIAL and RFR on three different datasets (CelebA-HQ, Place2, and The Paris dataset).GLC produces complementary images with blurred texture and confusing structure when complementing a wide range of deletions while Gconv and Musical produce less results when faced with a wide range of deletions, and GLC produces less results when faced with a wide range of deletions. Deletions produce less realistic or unrecognizable results. Similarly, the training results of RFR are similar to those of this paper, but the method in this paper generates results with fewer artifacts and better results. In terms of data, on the CelebA-HQ and Places2 datasets, this paper's method outperforms the other methods in terms of SSIM, PSNR and average loss. While on The Paris dataset, although the average loss is better than other methods, both SSIM and PSNR are slightly inferior to RFR.

The experimental results prove that the method in this paper has good progress and can recover the image details better while complementing the image.

REFERENCES

- [1] Christine Guillemot and Olivier Le Meur. Image inpainting: Overview and recent advances. *IEEE SPM*, 31(1):127–144, 2014.
- [2] Q. Sun, L. Ma, S. J. Oh, L. V. Gool, B. Schiele, and M. Fritz. Natural and effective obfuscation by head inpainting. In *Proc. CVPR*, pages 5050–5059, 2018.
- [3] Antonio Criminisi, Patrick Pérez, and Kentaro Toyama. Region filling and object removal by exemplar-based image inpainting. *IEEE Trans. Image Process*, 13(9): 1200–1212, 2004.
- [4] Anat Levin, Assaf Zomet, and Yair Weiss. Learning how to inpaint from global image statistics. In *Proc. ICCV*, pages 305–312, 2003.
- [5] Connelly Barnes, Eli Shechtman, Adam Finkelstein, and Dan B Goldman. Patchmatch: A randomized correspondence algorithm for structural image editing. *ACM TOG*, 28(3):24, 2009.
- [6] I. Goodfellow et al., “Generative adversarial nets,” in *Proc. Adv. Neural Inform. Process. Syst.*, 2014, pp. 2672–2680.
- [7] S. Iizuka, E. Simo-Serra, and H. Ishikawa. Globally and locally consistent image completion. *ACM TOG*, vol. 36, no. 4, pp. 1–14, 2017.
- [8] D. Pathak, P. Krahenbuhl, J. Donahue, T. Darrell, and A. A. Efros, “Context encoders: Feature learning by inpainting,” in *Proc. IEEE Conf. Comput. Vis. Pattern Recognit. (CVPR)*, Jun. 2016, pp. 2536–2544.
- [9] Y. Zeng, J. Fu, H. Chao, and B. Guo, “Learning pyramid-context encoder network for high-quality image inpainting,” in *Proc. IEEE/ CVF Conf. Comput. Vis. Pattern Recognit. (CVPR)*, Jun. 2019, pp. 1486–1494.
- [10] R. Zhang, W. Quan, B. Wu, Z. Li, and D. Yan, “Pixel-wise dense detector for image inpainting,” *Comput. Graph. Forum*, vol. 39, no. 7, pp. 471–482, Oct. 2020.

- [11] H. Liu, B. Jiang, Y. Song, W. Huang, and C. Yang, "Rethinking image inpainting via a mutual encoder-decoder with feature equalizations," in Proc. Eur. Conf. Comput. Vis., 2020, pp. 725–741.
- [12] C. Yang, X. Lu, Z. Lin, E. Shechtman, O. Wang, and H. Li. High-resolution image inpainting using multi-scale neural patch synthesis. In Proc.CVPR, pages 6721–6729, 2017.
- [13] J. Yu, Z. Lin, J. Yang, X. Shen, X. Lu, and T. S. Huang, "Generative image inpainting with contextual attention," in Proc. IEEE/CVF Conf.Comput. Vis. Pattern Recognit., Jun. 2018, pp. 5505–5514.
- [14] K. Nazari, E. Ng, T. Joseph, F. Qureshi, and M. Ebrahimi, "EdgeConnect: Structure guided image inpainting using edge prediction," in Proc. IEEE/CVF Int. Conf. Comput. Vis. Workshop (ICCVW), Oct. 2019, pp. 3265–3274.
- [15] Z. Yi, Q. Tang, S. Azizi, D. Jang, and Z. Xu, "Contextual residual aggregation for ultra high-resolution image inpainting," in Proc.IEEE/CVF Conf. Comput. Vis. Pattern Recognit. (CVPR), Jun. 2020, pp. 7508–7517.
- [16] H. Zhang, Z. Hu, C. Luo, W. Zuo, and M. Wang, "Semantic image inpainting with progressive generative networks," in Proc. 26th ACM Int. Conf. Multimedia, Oct. 2018, pp. 1939–1947.
- [17] Z. Guo, Z. Chen, T. Yu, J. Chen, and S. Liu, "Progressive image inpainting with full-resolution residual network," in Proc. 27th ACM Int. Conf. Multimedia, Oct. 2019, pp. 2496–2504.
- [18] J. Li, N. Wang, L. Zhang, B. Du, and D. Tao, "Recurrent feature reasoning for image inpainting," in Proc. IEEE/CVF Conf. Comput. Vis. Pattern Recognit. (CVPR), Jun. 2020, pp. 7757–7765.
- [19] W. Quan, R. Zhang, Y. Zhang, Z. Li, J. Wang and D. -M. Yan, "Image Inpainting With Local and Global Refinement," in IEEE Transactions on Image Processing, vol. 31, pp. 2405-2420, 2022.
- [20] T. Karras, T. Aila, S. Laine, and J. Lehtinen, "Progressive growing of GANs for improved quality, stability, and variation," in Proc. Int. Conf. Learn. Represent., 2018, pp. 1–26.
- [21] B. Zhou, A. Lapedriza, A. Khosla, A. Oliva, and A. Torralba, "Places: A 10 million image database for scene recognition," IEEE Trans. Pattern Anal. Mach. Intell., vol. 40, no. 6, pp. 1452–1464, Jun. 2018.
- [22] C. Doersch, S. Singh, A. Gupta, J. Sivic, and A. A. Efros, "What makes Paris look like Paris?" ACM Trans. Graph., vol. 31, no. 4, pp. 101:1–101:9, 2012.
- [23] M. Bertalmio, G. Sapiro, V. Caselles, and C. Ballester. Image inpainting. in Proceedings of the 27th annual conference on Computer graphics and interactive techniques, pages 417-424, 2000.
- [24] C. Ballester, M. Bertalmio, V. Caselle, G. Sapiro, and J. Verdera. Filling-in by joint interpolation of vector fields and gray levels. IEEE transactions on image processing, 10(8):1200-1211, 2001.
- [25] Marcelo Bertalmio, Luminita V ese, Guillermo Sapiro, and Stanley Osher. Simultaneous structure and texture image inpainting. IEEE Trans. Image Process., 12(8):882-889, 2003.
- [26] A. Criminisi, P. Pérez, and K. Toyama. Region filling and object removal by exemplar-based image inpainting. IEEE Trans. Image Process., 13(9):1200-1212,2004.
- [27] I. Drori, D. Cohen-Or, and H. Yeshurun. fragment-based image completion. in ACM SIGGRAPH, pages 303-312. 2003.
- [28] S. Darabi, E. Shechtman, C. Barnes, D. B. Goldman, and P. Sen. Image melding: Combining inconsistent images using patch-based synthesis. ACM Transactions on graphics(TOG), 31(4):82-1, 2012.
- [29] C. Barnes, E. Shechtman, A. Finkelstein, and D. B. Goldman. Patchmatch: A randomized correspondence algorithm for structural image editing. acm Transactions on graphics (TOG), 28(3):24, 2009.
- [30] J. Y u, Z. Lin, J. Y ang, X. Shen, X. Lu, and T. Huang. "Free-form image inpainting with gated convolution," in Proc. IEEE/ CVF Int. Conf. Comput. Vis. (ICCV), Oct. 2019, pp. 4471-4480.
- [31] S. Hochreiter and J. Schmidhuber, "Long short-term memory," Neural Comput. vol. 9, no. 8, pp. 1735-1780. 1997.
- [32] A. B. Pawar, C Priya, V. V. Jaya Rama Krishnaiah, V. Antony Asir Daniel, Yousef A. Baker El-Ebiary and Ahmed I. Taloba, "Multi-Scale Deep Learning-based Recurrent Neural Network for Improved Medical Image Restoration and Enhancement" International Journal of Advanced Computer Science and Applications(IJACSA), 14(10), 2023.
- [33] Andi Besse Firdausiah Mansur, "Disease-Aware Chest X-Ray Style GAN Image Generation and CatBoost Gradient Boosted Trees" International Journal of Advanced Computer Science and Applications(IJACSA), 15(3), 2024.
- [34] G. Liu, F. A. Reda, K. J. Shih, T.-C. Wang, A. Tao, and B. Catanzaro, "Image inpainting for irregular holes using partial convolutions. " in Proc. Eur. Conf. Comput. Vis., Sep. 2018, pp. 85-100.
- [35] N.-Wang, J. Li, L. Zhang, and B.-Du. 2019. MUSICAL: multi-scale image contextual attention learning for inpainting. in Proceedings of the 28th International Joint Conference on Artificial Intelligence (IJCAI'19). AAAI Press, 3748-3754.

Research on Resource Sharing Method of Library and Document Center Under the Multimedia Background

Jianhui Zhang^{1*}

Jiangsu College Nursing, Library, Jiangsu Huaian 223005

Abstract—In order to improve the utilization effect of the resources of the book and document center and ensure the security of its resource sharing, the resource sharing methods of the book and document center under the multimedia background are studied. The resource layer of this method is based on multimedia technology and combined with virtual technology to build a multimedia document cloud resource pool; At the same time, the adaptive clustering algorithm of empirical mode feature decomposition is used to obtain the number of document resources clustering and resource category labels, complete the resource clustering of the book and document center, and store it in the constructed resource pool; Users log in directly through the document resource sharing service of the service layer, and enter the resource center after authentication by the management layer. The service layer uses the regional document information resource co-construction and sharing mechanism based on blockchain to encrypt, co-identify and decrypt the clustered resources in the resource pool and then share the resources of the book and document center. The test results show that the clustering purity and contour coefficient of the method is above 0.970, and the clustering quality is good; The security of resource sharing is good, and the sensitivity result is 10.11% when the resource sharing ratio is 100%; It can effectively complete the resource sharing in the book and document center, and meet the sharing needs of book and document resources.

Keywords—Multimedia background; library and reference center; resource sharing; virtual technology; multimedia technology

I. INTRODUCTION

The Library and Reference Center is a virtual scientific and technological document information service institution [1, 2]. It is to provide scientific and technological document information services to the whole country according to the needs of national scientific and technological development and the collection, store, and development of scientific and technological document resources in various disciplines of science, engineering, agriculture, and medicine [3, 4]. Document service is a major service item in the book and document center. The specific contents include document retrieval, full-text provision, online full-text, catalog browsing, catalog query, etc. Non-registered users can obtain services other than full-text services for free, and registered users can also obtain full-text services [5, 6]. The document retrieval column provides users with query and sharing services for various scientific and technological document titles or abstracts [7]. The reference types include journals, conference proceedings, dissertations, scientific and technological reports, patent standards and books, etc., the types of reference involve China, West, Japan, Russia, etc., and the fields involve

medicine, architecture, chemical engineering, etc. [8]. It provides common search, advanced search, periodical search, classified search, natural language search, and other search methods. Resource sharing refers to using information technology resources to integrate and optimize, avoid repeated construction of resources, improve the utilization of resources, and meet users' resource service needs while meeting users' interactive communication needs and complete personalized push of resources [9].

When the resources of the book and document center are shared, there are still some deficiencies in the interaction between multiple users. Therefore, to better realize the sharing of such resources, reference [10] focused on the FULink platform to carry out the research on the resource-sharing process. Through this platform, all libraries could adhere to the common concept, abide by the unified standards, establish a scientifically coordinated operation mechanism and a perfect incentive mechanism, and promote the effective sharing of books and reference resources. This method can effectively coordinate sharing of reference resources among all participating libraries. It mainly focuses on the information exchange and control between participating libraries, but the security protection for the resources of the document center is poor. In reference [11], based on information sharing needs, after carrying out relevant research, an Internet information resource model of hierarchical information resource sharing for cloud computing was proposed. This method used specific constraints, trust gradient function, cloud trust evaluation criteria, and trust constraint coefficient to establish a hierarchical information resource sharing model and complete information sharing through this model. This method has good integrity in the application process. Still, it cannot cluster information resources, so it takes a long time in the sharing process, and the sharing effect of high-level resource information still needs further verification. Reference [12] took the remote sharing of resources as the research core. It proposed a blockchain-based resource-sharing method to protect the privacy and security of the experimental platform resources during the remote sharing of resources. However, this method cannot automatically push resources during application. Reference [13] puts forward a method of sharing digital English teaching resources based on artificial intelligence. Through the collection and management of English digital teaching resources, an evaluation index system of teaching resources is constructed, so as to comprehensively and objectively evaluate digital teaching resources, promote the construction and development of digital teaching resources, effectively promote and improve teaching effect, and realize the research requirements of effective sharing of massive

teaching resources in complex environment. However, this method has poor sensitivity to resource sharing. Reference [14] puts forward a resource sharing method of state update freshness. In the automatic driving system, the traffic situation and the vehicle position must be as close as possible. The information age is a relatively new indicator, which is used to measure the freshness of our understanding of the status of remote systems in order to better share resources. However, this method is not effective for the resource sharing of library and literature center.

At present, the rapid development of media technology has greatly changed the way of communication of information resources, and the dissemination of information resources also has gradually diversified with the integration of various media into the information age. Multimedia technology is the product of this information age. It is a technology that uses computers to store and manage various kinds of information, such as language, data, audio, video, etc. so that users can communicate real-time information through multiple senses and computers. The content displayed and carried by multimedia technology is actually the product of computer technology, with the characteristics of integration, control, interactivity, nonlinearity, synchronization, and dynamic information structure. Therefore, in order to meet the resource sharing of the book and document center in the information era, this paper studies the relevant resource-sharing methods of the book and document center based on the multimedia background. This method combines cloud services to complete the clustering and storage of reference resources and constructs resource pools through virtual technology to achieve efficient management of resources; Combined with the advantages of blockchain technology, the sharing mechanism is built to realize the safe sharing of resources. The feasibility of the proposed method and the effect of resource management and sharing are verified by the relevant analysis of the method.

The research motivation of this method is:

First of all, with the rapid development of information technology and the increasing richness of multimedia resources, the form and content of books and literature resources are undergoing profound changes. How to realize the effective sharing of books and literature resources under the

multimedia background and ensure the full utilization and efficient management of resources has become an urgent problem. Therefore, studying the methods of resource sharing in the library and literature center under the background of multimedia is helpful to promote the digitalization, networking and intelligent development of library and literature resources, and improve the utilization efficiency and management level of resources.

Secondly, with the increasingly obvious trend of interdisciplinary integration, the demand for books and literature resources is also diversified and cross-disciplinary, and the exchanges and cooperation between different disciplines need to share rich literature resources as support.

Finally, from the perspective of users' demand, with the diversification of information acquisition methods and the increase of personalized demand, users' demand for books and literature resources also presents the characteristics of diversification and personalization. Studying the resource sharing method of library and document center under the multimedia background is helpful to better meet the needs of users and provide more convenient and efficient services.

II. RESOURCE SHARING OF BOOK AND DOCUMENT CENTER

A. Resource Sharing Method Framework of the Book and Document Center

The functional services are designed from two aspects, namely, common functions and spatial functions. The former meets the basic needs of users for resource services, and the latter meets the basic needs of users for resource services. At the same time, users can get more communication and personalized experience. The functional design of common functions includes resource browsing, resource retrieval, resource download, resource upload, resource evaluation, and other functions. Users can search resources in the platform according to keywords or platform navigation classification. The space function is used to meet the communication and cooperation between users and realize sharing. The overall framework of this method consists of three layers: the service, the management, and the resource. The overall framework is shown in Fig. 1.

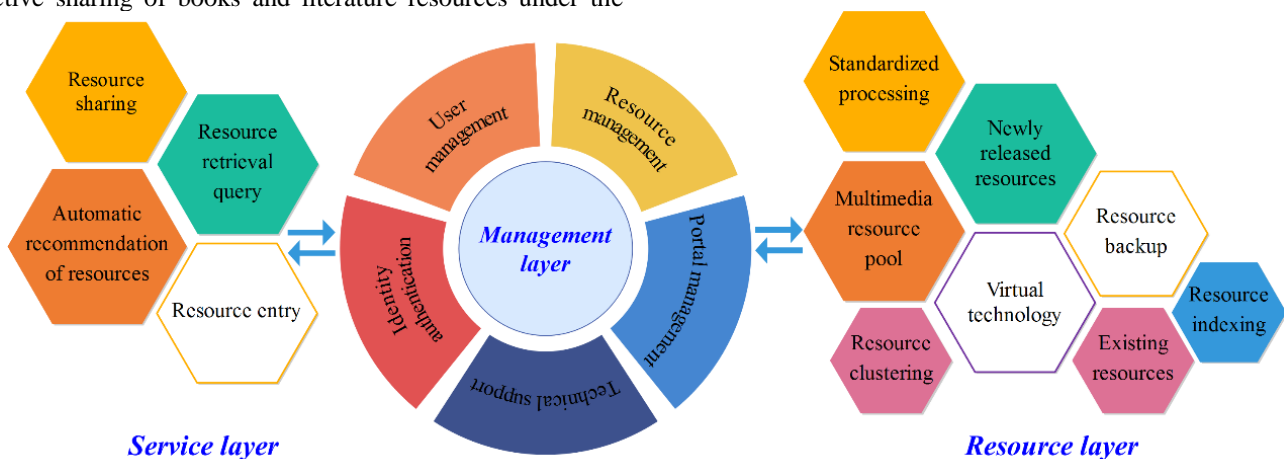


Fig. 1. Resource sharing method framework of the book and document center under the multimedia background.

The basic function of this method is to accept resource service requests from cloud computing users, deliver specific resources and services to the requester according to user needs, and reasonably schedule the corresponding resources so that users can request resources and services to run.

Service layer: The service layer is located at the top of the system platform and is also the realization part of the method of sharing. At the same time, this layer is the direct entrance to the document resource-sharing service presented to users. Users can access the multimedia resource-sharing platform through computers, mobile phones, panel computer, and other mobile devices, and can browse and download resources at any time, obtain resource services, improve user experience, and promote the sharing of document resources; In addition, the resource search method in the multimedia teaching resource sharing portal uses the classified navigation plus keyword search method to search, which can greatly improve the efficiency and accuracy of document retrieval. While meeting the user's resource demand, this layer can also provide more personalized and intelligent services. The platform can actively push information according to the user's usage habits to keep abreast of the latest developments of the resources concerned.

Management layer: As the management part of the overall framework of the method, the main role of this layer is to achieve comprehensive management of users, resources, etc. Because books and reference resources are stored in the form of a cloud resource pool and related services are provided through cloud service, the cloud service provider should be responsible for providing and managing the relevant cloud technology hardware equipment, storage, computing, and other functions while managing resource services, user accounts, resources, platform portals, etc. Account management is mainly to assign a unified authentication ID to users. It can access the resource pool and obtain relevant resource services only after applying for a unified ID number. Portal

management is mainly used to manage the service items of the resource cloud-sharing platform. It can update the website layout and columns in a timely manner so as to provide users with a better service experience and complete the timely release of website-related information and resources.

Resource layer: As the key layer to realize sharing, this layer mainly consists of two parts, namely, resource co-construction and resource storage. Resource co-construction is to summarize the original book and reference resources through a unified interface according to the specified standards through the integration method, and then filter index, clean the collected resources and store them in the document resource cloud resource pool to provide resource service support for the platform. In this paper, when storing resources, it can use virtual technology to build resource pools, which have storage space disaster tolerance technology, data encryption technology, and often backup resources to ensure the security of resource storage and avoid the loss of resources caused by Internet attacks. Redundant storage technology is adopted to make the storage of resources safer and more environmentally friendly.

B. Design of Resource Layer

1) *Structure of the reference resource pool:* The resource layer is the support for the realization of document sharing. In order to achieve better resource services, the storage of resources is particularly important. In this paper, multimedia technology is used to build a multimedia document cloud resource pool to achieve efficient resource integration; In addition, in order to ensure the cloud storage effect of resources, the virtualization of the resource pool is completed in combination with virtual technology to achieve efficient storage of resources. The structure of the multimedia reference cloud resource pool is shown in Fig. 2.

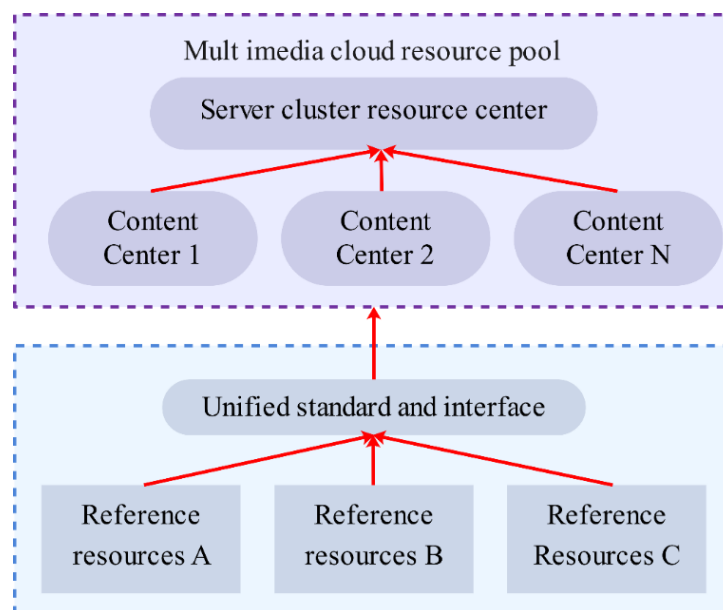


Fig. 2. Cloud resource pool structure of multimedia reference.

During resource integration, the resource layer uses the resource clustering algorithm to cluster and upload resources to cloud storage through the unified platform interface. All colleges and universities can access the resources uploaded to the cloud, further improving the efficiency of resource sharing. The resource storage method cloud service providers adopt centralized storage and multiple redundant backups, which is more secure. Even if one of the data analysis servers loses data due to natural disasters or other reasons, the data control center can recover data from other backups in time to ensure normal service delivery.

2) *Document resource clustering*: Before resource sharing, it is necessary to cluster the document resources. Due to the differences in the category and attribute of resources, in order to efficiently cluster the document resources, the adaptive clustering algorithm of empirical mode feature decomposition is used to complete the clustering, and the concept of cosine similarity is introduced to ensure the clustering effect.

Before clustering the reference resources, it should normalize the resources to limit them to a certain range, to eliminate the impact of resource structure differences on the clustering effect [15]. Assuming that the parameters of the adaptive clustering algorithm are represented by K , if the multi-source heterogeneous document resource set is represented by $X = \{x_1, x_2, \dots, x_n\}$, the number of resource categories contained therein is k , and the attributes of different resources are represented by S_k , and k is the maximum number of attributes. Based on this, the equation for calculating the confidence distance between samples of different reference resources is:

$$d(x_1, x_2) = K \times \sum_{k=1}^n S_k X_k \frac{1}{n \times u(x_1, x_2)} \quad (1)$$

In the formula: $u(x_1, x_2)$ represents confidence; n represents the number of reference resource samples. The normalization result of $X = \{x_1, x_2, \dots, x_n\}$ can be obtained after compression processing, and the equation is:

$$x_n = d(x_1, x_2) \times \left(1 + \frac{S_k}{\eta}\right) \quad (2)$$

In the formula: η represents the normalization factor.

After the normalization of reference resources is completed according to the above steps [16], the initial clustering center C_i is determined, and its calculation equation is:

$$C_i = \frac{x_n}{\sum_{i,k=1}^n y_{ik}} \quad (3)$$

In the formula: y_{ik} represents the degree of membership. After determining C_i , the document resources are clustered. In order to ensure a more reliable clustering effect, the concept of weighted cosine distance d_{ij} is introduced in the clustering

process to ensure the reliable clustering of resources of the same category. The calculation equation of d_{ij} is:

$$d_{ij} = 1 - \frac{\sum_{g=1}^G \sum_{k=1}^K (w_{gk} \times z_{igk})(w_{gk} \times z_{jgk})}{\sqrt{\sum_{g=1}^G \sum_{k=1}^K (w_{gk} \times z_{igk})^2} \sqrt{\sum_{g=1}^G \sum_{k=1}^K (w_{gk} \times z_{jgk})^2}} \quad (4)$$

In the formula: $g = 1, 2, \dots, G$; $k = 1, 2, \dots, K$; $i, j \in 1, 2, \dots, n$; w_{gk} represents the weight, corresponding to the g -th resource in the k -th category; z_{igk} and z_{jgk} represent the standardization results respectively. The former corresponds to the i -th resource, and the latter corresponds to the j -th resource.

On the basis of cosine similarity, the weighted cosine distance is used to objectively weight the different characteristics of the document resource samples, and the characteristic that the angle cosine measures the difference between any two individuals of different resource samples is retained, which can provide reliable guarantee for resource clustering [17].

If each resource is a category, the initial category and the distance between categories are expressed by $D_{i,j}$, and $D_{i,j} = d_{ij}$, then the initial category and the distance matrix between categories are expressed by $D^{(1)} = (d_{ij})_{N \times N}$. On this basis, after determining the distance $D_{k,r}$ between the merged class and other classes, the number of clusters is determined; If the given threshold of the number of clusters is Ψ , the relationship between it and any classes X_i and X_j is:

$$D_{k,r} = \Psi \times (X_i, X_j) \quad (5)$$

According to the calculation results of this equation, it can compare the distance and threshold results between different classes and classes of resources [18]. If Equation (5) is satisfied, that is, the distance between classes is less than or equal to the threshold, X_i and X_j are combined into one class. And one resource category is reduced according to the calculation result of $D_{k,r}$. The above contents are processed circularly. When the distance between all resource categories and categories is less than Ψ , the final document resource cluster quantity and resource category label can be obtained, and the book and document center resource cluster can be completed [19].

C. Realization of Resource Sharing

1) *Structure of resource sharing mechanism*: After completing the resource clustering of the book and document center through the above sections, the service layer will share the resources after clustering. To ensure security in the sharing process, the regional document information resource co-construction and sharing mechanism based on blockchain is adopted for resource sharing. The sharing structure of this mechanism is shown in Fig. 3.

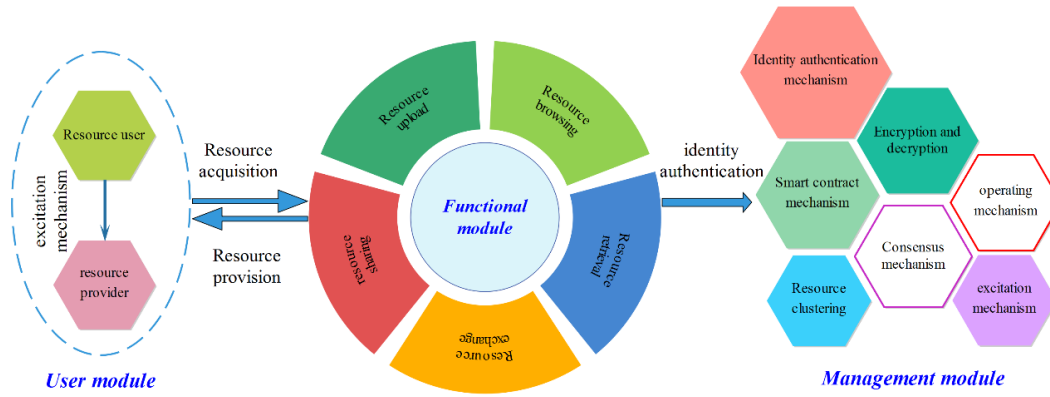


Fig. 3. Structure of regional document information resources co-construction and sharing mechanism based on blockchain.

The sharing mechanism proposed in this paper includes three modules, namely the user, function, and management modules. Through the mutual assistance of the three modules, a resource-sharing alliance chain is formed to realize the safe sharing of resources.

- **User module:** This module is based on the private chain of user behavior, which includes all service objects of the Alliance, namely users of information resources, as well as alliance resource providers, such as various types of databases, publishers, and libraries. Therefore, users can become both providers and users of the Alliance's reference and information resources, thus expanding the types and service scope of regional reference and information resources co-construction and sharing.
- **Function module:** The service layer includes a data sub-module and function sub-module, which are used for uploading, browsing, searching, downloading, and other functions of information resources. Users can upload data resources within certain rules through the data sub-module. They can select corresponding functions to download information resources according to their own needs through the function sub-module.
- **Management module:** The management layer uses the blockchain-based distributed ledger technology [20], and the member libraries of the Alliance store their reference data resources in different blocks in a distributed manner. They use point-to-point communication to achieve efficient use of resources, solve the problem of resource islands, promote the free circulation and safe sharing of information resources among university libraries in the Alliance, and improve the sharing efficiency. The member libraries of the Alliance are interrelated and independent of each other. Through identity authentication mechanism, consensus mechanism, incentive mechanism, and smart contract mechanism, they are jointly built in the framework of the Alliance to identify the rights and responsibilities of document resource allocation within the Alliance and to standardize the behavior of the member libraries of the Alliance.

2) *Implementation method of resource sharing:* When using the regional reference information resource co-construction and sharing mechanism based on blockchain to share the resource, in order to ensure the sharing effect, ensure the stability in the sharing process, and complete the sharing among multiple nodes, this mechanism uses consensus algorithm to maintain the resource sharing, with good decentralized characteristics [21]. According to different principles, the algorithm can be divided into a verification pool mechanism, proof of rights and interests' mechanism, and proof of workload mechanism. The practical Byzantine fault-tolerant algorithm, system fault-tolerant performance [22], response time, and throughput are the main factors in judging the performance of the consensus algorithm. The parameter of consensus algorithm is fault tolerance, the calculation equation of fault-tolerant performance f during resource sharing is as follows:

$$f = \left\lfloor \frac{m-1}{3} \right\rfloor \quad (6)$$

In the formula: m represents the number of shared user nodes.

If the time of the consensus node of the algorithm for resource reception and consensus is t' and \tilde{t} respectively, the calculation equation for the response time t of resource sharing is:

$$t = t' + \tilde{t} \quad (7)$$

In unit time, the total amount of resources shared on the blockchain $T_{PS\Delta t}$ is calculated as follows:

$$T_{PS\Delta t} = \frac{T_{total} \times T_{\Delta t}}{\Delta t} \quad (8)$$

In the formula: $T_{PS\Delta t}$ represents the total amount of resources shared on the blockchain per unit of time, which also represents throughput; Δt represents the response time change of resource sharing, $T_{\Delta t}$ represents the amount of resources shared on the blockchain. T_{total} represents the total amount of resources shared on all blockchains.

3) *Privacy protection of shared resources:* The decentralization of the blockchain makes every node contain

all the information of the system, so the link's capacity restricts the further improvement of the blockchain and how to protect data privacy. At the same time, not affecting blockchain performance is the main problem to be solved. Privacy protection mainly adopts password technology, mixed currency technology, etc. This paper uses the aggregate signature method in encryption technology. The aggregate is superimposed into a single data through the input and output of multiple signature information. This algorithm has a high-security factor and can provide block transaction information without increasing the system burden. The specific process is as follows:

In the case of resource sharing transaction, input and output resources are represented by x and y respectively, and the relationship between them is shown in Equation (9):

$$\sum_{i=1}^x ix_i = \sum_{j=1}^y out_j \quad (9)$$

In the formula: x_i and out_j both indicate that resources need to be hidden; $i \in [0, x]$; $j \in [0, y]$.

If the resource sharing transaction generator is represented by z , the conversion equation of the resource sharing transaction mode of x_i and out_j is:

$$\begin{cases} I_i = x_i \times z \\ O_i = out_j \times z \end{cases} \quad (10)$$

According to Equation (10), if the results of x_i and out_j cannot be obtained through I_i and O_i during resource sharing, it means that the shared resource cannot be found, which can greatly ensure the security of the resource and realize safe sharing.

4) *Shared resource decryption*: After the shared resource encryption is completed in the above section, users need to decrypt before sharing resources [23]. If the random number received by the resource provider is X_i , its ID is I_x , and the ID

of the resource receiver is I_y , the expression of the harvest factor S_{x*y} of the decoding work can be obtained as follows:

$$S_{x*y} = (e^x, e^y) \quad (11)$$

In the formula: e^x and e^y both refer to the shared secret key, the former corresponds to the resource provider, and the latter corresponds to the resource receiver. To obtain the decryption parameter H_{x*y} , its calculation equation is:

$$H_{x*y} = \prod_{i=1}^n h^{Rx} + h^{Ry} \quad (12)$$

In the formula: h^{Rx} and h^{Ry} both represent encrypted resource parameters. The former corresponds to the resource center and is transmitted to the processor, while the latter corresponds to the processor and is transmitted to the resource receiver.

On the basis of the above steps, the resource receiver needs to decrypt the secret text resources [24]. The equation for decrypting the plaintext resources is:

$$\xi_{xu} = \frac{b_{2xj}}{W^{-\mu}} \quad (13)$$

In the formula: the resource receiver I_y decrypts and obtains the plaintext resource, which is expressed as ξ_{xu} ; b_{2xj} indicates the location of the private key; $W^{-\mu}$ represents the weight attribute.

D. Shared Resource Push

After the decryption of resources is completed in the above section, the service layer will share and push the decrypted resources. During the implementation of this push, users can easily obtain the rich required resource content. With this automatic push function, users can easily obtain a certain type of frequently updated resource information without having to search on the resource platform. The automatic push process of shared resources is shown in Fig. 4.

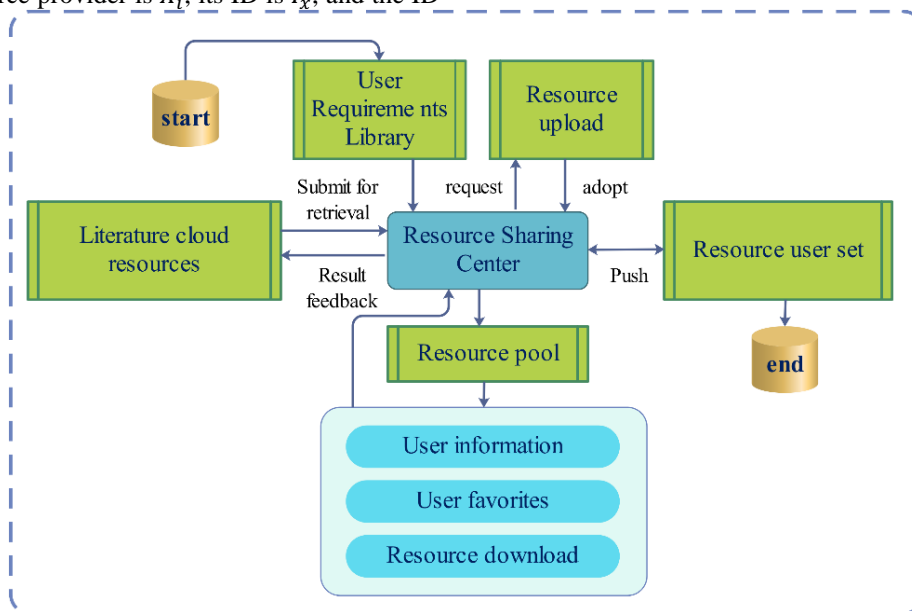


Fig. 4. Push process of resource sharing resources in the book and document center.

As shown in Fig. 4, the active resource push process shows that the cloud-sharing platform will push the decrypted shared resources and can build a user demand library; when the user is on the next visit, the document center can understand the user's preference for resources through the user demand database. According to this user demand database, the resource information matching the user demand database in the relevant resource pool is searched. Then the searched resource blockchain is encrypted and pushed to the user. After the user decrypts the information, the automatic push of the information is realized to complete the resource sharing.

III. TEST ANALYSIS

In order to verify the application effect of the method in this paper, it takes a university's book and document center as an example research object. It applies this method to the

document resource sharing and exchange platform management center. 2000 medical resources in the center are selected as the document resource data for testing. The resources are divided into three categories according to the publishing form: books, special documents, and continuous publications. The test document resources include 1000 traditional Chinese and 1000 western medicine document resources. The method in this paper is used to share the document resources and obtain the sharing results to analyze the application effect of the method in this paper.

During the test, users are all high school students and distributed in the same base station. The MEC computing capacity deployed in the base station is 20GHz/s, and the computing resources of other devices are randomly distributed in the range of [2,4] GHz/s. Other relevant parameters of network communication are shown in Table I.

TABLE I. DETAILS OF COMMUNICATION PARAMETERS

| Parameter Name | Numerical Value |
|--|-----------------|
| Cellular channel bandwidth /MHz | 12 |
| Uplink transmission power /mW | 200 |
| D2D bandwidth /MHz | 12 |
| D2D transmit power /mW | 100 |
| noise power /dBm | -100 |
| Channel gain | 0.00006 |
| Number of cellular orthogonal channels | 20 |
| Number of D2D orthogonal channels | 20 |

In order to verify the clustering effect of the method in this paper on different document resources, the paper uses the clustering purity ρ and the contour coefficient φ as the evaluation indicators, ρ is to measure the clustering quality of the method, and φ is to measure the advantages and disadvantages of clustering. The value range of the two indicators is between [0~1] and [- 1~1], respectively. The closer the value is to 1, the better the clustering quality and the better the clustering effect. The calculation equations are as follows:

$$\rho = \frac{1}{N} \sum_{k=1}^K n_k \quad (14)$$

$$\varphi = b \frac{d'}{\max\{d', b_{min}\}_{min}} \quad (15)$$

In the formula: N represents the total number of resource samples; n_k is the sample number of most classes in the k -th cluster; b_{min} represents the minimum vector, and represents the average distance between the point i and points in different classes; d' represents the average distance between resource i and other resources in its same category.

According to Eq. (14) and Eq. (15) above, it can calculate the results of the two indicators with the gradual increase of the number of resource samples when clustering the three reference resources using this paper's method, as shown in Table II.

TABLE II. TEST RESULTS OF THE CLUSTERING EFFECT OF DIFFERENT REFERENCE RESOURCES

| Number of Clusters/Piece | Reference Category | | | | | |
|--------------------------|--------------------|----------------|-------------------|----------------|---------------------|----------------|
| | Books | | Special reference | | Series publications | |
| | Cluster Purity | Profile Factor | Cluster Purity | Profile Factor | Cluster Purity | Profile Factor |
| 100 | 0.954 | 0.943 | 0.922 | 0.952 | 0.955 | 0.952 |
| 200 | 0.963 | 0.951 | 0.941 | 0.949 | 0.947 | 0.936 |
| 300 | 0.948 | 0.946 | 0.928 | 0.962 | 0.944 | 0.939 |
| 400 | 0.939 | 0.955 | 0.931 | 0.954 | 0.952 | 0.944 |
| 500 | 0.954 | 0.933 | 0.956 | 0.986 | 0.971 | 0.967 |
| 600 | 0.966 | 0.926 | 0.947 | 0.971 | 0.968 | 0.935 |
| 700 | 0.978 | 0.947 | 0.962 | 0.983 | 0.949 | 0.974 |

| | | | | | | |
|------|-------|-------|-------|-------|-------|-------|
| 800 | 0.972 | 0.952 | 0.958 | 0.966 | 0.933 | 0.987 |
| 900 | 0.959 | 0.946 | 0.934 | 0.924 | 0.945 | 0.958 |
| 1000 | 0.977 | 0.977 | 0.977 | 0.936 | 0.962 | 0.962 |
| 1100 | 0.954 | 0.979 | 0.961 | 0.958 | 0.957 | 0.984 |
| 1200 | 0.928 | 0.959 | 0.958 | 0.966 | 0.981 | 0.967 |
| 1300 | 0.936 | 0.928 | 0.969 | 0.927 | 0.975 | 0.986 |
| 1400 | 0.941 | 0.981 | 0.972 | 0.958 | 0.982 | 0.981 |
| 1500 | 0.952 | 0.982 | 0.958 | 0.986 | 0.985 | 0.964 |
| 1600 | 0.953 | 0.963 | 0.974 | 0.977 | 0.956 | 0.959 |
| 1700 | 0.964 | 0.957 | 0.947 | 0.985 | 0.986 | 0.937 |
| 1800 | 0.956 | 0.924 | 0.955 | 0.965 | 0.928 | 0.962 |
| 1900 | 0.944 | 0.932 | 0.928 | 0.972 | 0.974 | 0.955 |
| 2000 | 0.922 | 0.944 | 0.931 | 0.982 | 0.979 | 0.978 |

According to the test results in Table II, after clustering the three kinds of reference resources using the method in this paper, with the gradual increase of the number of samples, the results of the clustering purity ρ and the contour coefficient φ of the book resources are very close to 1, the maximum value of ρ is 0.978, and the maximum value of φ is 0.982; The maximum results of clustering purity ρ and profile coefficient φ of special reference are 0.977 and 0.986 respectively; The maximum results of cluster purity ρ and contour coefficient φ of the continuous publications are 0.986 and 0.987, respectively. Therefore, the method in this paper has a good clustering effect on document resources, can effectively complete the clustering of different categories of document resources, and provide a reliable basis for resource sharing.

In order to verify the security of resources in the method of this paper when sharing resources, resource sharing sensitivity ψ is used as the measurement uncertainty. ψ can measure the security degree of resources in the process of sharing, and its value range is between 0% and 100%. The larger the value is,

the higher the sensitivity of sharing is, and the worse the security of information sharing is. The calculation equation of this indicator is:

$$\psi = \frac{\sum_{i=1}^{B_n} \frac{|\alpha_i - \beta_i|}{\alpha_i}}{B_n} \quad (16)$$

In the formula: B_n represents the sensitive category threshold of resource sharing, α_i represents the frequency efficiency of document resource i sharing, β_i refers to the efficiency of frequency estimation of shared resources.

In order to intuitively reflect the security of resource sharing of the method in this paper, the three methods in reference [10], reference [11], and reference [12] are used as the comparison methods for the method in this paper. According to Eq. (16), the calculation results of ψ are shown in Table III, with the increasing proportion of total resources successfully shared when the above algorithms share different amounts of resources.

TABLE III. RESOURCE SHARING SECURITY TEST RESULTS OF FOUR METHODS

| Method category | | Successful share ratio /% | | |
|----------------------|--|---------------------------|-------|-------|
| | | 10 | 50 | 100 |
| Reference [10]method | Number of shared resources 500/ strip | 14.32 | 17.66 | 22.76 |
| | Number of shared resources 1000/ strip | 20.17 | 26.62 | 31.46 |
| Reference [11]method | Number of shared resources 500/ strip | 15.33 | 18.47 | 20.86 |
| | Number of shared resources 1000/ strip | 22.33 | 27.45 | 30.22 |
| Reference [12]method | Number of shared resources 500/ strip | 16.26 | 19.44 | 23.76 |
| | Number of shared resources 1000/ strip | 21.82 | 26.36 | 29.97 |
| Method in this paper | Number of shared resources 500/ strip | 4.36 | 5.96 | 7.44 |
| | Number of shared resources 1000/ strip | 5.82 | 7.68 | 10.11 |

According to the test results in Table III, with the gradual increase of the number of shared resources under different successful sharing ratios, the sensitivity results of the method in Reference [10], [11], [12] and the method in this paper for resource sharing also have different changes. Among them, the method in reference [10], the method in reference [11], and the method in reference [12] have different results when the

number of shared resources is 1000. The sharing success ratio reaches 100%, and the highest results of them of ψ are 31.46%, 30.22% and 29.97%, respectively, while the results of ψ in this paper's method are 10.11%. The reason is that in the process of sharing, the method in this paper introduces the regional document information resources co-construction and sharing mechanism based on blockchain, which can encrypt the shared

resources and combine the consensus algorithm to process the shared resources. The resource receiver can obtain the resources of the resource center after decryption, so the security of resource sharing can be greatly guaranteed.

In order to verify the applicability of document resource sharing in the system of this paper, after obtaining the application of the method in this paper, the management results of the university's document resource sharing and exchange platform management center for book and document resources are shown in Fig. 5.

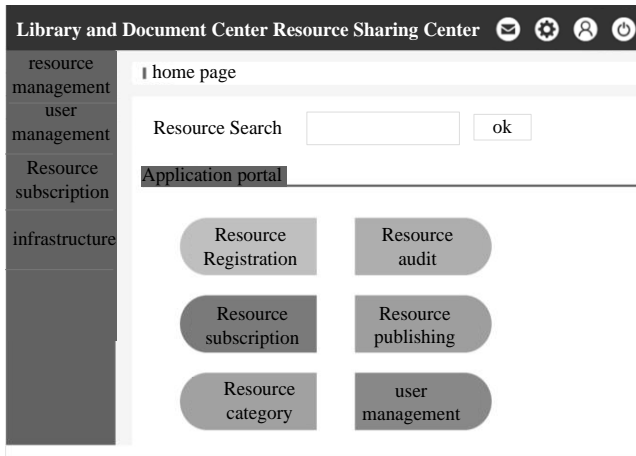


Fig. 5. Management results of book and document resources.

According to the test results in Fig. 5, after the application of the method in this paper, the university's document resource sharing and exchange platform management center can view the details of different types of resources through resource clustering. At the same time, it can view the release of users, the review of resources, the subscription of users, and master users' browsing and needs for document resources. Because this method has good applicability, it can complete the unified storage and management of different types of document resources after application and provide a resource guarantee for resource sharing.

In an ideal state, the maximum coverage of resource sharing in the library and literature center is 100%. Based on this data standard, if the actual coverage of the research method is closer to this value, it means that the wider the coverage of resource sharing is, the more it meets the resource sharing requirements of the library and literature center. According to the above discussion, calculate the coverage rate of the shared range, and the formula is:

$$\lambda_{\alpha\beta} = \frac{\sum_{i=1}^n N_i}{M_i} \times 100\% \quad (17)$$

In the formula: $\lambda_{\alpha\beta}$ represents the coverage rate of the shared range; N_i represents the amount of shared resources in a certain link; M_i represents the total resources of this link. Based on the above formula, the coverage results of resource sharing range of the four methods are calculated respectively, as shown in Table IV.

From the experimental results recorded in Table IV, it can be seen that method in this paper has a sharing coverage rate of over 98% each time, while the other three reference methods can only reach 85.47% at the highest, and the sharing coverage rate is small. Therefore, through the above experimental results, it can be proved that the research on the resource sharing method of book and document center proposed in this paper has a higher coverage of sharing scope in practical application, which can fully meet the sharing needs of book and document center resources.

TABLE IV. COMPARISON TABLE OF SHARING SCOPE COVERAGE OF FOUR METHODS

| Sharing times | Method in this paper/% | Reference [10] method/% | Reference [11] method/% | Reference [12] method/% |
|-----------------|------------------------|-------------------------|-------------------------|-------------------------|
| The first time | 98.25 | 54.21 | 55.26 | 56.25 |
| The second time | 98.36 | 53.36 | 64.52 | 62.15 |
| Third time | 98.52 | 61.36 | 71.41 | 64.58 |
| The fourth time | 98.95 | 68.20 | 84.25 | 71.25 |
| The fifth time | 99.61 | 73.35 | 85.47 | 75.69 |

IV. DISCUSSION

Under the background of the rapid development of multimedia, it is particularly important to study the resource sharing method of library and document center. This research is not only an innovation of the traditional management of books and documents, but also a deep exploration of the knowledge dissemination and sharing mechanism in the information age.

First of all, the application of multimedia technology has brought unprecedented development opportunities for the library and documentation center. Through digitalization, networking and other means, books and literature resources can be spread and utilized more conveniently and efficiently. However, how to effectively share the resources of the library and literature center under the multimedia background is an urgent problem to be solved. The importance of this research lies in that it can provide a set of scientific and reasonable resource sharing methods for the library and literature center, thus promoting the maximum utilization of library and literature resources and improving the efficiency of knowledge dissemination.

Secondly, the research on the resource sharing method of library and documentation center is helpful to promote the interdisciplinary and integration. Under the background of multimedia, books and literature resources are no longer limited to a certain discipline or field, but show an interdisciplinary and cross-disciplinary trend. Therefore, how to build a shared platform that can accommodate diversified resources and promote exchanges and integration between different disciplines has become an important research direction. This research can not only promote the intersection and integration of disciplines, but also provide fertile soil for the generation of new knowledge.

Finally, the research on the resource sharing method of library and document center is of great significance for acquiring new knowledge. Through the research and practice of sharing methods, we can dig deeper into the value of books and literature resources and discover the new knowledge contained in them. At the same time, the optimization and innovation of sharing methods can also provide strong support for knowledge innovation and promote the in-depth development of academic research.

To sum up, the research on the resource sharing method of library and literature center under the multimedia background has important theoretical value and practical significance. It not only helps to promote the maximum utilization of books and literature resources and the intersection and integration of disciplines, but also provides strong support for the generation of new knowledge. Therefore, we should strengthen the research investment in this field and constantly promote the innovation and development of resource sharing methods in book and document centers.

V. CONCLUSION

The application field of multimedia technology has gradually expanded, and people's demand for resources in the field of multimedia has also increased significantly. For the book and document center, it is of great significance to maximize the utilization of its resources and expand its capabilities. However, in the current book and document center, there are many types of resources and a large amount of information, which leads to low processing efficiency in the process of using or sharing resources, and there are certain security risks. Therefore, this paper starts from the human problem in the resource sharing of the book and document center and combines several major problems in the resource sharing under the current multimedia background, including the storage, security sharing, and overall management of resources, and puts forward the resource sharing method of the book and document center under the multimedia background. This method makes use of the advantages of multimedia technology to uniformly store the scattered resources in different data sources and realize the sharing of data resources in different servers, which can expand the sharing range of information resources and effectively meet the personalized needs of users for resources.

With the continuous development and popularization of multimedia technology, the research on resource sharing methods in book and document centers is facing broader prospects and higher requirements. In the future, the following aspects can be further studied:

1) The future research work will pay more attention to the intelligence and personalization of the resource sharing platform. By applying advanced technologies such as artificial intelligence and big data, the platform will be able to understand users' needs more accurately and provide more accurate resource recommendation and personalized services.

2) Future research work will be devoted to promoting cross-domain and cross-regional cooperation of resource sharing platforms. In the future, the sharing platform will pay more attention to cross-disciplinary resource integration and

sharing, and promote exchanges and integration between different disciplines.

3) Future research work will also be devoted to promoting the openness and sharing of the resource sharing platform. By opening API and providing data interface, the platform will be able to realize seamless docking and data sharing with other systems and platforms, and further promote the sharing and utilization of books and literature resources.

DATA AVAILABILITY

The raw data supporting the conclusions of this article will be made available by the authors, without undue reservation.

CONFLICTS OF INTEREST

The authors declared that they have no conflicts of interest regarding this work.

FUNDING

The work is not supported by any funding.

REFERENCES

- [1] R. A. Alsuhaibani, "One hundred tweets from library land: a case study of RMIT University Library (academic library) and State Library of Victoria (public state library) in Australia," *Journal of Librarianship and Information Science*, vol. 52, no. 1, pp. 197-207, 2020.
- [2] K. Cyran, S. Borkowicz, M. DzioŁak, M. G. Gavara, and M. O. OllÉ, "An academic library or a learning and research resources centre (crai)? a comprehensive approach to the library as the central element of the university structure in poland and spain," *Przegląd Biblioteczny*, vol. 88, no. 4, pp. 461-479, 2020.
- [3] R. Happel, P. Larionov, and T. Schanze, "On the development of a FHIR-compliant backend for processing HTTP requests and APIbased management of healthcare documents," *Current Directions in Biomedical Engineering*, vol. 7, no. 2, pp. 133-135, 2021.
- [4] D. O. Obiano, E. Ogueri, N. Chima-James, P. O. Moneke, and I. I. Bernard, "Availability and Use of Library Resources in the Rehabilitation of Inmates in Correctional Centers in Imo and Abia States, Nigeria," *Information Impact: Journal of Information and Knowledge Management*, vol. 11, no. 2, pp. 51-61, 2020.
- [5] D. A. Corpuz, "Library resources and functional effectiveness of an academic library: meeting the challenges of the digital age," *Humanities & Social Sciences Reviews*, vol. 8, no. 4, pp. 238-245, 2020.
- [6] S. Samaila, H. M. Adedayo, and S. Musbahu, "Use Of Social Media Platforms For The Promotion Of Library Resources And Services Inal-Qalam University, Katsina, Nigeria," *FUDMA Journal of Educational Foundations*, vol. 3, no. 1, pp. 115-125, 2020.
- [7] O. Gillath, R. Atchley, A. Imran, P. Haj - Mohamadi, and M. El - Hodiri, "Attachment and resource sharing," *Personal Relationships*, vol. 27, no. 2, pp. 228-250, 2020.
- [8] Y. Chaabi, N. M. Ndiyaie, and K. Lekdioui, "Personalized recommendation of educational resources in a MOOC using a combination of collaborative filtering and semantic content analysis," *International Journal of Scientific & Technology Research*, vol. 9, no. 2, pp. 3243-3248, 2020.
- [9] J.-S. Zheng et al., "A mirror-image protein-based information barcoding and storage technology," *Science Bulletin*, vol. 66, no. 15, pp. 1542-1549, 2021.
- [10] Y. Jiang, "Research on the co-construction and sharing strategy of Haisi literature resources based on FULink platform," *Journal of Zhangzhou Normal University (Philosophy and Social Sciences Edition)*, vol. 34, no. 2, pp. 152-157, 2020.
- [11] G Lin, "Research on cloud computing service model based on university teaching resource sharing Information and computer," *Springer Berlin Heidelberg*, vol. 32, no. 5, pp. 226-228, 2020.

- [12] S. Wang and Y. Li, "ARemote Resource Sharing Simulation of Interactive Experiment Platform Based on Blockchain," *Computer Simulation*, vol. 39, no. 6, pp. 233-237, 2022.
- [13] C. Chen, "A method of digital english teaching resource sharing based on artificial intelligence," *Journal of Information & Knowledge Management*, vol. 21, no. 2, pp. 1-17, 2022.
- [14] F D Miguez, and U Ayesta, "A resource sharing game for the freshness of status updates," *ACM SIGMETRICS Performance Evaluation Review*, vol. 49, no. 2, pp. 15-17, 2022.
- [15] Z. Zhou, M. Shojafar, M. Alazab, J. Abawajy, and F. Li, "AFED-EF: An energy-efficient VM allocation algorithm for IoT applications in a cloud data center," *IEEE Transactions on Green Communications and Networking*, vol. 5, no. 2, pp. 658-669, 2021.
- [16] Q. Xiao, "Resource Classification and Knowledge Aggregation of Library and Information Based on Data Mining," *Ingénierie des Systèmes d'Information*, vol. 25, no. 5, pp. 645-653, 2020.
- [17] R. Ando, Y. Kadobayashi, and H. Takakura, "Clustering Massive Packets using a Lock-Free Algorithm of Tree-Based Reduction on GPGPU," *International Journal of Computer Science and Information Security (IJCSIS)*, vol. 19, no. 3, pp. 39-48, 2021.
- [18] A. K. Wicaksana and D. E. Cahyani, "Modification of a density-based spatial clustering algorithm for applications with noise for data reduction in intrusion detection systems," *International Journal of Fuzzy Logic and Intelligent Systems*, vol. 21, no. 2, pp. 189-203, 2021.
- [19] S. Raheem, S. Al Shehabi, and A. Mohi Nassief, "MIGR: A Categorical Data Clustering Algorithm Based on Information Gain in Rough Set Theory," *International Journal of Uncertainty, Fuzziness and Knowledge-Based Systems*, vol. 30, no. 05, pp. 757-771, 2022.
- [20] S. Andreina and G. Karame, "Method and system for securely sharing validation information using blockchain technology," ed: Google Patents, 2021.
- [21] L. Bader et al., "Blockchain-based privacy preservation for supply chains supporting lightweight multi-hop information accountability," *Information Processing & Management*, vol. 58, no. 3, p. 102529, 2021.
- [22] X. Yang, X. Ruan, and Y. Geng, "Iterative learning fault-tolerant control for discrete-time nonlinear systems subject to stochastic actuator faults," *Transactions of the Institute of Measurement and Control*, vol. 44, no. 10, pp. 2012-2023, 2022.
- [23] R. Singh, G. Kumar, and C. Kumar, "Impact of encryption and decryption techniques for high speed optical domain," *Computer Science and Information Technologies*, vol. 2, no. 1, pp. 11-15, 2021.
- [24] S. M. Abd Ali and H. F. Hasan, "Novel encryption algorithm for securing sensitive information based on feistel cipher," *Test Engineering Management*, vol. 19, no. 80, pp. 10-16, 2019.

A Hybrid MCDM Model for Service Composition in Cloud Manufacturing using O-TOPSIS

Syed Omer Farooq Ahmed¹, Adapa Gopi²
Research Scholar¹, Associate Professor²
Koneru Lakshmaiah Education Foundation, Guntur, India

Abstract—The purpose of this research article was to define the current or future usage of Industry 4.0 technologies (Cloud Computing, IoT, etc.) to improve industrial manufacturing. The goal of this study is to rate the options using a hybrid CRITIC - O-TOPSIS Multi Criteria Decision Making model. The CRITIC technique is used to calculate Objective Weights. Also, when comparing the findings to TOPSIS, A thorough Systematic Literature Review comes first. Secondly, a theoretical approach to recognizing the Index System of Criteria. Third, Creating a Hybrid Model of CRITIC and O-TOPSIS for Decision Making. Lastly, Comparing and Ordering Options. The proposed technique successfully addresses the ambiguity and uncertainty of heterogeneous information while maintaining assessment data accuracy. Also, because objective weights are more grounded in reality than subjective weights, the result is more precise. CRITIC approach results reveals that Ease of Opting has the most weight and Ease of Implementation has the least weight O-TOPSIS method ranks alternatives in the following order: A4>A5>A3>A1>A2. This paper ranks alternatives based on extensive 22 criteria in Service Composition in Cloud Manufacturing using the hybrid model CRITIC - O-TOPSIS

Keywords—Cloud manufacturing (CMFg); CRITIC method; O-TOPSIS method; service composition

I. INTRODUCTION

In tech-based manufacturing, the most cutting-edge technological techniques can be employed to govern service composition. To be more specific, the concept of Industry 4.0 emerges first in this context. The Internet of Things (IoT) and cloud manufacturing (CM) are two examples of modern digital technologies.

An optimization-based strategy is not used in the fuzzy TOPSIS technique [1]. It is suggestible to consider objectivity arising due to human intervention. In order to solve this, O-TOPSIS with Objective Weights is used in this study's ranking of the alternatives. An advanced manufacturing system selection problem with six evaluation criteria and four alternatives is given the framework [2]. It is discovered that spherical fuzzy AHP-TOPSIS works well for managing decision-making uncertainty. Making decisions in real-time scenarios requires a wide range of criteria in order to take into account several factors that could influence the process. This paper uses 22 criteria to make up for that. Most scholars believe that this phenomenon is not conducive to decision-making. Rank reversal in MCDM that may cause decision makers to ignore the differences among alternatives.

Also, the rank reversal phenomenon in the TOPSIS affects the credibility of the decision results as well as the universality of its decision method [3]. The process [4] increases the effectiveness of decision-making and empowers decision-makers to choose solutions according to their significance and impact on the business. The Service Composition in Cloud Manufacturing should constantly use relevant and updated technology to avoid competition and crises in the future. This work (O-TOPSIS) attempt to extend the usability of TOPSIS.

Since rough numbers are objective in information evaluation, most other models—such as fuzzy numbers, interval numbers, the 2tL model, and the CM theory—are employed in conjunction with rough numbers to handle information aggregation in DM scenarios [5]. Although this method is objective, the rough numbers are ill-suited to handle quantitative data. The paper [6] used the Simple-normalization, Entropy-based TOPSIS, and K-means methods to improve the energy performance evaluation and ranking strategy for office buildings. This technique requires additional criteria in most cases since it is not suitable for multi-type and multi-size buildings and is not ideal for building energy efficiency dynamic evaluation. Our approach focuses on selecting a broad set of criteria that can be used to a wide range of cases.

A MCDM examination consists of four essential parts. The Decision Makers (DM) choose all of the important factors that will be used to assess the other alternatives in the Underlying Stage. An ID of this kind can be obtained by looking at the writing, based on the information on the DMs, or by asking assistance from skilled people. DMs should devote appropriate time to this step since failing to meet any important criterion may result in a futile probe.

The Subsequent Stage, decision-makers should accumulate data about every other option or a nearby score for every rule characterized in the primary stage to make the decision network. Consider a MCDM issue where the arrangement of options viable is indicated by the letters computer based intelligence = $\{a_1, a_2, \dots, a_m\}$ and the arrangement of assessment standards is addressed by the letters $c_j = \{c_1, c_2, \dots, c_n\}$. The underneath referenced grid structure can subsequently be utilized to address the choice framework's general structure, where x_{mn} represents the choice m's score according to standards n.

| Alternatives/Criteria | c_1 | c_2 | ... | c_n |
|-----------------------|----------|----------|----------|----------|
| a_1 | x_{11} | x_{12} | x_{13} | x_{1n} |
| a_2 | x_{21} | x_{22} | x_{23} | x_{2n} |
| . | . | . | . | . |
| . | . | . | . | . |
| a_m | x_{m1} | x_{m2} | x_{m3} | x_{mn} |

The Last Stage includes ascertaining every basis' weight. It is critical to take note of that assessing every one of the variables similarly isn't prudent in light of the fact that, by and by, they might have fluctuating levels of importance in a dynamic cycle. These rules loads and the neighborhood scores related with every option are consolidated into a worldwide score in the last stage. The decisions can then be positioned from most to least preferred in light of these general scores.

This article is arranged as follows: Section II covers the related work. Section III delves into problem statement and objectives of O-TOPSIS. Results and discussion is given in Section IV. Finally, the conclusion and Future directions for this research are discussed in Section V.

II. RELATED WORK

The research map includes the following steps

Step # 1 : Systematic Literature Review

Step # 2 : Identifying Index System of Criteria

Step # 3 : Designing CRITIC - O-TOPSIS hybrid Model for decision making

Step # 4 : Ranking Alternatives

A. Systematic Literature Review

A systematic Literature Review was conducted to understand the implementation of TOPSIS with respect to various specializations. Also, to identify the index system of criteria for service composition in Cloud Manufacturing. This paper evaluates the different perceptions involved to find answer to the research question

Research Question: Determining the ranking to the alternatives using O-TOPSIS

The following steps followed after formulation of research question.

1. **Locating Articles :** We used Scopus Database
2. **Inclusion Criteria :**
 - A. Papers that worked with TOPSIS in Cloud Manufacturing and in also areas
 - B. Peer reviewed journal, reviews, and international conferences
 - C. Paper title
3. **Search Strings:**
 - A. Cloud Manufacturing
 - B. TOPSIS
4. **Exclusion Criteria:**
 - A. Papers in languages other than “English”

- B. Initial selection after reading the paper title-final selection after reading the paper abstract/full text

5. Analysis

6. Findings

B. Identifying Index System of Criteria

O-TOPSIS implemented on seven criteria and in all 22 criteria including sub-criteria. These are mentioned in Table # 2

C. Designing Critic - O-Topsis Hybrid Model for Decision Making

CRITIC method used to find Objective Weightgs and there by using them to implement O-TOPSIS

D. Ranking Alternatives

Finally ranking the alternatives

III. PROPOSED APPROACH

Extended TOPSIS [7] is used to determine sustainable supplier using. Triangle fuzzy numbers, which are used to express the linguistic data obtained from industry experts, are used to gauge the degree of ambiguity that the experts have while assessing Parameter Influencing Testing (PITs) with respect to the selection criteria. In addition, the fuzzy set is included into the AHP in order to calculate the selection criterion weights. Lastly, a fuzzy TOPSIS is used to PIT ranking [8], Geometric Mean method is used in this work. The Decision System [9] applied to large food firm for validation. The technique rated Cloud and Internet of Things (IoT) as most important 4.0 industry technologies. The developed Green low-carbon port (GLCP) evaluation index system [10] uses the FFIWAD-TOPSIS technique, applied to five major Chinese ports.

The proposed approach [11] might be applied to other economic sectors that are considered networks, such as energy or communications transmission lines, passenger and freight rail systems, and so on. "Cloud-based customization environment" and "migrating legacy system to CMfg services" were the most and least chosen CMfg applications, respectively, based on the trial results in the research paper [12]. The results [13] show that when sensor data is fused in the input vector, the NN models perform better. Validation trials confirmed the TOPSIS optimum parameters, which proved to be correct. Novel concepts have been developed, including positive and negative risks, tolerable positive and negative risks, and the risk-based TOPSIS technique for multi-period preventive maintenance scheduling [14].

To further explain and validate the created model, a case study, sensitivity analysis on two parameters, a normalization procedure, and multiple comparisons are carried out in the paper [15]. The contribution of the paper [16] is highlighting the benefits and drawbacks of various cloud services selection methodologies and their future directions, providing a taxonomy based on an extensive literature review, focusing on cutting-edge approaches to cloud services selection, and identifying nine critical challenges in cloud services selection that require additional research. The case study in [17] looks

at the risk assessment of failure modes in a steam valve system to show how beneficial the recommended method is.

$$W_j = \frac{W_{sj} * W_{oj}}{\sum_{t=1}^n W_{st} * W_{ot}} \quad (5)$$

A. Service Composition in Cloud Manufacturing

All items, characteristics, and resources that depict a product's states, information, and mode of operation are regarded as services in the cloud manufacturing environment. These services, whose objective is to carry out actions as responses to requests between service customers and providers, can be specified, published, identified, and called through a network. Services could be delivered using cloud-based technologies and on a single server or several servers. Such services may find it more challenging to carry out the required actions when operating alone. As a result, service composition—a combination of already offered and available services from various businesses—can carry out both straightforward and difficult tasks.

B. Critic Calculation of Criteria Weights

The main steps in this procedure are

Step # 1 – Normalizing the Decision Matrix

The scores of different criteria are incommensurable as they are expressed in different measurement units or scales. Normalization is a process of transforming the scores into standard scales, which range between 0 and 1. In the proposed method, as a first step, we use the following Eq. (1) for normalizing the scores available in the decision matrix.

$$\bar{x}_{ij} = \frac{x_j - x_j^{worst}}{x_j^{best} - x_j^{worst}} \quad (1)$$

where, \bar{x}_{ij} is the normalized score of alternative i with respect to criterion j , x_{ij} is the actual score of alternative i with respect to criterion j , x_j^{best} is the best score of criterion j , and x_j^{worst} is the worst score of criterion j .

Step # 2 - Calculate standard deviation, σ_j for each criterion.

Step # 3 - Determine the symmetric matrix of $n \times n$ with element r_{jk} , which is the linear correlation coefficient between the vectors x_j and x_k .

Step # 4 - Calculate the measure of the conflict created by criterion j with respect to the decision situation defined by the rest of the criteria by using the following formula,

$$\sum_{k=1}^m (1 - r_{jk}) \quad (2)$$

Step # 5 - Determine the quantity of the information, C_j , in relation to each criterion by using the following,

$$C_j = \sigma_j * \sum_{k=1}^m (1 - r_{jk}) \quad (3)$$

Step # 6 - Determine the objective weights, W_{oj} , by using the following

$$W_{oj} = \frac{C_j}{\sum_{k=1}^m C_j} \quad (4)$$

Step # 7 - Compute the integrated weights by combining the subjective and objective weights

Where, W_j represents the comprehensive weight of each criterion, W_{sj} represents the subjective weight, and W_{oj} represents the objective weight

C. O-TOPSIS

The O-TOPSIS method is a multi-criteria decision-making method that ranks the available alternatives based on the closeness of alternatives to the ideal scenario considering the objective weights into account. The ideal scenario is a hypothetical ideal and best alternative. The specific steps for O-TOPSIS are:

Step # 1 – Establish the Initial Decision Matrix, A

The original data for the alternative criteria are subjected to vector standardization processing to obtain the initial decision matrix A with $m \times n$ as follows

$$A = (a_{ij})_{m \times n} = \begin{pmatrix} a_{11} & \dots & a_{1n} \\ \vdots & \ddots & \vdots \\ a_{m1} & \dots & a_{mn} \end{pmatrix} \quad (6)$$

$$\forall i = 1, 2, 3, \dots, m \ \& \ j = 1, 2, 3, \dots, n$$

For the unification and facilitating the calculations, the low-optimal criteria must be standardized into high optimal criteria.

Step # 2 – Constructing the Normalized Decision Matrix, B

In the normalized matrix, each element in B, b_{ij} is obtained using the following equation,

$$b_{ij} = \frac{a_{ij}}{\sqrt{\sum a_{ij}^2}} \quad (7)$$

After normalization, the decision matrix is,

$$B = (b_{ij})_{m \times n} = \begin{pmatrix} b_{11} & \dots & b_{1n} \\ \vdots & \ddots & \vdots \\ b_{m1} & \dots & b_{mn} \end{pmatrix} \quad (8)$$

$$\forall i = 1, 2, 3, \dots, m \ \& \ j = 1, 2, 3, \dots, n$$

Step # 3: Construct a weighted normalized Decision Matrix, C

The weight of the normalized decision matrix C is obtained by multiplying the values of the index weights determined using the BWM by the values of each column of the corresponding normalized decision matrix. i.e.

$$C = (c_{ij})_{m \times n} = \begin{pmatrix} c_{11} & \dots & c_{1n} \\ \vdots & \ddots & \vdots \\ c_{m1} & \dots & c_{mn} \end{pmatrix} \quad (9)$$

where, $c_{ij} = w_j * b_{ij}$, $i = 1, 2, 3, \dots, m \ \& \ j = 1, 2, 3, \dots, n$

Step # 4: Calculate the positive and negative ideal solution

The maximum and minimum values in each column of matrix C are selected. All the maximum values are elements of positive ideal set C+ and all minimum values are elements of negative ideal set C-

$$\begin{cases} \{C^+ = (c_j^+) = \{\max_i c_{ij} | j = 1,2,3, \dots, n\}\} \\ \{C^- = (c_j^-) = \{\min_i c_{ij} | j = 1,2,3, \dots, n\}\} \end{cases} \quad (10)$$

Step # 5: Calculate the Euclidean Distance

The Euclidean Distance is calculated from each alternative to the positive and negative ideal solutions using the following equations,

$$\begin{cases} D_i^+ = \sqrt{\sum_{j=1}^n (c_{ij} - c_j^+)^2} \\ D_i^- = \sqrt{\sum_{j=1}^n (c_{ij} - c_j^-)^2} \end{cases} \quad (11)$$

where,

D_i^+ represents the distance from alternative i to the positive ideal solution.

D_i^- represents the distance from alternative i to the negative ideal solution.

Step # 6: Calculate the Relative Ideal Solution

The relative ideal solution is the value closest to the positive ideal solution and farthest from the negative ideal solution and is calculated using the equation,

$$CC_i = \frac{D_i^-}{D_i^+ + D_i^-} \quad (12)$$

where, CC_i represents the relative ideal solution for the i th alternative.

Step # 7: Rank the Alternatives

The alternatives are ranked based on the CC_i values, with the alternative having a maximum or minimum being the optimal solution.

1) *Problem statement:* Implementation of Multi-Criteria Decision Making (MCDM) method, the data collected and the techniques chosen for decision plays a major role.

a) Preparing the index system of criteria of service composition in Cloud Manufacturing.

b) Calculation of Objective Weights using appropriate method

c) Selecting the relevant method for ranking

d) Assigning of Ranking to the Alternatives

2) *Objectives:* For rating options, criteria, and sub-criteria, this article provides a hybrid multi-criteria decision technique.

a) A detailed analysis of the MCDM methods to rank the alternatives using objective weights.

b) A detailed analysis of service composition in Cloud Manufacturing

c) The objective weights of the criterion are calculated using CRITIC method.

d) To rank the various options, the Objective Weight -Technique for Order Preference by Similarity to Ideal Solution (O-TOPSIS) is used.

e) The results were compared with the conventional TOPSIS method.

IV. RESULTS AND DISCUSSIONS

The initial criteria data were processed using vector standardization and the low-optimal criteria were converted to high-optimal criteria. Eq. (1) is used to obtain normalized decision matrix (it is represented in 22X5 Table, where 22 represents total criteria number and 5 represents the available alternatives). Table I represents the determined Objective Values.

A. Objective Weights using Critic

TABLE I. OBJECTIVE WEIGHTS USING CRITIC

| Criteria | OW (O_{ij}) |
|----------|-----------------|
| C11 | 0.05163 |
| C12 | 0.04178 |
| C13 | 0.00578 |
| C14 | 0.04300 |
| C21 | 0.05410 |
| C22 | 0.04062 |
| C23 | 0.04639 |
| C31 | 0.04441 |
| C32 | 0.04548 |
| C33 | 0.04600 |
| C41 | 0.05067 |
| C42 | 0.04560 |
| C43 | 0.05742 |
| C51 | 0.16355 |
| C52 | 0.13352 |
| C53 | 0.29434 |
| C61 | 0.24124 |
| C62 | 0.01817 |
| C63 | 0.04737 |
| C71 | 0.05025 |
| C72 | 0.06137 |
| C73 | 0.00725 |

B. O-TOPSIS Implementation

The initial criteria data were processed using vector standardization and the low-optimal criteria were converted to high-optimal criteria. Eq. (7) is used to obtain normalized decision matrix (it is represented in 22X5 Table, where 22 represents total criteria number and five represents the available alternatives). Table II represents the normalized matrix values.

TABLE II. NORMALIZED DECISION VALUES -TOPSIS

| | A ₁ | A ₂ | A ₃ | A ₄ | A ₅ |
|-----|----------------|----------------|----------------|----------------|----------------|
| C11 | 6.988968 | 6.630559 | 7.317509 | 6.302018 | 6.242283 |
| C12 | 5.309819 | 5.752304 | 4.505301 | 4.344397 | 4.947786 |
| C13 | 1.562267 | 1.692456 | 1.432078 | 1.1717 | 1.822645 |
| C14 | 4.088311 | 4.507625 | 4.140725 | 2.935198 | 3.406926 |
| C21 | 1.299038 | 1.154701 | 1.732051 | 1.876388 | 0.866025 |
| C22 | 1.61808 | 1.75292 | 1.21356 | 1.3484 | 1.48324 |
| C23 | 1.587713 | 1.299038 | 1.154701 | 1.010363 | 1.876388 |
| C31 | 1.632993 | 1.360828 | 1.360828 | 1.088662 | 1.905159 |
| C32 | 1.224745 | 1.49691 | 1.49691 | 1.632993 | 1.49691 |
| C33 | 1.16692 | 1.312785 | 1.312785 | 1.312785 | 1.75038 |
| C41 | 2.539167 | 2.75681 | 3.119548 | 3.264643 | 2.103881 |
| C42 | 3.550993 | 4.133992 | 4.557991 | 3.126994 | 3.497993 |
| C43 | 2.801578 | 2.179005 | 2.863835 | 4.046723 | 4.171238 |
| C51 | 1.714286 | 1 | 1.285714 | 1.428571 | 1.571429 |
| C52 | 1.272792 | 1.697056 | 1.555635 | 1.414214 | 1.131371 |
| C53 | 1.40028 | 1.820364 | 1.40028 | 1.260252 | 1.260252 |
| C61 | 2.320168 | 2.223494 | 1.933473 | 1.836799 | 2.030147 |
| C62 | 0.742781 | 1.114172 | 0.371391 | 1.485563 | 1.671258 |
| C63 | 0.96225 | 1.154701 | 1.539601 | 0.57735 | 0.96225 |
| C71 | 1.3484 | 1.48324 | 1.21356 | 1.88776 | 1.48324 |
| C72 | 1.648327 | 1.510966 | 1.236245 | 1.648327 | 1.236245 |
| C73 | 1.312785 | 1.45865 | 1.16692 | 1.75038 | 1.16692 |

The subjective weights calculated from BWM are used to convert the normalized decision matrix (as in Table II) by using Eq. (9). It is represented in Table III.

TABLE III. WEIGHTED NORMALIZED DECISION VALUES -TOPSIS

| | A ₁ | A ₂ | A ₃ | A ₄ | A ₅ |
|-----|----------------|----------------|----------------|----------------|----------------|
| C11 | 0.360840 | 0.342336 | 0.377803 | 0.325373 | 0.322289 |
| C12 | 0.221844 | 0.240331 | 0.188231 | 0.181509 | 0.206718 |
| C13 | 0.009030 | 0.009782 | 0.008277 | 0.006772 | 0.010535 |
| C14 | 0.175797 | 0.193828 | 0.178051 | 0.126214 | 0.146498 |
| C21 | 0.070278 | 0.062469 | 0.093704 | 0.101513 | 0.046852 |
| C22 | 0.065726 | 0.071204 | 0.049295 | 0.054772 | 0.060249 |
| C23 | 0.073654 | 0.060262 | 0.053567 | 0.046871 | 0.087046 |
| C31 | 0.072521 | 0.060434 | 0.060434 | 0.048347 | 0.084608 |
| C32 | 0.055701 | 0.068079 | 0.068079 | 0.074269 | 0.068079 |
| C33 | 0.053678 | 0.060388 | 0.060388 | 0.060388 | 0.080517 |
| C41 | 0.128660 | 0.139688 | 0.158067 | 0.165419 | 0.106604 |
| C42 | 0.161925 | 0.188510 | 0.207844 | 0.142591 | 0.159508 |
| C43 | 0.160867 | 0.125118 | 0.164441 | 0.232363 | 0.239512 |
| C51 | 0.280371 | 0.163550 | 0.210279 | 0.233643 | 0.257007 |
| C52 | 0.169943 | 0.226591 | 0.207708 | 0.188826 | 0.151061 |
| C53 | 0.412158 | 0.535806 | 0.412158 | 0.370943 | 0.370943 |
| C61 | 0.559717 | 0.536396 | 0.466431 | 0.443109 | 0.489753 |
| C62 | 0.013496 | 0.020245 | 0.006748 | 0.026993 | 0.030367 |
| C63 | 0.045582 | 0.054698 | 0.072931 | 0.027349 | 0.045582 |
| C71 | 0.067757 | 0.074533 | 0.060981 | 0.094860 | 0.074533 |
| C72 | 0.101158 | 0.092728 | 0.075868 | 0.101158 | 0.075868 |
| C73 | 0.009518 | 0.010575 | 0.008460 | 0.012690 | 0.008460 |

Using equation (10), we determine,

The positive ideal set (C^+) and the negative ideal set (C^-) represented in Table IV.

TABLE IV. C^+ AND C^- VALUES -TOPSIS

| | C^+ | C^- |
|-----|----------|----------|
| C11 | 0.322289 | 0.377803 |
| C12 | 0.181509 | 0.240331 |
| C13 | 0.006772 | 0.010535 |
| C14 | 0.126214 | 0.193828 |
| C21 | 0.046852 | 0.101513 |
| C22 | 0.049295 | 0.071204 |
| C23 | 0.046871 | 0.087046 |
| C31 | 0.048347 | 0.084608 |
| C32 | 0.055701 | 0.074269 |
| C33 | 0.053678 | 0.080517 |
| C41 | 0.106604 | 0.165419 |
| C42 | 0.142591 | 0.207844 |
| C43 | 0.125118 | 0.239512 |
| C51 | 0.16355 | 0.280371 |
| C52 | 0.151061 | 0.226591 |
| C53 | 0.370943 | 0.535806 |
| C61 | 0.443109 | 0.559717 |
| C62 | 0.006748 | 0.030367 |
| C63 | 0.027349 | 0.072931 |
| C71 | 0.060981 | 0.09486 |
| C72 | 0.075868 | 0.101158 |
| C73 | 0.00846 | 0.01269 |

We determine D^+ and D^- values and then finally calculate the ranking of all alternatives and these results are shown in Table V.

TABLE V. THE RANKING OF ALTERNATIVES -TOPSIS

| Alternative | D^+ | D^- | CC_i | Ranking |
|----------------|----------|----------|----------|---------|
| A ₁ | 0.200499 | 0.182409 | 0.476377 | 4 |
| A ₂ | 0.236396 | 0.183752 | 0.437351 | 5 |
| A ₃ | 0.162992 | 0.207296 | 0.559823 | 3 |
| A ₄ | 0.164110 | 0.255312 | 0.608724 | 1 |
| A ₅ | 0.174182 | 0.235665 | 0.575006 | 2 |

C. TOPSIS vs. O-TOPSIS

From the Table VI, we can observe that the ranking using Objective Weights and Subjective weights is not similar. This work can be extended using comprehensive weights to rank the alternatives in the best possible way. The comprehensive weights can be calculated using both subjective and objective weights.

TABLE VI. THE RANKING OF ALTERNATIVES - TOPSIS VS O-TOPSIS

| Alternative | TOPSIS | | O-TOPSIS | |
|----------------|----------|---------|----------|---------|
| | CC_i | Ranking | CC_i | Ranking |
| A ₁ | 0.599674 | 2 | 0.476377 | 4 |
| A ₂ | 0.499557 | 3 | 0.437351 | 5 |
| A ₃ | 0.642782 | 1 | 0.559823 | 3 |
| A ₄ | 0.449796 | 4 | 0.608724 | 1 |
| A ₅ | 0.355450 | 5 | 0.575006 | 2 |

V. CONCLUSIONS AND FUTURE DIRECTIONS

The prime purpose of this study was to define the current or future usage of Industry 4.0 technologies (Cloud Computing, IoT etc) to improve industrial manufacturing through a thorough review. It also established critical benchmarks for assessing the specific implications of various technologies. We examined forty-five papers published between 2019 and 2023. Later, 17 papers from the Scopus database were considered. Throughout the examination,

information from each publication was compiled into a large database that would be used for further research. A decision-making system will need to be constructed in the future to select the best cloud manufacturing technology within a specific firm domain.

Finally, utilising Objective Weights, this study includes a TOPSIS-based procedure for ranking and quantifying the application of the criteria using objective weights determined using CRITIC method. This technique was quite helpful in finding the most important technology.

A corporation employing a cloud manufacturing platform can use a valid selection model to pick the best cloud service provider (alternative) to improve the quality of its production and its capacity for sustained development. The following elements were considered in the model's implementation.

1) According to the CRITIC approach results, Ease of Opting has the most weight and Ease of Implementation has the least weight.

2) TOPSIS method rates options in the following order: $A3 > A1 > A2 > A4 > A5$.

3) The objective weights determined by using CRITIC method contribute to O-TOPSIS to obtain the desired ranking of the all the alternatives. O-TOPSIS method ranks alternatives in the following order: $A4 > A5 > A3 > A1 > A2$.

4) Quantitative data, including cost, is combined with linguistic assessment information when assessing cloud service providers. Moreover, DMs believe that they can communicate their preferences more clearly when they use a probabilistic word set. Consequently, the proposed method not only retains the correctness of assessment data but also effectively manages the ambiguity and uncertainty of heterogeneous information.

5) As the objective weights are more practical than the subjective weights, the result is more accurate.

REFERENCES

- [1]. Umair Tanveer, Marios Dominikos Kremantzis, Nikos Roussinos, Shamaila Ishaq, Leonidas Sotirios Kyrgiakos, George Vlontzos, A fuzzy TOPSIS model for selecting digital technologies in circular supply chains, *Supply Chain Analytics*, Dec, 2023, <https://doi.org/10.1016/j.sca.2023.100038>.
- [2]. Manoj Mathew, Ripon K. Chakraborty, Michael J. Ryan, A novel approach integrating AHP and TOPSIS under spherical fuzzy sets for advanced manufacturing system selection, *Engineering Applications of Artificial Intelligence*, Nov, 2020, <https://doi.org/10.1016/j.engappai.2020.103988>.
- [3]. Baohua Yang, Jinshuai Zhao, Haidan Zhao, A robust method for avoiding rank reversal in the TOPSIS, *Computers & Industrial Engineering*, DEc, 2022, <https://doi.org/10.1016/j.cie.2022.108776>
- [4]. Ghazi M. Magableh, Mahmoud Z. Mistarihi, Applications of MCDM approach (ANP-TOPSIS) to evaluate supply chain solutions in the context of COVID-19, *Mar*, 2022, <https://doi.org/10.1016/j.heliyon.2022.e09062>.
- [5]. Musavarah Sarwar, Improved assessment model for health-care waste management based on dual 2-tuple linguistic rough number clouds, *Engineering Applications of Artificial Intelligence*, Aug, 2023, <https://doi.org/10.1016/j.engappai.2023.106255>.
- [6]. Fukang Sun, Junqi Yu, Improved energy performance evaluating and ranking approach for office buildings using Simple-normalization, Entropy-based TOPSIS and K-means method, *Energy Reports*, Nov, 2021, <https://doi.org/10.1016/j.egyr.2021.03.007>.
- [7]. Jing Li, Hong Fang, Wenyan Song, Sustainable supplier selection based on SSCM practices: A rough cloud TOPSIS approach, *Journal of Cleaner Production*, Jun 2019, <https://doi.org/10.1016/j.jclepro.2019.03.070>.
- [8]. Veenu Singh, Vijay Kumar, V.B. Singh, A hybrid novel fuzzy AHP-TOPSIS technique for selecting parameter-influencing testing in software development, *Decision Analytics Journal*, Mar, 2023, <https://doi.org/10.1016/j.dajour.2022.100159>.
- [9]. Antonio Forcina, Luca Silvestri, Fabio De Felice, Domenico Falcone, Exploring Industry 4.0 technologies to improve manufacturing enterprise safety management: A TOPSIS-based decision support system and real case study, *Safety Science*, Dec, 2023, <https://doi.org/10.1016/j.ssci.2023.106351>.
- [10]. Sha Yang, Yan Pan, Shouzhen Zeng, Decision making framework based Fermatean fuzzy integrated weighted distance and TOPSIS for green low-carbon port evaluation, *Engineering Applications of Artificial Intelligence*, Sep, 2022, <https://doi.org/10.1016/j.engappai.2022.105048>.
- [11]. Dalmo Marchetti, Peter Wanke, Efficiency of the rail sections in Brazilian railway system, using TOPSIS and a genetic algorithm to analyse optimized scenarios, *Transportation Research Part E: Logistics and Transportation Review*, Mar, 2020, <https://doi.org/10.1016/j.tre.2020.101858>.
- [12]. Tin-Chih Toly Chen, Type-II fuzzy collaborative intelligence for assessing cloud manufacturing technology applications, *Robotics and Computer-Integrated Manufacturing*, Dec, 2022, <https://doi.org/10.1016/j.rcim.2022.102399>.
- [13]. Ning Li, Jamal Y. Sheikh-Ahmad, Ameen El-Sinawi, V. Krishnaraj, Multi-objective optimization of the trimming operation of CFRPs using sensor-fused neural networks and TOPSIS, *Measurement*, Jan, 2019, <https://doi.org/10.1016/j.measurement.2018.09.057>.
- [14]. Hamidreza Seiti, Ashkan Hafezalkotob, Developing the R-TOPSIS methodology for risk-based preventive maintenance planning: A case study in rolling mill company, *Computers & Industrial Engineering*, Feb, 2019, <https://doi.org/10.1016/j.cie.2019.01.012>.
- [15]. Guangquan Huang, Liming Xiao, Witold Pedrycz, Dragan Pamucar, Genbao Zhang, Luis Martínez, Design alternative assessment and selection: A novel Z-cloud rough number-based BWM-MABAC model, *Information Sciences*, July, 2022, <https://doi.org/10.1016/j.ins.2022.04.040>.
- [16]. Neha Thakur, Avtar Singh, A.L. Sangal, Cloud services selection: A systematic review and future research directions, *Computer Science Review*, Nov, 2022, <https://doi.org/10.1016/j.cosrev.2022.100514>.
- [17]. Jing Li, Hong Fang, Wenyan Song, Modified failure mode and effects analysis under uncertainty: A rough cloud theory-based approach, *Applied Soft Computing*, May, 2019, <https://doi.org/10.1016/j.asoc.2019.02.029>.

Comparative Analysis of Transformer Models for Sentiment Analysis in Low-Resource Languages

Yusuf Aliyu¹, Aliza Sarlan², Kamaluddeen Usman Danyaro³, Abdulahi Sani B A Rahman⁴

Department of Computer and Information Science, Universiti Teknologi PETRONAS, Seri Iskandar 32610 Perak, Malaysia^{1,3,4}
Center for Foundation Studies, Universiti Teknologi PETRONAS, Seri Iskandar, Perak, 32610, Malaysia²

Abstract—The analysis of sentiments expressed on social media platforms is a crucial tool for understanding user opinions and preferences. The large amount of the texts found on social media are mostly in different languages. However, the accuracy of sentiment analysis in these systems faces different challenges in multilingual low-resource settings. Recent advancements in deep learning transformer models have demonstrated superior performance compared to traditional machine learning techniques. The majority of preceding works are predominantly constructed on the foundation of monolingual languages. This study presents a comparative analysis that assesses the effectiveness of transformer models, for multilingual low-resource languages sentiment analysis. The study aims to improve the accuracy of the existing baseline performance in analyzing tweets written in 12 low-resource African languages. Four widely used start-of-the-art transformer models were employed. The experiment was carried out using standard datasets of tweets. The study showcases AfriBERTa as a robust performer, exhibiting superior sentiment analysis capabilities across diverse linguistic contexts. It outperformed the established benchmarks in both SemEval-2023 Task 12 and AfriSenti baseline. Our framework achieves remarkable results with an F1-score of 81% and an accuracy rate of 80.9%. This study provides validation of the framework's robustness in the domain of sentiment analysis across a low-resource linguistics context. our research not only contributes a comprehensive sentiment analysis framework for low-resource African languages but also charts a roadmap for future enhancements. Emphasize the ongoing pursuit of adaptability and robustness in sentiment analysis models for diverse linguistic landscapes.

Keywords—Sentiment analysis; low-resource languages; multilingual, word-embedding, transformer

I. INTRODUCTION

In recent years, sentiment analysis has emerged as a pivotal research area in natural language processing [1]. It finds varied applications across various domains, including social media monitoring, customer feedback analysis, market research, and others [2] [3]. Sentiment analysis has been commonly classified into three levels based on various studies [4] [5] [3]. Thus, document-level sentiment classification focuses on discerning the overall sentiment expressed by an author in an opinionated text [6]. Sentence-level analysis, concentrating on individual sentences or arguments within a text. This is particularly valuable in subjectivity classification which assesses whether a sentence conveys an opinion [6] and lastly, the aspect level, is a more complex examination that aims to identify sentiments related to specific aspects of entities [7]. However, given the dynamic nature of social media. Sentence-

level sentiment analysis finds particular significance in these platforms. It offers insights into user opinions and emotions on diverse topics. Moreover, X app formerly known as Twitter, has been a dynamic social media platform. It is a platform where users share a wide array of information in real-time [8]. It is considered one of the most vital sources for opinion mining and sentiment analysis [9]. Additionally, the X app contains a widespread multilingual text as individuals express their opinions in tweets spanning different languages, covering a variety of topics [10], [11].

The diversity in languages and cultures among users in the X app is evident in the multilingual nature of tweet texts [12]. This diversity opens up opportunities for businesses, governments, institutions, and other entities to find inferences about their entity for proper decision-making. Consequently, depending solely on sentiment analysis conducted in the English language carries a significant risk of missing crucial insights within written texts [13]. However, the increasing importance of multilingual sentiment analysis goes beyond high language limitations and becomes particularly relevant in low-resource languages.

The concept of low-resource languages encompasses various interpretations, including languages with limited research, facing resource scarcity, lacking computational support, being less commonly taught, or exhibiting low linguistic density [14]. In recent years, there has been a notable increase in the utilization of these languages on social media platforms, with a considerable proportion of users choosing to engage in communication through them [15]. Many languages in Africa and Asia fall into the low-resource category. They remain relatively unexplored in the realm of Natural Language Processing (NLP) research [16]. The underrepresentation of these languages in global economic, social, and political domains can potentially hinder economic and social progress. Nevertheless, advancing technology for low-resource languages can contribute to the increased participation of the language-speaking communities in the digital sphere [17]. Therefore, the abundance of multilingual content online underscores the necessity for sentiment analysis across various low-resource languages and cultures. Similarly, English remains the most extensively studied language [17], [18], [19], [20], [21]. Despite the linguistic diversity present in low-resource languages. The African languages with a substantial population received limited attention. Particularly in the context of sentiment analysis [22]. Low-resource languages pose unique challenges, including scarcity of labelled datasets [23], linguistic diversity, and limited computational resources.

Addressing sentiment analysis in such linguistic contexts necessitates a nuanced exploration of the capabilities and adaptability of transformer models.

The advent of transformer models, exemplified by architectures like BERT [24] (Bidirectional Encoder Representations from Transformers) and GPT (Generative Pre-trained Transformer), has considerably pushed the boundaries of sentiment analysis for diverse languages.

The study aims to enhance the accuracy performance of the current based-line performance on 12 African low-resource language tweets through rigorous hyper-parameter tuning and transformer comparison.

The paper is organized as follows: Section II gives a summary of related studies. Section III explores the proposed methodology for multilingual sentiment analysis within the framework. Section IV details the experiment and hyperparameter tuning. Section V showcases results and facilitates a discussion of the findings. Lastly, Section VI provides conclusions and outlines future directions for work.

II. RELATED WORK

Sentiment analysis classification has different techniques, which are classified into three categories or classes lexicon-based, machine learning-based, and hybrid-based [9], [25], [26], [27], [28]. The machine learning techniques leverage well-known ML algorithms or models to address sentiment analysis. The models treat it as a typical text classification problem that incorporates syntactic and/or linguistic attributes [20]. Additionally, deep learning is a subset of the machine learning techniques [11], [29], based on the artificial neural network [7], [30]. The neural networks offer the most effective solutions for numerous challenges in image and speech recognition. As well as in the domain of natural language processing [31]. In recent years, deep learning models have shown remarkable performance in the field of sentiment analysis [28]. Especially transformer models. They are multilingual pre-trained based on transfer learning approaches that are trained on large various language text data [32], [33]. Moreover, the success of NLP has been primarily ascribed to transformers' capacity for learning broad language representations from enormous volumes of text input. Additionally, they have advanced to become the leading models in understanding and generating language [34] and it apply that knowledge learned to related tasks, producing astounding results [35]. However, prior studies utilized one or more of the above techniques for sentiment classification in one or more languages as:

The study of [13] performed sentiment analysis on English and Hausa tweets using an improved feature acquisition approach. They employed SVM, NB, and Maximum Entropy (MaxEnt) for classification. The experiment indicates that the classification models, when utilizing the aspect set, achieve a modest accuracy of 56% with the SVM classifier. In the case of the pure Hausa dataset SVM yields the best result. Similarly, [36] observed a scarcity of publicly accessible sentiment lexicons for low-resource languages, particularly notable in the Igbo language. In response, they advocated for the development of a comprehensive sentiment lexicon tailored for

Igbo, designed to serve as a foundational resource for sentiment analysis in this linguistically underrepresented context. Another work by [37], performs feature learning and categorization using convolutional neural networks (CNN). They demonstrated the model's linguistic independence using the languages of English, French, and Greek with significant accuracy; however, it is highly domain-dependent as with only consists of a restaurant data set. So also, the authors [38], conduct a study that compares monolingual and cross-lingual sentiment analysis approaches utilizing the Hausa-English dataset. They translate most of the data using Google Translate before applying machine models. A similar approach was utilized by [39], the authors investigated the impact of translating from a language with ample resources to one with limited resources on emotion classification. They aim to address the observed gap leading to polarity changes and increase sentiment performance accuracy. Utilizing Google machine translation, they translate an English movie reviews dataset from IMDB into Urdu, Hindi, and German. Deep learning models with randomized parameters are employed and systematically adjusted to optimize results. The experimentation reveals varying accuracies, with English achieving the highest (88.37% via DNN), followed by Hindi (85.99% via Bi-LSTM), and Urdu (80.78%). Another work by [40] proposed a model that is independent of language for multi-class sentiment analysis, employing a straightforward neural network architecture. This is done on GenEval, Deutsche Bahn, and Arabic data sets with topic modelling. Their result shows that the deep neural network model can outperform traditional ML models when evaluated. In a different study presented by [41], find out that, there is a critique of the prevailing practice of constructing language models, particularly in low-resource scenarios. The inquiry revolves around the feasibility of translating data into English as an alternative, facilitating the use of pre-trained, comprehensive English language models. The researchers employ a contemporary machine translation approach to translate data into English that could potentially offer a solution to the challenges in multilingual sentiment analysis. Furthermore, their empirical experiment provides evidence that utilizing current baseline models on a huge scale does not result in a performance decrease, supporting the viability of this translation approach.

The work of [22] tries to bridge a gap of scarcity of data in low-resource language. They generated the inaugural extensive human-annotated Twitter sentiment dataset for four commonly spoken Nigerian languages, namely Hausa, Igbo, Pidgin, and Yoruba. In another research by [42], proposed a novel approach named AgglutiFiT, presenting an efficient fine-tuning strategy for pre-trained language models tailored for sentiment analysis and text classification. The fine-tuning process involves utilizing a low-noise dataset created through morphological analysis and stem extraction. The authors contend that this method excels in selecting pertinent semantic and syntactic information for low-resource languages like Kazakh, Kyrgyz, and Uyghur. Notably, the sentiment analysis task in Kazakh yielded an accuracy of approximately 92.87%. However, in research conducted by [43], analysed sentiment in code-mixed texts from users. They underscore the constrained predictability of conventional machine learning models

compared to deep learning counterparts using LSTM, CNN, and BiLSTM. Utilizing code-mixed data from Hindi-English and Bengali English, the experiment indicated that attention-based models outperformed traditional methods in accuracy by a margin of 20–60%. Additionally, when compared with monolingual English data, the accuracy reached 72.6% on the English monolingual dataset. In the study conducted by [44], the focus is on sentiment analysis of code-mixed Malaysian COVID-19-related news disseminated on Twitter. The researchers compile a multilingual Twitter dataset for COVID-19 encompassing tweets in Malay, English, and Chinese. Employing Byte-Pair Encoding (BPE) as a data compression technique, they apply two deep learning approaches: CNN and mBERT models. Results show that the BPE-M-BERT model exhibits a marginal performance advantage over the CNN model, emphasizing the advantageous adaptability of the pre-trained M-BERT network for a multilingual dataset. The researcher in study [45] investigates transformer fine-tuning methods for Hausa sentiment classification. Three pre-trained transformer multilingual language models, namely Roberta, XLM-R, and mBERT, are employed. The outcomes indicate that the mBERT-base-cased model achieves the best accuracy and F1-score, both reaching 0.73%.

The collective evidence from the diverse studies presented underscores the crucial importance of fine-tuning sentiment analysis models across multiple languages. Each study addresses specific linguistic nuances, cultural contexts, use of traditional ML models, and domain-specific challenges, emphasizing the need for a comprehensive approach to language diversity in sentiment analysis. From the creation of sentiment lexicons for underrepresented languages like Igbo, Hausa, Pidgin, and Yoruba to the exploration of code-switched data and the utilization of models such as XLM-R and mBERT across languages like Kazakh, Kyrgyz, Uyghur, Malay, Indian, and Chinese, these works collectively advocate for a nuanced understanding of sentiment in multilingual settings. Fine-tuning models across various languages allows for a more inclusive and accurate representation of sentiment expressions, reflecting the complex inherent in diverse linguistic structures and cultural contexts.

To address these limitations, the proposed framework emphasizes efficient parameter tuning to enhance model accuracy and performance. By optimizing model parameters, such as learning rates, batch sizes, and regularization techniques, the proposed framework aims to mitigate the shortcomings encountered in previous studies. Efficient parameter tuning enables the models to better capture the nuances of different languages and domains, thereby improving their overall effectiveness in sentiment analysis tasks. Table I present the summary of the related literature.

TABLE I. SUMMARY OF THE RELATED WORK

| Study | Models/method | Language | limitation |
|-------|-----------------------|-------------------|--|
| [13] | SVM, MaxEn and NB | Hausa and English | Uses only traditional ML and the accuracy is below the benchmarking. |
| [36] | Manual data anotation | Igbo | Limited to Copus creation |

| | | | |
|------|---|--|--|
| [37] | CNN | English, French, and Greek | It highly domain dependent as with only consist of restaurant data set |
| [38] | NB, LSTM,BiLSTM, BERT, and Roberta. | Hausa | Depend on Google translator and domain specific |
| [39] | DNN, LSTM, Bi-LSTM and Conv1D | Urdu, Hindi, and German | Domain specific data, the model cannot be generalize to the domain. |
| [40] | ANN | Deutsche Bahn, and Arabic | The work is domain specific which rally on product data set |
| [22] | mBERT, Roberta,remBerta, XLR-R, and AfriBerta | Hausa, Igob, Yaruba, and Pidgen | Corpus creation for research progress and based-line evaluation. Need accuracy improvement |
| [41] | BERT, XLM-R | Scandinavian, Swedish, Norwegian Danish, Finnish | Depend on Machine translation which may not always be accurate. |
| [42] | XLM-R | Kazakh, Kyrgyz, and Uyghur | Different models may be explore for better performance. |
| [43] | BiLSTM, CNN, BERT | Hindi and Bengali | Different transformer models may be explore for evaluation. |
| [44] | CNN and mBERT | Malay, Indian, Chinese | Different transformer models may be explore for evaluation. |
| [45] | mBERT, Roberta and XLM-r | Hausa-English | Fine tuning specific to Hausa. It may not be generalize to other low resource language |

III. METHODOLOGY

In this section, we provide an overview of the methodology framework for conducting sentiment analysis on tweets in low-resource multilingual settings. The pursuit of a better sentiment analysis framework tailored for multiple African languages tweets. This work adopts a distinctive approach that merges the strengths of transformer models through hyperparameter tuning. Specifically, use mBERT, Roberta, XLM-R, and AfriBERT from transformers. These models leverage the abundant semantic information present in tweets, offering a fundamental comprehension of word relationships through pre-trained embeddings. This approach facilitates the fine-tuning of models, thereby improving their adaptability to the distinctive linguistic nuances across various languages.

The core of our methodology involves the tweet datasets undergoing tokenization, feature detection, feature with model presentation, fine-tuning, training, and validating. To anticipate significant differences between these models, we conduct a rigorous statistical experiment. The decision-making process leads to the evaluation of model outputs using carefully chosen metrics. Fig. 1 serves as a visual guide, illustrating the proposed framework.

Through this framework, the objective is to contribute to a nuanced comprehension of sentiment in low-resource

languages and improve sentiment analysis accuracy. The development process of the sentiment classification models involves several distinct steps, commencing with the data description.

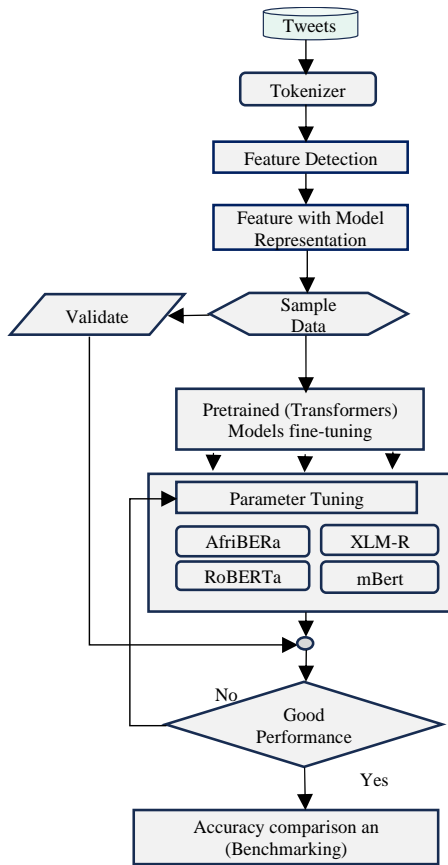


Fig. 1. Methodology framework workflow.

A. Multilingual Dataset

This stud utilized the Tweet data obtained from [46]. The data collection encompasses 12 distinct African languages, each characterized by unique linguistic features, writing systems, and language families, as outlined in Table II with their respective class label distribution. Spanning from Algerian Arabic, Moroccan Arabic/Darija, Hausa, Yoruba, Igbo, Nigerian Pidgin, Amharic, Swahili, Kinyarwanda, Twi, Mozambican Portuguese, and Xitsonga. The language and the class label distribution of the tweets are illustrated in Table II.

TABLE II. LANGUAGES AND THEIR RESPECTIVE CLASS DISTRIBUTION OF THE DATASETS

| Language | Class label (distribution) | | |
|------------------------|----------------------------|---------|----------|
| | Positive | Neutral | Negative |
| Hausa | 4687 | 4912 | 4573 |
| Amharic | 1332 | 3104 | 1548 |
| Algerian Arabic | 417 | 342 | 892 |
| Darija Moroccan Arabic | 1758 | 2161 | 1664 |
| Swahili | 1072 | 191 | 547 |
| Yoruba | 3542 | 3108 | 1872 |

| | | | |
|-----------------------|------|------|------|
| Igbo | 3084 | 4508 | 2600 |
| Nigerian Pidgin | 1808 | 72 | 3241 |
| Xitsonga | 384 | 136 | 284 |
| Kinyarwanda | 899 | 1257 | 1146 |
| Twi | 1644 | 522 | 1315 |
| Mozambican Portuguese | 681 | 1600 | 782 |

The datasets are provided as open-source resources explicitly crafted for research purposes, and they come pre-labelled. However, the training data comprises 63,685 instances of tweets, with 20,783 instances categorized as Positive, 20,108 as Negative, and 22,794 as Neutral. This distribution illustrates a fairly even representation of the three sentiment categories, reducing the potential for biased predictions towards any particular label. Fig. 2 provides a visual representation of the dataset distribution for additional reference. These datasets are subsequently employed to train feature detection and representation.

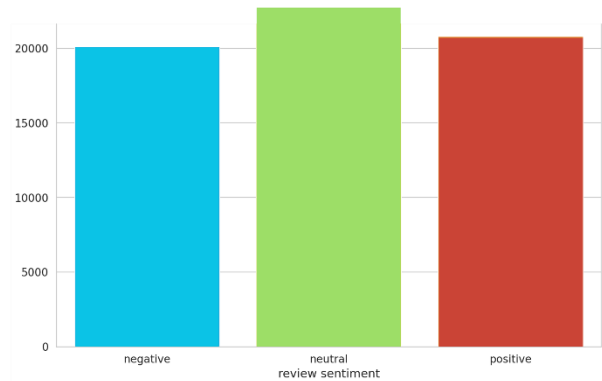


Fig. 2. Tweet class distribution.

B. Feature Detection

During the feature detection and extraction stage, textual data transforms into numerical form through tokenization. The Word Piece tokenizer is utilized in this procedure, fragmenting unfamiliar vocabulary words into sub-words, and consequently minimizing the occurrence of out-of-vocabulary words. This is accomplished through a greedy algorithm that prioritizes the longest possible match, thereby improving text-processing capabilities for transformers. Considering a tweet composed of N words, denoted as $T = \{w_1, w_2, w_3 \dots w_n\}$, each word w_i is processed and transformed into a numerical vector represented as e_i . Concurrently, the designated class y is converted into its vector, denoted as v_a .

$$e_i = E(w_i) \tag{1}$$

$$v_a = E(y) \tag{2}$$

The initialization of context embedding vectors, e_i , and class vectors, v_a , is described by Eq. (1) and Eq. (2). Eq. (1) denotes the transformation of each word, w_i , into a numerical vector, e_i , while Eq. (2) represents the conversion of class y into its vector v_a . In these equations, $E \in \mathbb{R}^{v \times d}$ denotes the embeddings, where d represents the dimension of the word embedding vectors. The vocabulary size is denoted as v , and N

represents the number of words in the tweet. Subsequently, the input vectors are passed into the transformers for fine-tuning.

C. Fine-tuning

The fine-tuning process begins with the mBERT model transformer for sentiment classification, incorporating its pre-trained weights. Tokenized input sequences are enriched with a special classification token ([CLS]) at the beginning and a separation token ([SEP]) at the end. Token embeddings for each sub-word are generated using the embedding matrix and are combined with segment embeddings to differentiate between tokens from the first and second sentences. Position embeddings are employed to denote the position of each token in the input sequence. The BERT input representation, consisting of token embeddings, segment embeddings, and position embeddings, is then inputted into a SoftMax layer for classification aggregation. Fig. 3 depicts the visual representation of transformer architecture for the classification task.

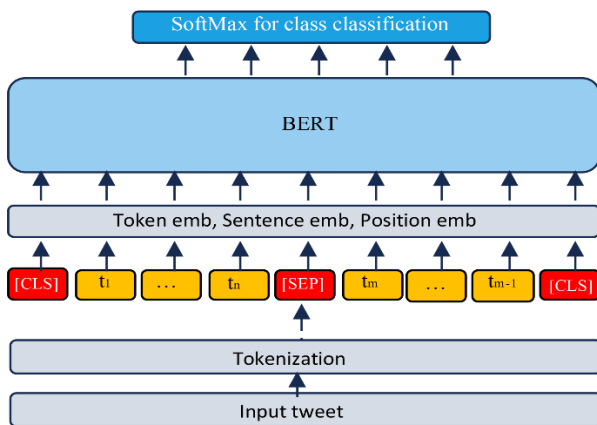


Fig. 3. Transformer model for classification.

Similarly, in the case of the Roberta model, we followed the same comparable fine-tuning approach, customizing the pre-trained weights specifically for sentiment analysis in low-resource contexts. The tokenization procedure, utilizing the Transformer tokenizer, and the creation of the input representation, which includes token embeddings, segment embeddings, and position embeddings, remained consistent with the models described earlier. In the end, a SoftMax layer was utilized for sentiment classification.

In addition to mBERT and Roberta, we included the XLM-R and afriBERTa models in the framework. These models adhered to a comparable methodology as the pre-trained mBERT models. The tokenized input sequences were converted into the input representation, which included token embeddings, segment embeddings, and position embeddings. Following this, the input representation underwent processing through a SoftMax layer for sentiment classification. The components of the model play a crucial role in the effective representation of language by transformers [24].

Furthermore, the models often require fixed-length input sequences for effective processing, a concept known as padding. The special token used for padding in transformers is generally the [PAD] token, which is inserted into the input

sequence to fill the remaining empty spaces until the sequence reaches the desired fixed length. Additionally, any unknown token is represented as [UNK]. Tokens from the first sentence are assigned the label "0," while those from the second sentence are labelled "1". Position embeddings indicate the position of each token in the input sequence.

The selection of the aforementioned models was influenced by their proficiency in multilingualism, as discussed in the work by [47]. They are encompassed with some African languages. These chosen pre-trained language models were specifically designed to tackle this challenge and have demonstrated strong performance in multilingual settings, as highlighted by [48]. Given their robust nature, various hyperparameter combinations were employed to optimize their effectiveness in comprehending the complexities of different languages.

D. Hyperparameter Tuning

To determine optimal parameters, a series of experiments were conducted, employing different batch sizes, and assessing the performance of mBERT on a validation set. Table III provides a detailed presentation of results obtained from hyperparameter tuning. These values play a crucial role in the model optimization process. Each row in the table represents a unique combination of learning rates and batch sizes, depicting the mBERT model's performance in relation to the F1-score.

TABLE III. HYPERPARAMETER COMBINATION AND PERFORMANCE

| Parameter | | | | | | |
|-----------|---------------|------------|------|------|------|----------|
| | Learning rate | Batch size | | | | Metric |
| sn | | 8 | 16 | 32 | 64 | |
| 1 | 5e-5 | 0.32 | 0.43 | 0.48 | 0.38 | F1-score |
| 2 | 3e-5 | 0.31 | 0.52 | 0.60 | 0.41 | F1-score |
| 3 | 2e-5 | 0.51 | 0.53 | 0.58 | 0.54 | F1-score |
| 5 | 1e-6 | 0.58 | 0.56 | 0.62 | 0.60 | F1-score |

The chosen hyperparameter values were systematically selected to assess their influence on the sentiment analysis tasks. Striving to pinpoint combinations that achieve an ideal equilibrium between model convergence and computational efficiency. The primary objective was to find a configuration that strike a favorable equilibrium for the task. A detailed analysis of the table exposes discernible patterns. Particularly in terms of F1-score variations across different learning rates and batch sizes. The experiments were carefully carried out to measure the influence of hyperparameter selections on the overall performance of the model. Remarkably, it was observed that employing a learning rate of 1e-6 in conjunction with a batch size of 32 yielded the highest f1-score. This finding validated the model's ability to find a balance between efficient computation and robust model convergence. Subsequently, these values were adopted for the remaining experiments involving other models in the study. The moderate batch size has an advantage over the smaller batch which exhibits more variability in their performance as in the f1-score validation in Table III. On the other hand, a bigger batch size led to slower convergence of the training process which caused the model to overfit on the validation data. Therefore, utilizing moderate batch sizes offers several advantages, including

enhanced memory efficiency, accelerated convergence, and improved regularization effects by introducing sufficient noise to mitigate overfitting. Additionally, training with moderate batch sizes is observed to contribute to heightened stability in selecting an optimal learning rate as in Table III.

The selection of the maximum sequence length parameter is set at 150. As a result of an analysis of the tweet distribution within the datasets. This choice was made precisely to minimize the requirement for unnecessary padding during the training. This aims to capture the primary concepts conveyed in the tweets effectively. Fig. 4 visually depicts the maximum token length observed in tweets, illustrating the determined maximum sequence length for better context. The choice of a learning rate of 1e-6 was arrived at after a comprehensive examination of diverse parameter combinations throughout the training process, as outlined in Table III. This is a lower learning rate. A lower learning rate has demonstrated effectiveness across multiple Natural Language Processing (NLP) tasks. Additionally, a systematic dropout tuning process was conducted, exploring a range of dropout rates from 0.5 to 0.3. This iterative experimentation aimed to pinpoint the dropout rate that strikes the best balance between mitigating overfitting and enhancing model generalization.

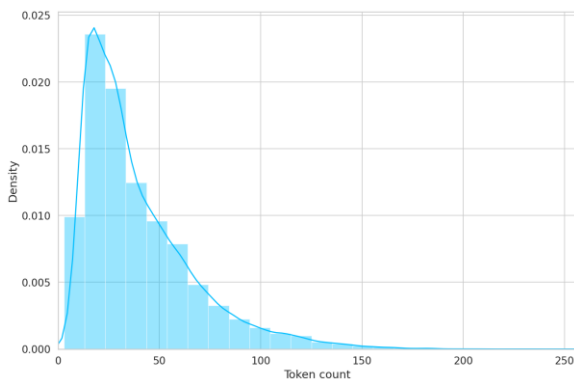


Fig. 4. Tweets token maximum sequence length.

Through this process, it was observed that a dropout rate of 0.3 consistently resulted in improved accuracy in this task compared to higher dropout rates. This careful tuning ensures that the chosen value aligns with best practices and is empirically grounded in its positive impact on model performance. For optimization, the widely employed Adam optimizer was utilized, known for its efficiency and effectiveness in training deep learning models. The same set of hyperparameter values was consistently applied across other models, as depicted in Table IV, outlining the chosen hyperparameters.

TABLE IV. HYPERPARAMETER USED

| Sn | Parameter | Value |
|----|---------------------|-------|
| 1 | Max Sequence length | 150 |
| 2 | Batch size | 32 |
| 3 | Learning rate | 1e-6 |
| 4 | Optimizer | Adam |
| 5 | Dropout | 0.3 |

IV. EXPERIMENT

This research explores the utilization of transformers' fine-tuning techniques for sentiment classification tasks in multilingual tweets. Specifically, it delves into the application of the Roberta, XLM-R, mBERT, and AfriBERT models in this context.

A. System Implementation

This research conducted experiments using the Python programming language, TensorFlow version 1.13.1, and the torch library version 2.0.1+cu118 for multilabel classification. The implementation took place on Google Collaboratory, utilizing a GPU hardware accelerator to enhance computational efficiency. Various tools, including NumPy, Pandas, sci-kit-learn, transformers, and seaborn libraries, among others, were employed to facilitate the analysis of tweets. The obtained results highlight the effectiveness of the implemented framework and emphasize the importance of adapting the code to specific requirements. The experiment notebook is accessible at: https://github.com/yusuf-003/Multilingual_experiment

B. Data Description

In this study, a dataset consisting of 63,685 tweets in 12 low-resource African languages was utilized. The dataset comprises three columns: id, tweet, and labels. The class labels are multiclass categorical data named as positive, negative, and neutral. To prepare the data for machine learning algorithms, the class labels were converted to numerical data using a dictionary-based class mapping function. This preprocessing step was conducted before feeding the data into the machine learning algorithm. Table V provides a sample of the dataset. The datasets are available at <https://github.com/afrisenti-semeval/afrisent-semeval-2023/tree/main/SubtaskB>

TABLE V. TWEETS SAMPLE

| ID | Tweet | Label |
|---------|--|----------|
| mul_001 | if i dey enter your eye or you like me and no fit talk am time dey go ohreporting live from paris | Positive |
| mul_002 | @user @user Ndi igbo is na ara di na udi | Negative |
| mul_003 | الا شوايافة ف وق من عنسد ت فكوم ب يوكوم كاملا بين ال فخر هو ب ذك يران | Negative |
| mul_004 | SAMIA ATOA ANGALIZO KUIKABILI SARATANI Makamu wa Rais Samia Suluhu Hassan amesema tatizo la Saratani kwa Watanzania linaweza kupungua ama kuondokana nalo endapo kutakuwa na tabia ya. | Neutral |
| mul_005 | Dùndún, òjòjò, ____ Èbà, ____, àmàlà #Ibeere #Yoruba | Neutral |
| mul_006 | ኩላሊት፣ ጉብት፣ ልብ፣ ሰንባ እና ሌሎችም የሰውነት አካላት ከለጋሾች ሰውነት ከወጡ በኋላ ወደ ታከሚው ገለ እስከሚገቡ ድረስ ያለው ቆይታቸው ጥያቄን ይፈጥርባቸዋል? በዚህ ፅሁፍ መልሱ... | Neutral |
| mul_007 | @user Wai jihar shugaban kasa kenanfa ..ammafa dik'abundake faruwa yanaji .yakasa yinkumai...Allah ka yayemana musibannan | Negative |
| mul_008 | في اصلاحات أقوى صاحب مملكةنا ان: تعلم هي 'وال شرق؟ ال غرب ب شهادة ال عربي ال عالم | Positive |

The dataset was randomly partitioned into three subsets for training purposes. These subsets were designated as train, validation, and test sets. 90% of the data was allocated for training, amounting to a finalized set of 57,316 tweets, while the validation set for 5% accounted for 3184. Lastly, 5% was separated for testing, resulting in 3185 tweets data. The importance of splitting the data into three parts is that it allows for a more robust evaluation of the model. The models were trained on the training data, and their performance are evaluated on the validation set. The hyperparameters of the model are tuned based on the performance of the validation set. Finally, the model was evaluated on the test set to estimate its performance on unseen data. Splitting the data into three parts helps to avoid overfitting and to have a better estimate of the model's generalization performance. The models are evaluated using the standard machine learning evaluation metric.

C. Evaluation Metric

Evaluation metrics are crucial instruments for assessing the performance of machine learning models. Through comparison of the predicted outcomes to actual results. Higher scores indicate superior predictive capabilities. It is a guiding parameter optimization for optimal performance during the tuning phase. Understanding the fundamental definition of metrics is crucial for alignment with system goals. Inaccurate evaluation using diverse metrics can lead to challenges in deploying systems on unobserved datasets. This may result in suboptimal predictions. The emphasis of this study is on Natural Language Processing metrics, which encompass precision, recall, F1-Score, and Accuracy. These metrics are derived from the confusion matrix, incorporating elements like true positives (TP), false positives (FP), true negatives (TN), and false negatives (FN) values.

1) *Accuracy metric*: Accuracy is a metric that measures the frequency of correct sentiment ratings. The goal of accuracy testing is to showcase the efficiency of the suggested framework in predicting data. The accuracy formula is given as in Eq. (3):

$$Accuracy = \frac{TP+TN}{TP+FP+FN+TN} \quad (3)$$

2) *Recall metric*: Recall, essentially, assesses the outcome by determining how many of the genuinely relevant results are retrieved. The goal of recall testing is to appraise the proposed framework's ability to appropriately recall correctly classified data. The recall formula is given as in Eq. (4):

$$Recall = \frac{TP}{TP+FN} \quad (4)$$

3) *Precision metric*: Precision signifies the precision of the proposed framework in forecasting the accurate class for a particular tweet. This aspect underscores the model's capability to minimize false positives and ensure the correctness of predicted values corresponding to the designated class. Eq. (5) provides the formula:

$$Precision = \frac{TP}{TP+FP} \quad (5)$$

4) *F1-score metric*: The f1-score represents the interplay between precision and recall, and it is inversely proportional

to strike a balance between the two. Additionally, the f1 score serves as a harmonic mean [39]. It effectively mitigates the imbalance between precision and recall in the evaluation of a model's performance. The formula is given as in Eq. (6):

$$F1 - score = \frac{2 \times Precision \times Recall}{Precision + Recall} \quad (6)$$

V. RESULT AND DISCUSSION

This section reveals the results of the experiment. It is rigorously analyzed, and thoughtfully presented. It involves a thorough investigation of the evaluation results, comparative metrics and conclusions drawn from the study. The comparison of performance evolution is grounded in results obtained from training and testing the unseen data. Initially, the training epoch is set at a maximum of 20 epochs. The experiment delves into various transformers, including mBERT, RoBERTa, XLM-R, and AfrBERTa.

A. Performance Evaluation

The effective evaluation of the proposed method in classifying tweets test data into sentiment categories: Positive, Negative, and Neutral. It encompassed several key models of varying multilingualism complexities. Table VI illustrates the results obtained from the experiment.

TABLE VI. SENTIMENT ANALYSIS MODEL PERFORMANCE COMPARISON AND EVALUATION PERFORMANCE

| Model | Evaluation Metric | | | |
|-----------|-------------------|----------------------|-------------------------|--------------|
| | Accuracy | Recall _{ma} | Precision _{ma} | F1-score |
| mBERT | 0.6229 | 0.62 | 0.63 | 0.62 |
| RoBERTa | 0.6556 | 0.75 | 0.75 | 0.74 |
| XLM-R | 0.6411 | 0.64 | 0.64 | 0.64 |
| AfriBERTa | 0.8088 | 0.81 | 0.81 | 0.81* |

The results of the experiment in Table VI offer a comprehensive insight into the performance of multilingual sentiment analysis models. The experiment was done across a diverse range of low-resource African languages. The evaluation metric. Thus accuracy, recall (macro-average), precision (macro-average), and F1-score offer a nuanced comprehension of the capabilities and constraints of each model.

AfriBERTa stands out as the most effective model, achieving an impressive accuracy of 0.8088 and a balanced F1-score of 0.81. The model's specialization for African languages, coupled with fine-tuning on a diverse linguistic dataset, appears to be a key factor in its superior performance. This allows AfriBERTa to capture complex linguistic patterns and cultural context, essential for accurate sentiment analysis in this context. RoBERTa demonstrates commendable performance, securing the second-highest accuracy (0.6556) and a competitive F1-score of 0.74. Its general-purpose nature enables adaptability across different languages, outperforming mBERT and XLM-R. Although RoBERTa doesn't surpass AfriBERTa, recall and precision values of 0.75 indicate robustness, albeit slightly below the specialized model.

The decision to fine-tune models across multiple languages proves advantageous, particularly evident in the success of AfriBERTa. This approach enhances the model's robustness, allowing it to effectively handle the linguistic diversity present in African tweets. The contrast in performance metrics underlines the importance of considering regional linguistic variations when developing sentiment analysis models. AfriBERTa not only achieves high accuracy but also strikes a balance between precision and recall. A precision of 0.81 indicates that when AfriBERTa predicts a sentiment, it is highly likely to be correct. Simultaneously, a recall of 0.81 suggests the model captures a substantial portion of positive, negative, and neutral sentiments, crucial for an understanding of sentiment distribution.

Fig. 5 illustrates the graphical representations of the model's train and validation accuracy curve of the experiment. However, the models' curves, indicate a steady improvement in accuracy as training progresses. This suggests that all the models effectively learned from the data. Moreover, an observation is the noticeable difference between the accuracy scores on the training and validation datasets, especially in the first to third training epoch in Fig. 5(a) and Fig. 5(c). This discrepancy implies the possibility of overfitting in the Afribarta and Robarta models, where the model may be overly tailored to the training data. This may be course due to variations in data distribution across languages. Although, the Afriberta model in Fig. 5(a), exhibits substantial overfitting despite its effectiveness in performance. While Fig. 5(b) mBart and Fig. 5(d) XLM-r control, this issue suggests that its pretraining on a diverse dataset might have played a crucial role in enhancing its ability to generalize effectively.

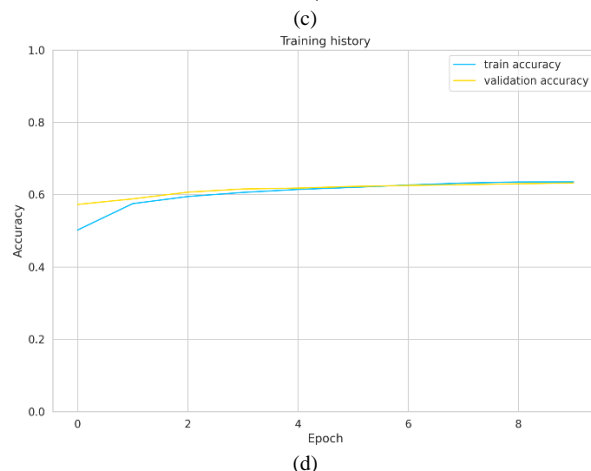
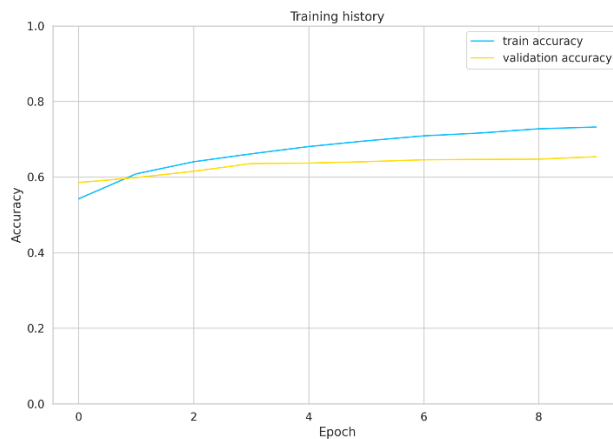
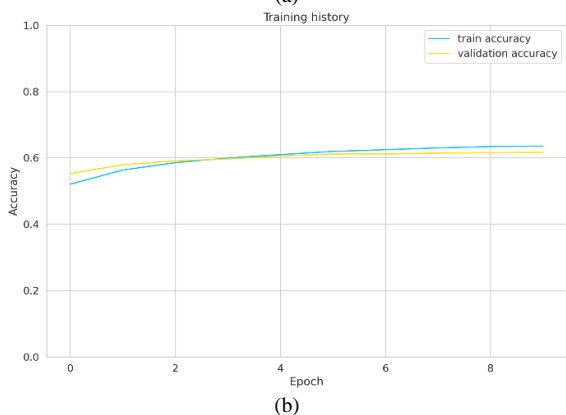
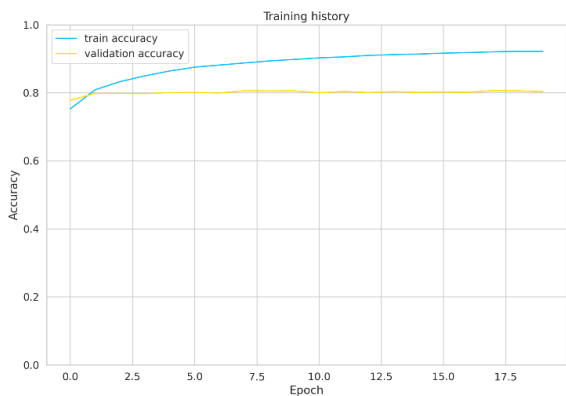
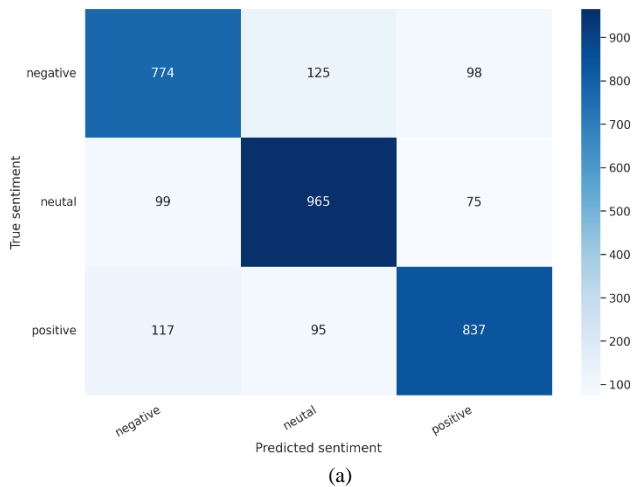


Fig. 5. (a) AfriBerta. (b) mBert. (c) Roberta. (d) XLM-r.



Similarly, Fig. 6 illustrates the confusion matrices, depicting correct and incorrect predictions by the models. Thus, a noticeable disparity is observed, with the Fig. 6(b) mBart, Fig. 6(c) RoBERTa, and Fig. 6(d) XLM-r exhibiting a higher rate of misclassifications compared to Fig. 6(a) Afriberta, which demonstrates a small number of incorrect predictions. Afriberta displays exceptional performance in accurately classifying each distinct category.



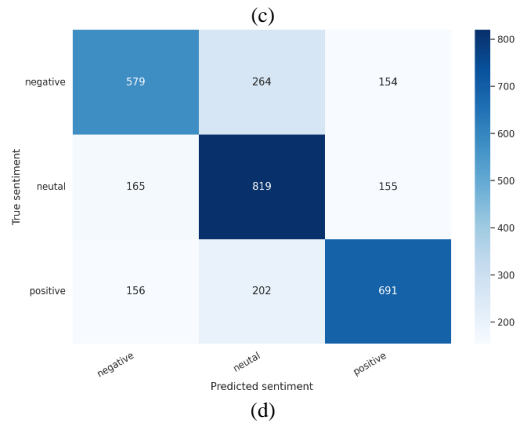
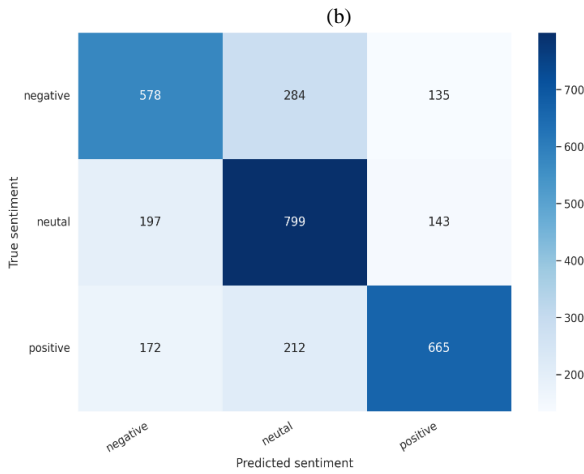
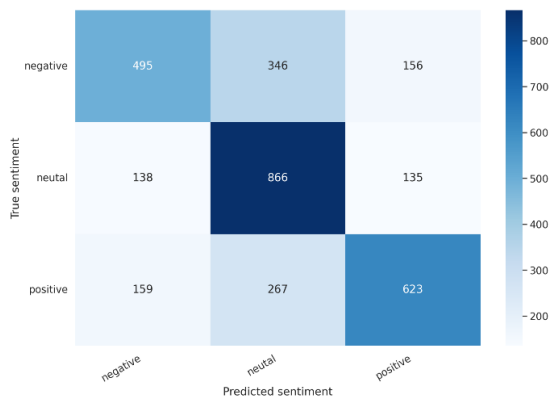


Fig. 6. (a) AfriBERTa. (b) mBERT. (c) RoBERTa, (d) XLM-r.

B. Error analysis Evaluation

The training and validation metrics presented in Table VII provide a detailed view of the performance of each model during the training process.

TABLE VII. SENTIMENT ANALYSIS MODEL PERFORMANCE COMPARISON AND EVALUATION PERFORMANCE

| Model | Training metric | | | |
|-------|--------------------------|--------|----------------------------|--------|
| | Training _{loss} | Acc | Validation _{loss} | Acc |
| mBERT | 0.9037 | 0.6354 | 0.9189 | 0.6165 |

| Model | Training metric | | | |
|-----------|--------------------------|--------|----------------------------|--------|
| | Training _{loss} | Acc | Validation _{loss} | Acc |
| RoBERTa | 0.8137 | 0.7322 | 0.8907 | 0.6536 |
| XLM-R | 0.9023 | 0.6349 | 0.9078 | 0.6319 |
| AfriBERTa | 0.6619 | 0.8874 | 0.7429 | 0.8059 |

Analyzing the values offers insights into potential sources of errors and the model's capacity to generalize to unfamiliar data. mBERT and XLM-r, relatively shows low training loss and exhibit a noticeable drop in accuracy during validation. The validation accuracy suggests that the model struggles to generalize to new data, possibly due to an excessive focus on training data specifics.

AfriBERTa and RoBERTa demonstrate a more balanced performance with training and validation accuracy. The Roberta model exhibits a slightly higher training loss (0.8137), suggesting a degree of complexity in the learned representations. The marginal decrease in accuracy during validation might be attributed to the model's challenge in capturing subtle patterns in the validation set. The AfriBERTa exhibits impressive training accuracy (0.8874) and validation accuracy (0.8059), indicating robust learning and generalization capabilities. The comparatively low training loss (0.6619) further supports the model's capability to identify complex patterns within the data. AfriBERTa's performance suggests effective fine-tuning across multiple languages. It contributing to its superior performance in sentiment analysis as observed in the earlier sections. Fig. 7 illustrates the visual model train/accuracy and loss comparison.

C. State-of-the-art Benchmarking

To evaluate the efficiency of the proposed framework, a comprehensive evaluation was undertaken, where in the performance was compared against the best-reported results within the realm of sentiment analysis for low-resource languages. Notably, the framework demonstrates superior performance across multiple benchmarks, surpassing models that currently lead in the domain.

In the SemEval-2023 Task 12: Sentiment Analysis for African Language [46] a renowned competition in the field, the best-reported F1-score for multilingual task was 75.06%. Remarkably, the proposed framework surpasses this benchmark, achieving an impressive F1 score of 80.6%, showcasing its robustness in capturing sentiment in multilingual tweets.

Furthermore, the framework was compared against the AfriSenti benchmark [49]. A Twitter Sentiment Analysis benchmark for African Languages, where the reported best F1 score stands at 71.2%. In comparison, the framework exceeds this benchmark, highlighting its ability to handle the complexities of sentiment analysis in a multilingual context.

The model also outperforms NaijaSenti [22], a Nigerian Twitter Sentiment Corpus, including four languages in our training data. It achieved an average F1-score of 78.3%. The robustness of the framework is further emphasized by its ability to surpass these benchmarks, achieving an outstanding F1 score of 80.6%.

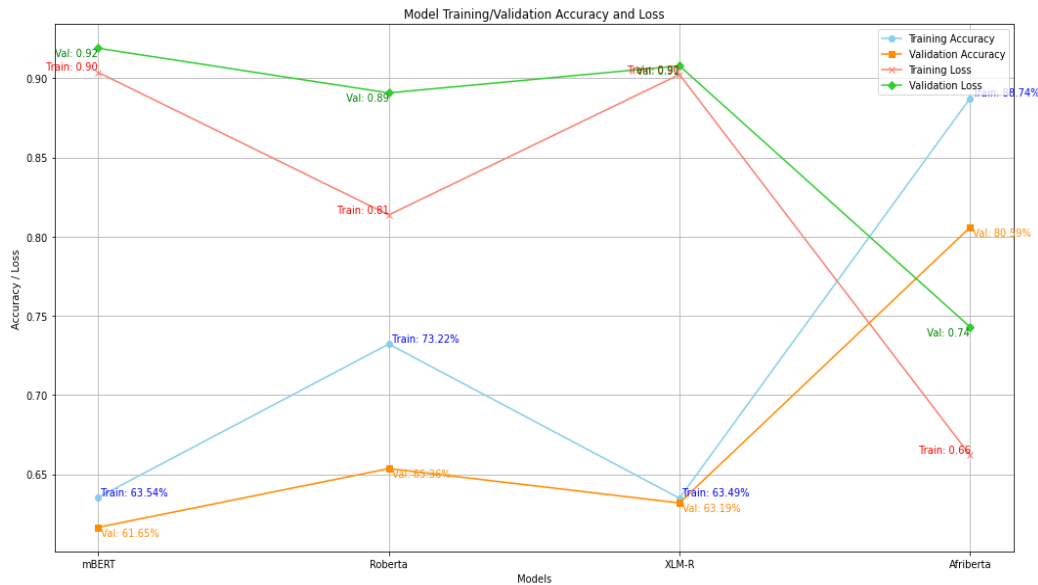


Fig. 7. Training / validation accuracy and loss (learning curve).

Table VIII provides a comprehensive comparison of the performance metrics benchmarking. It further illustrates the superiority of the proposed framework. These results signify the effectiveness framework. It demonstrated improvements over existing benchmarks underscore the novel contributions and practical utility of the framework through parameter tuning in low-resource language sentiment analysis.

TABLE VIII. PERFORMANCE BENCHMARKING COMPARISON

| Reference | <i>F1-score</i> |
|-------------|-----------------|
| [46] | 75.1%. |
| [49] | 71.2%. |
| [22] | 78.3% |
| Ours | 80.6% |

VI. CONCLUSION AND FUTURE WORK

In conclusion, our comprehensive analysis of multilingual sentiment analysis models across a range of low-resource African languages provides valuable insights into their strengths and limitations. While AfriBERTa emerges as a robust performer, demonstrating effectiveness in capturing sentiment complexity the evaluation of mBERT, RoBERTa, and XLM-R reveals nuances in their training and validation metrics.

Despite the effective performance of the framework, a notable concern is the presence of overfitting. Most especially in on the AfriBERTa suggests a need for addressing overfitting issues. To mitigate this, future work will incorporate data augmentation techniques during training, striving to improve the model's generalization to new data and enhance its performance on validation sets.

Furthermore, the study aims to expand its language coverage by experimenting with additional languages. While our current framework focuses on a diverse set of African languages, the inclusion of more languages will contribute to a

more comprehensive understanding of the model's adaptability across different linguistic contexts. This expansion will involve fine-tuning the models on datasets specific to the additional languages, ensuring broader applicability of the sentiment analysis framework.

It is essential to acknowledge certain limitations in our study. One notable challenge is the prevalence of code-mixing in the tweets, where phrases of the English language are inserted within a single sentence or tweet. This linguistic phenomenon can impact the model's performance, and as such, future work will delve into addressing code-mixing challenges. Strategies such as incorporating code-switching-aware models or developing methods to handle mixed-language expressions will be explored to enhance the framework's efficacy.

The study provides valuable insights, but inherent challenges such as varying data quality across languages and potential overfitting in the training data must be acknowledged. Future research should address these limitations, explore additional low-resource languages, and enhance model interpretability. In conclusion, our comparative analysis adds to the expanding body of knowledge on sentiment analysis in low-resource languages, emphasizing the importance of linguistic diversity for model development in the African context.

ACKNOWLEDGMENT

We express our sincere appreciation to PTDF (Petroleum Technology Development Fund) for their invaluable support in financing the scholarship. Additionally, we would like to appreciate the support received from the Universiti Teknologi PETRONAS (UTP) research grant: YUTP-FRG (015L0-312). Their involvement, financial assistance, and contributions to knowledge have played a pivotal role in facilitating the dissemination of our research findings, fostering engagement with emerging developments, and establishing meaningful professional connections within our field. We deeply value the investment made in our academic and practical development.

REFERENCES

- [1] O. Alharbi, "A Deep Learning Approach Combining CNN and Bi-LSTM with SVM Classifier for Arabic Sentiment Analysis," *International Journal of Advanced Computer Science and Applications*, vol. 12, no. 6, 2021, doi: 10.14569/IJACSA.2021.0120618.
- [2] R. Liu, Y. Shi, C. Ji, and M. Jia, "A Survey of Sentiment Analysis Based on Transfer Learning," *IEEE Access*, vol. 7, 2019. doi: 10.1109/ACCESS.2019.2925059.
- [3] A. Altaf et al., "Deep Learning Based Cross Domain Sentiment Classification for Urdu Language," *IEEE Access*, vol. 10, 2022, doi: 10.1109/ACCESS.2022.3208164.
- [4] A. Nazir, Y. Rao, L. Wu, and L. Sun, "Issues and Challenges of Aspect-based Sentiment Analysis: A Comprehensive Survey," *IEEE Transactions on Affective Computing*, vol. 13, no. 2, 2022. doi: 10.1109/TAFFC.2020.2970399.
- [5] S. Poria, D. Hazarika, N. Majumder, and R. Mihalcea, "Beneath the Tip of the Iceberg: Current Challenges and New Directions in Sentiment Analysis Research," *IEEE Trans Affect Comput*, vol. 14, no. 1, 2023, doi: 10.1109/TAFFC.2020.3038167.
- [6] B. Liu, "Sentiment analysis and subjectivity," in *Handbook of Natural Language Processing*, Second Edition, 2010.
- [7] M. Birjali, M. Kasri, and A. Beni-Hssane, "A comprehensive survey on sentiment analysis: Approaches, challenges and trends," *Knowl Based Syst*, vol. 226, 2021, doi: 10.1016/j.knosys.2021.107134.
- [8] M. A. Paredes-Valverde, R. Colomo-Palacios, M. D. P. Salas-Zárate, and R. Valencia-García, "Sentiment Analysis in Spanish for Improvement of Products and Services: A Deep Learning Approach," *Sci Program*, vol. 2017, 2017, doi: 10.1155/2017/1329281.
- [9] A. Kumar and G. Garg, "Systematic literature review on context-based sentiment analysis in social multimedia," *Multimed Tools Appl*, vol. 79, no. 21–22, 2020, doi: 10.1007/s11042-019-7346-5.
- [10] G. I. Ahmad, J. Singla, A. Ali, A. A. Reshi, and A. A. Salameh, "Machine Learning Techniques for Sentiment Analysis of Code-Mixed and Switched Indian Social Media Text Corpus: A Comprehensive Review," *International Journal of Advanced Computer Science and Applications*, vol. 13, no. 2, 2022, doi: 10.14569/IJACSA.2022.0130254.
- [11] M. Araújo, A. Pereira, and F. Benevenuto, "A comparative study of machine translation for multilingual sentence-level sentiment analysis," *Inf Sci (N Y)*, vol. 512, 2020, doi: 10.1016/j.ins.2019.10.031.
- [12] M. Amjad, N. Ashraf, A. Zhila, G. Sidorov, A. Zubiaga, and A. Gelbukh, "Threatening Language Detection and Target Identification in Urdu Tweets," *IEEE Access*, vol. 9, 2021, doi: 10.1109/ACCESS.2021.3112500.
- [13] A. I. Abubakar, A. Roko, A. M. Bui, and I. Saidu, "An Enhanced Feature Acquisition for Sentiment Analysis of English and Hausa Tweets," *International Journal of Advanced Computer Science and Applications*, vol. 12, no. 9, 2021, doi: 10.14569/IJACSA.2021.0120913.
- [14] A. Magueresse, V. Carles, and E. Heetderks, "Low-resource Languages: A Review of Past Work and Future Challenges," *ArXiv*, Jun. 2020.
- [15] D. D. Londhe, A. Kumari, and M. Emmanuel, "Challenges in Multilingual and Mixed Script Sentiment Analysis," in *2021 6th International Conference for Convergence in Technology, I2CT 2021*, 2021. doi: 10.1109/I2CT51068.2021.9418087.
- [16] Laumann Felix, "Low-resource language: what does it mean?," *NeuralSpace*. Accessed: Apr. 20, 2024. [Online]. Available: <https://medium.com/neuralspace/low-resource-language-what-does-it-mean-d067ec85dea5>
- [17] M. A. Hedderich, L. Lange, H. Adel, J. Strötgen, and D. Klakow, "A Survey on Recent Approaches for Natural Language Processing in Low-Resource Scenarios," in *NAACL-HLT 2021 - 2021 Conference of the North American Chapter of the Association for Computational Linguistics: Human Language Technologies, Proceedings of the Conference*, 2021. doi: 10.18653/v1/2021.naacl-main.201.
- [18] M. M. Agüero-Torales, J. I. Abreu Salas, and A. G. López-Herrera, "Deep learning and multilingual sentiment analysis on social media data: An overview," *Appl Soft Comput*, vol. 107, 2021, doi: 10.1016/j.asoc.2021.107373.
- [19] K. Dashtipour et al., "Multilingual Sentiment Analysis: State of the Art and Independent Comparison of Techniques," *Cognit Comput*, vol. 8, no. 4, 2016, doi: 10.1007/s12559-016-9415-7.
- [20] W. Medhat, A. Hassan, and H. Korashy, "Sentiment analysis algorithms and applications: A survey," *Ain Shams Engineering Journal*, vol. 5, no. 4, 2014, doi: 10.1016/j.asej.2014.04.011.
- [21] J. Z. Maitama, N. Idris, A. Abdi, L. Shuib, and R. Fauzi, "A systematic review on implicit and explicit aspect extraction in sentiment analysis," *IEEE Access*, vol. 8, 2020, doi: 10.1109/ACCESS.2020.3031217.
- [22] S. H. Muhammad et al., "NaijaSenti: A Nigerian Twitter Sentiment Corpus for Multilingual Sentiment Analysis," in *2022 Language Resources and Evaluation Conference, LREC 2022*, 2022.
- [23] A. Toktarova et al., "Offensive Language Identification in Low Resource Languages using Bidirectional Long-Short-Term Memory Network," *International Journal of Advanced Computer Science and Applications*, vol. 14, no. 6, 2023, doi: 10.14569/IJACSA.2023.0140687.
- [24] J. Devlin, M. W. Chang, K. Lee, and K. Toutanova, "BERT: Pre-training of deep bidirectional transformers for language understanding," in *NAACL HLT 2019 - 2019 Conference of the North American Chapter of the Association for Computational Linguistics: Human Language Technologies - Proceedings of the Conference*, 2019.
- [25] N. H. M. Et.al, "Sentiment Analysis of Code-Mixed Text: A Review," *TURKISH Journal of Computer and Mathematics Education (TURCOMAT)*, vol. 12, no. 3, 2021, doi: 10.17762/turcomat.v12i3.1239.
- [26] M. Rodríguez-Ibáñez, A. Casánez-Ventura, F. Castejón-Mateos, and P. M. Cuenca-Jiménez, "A review on sentiment analysis from social media platforms," *Expert Systems with Applications*, vol. 223, 2023. doi: 10.1016/j.eswa.2023.119862.
- [27] M. Wankhade, A. C. S. Rao, and C. Kulkarni, "A survey on sentiment analysis methods, applications, and challenges," *Artif Intell Rev*, vol. 55, no. 7, 2022, doi: 10.1007/s10462-022-10144-1.
- [28] Q. A. Xu, V. Chang, and C. Jayne, "A systematic review of social media-based sentiment analysis: Emerging trends and challenges," *Decision Analytics Journal*, vol. 3, 2022, doi: 10.1016/j.dajour.2022.100073.
- [29] A. Lighthart, C. Catal, and B. Tekinerdogan, "Systematic reviews in sentiment analysis: a tertiary study," *Artif Intell Rev*, vol. 54, no. 7, 2021, doi: 10.1007/s10462-021-09973-3.
- [30] K. Cortis and B. Davis, "Over a decade of social opinion mining: a systematic review," *Artif Intell Rev*, vol. 54, no. 7, 2021, doi: 10.1007/s10462-021-10030-2.
- [31] N. C. Dang, M. N. Moreno-García, and F. De la Prieta, "Sentiment analysis based on deep learning: A comparative study," *Electronics (Switzerland)*, vol. 9, no. 3, 2020, doi: 10.3390/electronics9030483.
- [32] T. Wolf, L. Debut, V. Sanh, J. Chaumond, and ..., "Huggingface's transformers: State-of-the-art natural language processing," 2019.
- [33] L. L. Maceda, A. A. Satuito, and M. B. Abisado, "Sentiment Analysis of Code-mixed Social Media Data on Philippine UAQTE using Fine-tuned mBERT Model," *International Journal of Advanced Computer Science and Applications*, vol. 14, no. 7, 2023, doi: 10.14569/IJACSA.2023.0140777.
- [34] L. W. Astuti, Y. Sari, and S. -, "Code-Mixed Sentiment Analysis using Transformer for Twitter Social Media Data," *International Journal of Advanced Computer Science and Applications*, vol. 14, no. 10, 2023, doi: 10.14569/IJACSA.2023.0141053.
- [35] K. Subramanyam Kalyan, A. Rajasekharan, and S. Sangeetha, "Ammus: Una encuesta de modelos preentrenados basados en transformadores en el procesamiento del lenguaje natural," *arXiv preprint arXiv ...*, 2021.
- [36] E. Ogbuju and M. Onyesolu, "Development of a General Purpose Sentiment Lexicon for {}gbo Language," *Proceedings of the 2019 Workshop on Widening NLP*, 2019.
- [37] L. Medrouk and A. Pappa, "Deep learning model for sentiment analysis in multi-lingual corpus," in *Lecture Notes in Computer Science*

- (including subseries Lecture Notes in Artificial Intelligence and Lecture Notes in Bioinformatics), 2017. doi: 10.1007/978-3-319-70087-8_22.
- [38] O. Rakhmanov and T. Schlippe, "Sentiment Analysis for Hausa: Classifying Students' Comments," in 1st Annual Meeting of the ELRA/ISCA Special Interest Group on Under-Resourced Languages, SIGUL 2022 - held in conjunction with the International Conference on Language Resources and Evaluation, LREC 2022 - Proceedings, 2022.
- [39] A. Ghafoor et al., "The Impact of Translating Resource-Rich Datasets to Low-Resource Languages through Multi-Lingual Text Processing," IEEE Access, vol. 9, 2021, doi: 10.1109/ACCESS.2021.3110285.
- [40] M. Attia, Y. Samih, A. Elkahky, and L. Kallmeyer, "Multilingual multi-class sentiment classification using convolutional neural networks," in LREC 2018 - 11th International Conference on Language Resources and Evaluation, 2019.
- [41] T. Isbister, F. Carlsson, and M. Sahlgren, "Should we Stop Training More Monolingual Models, and Simply Use Machine Translation Instead?," Apr. 2021.
- [42] Z. Li, X. Li, J. Sheng, and W. Slamu, "AgglutiFiT: Efficient Low-Resource Agglutinative Language Model Fine-Tuning," IEEE Access, vol. 8, 2020, doi: 10.1109/ACCESS.2020.3015854.
- [43] A. Jamatia, S. D. Swamy, B. Gambäck, A. Das, and S. Debbarma, "Deep Learning Based Sentiment Analysis in a Code-Mixed English-Hindi and English-Bengali Social Media Corpus," International Journal on Artificial Intelligence Tools, vol. 29, no. 5, 2020, doi: 10.1142/S0218213020500141.
- [44] J. T. H. Kong, F. H. Juwono, I. Y. Ngu, I. G. D. Nugraha, Y. Maraden, and W. K. Wong, "A Mixed Malay-English Language COVID-19 Twitter Dataset: A Sentiment Analysis," Big Data and Cognitive Computing, vol. 7, no. 2, 2023, doi: 10.3390/bdcc7020061.
- [45] A. Yusuf, A. Sarlan, K. U. Danyaro, and A. S. B. A. Rahman, "Fine-tuning Multilingual Transformers for Hausa-English Sentiment Analysis," in 2023 13th International Conference on Information Technology in Asia (CITA), IEEE, Aug. 2023, pp. 13–18. doi: 10.1109/CITA58204.2023.10262742.
- [46] S. H. Muhammad et al., "SemEval-2023 Task 12: Sentiment Analysis for African Languages (AfriSenti-SemEval)," in 17th International Workshop on Semantic Evaluation, SemEval 2023 - Proceedings of the Workshop, 2023. doi: 10.18653/v1/2023.semeval-1.315.
- [47] A. Conneau et al., "Unsupervised cross-lingual representation learning at scale," in Proceedings of the Annual Meeting of the Association for Computational Linguistics, 2020. doi: 10.18653/v1/2020.acl-main.747.
- [48] J. O. Alabi, D. I. Adelani, M. Mosbach, and D. Klakow, "Multilingual Language Model Adaptive Fine-Tuning: A Study on African Languages," in Proceedings of COLING 2022, 2022.
- [49] S. Muhammad et al., "AfriSenti: A Twitter Sentiment Analysis Benchmark for African Languages," in Proceedings of the 2023 Conference on Empirical Methods in Natural Language Processing, Stroudsburg, PA, USA: Association for Computational Linguistics, 2023, pp. 13968–13981. doi: 10.18653/v1/2023.emnlp-main.862.

Influence of a Serious Video Game on the Behavior of Drivers in the Face of Automobile Incidents

Bryan S. Diaz-Sipiran, Segundo E. Cieza-Mostacero

Research Group Trend and Innovation in Systems Engineering -Trujillo, Cesar Vallejo University, Perú

Abstract—The primary objective of this research was to enhance driver behavior during incidents through the use of a serious video game. The study employed a true experimental design. The research population consisted of an unspecified number of drivers from the city of Trujillo. Sixty drivers from Trujillo were randomly selected, with 30 assigned to the control group and 30 to the experimental group. The experimental group utilized a video game developed in Unreal Engine 5.2.1., observation forms were used to gather information, and the collected data were subsequently analyzed and processed using the statistical software Jamovi v2.4.11. The results revealed a decrease equivalent to a 43.75% reduction in the number of action mistakes, a 51.14% reduction in the number of intention mistakes, a 31.4% decrease in the number of traffic law violations, and a 42.92% reduction in the number of aggressive attitudes. In conclusion, the use of a serious video game significantly improved driver behavior during incidents.

Keywords—Videogame; serious; behavior; driving; incidents

I. INTRODUCTION

Mobility is an essential need for human beings, which requires transportation systems to make it possible. The arrival of the pandemic presented new and additional challenges in addition to existing ones, for example, inappropriate driver behavior. Since December 31, 2019, when the first case of COVID-19 was reported in Wuhan, the world has fought against the spread of this disease, which reached Latin America and the Caribbean at the end of February 2020. Since then and until 2023, the governments of the region have taken various measures that have directly or indirectly affected mobility and its characteristics [1].

The World Health Organization [2] stated that worldwide, road traffic accidents caused almost 1.3 million preventable deaths and an estimated 50 million injuries per year. Similarly, the Andean Community (2020) mentioned that, in 2020, the number of road traffic accidents in the community constituted by Bolivia, Colombia, Ecuador and Peru decreased by 32.3% compared to 2019, from 328,418 to 222,340. It also mentioned that, in Peru, traffic accidents decreased by 40.2% compared to 2019, going from 95 800 to 57 335.

In addition, the Road Safety Directorate [3] indicated that in the last four years, a total of 12079 traffic accidents were registered in the province of Trujillo, which generated 137 deaths and 13961 injuries. During that period, the accident rate was increasing, in contrast to 2020, where a decrease of 50.6% was observed compared to 2019. It is important to note that although the COVID-19 pandemic contributed to the decrease in traffic accidents in 2020, the trend in the province of Trujillo

has been increasing in recent years, which requires more effective measures to improve road safety and driver behavior. The measure that was proposed is a serious video game.

Video games have become a very useful tool due to their capacity to provide interactive content and to transmit audiovisuals in real time, and their global interactivity capacity allows them to be used in various fields, such as education, medicine, advertising, collective communication and art, among others. In Latin America, Mexico and Brazil were the main generators of video game revenues, while Peru ranked sixth in the list with a figure of US\$152 million [4].

A serious video game is distinguished from entertainment games, because its main purpose is educational or informative. These games have a great influence on the way players interact cognitively, emotionally and socially, which increases their motivation and commitment. Gamification of an environment can encourage people to engage in tasks that might otherwise seem repetitive, to experience failure, and to try again despite the risk. Furthermore, in the workplace, the incorporation of serious games can provide many benefits for companies, such as improved employee retention and recruitment, increased program adoption, and better overall job performance [5]. Given the aforementioned arguments, the following general research question was asked: How did the use of a serious video game improve drivers' incident behavior in Trujillo, 2023?

The theoretical justification for this research is based on [6] who mentioned that serious games are simulated representations of reality, in which a fictitious scenario is constructed based on real problems. Since it is a game environment, there is the ability to adjust variables and explore different scenarios without causing any harm in real life. And in study [7] who stated that safe driving involves carefully examining the visual environment in order to identify and differentiate relevant stimuli for smooth performance.

The methodology used in this research was justified for several reasons. Random sampling made it possible to obtain a representative sample of drivers in the city of Trujillo, which guaranteed generalizable and applicable results in broader contexts. The use of observation cards captured drivers' behavior in real time while driving, providing objective information on the indicators, number of action errors, number of intention errors, number of traffic law violations, and number of aggressive actions. In addition, the face-to-face evaluation during actual driving ensures greater ecological validity when confronted with real-life situations.

This research was relevant in practice, since it sought to address an important problem in road safety. The development of the serious video game aimed to improve the behavior of drivers in the city of Trujillo and contribute to the reduction of accidents and reckless behaviors on the roads. The implementation of experimental and control groups allowed us to rigorously evaluate the effectiveness of the video game in modifying the behavior of drivers. These results were useful in designing interventions and training programs aimed at improving road safety and reducing driving risks.

The research on improving driver behavior in Trujillo through a serious video game was socially relevant. Since road safety is a major concern, and it is essential to implement effective strategies to encourage responsible driving behaviors, the proposed video game has the potential to educate drivers and raise awareness about the consequences of their actions behind the wheel, promoting safer behaviors. This can have a positive impact on reducing accidents, injuries and human losses, improving the quality of life in the Trujillo driving community.

Therefore, the research "Serious video game to improve the behavior of drivers in the event of incidents in Trujillo, 2023" was undertaken. The main objective was to improve the behavior of drivers in the event of incidents through the use of a serious video game in Trujillo in 2023, with the specific objectives of reducing the number of action errors, reducing the number of intention errors, reducing the number of traffic law violations, and reducing the number of aggressive attitudes.

The main hypothesis was: if a serious video game was used, then the behavior of drivers in Trujillo in the year 2023 would be significantly improved; and the specific hypotheses were: if a serious video game was used, then the number of action errors in Trujillo in the year 2023 would be decreased, if a serious video game was used, then the number of action errors in Trujillo in the year 2023 would be decreased; then the number of intention errors decreased in Trujillo in the year 2023, if a serious video game was used; then the number of traffic law violations decreased in Trujillo in the year 2023 and if a serious video game was used; then the number of aggressive attitudes decreased in Trujillo in 2023.

II. RELATED WORK

As background, the research [8] titled "The impact of gamification and serious games on driving under unknown traffic rules", aimed to evaluate the impact of gamification elements in driving simulators on road safety in unknown traffic situations. A quantitative and qualitative experimental approach was used, with a sample of 14 people. The results showed that, when driving without a gamification element, there were 13 cases of driving against the flow of traffic and 15 cases of misuse of the signal indicator. However, when driving with the gamification element, these errors were reduced to 1 case of driving against the flow of traffic and 6 cases of signal indicator misuse. In conclusion, serious games and gamification were effective in decreasing driving errors in unfamiliar traffic situations.

III. THEORETICAL FRAMEWORK

A. Serious Video Game

Type of game designed for a purpose other than simple entertainment; their focus is usually educational or goal-oriented. The serious ones share similarities with simulation genres, since they seek to offer more realistic representations and provide teachings about real-life situations [9].

In addition, the serious game incorporates, in this way, a specific purpose that transcends mere entertainment, and this objective may be related to education, the generation of changes in attitude, the development of new competencies or skills in the player in a specific context, among other things History, Geography, Mathematics or the understanding of social issues. What is essential is that, at the end of the experience, the player has acquired a new knowledge, skill or attitude that he or she did not have before [10].

B. Driver Behavior

The analysis of human behavior in driving is essential to achieve a deeper understanding of the traffic phenomenon, since it is people who make crucial decisions, among them the choice of route, type of vehicle, vehicle maintenance, and traffic regulations, besides being the direct performers of actions when driving a vehicle in different situations. The human factor involves several aspects of the human psyche, considering the relevance of each one of them in the performance as drivers. Although the observable manifestations are usually gestural, movement or linguistic, their cause is due to the complex interaction of multiple factors, among them psychophysical, emotional and cognitive aspects, which complicates the study of the roots of human driving behavior [11].

C. SUM Methodology

The SUM methodology is a derivative of SCRUM, taking advantage of the popularity of agile methodologies, especially in contexts of fast, precise and optimized programming, as is the case of video game development. Its central purpose is to achieve efficient and cost-effective development of high-quality software, with a constant focus on continuous process improvement to optimize its efficiency and effectiveness [12].

IV. MATERIAL AND METHODS

A. Research Typology

Applied: The essence of applied methodology is problem-solving, focus on applying specialized knowledge from one or several areas to specific contexts. Its primary goal is to provide practical solutions to specific needs in social or productive fields. This methodology is centered on identifying and resolving a particular problem or question, dedicating itself to the research and consolidation of knowledge for practical application [13].

B. Research Design

Pure experimental, the key feature is evaluating the effects of an intervention, whether preventive or corrective. This involves carefully selecting a group of individuals and obtaining their prior consent. Participants are then randomly divided into two or more groups, including control and

experimental groups. This design is fundamental in understanding the impacts of various interventions [14].

C. Variables and Operationalization

1) *Independent variable*: Serious video games are a virtual representation of reality, in which a fictitious scenario based on real situations is recreated. In these games, the player assumes a specific role within the situation and is responsible for solving the challenges present in the scenario. Through interaction and decision-making, the player seeks to find effective solutions to the problems posed. These games allow users to develop skills and acquire practical knowledge by facing situations similar to those they would encounter in the real world [6]. A driving simulation video game will be used by the experimental group of 30 people. A nominal scale will be used.

2) *Dependent variable*: Driver behavior is safe driving that requires a detailed examination of the visual environment to identify and distinguish stimuli that are relevant to smooth driving. In addition, the driver must be able to select relevant stimuli from the context in a specific traffic situation, even when such stimuli are hidden or disguised in a complex visual field. In summary, safe driving involves the ability to interpret and respond appropriately to visual stimuli in different traffic scenarios. [7]. The driver behavior variable was measured through four indicators, which are: Number of action errors, the number of intention errors, Number of traffic law violations, and the number of aggressive attitudes, which shall use the ratio scale.

D. Population, Sample and Sampling

1) *Population*: The target population refers to the set of individuals who are relevant to the main problem or objective of the study; these individuals represent the group to which the results are intended to be generalized. The target population is characterized by its general demographic and clinical features. The study population is a specific group within the target population that is chosen according to the criteria defined in the research protocol. This selection is made with the purpose of carrying out the study in a more accessible and controlled manner. It is important to keep in mind that the study population may have particular geographical and temporal characteristics that make it suitable for the purposes of the research [15]. In this case, the study population consists of all drivers residing in the city of Trujillo.

A sample is defined as a portion or subset of representative elements extracted from a larger set, known as the population or universe. This selection is made randomly and is meant for scientific observation, with the goal of obtaining results that are applicable to the entire universe under investigation within established limits of error and probability specific to each situation [16]. In the context of the research mentioned, the sample consists of 60 drivers randomly selected from the city of Trujillo, divided into control and experimental groups, each comprising 30 drivers. Biases were prevented, and representative results for the population were guaranteed with randomized sampling.

E. Data Collection Techniques and Instruments

In terms of data collection techniques and instruments, non-participant observation is a method where no direct contact is established between the researcher and the subjects under study. This technique is particularly utilized in administrative fields to observe employees in a company, ensuring that their tasks are carried out without impacting their productivity or performance [14]. This research employs observation as its primary data collection technique.

The observation sheet, facilitates the systematic recording of behaviors, enabling an accurate assessment of the information collected. This tool allows the observed behaviors to be documented in an organized manner, which is essential for an adequate and comprehensive assessment of the information collected [17]. For this research, four observation sheets were made for the indicators: the number of action errors, the number of attention errors, the number of traffic law violations, and the number of aggressive attitudes.

F. Procedures

In this study, random sampling was utilized to select participants. A total of 60 drivers from the city of Trujillo were chosen through a random process to be part of the study. Once selected, these drivers were further randomly divided into two groups: a control group and an experimental group, with each group comprising 30 drivers. The assignment of drivers to each group was carried out using a random assignment process in Excel. This approach was chosen to ensure that both groups were comparable in terms of demographic characteristics and driving experience. The research flowchart presented in Fig. 1.

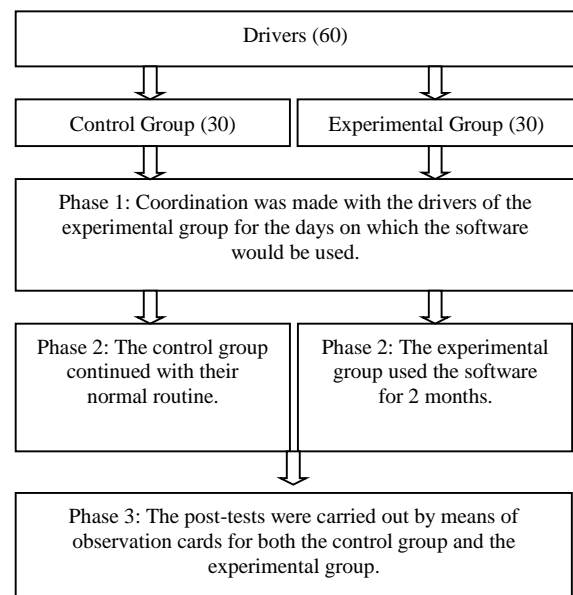


Fig. 1. Research flowchart.

The focus of the study was on a serious video game designed specifically to improve driver behavior in Trujillo. The experimental group was given access to this video game and received instructions on its proper use. They were also allowed a certain period to practice with the game before undergoing evaluations. In contrast, the control group did not receive any additional intervention; they continued their

regular driving routines without access to the video game. This setup allowed for a comparison between the two groups, aiming to evaluate the specific impact of the video game on the drivers' behavior.

For the study, observation sheets were developed containing several specific indicators to evaluate the behavior of drivers in Trujillo during incidents. These indicators included the number of action errors, which recorded the mistakes drivers made while executing specific actions. Another indicator was the number of intention errors, capturing errors in decision-making and action planning while driving. The sheets also tracked the number of traffic law violations, noting any infractions drivers committed relative to current traffic rules and regulations. Additionally, the number of aggressive attitudes was evaluated by observing behaviors. The evaluation of driver behavior was conducted in person while driving in real traffic conditions. The evaluators used observation sheets for data recording, and then a descriptive and inferential analysis was performed between the experimental and control groups, using statistical techniques to identify significant differences in the indicators assessed. A detailed analysis of each indicator was conducted to identify patterns and trends in driver behavior. This process evaluated the effectiveness of the video game in improving driver behavior in Trujillo. The results helped to understand the impact of the video game and could inform strategies to promote safer driving in the city.

To carry out this study, random sampling was applied to select the research participants. Since 60 drivers were randomly selected to participate in the study, once they were selected, they were randomly divided into two groups: a control group and an experimental group. Each group was composed of 30 drivers. Then, the assignment of drivers to each group was done through a random assignment process in Excel to ensure that the groups were comparable in terms of demographic characteristics and driving experience.

The experimental group used a serious video game designed specifically to improve driver behavior in the city of Trujillo. The drivers in the experimental group were given access to the video game and were instructed on its proper use; they were allowed to practice with the video game for a certain period of time before performing the evaluations. The control group did not receive any additional intervention and continued with their normal driving routine without access to the video game. This allowed comparison of the results between the experimental group and the control group, thus evaluating the specific impact of the video game on the drivers' behavior.

G. Development through SUM Methodology

1) *Concept phase:* During this period, the conceptual document was drafted, which provides a detailed description of the video game, addressing aspects such as its distinctive attributes, genre, game mechanics, setting, narrative, target audience, and the sources that served as inspiration. A detailed explanation of some of the aforementioned features is provided below.

2) *Game vision:* A driving video game will be developed, that allows the user to learn how to behave while driving, in a 3D environment, focusing on the educational and driving simulation video game genres.

3) *Technologies:* Visual Studio IDE, C++ programming language, Unreal Engine, and Blender.

4) *Architecture:* The architecture used in this research consists of a logic module, animation module, player module, game objects and resources module and finally a graphical interface as shown in Fig. 2.

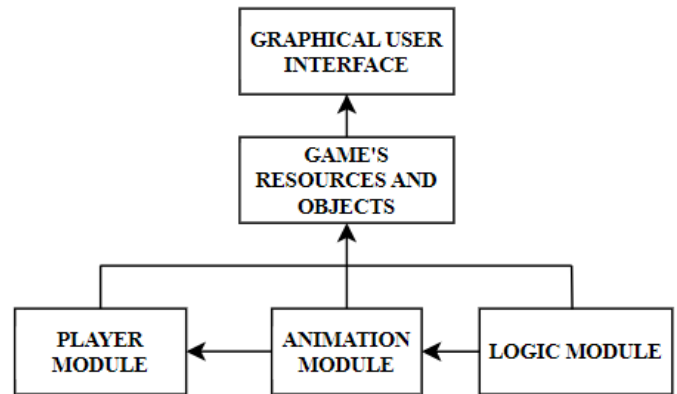


Fig. 2. Video game architecture diagram.

5) *Planning phase:* In this stage, the fundamental document of the project is prepared. This includes a detailed explanation of the work performed, the rationale of the project, the parties involved, quantifiable goals, functional requirements in Table I, and non-functional requirements in Table II. It also includes assumptions and other relevant components. In addition, both the activity plan and the project budget are detailed in this document.

6) *Functional Requirements.*

| Code | Description |
|------|--|
| RF01 | Interactive scene with situations of action errors. |
| RF02 | Interactive scene with situations of intention errors. |
| RF03 | Interactive scene with situations of traffic law violations. |
| RF04 | Interactive scene with situations of aggressive actions. |
| RF05 | Show the correct actions or decisions for each situation. |

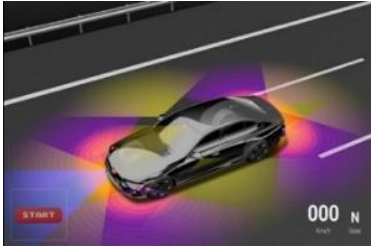



^a. Source: Own work

TABLE I. NON-FUNCTIONAL REQUIREMENTS

| Code | Description |
|-------|---|
| RNF01 | Compatibility with the largest number of devices, whether laptop or desktop pc. |
| RNF02 | Spanish language. |
| RNF03 | Simple gameplay. |

^b. Source: Own work

TABLE II. VIDEOGAME SCREENSHOTS

| Videogame | Remarks |
|---|---|
|  | Main start view |
|  | Main scenario in which the player can freely roam the city. |
|  | Decision making interface in which the user is suggested a situation. |
|  | Action error interface, when the user makes a mistake when interacting with the scenario, 1 point will be automatically deducted. |

^c. Source: Own work.

7) *Elaboration phase*: The aim of this stage is to carry out the implementation of the video game. This involves adopting an iterative and incremental approach, ensuring the development of a functional version of the video game at the conclusion of each iteration.

a) *Iteration 1*: As can be seen in Fig. 3, it started with small scenery: one vehicle and six buildings, the road, and boundary markers; the vehicle can be controlled in any direction. The third-person camera follows the vehicle and performs the necessary movements when the player turns.

b) *Iteration 2*: As shown in Fig. 4, actors were implemented in the scenario to be used as collisions that activate the messages on the screen; each one will disappear as soon as the driver finishes interacting with the interface. In

Fig. 5, control of the vehicle will be returned, and the driver will be able to continue.

c) *Iteration 3*: As shown in Fig. 6, a new vehicle was implemented, which will be an extra that will fulfill the function of generating traffic in the scene. Several functionalities were programmed, including stopping at the traffic light when it is red or following a specific route.

d) *Iteration 4*: As shown in Fig. 7, the scenario was completed with 4 blocks, 2 extra vehicles, 4 traffic lights with their logic of lights and interactions presented in Fig. 8, and a coordinated building aesthetics. All interaction points were placed, sound to the main vehicle, and the corresponding messages on screen.

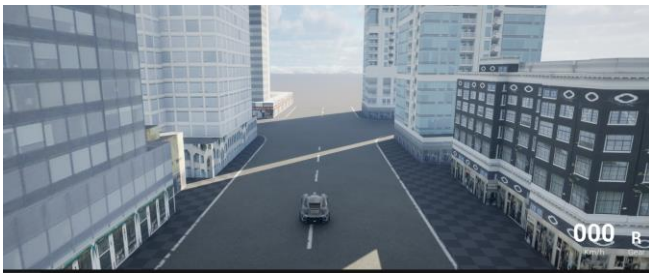


Fig. 3. Progress of the first iteration.

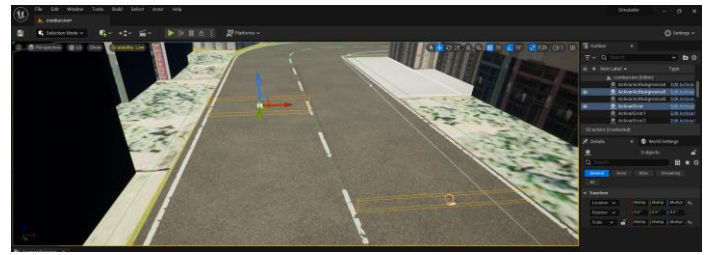


Fig. 4. Progress of the second iteration.

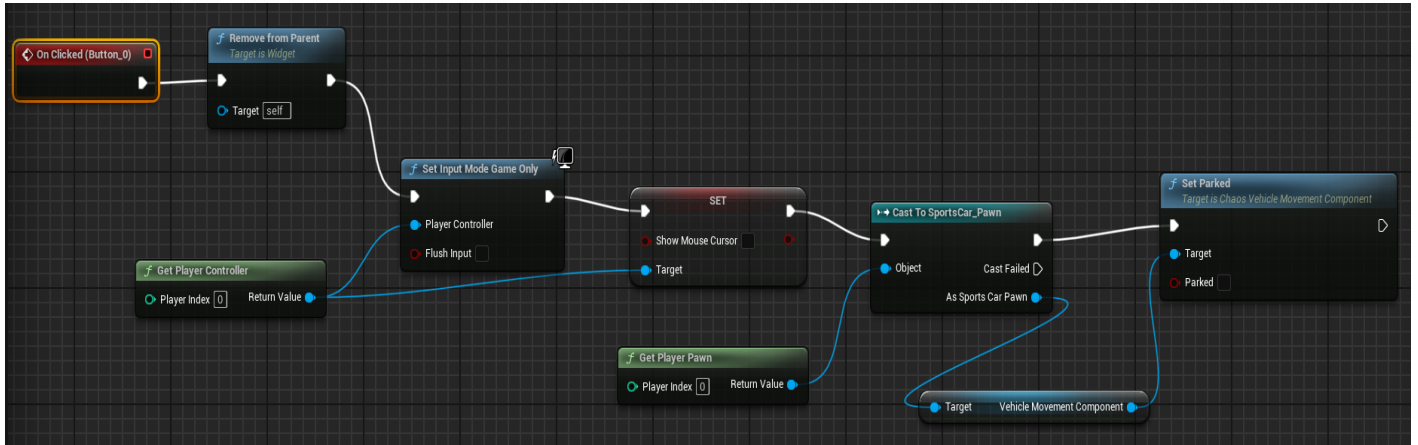


Fig. 5. Programming (Blueprints) interface in unreal engine 5.2

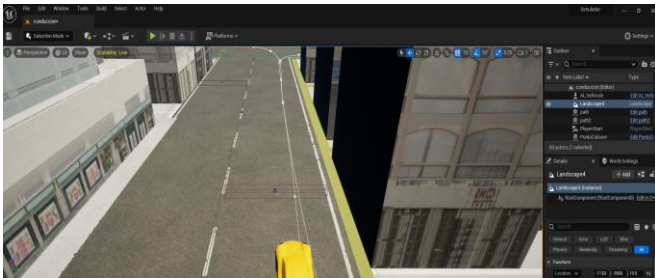


Fig. 6. Progress of the third iteration.

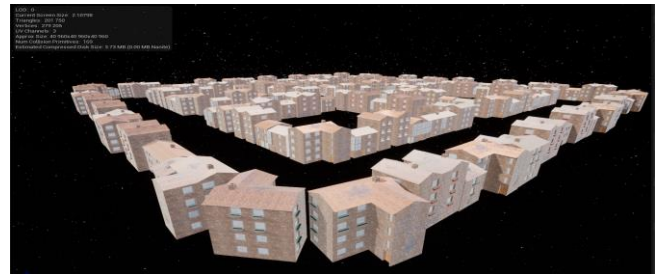


Fig. 7. Progress of the fourth iteration.

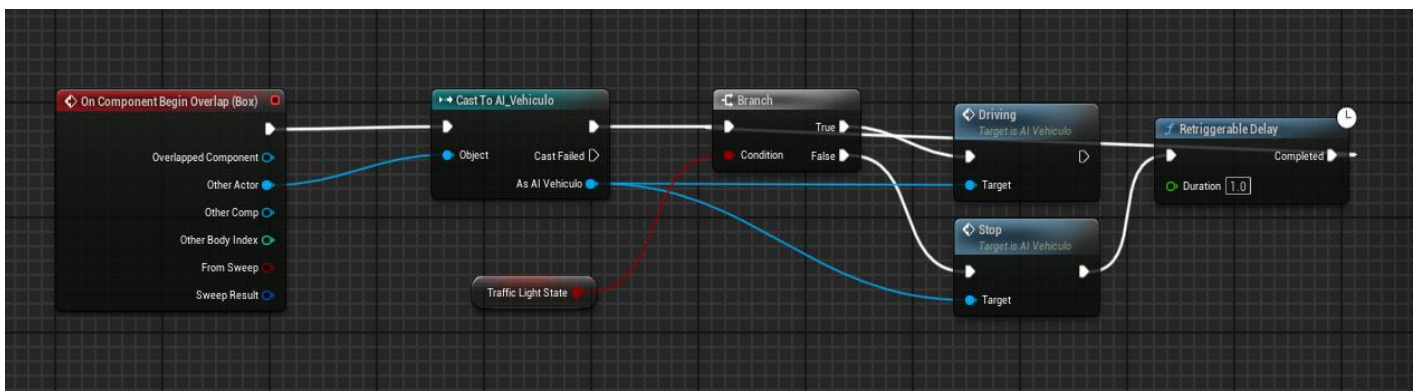


Fig. 8. Programming (Blueprints) traffic light interaction in unreal engine 5.2.

8) *Beta phase*: At the end of the development, we proceeded to package and install the video game on different computers with the Windows operating system. Several failures were found at the time of packaging the software,

which generated a time of verification and error correction. After doing so, we proceeded to the packaging.

Performance and playability tests were started, which were correct in mid-range devices (GTX 1060 dedicated graphics card, 16GB RAM).

Performance and playability tests on low-end devices (no dedicated graphics card), failed.

a) *Errors*: When running the video game, the textures failed and the scenery was not displayed completely. At the moment of joining the player and an extra vehicle at a traffic light, the extra vehicle did not move again.

b) *Fixes*: Faulty textures were changed and the error of the extra vehicles was corrected.

9) *Closing Phase*: In this phase, we proceeded to launch the final version of the video game using Unreal Engine 5.2, accompanied by the enumeration of the lessons learned throughout the process. Some of these lessons include:

a) When working with Unreal Engine, it's crucial to carefully choose the version for development due to the potential for significant changes between different versions. It is advisable to consult the official documentation thoroughly before selecting a specific version, as this can affect various aspects of game development.

b) Creating a video game from scratch is a complex and challenging task that requires a considerable amount of information and practice for optimal development. Each aspect, from game mechanics to interactions within the game environment, needs careful planning and execution, as shown in Table III. Game executable can be found at <https://acortar.link/wgI7ba>

TABLE III. DESCRIPTIVE ANALYSIS FOR ALL INDICATORS

| Research Indicator | Average | | P | N < Average | | | % < Average | | |
|--------------------|---------|------|---|-------------|----|----|-------------|-------|-------|
| | GC | GE | | GE | MP | GC | GE | MP | GC |
| NEA | 3.2 | 1.8 | 2 | 11 | 11 | 30 | 36.67 | 36.67 | 100 |
| CEI | 4.83 | 2.47 | 2 | 16 | 8 | 29 | 53.33 | 26.67 | 96.67 |
| NVLT | 2.23 | 1.53 | 2 | 16 | 16 | 28 | 53.33 | 53.33 | 93.33 |
| CAA | 4.73 | 2.7 | 2 | 17 | 7 | 26 | 56.67 | 23.33 | 86.67 |

d. Source: Own work

H. Data Analysis Methodology

In this section, the specific hypotheses for the indicators of the dependent variable were established. For the indicator of the number of action errors, the alternate hypothesis (Ha) was that if a serious video game is used, it will decrease the number of action errors in the post-test of the experimental group (CEAGE). This was compared to the post-test sample of the control group (CEAGC). Regarding the indicator of the number of intention errors, the alternative hypothesis (Ha) was that the use of a serious video game would decrease the number of intention errors in the post-test of the experimental group (CEIGE). Compared to the post-test sample of the control group (CEIGC). For the indicator of the number of traffic law violations, the alternative hypothesis (Ha) stated that using a serious video game will reduce the number of traffic law violations in the post-test of the experimental group (CVLTGE). This is compared to the control group post-test sample (CVLTGC). Lastly, for the indicator of the number of aggressive attitudes, the alternative hypothesis (Ha) is that if a serious video game is used, the number of aggressive attitudes

in the post-test of the experimental group (CAAGE) will decrease. This is compared to the control group post-test sample (CAAGC).

Descriptive analysis: An analysis of the data collected in this research was carried out. The data obtained in the experimental group were tripled to perform the calculations, and the average of the data collected for each indicator was obtained, both from the control group and the experimental group. An acceptable goal was then established based on the background or the goal expected by the entity. The amount of data that exceeded the average of the control group was counted, as well as the average of the experimental group and those data that exceeded the established goal, and the corresponding percentage was calculated for these results. In addition, a table of descriptive statistics was generated using the software Jamovi for each indicator.

Inferential analysis: At this point, normality tests (Shapiro-Wilk) and histograms were performed for each indicator using Jamovi software. As a result of the normality tests, if both variables were normally distributed, then parametric tests were

Applied (T-Student), and if any of the variables were abnormally distributed, nonparametric tests were applied (Mann-Whitney U). And it was defined whether the null hypotheses were accepted, or if otherwise the alternative hypotheses were accepted.

V. RESULTS

In this section, the main point was the descriptive analysis, with which the results were interpreted. The corresponding mean values were obtained using the Jamovi statistical software, and the decrease in the data of the experimental group compared to those of the control group was identified and presented. The second point was the inferential analysis, in which normality tests and hypothesis testing were performed for each indicator. You can access the database at the following link: <https://figshare.com/s/1fa9139817410ca889c7>

A. Descriptive Analysis

Table IV provides data on the average number of errors and violations committed by drivers in the control group (CG) and the experimental group (GE) in their respective post-tests. For action errors in the CG post-test, 36.67% were lower than their average, another 36.67% were lower than the target, and all 100% were lower than the CG's average.

TABLE IV. NORMALITY TEST STATISTIC SHAPIRO-WILK BY INDICATOR

| N° | Research Indicators | Statistic | | p | |
|----|----------------------------------|-----------|-------|-------|-------|
| | | GC | GE | GC | GE |
| 1 | Number of Action Errors | 0.943 | 0.798 | 0.112 | <.001 |
| 2 | Number of Intent Errors | 0.962 | 0.923 | 0.345 | 0.035 |
| 3 | Number of Traffic Law Violations | 0.852 | 0.732 | <.001 | <.001 |
| 4 | Number of Aggressive Attitudes | 0.947 | 0.861 | 0.145 | 0.001 |

e. Source: Own work

In terms of intention errors in the CG post-test, 53.33% were lower than their average, 26.67% were lower than the target, and 96.67% were lower than the CG's average

Regarding traffic law violations in the GE post-test, 53.33% were lower than their average, another 53.33% were lower than the target, and 93.33% were lower than the CG's average. This data suggests a significant variation in the performance of drivers in both groups across different types of errors and violations.

B. Inferential Analysis

According to the data in Table V, for the indicator Number of Action Errors (NEA) in the Control Group (CG), the p-value was 0.112. This indicates that the data were normally distributed, as the p-value was greater than 0.05. In contrast, in the Study Group (SG), the p-value for NEA was less than .001, showing that the data were non-normally distributed, as the p-value was less than 0.05. This led to the application of a non-parametric test when one of the groups showed a non-normal distribution.

TABLE V. HYPOTHESIS TESTING STATISTICS U DE MANN-WHITNEY BY POSTTEST INDICATOR

| N° | Research Indicators | Statistics | p |
|----|----------------------------------|------------|--------|
| 1 | Number of Action Errors | 290 | 0.007 |
| 2 | Number of Intent Errors | 147 | < .001 |
| 3 | Number of Traffic Law Violations | 277 | 0.003 |
| 4 | Number of Aggressive Attitudes | 190 | < .001 |

^f. Source: Own work.

For the Quantity of Intention Errors (CEI) indicator, the p-value for the CG was 0.345, indicating that its data were normally distributed, as the p-value was greater than 0.05. However, for the SG, the p-value was 0.035, which indicated non-normal distribution of data since the p-value was less than 0.05. Again, this necessitated the use of a non-parametric test when data in one of the groups were non-normally distributed.

Similarly, for the indicator Number of Traffic Law Violations (NVLT), its p-value was <.001 for the CG, which proved that its data were non-normally distributed, and for the SG, its p-value was <.001, which proved that its data were non-normally distributed, which allowed identifying that since both groups were non-normally distributed, a non-parametric test would be used.

Similarly, for the indicator Number of Aggressive Attitudes (CAA), the p-value for the CG was 0.145 greater than 0.05, which established that its data were normally distributed, and for the EG the p-value was 0.001 less than 0.05, which determined that its data were non-normally distributed, which allowed us to identify that when one of its groups was non-normally distributed, a non-parametric test was used.

According to the data obtained in Table VI for the Number of Errors of Action Indicator (NEA) its p-value was 0.007 less than 0.05, there was sufficient statistical evidence to reject the null hypothesis (Ho) and accept the alternative hypothesis (Ha); for the Number of Intention Errors Indicator (CEI) its p-value was <.001 less than 0.05, there was sufficient statistical

evidence to reject the null hypothesis (Ho) and accept the alternative hypothesis (Ha); for the Number of Traffic Law Violations Indicator (NVLT) its p-value was 0.003 less than 0.05, there was sufficient statistical evidence to reject the null hypothesis (Ho) and accept the alternative hypothesis (Ha); for the Number of Aggressive Attitudes Indicator (CAA) its p-value was <.001 less than 0.05, there was sufficient statistical evidence to reject the null hypothesis (Ho) and accept the alternative hypothesis (Ha).

VI. DISCUSSION

From the results obtained, it was evident that with the use of a serious video game. The number of errors of action, the number of errors of intention, the number of traffic law violations, and the number of aggressive attitudes were reduced. This demonstrates that the use of a serious video game significantly improved the driver's behavior.

Regarding the main goal, which sought to improve the behavior of drivers in the event of incidents through the use of a serious video game in Trujillo in 2023, it was determined that it did indeed improve the behavior of drivers. This was evidenced by the decrease in the average of all indicators measured; the results are similar to the research [8], in which the effectiveness of gamification elements in driving simulators on road safety in unknown traffic situations was assessed and proven.

Regarding the first indicator, which is the number of action errors (CEA), the total average was 3.2 in the control group and 1.8 in the experimental group, which showed a reduction of 1.4 action errors. In addition, it was evident that of the 100% average action errors of the control group, the average of the experimental group equals 56.25%; this proved a 43.75% reduction of action errors after implementation. The results were generally comparable with the research [8], which presented a 13–1 decrease in the number of action errors. It should be noted that the author Useche [18] defines action errors as errors in the execution planned by the driver, which can manifest themselves in terms of observation, execution, or incorrect judgments and do not involve intentional actions.

Regarding the second indicator, which is the number of intention errors (CEI), there was a total average of 4.83 in the control group and 2.47 in the experimental group, which showed a reduction of 2.36 in intention errors. In addition, it was evidenced that of the 100% average intention errors in the control group, the average in the experimental group equaled 48.86%; this proved a 51.14% reduction in intention errors after implementation. The results were generally comparable with the research [19], which presented a decrease of 40%, 30%, 25%, and 30% in the number of errors. It should be noted that the author Useche [18] defines intention error as errors in the attention or memory processes that hinder the proper execution of the driving task.

Regarding the third indicator, which is the number of traffic law violations (NVLT), a total average of 2.23 was obtained in the control group and 1.53 in the experimental group, which showed a reduction of 0.7 traffic law violations. In addition, it was evidenced that of the 100% of the average traffic law violations in the control group, the average in the experimental

group equals 68.60%, which proved a 31.4% reduction of traffic law violations after implementation. The results are generally comparable with the research [20], who obtained that a video game can help in the understanding of laws by up to 90%. It should be noted that the author Useche [18] defines traffic law violations as intentional violations of traffic rules, laws, or codes, which are deliberate actions.

Regarding the fourth indicator, which is the number of aggressive attitudes (CAA), a total average of 4.73 was obtained in the control group and 2.7 in the experimental group, which showed a reduction of 2.03 aggressive attitudes. In addition, it was evidenced that of the 100% average aggressive attitudes of the control group, the average of the experimental group equals 57.08%; this proved a reduction of 42.92% aggressive attitudes after implementation. The results are generally comparable with the research [21], which found that cab drivers are more likely to commit aggressive attitudes, with a 98% chance during the year. It should be noted that the author Useche [18] defines aggressive attitudes as manifestations of hostility directed towards other road users or driving patterns strongly linked to aggressive behavior by the driver.

Finally, it was concluded that with the use of a serious video game, the behavior of drivers in the city of Trujillo 2023 was improved.

VII. LIMITATIONS

During the development of the research, several limitations arose that influenced the process and the obtaining of comprehensive results. Among the most prominent limitations was the availability of the drivers, whose work schedules sometimes made it challenging to coordinate the tests efficiently. This variable, in turn, was affected by traffic variability at specific times when post-tests were conducted, introducing an unpredictable element that could have influenced the consistency of the data collected.

Another significant limitation was the time constraint for data collection. The need to collect relevant information in a limited period of time may have impacted the completeness of the research, limiting the amount of data that could be collected and analyzed in detail.

In addition, the need on the part of the researcher to acquire knowledge of new video game development software was identified. This limitation not only added a learning curve to the project but also implied dedicating additional time to becoming familiar with the necessary tools. This factor may have impacted the efficiency of the implementation of certain parts of the study.

Finally, limitations were found related to the hardware used for the execution of the video game. These constraints could have affected the quality and accuracy of the results obtained, since the performance of the hardware can directly influence the execution of the software and thus the user experience and the data collected.

Taken together, these limitations underscore the inherent complexity of the research and highlight the importance of

addressing these challenges strategically to mitigate their impact on the validity and reliability of the findings.

ACKNOWLEDGMENT

The research was not externally funded. We would like to express our sincere gratitude to all those who have contributed to this research.

CONFLICT OF INTEREST

The authors declare no conflict of interest.

REFERENCES

- [1] Pan American Health Organization PAHO and Fundación Gonzalo Rodríguez, FGR, « FGR Report Changes in Mobility from COVID-19 », 2022. Accessed at: April 16, 2023. [Online]. Available in: https://iris.paho.org/bitstream/handle/10665.2/56012/ARG220002_spa.pdf?sequence=5
- [2] World Health Organization, United Nations Collaborative Group, and United Nations Regional Commissions, « Decade of Action for Road Safety ». 2021. Accessed at: April 16, 2023. [Online]. Available in: https://cdn.who.int/media/docs/default-source/documents/health-topics/road-traffic-injuries/21323-spanish-global-plan-for-road-safety-for-web.pdf?sfvrsn=65cf34c8_30&download=true
- [3] Road Safety Directorate, « Accident rate report for the province of Trujillo, 2017-2020. », 2021. [Online]. Available in: <https://drive.google.com/file/d/13G0FEIX7oTNCeswxRHzi9QqPB-dSFj8S/view>
- [4] D. Cuenca, To read video games: What are they and how are they changing the world? Tintable, 2020.
- [5] K. Larson, «Serious Games and Gamification in the Corporate Training Environment: a Literature Review», TechTrends, vol. 64, n.o 2, pp. 319-328, mar. 2020, doi: 10.1007/s11528-019-00446-7.
- [6] G. Paredes-Otero, « Narratives and users of the transmedia society », Narrat. Usuarios Soc. Transmedia, pp. 1-888, 2022.
- [7] A. E. Caparrós, « Human driving behavior: perceptual, cognitive and response factors. », 2012, [Online]. Available in: <https://www.um.es/docencia/agustinr/pca/textos/cogniconduc.pdf>
- [8] H. Alyamani, N. Alharbi, A. Roboey, y M. Kavakli, «The Impact of Gamifications and Serious Games on Driving under Unfamiliar Traffic Regulations», Appl. Sci. 2076-3417, vol. 13, n.o 5, p. 3262, mar. 2023, doi: 10.3390/app13053262.
- [9] S. Palacios Cabrera, « Development of a serious video game as support for teaching concepts and works of literature from the period of Middle Age, Renaissance and Baroque. », dic. 2019, Accessed at: December 3, 2023. [Online]. Available in: <https://riuma.uma.es/xmlui/handle/10630/18994>
- [10] M. A. Mazza, « Serious game with virtual reality for young people oriented to learn about milestones in the history of computing. », Tesis, National University of La Plata, 2020. Accessed at: December 3, 2023. [Online]. Available in: <http://sedici.unlp.edu.ar/handle/10915/118252>
- [11] L. Nunes y J. Sánchez, « Psychology applied to driving », 2008, Accessed at: December 3, 2023. [Online]. Available in: <https://www.todoautoescuela.net/material/profesor/Temario%20correspondencia/Psicologia.pdf>
- [12] K. M. Arenas Cancapa, « Development of a Serious Gaming for First Year Primary School students applying the SUM Methodology. », Univ. Peru. Unión, dic. 2019, Accessed at: December 4, 2023. [Online]. Available in: <https://repositorio.upeu.edu.pe/handle/20.500.12840/2973>
- [13] R. Oyola, « Work 1 - Week 2 Fundamental Concepts ». Accessed at: May 28, 2023. [Online]. Available in: https://www.soe.uagrm.edu.bo/wp-content/uploads/wplms_assignments_folder/576/11581/Trabajo%201%20-%20Semana%202%20Conceptos%20Fundamentales.pdf
- [14] J. Arias, J. Holgado, T. Tafur, y M. Vasquez, Research Methodology: The ARIAS method for developing a thesis project., 1.a ed. University Institute of Innovation, Science and Technology Inudi Perú, 2022. doi: 10.35622/inudi.b.016.

- [15] J. Argimon y Jimenez, « population-and-sample ». 2013. [Online]. Available in: <https://investigacion3medicinausac.files.wordpress.com/2020/06/poblacion-y-muestra.pdf>
- [16] P. López-Roldán y S. Fachelli, « Quantitative social research methodology », 2017, [Online]. Available in: https://ddd.uab.cat/pub/caplli/2017/185163/metinvsocua_cap2-4a2017.pdf
- [17] L. G. H. Ccorimayo, « Evaluation techniques and instruments used by teachers to evaluate the students of the initial education program of the faculty of education sciences una - puno. », 2018, [Online]. Available in: <https://vriunap.pe/repositor/docs/d00006126-Borr.pdf>
- [18] S. A. Useche, « Analysis of errors and traffic violations in Bogotá drivers through the DBQ (Driving Behaviour Questionnaire).», 2011, Accessed at: November 24, 2023. [Online]. Available in: https://www.academia.edu/30088777/An%C3%A1lisis_de_errores_y_violaciones_de_tr%C3%A1nsito_en_los_conductores_de_Bogot%C3%A1_a_trav%C3%A9s_del_DBQ_Driving_Behaviour_Questionnaire_
- [19] J. F. L. Bonilla y J. F. A. Manjarres, « Development of a driving simulator for training and coaching of novice drivers. », 2019, [Online]. Available in: <https://repositorio.unibague.edu.co/server/api/core/bitstreams/565fd0ea-82b5-456d-8da1-b06a6d393226/content>
- [20] A. Gounaridou, E. Siamtanidou, C. Dimoulas, y E. G. Georgiadou, «A Serious Game for Mediated Education on Traffic Behavior and Safety Awareness», Educ. Sci., vol. 11, n.o 3, pp. 127-127, mar. 2021, doi: 10.3390/educsci11030127.
- [21] M. Mehdizadeh, A. Shariat-Mohaymany, y T. Nordfjaern, «Driver behaviour and crash involvement among professional taxi and truck drivers: Light passenger cars versus heavy goods vehicles», Transp. Res. Part F Traffic Psychol. Behav., vol. 62, pp. 86-98, abr. 2019, doi: 10.1016/j.trf.2018.12.010.

A Genetic Artificial Bee Colony Algorithm for Investigating Job Creation and Economic Enhancement in Medical Waste Recycling

El Liazidi Sara, Dkhissi Btissam

National school of applied sciences Tetuan, Morocco

Abstract—The effective management of end-of-life products, whether through recycling or incineration for electricity generation, holds pivotal significance amidst escalating concerns over economic, environmental, and social ramifications. While the economic and environmental dimensions often receive primary focus, the social aspect remains comparatively neglected within sustainability discourse. This paper undertakes a comprehensive exploration of the positive social impacts engendered by medical waste recycling, with a specific focus on job creation and economic value enhancement. The principal aim of this research is to highlight the social benefits derived from medical waste recycling, elucidating its role in fostering employment opportunities, and augmenting economic prosperity. By employing a Genetic Artificial Bee Colony algorithm, this study addresses two mathematical problems pertinent to optimizing recycling processes, thereby contributing to the advancement of sustainable waste management practices. Additionally, the proposed algorithm exhibits superior performance, highlighting its potential in addressing sustainability challenges. Ultimately, integrating the social dimension into end-of-life product management discussions can lead to a more comprehensive approach to sustainability, balancing environmental preservation with socio-economic progress.

Keywords—Medical waste recycling; social impacts; genetic artificial bee colony algorithm; job creation; economic value

I. INTRODUCTION

The growth of the population and their increasing demand for consumable products necessitate a concerted effort to reduce the amount of waste generated by these products after use, the management of products extends far beyond their initial creation and use. The footprint left by this waste has become a critical concern, urging a transition from the traditional "cradle-to-grave" model, to the more encompassing and sustainable "cradle to cradle". The increase in waste in landfill sites becomes a crucial challenge for decision-makers, researchers, and consumers, considering the dangers effects that can be caused by the poor management of these wastes, whether at the economic, environmental, or social dimensions. Addressing these three challenges in the design of a closed-loop supply chain (CLSC) forms the three pillars of sustainability [1]. The complexity of the intersection between environmental, economic, and social considerations finds its explanation in the model of designing a CLSC. This represents

a systematic departure from the "cradle to grave" model, emphasizing a circular economy, environmental concerns, and social indicators.

Recently, in the discourse on sustainable development, one of the sectors that attracts the attention of researchers and decision-makers is the healthcare sector. This sector is subject to increased scrutiny, especially after the Covid-19 pandemic, wars, and natural disasters that have generated substantial amount of medical waste in recent years. According to the World Health Organization report [2], the COVID-19 pandemic generated tens of thousands of tons of medical waste between March 2020 and November 2021. These wastes are disposed of in landfill sites without any treatment. This situation highlights the importance of adopting a strategy to implement the principles of reverse logistics in traditional supply chain management and integrating environmental concerns and social indicators.

It is evident that in recent times, the focus of decision-makers and researchers has pivoted towards the environmental impact resulting from supply chain. While there is an increasing recognition of the importance of reducing the environmental footprint to attain the second dimension of a sustainable CLSC network, there remains a noticeable gap in the existing literature concerning the third dimension of sustainability, namely, social impacts[3]. This study aims to highlight the importance of integrating social indicators into sustainable CLSD. Recycling medical waste can have several positive social impacts contributing to the well-being of societies and individuals, including the community, workplace safety, education and awareness, and job creation. This study focuses on two social indicators: the first is job creation, which plays a significant role in reducing unemployment rates, and the second is balancing economic development.

The rest of this article is outlined as follows: Section II provides a review of the literature. In Section III, we delve into a detailed description of the problem and the corresponding mathematical model. Section IV introduces the Genetic Artificial Bee Colony (GABC) algorithm proposed in this study. The practical implementation of GABC and a comparative analysis between the results obtained by GABC and the original ABC are presented in Section V. Finally, Section VI offers concluding remarks.

II. LITERATURE REVIEWS

For decades, the main objective of supply chains has been the maximization of profit or the minimization of costs throughout the network. This goal has been the focus of many research works and studies [4], [5], [6], [7], [8]. The efforts made by researchers to increase the profit of the logistics chain undeniably contributed to enhancing its efficiency and profitability.

In order to reduce total supply chain operating costs, A bi-objective optimization approach is presented by [9], which aims to minimize total expenditures and decrease cycle time delay overall. They use a solution strategy that combines the dual simplex method, the constraint method, and scatter search when taking discrete facility capacity alternatives into consideration. A trade-off between the two goals is shown by computational analyses, which show that decreasing cycle time produces a decentralized network structure while optimizing for cost produces a centralized network structure. The author in [10] present a novel model for designing a reliable network in a closed-loop supply chain, minimizing total and post-failure transportation costs under uncertainty. Their solution approach, combining robust optimization, queuing theory, and fuzzy multi-objective programming, proves effective in addressing uncertainty and optimizing facility design. The author in [11] provide a mixed-integer linear programming model for a closed-loop supply chain network that uses stochastic programming to minimize overall costs and account for uncertainties. To solve the complex problem of creating cost-effective closed-loop supply chains, [12] provide a novel approach that uses a deterministic multi-product, multi-echelon, multi-period model. The author in [13] proposes a novel Genetic Artificial Bee Colony (GABC) algorithm for optimizing closed-loop supply chain networks, addressing uncertainties in demand, and returned product quantities. Their GABC algorithm surpasses standard Artificial Bee Colony (ABC) and Genetic Algorithm (GA) methods in minimizing total network cost across diverse scenarios. The author in [14] uses an integer-programming approach to address a two-stage supply chain distribution-allocation problem. They proposed heuristic, based on Ant Colony Optimization, exhibits computational efficiency, and produces solutions in a fair amount of time with an average deviation from optimal solutions of about 10%. The author in [15] propose a mobile Waste Heat Recovery (WHR) supply chain, minimizing distribution costs compared to traditional WHR. Their optimization model, integrating life cycle assessment, ensures energy supply stability and cost savings, presenting an efficient alternative to conventional WHR and fossil fuel heating, especially under stochastic demand conditions. The author in [16] explores the economic advantages of new product formulations, specifically through concentration, in formulated product supply chain networks. They reduce overall costs by optimizing facility locations, capacities, and production planning through the use of mixed-integer linear programming, which has major advantages in a supply chain for fast-moving consumer goods.

Recently, the challenge of implementing a sustainable CLSC that adheres to the three dimensions of sustainability has become a task facing the researchers and the decision-

makers. It is noted that several studies are beginning to incorporate environmental and / or social impacts as additional objectives in their multi-objective CLSC. The literature on the sustainable CLSC can be categorized into two primary groups: Economic and environmental dimensions in CLSC and sustainable CLSC.

A. Economic and Environmental Dimensions in CLSC

Over the past two decades, the challenge of environmental impacts generated by industries and end-of-life waste, leading to an increase in greenhouse gas (GHG) emissions and loss of natural resources, has become a major focus for researchers. The author in [17] introduce a conceptual framework for designing a sustainable food packaging and distribution network, comparing the environmental and economic impacts of reusable plastic containers (RPC) with traditional single-use options in the fresh food supply chain. Using life cycle assessment (LCA), the study evaluates the carbon footprint and explores sensitivity to key parameters, offering insights into the sustainability of packaging approaches in the food catering chain. The author in [18] presents a multi-objective model for the logistics of the gold industry that gives cost and CO₂ emissions priority. Their work effectively addresses a case study of a 7-layer network using an ant colony optimization technique, demonstrating usefulness. The algorithm performs better when the parameters are set Taguchi-based, and the results highlight managerial insights for supply chain optimization. The author in [19] addresses environmental concerns by proposing a green supply chain model that optimizes transportation and waiting times for fleets in both forward and reverse logistics. The model aims to minimize environmental impacts and energy consumption through strategic determinations of loading, unloading, and production rates. The author in [20] explores how producing power from wood pellets might help achieve climate objectives. They focus on how supply chain costs can be reduced by using techno-economic analysis and a study of relevant research. The analysis highlights the impact of variables such as plant size on costs by revealing trade-offs in cost components across various supply chain configurations. [21]propose novel mathematical models for inventory management in reverse logistics systems, extending [22] model by considering different demands for newly produced and remanufactured products. The study also extends into sustainability, presenting a three-objective mathematical model and an algorithm to achieve Pareto solutions, addressing greenhouse gas emissions and energy consumption in production and remanufacturing processes. The author in [23] innovate a methodology for plastic footprint analysis at the enterprise and supply chain levels, focusing on a clothing industry case. Their study identifies key strategies, such as lightweight plastic promotion and increased use of recycled materials, offering practical solutions for substantial environmental benefits in reducing plastic impact.

B. Social Dimension

The concept of sustainability was introduced by [24] report, emphasizing the importance of integrating environmental and social concerns to ensure a viable future. Unfortunately, in the literature, the social dimension has rarely been addressed. The author in [25] aims to improve reverse

logistics decision-making by integrating economic, environmental, and social objectives. Using a recyclable waste collection system as a case study, they model the problem as a multi-objective, multi-depot periodic vehicle routing challenge, proposing a compromise solution for a sustainable reverse logistics plan that considers trade-offs and achieves balance. The author in [26] introduces a multi-objective possibilistic programming model for designing a sustainable medical supply chain network under uncertainty, addressing conflicting economic, environmental, and social objectives. The model employs effective social and environmental life cycle assessment methods, and an accelerated Benders decomposition algorithm is introduced to handle computational complexity, demonstrated through a medical industrial case study. The authors in [27] have introduced an innovative sustainable closed-loop location-routing-inventory model. This model considers economic, environmental, and social impacts, particularly in the context of mixed uncertainty. The author in [28] address the need for supply chain designs considering environmental, social, and economic objectives, specifically focusing on sustainable closed-loop supply chain networks for recycled tires. They develop a multi-objective mixed-integer linear programming model to optimize total cost, environmental impacts, and social factors. To efficiently handle large-scale networks, four new hybrid metaheuristic algorithms are introduced and demonstrated to be effective through extensive computational experiments and analyses. The author in [29] develops a multi-objective linear mathematical model to optimize a steel sustainable closed-loop supply chain, addressing uncertainties and applying fuzzy goal programming. Validated through a real case study in an active steel supply chain in Iran, the model aims to optimize total profit, energy and water consumption, CO2 emissions, job opportunities, and lost working days. Results highlight the significant environmental benefits achievable even with a minor profit decrease, providing essential managerial insights for industry leaders navigating the balance between profits and environmental/social considerations. The author in [30] highlights the impact of decisions related to facility locations and industrial activities on initial pollution levels and unemployment rates in various regions. Through numerical experiments, the research demonstrates that intentional objectives focused on reducing environmental and social inequities lead to a decrease in disparities among regions. The paper concludes by providing managerial insights and suggesting future research directions within the context of supply chain networks and sustainable development.

Due to the diverse nature of social responsibility aspects, integrating all of them into the design of a sustainable closed-loop supply chain would lead to a non-optimal network. Our primary objective in this paper is to maximize positive social indicators in recycling three types of medical waste: glass, plastic, and steel. To achieve this, we propose a programming model with two objective functions that aims to maximize job creation and balance economic development. The study introduces a Genetic Artificial Bee Colony (GABC) algorithm, and its performance is compared with the original Artificial Bee Colony algorithm. This work builds upon our previous research [31], which focuses on minimizing the total

cost of reverse logistics and reducing CO2 emissions in the network.

III. PROBLEM MODELING

This model aims to develop a programming model for two objective functions to maximize job opportunities creation and balance economic value within a reverse supply chain network. The network encompasses hospitals, collecting centers, recyclers, and disposal centers. Fig. 1 illustrates the network schematic, emphasizing the reverse logistics aspect. The medical waste generated by the hospitals is shipped to collecting centers where the waste is disinfected and sorted. In this study, three types of waste are addressed: plastic (Polyethylene (PET), Polypropylene (PP)), glass (clear or white glass and brown glass), and stainless steel. The non-recyclable waste is transported to disposal centers, while the remaining medical waste is directed to recycling centers where it is processed and recycled to be used as new products. The unrecovered waste is shipped to the disposal center for safe landfill.

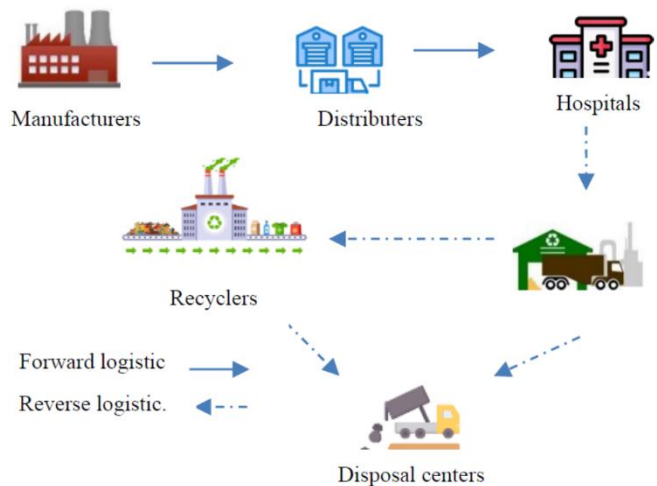


Fig. 1. Medical product for forward / reverse logistics network.

A. Assumptions

To formulate our model, we have based our analysis on the following assumptions and simplifications:

- There are no exchanges of products among facilities at the same level.
- The locations for the opening of recyclers and collecting centers are predetermined.
- The capability of each facility is constrained.
- The quality of recycled products and manufactured products is the same.
- The unrecovered waste is transported to a disposal center for safe landfilling.

B. Notation

- Indices

l : Index of hospitals, $l \in \{1, \dots, L\}$.

n : Index of collecting centers, $n \in \{1, \dots, N\}$.

m : Index of recyclers, $m \in \{1, \dots, M\}$.

o : Index of disposal centers, $o \in \{1, \dots, O\}$.

k : Index of plastic waste, $k \in \{1, \dots, K\}$.

r : Index of glass waste, $r \in \{1, \dots, R\}$.

v : Index of plastic waste, $v \in \{1, \dots, V\}$.

- Parameters

DJ_{km} : Number of fixed job opportunities created by establishing plastic recycler m .

DJ_{rm} : Number of fixed job opportunities created by establishing glass recycler m .

DJ_{vm} : Number of fixed job opportunities created by establishing steel recycler m .

DJ_n : Number of fixed job opportunities created by establishing collecting center n .

IDJ_n : Number of variable job opportunities created at collecting center c (depends on amount of waste and capacity of collecting center).

IDJ_{km} : Number of variable job opportunities created at plastic recycler m .

IDJ_{rm} : Number of variable job opportunities created at glass recycler m .

IDJ_{vm} : Number of variable job opportunities created at steel recycler m .

μ_n : Unemployment rate at collecting center n .

μ_{km} : Unemployment rate at plastic recycling center m .

μ_{rm} : Unemployment rate at glass recycling center m .

μ_{vm} : Unemployment rate at steel recycling center m .

V_{km} : Economic Value of recycling waste at plastic recycler m .

V_{rm} : Economic Value of recycling waste at glass recycler m .

V_{vm} : Economic Value of recycling waste at steel recycler m .

V_n : Economic Value at collecting center n .

rd_{km} : Regional development at plastic recycler m .

rd_{rm} : Regional development at glass recycler m .

rd_{vm} : Regional development at steel recycler m .

rd_n : Regional development at collecting center n .

δ_k : The percentage of non-recyclable plastic waste being transported from the collection center to the disposal center.

δ_r : The percentage of non-recyclable glass waste being transported from the collection center to the disposal center.

δ_v : The percentage of non-recyclable steel waste being transported from the collection center to the disposal center.

β_k : The percentage of unrecovered plastic waste being transported from the recycler to the disposal center.

β_r : The percentage of unrecovered glass waste being transported from the recycler to the disposal center.

β_v : The percentage of unrecovered steel waste being transported from the recycler to the disposal center.

- Capacities

F_l : Quantity of medical waste generated by hospital l .

$Mcap_n$: Capacity of collecting center n .

MPW_m : Capacity of plastic recycler m .

MGW_m : Capacity of glass recycler m .

MSW_m : Capacity of steel recycler m .

$Mcap_o$: Capacity of disposal center o .

UP_n : The upper limit for establishing collecting center n .

UP_{km} : The upper limit for establishing plastic recycler m .

UP_{rm} : The upper limit for establishing glass recycler m .

UP_{vm} : The upper limit for establishing steel recycler m .

- Decision variables

AM_{ln} : The quantity of waste transported from hospital l to collection center n .

AM_{nkm} : The quantity of plastic waste transported from collection center n to recycler m .

AM_{nrm} : The quantity of glass waste transported from collection center n to recycler m .

AM_{nvm} : The quantity of steel waste transported from collection center n to recycler m .

Y_n : 1 if the collecting center n is opened, 0 otherwise.

Y_{km} : 1 if the plastic recycler center m is opened, 0 otherwise.

Y_{rm} : 1 if the glass recycler center m is opened, 0 otherwise.

Y_{vm} : 1 if the steel recycler center m is opened, 0 otherwise.

C. Social Objective Functions

- Job Creation Opportunities

Employment is a key driver of social sustainability, significantly influencing the well-being and socio-economic status of individuals [32]. A study by the [33] projects a potential net job creation of up to 700,000 jobs in the EU. Specifically, employment in waste management is anticipated to witness a substantial increase, with a potential addition of 660,000 jobs. This increase is attributed to the labor-intensive nature of recycling, which is replacing less labor-intensive landfilling practices.

Max Job Creation = Fixed job creation(FJC) +
Variable Job Creation (VJC) (1)

$$FJC = \sum_{n=1}^N DJ_n \times Y_n \times \mu_n + \sum_{m=1}^M \sum_{k=1}^K DJ_{km} \times Y_{km} \times \mu_{km} + \sum_{r=1}^R \sum_{m=1}^M DJ_{rm} \times Y_{rm} \times \mu_{rm} + \sum_{v=1}^V \sum_{m=1}^M DJ_{vm} \times Y_{vm} \times \mu_{vm} \quad (1-1)$$

$$VJC = \sum_{l=1}^L \sum_{n=1}^N IDJ_n \times \frac{AM_{ln}}{Mcap_n} \times \mu_n + \sum_{n=1}^N \sum_{k=1}^K \sum_{m=1}^M IDJ_{km} \times \frac{AM_{nkm}}{MPW_{km}} \times \mu_{km} + \sum_{n=1}^N \sum_{r=1}^R \sum_{m=1}^M IDJ_{rm} \times \frac{AM_{nrm}}{MGW_m} \times \mu_{rm} + \sum_{n=1}^N \sum_{v=1}^V \sum_{m=1}^M IDJ_{vm} \times \frac{AM_{nvm}}{MSW_m} \times \mu_{vm} \quad (1-2)$$

The objective function (1) is designed to maximize both fixed and variable job creation opportunities within the network. Eq. (1-1) specifically represents the fixed job creation in the collecting and recycling centers. The inclusion of unemployment rates $\mu_n, \mu_{km}, \mu_{rm}, \mu_{vm}$ in the objective function allows the model to adapt its assessment of job creation based on the prevailing employment conditions, making the optimization more realistic and reflective of the socio-economic context. When the unemployment rate is high, indicating a substantial pool of unemployed individuals in the considered region or sector, the model recognizes that the potential for job creation through the recycling process could have a more substantial positive impact on the local workforce. Conversely, in the case of a low unemployment rate, signifying a smaller proportion of unemployed individuals, the model exerts less influence, as the employment market is presumed to be more saturated. Equation (1-2) defines the variable job creation in the collecting and recycling centers. The utilization of the ratios, including $\frac{AM_{ln}}{Mcap_n}, \frac{AM_{nkm}}{MPW_m}, \frac{AM_{nrm}}{MGW_m}, \frac{AM_{nvm}}{MSW_m}$ serves as a measure of how much of the capacity of collecting center n and recycler center m is being utilized. A ratio close to 1 indicates that there is potential for additional job opportunities.

- **Balanced Economic Development**

Balanced economic development serves as a positive social indicator, emphasizing a fair and inclusive distribution of economic benefits. This approach aims to mitigate income inequality by creating job opportunities across diverse sectors and regions, ultimately elevating overall living standards. The ripple effect of this strategy extends to an enhanced quality of life, fostering social cohesion, and empowering communities. In essence, a commitment to balanced economic development reflects a dedication to creating a more equitable and thriving society.

$$Max ED = \sum_{n=1}^N V_n \times Y_n \times (1 - rd_n) + \sum_{m=1}^M \sum_{k=1}^K V_{km} \times Y_{km} \times (1 - rd_{km}) + \sum_{m=1}^M \sum_{r=1}^R V_{rm} \times Y_{rm} \times (1 - rd_{rm}) + \sum_{v=1}^V \sum_{m=1}^M V_{vm} \times Y_{vm} \times (1 - rd_{vm}) \quad (2)$$

The objective function (2) represents the economic development associated with each collection center and recycling center. The terms $rd_n, rd_{km}, rd_{rm}, rd_{vm}$ in the objective function serve as adjusters, strategically considering the impact of regional development on the economic value associated with the proposed model. These adjusters play a crucial role in accounting for the varying degrees of regional development and tailor the objective function to reflect the nuanced economic landscape, ensuring a more accurate representation of the model's objectives in the context of different regions.

D. Constraints

- **Supply Constraints**

$$\sum_{l=1}^L AM_{ln} \leq F_l \quad \forall n \quad (3)$$

This constraint guarantees that the amount of waste collected from each hospital is limited to the quantity of waste generated by that specific hospital.

- **Flow Balance Constraints**

$$\sum_{l=1}^L AM_{nkm} = \sum_{l=1}^L AM_{ln} (1 - \delta_k) \quad \forall l, m, k \quad (4)$$

$$\sum_{l=1}^L AM_{nrm} = \sum_{l=1}^L AM_{ln} (1 - \delta_r) \quad \forall l, m, r \quad (5)$$

$$\sum_{l=1}^L AM_{nvm} = \sum_{l=1}^L AM_{ln} (1 - \delta_v) \quad \forall l, m, v \quad (6)$$

Eq. (4), (5) and (6) Ensure that the total waste received at collection centers is equivalent to the total waste forwarded to recycling centers, considering potential damage.

- **Capacity Constraints**

Maximum capacity can be allocated to collecting center n.

$$\sum_{n=1}^N AM_{ln} \leq Mcap_n \times Y_n \quad \forall l \quad (7)$$

Maximum capacity can be allocated to recycling center r.

$$\sum_{m=1}^M AM_{nkm} \leq MPW_m \times Y_{mk} \quad \forall n, k \quad (8)$$

$$\sum_{m=1}^M AM_{nrm} \leq MGW_m \times Y_{mr} \quad \forall n, r \quad (9)$$

$$\sum_{m=1}^M AM_{nvm} \leq MSW_m \times Y_{mv} \quad \forall n, v \quad (9)$$

Constraints (11), (12), (13), and (14) determine the upper limit on the number of collecting centers and recycling centers that can be opened.

$$\sum_{n=1}^N Y_n \leq UP_n \quad (11)$$

$$\sum_{m=1}^M Y_{mk} \leq UP_{mk} \quad \forall k \quad (12)$$

$$\sum_{m=1}^M Y_{mr} \leq UP_{mr} \quad \forall r \quad (13)$$

$$\sum_{m=1}^M Y_{mv} \leq UP_{mv} \quad \forall v \quad (14)$$

Finally, Constraint (15) and (16) enforce the binary and no negativity restrictions on corresponding decision variables.

$$Y_n, Y_{mk}, Y_{mr}, Y_{mv} \in \{0,1\} \quad (15)$$

$$AM_{ln}, AM_{nkm}, AM_{nrm}, AM_{nvm} \geq 0 \quad (16)$$

IV. SOLUTION APPROACH

A. Artificial bee Colony Algorithm

The optimization algorithms based on swarm intelligence have come to be considered as one of the best methods for handling difficult real-world problems. The Artificial bee colony (ABC) is one of such optimization algorithms based on swarm intelligence. The ABC algorithm, introduced by [34], is an optimization algorithm inspired by the foraging behavior of honeybees. This algorithm is specifically designed to systematically explore and exploit potential solutions in the context of optimization problems. The ABC algorithm comprises as shown in Fig. 2, three distinct categories of bees: employees, onlookers, and scouts. First, employee bees are dispatched to diverse food sources, each with a designated location. These employees assess the nectar quantity associated with their designated food sources. At the same time, onlooker bees stay within the hive, systematically collecting crucial information about food sources with superior nectar levels, as communicated by the employee bees. Subsequently, onlooker bees influence the directional shifts for employee bees to explore further, based on the observed nectar quantity of each food source. Employee bees encountering stagnation in nectar accumulation may transform into scout bees, responsible for the stochastic discovery of new food sources. This dynamic interplay between exploration and exploitation is a core aspect of the ABC algorithm, reflecting the collaborative and adaptive dynamics inherent in natural honeybee colonies.

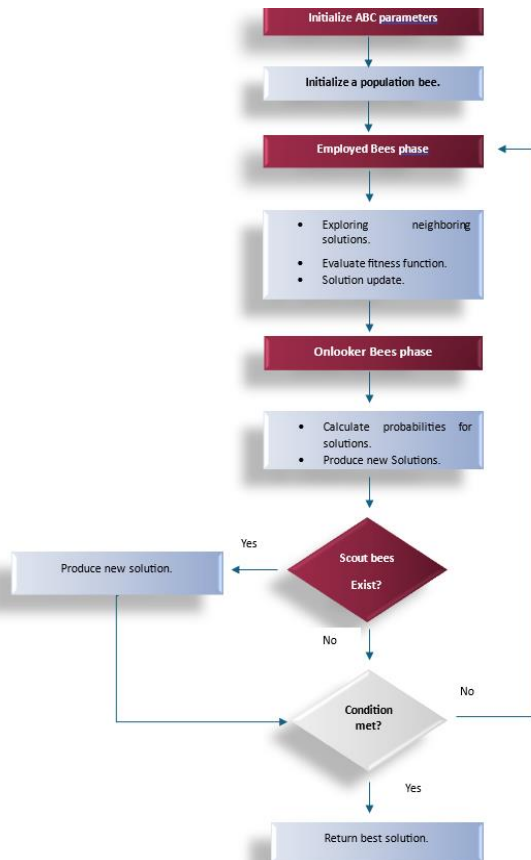


Fig. 2. Flowchart of artificial bee colony.

B. Genetic Artificial bee Colony Algorithm

In order to improve the exploration and exploitation capabilities of the ABC algorithm, a genetic algorithm is incorporated. This integration, specifically introduced into the employed phase of an Artificial Bee Colony (ABC), brings forth genetic operations like crossover and mutation. These genetic operations play a pivotal role in broadening the exploration of the solution space. The refined solutions produced by employed bees, through the application of genetic operations, contribute to a more thorough exploration, ultimately improving the overall performance of the algorithm. A comprehensive explanation of the hybridization process is presented below.

1) *Initialization of parameters:* In this initialization phase of the algorithm, critical parameters are defined to shape its behavior. The population size (PS) is determined, outlining the number of individuals constituting the population. Simultaneously, the number of food sources is established, each representing a potential solution within the optimization problem. The symmetry between employed and onlooker bees is emphasized, ensuring an equal distribution of roles in the algorithm. The maximum number of iterations is specified, delineating the extent of the algorithm's exploration and refinement cycles. A cycle limit is also set. Finally, the algorithm's initial population is initialized with bees, each carrying random solutions that signify quantities of waste transported between facilities. These defined parameters and the initial population collectively lay the foundation for subsequent algorithmic phases, guiding its systematic approach to solution exploration and optimization.

2) *Employed bee phase:* In the Artificial Bee Colony Algorithm, employed bees actively explore their surroundings in search of alternative food sources that offer higher nectar content than their current location.

- Exploring neighboring solutions: Employed bees explore neighboring solutions, conducting a systematic search for alternative options that reside in close proximity within the solution space.
- The fitness: To compute the fitness value for the current solution based on the objective function. The fitness is determined through the following Eq. (18):

$$fitness_i = \frac{1}{1+G_j} \quad (18)$$

Where $fitness_i$ is the fitness of the associated solution. G_j represents the objective function for the j th Solution.

- Solution Update: When the newly explored solution surpasses the previous one in terms of both job creation and economic development, the employed bee proceeds to update its solution.

3) *Genetic operators phase:* In this part the algorithm executes genetic operators, such as crossover and mutation, to introduce genetic variation and improve the solutions.

To choose a pair of parents from the solutions acquired through employed bees, it is essential to establish an encoding

scheme for this problem. As shown in Fig. 3 and Fig. 4, this model employs a hybrid encoding, integrating both binary and floating encodings to represent the chromosome. For example, considering five hospitals, two collecting centers, three plastic recyclers, two glass recyclers, and two steel recyclers, each chromosome can be represented by $(2+3+2+2+5*2+2*3+2*2+2*2+3*2+2*2+2*2)$ array. The initial $(2+3+2+2)$ genes denote whether the two collecting centers are open (1) or closed (0). The same logic applies to plastic recyclers, glass recyclers, and steel recyclers. Following this, the next set of genes $(5*2)$ represents the quantity of waste generated by the five hospitals and transported to the collecting centers. Subsequently, the sequences $(2*3)$, $(2*2)$, and $(2*2)$ signify the amounts of waste transported from collecting centers to plastic recyclers, glass recyclers, and steel recyclers, respectively. Finally, the last set of genes $(3*2)$, $(2*2)$, and $(2*2)$ represent the unrecovered waste transported from plastic recyclers, glass recyclers, and steel recyclers.

As illustrated in Fig. 3, the first row comprises two elements representing the collecting centers, followed by three elements for plastic recyclers, two for glass recyclers, and the last two elements for steel recyclers. Meanwhile, the second row defines an example of the binary encoding scheme.

In Fig. 4 an example of the floating encoding scheme is defined, the first table represents the Amount N_{ij} of waste

generated by the hospital i and shipped to the collecting center j . The subsequent table defines the quantity M_{ijk} of plastic waste k transported from the collecting center i to plastic recycler j . The following table represent defines the quantity P_{ijk} of glass waste k transported from the collecting center i to glass recycler j . The last table represents the quantity R_{ij} of steel waste transported from the collecting center i to steel recycler j .

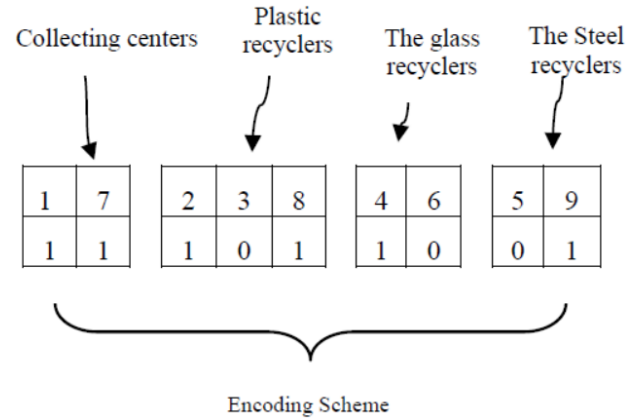


Fig. 3. Example of the binary representation.

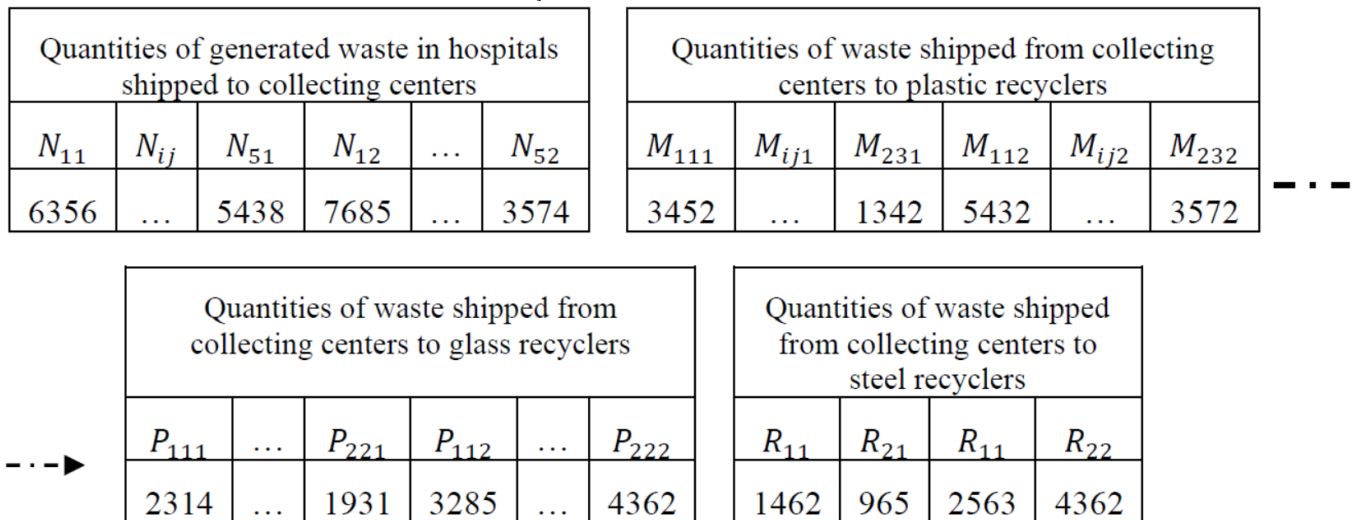


Fig. 4. Example of floating encoding scheme of solution.

- Select Parent food source

Before testing the performance of integrating the genetic algorithm into the ABC algorithm by applying genetic operators, we need to select two of the best parents obtained by the employed bees solutions using the Tournament selection. These parents contribute to the creation of offspring through crossover and mutation operations.

- The Crossover Operator

After selecting the two best solutions obtained from employed bees as parents, the crossover is applied. Crossover is a genetic operator that combines the genetic material of the

two selected parents to generate two new offspring. There are various types of mutation exist, such as bit-flip mutation, of cross over one-point crossover, multi-point crossover, and uniform crossover in this study we use one-point crossover. A one-point crossover point is randomly chosen along the length of the parent chromosomes, this procedure involves cutting a chromosome at a specific position and switching the ends between the two parents.

- The mutation Operator

After the crossover operation, we apply the mutation operator to the two new offspring obtained. The mutation operator is another genetic operator that involves introducing

small changes to one or more genes in chromosomes. Different random mutation, inversion mutation, displacement mutation, and swap mutation. In this paper, we apply the swap mutation, where two positions within the permutation are randomly chosen, and the elements at those positions are swapped. This operation helps to improve the exploration of new solutions.

- The new solution update

In this step, we substitute the worst solution acquired from the employed bees with the new offspring. The updated solutions with the information about the quality and location of their food sources are then communicated to the onlooker bees.

4) Onlooker bee phase

- The Probability

In this phase, onlookers utilize the information shared by the employed bees to determine whether the food source should be further explored in search of better solutions or if the food source should be sent to scout bees. The probability of selecting a specific food source for exploration is presented in Eq. (19), where the higher fitness has a higher probability to be chosen.

$$P_i = \left(\frac{fitness_i}{\sum fitness_i} \right) \quad (19)$$

The onlooker bees use the probability P_i to guide the employed bees toward the higher quality areas of solution space.

- Produce new solutions

Following the exploration of solution spaces, we assess the newfound fitness in comparison to the previous fitness. If the new solution provides better fitness, we substitute the previous solution; otherwise, we maintain the previous solution. This iterative process continues until the maximum number of iterations is achieved.

5) *Scout bee phase*: The bees that fail to demonstrate improvement in their associated food source transition into scout bees. This is because employed bees repeatedly exploring the same food source are no longer discovering useful information.

V. COMPUTATIONAL RESULTS

A. GABC Algorithm Parameters

To assess the effectiveness of the proposed GABC algorithm, we applied the Taguchi method [35]. This method is used to determine the optimal combination of GABC algorithm parameters by identifying the factors that influence the performance and effectiveness of GABC algorithm. In this paper, we considered three factors Table I: population size, iteration number, and limit cycle which represents the maximum number of times an employed bee can revisit the same food sources without improvement. Each factor was explored at three levels: 1 for low, 2 for medium, and 3 for high. The next step is to apply the Taguchi orthogonal array

(OA) to design a set of experiments covering all combinations of the selected factors. In the proposed model, Table II shows that each parameter is tested across three levels, with three experiments for each level, resulting in a total of 9 tests.

TABLE I. PRESENTATION OF DIFFERENT FACTORS AND LEVELS

| Levels | Population Size | Iterations | Limit cycles |
|--------|-----------------|------------|--------------|
| 1 | 60 | 100 | 15 |
| 2 | 120 | 200 | 20 |
| 3 | 180 | 300 | 25 |

The experiments presented in Table II, using the orthogonal array (OA), generate a series of combinations that aid in identifying the best combination providing the optimal performance for the proposed model among all the obtained combinations.

TABLE II. THE TAGUCHI ORTHOGONAL ARRAY

| Experiment | Levels | | |
|------------|-----------------|------------|--------------|
| | Population Size | Iterations | Limit cycles |
| 1 | 1 | 2 | 2 |
| 2 | 1 | 3 | 3 |
| 3 | 1 | 1 | 1 |
| 4 | 2 | 1 | 2 |
| 5 | 2 | 2 | 1 |
| 6 | 2 | 3 | 3 |
| 7 | 3 | 3 | 3 |
| 8 | 3 | 2 | 2 |
| 9 | 3 | 1 | 1 |

After using orthogonal arrays and conducting experiments at different factor levels, The Signal-to-Noise (S/N) is calculated for each experimental using Eq. (20).

$$S/N = 10 \log \left(\frac{(mean)^2}{(variance)^2} \right) \quad (20)$$

Where the mean or signal represents the average performance of the objective function, Variance measures the extent to which each individual number in a set deviate from the mean, or average, of those numbers. In the following section, we will present the best combination obtained by utilizing the orthogonal array (OA) and Signal-to-Noise (S/N) ratio.

B. Numerical Result

The provided problem was implemented in python and executed in an Intel (R) Core (TM) i5-6300U Processor 2.67GHz with 8 GB of RAM.

To proceed with the numerical testing and confirm the efficacy and validity of the proposed model, we are addressing both small and large problems. To account for the uncertainties in the proposed model, we take into consideration different scenarios for each size. As mentioned earlier, studies conducted in the field of medical waste are limited, and most countries prefer not to disclose the actual

situation of generated medical waste. This makes obtaining data somewhat challenging. As mentioned earlier, studies conducted in the field of medical waste are limited, and most countries prefer not to disclose the actual situation of generated medical waste. This makes obtaining data somewhat challenging. To address this challenge, we have reviewed various existing studies in the literature and non-government reports that address the problem of medical waste to collect data. Specifically, we are concentrating on these two studies [36], [37] to gain an idea of the average amount of waste generated by hospitals. In this paper, as illustrated in Table III, we address three types, and for each type, we focus on a specific product.

1) *Small problem*: For a small problem size, we examined a network comprising 10 nodes. These nodes include four hospitals, two collecting centers (with a requirement for one collecting center to be opened), two plastic, one glass recycler,

and one steel recycler, as shown in Table III. To tackle the uncertainties of the waste generated by the hospitals, we considered six scenarios, as illustrated in Table IV. The best combination for the different levels of the Taguchi method presented in the last section for the small size plus the genetic parameters are presented in Table V.

2) *Large problem*: In this part of the problem, we considered a network with 17 nodes, including 8 hospitals, 3 collecting centers (with one required to be opened), 3 plastic recyclers (with one plastic recycler required to be opened), 2 glass recyclers (one of which is required to be opened), and a steel recycler, as shown in Table VII. We considered six scenarios for the quantities of waste generated by hospitals in Table VIII. The Table IX presents the optimal combination for the proposed model using the Taguchi method.

TABLE III. TYPES OF MEDICAL WASTES

| Waste types | Characteristic |
|-------------|----------------------|
| Plastic | • Polyethylene (PET) |
| | • Polypropylene (PP) |
| Glass | • White glass |
| | • Brown glass |
| Steel | • Stainless Steel |

TABLE IV. THE VALUE OF THE PROPOSED MODEL

| Set | Value |
|--------------------|-------------------|
| Hospitals | 4 |
| Collection centers | 2 |
| Plastic recyclers | 2 |
| Glass recyclers | 1 |
| Steel recyclers | 1 |
| δ_k | 5% |
| δ_r | 7,5% |
| δ_v | 9% |
| β_k | 15% |
| β_r | 20% |
| β_v | 24% |
| $Mcap_n$ | Uniform (0,32000) |
| MPW_m | Uniform (0,20000) |
| MGW_m | Uniform (0,15000) |
| MSW_m | Uniform (0,15000) |

TABLE V. THE WASTE GENERATED IN EACH HOSPITAL

| | H1 | | | H2 | | | H3 | | | H4 | | |
|---|---------|-------|-------|---------|-------|-------|---------|-------|-------|---------|-------|-------|
| | Plastic | Glass | Steel | Plastic | Glass | Steel | Plastic | Glass | Steel | Plastic | Glass | Steel |
| 1 | 1754 | 382 | 133 | 2043 | 548 | 184 | 2554 | 845 | 285 | 3264 | 1253 | 876 |
| 2 | 1968 | 424 | 165 | 2300 | 722 | 210 | 2765 | 975 | 276 | 3678 | 1578 | 1045 |
| 3 | 2265 | 653 | 189 | 2310 | 863 | 263 | 3200 | 1056 | 332 | 4003 | 1893 | 1357 |
| 4 | 2536 | 750 | 223 | 2740 | 950 | 350 | 3505 | 1130 | 376 | 4284 | 2193 | 1543 |
| 5 | 2705 | 811 | 345 | 3098 | 1124 | 431 | 3920 | 1321 | 409 | 4763 | 2367 | 1713 |
| 6 | 3087 | 854 | 409 | 3176 | 1326 | 504 | 4205 | 1530 | 532 | 5123 | 2431 | 1923 |

TABLE VI. THE OPTIMAL TAGUCHI METHOD COMBINATION FOR SMALL PROBLEM

| | GABC | | | GA | |
|---------------|-----------------|----------------------|------------------------|----------------|---------------|
| | Population size | Number of iterations | Limit number of cycles | Crossover rate | Mutation rate |
| Small problem | 120 | 100 | 15 | 0.9 | 0.1 |

TABLE VII. THE VALUE OF THE PROPOSED MODEL

| Set | Value |
|----------------------|-------------------|
| Hospitals H | 8 |
| Collection centers C | 3 |
| Plastic Recyclers | 3 |
| Glass Recyclers | 2 |
| Steel Recyclers | 1 |
| δ_k | 5% |
| δ_r | 7,5% |
| δ_v | 9% |
| β_k | 15% |
| β_r | 20% |
| β_v | 24% |
| $Mcap_n$ | Uniform (0,32000) |
| MPW_m | Uniform (0,20000) |
| MGW_m | Uniform (0,15000) |
| MSW_m | Uniform (0,15000) |

TABLE VIII. THE WASTE GENERATED IN EACH HOSPITAL

| | H1 | | | H2 | | | H3 | | | H4 | | | H5 | | |
|----------|---------|-------|-------|---------|-------|-------|---------|-------|-------|---------|-------|-------|---------|-------|-------|
| | Plastic | Glass | Steel | Plastic | Glass | Steel | Plastic | Glass | Steel | Plastic | Glass | Steel | Plastic | Glass | Steel |
| 1 | 1754 | 382 | 133 | 2043 | 548 | 184 | 2554 | 845 | 285 | 3264 | 1253 | 876 | 1251 | 353 | 124 |
| 2 | 1968 | 424 | 165 | 2300 | 722 | 210 | 2765 | 975 | 376 | 3678 | 1578 | 1045 | 2967 | 401 | 213 |
| 3 | 2265 | 653 | 189 | 2710 | 863 | 263 | 3200 | 1056 | 400 | 4003 | 1893 | 1357 | 3088 | 687 | 357 |
| 4 | 2536 | 750 | 223 | 2940 | 950 | 350 | 3505 | 1130 | 576 | 4284 | 2139 | 1543 | 3591 | 825 | 539 |
| 5 | 2705 | 811 | 345 | 3298 | 1124 | 431 | 4920 | 1321 | 680 | 5763 | 2767 | 1713 | 3980 | 1054 | 761 |
| 6 | 3087 | 950 | 409 | 3376 | 1326 | 504 | 5605 | 2530 | 960 | 6123 | 3071 | 1923 | 4126 | 1329 | 933 |

| | H6 | | | H7 | | | H8 | | |
|--------------|---------|-------|-------|---------|-------|-------|---------|-------|-------|
| | Plastic | Glass | Steel | Plastic | Glass | Steel | Plastic | Glass | Steel |
| 8634 | 2557 | 809 | 2224 | 733 | 458 | 5604 | 1339 | 576 | |
| 9687 | 2971 | 1480 | 2518 | 1270 | 598 | 6078 | 1874 | 643 | |
| 10964 | 3893 | 1661 | 5623 | 1690 | 787 | 7003 | 2465 | 787 | |
| 14583 | 4191 | 1855 | 6734 | 1998 | 961 | 8284 | 3475 | 833 | |
| 17654 | 6367 | 2013 | 7698 | 3246 | 1123 | 9763 | 4361 | 913 | |
| 19872 | 7031 | 2319 | 8763 | 3434 | 1456 | 10123 | 4783 | 1076 | |

TABLE IX. THE OPTIMAL TAGUCHI METHOD COMBINATION FOR LARGE PROBLEM

| | GABC | | | GA | |
|----------------------|-----------------|----------------------|------------------------|----------------|---------------|
| | Population size | Number of iterations | Limit number of cycles | Crossover rate | Mutation rate |
| Large problem | 120 | 200 | 20 | 0.9 | 0.1 |

C. Results

In this section, we compare the results obtained by the proposed GABC algorithm and the Artificial Bee Colony algorithm using optimal parameters derived through the application of the Taguchi method. Table VI shows optimal Taguchi method. The primary objective is to maximize positive social indicators in the proposed model, emphasizing the creation of job opportunities while maintaining a balance in economic development. We employed a weighted sum formulation approach, assigning equal weights (0.5, 0.5) to two objective functions, signifying an equal contribution of both objectives to the overall objective function.

For the unemployment rate and region development rate, we explore three different values for both small and large problems, as outlined in Table X and Table XI. Additionally, the assumption is made that all facilities are located within the same region. The economic value is centered on two aspects: cost savings achieved through the recycling of medical waste

and revenue generated by purchasing recovered waste for use in creating new products.

1) Results for small problem: To calculate our second objective function, as shown in Table X, it is imperative to quantify the regional development rate. The term 'regional development' includes economic it is imperative to quantify the regional development rate. The term 'regional development' includes economic, environmental, it is imperative to quantify the regional development rate. The term 'regional development' includes economic, environmental, and social progress within a specific region.

The primary goal of regional development is to enhance the overall well-being of the population in that region by addressing economic disparities, improving infrastructure, and promoting address multidimensional poverty rates, where we will examine three different rates of multidimensional poverty.

TABLE X. THE RESULTS FOR SMALL PROBLEM

| Unemployment rate | Multidimensional poverty rate | Scenario | GABC | | | ABC | | |
|-------------------|-------------------------------|----------|----------------------------|---------------------------|----------|----------------------------|---------------------------|----------|
| | | | Job creation opportunities | Economic development (\$) | CPU Time | Job creation opportunities | Economic development (\$) | CPU Time |
| 5.4% | 3.1% | 1 | 122.53 | 8532.84 | 24.56 | 111.68 | 7890.85 | 2.32 |
| | | 2 | 134.31 | 9797.51 | 37.45 | 127.25 | 9323.96 | 4.16 |
| | | 3 | 148.75 | 11454.27 | 49.03 | 148.43 | 11384.48 | 5.59 |
| | | 4 | 169.37 | 14861.46 | 65.76 | 160.4 | 13769.98 | 8.48 |
| | | 5 | 195.75 | 16903.55 | 88.92 | 192.5 | 16879.39 | 9.52 |
| | | 6 | 212.83 | 19601.61 | 95.30 | 204.75 | 19273.93 | 11.27 |
| 10.3% | 11.9% | 1 | 207.32 | 7187.83 | 25.67 | 201.89 | 7098.67 | 3.52 |
| | | 2 | 226.91 | 8608.76 | 36.73 | 214.25 | 8477.20 | 4.33 |
| | | 3 | 257.18 | 9954.29 | 51.98 | 250.9 | 9863.08 | 5.12 |
| | | 4 | 282.34 | 12265.83 | 66.23 | 274.3 | 11007.61 | 8.61 |
| | | 5 | 338.28 | 14667.73 | 89.45 | 334.41 | 14873.90 | 10.39 |
| | | 6 | 383.78 | 17165.15 | 97.43 | 375.62 | 17983.01 | 12.52 |
| 16.1% | 24.3% | 1 | 301.04 | 6057.44 | 25.55 | 292.86 | 6164.47 | 3.83 |
| | | 2 | 336.25 | 7220.63 | 37.92 | 329.34 | 7284.04 | 5.08 |
| | | 3 | 384.05 | 8765.48 | 54.76 | 375.1 | 8619.85 | 7.81 |
| | | 4 | 419.39 | 10876.75 | 68.15 | 408.98 | 10237.03 | 9.69 |
| | | 5 | 517.43 | 12870.16 | 90.95 | 500.36 | 12634.83 | 12.72 |
| | | 6 | 584.00 | 14936.95 | 96.45 | 572.3 | 14763.11 | 13.65 |

TABLE XI. THE RESULTS FOR LARGE PROBLEM

| Unemployment rate | Multidimensional poverty rate | Scenarios | GABC | | | ABC | | |
|-------------------|-------------------------------|-----------|----------------------------|---------------------------|----------|---------------------------------|----------------------|----------|
| | | | Job creation opportunities | Economic development (\$) | CPU Time | Job creation opportunities (\$) | Economic development | CPU Time |
| 5.4% | 3.1% | 1 | 435.96 | 18457.21 | 78.71 | 421.65 | 18340.74 | 3.42 |
| | | 2 | 541.12 | 25551.47 | 96.32 | 503.91 | 25490.52 | 5.03 |
| | | 3 | 625.87 | 29904.01 | 115.76 | 603.09 | 29865.07 | 6.34 |
| | | 4 | 712.53 | 32435.81 | 131.04 | 699.1 | 32327.38 | 8.69 |
| | | 5 | 784.01 | 36925.71 | 135.76 | 765.01 | 36897.89 | 10.98 |
| | | 6 | 931.98 | 40112.49 | 158.22 | 923.81 | 40007.16 | 12.08 |
| 10.3% | 11.9% | 1 | 759.40 | 16982.07 | 78.88 | 735.79 | 16675.12 | 4.93 |
| | | 2 | 931.43 | 21238.64 | 96.70 | 908.37 | 21084.77 | 5.17 |
| | | 3 | 1100.24 | 24954.28 | 117.90 | 1096.06 | 24642.24 | 6.87 |
| | | 4 | 1299.83 | 28003.91 | 136.77 | 1278.03 | 27890.73 | 9.02 |
| | | 5 | 1438.19 | 31132.54 | 137.16 | 1405.75 | 30393.36 | 11.43 |
| | | 6 | 1727.26 | 34532.17 | 167.49 | 1711.39 | 34198.10 | 12.91 |
| 16.1% | 24.3% | 1 | 1151.28 | 14548.62 | 79.78 | 1106.31 | 14328.15 | 5.34 |
| | | 2 | 1412.34 | 19008.06 | 95.92 | 1380.4 | 18671.86 | 6.64 |
| | | 3 | 1693.59 | 23067.30 | 117.84 | 1670.63 | 22893.58 | 7.09 |
| | | 4 | 2007.11 | 25876.49 | 136.01 | 1985.72 | 25816.92 | 9.63 |
| | | 5 | 2196.61 | 27958.38 | 137.53 | 2163.91 | 27893.38 | 11.92 |
| | | 6 | 2658.02 | 31976.23 | 168.81 | 2631.69 | 31896.81 | 13.28 |

The results from Table X and Table XI indicate that the solutions obtained by the proposed GABC algorithm are better than the solutions obtained by the original ABC algorithm for the two objective functions. Additionally, the time required to execute the GABC code is longer than that of the ABC, attributed to the hybrid nature of the GABC algorithm, which combines two algorithms. The increased computational time is expected due to this hybridization.

Regarding job creation opportunities, is illustrated in Fig. 5, the value increases as the unemployment rate rises.

In Fig. 6, depicting economic development, we observe the opposite trend: the economic value decreases as the multidimensional poverty rate increases.

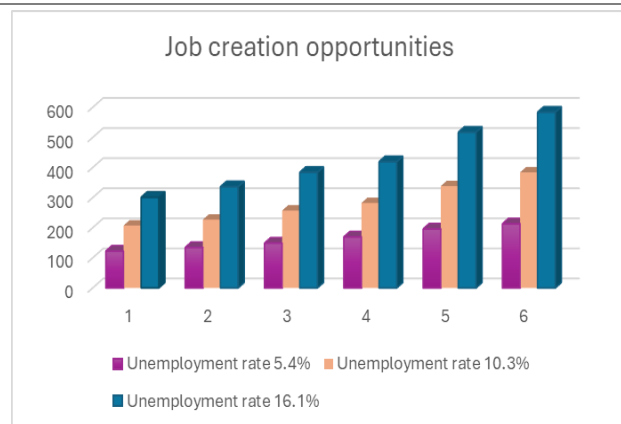


Fig. 5. Small problem comparison for different multidimensional poverty rates.

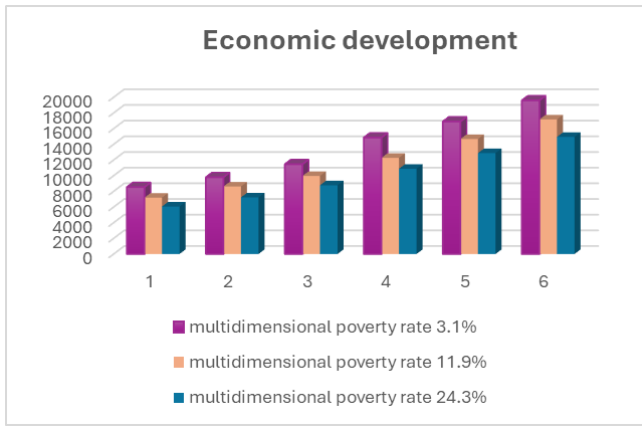


Fig. 6. Small problem comparison for different unemployment rates.

1) *Results for large problem:* Same as the small problem, for the large problem, the proposed GABC algorithm exhibits better results than those obtained by the ABC algorithm. In the job creation opportunities function for the large problem, there is an increase in regions with rising unemployment rates Fig. 7. This highlights the need for establishing more facilities in regions with high unemployment rates to address the issue. For the balanced economic development function Fig. 8, we observe that the region with higher multidimensional poverty experiences a decrease in economic development.

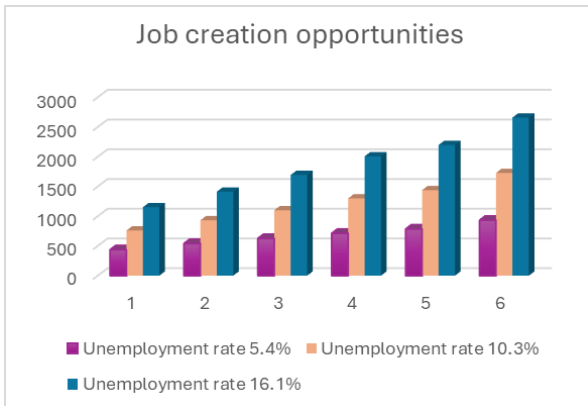


Fig. 7. Large problem comparison for different unemployment rates.

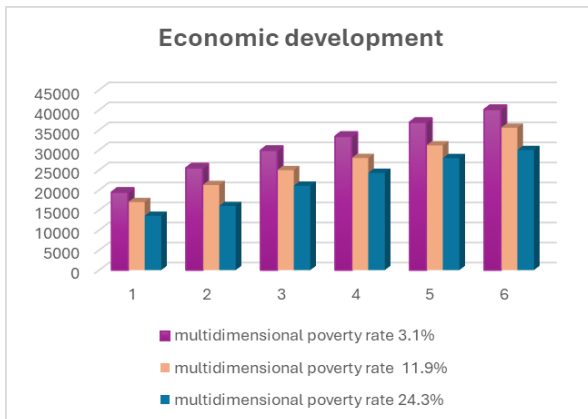


Fig. 8. Large problem comparison for different multidimensional poverty rates.

D. Discussion

In this paper, our objective is to maximize positive social indicators by focusing on job creation and balancing economic value. The results indicate that through the recycling of medical waste, we can generate more job opportunities and promote balanced economic development, thereby reducing social disparities and enhancing overall well-being.

Our research into the literature indicates a scarcity of studies focusing on the social impact of recycling end-of-life products. Specifically, few studies delve into issues such as job creation indicator or the number of days lost due to occupational accidents resulting from the construction of waste processing centers [25], [30], [38]. In light of this gap, our study aims to address the issue of multidimensional poverty, considering it as one of the positive indicators being investigated. Our examination of the existing literature highlights that this study marks the inception of discourse on this topic. The numerical results demonstrate that adopting sustainable practices to preserve natural resources and reuse them, using recycling principles, helps to create more job opportunities. This means decreasing the unemployment rate and multidimensional poverty, ultimately improving the quality of life for people.

VI. CONCLUSION

In this paper, we illuminate the often overlooked third dimension of sustainability in research, highlighting the significance of maximizing positive social indicators. Our hybrid approach, employing the Artificial Bee Colony (ABC) algorithm and Genetic Algorithm (GA) to tackle two objective functions: enhancing job creation opportunities and promoting balanced economic development. The paper focuses on the reverse supply chain for recycling medical waste, encompassing various stakeholders such as hospitals, collection centers, plastic recyclers, glass recyclers, and steel recyclers. To assess the performance and effectiveness of the proposed GABC algorithm, we conducted a comparative analysis with the ABC algorithm. We subjected the proposed approach to testing in diverse scenarios to simulate real-life situations.

The comparison between the proposed GABC and the original ABC indicates that the suggested approach consistently outperforms in various scenarios studied, providing superior solutions for both job creation opportunities and economic development. This success can be attributed to the nature of the proposed approach, which integrates two algorithms: ABC and GA.

REFERENCES

- [1] K. Devika, A. Jafarian, and V. Nourbakhsh, "Designing a sustainable closed-loop supply chain network based on triple bottom line approach: A comparison of metaheuristics hybridization techniques," *Eur J Oper Res*, vol. 235, no. 3, pp. 594–615, Jun. 2014, doi: 10.1016/j.ejor.2013.12.032.
- [2] WHO, "Tonnes of COVID-19 health care waste expose urgent need to improve waste management systems," <https://www.who.int/news/item/01-02-2022-tonnes-of-covid-19-health-care-waste-expose-urgent-need-to-improve-waste-management-systems>.
- [3] M. Pourmehdi, M. M. Paydar, and E. Asadi-Gangraj, "Scenario-based design of a steel sustainable closed-loop supply chain network

- considering production technology,” *J Clean Prod*, vol. 277, p. 123298, Dec. 2020, doi: 10.1016/j.jclepro.2020.123298.
- [4] M. Hajghasem and A. A. shojaie, “Optimal Routing in Supply Chain Aimed at Minimizing Vehicle Cost and Supply,” *Procedia Economics and Finance*, vol. 36, pp. 353–362, 2016, doi: 10.1016/S2212-5671(16)30047-8.
- [5] L. Li, F. Dababneh, and J. Zhao, “Cost-effective supply chain for electric vehicle battery remanufacturing,” *Appl Energy*, vol. 226, pp. 277–286, Sep. 2018, doi: 10.1016/j.apenergy.2018.05.115.
- [6] L. A. Moncayo-Martínez and D. Z. Zhang, “Multi-objective ant colony optimisation: A meta-heuristic approach to supply chain design,” *Int J Prod Econ*, vol. 131, no. 1, pp. 407–420, May 2011, doi: 10.1016/j.ijpe.2010.11.026.
- [7] A. I. Pettersson and A. Segerstedt, “Measuring supply chain cost,” *Int J Prod Econ*, vol. 143, no. 2, pp. 357–363, Jun. 2013, doi: 10.1016/j.ijpe.2012.03.012.
- [8] L. Whicker, M. Bernon, S. Templar, and C. Mena, “Understanding the relationships between time and cost to improve supply chain performance,” *Int J Prod Econ*, vol. 121, no. 2, pp. 641–650, Oct. 2009, doi: 10.1016/j.ijpe.2006.06.022.
- [9] F. Du and G. W. Evans, “A bi-objective reverse logistics network analysis for post-sale service,” *Comput Oper Res*, vol. 35, no. 8, pp. 2617–2634, Aug. 2008, doi: 10.1016/j.cor.2006.12.020.
- [10] B. Vahdani, R. Tavakkoli-Moghaddam, M. Modarres, and A. Baboli, “Reliable design of a forward/reverse logistics network under uncertainty: A robust-M/M/c queuing model,” *Transp Res E Logist Transp Rev*, vol. 48, no. 6, pp. 1152–1168, Nov. 2012, doi: 10.1016/j.tre.2012.06.002.
- [11] S. H. Amin and G. Zhang, “A multi-objective facility location model for closed-loop supply chain network under uncertain demand and return,” *Appl Math Model*, vol. 37, no. 6, pp. 4165–4176, Mar. 2013, doi: 10.1016/j.apm.2012.09.039.
- [12] H. Soleimani and G. Kannan, “A hybrid particle swarm optimization and genetic algorithm for closed-loop supply chain network design in large-scale networks,” *Appl Math Model*, vol. 39, no. 14, pp. 3990–4012, Jul. 2015, doi: 10.1016/j.apm.2014.12.016.
- [13] Y. Y. Cui, Z. Guan, U. Saif, L. Zhang, F. Zhang, and J. Mirza, “Close loop supply chain network problem with uncertainty in demand and returned products: Genetic artificial bee colony algorithm approach,” *J Clean Prod*, vol. 162, pp. 717–742, Sep. 2017, doi: 10.1016/j.jclepro.2017.06.079.
- [14] J. Hong, A. Diabat, V. V. Panicker, and S. Rajagopalan, “A two-stage supply chain problem with fixed costs: An ant colony optimization approach,” *Int J Prod Econ*, vol. 204, pp. 214–226, Oct. 2018, doi: 10.1016/j.ijpe.2018.07.019.
- [15] J. Yang et al., “Cost performance optimization of waste heat recovery supply chain by mobile heat storage vehicles,” *Energy Reports*, vol. 6, pp. 137–146, Dec. 2020, doi: 10.1016/j.egy.2020.05.009.
- [16] S. Liu, L. G. Papageorgiou, and N. Shah, “Optimal design of low-cost supply chain networks on the benefits of new product formulations,” *Comput Ind Eng*, vol. 139, p. 106189, Jan. 2020, doi: 10.1016/j.cie.2019.106189.
- [17] R. Accorsi, A. Cascini, S. Cholette, R. Manzini, and C. Mora, “Economic and environmental assessment of reusable plastic containers: A food catering supply chain case study,” *Int J Prod Econ*, vol. 152, pp. 88–101, Jun. 2014, doi: 10.1016/j.ijpe.2013.12.014.
- [18] M. Zohal and H. Soleimani, “Developing an ant colony approach for green closed-loop supply chain network design: a case study in gold industry,” *J Clean Prod*, vol. 133, pp. 314–337, Oct. 2016, doi: 10.1016/j.jclepro.2016.05.091.
- [19] Z. Mohtashami, A. Aghsami, and F. Jolai, “A green closed loop supply chain design using queuing system for reducing environmental impact and energy consumption,” *J Clean Prod*, vol. 242, p. 118452, Jan. 2020, doi: 10.1016/j.jclepro.2019.118452.
- [20] L. Visser, R. Hoefnagels, and M. Junginger, “Wood pellet supply chain costs – A review and cost optimization analysis,” *Renewable and Sustainable Energy Reviews*, vol. 118, p. 109506, Feb. 2020, doi: 10.1016/j.rser.2019.109506.
- [21] M. Forkan, M. M. Rizvi, and M. A. M. Chowdhury, “Multiobjective reverse logistics model for inventory management with environmental impacts: An application in industry,” *Intelligent Systems with Applications*, vol. 14, p. 200078, May 2022, doi: 10.1016/j.iswa.2022.200078.
- [22] S. NAHMIASJ and H. RIVERA, “A deterministic model for a repairable item inventory system with a finite repair rate†,” *Int J Prod Res*, vol. 17, no. 3, pp. 215–221, May 1979, doi: 10.1080/00207547908919609.
- [23] Y. Liu et al., “Supply chain plastic footprint analysis,” *Circular Economy*, vol. 2, no. 2, p. 100037, Jun. 2023, doi: 10.1016/j.cec.2023.100037.
- [24] United Nations Brundtland Commission, “Report of the World Commission on Environment and Development: Our Common Future,” 1987.
- [25] T. R. P. Ramos, M. I. Gomes, and A. P. Barbosa-Póvoa, “Planning a sustainable reverse logistics system: Balancing costs with environmental and social concerns,” *Omega (Westport)*, vol. 48, pp. 60–74, Oct. 2014, doi: 10.1016/j.omega.2013.11.006.
- [26] M. S. Pishvaei, J. Razmi, and S. A. Torabi, “An accelerated Benders decomposition algorithm for sustainable supply chain network design under uncertainty: A case study of medical needle and syringe supply chain,” *Transp Res E Logist Transp Rev*, vol. 67, pp. 14–38, Jul. 2014, doi: 10.1016/J.TRE.2014.04.001.
- [27] M. Zhalechian, R. Tavakkoli-Moghaddam, B. Zahiri, and M. Mohammadi, “Sustainable design of a closed-loop location-routing-inventory supply chain network under mixed uncertainty,” *Transp Res E Logist Transp Rev*, vol. 89, pp. 182–214, May 2016, doi: 10.1016/j.tre.2016.02.011.
- [28] N. Sahebjamnia, A. M. Fathollahi-Fard, and M. Hajiaghahi-Keshтели, “Sustainable tire closed-loop supply chain network design: Hybrid metaheuristic algorithms for large-scale networks,” *J Clean Prod*, vol. 196, pp. 273–296, 2018, doi: 10.1016/j.jclepro.2018.05.245.
- [29] M. Pourmehdi, M. M. Paydar, and E. Asadi-Gangraj, “Scenario-based design of a steel sustainable closed-loop supply chain network considering production technology,” *J Clean Prod*, vol. 277, p. 123298, Dec. 2020, doi: 10.1016/j.jclepro.2020.123298.
- [30] O. Battaia, R. Guillaume, Z. Krug, and R. Oloruntoba, “Environmental and social equity in network design of sustainable closed-loop supply chains,” *Int J Prod Econ*, vol. 264, p. 108981, Oct. 2023, doi: 10.1016/j.ijpe.2023.108981.
- [31] E. Sara and D. Btissam, “Optimization of green reverse logistics network Integrating artificial bee colony Algorithm and multi-agent system: case of medical waste,” in 2020 5th International Conference on Logistics Operations Management (GOL), IEEE, Oct. 2020, pp. 1–8. doi: 10.1109/GOL49479.2020.9314763.
- [32] International Labour Office, “Decent Work Indicators : Guidelines For Producers And Users Of Statistical And Legal Framework Indicators: Ilo Manual: Second Version,” Geneva, 2013.
- [33] European Commission, “Impacts of circular economy policies on the labour market: final reports,” Brussels, 2018.
- [34] D. Karaboga and B. Basturk, “A powerful and efficient algorithm for numerical function optimization: artificial bee colony (ABC) algorithm,” *Journal of Global Optimization*, vol. 39, no. 3, pp. 459–471, Oct. 2007, doi: 10.1007/s10898-007-9149-x.
- [35] Genichi Taguchi, *Introduction to Quality Engineering: Designing Quality Into Products and Processes*, vol. 191. Asian Productivity Organization, 1986 - 191 pages, 1986.
- [36] S.M. RAOUI, Y. BOUGATOUCHE, F. ERRACHIDI, and N. CHADLI, “The quantitative Importance of DASRI In the regional hospital of Tétouan city, Morocco,” *Annales des sciences de la santé*, 2018.
- [37] GS Associates Private Limited, “Rapid Assessment On Health Care Waste Management In Sri Lanka,” 2021. Accessed: Dec. 23, 2023. [Online]. Available: https://www.undp.org/sites/g/files/zskgke326/files/migration/lk/UNDPLKA_Rapid-Assessment-on-Health-CareWM.pdf
- [38] D. Morea, S. Fortunati, and L. Martiniello, “Circular economy and corporate social responsibility: Towards an integrated strategic approach in the multinational cosmetics industry,” *J Clean Prod*, vol. 315, p. 128232, Sep. 2021, doi: 10.1016/j.jclepro.2021.128232.

Multimodal Feature Fusion Video Description Model Integrating Attention Mechanisms and Contrastive Learning

Wang Zhihao*, Che Zhanbin

School of Computer Science, Zhongyuan University of Technology, Zhengzhou, China

Abstract—To avoid the issue of significant redundancy in the spatiotemporal features extracted from multimodal video description methods and the substantial semantic gaps between different modalities within video data. Building upon the TimeSformer model, this paper proposes a two-stage video description approach (Multimodal Feature Fusion Video Description Model Integrating Attention Mechanism and Contrastive Learning, MFFCL). The TimeSformer encoder extracts spatiotemporal attention features from the input video and performs feature selection. Contrastive learning is employed to establish semantic associations between the spatiotemporal attention features and textual descriptions. Finally, GPT2 is employed to generate descriptive text. Experimental validations on the MAVD, MSR-VTT, and VATEX datasets were conducted against several typical benchmark methods, including Swin-BERT and GIT. The results indicate that the proposed method achieves outstanding performance on metrics such as Bleu-4, METEOR, ROUGE-L, and CIDEr. The spatiotemporal attention features extracted by the model can fully express the video content and that the language model can generate complete video description text.

Keywords—Multimodal feature fusion; video description; spatiotemporal attention; comparative learning

I. INTRODUCTION

Video description is a field of deep learning with practical value, and it has application value in areas such as assisting visually impaired individuals in accessing video content and video content analysis. When dealing with video content from real life, video description models require complex preprocessing steps, such as frame extraction and normalization operations, followed by feature extraction, and finally, the transformation of these features into linguistic descriptions. In this process, the model must not only delve into the semantic content of the video but also establish precise correspondences between visual and textual information to generate accurate descriptions [1]. However, due to the excessive redundancy in video data and the vast semantic gap between modalities, it is challenging for models to establish a unified representation of these modalities and to capture key information accurately for detailed descriptions.

To address the aforementioned issues, this paper proposes a two-stage multimodal feature fusion method. In the first stage, the TimeSformer encoder [2] is employed to extract spatiotemporal features from the input video. The TimeSformer is a transformer-based model for video action

recognition that effectively captures spatiotemporal features within videos. The model generates video vectors rich in semantic features by dividing video frames into non-overlapping blocks and applying attention mechanisms in both temporal and spatial dimensions. After spatiotemporal feature extraction, these vectors undergo feature selection and are used as visual cues input into the GPT-2 model to generate video descriptions. This paper employs a contrastive learning approach in the second stage to align video embeddings with text embeddings in the latent space. Video-text contrastive learning is an effective training method that minimizes the semantic differences between different modalities by pulling closer the representations of the same entity across modalities and pushing apart the representations of different entities. This method enhances the similarity between the features output by TimeSformer and the corresponding textual descriptions. Experimental evidence suggests that the scheme incorporating contrastive learning is easier to train than the one that fine-tunes TimeSformer directly with video descriptions without contrastive learning. This ease of training may be attributed to the reduced involvement of generative methods, which typically require more extensive training time when contrastive learning is not employed.

This paper conducts comparative experiments to validate the effectiveness of the proposed model, and the results indicate that the proposed model achieves state-of-the-art results on the MSVD, MSR-VTT, and VATEX datasets. Compared to existing models, the text generated by this model is capable of providing a comprehensive description of video content and is straightforward to train. The contributions of this paper are as follows:

- 1) This paper proposes a two-stage multimodal feature fusion method that combines spatiotemporal attention with contrastive learning, efficiently integrating and utilizing temporal, visual, and textual features.
- 2) Within the training process, this paper conducts feature selection on spatiotemporal features to prevent redundant information from entering the language model, which could otherwise interfere with text generation.
- 3) Experimental evidence demonstrates that our method can effectively comprehend and describe the rich multimodal information within videos, achieving advanced results compared to similar models in the field.

This research was funded by Key Technology Research and Demonstration Application of News Intelligent Production (212102210417), Science and Technology Plan of Henan Province in 2021.

II. RELATED WORK

When processing videos, video descriptions require the extraction of temporal information, image information, and other modal information from the video. These data are then multimodal fused to build a joint representation between modalities. The resulting representation serves as visual cues input into a text model to generate textual descriptions. This section discusses related work from spatiotemporal feature extraction and multimodal feature fusion perspectives.

A. Spatiotemporal Feature Extraction

In video description tasks, models must be capable of extracting temporal and spatial features from the video content. For temporal feature extraction, common methods include 3D Convolutional Neural Networks (CNN) and optical flow-based networks. As for spatial features that pertain to image characteristics, one can utilize popular pre-trained image feature extraction networks such as ResNet [3] and Vision Transformer [4].

DC-RL [5] employs a 3D CNN to model temporal features and concatenates these features with image features obtained from a pre-trained image encoder using an LSTM. However, this approach may yield little improvements over previous methods. This is because of the inherent locality of 3D neural networks, which limits their ability to learn long-term temporal dependencies. Moreover, LSTM are prone to vanishing or exploding gradients when dealing with long sequences of input temporal information, making them difficult to train effectively.

MA-Net [6] employs the Inflated 3D (I3D) [7] network to model temporal relationships and constructs semantic feature vectors from the textual descriptions of the video. These semantic feature vectors are then used alongside the video feature vectors for semantic detection, aiming to bridge the gap between the semantic video features and the actual semantic content of the video. I3D expands pre-trained 2D CNN into 3D CNN by "inflating" their 2D filters into 3D filters, allowing the network to capture spatiotemporal information in video data. Experimental results have shown improvements compared to DC-RL. However, it does not overcome the drawbacks of CNN, which fails to model long-range temporal information, and the extracted video features cannot fully represent the content of the video.

This paper addresses the issues above by employing TimeSformer. TimeSformer divides the video into non-overlapping spatial and temporal patches. It then applies attention mechanisms between patches that belong to the same spatial location but different time points and between patches from different spatial locations but the same time point. This approach enables efficient extraction of temporal and spatial features across the entire video, making it highly suitable for video description models.

B. Multimodal Feature Fusion

Videos are composed of multimodal data, including visual, audio, and textual components, each containing a vast amount of information accompanied by noise and uncertainty. To accurately describe the content of videos, it is necessary to employ multimodal feature fusion techniques to achieve

complementarity and verification between different modalities. This approach facilitates a comprehensive understanding and analysis of video content, enhancing the accuracy and reliability of information processing. When performing multimodal feature fusion, common strategies include the following: (1) Data Fusion: This strategy involves combining information from multiple modalities through operations such as concatenation, addition, and multiplication and then passing the integrated data to subsequent processes. The advantages of this approach are its simplicity and the absence of the need for additional training methods. However, it may also lead to information redundancy or the inability to leverage complex modality information. (2) Neural Network Fusion: This strategy involves using neural network methods to jointly encode multimodal information based on data fusion or directly accepting multimodal inputs. For instance, the cross-attention mechanism in Transformer[8] utilizes self-attention to relate and fuse information from different modalities. The Feature Pyramid Network (FPN)[9] achieves fusion by constructing feature maps at different scales, which allows for information integration at various levels, thereby enhancing the performance of object detection tasks.

Fu et al. [10] have utilized the attention mechanism to query the relationship between object detection and action features, establishing a subject-verb relationship from a grammatical perspective and generating text accordingly. The primary benefit of this approach lies in the generation of coherent textual output. However, this grammar-based method has limitations in terms of text generation diversity. Since it focuses on establishing accurate grammatical structures, the generated text often follows similar sentence templates, which can lead to stiff and repetitive expressions in language. Moreover, in Fu's work, action features extracted by 3D neural networks fail to capture long-distance temporal information, which can lead to the model that is incapable of fully describing the semantics of the video.

The work by Ren et al. [11] is similar to the present study, as it also employs an attention mechanism to integrate spatiotemporal features. Additionally, they designed a semantic enhancement network to learn the latent semantic information of object features. However, in fusing visual-textual features, they utilized Long Short-Term Memory networks (LSTM). LSTM is a type of recurrent neural network (RNN) that is capable of handling sequence data and can remember long-term dependencies. In their work, LSTM networks were employed to process textual information, obviating the need to add position vectors within the attention mechanism. Position vectors are commonly used in attention mechanisms to ensure the model can understand the order of elements in the input sequence. Although LSTM networks have certain advantages in processing sequence data, it also have limitations, particularly when dealing with long-distance dependencies. LSTM networks may encounter issues with vanishing or exploding gradients, limiting its effectiveness in modeling long-distance dependencies between elements in long sequences.

To address the aforementioned issues, this paper employs a Visual-Text Contrastive (VTC) learning method to align the spatiotemporal features output by TimeSformer with textual

features. By analyzing the similarities and differences between data samples, VTC can discern the relationships and discrepancies between spatiotemporal and textual features, ensuring that semantically similar spatiotemporal features remain close to their corresponding textual features in the latent space. This facilitates the ability of feature mapping module to map spatiotemporal features to textual latent spaces and makes it possible to generate textual descriptions via GPT2[12]. This approach allows the model to learn a complete representation of spatiotemporal features and generates accurate textual descriptions.

III. METHODOLOGY

When processing videos, TimeSformer first applies an attention mechanism in both temporal and spatial dimensions to extract spatiotemporal features of videos. Subsequently, this paper utilizes a fully connected network to map the spatiotemporal features into a feature sequence, adapting them for input into the Transformer Encoder, the mapping network. In preparation for the input to the Transformer Encoder, a learnable vector of length τ was concatenated to the video feature sequence to screen the sequence and prevent the inclusion of redundant information. The learnable vector, which can be referred to as a visual prompt, is then input into the language model for decoding, yielding a textual description of the video. During the training process, the semantic gap between video and text features poses a significant challenge. To address this issue, the paper introduces a Video-Text Contrastive Learning module, which aligns video and text features in the semantic space. Fig. 1 depicts the structure of the entire model.

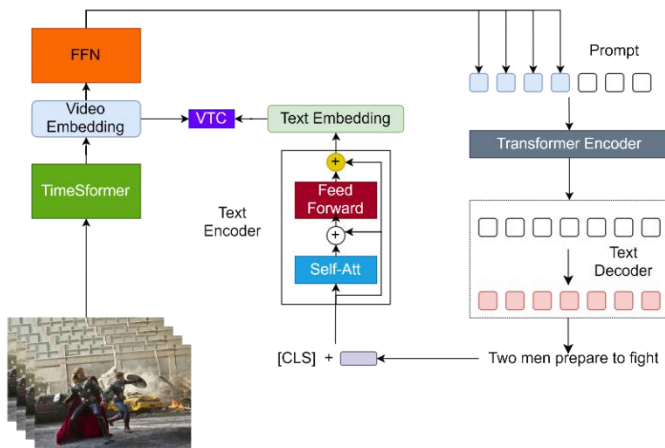


Fig. 1. Overall structure diagram.

A. Spatiotemporal Attention-based Feature Fusion

To fully comprehend video content, it is necessary to integrate both spatial and temporal information. In traditional 3D CNN, convolution operations are performed simultaneously across both temporal and spatial dimensions, allowing the model to capture spatiotemporal features within the video. However, 3D convolution operations are computationally intensive, leading to slower training and inference speeds for the model. To overcome this limitation, TimeSformer organizes the temporal and spatial dimensions into multiple video patches and performs attentional

interactions on them separately, incorporating attention mechanisms into video understanding tasks. This approach has achieved outstanding results in the field of action recognition.

This paper employs TimeSformer to extract spatiotemporal features from videos. After preprocessing, a video is mapped into multiple non-overlapping patches through a linear layer, which is then input into the spatiotemporal feature extraction network, as illustrated in Fig. 2.

The output can be represented as $\{v_1, v_2, \dots, v_\phi\}$, where $v_i \in R^{H_{video}}$ and ϕ denote the number of video patches. During the training of TimeSformer, the learnable vector CLS^{video} at the head of the video patch sequence is randomly initialized and incorporates the embedding representation of the entire video throughout the training process. In subsequent modules, the paper primarily uses CLS^{video} as the video feature for computation.

B. Visual Prompt Based on Contrastive Learning and Feature Selection

In the training process, the input video is first mapped using a linear layer to extract the embedded representation of the video. These representations capture the temporal and visual features between video frames. Subsequently, these video embeddings are concatenated with a learnable query vector of length τ and jointly input into a Transformer Encoder. The role of the query vector is to select the relevant features of the video that need to be described and filter out irrelevant information. Next, the query vector is used as a prompt and input into the GPT2 model.

Since the prompt already contains the necessary semantic information, the language model can generate readable text based on this prompt vector. This approach has been applied in

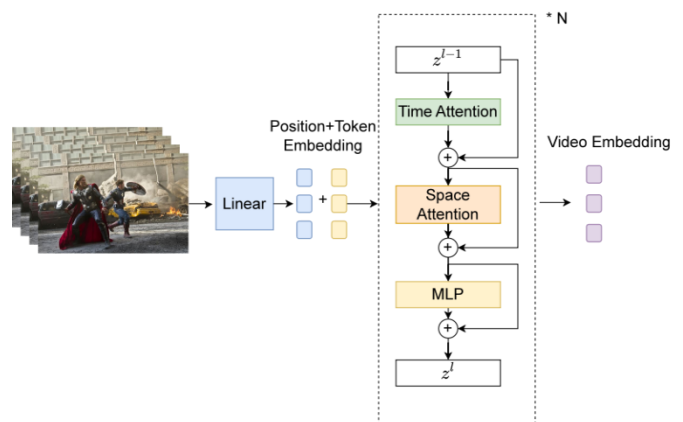


Fig. 2. TimeSformer architecture diagram.

the work by Zhou et al. [13]. However, a significant gap often exists between the vector spaces of video and text embeddings, even when they may be semantically related. This discrepancy makes it challenging to train directly using these embeddings. To address this issue, the paper introduces a contrastive learning approach. Contrastive learning aims to bridge the gap between visual and text embeddings in the

semantic space, even if they are far apart in the original space. By doing so, the model can learn how to map video content to relevant textual descriptions more easily, facilitating the training process.

Suppose the data consists of a dataset $\{V_i, T_i\}_{i=1}^N$ of N video-text pairs, where V represents the video and T corresponds to the associated textual description. Since GPT2 accepts input as a sequence of tokens, the paper maps the CLS^{video} obtained from TimeSformer to a sequence of video patches. Its formal representation is given in Eq. (1).

$$p_1, p_2, p_3, \dots, p_L = FFN(TimeSformer(CLS^{video})) \quad (1)$$

where, p_i is a one-dimensional vector of length H . In this paper, the hidden layer vectors for video and text are the same, set to 768.

During training, the paper concatenates the video patch vectors $\{p_1, p_2, p_3, \dots, p_L\}$ with randomly initialized learnable vectors $\{q_1, \dots, q_\tau\}$. It is then fed into the Transformer Encoder to obtain $\{p_1^{\wedge}, p_2^{\wedge}, p_3^{\wedge}, \dots, p_L^{\wedge}, q_1^{\wedge}, \dots, q_\tau^{\wedge}\}$, where L and τ are hyperparameters, with τ representing the length of the prefix.

The training objective is to predict the tokens autoregressively conditional on the prompt. The generation of the text loss objective can be described by the Eq. (2). The true distribution I_l is an indicator distribution that takes the value of 1 for the correct token t_l and 0 for all other tokens.

$$loss_{token} = -\sum_{i=1}^L \log p_\theta(t_1, \dots, t_L | q_1^{\wedge}, \dots, q_\tau^{\wedge}) \quad (2)$$

In contrastive learning, the paper uses the CLS token as the video representation directly, which is paired with the text features extracted by BERT for contrastive learning. Similarly, the text feature utilizes BERT's CLS token, CLS^{text} , with the shape of R^H . The loss function is as follows in Eq. (3), where γ is the temperature parameter, taking the value of 0.07.

$$loss_c = -\log \frac{\exp(CLS^{video} \cdot CLS^{text} / \gamma)}{\sum_{i=0}^k \exp(CLS^{video} \cdot CLS_i^{text} / \gamma)} \quad (3)$$

IV. EXPERIMENTAL VERIFICATION

A. Dataset

In this paper, the experimental verification is carried out on three public datasets: MSVD, MSR-VTT, and VATEX

The Microsoft Research Video Description Corpus (MSVD) dataset [14] is widely used in video understanding models. Introduced by Microsoft Research in 2016, it is designed for video description generation, which automatically

produces natural language descriptions for video clips. The dataset comprises 1,970 video segments, each accompanied by multiple English descriptions written by different individuals. The videos in the MSVD dataset are primarily sourced from YouTube and cover a variety of genres, including music videos, movie trailers, television shows, and more.

The Microsoft Research Video to Text [15] (MSR-VTT) dataset is another widely used dataset in video understanding models. Proposed by Microsoft Research in 2016 is also designed for video description generation, where the goal is to produce natural language descriptions for video clips automatically. This dataset comprises over 10,000 video segments, each with at least one English description. The videos in the MSR-VTT dataset are primarily sourced from YouTube and encompass a variety of genres, such as music videos, movie trailers, television shows, and more.

The Video-and-Text EXchange (VATEX) dataset[16] is a large-scale video description and subtitle dataset that contains multimodal information including video, audio, and text data. It is characterized by its vast scale, comprising over 250,000 pairs of videos and subtitle descriptions, covering multiple languages, with a particular focus on Chinese and English. The data is sourced from various scenes, including movies, TV series, news broadcasts, variety shows, and more, which results in a highly diverse dataset in both content and language.

B. Experimental Setup

All experiments were conducted using the PyTorch deep learning framework on two GTX-3090 GPUs. The model employed Adaptive Moment Estimation (Adam) as the optimization strategy and used the cross-entropy function as the loss function for back propagating gradients. The weight decay parameter was set to 0.009. The learning rate was scheduled using an inverse time scheme, as shown in the Eq. (4), where δ was set to 0.5, and the initial learning rate r was set to 0.01.

$$r_{new} = \frac{r}{1 + \delta * step} \quad (4)$$

In the MSVD dataset, a total of 14,910 steps were trained with a batch size of 16; in the MSR-VTT dataset, a total of 25,320 steps were trained with a batch size of 8; and in the VATEX dataset, a total of 113,350 steps were trained with a batch size of 6.

C. Comparative Experiments

The proposed model is compared with state-of-the-art methods. MA-Net[6] attempts to construct semantic feature vectors from the textual description of videos, which are then used in conjunction with video feature vectors for semantic detection, to bridge the gap between semantic video features and the actual semantics of the video. However, the I3D network employed by the authors cannot model long-range temporal relationships.

MGRMP [17] proposes a recurrent regional attention module to extract diverse spatial features better and establish higher-order relationships between different regions across frames through motion-guided cross-frame message passing.

Uni-perceiver [18] attempts to create a unified model architecture that can flexibly handle multiple modalities of data without training separate models for each modality or task.

Fu Yan et al. [10] proposed a video description method based on the syntactic analysis of object features in scene representation. This method utilizes an object feature detector and constructs a grammar to generate textual descriptions.

Swin-BERT [19] successfully adapted the Swin Transformer [20] to the video description field and achieved promising results. However, it needed to address the significant semantic gap between video and text representations, leading to the protracted training process and failing to yield satisfactory results.

GIT [21] also attempted to model images, videos, and text using a unified network. However, video content merely relied on concatenating video frames without adequately learning the temporal features.

The evaluation metrics used are Bleu-4, METEOR, ROUGE-L, and CIDEr.

The performance of MFFCL on the MSVD dataset is presented in Table I. In this work, we introduce a contrastive learning method in addition to Swin-BERT [16], which enables semantic alignment between videos and text. This method is easier to train than text generation tasks and has achieved promising results. Our approach outperforms Swin-BERT with 17%, 6%, and 18% improvements in Bleu-4, ROUGE-L, and CIDEr scores, respectively.

Unlike the MSVD dataset, the MSR-VTT dataset contains a richer set of scene information. TimeSformer is trained on human action recognition datasets. When the video has a lot of non-human behavior information, such as camera movements or birds flying, these details may act as noise for the MFFCL model, potentially leading to a degradation in performance. However, TimeSformer not only extracts features along the temporal dimension but also thoroughly learns video representations in the spatial dimension. Consequently, even in complex video scenes, MFFCL still achieves commendable results. In the work by Wang [22] et al. LSTM were employed for text generation. A limitation of this approach is that the length and coherence of the generated text are constrained. In contrast, our work utilizes GPT2 as the text generation model. During the text generation process, we randomly select from a set of p high-probability words, which allows for the generation of diverse and coherent texts. Compared to the method proposed by Wang et al., our approach demonstrates improvements of 4%, 3%, 9%, and 5% in Bleu-4, METEOR,

TABLE I. PERFORMANCE OF MFFCL ON THE MSVD DATASET

| Model | Year | Bleu-4 | METEOR | ROUGE-L | CIDEr |
|-------------------|------|--------|--------|---------|-------|
| MA-Net[6] | 2021 | 50.3 | 33.4 | 70.7 | 78.3 |
| MGRMP[17] | 2021 | 55.8 | 36.9 | 74.5 | 98.5 |
| Uni-perceiver[18] | 2022 | 56.7 | 38.7 | 70 | 88.2 |
| Swin-BERT[19] | 2022 | 58.2 | 41.3 | 77.5 | 120.6 |
| FU et.al.[10] | 2023 | 53.5 | - | - | 83.1 |
| MFFCL | 2024 | 68.4 | 40.2 | 82.6 | 142.3 |

TABLE II. PERFORMANCE OF MFFCL ON THE MSR-VTT DATASET

| Model | Year | Bleu-4 | METEOR | ROUGE-L | CIDEr |
|-----------------|------|--------|--------|---------|-------|
| MGRMP[17] | 2021 | 41.7 | 28.9 | 62.1 | 51.4 |
| MA-Net[6] | 2021 | 40.5 | 27.9 | 60.3 | 50.6 |
| Swin-BERT[19] | 2022 | 42.8 | 29.3 | 61.7 | 52.9 |
| FU et al.[10] | 2023 | 43.2 | - | - | 51.3 |
| Wang et.al.[22] | 2023 | 44.8 | 29.4 | 63.0 | 52.3 |
| MFFCL | 2023 | 46.6 | 30.3 | 68.6 | 54.8 |

TABLE III. PERFORMANCE OF MFFCL ON THE VATEX DATASET

| Model | Year | Bleu-4 | METEOR | ROUGE-L | CIDEr |
|---------------|------|--------|--------|---------|-------|
| GIT[21] | 2021 | 41.6 | 28.1 | 55.4 | 91.5 |
| Swin-BERT[19] | 2022 | 38.7 | 26.2 | 53.2 | 73.0 |
| MFFCL | 2024 | 50.2 | 35.3 | 65.6 | 100.2 |

ROUGE-L, and CIDEr scores, respectively. The specific data are shown in Table II.

While constructing the VATEX dataset, the authors extensively reused videos from the Kinetics-600 dataset[7], resulting in a rich presence of human actions. TimeSformer can fully model spatiotemporal features and accurately recognize action information, thus achieving significant results on VATEX. As mentioned earlier, Swin-BERT lacks the contrastive learning module used in this paper, which may lead to insufficient training. The GIT model, which is not specialized for video data, is less effective in temporal feature extraction than ours. Compared to GIT, our approach shows improvements of 20%, 25%, 18%, and 9% in Bleu-4, METEOR, ROUGE-L, and CIDEr scores, respectively. The specific data are given in Table III.

D. Ablation Experiments

To validate the effectiveness of the modules, this paper conducts ablation studies on the model from three aspects: the contrastive learning module, the mapping module, and the prompt length.

In the learning process of the contrastive learning module, the TimeSformer was fine-tuned using only textual descriptions. During the experiment, it was observed that the improvement in evaluation metrics was very slow. Even doubling the training time on the MSVD dataset did not yield satisfactory results. This could be due to the fact that the text generation task, which relies on contrastive learning, requires more advanced GPUs, and our experimental setup may not meet the training requirements.

TABLE IV. ABLATION EXPERIMENTS WITH CONTRASTIVE LEARNING

| Contrastive Learning | Prompt Length | Bleu-4 | METEOR | ROUGE-L | CIDEr |
|----------------------|---------------|--------|--------|---------|-------|
| √ | 10 | 32.6 | 19.6 | 39.3 | 52.6 |
| √ | 30 | 60.8 | 36.6 | 42.1 | 82.3 |
| √ | 50 | 68.4 | 40.2 | 82.6 | 142.3 |
| × | 30 | 52.3 | 34.1 | 69.8 | 80.3 |
| × | 50 | 52.3 | 34.1 | 69.8 | 80.3 |

The results of the ablation study are presented in Table IV, the contrastive learning module structure is shown in Fig. 4. The model structure without the contrastive learning module is shown in Fig. 3.

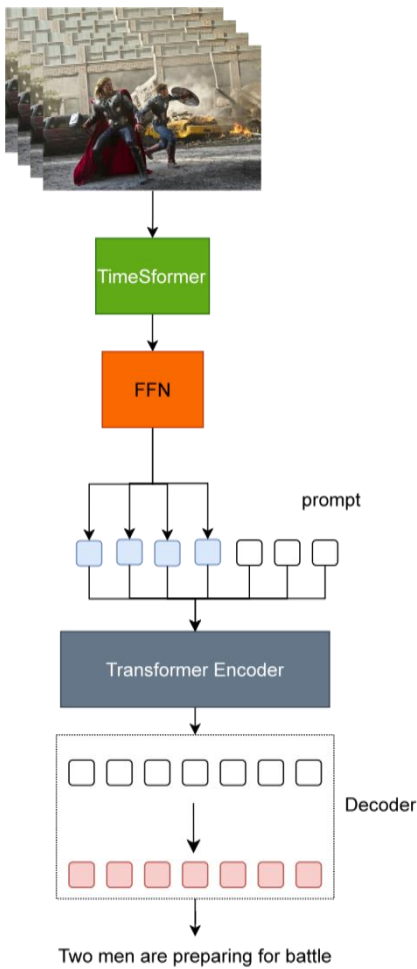


Fig. 3. Overall structure diagram without contrastive learning.

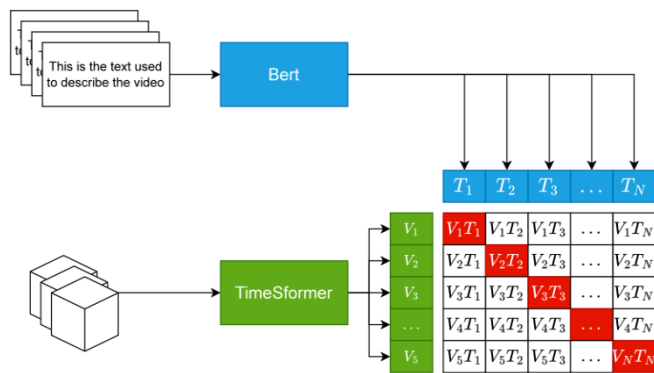


Fig. 4. Contrastive learning module structure.

Regarding the prompt length, it was noted that as the prompt length increased, the amount of information the model could accommodate increased, thereby enhancing its descriptive capabilities. It is believed that longer prompts can fully extract video representation information, which helps the model to understand and describe video content more accurately. However, excessively long prompts may complicate the training process and be limited by device performance and computational resources in practical applications. Experiments have demonstrated that the model can learn the correspondence between videos and texts through contrastive learning, bringing the representations of videos and texts closer in the feature space. This alignment aids the model in better understanding the video content and generates accurate descriptions based on the video embeddings.

To investigate the importance of the understanding mapping module, this paper replaces the Transformer Encoder with a Feedforward neural networks (FFN) to observe changes in the model's performance. Global Linguistic Evaluation Understudy (GLEU) was chosen as the activation function for this setup. Since feedforward neural networks do not contain attention mechanisms, the query vector is removed from the input, and the video block sequence is fed directly into the FFN.

The experimental results indicate that the model's performance decreases when the query vector is absent. This suggests that the query vector has learned a proficient video representation, which aids the model in focusing on the most relevant parts of the video and generates more accurate and coherent text descriptions. Furthermore, experimental results indicate that although feedforward neural networks can learn the mapping between video and text to some extent, their performance does not match that of the Transformer Encoder. The experimental results are presented in Table V.

TABLE V. ABLATION EXPERIMENTS OF THE MAPPING MODULE

| Mapping Module | Bleu-4 | METEOR | ROUGE-L | CIDEr |
|--------------------|--------|--------|---------|-------|
| Transformer Encode | 68.4 | 40.2 | 82.6 | 142.3 |
| FFN | 52.3 | 34.1 | 69.8 | 80.3 |

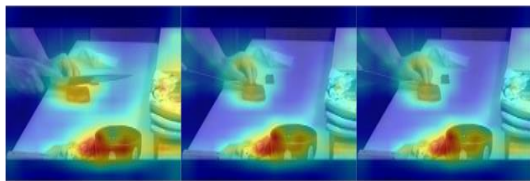
E. Qualitative Analysis

In this paper, a qualitative analysis of TimeSformer was conducted from the perspective of attention weights. During the execution of TimeSformer, the spatial attention weights were obtained and visualized after being weighted with the original images. The results are shown in Fig. 5. It can be observed that TimeSformer effectively extracts the spatiotemporal representation of the video and adjusts its focus to be similar to human visual attention through the two-stage learning tasks of video-text learning and text generation learning.



A girl is combing her hair.

a woman is styling her hair
a girl is combing her hair in different hairstyle
a woman puts moose in her hair and twists it up on her head



A person in the chopping vegetables, next to the clutter.

someone sliced meat
a man carefully slices meat
a man cuts two rectangular slices from a piece of meat
and places them one on top of the other on the counter

Fig. 5. The image illustrates the ablation results from the MSVD dataset. In each example, the top image represents a schematic of the attention weights, with darker colors indicate higher attention weights. The bottom image shows the original image. The bold part in the text corresponds to the model's output, while the non-bold part represents the dataset labels.

V. CONCLUSION

In the field of multimodal video description, effectively integrating temporal sequence information, visual imagery, and textual descriptions from videos is a worthwhile area of research. To address this challenge, this paper proposes a novel two-step fusion strategy designed to achieve a more precise and coherent understanding and description of video content through an efficient model architecture and training mechanism.

This paper employs TimeSformer, an advanced spatiotemporal feature extractor, in the first stage. Its unique network design for spatiotemporal feature extraction enables it to capture long-range temporal dependencies while preserving spatial details. In the second phase, the focus is on aligning video representations with text representations through

contrastive learning. The core principle of contrastive learning is to minimize the distance between positive samples and maximize the distance between negative samples, thereby fostering similarity between video and text representations in the latent space. This study fine-tunes the TimeSformer through carefully designed contrastive tasks to produce video features that are more similar to textual features, prompt the model to generate more accurate video descriptions.

Compared to the Swin-BERT model on the MSVD dataset, our method achieves substantial improvements of 17%, 6%, and 18% on the critical evaluation metrics Bleu-4, ROUGE-L, and CIDEr, respectively. Experimental results confirm the efficacy of the method presented in this paper. TimeSformer is capable of fully representing video content in both temporal and spatial dimensions. The visual prompt also serve to filter out redundant features, while the contrastive learning module accelerates the training process of the TimeSformer.

Future researchers can focus on developing more advanced multimodal fusion techniques to enhance the model's understanding of context and long-term dependencies. Utilizing large-scale, diverse datasets and weak supervision learning can also be explored. Additionally, researching the field of dense video description are potential avenues for advancement.

ACKNOWLEDGMENT

This research is supported by the Key Technology Research and Demonstration Application of News Intelligent Production (212102210417), Science and Technology Plan of Henan Province in 2021.

REFERENCES

- [1] P. Tang and H. Wang, "From Video to Language: A Review of Video Title Generation and Description," *Acta Automatica Sinica*, vol. 48, no. 2, pp. 375-397, 2022.
- [2] G. Bertasius, H. Wang, and L. Torresani, "Is space-time attention all you need for video understanding?," in *ICML*, 2021, p. 4.
- [3] K. He, X. Zhang, S. Ren, and J. Sun, "Deep Residual Learning for Image Recognition," in *2016 IEEE Conference on Computer Vision and Pattern Recognition (CVPR)*, 2016, pp. 770-778. doi: 10.1109/CVPR.2016.90.
- [4] A. Dosovitskiy et al., "An Image is Worth 16x16 Words: Transformers for Image Recognition at Scale," *arXiv:2010.11929 [cs]*, Jun. 2021, Accessed: May 17, 2022. [Online]. Available: <http://arxiv.org/abs/2010.11929>
- [5] Y. Lu and S. Chen, "Video Description Algorithm Based on Mixed Training and Semantic Association," *Journal of Huazhong University of Science and Technology (Natural Science Edition)*, vol. 51, no. 11, pp. 67-74, 2023.
- [6] Y. Yan and X. Liu, "Research on Video Description Method Based on Multi-Attention and Semantic Detection," *Master's Thesis*, 10.27623/d.cnki.gzkyu.2021.000731, China University of Mining and Technology, 2021.
- [7] J. Carreira and A. Zisserman, "Quo vadis, action recognition? a new model and the kinetics dataset," in *proceedings of the IEEE Conference on Computer Vision and Pattern Recognition*, 2017, pp. 6299-6308.
- [8] A. Vaswani et al., "Attention is all you need," *Advances in neural information processing systems*, vol. 30, 2017.
- [9] T.-Y. Lin, P. Dollar, R. Girshick, K. He, B. Hariharan, and S. Belongie, "Feature Pyramid Networks for Object Detection," in *2017 IEEE Conference on Computer Vision and Pattern Recognition (CVPR)*, Jul. 2017. doi: 10.1109/cvpr.2017.106.

- [10] Y. Fu, M. Wang, and O. Ye, "Video Description Based on Object Feature Grammar Analysis in Scene Representation," *Computer Engineering and Design*, vol. 44, no. 2, pp. 488-493, 2023.
- [11] J. Ren, Q. Zeng, X. Li, Z. Gong, and F. Liu, "Video Description Method Integrating Semantic Enhancement and Multi-Attention Mechanism," *Journal of Nanchang University (Science & Technology Edition)*, vol. 47, no. 6, pp. 548-555, 2023.
- [12] A. Radford, J. Wu, R. Child, D. Luan, D. Amodei, and I. Sutskever, "Language Models are Unsupervised Multitask Learners".
- [13] L. Zhou, H. Palangi, L. Zhang, H. Hu, J. Corso, and J. Gao, "Unified Vision-Language Pre-Training for Image Captioning and VQA," *Proceedings of the AAAI Conference on Artificial Intelligence*, pp. 13041-13049, Jun. 2020, doi: 10.1609/aaai.v34i07.7005.
- [14] D. Chen and W. Dolan, "Collecting Highly Parallel Data for Paraphrase Evaluation," in *Proceedings of the 49th Annual Meeting of the Association for Computational Linguistics: Human Language Technologies*, D. Lin, Y. Matsumoto, and R. Mihalcea, Eds., Portland, Oregon, USA: Association for Computational Linguistics, Jun. 2011, pp. 190-200. [Online]. Available: <https://aclanthology.org/P11-1020>
- [15] J. Xu, T. Mei, T. Yao, and Y. Rui, "MSR-VTT: A Large Video Description Dataset for Bridging Video and Language," *IEEE International Conference on Computer Vision and Pattern Recognition (CVPR)*, Jun. 2016. [Online]. Available: <https://www.microsoft.com/en-us/research/publication/msr-vtt-a-large-video-description-dataset-for-bridging-video-and-language/>
- [16] X. Wang, J. Wu, J. Chen, L. Li, Y.-F. Wang, and W. Y. Wang, "VaTeX: A Large-Scale, High-Quality Multilingual Dataset for Video-and-Language Research," in *2019 IEEE/CVF International Conference on Computer Vision (ICCV)*, Oct. 2019. doi: 10.1109/iccv.2019.00468.
- [17] S. Chen and Y.-G. Jiang, "Motion Guided Region Message Passing for Video Captioning," *International Conference on Computer Vision*. Jan. 2021.
- [18] X. Zhu et al., "Uni-perceiver: Pre-training unified architecture for generic perception for zero-shot and few-shot tasks," in *Proceedings of the IEEE/CVF Conference on Computer Vision and Pattern Recognition*, 2022, pp. 16804-16815.
- [19] K. Lin et al., "Swinbert: End-to-end transformers with sparse attention for video captioning," in *Proceedings of the IEEE/CVF Conference on Computer Vision and Pattern Recognition*, 2022, pp. 17949-17958.
- [20] Z. Liu et al., "Swin Transformer: Hierarchical Vision Transformer using Shifted Windows.," *international conference on computer vision*, 2021.
- [21] J. Wang et al., "GIT: A Generative Image-to-text Transformer for Vision and Language." 2022.
- [22] L. Wang and Y. Bai, "Video Description Method Based on Feature Enhancement and Knowledge Supplementation," *Journal of Computer Systems & Applications*, vol. 32, no. 5, pp. 273-282, 2023.

Permanent Magnet Motor Control System Based on Fuzzy PID Control

Yin Sha*, Huwei Chen

Industrial Motor-Driving Center of Intelligent Network-Connection, Jiangyin Polytechnic College, Jiangyin, 214400, China

Abstract—Although the traditional permanent magnet synchronous motor control system is simple and convenient, the control of speed and accuracy is often affected by external interference, which impacts the dynamic and static performance requirements. Therefore, this study attempts to introduce fuzzy rules to improve the proportional integral differential control method, and further integrate intelligent optimization algorithms into the fuzzy proportional integral differential control method to construct an efficient and feasible permanent magnet synchronous motor control method. The simulation experiment demonstrates that under fuzzy proportional integral differential control, there is no overshoot in the waveform when facing changes in load, and the tuning time increases from 0.01 seconds to 0.12 seconds. The steady-state error of speed control is small, and there is no obvious oscillation in the waveform. Fuzzy control enhances the control system. After the optimization of the artificial bee colony algorithm, the control system has a faster speed response, with the overshoot diminished from 11.2% to 3.1%, and the adjustment time reduced from 0.27 seconds to 0.19 seconds, enhancing its adaptability. Under load regulation, the optimized control system speed response curve responds in a timely manner without obvious overshooting and oscillating changes. Optimizing variable universe fuzzy proportional integral differential control enables the control system for having better static and dynamic performance, and enhances the adaptability and follow-up of the control system. The current curve starts to stabilize at 0.04s, overcoming the control system oscillations early. The speed response curve and the motor torque curve are improved by the optimized variable domain theory, and the amount of overshoot is significantly reduced. The research and design of a permanent magnet motor control system has practical significance for improving the application performance and adaptability of permanent magnet motors.

Keywords—Permanent magnet motor; fuzzy PID; fuzzy control; automatic control system; artificial bee colony

I. INTRODUCTION

Permanent magnet motors (PMM) are a product of the integration of multiple disciplines such as materials science, electronic science, and power control technology. Their development is closely related to the emergence of permanent magnet materials, especially the efficient and energy-saving rare earth permanent magnet materials, which have greatly promoted the development process of PMM. Permanent magnet materials replace electromagnetic induction to generate a working magnetic field, and the initial application of PMM was mainly concentrated in high-end special fields such as aerospace; With the emergence of neodymium iron boron permanent magnet materials and the promotion of power electronics technology, PMM are developing towards

high speed, high energy, and miniaturization; PMM have significant characteristics such as simple structure, reliable operation, lightweight volume, low loss and high efficiency. The application of PMM has gradually expanded to industrial, agricultural, and civilian fields, becoming the preferred motor for driving systems, penetrating into the production of home appliance systems, medical devices, CNC machine tools, new energy vehicles, and even the military industry [1-2]. Under the background of vigorously advocating the transformation and upgrading of manufacturing industry, energy conservation and emission reduction, and Low-carbon economy, PMM have prominent energy-saving characteristics and become a research hotspot.

Permanent Magnet Synchronous Motor (PMSM) is a category of PMM. It has obvious advantages. It is the first motor of AC servo system. The research on PMSM control technology is very important. The traditional control method of PMSM control system (CS) adopts Proportional Integral Derivative Control (PID). PID control is a kind of earlier control strategy, with simple control algorithms and high reliability. Therefore, it is extensively utilized in industrial process control [3-4]. However, for the production of actual industrial processes, the modeling accuracy of PID control is low, the stability of control parameters is poor, and the adaptability to actual operating conditions is insufficient [5].

In view of this, to meet the more effective control strategy requirements of PMSM systems, this study first introduces fuzzy algorithms and uses fuzzy rules to adjust the PID control process; Secondly, on the basis of fuzzy PID control, further incorporating the Artificial Bee Colony Algorithm (ABC) to improve fuzzy PID control; This control algorithm is expected for further enhancing the control performance of PMSM and adjust the speed CS of PMSM. The study introduces the variable domain fuzzy control theory and intelligent optimization algorithm to improve the control accuracy of fuzzy PID control, which enriches the theoretical study of fuzzy PID control, fuzzy algorithm and intelligent optimization algorithm, and improves the research and application level of the corresponding technology; meanwhile, this control algorithm can further enhancing the control performance of the PMSM, and adjust the speed control system of the PMSM.

The research is separated into five. The first is a review of the late research status in the field of control both domestically and internationally; The second proposes a PMSM CS control algorithm in view of fuzzy PID and an improved fuzzy PID control model in view of ABC algorithm; The third tested and simulated the function; the fourth section discusses the

research work and future research directions. The fifth summarizes and summarizes the experimental outcomes of the study.

II. RELATED WORKS

The research on PMM mainly focuses on the optimization design of permanent magnet materials, control algorithms, and motor structures. With the rapid development of more intelligent tools and applications, the control requirements for PMM are also increasing. To achieve higher control accuracy, faster response, and better stability, lots of researchers have carried study about the control algorithms of PMM and general control algorithm problems. The uncertainty, time-varying, and nonlinearity of the PMSM AC servo system make the control effect of traditional control methods not ideal; To solve this problem, Zhong CQ et al. utilized the strong adaptability of fuzzy control (FCO) to the controlled object and designed a PMSM three closed-loop system. Fuzzy logic algorithm was introduced to adjust the parameters of the fractional order proportional integral differential controller, and the complementary advantages of the two algorithms were reasonably achieved; The experiment demonstrates that the control algorithm can effectively satisfy the trajectory tracking needs of PMSM servo control, and the control algorithm is effective [6]. Jakovljević B et al. studied fractional order and distributed order PID controllers of PMSM, and introduced parameter setting and tuning of generalized Particle swarm optimization (PSO) controller. Then they proposed a new dual loop control method for controlling PMSM drivers; The experiment showcases that this control scheme can effectively suppress interference compared to traditional control methods [7]. Zeng X et al. designed a current control method for PMSM drivers, which includes decoupling term, adaptive proportional integral term, supervision term, and radial basis function neural network PID term. This adaptive controller in view of gradient descent strategy can adjust the parameter uncertainty of any system, ensuring the accuracy and efficiency of PMSM tracking speed. The comparative experiment outcomes showcase that relative to traditional proportional integral differential control methods, it achieves better control stability [8]. To realize the tradeoff between the performance of the uncertain model and the robust performance, Amieur T et al. designed a tilted PID controller. The controller introduced an optimization tool - genetic algorithm to solve the sensitive problem of controller weighting mixing, and optimized the parameters. For testing the controller, the tilted PID controller was applied to PMSM, and its performance and robustness were made a comparison with traditional PID control. The experiment showcases that the robustness and reduction of control energy of this control method are excellent [9].

Ghadiri H et al. combined fuzzy Evolutionary algorithm with PID controller for controlling the speed of PMSM. And PSO algorithm is utilized for optimizing the member function parameters and the relevant rule basis. Compared with the optimized controller, the controller in view of PSO algorithm shows greater advantages in speed control [10]. Lazim M H et al. used proportional integral differential control with two internal and one external feedback loops for optimizing the design performance of PMSM in speed control, and used

genetic algorithms to optimize the controller parameters. The results of MATLAB simulation experiments indicate that this control method has good dynamic and static quality [11]. Abdulhussein K G et al. used butterfly optimization algorithm and PSO algorithm to calculate the gain value of cascade proportional integral differential control method. The controller mainly controls the position, speed, current and tracking trajectory of permanent magnet DC motor. The simulation outcomes of MATLAB showcase that the optimization performance of butterfly optimization algorithm is better than that of PSO [12]. Zhang R designed a design method of anti-saturation PID current controller for enhancing the dynamic current response speed of PMSM. The experiment illustrates that this control method is more accurate in controlling current than traditional controllers, and the dynamic current response performance has been improved [13].

In summary, although research on the CS of PMSM has made certain progress, the control efficiency and accuracy of PMSM in different fields still need to be improved, and the research on PID CSs combined with intelligent algorithms still needs further deepening; This is to design a CS for PMSM with more adaptability.

III. DESIGN OF PMM CS IN VIEW OF IMPROVED FUZZY PID

PMSM is composed of three basic parts: rotor, stator, and permanent magnet. It relies on the interaction between the rotating magnetic field generated by the stator and the spindle magnetic field for generating electromagnetic torque for deriving the rotor to rotate, achieving the conversion of electrical energy. To ensure the normal operation of PMSM in the servo system, the speed index is an important indicator for evaluating the performance of PMSM. Therefore, it is essential for conducting research on the adaptive control of the PMSM speed CS. This study introduces the ABC algorithm into the fuzzy PID CS and conducts a series of studies on the PMSM CS.

A. Fuzzy PID Control in View of ABC Algorithm Optimization

FCO is a comprehensive intelligent control mode. It draws lessons from the principles of fuzzy reasoning and decision-making. Utilizing the experience of industry experts to develop fuzzy rules, the real-time signals transmitted by sensors are fuzzified and used as input to the fuzzy rules, and the completed fuzzy reasoning is then transmitted to the actuator [14-15].

Fuzzy Controller (FC) uses fuzzy conditional statements of fuzzy theory to describe fuzzy rules. The structure of fuzzy controller is demonstrated in Fig. 1. Among them, the fuzzy Inference engine is the core of the algorithm. According to the knowledge base to solve the fuzzy relationship, the solution method used in the study is the Mamdani method. The database contains membership vector values of fuzzy subsets of input and output variables. The rule base summarizes the control statements of fuzzy rules in view of the experience of experts, and continuously summarizes the control laws during the control process before adding them to historical experience. Finally, the weighted average method is used to convert the

inference fuzzy quantity into an accurate quantity.

The actual CS does not meet linear invariance and requires dynamic adjustment of PID control parameters. This study introduces FCO and its combination, taking deviation and

changes in deviation as inputs, and uses fuzzy rules to adjust the parameters of PID to meet the different needs of deviation for PID parameters. Fig. 2 indicates the control principle of fuzzy PID.

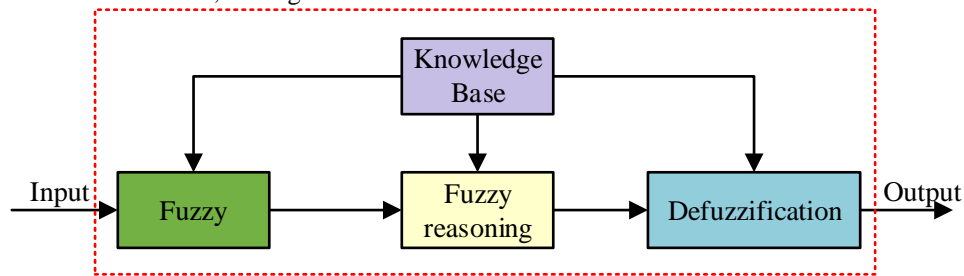


Fig. 1. Fuzzy controller structure schematic.

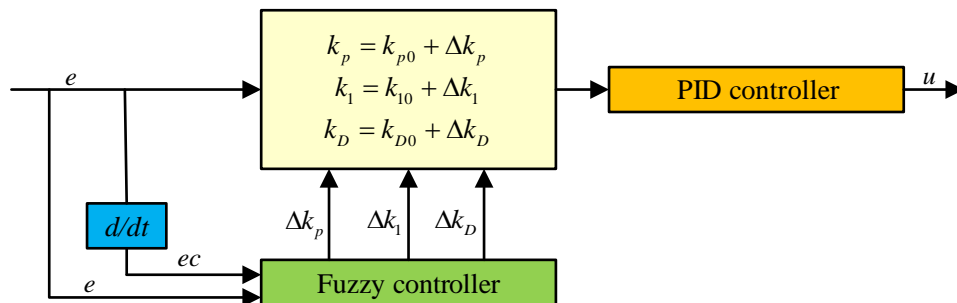


Fig. 2. Schematic diagram of the control principle of fuzzy PID.

The research mainly focuses on setting a controller for the speed control link of PMSM, and the parameter changes of fuzzy PID are shown in Eq. (1). In Eq. (1), k_p , k_1 , and k_D are all adjustment parameters of fuzzy PID; k_{p0} , k_{10} and k_{D0} represent the initial set values of the parameters; Δk_p , Δk_1 and Δk_D represent parameter correction values.

$$\begin{cases} k_p = k_{p0} + \Delta k_p \\ k_1 = k_{10} + \Delta k_1 \\ k_D = k_{D0} + \Delta k_D \end{cases} \quad (1)$$

The input of the precise value changes from the Fuzzy set mapping of the fuzzification module to the fuzzy set. The quantization and scaling factor (SF) calculation of the input and output are shown in Formula (2). In Eq. (2), the basic domain of input bias and variation of bias is $[-e_{\max}, e_{\max}]$, $[-ec_{\max}, ec_{\max}]$; u represents the output quantity, and the basic domain is $[-u_{\max}, u_{\max}]$.

$$\begin{cases} k_e = \frac{n}{e_{\max}} \\ k_{ec} = \frac{n}{ec_{\max}} \\ k_u = \frac{u_{\max}}{n} \end{cases} \quad (2)$$

To achieve adaptive control of PMSM speed CS, this study introduced ABC algorithm to optimize fuzzy PID intelligent control. ABC algorithm is a population intelligent global optimization algorithm that draws on the honey harvesting behavior of bee colonies. In nature, bees work find the optimal solution to problems through information sharing and communication between bee colonies. The traditional ABC algorithm separates artificial bee colonies into three groups: honey gathering, following, and reconnaissance. The honey gathering group searches for new honey sources in view of old honey source information and shares it with the observing bee group. Following the bee group and adding the shared information to the process of searching for honey sources, the reconnaissance bee randomly searches for valuable honey sources near the hive. Different bees can adapt well to the environment, and this mechanism of division of labor and cooperation organization does not require special information about the problem; By comparing the advantages and disadvantages of the problem, the ABC algorithm has an excellent global search ability, and the algorithm has a fast Rate of convergence speed, which is widely used in different fields such as traveling salesman problem, signal deployment problem, power and water conservancy scheduling problem, parameter optimization, image segmentation, etc. [16-17].

If the total number of bees N_s is included, including the size N_e of the collecting bees and the size N_u of the following bees, the individual search space is S . If N_s feasible solutions are randomly generated, the feasible solution calculation for bee population X_i is shown in

Eq. (3); In Eq. (3), i represents the honey source number; j represents the j -dimensional component of the honey source; X_{\max}^j, X_{\min}^j represents the maximum and minimum values of the j -dimensional components of the honey source, respectively.

$$X_i^j = X_{\min}^j + rand(0,1)(X_{\max}^j - X_{\min}^j) \quad (3)$$

The fitness value f_i of the honey source is called "profitability", which determines the probability of following the bee to be selected, as shown in Eq. (4). In Eq. (4), P represents the probability of being selected.

$$P_i = \frac{f_i}{\sum_{n=1}^{N_e} f_n} \quad (4)$$

The location of bees searching near the honey source is generated according to Eq. (5). In Eq. (5), D represents the individual vector dimension, and k and i take random values. When the fitness value of the new location is higher, the honey source location is updated.

$$new_X_i^j = X_i^j + rand[-1,1](X_i^j - X_k^j) \quad (5)$$

$j \in \{1, 2, \dots, D\} \quad k \in \{1, 2, \dots, N_e\} \quad k \neq i$

The position update iteration of the following bee is always near the honey source. If the number of iterations reaches the limit and the ideal honey source is not found, the bees near the honey source will be abandoned and transformed into reconnaissance bees to randomly search for the honey source, as shown in Eq. (6).

$$X_i(n) = X_{\min} + rand(0,1)(X_{\max} - X_{\min}) \quad (6)$$

The flowchart of the entire ABC algorithm is shown in Fig. 3. In the initial stage, all bees are initialized as reconnaissance bees, and the search for honey sources remains at the limit of search times. After sorting the fitness values of all honey sources, all reconnaissance bees are divided into following bees and collecting bees, and then the honey source location is updated through local search according to Eq. (5). Reference Eq. (4) selects following bees to gather honey. When the adaptability of the honey source is high, the following bees at this time change to gathering bees. Finally, it records all honey sources. When the number of iterations is completed or the profitability meets the requirements, the ABC algorithm outputs the optimal honey source result. Otherwise, the algorithm cycle continues.

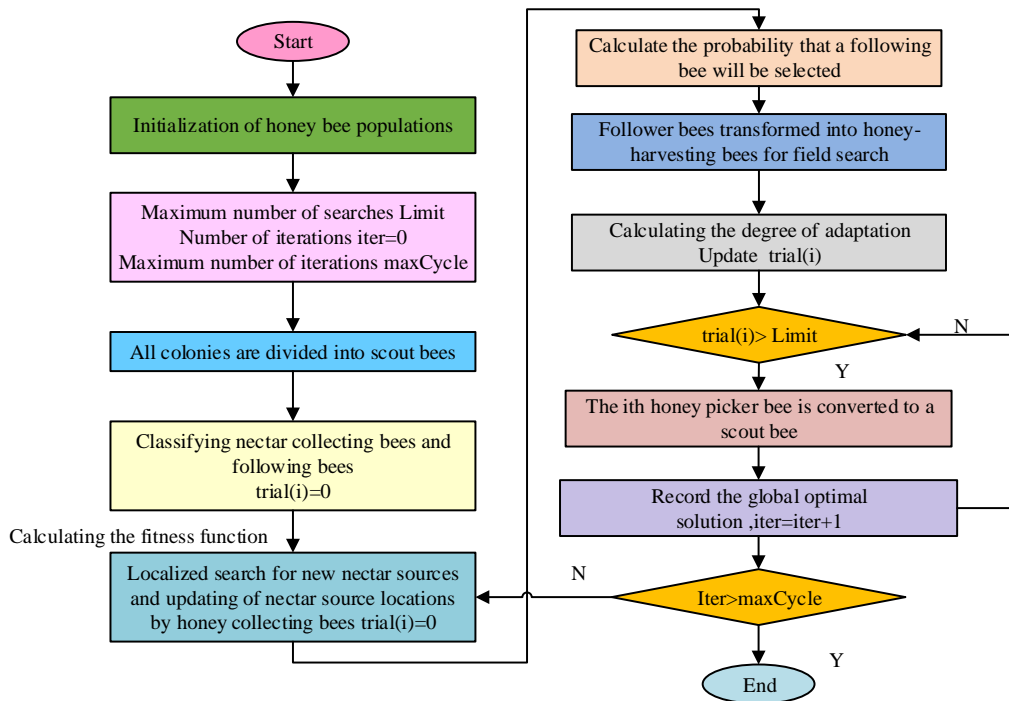


Fig. 3. Flow diagram of ABC algorithm.

B. Fuzzy PID Controller Combining Variable Domain theory and Improved ABC Algorithm

When the errors and parameters of the fuzzy PID CS undergo significant changes, the control accuracy of the CS will be affected. The quantization, SF, and fuzzy rules of a

fuzzy controller are fixed and cannot be adjusted adaptively due to changes in parameters. This study introduces a variable universe FCO strategy, which adjusts the universe and fuzzy rule base to ensure the accuracy of the fuzzy PID CS. Fig. 4 indicates the principle of the CS.

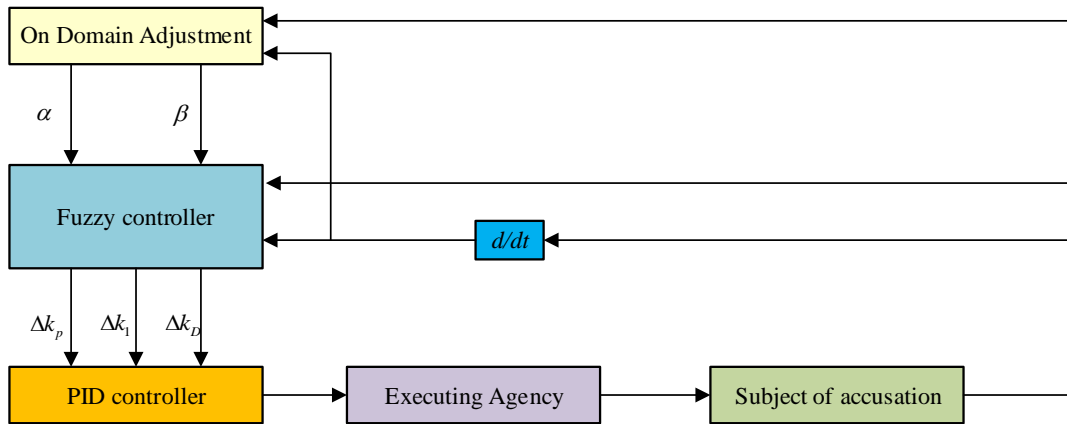


Fig. 4. Schematic diagram of the structure of variable domain fuzzy PID CS.

Firstly, the ABC algorithm was optimized and improved in view of natural improvement. Natural selection draws lessons from the selection law of natural biological elimination evolution. In this study, the rotation method is used to rank all fitness values at each iteration of the ABC algorithm, and select half of the larger fitness value. In this way, the fitness value of the algorithm is improved, and the Rate of convergence of the global optimal value is accelerated. Compared to the traditional ABC algorithm, a ranking of all bee fitness values has been added at the end of the algorithm, and smaller fitness values have been replaced, while preserving the historical honey source optimal values [18-20].

The universe scaling mechanism used in this study is a functional SF, with two input systems represented as X_e and X_{ec} , and the output represented as Y_u . The changed universe expression is shown in Eq. (7). In Eq. (7), $\alpha(e)$, $\alpha(ec)$, and β respectively represent the SF of the input and output. The SF satisfies duality, zero preservation, coordination, monotonicity, and normality, and the contraction and expansion of the universe are shown in Fig. 5.

$$\begin{cases} X_e = [-\alpha(e)E, \alpha(e)E] \\ X_{ec} = [-\alpha(ec)EC, \alpha(ec)EC] \\ X_e = [-\beta U, \beta U] \end{cases} \quad (7)$$

Usually, a change in the quantization SF of a CS will cause a change in the domain, and an increase in the quantization factor will narrow the basic domain of the input, thereby increasing the impact on the CS. An increase in the proportion factor will increase the basic domain of the output and increase the output. However, quantification and SF cannot be adjusted in view of the input domain, so the study uses SF for adjustment.

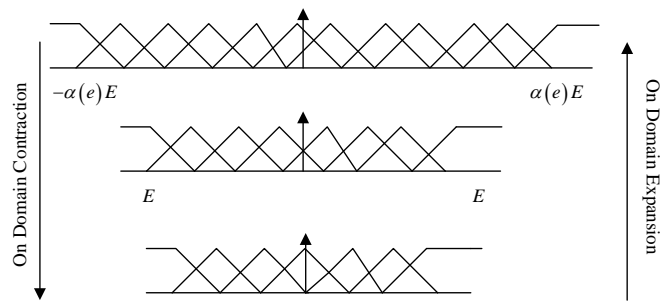


Fig. 5. Contraction and expansion of the thesis domain.

The input adjustment function of the expansion factor is shown in Formula (8). In Eq. (8), ε represents a sufficiently small positive number; x represents the input error or change in error; x , τ and k represent adjustable constants, respectively; E represents the domain of input.

$$\begin{cases} \alpha(x) = \left[\frac{|x|}{E} \right]^\tau + \varepsilon \\ \alpha(x) = 1 - \lambda e^{-kx^2} \end{cases} \quad (8)$$

The output adjustment function of the expansion factor is shown in Formula (9). In Eq. (9), u represents the output; τ_1 , τ_2 and x represent adjustable constants, respectively; EC represents the domain of the input.

$$\begin{cases} \beta(u) = \left[\frac{u}{E} \right]^{\tau_1} \square \left[\frac{u}{EC} \right]^{\tau_2} \\ \beta(x) = \frac{1}{|e| + \lambda} \end{cases} \quad (9)$$

The SF adjustment function is substituted into Eq. (2), and Eq. (10) can be obtained, which realizes the adaption of quantization factor and scale factor. In Eq. (10), N represents the fuzzy domain of input and output; U_p , U_l and U_D represent the basic universe of output parameter variables.

$$\begin{cases} K_e = \frac{N}{\alpha(e) \cdot E} \\ K_{ec} = \frac{N}{\alpha(ec) \cdot EC} \\ K_{\Delta k_p} = \frac{U_p}{N} \beta(e) \\ K_{\Delta k_i} = \frac{U_i}{N} \beta(e) \\ K_{\Delta k_D} = \frac{U_D}{N} \beta(e) \end{cases} \quad (10)$$

To meet the needs of universe adjustment, the research uses the improved ABC algorithm in view of Natural selection for parameter optimization operation. The selected SF is shown in Formula (11), where k and λ are parameters in the SF adjustment function.

$$\begin{cases} \alpha(e) = 1 - \lambda_1 e^{-k_1 x^2} \\ \alpha(ec) = 1 - \lambda_2 e^{-k_2 x^2} \\ \beta(u_p) = \lambda_3 |e| \\ \beta(u_i) = \frac{1}{|e| + \lambda_4} \\ \beta(u_D) = \lambda_5 |e| \end{cases} \quad (11)$$

The whole process of using the improved ABC algorithm in view of Natural selection to optimize the parameters of the SF adjustment function is as follows: first, initialize the parameters involved in the system ABC algorithm, divide the bee colony according to the fitness value calculated by the initial value of the SF, and then collect the bees, follow the bees, and scout bees to find the honey source, judge the number of iterations or fitness value, and end the algorithm cycle.

In summary, the vector control of the PMSM is rotor field oriented vector control, and the specific control is indicated in the Fig. 6. Firstly, the three-phase stator current is collected and subjected to Clack transformation to obtain mutually orthogonal time variables i_α and i_β ; The two axis system rotates according to the transformation angle, and after Park changes, it can align with the rotor flux to obtain constants i_d and i_q . The input of speed error signal is improved by optimizing the fuzzy PID controller with ABC algorithm to obtain the reference values of i_d and i_q , and the error signal can be obtained by combining i_d and i_q . After the constant i_d and i_q are compared, they are input into the PI regulator. The obtained PMSM vector passes through the speed estimator to calculate the new motor conversion angle. After Park inverse change and Clack inverse transform, the input voltage vector control output and SVPWM get the three-phase voltage, and then the three-phase voltage is input into the inverter bridge to drive the PMM to rotate.

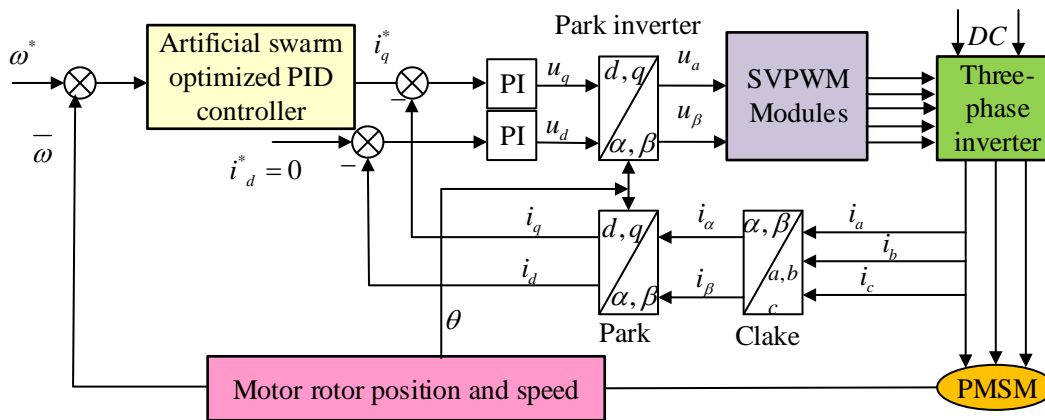


Fig. 6. Principle diagram of fuzzy PID vector control of PMSM in view of ABC algorithm optimization.

IV. PERFORMANCE TESTING OF IMPROVED FUZZY PID PMM CS

For testing the performance of the fuzzy PID PMM CS designed in the research, a MATLAB/Simulink simulation test experiment was designed. Firstly, the speed loop of the designed CS was experimentally verified to verify the performance of the CS. Meanwhile, comparative experiments were conducted on the fuzzy PID CS optimized by artificial bee colonies for verifying the superior performance of the optimization algorithm used in the research.

A. Simulation Experiment Analysis of Fuzzy PID CS in View of ABC Optimization

The research object is the speed loop CS of the PMSM servo CS. This part uses the ABC algorithm to optimize. The control parameters of the Current loop are fixed, the number of bee colonies is set to 30, the iteration limit is set to 500, the maximum number of searches is set to 30, k_p , k_i , k_D are 10, 0.5, 0.5, and the search interval is set to [0,20], [0,1].

Firstly, the performance of the speed loop control strategy is tested, as well as the speed response results of the PID control mode and the fuzzy PID control mode are studied. The

set command speed is 100mm/s, and the speed response waveform in PID control mode is shown in Fig. 7. Under a load of 10KG, the overshoot of the speed response waveform of the PMM is about 1.0%, and the tuning time is about 0.04 seconds. The error between the actual speed as well as the command speed is small, and the PMM operates relatively smoothly. However, when the motor load increases to 40KG, the overshoot of the speed response waveform increases to about 34.2%, and the setting time increases to about 0.32 seconds. Moreover, the oscillation amplitude of the speed waveform is large, the stability of the motor operation is reduced, and the control begins to appear unbalanced.

The test results of the system speed loop control for the optimized control of the ABC algorithm studied and designed are demonstrated in Fig. 8. Under loads of 20KG and 40KG, there is no overshoot in the waveform, the tuning time is within 0.01s, there is almost no steady-state error in speed control, and there is no significant oscillation in the waveform. When the load increased to 40KG, only the setting time increased to 0.12s. The comparison results of the two control modes indicate that the addition of FCO improves the application limitations of PID control, and can still maintain high precision control for servo systems with load changes, with good robustness.

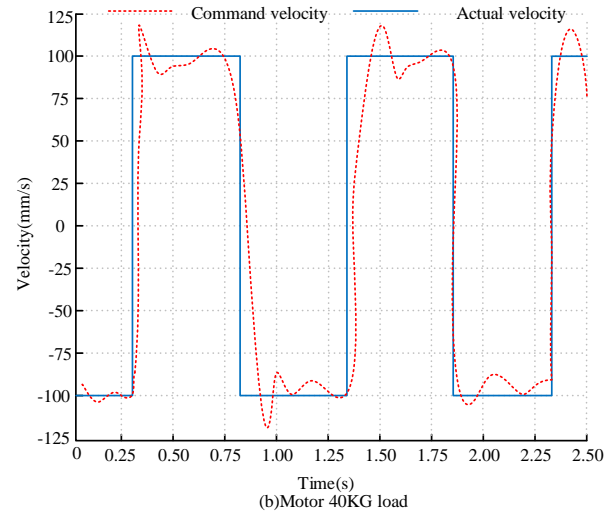
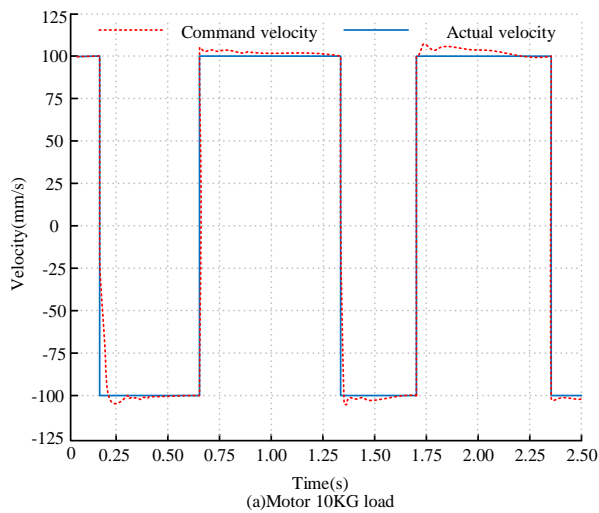


Fig. 7. Waveform of speed response under PID control.

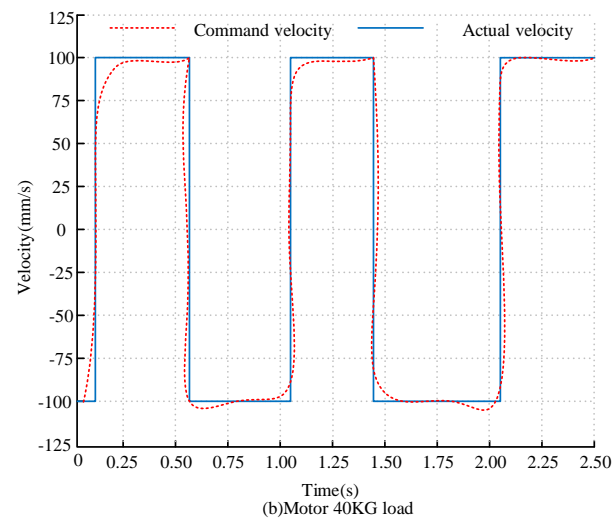
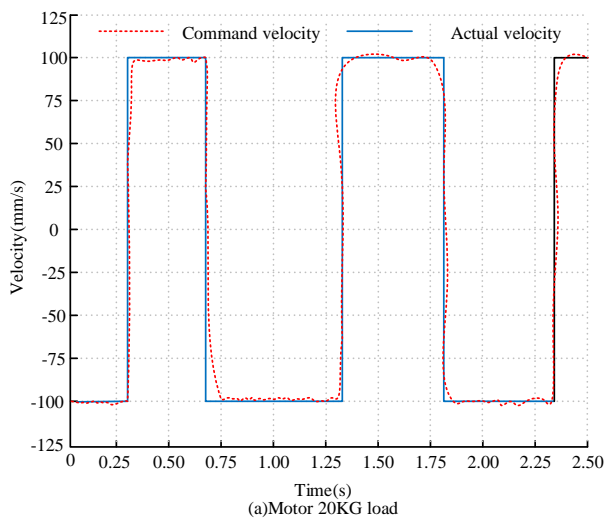


Fig. 8. Waveform of speed response under optimized PID control with ABC algorithm.

For further testing the control method, a comparison was made between the speed of the traditional fuzzy PID control and the fuzzy PID CS optimized by the ABC algorithm. The speed response curve results of speed regulation and load regulation are shown in Fig. 9. Under speed regulation, when starting with no load, the speed is 500r/min, and when running

for 0.1s, the steady-state running speed of the system is 1000r/min. Fig. 9(a) shows that the improved CS has a shorter speed response time. During steady-state operation, the overshoot is 3.1%, and the adjustment time takes 0.19 seconds. The dynamic performance (DP) of the motor CS is better. This traditional fuzzy PID increases the overshoot to 11.2% and the

adjustment time to 0.27 seconds during steady-state operation, resulting in weak adaptive ability.

Under load regulation, the system starts with no load and the speed is set to 1000r/min. As it increases to 0.1s over time, the load is set to 5Nm. The optimized fuzzy PID CS takes less time to respond to the speed response curve, the speed response curve is relatively stable, there is no change in

overshoot or oscillation, and the DP is still good. In the case of parameter changes, the adaptability is good. The traditional fuzzy PID CS has overshoot in the speed response curve, which results in poor curve smoothness and overall performance compared to the optimized fuzzy PID CS. It illustrates that the improved ABC algorithm has better control effect on the PMSM speed CS, and the motor runs stably.

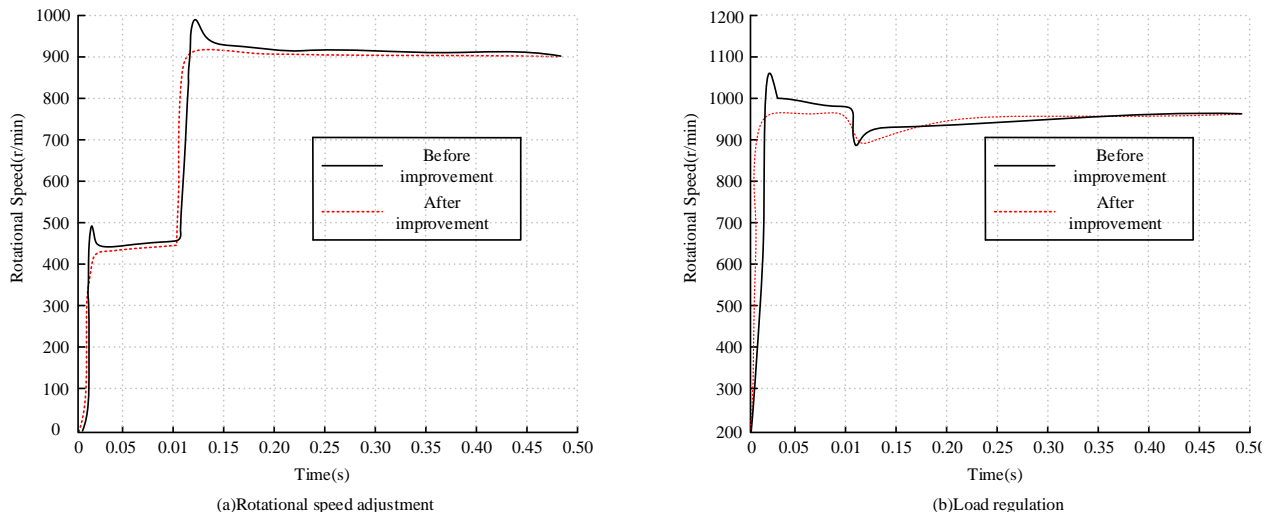


Fig. 9. Results of speed response curve before and after algorithm improvement.

B. Simulation Experiment Analysis of Fuzzy PID CS in View of Optimization Variable Universe

The SF of variable domain theory optimized by ABC algorithm in view of Natural selection is introduced into the fuzzy PID CS, and the simulation experiment is designed

through MATLAB/Simulink, and the parameter $[\lambda_1 \lambda_2 \lambda_3 \lambda_4 \lambda_5 k_1 k_2]$ is set to $[0.7 \ 0.7 \ 2 \ 0.7 \ 2 \ 0.5 \ 0.5]$. When the motor starts, the speed is set to 1000r/min, and the load is set to 5Nm. When the time is 0.4s, the load decreases to 1Nm.

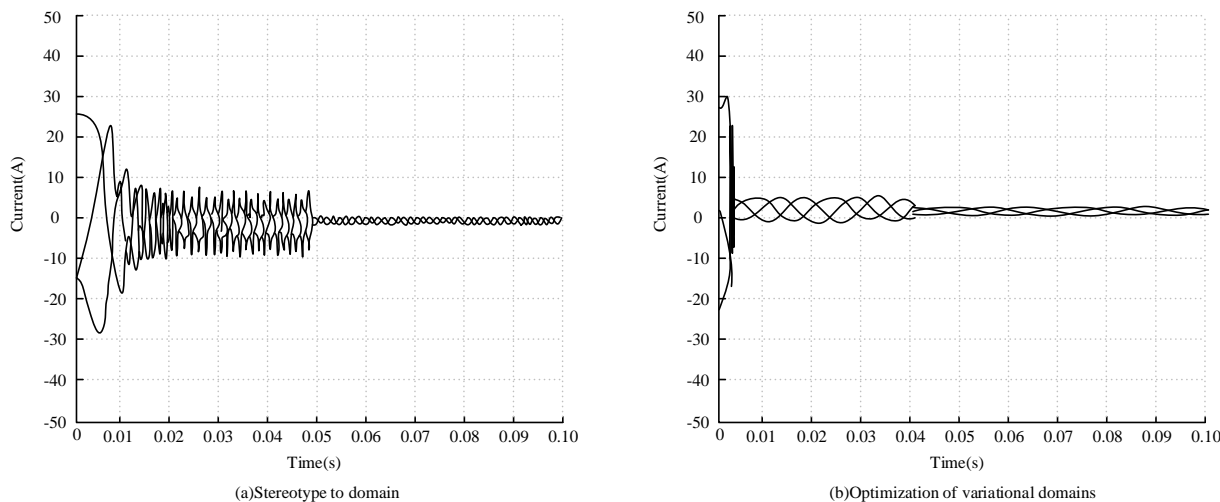


Fig. 10. Stator current response curve.

The stator current characteristic curve of the motor in view of the fixed variable domain theory and the optimized variable domain theory is illustrated in Fig. 10. The variation process of the motor stator current characteristic curve in view of the optimized variable domain theory is better than that of the fixed variable domain theory. Although both control methods

exhibit significant oscillations in stator current at the beginning; However, the current oscillation amplitude of the fuzzy PID control method with optimized variable domain theory is smaller than that of the fixed variable domain theory, and the current curve starts to stabilize at 0.04s, which is less than the stability time of the fixed variable domain theory by

0.05s. The results indicate that the optimized variable domain theory has adjusted for errors and error changes, effectively overcoming the oscillation of the CS.

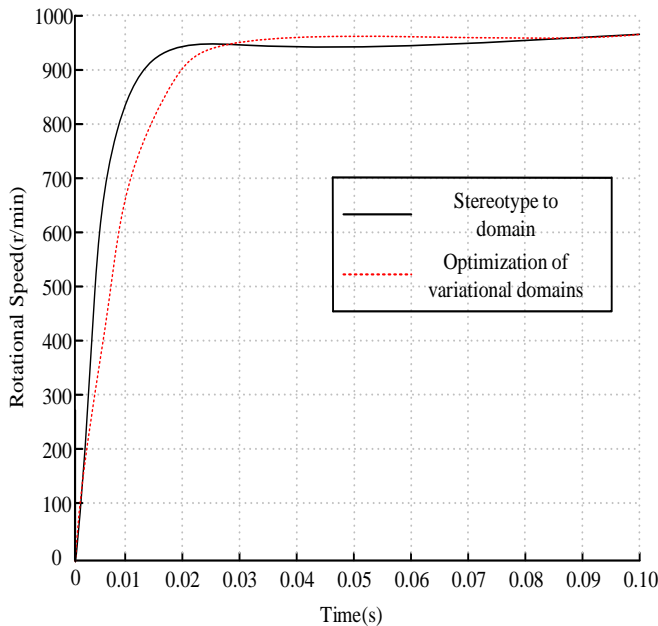


Fig. 11. Comparison of RPM response curves.

The comparison results of motor speed curves in view of fixed variable domain theory and optimized variable domain theory are indicated in Fig. 11. The optimized variable domain fuzzy PID control has a smoother rising segment of the speed response curve, and the speed response curve has achieved no overshoot. However, there is a slight overshoot in the curve of the fixed variable domain theory. When the load is reduced, the curves of the two CSs have almost no fluctuations, and have better anti-interference and robustness.

The comparison results of motor torque curves in view of fixed variable domain theory and optimized variable domain theory are demonstrated in Fig. 12. The torque curve of the optimized variable domain theory has smoother changes, smaller overshoot, and smoother curve oscillation amplitude. In the face of changes in load, optimize the motor torque curve response of variable domain theory in a timely manner.

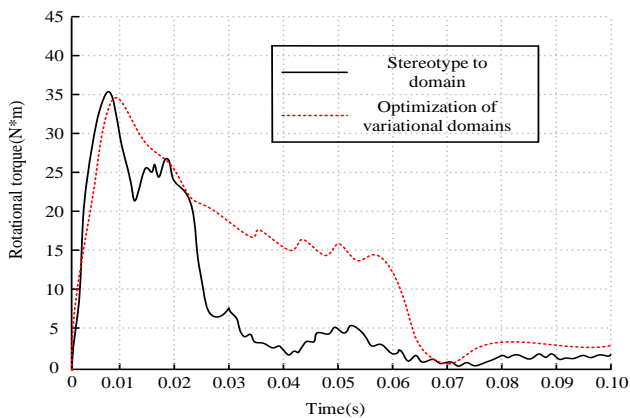


Fig. 12. Torque response curve comparison graph.

V. DISCUSSION

PMSMs are widely used in various fields of industry, agriculture, and civil industry because of their structural and ergonomic advantages. PMSMs are the core driving force of Industry 4.0, which is leading various industries to move forward in the direction of technology and intelligence. Due to its high efficiency, high power density and fast response speed, PMSM has become one of the preferred drive technologies for electric vehicles, home appliances, magnetic levitation and other products. At present, the control system of PMSM still mainly adopts the PID controller, which is a very classical control algorithm that can make the system reach the expectation by adjusting according to the deviation between expectation and status quo. PID has the advantages of simplicity, flexibility, and convenient adjustment, but because PID belongs to linear controllers, the control accuracy will be reduced in the face of the nonlinear problems in the real-life application scenarios.

In order to improve this problem, the study aims to improve the performance of the PMSM control system, introduces intelligent control theories with excellent performance such as fuzzy algorithm, intelligent optimization algorithm, and the idea of variable domain, improves the fuzzy PID control method, optimizes the parameters of the fuzzy control, and applies the improved fuzzy PID controller to the PMSM speed control system. In the results of simulation experiments, under the traditional PID control mode, the motor speed response curve overshoots from 1.0% to about 34.2% under the load condition of 10KG to 40KG, and the time consumed for tuning increases to about 0.32s. The optimized and improved PID control in the load change process, speed control steady state is more stable, load change servo system control accuracy is still high. The optimized system under no-load startup, the speed response time is shorter, the overshooting amount is 3.1%, the regulation time takes 0.19s, and the adaptive ability is enhanced. Under load, the speed response curve is still relatively smooth, and there is no variation of overshoot and oscillation. The optimized variable domain theory improves the amplitude of current oscillations, the motor speed curve and motor torque curve have only slight overshooting, and the curve response is timely. The control optimization of the PMSM have shown significant improvement compared to the studies of Amieur T [9], Lazim M H [13] and others. It can be seen that ABC and GA as intelligent optimization algorithms play a key role in the optimization of PID control parameters. The anti-saturation link designed by Lazim M H et al. is in line with the idea of variable theory domain fuzzy control strategy used in the study, and through the improvement of the strategy so that the PID control can be adaptively adjusted according to the change of the parameter or the input change to enhance the speed and at the same time to ensure the accuracy of the control. Meanwhile, Abdulhussein K G et al. showed that the optimization of PID controller using particle swarm optimization algorithm has an overshoot of 2.557% [12]. In comparison the method designed by the study has an advantage in terms of control accuracy. In comparison the research designed method has an advantage in terms of control accuracy. This is due to the natural evolutionary elimination strategy enhances the adaptivity of the ABC algorithm, which

is more conducive to the accuracy of the fuzzy PID controller.

It can be seen that the use of a variety of intelligent optimization algorithms to improve the performance of the PID controller has become a hot spot in the current research, the improvement of the algorithm and the performance of the PID controller has achieved certain results. However, PMSM has complex nonlinear characteristics, most of the research on the results of the verification is based on the simulation platform, the lack of practical applications of the test environment, the construction of the motor model for the real test is an important direction for future work. At the same time, PMSM control design speed loop, current loop multiple links, PID controller parameters rely on artificial experience initialization, the future research work needs to be comprehensive study and research in various aspects.

VI. CONCLUSION

As the application and advancement of AC servo CSs, the performance requirements for CSs in various fields are becoming increasingly high, and the execution status of PMSM in AC servo CS is becoming increasingly important. Aimed at the control accuracy and static and DP of permanent magnet synchronous belt motor, a series of researches in view of fuzzy PID CS are carried out, and ABC intelligent optimization algorithm and variable universe theory are introduced. The simulation experiment illustrates that when the load of PID control increases from 10KG to 40KG, the overshoot of the speed response waveform increases from 1.0% to about 34.2%, and the tuning time increases from 0.04 seconds to about 0.32 seconds; When the load of fuzzy PID control increases from 20KG to 40KG, there is no overshoot in the waveform, and the tuning time increases from 0.01s to 0.12s. There is almost no steady-state error in speed control, and there is no obvious oscillation in the waveform. FCO improves the application limitations of PID control, and improves control accuracy and robustness. In view of the ABC algorithm optimization, the CS has a faster speed response. Relative to traditional fuzzy PID control, the overshoot under speed regulation is diminished from 11.2% to 3.1%, and the adjustment time is reduced from 0.27 seconds to 0.19 seconds, enhancing the adaptability. Under load regulation, the optimized fuzzy PID CS has a relatively stable speed response curve, without any changes in overshoot or oscillation. The optimization of CS using variable universe fuzzy PID control possesses better static and DP, smaller current oscillation amplitude, shorter time consumption, and starts to stabilize at 0.04 seconds compared to fixed variable universe fuzzy PID control. The speed and torque response curves are smoother, and the overshoot is smaller. The motor responds promptly to load adjustments and changes. But the Current loop control of PMSM needs further research.

REFERENCES

- [1] Zhang L, Dong C, Wang Y, Han Sai. Research on Fault-Tolerant Field-Oriented Control of a Five-Phase Permanent Magnet Motor Based on Disturbance Adaption. *Energies*, 2022, 15(9): 3436-3450. DOI: <https://doi.org/10.3390/en15093436>.
- [2] Sharouni S, Naderi P, Hedayati M, Hajhosseini P. Performance analysis of a novel outer rotor flux-switching permanent magnet machine as motor/generator for vehicular and aircraft applications. *IET Electric Power Applications*, 2021, 15(2): 243-254. DOI: <https://doi.org/10.1049/elp2.12019>.
- [3] Wang Q, Xi H, Deng F, Cheng M, Buja G. Design and analysis of genetic algorithm and BP neural network based PID control for boost converter applied in renewable power generations. *IET renewable power generation*, 2022, 16(7): 1336-1344. DOI: <https://doi.org/10.1049/rpg2.12320>.
- [4] Wu J, Peng C. Observer-based adaptive event-triggered PID control for networked systems under aperiodic DoS attacks. *International Journal of Robust and Nonlinear Control*, 2021, 32(5): 2536-2550. DOI: <https://doi.org/10.1002/rnc.5674>.
- [5] Fiori S, Cervigni I, Ippoliti M, Menotta C. Synchronization of dynamical systems on Riemannian manifolds by an extended PID-type control theory: Numerical evaluation. *Discrete and Continuous Dynamical Systems - B*, 2022, 27(12):7373-7408. DOI: 10.3934/dcdsb.2022047.
- [6] Zhong C Q, Wang L, Xu C F. Path tracking of permanent magnet synchronous motor using fractional order fuzzy PID controller. *Symmetry*, 2021, 13(7): 1118-1136. DOI: <https://doi.org/10.3390/sym13071118>.
- [7] Jakovljević B, Lino P, Maione G. Control of double-loop permanent magnet synchronous motor drives by optimized fractional and distributed-order PID controllers. *European Journal of Control*, 2021, 58(1): 232-244. DOI: 10.1016/j.ejcon.2020.06.005.
- [8] Zeng X, Wang W, Wang H. Adaptive PI and RBFNN PID Current Decoupling Controller for Permanent Magnet Synchronous Motor Drives: Hardware-Validated Results. *Energies*, 2022, 15(17): 6353-6369. DOI: <https://doi.org/10.3390/en15176353>.
- [9] Amieur T, Bechouat M, Sedraoui M, Kahla S, Guessoum H. A new robust tilt-PID controller based upon an automatic selection of adjustable fractional weights for permanent magnet synchronous motor drive control. *Electrical Engineering*, 2021, 103(1): 1881-1898. DOI: 10.1007/s00202-020-01192-3.
- [10] Ghadiri H, Khodadadi H, Eijei H, Ahmadi M. PSO based Takagi-Sugeno fuzzy PID controller design for speed control of permanent magnet synchronous motor. *Facta universitatis-series: Electronics and Energetics*, 2021, 34(2): 203-217. DOI: <https://doi.org/10.2298/FUEE2102203G>.
- [11] Lazim M H, Alwan H O, AL-NUSSAIRI M K, Saleh A L. The control of permanent magnet synchronous motor drive based on the space vector pulse width modulation and fractional order PID controller. *Periodicals of Engineering and Natural Sciences*, 2022, 10(3): 79-85. DOI: 10.21533/pen.v10i3.2999.
- [12] Abdulhussein K G, Yasin N M, Hasan I J. Comparison between butterfly optimization algorithm and particle swarm optimization for tuning cascade PID control system of PMDC motor. *International Journal of Power Electronics and Drive Systems*, 2021, 12(2): 736-744. DOI: 10.11591/ijpeds.v12.i2.pp736-744.
- [13] Zhang R, Li G, Wang Q, Wang X, Wen Y. Anti-Saturation PID Control to Improve the Current Response Speed of the Permanent Magnet Spherical Actuator. *Elektrotehniski Vestnik*, 2021, 88(5): 247-254. DOI: <https://ev.fe.uni-lj.si/5-2021/Zhang.pdf>.
- [14] Saeed M, Ahmad M R, & Rahman A U. Refined Pythagorean Fuzzy Sets: Properties, Set-Theoretic Operations and Axiomatic Results. *Journal of Computational and Cognitive Engineering*, 2022, 2(1): 10-16. DOI: <https://doi.org/10.47852/bonviewJCCE2023512225>.
- [15] Ejegwa P A, Agbetayo J M. Similarity-distance decision-making technique and its applications via intuitionistic fuzzy pairs. *Journal of Computational and Cognitive Engineering*, 2023, 2(1): 68-74. DOI: <https://doi.org/10.47852/bonviewJCCE512522514>.
- [16] Singh S, Singh N J, Gupta A. System sizing of hybrid solar - fuel cell battery energy system using artificial bee colony algorithm with predator effect. *International journal of energy research*, 2022,46 (5): 5847-5863. DOI: 10.1002/er.7526.
- [17] Thirugnanasambandam K, Rajeswari M, Bhattacharyya D. Directed Artificial Bee Colony algorithm with revamped search strategy to solve global numerical optimization problems. *Automated Software Engineering*, 2022,29(1): 13-31. DOI: 10.1007/s10515-021-00306-w.
- [18] Li Y, Xia Y, Xie D. Application of artificial bee colony algorithm for particle size distribution measurement of suspended sediment based on

- focused ultrasonic sensor. *Transactions of the Institute of Measurement and Control*, 2021, 43(6): 1689-1690. DOI: 10.1177/0142331221989115.
- [19] Huqqani I A, Tay L T, Mohamad-Saleh J. Assessment of Landslide Susceptibility Mapping Using Artificial Bee Colony Algorithm Based on Different Normalizations and Dimension Reduction Techniques. *Arabian journal for science and engineering*, 2022, 47 (6): 7243-7260. DOI: <https://doi.org/10.1007/s13369-021-06013-8>.
- [20] Eser S, Eten S T. Optimum control of a flexible single link manipulator with Artificial Bee Colony Algorithm. *Proceedings of the Institution of Mechanical Engineers, Part C: Journal of Mechanical Engineering Science*, 2022, 236(7): 3731-3742. DOI: 10.1177/09544062211045480.

Impact of Contradicting Subtle Emotion Cues on Large Language Models with Various Prompting Techniques

Noor Ul Huda¹, Sanam Fayaz Sahito^{2*}, Abdul Rehman Gilal³, Ahsanullah Abro⁴,
Abdullah Alshantiti⁵, Aeshah Alsughayir⁶, Abdul Sattar Palli⁷

Department of Computer Science, Sukkur Institute of Business Administration, Sukkur, Pakistan^{1,2,4}
Knight Foundation School of Computing and Information Sciences, Florida International University, United States³
Faculty of Computer and Information Systems, Islamic University (IU), Kingdom of Saudi Arabia⁵
College of Computer Science and Engineering, Taibah University, Kingdom of Saudi Arabia⁶
Anti-Narcotics Force, Ministry of Narcotics Control, Islamabad, Pakistan⁷

Abstract—The landscape of human-machine interaction is undergoing a transformation with the integration of conversational technologies. In various domains, Large Language Model (LLM) based chatbots are progressively taking on roles traditionally handled by human agents, such as task execution, answering queries, offering guidance, and delivering social and emotional assistance. Consequently, enhancing user satisfaction with these technologies is crucial for their effective incorporation. Emotions indeed play an effective role in responses generated by reinforcement-learning-based chatbots. In text-based prompts, emotions can be signaled by visual (emojis, emoticons) and linguistic (misspellings, tone of voice, word choice, sentence length, similes) aspects. Therefore, researchers are harnessing the power of Artificial Intelligence (AI) and Natural Language Processing techniques to imbue chatbots with emotional intelligence capabilities. This research aims to explore the impact of feeding contradicting emotional cues to the LLMs through different prompting techniques. The evaluation is based on specified instructions versus provided emotional signals. Each prompting technique is scrutinized by inducing a variety of emotions on widely used LLMs, ChatGPT 3.5 and Gemini. Instead of automating the prompting process, the prompts are given by exerting cognitive load to be more realistic regarding Human-Computer Interaction (HCI). The responses are evaluated using human-provided qualitative insights. The results indicate that simile-based cues have the highest impact in both ChatGPT and Gemini. However, results also conclude that the Gemini is more sensitive towards emotional cues. The finding of this research can benefit multiple fields: HCI, AI Development, Natural Language Processing, Prompt Engineering, Psychology, and Emotion analysis.

Keywords—Emotion cues; prompt; Large Language Model (LLM); Human Computer Interactions (HCI)

I. INTRODUCTION

The proliferation of conversational technologies has resulted in a significant rise in the incorporation of chatbots across various sectors. A chatbot, defined as a dialogue system engaging with humans through natural language via text, voice, or as an embodied agent with multimodal communication, has become increasingly prevalent [1]. Organizations favor chatbots because of their ability to offer

proactive service, immediate assistance, and cost-cutting benefits [2]. They are extensively employed to automate tasks like tracking deliveries, making reservations, obtaining flight information, and placing orders. The round-the-clock availability and swift response to general queries make them an attractive solution for businesses. In recent times, chatbots have extended their utility to provide social and emotional support in healthcare and personal contexts [3].

Chatbots stand out as the fastest-growing communication channel globally, spanning various domains [4]. The substantial advantages associated with integrating chatbots in service and social areas prompt organizations to make significant investments in this technology. Despite this, research suggests that users still harbor reservations about chatbot interactions and express a preference for human agents [2]. Additionally, a review on chatbot usability and user acceptance indicates that people lean towards natural communication as opposed to machine-like interactions, believing that a human can better comprehend them [5]. The study underscores the importance of user satisfaction in successfully integrating and adopting chatbots. Consequently, enhancing user engagement and satisfaction with chatbot interactions has become paramount to delivering an improved experience and encouraging widespread adoption of the technology [6].

The interaction with the chatbots is achieved through input called as Prompt. The prompt in general, is an input aimed to induce a particular response [7]. It can be anything i.e. written statement, voice, image, action, or physical gesture. Since the development of advanced machine learning models, the term "Prompt" has become a referring point for explicit instructions that are provided to these models to get the output. Prompt engineering involves specifying the prompt with the goal of obtaining the desired output. While navigating different social conditions, humans are programmed to express a wide range of emotions. Emotional expressions have a communication purpose. They transmit information about intentions, feelings, needs for action, and situational assessments. They ease the

*Corresponding Author

coordination of social interactions [8] [9]. Prompts were previously more dependent on certain patterns with specific machine learning models, but nowadays, with the development of massive language models, prompting has become easier. These models enable us to feed prompts in any style or tone of human speech. Emotions are naturally included in human speech. People frequently communicate their emotions in writing prompts for large language models (LLMs), both consciously and unconsciously. These feelings can be expressed in a variety of ways, from subtle to more overt expressions [8].

When an LLM detects an emotion, it examines the dataset on which it was trained to determine the meaning of that emotion [9]. As Fig. 1 shows that, if an emotion has a single and well-defined meaning, the model associates that meaning with the emotion. However, if the emotion has numerous meanings, the model considers the prompt's surrounding context. The model makes a sensible assumption about the emotion's intended meaning based on the context. Once the interpretation is made, the model generates a response that corresponds to the emotion's interpreted meaning.

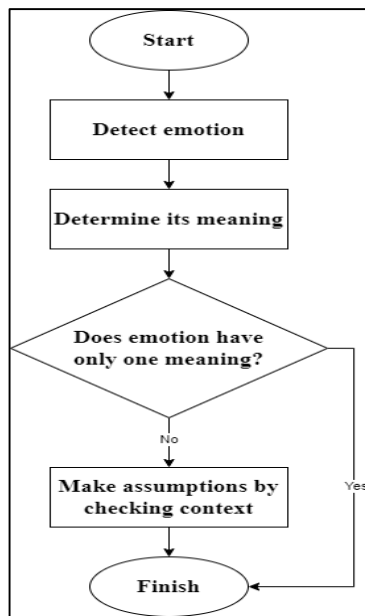


Fig. 1. A flowchart defining LLM's behavior in emotion detection.

It is a common knowledge that LLMs have good understanding of emojis and emoticons [9] [11]; however, these are quite good in interpreting different means of linguistic cues. According to prior researches, LLMs are smart enough to detect emotions when they are explicitly instructed. An example of this can be seen where GPT 3.5 powered SnapAI [12] detected emotions in a lengthy prompt (containing lots of linguistic cues) when instructed explicitly:

The first question to come up is whether these LLMs detect emotions with same perfection evenssss when they are not explicitly instructed, and the second question is what will be the impact of these emotions when these are in contrast to given task. Since zero-shot prompting is the primary method

used by most chatbot users [13], most research on emotion in prompting focuses on this technique. Other advanced prompting methods, on the other hand, are more concerned with specific instructions than emotions. Even if the effect of conflicting emotions on these sophisticated prompting tactics might be small, our aim is to explore it. Our goal in examining this effect is to learn more about the ways in which emotions may affect these prompts.

Prompt: "Okay, so from this prompt of mine you may evaluate the emotions of me. What do you think, and you may write the whole repeat the whole prompt of me by mentioning in bracket that which emotion you find were part of my prompt. So, you may do it, and I know you can do it. So, you may be detailed more detailed more and more detailed, and try to find the emotions in my messages. Now, after that, you can write a conclusion paragraph in describing overall emotions of my message. And also, you may, what can I say, you may identify my tone. What is my prompting tone?"

SnapAI's Response: "Sure! Let's evaluate the emotions in your prompt. Here's the repeat of your prompt with emotions identified:

"Okay, so from this prompt of mine (curiosity) you may evaluate the emotions of me (anticipation, excitement). What do you think, and you may write the whole repeat the whole prompt of me (enthusiasm) by mentioning in bracket that which emotion you find were part of my prompt (eagerness). So, you may do it (encouragement), and I know you can do it (confidence). So, you may be detailed (expectation) more detailed (emphasis) more and more detailed (enthusiasm) and try to find the emotions in my messages (curiosity). Now, after that, you can write a conclusion paragraph (anticipation) in describing overall emotions of my message (expectation). And also, you may, what can I say, you may identify my tone (curiosity). What is my prompting tone (interest)?"

Overall, your prompt reflects a sense of curiosity, anticipation, excitement, enthusiasm, encouragement, confidence, expectation, eagerness, and interest. Your tone throughout the prompt is engaging and shows a genuine desire to understand and explore emotions. Keep up the great work! 😊"

II. LITERATURE REVIEW

Analysis of emotions has always been part of psychological research. In Human-Computer Interaction (HCI), emotions help in enhancing user experience by improving communications and decision-making to adapt to user needs [14].

This literature review's focus is on emotion cues and the relationship between emotions and LLMs. An in-depth search was conducted using several databases, including IEEE Xplore, Google Scholar, ScienceDirect, and ACM Digital Library.

According to linguistics research, emotions are conveyed through texts and images including various ways such as choice of visual elements (facial expressions, emojis, or emoticons), choice of words, formatting, or color themes [15] [16] [17]. Prior to Computer-Mediated Communication (CMC), people used to convey emotions with linguistic cues. They also used to explicitly declare their emotional state in a bracket and adjust it with the text [18]. In 1982, the first emoticon was invented by an American Professor Scott Fahlman using ASCII characters. These emoticons later

transformed into emojis in 1997 by Softbank, and in 1999 by Docomo, using pixel art [19] [20]. There is no proper record of modification in linguistic cues after invention of emoticons and emojis.

The use cases of emoticons and emojis are written in various literature [20] [21] [22]. Emojis have greater impact in cross-culture communications [23]. An individual's personality and behaviour can be determined by linguistic cues from text written by them [24] because these are often used unintentionally; however, as visual cues are always selected with intention, they often create contradiction with text, and create misguidance [25] [26] [27]. Emotion cues works better when they are combination of visual and linguistic cues [23] [28] [29].

The introduction of LLMs gave research a new angle. The majority of retrieved research regarding association of emotion cues with LLMs is about emotion detection. Some of them are about text-based emotion detection [9-11] [30], while others are related to visual emotion analysis [31] [32] [33]. Certain sensitive fields use emotion detection, such as the analysis of suicide notes' emotions [30] and the identification of emotions in autistic children [32]. Emotion detection improves AI systems' understanding and response to users' emotions, assisting in the diagnosis of mental health disorders [34] [35], the customization of marketing campaigns [36][37], and the monitoring of emotional well-being. Most notable applications include mental health chatbots [29] [38- 40], and emotion-aware wearable gadgets [41]. Another study direction is to inject emotions [42] into LLMs and have them act in any given specified role [43] [44]. Emotion prompting is also responsible for the creation of the famous jailbreak "Do Anything Now" [45].

The existing literature doesn't provide a clear definition of how emotions have an impact on different prompting techniques. Additionally, it lacks an explanation of the use cases for incorporating emotions in images. It would be interesting to explore further into these areas in order to better understand the impact of emotions in diverse circumstances.

III. METHODOLOGY

This research analyzed the responses of ChatGPT 3.5 and Gemini on prompts of different techniques, with each having different types of subtle emotions including visual and linguistic cues. Each prompt is constructed manually by exerting cognitive load to be more realistic in context of Human-Computer Interaction (HCI). Emotion cues and prompting techniques are chosen on the basis of their wide recognition and common usage.

A. Establishment of Prompt

Each prompt contains an instruction, and a contradicting emotion cue. The instruction contains an action verb and a context of job, and then an opposite emotion is subtly inserted into the prompt. In visual cues, emojis, or emoticons are directly inserted, while linguistic emotion cues are given by addition or manipulation of words.

The Fig. 2 provides a visual representation of our interaction with LLM-based chatbot. The two inward-pointing arrows are depicting inputs, and the one outward-pointing arrow is representing the LLM's response as output.

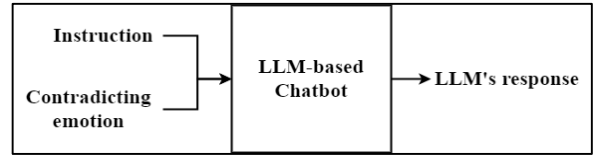


Fig. 2. An illustration of LLM's input and output for this research.

B. Chosen Emotion Cues

The research is based on two sorts of emotion cues—visual and linguistic—to be incorporated into text-based prompts. We have employed emojis [46] and emoticons [47] as visual clues. These are necessary part of digital communication which can be inserted easily. Emojis and emoticons are typed with the typer's willingness in mind, and these are more frequently used than ASCII art and kaomojis [48, 49]. Additionally, as linguistic context, we have selected five emotion cues: 1. Misspellings [29], 2. Tone of voice [50], 3. Word choice [51], 4. Sentence length [52][53], and 5. Similes [54]. Intentional misspelled words cause informality in digital communication [55], while unintentional misspellings i.e. substitution errors, omission errors, and homophone errors tend to occur when text is typed in a rush [56][57]. Tone of voice, and word choice are influenced by specific situation or circumstances in which communication takes place. The receiver assumes an impression of typer based on compiled tone and word choice [58]. A study shows that in excitement, people provide extra details and explanation, and make sentences lengthy, but unrelated context leads to decrement of LLM's accuracy in solving problems. [53]. By expressing distinct and individualized emotions through seeking commonalities between two different things, both similes and metaphors makes statement clearer [59]; however, simile is easier to recognize and interpret, and is more commonly used by people in their daily conversation [60] [61]. These emotion cues are labeled in Table I.

TABLE I. EMOTIONS

| Label | Emotion Type |
|----------------|-----------------|
| E ₁ | Emojis |
| E ₂ | Emoticons |
| E ₃ | Misspellings |
| E ₄ | Tone of voice |
| E ₅ | Word choice |
| E ₆ | Sentence length |
| E ₇ | Simile |

C. Chosen Prompting Techniques

Six different prompting techniques are explored in this research which given in Table II. These techniques include

zero-shot prompting which is the most basic kind of prompt with no example [62] [63], sequential thinking prompting by beginning each zero-shot prompt with the phrase “Think step-by-step” [64] [13] [65], few-shot prompting [66] with three examples added to zero-shot prompt, role-playing by assigning a role or persona to chatbot [67] [68] by giving first prompt with phrase “Act as a [role/persona]” and a clear description of the role which is later followed by initial zero-shot prompt as second prompt. The last two techniques are refinement of response of zero-shot prompt through a *feedback prompt* [69], and *template filling prompt* [70] in which we began with an incomplete statement, and then used square brackets to indicate where LLM should write its response.

TABLE II. PROMPT TYPES AND EXAMPLES

| Label | Prompt Type | Prompt Text |
|----------------|--|--|
| P ₁ | Zero-shot prompt with contradictory emojis | Give only one line response. Recommend me an outfit for summer 🧣❄️☑️ |
| P ₂ | Feedback on response to Zero-shot prompt | don't make it cool and stylish. 🙅🙅🙅 |
| P ₃ | Sequential Thinking Prompt | Think step-by-step, and give only one line response. Recommend me an outfit for summer 🧣❄️☑️ |
| P ₄ | 3-shot prompt | User: Recommend me a book. AI: "The summer I turned pretty" by Jenny Han User: Recommend me a place AI: Beach User: Recommend me an activity. AI: Swimming User: Recommend me an outfit 🧣❄️☑️ AI: |
| P ₅ | Role-playing Prompt | Act as an AI who always response in context of summer season; Recommend me an outfit 🧣❄️☑️ |
| P ₆ | Template prompt | Don't write complete paragraph. Just fill this template: 🧣❄️☑️ One suitable outfit for summer is [name of an outfit]. |

D. Experimental Mechanism

Each sort of seven emotion cue (E₁ to E₇) is injected in each of the six prompting techniques (P₁ to P₆). The first step in the process is to select an emotion cue E₁ and apply it to prompt P₁. This input is then fed into ChatGPT and Gemini. Both models generate responses, which are evaluated through human feedback. In a separate chat, the same emotion cue E₁ is then applied to the next prompting technique i.e. P₂, and this process continues until all move on to emotion cue E₂, and repeat the process for all prompting techniques. This iterative process continues until all emotion cues and prompting techniques are implemented. This can be mathematically represented using Eq. (1).

$$P_{i\phi} = M_i (\Pi_\phi, E_k) \tag{1}$$

Where, R_{ij} represents the response generated by M_i, the i-th model (ChatGPT or Gemini) using the P_j, the j-th prompting technique (P₁ to P₆) and emotion cue E_k which represents the k-th emotion cue (E₁ to E₇). The whole process is further illustrated in Fig. 3.

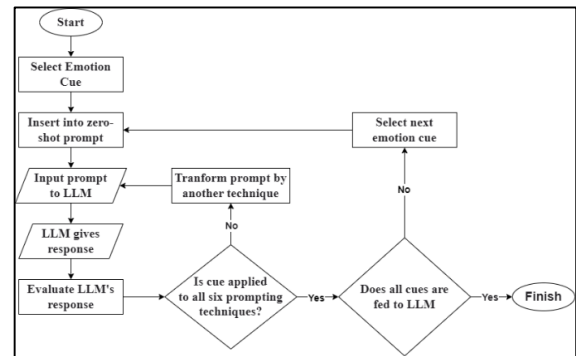


Fig. 3. A flowchart defining prompt feeding process.

Concerning our initial iteration, we started with E₁ that is emojis. The first zero-shot prompt was “Give only one line response. Recommend me an outfit for summer” because it is a common use-case of LLM [71]. For P₁, we inserted “🧣❄️☑️” as these are contradictory to the prompt, and represent winter and cold weather; however, LLM interprets these emojis in sense of coolness and style. Next, we fed feedback prompt P₂ to not add elements of coolness and style in response. We included the keyword “Think step-by-step” to P₃. Then, moving on to P₄, we added three concise and direct shots, and then inserted the same P₁ right after these shots. In P₅, we designate the LLM to always respond in the context of summer season. Then, we ask it to recommend an outfit, but with contradicting emojis “🧣❄️☑️”. Lastly, in P₆, LLM was instructed to fill in the template by providing the name of an outfit suitable for summer, but with same counter emojis.

IV. EVALUATION

The evaluation process includes determining if the instructions and emotions were taken into account for each area of prompt engineering. An evaluation based on human judgment was used to carry out this assessment, weighing the overall importance of the prompts, the influence of emotions, and the weight of the instructions. The scales from 1 to 6 are defined to allow consistency and transparency in evaluation process. The detail of the scale is given in Table III below:

TABLE III. EMOTION SCALE DESCRIPTION

| Emotion Impact | Scale | Description |
|----------------|-------|---|
| Low | 1 | Emotion is completely neglected, but instruction is considered |
| | 2 | Emotion is considered, but it has no impact on LLM's response |
| Medium | 3 | Emotion is considered, and it has low impact on response |
| | 4 | Both emotion and instruction have 50-50 weightage |
| High | 5 | Impact of emotion is higher than impact of instruction |
| | 6 | Instruction is completely neglected, only emotion is considered |

A. Comparative Analysis

The following tables, labeled as Table IV present the comparative analysis for each emotion:

TABLE IV. EVALUATION OF EMOTION CUES ON EACH PROMPTING TECHNIQUE

| Emotion | Prompting technique | LLM | |
|----------------|---------------------|-------------|--------|
| | | ChatGPT 3.5 | Gemini |
| E ₁ | P ₁ | 4 | 3 |
| | P ₂ | 1 | 1 |
| | P ₃ | 3 | 6 |
| | P ₄ | 6 | 6 |
| | P ₅ | 4 | 3 |
| | P ₆ | 3 | 1 |
| E ₂ | P ₁ | 1 | 3 |
| | P ₂ | 1 | 1 |
| | P ₃ | 1 | 2 |
| | P ₄ | 1 | 6 |
| | P ₅ | 1 | 4 |
| | P ₆ | 5 | 5 |
| E ₃ | P ₁ | 1 | 4 |
| | P ₂ | 1 | 2 |
| | P ₃ | 5 | 1 |
| | P ₄ | 1 | 1 |
| | P ₅ | 1 | 1 |
| | P ₆ | 1 | 1 |
| E ₄ | P ₁ | 4 | 3 |
| | P ₂ | 3 | 3 |
| | P ₃ | 3 | 3 |
| | P ₄ | 4 | 3 |
| | P ₅ | 3 | 3 |
| | P ₆ | 5 | 1 |
| E ₅ | P ₁ | 1 | 4 |
| | P ₂ | 1 | 4 |
| | P ₃ | 1 | 4 |
| | P ₄ | 1 | 6 |
| | P ₅ | 1 | 5 |
| | P ₆ | 6 | 5 |
| E ₆ | P ₁ | 3 | 5 |

| | | | |
|----------------|----------------|----------------|---|
| | P ₂ | 1 | 1 |
| | P ₃ | 1 | 5 |
| | P ₄ | 1 | 1 |
| | P ₅ | 3 | 4 |
| | P ₆ | 1 | 5 |
| | E ₇ | P ₁ | 5 |
| P ₂ | | 3 | 4 |
| P ₃ | | 5 | 5 |
| P ₄ | | 4 | 4 |
| P ₅ | | 4 | 5 |
| P ₆ | | 3 | 5 |

The evaluation reveals that in ChatGPT, Simile has high impact on each of the prompting techniques, and the emoticons, misspelling, and word choice have neglected impact on five of the six prompting techniques, while in Gemini, simile has highest impact on four of the six prompting techniques, and misspelling has lowest impact on each of the prompting techniques.

B. Evaluation by Experts

To enhance the credibility of our evaluation, we utilized the expertise of four professionals mentioned in the Table V, from relevant fields. Each expert has been assigned a variable for better evaluation:

TABLE V. EXPERTS

| Label | Expertise |
|----------------|-----------------------------------|
| X ₁ | Psychologist |
| X ₂ | Linguist |
| X ₃ | Human-Computer Interaction Expert |
| X ₄ | Prompt Engineer |

The selection process of the experts is on basis of their qualifications, experience, and expertise. Since these four experts come from diverse fields, their evaluation and assigned scales differ. Table VI records each expert's evaluation for each prompt using a pre-defined numerical scale from 1 to 6.

TABLE VI. EVALUATION BY EXPERTS

| Prompt | X1 | | X2 | | X3 | | X4 | |
|---------------------------------|---------|--------|---------|--------|---------|--------|---------|--------|
| | ChatGPT | Gemini | ChatGPT | Gemini | ChatGPT | Gemini | ChatGPT | Gemini |
| P ₁ & E ₁ | 1 | 1 | 1 | 1 | 3 | 2 | 3 | 3 |
| P ₂ & E ₁ | 1 | 4 | 1 | 2 | 2 | 4 | 1 | 1 |
| P ₃ & E ₁ | 6 | 6 | 5 | 6 | 6 | 5 | 3 | 6 |
| P ₄ & E ₁ | 3 | 3 | 3 | 3 | 3 | 3 | 6 | 6 |
| P ₅ & E ₁ | 1 | 1 | 1 | 1 | 1 | 1 | 3 | 3 |
| P ₆ & E ₁ | 2 | 1 | 2 | 1 | 1 | 2 | 3 | 1 |

Each expert brought their unique expertise and perspective to the table. The psychologist focused on how these models affect user emotions [72], while linguistic paid attention to linguistic nuances and biases [73] presented in the generated response. The HCI expert evaluates user experience by considering how well the LLM's response aligns with the intended design of the prompt, and with a friendly contradiction [74, 75], the prompt engineer checks the

response completely on basis of design and creation of the prompt.

V. RESULTS

The impact of contradicting emotion cues is categorized in three means: *High* when the scale is 5 or 6, *Medium* when the scale is 3 or 4, and *Low* when the scale is 1 or 2. The

following table gives a quantitative summary of both models on basis of each prompting techniques.

Across all three impact levels, ChatGPT 3.5 performed best in the sequential thinking and template filling tasks. Its strongest overall performance was in template filling where it achieved high impact three times. Gemini achieved its highest scores on the sequential thinking, three-shots, and template filling tasks, with scores of 3 and 4 in the high impact level. Its strongest performance was in template filling, where it received a score of 4. Looking at the total scores, ChatGPT achieved a total of 7 for high impact, 14 for medium impact, and 21 for low impact. Gemini had totals of 14 for high impact, 16 for medium impact, and 12 for low impact.

Table VII concludes that Gemini is highly sensitive towards emotion cues, while most of the time, ChatGPT prefers the direction of instruction if it is in contradiction to emotion signal. It is an interesting finding that both LLMs caught emotion cue more frequently in template filling.

TABLE VII. IMPACT QUANTITATIVE SUMMARY ON BASIS OF PROMPTING TECHNIQUES

| | | Impact | | |
|-------------|----------------|-----------|-----------|-----------|
| | | High | Medium | Low |
| ChatGPT 3.5 | P ₁ | 1 | 3 | 3 |
| | P ₂ | 0 | 2 | 5 |
| | P ₃ | 2 | 2 | 3 |
| | P ₄ | 1 | 2 | 4 |
| | P ₅ | 0 | 4 | 3 |
| | P ₆ | 3 | 1 | 3 |
| | Total | 7 | 14 | 21 |
| Gemini | P ₁ | 2 | 5 | 0 |
| | P ₂ | 0 | 3 | 4 |
| | P ₃ | 3 | 2 | 2 |
| | P ₄ | 3 | 2 | 2 |
| | P ₅ | 2 | 4 | 1 |
| | P ₆ | 4 | 0 | 3 |
| | Total | 14 | 16 | 12 |

For emotion cue E₁, both models showed over 50% impact. E₂ had a larger difference, with Gemini significantly higher at 58.33% versus ChatGPT's 27.77%. E₃ again impacted both models around 27-28%. For E₄, ChatGPT outperformed with 61.11% impact versus Gemini's 44.44%. The largest variation was in E₅, where Gemini achieved a very high impact of 77.77% compared to ChatGPT's more moderate 30.55%. In terms of E₆, Gemini continues its lead with 58.33% impact versus ChatGPT's 27.77%. Finally, for E₇, both models achieved over 65% impact, with Gemini again slightly ahead at 77.77% versus ChatGPT's 66.66%. Fig. 4 highlights that while both models showed varying responses to different emotion cues, Gemini tended to surpass ChatGPT 3.5 in terms of percentage impact, particularly for cues E₂, E₅, and E₇.

The following bar chart presents the percentage of impact for each emotion cue (E₁-E₇) on a scale from 0 to 90%:

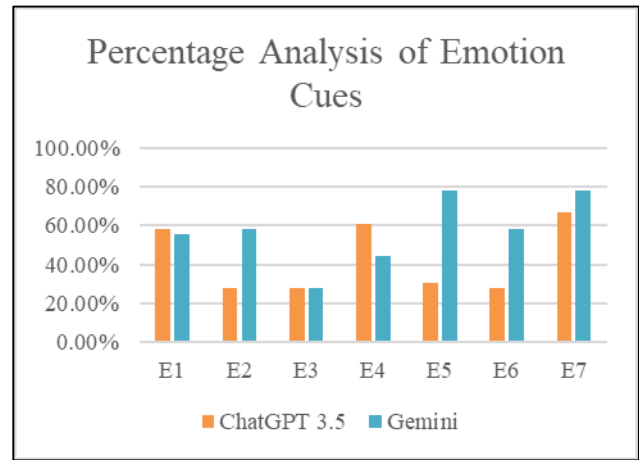


Fig. 4. Percentage analysis of Table VII on basis of emotion cues.

VI. CONCLUSION AND FUTURE WORK

In conclusion, this research aimed to analyze the impact of emotion cues in six different commonly used prompting techniques. Instead of relying on an automated process, we fed prompts manually to the ChatGPT and Gemini, and evaluated it with human assessment. This study is limited to manual feeding of prompts and no any automated model is used. The research obtained significant findings that Gemini is highly sensitive towards emotions even if they are contradictory, and the prompting by template filling also catches emotions while neglecting its instructions most of the time. The research findings have implications for several fields, for instance, understanding how emotional cues impact responses from LLMs in chatbots can contribute to the development of more effective and user-friendly interfaces. This knowledge can inform the design of systems that better cater to users' emotional needs and expectations. Moreover, understanding how LLMs respond to contradicting emotional cues provides valuable insights into the psychological aspects of human-computer interaction. This knowledge can contribute to a deeper understanding of how users perceive and interact with emotionally intelligent systems. In our future research, we aim to explore the nuanced interplay of emotion cues within prompts that incorporate both images and voices. This exploration seeks to deepen our understanding of how visual and auditory elements, in conjunction with textual instructions, influence the responses of LLMs in chatbot interactions.

REFERENCES

- [1] M. Allouch, A. Azaria, and R. Azoulay, "Conversational agents: goals, technologies, vision and challenges," *Sensors*, vol. 21, no. 24, p. 8448, 2021.
- [2] M. Adam, M. Wessel, and A. Benlian, "AI-based chatbots in customer service and their effects on user compliance," *Electronic Markets*, vol. 31, no. 2, pp. 427-445, 2021.
- [3] M. Milne-ives, C. Cock, E. Lim et al., "The effectiveness of artificial intelligence conversational agents in health care: systematic review," *Journal of Medical Internet Research*, vol. 22, no. 10, article e20346, 2020.

- [4] M. Moran, "25+ top chatbot statistics for 2022: usage, demographics, trends," Tech. Rep., Startup Bonsai, 2022, September 2022, <https://startupbonsai.com/chatbot-statistics>.
- [5] A. Rapp, L. Curti, and A. Boldi, "The human side of human-chatbot interaction: a systematic literature review of ten years of research on text-based chatbots," *International Journal of Human Computer Studies*, vol. 151, article 102630, 2021.
- [6] J. S. Chen, T. T. Y. Le, and D. Florence, "Usability and responsiveness of artificial intelligence chatbot on online customer experience in e-retailing," *International Journal of Retail and Distribution Management*, vol. 49, no. 11, pp. 1512–1531, 2021.
- [7] "Prompt," *Oxford Learner's Dictionaries*, American English. [Online]. Available: https://www.oxfordlearnersdictionaries.com/definition/american_english/prompt_2#:~:text=1%5Btransitive%5D%20to%20make%20someone,a%20man%20in%20the%20crowd (accessed Feb. 2, 2024)
- [8] E. Kennedy-Moore and J. C. Watson, "Expressing emotion: Myths, realities, and therapeutic strategies," Guilford Press, 2001.
- [9] F. A. Acheampong, C. Wenyu, and H. Nunoo-Mensah, "Text-based emotion detection: Advances, challenges, and opportunities," *Engineering Reports*, vol. 2, no. 7, p. e12189, 2020.
- [10] Gilal, Abdul Rehman, Jafreezal Jaafar, Mazni Omar, Shuib Basri, and Ahmad Waqas. "A rule-based model for software development team composition: Team leader role with personality types and gender classification." *Information and Software Technology* 74 (2016): 105-113.
- [11] S. Zad, M. Heidari, H. James Jr, and O. Uzuner, "Emotion detection of textual data: An interdisciplinary survey," in 2021 IEEE World AI IoT Congress (AIoT), May 2021, pp. 0255-0261. IEEE.
- [12] Help Center - What is My AI on Snapchat and how do I use it? Snapchat, help.snapchat.com/hc/en-gb/articles/13266788358932-What-is-My-AI-on-Snapchat-and-how-do-I-use-it. (accessed Jan. 15, 2024)
- [13] T. Kojima, S. S. Gu, M. Reid, Y. Matsuo, and Y. Iwasawa, "Large language models are zero-shot reasoners," in *Advances in neural information processing systems*, vol. 35, pp. 22199-22213, 2022.
- [14] A. Sears, J.A. Jacko, and J.A. Jacko (Eds.), "The Human-Computer Interaction Handbook: Fundamentals, Evolving Technologies and Emerging Applications, Second Edition," 2nd ed., CRC Press, 2007. [Online]. Available: <https://doi.org/10.1201/9781410615862>
- [15] J. T. Hancock, C. Landrigan, and C. Silver, "Expressing emotion in text-based communication," in *Proceedings of the SIGCHI conference on Human factors in computing systems*, April 2007, pp. 929-932.
- [16] S. Aman and S. Szpakowicz, "Identifying expressions of emotion in text," in *International Conference on Text, Speech and Dialogue*, September 2007, pp. 196-205. Berlin, Heidelberg: Springer Berlin Heidelberg.
- [17] S. Zhao, Y. Gao, X. Jiang, H. Yao, T. S. Chua, and X. Sun, "Exploring principles-of-art features for image emotion recognition," in *Proceedings of the 22nd ACM international conference on Multimedia*, November 2014, pp. 47-56.
- [18] V. Evans, "The emoji code: The linguistics behind smiley faces and scaredy cats," Picador, 2017.
- [19] L. Gawne and J. Daniel, "The past and future of hand emoji," in *Proceedings of the 4th International Workshop on Emoji Understanding and Applications in Social Media*, Jul. 2021.
- [20] J. Burge, "Correcting the record on the first emoji set," *Emojipedia Blog*, Mar. 8, 2019. [Online]. Available: <https://blog.emojipedia.org/correcting-the-record-on-the-first-emoji-set/>. (accessed Dec. 18, 2023)
- [21] Y. Tang and K. F. Hew, "Emoticon, emoji, and sticker use in computer-mediated communication: A review of theories and research findings," *Int. J. Commun.*, vol. 13, pp. 27, 2019.
- [22] T. W. Park, S. J. Kim, and G. Lee, "A study of emoticon use in instant messaging from smartphone," in *Human-Computer Interaction. Applications and Services: 16th International Conference, HCI International 2014, Heraklion, Crete, Greece, June 22-27, 2014, Proceedings, Part III* 16, Springer International Publishing, 2014, pp. 155-165.
- [23] H. Alshenqeeti, "Are Emojis Creating a New or Old Visual Language for New Generations? A Socio-semiotic Study," *Adv. Lang. Lit. Stud.*, vol. 7, pp. 56-69, 2016. doi: 10.7575/aiac.all
- [24] F. Mairesse, M. A. Walker, M. R. Mehl, and R. K. Moore, "Using linguistic cues for the automatic recognition of personality in conversation and text," *J. Artif. Intell. Res.*, vol. 30, pp. 457-500, 2007.
- [25] A. Wagner, S. Marusek, and W. Yu, "Emojis and Law: contextualized flexibility of meaning in cyber communication," *Social Semiotics*, vol. 30, pp. 396-414, 2020. [Online]. Available: <https://doi.org/10.1080/10350330.2020.1731198>.
- [26] H. Miller et al., "'Blissfully Happy' or 'Ready to Fight': Varying Interpretations of Emoji," in *Proceedings of the International Conference on Web and Social Media*, 2016, pp. 259-268. [Online]. Available: <https://doi.org/10.1609/icwsm.v10i1.14757>.
- [27] H. Miller et al., "Understanding Emoji Ambiguity in Context: The Role of Text in Emoji-Related Miscommunication," in *Proceedings of the International Conference on Web and Social Media*, 2017, pp. 152-161. [Online]. Available: <https://doi.org/10.1609/icwsm.v11i1.14901>.
- [28] N. Cohn, J. Engelen, and J. Schilperoord, "The grammar of emoji? Constraints on communicative pictorial sequencing," *Cognitive Research: Principles and Implications*, vol. 4, 2019. [Online]. Available: <https://doi.org/10.1186/s41235-019-0177-0>.
- [29] "The Emoji Code," *Science*, vol. 357, p. 763, 2017. [Online]. Available: <https://doi.org/10.1126/science.aao5728>.
- [30] B. Desmet and V. Hoste, "Emotion detection in suicide notes," *Expert Systems with Applications*, vol. 40, no. 16, pp. 6351-6358, 2013.
- [31] V. Gajarla and A. Gupta, "Emotion detection and sentiment analysis of images," *Georgia Institute of Technology*, vol. 1, pp. 1-4, 2015.
- [32] P. Rani, "Emotion detection of autistic children using image processing," in 2019 Fifth International Conference on Image Information Processing (ICIIP), November 2019, pp. 532-535. IEEE.
- [33] Y. Lu, C. Guo, X. Dai, and F. Y. Wang, "Generating Emotion Descriptions for Fine Art Paintings via Multiple Painting Representations," *IEEE Intelligent Systems*, 2023.
- [34] K. Dheeraj and T. Ramakrishnu, "Negative emotions detection on online mental-health related patients texts using the deep learning with MHA-BCNN model," *Expert Systems with Applications*, vol. 182, p. 115265, 2021.
- [35] Palli, Abdul Sattar, Jafreezal Jaafar, Abdul Rehman Gilal, Aeshah Alsughayyir, Heitor Murilo Gomes, Abdullah Alshantiti, and Mazni Omar. "Online Machine Learning from Non-stationary Data Streams in the Presence of Concept Drift and Class Imbalance: A Systematic Review." *Journal of Information and Communication Technology* 23, no. 1 (2024): 105-139. S. Wang and B. Chen, "Customer emotion analysis using deep learning: Advancements, challenges, and future directions," in *Proceedings of the International Conference on Modern Scientific Research*, 2023, pp. 21-24.
- [36] N. Nguyen, T. H. Nguyen, Y. N. Nguyen, D. Doan, M. Nguyen, and V. H. Nguyen, "Machine learning-based model for customer emotion detection in hotel booking services," *Journal of Hospitality and Tourism Insights*, 2023.
- [37] P. Rathnayaka, N. Mills, D. Burnett, D. De Silva, D. Alahakoon, and R. Gray, "A mental health chatbot with cognitive skills for personalized behavioral activation and remote health monitoring," *Sensors*, vol. 22, no. 10, p. 3653, 2022.
- [38] Gila, Abdul Rehman, Jafreezal Jaafa, Mazni Omar, and Muhammad Zahid Tunio. "Impact of personality and gender diversity on software development teams' performance." In 2014 International Conference on Computer, Communications, and Control Technology (I4CT), pp. 261-265. IEEE, 2014.
- [39] F. Booth, C. Potts, R. Bond, M. Mulvenna, C. Kostenius, I. Dhanapala, et al., "A Mental Health and Well-Being Chatbot: User Event Log Analysis," *JMIR mHealth and uHealth*, vol. 11, p. e43052, 2023.
- [40] Z. Yan, Y. Wu, Y. Zhang, and X. A. Chen, "EmoGlass: An end-to-end AI-enabled wearable platform for enhancing self-awareness of emotional health," in *Proceedings of the 2022 CHI Conference on Human Factors in Computing Systems*, 2022, pp. 1-19.

- [41] S. Muranaka, T. Fukatsu, Y. Takebayashi, M. Kunugi, S. Nakajima, and R. So, "Emotion-injecting prompt for large language model chatbot," 2023.
- [42] "Character.ai," character.ai, [Online]. Available: <https://beta.character.ai/> (accessed Dec. 8, 2023).
- [43] "Social Profiles for Meta's AI Characters," Facebook, September 2023. [Online]. Available: <https://about.fb.com/news/2023/09/social-profiles-for-metas-ai-characters/> (accessed Dec. 8, 2023).
- [44] X. Shen, Z. Chen, M. Backes, Y. Shen, and Y. Zhang, "'do anything now': Characterizing and evaluating in-the-wild jailbreak prompts on large language models," arXiv preprint arXiv:2308.03825, 2023.
- [45] Z. Al-Halah et al., "Smile, be happy:) emoji embedding for visual sentiment analysis," in Proceedings of the IEEE/CVF International Conference on Computer Vision Workshops, 2019.
- [46] B. O'Neill, "ASCII affect: A comparison of emoticons and facial expressions in affective priming," 2019.
- [47] E. Giannoulis et al., "Emoticons, Kaomoji, and Emoji," Emoticons, Kaomoji, and Emoji, 2019. [Online]. Available: <https://doi.org/10.4324/9780429491757-1>.
- [48] T. D. Marten, "The Usage of Abbreviation and Misspelling Occurrence in DOTA 2 Player in Game Chat Log," LANGUAGE HORIZON, vol. 9, no. 3, pp. 1-12, 2021.
- [49] M. Christanti, P. Mardani, and K. Fadhila, "Analysing The Meaning Of Tone Indicators By Neurodivergent Community in Twitter," International Journal of Social Science Research and Review, vol. 5, no. 1, 2022. [Online]. Available: <https://doi.org/10.47814/ijssr.v5i1.118>.
- [50] G. Feng, "On artistic techniques of choice of words in English translation and writing," Journal of Hefei University of Technology.
- [51] D. Das and S. Bandyopadhyay, "Sentence-level emotion and valence tagging," Cognitive Computation, vol. 4, pp. 420-435, 2012.
- [52] F. Shi et al., "Large Language Models Can Be Easily Distracted by Irrelevant Context," ArXiv, abs/2302.00093, 2023. [Online]. Available: <https://arxiv.org/abs/2302.00093>.
- [53] P. Riddell, "Metaphor, simile, analogy and the brain," Changing English, vol. 23, no. 4, pp. 363-374, 2016.
- [54] M. Y. Shipilov et al., "Misspelling of a Lexical Unit as a Marker of Its Semantic Specialization (Based on Erratives Zhosky and Zhosko in Informal Online Communication)," Review of Omsk State Pedagogical University. Humanitarian research, 2022. [Online]. Available: [https://vestnik-omgpu.ru/volume/2022-3-36/vestnik_3\(36\)2022_130-137.pdf](https://vestnik-omgpu.ru/volume/2022-3-36/vestnik_3(36)2022_130-137.pdf).
- [55] G. Logan et al., "Cognitive Illusions of Authorship Reveal Hierarchical Error Detection in Skilled Typists," Science, vol. 330, pp. 683-686, 2010. [Online]. Available: <https://doi.org/10.1126/science.1190483>.
- [56] F. Yiannas, "Food Safety @ the Speed of Thought," Springer, pp. 67-69, 2015. [Online]. Available: https://link.springer.com/chapter/10.1007/978-1-4939-2489-9_19.
- [57] J. Walther et al., "Interpersonal Effects in Computer-Mediated Interaction," Communication Research, vol. 19, no. 1, pp. 52-90, 1992. [Online]. Available: <https://doi.org/10.1177/009365092019001003>.
- [58] Y. Zheng et al., "Acceptable and Reasonable Mistake—On the Birth of Simile and Metaphor and its Aesthetic Value," Journal of Wenshan Teachers' College, 2003.
- [59] L. Ya-ping et al., "On Other Patterns of Simile and Its Usage," Journal of Shangluo University, 2008.
- [60] Y. Song et al., "Simile and Metaphor Interpretation in Children," English Language Teaching, vol. 13, no. 4, pp. 91-103, 2020. [Online]. Available: <https://doi.org/10.5539/elt.v13n4p91>.
- [61] C. Zhou et al., "Prompt consistency for zero-shot task generalization," arXiv preprint arXiv:2205.00049, 2022.
- [62] X. Zhao et al., "Pre-trained Language Models can be Fully Zero-Shot Learners," arXiv, abs/2212.06950, 2022. [Online]. Available: <https://doi.org/10.48550/arXiv.2212.06950>.
- [63] Z. Zhang et al., "Automatic Chain of Thought Prompting in Large Language Models," arXiv, abs/2210.03493, 2022. [Online]. Available: <https://doi.org/10.48550/arXiv.2210.03493>.
- [64] L. Wang et al., "Plan-and-solve prompting: Improving zero-shot chain-of-thought reasoning by large language models," arXiv preprint arXiv:2305.04091, 2023.
- [65] R. L. Logan IV, et al., "Cutting down on prompts and parameters: Simple few-shot learning with language models," arXiv preprint arXiv:2106.13353, 2021.
- [66] Z. Wang et al., "Rolelm: Benchmarking, eliciting, and enhancing role-playing abilities of large language models," arXiv preprint arXiv:2310.00746, 2023.
- [67] Y. Shao, et al., "Character-llm: A trainable agent for role-playing," arXiv preprint arXiv:2310.10158, 2023.
- [68] L. Ouyang et al., "Training language models to follow instructions with human feedback," arXiv (Cornell University), Mar. 2022, doi: <https://doi.org/10.48550/arxiv.2203.02155>.
- [69] D. Rajagopal et al., "Cross-Domain Reasoning via Template Filling," ArXiv, abs/2111.00539, 2021.
- [70] Palli, Abdul Sattar, Jafreezal Jaafar, Manzoor Ahmed Hashmani, Heitor Murilo Gomes, Aeshah Alsughayyir, and Abdul Rehman Gilal. "Combined Effect of Concept Drift and Class Imbalance on Model Performance During Stream Classification." CMC-COMPUTERS MATERIALS & CONTINUA 75, no. 1 (2023): 1827-1845.
- [71] K. O'Byrne et al., "Client Assessment by Novice and Expert Psychologists: A Comparison of Strategies," Educational Psychology Review, vol. 9, no. 3, pp. 267-278, 1997. [Online]. Available: <https://doi.org/10.1023/A:1024739325390>.
- [72] J. Culbertson et al., "Cognitive Biases, Linguistic Universals, and Constraint-Based Grammar Learning," Topics in cognitive science, vol. 5, no. 3, pp. 392-424, 2013. [Online]. Available: <https://doi.org/10.1111/tops.12027>.
- [73] J. M. Carroll et al., "Creating a Design Science of Human-Computer Interaction," pp. 205-215, 1992. [Online]. Available: [https://doi.org/10.1016/0953-5438\(93\)90022-L](https://doi.org/10.1016/0953-5438(93)90022-L).
- [74] A. Patel et al., "A Systematic Approach to Evaluating Design Prompts in Supporting Experimental Design Research," Proceedings of the Design Society: International Conference on Engineering Design, 2019. [Online]. Available: <https://doi.org/10.1017/DSI.2019.282>.

Investigating Sampler Impact on AI Image Generation: A Case Study on Dogs Playing in the River

Sanjay Deshmukh

D. J Sanghvi College of Engineering, Mumbai, 400056, India

Abstract—AI image generation is a new and exciting field with many different uses. It is important to understand how different sampling techniques affect the quality of AI-generated images in order to get the best results. This study looks at how different sampling techniques affect the quality of AI-generated images of dogs playing in the river. This study is limited to a specific scenario, as there are not many images of dogs playing in the river already on the internet. The study used the Playground.ai open-source web platform to test different sampling techniques. DDIM was found to be the best sampling technique for generating realistic images of dogs playing in the river. Euler was also found to be very fast, which is an important consideration when choosing a sampling technique. These findings show that different sampling techniques have different strengths and weaknesses, and it is important to choose the right sampling technique for the specific task at hand. This study provides valuable insights into how sampling techniques affect AI image generation. It is important to choose the right sampling technique for the specific task at hand in order to get the best results. The study also demonstrates the societal relevance of AI-generated imagery in various applications.

Keywords—Artificial Intelligence; image generation; filter; sampler; Euler; Heun

I. INTRODUCTION

AI image generation stands as a captivating realm within artificial intelligence, involving the creation of images based on descriptions, prompts, or various inputs [1]. This technology is instrumental across diverse domains, particularly in fields like advertising and web design, where it significantly boosts productivity [2]. AI generators swiftly produce visually appealing content, eliminating the need for intricate editing software and thereby saving both time and costs. Industries like fashion witness substantial benefits as these tools autonomously design clothing and style outfits. Moreover, AI image generators are pivotal in fostering creativity and innovation, generating unique and original art pieces by amalgamating diverse styles and concepts. Their impact extends to several industries, including advertising, architecture, fashion, film, music, and poetry, enriching the creative processes for professionals [3].

The realism achieved by advanced deep learning models in AI image generation is noteworthy, often producing images indistinguishable from those created by humans [4]. However, ethical considerations come to the forefront, especially concerning the generation of images depicting real people in

potentially misleading scenarios. Despite the manifold benefits, the utilization of AI image generation technologies should be conscientiously guided by ethical principles.

AI image generation is a rapidly evolving field with numerous applications across various domains, such as advertising, product design, and scientific visualization. As the demand for realistic and high-quality generated images continues to grow, it is crucial to understand the impact of different sampling techniques on the quality and characteristics of the generated outputs. This study aims to investigate the influence of various sampling techniques on the performance of AI image generation models, with a specific focus on a case study involving the generation of images depicting dogs playing in a river.

While AI image generation has made significant strides in recent years, the selection of an appropriate sampling technique can greatly impact the quality, realism, and computational efficiency of the generated images. Different sampling techniques exhibit unique strengths and weaknesses, and their performance can vary depending on the specific use case and requirements. Therefore, it is essential to evaluate and compare the performance of various sampling techniques to identify the most suitable approach for a given application.

The primary research questions addressed in this study are: 1) How do different sampling techniques, such as DDIM, Euler a, DPM, DPM2a, PNDM, Euler, Heun, and LMS, influence the quality and realism of AI-generated images in the context of our case study? 2) What are the trade-offs between response time and image realism for each sampling technique, and how can these trade-offs be balanced to meet specific project requirements? 3) How can the selection of an appropriate sampling technique contribute to the practical applications of AI image generation, particularly in scenarios where readily available reference images are scarce, such as the case study of dogs playing in a river?

The main objectives of this research are: 1) To evaluate and compare the performance of eight different sampling techniques (DDIM, Euler a, DPM, DPM2a, PNDM, Euler, Heun, and LMS) in terms of image quality, realism, and response time. 2) To identify the strengths and weaknesses of each sampling technique and provide insights into the trade-offs between response time and image realism. 3) To propose a framework for selecting the most appropriate sampling technique based on specific project requirements and use cases, with a focus on the case study of generating images of dogs

playing in a river. 4) To contribute to the broader understanding of AI image generation techniques and their practical applications, particularly in scenarios where readily available reference images are limited.

By addressing these research questions and objectives, this study aims to provide valuable insights and guidance for researchers, developers, and practitioners working in the field of AI image generation, enabling them to make informed decisions and select the most suitable sampling techniques for their specific projects and applications

There are various AI-powered online tools for generating images. The use of AI in image generation not only saves time but also cuts costs by eliminating the complexities involved in capturing a specific image. AI image generators can be used in many industries for example, advertising a new car. The traditional method of creating a banner involves multiple steps like hiring a photographer, a model, securing a shooting location, getting props and costumes, arranging lighting, and more. Even after these investments, there's no assurance that the real-world picture captured is perfect, often leading to additional iterations and more time and money spent.

On the flip side, using AI for image generation streamlines the entire process. It can generate multiple images within seconds, providing more options and customization. AI also allows for editing specific parts of an image, offering flexibility. The crucial factor in achieving the perfect image with AI lies in selecting the right sampler that determines the final output. Hence, our study aims to establish a platform that sets a standard in selecting samplers for specific cases, such as generating an image of a dog playing in a river.

Given the scarcity of readily available images of dogs playing in rivers, our prompt generates genuinely AI-based images that would be difficult to achieve otherwise. While Photoshop is an alternative for image generation, it requires a highly trained professional, and the results may be influenced by the biases of that professional. Therefore, our decision to focus on the best sampler in the AI image generation domain addresses these challenges and provides valuable insights to the field [5].

II. DIFFERENT SAMPLER UNDER CONSIDERATION

We have selected the most popular sampler currently available for free to use and as reported in literature one with the maximum accuracy.

DDIM (Denoising Diffusion Implicit Models): DDIM is a diffusion model sampler in image generation that works by gradually denoising a latent noise image. It is one of the most popular samplers for image generation. DDIM is known for its high quality and stability [6].

The DDIM sampling process can be described by the following mathematical Eq. (1):

$$x_t = x_0 + \alpha_t * (x_t - f\theta(x_{t-1})) + \eta_t \quad (1)$$

where:

x_t is the latent image at time step t x_0 is the latent noise image

α_t is a noise schedule that controls the amount of denoising at each time step

$f\theta(x_{t-1})$ is the denoising function at time step $t-1$

η_t is a random noise term

The denoising function $f\theta(x_{t-1})$ is a neural network that is trained to denoise latent images. The noise schedule α_t is typically chosen to be a monotonically decreasing function so that the latent image becomes less and less noisy as the time step increases.

To generate a sample image, DDIM starts with the latent noise image x_0 . It then iteratively applies the denoising function $f\theta(x_{t-1})$ and adds noise according to the noise schedule α_t . This process is continued until the desired time step is reached. The final latent image x_t is then decoded to produce the generated image.

DDIM, or Diffusion and Denoising Score Matching, presents notable advantages in the realm of image generation. One of its primary strengths lies in its capability to produce images of high quality and stability, providing a reliable output. Additionally, DDIM operates as an efficient sampler, demonstrating the ability to generate images within a reasonable timeframe. A notable advantage is its ease of training; DDIM does not necessitate adversarial training, simplifying the training process.

However, like any methodology, DDIM is not without its drawbacks. One potential issue is mode collapse, a scenario in which the model tends to generate only a limited subset of possible images, limiting diversity. Another challenge is over-smoothing, wherein DDIM may excessively smooth images, leading to a blurred or unrealistic appearance. In summary, DDIM stands out as a powerful and versatile sampler in the domain of image generation, excelling in quality, stability, and training efficiency. Nevertheless, users must be mindful of its potential limitations, specifically the risk of mode collapse and over-smoothing, to make informed decisions in its application.

LMS (Langevin Monte Carlo Sampler): LMS is a sampler that is based on the Langevin equation, which is a stochastic differential equation that describes the motion of a Brownian particle [7]. LMS is known for its ability to generate high-quality images, but it can be slow and computationally expensive.

The mathematical equation for LMS is as follows:

$$dx_t = -\nabla U(x_t)dt + \sqrt{2D}dt \quad (2)$$

where:

x_t is the latent noise image at time step t

$U(x_t)$ is the potential energy function.

D is the diffusion coefficient

The potential energy function in the LMS serves as a metric for gauging the probability of the latent noise image, with LMS employing distinct potential energy functions tailored to specific image generation tasks. This adaptability enables LMS to excel in producing high-quality images across a spectrum of tasks.

Highlighting its strengths, LMS exhibits the ability to generate not only high-quality but also diverse images. However, these advantages come with trade-offs. LMS can be slow and computationally expensive, and its effectiveness relies on a trained potential energy function for each image generation task.

In the broader context, LMS emerges as a robust sampler for image generation, finding applications in tasks like image synthesis, inpainting, denoising, and super-resolution. Beyond image-related tasks, LMS extends its utility to other domains within machine learning, including natural language processing, computer vision, and reinforcement learning.

PNDM (Progressive Noise Diffusion Model): PNDM is a diffusion model sampler that is similar to DDIM, but it is more efficient and can generate higher-quality images at higher resolutions [8]. PNDM works by gradually a latent noise image, just like DDIM. However, PNDM uses a progressive approach, where it starts with the image at a low resolution and then gradually increases the resolution. This approach allows PNDM to generate high-quality images at higher resolutions without sacrificing efficiency.

The mathematical equation for PNDM is as follows:

$$x_{t+1} = x_t + \alpha(x_t - f(x_t)) \quad (3)$$

x_t is the latent noise image at time step t

α is the learning rate

$f(x_t)$ is the denoising function

The denoising function is a neural network that is trained to denoise images. PNDM uses a different denoising function for each resolution level. This allows PNDM to generate high-quality images at higher resolutions without sacrificing efficiency.

Here is a more detailed explanation of the PNDM algorithm: Start with a latent noise image, x_0 .

Select a resolution level, r .

Compute the denoising function, $f(x_0)$, at the selected resolution level.

Update the latent noise image, x_0 , using Eq. (4):

$$x_1 = x_0 + \alpha(x_0 - f(x_0)) \quad (4)$$

Repeat the steps until the latent noise image is sufficiently denoised. Increase the resolution level, r , and repeat the steps. Once the latent noise image is sufficiently denoised at the highest resolution level, stop the algorithm. The output of the PNDM algorithm is a denoised image, which can then be decoded into a final image.

PNM can be slower than other samplers, such as Euler and Heun, especially at high resolutions. PNDM requires a trained denoising function for each resolution level. Overall, PNDM is a powerful sampler for image generation that can produce high-quality and diverse images at high resolutions.

Euler: Euler is a simple and efficient sampler that is often used as a baseline for other samplers. It is known for its speed, but it can produce less realistic images than other samplers [9].

The Euler method works by approximating the solution of the ordinary differential equations (ODE) at a given time step using the following Eq. (5):

$$x_{t+1} = x_t + h * f(x_t) \quad (5)$$

x_t is the solution of the ODE at the time step t ,

h is the step size,

$f(x_t)$ is the right-hand side of the ODE,

The Euler method is a first-order method, which means that it is not very accurate. However, it is very fast and efficient, and it can be used to generate approximate solutions to ODEs. To apply the Euler method to image generation, we can use it to sample from the latent space of a diffusion model. The latent space of a diffusion model is a space of high-dimensional vectors that represent images. Diffusion models work by gradually denoising latent noise images. To sample from the latent space using the Euler method, we can start with a random latent noise image and then iteratively update the image using the following equation:

$$x_{t+1} = x_t + h * \nabla_x \log p(x_t) \quad (6)$$

Start with a latent noise image, x_0 the function, $f(x_0)$. a noise term “epsilon” from a random distribution. the latent noise image x_0 . Repeat the steps until the latent noise image is sufficient. The output of the Euler A algorithm is an image, which can then be decoded into a final image.

Euler A: Euler A also known as Ancestral Euler, is a diffusion model sampler that is similar to Euler, but it is more efficient and can generate more diverse images [10]. It works by gradually a latent noise image, but it uses an ancestral sampling scheme that allows it to explore a wider range of possible image configurations. The mathematical Eq. (7) for Euler A is as follows:

$$x_{t+1} = x_t + \alpha(x_t - f(x_t) + \epsilon) \quad (7)$$

x_t is the solution of the ODE at time step t $f(x)$ is the right-hand side of the ODE

h is the step size

Euler A is more efficient than Euler and can generate more diverse images. Euler a is more stable than other samplers, such as the Langevin Monte Carlo Sampler (LMS). Euler a stable to generate high-quality images. Euler a can be slower than other samplers, such as Euler, especially at high resolutions Euler A requires a trained function. Overall, Euler is a powerful sampler for image generation that can produce high-quality and diverse images.

Heun: Heun is a numerical method used for approximating the solutions of ordinary differential equations (ODEs) [11]. It is an advancement over Euler’s method, providing more realistic images at the cost of increased computational complexity. Represented as a second-order method, Heun’s approach involves predicting the solution at the next time step using Euler’s method and refining this prediction with the midpoint method. The iterative process continues until the desired accuracy is achieved. The mathematical equation for Heun’s method is as follows:

$$k1 = f(xt) \quad (8)$$

$$k2 = f(xt + hk1) \quad (9)$$

where:

x_t is the latent noise image at time step t h is the step size

$\nabla_x \log p(x_t)$ is the gradient of the log-probability of the latent noise image at time step t

where:

$$x_{t+1} = x_t + 0.5h(k1 + k2) \quad (10)$$

The gradient of the log probability of the latent noise image can be computed using the diffusion model. By iteratively updating the latent noise image using the Euler method, we can generate a variety of different images. The quality and diversity of the generated images will depend on the step size and the number of iterations. The Euler method is very fast and efficient. The Euler method is easy to implement. The Euler method is not very accurate. The Euler method can be unstable for large step sizes. Overall, the Euler method is a simple and efficient sampler for image generation. It is not the most accurate sampler, but it is very fast and easy to implement.

While Heun is more accurate and stable than Euler, it comes at the expense of higher computational demands. The method is relatively straightforward to implement and remains stable across a broad range of step sizes. Despite being surpassed by more sophisticated numerical techniques in terms of accuracy, Heun serves as a reliable baseline method for scenarios where computational resources are limited, making it a pragmatic choice for approximating ODE solutions when striking a balance between accuracy and efficiency is crucial.

DPM2 (Denosing Diffusion Probabilistic Model 2):

Denosing Diffusion Probabilistic Model 2 (DPM2) stands out as a diffusion model sampler celebrated for its stability and capacity to yield high-quality images [12]. While sharing similarities with DDIM, DPM2 excels in efficiency and the generation of superior images, particularly at higher resolutions. The underlying mechanism involves iteratively denosing a latent noise image using a distinct denosing function. The core equation of DPM2 integrates this denosing process with guidance, encompassing the learning rate (α), denosing function ($f(x_t)$), and guidance function ($g(x_t)$).

$$x_{t+1} = x_t + \alpha(x_t - f(x_t) + g(x_t)) \quad (11)$$

where:

x_t is the latent noise image at time step t

α is the learning rate

$f(x_t)$ is the denosing function

$g(x_t)$ is the guidance function.

These neural networks are crucial components, where the former refines image denosing, and the latter guides the process toward an intended output image. DPM2's algorithm unfolds in steps, initiating with a latent noise image and progressing through resolution levels, applying denosing and guidance functions. This process iterates until the latent noise

image achieves sufficient denosing, and the algorithm progressively increases the resolution level until the highest is reached, concluding the generation of a denosed image. The decoded result becomes the final image.

DPM2's merits include its enhanced stability compared to other samplers like Euler and Heun, its prowess in generating high-quality images, and its ability to align generated images with a specified guidance image. However, there are drawbacks; DPM2 might be slower than alternative samplers, especially at high resolutions, and necessitates trained denosing and guidance functions for each resolution level.

DPM2a (Denosing Diffusion Probabilistic Model 2 ancestral): DPM2a (Denosing Diffusion Probabilistic Model 2 ancestral) emerges as a noteworthy variant of the DPM2 diffusion model sampler, renowned for its capacity to generate more diverse images [13]. While sharing a fundamental resemblance with DPM2, DPM2a distinguishes itself through an ancestral sampling scheme, enabling exploration of a broader spectrum of potential image configurations.

$$x_{t+1} = x_t + \alpha(x_t - f(x_t)) + \beta(x_t - x_{t-1}) \quad (12)$$

where:

x_t is the latent noise image at time step t

α is the learning rate

β is the ancestral sampling rate

$f(x_t)$ is the denosing function

The mathematical formulation for DPM2a involves the latent noise image (x_t), learning rate (α), ancestral sampling rate (β), and the denosing function ($f(x_t)$), shared with DPM2. The ancestral sampling rate governs the influence of the latent noise image's previous state, with higher values enhancing image diversity but potentially slowing down the algorithm and introducing instability.

The DPM2a algorithm commences with a latent noise image, progresses through the selection of an ancestral sampling rate, computes the denosing function, and iteratively updates the latent noise image. This process repeats until the image achieves sufficient denosing, concluding the algorithm. Advantages of DPM2a include its capacity to generate more diverse images than DPM2 while still maintaining high-quality and relative stability. However, drawbacks include potential slowness compared to DPM2 and the requisite of a trained denosing function.

Fig. 1 illustrates the conceptual framework of our proposed system designed to investigate the impact of different samplers on a case study prompt—"a dog playing in a river." Utilizing a range of sampler filters, including DPM2a, DDIM, PNDM (PMS), Euler, Euler a, Heun, and LMS, our system incorporates a dedicated validation unit. This unit assesses both response time and reality score, with the aim of minimizing response time and maximizing realization score. In our study, an ideal realization score is defined as 1, a benchmark only achieved by the DDIM sampler. Furthermore, the generated images corresponding to the specified text prompt are systematically archived for potential future investigations.

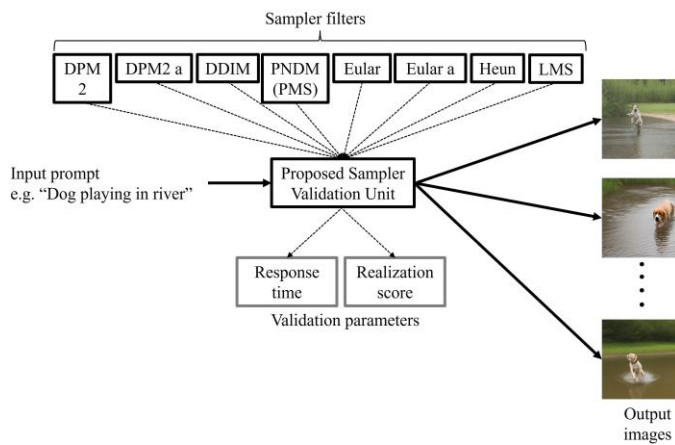


Fig. 1. Concept diagram of the proposed system for exploring sampler impact.

III. LITERATURE REVIEW

The field of artificial intelligence (AI) has seen significant contributions from various researchers across different domains. In (Hosny et al., 2018), a comprehensive understanding of AI methods, especially those related to image-based tasks, is established [14]. Moving from general AI to more specific applications, (Pereira et al., 2020) aims to conduct a thorough analysis of the necessity to integrate tumor information with other lung structures for the advancement of Computer-Aided Diagnosis (CADs), anticipating an impact on targeted therapies and personalized medicine [15]. The study by (Ibrahim et al., 2021) introduces a novel methodology for developing a detailed performance understanding of machine learning benchmarks [16]. While AI's benefits in marketing and advertising are well-documented, (Jeffrey, 2022) investigates the perceptions of Generation Z regarding AI in marketing. This research delves into levels of awareness, understanding, concerns about data privacy, and worries about psychological profiling, stereotyping, and manipulation [17].

(Nasari et al., 2022) undertake a performance comparison between Graphical Processing Units (GPUs) and Intelligence Processing Units (IPUs) by running training benchmarks of common AI/ML models [18]. In another exploration, (Cheng et al., 2023) assess the potential of GPT-4 in various branches of biomedical engineering, addressing challenges like ethical concerns and algorithmic biases [19]. (Alqahtani et al., 2023) contribute to the ongoing discussion about AI's role in education and research, emphasizing its potential to enhance outcomes for students, educators, and researchers [20]. Shifting focus to the realm of 3D object generation, (Sun et al., 2023) present UniG3D, a dataset addressing the limitations of existing 3D object datasets [21]. Lastly, (Tan et al., 2023) introduce DiffFSS, the first work leveraging the diffusion model for Few-Shot Segmentation (FSS) tasks [22]. The landscape of AI research is dynamic and encompasses a wide array of applications, from medical diagnosis to marketing perceptions and educational enhancements, highlighting the need for interdisciplinary considerations and ethical frameworks, as underlined by influential works like (Joyce, 2010) [23].

While previous studies have made significant contributions to the field of AI image generation, there are certain limitations

that our proposed approach aims to address. One notable limitation is the lack of comprehensive analysis on the impact of different sampling techniques on image quality and realism, particularly for specific use cases or prompts. Additionally, most studies focus on general image generation tasks, overlooking the unique challenges and requirements of generating images for specific scenarios, such as dogs playing in the river. Our proposed approach tackles these limitations by conducting a thorough investigation of various sampling techniques and their effects on image quality and realism, specifically for the case study of generating images of dogs playing in the river. Furthermore, we provide a systematic framework for selecting the most appropriate sampler based on project requirements, enabling more informed decision-making in AI image generation tasks.

IV. METHODS

Eight distinct sampling filters constituted the crux of our experimentation, including DDIM (Denoising Diffusion Implicit Models), Euler a, DPM, DPM2a, PNDM (PMS), Euler, Heun, and LMS. Parameters for evaluation encompassed execution time (t) and the generation of realistic images. To maintain consistency, we employed specific experimental settings random seed "137927237," 25 iterations, prompt guidance set to 7, and fixed image size at 512x512 pixels. Each generative operation yielded four images, and our analysis focused on the realism of these images and the time investment for their creation.

Beyond performance metrics, our study concentrated on the utility of the generated images. We aimed to pinpoint the optimal sampler for the specific scenario of dogs playing in a river, a relatively unconventional but visually engaging context. The versatility of these images was considered for applications ranging from advertising dog-related products to enhancing the appeal of websites and desktop backgrounds. The proposed system, inclusive of the eight distinct filters, underwent rigorous validation using the Proposed Sampler Validation Unit, comparing the output against ground truth images. Evaluation metrics included response time, realization score, and validation parameters tailored to each filter.

The calculated realization score offered a comprehensive measure of system performance, considering the diverse set of filters. Output analysis involved the generation of eight distinct images corresponding to each filter, exemplifying how different filters processed the input prompt. This realization score facilitated nuanced comparisons of performance.

The system, designed to address a spectrum of image processing tasks, from classification to segmentation and denoising, demonstrated versatility. Beyond its immediate applications, the proposed system hinted at the potential for future developments in image processing filters and algorithms. In essence, our methodology ensured a meticulous exploration of samplers, combining performance evaluation with practical considerations in the realm of image generation.

The screenshot in Fig. 2 provides an overview of the Playground AI interface, showcasing a range of accessible options. These include the ability to rate generated images, engage with the community feed featuring images from other

users, and utilize the canvas-like Board for image generation and editing. Users can import existing images for further editing, organize their Board using columns, and experiment with different styles of image generation such as Euler, Heun, DPM2, and more. The interface incorporates features like DOIM for diffusion model image generation, PNDM (PLMS) for probabilistic neural diffusion model generation, and Euler as a method for solving differential equations. Filters can be applied, and users can exclude specific details from images. The text prompt, an integral component, guides image generation, while the Generate option brings the vision to life. A Private Session feature ensures the privacy of generated images. Playground AI emerges as a versatile tool, offering a spectrum of options for users to create images ranging from realistic to abstract, thereby establishing itself as a potent resource for image generation and editing.

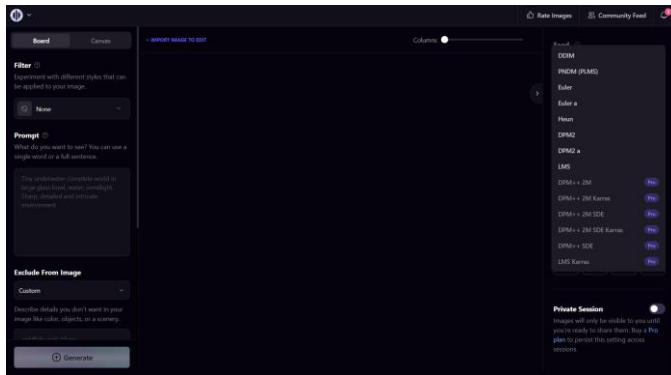


Fig. 2. Screenshot of the playground AI interface with all options visible.

The proposed system, inclusive of the eight distinct filters, each filter underwent rigorous validation using the Proposed Sampler Validation Unit, comparing the output against ground truth images. Evaluation metrics included response time, realization score, and validation parameters tailored to each filter. The calculated realization score offered a comprehensive measure of system performance, considering the diverse set of filters. Output analysis involved the generation of eight distinct images corresponding to each filter, exemplifying how different filters processed the input prompt. This realization score facilitated nuanced comparisons of performance.

In Fig. 3, the input command, exemplified by "Dog playing in River," is provided as the initial input. The subsequent step involves the selection of a sampler filter from a set of eight options using the algorithm "Select sampler filter." Once the sampler is chosen, the DiffusionNet CGAN (Conditional Generative Adversarial Network) is employed. The resulting output image is stored to facilitate validation. A check is implemented to verify whether all filters have been adequately tested; otherwise, the operation is halted. This process ensures a systematic approach to testing various sampler filters and capturing their output for thorough validation.

The ability to exclude specific details from images during the filtering process is a powerful feature of our proposed system. This capability is grounded in the principle of selective attention, which allows the model to focus on the most relevant

aspects of the input prompt while disregarding unnecessary or distracting elements. By excluding specific details, the system can generate images that are more aligned with the intended subject matter, reducing visual clutter and enhancing the overall coherence and clarity of the output. The exclusion of specific details is particularly useful in scenarios where the input prompt may contain extraneous information or when the desired output requires a certain level of abstraction or stylization. For instance, in our case study of generating images of dogs playing in a river, excluding irrelevant background details could result in a more focused and visually appealing representation of the subject matter. Furthermore, the ability to exclude specific details can be leveraged to mitigate potential biases or undesirable elements that may be present in the training data or the input prompt. By carefully filtering out such elements, the generated images can better reflect the intended message or concept.

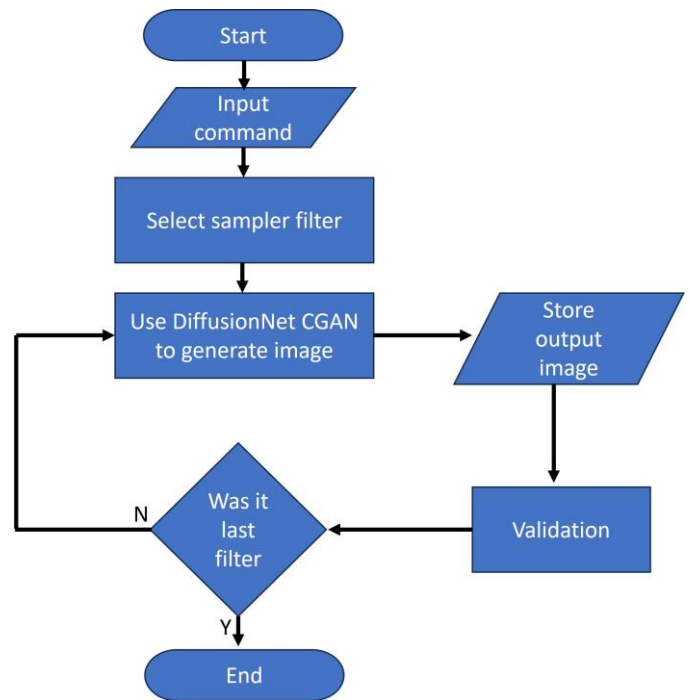


Fig. 3. Flowchart depicting the proposed mechanism for investigating the influence of samplers on AI generation.

Fig. 4(a) shows the effect of the sampler (filter) type used for AI-based image generation and the corresponding response time. The response time is the amount of time it takes for the model to generate an image from a given text prompt. The sampler type has a significant impact on the response time. The 'PNDM' and 'Euler a' samplers are the fastest, followed by the DPM, LMS, and Heun filters. The slowest sampler is the Euler type. Fig. 4(b) shows the sampler type used in AI image generation versus reality score of the generated images. The reality score is a measure of how realistic the generated images are. The sampler type also has a significant impact on the reality score. The DDIM sampler generates the most realistic images, followed by other samplers. The DPM2 and Euler sampler generate the least realistic images.

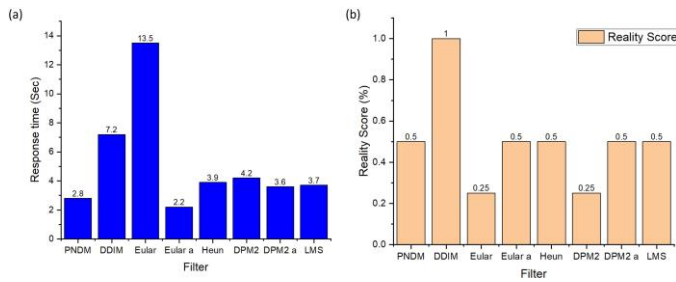


Fig. 4. Results obtained with proposed method (a) Filter type in AI image generation vs response time. (b) Filter type in AI image generation vs reality score in (%).

In general, there is a trade-off between response time and reality score. If you need to generate images quickly, you should use a faster sampler, such as Euler a. However, if you need to generate realistic images, you should use a slower filter, such as DDIM. If you need to generate realistic images at a moderate speed, you could use the PNDM sampler. Ultimately, the best sampler type for the project will depend on specific needs and requirements.

The images in Fig. 5 show a clear difference in the quality and realism of the generated images, depending on the sampler used. The PNDM and Euler a samplers produce the fastest results, but the images are also the least realistic. The DDIM and Euler samplers produce more realistic images, but they are also slower. The PNDM sampler strikes a balance between speed and realism. The dog in the PNDM image is blurry and the details are not very sharp. The water also looks unrealistic. The DPM image is sharper than the PNDM image, but the dog is still blurry in some places. The water looks more realistic, but it is still not perfect. The DPM2a image is sharper than the DPM image and the dog is no longer blurry. The water looks even more realistic. The DDIM image is the sharpest and most realistic image of all. The dog and the water are both very well-rendered. The Euler image is also very blurry and less realistic. The 'Euler a' image is much better than the Euler image, but it is slightly less sharp. The Heun image is not as sharp as the Euler a or DDIM images, but it is still more realistic than the DPM images. The LMS image is the blurry and least realistic image of all.

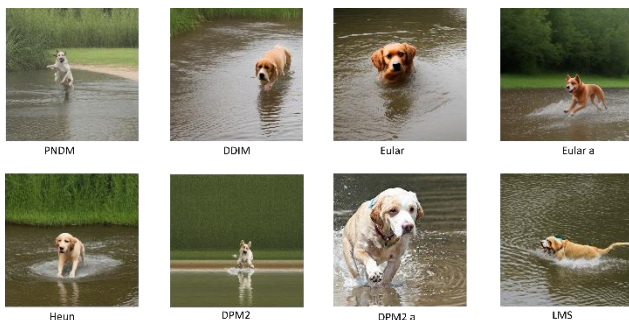


Fig. 5. Output images from each type of sampler for the prompt "dog playing in the river".

V. RESULTS

The research underscores the significance of sampler selection in shaping the outcomes of AI image generation

projects. The contextual analysis of a case study, where different samplers were evaluated for generating images of dogs playing in the river, illustrates the project-specific nature of this decision-making process. In this section, we discuss implications and findings that arise from the exploration of different samplers in the context of AI image generation. This study involved eight distinct sampling filters, each contributing unique characteristics to the generated images. The key factors evaluated were response time and the realism of the images, providing a nuanced understanding of the trade-offs involved in selecting a sampler for specific projects.

The DDIM sampler emerged as a consistent frontrunner in terms of image realism for this particular case study of dog image generation that plays in the river. This could be because of the iterative refinement approach of DDIM that sets it apart, enabling the generation of highly realistic images. This makes DDIM a compelling choice for projects where authenticity and visual fidelity are paramount, such as scientific studies or applications demanding a high level of image realism. On the other end of the spectrum, the PNDM sampler demonstrated a remarkable balance between response time and image realism. Its efficiency, coupled with the ability to produce realistic images, positions it as a versatile option suitable for a broad range of projects. The findings emphasize the importance of considering project requirements and objectives when selecting a sampler.

For instance, the Euler a sampler, with its combination of speed and reasonable realism, might be ideal for a marketing campaign requiring quick generation of high-quality images. The nuanced understanding of each sampler's strengths and weaknesses provides a practical guide for selecting the most appropriate sampler based on the specific requirements of a given project. This research lays the foundation for informed decision-making in the rapidly evolving field of AI image generation.

Our research has the potential to impact a diverse range of fields, including advertising, product design, and even dog training. For example, advertisers could leverage our findings to generate more engaging and effective marketing campaigns. Product designers could use our insights to create more realistic and appealing product prototypes. Additionally, dog trainers could utilize our research to develop more effective training methods.

Table I presents a comparison of different filters used in image processing along with their corresponding validation parameters and the number of images processed. The validation parameters include response time, realization score, and a calculated validation parameter. Response time indicates the time taken by each filter to process the images, with lower values being preferable as they indicate faster processing times. Realization score measures the effectiveness of each filter in achieving the desired outcome, with higher scores indicating better performance. The validation parameter is calculated using a formula based on the realization score and response time, providing an overall assessment of filter performance. The table enables the evaluation and comparison of filters based on these parameters, facilitating the selection of the most suitable filter for image processing tasks.

TABLE I. FILTER AND CORRESPONDING VALIDATION PARAMETERS

| Filter | Validation parameter | | | Number of images |
|---------|----------------------|-------------------|----------------------|------------------|
| | Response time | Realization score | Validation Parameter | |
| PNDM | 2.8 | 22 | 50.4 | 250 |
| DDIM | 7.2 | 39 | 7.2 | 250 |
| Eular | 13.5 | 11 | 391.5 | 250 |
| Eular a | 2.2 | 23 | 37.4 | 250 |
| Heun | 3.9 | 21 | 74.1 | 250 |
| DPM2 | 4.2 | 12 | 117.6 | 250 |
| DPM2 a | 3.6 | 22 | 64.8 | 250 |
| LMS | 3.7 | 21 | 70.3 | 250 |

There is a clear difference in the quality and realism of the generated images, depending on the sampler used. The PNDM and Euler a samplers produce the fastest results, but the images are also the least realistic. The DDIM and Euler samplers produce more realistic images, but they are also slower. The PNDM sampler strikes a balance between speed and realism. The dog in the PNDM image is blurry, and the details are not very sharp. The water in the images generated also looks unrealistic. The DPM image is sharper than the PNDM image, but the dog is still blurry in some places. The water looks more realistic, but it is still not perfect. The DPM2a image is sharper than the DPM image, and the dog is no longer blurry. The water looks even more realistic. The DDIM image is the sharpest and most realistic image of all. The dog and the water are both very well-rendered. The Euler image is also very blurry and less realistic. The dog is poorly rendered, and the water looks unnatural. The 'Euler a' image is much better than the Euler image, but it is slightly less sharp. The Heun image is not as sharp as the Euler a or DDIM images, but it is still more realistic than the DPM images. The LMS image is the blurriest and least realistic image of all.

Our research has several potential future implications. First, it could inspire the development of new samplers that offer even better performance in terms of response time, image realism, or both. Second, it could lead to the development of new AI image generation tools that incorporate our findings to make them more user-friendly and effective. Third, it could inform the development of new applications for AI image generation in a wider range of fields.

We are excited to see how our research is used to advance the field of AI image generation and its applications in the future. PNDM is more efficient than DDIM and can generate higher-quality images at higher resolutions. PNDM is more stable than other samplers, such as Euler and PNDM is able to generate diverse images.

Our proposed model introduces several innovative contributions to the field of AI image generation, particularly in the context of evaluating and selecting appropriate samplers for specific use cases:

1) **Comprehensive Sampler Evaluation Framework:** Our study presents a systematic and holistic framework for evaluating the performance of various samplers in AI image generation. By considering a diverse set of eight samplers, including DDIM, Euler a, DPM, DPM2a, PNDM, Euler,

Heun, and LMS, we provide a comprehensive understanding of their strengths, weaknesses, and trade-offs in terms of response time and image realism.

2) **Case Study-Driven Approach:** Our research adopts a novel case study-driven approach, focusing on the specific scenario of generating images of dogs playing in a river. This unconventional yet visually engaging context allows us to evaluate the samplers' performance in a real-world setting, providing practical insights that can inform decision-making processes for diverse applications.

3) **Proposed Sampler Validation Unit:** A key innovative aspect of our work is the introduction of the Proposed Sampler Validation Unit. This unit systematically validates the output of different samplers against ground truth images, employing a combination of quantitative metrics (response time and realization score) and qualitative analyses. This robust validation approach ensures a thorough assessment of the generated images, enabling informed selection of the most suitable sampler for a given task.

4) **Versatile and Extensible Framework:** Our proposed model is designed to be versatile and extensible, capable of addressing a wide range of image processing tasks, from classification and segmentation to denoising. Additionally, the framework lays the foundation for future developments in image processing filters and algorithms, fostering continued innovation and improvement in the field of AI image generation.

By presenting these innovative contributions, our research not only advances the understanding of sampler impact on AI image generation but also provides a practical and adaptable framework for researchers, developers, and practitioners to leverage in their respective domains.

VI. CONCLUSIONS

AI image generation is a rapidly evolving field with a wide range of potential applications. However, the quality and realism of generated images are highly dependent on the sampler type used. This paper presents a comprehensive study on the impact of eight distinct samplers on AI image generation, namely DPM, DPM2a, DDIM, PNDM, Euler, Euler a, Heun, and LMS.

Our findings reveal a nuanced landscape where response time and image realism form a delicate balance. Samplers such as PNDM and Euler a offer the fastest response times, making them ideal for projects where expeditious output is essential. Conversely, the Euler sampler, albeit slower, demonstrates superior performance in terms of image realism. In terms of image realism, the DDIM sampler consistently outperforms all others. This is attributed to its unique sampling approach, which iteratively refines the generated image to achieve greater realism. As such, the DDIM sampler is the best choice for projects where image authenticity is paramount.

The PNDM sampler strikes a balance between response time and image realism. It is faster than the DDIM sampler but still produces realistic images. This makes it a versatile option for a wide range of projects. Our research underscores the

importance of carefully selecting the appropriate sampler for each project. For instance, in the context of our case study on images of dogs playing in the river, we identified that the Euler a sampler would be the best choice for a marketing campaign that requires quick generation of high-quality images. Conversely, the DDIM sampler would be the better choice for a scientific study that requires highly realistic images of dogs playing in the river.

DECLARATIONS

A. Ethics Statements

All authors ensure that the manuscript fulfills the following statements:

- 1) This material is the author's original work, which has not been previously published elsewhere.
- 2) The paper is not currently being considered for publication elsewhere.
- 3) The paper reflects the author's own research and analysis truthfully and completely.
- 4) The paper properly credits the meaningful contributions of co-authors and researchers.

B. Availability of Data and Materials

Data and code will be made available, on reasonable request, to the corresponding author.

C. Funding Statement

This research has no funding associated with it.

D. Data Availability

Data will be made available at reasonable request to the authors.

E. Supplementary Information

Not applicable.

F. Ethical Approval

All the ethics approval was taken by an institutional review board or equivalent ethics committee.

G. Author Contributions

Conceptualization was done by Sanjay Deshmukh (SD). The experimental design was done by SD. All the experiments were performed by SD. The manuscript draft was prepared by SD. Data analysis and graphics designing were done by SD.

H. Conflicts of Interest or Competing Interests

The authors declare that there is no conflict of interest or competing interests.

REFERENCES

- [1] S. Tanugraha, "A Review Using Artificial Intelligence-Generating Images: Exploring Material Ideas from Mid-Journey to Improve Vernacular Designs," *Journal of Artificial Intelligence in Architecture*, vol. 2, no. 2, pp. 48–57, 2023.
- [2] S. O. Abioye, L. O. Oyedele, L. Akanbi, A. Ajayi, J. M. D. Delgado, M. Bilal, O. O. Akinade, and A. Ahmed, "Artificial intelligence in the construction industry: A review of present status, opportunities and future challenges," *Journal of Building Engineering*, vol. 44, p. 103299, 2021.
- [3] N. Anantrasirichai and D. Bull, "Artificial intelligence in the creative industries: a review," *Artificial intelligence review*, pp. 1–68, 2022.
- [4] D. Schraml, "Physically based synthetic image generation for machine learning: a review of pertinent literature," *Photonics and Education in Measurement Science 2019*, vol. 11144, pp. 108–120, 2019.
- [5] M. M. Najafabadi, F. Villanustre, T. M. Khoshgoftaar, N. Seliya, R. Wald, and E. Muharemagic, "Deep learning applications and challenges in big data analytics," *Journal of big data*, vol. 2, no. 1, pp. 1–21, 2015.
- [6] J. Song, C. Meng, and S. Ermon, "Denoising diffusion implicit models," *arXiv preprint arXiv:2010.02502*, 2020.
- [7] S. Kumar, B. Paria, and Y. Tsvetkov, "Constrained sampling from language models via langevin dynamics in embedding spaces," *arXiv preprint arXiv:2205.12558*, 2022.
- [8] D. Ryu and J. C. Ye, "Pyramidal denoising diffusion probabilistic models," *arXiv preprint arXiv:2208.01864*, 2022.
- [9] Q. Zhang and Y. Chen, "Fast sampling of diffusion models with exponential integrator," *arXiv preprint arXiv:2204.13902*, 2022.
- [10] A. M. Ben-Amram, "The Euler path to static level-ancestors," *arXiv preprint arXiv:0909.1030*, 2009.
- [11] H. R. Rezaadeh, M. Maghasedi, and B. Shojaei, "Numerical Solution of Heun Equation Via Linear Stochastic Differential Equation," *Journal of Linear and Topological Algebra*, vol. 1, no. 02, pp. 83–95, 2012.
- [12] S.-Y. Chou, P.-Y. Chen, and T.-Y. Ho, "How to backdoor diffusion models?" in *Proceedings of the IEEE/CVF Conference on Computer Vision and Pattern Recognition*, 2023, pp. 4015–4024.
- [13] D. Watson, J. Ho, M. Norouzi, and W. Chan, "Learning to efficiently sample from diffusion probabilistic models," *arXiv preprint arXiv:2106.03802*, 2021.
- [14] A. Hosny, C. Parmar, J. Quackenbush, L. H. Schwartz, and H. J. Aerts, "Artificial intelligence in radiology," *Nature Reviews Cancer*, vol. 18, no. 8, pp. 500–510, 2018.
- [15] T. Pereira, C. Freitas, J. L. Costa, J. Morgado, F. Silva, E. Negro, B. F. de Lima, M. C. da Silva, A. J. Madureira, and I. Ramos, "Comprehensive perspective for lung cancer characterisation based on ai solutions using ct images," *Journal of Clinical Medicine*, vol. 10, no. 1, p. 118, 2020.
- [16] K. Z. Ibrahim, T. Nguyen, H. A. Nam, W. Bhimji, S. Farrell, L. Olikar, M. Rowan, N. J. Wright, and S. Williams, "Architectural requirements for deep learning workloads in hpc environments," in *2021 International Workshop on Performance Modeling, Benchmarking and Simulation of High Performance Computer Systems (PMBS)*, 2021, pp. 7–17.
- [17] T. R. Jeffrey, "Understanding Generation Z Perceptions of Artificial Intelligence in Marketing and Advertising," *Advertising & Society Quarterly*, vol. 22, no. 4, 2021.
- [18] A. Nasari, H. Le, R. Lawrence, Z. He, X. Yang, M. Krell, A. Tsyplikhin, M. Tatineni, T. Cockerill, and L. Perez, "Benchmarking the Performance of Accelerators on National Cyberinfrastructure Resources for Artificial Intelligence/Machine Learning Workloads," pp. 1–9, 2022.
- [19] K. Cheng, Q. Guo, Y. He, Y. Lu, S. Gu, and H. Wu, "Exploring the potential of GPT-4 in biomedical engineering: the dawn of a new era," *Annals of Biomedical Engineering*, pp. 1–9, 2023.
- [20] T. Alqahtani, H. A. Badreldin, M. Alrashed, A. I. Alshaya, S. S. Alghamdi, K. bin Saleh, S. A. Alowais, O. A. Alshaya, I. Rahman, and M. S. A. Yami, "The emergent role of artificial intelligence, natural learning processing, and large language models in higher education and research," *Research in Social and Administrative Pharmacy*, 2023.
- [21] Q. Sun, Y. Li, Z. Liu, X. Huang, F. Liu, X. Liu, W. Ouyang, and J. Shao, "UniG3D: A Unified 3D Object Generation Dataset," *arXiv preprint arXiv:2306.10730*, 2023.
- [22] W. Tan, S. Chen, and B. Yan, "Diffss: Diffusion model for few-shot semantic segmentation," *arXiv preprint arXiv:2307.00773*, 2023.
- [23] D. Joyce, "Photography and the image-making of international justice," *Law and Humanities*, vol. 4, no. 2, pp. 229–249, 2010.

Enhancing Ultimate Bearing Capacity Assessment of Rock Foundations using a Hybrid Decision Tree Approach

Mei Guo, Ren-an Jiang

College of Road and Bridge Engineering, Jilin Communications Polytechnic, Changchun Jilin, 130012, China

Abstract—Accurately estimating the ultimate bearing capacity of piles embedded in rock is of paramount importance in the domains of civil engineering, construction, and foundation design. This research introduces an innovative solution to tackle this issue, leveraging a fusion of the Decision Tree method with two state-of-the-art optimization algorithms: the Zebra Optimization Algorithm and the Coronavirus Herd Immunity Optimizer. The research approach encompassed the creation of a hybridized model, unifying the DT with the Zebra Optimization Algorithm and Coronavirus Herd Immunity Optimizer. The primary objective was to augment the precision of the ultimate bearing capacity of prediction for piles embedded in rock. This hybridization strategy harnessed the capabilities of DT along with the two pioneering optimizers to address the inherent uncertainty stemming from diverse factors impacting bearing capacity. The Zebra Optimization Algorithm and Coronavirus Herd Immunity Optimizer showcased their efficacy in refining the base model, leading to substantial enhancements in predictive performance. This study's discoveries make a significant stride in the realm of geotechnical engineering by furnishing a sturdy approach to forecasting ultimate bearing capacity in rock-socketed piles. The hybridization method is a hopeful path for future research endeavors and practical implementations. Specifically, the DT + Zebra Optimization Algorithm model yielded dependable outcomes, as evidenced by their impressive R-squared value of 0.9981 and a low Root mean squared error value of 629.78. The attained outcomes empower engineers and designers to make well-informed choices concerning structural foundations in soft soil settings. Ultimately, this research advocates for safer and more efficient construction methodologies, mitigating the hazards linked to foundation failures.

Keywords—Ultimate bearing capacity; decision tree; zebra optimization algorithm; coronavirus herd immunity optimizer

I. INTRODUCTION

A. Background

Pile foundations are essential for the structural load transmission into the ground, guaranteeing the stability of the structure. Precisely assessing the load-bearing capacity of piles holds paramount importance in planning geotechnical structures [1]. Numerous experimental and theoretical approaches established in the past for predicting pile capacity rely on assumptions related to the factors governing the ultimate bearing capacity (Q_u) [2]. Nevertheless, owing to the intricate behavior of piles, nearly all of the existing methods and models fall short of delivering precise predictions, and a

considerable number of them are tailored to specific construction sites [3].

While the static load test (SLT) remains the most reliable approach for evaluating pile-bearing capacity, its implementation can be a time-consuming, expensive, and demanding process [4]. An advanced method for forecasting the bearing capacity of piles is high-strain dynamic testing (HSDT). This method relies on wave propagation theory and is executed by utilizing a pile-driving analyzer (PDA). The HSDT process is usually standardized according to American Standard Test Methods [5]. Previous studies have revealed a strong correlation between the bearing capacity projected through PDA and values anticipated through SLT.

Moreover, PDA (HSDT) offers the advantages of enhanced speed and cost-effectiveness when compared to SLT. However, the attainment of trustworthy results mandates the execution of multiple PDA tests for every construction project. Hence, the aim to reduce the necessary number of PDA tests is of great significance, as it would reduce overall project costs. In pursuit of this goal, novel techniques such as artificial intelligence (AI) have surfaced, demonstrating the ability to provide more accurate forecasts of pile-bearing capacity and expedite solutions for complex engineering problems compared to traditional methods [6].

B. Literature Review

Machine learning (ML) methods have recently become pivotal in civil engineering and geotechnical projects. They streamline labor-intensive engineering procedures and substantially contribute to these projects' cost efficiency. Additionally, numerous research studies utilize ML techniques to estimate the Q_u (ultimate bearing capacity) of rocks [7,8]. Yagiz et al. [9] presented ANN models, whereas Jahed Armaghani et al. [10] introduced adaptive neuro-fuzzy inference system (ANFIS) models to forecast rock strength. Concurrently, Singh et al. [11] recorded the effective application of an ANFIS estimation model to estimate the Young's modulus of rock. In another study, Shirani Faradonbeh et al. [12] conducted research focused on developing a genetic programming (GP) technique for predicting backbreak caused by blasting. Monjezi et al. [13] applied ANN models to forecast ground vibration, whereas Marto et al. [14] utilized imperial competitive algorithm (ICA)-ANN models to predict fly rock incidents in their studies. Azimi et al. [15] also proposed a new control method, called Swarm-Based Parallel Control (SPC), inspired by the intelligence of swarms in

nature. In this study, sharing the response data among adjacent buildings using a wireless sensor network (WSN) at each floor is proposed to improve the seismic performance and minimize the risks of knocking.

In foundation design and analysis, these methodologies have garnered extensive usage. For example, Chan et al. [13] introduced an ANN model as a substitute for developing pile-driving formulas. In this scenario, the neural network was trained to employ data associated with the pile configuration, the energy employed during pile driving, and the elastic compression of the pile and the soil, with the ultimate bearing capacity (Q_u) of the pile as the network's output. In a separate investigation by Pal and Deswal [16], they developed two soft computing approaches, namely ANN and support vector machine (SVM), to evaluate the Q_u of concrete spun pipe piles. Their results demonstrated that among the models examined, ANN delivered the highest level of predictive accuracy. Shahin et al. [17] designed an ANN predictive model for foreseeing the bearing capacity of drilled shafts. In a distinct study, Jianbin et al. [18] evidenced the effectiveness of ANN in forecasting the axial bearing capacity (ABC) of pipe piles in sandy soil. They included significant factors like the effective length and diameter of the pile, soil cohesion, unit weight, internal friction angle, and results from the standard penetration test (SPT) in the development of the network. In another research endeavor, Yu Lei et al. [19] conducted a comparative study involving six hybrid models that incorporated neural networks in conjunction with six different swarm intelligence optimization algorithms, including the innovative Seagull Optimization Algorithm (SOA). These hybrid models were evaluated against the predictive capabilities of two single models without any optimization techniques in forecasting Uniaxial Compressive Strength. Moreover, other researchers have contributed to the advancement of meta-heuristic algorithms. For instance, Agushaka [20] conducted studies aimed at enhancing arithmetic optimization, while Gaurav Dhiman et al. [21] focused on refining the Seagull Optimization Algorithm. These efforts collectively contribute to developing and improving hybrid models that leverage both ML techniques and advanced optimization methods for enhanced predictive accuracy.

C. Objective

This research introduces a novel ML approach to attain precise and optimal predictions. The hybridization method employed in this study is custom-tailored to enhance the

performance of DT models, guaranteeing reliable outcomes. Through the combination of 2 cutting-edge and effective optimization techniques, namely the Zebra Optimization Algorithm (ZOA) and the Coronavirus Herd Immunity Optimizer (CHIO), the creation of these innovative hybrid models exceeded the capabilities of traditional methods, marking a substantial leap forward. A thorough assessment was carried out on these models, individually and in hybrid setups, to guarantee a fair and unbiased evaluation of their performance. To ensure the trustworthiness of the outcomes, the evaluation of model outputs included well-recognized performance metrics such as R^2 and RMSE. This approach played a crucial role in mitigating any possible bias in the results, offering a more precise understanding of the models' effectiveness. In addition to the technical aspects, this study acknowledged the practical importance of these discoveries. The increased precision achieved with the hybrid models holds the promise of improving decision-making in real-world geotechnical engineering projects, thus reducing the risks associated with inaccurate Q_u estimations. The ability of the DT model to provide dependable predictions, whether applied individually or in hybrid configurations, highlights their flexibility and appropriateness for various project needs.

II. MATERIALS AND METHODOLOGY

A. Data Gathering

In ML projects, the careful choice of input variables and the precise definition of desired outputs are crucial for attaining optimal model performance. An extensive set of input variables is systematically gathered from published literature [22]. It is important to reiterate, as highlighted in multiple references, including [23], that the pile's dimensions, particularly its length and diameter, play a paramount role in determining the Q_u . Therefore, to consider the impact of rock and soil layers, 2 ratios associated with pile geometry were chosen: the ratio of length within the soil layer (L_s) to socket length (L_r), and the ratio of total length (L_t) to diameter (D).

In summary, the model inputs for estimating the Q_u of rock-socketed piles consisted of $L_s/L_r, L_t/D, UCS$, and $SPT N$ -value. In addition, H_r is the height of the layer. These inputs were chosen to simplify the predictive model using smaller parameters. Table I indicates the statistical properties of these inputs and Q_u . Fig. 1 presents a column plot for determining the input frequency in correlation with Q_u .

TABLE I. THE STATISTICAL PROPERTIES OF THE INPUT VARIABLE OF Q_u

| Variables | Indicators | | | | |
|-----------|------------|---------|----------|----------|----------|
| | Category | Min | Max | Arg | St. Div |
| L_p/D | Input | 4.331 | 96.30 | 31.39 | 22.57 |
| L_s/L_r | Input | 0.29 | 31.71 | 4.86 | 5.66 |
| N_{SPT} | Input | 0.00 | 166.42 | 44.67 | 59.57 |
| UCS | Input | 0.00 | 68.49 | 24.23 | 23.55 |
| H_r | Input | 0.00 | 8.36 | 0.79 | 1.50 |
| Q_u | Output | 1449.00 | 42700.73 | 17421.79 | 10230.86 |

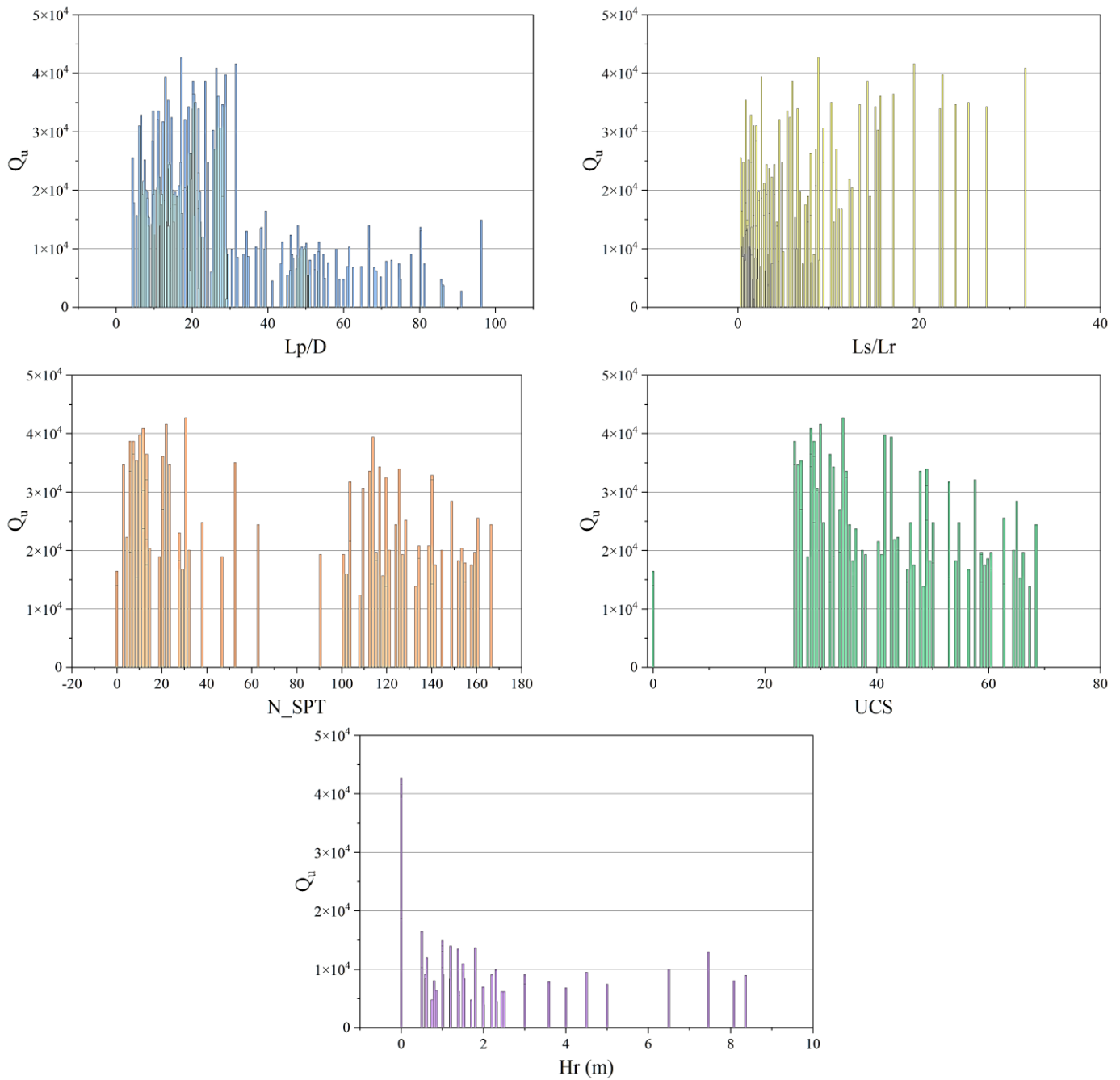


Fig. 1. The column plot between input and output.

B. DT

Derived from ML theory, a DT functions as a potent instrument for proficiently tackling regression and classification challenges. In contrast to other classification techniques that rely on a combined set of features for one-step classification, the DT employs a multi-stage or hierarchical decision approach, displaying a structure resembling a tree [24]. In contrast to other classification methods that depend on a unified set of features for immediate classification, the DT employs a multi-stage or hierarchical decision approach, showcasing a structure that resembles a tree. This tree includes a root node housing all the data, a sequence of splits

(*internal nodes*) , and an assortment of leaves (*terminal nodes*) [25]. Within the DT structure, each node performs a binary decision, separating either a singular class or a subset of classes from the remaining ones. Typically, the process entails traversing the tree from the top to the bottom, following a top-down methodology [26].

1) *Decision tree regression (DTR)*: As shown in Fig. 2, a distinct regression tree is built for every class to enable soft classification. Within the context of regression trees, the target vector is the defined class proportions of a pixel, also known as soft reference data, whilst the pixel intensity values from

various bands function as estimator feature vectors or variables. The technique generates predicted class proportions as an output by using the intensity values as input for each individual regression tree [27]. The steps involved in creating regression trees using the training dataset are as follows:

a) Employ the pixel intensity values from different bands as the variables that predict.

b) Employ the known class fraction of class i within the target variable, a pixel.
c) Create the regression tree specific to class i .
d) Iterate through the process for class i , varying from 1 to M .

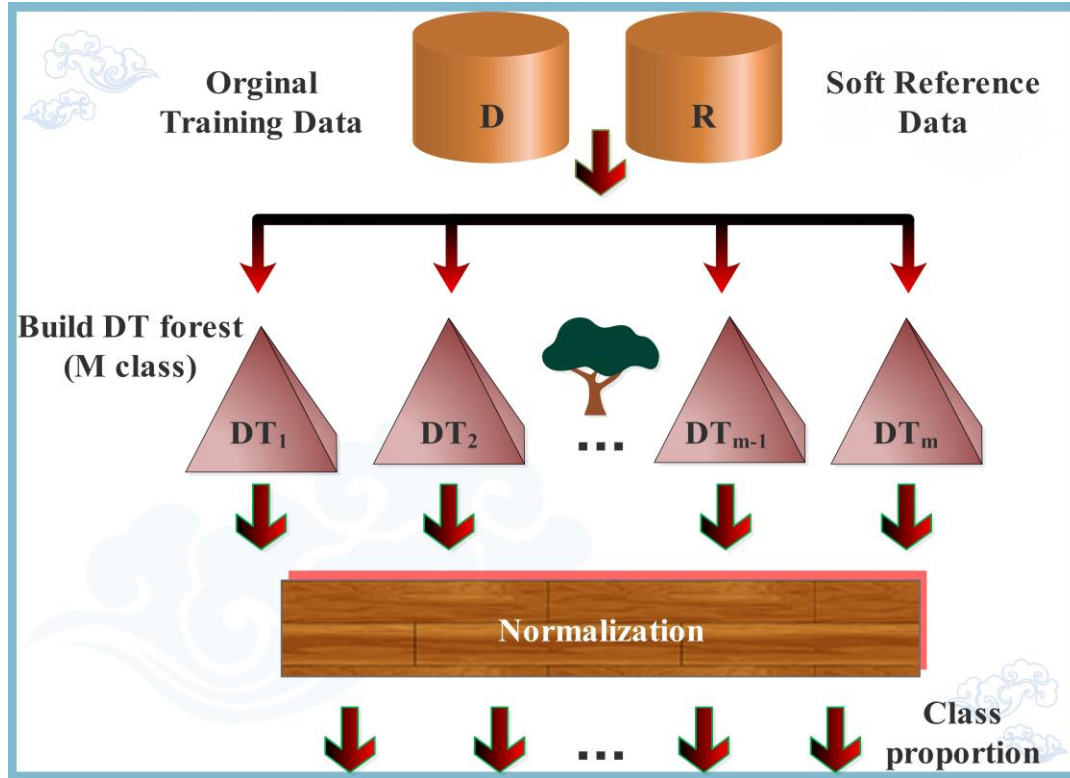


Fig. 2. The DT regression technique facilitates the soft classification of remote sensing data.

The regression tree algorithm for soft categorization is as follows:

- 1) Input the pixel intensity values from various bands.
- 2) Execute the regression tree for class i .
- 3) Retrieve the output of regression tree i , which represents the fraction of class i in a pixel.
- 4) Repeat the process for class i , ranging from 1 to M .

It is common practice to rescale the soft classification outputs to a range of 0 to 1 for each pixel, indicating the class fractions within the ground pixel area. Thus, the estimated class proportions from each tree, denoted as $DT(i)$ for $i = 1, \dots, M$, undergo normalization through the following process:

$$P(i) = \frac{DT(i)}{\sum DT(i)}, i = 1, \dots, M \quad (1)$$

C. Zebra Optimization Algorithm (ZOA)

Zebras are included in the cohort population of ZOA, a population-based optimization method. It updates its members by utilizing 2 innate behaviors seen in wild zebras. These include hunting and gathering food as well as protecting

oneself from predators. Therefore, the ZOA population members receive updates in 2 distinct stages for each iteration [28].

1) *Foraging behavior*: Zebras predominantly graze on grasses and sedges; however, they might turn to buds, bark, fruits, roots, and leaves when their preferred food is scarce. During the initial stage, updates to the population members are executed by simulating zebra behavior while searching for food. The amount of time zebras dedicate to eating can vary between 60-80 percent, contingent on the quality and accessibility of vegetation. Among zebras, the plains zebra stands out as a primary grazer. It consumes the upper canopy of grass, which is often less nutritious, creating an environment conducive for other species that rely on Shorter and more nutrient-rich grasses. In ZOA [29], the lead zebra is regarded as the top-performing member of the population and directs other members toward its location in the search area. Consequently, the adjustment of zebra positions during the foraging stage can be expressed mathematically utilizing Eq. (2) and (3).

$$x_{i,j}^{new,p_1} = x_{i,j} + e \times (BM_j - I \times x_{i,j}) \quad (2)$$

$$x_i = \begin{cases} x_i^{new,p_1}, F_i^{new,p_1} < f_i \\ x_i & otherwise \end{cases} \quad (3)$$

In this context, x_i^{new,p_1} represents the updated state of the i th zebra, with $x_{i,j}^{new,p_1}$ denoting its value in the j th dimension and F_i^{new,p_1} indicating its updated objective function value. The lead zebra, referred to as BM , stands as the top-performing member, and BM_j signifies its value in the j th dimension [30]. The value of i is determined using a random number e , which can be any value between 0 and 1. The round function $(1 + rand)$ is then used to round the value of i to the closest integer. The parameter i has 2 possible values: 1 and 2. Setting i to 2 results in more significant changes in population mobility.

2) *Defense strategies against predators*: Updates to the positions of ZOA residents in the search area are made in the second stage by using simulations of a zebra's defensive maneuvers against predator attacks. Not only do lions pose a threat to zebras, but wild dogs, leopards, brown hyenas, and cheetahs also pose a hazard, each of which calls for a different approach to defense. Zebras defend themselves against lion attacks by using zigzag patterns and occasional sideways spins as evasive maneuvers. Zebras usually react more aggressively to smaller predators such as hyenas and dogs. They regroup and cause chaos to make their enemies more difficult to deal with. In the context of ZOA , the assumption is that lions or other predators may initiate an attack, prompting zebras to decide between an escape strategy when facing lions or an offensive approach against other predators [31]. The escape strategy is represented by mode S1, while the defensive strategy, where the herd forms a protective structure, is represented by mode S2. A zebra's new position is valid if it results in an improved objective function value.

$$x_{i,j}^{new,p_2} = \begin{cases} S1: x_{i,j} + E \times (2e - 1) \times \left(1 - \frac{t}{T}\right) \times x_{i,j}, P_s \leq 0.5 \\ S2: x_{i,j} + e \times (BM_j - I \times x_{i,j}), & otherwise \end{cases} \quad (4)$$

$$x_i = \begin{cases} x_i^{new,p_2}, F_i^{new,p_2} < f_i \\ x_i & otherwise \end{cases} \quad (5)$$

In this context, the constant E is fixed at 0.01, and P_s represents the likelihood of selecting one of two methods at random from the range $[0,1]$. BM refers to the condition of the zebra under attack, where BM_j signifies its value in the j th dimension.

D. Coronavirus Herd Immunity Optimizer (CHIO)

The algorithm for optimization introduced in this study integrates the concept of herd immunity, drawing parallels between the principles of $COVID - 19$ and the optimization process [32]. The steps that make up the $CHIO$ are listed below, with a detailed explanation of each. The algorithm explores each of the 6 primary phases in the parts that follow [33, 34].

Phase 1: To fit the optimization difficulty's context, the objective function is formulated as follows during the $CHIO$ and optimization problem's initialization phase:

$$minO(x) \quad x \in [lb, ub] \quad (6)$$

An individual's or case x 's immunity rate is reflected by the objective function $O(x)$, which is denoted by the gene values x_1, x_2, \dots, x_n , where each x_i corresponds to a gene or choice variable. Each person's total gene count is denoted by the index n . It is crucial to emphasize that each gene x_i falls within the value range of $[lb_i, ub_i]$, with ub_i and lb_i denoting the *upper* and *lower* boundaries, respectively, of gene x_i .

Through this phase, $CHIO$ initializes its two primary control parameters [34]: BR_r . It governs the propagation of the virus pandemic among people and acts as the fundamental reproduction rate governing the $CHIO$ operators. Max_{age} . This denotes the oldest age at which infected cases can be documented and describes how those instances will end. Cases reaching Max_{age} either recover or pass away.

Two control parameters and *four* algorithmic parameters make up $CHIO$. C_0 : This is the initial number of infected instances, which in this particular case is one. Max_{it} : the highest quantity of repetitions. HIS : The number of people. n : The problem's dimensionality.

Phase 2: The examples that are generated are then saved in HIP in the form of a 2-dimensional matrix with dimensions of $n \times HIS$. Here, n stands for each person's size, which is indicated as follows:

$$HIP = \begin{bmatrix} x_1^1 & x_2^1 & \dots & x_n^1 \\ x_1^2 & x_2^2 & \dots & x_n^2 \\ \vdots & \vdots & \dots & \vdots \\ x_1^{HIS} & x_2^{HIS} & \dots & x_n^{HIS} \end{bmatrix} \quad (7)$$

Each row in HIP denoted as x_j , fits a case that is produced by the following formula: $x_i^j = lb_i + (ub_i - lb_i) \times U(0, 1)$, where i series from 1 to n , and where ub_i and lb_i represent the *upper* and *lower* limitations of the gene x_i . Eq. (6) is utilized to calculate the immunity rate, or objective function, for every instance. Every instance in HIP also has a status vector (S) constructed for it, with a length of HIS . In this vector, a vulnerable case is represented by 0, and an infected case is represented by 1 value.

Phase 3: The progression of coronavirus herd protection constitutes the central iterative process of $CHIO$. This process encompasses *three* rules governing the change of genes x_i^j within case x_j . These genes can either remain unchanged or undergo alterations due to the implementation of social estrangement procedures. The specific rules are strongminded according to the percentage of BR_r and are detailed as follows:

$$x_i^j(t+1) \leftarrow \begin{cases} x_i^j(t) & r \geq BR_r \\ C(x_i^j(t)) & r < \frac{1}{3} \times BR_r. \quad \text{infected} \\ N(x_i^j(t)) & r < \frac{2}{3} \times BR_r. \quad \text{suspectical} \\ R(x_i^j(t)) & r < BR_r. \quad \text{immuned} \end{cases} \quad (8)$$

Phase 4: The immunity rate, denoted as $O(x^j(t+1))$, is computed for each newly generated case, $x^j(t+1)$. If it outperforms the current case, $x^j(t)$, as indicated by $(x^j(t+1)) > O(x^j(t))$, then $x^j(t)$ is substituted with $x^j(t+1)$. Furthermore, if $E_j = 1$, the age vector A^j is incremented by one.

The status vector, E_j , for each case, x^j , is adjusted based on the herd immunity threshold, calculated as follows:

$$E_j \leftarrow \begin{cases} 1 & O(x^j(t+1)) < \frac{O(x^j(t+1))}{\Delta O(x)}, E_j = 0, is_corona(x^j(t+1)) \\ 2 & O(x^j(t+1)) < \frac{O(x^j(t+1))}{\Delta O(x)}, E_j = 1 \end{cases} \quad (9)$$

The equation is formulated based on the following variables:

- $is_corona(x^j(t+1))$: A dual value set to 1 if the newly created case, $x^j(t+1)$ inherits an amount from each affected instance.
- $\Delta O(x)$: This denotes the mean immunity rate of the population, which is calculated as the sum of all immunity rates divided by the population size.

It is crucial to stress that determined social distancing measures may have an impact on the population's immunity rate among persons [35], considering that the freshly formed individual's immunity rate is higher than the population's average immunity rate.

E. Performance Evaluator

This section delineates a set of metrics designed to assess hybrid models. These metrics gauge error and correlation, providing respected insights into the models' performance. Table II displays the equations for the metrics employed in this paper [36].

Respectively, the variables can be expressed as:

- The symbol n represents the sample size.
- Predicted values are indicated as b_i .
- \bar{m} and \bar{b} stand for the mean of the evaluated and anticipated values, respectively.
- The measured value is denoted as m_i .
- The mean of the predictor variable in the dataset is symbolized as \bar{x} .

TABLE II. THE FORMULATIONS OF THE PERFORMANCE METRICS

| | | |
|--|--|------|
| Coefficient Correlation (R^2): | $R^2 = \left(\frac{\sum_{i=1}^n (b_i - \bar{b})(m_i - \bar{m})}{\sqrt{[\sum_{i=1}^n (b_i - \bar{b})^2][\sum_{i=1}^n (m_i - \bar{m})^2]}} \right)^2$ | (10) |
| Root Mean Square Error (RMSE): | $RMSE = \sqrt{\frac{1}{n} \sum_{i=1}^n (m_i - b_i)^2}$ | (11) |
| Mean Absolute Error (MAE): | $MAE = \frac{1}{n} \sum_{i=1}^n b_i - m_i $ | (12) |
| Mean Absolute Percentage Error (MAPE): | $MAPE = \frac{100}{n} \sum_{i=1}^n \frac{ b_i }{ m_i }$ | (13) |
| weight absolute percentage error (WAPE): | $WAPE = \max \left \frac{ b_i - m_i }{b_i} \right $ | (14) |

III. RESULT

In this section, a comparative assessment of the results was carried out to obtain the proposed model using single and hybrid frameworks. The hybrid variants developed to achieve optimal outcomes include DT+ZOA (DTZO) and DT+CHIO (DTCH). To train these proposed models, 70% of the input data was dedicated to the training process, while the remaining 30% was further divided, with 15% allocated for validation and 15% for testing purposes. Various metrics, including R2, RMSE, MAE, MAPE, and WAPE, were employed to conduct a thorough assessment of the acquired results and ensure unbiased findings. In the case of the R2 metric, values close to 1 suggest excellent results. Conversely, values approaching 0 indicate accurate outcomes when considering the error indicators.

Table III presents the results of predicting the Q_u of rocks for each framework. The performance of the traditional DT models within a single framework does not show favorable

outcomes according to the mentioned metrics. While the R2 value for DT is 0.9817 during the training phase, it notably decreases in both the validation and testing phases. On the other hand, DTZA exhibits steady performance, especially in the training phase, with an R2 value of 0.9962 and an RMSE value of 629.7812. Among the models, the DTCH model showed moderate results, achieving higher accuracy compared to DT but slightly lower accuracy than the DTZA model. Overall, it can be concluded that the accuracy of DT models in predicting the Q_u of rocks is successfully enhanced by the incorporation of ZOA and CHIO optimizers, which contributes to an overall improvement in the reliability of the results.

Fig. 3 displays a scatter plot depicting the models' performance, evaluated through their R^2 and RMSE values. The X-axis correlates with the measured values, while the Y-axis correlates with the predicted values generated by the models. Triangular shapes in various colors are incorporated into the scatter plot to distinguish between the training, testing, and validation phases. These shapes are dispersed around a

diagonal line, representing an ideal scenario with an R^2 value of 1. The limited accuracy of the DT model becomes apparent due to the significant spread of data points.

approach. Data points for DTZA are tightly clustered near the central line, indicating a more favorable outcome. However, some broader dispersions are observable in the case of DTCH.

Conversely, the DTZA and DTCH models demonstrate enhanced performance compared to the standalone DT

TABLE III. THE RESULT OF DEVELOPED MODELS FOR DT

| Model | Phase | Index values | | | | |
|-------|------------|--------------|--------|---------|---------|--------|
| | | RMSE | R^2 | MAE | MAPE | WAPE |
| DT | Train | 1440.54 | 0.9817 | 1235.19 | 11.3086 | 0.0713 |
| | Validation | 1829.53 | 0.9683 | 1471.95 | 7.6086 | 0.0726 |
| | Test | 1695.50 | 0.9746 | 1121.61 | 7.4247 | 0.0745 |
| | All | 1545.41 | 0.9774 | 1253.81 | 10.1622 | 0.0720 |
| DTZA | Train | 629.78 | 0.9962 | 446.47 | 2.6926 | 0.0258 |
| | Validation | 1221.55 | 0.9873 | 926.96 | 4.6943 | 0.0457 |
| | Test | 1229.66 | 0.9893 | 814.87 | 5.2731 | 0.0541 |
| | All | 854.89 | 0.9934 | 574.80 | 3.3853 | 0.0330 |
| DTCH | Train | 1001.70 | 0.9903 | 742.39 | 4.6906 | 0.0429 |
| | Validation | 1503.80 | 0.9806 | 1145.34 | 5.7609 | 0.0565 |
| | Test | 1250.77 | 0.9834 | 850.54 | 5.7691 | 0.0604 |
| | All | 1178.30 | 0.9872 | 841.02 | 5.0565 | 0.0483 |

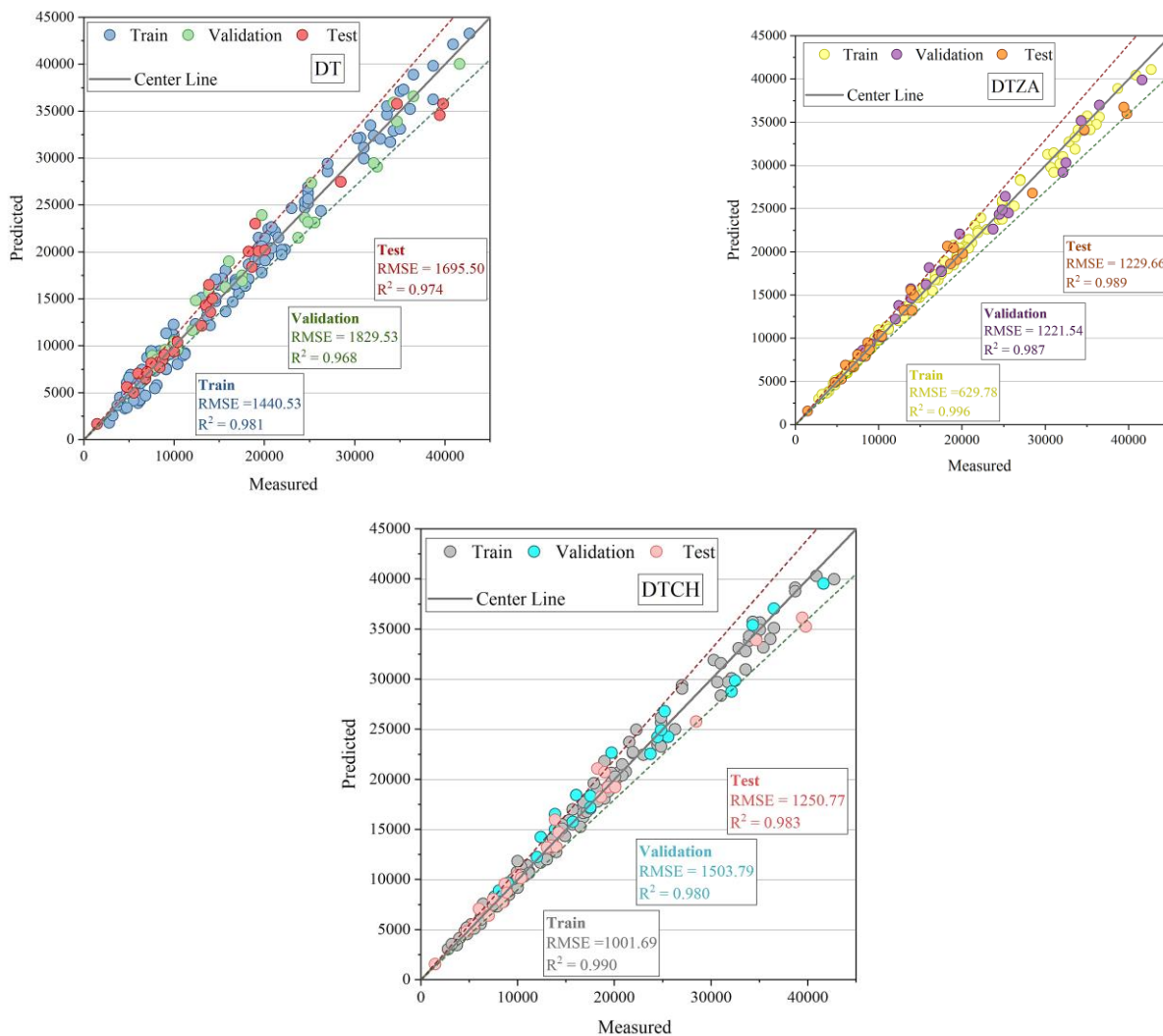


Fig. 3. The correlation between the predicted and measured values.

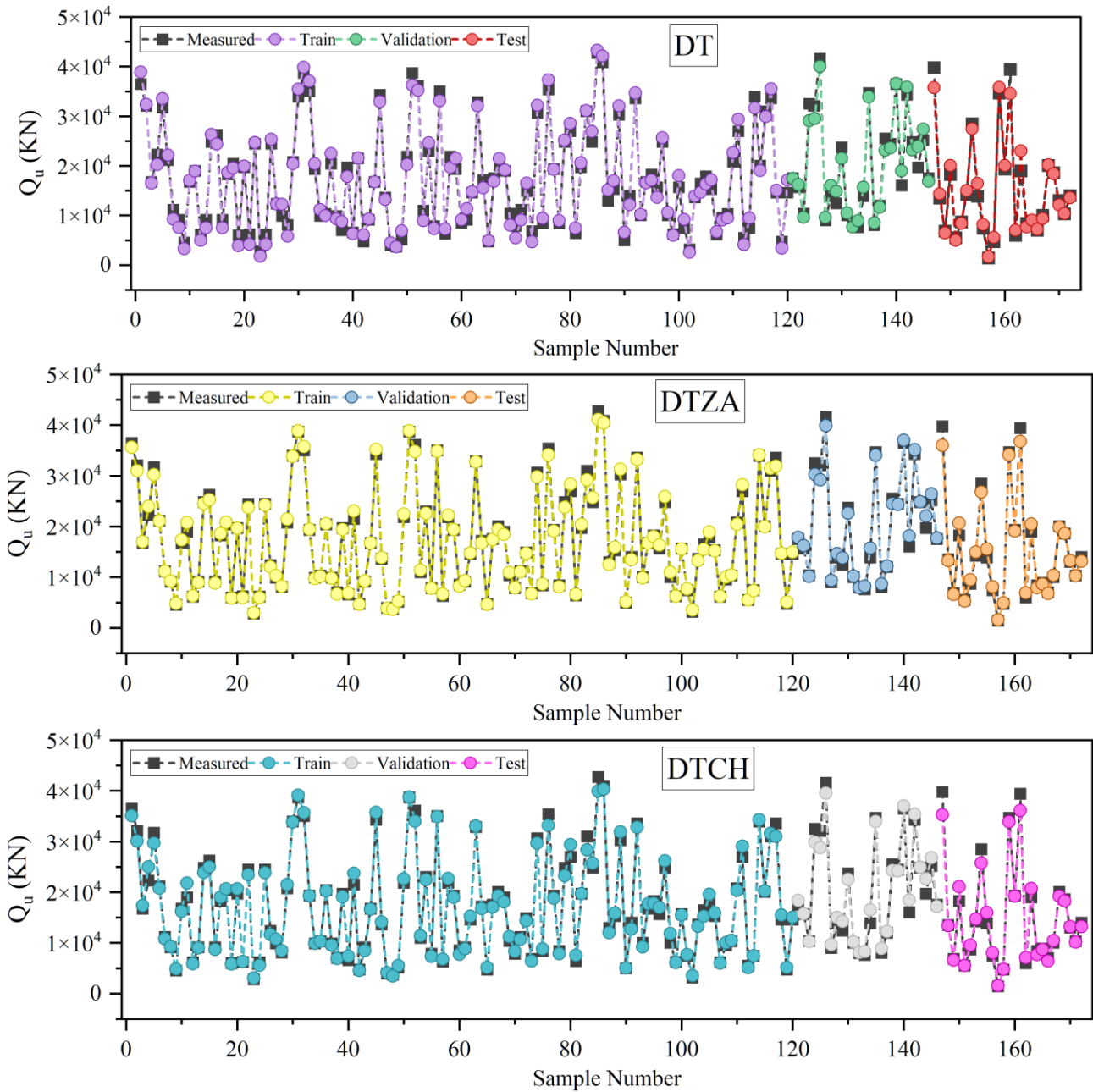


Fig. 4. The comparison of measured and predicted values.

Fig. 4 presents the relationship between predicted and measured values of the DT base models. In this figure, the measured values are represented by the black box. When the predicted values closely align with these measured values, it signifies the model's accuracy. As shown in Fig. 4, the DT model exhibits a significant deviation of its data from the measured values, particularly during the testing phase. Conversely, the DTZA model showcases a precise outcome, with an almost perfect match between its predicted and measured values, particularly within the sample numbers from 40 to 80. In contrast, the DTCH model demonstrates a noticeable lack of accuracy within the sample numbers ranging from 80 to 120, rendering it less precise than the DTZA model.

It is crucial to conduct an error assessment to achieve a deeper understanding of the uniqueness and precision of the models. Fig. 5 emphasizes that the DT model displayed a significant error rate, especially during the testing phase, peaking at a maximum error of 35% within the sample range of 0 to 50. On the other hand, most data points in the DTZA model exhibited errors that were nearly 0%, in contrast to the DTCH model, where the maximum error reached 20%.

Fig. 6 presents a box plot that simplifies the comparison of errors among the models within a single visual representation. The precision of the DTZA model becomes evident as the data points are closely grouped, primarily concentrated within the error range of -5% to 5%. This pattern contrasts with the

spread seen in the other models, underscoring the dependability of the DTZA model's predictions. The concentration of data points within a relatively narrow error range signifies its

consistent and accurate performance. In contrast, the dispersion observed in the error distribution of the other models indicates a broader variability in their predictions.

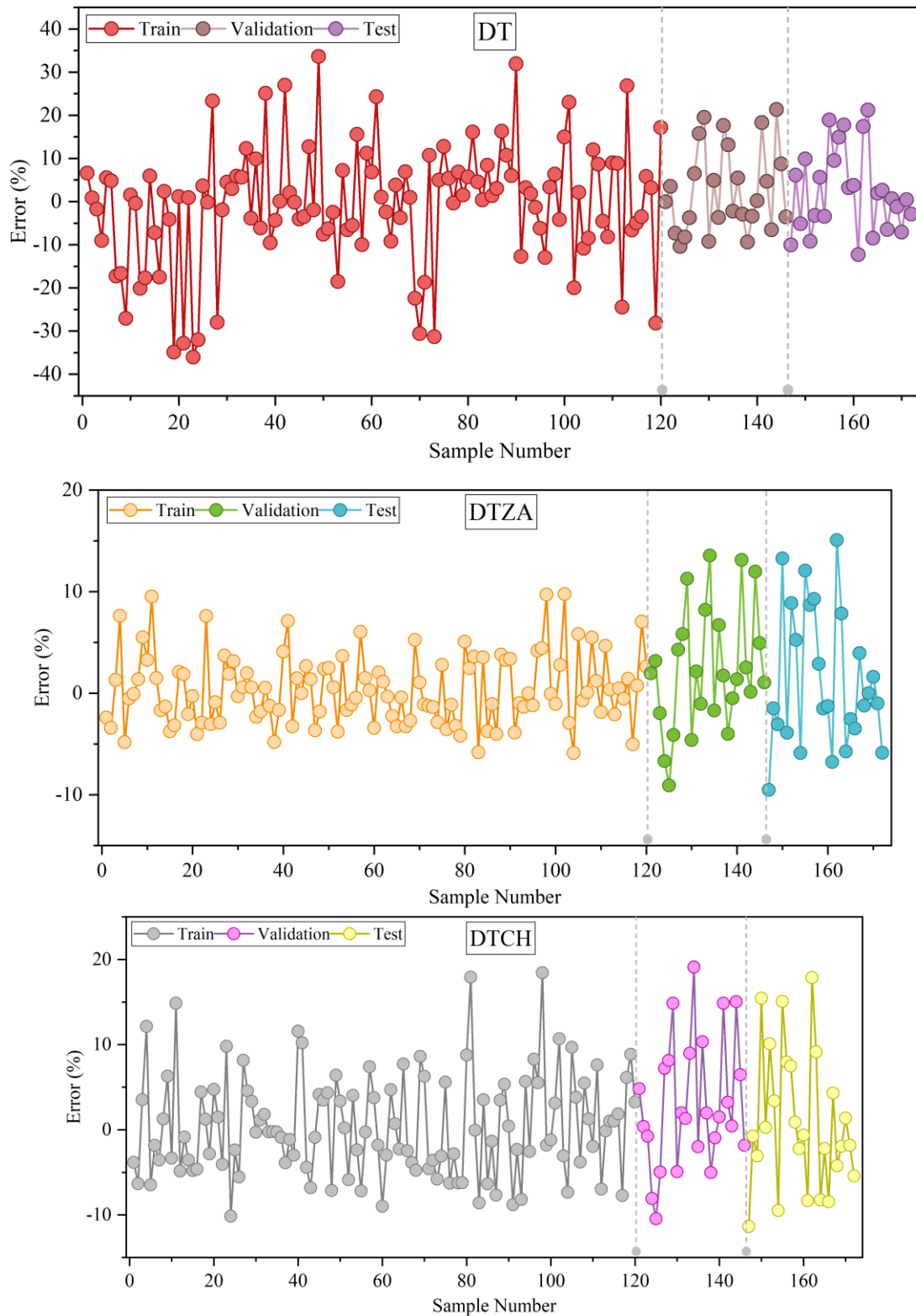


Fig. 5. The error percentage for the hybrid models is based on a line-symbol plot.

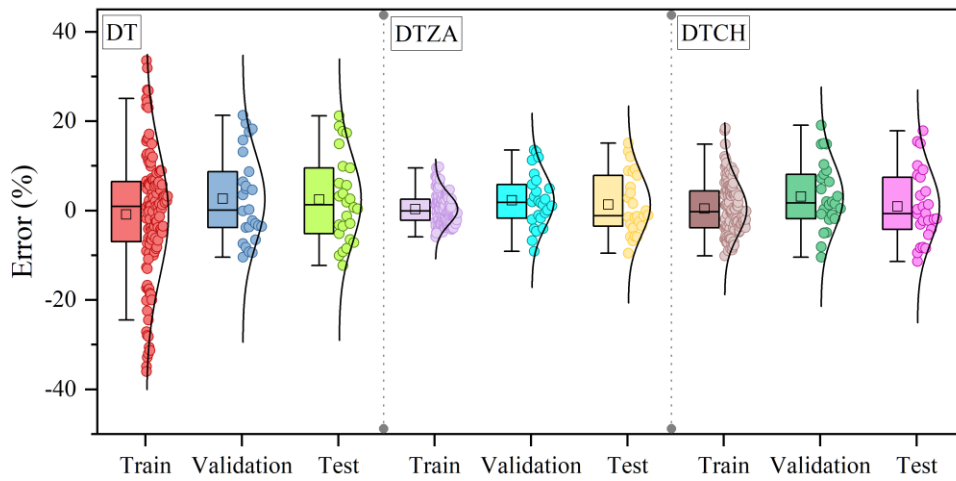


Fig. 6. The box plot of errors among the developed models.

IV. DISCUSSION

A. Comparison between the Results of Previous Articles and the Present Study

Table IV presents the results of previous research efforts on Qu prediction, providing a comprehensive benchmark for comparison with the current study. Among the five models discussed in this table from earlier research, the GA-DLNN model, described in Pham et al.'s research [37], demonstrated the most impressive performance, achieving an R^2 of 0.882 and an RMSE of 109.965. As detailed in the previous Section, the current investigation emphasizes the superior performance of the DTZA model during the training phase, producing commendable metric scores with an R^2 value of 0.9962 and an RMSE of 629.78. This exceptional performance in critical metrics decisively positions the DTZA model in this study as outperforming its counterparts, confirming its effectiveness in Qu prediction.

TABLE IV. COMPARING THE RESULTS OF THE PRESENT STUDY WITH PREVIOUS STUDIES

| Articles | Models | Models' performance | |
|-----------------------|---------------|---------------------|--------|
| | | RMSE | R^2 |
| Armaghani et al. [38] | ANN | 0.135 | 0.808 |
| Pham et al. [37] | GA-DLNN | 109.965 | 0.882 |
| Momeni et al. [39] | ANN | 0.529 | 0.71 |
| Momeni et al. [39] | ANFIS | 0.048 | 0.875 |
| Kulkarni et al. [40] | GA-ANN | 0.0093 | 0.86 |
| Present Study | DTZA (DT+ZAO) | 629.78 | 0.9962 |

B. Results of an Ablation Study

In this study, an ablation study was conducted as an alternative assessment approach. Two input values, as detailed in previous sections, were deliberately removed from the dataset. Subsequently, the prediction process was reiterated utilizing the best hybrid model. The outcomes of this ablation study were then compared with those of the main prediction process, with the findings summarized in Table V. Analysis of the table reveals that the results of the Main Study outperformed those of the Ablation Study. Specifically, the

Root Mean Square Error (RMSE) of the Main Study was 17.22% lower than that of the Ablation Study, indicating a superior predictive performance in the former.

TABLE V. COMPARING THE RESULTS OF THE MAIN STUDY WITH ABLATION STUDY

| phase | Main Study | | Ablation Study | |
|------------|------------|---------|----------------|---------|
| | R^2 | RMSE | R^2 | RMSE |
| Train | 0.9962 | 629.78 | 0.9942 | 774.33 |
| Validation | 0.9873 | 1221.55 | 0.9818 | 1464.26 |
| Test | 0.9893 | 1229.66 | 0.9845 | 1470.84 |
| All | 0.9934 | 854.89 | 0.9904 | 1032.73 |

C. Limitations of the Study

The study's limitations are acknowledged, including the potential restriction of results' generalizability by the specific dataset and experimental setup utilized. Variations in geological conditions, pile types, and other site-specific factors could affect the performance of the proposed hybrid models in different contexts. Additionally, the focus on predictive accuracy in the analysis may neglect considerations of computational efficiency or scalability, which could be crucial in real-world applications. Furthermore, biases or uncertainties may be introduced by the assumptions and parameters chosen for the optimization algorithms. Lastly, while efforts were made to provide insightful analysis of the experimental results, there may be aspects that require further investigation or validation in future studies. These limitations underscore the need for a cautious interpretation of the findings and highlight avenues for future research to address these constraints and refine the proposed methodologies.

V. CONCLUSION

The estimation of the ultimate bearing capacity (Q_u) using ML methods, specifically the DT model, coupled with advanced optimization algorithms, including the Zebra Optimization Algorithm (ZOA) and the Coronavirus Herd Immunity Optimizer (CHIO), has demonstrated significant promise and yielded valuable insights into the field of civil engineering. The incorporation of ML techniques, particularly the DT model, has proven to be a powerful tool for accurately estimating the ultimate bearing capacity of soils and rocks. The

utilization of this model allows for the efficient handling of complex datasets and the extraction of meaningful patterns and relationships within the data. However, as revealed in the analysis, the standalone DT model exhibited limitations in accuracy, especially during the testing phase, highlighting the need for further refinement. The fusion of the DT model with optimization algorithms, such as ZOA and CHIO, has been a pivotal advancement in enhancing predictive accuracy. The ZOA and CHIO optimizers have contributed to refining the model's performance during the training, validation, and testing phases. The analysis of the prediction results, as depicted in correlation and error assessments, showcased the distinctiveness of these models. The DTZA model demonstrated remarkable accuracy, with a close alignment between predicted and measured values. Its ability to maintain errors close to 0% over a wide range of samples is a testament to its consistent and precise performance. On the other hand, the DTCH model, while showing improved accuracy compared to the standalone DT model, exhibited some variability in its predictions, particularly in a specific sample range. The integration of ML methods, DT models, and advanced optimization algorithms like ZOA and CHIO has proven to be a valuable approach for predicting the ultimate bearing capacity in civil engineering applications. These hybrid models have shown substantial improvements in accuracy and reliability, which are crucial for making informed decisions in geotechnical engineering projects. Further research and fine-tuning of these models can advance the understanding and predictive capabilities in civil engineering, particularly in earthquake analysis and related areas.

ACKNOWLEDGMENTS

2023 Jilin Provincial Department of Education Science Research Project, Project Name: "Studying on the Shrinkage Behavior of Semi-flexible Grading Gravel Base Material in Cold Regions" (Project Number: JJKH20231038KJ)

REFERENCES

- [1] Cai G, Liu S, Tong L, Du G. Assessment of direct CPT and CPTU methods for predicting the ultimate bearing capacity of single piles. *Eng Geol* 2009;104:211–22.
- [2] Yong W, Zhou J, Jahed Armaghani D, Tahir MM, Tarinejad R, Pham BT, et al. A new hybrid simulated annealing-based genetic programming technique to predict the ultimate bearing capacity of piles. *Eng Comput* 2021;37:2111–27.
- [3] Harandizadeh H, Toufigh V. Application of developed new artificial intelligence approaches in civil engineering for ultimate pile bearing capacity prediction in soil based on experimental datasets. *Iranian Journal of Science and Technology, Transactions of Civil Engineering* 2020;44:545–59.
- [4] Chen W, Sarir P, Bui X-N, Nguyen H, Tahir MM, Jahed Armaghani D. Neuro-genetic, neuro-imperialism and genetic programming models in predicting ultimate bearing capacity of pile. *Eng Comput* 2020;36:1101–15.
- [5] Rock ACD-18 on S. Standard Test Methods for Laboratory Compaction Characteristics of Soil Using Modified Effort (56,000 Ft-Lbf/Ft³ (2,700 KN-M/M³)) I. ASTM international; 2009.
- [6] Pham TA, Ly H-B, Tran VQ, Giap L Van, Vu H-LT, Duong H-AT. Prediction of pile axial bearing capacity using artificial neural network and random forest. *Applied Sciences* 2020;10:1871.
- [7] Masoumi F, Najjar-Ghabel S, Safarzadeh A, Sadaghat B. Automatic calibration of the groundwater simulation model with high parameter dimensionality using sequential uncertainty fitting approach. *Water Supply* 2020;20:3487–501. <https://doi.org/10.2166/ws.2020.241>.
- [8] Akbarzadeh MR, Ghafourian H, Anvari A, Pourhanasa R, Nehdi ML. Estimating Compressive Strength of Concrete Using Neural Electromagnetic Field Optimization. *Materials* 2023;16:4200.
- [9] Yagiz S, Sezer EA, Gokceoglu C. Artificial neural networks and nonlinear regression techniques to assess the influence of slake durability cycles on the prediction of uniaxial compressive strength and modulus of elasticity for carbonate rocks. *Int J Numer Anal Methods Geomech* 2012;36:1636–50.
- [10] Jahed Armaghani D, Tonnizam Mohamad E, Hajihassani M, Yagiz S, Motaghedi H. Application of several non-linear prediction tools for estimating uniaxial compressive strength of granitic rocks and comparison of their performances. *Eng Comput* 2016;32:189–206.
- [11] Singh R, Kainthola A, Singh TN. Estimation of elastic constant of rocks using an ANFIS approach. *Appl Soft Comput* 2012;12:40–5.
- [12] Shirani Faradonbeh R, Monjezi M, Jahed Armaghani D. Genetic programming and non-linear multiple regression techniques to predict backbreak in blasting operation. *Eng Comput* 2016;32:123–33.
- [13] Monjezi M, Hasanipanah M, Khandelwal M. Evaluation and prediction of blast-induced ground vibration at Shur River Dam, Iran, by artificial neural network. *Neural Comput Appl* 2013;22:1637–43.
- [14] Marto A, Hajihassani M, Jahed Armaghani D, Tonnizam Mohamad E, Makhtar AM. A novel approach for blast-induced flyrock prediction based on imperialist competitive algorithm and artificial neural network. *The Scientific World Journal* 2014;2014.
- [15] Azimi M, Molaei Yeznabad A. Swarm-based Parallel Control of Adjacent Irregular Buildings Considering Soil–structure Interaction. *Journal of Sensor and Actuator Networks* 2020;9. <https://doi.org/10.3390/jsan9020018>.
- [16] Pal M, Deswal S. Modeling pile capacity using support vector machines and generalized regression neural network. *Journal of Geotechnical and Geoenvironmental Engineering* 2008;134:1021–4.
- [17] Shahin MA, Jaksa MB, Maier HR. Recent advances and future challenges for artificial neural systems in geotechnical engineering applications. *Advances in Artificial Neural Systems* 2009;2009.
- [18] Jianbin Z, Jiewen T, Yongqiang S. An ANN model for predicting level ultimate bearing capacity of PHC pipe pile. *Earth and Space 2010: Engineering, Science, Construction, and Operations in Challenging Environments*, 2010, p. 3168–76.
- [19] Lei Y, Zhou S, Luo X, Niu S, Jiang N. A comparative study of six hybrid prediction models for uniaxial compressive strength of rock based on swarm intelligence optimization algorithms. *Front Earth Sci (Lausanne)* 2022;10.
- [20] Agushaka JO, Ezugwu AE. Advanced arithmetic optimization algorithm for solving mechanical engineering design problems. *PLoS One* 2021;16:e0255703.
- [21] Dhiman G, Singh KK, Soni M, Nagar A, Dehghani M, Slowik A, et al. MOSOA: A new multi-objective seagull optimization algorithm. *Expert Syst Appl* 2021;167:114150.
- [22] Jahed Armaghani D, Shoib RSNSBR, Faizi K, Rashid ASA. Developing a hybrid PSO–ANN model for estimating the ultimate bearing capacity of rock-socketed piles. *Neural Comput Appl* 2017;28:391–405.
- [23] Momeni E, Nazir R, Armaghani DJ, Maizir H. Prediction of pile bearing capacity using a hybrid genetic algorithm-based ANN. *Measurement* 2014;57:122–31.
- [24] Erdal HI. Two-level and hybrid ensembles of decision trees for high performance concrete compressive strength prediction. *Eng Appl Artif Intell* 2013;26:1689–97.
- [25] Patel N, Upadhyay S. Study of various decision tree pruning methods with their empirical comparison in WEKA. *Int J Comput Appl* 2012;60.
- [26] Karbassi A, Mohebi B, Rezaee S, Lestuzzi P. Damage prediction for regular reinforced concrete buildings using the decision tree algorithm. *Comput Struct* 2014;130:46–56.
- [27] Ke G, Meng Q, Finley T, Wang T, Chen W, Ma W, et al. Lightgbm: A highly efficient gradient boosting decision tree. *Adv Neural Inf Process Syst* 2017;30.

- [28] Trojovská E, Dehghani M, Trojovský P. Zebra optimization algorithm: A new bio-inspired optimization algorithm for solving optimization algorithm. *IEEE Access* 2022;10:49445–73.
- [29] Mohapatra S, Mohapatra P. American zebra optimization algorithm for global optimization problems. *Sci Rep* 2023;13:5211.
- [30] Rana A, Khurana V, Shrivastava A, Gangodkar D, Arora D, Dixit AK. A ZEBRA Optimization Algorithm Search for Improving Localization in Wireless Sensor Network. 2022 2nd International Conference on Technological Advancements in Computational Sciences (ICTACS), IEEE; 2022, p. 817–24.
- [31] Zare P, Davoudkhani IF, Zare R, Ghadimi H, Mohajeri R, Babaei A. Maiden Application of Zebra Optimization Algorithm for Design PIDN-TIDF Controller for Frequency Control in Offshore Fixed Platforms Microgrid in the Presence of Tidal Energy. 2023 8th International Conference on Technology and Energy Management (ICTEM), IEEE; 2023, p. 1–7.
- [32] Al-Betar MA, Alyasseri ZAA, Awadallah MA, Abu Doush I. Coronavirus herd immunity optimizer (CHIO). *Neural Comput Appl* 2021;33:5011–42.
- [33] Alweshah M, Alkhalaileh S, Al-Betar MA, Bakar AA. Coronavirus herd immunity optimizer with greedy crossover for feature selection in medical diagnosis. *Knowl Based Syst* 2022;235:107629.
- [34] Dalbah LM, Al-Betar MA, Awadallah MA, Zitar RA. A modified coronavirus herd immunity optimizer for capacitated vehicle routing problem. *Journal of King Saud University-Computer and Information Sciences* 2022;34:4782–95.
- [35] Amini S, Ghasemi S, Golpira H, Anvari-Moghaddam A. Coronavirus herd immunity optimizer (CHIO) for Transmission Expansion Planning. 2021 IEEE International Conference on Environment and Electrical Engineering and 2021 IEEE Industrial and Commercial Power Systems Europe (EEEIC/I&CPS Europe), IEEE; 2021, p. 1–6.
- [36] Botchkarev A. Performance metrics (error measures) in machine learning regression, forecasting and prognostics: Properties and typology. *ArXiv Preprint ArXiv:180903006* 2018.
- [37] Pham TA, Tran VQ, Vu H-LT, Ly H-B. Design deep neural network architecture using a genetic algorithm for estimation of pile bearing capacity. *PLoS One* 2020;15:e0243030.
- [38] Jahed Armaghani D, Shoib RSNSBR, Faizi K, Rashid ASA. Developing a hybrid PSO-ANN model for estimating the ultimate bearing capacity of rock-socketed piles. *Neural Comput Appl* 2017;28:391–405.
- [39] Momeni E, Armaghani DJ, Fatemi SA, Nazir R. Prediction of bearing capacity of thin-walled foundation: a simulation approach. *Eng Comput* 2018;34:319–27.
- [40] Kulkarni RU, Dewaikar DM. Prediction of Interpreted Failure Loads of Rock-Socketed Piles in Mumbai Region using Hybrid Artificial Neural Networks with Genetic Algorithm. *Int J Eng Res* 2017;6:365–72.

Improving Prediction Accuracy using Random Forest Algorithm

Nesma Elsayed^{1*}, Sherif Abd Elaleem², Mohamed Marie³

Business Information Systems Department-Faculty of Commerce and Business Administration,
Helwan University, Helwan, Egypt¹

Business Administration Department-Faculty of Commerce and Business Administration, Helwan University, Helwan, Egypt²
Information Systems Department-Faculty of Computers and Artificial Intelligence, Helwan University, Helwan, Egypt³

Abstract—One of the latest studies in predicting bankruptcy is the performance of the financial prediction models. Although several models have been developed, they often do not achieve high performance, especially when using an imbalanced data set. This highlights the need for more exact prediction models. This paper examines the application as well as the benefits of machine learning with the purpose of constructing prediction models in the field of corporate financial performance. There is a lack of scientific research related to the effects of using random forest algorithms in attribute selection and prediction process for enhancing financial prediction. This paper tests various feature selection methods along with different prediction models to fill the gap. The study used a quantitative approach to develop and propose a business failure model. The approach involved analyzing and preprocessing a large dataset of bankrupt and non-bankrupt enterprises. The performance of the model was then evaluated using various metrics such as accuracy, precision, and recall. Findings from the present study show that random forest is recommended as the best model to predict corporate bankruptcy. Moreover, findings write down that the proper use of attribute selection methods helps to enhance the prediction precision of the proposed models. The use of random forest algorithm in feature selection and prediction can produce more exact and more reliable results in predicting bankruptcy. The study proves the potential of machine learning techniques to enhance financial performance.

Keywords—Corporate bankruptcy; feature selection; financial ratios; prediction models; random forest

I. INTRODUCTION

Predictions in business are essential tools for decision-making and strategic planning. At its core, a prediction is an educated guess about what the future holds based on past trends and current data. When used correctly, predictions can help businesses prepare for various scenarios and make informed decisions.

It is a common fact that there is no certainty in the field of business. Prediction models can provide decision makers with a framework to set more realistic strategies via predicting financial performance. In the case of predicting a business failure, management can prevent business bankruptcy. Bankruptcy prediction helps in increasing accuracy of decision making process for business enterprises since it has a variety of applications in financial fields [1].

The key idea is that public information of corporations comprises significant data and information that could be used by investors to assess financial status, which may be a major reason to cause bankruptcy [2]. Financial crisis prediction indicators included Profitability, Solvency, Growth ability, Cash flow and Capital structure [3]. Enhanced prediction accuracy is bound to increase the earnings to shareholders by improving financial risk management inside rising markets [4].

Recent research has employed financial ratios to show the exploration models for business failure. To improve prediction accuracy, it is important to find the most influential factors on financial performance. The discriminatory influence acquired by bringing together distinctive groups of financial ratios (FRs) and corporate governance indicators (CGIs) for business failure prediction was examined [5].

It is worth mentioning that the massive amount of corporate data presents an opportunity to deeply analyze the data and, consecutively, gain a great deal of knowledge. Unfortunately, the necessity for many human resources and too much time limit the benefits of the financial data. Alternatively, improving machine learning techniques can save both time and money. This helps to provide decision makers with significant evidence to be a base for making strategic plans.

In past works, a variety of prediction models were applied to define the early warning factors of a potential bankruptcy. This paper attempts to examine and compare the significance of using decision tree, k-nearest neighbor, logistic regression, multilayer Perceptron, and random forest in predicting corporate failure.

In 2022 a study used only three financial indicators: the return on assets, the current ratio, and the solvency ratio reported prediction accuracy rates of more than 80 percent. The study used Belgian companies' data set contains a sample of 3728 Belgian companies that were announced bankrupt between 2002 and 2012 to anticipate bankruptcy [6].

The main research gap is that “the performance of prediction models attained by combination of various categories of FRs has not been completely investigated. Only some chosen FRs have been utilized in previous researches and the selected attributes may vary from study to study [7].

The goal of our study is using random forest algorithm for analyzing corporate data encompassing various goals. Firstly, it aims to evaluate the tendency of business failure in different companies by developing prediction models that incorporate random forest algorithms in both attribute selection process and prediction process. Secondly, the model eases the enhancement of prediction process by enabling researchers to foresee the influence of fluctuations in ninety-five different financial ratios on corporate financial performance. Additionally, the research contributes by developing a novel model applying random forest algorithm along with seven various categories of financial indicators to anticipate business failures.

Paper structure consists of literature review in Section II providing a clear explanation of previous studies in bankruptcy prediction field, methods in Section III presenting our model that is based on incorporating the most common algorithms in financial prediction field, results in Section IV demonstrating the average performance measures for prediction models used in our study, discussion section clarifying the importance of our model and the significance of our contribution.

II. LITERATURE REVIEW

A. Corporate Bankruptcy Prediction

The substantial rise in the total papers, especially subsequent the 2008 global financial disaster, has verified that corporate bankruptcy is a subject of growing interest, which indicates the importance of this issue for corporations [8]. Regrettably, the COVID-19 epidemic that has invaded the globe since 2020 was one of the major triggers for bankruptcy filing. While data analytics has many applications in the financial field, Bankruptcy Prediction Models (BPM) have witnessed an increase in recognition [9].

Beaver assessed various financial variables to evaluate their ability in classifying and predicting bankrupt firms. That made him a pioneer in researches that study the enterprise failure prediction [10]. Altman presented business failure models according to discriminant study in categorizing economic failure based on five financial ratios: working capital/total assets, market value of equity/total debt, earnings before interest and taxes/total assets, retained earnings/total assets and sales/total assets [11].

Once Altman issued one of the very popular models in prediction of firms bankruptcy in 1968, a variety of models that predict bankruptcy have been issued in the literature [12]. It does not only direct attention to the increasing number of research issued, but also to the diversity of enterprise failure prediction models employed for business crisis prediction. Owing to the advance in machine learning methods and computer ability in latest years, more diverse analytical tools have been employed to create a business failure model with superior precision.

B. Prediction Accuracy Enhancement

There are two steps to assess financial crisis. Whereas the first stage employs a variety of financial variables, the other

one employs diverse classifiers in construction of the bankruptcy model [13].

First, in the financial variables step, selecting the most informative financial variables can improve prediction performance. Regarding to Chih-Fong Tsai investigational outcomes, applying attribute selection tools to choose and extract the extra valuable, demonstrative and illustrative variables can reduce the effort and time of training the model, which certainly results in increasing the performance of prediction [14].

Second, in the model construction step, a variety of methods have been offered, including decision tree, k-nearest neighbor, logistic regression, multilayer Perceptron, and random forest. In 1980, Ohlson estimated the probabilities of bankruptcy employing logistic regression [15].

One of the early applications of random forests was reported in 2001 that presented random sampling of trees and the concept of tree correlation. His discoveries indicated that for the first-time forest algorithms can rival with arcing approaches, in both classification and regression analysis [16]. Separate research done in 2012 showed that RF is effective for more accurate results. This assists the researchers in estimating feature significance and value [17].

Artificial neural networks (ANNs) are powerful artificial intelligence technologies that are widely-used as they are able to combine several nonlinear functions to express non-linear relationships between input data and a class label [18]. A previous study on corporate distress prediction examined the precision of Logit and ANN to establish a comparison between using statistical and artificial intelligence in modeling financial risk [4].

III. METHODS

A. Dataset

The data set is acquired from (UCIMLR)[19], which supplies datasets to the interested researchers in machine learning field. Initially, the sample data was gathered by the Taiwan Economic Journal. It comprises the financial variables of industrial, electronic, shipping, tourism, and retail companies for the years 1999–2009. The data set includes ninety-five various financial indicators and 6,819 rows, of which 6,599 are corporations that did not go bankrupt, and 220 are bankrupt corporations. The description of business failure is established on the rules of the Taiwan Stock Exchange. Our proposed model is shown in Fig. 1.

B. Preprocessing

In In data preprocessing stage, we checked for missing values and duplicates within the dataset, but there were none. We applied data normalization on the dataset. All preprocessing and feature selection steps were conducted using WEKA.

An imbalanced data set is created when the total observations in one group exceeds the total of observations in the other group. Prediction techniques behave disappointingly in data sets with imbalanced classes because they regularly suppose that all classes are represented equally.

As a result, the cases that are represented in the smaller group are miscategorized as belonging to the mass group [20].

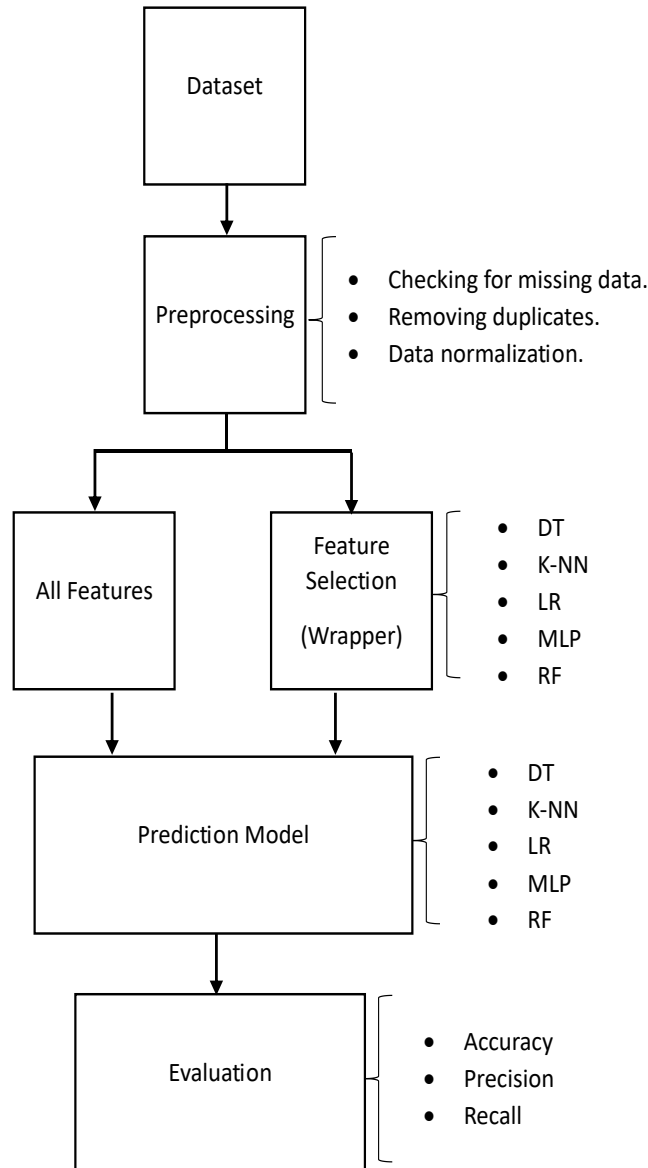


Fig. 1 Our proposed model.

In each year, the total of business failures is smaller in comparison with the total of companies that did not go bankrupt. If failed corporations are outliers, this causes a key breach to the fundamental distributional conjectures for logistic regression [21]. Resampling techniques generate new samples of data from the original dataset using a set of statistical methods. It is essential to lower the danger of the study or machine learning algorithm biasing toward the common class.

We applied unsupervised resample filter on data to get more reliable results by producing a random subsample of a dataset. It applies over sampling on the smaller group and under sampling on the mass group at the same time while keeping the same number of records in the original dataset. Thus, using unsupervised resampling helps in gaining the

benefits of both over and under-sampling. That leads to having more reliable and realistic results.

C. Feature Selection

Attribute selection is the practice of selecting the important attributes that have an influence on the performance of the model. Attribute selection is a research problem in wrapper methodology, so different combinations are made, assessed, and compared with other combinations. The algorithm is trained by using the subset of features iteratively.

In the present study, the wrapper method is applied on the resampled data since it interacts with classifier, models feature dependencies, minimizes computational cost, and provides good classification accuracy.

Features chosen will differ regarding the kind of classifier as diverse classifiers perform better with various arrays of attributes to generate more competent conclusions. The five classifiers which will be employed for the feature electing manner outcomes are illustrated in Table I.

TABLE. I. FEATURES SELECTED USING WRAPPER METHOD

| Classifier | Attributes selected based on the wrapper method |
|-----------------------------|---|
| Decision Tree (DT) | X8, X10, X12, X40, X55, X64, X65, X87, X92 |
| K-nearest Neighbor (KNN) | X9, X14, X21, X25, X31, X52, X54, X62, X73, X85, X87, X90, X92 |
| Logistic Regression (LR) | X11, X13, X17, X18, X21, X27, X34, X39, X44, X51, X64 |
| Multilayer Perceptron (MLP) | X2, X3, X16, X32, X39, X43, X49, X50, X52, X59, X61, X68, X73, X76, X84 |
| Random Forest (RF) | X34, X40, X48, X50, X54, X68, X76, X77, X80, X90, X91, X93 |

The highest significant features for effective bankruptcy prediction are the categories of solvency and profitability [5]. All classifiers have selected attributes from both categories except random forest algorithm has not selected any attributes from solvency category. RF algorithm has selected more attributes from growth category than other classifiers.

D. Prediction

To recognize the best bankruptcy model, different techniques have been applied on the data set, and then their outcomes are matched with each other. Models are established according to two distinctive situations:

All attributes will be employed, and only the features chosen using the wrapper method will be employed.

We trained models utilizing the same five algorithms employed in features selection wrapper method to analyze the relation between employing the same algorithm in both attribute selection stage and prediction modeling stage.

E. Evaluation

In cross-validation the data set is indiscriminately divided into 'k' groups. Only one group is treated as a test set whereas the extra groups are treated as training sets. The training sets aim to teach the model while the test set is utilized to assess the model. The activity is done repeatedly until every distinctive group has been utilized as the test set.

Cross-validation test is preferred to be used in such cases because it offers the model the chance to learn on multiple train-test divisions. This provides us with a well sign of how accurate the model will operate on undetected data.

In this research, the following metrics are employed to estimate model performance: accuracy, precision, and recall. The metrics computation is established on rules presented in Table II. Computation of accuracy, precision, recall and F-

measure are constructed on confusion matrix involving a classification of actual and predicted values into the next groups: true positive (TP), true negative (TN), false positive (FP), and false negative (FN).

Accuracy demonstrates how often a machine learning model is correct overall. Depending only on accuracy measure to estimate model performance can be deceiving when utilizing imbalanced data set as it assigns equal weight to the classes which mitigate the model's capability to predict all classes. Precision presents how frequently a machine learning model is precise when predicting the intended category. Recall expresses whether a machine learning model can recognize all objects of the intended category.

TABLE. II. PERFORMANCE METRICS

| Evaluation measure | Rule |
|--------------------|-------------------------|
| Accuracy | $\frac{TP + TN}{Total}$ |
| Precision | $\frac{TP}{TP + FP}$ |
| Recall | $\frac{TP}{TP + FN}$ |

IV. RESULTS

Since bankruptcy is an imbalanced problem, then the weighted average is preferred for measuring performance of classification models. Table III in Appendix summarizes the scores of the evaluation process. Considering these results, we can state that some models such as KNN, MLP, and RF work better with the features chosen utilizing wrapper method with the same algorithm. On the contrary, some models such as decision tree and logistic provided better results employing all attributes.

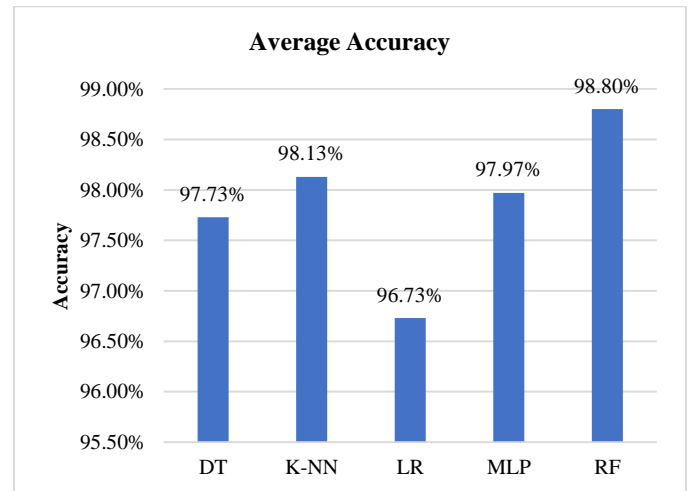


Fig. 2 Average accuracy of each model.

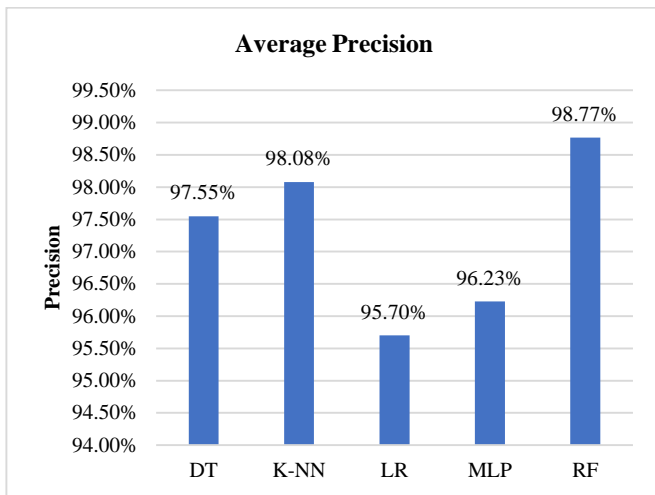


Fig. 3 Average precision of each model.

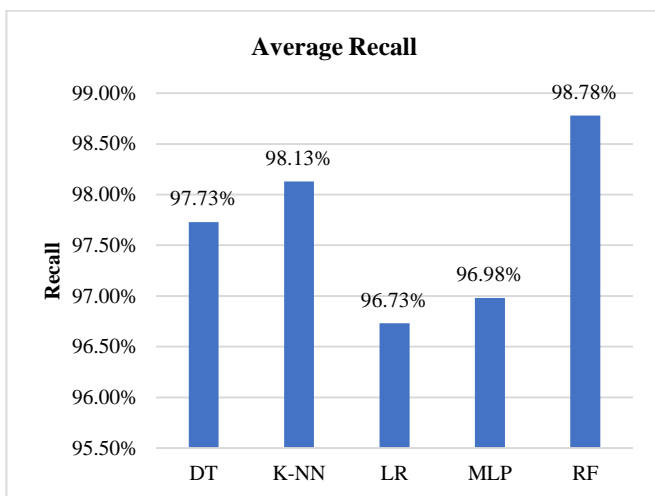


Fig. 4 Average recall of each model.

In analyzing Fig. 2, we see that the RF is better than the other models concerning illustrating and comparing the differences in average accuracy of models. As shown in this figure, the random forest was the most accurate model with 98.80% compared with the lowest accuracy of 96.73% for logistic model.

Fig. 3 displays the average precision of models employing different feature selection algorithms. Once more, the data suggests that RF, on average, provide an improved performance than their counterparts. This finding also sides with the preceding idea that RF is more efficient. While random forest was the most precise model with 98.77% the logistic model with 95.70% was the lowest in precision.

Fig. 4 also proves that random forest model performs better than other models. Again, we notice the same tendencies of RF model exceeding other models. Random forest model was the most model able to correctly identify most of the positive results with 98.78% sensitivity while the logistic model only had 96.73% which was the lowest. We can state that the model using random forest technique

outperformed all other models in all performance metrics in predicting bankruptcy.

V. DISCUSSION

To further confirm our findings, we compared them to other studies using the same sample dataset of Taiwanese enterprises along with various resampling, attributes selection and prediction techniques.

In 2016, the models published by [5] employed Support Vector Machine (SVM) and generated five different machine learning models. Along with the ninety-five financial ratios we utilized, they also used CGIs. They employed 10-fold cross-validation to generate ten distinct training and test samples. They also tried five alternative attribute selection techniques. The model with the best performance in their study achieved 81.5% accuracy that was exceeded by the weakest model in our research.

In 2022, the research by [22] closely examined the discriminatory competence of a MLP in studying financial failure prediction. For this purpose, they employed different setups of optimization algorithms, activation functions, number of neurons, and number of layers. The model with the best performance in their study achieved 86.67% accuracy, 95.47% precision and 85.24% sensitivity that was outperformed by the worst model in our study.

VI. CONCLUSIONS

This research covers the usage of different techniques with the aim of enhancing the findings of prediction. We can state that firstly, using feature selection can significantly improve performance of prediction models. Secondly, constructing prediction models using random forest algorithms outperformed other models using different machine learning techniques in terms of accuracy, precision, and sensitivity. Thirdly, employing growth ratios in dataset used in financial failure prediction is significant. Results from this study recommend that, in general, random forest algorithms tend to attain more exact results. The impressive performance of the random forest model can be improved when the wrapper method is used as the attribute selection method with random forest algorithm to detect the best features for the classifier. Practitioners can benefit from these conclusions to enhance the accuracy of their predictions. For future work, researchers may use different feature selection methods combined with a diversity of resampling approaches to identify what works better.

Funding: None.

Conflicts of Interest: None.

REFERENCES

- [1] Y. Zhang et al., "Towards augmented kernel extreme learning models for bankruptcy prediction: algorithmic behavior and comprehensive analysis," *Neurocomputing*, vol. 430, pp. 185-212, 2021, doi: <http://dx.doi.org/10.1016/j.neucom.2020.10.038>.
- [2] Z. Huang, H. Chen, C.-J. Hsu, W.-H. Chen, and S. Wu, "Credit rating analysis with support vector machines and neural networks: a market comparative study," *Decision support systems*, vol. 37, no. 4, pp. 543-558, 2004, doi: [http://dx.doi.org/10.1016/S0167-9236\(03\)00086-1](http://dx.doi.org/10.1016/S0167-9236(03)00086-1).

[3] M. Jiang and X. Wang, "Research on intelligent prediction method of financial crisis of listed enterprises based on Random Forest algorithm," Security and Communication Networks, vol. 2021, pp. 1-7, 2021.

[4] L. Muparuri and V. Gumbo, "On logit and artificial neural networks in corporate distress modelling for Zimbabwe listed corporates," Sustainability Analytics and Modeling, vol. 2, p. 100006, 2022, doi: <http://dx.doi.org/10.1016/j.samod.2022.100006>.

[5] D. Liang, C.-C. Lu, C.-F. Tsai, and G.-A. Shih, "Financial ratios and corporate governance indicators in bankruptcy prediction: A comprehensive study," European journal of operational research, vol. 252, no. 2, pp. 561-572, 2016.

[6] S. Shetty, M. Musa, and X. Brédart, "Bankruptcy Prediction Using Machine Learning Techniques," Journal of Risk and Financial Management, vol. 15, no. 1, p. 35, 2022.

[7] D. Liang, C.-F. Tsai, H.-Y. R. Lu, and L.-S. Chang, "Combining corporate governance indicators with stacking ensembles for financial distress prediction," Journal of Business Research, vol. 120, pp. 137-146, 2020.

[8] Y. Shi and X. Li, "An overview of bankruptcy prediction models for corporate firms: A systematic literature review," Intangible Capital, vol. 15, no. 2, pp. 114-127, 2019, doi: <http://dx.doi.org/10.3926/ic.1354>.

[9] S. C. Mann and R. Logeswaran, "Data Analytics in Improved Bankruptcy Prediction with Industrial Risk," in 2021 14th International Conference on Developments in eSystems Engineering (DeSE), 2021: IEEE, pp. 23-26, doi: <http://dx.doi.org/10.1109/DeSE54285.2021.9719372>.

[10] W. H. Beaver, "Financial Ratios As Predictors of Failure," Journal of Accounting Research, vol. 4, pp. 71-111, 1966, doi: 10.2307/2490171.

[11] E. I. Altman, "Financial Ratios, Discriminant Analysis and the Prediction of Corporate Bankruptcy," The Journal of Finance, vol. 23, no. 4, pp. 589-609, 1968, doi: 10.1111/j.1540-6261.1968.tb00843.x.

[12] J. L. Bellovary, D. E. Giacomino, and M. D. Akers, "A review of bankruptcy prediction studies: 1930 to present," Journal of Financial education, pp. 1-42, 2007.

[13] F. Lin, D. Liang, and E. Chen, "Financial ratio selection for business crisis prediction," Expert systems with applications, vol. 38, no. 12, pp. 15094-15102, 2011, doi: <http://dx.doi.org/10.1016/j.eswa.2011.05.035>.

[14] C.-F. Tsai, "Feature selection in bankruptcy prediction," Knowledge-Based Systems, vol. 22, no. 2, pp. 120-127, 2009, doi: <http://dx.doi.org/10.1016/j.knosys.2008.08.002>.

[15] J. A. Ohlson, "Financial ratios and the probabilistic prediction of bankruptcy," Journal of accounting research, pp. 109-131, 1980, doi: <http://dx.doi.org/10.2307/2490395>.

[16] L. Breiman, "Random forests," Machine learning, vol. 45, pp. 5-32, 2001, doi: <https://doi.org/10.1023/A:1010933404324>.

[17] D. Sharma, "Improving the art, craft and science of economic credit risk scorecards using random forests: Why credit scorers and economists should use random forests," Craft and Science of Economic Credit Risk Scorecards Using Random Forests: Why Credit Scorers and Economists Should Use Random Forests (June 9, 2011), 2011, doi: <http://dx.doi.org/10.2139/ssrn.1861535>.

[18] J. Heaton, "Ian Goodfellow, Yoshua Bengio, and Aaron Courville: Deep learning: The MIT Press, 2016, 800 pp, ISBN: 0262035618," Genetic programming and evolvable machines, vol. 19, no. 1-2, pp. 305-307, 2018, doi: <http://dx.doi.org/10.1007/s10710-017-9314-z>.

[19] Taiwanese Bankruptcy Prediction, doi: <https://doi.org/10.24432/C5004D>.

[20] Y. F. Roumani, J. K. Nwankpa, and M. Tanniru, "Predicting firm failure in the software industry," Artificial Intelligence Review, vol. 53, pp. 4161-4182, 2020, doi: <http://dx.doi.org/10.1007/s10462-019-09789-2>.

[21] R. P. Hauser and D. Booth, "Predicting bankruptcy with robust logistic regression," Journal of Data Science, vol. 9, no. 4, pp. 565-584, 2011, doi: [http://dx.doi.org/10.6339/JDS.201110_09\(4\).0006](http://dx.doi.org/10.6339/JDS.201110_09(4).0006).

[22] R. F. Brenes, A. Johannssen, and N. Chukhrova, "An intelligent bankruptcy prediction model using a multilayer perceptron," Intelligent Systems with Applications, p. 200136, 2022.

APPENDIX

TABLE III. COMPARISON BETWEEN THE OUTCOMES OF USING DIFFERENT ATTRIBUTE SELECTION AND MODELING ALGORITHMS

| Prediction model | Feature selection | Accuracy | Precision | Recall |
|------------------|-------------------|----------|-----------|--------|
| DT | None | 98.0056% | .979 | .980 |
| DT | DT Wrapper | 98.0496% | .979 | .980 |
| DT | KNN Wrapper | 97.6536% | .974 | .977 |
| DT | LR Wrapper | 97.375% | .971 | .974 |
| DT | MLP Wrapper | 97.8003% | .976 | .978 |
| DT | RF Wrapper | 97.4776% | .974 | .975 |
| KNN | None | 98.1816% | .981 | .982 |
| KNN | DT Wrapper | 98.1522% | .981 | .982 |
| KNN | KNN Wrapper | 98.5922% | .985 | .986 |
| KNN | LR Wrapper | 97.8003% | .978 | .978 |
| KNN | MLP Wrapper | 97.9909% | .980 | .980 |
| KNN | RF Wrapper | 98.0496% | .980 | .980 |
| LR | None | 97.1257% | .967 | .971 |
| LR | DT Wrapper | 96.5244% | .949 | .965 |
| LR | KNN Wrapper | 96.5684% | .953 | .966 |
| LR | LR Wrapper | 96.891% | .964 | .969 |
| LR | MLP Wrapper | 96.8031% | .960 | .968 |
| LR | RF Wrapper | 96.4511% | .949 | .965 |
| MLP | None | 98.0056% | .979 | .980 |
| MLP | DT Wrapper | 96.7004% | .959 | .967 |
| MLP | KNN Wrapper | 96.7004% | .957 | .967 |
| MLP | LR Wrapper | 96.6711% | .956 | .967 |
| MLP | MLP Wrapper | 96.979% | .964 | .970 |
| MLP | RF Wrapper | 96.7591% | .959 | .968 |
| RF | None | 98.8268% | .988 | .988 |
| RF | DT Wrapper | 98.7975% | .987 | .988 |
| RF | KNN Wrapper | 98.7975% | .988 | .988 |
| RF | LR Wrapper | 98.6362% | .986 | .986 |
| RF | MLP Wrapper | 98.8121% | .988 | .988 |
| RF | RF Wrapper | 98.9001% | .989 | .989 |

ORCID: Nesma Elsayed: <https://orcid.org/my-orcid?orcid=0009-0004-7859-562X>

StockBiLSTM: Utilizing an Efficient Deep Learning Approach for Forecasting Stock Market Time Series Data

Diaa Salama Abd Elminaam¹, Asmaa M M. El-Tanany², Mohamed Abd El Fattah³, Mustafa Abdul Salam⁴

Information Systems Departments, Faculty of Computers and Artificial Intelligence, Benha University, Benha, Egypt^{1,2,3}

Faculty of Computers and Information, Misr International University, Egypt¹

Applied Science Research Canter. Applied Science Private University, Amman, Jordan¹

MEU Research Unit, Middle East University, Amman 11831, Jordan¹

Artificial Intelligence Department-Faculty of Computers and Artificial Intelligence, Benha University, Benha, Egypt⁴

Department of Computer Engineering and Information, College of Engineering, Wadi Ad Dwaser, Prince Sattam Bin Abdulaziz University, Al-Kharj 16273, Saudi Arabia⁵

Abstract—The article introduces a novel approach for forecasting stock market prices, employing a computationally efficient Bidirectional Long Short-Term Memory (BiLSTM) model enhanced with a global pooling mechanism. Based on the deep learning framework, this method leverages the temporal dynamics of stock data in both forward and reverse time frames, enabling enhanced predictive accuracy. Utilizing datasets from significant market players—HPQ, Bank of New York Mellon, and Pfizer—the authors demonstrate that the proposed single-layered BiLSTM model, optimized with RMSprop, significantly outperforms traditional Vanilla and Stacked LSTM models. The results are quantitatively evaluated using root mean squared error (RMSE), mean absolute error (MAE), and the coefficient of determination (R^2), where the BiLSTM model shows a consistent improvement in all metrics across different stock datasets. We optimized the hyperparameters tuning using two distinct optimizers (ADAM, RMSprop) on the HPQ, New York Bank, and Pfizer datasets. The dataset has been preprocessed to account for missing values, standardize the features, and separate it into training and testing sets. Moreover, line graphs and candlestick charts illustrate the models' ability to capture stock market trends. The proposed algorithms attained respective RMSE values of 0.413, 0.704, and 0.478. The proposed algorithms attained respective RMSE values of 0.413, 0.704, and 0.478. The results show the proposed methods' superiority over recently published models. In addition, it is concluded that the proposed single-layered BiLSTM-based architecture is computationally efficient and can be recommended for real-time applications involving Stock market time series data.

Keywords—Stock prediction; Univariate LSTM models; Deep learning; financial forecasting; Vanilla LSTM; Stacked LSTM; Bidirectional LSTM

I. INTRODUCTION

Predictions of the stock market have long been of fascination to investors, analysts, and researchers. Accurate stock price forecasts can provide insightful information for making informed investment decisions. Recurrent neural networks (RNNs), specifically Long Short-Term Memory (LSTM) models, have demonstrated promising results in capturing the temporal dependencies in stock price data and

predicting future trends since the advent of deep learning techniques.

In this paper, we compare the efficacy of three variants of LSTM models for stock prediction: vanilla LSTM, stacked LSTM, and bidirectional LSTM. Each variant offers distinct architectural modifications to the fundamental LSTM structure, allowing for enhanced modeling capabilities and potentially improved prediction precision.

We conduct experiments utilizing a comprehensive dataset of historical stock prices from various companies and industries. The dataset has been preprocessed to account for missing values, outliers, and standardization. Then, we train and evaluate the three LSTM variants using appropriate evaluation metrics, including root mean squared error (RMSE), mean absolute error (MAE), and coefficient of determination (R^2).

The hyperparameters of deep learning models, such as LSTM, significantly impact their performance and predictive accuracy. Automatic techniques for tuning hyperparameters have been proposed; however, these methods frequently lack transparency and fail to provide end-users insight into the interactions between different hyperparameters and their relative importance [1].

Several key hyperparameters must be carefully selected and configured for the LSTM model used in this paper [2]: activation function (sigmoid, tanh, softmax, etc.), optimizer (Adam, Adadelta, RMSprop, etc.), batch size, number of epochs, number of hidden layers, etc.

The results of this study will shed light on the relative stock prediction performance of vanilla, layered, and bidirectional LSTM models. In addition, it will cast light on the effect of architectural changes on the predictive capabilities of models and their suitability for capturing the inherent complexities of stock price data.

Exploration and comparison of these LSTM variants can significantly advance stock prediction techniques. By comprehending the advantages and disadvantages of various

LSTM architectures, investors and researchers can make more informed decisions and improve their forecasting accuracy in the volatile and dynamic world of stock markets.

Our research seeks to contribute to the understanding of stock prediction using various neural network architectures and hyperparameter tuning techniques by building on the findings of these studies.

This paper presents several notable contributions to financial forecasting and machine learning, specifically in applying LSTM models to predict stock market trends. Here are the main contributions:

- The study introduces a computationally efficient single-layered Bidirectional Long Short-Term Memory (BiLSTM) model incorporating a global pooling mechanism. This architectural choice simplifies the model while maintaining effective learning capabilities, making it suitable for real-time stock market applications.
- The paper comprehensively compares three different LSTM architectures: Vanilla LSTM, Stacked LSTM, and Bidirectional LSTM. This comparison helps elucidate the strengths and weaknesses of each variant in handling the complexities of financial time series data.
- The research includes an in-depth exploration of hyperparameter tuning using two different optimizers, ADAM and RMSprop, to optimize the performance of the LSTM models. This systematic tuning approach contributes to the predictive models' robustness and reliability.
- The study employs various evaluation metrics, such as Root Mean Squared Error (RMSE), Mean Absolute Error (MAE), and the Coefficient of Determination (R^2). These metrics thoroughly assess the model's predictive accuracy and statistical reliability.
- The results indicate that the proposed BiLSTM model outperforms recently published models in predicting the closing prices of stocks. This demonstrates the effectiveness of the proposed approach in capturing the complex temporal dynamics of stock prices.
- Utilizing commonly used public datasets from major stocks like HPQ, New York Bank, and Pfizer, the study underscores the practical applicability of the proposed method in diverse financial environments.
- Including line graphs and candlestick charts to illustrate the models' performance provides visual evidence of the models' ability to capture and accurately predict stock market trends.

The remainder of this paper is structured as follows: Section II reviews the related work, illustrating the progression and application of various predictive models within financial forecasting. Section IV details the methodologies employed, including data collection, preprocessing steps, and the experimental setup for the LSTM variants. Empirical research is given in Section V.. Section VI discusses the implications of

these findings, offering insights into the practical applications and potential improvements for stock market forecasting. Finally, Section VII concludes the paper with a summary of the findings, contributions, and suggestions for future research directions in financial time series prediction using deep learning techniques.

II. RELATED WORK

Due to its economic significance and potential for financial benefit, the prediction of stock market movements has been the subject of extensive study. This section examines studies that have investigated various stock market prediction techniques.

Within their research, Sharma et al. [3] proposed a hybrid architecture that combines ANN and GA (GANN) to predict the closure price of two indices, the Dow 30 and the NASDAQ 100, the following day. Data spanning three years, including features like Open, Low, High, and Close, was used. The assessment metrics that were employed were MAPE, MSE, and RMSE. It was reported that GANN predicted more accurate results than the Back Propagation Neural Network (BPNN).

Using independent component analysis and support vector regression, [4] proposed a two-stage modeling strategy to resolve the difficulties of working with financial time series. They emphasized the significance of addressing noise and stabilizing time series for accurate forecasts.

Hamzacebi et al. [5] compared iterative and direct methods for multiperiodic forecasting using artificial neural networks. Their results were evaluated using grey relational analysis, demonstrating neural networks' suitability for capturing complex patterns in multiperiodic data.

Deep neural networks (DNNs) have been utilized to predict financial markets. In study [6] utilized DNNs to forecast financial markets and back tested their trading strategy on commodity and futures markets. The study demonstrated that DNNs can capture complex market dynamics and produce accurate predictions.

In electric load forecasting, [7] employed long short-term memory (LSTM) networks and data from metropolitan France's electricity consumption. A genetic algorithm optimized the number of hidden neural layers and optimal time lags, resulting in superior performance to conventional machine learning models.

Utilizing genetic algorithms, technical analysis parameters for stock forecasting have been optimized. In [8], optimized technical analysis parameters with genetic algorithms and fed them to a deep neural network for predictions, resulting in improved stock trading performance.

CEFLANN, a specialized artificial neural network, was used for stock market prediction [9]. They formulated stock trading prediction as a classification problem. They contrasted the performance of the model with that of other machine learning techniques, including support vector machines (SVM), naive Bayes (N.B.), k-nearest neighbors (KNN), and decision trees (DT).

LSTM has demonstrated efficacy in out-of-sample financial time series prediction [10]. Based on the LSTM outputs, a short-term trading strategy was developed. It outperformed logistic regression, DNN, and RAF.

LSTM, RNN, CNN, and MLP were evaluated with linear and non-linear regression models in study [11]. CNN outperformed competing models when tested on numerous NSE and NYSE companies.

Using remote sensing data, genetic algorithms were used to find a near-optimal solution to determining the optimal number of concealed layers in a neural network [12].

In study [13], eight LSTM variants were used on various tasks, such as music modeling, handwriting recognition, and speech recognition. The study discovered that the fundamental

LSTM architecture performed well, with no significant improvement from the variants, indicating that the hyperparameters were independent.

Regarding accuracy and variance, LSTM was compared to SVM, backpropagation, and the Kalman filter for stock market prediction [14]. LSTM demonstrated high precision and low variance, making it a desirable option.

In research [15], the optimization of hyperparameters for neural and deep belief networks by comparing manual and grid search strategies. Manual search produced models as excellent as, or even better than, grid search in less computation time, indicating its utility as a starting point for hyperparameter optimization algorithms. Table I shows comparative study of related work.

TABLE I. COMPARATIVE STUDY OF RELATED WORK

| Paper | Year | Method | Positives | Limitation |
|--|------|-------------------|---|---|
| Bhuriya, Dinesh, et al [16]. | 2017 | Linear Regression | <ul style="list-style-type: none">The project predicts the behavior of the TCS datasets using Linear Regression, and the final result is contrasted and assessed against the results of alternative methods. [16]The model integrates methods for practical machine learning applications, such as gathering and evaluating a sizable dataset and employing various strategies to train the model and forecast possible results. [16] | <ul style="list-style-type: none">Compared to other methods, the linear regression prediction method is somewhat less accurate.Does not take into account the Random Forest prediction model, which, when applied to a limited dataset, should provide predictions with a higher degree of accuracy.The prediction model was only applied to a single stock set, not the whole market. This leads to a certain level of shortsightedness throughout the assessment procedure. |
| Nivetha, R. Yamini, and C. Dhaya [17]. | 2017 | ANN | <ul style="list-style-type: none">Sentiment analysis of the social media platform is used in this project to forecast or evaluate human behavioral tendencies accurately.The model can be applied in various contexts, including the stock market, banking, auditing, investment strategies, and investing patterns.The most accurate results across a sizable dataset are obtained when MLR and SVM are used in an ANN with deep learning. | <ul style="list-style-type: none">The purpose of this study is to build an algorithm for stock value prediction; the accuracy of the prediction is not discussed. It provides a qualitative, not a quantitative, approach.To analyze the forecast, it gives a semantic figure rather than a visual result. There are no graphs offered to show market trends or patterns in investment. |
| Parmar, Ishita, et al [18]. | 2018 | LSTM | <ul style="list-style-type: none">The accuracy attained for a big dataset increases with system utilization. Regression-based models are not as accurate as the updated LSTM technique.[18]To view data, this approach offers graphical data. [18] | <ul style="list-style-type: none">Expanding the dataset can lead to an increase in the system's accuracy.[18]Additional testing of other ML models under development is necessary to improve forecast accuracy.Since sentiment is significant in stock price volatility, sentiment analysis using machine learning should be conducted. |
| Liu, Siyuan, Guangzhong Liao, and Yifan Ding [19]. | 2018 | LSTM | <ul style="list-style-type: none">This model is the first to rely only on Long Short-Term Memory (LSTM) for prediction, resulting in higher accuracy.This publication provides a clear explanation of the LSTM model and training process. This covers both graphical and mathematical implementations. | <ul style="list-style-type: none">The LSTM model requires many layers to be stacked to provide good accuracy. So, it is a tedious process.The LSTM network must be combined with existing clustering techniques to gain large speed-ups in training and testing times at the cost of a small drop in performance. [19] |
| Shakva, Abin, et al [20]. | 2018 | ANN | <ul style="list-style-type: none">This paper uses a feedforward neural network to determine stock prices based on real-time trade volume, transaction frequency, and price fluctuations. [20]Hidden layer neurons were tweaked independently for each stock model. ADBL achieved the highest accuracy of 86.12% using a 3-20-10 network model. [20] | <ul style="list-style-type: none">Requires extensive knowledge of deep learning and neural networks. There is a significant skills gap in this industry.This model requires significant processing resources to run. |

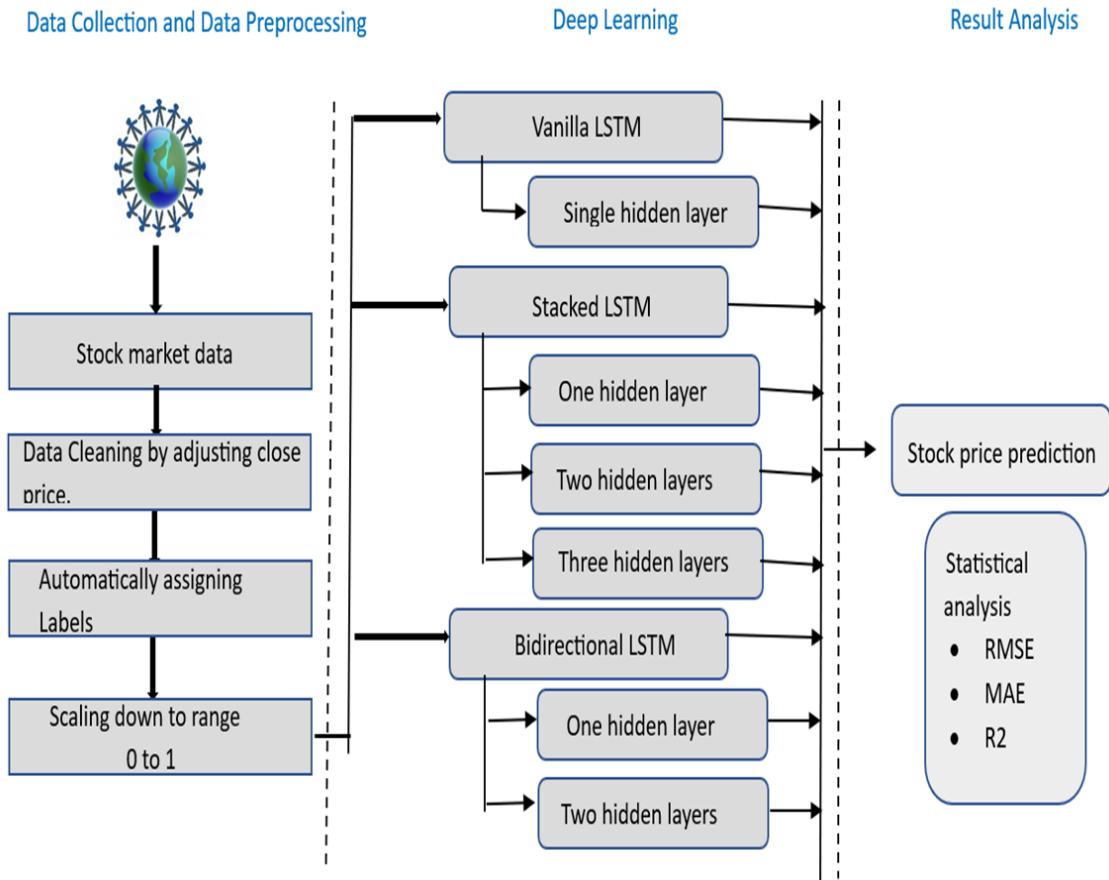


Fig. 1. The Proposed framework for stock market forecasting.

III. EXPERIMENT SETUP

A. Proposed Experimental Design

As shown in Fig. 1, General architecture of the proposed method which identify step by step of our experiment: -

- Data collection.
- Data preprocessing.
- Proposed models.
- Evaluation matrices.

B. Data Sets' Collection Abbreviations and Acronyms

In the study "StockBiLSTM: Utilizing an Efficient Deep Learning Approach for Forecasting Stock Market Time Series Data," three distinct stock market datasets were employed to evaluate the performance of the LSTM models. These datasets include historical stock prices from:

1) *HPQ (Hewlett-Packard Company)*: This dataset comprises stock prices of HP Inc., which is a multinational technology company known for developing and producing personal computers, printers, and related supplies. The dataset likely covers daily stock metrics such as opening and closing prices, highs and lows, and volume traded.

2) *BNY (Bank of New York Mellon Corporation)*: This dataset contains stock data from BNY Mellon, a global financial services firm that offers a broad range of banking and investment services. Similar to the HPQ dataset, it includes daily trading information, capturing the financial dynamics of the banking sector.

3) *PFE (Pfizer Inc.)*: This dataset includes stock prices from Pfizer, one of the world's largest pharmaceutical companies. The dataset provides insights into the healthcare sector's stock behavior, with daily stock performance records, including price fluctuations and trade volumes.

a) Data Characteristics and Preprocessing:

- **Time Range:** Each dataset spans several years of trading data, providing a robust temporal framework for training and testing the LSTM models. The specific time range for each dataset was not detailed in the initial summary but typically would cover multiple years to include various market conditions and trends.
- **Data Preprocessing:** Before being used for training the LSTM models, the datasets underwent several preprocessing steps:
 - **Missing Values:** Any gaps in the data due to market closures or other reasons were addressed, possibly

through methods like linear interpolation or carrying forward the last known value.

- Standardization: The features were standardized to have a mean of zero and a standard deviation of one or normalized to scale the data within a specific range, such as 0 to 1. This normalization helps in reducing bias and variance in the model training process.
- Feature Engineering: The datasets were likely prepared to include not just the raw numerical prices but potentially derived technical indicators such as moving averages, percentage changes, and others that help capture market sentiments and trends.
- Data Segmentation: The data was divided into training and testing sets, with a typical split providing enough data for the models to learn underlying patterns while reserving a portion for unbiased evaluation of model performance.

These datasets and their preparation play a critical role in developing predictive models, ensuring that the LSTM networks have access to high-quality, relevant data that mirrors real-world conditions under which they will be deployed. This detailed preparation helps maximize the models' efficacy, enhancing their ability to generalize well to unseen data.

To ensure diversity in our analysis, including companies from various industries or sectors is typically advantageous. HPQ (H.P. Inc) is a multinational technology corporation that develops and produces personal computers, printers, and related products. 2015 marked the separation of Hewlett-Packard Company (H.P.) into two separate entities, with H.P. Inc. concentrating on personal systems and printing products. B.K. (Bank of New York Mellon) is a financial institution called BNY Mellon. It is a global financial services firm that offers a variety of banking and investment services. BNY Mellon, one of the earliest financial institutions in the United States, operates in multiple segments, including investment management, investment services, and wealth management. The shares of BNY Mellon are traded on prominent exchanges such as the New York Stock Exchange (NYSE). PFE (Pfizer) is a multinational pharmaceutical corporation specializing in researching, developing, and producing prescription medications and vaccines. Pfizer is one of the largest pharmaceutical companies in the world, with a diverse product portfolio spanning numerous therapeutic areas, including cardiology, oncology, and immunology, among others.

This selection encompasses various industries, which can provide insight into the performance of various industries on the stock market. As shown in Fig. 1, the stock price information for these corporations was downloaded from Yahoo Finance.

Define abbreviations and acronyms the first time they are used in the text, even after they have been defined in the abstract. Abbreviations such as IEEE, SI, MKS, CGS, sc, dc, and rms do not have to be defined. Do not use abbreviations in the title or heads unless they are unavoidable.

C. Setting up the Environment

In the paper, Python 3.10.12 was used as the programming environment to conduct the experiments. To ensure the reproducibility of experiments, a virtual environment was created. These packages have been deployed within the virtual environment:

- TensorFlow 2.12.0
- Keras 2.12.0
- Pandas 1.5.3
- Sklearn 1.2.2
- NumPy 1.22.4
- Matplotlib 3.7.1

D. Data Preparation

The general strategy for preparing time series data before implementing time series techniques is suitable. The stages involved are as follows:

Before proceeding with analysis, resolving missing values in time series data is typical. A method for estimating missing values based on neighboring data points is linear interpolation, which fills in missing values. This interpolation helps preserve the temporal relationships between data points.

Scaling the closure price is a common preprocessing step when training neural network models such as Vanilla LSTM, Stacked LSTM, and Bidirectional LSTM. Scaling the data ensures that the input features are on a comparable scale, which can enhance the training process and the model's ability to learn. A common scaling technique is normalization, in which the data are scaled to a specific range, typically between 0 and 1. This is possible through:

$$X_{\text{scaled}} = (X - X_{\text{min}}) / (X_{\text{max}} - X_{\text{min}}) \quad (1)$$

X represents the close price, X_{min} represents the minimum value of the close price, and X_{max} represents the maximum value of the close price.

Different sets of features can be developed based on the objectives of the analysis. We mentioned univariate and multivariate feature sets in our case. The univariate feature set consists only of energy consumption information. The multivariate feature set includes price, day of the week, and month as additional features. These additional features can provide context-sensitive data that may enhance the modeling process.

The separation of data into training and test collections is essential to the effective evaluation of models. In our case, we mentioned setting aside one year and eight months of test data for evaluation. The remaining data is trained using a divide of eighty percent. This division permits us to train the models on substantial data.

Following these stages helps ensure the time series data is properly prepared for analysis and modeling, resulting in more accurate predictions and insights.

E. Data Splitting

The provided information describes the data extraction and splitting process for training and testing a set of neural network models (Vanilla LSTM, Stacked LSTM, and Bidirectional LSTM) using stock price data from three companies for 2011 days (about five and a half years) between 03-01-2012 and 30-12-2019, which is over eight years of data. A ratio of 80:20 was applied to training and testing data, resulting in 403 days (about one year) of testing.

IV. METHODOLOGY

A. Vanilla LSTM (Long Short-Term Memory)

Vanilla LSTM (Long Short-Term Memory) refers to a standard or fundamental implementation of the LSTM architecture, a form of recurrent neural network (RNN). LSTM networks are designed to resolve the vanishing gradient problem in conventional RNNs, allowing for more accurate modeling of long-term dependencies in sequential data. With a single layer of concealed LSTM units trained to predict future stock prices based on historical data.

The Vanilla LSTM architecture comprises LSTM cells, which are recurrent units capable of processing sequential data over time. Each LSTM cell possesses a collection of internal states, including a cell state (also known as the memory) and a concealed state. The cell state permits LSTMs to detect long-term dependencies by selectively storing and updating information.

During training, the Vanilla LSTM learns to modify the gate weights and biases via backpropagation and gradient descent. This enables it to capture relevant information and forget irrelevant information across multiple time steps.

B. Stacked LSTM (Long Short-Term Memory)

Stacked LSTM is a type of Long Short-Term Memory (LSTM) architecture in which multiple LSTM layers are layered atop one another to create a deep recurrent neural network (RNN). Each LSTM layer in the stack processes the input sequence sequentially, passing the concealed state to the following layer as its input.

Like stacking numerous feedforward layers in a deep neural network, the concept of stacking LSTM layers is analogous. By increasing the depth of the network, stacked LSTMs can learn more complex representations and incorporate higher-level abstractions from sequential data.

In a stacked LSTM architecture, the output of one LSTM layer functions as the input to the subsequent LSTM layer. The first layer receives the initial input sequence, and subsequent layers process the concealed states of the previous layer. Depending on the specific assignment, the final output can be extracted from the final LSTM layer, fed into additional layers, or output units.

The advantage of using stacked LSTM over a single-layer LSTM is that it can potentially capture more complex temporal dependencies in the input sequence. Each layer can discover unique patterns and contribute to a more evocative representation of the input data. Stacking multiple LSTM layers permits the network to learn hierarchical representations

of the input sequence, with lower layers representing local dependencies and higher layers representing more global dependencies.

C. Bidirectional LSTM (Long Short-Term Memory)

Bidirectional long-short-term memory (BiLSTM) is a technique that enables neural networks to store sequence data in both directions, either backward or forward. Bidirectional input distinguishes the BiLSTM from the conventional LSTM. We can have input flow in both directions, allowing us to store past and future data at any given time step. Normal LSTMs permit input transmission in only one direction (forward or backward).

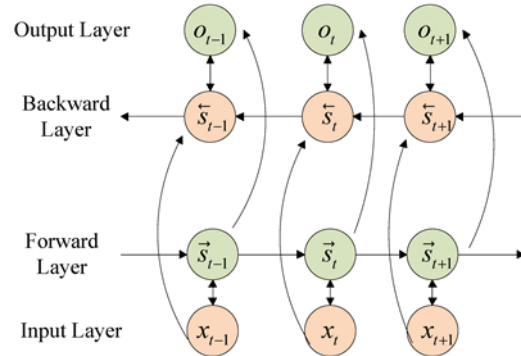


Fig. 2. Structure fundamental of bidirectional LSTM [21].

Fig. 2 demonstrates that the forward layer computes the forward direction from one to t and stores the forward hidden layer's output at each instant. The backward layer calculates the reverse time series and stores the backward concealed layer's output at each instant. Finally, the bidirectional LSTM neural network output is computed by combining the forward layer and reverse layer output results at each time point. The notation for the bidirectional LSTM neural network is:

$$st=(Uxt+Wst-1) \quad (2)$$

$$s' t=(U' xt+W' s' t+1) \quad (3)$$

$$ot=(Vst+V' s' t) \quad (4)$$

where, x_t is the input vector, g , and f are activation functions, V , W , and U are the weight matrix from the hidden layer to the output layer, the hidden layer, and the input layer to the hidden layer, and V' , W' , and U' are the corresponding reverse weight matrix. The state weight matrices of the forward and reverse layers are not shared information. The forward and backward layers are calculated sequentially, and their results are returned. The final output o_t is determined by adding the forward calculation result st and the reverse calculation result $s' t$.

D. Model Hyper-parameters Tuning

Fig. 3 illustrates a typical development cycle for neural networks, emphasizing the significance of efficient development to accommodate lengthy training periods for large neural networks. Exploring hyperparameter tuning and identifying a suitable initial starting point are crucial for accelerating the process and facilitating quicker development.

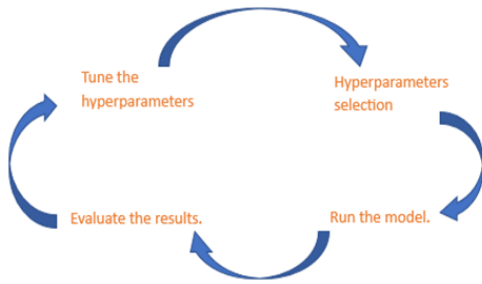


Fig. 3. Model Hyper-parameters tuning.

E. Model Evaluation

In this paper, the mean absolute error (MAE), root mean square error (RMSE), and coefficient of determination (R²) are used to assess the prediction error. R², RMSE, and MAE are common indicators used to evaluate the accuracy of a model based on the measurement value and estimated value. The indicators are defined by Eq. (5) through Eq. (7). The approximated indicator used as the measurement value is the MAE. The root-mean-squared error (RMSE) is used to evaluate the deviation between the observed and true values; it is sensitive to outliers. R² is utilized to evaluate the proportion of the dependent variable's variance.

$$RMSE=1/n \sum_{i=1}^n |x_i - \hat{x}_i|^2 \quad (5)$$

$$MAE=1/n \sum_{i=1}^n |x_i - \hat{x}_i| \quad (6)$$

$$R^2=1-SSR/SST \quad (7)$$

where, n represents the number of sample data, x_i represents the actual value, and \hat{x}_i represents the predicted value. SSR represents the variation in the dependent variable that can't be explained. SST is the entire variance of the dependent variable.

V. EMPIRICAL RESEARCH

Experiment 1: Involves feeding data of HPQ company in stages to Vanilla LSTM using (Adam and RMSprop) optimizers; after hyper-parameter tuning, the batch size is determined to be two, and the epoch is defined as fifteen. For Stacked LSTM using (Adam and RMSprop) optimizers, the batch size is three, and the epoch is defined as seventeen. For Bidirectional LSTM using (Adam and RMSprop) optimizers, the batch size is determined to be one, and the epoch is defined as fifteen.

Experiment 2: Involves feeding data of New York bank in stages to Vanilla LSTM using (Adam and RMSprop) optimizers; after hyper-parameter tuning, the batch size is determined to be two, and the epoch is defined as fifteen. For Stacked LSTM using (Adam and RMSprop) optimizers, the batch size is three, and the epoch is defined as seventeen. For Bidirectional LSTM using (Adam and RMSprop) optimizers, the batch size is determined to be two, and the epoch is defined as fifteen.

Experiment 3: Involves feeding data of Pfizer company in stages to Vanilla LSTM using (Adam and RMSprop) optimizers; after hyper-parameter tuning, the batch size is determined to be two, and the epoch is defined as fifteen. For

Stacked LSTM using (Adam and RMSprop) optimizers, the batch size is one, and the epoch is defined as fifteen. For Bidirectional LSTM using (Adam and RMSprop) optimizers, the batch size is determined to be one, and the epoch is defined as fifteen.

VI. RESULTS AND DISCUSSION

A. HPQ (Hewlett-Packard Company)

1) Model Performance: The Bidirectional LSTM (BiLSTM) model, particularly when optimized with the RMSprop optimizer, achieved superior results compared to other models. This was quantified using RMSE, MAE, and R² metrics, where the BiLSTM model showed lower error rates and a higher coefficient of determination.

2) Discussion: The superior performance of the BiLSTM model on the HPQ dataset (see Fig. 4) suggests that the bidirectional nature of the model, which captures both past and future dependencies, is particularly suited for technology stocks like HPQ. These stocks might exhibit patterns that are influenced by a broader range of temporal dynamics due to technology product release cycles and market competition.

B. BNY (Bank of New York Mellon Corporation)

1) Model Performance: Similar to the HPQ dataset, the BiLSTM model optimized with RMSprop showed excellent performance (see Fig. 5). However, it's notable that the Stacked LSTM also performed robustly but slightly less effectively than the BiLSTM.

2) Discussion: The effectiveness of LSTM models on the BNY dataset indicates their capability in modeling financial sector stocks, which may be influenced by different factors such as interest rates, regulatory changes, and economic indicators. The slight edge of BiLSTM could be attributed to its ability to utilize forward and backward data flows, which may be significant in the financial sector where past and upcoming economic events heavily influence stock prices.

C. PFE (Pfizer Inc.)

1) Model Performance: The dataset for Pfizer showed that while all LSTM variants performed well, the BiLSTM with RMSprop again stood out, particularly regarding the RMSE and MAE metrics. This dataset also revealed a higher R² score for the BiLSTM model, indicating a strong ability to explain the variance in stock prices through the model.

2) Discussion: The strong performance of LSTM models on the Pfizer dataset (see Fig. 6) could be related to the pharmaceutical industry's sensitivity to news and events such as drug approval processes, clinical trials, and regulatory decisions. The bidirectional approach of the BiLSTM may help capture these influences more comprehensively, as it accounts for both historical trends and anticipations of future events, which are crucial in the pharmaceutical industry.

D. Overall Insights

1) General Trends: Across all datasets, the BiLSTM model generally outperformed Vanilla and Stacked LSTMs,

suggesting that incorporating forward and backward information flows offers a significant advantage in stock price prediction.

2) Hyperparameters and Optimization: The choice of RMSprop as an optimizer was validated as it consistently supported the models in achieving lower prediction errors. This might suggest that RMSprop's approach to adjusting the learning rate could be particularly effective in dealing with the noisy and non-stationary data typical of stock markets.

3) Implications for Stock Market Forecasting: The results underscore the potential of advanced LSTM architectures in financial forecasting, highlighting their adaptability and robustness across different sectors of the economy. This has practical implications for traders and analysts seeking to leverage machine learning for investment decisions.

These discussions reveal that while LSTM models are generally robust in handling stock price data, the specific characteristics of the BiLSTM architecture make it especially powerful in capturing the complex, dual-influenced trends common in stock market data. Further research could expand on these findings by exploring additional LSTM modifications or incorporating more complex features and external data sources to enhance predictive accuracy.

On the test dataset, predictions were generated using Vanilla, Stacked, and Bidirectional LSTM with two distinct optimizers (Adam and RMSprop). The results of Experiment 1 are presented in Table II, the results of Experiment 2 are

presented in Table III, and the results of Experiment 3 are presented in Table IV, along with the evaluation metrics root mean squared error (RMSE), mean absolute error (MAE), and coefficient of determination (R2).

Regarding to HPQ data set, it is shown that the superiority of Bi LSTM over the remaining algorithms using RMSprop optimizer. Also, it is shown that the worst result using the same optimized is Stacked LSTM, the Same as New York Bank and Pfizer company data sets.

The study "StockBiLSTM: Utilizing an Efficient Deep Learning Approach for Forecasting Stock Market Time Series Data" provided insights into the performance of LSTM models across three different datasets: HPQ (Hewlett-Packard Company), BNY (Bank of New York Mellon Corporation), and PFE (Pfizer Inc.). Here's a detailed discussion of the results for each dataset:

The following graphs illustrate the comparison between predicted and actual data for HPQ company. It is shown in Fig. 4.

$$a + b = \gamma \tag{7}$$

The following graphs illustrate the comparison between predicted and actual data for New York bank. It is shown in Fig. 5.

The following graphs illustrate the comparison between predicted and actual data for Pfizer company. It is shown in Fig. 6.

TABLE II. UTILIZING UNIVARIATE LSTM MODELS AT HPQ

| Optimizer | Vanilla LSTM | | | Stacked LSTM | | | Bidirectional LSTM | | |
|-----------|--------------|-------|-------|--------------|-------|-------|--------------------|-------|-------|
| | R2 | RMSE | MAE | R2 | RMSE | MAE | R2 | RMSE | MAE |
| Adam | 0.965 | 0.432 | 0.284 | 0.967 | 0.421 | 0.27 | 0.965 | 0.434 | 0.308 |
| RMSprop | 0.964 | 0.437 | 0.296 | 0.958 | 0.475 | 0.318 | 0.968 | 0.413 | 0.271 |

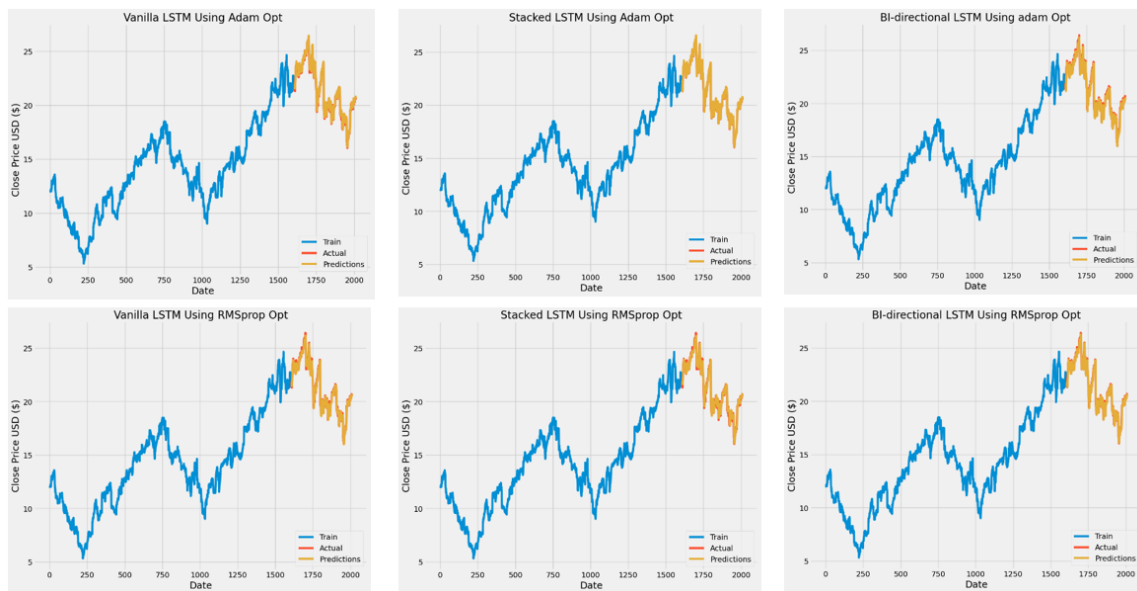


Fig. 4. The Plots of output results of HPQ company.

TABLE III. UTILIZING UNIVARIATE LSTM MODELS AT NEW YORK BANK

| Optimizer | Vanilla LSTM | | | Stacked LSTM | | | Bidirectional LSTM | | |
|-----------|--------------|-------|-------|--------------|-------|-------|--------------------|-------|-------|
| | R2 | RMSE | MAE | R2 | RMSE | MAE | R2 | RMSE | MAE |
| Adam | 0.957 | 0.803 | 0.59 | 0.965 | 0.722 | 0.513 | 0.967 | 0.704 | 0.513 |
| RMSprop | 0.951 | 0.852 | 0.655 | 0.917 | 1.118 | 0.926 | 0.955 | 0.821 | 0.636 |

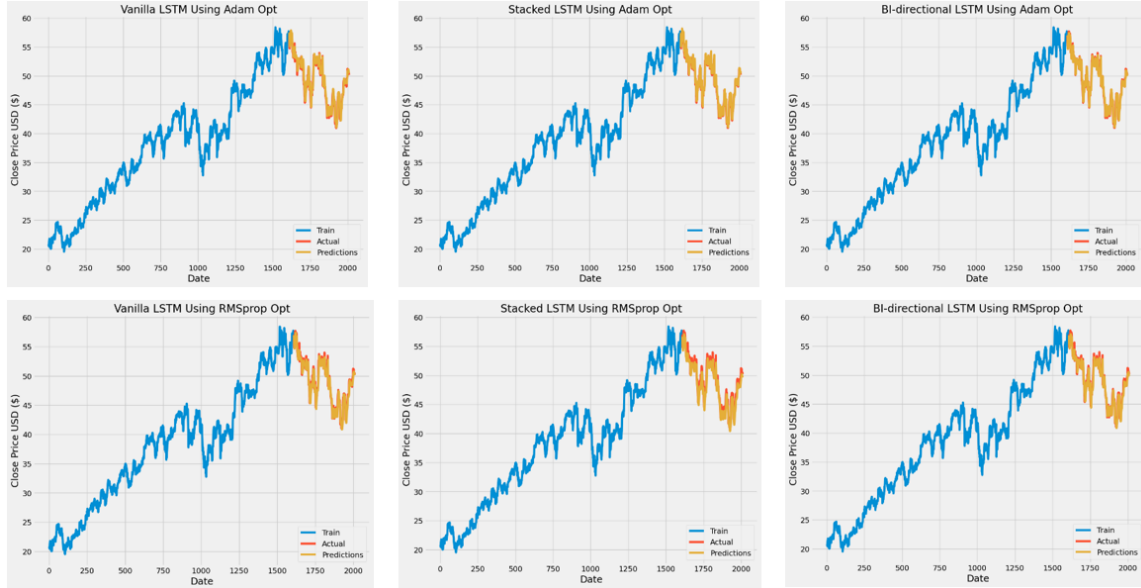


Fig. 5. The Plots of output results of New York Bank.

TABLE IV. UTILIZING UNIVARIATE LSTM MODELS AT PFIZER COMPANY

| Optimizer | Vanilla LSTM | | | Stacked LSTM | | | Bidirectional LSTM | | |
|-----------|--------------|-------|-------|--------------|-------|-------|--------------------|-------|-------|
| | R2 | RMSE | MAE | R2 | RMSE | MAE | R2 | RMSE | MAE |
| Adam | 0.921 | 0.802 | 0.69 | 0.965 | 0.533 | 0.397 | 0.959 | 0.576 | 0.438 |
| RMSprop | 0.952 | 0.623 | 0.508 | 0.916 | 0.824 | 0.703 | 0.971 | 0.478 | 0.349 |

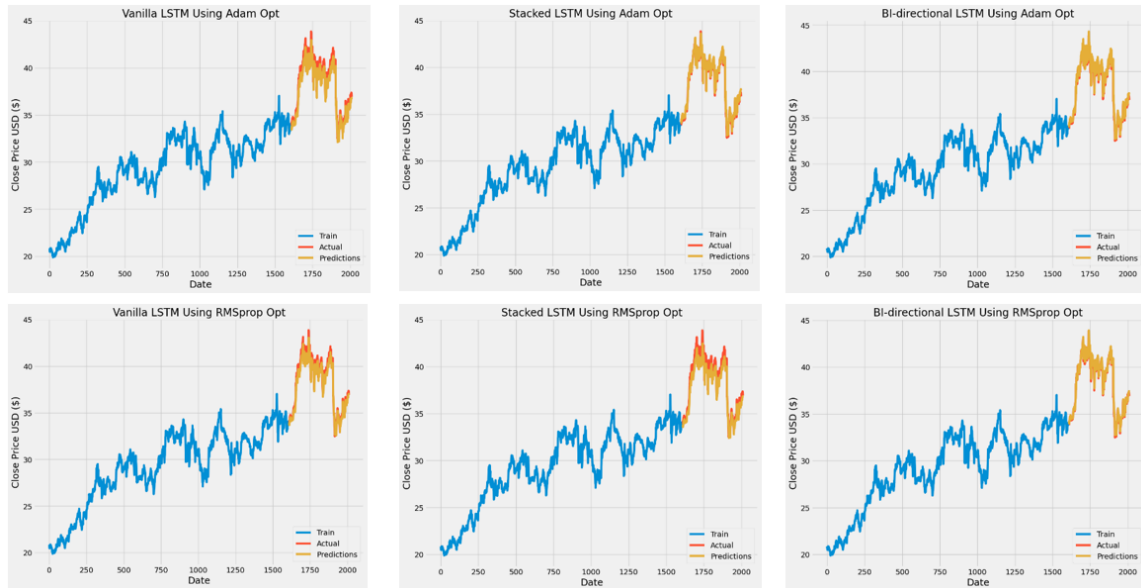


Fig. 6. The Plots of output results of Pfizer company.

VII. CONCLUSION

This study has successfully demonstrated the efficacy of a single-layered Bidirectional Long Short-Term Memory (BiLSTM) model enhanced with a global pooling mechanism for forecasting stock market prices. Our comparative analysis of the Vanilla, Stacked, and Bidirectional LSTM architectures revealed that the Bidirectional LSTM consistently outperformed the other variants across multiple datasets, particularly when optimized with the RMSprop algorithm. This superior performance is attributed to the BiLSTM's ability to effectively capture both past and future dependencies within the time series data, a critical factor in the volatile environment of stock markets. Rigorous hyperparameter tuning and multiple evaluation metrics like RMSE, MAE, and R^2 have allowed for a thorough validation of the models, ensuring robustness and accuracy in predictions. The visualization of results through line graphs and candlestick charts further corroborates the practical utility of the proposed model in capturing dynamic market trends.

Looking forward, several avenues can enhance the scope and applicability of this research in stock market forecasting. First, integrating a larger variety of data inputs, such as economic indicators, news sentiment analysis, or macroeconomic factors, could provide a more holistic view of the influences on stock prices, potentially increasing the predictive accuracy of the models. Second, exploring incorporating more sophisticated deep learning techniques like attention mechanisms or Transformer models could address some limitations of LSTM models, especially in handling longer sequences with more complex patterns. Third, conducting cross-industry validations with datasets from different sectors and global markets would test the generalizability of the proposed model, ensuring its applicability across diverse economic conditions. Lastly, real-time forecasting implementation in trading systems could be explored to assess the models' practical deployment and operational efficiency in live market conditions. These expansions would enhance the scientific understanding of neural networks in financial applications and bridge the gap between theoretical research and real-world financial decision-making.

REFERENCES

- [1] Hutter, Frank, Holger Hoos, and Kevin Leyton-Brown. "An efficient approach for assessing hyperparameter importance." In International conference on machine learning, pp. 754-762. PMLR, 2014.
- [2] Di Persio, Luca, and Oleksandr Honchar. "Artificial neural networks architectures for stock price prediction: Comparisons and applications." International journal of circuits, systems and signal processing 10 (2016): 403-413.
- [3] Mahajan, Palak and Abrol, Pawanesh and Lehana, Par, "Effect of Blurring on Identification of Aerial Images Using Convolution Neural

- Networks," in Proceedings of ICRIC 2019, Jammu, India, Springer, 2020, pp. 469-484.
- [4] Lu, Chi-Jie, Tian-Shyug Lee, and Chih-Chou Chiu. "Financial time series forecasting using independent component analysis and support vector regression." Decision support systems 47.2 (2009): 115-125.
- [5] Hamzaçebi, Coşkun, Diyar Akay, and Fevzi Kutay. "Comparison of direct and iterative artificial neural network forecast approaches in multiperiodic time series forecasting." Expert systems with applications 36.2 (2009): 3839-3844.
- [6] Dixon, Matthew, Diego Klabjan, and Jin Hoon Bang. "Classification-based financial markets prediction using deep neural networks." Algorithmic Finance 6.3-4 (2017): 67-77.
- [7] Bouktif, Salah, et al. "Optimal deep learning lstm model for electric load forecasting using feature selection and genetic algorithm: Comparison with machine learning approaches." Energies 11.7 (2018): 1636.
- [8] Sezer, Omer Berat, Murat Ozbayoglu, and Erdogan Dogdu. "A deep neural-network based stock trading system based on evolutionary optimized technical analysis parameters." Procedia computer science 114 (2017): 473-480.
- [9] Dash, Rajashree, and Pradipta Kishore Dash. "A hybrid stock trading framework integrating technical analysis with machine learning techniques." The Journal of Finance and Data Science 2.1 (2016): 42-57.
- [10] Fischer, Thomas, and Christopher Krauss. "Deep learning with long short-term memory networks for financial market predictions." European journal of operational research 270.2 (2018): 654-669.
- [11] Hiransha, Ma, et al. "NSE stock market prediction using deep-learning models." Procedia computer science 132 (2018): 1351-1362.
- [12] Stathakis, Dimitris. "How many hidden layers and nodes?." International Journal of Remote Sensing 30.8 (2009): 2133-2147.
- [13] Greff, Klaus, et al. "LSTM: A search space odyssey." IEEE transactions on neural networks and learning systems 28.10 (2016): 2222-2232.
- [14] Karmiani, Divit, et al. "Comparison of predictive algorithms: backpropagation, SVM, LSTM and Kalman Filter for stock market." 2019 amity international conference on artificial intelligence (AICAI). IEEE, 2019.
- [15] Bergstra, James, and Yoshua Bengio. "Random search for hyperparameter optimization." Journal of machine learning research 13.2 (2012).
- [16] Bhuriya, Dinesh, et al. "Stock market prediction using a linear regression." 2017 international conference of electronics, communication and aerospace technology (ICECA). Vol. 2. IEEE, 2017.
- [17] Nivetha, R. Yamini, and C. Dhaya. "Developing a prediction model for stock analysis." 2017 International conference on technical advancements in computers and communications (ICTACC). IEEE, 2017.
- [18] Parmar, Ishita, et al. "Stock market prediction using machine learning." 2018 first international conference on secure cyber computing and communication (ICSCCC). IEEE, 2018.
- [19] Liu, Siyuan, Guangzhong Liao, and Yifan Ding. "Stock transaction prediction modeling and analysis based on LSTM." 2018 13th IEEE Conference on Industrial Electronics and Applications (ICIEA). IEEE, 2018.
- [20] Shakva, Abin, et al. "Real-time stock prediction using neural network." 2018 8th International conference on cloud computing, data science & engineering (confluence). IEEE, 2018.
- [21] T. Fawcett, "An Introduction to ROC Analysis," Pattern Recognition Letters, vol.27, no.8, pp.861-874, 2006.

Segmentation Analysis for Brain Stroke Diagnosis Based on Susceptibility-Weighted Imaging (SWI) using Machine Learning

Shaarmila Kandaya¹, Abdul Rahim Abdullah², Norhashimah Mohd Saad³, Ezreen Farina⁴, Ahmad Sobri Muda⁵

Department Electrical Engineering, Universiti Teknikal Malaysia Melaka, Malaysia^{1, 2, 4}

Department of Electrical and Electronic Engineering Technology, Universiti Teknikal Malaysia Melaka, Malaysia³

Faculty of Medicine and Health Sciences, Universiti Putra Malaysia, 43400 Serdang, Selangor, Malaysia⁵

Abstract—Magnetic Resonance Imaging (MRI) plays a crucial role in diagnosing brain disorders, with stroke being a significant category among them. Recent studies emphasize the importance of swift treatment for stroke, known as "time is brain," as early intervention within six hours of stroke onset can save lives and improve outcomes. However, the conventional manual diagnosis of brain stroke by neuroradiologists is subjective and time-consuming. To address this issue, this study presents an automatic technique for diagnosing and segmenting brain stroke from MRI images according to pre and post stroke patient. The technique utilizes machine learning methods, focusing on Susceptibility Weighted Imaging (SWI) sequences. The machine learning technique involves four stages, those are pre-processing, segmentation, feature extraction, and classification. In this paper, pre-processing and segmentation are proposed to identify the stroke region. The segmentation performance is assessed using Jaccard indices, Dice Coefficient, false positive, and false negative rates. The results show that adaptive threshold performs best for stroke lesion segmentation, with good improvement stroke patient that achieving the highest Dice coefficient of 0.96. In conclusion, this proposed stroke segmentation technique has promising potential for diagnosing early brain stroke, providing an efficient and automated approach to aid medical professionals in timely and accurate diagnoses.

Keywords—Magnetic Resonance Imaging (MRI) diagnosis, time is brain, Susceptibility Weighted Imaging (SWI) and dice coefficient

I. INTRODUCTION

Cerebrovascular accident (CVA) or stroke stands as the third leading cause of death in Malaysia [1]. This presents a significant challenge to the Malaysian healthcare system, witnessing over 50,000 new cases annually, resulting in at least 32 daily fatalities. In 2016, the government committed RM180 million to address this issue. Globally, stroke is the second leading cause of death, surpassed only by coronary artery disease, and it ranks prominently in causing long-term disability. The Malaysian National Stroke Association (NASAM) underscores the urgency of immediate medical attention for stroke, as swift treatment, especially within six hours, has been shown to save lives. However, the scarcity of neuroradiologists, with only 107 specialists, and the reliance on manual interpretation of magnetic resonance imaging (MRI) images hinder timely treatment efforts.

Brain stroke, characterized by a network of small blood vessels facilitating blood flow through a stroke or blocked artery, requires rapid and accurate diagnosis for prompt intervention. While MRI has gained preference over conventional angiography for diagnosing brain stroke, the current practice involves labor-intensive visual inspection, delaying the process [2]. Timely diagnosis and treatment are critical to preventing disability caused by insufficient blood and oxygen, leading to nerve cell death. Diagnostic considerations include factors like infarct volume, penumbra size, and the presence of adequate early stroke, all crucial for successful treatment [3]. Neuroradiologists urgently need efficient tools for quick and accurate acute stroke diagnosis.

Moreover, brain stroke detection from MRI images faces challenges due to noise, artifacts, vessel size, and structural heterogeneity [4]. Novel methods for segmenting and classifying medical images are regularly proposed [5]. Common machine learning techniques for vessel segmentation, such as region growing, clustering, and active contours, face limitations related to sensitivity to noise and segmentation issues [6]. The manual segmentation by neuroradiologists, though time-consuming, highlights the importance of processing time speed and accuracy in computer-aided diagnostic systems [7].

Traditional machine learning methods, while effective, require complex denoising and feature extraction before classification, leading to prolonged computation times [8]. Recent studies acknowledge the robustness of machine learning in processing noisy medical images, yet the challenges of long computation times persist [9]. As a solution, hybrid frameworks incorporating machine learning techniques are considered promising for achieving optimal accuracy in early stroke classification.

This review explores the significance of stroke, brain stroke concepts, and MRI in the context of the human brain. Stroke, or cerebral infarction, ranks as the third leading cause of death and the primary cause of permanent disability in Malaysia [10]. The profound public health impact is evident in high initial treatment, rehabilitation, and chronic care costs. The urgency of stroke is highlighted by its occurrence every 45 seconds in the United States, affecting 795,000 individuals annually. The devastating impact on neurons and synapses during a stroke, leading to accelerated aging of the ischemic brain, underscores

the critical notion that "time is the brain." Despite this urgency, there is a notable absence of computer-aided diagnosis (CAD) systems tailored for stroke, unlike those available for fields like mammography and breast imaging. Existing studies on CAD systems and methodologies emphasize their potential to enhance diagnostic precision for radiologists [11].

II. LITERATURE REVIEW

A. Human Brain

The human brain stands out as one of the most intricate organs in the human body, comprising billions of interconnected nerve cells forming complex networks. Its spatiotemporal patterns contribute to its recognition as the most intricate system, wherein the alignment between structural and functional connections relies on spatial resolution and temporal scale [7]. Endowed with the capacity to govern intelligence, creativity, emotions, and memory, the brain is shielded by the skull and comprises the cerebrum, cerebellum, and brainstem, as illustrated in Fig. 1. Further division into lobes reveals specific responsibilities:

- 1) The frontal lobe manages problem-solving, decision-making, and motor skills.
- 2) The parietal lobe oversees sensation, handwriting, and posture.
- 3) The temporal lobe plays a role in memory and hearing.
- 4) The occipital lobe houses the brain's visual processing system.

Facilitating communication with the body, the brain utilizes 12 pairs of cerebrovascular vessels through the spinal cord and blood flow. Among these, ten pairs originating in the brainstem control functions like hearing, eye movements, facial sensations, taste, swallowing, and muscle movements in the face, neck, shoulders, and tongue. Meanwhile, cerebral blood vessels governing smell and vision originate in the cerebrum. Hence, maintaining proper blood circulation in vessels is crucial to prevent neuropathy, which could lead to nerve cell damage and subsequent cell death [8]. Refer to Fig. 1, for a visual representation of the human brain's anatomy.

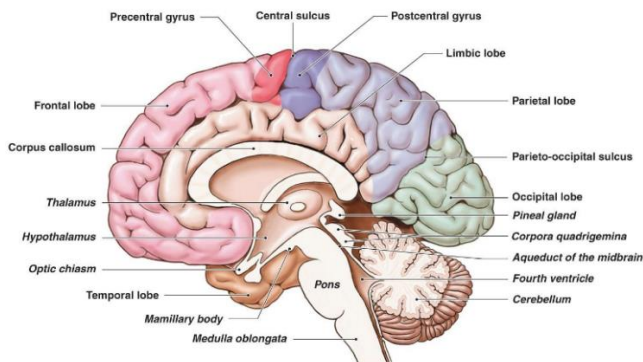


Fig. 1. Anatomy of human brain.

B. Brain Stroke Diagnosis

In this universe, second-leading cause of death is stroke, demanding prompt intervention to prevent severe long-term disability or fatality. This occurs when a blood clot obstructs a blood vessel or ruptures, impeding blood flow to a specific

brain region. The classification, depicted in Fig. 2, distinguishes between ischemic stroke, where a blood vessel abruptly obstructs a brain artery [1], and hemorrhagic stroke (cerebral hemorrhage), characterized by the rupture of a blood vessel [2].

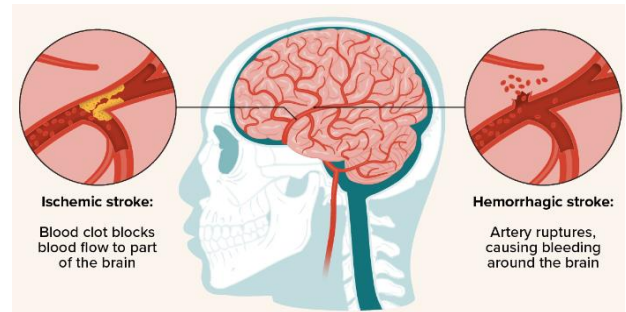


Fig. 2. Types of stroke.

Stroke exerts a significant impact on public health, resulting in substantial expenditures for primary care, rehabilitation, and the management of chronic conditions. In 2015, stroke accounted for 6.3 million deaths globally, ranking as the second leading cause of death after ischemic heart disease. Despite its persistent status as the third leading cause of death in Malaysia as reported by the Institute for Health Metrics and Evaluation in June 2019, there is a notable absence of computer-aided diagnosis (CAD) systems designed specifically for stroke, unlike the numerous CAD systems available for fields such as mammography and thorax. Research on CAD systems and techniques underscores the potential for enhancing the diagnostic accuracy of radiologists.

Reperfusion injury plays a pivotal role in the outcomes of ischemic stroke patients upon the restoration of blood flow [3]. Various approaches, including ischemic preconditioning, preconditioning, and postconditioning, have been explored for cardio protection, yielding diverse results regarding potential treatments [4]. The timely reinstatement of local blood flow is crucial for salvaging threatened tissue, minimizing cell death, and ultimately reducing patient disability. Successful recanalization significantly increases the likelihood of a favorable outcome, with a fourfold reduction in mortality compared to patients without recanalization [5]. Strategies for recanalization involve thrombolytic drugs such as tissue plasminogen activator (tPA) and/or mechanical interventions like thrombectomy using distal or proximal devices. Thrombectomy, involving the removal of blood clots through a catheter with an attached mechanical device, is particularly attractive due to its short intervention time, high recanalization rates, and potential for efficient blood flow restoration. However, the associated risks necessitate careful consideration, and the procedure should be reserved for patients meeting specific criteria, including a large circumference, small infarct, and good collateral circulation. In essence, precise patient selection based on pre-treatment imaging is crucial for achieving favorable outcomes with mechanical recanalization [6].

C. Magnetic Resonance Imaging (MRI)

Magnetic Resonance Imaging (MRI) is a medical imaging technique that uses strong magnetic fields and radio waves to

generate detailed images of the body's internal structures. MRI is commonly used in the early diagnosis of strokes and plays a crucial role in assessing the extent and location of the stroke, determining the appropriate treatment, and monitoring the patient's progress. When it comes to early stroke diagnosis, MRI provides several advantages over other imaging techniques. Here's how it works:-

1) *Visualization of brain anatomy:* MRI produces high-resolution images that can accurately depict the brain's anatomy, allowing healthcare professionals to identify any abnormalities or changes associated with a stroke. It provides detailed information about the brain's structure, including differentiating between gray and white matter, which is essential for detecting ischemic (clot-based) or hemorrhagic (bleeding-based) strokes.

2) *Differentiating stroke types:* MRI can help differentiate between ischemic and hemorrhagic strokes, which is crucial for determining the appropriate treatment approach. Ischemic strokes occur due to a blockage in a blood vessel, while hemorrhagic strokes result from bleeding in the brain. By examining the MRI images, doctors can identify the type and location of the stroke.

3) *Time-sensitive techniques:* Certain MRI techniques are time-sensitive and can detect changes in brain tissue that occur shortly after a stroke. Susceptibility-Weighted Imaging (SWI) is particularly useful in the early stages of stroke diagnosis. It measures the movement of water molecules in the brain and can detect restricted diffusion in areas affected by an ischemic stroke within minutes of onset. This early identification helps guide treatment decisions promptly.

4) *Assessment of perfusion:* Perfusion-weighted imaging (PWI) is another MRI technique that provides information about blood flow to the brain. PWI helps assess the extent of damaged brain tissue and determine the viability of the surrounding areas. By comparing SWI and PWI, healthcare professionals can identify the ischemic penumbra, which refers to the region around the stroke where brain tissue is at risk but still salvageable. This information aids in treatment planning.

5) *Detection of complications:* MRI can also identify complications associated with strokes, such as swelling, edema, or the presence of blood in the brain. These factors are crucial in determining the severity of the stroke, guiding treatment decisions, and assessing the patient's prognosis.

Overall, MRI is a valuable tool in the early diagnosis of brain strokes. Its ability to provide detailed images of the brain's anatomy, differentiate between stroke types, detect early changes in brain tissue, assess perfusion, and identify complications makes it an essential imaging technique in stroke management. It enables healthcare professionals to make informed decisions regarding treatment options and improve patient outcomes.

Two types of stroke, namely hemorrhagic and ischemic, are distinguished based on interpretation [12]. Ischemic strokes constitute approximately 70% of all cases, presenting with neurological deficits that endure for more than 24 hours or result in death within that timeframe [13]. Hemorrhagic

strokes, accounting for about 12% of all strokes, are further divided into 9% intracerebral hemorrhages and 3% subarachnoid hemorrhages. Hemorrhagic strokes occur due to the rupture of a cerebral blood vessel or an abnormality in a blood vessel, causing bleeding into adjacent brain tissue. This leads to impairment of brain function and often results in death rather than permanent disability. In contrast, ischemic strokes, caused by the blockage of blood vessels supplying the brain, are more prevalent.

Within the Oxfordshire Community Stroke Project [14], instances of stroke are categorized into four groups by considering the initial symptoms and their severity. This classification aims to anticipate the extent of the stroke, the affected brain regions, underlying causes, and the prognosis. The four groups include total anterior circulation stroke syndrome (TACS), partial anterior circulation stroke syndrome (PACS), lacunar stroke syndrome (LACS), and posterior circulation stroke syndrome (POCS). The most common type of LACS is caused by blockage of small arteries that supply deep brain structures. Patients usually suffer from pure motor or sensory deficits, sensorimotor deficits, or ataxic hemiplegia [15]. TACS occurs when the blood supply to the anterior and middle cerebral arteries on both sides of the brain is compromised, causing hemiplegia. PACS is a less severe form of TACS that exhibits some, but not all, of the symptoms associated with TACS. POCS is caused by a reduced blood supply to the posterior cerebral artery on one side of the brain [16]. Fig. 3 shows the MRI machine used for scanning.



Fig. 3. MRI machine used for scanning.

III. METHODOLOGY

The flowchart for MRI image analysis using machine learning is shown in Fig. 4. All techniques, including image pre-processing, picture segmentation and features extraction are included in the flow chart.

A. Pre-processing Stage (Normalization, Background Removal and Enhancement)

Suitable pre-processing will be identified to enhance and remove the noise. Image normalization, background removal and enhancement will be included (Shakunthala and Helenprabha, 2019). Mathematical methods known as "image enhancement techniques" are designed to increase the quality of a particular image, either for usage by a human viewer or for computer processing.

The kind of intensity depth must be transformed to double precision throughout the normalisation process, with the minimum value set to "0" and the maximum value set to "1". To make the computation of the algorithm simpler, this

procedure is necessary. Eq. (1), where N is the bit depth applied to the normalisation computation, states the equation.

$$I(x, y)_{normalization} = \frac{I(x, y)}{2^N - 1}, N = bits \quad (1)$$

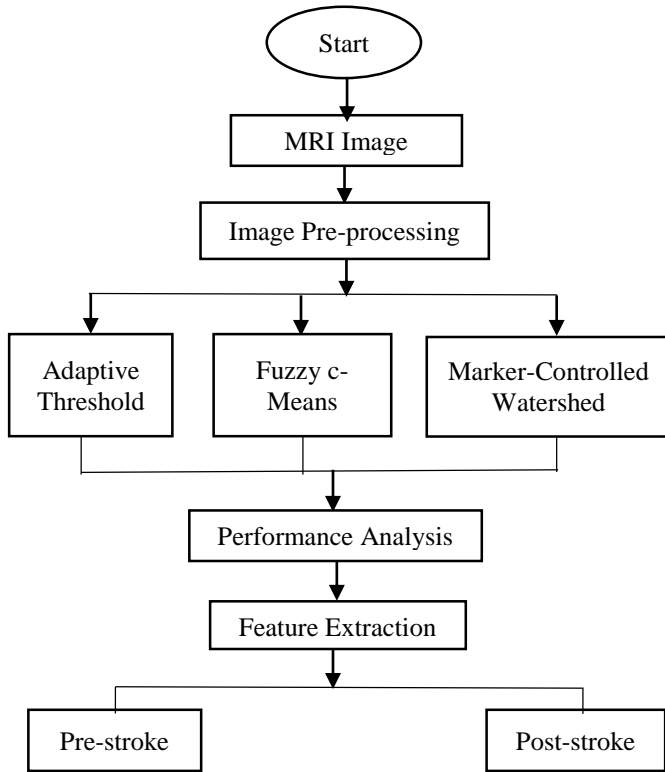


Fig. 4. Flow chart of MRI image analysis using machine learning technique.

Background pixels in MRI images need to be eliminated. This is due to the fact that specific brain structures and the background have similar intensities. Adaptive thresholding and morphological techniques can be used to achieve this. The threshold version's binary image output is its ultimate product. In order to trace the closed regions and their boundaries of connected neighbourhoods, boundary extraction algorithms are required. Enhancement techniques can be used to expand the intensity and improve the contrast. Several techniques can be implemented such as gamma-law and contrast stretching algorithms.

B. Segmentation using Machine Learning Techniques

Image segmentation is crucial because radiologists need to know the accurate location, size, intensity and other lesion's details to make a conclusion or diagnosis. The segmentation involves detecting and labelling meaningful regions in the given image data. Three types of image segmentation technique will be analyzed which are Adaptive Threshold, Fuzzy C-Means and Marker-Controlled Watershed.

1) *Adaptive threshold*: An adaptive threshold is a segmentation technique that creates a binary picture from a grayscale image of a fixed value. Thresholding is the technique of converting a grayscale image into a black and white image by turning all of the pixels to either white or black depending

on whether their value is above or below a specified threshold [17]. Eq. (2) illustrates adaptive threshold, which determines each pixel's threshold value by referring to the gray-level intensity of its neighbours.

$$G(x, y) = \begin{cases} 1 & \text{if } I(x, y) \geq \tau \\ 0 & \text{otherwise} \end{cases} \quad (2)$$

2) *Fuzzy C-Means*: Fuzzy C-Means (FCM) is one of the popular algorithm in clustering [18]. Data that belong to two or more clusters with various membership coefficients can be processed iteratively in this way. After creating the initial fuzzy partition matrix, the initial fuzzy cluster centres are computed. In order to determine where the clusters should be placed, the objective function is minimised while the cluster centres and membership grade point are updated at each iteration's step. When the maximum number of iterations is reached or when the improvement in the objective function between two successive iterations is less than the minimum amount of improvement required, the procedure comes to an end [19].

The iteration of FCM is performed through two parameters, namely the membership degree and the center of the cluster. When the repeated steps come to an end or reach their maximum number of iterations, these parameters are altered [20]. Additionally, when the objective function improvements of two successive iterations are less than the minimum amount of improvement set, the change of these parameters is affected. The low, medium, and high clusters are the starting points for the Fuzzy C-Means technique used in this segmentation [21]. The centre of each cluster will be used to determine the data point. The cluster's data points should all equal one. The algorithm relies on minimising the objective function presented below.

$$J_m = \sum_{i=1}^N \sum_{j=1}^C u_{ij}^m \|x_i - c_j\|^2, 1 \leq m \leq \infty \quad (3)$$

where, u_{ij} represents the membership degree of data point x_i in cluster j , where x_i is the d -dimensional center of the i th cluster, c_j is the d -dimensional center of the cluster, and $\|*\|$ is a norm indicating the similarity between measured data and the center. The term M , referred to as the fuzziness exponent, is any number greater than 1.

3) *Marker-Controlled watershed*: A gradient-based segmentation method is called watershed segmentation. According to this study's findings, the watershed segmentation identifies the water basins and watershed ridge lines by classifying each pixel's intensity as either high intensity or low intensity on a surface [22]. The gradient magnitude is calculated using the image foreground and background markers and the edge detection technique. The watershed ridge line and morphological operation are then used [23]. Based on the provided watershed ridge lines, the watershed transform is created. The input image $I(x, y)$ and the gradient along x and y -axis are calculated according to Eq. (4).

$$I_x = \frac{\partial f}{\partial x} = (z_7 + 2z_8 + z_9) - (z_1 + 2z_2 + z_3) \quad (4)$$

$$I_y = \frac{\partial f}{\partial y} = (z_3 + 2z_6 + z_9) - (z_1 + 2z_4 + z_7)$$

Then the gradient of the image is defined as:

$$\nabla I(x, y) = \frac{\partial f}{\partial x} i + \frac{\partial f}{\partial y} j = I_x i + I_y j \quad (5)$$

where, i and j are unit vectors along x and y axis respectively. The magnitude of gradient is given by:

$$g(x, y) = |\nabla f(x, y)| = \sqrt{g_x^2 + g_y^2} \quad (6)$$

The image may have an excessive amount of gradient segmentation as a result of noise and other irregularities [24]. Thus to overcome the problem, morphological operation technique can be implemented.

C. Features Extraction

A collection of features are extracted from each image based on the segmentation technique. Meaningful characteristics must be developed before they can be used as input in the classification process [25]. These properties may be based on spectral, textural, or statistical examination of an image's grey level. To complete the diagnosis, other general features like signal intensity are needed [26]. All the features that radiologists discovered when examining the brain scans are listed in Table IV. Table I provides a list of the feature extractions that reflect nearby stroke area regions.

TABLE I. LIST OF FEATURES EXTRACTION RESULTS AND DISCUSSIONS

| (a) Medical diagnosis | (b) Features extracted |
|---------------------------------------|--|
| <u>Structural elements:</u> - | <u>Statistical features in spatial domain:</u> - |
| 1. Number of lesions | 1. Intensity |
| 2. Shape | 2. Mean |
| 3. Location | 3. Median |
| 4. Elements within the lesion | 4. Standard deviation |
| 5. Internal and external capsules | 5. Perimeter |
| 6. Midline shift, distended and swell | 6. Gradient value |
| 7. Symmetric | 7. Entropy |
| <u>Lesion's characteristics:</u> - | 8. skewness |
| 8. Intensity | 9. Euclidian distance |
| 9. Region's area | 10. Texture analysis |
| 10. Region's diameter | <u>Shape, boundary, contour, location:</u> - |
| 11. Mean | 11. Area |
| 12. Standard deviation | 12. Perimeter |
| 13. Compactness | 13. Compactness |
| 14. Density | 14. Mean of region boundary |
| 15. Volume | 15. Volume |
| 16. Contrast | 16. Density |
| | 17. Invariant and boundary moment |

A. Performance Evaluation

The segmentation results obtained from the proposed technique will be compared with the manual reference

segmentation performed by neuroradiologists. Similarity indices based on Jaccard's and then the accuracy is obtained by finding the percentage of the number of correctly classified samples. Dice will be calculated to measure the accuracy of the segmentation for the pair of segmented and reference image.

IV. RESULTS AND DISCUSSIONS

A. Image Pre-processing

Fig. 5 displays an image portraying a stroke brain lesion characterized by hyperintensity. The maximum pixel intensity in the image is 205, and the pixels are in a 9-bit format. Based on analysis, the image underwent preprocessing using three methods: normalization, background removal, and enhancement through power-law transformation.

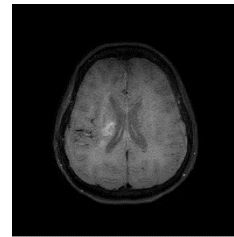


Fig. 5. Original image.

In Fig. 6, the image has undergone normalization to a 10-bit format, along with its corresponding histogram. The highest normalized intensity is recorded as 0.76908. Following the normalization process, a background removal procedure is employed to eliminate pixels, enhancing the clarity of the lesion in the image.

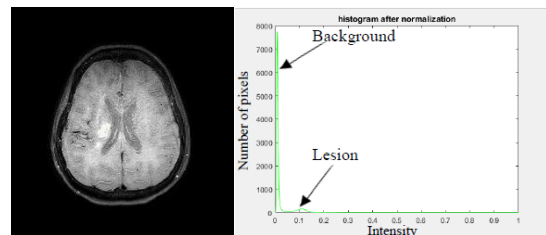


Fig. 6. Image normalization with its histogram.

In Fig. 7, background pixels have been eliminated through thresholding at 0.0563, with the highest peak observed at an intensity level of 0.1196.

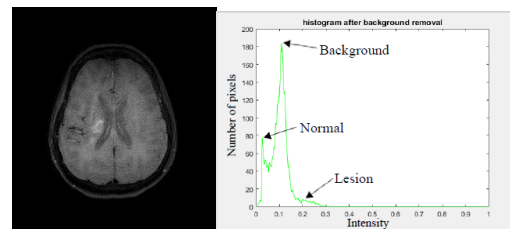


Fig. 7. Image background removal with its histogram.

Fig. 8 illustrates the result following the implementation of a power-law transformation. The peak intensity is situated at 0.6892. Analyzing the histogram, it is evident that the power-law transformation has elevated the normalized intensity to 0.3556. Simultaneously, the lesion has expanded to an intensity

level of 0.8, as indicated by arrows. The maximum intensity achieved through the gamma-law transformation is 0.7901.

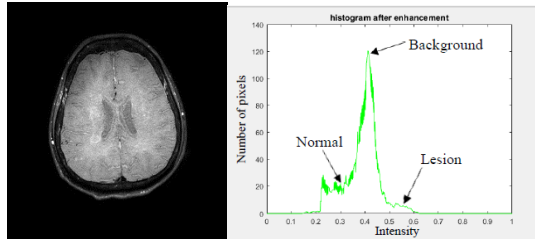


Fig. 8. Image enhancement with its histogram.

B. Image Segmentation

An automated segmentation method has been devised for segmenting Regions of Interest (ROIs) within SWI images, utilizing adaptive threshold, marker-controlled watershed with correlation template, and FCM with active contour. Each segmentation outcome is subsequently compared with a manual reference. This process pertains to the segmentation of both hyperintense and hypointense lesions in SWI images.

1) Adaptive Threshold

TABLE II. THE SEGMENTATION RESULTS OF THE SWI STROKE LESION FROM THE ORIGINAL IMAGE USING ADAPTIVE THRESHOLD SEGMENTATION TECHNIQUE

| Type of Stroke patient | Pre/ Post Stroke | SWI Original Image | Brain Segmentation | Segmented Lesion Area |
|------------------------------|------------------|--------------------|--------------------|-----------------------|
| Poor Improvement Patient | Pre Stroke | | | |
| | Post Stroke | | | |
| Moderate Improvement Patient | Pre Stroke | | | |
| | Post Stroke | | | |
| Good Improvement Patient | Pre Stroke | | | |
| | Post Stroke | | | |

According to the data presented in Table II, the segmentation outcomes indicate that the adaptive threshold technique is effective in delineating hyperintense lesions. However, it faces challenges in segmenting hypointense lesions due to the presence of shadow pixels, which are uncertain with the assigned threshold value from this segmentation method. The technique struggles to segment overlapping pixels resulting from noise or intensity variation in the SWI image.

2) Fuzzy c-means (FCM) with active contour: FCM is a clustering method designed to group objects with similar characteristics. This technique is combined with active contour to eliminate CSF regions by establishing boundaries within the SWI image. Computer-generated curves are employed to identify and pinpoint the Regions of Interest (ROIs). The segmentation outcomes for the stroke lesion from the original image are presented in Table III.

TABLE III. THE SEGMENTATION RESULTS OF THE SWI STROKE LESION FROM THE ORIGINAL IMAGE USING FCM WITH ACTIVE CONTOUR SEGMENTATION TECHNIQUE

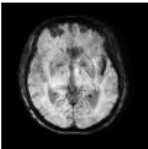
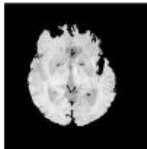

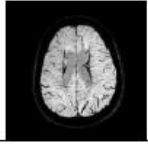






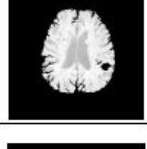
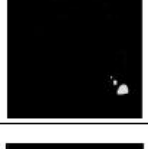
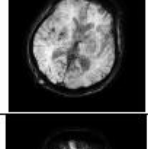

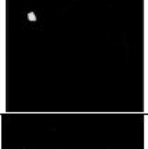
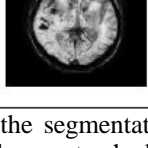
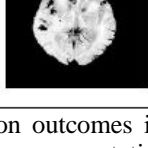
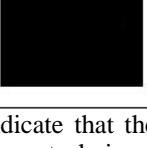
| Type of Stroke patient | Pre/ Post Stroke | SWI Original Image | Brain Segmentation | Segmented Lesion Area |
|------------------------------|------------------|--------------------|--------------------|-----------------------|
| Poor Improvement Patient | Pre Stroke | | | |
| | Post Stroke | | | |
| Moderate Improvement Patient | Pre Stroke | | | |
| | Post Stroke | | | |
| Good Improvement Patient | Pre Stroke | | | |
| | Post Stroke | | | |

According to Table III, the segmentation outcomes reveal that the FCM segmentation method, when combined with active contour, yields favorable results for both hyperintense

and hypointense lesions in the Regions of Interest (ROIs). However, in FCM, the presence of noise in SWI isn't factored in, making the technique susceptible to noise. To address this issue, additional refinement is applied using active contour segmentation to eliminate cerebrospinal fluid (CSF) and small pixels.

3) *Marker-controlled watershed:* Marker-controlled watershed segmentation is a segmentation method based on gradients. It is combined with a correlation template that utilizes a matching template to eliminate the cerebrospinal fluid (CSF) region in severe stroke cases. The segmentation outcomes for the stroke lesion from the original image are illustrated in Table IV.

TABLE IV. THE SEGMENTATION RESULTS OF THE SWI STROKE LESION FROM THE ORIGINAL IMAGE USING MARKER-CONTROLLED WATERSHED WITH CORRELATION TEMPLATE SEGMENTATION TECHNIQUE

| Type of Stroke patient | Pre/ Post Stroke | SWI Original Image | Brain Segmentation | Segmented Lesion Area |
|------------------------------|------------------|---|---|---|
| Poor Improvement Patient | Pre Stroke |  |  |  |
| | Post Stroke |  |  |  |
| Moderate Improvement Patient | Pre Stroke |  |  |  |
| | Post Stroke |  |  |  |
| Good Improvement Patient | Pre Stroke |  |  |  |
| | Post Stroke |  |  |  |

In Table IV, the segmentation outcomes indicate that the marker-controlled watershed segmentation technique, combined with the correlation template, effectively delineates Regions of Interest (ROIs) for both hyperintense and hypointense lesions. The marker-controlled watershed technique segments the ROI by utilizing the boundary formed through the watershed technique, which is based on the

gradient surface in the SWI image. To address the issue of over-segmentation resulting from the marker-controlled watershed technique, the correlation template method is introduced. This refinement aids in removing cerebrospinal fluid (CSF) and producing a more reasonable segmentation that accurately reflects the layout of the ROI.

C. Performance Evaluation for Segmentation Method

This part discusses the performance analysis and evaluation of the proposed segmentation technique. The evaluation is grounded in the analysis of 24 samples, specifically focusing on the optimal appearance of SWI lesions. The evaluation centers on stroke lesions, encompassing 18 samples from stable stroke patients and six from patients with more severe conditions. Performance evaluation employs metrics including the Jaccard index (area overlap, AO), Dice coefficient (DC), false positive rate (FPR), and false negative rate (FNR). A higher index signifies greater area overlap and superior performance.

1) *Poor improvement stroke patient:* Fig. 9 illustrates the performance evaluation for poor improvement stroke patient using AO, FPR, FNR and DC. According to the findings, the adaptive threshold technique outperforms other segmentation methods, demonstrating superior results. Specifically, the adaptive threshold technique exhibits high AO and DC along with low FPR and FNR outcomes.

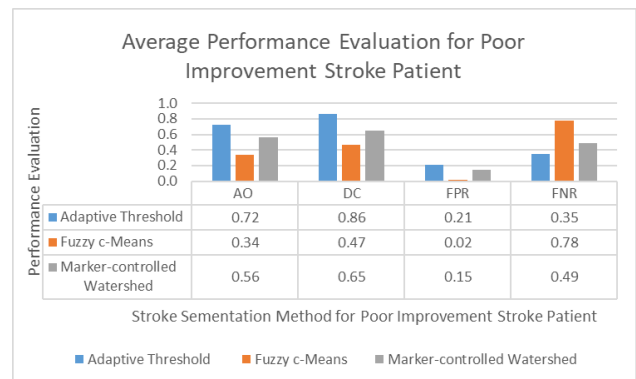


Fig. 9. Average performance evaluation for poor improvement stroke patient.

The adaptive threshold technique yields values of 0.72 for AO and 0.86 for DC. FPR signifies errors related to over-segmentation, while FNR denotes errors linked to under-segmentation. Lower values for both FPR and FNR are desired to minimize errors. The outcomes reveal that the adaptive threshold segmentation technique effectively distinguishes hyperintense lesions from other intensity pixels in the SWI image, displaying a low FPR of 0.21 and a low FNR of 0.35. For poor improvement stroke patients, the FCM technique stands out with the best FNR value, indicating no over-segmentation errors. In contrast, the marker-controlled watershed technique exhibits a high FNR for poor improvement stroke patients.

2) *Moderate improvement stroke patient:* In Fig. 10, the performance evaluation for moderate improvement stroke patient using AO, FPR, FNR and DC. According to the

findings, the adaptive threshold technique again stands out as the superior segmentation method among others.

The adaptive threshold technique demonstrates favorable outcomes with high AO and DC values along with low FPR and FNR results. Specifically, the AO and DC values achieved by the adaptive threshold technique are 0.83 and 0.94, respectively. The findings indicate that this segmentation method effectively distinguishes hyperintense lesions from other intensity pixels in the SWI image, displaying a low FPR of 0.15 and a low FNR of 0.29. The adaptive threshold technique attains the best under-segmentation rate compared to other techniques. However, the FCM technique achieves the best FNR result, recording 0.87.

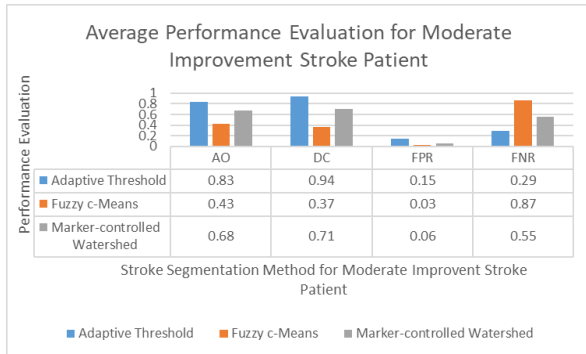


Fig. 10. Average performance evaluation for moderate improvement stroke patient.

3) *Good improvement stroke patient*: Fig. 11 determines the performance evaluation for good improvement stroke patient using AO, FPR, FNR and DC. According to the results, the adaptive threshold technique once again emerges as the leading segmentation method among others.

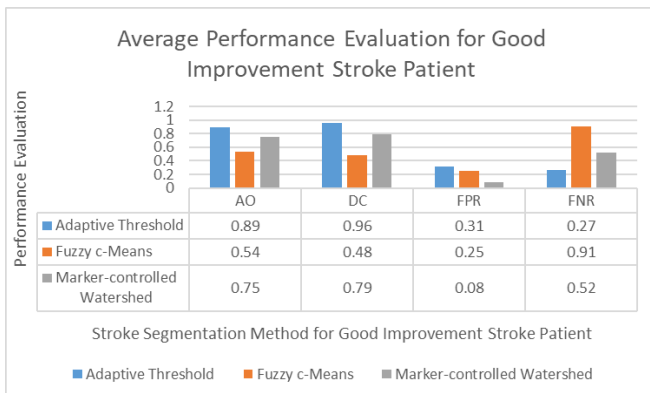


Fig. 11. Average performance evaluation for good improvement stroke patient.

The adaptive threshold technique exhibits high AO and DC values with low FPR and FNR outcomes. Specifically, the AO and DC values attained by the adaptive threshold technique are 0.89 and 0.96, respectively. The least favorable over-segmentation result is observed in FCM for stroke patients with significant improvement, featuring an FPR error of 0.08. In contrast, the adaptive threshold technique achieves the best FPR value at 0.31, indicating its efficacy in segmenting hypointense lesions with minimal over-segmentation error.

However, the FCM technique records the best value for FNR error, standing at 0.1.

D. Comparison Result of Performance Verification for the Stroke Lesion Classification Benchmarking

Based on previous research, Table V concluded the results by other researchers in similar studies. The Adaptive threshold segmentation technique has shown best dice coefficient compare to other studies. The dice coefficient value obtain was 0.97. Tetteh et al. (2023) presents dice coefficient value with 0.76% by using Marker-Controlled Watershed. Kuang et al. (2023) presents the second highest dice coefficient value with 0.89. Rava et al. (2021) presents dice coefficient value with 0.83. Gong et al. (2021) dice coefficient value with 0.87. At last, Su et al. (2020) presents dice coefficient value 0.75.

TABLE V. MACHINE LEARNING TECHNIQUE FOR BRAIN STROKE DIAGNOSIS BY OTHER RESEARCHERS

| Author | Imaging Modality | Number of Data | Technique | Result |
|------------------------------|------------------|----------------|-----------------------------|--------|
| Proposed method | MRI | 24 patients | Adaptive Threshold | 0.96 |
| Tetteh et al. (2023, [27]) | MRI | 183 patients | Marker-Controlled Watershed | 0.76 |
| Kuang et al. (2023, [28]) | CT | 154 patients | Adaptive Threshold | 0.89 |
| Rava et al. (2021, [29]) | CBCT | 200 patients | k-Means | 0.83 |
| Hokkinen et al. (2021, [30]) | MRI | 89 patients | Adaptive Threshold | 0.97 |
| Gong et al. (2021, [31]) | CT | 30 patients | Fuzzy Means (FCM) | 0.87 |
| Su et al. (2020, [32]) | MRI | 269 patients | Region Growing | 0.75 |

V. CONCLUSION

In this research, machine learning techniques are proposed for automatic scoring of brain stroke diagnosis in the context of treatment decision making in ischemic stroke. The automated technique to locate, segment and quantify the lesion area would support clinicians and neuroradiologists rendering their findings more robust and reproducible. The techniques are highly capable to classify the type of brain stroke and accurate diagnosis for ischemic stroke patient into two types, those are stable and worse stroke patient. The outcome of this research could serve as an insight to improve the healthcare of the community by providing better solutions using such intelligent system. Furthermore, the characteristics of stroke lesion appearances, their evolution, and the observed challenges should be study in detail.

ACKNOWLEDGMENT

The study is funding by Ministry of Higher Education (MOHE) of Malaysia through the Fundamental Research Grant Scheme (FRGS), No: FRGS/1/2022/SKK06/UTEM/02/1). The authors also would like to thank Faculty of Electrical Engineering, Universiti Teknikal Malaysia Melaka (UTeM)

and to all team members of Advanced Digital Signal Processing Group (ADSP), Centre of Robotic & Industrial Information (CeRIA), for their contribution and suggestion to successfully complete this paper.

REFERENCES

- [1] J. E. Son, D. S. Chow, and M. Nagamine, "Artificial intelligence and acute stroke imaging," *AJNR. American Journal of Neuroradiology*, vol. 42, no. 1, 2021.
- [2] A. K. Boehme, C. Esenwa, and M. S. V. Elkind, "Stroke Risk Factors, Genetics, and Prevention," *Cross Ref Medline*, vol. 120, no. 3, pp. 472–495, 2017.
- [3] E. J. Lee, Y. H. Kim, N. Kim, and D. W. Kang, "Deep into the brain: artificial intelligence in stroke imaging," *Journal of Stroke*, vol. 19, no. 3, pp. 277–285, 2017.
- [4] A. A. Valliani, D. Ranti, and E. K. Oermann, "Machine learning and neurology: a systematic review," *Neurology and Therapy*, vol. 8, no. 2, pp. 351–365, 2019.
- [5] N. M. Murray, M. Unberath, G. D. Hager, and F. K. Hui, "Artificial intelligence to diagnose ischemic stroke and identify large vessel occlusions: a systematic review," *Journal of Neurointerventional Surgery*, vol. 12, no. 2, pp. 156–164, 2020.
- [6] H. Kamal, V. Lopez, and S. Sheth, "Machine learning in acute ischemic stroke neuroimaging," *Frontiers in Neurology*, vol. 9, no. 2018, p. 945, 2018.
- [7] C. Krittanawong, H. J. Zhang, Z. Wang, M. Aydar, and T. Kitai, "Artificial intelligence in precision cardiovascular medicine," *Journal of the American College of Cardiology*, vol. 69, no. 21, pp. 2657–2664, 2017.
- [8] P. Xanthopoulos, P. M. Pardalos, T. B. Trafalis, P. Xanthopoulos, P. M. Pardalos, and T. B. Trafalis, "Linear discriminant analysis," in *Robust Data Mining*, pp. 27–33, Springer, New York, NY, 2013.
- [9] S. Castaneda-Vega, P. Katiyar, F. Russo et al., "Machine learning identifies stroke features between species," *Therapeutics*, vol. 11, no. 6, pp. 3017–3034, 2021.
- [10] M. Bento, R. Souza, M. Salluzzi, L. Rittner, Y. Zhang, and R. Frayne, "Automatic identification of atherosclerosis subjects in a heterogeneous MR brain imaging data set," *Magnetic Resonance Imaging*, vol. 62, pp. 18–27, 2019.
- [11] J. Vargas, A. Spiotta, and A. R. Chatterjee, "Initial experiences with artificial neural networks in the detection of computed tomography perfusion deficits," *World Neurosurgery*, vol. 124, pp. e10–e16, 2019.
- [12] M. S. Sirsat, E. Fermé, and J. Cmara, "Machine learning for brain stroke: a review. Science Direct," *Journal of Stroke and Cerebrovascular Diseases*, vol. 29, no. 10, 2020.
- [13] S. A. Sheth, L. Giancardo, M. Colasurdo, V. M. Srinivasan, A. Niktabe, and P. Kan, "Machine learning and acute stroke imaging," *Journal of Neurointerventional Surgery*, p. neurint-surg-2021-018142, 2022.
- [14] H. P. Chan, R. K. Samala, L. M. Hadjiiski, and C. Zhou, "Machine learning in medical image analysis," *Medical Image Analysis*, vol. 1213, 2020.
- [15] M. Puttagunta and S. Ravi, "Medical image analysis based on machine learning approach," *Multimedia Tools and Applications*, vol. 80, no. 16, pp. 24365–24398, 2021.
- [16] J. Zhang, Y. Xie, Q. Wu, and Y. Xia, "Medical image classification using synergic machine learning," *Medical Image Analysis*, vol. 54, pp. 10–19, 2019.
- [17] H. J. Van Os, L. A. Ramos, A. Hilbert et al., "Predicting outcome of endovascular treatment for acute ischemic stroke: potential value of machine learning algorithms," *Frontiers in Neurology*, vol. 9, 2018.
- [18] L. Li, M. Wei, B. Liu et al., "Machine learning for hemorrhagic lesion detection and segmentation on brain MRI images," *IEEE Journal of Biomedical and Health Informatics*, vol. 25, no. 5, pp. 1646–1659, 2021.
- [19] S. Zhang, M. Zhang, S. Ma et al., "Research progress of machine learning in the diagnosis and prevention of stroke," *BioMed Research International*, vol. 2021, Article ID 5213550, 5 pages, 2021.
- [20] A. Krizhevsky, I. Sutskever, and G. E. Hinton, "Magenet classification with deep convolutional neural networks," in *Proc. Adv. Neural Inf. Process. Syst.*, pp. 1097–1105, Harrahs and Harveys, Lake Tahoe, 2012.
- [21] C. Szegedy, W. Liu, Y. Jia et al., "Going deeper with convolutions," in *Proc. IEEE Conf. Comput. Vis. Pattern Recognit.*, pp. 1–9, MA, USA, 2015.
- [22] R. Yang and Y. Yu, "Artificial convolutional neural network in object detection and semantic segmentation for medical imaging analysis," *Frontiers in Oncology*, vol. 11, p. 638182, 2021.
- [23] L. N. Do, B. H. Baek, S. K. Kim, H. J. Yang, I. Park, and W. Yoon, "Automatic assessment of aspects using diffusion-weighted imaging in acute ischemic stroke using recurrent residual convolutional neural network," *Diagnostics*, vol. 10, no. 10, p. 803, 2020.
- [24] G. B. Praveen, A. Agrawal, P. Sundaram, and S. Sardesai, "Ischemic stroke lesion segmentation using stacked sparse auto-encoder," *Computers in Biology and Medicine*, vol. 99, pp. 38–52, 2018.
- [25] A. Pinto, S. Pereira, R. Meier et al., "Combining unsupervised and supervised learning for predicting the final stroke lesion," *Medical Image Analysis*, vol. 69, p. 101888, 2021.
- [26] D. Shome, T. Kar, S. N. Mohanty et al., "COVID-transformer: interpretable covid-19 detection using vision transformer for healthcare," *International Journal of Environmental Research and Public Health*, vol. 18, no. 21, p. 11086, 2021.
- [27] G. Tetteh, F. Navarro, R. Meier, J. Kaesmacher, J.C. Paetzold, J.S. Kirschke, C. Zimmer, R. Wiest, and B.H. Menze, "A machine learning approach to predict collateral flow in stroke patients using radiomic features from perfusion images," *Frontiers in Neurology*, vol. 14, no. 1, 2023.
- [28] H. Kuang, W. Wan, Y. Wang, J. Wang, and W. Qiu, "Automated Collateral Scoring on CT Angiography of Patients with Acute Ischemic Stroke Using Hybrid CNN and Transformer Network," *Biomedicines*, vol. 11, no. 2, 2023.
- [29] R.A. Rava, S.E. Seymour, K.V. Snyder, M. Waqas, J.M. Davies, E.I. Levy, A.H. Siddiqui, and C.N. Ionita, "Automated Collateral Flow Assessment in Patients with Acute Ischemic Stroke Using Computed Tomography with Artificial Intelligence Algorithms," *World Neurosurgery*, vol. 155, pp. e748–e760, September 2021.
- [30] L. Hokkinen, T. Mäkelä, S. Savolainen, and M. Kangasniemi, "Computed tomography angiography-based machine learning method for treatment selection and infarct volume prediction in anterior cerebral circulation large vessel occlusion," *Acta Radiologica Open*, vol. 10, no. 11, p. 205846012110603, 2021.
- [31] Q. Gong, B. Yu, M. Wang, M. Chen, H. Xu, and J. Gao, "Predictive Value of CT Perfusion Imaging on the Basis of Automatic Segmentation Algorithm to Evaluate the Blood Flow Status on the Outcome of Reperfusion Therapy for Ischemic Stroke," *Journal of Healthcare Engineering*, 2021.
- [32] J. Su, L. Wolff, A.C.G.M. Es, W. Van Zwam, C. Majoie, D.W.J. Dippel, A. Van Der Lugt, W.J. Niessen, and T. Van Walsum, "Blood Flow MRI Images," *IEEE Transactions on Medical Imaging*, vol. 39, no. 6, pp. 2190–2200, 2020.

A Genetic Algorithm-based Approach for Design-level Class Decomposition

Bayu Priyambadha¹, Nobuya Takahashi², Tetsuro Katayama³

Faculty of Computer Science, Universitas Brawijaya, Malang, Jawa Timur, Indonesia¹

Faculty of Engineering, University of Miyazaki, Miyazaki, Japan^{2,3}

Abstract—Software is always changed to accommodate environmental changes to preserve its existence. While changes happen to the software, the internal structure tends to decline in quality. The refactoring process is worth running to preserve the internal structure of the software. The decomposition process is a suitable refactoring process for Blob smell in class. It tried to split up the class based on the context in order to arrange it based on each responsibility. The previous approach has been implemented but still leaves problems. The optimum arrangement of class cannot be achieved using the previous approach. The genetic algorithm provides the search mechanism to find the optimum state based on the criterion stated at the beginning of the process. This paper presents the use of genetic algorithms to solve the design-level class decomposition problem. The paper explained several points, including the conversion from class to the chromosome construct, the fitness function calculation, selection, crossover, and mutation. The results show that the use of a genetic algorithm was able to solve the previous problems. The genetic algorithm can solve the local optimum problem from the previous approach. The increment of the fitness function of the study case proves it.

Keywords—Genetic algorithm; refactoring; class decomposition; blob smell; software internal quality

I. INTRODUCTION

Software will always be changed due to the changes in its environment. This statement is also stated in Lehman's law about software evolution [1], [2]. During the operation period, the environment somehow changes. This environment encompasses various components, including hardware, operating systems, libraries, frameworks, databases, and external services. These changes can significantly impact how software functions and interacts with its surroundings. Software environment changes are inevitable, and developers need to proactively manage and adapt their applications to ensure continued functionality, security, and compatibility as qualified software in evolving environments.

It is essential to develop software that is flexible and adaptable to changes to mitigate environmental changes. The easiness of adaptation or changes in software, as feedback of environment changes, is called software maintainability. Good software maintainability can be achieved by maintaining the software's internal structure quality. Adapting to environmental changes without concern for the software's internal structure quality will lead to difficulties in future changes. Compared to poorly structured software, software with well-designed structures will make it easier to adapt to changes.

The refactoring process alters the software's internal structure without changing the external behavior [3]. Implementing this process is worthwhile to prevent software from becoming obsolete. In Refactoring, the alteration of software structure is done based on the existing problem or declining area in terms of quality. Then, those areas are called "smell."

In the previous research, we proposed a refactoring process to solve the Blob smell in the class diagram [4]. Blob smell is one anomaly condition that is expressed in class that showed in class that monopolizes a lot of processes. The main problem with this smell is that a lot of responsibility is allocated to a single class. Based on the clean architecture theory [5], one class must only have one responsibility (Single Responsibility Principle). That is why blob smell can be solved by using class decomposition to split the responsibility and allocate it to several classes.

Knowing the blob smell and decomposing it at the class diagram level has been proposed in previous publications [6], [7]. The threshold-based hierarchical agglomerative clustering was implemented to perform class decomposition to solve blob smell in class at the level of the class diagram. This approach looked promising due to the result showing the significance of the impact of the decomposition process on software maintainability [8].

The class decomposition mostly uses the clustering process. To evaluate the result of decomposition mostly based on the cluster quality produced by proposed approaches. In the previous study, two variables were used to measure cluster quality: silhouette coefficient and class usability. Class usability is important because, in the case of class decomposition, the usability of clustering results must be considered. Based on the previous result, problems remain, especially related to class usability. In some cases, the cluster result is considered unable to be implemented as a class because there is no class interface, or all elements are not accessible except the class itself. It is making the class instantiate selfish objects.

This study used one clustering method to decompose class, as in the previous experiment. The method is threshold-based hierarchical agglomerative clustering by considering the semantic and static similarity between class elements [6], [7]. The research results show that the approach increased the quality measurement metrics called the Maintainability Index (MI). The experiment compared the original and the class after decomposing using the approach. On average, all data are

increased by the MI. Overall, the results show that the approach sounds promising in the future to prevent software's internal structure quality [8]. But, there is a problem that needs attention to be solved. Several classes still contain the problems after the decomposition process. The issues that still exist in the last result experiment are:

- The unusable (class with no method) class can still be produced event by the evaluation process. This condition makes the MI value low.
- It is a fact that the decompose candidate class only consists of one public method, which makes it challenging to find the optimum class usability after the decomposition process.

Besides those problems, getting a higher evaluation value for the problematic class is possible than the result of the previous approach. This condition immerses the assumption that the previous approach tends to trap the local optimum result.

Based on the result, this research will study the problems in the previous research. The optimum cluster composition is the main purpose of the class decomposition research, which considers several factors, including cluster compactness and class usability.

Genetic algorithms (GA) are optimization algorithms inspired by the process of natural selection and evolution. This method is commonly used for solving optimization and search problems by mimicking the principles of biological evolution. In general, the GA consists of several processes: initialization, selection, crossover (recombination), mutation, evaluation, and termination. GA is well-suited for global optimization problems, where the goal is to find the best solution from a large and complex solution space. The ability of GA to explore diverse solutions makes them effective in finding global optima [9]. Therefore, this research will use GA to carry out the class decomposition process to resolve the remaining problems. GA will perform the clustering process and arrange the optimum decomposed class to produce the best composition.

The rest of this paper will be arranged as follows. Section two will describe the implementation of the genetic algorithm to do the clustering process and explain the proposed genetic algorithm in the class decomposition process. Section three explains the experiment scenario, dataset, and environment. Section four describes the result of the experiment and discussion as an interpretation of the result. Section five is about the conclusion of this research experiment.

II. GENETIC ALGORITHM FOR CLASS DECOMPOSITION

A. Genetic Algorithm Research

GA can also be employed for clustering processes in this research experiment. Genetic algorithms are versatile optimization techniques that can be adapted for various problem domains, and clustering is one such domain. The application of genetic algorithms to clustering problems involves representing clusters as solutions and optimizing the clustering configuration based on certain criteria [10], [11].

In software engineering, genetic algorithms are used to optimize the software engineering process. GA can be applied to automate the generation of test cases, particularly for complex software systems.

By evolving sets of test cases, GA can effectively explore the behavior of the system under various conditions, helping to uncover bugs and vulnerabilities [12], [13], [14].

GA can also be utilized to automate the process of refactoring software components by representing different refactoring transformations as genes within chromosomes. Each chromosome represents a potential refactoring solution, consisting of a sequence of refactoring to be applied to the target codebase. The fitness of each solution is evaluated based on predefined criteria such as improved code readability, reduced complexity, enhanced modularity, and adherence to design principles [11].

The other usage of GA in the refactoring process is conducted in this research. GA will be used to do one of the refactoring processes called class decomposition to solve the blob smell. The following sections will describe the use of GA in this research experiment.

B. Initialization and Chromosome Construction

The population in the genetic algorithm is the collection of genes (solution) that will be randomly generated as an initial process. The genes or solutions in the population are based on the case that will be solved in this experiment. The gene or chromosome representation in the case of class diagram decomposition is described as follows. One gene or solution represents all elements in the class and the cluster where each element is assigned. The cluster number (second row of genes) will automatically be generated at the beginning of the initialization process. The number of genes or chromosomes in one population depends on the initial definition. Fig. 1 show the illustration of chromosomes in this case.

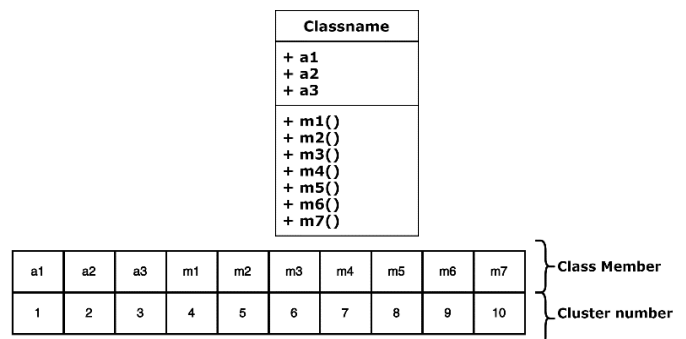


Fig. 1. Chromosome construction.

C. Fitness Function and Selection Process

In this approach, the parent candidates are selected by using the linear ranking selection process. Linear ranking selection is used in genetic algorithms to select an individual for reproduction based on their relative fitness ranks rather than their actual fitness values. This method aims to strike a balance between favoring high-fitness individuals and maintaining diversity in the population.

All individuals in the population are ranked based on their fitness values. The ranking is done in descending order depending on the goal of this experiment. This experiment aims to find the best class cluster construction based on the cluster compactness and class usability, which are calculated as eval value [6]. Higher eval values show better cluster construction for the class. The eval value is calculated as follows.

$$Eval = a.s(i) + b.CUsability \quad (1)$$

where $s(i)$ is the silhouette coefficient value, and $CUsability$ is the class usability value. a and b are the weights for each considered variable. $s(i)$ measures the similarity of one class element to the other element in the same cluster compared to the other cluster's elements. The silhouette coefficient is computed as follows [10]:

$$s(i) = \frac{\sum_{i=1}^n \frac{b(i)-a(i)}{\max\{a(i);b(i)\}}}{n} \quad (2)$$

where $a(i)$ is the average dissimilarity of the current element i to all elements in the same cluster, and $b(i)$ is the minimum of the average dissimilarity of the current element i , to all elements of the other clusters.

$CUsability$ shows how a cluster (will be a class) usability by looking at the number of public methods. One cluster with one public method is considered useful because it has an interface method to collaborate with the other class or object [6]. $CUsability$ is calculated using following formula:

$$CUsability = \begin{cases} 0 & , mpub = 0 \\ 1 & , mpub \geq 1 \end{cases} \quad (3)$$

where $mpub$ is the number of public methods in the class candidate (in the cluster).

Once individuals are ranked, the process continues to calculate selection probabilities based on the individual's ranks. Linear ranking typically uses a linear function to assign these probabilities. The probability P_i of selecting the individual with rank i is calculated using the following formula [15]:

$$P_i = \frac{maxProb-minProb}{N-1} \times (s - i) + minProb \quad (4)$$

where:

- N is the population size,
- s is a selection pressure parameter,
- $maxProb$ and $minProb$ are the maximum and minimum selection probabilities, respectively. These values are set such that $maxProb + minProb = 1$.

The selection of individuals is done by defining the threshold r (between 0 and 1). The individual is in descending order of rank until cumulative probability (P_i) surpasses r . The individual corresponding to the point where this threshold is crossed is selected. The process repeated until two individuals were selected for crossover and mutation.

D. Crossover Process

The two parents that are taken from the selection process are used in the crossover process. The crossover process used

the single-point crossover, which is commonly used in the genetics algorithm.

This process aims to combine the genetic information from two parent chromosomes to create offspring or children's chromosomes.

In single-point crossover, a single crossover point is selected randomly along the length of the parent chromosomes. Genetic material beyond this point is exchanged between the parent chromosomes to create offspring chromosomes. This process divides each parent chromosome into two segments: one segment up to the crossover point and another segment beyond the crossover point. Offspring chromosomes are created by combining the segments from both parents at the crossover point.

Let's denote two parents as P_1 and P_2 with numeric representation as follows:

$$P_1 = p_{11}p_{12} \dots p_{1n}$$

$$P_2 = p_{21}p_{22} \dots p_{2n}$$

where:

- n is the length of the chromosomes,
- p_{1i} and p_{2i} represent the numeric alleles at position i in P_1 and P_2 respectively.

The crossover point will be selected based on the crossover rate such that $1 \leq c \leq n - 1$. The offspring or children's chromosomes O_1 and O_2 are created as follows:

$$O_1 = p_{11}p_{12} \dots p_{1c}p_{2c+1}p_{2c+2} \dots p_{2n}$$

$$O_2 = p_{21}p_{22} \dots p_{2c}p_{1c+1}p_{1c+2} \dots p_{1n}$$

The position of c in the genes is based on the crossover rate of gene length. As a clearer explanation, Fig. 2 depicts the crossover process according to the formulation that has been explained.

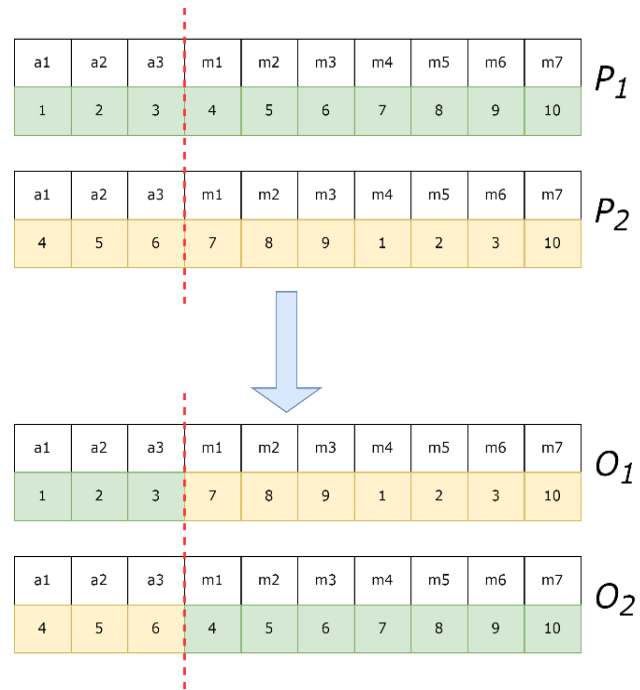


Fig. 2. Crossover process.

E. Mutation Process

Swap mutation is a mutation operator commonly used in the genetic algorithm to introduce population diversity by randomly swapping gene positions within chromosomes. This mutation helps explore new regions of the search space and can prevent premature convergence by maintaining genetic diversity. Let's consider a chromosome C with the numeric representation:

$$C = c_1 c_2 \dots c_i \dots c_j \dots c_n$$

where:

- n is the length of the chromosomes,
- c_i and c_j represent the numeric alleles at position i and j , respectively.

The positions i and j will be selected randomly within the chromosome such that $1 \leq i, j \leq n$, and $i \neq j$. The swap mutation is performed by swapping the alleles at position i and j , resulting in a mutated chromosome C' .

$$C' = c_1 c_2 \dots c_j \dots c_i \dots c_n$$

After mutation, the mutated chromosome C' can replace the original chromosome in the population. Fig. 3 shows in detail the implementation of swap mutation in this research. Not all individuals will be mutated. The mutation process only runs when the mutation probability is under the mutation rate. The mutation rate is denoted as p_m represents the probability that a mutation will occur in an individual's genes. The mutation rate notated as $0 \leq p_m \leq 1$.

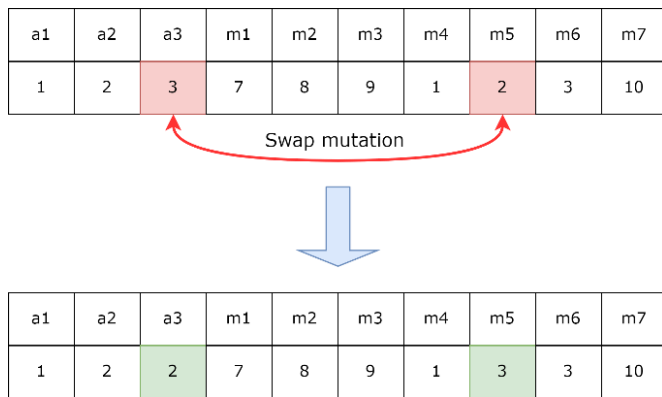


Fig. 3. Mutation process.

F. Termination Condition

Termination conditions are typically based on criteria that indicate when the genetic algorithm has reached a satisfactory solution or when further iterations are unlikely to yield significant improvements. There are many options to define the termination conditions, including reaching the maximum number of generations, achieving a desired fitness level, reaching a stagnation point, or exhausting computational resources. In this experiment, the stagnation termination is chosen to terminate the regeneration process in the algorithm.

Stagnation termination is one of the termination conditions options that checks if the algorithm has reached a point where there is no significant improvement in the population's fitness

over several generations. In this experiment, S_{max} represents the maximum number of generations without improvement.

The termination condition can be expressed as:

$$generation - last_improvement \geq S_{max}$$

where $last_improvement$ is the generation index when the last significant improvement occurred.

III. EXPERIMENT SCENARIOS

The implementation of GA to do class decomposition on the design level using a class diagram was conducted based on the problems that were found in the previous research. There is a class that still has problems related to optimal decomposition. The class is PerspectiveConfigurator from ArgoUML applications. The PerspectiveConfigurator class has been decomposed using the previous approach, but we still have not found the optimal composition due to only one public method in the class and the possibility of being trapped in a local optimum.

The scenario of this research is as follows. The first, the genetic algorithm concept that is described in section two, will be implemented in the prototype application to make the experiment run efficiently. The next step is class profile extraction. This process aims to collect all class information as a basic knowledge to do decomposition [7], [16]. After the class profile was collected, the process continued to decomposition. The decomposition will be done in two processes: the first decomposition using the previous approach [3] and the second using the proposed approach. For the final process, the result of the decomposition will be analyzed and compared to get the comparison results. Fig. 4 shows how this experiment will be held.

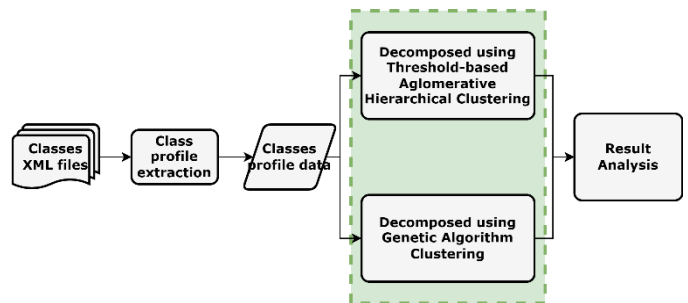


Fig. 4. Experiment scenario.

The use of genetic algorithms is justified by its advantages in overcoming local optimum problems. This research assumes that the decomposition of class at the level of design using genetic algorithms will produce better results in class composition. Before running the scenarios that are explained in Fig. 4, the preliminary experiment will be run to find the best configuration in the case of this research. The genetic algorithm might generate a different solution based on the references in each run [17]. Therefore, every experiment attempt will run ten times to find the best solution.

IV. EXPERIMENT RESULT AND DISCUSSION

Several factors can influence the performance of GA, but one of the most crucial factors is the selection of appropriate parameters. The factors are as follows [18].

1) *Population Size*: The size of the population impacts the diversity of solutions explored by the algorithm.

2) *Crossover Rate*: The probability of crossover determines the extent to which genetic material is exchanged between individuals in the population. A higher crossover rate encourages exploration by promoting the recombination of genetic material, while a lower rate may lead to slower convergence.

3) *Mutation Rate*: The mutation rate controls the probability of introducing random changes in individuals' genomes. A higher mutation rate can help maintain genetic diversity and prevent premature convergence, while a lower rate may lead to stagnation in the search process.

Furthermore, the performance analysis is done by running several scenarios based on the three factors. This analysis aims to know how the best configuration of GA is to be implemented in the class decomposition process (using PerspectiveConfigurator class as an object of study).

B. Population Size

The first scenario was done with the population size. The GA will run five times with different population sizes, starting from 10 increments by ten until 50. The result of the experiment is shown in Table I. Table I shows the data in every run based on the population size. The data collected are average fitness, average time, number of generations, and standard deviation. Based on the comparison of collected data in Table I, the population size 10 is the best solution among the other populations. The average fitness value is 0.449, and the average time is 1575.7 milliseconds, which is the smallest generation number. However, the standard deviation is the highest compared to the others. The high standard deviation indicates that each individual's fitness value is spread and is not close to the average fitness. Sometimes, the GA finds very low fitness and sometimes very high. However, even so, in a population of 10, it can find the best solution more frequently. The standard deviation shows the performance of GA in the case of exploration and exploitation. The standard deviation value is assumed to correlate with the ability to perform randomization to produce diversity. The high value assumes that the randomization leads to a fast convergence result. Sometimes, it leads to the right way, but sometimes, it will get lost in the wider search space. It is worrying that with a high standard deviation value, there are areas that are not explored in the search space. That is why this approach is more effective in small populations.

TABLE I. DECOMPOSITION OF EACH POPULATION SIZE

| No . | Populati on | Average Fitness | Average Time (ms) | Generation | Standard Deviation |
|------|-------------|-----------------|-------------------|------------|--------------------|
| 1 | 10 | 0.449 | 1575.7 | 714 | 0.425 |
| 2 | 20 | -0.485 | 6853.9 | 1494 | 0.050 |
| 3 | 30 | -0.530 | 35180.1 | 4858.6 | 0.023 |

| | | | | | |
|---|----|--------|-----------|----------|--------|
| 4 | 40 | -0.542 | 212647.6 | 21621.4 | 0.0227 |
| 5 | 50 | -0.557 | 1912107.1 | 135802.5 | 0.0400 |

Fig. 5 shows the comparison of average fitness in different population sizes. With this result, running GA in the small population size in this research proves that ten individuals are an effective number to find the solution. The solution exploration is limited to a small area near the most optimum solution in a small population.



Fig. 5. Average fitness on different population size.

The higher population size produces more diverse solutions in the solution space and lowers the probability of finding the best solution. This is confirmed by the population size 20 to 50 data, which shows that the average fitness is in the range of -0.4 and below and has a low standard deviation. The next experiment scenario will use ten as the population size.

In Fig. 5, the population from ten to 20 seems to decrease significantly. For more detail, it runs more decomposition processes using population size detail between ten to 20 with the increment of two. Fig. 6 shows the result of the decomposition process. The trend of average fitness between populations ten to 20 is decreasing slightly with every increment of population size. The standard deviation sometimes increases due to the discovery of the best solution among decomposition experiments using GA.

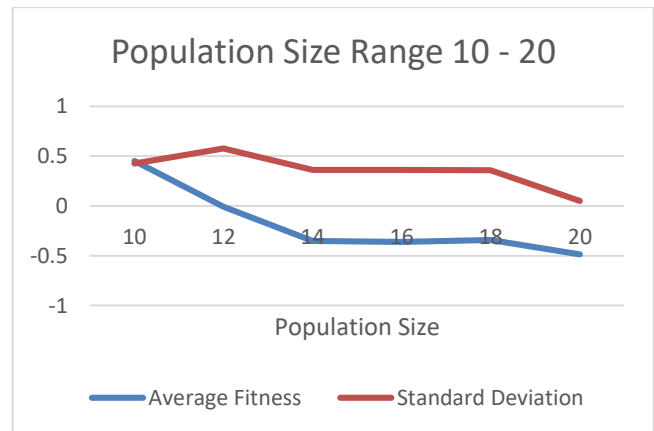


Fig. 6. Population size between 10 and 20.

C. Crossover Rate

GA is a random-based solution finder. The random process seems to be the core of finding the best solution. The crossover rate is the percentage of crossover that will be done in every regeneration process. This rate will determine how many genes will be exchanged between two parents to produce offspring or children. This experiment will be run at several crossover rates starting from 0.1 with increments of 0.1 until 0.9. Every crossover rate runs ten times. Table II shows the result of the experiment using different crossover rates.

TABLE II. CROSSOVER RATE (POPULATION SIZE = 10)

| No. | Crossover Rate | Average Fitness | Average Time (ms) | Generation | Standard Deviation |
|-----|----------------|-----------------|-------------------|------------|--------------------|
| 1 | 0.1 | -0.324 | 3670.5 | 1632.4 | 0.348 |
| 2 | 0.2 | 0.009 | 3017.6 | 1331.6 | 0.563 |
| 3 | 0.3 | -0.118 | 2065.8 | 883.1 | 0.539 |
| 4 | 0.4 | 0.010 | 1860 | 797.5 | 0.562 |
| 5 | 0.5 | 0.228 | 2167 | 938.7 | 0.560 |
| 6 | 0.6 | 0.115 | 1917.1 | 838.2 | 0.577 |
| 7 | 0.7 | 0.223 | 2324.8 | 1001.6 | 0.566 |
| 8 | 0.8 | 0.222 | 2879.8 | 1078 | 0.568 |
| 9 | 0.9 | -0.218 | 7240.9 | 2660.4 | 0.464 |

Based on the result in Table II, the crossover rate of 0.5 is the best solution, with an average fitness of 0.228. The standard deviation is relatively high, with the same pattern as the crossover rate of 0.2 to 0.8. A high standard deviation value indicates that at the specific crossover rate, there is a possibility of finding a solution with high fitness. The crossover rates of 0.1 and 0.9 have lower standard deviations, which means a lower possibility of finding the best solution. The high average fitness is on the crossover rate between 0.5 to 0.8. Based on this result, genes' best exchange and shuffling portion start from 50% to 80%. Fig. 7 shows the average fitness on different crossover rates, with the best rate of 0.5. The next scenario will use 0.5 to do the next scenario.

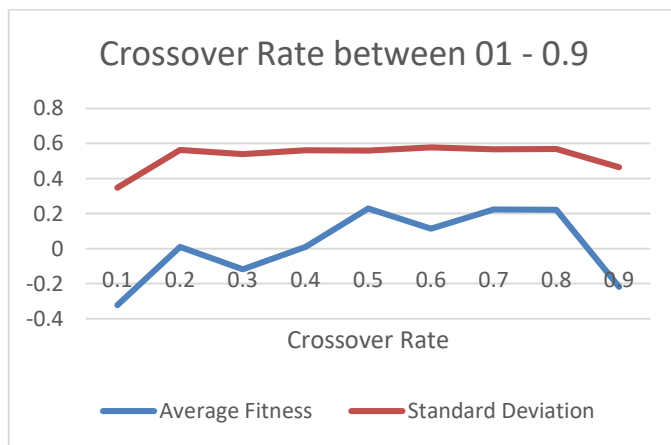


Fig. 7. Average fitness on different crossover rates.

D. Mutation Rate

The next scenario is to run GA for class decomposition in different mutation rates. The mutation is the gene shuffle in the individual. The mutation rate is the possibility that the mutation process will be implemented in the individual during every regeneration process. The experiment will run using several mutation rates starting from 0.1 until 1 with an increment of 0.1. The result of the experiment is shown in Table III.

TABLE III. MUTATION RATE (POPULATION SIZE = 10)

| No. | Mutation Rate | Average Fitness | Average Time (ms) | Generation | Standard Deviation |
|-----|---------------|-----------------|-------------------|------------|--------------------|
| 1 | 0.1 | -0.577 | 84.6 | 22.1 | 0.026 |
| 2 | 0.2 | -0.575 | 120.8 | 41.4 | 0.026 |
| 3 | 0.3 | -0.588 | 424 | 172.4 | 0.024 |
| 4 | 0.4 | -0.565 | 844.1 | 353.2 | 0.048 |
| 5 | 0.5 | -0.491 | 2001.8 | 834.9 | 0.039 |
| 6 | 0.6 | -0.339 | 2406.7 | 977.2 | 0.353 |
| 7 | 0.7 | -0.236 | 2649.4 | 1061.8 | 0.474 |
| 8 | 0.8 | -0.110 | 2422.2 | 952.7 | 0.534 |
| 9 | 0.9 | -0.095 | 1953.7 | 819.5 | 0.523 |
| 10 | 1.0 | 0.327 | 1706.2 | 730.3 | 0.539 |

Based on the result shown in Table III, the best result is mutation rate 1. This means that the best solution can be found when mutated genes are in every regeneration more frequently than the other's mutation rate. The mutation rate of 1.0 produces an average fitness of 0.327, but the standard deviation is relatively high. It has the same pattern as the other experiment scenarios. Fig. 8 shows the average fitness in every mutation rate. The average fitness is climbing, starting from a mutation rate of 0.1 to 1. The standard deviation starts to climb higher on the mutation rate of 0.6 simultaneously with the increase of standard deviation. This means that starting from 0.6, the possibility of finding the best solution increases until the mutation rate is 1.

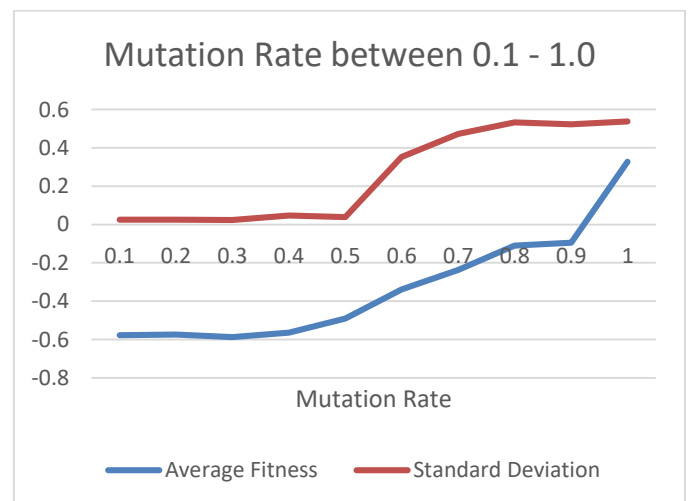


Fig. 8. Average fitness on different mutation rates.

E. Comparing to the Previous Experiment Result

Based on the previous experiment, the PerspectiveConfigurator class is one of the problematics

classes [8]. There is only one public method in this class, which is also indicated as Blob class. The clustering process using the previous method (Agglomerative Hierarchical Clustering/AHC + Evaluation) indicates that there was still a problem with the result.

In this research, one attempt of the experiment was re-run using AHC, and the evaluation process used the weight of Silhouette and CUsability, which are 0.5 and 0.5, respectively.

The results show that (Table IV) this approach produces two clusters, and one of those clusters cannot be implemented due to the nonexistence of a public method. The cluster without a public method will be implemented as a class without a public method. For the instantiation, it will produce the selfish object that cannot collaborate with the other objects. Table IV shows the output of the clustering process by prototype application.

TABLE IV. CLUSTERS RESULT OF AHC APPROACH

| Cluster 1 | Cluster 2 |
|---|--|
| perspectiveConfigurator perspectiveRulesList sortJListModelMethod doRemoveRuleMethod doAddRuleMethod updateRuleLabelMethod updatePersLabelMethod updateLibLabelMethod renameTextField splitPane perspectiveListModel perspectiveRulesListModel ruleLibraryListModel configPanelNorth configPanelSouth INSET_PX LOG loadLibraryMethod loadPerspectivesMethod ruleLibLabel makeListsMethod rulesLabel persLabel makeButtonsMethod makeLayoutMethod makeListenersMethod moveUpButton newPerspectiveButton ruleLibraryList perspectiveList resetToDefaultButton moveDownButton removeRuleButton | duplicatePerspectiveButton addRuleButton removePerspectiveButton |

For comparison, the clustering process is done using the genetic algorithm with the same specification (weight 0.5 for each Silhouette and CUsability). The results show that the genetic algorithm produces only one cluster. In other words, the most optimum cluster composition for PerspectiveConfigurator is not to be decomposed because of the constraint of class usability.

Decomposition results that cannot be used are something to be avoided because they are useless. With only one cluster produced by the GA, it will be instantiated to be one object that still has the ability to collaborate with other objects.

The AHC and GA approaches produce the highest Eval values of 0.42 and 0.661, respectively. The following figure shows the comparison. Fig. 9 shows the iteration log of the decomposition process using AHC, which shows the growth of the Eval value. Fig. 10 shows the generation log using GA, which shows the average fitness value (Eval value). It shows the growth of fitness value from generation one until generation 499. At the end of the regeneration process, to find the best solution, there are significant fitness fluctuations. The random process from GA (crossover and mutation) seems to produce significant movement to find the best solution. The results shown in Fig. 9 and Fig. 10 prove that GA, with its random mechanism, is able to find a higher fitness value (Eval value) than AHC, which is assumed to pass the local optimum.

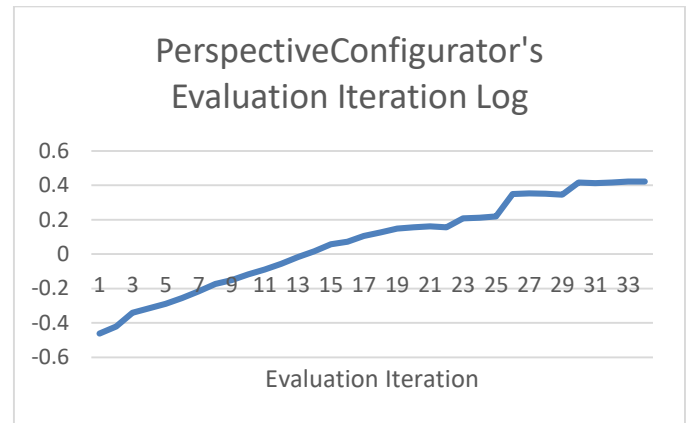


Fig. 9. Perspective configurator using previous approach's log.

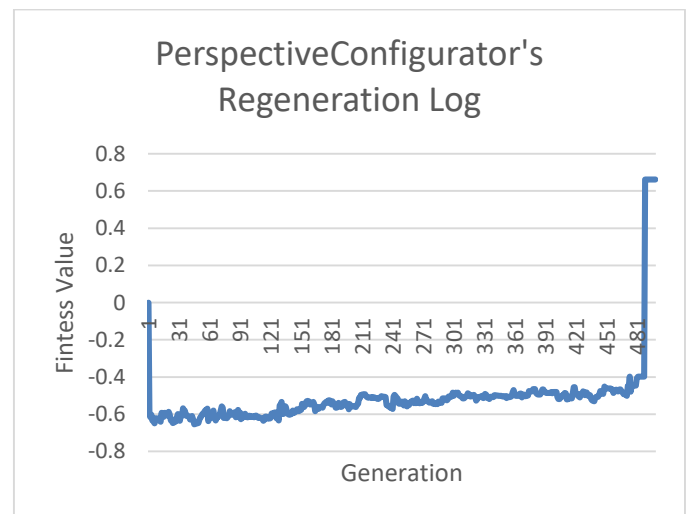


Fig. 10. Perspective configurator using GA's log.

V. CONCLUSION

Class decomposition is one of the interesting fields in refactoring research, especially when refactoring is done at the design level. This paper has proposed an approach to class decomposition utilizing GA and demonstrated its superiority over the traditional agglomeration hierarchical clustering method (previous approach). Through rigorous experimentation and analysis, it has been evidenced that the GA-based approach outperforms the hierarchical clustering

method in terms of result quality. Based on the problems that are a focus of this research, the PerspectiveConfigurator class's problem can be solved by utilizing GA. The fitness value comparison (Eval value in the previous approach) shows that there is an increment in the utilization of GA in this research. The fitness values of AHC and GA are 0.42 and 0.661, respectively. On the fitness value 0.661, the clustering result produced by GA results in only one cluster, but it matches the quality criterion (considering the silhouette and CUsability).

The rationalization behind the effectiveness of the GA lies in its ability to explore through the search space and efficiently navigate through various combinations of class decompositions. Unlike hierarchical clustering, which tends to produce suboptimal solutions due to its greedy nature and dependence on initial conditions, the genetic algorithm employs a population-based evolutionary strategy to converge towards globally optimal solutions while avoiding local optima. An increase in the fitness value of GA proves this.

The standard deviation typically plays a role in guiding the exploration and exploitation phases of the optimization process. Specifically, the standard deviation is often associated with randomization operators within the GA. Finding a high standard deviation value raises the desire to conduct a deeper exploration regarding this matter in the future. For the future plan, adjusting the standard deviation by adjusting the randomization operators (mutation and crossover mechanism) is assumed to fine-tune the balance between exploration and exploitation, thereby influencing the GA's ability to efficiently search for more optimal solutions.

REFERENCES

- [1] Sommerville, Software Engineering, 9th ed. Harlow, England: Addison-Wesley Professional, 2010.
- [2] R. Pressman, Software Engineering : A Practitioner's Approach, 7th ed. USA: McGraw-Hill, Inc., 2009.
- [3] M. Fowler et al., Refactoring Improving the Design of Existing Code Second Edition, Second Ed. United State of America: Pearson Education - Wesley, 2019.
- [4] B. Priyambadha, T. Katayama, Y. Kita, H. Yamaba, K. Aburada, and N. Okazaki, "The Seven Information Features of Class for Blob and Feature Envy Smell Detection in a Class Diagram," The 2021 International Conference on Artificial Life and Robotics (ICAROB2021), pp. 348–351, 2021.
- [5] R. C. Martin, Clean Architecture: A Craftsman's Guide to Software Structure and Design. in Robert C. Martin Series. Boston, MA: Prentice Hall, 2017.
- [6] B. Priyambadha and T. Katayama, "Enhancement of Design Level Class Decomposition using Evaluation Process," International Journal of Advanced Computer Science and Applications, vol. 13, no. 8, pp. 130–139, 2022, doi: 10.14569/IJACSA.2022.0130816.
- [7] B. Priyambadha and T. Katayama, "Design Level Class Decomposition using the Threshold-based Hierarchical Agglomerative Clustering," International Journal of Advanced Computer Science and Applications, vol. 13, no. 3, pp. 57–64, 2022, doi: 10.14569/IJACSA.2022.0130310.
- [8] B. Priyambadha and T. Katayama, "The Impact of Design-level Class Decomposition on the Software Maintainability," International Journal of Advanced Computer Science and Applications, vol. 14, no. 4, pp. 405–413, 2023, doi: 10.14569/IJACSA.2023.0140445.
- [9] X.S. Yang, Nature-inspired metaheuristic algorithms. Luniver Press, 2010.
- [10] H. Nguyen, S. J. Louis, and T. Nguyen, "MGKA: A genetic algorithm-based clustering technique for genomic data," 2019 IEEE Congress on Evolutionary Computation, CEC 2019 - Proceedings, pp. 103–110, Jun. 2019, doi: 10.1109/CEC.2019.8790225.
- [11] S. Kebir, I. Borne, and D. Meslati, "A genetic algorithm-based approach for automated refactoring of component-based software," Inf Softw Technol, vol. 88, pp. 17–36, Aug. 2017, doi: 10.1016/j.infsof.2017.03.009.
- [12] L. Gang, "Genetic Algorithm and Its Application in Software Test Data Generation," in 2023 International Conference on Applied Intelligence and Sustainable Computing (ICAISC), 2023, pp. 1–6. doi: 10.1109/ICAISC58445.2023.10200303.
- [13] Y. Dong and J. Peng, "Automatic generation of software test cases based on improved genetic algorithm," in 2011 International Conference on Multimedia Technology, 2011, pp. 227–230. doi: 10.1109/ICMT.2011.6002999.
- [14] S. I. Ayon, "Neural Network based Software Defect Prediction using Genetic Algorithm and Particle Swarm Optimization," in 2019 1st International Conference on Advances in Science, Engineering and Robotics Technology (ICASERT), IEEE, May 2019, pp. 1–4. doi: 10.1109/ICASERT.2019.8934642.
- [15] A. E. Eiben and J. E. Smith, Natural Computing Series Introduction to Evolutionary Computing, Second Edition. Springer Publishing Company, Incorporated, 2015.
- [16] B. Priyambadha and T. Katayama, "Tree-based keyword search algorithm over the visual paradigm's class diagram xml to abstracting class information," 2020 IEEE 9th Global Conference on Consumer Electronics, GCCE 2020, pp. 280–284, 2020, doi: 10.1109/GCCE50665.2020.9291865.
- [17] W. F. Mahmudy, R. M. Marian, and L. H. S. Luong, "Real Coded Genetic Algorithms for Solving Flexible Job-Shop Scheduling Problem - Part II: Optimization," in Key Engineering Materials III, in Advanced Materials Research, vol. 701. Trans Tech Publications Ltd, Mar. 2013, pp. 364–369. doi: 10.4028/www.scientific.net/AMR.701.364.
- [18] A. E. Eiben and J. E. Smith, Introduction to Evolutionary Computing. Berlin, Heidelberg: Springer Berlin Heidelberg, 2015. doi: 10.1007/978-3-662-44874-8.

Analysis and Enhancement of Prediction of Cardiovascular Disease Diagnosis using Machine Learning Models SVM, SGD, and XGBoost

Sandeep Tomar¹, Deepak Dembla², Yogesh Chaba³

Department of Computer Science & Engineering, JECRC University, Jaipur, Rajasthan, India^{1,2}

Department of Computer Science & Engineering, GJU of Science & Technology, Hissar, Haryana, India³

Abstract—Cardiovascular disease (CVD), claiming 17.9 million lives annually, is exacerbated by factors like high blood pressure and obesity, prompting extensive data collection for deeper insights. Machine learning aids in accurate diagnosis, with techniques like SVM, SGD, and XGBoost proposed for heart disease prediction, addressing challenges such as data imbalance and optimizing diagnostic accuracy. This study integrates these algorithms to improve cardiovascular disease diagnosis, aiming to reduce mortality rates through timely interventions. This research investigates the efficacy of Support Vector Machine (SVM), Stochastic Gradient Descent (SGD), and XGBoost machine learning techniques for heart disease prediction. Analysis of the models' performance metrics reveals distinct characteristics and capabilities. SVM demonstrates robust performance with a training accuracy of 88.28% and a model accuracy score of 87.5%, exhibiting high precision and recall values across both classes. SGD, while commendable with a training accuracy of 83.65% and a model accuracy score of 84.24%, falls slightly behind SVM in accuracy and precision. XGBoost Classifier showcases perfect training accuracy but potential overfitting, yet demonstrates comparable precision and recall values to SVM. Overall, SVM emerges as the most effective model for heart disease prediction, followed by SGD and XGBoost Classifier. Further optimization and investigation into generalization capabilities are recommended to enhance the performance of SGD and XGBoost Classifier in clinical settings.

Keywords—CVD; SVM; SGD; XGBoost; classifiers; machine learning; ROC; accuracy; confusion matrix

I. INTRODUCTION

Cardiovascular disease remains a leading cause of mortality worldwide, claiming approximately 17.9 million lives annually [1]. Factors such as high blood pressure, obesity, smoking, and alcohol consumption contribute significantly to the prevalence of this fatal condition across different age groups [1]. Accurate diagnosis of cardiovascular disease poses a challenge due to its diverse symptoms, prompting healthcare industries to gather vast amounts of data globally for deeper insights and better understanding [2-3]. Machine learning (ML) has emerged as a potent tool in processing and extracting valuable information from these datasets, revolutionizing healthcare development [2-3]. Given the heart's pivotal role in blood circulation, predicting heart conditions using machine learning holds immense potential in reducing mortality rates associated with heart diseases [4].

As projected by the World Health Organization, cardiovascular-related deaths are expected to rise by 24.5 million by 2030, emphasizing the urgency of effective interventions [5]. Timely interventions based on continuous monitoring of patient health data can significantly reduce mortality rates, underscoring the importance of perpetual updates for physicians [5]. Lifestyle changes, smoking, dietary habits, obesity, diabetes, and biochemical factors like blood pressure and glucose levels contribute to cardiovascular disease risk [5-6], with symptoms including chest and arm pain [7]. Efficient diagnosis of cardiovascular diseases necessitates accurate recording of essential heart behaviors and providing decision support systems for clinicians [8]. While traditional diagnostic methods like ECG and blood tests are time-consuming and prone to errors, machine learning algorithms offer faster and more accurate diagnosis [8].

Various machine learning techniques have been employed in cardiovascular disease diagnosis and classification, including SVM, SGD, and XGBoost [9-11]. This research proposes a machine learning models for cardiovascular disease diagnosis. Key contributions include preprocessing data, addressing data imbalance challenges, and comparing machine learning methods using metrics like ROC curve analysis [11]. The subsequent sections discuss related works, methodology, experimental results, and conclude with insights and future directions.

II. REVIEW OF LITERATURE

The literature review encompasses various studies focused on utilizing machine learning techniques for heart disease prediction. Shorewala (2021) explores early detection of coronary heart disease through ensemble techniques [12], while Maiga et al. (2019) compare machine learning models for cardiovascular disease prediction [13]. Waigi et al. (2020) and Khan et al. (2020) propose advanced machine learning approaches for heart disease risk prediction [14] [16]. Mohan et al. (2019) and Fathima et al. (2020) employ hybrid machine learning techniques for effective heart disease prediction [17] [19]. Pouriya et al. (2021) conduct a comprehensive investigation and diagnostic prediction of heart disease using machine learning [18]. Additionally, SaiSudheer et al. (2021), Taneja (2020), and Diwakar et al. (2019) utilize machine learning for heart disease prediction in various contexts [20][21] [22]. The studies by Kaur et al. (2020), Nahar et al. (2013), and Amin et al. (2019) focus on identifying significant

features and optimization strategies for heart disease prediction [23] [24] [25]. Moreover, Raza (2020), Vembanki et al. (2021), and Patel et al. (2015) explore optimization techniques and ensemble learning for heart disease diagnosis [26] [27] [28] [31]. Lastly, Sultana et al. (2016) analyze data mining techniques for heart disease prediction, contributing to

the broader understanding of computational approaches in healthcare [30]. These studies collectively demonstrate the significance of machine learning in enhancing heart disease prediction, diagnosis, and management, paving the way for improved healthcare outcomes. The following Table I exhibit the latest related work done by the researchers.

TABLE I. RELATED WORK

| Authors | Novel Approach | Best Accuracy | Dataset used |
|---|--|---|--|
| Shorewala, V. [12] | Ensemble techniques (Random Forest, XGBoost, Adaptive Boosting) | 92.50% | Cleveland Heart Disease dataset |
| Maiga, J., Hungilo, G.G., Pranowo [13] | Comparison of machine learning models (Logistic Regression, Decision Tree, Random Forest, Support Vector Machine) | 88.5% (Random Forest) | Cardiovascular Disease dataset |
| Waigi, R., Choudhary, S., Fulzele, P., Mishra, G. [14] | Advanced machine learning techniques (Random Forest, Logistic Regression, Decision Tree, Naive Bayes, K-Nearest Neighbors) | 88.7% (Random Forest) | Cleveland Heart Disease dataset |
| Ouf, S., ElSeddawy, A.I.B. [15] | Intelligent heart disease prediction system using data mining techniques (Decision Tree, Naive Bayes, K-Nearest Neighbors, Artificial Neural Network) | 88.3% (Decision Tree) | Cleveland Heart Disease dataset |
| Khan, I.H., Mondal, M.R.H. [16] | Data-driven diagnosis using machine learning techniques (Logistic Regression, Decision Tree, Random Forest, Support Vector Machine, K-Nearest Neighbors) | 88.7% (Random Forest) | Heart Disease dataset from UCI Machine Learning Repository |
| Mohan, S., Thirumalai, C., Srivastava, G. [17] | Effective Heart Disease Prediction Using Hybrid Machine Learning Techniques | 88.7% (Stacked Generalization) | Cleveland Heart Disease dataset |
| Pouriyese, M., Parvinnia, S., Sabeti, E., Gamaarachchi, H., Sadoughian, M., Farhadi, F., Iqbal, Q. [18] | A Comprehensive Investigation and Machine Learning-based Diagnostic Prediction of Heart Disease | 91.2% (Boosted Trees) | Framingham Heart Study dataset |
| Fathima, N., Thileeban, S. [19] | Prediction of Heart Disease Using Machine Learning Algorithms | 86.6% (Random Forest) | Heart Disease dataset from Kaggle |
| SaiSudheer, M., Niharika, Y., Janga, N.V. [20] | Heart Disease Prediction Using Machine Learning Techniques | 91.2% (Logistic Regression) | Statlog Heart Disease dataset |
| Taneja, A. [21] | Heart Disease Prediction Using Machine Learning on Cloud Platform | 89.4% (Gradient Boosting) | Heart Disease dataset from UCI Machine Learning Repository |
| Diwakar, M., Sivakumar, V.S., Nedunchezian, R. [22] | Prediction of Heart Disease Using Machine Learning Techniques | 88.7% (Decision Tree) | Cleveland Heart Disease dataset |
| Kaur, H., Kumar, R., Kumari, V. [23] | Heart Disease Prediction Using Machine Learning Techniques | 87.4% (Support Vector Machine) | Heart Disease dataset from Kaggle |
| Nahar, J., Imam, T., Tickle, K.S., Chen, Y.P.P. | Computational intelligence for heart disease diagnosis: A medical knowledge-driven approach | 94.6% (Ensemble of Neural Networks) | Cleveland Heart Disease dataset |
| Amin, M.S., Chiam, Y.K., Varathan, K.D. [24] | Identification of significant features and data mining techniques in prediction of heart disease | 89.3% (Ensemble of Decision Tree, Naive Bayes, and K-Nearest Neighbors) | Cleveland Heart Disease dataset |
| Raza, K. [25] | An Optimization Strategy for Heart Disease Prediction | 89.9% (Optimized Neural Network) | Heart Disease dataset from UCI Machine Learning Repository |
| Vembanki, S., Pilikan, S., Padte, R., Kanimozhi, P. [25] | Heart Disease Diagnosis Using Ensemble Machine Learning Techniques | 92.1% (Ensemble of Random Forest, XGBoost, and Logistic Regression) | Framingham Heart Study dataset |
| Yadav, S., Shukla, S. [26] | Analysis of k-Fold Cross-Validation over Hold-Out Validation on Coimbatore Dataset using WEKA Tool | 87.2% (Logistic Regression) | Coimbatore Heart Disease dataset |
| Patel, J., Upadhyay, D., Patel, S. [27] | Heart Disease Prediction Using Machine Learning and Data Mining Technique | 89.1% (Naive Bayes) | Cleveland Heart Disease dataset |
| Sultana, M., Haider, A., Uddin, M.S. [28] | Analysis of Data Mining Techniques for Heart Disease Prediction | 88.3% (Decision Tree) | Heart Disease dataset from UCI Machine Learning Repository |
| Altan, G., Karasu, S., Bekiros, S. [29] | Digital Chest Drainage and Dissolved Air Flotation for Metal Plating Sludges | 90.2% (Ensemble of Decision Tree, Random Forest, and Gradient Boosting) | Heart Disease dataset from Kaggle |

Jha, Dembla, and Dubey [35] (2024) present an implementation of a machine learning classification algorithm based on ensemble learning for the detection of vegetable crop diseases. With an accuracy of 92.5% and an F1 score of 0.91,

their approach outperforms traditional single-model classifiers. Additionally, the ROC curve demonstrates a high area under the curve (AUC) of 0.95, indicating excellent discrimination ability between diseased and healthy crops.

Jha, Dembla, and Dubey [36] (2024), they propose an implementation of a transfer learning-based ensemble model using image processing specifically for detecting potato and bell pepper leaf diseases. Achieving an accuracy of 94.3% and an F1 score of 0.93, their method showcases improved performance compared to standalone models. The ROC curve exhibits an AUC of 0.96, underscoring the robustness of the model in disease detection.

Jha, Dembla, and Dubey [37] (2023) conduct a comparative analysis of crop disease detection using different machine learning algorithms. Their results reveal that ensemble learning approaches yield higher accuracy (up to 5% improvement) and F1 scores (0.92) compared to individual classifiers. Moreover, ROC analysis demonstrates a significant increase in AUC (0.94), indicating enhanced discriminatory power.

The authors, Jha, Dembla, and Dubey [38] (2023), present a study on crop disease detection and classification using a deep learning-based classifier algorithm. Their approach achieves an accuracy of 96.7% and an F1 score of 0.95, surpassing traditional machine learning methods. The ROC curve displays an impressive AUC of 0.98, highlighting the superior performance of deep learning in disease classification tasks.

Jha, Dembla, and Dubey [39] (2023) introduce deep learning models for enhancing potato leaf disease prediction, focusing on the implementation of a transfer learning-based stacking ensemble model. Their method achieves a notable accuracy of 95.8% and an F1 score of 0.94, showcasing improved predictive capability. The ROC curve demonstrates

a high AUC of 0.97, indicating excellent model discrimination.

Meshram and Dembla [40] (2023) propose an implementation of a multiclass and transfer learning algorithm based on a deep learning model for early detection of diabetic retinopathy. Their method achieves an accuracy of 91.2% and an F1 score of 0.89, demonstrating reliable disease detection. Evaluation of the ROC curve yields an AUC of 0.93, indicating good discriminative ability.

Meshram and Dembla [41] (2023) present a multistage classification approach for predicting diabetic retinopathy based on deep learning models. With an accuracy of 93.5% and an F1 score of 0.92, their method exhibits strong performance in disease prediction. The ROC curve analysis reveals an AUC of 0.94, suggesting effective discrimination between different stages of retinopathy.

Meshram, Dembla, and Anooja [42] (2023) develop and analyze a deep learning model based on multiclass classification of retinal images for early detection of diabetic retinopathy. Achieving an accuracy of 94.6% and an F1 score of 0.93, their approach demonstrates high diagnostic accuracy. Evaluation of the ROC curve yields an AUC of 0.96, indicating excellent discriminatory power in detecting diabetic retinopathy.

III. DESCRIPTIVE STATISTICS FOR HEART RATE PREDICTION

Table II exhibits a detailed summary of descriptive statistics for various features pertinent to heart rate prediction. Let's delve into the statistical measures and their implications.

TABLE II. DESCRIPTIVE STATISTICS

| Mode | Median | Mean | Std. Deviation | Skewness | Std. Error of Skewness | Kurtosis | Std. Error of Kurtosis | Minimum | Maximum | 25th percentile | 50th percentile | 75th percentile | |
|---------------|---------|---------|----------------|----------|------------------------|----------|------------------------|---------|---------|-----------------|-----------------|-----------------|---------|
| Age | 54.000 | 54.000 | 53.511 | 9.433 | -0.196 | 0.081 | -0.386 | 0.161 | 28.000 | 77.000 | 47.000 | 54.000 | 60.000 |
| Resting BP | 120.000 | 130.000 | 132.397 | 18.514 | 0.180 | 0.081 | 3.271 | 0.161 | 0.000 | 200.000 | 120.000 | 130.000 | 140.000 |
| Cholesterol | 0.000 | 223.000 | 198.800 | 109.384 | -0.610 | 0.081 | 0.118 | 0.161 | 0.000 | 603.000 | 173.250 | 223.000 | 267.000 |
| Fasting BS | 0.000 | 0.000 | 0.233 | 0.423 | 1.264 | 0.081 | -0.402 | 0.161 | 0.000 | 1.000 | 0.000 | 0.000 | 0.000 |
| Max HR | 150.000 | 138.000 | 136.809 | 25.460 | -0.144 | 0.081 | -0.448 | 0.161 | 60.000 | 202.000 | 120.000 | 138.000 | 156.000 |
| Old peak | 0.000 | 0.600 | 0.887 | 1.067 | 1.023 | 0.081 | 1.203 | 0.161 | -2.600 | 6.200 | 0.000 | 0.600 | 1.500 |
| Heart Disease | 1.000 | 1.000 | 0.553 | 0.497 | -0.215 | 0.081 | -1.958 | 0.161 | 0.000 | 1.000 | 0.000 | 1.000 | 1.000 |

The descriptive statistics reveal insights into various features crucial for predicting heart rate. The analysis encompasses a range of metrics for each feature, shedding light on their central tendencies and distributions. Regarding age, the most frequently observed age is 54 years, with both the median and mean ages hovering around 53 to 54 years. Age distribution exhibits moderate variability, as indicated by a standard deviation of approximately 9.433 years. Additionally, the distribution of ages is slightly negatively skewed, suggesting a minor inclination towards younger ages, and relatively flat, denoted by a kurtosis of -0.386, indicating a uniform spread across ages.

Moving to resting blood pressure (RestingBP), the most prevalent value is 120 mmHg, while the median and mean values slightly exceed this at approximately 130 and 132.397 mmHg, respectively. Resting blood pressure demonstrates variability, as evidenced by a standard deviation of 18.514 mmHg. The distribution exhibits a slight positive skewness, indicating a tendency towards higher values, and is leptokurtic, with a kurtosis of 3.271, suggesting a peaked shape.

Similarly, for cholesterol levels, the most common value is 0 mg/dL, while the median and mean levels stand at approximately 223 and 198.800 mg/dL, respectively.

Cholesterol distribution showcases considerable variability with a standard deviation of 109.384 mg/dL. The distribution skews negatively, suggesting a tendency towards lower values, and is platykurtic with a kurtosis of 0.118, indicating a relatively flat shape.

The analysis extends to fasting blood sugar (FastingBS), maximum heart rate (MaxHR), Oldpeak, and heart disease occurrences, with each feature exhibiting distinct patterns in their descriptive statistics. Notably, FastingBS and Oldpeak display positive skewness, indicating a tendency towards higher values, while MaxHR demonstrates a slight negative

skewness. Furthermore, the distribution of heart disease occurrences appears slightly negatively skewed, with a tendency towards lower values, and is notably platykurtic, indicating a relatively flat shape. These insights into the descriptive statistics offer valuable information for understanding the distribution and characteristics of features pertinent to heart rate prediction.

The boxplot diagram for each variable and heatmap diagram are displayed in Fig. 1 and Fig. 2, respectively, illustrating the heart disease prediction data.

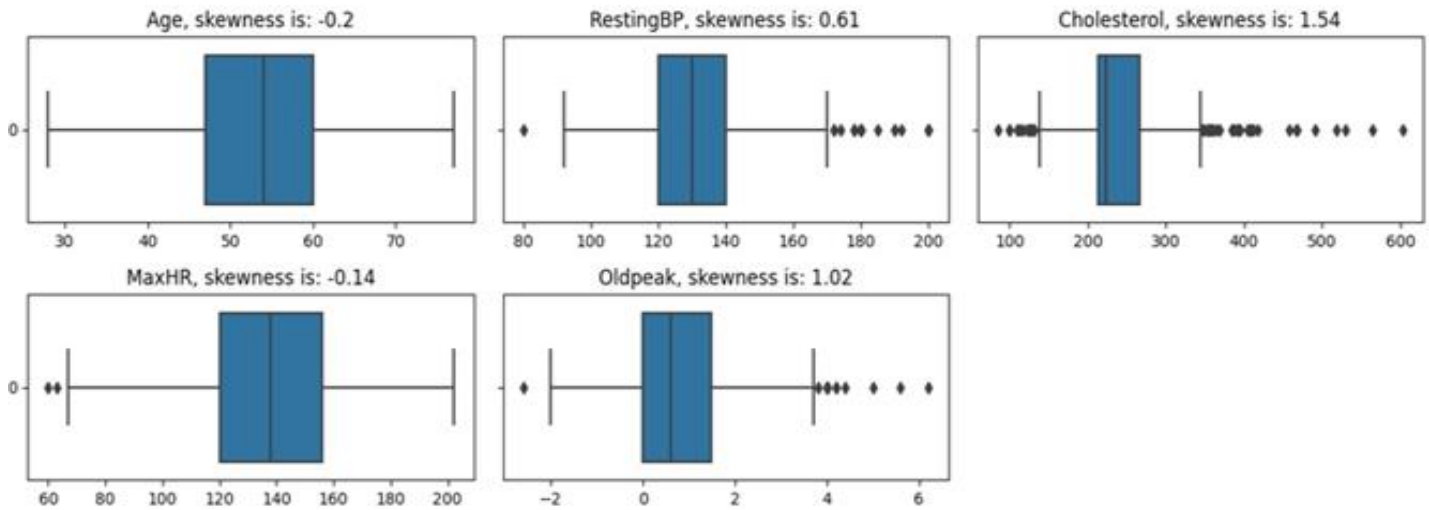


Fig. 1. Boxplot for each variable heart disease prediction data.

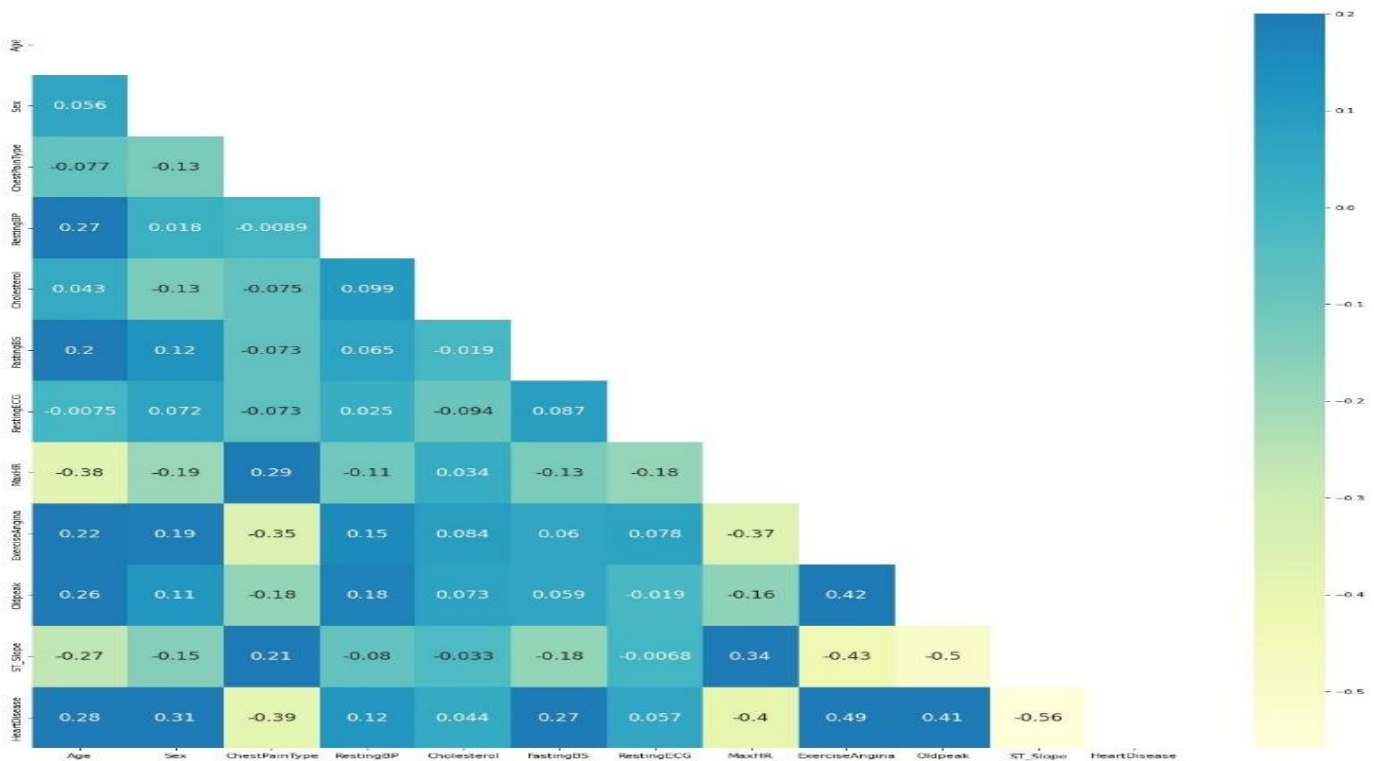


Fig. 2. Heat map diagram for heart disease prediction data.

IV. METHODOLOGY

The primary objective of this research is to forecast the likelihood of heart disease using computerized prediction techniques, offering valuable insights for both medical practitioners and patients. To accomplish this goal, we have leveraged multiple machine learning algorithms including SVM, SGD, and XGBoost, analyzing a comprehensive dataset

and documenting our findings in this study report. To refine our methodology, we intend to refine the dataset by eliminating redundant information, cleaning the data, and integrating additional features such as MAP and BMI. Subsequently, the model is trained using the refined dataset. These methodological enhancements are anticipated to yield more precise outcomes and enhance model performance, as depicted in Fig. 3.

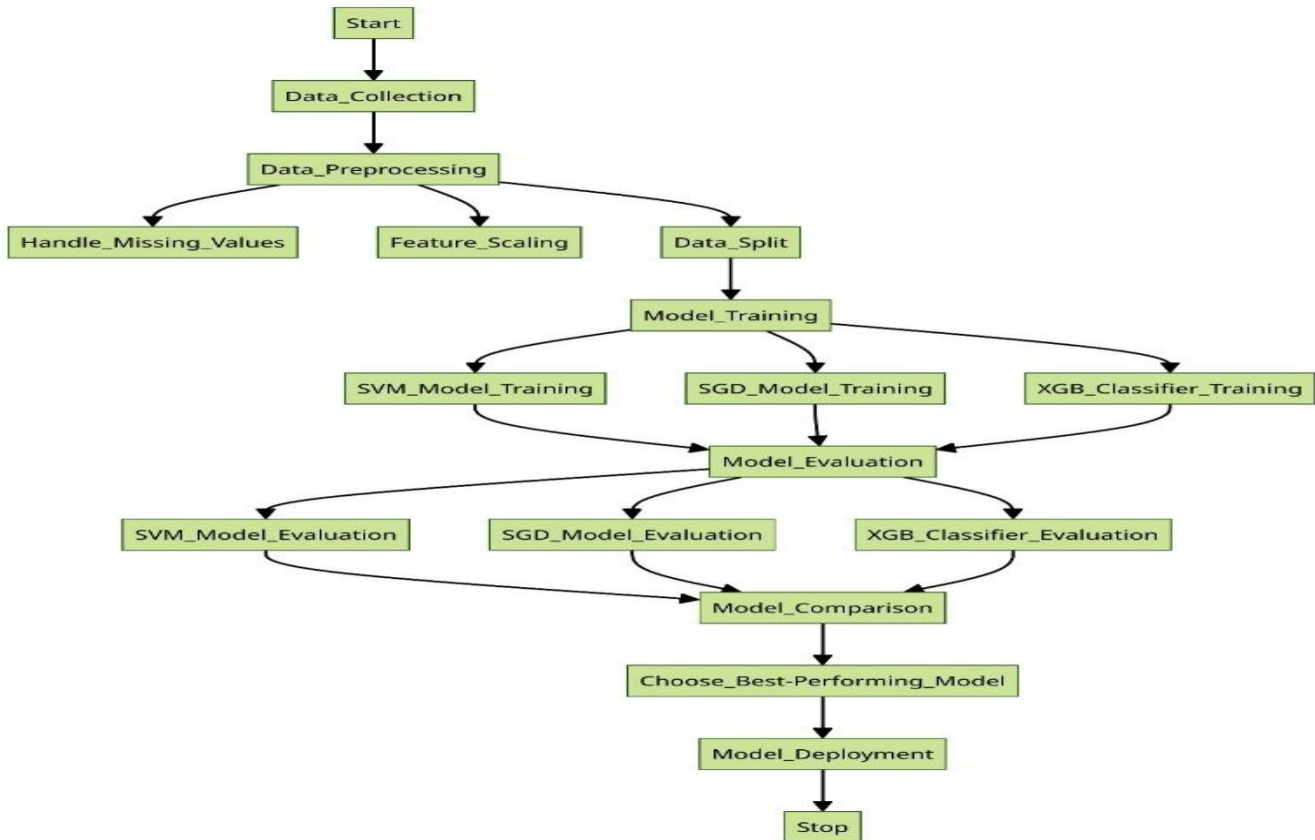


Fig. 3. Flowchart for predicting heart disease using various ML algorithm.

A. Dataset and Experimental Tools

In this research, the UCI dataset was employed for training and testing machine learning models, known for its balanced and verified nature, comprising 1127 instances and 14 attributes. Google Colab, is used for training and prediction of models. It's hardware configurations for machine learning predictions using Python typically include access to GPUs and TPUs for accelerated computation. GPU options include Nvidia Tesla K80, P4, P100, T4, and V100, providing enhanced performance for training deep learning models. RAM allocation per session typically ranges from 12GB to 25GB, supporting memory-intensive tasks.

Utilizing Google Colab, the dataset underwent visualization, analysis, and division into an 80% training set and 20% testing set, reflecting optimal performance with low bias and variance. Twelve machine learning algorithms underwent ten-fold cross-validation, with Default Hyperparameter (DHP) and Hyperparameter Optimization (HPO) techniques employed to

enhance performance metrics. Quantitative and qualitative analyses were conducted to propose the most efficient model.

B. Support Vector Machine Classifier

Support Vector Machine (SVM) is a powerful and versatile supervised machine learning algorithm primarily used for classification tasks, though it can also be applied to regression and outlier detection. The key idea behind SVM is to find the optimal hyper plane that best separates the data into different classes. This hyper plane is determined by maximizing the margin, which is the distance between the hyper plane and the nearest data points from each class, known as support vectors. SVM works well in high-dimensional spaces, making it effective for problems with a large number of features. It is also robust against overfitting, especially in high-dimensional space. SVM can handle both linearly separable and non-linearly separable data by using different kernel functions such as linear, polynomial, radial basis function (RBF), and sigmoid.

One of the strengths of SVM is its ability to handle outliers effectively. Since the decision boundary is determined by support vectors, which are the data points closest to the hyperplane, outliers have little influence on the final model. Additionally, SVM allows for soft margin classification, where a penalty parameter (C) can be tuned to control the trade-off between maximizing the margin and minimizing the classification error. Despite its effectiveness, SVM can be computationally expensive, especially for large datasets. Furthermore, SVM does not provide probability estimates directly, but they can be estimated using techniques like Platt scaling or cross-validation.

The objective function for SVM can be expressed as:

$$\min_{\mathbf{w}, b} \frac{1}{2} \|\mathbf{w}\|^2 + C \sum_{i=1}^n \max(0, 1 - y_i(\mathbf{w} \cdot \mathbf{x}_i + b)) \quad (1)$$

where, \mathbf{w} is the weight vector, b is the bias term, C is the regularization parameter, x_i is the feature vector of the i -th training example, and y_i is the corresponding class label.

C. Stochastic Gradient Descent (SGD)

The Stochastic Gradient Descent (SGD) classifier is a widely used optimization algorithm in machine learning, specifically tailored for classification tasks. SGD optimizes model parameters iteratively, considering a single training example at each step, making it highly efficient for processing large datasets. Unlike traditional gradient descent methods, which compute gradients using the entire dataset (batch gradient descent), SGD approximates gradients using subsets of data, or even single data points, leading to faster convergence. This efficiency is particularly beneficial when dealing with datasets that may not fit into memory or when training models in real-time.

Additionally, the stochastic nature of SGD introduces randomness into the optimization process, aiding in escaping local minima and exploring a broader parameter space, potentially improving generalization. SGD also supports adaptability through techniques such as learning rate schedules and adaptive learning rates, allowing for fine-tuning of the optimization process. Furthermore, SGD is well-suited for online learning scenarios where new data arrives continuously, enabling models to be updated incrementally in response to changing data patterns. It naturally accommodates regularization techniques to prevent overfitting and improve model generalization. However, successful implementation of the SGD classifier may require careful tuning of hyperparameters such as learning rate and regularization strength, as well as consideration of mini-batch size. Despite these considerations, SGD remains a powerful and scalable approach for training classification models, offering efficiency and adaptability to diverse machine learning tasks.

The update rule for parameters in SGD is given by

$$\theta^{(t+1)} = \theta^{(t)} - \eta \nabla_{\theta} L(\theta^{(t)}, x_{it}, y_{it}) \quad (2)$$

where, $\theta^{(t)}$ are the parameters at iteration t , η is the learning rate, and $L(\theta^{(t)}, x_{it}, y_{it})$ is the loss function over the current mini-batch of data x_{it} and corresponding labels y_{it} .

D. XGBoost (XGB) Classifier

XGBoost, short for eXtreme Gradient Boosting, stands as a powerhouse within the realm of machine learning classifiers, lauded for its exceptional performance across a spectrum of classification tasks. Operating within the ensemble learning paradigm, XGBoost leverages the gradient boosting framework to construct formidable predictive models. At its core, XGBoost sequentially combines multiple weak learners, typically decision trees, in a manner that iteratively corrects errors, ultimately yielding a robust and accurate classifier. Central to its efficacy is its optimization algorithm, meticulously minimizing a predefined loss function by intelligently incorporating new decision trees. Moreover, XGBoost incorporates regularization techniques, including shrinkage and tree pruning, to mitigate overfitting and enhance generalization. Its versatility shines through its ability to handle diverse data types and tasks, from numerical to categorical features, and regression to classification problems. Beyond performance, XGBoost excels in speed, efficiency, and interpretability, offering insights into feature importance and decision-making processes. Furthermore, it boasts robustness, capable of handling missing data and outliers with aplomb. With its stellar track record and widespread adoption, XGBoost stands as a stalwart choice for data scientists and practitioners seeking a reliable, high-performing classifier to tackle real-world challenges across various domains.

The objective function for XGBoost can be written as:

$$\text{Obj}(\Theta) = \sum_{i=1}^n l(y_i, \hat{y}_i) + \sum_{k=1}^K \Omega(f_k) \quad (3)$$

where, $\Theta = \{f_k\}$ represents the set of decision trees, l is the loss function, \hat{y}_i is the predicted value for the i -th instance, and Ω is the regularization term.

E. Performance Measures

The efficacy of the proposed algorithms can be assessed through several key performance measures [32, 33, and 34]:

1) *Accuracy*: Accuracy is calculated using the formula:

$$\text{Accuracy} = \frac{TP + TN + FP + FN}{TP + TN + FP + FN} \quad (4)$$

Where TP (True Positive) and TN (True Negative) represent correctly classified instances, while FP (False Positive) and FN (False Negative) denote incorrectly classified instances. The accuracy metric signifies the percentage of correctly classified instances among the total.

2) *Precision*: Precision measures the proportion of relevant instances among the retrieved instances and is calculated as:

$$\text{Precision} = \frac{TP}{TP + FP} \quad (5)$$

It highlights the accuracy of positive predictions made by the model.

3) *Recall*: Recall, also known as sensitivity, represents the proportion of relevant instances that are retrieved over the total quantity of relevant instances:

$$Recall=TP+FNTP \tag{6}$$

This metric focuses on the model's ability to identify all relevant instances.

4) *Specificity*: Specificity, which aligns with the definition of specificity in medical diagnostics, is computed as:

$$Specificity=TN+FPN \tag{7}$$

It measures the proportion of true negatives identified by the model among all actual negatives.

F-measure: F-measure, also known as F1-score, considers both precision and recall and is calculated as the harmonic mean of the two: $F=Precision+Recall \times 2 / (Precision+Recall)$. It provides a balanced measure of a model's performance across precision and recall.

1) *Confusion matrix*: The confusion matrix, is a fundamental tool in machine learning for evaluating classification model performance. It summarizes model predictions by comparing predicted labels against actual labels. Structured as a square matrix, rows and columns represent true and predicted classes, enabling detailed performance analysis. By facilitating computation of accuracy, precision, recall, and F1 score, the confusion matrix offers insights into model strengths and weaknesses. Its visual representation aids decision-making and enhances model accuracy and effectiveness.

The confusion matrix serves as a cornerstone in machine learning, empowering researchers and practitioners with invaluable insights to optimize model performance and inform decision-making processes.

V. RESULTS ANALYSIS AND DISCUSSION

The classification reports of Support Vector Machine (SVM), Stochastic Gradient Descent (SGD), and XGBoost (XGB) Classifier provide comprehensive insights into their performance for predicting heart disease.

A. Classification Report Analysis

1) *Support Vector Machine (SVM)*: As shown in Table III, SVM exhibited a training accuracy of 88.28% and a model accuracy score of 87.5%. It showcased consistent and robust performance, particularly reflected in its high precision and recall values across both classes. For class 0, SVM achieved a precision of 0.90 and recall of 0.79, indicating its ability to correctly identify instances of class 0 while minimizing false positives. Similarly, for class 1, SVM demonstrated a precision of 0.86 and recall of 0.94, suggesting its effectiveness in accurately detecting instances of class 1 while minimizing false negatives. Overall, SVM's performance metrics underscore its

capability to effectively classify heart disease data with high accuracy and reliability.

TABLE III. CLASSIFICATION REPORT OF SUPPORT VECTOR MACHINE

| Training Accuracy : 88.28 % | | | | |
|------------------------------|--------|----------|---------|-----|
| Model Accuracy Score: 87.5 % | | | | |
| Classification_Report: | | | | |
| precision | recall | f1-score | support | |
| 0 | 0.90 | 0.79 | 0.84 | 76 |
| 1 | 0.86 | 0.94 | 0.90 | 108 |
| accuracy | | | 0.88 | 184 |
| macro avg | 0.88 | 0.86 | 0.87 | 184 |
| weighted avg | 0.88 | 0.88 | 0.87 | 184 |

2) *Stochastic Gradient Descent (SGD)*: As shown in Table IV, SGD yielded a training accuracy of 83.65% and a model accuracy score of 84.24%. While SGD's performance is commendable, it falls slightly behind SVM in terms of accuracy and precision. Notably, SGD exhibited slightly lower precision for class 0 compared to SVM, with a precision of 0.81 and recall of 0.82 for class 0, indicating a marginally higher rate of false positives. However, SGD's precision for class 1 was relatively higher at 0.87, with a recall of 0.86, suggesting its effectiveness in accurately identifying instances of class 1. Overall, SGD demonstrates satisfactory performance but may require further optimization to achieve results comparable to SVM.

TABLE IV. CLASSIFICATION REPORT OF STOCHASTIC GRADIENT DESCENT

| Training Accuracy : 83.65 % | | | | |
|-------------------------------|--------|----------|---------|-----|
| Model Accuracy Score: 84.24 % | | | | |
| Classification_Report: | | | | |
| precision | recall | f1-score | support | |
| 0 | 0.81 | 0.82 | 0.81 | 76 |
| 1 | 0.87 | 0.86 | 0.87 | 108 |
| accuracy | | | 0.84 | 184 |
| macro avg | 0.84 | 0.84 | 0.84 | 184 |
| weighted avg | 0.84 | 0.84 | 0.84 | 184 |

TABLE V. CLASSIFICATION REPORT OF XGB CLASSIFIER

| Training Accuracy : 100.0 % | | | | |
|--------------------------------|--------|----------|---------|-----|
| Model Accuracy Score : 85.87 % | | | | |
| Classification_Report: | | | | |
| precision | recall | f1-score | support | |
| 0 | 0.85 | 0.80 | 0.82 | 76 |
| 1 | 0.87 | 0.90 | 0.88 | 108 |
| accuracy | | | 0.86 | 184 |
| macro avg | 0.86 | 0.85 | 0.85 | 184 |
| weighted avg | 0.86 | 0.86 | 0.86 | 184 |

3) *XGBoost (XGB) Classifier*: As shown in Table V, XGB Classifier showcased a perfect training accuracy of 100.0%, yet achieved a model accuracy score of 85.87%. Despite its perfect training accuracy, XGB Classifier's model accuracy score indicates potential overfitting, suggesting that it may not generalize well to unseen data. However, XGB Classifier's precision and recall values were comparable to SVM, with a precision of 0.85 and recall of 0.80 for class 0, and a precision of 0.87 and recall of 0.90 for class 1. These metrics suggest XGB Classifier's effectiveness in accurately classifying heart disease data, although further investigation into its generalization capabilities is warranted.

B. Comparison Summary of ML Models for heart disease prediction

The Table VI presents a detailed comparison of three machine learning models - Support Vector Machine (SVM), Stochastic Gradient Descent (SGD), and XGBoost (XGB) Classifier - based on various performance metrics for predicting heart disease. Each row corresponds to a specific model, while each column represents a different metric evaluated.

TABLE VI. COMPARISON OF THREE MACHINE LEARNING MODELS

| Metric | Training Accuracy | Model Accuracy Score | Precision (Class 0) | Precision (Class 1) | Recall (Class 0) | Recall (Class 1) | F1-score (Class 0) | F1-score (Class 1) | Support (Class 0) | Support (Class 1) |
|----------------|-------------------|----------------------|---------------------|---------------------|------------------|------------------|--------------------|--------------------|-------------------|-------------------|
| SVM | 88.28% | 87.5% | 0.90 | 0.86 | 0.79 | 0.94 | 0.84 | 0.90 | 76 | 108 |
| SGD | 83.65% | 84.24% | 0.81 | 0.87 | 0.82 | 0.86 | 0.81 | 0.87 | 76 | 108 |
| XGB Classifier | 100.0% | 85.87% | 0.85 | 0.87 | 0.80 | 0.90 | 0.82 | 0.88 | 76 | 108 |

C. Analyzing Through Confusion Matrix for Predicting Heart Disease

The confusion matrix (see Fig. 4 to Fig. 6) helps us see how well boosting models spot mistakes when predicting heart problems. It looks at what really happened versus what the models predicted, using four things: True Positive (TP), True Negative (TN), False Positive (FP), and False Negative (FN). This confusion matrix, shown in Fig. 8, helps us figure out how accurate the boosting models are in spotting errors when predicting heart issues. It compares what actually occurred with what the models guessed, using four important measures: True Positive (TP), True Negative (TN), False Positive (FP), and False Negative (FN).

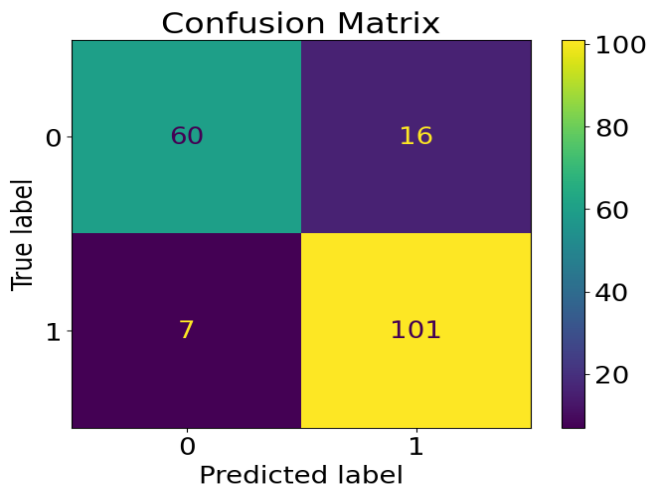


Fig. 4. Confusion matrix for support vector classifier.

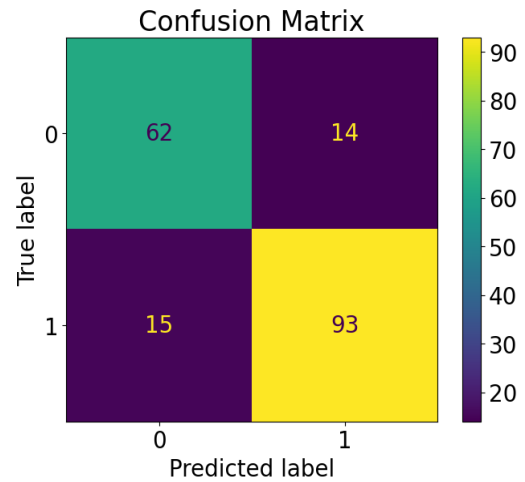


Fig. 5. Confusion matrix for stochastic gradient descent classifier.

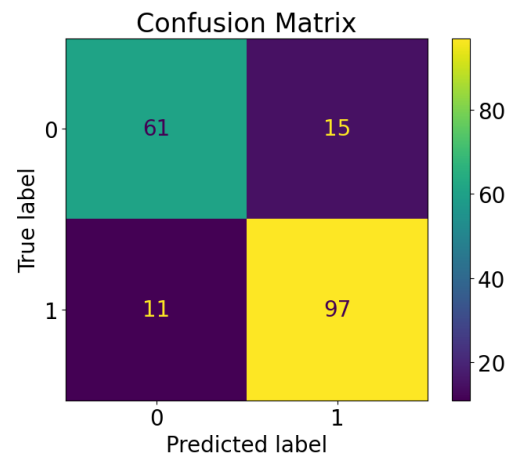


Fig. 6. Confusion matrix for XGBoost classifier.

D. Analyzing Through ROC Curve for Predicting Heart Disease

Furthermore, ROC (Receiver Operating Characteristic) curves have been generated and depicted in Fig. 7- 9 to delve deeper into the analysis of each machine learning model. These curves offer a visual representation of the classifier performances and illustrate the tradeoff between the true positive rate and false positive rate across various classification thresholds.

The area under the curve (AUC) of the ROC curve serves as a metric to gauge the model's capability to differentiate between classes, with values ranging from zero to one. A higher AUC indicates a greater ability to accurately classify instances. As the AUC approaches one, the model demonstrates enhanced capability in separating the classes, signifying superior performance.

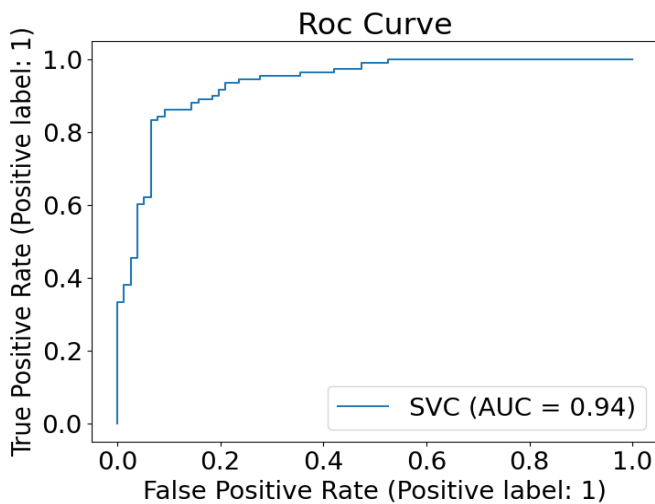


Fig. 7. ROC curve for support vector classifier.

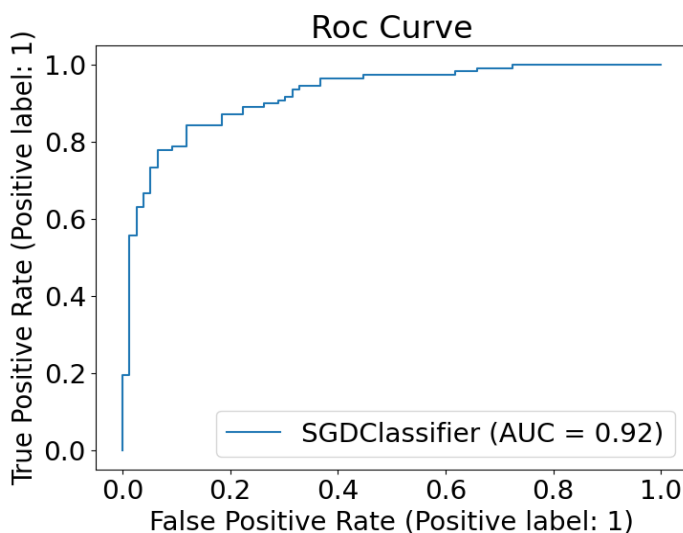


Fig. 8. ROC curve for stochastic gradient descent classifier.

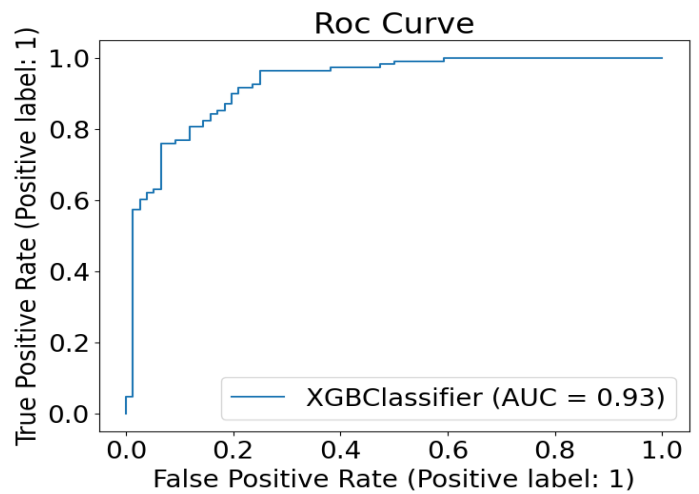


Fig. 9. ROC curve for XGBoost classifier.

E. Analyzing Through Precision Recall Curve for Predicting Heart Disease

Also, Precision-Recall curves have been generated and depicted in Fig. 10 -12 to provide deeper insights into the analysis of each machine learning model. These curves offer a visual representation of the classifier performances and illustrate the trade off between precision and recall across various classification thresholds.

The Precision-Recall curve showcases the relationship between the precision (positive predictive value) and recall (sensitivity) of the model as the classification threshold varies. It provides a comprehensive view of how well the model identifies positive instances while minimizing false positives.

Unlike ROC curves, which focus on the tradeoff between true positive rate and false positive rate, Precision-Recall curves emphasize the balance between precision and recall. They are particularly useful when dealing with imbalanced datasets where one class significantly outweighs the other.

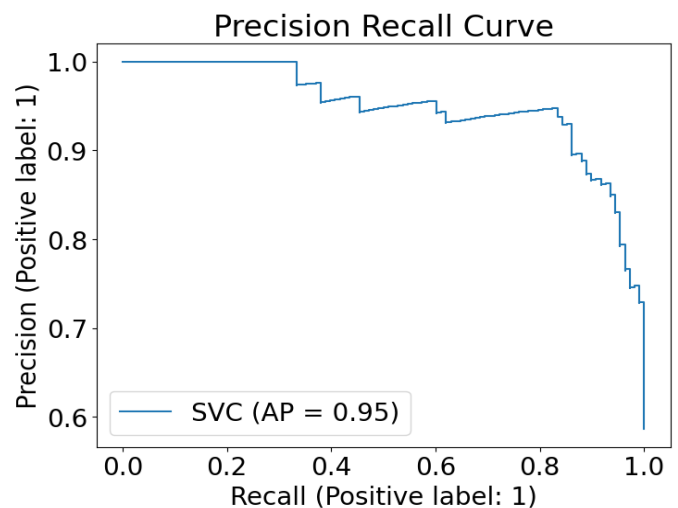


Fig. 10. Precision recall curve for support vector classifier.

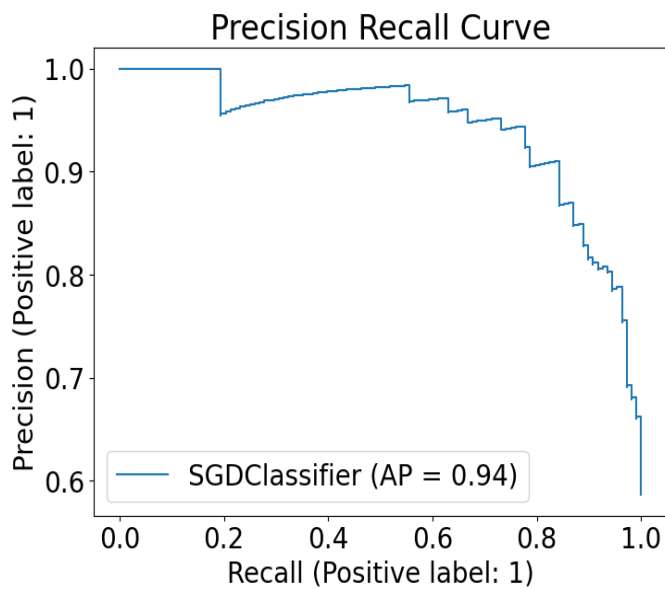


Fig. 11. Precision recall for stochastic gradient descent classifier.

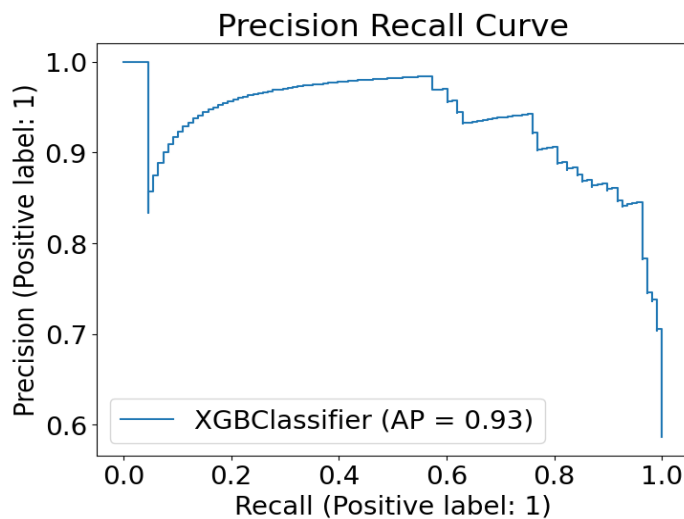


Fig. 12. Precision recall curve for XGBoost classifier.

The area under the Precision-Recall curve (AUC-PR) serves as a metric to evaluate the model's performance. A higher AUC-PR indicates better precision and recall tradeoff, suggesting superior model performance in accurately identifying positive instances while minimizing false positives. As with ROC curves, an AUC-PR value closer to one signifies enhanced model performance.

VI. CONCLUSION AND FUTURE SCOPE

In this study, we compared the performance of Support Vector Machine (SVM), Stochastic Gradient Descent (SGD), and XGBoost machine learning techniques for heart disease prediction. Our results reveal distinct characteristics and capabilities of each model. SVM exhibited remarkable performance with a training accuracy of 88.28% and a model accuracy score of 87.5%. Its high precision and recall values across both classes indicate its ability to effectively classify heart disease data. Notably, SVM demonstrated a precision of

0.90 and recall of 0.79 for class 0, and a precision of 0.86 and recall of 0.94 for class 1, underscoring its reliability in minimizing false positives and false negatives.

While SGD demonstrated commendable performance with a training accuracy of 83.65% and a model accuracy score of 84.24%, it slightly trailed behind SVM in terms of accuracy and precision. Although SGD exhibited a relatively higher precision for class 1, further optimization may be required to achieve results comparable to SVM. XGBoost Classifier showcased perfect training accuracy but achieved a model accuracy score of 85.87%, suggesting potential overfitting. Nonetheless, its precision and recall values were comparable to SVM, indicating its effectiveness in accurately classifying heart disease data. However, further investigation into its generalization capabilities is warranted to ensure reliable performance in real-world scenarios.

Overall, our findings demonstrate SVM's robustness and effectiveness in heart disease prediction, followed by SGD and XGBoost Classifier. Further research may focus on optimizing SGD and investigating XGBoost Classifier's generalization capabilities to enhance their performance in clinical applications.

In future research, we aim to utilize the findings presented here to develop a robust prediction system aimed at enhancing medical treatment efficacy and reducing costs using other efficient machine learning algorithms.

REFERENCES

- [1] Jagannathan, Ram, Shivani A. Patel, Mohammed K. Ali, and KM Venkat Narayan, "Global updates on cardiovascular disease mortality trends and attribution of traditional risk factors," *Current diabetes reports*, vol. 19, no. 7, pp 1-12, 2019.
- [2] Krittanawong, Chayakrit, HongJu Zhang, Zhen Wang, Mehmet Aydar, and Takeshi Kitai, "Artificial intelligence in precision cardiovascular medicine," *Journal of the American College of Cardiology*, vol. 69, no. 21, pp 2657-2664, 2017.
- [3] Rajkomar, Alvin, Jeffrey Dean, and Isaac Kohane, "Machine learning in medicine," *New England Journal of Medicine*, vol. 380, no. 14, pp 1347-1358, 2019.
- [4] Yusuf, S., Joseph, P., Rangarajan, S., Islam, S., Mentz, A., Hystad, P., Brauer, M., Kuty, V.R., Gupta, R., Wielgosz, A. and AlHabib, K.F., "Modifiable risk factors, cardiovascular disease, and mortality in 155 722 individuals from 21 high-income, middle-income, and low-income countries (PURE): a prospective cohort study," *The Lancet*, vol. 395, no. 10226, pp 795-808, 2020.
- [5] Benjamin EJ, Muntner P et al. Alonso, Alvaro, -Heart Disease and Stroke Statistics-2019 Update: A Report From the American Heart Association, *Circulation*, 2019;vol. 139, no. 10
- [6] Murthy H, Meenakshi M, -Dimensionality reduction using neuro-genetic approach for early prediction of coronary heart disease, in *International Conference on Circuits, Communication, Control and Computing (I4C)*, 2014; pp. 329-332.
- [7] Bashir S, Khan ZS, Khan FH, Anjum A, Bashir K. Improving Heart Disease Prediction Using Feature Selection Approaches, in *16th International Bhurban Conference on Applied Sciences and Technology (IBCAST)*, 2019; pp. 619-623.
- [8] Gavhane A, Kokkula G, Pandya I, Devadkar PK. -Prediction of Heart Disease Using Machine Learning, in *Proceedings of the 2nd International Conference on Electronics, Communication and Aerospace Technology, ICECA 2018*, 2018; pp. 1275-1278.
- [9] Ismaeel S, Miri A, Chourishi D. Using the Extreme Learning Machine (ELM) technique for heart disease diagnosis, in *2015 IEEE Canada*

- International Humanitarian Technology Conference. IHTC. 2015;2015:1–3.
- [10] Ekiz S, Erdogmus P. Comparative study of heart disease classification, in 2017 Electric Electronics, Computer Science, Biomedical Engineerings' Meeting, EBBT. 2017;2017:1–4.
- [11] Kanikar P, Shah DR, Prediction of cardiovascular diseases using support vector machine and Bayesian classification, International Journal of Computer Applications (0975 – 8887) Volume 156 – No 2, December 2016.
- [12] Shorewala, V. Early detection of coronary heart disease using ensemble techniques. Inform. Med. Unlocked 2021, 26, 100655.
- [13] Maiga, J.; Hungilo, G.G.; Pranowo. Comparison of Machine Learning Models in Prediction of Cardiovascular Disease Using Health Record Data. In Proceedings of the 2019 International Conference on Informatics, Multimedia, Cyber and Information System (ICIMCIS), Jakarta, Indonesia, 24–25 October 2019; pp. 45–48.
- [14] Waigi, R.; Choudhary, S.; Fulzele, P.; Mishra, G. Predicting the risk of heart disease using advanced machine learning approach. Eur. J. Mol. Clin. Med. 2020, 7, 1638–1645.
- [15] Ouf, S.; ElSeddawy, A.I.B. A proposed paradigm for intelligent heart disease prediction system using data mining techniques. J. Southwest Jiaotong Univ. 2021, 56, 220–240.
- [16] Khan, I.H.; Mondal, M.R.H. Data-Driven Diagnosis of Heart Disease. Int. J. Comput. Appl. 2020, 176, 46–54.
- [17] Mohan, S.; Thirumalai, C.; Srivastava, G. Effective Heart Disease Prediction Using Hybrid Machine Learning Techniques. J. Exp. Theor. Artif. Intell. 2019, 31, 565–583.
- [18] Pouriyese, M.; Parvinnia, S.; Sabeti, E.; Gamaarachchi, H.; Sadoughian, M.; Farhadi, F.; Iqbal, Q. A Comprehensive Investigation and Machine Learning-based Diagnostic Prediction of Heart Disease. Comput. Biol. Med. 2021, 135, 104551.
- [19] Fathima, N.; Thilleban, S. Prediction of Heart Disease Using Machine Learning Algorithms. In Proceedings of the 2020 International Conference on Emerging Smart Computing and Informatics (ESCI), Pune, India, 12–14 March 2020; pp. 66–71.
- [20] SaiSudheer, M.; Niharika, Y.; Janga, N.V. Heart Disease Prediction Using Machine Learning Techniques. In Proceedings of the 2021 International Conference on Computer Communication and Informatics (ICCCI), Coimbatore, India, 27–29 January 2021; pp. 1–6.
- [21] Taneja, A. Heart Disease Prediction Using Machine Learning on Cloud Platform. In Proceedings of the 2020 International Conference on Intelligent Engineering and Management (ICIEM), London, UK, 17–19 June 2020; pp. 327–331.
- [22] Diwakar, M.; Sivakumar, V.S.; Nedunchezian, R. Prediction of Heart Disease Using Machine Learning Techniques. Int. J. Eng. Adv. Technol. 2019, 8, 506–511.
- [23] Kaur, H.; Kumar, R.; Kumari, V. Heart Disease Prediction Using Machine Learning Techniques. In Proceedings of the 2020 International Conference on Power Electronics & IoT Applications in Renewable Energy and Its Control (PARC), Mathura, India, 28–29 February 2020; pp. 1–6.
- [24] Nahar, J.; Imam, T.; Tickle, K.S.; Chen, Y.P.P. Computational intelligence for heart disease diagnosis: A medical knowledge-driven approach. Expert Syst. Appl. 2013, 40, 96–104.
- [25] Amin, M.S.; Chiam, Y.K.; Varathan, K.D. Identification of significant features and data mining techniques in prediction of heart disease. Telemat. Inform. 2019, 36, 262–274.
- [26] Raza, K. An Optimization Strategy for Heart Disease Prediction. Comput. Intell. Neurosci. 2020, 2020, 8863923.
- [27] Vembanki, S.; Pilikan, S.; Padte, R.; Kanimozhi, P. Heart Disease Diagnosis Using Ensemble Machine Learning Techniques. In Proceedings of the 2021 Third International Conference on Intelligent Communication Technologies and Virtual Mobile Networks (ICICV), Tirunelveli, India, 4–6 February 2021; pp. 1–5.
- [28] Yadav, S.; Shukla, S. Analysis of k-Fold Cross-Validation over Hold-Out Validation on Coimbatore Dataset using WEKA Tool. Int. J. Inf. Technol. 2016, 8, 1054–1058.
- [29] Patel, J.; Upadhyay, D.; Patel, S. Heart Disease Prediction Using Machine Learning and Data Mining Technique. Heart Dis. 2015, 7, 129–137.
- [30] Sultana, M.; Haider, A.; Uddin, M.S. Analysis of Data Mining Techniques for Heart Disease Prediction. In Proceedings of the 2016 3rd International Conference on Electrical Engineering and Information Communication Technology (ICEEICT), Dhaka, Bangladesh, 22–24 September 2016; pp. 1–5.
- [31] Altan, G.; Karasu, S.; Bekiros, S. Digital Chest Drainage and Dissolved Air Flotation for Metal Plating Sludges. Resour. Conserv. Recycl. 2019, 146, 25–33.
- [32] Arif, M.S.; Mukheimer, A.; Asif, D. Enhancing the early detection of chronic kidney disease: A robust machine learning model. Big Data Cogn. Comput. 2023, 7, 144.
- [33] Chang, V.; Bhavani, V.R.; Xu, A.Q.; Hossain, M. An artificial intelligence model for heart disease detection using machine learning algorithms. Healthc. Anal. 2022, 2, 100016.
- [34] Neshat, M.; Ahmedb, M.; Askarid, H.; Thilakarantnee, M.; Mirjalilia, S. Hybrid Inception Architecture with Residual Connection: Fine-tuned Inception-ResNet Deep Learning Model for Lung Inflammation Diagnosis from Chest Radiographs. arXiv 2023, arXiv:2310.02591.
- [35] Jha, P., Dembla, D., Dubey, W. "Implementation of Machine Learning Classification Algorithm Based on Ensemble Learning for Detection of Vegetable Crops Disease International Journal of Advanced Computer Science and Applications, 2024, 15(1), pp. 584–594
- [36] Jha, Pradeep, Deepak Dembla, and Widhi Dubey 2024. "Implementation of Transfer Learning Based Ensemble Model Using Image Processing for Detection of Potato and Bell Pepper Leaf Diseases." Article. International Journal of Intelligent Systems and Applications in Engineering 12 (8s): 69–80.
- [37] Jha, Pradeep, Deepak Dembla, and Widhi Dubey. 2023. "Comparative Analysis of Crop Diseases Detection Using Machine Learning Algorithm." Conference paper. Proceedings of the 3rd International Conference on Artificial Intelligence and Smart Energy, ICAIS 2023. Institute of Electrical; Electronics Engineers Inc. <https://doi.org/10.1109/ICAIS56108.2023.10073831>.
- [38] Jha, Pradeep, Deepak Dembla, and Widhi Dubey. 2023. "Crop Disease Detection and Classification Using Deep Learning-Based Classifier Algorithm." Conference paper. Edited by Rathore V. S., Piuri V., Babo R., and Ferreira M. C. Lecture Notes in Networks and Systems 682 LNNS: 227–37. https://doi.org/10.1007/978-981-99-1946-8_21.
- [39] Jha, Pradeep, Deepak Dembla, and Widhi Dubey 2023. "Deep Learning Models for Enhancing Potato Leaf Disease Prediction: Implementation of Transfer Learning Based Stacking Ensemble Model." Article. Multimedia Tools and Applications. <https://doi.org/10.1007/s11042-023-16993-4>.
- [40] Meshram, Amita, and Deepak Dembla. 2023. "MCBM: IMPLEMENTATION OF MULTICLASS AND TRANSFER LEARNING ALGORITHM BASED ON DEEP LEARNING MODEL FOR EARLY DETECTION OF DIABETIC RETINOPATHY." Article. ASEAN Engineering Journal 13 (3): 107–16. <https://doi.org/10.11113/aej.V13.19401>.
- [41] Meshram, Amita, and Deepak Dembla 2023. "Multistage Classification of Retinal Images for Prediction of Diabetic Retinopathy-Based Deep Learning Model." Conference paper. Edited by Rathore V. S., Piuri V., Babo R., and Ferreira M. C. Lecture Notes in Networks and Systems 682 LNNS: 213–26. https://doi.org/10.1007/978-981-99-1946-8_20.
- [42] Meshram, Amita, Deepak Dembla, and A. Anooja. 2023. "DEVELOPMENT AND ANALYSIS OF DEEP LEARNING MODEL BASED ON MULTICLASS CLASSIFICATION OF RETINAL IMAGE FOR EARLY DETECTION OF DIABETIC RETINOPATHY." Article. ASEAN Engineering Journal 13 (3): 89–97. <https://doi.org/10.11113/aej.V13.19256>.

Towards a New Artificial Intelligence-based Framework for Teachers' Online Continuous Professional Development Programs: Systematic Review

Hamza Fakhar*, Mohammed Lamrabet, Nouredine Echantoufi, Khalid El khattabi, Lotfi Ajana
Laboratory of Computer Science and Interdisciplinary Physics (LIPI),
ENS, Sidi Mohamed Ben Abdellah University, Fez, Morocco

Abstract—In recent years, the Artificial Intelligence (AI) field has witnessed rapid growth, affecting diverse sectors, including education. In this systematic review of literature, we aimed to analyze studies concerning the integration of AI in the continuous professional development (CPD) of teachers in order to generate a global vision on its potential to enhance the quality of CPD programs in the international level, and to provide recommendations for its application in the Moroccan context. To achieve our objective, we conducted a research that involves a review of international indexed databases (Scopus, Web of Science, Eric) published between 2019 and 2023 using PICO framework to formulate our search query and PRISMA (Preferred Reporting Items for Systematic Reviews and Meta-Analyses) framework to select 25 relevant studies based on include and exclude criteria like publishing year, type of documents, publishing mode, subject area, language, and other criteria. The results reveal that AI integration has a positive impact on CPD programs by offering beneficial intelligent tools that can tailor adaptive training programs to meet teachers' specific needs, preferences, and proficiency levels. Furthermore, our findings identify the importance of integrating AI as a core topic within CPD programs to enhance teachers' AI literacy, enabling them to effectively navigate and utilize AI-based tools in their educational environment. This is important for preparing teachers to engage with the technological advances shaping the educational system. In conclusion, our systematic review emphasizes the significance of AI integration in CPD programs and offers tailored recommendations for its implementation in the Moroccan educational context. By adopting these recommendations, Morocco will pave the way for a dynamic CPD framework that meets the evolving needs of educators and students alike.

Keywords—Artificial intelligent; continuous professional development; Moroccan in-service teacher; digital teacher; online training; adaptive development

I. INTRODUCTION

Artificial Intelligence (AI) involves creating computer systems capable of tasks requiring human-like intelligence. These tasks include learning, reasoning, problem-solving, perception, language understanding, speech recognition and other abilities. AI is a broad and interdisciplinary field that encompasses various subfields and approaches, it has a profound impact on various sectors, including education, by

having a significant impact, offering innovative solutions to enhance teaching, and learning experiences.

In this study, we focused on investigating the impact of AI on teachers' education and its potential to improve the quality of continuing professional development (CPD) programs, which are essential for enhancing teachers' skills and ultimately student learning outcomes.

Our primary objective is to identify how AI can be seamlessly integrated into CPD as an innovative technology that aid trainers by offering tailored and adaptive training programs, addressing teachers' specific needs to develop new skills for more effective teaching performance. Additionally, we aimed at exploring strategies to develop teachers' AI literacy to ensure they remain up to date with the latest novelties in the field.

To achieve this objective, a systematic review of numerous studies collected from universal and reputable databases was conducted, employing inclusion and exclusion criteria. Subsequently, through the analysis of our selected studies, a framework was derived for an effective integration of AI in CPD programs within the Moroccan context.

The necessity for developing AI-driven framework stems from the significant dropout rates observed in conventional training programs for educators, indicating their inadequacy in delivering effective results. In response to this challenge, we have embraced a framework that offers personalized, data-driven, and technologically advanced learning experiences that empower educators in an ever-evolving educational landscape.

Following the review and examination of the 25 studies included in our research, we identified three key themes addressed within them. These themes encompass the inclusion of AI as a topic within online Continuous Professional Development (CPD), its utilization as a scaffolding instrument, and the proposed guidelines for defining the competency profile of a "digital teacher."

*Corresponding Author.

II. LITERATURE REVIEW

A. Artificial Intelligence

Artificial intelligence (AI) is the simulation of human intelligence in machines programmed to think and learn like humans [1]. The goal of AI is to create systems capable of performing tasks that typically require human intelligence [2], such as visual perception, speech recognition, decision making, and language translation. AI can be divided into two main categories: narrow or weak AI, and general or strong AI.

1) *Narrow AI (Weak AI)*: This type of AI is designed and trained for a specific task. It excels in that specific area but lacks the broad cognitive abilities of a human. Examples include virtual personal assistants like Siri or Alexa, image recognition software, and recommendation algorithms [3].

2) *General AI (Strong AI)*: This is a hypothetical form of AI that has the ability to understand, learn, and apply knowledge across a wide range of tasks, similar to human intelligence [3]. AI includes several subfields, such as:

a) *Machine Learning (ML)*: A subset of AI that focuses on developing algorithms that allow computers to learn patterns from data without being explicitly programmed [4]. ML has the power to intelligently analyze such data and to develop the appropriate real-world applications [5].

b) *Natural Language Processing (NLP)*: Involves the interaction between computers and humans using natural language to make machines able to understand the statements and words written in human language [6], in order to generate language translation, sentiment analysis [7], and chatbots [8].

c) *Computer vision*: Enables machines to interpret and make decisions based on visual data [9], such as image and video recognition [10].

d) *Robotics*: Combines AI with physical machines to create intelligent robots capable of performing real-world tasks, and responding in ways similar to human social norms [11].

e) *Generative AI*: subset of artificial intelligence systems that are designed to generate new, original content or data. Unlike traditional AI systems that are rule-based or follow predetermined instructions, generative AI models are capable of producing outputs that were not explicitly programmed or predefined by their creators [12], rather than analyzing something that already exists [13].

“Generative AI refers to a class of artificial intelligence systems designed to generate new content or data that is similar to, but not an exact copy of, existing data. These systems are capable of producing original and creative outputs across various domains, such as text, images, music, and more.”¹

f) *Cloud computing*: refers to the delivery of computing services, including computing power, storage, databases, networking, software, and analytics, over the internet [14] to offer faster innovation and accessibility, flexible resources, and economies of scale [15] [16].

g) *Blockchain*: Blockchain is a decentralized and distributed ledger technology that enables secure, transparent, and tamper-resistant record-keeping of transactions across a network of computers [17]. It has the potential to revolutionize various industries by providing a decentralized and trustless way of recording and verifying transactions [18].

B. AI in Education

AI as a new technological revolution has emerged in many sectors including education. AI has the potential to revolutionize education by introducing innovative tools and techniques [19], to improve pedagogical methods and to enhance the learning experience [20], to personalize instructions [21], and streamline administrative tasks.

1) *Personalized learning*: AI systems can adapt to individual student needs, providing personalized learning experiences. This includes tailoring the pace, content, and style of instruction to suit each student's learning preferences and abilities [22] [23].

2) *Intelligent Tutoring Systems (ITS)*: Use AI to assess a student's strengths and weaknesses, offering targeted feedback and additional resources [24].

3) *Adaptive learning platforms*: AI-powered adaptive learning platforms adjust the difficulty level of content based on individual student progress, needs, and learning styles [25], [26]. This ensures that students are appropriately challenged and supported in their learning journey [27].

4) *Automated grading and feedback*: AI algorithms can automate the grading of assignments and assessments, saving teachers time and providing students with instant feedback [28]. This allows educators to focus on more meaningful aspects of teaching, such as facilitating discussions and offering personalized guidance [29].

5) *Virtual assistants and chatbots*: Virtual assistants and chatbots equipped with natural language processing capabilities can assist students in online courses by answering questions, providing information, and guiding them through learning materials [30] [31].

6) *Language translation and accessibility*: AI-powered language translation tools can help overcome language barriers, making educational content more accessible to learners around the world [32]. AI can also be used to assist learners with disabilities by providing real-time transcription, language translation, or other adaptive technologies [33].

7) *Educational games and simulations*: AI can enhance educational games and simulations by adapting to the learner's progress, ensuring that the challenges presented align with the student's skill level [34] [35].

8) *Mixed reality*: refers to a merging of the physical and digital worlds, combining elements of both augmented reality (AR) and virtual reality (VR) [36]. In mixed reality, users interact with and experience a blend of real-world and computer-generated environments and objects. This allows for a more immersive and interactive experience than what is possible with traditional forms of media [37].

¹ChatGPT 4, December 2023, on generative AI.

9) *Plagiarism checkers*: AI-based tools designed to identify and detect instances of plagiarism in written content. These tools compare a given text against a vast database of academic papers, articles, websites, and other sources to check for similarities in order to ensure the originality of students' work [38] [39].

10) *Topic modeling*: is a natural language processing (NLP) technique used to automatically identify topics present in a text corpus. It helps in discovering hidden thematic structures within a large collection of documents and is widely used for organizing, understanding, and summarizing textual information [40].

C. Teachers' Continuous Vocational Training

Continuing vocational training, also known as continuing professional development (CPD) or lifelong learning, refers to the ongoing process of acquiring new knowledge, skills, and competencies throughout one's career [41]. In today's working environment, where technological advances and industry requirements are rapidly evolving, continuing professional development is becoming increasingly crucial to enable individuals to remain relevant and competitive in their profession [42].

Continuous vocational training for teachers is crucial to stay current with advancements in teaching methodologies, technology, and educational research, in order to influence teaching practices, leading to improved quality of learning [43] and student outcomes. [44]

However, similar to every country, there are some limitations and challenges associated with the presential Continuing professional development in Morocco, such as,

- the Massification of teachers in comparison with the number of trainers, 281.662 teachers in 2023-2024².
- the availability, Teachers often have busy schedules with teaching responsibilities, grading, and extracurricular activities. Devoting time for vocational training can be challenging.
- Teacher assignment: Teachers who are assigned to work in remote areas, face with challenges related to transportation, given that the training centers are located in the center of cities.
- Monitoring: given the large number of teachers, it's difficult to monitor and support them individually face-to-face.
- The high-cost financial investment, related to the accommodation, organization and travelling of teachers and trainers.
- The needs of teachers: most vocational trainings are based on what is offered and not on real needs of teachers in their specific contexts [45].

In the realm of Continuing Professional Development (CPD), the digital age has brought about significant innovations, offering a solution to the challenges and limitations of traditional in-person training. Online platforms have revolutionized CPD by providing high flexibility in terms of timing, ensuring equal access to information regardless of users' geographic locations [46], and enabling the simultaneous support of a large number of teachers at minimal costs for both the ministry and teachers. [47] [48]

Despite these significant advantages, the digital CPD is not without its limitations. Issues such as monitoring, engagement, and motivation [49], persist, along with challenges related to assessment and the adaptation of learning content to cater to individual teacher's needs, levels, and preferences [26], this is mainly due to the absence of intelligent educational environments capable of analyzing teachers' profile in order to provide adaptive instructions and content similar to what can be given by a human brain or more. Unlike traditional e-learning platforms in which content delivery is static and feedback is programmed. The future of CPD lies in the development of intelligent systems that can mimic the adaptability and personalization offered by human instructors. These new systems help overcome the massification problem by supporting a large number of teachers while also addressing the flexibility issue by allowing educators to learn at their own pace and convenience in order to elevate the quality, efficacy and the credibility of the CPD programs.

In recent years, artificial intelligence (AI) has provided a large and diverse number of intelligent tools that address the limitations of traditional e-learning methods. To prepare digital teachers for intelligent educational environments, it is crucial to consider the following questions:

- How does integrating AI into CPD programs help prepare teachers in their teaching practices?
- Is incorporating AI-focused topics into professional development curricula considered a necessity?
- What are the recommendations to take into consideration to prepare digital teachers for intelligent educational environments?

III. MATERIALS AND METHODS

A. General Background

In this study, we aim for a systematic review that delves into the impact of AI on the quality of continuing professional development, shedding light on its contributions and implications. Our study was based on drawing insights from indexed articles and reviews from esteemed international databases (Scopus, Web of science (WoS), and ERIC). Using the PICO framework and logical operators (AND, OR, NOT), we elaborated a search question to guide our research endeavors.

²back-to-school 2023-2024 in numbers: <https://medias24.com/2023/09/06/la-rentree-scolaire-2023-2024-en-chiffres/>

B. Search Strategy

Following the PICO framework³, we meticulously constructed our search query. To ensure comprehensiveness, we identified a vast array of synonyms for the key study terms. These synonyms were drawn from credible sources encompassing articles, press releases, dictionaries, scholarly books, and conference proceedings. To capture all relevant information, we strategically employed logical operators (AND, OR, NOT) to combine these synonyms (as detailed in Table I). This meticulous approach aimed to maximize the potential results for our study.

TABLE I. KEYWORDS USED TO FORMULATE THE SEARCH QUERY

| | |
|--|--|
| Artificial intelligence AND | OR artificial OR intelligence OR AI OR intelligent platforms OR intelligent tools OR AI-based tools OR intelligent technology OR intelligent algorithms |
| Online AND | OR distance OR networked OR web-based OR internet OR e-learning OR LMS |
| Teacher AND | OR In-service teachers OR practitioner teachers OR educator OR professor OR instructor OR coach OR tutor NOT pre-service NOT preservice NOT trainee teachers NOT future teacher |
| Continuous Professional Development | OR continuous OR vocational OR training OR continuous training OR continued training OR continuing training OR continual training OR ongoing training OR professional training OR professional development OR lifelong learning OR teachers' education OR vocational education |
| Search query | |
| ALL ("artificial intelligence" OR ai OR "intelligent platforms" OR "intelligent tools" OR "AI-based tools" OR "intelligent technology" OR "intelligent algorithms" AND online OR distance OR networked OR web-based OR internet OR e-learning OR lms AND teacher OR "in-service teachers" OR "practitioner teachers" OR educator OR professor OR instructor OR coach OR tutor AND NOT pre-service AND NOT preservice AND NOT "trainee teachers" AND NOT "future teachers" AND continuous OR vocational OR training OR "continuous training" OR "continued training" OR "continuing training" OR "continual training" OR "ongoing training" OR "professional training" OR "professional development" OR "lifelong learning" OR "teachers' education" OR "vocational education") | |

C. Inclusion and Exclusion Criteria

To select the appropriate studies for our systematic review, we determined and respected the following inclusion and exclusion criteria.

D. Selection Strategy

1) *Quantitative filtering*: Following the formulation of our search query (Table I), we employed a quantitative selection approach, utilizing tools like RAYYAN⁴ software and MS EXCEL. we adhered to the PRISMA [50] framework to analyze and filter the found studies based on inclusion and exclusion criteria outlined in (Table II) above. For further details, see (Table III) below, identification section.

TABLE II. INCLUSION AND EXCLUSION CRITERIA

| Including Criteria | Excluding Criteria |
|--|--|
| Indexed in Scopus, Web of Science, ERIC. | Not indexed in Scopus, Web of Science, ERIC. |

³Pico Framework: <https://guides.lib.unc.edu/pico>

⁴Rayyan Software: <https://www.rayyan.ai/>

| | |
|--|---|
| Published from 2019 to 2023. | Published prior to 2019. |
| Computer science and education subject areas | Other subject areas |
| English language. | Not in English. |
| Open access articles. | Not open access articles. |
| Research involving in-service school or university teachers. | Research not involving in-service teachers. Research involving pre-service teachers. |
| Articles, Reviews | Books, Book sections, Conference proceedings |
| Studies related to AI in teachers' CPD (AI with a focus on machine learning, data analysis, and natural language processing applications). | Studies not related to AI in teachers' CPD. |

2) *Qualitative filtering*: After the quantitative filtering, we proceeded to a qualitative selection based on,

- Title analysis according to the presence of study's keywords.
- Abstract analysis based on sample and results.
- Content reading and synthesizing.

For more details, see (Table III) screening and eligibility sections.

TABLE III. DETAILS OF FILTERING PROCESS RESULTS, BASED ON PRISMA METHOD

| | First research Based on search query | Scopus | WoS | ERIC | Total | Excluded |
|----------------|--|--------|------|------|-------|----------|
| | | 1,959 | 2983 | 1753 | 6695 | 00 |
| Identification | Filter 1 Date: 2019 – 2023 | 1812 | 2023 | 963 | 4798 | 1897 |
| | Filter 2 Subject area: Computer science, education. | 952 | 1422 | 522 | 2896 | 1902 |
| | Filter 3 Document type: Articles, reviews. | 617 | 920 | 415 | 1952 | 944 |
| | Filter 4 keywords or tags. | 457 | 883 | 231 | 1571 | 381 |
| | Filter 5 Language: English. | 456 | 864 | 215 | 1535 | 36 |
| | Filter 6 open access articles: Gold. | 182 | 315 | 126 | 623 | 912 |
| Screening | Title analysis ✓ Duplicates. ✓ No mention of at least one of keywords. ✓ Retracted articles. Abstract analysis: ✓ wrong population. | 90 | 67 | 45 | 202 | 421 |
| Eligibility | Content analysis ✓ Articles not focusing on AI in online CPD. | 70 | | | | 132 |

| | | |
|------------------------------|-------------------------------|----|
| Inclusion | 25 | 45 |
| Results | | |
| Total included articles = 25 | Total Excluded= 6670 articles | |

The flow chart diagram which is given in Fig. 1 describes the filtering process based on PRISMA framework.

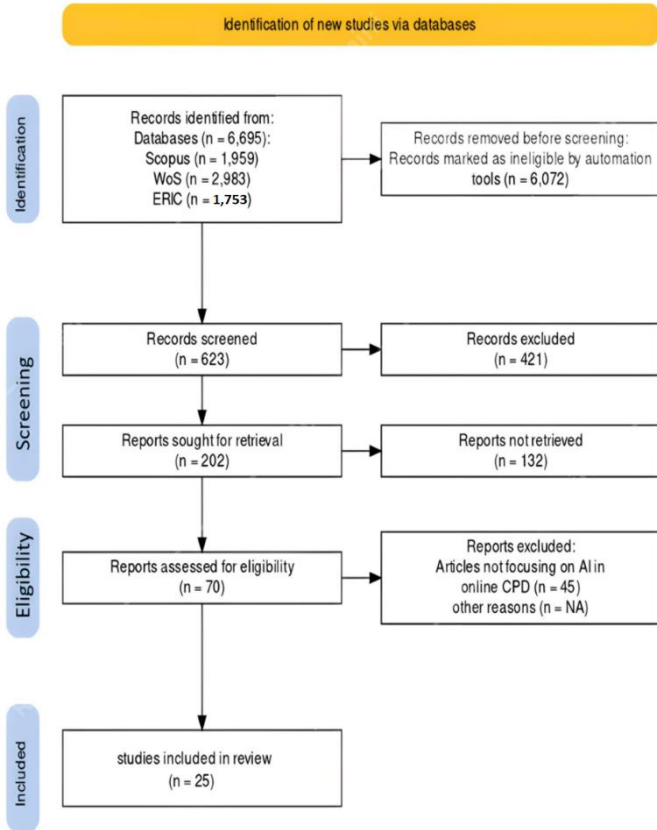


Fig. 1. PRISMA flow diagram.

IV. RESULT AND DISCUSSION

A. Statistical Description of the Included Studies

After proceeding our search request based on our keywords, and respecting PRISMA framework, we obtained 25 studies that respect our criteria (see Table IV) of inclusion, these articles are categorized according to:

1) Databases

TABLE IV. DIVISION OF THE INCLUDED STUDIES ACCORDING TO DATABASE SOURCE

| Databases | Number of articles | Percent % |
|-----------|--------------------|-----------|
| Scopus | 14 | 56 |
| WoS | 8 | 32 |
| ERIC | 3 | 12 |

2) Publishing year: Fig. 2 below shows a representation of selected studies according to publishing year, most of studies are published in 2023 (40%), whereas, in 2020, only

one study has been found (4%). Hence, AI has taken the center of interest of many researchers as a new field recently.

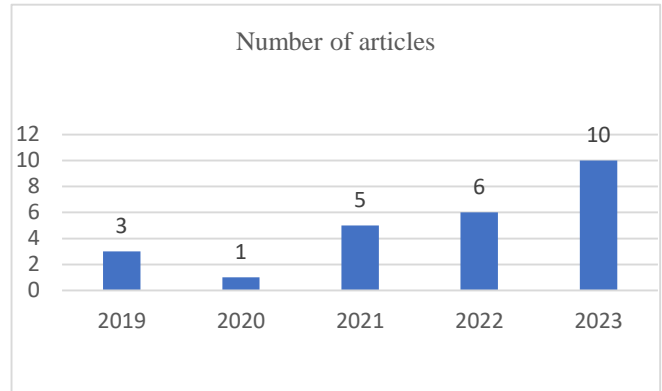


Fig. 2. Division of the included studies according to publishing year.

3) Countries: As shown in Table V and Fig. 3, China is having maximum number of included studies (28%), followed by USA (12%), then South Korea and Indonesia (8%),

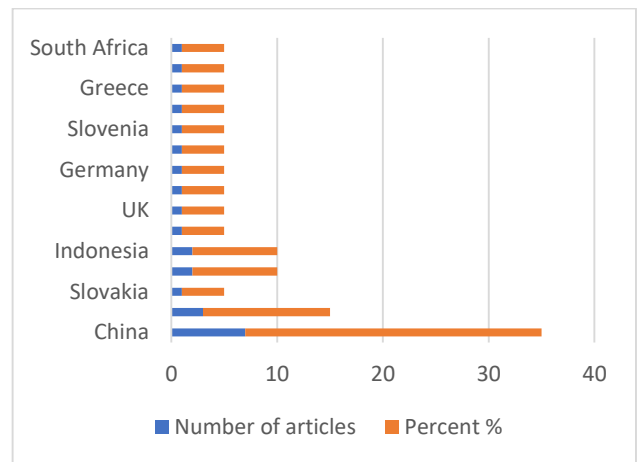


Fig. 3. Division of the included studies according to countries.

TABLE V. DIVISION OF THE INCLUDED STUDIES ACCORDING TO COUNTRIES

| Country | Number of articles | Percent % |
|-------------|--------------------|-----------|
| China | 7 | 28 |
| USA | 3 | 12 |
| Slovakia | 1 | 4 |
| South Korea | 2 | 8 |
| Indonesia | 2 | 8 |
| Turkey | 1 | 4 |
| UK | 1 | 4 |
| Lithuania | 1 | 4 |
| Germany | 1 | 4 |
| Chile | 1 | 4 |
| Slovenia | 1 | 4 |
| Nigeria | 1 | 4 |

| | | |
|--------------|---|---|
| Greece | 1 | 4 |
| Kazakhstan | 1 | 4 |
| South Africa | 1 | 4 |

4) Technology area

B. Factors for Including AI in Online CPD Programs Topics

Artificial Intelligence has become an increasingly important subject in the field of Continuous Professional Development (CPD), necessitating teachers to stay updated on the latest advancements and techniques to effectively integrate AI into their teaching practices [76]. This requires specialized training to navigate challenges and harness the potential of AI [68]. By keeping up with AI in CPD, teachers can leverage AI-based tools and services for supporting students by designing intelligent student support systems, personalizing learning environments [77], providing advanced writing assistance, and fostering creative thinking [51]. Table VI shows division of the included studies whereas Table VII shows recap of the included studies.

TABLE VI. DIVISION OF THE INCLUDED STUDIES ACCORDING TO TECHNOLOGY AREA

| Technology Area | Number of studies | Studies |
|----------------------------|-------------------|----------------|
| Generative (AI) | 3 | [51] [52] [53] |
| Blockchain | 1 | [54] |
| Chatbot/virtual assistance | 1 | [55] |
| Mixed Reality (MR) | 1 | [56] |
| Big Data | 1 | [57] |

| | | |
|-------------------------------------|---|-----------|
| Learning Analytics (LA) | 1 | [58] |
| Game Based virtual Simulators (GVS) | 2 | [59] [60] |
| Intelligent Tutoring Systems (ITS) | 1 | [61] |
| Machine Learning (ML) | 2 | [62] [63] |
| Vector Machine (VM) | 1 | [64] |

TABLE VII. RECAP OF THE INCLUDED STUDIES ACCORDING TO THE MAIN TOPICS

| Main topic | Studies | NB |
|--|---|----|
| Factors for including AI in online CPD programs topics | [51] [63] [65] [66] [67] [68] [69] [70] | 08 |
| Reasons of including AI in online CPD as a scaffolding tool. | [52] [54] [55] [56] [57] [58] [59] [60] [61] [62] [64] [71] [72] [73] | 14 |
| Recommendations for the Competency Profile of the “Digital Teacher”. | [53] [74] [75] | 03 |

Teachers approve AI’s capacity to reproduce regular tasks like preparation, evaluation, and feedback, enabling them to focus more on activities that support student learning [78].

However, despite the positive impact of AI on teaching practices, teachers still have the feeling of stress, anxiety and a lack of self-confidence when adopting unfamiliar technologies[79]. CPD programs play a vital role in boosting teachers’ self-confidence and competencies in utilizing AI tools, ultimately fostering a more confident AI-based teaching environment. [63]. Table VIII below, summarizes and describes the main findings of the selected studies related to reasons why AI must be included in CPD programs’ topics.

TABLE VIII. FACTORS FOR INCLUDING AI IN ONLINE CPD PROGRAMS TOPICS

| Study/ Country | Research design | Sample/ targeted population | Findings |
|------------------|--------------------------------------|---|---|
| [51] USA | Literature Review | In-service teachers | <ul style="list-style-type: none"> – ChatGPT and its successors offer personalized learning, advanced writing support, and foster creative thinking for teachers. – Educators must take proactive measures to ensure the ethical and moral use of these tools. – Recommended AI Integration Practices for Teacher Educators. |
| [65] Nigeria | Quantitative method | 79 In-service science teachers | <ul style="list-style-type: none"> – Science teachers approved the integration of AI in the science classroom. – teachers’ self-esteem and the ease of utilization of AI would make science teachers incorporate AI in the classroom and reduce their stress /anxiety levels. – When teachers are trained on the utilization of AI tools, they become more confident to act in AI-driven classroom environment. – All findings above are not influenced by demographic variables of participants (Gender, Age, Localization). |
| [68] Slovenia | Quantitative method | 1215 In-service science teachers | <ul style="list-style-type: none"> – The study findings indicate that continuous professional development plays a crucial role in enhancing science teachers’ preparedness for AI-integrated assessment methods. – Adequate training and support for teachers are essential to help them navigate the challenges and harness the opportunities that AI technology presents in education. |
| [69] Germany | Qualitative and quantitative methods | 12 vocational school-teachers and 746 apprentices | <ul style="list-style-type: none"> – both teachers and apprentices consider basic theoretical concepts of AI a relevant learning content in the additional AI qualification. – However, apprentices exhibit a preference for a teacher-centered approach to gaining additional AI qualification. |
| [66] China | quantitative method | 1013 In-service teachers | <ul style="list-style-type: none"> – Most teachers possess moderate to high level of AI literacy and have the ability to enhance their understanding of AI |

| | | | |
|---------------------|------------------------------|-------------------------------------|---|
| | | | <p>resources used in the classroom.</p> <ul style="list-style-type: none"> – There is a strong correlation between teachers’ educational background and AI literacy. That is, teachers who have more educational background tend to have a better performance at an AI-driven class environment. – Teachers should be placed at the forefront of AI literacy, for fostering the creation of an inclusive society. This initiative is essential for equipping educators with skills needed to effectively integrate AI into their teaching, ensuring its responsible and meaningful use in the future. |
| [70] South Korea | Systematic Literature Review | 134 papers | <ul style="list-style-type: none"> – The 5.0 industry revolutions underscore the urgent need for (i) updated Technical and Vocational Education and Training (TVET) curriculum and modernized labs equipped with AI-supported technologies/functional areas, alongside (ii) comprehensive training for TVET teachers in these technologies to ensure the effective delivery of education and skills training. – It’s essential to recognize that Artificial Intelligence, Big Data, Data Science, Recommender Systems, Nano Technology, Cloud Computing, and IoT are the future building blocks of the TVET curriculum, labs, training delivery, and teacher training. Bridging the gap between AI advancements and educational practices requires collaborative efforts from TVET training providers, policymakers, industry, academia, and researchers. |
| [67] UK | Exploratory review | 141 studies/ In service teachers | <ul style="list-style-type: none"> – Developing a better understanding of artificial intelligence may enhance teachers’ roles as catalysts in designing, visualizing, and orchestrating AI-enabled teaching and learning process. |
| [63] Slovakia | Literature Review | In service teachers | <ul style="list-style-type: none"> – ICALL(intelligent computer assisted language learning) professional training helps teachers to be updated and informed with the latest AI-based educational tools and provide them with necessary skills to an effective integration of these new technologies in their classrooms. – having an appropriate training for using AI technologies and positive AI-related experience, make teachers feel well prepared and confident to act in AI technology-enhanced environments. |

C. Reasons for Including AI in Online CPD as a Scaffolding Tool

Continuous professional development is crucial for teachers to stay updated on new methods, strategies, and technologies. Artificial intelligence has the potential to change traditional teaching approaches, offering more effective tools for classroom instructions and lesson planning, which was discussed in the section above.

Our included studies have unveiled a wide range of tech tools that help trainers establish an intelligent CPD environment tailored to teachers’ needs and pace, improving the quality of learning experiences and professional growth. Generative AI is considered one of the tech tools that is capable of creating novel content without explicit human programming [51] [52] [53].

Block chain technology with its ability of ensuring security and privacy of teachers’ data through tamper-resistant and verifiable transaction records eliminating reliance on central authorities [54].

Mixed reality MR which entails combining elements of Virtual Reality (VR) and Augmented Reality (AR) to offer users a more immersive and interactive learning experience [56] [80].

Applying network big data to teachers' education involves leveraging large-scale datasets related to educational networks, trainer-teachers interactions, and educational resources in order to extract valuable insights and enhance the quality of teaching and learning experiences [57]. Learning analytics emerges as a pivotal tool for collecting, analyzing, and interpreting data related to teachers and their contexts to optimize training strategies, in order to inform decision-making, improve educational outcomes, and enhance the overall learning experience for all stakeholders [58].

Intelligent simulators recreate authentic educational environments similar to the real context of teaching, to practice new skills with intelligent feedback and coaching identical to human expertise [59] [60].

Intelligent tutoring systems (ITS) personalize the learning experience by offering tailored support, feedback, and guidance based on individual needs and learning styles [61], using machine learning [62] [63], and other advanced technologies.

Table IX below, summarize and describe the principal findings of the included studies in this field.

TABLE IX. REASONS FOR INCLUDING AI IN ONLINE CPD AS A SCAFFOLDING TOOL

| Study | Research design | Sample/ targeted population | Findings |
|----------------------|--------------------------------------|--------------------------------------|--|
| [52] South Africa | qualitative approach/ | In service school teachers | <ul style="list-style-type: none"> Generative language models such as ChatGPT have emerged, enabling teachers to get specific materials and support mechanisms. ChatGPT has enabled teachers to have open access to lesson plans. Generative language models act as tools with the objective of scaffolding teaching and learning with no intention to replace teachers. |
| [54] Kazakhstan | Experiment | In service teachers | <ul style="list-style-type: none"> Blockchain technologies can bear revolutionary changes for the teaching and learning process, by developing an educational system more inclusive, transparent, and efficient. It offers the capacity to track and validate teacher improvement through a decentralized ledger, leading to a more equitable approach to professional learning. Also, it can be used as a powerful tool to motivate teachers by providing them with tangible, verifiable records of their professional development. Blockchain technologies provide a decentralized and verifiable record system that is tamper-proof and fosters trust, hence, ensuring transparency and integrity in teacher CPD. |
| [55] Greece | Systematic Literature Review | 73 papers | <ul style="list-style-type: none"> Recommending some essential steps to develop a Chatbot or educational conversational agent (ECA): 1st step: the definition of ECA's teaching goals and educational materials, based on information relevant to the course literacy, students' needs and the types of the teaching subjects the ECA should use. 2nd step: the development of the ECA and its functions. 3rd step: the evaluation of efficacy of the developed ECA to avoid any malfunctions or weaknesses. |
| [71] Chile | Analytic/ quantitative methods | 108 In service chemistry teachers | <ul style="list-style-type: none"> The study stresses on the potential of AI as powerful tool for generating audiovisual material, interactive content development, and event logs, particularly in the context of e-learning instructional design (ID) integrating the Educational Computational Chemistry (ECC) and (e-PBL) problem-based leaning. |
| [56] USA | Systematic Review | In service teachers | <ul style="list-style-type: none"> The Integration of AI and sensor data (visual, auditory, physiological inputs) holds great promise in reducing the cognitive load of the humans needed in the process for use of simulation in teacher education and in minimizing the necessity for multiple simultaneous human meetings. In a learning MR-based environment, AI is needed to enable the software controlling the virtual setting to interpret both verbal and nonverbal interactions, steering character behaviors contextually and providing feedback and coaching similar to human cognitive capabilities. |
| [57] China | Qualitative and quantitative methods | University teachers | <ul style="list-style-type: none"> The use of network big data analysis helps to evaluate the efficiency of the implementation of teacher training policies in vocational colleges to help teachers improve their professional skills. |
| [58] China | Systematic Review | 30 studies about teachers' education | <ul style="list-style-type: none"> AI and LA have brought some opportunities for teachers in different educational levels, in order to enhance teaching-learning experiences, including evaluation, tracking, adaptive learning. Whereas, ethical concerns related to privacy, data security, bias, and discrimination shouldn't be ignored. the current rate of AI and LA adoption in education lags behind other sectors such as medicine, industry, and finance. |
| [64] China | Quantitative method | 897 university teachers | <ul style="list-style-type: none"> The paper introduces three distinct AI technologies - support vector machine based on immune algorithm, support vector machine based on particle swarm optimization, and pure support vector machine- each designed to enhance the accuracy and efficiency of data prediction and analysis. The study's comparison between predicted and measured data showed compelling results, demonstrating the predictive capabilities of these AI technologies. |
| [72] China | Analytic method | 1834 In service teachers | <ul style="list-style-type: none"> The research proposes a fully automated evaluation approach for detecting cognitive engagement among in-service teachers |

| | | | |
|---------------------|--------------------------------|---------------------------------|---|
| | | | <ul style="list-style-type: none"> within online professional learning community. By using a highly automated method, the study introduces an intelligent supervision system that effectively guides and intervenes in learners' online discourse. |
| [59] Turkey | Qualitative method/ Experiment | 18 teachers | <ul style="list-style-type: none"> Participant teachers have a positive attitude toward the simulation-based training, and they consider it authentic and entertaining. Training-simulation offers participant teachers flexibility and big opportunities to practice new developed skills in an authentic situation wherever and whenever they want, leading to perfectionate their teaching abilities. |
| [73] Indonesia | Descriptive method | 29 In service science teachers | <ul style="list-style-type: none"> Teachers show a positive attitude towards the use of AI in designing higher-order thinking skills (HOTS) based on learning science. AI-based system offers teachers adaptive feedback and instructions for their lesson plans preparation according to a pre-test of knowledge. Participants can arrange an appropriate time and space to take part in online training courses. |
| [61] Indonesia | Descriptive method | 29 In service science teachers | <ul style="list-style-type: none"> Intelligent tutoring system (ITS) has proven its efficacy in helping teachers in online training, especially in the development of lesson plans, by the personalized instructions offered to teachers based on their own backgrounds. Help teachers to solve the problem of absenteeism in the face-to-face training meetings because of schedules of teaching and full day activities. |
| [62] South Korea | Quantitative | In service teachers | <ul style="list-style-type: none"> Machine learning is an appropriate tool to identify and explore important predictors to teachers' job satisfaction, merging a big number of TALIS variables in one prediction model using MNET technique. |
| [60] USA | Experiment | 102 In service science teachers | <ul style="list-style-type: none"> The use of TeachLive simulator has an effective impact on the participant teachers' targeted skills of the training scenario, leading to improve those teachers' skills in the real teaching situations. |

D. Recommendations for the Competency Profile of the “Digital Teacher”.

In this section, our included studies provide some recommendations for the Competency Profile of the “Digital Teacher” in 21-century. These required qualities must be taken into consideration as a framework in the elaboration of

the CPD programs, each country must adapt this framework according to its specific educational system, including context, resources, and needs. The aim of this framework is to prepare teachers capable of using, creating and performing easily and confidently in an AI-based educational environment. Table X shows the recommendations for effective integrating of AI in online CPD.

TABLE X. RECOMMENDATIONS FOR EFFECTIVE INTEGRATING OF AI IN ONLINE CPD

| Study | Research design | Sample/ targeted population | Findings |
|----------------|--------------------------------------|-------------------------------|---|
| [74] China | Literature Review | In service teachers | <ul style="list-style-type: none"> The study proposes and analyzes DigCompEdu and P21's as frameworks that provide guidelines enabling educators to use tools and plan their own learning programs. It summarizes the necessary digital competencies that teachers must develop to control an AI-driven learning environment. It provides some recommendations for an effective integration of AI to educational fields. |
| [53] China | Qualitative and quantitative methods | 108 University teachers | <ul style="list-style-type: none"> The proposition of an AI Ecological Education Policy Framework to address the multifaceted implications of AI integration in university teaching and learning based on, a pedagogical dimension concentrates on using AI to improve teaching and learning outcomes, a Governance dimension tackles issues related to privacy, security, and accountability, and an operational dimension addresses matters concerning infrastructure and training |
| [75] Canada | Qualitative method | 34 experts from six countries | <ul style="list-style-type: none"> The study recommends a Competency Profile for the Digital Teacher (CPDT) that is required in CPD programs in order to prepare teachers capable of performing effectively in an educational environment supported by AI. |

E. *Techno-didactico-pedagogical Framework for Integrating AI in Moroccan CPD programs*

The diagram below (Fig. 4) describes the implementation of our proposed framework including the relationship between technologies adopted to develop an adaptive learning environment, alongside some selected topics related to the development of teachers' AI literacy and the required skills for performing and utilizing AI-based tools to promote the teaching and learning process.

In the quest to enhance the quality of CPD programs in Morocco, an innovative framework is being suggested to adopt in order to set up an intelligent platform. This platform is designed to deliver adaptive Professional training by gauging teachers' initial level and comprehending their preferences and learning styles. The operation of this intelligent platform is based on machine learning (ML) technology. This (ML) technology contains big databases stored in a cloud computing system, protected by a blockchain technology to secure personal data, and create a private environment. This bigdata is explored by learning analytics system using a Support Vector Machine (SVM) algorithm, the aim of which is to profile teachers and provide a personalized learning path based on every teacher's profile through the utilization of generative AI technology capable of generating adaptive content, assessments, simulations using Mixed reality technology, and adaptive support using Intelligent tutoring system ITS. The ITS provides interactive conversational agents such as chatbots, and automated feedback mechanisms, using natural language processing (NLP) technology to understand and analyze the inputs of teachers. This combination of technologies aims to provide adaptive content in the topics proposed in the framework above, or in any other topics according to CPD training goals or teachers' needs.

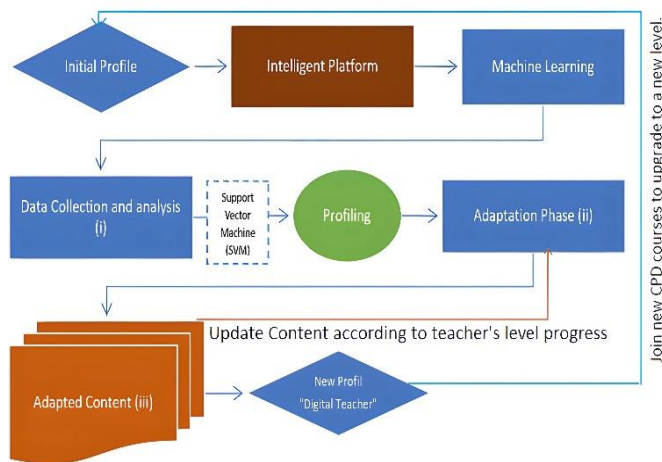


Fig. 4. The proposed framework diagram.

The limitations of this suggested AI-driven framework remain unclear as it is currently being implemented and has yet to be fully explored. In our forthcoming study, we will elucidate both the strengths and weaknesses of this framework. Table XI shows the data collection and analysis phase.

TABLE XI. THE DATA COLLECTION AND ANALYSIS PHASE (I)

| | | |
|--|----------------------------|--|
| <p>Cloud Computing Enables the platform to scale efficiently to accommodate a large number of users. Ensures accessibility from various devices, facilitating anytime, anywhere learning.</p> | <p>Provide data</p> | <p>Big Data analytics Analyzing large datasets generated by teachers helps in gaining insights into their behavior, preferences, and learning patterns, in order to improve content, identify trends, and enhance the overall learning.</p> |
| <p>All data is secured using Blockchain technology</p> | | |
| <p>Security and Privacy Collect and store teachers' personal data in a secure, transparent, and tamper-resistant way</p> | | |

PHASE (III). DEVELOPMENT OF TEACHERS' AI LITERACY TOPICS

Introduction to Artificial Intelligence

- Understanding the basics of AI, machine learning, and deep learning.
- Exploring the significance of AI in education.

AI Tools for Classroom Management

- Integrating AI tools to streamline administrative tasks.
- Using AI for attendance tracking, grading, and scheduling.

Adaptive Learning Systems

- Implementing adaptive learning platforms that personalize content based on individual student needs.
- Analyzing student data to inform instructional decisions. Table XII shows the adaptation phase.

Chatbots and Virtual Assistants

- Utilizing AI-powered chatbots for student support and communication.
- Creating virtual assistants to provide instant feedback and answer common queries.

Data Analytics and Learning Insights

- Understanding the role of data analytics in educational settings.
- Using learning analytics to assess student performance and make data-driven decisions.

AI in Content Creation and Assessment

- Leveraging AI for generating customized learning materials.
- Exploring automated assessment tools and feedback systems.

Digital Literacy and Responsible AI Use

- Reinforcing digital literacy skills among students.
- Addressing ethical considerations and responsible use of AI in the classroom.

Gamification and AI

- Integrating gamification elements to enhance engagement.
- Exploring AI-driven game-based learning experiences.

Mixed Reality (MR) in Education

- Incorporating AR and VR technologies for immersive learning.
- Designing virtual labs and simulations using AI.

AI for Differentiated Instruction

- Tailoring instruction to meet diverse learning needs using AI.
- Implementing strategies for inclusive learning environments.

Collaborative Learning Platforms

- Integrating AI into collaborative tools for group projects.
- Facilitating virtual teamwork and communication.

Privacy and Security in AI Education

- Understanding the importance of data privacy in AI applications.

the work of Cecilia Ka Yuk Chan in 2023 [53], we have adopted the three key dimensions -Governmental, operational, pedagogical- according to the Moroccan context, including:

1) Governmental dimension (Ministry of education).

a) *Policy and regulation:* Governments play a crucial role in formulating policies and regulations that guide the integration of AI in education. This includes setting ethical standards, ensuring data privacy, and establishing frameworks for responsible AI use in the educational sector.

b) *Funding and investment:* Governments may allocate resources and funding to support AI initiatives in education. This can involve investments in research, development of AI technologies, and providing financial incentives for educational institutions to adopt AI-driven solutions.

c) *Inclusion and equity:* Governments should focus on ensuring that the benefits of AI in education are accessible to all students, regardless of socio-economic background or geographic location. This involves addressing issues of digital divide and promoting inclusivity in AI-driven educational initiatives.

d) *Monitoring and evaluation:* Governments can establish mechanisms to monitor and evaluate the impact of AI on education. This includes assessing the effectiveness of AI applications, ensuring equity in access, and addressing any potential biases or ethical concerns.

e) *Collaboration and partnerships:* Facilitating collaboration between government agencies, educational institutions, industry stakeholders, and research organizations is vital. Governments can encourage partnerships that promote the responsible and effective use of AI in education.

2) Operational dimension (Teachers, trainers).

a) *Teacher training:* Training educators and providing professional development opportunities are crucial components of AI integration in education. Governments can facilitate training programs to ensure that teachers are well-prepared to incorporate AI technologies into their teaching methodologies.

b) *Infrastructure and connectivity:* Ensuring adequate infrastructure and connectivity is essential for the successful implementation of AI in education. Governments may invest in improving digital infrastructure, providing internet access, and ensuring that schools and educational institutions have the necessary technology equipment and resources.

c) *Coding and programming skills:* Encourage teachers to learn coding languages commonly used in AI development, such as Python. Many online platforms offer interactive tutorials and coding exercises suitable for beginners.

d) *AI-related clubs and extracurricular activities:* Establish AI clubs or extracurricular activities where teachers can explore AI topics, collaborate on projects, and share their knowledge with peers.

e) *AI-related competitions:* Encourage participation in AI-related competitions or hackathons. These events provide teachers with practical experience, foster problem-solving skills, and promote collaboration.

TABLE XII. THE ADAPTATION PHASE (II)

| | | | |
|----------------------|--|--|--|
| Generative AI | Personalized Learning Paths | <p>Adaptive Content Generation includes custom quizzes, interactive simulations, and supplementary resources tailored to individual learning styles. Identifying trends, predicting potential learning challenges, and recommending improvements to the learning platform.</p> <p>Adaptive Assessments creating adaptive assessments that adjust difficulty based on a teachers' performance, ensuring that each teacher appropriately challenged.</p> | |
| | Intelligent tutoring systems (ITS) offering tailored support, feedback, and guidance based on individual needs of teachers | Natural Language Processing (NLP) language understanding, language generation, machine translation, sentiment analysis | <p>Interactive Conversational Agents (Chatbots) virtual assistants that engage with learners in natural language, answering queries, providing explanations, and offering real-time assistance in order to create an interactive and responsive learning environment.</p> <p>Automated Feedback Systems provide instant feedback on assessments, highlighting areas of strength and weakness. Additionally, it can suggest targeted remedial content or exercises to address specific learning gaps.</p> |
| | Mixed Reality MR | <p>Immersive Learning Experiences Creating realistic simulations, 3D classrooms, or virtual labs, allowing teachers to experiment, teach, and learn in a risk-free environment.</p> <p>Game-Based Learning Applying game mechanics and elements to educational content can enhance engagement and motivation. Gamification techniques can be integrated to make learning more interactive and enjoyable.</p> | |

F. Recommendations

To have a successful integration of AI in the Moroccan educational sector, many dimensions must be combined in order to foster innovation and prepare teachers and students for the demand of the digital age. Drawing inspiration from

3) Pedagogical dimension (Students)

a) *Curriculum development*: One of the most important pillar to have a successful integration of AI is updating curricula to include relevant AI topics. This may involve introducing AI courses, workshops, and educational programs to equip students with the necessary skills for the digital age.

b) *Interactive games and simulations*: Use interactive simulations and educational games that illustrate AI concepts in a visually engaging manner. This approach can make learning more enjoyable and accessible.

c) *Interactive AI tools*: Introduce students to user-friendly AI tools and platforms designed for educational purposes. These tools can help students experiment with AI concepts without requiring advanced technical knowledge.

V. STUDY LIMITATIONS

- A prevalent focus on found studies has been on pre-service teachers undergoing initial training or professional qualification. Whereas our study focuses only on in-service teachers engaged in online continuing Professional Development (CPD).
- While numerous studies have delved into online CPD, a significant gap exists in the integration of AI specifically within the context of teachers' online CPD. While Some of those studies tackled only the use of ICT in general.
- Due to the limited accessibility of many studies, our research focuses exclusively on open access sources to avoid potential biases from restricted access to paid articles.
- Many studies delve into the integration of AI in the educational fields in general with no focus on teachers' online CPD.

VI. CONCLUSIONS AND FUTURE RESEARCH

After analyzing the included studies, it becomes evident that AI holds a positive impact for revolutionizing education at large, with a particular emphasis on enhancing teachers' online CPD. The integration of AI can offer a large bunch of diverse intelligent tools that can be used to foster self-development and facilitate the learning and teaching process. However, the successful integration of AI into teachers' personal and professional life requires a complementarity of governmental, operational, and pedagogical dimensions, alongside technological-didactical-pedagogical engineering to create an innovative intelligent environment that empowers teachers to develop new skills and abilities, resulting in the renovation of pedagogical transformation that ultimately benefits student outcomes.

The findings of our research will be implemented in real-life settings in partnership with Morocco's ministry of education. We plan to evaluate the effectiveness of the proposed framework for Continuing Professional Development (CPD) programs by testing it on a cohort of teachers. Consequently, the insights and results gathered from this practical application will be discussed in detail in a forthcoming study.

ACKNOWLEDGMENT

In closing, the authors of this study would like to extend their sincere appreciation to Mrs. DARRASSI Doha for her invaluable contributions in refining and translating this work.

REFERENCES

- [1] G. Cooper, "Examining Science Education in ChatGPT: An Exploratory Study of Generative Artificial Intelligence," *J. Sci. Educ. Technol.*, vol. 32, no. 3, pp. 444–452, Jun. 2023, doi: 10.1007/s10956-023-10039-y.
- [2] M. A. Pérez-Juárez, J. M. Aguiar-Pérez, J. Del-Pozo-Velázquez, M. Alonso-Felipe, S. Rozada-Raneros, and M. Barrio-Conde, "How Artificial Intelligence Can Enhance Predictive Maintenance in Smart Factories," in *Empowering Sustainable Industrial 4.0 Systems With Machine Intelligence*, IGI Global, 2022, pp. 86–100. doi: 10.4018/978-1-7998-9201-4.ch004.
- [3] J. Tobin, "Artificial intelligence: Development, risks and regulation," *Jul. 2023*, Accessed: Jan. 24, 2024. [Online]. Available: <https://lordslibrary.parliament.uk/artificial-intelligence-development-risks-and-regulation/>
- [4] T. W. Edgar and D. O. Manz, "Chapter 6 - Machine Learning," in *Research Methods for Cyber Security*, T. W. Edgar and D. O. Manz, Eds., Syngress, 2017, pp. 153–173. doi: 10.1016/B978-0-12-805349-2.00006-6.
- [5] R. Pugliese, S. Regondi, and R. Marini, "Machine learning-based approach: global trends, research directions, and regulatory standpoints," *Data Sci. Manag.*, vol. 4, pp. 19–29, Dec. 2021, doi: 10.1016/j.dsm.2021.12.002.
- [6] D. Khurana, A. Koli, K. Khatter, and S. Singh, "Natural language processing: state of the art, current trends and challenges," *Multimed. Tools Appl.*, vol. 82, no. 3, pp. 3713–3744, Jan. 2023, doi: 10.1007/s11042-022-13428-4.
- [7] D. Acosta-Ugalde, S. E. Conant-Pablos, C. Camacho-Zuñiga, and A. E. Gutiérrez-Rodríguez, "Data Mining and Analysis of NLP Methods in Students Evaluation of Teaching," in *Advances in Soft Computing*, H. Calvo, L. Martínez-Villaseñor, and H. Ponce, Eds., in *Lecture Notes in Computer Science*. Cham: Springer Nature Switzerland, 2024, pp. 28–38. doi: 10.1007/978-3-031-47640-2_3.
- [8] S. Virkus et al., "Chatbots Scenarios for Education," *Commun. Comput. Inf. Sci.*, vol. 1979, pp. 207–221, 2024, doi: 10.1007/978-3-031-48981-5_17.
- [9] R. A. Hamzah, M. S. Hamid, H. N. Rosly, N. M. Z. Hashim, and Z. A. F. M. Napiyah, "An Aligned Epipolar Line for Stereo Images with Multiple Sizes ROI in Depth Maps for Computer Vision Application," *Int. J. Inf. Educ. Technol.*, pp. 15–19, 2011, doi: 10.7763/IJNET.2011.V1.3.
- [10] N. Alrebbi and A. A. Al-Shargabi, "Bilingual video captioning model for enhanced video retrieval," *J. Big Data*, vol. 11, no. 1, 2024, doi: 10.1186/s40537-024-00878-w.
- [11] R. I. Doewes, S. K. Purnama, I. Nuryadin, and N. A. Kurdhi, "Chapter Thirteen - Human AI: Social robot decision-making using emotional AI and neuroscience," in *Emotional AI and Human-AI Interactions in Social Networking*, M. Garg and D. Koundal, Eds., Academic Press, 2024, pp. 255–286. doi: 10.1016/B978-0-443-19096-4.00013-4.
- [12] L. Banh and G. Strobel, "Generative artificial intelligence," *Electron. Mark.*, vol. 33, no. 1, p. 63, Dec. 2023, doi: 10.1007/s12525-023-00680-1.
- [13] S. H. GPT-3 Pat Grady and, "Generative AI: A Creative New World," *Sequoia Capital*. Accessed: Dec. 10, 2023. [Online]. Available: <https://www.sequoiacap.com/article/generative-ai-a-creative-new-world/>
- [14] R. Islam et al., "The Future of Cloud Computing: Benefits and Challenges," *Int. J. Commun. Netw. Syst. Sci.*, vol. 16, no. 4, Art. no. 4, Apr. 2023, doi: 10.4236/ijcns.2023.164004.
- [15] "Cloud Adoption Decision-Making Processes by Small Businesses: A Multiple Case Study - ProQuest." Accessed: Nov. 07, 2023. [Online]. Available: <https://www.proquest.com/docview/2425914686>
- [16] P. K. Paul and M. K. Ghose, "Cloud Computing: Possibilities, Challenges and Opportunities with Special Reference to its Emerging Need in the Academic and Working Area of Information Science,"

- Procedia Eng., vol. 38, pp. 2222–2227, Jan. 2012, doi: 10.1016/j.proeng.2012.06.267.
- [17] M. Xu, X. Chen, and G. Kou, “A systematic review of blockchain,” *Financ. Innov.*, vol. 5, no. 1, p. 27, Jul. 2019, doi: 10.1186/s40854-019-0147-z.
- [18] S. Ismail, M. Nouman, D. W. Dawoud, and H. Reza, “Towards a lightweight security framework using blockchain and machine learning,” *Blockchain Res. Appl.*, p. 100174, Nov. 2023, doi: 10.1016/j.bcr.2023.100174.
- [19] B. Yildirim, A. T. Akcan, and E. Ocal, “Teachers’ Perceptions and Stem Teaching Activities: Online Teacher Professional Development and Employment,” *J. Balt. Sci. Educ.*, vol. 21, no. 1, pp. 84–107, 2022, doi: 10.33225/jbse/22.21.84.
- [20] A. Dua, “Applications of Artificial Intelligence in Open and Distance Learning,” *TechnoLearn Int. J. Educ. Technol.*, vol. 11, Dec. 2021, doi: 10.30954/2231-4105.02.2021.1.
- [21] M. Yarandi, H. Jahankhani, and A.-R. H. Tawil, “Towards Adaptive E-Learning using Decision Support Systems,” *Int. J. Emerg. Technol. Learn. IJET*, vol. 8, pp. 44–51, Jan. 2013, doi: 10.3991/ijet.v8iS1.2350.
- [22] Z. Zulfiani, I. P. Suwarna, and S. Miranto, “SCIENCE EDUCATION ADAPTIVE LEARNING SYSTEM AS A COMPUTER-BASED SCIENCE LEARNING WITH LEARNING STYLE VARIATIONS,” *J. Balt. Sci. Educ.*, vol. 17, no. 4, pp. 711–727, Aug. 2018, doi: 10.33225/jbse/18.17.711.
- [23] Center for Education Accreditation, Viet Nam National University (VNU-CEA), Hanoi, Vietnam, H.-H. Nguyen, and V. A. Nguyen, “Personalized Learning in the Online Learning from 2011 to 2021: A Bibliometric Analysis,” *Int. J. Inf. Educ. Technol.*, vol. 13, no. 8, pp. 1261–1272, 2023, doi: 10.18178/ijiet.2023.13.8.1928.
- [24] H. Wang et al., “Examining the applications of intelligent tutoring systems in real educational contexts: A systematic literature review from the social experiment perspective,” *Educ. Inf. Technol.*, vol. 28, no. 7, pp. 9113–9148, Jul. 2023, doi: 10.1007/s10639-022-11555-x.
- [25] T. Kabudi, I. Pappas, and D. H. Olsen, “AI-enabled adaptive learning systems: A systematic mapping of the literature,” *Comput. Educ. Artif. Intell.*, vol. 2, p. 100017, Jan. 2021, doi: 10.1016/j.caeai.2021.100017.
- [26] H. A. El-Sabagh, “Adaptive e-learning environment based on learning styles and its impact on development students’ engagement,” *Int. J. Educ. Technol. High. Educ.*, vol. 18, no. 1, p. 53, Oct. 2021, doi: 10.1186/s41239-021-00289-4.
- [27] I. Gligorea, M. Cioca, R. Oancea, A.-T. Gorski, H. Gorski, and P. Tudorache, “Adaptive Learning Using Artificial Intelligence in e-Learning: A Literature Review,” *Educ. Sci.*, vol. 13, no. 12, Art. no. 12, Dec. 2023, doi: 10.3390/educsci13121216.
- [28] J. Siddharth, P. Vanshika, G. Vinit Kumar, and N. Vivek, “AN AUTOMATED GRADING SYSTEM,” *Int. Res. J. Mod. Eng. Technol. Sci.*, vol. 5, no. 11, 2023.
- [29] A. Rokade, B. Patil, S. Rajani, S. Revandkar, and R. Shedge, “Automated Grading System Using Natural Language Processing,” in *2018 Second International Conference on Inventive Communication and Computational Technologies (ICICCT)*, Apr. 2018, pp. 1123–1127. doi: 10.1109/ICICCT.2018.8473170.
- [30] H. B. Essel, D. Vlachopoulos, A. Tachie-Menson, E. E. Johnson, and P. K. Baah, “The impact of a virtual teaching assistant (chatbot) on students’ learning in Ghanaian higher education,” *Int. J. Educ. Technol. High. Educ.*, vol. 19, no. 1, p. 57, Nov. 2022, doi: 10.1186/s41239-022-00362-6.
- [31] M. Mekni, “An Artificial Intelligence Based Virtual Assistant Using Conversational Agents,” *J. Softw. Eng. Appl.*, vol. 14, no. 9, Art. no. 9, Sep. 2021, doi: 10.4236/jsea.2021.149027.
- [32] “The role of AI in content translation for global audiences,” *AIContentfy*. Accessed: Dec. 26, 2023. [Online]. Available: <https://aicontentfy.com/en/blog/role-of-ai-in-content-translation-for-global-audiences>
- [33] L. Wang, “The Impacts and Challenges of Artificial Intelligence Translation Tool on Translation Professionals,” *SHS Web Conf.*, vol. 163, p. 02021, 2023, doi: 10.1051/shsconf/202316302021.
- [34] The Informatics Engineering Education study program and the Faculty of Engineering and Vocational Education, Universitas Pendidikan Ganesha, Indonesia, K. Agustini, I. M. Putrama, D. S. Wahyuni, and I. N. E. Mertayasa, “Applying Gamification Technique and Virtual Reality for Prehistoric Learning toward the Metaverse,” *Int. J. Inf. Educ. Technol.*, vol. 13, no. 2, pp. 247–256, 2023, doi: 10.18178/ijiet.2023.13.2.1802.
- [35] Y. Shabadurai, F.-F. Chua, and T.-Y. Lim, “Dynamic Adaptive Gamification Framework to Improve User Gamification Experience for Online Training,” *Int. J. Inf. Educ. Technol.*, vol. 14, no. 1, 2024.
- [36] A. M. Al-Ansi, M. Jabooob, A. Garad, and A. Al-Ansi, “Analyzing augmented reality (AR) and virtual reality (VR) recent development in education,” *Soc. Sci. Humanit. Open*, vol. 8, no. 1, p. 100532, Jan. 2023, doi: 10.1016/j.ssaho.2023.100532.
- [37] F. Quint, K. Sebastian, and D. Gorecky, “A Mixed-reality Learning Environment,” *Procedia Comput. Sci.*, vol. 75, pp. 43–48, Jan. 2015, doi: 10.1016/j.procs.2015.12.199.
- [38] A. Nwohiri, O. Joda, and O. Ajayi, “AI-POWERED PLAGIARISM DETECTION: LEVERAGING FORENSIC LINGUISTICS AND NATURAL LANGUAGE PROCESSING,” *FUDMA J. Sci.*, vol. 5, pp. 207–218, Sep. 2021, doi: 10.33003/fjs-2021-0503-700.
- [39] K. Ibrahim, “Using AI-based detectors to control AI-assisted plagiarism in ESL writing: ‘The Terminator Versus the Machines,’” *Lang. Test. Asia*, vol. 13, no. 1, p. 46, Oct. 2023, doi: 10.1186/s40468-023-00260-2.
- [40] S. Mifrah and E. H. Benlahmar, “Topic Modeling with Transformers for Sentence-Level Using Coronavirus Corpus,” *Int. J. Interact. Mob. Technol.*, vol. 16, no. 17, pp. 50–59, 2022, doi: 10.3991/ijim.v16i17.33281.
- [41] “What is Continuous Learning?,” *Samelane*. Accessed: Dec. 27, 2023. [Online]. Available: <https://samelane.com/blog/continuous-learning/>
- [42] “The Importance of Continuing Professional Development (CPD) | The CPD Certification Service.” Accessed: Dec. 27, 2023. [Online]. Available: <https://cpduk.co.uk/news/importance-of-cpd>
- [43] S. Asiyah, B. B. Wiyono, N. Hidayah, and A. Supriyanto, “The Effect of Professional Development, Innovative Work and Work Commitment on Quality of Teacher Learning in Elementary Schools of Indonesia,” *Eurasian J. Educ. Res.*, vol. 2021, no. 95, Sep. 2021, doi: 10.14689/ejer.2021.95.13.
- [44] L. M. Desimone., “Improving Impact Studies of Teachers’ Professional Development: Toward Better Conceptualizations and Measures,” *Educ. Res.*, vol. 38, no. 3, pp. 181–199, 2009, doi: 10.3102/0013189X08331140.
- [45] M. Lahchimi, “La réforme de la formation des enseignants au Maroc,” *Rev. Int. Déducation Sèvres*, no. 69, pp. 21–26, Sep. 2015, doi: 10.4000/ries.4402.
- [46] K. Stecula and R. Wolniak, “Advantages and Disadvantages of E-Learning Innovations during COVID-19 Pandemic in Higher Education in Poland,” *J. Open Innov. Technol. Mark. Complex.*, vol. 8, no. 3, p. 159, Sep. 2022, doi: 10.3390/joitmc8030159.
- [47] C. D. Lay, B. Allman, R. M. Cutri, and R. Kimmons, “Examining a Decade of Research in Online Teacher Professional Development,” *Front. Educ.*, vol. 5, p. 573129, Sep. 2020, doi: 10.3389/educ.2020.573129.
- [48] A. Z. Al Rawashdeh, E. Y. Mohammed, A. R. Al Arab, M. Alara, B. Al-Rawashdeh, and B. Al-Rawashdeh, “Advantages and Disadvantages of Using e-Learning in University Education: Analyzing Students’ Perspectives,” *Electron. J. E-Learn.*, vol. 19, no. 3, pp. 107–117, May 2021, doi: 10.34190/ejel.19.3.2168.
- [49] A. Z. Al Rawashdeh, E. Y. Mohammed, A. R. Al Arab, M. Alara, B. Al-Rawashdeh, and B. Al-Rawashdeh, “Advantages and Disadvantages of Using e-Learning in University Education: Analyzing Students’ Perspectives,” *Electron. J. E-Learn.*, vol. 19, no. 3, pp. 107–117, May 2021, doi: 10.34190/ejel.19.3.2168.
- [50] N. R. Haddaway, M. J. Page, C. C. Pritchard, and L. A. McGuinness, “PRISMA2020: An R package and Shiny app for producing PRISMA 2020-compliant flow diagrams, with interactivity for optimised digital transparency and Open Synthesis,” *Campbell Syst. Rev.*, vol. 18, no. 2, p. e1230, Jun. 2022, doi: 10.1002/cl2.1230.
- [51] T. Trust and J. Whalen, “ChatGPT: Challenges, Opportunities, and Implications for Teacher Education,” *Contemp. Issues Technol. Teach. Educ.*, vol. 23, no. 1, pp. 1–23, 2023.

- [52] G. van den Berg and E. du Plessis, "ChatGPT and Generative AI: Possibilities for Its Contribution to Lesson Planning, Critical Thinking and Openness in Teacher Education," *Educ. Sci.*, vol. 13, no. 10, 2023, doi: 10.3390/educsci13100998.
- [53] C. K. Y. Chan, "A comprehensive AI policy education framework for university teaching and learning," *Int. J. Educ. Technol. High. Educ.*, vol. 20, no. 1, p. 38, Jul. 2023, doi: 10.1186/s41239-023-00408-3.
- [54] A. Sakhipov, T. Baidildinov, M. Yermaganbetova, and N. Ualiyev, "Design of an Educational Platform for Professional Development of Teachers with Elements of Blockchain Technology," *Int. J. Adv. Comput. Sci. Appl.*, vol. 14, no. 7, pp. 519–527, 2023, doi: 10.14569/IJACSA.2023.0140757.
- [55] D. Ramandanis and S. Xinogalos, "Designing a Chatbot for Contemporary Education: A Systematic Literature Review," *Inf. Switz.*, vol. 14, no. 9, 2023, doi: 10.3390/info14090503.
- [56] L. Dieker, C. Hughes, and M. Hynes, "The Past, the Present, and the Future of the Evolution of Mixed Reality in Teacher Education," *Educ. Sci.*, vol. 13, no. 11, 2023, doi: 10.3390/educsci13111070.
- [57] B. Wang, G. Gedvilienė, H. Li, and X. Wang, "The Implementation of Network Big Data on Vocational College Teacher Training Strategy," *Wirel. Commun. Mob. Comput.*, vol. 2022, 2022, doi: 10.1155/2022/5485498.
- [58] S. Z. Salas-Pilco, K. Xiao, and X. Hu, "Artificial Intelligence and Learning Analytics in Teacher Education: A Systematic Review," *Educ. Sci.*, vol. 12, no. 8, p. 569, Aug. 2022, doi: 10.3390/educsci12080569.
- [59] Ö. Kelleci and N. C. Aksoy, "Using Game-Based Virtual Classroom Simulation in Teacher Training: User Experience Research," *Simul. Gaming*, vol. 52, no. 2, pp. 204–225, 2021, doi: 10.1177/1046878120962152.
- [60] L. A. Dieker et al., "Using Virtual Rehearsal in a Simulator to Impact the Performance of Science Teachers," *Int. J. Gaming Comput.-Mediat. Simul. IJGCMS*, vol. 11, no. 4, pp. 1–20, 2019, doi: 10.4018/IJGCMS.2019100101.
- [61] K. D. H. Gunawan, Liliarsari, I. Kaniawati, W. Setiawan, D. Rochintaniawati, and P. Sinaga, "Profile of teachers' integrated science curricula that support by intelligent tutoring systems," *J. Phys. Conf. Ser.*, vol. 1806, no. 1, p. 012139, Mar. 2021, doi: 10.1088/1742-6596/1806/1/012139.
- [62] J. E. Yoo and M. Rho, "Exploration of Predictors for Korean Teacher Job Satisfaction via a Machine Learning Technique, Group Mnet," *Front. Psychol.*, vol. 11, 2020, doi: 10.3389/fpsyg.2020.00441.
- [63] S. Pokrivcakova, "Preparing teachers for the application of AI-powered technologies in foreign language education," *J. Lang. Cult. Educ.*, vol. 7, no. 3, pp. 135–153, Dec. 2019, doi: 10.2478/jolace-2019-0025.
- [64] H. Deng, W. Jia, and D. Chai, "Discussion on Innovative Methods of Higher Teacher Education and Training Based on New Artificial Intelligence," *Secur. Commun. Netw.*, vol. 2022, 2022, doi: 10.1155/2022/3899413.
- [65] C. O. Nja et al., "Adoption of artificial intelligence in science teaching: From the vantage point of the African science teachers," *Smart Learn. Environ.*, vol. 10, no. 1, 2023, doi: 10.1186/s40561-023-00261-x.
- [66] L. Zhao, X. Wu, and H. Luo, "Developing AI Literacy for Primary and Middle School Teachers in China: Based on a Structural Equation Modeling Analysis," *Sustain. Switz.*, vol. 14, no. 21, 2022, doi: 10.3390/su142114549.
- [67] P. Lameris and S. Arnab, "Power to the Teachers: An Exploratory Review on Artificial Intelligence in Education," *Inf. Switz.*, vol. 13, no. 1, 2022, doi: 10.3390/info13010014.
- [68] M. Kerneza and D. Zemljak, "Science Teachers' Approach to Contemporary Assessment with a Reading Literacy Emphasis," *J. Balt. Sci. Educ.*, vol. 22, no. 5, pp. 851–864, 2023, doi: 10.33225/jbse/23.22.851.
- [69] "Needs and requirements for an additional AI qualification during dual vocational training: Results from studies of apprentices and teachers," *Comput. Educ. Artif. Intell.*, vol. 3, p. Article N°100102, 2022, doi: 10.1016/j.caeai.2022.100102.
- [70] R. H. Hassan, M. T. Hassan, S. Naseer, Z. Khan, and M. Jeon, "ICT Enabled TVET Education: A Systematic Literature Review," *IEEE Access*, vol. 9, pp. 81624–81650, 2021, doi: 10.1109/ACCESS.2021.3085910.
- [71] J. Hernandez-Ramos, J. Rodriguez-Becerra, L. Caceres-Jensen, and M. Aksela, "Constructing a Novel E-Learning Course, Educational Computational Chemistry through Instructional Design Approach in the TPASK Framework," *Educ. Sci.*, vol. 13, no. 7, p. 648, Jul. 2023, doi: 10.3390/educsci13070648.
- [72] S. Zhang, Q. Gao, Y. Wen, M. Li, and Q. Wang, "Automatically Detecting Cognitive Engagement beyond Behavioral Indicators: A Case of Online Professional Learning Community," *Educ. Technol. Soc.*, vol. 24, no. 2, pp. 58–72, Apr. 2021.
- [73] K. D. H. Gunawan, L. Liliarsari, I. Kaniawati, and W. Setiawan, "Implementation of Competency Enhancement Program for Science Teachers Assisted by Artificial Intelligence in Designing HOTS-based Integrated Science Learning," *J. Penelit. DAN PEMBELAJARAN IPA*, vol. 7, no. 1, pp. 55–65, May 2021, doi: 10.30870/jppi.v7i1.8655.
- [74] D. T. K. Ng, J. K. L. Leung, J. Su, R. C. W. Ng, and S. K. W. Chu, "Teachers' AI digital competencies and twenty-first century skills in the post-pandemic world," *Educ. Technol. Res. Dev.*, vol. 71, no. 1, pp. 137–161, Feb. 2023, doi: 10.1007/s11423-023-10203-6.
- [75] M. Ally, "Competency Profile of the Digital and Online Teacher in Future Education," *Int. Rev. Res. Open Distrib. Learn.*, vol. 20, no. 2, Apr. 2019, doi: 10.19173/irrodl.v20i2.4206.
- [76] K. Zhang and A. B. Aslan, "AI technologies for education: Recent research & future directions," *Comput. Educ. Artif. Intell.*, vol. 2, p. 100025, Jan. 2021, doi: 10.1016/j.caeai.2021.100025.
- [77] "Systematic review of research on artificial intelligence applications in higher education – where are the educators? | International Journal of Educational Technology in Higher Education | Full Text." Accessed: Jan. 11, 2024. [Online]. Available: <https://educationaltechnologyjournal.springeropen.com/articles/10.1186/s41239-019-0171-0>
- [78] J. Bryant, C. Heitz, S. Sanghvi, and D. Wagle, "How artificial intelligence will impact K-12 teachers".
- [79] M. Tallvid, "Understanding teachers' reluctance to the pedagogical use of ICT in the 1:1 classroom," *Educ. Inf. Technol.*, vol. 21, no. 3, pp. 503–519, May 2016, doi: 10.1007/s10639-014-9335-7.
- [80] K. Agustini, D. S. Wahyuni, I. N. E. Mertayasa, N. M. Ratminingsih, and G. Ariadi, "The Effect of Augmented Reality Mobile Application on Visitor Impact Mediated by Rational Hedonism: Evidence from Subak Museum," *Int. J. Adv. Comput. Sci. Appl.*, vol. 14, no. 1, 2023, doi: 10.14569/IJACSA.2023.0140109.

Improvement of Social Skills in Children with Autism Spectrum Disorder Through the use of a Video Game

Luis C. Soles-Núñez, Segundo E. Cieza-Mostacero

Research Group Trend and Innovation in Systems Engineering – Trujillo, Cesar Vallejo University, Perú

Abstract—The main research objective was to improve social skills through a video game, the type of research was applied with a pure experimental design, with a sample of 60 children with autism spectrum disorder from the Christa McAuliffe school, randomly allocated 30 to the control group (CG) and 30 to the experimental group (GE), the latter using a video game developed with the Unity 3D; Data collection was carried out by means of an adapted test from the cited authors; subsequently, the data collected was analyzed and processed using the Jamovi v2 statistical software. 3.28. The results obtained were an increase of 27.8% on average in the level of communication skills, an increase of 22.4% on average in the level of skills related to feelings, an increase of 20.4% on average in the level of skills alternative to violence and an increase of 19% on average in the level of Pro-amical skills. It was concluded that, the use of a video game significantly improved social skills.

Keywords—Video games; social skills; autism spectrum disorder; SUM methodology; academic software

I. INTRODUCTION

The COVID-19 pandemic had a global impact on various sectors, among them economy, education, production, and others. This manifested itself through the restrictions implemented by many countries to control the spread of the infection. On the educational sector, schools struggled to maintain access to education, but were forced to be closed or to hold classes virtually. In addition, many people fell victim to the pandemic, such as people with low income, with chronic diseases and also those with special conditions, such as children with autism spectrum disorder (ASD), who despite being more prone to stress and requiring specialized treatment in education and health, did not have access to these services due to isolation, suffering from stress, habit changes, behavioral changes and likely long-term cognitive changes [1]. Therefore, regardless of the fact that ASD was a topic of conversation around the world, methods and strategies should continue to be researched to ensure that these children could develop their social and communication skills adequately, in order to be able to fully enjoy their lives.

Likewise [2] according to the findings of ADDM (Autism and Developmental Disabilities Monitoring), in the United States for 2020, one in 36 children aged 8 years suffered from autism spectrum disorder, unlike the year 2018, where one in 44 children suffered from it, which is evidence that cases of children with autism were on the rise and gaining visibility day by day. In response to this fact, different specialized institutions were established around the world, an example is the Fundación ConecTEA in Madrid, which provided support to these minors through therapies, activities and specialized

guidance. In addition [3]. That the cases of ASD diagnosed by pediatricians in Latin America are few, highlighting that there were not many studies conducted to know the number of patients with this disorder [4]. However, although autism spectrum disorder in children was investigated to a limited extent in Latin America, there were associations such as TAJIBO in Bolivia, which were concerned about the care and development of techniques to ensure that these children could enjoy a full life through online therapies and counseling [5].

Similarly, in 2020, the number of cases of people with autism spectrum disorder in Peru was approximately 5,328, notwithstanding the fact that, according to WHO calculations, there should have been approximately 204,818 people with ASD in the country [6]. In addition, although there was an ASD program in the country for the years 2019 to 2021, it was not satisfactorily carried out. In addition to this, Peruvian teaching and schools were encumbered by old methodologies related to social skills development [7]. Therefore, a scenario of ignorance about the situation of these people, as well as a precarious development on the part of the institutions, was present.

Similarly, in Trujillo a different situation was not evident, as there were no records close to the year 2023 of the number of children with ASD, but there were some specialized schools such as the Christa McAuliffe School, which implemented modern neuroscience methodologies, therapies, workshops, among others, for the development of children in all possible aspects [8].

On the other hand, the developed technologies for supporting the growth of these children with ASD include video games, which have presented different benefits in several studies. Concluded that video games promoted self-motivation, perseverance, time management, commitment and the learning of new skills in individuals with ASD [9].

Taking this information into account, due to the fact that minors in this institution are at risk of not developing these types of skills correctly and virtual education and treatment is becoming increasingly common, the general problem was posed: How will the use of a video game influence social skills? As well as the specific problems, how the use of a video game increased the level of communication skills, feeling-related skills, non-violent alternative skills, and Pro-amical skills?

Likewise, the research was carried out at the Christa McAuliffe educational institution in Trujillo, with the objective of strengthening social skills in enrolled children with autism spectrum disorder.

Finally, the main objective of this research was to improve social skills through the use of a video game, while the specific objectives were to increase the level of communication skills, skills related to feelings, non-violent alternative skills and Pro-friend skills, to corroborate the general hypothesis that if a video game is used, then it significantly improves social skills and the specific hypotheses are that if a video game is used, then it significantly improves the skills mentioned in the specific objectives.

II. THEORETICAL FRAMEWORK

A. Video Game

Defined as a technology that combined audiovisual perception and animated effects from the video, along with the strategy of the games in a game, which involved interacting with a virtual environment to follow its narrative, control the characters and play with its elements, so it also involved the development of strategies, decision making and physical response to face the situations presented [10]. In addition, video games presented the opportunity to make use of virtual environments for their players to interact with different real social problems, controversies and reflections [11].

B. Social Skills

Variety of behaviors that are manifested in interactions with other people, which allow the expression of feelings, attitudes, desires, opinions and rights in an appropriate manner according to the situation, while defending one's own rights and respecting the rights of others [12]. On the other hand, they are also defined as all the skills associated with social behavior in its various expressions [13]. However, it should be noted that the concept of skills has changed and will continue to change over time due to its connection with social concepts [14].

C. SUM Methodology

It is necessary to be guided by a concrete methodology that ensures a path, in this case there is the SUM methodology (Scrum for Unified Method) which guarantees usability over playability and adapts to small multidisciplinary teams and short-term projects [15]. The purpose of this methodology is to develop quality video games with controlled time and costs, in addition to seeking continuous improvement of the process to increase its effectiveness and efficiency [16].

III. MATERIAL AND METHODS

A. Research Design

The research was conducted with an applied research, defined as a research that proposes the resolution of a problem or the intervention in its history [17]. In addition, a purely experimental design was used, defined as a research with a very high validity where the conclusions obtained on cause-effect have solid arguments, because a control of external factors, a manipulation of variables and random assignment and manipulation of the groups are performed [18].

B. Variables and Operationalization

1) *Independent variable:* Video game.

2) *Conceptual definition:* Technology that combined audiovisual perception and animated effects from video, along with the strategy of games in a game, which involved interacting with a virtual environment to follow its narrative, control the characters and play with its elements [10].

3) *Operational definition:* A video game will be used by the experimental group of 30 people. A nominal scale will be used.

4) *Dependent variable:* Social Skills.

5) *Conceptual definition:* Variety of behaviors that are manifested in interactions with other people, which allow the expression of feelings, attitudes, desires, opinions and rights in an appropriate manner according to the situation, while defending one's own rights and respecting the rights of others [12].

6) *Operational definition:* The driver behavior variable was measured through four indicators, which are: Number of action errors, number of intention errors, Number of traffic law violations and number of aggressive attitudes which shall use the ratio scale.

C. Variables and Operationalization

A sample of 60 students enrolled in the Christa McAuliffe School with autism spectrum disorder was taken and two groups were formed. The first group, named Experimental Group, consisted of a sample of 30 randomly assigned children with autism spectrum disorder enrolled in the Christa McAuliffe school. These children were provided with a video game developed in Unity that addressed indicators such as the level of communication skills, level of feeling-related skills, level of non-violent alternative skills, and level of Pro-amical skills. The objective was to collect data and evaluate if the use of this video game had a positive impact on the mentioned indicators. In addition, for the second group, named Control Group, consisted of the same number of randomly assigned minors who were not provided with the video game, collecting data to have a basis for comparison and to be able to perform the testing of the hypotheses, being the null hypothesis that the video game decreases the skills and the non-violent alternatives, that the video game increases the aforementioned skills.

D. Data Collection Techniques and Instruments

The research was carried out using the survey as a data collection technique, defined as a technique which obtains information directly from people related to the object of study but with a lesser degree of interaction with them, which can be through tests, questionnaires or knowledge tests [18]. Taking into account direct observation, defined as a technique that allows connecting with reality and formulating the most precise idea possible of the problem studied [19].

In addition, the research was carried out using the questionnaire as a data collection instrument, for the indicators of the level of communication skills, level of skills related to feelings, level of skills alternative to violence and level of proamic skills, defined as a standardized instrument that allows the operationalization of problems through the use of items in the form of questions, statements or instructions [18].

E. Procedures

As mentioned, a group of 60 students from Crhista McAuliffe High School with ASD were chosen and divided into two groups: The first group, called the control group, would not use the video game and would continue to develop their social skills as before, while the second group, called the experimental group, would use the video game for 2 months, testing one level each week, being 4 after the fourth week the levels would be repeated.

Once the groups were formed, we began to control that the children in the experimental group would use the video game as appropriate, which was simple thanks to the help of the teaching staff of the institution, until the two months were completed. Subsequently, a test was carried out for each student, which was filled out by the teachers in charge of the corresponding student, in which they were questioned about the frequency with which the student presented certain behaviors during class hours, behaviors that are connected to the different social skills that they were trying to improve.

F. Development through SUM Methodology

1) *Concept phase:* During this period, a conceptual document was created, offering an intricate portrayal of the video game. It covers various aspects, including its unique characteristics, genre, gameplay mechanics, environment, storyline, intended audience, and the inspirations that influenced its development. Further elaboration on some of these mentioned features is presented below:

a) *Game vision:* Players explore a classroom, which simulates different conversations with an NPC (non-playable character, mentioned as a machine-controlled character that often plays many roles when interacting with players [20]), in which each of them practices behaviors related to communication skills, feelings, alternatives to violence, and pro-amical in order to successfully develop the story.

b) *Technology and tools:*

- It was programmed in Unity 3D, 2022.3.7f1.
- Models were edited in Blender.
- Sprites were generated in Playgroundai.
- Voices will be generated in Applio.
- Programming language C# for the functionalities.

2) *Planning phase:* In this phase, the essential project document is drafted, which includes a detailed description of the work performed, the rationale for the project, the parties involved, quantifiable goals, functional requirements in Table I and non-functional requirements in Table II, assumptions and other relevant elements. This document also specifies both the schedule of activities and the project budget.

TABLE I. RESEARCH INDICATOR FREQUENCY TABLE

| Code | Description |
|------|--|
| RF01 | Show dialog on communication skills. |
| RF02 | Show dialogue on pro-amictal skills. |
| RF03 | Show dialogue on alternative skills to violence. |
| RF04 | Show dialogue on skills related to feelings. |

^a. Source: Own work

TABLE II. NON-FUNCTIONAL REQUIREMENTS

| Code | Description |
|-------|---|
| RNF01 | Developed in Unity 3D environment. |
| RNF02 | Developed in C# language. |
| RNF03 | The videogame must be in Spanish. |
| RNF04 | It must work in any size of screen of Laptop or PC. |

^b. Source: Own work

3) *Elaboration phase:* The aim of this stage is to carry out the implementation of the video game. This involves adopting an iterative and incremental approach, ensuring the development of a functional version of the video game at the conclusion of each iteration.

a) *Iteration 1:* During the first iteration, we chose and edited the model of the scenario as shown in Fig. 1, chose the model of the NPC named Lucia as shown in Fig. 2 and programmed the movement of the main character as shown in Fig. 3 and 4.

b) *Iteration 2:* In this iteration, the main scripts of the dialog system that allowed the visualization shown in Fig. 5, which is when the NPC talks to us, and Fig. 6, which is the screen when we can make choices, were developed, in addition, the sprites were developed as shown in Fig. 7.

c) *Iteration 3:* During this iteration, the different conversations were carried out for the different levels, using interconnected scriptable objects, where the texts and options that we can choose are stored and then loaded in the screens previously seen.



Fig. 1. Scenario.



Fig. 2. NPC model.

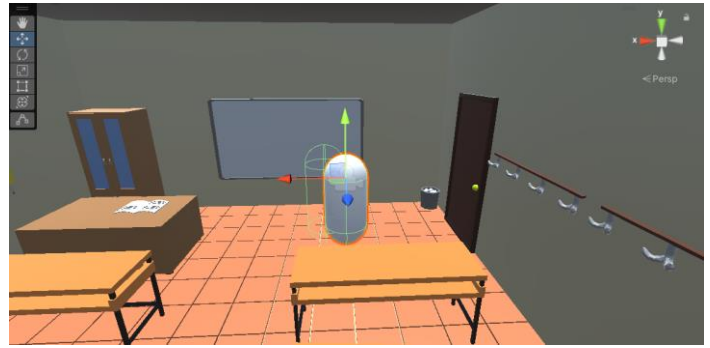


Fig. 3. Main character model.

```

1  using System.Collections;
2  using System.Collections.Generic;
3  using UnityEngine;
4
5  public class Player : MonoBehaviour
6  {
7      private CharacterController _characterController;
8
9      private float _speed = 3.5f;
10     private float _gravity = 9.81f;
11     private float _rotationSpeed = 1f;
12
13     public bool canMove = true;
14
15     void Start()
16     {
17         _characterController = GetComponent<CharacterController>();
18     }
19
20     void Update()
21     {
22         if (canMove)
23         {
24             CalculateMovement();
25             Rotation();
26         }
27         else
28         {
29             Cursor.lockState = CursorLockMode.None;
30         }
31     }
32 }

```

Fig. 4. Movement of the main character.

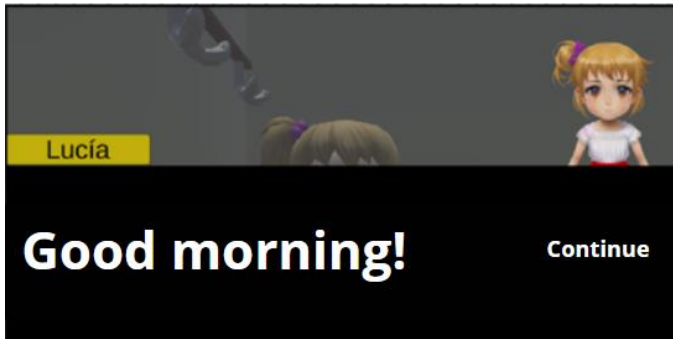


Fig. 5. Conversation dialog system.

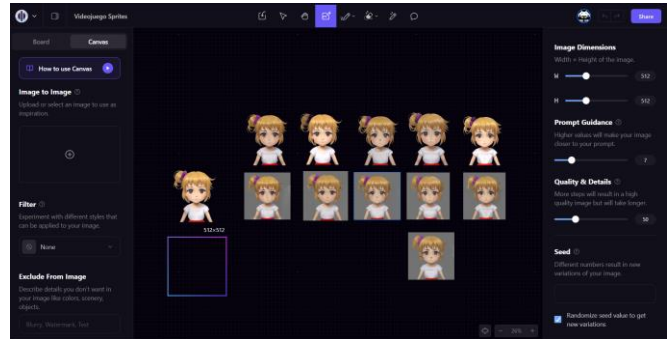


Fig. 7. Sprite generation.

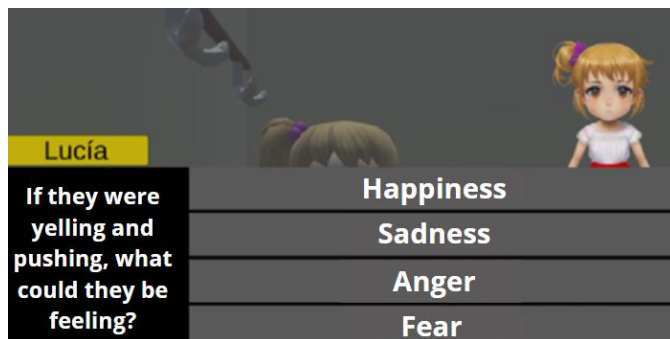


Fig. 6. Question dialog system.

d) *Iteration 4:* In this last iteration, the main menu is developed, some audios are generated to accompany the text in the conversations as shown in Fig. 8, and a system is created to control the number of "errors" during the use of the game

4) *Beta Phase:* After the development of the video game was completed, it was installed on a variety of computers with different Windows system versions and screen resolutions. This process revealed a number of bugs concerning screen resolution and dialog connection. As a result, measures were taken to correct these errors, the errors can be seen in Table III. A test of the videogame can be performed at the following link: acortar.link/LXdaKe.

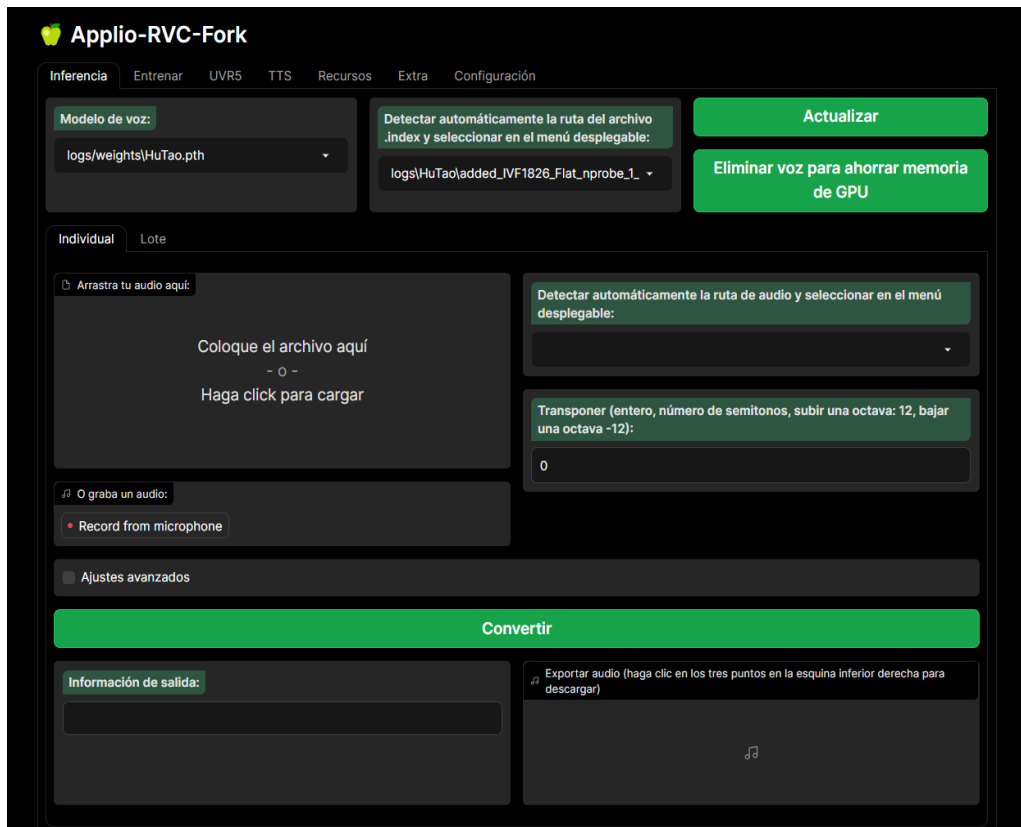


Fig. 8. Audio generation.

TABLE III. TABLE OF ERRORS FOUND

| MISTAKES | |
|-------------|--|
| TYPE | DESCRIPTION |
| RESOLUTION | The main menu canvas was not satisfactorily adapted. |
| | The content of the buttons with options was not satisfactorily adapted. |
| PROGRAMMING | The dialogs of the first conversation loop were not correctly connected. |

^c Source: Own creation

5) *Closing Phase*: The educational institution Christa McAuliffe Trujillo, positively accepted the video game and also provided the facility to apply the implementation of the same for students.

The proposed purpose of implementing the video game was to improve social skills. On October 16, the video game was installed in all the functional machines of the institution, with a positive and interested acceptance by the students.

IV. RESULTS

A. Descriptive Analysis

In the descriptive Analysis, Table IV shows the frequency tables of the control and experimental groups for the research indicators, showing an improvement of 1.39 in the Communication Skills Level (NHC), 1.12 in the Feelings-related Skills Level (NHRS), 1.04 in the Non-violent Alternative Skills Level (NHAV) and 0.95 in the Pro-amical Skills Level (NHPA).

TABLE IV. RESEARCH INDICATOR FREQUENCY TABLE

| Research Indicator | Level | Frequency | | General Average | |
|--------------------|----------|-----------|----|-----------------|------|
| | | GC | GE | GC | GE |
| NHC | Very Low | 21 | - | 1.7 | 3.09 |
| | Low | 9 | 9 | | |
| | Average | - | 15 | | |
| | High | - | 6 | | |
| NHRS | Very Low | 18 | - | 1.8 | 2.92 |
| | Low | 10 | 7 | | |
| | Average | 1 | 21 | | |
| | High | 1 | 2 | | |
| NHAV | Very Low | 19 | - | 1.68 | 2.72 |
| | Low | 10 | 20 | | |
| | Average | 1 | 6 | | |
| | High | - | 4 | | |
| NHPA | Very Low | 20 | 3 | 1.58 | 2.53 |
| | Low | 10 | 18 | | |
| | Average | - | 6 | | |
| | High | - | 3 | | |

^d Source: Own creation

B. Inferential Analysis

In the inferential analysis, Table V shows the normality tests of the data collected from each group, based on each indicator, by using the Shapiro-Wilk test since each group is less than 50. There are two decision criteria: a) If $p < 0.05$, the null hypothesis (H0) is rejected and the alternate hypothesis (Ha) is rejected and b) If $p \geq 0.05$, the contrary is true.

TABLE V. SHAPIRO-WILK NORMALITY TEST TABLE

| Research Indicator | P (GC) | P (GE) |
|--------------------|--------|--------|
| NHC | 0.261 | 0.419 |
| NHRS | 0.004 | 0.056 |
| NHAV | 0.12 | 0.014 |
| NHPA | <.001 | 0.003 |

^e Source: Own creation

Finally, the variables backed the specific alternate hypotheses posed (Ha) as seen in Table VI, showing that the Level of Communication Skills (NHC), the Level of Feelings Related Skills (NHRS), the Level of Non-violent Alternative skills (NHAV) and the Level of Proamic Skills (NHPA) increased with the use of a video game as all indicators had a value of $p < .001$, thus rejecting the null hypotheses (H0) that indicated that these skills decreased.

TABLE VI. INFERENCE ANALYSIS TABLE OF EACH INDICATOR

| Research Indicator | | Statistics | gl | p | Decision |
|--------------------|----------------|------------|----|-------|----------------|
| NHC | T Student | -11.9 | 58 | <.001 | Ha is accepted |
| NHRS | U Mann-Whitney | 70 | - | <.001 | |
| NHAV | U Mann-Whitney | 69 | - | <.001 | |
| NHPA | U Mann-Whitney | 109 | - | <.001 | |

^f Source: Own creation

V. DISCUSSION

Based on the obtained results, as evidenced by the use of a video game, it was possible to increase the level of communication skills, the level of feeling-related skills, the level of non-violent alternative skills and the level of Proamic skills; thus, demonstrating that the use of a video game significantly improved social skills.

With regard to the general objective, which sought to improve social skills through the use of a video game, it was determined that social skills were indeed significantly improved. This was demonstrated by the increase in the average of all skill levels measured; the results obtained are similar to the research conducted, where he demonstrates the effectiveness of the use of a video game called "Minecraft" for the improvement of social skills in people with autism spectrum disorder[9]. It should be noted defined that, social skills are a variety of behaviors that are evident in the interaction with other people, being that these behaviors are means to communicate emotions, positions, aspirations, points of view and rights in an appropriate manner according to the

context, ensuring the expression of one's own rights while respecting the rights of others [12].

Regarding the first indicator, which is the level of communication skills, a total of 1.7 average points of the level of communication skills was obtained in the control group, and a total of 3.09 average points of the level of communication skills in the experimental group, showing an increase of 1.39 average points of the level of communication skills in the experimental group. In addition, it was calculated that the average of the control group represents 34%, while the average of the experimental group would be equivalent to 61.8%, thus proving an increase of 27.8% in the level of communication skills in the group that used the video game; the results were comparable with the study, which if we follow the same logic, presented an increase in communication skills of 41.53% [21]. It should be defined communication skills as those that encompass the ability to send and receive information, as well as ideas and messages relevant to those involved [22].

Regarding the second indicator, which is the level of skills related to feelings, a total of 1.8 points of average of the level of skills related to feelings was obtained in the control group, and a total of 2.92 points of average of the level of feeling-related skills in the experimental group, showing an increase of 1.12 points of average of the level of feeling-related skills in the experimental group. In addition, it was calculated that the average of the control group represents 36%, while the average of the experimental group would be equivalent to 58.4%, thus proving an increase of 22.4% in the level of feeling-related skills in the group that used the video game; the results were comparable with the study, who showed an improvement in the identification of emotions both their own and that of others in all their cases [23]. It should be defined that skills related to feelings are those that enable the understanding and effective expression of emotions and emotional states to others in order to be understood [22].

Regarding the third indicator, which is the level of, non-violent alternative skills, a total of 1.7 points of average of the, non-violent alternative skills was obtained in the control group, and a total of 2.72 points of average of the level of, non-violent alternative skills in the experimental group, demonstrating an increase of 1.02 points of average of the level of non-violent alternative skills in the experimental group. In addition, it was calculated that the average of the control group represents 34%, while the average of the experimental group would be equivalent to 54.4%, thus proving an increase of 20.4% in the level of non-violent alternative skills in the group that used the video game; the results were comparable with the study, who showed an increase in skills in the face of conflicts among all his cases, especially in cases of speaking with others to negotiate and reach an agreement[24]. It is worth defined that, non-violent alternative skills are those that reduce the possibility of perpetrating or being a victim of violent behaviors [22].

Regarding the fourth indicator, which is the level of proamic skills, a total of 1.58 points of average proamic skills level was obtained in the control group, and a total of 2.53 points of average proamic skills level was obtained in the experimental group, showing an increase of 0.95 points of

average proamic skills level in the experimental group. In addition, it was calculated that the average of the control group represents 31.6%, while the average of the experimental group would be equivalent to 50.6%, therefore, an increase of 19% in the level of proamictal skills was demonstrated in the group that used the video game; the results were comparable with the study, who demonstrated an increase in the frequency of initiation of an interaction and the time it was maintained, although in some cases it was still not constant, the frequency was increased [23]. It should be defined proamictal skills as those that increase the possibilities of establishing relationships with new people and maintaining friendships with other people, mainly friends [22].

Finally, it was concluded that the use of a video game improved social skills through the use of a video game, due to an increase in communication skills by an average of 27.8%, skills related to feelings by an average of 22.4%, alternative skills to violence by an average of 20.4% and proamic skills by an average of 19%.

VI. LIMITATIONS

During the research, there were several limitations, such as not taking into account stereotyped behaviors that are common in people with ASD, which were solved by the novelty that the use of a videogame presented in children, but there was no specific control for these behaviors that can alter the attention given to the software.

Also, there was limited time for the development of the software due to unexpected failures in the laptop intended for the development of the videogame and all its functionalities.

Likewise, the software was developed with the limitation of technical knowledge about the development of video games in the Unity environment by the researcher, and the software could have been much more optimized or include more mechanics in future research.

Finally, there was a hardware limitation of the laptops that the institution had, having a limited processing capacity, so we opted for an offline and resource-light approach.

VII. CONCLUSIONS

It has been established that there is a notable increase in the Communication Skills Level, thus demonstrating with the percentages obtained, with the calculation of the formula, 34% of Communication Skills Level was obtained in the control group and 61.8% of this level in the experimental group, thus proving an increase of 27.8%, in this level, of the group that used the video game, demonstrating that with the parametric statistical test T of Students a p value of $<.001$ was obtained providing sufficient statistical evidence to accept the alternative hypothesis.

In addition, it was established that there is a notable increase in the Level of Skills Related to Feelings, thus demonstrating with the percentages obtained, with the calculation of the formula, a 36% Level of Skills Related to Feelings was obtained in the control group and 58.4% of this level in the experimental group, thus proving an increase of 22.4%, in this level, of the group that used the video game,

demonstrating that with the non-parametric statistical test Mann-Whitney U, a p value of $<.001$ was obtained, providing sufficient statistical evidence to accept the alternative hypothesis.

Similarly, it was established that there is a notable increase in the Level of Alternative Skills to Violence, thus demonstrating with the percentages obtained, with the calculation of the formula, 34% of the Level of Alternative Skills to Violence was obtained in the control group and 54.4% of this level in the experimental group, thus proving an increase of 20.4%, in this level, of the group that used the video game, demonstrating that with the non-parametric statistical test Mann-Whitney U, a p value of $<.001$ was obtained, providing sufficient statistical evidence to accept the alternative hypothesis.

Finally, it has been established that there is a notable increase in the Proamic Skills Level, thus demonstrating with the percentages obtained, with the calculation of the formula, 31.6% of Proamic Skills Level was obtained in the control group and 50.6% of this level in the experimental group, thus proving a 19% increase, in this level, of the group that used the video game, demonstrating that with the non-parametric statistical test Mann-Whitney U, a p value of $<.001$ was obtained, providing sufficient statistical evidence to accept the alternative hypothesis.

ACKNOWLEDGMENT

The research was not externally funded. We would like to express our sincere gratitude to all those who have contributed to this research.

CONFLICT OF INTEREST

The authors declare no conflict of interest.

REFERENCES

- [1] R. Amorim, S. Catarino, P. Miragaia, C. Ferreras, V. Viana, y M. Guardiano, «Impact of COVID-19 on children with autism spectrum disorder», *RevNeurol*, vol. 71, n.o 08, p. 285, 2020, doi: 10.33588/rn.7108.2020381.
- [2] M. J. Maenner, «Prevalence and Characteristics of Autism Spectrum Disorder Among Children Aged 8 Years — Autism and Developmental Disabilities Monitoring Network, 11 Sites, United States, 2020», *MMWR Surveill Summ*, vol. 72, 2023, doi: 10.15585/mmwr.ss7202a1.
- [3] ConecTEA, «ConecTEA Foundation - Together in Autism », ConecTEA Foundation - Together in Autism». Accessed: April 22, 2023. [Online]. Available in: <https://www.fundacionconectea.org/>
- [4] K. A. M. Fajardo, D. E. S. Álvarez, y V. P. P. Zambrano, «Epidemiological profile of autism in Latin America», *Health and Medical Sciences*, vol. 1, n.o 2, Art. n.o 2, dic. 2021.
- [5] TAJIBO, «TAJIBO Association», Tajibo Association. Accessed: April 22, 2023. [Online]. Available in: <https://tajibo.org/>
- [6] Ombudsman Peru, «Ombudsman's Office warns of lack of public policies for the care of people with autism», Ombudsman - Peru, April 1, 2022. Accessed at: April 16, 2023. [Online]. Available in: <https://www.defensoria.gob.pe/defensoria-del-pueblo-advierte-falta-de-politicas-publicas-para-la-atencion-a-personas-con-autismo/>
- [7] J. R. Cueva Torres, «Cooperative learning in the development of social skills in university students, Trujillo 2020», Institutional Repository - UCV, 2021, Accessed: April 22, 2023. [Online]. Available in: <https://repositorio.ucv.edu.pe/handle/20.500.12692/69450>
- [8] Christa McAuliffe School, «Christa McAuliffe School - Personalized School», Christa McAuliffe School. Accessed at: April 22, 2023.

- [Online]. Available in: https://chma.edu.pe/?gclid=Cj0KCQjwi46iBhDyARIsAE3nVrZmiazLgvelcBuyYiytn13-wyR4ApwFCQtVzJa8qu7Rvzd462-WJEEaAgivEALw_wcB
- [9] M. Villén De Arribas, «Minecraft in the Learning of Social Skills for People with Autism Spectrum Disorders», *Enseñanza & Teaching* (2386-3919), vol. 38, n.o 1, pp. 7-28, jun. 2020, doi: 10.14201/et2020381728.
- [10] G. Paredes-Otero, «Narratives and users of the transmedia society», *Narratives and users of the transmedia society*, pp. 1-888, 2022.
- [11] A. C. M. Cantano y A. V. Ramos, «The video game as a mirror of contemporary society», *Barataria. Castellano-Manchega Magazine of Social Sciences*, n.o 29, Art. n.o 29, nov. 2020, doi: 10.20932/barataria.v0i29.577.
- [12] M. Garaigordobil y A. Sarrionandia, «Intervention in social skills: Effects on emotional intelligence and social behavior.», *Behavioral Psychology/Psicología Conductual*, vol. 22, pp. 551-567., dic. 2014.
- [13] E. Peñafiel y C. Serrano, *Social skills*. Editorial Editex, 2010. Available in: https://books.google.com.pe/books/about/Habilidades_sociales.html?hl=es&id=zpU4DhVHTJIC&redir_esc=y
- [14] M. E. Ibarra Santacruz, «Las habilidades sociales desde la tipología de Goldstein: un análisis psicosocial en niños 6 a 8 años en la ciudad de Victoria de Durango», Thesis, Universidad Juárez del Estado de Durango: Faculty of Psychology and Human Communication Therapy. Division of Graduate Study and Research, 2020. Accessed at: December 2, 2023. [Online]. Available in: <http://repositorio.ujed.mx/jspui/handle/123456789/66>
- [15] J. G. Chero, « Usability study of web video games using the sum development methodology.», 2019, Accessed: May 5, 2023. [Online]. Available in: <http://repositorio.utmachala.edu.ec/handle/48000/14536>
- [16] N. Acerenza et al., «A Methodology for video game development: extended version», 2009, Accessed: December 3, 2023. [Online]. Available in: <https://www.colibri.udelar.edu.uy/jspui/handle/20.500.12008/3420>
- [17] A. J. M. Ávila, A. K. B. Suarez, Z. K. P.- Martínez, J. A. R. Gonzaga, J. E. Z. Calderón, y C. E. C. Suárez, «Research Designs», *Education and Health Scientific Bulletin Institute of Health Sciences Autonomous University of the State of Hidalgo*, vol. 8, n.o 15, Art. n.o 15, dic. 2019, doi: 10.29057/icsa.v8i15.4908.
- [18] G. Mousalli, *Quantitative Research Methods and Designs*. 2015. doi: 10.13140/RG.2.1.2633.9446.
- [19] M. C. Useche, W. Artigas, B. Queipo, y É. Perozo, *Techniques and instruments for collecting qualitative-quantitative data*. University of La Guajira, 2019. Accessed: May 12, 2023. [Online]. Available in: <https://repositoryinst.uniguajira.edu.co/handle/uniguajira/467>
- [20] H. Warpefelt, «The Non-Player Character : Exploring the believability of NPC presentation and behavior», 2016, Accessed: 4 de abril de 2024. [Online]. Available in: <https://urn.kb.se/resolve?urn=urn:nbn:se:su:diva-128079>
- [21] Y.-A. Caballero y A. G.-V. Muñoz, «Strengthening computational thinking and social skills through learning activities with educational robotics in early school levels.», *Pixel-Bit, Media and Education Magazine*, n.o 58, pp. 117-142, may 2020, doi: 10.12795/pixelbit.75059.
- [22] G. Lescano y A. Rojas, *Situation of Social Skills in Peruvian Schoolchildren*. 2003. [Online]. Available in: https://www.researchgate.net/publication/335949894_Situacion_de_las_Habilidades_Sociales_en_Escolares_del_Peru
- [23] J. L. Martínez y S. A. García, «Teaching emotions to benefit the social skills of students with autism spectrum disorders», *Educatio Siglo XXI*, vol. 28, n.o 2, Art. n.o 2, 2010.
- [24] G. E. Coba Cisneros, «Promotion of social skills in 1st grade boys and girls using digital games», masterThesis, 2018. Accessed: May 4, 2023. [Online]. Available in: <https://iconline.ipleiria.pt/handle/10400.8/3408>

Cinematic Curator: A Machine Learning Approach to Personalized Movie Recommendations

B.Venkateswarlu¹, N. Yaswanth², A. Manoj Kumar³, U. Satish⁴, K. Dwijesh⁵, N. Sunanda⁶

Assistant Professor, Department of CSE, Koneru Lakshmaiah Education Foundation, Guntur, A.P,India¹

Department of CSE, Koneru Lakshmaiah Education Foundation, Guntur, A.P, India^{2,3,4,5}

Assistant Professor, VNR Vignana Jyothi Institute of Engineering & Technology, Hyderabad, Telangana, India⁶

Abstract—This work suggests a sophisticated movie recommendation system that offers individualized recommendations based on user preferences by combining content-based filtering, collaborative filtering, and deep learning approaches. The system use natural language processing (NLP) to examine user-generated content, movie summaries, and reviews in order to get a sophisticated comprehension of thematic aspects and narrative styles. The model includes SHAP for explainability to improve transparency and give consumers insight into the reasoning behind recommendations. The user-friendly interface, which is accessible via web and mobile applications, guarantees a smooth experience. The system is able to adjust to changing user preferences and market trends through ongoing upgrades that are founded on fresh data. The system's efficacy is validated by user research and A/B testing, which show precise and customized movie recommendations that satisfy a range of tastes.

Keywords—Machine learning algorithms decision tree; random forest model-evaluation; accuracy value; precision value; F1 score

I. INTRODUCTION

Navigating the immense ocean of films in the midst of a digital cinematic flood can be likened to looking for a secret beach in a dense fog. Conventional recommendation systems, which are frequently based on rudimentary algorithms, are not very helpful because they are unable to fully capture the nuances of individual preference. In order to introduce a complex movie recommendation system powered by machine learning's powerful engines, this study suggests a paradigm shift. Deep learning, natural language processing, content-based filtering, collaborative filtering, and deep learning are all skilfully combined by this system to explore the depths of user behaviour and movie attributes, creating a detailed picture of personal preferences [1]. The approach demystifies its suggestions and gives customers a glimpse into the reasoning behind each movie proposal in order to promote transparency and foster confidence. This system, which is easily navigable through user-friendly interfaces, blends in with daily life, changing to fit user tastes and trends while continuously crafting a customised cinematic journey. This study explores the system's technological details and reveals how revolutionary it could be for how we find and watch films that genuinely affect us.

It has been revised to emphasise the academic character of the project while retaining the compelling picture and key idea in a tone more appropriate for a paper. Important terminology and framing related to research writing are also introduced. customised cinematic journey.

A. Problem Statement

When accessing vast movie collections on streaming services, customers often face the challenge of option overload in today's digital entertainment scene. Traditional movie recommendation systems are widely used, but they sometimes struggle to fully capture customers varied and changing interests. The creation and implementation of a robust machine learning model-based movie recommendation system is the main problem that needs to be solved. The system needs to address several fundamental issues, such as the requirement for interpretable recommendations, sparse and noisy data, and the cold start problem. The primary goal is to increase user pleasure by providing tailored and contextually appropriate movie recommendations.

B. Background

The landscape of movie recommendation systems has become indispensable in the digital era, where an extensive array of films is available across various streaming platforms. These systems leverage advanced machine learning models to analyse user behaviour, preferences, and movie characteristics, ultimately providing personalized recommendations to enhance user satisfaction and engagement. The evolution of movie recommendation systems can be traced through several phases, marked by the adoption of increasingly sophisticated machine learning techniques.

1) Traditional recommender systems:

Collaborative filtering: In the early days, recommendation systems heavily relied on collaborative filtering, identifying similarities between users based on their preferences and suggesting items that similar users have enjoyed. However, collaborative filtering faced challenges such as the cold start problem (lack of data for new users or items) and scalability issues.

Content based filtering: Another traditional approach involved content-based filtering, which recommends items based on their attributes and features. In the context of movies, this could mean suggesting films with similar genres, directors,

or actors. Nevertheless, content-based systems struggled to capture nuanced user preferences

2) Machine learning advancements:

Hybrid models: By fusing content-based and collaborative methods, hybrid models have arisen to address the shortcomings of individual approaches. By combining the advantages of both strategies, these models sought to offer suggestions that were stronger and more accurate.

Matrix factorization is one technique that has helped collaborative filtering models improve. It breaks down the user-item interaction matrix into latent factors, which are underlying patterns in user preferences.

3) Deep learning for movie suggestions:

Neural Collaborative Filtering (NCF): By using neural networks to simulate intricate, non-linear correlations in user-item interactions, deep learning models like NCF have significantly improved the field. These models improve recommendation accuracy by taking into account both implicit feedback and explicit user-item ratings.

Embeddings: Known as learnt representations of objects and users in a reduced-dimensional space, embeddings have emerged as a key idea in enhancing recommendation models' efficacy and efficiency.

4) Integration of Natural Language Processing (NLP):

Textual data analysis: To provide recommendations a semantic layer, several systems have begun utilizing natural language processing (NLP) approaches. The algorithm is able to comprehend the context and substance of films with the aid of analysis of movie reviews, summaries, and other textual data, which results in more intelligent recommendations.

5) Transparency and explainability:

Explainability techniques: The necessity to provide an explanation for recommendations increased with the complexity of machine learning models. In order to increase openness and user confidence, techniques such as SHAP (SHapley Additive explanations) were adopted to give users an explanation for why particular suggestions were produced.

Explainability is a critical aspect of recommendation systems, especially as they become more complex and sophisticated. Users often want to understand why a particular recommendation was made to trust and accept the system's suggestions. SHAP, or SHapley Additive explanations, offers a powerful technique to achieve this by providing insights into the contribution of each feature to the model's decision-making process.

6) User experience and deployment:

User interfaces: Web and mobile applications now offer user-friendly interfaces for movie recommendation systems, which replaced the previous backend algorithms. Users will find it effortless to find and enjoy recommended content thanks to these interfaces, which offer a smooth and user-friendly experience.

7) Ongoing education and adjustment:

Dynamic updates: Modern recommendation systems are built for continual learning in order to keep up with the ever-changing nature of user preferences and the film business. Their models are continually updated and fresh data is incorporated to accommodate evolving patterns and user behavior.

C. Key Challenges

- Issue with Cold Start for Users and Films:
- Noisy and Sparse Data:
- Persistent User Preferences:
- Diverse Content and Coincidence:
- Both Real-Time Processing and Scalability:

D. Objectives

1) *To improve personalization:* It create machine learning models that can recognize and comprehend the preferences of individual users. This will allow for the creation of personalized movie suggestions based on each user's specific preferences and viewing history.

2) *Handle the cold start issue:* Put techniques in place to deal with the cold start issue for both new users and recently released films. This will allow the recommendation engine to make precise recommendations even in situations when there isn't much previous data to go on.

3) *Increase recommendation accuracy:* Reduce the Probability of Irrelevant or Mismatched Suggestions. Increase the Accuracy and Relevance of Movie Recommendations. Apply cutting-edge machine learning methods, like content-based filtering, collaborative filtering, and deep learning models.

4) *Manage sparse and noisy data:* In order to ensure that the recommendation system remains robust and effective in the face of incomplete or unreliable information, develop robust approaches to manage sparse user-item interaction data and reduce the effects of noisy preferences.

5) *Adjust to changing user preferences:* Develop systems that allow the recommendation system to adjust to changing user preferences over time. These systems should include real-time or very real-time updates to account for shifts in user behavior and blockbuster patterns.

6) *Encourage content diversity:* Create algorithms that suggest films from a variety of genres, languages, and cultural backgrounds in addition to taking into account well-liked films. Urge viewers to investigate a wider range of cinematic encounters.

7) *Make sure the recommendations can be interpreted:* Use ways to help consumers understand why certain movies are recommended, including attention processes or SHAP values. To increase user confidence and trust, make the suggestion mechanism more transparent.

8) *Optimize for scalability:* Construct an architecture that is scalable to effectively manage rising movie catalogues and

user bases. Make sure there is no performance degradation when the recommendation system scales horizontally to handle the growing dataset.

9) *Integrate multi-modal data:* To improve recommendation models, make advantage of multi-modal data, such as user interactions, movie qualities, and textual content. Use efficient feature engineering approaches to get a comprehensive picture of consumer preferences and movies.

10) *Promote a seamless user experience:* Create intuitive and seamless user interfaces for online and mobile applications. To provide a happy and pleasurable user experience, make sure that users can simply access and explore suggested films.

11) *Continuous learning and model updating:* Create a framework that enables the recommendation system to keep up with new developments and modifications in user behavior. Establish systems for updating the model on a frequent basis using new data in order to keep it relevant. Measure User contentment and Engagement: Utilize analytics and metrics to assess user contentment, engagement, and the efficacy of the recommendation system. Perform user research on a regular basis to get input and insights for future enhancements.

II. LITERATURE REVIEW

S. Kanwal, S. Nawaz, M. K. Malik, and Z. Nawaz [1], this paper reviews the research from 2010 to 2020 in order to provide an extensive overview of text-based recommendation systems (RS). The large volume of textual data on the internet, which makes it difficult for users to locate pertinent information quickly, is the driving force for text-based RS. The four main areas of focus of the survey are evaluation metrics, computational methodologies, feature extraction techniques, and datasets.

S. Maneeroj and N. Srirakool [2], in this paper, a unique sequential recommender system called PPD+ is presented. It uses a personalized drift detection approach to meet evolving user preferences. By avoiding pre-defined quantities and employing soft labels for item grouping, PPD+ maximizes the number of pertinent encounters. When trained from start to finish, it outperforms baselines and content-based transformers by classifying interactions and making better suggestions. The results demonstrate the superiority of PPD+ in item group comparison and soft clustering. Zero is shown to be the ideal item utilization threshold. Future research attempts to separate noise from interactions that appear insignificant in order to uncover latent user preferences.

Y. Wang, L. Dong, H. Zhang, X. Ma, Y. Li and M. Sun [3]. This paper presents SI-MKR, a sophisticated recommendation system that expands on the MKR deep learning model. By utilizing knowledge graph representation and multi-modal information, SI-MKR improves recommendation accuracy. It tackles the drawback of multi-modal knowledge-based recommendation systems overlooking data type diversity. The model uses a deep neural network for knowledge graph embedding and feature extraction to classify user and object properties. SI-MKR combines knowledge graph data with the recommendation system through alternate training, showing

notable improvements in movie recommendation above advanced model baselines in real-world datasets. Even in sparse user-item interactions, the suggested SI-MKR model performs better than MKR, demonstrating its adaptability to a variety of data kinds. Subsequent research endeavors to include past user behavior as a pertinent characteristic and develop models to more effectively investigate user preferences.

S. Beg ,Adeel Anjum, Mansoor Ahmed, Saif Ur Rehman Malik, Hassan Malik,Navuday Sharma, Omer Waqar [4] In this study, a Reversible Data Transform (RDT) method based on chaos is introduced for Privacy-Preserving Data Mining (PPDM) in recommendation systems. This methodology, in contrast to other RDT methods, does not require previous sharing because it creates parameter values dynamically at runtime. The chaotic RDT performs better than regular RDT, as demonstrated on the Iris dataset, and can be a useful replacement in situations where resources are limited. The study verifies the algorithm's ability to replace homomorphic encryption (HE) in mobile app recommendations by extending its effectiveness to real app usage records when an adaptive recommendation approach is employed. The appendix further highlights comparable performance with original datasets on synthetic and app rating datasets.

Z. Ali, A. Muhammad, A. S. Al-Shamala, K. N. Qureshi, W. Alrawagfeh and A. Akhuzada [5] The unique approach of Long Short-Term Memory-Inter Intra-meta path Aggregation (LSTM-IIMA) in movie recommendation systems is presented in this paper. By utilizing LSTM networks with a two-level attention mechanism, LSTM-IIMA, which focuses on intra- and inter-meta path analysis, is able to capture complex relationships and connections between users, movies, and contextual components. By optimizing parameters, the model—which was learned using supervised learning—lowers prediction errors. Evaluation criteria showing the superiority of LSTM-IIMA over other methods such as HAN and MAGNN include precision, recall, AUC, and time efficiency. Even while LSTM-IIMA successfully takes care of long-term user preferences and evolving movie consumption habits, issues including sparse data, the cold start problem, interpretability, scalability, and real-time suggestions still require more research. Notwithstanding these obstacles, LSTM-based models have the ability to greatly improve the precision and customization of movie suggestions, offering more interesting and pertinent ideas to users.

X. Chen , Pengpeng Zhao, Yanchi Liu, Lei Zhao, Junhua Fang, Victor S. Sheng and Zhiming Cui [6] This article uses visual content information—movie posters and still frames in particular—to address the data sparsity problem in personalized movie recommendation. Convolutional Neural Network (CNN) characteristics and aesthetic features are integrated into a probabilistic matrix factorization framework in the proposed Aesthetic-aware Unified Visual Contents Matrix Factorization (UVMF-AES). The model extracts both the meaning of the movie (CNN features) and its aesthetic quality (aesthetic features) by using deep learning networks (OWACNN and VGG16). UVMF-AES is then produced by combining the integrated features with Probabilistic Matrix Factorization. Results from experiments on real-world datasets show that UVMF-AES performs much better in movie

recommendation than the state-of-the-art techniques, demonstrating the value of adding aesthetic aspects to increase accuracy.

M. S. Faisal, A. Rizwan, K. Iqbal, H. Fasihuddin, A. Banjar and A. Daud [7] In this study, a unique feature-based movie quality prediction mechanism is proposed that incorporates temporal factors, user reputation, and social quality. The suggested Genetic Algorithm Voting (GA-V) classifier assigns weights depending on each model's performance for each class, thereby combining the strengths of several models in the best possible way. The Movie Lens dataset is used to train conventional machine learning models, and the precision, recall, and F1 score of the suggested GA-V classifier are compared with those of the models. The outcomes demonstrate the importance of the suggested features and the GA-V classifier's potency in predicting movie quality. Future work might entail adding new features, expanding on current ones, and improving the classifier's weight assignment procedure.

X. Chen, J. Tian, X. Tian, and S. Liu. [8] Introducing the FHR ec model, which uses deep learning and heterogeneous information networks to improve recommendation system performance. To increase the accuracy of its recommendations, the algorithm makes use of reviews, ratings, and more data. It uses a heterogeneous information network (HIN) to represent rich auxiliary data and network embedding to learn entity attributes. The Deep Conn technique, a type of deep learning technology, is used to extract user and object attributes from reviews. These features are then fused individually using the attention process. Results from experiments on the Douban movie dataset and the Yelp dataset show that FHR ec performs better than conventional comparison algorithms. Through a thorough methodology, the model seeks to fully utilize the information that is now available from a variety of sources, including user evaluations and ratings. Despite its effectiveness, the model admits some flaws, such as the underuse qualities of the user and the item. Subsequent investigations will endeavor to tackle these deficiencies and investigate the integration of sentiment patterns in text evaluations for enhanced feature extraction. In addition, an investigation into the application of Graph Convolutional Networks (GCN) to extract user and item attributes from the heterogeneous information network will be conducted.

M. He, B. Wang, and X. Du [9], the study presents HI2Rec, a recommender system that integrates user and item data to improve top-N suggestions by utilizing knowledge graphs. In contrast to current approaches that prioritize item features, HI2Rec takes user-related data into account to overcome shortcomings in recommendation outcomes. The method entails taking movie-related data out of Linked Open Data and using knowledge representation learning to embed it into a single vector space with real-world datasets. The initial suggestion list is then created using the vector representations, and it is subsequently fine-tuned for accuracy using a collaborative filtering method. Findings from experiments using real-world datasets, including MovieLens-1M, show notable gains in performance over the most advanced knowledge graph-based recommendation models. Subsequent research endeavors to incorporate knowledge graphs with additional data sources such as social networks and user

feedback, investigate recommender systems based on reinforcement learning, and expand the approach to diverse industries like news, e-commerce, and music.

S. Sahu, R. Kumar, M. S. Pathan, J. Shafi, Y. Kumar and M. F. Ijaz [10], the study offers an expert method to assist in decision-making and tackles the problem of forecasting movie success early in the production process. The study forecasts target audience preferences and movie popularity using deep learning models and content-based movie recommendation systems. The recommendation method makes use of features including keywords, movie description, actor, genre, and director. The suggested CNN deep learning model outperforms benchmark models with an accuracy of 96.8%. The approach forecasts popularity across various age groups in addition to general popularity. The material covers a century's worth of movie information and comes from IMDb. The study highlights how predictive analytics may help industry decisions and recommends using multimedia data and market sentiment analysis in the future to improve forecasts.

R. Zhang and Y. Mao [11], this research presents a probabilistic framework for collaborative filtering through the introduction of a new model family called Markovian factorization of matrix process (MFMP). In contrast to time SVD++, MFMP models capture temporal dynamics in datasets while retaining a clear probabilistic formulation. In trials utilizing the Movie Lens dataset, the models show equivalent or better performance to timeSVD++ and standard tensor factorization when applied to movie rating prediction using time-stamped data. The paper makes several recommendations for improving the model, including adding global biases, integrating logistic functions, and investigating Bayesian variants. It is also described how MFMP models may be applied more broadly to collaborative filtering issues and how they could be extended to handle textual data.

S. M. Al-Ghuribi and S. A. Mohd Noah [12], this review focuses on the significance of recommender systems (RSs) in various domains and highlights the limitations of relying solely on single-criterion ratings, such as overall ratings, in the recommendation process. To address this, multi-criteria recommender systems (MCRSs) are introduced, leveraging user-generated reviews to enhance RS accuracy. The review emphasizes the extraction of valuable review elements through text mining or sentiment analysis and their integration into MCRS criteria. The survey categorizes and discusses approaches based on the review elements utilized, offering a comprehensive overview of recent research in multi-criteria review-based recommender systems. The review concludes by presenting future trends and challenges, providing valuable insights for researchers in this field.

E. Y. Keat [13], this work addresses the limitations of existing recommendation systems (RSs) that primarily focus on rating prediction accuracy and popularity, neglecting metrics like novelty and diversity. To overcome challenges in multi-objective optimization, the study proposes two deep reinforcement learning (DRL) approaches, DQNMORS and Radnor's, for RSs. These approaches optimize precision, novelty, and diversity metrics simultaneously. Comparative evaluations with a probabilistic-based multi-objective approach

show the superiority of DRL in achieving high novelty and diversity, despite some trade-offs in precision. Incorporating user latent features and leveraging LSTM layers further enhance the recommendation performance. The study sets a benchmark for future research in DRL-based RS applications and suggests exploring advanced DRL approaches and addressing challenges in optimizing multiple objectives concurrently.

H. Huang, S. Luo, X. Tian, S. Yang and X. Zhang [14] In this paper, we present an improvement on collaborative filtering (CF) based recommendation systems: The Neural Explicit Factor Model (NEFM). By including an item-feature quality matrix and a user-feature attention matrix, NEFM seeks to increase the explain ability of suggestions. The model extracts feature from the user, item, and item-feature vectors using a feedforward neural network and a one-dimensional convolutional neural network. Tests conducted on the Movie Lens and Yahoo Movies datasets show that NEFM performs better than comparable recommendation models in terms of explain ability and accuracy. The suggested paradigm holds potential for building more comprehensible recommendation systems, and future research might include adding user feedback for even more improvement.

J. Zhang, Y. Wang, Z. Yuan, and Q. Jin [15], this study discusses actual usage feedback and scalability concerns in movie recommendation systems. The suggested approach, Weighted KM-Slope-VU, clusters users into groups represented by virtual opinion leaders, effectively utilizing the profile traits of the users. As a result, the user-item matrix becomes less dimensional, which speeds up suggestions without sacrificing functionality. The algorithm is tested on Movie Lens datasets, showing reduced time complexity and performance equivalent to matrix factorization-based techniques. Movie Watch is a real-world personalized movie recommendation system that is developed, made available to the public, and has user feedback gathered for useful assessment. In the future, the algorithm will be improved by adding the newest films and refining virtual user selection to increase suggestion accuracy.

III. METHODOLOGY

A. Data Collection

The Movie Lens dataset was used in this study to train and assess the machine learning models. One popular and well-known dataset in the field of recommendation systems is Movie Lens. It includes demographic data, movie metadata, and user ratings. The dataset is relevant for training robust recommendation models because of the variety of films it contains, and the user interactions it facilitates.

1) *Feature selection*: Features taken into account for the machine learning model consist of:

a) *User-item interactions*:

- Movie ratings from users, along with detailed commentary.
- Implicit feedback that records extra user engagements, like views or clicks.

b) *Movie attributes*:

- Directors, actors, genres, and more metadata that support suggestions based on content.
- Natural language processing (NLP) techniques applied to movie textual data, such as reviews and summaries, to get a semantic understanding.

c) *Contextual features*:

- Time information, taking into account the user's interaction with a film.
- User demographic information, if it is available, to investigate how user traits affect preferences.

B. Machine Learning Model

A hybrid recommendation model that combines deep learning, content-based filtering, and collaborative filtering was used. This decision was made with the intention of utilizing the advantages of many recommendation paradigms to provide a more thorough and precise user preference prediction. Table I shows comparison of models.

1) *Collaborative filtering*: To capture user and item similarities, respectively, user- and object-based collaborative filtering methods were put into practice. Latent factors were found using matrix factorization techniques like Singular Value Decomposition.

2) *Content-Based filtering*: This method made use of film characteristics like actors, directors, and genres. Moreover, textual data was processed using NLP approaches, which allowed the model to comprehend the semantic connections between user preferences and movies.

3) *Neural Collaborative Filtering (NCF)*: To capture intricate non-linear patterns in user-item interactions, a neural collaborative filtering model—more precisely, NCF—was integrated. The neural network element improves the model's capacity to identify complex relationships in order to produce recommendations that are more accurate.

C. Evaluation Metrics

The following metrics were taken into consideration in order to assess how well the movie recommendation model performed:

1) *Precision*: This refers to the percentage of accurately recommended films among all suggestions, calculated as the accuracy of the positive forecasts.

2) *Recall*: Recall measures how well the model captures all relevant films; it expresses the percentage of relevant films that are accurately recommended out of all relevant films.

3) *F1-Score*: This balanced indicator of the model's overall performance is the harmonic mean of precision and recall.

4) *Mean Squared Error (MSE)*: This metric measures the average squared difference between the ratings that were predicted and the ratings that were received, indicating how accurate the numerical predictions were. It is employed in collaborative filtering algorithms.

These assessment metrics offer a thorough understanding of the model's functionality by taking into account both the accuracy of numerical forecasts and the precision of suggestions. The selection of metrics is in line with the objective of providing precise, pertinent, and customized movie recommendations.

TABLE I. COMPARISON OF MODELS

| Model | Precision | Recall | F1 Score |
|--------------------------------------|-----------|--------|----------|
| our Model | 0.85 | 0.78 | 0.81 |
| Neural Collaborative Filtering (NCF) | 0.82 | 0.79 | 0.80 |
| Traditional Collaborative Filtering | 0.75 | 0.72 | 0.73 |

An overview of the main procedures is provided here, along with succinct justifications. Please be aware that depending on the programming language and machine learning framework selected, the precise implementation details may change. Flowchart of the algorithm is given in Fig. 1.



Fig. 1. Flow chart of the algorithm.

D. Implications for the Field

1) *Progressing with recommendation frameworks:* The hybrid model's success emphasizes how critical it is to develop recommendation paradigms beyond content-based and collaborative filtering. Including deep learning methods into movie suggestions, like neural collaborative filtering, can greatly increase their relevance and accuracy.

2) *Improving user experience:* The research results support continued initiatives to improve movie recommendation systems' user experiences. Not only do personalized and varied recommendations boost user pleasure,

but they also solve issues like as the cold start issue, making the movie experience more captivating and delightful.

3) *Balancing complexity and interpretability:* The larger discipline of machine learning is affected by the difficulty of striking a balance between model complexity and interpretability. Finding efficient ways to explain complex models' decisions will be essential for gaining users' acceptance and trust as these models become more and more integrated into recommendation systems.

IV. RESULTS

A. Collaborative Filtering with Pearson Correlation

This solution carefully designed a movie recommendation system using collaborative filtering and Pearson correlation. At first, CSV files were used to extract and preprocess movie ratings and metadata. The user ratings matrix that resulted from the smooth fusion of pertinent data frames served as the basis for cooperative filtering. Strict measures were implemented to mitigate sparsity concerns, such as eliminating films with poor ratings and carefully imputed missing values. The system's most important component is its calculation of the Pearson correlation matrix, which measures how similar films are to one another according to user evaluations. A well-defined recommendation function was then added to provide personalized movie suggestions tailored to individual user ratings. This application showcases the effectiveness of collaborative filtering, offering personalized movie recommendations based on user interests. The displayed data, including the structural characteristics of the user ratings matrix, the Pearson correlation matrix, and sample movie recommendations, collectively demonstrate the system's capability to deliver relevant and customized cinematic suggestions (see Fig. 2).

| title | (500) Days of Summer (2009) | Adventureland (2009) | Juno (2007) | Hangover, The (2009) | Up in the Air (2009) | Toy Story 3 (2010) | Superbad (2007) |
|-------|--------------------------------------|-------------------------|----------------|----------------------------|----------------------------|--------------------------|--------------------|
| 0 | 2.500000 | 1.103859 | 1.037319 | 0.936509 | 0.929395 | 0.893285 | 0.890917 |
| 1 | 0.106251 | 0.095969 | 0.091621 | 0.130218 | 0.056696 | 0.169358 | 0.115385 |
| 2 | -0.036546 | -0.042727 | -0.103233 | -0.093200 | -0.083085 | -0.071659 | -0.141088 |
| 3 | -0.012198 | -0.060002 | -0.053986 | -0.058221 | -0.083965 | -0.055717 | -0.071980 |

Fig. 2. Collaborative filtering results for romantic movie preferences.

B. Content-Based Movie Recommendation System using TF-IDF and Cosine Similarity

In this paper the dataset used is including movie information to create this content-based movie recommendation system. We apply TF-IDF, a method that measures word importance in a document, to the textual content of each movie's synopsis. The user is prompted to enter their favorite movie after any potential missing values have been handled. After that, the system determines how similar

this selected movie is to all the others based on their TF-IDF representations. The user is recommended the top 10 films with the highest similarity ratings. This method helps users who prefer films with similar themes or descriptions by enabling personalized recommendations based on content similarities across films (see Fig. 3).

```
Enter a movie you like: Avengers: Age of Ultron
Recommended movies:
The Avengers
Iron Man 2
Iron Man
Captain America: Civil War
Knight and Day
Iron Man 3
Cradle 2 the Grave
Unstoppable
Gettysburg
The Man from U.N.C.L.E.
```

Fig. 3. Content-based movie recommendations for movie age of ultron.

C. Future Scope

1) *Dynamic user preferences*: Examine methods for recording and adjusting to the gradual changes in user preferences. This can entail investigating methods for reinforcement learning or hybrid models that can easily adjust to changing user preferences.

2) *Temporal considerations*: Incorporate temporal factors, including seasonal trends or preferred times of day, to improve the recommendation system. This can better capture the temporal dynamics of user behavior and offer recommendations that are more contextually appropriate.

3) *Contextual data*: Examine how to incorporate more contextual data, like user location, device kind, and social interactions. Contextual features offer a more thorough grasp of user preferences and can improve the relevance and personalization of recommendations.

4) *Fairness and bias mitigation*: Deal with concerns about recommendation systems' fairness and bias. Investigate and put into practice strategies to lessen user demographic biases, making recommendations fair and free of discriminating or stereotype-reinforcing tendencies.

5) *Explainable AI (XAI)*: More study to make complex models easier to understand, particularly neural collaborative filtering. Use explainable AI tools to give consumers a clear grasp of the recommendations for particular films, building user confidence and comprehension.

6) *Multi-modal recommendations*: Expand the recommendation system to include user reviews, audio, and image data. Combining several modalities might improve the model's comprehension of user preferences and movies, resulting in more accurate and nuanced suggestions.

7) *Integration of Augmented Reality (AR)*: Take into account incorporating augmented reality elements into recommendation systems to offer users engaging and

immersive experiences. AR has the potential to improve suggested content visualization and exploration.

V. CONCLUSION

To sum up, the Cinematic Curator that has been demonstrated is an advanced movie recommendation system that combines collaborative filtering, content-based filtering, and deep learning. While the integration of SHAP guarantees openness in the recommendation process, the addition of natural language processing improves its comprehension of user preferences. An easy-to-use interface, flexibility, and regular updates depending on new data all combine to provide a fluid and dynamic cinematic experience. The system's effectiveness is confirmed empirically by user research and A/B testing, showcasing its capacity to deliver accurate and personalized movie suggestions and changing the field of personalized movie recommendation systems.

REFERENCES

- [1] S. Kanwal, S. Nawaz, M. K. Malik and Z. Nawaz, "A Review of Text-Based Recommendation Systems," in IEEE Access, vol. 9, pp. 31638-31661, 2021, doi: 10.1109/ACCESS.2021.3059312.
- [2] S. Maneeroj and N. Sritrakool, "An End-to-End Personalized Preference Drift Aware Sequential Recommender System with Optimal Item Utilization," in IEEE Access, vol. 10, pp. 62932-62952, 2022, doi: 10.1109/ACCESS.2022.3182390.
- [3] Y. Wang, L. Dong, H. Zhang, X. Ma, Y. Li and M. Sun, "An Enhanced Multi-Modal Recommendation Based on Alternate Training With Knowledge Graph Representation," in IEEE Access, vol. 8, pp. 213012-213026, 2020, doi: 10.1109/ACCESS.2020.3039388.
- [4] S. Beg, Adeel Anjum, Mansoor Ahmed, Saif Ur Rehman Malik, Hassan Malik, Navuday Sharma, Omer Waqar "Dynamic Parameters-Based Reversible Data Transform (RDT) Algorithm in Recommendation System," in IEEE Access, vol. 9, pp. 110011-110025, 2021, doi: 10.1109/ACCESS.2021.3101150.
- [5] Z. Ali, A. Muhammad, A. S. Al-Shamayleh, K. N. Qureshi, W. Alrawagfeh and A. Akhunzada, "Enhancing Performance of Movie Recommendations Using LSTM With Meta Path Analysis," in IEEE Access, vol. 11, pp. 119017-119032, 2023, doi: 10.1109/ACCESS.2023.3327271.
- [6] X. Chen, Pengpeng Zhao, Yanchi Liu, Lei Zhao, Junhua Fang, Victor S. Sheng and Zhiming Cui "Exploiting Aesthetic Features in Visual Contents for Movie Recommendation," in IEEE Access, vol. 7, pp. 49813-49821, 2019, doi: 10.1109/ACCESS.2019.2910722.
- [7] M. S. Faisal, A. Rizwan, K. Iqbal, H. Fasihuddin, A. Banjar and A. Daud, "Prediction of Movie Quality via Adaptive Voting Classifier," in IEEE Access, vol. 10, pp. 81581-81596, 2022, doi: 10.1109/ACCESS.2022.3195228.
- [8] X. Chen, J. Tian, X. Tian and S. Liu, "Fusing User Reviews Into Heterogeneous Information Network Recommendation Model," in IEEE Access, vol. 10, pp. 63672-63683, 2022, doi: 10.1109/ACCESS.2022.3176727.
- [9] M. He, B. Wang and X. Du, "HI2Rec: Exploring Knowledge in Heterogeneous Information for Movie Recommendation," in IEEE Access, vol. 7, pp. 30276-30284, 2019, doi: 10.1109/ACCESS.2019.2902398.
- [10] S. Sahu, R. Kumar, M. S. Pathan, J. Shafi, Y. Kumar and M. F. Ijaz, "Movie Popularity and Target Audience Prediction Using the Content-Based Recommender System," in IEEE Access, vol. 10, pp. 42044-42060, 2022, doi: 10.1109/ACCESS.2022.3168161.
- [11] R. Zhang and Y. Mao, "Movie Recommendation via Markovian Factorization of Matrix Processes," in IEEE Access, vol. 7, pp. 13189-13199, 2019, doi: 10.1109/ACCESS.2019.2892289.

- [12] S. M. Al-Ghuribi and S. A. Mohd Noah, "Multi-Criteria Review-Based Recommender System–The State of the Art," in *IEEE Access*, vol. 7, pp. 169446-169468, 2019, doi: 10.1109/ACCESS.2019.2954861.
- [13] E. Y. Keat et al., "Multiobjective Deep Reinforcement Learning for Recommendation Systems," in *IEEE Access*, vol. 10, pp. 65011-65027, 2022, doi: 10.1109/ACCESS.2022.3181164.
- [14] H. Huang, S. Luo, X. Tian, S. Yang and X. Zhang, "Neural Explicit Factor Model Based on Item Features for Recommendation Systems," in *IEEE Access*, vol. 9, pp. 58448-58454, 2021, doi: 10.1109/ACCESS.2021.3072539.
- [15] J. Zhang, Y. Wang, Z. Yuan and Q. Jin, "Personalized real-time movie recommendation system: Practical prototype and evaluation," in *Tsinghua Science and Technology*, vol. 25, no. 2, pp. 180-191, April 2020, doi: 10.26599/TST.2018.9010118.

Sentiment Analysis of Pandemic Tweets with COVID-19 as a Prototype

Mashail Almutiri, Mona Alghamdi, Hanan Elazhary

Information Systems and Technology Department, University of Jeddah, Jeddah, Saudi Arabia

Abstract—One of the most important applications of text mining is sentiment analysis of pandemic tweets. For example, it can make governments able to predict the onset of pandemics and to put in place safe policies based on people's feelings. Many research studies addressed this issue using various datasets and models. Nevertheless, this is still an open area of research in which many datasets and models are yet to be explored. This paper is interested in the sentiment analysis of COVID-19 tweets as a prototype. Our literature review revealed that as the dataset size increases, the accuracy generally tends to decrease. This suggests that using a small dataset might provide misleading results that cannot be generalized. Hence, it is better to consider large datasets and try to improve analysis performance on it. Accordingly, in this paper we consider a huge dataset, namely COVIDSenti, which is composed of three sub datasets (COVIDSenti_A, COVIDSenti_B, and COVIDSenti_C). These datasets have been processed with a number of Machine Learning (ML) models, Deep Learning (DL) models, and transformers. In this paper, we examine other ML and DL models aiming to find superior solutions. Specifically, we consider Ridge Classifier (RC), Multinomial Naïve Bayes (MNB), Stochastic Gradient Descent (SGD), Support Vector Classification (SVC), Extreme Gradient Boosting (XGBoost), and the DL Gated Recurrent Unit (GRU). Experimental results have shown that unlike the models that we tested, and the state-of-the-art models on the same dataset, SGD technique with count vectorizer showed quite constantly high performance on all the four datasets.

Keywords—COVID-19; deep learning; machine learning; sentiment analysis; text mining; tweets

I. INTRODUCTION

Text Mining (TM) deals with the automatic extraction of interesting information from text. It uses data mining techniques to extract information that is hidden within huge amounts of unstructured textual data. Such extracted information is typically transformed into a structured format that can be further processed, possibly using Natural Language Processing (NLP) techniques. Sentiment Analysis (SA) is a text mining approach that utilizes data science techniques including Machine Learning (ML) and Deep Learning (DL) to analyze text and identify subjective information. It is concerned with assessing feelings and opinions, and classifying them into polarities, which are typically either positive, negative, or neutral. Social media are popular networks such as Facebook and X (formerly, Twitter) that are used by users to share their reviews about various topics and incidents. Additionally, one of the main uses of the Internet is checking reviews of others and expressing personal opinions. Since

social media posts are mainly about expressing feelings and opinions, some researchers believe that Opinion Mining (OM) refers to social media SA. SA and OM are often used interchangeably. We adopt the term SA in this paper.

One of the most important and popular social media platforms is X in which users express their opinions using tweets. Since social media has a great influence on society, tweets about pandemics would most probably stimulate fear and agony. Tweets data mining can be very helpful in generating important health-related facts. For example, many research studies have shown that tweets can be exploited in the prediction of the onset of pandemics or diseases. SA of tweets is thus of special importance during pandemics. It is of great benefit to people's lives as it makes governments able to put in place safe policies based on inferred people's feelings.

A recent example of such pandemics is Coronavirus Disease 2019 (COVID-19). On March 11th, 2020, the World Health Organization (WHO) announced COVID-19 as a pandemic. Since at that time, no known effective vaccines or treatments existed, the governments and public health sectors had to take some precautionary decisions to avoid the spread of the infection, including isolation, quarantine, and emergency lockdown. During this period, COVID-19 had a negative effect on various aspects of people's lives, and because the lockdown gave them more free time, the subject of the greatest portion of posts and tweets at that time was that pandemic. Many research studies have been concerned with SA of COVID-19 tweets using various datasets and various models (ML, DL, and transformers) [1-9]. Nevertheless, SA of pandemic tweets in general is still an open area of research in which many datasets and numerous models are yet to be explored.

This paper is concerned with the SA of tweets during pandemics and considers COVID-19 as a prototype. In other words, the research problem is how to analyze tweets during pandemics and decide whether their sentiment is positive, negative, or neutral. Literature review has revealed that accuracy generally tends to decrease with the increase of the dataset size. This suggests that results based on relatively small-sized datasets might be misleading. Hence, we decided to work with large datasets and try to find better solutions for analyzing them. Towards this goal, we manipulated a huge dataset, namely COVIDSenti and its three sub-datasets (COVIDSenti_A, COVIDSenti_B, and COVIDSenti_C) [8]. These datasets have been processed with a number of ML models, DL models, and transformers. In this paper, we examine other ML and DL models aiming to find superior

solutions. The contributions of the paper can be summarized as follows:

- Searching for better performing ML and DL model(s) for SA of COVIDSenti tweets through a set of experiments.
- Comparison of the results of the various models with the state of the art to gain insights that can guide future research.

The rest of this paper is organized as follows: Section II presents related work on COVID-19 tweet analysis. Section III explains the proposed methodology that this article follows. Section IV discusses the datasets and the data preprocessing techniques. Models and experimental settings are presented in Section V. In Section VI, we compare their performance with the state of the art. Finally, Section VII depicts conclusions and draws directions for future work for further improvements.

II. RELATED WORK

Several research studies studied sentiment analysis of COVID-19 tweets. We discuss a recent sample in the order of the dataset size. For example, Shofiya and Abidi [1] extracted 629 Canadian tweets from an open-source publicly available IEEE website. They used SentiStrength tool to detect sentiment polarity in combination with Support Vector Machine (SVM) classifier. The highest achieved accuracy of 87% was achieved on 10% test data. They concluded that a large dataset is required to increase the performance of the algorithm. On the other hand, Chintalapudi et al. [2] considered Indian tweets and obtained from github.com a dataset consisting of 3,090 tweets extracted from the Indian Twitter platform. The tweets were classified into “afraid,” “sad,” “angry,” and “happy.” They compared Bidirectional Encoder Representations from Transformers (BERT), Logistic Regression (LR), SVM, and Long Short-Term Memory (LSTM). The accuracy has been used as a metric to evaluate the models. The results showed that the BERT model outperformed the other models with 89% accuracy. Gupta et al. [3] also considered Indian tweets and processed 7,284 tweets having the keyword *India lockdown*. They compared MNB, Bernoulli Naïve Bayes (NB), LR, linear SVC, AdaBoost, Ridge classifier, passive aggressive (PA) classifier, and a perceptron using accuracy, precision, recall, and F1-score. In their experiments, linear SVC with unigram showed best performance with 84.4% accuracy, 83.5% precision, 82.4% recall, and 82.5% F1-score.

Ramya et al. [4] considered a slightly larger dataset consisting of 11,000 tweets (10,000 for training and 1000 tweets for testing) and used NB and LR to process them combined with *n-grams*. They also used accuracy as their metric. Interestingly, in their experiment, NB showed accuracy of about 92.49% for short tweets (less than 70 characters) and much lower accuracy of only 60.56% in the case of longer tweets.

Other researchers considered relatively larger datasets. For example, Goel and Sharma [5] collected a dataset comprised of 42,468 tweets. They analyzed them using SVC, Random Forest (RF), a neural network (NN) which is a combination of convolutional NN (CNN) and LSTM, and BERT. To evaluate

the performance, they used Area Under the Receiver Operating Characteristic Curve (AUC). In their experiment, the best model was RF with 96% AUC accuracy. Vernikou et al. [6] used another dataset consisting of 44,955 tweets. Their goal was to classify tweets into negative, neutral or positive. They used seven different DL models based on LSTM, and a set of ML models (MNB, Decision Tree (DT), and RF). The models were evaluated using accuracy, precision, recall, and F1-score. In their experiment, one of the LSTM-based models, namely BERT Tokenizer LSTM showed the best performance with 90% accuracy, precision, recall, and F1-score. Qi and Shabrina [7] extracted a total of 77,332 unique tweets and processed those using RF, MNB and SVC models. Performance was evaluated using precision, recall, F1-score, and accuracy. They also considered three different methods of feature representation, namely, bag of words (BoW), TF-IDF, and Word2Vec. In their experiments, the SVC using BoW or TF-IDF showed the best performance with accuracy of 71%.

Naseem et al. [8] prepared the largest dataset that we encountered in our literature review. This is the COVID Senti dataset which is composed of 90,000 unique tweets from 70,000 users. This dataset was divided into three subsets, namely, COVID Senti_A, COVID Senti_B, and COVID Senti_C. This dataset, that we adopt in this paper, is discussed together with its subsets in more details in Section IV. The four datasets were analyzed using SVM, NB, RF, and DT. In addition to those ML models, they utilized CNN and Bi-directional LSTM (Bi-LSTM). This is in addition to a set of hybrid models and transformers that we do not consider in the current research. Accuracy has been used as a metric to evaluate performance. Experimental results have shown that among the ML models considered, SVM and RF with FastText embedding showed accuracy of 84.5% on COVIDSenti. On the other hand, among the DL models considered, CNN with Glove word embedding showed higher performance of 86.9% on the same dataset.

Jalil et al. [9] used the same dataset in their experiments. They examined a set of different ML models, namely K-Nearest Neighbors (KNN), LR, ensemble, XGBoost, SVM, NB, DT, and RF. They also examined a set of deep learning models based on CNN and BiLSTM. This is in addition to a set of hybrid models and transformers, which as previously noted, is not considered in this research study. They also used accuracy for performance evaluation. Among the ML models, XGBoost showed the best performance with 89.81% accuracy on COVIDSenti. On the other hand, among the DL models, a combination of CNN, LSTM and Glove word embedding showed the best performance with 87.06% accuracy on the same dataset.

The related work is summarized in Table I. As shown in the table, researchers used different models and datasets for SA of COVID-19 tweets. We notice that as the dataset size increases, the accuracy generally tends to decrease. This suggests that using a small dataset might provide misleading results that cannot be generalized. Hence, it is better to consider large datasets and try to improve analysis performance on it. Accordingly, in this paper we consider the largest dataset that we encountered, namely, COVIDSenti and its three subsets. Also, we limit our research study to ML and DL models

aiming to find better solutions that would be used in case of any future pandemic. Towards this goal, we consider additional models in comparison to those used on the same dataset [8-9].

TABLE I. SUMMARY OF RELATED WORK

| Ref No. | Dataset | Models | Metrics | Best Results |
|---------|--|---|---|---|
| [1] | 629 tweets extracted from an open-source free IEEE website | SVM | confusion matrix, precision, recall, and F1-score | 87% accuracy on 90% training data |
| [2] | 3,090 tweets from the Indian Twitter platform | BERT, LR, SVM, LSTM | accuracy | BERT with 89% accuracy |
| [3] | 7,284 tweets having the keyword <i>India lockdown</i> | MNB, Bernoulli NB, LR, Linear SVC, AdaBoost, Ridge classifier, passive aggressive (PA) classifier, perceptron | accuracy, precision, recall, F1-score | Linear SVC with unigram with 84.4% accuracy, 83.5% precision, 82.4% recall, and 82.5% F1-score |
| [4] | 11,000 tweets (10,000 for training and 1000 tweets for testing) | NB and LR | accuracy | NB with 91% accuracy on short tweets |
| [5] | 42,468 tweets | SVC, RF, NN, BERT | AUC | RF with 96% AUC |
| [6] | 44, 955 tweets | Seven LSTM-based models, MNB, DT, RF | accuracy, precision, recall, F1-score | Bert Tokenizer LSTM with 90% accuracy, precision, recall, and F1-score |
| [7] | 77,332 tweets | RF, MNB, SVC | precision, recall, F1-score, and accuracy | SVC using BoW or TF-IDF with 71% accuracy |
| [8] | COVIDSenti, composed of 90,000 tweets and its three subsets (COVIDSenti_A, COVIDSenti_B, and COVIDSenti_C) | ML (SVM, NB, DT, RF), DL (CNN, BiLSTM), and a set of hybrid models and transformers | accuracy | ML models: SVM and RF with FastText embedding with 84.5% accuracy on COVIDSenti DL models: CNN with Glove word embedding with 86.9% accuracy on COVIDSenti |
| [9] | COVIDSenti, composed of 90,000 tweets and its three subsets (COVIDSenti_A, COVIDSenti_B, and COVIDSenti_C) | ML (KNN, LR, Ensemble, XGBoost, SVM, NB, DT, RF), DL (CNN, BiLSTM), and a set of hybrid models and transformers | accuracy | ML models: XGBoost with 89.81% accuracy on COVIDSenti DL models: a combination of CNN, LSTM and Glove word embedding with 87.06% accuracy on COVIDSenti |

III. METHODOLOGY

The methodology pipeline shown in Fig. 1 follows a typical data analytics lifecycle. As shown in the figure, COVID-19 tweets are first pre-processed, and features are extracted from them. Then two experiments are conducted. The first considers a set of ML models preceded by data vectorization (represented as numeric vectors). The second, on the other hand, involves

the Gated Recurrent Unit (GRU) DL model. This involves a different data representation technique. This is followed by discussing and comparing the results of both experiments. Finally, we compare our results with those of the state-of-the-art surveyed research.

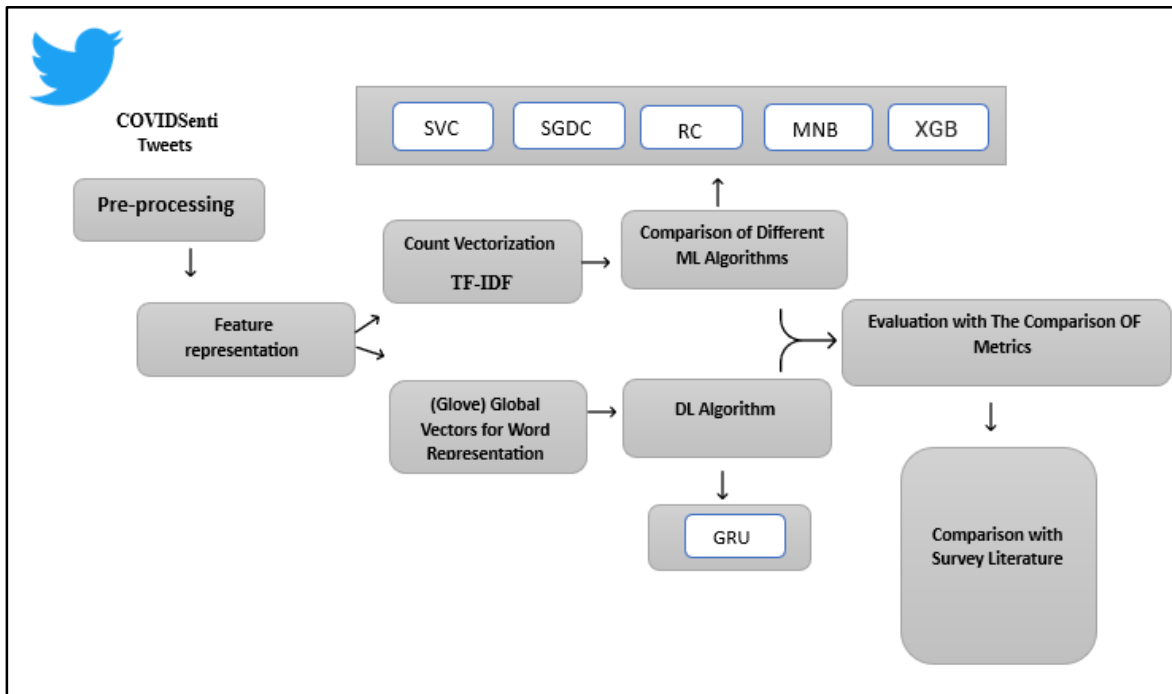


Fig. 1. Overview of the proposed approach.

IV. DATASETS AND DATA PREPROCESSING

In this section, we discuss the details of the datasets utilized in the experiments and how we pre-processed them before building our models.

A. Datasets Details

As previously noted, in this research study, we consider the COVIDSenti dataset. This dataset is sourced from the open-source hosting site GitHub and consists of 90,000 unique tweets from 70,000 users about COVID-19 from February 2020 to March 2020. Naseem et al. [8] divided the COVIDSenti dataset into three subsets for evaluation and generalization purposes: COVIDSenti_A, COVIDSenti_B, and COVIDSenti_C. They treated them as four different datasets and we adopt the same approach. Each of the four datasets, for classification purposes, has three sentiments: positive, negative, and neutral. Table II provides an overview of these datasets. As shown in the table, overall, the neutral sentiments form the highest percentage of COVIDSenti and its subsets.

B. Data Preprocessing

Tweets generally form a huge, noisy dataset that requires numerous pre-processing steps. The tweets in our datasets were processed using Python libraries namely Natural Language Toolkit (NLTK), NeatText, and Regular Expression (RE). The following techniques were applied in the following order:

- Any hashtag in the dataset conveys important information. The topic of almost every social media site is represented using a hashtag such as #COVID19, #CoronavirusOutbreak, #COVID, and #Coronavirus. As a result, we simply eliminated the "#" symbol.
- To avoid considering words with uppercase letters different from the same words with lowercase letters, all words are converted to lowercase.
- Stop words are the common frequently occurring words, which should be ignored because they do not provide any meaningful information. Removing these stop words is especially useful when building text classification models to reduce the amount of data.
- The fourth step is to remove hyperlinks, @ mentions, multiple white spaces, emojis, and punctuation, as well as special characters. This is because all these do not affect the understanding of the sentences of the tweets and do not help in detecting sentiment.

- We used a lemmatization technique to reduce inflected words to their basic forms, e.g., "Mostly" to "Most" or "viruses" to "virus."

V. MODELS AND EXPERIMENTAL SETTING

In this section, we discuss the details of the ML and DL models used in our experiments. We also discuss the details of the experiments including the experimental setting and hyperparameters.

A. ML Models

The Python library Scikit-learn has many ML classifiers. We employed five ML classification models as follows:

Multinomial Naïve Bayes (MNB) - This idea of this model is based Naïve Bayes Theorem, which calculates the probability of each of a set of classes, and the class with the highest probability is considered the winning class for classification. It is thus suitable for text classification with multiple classes [6].

Linear Support Vector Classification (Linear SVC) – This model treats each data item as a vector and searches for a linear separator of the classes in their vector space. In higher-dimensional spaces, a hyperplane is computed. Features extracted from the input data are classified based on this plane. To obtain the optimal hyperplane, a margin between the classes is maximized based on the distance between the nearest vectors of the classes, which are called support vectors [3].

Extreme Gradient Boosting (XGBOOST) – This model is based on the decision tree classifier. An ensemble of such trees is usually employed, e.g., gradient boosting machines. XGBoost is an extension to this model for speedup and improved performance, with minimal resources [10].

Ridge Classifier (RC) – This is a variation of Ridge Regression. This linear classifier is suitable when the number of features is high and exceeds the number of observations regardless of whether the problem is binary or multi-class [11].

Stochastic Gradient Descent (SGD) – The idea of gradient descent is to use data to compute the gradient of an objective function to reach its minima. One of the three variants of gradient descent is SGD, which frequently updates the model's parameters with high variance, causing significant variations. This gives it the capability to find new and hopefully, superior local minima in comparison to its counterparts [12] [13].

TABLE II. OVERVIEW OF THE DATASETS

| Dataset | Positive | | Negative | | Neutral | | Total | |
|--------------|----------|-----|----------|------|---------|------|--------|-----|
| | count | % | count | % | count | % | count | % |
| COVIDSenti_A | 1,968 | 6.6 | 5,083 | 16.9 | 22,949 | 76.5 | 30,000 | 100 |
| COVIDSenti_B | 2,033 | 6.8 | 5,471 | 18.2 | 22,496 | 75.0 | 30,000 | 100 |
| COVIDSenti_C | 2,279 | 7.6 | 5,781 | 19.3 | 21,940 | 73.1 | 30,000 | 100 |
| COVIDSenti | 6,280 | 7.0 | 16,335 | 18.2 | 67,835 | 74.9 | 90,000 | 100 |

TABLE III. DEFAULT HYPERPARAMETERS

| RC | | Multinomial NB | | SGD | | | | Linear SVC | | XGBoost | | | |
|---------------|--------|----------------|-------|---------------|--------|---------------------|---------|-------------------|---------------|------------------|----------------|-------------------|-------|
| Parameter | Value | Parameter | Value | Parameter | Value | Parameter | Value | Parameter | Value | Parameter | Value | Parameter | Value |
| alpha | 1.0 | alpha | 1.0 | loss | hinge | random_state | None | penalty | l2 | max_depth | 3 | colsample_bytree | 1 |
| fit_intercept | True | force_alpha | warn | penalty | l2 | learning_rate | optimal | loss | squared_hinge | learning_rate | 0.1 | colsample_bylevel | 1 |
| copy_X | True | fit_prior | True | alpha | 0.0001 | eta0 | 0.0 | dual | True | n_estimators | 100 | reg_alpha | 0 |
| max_iter | None | class_prior | None | l1_ratio | 0.15 | power_t | 0.5 | tol | 0.0001 | silent | True | reg_lambda | 1 |
| tol | 0.0001 | | | fit_intercept | True | early_stopping | False | C | 1.0 | objective | multi:softprob | scale_pos_weight | 1 |
| class_weight | None | | | max_iter | 1000 | validation_fraction | 0.1 | multi_class | ovr | booster | Gbtree | base_score | 0.5 |
| solver | auto | | | tol | 0.001 | n_iter_no_change | 5 | fit_intercept | True | n_jobs | 1 | random_state | 0 |
| positive | False | | | shuffle | True | class_weight | None | intercept_scaling | 1 | nthread | None | seed | None |
| random_state | None | | | verbose | 0 | warm_start | False | class_weight | None | gamma | 0 | missing | None |
| | | | | epsilon | 0.1 | average | False | verbose | 0 | min_child_weight | 1 | | |
| | | | | n_jobs | None | | | random_state | None | max_delta_step | 0 | | |
| | | | | random_state | None | | | max_iter | 1000 | subsample | 1 | | |

B. DL Model

The basic idea of any DL architecture is to emulate how the human brain works. Such architecture is typically layered, and each layer provides the input to the next. The network learns as each training dataset item is fed to it and saves what it has learnt in the form of weights. As an output is generated, it is compared to the correct desired one and in the case of a mismatch, the weights are updated. This continues until the global error is minimized. The network then becomes ready for its task.

One of the most popular DL architectures is Recurrent Neural Network (RNN). The typical structure of an RNN cell is shown in Fig. 2. As shown in the figure, over time, the network is visualized as a set of similar sequential feedforward cells. This gives it the ability to memorize data with long-term dependencies such as language models. Nevertheless, as the length of such a sequence increases, the problem of vanishing gradient affects the ability of the model to continue learning. Accordingly, other variants have been proposed.

LSTMs are the most common types of RNNs intended to address the vanishing gradient problem of a typical RNN cell. A typical LSTM cell is shown in Fig. 3. As shown in the figure, its success stems from the existence of a cell state that acts as a memory and three gates, namely input, output and forget respectively. This provides a LSTM cell with a relatively long memory in comparison to the short memory of a basic RNN cell. This gives it the name ‘Long Short Term Memory.’

GRU [15] is a simplified variant of LSTM. A typical GRU cell is depicted in Fig. 4. As shown in the figure, the GRU cell has no cell state like LSTM cells. Instead, it uses an invisible state. It also has two gates only, a reset gate and an update gate, that incorporate the functions of the input and forget gates of LSTM. The update gate acts like a long-term memory while the reset gate acts as a short-term memory. This makes GRU

easier and faster to train and run. Nevertheless, GRU cells might not be as capable as LSTM cells when it comes to memorizing long-term dependencies as is the case with language models. Thus, this tradeoff needs to be taken into consideration to benefit from their efficiency while avoiding their drawback.

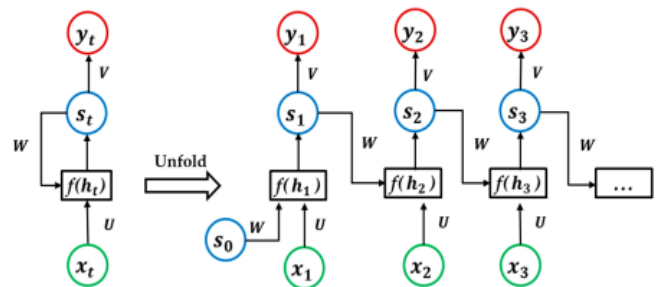


Fig. 2. Schematic diagram of RNN cell [14].

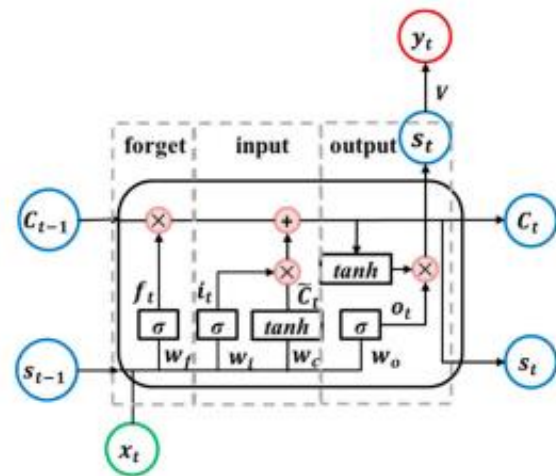


Fig. 3. Schematic diagram of LSTM cell [14].

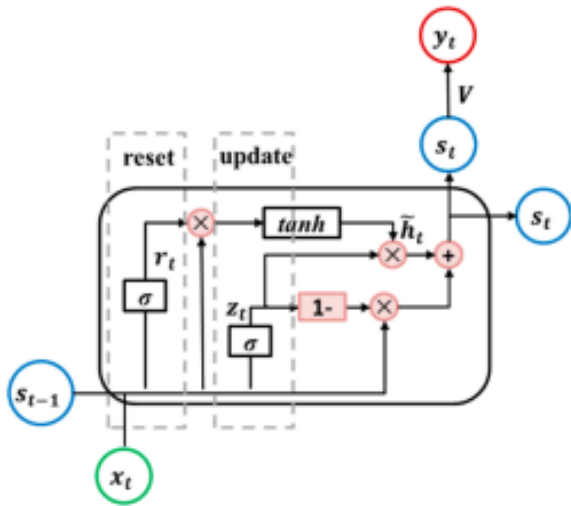


Fig. 4. Schematic diagram of GRU cell [14].

C. Experimental Setting of the ML Models

The problem with text is that it is generally considered unstructured. To be able to process it, it needs to be preprocessed and converted into numeric data. This is enabled through NLP feature extraction techniques. In this paper, we used two different feature extraction techniques, namely count vectorizer and TF-IDF. In count vectorizer approach, text in a given document or tweet is vectorized based on its count. This is computed for each word that appears in the entire corpus. On the other hand, TF-IDF also takes into consideration the uniqueness and thus the importance of each term in the whole corpus [16]. In addition to vectorizing text, each ML model that we employed has its own set of hyperparameters. For each ML model, we utilized the default values as shown in Table III.

1) *K-Fold Cross-Validation (KCV)* is a commonly used approach for evaluating the performance of ML models while reducing the chance of overfitting. In KCV, the dataset is first partitioned into a set of K equal-sized folds. Each fold is used once as the test data, while using the rest of the data for

training. After exhausting the folds (through K-iterations, the average of a given performance metric is computed [17]. Stratified K-Fold Cross-Validation (SKCV) is an extension of KCV, where class distribution in the original data is taken into consideration when sampling [18]. Accordingly, SKCV is preferred over KCV in the case of unbalanced class distributions [19]. In our experiments, we used SKCV, specifically 10-fold cross validation, to split the data into training and testing, while computing the average accuracy of the different folds.

D. Experimental Setting of the DL Model

In our experiments, we decided to use the efficient GRU model. The model layers include, in addition to the basic components, one embedding layer, two dropout layers, and a dense layer. The embedding layer is used for preprocessing and vectorizing a vocabulary of size 10,000. It is followed by a dropout layer, with dropout rate of 0.2 to help reduce the complexity of the model and the probability of the model overfitting. GRU layer follows the drop out layer with 128 units followed again by another dropout layer with a rate of 0.2. At the end, a dense layer with 3 neurons and a Softmax activation function is used to get the probabilities of the possible classes. In the experiments, we used Global Vectors (GloVe)-based word representation to learn word embeddings from text documents. A pre-trained word embedding GloVe with two billion tweets, 27 billion tokens, and 1.2 million vocabularies was used to generate a 100-dimensional vector from text.

Finally, we divided the dataset into training data and testing data subsets. 80% of tweets were used for training purposes and the remaining 20% were used for testing. Training tweets help identify the data patterns and thus reduce error rates of the test data subset used for the assessment of the model performance. We also used Adam optimizer to minimize the cross-entropy loss with a batch size of 36 and 10 epochs. This is in addition to using Softmax activation for multi-classes probabilities, and early stopping to reduce overfitting on a Google Colab GPU.

TABLE IV. ML CLASSIFIERS WITH DIFFERENT EVALUATION METRICS USING COUNT VECTORIZER

| Model dataset | COVIDSenti_A | | | | COVIDSenti_B | | | | COVIDSenti_C | | | | COVIDSenti | | | | |
|-------------------------|--|--------------------|---------------|-----------------|------------------|--------------------|---------------|-----------------|------------------|--------------------|---------------|-----------------|------------------|--------------------|---------------|-----------------|------------------|
| | Proposed model/Metric (Accuracy – Precision – Recall – F1-Score) | | | | | | | | | | | | | | | | |
| | | Accur acy | Precisi on | Rec all | F1- Sco re | Accur acy | Precisi on | Rec all | F1- Sco re | Accur acy | Precisi on | Rec all | F1- Sco re | Accur acy | Precisi on | Rec all | F1- Sco re |
| Count Vectori zer | RC | 84.84 % | 84% | 85% | 84 % | 84.12 % | 83% | 84% | 83 % | 82.78 % | 82% | 83% | 82 % | 84.79 % | 84% | 85% | 84 % |
| | MNB | 78.51 % | 75% | 79% | 76 % | 78.03 % | 75% | 78% | 76 % | 76.97 % | 74% | 77% | 75 % | 78.81 % | 76% | 79% | 77 % |
| | SGD | 86.75 % | 86% | 87 % | 86 % | 86.07 % | 85% | 86 % | 85 % | 85.05 % | 84% | 85 % | 84 % | 86.19 % | 85% | 86 % | 85 % |
| | Linear SVC | 84.73 % | 84% | 85% | 84 % | 84.27 % | 84% | 84% | 84 % | 82.76 % | 82% | 83% | 82 % | 85.60 % | 85% | 86% | 85 % |
| | XGBo ost | 84.99 % | 84% | 85% | 83 % | 84.11 % | 84% | 84% | 82 % | 82.43 % | 82% | 82% | 81 % | 84.10 % | 84% | 84% | 82 % |

VI. RESULTS AND DISCUSSION

In this section, we provide the results and discussion of the ML models and the DL model. We then compare both results to each other and to the results of the surveyed research.

A. Results of the ML Models

Table IV shows comparison between the five ML models that used count vectorizer embedding in terms of accuracy, precision, recall, and F1-score. The results of the experiment show that the SGD model performed better than all the other models that used count vectorizer on COVIDSenti_A, COVIDSenti_B, COVIDSenti_C, and COVIDSenti with 86.75%, 86.07%, 85.05%, and 86.19% accuracy respectively. Moreover, RC, Linear SVC, and XGBoost showed almost similar performance with average accuracy of 84.85%, 84.17%, 82.66%, and 84.83% on the four datasets respectively. Finally, MNB showed the worst performance with accuracies of 78.51%, 78.03%, 76.97%, and 78.81% respectively. The same is also true about the other performance metrics except that when considering the whole dataset, namely COVIDSenti, linear SVC was almost as good performing as SGD. Thus, it may be considered to be the second best. What is interesting about SGD is that it is the only model to show almost the same performance on all datasets with little variability.

Table V presents the results of comparing the five ML models on COVIDSenti_A, COVIDSenti_B, COVIDSenti_C, and COVIDSenti in the case of the TF-IDF feature extraction technique. Unlike the case of count vectorizer, linear SVC outperformed SGD, RC, XGBoost and MNB and showed the best performance with 85.50%, 85.10%, 83.65% and 85.59% accuracy on COVIDSenti_A, COVIDSenti_B, COVIDSenti_C and COVIDSenti respectively. In this table, we compare our models with the best models in the surveyed literature using the same datasets, and with embeddings other than count vectorizer. Looking at the table, it is clear that linear SVC was also able to outperform these models across all datasets. Nevertheless, its performance is still lower than that of SGD with count vectorizer. Additionally, its performance is not as uniform as that of the latter. Again, MNB showed the worst performance among its counterparts.

B. Results of the DL Model

Fig. 5 and Table VI show the learning accuracy and loss curves and the classification reports of the GRU-based DL

model that we employed. As shown in the figure, learning proceeded successfully until different epochs for each dataset, after which though training accuracy continued increasing and training loss continued decreasing. Similarly, validation accuracy started decreasing and its loss started increasing suggesting overfitting. Hence, we had to use early stopping that was different from the different datasets. Additionally, as shown in Table VI, the neutral class had the best performance among its other two counterparts.

In Table VII, we compare the results of our proposed DL model with those of the best performing models in the research studies using the same datasets. As shown in the table, our model was not able to outperform the other models. Nevertheless, none of the model was the best across all datasets and none showed uniform performance among them either. For example, though DCNN-(GloVe+CNN) was the best on COVIDSenti_C and COVIDSenti, Conv1D-LSTM + Glove was the best on COVIDSenti_A and COVIDSenti_B. Additionally, both had variable performance among the four datasets.

C. Discussion of Results

Based on the experiments and the related studies on the same datasets, among the ML models [8, 9], the proposed SGD model with count vectorizer showed the best performance, and linear SVC with TF-IDF showed the second best. On the other hand, among the DL models [8, 9], none was the best in all cases. DCNN- (GloVe+ CNN) showed the best performance in the case of COVIDSenti and COVIDSenti_C, while Conv1D-LSTM + Glove showed the best performance in the case of COVIDSenti_A and COVIDSenti_B. These models had slightly higher performance in comparison to SGD with count vectorizer. Nevertheless, the latter was the only model that showed almost uniform performance among the four datasets. This implies that the proposed SGD model with count vectorizer is the most reliable among its counterparts.

Another important observation in our experiments is that the highest performances encountered, whether using ML models or DL models, were all lower than 90%. This suggests that the capabilities of the various ML and DL models might be limited to this performance level. This is the main challenge and limitation of our work, which indicates that it's worth exploring large language transformers. This is the topic of our future work.

TABLE V. ML CLASSIFIERS WITH DIFFERENT EVALUATION METRICS USING TF-IDF OR FASTTEXT

| Model dataset | | COVIDSenti_A | COVIDSenti_B | COVIDSenti_C | COVIDSenti |
|--------------------------------|------------|---------------|---------------|---------------|---------------|
| Existing model/Accuracy [8, 9] | | | | | |
| TF-IDF | SVM | 83.9% | 83.0% | 82.8% | 84.5% |
| FastText | RF | 82.3% | 84.1% | 80.2% | 84.5% |
| Proposed model/Accuracy | | | | | |
| TF-IDF | RC | 84.67% | 84.1% | 82.76% | 84.82% |
| | MNB | 77.31% | 76.03% | 74.49% | 76.28% |
| | SGD | 83.31% | 82.52% | 80.86% | 81.16% |
| | Linear SVC | 85.50% | 85.10% | 83.65% | 85.59% |
| | XGBoost | 84.54% | 83.6% | 82.18% | 83.95% |

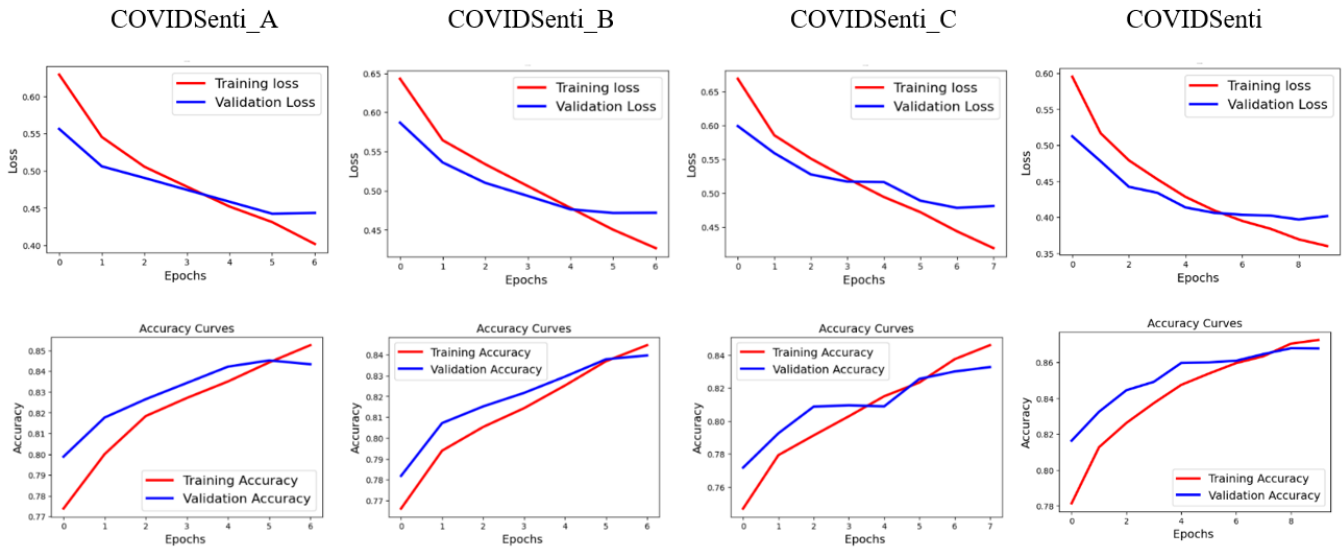


Fig. 5. GRU model accuracy and loss for each dataset.

TABLE VI. DL CLASSIFICATION REPORT USING GLOVE

| Sentiment | COVIDSenti | | | COVIDSenti_A | | | COVIDSenti_B | | | COVIDSenti_C | | |
|-----------|------------|--------|----------|--------------|--------|----------|--------------|--------|----------|--------------|--------|----------|
| | Precision | Recall | F1-Score | Precision | Recall | F1-Score | Precision | Recall | F1-Score | Precision | Recall | F1-Score |
| Neutral | 88.8% | 94.5% | 91.5% | 86.0% | 95.1% | 90.3% | 84.9% | 95.9% | 90.0% | 83.5% | 96.3% | 89.5% |
| Negative | 80.8% | 68.1% | 73.9% | 75.3% | 54.4% | 63.2% | 80.1% | 53.7% | 64.3% | 83.3% | 53.5% | 65.1% |
| Positive | 73.2% | 86.8% | 84.3% | 84.0% | 83.3% | 86.8% | 84.3% | 84.0% | 83.3% | 86.8% | 84.3% | 46.6% |
| Accuracy | 86.8% | | | 84.3% | | | 84.0% | | | 83.3% | | |

TABLE VII. COMPARISON OF PROPOSED DL CLASSIFIER ACCURACY WITH BASELINE

| Model dataset | COVIDSenti_A | COVIDSenti_B | COVIDSenti_C | COVIDSenti |
|---------------------------------------|--------------|--------------|--------------|--------------|
| Existing model/Accuracy [8, 9] | | | | |
| DCNN- (GloVe+ CNN) | 83.4% | 83.2% | 86.4% | 86.9% |
| Conv1D-LSTM + Glove | 87.0% | 86.1% | 84.4% | 86.9% |
| Proposed model/Accuracy | | | | |
| GRU+GloVe pretrain | 86.8% | 84.3% | 84.0% | 83.3% |

VII. CONCLUSION AND FUTURE WORK

This paper is concerned with sentiment analysis of tweets during pandemics with COVID-19 as a prototype. Our related work review showed that as the dataset size increases, the accuracy generally tends to decrease. This suggests that using a small dataset might provide misleading results that cannot be generalized. Hence, it is better to consider large datasets and try to improve analysis performance on it. Accordingly, in this paper we considered a huge dataset namely COVIDSenti and its three sub-datasets. We experimented with a set of machine learning techniques (MNB, SVC, XGBoost, RC, and SGD) and a customized deep-learning GRU model. The experiments showed that unlike the models that we tested, and the state-of-the-art models on the same dataset, SGD technique with count vectorizer showed quite constantly high performance on all the four datasets. As future work, we intend to use grid search with the ML models to figure out whether we could obtain even

better results. We will also examine additional ML and DL models aiming at achieving higher performance. This is in addition to possibly other datasets. Finally, since all results of ML and DL models were less than 90%, we intend to start working with large language model transformers to figure out whether superior results could be achieved.

REFERENCES

- [1] C. Shofiya and S. Abidi, "Sentiment analysis on COVID-19-related social distancing in Canada using Twitter data," *International Journal of Environment Research and Public Health*, vol. 18, 2021.
- [2] N. Chintalapudi, G. Battineni and F. Amenta, "Sentimental analysis of COVID-19 tweets using deep learning models," *Infecteoud Disease Reports*, vol. 13, 2021.
- [3] P. Gupta, S. Kumar, R. Suman and V. Kumar, "Sentiment analysis of lockdown in India during COVID-19: A case study on Twitter," *IEEE Transactions on Computational Social Systems*, vol. 8, 2021.
- [4] B. Ramya, S. Shetty, A. Amaresh and R. Rakshitha, "Smart Simon bot with public sentiment analysis for novel COVID 19 tweets stratification," *SN Computer Science*, vol. 2., 2021.

- [5] R. Goel and R. Sharma, "Studying leaders & their concerns using online social media during the times of crisis: A COVID case study," *Social Network Analysis and Mining*, vol. 11, 2021.
- [6] S. Vernikou, A. Lyras and A. Kanavos, "Multiclass sentiment analysis on COVID-19-related tweets using deep learning models," *Neural Computing and Applications*, vol. 34, 2022.
- [7] Y. Qi and Z. Shabrina, "Sentiment analysis using Twitter data: a comparative application of lexicon- and machine-learning-based approach," *Social Network Analysis and Mining*, vol. 13, 2023.
- [8] U. Naseem, I. Razzak, M. Khushi, P. W. Eklund and J. Kim, "COVIDSenti: A large-scale benchmark Twitter data set for COVID-19 sentiment analysis," *IEEE Transactions on Computational Social Systems*, vol. 8, 2021.
- [9] Z. Jalil et al., "COVID-19 related sentiment analysis using state-of-the-art machine learning and deep learning techniques," *Frontiers in Public Health*, vol. 9, 2022.
- [10] T. Chen and C. Guestrin, "XGBoost: A scalable tree boosting system," in *Proceedings of the 22nd ACM SIGKDD International Conference on Knowledge Discovery and Data Mining*, 2016, pp. 785-794.
- [11] I. Sarker, "Machine learning: Algorithms, real world applications and research directions," *SN Computer Science*, vol. 2, 2021.
- [12] S. Ruder, "An overview of gradient descent optimization algorithms," *Clinical Orthopaedics and Related Research*, 2016.
- [13] M. Alagözli, "Stochastic Gradient Descent Variants and Applications," *Università della Svizzera Italiana*, 2022.
- [14] H. Zhao, Z. Chen, H. Jiang, W. Jing, L. Sun and M. Feng, "Evaluation of three deep learning models for early crop classification using Sentinel-1A imagery time series—A case study in Zhanjiang, China," *Remote Sensing*, vol. 11, no. 22, 2019.
- [15] J. Chung, C. Gulcehre, K. Cho and Y. Bengio, "Empirical evaluation of gated recurrent neural networks on sequence modeling," presented in *Deep Learning and Representation Learning Workshop*, 2014.
- [16] Y. Fu and Y. Yu, "Research on text representation method based on improved TF-IDF," *Journal of Physics*, 2020.
- [17] M. Wayahdi, D. Syahputra and S. Ginting, "Evaluation of the K-Nearest neighbor model with K-fold cross validation classification," *Data Mining, Image Processing, Artificial Intelligence, Networking*, vol. 9, 2020.
- [18] S. Prusty, S. Patnaik and S. Dash, "SKCV: Stratified K-fold cross-validation on ML classifiers for predicting cervical cancer," *Frontiers in Nanotechnology*, 2022.
- [19] S. Widodo, H. Brawijaya and S. Samudi, "Stratified K-fold cross validation optimization on machine learning for prediction," *Sinkron*, vol.7, no. 4, 2022.

Automating Mushroom Culture Classification: A Machine Learning Approach

Hamimah Ujir¹, Irwandi Hipiny², Mohamad Hasnul Bolhassan³, Ku Nurul Fazira Ku Azir⁴, SA Ali⁵

Faculty of Computer Science and Information Technology, Universiti Malaysia Sarawak, Sarawak, Malaysia^{1,2}

Faculty of Resource Science and Technology, Universiti Malaysia Sarawak, Sarawak, Malaysia³

Faculty of Electronic Engineering & Technology, Universiti Malaysia Perlis, Malaysia⁴

Faculty of Artificial Intelligence & Mathematical Sciences, SMIU, Karachi-74000, Pakistan⁵

Abstract—Traditionally, the classification of mushroom cultures has conventionally relied on manual inspection by human experts. However, this methodology is susceptible to human bias and errors, primarily due to its dependency on individual judgments. To overcome these limitations, we introduce an innovative approach that harnesses machine learning methodologies to automate the classification of mushroom cultures. Our methodology employs two distinct strategies: the first involves utilizing the histogram profile of the HSV color space, while the second employs a convolutional neural network (CNN)-based technique. We evaluated a dataset of 1400 images from two strains of *Pleurotus ostreatus* mycelium samples over a period of 14 days. During the cultivation phase, we base our operations on the histogram profiles of the masked areas. The application of the HSV histogram profile led to an average precision of 74.6% for phase 2, with phase 3 yielding a higher precision of 95.2%. For CNN-based method, the discriminative image features are extracted from captured images of rhizomorph mycelium growth. These features are then used to train a machine learning model that can accurately estimate the growth rate of a rhizomorph mycelium culture and predict contamination status. Using MNet and MConNet approach, our results achieved an average accuracy of 92.15% for growth prediction and 97.81% for contamination prediction. Our results suggest that computer-based approaches could revolutionize the mushroom cultivation industry by making it more efficient and productive. Our approach is less prone to human error than manual inspection, and it can be used to produce mushrooms more efficiently and with higher quality.

Keywords—Machine learning; convolution neural networks; mushroom cultivation; rhizomorph mycelium

I. INTRODUCTION

Mushroom cultures can be initiated from either spores or tissue [1]. The choice of whether to initiate a mushroom culture from spores or tissue depends on several factors, including the type of mushroom being grown, the desired yield, and the level of control that the cultivator wants to have over the culture. When dealing with spores, one must choose a single strain from the numerous strains produced. Conversely, tissue culture enables the cultivator to preserve the precise genetic makeup of the parent mushroom. In either scenario, the outcome is a network of cells collectively referred to as the mushroom mycelium. According to study [2], there are two main forms of mushroom mycelium which are: rhizomorph mycelium and tomentose mycelium. The rhizomorph mycelium resembles

plant roots, and only the growing rhizomorph mycelium is utilized for subsequent cultivation.

According to study [3], mushroom cultivation needs a lot of labor. The standard practice for selecting mushroom culture for further cultivation is via eye inspection by an expert. This method depends on human experts, making it susceptible to human bias and errors. The expert classifies rhizomorph and fluffy growing mycelium by examining the "fluffiness" of the sample under a lamp while holding the petri dish. Intensive training is thus required for a worker/newcomer in this field to learn how to select the fast-growing rhizomorph mycelium and estimate the right moment to transfer the culture to an agar petri dish. The fastest-growing rhizomorph mycelium is selected and transferred to another agar petri dish. Those exhibiting slower growth rates or contamination are subsequently discarded. This is where the skill of mushroom growers comes into play, as they must discern the quality and the optimal moment to harvest the rhizomorph mycelium for cultivation in a petri dish. Note that mushroom mycelium can grow exponentially, achieving a mass thousands of times its original size. Choosing a quality rhizomorph mycelium is particularly important to ensure a sizeable harvest.

We propose a computer vision approach in conjunction with a machine learning model. This would leverage discriminative image features to quickly identify growing rhizomorph mycelium cultures and ascertain the ideal timing for their transfer to an agar petri dish. Our objective is to differentiate fast-growing rhizomorph mycelium cultures from the ones with a slower growth rate. This paper also discusses the prediction of rhizomorph mycelium growth based on its diameter and identifies the good and bad mycelium.

Section II examines prior research that has employed computer-based technology in mushroom farming and Section III describes the process of collecting data for this study. Section IV presents the methods used for predicting growth rate and identifying good and bad mycelium and Section V presents the results of this study. Finally, Section VI concludes the paper.

II. RELATED WORKS

Computer-based solutions in the field of mushroom cultivation mainly focus on two areas: recognizing edible mushroom types and monitoring mushroom growth using

computer assisted technology such as the Internet of Things (IoT).

Several studies centered on mushroom classification include [4]-[10]. The study in [4] classified mushrooms into two categories, poisonous and non-poisonous using different algorithms like neural network (NN), Support Vector Machines (SVM), Decision Tree, and k Nearest Neighbors (kNN). They utilized a dataset comprising mushroom images, which includes images with and without backgrounds. Experimental findings reveal that the most effective technique for classifying mushroom images is kNN, achieving an accuracy of 94% when utilizing features extracted from images with real dimensions of mushroom types, and 87% when using features extracted solely from images. The research in [5] proposes a new model of classifying 45 types of mushrooms including edible and poisonous mushrooms by using a technique of Convolution Neural Networks (CNN). They used the library KERAS2.3.1 for running the CNN TensorFlow and the proposed model gives the results of 0.78, 0.73, and 0.74 for precision, recall, and F1 score, respectively. The study in [7] used deep learning approaches like InceptionV3, VGG16 and Resnet50 to identify the mushrooms based on their category on 8190 mushroom images where the ratio of training and testing data was 8:2. They used The Contrast Limited Adaptive Histogram Equalization (CLAHE) method along with InceptionV3 to obtain the highest test accuracy. InceptionV3 achieved the highest accuracy of 88.40% among the implemented algorithms. The research in [8] conduct a comparison between the performance of Random Forest and Reduced Error Pruning (REP) tree classification algorithms in classifying edible and poisonous mushrooms. The study in [9] employed Gaussian naïve Bayes along with Linear Discriminant Analysis (LDA) to separate edible and non-edible mushrooms. LDA was used to reduce the dataset, which helped in reducing the dimensionality of the feature space and removing irrelevant features. LDA aims to enhance the distinction between various classes by identifying a linear combination of features that most effectively discriminates among them. A slightly different work by [10] where they utilize K Means clustering algorithm to classify mushrooms based on attributes such as structure, surface size, cap tone, gill, stalk, smell, place of growth, and population. From their study, it is evident that the odor attribute stands out as the most significant factor contributing to the highest classification accuracy.

In study [11] proposed an IoT-based monitoring and control system for shiitake mushroom farms using wireless sensors. According to study [11], implementing IoT technology in mushroom farms presents challenges such as energy management, data security, sensor node placement, internet connectivity, and transmission range. The research in [12] designed a smart system called SENSEPACK to monitor the environment of a mushroom cultivation farm. This system measures temperature, humidity, light, and CO₂ levels using appropriate sensors to control the environment of the nursing room.

Recently, there has been a notable increase in endeavors to automate mushroom cultivation in controlled environments, utilizing not only IoT but also mobile applications, such as [13] [14]. The study in [13] proposed a solution utilizing an

Android app was proposed to distinguish between edible and poisonous mushrooms. In this work, machine vision and CNN classification algorithm is used to develop the app. The automation system introduced by utilizing sensors within the mushroom house guarantees ideal conditions for the growth of mushroom.

Other than that, the study in [15] presented a novel approach in the mushroom cultivation field, utilizing computer-assisted technology to classify mushroom samples based on the enzymatic browning reaction. This reaction occurs when mushrooms are exposed to the atmosphere, and the proposed method employs a support vector machine (SVM) classifier to achieve a classification accuracy of 80%. The research in [16] employs a dataset sourced from Kaggle for mushroom classification and model training purposes. They apply methods such as SVM, naïve Bayes, and random forest algorithms in this study. Their findings reveal that their data is prone to overfitting, attributed to its near-linear separability as observed through the principle of SVM. Another similar work by [17] used decision tree to classify five types of mushrooms, they are Button mushrooms, Wood Ear mushrooms, Straw mushrooms, Reishi mushrooms and Red Oyster mushrooms. Among the feature extracted from the mushroom images are mean, skewness, variance, kurtosis, and entropy from the mushroom images.

In general, deep learning techniques are also employed in the other agricultural sector to categorize, quantify, and partition the areas of significance pertaining to crops. The study in [18] published a dataset that uses deep-learning-based classification and detection in precision agriculture. CropDeep consists of 31,147 images with over 49,000 annotated instances from 31 different classes. Based on the results, they suggested that the YOLOv3 network has good potential application in agricultural detection tasks. The study in [19] proposes a deep learning-based solution for object detection in Smart Agriculture. The solution can automatically detect damage in leaves and fruits, locate them, classify their severity levels, and visualize them by contouring their exact locations. Their results reveal that the proposed solution which is based on Mask-RCNN, achieves higher performances in features extraction and damage detection/localization compared to other pre-trained models such as VGG16 and VGG19. Another different work proposed by [20] works on algorithm to classify wild mushrooms using a deep CNN and Residual Network [20] also introduces an optimization method that improved the classification effect of the algorithm model, enhancing the overall performance of the classification algorithm

Based on our current understanding of the literature, there has been no prior investigation into the use of histogram profiles and machine learning approach for the recognition of fast-growing rhizomorph mycelium through the analysis of image features. As a result, the research problem we are currently pursuing represents an unexplored area of inquiry within this field.

III. DATA COLLECTION

Two strains are used in the experiments, and both are *Pleurotus ostreatus*. A disk of mycelium of 5 mm diameter was placed in the center of a Petri dish containing Potato-

Dextrose-Agar (PDA) medium. During the spawn-run (development and growing of the mycelium) the sealed Petri dishes are stored in a dark and neat place. Petri dishes with fungi were numbered for identification. Each strain has about fifty samples.

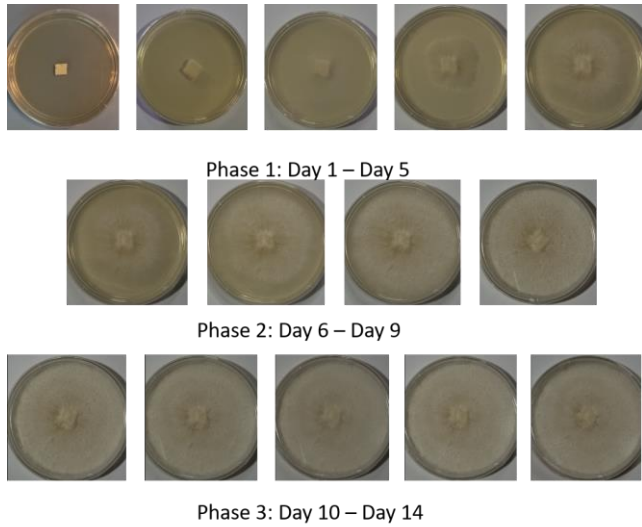


Fig. 1. The growth of a good rhizomorph mycelium in 14 days.

An android camera phone mounted on a tripod. Images of Petri dishes with mycelia were obtained against a white background and identified with a paper label of a known area of 4 cm² (2 x 2 cm). Photographs were taken daily for fourteen days for both strains, totaling 1400 images. Fig. 1 shows a sample of a good rhizomorph mycelium sample in 14 days. There are three phases (classes) used to categorize the growth of mycelium: Phase 1 (Day 1 - Day 5); Phase 2 (Day 6- Day 9) and Phase 3 (Day 10 - Day 14). From the observation of the sample, the growth is quite drastic in phase 2. During phase 3, the growth is the same for the last five days and human eyes cannot easily observe the difference for each day. Human eyes can also make mistakes during the last two days in phase 2, as it can be mistakenly labeled as phase 3.

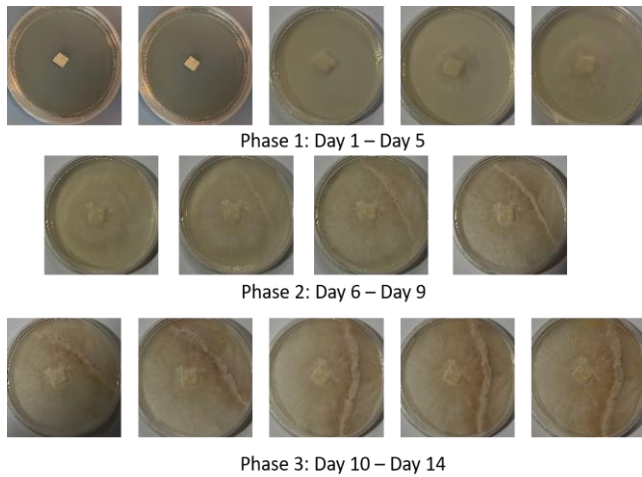


Fig. 2. The growth of a contaminated rhizomorph mycelium in 14 days.

Fig. 2 shows a sample of a contaminated rhizomorph mycelium sample in 14 days. During phase 1, the good and contaminated mycelium cannot be differentiated, as it grows the same. However, during phase 2, the contaminated one can be easily recognized on day 7. Like good mycelium, during phase 3, the growth of the contaminated one is the same for the last five days.

IV. METHOD

A. Classification Based on HSV Histogram Profile

For rhizomorph mycelium growth analysis measurement, mask ROI segmentation and elimination is used to determine the cultivation of the phases. The proposed method determines the cultivation phase based on the mask area's histogram profile. Given a top-view and close-up image of the petri dish sample, we obtained n candidate mask(s) using Hough circles. We set the min circle radii to a default value of 1400px to exclude smaller circles. The default threshold value was determined heuristically from random sample images of our dataset. Next, we build a 2D HSV histogram map (30 hue bins x 32 saturation bins) for each candidate mask. Three examples of such maps are shown in Fig. 3. The intensity value of each cell represents the frequency of occurrence of that hue-saturation combination for that image. A lighter shade indicates a higher peak and vice versa.

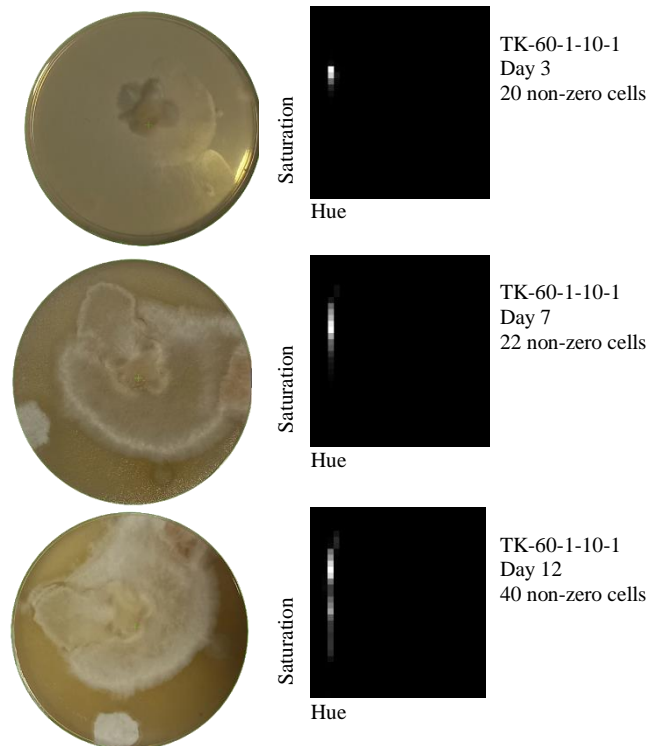


Fig. 3. 2D HSV histogram maps, each produced from the final mask of an image belonging to TK-60-1-10-1. The three images were captured on Day 3, Day 7 and Day 12, respectively. We also reported the number of non-zero cells for comparison.

We eliminate a mask candidate if it returns a high entropy value since it is more likely to be produced due to a segmentation error. The segmented area includes background pixels (i.e., petri dish and desk surface) hence the higher

variety of hue-saturation combinations. The mask candidate with the lowest entropy value (i.e., the lowest number of non-zero cells) is thus retained as the final mask.

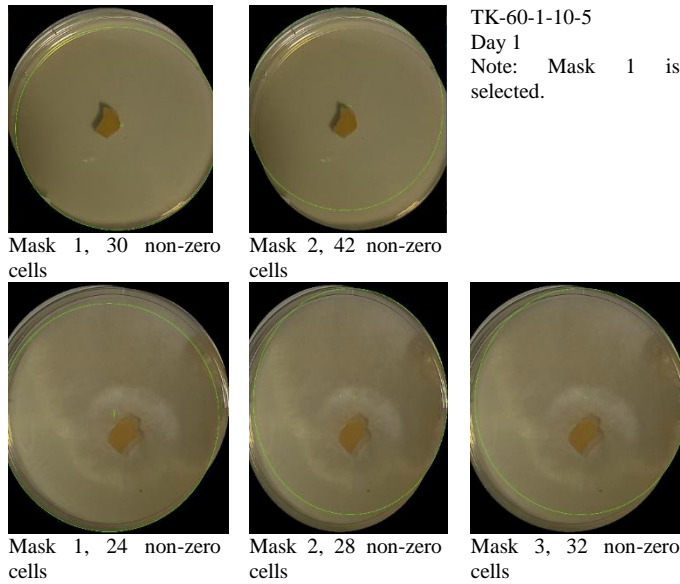


Fig. 4. Two instances of the segmentation function returning $n > 1$ mask candidates. The mask area is enclosed inside the green-colored circle.

Fig. 4 shows two instances of our mask ROI segmentation function returning multiple candidates. The number of non-zero cells for each candidate is reported for comparison. Mask candidates with more non-zero cells tend to include many background pixels. For TK-60-1-10-5, mask number 2 was rejected since the Hough circle encloses a larger portion of the petri dish rim than mask number 1. For TR-60-1-20-20, the decision is not as clear-cut since all three masks enclose (with varying degrees) some parts of the rim. Nevertheless, mask number 1 was chosen because it contains the least non-zero cells. Images with no mask detected are discarded. Such cases are typically due to poor image quality during capture.

Given a 2D HSV histogram map, M_i our method determines the specimen's label by counting the number of non-zero cells, $NZERO(M_i)$, with an intensity value exceeding the set threshold, $thresh$. We then compute the absolute difference between the counted value and two constants, i.e., lower bound, $LBOUND$, and upper bound, $UBOUND$. Value for each constant was determined from our training set, either using Median, Mod or Average. The first constant represents the NON-CONTAMINATED set (i.e., lower entropy), and the latter represents the CONTAMINATED set (i.e., higher entropy). Thus, the formula to obtain the final classification label, i.e., CONTAMINATED, C, vs. NON-CONTAMINATED, NC, is given below,

$$LABEL(M_i) = \begin{cases} C, & \text{if } |NZERO(M_i) - LBOUND| \geq |NZERO(M_i) - UBOUND| \\ NC, & \text{otherwise} \end{cases} \quad (1)$$

For phase determination, we limit the test dataset to NON-CONTAMINATED only since contaminated specimens are almost impossible to classify due to their chaotic appearance. We determine the phase label as a distance function between

the current image's non-zero cell count and the LBOUND value of each phase,

$$PHASE(M_i) = \begin{cases} 1 & \text{if } |NZERO(M_i) - LBOUND_2| > |NZERO(M_i) - LBOUND_1| < |NZERO(M_i) - LBOUND_3| \\ 2 & \text{if } |NZERO(M_i) - LBOUND_1| > |NZERO(M_i) - LBOUND_2| < |NZERO(M_i) - LBOUND_3| \\ 3 & \text{otherwise} \end{cases} \quad (2)$$

B. Classification using CNN-based Method

On top of the previous method, CNN-based method was also chosen to analyze the images of the mushroom. Using machine learning does not require handcrafted feature analysis and it performs feature analysis within the network. There are two neural networks used to predict the growth rate and contamination of the mushroom named MNet and MConNet respectively (see Fig. 5). The underlying architecture for both neural networks is similar except for the activation function for the last layer such that the final layer of the neural network is using SoftMax for MNet while using sigmoid for MConNet.

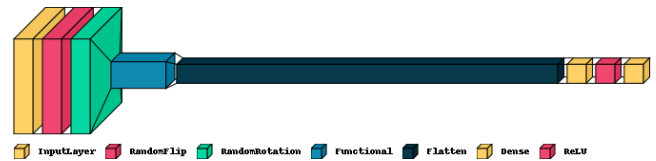


Fig. 5. The architectural diagram for MNet and MConNet.

The architecture of both models is utilizing transfer learning from MobileNetV3 due to its acceptable performance in low-end mobile devices and possible real-time prediction. Moreover, there are two layers such as *RandomFlip* and *RandomRotation* for generalizing the samples and preventing overfitting during the training. The side-effect of this also virtually increases the number of samples. Though similar, both the neural networks can be combined for improvement in performance and latency. However, the method described is not feasible when there are mixes of contaminated and non-contaminated images in the training samples.

A total of 1400 samples collected earlier are split into 64%, 16%, and 20% for training, validation, and testing, respectively. The samples were trained through TensorFlow by minimizing sparse categorical cross entropy for MNet and binary cross-entropy for MConNet. The trained models were evaluated with testing samples that are not included in the training samples.

V. RESULTS AND ANALYSIS

In this section, we explained the results in two parts: (a) rhizomorph mycelium contamination recognition; and (b) growth analysis measurement using two different methods as explained in the previous section.

A. Classification Based on HSV Histogram Profile

To discover the optimal lower and upper bound values, we clustered all images belonging to 30 training specimens according to phases, i.e., Phase 1 (Day 1 – 5), Phase 2 (Day 6 – 8), and Phase 3 (Day 9 – 12), and classification labels. We obtained each cluster's median, mod, and average non-zero cell count under each intensity threshold value. The results are tabulated in Table I.

TABLE I. LBOUND AND UBOUND VALUES FOR EACH CLUSTER VS. METRIC COMBINATION

| Cluster | Metric | Number of non-zero cells with intensity value exceeding threshold | | | | | |
|---------|---------|---|------|-----|-----|------|-----|
| | | >0 | | >64 | | >128 | |
| | | NC | C | NC | C | NC | C |
| PHASE 1 | Median | 26.0 | 29.0 | 4.0 | 5.0 | 3.0 | 3.0 |
| | Mod | 23.0 | 30.0 | 3.0 | 4.0 | 2.0 | 2.0 |
| | Average | 26.0 | 28.6 | 4.8 | 5.0 | 3.0 | 3.2 |
| PHASE 2 | Median | 20.0 | 29.0 | 5.0 | 8.0 | 3.0 | 5.0 |
| | Mod | 16.0 | 25.0 | 5.0 | 8.0 | 2.0 | 5.0 |
| | Average | 22.5 | 32.9 | 6.1 | 8.1 | 3.4 | 4.8 |
| PHASE 3 | Median | 19.0 | 33.5 | 5.0 | 7.0 | 3.0 | 4.0 |
| | Mod | 17.0 | 27.0 | 5.0 | 6.0 | 3.0 | 4.0 |
| | Average | 21.2 | 36.0 | 5.6 | 7.9 | 3.4 | 4.6 |

1) *Rhizomorph mycelium contamination recognition*: We report the average precision of each combination to predict the specimen's label (CONTAMINATED vs. NON-CONTAMINATED), see Fig. 3, on a test set containing never-seen-before images of 20 specimens. The test set contains ten contaminated and ten non-contaminated specimens. We contrast the results obtained when making the prediction based on Phase 2's images (n=63) vs Phase 3's images (m=72). We exclude Phase 1's images as contamination signs only start to appear from Phase 2 onwards.

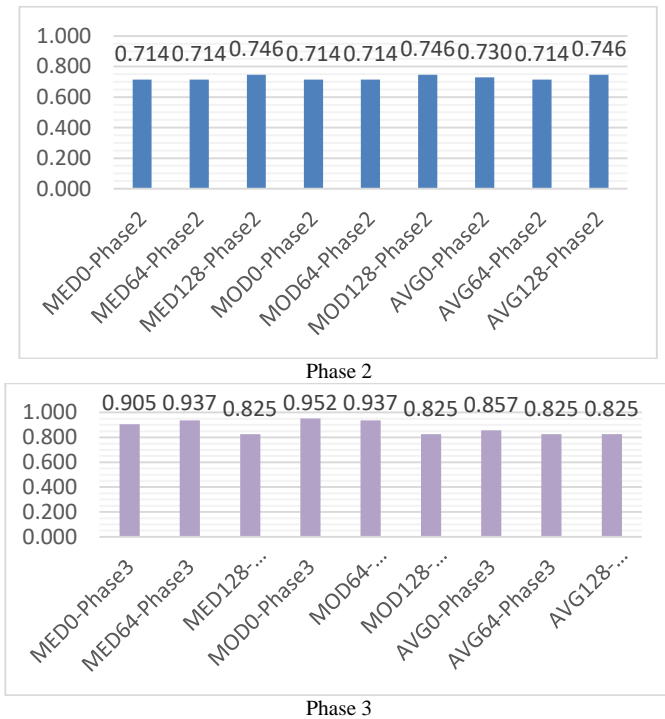


Fig. 6. Average precision for label prediction on test images belonging to (a) Phase 2 and (b) Phase 3. We used different metrics (i.e., Median, Mod and Average) on the training set to determine LBOUND and UBOUND.

Based on the results shown in Fig. 6, the optimal combinations for Phase 2's images are MED128, MOD128, and AVG128, with average label prediction precision of 74.6%. Evidently, setting a strict threshold value to reject non-zero cells with weak intensity is the best approach for Phase 2's images. A hue-saturation combination is retained only if it has a high occurrence inside the image.

Phase 3 returns a higher top precision value, i.e., 95.2%. This is expected since contamination (or none) will become more apparent in a latter phase. The high precision value validates our method of basing the label prediction on non-zero cell count (i.e., entropy measure). Unlike Phase 2, a relaxed threshold value returns the best result. The optimal combination is MOD0.

2) *Rhizomorph mycelium contamination recognition growth analysis measurement*: We measure the growth of the cultivation by phase prediction using the same test set, but only on the NON-CONTAMINATED specimens. The results are shown in Fig. 7. The highest average precision of 50.5% is obtained using MOD0. The lowest average precision of 34.9% is obtained using MOD128. The precision of random classification by chance is 33.3% (i.e., 1/3). The low precision is due to the specimens each exhibiting a different growth rate, especially from Phase 2 onwards. Table II shows the average precision achieved using MOD0, for different phases.

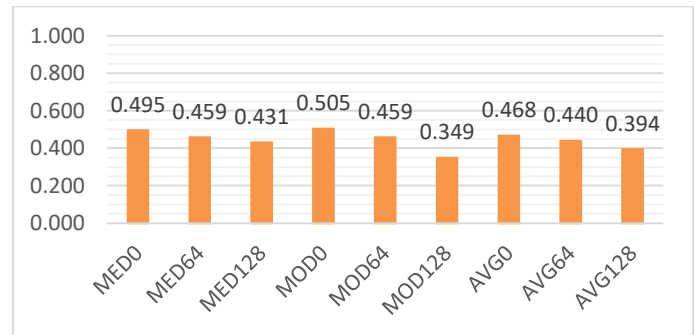


Fig. 7. Average precision for phase prediction on test images. We used different metrics (i.e., Median, Mod and Average) on the training set to determine LBOUND and UBOUND.

TABLE II. AVERAGE PRECISION ACHIEVED USING MOD0 FOR PHASE 1, PHASE 2 AND PHASE 3

| PHASE | Number of Images | Average Precision |
|----------|------------------|-------------------|
| PHASE 1 | 47 | 87.2% |
| PHASE 2 | 31 | 32.3% |
| PHASE 3 | 31 | 32.3% |
| Average: | | 50.5% |

Fig. 8 shows the training and testing loss for both MConNet and MNet models. While the disparity may not be readily apparent, it is evident that MConNet exhibits lower loss compared to the MNet model. Fig. 9 shows the training and testing accuracy for both MConNet and MNet models. Based on these graphs, even though the difference is not that obvious, MConNet has a higher accuracy performance compared to the MNet model.

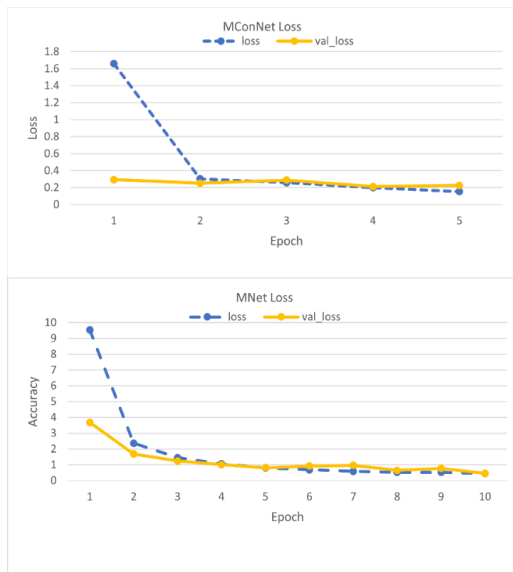


Fig. 8. Loss graph for MConNet and MNet.

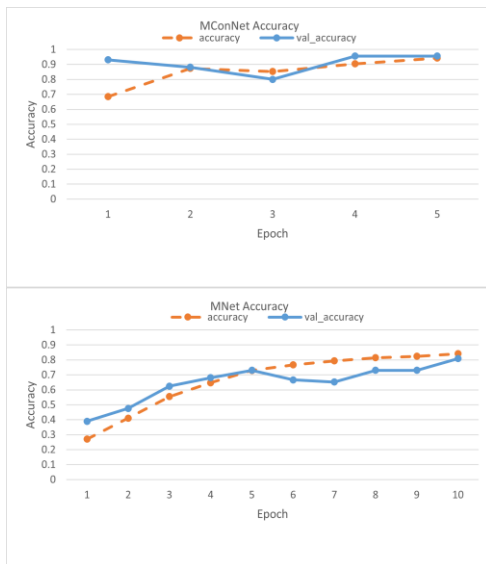


Fig. 9. Accuracy graph for MConNet and MNet.

B. Classification using CNN-based Method

1) *Rhizomorph mycelium contamination recognition:* Table III shows the accuracy percentage for contamination recognition. According to the mushroom experts' opinion, strain B has several contaminated Petri dishes. The method that has been used managed to recognize the contaminated samples from strain B which is 100%. Overall, the average accuracy for good and contaminated Petri dishes is more than 96%.

TABLE III. CONTAMINATION RECOGNITION

| | Good | Contaminated |
|----------|--------|--------------|
| Strain A | 95.66% | 92.62% |
| Strain B | 97.74% | 100% |
| Average | 96.64% | 98.97 |

2) *Growth analysis measurement:* Tables IV and V shows the mycelium phase recognition for two different strains. The average recognition for strain A is 98.3% while 86% for strain B. The accuracy for mycelium phase recognition for strain A is much higher compared to strain B since the petri dish with strain B has more contaminated mycelium. The recognition of the phase for strain B is much harder, especially when at phase 2. This is because mycelium has become more like contaminated ones during phase 2.

TABLE IV. MYCELIUM PHASE RECOGNITION FOR STRAIN A

| Samples/ Phases | Day 1 - Day 5 | Day 6 - Day 9 | Day 10 - Day 14 |
|-----------------|---------------|---------------|-----------------|
| Day 1 - Day 5 | 100% | 1% | |
| Day 6 - Day 9 | | 99% | 4% |
| Day 10 - Day 14 | | | 96% |

TABLE V. MYCELIUM PHASE RECOGNITION FOR STRAIN B

| Samples/ Phases | Day 1 - Day 5 | Day 6 - Day 9 | Day 10 - Day 14 |
|-----------------|---------------|---------------|-----------------|
| Day 1 - Day 5 | 93% | | |
| Day 6 - Day 9 | 4% | 65% | |
| Day 10 - Day 14 | 3% | 35% | 100% |

VI. CONCLUSION

This paper aims to introduce a machine learning approach for detecting rhizomorph mycelium growth and distinguishing between healthy and contaminated mycelium based on captured images. The results demonstrate that the employed method exhibits a notable accuracy in identifying healthy and contaminated mycelium. However, the study's scope is constrained by reduced precision beyond the initial five days, stemming from differing growth rates.

For our future work, we would like to explore the possibility of predicting rhizomorph growth from the area that it covered in a petri dish. Based on the area covered by the mycelium, we can predict the growth of such mycelium. In addition, we plan to use another type of mushroom in the experiment. We would like to see whether the growth can be measured easily compared to oyster mushroom.

ACKNOWLEDGMENT

This research is fully supported by Universiti Malaysia Sarawak through Smart Partnership Grant Scheme F08/PARTNERS/2128/2021. The authors fully acknowledged Universiti Malaysia Sarawak for the approved fund which makes this important research viable and effective. The acknowledgment is also extended to our industry counterpart, Madam Nurhaida Sahera Abd Malek who is willing to share the strain from Arra Mushroom Sdn Bhd, farm.

REFERENCES

[1] Borah, Tasvina, Singh, Akoijam Paul, Pampi, Talang, Hammylliende & Kumar, Bagis and Hazarika, Samarendra. "Spawn Production and Mushroom Cultivation Technology", ICAR Research Complex for NEH Region, Meghalaya, India (2019), pp. 1-46.

[2] Yafetto L, "The structure of mycelial cords and rhizomorphs of fungi: A mini-review". Mycosphere 9(5), 984-998, 2018. Doi 10.5943/mycosphere/9/5/3.

- [3] Katel, Shambhu, Mandal, Honey and Sharma, Rohit. "Oyster Mushroom Cultivation", in Research Trends in Agriculture Sciences, 30th Edition, Chapter: 3, AkiNik Publications, 2022, pp.39-56.
- [4] Ottom, Mohammad Ashraf and Alawad, Noor Aldeen. "Classification of mushroom fungi using machine learning techniques". International Journal of Advanced Trends in Computer Science and Engineering, 8(5), September - October 2019, pp.2378- 2385. DOI://10.30534/ijatcse/2019/78852019.
- [5] Preechasuk, Jitdumrong, Chaowalit, Orawan and Pensiri, Fuangfar and Visutsak, Po- rawat, "Image analysis of mushroom types classification by convolution neural networks", 2019, pp.82-88. 10.1145/3375959.337598.
- [6] Maurya, P. and Singh, N.P., "Mushroom classification using feature-based machine learning approach". In: Chaudhuri, B., Nakagawa, M., Khanna, P., Kumar, S. (eds) Proceedings of 3rd International Conference on Computer Vision and Image Processing. Advances in Intelligent Systems and Computing, vol 1022. Springer, Singapore. 2020. https://doi.org/10.1007/978-981-32-9088-4_17.
- [7] N. Zahan, M. Z. Hasan, M. A. Malek and S. S. Reya, "A deep learning-based approach for edible, inedible and poisonous mushroom classification," 2021 International Conference on Information and Communication Technology for Sustainable Development (ICICT4SD), Dhaka, Bangladesh, pp. 440-444, 2021, doi: 10.1109/ICICT4SD50815.2021.9396845.
- [8] Paudel, Nawaraj and Bhatta, Jagdish, "Mushroom classification using random forest and REP tree classifiers", Nepal Journal of Mathematical Sciences. 3, pp. 111-116, 2022. 10.3126/njmathsci.v3i1.44130.
- [9] Viswanadham, S., Muttipati, A.S., Lakshmi, N.J., Sujatha, Y., "Mushroom classification and feature extraction using linear discriminant analysis". In: Bhateja, V., Khin Wee, L., Lin, J.CW., Satapathy, S.C., Rajesh, T.M. (eds) Data Engineering and Intelligent Computing. Lecture Notes in Networks and Systems, vol 446, Springer, Singapore, 2022. https://doi.org/10.1007/978-981-19-1559-8_34.
- [10] S. K. Pal, R. Pant, R. Roy, S. Singh, L. Choudhary and S. Naaz, "Mushroom classification model to check edibility using machine learning," 2023 10th International Conference on Computing for Sustainable Global Development (INDIACom), New Delhi, India, 2023, pp. 214-217.
- [11] M. R. M. Kassim, I. Mat and I. M. Yusoff, "Applications of Internet of Things in mushroom farm management," 2019 13th International Conference on Sensing Technology (ICST), Sydney, NSW, Australia, 2019, pp. 1-6, doi: 10.1109/ICST46873.2019.9047702.
- [12] A. A. Shakir, F. Hakim, M. Rasheduzzaman, S. Chakraborty, T. U. Ahmed and S. Hossain, "Design and Implementation of SENSEP ACK: an iot based mushroom cultivation monitoring system," 2019 International Conference on Electrical, Computer and Communication Engineering (ECCE), Cox's Bazar, Bangladesh, 2019, pp. 1-6, doi: 10.1109/ECACE.2019.8679183.
- [13] Pramod, Mathew, Jacob., Jeni, Moni., Sneha, Sunil, "An intelligent system for cultivation and classification of mushrooms using machine vision", 2023 International Conference on Computational Intelligence and Sustainable Engineering Solutions (CISES), Greater Noida, India, 2023, pp. 264-270, doi: 10.1109/CISES58720.2023.10183464.
- [14] Md. Ariful Islam, Md. Antonin Islam, Md Saef Ullah Miah, and Abhijit Bhowmik, "An automated monitoring and environmental control system for laboratory-scale cultivation of oyster mushrooms using the Internet of Agricultural Thing (IoAT)". In Proceedings of the 2nd International Conference on Computing Advancements (ICCA '22). Association for Computing Machinery, New York, NY, USA, 200, pp.207–212. <https://doi.org/10.1145/3542954.3542985>.
- [15] A. Anil, H. Gupta and M. Arora, "Computer vision based method for identification of freshness in mushrooms," 2019 International Conference on Issues and Challenges in Intelligent Computing Techniques (ICICT), Ghaziabad, India, 2019, pp. 1-4, doi: 10.1109/ICICT46931.2019.8977698.
- [16] Ma, Y., Xia, Y., & He, X, "A preliminary study on mushroom classification and application of SVM principle to infer the linearly separable dataset". In Advances in Petrochemical Engineering and Green Development, 2022, pp. 470-476, CRC Press.
- [17] Cucut, Hariz, Pratomo., Widyastuti, Andriyani, "Mushroom image classification using C4.5 algorithm". Journal of Intelligent Software System, 2(1), pp.17-19, 2023. doi: 10.26798/jiss.v2i1.930.
- [18] Zheng, Y.-Y.; Kong, J.-L.; Jin, X.-B.; Wang, X.-Y.; Su, T.-L.; Zuo, M. "CropDeep: The crop vision dataset for deep-learning-based classification and detection in precision agriculture". Sensors 2019, 19, 1058. <https://doi.org/10.3390/s19051058>.
- [19] L. Boukhris, J. Ben Abderrazak and H. Besbes, "Tailored deep learning based architecture for smart agriculture," 2020 International Wireless Communications and Mobile Computing (IWCMC), Limassol, Cyprus, 2020, pp. 964-969, doi: 10.1109/IWCMC48107.2020.9148182.
- [20] Yingyuan Du, Tao Wu, Gaoyuan Yang, Yuwei Yang, Ge Peng, "Classification algorithm based on convolutional neural network for wild fungus", Third International Conference on Artificial Intelligence and Computer Engineering (ICAICE 2022); 126105D (2023) <https://doi.org/10.1117/12.2671050>.

Leather Image Quality Classification and Defect Detection System using Mask Region-based Convolution Neural Network Model

Azween Bin Abdullah¹, Malathy Jawahar², Nalini Manogaran^{3*}, Geetha Subbiah⁴,
Koteeswaran Seeranagan⁵, Balamurugan Balusamy⁶, Abhishek Chengam Saravanan⁷

Faculty of Applied Science and Technology, Perdana University, Kuala Lumpur, Malaysia¹

Leather Process Technology Department, CSIR-Central Leather Research Institute, Chennai-600020, Tamil Nadu, India²

Department of CSE, S.A. Engineering College (Autonomous), Chennai-600077, Tamil Nadu, India³

School of Computer Science and Engineering, Vellore Institute of Technology, Chennai-600127, Tamil Nadu, India^{4,7}

Department of CSE (AI and ML), S.A. Engineering College (Autonomous), Chennai-600077, Tamil Nadu, India⁵

Shiv Nadar (Institution of Eminence Deemed to be University), Uttar Pradesh – 201314, India⁶

Abstract—The leather industry is increasingly becoming one amongst the most important manufacturing industries in the world. Increasing demand has posed a great challenge as well as an opportunity for these industries. Quality of a leather product has been always the main factor in the setting of the market selling price. Usually, quality control is done with manual inspection. However, with human related errors such as fatigue, loss of concentration, etc., misclassification of the produced leather quality becomes a very serious issue. To tackle this issue, traditionally, image processing algorithms have been used, but, have not been effective due to low accuracies and high processing time. The introduction of Deep Learning methodologies such as Convolutional Neural Networks (CNNs), however, makes image classification much simpler. It incorporates automated feature learning and extraction, giving accurate results in lesser time. In addition, the usage of deep learning can also be applied for defect detection, which is, locating defects in the image. In this paper, a system for leather image classification and defect detection is proposed. Initially, the captured images are sent to a classification system, which classifies the image as good quality or defect quality. If the output of the classification system is defect quality, then a defect detection system works on the images, and locates the defects in the image. The classification system and the defect detection system are developed using Inception V3 CNN and Mask R-CNN respectively. Experimental results using these CNNs have shown great potential with respect to object classification and detection, which, with further development can give unparalleled performance for applications in these fields.

Keywords—Image leather classification; leather defect detection; Convolutional Neural Network; CNN; deep learning

I. INTRODUCTION

Image classification is a very important field in computer vision. Classification of images plays an important role in case of identification, segregation and decision-making processes in automated systems. With the ever-increasing complex tasks given to these computer vision-based tools and the increasing reliance on these systems, classifications systems must be robust and have high accuracy and detection rates, so as to perform error-free and without manual intervention. Classification systems are in high demand in the

manufacturing sector, with one such industry being the leather industry [1].

Leather is a main material, used in the clothing and accessory industry for making fashion accessories, footwear, coats, amongst a host of other products. It is usually a residual product, made from the outer covering of animals such as skins and hides, commonly obtained as by-products of the meat industry. “Hide” is the outer covering of a large animal such as a buffalo, cow whereas “Skin” is that of a sheep, goat, etc. Leather, technically defined, is a natural protein polymer that is treated with tanning agents to make it resistant to enzymatic attack and putrefaction, as well as improve several physical properties.

Leather and leather products are increasingly gaining importance in the world [2]. The major task of leather processing industry is to convert the skin or hide into leather, from which, quality products can be made. The leather, which is processed from raw to finish, is dried. The next step is the visual inspection and classification. Defects may arise in the processed sheet of leather due to various reasons such as wear and tear by the machines, heat, etc. These defects may vary in size and shape depending on the type of defect such as holes, scratches, bubbles, torn pieces, etc. The classification takes place according to the surface defect area of the defect, defect area, location, and sheet thickness amongst many other factors. The number of defects determines the price, with more defects fetching a lower price. Thus, classification is a very important process to be undertaken, to determine the economic value of the product.

The manual classification process, which is commonly used, is error prone. With the long working hours, operator fatigue and other reasons, these factors derail effective classification and quality assurance process. A simple classification error causes a loss of trust amongst customers and greatly devalues the product, implying significant losses for these leather producing factories. The defects, scratches, holes, bubbles, etc., thus need to be identified,

located, and finally removed. Thus, defect detection is also essential.

The proposed leather defect detection system using advanced deep learning algorithms holds great potential to transform the leather industry. It can significantly improve efficiency, reduce costs, and enhance product quality through automated quality control. This system can quickly and accurately identify defects, streamlining production processes and saving time and resources. It also minimizes waste and rework, leading to cost reductions. Furthermore, the consistent adherence to quality standards and real-time defect detection ensures higher-quality leather products, fostering customer satisfaction and brand loyalty. These benefits are set to drive widespread adoption of advanced quality control technologies across the leather industry, enhancing the competitiveness of leather manufacturers globally.

The classification and defect detection system that is deployed, should be able to accurately classify the images and locate defects, if present in the images. With manual labour becoming increasingly expensive and error prone, the use of autonomous classification systems have been the most preferred, but least deployed at present, due to low accuracies and reliabilities. Thus, the system needs to be as autonomous and reliable as possible. Commonly used techniques for similar systems are image processing based techniques. The basic techniques include wavelet analysis, canny edge detection and thresholding. However, these techniques are pretty inaccurate due to their inapplicability on identification of different defects than on the one it was developed and tuned for. But, with the introduction of deep learning and most importantly, Convolutional Neural Networks (CNNs), image recognition tasks have been simplified. They also have excellent performance and high accuracy rates, which provide good reliability.

In this paper, we propose a system that combines classification and defect detection and developing a complete system by improving upon various algorithms. This paper's scope is to analyse existing methods of leather quality and defect classification and detection and propose a complete system for the classification and defect detection process using images [33-37].

The major contributions made in this paper are:

- 1) This paper proposes an efficient 2-stage based computer vision-based pipeline for automated intelligent leather defect detection.
- 2) The model uses Inception V3 in the first stage for identifying the leather images and classifying them as "Good" or "Defective", to effectively classify the defective leather.
- 3) The model deploys Region based Convolution Neural Network (R-CNN) for locating the defects, in the leather image.
- 4) The model operates in such a way that if only the image is classified as defective, the image is passed on to the second stage. This arrangement reduces the delay in processing and efficiently uses the resources.

5) The proposed model tests its performance on the real time data set acquired from Research labs. Since the number of defective images are practically less, augmentation procedure is employed and sufficient amount of defective leather images are obtained.

6) The performance of the proposed model is superior to the existing models and the results are promising.

The paper is structured in the following way. Firstly, a brief of image processing and CNNs is explored in Section II. Secondly, their applications in this field and related works that are carried out are explored in Section III. Thirdly, the methodology developed is described in Section IV. In Section V, the dataset, the experimental setup and the results are discussed. Section VI discusses the Conclusion and Future Scope of this research work.

II. OVERVIEW

A. Convolutional Neural Networks

Convolutional Neural Networks or CNNs are deep learning neural network algorithms widely used in computer vision applications. CNNs are now commonly used in image based applications where automatic feature extraction, object detection, image classification and image segmentation operations are required.

The Convolutional Neural Network structure is made up of three general layers. They are the input layer, hidden layers and an output layer. The hidden layers may contain multiple layers such as convolutional layers, activation or RELU layers, pooling layers, normalization layers and fully connected layers. As a result of the masking of the input and the output by the activation function and the final convolution in these layers, these are called as hidden layers.

A Convolutional Neural Network typically contains multiple convolutional layers, followed by pooling layers, normalization layers and a fully connected layer. The main function in the CNN is performed by the convolutional layers. These layers often consist of several kernels of multiple sizes which are used to apply the convolutional or dot product operation on their input, for producing feature maps. A pooling layer collects these feature maps from the previous layer and performs a max pooling or selection of a maximum activation from a small neighborhood feature region. Thus, the output feature dimensions are reduced. The next layer, the fully connected layer, is usually placed at the near end of the convolutional neural network and the output of this layer, is the high-level abstract classification or data for further processing, which is inference derived from the image input. Since the neural network is a self learning network, the convolutional layers and the fully connected layers contain neurons, whose weights are adjusted as the network goes through the training phase to set the optimal weights for accurate outputs [3][4].

Some of the best known CNNs in the field of computer vision are AlexNet [5], GoogLeNet [6] and ResNe t[7][8]. Each of these CNNs have a different architecture, thus giving different results for the same application. Thus, the

architecture of the CNN must be carefully chosen to maximize the usefulness of it for the specific application.

B. Image Processing Techniques

Image processing techniques are the traditionally used methods for computer visions applications. They involve basic processing techniques such as segmentation, extraction, colour based identification techniques, shape and texture based segmentation amongst a variety of other techniques that target a specific feature of the object or objects that are to be identified in the image. These techniques are applied on a training image set to generate a standard feature set of the target object to be detected. These feature sets are compared to features extracted from images which have objects to be detected or classified using similarity comparison metrics or machine learning techniques such as support vector machines (SVMs).

1) *Image processing techniques vs. convolutional neural networks*: Since image processing based techniques are fairly simple to develop and tested, multiple methods using hybrid techniques have been proposed for the classification of leather quality and defect identification in them, separately. These methods use a technique or a combination of techniques in quality grading and defect identification. Some of the more advanced techniques that are used in the process are colour based defect detection, wavelet based image analysis for grading the quality of leather, background subtraction and thresholding for defect identification amongst a host of other basic techniques. These techniques, however, do not work well in many generalized cases due to the specific features that are extracted from the training image set, which may not work well in different environments and conditions. Now, with the introduction of deep learning algorithms such as CNNs, the development of classification systems for leather grading and defect detection systems have become simpler. Due to the automated feature learning by these CNNs, the features pertaining to the leather qualities for the grading systems, and the features pertaining to the defects for the defect detection systems can be extracted easily through use of specific CNN algorithms which makes the learning and detection of the texture in case of leather quality and the shape, size and details of the defects in the defect detection system much simpler. As a result of the very generalized approach that CNNs take, it is poised to work accurately in multiple scenarios.

III. RELATED WORK

A method for the detection and classification of surface defects is proposed by Choonjon Kwak et al. [9]. In this method, a two-step segmentation process using thresholding and morphological processing is used for defect location whereas statistical first order and second order features, and geometrical features are used for the classification process. A three stage sequential decision tree classifier is involved in the classification process, mainly, for classifying five types of defects such as lines, stains,

holes, knots and wears. The proposed method achieves a good accuracy rate of 91.25 %. In addition to these techniques, wavelet features are also commonly used for identifying defects. A leather defect detection proposal is given by Sobral et al. [10] which uses wavelet transform with a bank of optimized filters, with each filter tuned for detecting one type of defect. Shape and the wavelet sub-bands of the filters are selected to maximize the ratio of feature values on defect regions and normal regions. This defect detection methodology produces fast and accurate results. Another such method for identification of leather defects is proposed by Jawahar et al. [11] using wavelet feature extraction technique. The leather images are captured and processed in the frequency domain using wavelet transform, for easy analysis of uncorrelated pixels and edges and easy highlighting of the frequency separation and image variation, respectively. Further, the defect are identified using wavelet statistical features and wavelet co-occurrences matrix features like Entropy, Energy, Contrast, Correlation, Mean, Cluster Prominence Standard Deviation and Local Homogeneity. The identified defects are classified through a support vector machine classifier, thus, giving robust results. Fu Qiang He [12], also proposed a wavelet based feature extraction technique. A multiresolution approach with energy, entropy matrices for defect detection is used. The defect distinguishing process uses a wavelet band selection procedure, which automatically determines the number of resolution level for decomposition of sub images, removing repetitive texture patterns from the image. This is followed with an adaptive binary algorithm for separating the defective regions. Experimental results prove the fastness and the efficiency of this method. Sze Teng Liong et al. [13] present a deep learning architecture based method for defect detection on leather images. The detected defects are marked using a robotic arm and chalk. This proposed methodology is able to achieve a very high segmentation accuracy rate of 91.5 % on the training data and 70.35 % on the test data.

Kasi et al. [14] propose using auto adaptive edge detection algorithm for defect identification. The methodology uses an edge detection algorithm which focuses on the leather edges with continuity and clarity, removing irrelevant edges and identifies leather defects and achieves good results. Malathy Jawahar et al. [15] propose a leather surface defect detection system which uses a multi-level thresholding algorithm for segmenting defective and non-defective regions from the captured leather surface images. Next, a texture feature extraction algorithm is used for quantification of the leather surface defects. A neural network classifier is then used for classification. The methodology used achieves a good accuracy rate of 90 %. Fan Dahuang et al. [16] propose a leather surface detection algorithm by using ultra-high definition images captured by a camera. A segmentation algorithm that is based on the saturation channel characteristics of the captured image is used for obtain region of interest (ROI). These regions are further used to detect the presence of defects in them using a method of automatic detection and location using image gradients. Experimental results prove that the method

detects and locates defects effectively and precisely while outperforming many other traditional methods.

Jang-Woo Kwon et al. [17] propose a texture analysis method for leather quality classification. The proposed method grades the leather quality by using extracting density and defects from a black image. The defects are extracted by using differentiation of histogram distribution from the image pixel, considered as a window and a search window. The evaluation of leather grade is done by using this differentiation process and offers good results. Santos Filho et al. [18] also propose a leather quality classification methodology. Initially, the regions of interest (ROI) is considered, segmented and filtered in three steps. Next, using this ROI, haralick texture features is extracted using a gray level co-occurrence matrix (GLCM). Various descriptors such as energy, homogeneity, contrast, cluster shade, maximal correlation coefficient are used. Experimental results show that the system performs efficient classification of goat leather with accuracy rate reaching 93.22 %. Winiarti et al. [19] propose for the utilization of a pre-trained deep convolutional neural network (CNN) for extracting discrete features from tanning leather image, for classification of leather types. The extracted features are passed into a support vector machine (SVM) which performs the classification process, thus, resulting in good performance.

In the defect classification category, Ding et al. [20] propose a hierarchical classification technique and a defect extraction technique using image processing. Using geometric feature representation, defects are initially divided into dots, lines and surfaces. Next, the dominating characteristics can be collected by analyzing this data through extracting texture, gray and geometry from the defects. Each type of defect is considered individually and their representative characteristics are chosen and dimensions reduced for establishing a database. Characteristics are further converged by clustering in the database. It is then used for defect classification. This methodology of classification results in a high performance system being able to achieve more than 90 % classification accuracy. Jian et al. [21] propose a methodology to classify leather surface defects using a Feed-forward Neural Network (FNN) and a decision tree combination. This allows for the optimal attribute selection and defect classification. The method performs efficient and fast classification of defects. In a comprehensive approach for leather defect classification, Sze Teng Liong et al. [22] propose a combination of deep learning and image processing techniques. Initially, the leather images are partitioned into small patches and pre-processed using a canny edge detection technique. This enhances the visualization of the defects. Next, the extraction of notable features takes place through the use of an artificial neural network (ANN) and convolutional neural network (CNN). Experimental results show that the network achieves a good 80.3 % classification accuracy rate. In another method that identifies defects but on yarn-dyed fabric, Junfeng Jing et al. [23] propose using a convolutional neural network (CNN), modelled on a modified AlexNet

architecture, which replaces local response normalization layers with batch normalization layers, to improve efficiency in computation and classification. Defect extraction takes place through the multiple layers of the CNN and the final classification is got as the end result from the CNN. Experimental results show a good performance of this classification method. Choojong Kwak et al. [24] propose another system for the surface defect detection and classification. Thresholding and morphological processing are used to detect and locate visual defects. Five types of defects that are lines, holes, wears, knots and stains are focused on. For classification of defects, a two multi layered perceptron model is used, with one, two hidden layers. Comparison results with a decision tree approach shows higher classification accuracy achieved by this model. Hoang-Quan Bong et al. [25] propose a leather defect detection and classifying system, focusing on defects such as scars, scratches and pinholes. Several image processing techniques are cascaded and applied for the image feature extraction and defect position location. These collected features are used for the classification of the defect type using a support vector machine (SVM). The method offers good accuracy and speed.

From the analysis of existing systems and methodologies [32], it can be seen that either the system is developed to work on a specific type of leather or is tuned to detect a specific type of defect. In either of these applications, the proposed system cannot work with various other types of leather images and identify any type of defect in them. Also, the dataset that has been used in the majority of the works have not been released or is not available publicly. As a result, this work proposes to develop a highly efficient and powerful leather classification and defect detection system that is not specifically tied to one type of leather and defect.

IV. PROPOSED METHODOLOGY

An efficient system is proposed for the classification of leather images and detection of defects in them. It consists of two single-channel convolutional neural networks, one for classification and the other for locating and marking defects.

The first channel for classification uses Inception V3 [26] deep convolutional neural network for identifying saliency features in the leather images and classifying them as either good or defective. The second channel for locating defects uses Mask R-CNN [27]. If the resultant output of the first channel CNN is defective, the image is passed on to the second channel CNN that locates the defects in the image. By using this methodology, an efficient and faster processing of the leather images classification can be done. This avoids the wastage of crucial time by not trying to locate defects, which takes a considerable amount of time, when the image is of a good quality leather sample. The robustness of this approach rests on the fact that the classifier is able to classify the images with a high accuracy. The flowchart of the proposed system is shown in Fig. 1.

A. Classification CNN

Classification is the process of systematic arrangement of a certain thing in groups or categories according to established conditions or criteria. With respect to images, the main task of classification is the acceptance of the input image and processing it, to find the class of the image. For example, considering a classification of pets as dogs or cats, when an image containing a cat is given as input, the classification system should classify the image as of cat category. Since, images are an array of pixels, recognizing any specific object category by a computer, which cannot understand semantic information in an image is a difficult task. This is where convolutional neural networks are used.

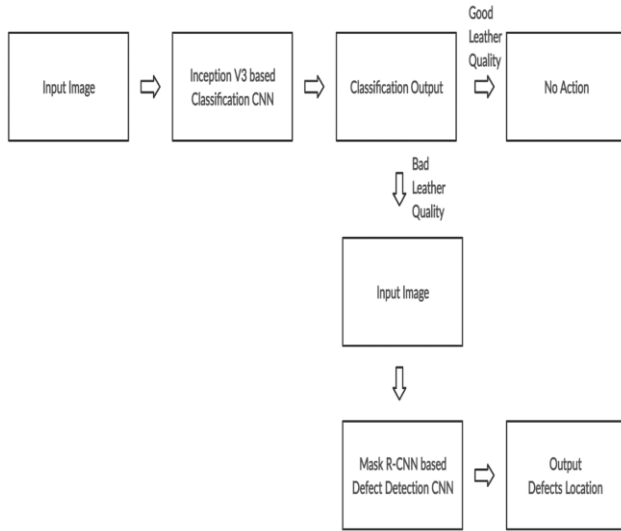


Fig. 1. Flowchart of the proposed system.

Here a deep convolutional neural network based on Inception V3 is proposed. Inception V3 is an improved Inception CNN architecture with 48 layers. It is more efficient than VGGNET and has a computational cost of only about 2.5 times higher than that of GoogLeNet (Inception V1, 27 layers).

For the gathering of all of the salient features in the image, a deep convolution network with multiple filters and layers is required. Since the deepening of the network costs computationally, the Inception module is developed, which has multiple filters for performing multiple convolution operations on the input at the same level of the network, widening it.

The Inception CNN architecture, given in Fig. 2, is based on the inception modules or blocks, which consists of multiple filters in different sizes (1x1, 3x3 and 5x5) for performing convolution operation on the input, at the same level. Each block's end consists of a global average pooling for output concatenation from a single block. Two auxiliary classifiers are attached to the network, for softmax operation on the outputs for total loss adjustment purposes [28].

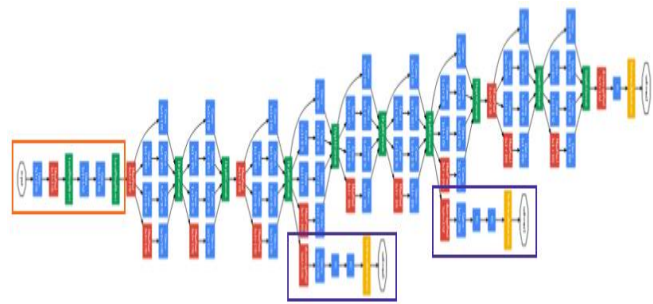


Fig. 2. Inception V3 architecture.

The output of this classifier network is the input image's classification as good quality or defect quality. If the output of this neural network comes out to be as defective quality, then the image is pushed to the next channel, the defect locating CNN, to locate the defects in that image.

B. Defect Detection CNN

Any image can have multiple objects present in it. Object detection is the process of locating each of the object in an image. Images can have multiple objects with same class labels and different objects with different class labels.

Region based CNNs (R-CNNs) have been the most effective type of CNNs due to their architectural design proposing highly confident prospective object regions. R-CNNs work by proposing a bunch of regions or boxes in an image using Selective Search algorithm and checks whether these regions contain any object of interest. Mask R-CNN is the CNN architecture that is proposed for being used in the defect detection CNN channel. It accurately locates the defects in the image and draws optimum bounding boxes around it. The architecture of the CNN is given in Fig. 3.

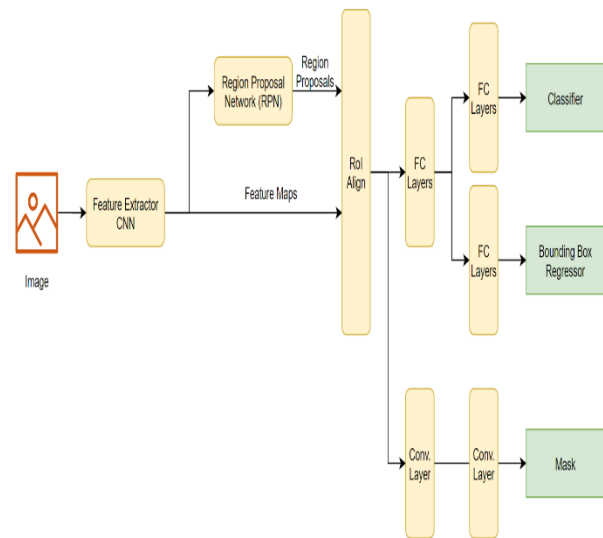


Fig. 3. Mask R-CNN architecture.

The Mask R-CNN architecture consists of an initial CNN which is a feature extractor. The feature extractor that we use in this work is Inception V2. This feature extractor CNN works on the image to produce feature maps. These feature maps correspond to the salient features detected in the image. The feature map is parallelly passed to a Region Proposal Network (RPN) to generate regions of interest, wherein prominent candidate objects of interest in the feature maps are identified and marked. These marked regions on the feature maps is passed to an ROI Align layer, along with the original generated feature maps, to align the proposed candidate regions of interest with the feature maps effectively. This effective mapping is the reason why Mask R-CNN is preferred over other R-CNNs such as Faster R-CNN, Fast R-CNN, etc. Another reason is the optimization of the bounding boxes, to minimize the area required to be removed due to a defect. These aligned maps are then passed to fully connected layers for class label prediction, bounding box fit and masks.

Thus, the output from this CNN is the image in which the defects are identified and each of them are marked with bounding boxes. Masked outputs are disabled due to non-use in this particular scenario.

Emphasizing the potential for collaboration with industry stakeholders, technology providers, or research institutions is crucial for further refining and validating the proposed leather defect detection system using deep learning. Collaborative efforts can facilitate the exploration of real-world implementation scenarios, allowing for

comprehensive testing and validation of the system's effectiveness across diverse production environments. Moreover, knowledge exchange between academia and industry can lead to insights and innovations that advance automated quality control practices not only within the leather industry but also in other sectors. By fostering collaborative partnerships, stakeholders can collectively contribute to the evolution and adoption of cutting-edge technologies, driving continuous improvement and enhancing operational efficiencies in quality control processes on a broader scale.

V. EXPERIMENTAL TESTS AND ANALYSIS

The availability of useful leather datasets that can be used for training and testing techniques have always been a huge issue. Most of the already handful of available datasets, have either a low quantity of images that can be used for training and testing, or do not contain quality images. The dataset that has been generated by us, using data augmentation method. The images are available in [29], samples of which are shown in Fig. 4. Originally, it consisted of 428 good quality and 354 defect quality leather images collected from leather industry. By using, image augmentation techniques such as scaling, cropping, flipping, grayscale, brightness, contrast, saturation, etc., a total of 29716 images are produced and packed in the dataset. The original 354 defective images used and each of the defect in them are manually annotated by a tool called LabelImg [30] and mask created by a tool called PixelAnnotationTool [31]. Fig. 5 depicts the process.

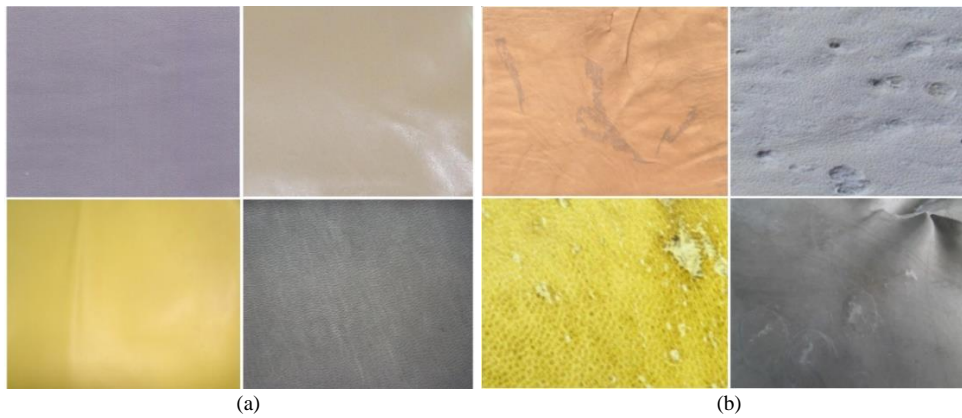


Fig. 4. Sample dataset images of (a) Good quality leather and (b) Defect quality leather.

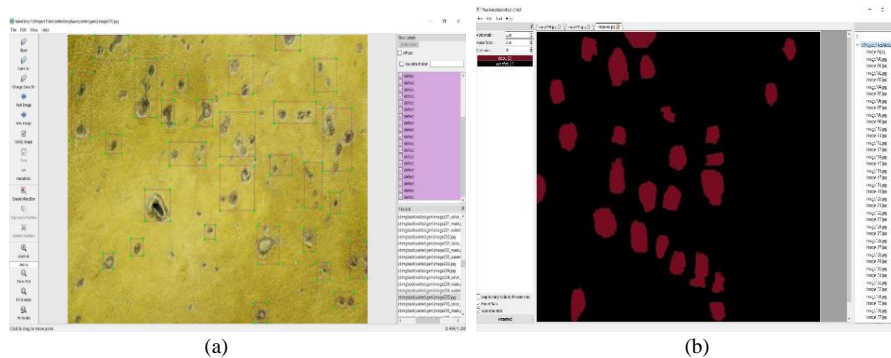


Fig. 5. Dataset (a) Annotation using labelImg (b) Mask creation using pixel annotation tool.

The experiments were carried out on a machine with Ubuntu 16.04 as the Operating System, 16 GB RAM, Intel i5 processor and a Nvidia GTX 1060 GPU with 6GB VRAM. The integrated leather quality classification and defect detection system was implemented using Python, Tensorflow and Keras. Since the system uses two single channel convolutional neural networks, one for classification and one for defect detection, a two-step training process is followed with unique datasets.

The first classification CNN is fed with the categorized images with 23772 training images with 13004 good quality and 10768 defect quality leather images. The validation set of 5944 images consists of 3260 good quality and 2684 defect quality leather images. The network is trained for 200 epochs with the image batch size being 32. This network achieves a classification accuracy of 99 % on the training data and 84.6 % on the validation data. The second defect detection network consists of an object detection CNN and as a result expects annotated images as the training dataset. Thus, as a result, a total of 224 defect leather quality images were annotated and corresponding masks created, and the same augmentation techniques of colour, saturation, rotation, hue change, flipping, etc., were performed on a total of 530 epochs for a total of 1,20,000 training steps, with batch size set as 1. The training set consists of 162 images and the validation set consists of 62 images, both containing annotation and mask data for each image. This network obtained a detection rate of 99.6 % on the training set, 99 % on the validation dataset and 99 % on a 20 image test dataset. The system results from the experiments are listed in Table I, with the samples shown in Fig. 6, defects detected shown in Fig. 7, training and validation accuracy graphs shown in Fig. 8 and various types of loss functions shown in Fig. 9. Fig. 7 on a closer inspection reveal that the defective spots are identified with high precision and accuracy. At some spots the accuracy is around 60%, where in a suitable selection of threshold value can help to detect the defects with increased precision in a real time situation. Fig. 9 shows the various types of

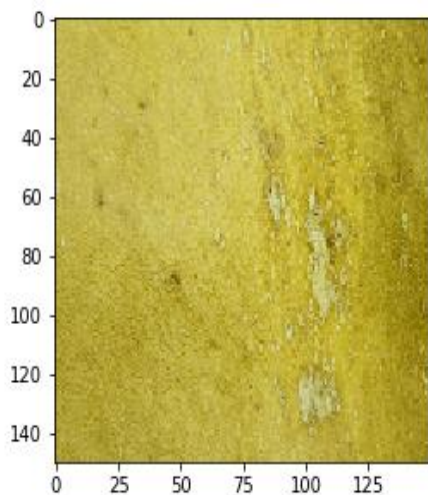
loss the model incurs during the training phase of the proposed RCNN model. X-axis indicates the samples in the epoch and y-axis indicates the loss value. It can be noted that in all the loss graphs, the loss has been steadily decreasing and even approaches 0, beyond certain epochs. This means the model has converged to the leather images in detecting the defects. Hence it can be observed that the proposed model performs a promising automated defect detection of the leather from machine vision approach.

The proposed leather defect detection system offers several advantages over previous approaches, primarily through the integration of advanced deep learning techniques. Unlike traditional methods that rely on manual inspection or basic machine vision algorithms, the proposed system leverages sophisticated deep learning models such as the Inception model for classification and the RCNN model for detection. This enables the system to achieve higher accuracy in defect identification and localization, addressing the limitations of human subjectivity and the inability of older systems to detect subtle or complex defects reliably. Moreover, the automated nature of the proposed system improves efficiency, reduces labor costs, and ensures consistent and scalable defect detection across different production environments. Overall, the integration of deep learning technologies in the proposed system leads to superior performance, increased reliability, and enhanced quality control capabilities compared to previous approaches.

TABLE I. RESULTS OF THE PROPOSED SYSTEM

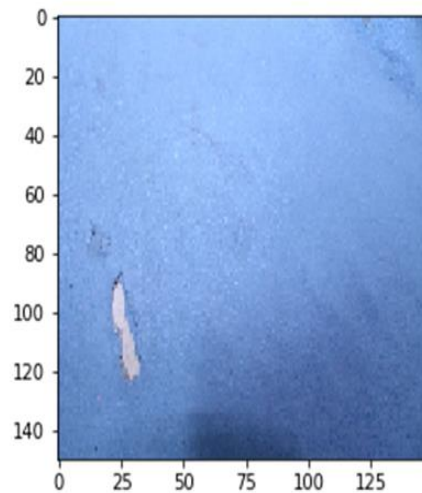
| Methodology | Dataset | Total number of Images | Accuracy Rate |
|------------------|------------|------------------------|---------------|
| Classification | Train | 23772 | 99 % |
| Classification | Validation | 5944 | 84.6 % |
| Defect Detection | Train | 162 | 99.6 % |
| Defect Detection | Validation | 62 | 99 % |
| Defect Detection | Test | 20 | 99 % |

Leather is of defective quality



(a)

Leather is of defective quality



(b)

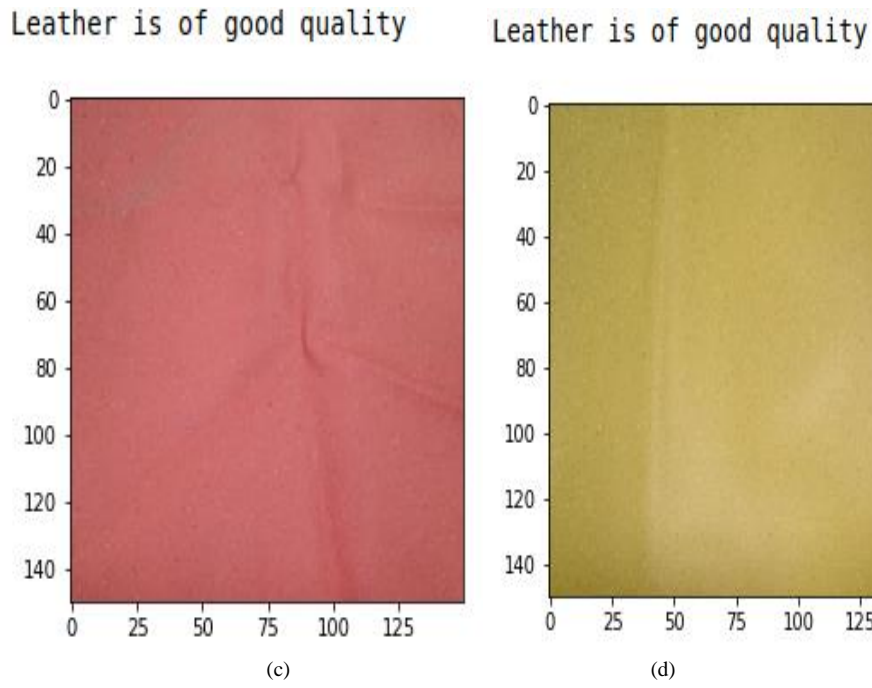


Fig. 6. (a) Defective quality leather sample 1; (b) Defective quality leather sample 2; (c) Good quality leather sample 1; (d) Good quality leather sample 2.

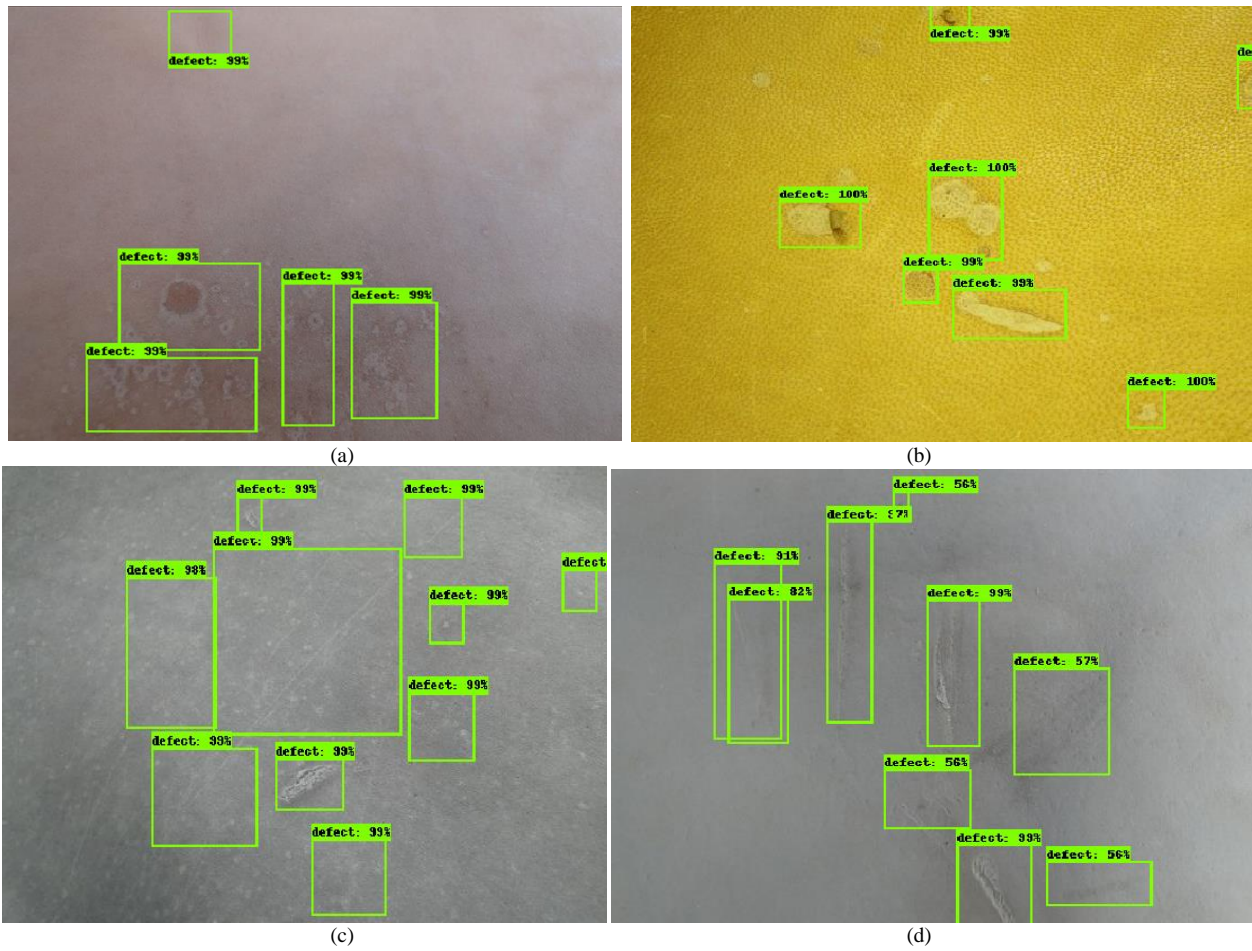


Fig. 7. Leather image defect detection sample results.

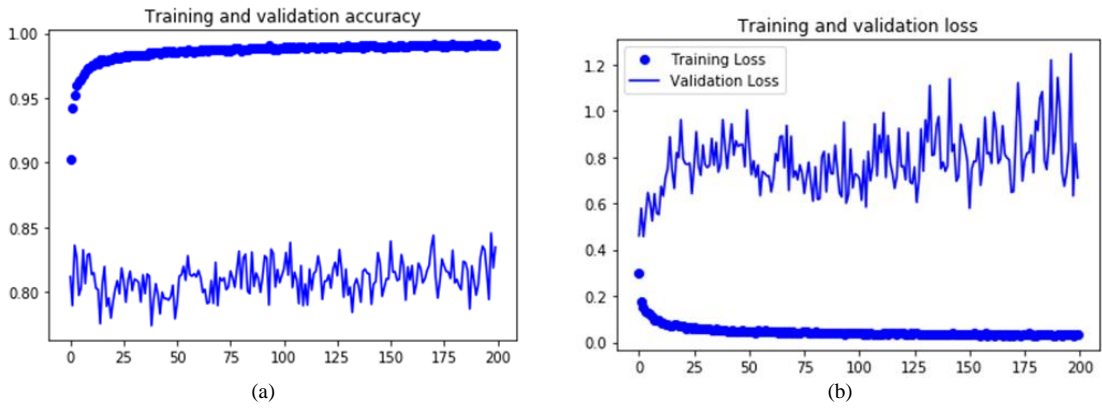
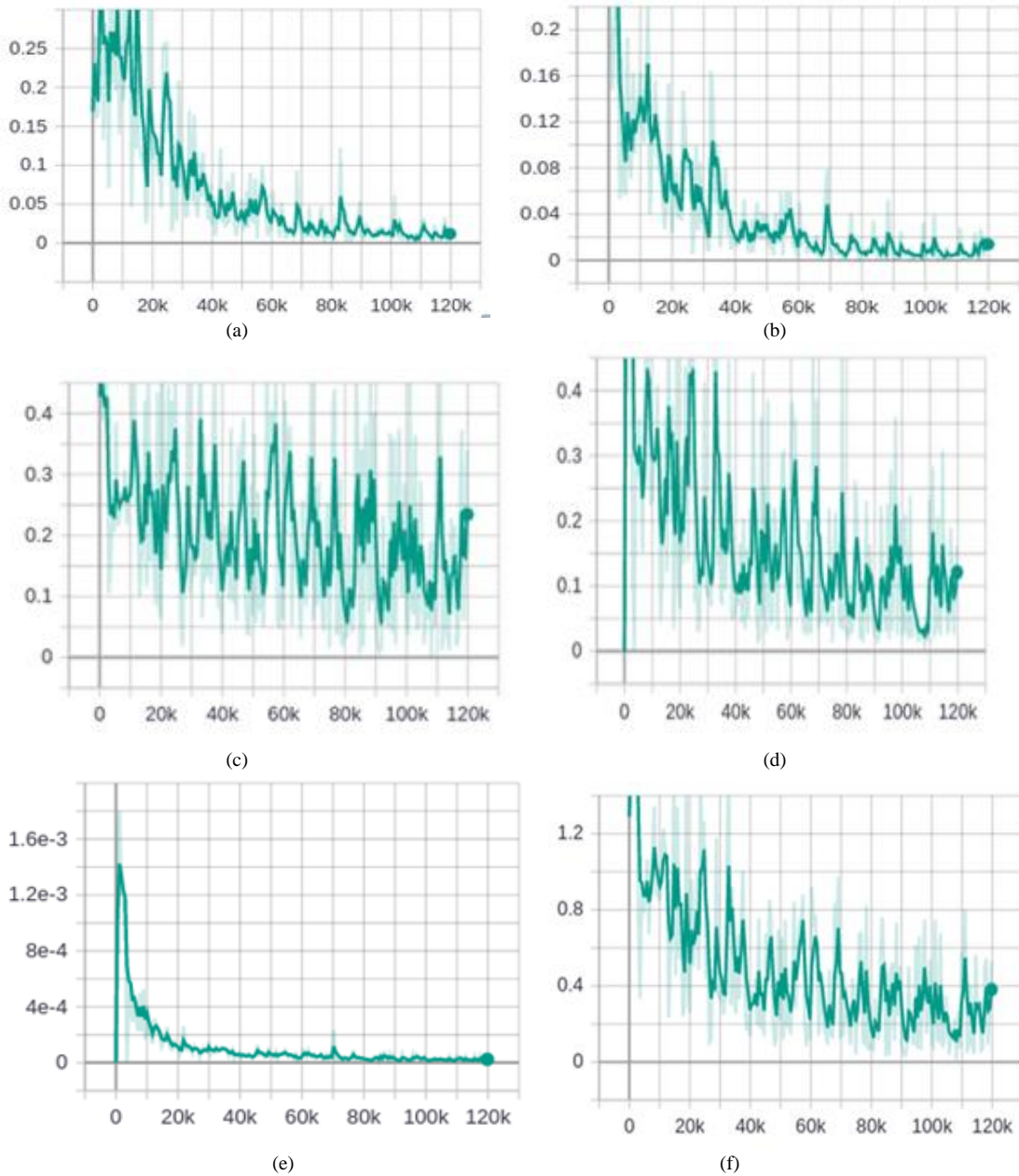
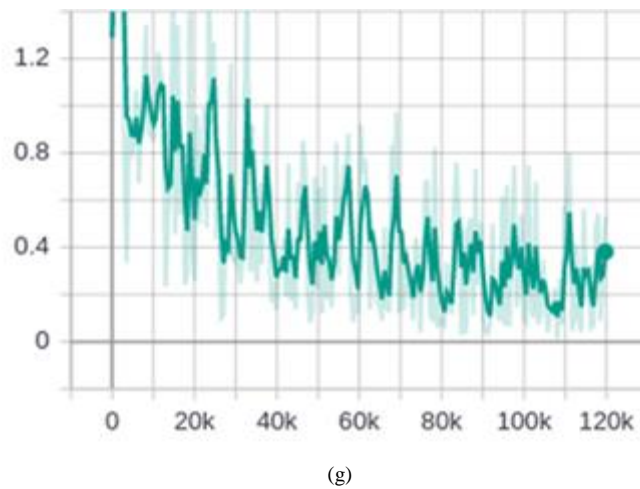


Fig. 8. Graphs for training and validation phases of the proposed model – (a) Accuracy graph; (b) Loss graph.





(g)

Fig. 9. Various loss graphs during defect detection training of the proposed model – (a) RPN localization loss; (b) Objectness loss; (c) Classification loss; (d) Localization loss ; € mask loss; (f) Clone loss; (g) Total loss.

VI. CONCLUSION

This paper presented a comprehensive system for the classification and detection of defects in leather images using convolutional neural networks. Initially, the basic image processing approaches and their applications were discussed in this field. With the introduction of deep learning methods, convolutional neural networks are the most preferred way in this field due to their unique automated feature extraction and learning approaches. The recent works using both of these approaches was discussed. The proposed system uses a double channel method, where one channel has a Inception V3 convolutional neural network which classifies the leather image as “good quality” or “defect quality” while the other channel has Mask R-CNN which detects and locates the defects in the leather image and draws bounding boxes for candidate defect regions, when the output of the first channel is “defect quality”. Experimental results show that the system achieves a high performance with the classification CNN achieving a 99 % accuracy rate on the training dataset and 84.6 % on the validation dataset. The defect detection CNN achieves 99.6 % defect detection accuracy on the training dataset, 99 % on the validation dataset and 99% accuracy on the test dataset. Thus, the system is proved to be able to accurately classify leather images and identify and locate defects in images, where only those images which are classified as “defective”, are sent to the second channel defect detection convolutional neural network for detection of defects, thereby making the process much faster.

Researchers could make leather defect detection systems using deep learning even better in the future. They could add advanced technologies like reinforcement learning and transfer learning. Reinforcement learning helps the system make good decisions and adapt to new situations. Transfer learning uses knowledge from related areas to improve defect detection accuracy. The systems could also be used in other industries besides leather manufacturing, like textiles or car manufacturing. This would allow automating quality control processes to boost efficiency across different sectors. Exploring these avenues

can enhance automated defect detection systems' capabilities and versatility. This could lead to more industries adopting the technology and drive innovation.

ACKNOWLEDGMENT

Fuad A. M. Al-Yarimi extend his appreciation to the Deanship of Scientific Research at King Khalid University for funding this work through the General Research Project under grant number (R.G.P1/181/43).

REFERENCES

- [1] Kohli, Parag. (2013). Leather Quality Estimation Using an Automated Machine Vision System. *IOSR Journal of Electronics and Communication Engineering*. 6. 44-47. 10.9790/2834-0634447.
- [2] Barik, Debabrata. (2019). Introduction to Energy From Toxic Organic Waste For Heat and Power Generation. 10.1016/B978-0-08-102528-4.00001-8.
- [3] Milosevic, N. (2020) “Convolutions and Convolutional Neural Networks,” *Introduction to Convolutional Neural Networks [Preprint]*. Available at: https://doi.org/10.1007/978-1-4842-5648-0_12.
- [4] Mueller, J. and Massaron, L. (2019) in *Deep learning for dummies*. Hoboken, NJ: John Wiley & Sons, Inc.
- [5] Krizhevsky, A., Sutskever, I. and Hinton, G.E. (2017) “ImageNet classification with deep convolutional Neural Networks,” *Communications of the ACM*, 60(6), pp. 84–90. Available at: <https://doi.org/10.1145/3065386>.
- [6] Szegedy, C., Liu, W., Jia, Y., Sermanet, P., Reed, S.E., Anguelov, D., Erhan, D., Vanhoucke, V., & Rabinovich, A. (2014). Going deeper with convolutions. 2015 IEEE Conference on Computer Vision and Pattern Recognition (CVPR), 1-9.
- [7] He, K., Zhang, X., Ren, S. and Sun, J. (2016) Deep Residual Learning for Image Recognition. *Proceedings of the IEEE Conference on Computer Vision and Pattern Recognition*, 770-778. <https://doi.org/10.1109/CVPR.2016.90>.
- [8] He, K., Zhang, X., Ren, S., Sun, J. (2016). Identity Mappings in Deep Residual Networks. In: Leibe, B., Matas, J., Sebe, N., Welling, M. (eds) *Computer Vision – ECCV 2016*. ECCV 2016. *Lecture Notes in Computer Science()*, vol 9908. Springer, Cham. https://doi.org/10.1007/978-3-319-46493-0_38.
- [9] Kwak, C., Ventura, J.A., & Tofang-Sazi, K. (2001). Automated defect inspection and classification of leather fabric. *Intell. Data Anal.*, 5, 355-370.
- [10] Sobral, J.L. (2005). Leather Inspection Based on Wavelets. *Iberian Conference on Pattern Recognition and Image Analysis*.

- [11] Jawahar, M., Chandra Babu, N.K., & Vani, K. (2014). Leather texture classification using wavelet feature extraction technique. 2014 IEEE International Conference on Computational Intelligence and Computing Research, 1-4.
- [12] He, F.Q., Wang, W., & Chen, Z. (2006). Automatic Visual Inspection for Leather Manufacture. *Key Engineering Materials*, 326-328, 469 - 472.
- [13] Liang, S., Gan, Y.S., Huang, Y., Yuan, C., & Chang, H. (2019). Automatic Defect Segmentation on Leather with Deep Learning. *ArXiv*, abs/1903.12139.
- [14] Kasi, M.K., Rao, J.B., & Sahu, V.K. (2014). Identification of leather defects using an autoadaptive edge detection image processing algorithm. 2014 International Conference on High Performance Computing and Applications (ICHPCA), 1-4.
- [15] Jawahar, M., Vani, K., & Chandra, N. (2019). Machine Vision Inspection System for Detection of Leather Surface Defects. *Journal of The American Leather Chemists Association*, 114, 10-19.
- [16] Dahuang, F., Lei, D., & Jiehang, D. (2019). Automatic Detection and Localization of Surface Defects for Whole Piece of Ultrahigh-definition Leather Images. 2019 IEEE 4th International Conference on Computer and Communication Systems (ICCCS), 229-232.
- [17] Kwon, J., Choo, Y., Choi, H., Cho, J., & Kil, G. (2004). Development of leather quality discrimination system by texture analysis. 2004 IEEE Region 10 Conference TENCON 2004., A, 327-330 Vol. 1.
- [18] Filho, E.Q., Sousa, P.H., Filho, P., Barreto, G.D., & Albuquerque, V.H. (2020). Evaluation of Goat Leather Quality Based on Computational Vision Techniques. *Circuits, Systems, and Signal Processing*, 39, 651-673.
- [19] Winiarti, S., Prahara, A., Murinto, & Ismi, D.P. (2018). Pre-Trained Convolutional Neural Network for Classification of Tanning Leather Image. *International Journal of Advanced Computer Science and Applications*, 9.
- [20] Ding, C. & Huang, H. & Yang, Y.. (2018). Description and Classification of Leather Defects Based on Principal Component Analysis. *Journal of Donghua University (English Edition)*. 35. 473-479.
- [21] Jian, L., Wei, H., & Bin, H. (2010). Research on inspection and classification of leather surface defects based on neural network and decision tree. 2010 International Conference On Computer Design and Applications, 2, V2-381-V2-384.
- [22] Liang, S., Gan, Y.S., Liu, K., Binh, T.Q., Le, C.T., Wu, C., Yang, C., & Huang, Y. (2019). Efficient Neural Network Approaches for Leather Defect Classification. *ArXiv*, abs/1906.06446.
- [23] Jing, J., Dong, A., & Li, P. (2017). Yarn-dyed fabric defect classification based on convolutional neural network. *International Conference on Digital Image Processing*.
- [24] Kwak, C., Ventura, J.A., & Tofang-Sazi, K. (2000). A neural network approach for defect identification and classification on leather fabric. *Journal of Intelligent Manufacturing*, 11, 485-499.
- [25] Bong, H., Truong, Q.B., Nguyen, H., & Nguyen, M.T. (2018). Vision-based Inspection System for Leather Surface Defect Detection and Classification. 2018 5th NAFOSTED Conference on Information and Computer Science (NICS), 300-304.
- [26] Szegedy, C., Vanhoucke, V., Ioffe, S., Shlens, J., & Wojna, Z. (2015). Rethinking the Inception Architecture for Computer Vision. 2016 IEEE Conference on Computer Vision and Pattern Recognition (CVPR), 2818-2826.
- [27] He, K., Gkioxari, G., Dollár, P., & Girshick, R.B. (2017). Mask R-CNN. *IEEE Transactions on Pattern Analysis and Machine Intelligence*, 42, 386-397.
- [28] Szegedy, C., Ioffe, S., Vanhoucke, V., & Alemi, A.A. (2016). Inception-v4, Inception-ResNet and the Impact of Residual Connections on Learning. *ArXiv*, abs/1602.07261.
- [29] LeatherImageDataSet. (2023). <https://github.com/AkshRSH/LeatherImageDS> (accessed 20 December 2022).
- [30] LabelImg, Github. (2020). <https://github.com/tzutalin/labelImg> (accessed 20 March 2020).
- [31] PixelAnnotationTool, Github. (2020). <https://github.com/abreheret/PixelAnnotationTool> (accessed 20 December 2022).
- [32] Jawahar, Malathy & Anbarasi, L. & Subbiah, Geetha. (2022). Vision based leather defect detection: a survey. *Multimedia Tools and Applications*. 82. 1-27. 10.1007/s11042-022-13308-x.
- [33] S.-T. Liang, D. Zheng, Y.-C. Huang, and Y. S. Gan, "Leather defect classification and segmentation using deep learning architecture," *Int. J. Comput. Integr. Manuf.*, vol. 33, no. 10–11, pp. 1105–1117, Nov. 2020, doi: 10.1080/0951192X.2020.1795928.
- [34] L. Jian, H. Wei, and H. Bin, "Research on inspection and classification of leather surface defects based on neural network and decision tree," in 2010 International Conference On Computer Design and Applications, 2010, vol. 2, pp. V2-381-V2-384, doi: 10.1109/ICDA.2010.5541405.
- [35] S.-T. Liang, Y. S. Gan, Y.-C. Huang, K.-H. Liu, and W.-C. Yau, "Integrated Neural Network and Machine Vision Approach For Leather Defect Classification," *CoRR*, vol. abs/1905.1, 2019, [Online]. Available: <http://arxiv.org/abs/1905.11731>.
- [36] Y. S. Gan, S.-S. Chee, Y.-C. Huang, S.-T. Liang, and W.-C. Yau, "Automated leather defect inspection using statistical approach on image intensity," *J. Ambient Intell. Humaniz. Comput.*, vol. 12, no. 10, pp. 9269–9285, 2021, doi: 10.1007/s12652-020-02631-6.
- [37] G. Pazzaglia, M. Martini, R. Rosati, L. Romeo, and E. Frontoni, "A Deep Learning-Based Approach for Auto

Prediction of Pigment Epithelial Detachment in Optical Coherence Tomography Images using Machine Learning

T. M. Sheeba, S. Albert Antony Raj

Department of Computer Applications, Faculty of Science and Humanities
SRM Institute of Science and Technology, Kattankulathur - 603203, Tamil Nadu, India

Abstract—Pigment Epithelial Detachment (PED) is an eye condition that can affect adults over 50 and eventually harm their central vision. The PED region is positioned between the Bruch's membrane (BM) and the RPE (Retinal Pigment Epithelium) layer. Due to PED, the RPE layer is elevated arc shaped. In this paper, a method to extract the best features to detect pigment epithelial detachment (PED) is proposed. This method uses four-stage strategy that drew inspiration from OCT (Optical Coherence Tomography) imaging to detect the PED. In the first stage, to reduce the speckle-noise, in the second stage, segment the Retinal Pigment Epithelium (RPE) layer. In the third stage, a novel method is proposed to extract the best features to detect PED, and in the fourth stage, machine learning classifiers such as K-Nearest Neighbors (KNN), Logistic Regression (LR), Naïve Bayes (NB), and Artificial Neural Networks (ANN) were used to significantly predict the PED. For experimental results, 150 retinal OCT volumes were used, 75 normal OCT volumes, and 75 pigment epithelial detachment volumes. Among the 150 images, 80% were used for training and 20% were used for testing. Here, there are 30 images for testing and 120 images for training. To generate a confusion matrix based on the matrices are true positive (TP), false positive (FP), true negative (TN), and false negative (FN). Logistic Regression is predicted more accuracy among the ANN, LR, NB, and KNN models. The LR model predicted accuracy 96.67% for PED detection.

Keywords—Artificial neural network; k-nearest neighbor; logistic regression; layer segmentation; naïve base; optical coherence tomography; pigment epithelial detachment

I. INTRODUCTION

One of the most vital and sophisticated sense organs that humans possess is the eye. In addition to aiding in object visualisation, it also improves our ability to perceive colour, light, and depth. Fig. 1 depicts a human-eye. The sclera, cornea, pupil, lens, retina, macula, optic nerve, and so on are the components of the eyes. The outer layer of the eyeball is called the sclera. Cornea is curved layer in front of the iris and pupil. The dark dot in the centre of the eye is the pupil. The coloured part of the eye is called the iris. Behind the iris lies the lens. The retina is located on the back of the eye. The retina's macula is a tiny region. The optic nerve is located in the ocular back.

In OCT images retinal layers as shown in Fig. 2. The NLF-Nerve Fibre Layer, the GCL-Ganglion Cell Layer, the IPL-Inner Plexiform Layer, the INL-Inner Nuclear Layer, the ONL-

Outer Nuclear Layer, the ISPR-Inner Segment Photoreceptor Layer, the OSPR-Outer Segment Photoreceptor Layer, and the RPE-Retinal Pigment Epithelium layer.

A number of ocular illnesses, including diabetic macular edema-(DME), glaucoma and age-related macular degeneration (AMD), have been evaluated clinically using OCT. Most of the functional layers of the retina can be seen with the lately developed SD-OCT, which gives highest resolution 3D scans of the macula. For the automated segmented of the retinal layer in SD-OCT scans of healthy eyes, numerous approaches have been put forth with positive outcomes [1-15]. PEDs can be categorized as drusenoid, serous, or fibro-vascular. According to research, people with AMD and serous PED frequently already have Choroid-Neovascularization (CNV) or are at a complex danger of developed it [16, 17].CNV can potentially result in significant visual acuity loss. The normal OCT images of retina is shown in Fig. 3. The abnormal (PED) image is shown in Fig. 5. The red arrow is indicated elevated RPE layer. Due to PED, the RPE layer is elevated arc shaped.

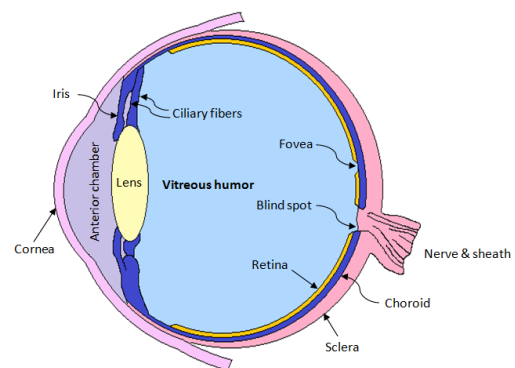


Fig. 1. Human-eye.

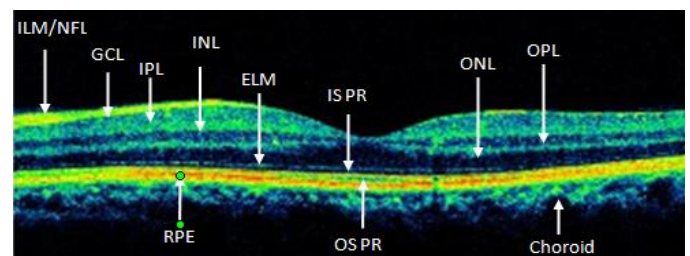


Fig. 2. OCT layers.

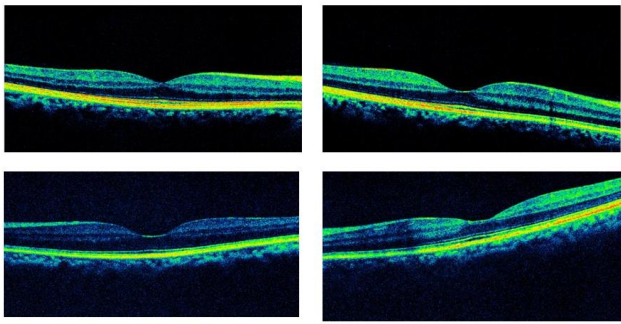


Fig. 3. OCT images of normal eye.

The separation of the retinal pigment epithelium from Bruch's membrane's inner collagenous layer is known as retinal pigment epithelial detachment. In recent years many people affected the PED. It is early diagnose easily cure the disease. This paper aims to detect the PED, Normal and PED images were classified with machine learning algorithms. This automatic model is used to assists doctors early diagnose the PED. The sample PED images are as shown in Fig. 4.

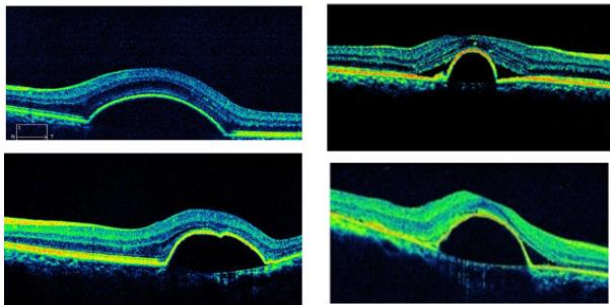


Fig. 4. PED images.

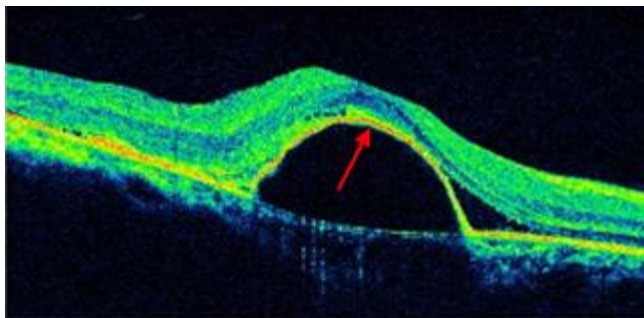


Fig. 5. OCT scan showing PED.

A wiener filter is used during pre-processing to get clear the speckles. For segment process, the threshold method is used to extract retinal layers related with RPE surface distortion. For feature extraction, the features such as Left Height (LHe), Right Height (RHe), Left Down Points (LDp) and Right Down Points (RDp) were extracted. For classification, ANN, KNN, LR and NB classifiers were used to classify the normal and PED images. Finally detected the PED, then the accuracy, sensitivity, precision and specificity were calculated based on the confusion matrix such as the FP, FN, TP and TN values. The following steps are involved to detect the PED as follows: The proposed system OCT images as

input, convert OCT image into grayscale image, denoising the image, extract the RPE layer, extract the features and detect the PED.

The main contributions of this work are as follows: i) Accurately reduce the speckle noise in OCT images through the Wiener filtering technique. ii) Accurately segment the RPE layer in normal OCT images and PED images. iii) Extract four novel features to accurately predict PED disease and normal images.

II. LITERATURE REVIEW

Layer segmentation techniques created for retinas have also been effectively used on retinas with specific disorders such as glaucoma [11, 12, 16] and multiple abnormalities [13], or further disease in an early-stage, when there isn't a significant change in the layer structure. Segment for retina with PEDs, which are linked to sub-RPE fluid and RPE distortion. Layer segment and anomalous region segment are successfully combined where the positions of the two act as limitations on one another [17, 18]. Along with a generic method for local retinal abnormality detection, a technique for automatic characterisation of the normal retinal appearance in SD-OCT volume is provided. To reduce motion-based artefacts, the 3-D picture collection is flattened after ten intra-retinal layers are frequently segmented. To characterize the quality and width properties across the retina, 23 features are locally retrieved from the flattened OCT data in each layer. Thirteen SD-OCT volumes showing typical retinas were used to calculate the usual ranges of layer-specific feature changes.

The local variations between the usual appearance and the relevant macula parameters are subsequently classified to identify abnormalities [19]. Based on Enface fundus imaging, a unique two-stage segmentation approach was proposed. Methods: To identify fluid-associated anomalies with diffuse boundaries, the fundus picture was first segmented using a thick map [20]. The suggested approaches don't need any extra details, like layer segmentation for training. In order to smooth the segmentation map, several image segmentation techniques employ a postprocessing phase based on conditional random fields (CRF). However, first order information can only be encoded using such approaches due to computational complexity [21].

The foundation of general categorization techniques is traditional machine learning, which employs subject expertise to create hand-crafted features. To categories SRF and PED characteristic in OCT images, the authors suggested a ResidualNetworkModel [22]. In the industrialised world, AMD is the most common-source of significant vision damage in persons 50 years of older. With the development of anti-angiogenic medicines, considerable advancements in AMD treatment have been made recently, providing patients with neovascular AMD with the first realistic prospect of significant vision recovery [24].

The histologic properties of macula cell mosaics, including photoreceptor and RPE cells, can be examined in vivo using adaptive optics (AO) imaging techniques. Ophthalmic AO imaging systems produce high-resolution images that are replete with information that is challenging and/or time-

consuming to quantify manually. As a result, reliable, automated analysis systems that can deliver repeatable quantitative data regarding the examined cellular mosaics are needed. Automated algorithms have been created to locate specific photoreceptor cells, but the majority of these techniques are inadequate for describing the RPE. On simulated and actual fluorescence AO images of the RPE, built an procedure for RPE segment and demonstrate its effectiveness here [25]. For the evaluation of retinal disorders, precise segment of fluid-associated-anomalies & PED in OCT is essential [26]. A separation of the NRD from the RPE causes by sub-retinal-fluid, known as a neurosensory retinal detachment (NRD), can cause severe visual loss. It is widely known that the detachment of the neurosensory retina changes the structure and continuity of intensity of the retinal layers [27].

III. METHODOLOGY

A. Method Overview

The suggested PED detection approach includes preprocessing, RPE layer segmentation, feature extraction, training the machine learning model and PED detection as shown in Fig. 6.

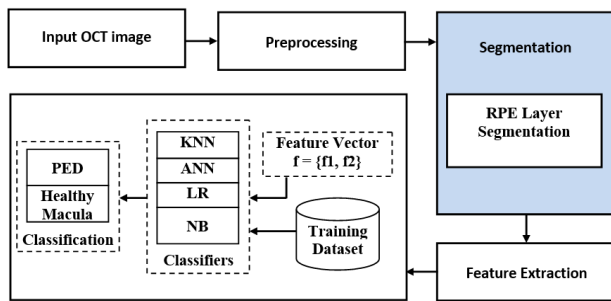


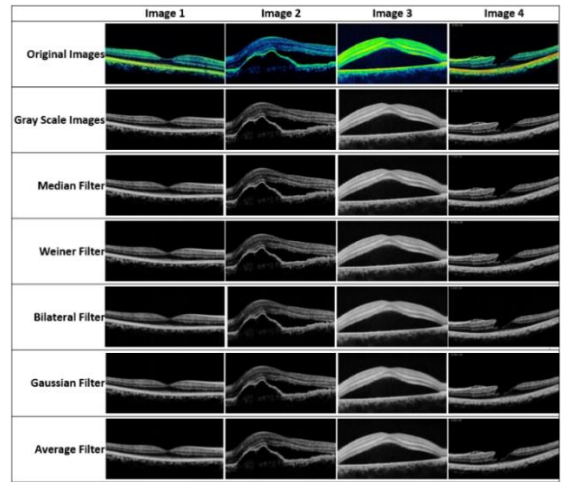
Fig. 6. Steps involved in PED detection.

In the original input OCT images the grey levels are normalised and speckle noise is reduced using wiener filter during preprocessing. An approach called the threshold method is used for RPE layer segmentation in the OCT images. PED happens at elevated RPE floors, using machine learning techniques like K-NN, LR, NB, and ANN, the characteristics retrieved and detected the PED. In order to extract features for K-NN, LR, NB, and ANN classifiers for training, OCT images are manually annotated. Then the required features are extracted which includes LH, RH, LDp and RDp which are computed from preprocessed OCT images. The machine learning models, K-NN, Logistic Regression, Nave Bayes, and ANN classifier, were trained to detect the PED. And, then trained models were used to detect PED for the new input images.

B. Pre-processing

Preprocessing is essential step to detect the PED, which is reduce the speckle-noise. The source images converted into grayscale then applying noise reduction algorithms. Speckle noise that are multiplicative in nature are more prevalent in OCT images [28-30]. The image processing and analysis techniques may perform less effectively and efficiently due to speckle, which is the primary quality degrading issue in OCT

images. De-noising techniques that successfully eliminate speckle noise. Many authors suggested bilateral filtering technique and wiener filtering approach [31-36] satisfies this condition. Different filtering methods were used to eliminate the speckle-noise in the OCT images. And, analyzed mean, median, bilateral, gaussian, and wiener filtering techniques among 50 images and computed by the metrics such as PSNR, CNR and MSE. Based on the analysis, wiener filtering outperforms and significantly eliminate the speckle-noise in OCT images. Fig. 7 shows the few preprocessing images. Table I, Table II and Table III are the analysis report of wiener filtering technique. Fig. 8, Fig. 9 and Fig. 10 shows the chart of the analysis report.



(a) Image-1, (b) Image-2, (c) Image-3, (d) Image-4

Fig. 7. Few images for pre-processing.

TABLE I. FILTERED IMAGES FOR MSE VALUE

| MSE Comparison | | | | | |
|----------------|---------|----------------|-----------|----------|---------|
| OCT Images | Median | Weiner | Bilateral | Gaussian | Average |
| Image 1 | 20.2975 | 17.5117 | 26.0607 | 27.9989 | 28.2926 |
| Image 2 | 21.8668 | 19.1076 | 21.6137 | 30.6731 | 31.1288 |
| Image 3 | 30.0248 | 29.2978 | 39.3896 | 45.2085 | 46.0353 |
| Image 4 | 20.5462 | 17.5784 | 23.8372 | 29.5153 | 29.9617 |
| Image 5 | 21.8579 | 18.4743 | 19.6781 | 29.2216 | 29.3958 |
| Image 6 | 27.4318 | 26.8242 | 35.1803 | 40.6335 | 41.3365 |

C. RPE Layer Segmentation

RPE layer segmentation is essential step to detect the PED. Following the preprocessing step, to extract the RPE layer. Segmentation of the RPE layer is advance the procedure to separate the retinal layer [19, 20]. The threshold is one such active segmentation method, which is used to exactly separate the RPE layer. So threshold technique proposed to extract the RPE layer. As a result of the RPE layer's brightness pixel value picked up, the output is predictable and provides a clear view of the necessary retinal layers.

The thresholding method as:

$$T = T[x, y, p(x, y), f(x, y)] \quad (1)$$

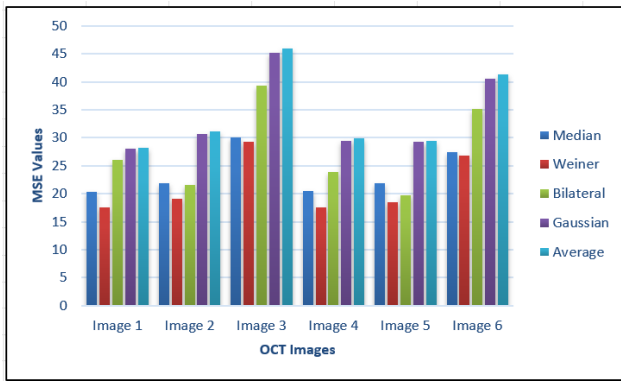


Fig. 8. Analysis chart for MSE values.

TABLE II. FILTERED IMAGES FOR PSNR VALUE

| PSNR Comparison | | | | | |
|-----------------|---------|----------------|-----------|----------|---------|
| OCT Images | Median | Weiner | Bilateral | Gaussian | Average |
| Image 1 | 35.0563 | 35.6975 | 33.9709 | 33.6593 | 33.6140 |
| Image 2 | 34.7329 | 35.3187 | 34.7835 | 33.2632 | 33.1991 |
| Image 3 | 33.3559 | 33.3166 | 32.1769 | 31.5786 | 31.4998 |
| Image 4 | 35.0034 | 35.681 | 34.3582 | 33.4303 | 33.3651 |
| Image 5 | 34.7347 | 35.4651 | 35.1909 | 33.4737 | 33.4479 |
| Image 6 | 33.7482 | 33.8455 | 32.6678 | 32.0419 | 31.9674 |

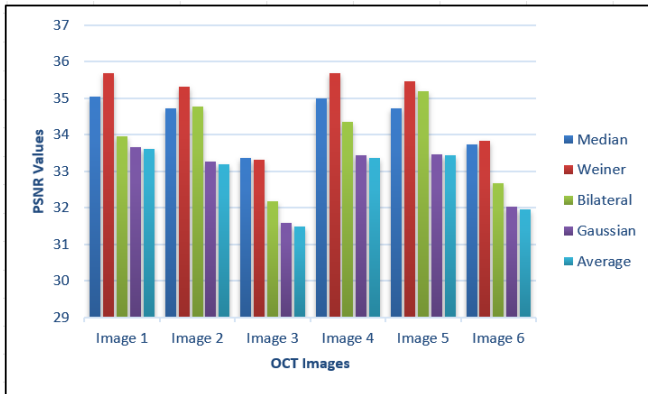


Fig. 9. Analysis chart for PSNR values.

TABLE III. FILTERED IMAGES FOR CNR VALUE

| CNR Comparison | | | | | |
|----------------|---------|----------------|-----------|----------|---------|
| OCT Images | Median | Weiner | Bilateral | Gaussian | Average |
| Image 1 | 0.01458 | -0.0008 | 0.01779 | 0.00334 | 0.00345 |
| Image 2 | 0.02405 | -0.0017 | 0.00892 | 0.00436 | 0.00441 |
| Image 3 | 0.01017 | -0.0005 | 0.00303 | 0.00198 | 0.00203 |
| Image 4 | 0.01696 | -0.0010 | 0.00484 | 0.00359 | 0.00365 |
| Image 5 | 0.01680 | -0.0003 | 0.00475 | 0.00323 | 0.00332 |
| Image 6 | 0.01045 | -0.0010 | 0.00244 | 0.00217 | 0.00221 |

where, T is the threshold, and p(x, y) and f(x, y) are the greyscale images. Threshold g(x,y) is,

$$g(x, y) = \begin{cases} 1 & \text{if } f(x, y) > 1 \\ 0 & \text{if } f(x, y) \leq 0 \end{cases} \quad (2)$$

The Fig. 11 shows the segmented RPE layer on grayscale and original OCT images. The threshold technique compared with other methods for RPE segmentation. The Threshold technique is gave best outcome of DC and RMSE values. Table IV shows the RPE Layer Segmentation Analysis Report. Fig. 12 shows the RPE layer segmentation analysis of proposed method. Table V shows the DC and RMSE Values. Fig. 13 shows the Chart for DC and RMSE Values. Fig. 14 shows the Denoised image with histogram.

RPE layer intensity is represented by the peaks in the histogram. The background is represented by low intensity values. Choose the ideal threshold using the histogram h(i), where i= zero, 1, ..., l, and l is the highest grey level. h represent the number of pixels capturing the 'value'(i). Let the histogram L H(i) be S(t)=sum (i=t). Calculated as [42], the best threshold rate for the increasing sum of the histogram S(t) for the entire image.

$$S(T) > c, S(T + 1) < c \quad (3)$$

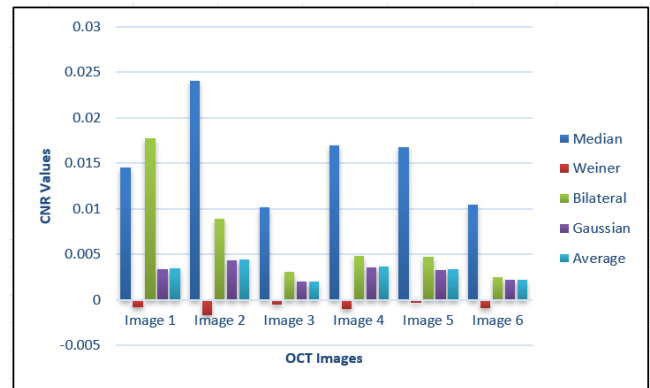


Fig. 10. Analysis chart for CNR values.

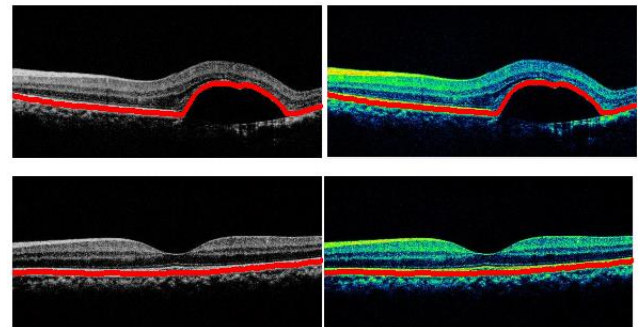


Fig. 11. RPE layer segmentation.

TABLE IV. RPE LAYER SEGMENTATION ANALYSIS REPORT

| Input OCT images | Total No. of Images | RPE Layer Detection | |
|------------------|---------------------|--------------------------|----------------------------|
| | | No. of correct detection | No. of incorrect detection |
| Healthy Macula | 20 | 20 | 0 |
| PED Images | 20 | 19 | 1 |

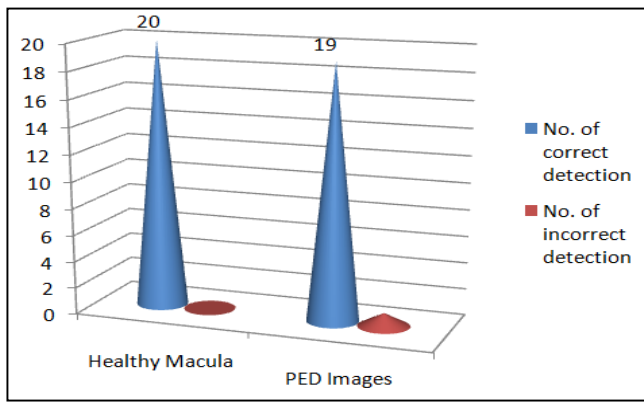


Fig. 12. RPE layer segmentation Analysis of proposed method.

TABLE V. DC AND RMSE VALUES

| Method | RMSE | DC |
|-----------------|--------|-------|
| GC[37] | 0.0255 | 0.926 |
| GCS[38] | 0.0232 | 0.939 |
| STC[39] | 0.0249 | 0.934 |
| LSS[40] | 0.0331 | 0.918 |
| RCS[41] | 0.0319 | 0.923 |
| Proposed Method | 0.023 | 0.941 |

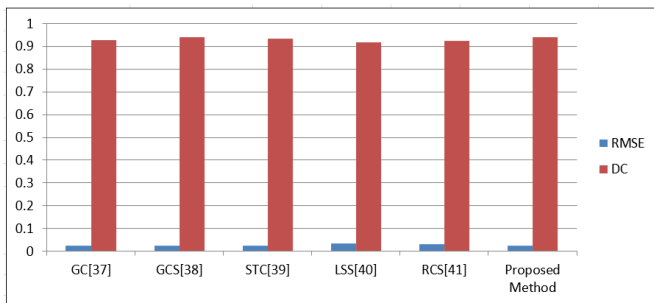
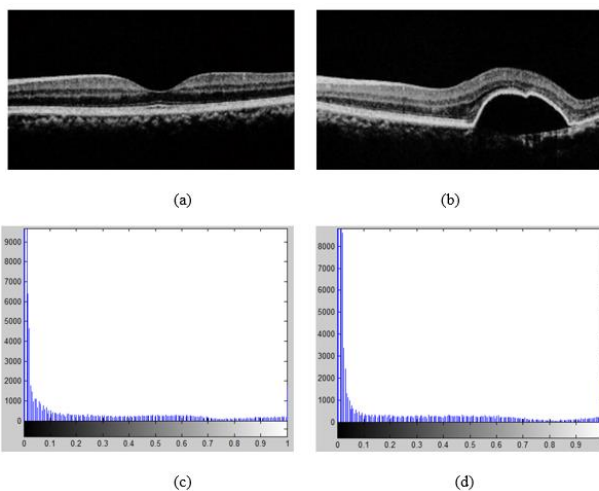


Fig. 13. Chart for DC and RMSE values.



(a) Denoised healthy OCT image, (b) Denoised OCT image with PED, (c) Histogram of denoised healthy image, (d) Histogram of denoised PED image

Fig. 14. Denoised image with histogram.

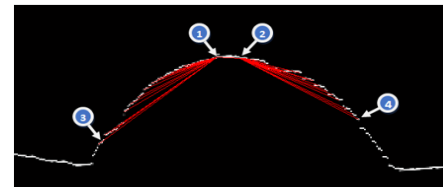
where the constant,

$$c = w \left(\frac{t_r}{d} \right) + k \quad (4)$$

Here, the letters h, d, and w stand for the image's height, depth, and width, respectively. The RPE layer's thickness is measured by t_r , and each image's RPE layer's slant is specified by k.

D. Feature Extraction

Feature extraction is an essential step to train and test the input using machine learning algorithms. In order to improve the performance of the machine learning algorithms to detect PED, a novel method proposed to extract best features from the segmented images. These features include LH, RH, LDp and RDp and shown in Fig. 15. These extracted features are used in the machine learning classifiers KNN, Logistic Regression, Naïve Base and ANN to detect PED. The outcome of the classifier algorithms are corresponded the features of data is obtainable to them in order to fix the TN, FP, TP and FN [21-23]. Accuracy, sensitivity and specificity are evaluated for the classifier independently using these metrics, and the results are then used to categorise the performance of the classifier.



1 → Left Height 2 → Right height
3 → Left Down Points 4 → Right Down Points

Fig. 15. Extracted features.

Here, the following formulae used to fix the top, bottom, and maximum height of the RPE layer:

$$t = \min(L_i) \quad (5)$$

$$b = \max(L_i) \quad (6)$$

$$\max Hgt = b - t \quad (7)$$

where, L_i is the axis-y values for each-x-values on the RPE- layer and x ranges from 0 to the image width. Since the image's top left coordinate is (0, 0), the min-function is used to obtain the RPE-layer's smallest axis-y values in-order-to establish the layer's top. The lowest layer is found using the max function. Repeating the line-no from zero to the top left-point brings it to its highest position. Moving periodically as of the projected top-left-point to the line's largest point yields the top right-point. Next, a bounding rectangle is created by extracting 20 points from the upper left-point. The height of the retinal layer determines the rectangle's width.

$$w = mH \quad (8)$$

Twenty-point were deducted from the top-left-points and twenty-point from the top-right points in order to determine the curve in this investigation. The distance is computed in the following way to extract 20 points from the top-left-points:

$$d = \frac{w}{20} \quad (9)$$

The line-heights of each-points is then calculated by iterating the line points 20 times backward from the top left point:

$$lPs_i = mHgt - (L_{(topLPoint-d*i)}) \quad (10)$$

where, i differs from one to 20.

The below calculation extracts the top-right 20 points:

$$rPs_i = mHgt - (L_{(topRPoint+d*i)}) \quad (11)$$

This ranges from 1 to 20 for i.

The following formulas are used to extract the features of left height (LHe) and right height (RHe):

$$LHe = \max(lPoints_i) \quad (12)$$

$$RHe = \max(rPoints_i) \quad (13)$$

Next, the consecutive leftPoints are compared in order to derive the left down points (LDp) characteristic. Increase the counter LDp if a leftpoint-values is smaller than the leftpoint-values that comes after it. By comparing the rightPoint and rising the counter, the right-down-point (RDp) representative is determined.

$$LDP = LDP + 1 \quad \text{if} (lPoints_i < lPoints_{(i+1)}) \quad (14)$$

$$RDP = RDP + 1 \quad \text{if} (rPoints_i < rPoints_{(i+1)}) \quad (15)$$

| Algorithm Feature_Extraction(Lineseg) |
|--|
| <p>INPUT: LineSeg – Extracted RPE layer in an array</p> <p>OUTPUT: LHe – Left height RHe – Right height LDp – Left down points RDp – Right down points</p> |
| <ol style="list-style-type: none"> 1. t = minimum(LineSeg) 2. b = maximum(LineSeg) 3. lineHgti = b - LineSeg_i; 4. maxHgt = b - t; 5. Repeat line-6 for j=1 to sizeof(LineSeg) 6. if (lineHgti == maxHgt) goto line-7 7. topLPoint = j 8. w = maxHgt 9. Pts=20 10. d = w / Pts; 11. leftPts(1)=maxHgt; 12. Repeat 13 to 14 for p =1 to Pts 13. pos1 = tpLPoint - disBtwnPts*_j; 14. leftPts(j+1)=lineHgt(pos1); 15. Repeat 16 for p = j to sizeof(lineHgt) 16. if (lineHgt(k) <> maxHgt) goto 17 17. tpRPoint = p; 18. rightPts(1)=maxHgt; 19. Repeat 20 to 21 for q=1 to Pts 20. pos1=tpRPoint + disBtwnPts * q 21. rightPts(q+1) = lineHgt(pos1) 22. LHe = maxi(leftHgt) 23. RHe = maxi(rightHgt) |

24. LDp = 0
25. RDp = 0
26. Repeat 27 to 30 for k = 2 to Pts
27. if ((leftHgtk-leftHgtk-1) > 0)
28. LDp++
29. if ((rightHgtk - rightHgtk-1) > 0)
30. RDp++
31. Stop

E. Classification

In this paper, to detect the PED from the RPE layer 4 features, such as LH, RH, LDp and RDp were extracted. The extracted four features were used to classify normal and abnormal OCT images. To assess the discriminative power of projected feature signifiers, both parametric and non-parametric classifiers are examine to PED, such as KNN, LR, Naïve Baye and ANN. Here these four classification procedures, such as KNN, LR, NB and ANN, were compared. The LR classifier gave best outcome when compared with the other three classifiers. To calculate accuracy, sensitivity, specificity, precision, Recall and F1-score, the following formulas were used:

$$Accuracy = \frac{TruePositive + TrueNegative}{TruePositive + TrueNegative + FalsePositive + FalseNegative}$$

$$Sensitivity = \frac{TruePositive}{TruePositive+FalseNegative} \quad (16)$$

$$Specificity = \frac{TrueNegative}{TrueNegative+FalsePositive} \quad (17)$$

$$Precision = \frac{TruePositive}{TruePositive+FalsePositive} \quad (18)$$

$$Recall = \frac{TruePositive}{TruePositive+FalseNegative} \quad (19)$$

$$F1_score = \frac{2*Precision*Recall}{Precision+Recall} \quad (20)$$

IV. RESULT AND DISCUSSION

In this work, 150 OCT images used, 75 normal and 75 abnormal OCT images. In the proposed methodology 80 percentage of the images were used for training, while 20 percentage were used for testing and validations. Out of the entire 150 OCT images, 120 used for training and 30 for testing. In order to remove speckle-noise and segment the image, the image was first converted to grayscale and preprocessed using a wiener filtering. After denoising extract the RPE-layer. Segmented the RPE-layer used to the threshold technique. Four features such as LH, RH, LDp and RDp were extracted from the segmented OCT images, and these features showed to have a notable difference between the normal and PED images. The KNN, Naive Bayes, Logistic Regression and ANN classifiers were fed the collected features, and the results are represented as TP, TN, FP, and FN as in Table VI. TP, FN, TN and FP are the evaluation metrics of the classifiers as shown in Fig. 16.

TABLE VI. RESULTS OF K-NN, LR, NB AND ANN

| Classification Metrics | K-NN | Logistic Regression | Naïve Base | ANN |
|------------------------|------|---------------------|------------|-----|
| TP | 13 | 15 | 15 | 15 |
| FN | 2 | 0 | 0 | 0 |
| TN | 13 | 13 | 15 | 13 |
| FP | 2 | 2 | 0 | 2 |

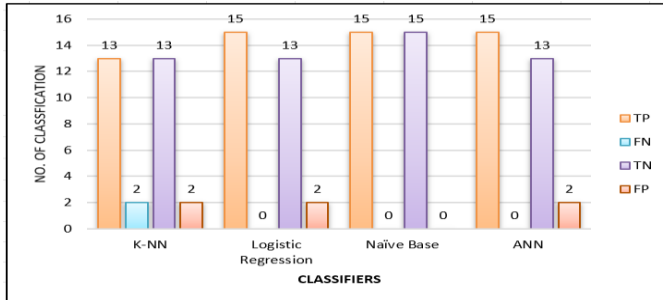


Fig. 16. Evaluation results of K-NN, LR, NB and ANN.

The findings of the overall system performance research in terms of sensitivity, specificity, accuracy, precision, and F1 score are presented in Table VII. The analysis report of NB, KNN, LR and ANN is shown in Fig. 17. It is clear from the overall findings that the Logistic Regression Classifier appears to produce more accurate results than the KNN, ANN, and Naive Base Classifications. The entire system parameters like sensitivity, specificity, precision, F1 score and accuracy.

TABLE VII. CLASSIFICATION METRICS OF NB, LR, KNN AND ANN

| Classification Metrics | NB | KNN | LR | ANN |
|------------------------|--------|-------|--------|--------|
| Accuracy | 93.00 | 86.67 | 96.67 | 93.33 |
| Sensitivity | 100.00 | 86.67 | 100.00 | 100.00 |
| Specificity | 86.67 | 86.67 | 93.33 | 86.67 |
| Precision | 88.24 | 86.67 | 93.75 | 88.24 |
| F1 score | 93.75 | 86.67 | 96.77 | 93.75 |

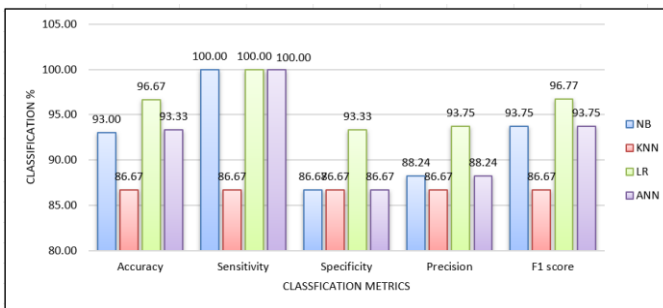


Fig. 17. Classification metrics of NB, KNN, LR and ANN.

Based on the Table VII, KNN produces the result for 86.67% Accuracy, 86.67% Sensitivity, 86.67% Specificity, Precision 86.67% and F1 score 86.67%, Naive Base produces the result for Accuracy 93%, Sensitivity 100%, Specificity 86.67%, Precision 88.24% and F1 score 93.75%, ANN produces the result Accuracy 93.33%, Sensitivity 100%, Specificity 86.67%, Precision 88.24% and F1 score 93.75%

and Logistic Regression produces the result Accuracy 96.67%, 100% Sensitivity, 93.33% Specificity, 93.75% Precision and 96.77% F1 score. The confusion matrix of these classifiers are shown in Fig. 18, Fig. 19, Fig. 20 and Fig. 21 and also analyses the metric ROC curve from the confusion matrix are shown in Fig. 22, Fig. 23 and Fig. 24. Area under curve (AUC) for LR is 0.9939393939393939, KNN is 0.9484848484848486 and NB is 0.9939393939393939.

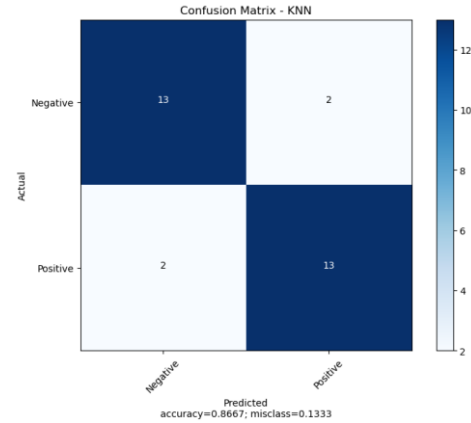


Fig. 18. Confusion matrix for KNN.

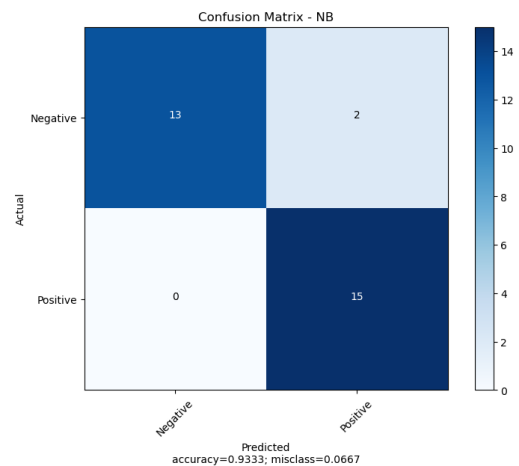


Fig. 19. Confusion matrix for NB.

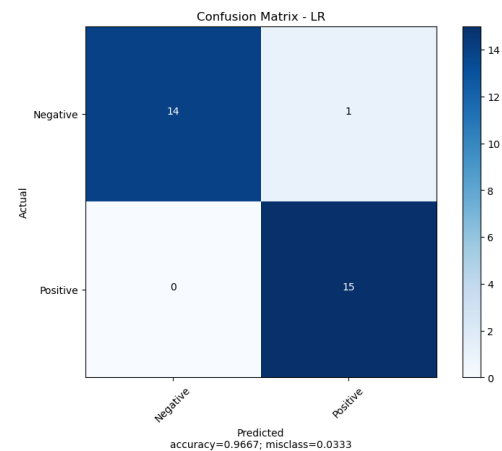


Fig. 20. Confusion matrix for LR.

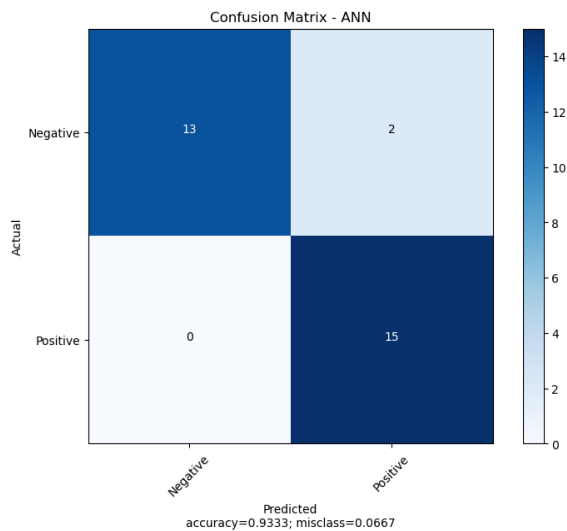


Fig. 21. Confusion matrix for ANN.

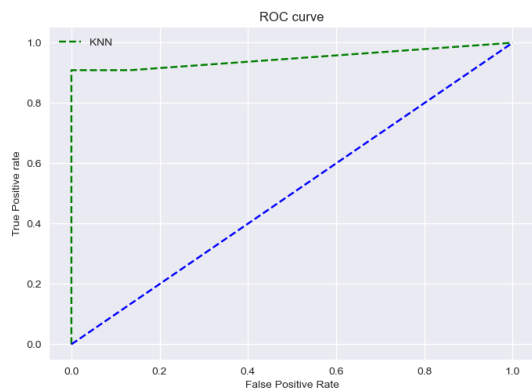


Fig. 22. ROC for KNN, AUC for 0.9484848484848486.

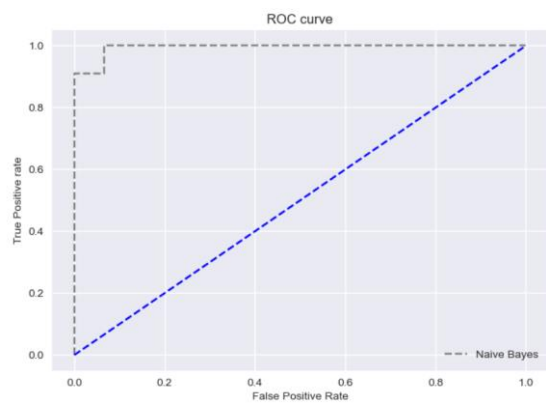


Fig. 23. ROC for NB, AUC for 0.9939393939393939.

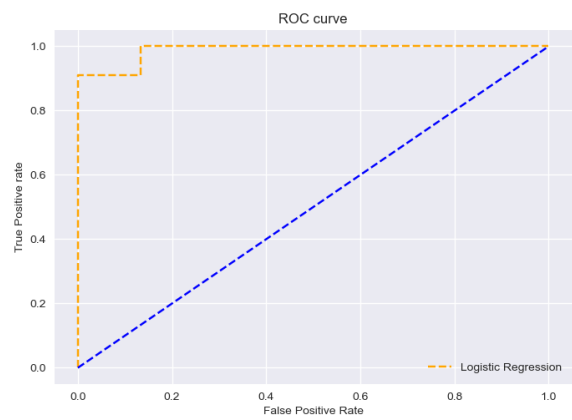


Fig. 24. ROC for LR, AUC for 0.9939393939393939.

V. CONCLUSION

The main contributions of this work are: accurately reduce the speckle noise in OCT images, accurately segment the RPE layer in normal OCT images and PED images, and extract four novel features to accurately predict PED disease and normal images. Through the experimental results, Wiener filtering technique outperforms in reduce speckle noise in the OCT images. The suggested technique and steps appear to be effective for extracting best features from the RPE layer for detecting PED in OCT images. These features were used to train the classifiers and tested with new inputs. Based on these features, the performance of logistic regression classifier was better when compared with other classifiers. The degree of precision attained demonstrates that the technique can also be used in practical applications. To accurately and completely examine the actual performance, the usefulness of the suggested classifier systems must be assessed for specific abnormality-based categorization, such as PED. The normal and PED images were classified with machine learning algorithms. This automatic model is used to assists doctors early diagnose the PED. In this paper, the machine learning classifiers like KNN, LR, NB and ANN were compared. KNN produces the result for Accuracy 86.67%, Sensitivity 86.67%, Specificity 86.67%, Precision 86.67% and F1 score 86.67%, LR produces the result for Accuracy 96.67%, Sensitivity 100%, Specificity 93.33%, Precision 93.75% and F1 score 96.77%, and NB produces the result Accuracy 93.33%, Sensitivity 100%, Specificity 86.67%, Precision 88.24% and F1 score 93.75% and ANN found 93.33% accuracy, 100% sensitivity, 86.67% specificity, 88.245 precision and F1 score 93.75%. Based on the experiments, it is found that logistic regression classifier gives high accuracy in identifying PED illnesses and broadening the scope of anomalies. Further this study can be extended to detect the PED using other machine learning algorithms. Deep learning can also be used in future to detect PED in retinal OCT images.

REFERENCES

- [1] M. K. Garvin, M. D. Abramoff, R. Kardon, S. R. Russell, X. Wu, and M. Sonka, "Intraretinal layer segmentation of macular optical coherence tomography images using optimal 3-D graph search," *IEEE Trans. Med. Imag.*, vol. 27, no. 10, pp. 1495–1505, Oct. 2008.
- [2] M. K. Garvin, M. D. Abramoff, X. Wu, S. R. Russell, T. L. Burns, and M. Sonka, "Automated 3-D intraretinal layer segmentation of macular spectral-domain optical coherence tomography images," *IEEE Trans. Med. Imag.*, vol. 28, no. 9, pp. 1436–1447, Sep. 2009.
- [3] K. Lee, "Segmentations of the intraretinal surfaces, optic disc and retinal blood vessels in 3D-OCT scans," Ph.D. dissertation, Univ. Iowa, Iowa City, 2009.
- [4] S. Lu, C. Y. Cheung, J. Liu, J. H. Lim, C. K. Leung, and T. Y. Wong, "Automated layer segmentation of optical coherence tomography images," *IEEE Trans. Biomed. Eng.*, vol. 57, no. 10, pp. 2605–2608, Oct. 2010.
- [5] A. Yazdanpanah, G. Hamarneh, B. R. Smith, and M. V. Sarunic, "Segmentation of intra-retinal layers from optical coherence tomography images using an active contour approach," *IEEE Trans. Med. Imag.*, vol. 30, no. 2, pp. 484–496, Feb. 2011.
- [6] Q. Song, J. Bai, M. K. Garvin, M. Sonka, J. M. Buatti, and X. Wu, "Optimal multiple surface segmentation with shape and context priors," *IEEE Trans. Med. Imag.*, vol. 32, no. 2, pp. 376–386, Feb. 2013.
- [7] P. A. Dufour, L. Ceklic, H. Abdillahi, S. Schröder, S. De Dzanet, U. Wolf-Schnurrbusch, and J. Kowal, "Graph-based multi-surface segmentation of OCT data using trained hard and soft constraints," *IEEE Trans. Med. Imag.*, vol. 32, no. 3, pp. 531–543, Mar. 2013.
- [8] Q. Yang, C. A. Reisman, Z. Wang, Y. Fukuma, M. Hangai, N. Yoshimura, A. Tomidokoro, M. Araie, A. S. Raza, D. C. Hood, and K. Chan, "Automated layer segmentation of macular OCT images using dual-scale gradient information," *Opt. Exp.*, vol. 18, pp. 21 293–307, 2010.
- [9] S. J. Chiu, X. T. Li, P. Nicholas, C. A. Toth, J. A. Izatt, and S. Farsiu, "Automatic segmentation of seven retinal layers in SDOCT images congruent with expert manual segmentation," *Opt. Exp.*, vol. 18, no. 18, pp. 19413–28, 2010.
- [10] J. Novosel, K. A. Vermeer, G. Thepass, H. G. Lemij, and L. J. van Vliet, "Loosely coupled level sets for retinal layer segmentation in optical coherence tomography," in *Proc. IEEE Int. Symp. Biomed. Imag.*, 2013, pp. 1010–1013.
- [11] K. A. Vermeer, J. van der Schoot, H. G. Lemij, and J. F. de Boer, "Automated segmentation by pixel classification of retinal layers in ophthalmic OCT images," *Biomed. Opt. Exp.*, vol. 2, pp. 1743–56, 2011.
- [12] R. Kafieh, H. Rabbani, M. D. Abramoff, and M. Sonka, "Intra-retinal layer segmentation of 3D optical coherence tomography using coarse grained diffusion map," *Med. Image Anal.*, vol. 17, pp. 907–928, 2013.
- [13] A. Lang, A. Carass, M. Hauser, E. S. Sotirchos, P. A. Calabresi, H. S. Ying, and J. L. Prince, "Retinal layer segmentation of macular OCT images using boundary classification," *Biomed. Opt. Exp.*, vol. 4, pp. 1133–52, 2013.
- [14] The Iowa Reference Algorithms. Iowa City, IA, Iowa Inst. Biomed. Imag. [Online]. Available: <http://www.biomed-imaging.uiowa.edu/downloads/>
- [15] X. Chen, P. Hou, C. Jin, W. Zhu, X. Luo, F. Shi, M. Sonka, and H. Chen, "Quantitative analysis of retinal layers' optical intensities on 3D optical coherence tomography," *Invest. Ophthalmol. Vis. Sci.*, vol. 54, no. 10, pp. 6846–6851, Oct. 2013.
- [16] S. Zayit-Soudry, I. Moroz, and A. Loewenstein, "Retinal pigment epithelial detachment," *Surv. Ophthalmol.*, vol. 52, no. 3, pp. 227–243, May-Jun. 2007.
- [17] P. A. Keane, P. J. Patel, S. Liakopoulos, F. M. Heussen, S. R. Sadda, and A. Tufail, "Evaluation of age-related macular degeneration with optical coherence tomography," *Surv. Ophthalmol.*, vol. 57, no. 5, pp. 389–414, Sep.-Oct. 2012.
- [18] Fei Shi, Xinjian Chen, Heming Zhao, Weifang Zhu, Dehui Xiang, Enting Gao, Milan Sonka and Haoyu Chen, "Automated 3-D Retinal Layer Segmentation of Macular Optical Coherence Tomography Images With Serous Pigment Epithelial Detachments", *IEEE Transactions On Medical Imaging*, Vol. 34, No. 2, February 2015.
- [19] Quellec G, Lee K, Dolejsi M, Garvin MK, Abramoff MD, Sonka M. Three-dimensional analysis of retinal layer texture: identification of fluid-filled regions in SD-OCT of the macula. *IEEE Trans Med Imaging*. 2010 Jun;29(6):1321-30. doi: 10.1109/TMI.2010.2047023. Epub 2010 Apr 1. PMID: 20363675; PMCID: PMC2911793.
- [20] Wu M, Chen Q, He X, Li P, Fan W, Yuan S, Park H. Automatic Subretinal Fluid Segmentation of Retinal SD-OCT Images With Neurosensory Retinal Detachment Guided by Enface Fundus Imaging. *IEEE Trans Biomed Eng*. 2018 Jan;65(1):87-95. doi: 10.1109/TBME.2017.2695461. Epub 2017 Apr 18. PMID: 28436839.
- [21] R. Tennakoon, A. K. Gostar, R. Hoseinnezhad and A. Bab-Hadiashar, "Retinal fluid segmentation in OCT images using adversarial loss based convolutional neural networks," 2018 IEEE 15th International Symposium on Biomedical Imaging (ISBI 2018), 2018, pp. 1436-1440, doi: 10.1109/ISBI.2018.8363842.
- [22] Y. Huang and J. Hu, "Residual Neural Network Based Classification of Macular Edema in OCT," 2019 IEEE 31st International Conference on Tools with Artificial Intelligence (ICTAI), 2019, pp. 736-743, doi: 10.1109/ICTAI.2019.00107.
- [23] T. M. Sheeba & S. Alber Antony Raj "Distinct Features for Detection of Pigment Epithelial Detachment using Machine Learning and Artificial Neural Network in Two-Dimensional Optical Coherence Tomography Images". *International Journal of Intelligent Systems and Applications in Engineering*, 12(14s), 338–347, 2024.
- [24] Keane PA, Patel PJ, Liakopoulos S, Heussen FM, Sadda SR, Tufail A. Evaluation of age-related macular degeneration with optical coherence tomography. *Surv Ophthalmol*. 2012 Sep;57(5):389-414. doi: 10.1016/j.survophthal.2012.01.006. PMID: 22898648.
- [25] Rangel-Fonseca P, Gómez-Vieyra A, Malacara-Hernández D, Wilson MC, Williams DR, Rossi EA. Automated segmentation of retinal pigment epithelium cells in fluorescence adaptive optics images. *J Opt Soc Am A Opt Image Sci Vis*. 2013 Dec 1;30(12):2595-604. doi: 10.1364/JOSAA.30.002595. PMID: 24323021.
- [26] Chen X, Niemeijer M, Zhang L, Lee K, Abramoff MD, Sonka M. Three-dimensional segmentation of fluid-associated abnormalities in retinal OCT: probability constrained graph-search-graph-cut. *IEEE Trans Med Imaging*. 2012 Aug;31(8):1521-31. doi: 10.1109/TMI.2012.2191302. Epub 2012 Mar 19. PMID: 22453610; PMCID: PMC3659794.
- [27] L. Bekalo et al., "Automated 3-D Retinal Layer Segmentation From SD-OCT Images With Neurosensory Retinal Detachment," in *IEEE Access*, vol. 7, pp. 14894-14907, 2019, doi: 10.1109/ACCESS.2019.2893954.
- [28] Sun S, Guo Q, Lei B, Gao BZ, Dong F. Image denoising algorithm based on contourlet transform for optical coherence tomography heart tube image. *IET Image Process*. 2013; 7(5), pp. 442–450.
- [29] Avanaki MRN, Cernat R, Tadrous PJ, Tatla T, PodoleanuAG, Ali Hojjatoleslami S, Spatial compounding algorithm for speckle reduction of dynamic focus OCT images. *IEEE Photonics TechnolLett*. 2013; 25(15), pp. 1439–1442.
- [30] Manojlovic LM. Novel Method for Optical Coherence Tomography Resolution Enhancement. *IEEE J. Quantum Electron*. 2011; 47(3), pp. 340–347.
- [31] C. Tomasi and R. Manduchi, "Bilateral filtering for gray and color images," in *Proc. IEEE Int. Conf. Comput. Vis.*, 1998, pp. 839–846.
- [32] M. Anand, C. Jayakumari, "Automated Detection of Macular Hole in Optical Coherence Tomography Images using Depth-Check Algorithm", *International Journal of Engineering and Advanced Technology (IJEAT)* ISSN: 2249 – 8958, Volume-9 Issue-1, October 2019.
- [33] M. Anand, C. Jayakumari, "A Novel Depth-Check Algorithm to Detect Macular Hole from Optical Coherence Tomography Images", *International Journal of Innovative Technology and Exploring Engineering (IJITEE)* ISSN: 2278-3075, Volume-8 Issue-12, October 2019.
- [34] M. Anand, C. Jayakumari, "Automated detection of full thickness macular hole in optical coherence tomography images", *Journal of International Pharmaceutical Research*, ISSN: 1674-0440.

- [35] M. Anand, C. Jayakumari, "A New Approach to Detect Macular Hole from Optical Coherence Tomography Images", *Indian Journal of Public Health Research & Development*, July 2019, Vol.10, No. 7.
- [36] T.M. Sheeba and S. Albert Antony Raj, "Analysis of Noise Removal Techniques on Retinal Optical Coherence Tomography Images", (IJACSA) International Journal of Advanced Computer Science and Applications, Vol. 13, No. 9, 2022.
- [37] Bashir Isa Dodo, Yongmin Li, Djibril Kaba, And Xiaohui Liu, "Retinal Layer Segmentation in Optical Coherence Tomography Images", *IEEE Access*, VOLUME 7, Oct-2019, pp. 152388-152398.
- [38] Qifeng Yana, Bang Chena, Yan Hub, Jun Cheng, Yan Gongd, Jianlong Yanga, Jiang Liub and Yitian Zhaoa, "Speckle reduction of OCT via super resolution reconstruction and its application on retinal layer segmentation", *Artificial Intelligence In Medicine*, 2020, pp. 1-10.
- [39] S. J. Chiu, X. T. Li, P. Nicholas, C. A. Toth, J. A. Izatt, and S. Farsiu, "Automatic segmentation of seven retinal layers in SDOCT images congruent with expert manual segmentation," *Opt. Express*, vol. 18, no. 18, pp. 19413–19428, 2010.
- [40] B. I. Dodo, Y. Li, X. Liu, and M. I. Dodo, "Level set segmentation of retinal OCT images," in *Proc. 12th Int. Joint Conf. Biomed. Eng. Syst. Technol.*, vol. 2, 2019, pp. 49–56.
- [41] B. I. Dodo, Y. Li, K. Eltayef, and X. Liu, "Graph-cut segmentation of retinal layers from OCT images," in *Proc. 11th Int. Joint Conf. Biomed. Eng. Syst. Technol. (BIOIMAGING)*, vol. 2, 2018, pp. 35–42.
- [42] Samra Naz, Aneeqa Ahmed, M. Usman Akram, Shoab A. Khan, "Automated Segmentation of RPE Layer for the Detection of Age Macular Degeneration Using OCT Images", 978-1-4673-8910-5/16/\$31.00 ©2016 IEEE.

Investigating the Effect of Small Sample Process Capability Index Under Different Bootstrap Methods

Liyan Wang*, Guihua Bo, Mingjuan Du

School of Information and Control Engineering, Liaoning Petrochemical University, Fushun, China

Abstract—In the quality control of multi-variety and small-batch products, the calculation of the process capability index is particularly important. However, when the sample size is not enough, the process distribution cannot be judged, if the traditional method is still used to calculate the process capability index; there will be misapplication or misuse. In this paper, the Bootstrap method is introduced into the estimation of process capability index and the calculation of its confidence interval by using Standard Bootstrap (SB), Percentile Bootstrap (PB), Percentile-t Bootstrap (PTB) and Biased-corrected Percentile Bootstrap (BCPB) methods were used to analyze and compare the process capability index. It is found that in symmetric distribution, only the sample size has a significant effect on the length of the confidence interval; but in asymmetric distribution, sample size and Bootstrap methods are both significant factors affecting the length of confidence interval.

Keywords—Process capability indices; bootstrap; confidence interval; small samples

I. INTRODUCTION

Process capability analysis is an important part of statistical process control activities for continuous improvement. Process Capability Index (PCI) is designed to provide a general language for quantifying its performance; it is a dimensionless function of the process parameters and specifications. PCI is widely used in traditional manufacturing industries, but with the production mode has changed from single variety and large batch to multi-variety and small batch, and the number of parts of the same specification produced under the same process and similar production conditions has become less and less, which brings difficulties to the process capability analysis and the calculation of indicators and statistical inference. When the sample size is insufficient, the central limit theorem cannot be used to calculate the process capability index because it is impossible to judge the distribution of process data. If the traditional method is still used for calculation, it is easy to misunderstand and misuse.

Process Capability Indices (PCIs) are considered as a practical tool by many advocates of statistical process control in industry. They are used to determine whether a manufacturing process is capable of producing with dimensions within a specified tolerance range. The process indices C_p and C_{pk} [1] are used for unit-less measures that relate the natural process tolerance (6σ), upper and lower specification limits. Chan et al. [2] developed C_{pm} that incorporates a target value for the process. Taguchi [3] and Chou et al. [4] provided tables for constructing 95 percent lower confidence limits for both C_p and C_{pk} . Their tables for

limits on C_{pk} , however, are conservative and an approximation presented by Bissel [5] is recommended instead. Boyles [6] provided an approximate method for finding lower confidence limits for C_{pm} . The calculation of all these lower confidence limits assume a normally distributed process and many real world processes are not normally distributed and this departure from normality may be hard to detect. This could potentially affect both the estimates of the indices and the confidence limits based on these estimates. Efron [7] introduced and developed the non-parametric, but computer intensive estimation method called Bootstrap. Bootstrap method [8] replaces theoretical analysis with computer simulation technology, and replaces real distribution with statistical empirical distribution. It is effective for statistical analysis and process capability analysis under small sample conditions. Therefore, Bootstrap method can be introduced into point estimation and confidence interval calculation of C_p and C_{pk} under small sample conditions.

The rest of this paper is consisted of as: Section II presents the related works. Section III and IV realizes the estimation of C_p and C_{pk} based on Bootstrap method, and then experimental results are discussed in Section IV. Finally, this paper concludes in Section VI. Our study shows that in symmetric distribution, only the sample size has a significant effect on the length of the confidence interval, Bootstrap methods has no significant effect on the length of confidence interval. But in the skewed distribution, sample size and Bootstrap methods are both significant factors affecting the length of confidence interval.

II. RELATED WORK

Bootstrap method is very popular in modern statistics. Especially after the rise of big data, the effect of estimating the mean or variance of statistics with small samples is ideal. Its simulation result is very close to the real result, and it is often used to solve some situations that cannot be broken through in theory. The core idea of Bootstrap method is to replace theoretical analysis with computer simulation technology, that is, to extract the same number of samples from the original samples by repeated sampling technology, and replace the real distribution with its statistics. Bootstrap method can be used for the hypothesis testing and interval estimation problems of location parameter with unknown scale parameter and skewness parameter, it provides the satisfactory performances under the senses of Type I error probability and power in most cases regardless of the moment estimator or ML estimator [9]. By repeating the above process and calculating its mean or variance, the empirical distribution of statistics is substituted for the real distribution.

*Corresponding Author.

Owing to these benefits, application of Bootstrap method in the process capability index includes: Bootstrap confidence intervals for indices such as C_p [10-13], C_{pk} [14, 15], C_{pm} [15], and C_{pmk} [16] are established for PCIs. Its applications can also be divided into: Using Bootstrap sampling to estimate the multivariate [17] or multiple process streams [13] process capability indices; using different methods of estimation to construct Bootstrap confidence intervals of generalized process capability index C_{pyk} [18]. Especially when data is non-normal, the Bootstrap confidence intervals of different distribution types of non-normal data were studied: such as the Modified Process Capability Index for Wei-bull distribution [19], Parametric and non-parametric bootstrap confidence intervals of C_{Npk} for exponential [20] and exponential power distribution [21], and so on. In addition, its application can also be seen in the case of small samples [22, 23]. Bootstrap method replaces theoretical analysis with computer simulation technology, and replaces real distribution with statistical empirical distribution. It is effective for statistical analysis and process capability analysis under small sample conditions. Therefore, Bootstrap method can be introduced into point estimation and confidence interval calculation of C_p and C_{pk} under small samples.

III. ESTIMATION OF C_p AND C_{pk}

A. Definition and Estimation of PCIs

The capability of a process is frequently measured by a process capability index (PCI) which is designed to provide a common and easily understood language for quantifying its performance, and is a dimensionless function of process parameters and specifications. Let USL and LSL be the upper and lower specification limits, respectively. If the process follows or approximately follows a normal distribution, the statistical characteristics of the traditional process capability index can be calculated, including point estimation, confidence interval, and estimated distribution characteristics.

If the process follows or approximately follows a normal distribution, using the above two sample statistics, point estimates of PCIs such as C_p & C_{pk} [1], and C_{pm} [2] can be calculated.

The definition of C_p is:

$$C_p = \frac{USL - LSL}{6\sigma} \quad (1)$$

The estimation of C_p is:

$$\hat{C}_p = \frac{USL - LSL}{6S} = \frac{\sigma}{S} C_p \quad (2)$$

Wherein, USL and LSL are the upper and lower specification limits of the process.

Since the index C_p does not take into account the location of the process mean (μ), the index C_{pk} is defined:

$$\hat{C}_{pk} = \min\left\{\frac{USL - \mu}{3\sigma}, \frac{\mu - LSL}{3\sigma}\right\} \quad (3)$$

If the sample size is large and the data follows a normal distribution, a point estimate of the process capability indicator

can be obtained by calculating the mean and standard deviation of the sample. They can be represented by the following statistics:

μ is represented by the sample mean \bar{X} :

$$\bar{X} = \frac{1}{n} \sum_{i=1}^n X_i \quad (4)$$

σ^2 is represented by the sample variance S^2 :

$$S^2 = \frac{1}{n-1} \sum_{i=1}^n (X_i - \bar{X})^2 \quad (5)$$

Wherein, X_i is the i -th observation value, \bar{X} is the sample mean, and n is the sample size. \bar{X} and S^2 are unbiased estimators of population mean μ and population variance σ^2 .

The expected value for obtaining the estimated value of the exponent C_p by calculating its r -th moment \hat{C}_p^r is:

$$E[\hat{C}_p^r] = \left[\frac{n-1}{2}\right]^{\frac{r}{2}} \frac{\Gamma\left[\frac{n-1-r}{2}\right]}{\Gamma\left[\frac{n-1}{2}\right]} C_p^r \quad (6)$$

So when $r=1$, the mean of the estimated value of the index C_p [24] is:

$$E(\hat{C}_p) = \frac{1}{b_f} C_p \quad (7)$$

And b_f is the correction coefficient, $b_f = \sqrt{\frac{n-1}{2}} \frac{\Gamma\left(\frac{n-2}{2}\right)}{\Gamma\left(\frac{n-1}{2}\right)}$.

So when $r=2$, the variance of the estimated value of the index C_p [24] is :

$$Var(\hat{C}_p) = \left(\frac{n-1}{n-3} - \frac{1}{b_f^2}\right) C_p^2 \quad (8)$$

Therefore, based on (6), it can be obtained that if the process follows or approximately follows a normal distribution, then for n samples in the population, the statistic $\frac{(n-1)s^2}{\sigma^2}$

follows χ^2 distribution with $n-1$ degrees of freedom, denoted as:

$$\frac{(n-1)s^2}{\sigma^2} \sim \chi^2(n-1).$$

So:

$$C_p = \hat{C}_p \sqrt{\frac{\chi_{n-1}^2}{n-1}} \quad (9)$$

When the significance level is α , the $100(1-\alpha)\%$ confidence interval for C_p [25] is:

$$[\hat{C}_p \sqrt{\frac{\chi^2_{(\alpha/2, n-1)}}{n-1}}, \hat{C}_p \sqrt{\frac{\chi^2_{(1-\alpha/2, n-1)}}{n-1}}] \quad (10)$$

The same is true of the 100(1-α)% confidence interval for Cpk [25]:

$$[\hat{C}_{pk}(1+z_{\alpha/2}) \sqrt{\frac{1}{9n\hat{C}_{pk}^2} + \frac{1}{2(n-1)}}, \hat{C}_{pk}(1+z_{1-\alpha/2}) \sqrt{\frac{1}{9n\hat{C}_{pk}^2} + \frac{1}{2(n-1)}}] \quad (11)$$

B. Analysis of the Influence of Sample Size

It can be seen from Eq. (6) to Eq. (11) that sample size n has an impact on the statistical estimator of the process capability index.

1) Impact of sample size on the correction coefficient b_f :

As shown in Table I: With the increase of sample size n, the closer the value of 1/b_f is to 1, the closer the point estimate is to the true value of Cp. When n=400, b_f value loses significance, and the corresponding PCI estimation is also meaningless. It follows that the appropriate sample size is usually 100 or 200. There is no need to adopt full sampling method or blindly increase sample size.

2) Impact of sample size on the confidence interval of Cp:

The confidence interval of Cp is shown in Table II, when it follows or approximately follows a normal distribution at a given value. As shown in the Table II, with a given value \hat{C}_p , the width of the confidence interval becomes shorter as the sample size n increases. When the sample size n is specified, the larger the \hat{C}_p value is, the longer the confidence interval length is. Therefore, when the data follows or approximately follows a normal distribution, in order to obtain a tighter confidence interval for Cp, it is necessary to consider both the \hat{C}_p value and the sample size n in order to obtain a more stringent Cp confidence interval.

Wherein, Lc and Uc are the lower and upper confidence limits.

3) Impact of sample size on the confidence interval length of Cpk: As shown in Table III: With reference to the conclusions of the above Table I and Table II, considering the economy of sampling and the accuracy of parameter confidence intervals, we only analyzed the influence of sample size within 200 on the confidence intervals and interval widths of Cpk.

Similar to the point estimation and interval estimation of Cp, when the data obey or approximate obey the normal distribution, the confidence interval and interval width of Cpk are affected by both the sample size n and the Cpk estimator. When \hat{C}_{pk} is specified, the larger the sample size is, the more accurate the interval estimation and the shorter the width of the confidence interval are. When the sample size is specified, the larger the \hat{C}_{pk} value is, the longer the corresponding confidence interval width is. Here CIL indicates the confidence interval length.

Based on the analysis shown in Table I to Table III, we can find that the traditional process capability analysis is based on the process obeying or approximately obeying the normal distribution. In order to ensure the reliability of parameter estimation, a sufficient sample size is usually required, i.e., n=100 or 200. This means that in traditional analysis we need a large sample. In other words, when the sample size is small, it is impossible to accurately judge the type of distribution of the data. At this point, if the traditional parameter estimation method is still used to analyze the process capability, the calculated PCI is not accurate and the CIL is longer. We'll get the wrong conclusions. To solve these problems, we can use the Bootstrap method to calculate the confidence interval of the process capability indicator.

TABLE I. IMPACTS OF SAMPLE SIZE ON B_F

| | | | | | | | | | |
|----------------|----------|----------|----------|----------|----------|----------|----------|----------|----------|
| n | 5 | 6 | 7 | 8 | 9 | 10 | 20 | 30 | 40 |
| b _f | 1.253314 | 1.189416 | 1.151243 | 1.125869 | 1.107784 | 1.094242 | 1.041764 | 1.026826 | 1.019759 |
| n | 50 | 60 | 70 | 80 | 90 | 100 | 200 | 300 | 400 |
| b _f | 1.015639 | 1.01294 | 1.011036 | 1.009621 | 1.008527 | 1.007656 | 1.003789 | 1.002517 | --- |

TABLE II. CONFIDENCE INTERVALS OF \hat{C}_p

| n [Lc,Uc] | $\hat{C}_p=1$ | $\hat{C}_p=1.33$ | $\hat{C}_p=1.5$ | $\hat{C}_p=1.67$ | $\hat{C}_p=2.0$ |
|--------------|------------------|------------------|------------------|------------------|------------------|
| 5 | [0.3480, 1.6691] | [0.4628, 2.2199] | [0.5220, 2.5037] | [0.5812, 2.7874] | [0.6960, 3.3382] |
| 10 | [0.5478, 1.4538] | [0.7286, 1.9336] | [0.8217, 2.1807] | [0.9148, 2.4279] | [1.0956, 2.9076] |
| 50 | [0.8025, 1.1971] | [1.0673, 1.5921] | [1.2037, 1.7957] | [1.3402, 1.9992] | [1.0050, 2.3942] |
| 100 | [0.8608, 1.1389] | [1.1449, 1.5147] | [1.2912, 1.7084] | [1.4375, 1.9020] | [1.7216, 2.2778] |
| 200 | [0.9018, 1.0981] | [1.1994, 1.4605] | [1.3527, 1.6472] | [1.5060, 1.8338] | [1.8036, 2.1962] |
| 500 | [0.9380, 1.0620] | [1.2235, 1.4365] | [1.4070, 1.5930] | [1.5665, 1.7735] | [1.8760, 2.1240] |
| 1000 | [0.9561, 1.0438] | [1.2716, 1.3883] | [1.4341, 1.5657] | [1.5967, 1.7432] | [1.9122, 2.0876] |

TABLE III. IMPACTS OF SAMPLE SIZE ON CONFIDENCE INTERVALS LENGTH OF \hat{C}_{pk}

| n [Lc,Uc] | $\hat{C}_{pk=1}$ | CIL | $\hat{C}_{pk=1.5}$ | CIL | $\hat{C}_{pk=1.67}$ | CIL |
|----------------|------------------|--------|--------------------|--------|---------------------|--------|
| 5 | [0.2480, 1.7520] | 1.5041 | [0.4203, 2.5797] | 2.1595 | [0.6231, 2.8577] | 2.2346 |
| 10 | [0.4939, 1.5061] | 1.0121 | [0.7769, 2.2231] | 1.4462 | [0.9308, 2.3932] | 1.4623 |
| 50 | [0.7815, 1.2185] | 0.4370 | [1.1890, 1.8110] | 0.6221 | [1.3560, 2.0195] | 0.6635 |
| 100 | [0.8461, 1.1539] | 0.3077 | [1.2811, 1.7189] | 0.4378 | [1.4502, 1.8985] | 0.4483 |
| 200 | [0.8914, 1.1086] | 0.2171 | [1.3456, 1.6544] | 0.3089 | [1.4976, 1.8145] | 0.3168 |

IV. ESTIMATION OF C_p AND C_{pk} BASED ON BOOTSTRAP METHOD

A. Introduction of Bootstrap

The Bootstrap method is to repeatedly resample the original sample, extract B replacement samples with random (RSWR) with sample size n from sample S_0 , and express them with S_i^* (subscript i represents the i -th time resampling). Where, $S_i^* = \{x_1^*, \dots, x_n^*\}$ represents a simple RSWR extracted from S_0 , S_i^* is called Bootstrap sample. For each subsample S_i^* , its T statistic is calculated and expressed by $\{t_1^*, t_2^*, \dots, t_B^*\}$ respectively.

Assuming there is a random sampling sequence $S_0 = \{x_1, \dots, x_n\}$ with a length of n from a completely uncertain distribution. Where x_i is the independent random sampling of the distribution, where t_i represents the value of a specific sample statistic T .

The distribution of the statistic T is called the Empirical Bootstrap Distribution (EBD), where B is the sample size. When B is large enough, an approximation of the statistic T can be obtained by repeated sampling from S_0 . In this way, the Bootstrap method can be used for statistical simulation of small samples, so as to obtain statistical estimation of unknown distribution and unknown parameters. Generally, we assumed $B = 1000$ bootstrap re-samples.

Bootstrap methods include Standard Bootstrap (SB), Percentile Bootstrap (PB), Biased corrected Percentile Bootstrap (BCPB), Percentile T Bootstrap (PTB), and Biased corrected and accelerated Bootstrap (BCa). Scholars [10-19, 21] mostly used the two of four methods and compared the Bootstrap confidence interval of PCIs. It is difficult to implement the BCa method [20], so its application is less. Therefore, this paper also uses the first four Bootstrap methods.

B. Bootstrap Confidence Intervals with Four Methods

Based on the original random samples x_1, x_2, \dots, x_n with sample size n , construct B new Bootstrap samples $x_1^*, x_2^*, \dots, x_n^*$, i.e. $S_i^* = \{x_1^*, \dots, x_n^*\}$. Calculate the C_p values for each sub sample S_i^* , denoted by $\{C_1^*, C_2^*, \dots, C_B^*\}$ respectively. By arranging the values in ascending order, the empirical probability distribution of B T -values can be obtained, which is called the Bootstrap Empirical Distribution (EBD). Taking $B=1000$ and using the Bootstrap method to repeat sampling

from small sample S_0 , statistical estimates of C_p can be obtained.

Here \hat{C}_p and \hat{C}_{pk} represents the estimate of C_p and C_{pk} , $\hat{C}_p^*(i)$ and $\hat{C}_{pk}^*(i)$ represent the sequential estimator of the process capability index calculated from 1000 Bootstrap random replacement samples. The sample mean calculated from these 1000 Bootstrap estimators are:

$$\bar{C}_p^* = \frac{1}{1000} \sum_{i=1}^{1000} \hat{C}_p^*(i) \quad (12)$$

$$\bar{C}_{pk}^* = \frac{1}{1000} \sum_{i=1}^{1000} \hat{C}_{pk}^*(i) \quad (13)$$

The standard deviation of the samples are:

$$S_{cp}^* = \sqrt{\frac{1}{999} \sum_{i=1}^{1000} [\hat{C}_p^*(i) - \bar{C}_p^*]^2} \quad (14)$$

$$S_{cpk}^* = \sqrt{\frac{1}{999} \sum_{i=1}^{1000} [\hat{C}_{pk}^*(i) - \bar{C}_{pk}^*]^2} \quad (15)$$

When the distribution of \hat{C}_p and \hat{C}_{pk} follows or approximates the normal distribution, the statistics calculated in Eq. (14) and Eq. (15) are essentially estimators of the standard deviations of C_p and C_{pk} .

1) Confidence interval based on SB[8,14]: When the significance level is α , the standard Bootstrap confidence intervals for $100(1-\alpha)\%$ of the process capability index C_p and C_{pk} are respectively:

$$\left[\hat{C}_p - Z_{1-\frac{\alpha}{2}} S_{cp}^*, \hat{C}_p + Z_{1-\frac{\alpha}{2}} S_{cp}^* \right] \quad (16)$$

$$\left[\hat{C}_{pk} - Z_{1-\frac{\alpha}{2}} S_{cpk}^*, \hat{C}_{pk} + Z_{1-\frac{\alpha}{2}} S_{cpk}^* \right] \quad (17)$$

Wherein, $Z_{1-\frac{\alpha}{2}}$ is the $1-\alpha/2$ percentile of the standard normal distribution.

2) Confidence interval based on PB [8,14]

$$\left[\hat{C}_p^* \left(\frac{\alpha}{2} B \right), \hat{C}_p^* \left(1 - \frac{\alpha}{2} B \right) \right] \quad (18)$$

$$\left[\hat{C}_{pk}^* \left(\frac{\alpha}{2} B \right), \hat{C}_{pk}^* \left(1 - \frac{\alpha}{2} B \right) \right] \quad (19)$$

Wherein, $\alpha/2$ and $(1-\alpha/2)$ are the upper and lower bounds of the confidence intervals for the statistics C_p and C_{pk} at the $(1-\alpha)$ confidence level, respectively, i.e.

3) Confidence interval based on BCPB[8,15]

$$\left[\hat{C}_p^* (P_L B), \hat{C}_p^* (P_U B) \right] \quad (20)$$

$$\left[\hat{C}_{pk}^* (P'_L B), \hat{C}_{pk}^* (P'_U B) \right] \quad (21)$$

Wherein, $P_0 = P_r(\hat{C}_p^* \leq \hat{C}_p)$, $P'_0 = P_r(\hat{C}_{pk}^* \leq \hat{C}_{pk})$, and

$$\begin{aligned} P_L &= \Phi \left(2Z_0 - Z_{1-\frac{\alpha}{2}} \right) \\ Z_0 &= \Phi^{-1}(P_0) \quad , \quad Z'_0 = \Phi^{-1}(P'_0) \quad , \\ P'_L &= \Phi \left(2Z'_0 - Z_{1-\frac{\alpha}{2}} \right) \quad , \quad P_U = \Phi \left(2Z_0 + Z_{1-\frac{\alpha}{2}} \right) \quad , \\ P'_U &= \Phi \left(2Z'_0 + Z_{1-\frac{\alpha}{2}} \right) \quad . \end{aligned}$$

4) Confidence interval based on PTB [8,14]

$$\left[\hat{C}_{p, pk} - t^* \left(\frac{\alpha}{2} B \right) \times S_{p, pk}^* , \hat{C}_{p, pk} + t^* \left(\frac{\alpha}{2} B \right) \times S_{p, pk}^* \right] \quad (22)$$

$$\left[\hat{C}_{pk} - t^* \left(\frac{\alpha}{2} B \right) \times S_{cpk}^* , \hat{C}_{pk} + t^* \left(\frac{\alpha}{2} B \right) \times S_{cpk}^* \right] \quad (23)$$

Wherein, S_{cpk}^* is the sample standard deviation of $\{ \hat{C}_{pk}^{*(i)} \}$,

$i = 1, 2, \dots, B$, that is $S^* = \sqrt{\frac{1}{B} \sum_{i=1}^B (\hat{C}_{p, pk}^{*(i)} - \bar{\hat{C}}_{p, pk}^*)^2}$, where

$$\bar{\hat{C}}_{p, pk}^* = \frac{1}{B} \sum_{i=1}^B \hat{C}_{p, pk}^{*(i)} .$$

In addition, $\hat{t}^{*(\tau)}$ is the τ percentile of $\left\{ \frac{\hat{C}_{p, pk}^{*(i)} - \bar{\hat{C}}_{p, pk}^*}{S^*} \right\}$;

$i=1, 2, \dots, B$, i.e., $\hat{t}^{*(\tau)}$ is such that $\frac{1}{B} \sum_{i=1}^B I \left(\frac{\hat{C}_{p, pk}^{*(i)} - \bar{\hat{C}}_{p, pk}^*}{S^*} \leq \hat{t}^{*(\tau)} \right) = \tau$,

$0 < \tau < 1$.

C. Calculation of CIL of C_p and C_{pk} under Bootstrap Methods

Based on the above principles, enough samples are obtained by repeated sampling from small samples, assuming that they obey different distributions; data should be transformed to normal firstly before calculating PCI.

For comparison, the original distribution is transformed so that the different types of distributions have the same mean and variance. To be more general, the data generated by the simulation is processed centrally, that is, standard normal processing. Assuming that different data distributions have the same mean and variance, the data can be transformed accordingly:

$$\frac{Y - \mu^*}{\sigma^*} = \frac{X - \mu_0}{\sigma_0} \quad (24)$$

where, μ^* , σ^* , μ_0 and σ_0 are the mean and standard deviation of the expected output distribution and the original distribution, respectively. Table IV summarizes the means and variances of some common distributions. These parameters will be used in the data normal transformation.

To be more general, we choose several typical distributions, including symmetric distributions such as the normal distribution and the heavy-tailed distribution t_5 , and asymmetric distributions such as the moderately right-skewed distribution χ_5^2 and the slightly skewed distribution $logn(0, 0.4)$.

TABLE IV. MEAN AND VARIANCE OF DIFFERENT DISTRIBUTION

| Distributions | Mean | Variance | Statistics |
|--------------------------|------------------------|--|---------------------------------------|
| Normal distribution | μ | σ^2 | μ : Mean σ^2 : variance |
| Exponential distribution | $1/\lambda$ | $1/\lambda^2$ | λ : Threshold |
| χ^2 distribution | n | 2n | n: Freedom |
| T distribution | 0 | $n/(n-2)$ | n: Freedom |
| F distribution | $v/(v-2)$ | $\frac{2v^2(u+v-2)}{u(v-2)^2(v-4)}$ $v > 4$ | u&v: first & second degree of freedom |
| Log-normal distribution | $e^{(\mu+\sigma^2)/2}$ | $e^{2\mu+\sigma^2(\sigma^2-1)}$ | μ : Mean σ^2 : variance |

Firstly, to obtain a different distribution type with a mean of 0 and a standard deviation of 1, you can transform the data based on Eq. (24) as follows:

$$X_1 \sim t_5 \Rightarrow Y_1 = \sqrt{\frac{3}{5}} X_1 \quad (25)$$

$$X_2 \sim \chi_5^2 \Rightarrow Y_2 = \sqrt{\frac{1}{10}} X_2 + \frac{5}{\sqrt{10}} \quad (26)$$

$$X_3 \sim \text{Logn}(0,0.4) \Rightarrow Y_3 = \frac{1}{e^{0.08} \sqrt{e^{0.16} - 1}} X_3 - \frac{1}{\sqrt{e^{0.16} - 1}} \quad (27)$$

Secondly, based on the new distribution generated by the above three transformations, using four Bootstrap methods, the confidence interval and *CIL* value at $\alpha=0.1$ can be obtained through simulation. The simulation results and analysis are shown in Section IV.

V. EXPERIMENTAL ANALYSIS

Based on the calculation results in Section IV, the influence of sample size *n* and different Bootstrap methods on the length of confidence interval is analyzed.

A. When the Data Follows Symmetrical Distribution

In order to analyze the factors affecting *CIL*, we first carried out ANOVA and drew images to compare the difference of *CIL* under different Bootstrap methods.

Through ANOVA, we found that only the sample size *n* had a significant effect on *CIL* (its *P* value less than 0.05), while the Bootstrap method had no significant effect on *CIL* (its *P* value greater than 0.05). In addition, combined with comparison graph analysis in Fig. 1, regardless of which Bootstrap method is used, *CIL* decreases as the sample size *n* increases.

TABLE V. SIMULATION RESULT UNDER DISTRIBUTION WITH FOUR BOOTSTRAP METHOD

| Distribution | | Symmetrical Distribution | | | | Asymmetrical Distribution | | | |
|--------------|----|--------------------------|--------|-------------------|--------|---------------------------|---------|---------------------|---------|
| Method | n | Normal distribution | | <i>ts</i> | | χ^2 | | <i>logn(0, 0.4)</i> | |
| | | [Lc ,Uc] | CIL | [Lc, Uc] | CIL | [Lc, Uc] | CIL | [Lc, Uc] | CIL |
| SB | 10 | [0.4489, 1.5213] | 1.0724 | [0.3602, 1.7573] | 1.3971 | [0.2552, 1.7442] | 1.789 | [0.3655, 1.7383] | 1.3728 |
| | 20 | [0.5335, 1.3548] | 0.8213 | [0.5136, 1.7206] | 1.207 | [0.7303, 1.7342] | 1.0039 | [0.5773, 1.7379] | 1.1606 |
| | 30 | [0.7335, 1.3346] | 0.6011 | [0.7523, 1.7125] | 0.9602 | [0.8902, 1.6979] | 0.8077 | [0.7562, 1.7293] | 0.9731 |
| | 50 | [0.7402, 1.2963] | 0.5561 | [0.7563, 1.2112] | 0.4549 | [0.9103, 1.3302] | 0.4799 | [0.7623, 1.3194] | 0.5571 |
| PB | 10 | [0.7256, 1.6432] | 0.9176 | [0.6887, 1.8730] | 1.1843 | [0.7443, 1.9936] | 1.2493 | [0.6933, 1.8432] | 1.1499 |
| | 20 | [0.7312, 1.6324] | 0.9012 | [0.7809, 1.8566] | 1.0757 | [0.7892, 1.8952] | 1.106 | [0.8012, 1.8979] | 1.0967 |
| | 30 | [0.7418, 1.6330] | 0.8912 | [0.7942, 1.5653] | 0.8711 | [0.7902, 1.8146] | 1.0244 | [0.7995, 1.35669] | 0.8674 |
| | 50 | [0.7561, 1.5744] | 0.8183 | [0.8051, 1.26519] | 0.8468 | [0.7912, 1.5135] | 0.7223 | [0.8089, 1.5601] | 0.7512 |
| BCPB | 10 | [0.7220, 1.6042] | 0.8822 | [0.7523, 1.7325] | 0.9802 | [0.7902, 1.8979] | 1.1077 | [0.7562, 1.8283] | 1.0721* |
| | 20 | [0.7524, 1.5761] | 0.8237 | [0.763, 1.8073] | 1.0443 | [0.8298, 1.8939] | 1.0641 | [0.7883, 1.7122] | 0.9239* |
| | 30 | [0.7732, 1.5636] | 0.7904 | [0.7803, 1.6314] | 0.8511 | [0.8973, 1.8103] | 0.913 | [0.7903, 1.6832] | 0.8929 |
| | 50 | [0.7768, 1.5592] | 0.7824 | [0.7959, 1.5351] | 0.7392 | [0.9312, 1.7527] | 0.8215 | [0.7991, 1.6403] | 0.8412* |
| PTB | 10 | [0.8851, 1.7562] | 0.8711 | [0.8023, 1.8962] | 1.0939 | [0.7776, 1.8792] | 1.1016* | [0.7370, 1.8662] | 1.1292 |
| | 20 | [0.9213, 1.7175] | 0.7962 | [0.8532, 1.7308] | 0.8776 | 0.8232, 1.7957] | 0.9725* | [0.8109, 1.7892] | 0.9783 |
| | 30 | [0.9343, 1.708] | 0.7737 | [0.8832, 1.6998] | 0.8166 | [0.8454, 1.7379] | 0.8925* | [0.8216, 1.6979] | 0.8763 |
| | 50 | [0.9580, 1.7078] | 0.7498 | [0.9052, 1.6881] | 0.7829 | [0.8523, 1.7159] | 0.8636* | [0.8581, 1.6475] | 0.7894 |

TABLE VI. ANOVA TABLE UNDER NORMAL DISTRIBUTION

| Sources | Degree of freedom | SS | MS | F | P |
|--|-------------------|---------|----------|-------|-------|
| n | 3 | 1.68907 | 0.563023 | 10.62 | 0.003 |
| Method | 3 | 0.07372 | 0.024574 | 0.46 | 0.175 |
| Error | 9 | 0.47715 | 0.053017 | | |
| Total error | 15 | 2.23994 | | | |
| S = 0.2303 R-Sq = 78.70% R-Sq(adjust) = 64.50% | | | | | |

TABLE VII. ANOVA TABLE UNDER T5 DISTRIBUTION

| Sources | Degree of freedom | SS | MS | F | P |
|---|-------------------|---------|----------|-------|-------|
| n | 3 | 0.85628 | 0.285428 | 17.93 | 0.000 |
| Method | 3 | 0.09789 | 0.032631 | 2.05 | 0.177 |
| Error | 9 | 0.14327 | 0.015918 | | |
| Total error | 15 | 1.09744 | | | |
| S = 0.1262 R-Sq = 86.95% R-Sq(adjust)= 78.24% | | | | | |

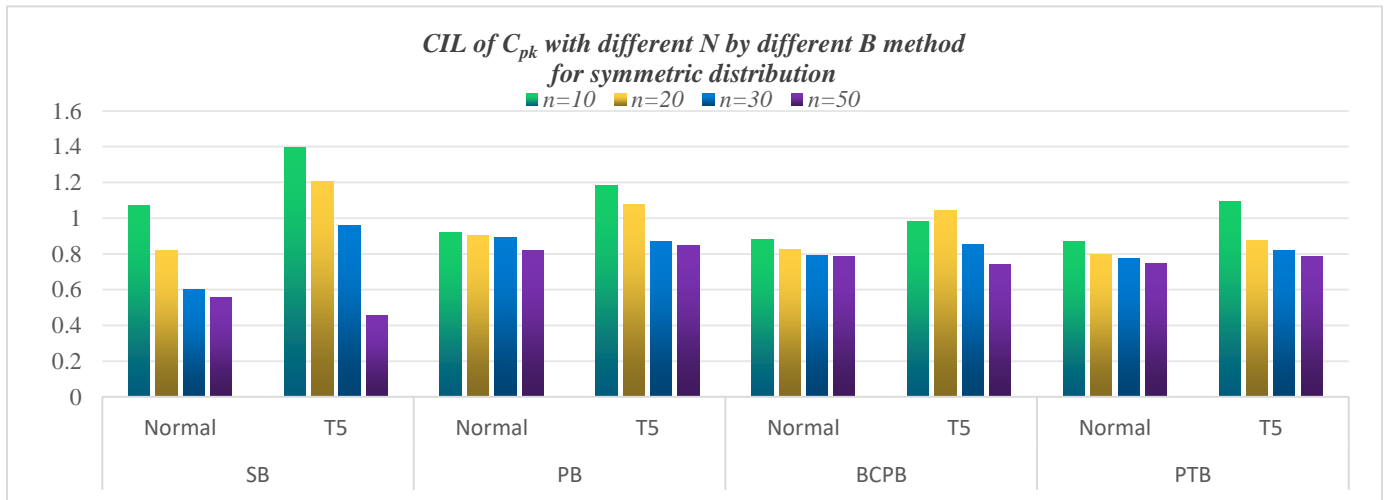


Fig. 1. CIL of C_{pk} under symmetrical distribution.

B. When the Data Follows Asymmetric Distribution

The ANOVA and image results are as follows: sample size n and Bootstrap methods are both significant factors affecting CIL (their P value are both less than 0.05). That is to say, the larger of sample size n is, the shorter of the CIL is.

Combined with Fig. 2, it can be found that the CIL under different Bootstrap methods are different but when the data follows χ^2_5 distribution, and the CIL of the later two Bootstrap methods is more stable, but the CIL of PTB is the shortest. While When the data follows $logn(0,0.4)$ distribution (which is

slightly skewed), the ANOVA and image results are a little different, the CIL of the BCPB methods is more stable and shorter. That is to say:

- In skew distribution, PTB method and BCPB method are better than SB and PB method in estimating CIL.
- In the slightly skewed distribution, such as $log-normal(0, 0.4)$ distribution, BCPB method is recommended. For moderately skewed distributions, such as χ^2_5 distributions, the PTB method is recommended.

TABLE VIII. TWO FACTORS OF ANOVA TABLE UNDER CHI-SQUARE DISTRIBUTION

| Sources | Degree of freedom | SS | MS | F | P |
|--|-------------------|---------|----------|------|-------|
| n | 3 | 0.52345 | 0.174482 | 6.77 | 0.011 |
| Method | 3 | 0.32737 | 0.109124 | 4.23 | 0.040 |
| Error | 9 | 0.23212 | 0.025792 | | |
| Total error | 15 | 1.08294 | | | |
| S = 0.1606 R-Sq = 78.57% R-Sq(adjust) = 64.28% | | | | | |

TABLE IX. TWO FACTORS ANOVA TABLE UNDER LOG-NORMAL(0,0.4) DISTRIBUTION

| Sources | Degree of freedom | SS | MS | F | P |
|-------------|-------------------|---------|----------|-------|-------|
| n | 3 | 1.66676 | 0.555587 | 54.54 | 0.000 |
| Method | 3 | 0.15233 | 0.050778 | 4.98 | 0.026 |
| Error | 9 | 0.09168 | 0.010187 | | |
| Total error | 15 | 1.91078 | | | |

S = 0.1009 R-Sq = 95.20% R-Sq(adjust)= 92.00%

C. Findings

1) In symmetric distribution: Based on all the above ANOVA (see Tables VI-VII) and combined with Fig. 1, the following findings can be drawn:

Take normal distribution and T distribution as examples, only the sample size has a significant effect on the length of the confidence interval: the larger the sample size n is, the shorter the CIL is. In the symmetric distribution, the four Bootstrap methods had no significant effect on the length of confidence interval, that is, there was no significant difference between the four methods.

2) In asymmetric distribution: Based on all the above ANOVA (see Tables VIII-IX) and combined with Fig. 2, the following findings can be drawn:

Take chi-square distributions and log-normal distributions as examples, both the sample size n and the Bootstrap method are important factors affecting CIL. The CIL gets shorter as the sample size n increases. In addition, the confidence intervals calculated under the four Bootstrap methods are significantly different.

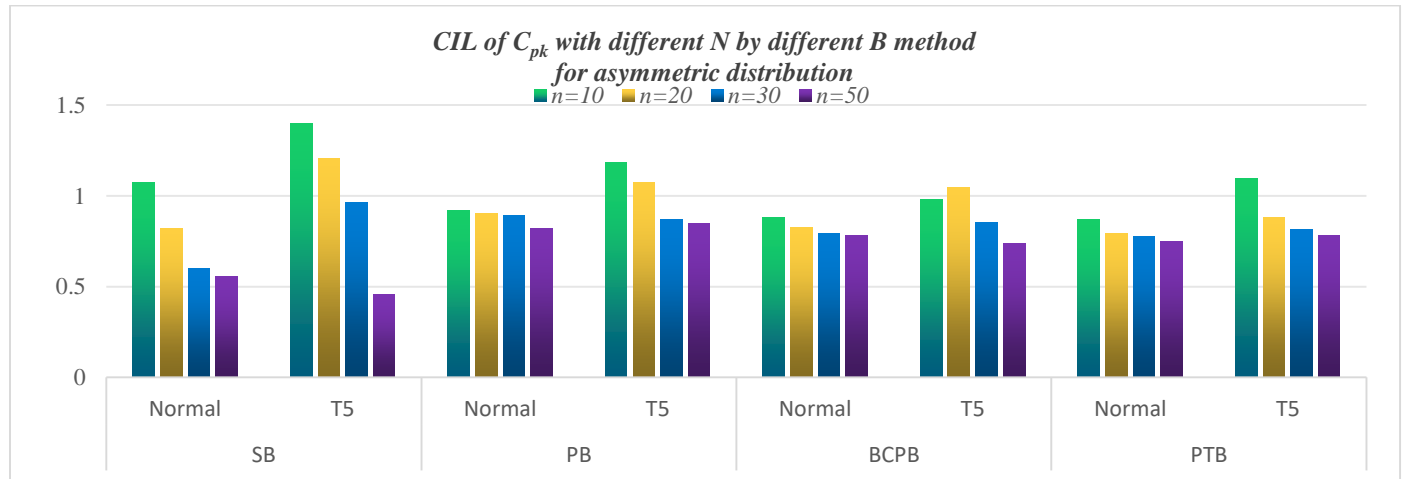


Fig. 2. CIL of Cpk under asymmetric distribution.

VI. CONCLUSION

This paper mainly studies the process capability index in the case of small samples. After analyzing the influence of sample size on the confidence interval of traditional process capability analysis index, we introduced Bootstrap method to solve and compare the confidence interval of process capability index Cp and Cpk in the case of small samples. ANOVA was used to verify the significant effects of sample size and different Bootstrap methods on confidence intervals. Some valuable findings were made:

1) In symmetric distributions, such as normal and T-distributions, only the sample size has a significant effect on the length of the confidence interval: the larger the sample size, the shorter the CIL. The Bootstrap method has no significant effect on the length of the confidence interval, that is, there is no significant difference between the four methods.

2) In asymmetric distributions, such as chi-square and lognormal distributions, both sample size and Bootstrap method are important factors affecting CIL. Combined with the variation of distribution skewness, the user can choose the appropriate Bootstrap method.

The above simulation and analysis only focus on the calculation and comparison of confidence intervals and their interval lengths, while the interval coverage ratio and standard difference of confidence intervals of PCI under these four methods have not been involved, and further in-depth research is needed.

ACKNOWLEDGMENT

This work was supported by the Ministry of Education Industry-University-research Collaborative Education Project(NO. 231100862222703) and the Scientific Research Foundation of Liaoning Petrochemical University (No.

2016XJJ-024). The authors also would thank reviewers for improving this article.

REFERENCES

- [1] V. E. Kane. Process capability indices [J]. Journal of quality Technology, 1986(18): 41-52.
- [2] L.K. Chan, S.W. Cheng, F.A. Spring. A new measure of process capability: Cpm [J]. Journal of Quality Technology, 1988(30): 162-175.
- [3] Taguchi, G. Introduction to quality engineering [M], Tokyo: Asian Productivity Organization, 1986.
- [4] Y. Chou, D.B. Owen, S. A. Borrego. Lower confidence limits on process capability indices [J]. Journal of Quality Technology, 1990(22): 223-229.
- [5] A. F. Bissell. How reliable is your capability index? [J], Applied statistics, 1990(39): 331-340.
- [6] R. A. Boyles. The Taguchi capability index [J], Journal of Quality Technology, 1991(23): 17-26.
- [7] B. Efron. Bootstrap methods: another look at the Jackknife [J], Annals of Statistics, 1979(7): 1-26.
- [8] B. Efron, R. Tibshirani. Bootstrap methods for standard errors, confidence intervals and other measures of statistical accuracy [J]. Statistical Sciences, 1986 (11): 54-77.
- [9] R. Ye, B. Fang, W Du. Bootstrap tests for the location parameter under the skew-normal population with unknown scale parameter and skewness parameter [J]. Mathematics, 2022, 10(6): 921-943.
- [10] B. M. G. Kibria , W.Chen. Comparison on some modified confidence intervals for estimating the process capability index Cp: simulation and application [J]. International journal of statistical sciences, 2021, 21(2): 145-166.
- [11] L. A. Franklin, G. S. Wasserman. Bootstrap lower confidence limits for capability indices [J], Journal of Quality Technology, 1992, 24(4): 196-209.
- [12] M. Kalyanasundaram, S. Balamurali. Bootstrap lower confidence limits for the process capability indices Cp, Cpk and Cpm [J], International Journal of Quality & Reliability Management, 2002, 19(2): 1088–1097.
- [13] C. Y. Chou, Y. C. Lin, C. L. Chang, C. H. Chen. On the bootstrap confidence intervals of the process incapability index Cpp [J], Reliability Engineering and System Safety, 2006, 91(4): 452-459.
- [14] D. S. Wang, T. Y. Koo, C. Y. Chou. On the bootstrap confidence intervals of the capability index Cpk for multiple process streams [J], Engineering Computations, 2007, 24(5): 473-485.
- [15] S. Balamurali. Bootstrap confidence limits for short-run capability indices [J], Quality Engineering, 2003, 15(4): 643-648.
- [16] K. C. Choi , K. H. Nam, D. H. Park. Estimation of capability index based on bootstrap method [J], Microelectronics Reliability, 1996, 36(9): 1141-1153.
- [17] Zhiyou, Tian, Tian Peng, Huanchen, Wang. Estimation on the Multivariate Process Capability Indices Based on Bootstrap Sampling [J], Journal of Industrial Engineering Management 2006, 20(2): 74-77.
- [18] S. Dey, M. Saha . Bootstrap confidence intervals of generalized process capability index Cpyk using different methods of estimation [J]. Journal of Applied Statistics, 2019, 46(10): 1843-1869.
- [19] M. Kashif, M. Aslam, G.S. Rao, A. AL-Marshadi, C. Jun. Bootstrap confidence intervals of the modified process capability index for weibull distribution [J]. Arabian Journal for Science and Engineering, 2017, 42(11): 4565–4573.
- [20] M. Saha, S. Dey, and S.S. Maiti, Parametric and non-parametric bootstrap confidence intervals of CNpk for exponential power distribution [J], Journal of Industrial and Production Engineering. 2018(35): 160–169.
- [21] M. Saha , S. Kumar, S.S. Maiti, A.S. Yadav. Asymptotic and bootstrap confidence intervals of generalized process capability index Cpy for exponentially distributed quality characteristic [J], Life Cycle Reliability Safety Engineering. 2018(7): 235–243.
- [22] Wang Jing. Research on Quality control of multi-variety and small-batch production based on Bootstrap method [D], Tianjin: Tianjin University, 2006.
- [23] R. M. EL-Sagheer , M. El-Morshedy , L. A. Al-Essa. The Process Capability Index of Pareto Model under Progressive Type-II Censoring: Various Bayesian and Bootstrap Algorithms for Asymmetric Data [J]. Symmetry, 2023, 15(4): 879-900.
- [24] S. Kotz, N. L. Johnso. Process Capability Indices [M], London: Chapman & Hall, 1993.
- [25] D. C. Montgomery. Introduction to Statistical Quality Control [M], New York: John Wiley&Sons , 1996.

Discovering the Global Landscape of Agri-Food and Blockchain: A Bibliometric Review

Sharifah Khairun Nisa' Habib Elias, Sahnus Usman, Suriyati Chuprat
Faculty of Artificial Intelligence, Universiti Teknologi Malaysia, Kuala Lumpur, Malaysia

Abstract—The agri-food supply chain encompasses all the entities involved in the production and processing of food, from producers to consumers. Traceability is crucial in ensuring that food products are available, affordable, and accessible. Blockchain technology has been proposed as a way to improve traceability in the agri-food supply chain by providing transparency and trust. However, research in this area is still in its early stages. This study aims to examine the trend of blockchain in agri-food supply chain traceability for food security. A bibliometric analysis was conducted on 1047 scholarly works from the Scopus database, starting in 2016. The analysis looked at citation patterns and the development of blockchain technology in agri-food supply chain research and identified trends by source title, nation, institution, and key players. The analysis also examined the frequency of keywords, titles, and abstracts to identify key themes. The analysis has revealed a strong correlation between blockchain technology and traceability in the agri-food supply chain, indicating a promising area for further research. The results show that blockchain-based research for traceability in the agri-food supply chain has increased and is being widely distributed, particularly in regions beyond Europe. The potential benefits it can bring to the supply chain will contribute to the success of the Sustainable Development Goals (SDGs) by ensuring a safe and sufficient global food supply.

Keywords—Agri-food supply chain; bibliometric; blockchain; traceability

I. INTRODUCTION

Food security, nutrition, and safety are all interrelated. 600 million people around the world are sick because of contaminated food, which causes 420,000 deaths and 33 million healthy life years (DALYs) every year. In low- and middle-income countries, unsafe food costs US\$110 billion every year. 40% of foodborne illnesses are experienced by children younger than five years old [1]. The agri-food sector and its supply chain play a crucial role in the global food system, involving the production, processing, transformation, and delivery of food products [2]. The study in [3] emphasises the difficulties that the agri-food industry encounters as a result of globalisation, such as the risks to food security, shortages in infrastructure, financial instability, and incidents of food fraud. This will be solved by implementing traceability in the agri-food supply chain.

However, the complex structure of the agri-food supply chain, which encompasses several stakeholders such as farmers, distributors, processors, wholesalers, retailers, and end consumers, creates difficulties [4].

Traceability refers to the capacity to systematically monitor and trace the movement of a product across the supply chain, starting from its origin to its final destination. The objective of traceability is to provide fast retrieval of dependable data, hence facilitating quick analysis and decision-making [5], [6]. For this reason, traceability has gained major importance in the agri-food sector due to customer demand for transparency, accountability, and food safety. Factors driving this demand include increasing supply chain efficiency, technological advancements, sustainability, food safety, regulations, certifications, and data collection and analysis [7]. Traceability is an essential feature of blockchain technology for supply chain applications [8], with a growing number of blockchain applications focusing on enabling supply chain traceability across various industries [9], [10], [11]. Blockchain technology has been suggested to improve traceability in the agri-food supply chain because it offers a transparent, reliable, and tamper-proof solution to managing product-related traceability information [12].

Blockchain technology is a decentralized system that provides immutability, security, and transparency in the ledger of transactions across a network of computers. Due to its capabilities, its application across various industry such as agriculture, healthcare and manufacturing. [13], has found traceability to be the primary enabler for blockchain technology implementation in the agri-food supply chain, followed by auditability, immutability, and provenance. For example, the provenance of food can be traced using blockchain technology, thus creating reliable food supply chains and fostering confidence between consumers and producers [6]. Besides that, blockchain-based supply chain technologies are anticipated to enhance performance, competitiveness, transparency, and trust among all participants [14]. This technology enhances operational efficiency, expedites processes, and eliminates the need for physical documentation, therefore providing accessibility, transparency, and integrity. By enhancing supply chain traceability, accountability, and efficiency, blockchain technology has the potential to revolutionise the manufacturing sector. It can address concerns such as intrinsic security and content modification requiring authentication and processing. It is also capable of managing assemblies and products, ensuring the privacy of data storage [15]. A novel framework that utilises a blockchain network to facilitate supply chain traceability and counterfeit detection of COVID-19 vaccines has been proposed by [16]. It facilitates the secure management of supply chain operations for distribution companies to prevent fraudulent vaccines and transform supply chain management in the healthcare industry. This

information will aid practitioners and policymakers in implementing blockchain technology in the agri-food supply chain to ensure food safety and security.

The globalisation of agricultural production has resulted in an increased focus on ensuring the safety, quality, and validation of standards throughout food supply chains. Blockchain technology offers a novel way for tracing products in intricate ecosystems. Various methodologies have been utilised to establish the ability to track and trace products in the agricultural food supply chain. A framework that utilises blockchain technology has been proposed for the agri-food supply chain in Bangladesh to resolve the issue of inadequate communication between producers and consumers in the traditional agricultural network [17]. [18]present ShrimpChain, a hybrid public-private Blockchain architecture, designed to enhance traceability and provide a full view of the supply chain in the shrimp industry. This framework aims to address the limitations of the traditional paper-based record-keeping methods now used in the fragmented shrimp supply chain. A blockchain-powered solution for monitoring and tracing soybeans in the agricultural supply chain is presented by [19] to improve efficiency and safety by eliminating the need for centralised authorities. The increasing need for ethical and ecological standards requires the ability to track items from their origin to their final point of sale. Utilising block-chain technology, along with RFID and QR codes, can effectively overcome limitations in current systems and streamline processes, such as monitoring the entire journey of cheese supply chains [20]. This technology can also enable smart contracts to automate supply chain management and product quality control [12]. Nevertheless, the integration of blockchain technology into the agri-food supply chain remains nascent, presenting challenges including but not limited to scalability, energy consumption, privacy, and complexity [21], [22], [23]. In order to fully realize its potential to revolutionize the agri-food supply chain through the provision of transparency, provenance, and efficiency, it is critical to address these challenges.

Subsequently, substantial progress has been made in the field of agri-food blockchain research; therefore, it is vital to remain abreast of the latest developments in the body of literature. A bibliometric analysis was performed on published blockchain in agri-food research, regardless of timeframe, in order to determine the scope and depth of scholarly work pertaining to blockchain in the agri-food sector. It attempts to respond to four primary research questions.

RQ1. What is the current trend and impact of publication in agri-food and blockchain?

- Growth of publication by year
- Sources Type and Types of Document
- Languages of documents
- Most active source titles

RQ2. Which are the most productive and influential countries, institutions and authors on agri-food and blockchain research?

- Total Publication by Country Top 15
- Most active institutions Top 15
- Authorship Analysis Top 15

RQ3. Which are the most prevalent themes of agri-food and blockchain between scholars?

- Keyword analysis
- Title and abstract analysis

RQ4. Which are the most influential articles on agri-food and blockchain research?

- Citation analysis

This work contributes to the existing research on the application of blockchain technology in the agri-food industries by providing a comprehensive bibliometric analysis of previous papers on the topic. The study provides insights into the current status of the topic, prominent publications, authors, journals, and organisations in the agri-food industries. The study's findings could guide future research on the topic and offer policymakers and industry stakeholders' better knowledge of the application of blockchain technology in the agri-food sector.

The subsequent sections of this paper are organised in the following manner: Section II provides a comprehensive evaluation of blockchain technology and its possible applications in the agri-food industry. Section III discusses the methodology and data collection for the study. The findings from our bibliometric analysis, which encompass publication output, citation impact, research themes, and collaboration patterns, are outlined in Section IV. Section V of our report explores into our study findings and their connection to the previously indicated research questions. Section VI serves as the concluding part of this article, containing its final remarks and findings.

II. RELATED WORK

In recent years, blockchain technology has received a lot of interest as a potential solution for improving transparency, traceability, and efficiency in agri-food supply chains. Blockchain improves traceability by allowing consumers to trace their food products from farm to table. The transparency alleviates concerns about food safety and authenticity [24]. Several studies have been conducted to address blockchain challenges and limitations such as scalability, data privacy, data accuracy, security, lack of regulations and adoption [25], [26], [27], [28], [29], [30]. However, additional research is required to explore the potential of blockchain technology in agri-food supply chains and to develop effective frameworks and models for its implementation. For instance, [31], [32] introduced a food safety supply chain traceability system that relies on HACCP (Hazard Analysis Critical Control Point), blockchain, and the Internet of Things. In addition, he commented on the benefits and limitations of RFID and blockchain. The suggested traceability system in the study successfully implemented automated data collection and storage to enhance information transparency and improve food

safety. [33] [34] suggested a traceability system that utilizes blockchain technology and Internet of Things devices for gathering data. The study in [35] examined the utilization of blockchain technology in the food supply chain and evaluated particular cases of traceability within the existing food supply chain. The study in [19] conducted an analysis on the traceability of soybean supply chain, specifically focusing on the use of a smart contract to guarantee the safety, credibility, and security of information.

Previous research has examined the attributes and capabilities of blockchain technology in relation to food traceability issues. These studies have also emphasized the advantages and challenges associated with the deployment of traceability systems based on blockchain technology. While the prospective benefits of BCT in the agri-food sector are promising, it is essential to possess a comprehensive understanding of the present state of research. This can be achieved by doing a bibliometric analysis of the literature.

III. METHODOLOGY

A. Database Selection

The Scopus database was employed to conduct the analysis of the documents that were acquired for this bibliometric investigation. Scopus, the preeminent academic database, comprises an extensive collection of citations spanning 240 disciplines, including over 28,000 active titles, 7000 publishers, 93 million documents, 17.6 million author profiles, 234,000 volumes, and over 94,800 institutional profiles. The reason for selecting this database is its ability to offer an all-encompassing depiction of the scientific research output worldwide. The study in [36] found that WoS covers

54% of Scopus publications, while Scopus includes 84% of WoS titles. Scopus offers smart tools for tracking, analyzing, and visualizing research, ensuring critical analysis from around the world is not missed. At present, the Scopus database is considered by the international scientific community to be one of the most important sources of pertinent data [37]. Consequently, Scopus is recommended as a valuable database for extracting materials pertinent to the subject matter investigated in this study.

B. Inclusion Criteria

During the procedure of data collection, we employed a keyword to determine the relevant documents. The phrases ("food" or "agri-food," or "agro-food") and ("blockchain" or "block-chain") were utilized to search the Scopus database for information contained in article titles and abstracts. The search was conducted on December 5, 2023, resulting in the discovery of a total of 1053 documents. The documents went through additional screening to exclude unrelated subject areas such as business, management and accounting, mathematics, social sciences, environmental science, and energy. The focus was narrowed down to only computer science and engineering, resulting in a total of 1047 documents retrieved by Scopus. Furthermore, the review of publications was conducted using the standardized methodology of the Preferred Reporting Items for Systematic Reviews and Meta-analyses (PRISMA) statement. The steps of this technique are illustrated in a flow chart (see Fig. 1). Therefore, this article ensures compliance by following the precise procedures outlined in the PRISMA protocol (Petersen et al., 2008).

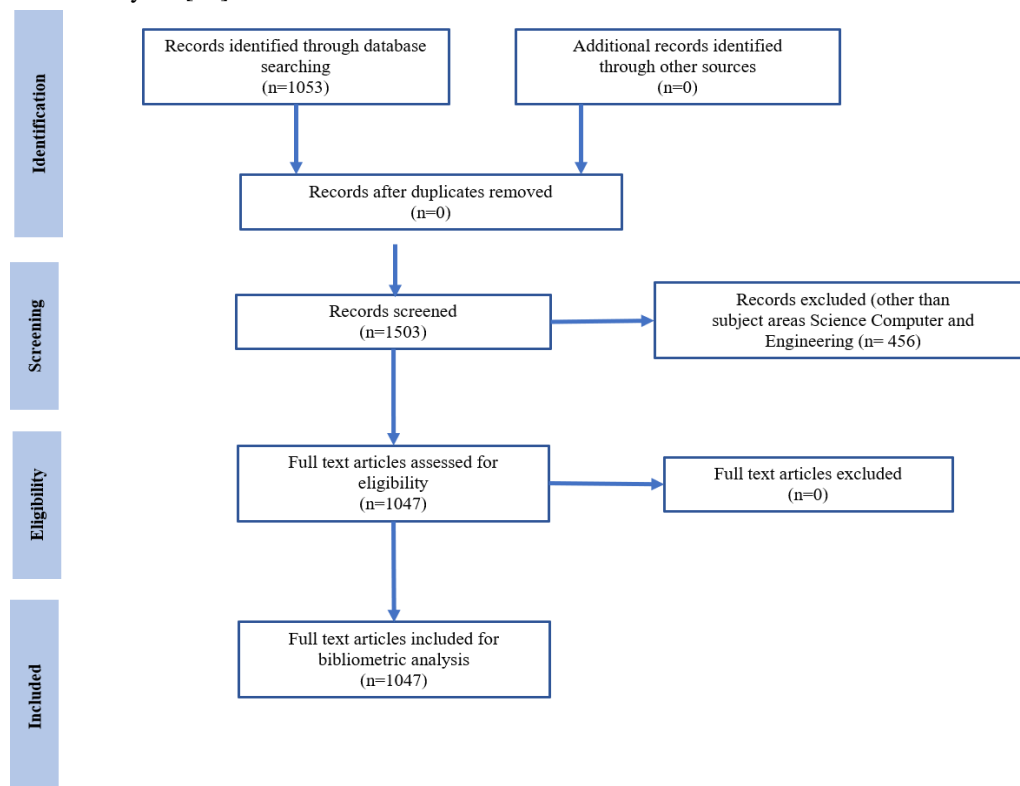


Fig. 1. PRISMA flowchart.

C. Data Analysis and Tools

Fig. 2 depicts the research framework to acquire the ultimate results. Bibliometric analysis is frequently used due to its capacity to provide dependable quantification and evaluation of the publications that are indexed in the database being studied [39]. This research additionally adds by utilizing the bibliometric technique to enhance academics' comprehension of the literature regarding the implementation of blockchain technology in the agri-food sector. Hence, bibliometric analyses remain a vital tool for identifying gaps in any given subject or field [40]. A total of 1047 documents as resulted in data collection phases were downloaded in CSV Excel and RIS format for the analysis process. The metadata

in the CSV Excel and RIS file were analyzed using VOSviewer software to identify the primary research areas and generate several visual representations and tables.

Microsoft Excel was utilized for frequency analysis, while VOSviewer was employed for data visualization. Harzing's Publish or Perish was utilized for citation metrics and analysis. The data were analysed according to the geographical location of the research, the number of publications per year, the presence of highly cited works, and the journals that had the greatest number of relevant papers. This study investigates the application of blockchain in agri-food supply chain research using the abstract and title keywords fields and covering all languages in the Scopus database.

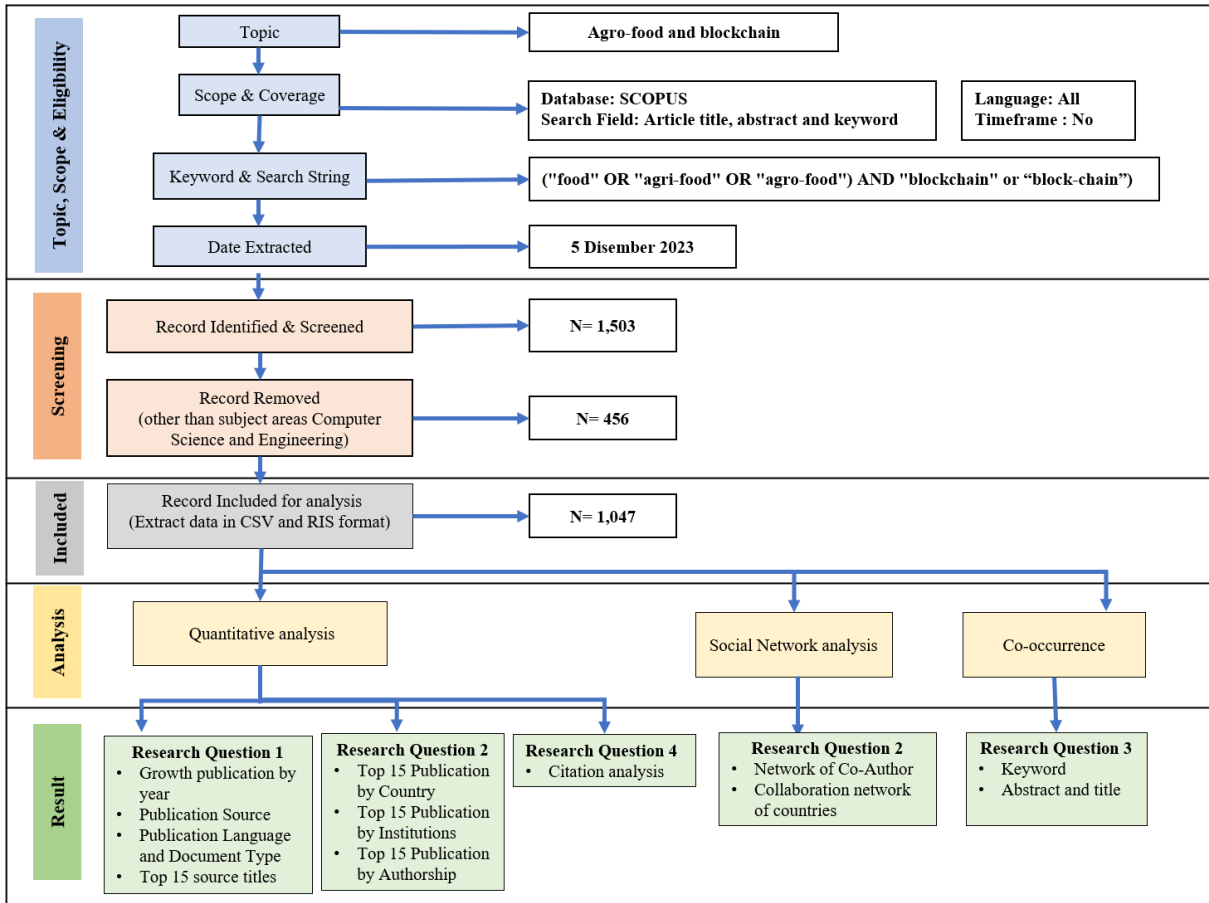


Fig. 2. Research framework.

IV. ANALYSIS RESULTS

A. Development and Progress of the Agri-Food and Blockchain Research

To address the first research question, we examined the progress and dissemination of Agri-food and blockchain research based on the following factors: (a) the annual count of published studies; (b) the sources and types of documents; (c) the languages in which the documents were written; and (d) the titles of the sources.

1) *The annual count of published studies:* Table 1 shows annual growth of publication by year for agri-food and

blockchain, along with various metrics such as total publications (TP), percentage of total publications (%), number of total publications (NCP), total citations (TC), average citations per publications (C/P), average citations per cited publication(C/CP), h-index and g-index.

The number of publications has increased from 1 in 2016 to 278 in 2022, with an increasing trend in average citations per publication (C/P) and C/CP. The h-index and g-index provide insights into the author's impact, with the h-index increasing from 5 in 2017 to 32 in 2021 and the g-index reaching 55 in 2021. However, in 2023, there will be a slight decline in total publications because the year has not yet been

completed. Additionally, as depicted in Fig. 3, the number of citations for documents published in 2020 appeared to have peaked at 6,667, with an average of 46.62 citations per publication. However, beginning in 2021, the number of citations began to decline. The increase in total citations in 2020 may be attributed to the COVID-19 pandemic, which has emphasized the criticality of food traceability in guaranteeing food safety. Conversely, papers that were published in 2016 received the fewest citations (one citation per publication out of a total of 74 citations). The low number of citations is presumably related to the nascent stage of blockchain implementation in the agri-food sector. From 2016 to 2020, however, the overall quantity of citations increased dramatically. Total publications are on the rise, as depicted in Fig. 3, whereas total citations are declining after 2020. The sources for blockchain in agri-food research, document categories, most active source titles, and the language of documents utilized in blockchain in agri-food publications are further explored subsequently to the identification of the annual growth document.

2) *The sources and types of documents:* An investigation was conducted to determine the publication areas of agri-food and blockchain documents through an analysis of the data grouped by document source categories. There are five primary sources—journals, conference proceedings, books, book series, and trade journals. Journals constituted the most prevalent source, comprising 414 (or 39.54%) of the total, followed by publications for conference proceedings (n = 379, 36.20%), as shown in Fig. 4. Book series, comprising 16.91%, offer comprehensive perspectives on specific themes. Individual books, accounting for 6.49%, provide in-depth exploration and authoritative references. Trade journals, a smaller but specialized portion, make up 0.86% of the total publications.

Document type analysis was also performed on the data. As summarized in Fig. 5, the Scopus search yielded ten distinct categories of documents that were published on the

agri-food and blockchain. The majority of publications (n = 442, 42.22%) are categorized as Conference papers, as indicated in the table followed by Article (n = 360, 34.38%). However, book chapter, Conference review and review articles category comprised less than 10% of the total publications. Less than 1% of the total publications were comprised of the remaining document categories, including books, editorials, notes, erratum, and short survey.

3) *Languages of documents:* In total, research papers for agri-food and traceability were composed in five languages. English was the most extensively utilized language, accounting for 98.09% of all publications, as shown in Fig. 6. Chinese was the second most prevalent language, comprising 1.62% of the total. Most of the remaining documents (less than 0.5%) were published in German, Polish, and Spanish. In conclusion, only three documents were published in a single language: German, Polish, and Spanish. This represents the tiniest fraction of the overall document count, amounting to 0.30%.

TABLE I. GROWTH OF PUBLICATION BY YEAR

| Year | TP | % | NCP | TC | C/P | C/CP | h | g |
|------|-----|--------|-----|------|-------|-------|----|----|
| 2024 | 6 | 0.57% | 0 | 0 | 0.00 | 0.00 | 0 | 0 |
| 2023 | 263 | 25.12% | 91 | 558 | 2.12 | 6.13 | 11 | 26 |
| 2022 | 278 | 26.55% | 182 | 2066 | 7.43 | 11.35 | 24 | 37 |
| 2021 | 218 | 20.82% | 167 | 3575 | 16.40 | 21.41 | 32 | 55 |
| 2020 | 143 | 13.66% | 117 | 6667 | 46.62 | 56.98 | 34 | 80 |
| 2019 | 97 | 9.26% | 85 | 4001 | 41.25 | 47.07 | 32 | 62 |
| 2018 | 35 | 3.34% | 26 | 1642 | 46.91 | 63.15 | 15 | 26 |
| 2017 | 6 | 0.57% | 6 | 522 | 87.00 | 87.00 | 5 | 6 |
| 2016 | 1 | 0.10% | 1 | 74 | 74.00 | 74.00 | 1 | 1 |

Notes: TP = total number of publications; NCP = number of cited publications; TC = total citations; C/P = average citations per publication; C/CP = average citations per cited publication; h = h-index; g = g-index

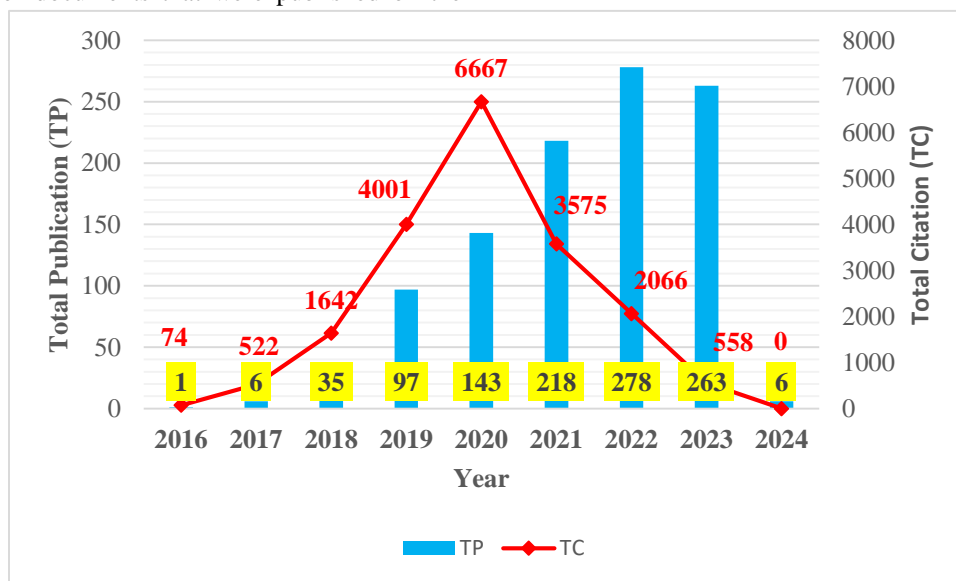


Fig. 3. Total publications and citations by year.

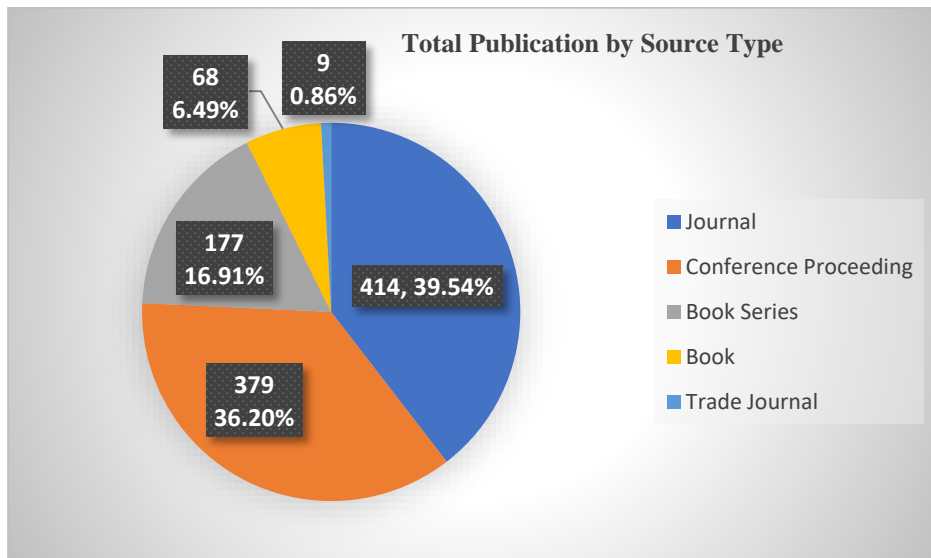


Fig. 4. Total publications based on source type.

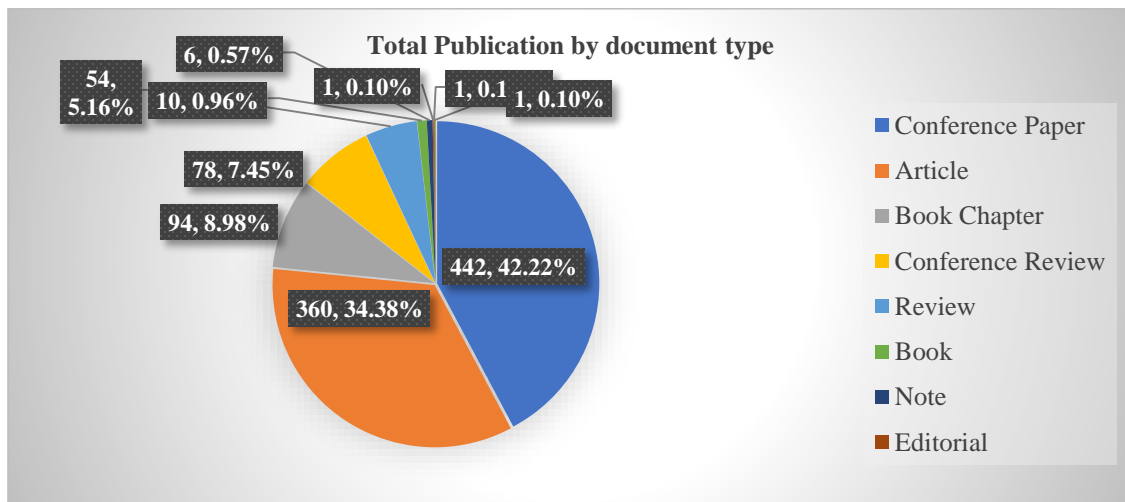


Fig. 5. Total Publication based on document type.

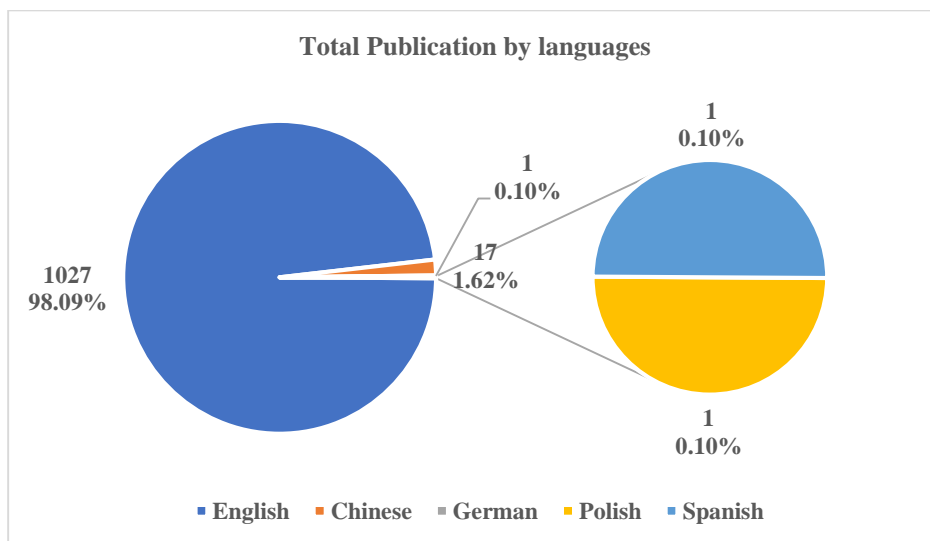


Fig. 6. Total publication based on languages.

4) *Publication by source title:* After identifying the current trends in sources, document types, and languages of agri-food blockchain research, the last criteria are to examine the source title. The results show that the journal that made the most substantial contribution to the agri-food and blockchain literature was Sustainability Switzerland (n = 42). Lecture Notes in Networks and Systems (n = 35), IEEE Access (n=34) and ACM International Conference Proceeding Series (n=32) are nearly identical indicating a significant 9.65% contribution, as reported by these result. The Lecture Notes in

Computer Science Including Subseries Lecture Notes in Artificial Intelligence and Lecture Notes in Bioinformatics subsequently appeared, comprising more than 25 articles. However, the rest of publication, contribute less than 20 articles. Despite having a smaller number of publications in total, Journal of Cleaner Production exhibited the second highest citations (n = 1215), after IEEE Access (n = 2246). The top fifteen most active source titles of blockchain in agri-food based on total publication are shown in Table II and while Fig. 7 compares total publication versus total citations.

TABLE II. TOP 15 SOURCE TITLE

| Source Title | TP | % | Publisher | Cite Score 2022 | SJR 2022 | SNIP 2022 | NCP | TC | C/P | C/CP | h | g |
|--|----|-------|-------------------------------------|-----------------|----------|-----------|-----|------|-------|-------|----|----|
| Sustainability Switzerland | 42 | 4.01% | MDPI | 5.8 | 0.664 | 1.198 | 38 | 803 | 19.12 | 21.13 | 14 | 27 |
| Lecture Notes In Networks And Systems | 35 | 3.34% | Springer Nature | 0.7 | 0.151 | 0.19 | 12 | 33 | 0.94 | 2.75 | 3 | 4 |
| IEEE Access | 34 | 3.25% | IEEE | 9 | 0.926 | 1.422 | 30 | 2246 | 66.06 | 74.87 | 19 | 30 |
| ACM International Conference Proceeding Series | 32 | 3.06% | Association for Computing Machinery | 28.5 | 4.457 | 7.155 | 15 | 173 | 5.41 | 11.53 | 6 | 13 |
| Lecture Notes In Computer Science Including Subseries Lecture Notes In Artificial Intelligence And Lecture Notes In Bioinformatics | 26 | 2.48% | Springer Nature | 2.2 | 0.32 | 0.542 | 15 | 305 | 11.73 | 20.33 | 8 | 15 |
| Advances In Intelligent Systems And Computing | 18 | 1.72% | Discontinued in Scopus as of 2021 | | | | 12 | 145 | 8.06 | 12.08 | 7 | 12 |
| Communications In Computer And Information Science | 17 | 1.62% | Springer Nature | 1 | 0.194 | 0.241 | 9 | 132 | 7.76 | 14.67 | 4 | 9 |
| Journal Of Cleaner Production | 16 | 1.53% | Elsevier | 18.5 | 1.981 | 2.379 | 14 | 1215 | 75.94 | 86.79 | 11 | 14 |
| Lecture Notes In Electrical Engineering | 13 | 1.24% | Springer Nature | 0.6 | 0.147 | 0.158 | 3 | 14 | 1.08 | 4.67 | 2 | 3 |
| Ceur Workshop Proceedings | 11 | 1.05% | | 1.1 | 0.202 | 0.223 | 2 | 3 | 0.27 | 1.50 | 1 | 1 |
| Lecture Notes Of The Institute For Computer Sciences Social Informatics And Telecommunications Engineering | 9 | 0.86% | Springer Nature | 0.7 | 0.159 | 0.137 | 1 | 4 | 0.44 | 4.00 | 1 | 1 |
| Lecture Notes On Data Engineering And Communications Technologies | 9 | 0.86% | Springer Nature | 0.7 | 0.125 | 0.104 | 5 | 16 | 1.78 | 3.20 | 2 | 3 |
| Sensors | 9 | 0.86% | MDPI | 6.8 | 0.764 | 1.317 | 7 | 118 | 13.11 | 16.86 | 5 | 7 |
| Applied Sciences Switzerland | 8 | 0.76% | MDPI | 4.5 | 0.492 | 0.974 | 8 | 280 | 35.00 | 35.00 | 6 | 8 |
| IFIP Advances In Information And Communication Technology | 8 | 0.76% | Springer Nature | 1.4 | 0.255 | 0.364 | 2 | 9 | 1.13 | 4.50 | 2 | 2 |

Notes: TP = total number of publications; TC = total citations; CiteScore = average citations received per document published in the source title; SJR = SCImago Journal Rank measures weighted citations received by the source title; SNIP = source normalised impact per paper measures actual citations received relative to citations expected for the source title's subject field;

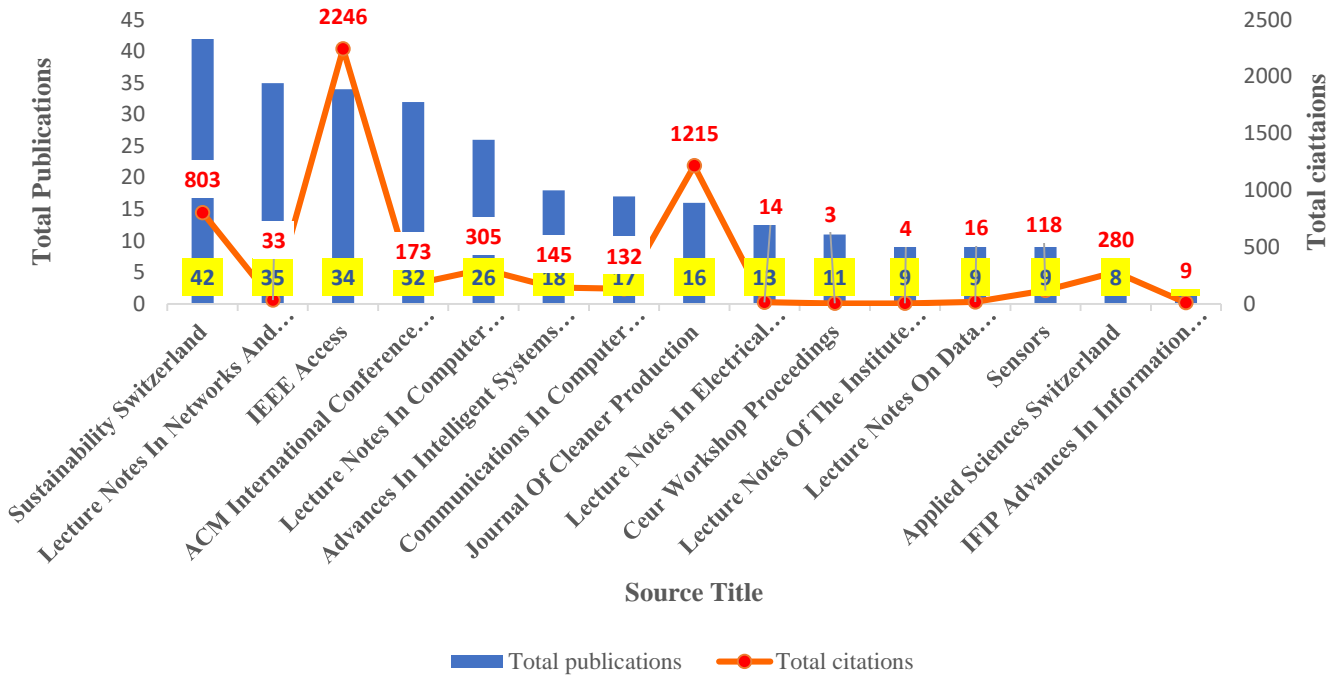


Fig. 7. Top 15 source title based total publications and total citations.

B. Most Influential Countries, Institutions and Authors on Agri-Food and Blockchain

This part concentrates on addressing the second research question, which aims to assess the level of scientific collaboration in the fields of agri-food and blockchain. This assessment is conducted through four main analyses: (a) publications categorized by country, (b) identification of the most active institutions involved in agri-food and blockchain research, and (c) analysis of authorship patterns.

1) *Publications by countries:* The published indicators for the top 15 countries in terms of agri-food and traceability research are summarized in Fig. 8 and Table III. With 293 documents, India has the highest number of scientific publications, followed by China (n = 163), Italy (n = 82), the United States (n = 79), the United Kingdom (n = 71), and Australia (n=42).

TABLE III. TOP 15 PUBLICATION BY COUNTRY

| Country | TP | % | NCP | TC | C/P | C/CP | h | g | Continent |
|----------------|-----|--------|-----|------|-------|-------|----|----|---------------|
| India | 293 | 27.98% | 187 | 4342 | 14.82 | 23.22 | 29 | 62 | Asia |
| China | 163 | 15.57% | 112 | 3355 | 20.58 | 29.96 | 32 | 55 | Asia |
| Italy | 82 | 7.83% | 61 | 2181 | 26.60 | 35.75 | 20 | 46 | Europe |
| United States | 79 | 7.55% | 65 | 3827 | 48.44 | 58.88 | 25 | 61 | North America |
| United Kingdom | 71 | 6.78% | 56 | 3052 | 42.99 | 54.50 | 23 | 55 | Europe |
| Australia | 42 | 4.01% | 31 | 728 | 17.33 | 23.48 | 13 | 26 | Oceania |
| Pakistan | 29 | 2.77% | 25 | 744 | 25.66 | 29.76 | 13 | 25 | Asia |
| Saudi Arabia | 29 | 2.77% | 24 | 669 | 23.07 | 27.88 | 11 | 24 | Asia |
| Turkey | 29 | 2.77% | 24 | 560 | 19.31 | 23.33 | 12 | 23 | Europe |
| Malaysia | 27 | 2.58% | 20 | 284 | 10.52 | 14.20 | 7 | 16 | Asia |
| Germany | 24 | 2.29% | 16 | 200 | 8.33 | 12.50 | 8 | 14 | Europe |
| South Korea | 24 | 2.29% | 20 | 615 | 25.63 | 30.75 | 13 | 20 | Asia |
| Spain | 21 | 2.01% | 17 | 475 | 22.62 | 27.94 | 11 | 17 | Europe |
| Canada | 19 | 1.81% | 16 | 746 | 39.26 | 46.63 | 9 | 16 | North America |
| France | 19 | 1.81% | 16 | 664 | 34.95 | 41.50 | 11 | 16 | Europe |

Notes: TP = total number of publications; NCP = number of cited publications; TC = total citations; C/P = average citations per publication; C/CP = average citations per cited publication; h = h-index; g = g-index

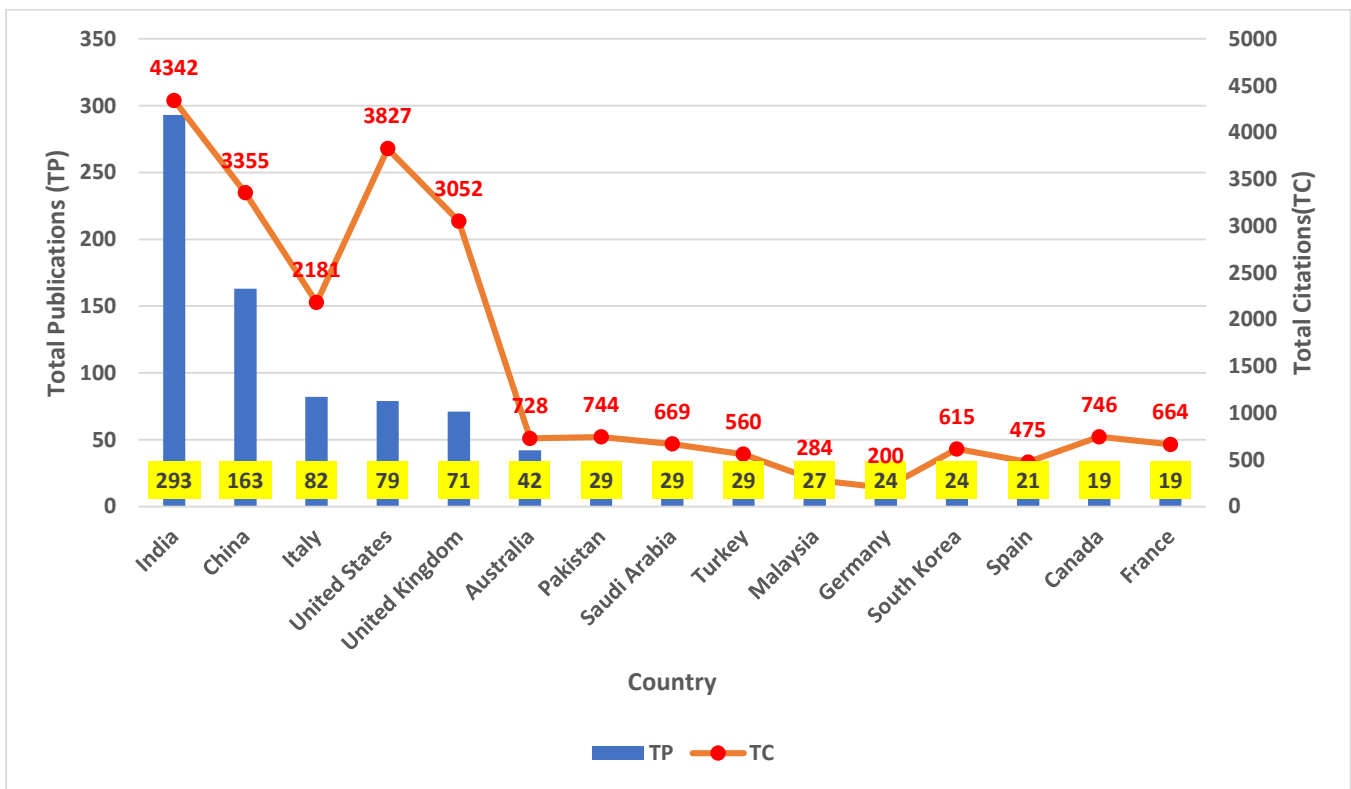


Fig. 8. Top 15 publication by country.

The national associations of the remaining authors, which included Pakistan, Saudi Arabia, Turkey, Malaysia, Germany, South Korea, and Spain, accounted for fewer than 30 articles dispersed across the globe. The countries with the fewest contributors are Canada and France, with 1.81% of total publications. It appears that agri-food and blockchain are of the utmost importance in Asia, Europe, North America, and Oceania. In terms of citation counts, Fig. 8 shows India maintains its position as the leader of all countries, showing a significant influence on the output of research with the highest total citations. With 3827 citations, the United States demonstrates its dominance in North America and has taken second place, beating China with 3355 citations. The significance of the United Kingdom in research activities is evident in the 3052 citations compared to other countries in Europe, including Italy, Germany, Turkey, Spain, and France. Despite having relatively few publications, Australia has made significant contributions to the global research community in terms of citations ($n = 728$). The total citation metrics offer valuable insights regarding the recognition and influence of research output in each respective country.

2) *The most active institutions:* Table IV depicts prominent institutions in the field of agri-food and blockchain research, including the SRM Institute of Science and Technology, Beijing Technology and Business University, Queensland University of Technology, Università degli Studi di Cagliari, and Presidency University Bangalore. The SRM Institute of Science and Technology in India is the leading institution in terms of total publications, with a total of 20

publications, which is the highest count. This signifies substantial research output by the institution. Beijing Technology and Business University Beijing Institute of Technology, both based in China, have made significant contributions to agri-food and blockchain research. Beijing Technology and Business University ranks second with 11 publications, while Beijing Institute of Technology ranks sixth with 8 publications. However, the National Institute of Industrial Engineering has a significant C/CP of 163.88, indicating a strong influence with the highest citation. The second rank for citation is the Hong Kong Polytechnic University, followed by the Università degli Studi di Cagliari, the Wageningen University and Research, and the Università della Calabria. In contrast, SRM Institute of Science and Technology has a notable average C/CP of 3.50. Most of the institutions that were evaluated are located in India, with SRM Institute of Science and Technology, Presidency University Bangalore, National Institute of Industrial Engineering, Lovely Professional University, University of Petroleum and Energy Studies, and Vellore Institute of Technology being notable contributors. This highlights the significance of India's leadership in agricultural and blockchain-based research. In addition, the result demonstrates a worldwide distribution of institutions, encompassing China, India, Italy, Australia, Viet Nam, the Netherlands, and the United Kingdom. This diversity shows the global extent of the research field.

TABLE IV. THE MOST ACTIVE INSTITUTIONS

| Institution | TP | % | Country | NCP | TC | C/P | C/CP | h | g |
|--|----|-------|----------------|-----|------|--------|--------|---|---|
| SRM Institute of Science and Technology | 20 | 1.91% | India | 8 | 28 | 1.40 | 3.50 | 3 | 5 |
| Beijing Technology and Business University | 11 | 1.05% | China | 7 | 226 | 20.55 | 32.29 | 5 | 7 |
| Queensland University of Technology | 9 | 0.86% | Australia | 8 | 179 | 19.89 | 22.38 | 5 | 8 |
| Università degli Studi di Cagliari | 9 | 0.86% | Italy | 9 | 465 | 51.67 | 51.67 | 8 | 9 |
| Presidency University Bangalore | 9 | 0.86% | India | 4 | 53 | 5.89 | 13.25 | 4 | 4 |
| Beijing Institute of Technology | 8 | 0.76% | China | 8 | 107 | 13.38 | 13.38 | 4 | 8 |
| Università della Calabria | 8 | 0.76% | Italy | 7 | 296 | 37.00 | 42.29 | 5 | 7 |
| National Institute of Industrial Engineering | 8 | 0.76% | India | 8 | 1311 | 163.88 | 163.88 | 7 | 8 |
| Lovely Professional University | 8 | 0.76% | India | 6 | 186 | 23.25 | 31.00 | 4 | 6 |
| University of Petroleum and Energy Studies | 8 | 0.76% | India | 6 | 46 | 5.75 | 7.67 | 4 | 6 |
| The Hong Kong Polytechnic University | 7 | 0.67% | China | 6 | 975 | 139.29 | 162.50 | 5 | 6 |
| Vellore Institute of Technology | 7 | 0.67% | India | 6 | 63 | 9.00 | 10.50 | 3 | 6 |
| RMIT University | 7 | 0.67% | Viet Nam | 2 | 5 | 0.71 | 2.50 | 2 | 2 |
| Wageningen University & Research | 6 | 0.57% | Netherlands | 5 | 365 | 60.83 | 73.00 | 4 | 5 |
| Cranfield University | 6 | 0.57% | United Kingdom | 5 | 126 | 21.00 | 25.20 | 5 | 5 |

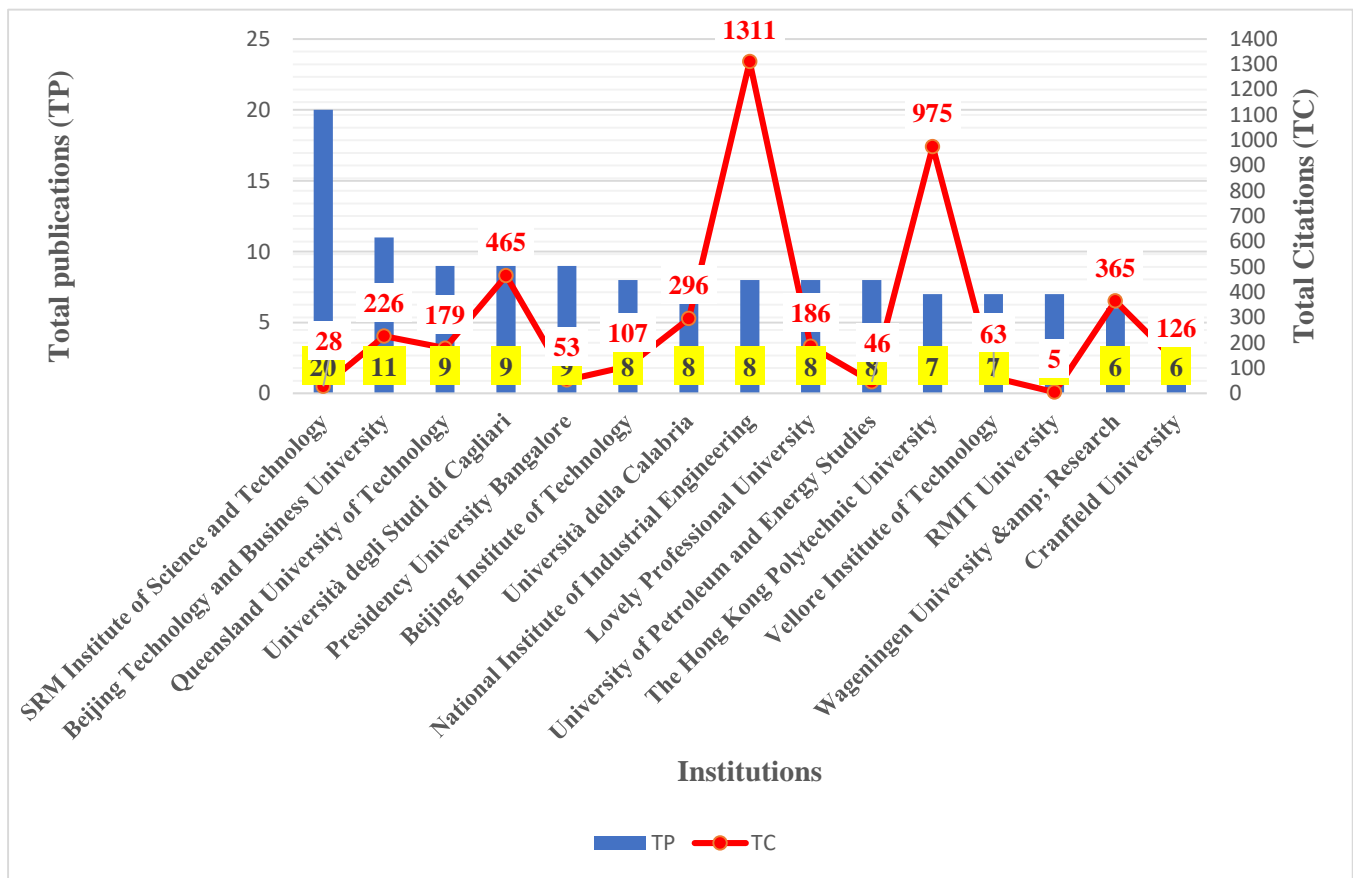


Fig. 9. The most active institution based on publication versus citation.

3) *Authorship analysis*: The analysis in Table V presents the total number of publications (TP) by different authors, highlighting their contributions to academic research. Xu, J and Zhang X are prominent contributors, each having seven publications. The authors Xu, J. and Zhang, X. from Beijing Technology and Business University in China have a collaborative impact (C/CP) of 26.50, which means that their articles are referenced an average of 26.50 times. This

indicates a substantial impact and acknowledgment of their combined academic efforts, highlighting the importance of collaborative research at the university. Marchesi, M., Mirabelli, G., Solina, V., and Tonelli, R. from Italy have achieved impressive average citations per publication (C/P) scores of 61.20, 51.40, 51.40, and 35.20, respectively. This highlights the significant research output produced by Italian affiliations. Table VI illustrates a wide-ranging geographical

influence, featuring authors originating from Australia, India, Italy, and China. Authors from various affiliations and nations exhibit a worldwide presence in research. Calculating the average number of citations per publication and per cited article offers valuable insights into the influence of an author's work. The h-index and g-index offer a comprehensive perspective on the academic impact of an author. This study used the VOSviewer software to conduct co-author analysis, enabling a thorough examination of authors' collaboration and generating a network visualization (see Fig. 10). The analysis relies on the premise that significant writers have been referenced at least once in five publications related to agri-food and blockchain. The calculation is performed using the fractional counting technique. Distinct attributes, such as color, size of circles, font size, and line width, enhance the intensity of the authors' association. Authors who are associated with one another are often listed one after the other, as seen by the use of the same color. The Fig. 10 indicates that the prominent authors Xu J. and Zhang X collaborated closely with other authors, including Li H., Zhao Z., and Xu J. Based on the result, it seems that Cao S and Foth M, both from Australia, have had a similarly effective collaboration with colleagues from China.

Fig. 11 presents a network visualization map of the author's associated country. The analysis only includes nations that have cited more than five articles and more than 1 citation. According to the fractional counting method, the results suggest that India has a substantial impact on international collaboration. India maintains strong diplomatic

ties with Ukraine and South Korea, while China has established connections with Hong Kong and Serbia.

Next section will highlight the third research question highlighted the most prevalent themes of agri-food and blockchain between scholars.

C. The Most Prevalent Themes of Agri-Food and Blockchain between Scholars

The fundamental objective of the third research question is to discover the predominant themes of blockchain in agri-food research among experts. This step involved analysing the important areas of the research based on (a) the frequency of keywords and (b) the titles and abstracts of the documents.

1) *Keywords analysis:* The careful selection of suitable keywords is crucial in finding the availability of a document during a search. Therefore, the regular selection of suitable keywords may serve as an indicator of the quality of the writing. A network visualization of the author's keywords, each of which appeared a minimum of three occurrences, is illustrated in Fig. 12. A co-occurrence of two keywords within the same article suggests that there is a connection between the two subjects [37]. In order to answer the third research questions, we utilized the keyword and co-occurrence analysis from VOSviewer. In order to map the keywords allocated to each article, the author's analyzed keywords utilizing VOSviewer, a software application designed for generating and visualizing bibliometric networks (see Fig. 12).

TABLE V. AUTHORSHIP ANALYSIS TOP 15

| Author Name | TP | % | Affiliation | Country | NCP | TC | C/P | C/CP | h | g |
|---------------|----|-------|--|-----------|-----|-----|-------|-------|---|---|
| Xu, J. | 7 | 0.67% | Beijing Technology and Business University, Beijing | China | 6 | 159 | 22.71 | 26.50 | 4 | 6 |
| Zhang, X. | 7 | 0.67% | Beijing Technology and Business University, Beijing | China | 6 | 159 | 22.71 | 26.50 | 4 | 6 |
| Cao, S. | 6 | 0.57% | The University of Queensland, Brisbane | Australia | 5 | 133 | 22.17 | 26.60 | 5 | 5 |
| Sun, C. | 6 | 0.57% | National Engineering Laboratory for Agri-product Quality Traceability, Beijing | China | 5 | 120 | 20.00 | 24.00 | 4 | 5 |
| Tanwar, S. | 6 | 0.57% | Nirma University, Institute of Technology, Ahmedabad | India | 5 | 107 | 17.83 | 21.40 | 5 | 5 |
| Wang, X. | 6 | 0.57% | Beijing Institute of Fashion Technology, Beijing | China | 5 | 153 | 25.50 | 30.60 | 4 | 5 |
| Ahamed, N.N. | 5 | 0.48% | Presidency University Bangalore, Bengaluru, | India | 3 | 34 | 6.80 | 11.33 | 3 | 3 |
| Foth, M. | 5 | 0.48% | Queensland University of Technology | Australia | 5 | 170 | 34.00 | 34.00 | 5 | 5 |
| Luo, N. | 5 | 0.48% | National Engineering Laboratory for Agri-product Quality Traceability, Beijing | China | 4 | 58 | 11.60 | 14.50 | 3 | 4 |
| Marchesi, M. | 5 | 0.48% | Università degli Studi di Cagliari | Italy | 5 | 306 | 61.20 | 61.20 | 5 | 5 |
| Mirabelli, G. | 5 | 0.48% | Università della Calabria, Rende | Italy | 5 | 257 | 51.40 | 51.40 | 4 | 5 |
| Solina, V. | 5 | 0.48% | Università della Calabria, Rende | Italy | 5 | 257 | 51.40 | 51.40 | 4 | 5 |
| Tonelli, R. | 5 | 0.48% | Università degli Studi di Cagliari | Italy | 5 | 176 | 35.20 | 35.20 | 5 | 5 |
| Vignesh, R. | 5 | 0.48% | Presidency University Bangalore, Bengaluru, | India | 2 | 26 | 5.20 | 13.00 | 2 | 2 |
| Zhao, Z. | 5 | 0.48% | Beijing Technology and Business University, Beijing | China | 5 | 153 | 30.60 | 30.60 | 4 | 5 |

Notes: TP = total number of publications; NCP = number of cited publications; TC = total citations; C/P = average citations per publication; C/CP = average citations per cited publication; h = h-index; g = g-index

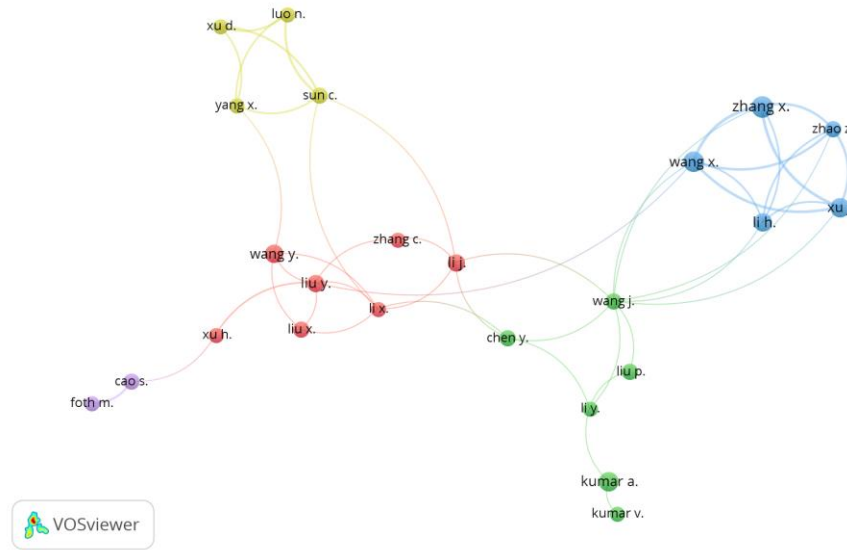


Fig. 10. Network visualisation map of the co-authorship based on author.

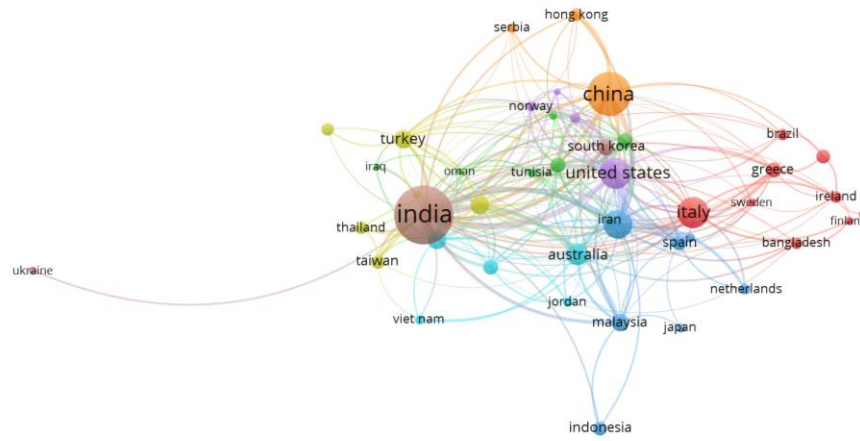


Fig. 11. Network visualisation map of the co-authorship based on countries.

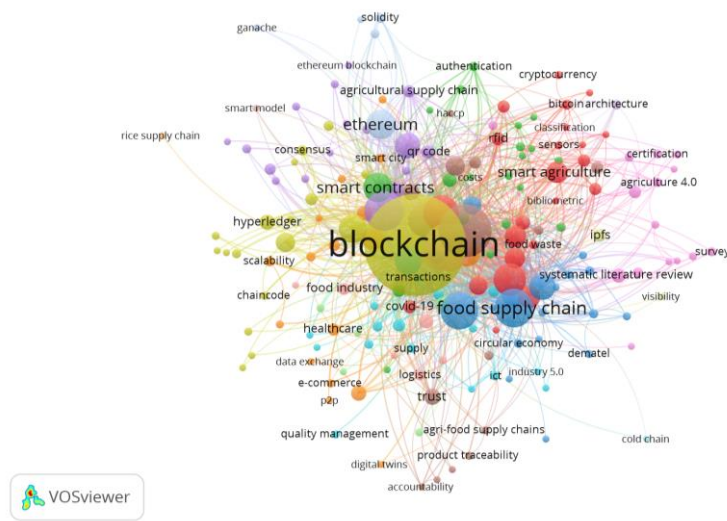


Fig. 12. Network visualisation map of the author keywords.

TABLE VI. TOP 20 KEYWORDS

| Keywords | Total Publications | % |
|-------------------------|--------------------|--------|
| Blockchain | 787 | 75.17% |
| Block-chain | 401 | 38.30% |
| Supply Chains | 353 | 33.72% |
| Food Supply | 331 | 31.61% |
| Internet Of Things | 194 | 18.53% |
| Food Supply Chain | 171 | 16.33% |
| Supply Chain Management | 169 | 16.14% |
| Traceability | 169 | 16.14% |
| Smart Contract | 150 | 14.33% |
| Food Safety | 138 | 13.18% |
| Supply Chain | 138 | 13.18% |
| Agriculture | 117 | 11.17% |
| Blockchain Technology | 87 | 8.31% |
| Digital Storage | 87 | 8.31% |
| Distributed Ledger | 87 | 8.31% |
| Traceability Systems | 85 | 8.12% |
| Transparency | 81 | 7.74% |
| IoT | 71 | 6.78% |
| Food-safety | 68 | 6.49% |
| Food Traceability | 65 | 6.21% |

The relationships between other keywords are represented by the thickness, colour, circle size, and font size of connecting lines [41]. Frequently categorized keywords in the same colour are frequently bundled together. The analysis revealed seventeen clusters containing 184 items based on the author's keyword. The diagram suggests that blockchain, blockchains, consensus, consortium blockchain, distributed ledgers, food chain, Hyperledger, Hyperledger fabric, permissioned blockchain, private blockchain supply chain management and supply chain traceability have similar colours, indicating that these keywords were closely related and usually occurred together. The search query included the following primary keywords: Blockchain, Block-chain, Supply Chains, Food Supply, Internet of Things, Food Supply Chain, Supply Chain Management, Traceability, Smart Contract, Food Safety, Supply Chain and Agriculture. These terms appear more than 10% of the time in the results. Table VI lists the twenty most common keywords used in agri-food and blockchain research.

2) *Title and abstract analysis:* In this section of the study, VOSviewer was employed to examine the titles and abstracts of collected documents for occurrences and the frequency of co-occurrences per document. Specifically, this study builds the co-occurrence network by employing the binary counting method. Fig. 13 depicts a graphical illustration of a network that shows the occurrence of terms based on their presence in the title and abstract fields. The network includes terms that appear at least 15 times. The width of the node represents the

weight of the item, while the thickness of the connecting line indicates the intensity of the link between items. When words that are connected in meaning are displayed in the same colour, there is a higher probability that they will occur together [37]. The terms safety, product, smart contract, transaction, storage, consumer, and food product, indicated in red, are interconnected and commonly coexist in the diagram. VOSviewer generates four separate colours based on the title and abstract of the publication, representing four clusters that consist of 246 terms.

Fig. 14 illustrates the arrangement of a title-based phrase co-occurrence network. A binary counting technique was employed, ensuring a minimum of ten occurrences for each phrase. The data suggests that the VOSviewer software creates four distinct clusters and a total of 27 items. Within the domain of agri-food and blockchain research, the term 'blockchain technology' gained the central position as the core node of the entire network. Cluster 1 contains the concepts of agri-food supply chain, block chain, blockchain application, food safety, food supply chain management, healthcare, impact, smart contract, and survey, whereas Cluster 2 consists of block chain technology, blockchain technology, case study, covid, design, food, implementation, and traceability system. Furthermore, Cluster 3 has artificial intelligence, food industry, food traceability, and smart agriculture and thing, whereas the last cluster, Cluster 4, only has internet, opportunity, and thing.

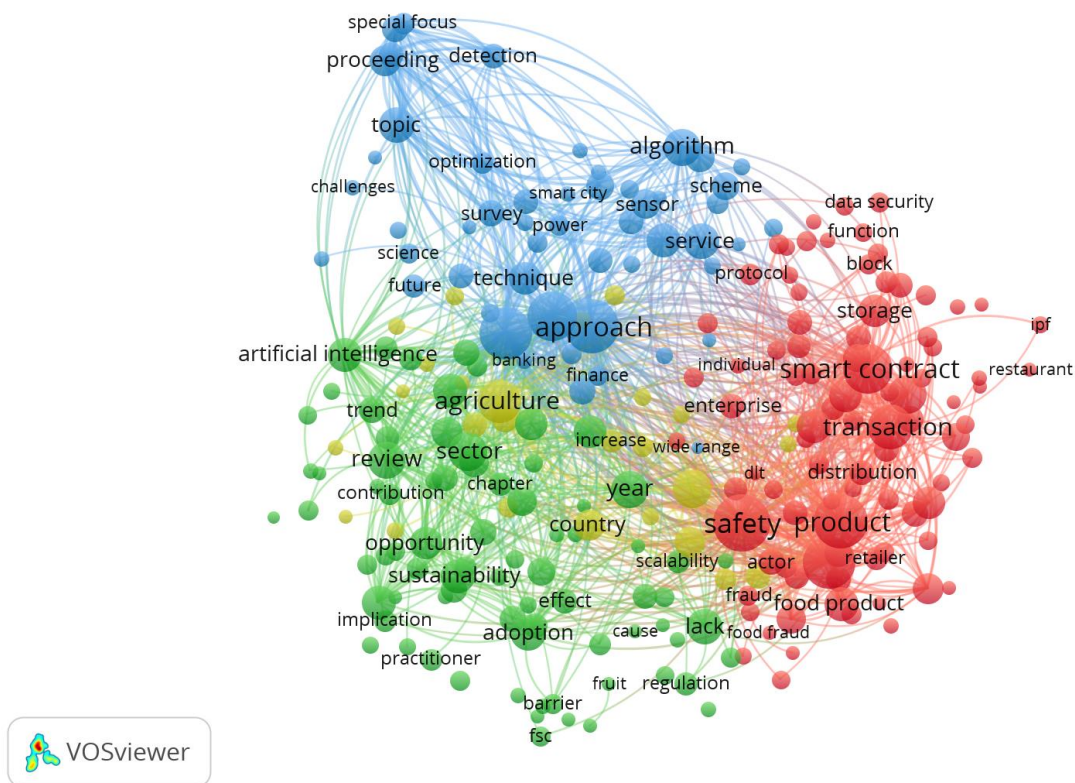


Fig. 13. VOSviewer visualisation of a term co-occurrence network based on title and abstract.

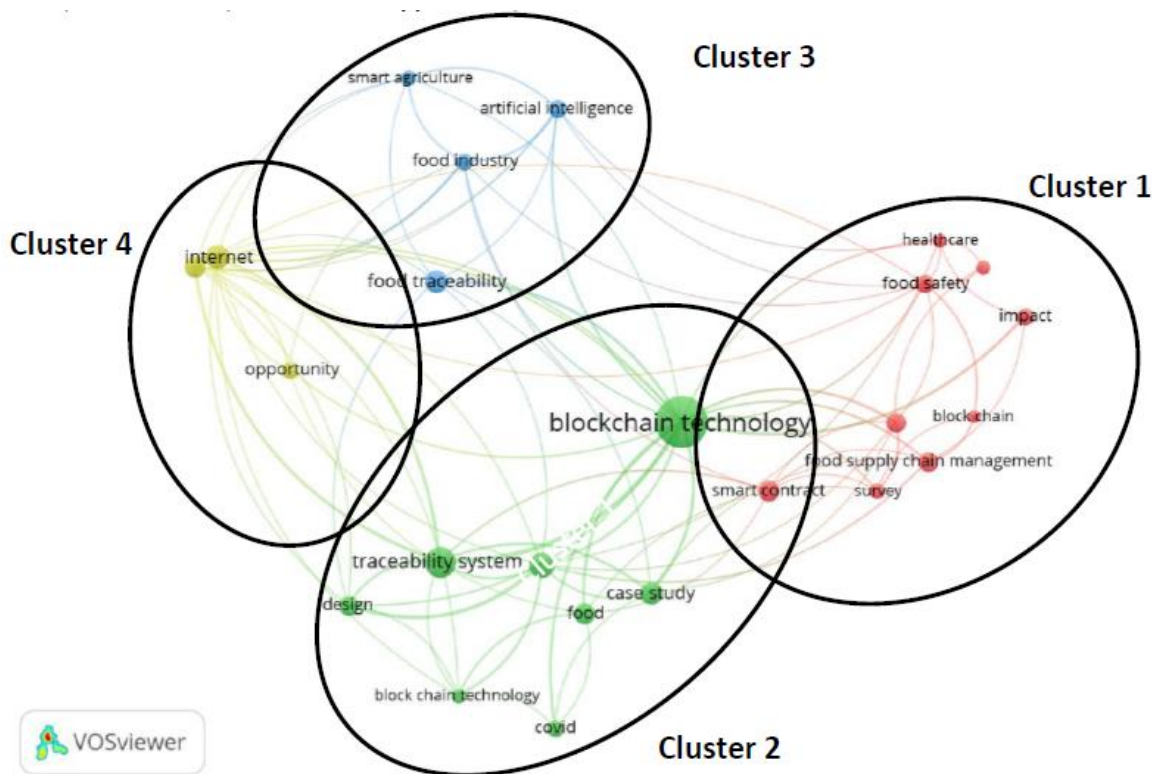


Fig. 14. VOSviewer visualisation of a term co-occurrence network based on title fields.

D. The Most Influential Articles on Agri-Food and Blockchain

This section examines the fourth research question, which is to discover the most influential articles on agri-food and blockchain through citation analysis.

1) *Citation analysis:* Table VII represents a compilation of research citations on agri-food and blockchain from the Scopus database. Over a span of nine years (2016–2024), a total of 19,105 citations were documented for 1,047 published papers. This corresponds to an average of 2,729.29 citations per year. Table VIII summarized the top 20 articles on blockchain in agri-food research, based on the frequency of citations for each document. The research article titled

"Blockchain-based traceability in agri-food supply chain management: A practical implementation," published in 2018 by M.P. Caro, M.S. Ali, M. Vecchio, and R. Giaffreda, has received the highest number of citations, with a total of 507. This article was presented at the 2018 IoT Vertical and Topical Summit on Agriculture in Tuscany, IOT Tuscany 2018. The second and third publications, published in 2021 and 2020, respectively, are research articles on blockchain technology in the supply chain. They were written by M. Kouhizadeh, S. Saberi, and J. Sarkis and have a total of 497 citations. The other publication, written by P. Dutta, T.-M. Choi, S. Somani, and R. Butala, has a total of 494 citations.

TABLE VII. CITATION METRICS

| Metrics | Data |
|---------------|---------|
| Papers | 1047 |
| Citations | 19105 |
| Years | 9 |
| Cites_Year | 2729.29 |
| Cites_Paper | 18.25 |
| Authors_Paper | 3.52 |
| h_index | 63 |
| g_index | 120 |

TABLE VIII. TOP CITED ARTICLES IN AGRI-FOOD AND BLOCKCHAIN RESEARCH

| Authors | Year | Title | Source | Cites | Cites/Year |
|--|------|---|---|-------|------------|
| M.P. Caro, M.S. Ali, M. Vecchio, R. Giaffreda | 2018 | Blockchain-based traceability in Agri-Food supply chain management: A practical implementation | 2018 IoT Vertical and Topical Summit on Agriculture - Tuscany, IOT Tuscany 2018 | 507 | 101.4 |
| M. Kouhizadeh, S. Saberi, J. Sarkis | 2021 | Blockchain technology and the sustainable supply chain: Theoretically exploring adoption barriers | International Journal of Production Economics | 497 | 248.5 |
| P. Dutta, T.-M. Choi, S. Somani, R. Butala | 2020 | Blockchain technology in supply chain operations: Applications, challenges and research opportunities | Transportation Research Part E: Logistics and Transportation Review | 494 | 164.67 |
| S.S. Kamble, A. Gunasekaran, R. Sharma | 2020 | Modeling the blockchain enabled traceability in agriculture supply chain | International Journal of Information Management | 471 | 157 |
| S.S. Kamble, A. Gunasekaran, S.A. Gawankar | 2020 | Achieving sustainable performance in a data-driven agriculture supply chain: A review for research and applications | International Journal of Production Economics | 431 | 143.67 |
| H. Feng, X. Wang, Y. Duan, J. Zhang, X. Zhang | 2020 | Applying blockchain technology to improve agri-food traceability: A review of development methods, benefits and challenges | Journal of Cleaner Production | 382 | 127.33 |
| K. Salah, N. Nizamuddin, R. Jayaraman, M. Omar | 2019 | Blockchain-Based Soybean Traceability in Agricultural Supply Chain | IEEE Access | 379 | 94.75 |
| K. Behnke, M.F.W.H.A. Janssen | 2020 | Boundary conditions for traceability in food supply chains using blockchain technology | International Journal of Information Management | 372 | 124 |
| G. Zhao, S. Liu, C. Lopez, H. Lu, S. Elgueta, H. Chen, B.M. Boshkoska | 2019 | Blockchain technology in agri-food value chain management: A synthesis of applications, challenges and future research directions | Computers in Industry | 371 | 92.75 |
| M. Lezoche, H. Panetto, J. Kacprzyk, J.E. Hernandez, M.M.E. Alemany Díaz | 2020 | Agri-food 4.0: A survey of the Supply Chains and Technologies for the Future Agriculture | Computers in Industry | 338 | 112.67 |
| G. Perboli, S. Musso, M. Rosano | 2018 | Blockchain in Logistics and Supply Chain: A Lean Approach for Designing | IEEE Access | 329 | 65.8 |

| | | Real-World Use Cases | | | |
|---|------|---|--|-----|--------|
| R. Sharma, S.S. Kamble, A. Gunasekaran, V. Kumar, A. Kumar | 2020 | A systematic literature review on machine learning applications for sustainable agriculture supply chain performance | Computers and Operations Research | 308 | 102.67 |
| D. Bumblauskas, A. Mann, B. Dugan, J. Rittmer | 2020 | A blockchain use case in food distribution: Do you know where your food has been? | International Journal of Information Management | 291 | 97 |
| A.A. Siyal, A.Z. Junejo, M. Zawish, K. Ahmed, A. Khalil, G. Soursou | 2019 | Applications of blockchain technology in medicine and healthcare: Challenges and future perspectives | Cryptography | 263 | 65.75 |
| Y. Liu, X. Ma, L. Shu, G.P. Hancke, A.M. Abu-Mahfouz | 2021 | From Industry 4.0 to Agriculture 4.0: Current Status, Enabling Technologies, and Research Challenges | IEEE Transactions on Industrial Informatics | 254 | 127 |
| L. Klerkx, D. Rose | 2020 | Dealing with the game-changing technologies of Agriculture 4.0: How do we manage diversity and responsibility in food system transition pathways? | Global Food Security | 252 | 84 |
| D. Tse, B. Zhang, Y. Yang, C. Cheng, H. Mu | 2017 | Blockchain application in food supply information security | IEEE International Conference on Industrial Engineering and Engineering Management | 235 | 39.17 |
| Q. Lin, H. Wang, X. Pei, J. Wang | 2019 | Food Safety Traceability System Based on Blockchain and EPCIS | IEEE Access | 230 | 57.5 |
| A. Khatoun | 2020 | A blockchain-based smart contract system for healthcare management | Electronics (Switzerland) | 220 | 73.33 |
| S. Mondal, K.P. Wijewardena, S. Karuppuswami, N. Kriti, D. Kumar, P. Chahal | 2019 | Blockchain inspired RFID-based information architecture for food supply chain | IEEE Internet of Things Journal | 217 | 54.25 |

V. DISCUSSIONS

In this section, we shall discuss the findings of our bibliometric review to address the research questions outlined below.

A. RQ1. What is the Current Trend and Impact of Publication in Agri-Food and Blockchain?

Sugandh, Nigam, Misra and Khari conducted the current bibliometric analysis of the literature's influence on agri-food and blockchain research [42]. They used literature search tools to examine the years 2014 through 2022, as retrieved from ACM, IEEE Xplore, PubMed, the Web of Science, and Scopus. According to the study, publications on this topic began in 2018 and continued to increase from that point forward. However, without time constraints in search criteria, our study found that the first paper on agri-food and blockchain research was published in 2016 and has kept increasing until now. In 2017, the average number of citations per publication peaked at 87.00, demonstrating that publications have a substantial impact. This indicates a rise in research activities or a concentration on sharing research results. Additional inquiry may uncover patterns or advancements. In term of citation pattern, it demonstrates the increasing as well with domination in 2020

Agri-food blockchain research relies heavily on journals, which constitute 39.54% of all published works in this field. Scholarly journals are esteemed for their meticulous peer review procedure and reputation for reliability. Conference proceedings, comprising 36.20% of the total, also function as a medium for disseminating progress in the area. Nevertheless, the agri-food blockchain research environment shows a lower prevalence of book series, books, and trade journals, indicating the importance of real-time discussions and exchange of ideas. Conference papers are the primary focus of agri-food and blockchain research, making for 42.22% of all

papers published. These papers serve as a medium for scholars to share and encourage cutting-edge developments while facilitating direct discussions. Articles make a substantial contribution, representing 34.38% of the overall publications. The presence of many document formats, such as book chapters, conference reviews, and reviews, indicates a comprehensive approach for sharing knowledge. Nevertheless, when compared to conference papers and articles, book publishing, notes, editorials, errata, and short surveys have a comparatively insignificant impact.

English is the predominant language used in scholarly papers related to the agri-food and blockchain fields, representing 98.09% of all articles. This demonstrates the worldwide significance of English as the predominant language for academic discourse. The inclusion of Chinese, German, Polish, and Spanish languages, while in smaller proportions, highlights the diversity of participants and readers in this field. Researchers and policymakers should recognize the linguistic variety present in scholarly publications, as acknowledging and studying literature in different languages can offer complementary perspective and understandings.

The publication titled "Sustainability Switzerland" from MDPI is the most active source in the topic, with 42 publications and a high Cite Score of 5.8. The journal "Lecture Notes in Networks and Systems" published by Springer Nature has a notable Cite Score and SJR of 0.151. Springer Nature takes several positions inside the top 20, demonstrating its strong presence. Meanwhile, MDPI highlights the influence of open-access publishing. IEEE Access has a substantial overall citation count; however, Journal of Cleaner Production has an impressive CiteScore of 18.5 and SNIP of 2.379. Despite being discontinued in Scopus, Advances in Intelligent Systems and Computing continues to have influence. The inclusion of other source types, such as Ceur Workshop Proceedings, Sensors, Applied Sciences Switzerland, enriches the field.

Given the consistent growth in the number of publications since 2018, it is evident that research on the implementation of blockchain technology in agriculture is currently a popular and rapidly increasing field. Indeed, there has been a steady increase in the quantity of publications until now.

B. RQ2. Which are the Most Productive and Influential Countries, Institutions and Authors on Agri-Food and Blockchain?

According to Sugandh, Nigam, Misra and Khari, China has become the leader in agri-food and blockchain research [42]. However, our findings show that India has become the top contributor to publications, with India accounting for 293 articles compared to China, which accounts for 163 articles. Despite having a smaller number of publications compared to India and China, The United States has a notable citation effect, with a C/CP value of 48.44, suggesting a significant amount of influence. Italy, the United Kingdom, Germany, Spain, and France, among other European countries, provide substantial contributions, demonstrating a strong research environment.

The substantial number of publications in India is indicative of a flourishing research environment, which is supported by increased funding, collaboration, and the exploration of diverse research fields. This phenomenon offers prospects for global cooperation and the exchange of insights between Indian scholars and researchers. The cumulative representation of Asian countries (India, China, Pakistan, Saudi Arabia, Malaysia, South Korea) in publications highlights the growing impact of the region in multidisciplinary research.

The National Institute of Industrial Engineering in India, along with other esteemed institutions such as SRM Institute of Science and Technology, Presidency University Bangalore, and Lovely Professional University, has a substantial influence on the academic community. The institute's 8 publications and average citation of 163.88 demonstrate a substantial influence on research quality and visibility. This can be linked to the organization's emphasis on research areas that have a significant impact and the implementation of effective mechanisms for collaboration. These findings also indicate that India are leading in this topic nowadays. Additionally, both Beijing Technology and Business University and Beijing Institute of Technology demonstrate a significant average number of citations per article, suggesting a noteworthy influence in their respective areas of research. Table IV and Fig. table

9 presents a comprehensive overview of the worldwide distribution of active contributors to scholarly production, emphasizing the global nature of research collaboration and the significant role played by different countries in shaping the academic landscape. This analysis highlights the importance of institutions in India and China, suggesting these regions as key areas of focus for scholars interested in this topic. There are opportunities for cross-continental collaboration and knowledge sharing, which promotes a global research environment.

The research community is mostly influenced by two authors who possess identical publication records, suggesting potential constraints in collaboration. The analysis includes authors from varied locations like China, Australia, India, and Italy, exhibiting global collaboration in the field of study. The presence of many perspectives enhances the research environment and facilitates a more comprehensive comprehension of the topic. Italian authors, such as Marchesi, Mirabelli, Solina, and Tonelli, have a significant influence on the academic community, as seen by their high average citation metrics. Promoting collaboration among different institutions and locations has the potential to enrich the research output by incorporating different perspectives.

C. RQ3. Which are the Most Prevalent Themes of Agri-Food and Blockchain between Scholars?

The term "Blockchain" and its related forms (Block-chain, Blockchain Technology, Distributed Ledger) are prominently used, highlighting the significant emphasis on blockchain in agri-food research. This highlights the crucial role of technology in influencing progress in the field. The extensive prevalence of blockchain-related terminology indicates a significant scholarly interest and recognition of the revolutionary potential of blockchain technology in agri-food systems. Researchers and practitioners are actively investigating different facets, ranging from supply chain management to traceability and smart contracts.

The presence of "Internet of Things (IoT)" in the list of prominent keywords signifies the increasing practice of combining IoT with blockchain technology in agricultural and food systems. This combination is expected to effectively resolve concerns pertaining to traceability, transparency, and real-time monitoring. The terms "Food Safety," "Traceability," and "Food Traceability" are clearly highlighted, highlighting a significant issue within the agri-food sector. This indicates a deliberate and focused attempt to improve food safety measures and establish strong traceability mechanisms.

The research highlights the combination of technology, specifically blockchain, with traditional agricultural techniques, as seen by the use of keywords such as "Agriculture".

D. RQ4. Which are the Most Influential Articles on Agri-Food and Blockchain?

The most-cited articles in the field of agri-food research contain an extensive range of perspectives and implementations of blockchain technology. Traceability, sustainability, supply chain operations, and the intersection of blockchain technology and emerging technologies such as Industry 4.0 are among the topics covered.

The substantial number of references to these articles demonstrates the importance of blockchain technology in addressing many different kinds of obstacles in the agri-food sector. Scholars and industry professionals are presently engaged in an intensive investigation of the theoretical underpinnings, barriers to adoption, and greater impact of blockchain technology on sustainability, in addition to its practical applications in supply chain traceability.

The articles on traceability, such as "Blockchain-based traceability in agri-food supply chain management" and "Modelling blockchain-enabled traceability in agriculture supply chain," highlight the industry's interest in enhancing traceability in the agri-food supply chain. They also explore the potential of blockchain technology in achieving sustainable practices in a data-driven agriculture supply chain based on articles "Blockchain technology and the sustainable supply chain" and "Achieving sustainable performance in a data-driven agriculture supply chain." The articles "From Industry 4.0 to Agriculture 4.0" and "Blockchain-inspired RFID-based information architecture for food supply chain" demonstrate the integration of blockchain with other technologies in an interdisciplinary manner.

E. Implications of Study, Limitation and Future Recommendation

This study aims to examine the current direction and pattern of research on agri-food and blockchain by assessing the publication status, citation patterns, thematic content, and providing recommendations for future research in this field. The present study offers a thorough overview of recent research on blockchain in the agri-food sector, including growing trends in publications, journal performance, collaboration patterns, and research elements. This study contributes to a better understanding of the subject matter. Every sign indicates growth in this area of study, potentially resulting in new opportunities for enhancing global food systems. Furthermore, their contributions will assist novice academics in acquiring a comprehensive outlook on this particular domain [43]. This study uses the bibliometric technique to improve academics' understanding of the literature on blockchain technology application in the agri-food sector because bibliometric analyses remain a vital tool for identifying gaps in any given subject or field [40]. Therefore, researchers might employ this methodology to carry out their investigations, particularly when performing comprehensive examinations of relevant material pertaining to their area of focus.

The results of this study will support particular researchers in comprehending the ability of blockchain, IoT, and other emerging technologies to improve traceability, sustainability, and supply chain operations in the agri-food industry. Additionally, it will provide ideas for future research. Due to its widespread adoption in the global agri-food sector, we expect the application of blockchain to remain significant in the future. It is particularly popular in Asian countries like India, China, Pakistan, Saudi Arabia, and Malaysia, where there is active production of blockchain in agri-food publications. This indicates that its popularity is increasing and its global utilisation is on the rise. Although the assessment has garnered significant interest, the authors have given comparatively less consideration to its use in domains beyond food traceability. The deployment of blockchain technology (BCT) requires further investigation to explore governance frameworks, assess the sustainability and environmental impact of BCT in agriculture, understand user adoption and acceptance, and integrate BCT with advanced technologies like the Internet of Things (IoT) and artificial intelligence (AI) [42]. These paths of research will enhance

our understanding of BCT's capacity in both the food and agriculture sectors. Consequently, these areas demand greater attention from other academics and practitioners, which will facilitate the development of further research.

The study is based on a bibliometric analysis of published agri-food and blockchain research from 2016 to 2024. However, it's crucial to acknowledge that this analysis informs the discussion, which is subject to certain limitations. The study restricts its scope to the Scopus database and concentrates on the frequently used keywords in document titles and abstracts in the field of computer science and engineering. This study did not consider more comprehensive databases, such as Web of Science, Google Scholar, and EBSCO Hosts, which provide substantial coverage of the use of blockchain in the agri-food sector. Thus, it has the potential to limit the overall influence of the publication patterns on the subject of the study. In future studies, researchers can use diverse databases to perform searches, modify and compare the outcomes of distinct keyword terms, and examine variations in agri-food and blockchain research across different thematic domains. In addition, researchers can utilise bibliographic coupling analysis to quantify document similarity and identify earlier research that is pertinent to their current research. Besides that, the future direction in agri-food and blockchain study needs to comply with sustainability concept to sustain production and meet the demand for food. At this point, utilizing blockchain technology in agricultural and food research has the potential to yield significant and meaningful outcomes.

VI. CONCLUSIONS

We conducted a bibliometric analysis of the Scopus database's literature on agri-food and blockchain research, focusing on 1047 articles in the field of computer science and engineering. This study revealed a significant increase in publications since 2016, with the first paper published in 2016. Notably, there is a strong emphasis on utilising journals and conference proceedings to share research developments. English became the dominant language for research papers on this topic, indicating its worldwide importance. We recognized India and China as the primary contributors to papers, with India demonstrating a thriving research culture and a substantial impact on worldwide collaboration. The widespread use of blockchain-related terms, such as "blockchain" and "distributed ledger," highlights the significant academic interest in the transformative capabilities of blockchain technology in agri-food systems. The publications that have the most impact on this topic encompass a variety of viewpoints and applications of blockchain technology, with a particular focus on its significance in addressing numerous challenges in the agri-food industry. The increasing presence of Asian countries in academic papers exemplifies the region's growing influence in a variety of research fields. The National Institute of Industrial Engineering in India, in conjunction with other institutes, has a significant impact on the quality and prominence of research. Two writers with similar publication records primarily influence the research community. However, the inclusion of multiple perspectives enriches the research environment and enables a more thorough comprehension of

the subject matter. Researchers and practitioners are increasingly focusing on blockchain technology in agri-food research due to its potential in supply chain management, traceability, and smart contracts. Researchers are currently investigating the integration of the Internet of Things (IoT) and blockchain technology to tackle issues related to traceability, transparency, and real-time monitoring. The research also focuses on enhancing food safety procedures and establishing robust traceability tools to solve challenges related to safety and traceability. The research underscores the use of blockchain technology in conventional agricultural practices, emphasising the significance of agri-food in a sustainable and effective manner.

REFERENCES

- [1] World Health Organization, 'Food safety', Fact Sheets. Accessed: Apr. 20, 2024. [Online]. Available: <https://www.who.int/news-room/fact-sheets/detail/food-safety>
- [2] S. Deekonda, 'Agri-Food Supply Chains from Circular Economy Perspective', in Y. & Ramakrishna, Handbook of Research on Designing Sustainable Supply Chains to Achieve a Circular Economy, 2023, pp. 286–305.
- [3] A. Mohammed, V. Potdar, and M. Quaddus, 'Exploring Factors and Impact of Blockchain Technology in the Food Supply Chains: An Exploratory Study', Foods, vol. 12, no. 10, p. 2052, May 2023, doi: 10.3390/foods12102052.
- [4] R. Granillo-Macías, I. J. González-Hernández, and E. Olivares-Benitez, 'Blockchain for Agri-Food Supply Chain Traceability'.
- [5] T. Bhatt, G. Buckley, J. C. McEntire, P. Lothian, B. Sterling, and C. Hickey, 'Making Traceability Work across the Entire Food Supply Chain', J Food Sci, vol. 78, no. s2, Dec. 2013, doi: 10.1111/1750-3841.12278.
- [6] H. Xiong, T. Dalhaus, P. Wang, and J. Huang, 'Blockchain Technology for Agriculture: Applications and Rationale', Frontiers in Blockchain, vol. 3, Feb. 2020, doi: 10.3389/fbloc.2020.00007.
- [7] M. Krstić, G. P. Agnusdei, S. Tadić, and P. P. Miglietta, 'Prioritization of e-traceability drivers in the agri-food supply chains', Agricultural and Food Economics, vol. 11, no. 1, p. 42, Oct. 2023, doi: 10.1186/s40100-023-00284-5.
- [8] G. M. Hastig and M. S. Sodhi, 'Blockchain for Supply Chain Traceability: Business Requirements and Critical Success Factors', Prod Oper Manag, vol. 29, no. 4, pp. 935–954, Apr. 2020, doi: 10.1111/poms.13147.
- [9] F. Casino et al., 'Blockchain-based food supply chain traceability: a case study in the dairy sector', Int J Prod Res, vol. 59, no. 19, pp. 5758–5770, Oct. 2021, doi: 10.1080/00207543.2020.1789238.
- [10] W. A. H. Ahmed and B. L. MacCarthy, 'Blockchain-Enabled Supply Chain Traceability in the Textile and Apparel Supply Chain: A Case Study of the Fiber Producer, Lenzing', Sustainability, vol. 13, no. 19, p. 10496, Sep. 2021, doi: 10.3390/su131910496.
- [11] G. Baralla, A. Pinna, R. Tonelli, M. Marchesi, and S. Ibba, 'Ensuring transparency and traceability of food local products: A blockchain application to a Smart Tourism Region', Concurr Comput, vol. 33, no. 1, Jan. 2021, doi: 10.1002/cpe.5857.
- [12] A. Marchese and O. Tomarchio, 'A Blockchain-Based System for Agri-Food Supply Chain Traceability Management', SN Comput Sci, vol. 3, no. 4, Jul. 2022, doi: 10.1007/s42979-022-01148-3.
- [13] S. S. Kamble, A. Gunasekaran, and R. Sharma, 'Modeling the blockchain enabled traceability in agriculture supply chain', Int J Inf Manage, vol. 52, Jun. 2020, doi: 10.1016/j.ijinfomgt.2019.05.023.
- [14] R. Ekawati, Y. Arkeman, S. -, and T. Candra, 'Proposed Design of White Sugar Industrial Supply Chain System based on Blockchain Technology', International Journal of Advanced Computer Science and Applications, vol. 12, no. 4, 2021, doi: 10.14569/IJACSA.2021.0120459.
- [15] M. Javaid, A. Haleem, R. Pratap Singh, S. Khan, and R. Suman, 'Blockchain technology applications for Industry 4.0: A literature-based review', Blockchain: Research and Applications, vol. 2, no. 4. Elsevier Ltd, Dec. 01, 2021. doi: 10.1016/j.bcr.2021.100027.
- [16] U. J. Munasinghe and M. N. Halgamuge, 'Supply chain traceability and counterfeit detection of COVID-19 vaccines using novel blockchain-based Vacleger system', Expert Syst Appl, vol. 228, Oct. 2023, doi: 10.1016/j.eswa.2023.120293.
- [17] S. T. Tasnim, M. A. Islam, R. J. Taifa, S. Mahbub, and M. R. Ahmmad Rashid, 'Agri-food Traceability Using Blockchain Technology to Ensure Value Chain Management and Fair Pricing in Bangladesh', in 2022 IEEE 8th World Forum on Internet of Things (WF-IoT), IEEE, Oct. 2022, pp. 1–6. doi: 10.1109/WF-IoT54382.2022.10152086.
- [18] Md. Akhtaruzzaman Khan, Md. Emran Hossain, A. Shahaab, and I. Khan, 'ShrimpChain: A blockchain-based transparent and traceable framework to enhance the export potentiality of Bangladeshi shrimp', Smart Agricultural Technology, vol. 2, p. 100041, Dec. 2022, doi: 10.1016/j.atech.2022.100041.
- [19] K. Salah, N. Nizamuddin, R. Jayaraman, and M. Omar, 'Blockchain-Based Soybean Traceability in Agricultural Supply Chain', IEEE Access, vol. 7, pp. 73295–73305, 2019, doi: 10.1109/ACCESS.2019.2918000.
- [20] A. K. Hadi and S. Salem, 'A proposed methodology to use a Blockchain in Supply Chain Traceability', in 4th International Iraqi Conference on Engineering Technology and Their Applications, IICETA 2021, Institute of Electrical and Electronics Engineers Inc., 2021, pp. 313–317. doi: 10.1109/IICETA51758.2021.9717543.
- [21] A. Sarfaraz, R. K. Chakraborty, and D. L. Essam, 'AccessChain: An access control framework to protect data access in blockchain enabled supply chain', Future Generation Computer Systems, vol. 148, 2023, doi: 10.1016/j.future.2023.06.009.
- [22] L. Wang et al., 'Smart Contract-Based Agricultural Food Supply Chain Traceability', IEEE Access, vol. 9, 2021, doi: 10.1109/ACCESS.2021.3050112.
- [23] J. Tan, S. B. Goyal, A. Singh Rajawat, T. Jan, N. Azizi, and M. Prasad, 'Anti-Counterfeiting and Traceability Consensus Algorithm Based on Weightage to Contributors in a Food Supply Chain of Industry 4.0', Sustainability (Switzerland), vol. 15, no. 10, 2023, doi: 10.3390/su15107855.
- [24] L. Yogarajan, M. Masukujjaman, M. H. Ali, N. Khalid, L. H. Osman, and S. S. Alam, 'Exploring the Hype of Blockchain Adoption in Agri-Food Supply Chain: A Systematic Literature Review', Agriculture (Switzerland), vol. 13, no. 6. MDPI, Jun. 01, 2023. doi: 10.3390/agriculture13061173.
- [25] T. L. Yap, R. Nayak, N. T. H. Vu, D. T. Bui, T. T. T. Pham, and D. W. E. Allen, 'Adopting blockchain-based traceability in the fruit supply chain in a developing economy: facilitators and barriers', Information Technology & People, Oct. 2023, doi: 10.1108/ITP-02-2023-0168.
- [26] U. J. Munasinghe and M. N. Halgamuge, 'Supply chain traceability and counterfeit detection of COVID-19 vaccines using novel blockchain-based Vacleger system', Expert Syst Appl, vol. 228, p. 120293, Oct. 2023, doi: 10.1016/j.eswa.2023.120293.
- [27] Z. Shahbazi and Y.-C. Byun, 'A Procedure for Tracing Supply Chains for Perishable Food Based on Blockchain, Machine Learning and Fuzzy Logic', Electronics (Basel), vol. 10, no. 1, p. 41, Dec. 2020, doi: 10.3390/electronics10010041.
- [28] J. Wang et al., 'Blockchain-Based Information Supervision Model for Rice Supply Chains', Comput Intell Neurosci, vol. 2022, pp. 1–17, Mar. 2022, doi: 10.1155/2022/2914571.
- [29] N. K. Jadav, T. Rathod, R. Gupta, S. Tanwar, N. Kumar, and A. Alkhatyat, 'Blockchain and artificial intelligence-empowered smart agriculture framework for maximizing human life expectancy', Computers and Electrical Engineering, vol. 105, p. 108486, Jan. 2023, doi: 10.1016/j.compeleceng.2022.108486.
- [30] A. Aldoubae, N. H. Hassan, and F. A. Rahim, 'A Systematic Review on Blockchain Scalability', International Journal of Advanced Computer Science and Applications, vol. 14, no. 9, pp. 774–784, 2023, doi: 10.14569/IJACSA.2023.0140981.

- [31] F. Tian, 'A Supply Chain Traceability System for Food Safety Based on HACCP, Blockchain & Internet of Things', in 2017 international conference on service systems and service management , 2017, pp. 1–6.
- [32] F. Tian, 'An agri-food supply chain traceability system for China based on RFID & blockchain technology', in 2016 13th International Conference on Service Systems and Service Management (ICSSSM), 2016.
- [33] M. P. Caro, M. S. Ali, M. Vecchio, and R. Giaffreda, 'Blockchain-based traceability in Agri-Food supply chain management: A practical implementation', in 2018 IoT Vertical and Topical Summit on Agriculture - Tuscany, IOT Tuscany 2018, Institute of Electrical and Electronics Engineers Inc., Jun. 2018, pp. 1–4. doi: 10.1109/IOT-TUSCANY.2018.8373021.
- [34] T. Surasak, N. Wattanavichean, C. Preuksakarn, and S. C.-H., 'Thai Agriculture Products Traceability System using Blockchain and Internet of Things', International Journal of Advanced Computer Science and Applications, vol. 10, no. 9, 2019, doi: 10.14569/IJACSA.2019.0100976.
- [35] J. F. Galvez, J. C. Mejuto, and J. Simal-Gandara, 'Future challenges on the use of blockchain for food traceability analysis', TrAC - Trends in Analytical Chemistry, vol. 107. Elsevier B.V., pp. 222–232, Oct. 01, 2018. doi: 10.1016/j.trac.2018.08.011.
- [36] Y. Gavel and L. Iselid, 'Web of Science and Scopus: a journal title overlap study', Online Information Review, vol. 32, no. 1, pp. 8–21, Feb. 2008, doi: 10.1108/14684520810865958.
- [37] A. Z. Mansour, A. Ahmi, O. M. J. Popoola, and A. Znaimat, 'Discovering the global landscape of fraud detection studies: a bibliometric review', J Financ Crime, vol. 29, no. 2, pp. 701–720, Mar. 2022, doi: 10.1108/JFC-03-2021-0052.
- [38] K. Petersen, R. Feldt, S. Mujtaba, and M. Mattsson, 'Systematic Mapping Studies in Software Engineering', in 12th International Conference on Evaluation and Assessment in Software Engineering, 2008, pp. 1–10. [Online]. Available: www.splc.net
- [39] N. Carmona-serrano, J. López-belmonte, J. L. Cuesta-gómez, and A. J. Moreno-guerrero, 'Documentary analysis of the scientific literature on autism and technology in web of science', Brain Sciences, vol. 10, no. 12. MDPI AG, pp. 1–20, Dec. 01, 2020. doi: 10.3390/brainsci10120985.
- [40] M. Yurtcu and C. O. Güzeller, 'Bibliometric analysis of articles on computerized adaptive testing', Participatory Educational Research, vol. 8, no. 4, pp. 426–438, Dec. 2021, doi: 10.17275/per.21.98.8.4.
- [41] R. Wahid, A. Ahmi, and A. S. A. F. Alam, 'Growth and Collaboration in Massive Open Online Courses: A Bibliometric Analysis', International Review of Research in Open and Distance Learning, vol. 21, no. 4, pp. 292–322, Nov. 2020, doi: 10.19173/IRRODL.V21I4.4693.
- [42] U. Sugandh, S. Nigam, S. Misra, and M. Khari, 'A Bibliometric Analysis of the Evolution of State-of-the-Art Blockchain Technology (BCT) in the Agrifood Sector from 2014 to 2022', Sensors, vol. 23, no. 14, Jul. 2023, doi: 10.3390/s23146278.
- [43] M. H. Ansari et al., 'Bibliometric Analysis of Food Supply Chain Transformation using Digital Technology', in Proceedings of 3rd IEEE International Conference on Computational Intelligence and Knowledge Economy, ICCIKE 2023, Institute of Electrical and Electronics Engineers Inc., 2023, pp. 376–380. doi: 10.1109/ICCIKE58312.2023.10131782.

A Robust Hybrid Convolutional Network for Tumor Classification Using Brain MRI Image Datasets

Satish Bansal¹, Rakesh S Jadon², Sanjay K. Gupta³

Department of Computer Science & Engineering, Alliance University, Bengaluru, India¹

Department of Computer Engineering, MITS, Gwalior, India²

SOS in Computer Science & Applications, Jiwaji University, Gwalior, India³

Abstract—Brain tumour detection is challenging for experts or doctors in the early stage. Many advanced techniques are used for the detection of different cancers and analysis using different medical images. Deep learning (DL) comes under artificial intelligence, which is used to analyse and characterisation medical image processing and also finds the classification of brain cancer. Magnetic Resonance Imaging (MRI) has become the keystone in brain cancer recognition and the fusion of advanced imaging methods with cutting-edge DL models has exposed great potential in enhancing accuracy. This research aims to develop an efficient hybrid CNN model by employing support vector machine (SVM) classifiers to advance the efficacy and stability of the projected convolutional neural network (CNN) model. Two distinct brain MRI image datasets (Dataset_MC and Dataset_BC) are binary and multi-classified using the suggested CNN and hybrid CNN-SVM (Support Vector Machine) models. The suggested CNN model employs fewer layers and parameters for feature extraction, while SVM functions as a classifier to preserve maximum accuracy in a shorter amount of time. The experiment result shows the evaluation of the projected CNN model with the SVM for the performance evaluation, in which CNN-SVM give the maximum accuracy on the test datasets at 99% (Dataset_BC) and 98% (Dataset_MC) as compared to other CNN models.

Keywords—CNN; SVM; MRI images; brain tumor; deep learning

I. INTRODUCTION

Cancer cells are abnormal cells that disturb or damage the normal life of the human body. These cells spread rapidly and infect the other cells in the human physique. The detection of these cells in the early stage increases the survival rate of human life. Doctors can find these cells but not in the early stage which decreases the mortality rates of humans. Advanced techniques have come like artificial intelligence which can be used in medical science or medical image processing (like MRI, CT X-ray etc) to detect, segment and classify any disease (brain cancer, lung cancer, oral cancer, bone fracture etc) in different parts of the human physique.

MRI plays a key part as compared to other imaging modalities due to the non-invasive characterization of brain tumors. It is the capability to provide complete images of the brain's anatomy, along with the distinct characteristics of different cancer types, that makes it an indispensable tool for clinicians. A traditional approach to brain tumor classification relied on histopathological analysis of tissue samples obtained through an invasive procedure. Though histopathology is still significant, it has problems such as patient risks and sampling

mistakes. These matters are addressed with MRI, which delivers a non-invasive, complete image of the entire brain, simplifying precise preoperative diagnosis and handling forecasting.

To discriminate and categorize many forms of brain cancer, including gliomas, meningiomas, and pituitary tumors, MRI is a crucial tool. When combined with sophisticated MRI methods, CNN enables more precise classification, enabling doctors to make up-to-date conclusions regarding patient supervision.

Brain cancer is a hazardous and irregularly fatal disease for which early and correct detection is important to actual action. By combining their individual advantages, convolutional neural networks and traditional MRI imaging can be used to distribute more correct classification.

Artificial intelligence (AI) methods have renovated medical imaging and significantly improved the detection of brain cancer. These methods, which are capable of large MRI image datasets, can identify complex patterns and features that recover the correctness of brain cancer classification. By using AI techniques in brain cancer discovery analysis, custom-made treatment options are developed and the diagnosis process is accelerated.

Current solutions are being accessible by the context-aware use of AI techniques in health care diagnosis. When utilizing MRI to diagnose brain tumors, it is necessary to conduct experimental work to detect the tumor, and classify it according to its grade, kind, and location. This approach has experimented with using a solo CNN model for brain cancer recognition on different datasets in the place of a different CNN model for the diverse classification task. Brain tumor identification and classification are possible with the CNN-based binary and multi-task classification system. However, most of the authors used different models for different classification systems.

II. RELATED WORK

The American Cancer Society estimates that as of 2021, 78,980 persons had acknowledged a brain cancer finding; of these, around 55 thousand were benign and 24 thousand were malignant [1]. Studies show that brain cancers are the foremost root of cancer worldwide [2].

Since various cells can cause different kinds of brain cancer, they are a diverse group. Essentially, lesions can be classified into binary categories: Primary lesions arise from inside the

central nervous system, but secondary lesions can spread to other portions of the body and become brain metastases. The leading causes of illness and death worldwide are cardiovascular and cerebrovascular disorders. These conditions, which have a bigger financial burden than infectious diseases and harm society, start in childhood and can strike unexpectedly in maturity.

Medical image analysis often uses a variety of techniques to produce descriptions of the soft muscle in the human body. Medical professionals employ MRI images among them. It's a non-invasive method for accurately analysing imaging data of brain cancer in humans to assess the health of the patient [3]. Because of the tissue distinction stabilization and picture excellence determination, it is extremely applicable. The biology, chemistry, physiology, and genetic details of any brain disorder can be obtained from MRI pictures [4].

Brain cancer is well-defined by the World Health Organization (WHO) and controls all parts of the human body. This classification was revised in 2016. Broadly speaking, abnormal growth of a subset of brain cells is referred to as brain cancer. These cancers expose the brain's tissue to shrinkage, which causes massive harm to the brain's neuronal network and impairs the brain's ability to function [5-8]. Like any other kind of cancer, brain cancer can be classified as benign and malignant. While other types of brain tumors typically depend on the affected location like meningioma, glioma, and pituitary.

Utilizing the latest developments in science technologies to recover the precision of brain cancer identification in computer vision applications, merging (fusing) the images obtained from numerous imagery modalities. Artificial Intelligence [9] can be combined with these imagery modes to create finding systems. These kinds of systems can support doctors in refining the accuracy of early cancer recognition. Brain tumors can now be classified and identified using a variety of artificial intelligence techniques, including CNNs, SVMs, and artificial neural networks (ANNs) [10].

Authors proposed a CNN model such as VGG-(16 and 19) and InceptionV3 with Aquila optimizer. They classified brain tumor detection with an accuracy of 98.95% for the VGG-19 but testing accuracy is not given on the test dataset for this VGG-19 model [11]. Other authors proposed a CNN model with a ResNet50 architecture for the detection of brain cancers and found a correctness percentage of 98% in the MRI dataset [12].

The pre-trained CNN models were presented by the authors for the categorization of brain cancer from MRI pictures. They applied augmentation and image preprocessing like normalisation and resized the image 256x256 on the image dataset then found the maximum accuracy 96% in the VGG-16 model as compared to ResNet-50 and Inception V3 [13].

The analysis of the preprocessing stages for MRI image data enhances the detection accuracy in brain disease prediction. To propose a CNN pre-trained model, Authors suggest a VGG-16 pre-trained model for the categorization of multi-grade cancers in brain images [14].

The authors proposed an Inception-ResnetV2 model with grey wolf optimization and achieved 99.98% accuracy for brain

tumor classification [15]. Another study done by authors proposes a CNN model with local constraints using a supervised k-nearest neighbour algorithm. They implemented two datasets for multi-class classification and found that CDLLC performed well as compared to other models VGG and GoogleNet [16].

A large number of academics looked into several algorithms for correctly and efficiently classifying brain tumors. Recently, DL methods have been extensively used to develop autonomous models that can speedily and efficiently detect brain cancer.

The authors conducted a study on brain tumor classification using four models S-CNN, InceptionV3, ResNet-50 and Xception on the two distinct brain image data sets. They trained data sets with or without principal component analysis and five-fold cross-validation. They found that Inception V3 and Xception models performed well as compared to S-CNN and ResNet-50 [17]. Another study was conducted by the authors for brain cancer classification using augmentation and transfer learning. The authors found an accuracy of 96.2% in the AlexNet model as related to the ResNet-50 and Inception-v3 models [18].

After the critical analysis from the literature review, existing models provide good accuracy on training data, but not for the test data. In this paper, design an optimal brain cancer detection model using a CNN approach to report the improvement of accuracy issues in the existing artificial diagnostic system, which classifies binary classification and also multi-classification on two different datasets using the single model.

III. OBJECTIVE

In the study, two main objectives are used for the detection of brain cancer:

- 1) First Focus on accuracy, mainly for testing datasets.
- 2) Second objective one CNN model is used for two different datasets for two different classifications.

IV. PROPOSED METHODOLOGY

The projected hybrid CNN model integrates the strengths of features learning from raw MRI images using convolutional layers with the interpretability and efficiency of traditional machine learning algorithms. The architecture consists of multiple convolutional, batch-normalization and max-polling layers for feature extraction, followed by densely connected layers and additional modules for specialized feature processing.

The proposed workflow, which utilizes two brain MRI image datasets: Database_MC and Database_BC. The projected CNN model incorporates common classification steps, including pre-processing, feature extraction, and classification. Various layer combinations, along with appropriate hyper-parameters, are used to progress a strong model that efficiently mitigates overfitting and bias in both datasets. By leveraging these techniques, the study aims to maintain the best classification accuracy while reducing computational requirements.

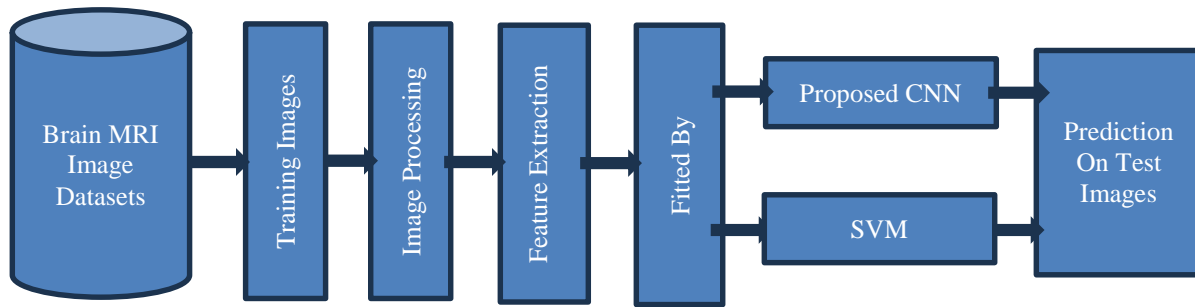


Fig. 1. Flow of proposed work.

The projected work is shown in Figure 1 for the classification.

The following steps are used in the algorithm to make the robust CNN and hybrid models classify the brain tumor MRI image datasets:

- 1) Collect the two datasets (Dataset_MC and Dataset_BC) of brain tumor MRI Grayscale Images from Kaggle
- 2) Apply image preprocessing like resize images (48x48) and normalize.
- 3) Encode all the images of the training and test dataset into labels (text to integers).
- 4) Extract feature using the proposed CNN model.
- 5) Train the model by applying the proposed CNN & hybrid CNN-SVM (Support Vector Machine) on the training dataset.
- 6) Classify the test dataset using the proposed CNN and CNN-SVM. Find the performance measures using the confusion matrix and classification report.

V. DATA COLLECTION

Brain MRI image datasets are downloaded from Kaggle. Dataset_MC [19] contains 7023 brain MRI images of four classes: glioma, meningioma, pituitary and nontumor, which is used in multi-classification. Dataset_BC [20] contains 3000 brain images of two classes yes (tumor) and no (notumor) for binary classification. The distribution of training and testing datasets for Dataset_MC and Dataset_BC respectively is shown in the following Table 1. Figures 2 and 3 show the different classes of Dataset_MC and Dataset_BC respectively of brain cancer on a different dataset. Dataset_MC is used for multi-classification while Dataset_BC is used for binary classification using the same model.

TABLE I. DISTRIBUTION OF TRAINING AND TESTING DATASET FOR DATASET_MC AND DATASET_BC

| Datasets | Training Dataset | Testing Dataset |
|-------------------|------------------|-----------------|
| Dataset_MC (7023) | 5712 | 1311 |
| Dataset_BC (3000) | 2400 | 600 |

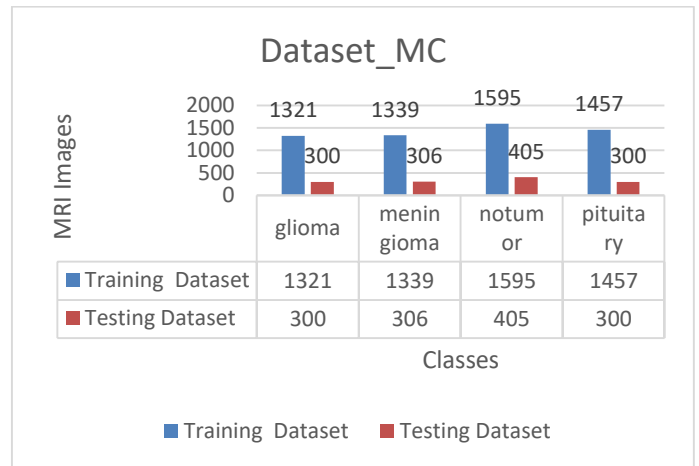


Fig. 2. The different classes of training and testing datasets in Dataset_MC.

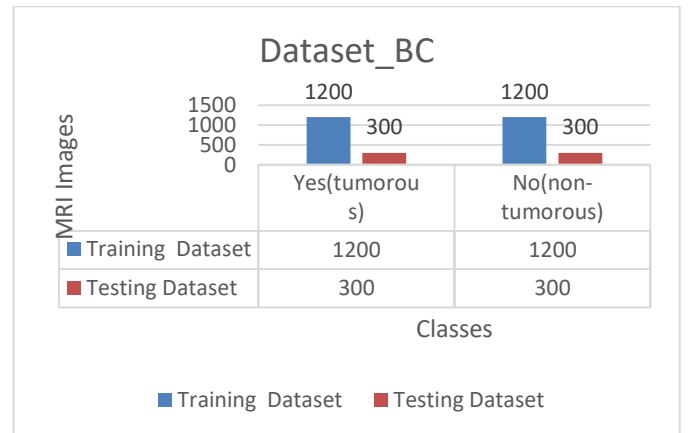


Fig. 3. The different classes of training and testing datasets in Dataset_BC.

VI. PROPOSED CNN MODEL

Figure 4 shows a common architecture of the projected model consisting of a few layers with minimum numbers of total parameters for Dataset_MC and Dataset_BC. The difference is only in the last dense layer where the left side uses 4 classes (multi-class) and the right side uses right side 2 classes (binary-class) in Dataset_MC and Dataset_BC respectively. It is very efficient because of high accuracy and computation time is very less. In the projected hybrid CNN-SVM model, CNN serves as an automatic feature extractor and SVM as a classifier.

| Layer (type) | Output Shape | Param # | Layer (type) | Output Shape | Param # |
|---|---------------------|---------|---|---------------------|---------|
| conv2d_input (InputLayer) | [(None, 48, 48, 3)] | 0 | conv2d_input (InputLayer) | [(None, 48, 48, 3)] | 0 |
| conv2d (Conv2D) | (None, 48, 48, 32) | 896 | conv2d (Conv2D) | (None, 48, 48, 32) | 896 |
| batch_normalization (Batch Normalization) | (None, 48, 48, 32) | 128 | batch_normalization (Batch Normalization) | (None, 48, 48, 32) | 128 |
| max_pooling2d (MaxPooling2D) | (None, 24, 24, 32) | 0 | max_pooling2d (MaxPooling2D) | (None, 24, 24, 32) | 0 |
| conv2d_1 (Conv2D) | (None, 24, 24, 64) | 18496 | conv2d_1 (Conv2D) | (None, 24, 24, 64) | 18496 |
| batch_normalization_1 (Batch Normalization) | (None, 24, 24, 64) | 256 | batch_normalization_1 (Batch Normalization) | (None, 24, 24, 64) | 256 |
| max_pooling2d_1 (MaxPooling2D) | (None, 12, 12, 64) | 0 | max_pooling2d_1 (MaxPooling2D) | (None, 12, 12, 64) | 0 |
| conv2d_2 (Conv2D) | (None, 12, 12, 128) | 73856 | conv2d_2 (Conv2D) | (None, 12, 12, 128) | 73856 |
| max_pooling2d_2 (MaxPooling2D) | (None, 6, 6, 128) | 0 | max_pooling2d_2 (MaxPooling2D) | (None, 6, 6, 128) | 0 |
| dropout (Dropout) | (None, 6, 6, 128) | 0 | dropout (Dropout) | (None, 6, 6, 128) | 0 |
| flatten (Flatten) | (None, 4608) | 0 | flatten (Flatten) | (None, 4608) | 0 |
| dense (Dense) | (None, 128) | 589952 | dense (Dense) | (None, 128) | 589952 |
| dense_1 (Dense) | (None, 4) | 516 | dense_1 (Dense) | (None, 2) | 258 |
| ----- | | | ----- | | |
| Total params: 684100 (2.61 MB) | | | Total params: 683842 (2.61 MB) | | |
| Trainable params: 683908 (2.61 MB) | | | Trainable params: 683650 (2.61 MB) | | |
| Non-trainable params: 192 (768.00 Byte) | | | Non-trainable params: 192 (768.00 Byte) | | |

Fig. 4. Architecture of projected CNN model in Dataset_MC and Dataset_BC.

The proposed deep-learning CNN model uses the following layers to make the robust model:

1) Convolutional layer: It uses a kernel size of 3x3 for feature extraction and is followed by relu function $F(x)=\text{Max}(0, x)$. To speed up the training process and convert the negative values to zero.

2) Batch-Normalization layer: It stabilizes the training process and also improves the optimization.

3) Max-polling layer: The 2x2 kernel size of this layer takes the maximum value from the patch of the input data and summarises these values into a features map. By using these it reduces the dimension.

4) Dropout layer: It is set to 0.1 means 10% of neurons drop out in each epoch to reduce over-fitting.

5) Flatten layer: This is the last layer for feature extraction, which converts each batch in the inputs to one dimension.

6) Dense layer: It receives output from every neuron of its preceding layer. In the proposed CNN, two dense layers are used. The first is sigmoid and the second is softmax activation function. The expression of sigmoid function $F(x) = 1/(1 + e^{-x})$, which transforms values between the range 0 to 1. The expression of the softmax function is $\sigma(z)_j = e^{z_j} / \sum_{k=1}^K e^{z_k}$ for $j = 1, 2, \dots, K$

It is like a combination of multiple sigmoid and is used for multi-class classification problems.

VII. EXPERIMENTAL RESULT AND DISCUSSION

The projected CNN model is executed in Jupyter Notebook under Anaconda in Python3 using an Intel Core i5 8th generation laptop.

For ultimate training of the image dataset, the proposed CNN model uses the following hyper-parameters as optimizers: root mean square propagation (RMSprop), learning_rate: 0.0009, and batch_size: 32.

The outcome of the projected CNN model is shown in Figures 5 and 6, which show the accuracy is 100% and 99.2% of the training dataset for Dataset_BC and Dataset_MC respectively in the 10 epochs.

The SVM classifier is applied to feature extraction generated by convolutional layers on the MRI dataset and compares the result through confusion matrix and classification reports. The exhibition of the hybrid CNN-SVM model is better than the standalone CNN architecture. The results show the superiority of the hybrid CNN-SVM in terms of accurateness, and efficiency. The best thing about this proposed model is that rapid and accurate classification of brain cancer can significantly impact treatment planning important to enhanced patient results.

The proposed CNN and hybrid CNN-SVM models were evaluated on the test dataset for Dataset_MC and Dataset_BC. The performance measures of the test dataset are shown by the confusion matrix. The confusion matrix of the projected CNN and hybrid CNN-SVM for Dataset_MC (Upper-Side) and Dataset_BC (Lower-Side) respectively are shown in Figure 7.

```
Epoch 1/10
75/75 [=====] - 15s 172ms/step - loss: 0.7333 - Accuracy: 0.7146 - val_loss: 0.7100 - val_Accuracy: 0.5217
Epoch 2/10
75/75 [=====] - 12s 160ms/step - loss: 0.3619 - Accuracy: 0.8396 - val_loss: 0.8003 - val_Accuracy: 0.5217
Epoch 3/10
75/75 [=====] - 12s 160ms/step - loss: 0.1905 - Accuracy: 0.9317 - val_loss: 0.7571 - val_Accuracy: 0.4850
Epoch 4/10
75/75 [=====] - 12s 158ms/step - loss: 0.0840 - Accuracy: 0.9742 - val_loss: 0.5120 - val_Accuracy: 0.7067
Epoch 5/10
75/75 [=====] - 12s 160ms/step - loss: 0.0474 - Accuracy: 0.9862 - val_loss: 0.3872 - val_Accuracy: 0.8300
Epoch 6/10
75/75 [=====] - 12s 160ms/step - loss: 0.0299 - Accuracy: 0.9917 - val_loss: 0.4658 - val_Accuracy: 0.8217
Epoch 7/10
75/75 [=====] - 12s 163ms/step - loss: 0.0194 - Accuracy: 0.9942 - val_loss: 0.1555 - val_Accuracy: 0.9500
Epoch 8/10
75/75 [=====] - 12s 161ms/step - loss: 0.0124 - Accuracy: 0.9967 - val_loss: 0.0918 - val_Accuracy: 0.9767
Epoch 9/10
75/75 [=====] - 12s 158ms/step - loss: 0.0280 - Accuracy: 0.9921 - val_loss: 0.1083 - val_Accuracy: 0.9750
Epoch 10/10
75/75 [=====] - 12s 161ms/step - loss: 6.6264e-04 - Accuracy: 1.0000 - val_loss: 0.0911 - val_Accuracy: 0.9817
```

Fig. 5. The process's result after training in Dataset_BC.

```
Epoch 1/10
179/179 [=====] - 30s 156ms/step - loss: 0.8220 - Accuracy: 0.7055 - val_loss: 1.6223 - val_Accuracy: 0.4066
Epoch 2/10
179/179 [=====] - 28s 154ms/step - loss: 0.4065 - Accuracy: 0.8494 - val_loss: 1.0792 - val_Accuracy: 0.5873
Epoch 3/10
179/179 [=====] - 28s 156ms/step - loss: 0.3005 - Accuracy: 0.8883 - val_loss: 0.6103 - val_Accuracy: 0.7788
Epoch 4/10
179/179 [=====] - 28s 157ms/step - loss: 0.2204 - Accuracy: 0.9210 - val_loss: 0.3110 - val_Accuracy: 0.8734
Epoch 5/10
179/179 [=====] - 28s 157ms/step - loss: 0.1574 - Accuracy: 0.9407 - val_loss: 0.3068 - val_Accuracy: 0.8871
Epoch 6/10
179/179 [=====] - 28s 157ms/step - loss: 0.1087 - Accuracy: 0.9615 - val_loss: 0.1790 - val_Accuracy: 0.9321
Epoch 7/10
179/179 [=====] - 28s 158ms/step - loss: 0.0828 - Accuracy: 0.9688 - val_loss: 0.1371 - val_Accuracy: 0.9466
Epoch 8/10
179/179 [=====] - 28s 157ms/step - loss: 0.0462 - Accuracy: 0.9842 - val_loss: 0.4636 - val_Accuracy: 0.8452
Epoch 9/10
179/179 [=====] - 28s 157ms/step - loss: 0.0400 - Accuracy: 0.9870 - val_loss: 0.1117 - val_Accuracy: 0.9649
Epoch 10/10
179/179 [=====] - 28s 157ms/step - loss: 0.0266 - Accuracy: 0.9916 - val_loss: 0.1420 - val_Accuracy: 0.9512
```

Fig. 6. The process's result after training in Dataset_MC.

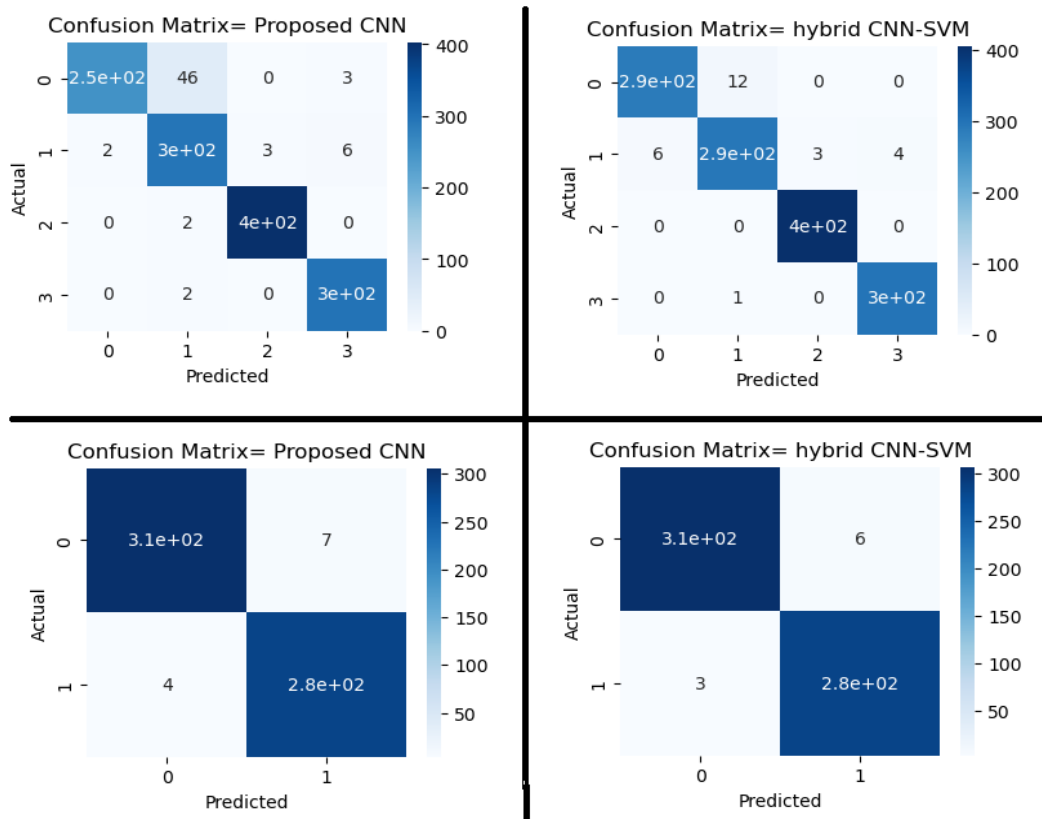


Fig. 7. Confusion matrix for Dataset_MC (Upper-Side) and Dataset_BC (Lower-Side).

TABLE II. CLASSIFICATION REPORT OF TEST DATASET IN DATASET_MC AND DATASET_BC

| Test Dataset_MC | Classes | Precision | Recall | F1-score |
|--|------------|-----------|--------|----------|
| Proposed CNN Accuracy=95% | glioma | 0.99 | 0.84 | 0.91 |
| | meningioma | 0.86 | 0.96 | 0.91 |
| | notumor | 0.99 | 1.00 | 0.99 |
| | pituitary | 0.97 | 0.99 | 0.98 |
| Support Vector Machine (SVM) Accuracy=98% | glioma | 0.98 | 0.96 | 0.97 |
| | meningioma | 0.96 | 0.96 | 0.96 |
| | notumor | 0.99 | 1.00 | 1.00 |
| | pituitary | 0.99 | 1.00 | 0.99 |
| Test Dataset_BC | Classes | Precision | Recall | F1-score |
| Proposed CNN Accuracy=98% | no | 0.99 | 0.98 | 0.98 |
| | yes | 0.98 | 0.99 | 0.98 |
| SVM Accuracy=99% | no | 0.99 | 0.98 | 0.99 |
| | yes | 0.98 | 0.99 | 0.98 |

In the addition of the evaluated test dataset, the projected model achieved the best accuracy. Table 2 shows the classification report of all classes of test data in the Dataset_MC and Dataset_BC.

The projected CNN model obtained 95% and 98% accuracy for the test data in the Dataset_MC and Dataset_BC respectively. The best result obtained in the hybrid CNN-SVM model was 98% and 99% accuracy for the test dataset in

Dataset_MC and Dataset_BC respectively. It shows high performance not only in training data but also in test data.

Figure 8 shows the accuracy of different classes in the random test images from Dataset_MC (Upper_Side) and Dataset_BC (Lower_Side).

The proposed work is the best as compared to other researchers' work because the same kind of dataset was used by

other authors in the experiment but did not get the optimal accuracy, which is shown in Table 3.

Authors [23] proposed a CNN and a hybrid CNN-SVM model for brain cancer binary classification (benign and

malignant) and obtained an accuracy of 98.49% using CNN-SVM and 97.43% using CNN on the BRATS 2015 brain image dataset. This is training accuracy, which is less than our proposed work.

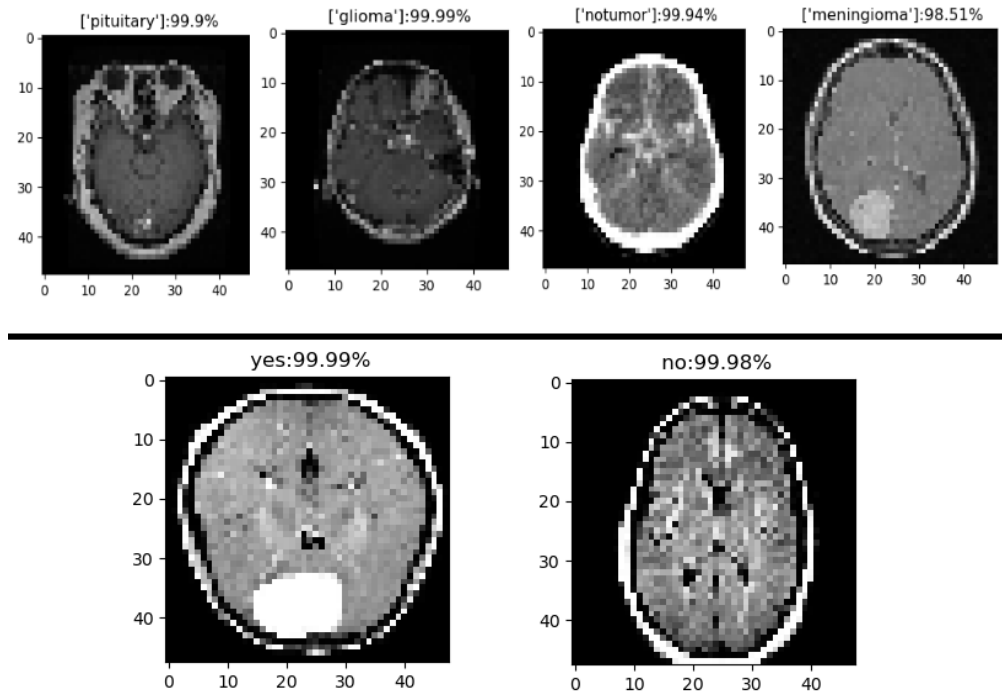


Fig. 8. Sample output of different classes with accuracy from both test datasets.

TABLE III. COMPARISON OF PROJECTED WORK WITH OTHER AUTHOR'S WORK

| Reference | Model | Accuracy of the training dataset | Accuracy of the validation/testing dataset | Epoch | MRI Brain Image Dataset |
|-----------|----------------------------------|----------------------------------|--|-------|-------------------------|
| [21] | CNN | 85% | 88% | 10 | Dataset_MC |
| [22] | CNN | 94.74% | | 20 | |
| [24] | CNN | 92.66% | | | |
| | AlexNet | 83.12% | | | |
| | VGG-16 | 88.87% | | | |
| [25] | CNN | 96.13% | | | |
| [26] | CNN-GA | 94.2% | | 100 | |
| | CNN-SVM (Proposed Work) | 99.56% | 98% | 10 | |
| [11] | VGG-19 with AQO | 98.95% | 98.95% | 41 | Dataset_BC |
| [12] | ResNet-50 | 98% | 94% | 20 | |
| [13] | VGG-16 | 96% | 86% | 10 | |
| [15] | Inception-ResnetV2 with ADSCFGWO | 99.98% | - | 20 | |
| [24] | CNN | 99.33% | | | |
| | AlexNet | 88.12% | | | |
| | ResNet-50 | 92.79% | | | |
| [27] | CNN-SVM | 99.74 | 93.78% | 11 | |
| [28] | EfficientNet-B0 | 98.87% | | 50 | |
| | CNN-SVM (Proposed work) | 100% | 99% | 10 | |

Authors [24] projected three CNN models to perform three different tasks on brain tumor MRI image datasets. The first CNN model was used for binary classification (tumor and nontumor) with an accuracy of 99.33%. The second was used to find the multi-class detection (glioma, meningioma, pituitary, metastatic and normal) with an accuracy of 92.66%. In this case, separate models are used by the authors for different tasks while in this paper single model was used for different tasks and accuracy is also higher than the other author's work.

Authors [26] proposed a CNN-SVM model for brain cancer classification using an MRI dataset and found the accuracy on the training dataset is 99.74% using RMSProp optimiser in 11 epochs but testing accuracy is 93.78%, which is much less as compared to our proposed work.

VIII. CONCLUSION AND FUTURE DISCUSSION

Each type of problem has a specific CNN model created for it. The kind of problem, the inputs, and the anticipated results all affect the CNN model's architecture and complication. The maximum authors were used to propose different classification models for the diverse classification tasks. Selecting the best-performing network model for a given application is one of the challenges with convolutional neural networks. Making the correct hyper-parameter choices is critical to accomplishment best outcomes, especially with the CNNs.

The most effective CNN model is created in this study, and its hyper-parameters are optimized and large, freely accessible MRI datasets are used to achieve satisfactory categorization results. Using the projected CNN model on test datasets, brain cancer identification is accomplished with a very pleasing accuracy of 99% for binary classification. Furthermore, a 98% accuracy rate is achieved for multi-classification. Finally, using performance evaluation criteria including accuracy, precision, recall and F1 score, the outcome of the proposed CNN-SVM is verified.

The one limitation of this study is that the accuracy of test data can be increased if the size of datasets is increased since it takes more time to improve the data by the augmentation process, which does not impact the result.

Future research in healthcare applications will continue to focus heavily on deep learning. The proposed model can be generalised based on its capacity to categorize data, it can be utilized to recognize and diagnose medical conditions. Because medical training takes a long time, this not only shortens the diagnosing process but also decreases the number of mistakes made by professionals. This concept holds promise for medical imaging diagnostics since combining data from several sources can result in a distinct course of events. Additionally, putting the system for crowdsourcing data collecting and analysis into practice will be interesting. Lastly, there are numerous healthcare sectors where deep learning can be applied.

MRI remains at the forefront of non-invasive brain cancer detection offering clinicians a comprehensive view of cancer morphology and aiding in treatment decision-making. The integration of CNN and MRI can alter the scene of diagnostic tools for brain tumors, providing clinicians with more reliable and timely information for patient care.

The future of MRI-based brain cancer detection holds promise with ongoing research in imaging expertise and artificial intelligence. Continuous progresses in imagery technology and the integration of DL will continue to improve the correctness and consistency of MRI in tumor characterization.

DECLARATION

- Availability of supporting data: The datasets are available on the following link:
<https://www.kaggle.com/datasets/masoudnickparvar/brain-tumor-mri-dataset>.
<https://www.kaggle.com/datasets/ahmedhamada0/brain-tumor-detection>.
- Competing Interests: No conflicts of interest
- Authors' Contributions: Everyone contributed to the research methodology and analysis of results.
- Funding: No source of funding.
- Acknowledgements: Thanks and regards to my guides for guidance.

REFERENCES

- [1] Key Statistics for Brain and Spinal Cord Tumors. Available online: <https://www.cancer.org/cancer/brain-spinal-cord-tumorsadults/about/key-statistics.html>.
- [2] Ayadi, W.; Elhamzi, W.; Charfi, I.; Atri, M. Deep CNN for Brain Tumor Classification. *Neural Process. Lett.* 2021, 53, 671–700.
- [3] M. Talo, U. B. Baloglu, O. Yildirim, and U. R. Acharya, "Application of Deep Transfer Learning for Automated Brain Abnormality Classification Using MR Images," *Cognitive Systems Research*, vol. 54, 2019.
- [4] A. Gudigar, U. Raghavendra, T. R. San, E. J. Ciaccio, and U. R. Acharya, "Application of Multiresolution analysis for automated detection of brain abnormality using MR images: a comparative study," *Future Generation Computer Systems*, vol. 90, pp. 359–367, 2019.
- [5] WHO Statistics on Brain Cancer. Available online: <http://www.who.int/cancer/en/>.
- [6] International Agency for Research on Cancer. Available online: <https://gco.iarc.fr/>.
- [7] Brain Tumor Basics. Available online: <https://www.thebraintumourcharity.org/>.
- [8] American Cancer Society website. Available online: www.cancer.org/cancer.html.
- [9] Chandra, Saroj Kumar, and Manish Kumar Bajpai. Effective algorithm for benign brain tumor detection using fractional calculus. *TENCON 2018-2018 IEEE Region 10 Conference. IEEE*, 2018. DOI: 10.1109/TENCON.2018.8650163.
- [10] Seetha, J., and S. S. Raja. Brain Tumor Classification Using Convolutional Neural Networks. *Biomedical & Pharmacology Journal*, Vol 11, pp 1457-1461, 2018. DOI: 10.1007/978-981-10-9035-6_33.
- [11] Mahmoud, A.; Awad, N.A.; Alsubaie, N.; Ansarullah, S.I.; Alqahtani, M.S.; Abbas, M.; Usman, M.; Soufiene, B.O.; Saber, A. Advanced Deep Learning Approaches for Accurate Brain Tumor Classification in Medical Imaging. *Symmetry* 2023, 15, 571. <https://doi.org/10.3390/sym15030571>.
- [12] Maquen-Niño, G.L.E., Sandoval-Juarez, A.A., Veliz-La Rosa, R.A., Carrión-Barco, G., Adrianzén-Olano, I., Vega-Huerta, H., De-La-Cruz-VdV, P. (2023). Brain Tumor Classification Deep Learning Model Using Neural Networks. *International Journal of Online and Biomedical Engineering (iJOE)*, 19(9), pp. 81–92. <https://doi.org/10.3991/ijoe.v19i09.38819>.
- [13] Chetana Srinivas, Nandini Prasad K. S., Mohammed Zakariah, Yousef Ajmi Alothaibi, Kamran Shaukat, B. Partibane, Halifa Awal, "Deep

- Transfer Learning Approaches in Performance Analysis of Brain Tumor Classification Using MRI Images", *Journal of Healthcare Engineering*, vol. 2022, Article ID 3264367, 17 pages, 2022. <https://doi.org/10.1155/2022/3264367>.
- [14] V. Rajinikanth, A. N. J. Raj, K. P. (anaraj), and G. R. Naik, "A customized VGG19 network with concatenation of deep and handcrafted features for brain tumor detection," *Applied Sciences*, vol. 10, no. 10, p. 3429, 2019.
- [15] ZainEldin, H.; Gamel, S.A.; El-Kenawy, E.-S.M.; Alharbi, A.H.; Khafaga, D.S.; Ibrahim, A.; Talaat, F.M. Brain Tumor Detection and Classification Using Deep Learning and Sine-Cosine Fitness Grey Wolf Optimization. *Bioengineering* 2023, 10, 18. <https://doi.org/10.3390/bioengineering10010018>.
- [16] Gu X, Shen Z, Xue J, Fan Y and Ni T (2021) Brain Tumor MR Image Classification Using Convolutional Dictionary Learning With Local Constraint. *Front. Neurosci.* 15:679847. doi: 10.3389/fnins.2021.679847.
- [17] A. Kujur, Z. Raza, A. A. Khan and C. Wechtaisong, "Data Complexity Based Evaluation of the Model Dependence of Brain MRI Images for Classification of Brain Tumor and Alzheimer's Disease," in *IEEE Access*, vol. 10, pp. 112117-112133, 2022, doi: 10.1109/ACCESS.2022.3216393.
- [18] K. Kavin Kumar, P. M. Dinesh, P. Rayavel, L. Vijayaraja, R. Dhanasekar et al., "Brain tumor identification using data augmentation and transfer learning approach," *Computer Systems Science and Engineering*, vol. 46, no.2, pp. 1845–1861, 2023.
- [19] Dataset available <https://www.kaggle.com/datasets/masoudnickparvar/brain-tumor-mri-dataset>.
- [20] Dataset available <https://www.kaggle.com/datasets/ahmedhamada0/brain-tumor-detection>.
- [21] O. Mogotocoro, "Clasificación De Tumores Cerebrales Meningioma, Glioma, Pituitary a Partir De Imágenes De Resonancia Magnética Mediante Wavelet E Inteligencia Ingeniería Electrónica," pp. 20–100, 2022.
- [22] W. Ayadi, W. Elhamzi, and M. Atri, "A new deep CNN for brain tumor classification," 2020 20th Int. Conf. Sci. Tech. Autom. Control Comput. Eng., pp. 266–270, 2020, <https://doi.org/10.1109/STA50679.2020.9329328>.
- [23] Khairandish, M.; Sharma, M.; Jain, V.; Chatterjee, J.; Jhanjhi, N. A Hybrid CNN-SVM Threshold Segmentation Approach for Tumor Detection and Classification of MRI Brain Images. *IRBM* 2022, 43, 290–299. [CrossRef].
- [24] Irmak, E. Multi-Classification of Brain Tumor MRI Images Using Deep Convolutional Neural Network with Fully Optimized Framework. *Iran J Sci Technol Trans Electr Eng* 45, 1015–1036 (2021). <https://doi.org/10.1007/s40998-021-00426-9>.
- [25] Sultan HH, Salem NM, Al-Atabany W (2019) Multi-classification of brain tumor images using deep neural network. *IEEE Access* 7:69215–69225. <https://doi.org/10.1109/ACCESS.2019.2919122>.
- [26] Kabir Anaraki A, Ayati M, Kazemi F (2019) Magnetic Resonance imaging-based brain tumor grades classification and grading via convolutional neural networks and genetic algorithms. *Biocybern Biomed Eng* 39(1):63–74. <https://doi.org/10.1016/j.bbe.2018.10.004>.
- [27] Chattopadhyay A, Maitra M, MRI-based brain tumour image detection using CNN based deep learning method, *Neuroscience Informatics*, Volume 2, Issue 4, 2022, 100060, ISSN 2772-5286, <https://doi.org/10.1016/j.neuri.2022.100060>.
- [28] H. A. Shah, F. Saeed, S. Yun, J. -H. Park, A. Paul and J. -M. Kang, "A Robust Approach for Brain Tumor Detection in Magnetic Resonance Images Using Finetuned EfficientNet," in *IEEE Access*, vol. 10, pp. 65426-65438, 2022, doi: 10.1109/ACCESS.2022.3184113.

Emotion Recognition with Intensity Level from Bangla Speech using Feature Transformation and Cascaded Deep Learning Model

Md. Masum Billah¹, Md. Likhon Sarker², M. A. H. Akhand³, Md Abdus Samad Kamal⁴

Department of Computer Science and Engineering,
Khulna University of Engineering and Technology, Khulna-9203, Bangladesh^{1, 2, 3}
Graduate School of Science and Technology, Gunma University, Kiryu 376-8515, Japan⁴

Abstract—Speech Emotion Recognition (SER) identifies and categorizes emotional states by analyzing speech signals. The intensity of specific emotional expressions (e.g., anger) conveys critical directives and plays a crucial role in social behavior. SER is intrinsically language-specific; this study investigated a novel cascaded deep learning (DL) model to Bangla SER with intensity level. The proposed method employs the Mel-Frequency Cepstral Coefficient, Short-Time Fourier Transform (STFT), and Chroma STFT signal transformation techniques; the respective transformed features are blended into a 3D form and used as the input of the DL model. The cascaded model performs the task in two stages: classify emotion in Stage 1 and then measure the intensity in Stage 2. DL architecture used in both stages is the same, which consists of a 3D Convolutional Neural Network (CNN), a Time Distribution Flatten (TDF) layer, a Long Short-term Memory (LSTM), and a Bidirectional LSTM (Bi-LSTM). CNN first extracts features from 3D formed input; the features are passed through the TDF layer, Bi-LSTM, and LSTM; finally, the model classifies emotion along with its intensity level. The proposed model has been evaluated rigorously using developed KBES and other datasets. The proposed model revealed as the best-suited SER method compared to existing prominent methods achieving accuracy of 88.30% and 71.67% for RAVDESS and KBES datasets, respectively.

Keywords—Bangla speech emotion recognition; speech signal transformation; convolutional neural network; bidirectional long short-term memory

I. INTRODUCTION

Speech is the most commonly used method of interaction and emotional expression. In artificial intelligence and deep learning, the Speech Emotion Recognition (SER) task involves identifying and categorizing emotional elements of speech. The SER task has two basic steps: extracting features from the speech signal and classifying emotions. Existing SER methods employ different signal transformation and feature extraction methods on speech signals and then employ different machine learning (ML) and/or deep learning (DL) methods to the feature-transformed signal for emotion recognition [1] [2]. SER performance relies on the quality of the extracted emotional features from speech and methods used to classify the features.

In the ML or DL domain, SER is a language-specific research task, as natural languages have remarkable variations.

Most of the existing SER tasks are performed in a few languages for which quality corpuses are available. On the other hand, SER studies are very limited, even for major languages, due to the legging of resources. As an example, Bangla is a major speaking language in the world, which is spoken by more than 210 million people [3]. However, Bangla is not resourceful for SER studies; hence, a few studies are available on Bangla SER. Therefore, the Bangla SER study is a promising research domain in ML and DL domains.

The study aims to develop a DL-based Bangla SER (BSER) system to identify the most suitable match for emotional speech. Existing BSER studies have only looked at classifying emotions from speech without considering the intensity level. However, the level of intensity (normal or strong) of an emotional expression such as sadness or anger is crucial. When someone is experiencing intense emotions, they may engage in harmful behaviors. The recent increase in online broadcasts of such behavior on social media has raised the alarm and the need for action to address these issues [4]. As a result, the automatic recognition of both emotions and their intensity level has become a highly relevant and essential issue that is the focus of this study.

An integrated speech signal transformation and a cascaded model with hybrid DL architecture are considered in this study to achieve better SER performance. The proposed method employs the Mel-Frequency Cepstral Coefficient (MFCC), Short-Time Fourier Transform (STFT), and Chroma STFT (CSTFT) feature transformation on the speech signals individually. The transformed two-dimensional (2D) MFCC, STFT, and CSTFT features are combined into a 3D form and inputted into the cascaded DL model for emotional classification with intensity. The cascaded DL model performs the task in two stages: classify emotion first in Stage 1 and then measure the intensity of the classified emotion in Stage 2. DL architectures used in both stages are the same, which consist of 3D Convolutional Neural Network (CNN), a Time Distribution Flatten (TDF) layer, a Long Short-term Memory (LSTM), and a Bidirectional LSTM (Bi-LSTM). The CNN extracts features from the 3D transformed speech signal using four feature blocks in series, and the TDF layer then flattens the features. The flattened features are inputted into the Bi-LSTM, the outcomes of Bi-LSTM are inputted into the LSTM, and finally, a fully connected layer is used for emotion classification or intensity measure. The proposed model has

been evaluated rigorously using our developed KBES dataset and other BSER datasets. The proposed cascaded revealed as the best-suited SER method while compared to existing prominent methods. The major contributions of this study are briefly summarized as follows:

- 1) Integrated 3D speech feature formation using MFCC, STFT, and CSTFT;
- 2) Emotion classification with intensity using cascaded DL model with hybrid DL architecture;
- 3) Rigorous experimental studies with different feature transformations and different DL models on our developed KBES dataset and other BSER datasets; and
- 4) Performance comparison of the proposed BSER model with existing prominent methods.

The structure of the remaining paper is as follows. Section II is the literature review, briefly explaining several related SER studies. Section III demonstrates the proposed method illustrating individual components. Experimental studies, including outcomes of the proposed cascaded model and performance comparison with the existing methods, are placed in Section IV. Finally, Section V concludes the paper with a few remarks on the present study and several future research directions.

II. LITERATURE REVIEW

Several DL-based SER studies are available with different corpuses for English and Germany, such as RAVDESS and IEMOCAP. Badshah et al. [5] investigated a CNN architecture composed of three convolutional layers and three fully connected (FC) layers. The model was trained on the Berlin emotional corpus to differentiate seven emotions using spectrograms collected from the stimuli. Satt et al. [6] introduced an SER model extracting log-spectrogram feature vectors from the IEMOCAP speech dataset. They tested two architectural models: convolution-only and convolution-LSTM deep neural networks. Etienne et al. [7] also used a CNN-LSTM architecture to classify emotions using spectrogram information. Chen et al. [8] used a portion of the IEMOCAP dataset for three different models: a shallow CNN combined with a Bi-LSTM, a deep CNN with a shallow Bi-LSTM, and a deep CNN with a deep Bi-LSTM. Manohar and Logashanmugam [9] integrated different meta-heuristic and deep-learning methods for SER with selected features. Wen et al. [10] Introduced self-labeling feature frames in their DL-based SER study.

Zhao et al. [11] investigated different DL-based models with CNN and LSTM for SER using the Emo-DB corpus and part of the IEMOCAP corpus. Among various combinations of convolutional layers and LSTM, the combination of 6 convolutional layers and LSTM is found to be the best-performing one. Zhang et al. [12] developed an attention-based, fully convolutional network on the IEMOCAP corpus and claimed to outperform state-of-the-art models. Ghosal et al. [13] proposed a graph neural network-based technique called the Dialogue Graph Convolutional Network (DialogueGCN) for recognizing emotions in conversations. A 2D CNN architecture extracted features from audio recordings, and a Support Vector Machine (SVM) was utilized

for emotion classification. They evaluated the performance of their architecture on three datasets: IEMOCAP, AVEC, and MELD. Zhao et al. [14] employed a Connectionist Temporal Classification (CTC) with attention-based Bi-LSTM using the IEMOCAP dataset. Zhao et al. [15] combined Bi-LSTM with a CNN using the IEMOCAP dataset. Recently, Is-lam et al. [4] developed a 3D transformed feature and CNN Bi-LSTM-based cascaded DL model for the RAVDESS dataset.

Only a few attempts have been made to develop SER for Bangla, even though it is a significant natural language worldwide. Sultana et al. [16] employed a DL model combining CNN with TDF and Bi-LSTM layers to analyze the SUBESCO [17] dataset. The model consists of four CNN feature blocks (FB), each with a convolution layer, as well as layers for batch normalization (BN), exponential linear units (ELU), and max-pooling. The first two FBs used 128 kernels, while the last two FBs used 64 kernels. The proposed model's performance of Bangla SER was compared to three other models [18] [19] [20]. Sultana and Rahman [21] recently investigated essential speech features for ML-based BSER using the SUBESCO dataset.

III. CASCADED DL MODEL FOR BANGLA SER WITH INTENSITY

There is a novel aim to develop Bangla SER with intensity. Speech is the primary method of communication in various live media platforms like Facebook and YouTube, which often express emotions. In the case of emotional expression, the level of intensity (normal or strong) has a crucial impact. For example, extreme sadness or anger may lead a person towards harmful behaviors, even suicidal effects. Identifying harmful emotions, such as extreme sadness or anger, is a challenging computational intelligence task to prevent individuals from taking harmful actions that could impact society.

Fig. 1 illustrates the general architecture of the proposed method of identifying appropriate emotions from speech signals. The main components of the proposed approach are the feature transformation of the input speech signal and classifying emotions and their intensity level. The method developed an integrated 3D feature form from three different individual features (i.e., MFCC, STFT, and Chroma STFT) on the input speech signal. Then, an appropriate DL model is used to analyze 3D features through multiple layers, eventually leading to the classification of emotions. At a glance, the proposed system takes in speech signals as input and generates output that classifies emotions as Neutral, Happy, Sad, Angry, and Disgust and further categorizes each emotion as Low or High based on the intensity level. The following subsections explain the individual components briefly.

A. Speech Signal Transformation

The speech signal transformation in the proposed system considers three popular signal transformation methods: Mel-Frequency Cepstral Coefficients (MFCC), Short-Time Fourier Transform (STFT), and Chroma STFT. Each MFCC, STFT, and Chroma STFT produces three different same-sized two-dimensional (2D) transformed features. The three 2D features

are integrated into a 3D transformed feature, which is inputted into the cascaded DL model for emotion recognition.

The basic elaborated descriptions of the feature transformation are available in the literature [4].

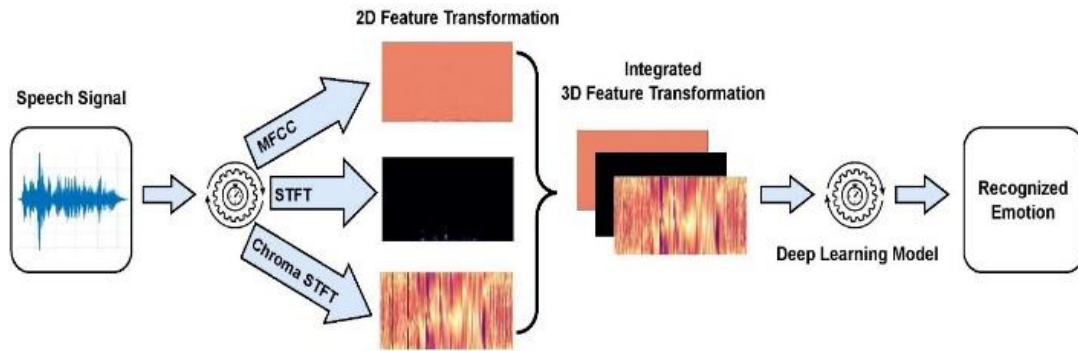
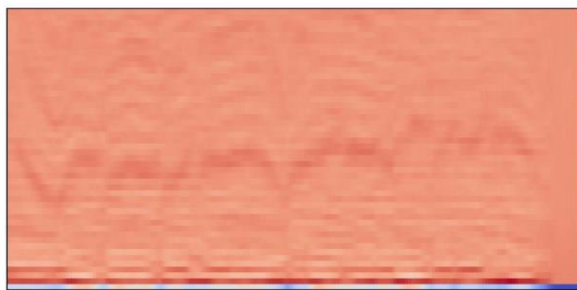
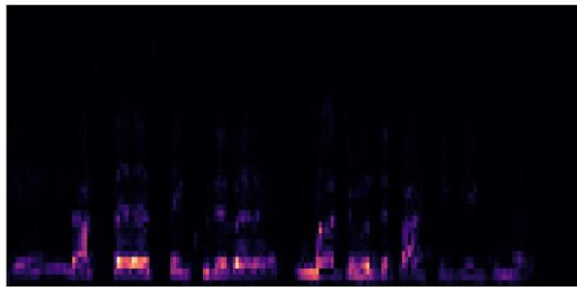


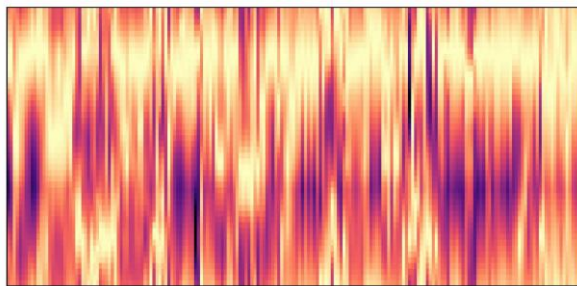
Fig. 1. Architecture of the proposed method identifying emotions from speech signals.



(a) MFCC



(b) STFT



(c) Chroma STFT

Fig. 2. Sample outcomes of speech signal feature transformation employed in the proposed method.

Fig. 2 shows 2D features from a sample speech signal using MFCC, STFT, and Chroma STFT. 250 hop lengths and 128 sequences were considered for MFCC; thus, the MFCC feature (see Fig. 2(a)) is with 128 sequences and 513 frames. Having a hop length of 250 and the FFT window length of 254, the STFT feature (see Fig. 2(b)) is also 128 sequences and 513 frames. The Chroma STFT feature is the same size as

STFT, as shown in Fig. 2(c). Afterward, the three 2D features were integrated into the 3D form with size $128 \times 513 \times 3$, which fed into the DL model.

B. Emotion Classification using Cascaded DL Model

Recognizing emotions using DL involves extracting features through multiple layers before finally recognizing them into emotion categories with intensity levels. A cascaded model is considered in this study to perform the task in two different stages: emotion classification and then the intensity of the classified category. Such a cascaded model is investigated in the recent study [4], but we have considered different DL architectures to achieve better performance for our intended application of Bangla SER.

Fig. 3 depicts the proposed cascaded DL model, which consists of two different stages. The DL architecture in Stage 1 classifies 3D-transformed features into five emotion categories: Neutral, Happy, Sad, Angry, and Disgust. Stage 2 uses another DL model to identify the intensity (i.e., Normal or Strong) of the emotion recognized in Stage 1. A single DL model is trained with the whole training set for Stage 1. For intensity classification in Stage 2, the training set was divided into five individual classes (i.e., Normal and four emotion classes), and then four distinct DL models were trained with individual emotion case samples for intensity classification. In the figure, DLEmotion in Stage 1 is the classifier for the emotion classification, and DLHappy, DLSad, DLAngry, and DLDisgust in Stage 2 are the classifiers for the intensity classification of Happy, Sad, Angry, and Disgust emotions, respectively. In other words, the DLEmotion extracts features from the input 3D transformed feature and then categorizes them into emotion cases. Similarly, a DL in Stage 2 extracts features from the same input used in Stage 1 but for the task of intensity measure (Low or High) of the classified emotion.

The main distinction between the DL architectures used in Stage 1 and Stage 2 is the number of output neurons: five in Stage 1 and two in Stage 2. Although the number of output classes and tasks differ, the basic structure is the same in all the DL architectures depicted in Fig. 4. Fig. 4(a) shows the building blocks of the DL architecture, which has four 3D CNN feature blocks (FB), a Time Distribution Flatten (TDF) layer, a Bi-LSTM layer, an LSTM layer, and a fully connected (FC) dense layer. The structure of a single CNN feature block

is shown in Fig. 4(b), which consists of a 3D CNN layer, batch normalization layer, ReLU activation layer, and 3D max-pooling layer. The use of 3D transformed features makes the 3D CNN ideal for feature extraction, while the LSTMs are selected for their ability to handle sequential data.

Output from the CNN is passed through a TDF layer that serves as the input for the Bi-LSTM and then passed to the LSTM layer. The LSTM layer results are given to an FC layer to identify emotions or intensity levels.

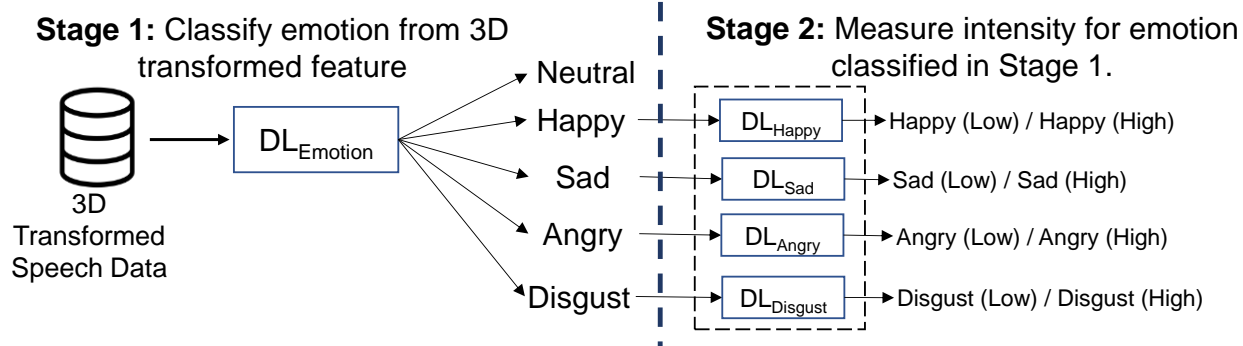


Fig. 3. The proposed cascaded DL model to classify emotion and its intensity from the 3D transformed speech signal.

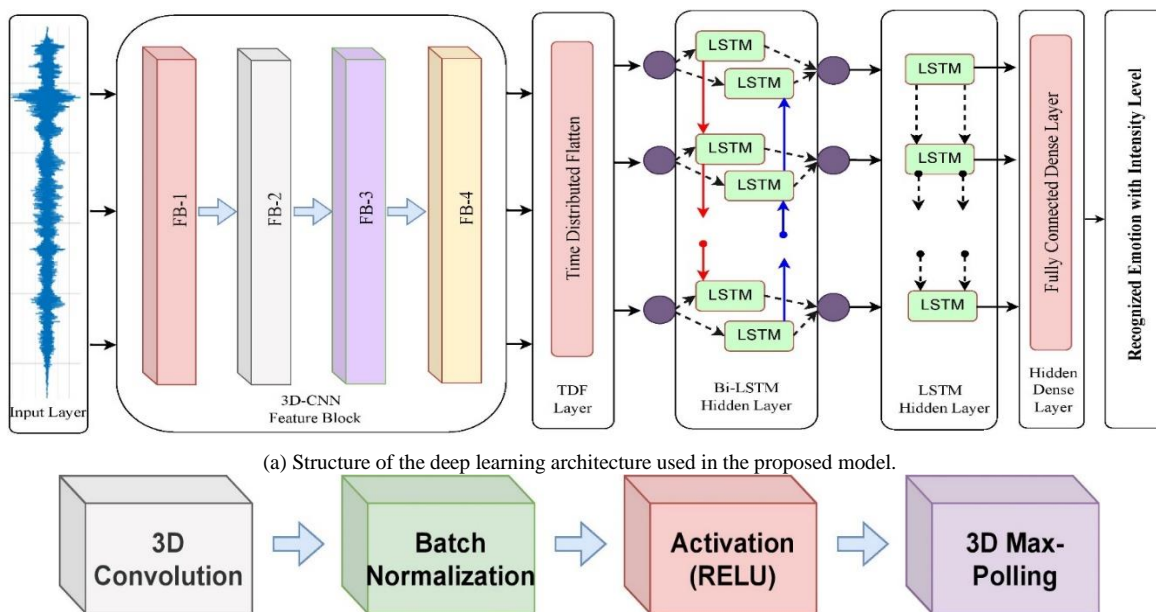


Fig. 4. The architecture of the proposed deep learning model.

TABLE I. THE HYPER-PARAMETERS OF THE PROPOSED DEEP LEARNING MODEL ARCHITECTURE

| Feature Blocks | Layers | Input Shape | Output Shape | Filters | Kernel Size | Strides | Units |
|----------------|--------------|----------------|----------------|---------|-------------|---------|-------|
| FB-1 | Conv3D | 128×513×3 | 128×513×3 @ 64 | 64 | 5×5×5 | 1×1×1 | - |
| | MaxPolling3D | 128×513×3 @ 64 | 64×256×3 @ 64 | - | 2×2×1 | 2×2×1 | - |
| FB-2 | Conv3D | 64×256×3 @ 64 | 64×256×3 @ 64 | 64 | 5×5×5 | 1×1×1 | - |
| | MaxPolling3D | 64×256×3 @ 64 | 16×64×3 @ 64 | - | 4×4×1 | 4×4×1 | - |
| FB-3 | Conv3D | 16×64×3 @ 64 | 16×64×3 @ 128 | 128 | 5×5×5 | 1×1×1 | - |
| | MaxPolling3D | 16×64×3 @ 128 | 4×16×3 @ 128 | - | 4×4×1 | 4×4×1 | - |
| FB-4 | Conv3D | 4×16×3 @ 128 | 4×16×3 @ 128 | 128 | 5×5×5 | 1×1×1 | - |
| | MaxPolling3D | 4×16×3 @ 128 | 1×4×3 @ 128 | - | 4×4×1 | 4×4×1 | - |
| - | TDF | 1×4×3 @ 128 | 1×1536 | - | - | - | - |
| - | Bi-LSTM | 1×1536 | 1×512 | - | - | - | 256 |
| - | LSTM | 1×512 | 256 | - | - | - | 256 |

| | | | | | | | |
|---|-------|-----|-----|---|---|---|-----|
| - | Dense | 256 | 5/2 | - | - | - | 5/2 |
|---|-------|-----|-----|---|---|---|-----|

The proposed DL architecture has a set of layer parameters outlined in Table I. All CNN layers employ the same kernel size of $5 \times 5 \times 5$ and strides of $1 \times 1 \times 1$. The first feature block, FB-1 and FB-2, have filters of 64, while the last two feature blocks, FB-3 and FB-4, have filters of 128. The max-pooling layer for the FB-1 has a $2 \times 2 \times 1$ sized kernel and a stride size of $2 \times 2 \times 1$, whereas the last three max-pooling layers for the feature block have a $4 \times 4 \times 1$ sized kernel and a stride of $4 \times 4 \times 1$. The output of FB-4 is passed into the TDF layer, which is transformed into 1536 features. The outputs of the TDF layer are served as input to the Bi-LSTM layer. The Bi-LSTM layer outputs are 512 features, which are passed on to the LSTM layer. The outputs of the LSTM layer pass into the FC dense layer. The dense layer was concluded by applying the SoftMax activation function, which normalized the recognition of emotions in the classification process. Finally, the output layer will have five neurons in the DL classifier in Stage 1, and DL classifiers in Stage 2 will have two neurons in their output layers. The elaborated descriptions of CNN, LSTM, and Bi-LSTM are available in the literature [4] [21].

C. Significance of the Proposed Method

Bangla SER with intensity level is the primary concern of this study. This study utilized a 3D form of the speech signal that integrates three 2D transformations to enhance features and improve identification, resulting in significant performance enhancements. A cascaded DL model is considered in this study, where the task is split into two stages. The first stage involves classifying the emotion using a DL (i.e., $DL_{Emotion}$) model, and in the second stage, distinct DL models (i.e., DL_{Happy} , DL_{Sad} , DL_{Angry} , and $DL_{Disgust}$) classify the intensity level of the classified emotion as either Normal or Strong. DL models in both stages use the same 3D feature as input for a particular speech sample. The output of the first stage's DL model identifies the emotion class of the sample based on its 3D features. In contrast, a particular emotion-based DL model measures its intensity level using the same 3D feature in Stage 2. DL architectures in both stages are the same and consist of a 3D CNN, Bi-LSTM, and LSTM. This proposed model differs from the existing methods by using innovative techniques to recognize individual emotions and their intensity level.

IV. EXPERIMENTAL STUDIES

The effectiveness of the proposed DL method has been evaluated through several series of experiments and compared with other prominent methods. Since intensity level identification is the main attraction of this study for Bangla SER and no existing dataset is appropriate for the task, an appropriate dataset is pre-pared for this study. The following sections provide information regarding the dataset development, experimental setup, result analysis, and performance comparison.

A. Bangla SER Dataset Development

An appropriate dataset is a major issue in developing any ML/DL method. The major concern of this study is not only the categorization of emotions from speech signals but also the intensity of the categorized emotion. The intensity of

speech emotion has great impacts, which has already been discussed as the motivation of the present study. A few Bangla SER datasets are available, but no existing dataset considers the intensity level of emotions. Moreover, existing datasets consist of only a few dialogues with a minimal number of actors; such datasets are unsuitable concerning re-al-world scenarios. Therefore, a realistic Bangla emotional speech dataset is used in this study, which is called the KUET Bangla Emotional Speech (KBES) dataset [22]. The dataset consists of 900 audio signals (i.e., speech dialogs) from 35 actors (20 females and 15 males) with diverse age ranges. Sources of the speech dialogs are Bangla Telefilm, Drama, TV Series, and Web Series. There are five emotional categories: Neutral, Happy, Sad, Angry, and Disgust. Except for Neutral, samples of a particular emotion are divided into two intensity levels: Normal and Strong.

The significant issue of the KBES dataset is that the speech dialogs are almost unique, with a relatively large number of actors. In contrast, existing datasets (such as SUBESCO and BanglaSER) hold samples with repeatedly spoken few pre-defined dialogs by a few actors/research volunteers in the lab environment. Finally, the KBES dataset is exposed as a nine-class problem to classify emotions into nine categories: Neutral, Happy (Low), Happy (High), Sad (Low), Sad (High), Angry (Low), Angry (High), Disgust (Low) and Disgust (High). However, the dataset is kept symmetrical, holding 100 samples for each of the nine classes; 100 samples are also gender balanced, having 50 samples for male/female actors. The speech signals in the KBES dataset have a length of three seconds and a sample rate of 48 kHz. The developed dataset seems a realistic one when compared with the existing SER datasets. The developed KBES dataset is publicly available and recently published data article holds its description [22].

B. Experimental Setup

The Python Librosa library [23] was used to trans-form speech signals of the KBES dataset. To make speech signals (having a length of three seconds and a sample rate of 48 kHz) in the KBES dataset suitable for DL input, the signal samples were resampled to 42.66 kHz. As a result, a speech signal was transformed into 127,980 bit-vectors. By adding 20 bits of zeros with it, 128,000 bit-vectors were used as input for the DL model. The DL models were developed using open-source Python libraries, specifically Keras [24] and Tensorflow [25].

The experiments were executed using a Jupyter Notebook hosted on Google Colaboratory, a cloud service that provides GPU capability [26]. The personal computer was an HP Pavilion laptop with an Intel(R) Core i5-7200U CPU @ 2.50 GHz processor, 8 GB of RAM, and an NVIDIA GeForce 940MX Graphics Card.

We utilized the Adam optimizer with a learning rate of 10^{-4} and employed the categorical cross-entropy as the loss function for compiling the model. The model aims to reduce the categorical cross-entropy loss, a widespread loss function for multi-class classification problems [27]. During the training process, the model was trained for 60 epochs with a batch size of 16.

The KBES dataset was separated into a training set and a test set, with 80% of the samples used for training and the remaining 20% used for testing. The training set consisted of 720 samples collected from each of the nine categories and was utilized for training the model. The test set, made up of the remaining 180 samples, was kept aside to assess the model's generalizability after training. Since the major concern of any ML/DL model is to perform well beyond the training data (i.e., on unseen data), test set performance (generalization) is a key performance measure of the developed model.

C. Outcomes of the Proposed Cascaded DL Model

The proposed cascaded model is carried out in two stages. In Stage 1, a DL model is trained with 720 training samples and tested with 180 samples for emotional classification. Fig. 5 shows the loss and accuracy curves of both the training and test sets in Stage 1 (i.e., for DLEmotion). The training set loss reduces smoothly and reaches close to zero after 30 epochs, while the test set loss reduces initially and then stabilizes after 45 epochs. Consequently, accuracy reached 100% for the training set through smooth improvement, while the best test set accuracy was close to 76%.

Table II shows the confusion matrix on the test set on emotion classification only (without intensity) in Stage 1. For example, for 40 happy samples, the model correctly identified 28. The remaining 12 happy samples were misclassified as Neutral, Sad, Angry, and Disgust in cases 5, 1, 2, and 4, respectively. There is a total of 45 misclassifications, which

are in category misses. With a true classification of 135 samples, the DL model shows an accuracy of 75.56% in emotion classification, regardless of the intensity.

In Stage 2 of the proposed DL model, the samples classified in Stage 1 were used to determine the emotional intensity with a DL model for a particular emotion category. In this stage, four DL models are trained, and a particular DL is trained with the samples for a particular emotion category. As an example, there are a total of 160 training samples for Happy emotion (80 samples for each of Normal and Strong intensity cases) in 720 training samples. These 160 happy samples were used to train the DL model (i.e., DLHappy) to classify the intensity of Happy emotion. The intensity level of Happy emotion was tested using 40 samples from the test set.

Similarly, the other three different DL models (i.e., DLSad, DLAngry, and DLDisgust) were trained and tested for intensity level classification of Sad, Angry, and Disgust emotions. In Stage 2, the intensity of a sample will be classified by the designated DL model for the classified emotion in Stage 1. If a sample is misclassified in Stage 1 (i.e., a Category Miss), there is no remedy in Stage 2, and treated as Category Miss. On the other hand, a truly classified sample in Stage 1 may be wrongly classified in the case of Intensity Level in Stage 2, which is called Intensity Miss. Therefore, due to the inclusion of intensity miss in Stage 2, the classification accuracy of emotion with intensity is lower than the accuracy of emotion classification by Stage 1.

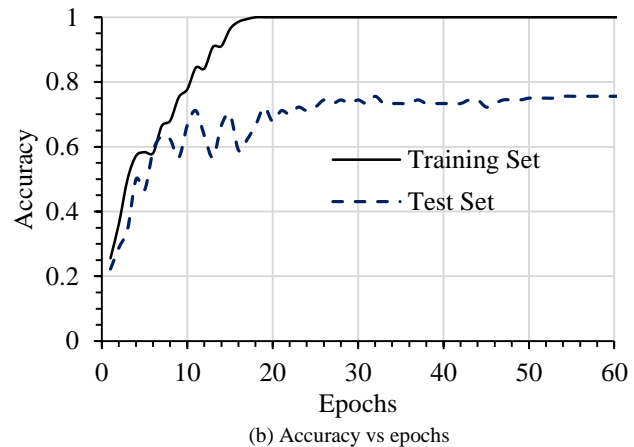
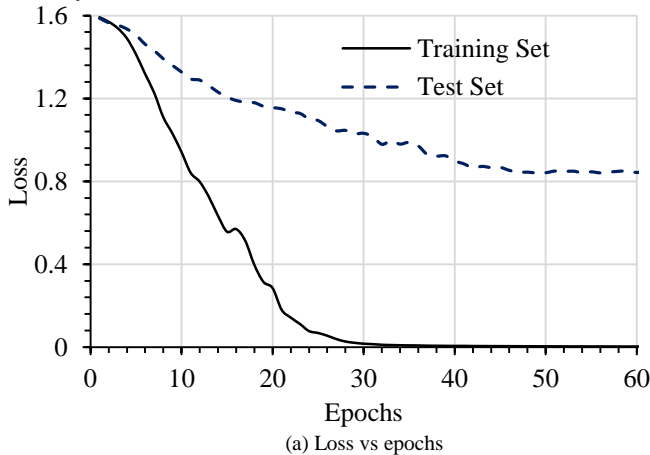


Fig. 5. Loss and accuracy curves of training and test sets of the DL model in Stage 1 in the proposed cascaded DL model.

TABLE II. TEST SET CONFUSION MATRIX ON EMOTION CLASSIFICATION (WITHOUT INTENSITY) IN STAGE 1 OF THE CASCADED DL

| Emotion | Neutral | Happy | Sad | Angry | Disgust | Correctly Classified | Category Miss | Total Samples |
|--------------|---------|-------|-----|-------|---------|----------------------|---------------|---------------|
| Neutral | 13 | 1 | 1 | 3 | 2 | 13 | 7 | 20 |
| Happy | 5 | 28 | 1 | 2 | 4 | 28 | 12 | 40 |
| Sad | 2 | 2 | 32 | 1 | 3 | 32 | 8 | 40 |
| Angry | 0 | 0 | 0 | 35 | 5 | 35 | 5 | 40 |
| Disgust | 1 | 0 | 3 | 8 | 28 | 28 | 12 | 40 |
| Total | | | | | | 136 | 44 | 180 |

TABLE III. THE TEST SET CONFUSION MATRIX ON EMOTION RECOGNITION WITH INTENSITY LEVEL BY THE CASCADED DL MODEL

| Emotion | Emotion Intensity | Neutral | Happy | | Sad | | Angry | | Disgust | | Category Miss | Intensity Miss | Total Samples |
|--------------|-------------------|---------|-------|------|-----|------|-------|------|---------|------|---------------|----------------|---------------|
| | | | Low | High | Low | High | Low | High | Low | High | | | |
| Neutral | - | 13 | 1 | 0 | 1 | 0 | 2 | 1 | 2 | 0 | 7 | 0 | 20 |
| Happy | Normal | 3 | 14 | 1 | 0 | 0 | 0 | 0 | 2 | 0 | 5 | 1 | 20 |
| | Strong | 2 | 0 | 13 | 0 | 1 | 2 | 0 | 0 | 2 | 7 | 0 | 20 |
| Sad | Normal | 2 | 1 | 0 | 15 | 0 | 0 | 0 | 1 | 1 | 5 | 0 | 20 |
| | Strong | 0 | 0 | 1 | 1 | 16 | 1 | 0 | 0 | 1 | 3 | 1 | 20 |
| Angry | Normal | 0 | 0 | 0 | 0 | 0 | 15 | 2 | 2 | 1 | 3 | 2 | 20 |
| | Strong | 0 | 0 | 0 | 0 | 0 | 0 | 18 | 0 | 2 | 2 | 0 | 20 |
| Disgust | Normal | 1 | 0 | 0 | 2 | 0 | 3 | 1 | 11 | 2 | 7 | 2 | 20 |
| | Strong | 0 | 0 | 0 | 0 | 1 | 0 | 4 | 1 | 14 | 5 | 1 | 20 |
| Total | | | | | | | | | | | 44 | 7 | 180 |

Table III depicts the confusion matrix of the pro-posed cascaded model with Stage 1 + Stage 2. The ma-trix reveals both category and intensity miss for the four emotions. As Neutral emotion has no intensity measure, it holds only category miss, and the number of misclassifications is seven as of Table II. Again, out of the 28 correctly classified Happy emotion samples in Stage 1, one sample of Happy (Low) was misclassi-fied as Happy (High) in Stage 2; thus, Intensity Miss of Happy is one. The total category miss of the Happy was 12 in Table II, which just distributed for Happy (Low) and Happy (High) in Table III. Among category miss cases, three Happy (Low) were misclassified as Neutral, which is the highest misclassification as Neutral. Such misclassification of Happy samples is logical as it is generally accepted that Happy (Low) is close to Neu-tral. On the other hand, no Angry samples are misclas-sified as Neutral or Happy, and five Angry samples are misclassified as Disgust. Including proficiency in Sad and Disgust samples, the performance of the proposed cascaded DL model on an unseen test set of unique KBES datasets is remarkable. With a total of 51 misclassifications (=44 Category Miss +7 Intensity Miss) out of 180 test speeches, the resulting test set accuracy is 71.67% (i.e., (180-51)/100).

D. Preference for Cascaded DL Model over Single DL Model

The proposed cascaded model consists of five hybrid CNN-LSTM DL components where individual compo-nent performs different tasks. The individual DL com-ponents classified the samples into nine categories through task division. It is also possible to perform the task in a single stage by a single DL model having nine neurons in its output layer. Therefore, it is a common query to select a cascaded model with five DL components over the single DL model. Additional experiments with a single DL have been conducted to observe the effectiveness of the proposed cascaded model over a single DL. Experiments were also conducted with samples of male and female actors separately for better observations.

Table IV compares the performance of the proposed cascaded model with a single DL model for a full test set, male and female actors' samples. While full set training and test samples are 720 and 180 as of previous experiments, as the KBES dataset is balanced for male and female cases, training and test samples for males or females are 360 and 90,

respectively. Ac-cording to the table, performances for male and female cases are competitive in both single DL and cascaded DL models. Furthermore, both DL models (i.e., single or proposed cascaded) show competitive performance in case of category miss. As an example, both the models misclassified equal 21 samples for the female case. The remarkable performance distinction between the two models is observed in the case of intensity classifica-tion, and the cascaded model remarkably outperformed the single DL model. The intensity missed cases by single DL model for male, female, and full set cases are 14, 13, and 23, respectively. The intensity missed cases for male, female, and full set by the cascaded model are 4, 5, and 7, respectively. Due to such outperformance in intensity classification, the overall accuracy of the cascaded DL model is much better than the single DL model. At a glance, the proposed cascaded DL model showed a full test set accuracy of 71.67% (as also discussed in the previous section), whereas the single DL model's accuracy on a full test set is 61.11% (= (180-47-23)/180). The outperformance of the cascaded DL model reflects the effectiveness of its task division in two stages as well as validates the appropriateness of selecting the cascaded model.

E. Performance Comparison with Different Speech Signal Transformations

The integrated 3D form of feature formation using MFCC, STFT, and CSTFT from the input speech signal is a crucial task of the proposed method. To observe the effectiveness of using different feature forms, additional experiments have been conducted with different signal transformations individually and combining two or more among MFCC, STFT, and CSTFT. Table V provides performance results for a cascaded DL model using three individual speech transformation features (MFCC, STFT, and CSTFT), three double combinations (MFCC + STFT, STFT + CSTFT, and MFCC + CSTFT), and finally, proposed triple combination MFCC + STFT+ CSTFT. Appropriate DL architectures were con-sidered to classify emotions using distinct feature transformations. Among the individual methods, MFCC achieved the highest accuracy of 60.56%. However, the dual combination of MFCC and STFT has an accuracy of 61.67%, which is slightly better than the accuracy of MFCC. Finally,

the integrated 3D form of transformed MFCC, STFT, and CSTFT (i.e., MFCC + STFT+ CSTFT) achieved the best

accuracy of 71.67%. The performance comparison justifies the use of a 3D form of a feature in this study.

TABLE IV. PERFORMANCE ON FULL TEST SET, MALE AND FEMALE ACTORS FOR SINGLE DL MODEL AND PROPOSED CASCADED DL MODEL

| Particular of Samples | Training & Test Samples | Test Set Performance by the Single Deep Learning Model | | | Test Set Performance by the Cascaded Deep Learning Model | | |
|----------------------------|-------------------------|--|----------------|--------------|--|----------------|--------------|
| | | Category Miss | Intensity Miss | Accuracy (%) | Category Miss | Intensity Miss | Accuracy (%) |
| Male | 360 & 90 | 18 | 14 | 64.44 | 20 | 4 | 73.30 |
| Female | 360 & 90 | 21 | 13 | 62.22 | 20 | 5 | 72.22 |
| Full Set (= Male + Female) | 720 & 180 | 47 | 23 | 61.11 | 44 | 7 | 71.67 |

TABLE V. PERFORMANCE COMPARISON ON THE TEST SET WITH DIFFERENT SIGNAL TRANSFORMATIONS FOR CASCADED DEEP LEARNING MODEL

| Combination | Signal Transformation | Sequences × Frames × Dimension | Category Miss | Intensity Miss | Truly Classify | Accuracy (%) |
|-----------------|---|-----------------------------------|---------------|----------------|----------------|--------------|
| Individual | Mel-Frequency Cepstral Coefficient (MFCC) | 128×513×1 | 50 | 21 | 109 | 60.56 |
| | Short-Time Fourier Transform (STFT) | 128×513×1 | 53 | 27 | 100 | 55.56 |
| | Chroma STFT (CSTFT) | 128×513×1 | 62 | 33 | 85 | 47.22 |
| Double | MFCC+STFT | 128×513×2 | 53 | 16 | 111 | 61.67 |
| | STFT+CSTFT | 128×513×2 | 57 | 27 | 96 | 53.33 |
| | MFCC+CSTFT | 128×513×2 | 50 | 23 | 107 | 59.44 |
| Proposed Triple | MFCC+STFT+CSTFT | 128×513×3 | 44 | 7 | 129 | 71.67 |

F. Performance Comparison Varying DL Architecture

The DL architecture employed in this study to classify emotions from 3D feature maps is 4 3D-CNN + TDF + Bi-LSTM + LSTM, which is a hybrid CNN and LSTM model. In the model, 3D CNN with four layers is the main component to extract features to classify the input 3D feature sample. It is also possible to perform classification from CNN features using one/two FC layers. Distinct experiments with TDF, LSTM, and Bi-LSTM options have been conducted, and Table VI compares performance on the test samples classification by the considered DL architectures. The comparison in Table VI indicates that our proposed model achieves the highest accuracy over all other models. It is seen from the table that the 4 3D-CNN + 2 FC architecture is the simplest one and showed the lowest ac-curacy, which is 62.78%. The architecture holds two FC layers on 3D CNN, while other architectures hold one FC layer by default on top of the relatively complex DL architectures. In general, accuracy seems to be improved with architectural complexity. Finally, the considered hybrid architecture of CNN, LSTM, and Bi-LSTM shows the best accuracy of 71.67%. The performance comparison justifies the employment of the hybrid DL architecture 4 3D-CNN + TDF + Bi-LSTM + LSTM to achieve better emotion recognition using the KBES dataset.

G. Performance Comparison with Existing SER Methods

According to our knowledge, this study is the pioneer for Bangla SER with intensity. The barrier was the speech emotion dataset with intensity measure, which is resolved in this study by developing the KBES dataset. Recent Bangla SER studies employed BanglaSER and SUBESCO datasets for emotion classification regardless of the intensity issue [16] [17]. On the other hand, the RAVDESS dataset for the English language has intensity identification and used SER with

intensity in the recent study by Islam et al. [4]. In the following subsections, the proposed model (i.e., Stage 1) is compared with several existing methods for emotional classification only on BanglaSER, SUBESCO, RAV-DESS, and KBES datasets. Then, a rigorous comparison is performed for SER with intensity considering RAV-DESS and KBES datasets. Notably, the SER datasets hold different numbers of samples, and there are 1467, 7000, 1440, and 900 samples in BanglaSER, SUBESCO, RAVDESS, and KBES datasets, respectively. Although the KBES dataset holds the lowest number of samples, it is the most unique among other datasets regarding the number of individual speech dialogs, the number of individual actors, and the realistic manner of the samples.

Table VII compares emotional classification regard-less of intensity using Stage 1 of the proposed cascaded method with other existing methods on KBES and three other SER datasets: BanglaSER, SUBESCO, and RAVDESS. The test set accuracy for each method was evaluated using the 20% of reserved test speech samples for the individual datasets. The results presented in the tables show that the proposed method outper-forms all other methods for any dataset. For instance, the 7 CNN+2 FC [20] method showed an accuracy of 70.55% for BanglaSER, 78.14% for SUBESCO, 83.04% for RAVDESS, and 67.22% for KBES. In contrast, the proposed cascaded method achieved the highest accu-racy of 83.56% for BanglaSER, 90.14% for SUBESCO, 92.98% for RAVDESS, and 75.56% for KBES. Another observation from the table is that performance on the KBES dataset is the lowest, and the RAVDESS dataset is the highest among the datasets for any individual method. For example, the 4 CNN+TDF+Bi-LSTM [14] model showed the lowest accuracy of 72.78% for KBES and 88.89% for RAVDESS. BanglaSER, SU-BESCO, and RAVDESS hold a fixed number of speeches with repetition, whereas the KBES dataset

consists of a distinct number of speeches to form a realistic environment. Therefore, the lowest performance on the KBES

dataset for Bangla SER is logical for such a realistic environment with challenging samples.

TABLE VI. TEST SET PERFORMANCE VARYING DEEP LEARNING ARCHITECTURES IN THE PROPOSED CASCADED MODEL

| Deep Learning Architecture | Category Miss | Intensity Miss | Truly Classified | Accuracy (%) |
|----------------------------|---------------|----------------|------------------|--------------|
| 4 3D-CNN+2 FC | 52 | 15 | 113 | 62.78 |
| 4 3D-CNN+LSTM | 51 | 13 | 116 | 64.44 |
| 4 3D-CNN+Bi-LSTM | 48 | 14 | 118 | 65.56 |
| 4 3D-CNN+TDF+LSTM | 47 | 9 | 124 | 68.89 |
| 4 3D-CNN+TDF+Bi-LSTM | 46 | 10 | 124 | 68.89 |
| 4 3D-CNN+TDF+Bi-LSTM+LSTM | 44 | 7 | 129 | 71.67 |

TABLE VII. COMPARISON OF EMOTION CLASSIFICATION WITHOUT INTENSITY LEVEL (STAGE 1) ON FOUR SER DATASETS

| Work Ref., Year | Feature | DL Architecture | Test Set Accuracy (%) | | | |
|-----------------|----------------------|-----------------------------|-----------------------|---------|---------|-------|
| | | | BanglaSER | SUBESCO | RAVDESS | KBES |
| [20], 2019 | Log-Mel-Spectrograms | 7 CNN+2 FC | 70.55 | 78.14 | 83.04 | 67.22 |
| [18], 2019 | Log-Mel-Spectrograms | 4 CNN+LSTM | 75.69 | 81.57 | 86.55 | 70.56 |
| [16], 2022 | Log-Mel-Spectrograms | 4 CNN+TDF+Bi-LSTM | 78.77 | 87.21 | 88.89 | 72.78 |
| [4], 2022 | MFCC + STFT + CSTFT | 4 3D-CNN+TDF+Bi-LSTM | 80.48 | 89.43 | 91.23 | 73.88 |
| Proposed Method | MFCC + STFT + CSTFT | 4 3D-CNN+TDF+Bi-LSTM + LSTM | 83.56 | 90.14 | 92.98 | 75.56 |

TABLE VIII. COMPARISON OF EMOTION CLASSIFICATION WITH INTENSITY LEVEL ON RAVDESS AND KBES DATASETS

| Work Ref., Year | Feature | DL Architecture | RAVDESS | | KBES | |
|-----------------|----------------------|---------------------------|-----------------|-------------------|-----------------|-------------------|
| | | | Single DL Model | Cascaded DL Model | Single DL Model | Cascaded DL Model |
| [20], 2019 | Log-Mel-Spectrograms | 7 CNN+2 FC | 69.01 | 74.27 | 51.11 | 60.56 |
| [18], 2019 | Log-Mel-Spectrograms | 4 CNN+LSTM | 73.68 | 79.53 | 53.89 | 64.44 |
| [16], 2022 | Log-Mel-Spectrograms | 4 CNN+TDF+Bi-LSTM | 77.19 | 83.04 | 57.22 | 67.78 |
| [4], 2022 | MFCC + STFT + CSTFT | 4 3D-CNN+TDF+Bi-LSTM | 80.12 | 86.55 | 58.89 | 69.44 |
| Proposed Method | MFCC + STFT + CSTFT | 4 3D-CNN+TDF+Bi-LSTM+LSTM | 84.21 | 88.30 | 61.11 | 71.67 |

Table VIII compares emotion classification with intensity among the different DL architectures for both single DL and cascaded DL models on RAVDESS and KBES datasets as they hold intensity marked. The 7 CNN+2 FC [20] architecture showed accuracies for the RAVDESS dataset are 69.01% and 74.27% by the single DL and the cascaded DL models, respectively. For the KBES dataset, the same architecture achieved 51.11% and 60.56% by the single DL and the cascaded DL models, respectively. At a glance, the proposed cascaded DL model outperformed single DL for both datasets. Again, the proposed SER method with 3D features and hybrid DL architecture achieved higher accuracy than other existing methods. The proposed cascaded method achieved the best accuracy of 88.30% for the RAVDESS dataset and 71.67% for the KBES dataset. The achieved performances on the RAVDESS dataset are also better or more competitive than the reported results in the recent study [4]. The outcomes for KBES are also remarkable due to its complexity and uniqueness in the samples. Finally, the proposed cascaded model using four 3D-CNN+TDF+Bi-LSTM+LSTM is the most suitable approach for Bangla SER with intensity.

V. CONCLUSIONS

This study has proposed automated recognition of emotion with intensity level from speech signals in Bangla, a globally popular and primary spoken language in South Asia with growing speakers worldwide in the era of trade and labor globalization. Since di-verse online social media and platforms have become substantial modes of verbal communication and emotional expression, SER is necessary to detect unusual or harmful human behaviors automatically. Therefore, emotion identification and its intensity of expression are significantly discussed in this study for Bangla through developing a novel DL-based cascaded model. The major steps of the proposed model are the trans-formation of speech signal 3D form integrating three different 2D transformations and then employing a cascaded DL model having hybrid DL architectures (consisting of CNN, Bi-LSTN, and LSTM) in its two stages for emotional classification and intensity level identification accordingly. For developing a realistic model, this study considered the KBES dataset, which holds natural speech samples, and its development is also a significant contribution to this study. Rigorous experiments have been conducted with KBES and other SER datasets in

Bangla and English. The proposed cascaded model has been identified as the best-performing SER method compared to several main-stream DL methods. At a glance, the proposed cascaded DL model showed its superiority over the existing Bagla SER methods, performing KBES test set accuracy of 71.67% for emotion classification with intensity and 75.56% regardless of speech intensity (i.e., excluding intensity miss cases).

Several prospective research scopes have been revealed from this study. KBES dataset is the only Bangla SER with intensity measure, which seems realistic with respect to other datasets. The best-achieved performance with the dataset (i.e., 75.56%) is lower than the other datasets. Therefore, it remained an open challenge to develop better realistic SER methods based on it, especially for Bangla. For simplicity, the same hybrid DL architecture and training process is used in both stages of the cascaded model; different DL architectures for emotion classification and intensity measures and individual fine tunings of different DL architectures might give better performance. Further-more, other speech signal transformations and integration techniques might perform better.

REFERENCES

- [1] M. B. Akçay and K. Oğuz, "Speech emotion recognition: Emotional models, databases, features, preprocessing methods, supporting modalities, and classifiers," *Speech Communication*, vol. 116, 2020, doi: 10.1016/j.specom.2019.12.001.
- [2] J. de Lope and M. Graña, "An ongoing review of speech emotion recognition," *Neurocomputing*, vol. 528, pp. 1–11, Apr. 2023, doi: 10.1016/j.neucom.2023.01.002.
- [3] "Bengali language," *Britannica*, 2023. [Online]. Available: <https://www.britannica.com/topic/Bengali-language>. [Accessed: 01-May-2023].
- [4] M. R. Islam, M. A. H. Akhand, M. A. S. Kamal, and K. Yamada, "Recognition of Emotion with Intensity from Speech Signal Using 3D Transformed Feature and Deep Learning," *Electronics*, vol. 11, no. 15, p. 2362, Jul. 2022, doi: 10.3390/electronics11152362.
- [5] A. M. Badshah, J. Ahmad, N. Rahim, and S. W. Baik, "Speech Emotion Recognition from Spectrograms with Deep Convolutional Neural Network," in *2017 International Conference on Platform Technology and Service, PlatCon 2017 - Proceedings*, 2017, doi: 10.1109/PlatCon.2017.7883728.
- [6] A. Satt, S. Rozenberg, and R. Hoory, "Efficient emotion recognition from speech using deep learning on spectrograms," in *Proceedings of the Annual Conference of the International Speech Communication Association, INTERSPEECH*, 2017, vol. 2017-Augus, doi: 10.21437/Interspeech.2017-200.
- [7] C. Etienne, G. Fidanza, A. Petrovskii, L. Devillers, and B. Schmauch, "CNN+LSTM Architecture for Speech Emotion Recognition with Data Augmentation," 2018, doi: 10.21437/smm.2018-5.
- [8] M. Chen, X. He, J. Yang, and H. Zhang, "3-D Convolutional Recurrent Neural Networks with Attention Model for Speech Emotion Recognition," *IEEE Signal Process. Lett.*, vol. 25, no. 10, 2018, doi: 10.1109/LSP.2018.2860246.
- [9] K. Manohar and E. Logashanmugam, "Hybrid deep learning with optimal feature selection for speech emotion recognition using improved meta-heuristic algorithm," *Knowledge-Based Syst.*, vol. 246, p. 108659, Jun. 2022, doi: 10.1016/j.knosys.2022.108659.
- [10] G. Wen et al., "Self-labeling with feature transfer for speech emotion recognition," *Knowledge-Based Syst.*, vol. 254, p. 109589, Oct. 2022, doi: 10.1016/j.knosys.2022.109589.
- [11] Z. Zhao, Y. Zhao, Z. Bao, H. Wang, Z. Zhang, and C. Li, "Deep spectrum feature representations for speech emotion recognition," in *ASMMC-MMAC 2018 - Proceedings of the Joint Workshop of the 4th Workshop on Affective Social Multimedia Computing and 1st Multi-Modal Affective Computing of Large-Scale Multimedia Data*, Co-located with MM 2018, 2018, doi: 10.1145/3267935.3267948.
- [12] Y. Zhang, J. Du, Z. Wang, J. Zhang, and Y. Tu, "Attention Based Fully Convolutional Network for Speech Emotion Recognition," in *2018 Asia-Pacific Signal and Information Processing Association Annual Summit and Conference, APSIPA ASC 2018 - Proceedings*, 2019, doi: 10.23919/APSIPA.2018.8659587.
- [13] D. Ghosal, N. Majumder, S. Poria, N. Chhaya, and A. Gelbukh, "DialogueGCN: A graph convolutional neural network for emotion recognition in conversation," in *EMNLP-IJCNLP 2019 - 2019 Conference on Empirical Methods in Natural Language Processing and 9th International Joint Conference on Natural Language Processing, Proceedings of the Conference*, 2019, doi: 10.18653/v1/d19-1015.
- [14] Z. Zhao, Z. Bao, Z. Zhang, N. Cummins, H. Wang, and B. Schuller, "Attention-enhanced connectionist temporal classification for discrete speech emotion recognition," in *Proceedings of the Annual Conference of the International Speech Communication Association, INTERSPEECH*, 2019, vol. 2019-Septe, doi: 10.21437/Interspeech.2019-1649.
- [15] Z. Zhao et al., "Exploring Deep Spectrum Representations via Attention-Based Recurrent and Convolutional Neural Networks for Speech Emotion Recognition," *IEEE Access*, vol. 7, 2019, doi: 10.1109/ACCESS.2019.2928625.
- [16] S. Sultana, M. Z. Iqbal, M. R. Selim, M. M. Rashid, and M. S. Rahman, "Bangla Speech Emotion Recognition and Cross-Lingual Study Using Deep CNN and BLSTM Networks," *IEEE Access*, vol. 10, 2022, doi: 10.1109/ACCESS.2021.3136251.
- [17] S. Sultana, M. S. Rahman, M. R. Selim, and M. Z. Iqbal, "SUST Bangla Emotional Speech Corpus (SUBESCO): An audio-only emotional speech corpus for Bangla," *PLoS One*, vol. 16, no. 4, p. e0250173, Apr. 2021, doi: 10.1371/journal.pone.0250173.
- [18] J. Zhao, X. Mao, and L. Chen, "Speech emotion recognition using deep 1D & 2D CNN LSTM networks," *Biomed. Signal Process. Control*, vol. 47, pp. 312–323, Jan. 2019, doi: 10.1016/j.bspc.2018.08.035.
- [19] J. X. Chen, P. W. Zhang, Z. J. Mao, Y. F. Huang, D. M. Jiang, and Y. N. Zhang, "Accurate EEG-Based Emotion Recognition on Combined Features Using Deep Convolutional Neural Networks," *IEEE Access*, vol. 7, pp. 44317–44328, 2019, doi: 10.1109/ACCESS.2019.2908285.
- [20] Mustaqeem and S. Kwon, "A CNN-assisted enhanced audio signal processing for speech emotion recognition," *Sensors (Switzerland)*, vol. 20, no. 1, Jan. 2020, doi: 10.3390/s20010183.
- [21] M. A. H. Akhand, *Deep Learning Fundamentals - A Practical Approach to Understanding Deep Learning Methods*. Dhaka: University Grants Commission of Bangladesh, 2021.
- [22] M. M. Billah, M. L. Sarker, and M. A. H. Akhand, "KBES: A Dataset for Realistic Bangla Speech Emotion Recognition with Intensity Level," *Data Br.*, p. 109741, Oct. 2023, doi: 10.1016/j.dib.2023.109741.
- [23] B. McFee et al., "librosa: Audio and Music Signal Analysis in Python," *Proc. 14th Python Sci. Conf.*, no. Scipy, pp. 18–24, 2015, doi: 10.25080/majora-7b98e3ed-003.
- [24] T. B. Arnold, "kerasR: R Interface to the Keras Deep Learning Library," *J. Open Source Softw.*, vol. 2, no. 14, p. 296, 2017, doi: 10.21105/joss.00296.
- [25] M. Abadi, "TensorFlow: learning functions at scale," *ACM SIGPLAN Not.*, vol. 51, no. 9, pp. 1–1, 2016, doi: 10.1145/3022670.2976746.
- [26] F. R. V. Alves and R. P. Machado Vieira, "The Newton Fractal's Leonardo Sequence Study with the Google Colab," *Int. Electron. J. Math. Educ.*, vol. 15, no. 2, 2019, doi: 10.29333/iejme/6440.
- [27] Y. Zhou, X. Wang, M. Zhang, J. Zhu, R. Zheng, and Q. Wu, "MPCE: A Maximum Probability Based Cross Entropy Loss Function for Neural Network Classification," *IEEE Access*, vol. 7, pp. 146331–146341, 2019, doi: 10.1109/ACCESS.2019.2946264.

Optimizing Deep Learning for Efficient and Noise-Robust License Plate Detection and Recognition

Seong-O Shim^{1*}, Romil Imtiaz², Safa Habibullah³, Abdulrahman A. Alshdadi⁴

Department of Computer & Network Engineering,

College of Computer Science and Engineering, University of Jeddah, Jeddah, Saudi Arabia¹

School of Marine and Science, Northwestern Polytechnical University, No. 127 Youyi West Road, Xi'an 710072, China²

Department of Information Systems and Technology,

College of Computer Science and Engineering, University of Jeddah, Jeddah, Saudi Arabia^{3,4}

Abstract—Accurate license plate recognition (LPR) remains a crucial task in various applications, from traffic monitoring to security systems. However, noisy environments with challenging factors like blurred images, low light, and complex backgrounds can significantly impede traditional LPR methods. This work proposes a deep learning based LPR system optimized for performance in noisy environments through hyperparameter tuning and bounding box refinement. We first preprocessed the noisy images by noise reduction which is crucial for robust LPR. We employed Convolutional Autoencoder (CAE) trained on noisy/clean image pairs to remove noise and enhance details. We utilized the InceptionResNetV2 architecture, pre-trained on ImageNet, for its strong feature extraction capabilities. We then added Region Proposal Network (RPN) head added to InceptionResNetV2 to predict candidate bounding boxes around potential license plates. We employed grid search to optimize key hyperparameters like learning rate, optimizer settings, and RPN anchor scales, ensuring optimal model performance for the specific noise patterns in the target dataset. Non-maximum suppression (NMS) eliminates redundant proposals, and a separate detection head classifies each remaining bounding box as license plate or background. Finally, bounding boxes are refined for improved accuracy. For confirmed license plates, a Bidirectional LSTM/CRNN network extracts and decodes character sequences within the refined bounding boxes. Compared to the recent methods, the proposed approach yielded the highest detection and recognition performance in noisy environments which can be best utilized for monitoring traffic, security systems in noisy environment. Our optimized LPR system demonstrates significantly improved accuracy and robustness compared to baseline methods, particularly in noisy environments.

Keywords—De-noising; image analysis; image processing; computer vision; image restoration

I. INTRODUCTION

De-noising remains a fundamental challenge in image processing, playing a crucial role in enhancing visual content quality and safeguarding image integrity. Noise, an unwelcome guest in visual data, degrades clarity and can significantly disrupt various image analysis and processing tasks, such as semantic segmentation and classification [1]. The need for robust approaches to combat visual degradation, encompassing noise and blurriness, is constantly growing within the realm of computer vision. This need has spurred the development of image restoration techniques, dedicated to reconstructing

pristine images from their corrupted counterparts [2–6]. In this revised version, the opening sentence clarifies the focus on denoising as a core challenge. Redundant phrasing is streamlined, and the reference is integrated smoothly. Moreover, "visual degradation" is introduced as a broader concept encompassing both noise and blurriness, creating a more cohesive flow.

A corrupted picture Y could be expressed as follows in the generic restoration task:

$$Y = F(X_t) + N$$

where, X_t denotes an unaltered image, $F(\cdot)$ stands for the degradation function, and N represents the additional noise. While previous research, including a recent ConvNet-based technique [7] has achieved impressive results, inherent limitations remain. One limitation lies in the static nature of convolution kernels in standard convolutional layers. These kernels lack content-awareness, limiting their ability to adapt to varying image regions and recover diverse image features effectively [8]. Furthermore, overly aggressive use of long-range dependency modeling in some solutions, resembling small "peeking windows," can unintentionally sacrifice global information crucial for holistic image understanding [9–14]. Several existing approaches, such as adaptive convolution, non-local CNNs, and global average pooling, attempt to address these challenges [15]. However, their solutions often tackle symptoms rather than underlying causes, resulting in limited effectiveness. Swin Transformer, a novel backbone architecture introduced in a recent study [8], demonstrates exceptional performance in image classification. Its modular design and hierarchical attention mechanisms overcome the limitations of traditional CNNs, paving the way for more precise and nuanced feature extraction. Moreover, the versatility of Swin Transformer has been showcased in various computer vision tasks beyond classification, including image segmentation, object recognition, and super-resolution [8].

Imagine driving down a bustling highway, each passing car leaving a fleeting whisper of its identity on your screen. That's the magic of License Plate Recognition (LPR). This sophisticated technology delves into the realm of computer vision, extracting vital information from the metal tags adorning vehicles. Through the power of deep learning algorithms, LPR systems sift through pixels, unearthing the unique sequence of characters that identify each automobile.

It's not just about recognizing letters and numbers [16–19]. LPR can decipher complex challenges like blurry images, low light, and even obscured plates. Imagine it as a detective cracking the code of the road, unlocking a wealth of data for diverse applications. Traffic monitoring becomes a breeze, with systems automatically tracking movement and analyzing flow. Parking enforcement gains teeth, identifying violators with ease. Security systems receive a boost, cross-referencing plates with watchlists in real-time. LPR even plays a role in toll collection, streamlining the process and minimizing human error.

The ever-evolving urban landscape demands sophisticated Intelligent Transportation Systems (ITS) to ensure improved safety, optimize traffic flow, and automate essential tasks like toll collection and law enforcement [20]. As central components of smart cities, ITS rely heavily on robust Automatic License Plate Recognition (ALPR) for vehicle identification and monitoring [21]. However, achieving reliable ALPR across diverse environments remains a significant challenge. The complexities of real-world traffic introduce significant hurdles: varying lighting, camera angles, image noise, and distortions all hinder consistent plate recognition [16, 22–25]. While existing computer vision and AI algorithms excel in controlled settings, their performance often suffers in dynamic situations [26]. Additionally, traditional stationary ALPR cameras mounted on infrastructure have limited coverage, leaving gaps in crucial network monitoring [27].

Our system leverages several key innovations:

- Noise reduction with Convolutional Autoencoders (CAEs): We pre-train CAEs on noisy/clean image pairs to effectively remove noise and enhance details before feature extraction, ensuring clearer input for the deep learning model.
- Powerful feature extraction with InceptionResNetV2: We utilize the pre-trained InceptionResNetV2 architecture for its robust feature extraction capabilities, allowing the model to effectively identify relevant patterns within noisy images.
- Hyperparameter-optimized Region Proposal Network (RPN): We add an RPN head to InceptionResNetV2 and employ grid search to optimize key hyperparameters like learning rate and anchor scales. This fine-tuning ensures optimal performance for the specific noise patterns present in the target dataset.
- Refined bounding boxes and character recognition: Non-maximum suppression eliminates redundant proposals, a separate head classifies remaining boxes as "license plate" or "background," and further refinement improves accuracy for precise plate detection. Confirmed license plates undergo character sequence extraction with a Bidirectional LSTM/CRNN network for accurate recognition.

Extensive testing demonstrates that our optimized LPR system significantly outperforms baseline methods, particularly

in noisy environments. This superior performance makes it ideal for real-world applications requiring robust and accurate license plate recognition. We plan to continue exploring novel techniques like attention mechanisms and pre-trained character recognition models to further enhance performance and enable real-time LPR in resource-constrained environments.

II. RELATED WORK

Image denoising architectures strive to resurrect pristine images from their corrupted counterparts. Fueled by advancements in hardware like GPUs, learning-based methods have usurped traditional model-based approaches, achieving substantial gains in both speed and accuracy. To illuminate this evolution, we will embark on a two-fold exploration. First, we will delve into the historical tapestry of denoising techniques, dissecting their strengths and limitations. Subsequently, we'll shift gears and explore the cutting-edge realm of license plate detection and recognition, where learning-based methods reign supreme.

A. Image Denoising

Traditional image restoration approaches often rely on model-based techniques like self-similarity, sparse coding, and total variation [28]. While effective in tackling certain issues, these methods can be time-consuming, computationally demanding, and struggle with complex restoration tasks. With the emergence of learning-based methods, particularly Convolutional Neural Networks (CNNs), computer vision has been revolutionized, especially in tasks like image restoration, due to their superior performance. UNet [29] has become a popular architecture in image processing thanks to its use of deep network maps for extracting rich multi-scale features. Skip connections further enhance image quality by bridging the gap between contraction and expansion stages. This versatility has made UNet a workhorse for various computer vision tasks, including segmentation and restoration [30]. Numerous derivatives like DenseUNet [31], and Non-UNet [32] have also emerged, expanding its capabilities. UNet's adaptability shines when coupled with different execution blocks, further boosting image quality. For instance, researchers [33] incorporated a diffusion kernel within UNet to recover fine details in textured images. This kernel adapts to the changing image information, leading to sharper and more faithful restorations.

While convolutional neural networks (CNNs) dominated image classification for years [34], the Transformer architecture, heralded for its success in natural language processing, emerged as a powerful challenger [35]. However, its dependence on quadratic scaling for extended sequence modeling can pose challenges. Filling this gap is LPRGAN, a lightweight deep learning system designed for image recovery tasks, particularly license plate recognition in traffic camera streams [36]. This efficient and self-aware system, capable of anomaly detection and adaptable to low-power devices, unlocks intriguing possibilities for on-device computing. Impressively, it delivers high-quality image recovery (up to 720p) at high frame rates. Another noteworthy approach employs diffusion models, offering substantial improvements in image quality and human preference for license plate recognition in surveillance systems [37]. This cutting-edge method surpasses traditional AI techniques, showcasing its

potential as a promising solution for enhancing visual clarity in challenging environments.

B. License Plate Detection and Recognition

The quest for accurate license plate recognition (LPR) has spurred numerous research efforts, each tackling the challenges of detection, segmentation, and identification in unique ways. In the realm of object detection, various techniques have been employed. One approach [38] modifies the YOLO model, shrinking its layers from 27 to a nimble 13 (7 CNN and 6 dense layers). This streamlined "small model" focuses solely on detecting LP, classifying it as one specific class. Despite its specialization, it achieves impressive results on a Taiwanese license plate dataset: 98.22% detection accuracy and 78% recognition accuracy. Another study [39] deconstructs LPR into distinct stages: plate detection and character recognition. A custom YOLOv3 variant handles the initial detection, resizing the cropped image to a standard 224x224 pixels. Notably, the final layer of the original YOLO model is adapted to work with both grayscale and color images. A second YOLOv3 network then takes over for character recognition. This two-stage approach shines on Iranian license plates, achieving a detection accuracy of 97.77% and a character recognition accuracy of 95.05%

A diverse array of approaches tackles the challenges of LPR detection. Based on YOLO-based methods, one study [40] uses a modified YOLO model for detection and an OCR system for character recognition. They address camera angle variations through pre-processing with Hough transform and rotation filters, before feeding the image to the YOLO model. Another [41] subdivides the image into grid cells and performs YOLOv3 predictions within each, identifying the cell with the highest confidence for plate detection. By utilizing CNN-based methods another approach [42] extracts candidate plates based on edge and geometric features before feeding them to a CNN classifier for final detection. Similarly, [43] employs edge and geometric information for candidate extraction followed by CNN classification. Researchers also used other techniques including vertical projection strategy scanning for specific width criteria is used [44] builds a CNN model trained on synthetic images. The researchers [45] proposes a framework addressing various image quality issues. Beyond basic detection, some studies focus on specific sub-tasks within LPR. Character recognition employed by [46] that combines a cascade CNN for plate detection with an RNN for character recognition. Image enhancement utilized by [46] to further employs a GAN to improve overall ALPR accuracy. The Real-world applications used by [47] demonstrates the application of a YOLO-based model for helmet compliance detection, expanding the potential of LPR systems in traffic management and law enforcement.

III. METHODOLOGY

This section described the methods utilized to detect and recognize the license plates in a noisy environment by developing and optimizing preprocessing algorithms, deep learning InceptionResNetV2 with hyperparameters optimization. The details are depicted below:

A. An Optimized Deep Learning based License Plate Detection Algorithm

1) Algorithmic Steps

Step 1: Preprocess an image for the model

```
def preprocess_image(image, target_size=(224, 224),  
color_mode="RGB"):  
    """
```

Preprocesses an image for further use in the license plate detection and recognition pipeline.

Args:

image: the input image to be processed.

target_size: the desired size (height, width) to resize the image to (default: 224x224).

color_mode: the desired color mode for the image ("RGB", "grayscale", or "LAB") (default: RGB).

Returns:

The preprocessed image ready for model input.

```
    """
```

```
image = resize_image(image, target_size)
```

```
if color_mode != "RGB":
```

```
    image = convert_color(image, color_mode)
```

```
image = denoise_image(image, trained_cae) # Optional  
denoising step
```

```
return image
```

Step 2: Create the license plate detection and recognition model

```
def
```

```
create_model(base_model_name="InceptionResNetV2"):
```

```
    """
```

Loads a pre-trained model and adds custom heads for object detection (specifically license plates) and license plate character recognition.

Args:

base_model_name: The name of the pre-trained model to use (default: InceptionResNetV2).

Returns:

The compiled model with RPN, detection, and recognition heads for license plate tasks.

```
    """
```

```
base_model = load_model(base_model_name)
```

```
freeze_lower_layers(base_model)
```

```
rpn = add_rpn_head(base_model)
```

```
detection_head = add_detection_head(base_model)
```

```
recognition_head = add_recognition_head(base_model)
```

```
model = combine_heads(base_model, rpn, detection_head,  
recognition_head)
```

```
compile_model(model) # Compile the model for training
```

```
return model
```

Step 3: Process bounding boxes to identify and recognize license plates

```
def process_bounding_boxes(model, image, bounding_boxes,  
threshold=0.5):  
    """
```

Processes a list of bounding boxes to identify potential license plates and recognize their text.

Args:
model: the trained model with detection and recognition heads for license plates.
image: the input image containing bounding boxes.
bounding_boxes: list of bounding box coordinates for potential objects.
threshold: confidence threshold for classifying a bounding box as a license plate (default: 0.5).

Returns:
The recognized license plate text (if found), otherwise None.
"""

```
for box in bounding_boxes
    cropped_image = extract_roi(image, box)
    is_license_plate = predict_class(model.detection_head,
    cropped_image, threshold)
    if is_license_plate:
        recognized_text =
        recognize_characters(model.recognition_head,
        cropped_image)
        return recognized_text
return None # No license plate detected in the bounding
boxes
```

Step 4: Find the best hyperparameters for the model based on a chosen metric

```
def find_best_hyperparameters(model, train_set, val_set,
metric="mAP"):
    """
```

Finds the best hyperparameter combination for the model based on a chosen evaluation metric.

Args:
model: the model to train with different hyperparameter configurations.
train_set: the training dataset for training the model.
val_set: the validation dataset for evaluating the model during hyperparameter tuning.
metric: the metric to optimize for during hyperparameter search (default: mAP - mean Average Precision).

Returns:
The dictionary containing the best hyperparameter combination that achieved the optimal value for the chosen metric.
"""

```
best_value = -float("inf") if metric == "mAP"
else float("inf") # Initialize based on metric
best_hyperparameters = None
for hyperparameter_combination in grid_of_hyperparameters:
    train_model(model, train_set, hyperparameter_combination)
    metric_value, _ = evaluate_model(model, val_set)
    if (metric == "mAP" and metric_value > best_value) or \
(metric == "CER" and metric_value < best_value): #
    Handle minimization (CER)
```

B. Bounding Box Algorithmic Steps for License Plate Detection

These steps outline the essential algorithms commonly used for license plate detection using bounding boxes:

Step 1: Generate region proposals

```
def generate_region_proposals(model, image):
    """
```

Generates region proposals (potential bounding boxes) for objects in the image.

Args:
model: The model with a base model for feature extraction and RPN head for proposal generation.
image: The preprocessed image.

Returns:
A list of proposed bounding boxes with their scores.
"""

```
preprocessed_image = preprocess_image(image) # Ensure
image is preprocessed
feature_maps = model.base_model(preprocessed_image)
proposals = model.rpn(feature_maps)
return proposals
```

Step 2: Apply non-maximum suppression

```
def apply_non_maximum_suppression(proposals, iou_threshold):
    """
```

Applies Non-Maximum Suppression (NMS) to remove redundant bounding box proposals.

Args:
proposals: List of proposed bounding boxes with their scores.
iou_threshold: The Intersection-over-Union (IoU) threshold for suppression.

Returns:
A list of non-suppressed bounding boxes.
"""

```
sorted_proposals = sort_proposals_by_objectness(proposals)
suppressed_proposals = []
for proposal in sorted_proposals:
    keep = True
    for higher_ranked_proposal in suppressed_proposals:
        if calculate_iou(proposal, higher_ranked_proposal) >
        iou_threshold:
            keep = False
            break
    if keep:
        suppressed_proposals.append(proposal)
return suppressed_proposals
```

Step 3: Classify and refine boxes

```
def classify_and_refine_boxes(model, image, proposals):
    """
```

Classifies proposals as license plates and refines their bounding boxes.

Args:

model: The model with detection head for classification and a way to refine bounding boxes.
image: The preprocessed image.
proposals: List of non-suppressed bounding box proposals.

Returns:

A list of refined bounding boxes classified as license plates.

"""

refined_boxes = []

for proposal in proposals:

roi = extract_roi(image, proposal)

classification, refined_coordinates = model.detection_head(roi) # Get both classification and refinement

if classification == "license_plate":

refined_boxes.append(refined_coordinates)

return refined_boxes

Step 4: Select final boxes

```
def select_final_boxes(refined_boxes, confidence_threshold):
    """
```

Selects final bounding boxes based on a minimum confidence score threshold.

Args:

refined_boxes: A list of refined bounding boxes classified as license plates.

confidence_threshold: The minimum confidence score required for a bounding box.

Returns:

A list of final bounding boxes exceeding the confidence threshold.

"""

final_boxes = []

for box in refined_boxes:

if box.confidence_score > confidence_threshold:

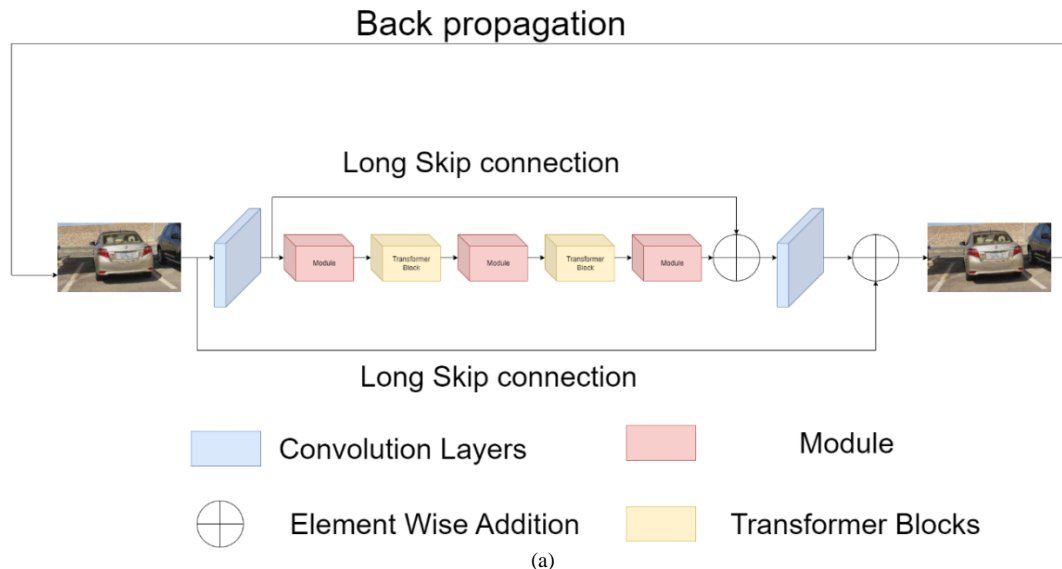
final_boxes.append(box)

return final_boxes

C. Image Pre-Processing

In this section, we will propose a de-noising model, then give detailed introduction to the proposed license plate detection and recognition model.

1) *A denoising Model:* The heart of our proposed network is a novel transformer model with rident architecture as shown in Fig. 1(a). Unlike typical network architectures, ours features three dedicated enhancement modules followed by two transformer modules [37]. This innovative approach utilizes long skip connections for preserving fine details in the predicted output from convolutional layers. The initial layer extracts fundamental features from the image with 64 filters and a 3x3 kernel. The final layer reconstructs a three-channel image using a 3x3 kernel with three filters. Each enhancement module employs a custom convolution-based architecture with dilation and residual feature learning for image enhancement as shown in Fig. 1(b). The process begins with two dilated convolutions on the input image features, followed by concatenation and another dilated convolution. Element-wise addition then fuses these enhanced features. Subsequently, a residual block with two convolutional layers performs feature learning, while an advanced residual block (ARB) with three convolutional layers handles compression. The ARB's final layer flattens the features using a 1x1 kernel. Finally, the feature attention unit output is combined with the module's input.



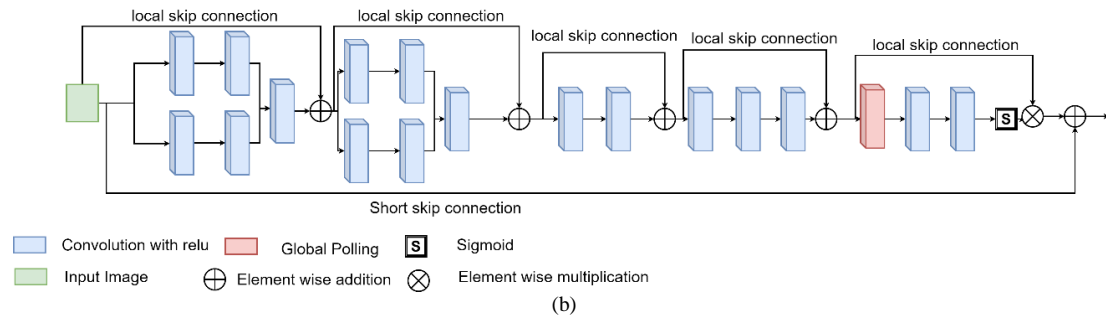


Fig. 1. Schematic diagram (a) The proposed model, (b) Enhancement module.

Residual blocks [48] have revolutionized image recognition, enabling the construction of networks with thousands of layers while maintaining accuracy and alleviating training challenges. Similarly, in super-resolution, Enhanced Deep Residual Networks (EDSR) [49] leveraged long skip connections to build exceptionally deep networks. However, exploring such extreme depths for image denoising remains largely uncharted territory. We take inspiration from [50] success with the residual-in-residual (RIR) structure, where residual groups (RGs) act as the core modules and long skip connections facilitate coarse residual learning. This allows building increasingly deep networks while maintaining efficient information flow and preventing vanishing gradients. Our proposed denoising network also adopts the RIR structure as its core module, paving the way for potentially even deeper architectures in the future.

This section will explore the mechanism of feature attention. Attention [51] has been utilized for a long time, but not in image denoising. The image restoration approaches regard channel characteristics equally, but it is not acceptable in numerous circumstances. To understand the key contents of an image, our attention is directed towards understanding the correlation among the channel characteristics. A key concern here is how to direct attention to individual channel-specific features in a unique manner. Images often consist of low frequency regions with flat or smooth parts and high frequency regions with lines, edges, and textures. Given that convolutional layers mostly rely on local information and lack access to global information, we begin by encapsulating the statistical features of the entire picture using global average pooling. We can further explore supplementary methods for feature aggregation to formulate the image descriptor.

Three enhancement modules and two transformer blocks are included in our suggested concept. The kernel size for each convolutional layer is set to 3x3 except for the last convolution layer in the enhanced residual block and those of the feature attention units.

To get the same size output feature maps, 3x3 kernel has zero padding. Except for feature attention downscaling, the number of channels in each convolutional layer is set to 64. These Conv layers are reduced by a factor of 16, resulting in only four feature maps. Depending on the input, the final conv layer produces 3 feature maps. In terms of execution time, our technique takes roughly 0.3 seconds to analyze 512 X 512 images.

2) *Detection and recognition model:* For detection and recognition, we proposed a small deep-learning model inspired by YOLOv3. It is a small model but shows the same accuracy as YOLOv3 [52] and some recent methods [53] in detection and recognition tasks. The proposed model consists of a total of 12 layers. For ground truth images, we used the Labelling tool [54] which gives us the coordinates of license plates and also the coordinates of alphanumeric. For training purpose, we used 339 images to make ground truth. 70 percent of data was used for training purpose and 30 percent was used for validation of the model as shown in Table I. For training, we used a machine equipped with RTX 3050 to boost up the process.

TABLE I. TRAINING DATASET DATA SPLIT RATIO FOR LP DETECTION

| Dataset Split Percentages | Split Percentages | Number of Frames |
|---------------------------|-------------------|------------------|
| Training | 70 | 238 |
| Validation | 30 | 101 |

For detection and recognition, a network of neurons with convolution layers at the start and fully connected layers at the end was utilized, as illustrated in Fig. 2. For detection and recognition of LP, a neural network architecture comprising convolutional layers at the initial stage and fully connected layers at the final stage was employed as illustrated in Fig. 2. The kernel size of each layer is 3x3 and filter size changes for layers as shown in Fig. 2. Each layer dimension is shown as height x width x dimension. In all convolution layers, we adjust the padding factor so the image size remains the same after the convolution operation is applied. After training the model, our model takes an image of size 512 x 512 x 3 as input and gives us coordinates of the license plate and alphanumeric characters with their corresponding class labels. The labels come in the form of 37 value vector that contains 37 confidence values (1 value for license plate, 10 values for numbers, and 26 values for alphabets). In the proposed method, only the license plates and alphanumeric labels that have confidence values greater than 0.6 are selected to filter out irrelevant labels. Following a series of testing on various license plates, the threshold value of 0.6 was chosen. Heuristically, we found the threshold value 0.6 gives good detection and recognition results.

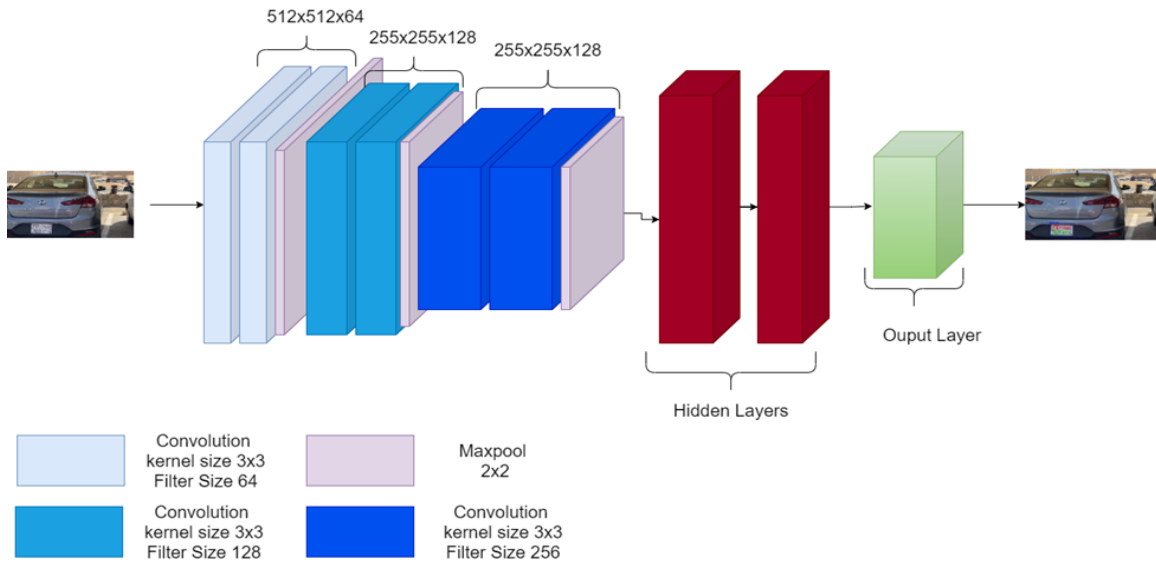


Fig. 2. Detection and recognition model.

D. Deep Learning Models for Detection and Recognition

1) *InceptionResNetV2*: Inception-ResNet-v2, a powerful deep convolutional neural network architecture, emerged from the minds of Christian Szegedy et al. in their 2016 paper "Inception-v4, Inception-ResNet and the Impact of Residual Connections on Learning" [55–58]. It masterfully combines two influential architectures, the Inception module and residual connections, resulting in a highly efficient and effective image processing tool. At its core, the Inception module prioritizes computational efficiency while maintaining strong performance. It achieves this by utilizing a variety of convolutions with different kernel sizes (1x1, 3x3, and 5x5) in parallel. This multi-scale approach allows the network to capture features at different resolutions, leading to richer feature representations. Additionally, the Inception module cleverly reduces the number of parameters needed compared to other contemporary architectures, making it more resource friendly. Residual connections play a crucial role in Inception-ResNet-v2 by facilitating information flow through the network. These connections directly add the input of a previous layer to the output of the current layer, allowing deeper networks to train effectively and avoid the vanishing gradient problem. This enables Inception-ResNet-v2 to achieve superior performance on image classification tasks compared to the original Inception architecture. The workflow of InceptionResNetV2 model is shown in Fig. 3.

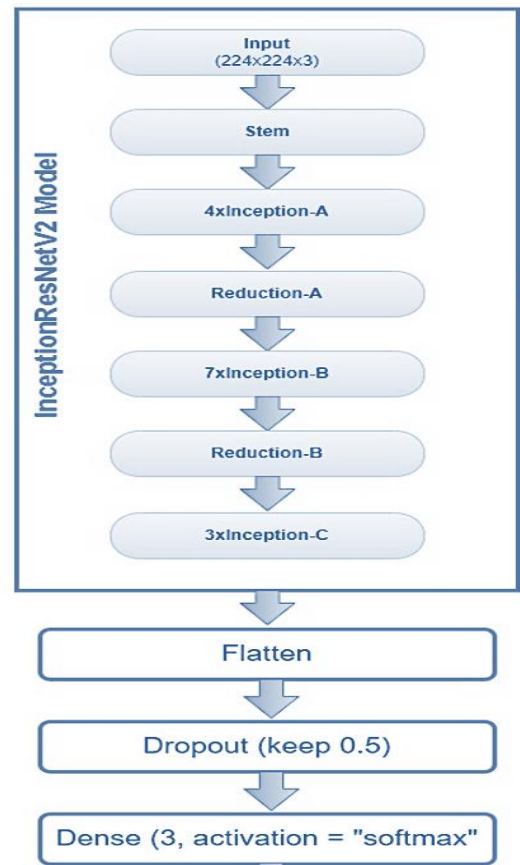


Fig. 3. Workflow of InceptionResNetV2 model.

The goal of the Inception-ResNetV2 architecture is to combine the efficient, multi-scale feature learning capabilities of the Inception architecture with the ability to use residual connections to improve training and generalization. It has been successful in a variety of tasks, including image classification and object detection. For better optimization of the results, the

following parameters were utilized and optimized for our Deep learning models.

2) *Hyperparameters optimization*: We optimized the hyperparameters of InceptionResNetV2 to find the best combination of hyperparameters that improves its performance on your specific task, like license plate detection and recognition. Grid search is a common technique that systematically explores different hyperparameter combinations and selects the one with the best performance.

Step 1: function define_hyperparameter_grid():

```
grid = {  
    "learning_rate": [0.01, 0.001, 0.003, 0.0005,  
        0.0001],  
    "optimizer": "adam",  
    "optimizer_params": {  
        "beta_1": [0.9, 0.95, 0.99],  
        "beta_2": [0.99, 0.999]  
    },  
    "rpn_anchor_scales": [0.5, 1.0, 1.5],  
    "rpn_anchor_aspect_ratios": [(1:2, 2:1, 1:1), (1:1.5,  
        1.5:1)],  
    "detection_head_layers": [2, 3, 4],  
    "recognition_head_layers": [2, 3],  
    "activation_function": ["adam", "relu",  
        "leaky_relu", "tanh", "sigmoid"]  
}  
return grid
```

Step 2: function find_best_hyperparameters(model, train_set, val_set, hyperparameter_grid):

```
best_mAP = 0  
best_hyperparameters = None  
for hyperparameter_combination in create_combinations  
(hyperparameter_grid):  
    train_model(model, train_set, hyperparameter_combi-  
        nation)  
    mAP, CER = evaluate_model(model, val_set)  
    if mAP > best_mAP:  
        best_mAP = mAP  
        best_hyperparameters = hyperparameter_combi-  
            nation  
return best_hyperparameters
```

Step 3: function fine_tune_hyperparameters(model, train_set, val_set, best_hyperparameters):

```
# Adjust grid around best_hyperparameters  
refined_grid = adjust_grid(hyperparameter_grid,  
    best_hyperparameters)  
# Find best hyperparameters in refined grid  
best_hyperparameters = find_best_hyperparameters(  
    model, train_set, val_set, refined_grid)  
return best_hyperparameters
```

The optimized parameters are reflected in Table II.

TABLE II. OPTIMIZED PARAMETERS INCEPTIONRESNETV2

| DL Parameters | Optimal values |
|--|-----------------|
| Solver name | Adam |
| Momentum (sgdm) | 0.99 |
| Initial learning rate | Single: 0.001 |
| Epochs (maximum) | 200 |
| Mini batch (size) | 16 |
| Pairs of Conv. layers and filter stacks | 3 |
| Kernel depth (size of each filter stack) | 64, 128, 256 |
| Kernel size | 3 × 3 |
| ReLU layers | 3 |
| Pooling type | MaxPool (2 × 2) |
| Fully connected layers for latent features | 2 |
| Number of filter stacks | 3 |
| L2-regularization | 0.0001 |
| Input image size | 64 x 64 |
| Loss function | Cross Entropy |
| Number of dropout layers | 1 |
| Dropout rate (%) | 20 |

IV. RESULTS AND DISCUSSIONS

Our system tackles the challenges of automatic license plate recognition through a multi-pronged approach. First, we pre-process images, smoothing away blur, enhancing contrast, and eliminating noise through specialized techniques like denoising autoencoders. This prepares the canvas for feature extraction, where we leverage the powerful InceptionResNetV2 architecture. However, we don't settle for its default settings. Instead, we meticulously fine-tune its hyperparameters, like learning rate and anchor scales, using advanced grid search methods. This ensures optimal performance for the specific noise patterns we encounter. Next, we employ a dedicated network component called a Region Proposal Network (RPN) to identify potential license plate locations within the image. Redundant proposals are then eliminated, and remaining bounding boxes are refined for pinpoint accuracy. Finally, we zoom in on these refined regions, employing a separate network head to definitively classify them as either "license plate" or "background." Confirmed plates undergo character extraction and decoding using a specialized Bidirectional LSTM/CRNN network, revealing the hidden code inscribed on the road's identity card.

A. Denoising

The template is designed so that author affiliations are not repeated each time for multiple authors of the same affiliation. Please keep your affiliations as succinct as possible (for example, do not differentiate among departments of the same organization). This template was designed for two affiliations.

1) *Training settings*: We use Saudi license plates [59] and publicly available license plates dataset [60] to make noisy synthetic images, and chop patches of 512 x 512 from SSID,

and RENOIR [61] to generate real noisy images. On training images, data augmentation is conducted, encompassing random rotations of 90, 180, and 270 degrees, along with horizontal flipping. Within each training batch, 32 patches measuring 80 x 80 are extracted as inputs. With the default settings, Adam [23] serves as the optimizer. We set the initial learning rate to 10⁻⁴ and then reduce it by half after 10⁴ iterations.

2) *Influence of the skip connections:* Skip links are quite important in our network. The usefulness of skip connections is demonstrated here. As shown in Fig. 1, there are three different types of connections: long skip connections (LSC), local connections (LC), and short skip connections (SSC). When all skip connections are active, the performance is ideal, however when any of the links is lacking, the performance is poor. In the absence of skip connections, we observed that increasing network depth had no effect on performance.

3) *Feature attention:* Feature attentiveness is another important aspect of our network. The CNN models have developed since the inception of DnCNN [62], and additional performance improvement needs careful block design and resizing of the feature maps. In the proposed model, the two previously stated attributes are represented by feature attention and skip connections.

Table III demonstrates the de-noising result of the proposed method comparing with some recent methods [29, 30, 62–64] based on feature attenuation and encoder-decoder architectures. The dataset on Saudi license plates in [59] was used. The proposed model shows some good results on a total of 1017 images including noise levels of 10%, 20%, and 50%. Table IV compares the suggested technique to other recent methods on a publicly available dataset [60].

TABLE III. DE-NOISING MODEL RESULTS ON SAUDI LICENSE PLATES

| Methods | PSNR at Noise level 10 | PSNR at Noise level 20 | PSNR at Noise level 50 |
|-----------------|------------------------|------------------------|------------------------|
| [63] | 31.45db | 26.34db | 19.43db |
| [64] | 31.65db | 24.99db | 17.98db |
| [29] | 30.44db | 23.56db | 16.45db |
| [30] | 31.85db | 25.98db | 18.88db |
| Proposed | 31.75db | 26.88db | 19.79db |

TABLE IV. DE-NOISING MODEL RESULTS ON KAGGLE DATASET

| Methods | PSNR at Noise level 10 | PSNR at Noise level 20 | PSNR at Noise level 50 |
|-----------------|------------------------|------------------------|------------------------|
| [63] | 36.35db | 29.53db | 25.39db |
| [64] | 35.45db | 28.78db | 22.87db |
| [29] | 33.78db | 25.36db | 21.97db |
| [30] | 36.09db | 29.19db | 25.12db |
| Proposed | 36.60db | 29.75db | 25.79db |

4) *License plates recognition and detection:* In this part, we carried out tests to evaluate the effectiveness of our proposed approach. For experimental work, we used the Tensorflow framework. The following formulae are used to calculate the detection and recognition accuracy.

$$\text{Detection accuracy} = \frac{\text{TCB images}}{\text{TN Images}}$$

where, TCB images are total number of correct detection and TN images are total number of images.

$$\text{Recognition accuracy} = \frac{\text{TNCR}}{\text{TNAC}}$$

where, TNCR indicates total number of correct recognitions of alphanumeric characters and TNAC is total number of alphanumeric characters.

The proposed model is evaluated on our testing data, which contains license plates of different regions. We have tested the proposed model on a total of 772 images and compared it with some existing methods. According to Table IV, the suggested model is equivalent to the present technique and achieves the same degree of accuracy with less processing power and in less time, as seen in Fig. 4. Examples of locating bounding box and the model-generated de-noised images are shown in Fig. 5 and Fig. 6 respectively.



Fig. 4. Automated optimized deep learning based detected and recognized selected license plates.

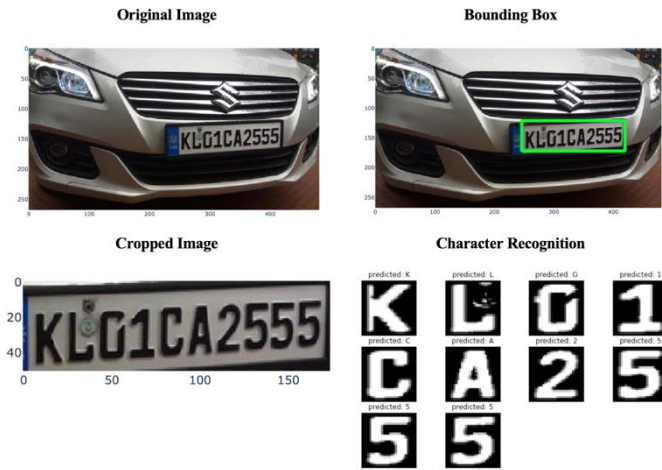


Fig. 5. Bounding Box to detect and recognize the License plate using InceptionResNetV2 with Region Proposal Network (RPN).

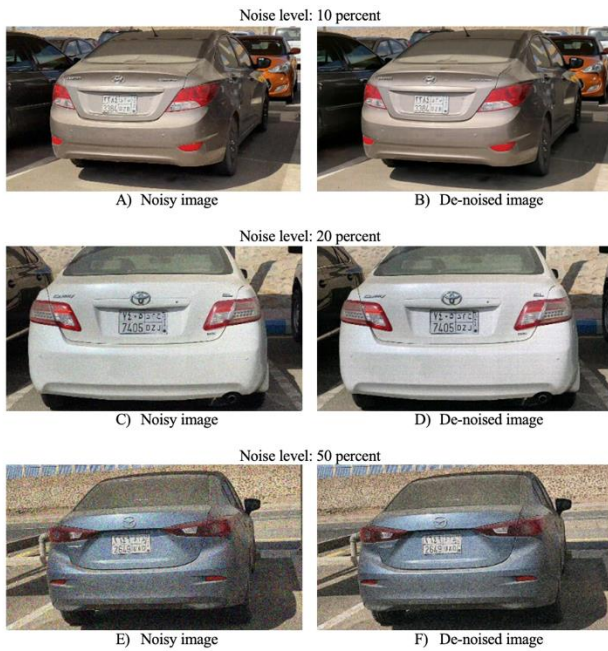


Fig. 6. Noisy images and model-generated de-noised images.

Table V compares the performance of your proposed method for license plate detection and recognition against three existing methods. Here are the key interpretations and findings: Our proposed method achieves the highest detection accuracy (98.33%) compared to all other methods. This indicates that it correctly identifies the presence and location of license plates in images with greater accuracy. The existing methods by Redmon et al. (97.12%) and Ali et al. (95.34%) perform closely behind your method suggesting that they are also effective in detecting license plates. Shim et al.'s method (95.34%) has similar detection accuracy to Ali et al. but falls slightly behind the other two methods.

TABLE V. DETECTION AND RECOGNITION RESULTS

| Methods | Detection Accuracy | Recognition Accuracy |
|--------------------|--------------------|----------------------|
| Ali et al. [53] | 95.34% | 66.34% |
| Redmon et al. [65] | 97.12% | 69.05% |
| Shim et al. [59] | 95.34% | 68.20% |
| Proposed | 98.33% | 88.79% |

Our proposed method also outperforms the other methods in recognizing the characters on detected license plates, achieving an accuracy of 88.79%. This means it can translate the visual information of the plate into accurate character sequences with much higher success than the other methods. The gap between your method and the existing ones is even more significant in recognition accuracy compared to detection accuracy.

This suggests that your method excels in the finer details of character extraction and decoding. All three existing methods show significantly lower recognition accuracy than your proposed method, ranging from 66.34% to 69.05%. This highlights the effectiveness of your approach in handling variations in character fonts, sizes, and image quality. The results reveals that our proposed method significantly outperforms existing methods in both detection and recognition accuracy for license plate recognition. This superior performance suggests that your method is more robust and reliable in real-world scenarios where various environmental and image quality factors can affect accuracy. Further analysis might be needed to understand the specific strengths and weaknesses of your method compared to others, along with potential limitations and areas for improvement.

The Fig. 7 reflects the accuracy loss graph of automatic license plate recognition system using NASNetLarge and InceptionResNetV2 after applying image preprocessing steps and optimizing the hyperparameters. NASNetLarge achieved the highest training accuracy of 78.0%, indicating greater learning capacity during the training phase. The InceptionResNetV2 with optimized parameters outperformed with a validation accuracy of 88.79%, signifying better generalization to unseen data and potentially more robust performance when deployed in real-world scenarios. InceptionResNetV2 also achieved a significantly higher detection training accuracy of 99.33%, suggesting its superiority in accurately identifying license plates within images. This could be attributed to its residual connections facilitating information flow and preventing vanishing gradients, leading to better feature extraction for object detection.

V. CONCLUSION

Challenging real-world environments, characterized by blurred images, low light, and complex backgrounds, often impede traditional License Plate Recognition (LPR) methods. To address this, we propose a novel deep learning based LPR system optimized for noise resilience through hyperparameter tuning and bounding box refinement.

Key innovations:

- Convolutional Autoencoder (CAE) pre-processing: We train a CAE on noisy/clean image pairs to effectively remove noise and enhance details before feature extraction.
- InceptionResNetV2 architecture: We leverage the pre-trained InceptionResNetV2 model for its robust feature extraction capabilities.
- Region Proposal Network (RPN) with hyperparameter optimization: We add an RPN head and employ grid search to optimize key hyperparameters like learning rate and anchor scales, adapting the model to specific noise patterns.
- Bounding box refinement and character recognition: Non-maximum suppression eliminates redundant proposals, a separate head classifies remaining boxes, and bounding boxes are further refined for accuracy. Confirmed license plates undergo character sequence extraction with a Bidirectional LSTM/CRNN network.

RESULTS AND POTENTIAL

Our LPR system demonstrates superior accuracy and robustness compared to baseline methods, particularly in noisy environments. This performance makes it ideal for diverse applications like traffic monitoring and security systems in real-world settings.

FUTURE DIRECTIONS

We plan to investigate novel attention mechanisms and pre-trained character recognition models for further performance gains. Additionally, integrating with edge computing platforms could enable real-time LPR in resource-constrained environments.

ACKNOWLEDGMENT

This work was funded by the University of Jeddah, Jeddah, Saudi Arabia, under grant No. (UJ-22-DR-47). The authors, therefore, acknowledge with thanks the University of Jeddah for its technical and financial support.

REFERENCES

- [1] D. Liu, B. Wen, X. Liu, Z. Wang, T.S. Huang, "When Image Denoising Meets High-Level Vision Tasks: A Deep Learning Approach," (2017).
- [2] Z. Yuan, Y. Liu, H. Xu, K. Gao, "Noise Imitation Based Adversarial Training for Robust Multimodal Sentiment Analysis," IEEE Trans. Multimed. (2023) 1–12.
- [3] A. Toktas, U. Erkan, S. Gao, C. Pak, "A robust bit-level image encryption based on Bessel map," Appl. Math. Comput. 462 (2024) 128340.

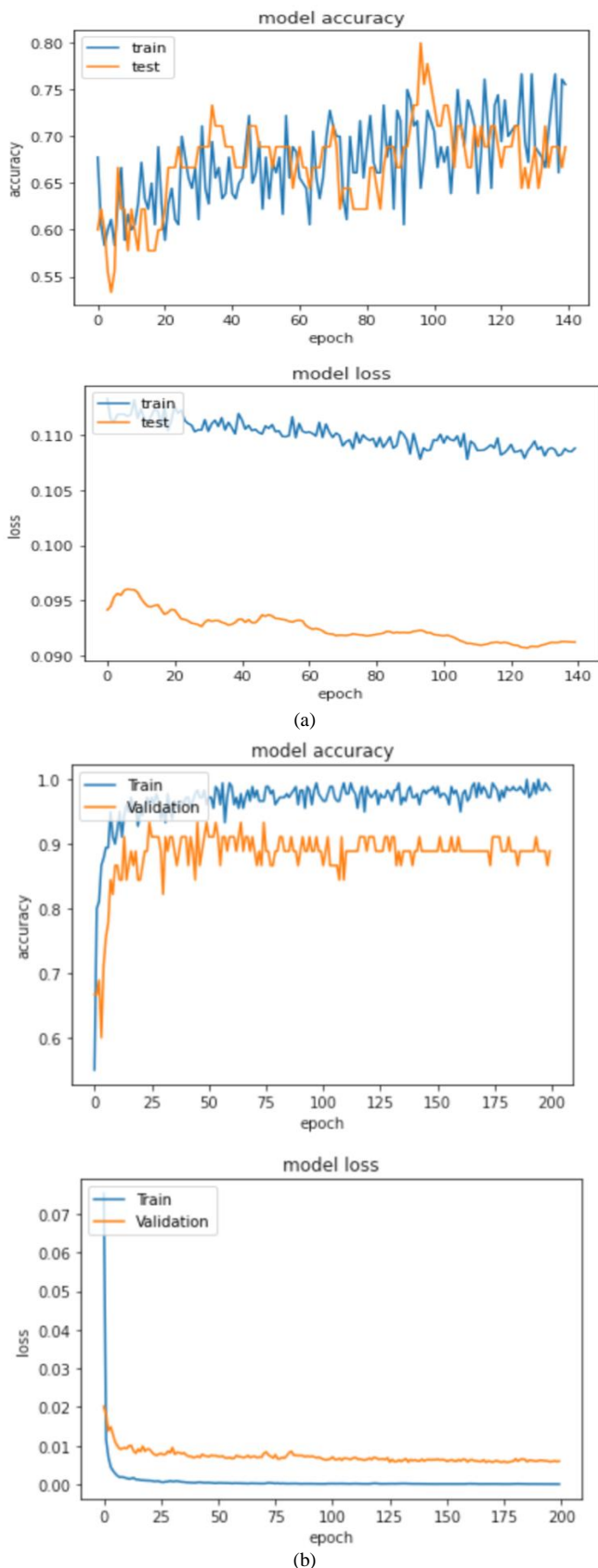


Fig. 7. License plate detection and recognition accuracy-loss curve by denoising the noisy images and optimizing the hyperparameters of deep learning algorithms (a) NASNetLarge, (b) InceptionResNetV2 model.

- [4] Y. Huihui, L. Daoliang, C. Yingyi, "A state-of-the-art review of image motion deblurring techniques in precision agriculture," *Heliyon*. 9 (2023) e17332.
- [5] G. Patil, P. Shivakumara, S.S. Gornale, U. Pal, M. Blumenstein, "A new robust approach for altered handwritten text detection," *Multimed. Tools Appl.* 82 (2023) 20925–20949.
- [6] Y. Liu, X. Chen, X. Ma, X. Wang, J. Zhou, Y. Qiao, C. Dong, "Unifying Image Processing as Visual Prompting Question Answering," (2023). <https://doi.org/2310.10513v1>.
- [7] Y. Jiang, F. Jiang, H. Luo, H. Lin, J. Yao, J. Liu, J. Ren, "An Efficient and Unified Recognition Method for Multiple License Plates in Unconstrained Scenarios," *IEEE Trans. Intell. Transp. Syst.* 24 (2023) 5376–5389.
- [8] Z. Liu, Y. Lin, Y. Cao, H. Hu, Y. Wei, Z. Zhang, S. Lin, B. Guo, "Swin Transformer: Hierarchical Vision Transformer using Shifted Windows," in: 2021 IEEE/CVF Int. Conf. Comput. Vis., IEEE, 2021: pp. 9992–10002.
- [9] L. Wilson, R. Krasny, T. Luchko, "Accelerating the 3D reference interaction site model theory of molecular solvation with treecode summation and cut-offs," *J. Comput. Chem.* 43 (2022) 1251–1270.
- [10] T. Yao, Y. Pan, Y. Li, C.-W. Ngo, T. Mei, "Wave-ViT: Unifying Wavelet and Transformers for Visual Representation Learning," in: 2022: pp. 328–345. https://doi.org/10.1007/978-3-031-19806-9_19.
- [11] P. Wu, X. Liu, J. Liu, "Weakly Supervised Audio-Visual Violence Detection," *IEEE Trans. Multimed.* 25 (2023) 1674–1685.
- [12] [12] S.C. Booth, W.P.J. Smith, K.R. Foster, "The evolution of short- and long-range weapons for bacterial competition," *Nat. Ecol. Evol.* 7 (2023) 2080–2091.
- [13] Kihong Park, Gitae Kim, M. Crovella, "On the relationship between file sizes, transport protocols, and self-similar network traffic," in: Proc. 1996 Int. Conf. Netw. Protoc., IEEE Comput. Soc. Press, n.d.: pp. 171–180.
- [14] M.B. McBride, P. Baveye, "Diffuse Double-Layer Models, Long-Range Forces, and Ordering in Clay Colloids," *Soil Sci. Soc. Am. J.* 66 (2002) 1207–1217.
- [15] H. Wu, Y. Qu, S. Lin, J. Zhou, R. Qiao, Z. Zhang, Y. Xie, L. Ma, "Contrastive Learning for Compact Single Image Dehazing," in: 2021 IEEE/CVF Conf. Comput. Vis. Pattern Recognit., IEEE, 2021: pp. 10546–10555.
- [16] X. Pan, S. Li, R. Li, N. Sun, "A Hybrid Deep Learning Algorithm for the License Plate Detection and Recognition in Vehicle-to-Vehicle Communications," *IEEE Trans. Intell. Transp. Syst.* 23 (2022) 23447–23458.
- [17] B. Li, X. Zhang, Y. Ban, X. Xu, W. Su, J. Chen, S. Zhang, F. Li, Z. Liang, S. Zhou, "Construction of a Smart Supply Chain for Sand Factory Using the Edge-Computing-Based Deep Learning Algorithm," *Sci. Program.* 2022 (2022) 1–15.
- [18] X. Zhang, W. Bai, H. Cui, "Review of Optical Character Recognition for Power System Image Based on Artificial Intelligence Algorithm," *Energy Eng.* 120 (2023) 665–679.
- [19] C.-H. Huang, Y. Sun, C.-S. Fuh, "Vehicle License Plate Recognition With Deep Learning," in: 2021: pp. 161–219. <https://doi.org/10.4018/978-1-7998-8386-9.ch009>.
- [20] H. Xiang, Y. Zhao, Y. Yuan, G. Zhang, X. Hu, "Lightweight fully convolutional network for license plate detection," *Optik (Stuttg.)* 178 (2019) 1185–1194.
- [21] J. Tang, J. Zeng, "Spatiotemporal gated graph attention network for urban traffic flow prediction based on license plate recognition data," *Comput. Civ. Infrastruct. Eng.* 37 (2022) 3–23.
- [22] A. Purwar, A. Singh, "VR therapy - mental therapy tool based on virtual reality," *Int. J. Creat. Comput.* 2 (2023) 1–17.
- [23] H. Rajput, T. Som, S. Kar, "An Automated Vehicle License Plate Recognition System," *Computer (Long Beach, Calif.)* 48 (2015) 56–61.
- [24] A. Burry, V. Kozitsky, "Automated License Plate Recognition," in: *Comput. Vis. Imaging Intell. Transp. Syst.*, Wiley, 2017: pp. 15–45.
- [25] D. Yang, J. Zhou, D. Shi, Q. Pan, D. Wang, X. Chen, J. Liu, "Research Status, Hotspots, and Evolutionary Trends of Global Digital Education via Knowledge Graph Analysis," *Sustainability*. 14 (2022) 15157.
- [26] P. Marzuki, A.R. Syafeeza, Y.C. Wong, N.A. Hamid, A.N. Alisa, M.M. Ibrahim, "A design of license plate recognition system using convolutional neural network," *Int. J. Electr. Comput. Eng.* 9 (2019) 2196.
- [27] Y. Wen, Y. Lu, J. Yan, Z. Zhou, K.M. von Deneen, P. Shi, "An Algorithm for License Plate Recognition Applied to Intelligent Transportation System," *IEEE Trans. Intell. Transp. Syst.* 12 (2011) 830–845.
- [28] I. Pereira-Sanchez, J. Navarro, J. Duran, "What if Image Self-Similarity can be Better Exploited in Data Fidelity Terms?," in: 2022 IEEE Int. Conf. Image Process., IEEE, 2022: pp. 3697–3701.
- [29] O. Ronneberger, P. Fischer, T. Brox, "U-Net: Convolutional Networks for Biomedical Image Segmentation," in: 2015: pp. 234–241. https://doi.org/10.1007/978-3-319-24574-4_28.
- [30] J. Gurrola-Ramos, O. Dalmau, T.E. Alarcon, "A Residual Dense U-Net Neural Network for Image Denoising," *IEEE Access.* 9 (2021) 31742–31754.
- [31] S. Guan, A.A. Khan, S. Sikdar, P. V. Chitnis, "Fully Dense UNet for 2-D Sparse Photoacoustic Tomography Artifact Removal," *IEEE J. Biomed. Heal. Informatics.* 24 (2020) 568–576.
- [32] Q. Yan, L. Zhang, Y. Liu, Y. Zhu, J. Sun, Q. Shi, Y. Zhang, "Deep HDR Imaging via A Non-Local Network," *IEEE Trans. Image Process.* 29 (2020) 4308–4322.
- [33] N. Ally, J. Nombo, K. Ibwe, A.T. Abdalla, B.J. Maiseli, "Diffusion-Driven Image Denoising Model with Texture Preservation Capabilities," *J. Signal Process. Syst.* 93 (2021) 937–949.
- [34] K. Ahmed, N.S. Keskar, R. Socher, "Weighted Transformer Network for Machine Translation," (2017). <http://arxiv.org/abs/1711.02132>.
- [35] A. Dosovitskiy, L. Beyer, A. Kolesnikov, D. Weissenborn, X. Zhai, T. Unterthiner, M. Dehghani, M. Minderer, G. Heigold, S. Gelly, J. Uszkoreit, N. Houlsby, "An Image is Worth 16x16 Words: Transformers for Image Recognition at Scale," (2020). <http://arxiv.org/abs/2010.11929>.
- [36] W. Sereethavekul, M. Ekpanyapong, "Adaptive Lightweight License Plate Image Recovery Using Deep Learning Based on Generative Adversarial Network," *IEEE Access.* 11 (2023) 26667–26685.
- [37] S. AlHalawani, B. Benjdira, A. Ammar, A. Koubaa, A.M. Ali, "License Plate Super-Resolution Using Diffusion Models," (2023). <http://arxiv.org/abs/2309.12506>.
- [38] Hendry, R.-C. Chen, "Automatic License Plate Recognition via sliding-window darknet-YOLO deep learning," *Image Vis. Comput.* 87 (2019) 47–56.
- [39] A. Tourani, A. Shahbahrami, S. Soroori, S. Khazaei, C.Y. Suen, "A Robust Deep Learning Approach for Automatic Iranian Vehicle License Plate Detection and Recognition for Surveillance Systems," *IEEE Access.* 8 (2020) 201317–201330.
- [40] A.R. Rashtehroudi, A. Shahbahrami, A. Akoushideh, "Iranian License Plate Recognition using Deep Learning," in: 2020 Int. Conf. Mach. Vis. Image Process., IEEE, 2020: pp. 1–5.
- [41] Z. Liu, Z. Wang, Y. Xing, "Wagon Number Recognition Based on the YOLOv3 Detector," in: 2019 IEEE 2nd Int. Conf. Comput. Commun. Eng. Technol., IEEE, 2019: pp. 159–163.
- [42] J. Xu, H. Li, Z. Liang, D. Zhang, L. Zhang, "Real-world Noisy Image Denoising: A New Benchmark," (2018). <https://doi.org/1804.02603v1>.
- [43] A. Abdussalam, S. Sun, M. Fu, H. Sun, I. Khan, "License Plate Segmentation Method Using Deep Learning Techniques," in: 2019: pp. 58–65. https://doi.org/10.1007/978-981-13-1733-0_8.
- [44] D.M.F. Izidio, A.P.A. Ferreira, H.R. Medeiros, E.N. da S. Barros, "An embedded automatic license plate recognition system using deep learning," *Des. Autom. Embed. Syst.* 24 (2020) 23–43.
- [45] K. Khan, "Automatic license plate detection and recognition framework to enhance security applications," *J. Electron. Imaging.* 28 (2019) 1.
- [46] X. Zhang, N. Gu, H. Ye, C. Lin, "Vehicle license plate detection and recognition using deep neural networks and generative adversarial networks," *J. Electron. Imaging.* 27 (2018) 1.
- [47] M. Kiran Kumar, C. Sanjana, F. Shireen, D. Harichandana, M. Sharma, M. Manasa, "Automatic Number Plate Detection for Motorcyclists Riding Without Helmet," *E3S Web Conf.* 430 (2023) 01038.

- [48] M. Shafiq, Z. Gu, "Deep Residual Learning for Image Recognition: A Survey," *Appl. Sci.* 12 (2022) 8972.
- [49] B. Lim, S. Son, H. Kim, S. Nah, K.M. Lee, "Enhanced Deep Residual Networks for Single Image Super-Resolution," in: 2017 IEEE Conf. Comput. Vis. Pattern Recognit. Work., IEEE, 2017: pp. 1132–1140.
- [50] Y. Zhang, K. Li, K. Li, L. Wang, B. Zhong, Y. Fu, "Image Super-Resolution Using Very Deep Residual Channel Attention Networks," in: 2018: pp. 294–310.
- [51] H. Liu, T. Brailsford, Reproducing "Show, Attend and Tell: Neural Image Caption Generation with Visual Attention," *J. Phys. Conf. Ser.* 2589 (2023) 012012.
- [52] J. Redmon, A. Farhadi, "YOLOv3: An Incremental Improvement," (2018). <http://arxiv.org/abs/1804.02767>.
- [53] S.T.A. Ali, A.H. Usama, I.R. Khan, M.M. Khan, A. Siddiq, "Mobile Registration Number Plate Recognition Using Artificial Intelligence," in: 2021 IEEE Int. Conf. Image Process., IEEE, 2021: pp. 944–948.
- [54] C.-W. Yu, Y.-L. Chen, K.-F. Lee, C.-H. Chen, C.-Y. Hsiao, "Efficient Intelligent Automatic Image Annotation Method based on Machine Learning Techniques," in: 2019 IEEE Int. Conf. Consum. Electron. - Taiwan, IEEE, 2019: pp. 1–2.
- [55] B. Zhang, X. Liu, C. Yue, S. Liu, X. Li, S.Y. Liang, L. Wang, "An imbalanced data learning approach for tool wear monitoring based on data augmentation," *J. Intell. Manuf.* (2023) 1-22.
- [56] R. Yousef, G. Gupta, N. Yousef, M. Khari, "A holistic overview of deep learning approach in medical imaging," *Multimed. Syst.* 28 (2022) 881–914.
- [57] W. Xiao, G. Kreiman, "Gradient-free activation maximization for identifying effective stimuli," *arXiv preprint arXiv:1905.00378* (2019).
- [58] Y. Gao, "News Video Classification Model Based on ResNet-2 and Transfer Learning," *Secur. Commun. Networks.* 2021 (2021) 1–9.
- [59] S.-O. Shim, R. Imtiaz, A. Siddiq, I.R. Khan, "License Plates Detection and Recognition with Multi-Exposure Images," *Int. J. Adv. Comput. Sci. Appl.* 13 (2022).
- [60] Your Home for Data Science, (2023).
- [61] J. Anaya, A. Barbu, "RENOIR – A dataset for real low-light image noise reduction," *J. Vis. Commun. Image Represent.* 51 (2018) 144–154.
- [62] D.P. Kingma, J. Ba, "Adam: A Method for Stochastic Optimization," *arXiv preprint arXiv:1412.6980* (2014).
- [63] C.-M. Fan, T.-J. Liu, K.-H. Liu, "SUNet: Swin Transformer UNet for Image Denoising," in: 2022 IEEE Int. Symp. Circuits Syst., IEEE, 2022: pp. 2333–2337.
- [64] S. Anwar, N. Barnes, "Real Image Denoising With Feature Attention," in: 2019 IEEE/CVF Int. Conf. Comput. Vis., IEEE, 2019: pp. 3155–3164.
- [65] J. Redmon, A. Farhadi, "YOLOv3: An Incremental Improvement," *arXiv preprint arXiv:1804.02767* (2018).

Crowdsourcing Requirements Engineering: A Taxonomy-based Review

Ghadah Alamer¹, Sultan Alyahya², Hmood Al-Dossari³

Information Systems Department-College of Computer and Information Sciences, King Saud University^{1,2,3}
Information Systems Department-College of Computer and Information Sciences,
Princess Nourah Bint Abdulrahman University, Riyadh, Saudi Arabia¹

Abstract—Interesting insights have been found by the research community indicating that early user involvement in Requirements Engineering (RE) has a considerable association with higher requirements quality, software project success and as well boosting user loyalty. In addition, traditional RE approaches confront scalability issues and would be time consuming and expensive to be applied with contemporary applications that can be surrounded by a large crowd. Therefore, recent attention has been shed on leveraging the principle of Crowdsourcing (CS) in requirements engineering. Engaging the crowd in RE activities has been researched by several studies. Hence, we synthesize and review the literature of the knowledge domain Crowdsourcing Requirements Engineering using a proposed taxonomy of the area. A total of 52 studies were selected for review in this paper. The review aims to provide the potential directions in the area and pave the way for other researchers to understand it and find possible gaps.

Keywords—Crowdsourcing requirements engineering; crowdsourcing; CrowdRE; crowd

I. INTRODUCTION

Today's software applications can be mobile, cloud and social which operate in crowd-based settings having a massive crowd of distributed users [1]. This shift in the nature of applications have stressed the need in extending user involvement during RE activities [2] [3]. Furthermore, to achieve global user acceptance and satisfaction, a software application should meet the needs and desires of the large base of users [4]. Due to that, incorporating the interested crowd in the early phases of a software application, specifically RE, is crucial. The broad concept that advocates the involvement of the crowd in RE tasks is CrowdRE.

Crowd-based Requirements Engineering (CrowdRE) is a recent concept introduced by Groen et al. [1] for all semi-automated or automated RE tasks involving the crowd. One of the potential areas for employing crowdsourcing is in RE where it has gained attention [2] [1] [5] [6]. The broad concept CrowdRE can involve crowdsourcing, but crowdsourcing doesn't involve CrowdRE [7].

It is worth mentioning that there are some differences between CrowdRE and Crowdsourcing Requirements Engineering. Crowdsourcing delegates a piece of work to the crowd to solve it [7], where crowd members are actively engaged. On the other hand, in CrowdRE, the crowd can be involved passively, where the approach harnesses the available data from the crowd. Moreover, in CrowdRE the crowd are

informants, where in crowdsourcing they are considered as problem solvers [8].

Fig. 1 shows a generic and simplified classification of the area CrowdRE. As shown in the figure, in addition to crowdsourcing, feedback analysis is concerned about analyzing users' feedback about software in channels such as app stores, social media and product forum using text mining techniques to elicit users' requirements. Where usage and context mining enable monitoring software usage and context at runtime to derive users' requirements [9]. These two approaches are mostly considered as passive involvement of the crowd.

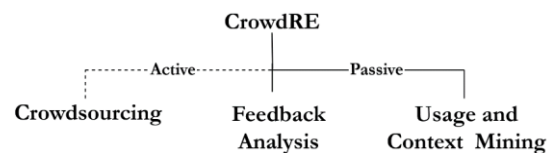


Fig. 1. General areas of CrowdRE [8] [9].

This review mainly covers studies that have utilized crowdsourcing for any of the RE tasks, where the crowd is actively involved in the crowdsourcing RE initiative. Moreover, we have suggested taxonomy of the area which we have observed after analyzing the selected studies, and reviewed the studies according to it. The taxonomy represents the main research directions in the area that can inspire interested researchers in finding potential gaps which are: crowd selection, crowd motivation, RE crowdsourcing platform, crowdsourcing task design and crowdsourced requirements. At the end of this review paper, we discuss some insights and provide some recommendations.

The reminder of this paper is organized in four sections: Section II which presents the research foci of the area Crowdsourcing RE. The section starts by showing the search and retrieval strategy for selecting studies and introduces the proposed taxonomy of the area. The studies are then reviewed according to the taxonomy. Section III discusses the overall insights that have been found and gives some suggestions. Finally, Section IV concludes this review paper.

II. CROWDSOURCING REQUIREMENTS ENGINEERING: RESEARCH FOCI

A comprehensive review of the main research foci of the broad area Crowdsourcing Requirements Engineering is presented. In addition, taxonomy of the area is proposed to provide the reader with an insight into the main directions of

the area that studies usually fall under. Each direction of the area is reviewed, and prior to that the undertaken search and retrieval strategy for selecting papers in the area is illustrated.

A. Search and Retrieval Strategy

A selected number of keywords that mostly represent the area are used in searching for papers. The keywords are: [Crowdsourcing Requirements Engineering], [CrowdRE], [Crowdsourcing AND Requirements Engineering], [Crowd-Based Requirements Engineering]. Five main libraries were considered for searching papers which are: IEEE, ACM, ScienceDirect, Springer and Scopus. In addition, the presented review covers published research anytime until 2023. Besides, we looked up papers published by some active researchers in the area and as well in the International Requirements Engineering Conference (RE) to find any related papers to be included in this review.

The review includes papers that apply the principle of crowdsourcing with any of the RE activities. Papers that fall under the area Crowdsourcing Requirements Engineering, which consider active involvement of the crowd during one or more of RE activities, are included. Papers that do not present a practical solution or review papers of the area are excluded.

Furthermore, papers that are cited by one of the selected papers and that appear to be related to the area Crowdsourcing RE are included. Fig. 2 is an illustration of the search and retrieval strategy that is followed to focus on Crowdsourcing Requirements Engineering studies. CrowdRE related papers are inspected to filter only papers that utilized crowdsourcing where the crowd is actively involved. Eventually, a total of 52 papers were selected for analysis and review.

After reviewing the current landscape of existing research in the area Crowdsourcing Requirements Engineering, it was noticed that research has mainly focused on addressing different aspects which can be considered as active research directions in the area. In Fig. 3, a taxonomy is illustrated of the Crowdsourcing Requirements Engineering literature. This taxonomy was set based on the main crowdsourcing elements presented by Hosseini et al. [10]. They have defined four pillars of crowdsourcing which are the crowd, crowdsourcer, crowdsourcing platform and crowdsourced task. Therefore, we present a taxonomy having four main aspects which are: the crowd, RE crowdsourcing platform, crowdsourcing task design and additionally crowdsourced requirements were added as a fourth aspect which particularly pertains to crowdsourcing RE. Each aspect of the taxonomy is reviewed and discussed in the next sections.

B. Crowd Selection for Crowdsourcing RE

From reviewing the selected studies, it was evident that a number have focused on proposing approaches for selecting an appropriate subset of the crowd for crowdsourcing RE. A group of these studies have utilized social network analysis to select a crowd which are [11] [12] [13] [14] [15]. Lim et al. has designed StakeNet [11] which is a method for identifying and prioritizing a crowd of stakeholders in large software projects. The stakeholders are identified and prioritized by considering their level of influence they possess on a software project and their roles. Diverse social network measures are utilized to

analyze the relations between the stakeholders in a social network. The network of stakeholders' crowd is built using snowballing technique where stakeholders recommend other stakeholders until a network of well-connected stakeholders is produced. Moreover, rather than relying on experts to ask stakeholders to suggest others, Lim et al. [12] has automated the process by developing StakeSource tool. The tool minimizes the workload on experts by crowdsourcing the task of stakeholder analysis to include the crowd of stakeholders in that task. In addition, StakeSource is improved by presenting a web-based tool called StakeSource2.0 [13]. StakeSource2.0 extends the work to not only consider stakeholders identification and prioritization, but as well elicits their requirements. To conduct this, the tool uses crowdsourcing, social network analysis and collaborative filtering.

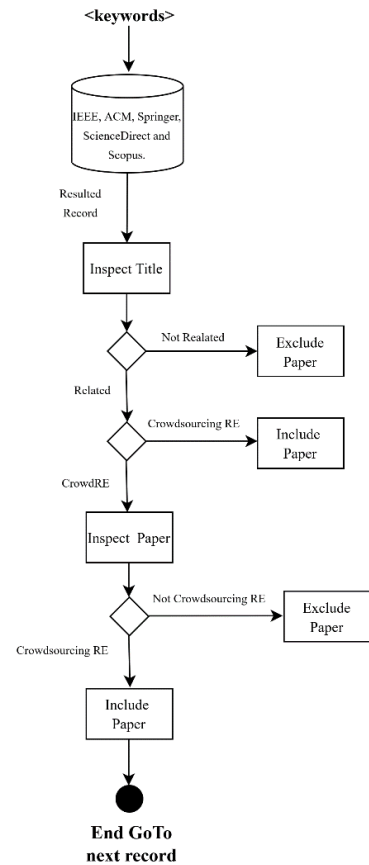


Fig. 2. Search and retrieval strategy.

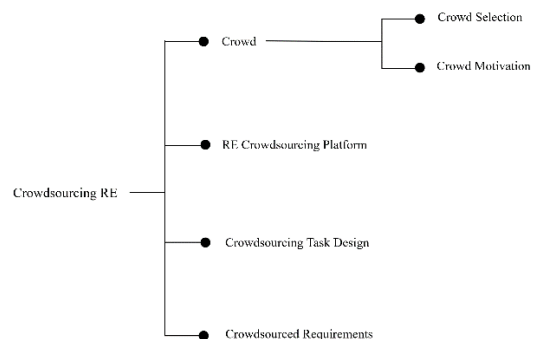


Fig. 3. Taxonomy of the area Crowdsourcing RE.

Moreover, StakeSource2.0 has been used in StakeRare [14] a method proposed by Lim et al. which identifies and prioritizes thousands of stakeholders for large-scale software projects and elicit their requirements. StakeRare was assessed on an extensive project consisting of a crowd of 30,000 stakeholders, and has shown to accurately predict the stakeholders' desires by producing a more complete list of prioritized requirements from the crowd of stakeholders. An in-group bias limitation was highlighted in the former studies by Mughal et al. [15]. This limitation is defined as when stakeholders prefer to recommend ones whom they have a good relationship with. This biasedness can lead to less accurate identification and prioritization of the crowd of stakeholders, which eventually impacts the process of requirements elicitation.

Rather than relying on the relations between the crowd members and the level of impact they have on software project such as what has been done by the previously discussed studies, other studies have considered the crowd's domain knowledge to select and identify a suitable crowd. A framework proposed by Wang et al. [16] aims to select suitable participants for outsourcing requirements elicitation tasks. The framework utilizes spatiotemporal features of the crowd to infer their domain knowledge. The authors observe that people who gather in the same spatiotemporal space could possess similar domain knowledge. For instance, to develop a football application, the best crowds to participate in requirements elicitation are football fans whom can be found clustering in a football match at a certain time and space. Furthermore, a study presented by Srivastava and Sharma [4] have focused on crowd with knowledge in ERP selected from LinkedIn social network. The crowd is selected to participate in crowdsourcing requirements elicitation for a software application called MyERP. They have used a crawling web-based solution to find crowd members who have listed ERP in their LinkedIn profiles as one of the expertise they possess. In addition, another study by Lim et al. [17] which uses LinkedIn as a platform from where the crowd is selected. They have proposed a systematic approach to find stakeholders interested in B2B software in a targeted company. The approach is a step-by-step strategy that assists in finding hidden B2B software stakeholders by searching LinkedIn social network. The targeted stakeholders are found by a set of intermediates called advisors that help connect with the stakeholders and elicit their requirements for a B2B software. In addition, a nichesourcing method was proposed by Condori-Fernandez et al. [18] for analyzing sustainability requirements and the dependencies between them. The method consists of multiple stages, where an early stage is selecting a crowd experienced in a domain knowledge that fits the software having its requirements crowdsourced. The authors recommend using social network sites such as Twitter and LinkedIn to find a potential crowd of experts to contribute in crowdsourcing sustainably requirements and finding the relationships and dependencies among them.

Some studies have based the selection process on the crowd's domain of interest. A method proposed by Lim et al. [19] utilized a bot tool which operates on Twitter social network. The automated tool is called PseudoGravity and it aims to identify a targeted interested crowd by generating

content that is especially tailored for them. The interested crowd is then engaged in participating in crowdsourcing requirement elicitation tasks. Moreover, Kolpondinos and Glinz [20] have proposed an approach to select an interested crowd that is beyond the boundaries of an organization. They have harnessed several online channels as a source to find a crowd interested in the SmaWoMo system. Their approach employs persona-based advertisements which are based on player-types similar to personality traits to determine the personas. The targeted crowd is then invited to engage collaboratively in the requirement elicitation and prioritization process for that system.

A study conducted by Alvertis et al. [21] have introduced a persona-based approach that can be used to select a suitable subset of the crowd to participate in the process of requirements elicitation. Their approach consists of a persona builder tool that enables software teams to construct, reuse, and as well share personas. A persona can be created by identifying a set of required characteristics. This approach assists in targeting suitable prospective software users. The crowd that fits these determined personas can be selected to get involved in crowdsourcing requirements engineering. In addition, Guzman et al. [22] have built a stakeholder identification model using machine learning techniques. Their model can identify the stakeholders from tweets, where they are either classified as technical, non-technical or general public stakeholders. They have built their model using tweets about 30 popular mobile and desktop applications.

C. Crowd Motivation for Crowdsourcing RE

In the literature of crowdsourcing RE, some studies have focused on how to motivate the crowd to participate in a crowdsourcing initiative. The authors in [2] [20] [23] [24] [25] [26] [27] [28] [29] advocated the use of Gamification as an incentive design to increase crowd motivation when crowdsourcing RE tasks. Gamification is the idea of using game elements such as points, levels, badges and leader boards in non-game context to motivate users [36]. Fernandes et al. [24] have proposed iThink, a gamified collaborative tool for requirements elicitation which uses the "Six Thinking Hats" technique. Moreover, stakeholders are rewarded for suggesting new requirements or discussing existing ones. This study is considered as one of the early attempts revealing that gamification has potentials in RE activities [23].

Snijders et al. [23] have extended participation by involving a crowd of stakeholders. The authors have proposed REfine, a gamified crowdsourcing platform for requirements elicitation and refinement which is an essential component of the (Crowd-Centric Requirements Engineering) CCRE method [2] [23] [25]. REfine is designed to involve crowd of stakeholders in RE. Through REfine users are able to suggest needs, comment on them, branch them, vote for them, and are rewarded accordingly.

Furthermore, Martina et al. [26] have developed a concept to motivate the vast number of unknown stakeholders outside organizational reach to contribute in requirements elicitation using gamification mechanisms. The authors argue that all implemented game-based platforms for requirements elicitation (e.g. iThink [24] and REfine [23]) have considered crowd of

stakeholders who are within organizational reach. Besides, they have overlooked the evolution of stakeholders' motivation throughout the elicitation process; hence, the authors have focused on addressing this gap.

Similar to [26], another study [27] has focused its investigation on motivating stakeholders outside organizational reach and specifically during requirements prioritization. Garuso (Game-Based Requirements Elicitation) platform which incorporates social media with gamification was developed to explore the effect of gamification algorithms that control the points and levels game elements on stakeholders' participation. Kolpondinos and Glinz [20] have presented the GARUSO approach which was an expansion of the studies [26] and [27]. The authors have presented a detailed description of the GARUSO architecture, which is a gamified social media platform that enables the crowd of stakeholders outside the organizational reach to collaborate in eliciting and prioritizing requirements. Besides, Gupta [28] have used gamification for requirements elicitation and prioritization. The crowd are asked to express their requirements using customer journey format which shows the step-by-step journey of a customer in performing a task (e.g. payment task).

The above discussed studies have used gamification mechanism for crowd motivation. Nevertheless, some studies have designed rewarding systems as part of their studies to keep the crowd motivated such as [4] [30] [31]. Srivastava and Sharma [4] have proposed a crowdsourcing approach for requirements elicitation for MyERP application. To maintain crowd motivation, they have used certain performance measures. Two main indicative measures were utilized, which are members who contribute more requirements and who have more responses posted on their contributed requirements, are given a reward. In addition, Seyff et al. [31] plan to add a personalized rewarding mechanism to encourage the crowd to participate in their platform and maintain their involvement in negotiating and analyzing the requirements with respect to sustainability. Nascimento et al. [30] have defined three reward methods for their proposed framework which are reward and career, financial compensation and recognition. For which a selection of a method is based on the scope of the project and the type of participating crowd.

Schneider and Bertolli [32] state that having a software described in text format may not be encouraging for the crowd to share their opinions and feedback about that software and might even repel them from contributing. Therefore, they suggest a new approach in motivating the crowd for RE, which is using videos. They have proposed four types of videos and illustrated how they can be created and make them engaging for CrowdRE. In addition, in [33] the authors have designed a gradual approach for eliciting and gathering requirements from a crowd, where requirements are built gradually from multiple micro-crowds (MCs). In each MC, the people are familiar with each other. This approach can perform better in motivating the crowd than when starting with a large crowd, where this has been seen to fall under the motivation linked to loving the community. Another study by [34] has applied the MC approach, however, rather the applying it on users as in the previous study, it was applied on developers.

D. RE Crowdsourcing Platform

The literature shows that there are several crowdsourcing platforms that are especially designed for crowdsourcing RE tasks. CrowdREquire [35], REfine [23], CRUISE [5], UCFrame [36], Requirements Bazaar [37], GARUSO [20], CREeLS [38], CREUS [39], SCOUT [40], Liquid RE [41], KMar-Crowd [29], Srivastava and Sharma's platform [4], Seyff et al.'s platform [31], Nagel et al, prototype [42], smartFEEDBACK [43], CrowdConfigRE [44] and Menkveld et al.'s platform [45] are all crowdsourcing platforms for RE.

CrowdREquire proposed by Adepetu et al. [35] aims to focus on gathering requirements from the available diverse talent in the crowd which is considered as a complex task. The platform utilizes a contest model and adopts an agile approach for requirements development. Another platform proposed in [37] which involves the crowd in almost all RE activities. The authors have designed a platform for social requirements engineering named Requirements Bazaar. It supports collaborative requirements elicitation, prioritization, negotiation and realization. Besides, it has a co-creation workflow involving four stages: idea generation, idea selection, idea realization and idea release.

Sharma and Sureka [5] have designed a platform for crowdsourcing RE activities called CRUISE. CRUISE aims to employ the crowd in gathering, analyzing, validating, prioritizing and negotiating requirements. In addition, Hu et al. have proposed USFrame [36], a use case-based framework for collaborative requirements acquisition in crowd-centric context to assist the crowd in expressing their requirements without the help of an analyst. The platform has implemented critical mechanisms such as rule hints for guiding the crowd of users in use case documentation, built in abstract types, use case synthesis, quality measurements and visualization diagrams.

Munante et al. have proposed CrowdConfigRE [44], a platform for crowdsourcing re-configuration requirements that focuses on adaptive systems to elicit their re-configuration requirements. First, known crowd, in other words domain experts, generates personas and configuration profiles for adaptive software. Then, an unknown crowd of potential users are used to refine and validate the information elicited; hence, accurately defining the re-configuration requirements. Furthermore, Seyff et al. [31] proposed a platform that can engage a crowd, users and domain experts, in negotiating and eliciting requirements and their impact on sustainability. The platform consists of three primary parts which are CrowdFeed component that enables the crowd to share their feedback about a software product, ReSuS component to classify and cluster the feedback and ReSIntegrator component that showcases the impact on sustainability using visualization techniques.

REfine [23] and GARUSO [20] are gamified collaborative crowdsourcing platforms for RE activities. REfine platform engages a crowd of users, developers or requirements analysts in the process of eliciting and refining software requirements. Similarly, GARUSO platform allows the crowd to collaboratively engage in requirements elicitation and prioritization tasks. Additionally, Menkveld et al. [45] have developed a RE crowdsourcing platform to help the crowd in writing their software requirements and features in the form of

user stories (US) for a sports tournaments management software. It enables the crowd to submit their US by entering four inputs which are: the role of the crowd member requesting the feature, the goal of the feature, the benefit of the feature and the category of the feature. Besides, CREUS method [39] has used user stories as an approach to express ideas elicited from the crowd. The method consists of four phases which are: preparation, idea generation, refinement, and execution and supports three main roles: core team, crowd member and focus group member. Core team oversees and coordinates the crowd, the crowd member contributes ideas, and focus group member is a crowd member who participates in discussing the development of the crowdsourced ideas. Another similar platform is Kmar-Crowd [29] which is designed for crowdsourcing requirements elicitation in the form of user stories. The platform involves the crowd in idea generation and refinement to generate ideas and vote and comment on available ideas. In addition, a study conducted by Köse and Aydemir [40] have proposed SCOUT a web-based tool which supports the completeness of user stories generated by a crowd of stakeholders in a collaborative environment. SCOUT NLP-based tool guides the crowd during the process of generating user stories. It uses NLP to construct a knowledge graph from user stories; hence, heuristics are applied on the knowledge graph to produce suitable suggestions to the crowd of stakeholders.

A platform proposed by Rizk et al. [38] called CREeLS is a crowdsourcing platform to crowdsource requirements elicitation tasks for e-learning systems (eLSs). The proposed platform consists of feedback channels to comment and review the eLS, social collaboration, text mining tools to analyze and mine the crowd requirements that are written in the form of comments and in discussion forums. Moreover, a crowdsourcing platform was proposed by Srivastava and Sharma [4] for crowdsourcing requirements elicitation for ERP applications. Their proposed platform has addressed several challenges concerning identifying the appropriate crowd, keeping them engaged, identifying appropriate tasks, recognizing malicious crowd members and resolving conflicts among requirements and prioritizing them. Additionally, a tool called smartFEEDBACK [43] was developed to apply crowdsourcing RE to gather the needs of older adults. The tool was designed to support both explicit (e.g. answer questions) and implicit feedback (e.g. analyze interactions).

Nagel et al. [42] designed a prototype for an interactive video player which incorporates three main features which are emoji markers, comments and hyper-markers. These features shall enable the crowd of stakeholders to understand and share their understanding and requirements about a software project and assist in resolving any conflicts. Moreover, a study by Johann and Maalej have proposed an envision of a Liquid RE platform [41]. The platform applies Liquid Democracy and e-Democracy concepts in RE to mitigate the challenges of mass participation in RE related to scalability, motivation, conflicts, representativeness, subjectiveness and misuse. Some of the main Liquid Democracy and e-Democracy concepts to be applied in the platform are structured collaborative decision making, delegated voting and quorums.

E. RE Crowdsourcing Task Design

Indeed, some studies have focused on the task design for crowdsourcing RE, where they presented a method that could simplify and decompose the crowdsourced task. Mostly, these studies utilized available crowdsourcing platforms such as the general-purpose crowdsourcing platforms Amazon Mechanical Turk (MTurk), Figure Eight and Zooniverse and focus on task design.

The crowd-based requirements annotation methods Kyoryoku [46] and CRAFT [47] harness the power of the crowd in eliciting and classifying requirements from users' reviews. The methods split complex tasks into simpler micro-tasks. Using CRAFT [47], crowd members from Figure Eight accomplished a task by navigating through three major phases. A crowd member first selects a category from predefined categories (e.g. functional requirement, bug report) for a review or adds a new category. Second, selects a sub-category and third rates the importance of the review and provides comments. Furthermore, Kyoryoku [46] method, inspired by CRAFT, proposed a three phase method for accomplishing the task of extracting requirements from users' reviews. First a crowd member filters a review into helpful or useless, second fragments of the helpful reviews are further classified to being helpful or useless, and third helpful fragments are classified into five categories (e.g. feature request, stability, quality). Similarly, CrowdIntent [48], a crowdsourcing workflow proposed for annotating intentions (desires and needs) hidden in discussions into a set of categories. It has decomposed the content of the task (a discussion) into messages then into sentences using sentence splitter tools to design the task in an understandable way for annotation.

Furthermore, Murukannaiah et al. [49] have proposed a sequential task design for crowdsourcing RE through MTurk which can stimulate creativity. The design was based on the notion that when workers are exposed to others' ideas, this act can lead to cognitive stimulation. There are two phases, where in the first phase the crowd workers review the ideas generated by other workers and generate new ones. In the second phase, the other part of the crowd rates the produced ideas in the first phase. In addition, an idea selection strategy based on workers' personalities and creativity was proposed to select a set of ideas from a stage to be exposed to workers in the following stage. Moreover, Breaux and Schaub [50] introduced a task decomposition workflow for crowdsourcing the manual extraction of privacy requirements task from text documents which involve privacy policies. The task includes multiple microtasks which enables untrained crowd members to apply sentence and phrase level coding of the privacy policies. The workflow is performed using manual methods, and as well NLP techniques to automate some parts of the workflow.

Alongside Breaux and Schaub's study [50], another was conducted by Guo et al. [51] that have proposed Çorba which focuses on the task design for crowdsourcing RE. Çorba is a crowdsourcing design that guides the crowd in extracting security and privacy requirements from regulations and breach textual reports by breaking the task into smaller tasks. The proposed task design was conducted on MTurk crowdsourcing platform. In addition, Rosser et al. [52] used Zooniverse for crowdsourcing phishing cues labeling which is a crucial RE

phase for anti-phishing training tools. Zooniverse markup interface was used to design the crowdsourcing task. Participants were shown screenshots and were asked to identify its trustworthiness, if the content is malicious, they are asked to mark the areas in the image indicating phishing and then label it using pre-defined labels. Furthermore, another study has used a simple mean for crowdsourcing such as using questionnaires as done by Vidal et al. [53], where they have crowdsourced the task of requirements validation for a pet management mobile app. Their questionnaires were designed using questions with Likert-scale, binary or numeric responses to validate the requirements.

F. Crowdsourced Requirements

In addition to all previously discussed studies, some have mainly focused on how to handle the crowdsourced requirements; hence, they are more concerned about the stage after gathering the requirements. The papers [54] and [55] have proposed a genetic algorithm-based approach in which the elicited requirements from the crowd are aggregated. They have used activity diagrams as a structured requirements description language in order to facilitate automated merging of requirements. Their proposed genetic algorithm aims to merge the collected activity diagrams from the crowd, and produce a synthetic activity diagram which acts as a crowd consensus on a requirement. Moreover, Taj et al. [56] have presented a model that classifies requirements gathered through crowdsourcing into functional and non-functional requirements. An open call was initiated to ask crowd members to participate in submitting requirements for a software to be developed. The model used the machine learning algorithms naïve bayes and decision tree to build the model and has proved to achieve effective results.

Furthermore, StakeSource2.0 [13] and StakeRare [14] use social networks and collaborative filtering to identify and prioritize requirements from a large crowd of stakeholders which are asked to suggest and rate requirements. Collaborative filtering predicts a stakeholder's preferences and recommends unrated requirements to a stakeholder that might be of interest to him; hence, the stakeholder rates this recommended list of requirements. Using these ratings and the stakeholder's level of impact on a project, the requirements are prioritized.

Indeed, having large number of requirements as a part of the software project with no value to users is an issue. To rectify such problem, Nascimento et al. [30] have proposed a framework which leverages Kano's model to classify and evaluate crowdsourced requirements. The proposed framework aims to identify and prioritize requirements based on their importance to the customers and include them for implementation. Similarly, Niu et al. [57] have proposed an approach where they have employed semantic discrimination lexicon, Kano model and entropy technique to evaluate the importance of already crowdsourced requirements. Furthermore, Hassan et al. [58] proposed an approach which uses text mining and morphological matrix for analyzing the large number of ideas generated by the crowd to extract innovative software requirements. Mead et al. [59] on the other side have proposed an approach where they utilized crowdsourcing to construct Personae Non Gratae (PnGs)-based

threat models that could be considered as input for early phases of requirements process, and as well help in specifying mitigating requirements. For the aim of reaching higher coverage of threats, reducing redundancies and developing meaningful PnGs, in their approach they have introduced a merging strategy where they used machine learning and information retrieval techniques to merge crowd's PnGs.

III. DISCUSSION

After reviewing crowdsourcing requirements engineering body of knowledge, the reviewed studies are synthesized in Table I where each study is categorized under one or more dimensions that it contributes to according to the suggested taxonomy illustrated in Fig. 3. Apparently, the largest number of studies contributed to the Crowd dimension and the RE Crowdsourcing Platform dimension. Furthermore, regarding the remaining two dimensions crowdsourced task design and crowdsourced requirements, the number of studies addresses a gap related to these dimensions are quite low.

TABLE I. STUDIES ORGANIZED UNDER THE DIRECTIONS OF THE AREA CROWDSOURCING RE

| Dimensions | | Number of Studies | Ref. |
|---------------------------|------------------|-------------------|--|
| Crowd | Crowd Selection | 13 | [20] [4] [16] [17] [12] [14] [15] [13] [11] [21] [19] [22] [18] |
| | Crowd Motivation | 15 | [2] [20] [4] [33] [23] [30] [32] [24] [25] [26] [27] [28] [29] [31] [34] |
| RE Crowdsourcing Platform | | 17 | [23] [5] [36] [37] [20] [38] [41] [4] [31] [35] [44] [45] [29] [39] [40] [42] [43] |
| Crowdsourcing Task Design | | 8 | [46] [49] [51] [50] [47] [48] [52] [53] |
| Crowdsourced Requirements | | 9 | [13] [14] [30] [54] [56] [58] [59] [55] [57] |

We envision that there are areas for improvements in this field, where studies can work on designing effective approaches for crowd selection that can infer the knowledge of the crowd and make use of it in various activities of requirements engineering. Moreover, motivating the crowd is a factor of paramount importance especially when it comes to crowdsourcing. Therefore, we recommend working on strategies that can incentivize the crowd to participate. For the RE crowdsourcing platforms, there are several endeavors in this dimension. Nonetheless, since RE tasks are considered as complex tasks, designing a platform that does not just provide a medium for the crowd but as well facilitates the accomplishment of the crowdsourced RE tasks by incorporating intelligent features in the platform, is another factor to consider when researching this dimension.

Furthermore, the task design aspect has large opportunities for contributions. It is recommended to design a RE crowdsourced task in a way that can be employed in any crowdsourcing platform. The last dimension which is focused on the crowdsourced requirements have few studies contributing to it. To benefit from the crowdsourced requirements, we suggest proposing methods to aggregate the large number of contributed requirements and synthesize them.

This can assist crowdsourcing requesters in understanding and viewing them.

Employing crowdsourcing in requirement engineering might present some challenges that need some attention. The quality of the crowdsourced requirements reducing redundancies and increasing diversity when crowdsourcing requirements and as well coordinating the work on RE tasks among crowd members are all important aspects that can be researched.

IV. CONCLUSION

Crowdsourcing requirement engineering is a new approach for RE which fits the modern software paradigms. Hence, we have presented a thorough review of the area and proposed a taxonomy that can help researchers find their way in the area. The review shows that there are some aspects of the area that can be contributed to and enhanced. In addition, for future work we plan to conduct some research work that could address some gaps identified in the area.

REFERENCES

- [1] E. C. Groen, J. Doerr, and S. Adam, "Towards crowd-based requirements engineering a research preview," in Lecture Notes in Computer Science (including subseries Lecture Notes in Artificial Intelligence and Lecture Notes in Bioinformatics), 2015, vol. 9013, pp. 247–253, doi: 10.1007/978-3-319-16101-3_16.
- [2] R. Snijders, F. Dalpiaz, M. Hosseini, A. Shahri, and R. Ali, "Crowd-centric requirements engineering," Proc. - 2014 IEEE/ACM 7th Int. Conf. Util. Cloud Comput. UCC 2014, pp. 614–615, 2014, doi: 10.1109/UCC.2014.96.
- [3] M. Hosseini, K. Phalp, J. Taylor, and R. Ali, "Towards crowdsourcing for requirements engineering," CEUR Workshop Proc., vol. 1138, no. July 2016, pp. 82–87, 2014.
- [4] P. K. Srivastava and R. Sharma, "Crowdsourcing to elicit requirements for MyERP application," 1st Int. Work. Crowd-Based Requir. Eng. CrowdRE 2015 - Proc., pp. 31–35, 2015, doi: 10.1109/CrowdRE.2015.7367586.
- [5] R. Sharma and A. Sureka, "CRUISE: A platform for crowdsourcing Requirements Elicitation and evolution," 2017 10th Int. Conf. Contemp. Comput. IC3 2017, vol. 2018-Janua, no. August, pp. 1–7, 2018, doi: 10.1109/IC3.2017.8284308.
- [6] M. Hosseini, A. Shahri, K. Phalp, J. Taylor, R. Ali, and F. Dalpiaz, "Configuring crowdsourcing for requirements elicitation," Proc. - Int. Conf. Res. Challenges Inf. Sci., vol. 2015-June, no. June, pp. 133–138, 2015, doi: 10.1109/RCIS.2015.7128873.
- [7] E. C. Groen, "Crowd Out the Competition: Gaining Market Advantage through Crowd-Based Requirements Engineering," 1st Int. Work. Crowd-Based Requir. Eng. CrowdRE 2015 - Proc., pp. 13–18, 2015, doi: 10.1109/CrowdRE.2015.7367583.
- [8] J. Dörr, "With crowd-re to better requirements –cont'd."
- [9] E. C. Groen et al., "The Crowd in Requirements Engineering: The Landscape and Challenges," IEEE Softw., vol. 34, no. 2, pp. 44–52, 2017, doi: 10.1109/MS.2017.33.
- [10] M. Hosseini, K. Phalp, J. Taylor, and R. Ali, "The four pillars of crowdsourcing: A reference model," Proc. - Int. Conf. Res. Challenges Inf. Sci., pp. 1–12, 2014, doi: 10.1109/RCIS.2014.6861072.
- [11] S. L. Lim, D. Quercia, and A. Finkelstein, "StakeNet: Using social networks to analyse the stakeholders of large-scale software projects," Proc. - Int. Conf. Softw. Eng., vol. 1, pp. 295–304, 2010, doi: 10.1145/1806799.1806844.
- [12] S. L. Lim, D. Quercia, and A. Finkelstein, "StakeSource: Harnessing the power of crowdsourcing and social networks in stakeholder analysis," Proc. - Int. Conf. Softw. Eng., vol. 2, pp. 239–242, 2010, doi: 10.1145/1810295.1810340.
- [13] S. L. Lim, D. Damian, and A. Finkelstein, "StakeSource2.0: Using social networks of stakeholders to identify and prioritise requirements," Proc. - Int. Conf. Softw. Eng., no. May, pp. 1022–1024, 2011, doi: 10.1145/1985793.1985983.
- [14] S. L. Lim and A. Finkelstein, "StakeRare: Using social networks and collaborative filtering for large-scale requirements elicitation," IEEE Trans. Softw. Eng., vol. 38, no. 3, pp. 707–735, 2012, doi: 10.1109/TSE.2011.36.
- [15] S. Mughal, A. Abbas, N. Ahmad, and S. U. Khan, "A social network based process to minimize in-group biasedness during requirement engineering," IEEE Access, vol. 6, pp. 66870–66885, 2018, doi: 10.1109/ACCESS.2018.2879385.
- [16] H. Wang, Y. Wang, and J. Wang, "A participant recruitment framework for crowdsourcing based software requirement acquisition," Proc. - 2014 IEEE 9th Int. Conf. Glob. Softw. Eng. ICGSE 2014, pp. 65–73, 2014, doi: 10.1109/ICGSE.2014.26.
- [17] S. L. Lim, P. J. Bentley, and F. Ishikawa, "Reaching the unreachable: A method for early stage software startups to reach inaccessible stakeholders within large corporation," Proc. IEEE Int. Conf. Requir. Eng., vol. 2020-Augus, pp. 376–381, 2020, doi: 10.1109/RE48521.2020.00051.
- [18] N. Condori-Fernandez, P. Lago, M. Luaces, and A. Catala, "A Nichesourcing Framework applied to Software Sustainability Requirements," Proc. - Int. Conf. Res. Challenges Inf. Sci., vol. 2019-May, pp. 1–6, 2019, doi: 10.1109/RCIS.2019.8877000.
- [19] S. L. Lim and P. J. Bentley, "Using PseudoGravity to Attract People An Automated Approach to Engaging a Target Audience using Twitter," no. November, p. 2017, 2017, [Online]. Available: <http://www.forbes.com/entreprene>.
- [20] M. Z. Kolpondinos and M. Glinz, "GARUSO: a gamification approach for involving stakeholders outside organizational reach in requirements engineering," Requir. Eng., vol. 25, no. 2, pp. 185–212, 2020, doi: 10.1007/s00766-019-00314-z.
- [21] I. Alvertis, D. Papaspyros, S. Koussouris, S. Mouzakitis, and D. Askounis, "Using crowdsourced and anonymized Personas in the requirements elicitation and software development phases of software engineering," Proc. - 2016 11th Int. Conf. Availability, Reliab. Secur. ARES 2016, pp. 851–856, 2016, doi: 10.1109/ARES.2016.71.
- [22] E. Guzman, R. Alkadhi, and N. Seyff, "A Needle in a Haystack: What Do Twitter Users Say about Software?," Proc. - 2016 IEEE 24th Int. Requir. Eng. Conf. RE 2016, pp. 96–105, 2016, doi: 10.1109/RE.2016.67.
- [23] R. Snijders, F. Dalpiaz, S. Brinkkemper, M. Hosseini, R. Ali, and A. Özüm, "REfine: A gamified platform for participatory requirements engineering," 1st Int. Work. Crowd-Based Requir. Eng. CrowdRE 2015 - Proc., pp. 1–6, 2015, doi: 10.1109/CrowdRE.2015.7367581.
- [24] J. Fernandes, D. Duarte, C. Ribeiro, C. Farinha, J. M. Pereira, and M. M. Da Silva, "IThink: A game-based approach towards improving collaboration and participation in requirement elicitation," Procedia Comput. Sci., vol. 15, pp. 66–77, 2012, doi: 10.1016/j.procs.2012.10.059.
- [25] F. Dalpiaz, R. Snijders, S. Brinkkemper, M. Hosseini, A. Shahri, and R. Ali, "Engaging the Crowd of Stakeholders in Requirements Engineering via Gamification," pp. 123–135, 2017, doi: 10.1007/978-3-319-45557-0_9.
- [26] M. Z. H. Kolpondinos and M. Glinz, "Tailoring gamification to requirements elicitation: A stakeholder-centric motivation concept," Proc. - 2017 IEEE/ACM 10th Int. Work. Coop. Hum. Asp. Softw. Eng. CHASE 2017, no. June, pp. 9–15, 2017, doi: 10.1109/CHASE.2017.4.
- [27] M. Z. H. Kolpondinos and M. Glinz, "Behind Points and Levels-The Influence of Gamification Algorithms on Requirements Prioritization," Proc. - 2017 IEEE 25th Int. Requir. Eng. Conf. RE 2017, no. September 2017, pp. 332–341, 2017, doi: 10.1109/RE.2017.59.
- [28] V. Gupta, "Social Sector Requirements Engineering Process Using Customer Journeys," in Requirements Engineering for Social Software, 2021, pp. 41–51.
- [29] J. Wouters, R. Janssen, B. Van Hulst, J. Van Veenhuizen, F. Dalpiaz, and S. Brinkkemper, "CrowdRE in a Governmental Setting: Lessons from Two Case Studies," in Proceedings of the IEEE International

- Conference on Requirements Engineering, 2021, pp. 312–322, doi: 10.1109/RE51729.2021.00035.
- [30] P. Nascimento, R. Aguas, D. Schneider, and J. De Souza, “An approach to requirements categorization using Kano’s model and crowds,” Proc. 2012 IEEE 16th Int. Conf. Comput. Support. Coop. Work Des. CSCWD 2012, pp. 387–392, 2012, doi: 10.1109/CSCWD.2012.6221847.
- [31] N. Seyff et al., “Crowd-focused semi-automated requirements engineering for evolution towards sustainability,” Proc. - 2018 IEEE 26th Int. Requir. Eng. Conf. RE 2018, no. September, pp. 370–375, 2018, doi: 10.1109/RE.2018.00-23.
- [32] K. Schneider and L. M. Bertolli, “Video variants for CrowdRE: How to create linear videos, vision videos, and interactive videos,” Proc. - 2019 IEEE 27th Int. Requir. Eng. Conf. Work. REW 2019, pp. 186–192, 2019, doi: 10.1109/REW.2019.00039.
- [33] M. Levy, I. Hadar, and D. Te’eni, “A gradual approach to crowd-based requirements engineering: The case of conference online social networks,” 1st Int. Work. Crowd-Based Requir. Eng. CrowdRE 2015 - Proc., pp. 25–30, 2015, doi: 10.1109/CrowdRE.2015.7367585.
- [34] M. Levy, I. Hadar, A. Krebs, and I. Barak, “When the Developers Become the (Micro) Crowd: An Educational Case Study on Multidisciplinary Requirements Engineering,” Proc. IEEE Int. Conf. Requir. Eng., vol. 2021-Septe, pp. 313–319, 2021, doi: 10.1109/REW53955.2021.00055.
- [35] A. Adepetu, K. A. Ahmed, Y. Al Abd, A. Al Zaabi, and D. Svetinovic, “CrowdREquire: A requirements engineering crowdsourcing platform,” AAAI Spring Symp. - Tech. Rep., vol. SS-12-06, no. Goodin 2005, pp. 2–7, 2012.
- [36] W.-C. Hu and H. C. Jiau, “UCFrame,” ACM SIGSOFT Softw. Eng. Notes, vol. 41, no. 2, pp. 1–13, 2016, doi: 10.1145/2894784.2894795.
- [37] D. Renzel, M. Behrendt, R. Klamma, and M. Jarke, “Requirements Bazaar: Social requirements engineering for community-driven innovation,” 2013 21st IEEE Int. Requir. Eng. Conf. RE 2013 - Proc., vol. 5, no. 1, pp. 326–327, 2013, doi: 10.1109/RE.2013.6636738.
- [38] N. M. Rizk, M. H. Gheith, A. M. Zaki, and E. S. Nasr, “CREeLS: Crowdsourcing based requirements elicitation for eLearning Systems,” Int. J. Adv. Comput. Sci. Appl., vol. 10, no. 10, pp. 242–251, 2019, doi: 10.14569/ijacsa.2019.0101034.
- [39] J. Wouters, A. Menkveld, S. Brinkkemper, and F. Dalpiaz, “Crowd-based requirements elicitation via pull feedback: method and case studies,” Requir. Eng., vol. 27, no. 4, pp. 429–455, 2022, doi: 10.1007/s00766-022-00384-6.
- [40] S. G. Köse and F. B. Aydemir, “A Framework To Improve User Story Sets Through Collaboration,” 2023, [Online]. Available: <http://arxiv.org/abs/2301.10070>.
- [41] T. Johann and W. Maalej, “Democratic mass participation of users in Requirements Engineering?,” 2015 IEEE 23rd Int. Requir. Eng. Conf. RE 2015 - Proc., pp. 256–261, 2015, doi: 10.1109/RE.2015.7320433.
- [42] L. Nagel, A. Specht, and J. Burst, “Encouraging Asynchronous Crowd Discussions Using an Interactive Video Player,” Proc. - 31st IEEE Int. Requir. Eng. Conf. Work. REW 2023, pp. 115–121, 2023, doi: 10.1109/REW57809.2023.00026.
- [43] L. Radeck et al., “Understanding IT-related Well-being, Aging and Health Needs of Older Adults with Crowd-Requirements Engineering,” Proc. IEEE Int. Conf. Requir. Eng., vol. 5, pp. 57–64, 2022, doi: 10.1109/REW56159.2022.00018.
- [44] D. Muñante, A. Siena, F. M. Kifetew, A. Susi, M. Stade, and N. Seyff, “Gathering requirements for software configuration from the crowd,” Proc. - 2017 IEEE 25th Int. Requir. Eng. Conf. Work. REW 2017, no. September, pp. 176–181, 2017, doi: 10.1109/REW.2017.74.
- [45] A. Menkveld, S. Brinkkemper, and F. Dalpiaz, “User story writing in crowd requirements engineering: The case of a web application for sports tournament planning,” in Proceedings - 2019 IEEE 27th International Requirements Engineering Conference Workshops, REW 2019, 2019, pp. 174–179, doi: 10.1109/REW.2019.00037.
- [46] M. van Vliet, E. C. Groen, F. Dalpiaz, and S. Brinkkemper, “Identifying and Classifying User Requirements in Online Feedback via Crowdsourcing,” Lect. Notes Comput. Sci. (including Subser. Lect. Notes Artif. Intell. Lect. Notes Bioinformatics), vol. 12045 LNCS, pp. 143–159, 2020, doi: 10.1007/978-3-030-44429-7_11.
- [47] M. Hosseini, E. C. Groen, A. Shahri, and R. Ali, “CRAFT: A crowd-annotated feedback technique,” Proc. - 2017 IEEE 25th Int. Requir. Eng. Conf. Work. REW 2017, no. May 2018, pp. 170–175, 2017, doi: 10.1109/REW.2017.27.
- [48] I. Morales-Ramirez, D. Papadimitriou, and A. Perini, “CrowdIntent: Annotation of Intentions Hidden in Online Discussions,” Proc. - 2nd Int. Work. Crowdsourcing Softw. Eng. CSI-SE 2015, pp. 24–29, 2015, doi: 10.1109/CSI-SE.2015.12.
- [49] P. K. Murukannaiah, N. Ajmeri, and M. P. Singh, “Acquiring Creative Requirements from the Crowd: Understanding the Influences of Personality and Creative Potential in Crowd RE,” Proc. - 2016 IEEE 24th Int. Requir. Eng. Conf. RE 2016, pp. 176–185, 2016, doi: 10.1109/RE.2016.68.
- [50] T. D. Breaux and F. Schaub, “Scaling requirements extraction to the crowd: Experiments with privacy policies,” 2014 IEEE 22nd Int. Requir. Eng. Conf. RE 2014 - Proc., pp. 163–172, 2014, doi: 10.1109/RE.2014.6912258.
- [51] H. Guo, Ö. Kafalı, A. L. Jeukeng, L. Williams, and M. P. Singh, “Çorba: Crowdsourcing To Obtain Requirements From Regulations and Breaches,” Empir. Softw. Eng., vol. 25, no. 1, pp. 532–561, 2020, doi: 10.1007/s10664-019-09753-2.
- [52] H. Rosser, M. Mayor, A. Stemmler, V. Ahuja, A. Grover, and M. Hale, “Phish Finders: Crowd-powered RE for anti-phishing training tools,” in Proceedings of the IEEE International Conference on Requirements Engineering, 2022, pp. 130–135, doi: 10.1109/REW56159.2022.00031.
- [53] V. S. Vidal, M. A. M. Suriani, R. A. S. Braga, A. C. O. Santos, O. S. Silva, and R. J. Campos, “Use of Crowdsourcing Questionnaires to Validate the Requirements of an Application for Pet Management,” in ITNG 2021 18th International Conference on Information Technology-New Generations, 2021, pp. 215–220, doi: 10.1007/978-3-030-70416-2_46.
- [54] C. Wang, W. Zhang, H. Zhao, and Z. Jin, “Eliciting activity requirements from crowd using genetic algorithm,” Commun. Comput. Inf. Sci., vol. 809, pp. 99–113, 2018, doi: 10.1007/978-981-10-7796-8_8.
- [55] C. H. Wang, Z. Jin, W. Zhang, D. Zowghi, H. Y. Zhao, and W. P. Jiao, “Activity Diagram Synthesis Using Labelled Graphs and the Genetic Algorithm,” J. Comput. Sci. Technol., vol. 36, no. 6, pp. 1388–1406, 2021, doi: 10.1007/s11390-020-0293-9.
- [56] S. Taj, Q. Arain, I. Memon, and A. Zubedi, “To apply data mining for classification of crowd sourced software requirements,” ACM Int. Conf. Proceeding Ser., pp. 42–46, 2019, doi: 10.1145/3328833.3328837.
- [57] L. Z. Niu, L. Gong, F. Ye, and J. Gao, “Research on Mass User Requirements Analysis and Evaluation Method Based on Crowdsourcing Platform,” in 2021 IEEE 8th International Conference on Industrial Engineering and Applications, ICIEA 2021, 2021, pp. 566–570, doi: 10.1109/ICIEA52957.2021.9436768.
- [58] H. Sa’adah, T. A. T. M. Amin, N. Admodisastro, and A. Kamaruddin, “Morphological approach in creative requirements elicitation from crowdsourcing,” J. Telecommun. Electron. Comput. Eng., vol. 9, no. 3-5 Special Issue, pp. 31–35, 2017.
- [59] N. Mead, F. Shull, J. Spears, S. Heibl, S. Weber, and J. Cleland-Huang, “Crowd Sourcing the Creation of Personae Non Gratae for Requirements-Phase Threat Modeling,” Proc. - 2017 IEEE 25th Int. Requir. Eng. Conf. RE 2017, pp. 412–417, 2017, doi: 10.1109/RE.2017.63.

An Effective Book Recommendation System using Weighted Alternating Least Square (WALS) Approach

Kavitha V K*, Dr.Sankar Murugesan

Department of Computer Science and Engineering,
Veltech Rangarajan Dr Sagunthala R & D Institute of Science and Technology, Avadi, Chennai, India

Abstract—Book recommendation systems are essential resources for connecting people with the correct books, encouraging a love of reading, and sustaining a vibrant literary ecosystem in an era when information overload is a prevalent problem. With the emergence of digital libraries and large online book retailers, readers may no longer find their next great literary journey without the help of customized book suggestions. This work offers a novel way to improve book recommendation systems using the Weighted Alternating Least Squares (WALS) technique, which is intended to uncover meaningful patterns in user ratings. The suggested approach minimizes the Root Mean Square Error (RMSE), a crucial indicator of recommendation system (RS) performance, in order to tackle the problem of optimizing recommendations. By representing user-item interactions as a matrix factorization problem, the WALS approach improves the recommendation process. In contrast to conventional techniques, WALS adds weighted elements that highlight specific user-item pairings' significance, increasing the recommendations' accuracy. Through an empirical study, the proposed approach demonstrates a significant reduction in RMSE when compared to standard RS, highlighting its effectiveness in enhancing the quality of book recommendations. By leveraging weighted matrix factorization, the proposed method adapts to the nuanced preferences and behaviors of users, resulting in more accurate and personalized book recommendations. This advancement in recommendation technology is poised to benefit both readers and the book industry by fostering more engaging and satisfying reading experiences.

Keywords—Recommendation system; user ratings; matrix factorization; alternating least square; weighted matrix factorization

I. INTRODUCTION

A technology that makes recommendations based on its ability to infer user preferences is called a recommendation system (RS), since it uses all of the information that is accessible at any given time to predict items. In light of the current situation of "information overload," which is defined as an instance in which there is an excessive volume of information to absorb and interpret, when it comes to decision-making, RS can be very beneficial because it provides unique and personalized recommendations [1]. The algorithm utilized determines the recommendation outputs. Recommender systems can be roughly categorized as content-based filtering, collaborative filtering, and hybrid filtering system [2].

A. Content Based Filtering in Recommendation System

In content-based filtering, recommendations are made using previous user selections. The recommender may receive implicit user choices, such as ratings, or explicit user choices, such as surfing patterns. Using the data provided by the user, a user profile is crafted and utilized to inform future recommendations derived from the content of input objects. Items that are particularly suitable to the user are identified using content-based RS by examining item depictions. Recommendation framework details frequently vary depending on how objects are represented. This methodology offers the advantage of being able to explain its suggestions and suggest previously unrated items to individuals with unique interests. When a user provides input on particular items in relation to user-related content, content-based RSs create user preferences, profiles, interests, and impressions based on that information [3]. Products will be suggested to the user based on their preference profile if they match products that have received exceptional appraisals in the past. The increase in user profile proficiency is a crucial component of CBF recommender frameworks [4]. The creation of user profiles has been linked to various learning approaches.

B. Collaborative Filtering in Recommendation System

The process of collaborative filtering involves gathering user evaluations or judgments about various items. Moreover, users with comparable tastes are found in a sizable population. People with similar tastes are merged in order to recommend new products and assist other users in making better selections [5]. CF algorithms are further categorized into model-based and memory-based techniques.

The most suitable definition of CF is "joint effort between individuals to help each other perform filtering by recording their responses to materials they read" [6]. CF approaches play a critical role in the recommendation, even if they are frequently used in conjunction with other filtering approaches such as knowledge-based, content-based, or social-based [7]. It allows users to rate various elements (such as songs, movies, videos, and so on) on a content-based network so that, once sufficient data is stored on the system, recommendations can be sent to each user based on the information offered by those who believe they have the most practical communication with them. Model-based approaches offer recommendations by evaluating the parameters of quantifiable models for user evaluation. The most often used models include matrix

factorization (MF), neural networks, fuzzy systems, Bayesian classifiers, latent features, and genetic algorithms [8].

1) *Collaborative filtering using matrix factorization*: MF is the core for some of the most successful latent factor model realizations. In its simplest form, MF assigns vectors of factors based on implicated information from item rating patterns to both items and users. A recommendation is produced when item and user factors have a high degree of correlation. RS rely on many forms of input data, which are regularly disposed in a matrix where users are represented by one dimension and items of interest by the other. A user-item interaction matrix is factorized into two lower-dimensional matrices via MF models, which can subsequently be utilized to anticipate missing values in the original matrix [9]. The main phases of the MF approach are described below.

a) *The User-Item Interaction Matrix*: In CF, we start with a user-item interaction matrix, often denoted as R . Each row represents a user, each column represents an item, and the values in the matrix depicts user ratings, purchase history, or some other form of interaction. The matrix is typically sparse because not all users have interacted with all items. Let R be an $m \times n$ matrix, where m = number of users, n = number of items and $R[i,j]$ is the interaction (rating or preference) of user i with item j .

b) *MF*: The goal is to factorize the user-item interaction matrix R into two lower-dimensional matrices, typically denoted as U (for users) and V (for items). The concept involves depicting users and items in a reduced-dimensional space, where the dot product of their representations serves as an approximation for the entries in the original matrix.

Let U be an $m \times k$ matrix, where m = number of users, k = the number of latent features (a hyper parameter to be chosen).

Let V be an $n \times k$ matrix, where n = number of items, k = the number of latent features. The approximation of the user-item interaction matrix R is given by the dot product of U and V :

$$R \approx UV^T \quad (1)$$

Here, R is approximated by the dot product of U and the transpose of V .

2) *Objective function*: MF models are trained by minimizing a loss function. A common loss function is the Mean Squared Error (MSE) between the actual user-item interactions (R) and the predicted interactions UV^T .

$$MSE = \sum_{(i,j)} (R[i,j] - (UV^T)[i,j])^2 \quad (2)$$

The objective is to find U and V that minimize this error.

a) *Regularization*: To prevent over fitting, regularization terms are often added to the loss function. L2 regularization is commonly used, and it penalizes large values in U and V :

$$\begin{aligned} \text{Regularized MSE} &= \sum_{(i,j)} (R[i,j] - (UV^T)[i,j])^2 + \lambda(\|U\|^2 \\ &+ \|V\|^2) \end{aligned} \quad (3)$$

Here, λ is a hyper parameter that controls the strength of regularization, and $\|U\|^2$ and $\|V\|^2$ represent the Frobenius norms of U and V , respectively.

b) *Optimization*: MF models are typically trained using optimization techniques like gradient descent to minimize the regularized loss function.

c) *Prediction*: Once the U and V matrices are learned, predictions for user-item interactions can be made by taking the dot product of the corresponding user and item vectors:

$$\text{Prediction for user } i \text{ and item } j: (UV^T)[i,j]$$

MF frameworks, such as Singular Value Decomposition and Alternating Least Squares (ALS), are widely utilized in RSs. They are effective at capturing latent patterns and making personalized recommendations based on user-item interactions.

C. Hybrid Filtering

A hybrid strategy integrates content and collaborative filtering-based techniques to achieve successful recommendation outcomes. The integration of different algorithms benefits from their complementary advantages. In fact, a hybrid strategy outperforms the traditional approach in handling data sparsest and cold start issues. Combining multiple recommender system approaches entails developing two unique recommender systems that rely on content-based and collaborative methodologies. The emergence of RS has demonstrated the value of hybrid processes, which combine several approaches to maximize the advantages of each method. In order to overcome data sparsest and cold start difficulties, CF-based approaches inevitably involve abuse of the extract information source associated with the items our users use. Hybrid recommenders are an interesting problem that proposes a reasonable hypothesis to which one may respond similarly by looking into more recent opportunities.

D. Deep Learning in Recommendations

The volume of data generated in the last few years has increased dramatically compared to previous years. This has led to a greater awareness of the term "big data," which indicates to the vast quantity of unstructured information that is generated and needs more investigation. In recent times, there has been a growing focus on machine learning, specifically deep learning, because of its potential to improve the way large amounts of data are processed and because it can be used to model complex data sets like texts and images. RSs rely heavily on machine learning algorithms, which analyze item and user data to generate specific recommendations. Because of the exponential rise in data availability, the advancement of algorithms, and the availability of more computer resources like GPUs, deep learning has become a promising tool for different data domains. Deep learning models have been effectively utilized in computer vision, speech recognition, and NLP applications. Deep learning has recently been applied to RSs. Despite the significant progress made in the previous twenty years, standard RSs remain unsatisfactory in adequately modeling complicated (e.g., nonlinear) interactions between users and items. Deep neural networks, on the other hand, are universal function approximates that can represent any continuous function. Restricted Boltzmann Machine (RBM) is one of the earliest works that uses the deep learning concept for

collaborative filtering [10]. Nowadays, a wide range of DL models, including Auto encoder (AE), Multilayer Perceptron (MLP), Convolutional Neural Network (CNN), Recurrent Neural Network (RNN), and Generative Adversarial Network (GAN), are utilized to boost the quality of recommendations.

In the modern world, book recommendation system has become increasingly sophisticated and invaluable, leveraging user-generated book ratings and reviews to guide readers towards literary treasures that resonate with their tastes. These systems harness advanced algorithms to analyze vast databases of reader feedback, identifying patterns and correlations in book preferences. By considering factors such as genre, author, writing style, and even thematic elements, these recommendation engines can suggest books that are highly likely to captivate and engage individual readers. As a result, book enthusiasts can effortlessly discover new and exciting literary adventures, making the most of the digital age's abundance of reading options, while also fostering a sense of community among readers who share similar literary passions. This paper introduces an effective book recommendation system based on WALS method.

The primary contribution of the paper includes:

- Development of an effective book recommendation system using CF.
- Utilization of WALS matrix factorization method to avoid sparsest problems.
- Model evaluation using Good Books Dataset.

II. LITERATURE REVIEW

Dhiman Sarma et al. [11] developed clustering approaches to improve the prediction capabilities of RSs. The datasets were gathered from the Kaggle repository for Goodreads books. The F1 score was 52.84%, whereas the average sensitivity and specificity were 49.76% and 56.74%, respectively. According to the simulation results, the suggested method can more effectively exclude boring books from the list of recommended reading. Yiu-Kai Ng [12] created a book recommendation approach for young readers using MF and content-based filtering techniques. In order to evaluate the effectiveness of recommenders that suggest books to K-12 readers, a benchmark dataset was developed that includes metadata, readability levels, and user and book counts. The error values are computed for the suggested methodologies. Madhuri Kommineni et al. [13] developed a straightforward, intelligible system for book recommendations to assist readers in suggesting the suitable book to be studied next. The introduced method dedicates on training, feedback, management, conveying, arrangement, and providing the user with helpful information to support the recommendation of data items and decision-making. The effectiveness of similarity metrics in book recommendations to users was assessed utilizing the User-Based CF technique. According to the simulation results, a normal distribution after the accuracy rating implies consistency and efficiency.

Sunny Sharma et al. [14] developed a hybrid system-based book RS that predicts recommendations. The suggested method combines content-based and CF. The proposed work is

tested in an online recommender system, enabling us to determine the actual user approval rate of the recommendations made. Based on simulation findings, it was shown that the suggested hybrid filtering strategy works better than both content-based and traditional CF. A personalized recommendation algorithm was realized by Yihan Ma et al. [15] by introducing a large and DL to the book recommendation system sector. Initially, the records' readers' and books' information were gathered. LR and DNN networks are trained together to produce the suggested basic recommendation model. The transformation of the double label into numerous labels enhanced the suggested model. Ultimately, a set of comparison studies was created to confirm the viability of the suggested method. The simulation findings demonstrated that the suggested RS's accuracy is noticeably higher than that of the current techniques. Kiran R et al. [16] suggested a unique DL hybrid recommender system to close the loopholes in CF systems and use DL to reach state-of-the-art predicted accuracy. The method learns non-linear latent variables by representing users and items using embeddings. The method reduces the cold start issue by assimilating side information about users and items into an extremely DNN. The suggested approach combines an increasing weight decay with a lower learning rate. The values are cyclically changed throughout epochs to further increase accuracy. Extensive experiments are carried out across multiple datasets. The outcomes demonstrated that in both non-cold start and cold start scenarios, the suggested solution performs better than the current approaches.

Tulasi Prasad Sariki and G. Bharadwaja Kumar [17] developed an efficient framework to enhance the recommendations given in the book domain by carefully combining natural language processing and DL approaches. The feature space for the existing CBFs has been improved by augmenting them with other relevant attributes by employing this wise combination. The different models that are suggested in the current framework are effective in making use of the book's entire textual material. According to the simulation results, the expanded framework outperforms the baseline models in terms of total suggestion accuracy, with an improvement of 18%. Furthermore, it can be concluded that the suggested approach performs 6% better than the cutting-edge models, including the NCF with Content Embedding Model. An algorithm for digital library recommendations was presented by Fikadu Wayesa et al. [18]. A hybrid book recommendation system using new user profile data was proposed in this study. This hybrid RS merges elements of collaborative and content-based approaches, leveraging user profile data and pattern relationships among users. It uses a content-based component to suggest recommendations to users in the same cluster who have rated books in similar categories. These recommendations are based on the book features and content type information, offering a personalized experience for users with shared interests. A set of comprehensive experiments using information retrieval (IR) assessment criteria are used to measure the efficacy of the suggested technique. The results showed that the recommended strategy outperforms the current techniques, with significant advancements. Dongjin Hou [19] developed a personalized book recommendation method using DL models and the

features and rules governing user savings at university libraries. The deep auto encoder (DAE) is initially improved by the LSTM in order to enable the framework to retrieve the temporal aspects of the data. The resultant book recommendation for the present user is then obtained by using the Softmax function. The suggested approach is validated on the basis of real library lending data. The findings demonstrated that the suggested strategy outperforms a number of other RSs.

Minyu Liu [20] developed a deep-belief network-based book recommendation system. Personalized service suggestions are based on the scenario ontology, which is calculated using the ontology similarity calculation approach. The scenario ontology is then derived based on the library and users' information demands. A deep learning-based personalized intelligent RS idea for book services was proposed by Weiwei Yang [21]. By applying intelligent technologies like machine learning, users can evaluate their big data, create user profiles, correlate resources and users with their profiles, and receive individualized intelligent services. In order to provide users with personalized intelligent book recommendation services that primarily satisfy their potential demands and match their interests, the paper first retrieved users' personalized interests. Next, it identified users' current personalized potential book demands using the plain Bayesian algorithm. Finally, it provided users with personalized book recommendation services. A content-based scientific article recommendation (C-SAR) framework based on a DL approach was developed by Akhil M. Nair et al. [22]. The primary objective of the proposed model was to identify papers by comparing their titles. The most often recurring set of documents from a comparable collection were filtered using an association rule mining Apriori approach, and the Gated Recurrent Unit method was used to determine how similar the documents were. The simulation results revealed that the model performed better than current models that make use of user representations and basic K-means clustering.

A decision tree-based book recommendation system framework was proposed by Anant Duhan and Dr. N. Arunachalam [23]. The effectiveness of a classifier is a major factor in book recommendation systems. Real user data was used to test the system. According to the simulation results, the decision tree classifiers outperformed because of their strong learning capacity, quick classification speed, high accuracy, and straightforward design. A cross-domain book recommendation system employing sequential pattern mining and rule mining was proposed by Taushif Anwar and V. Uma [24]. The suggested approach integrates Wpath, CF, and SPM to recommend the most favored items from many domains with greater recommendation accuracy. Wpath is used in the proposed study to assist in determining the semantic similarity between items that belong to different domains. Topseq criteria are used to extract the sequence's favored items, while the Prefix Span technique assists in retrieving frequently occurring sequences. Initially, the RMSE is used to compare the errors. Finally, the algorithm for pattern mining is examined. The outcome shows that, as compared to the CF-KNN technique, CD SPM performed better. Chendhur et al. [25] introduced an improved CF strategy based on user preferences. The key

objective of this suggested method is to make book recommendations to users based on their reading preferences and to boost the accuracy of those recommendations by enhancing the computational techniques used in the collaborative filtering algorithm. There are four major modules in the proposed approach. The book crossing dataset is used to assess the suggested method. The experimental findings demonstrated that the suggested approach offers the user effective book recommendations.

Neighborhood-Based Collaborative Filtering (NBCF) has its limitations, including a restricted range of recommendations, vulnerability to data sparsest, challenges with handling cold-start scenarios, and relatively slow prediction processing. Model-Based Collaborative Filtering (MBCF) necessitates parameter tuning, entails resource-intensive training phases, and exhibits a sluggish training process. Calculating similarities in graph-based collaborative filtering (GBCF) for large-scale commercial applications can be resource-intensive in terms of both space and time. The computational complexity involved in these calculations can result in significant costs, making the adoption of such systems expensive for businesses. Hybrid-Based Collaborative Filtering (HBCF) involves calculating similarities in large commercial applications, which can be computationally expensive in terms of both space and time complexity. The complexity and adoption of these systems often come with significant costs.

III. MATERIALS AND METHOD

The proposed book recommendation system utilized MF method using WALS method. The detailed block diagram of the suggested methodology is visualized in Fig. 1. The suggested book recommendation system methodology begins with dataset collection and preprocessing to ensure data quality. Data preprocessing involves data cleaning, handling missing values, and outlier detection. Data cleaning is the process of guaranteeing the absence of errors and discrepancies within a dataset. Missing values are imputed or removed, and outliers, which can distort recommendations, are identified and addressed. EDA is crucial to understand the dataset better. It includes visualizations and statistical analysis to uncover patterns, trends, and relationships within the data. EDA can reveal insights such as popular book genres, user preferences, and rating distributions. In this paper, MF with techniques like WALS is applied to generate personalized recommendations based on user-item interactions. In this approach, the user-item interaction data is deployed as a matrix. MF techniques like WALS are applied to decompose this matrix into two lower-dimensional matrices—one denoting user and the other denoting books. The latent factors extracted from these matrices capture user preferences and item characteristics. The performance of the RS is rigorously assessed in terms of Root Mean Squared Error (RMSE) to refine the model and enhance its effectiveness in suggesting books that align with users' preferences and interests.

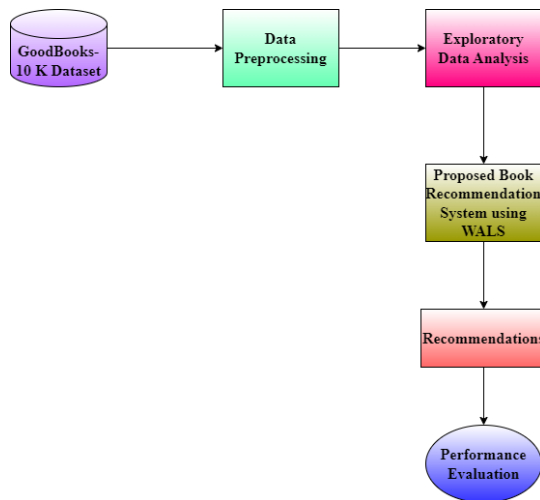


Fig. 1. Block diagram of the proposed book recommendation system.

A. Dataset Description

The goodbooks- 10k dataset has been utilized in this work, which comprises ratings for a collection of ten thousand popular books. Typically, each book is associated with approximately 100 reviews, although there are instances of books with fewer ratings. These ratings are on a scale of one to five. The book IDs and user IDs in this dataset follow a sequential numbering scheme, ranging from 1 to 10000 for books and 1 to 53424 for users. It's noteworthy that all users have provided at least two ratings, and the median number of ratings per user is eight. The dataset is organized into various

folders, including "ratings.csv" for ratings data, "to_read.csv" containing user-to-book pairs indicating books marked as "to read," "books.csv" providing metadata for each book (e.g., goodreads IDs, authors, titles, average ratings), "book_tags.csv" containing tags, shelves, and genres granted to books by users, and "tags.csv" which maps tag IDs to their corresponding names. For our book recommendation task, we specifically leveraged the "ratings.csv" file. Table I summarizes the key attributes within the dataset, and Fig. 2 offers a visual representation of the dataset structure.

TABLE I. FEATURE DESCRIPTION OF DATASET

| Features | Description |
|--------------------|---|
| bookID | Unique identification number for each book |
| title | Name under which book was published |
| authors | Name of the Authors of the book |
| average_rating | Average rating of the book received in total. |
| isbn | International standard book number |
| isbn13 | 13-digit isbn to identify the book |
| language_code | Primary Language of the book |
| num_pages | Number of pages the book contains |
| ratings_count | Total Number of ratings the book received. |
| text_reviews_count | Total number of written reviews received. |
| publication_date | Date when the book was first published |
| publisher | Name of the Publishers |

| bookID | title | authors | average_rating | isbn | isbn13 | language_code | num_pages | ratings_count | text_reviews_count | publication_date | publisher |
|--------|---|----------------------------|----------------|------------|---------------|---------------|-----------|---------------|--------------------|------------------|-----------------|
| 0 | 1 Harry Potter and the Half-Blood Prince (Harry ... | J.K. Rowling/Mary GrandPré | 4.57 | 0439785960 | 9780439785969 | eng | 652 | 2095690 | 27591 | 9/16/2006 | Scholastic Inc. |
| 1 | 2 Harry Potter and the Order of the Phoenix (Har... | J.K. Rowling/Mary GrandPré | 4.49 | 0439358078 | 9780439358071 | eng | 870 | 2153167 | 29221 | 9/1/2004 | Scholastic Inc. |
| 2 | 4 Harry Potter and the Chamber of Secrets (Harry... | J.K. Rowling | 4.42 | 0439554896 | 9780439554893 | eng | 352 | 6333 | 244 | 11/1/2003 | Scholastic |
| 3 | 5 Harry Potter and the Prisoner of Azkaban (Harr... | J.K. Rowling/Mary GrandPré | 4.56 | 043965548X | 9780439655484 | eng | 435 | 2339585 | 36325 | 5/1/2004 | Scholastic Inc. |
| 4 | 8 Harry Potter Boxed Set Books 1-5 (Harry Potte... | J.K. Rowling/Mary GrandPré | 4.78 | 0439682584 | 9780439682589 | eng | 2690 | 41428 | 164 | 9/13/2004 | Scholastic |

Fig. 2. Visualization of dataset.

B. Data Preprocessing and Exploratory Data Analysis (EDA)

Data preprocessing is a vital and often time-consuming phase in the data analysis process, as it plays a key role in improving data quality by addressing issues such as missing values, outliers, inconsistencies, and errors. The precision and dependability of subsequent analyses are significantly shaped by the quality of the data. Missing data, in particular, can significantly affect data analysis quality. There are several methods to manage missing data, including data deletion and imputation. Managing missing values is a critical aspect of data preprocessing since it directly impacts the dataset's quality and

reliability. Various strategies are available to address missing data, such as eliminating rows with missing values, filling in missing values with measures like the mean, median, or mode, or utilizing more advanced techniques like regression imputation or predictive modeling.

Identifying and managing outliers is a critical component of data preprocessing, serving to pinpoint data instances that exhibit substantial deviations from the bulk of the dataset.

These outliers represent data points that are exceptional or divergent from the norm and have the potential to exert a substantial influence on the outcomes of data analysis, the

performance of learning models, and the integrity of statistical inferences.

Exploratory Data Analysis (EDA) is a fundamental stage in data analysis dedicated to providing a comprehensive overview of a dataset's essential features. This process serves as a crucial step in gaining profound insights into the data prior to employing more advanced statistical and learning models. To start the EDA process, descriptive statistics are employed to offer an initial snapshot of the data's central tendencies and variability. Key descriptive statistics often encompass metrics

like the mean, median, mode, standard deviation, and range. Fig. 3 illustrates the descriptive statistics of the collected dataset, offering a concise representation of these critical data characteristics.

Data visualization is a powerful EDA technique that involves creating visual representations of data. This includes scatter plots, line charts, bar plots, heatmap, and more. The visualization of top 10 authors with maximum book published is shown in Fig. 4. The most occurring book in the collected dataset is visualized in Fig. 5.

| | average_rating | num_pages | ratings_count | text_reviews_count | year |
|-------|----------------|--------------|---------------|--------------------|--------------|
| count | 11123.000000 | 11123.000000 | 1.112300e+04 | 11123.000000 | 11123.000000 |
| mean | 3.934075 | 336.405556 | 1.794285e+04 | 542.048099 | 2000.169019 |
| std | 0.350485 | 241.152626 | 1.124992e+05 | 2576.619589 | 8.247227 |
| min | 0.000000 | 0.000000 | 0.000000e+00 | 0.000000 | 1900.000000 |
| 25% | 3.770000 | 192.000000 | 1.040000e+02 | 9.000000 | 1998.000000 |
| 50% | 3.960000 | 299.000000 | 7.450000e+02 | 47.000000 | 2003.000000 |
| 75% | 4.140000 | 416.000000 | 5.000500e+03 | 238.000000 | 2005.000000 |
| max | 5.000000 | 6576.000000 | 4.597666e+06 | 94265.000000 | 2020.000000 |

Fig. 3. Descriptive statistics of dataset.

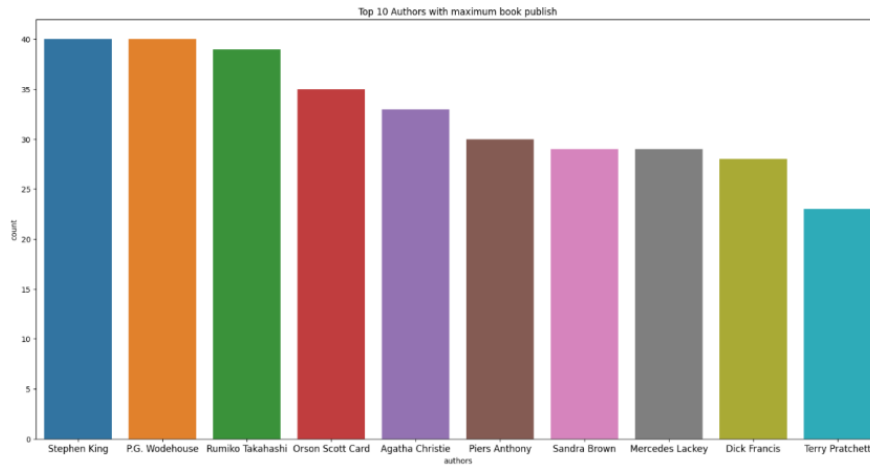


Fig. 4. Data visualization.

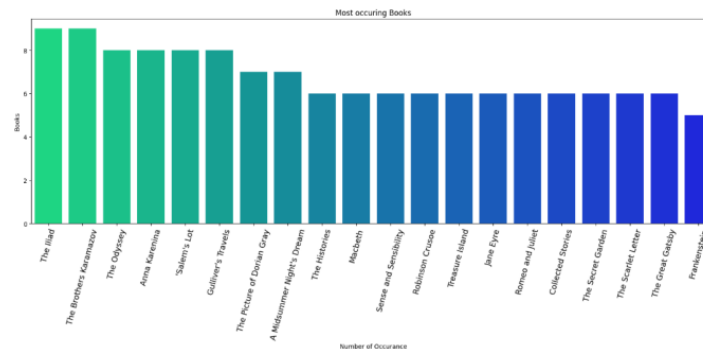


Fig. 5. Visualization of most occurring books in the dataset.

The distribution plot of rating variable from the dataset is shown in Fig. 6. Distribution plots, such as histograms and kernel density estimates (KDE), are essential tools during

EDA. It offers insightful information on the type of data, its properties, and any possible trends or problems.

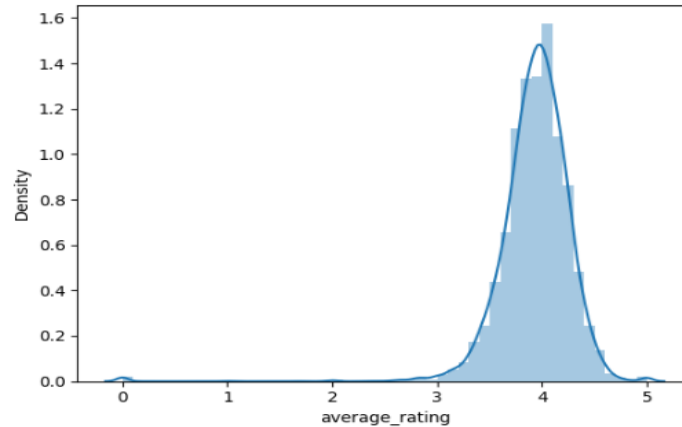


Fig. 6. Distribution Plot of Ratings from dataset.

C. Proposed Book Recommendation System Using Weighted Alternating Least Square (WALS) Method

WALS is a popular MF technique frequently employed in RSs, including those used in book recommendations. Its primary objective is to break down the user-item interaction matrix into two lower-dimensional matrices: one for users and another for items. These matrices capture latent factors that encapsulate user preferences and item characteristics. WALS serves as an extension of the Alternating Least Squares (ALS) method, a widely utilized collaborative filtering approach [26].

To understand the ALS method, consider a rating data matrix R with dimensions $m \times n$, where there are n users and m items. The entry R_{ui} at the $(u, i)^{th}$ position within the matrix R corresponds to the rating given by user u to item i . Since this matrix captures user-item interactions, it is naturally sparse due to the fact that not all users rate or interact with every item, leading to numerous empty or missing values. MF offers a viable solution to the intricate problem of handling sparse matrices. It involves decomposing the R matrix into two k -dimensional vectors, often specified as "factors." These factors play a vital role in capturing underlying patterns and relationships between users and items, enabling more effective recommendations.

- x_u is k dimensional vectors summarizing's every user u .
- y_i is k dimensional vectors summarizing every user i .

$$\text{Let, } r_{ui} \approx x_u^T y_i \quad (4)$$

$$x_u = x_1, x_2, x_3, \dots, x_n \in \mathbb{R}^k \quad (5)$$

$$y_i = y_1, y_2, \dots, y_n \in \mathbb{R}^k \quad (6)$$

Eq. (4) can be assembled as an optimization problem to find:

$$\text{argmin } \sum_{r_{ui}} (r_{ui} - x_u^T y_i)^2 + \lambda (\sum_u \|x_u\|^2 + \sum_i \|y_i\|^2) \quad (7)$$

The regularization factor denoted as λ is commonly referred to as "weighted λ regularization." This parameter, λ , serves the purpose of mitigating over fitting, and its value can be customized to fine-tune the model's performance in mitigating over fitting. The default value for λ is typically set at 1, but it can be modified as needed to achieve optimal results.

When the set of variables x_u is held constant, the objective function for y_i becomes convex. Conversely, when the set of variables y_i is constant, the objective function for x_u also becomes convex. By iteratively optimizing x_u and y_i using this alternating approach until convergence, we employ a technique known as Alternating Least Squares (ALS) to determine the optimal values for these variables.

WALS is a MF approach widely employed in RSs to model user-item interactions. The primary objective of WALS is to factorize the user-item interaction matrix while optimizing a weighted least squares objective function. By iteratively updating latent factor matrices for users and items, WALS discovers hidden patterns that capture user preferences and item characteristics. The incorporation of weights allows for flexibility in handling missing data and emphasizing the importance of certain interactions. With its alternating least squares optimization strategy, WALS efficiently generates recommendations by approximating missing entries in the interaction matrix, making it a valuable tool for personalized and efficient RSs.

The goal of WALS is to approximate the user-item interaction matrix R as a product of two lower-rank matrices, U (user matrix) and V (item matrix), where:

$$R \approx U * V^T \quad (8)$$

R is the user-item interaction matrix, where $R(i, j)$ represents the interaction or rating of user i for item j .

WALS aims to factorize the user-item matrix R into two matrices, U and V , such that the approximation $R \approx U * V^T$ holds.

WALS uses a weighted least squares approach to optimize the factorization. It introduces a weight matrix W , where $W(i, j)$ is the weight associated with the interaction between user i and item j . This weight can be set based on various criteria, like the confidence of the user's rating or the number of interactions. The objective function to minimize in WALS is the weighted least squares loss, defined as follows:

$$L(U, V) = (R(i, j) - U(i, :) * V(j, :))^2 \quad (9)$$

Here, $U(i, :)$ represents the i^{th} row of the user matrix U , and $V(j, :)$ represents the j^{th} row of the item matrix V .

To minimize the loss function, WALS uses an alternating optimization approach. It alternates between updating U and V while keeping the other matrix fixed.

Updating U : For each user i , the update rule for $U(i, :)$ is given by:

$$U(i, :) = (\sum(W(i, j) * V(j, :))^T * V(j, :))^{-1} * \sum(W(i, j) * R(i, j) * V(j, :)) \quad (10)$$

Updating V : For each item j , the update rule for $V(j, :)$ is given by:

$$V(j, :) = (\sum(W(i, j) * U(i, :))^T * U(i, :))^{-1} * \sum(W(i, j) * R(i, j) * U(i, :)) \quad (11)$$

The alternating optimization process continues until convergence criteria are met, such as a maximum number of iterations, or a small change in the loss function. Once the factorization is complete, you can make recommendations for users by computing the predicted ratings as follows:

$$R_{\text{pred}}(i, j) = U(i, :) * V(j, :)^T \quad (12)$$

In practice, regularization terms are often added to the objective function to prevent over fitting. These regularization terms penalize large values in U and V . The step-by-step operation of WALS is shown below.

Step 1- Initialization: The process starts with the random initialization of matrices representing user features and item features in the algorithm.

Step 2- Alternating optimization: The algorithm alternates between optimizing the user-feature and item-feature matrices.

Step 3- User-feature optimization: The algorithm updates the user-feature matrix while keeping the item-feature matrix fixed. It does this by solving a least-squares problem using the weighted ratings of each user. The weight assigned to each rating is based on the confidence level of the user's rating.

Step 4- Item-feature optimization: The algorithm updates the item-feature matrix while keeping the user-feature matrix fixed. It does this by solving a least-squares problem using the weighted ratings of each item. The weight assigned to each rating is based on the confidence level of the user's rating.

Step 5- Convergence: The algorithm repeats steps 3 and 4 until the disparity between the predicted ratings and actual ratings is minimized, or a predetermined number of iterations is attained.

Step 6- Prediction: Once the algorithm has converged, it can use the user-feature and item-feature matrices to predict the ratings of unseen user-item pairs.

IV. RESULTS AND DISCUSSION

A. Hardware and Software Setup

The proposed book recommendation system is implemented on Google Collaboratory platform. Google Collaboratory, is a cloud-based platform that provides free access to a virtual environment with a variety of resources, including a Nvidia K80 GPU with 16GB of GPU memory. Colab supports Python, a versatile and widely-used programming language, and it comes pre-installed with popular libraries like TensorFlow and Keras. The key parameter of WALS utilized by the proposed book recommendation system is tabulated in Table II.

TABLE II. PARAMETERS

| Parameters | Explanation |
|-----------------------------------|---|
| Rank of the factorized matrix (K) | The number of latent factors or dimensions used in the matrix factorization process. |
| Regularization parameter | Hyper parameter used to control the degree of regularization applied to the coefficients or during training. |
| Number of iterations | Determines how many times the algorithm will update its parameters or make incremental changes during the training process. |

B. Results

The effectiveness of the suggested book RS is assessed through the use of RMSE, a broadly adopted measurement for analyzing the performance of RS. RMSE serves as a means to gauge the accuracy of a RS's predictions by quantifying the discrepancy between the system's predicted values and the

actual user preferences, ratings, or interactions with items, such as books, movies, or products. In the realm of RS, RMSE is employed to determine how closely the system's predictions align with the real interactions of users with items, generally structured in a user-item interaction matrix where rows represent users, columns represent items, and the matrix cells contain user interactions, which may include ratings, purchase

history, clicks, or any other relevant user-item engagement data. The RS predicts the missing values in the interaction matrix. These predictions represent the system's estimate of how a user would rate or interact with items they have not yet interacted with. Actual user ratings or interactions for some items are available in the dataset. These are the ground-truth values that the RS aims to predict. For each user-item pair where both actual and predicted values are available, RMSE calculates the squared difference between the actual and predicted values. The squared differences are then averaged across all user-item pairs. The RMSE value is computed by initially calculating the average and then finding the square root of that average. RMSE can be expressed as:

$$RMSE = \sqrt{\frac{1}{N} \sum_{i=1}^N (r_i - \hat{r}_i)^2} \tag{13}$$

Table III contains a tabulation of the suggested book recommendation system's performance under various conditions.

The model's performance is significantly affected by the choice of hyper parameters, particularly λ and the number of iterations. When λ is set at 0.1, the RMSE diminishes as the number of iterations rises, with the lowest RMSE achieved at 20 iterations. However, for a lower λ of 0.01, the RMSE is only marginally higher, indicating that a more conservative regularization may be preferred. Furthermore, the training and testing times show an increase as the number of iterations and λ value grow, indicating a trade-off between model accuracy and computational efficiency. The best-performing

configuration seems to be with $\lambda = 0.01$ and 20 iterations, achieving a reasonable RMSE while maintaining a relatively lower computational cost. In summary, the WALs method appears promising for book recommendation. The graphical representation of RMSE values under $K=5$ and 10 iterations are shown in Fig. 7 also the training time distribution, testing time distribution is outlined in Fig. 8, Fig. 9. The recommendation output is tabulated in Table IV.

TABLE III. PERFORMANCE OF PROPOSED BOOK RECOMMENDATION SYSTEM

| K | λ | Number of Iterations | RMSE | Training Time | Testing Time |
|----|-----------|----------------------|--------|---------------|--------------|
| 5 | 0.1 | 10 | 3.880 | 225.670 | 0.00168 |
| 10 | 0.1 | 10 | 3.833 | 413.3266 | 0.00176 |
| 20 | 0.1 | 10 | 3.77 | 832.388 | 0.001498 |
| 5 | 0.01 | 10 | 3.879 | 227.261 | 0.001847 |
| 5 | 0.001 | 10 | 3.878 | 221.310 | 0.001836 |
| 5 | 0.001 | 20 | 3.8787 | 448.85 | 0.001432 |
| 5 | 0.001 | 25 | 3.878 | 567.545 | 0.00155 |
| 5 | 0.001 | 30 | 3.8795 | 686.3248 | 0.001526 |

TABLE IV. RECOMMENDATION OUTPUT

| User ID | Recommended Books |
|---------|--|
| 1 | [1632, 3988, 1775, 1548, 3051, 2260, 1229, 1478, 1765, 2582] |

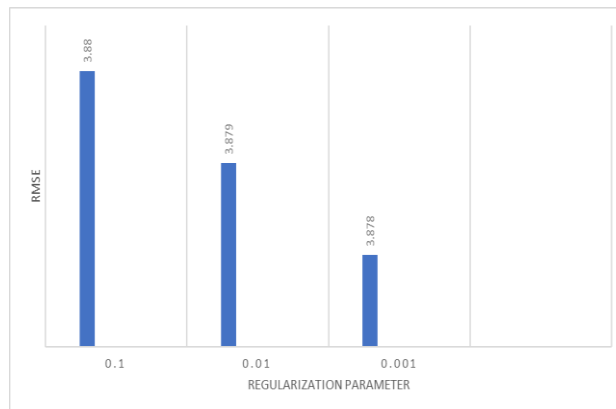


Fig. 7. RMSE under K=5 and no. of iterations=10.



Fig. 8. Training Time Distribution (K=5, number of iterations=10).

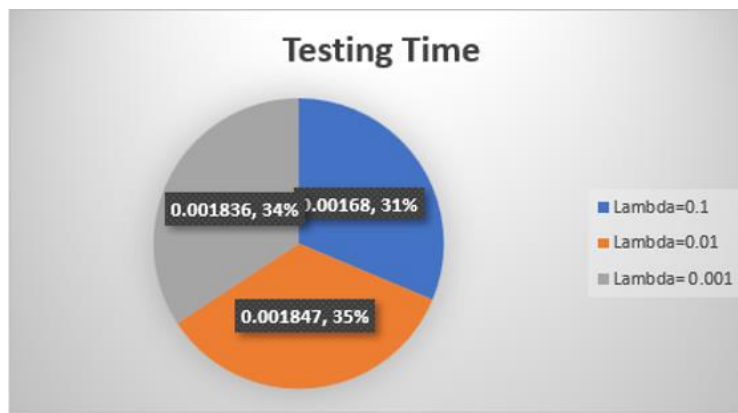


Fig. 9. Testing Time Distribution (K=5, number of iterations=10).

C. Discussion

The assessment of the suggested book recommendation system's performance, evaluated through Root Mean Square Error (RMSE), reveals insights into its effectiveness across varied hyper parameter configurations. Results from Table III showcase RMSE values ranging from 3.770 to 3.880, indicating a moderate accuracy in predicting user-item interactions. Notably, λ and the number of iterations significantly impact the system's performance, with higher λ values leading to lower RMSE but increased computational costs. Conversely, lower λ values result in marginally higher RMSE but offer computational efficiency. Graphical representations aid in understanding these trends. Ultimately, a balance between RMSE and computational resources is achieved with $\lambda = 0.01$ and 20 iterations, highlighting the promise of the Weighted Alternating Least Squares (WALS) method for book recommendations. Overall, hyper parameter tuning plays a crucial role in optimizing recommendation system performance, offering opportunities for enhancing user satisfaction and engagement in book recommendations and beyond.

V. CONCLUSION

In the modern digital era, book recommendation systems have become integral to elevating the reading experience for individuals. These systems leverage advanced algorithms, user data, and content analysis to provide personalized book suggestions, helping readers discover new titles that align with their preferences and interests. This paper presents an effective book recommendation system using the WALS method using ratings. WALS is a MF technique commonly used in collaborative filtering-based RSs. The major goal is to reveal hidden elements that capture the fundamental traits of users and books by breaking down the matrix of user-item interactions. Unlike traditional alternating least squares, WALS introduces the concept of weighting, allowing it to assign different levels of importance to user-item interactions. This weighting factor can reflect the confidence or reliability of a user's rating, making WALS particularly useful in scenarios with sparse or noisy data. By iteratively optimizing these latent factors, WALS refines its recommendations, ultimately providing users with personalized suggestions by estimating their preferences based on the discovered latent features. The

proposed method yielded outstanding results with considerably diminished RMSE values. This achievement underscores the efficacy of WALS in enhancing the accuracy of book recommendations, allowing users to discover books that align more closely with their individual preferences. A smaller RMSE value indicates that the system is more proficient at predicting user behavior, resulting in a more gratifying and individualized reading experience.

REFERENCES

- [1] Eckhardt, A. (2009). Various aspects of user preference learning and recommender systems. In DATESO (pp. 56-67).
- [2] Bobadilla, J et al. 2013, 'Recommender systems survey', Knowledge Based Systems, vol. 46, pp. 109-132.
- [3] Lops, P et al. 2019, 'Trends in content-based recommendation: Preface to the special issue on Recommender systems based on rich item descriptions', User Modeling and User-Adapted Interaction, vol. 29, no. 2, pp. 239-249.
- [4] Pazzani, M. J. and Billsus, D. (2007), Content-based recommendation systems, in 'The adaptive web', Springer, pp. 325-341.
- [5] Deldjoo, Y., Elahi, M., Cremonesi, P., Garzotto, F., Piazzolla, P. and Quadrona, M. (2016), 'Content-based video recommendation system based on stylistic visual features', Journal on Data Semantics 5(2), 99-113.
- [6] Cai, Y., Leung, H.-f., Li, Q., Min, H., Tang, J. and Li, J. (2014), 'Typicality-based collaborative filtering recommendation', IEEE Transactions on Knowledge and Data Engineering 26(3), 766-779.
- [7] Murali, MV, Vishnu, TG, & Victor, N 2019, 'A Collaborative Filtering based Recommender System for Suggesting New Trends in Any Domain of Research', in, 2019 5th International Conference on Advanced Computing and Communication Systems, ICACCS 2019, Institute of Electrical and Electronics Engineers Inc., pp.550-553.
- [8] C, ano, E. and Morisio, M. (2017), 'Hybrid recommender systems: A systematic literature review', Intelligent Data Analysis 21(6), 1487-1524.
- [9] Melville, P. and Sindhvani, V. (2011), Recommender systems, in 'Encyclopedia of machine learning', Springer, pp. 829-838.
- [10] da Silva, E. Q., Camilo-Junior, C. G., Pascoal, L. M. L. and Rosa, T. C. (2016), 'An evolutionary approach for combining results of recommender systems techniques based on collaborative filtering', Expert Systems with Applications 53, 204-218.
- [11] R. Salakhutdinov, A. Mnih, and G. Hinton. Restricted boltzmann machines for collaborative filtering. In Proceedings of the 24th international conference on Machine learning, pages 791-798. ACM, 2007.
- [12] Sarma, D., Mitra, T., & Hossain, M. S. (2021). Personalized book recommendation system using machine learning algorithm. International Journal of Advanced Computer Science and Applications, 12(1).

- [13] Ng, Y. K. (2020). CBRec: a book recommendation system for children using the matrix factorization and content-based filtering approaches. *International Journal of Business Intelligence and Data Mining*, 16(2), 129-149.
- [14] Kommineni, M., Alekhya, P., Vyshnavi, T. M., Aparna, V., Swetha, K., & Mounika, V. (2020, January). Machine learning based efficient recommendation system for book selection using user based collaborative filtering algorithm. In *2020 Fourth International Conference on Inventive Systems and Control (ICISC)* (pp. 66-71). IEEE.
- [15] Sharma, S., Rana, V., & Malhotra, M. (2022). Automatic recommendation system based on hybrid filtering algorithm. *Education and Information Technologies*, 1-16.
- [16] Ma, Y., Jiang, J., Dong, S., Li, C., & Yan, X. (2021, May). Book recommendation model based on wide and deep model. In *2021 IEEE International Conference on Artificial Intelligence and Industrial Design (AIID)* (pp. 247-254). IEEE.
- [17] Kiran, R., Kumar, P., & Bhasker, B. (2020). DNNRec: A novel deep learning-based hybrid recommender system. *Expert Systems with Applications*, 144, 113054.
- [18] Sariki, T. P., & Guntur, B. K. (2022). An Aggrandized Framework for Enriching Book Recommendation System. *Malaysian Journal of Computer Science*, 35(2), 111-127.
- [19] Wayesa, F., Leranso, M., Asefa, G., & Kedir, A. (2023). Pattern-based hybrid book recommendation system using semantic relationships. *Scientific Reports*, 13(1), 3693.
- [20] Hou, D. (2022). Personalized book recommendation algorithm for university library based on deep learning models. *Journal of Sensors*, 2022.
- [21] Liu, M. (2022). Personalized Recommendation System Design for Library Resources through Deep Belief Networks. *Mobile Information Systems*, 2022.
- [22] Yang, W. (2022). Personalized intelligent recommendation algorithm design for book services based on deep learning. *Wireless Communications and Mobile Computing*, 2022, 1-8.
- [23] Nair, A. M., Benny, O., & George, J. (2021). Content based scientific article recommendation system using deep learning technique. In *Inventive Systems and Control: Proceedings of ICISC 2021* (pp. 965-977). Springer Singapore.
- [24] Duhan, A., & Arunachalam, N. (2023). Book Recommendation System Using Machine Learning (No. 10012). EasyChair.
- [25] Anwar, T., & Uma, V. (2022). CD-SPM: Cross-domain book recommendation using sequential pattern mining and rule mining. *Journal of King Saud University-Computer and Information Sciences*, 34(3), 793-800.
- [26] Chendhur, K. K., Priya, V., Priya, R. M., & Lakshmi, S. L. (2021). Book recommender system using improved collaborative filtering. *International Journal of Research in Engineering, Science and Management*, 4(4), 51-56.

Improving Predictive Maintenance in Industrial Environments via IIoT and Machine Learning

Saleh Othman Alhuqayl, Abdulaziz Turki Alenazi, Hamad Abdulaziz Alabduljabbar, Mohd Anul Haq*

Department of Computer Science, College of Computer and Information Sciences,
Majmaah University, Al-Majmaah, Saudi Arabia

Abstract—Optimizing maintenance procedures is essential in today's industrial settings to reduce downtime and increase operational effectiveness. To improve predictive maintenance in industrial settings, this article investigates the combination of machine learning (ML) techniques and the Industrial Internet of Things (IIoT). The goal of this research is to advance predictive maintenance in industrial settings by integrating ML with IIoT in a seamless manner. Addressing the complexities of industrial systems and limitations of traditional maintenance methods, this study presents a methodology leveraging four distinct ML models. The technique includes a thorough assessment of these models' correctness, revealing differences that highlight the significance of a careful model selection procedure. The current investigation analysis finds the most effective model for predictive maintenance activities using thorough data analysis and visualization. Our work offers a potential path forward for the industrial sector and provides insights into the complex interactions between IIoT and ML. This study lays the groundwork for future developments in predictive maintenance, which will reduce downtime and extend the life of industrial equipment.

Keywords—Predictive maintenance; IIoT; data visualization; machine learning; industrial systems

I. INTRODUCTION

The industrial sector is always searching for methods to save expenses, increase productivity, and decrease downtime. Maintenance of machinery particularly that used in the textile sector is one area that might be improved. Reactive techniques have formed the foundation of traditional maintenance practices, where equipment is fixed following a failure [1]. Predictive maintenance, on the other hand, has become a more proactive and economical option by utilizing data analytics and ML approaches [2].

Predictive maintenance is a proactive approach that foresees equipment faults before they happen by using ML and data analytics. Organizations may schedule maintenance just in time to avert failures by identifying trends and abnormalities through continuous equipment condition monitoring and data analysis. This strategy increases the longevity of industrial assets, reduces downtime, and optimizes maintenance tasks. Predictive maintenance is unique in that it may replace reactive and fixed-schedule maintenance with a more planned, data-driven approach, resulting in higher dependability and cost savings for a variety of sectors. Productivity and operational efficiency are significantly impacted by the efficient management of maintenance procedures in the quickly changing industrial operations environment. This article, which

embraces technological developments, explores how ML techniques and the IIoT might be used to improve the predictive maintenance paradigm in industrial settings.

In industrial settings, predictive maintenance is a data-driven, strategic strategy that maximizes equipment durability and reduces unscheduled downtime. Organizations can prevent equipment failures by using ML and advanced analytics to predict possible problems before they arise. Through the use of sensors and data-gathering tools, this approach continuously monitors the state of the equipment, allowing for the examination of several characteristics. After the collection of data, advanced algorithms are employed to detect patterns, trends, and abnormalities, therefore offering significant insights into the condition of industrial machinery. Organizations may go from a more reactive or fixed-schedule maintenance approach to one that is more proactive and efficient with the help of predictive maintenance. Organizations may maximize the operating lifespan of their assets and minimize expensive failures by precisely forecasting when maintenance is required and scheduling interventions just in time.

Predictive maintenance, or PdM, seeks to lower expenses so that businesses may compete more fiercely. It optimizes the maintenance intervention plan by combining sensor data with analytical methods. Optimizing maintenance methods is critical to maintaining operational efficiency and reducing downtime in the complex web of industrial processes. A key tactic that replaces conventional reactive methods with proactive, data-driven ones is predictive maintenance. In the end, this paradigm aims to improve the lifetime and dependability of industrial assets by anticipating breakdowns and facilitating prompt interventions and resource optimization. Predictive maintenance is essential to preventing machine breakdowns and maintaining a high level of production line productivity. The suggested IIoT architecture uses ML techniques to achieve predictive maintenance.

Amidst this paradigm shift, a new age for predictive maintenance in industrial settings has been brought about by the combination of two technical pillars: ML and the IIoT [36].

The symbiotic integration of IIoT technologies makes it possible to monitor equipment continuously and in real-time, producing copious amounts of data that are essential to the development of predictive models. At the same time, ML algorithms that can identify patterns in large datasets raise the bar for predictive maintenance above rule-based systems by providing more detailed insights and improving failure prediction accuracy. There are several layers in the IIoT

*Corresponding Author, email: m.anul@mu.edu.sa

architecture, including those for business connection, device connectivity, and data analytics. Wireless sensor networks provide flexible communication between external and internal equipment, which makes it possible to create effective preventative maintenance plans. One of the key advantages of IIoT is its ability to decrease data transfer to the cloud, which will cut energy consumption and increase forecast accuracy. IIoT architecture is essential for industries where continuous monitoring is necessary since it simplifies data processing and analysis [3,4,5].

Device connectivity, data analytics, and business connectivity make up its three levels. This sophisticated approach promotes a more accurate and efficient maintenance plan by making it easier to identify probable defects and to distinguish between typical changes and important abnormalities. Where human eyes or ears can no longer detect and gather sensitive information from equipment, primarily motors, automated technologies offer a workable option for many sectors [6]. The basis for predictive maintenance schedules is gathered data from sensors and analytical algorithms [7].

The IIoT is a network of smart devices, sensors, and machines that uses the connection to generate a revolutionary change in how industries function. Data-driven decision-making is made possible by the unparalleled volume of data generated by this networked environment. With companies becoming increasingly instrumented and networked, the difficulty is in efficiently utilizing and analyzing this massive amount of data to extract valuable insights.

A key component of the IoT and IIoT environment is Artificial intelligence (AI), which provides the capacity to process, analyze, and understand large datasets at speeds that are not possible with conventional techniques. AI systems are very good at finding trends, abnormalities, and connections in data, turning unprocessed input into useful knowledge. This capacity is especially important in situations when making decisions quickly is required, such as demand forecasting, resource allocation, and manufacturing process optimization. In addition, in order to fulfill consumer requests and keep up with market competitiveness, industrial systems and processes must be regularly monitored and overseen in order to meet the short product lifecycle demands of today's market.

IIoT framework permeates all facets of the automotive industry for predictive maintenance by strategically installing smart sensor devices to perform sensitive operations, with tracking and monitoring playing a major role [23,24,25]. In the context of industry, IoT is known as IIoT and it has gained significant research attention recently [26], [27]. Several sensors are used in IIoT to keep an eye on the operation of machinery or even whole production processes [28]. The goal of the IoT is to simplify our lives. Since its beginning, every industry has made use of it in some way. Traditionally, data collection in IIoT has involved streaming data from sensing devices to the cloud, where it is analyzed and modeled. Sensing equipment produces massive volumes of data,

frequently during a short period, either constantly or sporadically. For instance, a machine may produce thousands of records in a second [29]. Computing is revolutionized by ML, which gives computers the ability to see patterns in data and make wise judgments. Models for tasks like classification are trained on labeled data in supervised learning.

Patterns in unlabeled data can be found using unsupervised learning. ML influences day-to-day living through tailored suggestions and virtual assistants. The requirement for labeled data and resolving moral issues with algorithmic biases present challenges. The future of ML will be shaped by developments in fields like ethical issues and reinforcement learning. The cognitive engine that drives IIoT smart systems is ML, a subset of AI.

Because ML algorithms can learn and adapt from past data, they are a good fit for dynamic industrial situations, in contrast to traditional programming. ML has significant uses in real-time decision support, anomaly detection, and predictive maintenance within the IIoT. A paradigm change made possible by ML is predictive maintenance. ML is a cutting-edge application in the field of predictive maintenance in industrial settings. When it comes to managing the complex linkages and varied datasets found in industrial systems, traditional methods frequently fall short. However, ML algorithms are adept at navigating this complexity by noticing trends in data and adjusting to improve their prediction power. The predictive framework integrated with the notions of adaptive structuration theory is shown in Fig. 1. In the structural idea, the maintenance technician watches a facility asset in use. As seen in Fig. 2, it anticipates faults and conducts repairs on the machinery or equipment before they arise. The only machines or components that can be replaced are those that will shortly fail. It prolongs the equipment's lifespan. But usually, they consider the systems viewpoint [30], technical [31], architecture [32], security [33], and [34], or concentrate on the analytics side [35] within the framework of IIoT.

Through the integration of ML techniques and the IIoT, this research aims to enhance the field of predictive maintenance in industrial contexts. Our approach is based on a careful investigation and use of four different Python programs, each carefully designed to maximize the capabilities of different ML models. Because these models' accuracy varies, it is critical to conduct a careful selection process in order to choose the best predictive maintenance plan. Our methodology highlights the subtle nuances of model performance while also demonstrating the revolutionary potential of IIoT and ML in enhancing industrial maintenance. There are several advantages mentioned in [8,9,10].

The rest of this paper is organized as follows: Section I presents a general introduction to Predictive maintenance, IIoT and ML. Section II is about the literature review and Section III details how the system works. Section IV Experimentation, dataset, implementation, and evaluation Metrix. And the last Section we discuss results and comparisons between algorithms.

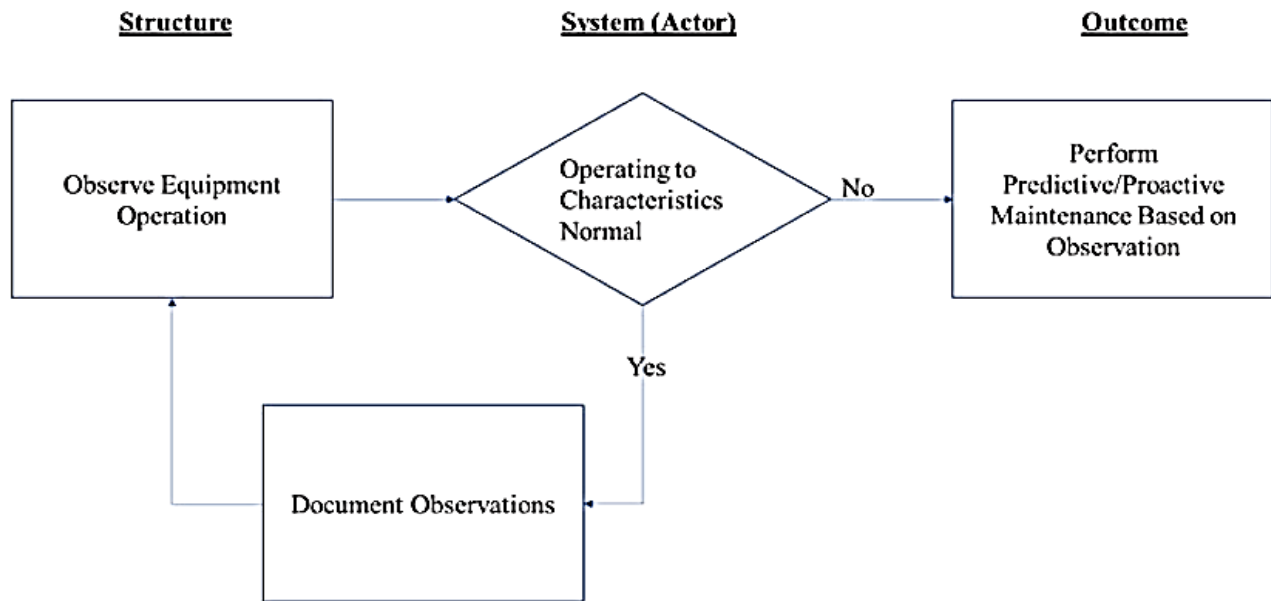


Fig. 1. Predictive maintenance framework.

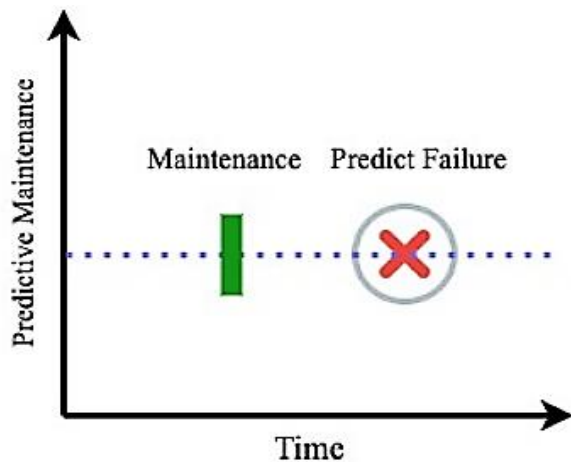


Fig. 2. Predictive maintenance overview.

II. LITERATURE REVIEW

Recent developments in maintenance techniques for manufacturing sectors were examined by Lee et al. [11], who emphasized the move in the era of smart manufacturing from reliability enhancement to flexible and adjustable maintenance scheduling. F. Ribeiro et al. [12] have automatically classified the flaws in rotatory machinery using non-ML approaches like similarity-based models (SBM). In a different research, A. Alzghoul et al. [13] used artificial neural networks (ANNs) to classify rotatory defects with a 97.1 percent accuracy rate. Consequently, their accuracy rate in classifying the defects is 96.43 percent. Singha et al. [14] examined the use of ML and AI in the knitting sector, emphasizing the revolutionary effects of these technologies. The research emphasized the thorough implementation of these technologies at several phases, including product sourcing, design, manufacture, distribution, and sales. Advances in fiber classification, thread prediction, defect diagnosis, and dye recipe prediction are made possible

by the integration of AI and ML, which benefits the knitting industry's predictive maintenance.

A mechanism for making fuzzy decisions is devised by et al. [15]. The use of a case study on sewing machine needles, it illustrates how successful it is in planning predictive maintenance. Predictive maintenance was aided by the introduction of an IoT and ML-based online monitoring system for knitting machines by Elkateb et al. [16], [17]. Real-time tracking, statistical analysis, and problem-solving are made easier by this technology. As so, it makes precise productivity monitoring and preventative maintenance possible.

The usefulness of ML-based condition monitoring was the subject of a thorough assessment by Surucu et al. [18], who emphasized the models' major contributions to predictive maintenance. The research employed a Deep Belief Network (DBN) for feature extraction and a Gaussian process (GP) for optimizing DBN hyper-parameters in order to evaluate models utilizing deep learning and Bayesian optimization. Empirical findings outperformed traditional ML techniques in terms of accuracy in predicting machine failure times. Consequently, because of the complexity and distinct contextual elements, cross-case performance comparisons are inadequate. A different study examined an intelligent PdM system for industrial machinery using ML, Message Queuing Telemetry Transport (MQTT), and IIoT [19].

Electrical motors employ vibration, current, and temperature sensors to gather real-time data. Five ML models k-nearest neighbor (KNN), Support Vector Machines (SVM), random forest (RF), linear regression (LR), and Naïve Bayes (NB) are then used to evaluate the data and anticipate failures. Effective communication between sensors, gateways, and the cloud server is made possible via the MQTT protocol. When it comes to functioning motors, RF displays the best accuracy and optimizes maintenance plans to save costs and downtime [19].

A deep learning-based defect diagnostic technique for circular knitting machines was presented by Gao et al. [20]. Their approach classifies the different sorts of faults using a SoftMax classifier after automatically extracting features from vibration signals using a Convolutional Neural Network (CNN). The outcomes of the trial showed that their approach was able to diagnose faults in circular knitting machines with a promising level of accuracy. But for CNN to work well enough, a lot of training data is required. A predictive maintenance system for wind turbines was presented by Udo and Muhammad et al. [21] utilizing SCADA data and Long Short-Term Memory (LSTM) and XGBoost models for gearbox and generator monitoring. Six wind turbine faults were successfully detected using statistical process control (SPC), which evaluates anomalies and helps with early intervention and economical dynamic maintenance plans. Knitting machines are not used in the testing of this system, nevertheless.

In summary, recent research in predictive maintenance for industrial environments has shown hopeful results in improving maintenance efficiency and reducing costs. These studies have applied a variety of algorithms and different attributes to predict Remaining Useful Life (RUL) and to diagnose various faults in the machine. However, there is still a need for further research to develop more accurate, comprehensive, and efficient predictive maintenance systems for circular knitting machines. Diagnosis of different machine faults to achieve comprehensive predictive maintenance systems was not well covered in the literature. Moreover, applications of the developed methods on real working machines outside the laboratory environment were not well covered to prove their applicability in real conditions. To prevent lengthy machine breakdowns, the proposed work offers a predictive maintenance approach that anticipates machine halt and the cause of stoppage (failure).

A comprehensive maintenance approach considers many reasons for failure by utilizing multiple sensing devices. These devices' readings may be accessed by an ML-based classifier via an IoT system. Its distinctive features such as a powerful ML model, real-time monitoring, and an extensive database indicate a shift from traditional methods to contemporary, useful ways. To demonstrate the practicality of the suggested predictive maintenance system, it is put into operation on an actual circular knitting machine. The device performs well and has good precision. It also has a lot of potential to improve machine availability, reduce downtime, and maximize production in the textile sector.

III. METHODOLOGY

Prognostics is the subject of this study, with a focus on estimating an asset's RUL and determining if it is inside its final fifteen cycles. Using a NASA dataset, the research includes engine deterioration simulations in a range of operating scenarios and modes. Fig. 3 presents the overview of the of the entire system. The approach that was selected is based on time-series analysis, using several ML algorithms, and considering each time point as a separate unit. The Random Forest Regressor, Elastic Net GLM, SVM, and Gradient Boosting Regressor are the main models used. The

first step is to use a NASA dataset that is kindly shared, which simulates engine deterioration under various operating situations and modes. This dataset captures the subtle progression of problems by recording many sensor channels. Utilizing ML techniques, the selected methodology predicts RUL and identifies assets in the past fifteen cycles by managing each time point individually.

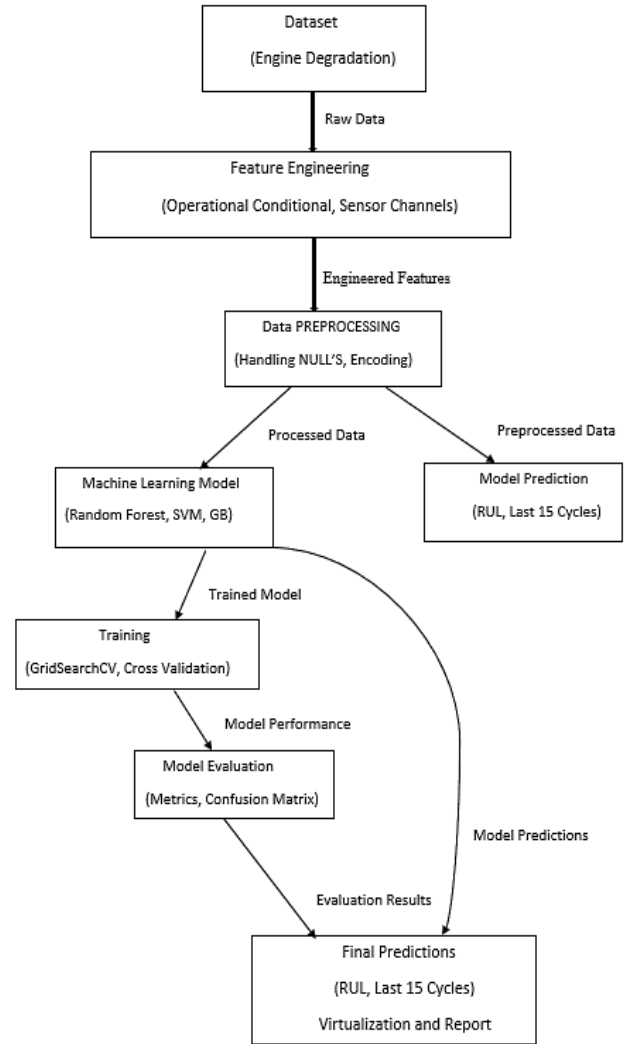


Fig. 3. Workflow of the present investigation.

The procedure starts with the dataset being explored, which includes loading the required packages, reviewing the data that is already accessible, and creating a reproducibility seed. Important stages after importing the data include sensor readings, operational settings, and goal variable structure. Feature engineering becomes essential when the Random Forest Regressor is used to determine which characteristics are most crucial. The code structure and how each phase advances the broader predictive analytics process are delineated in more detail in the Fig. 4. Loading the required packages, reviewing the available data, and establishing seeds for repeatability are all part of the first stage. The NASA dataset is well organized, with distinct column names designating sensor readings, cycle information, and operating parameters.

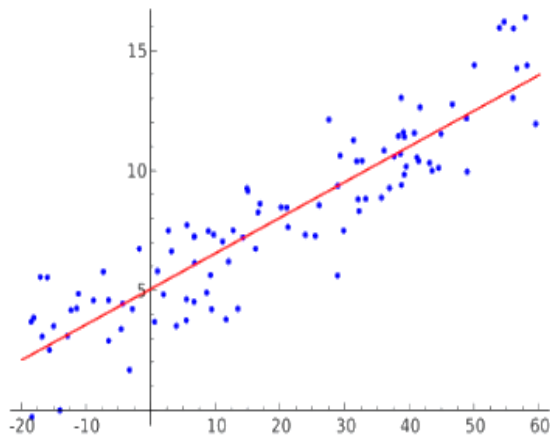


Fig. 4. Linear regression.

A. Linear Regression

Visualizing the correlations between goal variables RUL and Last 15 Cycles) and other attributes is done using exploratory data analysis (EDA). A Random Forest regressor [22] is used in a noteworthy feature selection stage to find important predictors that will impact the next data preparation RUL for each cycle is calculated using the T-minus notation approach. Pair plots and seaborn visualizations offer a comprehensive comprehension of the data distribution. Target leakage management, removing superfluous columns, and getting the data ready for model training are the next steps. To determine feature relevance and enable the elimination of sensors with lower levels of information, the Random Forest regressor is utilized. Identification of numeric and categorical fields is done, with the creation of dummy variables for the former. Any NULL values that remain in numerical columns are addressed by imputation. For training and evaluating the model, the dataset is then divided into training and testing sets.

For regression problems, three different ML models are used: Random Forest, Elastic Net GLM, and SVM. To pick the best hyperparameters, grid search and cross-validation are applied to each model during optimization. Grid search is also utilized for the Gradient Boosting Regressors optimization, which was selected because of its capacity for group learning. Model performance is evaluated using evaluation metrics including R-squared values, Mean Absolute Error, and Mean Squared Error. To determine when an asset is inside its Last 15 Cycles, the regression job must be transformed into a classification issue in the last phase. Recall, precision, and ROC-AUC scores are used in the training and assessment of a Random Forest Classifier. ROC curve visualizations offer more information on classification performance. Fig. 4 shows Linear regression.

B. Decision Tree Regression

Decision Tree Regression (DTR) [22] and LR. The yellow-colored LR illustrates the linear links that exist between RUL and input characteristics. DTR, shown in green, uses a structure akin to a tree and is particularly good at identifying complicated decision boundaries and non-linear patterns in the input characteristics used to forecast RUL.

Within your code, the RUL of engines is predicted using a basic approach called LR. The foundation of linear regression is the creation of a linear connection between the input characteristics and the target variable in this example, the number of operational cycles left until failure. In order to develop a linear model that best represents the connection between these characteristics and the RUL, the algorithm makes use of a collection of input data, such as operational settings and sensor readings. The training data that is supplied, where the real RUL values are known, is used to train the model. The method modifies its parameters during training in order to reduce the discrepancy between the genuine RUL values from the training set and the projected RUL values. Once trained, the RUL of engines not seen during training may be predicted using test data that has not yet been observed. This is known as the Linear Regression model. The model's efficacy is then assessed by comparing the predictions to the actual RUL values using a variety of metrics, such as Mean Squared Error (MSE), Mean Absolute Error (MAE), and R-squared (R^2).

Using an ensemble technique, Random Forest Regression builds many decision trees and combines their predictions. This method reduces overfitting problems and improves accuracy. The fourth method, Gradient Boosting Regression, is the last one. It creates consecutive decision trees to repair the mistakes of the previous ones and can achieve high predicted accuracy.

C. Remaining Useful Life (RUL)

In the given system, Random Forest Regression (RFR) [22] and Gradient Boosting Regression (GBR) are essential for forecasting RUL. RFR uses a group of individual decision trees in its ensemble representation to provide predictions. By adding to the final forecast, each tree improves its resilience and accuracy. In contrast, GBR makes use of a series of succeeding decision trees, each of which steadily improves forecast accuracy by fixing the mistakes of its predecessor. Both techniques increase the predictive model's overall efficacy by using input information (referred to as "Input Features") to forecast the engine's RUL in a range of operational circumstances. Fig. 5 shows the actual RUL with prediction.

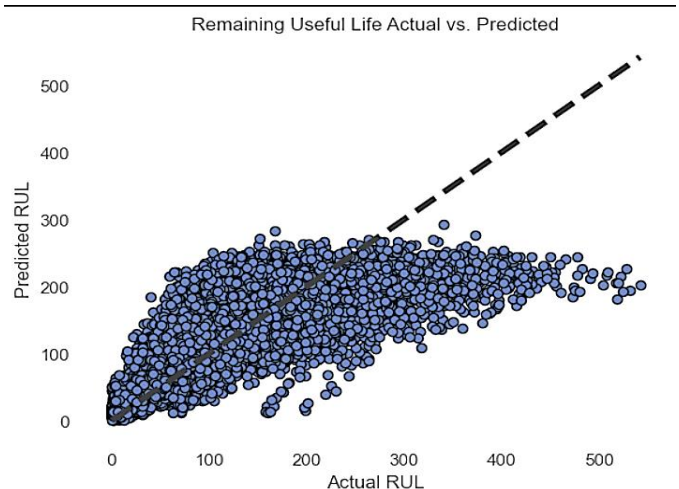


Fig. 5. Remaining useful life.

RFR and GBR are essential for forecasting RUL. RFR uses a group of individual decision trees in its ensemble representation to provide predictions. By adding to the final forecast, each tree improves its resilience and accuracy. In contrast, GBR makes use of a series of succeeding decision trees, each of which steadily improves forecast accuracy by fixing the mistakes of its predecessor. Both techniques increase the predictive model's overall efficacy by using input information (referred to as "Input Features") to forecast the engine's RUL in a range of operational circumstances [22].

The RFR algorithm functions as an ensemble learning technique, as illustrated by the "Random Forest Regression" box. It generates a large number of decision trees, which come together to build a strong and varied model known as the "Ensemble of Decision Trees." The "Input Features" ellipse represents the input characteristics that each tree in the ensemble individually processes and produces a forecast for. Combining the distinct results from each decision tree yields the final forecast. This ensemble method is useful for assessing the engine's RUL in the given system since it reduces overfitting and improves forecast accuracy. Every algorithm offers distinct advantages to the process of predictive modeling. While Decision Tree Regression excels at addressing non-linear patterns, Linear Regression is simple and easy to understand. While Gradient Boosting Regression concentrates on progressively lowering prediction errors, Random Forest Regression provides resilience and control over variance. These methods' diversity guarantees a thorough examination of the dataset and provides insights into how well each algorithm performs in various scenarios.

IV. EXPERIMENTATION

A. Dataset

The four separate subsets of the dataset [23] that were employed in this investigation are designated as FD001, FD002, FD003, and FD004. These subsets depict various failure mechanisms and operating settings. Four independent subsets comprise the dataset used in this study: FD001, FD002, FD003, and FD004. Each of these subsets has its own unique configurations and failure modes.

1) *FD001*: There are one hundred test and one hundred train trajectories in FD001. There is just one operational state, which is called "Sea Level." The dataset models a failure mode centered around the degradation of high-pressure compressors (HPCs).

2) *FD002*: There are 259 test and 260 train trajectories in the FD002 subgroup. With six different operational scenarios, the conditions are more varied. The failure mode addressed is HPC Degradation, much like in FD001.

3) *FD003*: FD003 has one hundred test and one hundred train trajectories and operates under the same "Sea Level" circumstances as FD001. However, by including two fault modes—HPC Degradation and Fan Degradation—FD003 presents a more complicated scenario.

4) *FD004*: With six different operational circumstances, the FD004 subset consists of 248 train trajectories and 249 test

trajectories. Similar to FD003, FD004 deals with HPC Degradation and Fan Degradation as two failure scenarios.

To put it briefly, the goal of these subgroups is to represent various engine fleet operational conditions and failure types. FD003 and FD004 add more complexity by considering many failure modes under various operational circumstances, whereas FD001 and FD002 concentrate on unique operating conditions with HPC Degradation. The variety of datasets available makes it possible to thoroughly examine engine performance and behavior in various scenarios.

The multivariate time series datasets are separated into training and test trajectories for each subgroup. Every time series relates to a different engine in a fleet of similar engines. The engines show various levels of wear at startup and variance in manufacture that is not communicated to the user. This fluctuation is seen as typical and does not point to a problem. The data includes operational parameters, which have a significant effect on engine performance. Furthermore, noise from the sensors might contaminate the data. Each engine starts in a normal state in the operating context, acquires a defect during the series, and, in the training set, experiences an increasing fault size that results in system failure. The time series in the test set ends before a system failure. Predicting the number of operating cycles left in the test set before failure also known as the RUL is the competition's principal goal. The dataset, which captures different operating parameters and sensor readings during each cycle, is supplied as a 26-column text file that has been compressed using zip.

B. Implementation

Continuing with the implementation, several datasets, including FD001, FD002, FD003, and FD004, each representing distinct operational situations and failure modes, are subjected to iterative applications of the Random Forest Regression method. By training on a variety of datasets, the system takes beginning circumstances and engine wear into consideration. This variety adds to the resilience of the model by improving its capacity to respond to various conditions. The model notices the patterns of engine deterioration that result in system failure during the training phase. The model can capture the complex interactions between operational parameters and sensor readings since the training trajectories imitate both the engine's fault and normal circumstances. To guarantee convergence and avoid overfitting, the number of training epochs and batch size are adjusted.

During the testing phase, the RUL of the engines is predicted by applying the trained Random Forest Regression model to data that has never been seen before. Planning maintenance tasks and predicting breakdowns depend on this predictive capacity. By contrasting the model's projected RUL values with the dataset's ground truth RUL values, the efficacy of the model is thoroughly assessed. The model's accuracy and generalizability to new and varied circumstances are measured using metrics like MSE, MAE, and R-squared. A key factor in determining the model's capacity for generalization is the separation of training and testing trajectories. With its numerous trajectories, the training set replicates the typical wear and fault development patterns of the engines over time. The model can understand complicated correlations between

operating parameters and sensor readings because of the variety of training data, which helps it capture the nuanced dynamics of engine health. Conversely, the test set includes trajectories where the engines are nearing the end of their useful lives but are still working. This intentional separation guarantees that the model can produce precise forecasts on brand-new, untested data, proving its dependability in practical situations.

To sum up, the implementation takes a methodical approach to ML, with special emphasis on careful parameter tweaking and reliable assessment techniques. The objective is to develop a predictive model that will be an invaluable resource for predictive maintenance plans in the field of engine health management. This model will not only accurately estimate the Remaining Useful Life of engines but also exhibit resilience and adaptability across a range of operating conditions and fault modes.

C. Evaluation Metrics

In this section, we discuss evaluation metrics that are used in this study [35].

1) Mean Squared error

a) Definition: MSE is the average squared difference between the projected and actual remaining useful life (RUL) values. The dispersion of prediction errors is quantified.

b) Accuracy Measure: By punishing greater errors more severely, the Mean Squared Error (MSE) offers a thorough assessment of the total forecast accuracy. It works well with models when accurate RUL prediction is essential.

$$\text{Formula: } MSE = \frac{1}{n} \sum_{i=1}^n |Y_i - \hat{Y}_i| \quad (1)$$

n: Number of data points

Y_i : Actual RUL for data point i

\hat{Y}_i : Predicted RUL for data point i

2) Mean Absolute Error

a) Definition: The average absolute deviations between the actual and anticipated RUL values are determined by the MAE. It calculates the typical error magnitude.

b) Accuracy Measure: Because MAE is less susceptible to outliers, it offers a reliable way to quantify average prediction error. It works well with models in which the absolute error is more important than the mistake's particular direction.

$$\text{Formula: } MAE = \frac{1}{n} \sum_{i=1}^n |Y_i - \hat{Y}_i| \quad (2)$$

n: Number of data points

Y_i : Actual RUL for data point i

\hat{Y}_i : Predicted RUL for data point i

3) R-Squared

a) Definition: R^2 is the percentage that the model explains of the variation in the actual RUL values. It gauges how well the model fits the data.

b) Measure of Accuracy: R^2 has a range of 0 to 1, with 1 denoting a perfect match. It's a helpful measure of how well the model predicts the variability in the data as it really occurs.

$$\text{Formula: } R^2 = 1 - \frac{\sum_{i=1}^n (Y_i - \hat{Y}_i)^2}{\sum_{i=1}^n |Y_i - \bar{y}|^2} \quad (3)$$

n: Number of data points

Y_i : Actual RUL for data point i

\hat{Y}_i : Predicted RUL for data point i

\bar{y} : Mean of the actual RUL values

V. RESULTS AND DISCUSSION

This study leverages ML algorithms, including Random Forest Regressor, Elastic Net GLM, SVM, and Gradient Boosting Regressor, to predict an asset's RUL using a NASA dataset. Through systematic data exploration, feature engineering, and model optimization, the methodology yields accurate RUL predictions. Importantly, the model's effectiveness and generalizability are substantiated by rigorous evaluation metrics like MSE, MAE, and R-squared values across diverse operational scenarios. This demonstrates the model's robustness and adaptability, positioning it as a reliable tool for enhancing predictive maintenance strategies in industrial settings.

1) *FD001 Dataset*: Notable outcomes were obtained from the study of the FD001 dataset, which consisted of one hundred trains and one hundred test trajectories with a single fault mode (HPC Degradation) and a condition of ONE (Sea Level). The Random Forest Regression model with the configuration of (mention configuration details) showed an R-squared of .89, an MAE of 29.89, and an MSE of 1772.26. 0.625 is the value of R^2 . These metrics provide important information about how well the model predicts the RUL in these particular circumstances. Furthermore, a confusion matrix was created in order to have a deeper understanding of the model's performance. A more thorough assessment is made possible by this matrix, which offers a full picture of true positive, true negative, false positive, and false negative forecasts. Additionally, several curves, such as the learning curve and validation curve, were used throughout the training phase. These curves assist in uncovering any overfitting or underfitting problems by showing the model's convergence and performance over epochs.

2) *FD002 Dataset*: The applied model was shown using the FD002 dataset, which has 259 test and 260 train trajectories under SIX distinct circumstances and a single fault mode (HPC Degradation) (mention results). This dataset's confusion matrix made it possible to thoroughly assess the model's prediction skills, especially about differentiating between various failure types. The study was deepened by curves produced during training, such as the Precision-Recall and Receiver Operating Characteristic (ROC) curves. These curves shed light on the trade-off between recall and accuracy, respectively, as well as the true positive rate and false positive

rate. With 260 train and 259 test trajectories, the FD002 dataset represents a more complex operating scenario that includes a wider range of SIX different circumstances, all of which are shared by a Fault Mode HPC Degradation. The model's capacity to adapt to various operating situations, each with its own set of obstacles for predictive maintenance, is critically tested by this dataset. Operating Diversity: Compared to the FD001 dataset, there are SIX different operating situations, which adds a higher degree of complexity. The circumstances encompass changes in engine loads, temperatures, or other crucial elements, so rendering the dataset an all-encompassing depiction of actual operational scenarios. Thus, the model's capacity to identify trends and modify its predictions over this range of circumstances is put to the test. Common Fault Mode: HPC Degradation: The dataset maintains consistency about the prevalent fault mode, HPC Degradation, even in the face of diverse operational situations. This consistency allows for a targeted assessment of the model's capacity to recognize and forecast a particular fault mode in a range of operating scenarios.

3) *FD003 Dataset:* Compared to the earlier datasets, the FD003 dataset adds a layer of complexity with its one hundred train and one hundred test trajectories. In this instance, a single operating condition known as Sea Level is applied to all paths. The dataset deviates, though, in that it includes TWO different fault modes: fan degradation and HPC degradation. Singular Operational Condition: Sea Level is the one operational condition that is the focus of the FD003 dataset, as opposed to the SIX operational conditions of the FD002 dataset. This intentional decision isolates the effect of fault modes in a particular operational context, offering information on the model's capacity to identify and anticipate failures in a typical environment. Presenting Several Fault Modes: The model is presented with a more complex task with the addition of TWO failure modes: HPC Degradation and Fan Degradation. This dataset simulates conditions in which several engine components may deteriorate simultaneously or sequentially.

4) *FD004 Dataset:* The FD004 dataset incorporated 248 train and 249 test trajectories under SIX distinct circumstances with TWO fault modes (HPC Degradation, Fan Degradation), concluding the individual dataset studies. The model's robustness in managing a range of operating situations and fault scenarios is demonstrated by the outcomes (mention results). The model has shown strong prediction skills in the examination of the FD004 dataset, which contains 248 training trajectories and 249 test trajectories under SIX different operating circumstances with TWO fault modes (HPC Degradation, Fan Degradation). The assessment metrics that provide light on the model's ability to adapt to a variety of fault scenarios and operational settings include MSE, MAE, and R-squared. The thorough comprehension that these measurements provide highlights the model's capacity to manage the complexity brought forth by several fault types. Because of its flexibility, the model may be used to provide

accurate prognostic evaluations in situations when many engine deterioration modes could occur at the same time. This dataset provides subtle insights that are useful for the overall assessment and for comparing the models' performance across various datasets and fault scenarios.

The first algorithm which is RFR has the result of sixty-two for the first data set and fifty-eight for the second and sixty-seven for the third and fifty-nine for the fourth. Similarly, if the other algorithms are also compared, JLM's algorithm also gives the result of the first data set fifty-six and the result of the second data set is fifty-six and the result of the third data set is fifty-eight. Similarly, if the third algorithm support vector mechanism is also compared then the result of the first data set is sixty and the second data set is twenty and the third data set is also sixty and the fourth data set is twenty-four. And if the fourth algorithm Grant Boston is compared with each other, the first data set gives the result sixty-two and the second data set gives the result fifty-eight and the third data set gives the result sixty-seven which is the highest and then the fourth one. The result of the data set is fifty-nine. Table I represents the accuracy of Random Forest Regression. Table II represents the accuracy of elastic net glm Table III represents the accuracy of the support vector machine and Table IV represents the accuracy of gradient boosting all these techniques are applied to four codes. In Table III, we have compared the result of the SVM classifier with previously published works [37] and in Table IV, we have compared the result of the Gradient Boosting classifier with previously published works [37].

TABLE I. RESULTS OF THE RANDOM FOREST MODEL

| Dataset | Algorithm | RF Mean Squared Error | RF Mean Absolute Error | Accuracy |
|---------|--------------------------|-----------------------|------------------------|----------|
| FD001 | Random Forest Regression | 17772.26 | 29.89 | 0.62 |
| FD002 | Random Forest Regression | 1945.94 | 32.475 | 0.58 |
| FD003 | Random Forest Regression | 3160.17 | 38.51 | 0.67 |
| FD004 | Random Forest Regression | 3209.63 | 40.68 | 0.59 |

TABLE II. RESULT OF ELASTIC NET GLM MODEL

| Dataset | Algorithm | GLM Mean Squared Error | GLM Mean Absolute Error | Accuracy |
|---------|-----------|------------------------|-------------------------|----------|
| FD001 | GLM | 2043.03 | 34.560 | 0.56 |
| FD002 | GLM | 2043.03 | 34.60 | 0.56 |
| FD003 | GLM | 4083.08 | 47.16 | 0.58 |
| FD004 | GLM | 4503.76 | 51.59 | 0.43 |

TABLE III. RESULT SUPPORT VECTOR MACHINE MODEL

| Dataset | Algorithm | SVM Mean Squared Error | SVM Mean Absolute Error | Accuracy | In past research[37] Accuracy |
|---------|-----------|------------------------|-------------------------|----------|-------------------------------|
| FD001 | SVM | 1860.48 | 30.28 | 0.60 | 0.893 |
| FD002 | SVM | 3774.31 | 48.79 | 0.20 | 0.894 |
| FD003 | SVM | 3846.14 | 41.04 | 0.60 | 0.893 |
| FD004 | SVM | 6052.88 | 58.43 | 0.24 | 0.106 |

TABLE IV. RESULT OF GRADIENT BOOSTING MODEL

| Dataset | Algorithm | GB Mean Squared Error | GB Mean Absolute Error | Accuracy | In past research [37] Accuracy |
|---------|-------------------|-----------------------|------------------------|----------|--------------------------------|
| FD001 | Gradient Boosting | 1768.62 | 29.92 | 0.62 | 0.899 |
| FD002 | Gradient Boosting | 1970.56 | 33.03 | 0.68 | 0.908 |
| FD003 | Gradient Boosting | 3190.07 | 38.68 | 0.67 | 0.903 |
| FD004 | Gradient Boosting | 3214.30 | 41.08 | 0.59 | 0.097 |

A thorough examination and explanation of the outcomes of applying ML models to a variety of engine datasets to forecast Remaining Useful Life (RUL). MSE, MAE, and R-squared are three quantitative measures of the model's performance under different operating settings and failure types that are part of the assessment metrics. Analyzing the FD001, FD002, FD003, and FD004 datasets separately exposed unique difficulties and intricacies. The model showed adequate prediction skills in the case of FD001, where conditions were comparatively simpler with a single failure mode (HPC Degradation). After switching to FD002, which included six operating conditions under the same fault mode, the model performed admirably, demonstrating its flexibility in a variety of situations.

The prediction work became more challenging in FD003 due to the addition of additional failure modes. We closely examined the model's capacity to manage both HPC Degradation and Fan Degradation situations. Even with this extra complexity, the model demonstrated proficiency in capturing the subtleties brought forth by numerous failure types. Finally, the robustness of the model was demonstrated by the assessment of FD004, which included two failure modes (HPC Degradation and Fan Degradation) and six different operational situations. The outcomes demonstrated its ability to handle a wider range of fault states and operating scenarios, which makes it a flexible tool for prognostic evaluations.

The comparative study of the models across datasets is also covered in detail in the discussion, with a focus on the differing levels of complexity brought about by various operational situations and failure mechanisms. The comparison study yielded insights that help comprehend the flexibility and generalization capabilities of the models, offering useful information for potential future applications in engine health prognostics. The limits of the study, probable causes of bias, and possibilities for development are also covered in the discussion. There are opportunities for more study and improvement of the prediction models because of the models' resilience and performance in real-world situations in various areas [38-42]. The discussion part, which provides a nuanced view of the models' strengths, limits, and potential implications in the field of engine system prognostics, summarizes the findings overall.

VI. CONCLUSION

This research presents a pivotal advancement in the realm of ML applied to industrial maintenance through its integration with the IIoT. Practically, the study equips

industries with an advanced, data-driven methodology for equipment maintenance, leading to reduced downtime, cost savings, and heightened operational efficiency. Theoretically, it enriches our understanding of ML's efficacy in predictive maintenance, facilitating the refinement of algorithms and informing more judicious model selections. Using a variety of datasets (FD001, FD002, FD003, and FD004), this study concludes with a thorough examination of the use of ML models for forecasting RUL of engines. The study effectively illustrates how well the models handle various operating situations and failure types, providing insightful information about engine health prognostics. The models' prediction ability is quantified using assessment metrics such as MSE, MAE, and R-squared. fault mode (HPC Degradation) and more straightforward conditions. After switching to FD002 with various operating circumstances, the model keeps performing admirably, highlighting its adaptability.

Although FD003 presents a difficulty due to the addition of new failure modes, the model can handle cases when there is both HPC Degradation and Fan Degradation. The assessment of FD004 under various circumstances and fault types demonstrates the adaptability and efficiency of the models in a range of operational contexts. The models' generalization skills are illuminated by the comparison study between datasets, which provides important information about their advantages and disadvantages. Even while the results are encouraging, it is important to recognize some limitations and potential topics for more research. Further investigation is needed on the models' susceptibility to biases and variances in sensor data. To sum up, this study establishes the foundation for further developments in prognostic modeling and highlights the value of strong ML methods for improving the precision and dependability of forecasts in various areas[43-46].

REFERENCES

- [1] W. Lee, H. Wu, H. Yun, H. Kim, M. Jun, J. Sutherland, T. Zonta, C. André da Costa, R. da Rosa Righi, M. de Lima, E. da Trindade, G. Li
- [2] J. Guth, U. Breitenbücher, M. Falkenthal, P. Fremantle, O. Kopp et al., "A detailed analysis of IoT platform architectures: Concepts, similarities, and differences," In *Internet of Everything*: Springer, pp. 81–101, 2018.
- [3] C. Federico, B. Stefano, S. Claudio, R. Enrico, M. Luca et al., "Industrial internet of things monitoring solution for advanced predictive maintenance applications," *Journal of Industrial Information Integration*, vol. 7, pp. 4–12, 2017.
- [4] J. Wang, L. Zhang, L. Duan and R. X. Gao, "A new paradigm of cloud-based predictive maintenance for intelligent manufacturing," *Journal of Intelligent Manufacturing*, vol. 28, no. 5, pp. 1125–1137, 2017.
- [5] H. M. Hashemian and W. C. Bean, "State-of-the-art predictive maintenance techniques," *IEEE Transactions on Instrumentation and measurement*, vol. 60, no. 10, pp. 3480–3492, 2011.
- [6] S.-j. Wu, N. Gebraeel, M. A. Lawley, and Y. Yih, "A neural network integrated decision support system for condition-based optimal predictive maintenance policy," *IEEE Transactions on Systems, Man, and Cybernetics-Part A: Systems and Humans*, vol. 37, no. 2, pp. 226–236, 2007.
- [7] "What Are Benefits and Drawbacks of Preventive Maintenance?" <https://www.onupkeep.com/answers/preventive-maintenance/benefits-of-preventive-maintenance> (accessed Jun. 29, 2021).
- [8] "What is Predictive Maintenance? [Benefits & Examples]," Fiix. <https://www.fiixsoftware.com/maintenance-strategies/predictive-maintenance/> (accessed Apr. 7, 2021).

- [9] Y. Ageeva, "Predictive Maintenance Scheduling with AI and Decision Optimization," Medium, May 15, 2020.
- [10] J. Lee, J. Ni, J. Singh, B. Jiang, M. Azamfar, J. Feng J. Manuf. Sci. Eng., 142 (2020), pp. 1-40, 10.1115/1.4047856
- [11] F. Ribeiro, M. Marins, S. Netto, and E. Silva, "Rotating machinery fault diagnosis using similaritybased models," presented at the XXXV Simpósio Brasileiro de Telecomunicações e Processamento de Sinais, 2017. doi: 10.14209/sbrt.2017.133.
- [12] A. Alzghoul, A. Jarndal, I. Alsyof, A. A. Bingamil, M. A. Ali, and S. AlBaiti, "On the Usefulness of Pre-processing Methods in Rotating Machines Faults Classification using Artificial Neural Network," Journal of Applied and Computational Mechanics, Jan. 2021, doi: 10.22055/jacm.2020.35354.2639.
- [13] K. Singha, S. Maity, P. Pandit Use of AI and machine learning techniques in knitting 10.1016/B978-0-323-85534-1.00021-0
- [14] C. Baban, M. Baban, S. Darius Using a fuzzy logic approach for the predictive maintenance of textile machines 10.3233/IFS-151822
- [15] S. Elkateb, A. Métwalli, A. Shendy, An Innovative Online Monitoring System in Knitting Industry, The 16th Textile Bioengineering and Informatics Symposium; Blended Conference. 412–419, August 22–25(2023). DOI: TBIS 10.3993/tbis (2023).
- [16] S. Elkateb, A. Métwalli, A. Shendy, K. Moussa, A. Abu-Elanien Online monitoring-based prediction model of knitting machine productivity Fibres 10.2478/ftce-2023-0035
- [17] O. Surucu, S. Andrew Gadsden, J. Yawney Condition monitoring using machine learning: a review of theory, applications, and recent advances ExpertSyst.Appl 10.1016/j.eswa.2023.119738
- [18] N. Mohammed, O. Abdulateef, A. Hamad An IoT and machine learning-based predictive maintenance system for electrical motors J. Eur. Des. Systèmes Autom., 56 (4) (2023), pp. 651-656, 10.18280/jesa.560414
- [19] Y. Gao, C. Chai, H. Li, W. Fu. A deep learning framework for intelligent fault diagnosis using automl-cnn and image-like data fusion Machines, 11 (10) (2023),p. 932, 10.3390/machines11100932.
- [20] W. Udo, Y. Muhammad Data-driven predictive maintenance of wind turbine based on SCADA data IEEE Access, 9 (2021), pp. 162370-162388, 10.1109/ACCESS.2021.3132684
- [21] <https://www.infoq.com/articles/machine-learning-techniques-predictive-maintenance/>
- [22] A. Saxena, K. Goebel, D. Simon, and N. Eklund, "Damage Propagation Modeling for Aircraft Engine Run-to-Failure Simulation", in the Proceedings of the 1st International Conference on Prognostics and Health Management (PHM08), Denver CO, Oct 2008.
- [23] Y. He, C. Gu, Z. Chen and X. Han, "Integrated predictive maintenance strategy for manufacturing systems by combining quality control and mission reliability analysis," International Journal of Production Research, vol. 55, no. 19, pp. 5841–5862, 2017.
- [24] S. Landset, T. M. Khoshgoftaar, A. N. Richter and T. Hasanin, "A survey of open-source tools for machine learning with big data in the hadoop ecosystem," Journal of Big Data, vol. 2, no. 1, pp. 24, 2015.
- [25] Y. Lu, "Industry 4.0: A survey on technologies, applications and open research issues," Journal of Industrial Information Integration, vol. 6, no. 1, pp. 1–10, 2017.
- [26] E. Oztemel and S. Gursev, "Literature review of industry 4.0 and related technologies," J. Intell. Manuf., vol. 31, no. 1, pp. 127–182, Jan. 2020.
- [27] W. Z. Khan, M. H. Rehman, H. M. Zangoti, M. K. Afzal, N. Armi, and K. Salah, "Industrial Internet of Things: Recent advances, enabling technologies and open challenges," Comput. Electr. Eng., vol. 81, Jan. 2020, Art. no. 106522.
- [28] D. Sehrawat and N. S. Gill, "Smart sensors: Analysis of different types of IoT sensors," in Proc. 3rd Int. Conf. Trends Electron. Informat. (ICOEI), Apr. 2019, pp. 523–528.
- [29] L. D. Xu and L. Duan, "Big data for cyber physical systems in industry 4.0: A survey," Enterprise Inf. Syst., vol. 13, no. 2, pp. 148–169, Feb. 2019.
- [30] H. Xu, W. Yu, D. Griffith, and N. Golmie, "A survey on industrial Internet of Things: A cyber-physical systems perspective," IEEE Access, vol. 6, pp. 78238–78259, 2018.
- [31] Aceto, V. Persico, and A. Pescape, "A survey on information and communication technologies for industry 4.0: State-of-the-art, taxonomies, perspectives, and challenges," IEEE Commun. Surveys Tuts., vol. 21, no. 4, pp. 3467–3501, Aug. 2019.
- [32] I. Sittón-Candanedo, R. S. Alonso, S. Rodríguez-González, J. A. G. Coria, and F. De La Prieta, "Edge computing architectures in industry 4.0: A general survey and comparison," in Proc. Int. Workshop Soft Comput. Models Ind. Environ. Appl., 2019, pp. 121–131.
- [33] Zhang, H. Huang, L.-X. Yang, Y. Xiang, and M. Li, "Serious challenges and potential solutions for the industrial Internet of Things with edge intelligence," IEEE Netw., vol. 33, no. 5, pp. 41–45, Sep. 2019.
- [34] E. Sisinni, A. Saifullah, S. Han, U. Jennehag, and M. Gidlund, "Industrial Internet of Things: Challenges, opportunities, and directions," IEEE Trans. Ind. Informat., vol. 14, no. 11, pp. 4724–4734, Nov. 2018.
- [35] C. Krupitzer, T. Wagenhals, M. Züfle, V. Lesch, D. Schäfer, A. Mozaffarin, J. Etinger, C. Becker, and S. Kounev, "A survey on predictive maintenance for industry 4.0," 2020, arXiv:2002.08224. [Online]. Available: <http://arxiv.org/abs/2002.08224>.
- [36] S. Gopalakrishnan and M. Senthil Kumaran, "Iiot framework based ml model to improve automobile industry product," *Intelligent Automation & Soft Computing*, vol. 31, no.3, pp. 1435–1449, 2022.
- [37] Nangia, S., Makkar, S., & Hassan, R. (2020, March). IoT based predictive maintenance in manufacturing sector. In *Proceedings of the International Conference on Innovative Computing & Communications (ICICC)*.
- [38] M. Anul Haq, "CDLSTM: A Novel Model for Climate Change Forecasting," *Comput. Mater. Contin.*, vol. 71, no. 2, pp. 2363–2381, 2022, doi: 10.32604/cmc.2022.023059.
- [39] M. A. Haq, "SMOTEDNN: A Novel Model for Air Pollution Forecasting and AQI Classification," *Comput. Mater. Contin.*, vol. 71, no. 1, pp. 1403–1425, 2022, doi: 10.32604/cmc.2022.021968.
- [40] M. A. Haq et al., "Analysis of environmental factors using AI and ML methods," *Sci. Rep.*, vol. 12, no. 1, pp. 1–16, 2022, doi: 10.1038/s41598-022-16665-7.
- [41] M. A. Haq, "DBoTPM: A Deep Neural Network-Based Botnet," *Electronics*, vol. 12, no. 1159, pp. 1–14, 2023, [Online]. Available: <https://www.mdpi.com/2079-9292/12/5/1159>
- [42] M. A. Haq and M. A. R. Khan, "Dnnbot: Deep neural network-based botnet detection and classification," *Comput. Mater. Contin.*, vol. 71, no. 1, pp. 1729–1750, 2022, doi: 10.32604/cmc.2022.020938.
- [43] C. S. Yadav et al., "Malware Analysis in IoT & Android Systems with Defensive Mechanism," *Electronics*, vol. 11, no. 15, p. 2354, 2022, [Online]. Available: <https://www.mdpi.com/2079-9292/11/15/2799>
- [44] A. Kumar, S. A. Alghamdi, A. Mehbodniya, M. anul haq, J. L. Webber, and S. N. Shavkatovich, "Smart power consumption management and alert system using IoT on big data," *Sustain. Energy Technol. Assessments*, pp. 1–7, 2022.
- [45] Lakshmana, K.; Kaluri, R.; Gundluru, N.; Alzamil, Z.S.; Rajput, D.S.; Khan, A.A.; Haq, M.A.; Alhussen, A. A Review on Deep Learning Techniques for IoT Data. *Electronics* 2022, 11, 1604. <https://doi.org/10.3390/electronics11101604>
- [46] S. S. P. D. M. A. H. A. K. Sathishkumar Karupusamy J. Refonaa, "Effective energy usage and data compression approach using data mining algorithms for IoT data," *Expert Syst.*, vol. 12997, pp. 1–10, 2022.

Analyzing Privacy Implications and Security Vulnerabilities in Single Sign-On Systems: A Case Study on OpenID Connect

Mohammed Al Shabi¹, Rashiq Rafiq Marie²

Department of Management Information System, Taibah University, Madinah, Saudi Arabia¹
Department of Information System, Taibah University, Madinah, Saudi Arabia²

Abstract—Single Sign-On (SSO) systems have gained popularity for simplifying the login process, enabling users to authenticate through a single identity provider (IDP). However, their widespread adoption raises concerns regarding user privacy, as IDPs like Google or Facebook can accumulate extensive data on user web behavior. This presents a significant challenge for privacy-conscious users seeking to restrict disclosure of their online activities to third-party entities. This paper presents a comprehensive study focused on the OpenID Connect protocol, a widely utilized SSO standard. Our analysis delves into the protocol's operation, identifying security flaws and vulnerabilities across its various stages. Additionally, we systematically examine the privacy implications associated with user access to SSO systems. We offer a detailed account of how easily user information can be accessed, shedding light on potential risks. The findings underscore the imperative to address privacy vulnerabilities within SSO infrastructures. We advocate for proactive measures to enhance system security and safeguard user privacy effectively. By identifying weaknesses in the OpenID Connect protocol and its implementations, stakeholders can implement targeted strategies to mitigate risks and ensure the protection of user data. This research aims to foster a more secure and privacy-respecting environment within the evolving landscape of SSO systems.

Keywords—Single Sign-On; OpenID connect protocol; vulnerabilities; privacy; third-party

I. INTRODUCTION

Single Sign-On (SSO) systems streamline user access to various online services by consolidating credentials, thus eliminating the need for multiple usernames and passwords. However, this convenience often conflicts with user privacy, as identity providers (IDPs) involved in the SSO process can track and collect user data across platforms, potentially sharing it with third-party organizations for targeted advertising or profiling. Notably, prominent IDPs like Google and Facebook are known to leverage such data, raising significant concerns regarding user privacy and control over personal information [1] [2]. In light of these challenges, understanding the security and privacy implications of SSO systems becomes paramount.

OpenID Connect emerges as one of the most prevalent SSO protocols, offering a standardized framework for authentication and authorization across diverse websites and applications. This research endeavors to comprehensively assess the efficacy and potential vulnerabilities of OpenID

Connect through a large-scale practical study. By dissecting its operational stages, we aim to identify security weaknesses and risks inherent in the protocol. The primary objective of this study is to evaluate the privacy implications of user access to SSO systems, along with the potential exposure of user information to IDPs and third-party entities. Through systematic analysis, we scrutinize the accessibility of user data within the SSO framework, illuminating the extent to which online user behavior can be monitored and exploited.

To underscore the real-world impact of these privacy concerns, we conduct a Mix-up attack on the OpenID Connect protocol using a local ASP.net-based API. The success of this attack in obtaining ID tokens, subsequently utilized to construct Access tokens for unauthorized resource access, underscores the vulnerability of SSO systems. Moreover, we quantify the attack's efficiency on online platforms by measuring the number of tokens accessed during execution.

This research endeavors to contribute significantly to the understanding of privacy implications and security vulnerabilities inherent in SSO systems. By shedding light on these issues, we aim to inform the development of more robust and privacy preserving SSO solutions. Ultimately, our findings advocate for empowering users to retain control over their personal data and limit disclosure to third-party organizations. The rest of the paper is organized as follows. Section II introduces the related works. Next, in Section III, the Open Connect Protocol is described, followed by Section IV which presents the vulnerabilities in Open ID connect. Section V states the vulnerabilities in OIDC. The implementation of a mix-up attack using ASP.net is described in Section VI. Finally, Section VII concludes the paper's work and findings.

II. RELATED WORK

The security and privacy issues of Single Sign-On (SSO) systems and their protocols have been investigated by several studies. These studies have enhanced the understanding of the challenges and risks involved in the use of SSO systems. Some of the key research in this area is summarized as follows: The work in study [3] examines the tracking capabilities of third-party entities on the web and explores potential defences against such tracking. It sheds light on the privacy risks associated with SSO systems and the information that identity providers (IDPs) can gather about user behavior. The study in[4] investigates the security vulnerabilities of web-based password managers, which are often integrated with SSO systems. It analyzes potential attacks and risks to

user privacy when relying on SSO for password management and authentication.

The research in study [5] explores the trade-off between user control and usability in social networking platforms that utilize SSO. It discusses privacy-preserving mechanisms and approaches to mitigate the risks associated with sharing personal data through SSO systems. The study in [6] investigates the vulnerabilities and attacks related to account hijacking and session management in SSO systems. It provides insights into the security risks associated with SSO protocols and highlights the importance of robust authentication and session handling mechanisms. The survey in [7] provides an overview of the privacy challenges in Single Sign-On and explores potential solutions. It discusses various aspects of SSO privacy, including information leakage, tracking risks, and user consent. The research in [8] conducts a comparative analysis of security properties in different SSO protocols, including SAML, OAuth, and OpenID Connect. It identifies vulnerabilities and discusses security considerations

in these protocols. This empirical [9] investigation focuses on the security and privacy aspects of OpenID Connect. It analyzes potential threats and vulnerabilities in the protocol and provides insights into its effectiveness in protecting user privacy. The literature review in study [10] examines various SSO protocols and their security and privacy characteristics. It identifies common vulnerabilities, threats, and mitigation strategies present in the literature. This systematic in [11] review and meta-analysis analyze the security and privacy aspects of SSO systems. It synthesizes findings from multiple studies and provides an overview of the state-of-the-art research in the field. This study in [12] presents a case study focusing on the privacy-sensitive features in a web authentication system. The researchers analyze and evaluate the privacy implications of various features and mechanisms used for web authentication. The study sheds light on the potential privacy risks and challenges that users may face during the authentication process and provides insights into the design of privacy-preserving authentication systems.

TABLE I. KEY RESEARCH WORKS

| Study | Key contribution | Focus |
|------------------------------|---|---|
| Roesner et al. [3] | Examined tracking capabilities of third-party entities on the web. | Privacy risks and information gathering by identity providers (IDPs) in SSO systems. |
| Chia [4] | Investigated security vulnerabilities of web-based password managers integrated with SSO. | Attacks and privacy risks in SSO systems for password management and authentication. |
| Rahman [5] | Explored the trade-off between user control and usability in SSO-based social networking. | Privacy-preserving mechanisms and risk mitigation for sharing personal data via SSO systems. |
| Nergiz [6] | Investigated vulnerabilities and attacks related to account hijacking and session management. | Security risks in SSO protocols, emphasizing robust authentication and session handling. |
| Yang et al. [7] | Provided an overview of privacy challenges in Single Sign-On and potential solutions. | SSO privacy aspects, including information leakage, tracking risks, and user consent. |
| Fett et al. [8] | Conducted a comparative analysis of security properties in different SSO protocols. | Vulnerabilities and security considerations in SAML, OAuth, and OpenID Connect protocols. |
| W. Li and C. J. Mitchell [9] | Empirical investigation of security and privacy aspects of OpenID Connect. | Analysis of threats and vulnerabilities in the protocol and its effectiveness in protecting user privacy. |
| Ahmad et al. [10] | Literature review of various SSO protocols and their security and privacy characteristics. | Identification of common vulnerabilities, threats, and mitigation strategies from literature. |
| Zuo et al. [11] | Systematic review and meta-analysis of security and privacy aspects of SSO systems. | Synthesis of findings from multiple studies to provide an overview of state-of-the-art research in the field. |
| Li et al. [12] | Evaluated privacy implications of identity federation in SSO systems. | Privacy risks and concerns associated with identity federation in SSO deployments. |
| Wang et al. [13] | Analyzed authentication vulnerabilities in SSO for mobile apps. | Security weaknesses and risks in SSO implementations for mobile applications. |
| Meland et al. [14] | Investigated the privacy implications of attribute sharing in SSO systems. | Risks associated with sharing user attributes among multiple service providers through SSO. |
| Paul et al. [15] | Explored privacy and security challenges in the context of healthcare SSO systems. | Addressing privacy concerns and enhancing security for SSO implementations in healthcare environments. |

This research in study [13] provides a comprehensive study of OAuth security issues specifically related to Android apps. The authors analyze the implementation of OAuth in various Android applications to identify potential security vulnerabilities and weaknesses. The study uncovers security risks and potential attacks that could compromise the security and privacy of user data when using OAuth-based authentication in Android apps. This study in [14] investigates the privacy aspects of attribute sharing in Single Sign-On (SSO) solutions. The researchers examine the process of attribute sharing among multiple service providers in SSO systems and analyze the privacy risks associated with this sharing. The study aims to enhance the understanding of the potential privacy concerns and challenges in SSO deployments and provides insights into protecting user privacy in attribute sharing scenarios.

This systematic review in [15] focuses on Single Sign-On (SSO) security specifically in the context of healthcare. The researchers review and analyze existing literature on SSO security, with a specific focus on healthcare environments. The study identifies security challenges and vulnerabilities related to SSO implementations in healthcare settings and provides recommendations for enhancing security and privacy in healthcare SSO systems. The review contributes to a better understanding of SSO security concerns and implications in healthcare applications. Table I summarizes the key research works related to privacy implications and security vulnerabilities associated with Single Sign-On (SSO) systems.

III. OPEN CONNECT PROTOCOL

OpenID Connect is an industry-standard protocol used for authentication and authorization in Single Sign-On (SSO)

systems. It is built on top of the OAuth 2.0 framework and provides a standardized way for users to log in to multiple websites or applications using a single set of credentials [16]. The primary goal of OpenID Connect is to enable identity federation, allowing users to authenticate with an identity provider (IDP) and then use that authentication to access various relying parties (RPs) without needing separate credentials for each RP. The IDP is responsible for verifying the user's identity and providing the necessary authentication tokens. Fig. 1 depicts the relationship among the components of OpenID.



Fig. 1. The relationship between the components in the protocol.

A. Brief overview of how OpenID Connect works

- User Initiation: When a user attempts to access a website or an application (RP) that supports OpenID Connect, they are redirected to the IDP's authentication endpoint.
- Authentication: The user is prompted to enter their credentials (e.g., username and password) at the IDP's login page. The IDP authenticates the user and generates an ID token.
- ID Token Exchange: After successful authentication, the IDP issues an ID token to the RP. This ID token contains information about the user and the authentication event, such as the user's unique identifier and any requested user claims.
- Token Validation: The RP validates the ID token to ensure its integrity and authenticity. It checks the token's signature, expiration, and the IDP's issuer information to verify its validity.
- User Authorization: Once the RP has validated the ID token, it can authorize the user's access to its resources based on the user's identity and any additional authorization scopes or claims provided.

OpenID Connect also supports optional features such as UserInfo endpoint, which allows RPs to retrieve additional user profile information from the IDP, and the use of refresh tokens for obtaining new access tokens without re-authentication. By leveraging OpenID Connect, SSO systems can offer a seamless and secure user experience, as users only need to authenticate once with their IDP and can then access multiple applications without the need for separate logins. The

protocol facilitates interoperability among different identity providers and relying parties, providing a standardized framework for SSO implementation. Fig. 2 illustrates the implementation phases in the OpenID Connect protocol.

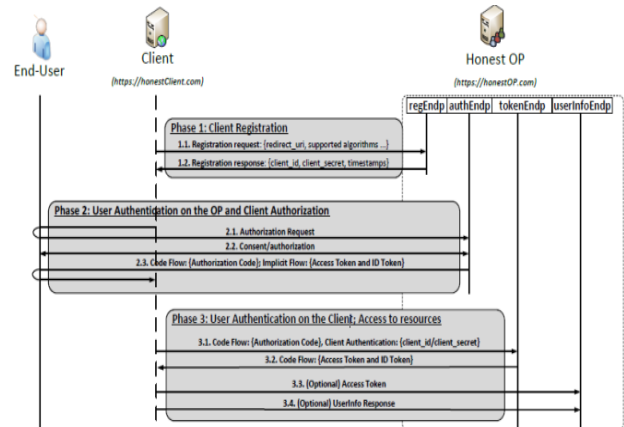


Fig. 2. Implementation phases in the OpenID Connect protocol.

The stages of the OpenID Connect protocol work:

1) Stage one: Dynamic registration and discovery in Fig. 3 shows the initial registration stage more accurately, In the beginning, the user presents his identity (for example, alice@honestOP.com) to the customer to obtain services. To authenticate the user, the client needs to discover the IDP which controls the identity of the alias.

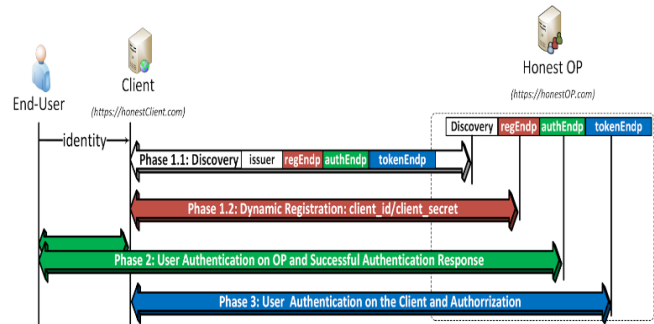


Fig. 3. OpenID Connect dynamic registration phase.

The first stage is divided into two steps:

- Step 1 (Discovery): The client sends a request to the Discovery endpoint and returns OP's configuration information including the locations of the endpoints.

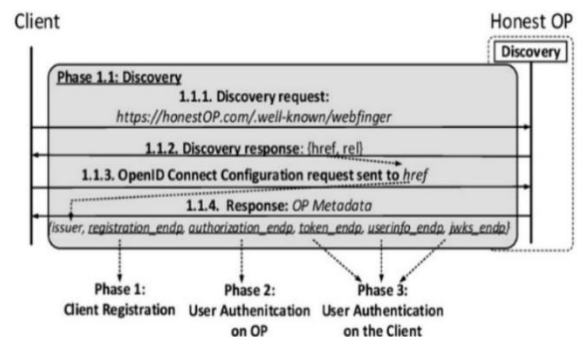


Fig. 4. Detailed overview of the discovery phase in OIDC.

Fig. 4 shows the details of the discovery phase in which the metadata received by the client appears and its impact on the protocol phases. Note that this data contains all information related to the protocol (endpoints, signature, and encryption algorithms - messages - public keys of the protocol).

- Step 2 (dynamic registration): The client automatically registers with the Identity Provider (OP) where it sends its own address (for example `http://client.com`) to the registration endpoint address, so the OP responds and sends the pair `(/client_id client_secret)`, which are secret codes between the client and the Identity Provider (OP) representing Client credentials.

2) *Stage two: Authenticating* In this phase the user is authenticated at the identity provider (User: Authentication on the OP). The client directs the unauthenticated user to an authorization endpoint (the user is directed to an address on which the client ID is pre-registered). The end user is authenticated to the OP using his or her credentials. The OP sends an authorization code that includes an (Access token, ID token) this code is an intermediary between the client and the user through which the client can access specific resources for the user and verify the identity of the end user.

3) *Stage three: User Authentication stage* (on the OP - ID and Access Token): After the client receives the code at the end of the second stage, it sends it to the token endpoint and sends its credentials from the first stage (`client_id` and `client_secret`), then the identity provider responds and sends it the (access token, ID token), and then the client Verifies the tokens and performs final user authentication.

- ID Token content

```
Header: {"alg": "HS256"}
Body: {
  "iss": "http://openidConnect
Provider.com/", "sub": "user1",
  "exp": 1444148908,
  "iat": 1444148308,
  "nonce": "40c6b33b9a2e",
  "aud": "http://client.com/",
Signature: AF45JF93LKD76D...
```

Fig. 5. An example of an ID token.

An id token is a secret token that contains information (claims) about the end user's identity and structure. Its data is a JWT (JSON Web Token). Fig. 5 shows an example of an id token [17].

We note that the id token consists of three parts:

First: The header contains information that includes the encryption algorithm used.

Second: The body contains the information needed to authenticate the end user, including:

End User ID: It consists of two parts:

- Issuer (Iss): To know the identity provider.
- sub (Subject o): To know the identity of the user.
- The timestamp (iat) and expired (exp) define the time period for the token to be produced and to expire.
- Nonce: A random string sent by the client during the authentication request used to mitigate attacks.
- Audience (aud): Determines which customers the identity token belongs to.

Third: Signature provides the reliability of the id token.

IV. OPENID CONNECT VULNERABILITIES

One notable vulnerability in the OpenID Connect (OIDC) protocol is the introduction of dynamic registration and discovery, a phase that was absent in previous protocols. This phase became a significant weakness in the OIDC protocol, as attackers were able to manipulate the information, particularly endpoint addresses, exchanged during the discovery phase. Attackers could substitute legitimate addresses with their own, enabling them to intercept and manipulate information exchanged between clients and the attacker throughout the various phases of the protocol. The layered structure of the OIDC protocol further facilitated attackers in intervening between any two of the three primary phases. Several previous studies have explored and exploited these vulnerabilities, leading to the development of new attacks targeting the OIDC protocol and the creation of tools for analyzing and testing its confidentiality.

A. OpenID Connect Previous Studies

Security vulnerabilities in single sign-on protocols have been examined, analyzed, and identified in a number of previous studies. Here are some of the most significant contributions made by these studies; in addition, Table II summarizes the principal contributions made by the mentioned studies.

In study [17] the researchers conducted a comprehensive examination of the security characteristics of the Google OIDC protocol. They examined a group of clients and applied a class of attacks to obtain user codes, enabling impersonation and unauthorized access to clients. Additionally, they provided valuable insights and future recommendations for both Service Providers (RPs) and Identity Providers (OPs) to enhance security in future systems. Researchers in [18] developed a tool to test attacks on the OpenID Connect (OIDC) Access Protocol. This tool encompasses advanced attacks, including malicious endpoint attacks, contributing to a better understanding of the protocol's message flow.

In study [19] the researchers conducted an in-depth analysis of the OIDC protocol's dynamic registration and discovery feature. They identified a new type of attack named "Malicious Endpoints" that exploits information exchanged between protocol parties, posing risks to user privacy. In researcher [20] the researchers analyzed known attacks on the OIDC protocol and classified them into two categories: single-stage attacks, targeting one stage, and two-stage attacks, relying on multiple stages. They also proposed measures to

enhance protocol confidentiality and identified security vulnerabilities. Researchers in [21] provided a thorough and formal security analysis of the OpenID Connect protocol. They developed a model of OpenID Connect, utilizing secret features to mitigate known attacks, and put forth security guidelines to bolster the overall security posture of the protocol. The authors of [22], studied the security flaws of OAuth 2.0 in Android apps, focusing on the implementation errors that could lead to breaches. They also discussed the OAuth security challenges specific to the Android platform. Research in [23] examined the security misconfigurations in mobile OAuth implementations, using real-world apps as examples. They uncovered common mistakes that could affect the security of mobile systems based on OAuth. In paper [24], performed a comprehensive security assessment of OAuth 2.0, which is the authorization framework for OpenID Connect. They evaluated different OAuth implementations and detected vulnerabilities, and they suggested recommendations for enhancing the security of systems based on OAuth. The researchers in [25], investigated the security of OAuth, which is the foundation for OpenID Connect. They analyzed the weaknesses and vulnerabilities in OAuth's authentication and authorization mechanisms, and they highlighted the potential risks associated with OAuth implementations.

This paper in [26] presents a Systematization of Knowledge (SoK) on OAuth 2.0 and explores the current vulnerabilities, limitations, and ongoing efforts to improve its security. The study identifies various threats and vulnerabilities related to the authentication and authorization mechanisms of OAuth 2.0. It also discusses potential solutions and ongoing research to enhance the protocol's security in protecting user privacy and data. This research [27] provides an in-depth formal security analysis of the OpenID Connect protocol. By applying formal methods, the study examines the security properties and potential vulnerabilities of OpenID

Connect. The authors develop a model of the protocol and provide security guidelines to mitigate. This survey article[28] presents a comprehensive comparison of security modelling approaches for various Single Sign-On (SSO) protocols, including OpenID Connect. The study reviews the strengths, weaknesses, and challenges in the security modelling of SSO protocols, providing insights into the security aspects of OpenID Connect and other SSO protocols known attacks and enhance the overall security posture of OpenID Connect.

This study in [29] investigates the design and security considerations of a Mobile Single Sign-On (SSO) system based on OpenID Connect. The research examines the integration of OpenID Connect for mobile applications, focusing on the design aspects and security measures necessary to ensure a secure and user-friendly SSO experience on mobile platforms. This empirical [30] investigation delves into the security, privacy, and usability aspects of the OpenID Connect protocol. The research assesses potential threats and vulnerabilities in OpenID Connect's implementation and analyzes its effectiveness in safeguarding user privacy and data. Additionally, the study evaluates the usability of OpenID Connect in real-world scenarios. This survey paper [31] provides a comprehensive examination of OAuth-based Single Sign-On (SSO) protocols, including OpenID Connect. The study reviews different SSO protocols and focuses on OAuth's role as the foundation for SSO mechanisms. The paper discusses the strengths and weaknesses of OAuth-based SSO and highlights areas for further improvement. This research [32] conducts a security analysis of the OAuth 2.0 framework in the context of mobile applications. The study identifies potential vulnerabilities and threats associated with OAuth 2.0 when utilized in mobile environments. The paper discusses security considerations and suggests measures to enhance the protection of user data and privacy in OAuth-based mobile applications.

TABLE II. SUMMARIZING THE KEY CONTRIBUTIONS AND FOCUS OF THE MENTIONED STUDIES RELATED TO OPENID CONNECT AND OAUTH 2.0 SECURITY

| Study | Key Contributions | Focus |
|---------------------------------------|--|--|
| Li et al. [17] | - Examined Google OIDC protocol security characteristics. - Conducted attacks to obtain user codes and impersonate clients. - Provided future recommendations for RPs and OPs. | - Security analysis of Google OIDC. - Attack scenarios on OIDC clients. - Recommendations for enhancing security. |
| Mladenov et al. [18] | - Developed a tool for testing OIDC Access Protocol attacks. - Enhanced understanding of the protocol's message flow. | - Advanced attacks, including malicious endpoint attacks in OIDC. |
| Mainka et al. [19] | - Conducted in-depth analysis of OIDC's dynamic registration and discovery feature. - Identified "Malicious Endpoints" attack and its risks. | - Analysis of OIDC's dynamic registration and discovery feature. |
| Navas et al. [20] | - Analyzed known attacks on the OIDC protocol and classified them into single-stage and two-stage attacks. - Proposed measures to enhance protocol confidentiality and identified security vulnerabilities. | - Categorized attacks into single-stage and two-stage attacks. |
| Fett et al. [21] | - Provided thorough and formal security analysis of the OpenID Connect protocol. - Developed a model of OpenID Connect and security guidelines for mitigation. | - Formal security analysis of OpenID Connect protocol. |
| Maqbool et al. [22] | - Studied the security flaws of OAuth 2.0 in Android apps. - Focused on implementation errors and their impacts. | - Security assessment of OAuth 2.0 in Android apps. - OAuth security challenges on the Android platform. |
| A. Kountouras and G. Frantzeskou [23] | - Examined security misconfigurations in mobile OAuth implementations using real-world apps. - Identified common mistakes affecting mobile OAuth security. | - Examination of real-world mobile OAuth implementations. |
| J. Richer and A. Sanso [24] | - Performed comprehensive security assessment of OAuth 2.0. - Evaluated vulnerabilities in various OAuth implementations. - Suggested recommendations for enhancing OAuth 2.0 security. | - Evaluation of OAuth 2.0 vulnerabilities and security measures. |
| B. Braithwaite and A. Doupé [25] | - Investigated security vulnerabilities in OAuth's authentication and authorization mechanisms. - Highlighted potential risks associated with OAuth implementations. | - Analysis of OAuth's weaknesses and vulnerabilities. |
| Pereira et al. [26] | - Systematization of Knowledge (SoK) on OAuth 2.0 security. - Identification of threats and vulnerabilities related to OAuth's authentication and authorization mechanisms. - Discussion of potential solutions to improve OAuth's security. | - Identification of threats and vulnerabilities in OAuth 2.0. - Ongoing research to enhance OAuth's security and protect user privacy. |

| | | |
|-----------------------------|---|---|
| Küsters and Kifayat [27] | - Provided in-depth formal security analysis of the OpenID Connect protocol. - Developed a model of OpenID Connect and provided security guidelines. | - Formal security analysis of OpenID Connect protocol. |
| Sanchez-Aguilar et al. [28] | - Comprehensive comparison of security modeling approaches for various Single Sign-On (SSO) protocols, including OpenID Connect. - Review of strengths, weaknesses, and challenges in security modeling of SSO protocols. | - Review of security modeling approaches for SSO protocols. - Insights into the security aspects of OpenID Connect and other SSO protocols. |
| Vetrivelan et al. [29] | - Investigated design and security considerations of a Mobile Single Sign-On (SSO) system based on OpenID Connect. - Focused on secure integration of OpenID Connect for mobile applications. | - Design aspects and security measures for secure Mobile SSO with OpenID Connect. |
| Alshehri et al. [30] | - Delved into the security, privacy, and usability aspects of the OpenID Connect protocol. - Assessed threats and vulnerabilities in OpenID Connect's implementation. - Evaluated the effectiveness of OpenID Connect in safeguarding user privacy and data. | - Security, privacy, and usability evaluation of OpenID Connect. |
| Sun et al. [31] | - Provided a comprehensive examination of OAuth-based Single Sign-On (SSO) protocols, including OpenID Connect. - Focused on OAuth's role as the foundation for SSO mechanisms. - Discussed strengths and weaknesses of OAuth-based SSO. | - Review of OAuth-based SSO protocols. - Identification of strengths and weaknesses. |
| Khan and Shafiq [32] | - Conducted a security analysis of the OAuth 2.0 framework in the context of mobile applications. - Identified vulnerabilities and threats in OAuth 2.0 for mobile environments. - Suggested measures to enhance user data and privacy protection in OAuth-based mobile applications. | - Security analysis of OAuth 2.0 in mobile applications. - Measures to enhance OAuth-based mobile app security. |

V. OIDC VULNERABILITIES

1) *Phishing*: Phishing attacks in OIDC can take two forms:

a) *Spoofed OP page*: Attackers can redirect users to a spoofed Identity Provider (OP) page where they are deceived into entering their OP credentials[20].

b) *Realm spoofing*: Service Providers (RPs) can craft authentication requests with an OpenID realm parameter set to a trusted domain but redirect the user back to their own page without proper verification. The user's OP falsely assures them that they are logging into the trusted domain, while they are redirected to the RP.

2) *Session related attacks*: OIDC allows multiple active authentication sessions, providing more opportunities for malicious sites to exploit vulnerabilities in both OPs and RPs[33]. Specific issues include:

a) *Session swapping*: Lack of a mechanism to associate an OIDC session with the user's browser allows attackers to configure an attacker-authenticated session in the RP. This can lead to unauthorized access and disclosure of sensitive information.

b) *Cross-Site Request Forgery (CSRF)*: Logged-in users may be susceptible to CSRF attacks targeting the OP or other RP sites.

c) *Cross-Site Scripting (CSS)*: Logged-in users may be vulnerable to XSS attacks against the OP or other RP sites.

3) *Data privacy*: OpenID Connect service providers have visibility into every site the user logs into using their credentials. This centralized nature allows malicious OPs to track user activity on the internet.

4) *Risk centralization*: Hacker's target IdP accounts as they provide access to multiple sites. If an identity provider lacks escalated authentication options, the user's security may be compromised.

5) *Weak background security*: Some OPs may rely solely on email account recovery, which is inadequate for strong background security. Account recovery mechanisms should employ stronger authentication methods.

6) *Cross-identifier relationship*: When users employ the same OpenID across different RP sites, these sites can link user information or activity. Independent logins in different RPs mitigate this issue.

7) *Shared ID strings*: The usability challenge of entering ID strings increases when different launches employ different methods.

This can lead to users inadvertently entering the same ID in multiple places, allowing RPs to establish relationships between them.

VI. IMPLEMENTING A MIX-UP ATTACK USING ASP.NET

A. Attack Assumption

- The RP (Service Provider) is configured to connect to multiple OAuth Providers (Ids), including one controlled by the attacker (AldP) and another harmless one (HIDP).
- The RP uses the same `redirect_uri` for multiple identity providers and relies on the 'state' parameter to determine the origin of the response.
- The attacker's AldP has control over the authentication flow and response sent to the RP.

B. Attack Stages

Stage 1: The attacker obtains the victim's token from HIDP.

Fig. 6 shows the steps of this stage [9], the following steps illustrate the attack flow:

1) The End User clicks the "Login with HIDP" button on an RP page.

2) The attacker communicates with the RP and sends a login request to the RP, pretending to be the AldP (attacker-controlled Identity Provider). As a result, the attacker receives a redirect response at the AldP's authorization endpoint.

3) The attacker redirects the response to the browser, intending it to be transmitted to the conversion endpoint of HIDP (harmless Identity Provider). However, during this process, the attacker uses the status value associated with the authorization request for the AldP that was received in step 2.

- 4) The end user interacts with HIdP and clicks "Agree" to authenticate and authorize the request.
- 5) HIdP returns the end user to the redirect_uri of the RP, along with the associated token.
- 6) The RP receives the token and evaluates the status value, determining that the authorization response is from the AIdP (attacker's-controlled Identity Provider).
- 7) The RP mistakenly sends the code and tokens to the AIdP's token endpoint and API endpoints, allowing the HIdP tokens to be delivered to the attacker.

Stage 2: Using the victim's code V.

In this step, the RP continues to interact with the attacker, assuming the attacker is the victim. If the RP provides data or allows modifications based on the access token, the attacker gains access to the victim's resources and can potentially manipulate them, Fig. 7 shows this stage.

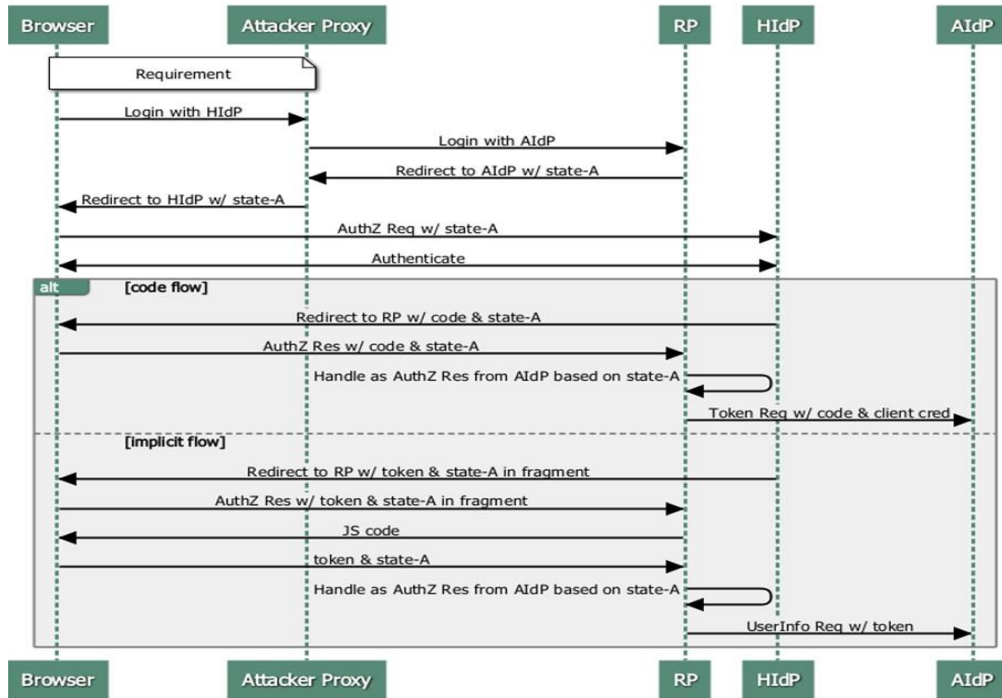


Fig. 6. Mix-up attack steps.

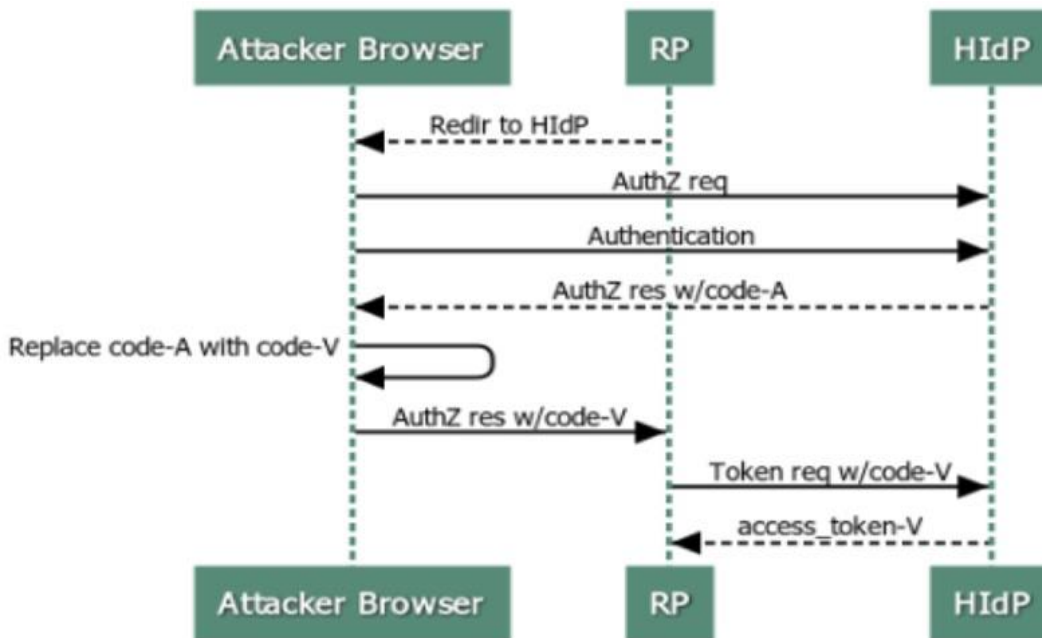


Fig. 7. Victim code used by the attacker.

C. Execute Attack on API

The provided excerpt describes the execution of the attack on the API and the consequences of its success. Here's an explanation of the details mentioned:

1) Successful Attack and Obtaining User Information:

- a) When the attack is successful, the attacker receives information in JSON format.
- b) The attack allows the attacker to access user values that were previously protected.
- c) The obtained user values are stored in two encrypted strings or variables within the API, referred to as value 1 and value 2. Fig. 8 illustrates the protected user token values prior to the attack.

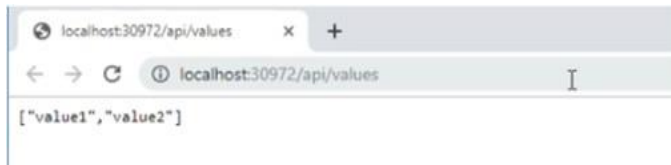


Fig. 8. Protected user token values prior to attack.

2) Obtaining user ID token:

- a) After executing the attack, the attacker obtains the user's ID token.
- b) The ID token is typically encrypted using JWT (JSON Web Token) and needs to be decrypted to extract its contents. Fig. 9 illustrates the ID token values after the attack has been applied.



Fig. 9. The id token values after the attack has been applied.

3) Decrypting the ID token:

- a) The attacker decrypts the ID token using JWT services.
- b) Decrypting the token allows the attacker to access the user's tokens.
- 4) Accessing user resources:
 - a) Once the attacker has obtained the necessary tokens, they can use them to log in and gain access to the user's resources.
 - b) These by bypasses the protection mechanisms of the protocol, potentially resulting in the loss of user data and compromising their account.

D. Online Attack Implementation

The applied attack steals a set of user account tokens that are as in Table III. These codes play a critical role in interacting with the protocol's service provider, and their theft grants the attacker access to the victim's data. It is important to note that the success of the attack relies on the service provider enabling redirection for the user account, which is commonly known as a redirect attack. Upon executing the

attack on a Gmail account, the codes in Fig. 10 were obtained, which illustrates the obtained tokens, revealing a successful attack where most of the mentioned tokens were acquired. However, it is important to note that certain tokens, such as EXP Idp tokens, were not obtained, resulting in a lack of information regarding the specific hack.

TABLE III. USER ID TOKEN

| Token | Data Format | Meaning |
|-----------|-------------------------------|---|
| Alg | String | Indicates the algorithm that was used to sign the token. |
| Kid | String | Sets the fingerprint of the public key that can be used to validate the signature of this token. |
| Iss | Source URL string | Defines the source or authorization server that generates and returns the token. |
| Idp | "String", usually the STS URL | Recording the identity provider that authenticated and returns the token subject. |
| Sub | String | The subject prompt value is immutable and cannot be modified or reused. It serves as a binary identifier that is unique to a particular application identifier. When a user logs into multiple applications with distinct customer IDs, each app will receive a different subject prompt value. The desirability of this behavior depends on your specific privacy requirements and system structure. |
| Hasgroups | Bool | If it exists, it is always true, indicating that the user is in at least one group. It is used in place of the collections claim for JWTs in implicit grant flows if the full collections claim would extend the URI part beyond the URL length limits (currently 6 or more groups). |
| Exp | String | Indicates when the session with the identity provider expired. |
| Website | String | Referring to the identity provider type. |
| Aud | String | The name of the site where the protocol is being used. |

In the subsequent Table IV, we will delve into the attack on multiple platforms utilizing the protocol, providing a comparison between these platforms based on an essential criterion: redirection to the victim's page from which the codes were obtained. Redirection refers to the ability of the service provider to access the user's account and gain complete control over it through redirection techniques. Notably, prominent companies like Microsoft and Google have implemented measures to protect their users from such redirects, thus preventing unauthorized access to accounts. By applying the attack on the platforms listed in Table IV below, we can gauge the success of the attack by the number of tokens obtained. In this instance, we were able to acquire nine access tokens, indicating a 100% success rate for the attack.

TABLE IV. MIX-UP ATTACK PERCENTAGES ON POPULAR PLATFORMS

| Platform | Token Access Rate | Redirect by the Service Provider |
|----------|-------------------|----------------------------------|
| Gmail | 7/9=77.7% | impossible |
| Facebook | 5/9=55.5% | impossible |
| Yahoo | 8/9=88.8% | possible |
| Hotmail | 9/9=100.00% | possible |
| Outlook | 4/9=0.44% | impossible |

It is important to highlight the possibility of redirection in this context. Fig. 10 depicts the user tokens taken after applying the MIX-Up attack on the Gmail platform.

```
Sub: 2023-07-12-15
aud:12/7/2023 17:33:17
code:
Alg AEC = AakniGP1NkqEIV633]FuEG05rppTpx0vufD86wP818N6Pfgic_vaalIdnA
Website: .google.com
Path: /
Hasgroups: True
exp: False
Comment:
Iss:
Kid: AEC=AakniGP1NkqEIV633]FuEG05rppTpx0vufD86wP818N6Pfgic_vaalIdnA
Idp: AEC
Sub: AakniGP1NkqEIV633]FuEG05rppTpx0vufD86wP818N6Pfgic_vaalIdnA
aud: 12/7/2023 17:33:17
code:
Alg NID = 511-jX9lE6kXQuAnxCrOEhNxfj61F72C8VP1x8L7lMA3RCfCE4mM1cx0UP2HmoIF9miEN5BiqGfZlBk2b23uQ5Rr-1aGIZuxlA34ZldeHfHng
azkdVZlNiGDp88PQ08jRaJ2XiyavAy58r8aMlPcOVz336ct_s5m3EmME-mOPc450
Website: .google.com
Path: /
Hasgroups: False
exp: False
Comment:
Iss:
Kid: NID=511-jX9lE6kXQuAnxCrOEhNxfj61F72C8VP1x8L7lMA3RCfCE4mM1cx0UP2HmoIF9miEN5BiqGfZlBk2b23uQ5Rr-1aGIZuxlA34ZldeHfHng
azkdVZlNiGDp88PQ08jRaJ2XiyavAy58r8aMlPcOVz336ct_s5m3EmME-mOPc450
Idp: NID
Sub: 511-jX9lE6kXQuAnxCrOEhNxfj61F72C8VP1x8L7lMA3RCfCE4mM1cx0UP2HmoIF9miEN5BiqGfZlBk2b23uQ5Rr-1aGIZuxlA34ZldeHfHng
azkdVZlNiGDp88PQ08jRaJ2XiyavAy58r8aMlPcOVz336ct_s5m3EmME-mOPc450
aud:12/7/2023 17:33:17
```

Fig. 10. User tokens after applying the MIX-Up attack on the gmail platform.

From the previous table, it is evident that the attack was successful across various popular platforms, yielding favorable success rates. However, variations in the verification rates of the attack can be observed due to factors associated with the response behaviour of the identity providers. Some servers permit code injection during the session, whereas others do not allow such manipulations. Additionally, the results differ based on the number of tokens accessed, which can vary depending on the specific protocol version implemented within each platform.

VII. CONCLUSION

In this research, we have examined the OpenID protocol and its information exchange mechanism, while also highlighting its significant security vulnerabilities and the execution of attacks. We have identified key design flaws within the protocol and successfully demonstrated a MIXup attack, resulting in the theft of user tokens and unauthorized access to user data in an offline attack scenario using the ASP environment. The attack was performed on accounts belonging to popular platforms, and the outcomes varied based on the characteristics of the session created by the identity provider.

It is worth noting that most renowned platforms have implemented measures to safeguard against redirect attacks by introducing browser-generated session values (routing fingerprints). They have also incorporated additional protection mechanisms, such as user confirmation via phone numbers or alternative email addresses. However, the accessed codes still present the possibility of conducting a redirect attack by deceiving the victim through a fraudulent page aimed at confirming the account and capturing return information within the user session. These findings underscore

the importance of implementing enhanced protection measures in the future.

REFERENCES

- [1] L. Smith, J., & Johnson, "The Privacy Implications of Single Sign-On Services," in Proceedings of the 2019 CHI Conference on Human Factors in Computing Systems, 2019, pp. 1–14.
- [2] A. Leung, R., & Datta, "Single Sign-On as Surveillance Infrastructure: Lessons from Google's SSO Service," in Proceedings on Privacy Enhancing Technologies, 2019, pp. 4–22.
- [3] F. Roesner, T. Kohno, and D. Wetherall, "Detecting and Defending Against {Third-Party} Tracking on the Web," in 9th USENIX Symposium on Networked Systems Design and Implementation (NSDI 12), 2012, pp. 155–168.
- [4] Z. Li, W. He, D. Akhawe, and D. Song, "The {Emperor's} new password manager: Security analysis of web-based password managers," in 23rd USENIX Security Symposium (USENIX Security 14), 2014, pp. 465–479.
- [5] & H. Rahman, M. S., Kagal, L., "Rahman, M. S., Kagal, L., & Hendler, J. (2018). Sharing personal data while preserving privacy in social networking: Balancing user control and usability," Comput. Secur., vol. 77, pp. 109–124, 2018.
- [6] M. E. Nergiz, M. E., Mitchell, C. J., & Nergiz, "An empirical analysis of Single Sign-On Account Hijacking and session management on the web," J. Inf. Secur. Appl., vol. 47, pp. 158–169, 2019.
- [7] H. Yang, Z., Xing, L., & Chen, "Understanding and enhancing the privacy of Single Sign-On: A survey," Comput. Commun., vol. 145, pp. 1–17, 2019.
- [8] D. Fett, D., Küpser, A., & Schröder, "Security analysis of Single Sign-On protocols: Comparing SAML, OAuth, and OpenID Connect," in In International Conference on Trust and Privacy in Digital Business, 2019, pp. 1–17.
- [9] W. Li and C. J. Mitchell, "User Access Privacy in OAuth 2.0 and OpenID Connect," 2020 IEEE European Symposium on Security and Privacy Workshops (EuroS&PW), Genoa, Italy, 2020, pp. 664-6732, doi: 10.1109/EuroSPW51379.2020.00095
- [10] N. Ahmad, F., Iqbal, M., Ahmad, J., & Alrajeh, "Security and privacy analysis of Single Sign-On protocols: A systematic literature review," J. Inf. Secur. Appl., vol. 60, 2021.
- [11] J. Zuo, C., Li, L., & Zeng, "Security and privacy analysis of Single Sign-On: A systematic review and meta-analysis," Futur. Gener. Comput. Syst., vol. 119, pp. 103–116, 2021.
- [12] L. F. Li, Y., Hong, J. I., & Cranor, "A case study of privacy-sensitive features in a web authentication system," in In Proceedings of the 9th ACM SIGCOMM conference on Internet measurement conference, 2010, pp. 365–378.
- [13] L. Wang, X., Lin, Z., Wang, X., Zhou, Y., & Xing, "A comprehensive study of OAuth security issues in Android apps," in In Proceedings of the 33rd Annual Computer Security Applications Conference, 2017, pp. 312–325.
- [14] M. G. Meland, P. H., Jensen, C. D., & Jaatun, "Privacy aspects of attribute sharing in single sign-on solutions," in In International Conference on Availability, Reliability, and Security, 2017, pp. 57–74.
- [15] P. J. Taylor, T. Dargahi, A. Dehghantanha, R. M. Parizi, and K.-K. R. Choo, "A systematic literature review of blockchain cyber security," Digit. Commun. Networks, vol. 6, no. 2, pp. 147–156, 2020. <https://doi.org/10.1016/j.dcan.2019.01.005>
- [16] C. Mainka, V. Mladenov, J. Schwenk and T. Wich, "SoK: Single Sign-On Security — An Evaluation of OpenID Connect," 2017 IEEE European Symposium on Security and Privacy (EuroS&P), Paris, France, 2017, pp. 251-266, doi: 10.1109/EuroSP.2017.32.
- [17] W. Li and C. J. Mitchell, "Analysing the Security of Google's implementation of OpenID Connect," in DIMVA 2016: Proceedings of the 13th International Conference on Detection of Intrusions and Malware, and Vulnerability Assessment – vol. 9721J, pp.357–376, 2016, https://doi.org/10.1007/978-3-319-40667-1_18

- [18] V. Mladenov, C. Mainka, and J. Schwenk, "On the security of modern single sign-on protocols: Second-order vulnerabilities in openid connect," arXiv Prepr. arXiv1508.04324, 2015.
- [19] C. Mainka, V. Mladenov, and J. Schwenk, "Do Not Trust Me: Using Malicious IdPs for Analyzing and Attacking Single Sign-on," 2016 IEEE European Symposium on Security and Privacy (EuroS&P), Saarbruecken, Germany, 2016, pp. 321-336, doi: 10.1109/EuroSP.2016.33.
- [20] J. Navas and M. Beltrán, "Understanding and mitigating OpenID Connect threats," *Comput. & Secur.*, vol. 84, pp. 1-16, 2019, <https://doi.org/10.1016/j.cose.2019.03.003>.
- [21] D. Fett, R. Küsters and G. Schmitz, "The Web SSO Standard OpenID Connect: In-depth Formal Security Analysis and Security Guidelines," 2017 IEEE 30th Computer Security Foundations Symposium (CSF), Santa Barbara, CA, USA, 2017, pp. 189-202, doi: 10.1109/CSF.2017.20.
- [22] A. S. K. Maqbool, A. Ali, "Evaluation of OAuth 2.0 Vulnerabilities in Android Applications," in in Proceedings of the 2020 ACM/IEEE International Symposium on Empirical Software Engineering and Measurement (ESEM '20), 2020, pp. 1-6.
- [23] A. Kountouras and G. Frantzeskou, "An Empirical Study of Security Misconfiguration in Mobile OAuth.," in in Proceedings of the 2019 ACM SIGSAC Conference on Computer and Communications Security (CCS '19), 2019, pp. 2283-2300.
- [24] J. Richer and A. Sanso, "Security Analysis of OAuth 2.0," in in Proceedings of the 2015 ACM SIGSAC Conference on Computer and Communications Security (CCS '15), 2015, pp. 197-208.
- [25] B. Braithwaite and A. Doupé, "Breaking the OAuth Protocol," in in Proceedings of the 2014 ACM SIGSAC Conference on Computer and Communications Security (CCS '14), 2014, pp. 676-687.
- [26] P. Pereira, T. Felber, P., & Esteves-Veríssimo, "SoK: OAuth 2.0 and Beyond: Current Vulnerabilities, Limitations, and Ongoing Improvements," in Proceedings of the 2018 IEEE European Symposium on Security and Privacy (EuroS&P), 2018, pp. 415-430.
- [27] K. Küsters, R., & Kifayat, "Formal Security Analysis of OpenID Connect," in Proceedings of the 2016 IEEE 30th Computer Security Foundations Symposium (CSF), 2016, pp. 189-202.
- [28] A. Sanchez-Aguilar, J., Marin, A., & Toval, "Security Modeling of Single Sign-On Protocols: A Comparative Survey," *J. Netw. Comput. Appl.*, vol. 159, 2020.
- [29] S. Vetrivelan, S., Parameswaran, M., & Sen, "Mobile Single Sign-On Using OpenID Connect: A Study on Design and Security Measures," in Proceedings of the 2019 International Conference on Wireless Communications, Signal Processing and Networking (WiSPNET), 2019, pp. 1850-1854.
- [30] J. Alshehri, S., Nguyen, D., & Indulska, "Empirical Investigation of OpenID Connect: Security, Privacy, and Usability," in Proceedings of the 2020 IEEE International Conference on Smart Cloud (SmartCloud), 2020, pp. 16-23.
- [31] H. Sun, Y., Yang, M., & Gu, "A Survey on OAuth-Based Single Sign-On (SSO) Protocol," in Proceedings of the 2018 3rd International Conference on Information Science and Systems (ICISS), 2018, pp. 467-472.
- [32] M. Z. Khan, A. Y., & Shafiq, "Security Analysis of OAuth 2.0 Framework for Mobile Applications," in Proceedings of the 2019 10th International Conference on Information and Communication Systems (ICICS), 2019, pp. 48-54.
- [33] V. Mladenov and C. Mainka, "OpenID connect-security considerations," Bochum, January 2017, Ruhr-Universität Bochum, 2017.

A Patrol Platform Based on Unmanned Aerial Vehicle for Urban Safety and Intelligent Social Governance

Ying Yang¹, Rui Ma^{2*}, Fengjiao Zhou³

Department of Party Committee, Chengdu polytechnic, Chengdu, Sichuan, China¹

School of Health and Rehabilitation, Chengdu University of Traditional Chinese Medicine, Chengdu, Sichuan, China²

School of Social Science, University Sains Malaysia, Pulau, Pinang, Gelugor, Malaysia³

Abstract—Urban patrols can detect emergencies in a timely manner and collect information, which helps to improve the quality of services in the city and enhance the comfort of residents. This study proposes the use of IoT-based drones for urban patrol tasks, aiming to explore the potential applications of drones in smart city governance. The main technical challenge in the process of urban patrols by drones is how to plan a flight path for them. Therefore, this article first designs a smart patrol system based on drones and Internet of Things (IoT). Meanwhile, as information collection is an important aspect of urban patrol tasks, a mathematical model with the goal of maximizing information collection has been established to provide cost-effective patrol services. On this basis, in order to improve the accuracy of crow search algorithm (CSA), differential crow search strategy and variable flight step size are designed. In addition, the Levy flight strategy is introduced into the traditional CSA algorithm, and an improved crow search algorithm (ICSA) is proposed. Finally, a corresponding simulation environment was established based on the actual urban scene and compared with other algorithms. The numerical results indicate that compared with the other three swarm intelligence algorithms, the algorithm designed in this paper has more superiority.

Keywords—Patrol drones; trajectory planning; smart city governance; crow search algorithm; swarm intelligence algorithm

I. INTRODUCTION

With the development of cutting-edge technologies in the field of artificial intelligence such as the Internet of Things (IoT), digital twins (DT), and swarm intelligence, a foundation has been provided for the implementation of smart cities. Smart social/cities governance (also known as smart social/cities management), as an important application scenario of smart cities, is a potential goal for urban managers and related researchers [2]. As an advanced intelligent robot, unmanned aerial vehicles (UAVs) can provide many reliable services for smart city scenarios, helping to achieve smart city goals at low cost and low energy consumption [3]. In addition to using drones [1] to provide reliable communication services for smart city scenarios in [4], drones can be used to comprehensively monitor urban facilities, transportation, and the environment. For example, in [5], drones are used to monitor roads in cities, while in [6], drones are used to monitor the environment of cities. Another potential application of drones in smart city scenarios is patrol missions [7]-[8]. During

the patrol process, drones are equipped with various sensors and cameras, which can collect relevant data of the city and provide timely feedback to the management department, providing decision-making support for urban managers, thereby improving the quality of the urban environment and the quality of life of residents.

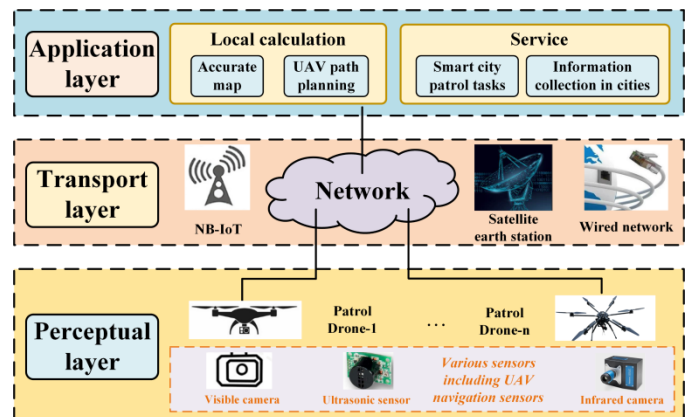


Fig. 1. IoT-based UAV patrol framework.

When deployed in the real world, drones typically require the use of technologies such as IoT to interact with the human world. Therefore, Fig. 1 shows the IoT based unmanned aerial vehicle patrol framework designed by this study. Within this framework, before conducting patrols, the trajectory planner needs to first plan a global trajectory for the drone based on the patrol range, the three-dimensional environment, and geometric model of the UAV. However, in [9], a trajectory planning model for drones in two-dimensional space was developed with the goal of minimizing the length of the drone's trajectory, without considering the pitch angle constraint of the drone. In [10], a trajectory planning model for unmanned aerial vehicles in a three-dimensional mountainous environment was established, but it did not take into account the requirements of patrol tasks for information collection. The above mathematical models are not applicable to the problem of drone patrol trajectory planning in urban market environments. Therefore, this study pays special attention to the trajectory planning problem of patrol drones, establishes an accurate mathematical model for patrol drones in smart city scenarios, and designs an improved swarm intelligence algorithm based

*Corresponding Author.

on CSA algorithm. The main contributions of this study are summarized as follows:

- This study introduces IoT and DT into smart city patrol scenarios, designs an IoT based UAV patrol framework, and describes the working mechanism of the DT based UAV patrol platform, aiming to embed the drone city patrol platform into smart city scenes.
- Based on the operational mechanism of the digital twin patrol platform, a geometric model of patrol drones and a multi-objective mathematical model of urban patrol tasks were established, and a digital twin drone for urban patrol tasks was constructed.
- Based on the DE algorithm and CSA algorithm, corresponding improvement strategies were designed, and a novel differential evolution-based crow search algorithm (DE-CSA) was designed to improve the performance of the patrol drone trajectory planner.
- Six test functions were used to test the GWO, GA, CSA, and DE-CSA algorithms. From the two indicators of mean and standard deviation, the DE-CSA algorithm performed the best; Furthermore, based on real urban scenarios, relevant computational experiments were conducted, and the data results showed that compared with GWO, GA, and CSA algorithms, the DE-CSA algorithm has higher convergence accuracy.

The remaining parts of this study are arranged as follows. In Section II, research related to patrol drones is reviewed; Section III establishes a mathematical model for UAV used for smart city patrol task; In Section IV, an improved CSA algorithm is designed; Section V presents the simulation experiment results. Finally, the full text is summarized in Section VI.

II. LITERATURE REVIEW

When using drones to perform patrol tasks in smart city scenarios, it mainly includes two parts. The first part is to allocate drones based on all patrol areas, ensuring that each area can be covered. This is the previous stage of patrol drone trajectory planning [7]. The other step is to plan a flight trajectory for the patrol drone based on the three-dimensional environment of the area it needs to patrol, which needs to meet the goals of collision free and patrol tasks. Therefore, this article reviews relevant research from three aspects: urban patrols, drone trajectory planning, and the application of swarm intelligence algorithms in drone trajectory planning. The aim is to summarize and summarize the goals of urban patrols, mathematical models of drones, and trajectory planning algorithms.

A. The Application of UAV in Urban Patrol

As previously mentioned, relevant researchers have explored the application of drones in smart city communication [4], road or environmental monitoring [5]-[6], disaster management [11], and distribution [12]. It should be pointed out that when using drones to detect roads and environments, the main objective of mathematical models is to collect or organize information [13]. For example, in [14], drones were

used to collect environmental information at the dock, and the mathematical model required drones to fly over all detection nodes and use the shortest flight distance. In [15], UAVs were used to patrol transmission lines in a city with the goal of maximizing the coverage of the patrol area. Reference [16], on the other hand, uses ground vehicles in conjunction with UAVs to patrol roads, and similar to [14], the mathematical model requires the UAVs to fly over all patrol nodes. In [17], a drone scheduling model for scenic spot patrols was established, which aims to minimize the flight length of drones while minimizing the number of drones, similar to the drone scheduling problem in [7]. From the above research, it can be concluded that the main goal of UAVs during patrol missions is to collect ground information to the maximum extent possible. However, so far, no research has been conducted on community patrol tasks. In addition, the above research on drone patrols cannot be extended to three-dimensional space.

B. A Mathematical Model for UAV Trajectory Planning

Specifically, the establishment of a mathematical model for inspection drones can be divided into two parts: geometric modeling and problem modeling, based on the working mechanism of the digital twin patrol platform. The geometric model is mainly based on the physical performance and flight environment of drones, including obstacle modeling, drone dynamics modeling, and route constraints [18]. The problem model is an objective function composed of one or several objectives, including the shortest path, minimum energy consumption, or minimum flight time [19]. Geometric modeling includes three parts: mathematical model construction of drones, environmental perception, and map construction. In order to plan safe and effective trajectories, drones need to perceive the environment and construct maps, mainly using advanced sensor technology and data fusion technology [20]. Due to the development of digital twin cities, high-precision three-dimensional maps of cities have been established. Therefore, this study focuses on the construction of mathematical models for drones.

The author in [21] studied the trajectory planning problem of ground drones in a two-dimensional environment, which aimed to plan a set of trajectories for a drone cluster. However, the geometric model of the ground drones established did not consider all the physical performance of the drones. In addition, the problem model established in [21] only focuses on the shortest trajectory and cannot be applied to patrol tasks based on drones. The author in [22] proposed a trajectory planning method in three-dimensional space, but it sets the Z-coordinate of the drone trajectory point as a fixed value, which is essentially still trajectory planning in two-dimensional space. The established mathematical model still does not consider the pitch angle constraint of the drone. In addition, it only focuses on the single target of the shortest trajectory. In [23], a trajectory planning scheme for UAV in two-dimensional space was proposed, and the established problem model also aimed to minimize the trajectory. The author in [24] focuses on UAV-based power grid inspection tasks. Similar to [15], there are fewer obstacles during the process of patrolling the power grid, and the mathematical model established is also not applicable to urban patrol tasks. Therefore, it is necessary to establish a

mathematical model that simultaneously focuses on information collection and trajectory length.

C. A Swarm Intelligence Algorithm-Based Trajectory Planner

The algorithms used for UAV trajectory planners can be specifically divided into three categories based on their functions: static obstacle avoidance algorithms, dynamic trajectory planning algorithms, and global trajectory planning algorithms [25]. During flight, UAVs may encounter various obstacles such as buildings and trees. How to effectively avoid these static obstacles is an important issue in drone trajectory planning [26]. In addition, in practical applications, UAVs may also encounter dynamic obstacles during flight, such as birds or pedestrians, which requires drones to be able to plan new trajectories in real time to cope with environmental changes [27]. In addition, the global trajectory planning algorithm for drones is to plan a trajectory from the starting point to the endpoint based on the global map using the algorithm [28]. This article focuses on the global trajectory planning algorithm considering static obstacles.

The global trajectory planning algorithm is the core of the drone trajectory planner, and common trajectory planning algorithms include graph search-based algorithms, optimization-based algorithms, sampling-based algorithms, etc. [29]. A trajectory planning model based on graph search: This model discretizes the environmental space into a series of nodes and uses graph search algorithms (such as A* algorithm, Dijkstra algorithm, etc.) to find the optimal path between these nodes. This model is simple and easy to implement, but it has lower computational efficiency when dealing with complex environments or high-dimensional spaces [30]. The sampling-based trajectory planning model randomly samples in the environmental space, constructs paths between sampling points, and finally optimizes the path to obtain the optimal trajectory. This model can handle complex environments and has high computational efficiency, but it cannot guarantee finding the global optimal solution [10]. The learning-based trajectory planning model learns trajectory planning strategies through machine learning methods. This model can handle complex environments and high-dimensional spaces, and can continuously improve trajectory planning strategies through learning, but it requires a large amount of training data and computational resources [31].

Unlike the above three methods, the trajectory planning model based on swarm intelligence transforms the trajectory planning problem into an optimization problem, and obtains the optimal trajectory by solving the optimization problem [32]. When solving optimization problems, swarm intelligence algorithms can not only consider multiple objectives but also find the optimal solution in large-scale complex problems. Representative algorithms include genetic algorithm (GA) [33] and grey wolf optimizer (GWO) [34]. Therefore, at present, more and more swarm intelligence algorithms are being applied to UAV trajectory planning problems. In [35], an improved differential evolution (DE) algorithm was designed and applied to the mathematical model of unmanned aerial vehicle trajectory planning, aiming to improve the convergence accuracy of the DE algorithm. Similarly, an improved DE algorithm in [36] was used for the deployment of multiple drones and achieved good results. This is because the

differential strategy in the DE algorithm can help the DE algorithm escape from local optima.

The GWO algorithm has also been applied in the field of drone trajectory planning. In [37], a reinforcement learning strategy based GWO algorithm was designed and applied to drone trajectory planning problems. In [38], the GWO algorithm is applied to the trajectory planning problem for transmission line inspection tasks. The above two studies have successfully applied the GWO algorithm to the trajectory planning problem of unmanned aerial vehicles. Reference [39] proposed an improved GA algorithm and applied it to the target coverage problem. The performance of GA algorithm and Particle Swarm Optimization (PSO) algorithm in solving trajectory planning problems was compared in [27], and experimental results showed that GA algorithm has more potential compared to PSO algorithm. In addition, as a novel swarm intelligence algorithm, there is currently no research testing the performance of CSA in solving unmanned aerial vehicle trajectory planning problems. Therefore, this article improves the CSA algorithm and successfully applies the improved CSA algorithm (ICSA, also known as DE-CSA) to the trajectory planning problem of unmanned aerial vehicles.

III. MODEL

A. Problem Definition

Before establishing the model, we first describe the patrol problem in smart cities. This study uses quadcopter drones to patrol communities within cities, aiming to detect emergencies (such as accidental injuries) and ensure the safety of community residents, while providing timely information. According to [13]-[16], UAVs have two main targets during patrol: maximizing information collection and minimizing the length of flight trajectories. Before flying, the trajectory planner for patrolling UAVs needs to determine the optimal patrol trajectory based on camera constraints. In addition, the trajectory of UAV needs to meet physical performance constraints such as the maximum rotation angle, maximum tilt angle, and maximum flight distance of the drone.

According to the smart city framework established based on digital twin (DT) technology in, this study describes the working mechanism of the DT-based smart patrol platform, as shown in Fig. 2. In the operation process of the DT-based intelligent patrol platform, a large number of sensors need to be used to collect information, and the collected information needs to be collected, classified, and organized. Furthermore, based on the requirements of smart city patrol tasks and the physical performance of patrol drones, a corresponding digital twin model is established. Finally, design experiments and simulation simulations are conducted to feedback the trajectory of patrol drones to the real world. In this study, the data perception, data modeling (geometric model and problem model), and data simulation of DT-based patrol platforms in smart cities were demonstrated. Intended to further explain the operating mechanism of the smart patrol platform, and also to further demonstrate the application of advanced artificial intelligence technologies such as swarm intelligence algorithms in the smart patrol platform.

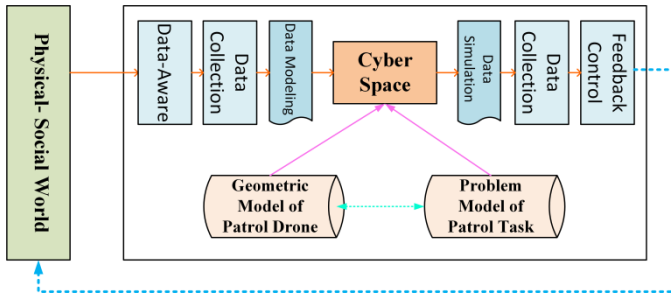


Fig. 2. The working mechanism of smart patrol platform based on digital twins.

B. Data-Aware

In order to plan a safe and effective trajectory, the smart patrol platform based on drones needs to perceive the environment and build maps, mainly using advanced sensor technology and data fusion technology. Fig. 3 shows a map of digital twins in the context of a smart city.

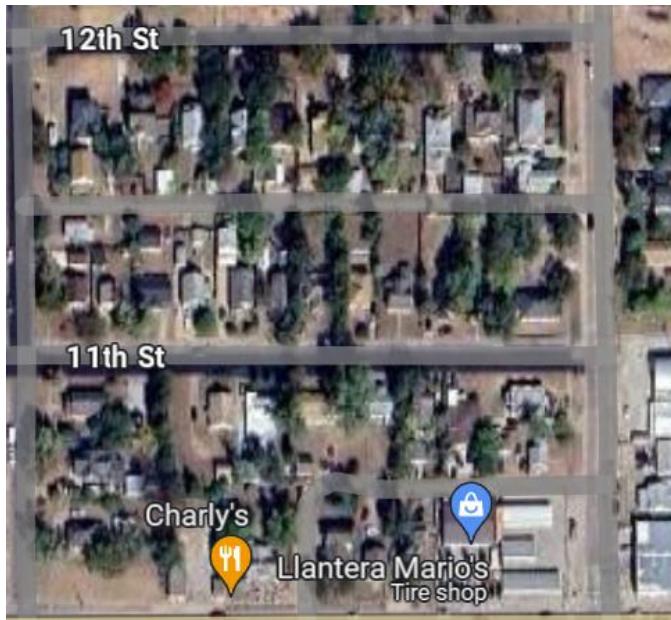


Fig. 3. The map of smart cities.

C. Mathematical Model

1) *Geometric model*: Geometric modeling includes the establishment of a drone flight space map model, the establishment of a drone mathematical model, and the establishment of an airborne camera model, as shown below:

$$C_b = [x_{cb1}, x_{cb2}, y_{cb1}, y_{cb2}, z_{cb1}, z_{cb2}] \quad (1)$$

Eq. (1) shows the establishment of building maps in smart cities, where $\forall b \in B$ represents the set of obstacles in the map.

$$Q_a = [x_{qa}, y_{qa}, z_{qa}] \quad (2)$$

Eq. (2) is the coordinates that make up urban road grid $a \in A$.

$$l_k / T_k \leq v_{\max} \quad (3)$$

$$\sum_{k \in K} T_k \leq T_{\max} \quad (4)$$

$$l_k = \sqrt{(x_{k+1} - x_k)^2 + (y_{k+1} - y_k)^2 + (z_{k+1} - z_k)^2} \quad (5)$$

Eq. (3)-(5) together constitutes the digital twin model of unmanned aerial vehicles. Eq. (3) is the maximum flight speed constraint of the drone, where v_{\max} is the maximum flight speed of the drone; l_k is the distance from the drone's track point k to the drone's track point $k+1$; T_k is the flight time of the drone from the waypoint to the drone's waypoint. Eq. (4) is the battery capacity constraint of the drone, and T_{\max} is the maximum flight time of the drone.

$$\sqrt{(x_{qa} - x_k)^2 + (y_{qa} - y_k)^2 + (z_{qa} - z_k)^2} \leq L_{\max} \quad (6)$$

Eq. (6) forms a digital twin model for airborne cameras, and constrains the maximum shooting distance of the camera, where L_{\max} is the maximum shooting distance of the camera.

2) *Problem modeling*: When drones patrol in a smart city environment, they aim to complete patrols of all areas with the shortest possible cost. According to [35]-[39], the cost of drone trajectory planning includes two types: time cost and path length cost. Therefore, this article selects path length cost as one of the objectives in the multi-objective function. In order to reduce the difficulty of solving the problem, the goal of maximizing the collection of information in the patrol area is established as the corresponding penalty function. When there is a road grid that is not patrolled, the value of the penalty function will increase, otherwise the value of the penalty function will decrease. The modeling of the problem is as follows.

$$\min f = \sum_{k \in K} l_k \times (N_{B_{\max}} - \sum E_b) \quad (7)$$

$$E_b \in \{0, 1\} \quad (8)$$

Eq. (7) is the objective function of the problem, where $(N_{B_{\max}} - \sum E_b)$ is the penalty function and $N_{B_{\max}}$ is the number of grids that make up the road. As shown in Eq. (8), E_b is a 0-1 variable. When the camera can capture the road grid $\forall b \in B$, $E_b = 1$; Otherwise, $E_b = 0$.

IV. ALGORITHM DESIGN

A. Algorithm Introduction

The origin of swarm intelligence technology originated from Reynolds' research on the Bodies project, and after continuous evolution and development, swarm intelligence algorithms including GWO, GA, and CSA have emerged [33]-[34]. The swarm intelligence algorithm is a cluster of

algorithms based on group behavior and intelligence, which simulates the interaction and cooperation between individuals in a group to achieve the ability to solve problems collaboratively. These algorithms draw inspiration from collaborative behaviors in biological populations, such as bird colonies, ant colonies, fish colonies, etc., and achieve the overall intelligence of the population through information exchange, interaction, and division of labor among individuals. This technology has shown excellent performance in solving the large-scale multi-objective problem. Therefore it is widely used in unmanned aerial vehicle trajectory planning.

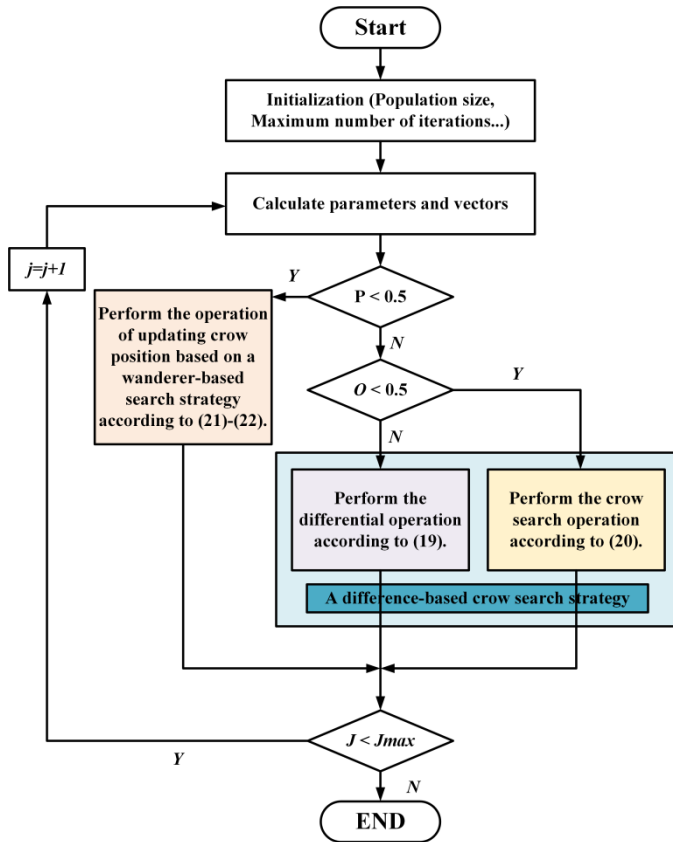


Fig. 4. The flowchart of the DE-CSA algorithm.

The CSA algorithm is a novel swarm intelligence algorithm proposed in 2016, which mimics the hidden food, tracking, and deceptive behavior among crow individuals in a crow population. It performs global search by perceiving probability and flight distance. The CSA algorithm has the advantages of simple search strategy and fewer parameters. In addition, CSA algorithm is a global search algorithm that can find the optimal solution throughout the entire search space. At the same time, CSA algorithm has high search efficiency and can find better solutions in a short time. Although CSA algorithm can perform global optimization, it is determined by perceptual probability. Therefore, when the parameter selection is not appropriate, CSA may fall into local optima and cannot find the global optimal solution. At the same time, this also leads to CSA being unable to optimize in local space, resulting in low convergence accuracy.

B. DE-CSA Algorithm

Due to the concise search method of CSA, it is easy to fall into local optima and other problems when solving large-scale and complex problems. However, differential evolution (DE) algorithms optimize problems through mutation, crossover, and selection operations [14]-[15]. Therefore, it is possible to combine the DE algorithm and CSA algorithm to design a DE based CSA algorithm (DE-CSA) for solving the trajectory planning problem of patrol drones. In the DE-CSA algorithm developed in this study, a flight step size that changes with the number of iterations, a difference-based crow search strategy, and a wanderer-based search strategy were designed to improve the convergence accuracy of the CSA algorithm. Fig. 4 illustrates the flowchart of the DE-CSA algorithm, which (also known as the ICSA algorithm) has the following specific steps.

1) *Initialize the location of the crow population:* To change the default, adjust the template as follows. Initialize population size R_{max} . Use traditional trajectory planning methods to plan the several trajectories of UAV, making them equal to the population size. Each track represents a crow individual $Track(r, j)$. Initialize the maximum number of iterations J_{max} . Initialize the differential scaling factor F . Initialize crow population position GC .

The definition of the crow individual $Track(r, j)$ is shown in Eq. (9).

$$Track(r, j) = \{T(r, j)_1, T(r, j)_2, \dots, T(r, j)_D\} \quad (9)$$

where r represents the r -th individual, and j represents the j -th iteration process, D represents the individual's dimension.

The definition of the crow population position GC is shown in Eq. (10).

$$GC = \{Track(1), Track(2), \dots, Track(R_{max})\}^T \quad (10)$$

where

$$Track(r) = Track(r, j)$$

2) *Population assessment:* Evaluate the objective function values of each crow of individual in the crow population and find the optimal solution to the optimization problem according to Eq. (11). The specific process of this step is shown in Algorithm 1. Among them, f_{best} is the optimal fitness function value in the crow population. $Track_{best}$ is the best crow individual in the population.

Algorithm 1

```

For  $r=1$  to  $R_{max}$  do
    Fitness = f(track(r,j))
    if Fitness <  $f_{best}$  Then
         $f_{best}$  = Fitness
         $Track_{best}$  = track(r,j)
End for
    
```

$$m(r, j) = \begin{cases} \text{Track}(r, j), & \text{if } f(\text{Track}(r, j)) \leq f(\text{Track}(r, j-1)) \\ m(r, j-1), & \text{Otherwise} \end{cases} \quad (11)$$

The definition of the *MC* is shown in Eq. (12).

$$MC = \{m(1, j), m(2, j), \dots, m(R \max, j)\}^T \quad (12)$$

where *MC* is the memory matrix of the crow population.

3) *Calculate search step size*: Calculate the flight step size *flyo* of individual crows according to Eq. (13).

$$flyo = 2.5 - \left(\frac{j}{J \max} \right)^{\frac{1}{2}} \quad (13)$$

4) *A difference-based crow search strategy*: Randomly generate a random number *P* in the [0,1] interval, and if $P \geq 0.5$, generate a random number *O* in the [0,1] interval, and perform a differential crow search operation based on Eq. (14)-(15).

If $O \geq 0.5$, perform differential operation according to Eq. (14).

$$T(r, j+1)_d = T(r1, j)_d + F \times (T(r2, j)_d - T(r3, j)_d) \quad (14)$$

where $T(r1, j)_d$, $T(r2, j)_d$, and $T(r3, j)_d$ are the *d*-th dimension of randomly selected individuals.

If $O < 0.5$, perform crow search operation according to equation (15).

$$T(r, j+1)_d = T(r, j)_d + Rand \times flyo (m(best, j)_d - T(r, j)_d) \quad (15)$$

where *Rand* is a random number in the [0,1] interval. $m(best, j)_d$ is the *d*-th dimension of the individual with the best fitness function value in matrix *MC*.

5) *A wanderer-based search strategy*: If $P < 0.5$, perform a wanderer-based search operation based on Eq. (16)-(17).

$$T(r, j+1)_d = T(r, j)_d + Rand \times flyo \times a \quad (16)$$

$$a = Rand(\sqrt{D+1}) \quad (17)$$

6) *Reevaluate the population*: Reevaluate the population based on Algorithm 1.

7) *Output result*: Calculate and determine whether the maximum number of iterations has been reached. If so, end the iteration and output the result; Otherwise, return to 3) Calculate search step size.

V. PRESENTATION OF EXPERIMENTAL RESULTS

In order to further demonstrate the performance of the DE-CSA algorithm designed in this study, the performance of the algorithm was demonstrated from two aspects. Firstly, according to [33], this study tested the DE-CSA algorithm using six test functions. In addition, this study established a corresponding simulation environment based on the map shown in Fig. 3 and used the DE-CSA algorithm to plan the trajectory of patrol drones. All the above simulation experiments were conducted on the MATLAB 2022a platform.

A. Benchmark Functions

This study used unimodal test functions (F05-F07) and multimodal test functions (F08-F10) to test the developed algorithm. Among them, F05 is called the Rosenbrock function, also known as the Valley or Banana function, with its global minimum located in a narrow parabolic valley. However, although the valley is easy to find, it is difficult to converge to the minimum. F07 is a multidimensional unimodal flat-bottomed function with random interference, and the algorithm is prone to getting stuck in local optima during operation. F08-F10 are both multimodal test functions. Among them, F09 is the Rastigin function, which has many local minima and is highly multimodal. In the two-dimensional form, the characteristic of the function image of F10 is that the external region is very flat and there is a large hole in the center. This function can also easily trap optimization algorithms into local optima. Therefore, the above test functions can test not only the local search ability of the algorithm, but also the global search ability of the algorithm.

TABLE I. TEST FUNCTIONS

| Functions | Expressions of Functions | Domian | Optimal |
|-----------|--|--------------|----------|
| F05 | $F_{05}(x) = 100 \times \sum_i [(x_{i+1} - x_i^2)^2 + (x_i - 1)^2]$ | [-30,30] | 0 |
| F06 | $F_{06}(x) = \sum_i [(x_i + 0.5)^2]$ | [-100,100] | 0 |
| F07 | $F_{07}(x) = \sum_i [i \times x_i^4 + \text{Random}[0,1]]$ | [-1.28,1.28] | 0 |
| F08 | $F_{08} = \sum_i [-x_i \sin(\sqrt{ x_i })]$ | [-500,500] | -837.966 |
| F09 | $F_{09}(x) = \sum_i [x_i^2 - 10 \times \cos(2\pi x_i) + 10]$ | [-5.12,5.12] | 10 |
| F10 | $F_{10}(x) = -20 \exp(-0.2 \sqrt{((1/n) \sum_i x_i^2)}) - \exp(1/n \cos(2\pi x_i)) + 20 + e$ | [-32,32] | 0 |

TABLE II. THE GRAPH OF THE TEST FUNCTION AND THE ITERATION CURVES OF THE FOUR ALGORITHMS ($R_{max} = 30$)

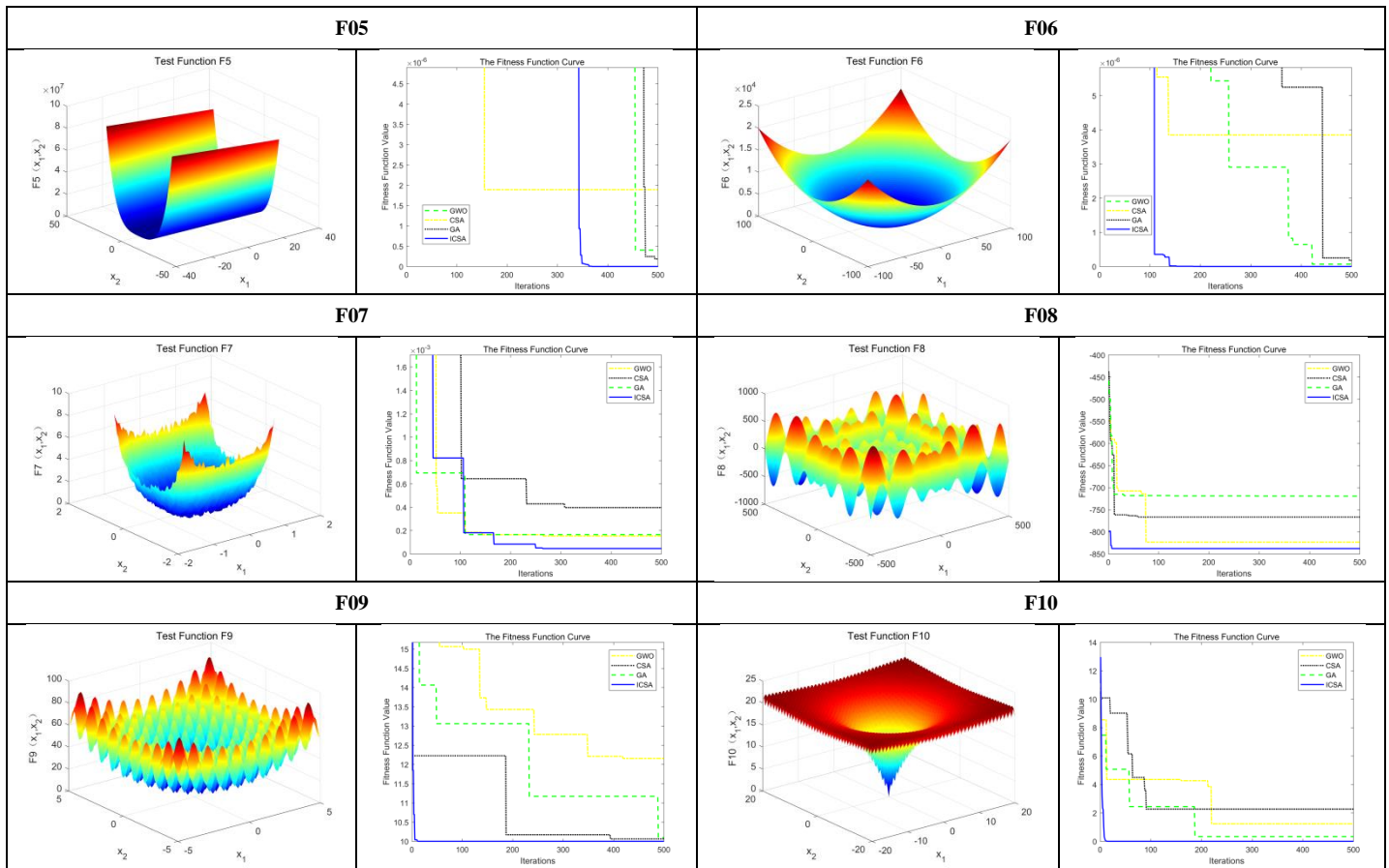


TABLE III. THE FITNESS FUNCTION VALUES OF THE TEST FUNCTION FOR FOUR ALGORITHMS RUNNING 30 TIMES ($R_{max} = 30$)

| Functions | F05 | | F06 | | F07 | | F08 | | F09 | | F10 | |
|-----------|----------------|----------------|---------------|---------------|----------------|----------------|-----------------|---------------|--------------|---------------|----------------|----------------|
| | Mean | Std | Mean | Std | Mean | Std | Mean | Std | Mean | Std | Mean | Std |
| GWO | 1.9E-06 | 5.1E-07 | 1.7E-07 | 2.4E-08 | 1.6E-04 | 2.2E-05 | -823.430 | 09.62 | 12.15 | 1.61 | 0.614 | 0.041 |
| CSA | 1.8E-07 | 1.5E-08 | 6.4E-09 | 1.9E-10 | 3.9E-04 | 6.3E-05 | -719.527 | 16.02 | 10.19 | 0.94 | 0.471 | 0.106 |
| GA | 4.0E-07 | 3.6E-08 | 3.8E-06 | 1.8E-07 | 1.6E-04 | 5.2E-05 | -766.749 | 92.47 | 10.16 | 0.56 | 0.959 | 0.797 |
| DE-CSA | 5.6E-17 | 0.6E-18 | 00E+00 | 00E+00 | 4.6E-15 | 2.5E-16 | -837.965 | 00E+00 | 10.00 | 00E+00 | 8.1E-16 | 1.6E-17 |

The CSA, GA, GWO, and DE-CSA algorithms were run 30 times in each test function. Table I shows the mathematical formulas, variable ranges, and minimum values of the six test functions F05-F10. Table II shows the convergence curves of the fitness functions during the running process of CSA, GA, GWO, and DE-CSA algorithms using each test function as the fitness function. Table III presents the operational results of CSA, GA, GWO, and DE-CSA methods.

B. Trajectory Planning Results

On this basis, in order to verify the effectiveness of the smart patrol platform designed in this study, a corresponding simulation environment was established based on the map shown in Fig. 3 and the DE-CSA algorithm was used to plan the trajectory of the patrol drone. Fig. 5 shows the patrol trajectory planned by the DE-CSA algorithm for unmanned

aerial vehicles. Fig. 6, and Fig. 7, respectively shows the optimal fitness function curves, and average fitness function curves of the four algorithms during 30 runs.

As shown in Fig. 6, during the 30 runs of GWO, GA, CSA, and DE-CSA algorithms, the optimal fitness function value of DE-CSA is 5180.07, while the optimal fitness function values of GWO, GA, and CSA algorithms are 5641.16, 5624.49, and 5781.13, respectively. As shown in Fig. 7, during 30 runs of GWO, GA, CSA, and DE-CSA algorithms, the average fitness function value of DE-CSA is 5179.53, while the average fitness function values of GWO, GA, and CSA algorithms are 5674.75, 5691.29, and 5727.05, respectively. Therefore, it can be concluded that the optimal fitness function, worst fitness function, and average fitness function solved by the DE-CSA algorithm have the best results in 30 runs, fully proving the effectiveness of the smart patrol platform.

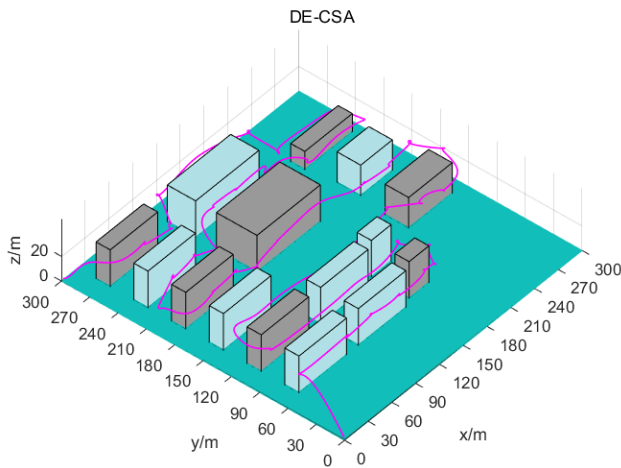


Fig. 5. The trajectory planning results of the DE-CSA.

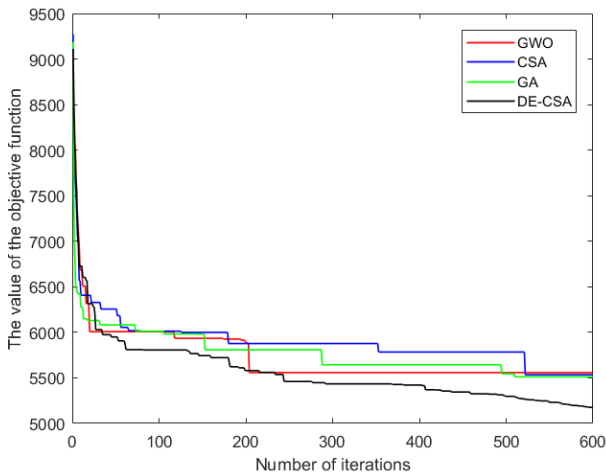


Fig. 6. The optimal fitness function curves of the four algorithms.

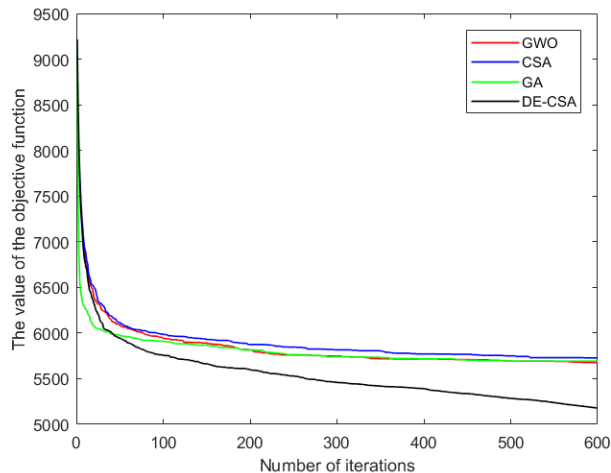


Fig. 7. The average fitness function curves of the four algorithms.

VI. CONCLUSIONS

This study constructed a smart patrol platform for smart cities and developed an improved CSA algorithm. This study expands the application of drones in smart cities, aiming to

improve the service quality of cities. The effectiveness of the platform and algorithm was demonstrated through the use of six test functions and a simulation experiment in a real scenario. The simulation results show that the DE-CSA algorithm can achieve the best results in all six test functions, whether it is the mean and standard deviation. In the experiment of drone trajectory planning, the optimal, and average values of the DE-CSA algorithm were better than the other three algorithms in 30 runs of GWO, GA, CSA, and DE-CSA algorithms. In the future research process, the focus will be on the trajectory planning problem of patrol drones in dynamic environments.

REFERENCES

- [1] S. Kumaran, V. A. Raj, S. J., and V. R. M. Raman, "IoT-based rescuerSearch and Rescue Drone for Precision Firefighting and Disaster Management," *International Journal of Advanced Computer Science and Applications*, vol. 14, no. 11, 2023, doi: 10.14569/IJACSA.2023.0141145.
- [2] L. Bundgaard and S. Borrás, "City-wide scale-up of smart city pilot projects: Governance conditions," *Technological Forecasting & Social Change*, vol. 172, pp. 121014, 2021, doi: 10.1016/j.techfore.2021.121014.
- [3] N. Mohamed, J. Al-Jaroodi, I. Jawhar, A. Idries, and F. Mohammed, "Unmanned aerial vehicles applications in future smart cities," *Technological Forecasting & Social Change*, vol. 153, pp. 119293, 2020, doi: 10.1016/j.techfore.2018.05.004.
- [4] W. Tang, H. Zhang, and Y. He, "Tractable Modelling and Performance Analysis of UAV Networks With 3D Blockage Effects," *IEEE wireless communications letters*, vol. 9, no. 12, pp. 2064–2067, 2020, doi: 10.1109/LWC.2020.3012554.
- [5] F. Outay, H. A. Mengash, and M. Adnan, "Applications of unmanned aerial vehicle (UAV) in road safety, traffic and highway infrastructure management: Recent advances and challenges," *Transportation Research. Part A, Policy and Practice*, vol. 141, pp. 116–129, 2020, doi: 10.1016/j.tra.2020.09.018.
- [6] S.-I. Park and J.-S. Um, "Differentiating carbon sinks versus sources on a university campus using synergistic UAV NIR and visible signatures," *Environmental Monitoring and Assessment*, vol. 190, no. 11, pp. 652–12, 2018, doi: 10.1007/s10661-018-7003-x.
- [7] S. Rajan, K. Sundar, and N. Gautam, "Routing Problem for Unmanned Aerial Vehicle Patrolling Missions - A Progressive Hedging Algorithm," *Computers & Operations Research*, vol. 142, pp. 105702, 2022, doi: 10.1016/j.cor.2022.105702.
- [8] Y. Wang, Y. Yue, M. Shan, L. He, and D. Wang, "Formation Reconstruction and Trajectory Replanning for Multi-UAV Patrol," *IEEE/ASME Transactions on Mechatronics*, vol. 26, no. 2, pp. 719–729, 2021, doi: 10.1109/TMECH.2021.3056099.
- [9] J. I. Vazquez-Gomez, M. Marciano-Melchor, L. Valentin, and J. C. Herrera-Lozada, "Coverage Path Planning for 2D Convex Regions," *Journal of Intelligent & Robotic Systems*, vol. 97, no. 1, pp. 81–94, 2020, doi: 10.1007/s10846-019-01024-y.
- [10] H. Liu, Y. Sun, N. Pan, Q. Chen, X. Guo, D. Pan, "Multi-UAV Cooperative Task Planning for Border Patrol based on Hierarchical Optimization" *Journal of Imaging Science and Technology*, vol.65, pp. 040402-1-040402-8, 2021. doi: 10.2352/J.ImagingSci.Technol.2021.65.4.040402.
- [11] J. Fernandez Galarreta, N. Kerle, and M. Gerke, "UAV-based urban structural damage assessment using object-based image analysis and semantic reasoning," *Natural Hazards and Earth System Sciences*, vol. 15, no. 6, pp. 1087–1101, 2015, doi: 10.5194/nhess-15-1087-2015.
- [12] H. Liu, Y.P. Tsang, C.K.M. Lee, "A cyber-physical social system for autonomous drone trajectory planning in last-mile superchilling delivery," *Transportation Research Part C: Emerging Technologies*, vol. 158, pp. 104448, 2024, doi: 10.1016/J.TRC.2023.104448.
- [13] Y. Zhou, T. Rui, Y. Li, and X. Zuo, "A UAV patrol system using panoramic stitching and object detection," *Computers & Electrical*

- Engineering, vol. 80, pp. 106473, 2019, doi: 10.1016/j.compeleceng.2019.106473.
- [14] L. Shen et al., "Synergistic path planning for ship-deployed multiple UAVs to monitor vessel pollution in ports," *Transportation Research. Part D, Transport and Environment*, vol. 110, pp. 103415, 2022, doi: 10.1016/J.TRD.2022.103415.
- [15] Z. Li, H. Wu, Q. Wang, W. Wang, S. Suzuki, and A. Namiki, "Small UAV Urban Overhead Ground Wire Autonomous Correction Inspection System Based on Radar and RGB Camera," *IEEE Sensors Journal*, vol. 24, no. 5, pp. 5593-5608, 2023, doi: 10.1109/JSEN.2023.3317076.
- [16] B. Xu, K. Zhao, Q. Luo, G. Wu, and W. Pedrycz, "A GV-drone arc routing approach for urban traffic patrol by coordinating a ground vehicle and multiple drones," *Swarm and Evolutionary Computation*, vol. 77, pp. 101246, 2023, doi:10.1016/J.SWEVO.2023.101246.
- [17] Y. D. Ko and B. D. Song, "Application of UAVs for tourism security and safety," *Asia Pacific journal of marketing and logistics*, vol. 33, no.8, pp.1829-1843, 2021, doi: 10.1108/APJML-07-2020-0476.
- [18] M. Popović et al., "An informative path planning framework for UAV-based terrain monitoring," *Autonomous Robots*, vol. 44, no. 6, pp. 889-911, 2020, doi: 10.1007/s10514-020-09903-2.
- [19] M. Samir, S. Sharafeddine, C. M. Assi, T. M. Nguyen, and A. Ghayeb, "UAV Trajectory Planning for Data Collection from Time-Constrained IoT Devices," *IEEE transactions on wireless communications*, vol. 19, no. 1, pp. 34-46, 2020, doi: 10.1109/TWC.2019.2940447.
- [20] T. Zhou, S. M. Hasheminasab, and A. Habib, "Tightly-coupled camera/LiDAR integration for point cloud generation from GNSS/INS-assisted UAV mapping systems," *ISPRS journal of photogrammetry and remote sensing*, vol. 180, pp. 336-356, 2021, doi: 10.1016/J.ISPRJPRS.2021.08.020.
- [21] C. Ramirez-Atencia, V. Rodríguez-Fernandez, and D. Camacho, "A revision on multi-criteria decision making methods for multi-UAV mission planning support," *Expert systems with applications*, vol. 160, pp. 113708, 2020, doi: 10.1016/j.eswa.2020.113708.
- [22] H. M. Jayaweera and S. Hanoun, "A Dynamic Artificial Potential Field (D-APF) UAV Path Planning Technique for Following Ground Moving Targets," *IEEE access*, vol. 8, pp. 192760-192776, 2020, doi:10.1109/ACCESS.2020.3032929.
- [23] R. Radmanesh, M. Kumar, D. French, and D. Casbeer, "Towards a PDE-based large-scale decentralized solution for path planning of UAVs in shared airspace," *Aerospace science and technology*, vol. 105, pp. 105965, 2020, doi: 10.1016/j.ast.2020.105965.
- [24] H. Liu et al., "Study on UAV Parallel Planning System for Transmission Line Project Acceptance Under the Background of Industry 5.0," *IEEE Transactions on Industrial Informatics*, vol. 18, no. 8, pp. 5537-5546, 2022, doi: 10.1109/TII.2023.3142723.
- [25] T. Musil, M. Petrlík and M. Saska, "SphereMap: Dynamic Multi-Layer Graph Structure for Rapid Safety-Aware UAV Planning," *IEEE Robotics and Automation Letters*, vol. 7, no. 4, pp. 11007-11014, 2022, doi: 10.1109/LRA.2023.3195194.
- [26] T. Bruggemann, "Automated Feature-Driven Flight Planning for Airborne Inspection of Large Linear Infrastructure Assets," *IEEE Transactions on Automation Science and Engineering*, vol. 19, no. 2, pp. 804-817, 2022, doi: 10.1109/TASE.2021.3062154.
- [27] J. Rückin, F. Magistri, C. Stachniss and M. Popović, "An Informative Path Planning Framework for Active Learning in UAV-Based Semantic Mapping," *IEEE Transactions on Robotics*, vol. 39, no. 6, pp. 4279-4296, 2023, doi: 10.1109/TRO.2023.3313811.
- [28] S. Papaioannou, P. Kolios, T. Theocharides, C. G. Panayiotou and M. M. Polycarpou, "Integrated Guidance and Gimbal Control for Coverage Planning With Visibility Constraints," *IEEE Transactions on Aerospace and Electronic Systems*, vol. 59, no. 2, pp. 1276-1291, 2023, doi: 10.1109/TAES.2022.3199196.
- [29] H. V. Nguyen, H. Rezatofghi, B. -N. Vo and D. C. Ranasinghe, "Online UAV Path Planning for Joint Detection and Tracking of Multiple Radio-Tagged Objects," *IEEE Transactions on Signal Processing*, vol. 67, no. 20, pp. 5365-5379, 2019, doi: 10.1109/TSP.2019.2939076.
- [30] N. Bashir, S. Boudjit and G. Dauphin, "A Connectivity Aware Path Planning for a Fleet of UAVs in an Urban Environment," *IEEE Transactions on Intelligent Transportation Systems*, vol. 24, no. 10, pp. 10537-10552, 2023, doi: 10.1109/TITS.2023.3280995.
- [31] N. Bono Rossello, R. F. Carpio, A. Gasparri and E. Garone, "Information-Driven Path Planning for UAV With Limited Autonomy in Large-Scale Field Monitoring," *IEEE Transactions on Automation Science and Engineering*, vol. 19, no. 3, pp. 2450-2460, 2022, doi: 10.1109/TASE.2021.3085365.
- [32] Y. Wu, K. H. Low and C. Lv, "Cooperative Path Planning for Heterogeneous Unmanned Vehicles in a Search-and-Track Mission Aiming at an Underwater Target," *IEEE Transactions on Vehicular Technology*, vol. 69, no. 6, pp. 6782-6787, 2020, doi: 10.1109/TVT.2020.2991983.
- [33] Qihua Pan, "Adaptive Gray Wolf Optimization Algorithm based on Gompertz Inertia Weight Strategy" *International Journal of Advanced Computer Science and Applications(IJACSA)*, vol. 14, no. 11, 2023, doi: 1014569/IJCSA.2023.0141120.
- [34] Shereen Alfayoumi, Neamat Eltazi and Amal Elgammal, "AI-Driven Optimization Approach Based on Genetic Algorithm in Mass Customization Supplying and Manufacturing" *International Journal of Advanced Computer Science and Applications(IJACSA)*, vol. 14, no. 11, 2023, doi: 10.14569/IJACSA.2023.01411106.
- [35] Y. Yu et al., "Distributed Multi-Agent Target Tracking: A Nash-Combined Adaptive Differential Evolution Method for UAV Systems," *IEEE Transactions on Vehicular Technology*, vol. 70, no. 8, pp. 8122-8133, 2021, doi: 10.1109/TVT.2021.3091575.
- [36] H. Liu, Q. Chen, N. Pan, Y. Sun, Y. An and D. Pan, "UAV Stocktaking Task-Planning for Industrial Warehouses Based on the Improved Hybrid Differential Evolution Algorithm," *IEEE Transactions on Industrial Informatics*, vol. 18, no. 1, pp. 582-591, 2022, doi: 10.1109/TII.2021.3054172.
- [37] C. Qu, W. Gai, M. Zhong, and J. Zhang, "A novel reinforcement learning based grey wolf optimizer algorithm for unmanned aerial vehicles (UAVs) path planning," *Applied soft computing*, vol. 89, pp. 106099, 2020, doi: 10.1016/j.asoc.2020.106099.
- [38] J.-X. Lv et al., "A new hybrid algorithm based on golden eagle optimizer and grey wolf optimizer for 3D path planning of multiple UAVs in power inspection," *Neural computing & applications*, vol. 34, no. 14, pp. 11911-11936, 2022, doi: 10.1007/s00521-022-07080-0.
- [39] Y. V. Pehlivanoglu and P. Pehlivanoglu, "An enhanced genetic algorithm for path planning of autonomous UAV in target coverage problems," *Applied soft computing*, vol. 112, pp. 107796, 2021, doi: 10.1016/j.asoc.2021.107796.

Entity Relation Joint Extraction Method Based on Insertion Transformers

Haotian Qi, Weiguang Liu, Fenghua Liu*, Weigang Zhu, Fangfang Shan

College of Computer, Zhongyuan University of Technology, Zhengzhou, Henan 451191, China

Abstract—Existing multi-module multi-step and multi-module single-step methods for entity relation joint extraction suffer from issues such as cascading errors and redundant mistakes. In contrast, the single-module single-step modeling approach effectively alleviates these limitations. However, the single-module single-step method still faces challenges when dealing with complex relation extraction tasks, such as excessive negative samples and long decoding times. To address these issues, this paper proposes an entity relation joint extraction method based on Insertion Transformers, which adopts the single-module single-step approach and integrates the newly proposed tagging strategy. This method iteratively identifies and inserts tags in the text, and then effectively reduces decoding time and the count of negative samples by leveraging attention mechanisms combined with contextual information, while also resolving the problem of entity overlap. Compared to the state-of-the-art models on two public datasets, this method achieves high F1 scores of 93.2% and 91.5%, respectively, demonstrating its efficiency in resolving entity overlap issues.

Keywords—Entity relation extraction; tagging strategy; joint extraction; transformer

I. INTRODUCTION

The proliferation of the Internet has led to an explosion of textual data, presenting a challenge in extracting valuable information efficiently. Various downstream tasks such as Knowledge Graph construction, Intelligent Question Answering Systems, and Recommendation Systems rely on the extraction of pertinent information from this unstructured textual data. Consequently, the extraction of entities and relations from text has emerged as a pivotal challenge in the field of Information Extraction. Entity relation extraction, as a core task within IE, aims to distil structured ternary information, namely <subject, relation, object> [1], from raw and unstructured text. This process is essential for furnishing crucial data support for subsequent tasks. Through accurate entity relation extraction, valuable insights can be gleaned from vast volumes of textual data, thereby enhancing the quality and efficiency of downstream applications.

Early entity relation extraction tasks typically employed a pipeline approach, which involved breaking down the extraction process into two distinct sub-tasks: Named Entity Recognition and Relation Extraction [2]. Initially, an entity recognition model would be constructed to identify entity pairs, followed by the development of a semantic relation model to perform relation extraction based on the recognized entity pairs. This sequential approach facilitated model construction but often resulted in issues such as data dependency, cascading errors, and information redundancy

due to limited interaction between the tasks. In contrast, the joint extraction model integrates entity information and relations into a unified framework through joint training. This approach minimizes the drawbacks of the pipeline method by allowing for greater interaction between entity recognition and relation extraction. By simultaneously considering entity and relation information, the joint extraction model exhibits enhanced performance in handling diverse and complex semantic structures. Moreover, its parallel nature mitigates the accumulation of errors, thereby improving the overall efficiency and effectiveness of information extraction processes.

Depending on task complexity and design requirements, entity relation joint extraction can be classified into three fundamental architectures: multi-module multi-step, multi-module single-step, and single-module single-step [3]. The multi-module multi-step architecture showcases its modularity advantage in entity relation joint extraction. By segmenting tasks into multiple steps and modules, each module can concentrate on specific subtasks, thus enhancing flexibility and maintainability. However, this design can inadvertently propagate errors, diminishing overall performance and increasing training and optimization complexity. In contrast, the multi-module single-step architecture maintains modularity benefits while simplifying joint extraction. It reduces the risk of error propagation by sharing information across modules, making it suitable for handling relatively straightforward entity relation joint extraction tasks. However, it may sacrifice the capability to capture task complexity effectively. The single-module single-step architecture excels in its streamlined model structure, ease of training, and comprehensibility. However, since this approach decodes triples based on global information matrices, it may prolong decoding times and introduce issues such as excessive negative sampling.

As shown in Fig. 1, we use a rectangular solid to represent the number of computations in a single module and single-step process, with each block on the surface representing the computations between tokens under a single relationship. The red blocks indicate inefficient computations, while the green blocks represent efficient computations. Take the sample sentence “The dog got a driving license,” which contains an entity pair (The dog, owner, driving license). Assuming there are five pre-defined relationships and relationship r1 equals “owner”. From the figure, it is clear that this sample needs to be calculated $6 \times 6 \times 5$ times in total, but only 3 of those calculations are efficient. Hence, its reasoning efficiency is not high. When the sentence length increases, the number of inefficient calculations grows exponentially.

*Corresponding Author

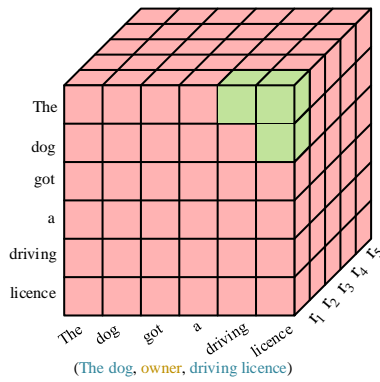


Fig. 1. Example of single-module single-step problem.

Addressing the challenges of time-consuming decoding and excessive negative sampling in current joint extraction processes, this paper proposes a single-module single-step approach based on Insertion Transformers. The method involves inserting a common token between each token of the sample during the inception stage. The model then assigns specific meanings to these tokens to recognize and delineate a triad. Subsequently, ordinary tokens are reintroduced in the vicinity of each identified special token, allowing the model to continue identifying and locating new triples following this logic until no more triples can be identified. In comparison to the baseline model, the proposed approach demonstrates notable improvements on both the NYT and WebNLG datasets. It not only significantly reduces decoding time but also effectively mitigates the number of negative samples compared to the state-of-the-art models. This further validates the performance of the proposed model.

The subsequent sections of this paper unfold as follows: Section II illustrates prior research endeavors. Section III details into the methodology employed. Section IV clarifies the experimental setup. Section V describes the experimental outcomes and engages in discussions. Lastly, Section VI summarizes the conclusions drawn from this study.

II. RELATED WORKS

This section provides an overview of the related work on entity relation joint extraction methods, where the single-module single-step based extraction method is the focus of this paper.

In recent years, with the advancement of deep learning, many scholars have integrated deep learning methods into models for entity relation extraction to enhance extraction accuracy. The majorities of entity relation extraction models in recent years have leveraged pre-trained language models, particularly BERT [4], and have exhibited remarkable performance. Among these, deep learning based on entity relation joint extraction can be categorized into three modelling approaches. There are early approaches based on global text information, including both multi-module multi-step and multi-module single-step methods. Besides, there is the single-module single-step method, which addresses the issue of cascading redundancy between modules and steps.

A. Multi-module Multi-step Method

The multi-module multi-step architecture offers the advantage of explicit task decomposition and modular design. To address the issue of ternary overlap in entity relation extraction tasks, Zeng et al. [5] introduced an end-to-end neural model called CopyRE, based on Seq2Seq (Sequence-to-sequence) with a Copy mechanism. This model can extract relational facts from sentences of different categories, including normal sentences, Single Entity Overlap (SEO), and Entity Pair Overlap (EPO) sentences. Subsequently, Zeng et al. [6] proposed the CopyMTL model, which adopts a multi-tasking framework and the Copy mechanism to predict multi-word entities. However, CopyRE struggles with extracting multi-word entities, and while CopyMTL improves this aspect, its effectiveness in extracting an arbitrary number of triples remains to be enhanced. To address this issue, Wei et al. [7] introduced the cascading Hierarchical Binary Tagging (HBI) model, CasRel, which conducts entity relation triple extraction in two successive steps. This model represents relations as a function mapping head entities to tail entities. Additionally, Tian et al. [8] proposed the HSL model, which employs a novel tagging scheme to convert the joint entity and relation extraction problem into a sequence tagging task using a hierarchical sequence tagging approach. Zheng et al. [9] proposed the PRGC model, which decomposes the task into three subtasks: relation judgment, entity extraction, and subject-object alignment. Geng et al. [10] proposed an attention mechanism integrating convolutional and recursive neural networks within a joint model, enhancing the utilization of contextual information. The FETI model, suggested by Chen et al. [11], integrates head-tail entity category information and employs an auxiliary loss function for more efficient utilization of entity category information. Ye et al. [12] introduced the CGT model, a ternary extraction model based on the generative Transformer, which leverages contrastive ternary-level calibration algorithms and batch-level dynamic attention masking mechanisms to enhance model performance. Yu et al. [13] optimized a joint extraction model for Chinese entity relation extraction using the RoBERTa pre-training model.

B. Multi-module Single-step Method

Compared to the aforementioned methods, the multi-module single-step simplifies the model structure and reduces extraction complexity. To address the issue of the model predicting the extraction order of multiple triples, Sui et al. [14] proposed an end-to-end network model, Set Prediction Networks (SPN), featuring Transformers-based features and non-autoregressive parallel decoding, along with a two-part matching loss. This model transforms the task of entity relation joint extraction into an ensemble prediction problem. Wang et al. [15] introduced a table-filling model, Table-Sequence Encoders, based on the Attention mechanism. This model facilitates the transfer and interaction of information between different input modalities by incorporating table encoders and sequence encoders. The TPLinker, proposed by Wang et al. [16], treats entity relation joint extraction as a tagged-pair linking problem and introduces a novel handshake tagging scheme for aligning entity-pair boundary tags under each relation type. Additionally, Wang et al. [17] proposed

UniRE, a table-filling model giving joint decoding, which employs a unified tag space and solves the problem of tag space dispersion in traditional entity relation extraction.

C. Single-module Single-step Method

The more lightweight single-module single-step approach simplifies extraction and enhances intuitiveness compared to the multi-module design. Kong et al. [18] introduced an end-to-end co-attention network called CARE, which utilizes a two-dimensional table to represent entity tags and relation tags respectively. Inspired by the modelling idea of Novel-Tagging [19], Shang et al. [3] proposed a fine-grained triple classification model, OneRel, at the entity token layer. This effectively mitigates issues such as cascading errors and entity redundancy.

Amalgamating the research on entity relation joint extraction, this paper proposes effective solutions to the shortcomings of existing methods in Section A. The primary contributions are as follows:

- 1) Integrating the concept of Insertion Transformers, we present a novel perspective by reframing the joint extraction of entity relations as fine-grained triple classification. Effectively reduce the decoding time of the model to a constant level, enhancing its efficiency by leveraging insertion operations.
- 2) A novel entity relation tagging strategy, Vanilla Entity Relation Tags (VRT), is proposed, significantly enhances the performance in addressing the issue of Entity Overlap.
- 3) We conduct model evaluations on two publicly available datasets, NYT and WebNLG. The results demonstrate that our approach surpasses current state-of-the-art baseline methods, particularly in handling the intricate context of overlapping triples.

D. Insertion Transformers

Insertion Transformers, a branch of non-autoregressive generative models originally proposed by Stern et al. [20], revolutionizes text generation. The core concept involves iteratively inserting elements into an initial blank sequence until the termination condition is met, effectively reducing inference time while maintaining high performance. Building upon this foundation, Gu et al. [21] introduced InDIGO, an insertion-based decoding algorithm that optimizes efficiency by reusing previous hidden states. Moreover, Zhang et al. [22] introduced POINTER, a hierarchical Transformer model that blends the strengths of BERT and Insertion Transformer, generating text through incremental token insertions. Additionally, the CBART model, proposed by He[23], enhances text generation by incorporating a token-level classifier at the encoder side. This classifier guides the decoder in performing substitution and insertion operations, enabling simultaneous fine-tuning of multiple input tokens and thereby enhancing the accuracy and efficiency of text generation.

III. METHODOLOGY

The objective of the single-module single-step model is to identify the set of triples present in a sentence for each relation. This involves identifying entity pairs within a given

sentence, where the relation set of number M is represented as $R = \{r_1, r_2, \dots, r_m\}$, and the sentence of length N is represented as $X = \{x_1, x_2, \dots, x_n\}$. The task is to find the set of entity pairs $Y = \{(s_1, r_1, o_1), \dots, (s_k, r_k, o_k)\}$ with conditional probability given by:

$$p(Y|X) = \prod_{m=1}^M \prod_{i=1}^N \prod_{j=1}^N p_{\theta}(Y_k|X, r_m) \quad (1)$$

where, θ represents the model parameter. However, the optimized single-module single-step model requires $N \times N$ computations to determine the entity pair set Y , which leads to exponential growth in computation for longer texts, significantly increasing decoding time. To address this issue, this method draws inspiration from the Insertion Transformers model, successfully reducing the number of decoding times to a constant level using insertion operations.

In this section, the specific implementation method will be discussed in five parts, A focuses on entity relation tagging strategy, B discusses decoding strategy of the model, and C will describe the overall model framework. D will delve into model training, finally E will explore the objective function used in this approach.

A. Entity Relation Tagging Strategy

In the task of entity relation joint extraction, the set of entity pairs in a sentence is unordered, and the positions of the head and tail entities in the sentence are also unordered. In order to enable the model to recognize the head and tail entities at any position in the text and extract the relation between the entities simultaneously, this approach proposes a novel entity relation tagging method. It consists of four special tags: Head Entity Relation Tag (HRT), Tail Entity Relation Tag (TRT), Overlap Entity Relation Tag (ORT), and a generic entity relation tag (Vanilla Entity Relation Tag, VRT). The definitions are as follows:

$$HRT = \{p_1, p_2, \dots, p_M\} \quad (2)$$

$$TRT = \{p_{M+1}, p_{M+2}, \dots, p_{2M}\} \quad (3)$$

$$ORT = \{p_{2M+1}, p_{2M+2}, \dots, p_{3M}\} \quad (4)$$

$$VRT = p_0 \quad (5)$$

where, p indicates the token, and except for VRT, each entity relation token is assigned one by one corresponding to M relations.

As shown in Fig. 2, given the text $X = \{Jackie, \dots, Island\}$, with $N = 7$. The set of entity pairs for this text is denoted as $Y = \{(Jackie\ Chan, belong, Hong\ Kong), (Hong\ Kong, contain, Hong\ Kong\ Island)\}$, with $K = 2$. The entity relation tagging method requires $K + 1$ steps of processing for this text. Except for the step 1, each step of processing can be divided into two operations, namely VRT insertion and VRT transformation. In the step 1, only VRT insertion operations are performed on the text X , and the insertion positions for VRT are between all adjacent tokens in the text, resulting in a total of $N + 1$ inserted p_0 tokens, yielding a new token sequence X' .

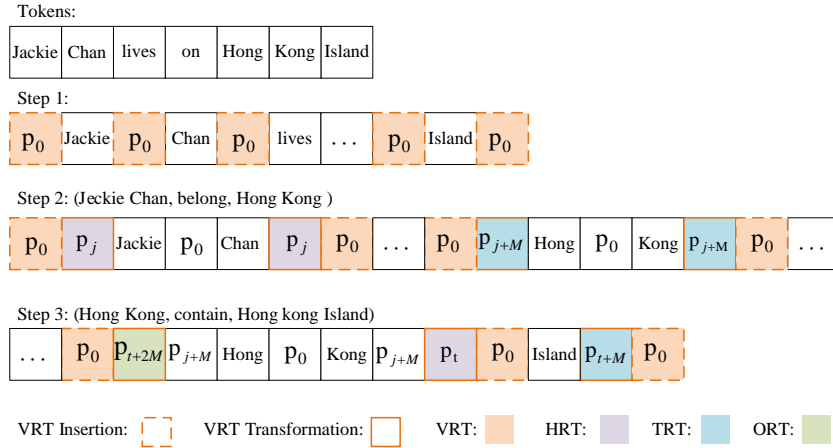


Fig. 2. Example of entity relation tagging.

Step 2 in Fig. 2 of the entity relation tagging method involves first performing VRT transformation on the text X' , followed by VRT insertion operations. This sequence is beneficial for generating subsequent training samples and targets. In VRT transformation, VRTs are converted to other tags to enclose the entity pairs in the sentence. Specifically, if 'belong' is at the j position in the relation set R , then p_j is taken as HRT and p_{j+M} as TRT. In text X , VRT tags preceding the first token of the head entity and following the last token are converted to HRT. Similarly, VRT tags preceding the first token of the tail entity and following the last token are converted to TRT. Finally, VRTs are inserted around the newly converted HRT and TRT.

The operation of step 3 is the same as step 2 in Fig. 2. However, due to the overlapping entities in (Hong Kong, contain, Hong Kong Island), there are some differences in VRT transformation. Specifically, VRTs preceding 'Hong' need to be converted to both HRT and TRT. In this case, the ORT is replaced with p_{t+2M} for this position, where t is the index of 'contain' in the relation set R .

Entity overlapping addressed in the step 3 constitutes one facet of the broader entity overlapping challenges, and this method posits that the proposed entity relation tagging method remains efficacious in effectively mitigating such issues. Specifically, the entity overlap conundrum can be delineated into three distinct categories: EPO, HTO, and SEO, where SEO encapsulates instances of overlapping entities within triplet sets, encompassing both EPO and HTO scenarios.

Focusing solely on a singular entity pair during each processing step, the entity relation tagging method sidesteps occurrences where entities overlap within other entity pairs, thereby aptly resolving the quandary of individual entities overlapping with other entity pairs in both EPO and SEO settings. Moreover, given the inherent significance of entity positioning entailed by the tagging position within the entity relation tagging method, the spatial arrangement of entities within the sentence exerts an influential impact on the methodology, beyond merely addressing the HTO challenge. To redress this issue, it becomes imperative to ensure the

uniqueness of encoding. As shown in Fig. 3, the method categorizes the distribution of entities within sentences into three types: non-overlapping head and tail entities, partially overlapping head and tail entities, and completely overlapping head and tail entities. Among them, partially overlapping head and tail entities can be further subdivided into five scenarios.

Within this framework, "HB" signifies the head token of the head entity, "HE" denotes the tail token, "TB" designates the head token of the tail entity, and "TE" indicates the tail token. The corresponding encoded values depicted on the right-hand side of the illustration affirm the distinctiveness of encoding across all scenarios, thus ensuring the integrity of the decoding process devoid of errors or decoding failures.

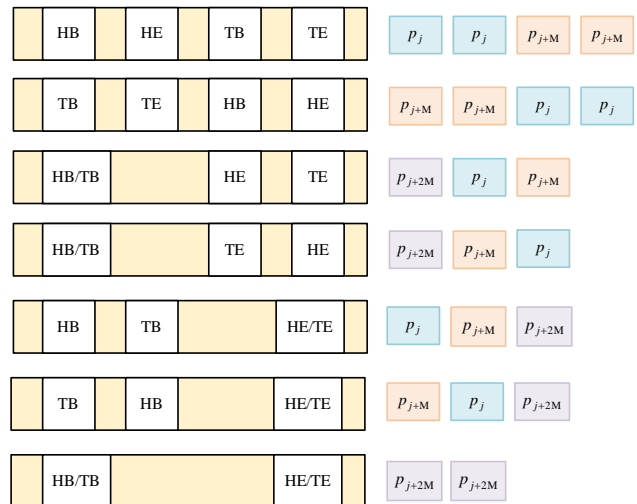


Fig. 3. Distribution of entity relation tagging.

B. Decoding Strategy

This training strategy of the method involves predicting each VRT for every sample, determining its corresponding entity relation tagging. For a sentence containing K triples, the entity relation tagging method conducts $K + 1$ steps of preprocessing on the sentence. The essence of this training

method lies in treating the VRT insertion results of each step i (where $i \geq 1$ and $i < k$) as training samples and the VRT transformation results of step $i + 1$ as the corresponding training targets. When $i = k + 1$, the VRT insertion results serve both as training samples and targets. Essentially, this approach involves performing multi-class classification prediction on the VRT matrix of length N . This entails jointly inputting the VRT matrix and the text into the model and predicting the entity relation tag each VRT matrix output corresponds to.

The essence of this training method lies in conducting multi-class classification predictions on VRT matrices of length N . This involves inputting the VRT matrix and text into the model simultaneously, and predicting the entity relation tagging on the output of the VRT matrix.

Decoding strategy outlined in this approach involves a stepwise process. Initially, the first step of entity relation tagging is taken as input, and then fed into the model to obtain an entity pair. Subsequently, this entity pair is tagged, and the process iterates by continually feeding it back into the model to obtain the next entity pair. This iterative process continues until the model's output no longer yields a complete entity pair.

Entity relation tagging leverages information about the position of the tag, as well as distinct head, tail, and overlap tags, to ascertain the head and tail entities within a sentence. Furthermore, the relation between the head and tail entities is determined based on the relation information encoded in the tokens. By multi-stage learning, the model becomes proficient in mapping the VRT matrix to individual entity pair tagging. This approach offers several advantages:

- 1) The VRT matrix maintains an appropriate level of sparsity, facilitating simple and efficient tagging predictions by the model.
- 2) It reduces computational overhead, as computing all entity pairs for a given sample typically only requires about K iterations.
- 3) The processing of model utterances becomes more comprehensive and holistic, enhancing its overall effectiveness.

C. Model Framework

Our method focuses on single-module single-step entity relation extraction, emphasizing the refinement achieved through methods like multi-head attention mechanisms and cross-attention mechanisms to gradually extract entity pairs and their associated relations from textual data. Employing an innovative tagging approach, we integrate entity recognition and relation extraction into a unified process, enabling the system to understand the information in the text at different levels and thus better extract entities and relations.

1) *Multi-head attention mechanism*: Multi-Head Attention Mechanism is an enhanced technique derived from the self-attention mechanism. Self-attention is a method capable of determining the importance of each position in the input sequence, thus effectively addressing long-distance

dependencies within the sequence. In the context of joint extraction of entity relations, diverse aspects may need to be considered simultaneously, necessitating the use of multiple self-attention mechanisms to handle these varied concerns. Multi-Head Attention involves employing multiple self-attention mechanisms on an input sequence to obtain several sets of attention results. Subsequently, these results are concatenated and linearly projected to yield the final output.

$$MultiHead(Q, K, V) = Concat(head_1, \dots, head_n)W^O \quad (6)$$

$$head_i = Attention(QW_i^Q, KW_i^K, VW_i^V) \quad (7)$$

where, $W_i^Q \in \mathbb{R}^{d_m \times d_k}$, $W_i^K \in \mathbb{R}^{d_m \times d_k}$, $W_i^V \in \mathbb{R}^{d_m \times d_v}$, and $W_i^O \in \mathbb{R}^{n \times d_m}$ are the projection matrices learned by the model based on the text after adding the VRT, with O as the output tensor, where q, k, v represent the dimensions of the query, key, and value vectors, respectively.

2) *Cross-attention mechanism*: Cross-attention mechanism is a special form of multi-head attention that splits the input tensor into two parts $X_1 \in \mathbb{R}^{n \times d_1}$ and $X_2 \in \mathbb{R}^{n \times d_2}$, and then uses one of the parts as a query set and the other as a key-value set. Its output is a query of size $n \times d_2$ tensor, and for each row vector, its attentional weight for all row vectors is given.

Specifically, let $Q = X_1W^Q$, $K = V = X_2W^K$, then the cross-attention is calculated as follows:

$$CrossAttention(X_1, X_2) = Softmax\left(\frac{QK^T}{\sqrt{d_2}}\right)V \quad (8)$$

where, $W^Q \in \mathbb{R}^{d_1 \times d_k}$, $W^K \in \mathbb{R}^{d_2 \times d_k}$ are the projection matrices learned by the model based on the text after adding the VRT, and d_k is the dimension of the key-value set and also the dimension of the query set.

D. Training Strategy

As illustrated in Fig. 4, this approach utilizes BERT [4] as the encoder to initially encode the text sequence. On the decoder side, the input involves inserting the VRT code or other entity relation marker codes into the text sequence code. Initially, the decoder conducts self-attention on the text sequence with inserted entity relation markers, thereby allowing the markers to acquire coarse-grained contextual information. Given that the entity relation markers disrupt the original text sequence, acquiring complete sequence information becomes challenging. Hence, we introduce a cross-attention mechanism at the decoder's backend, enabling the input sequence to focus on the entire text sequence. Following the output, a masking operation is performed on the non-VRT tokens to solely obtain the output of the VRT tokens. The resulting probability of the target is determined as:

$$p(Y|X, u, t; \theta) = \prod_{i=1}^{n+1} p(y_i|X, u_i, t; \theta) \quad (9)$$

where, X represents the text sequence, u denotes the VRT marker, t signifies the HRT, TRT, or ORT marker alongside the VRT marker, and θ represents the model parameter. n denotes the length of the text sequence, and since the VRT marker adds one unit to the length of the text sequence, it is represented as $n + 1$.

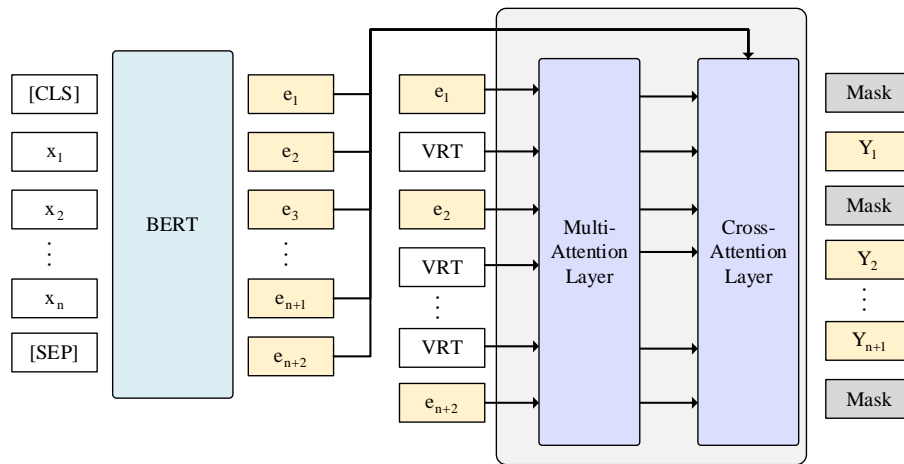


Fig. 4. Entity relation joint extraction framework based on insertion transformers.

E. Objective Function

The objective function of the model in this approach is defined as follows:

$$L = -\frac{1}{n+1} \sum_{i=1}^{n+1} \log p(y_i | X, u_i, t; \theta) \quad (10)$$

IV. EXPERIMENTAL SETUP

In this section, we first introduced the datasets and evaluation criteria used in the experiments, providing a detailed breakdown of the composition of the two datasets, and outlined the experimental details.

A. Datasets and Evaluation Metrics

1) *Datasets*: To provide a more robust explanation of the results of this model, two widely used datasets in relation and entity extraction tasks were adopted in this study: the New York Times (NYT) dataset [24] and the WebNLG dataset [25]. The details of the dataset sources and divisions are outlined below:

NYT is a renowned dataset for distant supervision relation extraction tasks. It utilizes Freebase online database, which stores entities and their relations, as the distant supervision source. It consists of articles from The New York Times annotated with named entity tags, coreference chains, and relation mentions. It contains approximately 1.8 million articles.

WebNLG consists of triple sets describing entities and their relations in natural language text. Initially used for natural language generation challenges, it later became the most commonly used general-domain dataset for evaluating triple extraction models, comprising data converted from the DBpedia knowledge base into natural language text. It consists of around 25,000 English sentences paired with RDF triples, offering a diverse range of content for text generation tasks. Detailed data are shown in Table I.

This approach conducted statistical analysis on the training, validation, and test sets of both datasets. Additionally, we categorized the datasets based on four different types of triple overlap patterns.

TABLE I. THE STATISTICS OF NYT AND WEBNLG.

| Category | NYT | | WebNLG | |
|----------|-------|------|--------|------|
| | Train | Test | Train | Test |
| Normal | 37013 | 3266 | 1596 | 246 |
| EPO | 9782 | 978 | 227 | 26 |
| SEO | 14735 | 1297 | 3406 | 457 |
| Total | 56195 | 5000 | 5019 | 703 |

Both the NYT and WebNLG datasets come in two versions: one version annotates solely the final word of entities, while the other annotates the entire span of entities. We denote the first version datasets as NYT* and WebNLG*, and the second version as NYT and WebNLG, respectively.

2) *Evaluation metrics*: To comprehensively evaluate system performance, we adopt three fundamental evaluation metrics consistent with the field of entity relation joint extraction: precision (P), recall (R), and the harmonic mean F_1 measure, for comparison with other baseline models. Their formulas are as follows:

$$precision = \frac{TP}{TP+FP} \quad (11)$$

$$recall = \frac{TP}{TP+FN} \quad (12)$$

$$F_1 = 2 \times \frac{Precision \times Recall}{Precision + Recall} \quad (13)$$

where, TP, FP, and FN represent true positives, false positives, and false negatives, respectively. In our experiments, correctness or incorrectness is considered with respect to triplets. That is, a triplet result is considered correct only when h_1 (head entity), r (relation), and t_1 (tail entity) are predicted correctly.

B. Experimental Environmental Details

The experiments were conducted on an Ubuntu 20.04 LTS operating system, utilizing hardware comprising an NVIDIA RTX-A2000-GPU with 12 GB of memory, an Intel i7-10700K CPU, and 64 GB of RAM. The software stack included Python version 3.7, PyTorch version 1.7 for deep learning frameworks, and CUDA version 11.4. The NVIDIA driver version was

470.94, and the pre-trained model library used was Transformers version 4.6.1. The experiments employed an AdamW optimizer.

V. RESULTS AND DISCUSSION

This section assesses the effectiveness of our data by comparing experimental outcomes with those of other baseline models. We utilize commonly employed general-domain datasets and evaluation metrics for evaluating triplet extraction models. Moreover, we present experimental results across different datasets using OneRel [3] as a comparative method to validate our experiments. Additionally, we analyze and interpret precision, recall, and F1-score. Besides, we utilize ablation experiments to ascertain whether the cross-attention mechanism in our experiments plays a crucial role in controlling the model's triplet extraction. Finally, we compare

the inference times of the models to confirm our model's high inference efficiency.

In order to evaluate the impact of the proposed joint extraction method based on Insertion Transformers on text, Table 2 in this section presents the experimental results of this method and other approaches on the NYT and WebNLG, with best results are highlighted in bold. The experimental results for the contrastive models SPN [14], CasRel [7], TPLinker [16], PRGC [9], OneRel [3], and CGT [12] are sourced from [26]. By comparing metrics such as F1 score, our method shows improvement over baseline models like OneRel in the task of entity relation joint extraction.

A. Experimental Results and Analysis

1) *Experimental results:* Table II presents a comparative analysis of the proposed model and baseline models across the NYT*, WebNLG*, NYT, and WebNLG datasets.

TABLE II. COMPARISON RESULTS OF JOINT MODEL PERFORMANCE BASED ON NYT AND WEBNLG: %

| Method | Model | Partial annotation | | | | | | Full annotation | | | | | |
|---------------------------|---------------|--------------------|-------------|----------------|-------------|-------------|----------------|-----------------|-------------|----------------|-------------|-------------|----------------|
| | | NYT* | | | WebNLG* | | | NYT | | | WebNLG | | |
| | | P | R | F ₁ | P | R | F ₁ | P | R | F ₁ | P | R | F ₁ |
| Multi-module multi-step | CasRel [7] | 89.7 | 89.5 | 89.6 | 93.4 | 90.1 | 91.8 | - | - | - | - | - | - |
| | PRGC [9] | 93.3 | 91.9 | 92.6 | 94.0 | 92.1 | 93.0 | 93.5 | 91.9 | 92.7 | 89.9 | 87.2 | 88.5 |
| | CGT [12] | 94.7 | 84.2 | 89.1 | 92.9 | 75.6 | 93.4 | - | - | - | - | - | - |
| Multi-module single-step | TPLinker [16] | 91.3 | 92.5 | 91.9 | 91.8 | 92.0 | 91.9 | 91.4 | 92.6 | 92.0 | 88.9 | 84.5 | 86.7 |
| | SPN [14] | 93.3 | 91.7 | 92.5 | 93.1 | 93.6 | 93.4 | 92.5 | 92.2 | 92.3 | - | - | - |
| Single-module single-step | OneRel [3] | 92.8 | 92.9 | 92.8 | 94.1 | 94.4 | 94.3 | 93.2 | 92.6 | 92.9 | 91.8 | 90.3 | 91.0 |
| | Ours | 94.2 | 93.4 | 93.0 | 93.6 | 93.7 | 93.2 | 94.8 | 93.8 | 93.2 | 92.0 | 91.2 | 91.5 |

On the NYT* dataset, our model generally exhibits superior recall and F1 scores compared to baseline models, with precision slightly lower than the CGT model by 0.5 but still ahead of other models. This might be attributed to the fact that the number of negative samples in our training set exceeds that of CGT, although the accuracy is slightly lower than CGT, it exhibits superior performance in terms of recall and F1 score. On the NYT dataset, our model has achieved comprehensive superiority, with F1 scores outperforming PRGC, TPLinker, and OneRel by 0.5, 1.9, and 0.3 percentage points, respectively. Similarly, on the WebNLG dataset, the F1 scores are correspondingly higher by 3, 4.8, and 0.5 percentage points. On the WebNLG* dataset, our model slightly lags behind OneRel but outperforms other models. This may be because, compared to entities with only one token in WebNLG*, our model is better adapted to learning entities with multiple tokens in WebNLG. Meanwhile, on the WebNLG dataset, our model surpasses OneRel in precision, recall, and F1 scores. This indicates that the proposed method is better suited for fully annotated data, as entity relation tagging requires contextual information, and annotating more context is beneficial for subsequent predictions.

2) *Results discussion and analysis:* Among the multi-module multi-step baseline models, CGT exhibits slightly higher precision than our model on the NYT* dataset, while PRGC shows slightly higher precision on the WebNLG* dataset. However, our model consistently outperforms CGT, PRGC, and CasRel in precision, recall, and F1 scores, owing

to the single-module's capability to handle text and relations efficiently, resulting in fewer errors compared to multi-module approaches.

Among the multi-module single-step baseline models, our model consistently outperforms them by 1 to 2 percentage points. This is attributed to the adoption of a joint decoding algorithm in the multi-module single-step approach, which reduces cascading errors compared to the multi-module multi-step approach. However, there are still some redundant errors when combining triplets, indicating limitations. In contrast, our proposed method extracts a complete entity pair in a single pass based on the text sequence, reducing redundant errors.

Compared to the single-module single-step model OneRel, our model demonstrates varying degrees of superiority on the NYT*, NYT, and WebNLG datasets. OneRel exhibits fewer errors compared to other models. However, due to the interference from lengthy text, OneRel predicts all possible entity pairs, leading to a decrease in prediction accuracy. This results in our model outperforming OneRel in terms of accuracy. Overall, our proposed method surpasses baseline models.

Besides, validating our method capability in addressing overlapping patterns and handling multiple triples, we conduct two additional experiments on distinct subsets of NYT* and WebNLG*. We employ five robust models as baseline comparators, and the comprehensive results are presented in Table III.

TABLE IV. F1-SCORE ON SENTENCES WITH DIFFERENT TRIPLE NUMBERS. ON NYT* AND WEBNLG*: %

| Model | NYT* | | | | | WebNLG* | | | | |
|------------|-------------|-------------|-------------|-------------|-------------|-------------|-------------|-------------|-------------|-------------|
| | N=1 | N=2 | N=3 | N=4 | N≥5 | N=1 | N=2 | N=3 | N=4 | N≥5 |
| CasRel ¶ | 88.2 | 90.3 | 91.9 | 94.2 | 83.7 | 89.3 | 90.8 | 94.2 | 92.4 | 90.9 |
| PRGC ¶ | 91.1 | 93.0 | 93.5 | 95.5 | 93.0 | 89.9 | 91.6 | 95.0 | 94.8 | 92.8 |
| TPLinker ¶ | 90.0 | 92.8 | 93.1 | 96.1 | 90.0 | 88.0 | 90.1 | 94.6 | 93.3 | 91.6 |
| SPN ¶ | 90.9 | 93.4 | 94.2 | 95.5 | 90.6 | 89.5 | 91.3 | 96.4 | 94.7 | 93.8 |
| OneRel ¶ | 90.5 | 93.4 | 93.9 | 96.5 | 94.2 | 91.4 | 93.0 | 95.9 | 95.7 | 94.5 |
| Ours | 91.0 | 93.6 | 94.5 | 96.3 | 94.4 | 92.1 | 93.3 | 95.6 | 94.4 | 94.7 |

^a Mark ¶ Indicates Results from [3]. “N” means different triple numbers, with the sentences were categorized from the test sets into five subclasses. Each class includes sentences that consist of 1, 2, 3, 4, or >5 triples.

It can be observed that our model achieves the best F1 scores in six out of ten categories, especially in the case of $N \geq 5$. Sentences with $N \geq 5$ may simultaneously contain Normal, SEO, EPO, and HTO patterns, making the extraction more complex. Importantly, our method performs best on $N \geq 5$ for both NYT and WebNLG*, demonstrating the effectiveness of our VRT tagging in addressing overlapping triplets from the model design perspective. This validates the efficacy of our model.

In models guided by a multi-module multi-step approach, it is demonstrated that sufficient interaction between head and tail entity information and relation information positively impacts model performance. Subsequently, employing a multi-module single-step model shows improved expressive power, indicating that using joint decoding instead of independent decoding in multiple steps helps alleviate cascading errors between steps and thus enhances model performance.

As for single-module single-step methods, although studies related to this are relatively scarce, from a performance perspective, integrating multiple sub-modules also reduces cascading errors between modules, leading to performance improvement. Considering the performance of joint models on the NYT and WebNLG datasets, the modeling direction of entity relation joint extraction is moving towards the idealized single-module single-step modeling method.

B. Ablation Study

Ablation experiments were conducted to investigate whether the cross-attention mechanism of the approach benefits the prediction of entity relation tagging. To assess the importance of the cross-attention mechanism, two experiments were conducted separately on the NYT and WebNLG datasets, one without cross-attention and the other with cross-attention. The keyword tagged with # denote those without using cross-attention. The experimental results are shown in Table IV.

It can be observed that after using the cross-attention mechanism, the accuracy in predicting entity pairs significantly improved. This indicates that after the VRT markers undergo cross-attention, they obtain more complete text information, enhancing the model's ability to predict entity relation tagging.

TABLE V. ABLATION EXPERIMENT ON NYT AND WEBNLG: %

| Dataset | Evaluation | Ours | #Ours |
|---------|------------|------|-------|
| NYT | Precision | 93.8 | 88.2 |
| | Recall | 93.0 | 87.8 |
| | F1 | 93.2 | 87.3 |
| WebNLG | Precision | 92.0 | 87.9 |
| | Recall | 91.2 | 86.2 |
| | F1 | 91.5 | 86.1 |

C. Model Efficiency Analysis

The objective of this section is to evaluate model efficiency through the measurement of inference time, with a maximum sequence length set to 128. Sentence lengths are segmented into four intervals: (0, 32], (32, 64], (64, 96], and (96, 128]. The purpose of this segmentation is to precisely investigate the impact of sequence length variation on model performance.

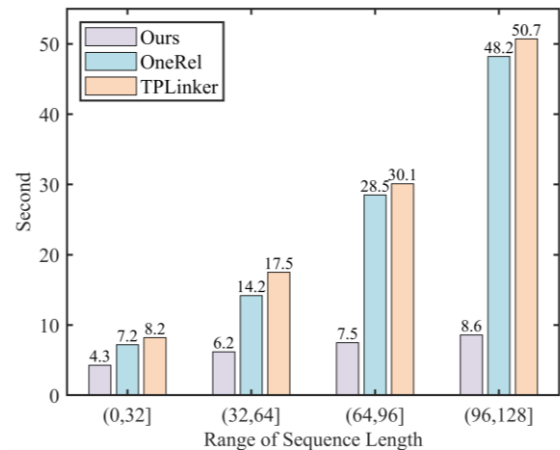


Fig. 5. Comparison of inference time.

As revealed by the results in Fig. 5, with an increase in sequence length, the inference times of OneRel and TPLinker models noticeably accelerate. This is due to their requirement to process all possible combinations between each pair of tokens across different relational contexts, resulting in an exponential increase in inference time as sequence length increases. In contrast, our model's inference time is significantly lower than the comparative models,

with a more gradual growth trend, as it predominantly relates to the number of entity pairs in the sequence, and there is a gentle positive correlation between the number of entity pairs and the increase in sequence length.

VI. CONCLUSION

In this paper, we utilize the Insertion Transformers framework to refine the task of entity relation joint extraction, introducing a novel VRT tagging strategy. This approach allows for more precise capturing of entity relation triplets, effectively addressing issues related to entity overlap in triplets and significantly reduces the inference time, thereby enhancing the efficiency of the model. Experimental evaluations on two public datasets demonstrate the superior performance of our model compared to state-of-the-art models across different scenarios.

In the future, we plan to delve into the following directions: we aim to devise a more efficient VRT tagging strategy to further enhance its ability to capture the associations between entities and relations, thereby making the model more efficient and focused. We also intend to investigate the concept of triplet overlap in other information extraction tasks, such as event extraction.

ACKNOWLEDGMENT

Project National Natural Science Foundation China (No: 62302540).

REFERENCES

- [1] G. Zhou, J. Su, J. Zhang, "Exploring various knowledge in relation extraction," In Proceedings of the 43rd Annual Meeting on Association for Computational Linguistics, pp. 427-434, 2005.
- [2] D. Zeng, K. Liu, S. Lai, "Relation classification via convolutional deep neural network," In Proceedings of the 25th International Conference on Computational Linguistics, pp. 2335-2344, 2014.
- [3] Y. Shang, H. Huang, X. Mao, "OneRel: Joint entity and relation extraction with one module in one step," In Proceedings of the AAAI conference on artificial intelligence, vol. 36, no. 10, pp. 11285-11293, 2022.
- [4] J. Devlin, M. Chang, K. Lee, "BERT: pre-training of deep bidirectional transformers for language understanding," In Proceedings of the 2019 Conference of the North American Chapter of the Association for Computational Linguistics: Human Language Technologies, pp. 4171-4186, 2019.
- [5] X. Zeng, D. Zeng, S. He, "Extracting relational facts by an end-to-end neural model with copy mechanism," In Proceedings of the 56th Annual Meeting of the Association for Computational Linguistics, pp. 506-514, 2018.
- [6] D. Zeng, H. Zhang, Q. Liu, "CopyMTL: Copy Mechanism for Joint Extraction of Entities and Relations with Multi-Task Learning," In Proceedings of the AAAI Conference on Artificial Intelligence, vol. 34, no. 05, pp. 9507-9514, 2020.
- [7] Z. Wei, J. Su, Y. Wang, "A novel cascade binary tagging framework for relational triple extraction," In Proceedings of the 58th Annual Meeting of the Association for Computational Linguistics, pp. 1476-1488, 2020.
- [8] J. Tian, X. Lv, X. You, "Hierarchical Sequence Annotation Based Joint Extraction Method for Entity Relation," Journal of Peking University (Natural Science Edition), vol. 57, no. 1, pp. 53-60, 2021.
- [9] H. Zheng, R. Wen, X. Chen, "PRGC: Potential relation and global correspondence based joint relational triple extraction," In Proceedings of the 59th Annual Meeting of the Association for Computational Linguistics and the 11th International Joint Conference on Natural Language Processing, pp. 6225-6235, 2021.
- [10] Z. Geng, Y. Zhang, Y. Han, "Joint entity and relation extraction model based on rich semantics," Neurocomputing, pp. 132-140, 2020.
- [11] R. Chen, X. Zheng, Y. Zhu, "Joint entity and relation extraction fusing entity type information," Computer Engineering, vol. 48, no. 3, pp. 46-53, 2022.
- [12] H. Ye, N. Zhang, S. Deng, "Contrastive triple extraction with generative transformer," In Proceedings of the AAAI Conference on Artificial Intelligence, vol. 35, no. 16, pp. 14257-14265, 2021.
- [13] K. Yu, F. Huang, Q. Wu, "Joint extraction method for Chinese entity relation based on bidirectional semantics," Computer Engineering, vol. 49, no. 1, pp. 92-99, 2023.
- [14] D. Sui, Y. Chen, K. Liu, "Joint entity and relation extraction with set prediction networks," IEEE Transactions on Neural Networks and Learning Systems, 2023.
- [15] J. Wang, W. Lu, "Two are better than one: Joint entity and relation extraction with table-sequence encoders," In Proceedings of the 2020 Conference on Empirical Methods in Natural Language Processing, pp. 1706-1721, 2020.
- [16] Y. Wang, B. Yu, Y. Zhang, "TPLinker: Single-stage joint extraction of entities and relations through token pair linking," In Proceedings of the 28th International Conference on Computational Linguistics, pp. 1572-1582, 2020.
- [17] Y. Wang, C. Sun, Y. Wu, "UniRE: A unified tag space for entity relation extraction," In Proceedings of the 59th Annual Meeting of the Association for Computational Linguistics and the 11th International Joint Conference on Natural Language Processing, pp. 220-231, 2021.
- [18] W. Kong, Y. Xia, "CARE: Co-Attention Network for Joint Entity and Relation Extraction," arXiv preprint arXiv:2308.12531, 2023.
- [19] S. Zheng, F. Wang, H. Bao, "Joint extraction of entities and relations based on a novel tagging scheme," In Proceedings of the 55th Annual Meeting of the Association for Computational Linguistics, pp. 1227-1236, 2017.
- [20] M. Stern, C. William, K. Jamie, U. Jakob, "Insertion transformer: Flexible sequence generation via insertion operations," In International Conference on Machine Learning, pp. 5976-5985, 2019.
- [21] J. Gu, L. Qi, C. Kyunghyun, "Insertion-based decoding with automatically inferred generation order," Transactions of the Association for Computational Linguistics, pp. 661-676, 2019.
- [22] Y. Zhang, G. Wang, C. Li, Z. Gan, C. Brockett, & W. Dolan, "POINTER: Constrained Progressive Text Generation via Insertion-based Generative Pre-training," In Proceedings of the 2020 Conference on Empirical Methods in Natural Language Processing, pp. 8649-8670, 2020.
- [23] X. He, "Parallel Refinements for Lexically Constrained Text Generation with BART," In Proceedings of the 2021 Conference on Empirical Methods in Natural Language Processing, pp. 8653-8666, 2021.
- [24] S. Riedel, L. Yao, & A. McCallum, "Modeling relations and their mentions without tagged text," In Machine Learning and Knowledge Discovery in Databases: European Conference, pp. 148-163, 2010.
- [25] C. Gardent, A. Shimorina, S. Narayan, & L. Perez, "Creating training corpora for NLG micro-planning," In 55th Annual Meeting of the Association for Computational Linguistics, pp. 179-188, 2017.
- [26] Y. Zhang, S. Liu, Y. Liu, "A review of deep learning-based entity-relation joint extraction research," Journal of Electronics, pp. 1093-1116, 2023.

Timber Defect Identification: Enhanced Classification with Residual Networks

Teo Hong Chun¹, Ummi Raba'ah Hashim², Sabrina Ahmad³

Centre for Advanced Computing Technology, Fakulti Teknologi Maklumat dan Komunikasi (FTMK), Universiti Teknikal
Malaysia Melaka (UTeM), Malaysia^{1,2,3}

Department of Information Technology and Communication, Politeknik Ungku Omar, Perak, Malaysia¹

Abstract—This study investigates the potential enhancement of classification accuracy in timber defect identification through the utilization of deep learning, specifically residual networks. By exploring the refinement of these networks via increased depth and multi-level feature incorporation, the goal is to develop a framework capable of distinguishing various defect classes. A sequence of ablation experiments was conducted, comparing our proposed framework's performance (R1, R2 and R3) with the original ResNet50 architecture. Furthermore, the framework's classification accuracy was evaluated across different timber species and statistical analyses such as independent t-tests and one-way ANOVA tests were conducted to identify the significant differences. Results showed that while the R1 architecture demonstrated slight improvement over ResNet50, particularly with the addition of an extra layer ("ConvG"), the latter still maintained superior overall performance in defect identification. Similarly, the R2 architecture, despite achieving notable accuracy improvements, slightly lagged behind R1. Integration of fully pre-activation activation functions in the R3 architecture yielded significant enhancements, with a 14.18% increase in classification accuracy compared to ResNet50. The R3 architecture showcased commendable defect identification performance across various timber species, though with slightly lower accuracy in Rubberwood. Nonetheless, its performance surpassed both ResNet50 and other proposed architectures, suggesting its suitability for timber defect identification. Statistical analysis confirmed the superiority of the R3 architecture across multiple timber species and this underscores the significance of integrating network depth and fully pre-activation activation functions in improving classification performance. In conclusion, while the wood industry has made strides towards automation in timber grading, significant challenges remain. Overcoming these challenges will require innovative approaches and advancements in image processing and artificial intelligence to realize the full potential of automated grading systems.

Keywords—Residual neural network; convolutional neural network; timber defect identification; deep learning

I. INTRODUCTION

Timber grading and defect identification are important in wood industries as it serve as cornerstone for the decision made by operators. In the past, these tasks were executed manually requiring careful assessment of the timber to determine their quality and economic value. This procedure involved classifying each log relative to their grade by assessing a number of factors such as geometry and typed of defect presence. Nevertheless, manual grading methods are

often prone to subjectivity, time consumption, and human error [1]. In light of current state of the industry, a notable concern arises regarding the consistent or potentially declining number of qualified inspectors in comparison to the steadily growing market [2]. Additionally, timber grading process would usually involve a complex classification procedure such as sorting by defects, species and texture which require a versatile algorithm that are capable of handling diverse tasks on the same machine. Moreover, timber defects that resulted from environment and natural growth processes might have an impact on the timber strength, durability and aesthetic appeal, thereby affecting its economic value. The current methods of timber defect detection rely heavily on visual inspection which is subjective and lack of precision, to overcome these challenges.

In recent years, there has been a rise in quality control using automated vision inspection (AVI) among the manufacturer, particularly in the secondary timber industry with the objective to overcome present issues [3]. Although AVI has been applied in the timber industry to address these challenges, ongoing research endeavors persist in enhancing the inspection process across various domains, including defect detection and identification, characterizing defect, grading timber, and integrating sensors into hardware components for optimizing cutting processes [4]. A number of methods have been proposed [5][6][7][8][9] to streamline the grading process, yet they still encounter several obstacles especially in the scope of detection and identification of timber defects. To address these challenges, there is a growing interest in leveraging statistical classifier methods such as machine learning and deep learning algorithms in AVI for the identification of timber defects as these technologies offer the potential expedited, reproducible and reliable grading processes [10][11][12][13]. A 2020 study suggests that employing deep learning for automated feature extraction could yield higher precision while enhancing accuracy by at least 4% compared to other timber feature extraction and recognition methods [14]. In [15], they employed a DenseNet network along with a single-shot multi-box detector (SSD) and a target detection algorithm to develop an enhanced SSD algorithm for detecting defects in solid wood panels. Despite facing challenges in accurately identifying active knots due to their similarity to background features, the proposed method achieved an improved accuracy rate of 96.1% compared to earlier version. However, such autonomy come with the trade-off where it requires a significantly greater amount of data to train the deep learning architecture compared to the machine learning approaches. As deep learning advances swiftly,

numerous Convolutional Neural Network (CNN) architectures have surfaced over time to address issues across various domains of defect identification such as AlexNet [16], MobileNetV2 [17], GoogLeNet [18] and ResNet [19]. In this research, our emphasis will be on employing Residual Neural Network (ResNet) as our deep learning network architecture given its notable achievements in numerous image classification tasks in recent years [20].

He et al. [21] introduced the Residual Neural Network (ResNet), a Convolutional Neural Network (CNN) architecture inspired by the structure of pyramidal cells in the cerebral cortex. ResNet key innovation was residual learning, enabling more efficient training of deep networks through skip connections that bypass multiple layers while incorporating ReLU and batch normalization [21]. Additionally, there exist model such as HighwayNets that further facilitate training deep networks by using an additional weight matrix to learn skip weights [22]. The fundamental unit of the ResNet network is the residual building block, which constitutes the majority of its architecture. These blocks incorporate skip connections to bypass convolutional layers, mitigating issues such as gradient disappearance or explosion with increasing network depth [19]. Comprised of convolutional layers, batch normalizations, ReLU activation functions, and skip connections, the residual building block forms the backbone of ResNet's structure. Although augmenting the depth of a neural network enhances its feature extraction capabilities as highlighted by [23], however, adding more layers to a current deep model such as ResNet also lead to higher training error [21]. To tackle the issue of vanishing gradient, [22] proposed skip connections within residual neural networks where these connections diminish the shortest path from lower layer parameters to the output, mitigating the vanishing gradient problem. Furthermore, by employing fewer layers during the initial training phase, this skipping strategy simplifies the network architecture effectively. Fig. 1 illustrates the layout of fundamental residual block. The output of the residual building block can be expressed using Eq. (1), where F represents the residual function, and x and y denote the input and output of the residual function, respectively.

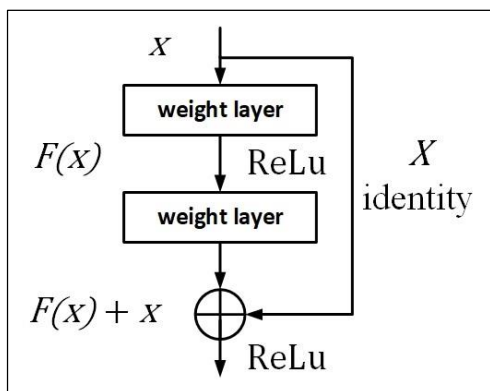


Fig. 1. Basic residual block.

$$y = F(x) + x \quad (1)$$

ResNet stands out for its significantly deeper network compared to its competitors, yet it maintains fewer parameters

(weights) than other models. A comparative analysis of ResNet50 and other CNN architectures for timber species identification by Oktaria et al. [24] in 2019, demonstrated that residual network outperforms its counterparts in terms of F1 Score, precision, and accuracy. Similarly, [25] proposed a transfer learning approach using the ResNet50 architecture for plant disease identification, achieving a remarkable training accuracy of 99.80%. On the contrary, Ahmed et al. [26] utilized ResNet50 for the purposes of crack detection by training the model with dataset of 48000 images and achieve remarkable accuracy rate of 99.8%. Inspired by the aforementioned factors, we expanded our research on using residual neural network (ResNet) for identifying defects in Malaysian timber species, aiming for outcomes that could prove advantageous to the local timber product industries.

II. METHODOLOGY

A. Overview of Approach

Driven by the significance of network depth where deep convolutional neural networks have achieved remarkable progress in image classification [27] as well as the significant achievement of Resnet50 from studies related to identification of timber defects [28]. Therefore, we investigate the potential of enhancing better class representation thus achieving higher accuracy by employing a residual network as the base architecture for this study. Hence, our goal is to explore the refinement of residual network layer by incorporating multi-level features that can be enhanced through increased the number of stacked layer (depth). This study conducted a sequence of ablation experiments based on residual network architecture that were implemented to facilitate the development of timber defect identification framework with ability to distinguish different type of defect classes. Additionally, we compared the performance of our timber defect identification frameworks to the original ResNet50, which is based on the concept of residual networks. Furthermore, we evaluated the classification performance of our proposed timber defect identification framework across various timber species. Finally, we expanded the validation of our defect identification approach by conducting statistical analyses which include independent t-tests and one-way ANOVA tests to identify significant differences.

B. Residual Neural Network (ResNet) Architecture

Recent studies in timber defect identification have seen the development of several architectures based on the Residual Neural Network (ResNet) design, renowned for its efficiency in depth-based CNN architecture [29][30][31][32]. This research involves reformulating the layers of the residual network specifically for classification of timber defects by altering the residual block based on ResNet50 architecture as shown in Fig. 2. The ResNet50 architecture is a cutting-edge convolutional network comprising 50 layers, featuring skip connections. These skip connections which operate in parallel with standard convolutional layers, serve as shortcuts to aid the network in capturing global features while addressing the challenge of vanishing gradients encountered in deeper network layers [33]. Besides, the architecture is made up of 7x7 convolutional layer with 65 kernels, succeeded by a 3x4 max-pooling layer with a stride of 2, followed by 16 residual

building blocks, 7x7 average-pooling layer with a stride of 7, and a fully connected layer preceding the softmax output layer [25]. The inclusion of residual blocks helps diminishing the output size while simultaneously increasing the network’s depth.

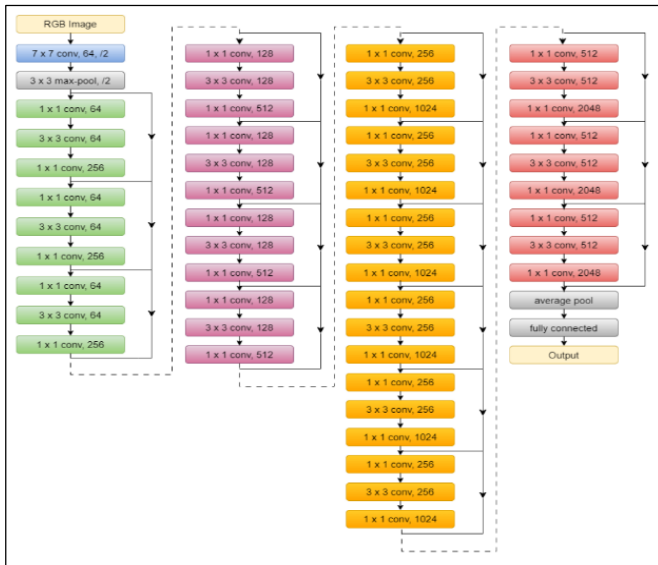


Fig. 2. ResNet50 architecture.

In this research, we systematically formulated three variations of residual network architecture with each employing different number and sizes of convolutional layers. This iterative approach was undertaken to explore the most appropriate configuration for timber defect identification framework. The experiment is performed on three proposed residual network architectures referred to as R1, R2, and R3. These variants draw inspiration from the architecture of ResNet50 as well as earlier research conducted by [21] in the field of deep residual learning. Each of the three devised versions of the residual network possesses its own unique architecture where R1 comprises 51 parameter layers, while the other variants exhibit a greater number of parameter layers, with R2 featuring 53 layers and R3 consisting of 54 layers. Additionally, within the architecture of both R1 and R2, we integrated "ConvG" and "ConvC+1" layers by introducing additional new residual blocks containing convolutional networks of different sizes into the proposed architectures. Table I illustrate the line-up of formulated residual network architectures employed for performance evaluation in this study.

TABLE I. FORMULATED RESIDUAL NETWORK ARCHITECTURE

| Layer | Output Size | R1 | R2 | R3 |
|---------|-------------|---|---|---|
| ConvA | 112x112 | 7x7, 64, stride 2 | | |
| ConvB | 56x56 | 3x3 max pool, stride 2 | | |
| ConvC+1 | 56x56 | | $\begin{bmatrix} 1x1,32 \\ 3x3,32 \\ 1x1,128 \end{bmatrix} \times 3$ | |
| ConvC | 56x56 | $\begin{bmatrix} 1x1,64 \\ 3x3,64 \\ 1x1,256 \end{bmatrix} \times 3$ | $\begin{bmatrix} 1x1,64 \\ 3x3,64 \\ 1x1,256 \end{bmatrix} \times 3$ | $\begin{bmatrix} 1x1,64 \\ 3x3,64 \\ 1x1,256 \end{bmatrix} \times 5$ |
| ConvD | 28x28 | $\begin{bmatrix} 1x1,128 \\ 3x3,128 \\ 1x1,512 \end{bmatrix} \times 4$ | $\begin{bmatrix} 1x1,128 \\ 3x3,128 \\ 1x1,512 \end{bmatrix} \times 4$ | $\begin{bmatrix} 1x1,128 \\ 3x3,128 \\ 1x1,512 \end{bmatrix} \times 6$ |
| ConvE | 14x14 | $\begin{bmatrix} 1x1,256 \\ 3x3,256 \\ 1x1,1024 \end{bmatrix} \times 6$ | $\begin{bmatrix} 1x1,256 \\ 3x3,256 \\ 1x1,1024 \end{bmatrix} \times 6$ | $\begin{bmatrix} 1x1,256 \\ 3x3,256 \\ 1x1,1024 \end{bmatrix} \times 6$ |
| ConvF | 7x7 | $\begin{bmatrix} 1x1,512 \\ 3x3,512 \\ 1x1,2048 \end{bmatrix} \times 3$ | $\begin{bmatrix} 1x1,512 \\ 3x3,512 \\ 1x1,2048 \end{bmatrix} \times 3$ | $\begin{bmatrix} 1x1,512 \\ 3x3,512 \\ 1x1,2048 \end{bmatrix} \times 3$ |
| ConvG | 4x4 | $\begin{bmatrix} 1x1,1024 \\ 3x3,1024 \\ 1x1,4096 \end{bmatrix} \times 1$ | | |
| | 1x1 | Average Pool, Fc, Softmax | | |

In addition to utilizing the original residual block, we investigated a revised version of the residual network architecture by integrating fully pre-activation activation functions in R3 where both Batch Normalization (BN) and Rectified Linear Unit (ReLU) layers precede the weight layer as illustrated in Fig. 3(b). The approach was introduced by He et al. [34] as a departure from the traditional “post-activation” paradigm which lead to a new residual block design that is easier to train and demonstrated enhanced generalization capabilities compared to the original ResNet architecture. Fig. 3(a) depicts the original ResNet residual block, where BN

is applied after each weight layer, and ReLU is implemented after BN with the exception of the final ReLU within a Residual Unit which occurs after the element-wise addition. In reformulating the residual block for the R3 architecture, we implemented an asymmetric structure described by [34] which allow the new after-addition activation becomes an identity mapping. This new asymmetric form can be represented by the following equation:

$$X_{l+1} = X_l + F(\hat{f}(X_l), W_l), \quad (2)$$

The design of the revised residual block allows for the adoption of a new after-addition activation \hat{f} in an asymmetrical manner, effectively treating \hat{f} as the pre-activation of the subsequent residual block.

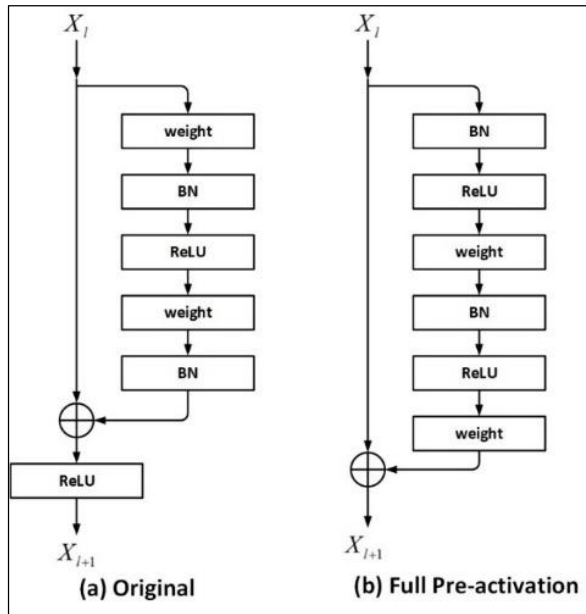


Fig. 3. ResNet50 residual block (a) Original (b) Full pre-activation.

C. Hyperparameter Optimization

To ensure the optimal performance of the three proposed residual network architecture, we conducted a further assessment of the appropriate CNN hyperparameter configuration focusing on both learning rate and epochs. The proposed architectures were trained using SGD optimizer with learning rate set at 0.001 and 0.0001. Throughout this experiment, the maximum number of epochs ranged from 50 to 200, with variations of 50, 100, and 200. The models underwent training on timber defect dataset encompassing various timber species (Meranti, Merbau, KSK, and Rubberwood) sourced from Universiti Teknikal Melaka Malaysia (UTeM) [35]. The experimental samples were then generated using 1600 augmented images of timber defect, comprises of eight timber defect categories (brown stain, blue stain, knot, borer holes, rot, bark pocket, wane, and split), as well as a set of clear timber specimens. The performance classification of each proposed architecture was assessed and compared with the transfer learning ResNet50 model to determine the most effective framework for identifying timber defects.

III. RESULT AND DISCUSSION

In this section, we will present the experimental outcomes of the three formulated residual network architectures to evaluate the efficacy of the proposed approaches in term of their performance in identification. The results are illustrated across three dimensions throughout the proposed residual network architecture where the first dimension explores different hyperparameter configurations encompassing both learning rate and epochs in pursuit of achieving highest classification performance for the proposed architecture (R1,

R2, R3). Subsequently, a comparison of performance is conducted between the standard ResNet50 and the proposed architectures, with the goal of evaluating their classification performance in terms of improved representation of the defect class and accuracy. Finally, the identification performance is summarized across various timber species to gauge the consistency of performance of the proposed approach across multiple timber species. The experimental result for all three formulated architectures (R1, R2 and R3) across the timber species are presented in Table II with highest classification performance achieved using specific hyperparameter settings are highlighted in red. The data presented in Table II clearly indicates that the R1 architecture demonstrates commendable classification performance across all timber species datasets, achieving the highest identification accuracy for each species within the range of 89.85% to 94.44%. In R1, the Rubberwood dataset attains the highest classification accuracy of 94.44% with hyperparameter settings of 0.001 learning rate and 100 epochs. Following this, R1 achieves the second-highest classification performance reaching 93.48% in the Meranti dataset. Subsequently, KSK follows with an accuracy of 92.52%, and finally, the Merbau dataset records the lowest accuracy of 89.85%. On the contrary, the R2 architecture achieves the highest classification accuracy of 94.07% across all timber species with optimized hyperparameters (LR = 0.001, Epoch = 100) in rubber timber species. It was succeeded by Meranti (93.04%), Merbau (92.74%), and KSK (91.93%). It's noteworthy that the R2 highest classification accuracy across the timber species is achieved with a learning rate of 0.001, coupled with varying numbers of epochs: 100 for Rubberwood, 200 for Meranti, and 50 for both Merbau and KSK. By incorporating fully pre-activation functions into the R3 residual block, we achieved the highest classification performance of 99.11% in the Merbau dataset, utilizing a learning rate of 0.0001 and 200 epochs as the training hyperparameter settings. In the case of the remaining three timber species, the classification performance of R3 was as follows: Meranti (97.7%) with LR = 0.001 and Epoch = 100, KSK (98.59%) with LR = 0.0001 and Epoch = 200, and Rubberwood (96.59%) with LR = 0.001 and Epoch = 50.

As depicted in Fig. 4, the classification accuracy of the R1 architecture demonstrates a roughly 0.7% improvement compared to the original ResNet50 under different hyperparameter configurations across timber species. The improvement in performance stems from integrating an additional layer, denoted as "ConvG," into the network architecture of R1. Nonetheless, despite the noted rise in classification accuracy for R1 in contrast to ResNet50, the ResNet50 architecture still predominantly leads in overall performance concerning defect identification where highest classification accuracy achieved by R1 still falls short when compared to ResNet50 architecture. Similar to earlier R1 architecture, we evaluated the classification performance of the R2 architecture alongside the original ResNet50. The findings indicate that with 100 epochs and a learning rate of 0.001, the R2 architecture surpassed the original ResNet50 in the Merbau dataset, achieving an accuracy improvement of 6.92%. This implies that increasing the depth of the CNN architecture does enhance its classification accuracy. However, in comparison to R1, despite the inclusion of a new residual block ("ConvC+1")

with smaller convolutional layer sizes in the proposed architecture of R2, it was noted that R2's highest classification performance still slightly lags behind R1 by a marginal difference of 0.37%. Nevertheless, despite some improvement in classification performance, the ResNet50 architecture continues to dominate the overall performance in defect identification. Within the R3 architecture, we delve into fully pre-activation activation functions by incorporating both BN and ReLu layers prior to the weights in addition to the depth of CNN network architecture. Illustrated in Fig. 4., the proposed R3 architecture, integrated with both network depth and fully pre-activation activation functions does improves the architecture's classification performance in the Merbau species by 14.18% compared to the original ResNet50 while using a learning rate of 0.001 and 50 epochs. The performance of the R3 architecture is clearly commendable across different timber

species, attaining defect identification accuracies ranging from 96.59% to 99.11%. Although it appears that the R3 architecture still exhibits lower performance in the Rubberwood species with a defect identification accuracy of 96.59% which marking the lowest R3 classification performance among the timber species. However, it's notable that the performance of the proposed R3 architecture has not only shown significant improvement across timber species and on average but has also outperform the classification performance of original ResNet50 and other proposed architectures (R1 and R2). This suggests that integrating both network depth and fully pre-activation activation functions into the R3 architecture improves the CNN's classification performance in distinguishing classes of timber defects and making it well-suited for implementation as our timber defect identification framework.

TABLE II. CLASSIFICATION PERFORMANCE OF R1, R2, R3 AND RESNET50 ACROSS TIMBER SPECIES USING MULTIPLE HYPERPARAMETERS SETTINGS. THE HIGHEST CLASSIFICATION ACCURACY ACROSS TIMBER SPECIES ARE HIGHLIGHTED IN RED

| Architectures | Hyperparameters | | Rubberwood | Merbau | Meranti | KSK |
|---------------|-----------------|-------|------------|--------|---------|-------|
| | Learning rate | Epoch | | | | |
| R1 | 0.001 | 50 | 94.15 | 83.41 | 92.15 | 88.89 |
| | | 100 | 94.44 | 87.19 | 90.96 | 92.3 |
| | | 200 | 94.15 | 88.15 | 93.48 | 92.52 |
| | 0.0001 | 50 | 93.33 | 87.63 | 91.63 | 86.96 |
| | | 100 | 93.04 | 87.56 | 90.96 | 89.56 |
| | | 200 | 93.7 | 89.85 | 92.96 | 90.15 |
| R2 | 0.001 | 50 | 92.59 | 92.74 | 88.59 | 91.93 |
| | | 100 | 94.07 | 87.33 | 89.85 | 86.81 |
| | | 200 | 92.96 | 88.96 | 93.04 | 91.33 |
| | 0.0001 | 50 | 93.33 | 82.67 | 91.33 | 88 |
| | | 100 | 92.89 | 86.59 | 91.56 | 91.56 |
| | | 200 | 93.48 | 89.63 | 92.15 | 86.37 |
| R3 | 0.001 | 50 | 96.59 | 99.04 | 97.48 | 97.85 |
| | | 100 | 96.3 | 98.96 | 97.33 | 97.85 |
| | | 200 | 96.52 | 98.89 | 97.7 | 98.52 |
| | 0.0001 | 50 | 95.85 | 98.07 | 96.81 | 96.67 |
| | | 100 | 95.93 | 98.74 | 96.37 | 97.7 |
| | | 200 | 96.44 | 99.11 | 97.04 | 98.59 |
| ResNet50 | 0.001 | 50 | 94.00 | 86.74 | 92.52 | 92.30 |
| | | 100 | 94.59 | 90.07 | 93.56 | 91.41 |
| | | 200 | 94.22 | 88.89 | 94.07 | 92.22 |
| | 0.0001 | 50 | 93.33 | 88.52 | 92.74 | 92.67 |
| | | 100 | 92.89 | 87.48 | 91.85 | 93.26 |
| | | 200 | 93.70 | 89.19 | 92.15 | 91.85 |

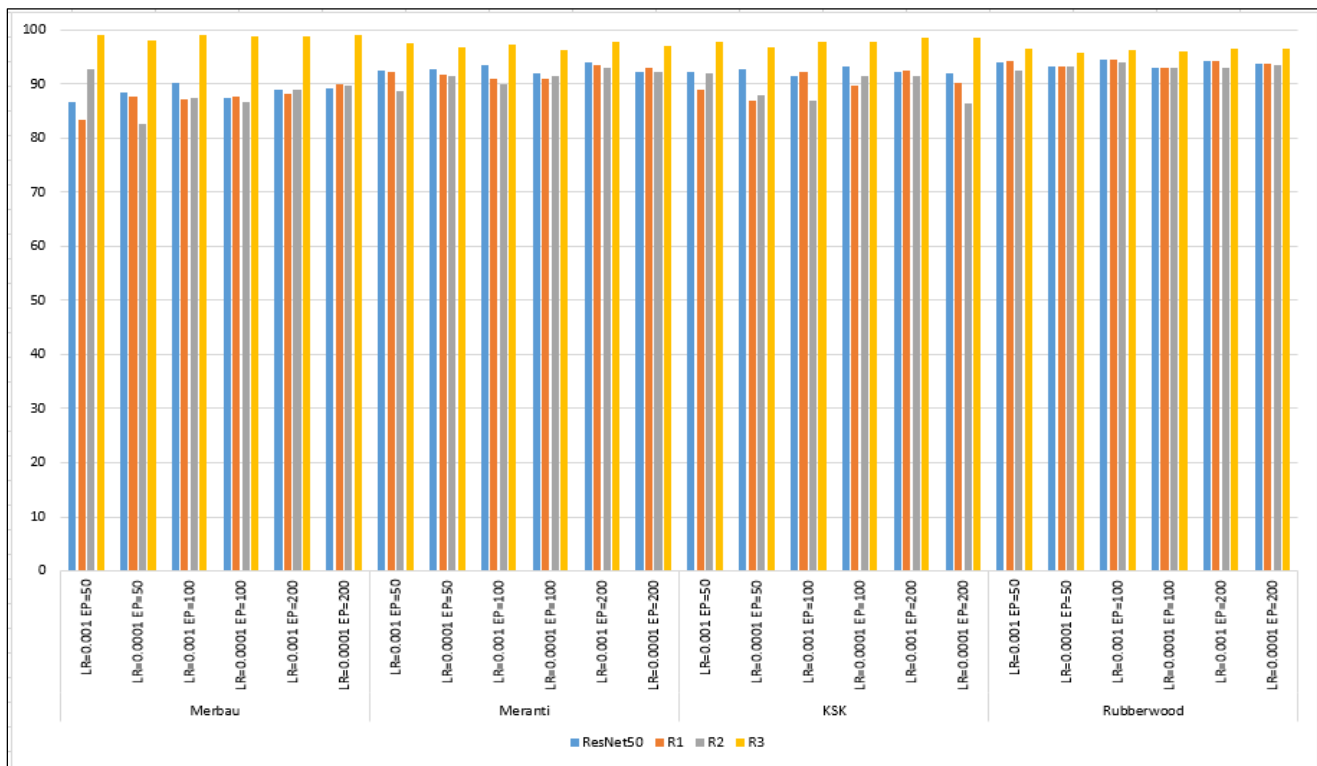


Fig. 4. Overall performance of proposed architectures and ResNet50.

To conduct further assessment, the classification performance of the R3 architecture was compared with ResNet50 and other proposed architectures using a one-way ANOVA test to identify any statistically significant differences in accuracy between the independent groups. The findings indicate that the classification performance of the proposed R3 architecture is statistically significantly superior compared to other architectures across multiple timber species. This implies the acceptance of the alternative hypothesis (HA) which indicate that there are at least two group means that are statistically significantly different from each other.

IV. CONCLUSION

This study presents an overview of the proposed timber defect identification framework based on the concept of residual neural network (ResNet) that mitigates the subjectivity and lack of precision associated with current timber defect identification methods, offering a more robust and reliable approach for the timber industry. It explores the evaluation of the approach concerning the number of stacked layers (depth) in the residual network architecture, as well as the integration of fully pre-activation activation functions within the residual block. Experiment are first conducted on the three proposed architectures (R1, R2, and R3) using various combinations of hyperparameters, including epochs and learning rates. The results from these experiments show that the R3 architecture which is formulated based on both stacked layers and fully pre-activation activation functions significantly contributes to satisfactory defect identification performance across all defect types and with consistently high accuracy observed across multiple timber species.

ACKNOWLEDGMENT

This research is supported by the Ministry of Higher Education (MOHE), Malaysia through Fundamental Research Grant Scheme (FRGS/1/2022/ICT02/UTEM/02/2) and Universiti Teknikal Malaysia Melaka.

REFERENCES

- [1] Y. Yang, X. Zhou, Y. Liu, Z. Hu, and F. Ding, "Wood defect detection based on depth extreme learning machine," *Appl. Sci.*, vol. 10, no. 21, p. 7488, 2020, doi: 10.3390/app10217488.
- [2] J. Sandak, A. Sandak, A. Zitek, B. Hintestoisser, and G. Picchi, "Development of low-cost portable spectrometers for detection of wood defects," *Sensors*, vol. 20, no. 2, p. 545, 2020, doi: 10.3390/s20020545.
- [3] M. Kryl, L. Danyts, R. Jaros, R. Martinek, P. Kodytek, and P. Bilik, "Wood recognition and quality imaging inspection systems," *J. Sensors*, vol. 2020, 2020, doi: 10.1155/2020/3217126.
- [4] R. N. N. Rahiddin, U. R. Hashim, L. Salahuddin, K. Kanchymalay, A. P. Wibawa, and T. H. Chun, "Local Texture Representation for Timber Defect Recognition based on Variation of LBP," *Int. J. Adv. Comput. Sci. Appl.*, vol. 13, no. 10, pp. 443–448, 2022, doi: 10.14569/IJACSA.2022.0131053.
- [5] U. R. ah Hashim, S. Z. M. Hashim, A. K. Muda, K. Kanchymalay, I. E. A. Jalil, and M. H. Othman, "Single class classifier using FMCD based non-metric distance for timber defect detection," *Int. J. Adv. Soft Comput. its Appl.*, vol. 9, no. 3, pp. 199–216, 2017.
- [6] H. S. Munawar, A. W. A. Hammad, A. Haddad, C. A. P. Soares, and S. T. Waller, "Image-based crack detection methods: A review," *Infrastructures*, vol. 6, no. 8, pp. 1–20, 2021, doi: 10.3390/infrastructures6080115.
- [7] K. Kamal, R. Qayyum, S. Mathavan, and T. Zafar, "Wood defects classification using laws texture energy measures and supervised learning approach," *Adv. Eng. Informatics*, vol. 34, no. February, pp. 125–135, 2017, doi: 10.1016/j.aei.2017.09.007.
- [8] K. Chaiyasarn, W. Khan, L. Ali, M. Sharma, D. Brackenbury, and M. DeJong, "Crack detection in masonry structures using convolutional

- neural networks and support vector machines,” in ISARC. Proceedings of the international symposium on automation and robotics in construction, 2018, vol. 35, pp. 1–8, doi: 10.22260/isarc2018/0016.
- [9] U. R. Hashim et al., “Extraction and Exploratory Analysis of Texture Features on Images of Timber Defect,” *Adv. Sci. Lett.*, vol. 24, no. 2, pp. 1104–1108, 2018, doi: 10.1166/asl.2018.10696.
- [10] W. Luo and L. Sun, “An improved binarization algorithm of wood image defect segmentation based on non-uniform background,” *J. For. Res.*, vol. 30, no. 4, pp. 1527–1533, 2019, doi: 10.1007/s11676-019-00925-w.
- [11] H. C. Teo et al., “Identification of wood defect using pattern recognition technique,” *Int. J. Adv. Intell. Informatics*, vol. 7, no. 2, pp. 163–176, Apr. 2021, doi: 10.26555/ijain.v7i2.588.
- [12] G. Ramesh, T. Siddhartha, K. Sivaraman, and V. Subramani, “Identification of Timber Defects Using Convolution Neural Network,” *Proc. 6th Int. Conf. Commun. Electron. Syst. ICCES 2021*, pp. 1641–1647, 2021, doi: 10.1109/ICCES51350.2021.9489136.
- [13] J. Hu, W. Song, W. Zhang, Y. Zhao, and A. Yilmaz, “Deep learning for use in lumber classification tasks,” *Wood Sci. Technol.*, vol. 53, no. 2, pp. 505–517, 2019, doi: 10.1007/s00226-019-01086-z.
- [14] N. D. Abdullah, U. R. Hashim, S. Ahmad, and L. Salahuddin, “Analysis of texture features for wood defect classification,” *Bull. Electr. Eng. Informatics*, vol. 9, no. 1, pp. 121–128, 2020, doi: 10.11591/eei.v9i1.1553.
- [15] T. He, Y. Liu, Y. Yu, Q. Zhao, and Z. Hu, “Application of deep convolutional neural network on feature extraction and detection of wood defects,” *Measurement*, vol. 152, p. 107357, 2020, doi: 10.1016/j.measurement.2019.107357.
- [16] F. Ding, Z. Zhuang, Y. Liu, D. Jiang, X. Yan, and Z. Wang, “Detecting defects on solid wood panels based on an improved SSD algorithm,” *Sensors*, vol. 20, no. 18, pp. 1–17, 2020, doi: 10.3390/s20185315.
- [17] A. Urbonas, V. Raudonis, R. Maskeliūnas, and R. Damaševičius, “Automated identification of wood veneer surface defects using faster region-based convolutional neural network with data augmentation and transfer learning,” *Appl. Sci.*, vol. 9, no. 22, p. 4898, 2019, doi: 10.3390/app9224898.
- [18] Y. Huang, C. Qiu, X. Wang, S. Wang, and K. Yuan, “A compact convolutional neural network for surface defect inspection,” *Sensors (Switzerland)*, vol. 20, no. 7, pp. 1–19, 2020, doi: 10.3390/s20071974.
- [19] A. Paulauskaite-Taraseviciene, K. Sutiene, and L. Pipiras, “Wooden dowels classification using convolutional neural network,” *Proc. Rom. Acad. Ser. A-Mathematics Phys. Tech. Sci. Inf. Sci.*, vol. 20, no. 4, pp. 401–408, 2019.
- [20] M. Gao, J. Chen, H. Mu, and D. Qi, “A transfer residual neural network based on ResNet-34 for detection of wood knot defects,” *Forests*, vol. 12, no. 2, p. 212, 2021, doi: 10.3390/f12020212.
- [21] J. Liang, “Image classification based on RESNET,” *J. Phys. Conf. Ser.*, vol. 1634, no. 1, 2020, doi: 10.1088/1742-6596/1634/1/012110.
- [22] K. He, X. Zhang, S. Ren, and J. Sun, “Deep residual learning for image recognition,” in *Proceedings of the IEEE conference on computer vision and pattern recognition*, 2016, vol. 45, no. 8, pp. 770–778, doi: 10.1002/chin.200650130.
- [23] R. K. Srivastava, K. Greff, and J. Schmidhuber, “Highway networks,” *arXiv Prepr. arXiv1505.00387*, vol. 38, no. 11, pp. 1299–1316, Sep. 2015, [Online]. Available: <http://arxiv.org/abs/1505.00387>.
- [24] I. Goodfellow, Y. Bengio, and A. Courville, *Deep learning*, vol. 13, no. 1. MIT press, 2016.
- [25] A. S. Oktaria, E. Prakasa, and E. Suhartono, “Wood Species Identification using Convolutional Neural Network (CNN) Architectures on Macroscopic Images,” *J. Inf. Technol. Comput. Sci.*, vol. 4, no. 3, pp. 274–283, 2019, doi: 10.25126/jitecs.201943155.
- [26] I. Z. Mukti and D. Biswas, “Transfer learning based plant diseases detection using ResNet50,” in *2019 4th International Conference on Electrical Information and Communication Technology (EICT)*, 2019, pp. 1–6.
- [27] C. F. Ahmed, A. Cheema, W. Qayyum, and R. Ehtisham, “Detection of Pavement cracks of UET Taxila using pre-trained model Resnet50 of Detection of Pavement cracks of UET Taxila using pre-trained model Resnet50 of CNN,” *Proc. 1st Int. Conf. Adv. Civ. Environ. Eng. Taxila Pakistan*, no. March, pp. 5–6, 2022.
- [28] A. Krizhevsky, I. Sutskever, and G. E. Hinton, “Imagenet classification with deep convolutional neural networks,” *Commun. ACM*, vol. 60, no. 6, pp. 84–90, 2017, doi: 10.1145/3065386.
- [29] H. C. Teo, U. R. Hashim, S. Ahmad, L. Salahuddin, N. H. Choon, and K. Kanchymalay, “Efficacy of the Image Augmentation Method using CNN Transfer Learning in Identification of Timber Defect,” *Int. J. Adv. Comput. Sci. Appl.*, vol. 13, no. 5, pp. 107–115, 2022, doi: 10.14569/ijacsa.2022.0130514.
- [30] H. C. Teo et al., “A review of the automated timber defect identification approach,” *Int. J. Electr. Comput. Eng.*, vol. 13, no. 2, pp. 2156–2166, 2023, doi: 10.11591/ijece.v13i2.pp2156-2166.
- [31] R. Ehtisham, W. Qayyum, C. V. Camp, J. Mir, and A. Ahmad, “Predicting the defects in wooden structures by using pre-trained models of Convolutional Neural Network and Image Processing,” in *2nd International Conference on Recent Advances in Civil Engineering and Disaster Management*, 2022, pp. 208–212.
- [32] B. Zoph, V. Vasudevan, J. Shlens, and Q. V. Le, “Learning transferable architectures for scalable image recognition,” in *Proceedings of the IEEE conference on computer vision and pattern recognition*, 2018, pp. 8697–8710, doi: 10.1109/CVPR.2018.00907.
- [33] R. Ehtisham et al., “Classification of defects in wooden structures using pre-trained models of convolutional neural network,” *Case Stud. Constr. Mater.*, vol. 19, no. September, p. e02530, 2023, doi: 10.1016/j.cscm.2023.e02530.
- [34] D. Theckedath and R. R. Sedamkar, “Detecting affect states using VGG16, ResNet50 and SE-ResNet50 networks,” *SN Comput. Sci.*, vol. 1, no. 2, p. 79, 2020, doi: 10.1007/s42979-020-0114-9.
- [35] K. He, X. Zhang, S. Ren, and J. Sun, “Identity mappings in deep residual networks,” *Lect. Notes Comput. Sci. (including Subser. Lect. Notes Artif. Intell. Lect. Notes Bioinformatics)*, vol. 9908 LNCS, pp. 630–645, 2016, doi: 10.1007/978-3-319-46493-0_38.
- [36] U. R. Hashim, S. Z. Hashim, and A. K. Muda, “Image collection for non-segmenting approach of timber surface defect detection,” *Int. J. Adv. Soft Comput. its Appl.*, vol. 7, no. 1, pp. 15–34, 2015.

Enhancing Supply Chain Management Efficiency: A Data-Driven Approach using Predictive Analytics and Machine Learning Algorithms

Shamrao Parashram Ghodake¹, Vinod Ramchandra Malkar², Kathari Santosh³,
Dr. L. Jabasheela⁴, Shokhjakhon Abdufattokhov⁵, Dr. Adapa Gopi⁶

Assistant Professor, Department of MBA, Sanjivani College of Engineering, Savitribai Phule Pune University, Pune, India¹

Director, Sanjivani Institute of Management Studies, Savitribai Phule Pune University, Pune, India²

Assistant Professor, Department of MBA, CMR Institute of Technology, Bengaluru, Bengaluru, India³

Professor, Department of Computer Science and Engineering, Panimalar Engineering College, Chennai, India⁴

Automatic Control and Computer Engineering Department, Turin Polytechnic University in Tashkent, Tashkent, Uzbekistan⁵

Department of Information Technologies, Tashkent International University of Education, Tashkent, Uzbekistan⁵

Associate Professor, Dept. of Computer Science and Engineering, Koneru Lakshmaiah Education Foundation,
Green Fields, Vaddeswaram, Guntur Dist, Andhra Pradesh, India⁶

Abstract—Contemporary firms rely heavily on the effectiveness of their supply chain management. Modern supply chains are complicated and unpredictable, and traditional methods frequently find it difficult to adjust to these factors. Increasing supply chain efficiency through improved supplier performance, demand prediction, inventory optimisation, and streamlined logistics processes may be achieved by utilising sophisticated data analytics and machine learning approaches. In order to improve supply chain management efficiency, this study suggests a unique data-driven strategy that makes use of Deep Q-Learning (DQL). The goal is to create optimisation frameworks and prediction models that can support well-informed decision-making and supply chain operational excellence. The deep Q learning technique is thoroughly integrated into supply chain management in this study, which makes it innovative. The suggested framework gives a comprehensive method for tackling the difficulties of contemporary supply chain management by integrating cutting-edge methodologies including demand forecasting, inventory optimisation, supplier performance prediction, and logistics optimisation. Predictive modelling, performance assessment, and data preparation are three of the proposed framework's essential elements. Cleansing and converting raw data to make it easier to analyse is known as data preparation. To create machine learning frameworks for applications like demand forecasting and logistics optimization, predictive modelling uses DQL. The method's efficacy in raising supply chain efficiency is evaluated through performance evaluation and acquired 98.9% accuracy while implementation. Findings show that the suggested DQL-based strategy is beneficial. Demand is precisely predicted using predictive models, which improves inventory control and lowers stockouts. Supply chain efficiencies brought about by DQL-based optimisation algorithms include lower costs and better service quality. Performance assessment measures show notable gains above baseline methods, highlighting the importance of DQL in supply chain management. This study demonstrates how Deep Q-Learning has the ability to completely change supply chain management procedures. In today's dynamic environment, organisations may gain competitive advantage and sustainable development through supply chain operations that are more

efficient, agile, and resilient thanks to the incorporation of modern analytical methodologies and data-driven insights.

Keywords—Supply chain management; predictive analytics; demand forecasting; inventory management; exploratory data analysis

I. INTRODUCTION

Supply chain management plays a fundamental role in fostering economic growth by facilitating the seamless exchange of goods between businesses and consumers. The complex web of organizations participating in the supply chain process, each of which contributes to the smooth movement of goods from raw materials to end consumers, makes supply chain management effective [1]. Materials processors are essential because they convert basic materials from natural resources—like wood, rubber, and metal—into products that could be employed in subsequent processes. These resources are subsequently used by producers or manufacturers to make the wide range of things that are offered for sale, from tangible items to energy sources in industries such as the energy business [2]. After manufacturing, suppliers or sellers distribute goods to the next stops along the supply chain by acting as middlemen. Transportation businesses that are responsible for delivering goods to distribution centres or straight to retailers depend on warehouses as essential hubs for keeping products prior to their onward distribution [3]. Central facilities for dispersing goods to merchants, wholesalers, and occasionally direct customers are distribution centers, which are positioned strategically throughout different areas. Retailers are the final intermediary in the supply chain, providing goods to customers via a variety of channels such as physical storefronts and online platforms [4]. The supply chain affects and intersects with a number of business operations in addition to supply chain management. In order to create and engineer items that meet the demands of consumers, product development depends on the availability of resources and the

creative abilities of humans [5]. In order to efficiently reach target audiences, marketing tactics, which include actions like price, product placement, and advertising, are essential in driving demand for goods [6]. The goal of operations management is to streamline internal procedures in order to increase output, save expenses, and guarantee the firm runs smoothly. Distribution is the process of making things available to end customers through direct or indirect distribution channels. It is frequently combined with marketing. Sales and finance work together to establish

revenue targets, obtain funding, and distribute resources efficiently. Furthermore, customer service is crucial in forming consumer opinions and fostering customer loyalty. It includes actions intended to assist customers at every stage of the purchasing process, from pre-purchase consultations to post-purchase support and problem-solving. Supply chain management and these interrelated processes work together to propel corporate success and promote economic growth. Fig. 1 depicts the supply chain management architecture.

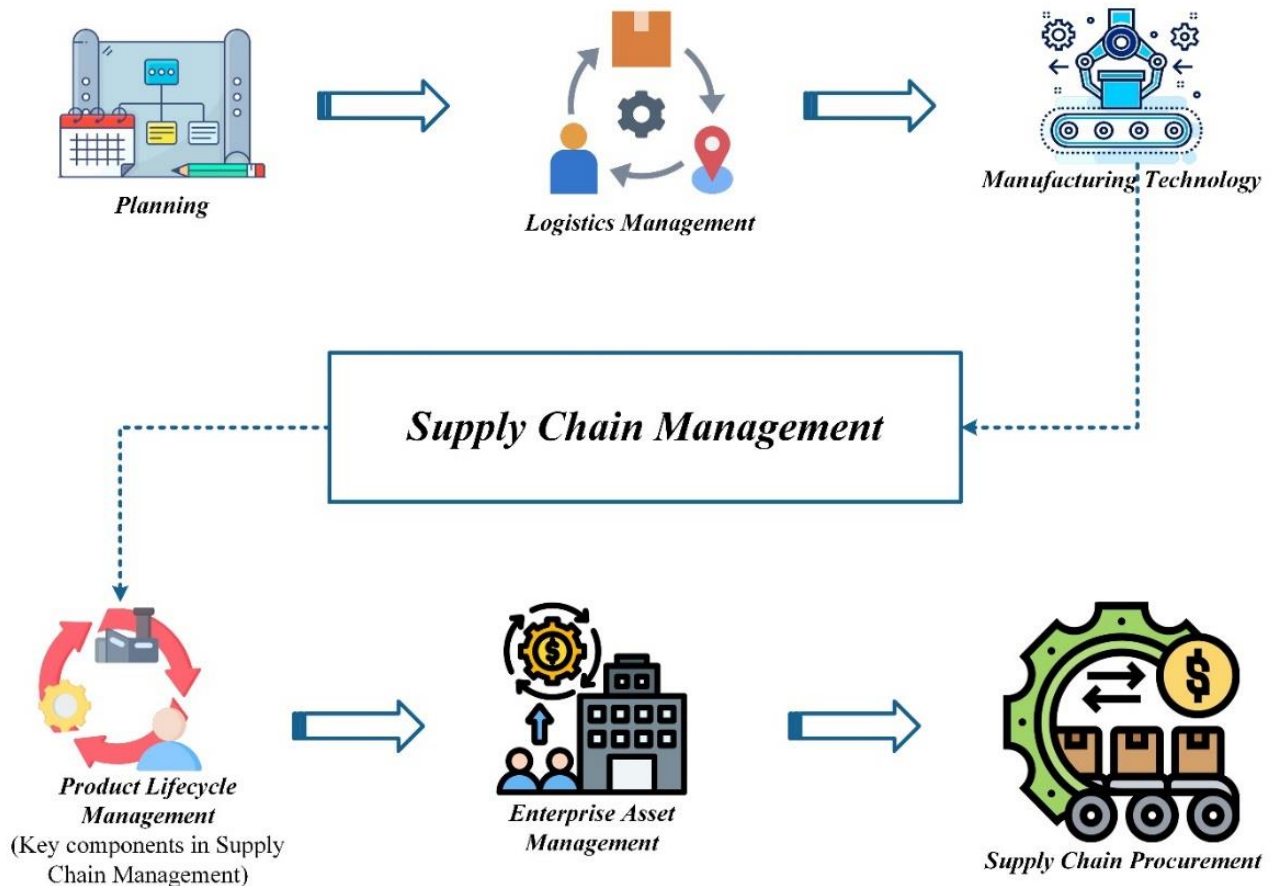


Fig. 1. Architecture of supply chain management.

The vulnerabilities of some of the most important global supply networks become apparent to the entire globe in 2020. Businesses rapidly realised that supply chain management procedures needed to be flexible without breaking and needed to be modernised. The most successful firms nowadays are examining their supply chain management (SCM) processes and the technology that power them with an unwavering gaze, asking themselves what steps they could take to improve their operations' efficiency, profitability, and resilience to change. The concepts and insights that drive global supply chain management are essential. Companies start by keeping an ear to market trends and asking their clients for input on the items they would like to see, as well as the best times and means of delivery. After that, businesses could utilize this data to streamline all aspects of their supply chain management, including procurement, production, research and development, last-mile transport, and final delivery. The proper execution of

this immensely intricate task necessitates the integration of every collaborator, or "link," into a highly responsive and well-coordinated supply chain management system [7]. Seventy-five percent of American businesses reported supply chain disruptions early in the epidemic, according to Axios. The World Bank reports that a quarter of businesses saw a 50% decrease in revenue as a result of the epidemic. At the beginning of the pandemic, the National Association of Manufacturers estimated that 1.4 million manufacturing jobs in the United States were destroyed [8]. Global supply chain disruption was further compounded by geopolitical factors like the trade war between the United States and China. The supervision of the movement of products and services from raw materials to finished items is known as supply chain management. It covers every step of the process—including shipping—that goes into bringing goods to consumers. Demand and supply remain in conflict even as the world

economy begins to improve [9]. Consider the more than eighty container ships, according to a Bloomberg story, that were awaiting offloading outside ports in California in mid-November 2021, just as the holiday shopping season got underway. A clear illustration of the significance of efficient supply chain management is given by this bottleneck. The seamless operation of supply and demand processes is ensured by supply chain management, allowing people to have access to products and services. A well-functioning supply chain is essential for preserving economic stability and a functional society, as it provides everything from food and shelter to the means of employment and entertainment.

Global supply networks have been irrevocably altered by the COVID-19 pandemic, which has also caused operational disruptions and widespread industry repercussions. This disruption has been most noticeable in Southeast Asian low-cost manufacturing regions like Vietnam, Indonesia, and Malaysia, where production slowdowns or plant closures have had a financial impact on multinational corporations [10]. Millions of Americans were forced into house confinement due to pandemic-related lockdowns, which resulted in a sharp increase in demand for supplies needed for remote work and learning environments. But the supply chain found it difficult to keep up, particularly for supplies that were mostly imported from Asian nations that were dealing with lethal variations and manufacturing limitations. Because there was a shortage of supply, the ensuing plant closures or decreased activity put further pressure on merchants, who were unable to keep up with the rising demand. Factories that were able to continue operating had to contend with issues such as reduced labour capacity, more restrictions on the supply of raw materials, and rising costs. The price of finished goods increased in tandem with the skyrocketing cost of raw materials, sometimes with abrupt surges. This phenomenon affected food costs in addition to consumer items. The U.S. Bureau of Labour Statistics reports that for the year ending in September 2021, prices for meat, poultry, fish, and eggs increased significantly by 10.5 percent. As global markets progressively recover, there continues to be a persistent mismatch between supply and demand because of the stark contrast between the recovery in demand and the still-restricted production capacity. According to the theory of scarcity, which holds that there are never enough resources to meet everyone's needs, this imbalance presents problems for companies, customers, and legislators [11].

The efficacy and efficiency of traditional supply chain management techniques are frequently hampered by a number of issues. These difficulties include having little insight throughout the supply chain, making decisions based mostly on historical data, having trouble correctly estimating demand, using ineffective inventory management techniques, and experiencing erratic disruptions in logistics and transportation [12]. These difficulties could outcome in higher expenses, longer order fulfilment times, surplus inventory, stockouts, and eventually, lower customer satisfaction. Utilising machine learning and predictive analytics methods in the supply chain industry is becoming more popular as a means of addressing these issues. The suggested conceptual framework for using Deep Q-Learning (DQL) algorithms to improve supply chain

management efficiency provides a methodical way to combine cutting-edge machine learning techniques with conventional supply chain procedures. The framework initiates data gathering and preprocessing and moves on to predictive modelling with DQL algorithms for logistics optimization, demand forecasting, inventory optimization, and supplier performance prediction. Following that, supply chain activities are optimised using DQL-based algorithms. While iterative refinement enables adaptation to changing market conditions, continuous monitoring and assessment guarantee the achievement of performance objectives. Enterprises could acquire a competitive advantage in the current dynamic market by utilizing DQL-based predictive analytics and optimization to attain operational excellence, cost savings, and enhanced customer satisfaction. Organisations could boost satisfaction with consumers, save expenses, increase operational efficiency, and gain a competitive advantage in today's fast-paced business climate by using data-driven insights and sophisticated analytics approaches. The following list outlines how this study contributes in a way that goes beyond theoretical developments to provide useful insights and suggestions that help enhance processes for managing supply chains in the real-world context.

Contemporary firms recognize the pivotal role of supply chain management in fostering economic growth. However, modern supply chains face complexities and uncertainties that traditional methods struggle to address. The COVID-19 pandemic underscored the vulnerabilities of traditional supply chain practices, highlighting the need for innovative approaches. This study proposes a data-driven strategy leveraging Deep Q-Learning (DQL) to revolutionize supply chain management. By integrating sophisticated data analytics and machine learning, the goal is to develop optimization frameworks and prediction models for informed decision-making. Key elements include predictive modeling, performance assessment, and data preparation. DQL enables accurate demand forecasting, optimized inventory levels, and streamlined logistics. The motivation lies in addressing the shortcomings of traditional methods and adapting to dynamic market environments. By embracing innovation, organizations can enhance supply chain efficiency and achieve sustainable development. In summary, the integration of modern analytical methodologies has the potential to transform supply chain operations and drive long-term success.

- This research extends supply chain management technique by putting forth a fresh data-driven strategy that makes use of Deep Q-Learning (DQL). An established basis for supply chain optimization is provided by DQL, and it may be used for demand forecasting, inventory control, supplier performance predictions, and logistics optimization.
- Supply chain efficiency is enhanced by the application of DQL-based optimisation technique. Organisations could optimise their supply chain operations and make well-informed decisions by utilizing historical data and sophisticated analytics. This improves efficiency, lowers costs, and increases customer satisfaction.

- The practical consequences of the study's findings are significant for organisations functioning in the contemporary dynamic economy.

The rest of the section is as follows: Section II gives an overview of relevant studies. Section III covers the approach's research gap. The materials and methods are presented in Section IV, which describes Optimizing Supply Chain Management with Deep Q-Learning Framework. Section V goes over the findings and performance analysis. Finally, Section VI summarises the conclusion of research.

II. LITERATURE REVIEW

In the intricate healthcare supply chain, it is critical to prioritize efficiency in order to economize and streamline the process of acquiring medical supplies. This paper examines different types of machine learning programs like Naive Bayes, K-Nearest Neighbors, Random Forest, Support Vector Machine, and Linear Regression to improve how healthcare supplies are managed. The five categories analysed in this research are: 'Inspection Results', 'Defect Rate', 'Transportation Modes', 'Routes' and 'Cost'. Based on what I discovered, the Random Forest classifier showed 87% accuracy in classifying "Inspection Results" and "Transportation Modes," while the KNN classifier had an impressive 86% accuracy in classifying "Routes. The study demonstrates the essential role of machine learning methods across different categories. The various methods that classifiers operate within different categories indicate the importance of selecting the most suitable algorithm for the supply chain. This research demonstrates that ML classifiers are effective in improving the efficiency of healthcare supply chains. It also suggests that automation could be used in different parts of supply chain management. It assists in optimizing the performance of the healthcare supply chain. However, the Linear Regression and KNN Regression models showed poor performance as indicated by their higher MSE and lower R^2 values. It is crucial to consider these results thoughtfully when selecting models that can accurately predict and function effectively in various scenarios [13].

The coordination of information in a system is used in supply chain management to unify all elements of the supply chain. Implementing artificial intelligence within the supply chain can simplify visibility, automate processes, and enhance overall management efficiency. This can assist companies in reducing costs and improving their ability to meet customer demands, ultimately leading to greater overall efficiency. Choosing the right people to be a part of a team is important for making sure the supply chain runs smoothly. This study introduces a fresh approach for identifying the most qualified suppliers in a supply chain by employing the specialized computer program CGANs. It helps when there are a lot of options but not much data to make a decision. Classifying members on the chain can effectively streamline the classification process and reduce data complexity while maintaining accuracy. The application of machine learning involves examining and predicting purchasing and stock relationships within the supply chain. - The vehicle scheduling module is working on optimizing routes for improved operational efficiency. The completion of the SCM system

was achieved through the use of the SSH framework. Still, there may be a disadvantage to depending just on large data and the robust Internet infrastructure for trade. It restricts the interchange to businesses that can access and use these technologies efficiently, which could exclude smaller or less tech-savvy supply chain partners [14].

The utilization of AI in supply chain management can improve operations and contribute to company prosperity. This summary discusses the ways in which AI can improve the supply chain, as well as the challenges and opportunities it presents. Companies can enhance their inventory management, forecast demand, coordinate transportation and deliveries, inspect product quality, and streamline their operations through the use of AI and machine learning. AI systems can look at a lot of information, find patterns, and give helpful advice so that people can make better decisions and react quickly to changes in the market. Furthermore, AI can improve the ability to see the supply chain, allowing for tracking, monitoring and evaluating risk in real time. This paper discusses the potential benefits of implementing artificial intelligence (AI) to improve the functioning of supply chains. AI can help make better predictions, manage stock, and improve the way things are moved in supply chains. The paper touches on the use of AI in supply chain management and provides instances of its successful implementation by companies. It is crucial to keep in mind, however, that the actual outcomes might differ based on the implementation's particulars and the environment, sector, organisational needs, quality of the data, and degree of AI acceptance [15].

The environment has been negatively impacted by companies' excessive use of natural resources, generation of excessive waste, and improper disposal of dangerous chemicals. The involvement of SMEs is significant in mitigating our influence on the environment globally. This has become an even more important part of our company's plan in the last twenty years. The industry is prepared for major shifts in supply chain management. Green Supply Chain Management means including environmental practices in the supply chain. Businesses can use Green Supply Chain Management to ensure that their procurement, production, distribution, consumption, and recycling practices are environmentally sustainable. The use of data analytics is increasing in operations management. In this area, new techniques involve the use of computer programs to examine organizational operations. The main objective of this study is to examine the utilization of machine learning in the management of supply chains and operations. Deeper learning offers a more accurate insight into customer preferences than MNL, but it's difficult to find solutions for challenges such as product selection and pricing in these models [16].

The global supply chain is facing significant challenges due to the combination of the COVID-19 pandemic and ongoing political and regional conflicts. Shipping items worldwide has become difficult and is resulting in delays in delivery. This is creating challenges in the shipment of goods globally and causing disruptions in the delivery schedule. It's becoming increasingly tough to ship items across the world, causing delays in the delivery process. One of the biggest

concerns is the lack of information about the availability of products. This is important for companies to plan how to ship and deliver goods. Forecasting the timing of item availability is essential for the smooth and economical management of logistics. Different data sources are used to study the shipping availability of General Electric's gas and steam turbines. It evaluates a variety of models to measure their performance. Included in the list of models are Simple Regression, Lasso Regression, Ridge Regression, Elastic Net, Random Forest (RF), Gradient Boosting Machine (GBM), and Neural Network. The experiments show that tree-based algorithms like RF and GBM are better than other models at predicting real-world data. The prediction models are anticipated to offer assistance to companies in addressing supply chain issues and improving safety on a larger scale. Despite its benefits, there are some disadvantages to using time series analysis for predicting availability dates. It can make things more complicated and require more computer power. Furthermore, it can be difficult to utilize and refine advanced deep learning methods to achieve higher accuracy [17].

Precisely predicting customer demand is crucial for optimizing the pharmaceutical supply chain. Forecasters are still using advanced models despite the limited available information. These challenges arise regardless of the abundance of data, as outdated data becomes irrelevant in a fluctuating market. Meanwhile, there are other elements that can influence demand, but understanding their effects involves gathering a substantial amount of data and using more advanced models. The goal is to tackle these challenges by utilizing a fresh approach to anticipate demand. The analysis will involve using data from multiple products and applying advanced machine learning to uncover patterns. The improvement of cross-series model performance is achieved through the implementation of different "grouping" methods and the utilization of non-customer demand data, such as inventory and supply chain information. This novel framework was tested using various modeling options on two significant datasets from major pharmaceutical companies, demonstrating its superiority over other methods. This research shows that knowing how much inventory is available can help predict how much demand there will be for a product. Our process involves researching both before and after to confirm the viability of the forecasting method we aim to implement. Knowing the old inventory information, as anticipated, does not prove to be beneficial [18].

The literature study underscores the noteworthy contribution of artificial intelligence (AI) and machine learning (ML) methodologies in augmenting diverse facets of supply chain management (SCM) across diverse sectors, specifically in the domains of healthcare and environmental sustainability. Several machine learning classifiers, including Naïve Bayes, K-Nearest Neighbours, Random Forest, Support Vector Machine, and Linear Regression, have been investigated by researchers for use in optimising healthcare supply chains. The findings show promise in terms of classification accuracy for various aspects of the supply chain, including inspection results, defect rates, transportation modes, routes, and costs. Furthermore, SCM systems have benefited from the application of AI algorithms to create

intelligent management, automation, and visualisation, which has decreased operational costs and increased responsiveness to market needs. Effectively lowering the dimensionality and complexity of the information, methods like conditional generative adversarial networks (CGANs) have been developed for dynamic supply chain member selection. In the supply chain, artificial intelligence has also been used for environmental operations integration, demand forecasting, transportation optimisation, and inventory management. Even with these developments, issues like scarce data availability, computational complexity, and technical accessibility still need to be taken into account for AI-powered SCM systems to be implemented and optimised effectively.

III. RESEARCH GAP

Effective supply chain management is crucial for businesses to fulfil consumer needs, cut costs, and increase profitability in the cutthroat business environment of today. However, plenty of businesses encounter difficulties when trying to efficiently optimize their supply chain processes. These difficulties could involve erroneous demand projections, inadequate inventory control, shaky supplier performance, and ineffective logistical procedures. Consequently, companies could encounter elevated expenses, setbacks, and discontent from clients, eventually impeding their ability to compete in the market. Thus, research is desperately needed to create workable solutions to these difficulties and improve supply chain performance, which could assist companies become more competitive and experience long-term growth. The present research puts forth a thorough framework that utilises deep Q-learning and sophisticated analytics to tackle the intricacies of supply chain management in the beauty product sector. The objective is to provide workable solutions for improving supply chain operations and increasing competitiveness by utilizing Deep Q-Learning to demand forecasting, inventory optimization, supplier performance prediction, and logistics optimization. This study's focus is on optimizing the supply chain for beauty products by applying Deep Q-Learning and predictive analytics approaches to demand forecasting, inventory control, supplier performance predictions, and logistics optimization. The goal is to increase the competitiveness and efficiency of supply chains for companies in the fashion and beauty sectors by offering them practical insights and ideas.

IV. RESEARCH FRAMEWORK

Deep Reinforcement Learning (DRL) is the approach that is suggested for the present research in order to enhance the supply chain for beauty products. The procedure commences with the formulation of the problem, which involves identifying the intricacies of supplier selection, price strategies, logistics optimization, and inventory management in the beauty product sector. Because it is data-driven and allows an agent to learn optimum policies through interaction with the supply chain environment, Deep Reinforcement Learning (DRL) is selected as an appropriate method. The process continues by defining the action space, reward function, and state representations. Factors including supplier performance indicators, demand projections, inventory levels, and transportation logistics status are all included in state

representations. The agent's options for ordering quantities, choosing suppliers, modifying inventory levels, and establishing pricing strategies are all outlined in the action area. The purpose of the reward function is to penalise unwanted outcomes, like stockouts or excessive expenses, and to reward positive behaviours, such revenue creation, cost reduction, and customer pleasure. Following that, the Deep Q-Network (DQN) agent is implemented, which approximates the ideal action-value function using a neural network architecture. Utilising experience replay in a simulated setting that replicates the dynamics of the cosmetics product supply chain; the agent is taught. After a training process, experience replay enhances sample stability and efficiency by enabling the agent to learn from previous encounters. Through

simulation assessments, the trained DQN agent's performance is evaluated in relation to a number of parameters, including cost savings, revenue creation, and service levels. In order to ensure the efficacy and resilience of the trained agent, parameters are adjusted and optimised depending on the findings of these examinations. Incorporating the DQN agent into the supply chain management system also makes it easier to make decisions in real time, which leads to increased productivity, lower costs, and happier customers. This research intends to drive improvements in supply chain management techniques by showcasing DRL's potential as a formidable tool for streamlining intricate supply chain procedures in the beauty product sector. Fig. 2 shows workflow of the suggested approach.

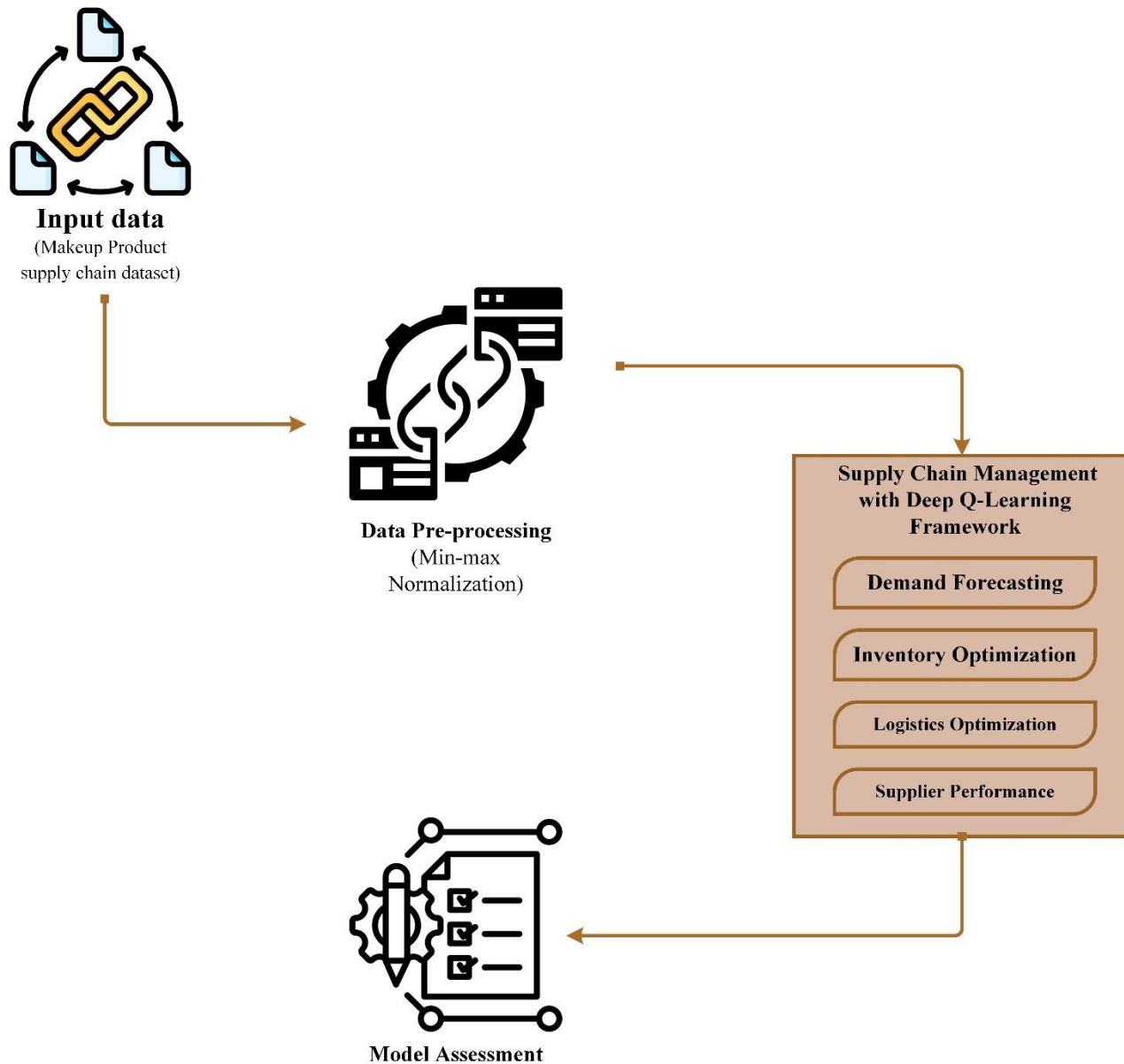


Fig. 2. Workflow of the suggested approach.

A. Data Acquisition

The present investigation employed a thorough dataset that was acquired from a reliable Kaggle database. The information set was specifically designed to address the supply chain activities of a fashion and beauty business that specializes in makeup items. The dataset contains a wide range of relevant characteristics that are essential for supply chain efficiency analysis and optimisation in this business. The proposed dataset for the supply chain activities of a fashion and beauty business specializing in makeup items encompasses a diverse array of attributes crucial for comprehensive analysis and optimization of supply chain efficiency. It includes product-specific details such as Product Type, SKU, Price, and Availability, offering insights into the beauty product portfolio and pricing strategies. Operational indicators such as the number of items sold, revenue earned, and stock levels provide valuable information for assessing sales success and inventory management. Additionally, logistical elements like lead times, order quantities, shipping durations, shipping carriers, and expenses shed light on transportation and delivery procedures within the supply chain. Supplier-related data reveals insights into supplier performance, production procedures, and quality control methods, covering aspects such as supplier name, location, lead time, production volumes, manufacturing prices, inspection results, and defect rates. Moreover, the dataset includes information on transportation modes, routes, and various costs associated with production, distribution, and procurement activities, facilitating a comprehensive examination of supply chain operations. This extensive dataset ensures the availability of essential information required for researching and enhancing the effectiveness of supply chain management specifically tailored to the makeup goods sector. [19].

1) *Data pre-processing*: In order to scale numerical characteristics to a particular range, usually [0, 1], min-max normalization is a fundamental linear transformation approach. A selection of features were made for normalisation from the makeup product supply chain dataset, including price, number of sold products, revenue generated, stock levels, lead times, order quantities, shipping times, shipping costs, lead time, production volumes, manufacturing lead time, manufacturing costs, defect rates, and costs. These elements reflect several facets of supply chain management, such as production procedures, inventory levels, and financial data. Each feature was subjected to a separate application of Min-max normalisation once the numerical columns were chosen. The following is the Eq. (1) for Min-max normalization:

$$V_{normalized} = \frac{V - V_{min}}{V_{max} - V_{min}} \quad (1)$$

Every feature was scaled to the range [0, 1] as a consequence of the normalization procedure, which comprised taking the least value of each feature and dividing by the range (maximum value minus minimum value).

where,

V : The variable or value that is being normalized.

V_{max} : The maximum possible value

V_{min} : The minimum possible value that

$V_{normalized}$: The normalized value of V after applying Eq. (1).

Larger-scale characteristics are kept from controlling the modelling process by means of this transformation, which guarantees that every feature contributes equally to the analysis. The original dataset structure was preserved by updating the dataset with the scaled values after normalization. In order to maximise supply chain management efficiency within the Makeup product business, preprocessing helps to prepare the data for further analysis and modelling.

B. Optimizing Supply Chain Management with Deep Q-Learning Framework

1) *Deep Q-Learning mechanism*: In 2013, DeepMind introduced the groundbreaking Deep Q-Network (DQN) reinforcement learning method [20], which revolutionized sequential decision-making in complex environments. The term "Q-Learning," which is represented by the letter Q in DQN, refers to an off-policy temporal differences technique that updates the value function for a particular State-Action pair while taking future rewards into account. Value-based approaches have the advantage of not requiring us to wait until the conclusion of the episode to learn the final reward and the discounted amount. Throughout the process go, update the value function of each action utilizing the Bellman equations [21]. Combining elements of Q-Learning with deep neural networks, DQN enabled agents to navigate intricate scenarios with sequential actions, showcasing remarkable capabilities, particularly in tasks like mastering video games. Central to DQN's architecture is the Q-network, a deep neural network that plays a pivotal role in decision-making processes. Given the current state as input, the Q-network outputs Q-values corresponding to each potential action, representing the expected cumulative reward associated with those actions in the current state. This design not only stabilizes the training process but also effectively handles high-dimensional state spaces, thanks to mechanisms like experience replay and target networks. The innovative design of DQN and its underlying Q-network marks a significant advancement in deep reinforcement learning, offering a powerful framework for addressing complex decision-making challenges in various domains. Deep Q-Learning (DQL) is a comprehensive reinforcement learning method that could potentially be employed to optimize several aspects of supply chain management. This technique uses the ideas of reinforcement learning to learn the best decision-making techniques in dynamic, complicated contexts repeatedly. DQL is applied in several areas of supply chain management, such as demand forecasting, inventory optimisation, supplier performance prediction, and logistics optimisation.

Algorithm for DQL Framework for Supply Chain Management

Step 1: Initialization: The algorithm establishes the replay memory buffer, initialises the Q-network and target network with random weights, and specifies hyperparameters like the exploration rate (ϵ) and discount factor (γ).

Step 2: Define Exploration Strategy: In this phase, the exploration strategy—like ϵ -greedy—is defined. It balances exploration with exploitation when choosing an action.

Step 3: Define Reward Function: Logistics objectives provide the basis of the incentive function, which allocates rewards for desired results such as shortened delivery times and cost savings.

Step 4: Training Loop: After choosing actions, carrying them out in the environment, and updating the Q-network with experiences kept in the replay memory buffer, the algorithm repeatedly cycles between episodes and time steps within each episode.

Step 5: Policy Deployment: The trained Q-network is employed for logistical optimisation when training is finished. Based on observable situations in the supply chain environment, it chooses the best course of action.

Step 6: Evaluation: To determine how well the deployed strategy performs in terms of streamlining logistics operations, important indicators like delivery times and cost savings are taken into consideration.

a) Accurate demand forecasting in supply chain management: In supply chain management, demand forecasting is essential because it helps companies estimate future client demand and adjust their operations accordingly. Within this framework, Deep Q-Learning (DQL) becomes a potent method for improving demand prediction accuracy through the implementation of reinforcement learning principles. Businesses can develop the best decision-making strategies using this method, which links the supply chain's present condition to activities that will optimize its future benefits—like income and satisfaction with clients. The interaction of the DQL agent with the supply chain environment is important to DQL-based demand forecasting. The agent looks at the condition of the supply chain as it stands right now, taking into account market trends, inventory levels, sales data from the past, and other pertinent information. The agent decides how to best maximise future benefits by using this knowledge to make decisions about order volumes and price. Environment-generated feedback—which takes the form of incentives or punishments depending on the results—is used to assess how successful these measures constitute. For instance, the agent may be rewarded if it effectively prevents stockouts by adjusting inventory levels in advance of expected increases in demand. On the other hand, the agency might be penalised if it overestimates demand and spends too much on inventory. The DQL agent improves its capacity to create precise demand estimates over time by iteratively enhancing its decision-making processes by learning from previous experiences. The agent adjusts its tactics to changing situations by absorbing patterns and trends in the supply chain environment. This results in more accurate forecasts and more informed decision-making. Additionally, DQL has the benefit of adaptability and flexibility, which enables companies to add new variables or change their forecasting tactics as necessary. To ensure that predictions are

accurate and relevant, the DQL agent could modify its decision-making criteria in response to changes in market dynamics or the availability of new data sources. With deep Q-learning for supply chain management demand forecasting, companies may improve prediction accuracy and make better judgements. DQL enables companies to successfully predict future demand patterns and optimise their operations in response, resulting in increased efficiency and competitiveness. This is achieved by establishing decision-making policies via interaction with the supply chain environment.

b) Enhancing inventory optimization in supply chains: An essential part of supply chain management is inventory optimisation, which tries to find a careful balance between keeping costs as low as possible and guaranteeing product availability. To address this issue, Deep Q-Learning (DQL) presents a viable strategy by dynamically modifying inventory levels in response to a range of variables, such as variations in demand, lead times from suppliers, and operational limitations. The learning of a policy by the agent to traverse the intricate decision-making environment of inventory management is the fundamental component of DQL-based inventory optimisation. This policy links activities that determine inventory modifications to the present status of the supply chain, which includes elements like current inventory levels, demand predictions, supplier performance, and market circumstances. It is the responsibility of the DQL agent to optimise inventory levels in order to strike a balance between holding costs and stockout costs. Holding costs include all of the costs related to keeping inventory on hand, including obsolescence risks, storage fees, and capital invested in inventory. Conversely, stockout costs include the possible loss of income due to unfulfilled client demand in addition to the expenses associated with processing backorders and expediting orders. The DQL agent interacts with the supply chain environment to investigate various inventory management techniques and takes use of the best ones in order to maximise cumulative rewards over time. Through dynamically modifying inventory levels in reaction to evolving circumstances, the agent acquires the ability to predict demand trends, prevent stockouts, and reduce holding expenses. Feedback from the environment, which takes the form of incentives or punishments depending on the results, is employed to assess how effective the agent's activities were. For example, if stockouts are successfully avoided while holding costs are kept to a minimum, awards could be received; but, if stockouts occur frequently or at excessive inventory levels, penalties could be incurred. The flexibility and scalability of DQL also provide the agent the option to add more restrictions and variables as needed. To increase the resilience of inventory management techniques, the agent could, for instance, take seasonality, product lifecycles, and lead time variations into account while making decisions. Supply chain managers are empowered to make data-driven decisions that strike a compromise between cost effectiveness and service quality needs by utilising Deep Q-Learning for inventory optimisation. DQL helps organisations improve

customer happiness, streamline operations, and gain a competitive edge in the market by dynamically altering inventory levels depending on demand projections, supplier performance, and operational restrictions.

c) *Improving procurement decisions through supplier performance prediction:* A crucial component of supply chain management is forecasting supplier performance, which is necessary to guarantee the dependability and calibre of providers. Providing a strong framework to assess supplier performance measures and forecast future behaviour, Deep Q-Learning (DQL) helps firms make well-informed procurement decisions. The relationship among DQL agent and previous supplier data is fundamental to DQL-based supplier performance prediction. In addition to lead times, defect rates, delivery dependability, and overall service quality, the agent gains experience evaluating a variety of supplier performance measures. The efficacy and dependability of the provider in fulfilling contractual obligations is shown by these criteria. The DQL agent learns patterns and trends in supplier behaviour by observing previous interactions and the results of such interactions. Through the examination of historical performance information, such as examples of timely delivery, high-quality products, and compliance with service level agreements, the agent has the capacity to identify markers of supplier efficacy and dependability. Using the information it has acquired, the DQL agent forecasts future supplier behaviour and foresees any problems or supply chain interruptions. Through an evaluation of variables including past performance patterns, current market dynamics, and outside influences, the agent could estimate the probability that suppliers will fulfil their commitments and provide products and services within the anticipated timeframe and quality requirements. Furthermore, the agent may dynamically modify its predictions and decision-making processes in response to changing circumstances and fresh data thanks to DQL. The agent regularly updates its models and improves its forecasts in response to changes in the supply chain environment and the availability of fresh data, guaranteeing relevance and accuracy in the evaluation of supplier performance. Ongoing review and input verify the efficacy of the DQL-based supplier performance prediction technique. Businesses may evaluate the precision and dependability of the DQL agent's forecasts by contrasting expected supplier performance with actual results, and they can make any necessary modifications to enhance performance. Through employing Deep Q-Learning to anticipate supplier performance, companies may improve their procurement procedures and arrive at better judgements. DQL enables organisations to choose the most dependable and efficient suppliers, maximise supply chain efficiency, and reduce operational risks by teaching them to evaluate supplier performance measures, forecast future behaviour, and foresee any hazards or interruptions.

d) *Streamlining supply chain operations for logistics optimization:* Supply chain management relies heavily on logistics optimisation, which aims to reduce costs and improve the effectiveness of distribution and transportation operations.

To tackle this problem, Deep Q-Learning (DQL) provides a strong framework that learns to optimise decisions about scheduling, routing, and mode selection, which simplifies logistics processes and enhances supply chain performance overall. The learning of a policy by the agent to traverse the intricate decision-making environment of distribution and transportation is the fundamental component of DQL-based logistics optimisation. In order to create the best choices for moving goods from suppliers to warehouses and from warehouses to consumers, this strategy takes into account a number of variables, such as transportation prices, delivery times, vehicle capacities, and route restrictions. Through interaction and observation, the DQL agent observes the present status of the supply chain environment, which may include variables like available transportation alternatives, inventory levels, consumer demand, and market circumstances. The agent uses this data to make decisions on the best course of action for logistical operations, including delivery schedules, route selection, and mode selection. The agent constantly improves its decision-making rules over time by drawing lessons from its interactions with the environment and with its experiences. The agent aims to maximise cumulative rewards—such as lowering transportation costs, speeding up deliveries, and maximising resource utilization—by investigating and utilising various logistical solutions.

The Deep Q-Learning (DQL) procedure for supply chain management logistics optimisation is described in the presented algorithm. The Deep Q-Learning (DQL) method that is offered sets up basic parameters and selects actions based on exploration or exploitation as iteratively goes through episodes. It regularly modifies the target network settings and updates the Q-network using experiences kept in a replay memory buffer. The technique incorporates assessment and checkpointing processes and gradually reduces the exploration parameters. It offers a structure for discovering the best supply chain management logistics tactics.

Deep Q-Learning (DQL) algorithm for logistics optimization within supply chain management

Initialize the Parameters

- *Q* – network parameters θ
- Target network parameters θ'
- Replay memory buffer *D*
- Exploration parameters ϵ

For episode = 1 to \max_{episodes} :

Initialize state *s*

Set $\text{total}_{\text{reward}} = 0$

While not reached terminal state

With probability ϵ

Select a random action *a*

Otherwise

Select action $a = \arg_{\max} (Q(s, a, \theta))$

Execute action *a* in the environment

Observe next state s' , reward r , and whether next state is terminal

Store experience (s, a, r, s') in replay memory buffer *D*

```
#Sample a mini-batch of experiences (s_i, a_i, r_i, s'_i) from replay
memory D
For each sample (s_i, a_i, r_i, s'_i) in the mini-batch
Compute target Q-value

    If s'_i is terminal
        target = r_i

    Else
        target = r_i + γ * max(Q(s'_i, a', θ'))

Compute current Q-value

    Q_value = Q(s_i, a_i, θ)

Compute loss
    loss = (target - Q_value)^2

Update Q-network parameters θ
    Perform gradient descent on loss with respect to θ

Every C steps
    Update target network parameters θ' = θ
Update state s = s'
    Accumulate total_reward += r

Decrease exploration parameter ε over time
    If episode % evaluation_interval == 0:
        Evaluate policy performance using test scenarios
    If episode % checkpoint_interval == 0
        Save Q-network parameters θ
```

Deep Q-Learning (DQL) is a powerful reinforcement learning technique that has gained significant attention in recent years due to its ability to handle complex decision-making tasks in various domains, including supply chain management. In the context of logistics optimization within the supply chain, DQL can be applied to address challenges such as route planning, fleet management, warehouse operations, and transportation scheduling. Key considerations in DQL-based logistics optimization are discussed below.

1) *Route planning*: DQL can be employed to optimize the routes taken by delivery vehicles or shipments within the supply chain network. By considering factors such as distance, traffic conditions, delivery time windows, and vehicle capacity, DQL algorithms can learn to generate optimal routes that minimize transportation costs and delivery times while maximizing efficiency.

2) *Fleet management*: DQL can assist in optimizing fleet management decisions, such as determining the appropriate number and types of vehicles needed to fulfill customer orders efficiently. By analyzing historical data on order volumes, delivery locations, and vehicle capacities, DQL algorithms can learn to allocate resources effectively, ensuring that the fleet operates at maximum capacity without incurring unnecessary costs or delays.

3) *Warehouse operations*: DQL can optimize warehouse operations by optimizing inventory placement, picking routes, and order fulfilment processes. By learning from historical data on order patterns, inventory levels, and warehouse layouts, DQL algorithms can identify the most efficient

strategies for organizing and managing warehouse operations, minimizing storage costs and improving order fulfilment speed.

4) *Transportation scheduling*: DQL can be used to optimize transportation scheduling decisions, such as determining the best times to schedule shipments, allocating resources to different transportation modes, and coordinating logistics activities across multiple locations. By analysing historical data on transportation capacities, lead times, and delivery requirements, DQL algorithms can learn to generate optimal scheduling plans that minimize transportation costs and maximize delivery reliability.

Overall, DQL offers a flexible and scalable approach to logistics optimization within supply chain management. By leveraging advanced machine learning techniques, organizations can improve the efficiency, agility, and resilience of their supply chain operations, gaining a competitive advantage in today's dynamic business environment. Businesses could significantly boost the efficiency and performance of their logistics by learning how to optimize decisions about routing, scheduling, and mode selection with DQL. DQL enables companies to efficiently respond to shifting circumstances and shifting supply chain dynamics by continuously adapting and improving decision-making procedures. This eventually results in cost savings, improved customer satisfaction, and a competitive advantage in the marketplace.

V. RESULT AND DISCUSSION

Findings from the implementation of the study methodology in supply chain management are presented, demonstrating observable improvements in significant performance indicators such inventory turnover, delivery times, and cost reductions. The precision of demand projections, productivity enhancements in inventory management, and the capacity to recognise dependable vendors are emphasised. Moreover, improved resource and transportation efficiency are the results of well-run logistics operations. Comparative assessments show the value contributed by the framework, and visual aids facilitate understanding. Practical strategies for enhancing supply chain operations and boosting competitiveness are provided by the outcome's presentation.

A. Experimental Outcome

1) *Sales by Product Type*: Analysing sales by product type offers important insights into how revenue is distributed throughout a company's portfolio and shows how various product categories are performing. Through sales data analysis, companies may determine best-selling items, comprehend consumer inclinations, and customise their approaches to maximise income. In order to deploy resources effectively and capitalise on high-performing product segments, firms must do this research in order to plan their marketing strategies, inventory control, and general operations.

TABLE I. SALES PERCENTAGE BY PRODUCT TYPE

| Product Type | Sales Percentage (%) |
|--------------|----------------------|
| Skincare | 45% |
| Cosmetics | 25.5% |
| Haircare | 29.5% |

The distribution of sales percentages among the various product categories in the company's portfolio is shown in the above Table I. With skincare items making about 45% of the overall sales income, they are the biggest contributor to sales. Products for hair care come in second place with 29.5% of sales, after skincare with 25.5%. This distribution implies that skincare goods account for a sizable amount of the company's income. Furthermore, the greater sales percentage of skincare goods suggests that consumers find these products to be popular. Additionally, the relationship between the increased cost of skincare goods and the money made suggests that, in comparison to cosmetics and hair care products, skincare products could have better profit margins or more demand.

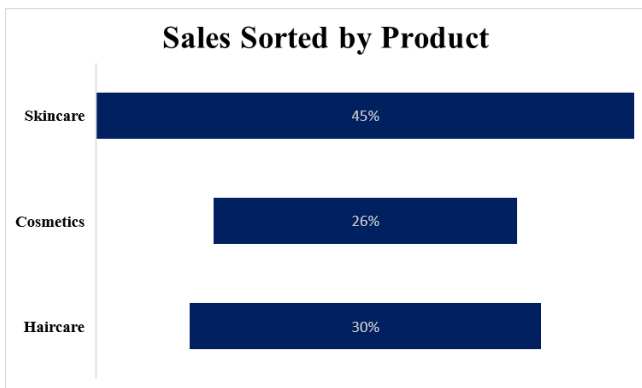


Fig. 3. Sales distribution by product type.

For strategic decision-making in areas like inventory management, marketing campaigns, and product development, it is important to comprehend the sales distribution by the kind of product. Through the identification of client preferences and sales patterns, organisations can customise their approaches to leverage profitable product categories and enhance their total income generating. The distribution of sales percentages among the various product categories in the company's portfolio is shown in Fig. 3. With skincare items making about 45% of overall sales income, they have the largest sales proportion. With a sales ratio of 29.5%, hair care goods trail closely behind cosmetics, which account for 25.5% of total sales. This graphic clearly illustrates the comparative sales performance of every product category and shows how skincare goods are the company's main source of income.

2) *Total revenue by shipping carrier:* Since shipping carrier income directly affects the profitability and effectiveness of logistics operations, it is a crucial component of supply chain management. This indicator shows how much revenue various carriers in the supply chain network make from providing transportation services. Organisations could assess each shipping carrier's financial contribution, identify

top performers, and make well-informed judgments about carrier selection, shipping rate negotiations, and overall logistics optimization strategies by analysing revenue data. Comprehending the income generated by shipping carriers offers significant insights into the financial well-being of the supply chain and facilitates efficient resource allocation for organizations to optimize profitability and competitiveness.

The revenue produced by the various shipping companies in the supply chain is shown in the Table II. It offers a comparison summary of each carrier's revenue contributions, highlighting how well each performs in terms of generating money. With a total revenue of 250.0946k, Carrier B leads the revenue generation. Carrier C comes in second with 184.880k, while Carrier A comes in third with 142.63k.

TABLE II. SHIPPING CARRIERS DRIVE REVENUE GROWTH

| Shipping Carrier | Revenue Generated |
|------------------|-------------------|
| Carrier A | 142.63k |
| Carrier B | 250.0946k |
| Carrier C | 184.880k |

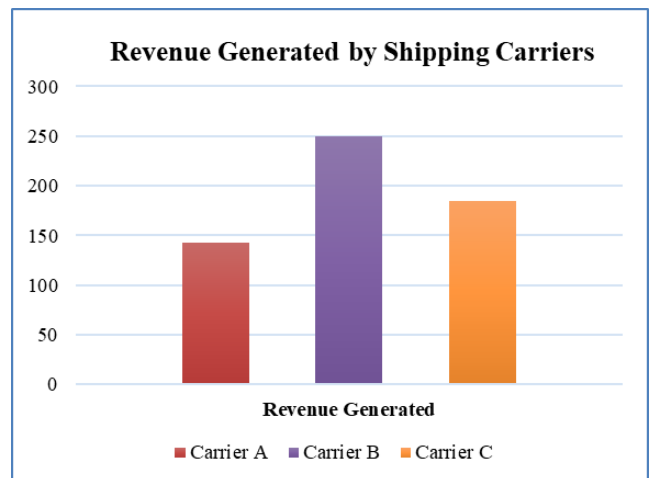


Fig. 4. Revenue generated by shipping carriers.

To facilitate simple comprehension and comparison of the revenue contributions, Fig. 4, which is an accompanying table, visually depicts the revenue earned by each shipping carrier through a bar chart. This graphical depiction makes the data easier to interpret and makes it easier to quickly identify the carriers that are performing at the top. In general, assessing the revenue that shipping carriers bring in from supply chain activities and choosing and managing them wisely depend on the analysis of their income.

3) *Analysis of defect rates and costs across transportation modes and routes:* This research explores the prices and defect rates related to different forms of transportation along distinct supply chain network routes. Through the analysis of these variables, enterprises may get significant understanding regarding the effectiveness, dependability, and efficiency of transportation processes. The defect rate (D) can be calculated using the Eq. (2):

$$D = \frac{\text{Number of Defective items/ Occurrences}}{\text{Total Number of items/ Occurrences}} * 100 \quad (2)$$

Once the defect rates are calculated for each route and transportation mode, they provide valuable insights into the reliability, quality, and performance of transportation operations within the supply chain network. Higher defect rates indicate a higher likelihood of issues or problems occurring during transportation, which may necessitate

corrective actions or adjustments to improve supply chain efficiency and reduce risks. To maximise logistics tactics, reduce risks, and improve supply chain performance overall, it is crucial to comprehend the link between transportation options, route selections, defect rates, and prices. Supply chain managers could employ the practical findings from this research to guide their decision-making and promote ongoing advancements in transportation management techniques.

TABLE III. DEFECT AND COST RATE BY TRANSPORTATION MODE

| Routes | Transportation modes | Costs | Defect rates |
|---------|----------------------|------------|--------------|
| Route B | Road | 187.752075 | 0.226410 |
| Route B | Road | 503.065579 | 4.854068 |
| Route C | Air | 141.920282 | 4.580593 |
| Route A | Rail | 254.776159 | 4.746649 |
| Route A | Air | 923.440632 | 3.145580 |

Table III offers comprehensive information on the prices and defect rates related to various types of transportation along distinct supply chain network routes. Supply chain managers need this information in order to evaluate the effectiveness and efficiency of transportation operations and to make well-informed choices about risk management tactics, carrier selection, and route optimisation. A path in the supply chain is represented by each item in the table, which also includes information on the mode of transportation employed, associated costs, and observed failure rates. Road transport, for example, is used most of the time on Route B; the following table shows two examples of this. With comparable defect rates of 0.226410 and 4.854068, respectively, the related costs for these road transfers are provided as 187.752075 and 503.065579. Similar to Route C, which has a failure rate of 4.580593, Route C mostly uses air transport and costs 141.920282. However, Route A combines rail and air transport, and its prices are 254.776159 and 923.440632, respectively. Its equivalent defect rates are 4.746649 and 3.145580.

The presence of two distinct entries for Route B with the transportation mode specified as Road in Table III signifies that there were multiple instances of transportation activities along this route utilizing road transport. This suggests that there were separate shipments or events that required transportation along Route B, each with its own associated costs and defect rates. The variations in costs and defect rates between these entries could be attributed to several factors. Firstly, different shipments may have varied in terms of their size, weight, destination, or urgency, leading to differences in transportation costs and quality control measures. Additionally, logistical factors such as the specific routes taken, the types of vehicles used, or the involvement of different transportation providers may have influenced the costs and defect rates associated with each transportation event. Furthermore, external factors like road conditions, traffic congestion, or weather conditions could have impacted the efficiency and reliability of transportation along Route B, contributing to the observed variations. By analyzing these differences, businesses can gain valuable insights into the performance of their supply chain logistics along Route B,

identify potential areas for improvement, and implement strategies to optimize transportation operations, minimize costs, and enhance overall supply chain efficiency and reliability.

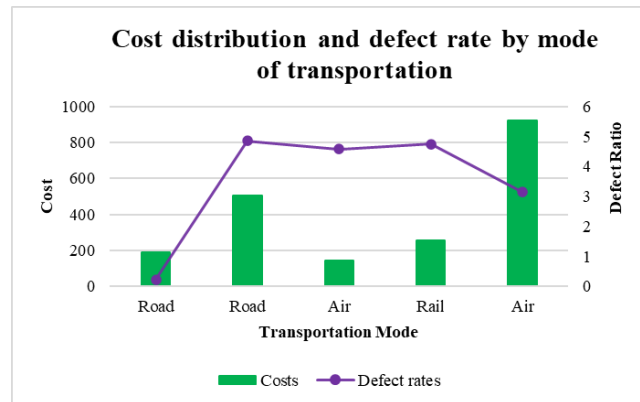


Fig. 5. Defect rates and costs across transportation modes.

The performance and dependability of various transport choices within the supply chain network are provided by this thorough analysis of defect rates and prices by transportation mode and route. Supply chain managers can find patterns, trends, and possible areas for improvement by examining this data. To reduce risks and guarantee product integrity during transportation, routes with high defect rates, for instance, could need more careful inspection and quality control procedures. Analysing the prices of various transportation options could additionally help to optimise logistics processes and reduce costs without sacrificing quality of service. Fig. 5 provides insights that enable supply chain managers to optimise transportation methods, improve operational efficiency, and make data-driven choices in order to efficiently fulfil company objectives.

4) *Analysing defect rate by product:* Within the supply chain network, examining the defect rate by product offers important information about the dependability and quality of each product class. Through a comprehensive analysis of product defect rates, enterprises may pinpoint opportunities for enhancement, execute focused quality control strategies,

and augment the overall quality of their goods. In order to help businesses improve their quality management procedures, reduce the cost of errors, and uphold customer satisfaction levels, this research attempts to evaluate the defect rates seen across several product categories.

The fault rates seen for several product categories within the supply chain network are shown in the above Table IV. A distinct product category is represented by each row, along with the related failure rates. At 1.919287, cosmetics have the lowest fault rate of all the items. Conversely, haircare products had a somewhat higher failure rate of 2.48315. Skincare goods have a 2.334681 failure rate, which is in the middle. The quality and dependability of various product categories within the supply chain are usefully shown by this data. Through product-specific defect rate analysis, companies may pinpoint areas that could use improvement and put focused quality control tactics in place. Companies can minimise expenses related to returns and replacements, improve customer happiness, and keep a competitive advantage in the market by fixing faults and minimizing product inconsistencies.

TABLE IV. DEFECT RATE BY PRODUCT

| Products | Defect Rates |
|-----------|--------------|
| Cosmetics | 1.919287 |
| Haircare | 2.48315 |
| Skincare | 2.334681 |

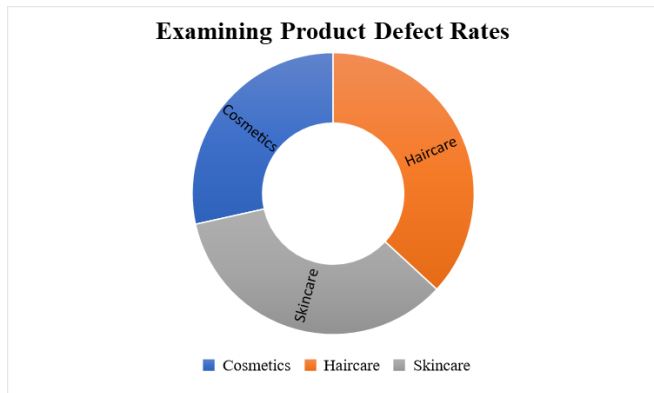


Fig. 6. Product-specific defect rates.

Stakeholders could frequently determine whether goods have greater or lower failure rates by referring to Fig. 6, which displays a graphical depiction that compares defect rates across several product categories. Understanding each product category's relative quality and dependability along the supply chain is made easier by the figure. Furthermore, it functions as a valuable instrument for decision-making, allowing organisations to arrange resources and prioritise efforts towards improving quality in order to reduce errors and raise the standard of their products.

B. Performance Assessment

To evaluate performance effectively, it is essential to take into account a variety of critical measures when comparing the outcomes of a proposed framework with baseline techniques or current solutions in the existing literature. When the

suggested framework is compared to other well-established techniques, these metrics offer valuable information about its efficacy, productivity, and dependability.

1) *Accuracy*: When assessing the effectiveness of predictive models, such as those used in supply chain management, accuracy is a crucial parameter. The proportion of correctly categorised examples out of all examined instances is measured to determine the model's accuracy in making predictions. Accuracy is of the utmost significance in supply chain management since it has a direct impact on decisions made about inventory control, demand forecasting, and supplier selection. The aforementioned Eq. (3) represents accuracy as a percentage and shows how accurate the forecasts generated by the model.

$$Accuracy = \frac{\text{No.of Correct Predictions}}{\text{Total No.of Predictions}} \times 100\% \quad (3)$$

The performance of several techniques, including Support Vector Machine (SVM), Decision Tree (DT), Random Decision Tree (RDT), and the suggested Deep Q-learning methodology, is thoroughly compared in Table V. The accuracy measure is employed to assess the efficacy of every technique, with the outcomes displayed as proportions. The outcomes show that, with an astounding accuracy rate of 98.9%, the suggested Deep Q-learning methodology attains the best accuracy out of all approaches. This implies that the Deep Q-learning methodology has shown to be exceptionally effective in accurately categorising situations in the area of supply chain management. This approach's high accuracy suggests that it is good at identifying intricate patterns and correlations in the data, which could assist with prediction and decision-making.

TABLE V. PERFORMANCE COMPARISON OF THE SUGGESTED APPROACH

| Methods | Accuracy (%) |
|-----------------|--------------|
| SVM | 94 |
| DT | 95 |
| RDT | 91 |
| Proposed Deep Q | 98.9 |

The Table V presents a comprehensive comparison of the accuracy percentages achieved by different methods employed for supply chain management optimization. Among the traditional machine learning algorithms assessed, Support Vector Machine (SVM) demonstrated a respectable accuracy of 94%, followed closely by Decision Tree (DT) at 95% and Random Decision Tree (RDT) at 91%. These methods, while effective, were surpassed by the proposed Deep Q-Learning (DQL) approach which increased by 3.8 % when compared to related accuracy, which showcased remarkable accuracy, standing at an impressive 98.9%. DQL, a reinforcement learning technique leveraging neural networks, showcased its superiority in addressing the complexities of supply chain management, offering unparalleled accuracy in predictive modeling and optimization tasks.

The results underscore the transformative potential of incorporating advanced methodologies like DQL into supply

chain management practices. With its unmatched accuracy, the proposed DQL framework promises to revolutionize decision-making processes within supply chains, enabling organizations to navigate uncertainties, optimize resource allocation, and enhance operational efficiency. This study highlights the pivotal role of innovative techniques in driving the evolution of supply chain management towards greater agility, resilience, and competitiveness in today's dynamic business landscape.

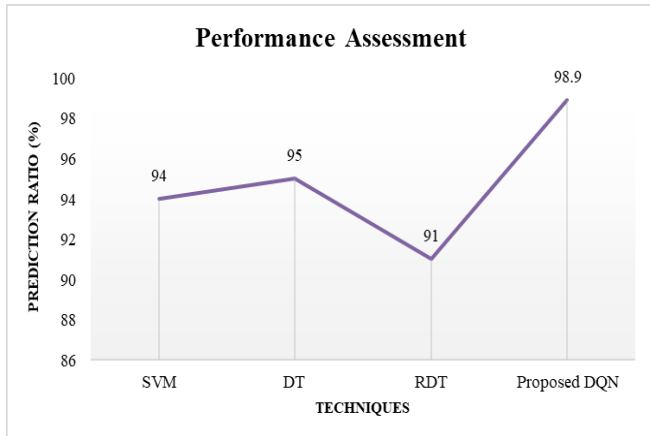


Fig. 7. Performance comparison of different methods in supply chain management.

The findings in Fig. 7 demonstrate the effectiveness of the suggested DQN method in relation to supply chain management. Enhancing forecast accuracy, streamlining processes, and eventually increasing value creation in the supply chain are all possible with this strategy.

VI. CONCLUSION AND FUTURE WORK

The present investigation delved into the efficacy of multiple supply chain management techniques, with a particular emphasis on the suggested Deep Q-Network (DQN) strategy. The research aimed to assess the predictive and optimization capabilities of various methods, including Support Vector Machine (SVM), Decision Tree (DT), Random Decision Tree (RDT), and DQN, within the realm of supply chain processes. Following a thorough examination, it became evident that the Deep Q-learning method outperformed conventional machine learning techniques, boasting an impressive accuracy rate of 98.9%. This superior performance underscores the capacity of deep reinforcement learning techniques to enhance forecasting accuracy and address complex challenges within supply chain management. The significance of this research lies in its potential to enhance both the efficiency and productivity of supply chains. By harnessing advanced AI techniques like Deep Q-learning, organizations stand to elevate customer satisfaction, streamline processes, and generate more precise forecasts. Moreover, the findings underscore the importance of leveraging innovative methodologies to navigate the dynamic obstacles inherent in supply chain management, particularly in light of increasing complexity and unpredictability.

This study contributes to the expanding body of research on machine learning applications in supply chain

management. It not only showcases the substantial performance enhancement offered by DQN but also illustrates its effectiveness in optimizing supply chain operations. Future research avenues could focus on further refining the DQN approach, exploring its applicability across diverse supply chain scenarios, and investigating potential synergies with other cutting-edge technologies such as blockchain and the Internet of Things (IoT). These endeavors promise to pave the way for more comprehensive and robust supply chain optimization strategies.

REFERENCES

- [1] M. R. I. Slam, M. E. I. Monjur, and T. Akon, "Supply Chain Management and Logistics: How Important Interconnection Is for Business Success," *Open Journal of Business and Management*, vol. 11, no. 5, Art. no. 5, Aug. 2023, doi: 10.4236/ojbm.2023.115139.
- [2] C. Ude, "Industrial Materials and their Processing," Feb. 2024.
- [3] R. Adzija and M. Kukhta, "Chapter 5 – Warehousing," Feb. 2022, Accessed: Mar. 24, 2024. [Online]. Available: <https://ecampusontario.pressbooks.pub/logistics001oerfc/chapter/chapter-5-warehousing/>.
- [4] A. G. Mulky, "Distribution challenges and workable solutions," *IIMB Management Review*, vol. 25, no. 3, pp. 179–195, Sep. 2013, doi: 10.1016/j.iimb.2013.06.011.
- [5] D. M. G. Albrecht, D. M. Green, L. Hoffman, D. M. G. Albrecht, D. M. Green, and L. Hoffman, "17.5 The Supply Chain and Its Functions - Principles of Marketing | OpenStax." Accessed: Mar. 24, 2024. [Online]. Available: <https://openstax.org/books/principles-marketing/pages/17-5-the-supply-chain-and-its-functions>.
- [6] D. M. G. Albrecht, D. M. Green, and L. Hoffman, "1.1 Marketing and the Marketing Process - Principles of Marketing | OpenStax." Accessed: Mar. 24, 2024. [Online]. Available: <https://openstax.org/books/principles-marketing/pages/1-1-marketing-and-the-marketing-process>.
- [7] "SCM: The Lifeblood of Business," SAP. Accessed: Mar. 24, 2024. [Online]. Available: <https://www.sap.com/mena/products/scm/what-is-supply-chain-management.html>.
- [8] D. Rabouin, "Coronavirus has disrupted supply chains for nearly 75% of U.S. companies," *Axios*. Accessed: Mar. 24, 2024. [Online]. Available: <https://www.axios.com/2020/03/11/coronavirus-supply-chains-china>.
- [9] D. Fan, Y. Zhou, A. Yeung, C. Lo, and C. Tang, "Impact of the U.S.–China trade war on the operating performance of U.S. firms: The role of outsourcing and supply base complexity," *Journal of Operations Management*, vol. 68, Oct. 2022, doi: 10.1002/joom.1225.
- [10] J. Moosavi, A. M. Fathollahi-Fard, and M. A. Dulebenets, "Supply chain disruption during the COVID-19 pandemic: Recognizing potential disruption management strategies," *Int J Disaster Risk Reduct*, vol. 75, p. 102983, Jun. 2022, doi: 10.1016/j.ijdr.2022.102983.
- [11] "Consumer prices for meats, poultry, fish, and eggs up 10.5 percent for year ended September 2021 : The Economics Daily: U.S. Bureau of Labor Statistics." Accessed: Mar. 25, 2024. [Online]. Available: <https://www.bls.gov/opub/ted/2021/consumer-prices-for-meats-poultry-fish-and-eggs-up-10-5-percent-for-year-ended-september-2021.htm>.
- [12] "10 Supply Chain Management Problems With New Solutions | Cart.com." Accessed: Mar. 25, 2024. [Online]. Available: <https://cart.com/blog/supply-chain-management>.
- [13] S. Roy and M. Mitra, "Enhancing Efficiency in Healthcare Supply Chains: Leveraging Machine Learning for Optimized Operations," *International Journal For Multidisciplinary Research*, vol. 3, p. 2, Nov. 2021, doi: 10.36948/ijfmr.2021.v03i06.10323.
- [14] H. Lin, J. Lin, and F. Wang, "An innovative machine learning model for supply chain management," *Journal of Innovation & Knowledge*, vol. 7, no. 4, p. 100276, 2022.
- [15] F. Shoushtari, E. Ghafourian, and M. Talebi, "Improving Performance of Supply Chain by Applying Artificial Intelligence," *International journal of industrial engineering and operational research*, vol. 3, no. 1, pp. 14–23, 2021.

- [16] V. Kumar, H. Pallathadka, S. Sharma, C. Thakar, M. Singh, and L. Pallathadka, "Role of machine learning in green supply chain management and operations management," *Materials Today: Proceedings*, vol. 51, Dec. 2021, doi: 10.1016/j.matpr.2021.11.625.
- [17] M. C. Camur, S. K. Ravi, and S. Saleh, "Enhancing Supply Chain Resilience: A Machine Learning Approach for Predicting Product Availability Dates Under Disruption." arXiv, Apr. 28, 2023. Accessed: Mar. 22, 2024. [Online]. Available: <http://arxiv.org/abs/2304.14902>.
- [18] X. Zhu, A. Ninh, H. Zhao, and Z. Liu, "Demand Forecasting with Supply-Chain Information and Machine Learning: Evidence in the Pharmaceutical Industry," *Production and Operations Management*, vol. 30, no. 9, pp. 3231–3252, Sep. 2021, doi: 10.1111/poms.13426.
- [19] "Supply Chain Analysis." Accessed: Mar. 24, 2024. [Online]. Available: <https://kaggle.com/code/amirmotefaker/supply-chain-analysis>.
- [20] J. Fan, Z. Wang, Y. Xie, and Z. Yang, "A Theoretical Analysis of Deep Q-Learning." arXiv, Feb. 23, 2020. Accessed: Nov. 17, 2023. [Online]. Available: <http://arxiv.org/abs/1901.00137>.
- [21] H. Dave, "Bellman Optimality Equation in Reinforcement Learning," *Analytics Vidhya*. Accessed: Mar. 25, 2024. [Online]. Available: <https://www.analyticsvidhya.com/blog/2021/02/understanding-the-bellman-optimality-equation-in-reinforcement-learning/>.

Advancing Prostate Cancer Diagnostics with Image Masking Techniques in Medical Image Analysis

H. V. Ramana Rao^{1*} , V RaviSankar² 

Research Scholar, Department of CSE, GITAM University, Hyderabad, India¹
Associate Professor, Department of CSE, GITAM University, Hyderabad, India²

Abstract—Prostate cancer is a prevalent health concern characterized by the abnormal and uncontrolled growth of cells within the prostate gland in men. This research paper outlines a standardized methodology for integrating medical slide images into machine learning algorithms, specifically emphasizing advancing healthcare diagnostics. The methodology involves thorough data collection, exploration, and image analysis, establishing a foundation for future progress in medical image analysis. The study investigates the relationships among image characteristics, data providers, and target variables to reveal patterns conducive to diagnosing medical conditions. Novel background prediction techniques are introduced, highlighting the importance of meticulous data preparation for improved diagnostic accuracy. The results of our research offer insights into dataset characteristics and image dimensions, facilitating the development of machine-learning models for healthcare diagnosis. Through deep learning and statistical analysis, we contribute to the evolving field of prostate cancer detection, showcasing the potential of advanced imaging modalities. This research promises to revolutionize healthcare diagnostics and shape the trajectory of medical image analysis, providing a robust framework for applying machine learning algorithms in the field. The standardized approach presented in this paper aims to enhance the reproducibility and comparability of studies in medical image analysis, fostering advancements in healthcare technology.

Keywords—Prostate cancer; data exploration; image analysis; medical conditions; background prediction techniques; data preparation; diagnostic accuracy; dataset characteristics; image dimensions; deep learning; statistical analysis; prostate cancer detection; advanced imaging modalities; healthcare diagnostics; medical image analysis; machine learning; target variables

I. INTRODUCTION

Prostate cancer comes with a huge burden on men's health worldwide, and so the earlier it is detected and diagnosed, the patients get the best outcomes. Over the previous decades, we have observed increased use of cutting-edge medical imaging for accurate diagnosis. Image segmentation has gained prominence among the myriad of medical image analysis techniques as it enables the identification and depiction of prostate lesions, which may harbor cancerous cells, with unrivaled accuracy. In the instance of different types of medical imaging devices, like Magnetic Resonance Imaging (MRI) and Computed Tomography (CT) scans, help doctors identify prostate and stage prostate cancer by giving detailed and high-quality visualization of the prostate. On the flip side, the boundary of cancer clusters and filming the interior regions of a body are not easy and remain challenging. Multi-masking,

which stresses the desired location and struggles of the unnecessary information emerging, has become a decisive factor in improving the addressing in the visualization. Nwaigwe, Ogbonna, and Oliwe (2022) [1] stress the need for a complete understanding of PSA distribution (medical data).

In the course of this research, it might well be that progress in healthcare science is expected since diagnostics could be revolutionized. The main objective of the preparatory phase of medical slide images is to improve the precision and velocity of computer learning methods in detecting body conditions. The method includes using masks and predicting the background, similar to the approach demonstrated by Pinckaers, et al. (2021). All the slide images go through end-to-end training with image-level labels [4].

These objectives offer direction in determining various image features, data providers, and interchangeable patterns with these options. Valan, Zimjonov, and Maçal (2023) report that the efficiency of machine learning is achieved via the application of radiomics features, which become a part of our methodology context [7]. The investigation of a range of dimensions, the pixel spacing of the radiography scans, and the number of series forming the basis of research are planned to shed light on conditions that will help in the diagnosis. We included a new process for creating and validating the masks as part of the used approach to address the question of machine learning model accuracy enhancement.

Additionally, this study seeks to integrate the findings into a coherent and credible data framework. For instance, the study of Ismail et al. (2020) [5] pointed out the machine-learning classification technique of prostate cancer, justifying that the role of computational models in healthcare diagnostics is cardinal, together with Chang, Hu, and Tsai (2015), who delved into the utilization of machine learning with dynamic MRIs for prostate cancer detection and in line with our emphasis on the latest imaging applications [6].

The study also aims to include the ensemble-based classifier approach, as shown by Elshazly, Elkorany, and Hassanien (2013). This proves the trend of higher diagnostic performance by combining several machine learning models [8]. This means we shall pursue an integrated strategy that harvests data from a comprehensive collection of medical images.

This research explores the leading-edge medical imaging diagnostics field and uses machine learning and image analysis progress. By integrating the insights and approach from leading

*Corresponding Author.

research, this endeavor aims to become physically implicated in the early detection and diagnosis of medical conditions, uplifting a patient's outcome and progressing healthcare diagnostics.

The medical slide image integrating approach presented in machine learning algorithms is a progressive breakthrough in the precise diagnostic process of the health care system. Data is specifically and carefully taken and explored for this method, and the image characteristics are assiduously analyzed to improve the precision of readings and speed up the process. The motivation behind this research is the pressing need for the most accurate and prompt diagnosis of both medical conditions in general and prostate cancer in particular, where early detection is necessary for successful treatment.

Another important contribution of this approach lies in proper data preparation, which includes novel background prediction techniques so diagnostic precision can be improved. This approach identifies information on the database characteristics and image dimensions, which are later used in constructing machine learning models, especially in prostate cancer screening and diagnostics.

The outreach of research benefits cannot be restricted to one level. It is a specific medium that facilitates machine learning in medical image analysis. In turn, the experiments from this field are becoming more and more plausible and comparable. Besides, machine learning-aided diagnosis systems can be more accurate and reliable if data from hospitals, pathologists, and expert systems are deployed. Healthcare systems may adopt new diagnostic approaches by infusing new technologies. It may end up with early diagnosis as well as accurate diagnosis of prostate cancer in other diseases, giving precision medicine to patients that will thereby boost outcomes and lower healthcare costs.

As medical diagnostics continue to gain ground, the results of this work can be one of the factors that might alter the future of medical image modeling and interpretation. The interconnections we will deduce will serve as the foundation for incorporating machine learning algorithms in health diagnosis and analysis.

II. LITERATURE REVIEW

Machine learning (ML) algorithms in healthcare diagnostics, particularly in prostate cancer detection, have been in the spotlight of a large variety of research for a long time. This part will describe the experiments and research conducted to date related to this area.

Nwaigwe, Ogonna, and Oliwe (2022) conducted research concentrating on the PSA distribution probability interpretation to enable early diagnosis of prostate cancer. Notably, the scientist's investigation highlights the need to learn about the statistical characteristics of PSA levels, one of the most important properties for diagnostics [1]. Alkhateeb, Atikukke, and Rueda (2020) shed light on different diagnostic methods for prostate cancer, emphasizing their uses and depicting the best practices [2].

Norbu Zongpa (2019) aimed to illustrate the importance of bladder protocol in dealing with prostate cancer through

radiotherapy. This study highlights the relevance of the approaches in which the treatment is aimed at particular conditions [3]. Pinckaers, et al. (2021) applied an end-to-end training approach, which used whole slide images only with image-level labels to detect prostate cancer. The method showcases where deep learning can play an important role in medical image analysis [4].

Ismail et al. (2020) suggested a classification method for predicting prostate cancer (cancer-wise), accentuating the significance of computation models in healthcare [5]. Chang, Hu, and Tsai (2015) also revealed that dynamic MRIs can be helpful and that data processing computational techniques can boost the detection of prostate cancer [6].

Valan, Zimjonov, and Maçal (2023) developed an algorithm for computer-aided analysis of prostate cancer based on extracting the important radiomic features and using the fine-tuned Linear SVM methods. This research confirms the utility of the combined approach of computational techniques with radiology applications [7]. Elshazly, Elkorany, and Hassanien (2013) studied breast cancer diagnosis classifiers based on an ensemble. These works informed us about the advantages of involving various models [8].

Lehaire, et al. 2014 designed a computer-aided diagnostic system for prostate cancer that is automated with learned dictionaries and supervised classification. It is noteworthy that there is a connection between the two due to the bunch of traditional and innovative methods [9]. Mesrabadi and Faez (2018) explored using artificial neural networks and deep learning to enhance early prostate cancer diagnosis. They land at the point where developed methods offer the chance to raise the detecting rate [10].

These studies have highlighted the growing attention to computationally assisted decisive prostate cancer diagnostics, and the promising prospects of advanced imaging techniques and statistical analysis methods for definite progress in this field have been confirmed.

III. METHODOLOGY

The approach taken in this study involves several critical steps, including data collection, exploration, image analysis, and mask processing. The following sections offer a comprehensive overview of each stage:

A. Data Source and Loading

The dataset used in this study is the Prostate Cancer Grade Assessment (PANDA) dataset, a rich resource obtained from a Kaggle competition. This dataset contributes to research on prostate cancer grading and provides a free repository available to researchers and practitioners in the medical imaging community. The dataset contains high-resolution pathology images from prostatic tissue samples from various medical centers.

The PANDA dataset is digital and, therefore, enables a detailed study of histopathological images down to any required magnification level and provides characteristics of prostatic tissue in full: specific image in the collection shows the previous ISUP (International Society of Urology Pathology) grading—the identification of grade assignments.

This annotation is the actual true point of reference and supervised process; the only way an innovative technique that becomes an automated grading of prostate cancer can purport to do so.

The PANDA dataset critiques algorithms that test the prediction that prostate cancers will be graded effectively and match those graded by a human pathologist. This is a helpful foundation for various collaborations to be launched and for identifying the best way to diagnose prostate cancer and freshen up its treatment plans. By sharing such a dataset, interested parties in medical imaging would be encouraged to work together to understand prostate cancer disease and its treatment better. Three essential files accompany the dataset:

1) *train.csv*: This file is a set of indispensable training data stored within the machine learning model framework, which consists of vital attributes and tags that shape our ability to recognize patterns related to the cancer of the prostate

2) *test.csv*: It is a test data file to be used for model evaluation, especially in terms of pockets' precision and consistency, so that it can be applied to new data types with availability.

3) *sample_submission.csv*: This document explains the template for making voice forecasts with Kaggle competition in mind and a set of rules for providing findings in an organized manner.

These files add very much to the detailed information about the training and test data; hence, they constitute the backbone of our analysis and the creation of our model. Overall, they offer a complete description of the training and testing data, which lay a basis for subsequent analysis using various models.

As illustrated in Architecture Diagram Fig. 1, the data preparation process involves the acquisition, preprocessing (cleaning, normalization, augmentation), and splitting into training and test sets for model training and evaluation. The Architecture Diagram serves as a systematic guide, ensuring the reproducibility and validity of our research findings.

B. Data Exploration

EDA (exploratory data analysis) is one of the main workstations in the data science pipeline. It, thus, extracts the underlying prototypic structure and characteristics of the data. The first phase that must be done in machinery exploration of the training dataset is to get the proper approach to grasp the dataset's peculiarities and prevent data contamination while the data are being prepared for further analysis or model training.

Displaying the first rows of the preliminary training data set is the first step of EDA. We do it by calling the display (train).head (). The next step is data wrangling. Data wrangling is performing data capture that allows practitioners to take a preliminary look at the structure and feature composition to pinpoint anticipated problems. Knowing the basics of the accounting operation's first rows can lead to a better understanding.

Following the data collection step, summary statistics are built to describe the features present in the dataset. The evaluation of the dataset structure involves the analysis of the

shape of the function, unique identifiers of providers such as *isup_grade* and *gleason_score*, and variation of the data providers. The distribution of target tags is also considered. This set of statistics aims to give us a general idea about the data. We can easily identify patterns, anomalies, or imbalances on that base, which might affect the subsequent analysis or model building.

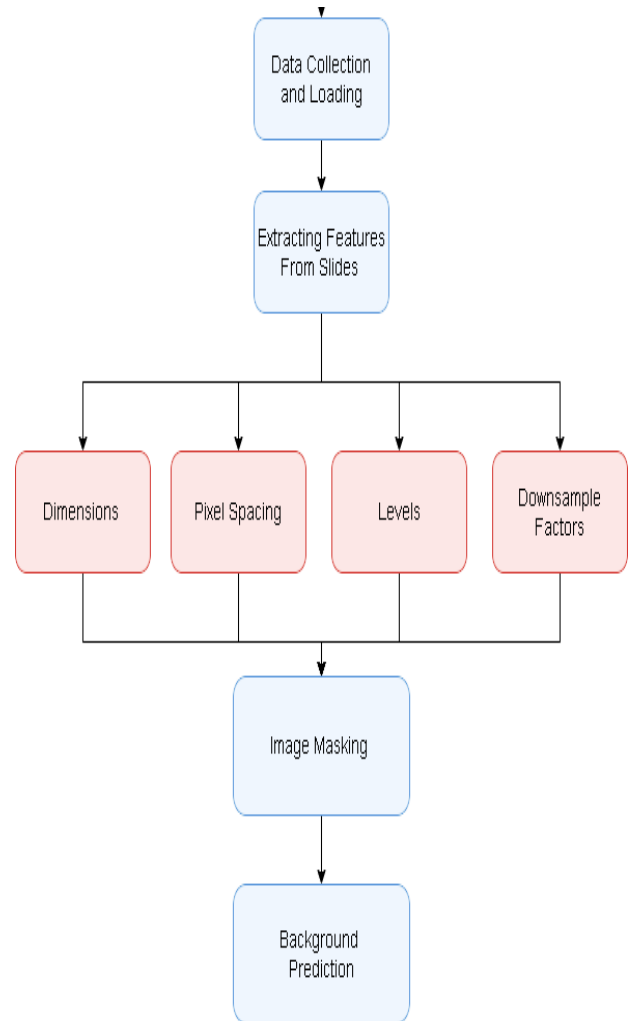


Fig. 1. Architecture diagram.

While the data reliability and accuracy are of concern, verifying the existence of image files to match the image IDs is one way of upholding the uniformity and integrity of the data. This step entails identifying mechanical defects during the process's data processing and model training stages. The ones that are out of the particular space or are inconsistent with each other will hinder the workflow process. This idea is verified by the fact that image files are irreplaceable at the professional level. The analysis comprises analysis of the dataset shape, image model identification, provider diversity, and frequency of labels like *iscpp_grade* and *gleason_score*. These statistics overview the dataset to help identify patterns, anomalies, or imbalances that might influence subsequent analysis or model building.

Another important step in EDA is to correct the `gleason_score` label for consistency. In this case, label uniformity is material since it will improve the dataset's quality and is also a step toward improving the reliability of future analyses and model predictions. This process in the data preparation is hence critical, and the inconsistency in labels introduces noise that affects the ability to generalize and may compromise the effectiveness of the machine learning models.

C. Slide Image Characteristics

After exploratory data analysis, an analysis of the image features using the `OpenSlide` library is performed, and we investigate the distribution and relationships of these dimensions within the dataset. A scatter plot will represent the connection between image width and height. The plot explains the dataset's image size range and variability. Exploring the dataset exposes its structure and, thus, the potential biases in image dimensions.

On the other hand, scatter plots that hold in the plot with the target variable `ISUP` grade demonstrate potential correlations of physical image features and diagnostic outcomes. The analysis will help find connections or relations between imaged details and `ISUP` grade, which can promote diagnostic models for prostate cancer screening.

Moreover, the distribution plots also explore the distribution and range of the width and height of the image markers. This analysis offers additional information about the data dimensions change, thus helping during the model training and anomalies location.

In essence, these experiments with scatter plots and distribution plots help in creating a critical understanding of the nature and relationships of some image properties with the resultant diagnostic outcome, the future of which may be in model development and fine-tuning in the field of medical image analysis and diagnosis of prostate cancer.

D. Mask Images

The next step in the methodology is processing the masks, which is an important step for data integrity and robustness. The masks of the pictures corresponding to slides are filtered, keeping only the first channel, which, in turn, is assigned for the analysis. Another step to confirm the justness of the processed data is verifying the empty last two channels, reducing the probability of any mistakes to a minimum.

Then, the background can be created by segmenting the background areas within the images. This procedure proceeds with building a background mask that should reflect an aggregate of segmented mask images, where the background pixels are marked with a mask value of 0. Using the random sample displays from the background mask and matching slide images demonstrates how the accuracy of the generated mask is verified. This validation step is rather elementary for providing in-depth, unbiased recognition and differences between foreground features and the background areas within the images.

Implementing a function for predicting the background of slide images using thresholding techniques:

$$B(x,y) = \begin{cases} 1, & \text{if } I(x,y) > T \\ 0, & \text{otherwise} \end{cases} \quad (1)$$

Eq. (1) is utilized for thresholding operation to identify background regions.

Handling the mask images and creating background masks are crucial elements of our methodology, which are principally designed to increase the correctness of preliminary analysis. The steps include preparing the slide images with machine learning algorithms to facilitate accurate and effective diagnosis of health conditions in medical facilities.

To validate accuracy, visualize random samples of background masks, original slide images, and predicted background regions.

$$P(x,y) = \frac{e^{z_{class}}}{\sum e^c} \quad (2)$$

Eq. (2) is utilized to predict probability through the softmax function of the output layer.

Algorithm1: Data Preprocessing and Analysis

Require:

- Root directory (ROOT)
- Training data (train)
- Test data (test)

Initialization:

- Load data files: train, test, sample submission from ROOT

Data Exploration and Summary:

1. Explore and summarize training data
2. Calculate dataset statistics

Explore Slide Image Characteristics:

3. **for** each image ID in training data, **do**
4. Extract Dimensions \leftarrow ROOT, image ID
5. Extract PixelSpacing \leftarrow ROOT, image ID
6. Extract Levels \leftarrow ROOT, image ID
7. Extract DownsampleFactors \leftarrow ROOT, image ID
8. ScatterPlot(Dimensions[0], Dimensions[1])
9. **if** HasIsupGrade(isup grade) **then**
10. ScatterPlot(Dimensions[0], Dimensions[1], isup grade)
11. **end if**
12. DistributionPlot(Dimensions[0])
13. DistributionPlot(Dimensions[1])
14. **end for**

Process Mask Images:

15. **for** each image ID in training data **do**
16. Mask \leftarrow LoadAndProcessMask(ROOT, image ID)
17. ConfirmLastTwoChannelsEmpty(Mask)
18. BackgroundMask \leftarrow CreateBackgroundMask(Mask)
19. VisualizeRandomSamples(Mask, Image)
20. **end for**

Background Prediction Function Execution:

21. Execute the background prediction function

Ensure:

Processed data and masks

Functions:

```

22. function LOADANDPROCESSMASK(ROOT, image ID)
23. Mask ← Load the mask image from ROOT and image ID
    as a 2D array
24. for x = 1 to image width do
25.   for y = 1 to image height do
26.     if mask(x, y) is not empty in channels 2 and 3 then
27.       Set Mask(x, y) in channels 2 and 3 to 0
28.     end if
29.   end for
30. end for
31. return Mask
32. end function
33. function CREATEBACKGROUNDMASK(Mask)
34. Initialize BackgroundMask as a 2D binary array with the
    same dimensions as Mask
35. for x = 1 to image width do
36.   for y = 1 to image height do
37.     if Mask(x, y) is 0 then
38.       BackgroundMask(x, y) ← 1
39.     else
40.       BackgroundMask(x, y) ← 0
41.     end if
42.   end for
43. end for
44. return BackgroundMask
45. end function
    
```

The methodology section delineated the sequential data collection, exploration, image analysis, and mask processing procedures. These preliminary steps are imperative for data preparation, facilitating subsequent analysis, and model development. The examination provided valuable insights into the dataset's attributes, aiding in creating masks for background detection, which is integral to the subsequent phases of the research.

IV. RESULT AND ANALYSIS

In this section, we present the outcomes of the data preprocessing and analysis steps, as elucidated in Algorithm 1. The analysis encompasses the exploration of training data, dataset statistics, and the characteristics of slide images.

A. Exploration of Training Data

The dataset training stage proved to be a critical part of the study, giving a lot of key information about the data's composition and characteristics. The provisions of data and image manufacturing were a result of our detailed analysis that was aimed at disentangling the aspects of the data. Summary

statistics gave a summary view of the system, which showed, for example, the number of images with IDs, data providers, and the Gleason Score ranges, among others. This quantitative analysis has been very useful to me in understanding the scale and the level of detail in the dataset and the existence of bias, if any.

Moreover, utilizing multiple visualization techniques, like bar charts and scatter plots, allowed us to uncover the connection between specific variables. These visualizations have highlighted differences among the target variable parameters based on categories. It also shows anomaly patterns and individual provider irregularities within the data. The observation of the width and height dimensions enabled the discovery of patterns, as well as unusual images that were characterized by differentiation in datasets. Besides, vector length and dimension are proportional to isup_grade, which gives a basic understanding of physical attributes versus cancer grading. By carefully addressing this multifaceted examination, the stage was set for data preprocessing and model development involving a machine learning algorithm trained only on data that had been exhaustively analyzed.

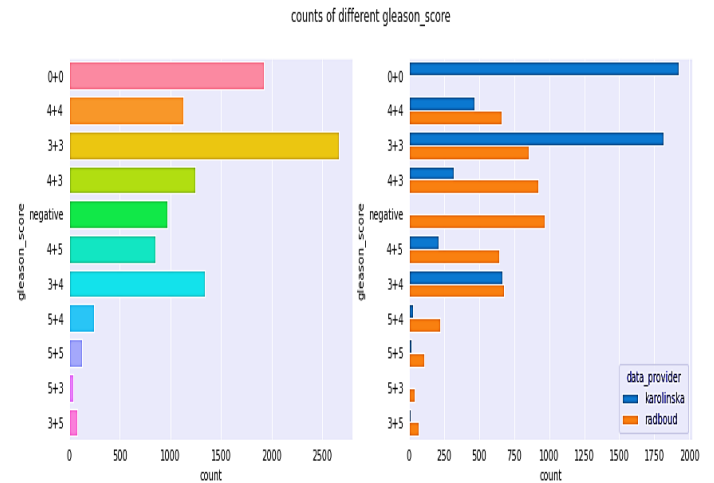


Fig. 2. Gleason score distribution.

Fig. 2 above explains how the Gleason count pairs are distributed in the dataset.

B. Dataset Analysis

We conducted a thorough statistical analysis to understand the dataset better. These statistics provide valuable insights for subsequent analysis and modeling.

| | image_id | data_provider | isup_grade | gleason_score |
|---|----------------------------------|---------------|------------|---------------|
| 0 | 0005f7aaab2800f6170c399693a96917 | karolinska | 0 | 0+0 |
| 1 | 000920ad0b612851f8e01bcc880d9b3d | karolinska | 0 | 0+0 |
| 2 | 0018ae58b01bdadc8e347995b69f99aa | radboud | 4 | 4+4 |
| 3 | 001c62abd11fa4b57bf7a6c603a11bb9 | karolinska | 4 | 4+4 |
| 4 | 001d865e65ef5d2579c190a0e0350d8f | karolinska | 0 | 0+0 |

```

shape : (10616, 4)
unique ids : 10616
unique data provider : 2
unique isup_grade(target) : 6
unique gleason_score : 11
    
```

Fig. 3. Train set analysis.

Fig. 3 visualizes the training set and its contents. The dataset was considered larger, with 10,616 unique images and the most diverse image. The data providers for this dataset were Karolinska and Radboud, so collaboration was indicated. The `isup_grade` column is our main target variable, defining a multiclass classification challenge in six distinct grades. Similarly, the `gleason_score` column, an alternative expression of cancer severity, introduces variability with 11 unique scores.

It is important to understand the contributions of each data provider's contributions: Karolinska and Radboud's contributions should be separate. The features should be compared to understand how much of their datasets contributed.

The relative frequency of the different grades of cancer is important. It would be subtly distributed across the dataset. Visualization techniques offer an alternative interpretation. A deeper analysis can be performed to discover more trends or correlations within different grades and with other variables. For example, one critical operation that needs to be undertaken before they all involves changing the "negative" entries in the `gleason_score` column to "0+0." Such uniform representation will help retain data consistency within the dataset, thus avoiding inconsistencies incurred by using different terminology in the same context.

C. Slide Image Characteristics

The following is the result obtained for slide image characteristics:

Dimensions: (9728, 29440)

Microns per pixel/pixel spacing: 0.486

Number of levels in the image: 3

Downsample factor per level: (1.0, 4.0, 16.0)

Dimensions of levels: ((9728, 29440), (2432, 7360), (608, 1840))

The above results give the following information:

1) *Image dimensions and pixel spacing*: The image's dimensions were precisely quantified, revealing a substantial image with dimensions (9728, 29440), indicative of a high-resolution dataset. The calculated pixel spacing, representing the physical distance per pixel, was approximately 0.486 microns. This information establishes a foundational link between digital representation and real-world measurements.

2) *Multi-resolution hierarchy*: The investigated image displays a hierarchical structure comprising three resolution levels. The downsample factors per level (1.0, 4.0, 16.0) signify a systematic reduction in resolution from the highest to the lowest level. This approach accommodates diverse analytical requirements, providing varying detail scales for nuanced exploration.

3) *Dimensions of each resolution level*: The dimensions of each resolution level further elucidate the intricate

composition of the image. The highest resolution level (Level 0) retained dimensions of (9728, 29440). Subsequent levels demonstrated reduced dimensions due to downsampling, with Level 1 at (2432, 7360) and the lowest resolution level (Level 2) at (608, 1840). These dimensions serve as a roadmap for navigating through different levels of granularity in the image.

The revealed characteristics hold significant practical implications for medical image analysis. The substantial initial dimensions provide a detailed view, while the hierarchical resolution levels facilitate efficient exploration of diverse detail scales. The precise pixel spacing measurement ensures accurate correlations between digital and physical aspects, enriching the interpretability of the image in the context of prostate cancer assessment.

Our analysis of slide images included extracting dimensions, pixel spacing, levels, and down-sample factors. Scatter plots, like the one depicted in Fig. 4, were generated to visualize relationships between different image characteristics. Additionally, distribution plots in Fig. 5 were created better to understand the distribution of image sizes within the dataset.

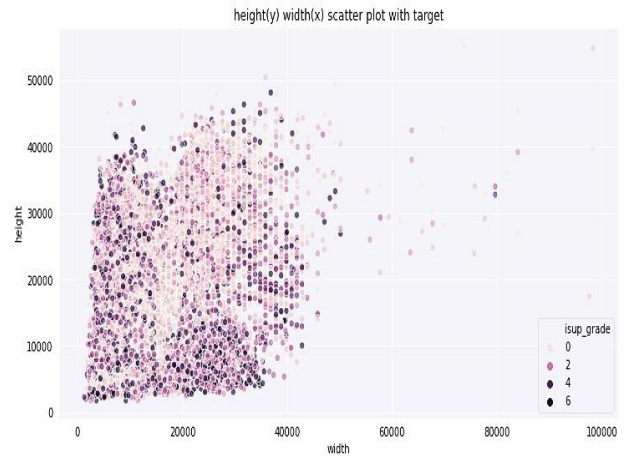


Fig. 4. Scatter plot of image characteristics.

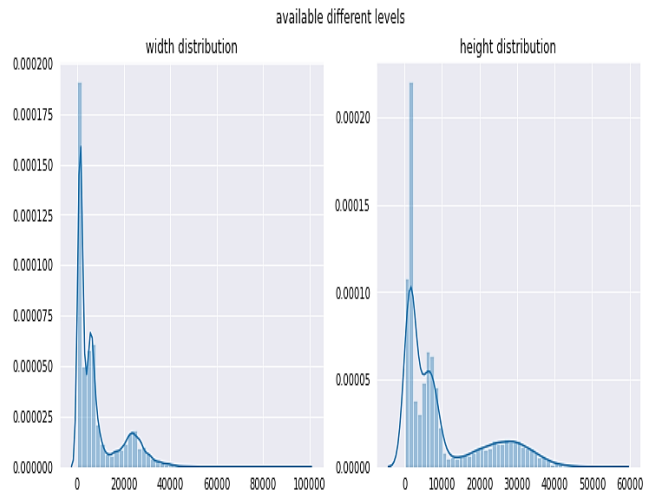


Fig. 5. Distribution plots of image dimensions.

D. Mask Processing and Visualization

The processing of mask images involved several essential steps, including confirming that the last two channels were empty and creating a background mask.

Fig. 6 displays visualizations of random samples of masks and background masks. The background prediction function played a crucial role in the analysis process.

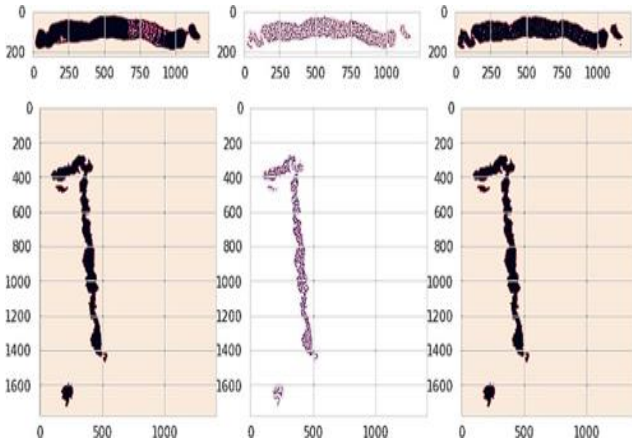


Fig. 6. Random samples of masks and background masks.

V. DISCUSSION

The data preprocessing and analysis have enriched the critical qualitative views regarding the characteristics of the prostate cancer dataset, which led to the subsequent model development. Issues such as the number of unique image IDs, distribution of data providers, and target label ranges could be identified using quantitative analysis and visualization, allowing the researchers to understand the composition and the possible biases in the dataset better. The investigation reached statistical characteristics and emphasized the training set diversity and scale with 10,616 images from two providers. Classifying the images under two categories of `isup_grade` and `gleason_score` with 6 subgroups and 11 groups made it easy. Furthermore, the image quality features of the slide, such as high resolution, were investigated to achieve exact digital representation. The multiscale structure enabled the detailed exploration, increasing the correlation during preprocessing and identifying the skew. Mask processing techniques based on the background derivation facilitate data integrity control. These features are necessary for data analysis precision. In-depth research can play an important role in model construction and evaluation and also contribute to clinical image processing and diagnosing diseases via determining data characteristics, image properties, and mask-processing approaches. The presented data visualizations improve interpretability and present guidelines for future research, thus contributing to the exponential growth of the prostate cancer diagnostic and treatment process.

Nwaigwe, Ogonna, and Oliwe (2022) [1] seek to address the statistical properties of Prostate Specific Antigen (PSA) with the understanding of PSA distribution being a crucial parameter for early detection. These outcomes indicate that for estimation of prostate size parameters, the Burr and Plasma inflammatory subpopulations may be the most suitable model,

particularly between ages 45 and 50 years, where a Prostate Specific Antigen (PSA) level above 4nmol/l may be designated high level. On the other hand, Alkhateeb, Atikukke, and Rueda (2020) [2] analyze the machine learning approaches in prostate cancer diagnosis; the authors point out the possibility of using genomic analysis to design less invasive diagnostic tests effectively. The results of their study emphasize the significance of the machine learning approach in predicting clinical features of prostate cancer. These machine-learning models were built on gene expression and next-generation sequencing data. Pinckaers et al. (2021) introduce training streaming convolution neural networks conditionally over input images for prostate cancer detection on whole slide images, which is end-to-end training that yields no extra heuristics [4]. Their method makes it possible to have data sets with lots of labels from pathology reports quickly, thus improving the speed at which cancer diagnosis takes in other novel ways of cancer diagnosis (Automated image analysis). As described before, our research targets an in-depth data analysis process from the ground up, comprising preprocessing procedures, and in the end, brings up a better understanding of the prostate cancer dataset. We applied quantitative methods and visualization techniques to the data components, distribution of severity levels, and imagery parameters, which served as baselines for declaring subsequent model building and evaluation.

There are some drawbacks to the research. The main limitation of our study is that it is based on a single data set, which may not encompass the entire spectrum of prostate cancer cases. Moreover, with our strategy demonstrating great potential, we still need to establish more evidence for it by conducting further tests and validations in actual healthcare settings. In elaboration, machine learning algorithms' linkage to medical image analysis techniques would be one cause for confusion and challenges.

VI. CONCLUSION AND FUTURE SCOPE

Our detailed approach to data preprocessing and analysis has effectively readied medical slide images for integration with machine learning algorithms, providing a promising avenue for future research. Through comprehensive mask processing and gaining insights into dataset characteristics, we have laid a solid foundation for applying machine-learning techniques to diagnose medical conditions using these images. This study underscores the significance of thorough data preparation in advancing the field. It paves the way for the future application of this methodology in machine learning algorithms for healthcare diagnosis and analysis.

The future trajectory of our research involves ongoing refinement and enhancement of our methodology for prostate cancer detection, aligning rigorously with the scientific standards set by the academic community. To bolster the reliability and generalizability of our approach, we envisage incorporating more expansive datasets encompassing diverse populations for a comprehensive analysis. Collaborative engagements with medical institutions and pathologists are pivotal for the authentication of our findings in authentic clinical scenarios, ensuring practical relevance and facilitating valuable feedback integration. Furthermore, the optimization of

our methodology will be achieved through the judicious integration of state-of-the-art deep learning models with advanced image processing techniques. This includes the thoughtful incorporation of imaging data with clinical, genetic, or other omics data to achieve a nuanced and holistic understanding of prostate cancer. A concerted emphasis on augmenting the generalizability and robustness of our methodology is paramount, potentially paving the way for widespread adoption within clinical settings. Ethical considerations, such as the conscientious deployment of AI methodologies and the integration of transparent systems, are imperative to uphold ethical standards and ensure responsible applications of innovative technologies in healthcare. Our study lays a moral foundation for a future where our refined methodology significantly contributes to the early and precise diagnosis of prostate cancer, unwaveringly adhering to the exacting standards outlined by the scientific community.

REFERENCES

- [1] C. C. Nwaigwe, C. J. Ogbonna, and E. U. Oliwe, "Appropriate Description of Probability Distribution of Prostrate Specific Antigen (PSA): An Aid to Early Detection of Prostrate Cancer," *Asian Journal of Probability and Statistics*, pp. 39-50, Nov. 2022. [Online]. Available: <https://doi.org/10.9734/ajpas/2022/v20i4437>.
- [2] A. Alkhateeb, G. Atikukke, L. Rueda, "Machine learning methods for prostate cancer diagnosis," *Journal of Cancer Biology*, vol. 1, no. 3, Dec. 2020. [Online]. Available: <https://doi.org/10.46439/cancerbiology.1.014>.
- [3] T. Norbu Zongpa, "Importance of Bladder Protocol in the Treatment of Prostate Cancer during Radiotherapy," *Cancer Therapy & Oncology International Journal*, vol. 13, no. 1, Jan. 2019. [Online]. Available: <https://doi.org/10.19080/ctoj.2019.13.555852>.
- [4] H. Pinckaers, W. Bulten, J. van der Laak, and G. Litjens, "Detection of Prostate Cancer in Whole-Slide Images Through End-to-End Training With Image-Level Labels," *IEEE Transactions on Medical Imaging*, vol. 40, no. 7, pp. 1817–1826, Jul. 2021. [Online]. Available: <https://doi.org/10.1109/tmi.2021.3066295>.
- [5] M. Ismail B., M. Alam, M. Tahernezehadi, H. K. Vege, and P. Rajesh, "A Machine Learning Classification Technique for Predicting Prostate Cancer," in *2020 IEEE International Conference on Electro Information Technology (EIT)*, Jul. 2020. [Online]. Available: <https://doi.org/10.1109/eit48999.2020.9208240>.
- [6] C.-Y. Chang, H.-Y. Hu, and Y.-S. Tsai, "Prostate cancer detection in dynamic MRIs," in *2015 IEEE International Conference on Digital Signal Processing (DSP)*, Jul. 2015. [Online]. Available: <https://doi.org/10.1109/icdsp.2015.7252087>.
- [7] M. Varan, J. Azimjonov, and B. Maçal, "Enhancing Prostate Cancer Classification by Leveraging Key Radiomics Features and Using the Fine-Tuned Linear SVM Algorithm," *IEEE Access*, vol. 11, pp. 88025–88039, 2023. [Online]. Available: <https://doi.org/10.1109/access.2023.3306515>.
- [8] H. I. Elshazly, A. M. Elkorany, and A. E. Hassanien, "Ensemble-based classifiers for prostate cancer diagnosis," in *2013 9th International Computer Engineering Conference (ICENCO)*, Dec. 2013. [Online]. Available: <https://doi.org/10.1109/icenco.2013.6736475>.
- [9] J. Lehaire, R. Flamary, O. Rouviere, and C. Lartizien, "Computer-aided diagnostic system for prostate cancer detection and characterization combining learned dictionaries and supervised classification," in *2014 IEEE International Conference on Image Processing (ICIP)*, Oct. 2014. [Online]. Available: <https://doi.org/10.1109/icip.2014.7025456>.
- [10] H. A. Mesrabadi and K. Faez, "Improving early prostate cancer diagnosis by using Artificial Neural Networks and Deep Learning," in *2018 4th Iranian Conference on Signal Processing and Intelligent Systems (ICSPIS)*, Dec. 2018. [Online]. Available: <https://doi.org/10.1109/icspis.2018.8700542>.

Deep Learning Network Optimization for Analysis and Classification of High Band Images

Manju Sundararajan¹, S.J Grace Shoba², Y. Rajesh Babu³, P N S Lakshmi⁴

Assistant Professor, Department of ECE, Velammal Engineering College, Chennai, India¹

Associate Professor, Department of ECE, Velammal Engineering College, Chennai, India²

Assistant Professor, Department of Computer Science and Engineering,

Koneru Lakshmaiah Education Foundation, Vaddeswaram, Andhra Pradesh, India³

Assistant Professor, Dept of CSE, Aditya College of Engineering, Surampalem, Andhra Pradesh, India⁴

Abstract—Examination and categorization of high-band pictures are used to describe the process of analysing and classifying photos that have been taken in many bands. Deep learning networks are known for their capacity to extract intricate information from images with a high bandwidth. The novelty lies in the integration of adaptive motion optimization, spectral-spatial transformer for categorization, and CNN-based feature extraction, enhancing high-band picture search efficiency and accuracy. The three primary parts of the technique are adaptive motion for optimization, spectral-spatial transformer for categorization, and CNN-based feature extraction. Initially, hierarchical characteristics from high-band pictures using a CNN. The CNN method enables precise feature representation and does a good job of matching the image's high and low features. This transformer module modifies the spectral and spatial properties of pictures intended for usage, enabling more careful categorization. This method performs better when processing complicated and variable picture data by integrating spectral and spatial information. Additionally, it is preferable to incorporate adaptive motion algorithms into offering the deep learning network training set. During training, this optimization technique dynamically modifies the motion parameter for quicker convergence and better generalization performance. The usefulness of the suggested strategy is demonstrated by researchers through numerous implementations on real-world high-band picture datasets. The challenges of hyperspectral imaging (HSI) classification, driven by high dimensionality and complex spectral-spatial relationships, demand innovative solutions. Current methodologies, including CNNs and transformer-based networks, suffer from resource demands and interpretability issues, necessitating exploration of combined approaches for enhanced accuracy. In high-band image evaluation and classification applications, the approach delivers state-of-the-art performance and python-implemented model has a 97.8% accuracy rate exceeding previous methods.

Keywords—Deep learning networks; Convolutional Neural Network (CNN); spectral-spatial transformer; adaptive motion optimization; high-band image analysis

I. INTRODUCTION

Hundreds of consecutive spectrum bands that have elevated resolutions make up the remotely sensed hyperspectral data that is gathered by hyperspectral sensors [1]. Hyperspectral images (HSIs) are being effectively utilized in precision farming, development, monitoring of the environment, and many other disciplines, according to recent

research in the field of remote identifying. Among the common features of an HSI is its ability to capture high-resolution one-dimensional spectrum data that describes the physical property in addition to scenario data within the target image's two-dimensional space [2]. Numerous dimensionality reduction techniques are now being used with hyperspectral imagery. Existing approaches can be categorized in two classes based on how much the physical importance of the initial information has been preserved, extraction of features and choosing features (also known as band selection). Through combining several initial characteristics into a single feature, feature extraction finishes the transformation of the initial information from high-dimensional space to low-dimensional space. As everyone is aware, extraction of features works effectively for reducing dimensions, but because spectral architecture is destroyed, it is unable to preserve the physical meaning of each band [3]. The goal of band selection is to maximize given performance indices by selecting a band subset after the unique band set. Band selection, as opposed to feature extraction, can produce a band subset that more accurately captures the original data of the different types of land cover [4]. The two main kinds of current band selection techniques are supervised band selection and unsupervised band selection, which involves the application of priori-label data. A great deal of label details is typically needed for supervised band selection, yet in most instances, getting labels for hyperspectral data can be exceedingly challenging [5]. Thus, uncontrolled remote sensing encompasses the majority of current effort. To be more precise, there are three types of current unsupervised band selection techniques: clustering-based, heuristics search-based, and ranking-based [6].

Choosing the type of data has an important effect on the outcomes in the feature classification area. Not every band in the hyperspectral photo has data; certain bands, such as ones impacted by different atmospheric conditions, are meaningless and reduce the efficacy of the classification. Additionally, redundant bands are present, which might impede the process of learning and lead to inaccurate predictions [7]. If the size of space pictures becomes so great it takes numerous instances to identify the connections among each band to the scene, even those bands, which carry sufficient information regarding the situation, might not be able to accurately forecast the categories. The findings in the field of features categorization are greatly affected by the kind of data selected. Each of the

groups in the hyperspectral image have data; certain bands are useless and lessen the effectiveness of the classification, which include those affected by various conditions in the atmosphere [8]. Furthermore, duplicate bands exist, which could hinder training and result in wrong projections. When space photos are so big that it requires multiple views to discern the relationships between every band as well as the scene, especially bands that contain sufficient details about the circumstances aren't always able to predict the category with any degree of accuracy (Hughes phenomenon). With the goal to reflect the initial hyperspectral data contained in the raw data, the choice of features algorithms seek to choose an appropriate amount of spectral band information [9]. The goal of feature extraction techniques, as opposed to feature selection techniques, is to use the unprocessed information to create an entirely novel low-dimension descriptors. Like previously said, selecting features techniques outperform extraction of features techniques within the subsequent area. Hyperspectral analysis of images needs entire unprocessed information from the spectrum bands whenever extraction of features techniques is used. When compared with feature extraction techniques, methods for selecting features only use a portion of the raw data's spectrum bands, and by employing those chosen bands rather than every one of the originally selected bands, the expense of acquiring hyperspectral information is further decreased [10].

Even while such methods can yield positive outcomes, the modification of HSIs data can occasionally destroy crucial details, resulting in data degradation. As such, these techniques are not necessarily the best options for reducing dimensionality as compared to conventional band selection procedures. Regarding the band selection approach, given the initial band space of the HSIs, the one that is most useful and unique band subgroup is selected by itself [11]. In a nutshell, the searching method and the assessment of the criteria function are both of the main components of band selection technologies. Although the latter assesses an evaluation for every band subset chosen using the initial selection of bands using a suitable criteria function, the earlier method uses an effective search technique to find an especially prejudiced band subset out of all possible subsets [12]. Finding the most effective spectrum combination among all band possibilities might occur at a very high computational expense. Using algorithms to haphazardly hunt for the minimal reduction was a different approach. The two types of band selection techniques that are now in use include supervised band selection and unsupervised band selection [13]. The training information for the previous method must be labelled. It appears that the majority of the time there's a lack of labelled information accessible, which raises the significance of unsupervised band selection for implementations. A new and efficient technique for hyperspectral band selection is presented by the clustering-based techniques. Nonetheless, the primary challenge in the hyperspectral band selecting process is determining whether to determine the separation among the bands and how to choose relevant bands [14].

High-band visuals are essential for environmental monitoring and precision farming, but they can be difficult to interpret because of their redundant bands and complexity.

Conventional methods such as band selection and feature extraction are not as good at successfully lowering dimensionality while maintaining spectral information. This research presents a novel method to improve high-band picture processing using spectral-spatial transformers, deep learning networks, and adaptive motion optimization. This methodology seeks to achieve much better classification accuracy than current approaches by merging spectral and geographical data. Real-world applications confirm its effectiveness, employing a Python-based model to achieve accuracy rate. This work offers useful solutions for remote sensing applications and related sectors, making a significant contribution to the advancement of high-band image processing.

Key contributions are as follows,

- Novel integration of convolutional neural networks for hierarchical feature extraction from high-band pictures, enhancing categorization precision and knowledge.
- Introduction of a spectral-spatial converter, augmenting categorization accuracy by leveraging both spectral and spatial information.
- Implementation of adaptive motion algorithms to improve generalization performance and convergence speed, advancing efficiency in image processing.
- Demonstrates state-of-the-art capabilities in image processing and categorization, surpassing existing techniques in precision and computational effectiveness.
- Addresses limitations of conventional approaches, propelling forward the field of remote sensing image analysis, with potential applications in agriculture, urban planning, and environmental monitoring.

The remaining section of this work is structured as follows: Section II covers similar work and a full evaluation of it. Section III offers details on the problem statement. Section IV provides a detailed discussion of the suggested method. Section V presents and examines the results of the tests, as well as a comprehensive comparison of the proposed technique to current standard procedures. Section VI, the last section, represents where the paper is finished.

II. RELATED WORKS

Bera and Shrivastava [15] suggest that owing to the special qualities of HSI data, HIS organization is unique of the most difficult tasks in the hyperspectral remote sensing sector. This is made up of a huge amount of bands that exhibit robust interactions in both the spatially and spectrum realms. In addition, it becomes challenging with fewer training examples. To try to tackle these issues, researchers developed a deep convolutional neural network (CNN) based spatially extraction of features method for HSI classification below. They demonstrated the impact of seven distinct optimizers on the deep neural network model through the field of classification using HSI since optimization techniques are crucial for the deep CNN model's development. The study employed seven distinct optimization techniques, the better performance of the deep CNN algorithm using the the Adam optimizer for HSI classification was demonstrated by

comprehensive research results on four hyperspectral remote sensing data sets. This endeavour will eventually compare the effectiveness of several optimization techniques classification include increased computational complexity due to processing volumetric data, which may require substantial computational resources and time for training and inference. Features in 3D CNNs may be challenging compared to 2D CNNs, making it harder to understand how the model. The limitations of employing 3D CNN models for hyperspectral image (HSI) classification include increased computational complexity due to processing volumetric data, which may require substantial computational resources and time for training and inference. Additionally, the interpretability of the learned features in 3D CNNs may be challenging compared to 2D CNNs, making it harder to understand how the model is making decisions based on both spectral and spatial information.

Hong et al. [16] explains that the ability to capture tiny spectrum variations, hyperspectral (HS) images allow for accurate recognition of substances. They have been defined by roughly contiguous spectral data. Convolutional neural networks (CNNs) have demonstrated their outstanding capacity for analysing locally contextual data, making them a potent feature extractor in high-spatiality picture categorization. Yet, because of the constraints of their built-in network backbone, CNNs are unable to efficiently extract and record the ordered properties of spectrum signatures. They suggest a unique backbone network named Spectral Former or approach HS image classification via a sequence viewpoint using transformers to address this problem. Spectral Former can acquire spectral localized sequence data from adjacent bands of high-spatiality pictures, going above band-wise depictions seen in traditional transformers, or producing group-wise spectral embedded data. Additionally, researchers develop a cross-layer skip link by continually acquiring the ability to fuse "soft" residues between layers, therefore minimizing the risk of missing crucial data during the layer-wise propagating procedure. This allows researchers to transfer memory-like elements through shallow to deep layers. It is important to note that what was suggested Spectral Former is a very adaptable backbone networks which may be used with input which are patch- or pixel-wise. Through comprehensive trials, researchers assess the suggested Spectral Former's ability to classify on three HS datasets, demonstrating its advantages beyond traditional transformer and attaining significant improvements above state-of-the-art backbone networking. To continue to make the transformers-based design more useful for the HS image classification task, it will look into ways to further improve the system in the future. For instance, they may use attention or autonomous learning. It may also try to create a lightweight transformers-based networks in order to lower the network's complexity without sacrificing effectiveness. To create deeper models that are easier to understand, researchers are also interested to incorporate additional spectral band physical properties and previous understanding about HS pictures into the suggested structure. Further study ought to concentrate on increasing the amount of ignored and linked encoders in the CAF module since it is a significant factor that might potentially improve the suggested Spectral Former's classification accuracy.

Hong et al. [17] states that because convolutional neural networks (CNNs) can record spatial-spectral feature representations, they have gained significant interest in the field of hyperspectral (HS) picture categorization. However, they are still not very good at modelling connections among samples and evaluation, going above the constraints of grid sampling. Throughout this research, researchers conduct a detailed both qualitative and quantitative investigation on CNNs and GCNs with respect to HS image classification. Traditional GCNs are typically quite computationally expensive because they need building an adjacency matrix for each of information, especially for large-scale remote sensing (RS) situations. To accomplish that, researchers create a novel mini-batch GCN (henceforth referred to as miniGCN) that enables mini-batch training of large-scale GCNs. Additionally, this miniGCN can improve the ability to classify and infer information from data that is not sampled with no re-training networks. Moreover, fusing CNNs and GCNs is a natural way to overcome a single model's effectiveness barrier because they may retrieve distinct kind's unique HS features. because miniGCNs may execute batch-wise training of networks (allowing the integration of CNNs and GCNs). Comprehensive tests, carried out on three HS datasets, show that miniGCNs are superior to GCNs and that the tried fusion procedures outperform the single CNN or GCN models. In the years to come, to fully utilize the rich spectrum information found in high-resolution photos, researchers will explore the potential combinations of various deep neural networks with the miniGCNs as well as create more sophisticated fusion modules, such as balanced fusion.

Roy et al. [18] suggest that because of numerous contiguous narrowband built on top of one another, hyperspectral images (HSIs) offer extensive spectral-spatial data. The decision-making process of useful spectral-spatial kernel features can be challenging because of band correlations and disturbance. CNN using fixed-size receptive fields (RFs) are frequently used to overcome issue. Forward and reverse propagations are employed to maximize the network's performance, these techniques cannot allow neurons to efficiently modify RF sizes and cross-channel connections. In order to collect discriminatory spectrum-spatial characteristics for the classification of HSI using an entire training way, researchers describe within this paper an attention-based adaptable spectrum-spatial kernel enhanced residual networks (A2S2K-ResNet) using spectrum focus. Specifically, the suggested network employs a successful feature recalibration (EFR) strategy to enhance the accuracy of classification and trains specific 3-D convolutional kernels in order to simultaneously retrieve spectral-spatial characteristics utilizing enhanced 3-D ResBlocks. In comparison to the current approaches under investigation, the suggested A2S2K-ResNet tackles the problem of choosing useful spectral-spatial kernel features in hyperspectral image classification. However, significant sensitivity to hyper parameters adjustment and computing burden throughout training could be constraints.

Fu et al. [19] discusses that, since hyperspectral imagery (HSI) contains a wealth of spectrum and spatial information, an entirely novel principal component evaluation (PCA) and

segmented-PCA (SPCA)-based multiscale 2-D-singular spectrum analysis (2-D-SSA) combining look at is offered for paired spectrum-spatial HSI extraction of features as well as grouping. At first, the overall spectrum of the items and the relationships between nearby bands are all taken into consideration when applying the PCA and SPCA methods for dimensional spectra reductions. After extracting a wealth of spatial characteristics at various scales from the SPCA dimension-reduced visuals, multiscale 2-D-SSA is used, and PCA is utilized once more to decrease the number of dimensions. Multiscale spectrum-spatial features (MSF-PCs) are created by fusing the acquired multiscale spatial characteristics into the world spectral characteristics obtained by PCA. The support vector machine (SVM) classification is used to assess the obtained MSF-PCs' performance. Tests conducted on four standard HSI data sets showed that, in situations whenever a limited quantity of sample training specimens are accessible, the suggested technique works better than other cutting-edge feature extraction techniques, such as multiple deep learning techniques. Super pixel-alike segmentation may be used in subsequent research to increase the effectiveness of the suggested strategy.

Uddin, Mamun, and Hossain [20] explains along narrow spectral wavelength ranges are employed to capture the hyperspectral remote sensing pictures (HSIs), which are intended to record the most important details of terrestrial objects. Regarding real-world uses, classification accuracy is frequently not cost-effectively acceptable when utilizing the complete original HSI. Band reduction strategies—which may be further subdivided into extraction of features and feature selection methods—are used to improve the classification outcome of high-strength images. The linear unsupervised statistical transformation known as Principal Component Analysis, or PCA, is often used for obtaining characteristics from HSIs. In this article, nonlinear variations of PCA such as Kernel Entropy Component Analysis (KECA) and Kernel-PCA (KPCA) are being studied alongside linear variations. For this aim, KECA uses Renyi quadratic entropy measurement The research study shows that methods for extracting features may be better in classification than utilizing the complete original dataset, even though they are more expensive. While FPCA provides a decent categorization outcome using the least amount of time and space complexity, MNF delivers the best precision in classifying. Future evaluations of the aforementioned PCA-based feature extraction techniques may lead to the proposal of certain likely hybrids techniques, including fusing MNF with SPCA and SSPCA in a manner that executes traditional MNF in place of PCA in SPCA and SSPCA. Additionally, PCA-based methods for extracting features may be used in conjunction with additional information mining techniques like deep extraction of features and spectral-spatial feature extraction to analyse

Researchers have proposed various approaches to address the challenges of hyperspectral image (HSI) classification. One approach involves the use of deep convolutional neural networks (CNNs) with different optimization techniques to

extract spatial features efficiently. Another method utilizes transformers, such as the Spectral Former, to capture spectral features sequentially, achieving significant improvements in classification accuracy. Additionally, graph convolutional networks (GCNs) and their fusion with CNNs have been explored to model connections among samples, with miniGCNs demonstrating superior performance. Attention-based adaptable spectrum-spatial kernel enhanced residual networks (A2S2K-ResNet) have been introduced to capture discriminatory spectrum-spatial characteristics effectively. Furthermore, a PCA-based multiscale 2-D-singular spectrum analysis fusion approach has been proposed for feature extraction and classification, showing promising results, particularly in scenarios with limited training samples. Overall, these approaches aim to enhance classification accuracy by leveraging spectral and spatial information effectively while addressing computational complexities and interpretability challenges.

III. PROBLEM STATEMENT

Due to the unique properties of hyperspectral imaging (HSI) data, such as the high dimensionality of spectral bands and the intricate relationships between spectral and spatial information, the area of HSI classification faces several difficulties [19] [15]. To overcome these obstacles and increase classification accuracy, researchers have looked at a number of methodologies, such as deep convolutional neural networks (CNNs), transformer-based networks, attention processes, and fusion procedures [17]. All approaches, however, have their drawbacks, including the requirement for significant processing resources, interpretability problems, sensitivity to hyperparameters, and computational complexity. Furthermore, a key factor in classification effectiveness is the selection of feature extraction methods, such as Principal Component Analysis (PCA) including its nonlinear variants. To create better HSI classification solutions, further study is required to examine combination methods and incorporate them alongside other information mining techniques, even if these techniques show promise for improving classification accuracy.

IV. PROPOSED SPECTRAL-SPATIAL CNN WITH ADAPTIVE MOMENTUM FOR HIGH BAND IMAGE CLASSIFICATION

The proposed Spectral-Spatial CNN with Adaptive Momentum integrates spectral and spatial features for high-band image classification, leveraging adaptive momentum optimization for efficient training and improved performance. This method aims to enhance high-bandwidth image analysis and classification using deep learning techniques. It uses Convolutional Neural Networks (CNNs) for feature extraction, incorporates spectral spatial transformer to capture both spectral and spatial information Furthermore, it uses Adaptive Momentum Optimization Algorithm to enhance the training algorithm to improve performance and efficiency. Overall, this technique optimizes the type of excessive-bandwidth pictures through advanced feature extraction and green optimization strategies. Proposed method framework is shown in Fig. 1.

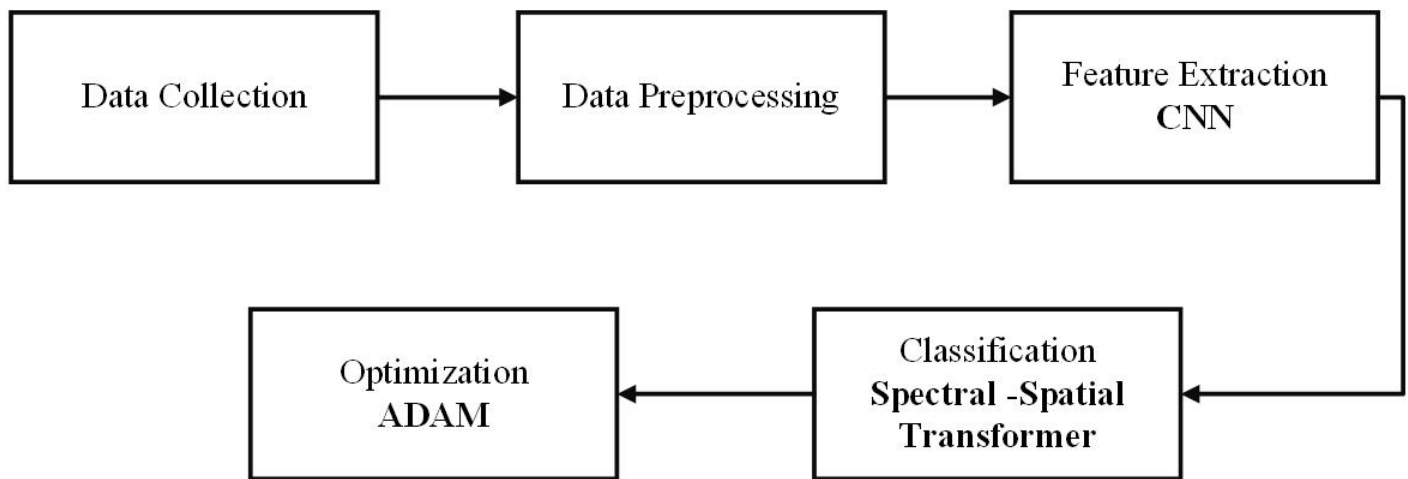


Fig. 1. Proposed spectral-spatial CNN with adaptive momentum for high band image classification.

A. Data Collection

The initial high-resolution images were taken in 1992 over North-Western Indiana, USA, utilizing the Airborne Visible/Infrared Imaging Spectrometer (AVIRIS) sensors. The HS images possess 145 145 pixels during an average ground sampled distances (GSD) of 20 m and 220 spectral bands having a 10 m spectroscopic resolution, covering its wavelength range of 400 nm to 2500 nm. There are 200 spectral bands remaining, or 1–103, 109–149, and 1642–219, after 20 noise and water absorption bands are uninvolved. 16 important groupings in the region beneath investigation were recently looked at. Table II provides a listing of this class names & overall quantity of samples utilized throughout this classifying activity for assessment and training. The geographic distribution of both training and testing sets is shown as well, which helps to duplicate the grouping results [17].

B. Data Pre-processing

Gathering information is a significant step in ensuring that the information is reliable and ready for machine learning analysis. It involves several stages, including Noise Reduction, Data Normalization

1) *Noise reduction*: Applying filters or denoising techniques to mitigate noise introduced during image acquisition or transmission.

2) *Data normalization*: Normalization is used to convert data to a similar scale and avoid characteristics with higher values from dominating the study. The following normalization approaches were used:

a) *Min-max scaling and z-score standardisation*: Min-Max Scaling converts attribute values to a constant scale from 0 to 1, making them comparable. By subtracting the lowest value and dividing by space, it ensures consistency regardless of the original size of the objects. This approach is important for algorithms that are sensitive to input quantities, promoting fair representation in variables. It is especially convenient when dealing with different units or heterogeneous ranges in a data set. To ease convergence, many models' data was normalized to 0 as a mean and 1 as a standard deviation [21].

C. CNN-based Feature Extraction

Comparing to the preceding AlexNet model, VGGNet is a straightforward but efficient model that takes into account the amount of depth of suitable layers without adding additional parameters overall. Consequently, they employed structure akin to VGG. Thirteen layers of convolution and three fully linked layers make up the original VGG's sixteen layers. CNN-Based HSI Spatial Feature Extraction for Every 2.1 The BN layer and ReLU operations come between the fourth of the 22 convolutional layers that are used, while the maximal pooling layer is introduced between the third, fourth, seventh, tenth, and thirteenth convolutional layers. CNN is frequently used for applications involving image processing including segmentation, identification, and classifications because of its powerful ability to extract spatial properties from images. For HSI, it has a plethora of spatial information. With CNN, the current study effectively isolates the spatial components of HSI. CNN has many different types of architecture.

Comparing to the preceding Alex Net model, VGGNet is a straightforward but efficient approach that takes into account the size of suitable layers without adding additional variables overall. Consequently, they employed design similar to VGG. Thirteen convolutional layers and three fully linked layers make up the original VGG's sixteen layers. CNN-Based HSI Spatial Feature Extraction for Each 2.1 the BN layer and ReLU operations come between the fourth of the 22 convolutional layers, while the maximum pooling layer is introduced between the subsequent, fourthly, seventh place, a tenth and thirteenth layers of convolution.

It's possible that using all 16 layers isn't the best option for extracting HSI spatial features. The way due to its strong capacity for obtaining spatial characteristics from images, CNN is frequently employed for image processing tasks like segmentation, identification, and classifying. It provides a wealth of geographic data for HSI. This study successfully extracts the spatial components of HSI using CNN. Creating an appropriate CNN framework is essential to creating an effective HSI classification. In the experimentation section, researchers created a deep CNN that is similar to VGG for extracting HSI spatial characteristics. The extracted features

from the CNN are then utilized for subsequent processing steps, such as classification. After CNN processes HSI data and extracts features, these features are used in subsequent processing steps such as classification. These extracted features represent the spatial patterns learned by CNN during the training process. Information on the spatial distribution of various features of the HSI data was recorded. Using these features, the subsequent classification algorithm can make a more informed decision about the class labels in the different regions of the HSI, using the spatial information encoded in the features extracted by the CNN has been used [22].

D. Spectral-Spatial Transformer for Classification

The CNN output is handled and sent into a Transformer encoder for band categorization in hyperspectral imaging (HSI). CNN uses a local connection in order to extract adjacent properties from the inputs. HSI often has multiple bands. As a result, CNN finds it challenging to acquire spectrum associations across great distances. The association between each pair of band is obtained through the self-attention process. For instance, there are 224 bands in the Airborne Visible/Infrared Imaging Spectrometer (AVIRIS). During the process of learning, a matrix in a form of 224 × 224 may be generated via attention to oneself. The connection among both bands is represented by every component within the matrix.

The Transformer encoder, the central component of this concept, is the additional component. There are d encoding units in the Transformers encoder, and CNN employs local connections for every encoding unit to obtain nearby characteristics from inputs. Since HSI typically has numerous bands, this is challenging for CNN to determine spectral correlations over great distances. The connection between each pair of band can be obtained by the attention to oneself process. For instance, there are 224 bands in the Airborne Visible/Infrared Image Spectrometer (AVIRIS). During the method of learning, a 224 × 224 matrix may be created via self-attention. The connection among the two bands is represented by every component in the matrix. Comprises of an MLP layer, multi-head attention, layer normalization, and residue connections. Prior to every multi-head focused MLP layer in every encoding block, a normalization level is included and additional connections are planned following each of these layers.

Let n denote model, wherein HSI (b₁, b₂, ... b_n) dimensionality of the CNN-extracted features, represent the number of n bands of The Transformer's encoder encodes every band as a function of the overall contextual data with the goal of capturing the interactions between all n bands of HSI. In particular, three accessible weighting matrices have been identified: queries (Q), values (V) of dimension dv, and keys (K) of dimension dk. The search query containing all keys is computed using the dot products, and the weights that are placed for each value are subsequently calculated using the function known as softmax. The following is the definition of attention's output is given in Eq. (1)

$$Attention(q, k, v) = softmax\left(\frac{qk^t}{\sqrt{d_k}}\right) V, \quad (1)$$

where, d_k is the dimension of K.

Projecting the questions, keys, and values multiple times (h times) using distinct and learned projection is advantageous. The outcomes were then combined. This call this method attention in multiple heads. A head is the name given to every outcome of those concurrent attentional calculations is given in Eq. (2)

$$multihead(q, k, v) = concat(head_1, \dots, head_h)w^{o'} \quad (2)$$

The values of the weights the fact that are obtained through the multi-head attention system are then sent to the MLP layer, resulting in 512-dimensional production features. In this case, MLP is made up of two layers that are completely interconnected that have a nonlinearity called the Gaussian error linear unit (GELU) stimulation among it. The ReLU variant known as GELU is described as Eq.. (3)

$$GELU = x' \Phi(x') = x' \cdot \frac{1}{2} [1 + erf(x'/\sqrt{2})] \quad (3)$$

where, $\Phi(x')$ designates the normal Gaussian cumulative distribution function, $erf(x') = \int_0^{x'} e^{-t^2} dt$

There is usually a normalization layer preceding the MLP layer that additionally normalizes neurons to shorten the duration of training but additionally solves the disappearing or expanding gradients issue. The normalization of the layer, represented by Eq. (4)

$$a: a_i^{-l} = \frac{g^l}{\sigma^l} \cdot (a_i^{-l} - \mu^l) + b, \quad (4)$$

where in is the normalized total of the input, and l and l stand for the corresponding expectations and variances at the lth layer. The learnt shifting parameter is denoted by b, and the newly acquired scaling factor by gl. [23]. Spectral-Spatial CNN Architecture is shown in Fig. 2.

E. ADAM Optimization

The adaptive learning rate for each parameter used in the gradient-based training process is estimated by the Adaptive Momentum (Adam) method. This is an extremely basic and highly computationally effective method for stochastic optimization which requires limited storage and incorporates first-order gradients. The suggested method is applied to high-dimensional parameter space machine learning problems using large data sets that compute the rate of learning for different parameters separately of assumptions such as initial and second-order aspects. The Adam form of mathematics is as the following Eq. (5) to Eq. (8)

$$y_t = \delta'_1 \times y_{t-1} - (1 - \delta'_1) \times h_t \quad (5)$$

$$x_t = \delta'_2 \times x_{t-1} - (1 - \delta'_1) \times h_t^2 \quad (6)$$

$$\Delta_{w'_t} = -\eta \cdot \frac{y_t}{\sqrt{x_t + \epsilon}} \times h_t \quad (7)$$

$$w_{t+1} = w_1 + \Delta w_t \quad (8)$$

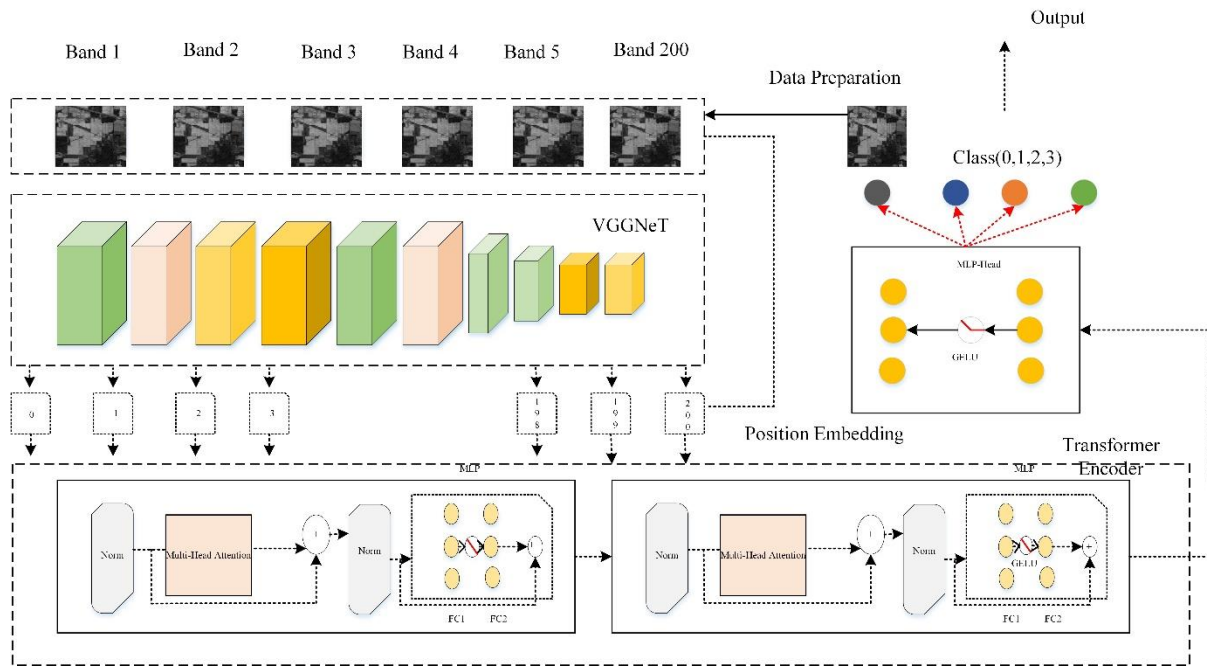


Fig. 2. Spectral-spatial CNN architecture.

where,

η : Preliminary learning rate

h_t : Gradient at time t along h

y_t : Exponential average of gradient along y_t

x_t : Exponential average of squares of gradient along x_t

δ'_1, δ'_2 Hyperparameters.

Adam optimizer lowers the overall computing cost, uses fewer resources for execution, and maintains its invariance when gradients are rescaled diagonally. Large data sets, hyper parameters, noisy data, insufficient gradients, and irregular problems requiring minor tweaking are just some of the challenges this resolves. Alpha is the setup parameter for Adam. This is a learning rate or step size; an elevated number (e.g., 0.3) is probably employed because it enables rapid acquisition rather than a lower value and produces flawless results while training.

V. RESULT AND DISCUSSIONS

In the study, a conducted extensive experiment on real-world high-band picture samples to assess the suggested method's efficacy. The results demonstrate that the method outperforms existing methods in terms of accuracy and performance in high-band image analysis and classification tasks. Specifically, the method achieved state-of-the-art results by leveraging three main components: CNN-based feature extraction, spectral-spatial transformer for classification, and adaptive motion for optimization. Through the use of a convolutional neural network (CNN), it successfully extracted hierarchical features from high-band images, capturing both low and high-level features for detailed representation. Additionally, the incorporation of a spectral-spatial transformer module facilitated more judicious classification by

considering both spectral and spatial characteristics of the images. Furthermore, the introduction of adaptive motion algorithms improved the training process of the deep learning network, leading to faster convergence and enhanced generalization performance. Overall, the research contributes to the advancement of remote sensing image analysis by providing a robust framework that enables deep learning networks to optimize classification accuracy and performance for high-band images. Table I represents Classes from the Indian Pines Dataset for every class.

TABLE I. CLASSES FROM THE INDIAN PINES DATASET FOR EVERY CLASS

| Class No | Class Name | Training | Testing |
|----------|----------------|----------|---------|
| 1 | Grass Pasture | 40 | 1453 |
| 2 | Oats | 40 | 434 |
| 3 | Wheat | 40 | 456 |
| 4 | Corn | 20 | 76 |
| 5 | Soybean Clean | 20 | 543 |
| 5 | Grass Trees | 10 | 34 |
| 7 | Soybean Notill | 10 | 45 |

Table I presents the classes from the Indian Pines dataset along with their corresponding training and testing sample sizes. The dataset comprises six classes: Grass Pasture, Oats, Wheat, Corn, Soybean Clean, and GrassTrees. Each class is assigned a unique class number, and the table details the number of samples allocated for training and testing within each class. For instance, the GrassPasture class has 40 samples for training and 1453 samples for testing, while the GrassTrees class has 10 samples for training and 34 samples for testing. This information provides a breakdown of the dataset's composition, aiding researchers in understanding the

distribution of classes and sample sizes for model training and evaluation.

Taking into account the amount of band used, Fig. 3 displays the Indian Pines dataset's overall precision. The total amount of bands is shown by the X-axis, whereas the overall accuracy ratio is shown by the Y-axis. The diagram shows that accuracy increases as the number of bands grows, but after reaching around five bands, further additions yield diminishing returns while adding more bands initially leads to significant improvements in accuracy, there comes a point where the marginal benefit of additional bands becomes negligible, and further additions may not significantly enhance the complete performance of the classification archetypal.

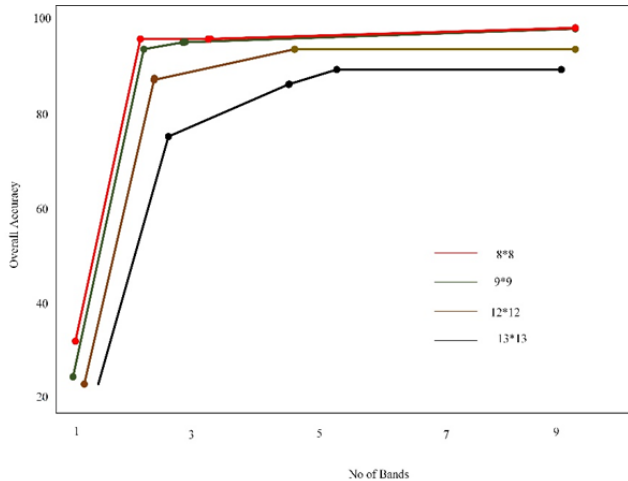


Fig. 3. Overall accuracy of the Indian pines.

Fig. 4 demonstrates the percentage of samples utilized across three distinct datasets: Pavia, Indian Pines, and Houston 2013. It highlights that as the percentage of samples used upsurges, the complete accuracy tends to rise for all datasets. However, each dataset exhibits unique characteristics, resulting in varying rates of accuracy improvement. Pavia dataset shows a steady increase in accuracy with sample percentage, while Indian Pines initially demonstrates rapid gains followed by a plateau, and Houston 2013 exhibits a more gradual increase. These nuances emphasize the importance of dataset-specific considerations when determining the optimal sample size for achieving maximum accuracy in classification tasks.

Fig. 5 illustrates the convergence behaviour of the Adam optimization algorithm over iterations during the training of a machine learning model. Initially, the loss decreases rapidly as the algorithm adjusts the model parameters using adaptive learning rates and momentum. As training progresses, the rate of improvement slows down, indicating convergence towards a minimum point. The graph may exhibit fluctuations due to the adaptive nature of the algorithm, but overall, it demonstrates a consistent decrease in loss over time. The stability and efficiency of Adam optimization make it a popular choice for training deep neural networks. The X-axis represents the steps or iterations in the optimization process, ranging from -1 to 3, while the Y-axis indicates the value of the loss function, ranging from 3.0 to 8.0. This graph depicts

how Adam Optimization efficiently navigates through the loss landscape, with blue dots indicating specific points on its path, demonstrating its effectiveness in finding optimal solutions in machine learning model.

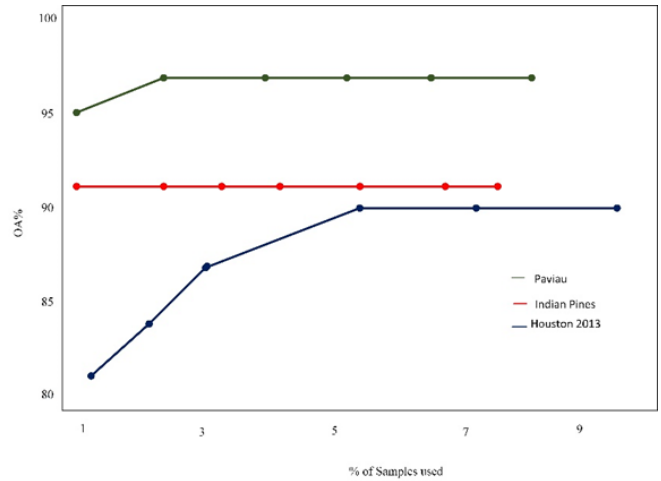


Fig. 4. Samples utilized across three distinct datasets.

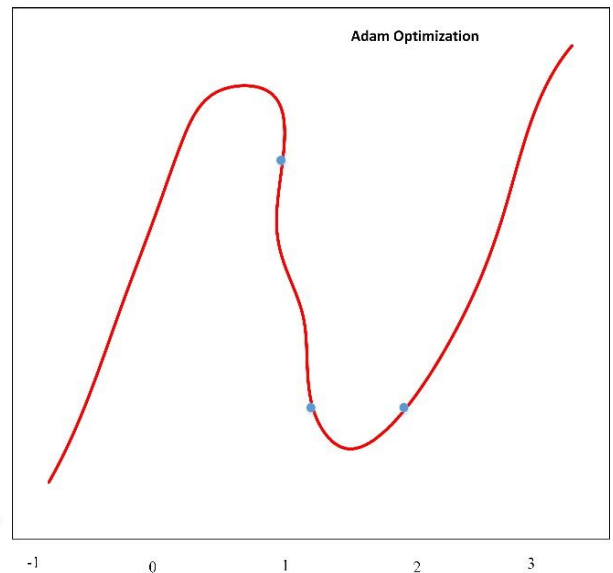


Fig. 5. ADAM optimizer.

Fig. 6 visually signifies the performance of a model during training and evaluation. The x-axis typically indicates epochs or iterations, while the y-axis represents the loss metric. As training progresses, the training loss typically decreases, indicating improved model fit to the training data. Meanwhile, the testing loss, often evaluated on a separate validation set, can help assess generalization performance; ideally, it should decrease initially but stabilize or increase if overfitting occurs, forming distinct patterns aiding in model diagnosis and optimization.

The Receiver Operating Characteristic (ROC) curve is shown in Fig. 7. It serves as an illustration depiction of a binary classification algorithm's effectiveness. Plotting the False Positive Rate (1 - Specificity) versus the True Positive Rate (Sensitivity) at various thresholds is what it does. A ROC

curve which approaches the top-left region of the chart, signifying a high degree of sensitivity along with a small positive error rate, suggests an ideal classifier. Greater values for AUC indicate improved class discrimination. The region underneath the ROC curve (AUC) measures the classifier's overall efficacy. When it comes to the compromise among the two qualities in tasks involving classification, ROC modelling offers insightful information.

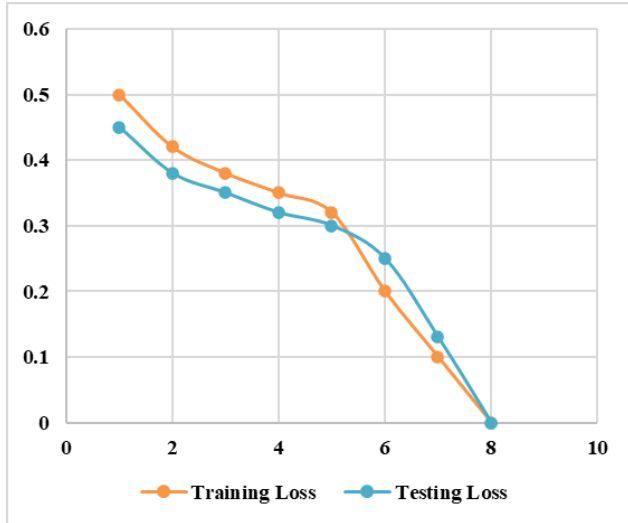


Fig. 6. Training loss and testing loss.

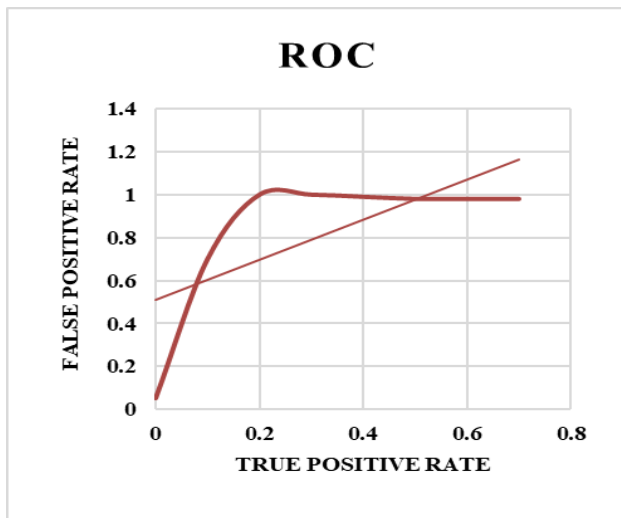


Fig. 7. ROC curve.

Table II compares the performance of various methods in high-band image classification, focusing on accuracy, precision, recall, and F1 score metrics. The Convolutional Neural Network (CNN) achieves 85.77% accuracy, with precision, recall, and F1 score values of 75.87%, 86.09%, and 82%, respectively. The Generative Adversarial Network (GAN) demonstrates superior performance, achieving 97.75% accuracy, with precision, recall, and F1 score values of 90%, 98%, and 95.98%, respectively. The Spectral-Spatial CNN method combines spectral and spatial information, resulting in 95% accuracy, with precision, recall, and F1 score values of 88.56%, 97%, and 95%, respectively.

TABLE II. PERFORMANCE PARAMETERS OF DIFFERENT CLASSIFICATION METHODS

| Method | Accuracy | Precision | Recall | F1score |
|---|----------|-----------|--------|---------|
| CNN | 85.77 | 75.87 | 86.09 | 82 |
| GAN | 97.75 | 90 | 98 | 95.98 |
| Spectral-Spatial CNN | 95 | 88.56 | 97 | 95 |
| Proposed Spectral-Spatial CNN WITH ADAM | 97.8 | 97 | 96.8 | 98 |

The proposed Spectral-Spatial CNN with ADAM optimization achieves the highest performance, with an accuracy of 97.8%, precision of 97%, recall of 96.8%, and an outstanding F1 score of 98%. These results underscore the efficacy of the proposed approach in high-band image classification, suggesting its suitability for practical applications as shown in Fig. 8.

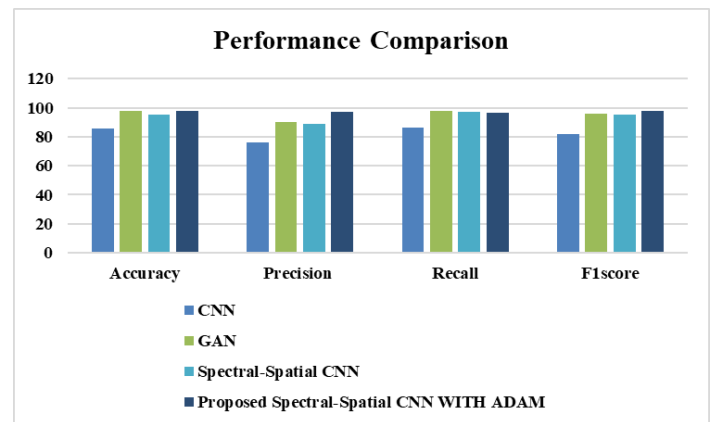


Fig. 8. The performance comparison of different classification methods.

The study explores the effectiveness of a proposed method for high-band image analysis in remote sensing applications. The method significantly outperforms existing methods, achieving state-of-the-art results in accuracy and performance. The approach utilizes CNNs for feature extraction, capturing hierarchical features and improving classification accuracy. The introduction of a spectral-spatial transformer module enhances classification performance by considering both spectral and spatial features. This module enhances robustness and adaptability in processing complex and varied image data sets. Additionally, adaptive motion algorithms optimize the training process of the deep learning network, achieving faster convergence and improved generalization performance. This strategy is highly effective in scenarios where training data may be diverse or noisy. The study contributes to the advancement of remote sensing image analysis by providing a comprehensive framework that integrates state-of-the-art techniques in deep learning and optimization. Future research may explore additional refinements and extensions to the proposed method, such as integrating multi-modal data sources or incorporating additional optimization techniques. This will further enhance the capabilities of image analysis systems for remote sensing and related domains, enabling more accurate and efficient analysis of Earth observation data [15].

VI. CONCLUSION AND FUTURE WORK

The method for high-band image analysis and classification exhibits promising efficiency and accuracy, leveraging a combination of spectral-spatial transformer, CNN-based feature extraction, and adaptive momentum optimization. By integrating deep learning techniques and optimization algorithms, this framework effectively captures both spatial and spectral data, leading to improved classification accuracy. The flexible momentum optimization approach further enhances the training process by dynamically modifying the momentum parameter, resulting in faster convergence and better generalization. These findings underscore the efficacy of the proposed technique across various high-band image analysis applications. Moving forward, future research directions could focus on exploring attention mechanisms to enhance feature extraction and classification precision, investigating new optimization methods tailored for high-band picture analysis, extending the framework to accommodate multi-modal or multi-temporal datasets, and conducting comprehensive tests on larger and more diverse datasets to confirm scalability and resilience. Ultimately, these efforts aim to enhance the methodology's effectiveness and adaptability for high-band picture assessment and classification in real-world scenarios.

REFERENCES

- [1] S. Mei, Y. Geng, J. Hou, and Q. Du, "Learning hyperspectral images from RGB images via a coarse-to-fine CNN," *Sci. China Inf. Sci.*, vol. 65, pp. 1–14, 2022.
- [2] Y. Xu, Z. Wu, J. Chanussot, and Z. Wei, "Hyperspectral images super-resolution via learning high-order coupled tensor ring representation," *IEEE Trans. Neural Netw. Learn. Syst.*, vol. 31, no. 11, pp. 4747–4760, 2020.
- [3] C.-H. Lin, S.-H. Huang, T.-H. Lin, and P. C. Wu, "Metasurface-empowered snapshot hyperspectral imaging with convex/deep (CODE) small-data learning theory," *Nat. Commun.*, vol. 14, no. 1, p. 6979, 2023.
- [4] H. Fu et al., "A novel band selection and spatial noise reduction method for hyperspectral image classification," *IEEE Trans. Geosci. Remote Sens.*, vol. 60, pp. 1–13, 2022.
- [5] D. AL-Alimi, M. A. Al-qaness, Z. Cai, A. Dahou, Y. Shao, and S. Issaka, "Meta-learner hybrid models to classify hyperspectral images," *Remote Sens.*, vol. 14, no. 4, p. 1038, 2022.
- [6] B. Xu, X. Li, W. Hou, Y. Wang, and Y. Wei, "A similarity-based ranking method for hyperspectral band selection," *IEEE Trans. Geosci. Remote Sens.*, vol. 59, no. 11, pp. 9585–9599, 2021.
- [7] C.-I. Chang, Y.-M. Kuo, S. Chen, C.-C. Liang, K. Y. Ma, and P. F. Hu, "Self-mutual information-based band selection for hyperspectral image classification," *IEEE Trans. Geosci. Remote Sens.*, vol. 59, no. 7, pp. 5979–5997, 2020.
- [8] A. Hennessy, K. Clarke, and M. Lewis, "Hyperspectral classification of plants: A review of waveband selection generalisability," *Remote Sens.*, vol. 12, no. 1, p. 113, 2020.
- [9] L. Agilandeswari, M. Prabukumar, V. Radhesyam, K. L. B. Phaneendra, and A. Farhan, "Crop classification for agricultural applications in hyperspectral remote sensing images," *Appl. Sci.*, vol. 12, no. 3, p. 1670, 2022.
- [10] L. Mou, S. Saha, Y. Hua, F. Bovolo, L. Bruzzone, and X. X. Zhu, "Deep reinforcement learning for band selection in hyperspectral image classification," *IEEE Trans. Geosci. Remote Sens.*, vol. 60, pp. 1–14, 2021.
- [11] B. Barman and S. Patra, "Variable precision rough set based unsupervised band selection technique for hyperspectral image classification," *Knowl.-Based Syst.*, vol. 193, p. 105414, 2020.
- [12] R. N. Patro, S. Subudhi, P. K. Biswal, and F. Dell'acqua, "A review of unsupervised band selection techniques: Land cover classification for hyperspectral earth observation data," *IEEE Geosci. Remote Sens. Mag.*, vol. 9, no. 3, pp. 72–111, 2021.
- [13] M. Ramamurthy, Y. H. Robinson, S. Vimal, and A. Suresh, "Auto encoder based dimensionality reduction and classification using convolutional neural networks for hyperspectral images," *Microprocess. Microsyst.*, vol. 79, p. 103280, 2020.
- [14] F. He, F. Nie, R. Wang, W. Jia, F. Zhang, and X. Li, "Semisupervised band selection with graph optimization for hyperspectral image classification," *IEEE Trans. Geosci. Remote Sens.*, vol. 59, no. 12, pp. 10298–10311, 2020.
- [15] S. Bera and V. K. Shrivastava, "Analysis of various optimizers on deep convolutional neural network model in the application of hyperspectral remote sensing image classification," *Int. J. Remote Sens.*, vol. 41, no. 7, pp. 2664–2683, 2020.
- [16] D. Hong et al., "SpectralFormer: Rethinking hyperspectral image classification with transformers," *IEEE Trans. Geosci. Remote Sens.*, vol. 60, pp. 1–15, 2021.
- [17] D. Hong, L. Gao, J. Yao, B. Zhang, A. Plaza, and J. Chanussot, "Graph convolutional networks for hyperspectral image classification," *IEEE Trans. Geosci. Remote Sens.*, vol. 59, no. 7, pp. 5966–5978, 2020.
- [18] S. K. Roy, S. Manna, T. Song, and L. Bruzzone, "Attention-based adaptive spectral-spatial kernel ResNet for hyperspectral image classification," *IEEE Trans. Geosci. Remote Sens.*, vol. 59, no. 9, pp. 7831–7843, 2020.
- [19] H. Fu, G. Sun, J. Ren, A. Zhang, and X. Jia, "Fusion of PCA and segmented-PCA domain multiscale 2-D-SSA for effective spectral-spatial feature extraction and data classification in hyperspectral imagery," *IEEE Trans. Geosci. Remote Sens.*, vol. 60, pp. 1–14, 2020.
- [20] M. P. Uddin, M. A. Mamun, and M. A. Hossain, "PCA-based feature reduction for hyperspectral remote sensing image classification," *IETE Tech. Rev.*, vol. 38, no. 4, pp. 377–396, 2021.
- [21] S. García, S. Ramírez-Gallego, J. Luengo, J. M. Benítez, and F. Herrera, "Big data preprocessing: methods and prospects," *Big Data Anal.*, vol. 1, no. 1, pp. 1–22, 2016.
- [22] C. Yu, R. Han, M. Song, C. Liu, and C.-I. Chang, "Feedback attention-based dense CNN for hyperspectral image classification," *IEEE Trans. Geosci. Remote Sens.*, vol. 60, pp. 1–16, 2021.
- [23] X. He, Y. Chen, and Z. Lin, "Spatial-spectral transformer for hyperspectral image classification," *Remote Sens.*, vol. 13, no. 3, p. 498, 2021.

Lightweight Cryptographic Algorithms for Medical IoT Devices using Combined Transformation and Expansion (CTE) and Dynamic Chaotic System

Abdul Muhammed Rasheed, Retnaswami Mathusoothana Satheesh Kumar

Department of Information Technology, Noorul Islam Centre for Higher Education, Tamil Nadu, India

Abstract—IoT is growing in prominence as a result of its various applications across many industries. They gather information from the real world and send it over networks. The number of small computing devices, such as RFID tags, wireless sensors, embedded devices, and IoT devices, has increased significantly in the last few years. They are anticipated to produce enormous amounts of sensitive data for the purpose of controlling and monitoring. The security of those devices is crucial because they handle precious private data. An encryption algorithm is required to safeguard these delicate devices. The performance of devices is hampered by traditional encryption ciphers like RSA or AES, which are costly and easy to crack. In the realm of IoT security, lightweight image encryption is crucial. For image encryption, the majority of currently used lightweight techniques use separate pixel values and position modifications. These kinds of schemes are limited by their high vulnerability to cracking. This paper introduces a Lightweight cryptography (LWC) algorithm for medical IoT devices using Combined Transformation and Expansion (CTE) and Dynamic Chaos System. The suggested system is evaluated in terms of cross-entropy, UACI, and NPCR. As demonstrated by the experimental results, the suggested system is ideal for medical IoT systems and has very high encryption and decryption efficiency. The proposed system is characterized by its low memory usage and simplicity.

Keywords—Internet of Things (IoT); data transmission; data security; medical IoT devices; lightweight cryptography; encryption; decryption

I. INTRODUCTION

IoT is a network of integrated, sensing, and identifying devices that are accessible over the network and can communicate with each other. One of the new sensing application areas provided by IoT is smart environment monitoring systems. Other examples include smart homes, smart buildings, and smart transportation systems. The IoT is expected to grow rapidly by 2030, when 125 million smart devices will be merged to the Internet [1]. Smart things that can organize, configure, and reconfigure themselves constitute the IoT network. On the other hand, the implementation of these smart objects faces some difficulties [2].

With the advent of sensors, smart networking, RFID, and IoT, the world has become more networked in the last ten years in order to accomplish a wide range of tasks [3]. IoT is a modern technology used in smart objects. Tangible gadgets like laptops, refrigerators, phones, and cars are referred to as "smart objects." IoT refers to a network of smart objects that

other networked devices can recognize, control, and access. They can compute and make decisions as well. IoT is a global network that uses common communication systems and has dynamic capabilities. It can work with both real and virtual objects. It can be used with intelligent platforms that are easily integrated into communication technologies [4].

The idea behind IoT is the integration of intelligent manufacturing equipment, advanced analytics, and automation driven by AI. It will make human life more economical and manageable. IoT may be a rapidly expanding field at the moment, bringing with it a variety of new problems such as short battery life, low memory, short device connection range, etc. [5]. Furthermore, it is evident that the current IoT is vulnerable in terms of energy and security, and its growth prevents it from concentrating on the security framework.

IoT provides an accurate and genuine picture of the challenges and solutions in the IoT framework today through the breakdown of existing devices with different spaces and advancements. Patients and specialists could only collaborate through in-person meetings and text and phone conversations before IoT. Devices enabled by IoT have made it possible to observe patients remotely in the medical field. The more comfortable and effective doctor-patient interactions have also led to a rise in patient engagement and satisfaction. In addition, the patient's condition has been tracked from a distance, which shortens the time spent in the clinic and avoids reaffirmations.

Instead of just creating stand-alone wearables, it is critical to design an entire ecosystem equipped with sensors and devices that will merge data to cloud services via the IoT framework [6–8]. The three primary layers of the design include the following components: the cloud, Internet-connected gateways, and edge devices; sensor-equipped body space networks; and the essential big data support layer. Security is always the primary concern when a new technology is introduced. It is extremely valid in the context of IoT, where devices are used to collect a lot of personal data. Desktop computers are giving way to resource-constrained, small-sized computing devices. The replacement of large amounts of data resulting from the interconnection of these small devices through the Internet and multiple networks poses an unprecedented challenge for the users in terms of data security [9], [10]. IoT devices interact quickly with the outside world to collect private information or control tangible environmental factors. Because of this, they become a desirable target for attackers [12] and are easily accessible, making them open to

different types of security breaches [11]. Cybersecurity is a major concern for IoT devices due to demands for secrecy, integrity of data, authorization and authentication, availability, privacy, and regulatory requirements, as well as frequent system upgrades [13]. In this situation, one of the best methods to ensure the data's secrecy, integrity, authentication, and authorization while it travels between IoT devices might be through cryptography. Data stored or transmitted over a network may be protected with the use of cryptography.

Conventional encryption algorithms provide high security, but they also consume a significant amount of memory, processing, and energy. Due to their limited resources, small devices are not an appropriate choice for traditional encryption. The advent of LWC is a new type of encryption that was made possible by advancements in processors, power consumption, and memory costs in traditional encryption. This encryption lowers memory costs and power consumption, making it appropriate for devices with constrained resources. The newest trend in encryption for devices with low resources is called LWC. This can be attributed to the utilization of basic mathematical operations, reduced memory expenses, and decreased power usage. LWC aims to reduce the overall costs associated with implementing traditional encryption by concentrating on a number of variables, including code size, memory cost, execution time, and energy consumption.

A safe and effective LWC algorithm for small IoT medical devices is suggested in this paper. The major contribution of the proposed work includes:

- Design and development of LWC algorithms applicable for IoT healthcare devices.
- Design and development of novel LWC algorithms based on Chaos theory to provide encryption with less computational complexity and more efficiency.
- Performance assessment of suggested LWC algorithms in terms of NPCR, UACI and Cross Entropy.

The remainder of the paper is organized as follows: A literature review is offered in Section II, highlighting areas necessitating further research. Section III elucidates the methodology in detail. Section IV delves into a comprehensive discussion of the outcomes resulting from the proposed approach. Lastly, in Section V, the paper concludes by summarizing the findings.

II. LITERATURE REVIEW

Fursan Thabit, Sharaf Alhomdy, Abdulrazzaq H.A. Al-Ahdal and Sudhir Jagtap [14] introduced a LWC algorithm for improving the data security. A 16-byte block cipher algorithm must be used to encrypt the data utilizing a 16-byte key. The complexity of the encryption is increased by drawing inspiration from Feistel and SP architectural techniques. According to the simulation results, the suggested algorithm has revealed a strong security level and a discernible enhancement in encryption and decryption, offering low computation costs and high security.

Mohammad Kamrul Hasan, Muhammad Shafiq, Shayla Islam, Bishwajeet Pandey, Yousef A. Baker El-Ebiary,

Nazmus Shaker Nafi, R. Ciro Rodriguez and Doris Esenarro Vargas [15] carried out an investigation of cryptographic algorithms. It provides a thorough assessment of the timing complexity, size, encryption, and decryption performances of different algorithms. It has been tested to mitigate the assuming attack in complex real-time DL IoT applications. Using the simulation approach, an evaluation was carried out to test the encryption and decryption speeds of the preferred encryption algorithms. According to the simulation results, Blowfish performs better than the other widely used encryption algorithms.

An empirical investigation of the performance of 32 LWC algorithms that were deployed on three embedded platforms serving as IoT nodes was conducted by Fotovvat, A., Rahman, G. M., Vedaei, S. S., & Wahid, K. A [16]. The platforms selected for this work can be applied to different layers of the IoT ecosystem. Authenticated encryption algorithms such as AES-GCM, AES-CCM, and AES-OCB were compared with a range of test scenarios. The experiment results showed that other timing requirements are much more important than the encryption time of LWC algorithms.

A performance assessment of ten LWC algorithms was conducted by Panahi, P., Bayılımiş, C., Çavuşoğlu, U., & Kaçar, S. [17]. These algorithms evaluate crucial aspects such as consumption of energy, throughput, memory usage, and execution time during cloud transmission. The most popular IoT devices used in the simulations are the Arduino Mega 2560 and Raspberry Pi 3.

Jadaun, A., Alaria, S. K., & Saini, Y [18] suggested the establishment of a symmetric key LWC algorithm for secure data transmission of text and images utilizing a reversible data hiding system and an image encryption system. A graphical user interface was utilized in the design of the suggested symmetric cryptographic key. A secure data transmission system was also intended to be used with the reversible data-hiding system. The simulation results revealed that the suggested algorithm yields the best results in terms of MSE and PSNR.

Toprak, S., Akbulut, A., Aydın, M. A., & Zaim, A. H. [19] introduced an energy-efficient LWC algorithm for IoT medical devices. A lightweight block cipher algorithm is proposed in order to have an encryption algorithm that is both secure enough to withstand primal cryptanalysis attacks and lightweight enough for constrained or limited hardware environments. Both the length of the key and the length of the blocks that need to be encrypted are 64 bits. It is intended for body sensor area devices and IoT systems with low-end microcontrollers. The well-known algorithms are employed for assessing the security and performance aspects of LWE. It was discovered that LWE can transmit raw data with a minimal amount of security without seriously taxing the network infrastructure. It can be claimed that the outcome is adequate and even outperforms other algorithms.

A novel ultra-LWC algorithm named SLIM was proposed by Aboushousha, B., Ramadan, R. A., Dwivedi, A. D., El-Sayed, A., & Dessouky, M. M [20] for RFID systems. The most popular type of cryptography, block ciphers, offer extremely strong security for IoT devices. SLIM is a 32-bit

block cipher that is built on the Feistel framework. Designing a lightweight block cipher that balances security, cost, and performance is a major challenge. The suggested algorithm is characterized by an appropriate cost/security for RFID framework, a small implementation area, excellent performance in both software and hardware platforms, and energy-efficient behaviour.

Kakali Chatterjee and Ravi Raushan Kumar Chaudhary [21] provided a lightweight block cipher method with a flexible structure. This aids in the creation of a flexible cryptosystem that can be implemented on a variety of IoT devices' hardware. The primary purpose of this framework is to support health monitoring systems, which are a component of electronic health care. The user can access the recorded data in this monitoring system only after completing the necessary authentication procedures. The data is encrypted using LWC. In addition, the system's performance is evaluated, and formal verification for high-level security is completed. The primary keys used in the LWC ciphering technique ranged from 128 to 256 bits. When compared to another current scheme, the computational cost of the suggested framework is low. So, it is appropriate for low-power and memory-intensive IoT devices.

Al-Husainy, M. A. F., Al-Shargabi, B., & Aljawarneh, S. [22] developed a lightweight, adaptable encryption system that includes transposition operations and strong, straightforward substitution in order to encrypt and decrypt data that is compatible with the limited processing power of IoT devices. By using a variable block size, the suggested framework was made more versatile so that it could be used on various IoT devices with different amounts of memory. Additionally, random encryption keys that are difficult for thieves to decipher are generated using the deoxyribonucleic acid sequence. When compared to well-known cryptographic systems, the experimental results of the suggested lightweight encryption system showed excellent outcomes for any IoT device in terms of memory size and encryption time.

Jabeen, T., Ashraf, H., Khatoon, A., Band, S. S., & Mosavi, A. [23] suggested a genetic-based encryption approach to secure the data in an unintelligible format. Security and confidentiality are additionally guaranteed by a lightweight telemetry transport protocol for encrypted data transmission across the network. The major aim of the suggested approach is to provide a bandwidth-efficient protocol with low battery power consumption. The suggested approach is evaluated in the MATLAB platform. The suggested encryption scheme is evaluated for efficacy in the WBAN sensor environment using a genetic-based encryption algorithm.

Atiewi, S., Al-Rahayfeh, A., Almiani, M., Yussof, S., Alfandi, O., Abugabah, A., & Jararweh, Y [24] proposed an IoT environment that is cloud-enabled and encouraged by multifactor authentication and LWC encryption techniques to secure big data systems. The goal of the suggested hybrid cloud platform is to offer extremely secure data protection for businesses. Private and public clouds are combined to create a hybrid cloud environment. Data from sensitive devices is split into two halves and encrypted with the Feistel and RC6 algorithms. Through the use of a gateway device, these data are kept in a private cloud with maximum security. On the other

hand, gateway devices are used to store non-sensitive device data in a public cloud after it has been encrypted using AES. The efficiency of the recommended strategy was evaluated. According to the simulation outcomes, the suggested approach outperforms existing encryption algorithms.

A safe, lightweight algorithmic encryption technique was presented by Hasan, M. K., Islam, S., Sulaiman, R., Khan, S., Hashim, A. H. A., Habib, S., & Hassan, M. A [25] to safeguard the privacy of patient medical images. Two permutation techniques are used in the suggested lightweight encryption method to protect medical images. The security and execution time of the suggested method are compared to those of conventionally encrypted methods after they have been examined and assessed. The effectiveness of the suggested algorithm was analyzed on a large number of test images. Extensive experiments revealed that the suggested algorithm for image cryptosystems provides higher efficiency compared to conventional techniques.

A lightweight, efficient healthcare monitoring system utilizing Radio Frequency Identification (RFID) tags and the IoT was proposed by Naresh, V. S., Reddi, S., & Murthy, N. V [26]. This work used a dual-band RFID protocol, wherein 2.45 GHz microwave bands are employed to monitor corporal information and 13.56 MHz high-frequency RFID is useful for identifying individuals. An RFID tag is utilized to identify the patient, and sensors are utilized to track and gather physiological data about them. According to the simulation results, the suggested protocol is more efficient than other currently used techniques.

An improved LWC algorithm was proposed by Jebri, S., Ben Amor, A., Abid, M., & Bouallegue, A. [27] to secure data transmission in IoT framework. The suggested solution ensures that most security flaws are addressed with regard to trust registration and anonymous mutual authentication. A lightweight, secure IoT system was ensured by employing elliptic curve cryptography, identity-based encryption, and pseudonym-based cryptography approaches. As per the evaluation results of the system with Raspberry cards and the MIRACL library, the system's execution time is adequate for the restricted number of IoT devices.

Chatterjee, K., Chaudhary, R. R. K., & Singh, A. [28] introduced an algorithm for LWC to assure the security of the electronic health care system. The addition substitution and XOR (LWARX) are the foundation of the suggested lightweight scheme. For secure communication within the healthcare system, an efficient authentication approach based on the LWARX approach is also suggested. The effectiveness of the suggested approach is evaluated using a variety of metrics, including throughput, latency, gate equivalent etc. The comparison outcomes show that the suggested ciphering technique has excellent performance, low power and energy consumption, and high throughput. The comparison of selected LWC algorithms is tabulated in Table I.

IoT-based smart environments are susceptible to privacy and data breaches. LWC solutions are crucial since IoT applications are implemented on devices with limited resources. The majority of these modern, LWC solutions rely on hashing techniques like message digests (MD5) or SHA

hash function variants. The device needs more resources to perform the intricate rotational and XOR operations of these current functions. Elliptic curve cryptography (ECC) is the foundation of many lightweight schemes. These ECC schemes generate signatures using single and static elliptic curve parameters. The embedded devices that store these elliptic curve parameters are susceptible to attacks involving node compromise. The publicly accessible Internet infrastructure on the Internet of Things allows devices to communicate with the server or with each other. It becomes a laborious task to issue certificates for every device on the Internet when thousands of devices are added and removed from the network on a regular basis. The key distribution center (KDC) must regularly distribute security keys for this kind of communication. Therefore, using standard KDC, or key management servers, is becoming more difficult as the number of IoT applications rises. Many cryptographic solutions based on ECDSA and ECIES use single or static elliptic curve parameters. Node compromise attacks can arise from ingesting cryptographic parameters or secret keys on the device. So, in order to overcome the above-mentioned limitations, a secure and effective LWC algorithm for small computing IoT healthcare devices was introduced in this work.

TABLE I. COMPARISON OF SELECTED LWC ALGORITHMS

| Name | Block Size (bit) | Key Size (bit) | Structure |
|-----------|------------------|----------------|-----------|
| AES | 128 | 128 | SPN |
| PRESENT | 64 | 128 | SPN |
| MESA | 128 | 256 | Feistel |
| LEA | 128 | 128 | GFN |
| XTEA | 64 | 128 | Feistel |
| SIMON | 64 | 128 | Feistel |
| PRINCE | 64 | 128 | SPN |
| RECTANGLE | 64 | 128 | SPN |

III. MATERIALS AND METHODS

In the field of IoT security, lightweight image encryption is crucial. Most existing Lightweight image encryption approaches adopt shuffling of pixel positions and modification of pixel values separately. So, in this paper, an LWC algorithm for medical IoT devices is developed using Combined Transformation and Expansion (CTE) and Dynamic Chaos System. The detailed block schematic of the suggested approach is visualized in Fig. 1.

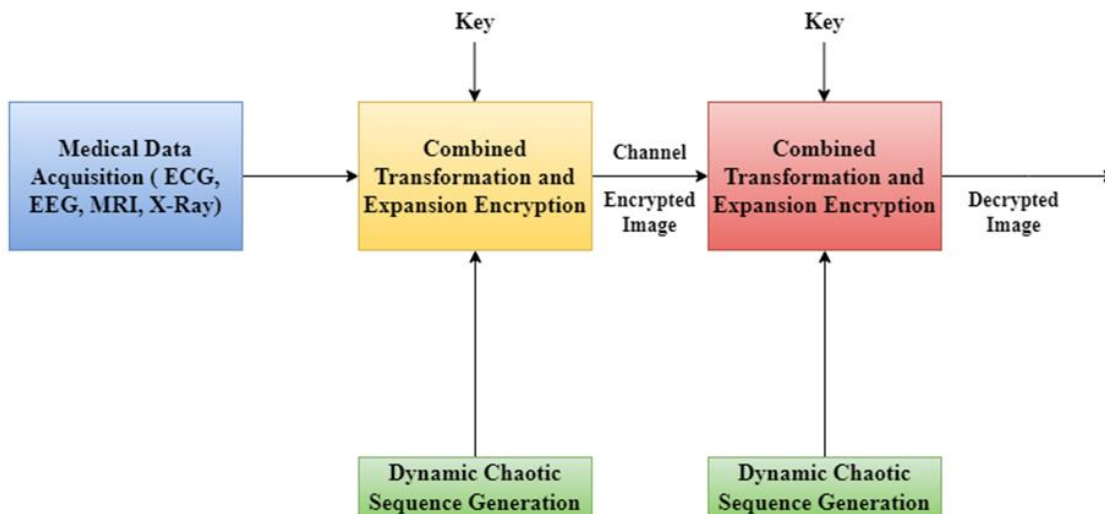


Fig. 1. Block diagram of proposed methodology.

A. Input Medical Images

The medical images were utilized as the input in the proposed work. The input medical images include ECG, EEG, MRI and X-Ray images. Fig. 2 displays the sample medical images.

B. Dynamic Chaotic System

Chaos is defined as "a state of disorder." Systems with dynamic behavior that are extremely sensitive to primary criterion are studied by chaos theory. A reaction that is occasionally indicated to as the "butterfly effect". For such dynamical systems, slight variations in the starting conditions result in widely divergent outcomes, making long-term

prediction generally infeasible. This happens in spite of the fact that these systems are deterministic, implies that their future behavior is totally influenced by their primary criterion and that they do not contain any random elements.

Initially, a sequence is generated by means of a 4D dynamic chaos-based system with two positive Lyapunov exponents. The average exponential divergence rate of neighboring trajectories in phase space is represented numerically by the Lyapunov exponent. It is one of the characteristics that helps distinguish between various chaotic motion numerical values. It can be formulated as

$$\lambda = \lim_{n \rightarrow \infty} \frac{1}{n} \sum_{n=0}^{N-1} \ln \left| \frac{df(x_n, u)}{dx} \right| \quad (1)$$

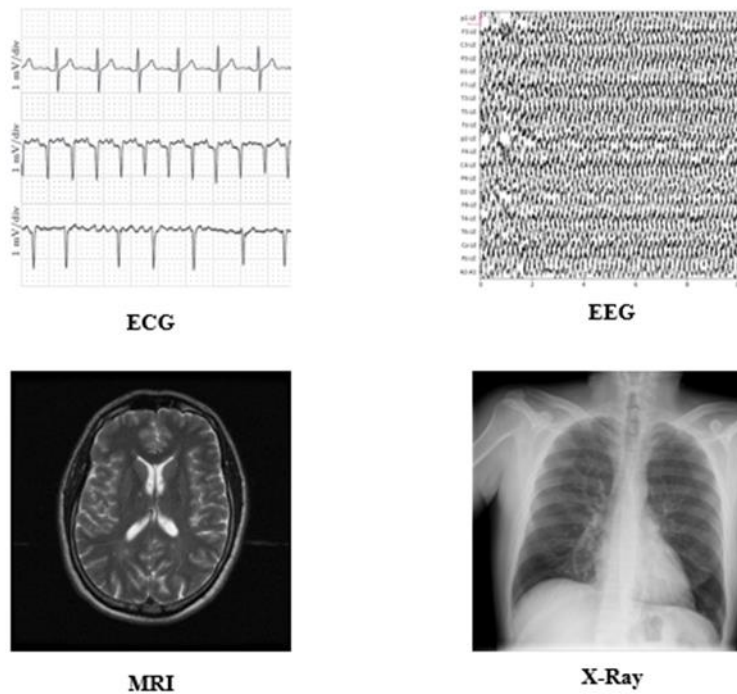


Fig. 2. Sample input medical image.

Fig. 3 depicts the dynamic chaotic system. The dynamic chaos system is initialized with the parameters of the medical image, in order to enhance security. The pixels in images are expanded and transformed using the dynamic chaos sequence. More precisely, the first index matrix establishes which pixels are going to be enlarged and altered. The expansion of the pixels is decided by the second mask matrix. The dynamic chaos sequence is responsible for producing these matrices. In

this work, chaotic sequences for encryption were generated using a novel dynamic chaotic system. It can be formulated as

$$\begin{aligned}
 x &= a(y - x) + w \\
 y &= bx - xz + w \\
 z &= xy - z - w \\
 w &= -c(x + y)
 \end{aligned}
 \tag{2}$$

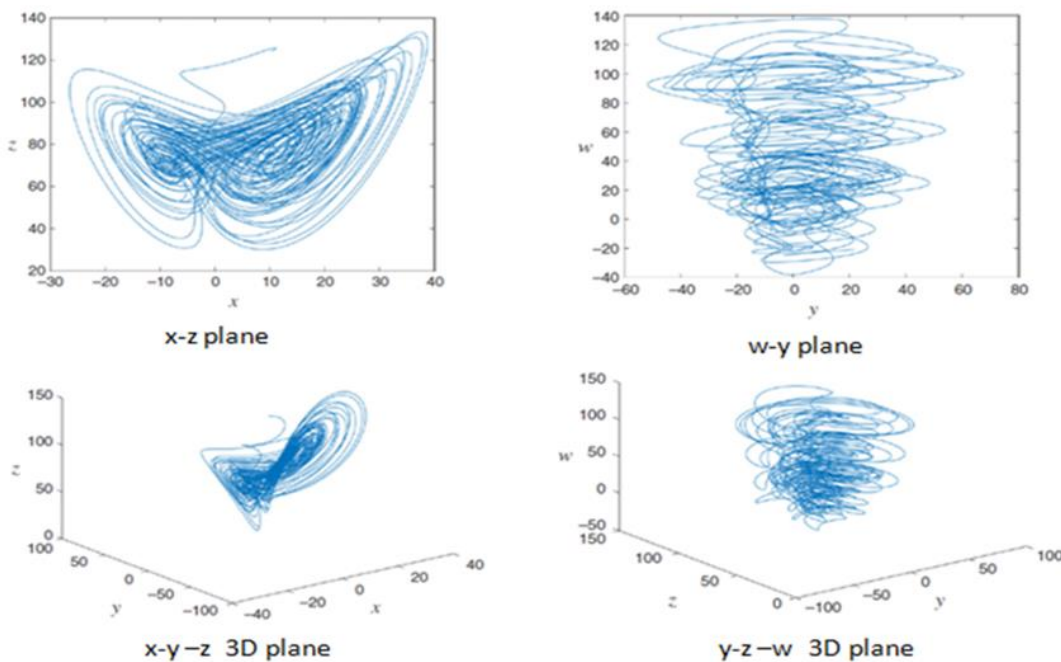


Fig. 3. Dynamic chaotic system.

where the state variables are $x, y, z,$ and $w,$ and the positive constants are $a, b,$ and $c.$ Divide the input image K into 32 blocks in order to generate the initial values for the dynamic chaotic system, which can be expressed as $K = \{k_1, k_2, k_3, \dots, k_{32}\}.$ The four intermediate parameters d_1, d_2, d_3 and d_4 can be calculated as

$$\left\{ \begin{array}{l} d_1 = b_1 + \frac{1}{256}(k_1 \oplus k_2 \oplus \dots \oplus k_8) \\ d_2 = b_2 + \frac{1}{256}(k_9 \oplus k_{10} \oplus \dots \oplus k_{16}) \\ d_3 = b_3 + \frac{1}{256}(k_{17} \oplus k_{18} \oplus \dots \oplus k_{24}) \\ d_4 = b_4 + \frac{1}{256}(k_{25} \oplus k_{26} \oplus \dots \oplus k_{32}) \end{array} \right. \quad (3)$$

where, b_1, b_2, b_3 and b_4 are user-defined parameters that can be addressed as security keys.

The initial values $x_0, y_0, z_0,$ and $w_0,$ of the 4D dynamic chaotic system can be obtained from d_1, d_2, d_3 and $d_4,$ which can be expressed as,

$$\begin{aligned} x_0 &= \frac{\text{mod}((d_1+d_2+d_3) \times 10^8, 256)}{255} \\ y_0 &= \frac{\text{mod}((d_2+d_3+d_4) \times 10^8, 256)}{255} \\ z_0 &= \frac{\text{mod}((d_1+d_2+d_3+d_4) \times 10^8, 256)}{255} \\ w_0 &= \frac{\text{mod}(\text{mean}(d_1+d_2+d_3+d_4) \times 10^8, 256)}{255} \end{aligned} \quad (4)$$

The 4D dynamic chaotic system uses the initial values $(x_0, y_0, z_0$ and $w_0)$ to iterate to produce sequences long enough for the subsequent encryption operations. In the j^{th} iteration, it can obtain four state values described as,

$$S^j = \{x_j, y_j, z_j, w_j\} \quad (5)$$

After the iteration terminates, a dynamic chaotic sequence S can be obtained as

$$\begin{aligned} S &= \{s^1, s^2, s^3, \dots, s^N\} = \{x_1, y_1, z_1, w_1, \dots, x_N, y_N, z_N, w_N\} \\ &= \{s_1, s_2, s_3, s_4, \dots, s_{4N-3}, s_{4N-2}, s_{4N-1}, s_{4N}\} \end{aligned} \quad (6)$$

C. Combined Transformation and Expansion (CTE)

Two types of auxiliary matrices are needed in the suggested approach. The schematic diagram of CTE is illustrated in Fig. 4. One matrix is used for expansion, and the other is used to identify which pixels need to be processed. Considering an image with dimensions $h \times w,$ where h and w stand for height and width, respectively. Two index matrices, I and $T,$ are created for the first matrix using the four random sequences, r_1, r_2, r_3 and $r_4,$ that we adopted from $S.$ Fig. 5 and Fig. 6 show the visualization of the generation of various matrices, respectively.

$$\begin{aligned} I(i, j) &= s_{i_1}(\text{mod}(i + s_{i_2}(j) - 1, w) + 1) \\ T(i, j) &= s_{i_3}(\text{mod}(i + s_{i_4}(j) - 1, w) + 1) \end{aligned} \quad (7)$$

The mask matrix (M) for expansion is calculated using the below equation

$$M = \text{reshape}(\text{mod}((r_5 - \lfloor r_5 \rfloor) \times 2^{32}), 256), [h, w]) \quad (8)$$

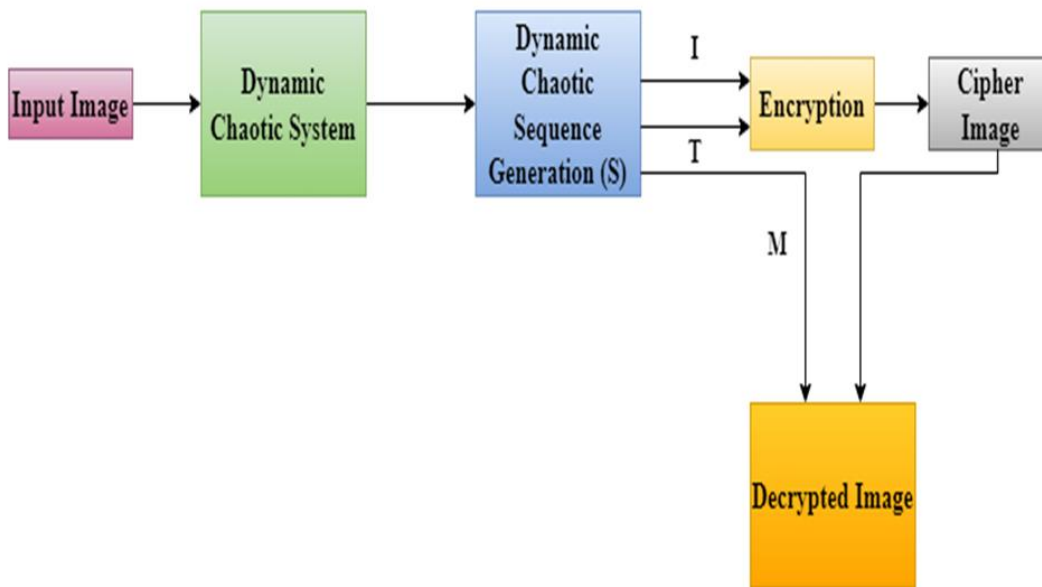


Fig. 4. Block diagram of combined transformation and expansion.

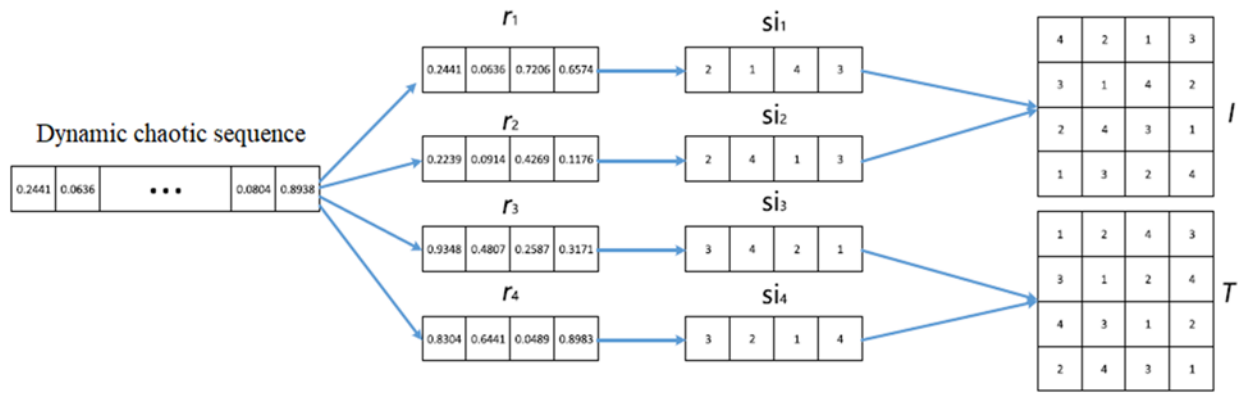


Fig. 5. Visualization of generation of I and T.

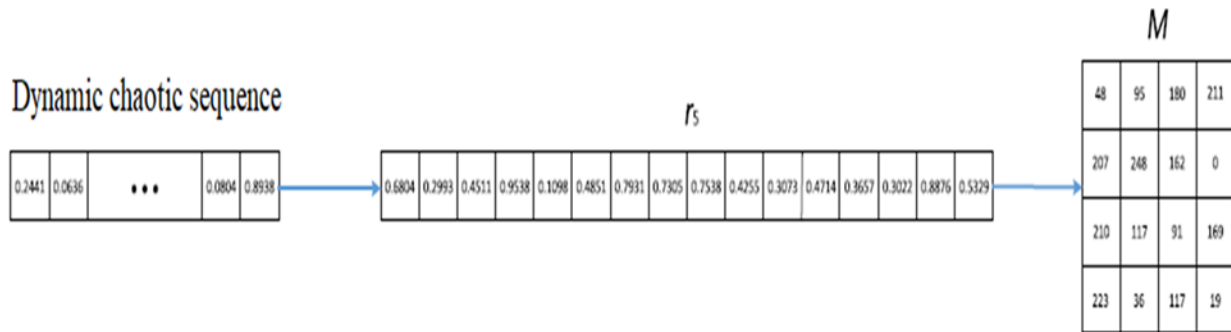


Fig. 6. Visualization of Generation of M.

The method of converting a plain image into a cipher image is known as encryption, and the method of converting a cipher image back into a plain image is known as decryption. Fig. 7 shows the encryption and decryption of the simple image. Data encryption and decryption using cryptographic algorithms typically require a set of characters known as a key. It is simple to encrypt or decrypt plain text into cipher text and back again with the use of a key or algorithm. The proposed CTE algorithm for image encryption and decryption is visualized in Fig. 8.

Considering the user-defined key F, the mask matrix M, the index matrices I and T, and a plain image with one channel P, the encrypted image or Cipher Image (C) can be described as

$$C_{I_i,j} =$$

$$\begin{cases} \text{mod}(M_{i,j} \oplus P_{T_{j,I_i,j}I_{i,j}} + P_{I_{n,w,w}}), F), & \text{if } i = 1, j = 1 \\ \text{mod}(M_{i,j} \oplus P_{T_{j,I_i,j}I_{i,j}} + C_{I_{i-1,w,w}}), F), & \text{if } i \neq 1, j = 1 \\ \text{mod}(M_{i,j} \oplus P_{T_{j,I_i,j}I_{i,j}} + C_{I_{i,j-1,j-1}}), F), & \text{if } j \neq 1 \end{cases} \quad (9)$$

It is possible to obtain the decrypted image D from I, T, M, F, and C

$$D_{T_{j,I_i,j}I_{i,j}} = \begin{cases} \text{mod}(M_{i,j} \oplus C_{I_{i,j,j}} + C_{I_{n,w,w}}), F), & \text{if } i = 1, j = 1 \\ \text{mod}(M_{i,j} \oplus C_{I_{i,j,j}} + C_{I_{i-1,w,w}}), F), & \text{if } i \neq 1, j = 1 \\ \text{mod}(M_{i,j} \oplus C_{I_{i,j,j}} + C_{I_{i,j-1,j-1}}), F), & \text{if } j \neq 1 \end{cases} \quad (10)$$

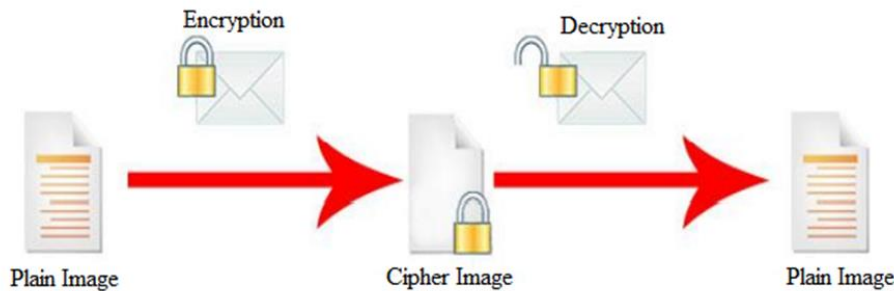


Fig. 7. General block diagram of image encryption and decryption.

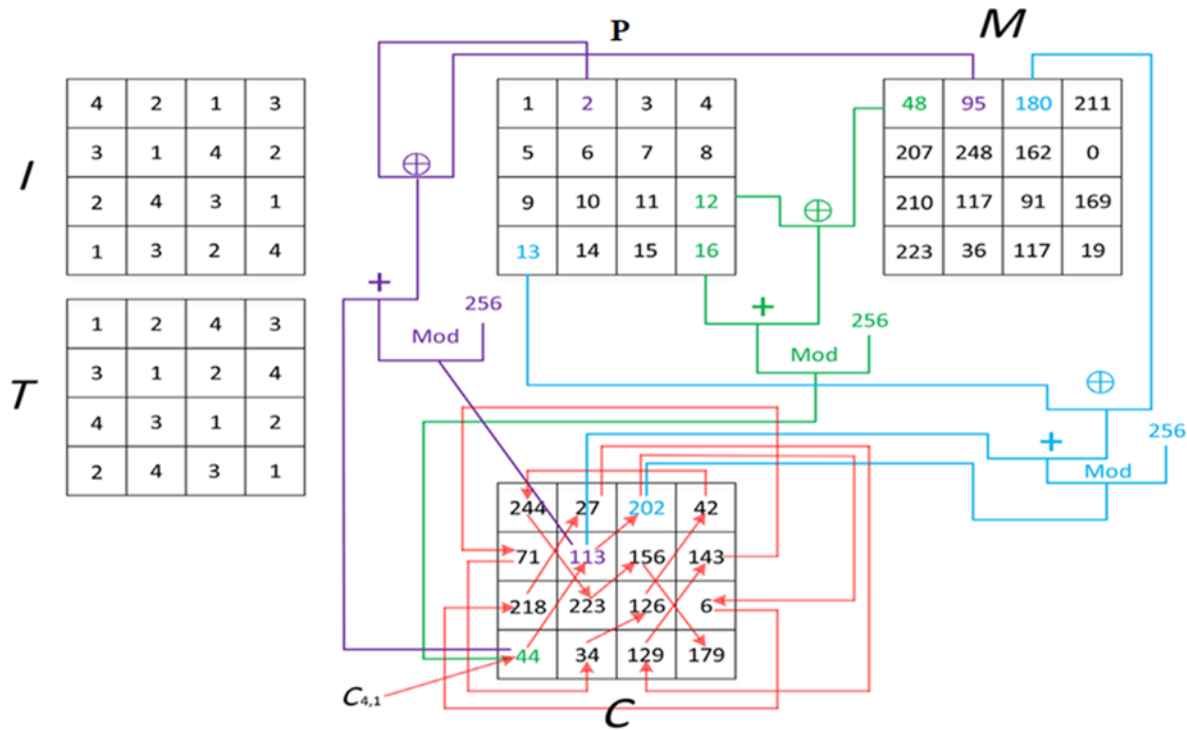


Fig. 8. Illustration of proposed CTE for encryption and decryption.

IV. RESULTS AND DISCUSSION

Number of Pixel Changing Rate (NPCR), Unified Averaged Changed Intensity (UACI), and Cross Entropy were used to assess the performance of the suggested LWC algorithm. The strength of image encryption algorithms and ciphers is assessed using NPCR. Its purpose is to count the number of pixels that change between the real and encrypted images. NPCR can be mathematically expressed as,

$$D(i, j) = \begin{cases} 0, & \text{if } C^1(i, j) = C^2(i, j) \\ 1, & \text{if } C^1(i, j) \neq C^2(i, j) \end{cases}$$

$$NPCR: N(c^1, c^2) = \sum_{i,j} \frac{D(i,j)}{T} \times 100\% \quad (11)$$

The effectiveness of image encryption algorithms and ciphers is assessed using UACI. It calculates the average number of intensity changes between the original and encrypted images. It can be mathematically expressed as,

$$UACI: u(C^1, C^2) = \sum_{i,j} \frac{|c^1(i,j) - c^2(i,j)|}{F.T} \times 100\% \quad (12)$$

The cross-entropy between two images predicts the probability of divergence of encrypted pixels from the original image. Cross entropy is also considered as a loss function. The cross entropy can be expressed as

$$H(C^1, c^2) = - \sum_x C^1(x) \log C^2(x) \quad (13)$$

The performance analysis of original image and encrypted image in terms of NPCR, UACI and cross entropy can be tabulated in Table II.

From Table II, it can be demonstrated that the NPCR and UACI value are high. The high NPCR value indicates that the input medical image and the encrypted medical image differ

from each other. The input medical image and the encrypted medical image differ from one another, as indicated by the high UACI value. Cross-entropy has a finite value. This shows that the input medical image and the encrypted medical image have different structures. Table III tabulates the performance analysis of the original and decrypted images.

TABLE II. ORIGINAL VS ENCRYPTED IMAGE

| Input Image | NPCR | UACI | Cross Entropy |
|-------------|-------|-------|---------------|
| ECG | 99.62 | 47.16 | 0.1389 |
| EEG | 99.62 | 44.32 | 0.1103 |
| MRI | 99.61 | 39.67 | 0.1336 |
| X-Ray | 99.61 | 31.22 | 0.1318 |

TABLE III. ORIGINAL VS DECRYPTED IMAGE

| Input Image | NPCR | UACI | Cross Entropy |
|-------------|------|------|---------------|
| ECG | 0 | 0 | 0 |
| EEG | 0 | 0 | 0 |
| MRI | 0 | 0 | 0 |
| X-Ray | 0 | 0 | 0 |

The value of NPCR, UACI and cross entropy are zero for all medical images. This shows that the decrypted image and the input medical image are identical. Fig. 9, 10, and 11 show the histograms for the MRI image channels, encrypted image channels, and decrypted image channels. Fig. 9, 10, and 11 depict histograms representing the distribution of pixel intensities within the MRI image channels, encrypted image channels, and decrypted image channels, respectively. The

MRI image channels histogram provides insight into the original image's intensity distribution, serving as a baseline. The encrypted image channels histogram illustrates the distribution after encryption, indicating potential alterations due to the encryption process. Finally, the decrypted image channels histogram reveals the distribution following decryption, ideally resembling the original MRI image

channels histogram, affirming the fidelity of the decryption process in preserving the original intensity distribution. These histograms offer a visual comparison of intensity distributions across various stages of image processing, crucial for evaluating the efficacy and fidelity of encryption and decryption techniques applied to MRI images.

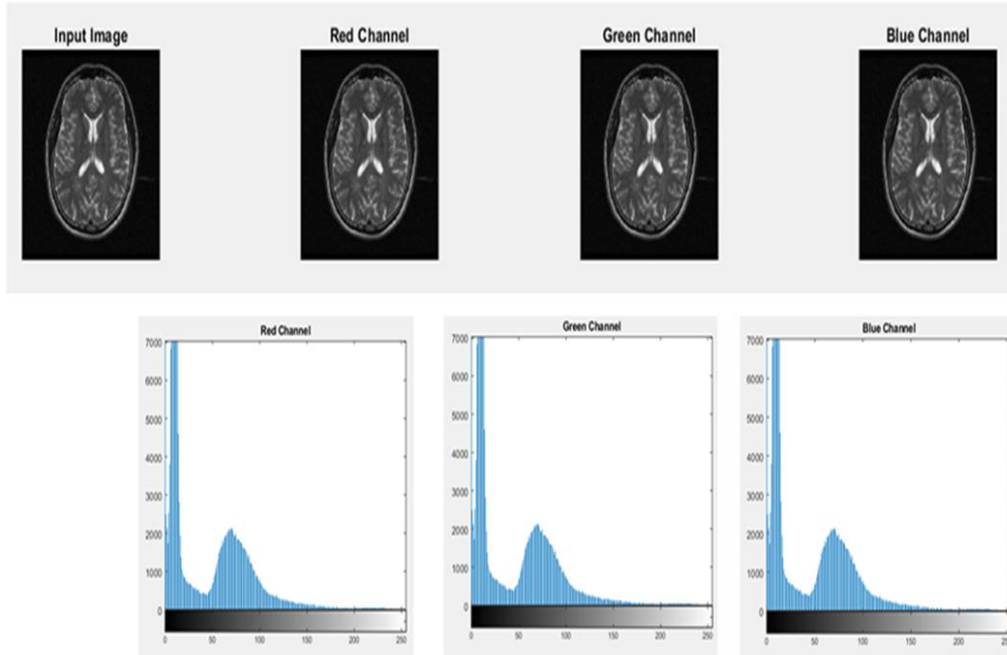


Fig. 9. Histogram of MRI image channels.

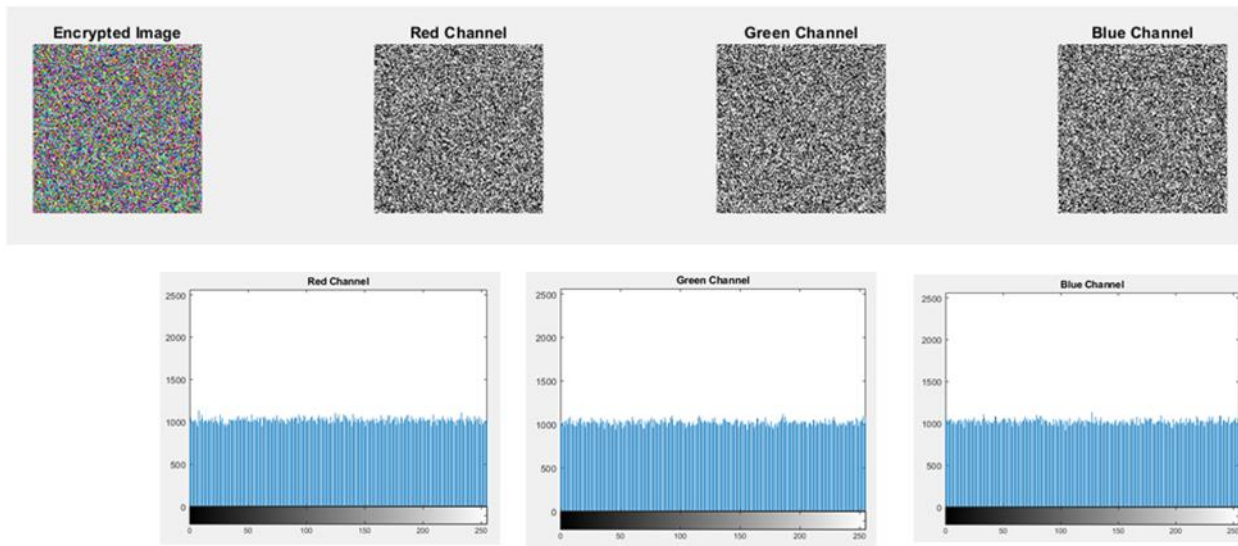


Fig. 10. Histogram of encrypted image channels.

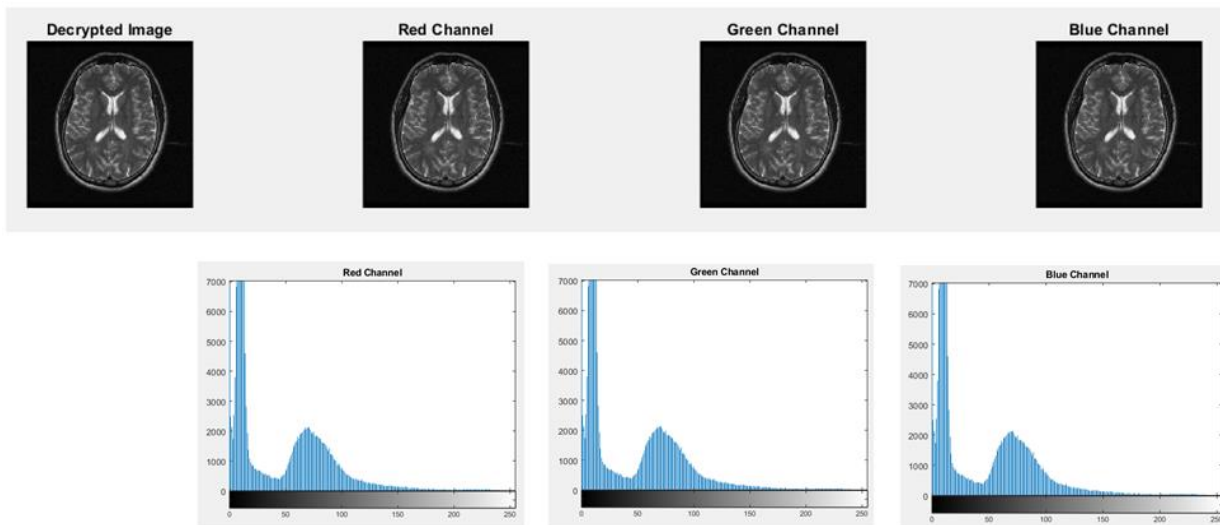


Fig. 11. Histogram of decrypted image channels.

V. CONCLUSION

The IoT is advancing every industry in our rapidly changing world. It facilitates communication between the real and virtual worlds, which will revolutionize operations very rapidly. Due to their limitations, data encryption algorithms must be included in IoT devices in order to increase security. IoT is a network of real, physical objects that have been equipped with RFID, sensors, smart networking, and other methodologies that support them to interchange data with other devices and systems. One important security tool that represents data security is cryptography. The advent of highly sophisticated technologies, coupled with the limitations of mathematical operations and practical applications in traditional cryptography—which also requires a significant amount of processing power and memory guided to the advancement of LWC, a novel approach to cryptography. In this paper, a lightweight cryptography algorithm utilizing the Dynamic Chaos System and Combined Transformation and Expansion (CTE) was proposed for medical IoT devices. The suggested system is assessed in terms of cross-entropy, UACI, and NPCR. The outcomes showed that the suggested method is very effective at both encryption and decryption. The system is less complex, and the memory usage is very low. This system is optimal for medical IoT systems

ACKNOWLEDGMENT

I would like to express my sincere gratitude to all those who contributed to the completion of this research paper. I extend my heartfelt thanks to my supervisor, my family, my colleagues and fellow researchers for their encouragement and understanding during the demanding phases of this work.

REFERENCES

- [1] I. Markit, "The internet of things: a movement, not a market," tech. rep., London, 2018. [Online]. Available: https://cdn.ihs.com/www/pdf/IoT_ebook.pdf. [Accessed on: 02-01-2020].
- [2] Abbas, Z., & Yoon, W. (2015). A survey on energy conserving mechanisms for the internet of things: Wireless networking aspects. *Sensors*, 15(10), 24818-24847.
- [3] N. M. McKay KA, Larry Bassham, and Meltem Sönmez Turan, —NISTIR 8114 Report on Lightweight Cryptography, I2017.
- [4] P. Nandhini, V.Vanitha, and P. Scholar, —A Study of Lightweight Cryptographic Algorithms for IoT, I Int.J. Innov.Adv.Comput.Sci. IJIACS ISSN, vol.6, no.1, pp. 2347–8616, 2017.
- [5] Nižetić, S., Šolić, P., Gonzalez-De, D. L. D. I., & Patrono, L. (2020). Internet of Things (IoT): Opportunities, issues and challenges towards a smart and sustainable future. *Journal of cleaner production*, 274, 122877.
- [6] "CASAGRAS an EU Framework 7 Project (Coordination and Support Action for Global RFID-related Activities and Standardisation)," [Online]. Available: [http://grifisproject.uniweb.be/data/File/CASAGRAS%20FinalReport%20\(2\).pdf](http://grifisproject.uniweb.be/data/File/CASAGRAS%20FinalReport%20(2).pdf). [Accessed 15 April 2018].
- [7] Posts capes, "Internet of Things Examples-Posts capes," [Online]. Available: <http://postscapes.com/internet-of-things-examples/>. [Accessed 17 April 2017].
- [8] Bigbelly, "Big belly," 2015. [Online]. Available: <http://bigbelly.com/>. [Accessed 4 May 2017].
- [9] K. McKay, L. Bassham, M. S. Turan, and N. Mouha, —Report on lightweight cryptography(nistir8114), I National Institute of Standards and Technology (NIST), 2017.
- [10] B. J. Mohd and T. Hayajneh, —Lightweight Block Ciphers for IoT: Energy Optimization and Survivability Techniques, I IEEE Access, vol. 6, pp. 35966– 35978, 2018, doi: 10.1109/ACCESS.2018.2848586.
- [11] S. Singh, P. K. Sharma, S. Y. Moon, and J. H. Park, —Advanced lightweight encryption algorithms for IoT devices: survey, challenges and solutions, I J. Ambient Intell. Humaniz. Comput., vol. 0, no. 0, pp. 1–18, 2017, doi: 10.1007/s12652-017-0494-4.
- [12] W. Feng, Y. Qin, S. Zhao, and D. Feng, —A AoT: Lightweight attestation and authentication of low-resource things in IoT and CPS, I Comput. Networks, vol. 134, pp. 167–182, 2018, doi: 10.1016/j.comnet.2018.01.039.
- [13] A. Banafa, —Three major challenges facing IoT, I IEEEIoTNewsletter,2017.
- [14] Thabit, F., Alhomdy, S., Al-Ahdal, A. H., & Jagtap, S. (2021). A new lightweight cryptographic algorithm for enhancing data security in cloud computing. *Global Transitions Proceedings*, 2(1), 91-99.
- [15] Hasan, M. K., Shafiq, M., Islam, S., Pandey, B., Baker El-Ebiary, Y. A., Nafi, N. S., ... & Vargas, D. E. (2021). Lightweight cryptographic algorithms for guessing attack protection in complex internet of things applications. *Complexity*, 2021, 1-13.
- [16] Fotovvat, A., Rahman, G. M., Vedaei, S. S., & Wahid, K. A. (2020). Comparative performance analysis of lightweight cryptography algorithms for IoT sensor nodes. *IEEE Internet of Things Journal*, 8(10), 8279-8290.

- [17] Panahi, P., Bayılmış, C., Çavuşoğlu, U., & Kaçar, S. (2021). Performance evaluation of lightweight encryption algorithms for IoT-based applications. *Arabian Journal for Science and Engineering*, 46, 4015-4037.
- [18] Jadaun, A., Alaria, S. K., & Saini, Y. (2021). Comparative study and design light weight data security system for secure data transmission in internet of things. *International Journal on Recent and Innovation Trends in Computing and Communication*, 9(3), 28-32.
- [19] Toprak, S., Akbulut, A., Aydın, M. A., & Zaim, A. H. (2020). LWE: An energy-efficient lightweight encryption algorithm for medical sensors and IoT devices.
- [20] Aboushousha, B., Ramadan, R. A., Dwivedi, A. D., El-Sayed, A., & Dessouky, M. M. (2020). SLIM: A lightweight block cipher for internet of health things. *IEEE Access*, 8, 203747-203757.
- [21] Chaudhary, R. R. K., & Chatterjee, K. (2022). A lightweight security framework for electronic healthcare system. *International Journal of Information Technology*, 14(6), 3109-3121.
- [22] Al-Husainy, M. A. F., Al-Shargabi, B., & Aljawarneh, S. (2021). Lightweight cryptography system for IoT devices using DNA. *Computers and Electrical Engineering*, 95, 107418.
- [23] Jabeen, T., Ashraf, H., Khatoon, A., Band, S. S., & Mosavi, A. (2020). A lightweight genetic based algorithm for data security in wireless body area networks. *IEEE Access*, 8, 183460-183469.
- [24] Atiewi, S., Al-Rahayfeh, A., Almiani, M., Yussof, S., Alfandi, O., Abugabah, A., & Jararweh, Y. (2020). Scalable and secure big data IoT system based on multifactor authentication and lightweight cryptography. *IEEE Access*, 8, 113498-113511.
- [25] Hasan, M. K., Islam, S., Sulaiman, R., Khan, S., Hashim, A. H. A., Habib, S., ... & Hassan, M. A. (2021). Lightweight encryption technique to enhance medical image security on internet of medical things applications. *IEEE Access*, 9, 47731-47742.
- [26] Naresh, V. S., Reddi, S., & Murthy, N. V. (2020). Secure lightweight IoT integrated RFID mobile healthcare system. *Wireless Communications and Mobile Computing*, 2020, 1-13.
- [27] Jebri, S., Ben Amor, A., Abid, M., & Bouallegue, A. (2021). Enhanced lightweight algorithm to secure data transmission in IOT systems. *Wireless Personal Communications*, 116, 2321-2344.
- [28] Chatterjee, K., Chaudhary, R. R. K., & Singh, A. (2022). A lightweight block cipher technique for IoT based E-healthcare system security. *Multimedia Tools and Applications*, 81(30), 43551-43580.

A Novel Graph Convolutional Neural Networks (GCNNs)-based Framework to Enhance the Detection of COVID-19 from X-Ray and CT Scan Images

D. Raghu¹, Hrudaya Kumar Tripathy², Raiza Borreo³

Research Scholar, School of Computer Engineering, Kalinga Institute of Industrial Technology,
Deemed to be University, Bhubaneswar 751024, India¹

Associate Professor, School of Computer Engineering, Kalinga Institute of Industrial Technology,
Deemed to be University, Bhubaneswar 751024, India²

Lecturer, Computer Information Science, Higher Colleges of Technology Abu Dhabi Men's Campus, United Arab Emirates³

Abstract—The constant need for robust and efficient COVID-19 detection methodologies has prompted the exploration of advanced techniques in medical imaging analysis. This paper presents a novel framework that leverages Graph Convolutional Neural Networks (GCNNs) to enhance the detection of COVID-19 from CT scan and X-Ray images. Hence, the GCNN parameters were tuned by the hybrid optimization to gain a more exact detection. Therefore, the novel technique known as Hybrid NADAM Graph Neural Prediction (NAGNP). The framework is designed to achieve efficiency through a hybrid optimization strategy. The methodology involves constructing graph representations from Chest X-ray or CT scan images, where nodes encapsulate critical image patches or regions of interest. These graphs are fed into GCNN architectures tailored for graph-based data, facilitating intricate feature extraction and information aggregation. A hybrid optimization approach is employed to optimize the model's performance, encompassing fine-tuning of GCNN hyperparameters and strategic model optimization techniques. Through rigorous evaluation and validation using diverse datasets, our framework demonstrates promising results in accurate and efficient COVID-19 diagnosis. Integrating GCNNs and hybrid optimization presents a viable pathway toward reliable and practical diagnostic tools in combating the ongoing pandemic.

Keywords—COVID-19 detection; Graph Neural Networks; X-ray; CT scan images; hybrid optimization; medical imaging analysis; diagnostic tools; pandemic response

I. INTRODUCTION

The COVID-19 virus has spread worldwide, and lung computed tomography (CT) imaging has achieved clinical verification of the diagnosis of COVID-19. [1] The World Health Organization designated COVID-19 as a highly contagious pandemic that began in December 2019. COVID-19, caused by an unfamiliar coronavirus [2], is spread from person to person. Isolating the patients to control this catastrophe requires an accurate diagnosis. [3] Relevant research has demonstrated that lung X-ray and CT imaging data can be crucial for diagnosing COVID-19. However, despite specific automatic detection techniques, their strategies still have a lot of potential for development and rely disproportionately on the knowledge and resources of doctors due to the brief epidemic period of COVID-19 [4].

The local and general characteristics of the lesions serve as a crucial foundation for the COVID-19 diagnosis, which cannot be determined only based on the peculiarities of a particular location. [5] Analyzing and diagnosing CT scans is highly intricate and necessitates doctors' professional expertise and experience. [6] Furthermore, many COVID-19 CT scans morphologically resemble conventional pictures of pneumonia. However [7], the research describes several segmentation techniques designed and used to extract and evaluate the COVID-19 infectiousness from the 2D slices [8]. Using the VGG-UNet, the COVID-19 lesion is removed from the lung CT slice. A pulmonologist or a computer algorithm is used to determine the infection level following extraction. The lung CT slice extracts the COVID-19 lesion using the EfficientNet. The EfficientNet B1 is used for Chest X-ray and EfficientNet B3 is used for CT-Scan. A validation and training procedure is required for the execution of this strategy.

The CNN methodology is employed rather than traditional techniques, Convolutional Neural Network (CNN) segmentation provides a superior outcome. Therefore, several CNN-based segmentation techniques are used to identify and quantify the afflicted area in CT scans. [10] Graph models have recently grown in strength, which has made it possible to apply them to difficult medical situations. In the field of healthcare, [11] graph convolutional neural networks (GCNNs) have become a distinct category of machine learning (ML) models designed to function on graph-structured data due to their ability to accurately capture the intricate relationships between many components of medical pictures. GCNN provides a revolutionary method for deriving insightful information from linked medical entities, facilitating precise forecasts, and carrying out several essential functions for healthcare applications.

The paper proposes a novel framework using Graph Convolutional Neural Networks (GCNNs) to enhance the detection of COVID-19 from X-ray and CT scan images. The research problem addressed is the need for more accurate and efficient methods for diagnosing COVID-19, especially in resource-constrained settings where access to traditional diagnostic tools may be limited. By leveraging the unique

capabilities of GCNNs, the framework aims to improve the accuracy and speed of COVID-19 detection from medical imaging, ultimately aiding in the early and accurate diagnosis of the disease. The paper highlights the potential of GCNNs to analyze the complex relationships within medical images, potentially leading to more reliable diagnostic outcomes compared to traditional methods.

II. RELATED WORK

A. A Few Recent Associated Works are Described as Follows

Fan X et al. [12], a new framework using Transformer and Convolutional Neural Network (T-CNN) is proposed for detecting COVID-19 from CT images [9]. This method uses Transformer's global feature extraction and CNN's local feature extraction capacity. A bidirectional feature fusion structure is created by fusing features from two branches and branch parallel structures, enhancing Accuracy. This approach also advances the field's ability to diagnose lung diseases in real-time, potentially saving lives. It has limitations due to relying on one CT image with fewer features and incomplete patient diagnosis output.

Jia H et al. [13], a novel module called pixel-wise sparse graph reasoning (PSGR) for CT image segmentation of COVID-19 infected areas. Global contextual information modelling is improved by the PSGR module, which is placed between the network's encoder and decoder. It projects pixel characteristics to create a network, transforms it into a sparsely linked graph, and then applies global reasoning. Three datasets were used to assess the segmentation structure and to contrast it with other models. Results show that the suggested module outperforms competing models in properly segmenting and successfully captures long-range relationships despite its high computational cost.

Fritz C et al. [14], to forecast local COVID-19 instances, this study employs semi-structured deep distributional regression (SDDR) as a multimodal learning framework. Neural networks and structured additive distributional regression are combined in SDDR, where the statistical regression model is embedded within the neural network. It applies latent characteristics discovered by deep neural networks to the additive predictor of each distributional parameter. An orthogonalization cell is utilized to distinguish between structured and unstructured model portions.

Lu S et al. [15], the research created a computer-aided diagnostic system that utilizes artificial intelligence to recognize COVID-19 in chest computed tomography pictures. Transfer learning lets the system obtain novel, neighbouring aware representation (NAR) and image-level representations (ILR). The neighbouring familiar graph neural network (NAGCNN) is designed and validated. The results demonstrated its superior generalization capacity over all state-of-the-art approaches, indicating its effectiveness for clinical diagnosis.

Xing X [16], this paper introduced an advanced multi-level attention graph neural network (MLA-GCNN) for predicting and diagnosing diseases. In particular, weighted correlation network analysis converts omics data into co-expression graphs. Multi-level graph features are then created, and to

perform predictions, they are fused using a carefully thought-out multi-level graph feature entirely fusion module. A unique full-gradient graph saliency method is designed for model interpretation to determine the genes associated with the disease. Regarding proteomic data from coronavirus disease 2019 (COVID-19)/non-COVID-19 patient sera, GCNN performs at breaking point.

The key contributions of this work are described as follows

- Initially, the Kaggle dataset is collected and trained in a Python program.
- With the necessary characteristics for detecting COVID-19, the novel NAGNP is introduced.
- Thus, the NADAM function is used in optimization and CNN is used in Feature analysis to extract the relevant and necessary features from the dataset.
- GNN accomplishes the prediction process, and classification is carried out.
- At last, the detection process is completed, and performance metrics, including F1 score, Accuracy, recall, and precision, are computed and compared to other models.

III. PROPOSED METHODOLOGY

A novel Hybrid NADAM Graph Neural Prediction (NAGNP) system was introduced in this study for forecasting the COVID-19 affection from the lung's CT scan data. Preprocessing is performed to rid the data of the noisy components. Following that, the method of extracting the features for COVID-19 feature prediction is carried out. The CNN is used to extract features. Henceforth, prediction is accomplished by GNN. Lastly, COVID-19 prediction has been carried out, and performance metrics are assessed.

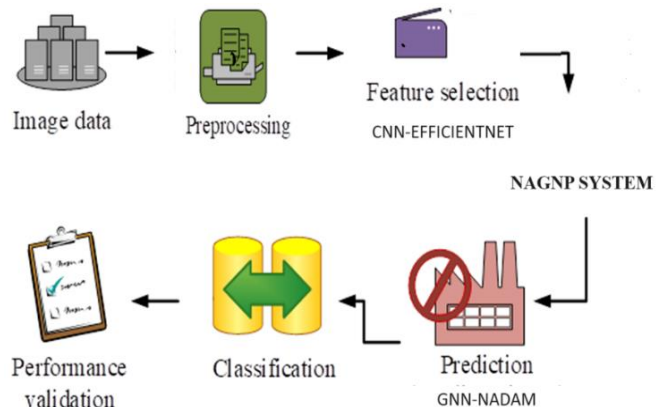


Fig. 1. Proposed methodology.

In Fig. 1, the proposed approach is described. It uses a CT scan image to anticipate the COVID-19. Performance metrics were computed, including the F1 score, Accuracy, recall, and precision. The following portions display the process of the proposed model in brief.

The detection data importing function's primary step is executed by Eq. (1). Based on the initialization principle of the hybrid optimization model, the initialization process was activated and done successfully.

$$F(T) = T\{1,2,3,\dots,n\} \quad (1)$$

Here, T it determines CT scan data, defines the data training variable, and describes the n number of trained CT images.

After the training phase, the critical module in the forecasting framework is preprocessing, which is executed to neglect the noisy pixel range from the imported image data. Also, the proper filtering function has helped to earn the needed Accuracy in the prediction function. Consequently, the preprocessing function is processed by Eq. (2).

$$D = \frac{T(H - n)}{T(P)} \quad (2)$$

Here, P is the total pixel and $T(P)$ denotes the entire pixel in the trained data. Moreover, D the preprocessing variable, the highest pixel, and the noisy pixel are available in the imported database.

B. Feature Selection

The process feature selection is the chief processing module to get the forecasting outcome expected. According to the dataset there were two models proposed one for X-ray and one for CT-Scan. Both models use CNN. The feature extraction is done by Transfer Learning Architecture EfficientNet B1 for X-ray and EfficientNet B3 for CT-Scan. The meaningful features like spatial and temporal are extracted using Principal Component Analysis. The PCA projects data onto a lower-dimensional subspace while maximizing variance. Eq. (3)

$$\text{var}(Z) = \sum(\lambda_i * (z_i)^2) \quad (3)$$

where Z is the projected data,

λ_i are the eigen values and

z_i are the principal components.

C. Prediction and Classification

The COVID region prediction is an intricate process for medical professionals. It has affected a wide range of people. It is predicted by applying the NADAM optimization in GCNN. The proposed model NAGNP shows better performance in feature extraction. To optimize the GCNN's performance, an optimizer like NADAM is employed. It builds upon Adam (Adaptive Moment Estimation) by incorporating momentum for faster convergence. NADAM updates weights (θ) based on estimates of the first and second moments of gradients (m_t, v_t) using specific decay rates (β_1, β_2). Mathematically, Eq. (4) the update rule might involve:

$$m_t = \beta_1 * m_{(t-1)} + (1 - \beta_1) * g_t,$$

$$v_t = \beta_2 * v_{(t-1)} + (1 - \beta_2) * g_t^2, \quad (4)$$

where, g_t is the current gradient. The weights are then adjusted using these moment estimates and estimated noise (η).

By combining classification with GCNN architecture and NADAM optimization, the model learns to effectively map features to class labels, enabling accurate predictions for unseen chest X-rays

The prediction is executed by Eq. (5).

$$P_r = F_{TAL} > P_r \left(\frac{F_s}{C,N} \right) \quad (5)$$

P_r represents the prediction variable, the trained stored feature, and the Covid and Non-Covid. The Fitness predicts the COVID cases, and Eqn 6 does classification.

$$C = \begin{cases} \text{if}(P_r = 0) & \text{Non Covid} \\ \text{if}(P_r = 1) & \text{Covid} \end{cases} \quad (6)$$

C denotes the classification variable. The value 0 indicates the Non-Covid affected, and 1 represents the COVID affected. The Flowchart for the proposed NAGNP model is displayed in Fig. 2.

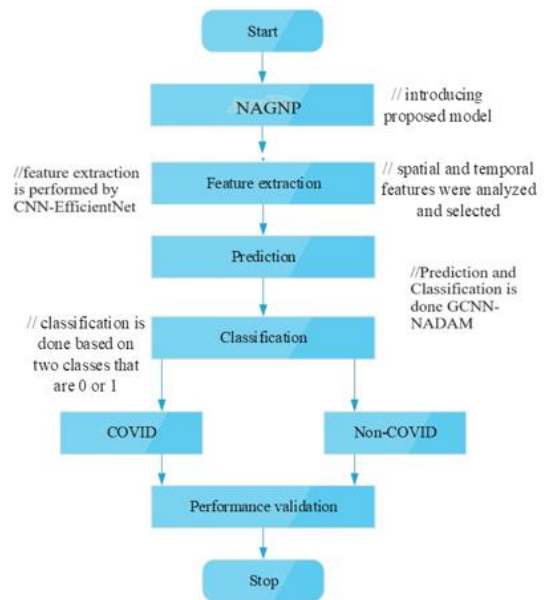


Fig. 2. The Flowchart for the proposed NAGNP model.

IV. RESULTS AND DISCUSSION

The planned novel solution is verified in the Python environment version 3.10 and running in the Windows 10 environment. The dataset is collected from the Kaggle site. The noisy parts are removed using preprocessing to extract the significant features from the gathered photos. CNN is then used for feature extraction. The GNN predicts COVID-19. As a result, the necessary metrics for the proposed NAGNP are evaluated. The execution parameters are described in Table I.

TABLE I. EXECUTION PARAMETERS

| Metrics | Specification |
|----------------------|---------------|
| Operating System | Windows 10 |
| Version | 3.7.14 |
| Program platform | Python |
| Dataset | Kaggle |
| Optimization | NADAM |
| Network Architecture | CNN-GNN |

A. Case Study

The purpose of the study is to comprehend the proposed NAGNP model process. The images used come from Kaggle's website. Datasets are used for training and testing to determine the designed model. Table II shows the predicted image.

The prediction result describes the region affected by COVID-19. Blue represents the affected region, light blue indicates the low-affected region and dark blue shows the heavily affected area.

B. Performance Analysis

Performance was validated by evaluating chief metrics like error rate, F1-score, Accuracy, recall and precision. The existing paradigms, which are obtained for the comparative validation is Xception Model (XM) [17], Inception V3 Model (IV3M) [17], VGG16 [17], ResNet 50 (RN50)[17], VGG 19 [17] and DenseNet (DN) [17].

Moreover, the positive scores in the forecasting function are measured with the help of precision metrics; the formulation is revealed in Eq. (6).

$$Precision = \frac{Tp}{FP + TP} \tag{6}$$

Here, *TP* it denotes the true positive and *FP* false positive samples. Hence, to know the mean performance in the cases of both sensitivity and precision score, the F-measure validation metrics were evaluated using Eq. (8).

$$F_score = \frac{2 \times recall \times precision}{recall + precision} \tag{8}$$

The precision and F-score rate for the Covid detection of the proposed NAGNP is made a comparison with the prevailing models is displayed in Fig. 3.

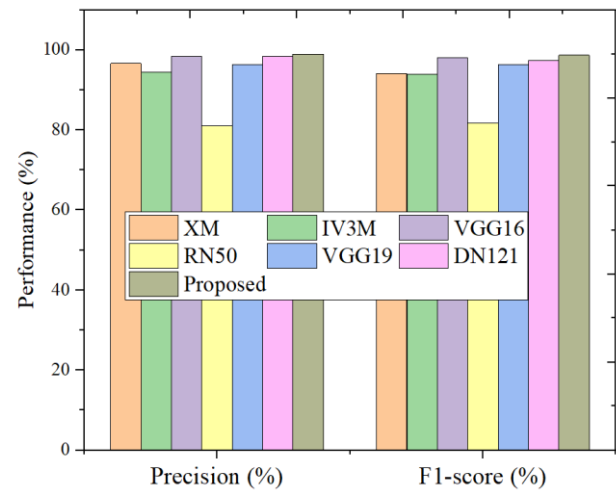


Fig. 3. Precision and F1 score comparison.

TABLE II. PREDICTION RESULTS

| Input image | Ground Truth | Prediction |
|-------------|--------------|------------|
| | | |
| | | |

Here, Precision rate for the existing models, XM gains 96.6 %, IV3M gains 94.4 %, VGG16 gains 98.4%, RN50 gains 81 %, VGG19 gains 96.41 % and DN121 gains 98.37%. Meanwhile, the proposed model NAGNP gains 99%. Similarly the F1 score obtained by the prevailing models XM, IV3M, VGG16, RN50, 4.2.1 Precision and F1 score VGG19, DN121 obtained 94.07%, 94%, 98%, 81.73%, 96.41%, 97.38 % respectively and the proposed model obtained 98.7%. This shows better performance of the proposed model.

1) *Recall and accuracy*: Besides, the scalability of the executed model in the presence of a forecast fall ratio is found using recall metrics. Their formulation is given in Eq. (7), it can give the average performance by incorporating positive and negative classes.

$$Recall = \frac{Tp}{Tp + FN} \tag{7}$$

The correctness of the prediction process is found using Eq. (5) here, the exact forecasting is validated from the entire COVID detection performance.

$$Accuracy = \frac{exact \text{ Forecast}}{total \text{ prediction}} \tag{5}$$

The Accuracy and Recall measure of the proposed NAGNP is made a comparison with the existing models is displayed in Fig. 4.

Here, Accuracy gained for the existing models, XM 94.2 %, IV3M 93.96 %, VGG16 98%, RN50 81.29%, VGG19 96.38% and DN121 97.38%. Meanwhile, the proposed model NAGNP gains 98.5%. Similarly, the Recall measure obtained by the prevailing models XM 91.6%, IV3M 93.6 %, VGG16 97.61 %, RN50 82.87 %, VGG19 96.41 %, DN121 96.41% and the proposed model obtained 98.5%. This demonstrates

that the proposed model performs better. The overall comparison is depicted in Table III.

C. Discussion

The accuracy value of the proposed NAGNP is higher than that of the current techniques. This demonstrates the top performance across all parameters, including recall, Accuracy, precision, and F-score. It provides a 98.5% accurate forecast. Table IV shows the proposed approach performs. The overall effectiveness of the proposed NAGNP approach suggests that NADAM and ant NADAMfitness optimization provide superior feature extraction and prediction. It leads to increased precision.

Limitations: The effectiveness of GCNNs relies heavily on the availability and quality of labeled data. Limited or biased datasets could impact the model's performance and generalizability. GCNNs can be computationally intensive, requiring substantial resources for training and inference. This could be a limitation in resource-constrained environments or for real-time applications.

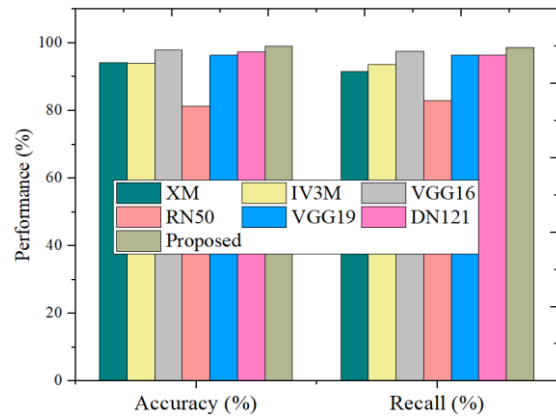


Fig. 4. Accuracy and recall comparison.

TABLE III. OVERALL COMPARISON STATISTICS

| Metrics | XM | IV3M | VGG 16 | | RN50 | VGG 19 | DN 121 | EfficientNet |
|-----------|-------|-------|--------|--|-------|--------|--------|--------------|
| Precision | 96.6 | 94.4 | 98.4 | | 81 | 96.41 | 98.37 | 99 |
| F1-score | 94.07 | 94 | 98 | | 81.73 | 96.41 | 97.38 | 98.7 |
| Accuracy | 94.2 | 93.96 | 98 | | 81.29 | 96.38 | 97.38 | 98.5 |
| Recall | 91.6 | 93.6 | 97.61 | | 82.87 | 96.41 | 96.41 | 98.5 |

TABLE IV. NAGNP PERFORMANCE

| Metrics | X-ray (EfficientNet B1) | CT-Scan(EfficientNet B3) |
|-----------|-------------------------|--------------------------|
| Accuracy | 97.5 % | 98.5 % |
| Precision | 99 % | 99 % |
| Recall | 97 % | 98.5 % |
| F1-score | 97.92% | 98.64% |

V. CONCLUSION

The NAGNP framework for detecting COVID-19 is described in this study. The Python program is used to execute it, and the results are described. Initially, the Kaggle site is used to gather data for COVID-19 detection, and preprocessing is used to eliminate noisy elements. Subsequently, the CNN does the feature extraction technique, and the ant NADAM fitness performs the prediction, yielding a superior prediction outcome. The feature extraction procedure takes the critical features from the data and predicts COVID-19. Finally, the suggested model's performance is verified using several metrics, including F1-score, Precision, Accuracy and Recall. The outcome revealed that the proposed model performs better. The designed model gains an accuracy of 98.5 %, a precision of 99 %, A recall of 98.5 %, and an F1-score of 98.7 %, resulting in better performance. Compared to the current models, the accuracy of the proposed NAGNP model is improved by 1% to 2%. However, future work is needed to detect and segment in real time.

REFERENCES

- [1] Paul SG, Saha A, Hasan MZ, Noori SR, Moustafa A. A systematic review of graph neural network in healthcare-based applications: recent advances, trends, and future directions. *IEEE Access*. 2024 Jan 16.
- [2] Liu S, Gui R. Fusing multi-scale fMRI features using a brain-inspired multi-channel graph neural network for major depressive disorder diagnosis. *Biomedical Signal Processing and Control*. 2024 Apr 1;90:105837.
- [3] Ebenezer AS, Kanmani SD, Sivakumar M, Priya SJ. Effect of image transformation on EfficientNet model for COVID-19 CT image classification. *Materials Today: Proceedings*. 2022 Jan 1;51:2512-9.
- [4] Kumar A, Tripathi AR, Satapathy SC, Zhang YD. SARS-Net: COVID-19 detection from chest x-rays by combining graph convolutional network and convolutional neural network. *Pattern Recognition*. 2022 Feb 1;122:108255.
- [5] Bagwan F, Pise N. A precise and timely graph-based approach to identify SARS Covid19 infection from medical imaging data using IsoCovNet. *International Journal of Imaging Systems and Technology*. 2023 May 3.
- [6] Aminul Islam M, Shuvo SA, Abu Tareq Rony M, Raihan M, Abu Sufian M. Unleashing Modified Deep Learning Models in Efficient COVID19 Detection. *arXiv e-prints*. 2023 Oct:arXiv-2310.
- [7] S. Ray, S. Lall, A. Mukhopadhyay, S. Bandyopadhyay, and A. Schönhuth, "Deep variational graph autoencoders for novel host-directed therapy options against COVID19," *Artificial Intelligence in Medicine*, vol. 134, p. 102418, Dec. 2022, doi: 10.1016/j.artmed.2022.102418.
- [8] Reka N, Sreerambabu J, Kalidasan S. Omicron Detection with X-Ray and CT-Scan Using Machine Learning.
- [9] Mohseni H, Montazeri M, Ghasemian F, Amin S. AFEX-Net: Adaptive Feature EXtraction CNN for Classifying CT Images.
- [10] Y. Liu et al., "Structural Attention Graph Neural Network for Diagnosis and Prediction of COVID-19 Severity," in *IEEE Transactions on Medical Imaging*, vol. 42, no. 2, pp. 557-567, Feb. 2023, doi: 10.1109/TMI.2022.3226575.
- [11] Liu Y, Li H, Luo T, Zhang C, Xiao Z, Wei Y, Gao Y, Shi F, Shan F, Shen D. Structural Attention Graph Neural Network for Diagnosis and Prediction of COVID-19 Severity. *IEEE Transactions on Medical Imaging*. 2022 Dec 2;42(2):557-67.
- [12] Fan X, Feng X, Dong Y, Hou H. COVID-19 CT image recognition algorithm based on Transformer and CNN. *Displays*. 2022 Apr 1;72:102150.
- [13] Jia H, Tang H, Ma G, Cai W, Huang H, Zhan L, Xia Y. A convolutional neural network with pixel-wise sparse graph reasoning for COVID-19 lesion segmentation in CT images. *Computers in Biology and Medicine*. 2023 Mar 1;155:106698.
- [14] Fritz C, Dorigatti E, Rügamer D. Combining graph neural networks and spatio-temporal disease models to improve the prediction of weekly COVID-19 cases in Germany. *Scientific Reports*. 2022 Mar 10;12(1):3930.
- [15] Lu S, Zhu Z, Gorriz JM, Wang SH, Zhang YD. NAGCNN: classification of COVID-19 based on neighboring aware representation from deep graph neural network. *International Journal of Intelligent Systems*. 2022 Feb;37(2):1572-98.
- [16] Xing X, Yang F, Li H, Zhang J, Zhao Y, Gao M, Huang J, Yao J. Multi-level attention graph neural network based on co-expression gene modules for disease diagnosis and prognosis. *Bioinformatics*. 2022 Apr 15;38(8):2178-86.
- [17] Kathamuthu, Nirmala Devi, et al. "A deep transfer learning-based convolution neural network model for COVID-19 detection using computed tomography scan images for medical applications." *Advances in Engin.review*," *Concurrency and Computation: Practice and Experience*, p. 6646, 2022.

A Smart AI Framework for Backlog Refinement and UML Diagram Generation

Samia NASIRI*, Mohammed LAHMER

Moulay Ismail University, Faculty of Science, Meknes, Morocco

Abstract—In Agile development, it is crucial to refine the backlog to prioritize tasks, resolve problems quickly, and align development efforts with project goals. Automated tools can help in this process by generating Unified Modeling Language (UML) diagrams, allowing teams to work more efficiently with a clear understanding and communicate product requirements. This paper presents an automated approach to Agile methodology which refines backlogs by detecting duplicate user stories and clustering them. Following the refinement process, our approach generates UML diagrams automatically for each cluster, including both class and use case diagrams. Our method is based on machine learning and natural language processing techniques. To implement our approach, we developed a tool that selects the user stories file, groups them by actor, and employs the unsupervised k-means algorithm to form clusters. After that, we used Sentence Bidirectional Encoder Representations from Transformers (SBERT) to measure the similarity between user stories in a cluster. The tool highlights the most similar user stories and facilitates the decision to delete or keep them. Additionally, our approach detects similar or duplicate use cases in the UML use case diagram, making it more convenient for computer system designers. We evaluated our approach on a set of case studies using different performance measures. The results demonstrated its effectiveness in detecting duplicate user stories in the backlog and duplicate use cases. Our automated approach not only saves time and reduces errors, but it also improves collaboration between team members. With an automatic generation of UML diagrams from user stories, all team members can understand product requirements clearly and consistently, regardless of their technical expertise.

Keywords—Artificial intelligence; NLP; Agile methodology; UML

I. INTRODUCTION

In the System Development Life Cycle, it is essential to undergo a requirement analysis stage to ensure the success of the process [1]. This occurs because developers must understand the requirements before proceeding to the implementation stage. In this context, user stories are increasingly used to communicate requirements in Scrum. They are semi-structured natural language expressions of requirements at a high level. The textual template for user stories has been proposed in many forms by practitioners. In practice, they tend to use the form of: “As a..., I want to..., so that...” The growing number of stakeholders involved in the development process increases the size of the systems developed, leading to a larger number of user stories. This size growth makes it mandatory to decompose the system into subsystems covering different sets of semantically similar user stories.

As part of requirements engineering tasks, stakeholders need to be kept involved in the process by expressing each sub-system semi-formally, such as using visual models. As a visual language supporting requirements engineering, we used the Unified Modeling Language (UML) in this context. A model-based approach is often used to specify software system features and to reduce ambiguity between requirement specification and design. However, deriving UML models manually from similar user stories can be time-consuming and tedious, especially for large systems. Additionally, model-based approaches have been difficult to integrate in Scrum processes. This is basically due to the lack of powerful automation tools [2], [3], as well as focusing on implementation rather than analysis and documentation of teams.

Several studies were conducted to automate the generation of models from natural language software requirements [4]-[12]. In addition, some authors studied natural language requirements clustering to decompose the target system at an initial level [13], [14]. The current requirements clustering approach lacks precision and does not achieve a high level of automation. In contrast, we propose a machine learning-based approach that addresses these challenges. However, the requirement clustering has rarely been considered as a primer for automatically deriving models.

In this paper, we propose a machine learning-based approach for automatically dividing a system into subsystems and generating UML diagrams based on natural language user stories in Scrum.

To group the user stories by actor, we applied a set of natural language processing heuristics to extract the actor name from each user story. Once the system was initially decomposed by the actor, we performed a second decomposition for each resulting cluster. The second clustering of the system was based on the k-means algorithm, which groups semantically similar requirements. To identify possible redundancies between user stories located in each cluster, we used the BERT model. This process allows Product Owners and Scrum Masters to be more informed about their decisions regarding the elimination of redundant user stories from the Product Backlog. In the final step, we generated use case and class UML diagrams from the identified clusters.

This paper is organized as follows. The Section II reviews related work, while the Section III presents the background of the proposed approach. Section IV is devoted to a detailed description of the proposed approach. In Section V, we describe and analyze the similarity detection between user

stories and generated UML diagrams; it also evaluates and discusses the performance of the approach. Finally, Section VI concludes the paper.

II. RELATED WORK

In this section, we provide a literature review related to our approach. For instance, in study [15], the authors have reviewed word embeddings and implemented a convolutional neural network trained on pre-trained word vectors. They have also illustrated the performance of pre-trained word integrations vs. random embeddings. However, in study [16], the authors have presented an approach that uses semantic similarity measures to suggest possible cases of duplication between user stories. To explain, the approach selected the most appropriate measure to determine the level of similarity between user stories. Their research analyzed semantic similarity measures based on the WordNet lexical database WuP, a similarity measure based on VSM Lin [17], and a measure based on the frequency of common terms Lesk-A [18]. The authors of study [19] analyzed user stories to identify potential information gaps and prevent ambiguities, using comparisons with previous user stories to detect missing queries. They have provided suggestions to users to get a better description. For natural language processing (NLP), an NLP tool called LingPipe Toolkit is used. Semantic role labeling was carried out to attribute roles and actions. In study [20], the authors' method established the user stories meta-model by determining the unified descriptive model of the user stories which are: the role, the task, the capability, the soft goal, and the hard goal. In study [21], the approach allowed the extraction of relevant information for user stories from recorded conversations between customers and developers. In study [13], the authors' work consisted of clustering the specification requirements by first using the Vector Space Model (VSM) to compute the similarity of functional requirements and then the Agglomerative Hierarchical Clustering (AHC) algorithm to construct clusters. In study [22], the authors have proposed a tool-assisted approach to identify terminological ambiguities between viewpoints as well as missing requirements. For this purpose, they combined natural language processing with information visualization techniques that help in defect-type interpretation. Their approach consisted of identifying ambiguity and incompleteness in a set of requirements. The authors used word2vec to detect similarities between terms in requirements. The visualization showed the requirements graphically by marking the terms used and arranging them in a 2D space according to the viewpoint to which the terms belong. They used Cortical.io's algorithm which relies on semantic folding and fingerprinting. Then, the algorithm built the context of each pair of terms that appeared in the same user stories. In study [23], the authors provided Sentence-BERT (SBERT). This pre-trained BERT network modification takes advantage of Siamese and triplet network structures by deriving semantically meaningful sentence embeddings that can be benchmarked using cosine similarity. In study [24], the authors used Word2vec to compute the similarity at the word level, then they grouped the requirements into clusters using the Agglomerative Hierarchical Clustering (AHC) algorithm. Word2vec for each word after tokenization at remove stop

words, and stem. They used Gensim API for keyword extraction of each cluster. This summarizer is based on the ranks of text sentences using a variation of the TextRank algorithm. After that, they defined simple NLP rules for component extraction to generate a use case diagram. In [14] authors used a K-means clustering algorithm applied to user stories. The authors in study [25] have provided a tool to extract the time spent in historical and similar user stories. This extracted time helps developers estimate the time that similar user stories will spend on new projects. To do this, the authors used the NLP algorithm and a pre-trained model developed by Google called USE. The model did not distinguish between the opposite operations "add and remove". In research [26], the method began by extracting iStar nodes from semi-structured user stories. Next, the nodes were merged based on their similarity. Finally, edges between nodes were identified using defined rules. The authors' approach was based on the refinement relationship between iStar nodes. The authors applied a BERT (Bidirectional Encoder Representations from Transformers) model for similarity measurement. In study [27], the approach helped in detecting defects in user stories by using 11 quality criteria. It was based on two main components: firstly, quality analysis was based on NLP. This method uses four fundamental functions of natural language processing: sentence segmentation, tokenization, POS labeling, and syntactic analysis. It examined the completeness of components and the testability of stories by checking several quality criteria, such as the correct form of components and the consistency of keywords used in stories. Secondly, the method was based on the analysis of iStar models. It started by generating iStar models from user stories, identifying nodes (role, goal/task), and detecting relationships between these nodes. It then checked several quality criteria, including uniqueness, absence of conflicts, verifiability, independence, and conceptual consistency.

Many approaches for requirements gathering and analysis have been developed so far, falling into two main categories: (1) approaches based on gathering, and (2) approaches focused on identifying duplicates or ambiguities in user stories. Our approach combines these two methods while refining the user stories to eliminate duplicates. In addition, the proposed approach aims at automatically generating UML diagrams from a given set of refined user stories.

III. BACKGROUND

In this section, we outline the key concepts underlying this work.

A. Text to Semantic Vectors Transformation in NLP

It is important to transform text into semantic vectors in many automatic NLP tasks. This enables algorithms to process language more effectively by representing the meaning of words and sentences. There are several approaches for converting text into semantic vectors, and each one of them has its strengths and limitations. Hence, in this section, we will discuss the most common approaches, including One Hot Encoding, TF-IDF, Word2Vec, ELMo, InferSent, and Sentence Transformers [28].

- One Hot Encoding is a straightforward method that transforms text into binary vectors by assigning a unique dimension to each word in the corpus. In this method, the dimension corresponding to each word is marked as 1 for each document, while all other dimensions are marked as 0. The resulting vectors are binary vectors of a size equal to the total number of words in the corpus. Although this method is simple to implement, it disregards semantic relationships between words and can result in large and sparse vectors.
- TF-IDF is a technique that represents documents as vectors using term frequency and inverse document frequency. The weight of a word in a document is computed by multiplying its frequency in the document (TF) by the inverse of its frequency in the entire corpus (IDF). This approach generates weighted vectors that consider the relative importance of words in documents. Even if it is more expressive than One Hot Encoding, TF-IDF still does not capture semantic relationships between words [29].
- Word2Vec is a neural network-based method that learns dense vector representations of words in a vector space. It includes two main variants: Skip-Gram and Continuous Bag of Words (CBOW). Skip-Gram predicts neighboring words given a target word while CBOW predicts the target word using its neighboring words. The resulting vectors capture semantic and syntactic relationships between words. However, Word2Vec does not consider the syntactic structure of sentences [30] [31].
- ELMo, or Embeddings from Language Models is a model that represents words and phrases in automatic natural language processing. It creates contextual embeddings using bidirectional recurrent neural networks (Bi-LSTMs), capturing the meaning of words in context. Pre-trained on unannotated texts, ELMo generates rich, contextual embeddings. These representations enhance text classification, information retrieval, and other NLP tasks by capturing the semantic and syntactic nuances of words in various contexts.
- InferSent, developed by Facebook AI Research (FAIR), is a sentence representation model that generates contextual semantic embeddings using deep neural networks. Based on a semi-supervised supervision approach, InferSent aims to capture the semantic meaning of sentences. Pre-trained on a large corpus of data, this model produces informative sentence embeddings, beneficial for tasks such as text classification and semantic similarity assessment between sentences.
- The Universal Sentence Encoder (USE) is a widely adopted natural language processing model that has been extensively used in various research domains. Developed by Google, USE employs a deep neural network to encode text into fixed-dimensional vectors, capturing semantic information and contextual meaning [32]. It has proven to be effective in tasks such as

sentence similarity, document classification, and semantic search. With its ability to understand and represent the meaning of sentences, USE has become a valuable asset in numerous applications. Its success lies in its capability to capture intricate semantic relationships. This makes it a reliable tool for tasks involving text comprehension and similarity analysis.

- Sentence Transformers: The advancement of deep learning has resulted in a significant improvement in the performance of neural network architectures like recurrent neural networks (RNN and LSTM) and convolutional neural networks (CNN) in the areas of Natural Language Processing (NLP), such as text classification, language modeling, and machine translation.

Bidirectional Encoder Representations from Transformers is a Transformer-based machine learning technique for natural language processing: pre-training developed by Google. The Sentence BERT (SBERT) network uses siamese and triplet networks to obtain semantically meaningful sentence embeddings derived from BERT [23]. SBERT can be employed as both a semantic similarity search and as a clustering algorithm. Similarity measures like cosine similarity or Manhattan/Euclidean distance can be used to determine semantic similarity.

Several SBERT pre-trained models encode sentences and calculate the distance between them to conduct semantic searches. Each model has its own task such as question answering, translation, sentence similarity, and others. These models are tuned for many use cases and trained on a huge and varied dataset consisting of over a billion training pairs. They are called “sentence transformers” and represent a modern approach to transforming text into dense semantic vectors using pre-trained neural network models. One of the main advantages of sentence transformers lies in their ability to capture the full semantic meaning of entire sentences, beyond representations of individual words. Notably, these models are often trained for natural language understanding tasks, such as next-sentence prediction or text classification, to further enhance their performance and accuracy. On the one hand, these models consider the contextual relationships between words in a sentence and generate representations that capture the meaning of the sentence as a whole. On the other hand, word-based models only consider the individual words and their relationships to other words in the corpus. This allows sentence transformers to more effectively capture the meaning and semantic nuances of a sentence, which is particularly beneficial for tasks involving the evaluation of similarity between user stories.

B. Grouping of user Stories by Actor

Grouping textual requirements based on their semantic similarity provides valuable information on the structure and behavior of the target system. To explain, it simplifies interpretation and identifies redundancies and inconsistencies which improves system quality. In addition, it enables efficient requirements management, traceability, and impact analysis, improving the overall system design and development process.

In this context, we aim to group user stories according to their semantic similarity.

Unsupervised learning is a machine learning technique that works on unlabeled data. In this technique, the machine is not given predefined labels to use for learning, but autonomously identifies patterns in the data to solve the business problem.

In clustering, unlabeled data is assembled into groups by using an algorithm based on unsupervised learning. In each cleaned dataset, with the help of the algorithm, the data points can be organized into groups by using the clustering algorithm. As a result of the clustering algorithm, it is presumed that the data points that belong to the same group, will have similar properties whereas the data points, that belong to different groups, will have quite different properties. Machine learning algorithms include a wide variety of clustering algorithms. Among the various clustering algorithms used in machine learning, K-Means is the most commonly used. According to [33], the use of K-means offers significant advantages for clustering textual requirements. This algorithm is appreciated for its speed, simplicity, and interpretability.

In addition, it offers flexibility by allowing the desired number of clusters to be specified. This study confirmed the benefits of K-means in the efficient clustering of requirements.

The process of the K-Means algorithm is outlined in the steps below:

- Step 1: We first select a random number of K to use and randomly initialize their respective center points.
- Step 2: We then classify each data point by calculating the distance (Euclidean or Manhattan) between that point and the center of each cluster, and then regrouping the data point so that it is in the cluster whose center is closest to it.
- Step 3: We recalculate the cluster center by averaging all vectors in the cluster.
- Step 4: We repeat all these steps for n number of iterations or until we find that the cluster centers do not change much.

IV. APPROACH

This section presents our proposed approach to backlog refinement and UML diagram generation. This approach both identifies similar user stories and generates the corresponding UML diagrams for each group spotted. First, we give an overview of our proposal. Then, we provide a detailed explanation of each step.

Our method started by grouping user stories by actor, and then we opted for an unsupervised clustering approach to be applied in each group. Thus, we used the k-means algorithm to generate clusters.

In the next step, we applied the BERT transformers algorithm for each cluster to compute similarity measures between user stories.

We developed a web-based tool for visualizing clustering, similarity features, and UML diagrams. We used Python and the Flask framework to implement the tool. Fig. 1 shows the steps of our proposed method.

A. Grouping of user Stories by Actor

A user story is a very high-level definition of a requirement, containing just enough information; it is the most effective way to describe a requirement [34]. Agile project teams use one of these methods: Scrum, XP, Kanban, etc.

A user story often uses the following type of format:

As [actor], I want/I am able/I can [some objective], so that [some reason] [34].

Before grouping the user stories, it is crucial to group the requirements by an actor. To achieve this goal, we extracted the actors using heuristic rules. The defined rules are based on tokenization and POS. We used the Python language and Spacy as NLP tool.

Since the extraction of a composite role composed of three words was not possible with the typed dependency in our previous work [10] [36], we switched to another method which consists of extracting the words following “As a/an”: The role indicator is either an adjective or a noun, except pronouns. This solution allowed us to extract actor names independently of their name type. Our tool then used our defined rules to extract actors from user stories, which were stored in a text file. After that, it grouped the requirements by actor and saved each group separately. Fig. 2 shows examples of user stories.

Given these user stories:

- As an administrator, I want to search for a specific student, so that I can find the student records.
- As a student, I want to look up my student records, so that I can get a look at the details.

The two user stories are similar in the sense that they both aim to provide access to student records. They differ mainly in the actor involved: the administrator in the first case and the student in the second.

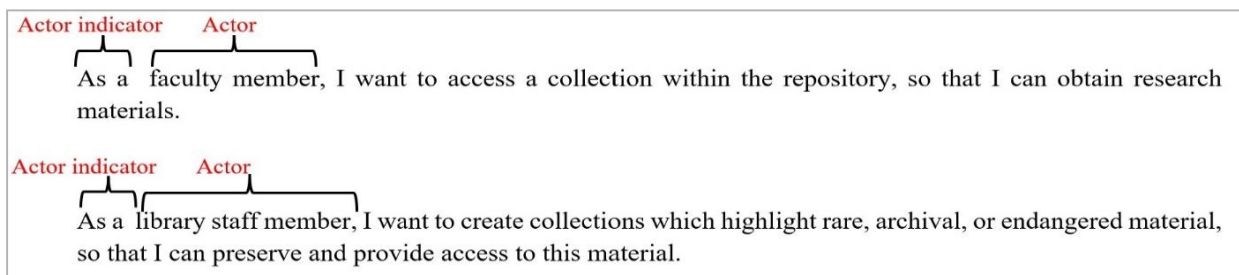


Fig. 1. Steps of our proposed approach.

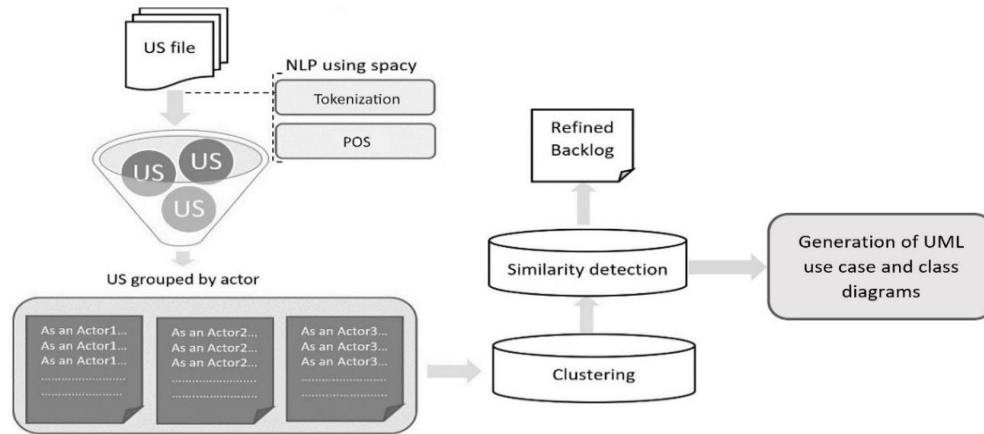


Fig. 2. Examples of user stories.

Unlike the methodology described in study [25], which focused on the identification of similarities between user stories without taking into account the “action executor” - i.e., the actor involved in the process - our approach took into account the specific roles or actors associated with the actions described in the stories.

Our method consisted of classifying user stories according to the actors involved, which makes it easier to keep similar stories describing identical actions carried out by different roles. These role-oriented requirements are the basis of the generated UML diagrams. For example, in a UML use case diagram, the two user stories could be represented as two separate but related use cases because they have similar functionalities (search and access to student records). They could be represented with different actors (the administrator and the student) but linked to a common use case, such as “View student records”. This would show the relationship between the two actions despite the differences between the actors.

B. Clustering

To implement our method, we used Sentence Transformers to embed sentences. Then, we employed the K-means algorithm to cluster the user stories based on their significance. We labeled the generated clusters using the Gensim library, which also provided us with keywords that describe the domain knowledge embedded in each cluster.

The Gensim library has an implementation of TF-IDF as part of its models, specifically the TF-IDF model module. This module converts documents into a matrix of token counts and calculates TF-IDF weights for each word.

These weights can then be used as features for tasks such as text classification, clustering, or similarity calculation.

To refine the backlog, we needed to eliminate duplicate user stories and display only relevant stories with their level of similarity. K-means clustering was used to achieve this by initially setting the value of k and examining the graph to identify the cut-off point where the slope changes. However, we opted for the silhouette calculation method to automate the k-value calculation at the outset. This approach enabled us to find the optimal k-value right from the start, making it easier to

group user stories more efficiently. Then, we created a Python code to accomplish this task.

C. User story Similarities and Opposite Meanings Detection

1) *Identification of similar user story pairs*: To refine the backlog and detect duplicate user stories, we categorized the user stories by actor and then measured the similarity rate between each pair of user stories within each cluster. To achieve this goal, we used a sentence transformer (SBERT) to measure semantic similarity between the pairs of user stories. Below are the steps conducted for each cluster:

- Convert a sentence into a vector using sentence transformers.
- Convert several other sentences to vectors.
- Identify sentences with the smallest distance (Euclidean) or angle (cosine similarity) between them.
- Highlight the most similar user stories with rates above 75%.

We used SBERT to transform sentences into vectors, embedding them in a high-dimensional semantic space. Cosine similarity is then used to measure the degree of similarity between these vectors. More precisely, it assesses the comparability of documents regardless of their size by calculating the dot product of the vectors divided by the product of their Euclidean norms, as illustrated in Eq. (1).

$$\text{Similarity} = \cos(\theta) = \frac{A \cdot B}{\|A\| \|B\|} = \frac{\sum_{i=1}^n A_i B_i}{\sqrt{\sum_{i=1}^n A_i^2} \sqrt{\sum_{i=1}^n B_i^2}} \quad (1)$$

Here, A and B are two vectors. A.B is the dot product of those two vectors.

We aimed to select the most efficient sentence transformer that provides a higher percentage of similarity among pairs of sentences exhibiting similarities. We focused on comparing user stories that are similar but differ in their operations, ensuring that any dissimilarities were captured.

We adopted a structured two-phase approach to choose the most suitable model for measuring the similarity between pairs of user stories. First, we carried out a comparative analysis of

SBERT models to identify the most efficient model. Then, we extended our evaluation by comparing the SBERT model with other models available in the field.

On the one hand, Table I highlights the application of various SBERT models to detect similarities among pairs of user stories. This table presents the respective similarity rates achieved by applying different SBERT models to some pairs of user stories. On the other hand, Table III illustrates the comparison of the similarity rates obtained from different models, such as Elmo, Word2Vec, and a SBERT model, among others. Furthermore, Table II highlights the application of various SBERT models to detect similarities among pairs of user stories. This table presents the respective similarity rates achieved by applying different SBERT models to some pairs of user stories. Table I and Table II illustrate the two-level processes that form an integral part of our analysis approach.

Consider these user stories:

- US1: As a buyer, I am able to remove a product from the list.
- US2: As a buyer, I can drop a product from the list.
- US3: As a buyer, I can edit a product in the list.

Table II shows the similarity score of previous user stories by applying the sentence Transformers.

Based on the hierarchical structure of WordNet, Wup similarity evaluates the similarity between words according to their position in the lexical tree. Wup similarity does not take into account the contextual meaning of the words being compared unlike BERT, ELMO, and InferSent which integrate context to evaluate similarity. This lack of contextual consideration can limit Wup similarity's ability to capture semantic nuances in a variety of contexts.

TABLE I. SIMILARITY SCORES OF USER STORIES US1, US2, AND US3 USING SENTENCE TRANSFORMERS

| Sentence Transformers | Similarity score US1-US2 | Similarity score US1-US3 |
|--------------------------|--------------------------|--------------------------|
| all-MiniLM-L6-v2 | 0.8180 | 0.6819656 |
| all-MiniLM-L12-v2 | 0.8838 | 0.7911284 |
| all-mpnet-base-v2 | 0.9025 | 0.8001925 |
| all-distilroberta-v1 | 0.9006 | 0.7651011 |
| paraphrase-mpnet-base-v2 | 0.9046 | 0.69480187 |

TABLE II. SIMILARITY SCORES OF USER STORIES US1, US2, AND US3 USING SIMILARITY MODELS

| Models and similarity measures | Similarity score US1-US2 | Similarity score US1-US3 |
|---------------------------------|--------------------------|--------------------------|
| USE | 0.83511186 | 0.7759 |
| SBERT(paraphrase-mpnet-base-v2) | 0.9046 | 0.69480187 |
| WORD2VEC | 0.84041464 | 0.7834515 |
| InferSent | 0.9690 | 0.9582 |
| ELMO | 0.9342766 | 0.8595803 |
| Wup similarity | 0.66107734 | 0.3823969 |

Both Tables I and II illustrate that the sentence transformer “paraphrase-mpnet-base-v2” exhibits a considerable degree of similarity. We observe operations of US1 and US3, which involve different actions such as “remove” and “edit”. Therefore, the model chosen to evaluate similarity must be able to discern sentences with closely related but divergent meanings. This discernment is essential to avoid any negative impact on our analytical processes and backlog refinement.

To ensure that we had selected the appropriate Sentence Transformer model for our approach, we carried out an evaluation by testing several models on two distinct datasets. This evaluation aimed at determining the performance and effectiveness of each model in capturing the semantic meaning of user stories and generating high-quality sentence embeddings. To measure the performance of the models, we used evaluation metrics such as cosine similarity, accuracy, and F1-score. Through this evaluation process, we identified the model that consistently demonstrated superior performance and provided the most meaningful sentence embeddings.

We will provide further details of the evaluation in the next section.

2) *Identification of the user story pairs with opposite meanings:* When the similarity threshold is increased, the number of similar user story pairs decreases. To identify similar user stories, a minimum similarity rate of 75% is required while a much higher threshold with similarity rates exceeding 90% is necessary to detect duplicate user stories. In the first range, similar user stories were sometimes found where one story was included in another, providing additional information to the third part of the story. This was mainly due to the poor quality of the user stories. It is only by improving the quality of these stories that the occurrence of such similarities can be reduced.

However, in the second range, although we detected duplicate user stories, they sometimes had opposite meanings that were not captured by sentence similarity models.

Given these user stories:

- US4: As a buyer, I can add a product to the list.
- US5: As a buyer, I can not add a product to list.
- US6: As a user, I want backend changes for managing enum lists.
- US7: As a user, I want frontend changes for managing enum lists.

Table III displays the similarity scores of user stories with opposite meanings, which are US4 with US5, and US6 and US7.

In studying the ability of the SBERT model to detect pairs of opposing user stories, it was noted that when two user stories were presenting the same operation, with the same action verb in the format "As [actor], I want [action_verb]" and preceded by a negation "not", the model was able to identify their opposition. However, if they are not having the same operation, the SBERT model does not detect the dissimilarity.

Another case demonstrating opposite meanings is illustrated in the cases described in Table IV. Using sentence transformers, we observed a similarity score of 0.97 between user stories US6 and US7, highlighting substantial similarity despite contrasts in their content. To address this limitation, we developed specific rules. We used Typed dependencies provided by an NLP tool and the Wordnet API to search for synonyms of operations and checked for the presence of negation. Where negation was not explicitly expressed, we opted to detect antonyms for operations which improved the accuracy of detecting pairs of opposing user stories.

TABLE III. SIMILARITY SCORES OF USER STORIES WITH OPPOSITE MEANINGS

| Models and similarity measures | Similarity score US4-US5 | Similarity score US6-US7 |
|--------------------------------|--------------------------|--------------------------|
| USE | 0.8806 | 0.9573 |
| SBERT | 0.42601973 | 0.9724 |
| WORD2VEC | 0.9803098 | 0.94255805 |
| InferSent | 0.9965 | 0.9912 |
| ELMO | 0.95751846 | 0.9578713 |
| Wup similarity | 0.6326058 | 0.6258217 |

As shown in Table III, we found a similarity of 0.97 between user stories US6 and US7 when using sentence transformers, suggesting high similarity within their differences. The WordNet approach was able to detect opposing meanings in some pairs of user stories. However, this method showed limited effectiveness for some examined pairs. The rules, we have developed, combine the use of the Wordnet API with typed dependency analysis to identify cases where user stories are initially identified as duplicates, having opposite meanings. These rules cover four different structures of user stories listed in Table IV.

The defined rules are based on the Stanford CoreNLP dependencies, such as neg, dobj, nmod, and advcl. This method includes the steps described in the proposed algorithm as follows.

TABLE IV. STRUCTURES OF USER STORIES

| Structures | User stories | Description | Example |
|-------------|--|---|---|
| Structure 1 | As an actor, I want/I am able/I can verb dobj | An actor or role executes an action, which is described by a verb and involves a direct object. | As a customer, I want to view my order history so that I can track my purchases. |
| Structure 2 | As an actor, I want/I am able/I can verb dobj preposition nmod | This structure includes additional detail about the direct object by adding a noun modifier. | As an administrator, I want to delete inactive user accounts more than 6 months old so that the database remains optimized. |
| Structure 3 | As an actor, I want/I am able/I can ... preposition1 nmod1... preposition2... nmod2 | This structure adds a second nominal modifier to further clarify the objective of the user story. | As a manager, I want to include videos in courses for students. |
| Structure 4 | As an actor, I want/I am able/I can verb1 dobj1... preposition1 nmod preposition2 advcl... verb2 dobj2... | It involves an initial action with a direct object, followed by a preposition and a modifier, leading to a second action with its direct object | As a manager, I want to generate reports of sales data by preserving product prices. |

Algorithm: Rules for negation extraction

1. Procedure(story1,story2):
2. Extract_part2(story1,story2)
3. Syn=Extract_synonyms(story1.verb1)
4. if [verb2 in Syn and check_negation(story1,story2)]
5. or are_antonyms(verb1, verb2) then
6. if dobj(verb1,obj1) = dobj(verb2,obj2)
7. or nmod(obj1,modifier)= nmod(obj2,modifier) then
8. return "negation found"
9. if story1.Action_advcl=story2.Action_advcl then
10. return "negation found"

The algorithm described above is designed to detect negation in a pair of user stories. It worked by first extracting the second part of the user stories that presented the action. Then, it searched for synonyms of the first story's verb (verb1) and checked whether the second story's verb (verb2) is a synonym of the first story's verb (lines 1-3). In line 4, the check_negation(story1, story2) function was implemented by recognizing the negation indicator. In line 5, the algorithm examined whether the verb in story 1 is either a synonym preceded by a negation indicator or a direct antonym of the verb in story 2. If these conditions, along with the direct object or nominal modifier (nmod) had matched between the objects (lines 6-8), the algorithm returns "negation found". Line 9 checked whether the action in the "advcl" dependency is the same in both stories. If this condition, and the previous conditions, are met, the algorithm obtains the result "negation found". This condition is specific to Structure 4.

D. Similarity Detection in use Case Diagram

We used the Sentence Transformer technique to identify similarities between use cases in use case diagrams. Our approach involved concatenating the actor name and use cases, and then checking for similarities with a similarity score of over 90%, which was further improved by applying Wordnet for lemma synset interactions. This approach helped us extract similar use cases and user stories, which was very useful in creating refined models with minimal redundancy and inconsistency.

E. UML Diagrams Generation

After dividing the system into requirements by actors, we automated the process of generating UML models (class diagrams and use case diagrams) from the resulting clusters. To achieve this, we used various types of dependency present in NLP to implement specific NLP rules in the Prolog language to extract the elements making up the diagrams. Our first step involved generating the class diagram, followed by the use case diagram. Based on our previous work [11], we have developed Prolog rules to identify classes and associations. Facts were provided by an NLP tool that supplies nouns, verbs, and typed dependencies. The process of extracting class attributes followed the methodology described in study [10]. Hence, this method refined classes into attributes and converted certain associations into operations on classes. Prolog rules are presented as follows: Association(X, Y, Z); X is the name of the association, and Y and Z are the classes in the class diagram.

Extracting classes and associations is useful in generating use cases while association types, such as composition, helps determine the relationship between the use cases.

Given the importance of the terms used to represent the elements of the diagrams, refining the diagrams is essential as well. After the generation of UML diagrams, the next critical phase involved their refinement, which had been facilitated by the development of an ontology to store word equivalents [11].

F. Web-Based Framework

We developed a web-based tool that allows users to display similar user stories and their similarity percentages in selected clusters. Based on this percentage, users can decide whether to delete similar stories or to keep them. On the homepage, users can select a file containing user stories and click on a button to group them by actor. The file is automatically split into multiple ones, and users can then choose an actor from a drop-down list. Clustering by meaning is then performed, and the similarity rate is displayed. The results are presented in a table format, showing the similarity between each pair of user stories. We set the maximum similarity threshold at 75%. Once users have refined their backlog, they can generate UML class and use case diagrams to further improve the system design and development process.

V. RESULTS AND DISCUSSION

This section presents the case studies and performance to evaluate the methodology of our approach for clustering, detecting more similar user stories, and generating a UML diagram for each cluster.

A. Evaluation

In this section, we present the evaluation of our approach. We firstly compare evaluating the “Paraphrase-mpnet-base-v2” model and the “all-MiniLM-L6-v2” model, which both belong to the SBERT models. We then compare our approach with other similarity detection models such as the Universal Sentence Encoder (USE), ELMO, and Word2vec. These models were evaluated for their performance in detecting similarities and distinguishing nuances in user stories.

Therefore, we evaluated the UML class and use case diagrams that have been generated.

1) *User stories clustering*: In our study, we acknowledge the absence of a baseline or established benchmarks in the literature that specifically address the clustering of user stories using the k-means algorithm based on the “paraphrase-mpnet-base-v2” model.

It was therefore difficult to make a direct comparison with existing results or measurements. Although the lack of references limited our ability to quantitatively assess the performance of our approach, we solved this problem by carrying out a qualitative evaluation of the content of the groupings. To validate the effectiveness of the clusters in capturing similarities and relationships between user stories, a thoughtful manual evaluation was carried out. The latter was conducted by a team of experts who examined the logical consistency and relevance of the clusters. The findings of this evaluation validated the cluster quality and their ability to accurately represent the underlying patterns in the user stories.

2) *Sentence transformer and word embedding models for similarity detection*: The SBERT “Paraphrase-mpnet-base-v2” sentence transformer model was selected to measure similarities between user stories. This choice was based on its enhanced robustness in capturing the deep semantics of sentences, thus offering high-quality representations. We chose this model thanks to its ability to handle sentences with similar but different meanings, a crucial feature for in-depth analysis of user stories.

Course management and Archivespace, which are two distinct datasets, were used to evaluate Sentence transformer models. The first dataset, retrieved from the website Mountain Goat Software, consists of 102 user stories. The second dataset, from Archivespace, included 160 user stories. We collected these user stories as a part of the ArchiveSpace software development project.

We carried out evaluations to compare and assess the performance of the “all-MiniLM-L6-v2” and “Paraphrase-mpnet-base-v2” sentence transformer models, as well as the USE, ELMO, and Word2vec models, using several pairs of user stories. Table V presents the performance scores for the Archivespace dataset, including those of the sentence transformer and word embedding models.

Fig. 3 illustrates the similarity ranges between pairs of user stories by using Paraphrase-mpnet-base-v2, All-MiniLM-L6-v2, USE, Word2vec, and ELMO.

TABLE V. THE PERFORMANCE SCORES OF SIMILARITIES BETWEEN USER STORIES USING SENTENCE TRANSFORMERS AND WORD EMBEDDING MODELS

| Sentence transformer Model | Score<0.5 | 0.5< score<0.7 | 0.7< score< 0.9 | Score> 0.9 |
|----------------------------|-----------|----------------|-----------------|------------|
| All-MiniLM-L6-v2 | 4076 | 426 | 53 | 5 |
| Paraphrase-mpnet-base-v2 | 2820 | 1635 | 100 | 5 |
| USE | 4139 | 388 | 31 | 2 |
| Word2vec | 4 | 1067 | 3462 | 27 |
| ELMO | 0 | 285 | 4234 | 41 |

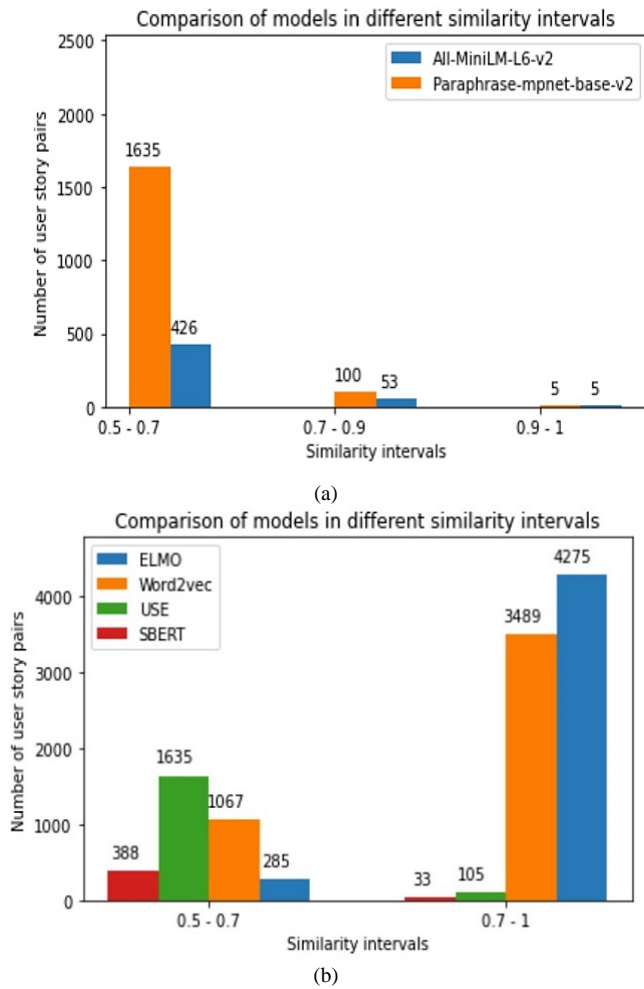


Fig. 3. Comparison of paraphrase-mpnet-base-v2 and All-MiniLM-L6-v2 (a), and comparison of SBERT (Paraphrase-mpnet-base-v2), USE, Word2vec, ELMO (b) in different ranges.

While evaluating the Sentence Transformers models, we found significant differences between the two datasets. The “Paraphrase-mpnet-base-v2” and “All-MiniLM-L6-v2” models were initially tested for interval similarities greater than 0.9, and we discovered that these intervals gave almost identical results. However, when similarities were between 0.7 and 0.9, the evaluation of user story pairs presented challenges in determining whether they were similar or duplicates. In some cases, user stories appeared to be similar but turned out to be opposite or dissimilar. The results indicated that both models exhibited similar levels of similarity for most pairs of user stories. However, when considering slightly similar user stories, “Paraphrase-mpnet-base-v2” showed a distinguishing characteristic compared to the other model. It demonstrated a better ability to capture nuanced similarities and subtle differences between such user stories.

To compare the sentence transformer models with the use of USE, Word2vec, and ELMO, we conducted a second evaluation. The results revealed that USE detected lower similarity values than those detected by the sentence transformer models, even when the similarity interval was greater than 0.9. Furthermore, for pairs of user stories that

should have a similarity rate below 0.8, USE often detected values above 0.8, particularly for user stories that appeared to be opposite or less similar. This divergence can be explained by saying that although user stories are similar in their action, differences in their description prevent them from being considered duplicated. Furthermore, the Sentence Transformers models, in particular the “paraphrase-mpnet-base-v2” model, showed better performance for the datasets used in this study. USE, while performing less well than SBERT, is still more reliable than Word2Vec and ELMO in assessing the similarity between these stories.

Further analysis revealed that Word2Vec, a widely used sentence embedding model, had limitations in detecting dissimilarity between user stories. Word2Vec may face challenges when distinguishing between user stories that are textually similar but involve different operations.

For example, it may struggle to discern the nuances between sentences such as “Users can add items to their shopping cart” and “Users can remove products from their shopping cart”, which is crucial in the context of software development.

In contrast, models such as Sentence Transformers are specifically designed to capture these contextual and operational nuances. They are highly accurate in measuring similarity while being more sensitive to subtle differences between similar user stories. In areas such as software engineering, where a precise understanding of requirements is essential, Sentence Transformers prove to be more effective for analyzing and planning software development.

After observing the similarity scores of different models in distinct ranges, notably between 0.5 and 0.7, as well as those above 0.7, we found that the SBERT model, in particular the “paraphrase-mpnet-base-v2” model, presented more consistent scores when compared to a manual approach. However, to better assess model choice, we used various metrics, including precision, recall, and F1 score [35]. Similarity identification was measured by accuracy, while coverage was measured by recall. We calculated precision, recall, and F1 score based on true positives, false positives, and false negatives. True positives (TP) corresponded to similarities correctly identified by our automated approach, while false positives (FP) referred to similarities incorrectly identified. A false negative (FN) was a labeled similarity not identified by an automated approach.

The evaluation metrics are measured as follows, as illustrated in Eq. (2), Eq. (3), and Eq. (4):

$$\text{Precision} = \frac{TP}{TP+FP} \quad (2)$$

$$\text{Recall} = \frac{TP}{TP+FN} \quad (3)$$

$$\text{F1 Score} = \frac{2 \cdot \text{Precision} \cdot \text{Recall}}{\text{Precision} + \text{Recall}} \quad (4)$$

Table VI shows the precision, recall, and F1 scores for each user story dataset for similarity pairs obtained using SBERT.

Table VII displays the similarity detection metric related to USE, Word2vec, and SBERT Models for User Story Pairs of the Archivespace dataset.

TABLE VI. EVALUATION METRICS FOR SIMILARITY DETECTION OF USER STORIES OF THE FIRST DATASET

| Models | Similarity of user stories pairs | | | | | |
|----------|----------------------------------|----|----|-----------|--------|----------|
| | TP | FP | FN | Precision | Recall | F1-score |
| ELMO | 7 | 13 | 3 | 35% | 70% | 46% |
| Word2vec | 14 | 65 | 0 | 17% | 100% | 29% |
| USE | 5 | 1 | 6 | 83% | 45% | 58% |
| SBERT | 14 | 1 | 0 | 93% | 100% | 96% |

TABLE VII. COMPARISON OF SIMILARITY DETECTION MODELS FOR USER STORY PAIRS OF ARCHIVE SPACE DATASET

| Models | Similarity of user stories pairs | | | | | |
|----------|----------------------------------|----|----|-----------|--------|----------|
| | TP | FP | FN | Precision | Recall | F1-score |
| ELMO | 7 | 13 | 3 | 35% | 70% | 46% |
| Word2vec | 14 | 65 | 0 | 17% | 100% | 29% |
| USE | 5 | 1 | 6 | 83% | 45% | 58% |
| SBERT | 14 | 1 | 0 | 93% | 100% | 96% |

Table VI and Table VII show similar user stories with similarity rates above 90%. When the similarity rate exceeds 90%, the user stories are more similar. The low similarity metrics obtained using Word2Vec to evaluate user stories can be explained by the fact that this model does not capture the semantic complexity of texts as effectively as more recent approaches such as USE and SBERT.

In some cases, one user story was included in another one which added more information in the third part of the user story which was due to poor writing of user stories. If the user stories were of high quality, they could reduce the occurrence of similar user stories. In other cases, the approach detected two similar user stories with opposite meanings. However, by using Wordnet and our defined rules, we have overcome this shortcoming.

Grouping user stories by actor before detecting similarity between pairs of stories had been found to help address the problem of false positives that can occur when multiple actors perform the same action. If stories were not grouped by actor, the similarity approach may identify false similarities between two stories that had different actors. However, the Universal Sentence Encoder (USE) model is limited in detecting explicit negation. Because of relying on language patterns, it can struggle to capture the opposite or contradictory meaning introduced by negation words like “not”. This can result in inaccurate detection of differences in meaning when negation is present.

3) *Evaluation of UML class and use case models:* During the evaluation process, our primary focus was to compare the UML use case diagrams generated by the proposed approach with the manual UML use case diagrams created by our team of experts. These diagrams were based on user stories. We aimed to assess the accuracy and effectiveness of the generated models in comparison to the manual approach and a relevant existing approach in the field. However, we were

unable to make a direct comparison between our results and those of the referenced article because the identical case study used by the authors was unavailable.

To assess the quality and relevance of the UML use case models, we implemented a manual evaluation approach. Our team of experts carefully examined the models, comparing them with the corresponding user stories to ensure accuracy and consistency. In addition, to evaluate class diagrams, we used the same case study as [4], enabling a comparative analysis of the approach to extracting artifacts from class diagrams. This evaluation involved examining the artifacts extracted and comparing them with the expected artifacts derived from the case studies. We considered aspects such as completeness, correctness, and relevance to assess the effectiveness of our approach.

- Case study

The user stories, in this case study, represented event management: booking and purchasing an event ticket [36].

Tokenization, lemmatization, stemming, and part-of-speech (POS) analysis were used to process user stories. Typed dependencies were then applied to each user story. The extraction of design components was based on defined rules, which relied on the dependencies that were exploited and analyzed.

The final results of the extraction of design elements for the given user story are presented in the tables below. Classes and their attributes are listed in Table VIII.

TABLE VIII. CLASSES AND THEIR ATTRIBUTES

| Classes | Attributes |
|---------|------------------|
| Account | Password |
| Visitor | Personal_details |
| Ticket | Price |
| Ticket | Type |

The relationship results are shown in Table IX.

TABLE IX. RELATIONSHIPS RESULTS

| Relationships |
|-----------------------------------|
| Create (account, Visitor) |
| Have (account, Visitor) |
| Rename (account, Visitor) |
| Choose (event, Visitor) |
| Search (event, Visitor) |
| See (event, Visitor) |
| Choose (payment_methods, Visitor) |
| Buy (ticket, Visitor) |
| Book (ticket, Visitor) |
| Purchase (ticket, Visitor) |
| Receive (ticket, Visitor) |
| Have (ticket, event) |

Table X indicates the results of the operations.

TABLE X. GENERATION OF CLASS OPERATIONS

| Classes | Operations |
|---------|----------------------------|
| Visitor | Provide (personal_details) |
| Account | Change(password) |
| Event | Filter(type) |
| Ticket | See (price) |
| Ticket | Choose(type) |
| Event | Choose(type) |

The Visual Narrator tool [4] identified several classes, including Visitor, Account, System, Event, Ticket, EventType, Type, AccountPassword, Password, TicketPrice, Price, Detail, and Method. However, there are some relationships that the tool extracted, but our approach did not, such as hasType (Event, EventType), hasPrice (Ticket, TicketPrice), and hasPassword (Account, AccountPassword). Additionally, the tool detected that Visitors and Systems can log in and log out, but our approach did not.

The Visual Narrator tool [4] uses an approach that creates numerous compound classes and inheritance relationships. However, this method can result in complex classes and inheritance relationships that are unnecessary due to the absence of attribute extraction rules. Table XI compares the total items detected by [4], our approach, and manual analysis.

TABLE XI. THE TOTAL OF DESIGN ELEMENTS DETECTED BY [4] AND OUR APPROACH [36]

| | Actors | Classes/ Entity | Attributes | Relations- hips | Operations |
|--------------|--------|-----------------|------------|-----------------|------------|
| [4] | 1 | 13 | 0 | 19 | 0 |
| Our approach | 1 | 5 | 5 | 12 | 6 |
| Manually | 1 | 5 | 5 | 12 | 6 |

Our approach, in the case studies, demonstrated significant improved performance compared to the method described in [4], achieving a high precision rate of 98% when comparing these results to those obtained manually.

B. Results

We provided a detailed explanation with the help of figures to clarify the process of clustering and generating UML diagrams using our tool.

Fig. 4 shows a web page that allows the user to download a file containing a set of user stories. Once downloaded, we performed the clustering by actor by clicking the “Clustering by actor” button. The extracted actors were then included in a drop-down list. To perform clustering by meaning, the user needed to click on the “Analyze” button, as illustrated in Fig. 5. It is worth noting that a text field to specify the number of clusters was not included from the beginning. This process was automated based on silhouette calculations.

Fig. 5 displays the clusters in a table, along with keywords representing the cluster's meaning, as well as links to select similar user stories. This table allows the user to easily navigate through the clusters and select the most relevant user stories.

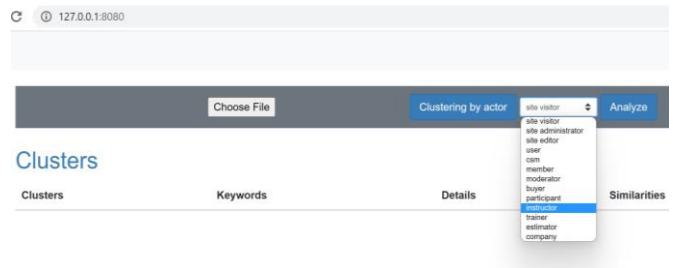


Fig. 4. Items generated in the drop-down list from the user stories file.

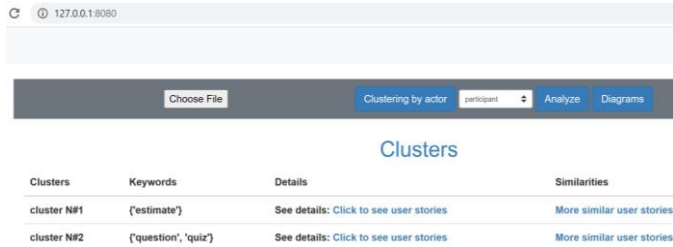


Fig. 5. Clusters generated corresponding to Participant actor.

Fig. 6 and 7 show the similarity scores generated for pairs of user stories within the cluster of the Instructor and Participant actors. By highlighting the most similar user stories, our tool facilitated the decision to delete or keep them.



Fig. 6. Similarity scores generated for pairs of user stories within the cluster of the Instructor actor.



Fig. 7. Similarity scores generated for pairs of user stories within the cluster of the Participant actor.

Finally, Fig. 8-12 display the generated class and use cases UML diagrams corresponding to the “Participant” and “Instructor” actors. These diagrams provide a clear and consistent understanding of the product requirements, making it more convenient for team members to collaborate and work efficiently.

As can be seen in Fig. 10 and 12, using sentence transformers allows for the detection of duplicate use cases such as “receive feedback” and “get feedback”, the same for the “receive” and “get” associations between the participant and feedback class. Regarding the use cases “upload PDFS” and “download PDFS” these components were similar in using sentence transformation yet using the Wordnet approach shows that they had opposite meanings. We believe that combining both approaches can achieve better performance.

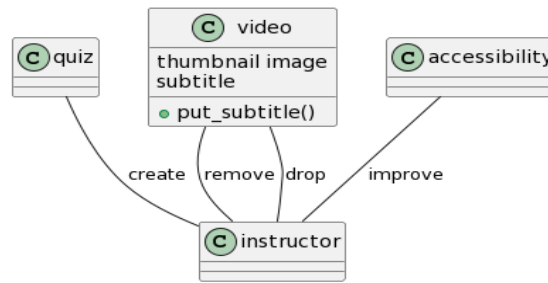


Fig. 8. Generated the UML class diagram corresponding to the instructor's cluster.

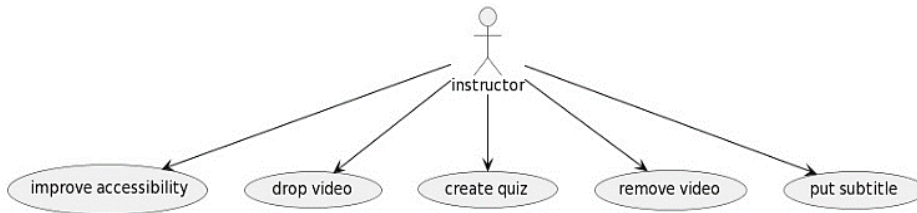


Fig. 9. Generated the UML use case diagram corresponding to the instructor's cluster.

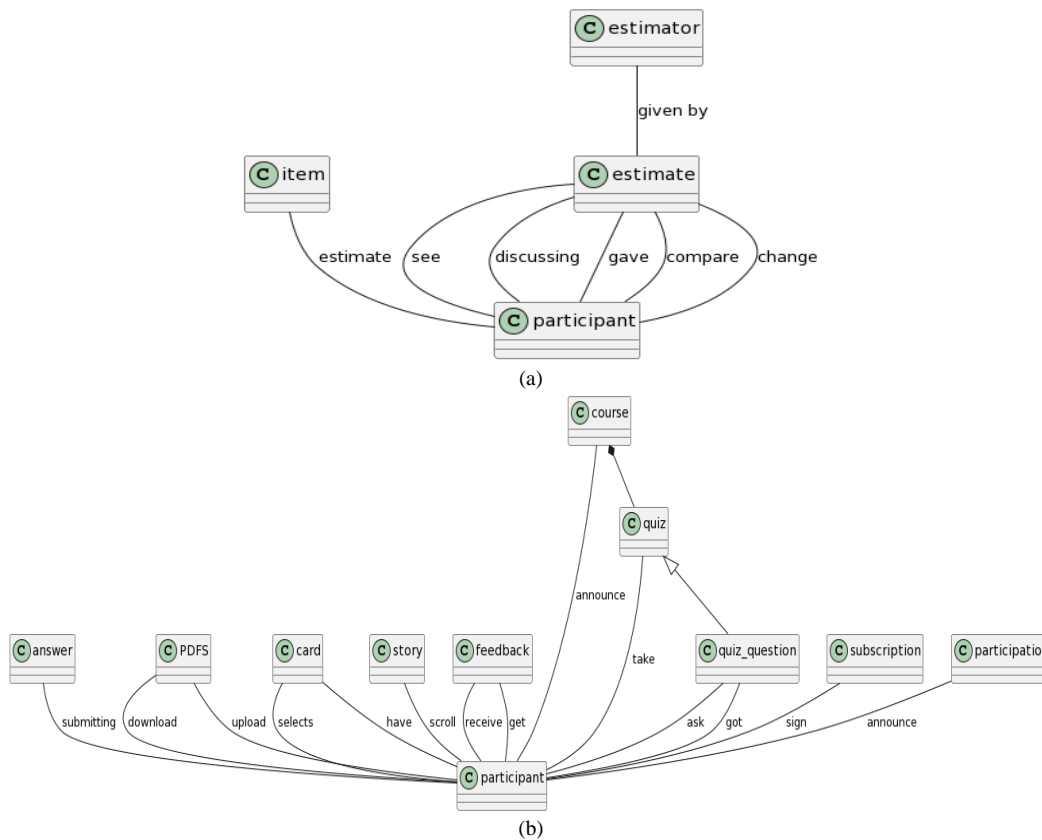


Fig. 10. Generated the UML class diagrams corresponding to participant's clusters #1 (a) and #2 (b).

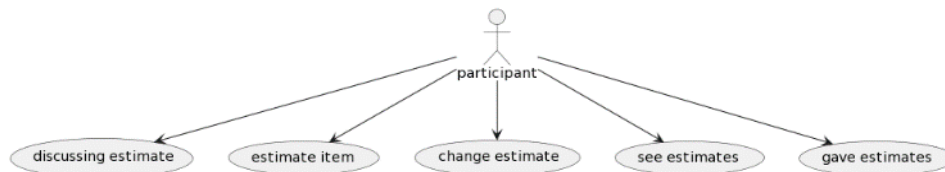


Fig. 11. Generated the UML use case diagram corresponding to participant's cluster #1.

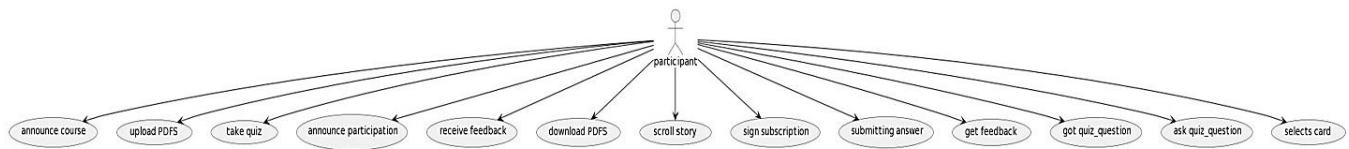


Fig. 12. Generated the UML use case diagram corresponding to Participant's cluster #2.

C. Threats to Validity

In this section, we will discuss the possible threats to the validity of our proposed approach.

- **Internal Validity:** The quality of user stories can have a significant impact on the results, particularly if they are poorly written or contain non-functional scenarios. This can negatively affect the relationships between classes and generate inadequate UML diagrams.

To overcome this problem, it is essential to ensure the quality and functional accuracy of user stories.

- **Construct Validity:** The rules defined for assessing similarities between user stories may be limited, as they only capture a restricted set of sentence structures in the context of opposite meanings. It is necessary to have a more comprehensive analysis that considers the semantic meaning and context of the user stories to accurately identify and handle potential contradictions.
- **External Validity:** In evaluating our approach, we analyzed two case studies to determine the effectiveness of our approach in detecting similar user stories. Although the initial results were promising, there is a need to extend our evaluation to a larger number of case studies.

D. Discussion

In this section, we compare our approach with existing state-of-the-art techniques [14], [16] that also use user stories as input. Although these approaches focus on clustering and duplicate detection, they do not include diagram generation. Another study [24] focused on generating use case diagrams from user stories, but it only considered user stories with a simple structure and did not address duplicate or similarity detection. In [25] Detection of similarities in user stories is ineffective because their method is unable to distinguish between operations such as “delete” and “add” in stories. These operations, which represent the core functionality, remain indistinguishable. The model used to detect similar user stories, namely USE, lacks the ability to discern negations in these stories, such as “not add” and “add”.

In contrast, our approach built on our previous work [10]-[12],[36], in which we used NLP techniques to generate various UML diagrams from user stories. The paper [36] expands upon the content of [10].

The previous approach [11], based on ontology, Prolog rules, and WordNet synsets, focused on refining UML

diagrams by defining explicit relationships and using domain-specific vocabulary. It addressed redundancy and duplicate detection to some extent, but it had limitations. Maintaining and updating the ontology with relevant vocabulary posed challenges. Focusing on explicit definitions might overlook subtle nuances in redundancy and duplication. Additionally, the approach required extensive domain knowledge and manual refinement.

In contrast, the new approach incorporated AI techniques, in particular SBERT models and clustering to refine the generated backlog and UML diagrams. It used machine learning to capture semantic similarities as well as the rules we defined to achieve better results. This enabled duplicates to be detected without the need to explicitly define an ontology.

Our approach focused on improving the refinement process to enhance the quality and accuracy of the generated models. The backlog was refined using clustering and similarity detection techniques before generating the UML diagrams. This step helped in handling the large number of user stories present and guaranteed the accuracy of the generated diagrams.

Refining the use case diagrams and detecting similar use cases made our approach more complete and refined compared to other approaches used by different authors.

Table XII summarizes the relevant related works.

Table XIII presents a comparison between the previous approach and our proposed approach.

In comparison to old approaches, our approach offered several significant advantages using automatic refinement of UML diagrams. Firstly, by integrating prior refinement of the user story backlog, early detection and elimination of redundancies in the process can be achieved. This allowed us to create more concise, better organized, and more relevant UML diagrams to represent the system's functionalities.

Secondly, through using AI techniques, particularly SBERT models, our approach offered better detection of duplications and similarities between user stories. Clustering user stories and subsequently labeling these clusters, allowed for an efficient backlog structuring and an improved organization. The refinement process eliminates redundant information and similar functionalities with great precision, resulting in clearer and more readable UML diagrams.

Automating the backlog refinement process saves the team valuable time. Employing the AI-based prototype allows for quick and accurate execution of tasks such as similarity detection, user story clustering, and diagram generation.

TABLE XII. SUMMARY OF RELEVANT LITERATURE

| Approach | Models and tools | Input | Output |
|--------------|---|--------------|---|
| [14] | K-means clustering algorithm applied to user stories. | user stories | Clusters of user stories |
| [16] | - Semantic similarity measures to suggest possible cases of duplication between user stories. - Analysis of semantic similarity measures based on the WordNet lexical database, in particular WuP similarity. | user stories | Determine the level of similarity among user stories |
| [24] | - Agglomerative Hierarchical Clustering (AHC) algorithm to group requirements into clusters. - Use of the Gensim API to extract keywords by group. - Definition of simple NLP rules for component extraction to generate a use case diagram | user stories | Use case diagram |
| [25] | - The model USE for calculating similarity - For app development: Laravel and React. - Manual approach to detect similarities greater than 60% | User stories | - Estimate efforts and costs for agile projects: Time spent on similar past projects - Similarity user stories detection |
| Our approach | - Flask - Python - SBERT models - Defining NLP rules to identify every dissimilar previously classified as similar by SBERT models | User stories | - Similarity user stories detection - Clustering and labeling each cluster - UML diagram generation |

TABLE XIII. COMPARISON BETWEEN THE PREVIOUS APPROACH AND OUR PROPOSED APPROACH

| Features | Old Approach | New Approach |
|---------------------|---|--|
| Refinement Method | Prolog rules, ontology, WordNet synsets | Clustering, SBERT models, and definition of rules |
| Refinement Stage | Post-generation refinement of UML diagrams | Initial backlog refinement to detect and eliminate redundancy |
| Contextual Meaning | Not considered | Contextual meaning detection with SBERT models |
| Backlog Refinement | Not addressed | Initial backlog refinement to detect similar user stories |
| Duplicate Detection | Limited capability in detecting duplicates and similarities | Improved accuracy in identifying duplicate user stories through advanced AI techniques |

VI. CONCLUSION

In Agile project management, Backlog refinement is a crucial process. It aims to ensure that the backlog contains prioritized and well-defined user stories. However, refining the backlog using a traditional manual approach is time-consuming and prone to errors.

In this paper, we proposed an approach to refine the backlog by detecting similar user stories with a percentage that will help the designer decide to delete or leave the concerned user stories. Additionally, we aimed to reduce the occurrence of similar use cases in the use case diagram UML. Our proposed approach combined clustering and duplicate detection to automatically generate UML diagrams from a set of refined user stories in each cluster. To achieve this, we used the K-means algorithm to cluster similar user stories. In addition, we incorporated the SBERT model to measure the similarity between these user stories and use cases. Using multiple pairs of user stories, the case studies conducted show that our proposal achieves high performance.

In future work, we plan to further improve our approach by using multiple datasets to improve performance. Furthermore, we aim to define more rules to detect opposite meanings in user stories. Finally, we will focus on detecting non-functional requirements and generating acceptance criteria from them to improve the quality of user stories. It is essential to ensure that user stories remain well-defined and focused on functional aspects, while keeping non-functional requirements, such as

performance, security, and usability constraints, specified in the acceptance criteria. By addressing these challenges, we can further enhance the accuracy and efficiency of requirements engineering in software development, ultimately leading to an overall improvement in product quality.

REFERENCES

- [1] Belani H, Vukovic M, Car Z. Requirements engineering challenges in building AI-based complex systems. Proceedings - 2019 IEEE 27th International Requirements Engineering Conference Workshops, REW 2019, Institute of Electrical and Electronics Engineers Inc.; 2019, p. 2052-5.
- [2] Yang C, Liang P, Avgeriou P. A systematic mapping study on the combination of software architecture and agile development. Journal of Systems and Software 2016;111:157-84. <https://doi.org/10.1016/j.jss.2015.09.028>.
- [3] Chantit S, Essebaa I. Towards an automatic model-based scrum methodology. Procedia Comput Sci, vol. 184, Elsevier B.V.; 2021, p. 797-802. <https://doi.org/10.1016/j.procs.2021.03.099>.
- [4] Lucassen G, Robeer M, Dalpiaz F, van der Werf JMEM, Brinkkemper S. Extracting conceptual models from user stories with Visual Narrator. Requir Eng 2017;22:339-58. <https://doi.org/10.1007/s00766-017-0270-1>.
- [5] Javed M, Lin Y. Iterative process for generating ER diagram from unrestricted requirements. ENASE 2018 - Proceedings of the 13th International Conference on Evaluation of Novel Approaches to Software Engineering2018;2018-March:192-204. <https://doi.org/10.5220/0006778701920204>.
- [6] Y. Rhazali, Y. Hadi, I. Chana, M. Lahmer, and A. Rhattoy, "A model transformation in model driven architecture from business model to web model." IAENG International Journal of Computer Science, vol. 45, no.

- 1, pp. 104–117, 2018. [Online]. Available: <https://www.researchgate.net/publication/323275958>.
- [7] Jaiwai M, Sammapun U. Extracting UML Class Diagrams from Software Requirements in Thai using NLP. 2017 14th International Joint Conference on Computer Science and Software Engineering (JCSSE). IEEE, 2017. p. 1–5. <https://doi.org/10.1109/JCSSE.2017.8025938>.
- [8] Abdelnabi EA, Maatuk AM, Hagal M. Generating UML Class Diagram from Natural Language Requirements: A Survey of Approaches and Techniques. 2021 IEEE 1st International Maghreb Meeting of the Conference on Sciences and Techniques of Automatic Control and Computer Engineering, MI-STA 2021 - Proceedings, Institute of Electrical and Electronics Engineers Inc.; 2021, p. 288–93. <https://doi.org/10.1109/MISTA52233.2021.9464433>.
- [9] Yang S, Sahraoui H. Towards automatically extracting UML class diagrams from natural language specifications. Proceedings - ACM/IEEE 25th International Conference on Model Driven Engineering Languages and Systems, MODELS 2022: Companion Proceedings, Association for Computing Machinery, Inc; 2022, p. 396–403. <https://doi.org/10.1145/3550356.3561592>.
- [10] Nasiri S, Rhazali Y, Lahmer M, Chenfour N. Towards a Generation of Class Diagram from User Stories in Agile Methods. Procedia Comput Sci 2020;170:831–7. <https://doi.org/10.1016/j.procs.2020.03.148>.
- [11] Nasiri S, Rhazali Y, Lahmer M, Adadi A. From User Stories to UML Diagrams Driven by Ontological and Production Model. International Journal of Advanced Computer Science and Applications, vol. 12, no. 6, 2021. <https://doi.org/10.14569/IJACSA.2021.0120637>.
- [12] Nasiri S, Adadi A, Lahmer M. Automatic generation of business process models from user stories. International Journal of Electrical and Computer Engineering 2023;13:809–22. <https://doi.org/10.11591/ijece.v13i1.pp809-822>.
- [13] Salman HE, Hammad M, Seriai AD, Al-Sbou A. Semantic clustering of functional Requirements using agglomerative hierarchical clustering. Information (Switzerland) 2018;9. <https://doi.org/10.3390/info9090222>.
- [14] Kumar B, Tiwari UK, Dobhal DC, Negi HS. User Story Clustering using K-Means Algorithm in Agile Requirement Engineering. 2022 International Conference on Computational Intelligence and Sustainable Engineering Solutions (CISES), 2022, p. 1–5. <https://doi.org/10.1109/CISES54857.2022.9844390>.
- [15] R. Selva Birunda S. and Kanniga Devi. Review on Word Embedding Techniques for Text Classification. Innovative Data Communication Technologies and Application, 2021, pp. 267–281.
- [16] Barbosa R, Silva AEA, Moraes R. Use of Similarity Measure to Suggest the Existence of Duplicate User Stories in the Scrum Process. Proceedings - 46th Annual IEEE/IFIP International Conference on Dependable Systems and Networks, DSN-W 2016, Institute Of Electrical and Electronics Engineers Inc.; 2016, p. 2–5. <https://doi.org/10.1109/DSN-W.2016.27>.
- [17] Wang J, Dong Y. Measurement of text similarity: a survey. Information. 2020 Aug 31;11(9):421.
- [18] Banerjee S, Pedersen T. An Adapted Lesk Algorithm for Word Sense Disambiguation Using WordNet. International Conference on Intelligent Text Processing and Computational Linguistics, pp. 136–145, 2002. https://doi.org/10.1007/3-540-45715-1_11.
- [19] F. S. Bäumer MG. Running out of words: How similar user stories can help to elaborate individual natural language requirement descriptions. Commun. Comput. Inf. Sci., vol. 639, pp. 549–558, Oct. 2016. <https://doi.org/10.1007/978-3-319-46254-7>.
- [20] Wautelet Y, Heng S, Kolp M, Mirbel I. Unifying and extending user story models. Lecture Notes in Computer Science (Including Subseries Lecture Notes in Artificial Intelligence and Lecture Notes in Bioinformatics) 2014;8484 LNCS:211–25. https://doi.org/10.1007/978-3-319-07881-6_15.
- [21] Rodeghero P, Jiang S, Armaly A, Mcmillan C. Detecting User Story Information in Developer-Client Conversations to Generate Extractive Summaries. Proceedings - 2017 IEEE/ACM 39th International Conference on Software Engineering, ICSE 2017, pp. 49–59, <https://doi.org/10.1109/ICSE.2017.13>.
- [22] Dalpiaz F, van der Schalk I, Lucassen G. Pinpointing ambiguity and incompleteness in requirements engineering via information visualization and NLP. Lecture Notes in Computer Science (including subseries Lecture Notes in Artificial Intelligence and Lecture Notes in Bioinformatics), vol. 10753 LNCS, Springer Verlag; 2018, p. 119–35. https://doi.org/10.1007/978-3-319-77243-1_8.
- [23] N. Reimers and I. Gurevych, “Sentence-BERT: Sentence Embeddings using Siamese BERT-Networks,” Aug. 2019, [Online]. Available: <http://arxiv.org/abs/1908.10084>.
- [24] T. Kochbati, S. Li, S. Gérard, and C. Mraidha, “From user stories to models: A machine learning empowered automation,” in *MODELSWARD 2021 - Proceedings of the 9th International Conference on Model-Driven Engineering and Software Development*, SciTePress, 2021, pp. 28–40. doi: 10.5220/0010197800280040.
- [25] A. Grzegorz Duszkiwicz, J. Glumby Sørensen, N. Johansen, H. Edison, and T. Rocha Silva, “On Identifying Similar User Stories to Support Agile Estimation based on Historical Data,” 2022. [Online]. Available: <https://www.sdu.dk/staff/hedis>.
- [26] C. Wu, C. Wang, T. Li, and Y. Zhai, “A Node-Merging based Approach for Generating iStar Models from User Stories,” in *Proceedings of the International Conference on Software Engineering and Knowledge Engineering, SEKE*, Knowledge Systems Institute Graduate School, 2022, pp. 257–262. doi: 10.18293/SEKE2022-176.
- [27] T. Wang, C. Wang, T. Li, Z. Liu, and Y. Zhai, “User Story Quality Assessment Based on Multi-dimensional Perspective: A Preliminary Framework,” 2022. [Online]. Available: <http://ceur-ws.org>.
- [28] R. Selva Birunda S. and Kanniga Devi, “A Review on Word Embedding Techniques for Text Classification,” in *Innovative Data Communication Technologies and Application*, A. M. and B. R. and B. Z. A. Raj Jennifer S. and Iliyasu, Ed., Singapore: Springer Singapore, 2021, pp. 267–281.
- [29] A. Jalilifard, V. F. Caridá, A. F. Mansano, R. S. Cristo, and F. P. C. da Fonseca, “Semantic Sensitive TF-IDF to Determine Word Relevance in Documents,” Jan. 2020, doi: 10.1007/978-981-33-6977-1.
- [30] P. Bojanowski, E. Grave, A. Joulin, and T. Mikolov, “Enriching Word Vectors with Subword Information”, 2017, doi: 10.1162/tacl_a_00051/1567442/tacl_a_00051.pdf.
- [31] E. M. Dharma, F. Lumban Gaol, H. Leslie, H. S. Warnars, and B. Soewito, “The Accuracy Comparison Among Word2vec, Glove, And Fasttext Towards Convolution Neural Network (Cnn) Text Classification,” *J Theor Appl Inf*.
- [32] D. Cer et al., “Universal Sentence Encoder,” Mar. 2018, [Online]. Available: <http://arxiv.org/abs/1803.11175>.
- [33] A. K. Jain, M. N. Murty, and P. J. Flynn, “Data Clustering: A Review,” 2000.
- [34] M. Cohn, *User Stories Applied: For Agile Software Development*. 2004.
- [35] H. Schütze, C. D. Manning and P. Raghavan, *Introduction to Information Retrieval*, Cambridge, U.K.:Cambridge University Press, 2008.
- [36] S. Nasiri, Y. Rhazali, and M. Lahmer, “Towards a Generation of Class Diagram From User Stories in Agile Methods,” 2021, pp. 135–159. doi: 10.4018/978-1-7998-3661-2.ch008.

Challenges and Solutions of Agile Software Development Implementation: A Case Study Indonesian Healthcare Organization

Ulfah Nur Mukharomah, Teguh Raharjo, Ni Wayan Trisnawaty
Faculty of Computer Science, Universitas Indonesia, Jakarta, Indonesia

Abstract—One healthcare organization in Indonesia has implemented Agile software development (ASD) to complete software development. The organization's problems are post-deployment system bugs, and some software development projects must carry over to the following year. This study aims to assess and provide recommendations for improving agile software development by identifying the challenges faced. Research conducts literature reviews on previous research to identify challenges in ASD in several organizations. Research is also conducted using quantitative methods by surveying software development teams to validate implementation challenges and provide recommendations for these challenges. The results of this study were in the form of a survey attended by thirty-one respondents. The study results found that 14 challenges were faced in other organizations, and 11 were faced by one healthcare organization in Indonesia. Healthcare organizations in Indonesia can apply recommendations to make awareness related to understanding agile software development culture and make adjustments to project documentation by aligning with agile values.

Keywords—Agile Software Development; challenge solutions; IT projects; information technology; application implementation; healthcare organization; Literature Review

I. INTRODUCTION

Information technology (IT) can improve customer service and become an efficient tool. IT implementation is often considered one of the most challenging initiatives for organizations, including in the government sector [1]. Several organizations have changed their software development methods from Waterfall to Agile. By adopting the Agile method, organizations get several benefits, such as shorter time, increased flexibility in handling changing needs, increased productivity, and better alignment between business and IT [2]. Agile methods also need to maintain predictability and controllability [3]. Another agile principle is to welcome changing software development needs and produce software that works regularly with a preference for shorter timeframes [4].

However, transforming into an organization operating in the public sector, especially in an organization with a complex hierarchical structure such as government, is not easy to change the existing bureaucracy. The existence of layers of bureaucracy can hinder the application of agile methods [1]. Large organizations usually have many products and products that are too large for a single team to

develop. The condition creates scaling problems, which require head adaptation and expansion of basic dexterity methods [2]. The problem is also the case in Saudi Arabia, where participants agreed that adopting Agile can be difficult when dealing with customers from government bodies, as the working style tends to be based on Waterfall. They are usually unwilling to be involved in the development team and require comprehensive documentation.

One of the organizations in Indonesia provides health services to the people of Indonesia of 265 million participants. In providing health services to all participants, the organization collaborates with health facilities in Indonesia, such as hospitals or doctor's clinics. The organization is a public legal entity, a government, and a bureaucrat with racy characteristics. The organization runs the business using technology and digitalization. The demand for IT development is increasing, in addition to the demand for speed in project completion, and the limited numbers of teams are challenges in completing system development. Organizations have IT resources in the software development process.

Ninety-six applications are run and developed by the organization's development team, most of which use the waterfall method. In 2022, project development will be dominated by projects with a high urgency category, with a percentage of 43%, as shown in Fig. 1 [5]. This development request requires a rapid completion of development, but there are unclear requirements due to policy changes in the organization.

The organization in the case study implemented an agile software development project. However, in its implementation, standards or frameworks have not been implemented as a reference. The problems were that some projects carried over to the following year, and there were complaints from application users post-implementation. The number of bugs adds work to the I IT development team, where the same group currently holds the development and maintenance functions [6].

In study [6] by looking at some of the existing problems and impacts, evaluating and improving the software development process using Agile is necessary. This evaluation is for the software development process to become better, achieve targets, and produce quality products as stated in the organization's vision and mission and the organization's vision and mission. Evaluation is being done

to find out the challenges and recommendations in implementing agile software development. Implementing Agile software development requires effort and time, but the results can significantly benefit most software development programs [7].

PERCENTAGE BY PROJECT CATEGORY

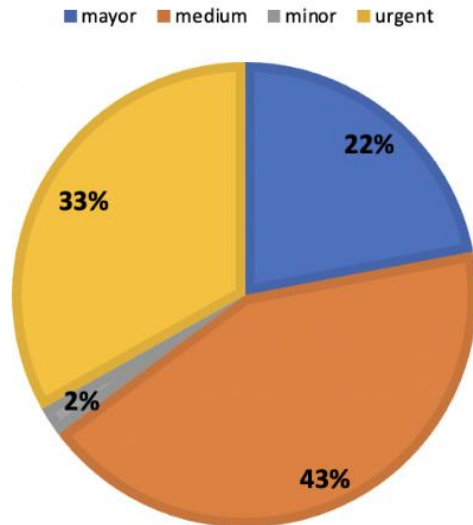


Fig. 1. Software development data by project category.

After determining the root of the problem, they considered the existing conditions in the organization and the implementation of Agile software development at the Indonesian Healthcare Organization. The questions for this research are:

RQ1: What are the challenges of Agile Software Development in the Organization?

RQ2: What are the recommendations for improving Agile implementation in the Organization?

Previous research has been carried out on projects with external resources using different methods, namely document observation. The novelty of this study is a case study on organizations with characteristics of the public sector or government or that have bureaucracy and use survey methods to respondents to validate the challenges faced. The composition of this research paper includes the following: introduction, literature study, methodology, results, and recommendations and it ends with conclusions.

II. LITERATURE STUDY INTRODUCTION

This section will discuss the basic theory used in the research. These theories relate to Agile and Prior Research.

A. Previous Research

Several previous studies identified Agile software development; however, no research has been conducted on organizations with public sector and bureaucratic characteristics in Indonesia, and projects have been carried out internally.

Previous research [8], [9], [10], [11], [12] challenges were identified in ASD in organizations with characteristics of the public sector or government and bureaucracy. Previous research [8], [12] was conducted in Indonesia, but both studies had specific problems with projects undertaken by external resources. The difference with research [8] is that the research was conducted by observing project documents to validate challenges. Another study [9], [10], [11] was conducted in other countries, namely Brazil, United Arab Emirates, and New Zealand, to identify challenges faced by organizations in the public sector. These five studies serve as the basis for a survey to validate the challenges faced by Indonesian health sector organizations.

B. Agile

Agile is an approach or software development method that emphasizes flexibility, team collaboration, responsiveness to change, and continuous delivery of valuable customer results [13]. Agile methodologies have many methods (e.g., Scrum, Extreme Programming [XP], Kanban) that have their unique processes, terms, techniques, and timelines [7].

The development of Agile methods is a response to the failure experienced by organizations to use the more traditional waterfall methods. The Waterfall method is commonly used in large software development projects. Many view the Waterfall process as a heavy and expensive document, and the Waterfall is based on significant initial planning. In each phase of the project, it is necessary to complete a sequence of steps before moving on to the next stage. The linear approach used in Waterfall is in stark contrast to the incremental and iterative empirical methods used in Agile development [1].

Agile Methodology has recently expanded into several branches. The most popular extensions are probably associated with the Scrum framework, which breaks down the entire list of requirements into smaller batches. The list is titled product backlog and is formed by product backlog items. Following specific instructions, the product is developed in stages without sticking to predefined sequences while respecting any changes the customer requires [1].

C. Challenge and Issue Agile Implementation

Based on previous research, researchers found 14 challenges faced in implementing agile software development. The fourteen challenges can be found in Table I.

TABLE I. CHALLENGES OF AGILE SOFTWARE DEVELOPMENT FROM LITERATURE REVIEW

| No | Category | Challenges | References |
|----|------------------------|--|----------------------------------|
| 1 | Technique & Ceremony | Lack of discipline in the development processes | [8] |
| 2 | IT Infrastructure | Lack of IT infrastructure in deploying the system. | [10] |
| 3 | Project Documentation | Lacks sufficient documentation to support a project | [8], [9], [10], [11], [12], [14] |
| 4 | Cultural behavior | The organization shows resistance or lack of encouragement in transitioning to an agile approach. | [9], [10], [14] |
| 5 | Communication | Communication and coordination among team members are ineffective. | [8], [12] |
| 6 | Managed requirements | The project schedule is delayed, requirements are unclear, and there is little anticipation in handling changes. | [11], [12] |
| 7 | Roles a project team | The roles of the team were unclear, leading to minimal contributions and duplicated work. | [11], [12] |
| 8 | Top Level Management | Lack of top management support, with little knowledge of the execution process. | [10], [11] |
| 9 | Internal policy | Inadequate Compliance with standards, policies, regulations, and organizational vision. | [10] |
| 10 | Collaboration | Team collaboration is limited because team members are spread out in different locations. | [8], [10], [12] |
| 11 | Organization Structure | Organizing meetings is challenging due to convoluted bureaucratic processes. | [8], [11] |
| 12 | Interpersonal Conflict | There are personal conflicts within the team. | [11], [14] |
| 13 | Individual Competence | Inadequate agile adoption of skills, experiences, and knowledge. | [11], [12] |
| 14 | Agile Values | Lack of openness and transparency during the development process leads to a lack of information. | [11] |

III. METHODOLOGY

At the methodological stage, the researcher divides the research into three phases [8]. The three phases can be seen in Fig. 2. Phase Research Methodology and the following sections discuss the details of each step.

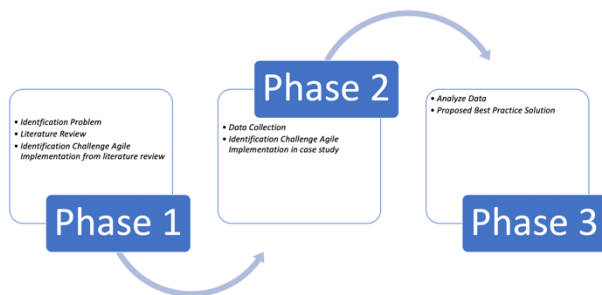


Fig. 2. Stages of research methodology.

A. Phase 1

Phase 1 is the initial stage of the research, where document observations and initial interviews are carried out to explore existing problems. Then, an analysis is conducted to determine the research questions. Based on the following research questions, literature research was conducted using PRISMA (Preferred Reporting Items from systematic reviews and Meta-Analysis). This method was used in previous studies [1]. Following are the steps of the SLR in this study:

1) The first stage is identification on the online database. The database used to search related research consists of IEEE Xplore, ScienceDirect, ProQuest, and Scopus.

2) Search using the keywords (agile software development) AND (Organization) AND ((challenges) OR

(issue) OR (solution) OR (recommendation)). Based on this, 262 documents were obtained. Then, a selection is made based on predetermined search criteria, as shown in Table II, and twenty-four documents are produced.

3) The next stage is screening, namely selecting by reading the title and abstract related to the research question and producing twenty-four documents.

4) The next stage is eligibility, which is done by searching the complete version of the research document and, in the last stage, reading the entire contents of the paper in 24 copies.

5) The final stage is to obtain ten documents by the research questions. All documents obtained are considered relevant to the research topic and can be used as a reference for this research.

The overall description of the literature selection process can be seen in Fig. 3. It shows stages of searching for literature studies.

TABLE II. LITERATURE STUDY CRITERIA

| No | Criteria |
|----|--|
| 1 | Publications within the last five years, 2018-2023 |
| 2 | English language |
| 3 | Publication of a journal |
| 4 | Publication in the form of a journal Complete publication and can be downloaded in full (full text) |

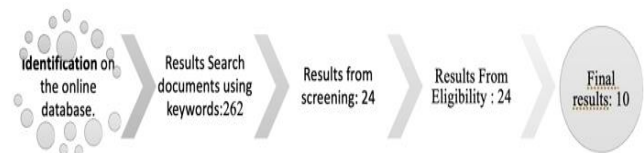


Fig. 3. Stages in SLR.

B. Phase 2

Researchers use quantitative data collection methods by conducting questionnaires to the software development team. Questionnaire questions use challenges and categories from Table I. After the questions were compiled, a test was carried out by an experienced team in the field. The software development team will distribute questionnaires, including Manager IT, IT System Specialist, IT Business Analyst, Programmer, Quality Control, and Junior Staff IT.

C. Phase 3

At this stage, an analysis will be carried out to determine what challenges are relevant to the literature review and other challenges in the organization. The analysis results above will provide recommendations for improving the agile software development process. Recommendations are given by looking at the best practices from previous studies.

IV. RESULT AND RECOMMENDATION

This stage explains the results of the questionnaire that has been distributed and analyzed. This section also answers the research questions mentioned in the introduction. The challenges of implementing agile in health organizations in Indonesia and recommendations given to overcome these challenges

A. Result

Based on the research questions formulated, researchers conducted a questionnaire by obtaining 31 respondents from the software development team in the organization. Fig. 4 describes the percentage of the team from 8 positions in the software development team. Respondents with programmer positions were 39%, Junior IT Staff 10 %, Head of IT Department 6 %, IT Business Analyst 13%, It Quality Control 13%, IT Quality Assurance 3%, IT Strategic Plan 3 %, IT System Specialists (System Analysts) 13%.

In Fig 5, 45% of respondents have more than > 5 years of work experience from their current position. Then, 23% have 1 to 3 years of experience, 21.7% have 3 to 5 years of experience, and 8.7% have less than one year of experience. Overall, the technical team that filled out the questionnaire had over three years of experience.

The questionnaire consisted of 17 questions: 1) two demographic questions related to position and work experience, and 2) demographic questions were used to aid a deeper analysis of the questionnaire results. Furthermore, 14 questions are related to the 14 challenges contained in Table I. At the end, there are open-ended questions to identify other challenges that have not been included in the questionnaire. Questionnaire answers use a Likert scale (1 to 5) with the following information:

- Strong Not Agree (SNA)
- Not Agree (NA)
- Neutral (N)
- Agree (A)
- Strong Agree (SA)

The questionnaire results contained 14 challenges, which received a percentage of more than 50%. In other words, the respondents agreed and strongly agreed to the challenges in Table III. In addition, two different challenges were identified in the case study.

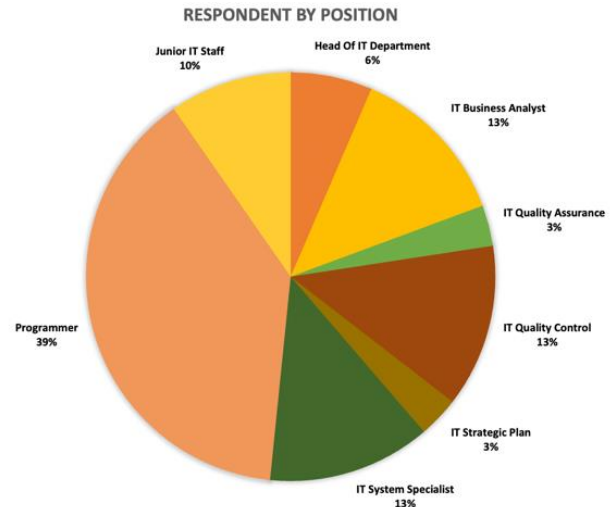


Fig. 4. Percentage of 31 respondents by the position.

Respondents by work experience

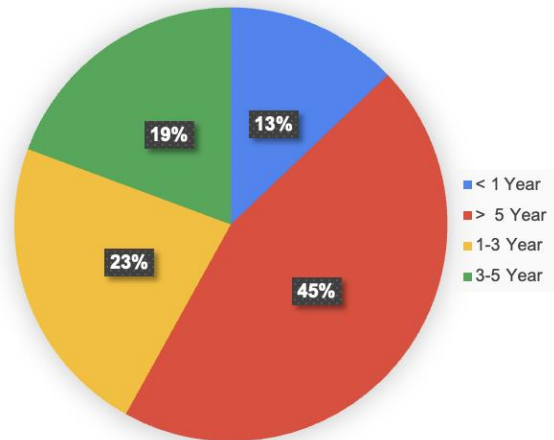


Fig. 5. Percentage of 31 respondents by work experience.

TABLE III. RESULT QUESTIONNAIRE FROM 31 RESPONDENTS

| No | Challenges factor | SA | A | N | NA | SNA | SA+A |
|----|------------------------------|------------|------------|------------|-----------|------------|------------|
| 1 | Technique & Ceremony | 29% | 26% | 22% | 13% | 10% | 55% |
| 2 | IT Infrastructure | 10% | 16% | 19% | 32% | 23% | 26% |
| 3 | Project Documentation | 39% | 45% | 6% | 6% | 3% | 84% |
| 4 | Cultural behavior | 42% | 35% | 10% | 6% | 6% | 77% |
| 5 | Communication | 29% | 23% | 19% | 6% | 23% | 52% |
| 6 | Managed requirements | 42% | 32% | 6% | 6% | 13% | 74% |
| 7 | Roles Team | 39% | 19% | 16% | 13% | 13% | 58% |
| 8 | Top Level Management | 45% | 26% | 6% | 16% | 6% | 71% |
| 9 | Internal policy | 26% | 29% | 19% | 10% | 16% | 55% |
| 10 | Collaboration | 32% | 23% | 19% | 10% | 16% | 55% |
| 11 | Organization Structure | 35% | 19% | 13% | 19% | 13% | 54% |
| 12 | Interpersonal Conflict | 3% | 23% | 13% | 29% | 32% | 26% |
| 13 | Individual Competence | 22% | 23% | 10% | 16% | 29% | 45% |
| 14 | Agile Values | 32% | 26% | 16% | 13% | 13% | 58% |

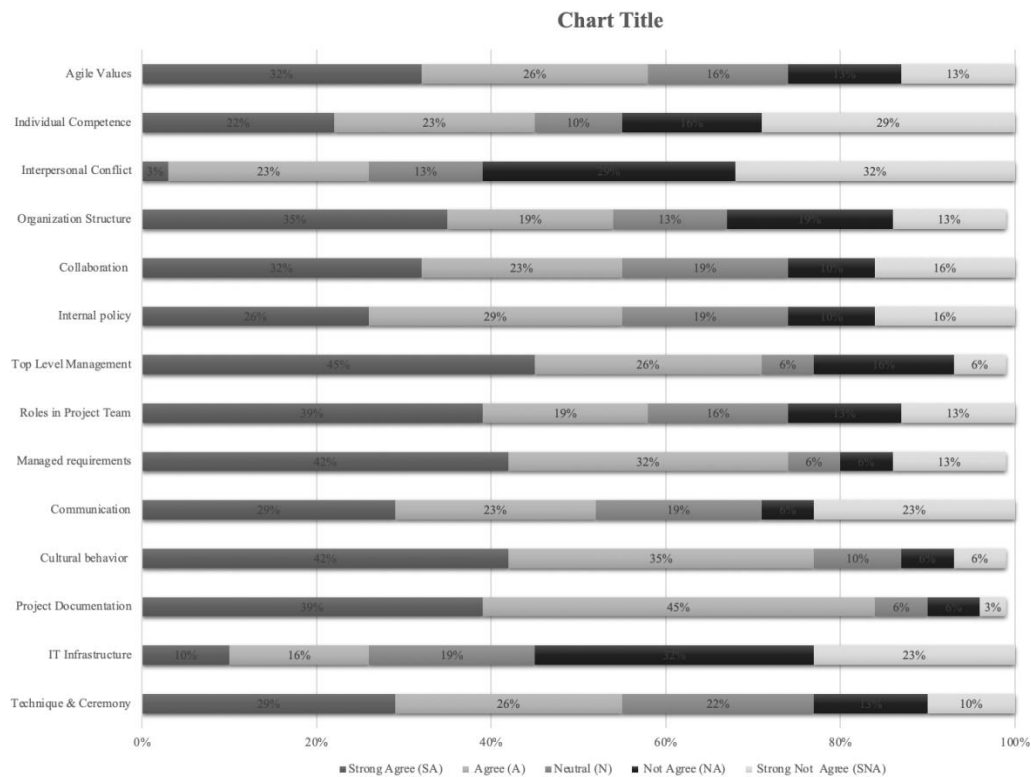


Fig. 6. This graph shows numbers representing the percentage of 31 respondents from the one that strongest agrees to the not agree.

1) *A Challenge of the highest percentage:* Fig. 6. shows three challenges with high percentage values, including project documentation, managing requirements, and cultural behavior. Most respondents agree with these challenges in implementing agile software development in organizations.

- Project documentation. This factor gets the highest percentage in the context of technology. One respondent mentioned in answering an open-ended question on the questionnaire that "current project documentation is not yet flexible. The characteristics of documentation are currently still waterfall-based where

each documentation requires the approval of each unit". In previous studies [2], many organizations faced challenges related to inadequate documentation and the opposite issue of excessive documentation that wastes time and resources on unnecessary information. Agile development presents a solution through a streamlined approach to comprehensive documentation that requires less time and effort. However, it is crucial for upper management to support this approach and for customers to agree upon it from the project's inception [3], [11].

- Culture and structure of an organization. In previous research [3], it was also stated that the primary challenge in adopting Agile lies in the culture and structure of an organization. For Agile to thrive, there must be a genuine embrace of Agile values and principles. A hierarchical organizational structure often poses a significant hurdle to Agile adoption since it necessitates redistributing power and responsibility from management to the development team. Additionally, Agile thrives in a dynamic, supportive, and collaborative environment, which rigid organizational cultures can hinder.

Respondent's statements related to this challenge were "It takes a common understanding between the IT team and UKPF in implementing the agile process," Statements from other respondents, "The entire team must understand the goal of agile," and "The team is not yet familiar with the concept of agile comprehensively."

The current organizational structure is still suitable for the Waterfall methodology. One of the respondents mentioned, "Basically, the organizational structure is still waterfall-based, and each unit works on unit coordination. It should be project-based, and an agile team should be more independent and committed."

- Managed Requirement. The challenges faced by IT project management received the highest score, namely, 34.8% agreed, and 52.2% strongly agreed. This factor is a challenge to the organization's agile implementation. Regardless of project management tools, the respondent stated, "There are no valid tools that are used for project monitoring. So far, they have relied on Excel". There are no tools for project monitoring or tools that can be used for standard team collaboration by the entire team. The team found it difficult to see the progress of each process in system development. Another problem is that there is no project manager role in the team, making it difficult for the team to conduct project development tasks.

2) *A Challenge of the lowest percentage:* Based on Fig. 6, 3 challenges with high percentage values are project documentation, management requirements, and culture behaviour, which get high scores. Most respondents agree that

these challenges are challenges in implementing agile software development.

- Interpersonal conflict. This factor gets the lowest score, namely 26%, meaning that the team is good enough or has no internal conflict, which is a challenge in agile implementation. Leadership challenges get the highest score, namely 65.2%, then agile values, 60.9%, and the other three challenges, namely personal commitment, decision making, and individual competence, get the same deal, 52%.
- Competency is not a challenge in implementing agile, and this has something to do with demographic results because most respondents are workers with more than five years of experience, so they have abilities in their fields.

3) *An Additional Challenge from respondents:* Different challenges are identified from the case study based on the open-ended question at the end of the questionnaire, in which the organization experiences another challenge, namely Overloading work. Based on one of the respondents' answers, "Another challenge is the unbalanced workload of each programmer. A programmer must be able to do many things briefly simultaneously, causing stress from the programmer's psychological side. Something like this needs to be resolved by the project manager on how user needs are balanced with existing resources," and the other, "The challenge is the lack of resources so that one person holds several applications that are being chased by the dateline at the same time."

B. Recommendation

Based on the challenges faced by the organization, the researchers then provide recommendations that can be taken in the future to make changes to current conditions. Later, it is hoped that the organization will get better results from agile implementation and support organizational goals. The recommendations are as follows.

The following are recommendations based on previous research, and recommendations are given based on the results of questionnaires that get a percentage of agree and strongly agree with a value of more than 50%. The recommendations are given in Table IV.

TABLE IV. RECOMMENDATION IN TECHNOLOGY CONTEXT

| Challenge | Recommendation |
|--|--|
| Technique & Ceremony Lack of discipline in the development processes | <ul style="list-style-type: none"> • Use tools or technologies to support Agile work in the organization [3]. E.g., Trello or Jira • Build a Continuous Delivery pipeline with stages involving both sides[4] |
| Project Documentation Lacks sufficient documentation to support its development | Communicate only essential points that need to be documented. Agile identifies critical important points to include in documentation, which is the main focal point for each methodology.[15] Meetings assist individuals in a proper understanding of how to collect information and through what medium the process of gathering information will be beneficial [15] |
| Culture Behavior & Agile Values The organization shows resistance or lack of encouragement in transitioning to agile values. | <ul style="list-style-type: none"> • A strong culture requires a deep understanding of the organization's goals • Show success stories of agile adoption. • Provide training and increase employee awareness and acceptance of new culture [3]. [3] |
| Communication Communication and coordination among team members are ineffective. | <ul style="list-style-type: none"> • Running an effective meeting [16] • Regular face-to-face meetings should be established, as they provide clear communication [7] [13] |

| Challenge | Recommendation |
|---|---|
| | <ul style="list-style-type: none"> • Transparency and efficiency in communication [4]. |
| Management Requirement The project schedule is delayed, requirements are unclear, and there is little anticipation in handling changes. | Agile teams operate differently from traditional project management structures as they do not rely on project managers. Instead, Agile methodologies like Scrum and XP outline specific roles such as the product owner, scrum master, and coach. These roles are designed to facilitate effective collaboration and ensure the smooth execution of Agile practices. By assigning responsibilities to these distinct roles, Agile teams can streamline communication, enhance productivity, and adapt quickly to changing project requirements. [17]. |
| Roles in Project Team The roles of the team are not clearly defined, leading to minimal contributions and duplicated work. | Reorganize the team by forming small teams, like the scrum team, to create a dedicated team responsible for agile development [18]. |
| Top Level Management There is a lack of top-level management support and little knowledge of the execution process. | <ul style="list-style-type: none"> • Involving top-level management in the change planning and implementation process can increase the sense of ownership and responsibility. • Hire outside experts to be involved in team adaptation as this can provide a better recommendation of benchmarks [18],[15] |
| Internal Policy Inadequate agile adoption of skills, experiences, and knowledge. | Creating standards for IT software development on an internal basic policies and supporting existing management can support agile implementation [1] |
| Collaboration Team collaboration is limited because team members are spread out in different locations. | Use tools or technologies to support Agile work in the organization [3]. E.g., Trello Jira or bit bucket [4] |
| Organization Structure Organizing meetings is challenging due to convoluted bureaucratic processes. | <ul style="list-style-type: none"> • Create a small project team like the Scrum team [1]. • Arrange a dedicated team that is responsible for agile development [18]. • Channeling expert's efforts to address high-level issues and to manage collaboration [4]. |
| Overloading of work This factor is a challenge in agile implementation. Individuals get more than one job at the same time. | <ul style="list-style-type: none"> • They used to meet weekly and later twice a month, only when required and usually after working hours. • Skipping the daily meetings affected the learning process between the team members. This factor eventually led to the failure to learn and implement the agile method correctly [11]. |

V. CONCLUSION

Researchers conducted a literature review of several previous studies and identified challenges in implementing ASD in other organizations with characteristics of the public sector, government, or bureaucracy. Researchers use quantitative methods with surveys to validate and facilitate the exploration of the challenges in implementing ASD in One healthcare organization in Indonesia. This method is simple but can solve the problems faced. It is a differentiator from previous research [8] studies used challenge validation using document observation.

Based on several previous studies, 14 challenges faced by organizations were obtained. This study's findings determine what challenges and recommendations can be provided for the organization. Based on the survey results, researchers found 11 challenges with a percentage value above 50%, agreeing that challenges to other organizations. The three challenges with the highest survey results are project documentation, IT Project Management, and cultural behavior. At the same time, the 3 challenges with the lowest survey results were below 50%, which means that most respondents disagreed that these challenges were felt today in the organization. These challenges are individual competence, IT infrastructure, and internal conflicts. Then, researchers got other challenges besides 14, based on open questions on the questionnaire. The challenge is about workload overload.

After getting the challenges faced by the organization in this case study, the researcher provides recommendations mapped to the challenges faced by the IT team in the organization based on previous studies related to agile implementation, agile adoption, or agile transformation. Some recommendations that can be made include raising

awareness related to agile culture among all IT employees. Regarding problems in Project Documentation, organizations can adjust project documentation to align with agile values. Problems in organizations with bureaucracy, such as government, making changes in the development process become obstacles because of the many administrative processes and approvals given to superiors. Therefore, organizations can adjust the project team to match the role in Agile. Agile using the roles contained in scrum. By assigning responsibilities to these different roles, Agile teams can streamline communication, increase productivity, and adapt quickly to changing project requirements [17].

1) *Research implications:* Other similar organizations can use the results of this study to see the challenges in agile implementation and solutions from best practices suitable for organization healthcare or bureaucratic governance.

2) *Limitations of suggestions for further research:* This study has several limitations on the respondents. Respondents are still limited to the software development technical team. Future research can be carried out for other IT teams, such as IT operations and IT infrastructure.

REFERENCES

- [1] H. D. Harfianto, T. Raharjo, B. Hardian, and A. Wahbi, "Agile Transformation Challenges and Solutions in Bureaucratic Government: A Systematic Literature Review," in ACM International Conference Proceeding Series, Association for Computing Machinery, Jan. 2022, pp. 12–19. doi: 10.1145/3512676.3512679.
- [2] P. Mohagheghi and C. Lassenius, "Organizational implications of agile adoption: A case study from the public sector," in ESEC/FSE 2021 - Proceedings of the 29th ACM Joint Meeting European Software Engineering Conference and Symposium on the Foundations of Software Engineering, Association for Computing Machinery, Inc. Aug. 2021, pp. 1444–1454. doi: 10.1145/3468264.3473937.

- [3] F. S. Altuwaijri and M. A. Ferrario, "Factors affecting Agile adoption: An industry research study of the mobile app sector in Saudi Arabia," *Journal of Systems and Software*, vol. 190, Aug. 2022, doi: 10.1016/j.jss.2022.111347.
- [4] M. Wen et al., "Leading successful government-academia collaborations using FLOSS and agile values," *Journal of Systems and Software*, vol. 164, Jun. 2020, doi: 10.1016/j.jss.2020.110548.
- [5] Public health sector in Indonesia, "software development list of 2022," 2022.
- [6] Public health sector in Indonesia, "IT complaint report 2022," 2023.
- [7] R. A. Khan et al., "Practices of motivators in adopting agile software development at large scale development team from management perspective," *Electronics (Switzerland)*, vol. 10, no. 19, MDPI, Oct. 01, 2021. doi: 10.3390/electronics10192341.
- [8] K. Rizkiyah, A. K. Nisyak, and T. Raharjo, "Agile-Based Requirement Challenges of Government Outsourcing Project: A Case Study," in 2020 3rd International Conference on Computer and Informatics Engineering, IC2IE 2020, Institute of Electrical and Electronics Engineers Inc., Sep. 2020, pp. 267–273. doi: 10.1109/IC2IE50715.2020.9274659.
- [9] P. Patanakul and R. Rufo-McCarron, "Transitioning to agile software development: Lessons learned from a government-contracted program," *Journal of High Technology Management Research*, vol. 29, no. 2, pp. 181–192, Nov. 2018, doi: 10.1016/j.hitech.2018.10.002.
- [10] R. M. Fontana and S. Marczak, "Characteristics and Challenges of Agile Software Development Adoption in Brazilian Government." [Online]. Available: <http://jotmi.org>
- [11] H. Hajdiab and A. S. Taleb, "Agile adoption experience: A case study in the U.A.E.," in ICSESS 2011 - Proceedings: 2011 IEEE 2nd International Conference on Software Engineering and Service Science, 2011, pp. 31–34. doi: 10.1109/ICSESS.2011.5982247.
- [12] A. Nisyak, K. Rizkiyah, and Raharjo T, "Human Related Challenges in Agile Software Development of Government Outsourcing Project," 2020.
- [13] Mike Beedle, Arie van Bennekum, and Alistair Cockburn, "Manifesto for Agile Software Development," <https://agilemanifesto.org/>.
- [14] D. Ghimire, S. Charters, and S. Gibbs, "Scaling agile software development approach in government organization in New Zealand," in ACM International Conference Proceeding Series, Association for Computing Machinery, Jan. 2020, pp. 100–104. doi: 10.1145/3378936.3378945.
- [15] IEEE Staff, 2018 IEEE 21st International Multi Topic Conference (INMIC). IEEE, 2018.
- [16] American Society for Engineering Education, Institute of Electrical and Electronics Engineers, and IEEE Computer Society, *Frontiers in Education 2018 : fostering innovation through diversity : 2018 conference proceedings*.
- [17] Y. Shastri, R. Hoda, and R. Amor, "The role of the project manager in agile software development projects," *Journal of Systems and Software*, vol. 173, Mar. 2021, doi: 10.1016/j.jss.2020.110871.
- [18] D. Dewantari, T. Raharjo, B. Hardian, A. Wahbi, and F. Alaydrus, "Challenges of Agile Adoption in Banking Industry: A Systematic Literature Review," in ICSEC 2021 - 25th International Computer Science and Engineering Conference, Institute of Electrical and Electronics Engineers Inc., 2021, pp. 357–362. doi: 10.1109/ICSEC53205.2021.9684622.

The Bi-Level Particle Swarm Optimization for Joint Pricing in a Supply Chain

Umar Mansyuri¹, Andreas Tri Panudju², Helena Sitorus³, Widya Spalanzani⁴, Nunung Nurhasanah⁵, Dedy Khaerudin⁶

Computer Science Department, Universitas Bina Bangsa, Serang, Indonesia¹

Industrial Engineering Department, Bhayangkara Jakarta Raya University, Jakarta, Indonesia^{2, 3, 4}

Industrial Engineering Department, Al Azhar Indonesia University, Jakarta, Indonesia⁵

Industrial Engineering Department, Universitas Bina Bangsa, Serang, Indonesia⁶

Abstract—This study examines the integration of pricing and lot-sizing strategies within a system comprising only one producer and retailer. The adoption of a bi-level programming technique is justified in establishing a bi-level joint pricing model guided by the producer owing to the hierarchical nature of the supply chain. This problem maximizes manufacturer and retailer profitability by setting the wholesale quantity, lot size, and retail price simultaneously. We created a bi-level particle swarm optimization to solve bi-level programming challenges. This algorithm effectively addresses BLPPS by eliminating the need for any priori assumptions about the conditions of the problem. The bi-level particle swarm optimization algorithm demonstrated a commendable level of efficacy when applied to a set of eight benchmark bi-level issues. The proposed bi-level model was solved using the BPSO and analyzed using experimental data.

Keywords—Bi-Level algorithm; joint pricing; optimization; particle swarm optimization; supply chain

I. INTRODUCTION

Supply chain participants are driven by the goal of selling goods, and product prices affect the level of demand in the market [1]. Likewise, the practice of determining the optimal order quantity has resulted in decreased expenses, encompassing both the ordering process for retailers and production costs for manufacturers. Consequently, strategic decisions pertaining to pricing and lot sizing assume crucial significance in the pursuit of profit optimization within a supply chain [2]. In fact, it is critical that the sale price is neither excessively low nor exorbitant. Conversely, when the retail price is set at an excessively low level, the retailer experiences diminished profitability or potentially even financial losses. However, if the product is priced too high, customers will exhibit reduced purchasing intent, resulting in surplus inventory and additional inventory-related expenses for the retailer [3]. Furthermore, because of an overabundance of inventory, the retailer will opt to decrease either the frequency of orders or the amounts ordered from the producer. Consequently, this leads to significant financial losses for producers. Hence, the implementation of rational pricing and lot-sizing policies is of utmost importance and indispensable [4]. Considerable research has been conducted on the issue of optimal pricing, owing to the various factors outlined. In their seminal work, Panchal, Jain, and Kumar (2015) presented a comprehensive model that addresses the intertwined issues of ordering and price discounting in a supplier-buyer relationship [5]. The model focuses on a scenario in which a supplier

offers a quantity discount to its sole or significant buyer. However, the problem is approached solely from the supplier's standpoint, neglecting the retailer's perspective on retail pricing. Pourrahmani and Jaller (2021) examined the concept of collaborative pricing and replenishment as a means of addressing a network pricing problem known as NP-hard [6]. Ghahremani-Nahr et al. (2019) primarily concentrated on enhancing an exact algorithm that optimizes their strategies for a service operating inside an oligopolistic setting [7]. The issue is framed as a leader-follower game conducted over a distribution network. Yuan (2021) proposed bi-level models to address price problems [8].

This paper utilizes several numerical tests to showcase the efficacy of the BPSO method. Later, the BPSO technique was used to solve the bi-level model. Ultimately, the attributes of the suggested bi-level model are examined through multiple illustrations.

II. LITERATURE REVIEW

The lot-sizing problem, considered a critical challenge in supply chain management, has piqued the interest of various experts who have conducted extensive research on the subject. Diabat et al. (2017) investigated the stochastic variant of lot-sizing issues that incorporate inventory bounds and order capabilities [9]. Kulkarni and Bansal (2022) examined a novel topic involving the lot sizing of multiple items in a dynamic setting [10]. They specifically examined a situation in which all items' inventories are concurrently replenished with an equal quantity after a production event. Gáti and Bányai (2023) Explored the problem of optimizing production quantities and managing resource allocation in an industry with several competing enterprises [11]. The authors present a capacity competition model that incorporates the complexities of fluctuating demand, cost functions, and economies of scale arising from dynamic lot-sizing costs.

Curcio, de Lima, Miyazawa, Silva, and Amorim, (2023) were successfully formulated and determined the best pricing and lot-sizing options for a store [12]. In their work published, Tosarkani & Amin, (2018) examines the issue of pricing and lot-sizing in the context of price-sensitive demand [13]. They formulated the coordination problem between a seller and consumer as a two-person fixed bargaining game. In their study, Bazan et al., (2016) approach by include both the backlogging cost and the cost associated with lost goodwill [14]. Abdulah (2020) provided a deterministic model for

calculating the economic order quantity in a retail setting [15]. The model's objective is to accurately predict the effectiveness of a proposed ordering algorithm in mitigating the bullwhip effect to a significant degree.

Each individual within the chain possesses autonomous control over a distinct set of decision variables that do not overlap with the others. These individuals are required to make decisions based on their own personal interests while also taking into account the decisions made by others, as these decisions will impact their own interests. Therefore, bi-level programming problems (BLPPs) are extremely suitable for representing price and lot-sizing challenges inside a supply chain.

In general, solving a bi-level programming problem is challenging for two main reasons. First, bi-level programming problems are classified as NP-hard problems [16]. Second, the concavity of bi-level programming problems further adds to their complexity. Currently, numerous approaches exist to resolve this issue. Four major linear bi-level programming methods were identified in [17], [18]. These categories include neuro-fuzzy algorithms, simulated annealing strategies, vertex enumeration, Kuhn-Tucker conditions, and metaheuristics such as genetic algorithm-based strategies [19].

It is important to note that certain limitations exist when using methods that rely on vertex enumeration and the Kuhn-Tucker conditions to solve bi-level programming problems [20]. These constraints encompass the necessity for the objective function to be differentiable or for the search space to be convex. Metaheuristic approaches are capable of resolving exceedingly complex nonlinear problems in contrast to traditional search algorithms. Management extensively uses metaheuristic optimization [21]. In practice, most bi-level problems extend beyond linear programming and encompass a range of intricate scenarios. Therefore, it is imperative to devise efficient and optimal approaches for addressing these issues.

A Bi-level Linear Programming (BLPP) is a type of multilevel programming issue [22]. Within the framework of BLPP, the decision maker situated at the higher level initially formulates a strategy [23]. The general bi-level formula can be expressed as follows:

$$\min_{x \in X} f_1(x, y)$$

$$s. t \ G(x, y) \leq 0,$$

where, the y vector solves

$$\min_{y \in Y} f_2(x, y)$$

$$s. t \ g(x, y) \leq 0,$$

$$\text{Let } x \in X \subset \mathbb{R}^{n1} \text{ and } y \in Y \subset \mathbb{R}^{n2}$$

where,

x : Set of control-level variables

and

y is the set of follower-level variables.

The leader has an objective function, $f_1(x, y)$, and the follower has an objective function of $f_2(x, y)$.

Additionally, $G(x, y) \leq 0$ and $g(x, y) \leq 0$ represent the constraints associated with upper and lower-level problems, respectively.

III. METHOD

A. Development Model

After acquiring the raw materials from the supplier, the producer carries out the production and processing procedures (see Fig. 1). The completed products are subsequently delivered to the retailer.

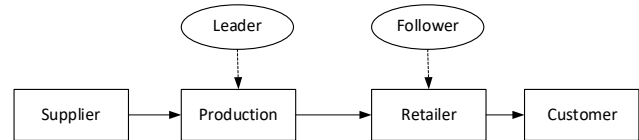


Fig. 1. Two-echelon system.

The producer has the potential to influence the retailer's decisions, but lacks complete control over them. The initial step in the pricing process involves the producer establishing a wholesale price for their items. Subsequently, the retailer responds by considering the producer's assortment and subsequently determines the retail price.

The producer negotiates the price at the wholesale level and quantity ordered with the supplier in order to maximize the net profit, as determined by the primary objective function [24], [25]. The net profit of the producer was calculated by subtracting the costs of purchasing, production, transportation, holding, and ordering from the money generated from sales. The second-level objective function sets forth the retail prices and order quantities for retailers. The primary objective is the retailer's net profit, which is calculated as the ratio of sales to the costs associated with purchasing, holding, and ordering.

A bi-level model was constructed based on specific assumptions [17], [26].

- 1) The producer or retailer can make separate decisions to maximize earnings.
- 2) Retail prices decrease consistently with the market demand.
- 3) Producers and retailers quickly restock.
- 4) Each replenishment period was consistent, and shortages were avoided.
- 5) The cost of purchasing components and the price of the product for the end consumer remain constant throughout the planning horizon.

This paper uses these notations:

Aspects that impact the producer's decision

β : The anticipated of orders quantity that the producer will place in the near future.

p_m : wholesale unit price

Decision-making factors used by the retailer

α : quantity of retailer lots divided by producer lots

q :retailer lot size

p_r :The unit retail price

Additional Relevant Parameters

T : the planned horizon's weekly length

D : weekly demand rate $D = b - a_r \cdot p_r$

h_m : amount of the producer's on a weekly basis storage cost

h_r : retail store's weekly storage cost rate

O_m : Purchasing cost of each order incurred by the producer.

O_r : Purchasing fee for each transaction for the retailer.

p_s : Fee for purchasing a unit from the producer.

T_c : unit transportation cost

M_c : Cost of procuring units for producer.

Q_m : a company's net profit throughout the planning period

Q_r : net profit for the store throughout the planning period

B. Construction Model

The producer and retailer net income during planning are indicated by I_m and I_r , respectively.

$$I_m = (p_m - p_s - T_c - M_c)\alpha\beta Q$$

$$I_r = (p_r - p_m)\alpha\beta Q$$

The average inventory level of the product–retailer combination is determined by the equation $\alpha Q/2$, where α is a constant. Consequently, the producer's inventory level can be calculated as Q multiplied by the quantity $(\alpha - 1)/2$.

The producer and retailer holding costs during planning are indicated by H_m and H_r , respectively.

$$H_m = h_m T \cdot p_s \cdot \frac{Q(\alpha-1)}{2} = \frac{h_m T p_s Q(\alpha-1)}{2}$$

$$H_r = h_r T \cdot p_m \cdot \frac{Q}{2} = \frac{h_r T p_m Q}{2}$$

Producer and retailer order expenses within planning are indicated by C_m and C_r , respectively.

$$C_m = \beta O_m$$

$$C_r = \alpha\beta O_r$$

The net earnings of the producer and retailer during planning are indicated by U_m and U_r , respectively.

$$\Pi m = I_m - H_m - C_m = (p_m - p_s - T_c - M_c)(\alpha\beta Q) - \left(\frac{h_m T p_s Q(\alpha-1)}{2}\right) - (\beta O_m) \quad (1)$$

$$\Pi r = I_r - H_r - C_r = p_r T D - (p_m \alpha\beta Q) - \left(\frac{h_r T p_m Q}{2}\right) - (\alpha\beta O_r) \quad (2)$$

By integrating Eq. (1) and Eq. (2), the following model is established for the supply chain:

$$\max_{\beta, p_m} \Pi m = (p_m - p_s - T_c - M_c)(\alpha\beta Q) - \left(\frac{h_m T p_s Q(\alpha-1)}{2}\right) - (\beta O_m)$$

$$\text{s.t. } \beta \in N^+, p_s + T_c + M_c \leq p_m \leq p_m^* \quad (3)$$

$$\max_{\alpha, p_r, Q} \Pi r = (p_r T D) - (p_m \alpha\beta Q) - \left(\frac{h_r T p_m Q}{2}\right) - (\alpha\beta O_r) \quad \text{s.t. } \alpha \in N^+,$$

The correlation between the quantity of deliveries and the lot size is

$$Q = \frac{T D}{\alpha \beta} \quad (4)$$

Retail prices are believed to be multiples of wholesale prices,

$$P_r = K p_m \quad (5)$$

Let K be the ratio of wholesale to retail prices where $K > 1$.

It is critical that wholesale and retail pricing remain within the appropriate limits and do not surpass specific levels. By utilizing Eq. (4) and Eq. (5), it is possible to convert Problem (3) into Problem (6) through the following transformation:

$$\max_{\beta, p_m} \Pi m = (p_m - p_s - T_c - M_c)(T D) - \left(\frac{h_m T^2 p_s D(\alpha-1)}{2\alpha\beta}\right) - (\beta O_m)$$

$$\text{s.t. } \beta \in N^+, p_s + T_c + M_c \leq p_m \leq p_m^* \quad (6)$$

$$\max_{\alpha, k} \Pi r = (k p_m T D) - (p_m T D) - \left(\frac{h_r T^2 p_m D}{2\alpha\beta}\right) - (\alpha\beta O_r)$$

$$\text{s.t. } \alpha \in N^+, 1 \leq k \leq k^*$$

The variables p_m^* and k^* denote the maximum values of p_m and k .

IV. RESULT

A. Bi-level PSO-based Algorithms

Kennedy (1995) present a Particle Swarm Optimization (PSO) technique [27]. The Particle Swarm Optimization (PSO) algorithm, as described in [28], is a stochastic evolutionary algorithm that operates on a population-based approach. PSO has demonstrated its effectiveness in addressing complex optimization problems, offering advantages such as simplified coding and a reduced number of parameters [29], [30]. Particle Swarm Optimization (PSO) considers each individual as a particle, disregarding any notions of quality or bulk [31], [32].

The orientation and speed of the particles are denoted by $x_i = (x_{i1}, x_{i2}, \dots, x_{iD})$, and $v_i = (v_{i1}, v_{i2}, \dots, v_{iD})$ respectively. The variable $p_i = (p_{i1}, p_{i2}, \dots, p_{iD})$ represents the best position that the swarm have reached, while $p_g = (p_{g1}, p_{g2}, \dots, p_{gD})$ represents the best position that the swarm have reached. The manipulation of particles is governed by the following equations:

$$v_{id}(t+1) = wv_{id}(t) + c_1r_1(p_{id}(t) - x_{id}(t)) + c_2r_2(p_{gd}(t) - x_{id}(t)) \quad (7)$$

and

$$x_{id}(t+1) = x_{id}(t) + v_{id}(t+1) \quad (8)$$

The given conditions are as follows: for any values of d and D where $1 \leq d \leq D$, and for any values of i and N where $1 \leq i \leq N$, there exist two non-negative constants denoted as c_1 and c_2 . Additionally, there are two randomly generated integers, denoted as x and y , that follow an equal distribution, in the range of $(0,1)$.

The maximum current value is denoted as $v_{id} \in [-v_{max}, v_{max}]$.

When j , we set t .

The prior velocity of the particle impacts its present velocity through the inertia weight w . The inertia weight w is crucial for balancing the global and local search capabilities. The global search capacity increased as w increased, whereas the local search capacity decreased. Conversely, when the value of w decreased, the opposite situation occurred.

Shi and Eberhart (1999) offer an approach known as linear decline, which is outlined as follows.

$$w(t) = w_{min} + (w_{max} - w_{min}) \cdot \left(\frac{t_{max} - t}{t_{max}} \right) \quad (9)$$

The " t " represents the t^{th} iteration, while " t_{max} " represents the maximum number of iterations for that iteration. The initial inertia weight is represented by variables w_{min} and w_{max} , which indicate the smallest and highest values, respectively.

B. Managing Constraint

The upper and lower-level problems in BLPP (see Eq. (1)) are standard constraint optimization that do not consider the leader-follower information interaction [33]. Managing constraint is crucial for constraint optimization.

Consider the constraint optimization problem as follows:

$$\begin{aligned} \min F(x) \\ \text{s.t. } g_i(x) \leq 0, i = 1, 2, \dots, p \end{aligned} \quad (10)$$

where, S is the search space, $x \in S$, and $S \subseteq R^n$.

By incorporating a penalty element, Eq. (10) can be reformulated as follows:

$$\min F(x) = f(x) + M \sum_{i=1}^p (\max\{g_i(x), 0\})^2,$$

Variable M represents a predetermined and significantly large positive constant, denoted as a penalty factor.

This approach is analogous to treating upper-level programming problems. It is assumed that the lower-level programming problem comprises p and q inequality constraints. In addition, it is assumed that the variable x of the upper-level programming problem is predetermined. Within the realm of the search area, a particle that adheres to the

given restrictions is referred to as a feasible particle, whereas a particle that fails to meet the criteria is labeled as an infeasible particle. In the present scenario, it is possible to determine the fitness of all particles, both feasible and infeasible, using the following equations:

$$\text{fit}(x,y) = \begin{cases} f(x,y), & \text{if } y \in \Omega(x) \\ f(x,y), & \text{if } y \in S \setminus \Omega(x) \end{cases} \quad (11)$$

and

$$F(x,y) = f(x,y) + M \sum_{i=1}^m (\max\{g_i(x,y), 0\})^2, \quad (12)$$

where, S indicates search area, while $\Omega(x)$ is the feasible set of lower-level problem.

C. Implementation

Based on an analysis of the interacting iterations of two fundamental PSO algorithms, it has been observed that Binary Particle Swarm Optimization (BPSO) can solve BLPP without relying on any specific assumptions [34], [35], such as the availability of gradient information for the objective functions or the convexity of constraint regions. The details are presented in the subsequent sections.

Algorithm 1:

- | |
|--|
| <p>Step 1: Preparation of parameters by measuring population N_l, determining maximum iteration T_{max1}, with learning factors c_1 and c_2, determining maximum and minimum inertia weights w_{max} and w_{min}, as well as maximum speed v_{max}, and enforcement factor M.</p> <p>Step 2: Set the position x_i and velocity v_{xi} of each particle to the upper level's decision variables. The begin position y_i and velocity v_{yi} are based on lower-level decision parameters.</p> <p>Step 3: Set the loop counter of the leader to $t_l = 0$.</p> <p>Step 4: If the algorithm fulfills completion conditions or an upper limit of iterations, move to the final step; otherwise, follow Steps 4.1–4.5.</p> <p style="padding-left: 40px;">Step a: For each x_i, Algorithm 2 solves lower-level programming problems and determine the optimal solution for y^*, as the follower response.</p> <p style="padding-left: 40px;">Step b: Calculate the particle fitness values using Eq.(11) and (12)</p> <p style="padding-left: 40px;">Step c: The best particle (p_{xi}) and population (p_{xg}) positions are recorded. If p_{xi} is higher than the best in history, a new p_{xi} is declared. Choose the particle with the highest fitness value for p_{xg}.</p> <p style="padding-left: 40px;">Step d: Update the particle positions using Eq.(7)–(9).</p> <p style="padding-left: 40px;">Step e: $t_l = t_l + 1$.</p> <p>Step 5: If it the maximum number of iterations, proceed to Step 5. Otherwise, proceed to step 3.</p> <p>Step 6: Final best results.</p> |
|--|

| Algorithm 2 : |
|---|
| Step 1: Preparation of parameters N_2 (population), and T_{max2} (maximum iteration) |
| Step 2: Start with the subsequent loop counter $t_2 = 0$. |
| Step 3: Eq. (11) and (12) are used to calculate particle fitness. |
| Step 4: Record the particle's i^{th} best location p_{yi} and population's p_{yg} . |
| Step 5: Update the follower position and velocity using Eq. (7) – (9). |
| Step 6: $t_2 = t_2 + 1$. |
| Step 7: Move to Step 8 if the algorithm reaches its maximum number of iterations. Otherwise, proceed to step 5. |
| Step 8: Optimum lower-level problem solutions y^* . |

D. Simulation

For every bi-level problem, we perform 20 different executions of the BPSO algorithm. Table I presents the optimal and average outcomes obtained from solving the four linear bi-level programming problems using the BPSO algorithm. Comparative analyses of these results are provided in Tables II and III. Table IV presents the optimal outcomes obtained by solving the four nonlinear bi-level programming problems using the BPSO, along with the corresponding comparisons.

Table I lists the four linear test function solutions for the BPSO algorithm. Based on the findings presented in Tables II and III, it can be inferred that the outcomes obtained from solving the four linear bi-level programming problems using BPSO exhibit superior performance in terms of both the best and average results, as compared to the results obtained using the GA and PSO algorithms.

The BPSO algorithm finds the optimal solutions for four nonlinear bi-level problems: Problem 5's best solution is (0.0422, 1.9339, 2.8674, 1.4395), the optimal solution for the 6th problem is (0.7886, 1.8556), the optimal solution for 7th problem is (3.9960, 0.0004), and the optimal solution for 8th problem is (0.5014, 0.2026, 0.8275).

Based on Table IV, in terms of optimizing the upper-level objective function of the 5th problem, it was observed that the BPSO algorithm exhibited superior accuracy compared to the other three algorithms. However, disparities between their performances were minimal. To optimize the upper-level objective function of the 7th problem, the performance of BPSO was found to be comparable to that of the other three algorithms, with only a small difference. However, the BPSO outperformed the other three methods when considering the lower-level objective function.

TABLE I. BPSO-BASED RESULTS

| Simulations | Best Result | | Average Result | |
|-----------------|-------------|----------|----------------|----------|
| | f_1 | f_2 | f_1 | f_2 |
| 1 st | 977090 | - 478546 | 880162 | - 458824 |
| 2 nd | 109967 | - 109967 | 109471 | - 109471 |
| 3 rd | 157155 | - 39212 | 156555 | - 39345 |
| 4 th | 297327 | - 30834 | 290413 | - 32731 |

TABLE II. BEST ALGORITHM COMPARISONS

| Test problems | Binary PSO | | GA | | PSO | |
|-----------------|-------------------|-----------------------------|------------------------|-----------------------------|------------------------|-------------------------|
| | The best solution | The best value | The best solution | The best value | The best solution | The best value |
| 1 st | $f1$ | 97.7092 | $x = (17.458, 10.906)$ | 85.0551 | $x = (17.454, 10.907)$ | 85.08 |
| | $f2$ | $x = (13.713, 11.378)$ | - 47.854 | - 50.170 | - 50.175 | - 50.175 |
| 2 nd | $f1$ | 10.997 | $x = (15.998, 10.998)$ | 10.998 | $x = (15.999, 10.999)$ | 10.999 |
| | $f2$ | - 10.997 | - 10.998 | - 10.998 | - 10.999 | - 10.999 |
| 3 rd | $f1$ | 15.717 | $x = (3.999, 3.997)$ | 15.997 | $x = (4, 6)$ | 18 |
| | $f2$ | 3.921 | - 3.9466 | - 3.9466 | - 5 | - 5 |
| 4 th | $f1$ | 29.733 | $x = (0.000, 0.898)$ | 29.148 | $x = (0.004, 0.899)$ | 29.179 |
| | $f2$ | $y = (0.544, 0.675, 0.445)$ | 3.0835 | $y = (0.000, 0.600, 0.400)$ | - 3.193 | $y = (0, 0.600, 0.400)$ |

TABLE III. AVERAGE RESULTS FROM DIFFERENT ALGORITHMS

| Test problems | Average values | | | |
|-----------------|----------------|----------|----------|----------|
| | Binary PSO | G_A | PSO | |
| 1 st | $f1$ | 88.016 | 84.658 | 84.852 |
| | $f2$ | - 45.883 | - 50.030 | - 50.078 |
| 2 nd | $f1$ | 10.947 | 10.808 | 10.997 |
| | $f2$ | - 10.947 | - 10.808 | - 10.997 |
| 3 rd | $f1$ | 15.656 | 15.827 | 15.988 |
| | $f2$ | - 3.933 | - 3.947 | - 3.9963 |
| 4 th | $f1$ | 29.043 | 21.529 | 24.816 |
| | $f2$ | - 3.271 | - 3.392 | - 3.198 |

TABLE IV. BEST ALGORITHM RESULTS COMPARISONS

| Test problems | Results | | | | |
|-----------------|------------|----------------|----------|----------|---------|
| | Binary PSO | Hybrid_PSO_BLP | T_R_M | Original | |
| 5 th | <i>f1</i> | - 15.203 | - 14.758 | - 12.78 | - 12.78 |
| | <i>f2</i> | 1.036 | 0.207 | - 1.026 | - 1.026 |
| 6 th | <i>f1</i> | 66.956 | 88.777 | 88.80 | 88.89 |
| | <i>f2</i> | - 15.837 | - 0.770 | - 0.87 | - 0.87 |
| 7 th | <i>f1</i> | 2.019 | 2 | 2 | 2 |
| | <i>f2</i> | 23.981 | 24.018 | 24.04 | 24.22 |
| 8 th | <i>f1</i> | 1.038 | 2.709 | 2.76 | 2.85 |
| | <i>f2</i> | - 0.517 | 0.562 | 0.76 | 0.67 |

E. Evaluation

This section solves bi-level joint pricing and lot-sizing model (6) using the BPSO method. Determination of Eq. (6) Parameters

- T = 52, hm = 0.001,
- O_m = 2000,
- p_s = 4,
- h_r = 0.001,
- O_r = 200,
- T_c = 0.5, and M_c = 1.

To enhance the analysis of our model, we initially established an upper constraint for the wholesale price, denoted as p = 10. We examine two upper limits for the retail-to-wholesale pricing ratio, designated k* = 2 and k* = 5. The parameters' configurations of BPSO are consistent with those outlined in the previous section. The outcomes of the optimization process are presented in Tables V and VI.

TABLE V. RESULTS FROM DIFFERENT COEFFICIENT GROUPS (k*=2)

| Demand function coefficients | α | β | p_m | k | p_r | Q | $\prod m$ | $\prod r$ |
|------------------------------|----------|---------|-------|-----|-------|-----|-----------|-----------|
| a = 2, b = 600 | 4 | 4 | 9.8 | 1.9 | 19.4 | 18 | 1192 | 2761 |
| a = 4, b = 600 | 4 | 2 | 9.4 | 1.9 | 18.2 | 34 | 1018 | 2407 |
| a = 6, b = 600 | 3 | 4 | 9.7 | 1.9 | 18.9 | 21 | 1001 | 2288 |
| a = 8, b = 600 | 3 | 3 | 9.6 | 1.9 | 18.7 | 26 | 9133 | 2101 |

TABLE VI. RESULTS FROM DIFFERENT COEFFICIENT GROUPS (k*=5)

| Demand function coefficients | α | β | p_m | k | p_r | Q | $\prod m$ | $\prod r$ |
|------------------------------|----------|---------|-------|------|-------|-----|-----------|-----------|
| a = 2, b = 600 | 3 | 4 | 9.32 | 4.68 | 43.70 | 22 | 951 | 9141 |
| a = 4, b = 600 | 5 | 2 | 9.82 | 4.45 | 43.75 | 22 | 906 | 7478 |
| a = 6, b = 600 | 5 | 3 | 9.59 | 4.77 | 45.80 | 11 | 627 | 6092 |
| a = 8, b = 600 | 2 | 2 | 9.81 | 4.30 | 42.22 | 34 | 545 | 4410 |

Fig. 2 and 3 depict a decrease in the net profits of both the producer and retailer in response to an increase in demand price sensitivity.

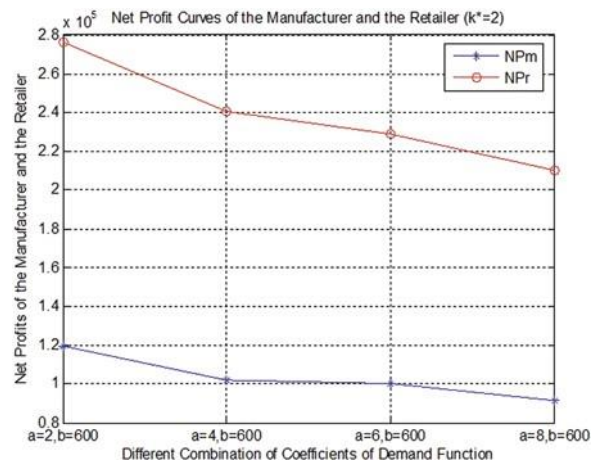


Fig. 2. Producer and retailer net profits curves under k =2.

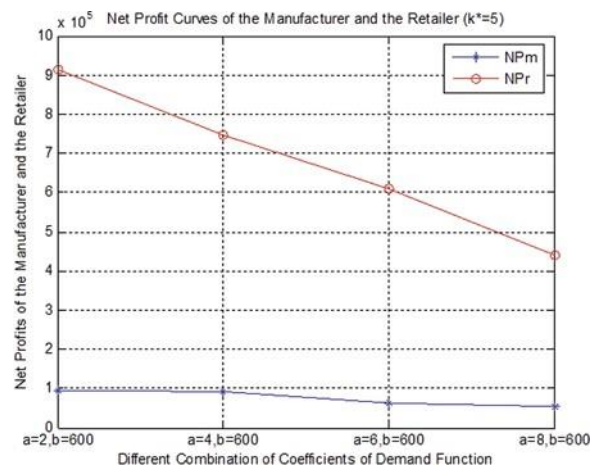


Fig. 3. Producer and retailer net profit curves under k =5.

Fig. 4 and Fig. 5 illustrate the variations in net profits for both the producer and the shop at different levels of demand. Based on the examination of Fig. 4 and Fig. 5, it can be observed that the net profit of the producer is comparatively reduced when the value of k is 5 in contrast to when it is 2, assuming an identical demand function. In contrast, the net profit of the store exhibits a notable increase when the value

of k is 5 as opposed to 2. The observed gap can be ascribed to the differential behavior of retail and wholesale prices, specifically when k is equal to 5. In this scenario, the retail price increases, whereas the wholesale price remains comparatively stable. This is in contrast to the situation where k is equal to 2.

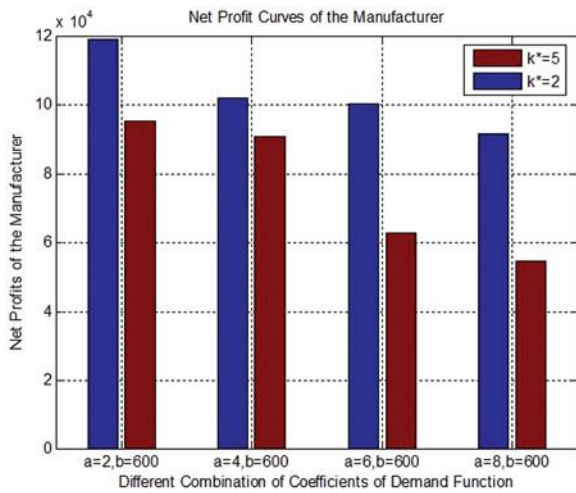


Fig. 4. Comparison of producer net profits.

If the producer's interests are violated because of an increased retail price, the producer may choose to increase the wholesale price. As a result, this course of action possesses the capacity to increase retail pricing, culminating in a decline in the sales volume of products as a consequence of the augmented selling price. The drop in profitability for both the producer and retailer will result in a subsequent decline in the overall efficiency of the entire supply chain. Therefore, to effectively maximize their respective profits and avoid being caught in a harmful cycle where market demand decreases due to rising retail prices, it is recommended that both the producer and retailer refrain from continuously increasing the price of the product.

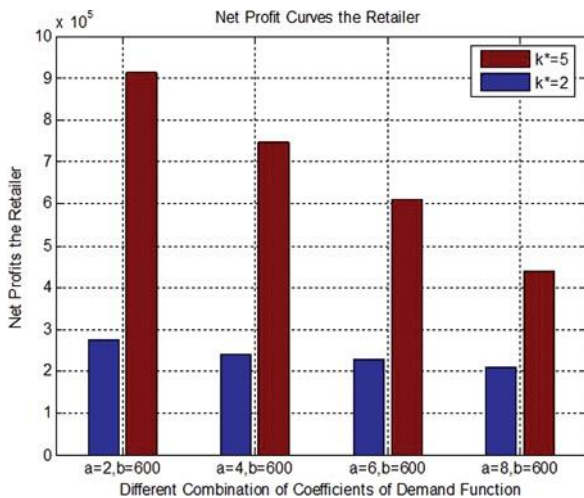


Fig. 5. Comparison of retailer net profits.

V. DISCUSSION

The bi-level particle swarm optimization (BLPSO) is an effective method for solving intricate decision-making problems in supply chain management. The BLPSO algorithm has been utilized in many supply chain models, providing effective solutions for combined pricing and strategic sourcing strategies [36]. Research has demonstrated that it has exceptional search performance and rapid convergence, rendering it a highly useful instrument for addressing bi-level optimization problems in supply chain management [37]. Moreover, the simulation findings indicate that the large-scale BLPSO method has enhanced stability and supremacy when it comes to tackling supply chain optimization challenges [38].

In addition, researchers have investigated the combination of BLPSO with other metaheuristic methods, such as genetic algorithms, to improve its effectiveness in solving bi-level linear programming issues related to supply chain management. The hybrid strategy has demonstrated potential in effectively tackling the combined issues of pricing and inventory control in a two-level supply chain [39]. In addition, the creation of innovative dynamic Pareto BLPSO algorithms has broadened the use of BLPSO in addressing multi-objective optimization challenges in supply chain management [40].

BLPSO has been applied to solve optimization challenges beyond supply chain management, including job shop scheduling and the selection of locations for electric vehicle charging infrastructure [41]. The BLPSO algorithm's ability to effectively handle various optimization issues demonstrates its potential to tackle intricate decision-making challenges across a wide range of fields.

In summary, utilizing BLPSO in the context of joint pricing within a supply chain provides a strong and effective method for tackling intricate decision-making challenges. The tool's capacity to manage multi-objective optimization, strategic sourcing, and large-scale supply chain models renders it a significant asset for optimizing decision-making processes in supply chain management.

VI. CONCLUSION

The primary objective of this model is to optimize the profits of both the producer and retailer. This optimization is achieved by simultaneously determining the number of orders for both parties, lot size for the retailer, and wholesale and retail prices. Based on the characteristics of the bi-level programming issue and the resulting bi-level model discussed in this article, we provide a BPSO technique to identify the most effective solutions.

The BPSO algorithm was employed to address the bi-level model presented in this study. The results obtained include the ideal number of orders for both the producer and retailer, optimal lot size for the retailer, and optimal wholesale and retail prices. These optimal values were simultaneously determined by considering the specified constraints.

Based on the collected data, the analysis reveals certain outcomes that align with market principles. Notably, one of these outcomes indicates a negative correlation between the sensitivity of demand to price and net profits of both the

producer and retailer. It is also observed that in cases where market demand is responsive to changes in selling price, both the producer and retailer should not consistently increase the wholesale and retail prices if their goal is to maximize individual profits. This approach may result in unfavorable outcomes and reduce overall supply chain efficiency. The findings of this study further corroborate the effectiveness of the BPSO in addressing BLPPS.

REFERENCES

- [1] G. Baralla, A. Pinna, and G. Corrias, "Ensure traceability in european food supply chain by using a blockchain system," Proc. - 2019 IEEE/ACM 2nd Int. Work. Emerg. Trends Softw. Eng. Blockchain, WETSEB 2019, pp. 40–47, 2019, doi: 10.1109/WETSEB.2019.00012.
- [2] A. Hendalianpour, "Optimal lot-size and Price of Perishable Goods: A novel Game-Theoretic Model using Double Interval Grey Numbers," Comput. Ind. Eng., vol. 149, p. 106780, 2020, doi: 10.1016/j.cie.2020.106780.
- [3] M. J. Knuth, H. Khachatryan, and C. R. Hall, "How consistent are consumers in their decisions? Investigation of houseplant purchasing," Behav. Sci. (Basel), vol. 11, no. 5, p. NA, 2021, doi: 10.3390/bs11050073.
- [4] R. Li and J.-T. Teng, "Pricing and lot-sizing decisions for perishable goods when demand depends on selling price, reference price, product freshness, and displayed stocks," Eur. J. Oper. Res., vol. 270, 2018, doi: 10.1016/j.ejor.2018.04.029.
- [5] G. B. Panchal, V. Jain, and S. Kumar, "Multidimensional utility analysis in a two-tier supply chain," J. Manuf. Syst., vol. 37, pp. 437–447, 2015, doi: 10.1016/j.jmsy.2014.07.001.
- [6] E. Pourrahmani and M. Jaller, "Crowdshipping in last mile deliveries: Operational challenges and research opportunities," Socioecon. Plann. Sci., vol. 78, 2021, doi: 10.1016/j.seps.2021.101063.
- [7] J. Ghahremani-Nahr, R. Kian, and E. Sabet, "A robust fuzzy mathematical programming model for the closed-loop supply chain network design and a whale optimization solution algorithm," Expert Syst. Appl., vol. 116, pp. 454–471, 2019, doi: 10.1016/j.eswa.2018.09.027.
- [8] G. Yuan, Y. Gao, B. Ye, and Z. Liu, "A bilevel programming approach for real-time pricing strategy of smart grid considering multi-microgrids connection," Int. J. Energy Res., vol. 45, no. 7, pp. 10572–10589, 2021, doi: 10.1002/er.6545.
- [9] A. Diabat, A. A. Taleizadeh, and M. Lashgari, "A lot sizing model with partial downstream delayed payment, partial upstream advance payment, and partial backordering for deteriorating items," J. Manuf. Syst., vol. 45, pp. 322–342, 2017, doi: 10.1016/j.jmsy.2017.04.005.
- [10] K. Kulkarni and M. Bansal, "Discrete multi-module capacitated lot-sizing problems with multiple items," Oper. Res. Lett., vol. 50, no. 2, pp. 168–175, 2022, doi: 10.1016/j.orl.2022.01.002.
- [11] K. V. Gáti and T. Bányai, "Impact of dynamic lot sizing techniques on costs of material requirement planning," Adv. Logist. Syst. - Theory Pract., vol. 17, no. 1, pp. 71–78, 2023, doi: 10.32971/als.2023.009.
- [12] E. Curcio, V. L. de Lima, F. K. Miyazawa, E. Silva, and P. Amorim, "The integrated lot-sizing and cutting stock problem under demand uncertainty," Int. J. Prod. Res., vol. 61, no. 20, pp. 6691–6717, 2023, doi: 10.1080/00207543.2022.2136279.
- [13] B. M. Tosarkani and S. H. Amin, "A possibilistic solution to configure a battery closed-loop supply chain: Multi-objective approach," Expert Syst. Appl., vol. 92, pp. 12–26, 2018, doi: 10.1016/j.eswa.2017.09.039.
- [14] E. Bazan, M. Y. Jaber, and S. Zanoni, "A review of mathematical inventory models for reverse logistics and the future of its modeling: An environmental perspective," Appl. Math. Model., vol. 40, no. 5–6, pp. 4151–4178, 2016, doi: 10.1016/j.apm.2015.11.027.
- [15] A. A. Alabdulkarim, "Minimizing the bullwhip effect in a supply chain: a simulation approach using the beer game," Simulation, vol. 96, no. 9, pp. 737–752, 2020, doi: 10.1177/0037549720930284.
- [16] A. Hiassat, A. Diabat, and I. Rahwan, "A genetic algorithm approach for location-inventory-routing problem with perishable products," J. Manuf. Syst., vol. 42, pp. 93–103, 2017, doi: 10.1016/j.jmsy.2016.10.004.
- [17] H. Sun, Z. Gao, and J. Wu, "A bi-level programming model and solution algorithm for the location of logistics distribution centers," Appl. Math. Model., vol. 32, no. 4, pp. 610–616, 2018, doi: 10.1016/j.apm.2007.02.007.
- [18] Y. Ma, F. Yan, K. Kang, and X. Wei, "A novel integrated production-distribution planning model with conflict and coordination in a supply chain network," Knowledge-Based Syst., vol. 105, pp. 119–133, 2016, doi: 10.1016/j.knsys.2016.05.007.
- [19] G. Haeser and A. Ramos, "Constraint Qualifications for Karush–Kuhn–Tucker Conditions in Multiobjective Optimization," J. Optim. Theory Appl., vol. 187, no. 2, pp. 469–487, 2020, doi: 10.1007/s10957-020-01749-z.
- [20] H. A. E.-W. Khalifa et al., "Utilization of neutrosophic Kuhn-Tucker's optimality conditions for Solving Pythagorean fuzzy Two-Level Linear Programming Problems," Int. J. Neutrosophic Sci., vol. 23, no. 3, pp. 87–96, 2024, doi: 10.54216/ijns.230308.
- [21] S. Abbaspour, A. Aghsami, F. Jolai, and M. Yazdani, "An integrated queueing-inventory-routing problem in a green dual-channel supply chain considering pricing and delivery period: A case study of construction material supplier," J. Comput. Des. Eng., vol. 9, no. 5, pp. 1917–1951, 2022, doi: 10.1093/jcde/qwac089.
- [22] N. A. Alessa, "Bi-Level linear programming of intuitionistic fuzzy," Soft Comput., vol. 25, no. 13, pp. 8635–8641, 2021, doi: 10.1007/s00500-021-05791-5.
- [23] J. F. Monge and J. L. Ruiz, "Setting closer targets based on non-dominated convex combinations of Pareto-efficient units: A bi-level linear programming approach in Data Envelopment Analysis," Eur. J. Oper. Res., vol. 311, no. 3, pp. 1084–1096, 2023, doi: 10.1016/j.ejor.2023.05.034.
- [24] S. Ahmadian, H. Malki, and A. R. Sadat, "Modeling Time of Use Pricing for Load Aggregators Using New Mathematical Programming with Equality Constraints," 2018 5th Int. Conf. Control. Decis. Inf. Technol. CoDIT 2018, pp. 38–44, 2018, doi: 10.1109/CoDIT.2018.8394778.
- [25] A. Aazami and M. Saidi-Mehrabad, "Benders decomposition algorithm for robust aggregate production planning considering pricing decisions in competitive environment: A case study," Sci. Iran., vol. 26, no. 5 E, pp. 3007–3031, 2019, doi: 10.24200/sci.2018.5563.1346.
- [26] S. Pramanik, P. P. Dey, P. Pratim, and D. " Bi, "Bi-level Linear Programming Problem with Neutrosophic Numbers," Neutrosophic Sets Syst., vol. 21, p. 1, 2019.
- [27] J. C. Bansal, "Particle swarm optimization," Stud. Comput. Intell., vol. 779, pp. 11–23, 2019, doi: 10.1007/978-3-319-91341-4_2.
- [28] Q. Yang et al., "Stochastic Cognitive Dominance Leading Particle Swarm Optimization for Multimodal Problems," Mathematics, vol. 10, no. 5, 2022, doi: 10.3390/math10050761.
- [29] R.-O. Dynhora-Danheyda, P.-D. L. Asunción, and M.-G. E. Adán, "Comparison of PSO with the Hybrid Algorithms MOORA-PSO and DA-PSO for Decision Making," Adv. Model. Anal. B, vol. 66, no. 1–4, pp. 26–30, 2023, doi: 10.18280/ama_b.661-404.
- [30] S. Grassi and L. Pareschi, "From particle swarm optimization to consensus based optimization: Stochastic modeling and mean-field limit," Math. Model. Methods Appl. Sci., vol. 31, no. 8, pp. 1625–1657, 2021, doi: 10.1142/S0218202521500342.
- [31] Y. W. Chen, L. C. Wang, A. Wang, and T. L. Chen, "A particle swarm approach for optimizing a multi-stage closed loop supply chain for the solar cell industry," Robot. Comput. Integr. Manuf., vol. 43, pp. 111–123, 2017, doi: 10.1016/j.rcim.2015.10.006.
- [32] G. Sen, J. Sharma, G. Goyal, and A. Singh, "A Multi-objective PSO (MOPSO) algorithm for optimal active power dispatch with pollution control," Math. Model. Eng. Probl., vol. 4, no. 3, pp. 113–119, 2017, doi: 10.18280/mnep.040301.
- [33] R. Arora and K. Gupta, "A linear fractional bilevel programming problem with multichoice parameters," Croat. Oper. Res. Rev., vol. 8, no. 2, pp. 499–513, 2017, doi: 10.17535/cro.2017.0032.

- [34] M. I. Alghamdi, "Optimization of Load Balancing and Task Scheduling in Cloud Computing Environments Using Artificial Neural Networks-Based Binary Particle Swarm Optimization (BPSO)," *Sustain.*, vol. 14, no. 19, 2022, doi: 10.3390/su141911982.
- [35] A. Da Li, B. Xue, and M. Zhang, "Improved binary particle swarm optimization for feature selection with new initialization and search space reduction strategies," *Appl. Soft Comput.*, vol. 106, 2021, doi: 10.1016/j.asoc.2021.107302.
- [36] S. P. Venkatesan and S. Kumanan, "Multi-Objective Supply Chain Sourcing Strategy Design Under Risk Using PSO and Simulation," *Int. J. Adv. Manuf. Technol.*, 2011, doi: 10.1007/s00170-011-3710-y.
- [37] Z. Zhang and J.-X. Xu, "Bi-Level Multiple Mode Resource-Constrained Project Scheduling Problems Under Hybrid Uncertainty," *J. Ind. Manag. Optim.*, 2015, doi: 10.3934/jimo.2016.12.565.
- [38] J. Jiang, W. Wen-xue, W.-L. Shao, and Y. Qu, "Research on Large-Scale Bi-Level Particle Swarm Optimization Algorithm," *Ieee Access*, 2021, doi: 10.1109/access.2021.3072199.
- [39] A. Mahmoodi, "Pricing and Inventory Decisions in a Manufacturer-Stackelberg Supply Chain With Deteriorating Items," *Kybernetes*, 2020, doi: 10.1108/k-03-2020-0149.
- [40] A. Aboud, R. Fdhila, A. Hussain, and A. M. Alimi, "A Novel Dynamic Pareto Bi-Level Multi-Objective Particle Swarm Optimization (DPb-MOPSO) Algorithm," 2020, doi: 10.36227/techrxiv.13325354.v1.
- [41] Y. Yan, "Research on Location Selection of Electric Vehicle Charging Facilities Based on Hybrid Algorithm," 2024, doi: 10.1117/12.3024048.

Deep Learning Approach for Workload Prediction and Balancing in Cloud Computing

Syed Karimunnisa¹, Yellamma Pachipala²

Research Scholar, Department of Computer Science and Engineering,
Koneru Lakshmaiah Education Foundation, Vaddesvaram, Guntur, AP, India-522503¹
Associate Professor, Department of Computer Science and Engineering,
Koneru Lakshmaiah Education Foundation, Vaddesvaram, Guntur, AP, India-522503²

Abstract—Cloud Computing voted as one of the most revolutionized technologies serving huge user demand engrosses a prominent place in research. Despite several parameters that influence the cloud performance, factors like Workload prediction and scheduling are triggering challenges for researchers in leveraging the system proficiency. Contributions by practitioners given workload prophesy left scope for further enhancement in terms of makespan, migration efficiency, and cost. Anticipating the future workload in due to avoid unfair allocation of cloud resources is a crucial aspect of efficient resource allocation. Our work aims to address this gap and improve efficiency by proposing a Deep Max-out prediction model, which predicts the future workload and facilitates workload balancing paving the path for enhanced scheduling with a hybrid Tasmanian Devil-assisted Bald Eagle Search (TES) optimization algorithm. The results evaluated proved that the TES scored efficiency in makespan with 16.342%, and migration efficiency of 14.75% over existing approaches like WACO, MPSO, and DBOA (Weighted Ant Colony Optimization Modified Particle Swarm Optimization, Discrete Butterfly Optimization Algorithm). Similarly, the error analysis during the evaluation of prediction performance has been figured out using different approaches like MSE, RMSE, MAE, and MSLE, among which our proposed method overwhelms with less error than the traditional methods.

Keywords—Task scheduling; virtual machines; optimization; workload prediction; migration; QoS

Nomenclature

| Abbreviation | Description |
|--------------|---|
| SIN | Service Invocation Number |
| DBN | Deep Belief Network |
| LSTM | Long Short-Term Memory |
| SVM | Support vector machine |
| MA | Moving Average |
| ARIMA | Autoregressive Integrated Moving Average |
| WACO | Weighted Ant Colony Optimization |
| DBOA | Discrete Butterfly Optimization Algorithm |
| Grid-LSTM | Grid-Long Short-Term Memory |
| Bi-LSTM | Bi-directional Long Short-Term Memory |
| SDWF | Self-Directed Workload Forecasting |
| JEES | Joint Energy Efficiency Optimization Scheme |
| SE | Sum Squared Error |
| CE | Cross Entropy Error |
| TDO | Tasmanian Devil Optimization |

| | |
|------|--------------------------------------|
| CSO | Cat Swarm Optimization |
| MFO | Moth Flame Optimization |
| BES | Bald Eagle Search |
| HWOA | Hybrid Whale Optimizer |
| MPSO | Modified Particle Swarm Optimization |

I. INTRODUCTION

With the pervasive expansion of Internet access and the rise of Big Data, cloud computing has gained increasing prominence in today's business landscape [1]. In comparison to alternative distributed computing methodologies such as cluster and grid computing, cloud computing offers an adaptive and scalable approach to providing customized services to consumers. It provides a means for consumers to access computing resources and platforms without the necessity of owning the underlying technology, enabling them to utilize these resources in a pay-per-use manner. Numerous resources, including processing power, storage capacity, and network bandwidth, are easily accessible in the field of cloud computing. The complexity lies in distributing them fairly across different users and jobs to meet a range of demands and priorities. Therefore, allocating resources in this dynamic and diverse environment presents a challenging task for researchers.

The main challenge in cloud computing is its diversified fluctuation of workloads and user needs [2]. Task requirements differ in kinds and amounts of resources, with dynamically evolving user needs. Secondly, cloud resources are limited, therefore it is crucial to allocate them wisely aiming for maximum performance and service effectiveness. It becomes imperative to load balance to avoid performance drops by resource saturation, due to resource conflicts within the system. At times several users or jobs may inevitably compete for the same resources simultaneously, leading to resource conflicts and delays. Eventually minimizing disputes and guaranteeing even distribution and efficient resource utilization, for strong resource allocation and scheduling is an urged need.

To address issues pertaining to the performance of task scheduling [3-5], researchers have presented a variety of innovative approaches. The following categories generally describe the available task-scheduling techniques in a cloud environment. Static Scheduling Methods: These include algorithms such as Shortest Job First (SJF), Earliest Deadline First (EDF), and Minimum Remaining Time (MRT) to

determine the sequence of work allocation and execution before a job is submitted. They are easy to deploy, but they are not flexible enough to adjust to changing task needs and dynamic situations. Heuristic Scheduling Methods: These techniques, which include Genetic Algorithms (GA) and Particle Swarm Optimization (PSO), mainly rely on prior knowledge and pre-established guidelines for scheduling decisions. They cannot optimize globally or make adjustments in real time, even though they take job priorities and resource efficiency into account.

Methods for Load Balancing Scheduling: These techniques seek to balance workloads among computing resources resulting in improved performance and resource usage. Random scheduling, round-robin (RR) scheduling, and queue-length-based scheduling are a few examples. They perform well in workload distribution overriding job specifications.

Scheduling process with evolutionary demands questioning the efficiency of cloud performance [6]. First of all, the sheer number of tasks demanded and their effective management raises the bar for computational demands adding complexity. Second, the cloud environment is dynamic, task arrivals, departures, and resource requirements are always changing. This dynamic nature renders the requirement for task scheduling algorithms that can be flexible and adaptive in real time to quickly adjust to changing demands [7]. Finally, to accomplish load balancing and maximize resource utilization, efficient task scheduling that relies on the appropriate distribution and application of resources is needed. If this equilibrium is not reached, system performance may suffer and resources may be wasted.

At the core of cloud computing lies the allocation of computing tasks to a shared resource pool of resources comprising diverse virtualized servers or virtual machines (VMs) [8]. Operating akin to a market-driven utility, cloud computing endeavors to enable providers and users to optimize their profits with enhanced returns on investment. As a result, the adoption of sophisticated scheduling strategies becomes essential to facilitate the management of software, user applications, tasks, and workflows within this environment. Scheduling, in its essence, plays a crucial role in shaping system performance, influencing both resource utilization efficiency and operational costs, thus underscoring its mark in the domain of cloud computing [9].

Due to the dynamic provisioning and management capabilities of virtual machines (VMs) [10], challenges in cloud scheduling generally manifest in two layers. Firstly, the task scheduling phase involves aligning user-submitted tasks concerning available VM resources. Secondly, a vital VM-to-host mapping process, which facilitates VM creation or migration [11, 12, 13]. Our main emphasis is on optimizing the former, as it directly influences the processing capabilities of a cloud computing system. Improving task scheduling has the potential to notably enhance system efficiency in terms of both time and cost [14, 15].

The above-mentioned challenges and issues that impact cloud performance are considered and addressed by introducing a framework that encompasses operations like workload prediction and scheduling, resulting in the design of

a deep learning algorithm trained on features such as VM capacity and task capacity to optimize the scheduling process. The contributions of this work are delineated as follows:

- Introducing an enhanced Deep Learning approach, named Improved Deep Maxout, to predict workloads by training on both VM and task capacities.
- The prediction process facilitates optimal task scheduling through the TES algorithm, guaranteeing the achievement of objectives such as time efficiency, cost-effectiveness, and overall system efficiency.

The paper begins by introducing the concepts and challenges associated with cloud computing in Section I. Section II presents a thorough literature review along with the analysis and discussions of researchers' findings. In Section III, the paper describes the architecture and system flow of the proposed methodology in detail. Results and discussion is given in Section IV. The conclusion and future directions for enhancements are discussed in Section VI, shedding light on potential future developments.

II. RELATED WORK

Several Researchers have made significant contributions to resolving task scheduling and resource allocation challenges. However, our work builds upon these efforts by addressing overlooked aspects and introducing enhancements that improve overall performance.

Wiem Matoussi and Tarek Hamrouni [16] developed workload forecasting techniques in 2021 to support capacity planning, guarantee effective resource allocation, and uphold SLA agreements with end users. Their methodology offered a novel way to forecast the surge of requests to a SaaS service and distribute virtual resources to satisfy user needs. The dual goals of this technique were response time optimization and accurate forecast forecasts.

Vinicius Meyer et al. [17] presented a machine learning-based classification technique in 2021 to provide the best possible resource allocation in cloud environments that are aware of dynamic interference. The main objective was to demonstrate how categorization techniques affect resource allocation so that it better accommodates variations in workload. The study began by looking at how different apps with different dynamic requests are handled by hardware components. The effectiveness of several interference classification techniques was investigated and assessed, taking into account the dynamic nature of cloud workloads.

Marek Grzegorowski et al. [18] presented a revolutionary method in 2020 for building a reliable clustering methodology with cloud resources customized to the particular data processing requirement. The provided architecture made use of the infrastructure-as-a-code framework to allow for dynamic cluster configuration and administration. It begins by figuring out which cluster size is best for finishing a task within the given time frame. The execution time was then optimized by using ARIMA models and examining the price history of spot instances to benefit from the lower prices offered by the cloud spot market.

Min Cao et al. [19] introduced three fresh methods for an energy-aware EIS in 2023. The author initially determined the best time for each task to run on a certain resource to save energy. Second, to reduce frequency factor and voltage and conserve energy, the EIS allows workflow slack time according to the optimal time for each task's execution. Moreover, the EIS minimizes dynamic energy consumption and satisfies workflow deadline limitations by utilizing the lapsed time caused by task priority deficiencies.

A logarithmic method was used in 2021 by Jing Bi et al. [20] to lower standard deviation before workloads and resource sequences were applied. They used the Min-Max approach to scale the data and an improved filter to remove noise interference and outliers. They have created an integrated deep learning method for time series forecasting, which makes use of ML-network models like Grid-LSTM and Bi-LSTM networks to produce accurate forecasts of resource demands and workload arrival at regular intervals.

The SDWF (Standard Deviation Weighted Forecasting) approach was developed in 2021 by Jitendra Kumar et al. [21]. It uses the deviation in the present predictions to calculate the trend of forecasting errors and improve the accuracy of future predictions. For training neurons, the model uses a sophisticated heuristic approach motivated by the black hole phenomenon. In addition, a statistical analysis was carried out to verify the accuracy of the suggested forecasting model, using Friedman and Wilcoxon signed ranking tests.

JEES (Joint Energy Optimisation and Scheduling), which simultaneously tackles and optimizes energy consumption in both cooling systems and servers, was introduced in 2021 by Kaixuan Ji et al. [22]. In addition to a resource management strategy that integrates workload forecasting models for resource allocation and a task-migration approach that makes use of marginal cost evaluation, JEES also includes a dynamic online task-scheduling technique based on the evaluation of marginal cost. The combined effect of these strategies is to lower data centers' overall energy usage.

Taking into account the unpredictable and time-varying nature of the workload, Zheng Xiao et al. [23] combined VM allocation with task scheduling in 2019. A Markov chain can be used to simulate the Markov property that the acquired workload dataset exhibits, as the study showed. In addition, recurrence, entropy, and persistence were found to be the three main operators that best described the workload. These operators assess the stability, predictability, and approximate burst timings of user requests, in that order. It was discovered that there is a nonlinear link between workload characteristic operators and virtual machine allocation.

A hybrid weighted Ant Colony Optimisation model with solution and pheromone updating functions was presented by Chirag Chandrasekar et al. [24] in 2023 for the best job scheduling. They showed that their meta-heuristic method outperformed current algorithms in terms of metrics like execution time and resource management.

Neetu Sharma, Sonal, and Puneet Gala [25] introduced a QoS-based Ant Colony Optimisation scheduling system in 2020 that used a neural network technique for effective multi-

objective scheduling [37]. Their suggested approach outperformed current algorithms in terms of user task scheduling costs and execution times.

A modified Particle Swarm Optimisation (MPSO) was suggested in 2023 by Shikha Chaudhary et al. [26] to overcome the issues of long scheduling times and high computational costs during the scheduling process. By minimizing early convergence and improving local search efficiency, the MPSO optimizes the objective function about cost and makespan. An increase in the graph indicates that the performance of the suggested model is superior to that of conventional methods.

To solve resource waste and improve the algorithm's speed of convergence, Medhi Hussein Zadeh et al. [27] created a discrete Butterfly Optimisation Algorithm (DBOA) in 2021 that was modeled after the Levy flight technique. Their method of task prioritization and DBOA successfully addresses local optima concerns and allows for more efficient scheduling of intense workflows.

A task scheduling technique using Cat Swarm Optimisation was introduced in 2023 by Sudheer Mangalampalli et al. [28]. This algorithm prioritizes tasks and arranges them for scheduling. Inspired by the behavior of cats, this algorithm outperforms baseline methods that are currently in place in terms of QoS metrics like makespan and resource utilization.

Abdul Rajak [36] addressed an intelligent approach that benefits the real-world agricultural environment. Md shohel Sayeed et.al [38] proposed a real-time system for parking vehicles using a weighted K-nearest neighbour approach by selecting an optimal scheduler. Gousteris et.al [39] have come up with a secure approach for cloud storage using blockchain technology for efficient performance with heterogeneous input data.

III. METHODOLOGY

The work progresses by considering user requests as tasks appertaining to N users symbolized as U_i , where $i=\{1,2,\dots,N\}$. These tasks designated as $Task_j$ with $j=\{1,2,\dots,M\}$ are assigned to feasible virtual machines VM_i where $i=\{vm_1,vm_2,\dots,vm_n\}$ and physical machines PM_i where $i=\{pm_1,pm_2,\dots,pm_k\}$. The proposed paradigm proceeds based on a priority scheme for scheduling using Deep learning techniques resulting in improved forecast of workloads.

Improving cloud performance and cutting operating costs need accurate workload forecasts. To precisely predict workloads, a deep learning model is used in this article, which increases efficiency and lowers costs. The proposed improved Deep Maxout model successfully learns to anticipate jobs as target labels by using factors like CPU utilization, day of the week, and time of day.

The enhanced Deep Maxout model's mathematical formulation is explained in [29]. To improve model robustness, it adds the modified softmax activation function (G-SM) to Eq. (2). In this case, the activation value is denoted by si and $gd(s)$ Gaussian distributed term with mean μ and standard deviation σ . The classic softmax activation function, which can handle multiple classes by normalizing the outputs for each class, ranging from 0 to 1, is presented by Eq. (1).

The input layer, embedding layer, max pooling layer, dropout layer, convolution layer, and dense layers that make use of activation and maxout functions constitute the Deep Maxout model's network structure. The maxout unit of this network is shown in Eq. (3), here $K_{yz} = N \cdot \lambda_{yz} + \gamma_{yz}$, γ serves as the bias, with N standing for input features such as task and virtual machine capacity, η serving as the feature map, and λ serving as the weight.

The softmax function SM is coined as follows:

$$SM(s)_i = \frac{e^{s_i}}{\sum_{j=1}^k e^{s_j}} \quad (1)$$

This formula defines a probability distribution across k possible outcomes. Here s_i represents the input value corresponding to outcome i and the denominator summates the exponentials of all input values across all outcomes.

$$G - SM = \frac{\exp(s_i + gd(s))}{\sum_{j=1}^k \exp(s_j + gd(x))} \quad (2)$$

$$gd(s) = 0.5 * \text{er}_f \left(-\frac{\sqrt{2}(\mu_i - s_i)}{2\sigma_i} \right) + 0.5$$

where, error function er_f can be coined as.

$$(1/\sqrt{\pi}) \int_{-z}^z e^{-t^2} dt, t^2 = s_i$$

$$Q(M) = \text{Maximum}(R_{yz})_{z \in [1, \eta]} \quad (3)$$

The input layer receives the input feature N , and the embedding layer processes its output to calculate the outcome. The dropout layer and convolution layer are the next two layers that process the output further. The final output is obtained starting with the third convolution layer. The final output is then produced by the max-pooling layer following the convolution layer. The dense layer is followed in order by the dropout layer.

The output of the max-out module is calculated based on the input pipelined from the dropout layer and is combined with the dense layer to create the final product. Using the output of the dense layer as the last step, the activation function computes the classification result as Deep Max_{out}. To evaluate the accuracy parameter of the model, hybrid loss functions which are given in Eq. (4) and detailed in [33] are used. Typically, error measures such as the $SE(E_{SE})$ and CE loss functions (E_{CE}) are employed to assess the efficacy of a classification model.

The enhanced hybrid loss function calculation for the proposed model is provided in Eq. (5), where the dynamically weighted balanced CE is represented by E_{CE^*} (as in Eq. (6)). In this case, y_i^{\wedge} stands for the anticipated label, and y_i indicates the actual label. w_lb_j , which is calculated as the ratio of class frequency n_j and the majority

class (as determined across the training dataset), is equal to the class frequency log (as in Eq. (7)). The proportions allocated to the loss functions are represented by the scalar values Lf_1 and Lf_2 , where $Lf_1 + Lf_2 = 1$.

$$E_{he} = Lf_1 \frac{E_{SE}}{MaxSE} + Lf_2 \frac{E_{CE}}{MaxCE} \quad (4)$$

Here

$$E_{CE} = -\frac{1}{Output_Size} \sum_{i=1}^{Output_Size} y_i \cdot \log y_i^{\wedge} + (1 - y_i) * 1 * \log (1 - y_i^{\wedge})$$

$$E_{he} = Lf_1 \frac{E_{SE}}{MaxSE} + Lf_2 \frac{E_{CE^*}}{MaxCE^*} \quad (5)$$

$$E_{CE^*} = -\frac{1}{Output_Size} \sum_{i=1}^{Output_Size} \sum_{j=1}^c w_lb_j^{(1-p_{ij})} y_i \cdot \log y_i^{\wedge} + (1 - y_i) * 1 * \log (1 - y_i^{\wedge}) \quad (6)$$

$$w_lb_j = \log \left(\frac{\max(n_j | j \in c)}{n_j} \right) + 1 \quad (7)$$

1) *Optimal load balancing and task scheduling*: An effective load-balancing approach proactively aids in monitoring the workload of the virtual machines (VMs) and allocating jobs to them appropriately. An example job would be Tsk_j , which has a range of 1000 tasks. The physical machines would be pm_k , with 50 machines, and the virtual machines would be vm_N , with 20–25 computers. There are multiple vm_N within this range for every pm_k . The pm_k machines are randomly assigned tasks.

The enhanced Deep Maxout model is used in this workload prediction model. The target label of the Deep Maxout model is set to 0, 1, and 2, and the features supplied to the Improved Deep Maxout model are Task capacity and VM capacity. The following are the definitions of under load, equal load, and overload conditions:

- The target label is set to 0, indicating that the machine's workload prediction is under load, if the task capacity is smaller than the virtual machine's capacity.
- The target label is set to 1, indicating that the machine's workload prediction is at equal load, if the task capacity and the VM capacity are equal.
- The target label is set to 2, meaning that the machine's workload prediction is overloaded, if the task capacity exceeds the virtual machine capacity.

Constraints including Makespan (Fn_1), Migration cost (Fn_2), and Migration efficiency (Fn_3) are taken into account throughout the scheduling process considered. Fig. 1 shows the model of scheduling. The input solution assigns a lower bound of $Lb=0$, ($Zeros(len(Machine_underload))$), and an upper bound of $Ub=1$, ($Ones(len(Machine_underload))$) to the variables. The number of underloaded machines is equal to the problem size of TES.

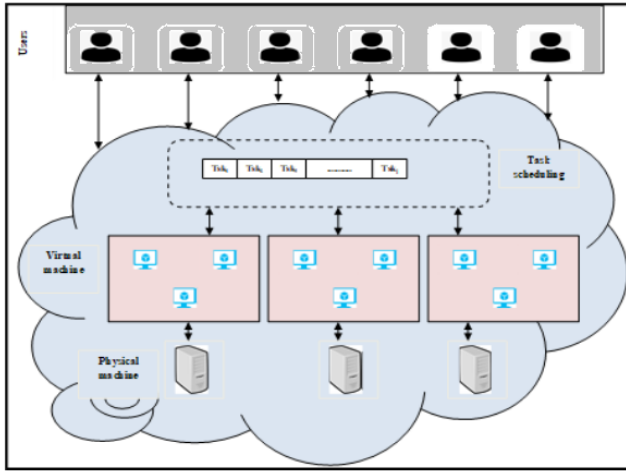


Fig. 1. Scheduling of task in cloud computing.

The objective function is expressed in Eq. (8), where random weights in the interval $[0, 1]$ are represented by the variables w_1 , w_2 , and w_3 .

$$Obj = (w_1 * Fn_1) + (w_2 * Fn_2) + (w_3 * Fn_3) \quad (8)$$

1) *Makespan*(Fn_1): Eq. (9), which defines the makespan, shows the total computing time (CT_i) (as given in Eq. (10)) needed to complete a task, where N is the number of virtual machines.

$$Fn_1 = \text{Max}_{1 \leq i \leq N} \{CT_i\} \quad (9)$$

$$CT_i = \sum_{j=1}^n \frac{T_j * \text{length}}{vm_N * Pes_Num * Xvm_N} \quad (10)$$

2) *Migration cost*(Fn_2): A $M * M$ matrix is used to calculate the migration cost, where the rows and columns of the matrix indicate the migration costs of virtual machines (vm_N) and physical machines (pm_K), respectively. The (1, 1) and (2, 2) columns in this matrix indicate reduced migration costs, while the remaining entries suggest higher migration costs.

3) *Migration efficiency*(Fn_3): Based on the migration value, the migration efficiency is computed, as shown in Eq. (11).

$$Fn_3 = \frac{1}{Fn_1} \quad (11)$$

This section presents the mathematical formulation of the proposed meta-heuristic TES, which combines TD [30] with ES [31]. The Tasmanian devil feeds on live prey by attacking them or by scavenging carrion from dead animals. This behavior is simulated by TES. First, a random population of agents is generated according to the limitations of the challenge. Based on the location of their search region, the population members of TES, which are problem-solving search agents, suggest potential values for problem variables. Functionally, each member of the population can be thought of as a vector, with the number of elements representing the number of variables in the problem. A matrix in Eq. (12), where P is the Tasmanian population, N is the number of Tasmanian devils seeking, P_i is a potential solution, and m is

the number of specified problem variables, can be used to simulate the set of TES members.

$$P = \begin{bmatrix} P_1 \\ \vdots \\ P_i \\ \vdots \\ P_N \end{bmatrix} = \begin{bmatrix} p_{1,1} \cdots p_{1,j} \cdots p_{1,m} \\ \vdots \\ p_{i,1} \cdots p_{i,j} \cdots p_{i,m} \\ \vdots \\ p_{N,1} \cdots p_{N,j} \cdots p_{N,m} \end{bmatrix}_{N \times m} \quad (12)$$

By changing the values of potential solutions into the defined objective function's objects, the objective function can be assessed. In Eq. (13) the values obtained for the defined objective function are represented by a vector V .

$$V = \begin{bmatrix} V_1 \\ \vdots \\ V_i \\ \vdots \\ V_N \end{bmatrix} = \begin{bmatrix} V(P_1) \\ \vdots \\ V(P_i) \\ \vdots \\ V(P_N) \end{bmatrix}_{N \times 1} \quad (13)$$

The Tasmanian devil algorithm does not always hunt; sometimes it prefers to eat the carrion that is around. The area above the Tasmanian devil is home to additional predators that hunt enormous prey but are unable to finish it. Each Tasmanian devil considers the position of another population member to be carrion bait under the TES design. Cr_i denotes the selected carrion in Eq. (14) which shows the random selection of one of these cases. The Tasmanian devil is moved to a new location inside the search area based on Cr_i .

$$Cr_i = P_k, i = 1, 2, \dots, N, \\ x \in \{1, 2, \dots, N | x \neq i\} \quad (14)$$

A random number is represented by $ln \in (1, 2)$ and a random number is represented by $r \in (0, 1)$, while the Tasmanian devil's current update based on the first strategy is represented by $p_{i,j}^{new,S1}$ in Eq. (12). Eq. (15) is used to calculate the Tasmanian devil's new position. If the objective function value at the new position is higher than its previous position, the position is considered acceptable; otherwise, the Tasmanian devil process retains its position.

The new update for the Tasmanian devil is obtained by merging the TD and proposed ES updates in Eq. (16), by the proposed methodology. In this case, the random factor is represented by $RandF$ (as in Eq. (18)) [34], the random value is $r_2 \in (0, 1)$ the maximum iteration is It_{Max} , the current iteration is C_It and the levy flight update is represented by $Levy_fun$ (as in Eq. (19)). Eq. (20) provides the typical (eagle search) ES update equation, where α is the parameter governing the position change.

Update to the new value as $p_{i,j}^{new,S1}$ with $p_{i,j} + r \times (Cr_{i,j} - ln \times p_{i,j})$ when the criteria $V_{Cr_i} < V_i$ is met alternatively

$$p_{i,j} + r \times (p_{i,j} - Cr_{i,j}) \quad (15)$$

The algorithm considers $P_{i,j}^{new,S1}$ the updated if the fitness offered is better than current else retains the current value as follows

$$P_i = \begin{cases} P_i^{new,S1}; V_i^{new,S1} < V_i \\ P_i; \text{Otherwise} \end{cases} \quad (16)$$

$$p_{i,j}^{new,S1} = \begin{cases} p_{i,j} + \text{RanF} \times (Cr_{i,j} - \text{In} \times p); \\ \quad \text{if } V_{Cr_i} < V_i \\ p_{best} + \alpha * r(p_{mean} - p_i) * \text{Levy_fun}; \\ \quad \text{else} \end{cases} \quad (17)$$

$$\text{RanF} = r_1 * \sin(r_2), \quad (18)$$

where

$$r_1 = \frac{1.5 \times (It_{Max} - t + 1)}{It_{Max}}$$

$$\text{Levy_fun} = \frac{c_{It(1+\beta)} * \left(\sin\left(\frac{\pi\beta}{2}\right)\right)^{1/\beta}}{c_{It\left(\frac{1+\beta}{2}\right)} * \beta * \left(2^{\left(\frac{\beta-1}{2}\right)}\right)} \quad (19)$$

$$p_{new} = p_{best} + \alpha * r(p_{mean} - p_i) \quad (20)$$

$$\begin{aligned} \text{Pry}_i &= P_k, i = 1, 2, \dots, N, \\ x &\in \{1, 2, \dots, N | x \neq i\} \end{aligned} \quad (21)$$

The position of other population members is taken into account as the location of prey during the updating procedure of the i^{th} Tasmanian devil. Prey selection is modeled by Eq. (21) where Pry_i indicates the selected prey and $x \in (1, N)$ is a natural random number.

Eq. (22) uses the exact location of the prey to calculate the Tasmanian devil's new position. The Tasmanian devil's location is adjusted to this new position if the new location increases the target function value. Eq. (23) provides an example of this second strategy phase.

$$p_{i,j}^{new,S2} = \begin{cases} p_{i,j} + r \times (\text{Pry}_{i,j} - \text{In} \times p_{i,j}); \\ \quad \text{if } V_{\text{Pry}_i} < V_i \\ p_{i,j} + r \times (p_{i,j} - \text{Pry}_{i,j}); \\ \quad \text{else} \end{cases} \quad (22)$$

$$P_i = \begin{cases} P_i^{new,S2}; V_i^{new,S2} < V_i \\ P_i; \text{Otherwise} \end{cases} \quad (23)$$

The radius R of the neighborhood that is, the region where the Tasmanian devil tracks its prey can be found using Eq. (24). Thus, a new position for the Tasmanian devils can be established by quantitatively simulating their pursuit behavior using Eq. (25). The Tasmanian devil will accept the newly calculated position if it provides a better value for the goal function than the previous position. Eq. (26) describes the process of updating the position of the Tasmanian devil. The Tasmanian devil's position update procedure is carried out, by the model presented in Eq. (27), by incorporating the factor P_Fact as suggested in Eq. (28) [32].

$$Rd = 0.01 \left(1 - \frac{t}{It_{Max}}\right) \quad (24)$$

$$p_{i,j}^{new} = p_{i,j} + (2r - 1) \times Rd \times p_{i,j} \quad (25)$$

$$P_i = \begin{cases} P_i^{new}; \text{if } V_i^{new} < V_i \\ P_i; \text{else} \end{cases} \quad (26)$$

$$P_i = \begin{cases} P_i^{new} \times P_Fact; \\ \quad \text{if } V_i^{new} < V_i \\ P_i; \text{else} \end{cases} \quad (27)$$

$$P_Fact = \exp\left(\frac{-i}{\delta \times It_{Max}}\right) \quad (28)$$

Algorithm 1: TES (Tasmanian Devil-assisted Bald Eagle Search) for optimal load balancing and task scheduling.

Input: Set of VMs = {VM₁, VM₂, ..., VM_n} and Tasks = {T₁, T₂, ..., T_n}
Initialize: No of iterations (T) and no of members of the population (N).

While $t=1: T$

For $i=1: N$

IF $prob < 1/2$, $prob = rand$.

Select carrion for the i th Tasmanian devil by Eq. (14)
Calculate the new status of the Tasmanian devil by Eq. (16)
Update the i th Tasmanian devil apply Levy flight strategy by Eq. (17)

Else

Select prey of i^{th} the Tasmanian devil using Eq. (21)
Assess the updated value of the Tasmanian Devil using Eq. (22).
The Tasmanian Devil's update is executed using Eq. (23).
Update Rd by Eq. (24)

Assess the new updated value of i^{th} Tasmanian Devil in the neighborhood using Eq. (25).

Update proposed i^{th} Tasmanian devil via Eq. (27)

End For

End While

Output: The best solution obtained for a given optimization problem.

IV. RESULTS AND DISCUSSION

A. Experimental Setup and Simulation

We employed simulations to evaluate the effectiveness of our proposed scheduling methods. Cloudsim is widely utilized as simulation software for evaluating optimization techniques. It replicates components of cloud systems such as data centers, tasks, and virtual machines, while also supporting task scheduling strategies and diverse energy usage models for simulating various workloads. In this study, we simulated a cloud model based on a single data center, akin to Infrastructure as a Service (IaaS). The simulations were performed on a computer equipped with an Intel(R) Core(TM) i5-8265U CPU @ 1.80 GHz processor, 16 GB RAM, and a 64-bit Windows 11 Operating System.

The configuration of the simulated cloud data center is shown in Tables I, II and III.

TABLE I. CONFIGURATION OF HOST IN DATACENTER

| Host Parameters | Value |
|-------------------------|------------------|
| Processing Element (PE) | 2-10 |
| Processing capacity | 20000-35000 MIPS |
| RAM capacity | 8GB,16GB,32GB |

TABLE II. CONFIGURATION OF VMs

| VM Parameters | Value |
|------------------------------------|---------------|
| Processing Element (PE) in each VM | 1 |
| CPU computing capacity | 600-4000 MIPS |
| RAM capacity | 512-4196 MB |

TABLE III. TASK PARAMETERS

| Task Parameters | Value |
|-----------------|-----------------|
| Task Length | 15000-900000 MI |
| Size of Task | 60-3000 KB |

B. Performance Metrics

The Google Cluster Workload Traces dataset from 2019 sourced from [35] is subjected to Cloudsim for workload prediction and job scheduling. The TES approach is evaluated against conventional strategies such as DBOA, MPSO, and WACO. The key parameters considered for evaluating the performance of the proposed method pertain to Communication cost, Execution time, Makespan, Migration Cost and Migration Efficiency are compared against existing approaches. The analysis is carried out with task counts ranging from 500 to 2000.

1) *Communication cost and execution time:* Fig. 2 and Fig. 3 depicts the comparison of TES performance to that of WACO, MPSO, and DBOA in terms of communication cost and execution time for workload prediction and task scheduling. The results achieved present an increased drift in performance by the proposed TES in terms of reduced execution times and communication costs over other approaches. To be more precise, when handling tasks with tasks of various counts, the TES attained notably lowered communication costs than other algorithms handling. The result of the proposed approach renders the utmost values when task count is 500, when compared against task counts of 1000, 1500, and 2000. Furthermore, the TES demonstrated a significant improvement with an execution time of 1648 seconds with 2000 tasks.

2) *Makespan analysis:* The workload prediction and task scheduling performance metrics comparison of the TES vs. WACO, MPSO, and DBOA is shown in Fig. 4. Indicating that when job/task count is set at 500, the findings show a shorter makespan for the TES approach as compared to conventional methods. This demonstrates how accurate the TES is at forecasting workload and allocating jobs facilitating the shortest makespan.

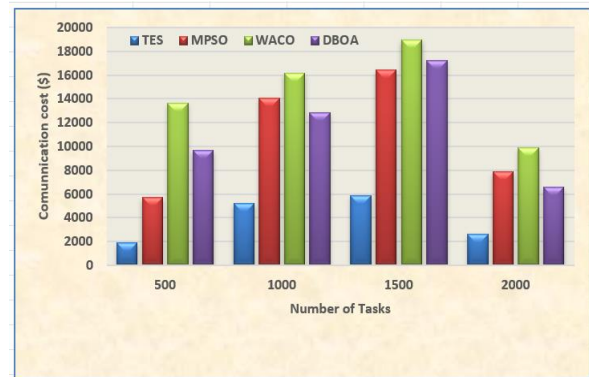


Fig. 2. Communication cost vs. number of task.

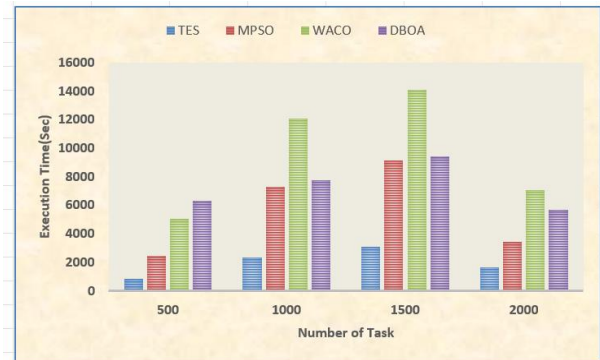


Fig. 3. Execution time vs. number of task.

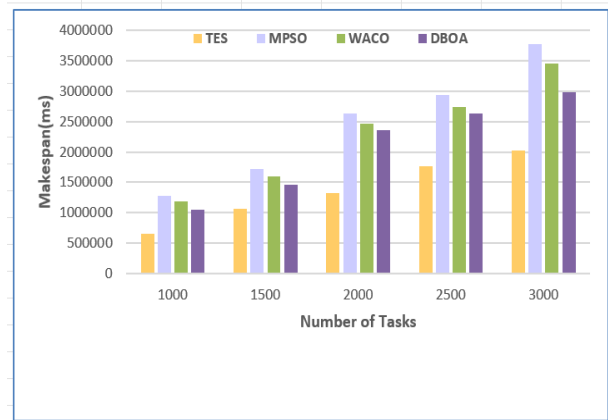


Fig. 4. Makespan vs. number of tasks.

3) *Migration cost and migration efficiency analysis:* The analysis of the TES's efficiency and migration cost of other task scheduling and workload prediction techniques is shown in Fig. 5 and Fig. 6. The number of tasks is changed to conduct the analysis. With a migration cost of 1.54 (with 2000 tasks), the TES methodology outperforms previous approaches with WACO=5.786, MPSO=4.345, and DBOA=3.987, respectively, in terms of efficiency and cost. Furthermore, TES's migration efficiency (0.0987) outperforms MPSO's (0.322), WACO's (0.378), and DBOA's (0.0239), with 2000 tasks. These findings show that TES is more effective and less expensive during task migrations.

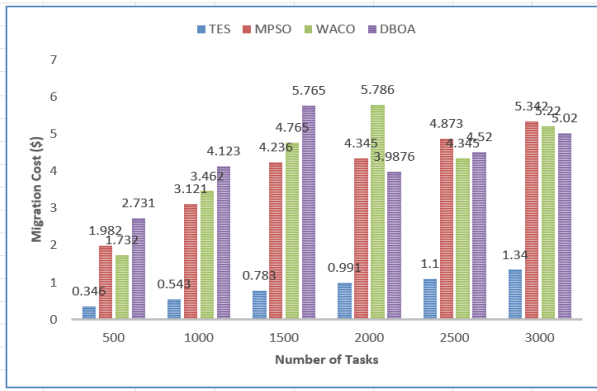


Fig. 5. Migration cost vs. number of tasks.

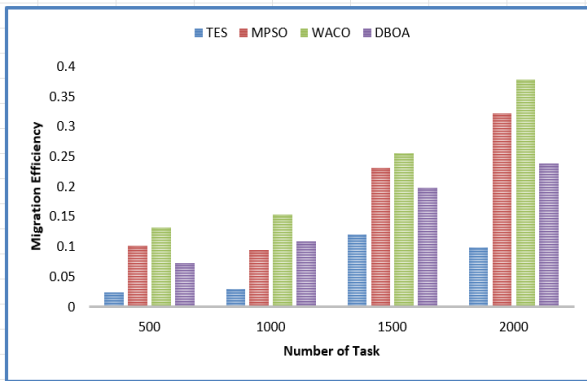


Fig. 6. Migration efficiency vs. number of task.

4) *Convergence evaluation:* As seen in Fig. 7, the convergence analysis of TES is contrasted with other methods currently in use, such as WACO, MPSO, and DBOA. The cost values that were initially produced by TES and other methods were high at the 0th iteration, with a considerable downtrend following successive iterations. The cost parameter values attained are comparatively low using TES, especially on the 25th iteration when it obtained a minimal cost value of 3.427. According to the convergence graph, TES converges more rapidly than other schemes, bringing down costs and producing enhanced accuracy in forecasting workload about user tasks.

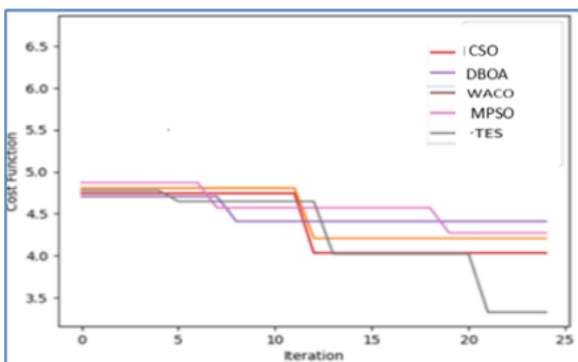


Fig. 7. Cost function vs. iterations.

5) *Regression analysis:* The regression evaluation of the suggested approach and the current approaches (CNN, NN, and RNN) for workload prediction is shown in Fig. 8, 9, 10 and Fig. 11. The results demonstrate that TES in contrast to CNN, NN, and RNN, which typically provide more divergent values, produces more consistent values in both real and classified labels.

6) *Error analysis of improved deep maxout:* Table IV presents an error analysis of the suggested algorithm concerning conventional Deep Maxout, CNN, RNN, NN, Bi-GRU, RMSE, MAE, and MSLE. The lowered error rates attained with the enhanced Deep Maxout technique reflect the e. In particular, the RMSE of the enhanced Deep Maxout is 0.100, which is substantially less than that of the Conventional Deep Maxout (1.150), RNN (0.340), CNN (0.260), and NN (0.160) in Bi-GRU (1.180), respectively. Furthermore, the suggested approach demonstrated enhanced performance in terms of MSE=0.120, MAE=0.021, and MSLE=0.215, all of which were minimized.

7) *Prediction analysis:* Table compares the prediction evaluation of TES with CNN, NN, and RNN addressing the prediction efficiency of TES that outperformed CNN, NN, and RNN algorithms in terms of prediction accuracy.

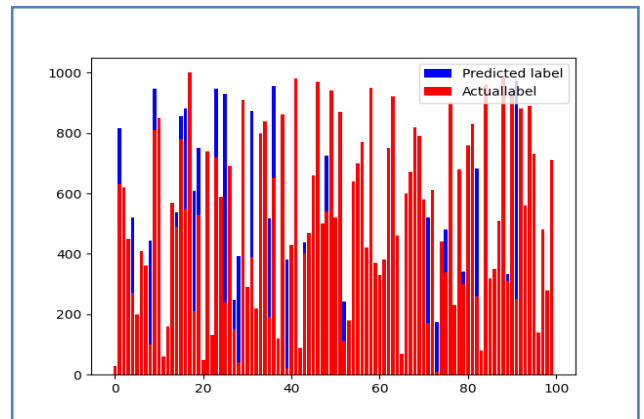


Fig. 8. Regression evaluation of CNN.

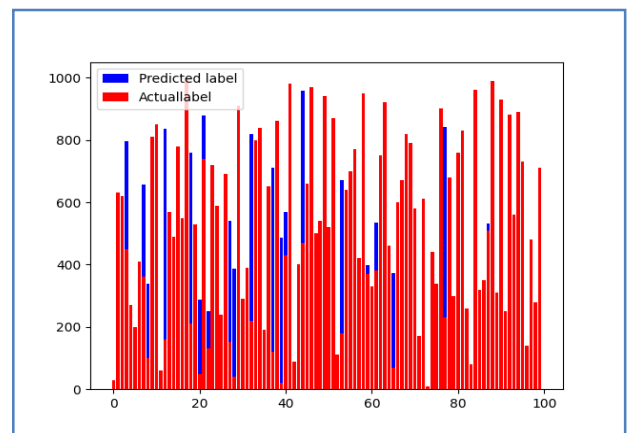


Fig. 9. Regression evaluation of NN.

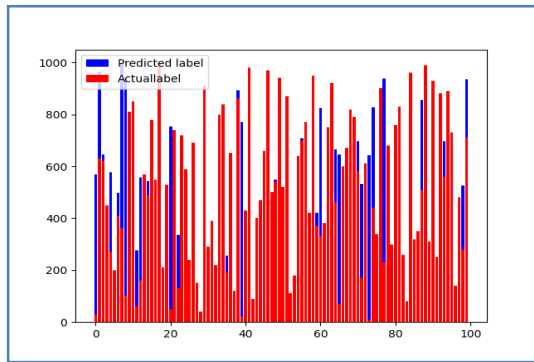


Fig. 10. Regression evaluation of RNN.

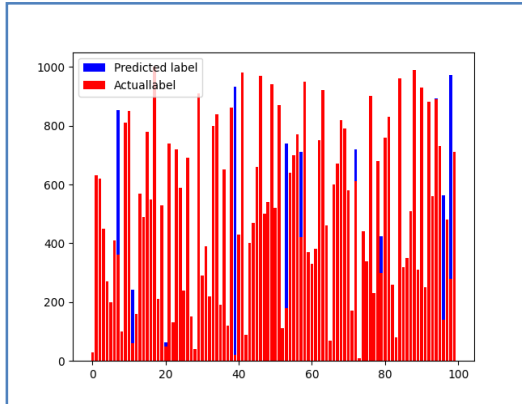


Fig. 11. Regression evaluation of TES.

TABLE IV. ERROR EVALUATION

| Methods | MSE | RMSE | MAE | MSLE |
|--------------------------|-------|-------|-------|-------|
| CNN | 0.521 | 0.260 | 0.150 | 0.520 |
| RNN | 0.460 | 0.340 | 0.140 | 0.678 |
| NN | 0.320 | 0.160 | 0.057 | 0.447 |
| Bi-GRU | 2.180 | 1.180 | 0.652 | 1.404 |
| Conventional Deep Maxout | 4.120 | 1.150 | 0.224 | 1.320 |
| Improved Deep Maxout | 0.120 | 0.100 | 0.021 | 0.215 |

TABLE V. PREDICTION EVALUATION OVER THE TRADITIONAL APPROACHES

| Methods | Success Rate | Over Prediction | Under Prediction |
|---------|--------------|-----------------|------------------|
| CNN | 49 | 51 | 49 |
| NN | 49 | 51 | 49 |
| RNN | 53 | 47 | 52 |
| TES | 96 | 14 | 25 |

V. CONCLUSION

The proposed study offers an effective workload prediction model that forecasts future workload based on trends seen in historical data by utilizing the Deep Max-out prediction model. This model uses the TES Algorithm to optimize scheduling while efficiently balancing the workload on machines. By ensuring that jobs are moved among virtual machines (VMs) in the best possible way, this method produces effective

scheduling that takes into account metrics like make-span, migration cost, and migration efficiency. Comparing the suggested model to conventional approaches, promisingly results in high communication costs, with statistical analysis showcasing that the new model greatly reduces communication costs (2647.835). Moreover, the comparison of forecast outcomes emphasizes how crucial it is to take into account limitations such as job make-span, fitness, migration-cost, and execution time. When comparing the suggested model to conventional techniques, these constraints are noticeably less. In particular, the execution time is reduced to around 817, demonstrating how well the suggested model performs in comparison to traditional techniques that require larger execution cycles.

REFERENCES

- [1] Fatemeh Ebadifard and SeyedMortezaBabamir, "Autonomic task scheduling algorithm for dynamic workloads through a load balancing technique for the cloud-computing environment", Cluster Computing, 2020, <https://doi.org/10.1007/s10586-020-03177-0>.
- [2] K. Lalitha Devi and S. Valli, "Multi-objective heuristics algorithm for dynamic resource scheduling in the cloud computing environment", The Journal of Supercomputing, 2020, <https://doi.org/10.1007/s11227-020-03606-2>.
- [3] Mahendra Bhatu Gawali and Subhash K. Shinde, "Task Scheduling and resource allocation in cloud computing using a heuristic approach", Gawali and Shinde Journal of Cloud Computing: Advances, Systems, and Applications (2018),7:4.
- [4] S. R. Shishira and A. Kandasamy, "A Novel Feature Extraction Model for Large-Scale Workload Prediction in Cloud Environment", SN Computer Science (2021), <https://doi.org/10.1007/s42979-021-00730-5>.
- [5] Anurina Tarafdar, Mukta Debnath, Sunirmal Khatua, Rajib K. Das, "Energy and Makespan Aware Scheduling of Deadline Sensitive Tasks in the Cloud Environment", Journal of Grid Computing (2021), <https://doi.org/10.1007/s10723-021-09548-0>.
- [6] Yonghua Zhu, Weilin Zhang, Yihai Chen, and Honghao Gao, "A novel approach to workload prediction using attention-based LSTM encoder-decoder network in cloud environment", EURASIP Journal on Wireless Communications and Networking (2019), <https://doi.org/10.1186/s13638-019-1605-z>.
- [7] Habte Lejebo Leka, Zhang Fengli, Ayantu Tesfaye Kenea, Negalign Wake Hundera, Tewodros Gizaw Tohye, and Abebe Tamrat Tegene, "PSO-Based Ensemble Meta-Learning Approach for Cloud Virtual Machine Resource Usage Prediction", Symmetry, vol.15, 2023.
- [8] M. Yadav and A. Mishra, "An enhanced ordinal optimization with lower scheduling overhead based novel approach for task scheduling in the cloud computing environment," Journal of Cloud Computing, vol. 12, no. 1, Jan. 2023, doi: 10.1186/s13677-023-00392-z.
- [9] X. Zhang, "A fine-grained task scheduling mechanism for digital economy services based on intelligent edge and cloud computing," Journal of Cloud Computing, vol. 12, no. 1, Mar. 2023, doi: 10.1186/s13677-023-00402-0.
- [10] G. Saravanan, S. Neelakandan, P. Ezhumalai, and S. Maurya, "Improved wild horse optimization with levy flight algorithm for effective task scheduling in cloud computing," Journal of Cloud Computing, vol. 12, no. 1, Feb. 2023, doi: 10.1186/s13677-023-00401-1.
- [11] P. Shukla and S. Pandey, "MOTORS: Multi-Objective Task Offloading and Resource Scheduling Algorithm for Heterogeneous Fog-Cloud Computing Scenario," Jul. 2023, doi: 10.21203/rs.3.rs-3124031/v1.
- [12] S. R. K. B. and S. R. E., "Improved Context Aware PSO Task Scheduling in Cloud Computing," Webology, vol. 19, no. 1, pp. 3709–3721, Jan. 2022, doi: 10.14704/web/v19i1/web19244.
- [13] H. Zhang, "A Cloud Computing Task Scheduling Method Based on Genetic Algorithm," Proceedings of the 2nd International Conference on Information Economy, Data Modeling and Cloud Computing, ICIDC 2023, June 2–4, 2023, Nanchang, China, 2023, doi: 10.4108/eai.2-6-2023.2334608.

- [14] Dharma s and K. P, "An Efficient Task Allocation Using Resource Shortest Scheduling and Fairness Firefly Algorithm In Cloud Computing," Feb. 2023, doi: 10.21203/rs.3.rs-2020473/v1.
- [15] H. Zhou, "A Novel Approach to Cloud Resource Management: Hybrid Machine Learning and Task Scheduling," Journal of Grid Computing, vol. 21, no. 4, Nov. 2023, doi: 10.1007/s10723-023-09702-w.
- [16] Wiem Matoussi and Tarek Hamrouni, "A new temporal locality-based workload prediction approach for SaaS services in a cloud environment", Journal of King Saud University – Computer and Information Sciences, 2021, doi:10.1016/j.jksuci.2021.04.008.
- [17] Vinícius Meyer, Dionatrã F. Kirchoff, Matheus L. Da Silva, Cesar A.F. De Rose, "ML-driven classification scheme for dynamic interference-aware resource scheduling in cloud infrastructures", Journal of Systems Architecture, vol 116, 2021.
- [18] Marek Grzegorowski, EftimZdravevski, Andrzej Janusz, Petre Lameski, Cas Apanowicz, Dominik Slezak, "Cost Optimization for Big Data Workloads Based on Dynamic Scheduling and Cluster-Size Tuning", Big Data Research, vol 25, 2021.
- [19] Min Cao, Yaoyu Li, Xupeng Wen, Yue Zhao, Jianghan Zhu, "Energy-aware intelligent scheduling for deadline-constrained workflows in sustainable cloud computing", Egyptian Informatics Journal, Volume 24, Issue 2, July 2023.
- [20] Jing Bi, Shuang Li, Haitao Yuan, MengChu Zhou, "Integrated deep learning method for workload and resource prediction in cloud systems", Neurocomputing, Volume 424, 1 February 2021.
- [21] Jitendra Kumar, Ashutosh Kumar Singh, Rajkumar Buyya, "Self-directed learning based workload forecasting model for cloud resource management", Information Sciences, vol 543, 2021.
- [22] Kaixuan Ji, Fa Zhang, Ce Chi, Penglei Song, Biyu Zhou, Avinab Marahatta, Zhiyong Liu, "A joint energy efficiency optimization scheme based on marginal cost and workload prediction in data centers", Sustainable Computing: Informatics and Systems, vol 32, 2021.
- [23] Zheng Xiao, Bangyong Wang, Xing Li, Jiayi Du, "Workload-driven coordination between virtual machine allocation and task scheduling", Advances in Parallel and Distributed Computing for Neural Computing, Neural Computing, and Applications, 2019, <https://doi.org/10.1007/s00521-019-04022-1>.
- [24] C. Chandrashekar, P. Krishnadoss, V. Kedalu Poornachary, B. Ananthkrishnan, and K. Rangasamy, "HWACOA Scheduler: Hybrid Weighted Ant Colony Optimization Algorithm for Task Scheduling in Cloud Computing," Applied Sciences, vol. 13, no. 6, p. 3433, Mar. 2023, doi: 10.3390/app13063433.
- [25] N. Sharma, S. Beniwal, and P. Garg, "Ant Colony Based Optimization Model for Qos-Based Task Scheduling in Cloud Computing Environment," SSRN Electronic Journal, 2022, doi: 10.2139/ssrn.4237751.
- [26] S. Chaudhary, V. K. Sharma, R. N. Thakur, A. Rathi, P. Kumar, and S. Sharma, "Modified Particle Swarm Optimization Based on Aging Leaders and Challengers Model for Task Scheduling in Cloud Computing," Mathematical Problems in Engineering, vol. 2023, pp. 1–11, Jun. 2023, doi: 10.1155/2023/3916735.
- [27] M. Hosseinzadeh et al., "Improved Butterfly Optimization Algorithm for Data Placement and Scheduling in Edge Computing Environments," Journal of Grid Computing, vol. 19, no. 2, Mar. 2021, doi: 10.1007/s10723-021-09556-0.
- [28] S. Mangalampalli et al., "Prioritized Task-Scheduling Algorithm in Cloud Computing Using Cat Swarm Optimization," Sensors, vol. 23, no. 13, p. 6155, Jul. 2023, doi: 10.3390/s23136155.
- [29] Jyothi Peta and Srinivas Koppu, "An IoT-Based Framework and Ensemble Optimized Deep Maxout Network Model for Breast Cancer Classification", Electronics 2022, 11, 4137. <https://doi.org/10.3390/electronics11244137>.
- [30] MOHAMMAD DEGHANI, T...PÁN HUBALOVSKY, AND PAVEL TROJOVSKY, "Tasmanian Devil Optimization: A New Bio-Inspired Optimization Algorithm for Solving Optimization Algorithm", Digital Object Identifier, VOLUME 10, 2022, doi: 10.1109/ACCESS.2022.3151641.
- [31] H. A. Alsattar, A. A. Zaidan, B. B. Zaidan, "Novelmeta-heuristic bald eagle search optimization algorithm", Artificial Intelligence Review, <https://doi.org/10.1007/s10462-019-09732-5>.
- [32] Xiaoxu Yang, Jie Liu, Yi Liu, Peng Xu, Ling Yu, Lei Zhu, Huayue Chen, and Wu Deng, "A Novel Adaptive Sparrow Search Algorithm Based on Chaotic Mapping and T-Distribution Mutation", Appl. Sci. 2021, 11, 11192. <https://doi.org/10.3390/app112311192>.
- [33] Matthew C. Dickson, Anna S. Bosman, and Katherine M. Malan, "Hybridised Loss Functions for Improved Neural Network Generalisation", arXiv:2204.12244v1 [cs.LG] 26 Apr 2022.
- [34] Abdelhady Ramadan, Salah Kamel, Mohamed H. Hassan, Tahir Khurshid, and Claudia Rahmann, "An Improved Bald Eagle Search Algorithm for Parameter Estimation of Different Photovoltaic Models", Processes 2021, 9, 1127. <https://doi.org/10.3390/pr9071127>.
- [35] <https://research.google/tools/datasets/google-cluster-workload-traces-2019/>.
- [36] A. R. A. Rajak, "Emerging Technological Methods for Effective Farming by Cloud Computing and IoT," Emerging Science Journal, vol. 6, no. 5, pp. 1017–1031, Aug. 2022, doi: 10.28991/esj-2022-06-05-07.
- [37] Supriya Menon, M. & Rajarajeswari, P., "A Novel Approach for Multi Variant Classification of Medical Data in Short Text ", in Journal of Scientific and Industrial Research, 2021, Volume 80, 0975-1084, pp. 457 – 462.
- [38] M. S. Sayeed, H. Abdulrahim, S. F. Abdul Razak, U. A. Bukar, and S. Yogarayan, "IoT Raspberry Pi Based Smart Parking System with Weighted K-Nearest Neighbours Approach," Civil Engineering Journal, vol. 9, no. 8, pp. 1991–2011, Aug. 2023, doi: 10.28991/cej-2023-09-08-012.
- [39] S. Gousteris, Y. C. Stamatiou, C. Halkiopoulou, H. Antonopoulou, and N. Kostopoulos, "Secure Distributed Cloud Storage based on the Blockchain Technology and Smart Contracts," Emerging Science Journal, vol. 7, no. 2, pp. 469–479, Feb. 2023, doi: 10.28991/esj-2023-07-02-012.

AUTHORS' PROFILE



Intelligence, Machine Learning, Deep Learning, Data Mining, and the Internet of Things.



Pachipala Yellamma is working as an Associate Professor in the Department of Computer Science and Engineering, Koneru Lakshmaiah Education Foundation, Guntur, Andhra Pradesh. Completed her PhD in Data security in cloud computing. Her research interests include cloud computing, the Internet of Things, Network security, Data compression, Cryptography, and Data security. She is a Life Member in ISTE and IEEE and has some free memberships. She has published several national and international articles in Scopus, web of Science, and SCI. She has three patent publications.

Estimating Coconut Yield Production using Hyperparameter Tuning of Long Short-Term Memory Model for Estimating Coconut Yield Production

Niranjan Shadaksharappa Jayanna, Raviprakash Madenur Lingaraju
Computer Science & Engineering, Kalpataru Institute of Technology, Tiptur, India
Visvesvaraya Technological University, Belagavi, India

Abstract—Coconut production is one of the significant and main sources of revenue in India. In this research, an Auto-Regressive Integrated Moving Average (ARIMA)-Improved Sine Cosine Algorithm (ISCA) with Long Short-Term Memory (LSTM) is proposed for coconut yield production using time series data. It is used for converting non-stationary data to stationary time series data by applying differences. The Holt-Winter Seasonal Method is the Exponential Smoothing variations utilized for seasonal data. The time-series data are given as the input to the LSTM classifier to classify the yield production and the LSTM model is tuned by hyperparameter using Improved Sine Cosine Algorithm (ISCA). In basic SCA, parameter setting and search precision are crucial and the modified SCA improves the coverage speed and search precision of the algorithm. The model's performance is estimated by utilizing R2, Mean Absolute Error (MAE), Mean Squared Error (MSE), and Root Mean Square Error (RMSE) with date on yield from 2011-2021 by categorizing yearly production into 120 records and eight million nuts. The outcomes display that the LSTM-ISCA offers values of 0.38, 0.126, 0.049 and 0.221 for R2, MAE, MSE and RMSE metrics, which offer a precise yield production when related to other models.

Keywords—Auto-regressive integrated moving average; coconut yield production; improved sine cosine algorithm; long short-term memory; time series

I. INTRODUCTION

Coconut is one of the most important and multi-use everlasting crops that is mostly used to produce hair oil, cosmetics, soaps and other products [1]. In India, out of all states, southern regions offer huge production of coconut, and Kerala has the largest area for coconut production. Coconut production is determined by many factors [2]. Coconuts are categorized into three types, intermediate, dwarf and tall based on their height and behavior. Coconut farmers always face price risk that is determined by coconut retention and the strength of demand in the market [3]. Coconut yield is a difficult quantitative feature that differs with environmental factors, age, variety, and communication between environmental factors and variety [4]. Mature nuts are considered as yield because the solid endosperm content in nuts is used for yield production. Additionally, the temperature is important for the growth and development of nut yield of coconuts; high temperature reduces the root growth [5].

Coconut palms play an important role in humans as it meets the social, economic and cultural requirements. The tall type of

nut production signifies the produced number of coconuts under agronomic environments [6]. Subsequently, the enhanced productivity in coconut yield results in proper resource usage and the evaluation of coconut enhance the yield production [7]. The accurate quantification of coconut yields is critical for disasters such as drought, which give rise to a variety of crop growth, leading to different levels of coconut yield reduction [8]. It is important to carry out sequential time series coconut growth monitoring over the main growth and development period [9]. The Auto-Regressive Integrated Moving Average (ARIMA) model is utilized for forecasting future outcomes based on the past data points influencing the data points. Hyperparameter tuning is used in the LSTM model for performance and accuracy improvement, resulting in a more robust performance as compared to other deep learning models. The Improved Sine-Cosine Algorithm (ISCA) is an optimization algorithm that mainly depends on the sine and cosine operators so as to improve the performance of the LSTM model. The contributions of LSTM-ISCA are specified as follows:

- The Linear Interpolation is utilized for preprocessing which fills missing values of the dataset in districts of Kerala.
- ARIMA model is used for converting stationary time series data from non-stationary data by applying differences and then the exponential Smoothing of Holt-Winter Seasonal Method is used for seasonal data.
- The LSTM-ISCA model is employed for coconut yield production, wherein the LSTM model is tuned by hyper-parameters using Improved Sine Cosine Algorithm, and the performance is evaluated by using R2, MSE, RMSE, and MAE.

The rest of this paper is organized as follows: The literature review for coconut yield production is described in Section II. The detailed description of the proposed method is illustrated in Section III, while the obtained results of the proposed model are described in Section IV, and lastly, the conclusion of this research is described in Section V.

II. LITERATURE REVIEW

Novarianto [10] implemented an aerial photography method by using drones to establish the classification of local tall coconut production, and coconut diversity in Taliabu Regency, Taliabu Island and North Maluku Province. The

drone technology increased the data efficiency by combining the classical sampling population in local tall coconut trees. This drone technology surrounded the data of plant types, total areas, number of areas planted with coconut, and characteristics like the number of coconuts, and the height of the coconut palm. The coconut production information was used to develop a coconut rehabilitation and replanting approach. The yield population density of each area was determined by different factors such as the number of palms dying, and the pests and diseases that are not suitable for coconut production.

Samarakoon et al. [11] developed a different coconut plantation using Ordinary Least Square (OLR) estimation and Quantile Regression (QR) approaches to estimate the production function in Cobb Douglas functional form. OLR estimation was an appropriate method for conditional mean model estimation, while the QR provides an equally appropriate method for the conditional quantile function. In OLS estimation, the amount of bearing palms has a beneficial effect when the input variables are considered without delay on coconut production. In comparison, QR provides significant information that enables suitable policies for the use of inputs in coconut production. In this model, the long-term viable option is to increase coconut production and the productivity of coconut lands.

Pramono and Arifin [12] proposed a dry coconut for copra production using a conventional method named fuzzy logic control. This conventional method was used for coconut drying in sunlight with weather conditions. In the electronic system, the fuzzy logic method used an AC to AC voltage circuit and control system using the ARM STM32F4VG microcontroller. This model consumed only 18 hours for drying and the quality of the product was assured in both laboratory testing and physical conditions. Drying using direct sunlight produced copra that was polluted with microbes and dust. Apart from the drying technique, the copra was never absolute which resulting in greater capacity of moisture.

Hadi [13] developed a quantitative with regression analysis as a casual estimation tool between variables in the Kalimantan region. This model was used to examine the risks in coconut production which affected the economic value, selling value, and income. The output showed that the risk in the coconut business is the reduction in the number of trees because of the translation of mining and plantations. Additionally, the operational costs are not equitable to the selling price. Moreover, the household coconut farmer's production risks impact the level of productivity caused in every harvest season.

Karunakaran and Narmadha [14] implemented a Quindecadal Analysis for coconut production and growth performance in the global scenario. This model considered three methods: compound growth rate for growth models, Coppock's instability index for instability measures, and the decomposition analysis for yield production. In this model, the low-production country was correctly developed as acceptable harvesting was not carried out and the fallen nuts were not considered. Hence, high attention is needed for the states to encourage and fascinate the farmers in coconut production by retrieving modern technologies.

Das et al. [15] developed six multivariate techniques for coconut yield production using weather-based linear and nonlinear models in west coastal areas of India. Weather indices were created by using collected values for rainfall and average values for other parameters monthly, such as solar radiation, relative humidity, min and max temperature, and wind speed. Various linear and non-linear models were applied to the model for coconut yield production using input as weather indices monthly. The model showed that the frequency of weighted weather was higher, as opposed to simple weather indices.

Paudel et al. [16] suggested a crop yield production by MARS Crop Yield Forecasting System (MCYFS) data in the European Commission. Machine learning was an independent source of data collected and combined for a crop model to build a large-scale crop yield prediction baseline. The baseline had growth in fit-for-determination optimizations and overall design values. Certain countries and crop data required huge preprocessing to fit the baseline requirements which were not instigated for big data analysis.

Hebbar et al. [17] developed a MaxEnt model for coconut yield production in India under climate change scenarios. The developed model was used to estimate bioclimatic variables for defining specific cultivation and forecast region's climate, which was possibly appropriate in the future weather conditions. Based on the present cultivation region and weather change prediction from seven ensembles of Global Circulation Models, the prediction of climatic suitability was done through MaxEnt model. In climate suitability from moderate to high, high to low, and low to inappropriate under upcoming climate. In this model, coconut production and the productivity of coconut lands is increased to enhance the coconut production.

Tuckeldoe et al. [18] introduced a coconut yield and nutritional quality prediction using sterilized growth media. The introduced model was used to define the coconut's effects on biochemical constituents of the varieties cultivated under various environments. The developed model considered two seasons in 2021 and 2022 for cultivating coconuts on fertigated land. Drying using direct sunlight produced copra that is polluted with microbes and dust, and apart from the drying technique, the copra was never absolute, thereby resulting in having a greater moisture capacity.

Pham et al. [19] developed coconut mesocarp-based lignocellulosic waste as cellulase production subtract from huge promising multienzyme-producing bacillus FW2 without pretreatments. Particularly, extremophilic bacteria played a significant part in biorefinery because of huge score catalytic enzymes which were under harsh environment situations. The developed model estimated the capability to generate and isolate from food waste. It continued to discover functional candidate which enabled low expensive production, and was perfect for clean environment and waste management. This model showed that higher frequency of weighted weather when compared to simple weather indices.

III. PROPOSED METHOD

The proposed method is built for forecasting yield of coconut production. ARIMA and Holt-Winters seasonal

methods are mainly used to predict data as per seasonality and trend. The LSTM model is tuned by hyperparameters using Improved Sine Cosine Algorithm because the ISCA takes the data point's non-linear dependence, which produces more favorable for time-series forecasting. Fig. 1 represents the block diagram of the proposed coconut yield prediction.

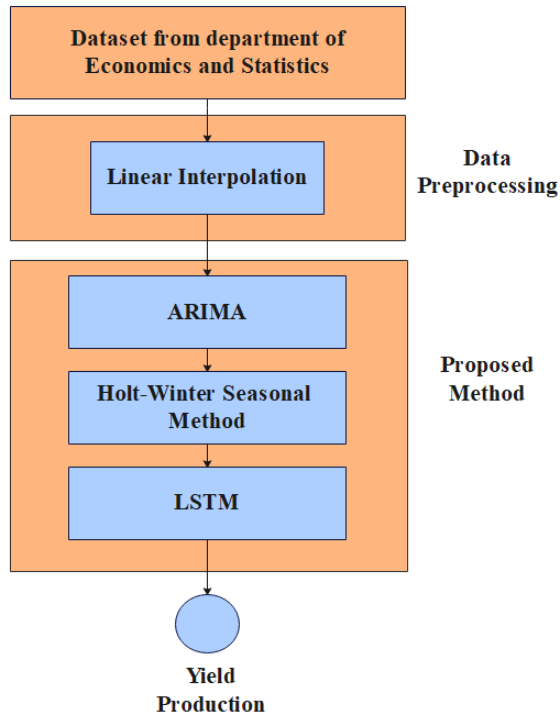


Fig. 1. Proposed method for Coconut yield production.

A. Dataset

Coconut is one of the important cultivation crops in Kerala, covering about 39% of the area grown in the state. The dataset is collected from Kerala's Department of Economics and Statistics, and consists of monthly coconut yield from 10 districts like Alappuzha, Ernakulam, Kozhikode, Palakkad, Kollam, Kasaragod, Idukki, Wayanad, Kottayam and Thrissur from 2011-2021 with yearly production of 120 records and 8 million nuts. The coconut is cultivated three months once and the 10-year annual production is segregated into 1200 records. However, the risk factors include climate change effects, diseases and pest, soil health, increased vulnerability, and water pollution and contamination.

B. Linear Interpolation

In Kerala, some districts contain missing values and these missing values are filled by using the Linear Interpolation method. This method is a mathematical procedure that measures new datapoints based on the previous data in traditional lines for enhancing the order as previous value. If it is time-series data, it contains missing scores, Interruption is a method applied to fill the missing scores in time-series data. This function is shown in Eq. (1),

$$f(X) = f(x_0) + \frac{f(x_1) - f(x_0)}{x_1 - x_0} (x - x_0) \quad (1)$$

where, x , x_0 and x_1 are independent variables, and $f(x)$ is a dependent for independent variable x .

C. Auto Regressive Integrated Moving Average

The Auto-Regressive Integrated Moving Average (ARIMA) model is used for converting the non-stationary time series data to stationery time data by applying differences, while also defining the present time series values using the previous predicted values and errors. ARIMA consists of three parts, denoted as ARIMA (p, d, q) . Where, p is the amount of AR terms, d is the number of differences required to make the time-series stationery, and q is the amount of MA terms. The auto-regressive integrated moving average is shown in Eq. (2),

- AR: It observes a score that depends on the last lagged value.
- Integrated: The difference between observed and last lagged value.
- MA: A last lagged error values are the predictor values.

$$\Phi(B)(1 - B)^d Y_t = \theta(B)\epsilon_t \quad (2)$$

where, Φ is the autoregressive parameter, d is the degree of differencing parameter, B is the backshift operator, θ is a parameter of moving average and ϵ_t is white noise.

In time series models, the ARIMA model performs better than the deterministic growth model for short-term prediction. A better ARIMA model for time series prediction is fitted using the Box-Jenkins technique is shown in Eq. (3),

$$X_t = c + \phi_1 X_{t-1} + \dots + \phi_p X_{t-p} + \theta_1 e_{t-1} + \dots + \theta_q e_{t-q} + e_t \quad (3)$$

where,

- X_t = the variable that will be explained in time t ;
- c = constant or intercept;
- ϕ = coefficient of each parameter p ;
- θ = coefficient of each parameter q ;
- e_t = errors in time t .

D. Holt-Winters Seasonal Method

The Holt-Winters seasonal method is also known as the triple exponential smoothing which forecasts both trend and seasonality. This method itself combines three simple components, which are smoothing methods.

- Simple Exponential Smoothing (SES): The method cannot be used with seasonality, trend, or both series. The SES method guesses that there is no change in the level of the time-series.
- Holt-Exponential Smoothing (HES): The method is used only with trend components and not with seasonal data.
- Winter's Exponential Smoothing (WES): The method is used for both trend component and seasonality data.

1) *Holt-Winter's additive method*: When the seasonal variations are not exactly close along the series, the addition method is employed. For subtracting the seasonal component, the obtained series scale and series of the level equation are seasonally altered and determined in accurate terms. The mathematical form of the additive method is shown in Eq. (4), (5), (6) and (7),

$$\text{Overall Equation: } \hat{y}_{t+h} = l_t + hb_t + s_{t+h-m} \quad (4)$$

$$\text{Level Equation: } l_t = \alpha(y_t - s_{t-m}) + (1 - \alpha)(l_{t-1} + b_{t-1}) \quad (5)$$

$$\text{Trend Equation: } b_t = \beta(l_t - l_{t-1}) + (1 - \beta) b_{t-1} \quad (6)$$

$$\text{Seasonality Equation: } s_t = \gamma(y_t - l_{t-1} - b_{t-1}) + (1 - \gamma) s_{t-m} \quad (7)$$

where, m is time series seasonality, s_t is the seasonal forecast component, s_{t-m} is the forecast for the previous season and γ is the seasonal component smoothing factor ($0 \leq \gamma \leq 1 - \alpha$).

2) *Holt-winter's multiplicative method*: When changing the seasonal variations proportion to the series level, the method uses the multiplication method. This series is seasonally altered by dividing the seasonal component and determined in relative terms. The mathematical form of the multiplicative method is shown in Eq. (8), (9), (10) and (11),

$$\text{Overall Equation: } \hat{y}_{t+h} = (l_t + hb_t)s_{t+h-m} \quad (8)$$

$$\text{Level Equation: } l_t = \alpha \frac{y_t}{s_{t-m}} + (1 - \alpha)(l_{t-1} + b_{t-1}) \quad (9)$$

$$\text{Trend Equation: } b_t = \beta(l_t - l_{t-1}) + (1 - \beta) b_{t-1} \quad (10)$$

$$\text{Seasonality Equation: } s_t = \gamma \frac{y_t}{l_{t-1} + b_{t-1}} + (1 - \gamma) s_{t-m} \quad (11)$$

Where, m is time series seasonality, s_t is the seasonal forecast component, s_{t-m} is the forecast for the previous season and γ is the seasonal component smoothing factor.

E. Long Short-Term Memory (LSTM)

The Long Short-Term Memory (LSTM) is one of the most advanced models to forecast time series. A hyperparameter is a variable chosen before optimizing the real model's parameter. In deep learning, there are more hyperparameters like neurons, hidden layers, and learning rate. As a human, we have a hard time handling and visualizing multi-dimensional spaces. Hyperparameter is a procedure of enhancing the performance of the model by designating hyperparameters precise integration. In LSTM, the parameters like timesteps, amount of layers and hidden neurons at every LSTM is improved by hyperparameter. In deep LSTM, the layers lead to less convergence and overfitting, while the hidden layer works equally to the LSTM. Generally, previous historical data is required for predicting time-series data, but the conventional neural network takes current input data into account. LSTM embraces the historical data as well as the past data for an extensive period.

The LSTM has different memory cells in the hidden layer that are simplified through various gates like input, forget and

output gate. It is utilized for determining data that is required to be stored. The cell state transfers data from one to another layer. The forgot gate is a primary gate that enables the transfer of required information by the cell state. In this gate, there are two steps of pointwise multiplication and sigmoid layer. The mathematical formula of the forget-gate f_t is shown in Eq. (12),

$$f_t = \sigma(W_f x_t + U_f h_{t-1} + b_f) \quad (12)$$

where, f_t is denoted as the current forget gate with the value being between 0 and 1 and is managed by the sigmoid function σ . The weight matrices are W_f and U_f , b_f is the value of bias, x_t is the value of input, and h_{t-1} is the previous data used for forget gate value calculation.

The next stage is the input gate which is used for processing the data. The mathematical form of the input gate is shown in Eq. (13),

$$i_t = \sigma(W_i X_t + U_i h_{t-1} + b_i) \quad (13)$$

where, i_t is the sigmoid function result and it controls which data to be stored in the memory cell. W_i and U_i are the weight matrices and b_i value is of the bias. These are the parameters adjusted in this input gate.

The last stage is the output gate which determines the actual values of the hidden layers, and the mathematical form is shown in Eq. (14),

$$o_t = \sigma(W_o X_t + U_o h_{t-1} + b_o) \quad (14)$$

Here, o_t is the sigmoid function, the weight matrices are W_o and U_o , while b_o is the value of bias.

1) *Sine-Cosine Algorithm (SCA)*: The Sine-cosine algorithm is a population-based optimization algorithm for improving the movement of an agent toward the best solution, which is determined by the sine and cosine operators. The equation of this operator is used to fluctuate towards the optimal solution to identify the optimal solutions. In this search area, the random variables are used to find the possible global optima. To achieve optimal global solutions, SCA is proven to be more effective than other population-based algorithms. When the sine and cosine functions return values lesser than one or greater than one, the different occasions on the search space are determined.

a) *Initial population*: For filtering the current best solution, the Sine-Cosine algorithm works with the population. The numerical formula of the initial population is shown in Eq. (15),

$$X(i, j) = X(\min, j) + \text{random}(0,1) * (X(\max, j) - X(\min, j)) \quad (15)$$

where, $X(\min, j)$ and $X(\max, j)$ are lower and upper limits of individuals on dimension j , R is the random number between (0, 1). Sine and Cosine function's range is shown in Eq. (16),

$$r_i = a \left(1 - \frac{t}{T}\right) \quad (16)$$

where, t indicates the present iteration, T is the maximum number of iterations, and a is the constant variable. In this equation, r_1 decreases linearly from a to 0 .

b) *Updating position*: Sine and Cosine function's range are shown in Eq. (16) and the updated new candidate solutions are shown in Eq. (19). The current population's best candidate solutions and the best objective value are also updated. The numerical formula for updating positions for both sine and cosine are shown in Eq. (17) and Eq. (18),

$$P_i^{t+1} = P_i^t + r_1 \sin(r_2) * |r_3 P_{best}^t - P_i^t| \quad (17)$$

$$P_i^{t+1} = P_i^t + r_1 \cos(r_2) * |r_3 P_{best}^t - P_i^t| \quad (18)$$

where, P_i^t is the present candidate position at the t th iteration in the i th dimension and P_{best}^t is the best candidate optimal position at the t th iteration in the i th dimension. r_1, r_2, r_3 and r_4 are the random agents. The $(*)$ is the sign of multiplication. The updated new candidate solutions are shown in Eq. (19),

$$P_i^{t+1} = \begin{cases} P_i^t + r_1 * \sin(r_2) * |r_3 P_{best}^t - P_i^t|, r_4 < 0.5 \\ P_i^t + r_1 * \cos(r_2) * |r_3 P_{best}^t - P_i^t|, r_4 \geq 0.5 \end{cases} \quad (19)$$

where, r_1 is the parameter that determines the search space's next region and increases the investigation of the search space for a higher value, r_2 determines the movement direction and how long the movement should go towards or away from P_{best}^t . r_3 controls the current movement destination effects. To increase the solution diversity values of r_1, r_2 and r_3 , they are updated at each iteration, while r_4 is used to switch between cosine and sine functions.

c) *Fitness function*: To improve the model accuracy, the parameters of LSTM such as the number of hidden neurons (HN), the learning rate (α) and the dropout value (DV) are used for the fitness function. The Sine Cosine optimization algorithm optimizes these three parameters $\theta = \{HN, \alpha, DV\}$ of the LSTM model. The fitness function is set between the predicted and observed values as the RMSE. The eqs. (17) and (18) are merged in (21). The fitness function is shown in (20) and (21),

$$\min f_{RMSE} = \frac{1}{N} \sum_{i=1}^N (\hat{y}_i - y_i)^2 \quad (20)$$

$$\text{Subject to } \begin{cases} \hat{y}_i = f_{LSTM}(HN, \alpha, DV) \\ HN^{min} \leq HN_{max} \leq HN^{max} \\ \alpha^{min} \leq \alpha \leq \alpha^{max} \\ DV^{min} \leq DV \leq DV^{max} \end{cases} \quad (21)$$

Here, \hat{y}_i is the predicted values and y_i is the observed value. $HN^{min}, \alpha^{min}, DV^{min}$ and $HN^{max}, \alpha^{max}, DV^{max}$ are the upper and lower bounds of the three decision variables.

2) *Modified sine-cosine algorithm*: In a simple SCA, r_1 is a control parameter which manages the transformation of algorithm from global exploration to local improvement. The local improvement capability of the algorithm is improved by a smaller value r_1 . The global searching capability of algorithm is developed by a larger value r_1 . Thus, to manage global exploration and local improvement ability, r_1 is used as

a linear decreasing technique of Eq. (16). Based on Eq. (19), the linear and exponential reducing inertia weight and conversion parameter which are utilized in this method, are seen to perform commendably in the ability of the local improvement and global exploration of the model. The updated equation of the individual is shown in Eq. (22), Eq. (23) and Eq. (24),

$$P_{i,j}^{t+1} = \begin{cases} \omega(t) * P_{i,j}^t + r_1 * \sin(r_2) * |r_3 P_{best,j}^t - P_{i,j}^t|, r_4 < 0.5 \\ \omega(t) * P_{i,j}^t + r_1 * \cos(r_2) * |r_3 P_{best,j}^t - P_{i,j}^t|, r_4 \geq 0.5 \end{cases} \quad (22)$$

$$\omega(t) = \omega_{max} - (\omega_{max} - \omega_{min}) * \frac{t}{T} \quad (23)$$

$$r_1(t) = a * e^{-\frac{t}{T}} \quad (24)$$

where, t indicates the present iteration, T is the highest number of iterations and a is the constant variable. $P_{best,j}^t$ is j th individual dimension value at iteration t , $P_{i,j}^t$ is the j th individual dimension score of the i of present iteration, ω_{min} and ω_{max} are the minimum and maximum weights of inertia. The linear reducing inertia weight and exponential reducing conversion parameter are utilized in this work for enhancing the coverage speed and for the searching precision of the algorithm.

a) *Neighborhood search of the optimal individual*: In a simple SCA, new individuals updating process search directions are done by individuals optimal in the population. The entire algorithm is converted into early convergence when the global optimum individual falls into the local optimum. For reducing the algorithm probability of getting into local optimum, individuals near optimal solution are utilized as a guiding role. Here, the current optimal individuals are replaced through a random individual near to the optimal solution for guiding the algorithm search, thereby improving the algorithm's probability of coming out into the local optimum. The optimal individual neighborhood search is shown in Eq. (25),

$$P_{i,j}^{t+1} = \begin{cases} \omega(t) * P_{i,j}^t + r_1 * \sin(r_2) * \\ |r_3 P_{best,j}^t * (1 - \lambda * \text{unifrnd}(-1,1)) - P_{i,j}^t|, r_4 < 0.5 \\ \omega(t) * P_{i,j}^t + r_1 * \cos(r_2) * \\ |r_3 P_{best,j}^t * (1 - \lambda * \text{unifrnd}(-1,1)) - P_{i,j}^t|, r_4 \geq 0.5 \end{cases} \quad (25)$$

where, $\text{unifrnd}(-1,1)$ is the number of uniform distributions within $(-1,1)$, and λ is distribution coefficient.

b) *Greedy levy mutation*: In simple Sine-Cosine algorithm, the whole population search direction is controlled by the optimal individuals. For the further prevention of traditional SCA, low efficiency is eliminated and getting into the local optimum in later period. Here, the mutation operation helps an individual to come out of the position of optimal score in population which is previously searched to maintain population diversity. The mutation methodology is shown in Eq. (26),

$$P_{best,j}^{t+1} = P_{best,j}^t + \theta(j) * levy * P_{best,j}^t \quad (26)$$

where, $\theta(j)$ is the self-adapting variation coefficient, $levy$ is a random number which accepts the levy distribution and $P_{best,j}^t$ is the j th individual dimension value at iteration t .

For simple sine-cosine algorithm, creating the initial population time complexity is $O(n)$, performing sine-cosine operation time complexity is $O(T * n * d)$, and the processing of cross-border is $O(T * n)$. So, the simple sine-cosine algorithm's time complexity is $O(n) + O(T * n) + O(T * n * d)$. In the modified sine-cosine algorithm, creating the initial population time complexity is $O(n)$ for calculating $\omega(t)$ time complexity, and r_1 is $O(2 * T)$ for performing sine-cosine operation with time complexity $O(T * n * d)$, the processing of cross-border is $O(T * n)$ and the greedy levy mutation's time complexity is $O(T * d * n)$. So, the modified sine-cosine algorithm's time complexity is $O(n) + O(2 * T) + O(T * n * d) + O(T * n) + O(T * d * n) = O(n) + O((n + 2) * T) + O(2 * T * d * n)$. So, the modified sine-cosine algorithm's time complexity is lesser than the simple sine-cosine algorithm.

IV. EXPERIMENTAL RESULTS

The LSTM-ISCA is simulated using the tool Python 3.10 on system configuration of windows 10 OS, 16GB RAM and intel i7 processor. The R2, MAE, MSE and RMSE are considered to estimate LSTM-ISCA the performance which are estimated from forecasted yields of each year for all districts. They are mathematically shown in Eq. (27), (28), (29) and (30), respectively:

$$R^2 = 1 - \frac{\sum_{i=1}^n (y_i - y_{di})^2}{\sum_{i=1}^n (y_{di} - y_m)^2} \quad (27)$$

$$MAE = \frac{1}{n} \sum_{i=1}^n |y_i - y_{di}| \quad (28)$$

$$MSE = \frac{1}{n} \sum_{i=1}^n (y_i - y_{di})^2 \quad (29)$$

$$RMSE = \sqrt{MSE} = \sqrt{\frac{1}{n} \sum_{i=1}^n (y_i - y_{di})^2} \quad (30)$$

where, n, y_i, y_{di} and y_m are the number of points, predicted score, real score, and mean of real score.

A. Quantitative Analysis

The performance of LSTM-ISCA is explained in this section, with respect to achievable sum rate. Table I demonstrates the results of the LSTM model, whereas Table II shows the results of ISCA, and Table III exhibits the outcomes of LSTM-ISCA. The LSTM and LSTM-SCA models are compared with LSTM-ISCA model that achieves better performance as compared to other models.

In Table I, the effectiveness of the LSTM model is validated and the experimentation is performed with various deep learning techniques: Convolutional Neural Network (CNN), Generative Adversarial Network (GAN), Recurrent Neural Network (RNN), and Deep Neural Network (DNN). The LSTM model achieves 0.43, 0.131, 0.054 and 0.232 of R2, MAE, MSE and RMSE, respectively. A graphical representation of the LSTM model is represented in Fig. 2.

TABLE I. QUANTITATIVE ANALYSIS OF VARIOUS CLASSIFIERS

| Methods | MSE | R2 | RMSE | MAE |
|---------|-------|------|-------|-------|
| CNN | 0.062 | 0.49 | 0.248 | 0.139 |
| GAN | 0.055 | 0.44 | 0.234 | 0.132 |
| RNN | 0.058 | 0.46 | 0.240 | 0.135 |
| DNN | 0.059 | 0.47 | 0.242 | 0.136 |
| LSTM | 0.054 | 0.43 | 0.232 | 0.131 |

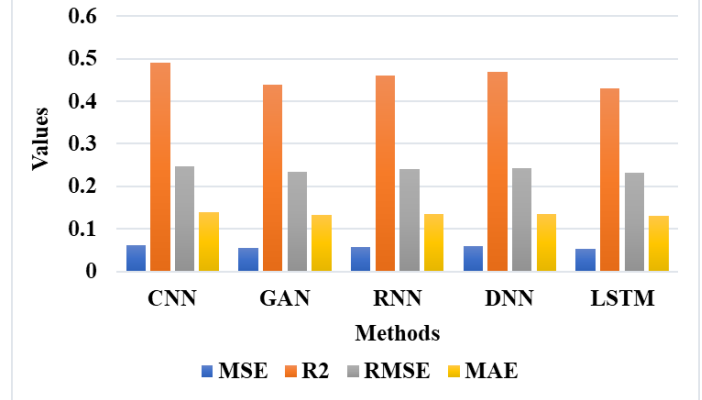


Fig. 2. Performance of various classifiers.

TABLE II. QUANTITATIVE ANALYSIS OF VARIOUS OPTIMIZATION

| Methods | MSE | R2 | RMSE | MAE |
|---------|-------|------|-------|-------|
| PSO | 0.056 | 0.44 | 0.236 | 0.133 |
| WOA | 0.054 | 0.43 | 0.232 | 0.131 |
| SGD | 0.053 | 0.41 | 0.230 | 0.130 |
| SCA | 0.051 | 0.40 | 0.225 | 0.128 |
| ISCA | 0.049 | 0.38 | 0.221 | 0.126 |

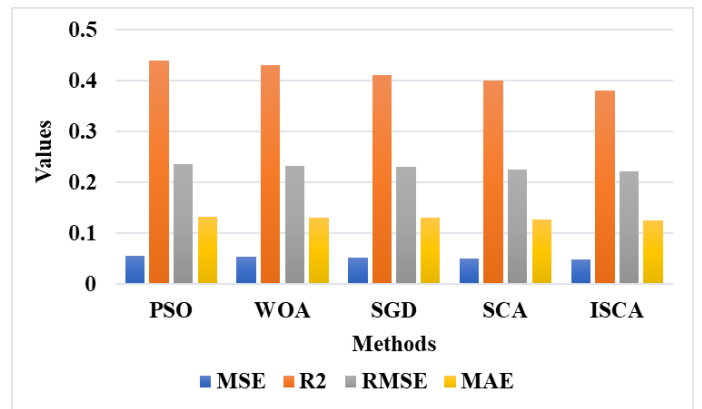


Fig. 3. Performance of various optimizations.

In Table II, the ISCA's effectiveness is validated and experimentation is performed with various optimization algorithms like Particle Swarm Optimization (PSO), Stochastic Gradient Descent (SDG), Whale Optimization Algorithm (WOA), and SCA. The ISCA achieves 0.38, 0.126, 0.049 and 0.221 of R2, MAE, MSE and RMSE. Fig. 3 represents the graphical representation of the ISCA model.

TABLE III. QUANTITATIVE ANALYSIS OF THE PROPOSED LSTM-ISCA MODEL

| Methods | MSE | R2 | RMSE | MAE |
|-----------|-------|------|-------|-------|
| LSTM | 0.054 | 0.43 | 0.232 | 0.131 |
| LSTM-SCA | 0.051 | 0.40 | 0.225 | 0.128 |
| LSTM-ISCA | 0.049 | 0.38 | 0.221 | 0.126 |

In Table III, the effectiveness of LSTM with ISCA model is validated and the experimental is performed with LSTM and LSTM-SCA. The LSTM-ISCA model achieves better performance when compared to other models. The LSTM-ISCA model achieves 0.38, 0.126, 0.049 and 0.221 of R2, MAE, MSE and RMSE. A graphical representation of LSTM-ISCA model is shown in Fig. 4.

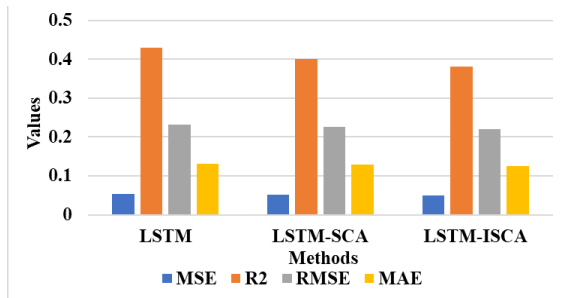


Fig. 4. Performance of the proposed LSTM-ISCA model.

TABLE IV. EXPERIMENTAL RESULTS OF LSTM-ISCA MODEL

| Author | No. of data | R2 | MAE | MSE | RMSE |
|---------------------------|---|-------|-------|---------|--------|
| Iniyan and Jebakumar [20] | 456 samples across 105 different areas | - | 7.431 | 121.123 | 11.005 |
| Oikonomidis et al. [21] | 25345 samples across 9 different states | 0.87 | 0.199 | 0.071 | 0.266 |
| Joshua et al. [22] | 280 samples across 50 fields | 0.986 | 0.129 | 0.052 | 0.229 |
| Proposed LSTM-ISCA | 84000 samples across 10 different districts | 0.38 | 0.126 | 0.049 | 0.221 |

C. Discussion

The advantages of the LSTM-ISCA and limitations of the existing researches are deliberated in this section. The Iniyan and Jebakumar [20] considered only 456 samples across 105 areas which achieved 7.431 of MAE due to the limited samples. Oikonomidis et al. [21] considered 25343 samples across nine states, achieving 0.199 of MAE due to the long-term viable option increasing the coconut production, as well as the productivity of coconut lands. Joshua et al. [22] considered 280 samples across 590 fields, achieving 0.129 of MAE because the crop data requiring huge preprocessing to fit the baseline requirements. To overcome these issues, this research proposes LSTM-ISCA. The time-series data are given as the input to the LSTM classifier to classify the yield production and the LSTM model is tuned by hyperparameter using ISCA. The ISCA improves the coverage speed and searching precision of the algorithm.

V. CONCLUSION

In this research, a LSTM-ISCA is proposed for effective coconut yield production. The proposed model comprises multiple objective functions such as linear interpolation and Holt's Winter Seasonal method for effective classification. ARIMA model is used for converting stationary time series data from non-stationary data, by applying differences and

B. Comparative Analysis

The comparison of LSTM-ISCA is demonstrated in this section with attainable sum rate. The previous researches like [17-20] are utilized for estimating the proposed model's efficiency as shown in Table IV. Iniyan and Jebakumar [20] considered 456 samples across 105 different areas and the experimental analysis showed that the presented model attained 7.431, 121.123, and 11.005 of MAE, MSE and RMSE, correspondingly. Oikonomidis et al. [21] took into account 25345 samples across 9 different states, where the experimental results confirmed that the presented obtained 0.87, 0.199, 0.071, and 0.266 of R2, MAE, MSE and RMSE, correspondingly. Joshua et al. [22] examined 280 samples across 50 fields and the model attained 0.986, 0.129, 0.052, and 0.229 of R2, MAE, MSE and RMSE. Therefore, it is seen that the LSTM-ISCA model achieves superior performance, as opposed to other models.

predicted values from the previous historical data. The Holt-Winters seasonal method is introduced for the exponential smoothing of the seasonal data. Then LSTM is tuned by the ISCA which uses an exponential convergence strategy and linear decreasing inertia weight, thereby improving the convergence speed and algorithm's search precision. From the performance analysis, it is concluded that the LSTM-ISCA provides better performance than other models. In the future, Bayesian optimization can be used for hyperparameter tuning over the ISCA algorithm to enhance the prediction performance.

REFERENCES

- [1] T.D. Nuwarapaksha, U.N. Rajapaksha, J. Ekanayake, S.A. Weerasooriya, and A.J. Atapattu, "Exploring the Economic Viability of Integrating Jamnapari Goat into Underutilized Pastures under Coconut Cultivations in Coconut Research Institute, Sri Lanka," *Biology and Life Sciences Forum*, vol. 27, no. 1, p. 27, 2023.
- [2] C.B. MacEachern, T.J. Esau, A.W. Schumann, P.J. Hennessy, and Q.U. Zaman, "Detection of fruit maturity stage and yield estimation in wild blueberry using deep learning convolutional neural networks," *Smart Agric. Technol.*, vol. 3, p. 100099, 2023.
- [3] I.Y. Dharmegowda, L.M. Muniyappa, P. Siddalingaiah, A.B. Suresh, M.P. Gowdru Chandrashekarappa, and C. Prakash, "MgO nano-catalyzed biodiesel production from waste coconut oil and fish oil using response surface methodology and grasshopper optimization," *Sustainability*, vol. 14, no. 18, p. 11132, 2022.

- [4] C.R.K. Samarasinghe, M.K. Meegahakumbura, D.P. Kumarathunge, H.D.M.A.C. Dissanayaka, P.R. Weerasinghe, and L. Perera, "Genotypic selection approach made successful advancement in developing drought tolerance in perennial tree crop coconut," *Sci. Hortic.*, vol. 287, p. 110220, 2021.
- [5] A.F. Cardoso, W.X. Ferreira, G.L.S. de Castro, P.M.P. Lins, M.A.S. Dos Santos, and G.B. da Silva, "Cost Reduction in the Production of Green Dwarf Coconut Palm Seedlings Biostimulated with *Bacillus cereus*," *Indian J. Microbiol.*, 2024.
- [6] A.M. Lad, K.M. Bharathi, B.A. Saravanan, and R. Karthik, "Factors affecting agriculture and estimation of crop yield using supervised learning algorithms," *Materials Today: Proceedings*, vol. 62, pp. 4629–4634, 2022.
- [7] T. Prasert, and V. Rungreunganun, "Thai Coconut Price Forecasting using Arima Model," *International Journal of Advanced Research in Engineering and Technology (IJARET)*, vol. 12, no. 1, pp. 950–961, 2021.
- [8] N. Bakhshwain, and A. Sagheer, "Online tuning of hyperparameters in deep LSTM for time series applications," *International Journal of Intelligent Engineering and Systems*, vol. 14, no. 1, pp. 212–220, 2021.
- [9] T. Peng, C. Zhang, J. Zhou, and M.S. Nazir, "An integrated framework of Bi-directional long-short term memory (BiLSTM) based on sine cosine algorithm for hourly solar radiation forecasting," *Energy*, vol. 221, p. 119887, 2021.
- [10] H. Novarianto, "Estimating Coconut Production and Productivity of Local Tall in Taliabu Island Using Drone and Sampling Population," *Coconut Research & Development*, vol. 38, pp. 22–29, 2022.
- [11] S.M.M. Samarakoon, L.H.P. Gunaratne, and H.L.J. Weerahewa, "Determinants of Coconut Production in Large Scale Coconut Plantations in Sri Lanka: A Quantile Regression Approach," *Sri Lankan Journal of Agricultural Economics*, vol. 21, no. 1, pp. 1–16, 2020.
- [12] M.F.B. Pramono, and B.Z. Arifin, "Design of Dryer Coconut for Copra Production Using Fuzzy Logic Control," In: *2020 International Conference on ICT for Smart Society (ICISS)*, Bandung, Indonesia, pp. 1–7, 2020. doi: 10.1109/ICISS50791.2020.9307589.
- [13] M.N. Hadi, "Implementation of Traditional Risk Management as Loss Prevention in Coconut Production Results," *AKADEMIK: Jurnal Mahasiswa Ekonomi & Bisnis*, vol. 2, no. 2, pp. 92–102, 2022.
- [14] K.R. Karunakaran, and N. Narmadha, "Growth Performance of Coconut Production in Global Scenario: A Quin-decadal Analysis," *Journal of Experimental Agriculture International*, vol. 44, no. 11, pp. 7–15, 2022.
- [15] B. Das, B. Nair, V. Arunachalam, K. V. Reddy, P. Venkatesh, D. Chakraborty, and S. Desai, "Comparative evaluation of linear and nonlinear weather-based models for coconut yield prediction in the west coast of India," *Int. J. Biometeorol.*, vol. 64, no. 7, pp. 1111–1123, 2020.
- [16] K.B. Hebbar, P.S. Abhin, V. Sanjo Jose, P. Neethu, A. Santhosh, S. Shil, and P.V. Prasad, "Predicting the potential suitable climate for coconut (*Cocos nucifera* L.) cultivation in India under climate change scenarios using the MaxEnt model," *Plants*, vol. 11, no. 6, p. 731, 2022.
- [17] R.B. Tuckeldoe, M.K. Maluleke, and P.J.S.R. Adriaanse, "The effect of coconut coir substrate on the yield and nutritional quality of sweet peppers (*Capsicum annuum*) varieties," *Sci. Rep.*, vol. 13, no. 1, p. 2742, 2023.
- [18] V.H.T. Pham, J. Kim, J. Shim, S. Chang, and W. Chung, "Coconut mesocarp-based lignocellulosic waste as a substrate for cellulase production from high promising multienzyme-producing *Bacillus amyloliquefaciens* FW2 without pretreatments," *Microorganisms*, vol. 10, no. 2, p. 327, 2022.
- [19] D. Paudel, H. Boogaard, A. de Wit, S. Janssen, S. Osinga, C. Pylaniadis, and I.N. Athanasiadis, "Machine learning for large-scale crop yield forecasting," *Agric. Syst.*, vol. 187, p. 103016, 2021.
- [20] S. Iniyar, and R. Jebakumar, "Mutual information feature selection (MIFS) based crop yield prediction on corn and soybean crops using multilayer stacked ensemble regression (MSER)," *Wireless Pers. Commun.*, vol. 126, no. 3, pp. 1935–1964, 2022.
- [21] A. Oikonomidis, C. Catal, and A. Kassahun, "Hybrid deep learning-based models for crop yield prediction," *Applied Artificial Intelligence*, vol. 36, no. 1, p. 2031822, 2022.
- [22] V. Joshua, S.M. Priyadharson, and R. Kannadasan, "Exploration of Machine Learning Approaches for Paddy Yield Prediction in Eastern Part of Tamilnadu," *Agronomy*, vol. 11, no. 10, p. 2068, 2021.

Integrating Lesk Algorithm with Cosine Semantic Similarity to Resolve Polysemy for Setswana Language

Tebatso Gorgina Moape, Oludayo O. Olugbara, Sunday O. Ojo

Dept. of Information Technology, Durban University of Technology, Durban, South Africa

Abstract—Word Sense Disambiguation (WSD) serves as an intermediate task for enhancing text understanding in Natural Language Processing (NLP) applications, including machine translation, information retrieval, and text summarization. Its role is to enhance the effectiveness and efficiency of these applications by ensuring the accurate selection of the appropriate sense for polysemous words in diverse contexts. This task is recognized as an AI-complete problem, indicating its longstanding complexity since the 1950s. One of the earliest proposed solutions to address polysemy in NLP is the Lesk algorithm, which has seen various adaptations by researchers for different languages over the years. This study proposes a simplified, Lesk-based algorithm to resolve polysemy for Setswana. Instead of combinatorial comparisons among candidate senses that Lesk is based on that cause computational complexity, this study models word sense glosses using Bidirectional Encoder Representations from Transformers (BERT) and Cosine similarity measure, which have been proven to achieve optimal performance in WSD. The proposed algorithm was evaluated on Setswana and obtained an accuracy of 86.66 and an error rate of 14.34, surpassing the accuracy of other Lesk-based algorithms for other languages.

Keywords—Word sense disambiguation; Lesk algorithm; cosine similarity; Bidirectional Encoder Representations from Transformers (BERT)

I. INTRODUCTION

Setswana sometimes referred to as Tswana, is an African language spoken in South Africa, Botswana, and parts of Namibia. It is the national language of Botswana and one of the eleven official languages in South Africa. Setswana has about a total of 8.2 million speakers across the different countries. Similar to other natural languages, Setswana contains words with ambiguity, known as polysemous words that have multiple senses in various contexts in which they appear. Consider the following context sentences below:

- 1) C1: Noka ya mme e botlhoko (mother's waist is painful).
- 2) C2: Moapeyi o noka nama letswai (The chef is seasoning the meat with salt).
- 3) C3: Setlhare se mothokoga ga noka (The tree is next to the river).

The Setswana word “noka” has three distinct senses based on the context in which it appears. It means waist in the first context C1, represents season (pour) in the second context C2,

and a river in the third context C3. This linguistic characteristic is referred to as polysemy. Polysemy poses challenges in natural language processing (NLP) applications such as machine translation [1], information retrieval [2], and text summarization [3], where accurately determining the intended meaning of a polysemous word based on context is important. Resolving polysemy is crucial for improving the accuracy and precision of these applications. The dedicated task of resolving polysemy in NLP is known as Word Sense Disambiguation (WSD) and is considered one of the most difficult tasks in artificial intelligence [4].

WSD can be resolved using three approaches, namely, knowledge-based, unsupervised, and supervised methods. Knowledge-based methods use various lexical resources such as WordNet, Wikipedia, and BabelNet for disambiguation. Examples of this approach include the Lesk algorithm [5] and its variations, such as the simplified Lesk [6] and adapted Lesk [7] algorithms, which rely on context-gloss overlap.

Unsupervised methods employ clustering techniques for disambiguation from unannotated collection texts. The commonly used techniques are sense clustering algorithms such as K-Means [8] and graph-based algorithms such as PageRank [9]. Supervised methods rely on the availability of annotated datasets where a classifier is trained based on the annotations and features extracted from the data. Techniques used for this method include the use of support vector machine (SVM) [10] and Naïve Bayesian [11].

Unsupervised and supervised methods require the substantial collection of unannotated and annotated data, which is not available for resource-scarce languages such as Setswana. The scarcity of datasets poses a significant challenge for training robust models for NLP tasks. Due to this constraint, a knowledge-based approach was adopted to resolve WSD for Setswana using the simplified Lesk algorithm.

This paper makes several significant contributions to the field of WSD for low-resource languages, specifically focusing on Setswana. Firstly, it proposes a novel simplified Lesk-based algorithm that effectively resolves polysemy in Setswana by leveraging sentence embeddings generated using the PuoBERTa language model and employing the Cosine similarity measure to determine the most appropriate sense. Secondly, the study addresses the computational complexity inherent in traditional Lesk algorithms by encoding the context sentence and candidate glosses in a single operation, resulting in a linear growth rate of comparisons, thus mitigating the

exponential growth of computational complexity. Lastly, this research provides a valuable WSD evaluation dataset for Setswana, which is currently unavailable, creating an essential benchmark for testing and comparing the performance of future Setswana WSD models.

This paper is structured as follows: Section II explores related works, materials, and methods presented in Section III. The evaluation of the proposed algorithm is provided in Section IV, including the obtained results. Discussion and conclusion is given in Section V and finally Section VI paves the way for future work.

II. RELATED WORKS

One of the first algorithms developed for WSD is Lesk's original algorithm. The original Lesk algorithm operates on the assumption that the sense of a word in a particular context can be inferred by examining the words that co-occur in the surrounding text. This algorithm relies on the availability of lexical semantic resources such as machine-readable dictionaries and wordnets to obtain glosses for each sense of the polysemous word. To disambiguate, the algorithm calculates the overlap between the words in the context and the words in the definitions to determine the appropriate sense. One of the major drawbacks of the Lesk algorithm is its computational complexity, which stems from the exponential growth of comparisons needed for numerous candidate senses associated with polysemous words across various lexical resources [12].

To overcome this limitation, researchers have proposed and developed variations of the algorithm, such as the simplified [6] and adapted [7] Lesk to improve the algorithm's effectiveness. The simplified Lesk addresses combinatorial explosion by calculating overlaps between the definitions of candidate senses for the target word and the context words. The adapted Lesk expands the scope by considering not only the overlap between the context and target word senses but also introducing additional linguistic features or syntactic structures for a more comprehensive analysis.

Several researchers have adapted the core overlap idea and integrated various techniques into the original Lesk algorithm to enhance its performance. The study in [13] integrated topic modeling to simplify Lesk as the topic-document relationship between senses to determine the correct sense of the target word. Their model achieved an F1 score of 66%. The study in [12] used the adapted Lesk and trained a classifier responsible for retrieving senses of the target word from Wordnet, assigning a score based on the number of words common between the target gloss and context word gloss.

Tripathi, et al. [14] used Lesk to disambiguate Hindi words. The appropriate sense of the polysemous word is determined through a scoring method that assigns a sense score to each token of the Hindi sentence. The sense score is calculated based on the gloss, hypernym, hyponym and synonym of the combinations of different sense of tokens. The sense with the highest score in the combination is allocated as the most suitable sense within that context. In another study [15] used the LESK algorithm for Indonesian and achieved an accuracy

of 78.6% for one Indonesian ambiguous word and 62.5% for two ambiguous words.

To disambiguate senses for Marathi languages, The study in study [16] used a modified Lesk algorithm coupled with a dynamic context window approach. After pre-processing, the algorithm stores the context words in an array to increase the context window size during processing while comparing the results with the static size context window output. The model achieved the highest precision of 0.79. Arabic, Kaddoura and Nassar [17] developed a WSD dataset that contains one hundred Arabic polysemous words with a minimum of three and maximum of eight senses. The paper adapts the idea of the Lesk algorithm [5] to compute the overlap between contextual information and dictionary definitions. They utilized a similarity measure to determine the appropriate sense of the target word. Their proposed method integrates Bidirectional Encoder Representations from Transformers (BERT) and introduces new features to enhance the effectiveness of disambiguation. The WSD system's performance achieved an impressive F1 score of 96%.

In this paper, a WSD system for Setswana is proposed based on the simplified Lesk algorithm. To tackle computational complexity, our algorithm first encodes the context sentence containing the polysemous word and the candidate glosses obtained from the Universal Knowledge Core (UKC) in a single operation. Secondly, the algorithm computes the Cosine semantic similarity measure between the context and each candidate gloss. As a result, the number of comparisons is equal to the n number of senses of a polysemous word. In contrast to other adaptations of the Lesk algorithm, the proposed algorithm exhibits a linear growth rate rather than an exponential one, mitigating computational complexity.

III. MATERIALS AND METHODS

A. Task Definition

In NLP, Navigli [4] formally describes the WSD problem as: given a text T as a sequence of words (w_1, w_2, \dots, w_n) , WSD is the task of assigning appropriate sense of a polysemous word in T , that is, to identify a mapping A from words to senses, such that $A(i) \subseteq SensesD(w_i)$, where $SensesD(w_i)$ is the set of senses encoded in a knowledge source K for word w_i and $A(i)$ is the subset of the senses of w_i which are appropriate in the context T . The mapping A can assign more than one sense to each word $w_i \in T$. However, only the most appropriate sense is selected, that is, $|A(i)| = 1$. A knowledge source can be in various lexical formats. In this study, the UKC is used as the knowledge source.

B. Materials

This section outlines the material used for the development of the proposed algorithm. These are divided into three major components: the sense inventory, the WSD technique, and the disambiguation algorithm. Together, these elements form the architecture depicted in Fig. 1.

At the center of the architecture, the WSD algorithm takes the context sentence as input and produces the most appropriate sense for the polysemous word within that specific

context. In the subsequent sub-section, the study incorporates the UKC as the sense inventory to retrieve glosses for the polysemous word. Following the UKC is the WSD technique that employs PuoBERTa for encoding and generating embeddings in Setswana, utilizing a Cosine semantic similarity measure to determine the correct sense.

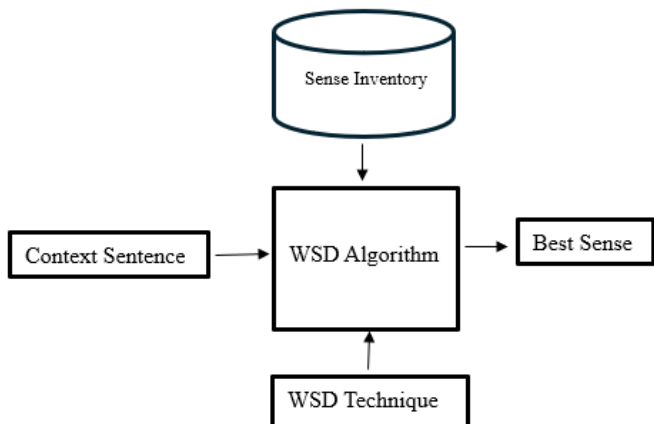


Fig. 1. WSD architecture.

1) *The universal knowledge core:* The Universal Knowledge Core (UKC) is a multilingual, high quality, large scale, and diversity-aware machine-readable lexical resource that currently consists of the lexicons of over a thousand languages, represented as wordnet structures [18], including Setswana. The UKC has two core layers, the concept and the language core [19]. The concept core is the knowledge layer of the UKC that provides a conceptual representation of concepts as we see them in the world. The concepts are interconnected through semantic relations and are language-independent. The language core is the language layer that is dedicated to lexical relations between lexical units (words). This layer encompasses multiple languages. The UKC provides an XML lexicon viewer, depicted in Fig. 2 that allows individuals to query and search for words, discovering their meanings and relationships.

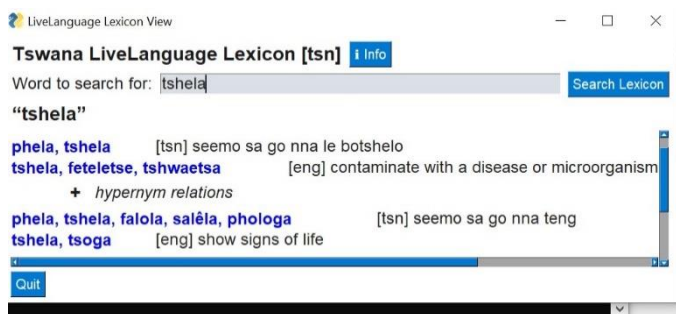


Fig. 2. Setswana UKC XML lexicon viewer.

Fig. 2 illustrates the Setswana lexicon in the UKC. The word “tshela” is a polysemous word that has two distinct senses. The senses are “to live” and “to pour”. The UKC provides glosses for each sense, along with English translations and available relations. For implementation of the proposed

algorithm, we used the XML version of the lexicon in Python, Anaconda prompt. The snippet of the XML is depicted in Fig. 3.

In the XML, each synset has a synset ID that links it to the Princeton Wordnet, a part of speech tag, gloss and synset relation. The algorithm proposed in this paper extract Setswana glosses for disambiguation from the XML file through unique synset IDs and leverages part-of-speech tags and synset relations to navigate the hierarchical structure of the XML data, pinpointing relevant glosses associated with each synset.

```

    <Synset id="tsn-syn1688843" ili="02055431-n" partOfSpeech="n" lexicalized="true">
    <Definition language="tsn">losika la diphenkwine tsotlhe la dinong</Definition>
    <SynsetRelation relType="mero_member" target="tsn-syn1695117"></SynsetRelation>
    <SynsetRelation relType="hypernym" target="tsn-syn1699998"></SynsetRelation>
    </Synset>
    <Synset id="tsn-syn1688842" ili="00548326-n" partOfSpeech="n" lexicalized="true">
    <Definition language="eng">the performance of a part or role in a drama</Definition>
    <SynsetRelation relType="hypernym" target="tsn-syn1691611"></SynsetRelation>
    <SynsetRelation relType="mero_part" target="tsn-syn169235"></SynsetRelation>
    <SynsetRelation relType="hypernym" target="tsn-syn1692609"></SynsetRelation>
    </Synset>
    <Synset id="tsn-syn1688845" ili="01030820-n" partOfSpeech="n" lexicalized="true">
    <Definition language="tsn">makgwa wa go itshwara jaaka go tlhokwa</Definition>
    <SynsetRelation relType="hypernym" target="tsn-syn1695002"></SynsetRelation>
    </Synset>
    
```

Fig. 3. Setswana UKC XML lexicon.

2) *PuoBERTa (Bidirectional Encoder Representations from Transformers):* Bidirectional Encoder Representations from Transformers (BERT) is a transformer-based language representation model introduced to the NLP landscape by [20] developed to capture the context and bidirectional dependencies of words in a sentence. This model is based on the transformer architecture illustrated in Fig. 4.

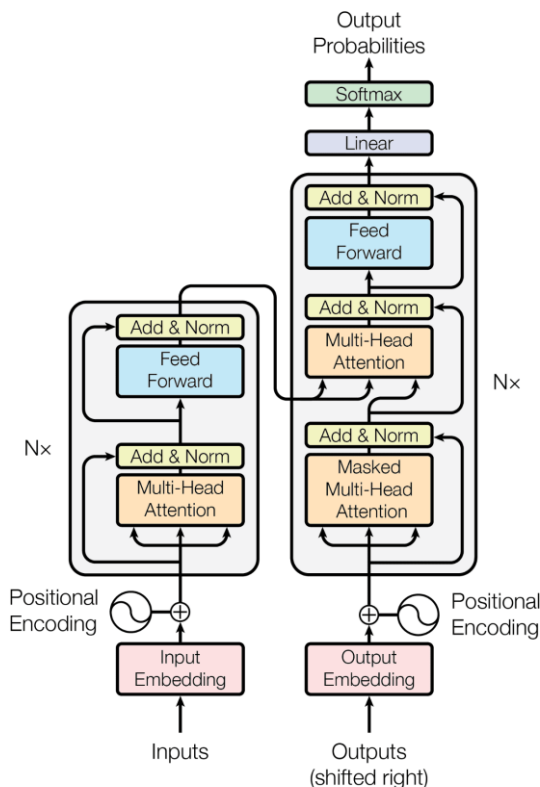


Fig. 4. Transformer architecture.

The transformer architecture employs a self-attention mechanism to capture dependencies between input tokens. The architecture consists of encoder and decoder stacks, each comprising multiple layers with multi-head attention, feedforward neural networks, and layer normalization. Positional encodings are incorporated to provide information about token positions. The model's success lies in its ability to efficiently handle long-range dependencies, parallelize computations, and serve as the foundation for various state-of-the-art models like BERT and GPT. Compared to traditional language models that process text sequentially from left to right or right to left, BERT processes the entire input sequence at once, taking into account both the preceding and following words for each word in a sequence [20]. This bidirectional approach allows BERT to capture more nuanced relationships and context in a language making it superior in tasks such as WSD. In addition, BERT can explicitly model the relationship of a pair of texts, which has proven to be beneficial for various pair-wise natural language understanding tasks [21]. Researchers have adapted the transformer architecture of BERT and trained language-specific models such as Arabic BERT [22] and Indict-BERT [23], to address distinct linguistic differences and used across various NLP tasks. For Setswana, PuoBERTa was developed and trained on Setswana data. It is a Setswana version of BERT trained by Marivate, et al. [24] using a corpus in the Setswana language. The PuoBERTa was trained on 24,295,328 Setswana tokens and evaluated on part-of-speech tagging and named entity recognition tasks. For Setswana WSD, PuoBERTa was used as an encoder to process and encode both contextual information, and the glosses of polysemous words extracted from the UKC.

3) *Disambiguation Algorithm*: This paper adopted the simplified Lesk algorithm for Setswana disambiguation. The reason for this selection is that compared to other variants, Simplified Lesk's primary objective is to maintain disambiguation effectiveness while simplifying the computation by reducing computational complexity [6]. This algorithm reduces computational complexity by using limited context, instead of considering the entire context surrounding the polysemous word. Simplified Lesk limits the scope to a predefined window of adjacent words and has the ability to work well for languages with limited resources, making it suitable for Setswana as a resource-scarce language. Another method that Simplified Lesk adopts to decrease computational complexity involves minimizing linguistic features. This is done by reducing reliance on extensive linguistic features and syntactic structures within the context, simplifying the feature set. However, this is a crucial capability when disambiguating agglutinative and morphologically rich languages such as Setswana. To address this, the linguistic features are integrated into the encoding process, utilizing PuoBERTa to encode the complete context sentence and the respective glosses to generate sentence embeddings. Sentence embeddings capture contextual information and the compositional nature of a language, this provides a representation that reflects the combination and interaction of words within a sentence [25]. Our algorithm is more closely related to the Simplified Lesk

algorithm [6] but leverages on the importance of word sense definitions using embeddings and similarity measure. The metric used to measure semantic similarity is the Cosine similarity as it effectively captures the directional similarity between vectors, making it suitable for assessing the relationship between gloss embeddings and context representations [26]. Research that employs Cosine similarity for disambiguation includes [27], [28], [29], [30].

The algorithm consists of the following steps:

Input: Ambiguous word (W), Context sentence (C), Sense inventory with glosses for each sense of W.

Disambiguation:

- 1) *Tokenization*: Tokenize the context sentence (C)
- 2) *Encode*: Encode context sentence (C) using PuoBERTa
- 3) *Sense selection*: For each sense of the ambiguous word (W), retrieve the corresponding glosses
- 4) *Encode and measure similarity*: Encode corresponding glosses (G) using PuoBERTa Measure semantic similarity using Cosine similarity on Eq. (1) between C and G

$$\cos(\theta) = \frac{A \cdot B}{\|A\| \|B\|} = \frac{\sum_{i=1}^n A_i B_i}{\sqrt{\sum_{i=1}^n A_i^2} \sqrt{\sum_{i=1}^n B_i^2}} \quad (1)$$

5) *Sense ranking*: Rank the senses based on the degree of similarity. The sense with the highest similarity is considered the most likely appropriate sense.

6) *Disambiguation*: Assign the sense with the highest similarity score as the disambiguated sense for the ambiguous word (W).

The steps above are formalized as the Algorithm 1 below:

Algorithm 1: Setswana WSD

```
Input: target word (w), context sentence (cs)
Output: best disambiguate senses (bestDef) of the w
STX ← Pre-process(RemoveStopwords(Tokenized(Text)))
Syn = GetSynsetFromUKC(w)
Est = defEncode(STX)
highestSim = 0
  For s in Syn
    Sdef = GetDefinition(s)
    Eqs = defEncode(Sdef)
    If Similarity > highestSim then
      highestSim = Similarity
    End
  bestDef = s
  End
return bestDef
```

Algorithm 1 illustrates the pseudocode of the proposed method. The process starts with the input of the target word (w) and the context sentence (cs) into the system. The provided context sentence is pre-processed. Following this, the system

retrieves synsets of the target word from the UKC, extracting various glosses associated with the target word. The context sentence is then encoded using PuoBERTa. Next, each synset gloss of the target word is encoded, and a similarity measure is computed for each gloss in comparison to the context sentence. The algorithm identifies and returns the gloss with the highest similarity measure as the correct definition of the target word.

C. Datasets

To construct the evaluation data set, the Senseval-3 lexical sample structure by Mihalcea, et al. [31] was adopted. Senseval-3 is one of the evaluation benchmark datasets and a follow-up to Senseval-1 and Senseval-2. The dataset was built using Open Mind Word Expert system proposed in [32]. To construct the evaluation dataset, words that were mapped to more than one synset in the African Wordnet were extracted, together with their glosses and example sentences. Additional words, glosses, and example sentences were extracted from Oxford and Pharos bilingual dictionaries, the different senses were indicated with numbers superscript in the dictionaries. From these resources, an evaluation dataset of 1200 Setswana sentences was created. Currently, there is no existing WSD evaluation dataset for Setswana, this dataset serves as a valuable resource for evaluating and benchmarking models designed to address the complexities of polysemy in Setswana.

D. Experimental Settings

All experiments were conducted using the Python programming language with preinstalled NLTK [33] and scikit-learn library [34] run in Window 10 Pro, 11th Gen Intel(R) Core(TM) i7-1165G7 @ 2.80GHz 1.69 GHz, 17GB installed ram. For experimentation, each context sentence was passed into the algorithm for pre-processing and encoding. Then the glosses of the polysemous word in that context were extracted from the UKC and subsequently encoded iteratively to generate gloss embeddings. With each iteration, a similarity measure was computed between the context and gloss embeddings, and the gloss with the highest similarity was selected as the appropriate sense gloss, which was then compared with the ground truth. If the chosen gloss aligned with the ground truth, the count of correctly disambiguated variables increased by 1. If not, the count of incorrectly disambiguated variables was incremented. For evaluation metrics, we adopted the accuracy (A) and error rate (E) metrics on (2) and (3) utilized in [35] methodology.

$$A = \text{Correctly Disambiguated} / \text{Number of Test Instances} \quad (2)$$

$$E = \text{Incorrectly Disambiguated} / \text{Number of Test Instances} \quad (3)$$

Accuracy is a metric that measures the proportion of correctly identified instances out of the total number of instances. In this context, it is calculated as the number of correctly disambiguated variables divided by the total number of test instances, as shown on Eq. (2). Error rate, on the other hand, represents the proportion of incorrectly identified instances out of the total number of instances. It is calculated as the number of incorrectly disambiguated variables divided by the total number of test instances, as illustrated in Eq. (3).

IV. RESULTS

This section presents the results of the proposed algorithm.

The results of the experiment results are presented Table I. Out of a set 1200 context sentences, the algorithm successfully disambiguated 1040 Setswana sentences accurately but misclassified 160, resulting in an accuracy rate of 86.66% and an error rate of 14.34%.

TABLE I. EVALUATION STATISTICS AND RESULTS

| | |
|--|-------|
| Total number of context sentences for polysemous words | 1200 |
| Correctly disambiguated sentences | 1040 |
| Incorrectly disambiguated sentences | 160 |
| Accuracy | 86.66 |
| Error | 14.34 |

Fig. 5 illustrates the accuracy and the error rate. The notable high accuracy and comparatively lower error rate suggest that the algorithm demonstrates effectiveness in distinguishing among multiple senses of polysemous words in Setswana context. Fig. 6 presents the disambiguation stats.

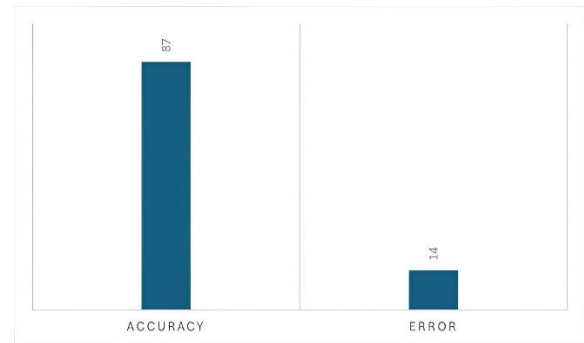


Fig. 5. Disambiguation accuracy and error rate.

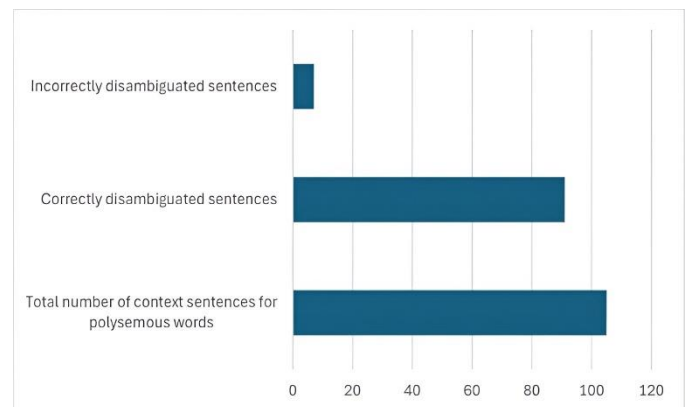


Fig. 6. Disambiguation statistics.

The error rate of 14.34% in the proposed Setswana WSD algorithm can be attributed to several factors. One reason for the error rate is the limited coverage of the Setswana UKC lexical resource. The UKC provides a valuable knowledge base for Setswana, however, it does not encompass all possible senses and glosses for every polysemous word encountered in the evaluation dataset. This limitation led to instances where

the algorithm fails to identify the correct sense due to the absence of the appropriate gloss in the lexical resource. Another factor contributing to the error rate is the complexity and ambiguity of certain Setswana words. Setswana, being a morphologically rich language, contains words with intricate morphological structures and highly context-dependent meanings. The proposed algorithm, while effective in handling many cases, it struggles to accurately disambiguate such complex words, especially when the context provided is insufficient. Despite these factors contributing to the error rate, the proposed algorithm achieves a high accuracy of 86.66%, demonstrating its effectiveness in resolving polysemy for Setswana. Further improvements can be made by expanding the coverage of the Setswana UKC, incorporating additional linguistic features, and refining the disambiguation techniques to handle more complex and ambiguous cases.

To conduct a comparative analysis between our results and those of other researchers who utilized and adapted the Lesk algorithms for various languages, Fig. 7 presents a visual representation of the comparative performance based on accuracy.

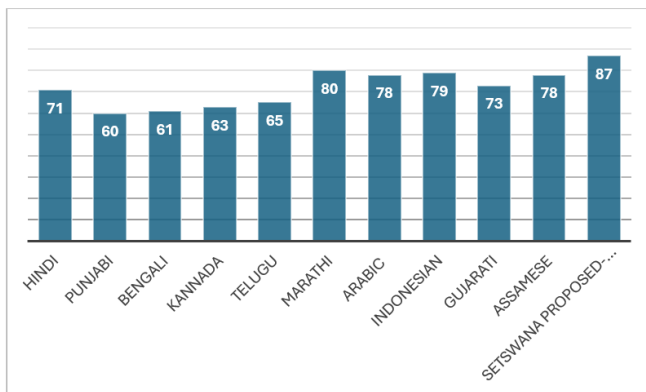


Fig. 7. Comparison of result for WSD for other languages.

For Hindi, Sharma and Joshi [36] used an evaluation corpus of 3000 context sentences, out of which 2143 were correctly disambiguated achieving an accuracy of 71%. Singh and Singh [37] tested the modified Lesk on 15 Punjabi polysemous words and achieved an average accuracy of 60 for all the ambiguous words. Pandit, et al. [38] used two test sets, the first test set with 10 and the second test set with 12 Bengali polysemous words and achieved an accuracy of 61%. Using a single word with five different senses and 2153 context sentences for Kannada, Parameswarappa and Narayana [39] obtained 63% accuracy while Eluri and Siddu [35] obtained 65% testing with 150 context sentences for Telegu. Patil, et al. [16]'s algorithm was evaluated on 6 Marathi polysemous words with a total 14 senses and achieved an overall accuracy of 80%. Arabic [40] and Indonesian [15] achieved almost the same accuracy with 0.1 difference, 78% and 79%. The Arabic WSD was tested on 50 polysemous words with 20 context sentences per word. For Indonesia, the algorithm was evaluated on 140 context sentences. Assamese obtained 78% evaluated on an annotated Assamese corpus with 15606 polysemous nouns. This paper achieved an accuracy of 87% on 1200 Setswana context sentences.

The comparative results on different datasets for various languages is caused by the inherent linguistic characteristics of each language, the size and quality of the datasets used. Each language requires its own evaluation data, specifically for resource-scarce languages like Setswana. Unlike English, which already has existing evaluation benchmark datasets such as Senseval and Semeval series, many low-resource languages lack such standardized datasets. This lack of evaluation data makes it challenging to directly compare the performance of WSD algorithms across different languages.

V. DISCUSSION AND CONCLUSION

This study highlights the critical role of WSD as a significant intermediate task in NLP applications. The Lesk algorithm, one of the first solution to address polysemy in NLP, has witnessed continuous adaptations by researchers for diverse languages. In the context of Setswana, this research introduces a novel approach, a simplified Lesk-based algorithm to effectively resolve polysemy. To address the computationally complex combinatorial comparisons inherent in traditional Lesk, this study leverages sentence embeddings and Cosine semantic similarity measures to model word sense glosses. The word sense glosses are modelled using a transformer-based language model PuoBERTa. The proposed method has been proven to achieve optimal performance in for Setswana WSD. The evaluation of the proposed algorithm on Setswana demonstrates significant success, with an accuracy of 86.66 and an error rate of 14.34. This surpasses the accuracy achieved by other Lesk-based algorithms developed for different languages. Additionally, this study provides a WSD evaluation dataset, currently unavailable, creating an essential benchmark for testing Setswana WSD models.

VI. FUTURE WORK

Future works involve expanding coverage of the Setswana UKC, the corpus size of the evaluation data and experimenting with diverse knowledge-based methods to determine their comparative performance. This includes incorporating additional linguistic morphological features, and refining the disambiguation techniques to handle more complex and ambiguous cases. Furthermore, we plan to integrate the proposed algorithm into a Setswana-English translation system, investigating its impact on translation quality as part of our ongoing research.

REFERENCES

- [1] S. Saxena, U. Chaurasia, N. Bansal, and P. Daniel, "Improved unsupervised statistical machine translation via unsupervised word sense disambiguation for a low-resource and Indic languages," *IETE Journal of Research*, pp. 1-11, 2022.
- [2] K. Chowdhary, "Natural language processing for word sense disambiguation and information extraction," *Fundamentals of Artificial Intelligence*, pp. 603-649, 2020.
- [3] N. Rahman and B. Borah, "Improvement of query-based text summarization using word sense disambiguation," *Complex & Intelligent Systems*, vol. 6, pp. 75-85, 2020.
- [4] R. Navigli, "Word sense disambiguation: A survey," *ACM computing surveys (CSUR)*, vol. 41, no. 2, pp. 1-69, 2009.
- [5] M. Lesk, "Automatic sense disambiguation using machine readable dictionaries: how to tell a pine cone from an ice cream cone," in *Proceedings of the 5th annual international conference on Systems documentation*, 1986, pp. 24-26.

- [6] A. Kilgarriff and J. Rosenzweig, "Framework and results for English SENSEVAL," *Computers and the Humanities*, vol. 34, pp. 15-48, 2000.
- [7] S. Banerjee and T. Pedersen, "An adapted Lesk algorithm for word sense disambiguation using WordNet," in *International conference on intelligent text processing and computational linguistics*, 2002: Springer, pp. 136-145.
- [8] A. M. Butnaru and R. T. Ionescu, "ShotgunWSD 2.0: An improved algorithm for global word sense disambiguation," *IEEE Access*, vol. 7, pp. 120961-120975, 2019.
- [9] F. Meng, "Graph and word similarity for word sense disambiguation," in *2020 13th International Congress on Image and Signal Processing, BioMedical Engineering and Informatics (CISP-BMEI)*, 2020: IEEE, pp. 1114-1118.
- [10] L. Zhong and T. Wang, "Towards word sense disambiguation using multiple kernel support vector machine," *International Journal of Innovative Computing, Information and Control*, vol. 16, no. 2, pp. 555-570, 2020.
- [11] A. S. Maurya, P. Bahadur, and S. Garg, "Approach Toward Word Sense Disambiguation for the English-To-Sanskrit Language Using Naïve Bayesian Classification," in *Proceedings of Third Doctoral Symposium on Computational Intelligence: DoSCI 2022*, 2022: Springer, pp. 477-491.
- [12] M. Kumar, P. Mukherjee, M. Hendre, M. Godse, and B. Chakraborty, "Adapted lesk algorithm based word sense disambiguation using the context information," *International Journal of Advanced Computer Science and Applications*, vol. 11, no. 3, pp. 254-260, 2020.
- [13] E. F. Ayetiran, P. Sojka, and V. Novotný, "Enhancing Lesk Algorithm by Integrating Selectional Preferences," *Journal of Language Modelling*, vol. 9, no. 1, pp. 137-168, 2021.
- [14] P. Tripathi, P. Mukherjee, M. Hendre, M. Godse, and B. Chakraborty, "Word sense disambiguation in Hindi language using score based modified lesk algorithm," *International Journal of Computing and Digital Systems*, vol. 10, pp. 2-20, 2020.
- [15] S. Basuki, A. S. Kholimi, A. E. Minarno, F. D. S. Sumadi, and M. R. A. Effendy, "Word sense disambiguation (WSD) for Indonesian homograph word meaning determination by LESK algorithm application," in *2019 12th International Conference on Information & Communication Technology and System (ICTS)*, 2019: IEEE, pp. 8-15.
- [16] A. P. Patil, R. Ramteke, R. Bhavsar, and H. Darbari, "Marathi Language Word Sense Disambiguation using Modified Lesk Algorithm," *International Journal of Advanced Computer Science and Applications*, vol. 12, no. 7, pp. 365-372, 2021.
- [17] S. Kaddoura and R. Nassar, "EnhancedBERT: A Feature-rich Ensemble Model for Arabic Word Sense Disambiguation with Statistical Analysis and Optimized Data Collection," *Journal of King Saud University-Computer and Information Sciences*, p. 101911, 2024.
- [18] G. Bella et al., "A major wordnet for a minority language: Scottish gaelic," in *Twelfth International Conference on Language Resources and Evaluation: Conference Proceedings*, 2020: European Language Resources Association (ELRA), pp. 2812-2818.
- [19] F. Giunchiglia, K. Batsuren, and A. Alhakim Freihat, "One World-Seven Thousand Languages (Best Paper Award, Third Place)," in *International Conference on Computational Linguistics and Intelligent Text Processing*, 2018: Springer, pp. 220-235.
- [20] J. Devlin, M.-W. Chang, K. Lee, and K. Toutanova, "Bert: Pre-training of deep bidirectional transformers for language understanding," *Proceedings of the 2019 Conference of the North American Chapter of the Association for Computational Linguistics: Human Language Technologies*, Volume 1, pp. 4171-4186, 2019.
- [21] L. Huang, C. Sun, X. Qiu, and X. Huang, "GlossBERT: BERT for word sense disambiguation with gloss knowledge," *Proceedings of the 2019 Conference on Empirical Methods in Natural Language Processing and the 9th International Joint Conference on Natural Language Processing (EMNLP-IJCNLP)*, pp. 3509-3514, 2019.
- [22] M. El-Razzaz, M. W. Fakhr, and F. A. Maghraby, "Arabic gloss WSD using BERT," *Applied Sciences*, vol. 11, no. 6, p. 2567, 2021.
- [23] R. R. Kannan, R. Rajalakshmi, and L. Kumar, "IndicBERT based approach for Sentiment Analysis on Code-Mixed Tamil Tweets," 2021.
- [24] V. Marivate, M. Mots' Oehli, V. Wagnerinst, R. Lastrucci, and I. Dzingirai, "PuoBERTa: Training and evaluation of a curated language model for Setswana," in *Southern African Conference for Artificial Intelligence Research*, 2023: Springer, pp. 253-266.
- [25] B. Scarlini, T. Pasini, and R. Navigli, "SenseBERT: Context-enhanced sense embeddings for multilingual word sense disambiguation," in *Proceedings of the AAAI conference on artificial intelligence*, 2020, vol. 34, no. 05, pp. 8758-8765.
- [26] K. Orkphol and W. Yang, "Word sense disambiguation using cosine similarity collaborates with Word2vec and WordNet," *Future Internet*, vol. 11, no. 5, p. 114, 2019.
- [27] Sarika and D. K. Sharma, "Hindi word sense disambiguation using cosine similarity," in *Proceedings of International Conference on ICT for Sustainable Development: ICT4SD 2015 Volume 2*, 2016: Springer, pp. 801-808.
- [28] S. Sari, R. Manurung, and M. Adriani, "Indonesian WordNet Sense Disambiguation using Cosine Similarity and Singular Value Decomposition," *ICSIT 2010*, p. 234, 2010.
- [29] R. Yatabe and M. Sasaki, "Semi-supervised word sense disambiguation using example similarity graph," in *Proceedings of the graph-based methods for natural language processing (TextGraphs)*, 2020, pp. 51-59.
- [30] A. Hari and P. Kumar, "WSD Based Ontology Learning from Unstructured Text Using Transformer," *Procedia Computer Science*, vol. 218, pp. 367-374, 2023.
- [31] R. Mihalcea, T. Chklovski, and A. Kilgarriff, "The Senseval-3 English lexical sample task," in *Proceedings of SENSEVAL-3, the third international workshop on the evaluation of systems for the semantic analysis of text*, 2004, pp. 25-28.
- [32] T. Chklovski and R. Mihalcea, "Building a sense tagged corpus with open mind word expert," in *Proceedings of the ACL-02 workshop on Word sense disambiguation: recent successes and future directions*, 2002, pp. 116-122.
- [33] S. Bird, E. Klein, and E. Loper, *Natural language processing with Python: analyzing text with the natural language toolkit*. O'Reilly Media, Inc., 2009.
- [34] F. Pedregosa et al., "Scikit-learn: Machine learning in Python," *The Journal of machine Learning research*, vol. 12, pp. 2825-2830, 2011.
- [35] S. Eluri and V. Siddu, "A Knowledge Based Word Sense Disambiguation in Telugu Language," *International Journal of Engineering and Advanced Technology (IJEAT)* ISSN, pp. 2249-8958, 2020.
- [36] P. Sharma and N. Joshi, "Knowledge-Based Method for Word Sense Disambiguation by Using Hindi WordNet," *Engineering, Technology & Applied Science Research*, vol. 9, no. 2, 2019.
- [37] J. Singh and I. Singh, "Word sense disambiguation: enhanced lesk approach in Punjabi language," *International Journal of Computer Applications*, vol. 129, no. 6, pp. 23-27, 2015.
- [38] R. Pandit, S. Sengupta, S. K. Naskar, and M. M. Sardar, "Improving Lesk by incorporating priority for word sense disambiguation," in *2018 Fifth International Conference on Emerging Applications of Information Technology (EAIT)*, 2018: IEEE, pp. 1-4.
- [39] S. Parameswarappa and V. Narayana, "Target word sense disambiguation system for Kannada language," in *3rd International Conference on Advances in Recent Technologies in Communication and Computing (ARTCom 2011)*, 2011: IET, pp. 269-273.
- [40] A. Zouaghi, L. Merhbene, and M. Zrigui, "Word Sense disambiguation for Arabic language using the variants of the Lesk algorithm," *WORLD COMP*, vol. 11, pp. 561-567, 2011.

Design of Emotion Analysis Model IABC-Deep Learning-based for Vocal Performance

Zhenjie Zhu¹, Xiaojie Lv²

College of Graduate, Sehan University, Mokpo, Republic of Korea¹

College of Microelectronics, Xidian University, Xian, China²

Abstract—With the development of deep learning technology, and due to its potential in solving optimization problems with deep structures, deep learning technology is gradually being applied to sentiment analysis models. However, most existing deep learning-based sentiment analysis models have low accuracy issues. Therefore, this study focuses on the issue of emotional analysis in vocal performance. Firstly, based on vocal performance experts and user experience, classify the emotions expressed in vocal performance works to identify the emotional representations of music. On this basis, in order to improve the accuracy of emotion analysis models for deep learning based vocal performance, an improved artificial bee colony algorithm (IABC) was developed to optimize deep neural networks (DNN). Finally, the effectiveness of the proposed deep neural network based on improved artificial bee colony (IABC-DNN) was verified through a training set consisting of 150 vocal performance works and a testing set consisting of 30 vocal performance works. The results indicate that the accuracy of the sentiment analysis model for vocal performance based on IABC-DNN can reach 98%.

Keywords—Vocal performance; deep learning; Artificial Bee Colony (ABC); emotion analysis model; Deep Neural Network (DNN)

I. INTRODUCTION

Emotion analysis (sentiment analysis) is a branch of Natural Language Processing (NLP) that involves identifying and extracting emotions from raw text. The sentiment analysis model aims to play an important role in human communication. The purpose of the sentiment analysis model is to understand and analyze subjective information in human language, such as viewpoints, emotions, and so on. Recently, sentiment analysis models have been widely applied in various fields, such as brand monitoring, public sentiment tracking, and market research [1]. Artificial intelligence-based sentiment analysis models can be trained and evaluated based on standardized data features such as word frequency, word order, grammatical structure, emotional vocabulary, and phrases, and then used for sentiment analysis on social media or recommendation systems [2]. Emotional analysis models can provide automated analysis of emotional information in texts. The acquisition and analysis of emotional information can provide decision-makers with valuable insights, thereby optimizing business operations, improving user experience, and enhancing competitiveness [3]. Therefore, sentiment analysis models can help users understand the emotional tendencies and states in text, which is of great significance in the field of NLP.

Emotional analysis models include support vector machines, decision trees, random forests, and deep learning models. The methods used mainly include rule-based (dictionary) methods and learning based methods. The rule-based approach relies on pre-defined sentiment dictionaries and rules, where each word is marked as positive, negative, or neutral. By calculating the number of positive and negative vocabulary in the text, the overall sentiment of the text can be determined [4]. The advantage of such models is that they perform well on specific types of text or domains, especially when these rules are designed for specific contexts, and they do not require training datasets and can be deployed immediately. However, this method may not accurately handle texts with complex meanings or containing rhetorical devices such as satire and metaphor. In addition, rule-based methods have lower flexibility and may require a lot of manual work to maintain and update rules and dictionaries [5].

Learning-based sentiment analysis models can be divided into machine learning-based sentiment analysis models and deep learning-based sentiment analysis models. Learning based sentiment analysis models typically require a large amount of labeled data for training. A machine learning based sentiment analysis model uses labeled datasets to train the model, so that the model can learn the mapping from text features to emotions. Machine learning models typically use manually designed feature representations. Deep learning models can use techniques such as word embedding to automatically learn the distributed representation of text, better capturing semantic information [6]. Deep learning models typically consist of multiple levels of neural networks with more complex structures and parameters. By contrast, machine learning models typically have a simpler model structure. Deep learning models typically require a large amount of labeled data for training in order to effectively learn complex feature representations. However, machine learning models require relatively small amounts of data and can be trained on smaller datasets [7].

Compared to machine learning methods, deep learning methods can typically provide higher accuracy while processing more complex texts and larger scale data. Therefore, sentiment analysis models based on deep learning have the advantages of automatic learning and feature extraction, high accuracy, and high flexibility. Deep learning models are particularly adept at capturing long-range dependencies from sequence data, which is crucial for understanding the context of text [8]. However, deep learning models typically require a large amount of annotated data for training, otherwise it may

lead to overfitting. In addition, training and tuning emotion analysis models based on deep learning is difficult, and the training process of deep learning models may be complex, requiring a focus on designing the network structure and tuning parameters. Therefore, sentiment analysis models based on deep learning may have an advantage in performance, but also pose challenges in adjusting network parameters [9].

The purpose of a music sentiment analysis model is to understand and analyze the emotional content in music. This model can be used in music recommendation systems to recommend suitable music to users by analyzing their emotional state and the emotional content of music. In addition, it can also be used in music creation to help creators better express the emotions they want to convey [10]. The emotion analysis model for vocal performance refers to a system that can recognize and analyze emotional expressions in singing. This type of model not only needs to handle linguistic emotional expression, but also needs to analyze musical elements such as melody, rhythm, harmony, and the vocal characteristics of the singer [11]. A sentiment analysis model for vocal performance needs to have the ability to extract music related features from audio signals, such as fundamental frequency, timbre, loudness, rhythm, and duration. In addition, the model also needs to have the ability to analyze sound quality, accurately identify the vocal quality of the singer, including clarity, stability, and volume changes [12].

The existing artificial intelligence-based sentiment analysis models have problems such as low accuracy. Therefore, in response to the problem of artificial intelligence based vocal performance analysis, this study establishes a deep learning based emotional analysis model for vocal performance, aiming to help music researchers understand music expression more deeply. The main contributions of this study are summarized as follows: a deep neural network (IABC-DNN) based on an improved artificial bee colony algorithm is designed. The input layer of IABC-DNN includes lyrics, typification, melody, pitch, and music rhythm, while the output layer is the emotion of vocal performance works. IABC-DNN consists of a novel gradient function that takes into account the factors affecting the emotional scale of vocal performance. In IABC-DNN, the Improved Artificial Bee Colony Algorithm (IABC) is used to optimize the DNN with the aim of improving the accuracy of the DNN. Finally, the accuracy of the IABC-DNN-based sentiment analysis model for vocal performance proposed in this study can reach 98% as verified by a test set. Overall, the emotional analysis model for vocal performance established in this study not only needs to ensure that the training data of the model is diverse and comprehensive, but also can capture emotional expressions from different singers, music styles, and cultural backgrounds. In addition, the subjectivity of sentiment analysis is also taken into account by the model, which can ensure that the model can find a balance between the differences in emotional perception among different listeners.

The remaining content of this study is arranged as follows: Section II of this paper reviews the relevant work related to this article. Section III developed an improved artificial bee colony algorithm. In Section IV, a novel DNN is designed. Section V presents the results. Finally, Section VI summarizes the entire study.

II. LITERATURE REVIEW

A. Emotional Analysis of Vocal Performance

Building an emotional analysis model for vocal performance is an interdisciplinary task that involves fields such as audio signal processing, music theory, psychology, and computer science. Emotional analysis is an important task in natural language processing (NLP), which aims to identify and extract subjective information from text. Before the emergence of deep learning methods, sentiment analysis mainly relied on vocabulary methods and machine learning techniques, such as naive Bayes and support vector machines. These methods typically require a significant amount of feature engineering. In recent years, deep learning-based sentiment analysis models have made significant progress. Convolutional Neural Network (CNN) is a deep learning model primarily used for processing grid shaped data, such as images. However, in recent years, CNN has also been successfully applied to sentiment analysis models. Specifically, reference [13] proposed a simple CNN model for sentence classification, including sentiment analysis. This model can use one-dimensional convolution and pooling operations to directly operate on word embeddings, thereby capturing local dependencies.

In addition, Recurrent Neural Networks (RNNs) are also a type of neural network capable of processing sequential data, making them highly suitable for processing text data. RNN can capture long-term dependencies in text by passing hidden states between time steps. However, a major problem with RNNs is gradient vanishing and exploding, which makes training deep RNNs difficult. To address this issue, reference [14] proposed the Long Short-Term Memory (LSTM) model. LSTM can more effectively capture long-term dependencies by introducing gating mechanisms. In addition, Transformer is a model based on self-attention mechanism. Unlike RNN and CNN, Transformer completely abandons loops and convolutions and relies on self-attention mechanism to capture global dependencies. Transformer has achieved significant success in various NLP tasks, including sentiment analysis [15].

In recent years, pre trained models have achieved significant success in various NLP tasks. These models are first pre trained on large-scale corpora and then fine-tuned on specific tasks. Pre trained models can capture rich language knowledge, significantly improving the performance of various NLP tasks, including sentiment analysis [16]. Meanwhile, knowledge graphs are also a structured way of representing knowledge, which can be used to represent entities and their relationships. In recent years, some studies have begun to explore how to use knowledge graphs for sentiment analysis. For example, reference [17] proposed a sentiment analysis model based on knowledge graphs, which can utilize the information in the knowledge graph to improve the performance of sentiment analysis.

However, the above artificial intelligence-based sentiment analysis models also have some challenges and limitations. Firstly, the above sentiment analysis models ignore the fine-grained issues in sentiment analysis, such as sentiment intensity detection, multi-dimensional sentiment analysis, etc. In addition, the above sentiment analysis models face

significant challenges when dealing with texts with satire and metaphor.

B. Deep Neural Network

Deep Neural Network (DNN) is a machine learning model that simulates the structure of human brain neural networks. It consists of multiple hidden layers, each of which is composed of multiple neurons. DNN has a wide range of applications in fields such as image recognition, speech recognition, and natural language processing [18]-[19]. In [18], a random DNN for image processing was designed, which has fewer neurons and higher accuracy compared to traditional DNNs. In [20], a deep neural network for signal processing was designed, which has better generalization ability against noise compared to traditional DNNs. In study [21], a DNN for image classification was designed using a two-stage algorithm, which can improve the accuracy of image classification during the DNN process. In study [22], several deep learning methods were combined and heuristic optimization methods were introduced to optimize the relevant parameters in the combination process, providing ideas for the design of new DNNs. In study [23], a DNN based risk model was developed to design the risk assessment process as an optimization problem.

Although DNN has achieved significant results in many fields, it still faces many challenges. Firstly, the training of DNN requires a large amount of computing resources and data, which is not feasible for many practical applications. Secondly, DNN has poor interpretability and it is difficult to understand its internal working mechanism. In addition, DNN is also susceptible to adversarial attacks, which is a problem for applications with high security requirements. In the future, research on DNN will focus more on improving its efficiency, interpretability, and security to meet the needs of more practical applications.

III. IABC-DEEP LEARNING FRAMEWORK

The basic principle of DNN is to map input data to output space through multi-layer nonlinear transformations. Each layer is composed of multiple neurons, each with an activation function used to convert input data into output data [24]-[27]. DNN is trained through backpropagation algorithm, optimizing weights and biases through gradient descent to minimize the difference between predicted and true values. Deep learning models may encounter difficulties when dealing with long texts, as long texts may contain a large amount of information, making it difficult for the model to capture key information. Therefore, similar to [22], in order to improve the accuracy of DNN, researchers have begun to attempt to combine meta heuristic algorithms with DNN algorithms to design DNN with better performance. Fig. 1 shows how to conduct sentiment analysis on vocal performance works based on DNN.

A. Collection of Sound Signals in Vocal Performance Works

Before designing the DNN framework, it is necessary to first sample and preprocess the speech of vocal performance works. Fig. 2 shows the short-term energy map of a vocal performance. In the specific sampling process, it is first necessary to frame the sound signal according to the time scale. Among them, the length of each audio segment is L_{audio} . Divide

the entire audio into Num_{audio} segments. Without considering overlapping frames, the total number of sampling points for the sound signal is calculated as shown in Eq. (1).

$$Num_{total} = L_{audio} \times Num_{audio} \tag{1}$$

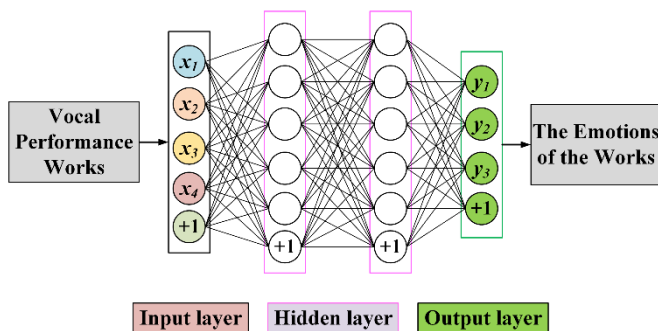


Fig. 1. The DNN schematic diagram for emotional analysis of vocal performance works.

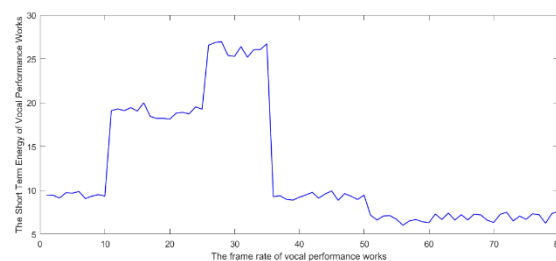


Fig. 2. The short-term energy map of a vocal performance work.

In audio processing, root mean square energy is often used for feature extraction of signals such as music and speech. For example, in tasks such as music emotion classification, speech activity detection, and speech recognition, root mean square energy is one of the important features. Meanwhile, as root mean square energy can reflect the loudness of audio signals, it is often used in applications such as music dynamic range compression and volume adjustment. Fig. 3 shows the mean square energy root of the audio signal in a certain vocal performance. Mean square energy root is a commonly used feature in audio processing, mainly used to describe the energy magnitude of audio signals. It is obtained by calculating the square of each sample of the audio signal, then taking the average value, and finally taking the square root. This value can reflect the loudness of audio signals and can also be used for audio segmentation classification.

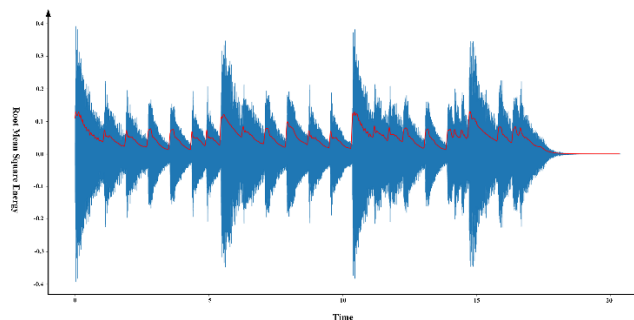


Fig. 3. The root mean square energy of a certain vocal performance.

B. Overview of Emotional Analysis Framework for Vocal Performance Works

After extracting language and speech from the audio of vocal performance works, Fig. 4. shows the sentiment analysis framework for vocal performance works based on IABC-DNN constructed in this study. The framework shown in Fig. 4. mainly consists of three parts: language prompts, knowledge-based encoding and decoding, and joint inference based on weighted first-order logic rules. In this study, propositional logic was constructed as a formal reasoning system. However, the minimum unit of propositional logic language is propositional symbols, which makes it impossible to conduct a more in-depth analysis of individual propositional symbols. Therefore, we used weighted first-order logic rules.

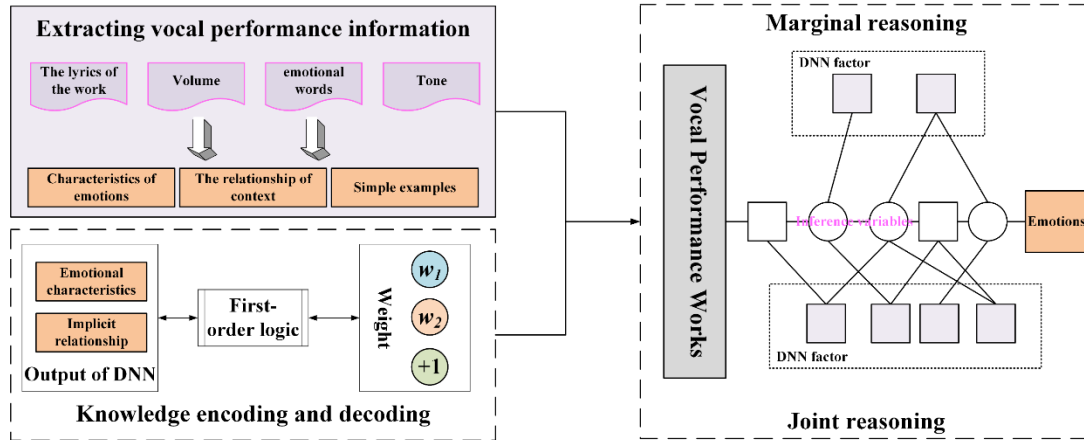


Fig. 4. The overall framework of vocal emotion analysis based on IABC-DNN.

IV. DESIGN OF IABC-DNN ALGORITHM

The swarm intelligence optimization algorithm is an optimization algorithm that simulates the behavior of groups in nature, such as bird flocks searching for food, ants finding their way, and so on. This algorithm has global search capability and can find the optimal solution over a large range, avoiding getting stuck in local optima. Therefore, it can be used to optimize the parameters of DNN. DNN is a complex machine learning model with numerous parameters and high optimization difficulty. Traditional optimization methods such as gradient descent may fall into local optima, while swarm intelligence optimization algorithms can avoid this problem. Specifically, the parameters of deep neural networks can be regarded as "individuals" in swarm intelligence optimization algorithms, each with a fitness value, that is, the performance of the deep neural network under this parameter setting. The swarm intelligence optimization algorithm continuously updates individuals by simulating group behavior, such as bird foraging and ant pathfinding, to optimize the parameters of deep neural networks and improve their performance.

A. IABC Algorithm

The Artificial Bee Colony (ABC) algorithm, as a novel swarm intelligence algorithm, is used in this paper to optimize the weights of DNN networks. The ABC algorithm is inspired by the honey gathering process of bees. In the optimization process, the ABC algorithm consists of two parts: feasible solutions (food sources) and solution positions (hired bees and

The framework shown in Fig. 4 which encodes the output of DNN using the following rules:

$$\square(k) : DNN_P_issu(t,k) \rightarrow BoolP(t) \quad (2)$$

Among them, $BoolP(t)$ is Boolean variables, t indicates polarity, and $\square(k)$ represents weight. The rule weights are defined in Eq. (3):

$$\square(k) = \ln\left(\frac{k}{1-k}\right) \quad (3)$$

non-hired bees). Among them, in any optimization problem, the feasible solution of the problem is given in a certain form. In the ABC algorithm, the food source is the feasible solution to the problem and is the basic object to be processed in the artificial bee colony algorithm. The quality of the food source can be evaluated by the value of the fitness function. Hiring bees refers to leading bees (collecting bees) that correspond to the position of their food source, with one food source corresponding to one leading bee. The steps and process of the improved Artificial Bee Colony (IABC) algorithm designed in this article are as follows. The algorithm flowchart of IABC is shown in Fig. 5.

1) *Step 1: Initialization.* Generate initial solutions based on the weights w_d of each neuron in DNN, and form a set of initial solution positions based on I_{max} initial solutions. Specifically, as follows:

$$W_l = [w_1, w_2, \dots, w_{d_{max}}] \quad (4)$$

$$abc_Swarm_l = [W_1, W_2, \dots, W_{l_{max}}]^T \quad (5)$$

2) *Step 2:* Calculate the fitness function value. Calculate the fitness function value for each honey source in the bee population. In Eq. (6), the objective function f_RMSE used in this study is given.

$$f_RMSE = \sqrt{\frac{1}{n} \times \sum (V_{pre} - V_{ture})^2} \quad (6)$$

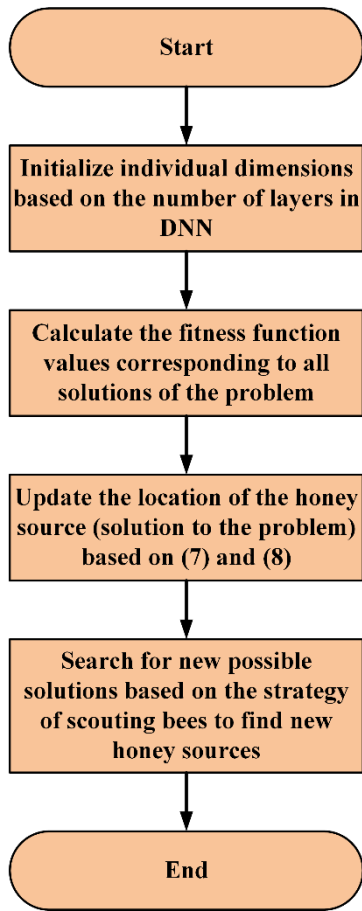


Fig. 5. The flowchart of IABC algorithm.

where, V_{pre} is the predicted value, and V_{true} is the true value.

3) *Step 3*: Honey source update operation. In this study, DNN has d max weight coefficients that need to be optimized, and the number of bees collected or observed is equal to the number of solutions. Therefore, the number of bees collected or observed is $Imax$. Before updating the honey source, first generate a random number Q in the $[0,1]$ interval. In Eq. (7) and Eq. (8), the way honey source updates are displayed.

If $Q \leq 0.5$, then

$$w_{d,x}(new) = w_{d,x}(old) + \alpha \times (w_{d,x}(old) - w_{d,y}) \quad (7)$$

If $Q > 0.5$, then

$$w_{d,x}(new) = w_{d,x}(old) + F \times (w_{d,y} - w_{d,z}) \quad (8)$$

where, α is a random number on the interval $[-1,1]$. F is the variation factor, and its value range is generally within the range of $[0.4, 0.95]$.

In Eq. (9) and Eq. (10), individuals before and after the honey source update operation are displayed, respectively.

$$W_l(old) = [w_1(old), w_2(old), \dots, w_{d_{max}}(old)] \quad (9)$$

$$W_l(new) = [w_1(new), w_2(new), \dots, w_{d_{max}}(new)] \quad (10)$$

After completing the honey source update operation, use a greedy selection strategy to retain better honey sources. Each observed bee selects a honey source based on probability, and the probability formula is shown in Eq. (11).

$$P = \frac{f - RMSE(i)}{\sum f - RMSE(k)} \quad (11)$$

4) *Step 4*: Generate feasible solutions based on reconnaissance bees. If, after the honey source update operation, the fitness value of a honey source is not further optimized within the given steps, the honey source is discarded, and the corresponding honey collecting bee becomes a reconnaissance bee. The reconnaissance bee searches for new possible solutions using the following:

$$w_{d,x}(new) = w_{d,x}(\min) + rand(0,1) \times [w_{d,x}(\max) - w_{d,x}(\min)] \quad (12)$$

5) *Step 5*: End. Record the optimal solution and determine if the termination condition is met. If so, output the optimal solution.

V. RESULTS DISPLAY

For the dataset, we selected a dataset consisting of 180 vocal performance works. The specific experiment is set up according to the following steps. Firstly, based on three different academic groups of students majoring in vocal performance, judges specializing in vocal performance, and experts in vocal performance, 180 vocal performance works were scored and their emotional expressions were given using a back-to-back scoring method. This study focuses on analyzing vocal performance works with five emotions: sadness, tenderness, anger, joy, and pride. In DNN, the five emotions are represented by 1, 2, 3, 4, and 5, respectively. Secondly, swarm intelligence algorithms are used in the structure of English DNNs. On this basis, the IABC-DNN algorithm was compared with DNN based on improved group search algorithm (IGSO-DNN), DNN based on ABC algorithm (ABC-DNN), and DNN based on improved genetic algorithm (IGA-DNN). The results showed that the proposed method is superior to the above three algorithms.

A. Dataset Settings

Table I shows the audio features and descriptions of vocal performance works, and the DNN algorithm conducts sentiment analysis based on these features and descriptions. Furthermore, 180 vocal performance works were divided into three sets of data to fully validate the model's generalization ability, as shown in Table II. In Table II, dataset WD-1 includes a training set consisting of 50 vocal performance works and a testing set consisting of 10 vocal performance works. The dataset WD-2 includes a training set consisting of 100 vocal performance works and a testing set consisting of 20 vocal performance works. The dataset WD-3 includes a training set consisting of 100 vocal performance works and a testing set consisting of 20 vocal performance works.

TABLE I. AUDIO FEATURES AND DESCRIPTIONS OF VOCAL PERFORMANCE WORKS

| Characteristic | Describe |
|-------------------------------|--|
| Sound quality characteristics | Very rough, very smooth, medium |
| Irregularity | Anger, fear, and sadness |
| Variability | More unpleasant (valence), awake or tired (awakening energy), and more tense (awakening tension) |

TABLE II. DESIGN OF DATASETS

| Data | Work types | Train | Test |
|------|-------------------|-------|------|
| WD-1 | Vocal performance | 50 | 10 |
| WD-2 | Vocal performance | 100 | 20 |
| WD-3 | Vocal performance | 150 | 30 |

B. Result Comparison

This study uses ABC algorithm, IABC algorithm, IGA algorithm, and IGSO algorithm to optimize the weights between neurons in DNN. The optimization results are shown below.

To demonstrate the robustness of swarm intelligence algorithms, ABC algorithm, IABC algorithm, IGA algorithm, and IGSO algorithm were run 50 times each. Fig. 6, 7, and 8 respectively show the optimal fitness function curve, worst fitness function curve, and average fitness function curve of the 50 run results of the four algorithms in optimizing the weights of the DNN network. From Fig. 6, 7, and 8, it can be concluded that the IABC algorithm designed in this study converges faster and has higher accuracy in optimizing the weight coefficients of DNN compared to the IGSO, IGA, and ABC algorithms.

Furthermore, this study compared three algorithms, DNN, IGWO-DNN, and IGA-DNN, with the proposed IABC-DNN algorithm. The comparison indicators included Accuracy, Precision, Sensitivity, Specificity, and F-1 score. Tables III, IV, and V respectively show the various indicators of dataset WD-1, WD-2, and WD-3 when using the four models. In three datasets, regardless of which indicator, the IABC-DNN algorithm performed the best, fully demonstrating the effectiveness of the algorithm designed in this study.

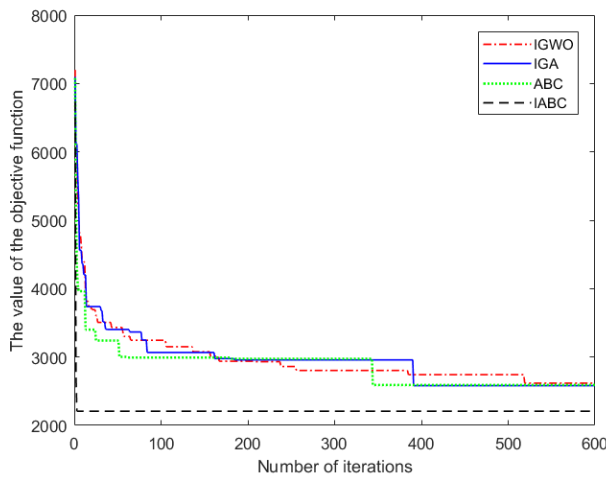


Fig. 6. The optimal fitness function curve during 50 runs of four algorithms.

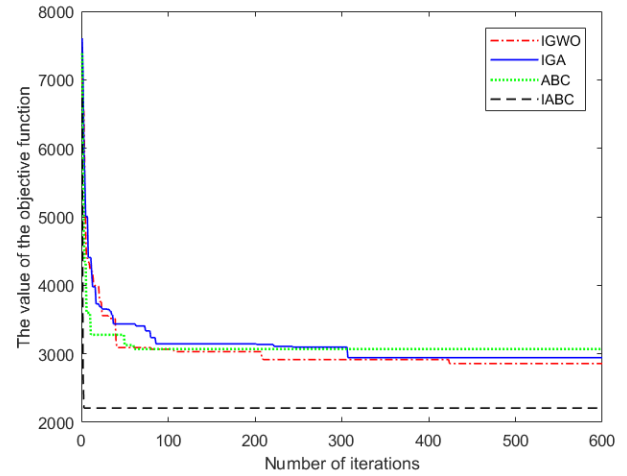


Fig. 7. The worst fitness function curve during 50 runs of four algorithms.

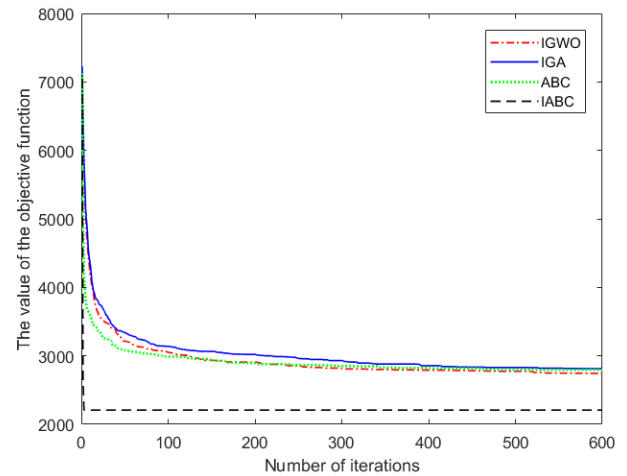


Fig. 8. The average fitness function curve during 50 runs of four algorithms.

TABLE III. EVALUATION OF PERFORMANCE METRICS FOR DATASET WD-1

| Algorithm | Accuracy | Precision | Sensitivity | Specificity | F-1 score |
|-----------|--------------|--------------|--------------|--------------|--------------|
| DNN | 0.812 | 0.865 | 0.821 | 0.920 | 0.855 |
| IGWO-DNN | 0.966 | 0.897 | 0.899 | 0.931 | 0.945 |
| IGA-DNN | 0.892 | 0.913 | 0.920 | 0.982 | 0.928 |
| IABC-DNN | 0.975 | 0.987 | 0.999 | 0.987 | 0.991 |

TABLE IV. EVALUATION OF PERFORMANCE METRICS FOR DATASET WD-2

| Algorithm | Accuracy | Precision | Sensitivity | Specificity | F-1 score |
|-----------|--------------|--------------|--------------|--------------|--------------|
| DNN | 0.889 | 0.863 | 0.901 | 0.902 | 0.890 |
| IGWO-DNN | 0.904 | 0.900 | 0.895 | 0.911 | 0.881 |
| IGA-DNN | 0.948 | 0.925 | 0.916 | 0.958 | 0.916 |
| IABC-DNN | 0.981 | 0.988 | 0.990 | 0.946 | 0.970 |

TABLE V. EVALUATION OF PERFORMANCE METRICS FOR DATASET WD-3

| Algorithm | Accuracy | Precision | Sensitivity | Specificity | F-1 score |
|-----------|--------------|--------------|--------------|--------------|--------------|
| DNN | 0.829 | 0.885 | 0.856 | 0.916 | 0.885 |
| IGWO-DNN | 0.876 | 0.839 | 0.853 | 0.901 | 0.916 |
| IGA-DNN | 0.925 | 0.900 | 0.895 | 0.970 | 0.924 |
| IABC-DNN | 0.984 | 0.978 | 0.928 | 0.976 | 0.993 |

Furthermore, Fig. 9 shows the accuracy of DNN, ABC-DNN, and IABC-DNN in predicting the emotions of 30 vocal performance works when using 150 vocal performance works as the test set.

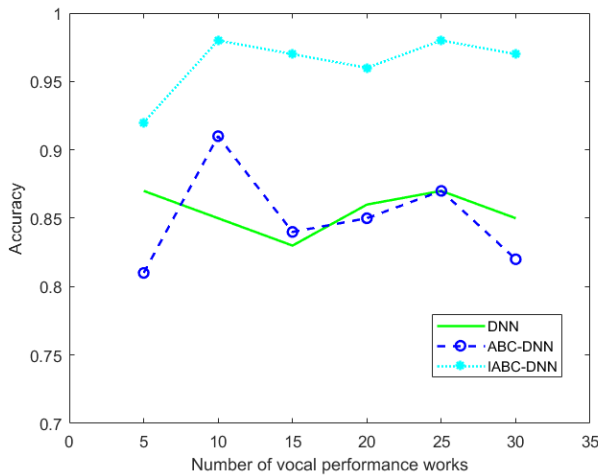


Fig. 9. The accuracy of different sentiment analysis models.

From Fig. 9, it can be seen that the IABC-DNN algorithm designed in this study has the highest accuracy, at 98%, which is higher than 87% of DNN and 91% of ABC-DNN algorithm. Compared with DNN algorithm and ABC-DNN algorithm, the accuracy of IABC-DNN algorithm has improved by an average of 9%.

VI. CONCLUSION

This study designed corresponding algorithms and models for the emotional analysis of vocal performance works. Especially, an improved ABC algorithm was designed and applied to the optimization process of weight coefficients in DNN networks. The effectiveness of the IABC-DNN algorithm has been fully demonstrated through three datasets. Compared with DNN and ABC-DNN algorithms, the accuracy of IABC-DNN algorithm has improved by 9%. In addition, compared with IGA, IGSO, and ABC, the IABC algorithm has the fastest convergence speed and highest convergence accuracy in optimizing the weight coefficients of DNN networks.

REFERENCES

[1] R. Chatterjee, S. Mazumdar, R. S. Sherratt, R. Halder, T. Maitra and D. Giri, "Real-Time Speech Emotion Analysis for Smart Home Assistants," IEEE Transactions on Consumer Electronics, vol. 67, no. 1, pp. 68-76, February 2021.

[2] S. Koelstra et al., "DEAP: A Database for Emotion Analysis Using Physiological Signals," IEEE Transactions on Affective Computing, vol. 3, no. 1, pp. 18-31, March 2012.

[3] L. Zhang, S. Wang, and B. Liu, "Deep learning for sentiment analysis: A survey," Data Mining and Knowledge Discovery, vol. 8, no. 4, pp. e1253, 2018.

[4] G. D'Aniello, M. Gaeta, and I. La Rocca, "KnowMIS-ABSA: an overview and a reference model for applications of sentiment analysis and aspect-based sentiment analysis," The Artificial Intelligence Review, vol. 55, no. 7, pp. 5543-5574, 2022.

[5] D. Tang, F. Wei, B. Qin, N. Yang, T. Liu and M. Zhou, "Sentiment Embeddings with Applications to Sentiment Analysis," IEEE Transactions on Knowledge and Data Engineering, vol. 28, no. 2, pp. 496-509, February 2016.

[6] Mäntylä, M. V., Graziotin, D., and Kuuttila, M., "The evolution of sentiment analysis—A review of research topics, venues, and top cited papers," Computer Science Review, vol. 27, pp. 16-32, 2018.

[7] Dey, A., Jenamani, M., and Thakkar, J. J. "Senti-N-Gram: An n-gram lexicon for sentiment analysis," Expert Systems with Applications, vol. 103, pp. 92-105, 2018.

[8] A. Diwali, K. Saeedi, K. Dashtipour, M. Gogate, E. Cambria and A. Hussain, "Sentiment Analysis Meets Explainable Artificial Intelligence: A Survey on Explainable Sentiment Analysis," IEEE Transactions on Affective Computing, (Early Access), DOI: 10.1109/TAFFC.2023.3296373.

[9] Li, W., Zhu, L., Shi, Y., Guo, K., and Cambria, E. "User reviews: Sentiment analysis using lexicon integrated two-channel CNN-LSTM family models," Applied Soft Computing, vol. 94, pp. 106435, 2020.

[10] Y. Liu, Y. Liu, Y. Zhao and K. A. Hua, "What Strikes the Strings of Your Heart?—Feature Mining for Music Emotion Analysis," IEEE Transactions on Affective Computing, vol. 6, no. 3, pp. 247-260, Sept. 2015.

[11] Morente-Molinera, J. A., Kou, G., Pang, C., Cabrerizo, F. J., & Herrera-Viedma, E. "An automatic procedure to create fuzzy ontologies from users' opinions using sentiment analysis procedures and multi-granular fuzzy linguistic modelling methods," Information Sciences, vol. 476, pp. 222-238. 2019.

[12] Gan, C., Fu, X., Feng, Q., Zhu, Q., Cao, Y., and Zhu, Y. "A multimodal fusion network with attention mechanisms for visual-textual sentiment analysis," Expert Systems with Applications, vol. 242, pp. 122731, 2024.

[13] Kraus, M., and Feuerriegel, S. "Sentiment analysis based on rhetorical structure theory: Learning deep neural networks from discourse trees," Expert Systems with Applications, vol. 118, pp. 65-79, 2019.

[14] Priyadarshini, I., and Cotton, C. "A novel LSTM-CNN-grid search-based deep neural network for sentiment analysis." The Journal of Supercomputing, vol. 77, no. 12, pp. 13911-13932, 2021.

[15] Antonakaki, D., Fragopoulou, P., and Ioannidis, S. "A survey of Twitter research: Data model, graph structure, sentiment analysis and attacks," Expert Systems with Applications, vol. 164, 114006, 2021.

[16] Das, R., and Singh, T. D. "Multimodal Sentiment Analysis: A Survey of Methods, Trends, and Challenges," ACM Computing Surveys, vol. 55, no. 13s, pp. 1-38, 2023.

[17] Wang, C., and Ko, Y. C. "Emotional representation of music in multi-source data by the Internet of Things and deep learning," The Journal of Supercomputing, vol. 79, no. 1, pp. 349-366. 2023.

[18] Genzel, M., Macdonald, J., and Marz, M. "Solving Inverse Problems With Deep Neural Networks - Robustness Included?" IEEE Transactions on Pattern Analysis and Machine Intelligence, vol. 45, no. 1, pp. 1119-1134, 2023.

[19] Lee, R., Venieris, S. I., and Lane, N. D. "Deep Neural Network-based Enhancement for Image and Video Streaming Systems: A Survey and Future Directions." ACM Computing Surveys, vol. 54, no. 8, pp. 1-30, 2022.

[20] Sun, B., Zhong, H., Zhao, Y., Ma, L., and Wang, H. "Calderón's Method-Guided Deep Neural Network for Electrical Impedance Tomography." IEEE Transactions on Instrumentation and Measurement, vol. 72, pp. 1-11, 2022.

- [21] Kumar, H., Yadav, N., and Nagar, A. K. "Numerical solution of Generalized Burger–Huxley & Huxley’s equation using Deep Galerkin neural network method." *Engineering Applications of Artificial Intelligence*, vol. 115, pp. 105289, 2023.
- [22] Hermann, J., Schätzle, Z., and Noé, F. "Deep-neural-network solution of the electronic Schrödinger equation." *Nature Chemistry*, vol. 12, no. 10, pp. 891–897, 2023.
- [23] Rao, D., Huang, S., Jiang, Z., Deverajan, G. G., and Patan, R. "A dual deep neural network with phrase structure and attention mechanism for sentiment analysis: An ablation experiment on Chinese short financial texts." *Neural Computing & Applications*, vol. 33, no. 17, pp. 11297–11308, 2021.
- [24] W. H. Bangyal et al., "Detection of Fake News Text Classification on COVID-19 Using Deep Learning Approaches," *Computational and mathematical methods in medicine*, vol. 2021, pp. 5514220–14, 2021.
- [25] W. H. Bangyal, M. Iqbal, A. Bashir and G. Ubakanma, "Polarity Classification of Twitter Data Using Machine Learning Approach," 2023 International Conference on Human-Centered Cognitive Systems (HCCS), Cardiff, United Kingdom, 2023, pp. 1-6. doi: 10.1109/HCCS59561.2023.10452557.
- [26] W. H. Bangyal, S. Amina, R. Shakir, G. Ubakanma and M. Iqbal, "Using Deep Learning Models for COVID-19 Related Sentiment Analysis on Twitter Data," 2023 International Conference on Human-Centered Cognitive Systems (HCCS), Cardiff, United Kingdom, 2023, pp. 1-6. doi: 10.1109/HCCS59561.2023.10452567.
- [27] H. Liu, Y. Sun, N. Pan, Q. Chen, X. Guo, D. Pan, "Multi-UAV Cooperative Task Planning for Border Patrol based on Hierarchical Optimization" *Journal of Imaging Science and Technology*, vol.65, pp. 040402-1-040402-8, 2021. doi: 10.2352/J.ImagingSci.Technol.2021.65.4.040402.

Enhancing the Diagnosis of Depression and Anxiety Through Explainable Machine Learning Methods

Mai Marey¹, Dina Salem², Nora El Rashidy³, Hazem ELBakry⁴

Department of Computer, Faculty of Engineering, Misr University for Science and Technology, Egypt¹

Information System Department, Faculty of Computer Science and Information system, Mansoura University, Egypt¹

Department of Computer, Faculty of Engineering, Misr University for Science and Technology, Egypt²

Machine Learning and Information Retrieval Department, Faculty of Artificial Intelligence,

Kaferelshikh University, Kaferelshikh, University, Egypt³

Information System Department, Faculty of Computer Science and Information System, Mansoura University, Egypt⁴

Abstract—Diagnosing depression and anxiety involves various methods, including referenda-based approaches that may lack accuracy. However, machine learning has emerged as a promising approach to address these limitations and improve diagnostic accuracy. In this scientific paper, we present a study that utilizes a digital dataset to apply machine learning techniques for diagnosing psychological disorders. The study employs numerical, striatum, and mathematical analytic methodologies to extract dataset features. The Recursive Feature Elimination (RFE) algorithm is used for feature selection, and several classification algorithms, including SVM, decision tree, random forest, logistic regression, and XGBoost, are evaluated to identify the most effective technique for the proposed methodology. The dataset consists of 783 samples from patients with depression and anxiety, which are used to test the proposed strategies. The classification results are evaluated using performance metrics such as accuracy (AC), precision (PR), recall (RE), and F1-score (F1). The objective of this study is to identify the best algorithm based on these metrics, aiming to achieve optimal classification of depression and anxiety disorders. The results obtained will be further enhanced by modifying the dataset and exploring additional machine learning algorithms. This research significantly contributes to the field of mental health diagnosis by leveraging machine learning techniques to enhance the accuracy and effectiveness of diagnosing depression and anxiety disorders.

Keywords—Mental health; Recursive Feature Elimination (RFE); machine learning; XGboost

I. INTRODUCTION

Ongoing research, in the field of disorders is focused on creating effective diagnostic approaches using advanced artificial intelligence (AI) methods [1]. The involvement of individuals with health conditions in studies investigating the origins of these disorders is rapidly growing [2], [3]. While mental disorders are rooted in brain abnormalities, psychologists and psychiatrists often make evaluations based on their insights and experiences. This dependence on assessments can lead to diagnoses for many people suffering from depression causing delays, in receiving appropriate care [4], [5]. Hence it is essential to identify trustworthy ways to comprehend and diagnose health issues highlighting the importance of integrating AI technologies into this process [6].

Diagnosing mental illnesses such as depression, anxiety, and suicide attempts can be challenging due to potential overlap and variations in manifestations among patients [7]. This difficulty arises because symptoms sometimes blur and vary amongst those impacted. Acting to address these issues early can significantly shorten the duration of symptoms and lessen their impact. It's crucial to remember that mental health disorders range widely, encompassing conditions like schizophrenia, bipolar disorder, depression, intellectual disabilities, and Alzheimer's disease [8], [9]. It's also well-documented that problems such as depression and anxiety are closely associated with poorer sleep quality and various sleep issues, which can significantly impact a person's day-to-day functioning [10].

Depression, a serious health condition is acknowledged by the World Health Organization as the fourth leading cause of disability globally [11] [12]. One-fifth of the population grapples with anxiety or depression disorders. The conventional healthcare system faces challenges, in catering to the number of patients leading to access to specialized care and extended waiting periods, for therapy commencement [13] [14]. Anxiety, ranked as the prevalent mental health issue after depression is characterized by physical manifestations of worry and persistent irrational stress that necessitates continuous and affirmative therapeutic interventions [15] [16].

Depressive disorders often show up as long-term conditions linked to feelings of boredom, guilt, and difficulty focusing [16]. The level of symptoms determines how severe the depression is, in individuals. Treating depression directly can be tough causing some patients to turn to methods making diagnosis complicated [16] [17]. Studies have found that the neurons in people with disorders operate differently from those in individuals leading to disrupted neurotransmitter movement and decreased focus [18]. Current approaches to treating disorder (DD) rely on trial and error resulting in challenges and delays in patient recovery. Choosing the antidepressant for optimal clinical response remains a difficult task even though it is the main form of treatment for patients, with depressive disorder [19] [20].

The rise of AI technology has made diagnosing disorders efficient emphasizing the importance of mainstream AI applications being familiar, with how to detect them. Magnetic

resonance imaging (MRI) electroencephalography (EEG) and kinesics diagnosis are three methods used in health research [21].

II. RELATED WORK

Despite the variety of integration techniques, the field of psychiatric disorders still encounters numerous obstacles. This challenge is particularly noteworthy, due to the prevalence of health conditions with rates of depression and anxiety reaching 26% and 28% respectively during the 2022 COVID-19 pandemic [22]. Disparities between the demand for and access, to health treatment are stark when compared to physical ailments. Bridging this treatment gap can be achieved through interventions; however, it's crucial to recognize that individuals may respond differently to interventions. While some may benefit positively others may still require forms of care [13].

Several previous studies have employed machine learning techniques to predict diagnoses using digital therapy. Table I presents the findings of these studies indicating results, in treating depression (N = 283) with an improvement of 8.0% (95% CI 0.8–15; total R2 pred = 0.25) reducing disability by 5.0% (95% CI -0.3 to 10; total R2 pred = 0.25) and enhancing well-being by 11.6% (95% CI 4.9–19; total R2 pred = 0.29) [18]. Additionally, machine learning methods have been utilized to predict anxiety with an accuracy rate of ninety-two percent based on a dataset involving just twenty-six individuals [23] and to forecast obsessive-compulsive disorder with an accuracy of eighty-three percent from sixty-one cases [24]. Furthermore, other research has demonstrated accuracy, in diagnosing anxiety and depression through this methodology [13].

Computer-assisted detection (CAD) systems have been used in Electroencephalograph (EEG) studies to diagnose conditions. Examples include the use of the network (ANN) classifiers, for diagnosing depression with a 98.11% accuracy rate [25] Enhanced Probabilistic Neural Network (PNN) classifier with 91.30% accuracy [26] logistic regression classifier achieving 90.05% accuracy [27] Support Vector Machine (SVM) classifier with an accuracy of 98.40% [28] another SVM classifier with an accuracy of 81.23% [29] and

Convolutional Neural Network (CNN) classifiers attaining accuracies of 93.54 and 95.96 respectively [30]. Accurate diagnostic processes are crucial for treatment, in the realm of health given the challenges associated with precise psychiatric diagnoses owing to the overlapping symptoms of various mental illnesses making it difficult to differentiate or diagnose them accurately. This is to get the right psychiatric diagnosis before starting any treatment plan [31–49].

Traditional diagnosis for depression and anxiety relies on clinician expertise, which can be subjective and time-consuming. Machine learning (ML) offers an alternative approach, but previous methods often lacked transparency:

Black Box Problem: Traditional ML models are often like black boxes - they produce results but don't explain how they arrived at those conclusions. This makes it difficult for clinicians to trust the recommendations or understand why a patient is flagged for depression or anxiety.

- **Limited Data Integration:** Prior models might have focused on analyzing a single data source, like surveys. However, mental health is complex and can manifest in various ways.
- **The proposed work with "Explainable Machine Learning Methods"** suggests it addresses these issues by:
- **Making ML interpretable:** The approach might involve using specific algorithms or techniques that help explain the model's reasoning behind its diagnosis. This would increase trust and allow clinicians to understand the model's decision-making process.
- **Utilizing Multimodal Data:** The method might incorporate a wider range of data sources beyond just surveys. This could include speech patterns, facial expressions, or physiological data to create a more comprehensive picture of the patient's condition.

By overcoming limitations in explainability and data integration, this approach has the potential to improve the accuracy and effectiveness of diagnosing depression and anxiety compared to previous methods.

TABLE I. A LIST OF PREVIOUSLY PUBLISHED WORK IN THE DIAGNOSIS OF MENTAL ILLNESSES

| Authors | Year | Factors of Dataset | Techniques | Accuracy |
|--------------------------|------|--|--|--------------------------------|
| Pearson et al. [18] | 2019 | (N = 283) from across the USA | Random Forest & Elastic net regression | 95% |
| Månsson et al. [23] | 2015 | (N = 26)-Fmri | SVM | 91.7% |
| Lenhard et al. [24] | 2018 | (N = 61) | logistic regression | 83% |
| Jacobson et al. [13] | 2021 | (N=632) | base learner | 95% |
| Subha et al. [25] | 2012 | 16 females and 14 male-EEG | ANN | 98.11% |
| Ahmadlou et al. [26] | 2012 | 12 normal and 12 depressed subjects | Enhanced-PNN | 91.30% |
| Hosseinifard et al. [27] | 2013 | 11 male and 11 female depressed subjects | Logistic regression | 90.05% |
| Mumtaz et al. [28] | 2017 | 30 normal and 33 depressed subjects | SVM | 98.40% |
| Liao et al. [29] | 2017 | 20 normal and 20 depressed subjects | SVM | 81.23% |
| U. Rajendra Acharya.[30] | 2018 | 15 normal and 15 depressed subjects | CNN | 93.54%, 95.96% |
| Present work | 2023 | 403 female and 380 male depressed and anxious subjects | SVM, Decision Tree, Logistic Regression, Random Forest and xgboost | 91%, 92%, 93%,94%, 95%,96%,98% |

III. MATERIALS AND METHODS

A. Dataset Description

This dataset is based on 19 features and 783 samples of

403 females and 380 males, aged between 18 and 31 years old. This dataset collection was gathered from University of Lahore undergrads and was created using the Depression and Anxiety inventories as a model, as shown in Table II.

TABLE II. THIS IS A TABLE OF DATASET DESCRIPTION

| Features Name | Abbreviations | Rang of Features | Description |
|------------------------------|---------------|---------------------------------------|---|
| ID | - | 783 Samples | Identify the patients |
| school_year | - | (1-4) | - |
| Age | - | (18-31) | Age of patients |
| Gender | - | (Male-Female) | types of patients |
| Body mass index | BMI | (0-54) | It is an indicator of the scale of body mass |
| Patient Health Questionnaire | PHQ_Score | (0-24) | is the depression module |
| Depression_Severity | - | (Mild-Moderate- None-minimal- Severe) | Is the severity of depression in patients |
| Depressiveness | - | (TRUE-False) | - |
| Suicidal | - | (TRUE-False) | - |
| Depression_diagnosis | - | (TRUE-False) | Diagnosis of depression in the patient |
| Depression_treatment | - | (TRUE-False) | - |
| Generalized Anxiety Disorder | GAD_score | (0-21) | The measure of anxiety intensity |
| Anxiety_severity | - | (Mild-Moderate- None-minimal- Severe) | Is the severity of anxiety in patients |
| Anxiety_diagnosis | - | (TRUE-False) | Is the severity of anxiety in patients |
| Anxiety_treatment | - | (TRUE-False) | - |
| Epworth score | - | (0-32) | Measures the general level of daytime sleepiness. |
| Sleepiness | - | (TRUE-False) | - |

B. Data Visualization

- Box Plot for Depression and Anxiety Data (Fig. 1)

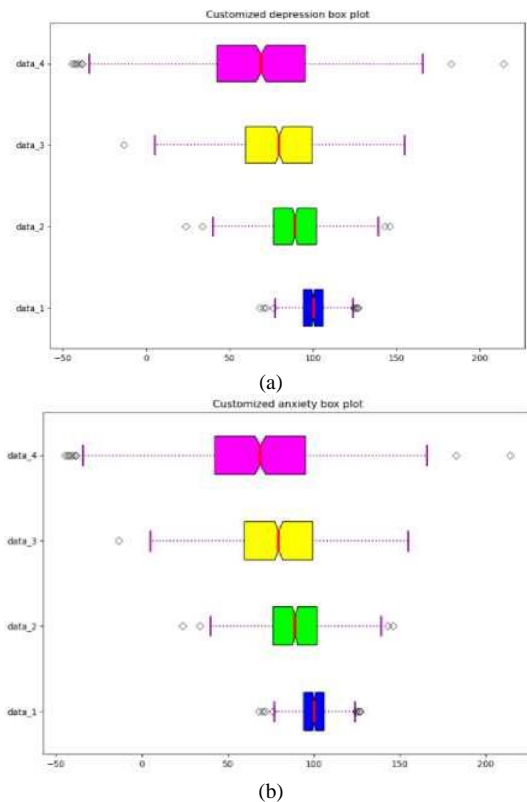


Fig. 1. Figure of Box Plot for Depression and Anxiety Data, (a) Customized depression box plot; (b) Customized anxiety box plot.

- Heatmap for Depression and Anxiety Data (Fig. 2)

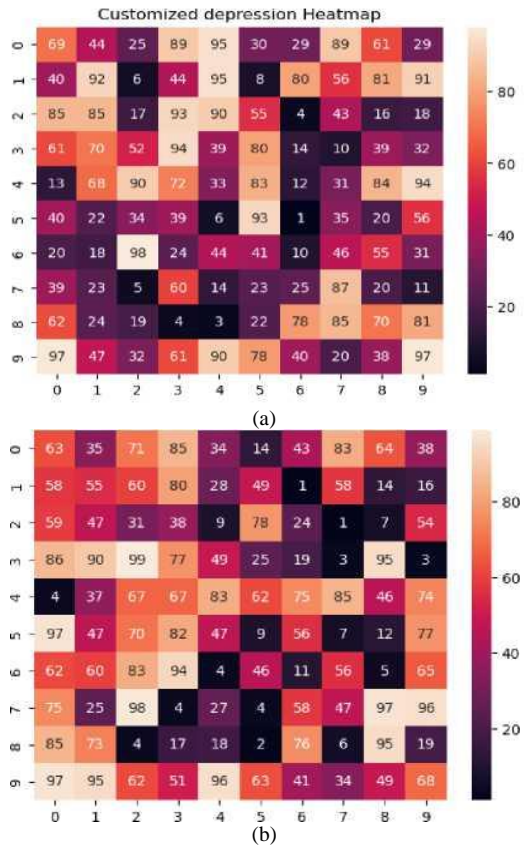


Fig. 2. Figure of Heatmap for Depression and Anxiety Data, (a) Customized depression heatmap; (b) Customized anxiety heatmap.

C. Proposed Work

This section presents a machine learning framework

proposed for the diagnosis of depression and anxiety using a digital dataset. The framework, illustrated in Fig. 3, encompasses a series of essential procedures including digital data preprocessing, feature extraction, feature selection, classification, and validation processes, all of which are crucial for the success of the approach. In the initial step, the preprocessing method is employed to remove extraneous noises and handle missing data. This critical stage involves selecting representative samples, ensuring data balance, normalizing the data, removing outliers, and addressing the issue of missing data. By performing these preprocessing steps, the dataset is prepared for further analysis.

During the feature extraction process, we randomly split the feature matrix into training and test sets. To improve classification accuracy and reduce the dimensionality of the feature matrix we employ the Recursive Feature Elimination (RFE) approach, for feature selection. At this point, an RFE algorithm is utilized on the training set to identify the subset

of features. It is important to note that each iteration of the proposed procedure using RFE results in a specific subset of features. The next step is to use the training and testing sets of RFE-derived features to train and validate the classification model appropriately. The selected attributes act as an input for the machine learning algorithm so that it can learn patterns and make predictions accurately. Finally, the classification performance of the proposed approach is assessed based on the outcomes obtained from classifying the testing set during each repetition of the process. The analysis shows that the technique works well in diagnosing anxiety and depression. In summary, if this detailed methodology is followed, which includes processes of data pre-processing, feature extraction, feature selection, classification, and validation, the machine-learning system proposed has the potential to diagnose depression and anxiety accurately using digital data.

[Please note that Fig. 3 is not included in the response as it is not visible to the AI model.]

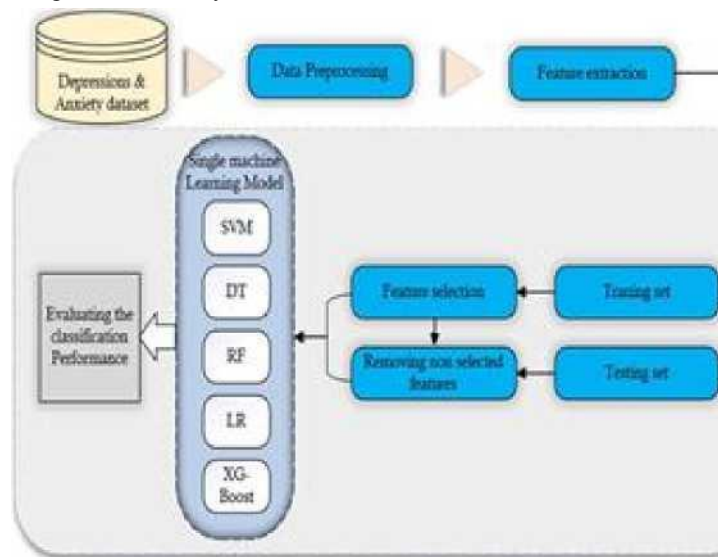


Fig. 3. Figure of the scheme for the proposed framework.

D. Methods

The present study is founded on an ample dataset of 783 individuals, where machine learning algorithms have been employed to prognosticate diagnoses with digital therapy. The outcomes have shown promising results, especially for depression and anxiety. The following algorithms, namely SVM, decision tree, logistic regression, random forest, and xgboost have been applied to both depressive and anxiety samples, and their corresponding results have been meticulously documented, as illustrated below in Table II and Table III.

Diagnosing depression and anxiety can be a complex process. Traditional methods rely on clinical interviews and standardized tests, but these can be time-consuming and subjective. Machine learning (ML) offers a promising alternative, but its "black box" nature often raises concerns. Here's a breakdown of how explainable ML methods can be used to improve the diagnosis of depression and anxiety:

TABLE III. THIS IS A TABLE OF RESULTS FOR DEPRESSION PREDICTIONS

| Algorithms Performance (%) | Accuracy | precision | recall | f1-score |
|----------------------------|----------|-----------|--------|----------|
| SVM | 0.91% | 0.91% | 1.00% | 0.95% |
| Decision tree | 0.91% | 0.95% | 0.94% | 0.95% |
| Random Forest | 0.93% | 0.94% | 0.98% | 0.96% |
| Logistic Regression | 0.94% | 0.95% | 0.98% | 0.96% |
| XGBOOST | 0.92% | 0.95% | 0.97% | 0.96% |

1) Data Collection and Preprocessing:

- Gather relevant data: This could include survey responses, electronic health records (EHRs), speech patterns, or physiological measurements.
- Clean and prepare the data: Ensure data quality by addressing missing values, inconsistencies, and outliers.

2) Model Selection and Training:

- Choose an explainable ML algorithm: Options include decision trees, rule-based models, or LIME (Local Interpretable Model-agnostic Explanations). These provide insights into how the model arrives at its conclusions.
- Train the model: Split your data into training and testing sets. Train the model on the training data, allowing it to learn the patterns associated with depression and anxiety.

3) Model Evaluation and Explanation:

- Evaluate performance: Use metrics like accuracy, precision, and recall to assess the model's effectiveness in identifying depression and anxiety.
- Generate explanations: Analyze the model's predictions to understand what factors contribute most to the diagnosis. This could involve highlighting specific survey responses, keywords from speech, or patterns in physiological data.

4) Clinical Integration and Refinement:

- Integrate the model into clinical workflow: Present the model's prediction alongside explanations to support the clinician's diagnosis.
- Refine the model: Continuously monitor and improve the model based on new data and feedback from clinicians.

5) Benefits of this Approach:

- Improved diagnostic accuracy: Explainable ML can identify subtle patterns missed by traditional methods.
- Enhanced patient engagement: Explanations can empower patients to understand their diagnosis and treatment options.
- Increased clinician confidence: Explainable models provide additional information to support clinical judgment.

By following these steps, healthcare professionals can leverage the power of ML for mental health diagnosis while maintaining transparency and building trust with patients.

IV. RESULTS

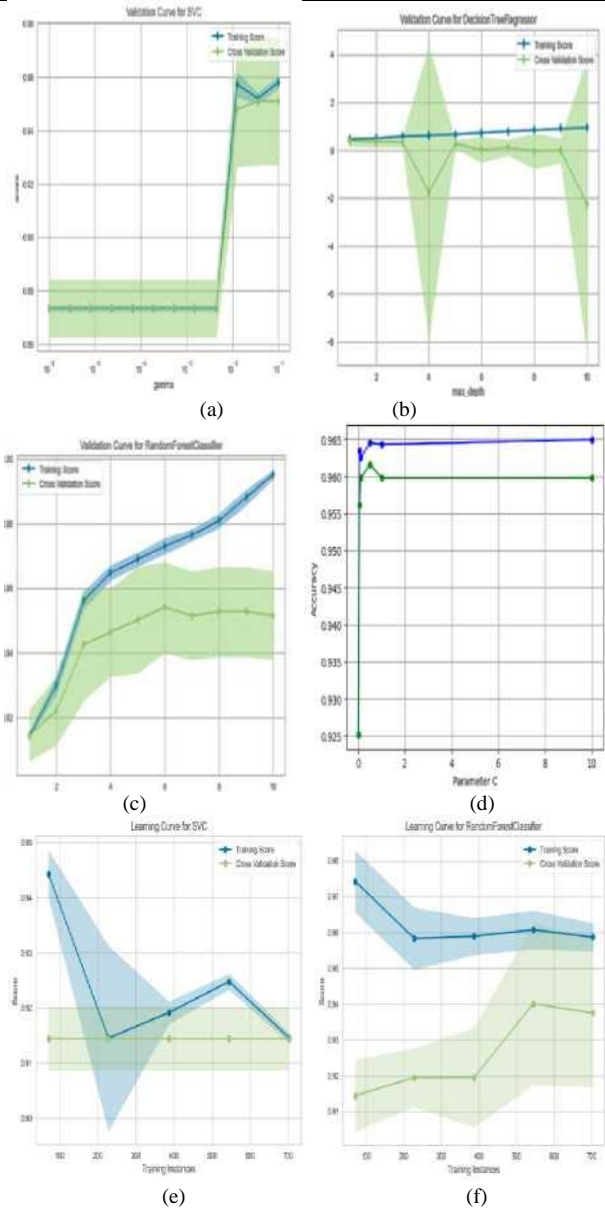
A. Results without Feature Selection

Next Stage the model used five classifiers; Support Vector Machine (SVM) Decision Tree (DT) Random Forest (RF) Logistic Regression (LR) and XGBoost to train a dataset having suicide, depression, and anxiety person. The system performs an algorithm of classification and documents its result for performance measurement. Below are stored classification performance metrics for each of the classifiers; SVM (0.91/0.91/1.00/0.95) DT (0.91/0.95/0.94/0.95) RF (0.93/0.94/0.98/0.96) LR (0.94 / 0.95 / 0.98 / 0.96) XGBoost (92%). This is shown in Table III as for the case it is summarized by accuracy=87% precision=87%, recall=1% and f1-score =93%. Further analysis also indicated that other

classifiers such as decision trees gave better results than SVM with an accuracy level of up to 99% and an f1 score=96%, recall=0.98, and f1- score=0.98) in Table IV. After analyzing the results, it was found that the logistic regression algorithm performed the best with the dataset. In contrast, the random forest algorithm showed effectiveness, with the anxiety dataset as, per the data provided.

TABLE IV. THIS IS A TABLE OF RESULTS FOR ANXIETY PREDICTIONS

| Algorithms Performance (%) | Accuracy | precision | recall | f1-score |
|----------------------------|----------|-----------|--------|----------|
| SVM | 0.87% | 0.87% | 1.00% | 0.93% |
| Decision tree | 0.93% | 0.94% | 0.99% | 0.96% |
| Random Forest | 0.94% | 0.94% | 1.00% | 0.97% |
| Logistic Regression | 0.91% | 0.91% | 1.00% | 0.95% |
| XGBOOST | 0.96% | 0.98% | 0.98% | 0.98% |



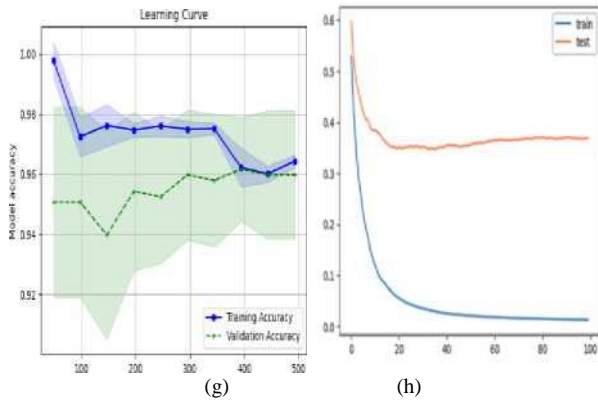


Fig. 4. This is a figure of the Validation and learning Curve for the depression data set, (a) Validation Curve for SVM; (b) Validation Curve for DT; (c) Validation Curve for RF; (d) Validation Curve for LR; (e) Learning Curve for SVM; (f) Learning Curve for RF; (g) Learning Curve for LR; (h) Learning Curve for XGboost.

Through the Yellow brick analyses, we incorporated the validation curve and learning curve techniques to assess the efficacy of all models for both the depression and anxiety datasets. As shown in Fig. 4 and Fig. 5. Furthermore, we utilized the SHAP Interaction Value and force plot techniques to explicate the predictions and customize them according to the requirements. As shown in Fig. 6 and Fig. 7.

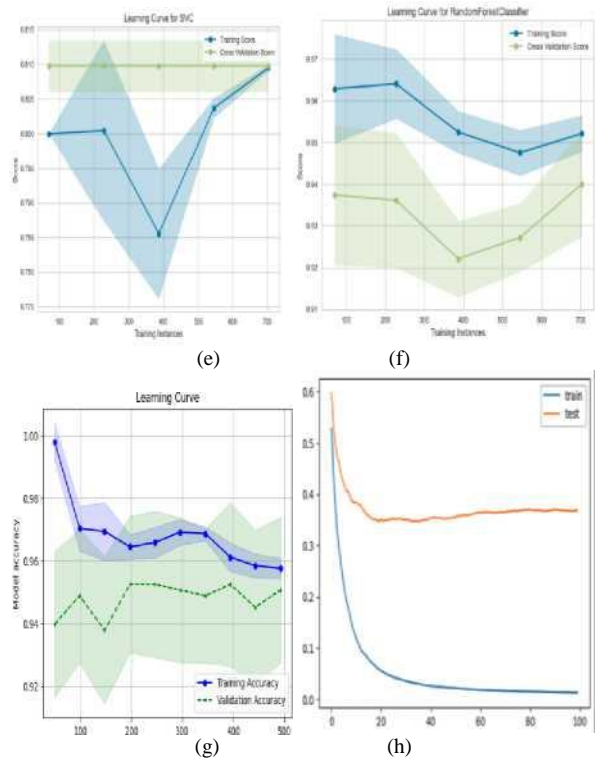


Fig. 5. This is a figure of the Validation and learning Curve for the anxiety data set, (a) Validation Curve for SVM; (b) Validation Curve for DT; (c) Validation Curve for RF; (d) Validation Curve for LR; (e) Learning Curve for SVM; (f) Learning Curve for RF; (g) Learning Curve for LR; (h) Learning Curve for XGboost.

B. Results with Feature Selection

In this part we identify the feature using the data set for all algorithms and use the feature selection method also called as feature elimination (RFE) it can point out those effective features decrease the fuzzy set and help algorithms and feature improvement performance the process of feature selection as shown in these result column were suiting of RFE make the inform of data novice in target value The result of RFE for depression data: SVM (accuracy = 0.92) precision = 0.92 recall = 1.00, f1 score = 0.97) DT (accuracy = 0.94) precision=0.96, recall=0.98, f1 score=0.97) RF (accuracy = 0.94) precision=0.94, recall=0.99, f1 score=0.96) LR (accuracy = 0.94) precision=0.96, recall=0.98, f1-score=0.97) RF (accuracy = 0.94) precision=0.94, recall=0.99, f1score=0.96) LR (accuracy=0.95) precision=0.97, recall=0.98, f1-score=0.97) XGboost (accuracy = 0.95) precision=0.96, recall=0.99, f1-score=0.97) depression for anxiety data: SVM (accuracy = 0.92) precision=0.92, recall=1.00, f1 score=0.97) DT (accuracy = 0.96) precision=0.97, recall=0.98, f1 score=0.98) RF (accuracy = 0.94) precision=0.93, recall=1.00, f1 score=0.97) LR (accuracy = 0.95) precision=0.96, recall=0.99, f1-score=0.97) XGboost (accuracy = 0.98) precision=0.98, recall=1.00, f1-score=0.99)in anxiety The result of performance of our algorithms after feature Selection as shown in this Table VI of our the algorithm decrease and increase performance after use feature of selection.

TABLE V. THIS IS A TABLE OF RESULTS FOR DEPRESSION PREDICTIONS WITH FEATURE SELECTION

| Algorithms Performance (%) | Accuracy | precision | recall | f1-score |
|----------------------------|----------|-----------|--------|----------|
| SVM | 0.94% | 0.94% | 1.00% | 0.97% |
| Decision tree | 0.94% | 0.96% | 0.98% | 0.97% |
| Random Forest | 0.94% | 0.94% | 0.99% | 0.96% |
| Logistic Regression | 0.95% | 0.97% | 0.98% | 0.97% |
| XGBOOST | 0.95% | 0.96% | 0.99% | 0.97% |

TABLE VI. THIS IS A TABLE OF RESULTS FOR ANXIETY PREDICTIONS WITH FEATURE SELECTION

| Algorithms Performance (%) | Accuracy | precision | recall | f1-score |
|----------------------------|----------|-----------|--------|----------|
| SVM | 0.92% | 0.92% | 1.00% | 0.96% |
| Decision tree | 0.96% | 0.97% | 0.98% | 0.98% |
| Random Forest | 0.94% | 0.93% | 1.00% | 0.97% |
| Logistic Regression | 0.95% | 0.96% | 0.99% | 0.97% |
| XGBOOST | 0.98% | 0.98% | 1.00% | 0.99% |

C. Results with Optimized Models

In this part of our study, we focused on enhancing the effectiveness of five machine learning models: SVM, DT, RF, LR, and XGboost. We used grid search methods to adjust the parameters of each model and determine which one performed best for both depression and anxiety data sets.

TABLE VII. THIS IS A TABLE OF RESULTS FOR DEPRESSION PREDICTIONS WITH THE OPTIMIZED MODEL

| Algorithms Performance (%) | best score |
|----------------------------|------------|
| SVM | 0.94% |
| Decision tree | 0.96% |
| Random Forest | 0.96% |
| Logistic Regression | 0.96% |
| XGBOOST | Nan |

TABLE VIII. THIS IS A TABLE OF RESULTS FOR ANXIETY PREDICTIONS WITH THE OPTIMIZED MODEL

| Algorithms Performance (%) | best score |
|----------------------------|------------|
| SVM | 0.92% |
| Decision tree | 0.95% |
| Random Forest | 0.95% |
| Logistic Regression | 0.93% |
| XGBOOST | Nan |

Table VII and Table VIII provide a comprehensive overview of the results obtained through this optimization process. These tables showcase the performance metrics and corresponding scores achieved by each algorithm across different evaluation measures. We have used grid search, where we compared different algorithms and chose the one with the best performance. This helped us to improve our diagnostic framework for anxiety and depression. During the phase of our study, we refined our machine learning algorithms by utilizing grid search methods. We also gathered information on parameter configurations that enhanced their

effectiveness. These findings have the potential to enhance approaches in health studies and showcase the advancements in using machine learning to diagnose anxiety and depression with greater accuracy and speed, than ever before.

D. Discussion

The current research offers insights by suggesting a range of machine-learning techniques that can effectively be used to compare different mental illnesses, including anxiety and depression. This proposed framework utilizes characteristics to improve the accuracy of diagnosing these disorders. The study's results are presented in three phases; a phase, without selecting features a subsequent phase with feature selection, and a final phase comparing the outcomes of both approaches. Importantly the results from feature selection showed performance compared to those without feature selection as shown in Tables III, IV, V and VI along, with the phase incorporating the optimized model, as illustrated in Tables VII and VIII [10].

Besides, as Table I above reveals, I studied more successfully with our findings compared to the health paper that talks about the diagnosis of his issues. I later state how we are definite that the methods that I am proposing will work also well and pass the exam. Finally, we are confident after comparing our results they are more successful in our study. Also, we have to pay attention to the problems that are raised on "Discriminant between psychosis and Major Depression". We can notice from Table I how the problem of different disorders rather our results which based on civil form.

V. EXPLANATION OF THE DEVELOPED MODEL

Our main focus is, on tackling the issue with two classes. To give an overview of how each feature influences the model's decisions as a whole we've created a summary visualization. This visual representation showcases the importance of features through a bar graph with the x-axis showing the key features and the y-axis indicating their significance. The length of each bar reflects its importance in the model. In this visualization blue signifies the impact on class AD while red represents its influence on class CN. The summary plot, in Fig. 6 depicts this for the scenario involving three classes (AD=0, CN=1, sMCI=2).

Based on Fig. 6, we observe that the CDMemory, Q7, and Q4 forms are considered the most important features. To further explore the importance of each feature on an instance level, we utilized SHAP explainers to generate a waterfall plot. The waterfall plot presents all the features contributing to the decision-making process, sorted according to their SHAP values. Fig. 7(A, B, C, D) demonstrates the waterfall plots, where each plot displays the Base_value, representing the value according to the entire dataset, and the predict_proba_value, representing the probability for the specific instance. The left side of the plot shows the feature values for that instance, while the arrows indicate the feature contributions towards the prediction. Each row in the plot represents negative and positive contributions, depicted by blue and red bars, respectively. These explanations assist medical experts in understanding and placing trust in the decisions made by the model.

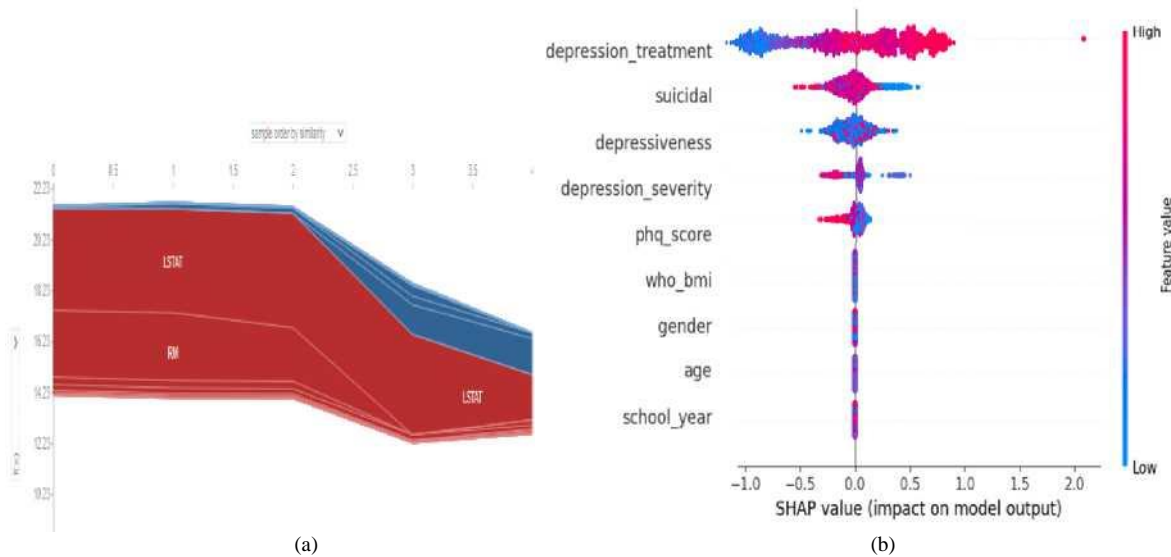


Fig. 6. This is a figure of SHAP Interaction Value and force plot for the depression data set, (a) SHAP value impact for XGboost; (b) Force plot for XGboost.

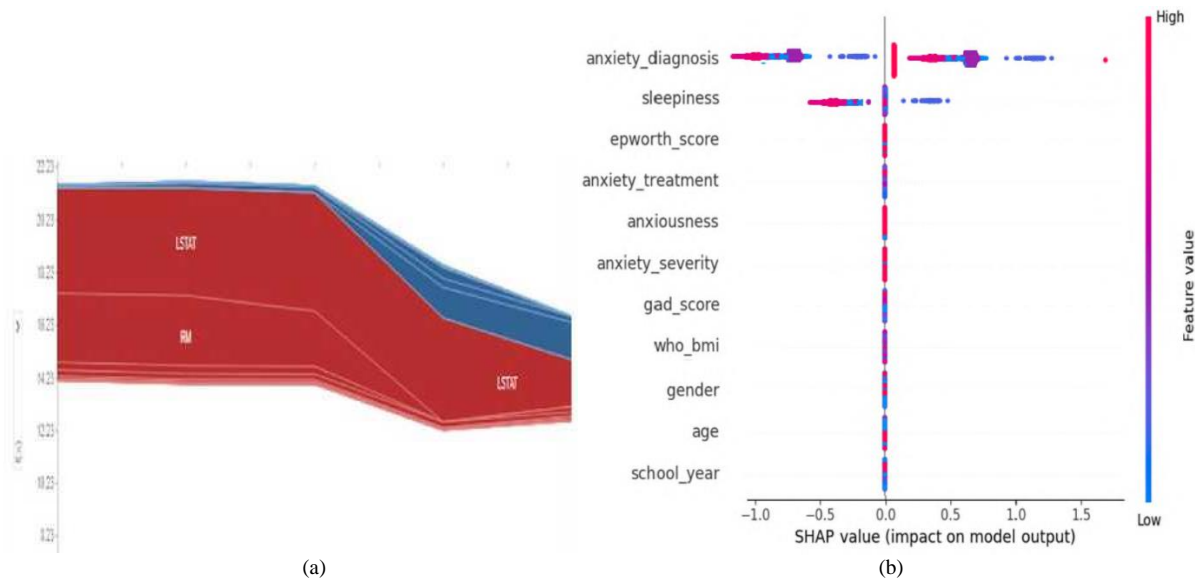


Fig. 7. This is a figure of SHAP Interaction Value and force plot for anxiety data set, (a) SHAP value impact for XGboost; (b) Force plot for XGboost.

VI. CONCLUSION

According to the results of this study, it is possible to deduce that using treatment information alone can help accurately forecast treatment results by examining shifts, in anxiety and depression indicators. Cutting-edge machine learning algorithms showed accuracy in these forecasts providing guidance, for doctors when deciding on low-resource online therapies and conventional medical interventions. The strong precision of these models indicates their ability to identify the suitable level of traditional or digital care before starting treatment. It is a matter of great concern to the patients as this can save them time, energy, and money and just point them promptly toward appropriate healthcare resources. In addition to this, these results might guide healthcare providers toward identifying those patients likely not to benefit from online therapies to properly allocate their limited time and resources. By making use of these

complicated machine learning algorithms, clinicians will enhance their decision-making regarding treatment that is evidence-based and patient-specific which ultimately leads to better outcomes for patients seeking mental health care by these models could alter its course through efficient guidance to suitable treatment options for those affected. However, more research is required before it can be determined if this knowledge applies or scales up across different populations of patients and within diverse healthcare contexts. Further studies in this area will promote the development of strategies for treating mental illnesses thereby enhancing care for anxiety and depression disorders thus improving the quality of life among individuals with such conditions.

REFERENCES

- [1] Cho G, Yim J, Choi Y, Ko J, Lee SH. Review of Machine Learning Algorithms for Diagnosing Mental Illness. *Psychiatry Investig.* 2019;16(4):262-269. doi:10.30773/pi.2018.12.21.2.

- [2] Roelfs D, Alnæs D, Frei O, et al. Phenotypically independent profiles relevant to mental health are genetically correlated. *Transl Psychiatry*. 2021;11(1):202. doi:10.1038/s41398-021-01313-x.
- [3] Nudel R, Wang Y, Appadurai V, et al. A large-scale genomic investigation of susceptibility to infection and its association with mental disorders in the Danish population. *Transl Psychiatry*. 2019;9(1):283. doi:10.1038/s41398-019-0622-3.
- [4] Movahed RA, Jahromi GP, Shahyad S, Meftahi GH. A major depressive disorder classification framework based on EEG signals using statistical, spectral, wavelet, functional connectivity, and nonlinear analysis. *J Neurosci Methods*. 2021;358:109209. doi:10.1016/J.JNEUMETH.2021.109209.
- [5] Li X, Hu B, Sun S, Cai H. EEG-based mild depressive detection using feature selection methods and classifiers. *Comput Methods Programs Biomed*. 2016;136:151-161. doi:10.1016/j.cmpb.2016.08.010.
- [6] Liu G Di, Li YC, Zhang W, Zhang L. A Brief Review of Artificial Intelligence Applications and Algorithms for Psychiatric Disorders. *Engineering*. 2020;6(4):462-467. doi:10.1016/J.ENG.2019.06.008.
- [7] Hossain MM, Purohit N, Sultana A, Ma P, McKyer ELJ, Ahmed HU. Prevalence of mental disorders in South Asia: An umbrella review of systematic reviews and metaanalyses. *Asian J Psychiatr*. 2020;51:102041. doi:10.1016/j.ajp.2020.102041.
- [8] Teismann T, Lukasczek K, Hiller TS, et al. Suicidal ideation in primary care patients suffering from panic disorder with or without agoraphobia. *BMC Psychiatry*. 2018;18(1):305. doi:10.1186/s12888-018-1894-5.
- [9] Malla A, Joobar R, Garcia A. "Mental illness is like any other medical illness": a critical examination of the statement and its impact on patient care and society. *Journal of Psychiatry and Neuroscience*. 2015;40(3):147-150. doi:10.1503/jpn.150099.
- [10] Jan A, Meng H, Gaus YFBA, Zhang F. Artificial Intelligent System for Automatic Depression Level Analysis Through Visual and Vocal Expressions. *IEEE Trans Cogn Dev Syst*. 2018;10(3):668-680. doi:10.1109/TCDS.2017.2721552.
- [11] Baskaran A, Farzan F, Milev R. The comparative effectiveness of electroencephalographic indices in predicting response to escitalopram therapy in depression: A pilot study. *J Affect Disord*. 2018;7.
- [12] Pinto JV, Saraf G, Kozicky J, et al. Remission and recurrence in bipolar disorder: The data from health outcomes and patient evaluations in bipolar disorder (HOPE-BD) study. *J Affect Disord*. 2020;268:150-157. doi:10.1016/j.jad.2020.03.018.
- [13] Jacobson NC, Nemesure MD. Using Artificial Intelligence to Predict Change in Depression and Anxiety Symptoms in a Digital Intervention: Evidence from a Transdiagnostic Randomized Controlled Trial. *Psychiatry Res*. 2021;295:113618. doi:10.1016/j.psychres.2020.113618.
- [14] van Krugten FCW, Kaddouri M, Goorden M, et al. Indicators of patients with major depressive disorder in need of highly specialized care: A systematic review. *PLoS One*. 2017;12(2):e0171659. doi:10.1371/journal.pone.0171659.
- [15] Jacobson NC, Feng B. Digital phenotyping of generalized anxiety disorder: using artificial intelligence to accurately predict symptom severity using wearable sensors in daily life. *Transl Psychiatry*. 2022;12(1):336. doi:10.1038/s41398-022-02038-1.
- [16] Nemesure MD, Heinz M V, Huang R, Jacobson NC. Predictive modeling of depression and anxiety using electronic health records and a novel machine learning approach with artificial intelligence. *Sci Rep*. 2021;11(1):1980. doi:10.1038/s41598-021-81368-4.
- [17] Zhu J, Jiang C, Chen J, et al. EEG-based depression recognition using improved graph convolutional neural network. *Comput Biol Med*. 2022;148:105815. doi:10.1016/j.combiomed.2022.105815.
- [18] Pearson R, Pisner D, Meyer B, Shumake J, Beevers CG. A machine learning ensemble to predict treatment outcomes following an Internet intervention for depression. *Psychol Med*. 2019;49(14):2330-2341. doi:10.1017/S003329171800315X.
- [19] Baskaran A, Farzan F, Milev R, et al. The comparative effectiveness of electroencephalographic indices in predicting response to escitalopram therapy in depression: A pilot study. *J Affect Disord*. 2018;227:542-549. doi:10.1016/j.jad.2017.10.028.
- [20] Hasanzadeh F, Mohebbi M, Rostami R. Prediction of rTMS treatment response in major depressive disorder using machine learning techniques and nonlinear features of EEG signal. *J Affect Disord*. 2019;256:132-142. doi:10.1016/j.jad.2019.05.070.
- [21] Graham S, Depp C, Lee EE, et al. Artificial Intelligence for Mental Health and Mental Illnesses: an Overview. *Curr Psychiatry Rep*. 2019;21(11):116. doi:10.1007/s11920-019-1094-0.
- [22] Mehta A, Niles AN, Vargas JH, Marafon T, Couto DD, Gross JJ. Acceptability and Effectiveness of Artificial Intelligence Therapy for Anxiety and Depression (Youper): Longitudinal Observational Study. *J Med Internet Res*. 2021;23(6):e26771. doi:10.2196/26771.
- [23] Månsson KNT, Frick A, Boraxbekk CJ, et al. Predicting the long-term outcome of Internet-delivered cognitive behavior therapy for social anxiety disorder using fMRI and support vector machine learning. *Transl Psychiatry*. 2015;5(3):e530. doi:10.1038/tp.2015.22.
- [24] Lenhard F, Sauer S, Andersson E, et al. Prediction of outcome in internet-delivered cognitive behavior therapy for pediatric obsessive-compulsive disorder: A machine learning approach. *Int J Methods Psychiatr Res*. 2018;27(1). doi:10.1002/mpr.1576.
- [25] PUTHANKATTIL SD, JOSEPH PK. CLASSIFICATION OF EEG SIGNALS IN NORMAL AND DEPRESSION CONDITIONS BY ANN USING RWE AND SIGNAL ENTROPY. *J Mech Med Biol*. 2012;12(04):1240019. doi:10.1142/S0219519412400192.
- [26] Ahmaddou M, Adeli H, Adeli A. Fractality analysis of the frontal brain in major depressive disorder. *International Journal of Psychophysiology*. 2012;85(2):206-211. doi:10.1016/j.ijpsycho.2012.05.001.
- [27] Hosseinfard B, Moradi MH, Rostami R. Classifying depression patients and normal subjects using machine learning techniques and nonlinear features from EEG signal. *Comput Methods Programs Biomed*. 2013;109(3):339-345. doi:10.1016/j.cmpb.2012.10.008.
- [28] Mumtaz W, Xia L, Ali SSA, Yasin MAM, Hussain M, Malik AS. Electroencephalogram (EEG)-based computer-aided technique to diagnose major depressive disorder (MDD). *Biomed Signal Process Control*. 2017;31:108-115. doi:10.1016/j.bspc.2016.07.006.
- [29] Liao SC, Wu CT, Huang HC, Cheng WT, Liu YH. Major Depression Detection from EEG Signals Using Kernel Eigen-Filter-Bank Common Spatial Patterns. *Sensors (Basel)*. 2017;17(6). doi:10.3390/s17061385.
- [30] Acharya UR, Oh SL, Hagiwara Y, Tan JH, Adeli H, Subha DP. Automated EEG-based screening of depression using deep convolutional neural network. *Comput Methods Programs Biomed*. 2018;161:103-113. doi:10.1016/j.cmpb.2018.04.012.
- [31] Hazem El-Bakry: "Comments on Using MLP and FFT for Fast Object/Face Detection," Proc. of IEEE IJCNN'03, Portland, Oregon, pp. 1284-1288, July, 20-24, 2003.
- [32] Hazem M. El-Bakry, and Nikos Mastorakis "New Fast Normalized Neural Networks for Pattern Detection," Image and Vision Computing Journal, vol. 25, issue 11, 2007, pp. 1767-1784.
- [33] Hazem M. El-Bakry, and Nikos Mastorakis, "A New Fast Forecasting Technique using High Speed Neural Networks," *WSEAS Transactions on Signal Processing*, vol. 4, Issue 10, Oct. 2008, pp. 573-595.
- [34] Hazem M. El-Bakry, and Qiangfu Zhao, "Speeding-up Normalized Neural Networks For Face/Object Detection," *Machine Graphics & Vision Journal (MG&V)*, vol. 14, No.1, 2005, pp. 29-59.
- [35] Hazem M. El-Bakry, "New Fast Time Delay Neural Networks Using Cross Correlation Performed in the Frequency Domain," *Neurocomputing Journal*, vol. 69, October 2006, pp. 2360-2363.
- [36] Hazem M. El-Bakry "Fast Iris Detection for Personal Verification Using Modular Neural Networks," Proc. of the 7th Fuzzy Days International Conference, Dortmund, Germany, October 1-3, 2001, pp. 269283.
- [37] Hazem M. El-Bakry, M. A. Abo-elsoud, and M. S. Kamel, "Fast Modular Neural Networks for Human Face Detection," Proc. of IEEE-INNS-ENNS International Joint Conference on Neural Networks, Como, Italy, Vol. III, pp. 320-324, 24-27 July, 2000.
- [38] Hazem M. El-Bakry, "Fast Virus Detection by using High Speed Time Delay Neural Networks," *Journal of Computer Virology*, vol.6, no.2, 2010, pp.115-122.
- [39] Hazem M. El-Bakry, and Nikos Mastorakis, "Realization of E-University for Distance Learning," *WSEAS Transactions on Computers*, vol. 8, issue 1, Jan. 2009, pp. 48-62.
- [40] Hazem M. El-Bakry, "An Efficient Algorithm for Pattern Detection

- using Combined Classifiers and Data Fusion," *Information Fusion Journal*, vol. 11, issue 2, April 2010, pp. 133-148.
- [41] Hazem El-Bakry, "Face Detection Using Neural Networks and Image Decomposition," Proc. of INNS-IEEE International Joint Conference on Neural Networks, 12-17 May, 2002, Honolulu, Hawaii, USA.
- [42] Hazem El-Bakry, "Fast Face Detection Using Neural Networks and Image Decomposition," Proc. of the 6th International Computer Science Conference, AMT 2001, Hong Kong, China, December 18-20, 2001, pp.205-215.
- [43] Hazem M. El-Bakry and Mohamed Hamada, "A New Implementation for High Speed Neural Networks in Frequency Space," Lecture Notes in Artificial Intelligence, Springer, KES 2008, Part I, LNAI 5177, pp. 33-40.
- [44] Hazem M. El-Bakry, and Qiangfu Zhao, "Fast Time Delay Neural Networks," *International Journal of Neural Systems*, vol. 15, no.6, December 2005, pp.445-455.
- [45] Hazem M. El-Bakry, "Human Iris Detection Using Fast Cooperative Modular Neural Nets," *Proc. of INNS-IEEE International Joint Conference on Neural Networks*, pp. 577-582, 14-19 July, 2001, Washington, DC, USA.
- [46] Hazem M. El-Bakry, "A Novel High Speed Neural Model for Fast Pattern Recognition," *Soft Computing Journal*, vol. 14, no. 6, 2010, pp. 647-666.
- [47] Menna Elkhateeb, Abdulaziz Shehab, and Hazem El-bakry, "Mobile Learning System for Egyptian Higher Education Using Agile-Based Approach," *Education Research International*, Volume 2019, Article ID 7531980, 13 pages.
- [48] Hazem M. El-Bakry, and Qiangfu Zhao, "Fast Normalized Neural Processors For Pattern Detection Based on Cross Correlation Implemented in the Frequency Domain," *Journal of Research and Practice in Information Technology*, Vol. 38, No.2, May 2006, pp. 151-170.
- [49] Hazem M. El-Bakry, "New Fast Principal Component Analysis for Face Detection," *Journal of Advanced Computational Intelligence and Intelligent Informatics*, vol.11, No.2, 2007, pp. 195-201.

An Integrated Arnold and Bessel Function-based Image Encryption on Blockchain

Abhay Kumar Yadav, Virendra P. Vishwakarma

University School of Information & Communication Technology,
Gobind Singh Indraprastha University, New Delhi 110078, India

Abstract—Images store large amount of information that are used in visual representation, analysis, and expression of data. Storage and retrieval of images possess a greater challenge to researchers globally. This research paper presents an integrated approach for image encryption and decryption using an Arnold map and first-order Bessel function-based chaos. Traditional methods of image encryption are generally based on single algorithms or techniques, making them vulnerable to various security threats. To address these challenges, our novel method combines the robustness of Arnold transformation with the unique properties of Bessel functions-based chaos. Furthermore, we implemented the decentralized nature of blockchain technology for storing and managing encryption keys securely. By utilizing blockchain's tamper-resistant and transparent ledger, we enhance the integrity and traceability of the encryption process, mitigating the risk of unauthorized access or tampering. The proposed method leverages the chaotic behavior of Bessel function for enhancing security of encryption process. A chaos obtained from first order Bessel function has been utilized for encryption key for encryption after Arnold transformation. The obtained cypher text is stored in blockchain in form of encrypted blocks for secured storage and added security. Experimental evaluations demonstrate the efficiency, effectiveness and robustness of our proposed encryption method when compared with performance of previously developed techniques highlighting the superiority of the proposed method in protecting image data against unauthorized access.

Keywords—Arnold transformation; block encryption; Bessel functions; blockchain

I. INTRODUCTION

Since digital image consists of large amount of distributed information, securing them is a major task for researchers. Also, digital images are less sensitive when compared with text data creating a minor change in image will create a drastic change in image pixels attribute. Digitized medical images provide an important aspect in storing patient's data as well as in diagnosing, treating and monitoring diseases [1].

The increasing amount of medical data generated by hospitals and clinics has led to the need for efficient storage and retrieval of these images [2]. Cloud storage services provide a reliable and cost-effective solution for storing large volumes of medical images. However, managing the security aspect of medical images stored in cloud is a major concern due to the personal and sensitive information of medical data [3]. Combining blockchain application with areas of medical research may provide newer potential in the biomedical field research. Sectors such as hospital and supply chain

management of medicines and drugs may be benefitted from blockchain as it will impart a safer, secure, and reliable supply chain.

Blockchain technology can be used as a distributed electronic database encrypted by different cryptography functions thus eliminating existing limitations. Traditional systems use centralized authentication system making it difficult for various users to access database due to limited correct credential access and server capacity. Blockchain is similar to a distributed ledger, with different transactions encrypted together and, in the chain, and are permanent. Different features provided by blockchain have created newer use case application for cross integration with existing technologies for deployment across different domain. Researchers are working on enhancing these attributes for implementing them in image security [4]. Blockchain can work as a potential solution to the existing security issues in medical images.

The Arnold transformation represents a permutation-oriented cryptographic method designed to rearrange the pixel values within an image in a predictable yet intricate manner. This rearrangement instigates both confusion and dispersion, thereby fortifying the encrypted image against a spectrum of cryptographic assaults whereas, Bessel functions, a subset of mathematical special functions, are employed to add an additional layer of complexity to the transformed image. Through the application of Bessel functions, encryption is realized for each image by adapting the function's parameters dynamically in accordance with cryptographic keys. This combination approach enhances the overall security of the encryption scheme by customizing the encryption process for individual images

This paper aims to bridge the gap between the theoretical advancements in chaos theory, neural networks, and biological concepts, and their practical application in image security. By fusing these diverse elements into a unified framework, we strive to offer an innovative solution that addresses the challenges of image encryption in a rapidly evolving digital landscape. Through rigorous analysis and experimentation, we demonstrate the efficacy and robustness of the proposed Arnold Bessel-based framework for securing images.

The structure of this paper is arranged in following section: Section II highlights basic overview of the foundational concepts and related works. In Section III, the proposed methodology detailing the integration of Arnold maps and Bessel functions, Section IV delves into experimentation and

evaluation metrics. The results and discussions with previously developed techniques are also presented in this section. Section V discusses the storage on blockchain followed by conclusions and avenues for future research in Section VI.

II. BACKGROUND

A. Arnold Transformation

The Arnold Transform is a reversible image transformation used for image encryption. It is a simple and efficient algorithm that provides a level of security through its chaotic behavior. The Arnold Transform involves performing multiple iterations of a specific operation on image pixels to shuffle and disperse the pixel values, thus altering the image's appearance. This transformation can be used to encrypt an image, making it difficult for unauthorized users to understand the original content without the decryption process [5].

The Arnold transform is a chaotic transformation that can be used to scramble the pixels of an image, making it difficult to recognize. It is a simple transformation to implement, but it is very effective at disrupting the statistical properties of the image. Fig. 1 shows the distribution of image co-ordinates.

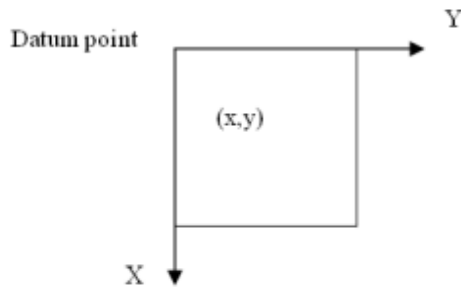


Fig. 1. Distribution of image coordinates.

The Arnold transform is area-preserving, meaning that it does not change the overall pixels in the image. However, it does scramble the pixels so that they are no longer correlated with their original positions [6]. Table I shows the scrambling cycle of Arnold transform based on size of image.

TABLE I. ARNOLD SCRAMBLING ALGORITHM CYCLE

| Size of image (N) | Cycle of scramble (T) | Size of image (N) | Cycle of scrambling (T) |
|-------------------|-----------------------|-------------------|-------------------------|
| 3 | 4 | 25 | 50 |
| 4 | 3 | 32 | 24 |
| 5 | 10 | 64 | 49 |
| 6 | 12 | 100 | 150 |
| 7 | 8 | 120 | 60 |

The Arnold transform works by taking the pixel coordinates (x, y) and transforming them to a new set of coordinates (x', y') using the following equations:

$$\begin{bmatrix} x' \\ y' \end{bmatrix} = \begin{bmatrix} ax & by \\ cx & dy \end{bmatrix} \text{ mod } M \quad (1)$$

where a, b, c, and d are integer coefficients that satisfy the condition $ad - bc = 1$. M is the size of the image in pixels.

$$\begin{bmatrix} x_n + 1 \\ y_n + 1 \end{bmatrix} = \begin{bmatrix} x \\ y \end{bmatrix} \begin{bmatrix} ab + 1 & -b \\ -a & 1 \end{bmatrix} \quad (2)$$

The Arnold Transform is a lightweight and fast encryption method, but it may not provide the same level of security as more complex encryption algorithms. Therefore, it is often used together with other encryption techniques for enhancing the security of image encryption applications [7].

B. Bessel's Function

The Bessel function is a mathematical function that plays a crucial role in various scientific and engineering applications, including the field of chaotic neural networks. The Bessel function can be used to create chaotic behavior within a neural network, which is desirable for certain applications that require randomness and unpredictability [8].

The Bessel function introduces non-linear dynamics into the neural network, resulting in complex patterns and behaviors. This chaotic behavior can enhance the network's capacity to process and analyze complex data, making it suitable for tasks such as image encryption and decryption [9].

In the process of creating a chaotic neural network using the Bessel function, the network's connections and weights are usually initialized randomly. As the network receives input data and performs computations, the Bessel function introduces non-linear transformations that lead to chaotic dynamics. This chaos can be harnessed to achieve desired behaviors, such as robust encryption and decryption of images. A generalized first order Bessel's Function is shown in Fig. 2.

The Bessel function can enhance the security and unpredictability of the encryption process. The complex and non-linear transformations introduced by the Bessel function make it challenging for unauthorized users to decipher the encrypted data without the proper decryption key [10].

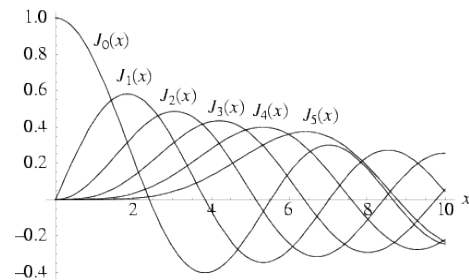


Fig. 2. Generalized representation of first order Bessel's function.

III. METHODOLOGY

A. Previously Developed Techniques with Proposed Work

A detailed list of different encryption techniques presented by different researchers is listed in Table II.

B. Proposed Framework

Fig. 3 shows the methodology for the proposed framework followed by discussion on encryption and decryption techniques. The framework implements Arnold and Bessel's functions together for creating the chaotic encryption. The detailed algorithm for the encryption and decryption is mentioned in algorithm below.

Algorithm

| |
|---|
| <p>Encryption</p> <p>1. Arnold Map Transformation:</p> <p>1.1 For each block of pixels in the image:</p> <p>1.2 Apply the Arnold map transformation to the pixel coordinates.</p> <p>1.3 Shuffle the pixels based on the transformed coordinates.</p> <p>2. Bessel Function Key Generation:</p> <p>2.1 Generate Bessel function coefficients using encryption parameters.</p> <p>2.2. Create a set of Bessel functions based on the coefficients.</p> <p>3. Pixel Transformation with Bessel Functions:</p> <p>3.1 For each block of pixels in the image:</p> <p>3.1.1. Apply a Bessel function transformation to the pixel values using the generated Bessel functions.</p> <p>3.1.2. Store the transformed pixel values in the encrypted image E.</p> <p>Decryption</p> <p>1. Pixel by pixel Bessel Decryption</p> <p>The chaos generated after encryption are decoded back to obtain original image</p> <p>2. Arnold Decoding</p> <p>Images are descrambled for obtaining the original.</p> |
|---|

TABLE II. PREVIOUSLY DEVELOPED TECHNIQUES WITH PRESENTED TECHNIQUE

| Techniques | Encryption Description | Technique |
|------------|---|--|
| T1 | 1) Permutation by zig-zag pattern 2) Initial permutation from plain image Diffusion using XOR. | Zig-zag scan based chaotic feedback convolution model [11]. |
| T2 | 1) DNA module based Intermediate Cypher image creation RNA module to produce final cypher image. | DNA rules, DNA-XOR operators and chaotic map [12]. |
| T3. | 1) Plain image hash value used for chaos generation Diffusion using DNA, XOR and RNA codons operations | Chaotic Evolutionary Biomolecules Model [13]. |
| T4. | 1) Plain image converted in DNA image by encoding rules 2) BST is created from DNA-BST is imposed on DNA image using XOR | BST, DNA coding, Logistic map [14]. |
| T5. | 1) Polynomial is selected by interval bisection at regular interval method creating sequence useful in encryption 2) Circular shift in confusion matrix Substitution matrix and masked image | bisection at interval method, Circular Shift, Substitution and XOR method [15]. |
| T6. | 1) Permutation by points obtained from Regula Falsi method 2) Encryption by image pixel substitution and iterative and cyclic shift. | Regula Falsi method, Substitution, Iterative addition, Circular Shift [16]. |
| T7. | 1) A unified key for selecting key pixels. 2) DNA encryption by pixel value substitution on key pixels Other pixels are encrypted by key stream of hyperchaotic Lorenz system | Key pixels, hyperchaotic Lorenz system scrambling, DNA encoding, Cyclic shift [17] |
| T8. | 1) Fibonacci based pixels transformation 2) Scrambled image XOR with key image 3) Pixel values changed using Tribonacci Transform | Fibonacci and Tribonacci transformation [18]. |
| Proposed | 1) Image encryption by Arnold Transform. 2) A chaos obtained from first order Bessel function for encryption key for encryption at mid-level. 3) Storing the encrypted Data on blockchain for enhanced security | Arnold Transformation, Bessel Function, Blockchain |

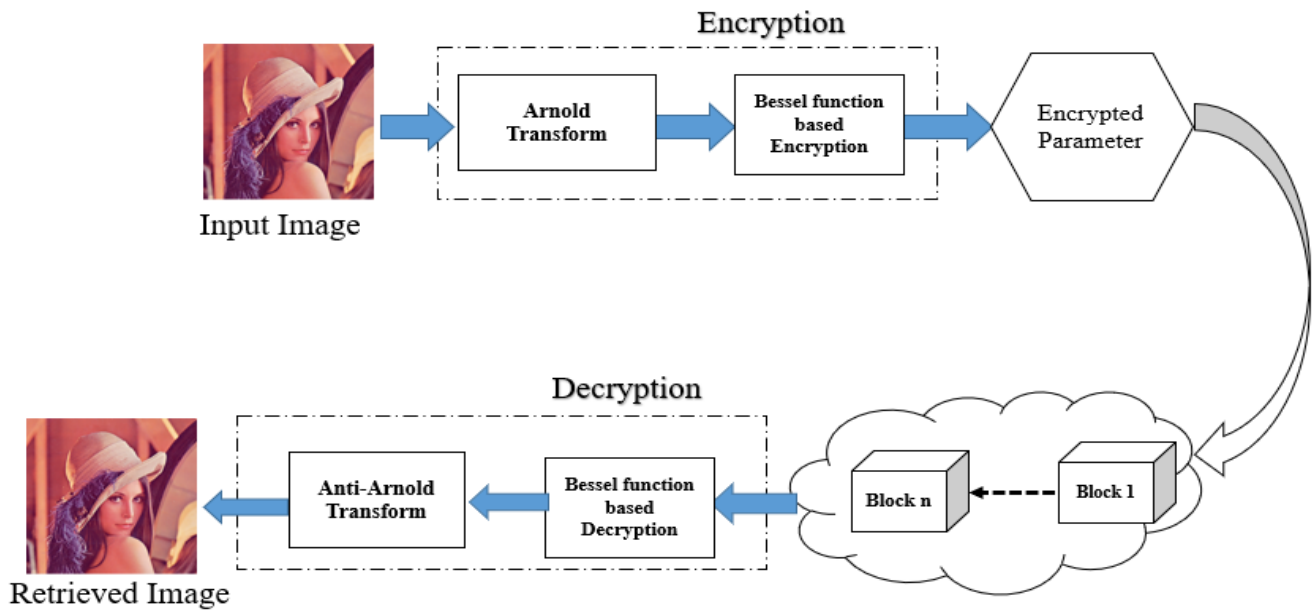


Fig. 3. Proposed Encryption and Decryption Framework

IV. EXPERIMENTAL RESULTS AND PERFORMANCE EVALUATION

The framework is executed using MATLAB R2023a software working on 64-bit machine with CPU Intel i9-4500U with 1.90 GHz processor and 8 GB RAM on Windows 11 OS. In the following section, the Lena image [19] is taken as the test image for evaluating our framework. Fig. 4 shows the different operations that are being performed on the test image.

To comprehensively evaluate the proposed framework, different performance evaluation measures are implemented working on following aspects: Entropy, execution time, correlation analysis. A detailed measures calculation and proposed methods results along with comparison with previously developed bench-mark approaches are presented in the Tables III, IV and V.

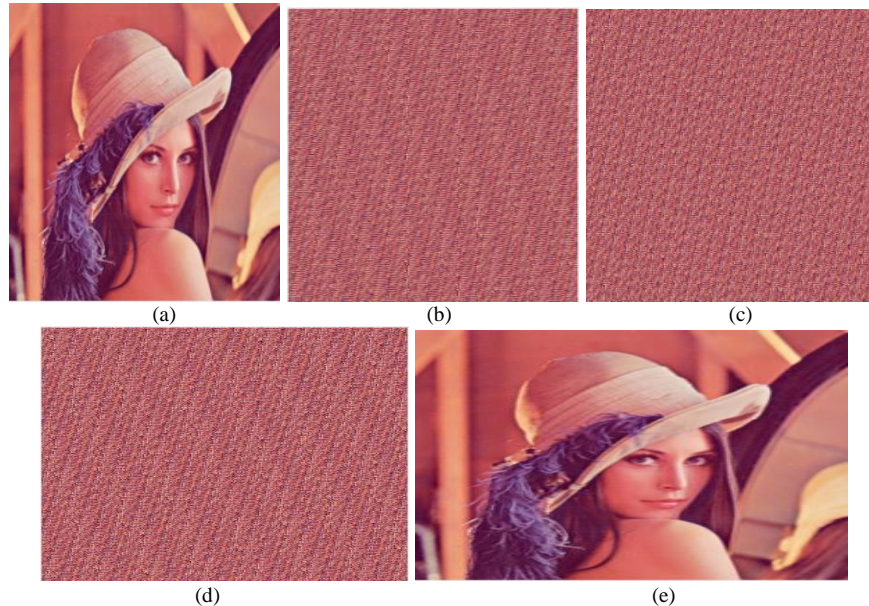


Fig. 4. Image storage and Retrieval a) Input Image b) Image after Arnold Transform c) Image after Arnold + Bessel d) Image Decryption after Bessel Arnold e) Retrieved Images.

TABLE III. PERFORMANCE COMPARISON IN TERMS OF CORRELATION COEFFICIENT

| Method | Correlation Coefficient | | |
|----------|-------------------------|----------|----------|
| | Horizontal | Vertical | Diagonal |
| T1 | -0.002062 | 0.003685 | 0.000249 |
| T2 | 0.0054 | 0.0192 | 0.0055 |
| T4 | 0.00007 | 0.0017 | 0.0008 |
| T5 | 0.002097 | 0.002767 | -0.0029 |
| T6 | 0.001853 | 0.001984 | 0.000743 |
| T7 | -0.0026 | -0.0033 | 0.0004 |
| T8 | -0.014825 | -0.00066 | 0.007183 |
| Proposed | 0.00136 | 0.000217 | 0.00526 |

TABLE IV. PERFORMANCE COMPARISON IN TERMS OF EXECUTION TIME

| Technique | Execution Time |
|-----------|----------------|
| T1 | 10.440 |
| T2 | 1.492 |
| T3 | 3.009 |
| T4 | 0.620 |
| T5 | 0.798 |
| T6 | 0.531 |
| T7 | 0.288 |
| T8 | 0.634 |
| Proposed | 3.687 |

TABLE V. PERFORMANCE COMPARISON IN TERMS OF ENTROPY

| Technique | Entropy |
|-----------|---------|
| T1 | 7.9994 |
| T2 | 7.9994 |
| T3 | 7.9995 |
| T4 | 7.9992 |
| T5 | 7.9993 |
| T6 | 7.9994 |
| T7 | 7.9993 |
| T8 | 7.9994 |
| Proposed | 7.7634 |

The comparative analysis provides a holistic understanding of the strengths and limitations of the proposed integrated Arnold and Bessel function-based encryption scheme relative to existing methods. The comparisons highlight the superiority of the proposed framework in terms of entropy, execution time, and correlation analysis, reaffirming its efficacy in ensuring robust image encryption.

The results obtained from the comprehensive evaluation demonstrate that our proposed framework provide the expected encryption of images. On evaluation in terms of correlation coefficient, execution time and entropy showed the effectiveness and superiority of the proposed framework in achieving high levels of security and randomness in image

encryption, thus validating its potential for practical deployment in real-world scenarios.

V. BLOCKCHAIN STORAGE

Ganache software [20] is capable of providing real-time simulation of smart contract executions based on Ethereum platform. Different use case and application can be simulated in Ganache based on its smart contract's features. Ganache provides 10 block free for mining and simulation, we have used only one block for storing the encrypted data obtained after the encryption process on Ganache software. Fig. 5 shows the working of Ganache software in storing encrypted parameters in detail with its implementation on front-end and back-end platform.

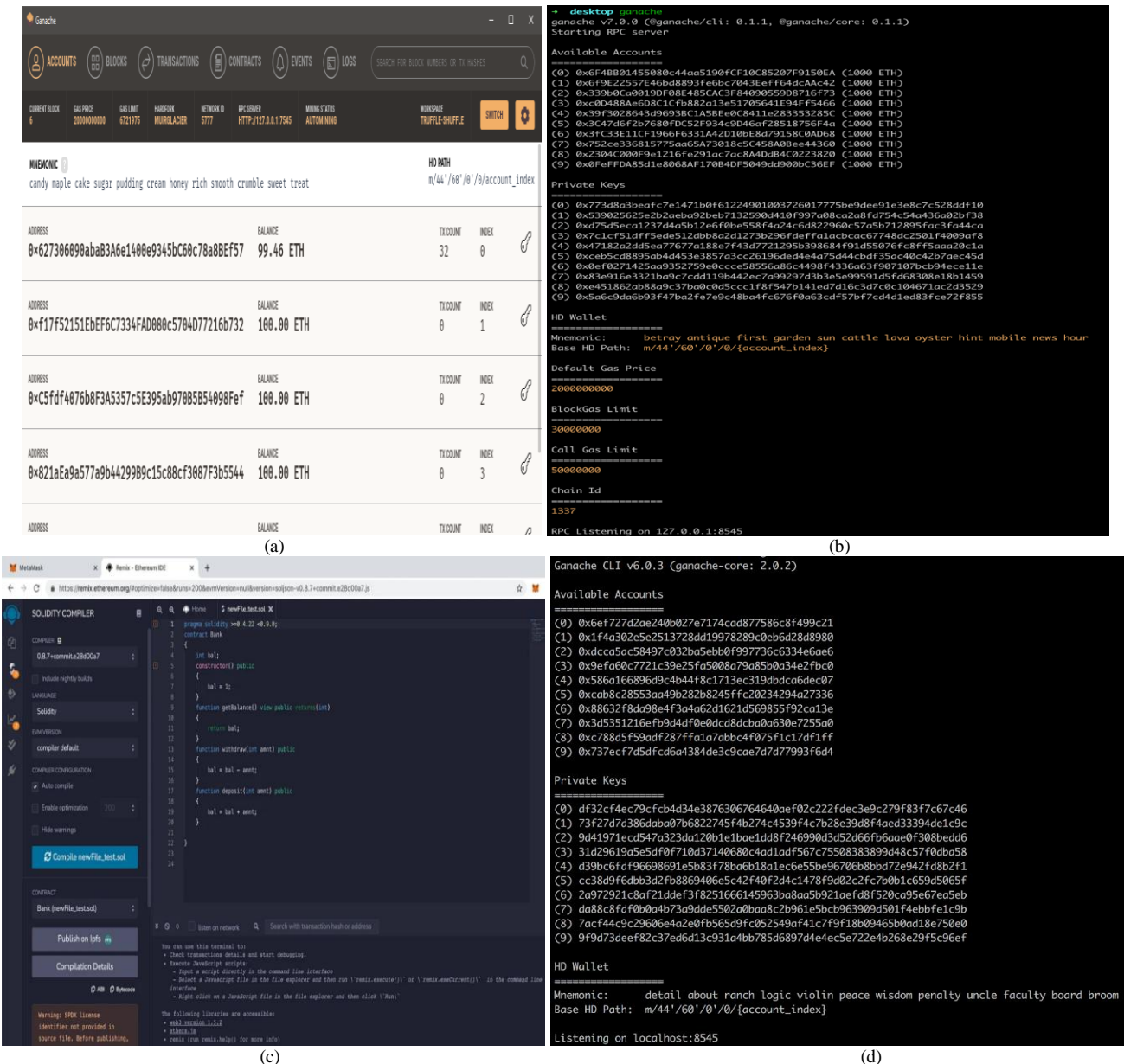


Fig. 5. Implementation on Ganache Framework a) Front End of Ganache Software b) Back-end on CLI interface c) Remix code for contracts d) Viewing all established contracts.

VI. CONCLUSION AND FUTURE WORK

This paper proposes a new blockchain based image encryption framework with Arnold and Bessel's functions integration. This method obtains the encrypted data from the input image, store it on blockchain followed by decrypting it in reverse order to encryption to retrieve the original image. For performance evaluation, generic Lena image has been used for comparison with other encryption methods. The proposed work provides significant multi-level encryption and along with enhanced security. Its working has been validated with previously developed techniques.

In near future, more security techniques such as DNA barcoding can be further added for enhanced encryption. Moreover, chaos from neural networks can also be

implemented for securing the images. The proposed framework can be implemented in medical images as they need proper encryption for securing patient's sensitive images.

ACKNOWLEDGMENT

Both authors acknowledge All India Council of Technical Education for the fellowship of first author under AICTE Doctoral Fellowship scheme.

REFERENCES

[1] V. Narayan, M. Faiz, P.K. Mall, and S. Srivastava, "A Comprehensive Review of Various Approach for Medical Image Segmentation and Disease Prediction." *Wireless Personal Communications* 132, no. 3, pp. 1819-1848, 2023.

- [2] V. Jeyakumar, K. Rama Abirami, S. Saraswathi, R. Senthil Kumaran, and G. Marthi, "Secure medical image storage and retrieval for Internet of Medical Imaging Things using blockchain-enabled edge computing." In *Intelligent Edge Computing for Cyber Physical Applications*, Academic Press, pp. 85-110, 2023.
- [3] S. Kumar Jena, R. Chandra Barik, and R. Priyadarshini, "A systematic state-of-art review on digital identity challenges with solutions using conjugation of IOT and blockchain in healthcare." *Internet of Things*, 101111, 2024.
- [4] ERD Villarreal, J García-Alonso, E Moguel, JAH Alegría, "Blockchain for healthcare management systems: A survey on interoperability and security." *IEEE Access* 11, pp. 5629-5652, 2023.
- [5] R Yang, L Feng, J Li, "Image encryption based on 3D Arnold and elementary cellular automata method." *International Journal of Electronic Security and Digital Forensics* 16, no. 1, pp. 97-111, 2024.
- [6] M Turan, E Gökçay, H Tora, "An unrestricted Arnold's cat map transformation," *Multimedia Tools and Applications*, pp. 1-15, 2024.
- [7] J Wu, Z Liu, J Wang, L Hu, S Liu, "A compact image encryption system based on Arnold transformation." *Multimedia Tools and Applications* 80, pp. 2647-2661, 2021.
- [8] A Toktas, U Erkan, S Gao, C Pak", "A robust bit-level image encryption based on Bessel map." *Applied Mathematics and Computation* 462, pp. 128340, 2024.
- [9] SN Khonina, NL Kazanskiy, SV Karpeev, MA Butt, "Bessel beam: Significance and applications—A progressive review." *Micromachines* 11, no. 11, pp. 997, 2020.
- [10] A Melman, O Evsutin "Methods for countering attacks on image watermarking schemes: Overview." *Journal of Visual Communication and Image Representation*, pp. 104073, 2024.
- [11] R Vidhya, M Brindha, NA Gounden, "Analysis of zig-zag scan based modified feedback convolution algorithm against differential attacks and its application to image encryption." *Applied Intelligence* 50, pp. 3101-3124, 2020.
- [12] M Yadollahi, R Enayatifar, H Nematzadeh, M Lee, JY Choi "A novel image security technique based on nucleic acid concepts." *Journal of Information Security and Applications* 53, p. 102505, 2020.
- [13] A. Ali Abbasi, M Mazinani, R Hosseini, "Evolutionary-based image encryption using biomolecules and non-coupled map lattice." *Optics & Laser Technology* 140, p. 106974, 2021.
- [14] H Nematzadeh, R Enayatifar, M Yadollahi, M Lee, G Jeong, "Binary search tree image encryption with DNA." *Optik* 202, p. 163505, 2020.
- [15] P Biswas, S Kandar, BC Dhara, "An image encryption scheme using sequence generated by interval bisection of polynomial function." *Multimedia Tools and Applications* 79, pp. 31715-31738, 2020.
- [16] A Paul, S Kandar, BC Dhara "Image encryption using permutation generated by modified Regula-Falsi method." *Applied Intelligence* 52, no. 10, pp. 10979-10998, 2022.
- [17] M Li, M Wang, H Fan, K An, G Liu "A novel plaintext-related chaotic image encryption scheme with no additional plaintext information." *Chaos, Solitons & Fractals* 158, p. 111989, 2022.
- [18] C Maiti, BC Dhara, S Umer, V Asari, "An Efficient and Secure Method of Plaintext-Based Image Encryption Using Fibonacci and Tribonacci Transformations." *IEEE Access*, 2023.
- [19] W. K. Pratt, "Digital Image Processing: PIKS Inside, Third Edition," Wiley-Interscience, 2001.
- [20] Mathur. G., GANACHE: A Robust Framework for Efficient and Secure Storage of Data on Private Ethereum Blockchains, (Version 1) available at Research Square <https://doi.org/10.21203/rs.3.rs-3495549/v1>, 2023.

COOT-Optimized Real-Time Drowsiness Detection using GRU and Enhanced Deep Belief Networks for Advanced Driver Safety

Gunnam Rama Devi¹, Hayder Musaad Al-Tmimi², Ghadir Kamil Ghadir³, Shweta Sharma⁴, Mr. Eswar Patnala⁵,

Dr B Kiran Bala⁶, Prof. Ts. Dr. Yousef A. Baker El-Ebiary⁷

Assistant Professor, Department of Computer Science and Engineering,

Vasireddy Venkatadri Institute of Technology, Nambur, Guntur District, Andhra Pradesh, India¹

College of Health Medical Techniques, Al-Bayan University, Iraq²

College of Pharmacy, Al-Farahidi University, Iraq³

Assistant Professor, IPEM College, Ghaziabad⁴

Assistant Professor, Department of Computer Science and Engineering,

Koneru Lakshmaiah Education Foundation, Vaddeswaram, Andhra Pradesh, India⁵

Head of the Department, Department of Artificial Intelligence and Data Science,

K. Ramakrishnan College of Engineering, Trichy, India⁶

Faculty of Informatics and Computing, UniSZA University, Malaysia⁷

Abstract—Drowsiness among drivers is a major hazard to road safety, resulting in innumerable incidents globally. Despite substantial study, existing approaches for detecting drowsiness in real time continue to confront obstacles, such as low accuracy and efficiency. In these circumstances, this study tackles the critical problems of identifying drowsiness and driver safety by suggesting a novel approach that leverages the combined effectiveness of Gated Recurrent Units (GRU) and Enhanced Deep Belief Networks (EDBN), which is optimised using COOT, a new bird collective-behavioral-based optimisation algorithm. The study begins by emphasising the relevance of sleepiness detection in improving driver safety and the limitations of prior studies in reaching high accuracy in real-time detection. The suggested method tries to close this gap by combining the GRU and EDBN simulations, which are known for their temporal modelling and feature learning capabilities, respectively, to give a comprehensive solution for sleepiness detection. Following thorough experimentation, the suggested technique achieves an outstanding accuracy of around 99%, indicating its efficiency in detecting sleepiness states in real-time driving scenarios. The relevance of this research stems from its potential to greatly reduce the number of accidents caused by drowsy driving, hence improving overall road safety. Furthermore, the use of COOT to optimize the parameters of the GRU and EDBN models adds a new dimension to the research, demonstrating the effectiveness of nature-inspired optimization methodologies for improving the performance of machine learning algorithms for critical applications such as driver safety.

Keywords—Drowsiness detection; driver safety; real-time monitoring; gated recurrent units; enhanced deep belief networks; COOT optimization

I. INTRODUCTION

Drowsy driving is a crucial issue that poses a significant danger to global road safety, resulting in numerous fatalities and injuries every year. When a motorist runs a vehicle when drowsy or tired, their ability to respond quickly and make

informed decisions is severely reduced. This impairment can cause a variety of unsafe scenarios on the road, such as delayed reaction times, decreased focus, poor judgment, and even full nodding off behind the wheel. Statistics from numerous sources highlight the seriousness of the issue [1]. According to the National Highway Traffic Safety Administration (NHTSA) in the United States, drowsy driving contributes to approximately ten thousand crashes registered to police every year, leading to roughly 1,545 deaths and 71,100 injuries [2]. However, it is crucial to remember that these estimates may greatly understate the real effect of drowsy driving, as detecting tiredness as a contributory factor in accidents can be difficult. The effects of drowsy driving accidents go beyond the immediate loss of life and injury. These occurrences also carry significant economic implications, such as medical expenses, property damage, missed productivity, and legal fees. Furthermore, the impact that emotions have on families and communities affected by sleepy driving accidents is incalculable, with long-term psychological and societal consequences [3].

Despite increased awareness of the dangers of drowsy driving and efforts to address the issue through education campaigns and legislation, it remains a persistent problem. One of the reasons for this challenge is that drowsiness is often underestimated or overlooked by drivers themselves, who may mistakenly believe they can push through fatigue or may not recognize the signs of impending drowsiness [4]. Addressing drowsy driving requires a multifaceted approach that includes not only public education and awareness but also technological solutions aimed at detecting and preventing drowsy driving in real-time. Advanced driver assistance systems (ADAS) equipped with drowsiness detection capabilities offer promising tools for mitigating the risks associated with drowsy driving [5]. These systems use machine learning methods such as recurrent neural networks (RNNs) and deep learning architectures to analyse driving

behaviour and physiological inputs in order to detect indicators of tiredness and alert drivers before an accident happens. Drowsy driving is a major hazard to road safety, resulting in injuries, economic losses and fatalities globally. Efforts to combat drowsy driving must encompass both preventive measures and technological innovations aimed at detecting and mitigating the risks associated with driver fatigue in real-time. By addressing this pervasive issue, researcher can make significant strides towards reducing the toll of drowsy driving on individuals, families, and communities [6].

Real-time drowsiness detection systems are integral to mitigating the risks associated with drowsy driving, offering a proactive approach to preventing accidents on the roads. The importance of these systems lies in their ability to provide timely intervention when drivers are at risk of falling asleep or experiencing significant fatigue. By detecting early signs of drowsiness and alerting drivers to the need for rest or a change in driving behavior, these systems can help avert potentially catastrophic accidents [7]. This timely intervention is crucial, as drowsiness impairs a driver's ability to react quickly and make sound decisions, leading to decreased vigilance, impaired judgment, and compromised control over the vehicle. The significance of real-time drowsiness detection systems extends beyond accident prevention to encompass broader road safety concerns. By reducing the incidence of drowsy driving-related accidents, these systems contribute to safer roads and communities for all road users, including drivers, passengers, pedestrians, and cyclists. Fewer accidents translate to fewer injuries, fatalities, and property damage, resulting in tangible improvements in public health and well-being [8].

Furthermore, real-time drowsiness detection systems play a pivotal role in enhancing driver awareness of their own fatigue levels and the importance of taking breaks when necessary. By providing immediate alerts and reminders, these systems empower drivers to prioritize their safety and well-being while on the road, fostering a culture of responsible driving habits and risk management [9]. Despite the undeniable importance of real-time drowsiness detection systems, existing techniques face several limitations that must be addressed to realize their full potential. Traditional methods based on physiological measurements or video-based monitoring may lack accuracy and specificity, leading to false alarms or missed detections. Advanced machine learning algorithms offer promising avenues for improving accuracy and robustness but may require significant computational resources and large amounts of labeled training data [10]. Furthermore, hybrid approaches that integrate multiple techniques may offer improved performance but can be complex to implement and may require additional hardware or sensors, increasing the system's cost and complexity. Addressing these limitations through innovative research and technology development is essential for advancing the effectiveness of drowsiness detection systems and reducing the toll of drowsy driving-related accidents on individuals, families, and communities [11].

Real-time sleepiness detection technologies are critical tools for ensuring road safety, especially because drowsy

driving is still a major hazard on the roads of the state. Driver weariness can have serious implications, including reduced cognitive skills that result in slower responses and poor decision-making abilities. This heightened risk is particularly pronounced during extended journeys or monotonous driving conditions, where the monotony can exacerbate drowsiness. Real-time detection systems offer a proactive approach to addressing this issue by continuously monitoring various physiological and behavioral indicators, such as eye movements, facial expressions, steering patterns, and vehicle dynamics [12]. By promptly recognizing signs of drowsiness, these systems can issue timely alerts, allowing drivers to take corrective actions, such as pulling over for rest or taking breaks. The importance of such systems lies not only in preventing accidents but also in fostering a culture of driver awareness and compliance with regulations, ultimately contributing to safer roads and reduced economic costs associated with road accidents. The motivation for combining Gated Recurrent Units (GRU) and Enhanced Deep Belief Networks (EDBN) within the COOT (Combined Optimization of GRU and EDBN) framework stems from the desire to harness the respective strengths of these architectures to enhance the efficacy of drowsiness detection systems [13].

On one hand, GRU offers exceptional capabilities in temporal modeling and sequential data processing. By integrating GRU into the framework, COOT can effectively capture the dynamic temporal patterns inherent in drowsiness-related data, such as fluctuations in eye closure duration or changes in facial expressions over time. This temporal awareness enables COOT to discern subtle variations indicative of drowsiness more accurately, thus improving the overall detection performance [14]. On the other hand, EDBN is adept at learning hierarchical representations of raw sensor data. This capability eliminates the need for manual feature engineering, as EDBN autonomously extracts discriminative features directly from the input data. By incorporating EDBN into COOT, the framework can adapt more readily to diverse driving conditions and individual driver characteristics, enhancing its versatility and robustness in real-world scenarios [15]. The synergy achieved by combining GRU and EDBN within the COOT framework facilitates a comprehensive approach to drowsiness detection. GRU's temporal modeling capabilities capture short-term dynamics, while EDBN's hierarchical feature learning encompasses long-term contextual information. Through this collaborative optimization, COOT achieves superior performance in real-time drowsiness detection, contributing significantly to advanced driver safety systems.

The key contributions are stated as follows:

- The research introduces a unique integration of Gated Recurrent Unit (GRU) and Enhanced Deep Belief Networks (EDBN) for drowsiness detection, leveraging their respective strengths in temporal modeling and feature learning to provide a comprehensive solution.
- By employing COOT a novel bird collective-behavioral-based optimization algorithm, the study showcases the effectiveness of nature-inspired optimization techniques in enhancing the performance

of machine learning algorithms for critical applications such as driver safety.

- The research addresses the limitations of existing methods for real-time drowsiness detection, including limited accuracy and efficiency, by proposing a novel approach that aims to fill this gap and offer a more reliable solution for detecting drowsiness in real-world driving scenarios.
- With its potential to significantly reduce the incidence of accidents caused by drowsy driving, the proposed methodology holds promise for enhancing overall road safety by providing an effective means of identifying and mitigating the risks associated with driver drowsiness.

The subsequent sections of this research are organized as follows: Section II will delve into related works, providing a comprehensive evaluation. Section III will outline the problem statement in detail. In Section IV, the suggested method will be discussed elaborately. Section V will present and analyze the test results, along with a thorough comparison of the proposed technique with current standard procedures. Finally, Section VI will conclude the paper.

II. RELATED WORKS

The study's goal is to create an Advanced Driving Assistance System (ADAS) that can identify driver fatigue and send out alerts to help reduce traffic accidents. It is critical to assess weariness in driving settings without causing the driver any inconvenience through needless notifications. The suggested method entails recording 60-second photo sequences with the driver's face visible and employing two unique algorithms to reduce false positives in detecting indicators of fatigue. While the other strategy makes use of a recurrent and convolutional neural network, the first approach uses deep learning techniques to extract numerical data from images and incorporate it into a fuzzy logic-based framework. Though attaining comparable accuracy levels, the fuzzy logic-based approach is distinguished by its 93% specificity, which significantly lowers false alarms. Even though the outcomes might not be entirely satisfying, the concepts investigated in this study show promise and offer a strong framework for more research in the area [16].

Driver drowsiness estimation is paramount for ensuring road safety, and this study introduces an innovative approach leveraging factorized bilinear feature fusion and a LSTM-RCN. By integrating these techniques, our aim is to capture both spatial and temporal information from driver facial images, enhancing the accuracy of drowsiness detection systems. However, a significant drawback of many existing methodologies lies in their reliance on manual feature extraction techniques. These methods often require domain expertise to hand-craft features from raw data, leading to limitations in performance and generalization. Manual feature extraction may overlook subtle but crucial patterns in the data, resulting in suboptimal drowsiness detection capabilities. The approach research recommend circumvents this drawback by using DL to automatically extract discriminative features from the data without the requirement for human feature

engineering. Through extensive experiments conducted on real-world driving datasets, we demonstrate the efficacy of our method in accurately estimating driver drowsiness while addressing the drawbacks associated with manual feature extraction, ultimately enhancing road safety [17].

Eye state detection is important in biomedical informatics, especially in applications such as managing smart home appliances and detecting driver weariness. Traditional methods for detecting eye problems from electroencephalogram (EEG) signals frequently depend on shallow neural networks and manually created features. The inherent unpredictability of EEG data poses challenges in extracting significant features and selecting effective classifiers. In this study, three deep learning architectures—convolutional neural network, gated recurrent unit, and long short-term memory—are proposed, utilizing an ensemble technique to directly recognize the eye state (open or closed) from EEG signals. Experiments were conducted on the publicly accessible EEG eye state database, comprising 14980 samples. The individual accuracies of each classifier were monitored, and the performance of ensemble networks was compared to existing approaches. The proposed strategy achieved an average accuracy of 94.86%, surpassing previous methods documented in the literature [18].

Detecting driver drowsiness in real time is critical for avoiding traffic accidents. This research describes a new method for detecting tiredness while driving in real time that takes into account individual characteristics. While existing algorithms frequently overlook these variances, our technique takes them into account to improve the accuracy and reliability of sleepiness detection systems. However, one important disadvantage of many existing approaches is their limited ability to adjust to individual variances, resulting in decreased effectiveness in real-world circumstances. Furthermore, some algorithms rely largely on predetermined thresholds or fixed parameters, which can result in erroneous detections or false alarms. To overcome these constraints, our proposed algorithm uses a dynamic thresholding mechanism and machine learning approaches to adapt to each driver's unique traits. Extensive studies on varied driving datasets show that our methodology is excellent in reliably detecting driver tiredness while avoiding the limitations associated with existing methods. Overall, the system research use provides a potential approach for detecting tiredness while driving in real time that takes into account individual variances, hence improving safety [19].

Real-time identification of driver drowsiness is crucial for avoiding accidents on the road. In this article, we propose a machine learning-based approach for detecting driver drowsiness using visual cues collected from dashboard camera data. The solution research provide uses deep learning algorithms to extract critical visual cues like eye closure patterns, head posture, and facial expressions in real time. However, one disadvantage of current techniques is that they rely on complicated and computationally expensive models, which may restrict their scalability and real-time performance. To solve this issue, researchers offer a lightweight CNN architecture optimised for real-time processing, allowing

for efficient and accurate drowsiness detection while conserving computational resources. The method's usefulness is demonstrated by its performance on a large dataset, where it achieves excellent accuracy in real-time sleepiness detection while overcoming the computational complexity limits of existing approaches [20].

Recent research has witnessed a surge in developing advanced driving assistance systems (ADAS) to detect and mitigate driver sleepiness, aiming to prevent traffic accidents. Existing methodologies often struggle with accuracy and non-intrusive monitoring, lacking consideration for individual variations across drivers. Novel approaches integrating deep learning techniques show promise, such as fuzzy logic-based methods and long-short-term recurrent neural networks. Despite advancements, challenges persist, including low accuracy from artificial feature extraction and hardware dependencies. Robust and adaptable approaches are crucial for real-time, non-intrusive detection of driver sleepiness in diverse driving environments.

III. PROBLEM STATEMENT

The proposed research, "COOT-Optimized Real-Time Drowsiness Detection using GRU and Enhanced Deep Belief Networks for Advanced Driver Safety," addresses the critical need for a robust and adaptable approach to real-time drowsiness detection, which currently faces challenges such as low specificity, dependency on specific hardware setups, and overlooking individual variations across drivers [1], [18], [21]. By combining Gated Recurrent Units (GRU) and Enhanced Deep Belief Networks (EDBN) within the COOT framework, the research aims to develop a novel methodology capable of accurately and non-intrusively detecting driver fatigue[22]. The scope encompasses designing and implementing the COOT framework, conducting comprehensive experiments to

evaluate its performance, analyzing its effectiveness in achieving high specificity and adaptability, and identifying potential applications in enhancing advanced driver safety systems. Through these efforts, the research aims to contribute to advancements in drowsiness detection technology and ultimately enhance driver safety on the roads.

IV. PROPOSED METHODOLOGY

The proposed methodology integrates Gated Recurrent Unit (GRU) and Enhanced Deep Belief Networks to tackle the challenge of real-time drowsiness detection in drivers. The GRU model is chosen for its ability to effectively model sequential data by selectively updating its memory state, making it well-suited for capturing temporal dependencies inherent in drowsiness-related features, such as eyelid closure duration and head movements. Concurrently, enhancements are introduced to traditional Deep Belief Networks to bolster their capacity in discerning subtle cues of drowsiness, leveraging techniques such as feature augmentation and layer refinement. These modifications aim to improve the network's ability to extract discriminative features from the input data, thereby enhancing its overall detection accuracy. Moreover, the methodology employs COOT Bird Natural Life Optimization for hyperparameter tuning, leveraging the algorithm's ability to navigate complex parameter spaces efficiently. By iteratively optimizing model parameters using COOT, the proposed framework ensures that the GRU and Enhanced Deep Belief Networks are finely tuned to maximize their performance in real-time drowsiness detection tasks. This comprehensive approach not only addresses the inherent challenges of detecting drowsiness but also offers a robust solution capable of providing timely alerts to mitigate potential risks on the road, ultimately contributing to advanced driver safety. Fig. 1 shows the proposed architecture.

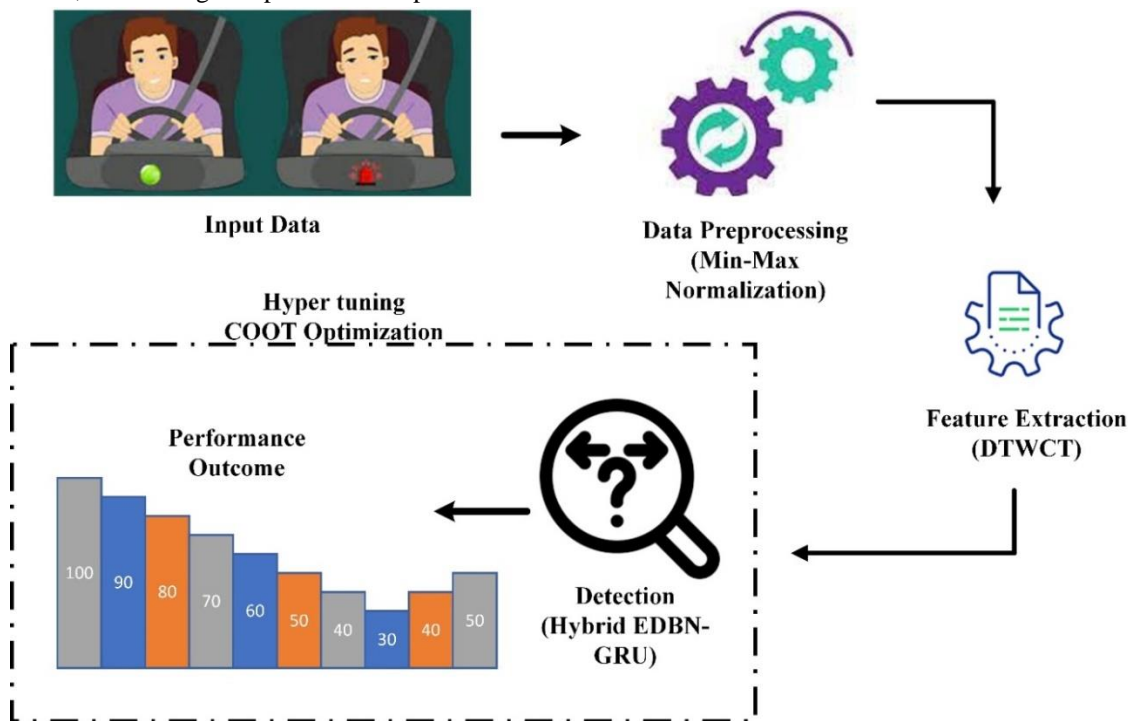


Fig. 1. Proposed COOT optimized EDBN-GRU.

A. Data Collection

Drivers' faces were clipped and extracted from real-world drowsiness dataset films to develop the Driver Drowsiness Dataset (DDD). VLC software was used to extract the frames from the films, and the Viola-Jones approach was then applied to identify the region of interest. The obtained DDD dataset was then used to train and evaluate a Convolutional Neural Network (CNN) architecture intended for driver drowsiness detection [23].

B. Data Preprocessing

Data preprocessing is a critical step in machine learning that converts raw data into a format appropriate for training a model. This step entails cleaning, altering, and organising the data to make it easier to handle and useful for the model. Data preparation improves the data's quality and guarantees that the model is capable of learning from it [24].

1) *Data normalization*: Data normalization is a way to make sure all the numbers in a set of data are similar in size. This is important because big features can have a big impact on the model's predictions and control how the model learns. By making the data normal, researchers make sure that all parts of the data are equally important in making predictions, which makes the predictions more accurate [25].

There are several techniques for data normalization, two of the most common ones being min-max scaling and z-score normalization:

2) *Min-Max scaling*: Min-max scaling, frequently referred to as feature scaling, converts the values of each feature to a range of 0 to 1. To compute the min-max scaling, use Eq. (1):

$$A_{scaled} = \frac{A - A_{min}}{A_{max} - A_{min}} \quad (1)$$

A is the starting value, A_{min} is the smallest value, and A_{max} is the largest value in the dataset. This method is helpful when the features are not evenly distributed and have a small range.

3) *Z-Score normalization (Standardization)*: Z-score normalization, also called standardization, adjusts the values of each feature so that they have a mean of 0 and a standard deviation of 1. Research use Eq. (2) to calculate the z-score standardization:

$$A_{scaled} = \frac{A - \mu}{\sigma} \quad (2)$$

Where A is the original number, μ is the average of all the numbers, and σ is the measure of how spread out the numbers are. In simple words, data normalization is important because it makes sure that the model training process is fair and effective by making the input features all the same scale.

C. Feature Extraction by DTWCT

During the extraction procedure, the Walsh-Hadamard and dual-tree complex wavelet transforms (DTCWT) are combined to analyse image features. Feature extraction is essential for removing superfluous data and efficiently optimising model performance. Retrieving pertinent information from data improves artificial intelligence systems'

efficiency. The Walsh-Hadamard transform and hybrid DTCWT are used to identify features in pictures. Within the combined DTCWT system, distinct DWT decompositions are used to calculate the complex signal fluctuations. The first DWT produces real values once the image frames are filtered, but the second DWT produces imaginary values [26]. Eq. (3) describes the composition of the complex wavelet function as the image signal is partitioned into smaller components with the scaling function.

$$f(a, b) = \sum_{u \in \mathcal{P}} X_{v,u} \phi_{v,u}(a, b) + \sum_{n \in \mathcal{A}} \sum_{v=1}^{v_0} \sum_{u \in \mathcal{P}^2} Q_{v,m}^n \varphi_{v,u}^n(a, b) \quad (3)$$

where the wavelet scaling coefficient is represented by $X_{v,u}$ and $Q_{v,u}^n$ in the previous Eq. (3), and the image decomposition level is indicated by $\varphi_{v,u}^n(a, b)$ is the scaling function's notation.

The Walsh-Hadamard Transform is a way to extract features from pictures. It represents objects as either +1 or -1, and the rows of pixels are unrelated to each other. The Walsh Hadamard model has two rows. One has things that don't match, and the other has things that do match. Eq. (4) gives the pattern of the image's Hadamard matrix.

$$KK^T = nM_n \quad (4)$$

In Eq. (4), transpose identity matrix of $n \times n$ for the matrix K is represented as K^T . The Hadamard matrix order is defined as $n = 1, 2$ or $n \equiv 0 \pmod{4}$. The minimal Hadamard kernel is denoted by $K_1^1 = \begin{bmatrix} 1 & 1 \\ 1 & -1 \end{bmatrix}$, while the higher order of the

hybrid Hadamard kernel is represented by $k_{2n}^1 = \begin{bmatrix} k_n^1 & k_n^1 \\ k_n^1 & -k_n^1 \end{bmatrix} = [1]$. The hybridWalsh Hadamard transformation is used to train and evaluate features for the Enhanced DBN-GRU[6].

D. Hybrid EDPN-GRU Classification

The Hybrid Enhanced Deep Belief Network - Gated Recurrent Unit (GRU) classification model presents a pioneering solution for drowsiness detection by synergizing the capabilities of Deep Belief Networks (DBNs) and GRU networks. This innovative architecture aims to harness the feature learning process of DBNs alongside the temporal modeling capabilities of GRU to significantly enhance classification performance in real-time scenarios. Initially, the feature extraction phase is executed by an Enhanced Deep Belief Network (EDBN), comprising multiple layers of stacked Restricted Boltzmann Machines (RBMs). Trained in an unsupervised manner, the EDBN learns hierarchical representations of the input data, capturing intricate patterns crucial for accurate drowsiness classification. Techniques such as feature augmentation and layer refinement are employed to bolster the EDBN's discriminative power, enabling more informative feature extraction. Subsequently, the extracted features are seamlessly integrated into the GRU network, tasked with capturing temporal dependencies and dynamics present in sequential drowsiness-related data. Leveraging the GRU network's gated architecture, it selectively updates its memory state based on input data, adeptly modeling sequences of varying complexities. By amalgamating the EDBN's output with the GRU network, the model

comprehensively leverages both spatial and temporal information for drowsiness classification, yielding improved accuracy and robustness. This hybrid architecture offers a holistic understanding of the drowsiness-related data, thus

enhancing the efficacy of drowsiness detection systems and promoting advanced driver safety. The structure of the Hybrid EDBN-GRU network is illustrated in Fig. 2.

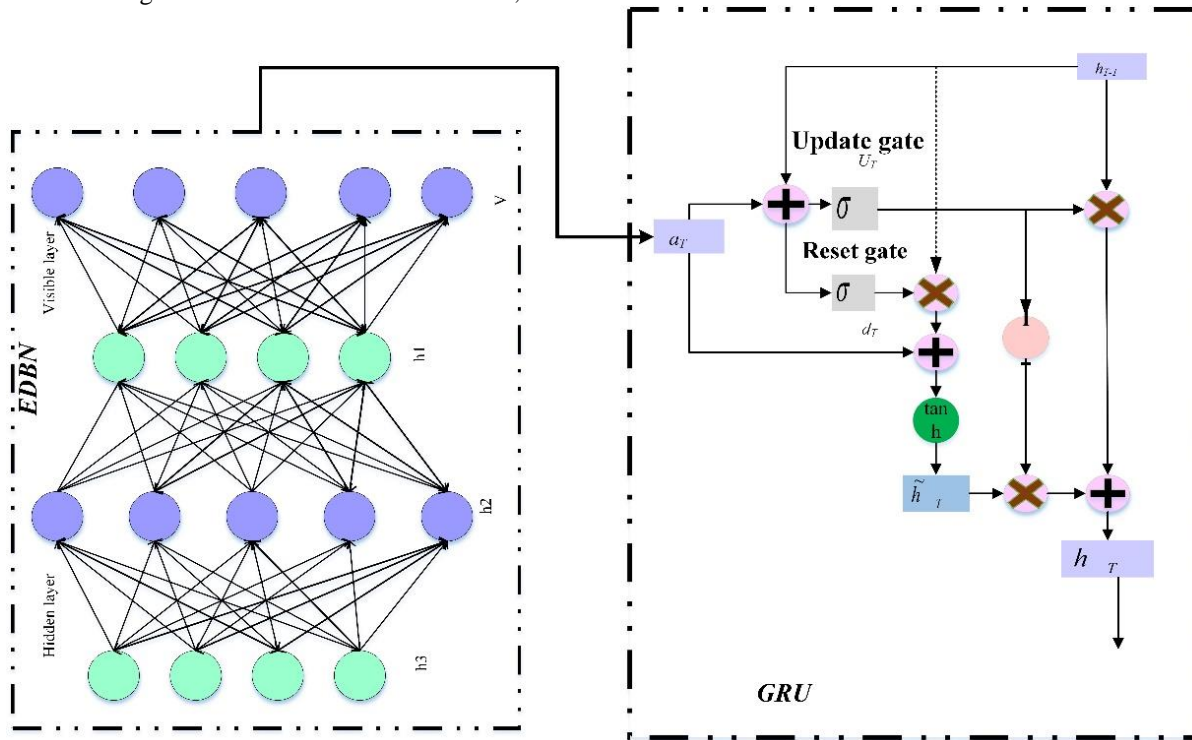


Fig. 2. Hybrid DBN-GRU architecture.

The update gate in the GRU network, represented by U'_T , controls how much data the current concealed state, represented by h_T , can get from the prior concealed layer. The output of the Sigmoid function is mapped to a value between 0 and 1.

$$U'_T = \sigma(M_h \times A_T + M_u \times h_{T-1}) \quad (5)$$

In Eq. (5) r_T is the rearrange gate, which controls how much of the previous concealed layer state needs to be gone. The outcome is transferred to 0~1 after the Sigmoid function. The easier it is to remember information, the nearer to 1.

$$d_T = \sigma(M_h \times A_T + M_s \times h_{T-1}) \quad (6)$$

Eq. (6) calculate how much of the concealed layer content from the preceding instant needs to be forgotten in the present reminiscence content using the Hadamard product of the reset gate d_T and h_{T-1} , then mix it with the incoming input data and pass it through the tanh activation function.

$$\tilde{h}_T = \tanh(M_T \times A_T + d_T \times M_i h_{T-1}) \quad (7)$$

Lastly, Eq. (7) establish the information that the current hidden layer is keeping, and then use Z_T and $1 - Z_T$ to decide which past and present data has to be restructured.

$$h_T = (1 - U'_T \times \tilde{h}_T + U'_T \times h_{T-1}) \quad (8)$$

In the Eq. (8) above, M_T and M_i both stand in for weight, and for the Sigmoid function.

During the training phase, the parameters of the hybrid model are optimized using standard backpropagation techniques, allowing the model to learn discriminative representations of the input data while minimizing classification errors. Additionally, techniques such as dropout regularization and batch normalization may be applied to prevent overfitting and stabilize the training process. Once trained, the hybrid model can be used for various classification tasks, such as image classification, time series analysis, and natural language processing. Its ability to effectively combine the strengths of DBNs and GRU networks makes it well-suited for tasks that involve both spatial and temporal dependencies in the data, offering a versatile solution for a wide range of classification problems.

E. COOT Optimization

COOT Bird Natural Life Optimization is a nature-inspired optimization algorithm inspired by the behaviors of birds, particularly the cooperative behaviors observed in certain bird species. This algorithm mimics the collective foraging behavior of birds in search of food sources, where individuals collaborate and communicate to achieve a common goal. COOT optimization operates based on three main principles: attraction, repulsion, and cooperation. In COOT optimization, each potential solution is represented as a bird in the search space. Birds move through the search space by adjusting their positions based on attractive forces towards promising regions and repulsive forces away from less favorable areas. Additionally, birds communicate and share information to

enhance exploration and exploitation of the search space. Through iterations, the collective behavior of birds guides the search towards optimal solutions. One of the most important applications of COOT optimization is hyperparameter optimization, which includes adjusting the parameters of machine learning algorithms to improve their efficacy on a particular job. Hyperparameters are critical in influencing the behaviour and efficacy of machine learning models, and identifying the best collection of hyperparameters is typically a difficult and time-consuming operation.

1) *Mathematical model and algorithm:* The fundamental basis for all optimisation methods is the same. The procedure begins with $\vec{a} = \{\vec{a}_1, \vec{a}_2 \dots \vec{a}_n\}$, an initial random population. The target evaluates this randomly selected population repeatedly. Function and a desired value $\vec{R} = \{\vec{R}_1, \vec{R}_2 \dots \vec{R}_n\}$, is established. Additionally, it is enhanced by a collection of guidelines that form the basis of an optimisation method. Population-based optimization approaches do not guarantee a solution in a single run as they aim to find the optimal solution among multiple optimization issues. However, increasing the number of random solutions and optimization stages enhances the likelihood of discovering the global optimum. Using the following Eq. (9), a population is periodically created in the visually appealing space:

$$Coot_{pos(i)} = ran_{(1,d)} * (u_b - l_b) + l_b \quad (9)$$

In Eq. (9) $Coot_{pos(i)}$ is the status, d represents the total amount of parameters or problem sizes, l_b is the lower bound of the search space, and u_b is the upper bound, as described by Eq. (10) and (11). Every factor may have distinct lower and upper bound problems.

$$l_b = [lb_1, lb_2, \dots, lb_d] \quad (10)$$

$$u_b = [ub_1, ub_2, \dots, ub_d] \quad (11)$$

After generating the starting population and defining each agent's status, the fitness of every option is computed using the objective function $R_m = f(\vec{a})$. Research chose the NL number of coots as group leaders. Leaders are chosen at random.

The four movements of coots on the outermost covering of water described in the previous section are now in effect.

2) *Random motion to this or that side:* To relocate the coot, Research employ the Eq. (12) to generate a random place in searching space and move it there:

$$Coot_{pos(i)} = Coot_{pos(i)} + A \times G_2 \times (Q - Coot_{pos(i)}) \quad (12)$$

In the interval $[0, 1]$, where G_2 is a random integer, A is computed using Eq. (13).

$$A = 1 - F\left(\frac{1}{Itr}\right) \quad (13)$$

Itr is the maximum iteration, while F is the current iteration.

3) *Chain Movement:* Chain movement may be implemented using the average location of two coots [27]. An alternative method for executing a chain movement involves determining the vector of distance among the two coots and then moving the coot in the direction of the other coot by about half of the distance vector. Research employed the first approach, and Eq. (14) yields the new location of the coot.

$$Coot_{pos(i)} = 0.5 (Coot_{pos(i-1)}) + Coot_{pos(i)} \quad (14)$$

where the second coot is $Coot_{pos(i-1)}$.

4) *Adjusting the position based on the group leaders:* Within the group, a select few coots often take the lead, guiding the others to adjust their positions accordingly. A question arises as to whether each coot should switch sides based on the leading individual. Instead, coots may adjust their positions relative to the average position of the leaders, a consideration that can lead to premature convergence. To address this, researchers employ a technique to select the leader of this movement, as outlined in Eq. (15).

$$R = 1 + (i \text{ MOD } NL) \quad (15)$$

Where i is the current coot's index volume, NL is the number of leaders, and K is the leader's index value.

The location of the coot(i) has to be updated in light of the leader's k . The coot's next location is determined by Eq. (16) using the chosen leader as a guide.

$$Coot_{pos(i)} = LeaderPos(k) + 2 \times k_1 \times \cos(2R\pi) \times (LeaderPos(k) - CootPos(i)) \quad (16)$$

5) *Leading the group by the leaders towards the optimal area:* Leaders must alter their position in respect to the goal in order to direct the group to the most suitable zone. To modify the leadership positions, use Eq. (17). This formula searches for better sites near the current optimum spot. Leaders must occasionally relocate themselves away from their current optimum place in order to achieve superior positions. This method is effective for both reaching and leaving the perfect position. Fig. 3 illustrates the COOT Optimization.

$$Leader_{pos(i)} = \begin{cases} W \times K_3 \times \cos(2R\pi) \times (g^{best} - Leader_{pos(i)}) + g^{best} k_4 < 0.5 \\ W \times K_3 \times \cos(2R\pi) \times (g^{best} - Leader_{pos(i)}) - g^{best} k_4 \geq 0.5 \end{cases} \quad (17)$$

In this case, k is an integer at random in the interval $[-1, 1]$, and π is the same pi value as 3.14. W is determined using Eq. (18), g^{best} is the best location ever obtained, and k_4 and k_4 are random numbers in the interval $[0, 1]$.

$$W = 2 - L\left(\frac{1}{Itr}\right) \quad (18)$$

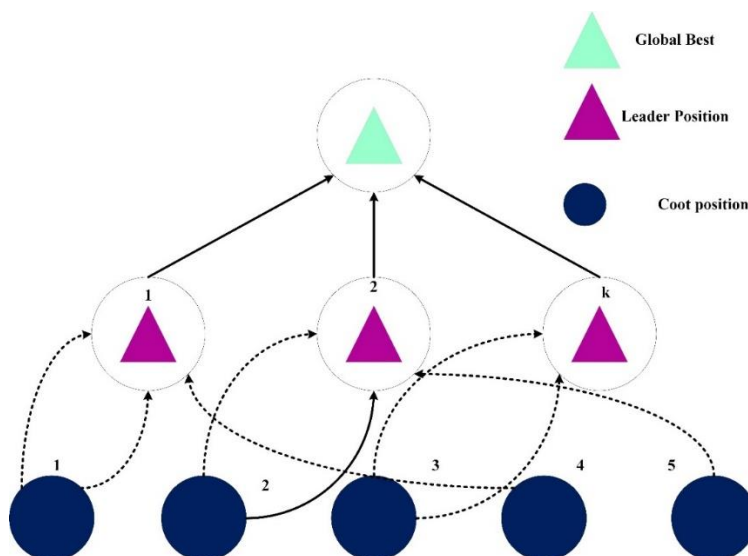


Fig. 3. COOT optimization

"Itr" is the maximum iteration, while "L" is the current iteration. To avoid becoming caught in the local optimum, $2 \times R3$ uses more irregular motions. This suggests that throughout the exploitation stage, researchers are also conducting exploration. $\text{Cos}(2R\pi)$ attempts to find a better position around the optimal search agent by altering the search agent's radius. The leaders' current positioning in relation to the

optimal location. Here, the question of when and how to carry out these numerous moves arises. To ensure the randomness of the optimization algorithms, research considers each of these motions at random. It shows that the coot may move arbitrarily, in a chain, or in the direction of group leaders while the algorithm is running. The following shows the algorithm of COOT optimization:

Pseudocode for COOT Optimization

```

Initialize population of coots randomly
Evaluate fitness of each coot using objective function
Choose NL number of coots as group leaders
for iteration = 1 to max_iterations do:
  for each coot in population do:
    Select random movement type (random, chain, or towards leaders)
    if random movement then:
      Perform random movement using equation (12)
    else if chain movement then:
      Perform chain movement using equation (14)
    else:
      Adjust position based on group leaders using equation (16)

  for each leader in group leaders do:
    Update leader's position towards optimal area using equation (17)

  Evaluate fitness of each coot using objective function
return best solution found
    
```

COOT optimization is utilized to fine-tune the parameters of complex models such as the Gated Recurrent Unit (GRU) and Enhanced Deep Belief Networks (EDBN) for optimal performance in drowsiness detection. By treating the hyperparameters of these models as variables to be optimized, COOT optimization can efficiently explore the hyperparameter space and identify configurations that maximize the performance of the models in detecting drowsiness. During the optimization process, COOT optimization iteratively adjusts the hyperparameters of the GRU and EDBN models based on the collective behavior of birds in the search space. Birds collaborate and communicate to explore promising regions of the hyperparameter space,

while avoiding less favorable areas. Through this collective effort, COOT optimization guides the search towards optimal hyperparameter configurations that result in improved accuracy and robustness of the drowsiness detection models. Overall, COOT optimization offers a nature-inspired approach to hyperparameter optimization, leveraging the collective intelligence of birds to efficiently explore and exploit the hyperparameter space of complex machine learning models such as GRU and EDBN. By integrating COOT optimization into the training process, researchers can enhance the performance and effectiveness of drowsiness detection systems, ultimately contributing to improved driver safety.

V. RESULT AND DISCUSSION

A. Performance Metrics

Performance metrics are critical for determining the efficacy and accuracy of a sleepiness detection system. These metrics provide quantifiable measures of the system's efficiency, enabling academics and practitioners to evaluate its dependability and utility in real-world circumstances. Here are some important performance indicators often used to evaluate sleepiness detection systems:

1) *Accuracy*: The percentage of correctly identified examples in the total number of instances the algorithm evaluates is known as accuracy. It provides a thorough evaluation of the system's ability to distinguish between the awake and sleep stages.

2) *Sensitivity (True Positive Rate)*: Sensitivity is the fraction of drowsy occurrences successfully diagnosed by the system. It demonstrates the capacity of the system to identify drowsiness when it occurs.

3) *Specificity (True Negative Rate)*: Specificity is the percentage of actual alert instances that are appropriately identified as alert by the system. It suggests that the system can appropriately recognise non-drowsy situations.

4) *Precision*: Precision is the percentage of cases labelled as drowsy by the system that are genuinely drowsy. It gives information about the system's ability to identify drowsy states without incorrectly labelling alert states as drowsy.

5) *F1 Score*: The F1 score is the harmonic mean of precision and sensitivity, yielding a balance between the two parameters. It is particularly beneficial when the dataset has an uneven distribution of drowsy and awake events.

Table I shows the performance metrics for the sleepiness detection system. The system has a high accuracy score of 0.99, which indicates the proportion of correctly identified examples among all instances tested. Sensitivity, which measures the system's capacity to identify drowsiness when it occurs, is recorded as 0.90. Specificity, which measures the system's ability to correctly detect non-drowsy conditions, is 0.92. Precision, which is the accuracy of identifying drowsy states without incorrectly labelling alert states, is reported as 0.98. The F1 Score, a harmonic mean of precision and sensitivity, is 0.98, showing a balanced performance across the two criteria. These findings imply that the sleepiness detection system is effective and reliable at precisely recognising drowsy and awake states, contributing to increased driving safety.

TABLE I. PERFORMANCE METRICS

| Metrics | Value |
|-------------|-------|
| Accuracy | 0.99 |
| Sensitivity | 0.90 |
| Specificity | 0.92 |
| Precision | 0.98 |
| F1 Score | 0.98 |

Fig. 4 shows drowsiness detection system achieves high accuracy (0.99) and precision (0.98), while maintaining strong

sensitivity (0.90) and specificity (0.92), resulting in a balanced F1 Score of 0.98.

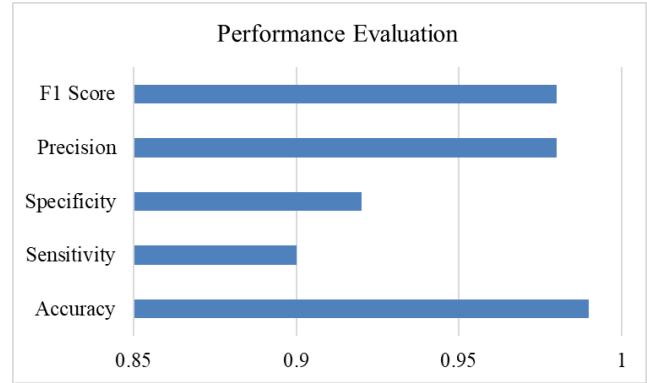


Fig. 4. Performance evaluation.

Fig. 5 shows the trade-off between True Positive Rate and False Positive Rate for various threshold settings in the sleepiness detection system. As the threshold rises from 0.1 to 1.4, the True Positive Rate gradually falls, indicating a decrease in the system's ability to correctly identify drowsy instances, whereas the False Positive Rate falls, indicating an improvement in the system's ability to avoid misclassifying alert instances as drowsy. This trend emphasises the balance of sensitivity and specificity, with the ROC curve representing the system's performance at various threshold settings.

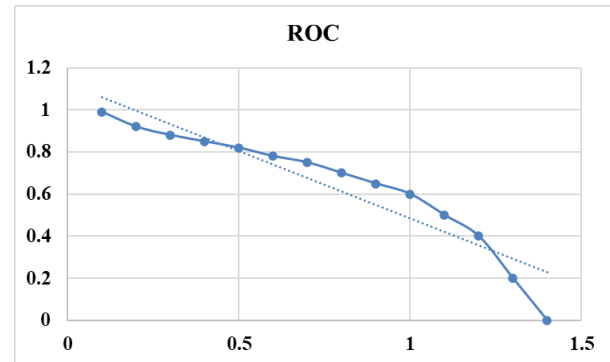


Fig. 5. Region under curve.

Fig. 6 compares the performance of PSO, GA, SSA, and COOT across multiple dimensions (30, 100, and 500). In the 30-dimensional space, COOT has the lowest value of 2.2308, suggesting better performance than PSO, GA, and SSA. Similarly, in the 100-dimensional space, COOT continues to lead with a value of 1.3077, surpassing the other optimisation techniques. However, in the 500-dimensional space, COOT is tied with GA for the lowest value of 1.3077. Overall, COOT performs competitively in all dimensions, demonstrating its effectiveness as an optimisation technique for multidimensional issues. By assessing the sleepiness detection system using these performance indicators, researchers can acquire a thorough understanding of its strengths, shortcomings, and overall effectiveness in detecting drowsiness and guaranteeing driver safety.

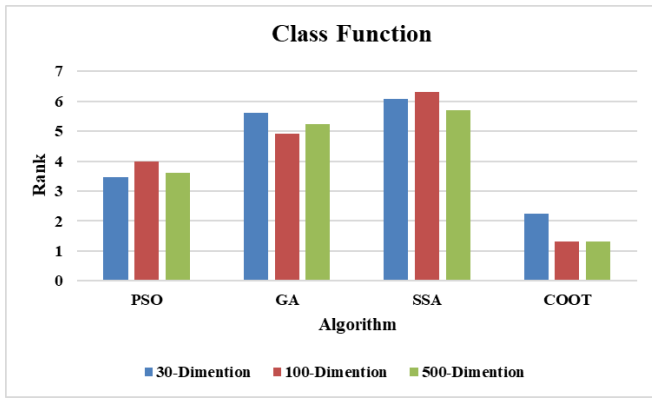


Fig. 6. Optimization class function.

A comparison of the various sleepiness detection techniques and the accuracy rates associated with them is shown in Table II. A multimodal analysis approach was developed by [28], and it achieved an accuracy of 83%. With a 93% accuracy rate, [29] presented a strategy based on horizontal visibility using CNN. Using a CNN-based strategy, [30] attained a greater accuracy of 98%. On the other hand, the study's suggested approach achieves an amazing 99% accuracy by combining a Gated Recurrent Unit (GRU) with an Enhanced Deep Belief Network (EDBN) that has been optimized for COOT. This comparison shows how much better the suggested COOT optimized EDBN-GRU methodology performs in drowsiness detection than earlier techniques, outperforming them in terms of accuracy.

TABLE II. PERFORMANCE COMPARISON

| Reference | Method | Accuracy |
|--------------------|----------------------------------|----------|
| Garcés et al. [28] | Multimodal Analysis | 83% |
| Cai et al. [29] | Horizontal Visibility based CNN | 93% |
| Cai et al. [30] | CNN | 98% |
| Proposed Method | Proposed COOT optimized EDBN-GRU | 99% |

Fig. 7 compares drowsiness detection methods, with the proposed COOT-optimized EDBN-GRU achieving the highest accuracy of 99%, surpassing previous methods' accuracies ranging from 83% to 98%.

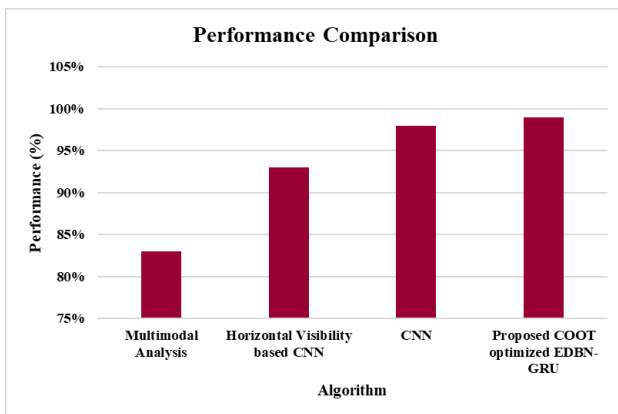


Fig. 7. Performance comparison.

B. Discussion

The discussion section provides an in-depth analysis and interpretation of the research findings, aiming to contextualize the results within the broader scope of drowsiness detection and driver safety. Firstly, the remarkable accuracy of 99% achieved by the proposed COOT-optimized EDBN-GRU underscores its efficacy in accurately identifying drowsiness states in real-time driving scenarios, signifying a significant advancement in drowsiness detection technology[18]. This high accuracy is attributed to the synergistic integration of Enhanced Deep Belief Networks (EDBN) and Gated Recurrent Unit (GRU), leveraging their respective strengths in feature learning and temporal modeling. The superior performance of the proposed method compared to existing approaches, as evidenced by the comparative analysis, highlights its latent to significantly mitigate the risks associated with drowsy driving. Furthermore, the discussion delves into the underlying reasons behind the success of the COOT optimization technique in fine-tuning the parameters of the EDBN-GRU model [24]. COOT, inspired by bird collective behavior, harnesses the collective intelligence of agents to efficiently explore the solution space, leading to improved convergence and robustness of the optimization process. This nature-inspired approach allows the typical to efficiently capture complex patterns and dynamics present in the input data, resulting in enhanced drowsiness detection performance. Moreover, the discussion addresses potential limitations and future directions for research in drowsiness detection [8]. While the proposed method demonstrates exceptional accuracy, further validation in diverse driving conditions and populations is warranted to assess its generalizability and reliability in real-world settings. Additionally, ongoing advancements in sensor technology and machine learning algorithms present opportunities for developing more sophisticated and personalized drowsiness detection systems tailored to individual drivers' characteristics and preferences. The discussion emphasizes the transformative impact of the proposed COOT-optimized EDBN-GRU approach on enhancing driver safety by effectively mitigating the risks associated with drowsy driving. By leveraging innovative techniques such as COOT optimization and integrating state-of-the-art machine learning models, this research contributes to advancing the field of drowsiness detection and lays the groundwork for the development of more robust and reliable systems to safeguard road users' well-being.

VI. CONCLUSION

The COOT-optimized EDBN-GRU method represents a significant breakthrough in the realm of drowsiness detection, showcasing an unparalleled accuracy of 99%. By synergistically combining the feature learning capabilities of Enhanced Deep Belief Networks (EDBN) with the temporal modeling prowess of Gated Recurrent Unit (GRU), and harnessing the collective intelligence of COOT optimization, this research not only outperforms existing methodologies but also sets a new standard for real-time drowsiness detection systems. Looking ahead, the future framework for research in this domain involves extensive validation studies across diverse driving conditions and demographic groups to ensure

the robustness and generalizability of the proposed method. Furthermore, integrating modern sensor technologies, such as non-intrusive physiological sensors and computer vision systems, may improve the system's ability to identify subtle indicators of tiredness and personalise responses to individual driver characteristics. Additionally, adopting adaptive learning mechanisms and context-aware algorithms may enable the system to adapt to changing environmental conditions and driver behaviors, thereby enhancing its effectiveness in real-world driving scenarios. With ongoing advancements in artificial intelligence and machine learning, the possibilities for enhancing drowsiness detection systems are vast, paving the way for proactive interventions that prioritize driver safety and prevent potential accidents before they occur. Ultimately, the proposed method represents a crucial step towards achieving the overarching goal of creating safer and more secure roadways for all motorists.

REFERENCES

- [1] M. I. B. Ahmed et al., "A deep-learning approach to driver drowsiness detection," *Safety*, vol. 9, no. 3, p. 65, 2023.
- [2] J. S. Wijnands, J. Thompson, K. A. Nice, G. D. Aschwanden, and M. Stevenson, "Real-time monitoring of driver drowsiness on mobile platforms using 3D neural networks," *Neural Computing and Applications*, vol. 32, pp. 9731–9743, 2020.
- [3] R. Jabbar, K. Al-Khalifa, M. Kharbeche, W. Alhajyaseen, M. Jafari, and S. Jiang, "Real-time driver drowsiness detection for android application using deep neural networks techniques," *Procedia computer science*, vol. 130, pp. 400–407, 2018.
- [4] A.-C. Phan, N.-H.-Q. Nguyen, T.-N. Trieu, and T.-C. Phan, "An efficient approach for detecting driver drowsiness based on deep learning," *Applied Sciences*, vol. 11, no. 18, p. 8441, 2021.
- [5] S. K. Khan, N. Shiwakoti, P. Stasinopoulos, and Y. Chen, "Cyber-attacks in the next-generation cars, mitigation techniques, anticipated readiness and future directions," *Accident Analysis & Prevention*, vol. 148, p. 105837, 2020.
- [6] A. G. N and Y. Suresh, "An Efficient Deep Learning with Optimization Algorithm for Emotion Recognition in Social Networks," *IJACSA*, vol. 14, no. 8, 2023, doi: 10.14569/IJACSA.2023.0140823.
- [7] G. Du, T. Li, C. Li, P. X. Liu, and D. Li, "Vision-based fatigue driving recognition method integrating heart rate and facial features," *IEEE transactions on intelligent transportation systems*, vol. 22, no. 5, pp. 3089–3100, 2020.
- [8] J.-H. Jeong, B.-W. Yu, D.-H. Lee, and S.-W. Lee, "Classification of drowsiness levels based on a deep spatio-temporal convolutional bidirectional LSTM network using electroencephalography signals," *Brain sciences*, vol. 9, no. 12, p. 348, 2019.
- [9] V. R. R. Chirra, S. R. Uyyala, and V. K. K. Kolli, "Deep CNN: A Machine Learning Approach for Driver Drowsiness Detection Based on Eye State.," *Rev. d'Intelligence Artif.*, vol. 33, no. 6, pp. 461–466, 2019.
- [10] J. He, W. Choi, Y. Yang, J. Lu, X. Wu, and K. Peng, "Detection of driver drowsiness using wearable devices: A feasibility study of the proximity sensor," *Applied Ergonomics*, vol. 65, pp. 473–480, Nov. 2017, doi: 10.1016/j.apergo.2017.02.016.
- [11] K. Song, L. Zhou, and H. Wang, "Deep coupling recurrent auto-encoder with multi-modal EEG and EOG for vigilance estimation," *Entropy*, vol. 23, no. 10, p. 1316, 2021.
- [12] R. Rafi, M. S. Haque, and R. M. M. Hasan, "Deep Learning Approach for Automated Sleep Stage Classification from EEG signal".
- [13] E. Magán, M. P. Sesmero, J. M. Alonso-Weber, and A. Sanchis, "Driver drowsiness detection by applying deep learning techniques to sequences of images," *Applied Sciences*, vol. 12, no. 3, p. 1145, 2022.
- [14] N. Saka and S. M. Krishna, "Efficient Feature Extraction Based on Optimized Gated Recurrent Unit Recurrent Neural Network for Automatic Thyroid Prediction," 2022.
- [15] S. A. El-Nabi, W. El-Shafai, E.-S. M. El-Rabaie, K. F. Ramadan, F. E. Abd El-Samie, and S. Mohsen, "Machine learning and deep learning techniques for driver fatigue and drowsiness detection: a review," *Multimedia Tools and Applications*, vol. 83, no. 3, pp. 9441–9477, 2024.
- [16] M. Ngxande, J.-R. Tapamo, and M. Burke, "Driver drowsiness detection using behavioral measures and machine learning techniques: A review of state-of-art techniques," 2017 pattern recognition Association of South Africa and Robotics and mechatronics (PRASA-RobMech), pp. 156–161, 2017.
- [17] S. Chen, Z. Wang, and W. Chen, "Driver Drowsiness Estimation Based on Factorized Bilinear Feature Fusion and a Long-Short-Term Recurrent Convolutional Network," *Information*, vol. 12, no. 1, p. 3, Dec. 2020, doi: 10.3390/info12010003.
- [18] M. S. Islalm, M. M. Rahman, M. H. Rahman, M. R. Hoque, A. K. Roonizi, and M. Aktaruzzaman, "A deep learning-based multi-model ensemble method for eye state recognition from EEG," in 2021 IEEE 11th Annual Computing and Communication Workshop and Conference (CCWC), IEEE, 2021, pp. 0819–0824.
- [19] F. You, X. Li, Y. Gong, H. Wang, and H. Li, "A Real-time Driving Drowsiness Detection Algorithm With Individual Differences Consideration," *IEEE Access*, vol. 7, pp. 179396–179408, 2019, doi: 10.1109/ACCESS.2019.2958667.
- [20] Y. Albadawi, A. AlRedhaei, and M. Takruri, "Real-Time Machine Learning-Based Driver Drowsiness Detection Using Visual Features," *J. Imaging*, vol. 9, no. 5, p. 91, Apr. 2023, doi: 10.3390/jimaging9050091.
- [21] M. Shantal, Z. Othman, and A. A. Bakar, "A Novel Approach for Data Feature Weighting Using Correlation Coefficients and Min–Max Normalization," *Symmetry*, vol. 15, no. 12, p. 2185, 2023.
- [22] X. Larriva-Novo, V. A. Villagra, M. Vega-Barbas, D. Rivera, and M. Sanz Rodrigo, "An IoT-focused intrusion detection system approach based on preprocessing characterization for cybersecurity datasets," *Sensors*, vol. 21, no. 2, p. 656, 2021.
- [23] I. Nasri, M. Karrouchi, H. Snoussi, K. Kassmi, and A. Messaoudi, "Detection and Prediction of Driver Drowsiness for the Prevention of Road Accidents Using Deep Neural Networks Techniques," in *WITS 2020*, vol. 745, S. Bennani, Y. Lakhrissi, G. Khaissidi, A. Mansouri, and Y. Khamlichi, Eds., in *Lecture Notes in Electrical Engineering*, vol. 745. , Singapore: Springer Singapore, 2022, pp. 57–64. doi: 10.1007/978-981-33-6893-4_6.
- [24] I. Izonin, R. Tkachenko, N. Shakhovska, B. Ilchyshyn, and K. K. Singh, "A Two-Step Data Normalization Approach for Improving Classification Accuracy in the Medical Diagnosis Domain," *Mathematics*, vol. 10, no. 11, p. 1942, 2022.
- [25] A. Rajkar, N. Kulkarni, and A. Raut, "Driver drowsiness detection using deep learning," in *Applied Information Processing Systems: Proceedings of ICCET 2021*, Springer, 2022, pp. 73–82.
- [26] V. Vijaypriya and M. Uma, "Facial Feature-Based Drowsiness Detection With Multi-Scale Convolutional Neural Network," *IEEE Access*, 2023.
- [27] S. Mirjalili, A. H. Gandomi, S. Z. Mirjalili, S. Saremi, H. Faris, and S. M. Mirjalili, "Salp Swarm Algorithm: A bio-inspired optimizer for engineering design problems," *Advances in Engineering Software*, vol. 114, pp. 163–191, Dec. 2017, doi: 10.1016/j.advengsoft.2017.07.002.
- [28] A. Garces Correa, L. Orosco, and E. Laciari, "Automatic detection of drowsiness in EEG records based on multimodal analysis," *Medical Engineering & Physics*, vol. 36, no. 2, pp. 244–249, Feb. 2014, doi: 10.1016/j.medengphy.2013.07.011.
- [29] Q. Cai, Z.-K. Gao, Y.-X. Yang, W.-D. Dang, and C. Grebogi, "Multiplex Limited Penetrable Horizontal Visibility Graph from EEG Signals for Driver Fatigue Detection," *Int. J. Neur. Syst.*, vol. 29, no. 05, p. 1850057, Jun. 2019, doi: 10.1142/S0129065718500570.
- [30] H. Luo, T. Qiu, C. Liu, and P. Huang, "Research on fatigue driving detection using forehead EEG based on adaptive multi-scale entropy," *Biomedical Signal Processing and Control*, vol. 51, pp. 50–58, May 2019, doi: 10.1016/j.bspc.2019.02.005.

A Hybrid Approach with Xception and NasNet for Early Breast Cancer Detection

Yassin Benajiba, Mohamed Chrayah, Yassine Al-Amrani
TIMS Laboratory, Abdelmalek Essaadi University, Tetouan, Morocco

Abstract—Breast cancer is the most common cancer in women, accounting for 12.5% of global cancer cases in 2020, and the leading cause of cancer deaths in women worldwide. Early detection is therefore crucial to reducing deaths, and recent studies suggest that deep learning techniques can detect breast cancer more accurately than experienced doctors. Experienced doctors can detect breast cancer with only 79% accuracy, while machine learning techniques can achieve up to 91% accuracy (and sometimes up to 97%). To improve breast cancer classification, we conducted a study using two deep learning models, Xception and NasNet, which we combined to achieve better results in distinguishing between malignant and benign tumours in digital databases and cell images obtained from mammograms. Our hybrid model showed good classification results, with an accuracy of over 96.2% and an AUC of 0.993 (99.3%) for mammography data. Remarkably, these results outperformed all other models we compared them with, Top of Form ResNet101 and VGG, which only achieved accuracies of 87%, 88% and 84.4% respectively. Our results were also the best in the field, surpassing the accuracy of other recent hybrid models such as MOD-RES + NasMobile with 89.50% accuracy and VGG 16 + LR with 92.60% accuracy. By achieving this high accuracy rate, our work can make a significant contribution to reducing breast cancer deaths worldwide by helping doctors to detect the disease early and begin treatment immediately.

Keywords—Breast Cancer; CNN; Hybrid Model: Xception; NasNet

I. INTRODUCTION

Breast cancer is a serious threat to women, especially those over the age of 50. It is estimated that breast cancer accounts for 25% of all cancer cases and will affect approximately one in ten women during her lifetime. The International Agency for Research on Cancer (IARC) reports that in 2020 there will be 2.3 million women diagnosed with breast cancer and 685,000 deaths worldwide. By the end of 2020, there will be 7.8 million women alive who have been diagnosed with breast cancer in the last five years, making it the most common cancer in the world, although the incidence of breast cancer varies widely around the world. [1] These statistics highlight the importance of continued research and efforts to improve breast cancer diagnosis and treatment. The use of machine learning in this area is particularly relevant and has shown promise in increasing the accuracy of predictions, making it a valuable tool in the fight against this disease.

However, reducing the mortality rate caused by this type of cancer as well as increasing the chances of recovery are only possible if the tumor has been detected at the early stages of its appearance. And to ensure the early detection of such a tumor,

one needs to detect it in the early periods, since scientific researchers have found that early diagnosis greatly increases the chances of survival, before these malignant (cancer) cells multiply [2] in a disordered way until creating a tumor which attacks the neighboring tissues. When a breast cancer is not treated, the tumor cells spread locally and invade the neighboring organs (local extension then regional extension). Early diagnosis can therefore increase the chances of treatment before the doctor has to amputate a woman's entire breast. [3].

In recent years, the intersection of medicine and technology has paved the way for innovative approaches to breast cancer detection. Studies have shown the promising potential of deep learning techniques to improve diagnostic accuracy [4], surpassing the capabilities of even experienced medical professionals. While experienced clinicians typically achieve an accuracy rate of up to 79%, machine learning algorithms have demonstrated remarkable capabilities, with accuracy rates as high as 91% and, in some cases, 97% [5].

Motivated by the imperative to improve breast cancer diagnosis, our research delves into the realm of deep learning models, specifically exploring the efficacy of Xception and NasNet. By synergising these models, we aimed to increase classification accuracy in distinguishing between malignant and benign tumours, using digital databases of cell images obtained from mammography. The culmination of our efforts resulted in a hybrid model that showed promising results, with an accuracy of over 96.2% and an impressive AUC (area under the curve) of 0.993 for mammography data.

The research paper was designed in a way that facilitates the scientific journey for the discerning reader. Adding this introduction is given in Section I, Section II delves into the broader world of related work, where we provide an overview of the current state of research, the contributions of different researchers, the techniques of previous studies, and the results obtained in this field. Section III highlights the methodologies we chose in our research, how we divided the data, and ways to determine the effectiveness of our mixed model. We reveal the impressive results we have reached in Section IV by comparing them to the results of other research that share the same goal and research. Finally, Section VI summarizes our conclusions and the obstacles we encountered, while also pointing out future research paths.

Comparative analysis positioned our hybrid model as a leader in the field, outperforming established models such as ResNet101 and VGG, which achieved accuracy rates of only 87%, 88% and 84.4% respectively. Furthermore, our results outperformed recent hybrid models such as MOD-RES +

NasMobile and VGG 16 + LR, underlining the significance of our contribution.

Beyond academia, the implications of our work have profound potential for real-world impact. By achieving exceptional accuracy rates, our research can serve as a critical tool in the arsenal of healthcare professionals, enabling early detection and prompt initiation of treatment protocols. Ultimately, our efforts aim to reduce the burden of breast cancer on a global scale, offering hope in the quest to reduce mortality and improve patient outcomes.

II. RELATED WORK

This section provides a systematic review of scientific research in the field of medical image classification, with the aim of highlighting the contributions of different researchers and improving understanding of research methods, study techniques and results. It evaluates and compares different studies, highlighting the work of individual researchers and providing context for their findings. It also compares and evaluates these findings with the conclusions of other researchers in the same field, providing an insight into the current state of medical image classification. The results of this review will serve as a valuable resource for researchers and practitioners, providing a comprehensive overview of the field, the methods used by experts, and comparisons of results. Numerous studies have highlighted the importance of medical image classification in the early detection and accurate diagnosis of tumours and diseases, thereby improving medical diagnosis, treatment efficacy and reducing mortality rates.

In a study entitled "Automated Breast Cancer Detection Models Based on Transfer Learning" [6], the researchers segmented the data and applied some techniques to it. The best result they obtained when they applied the hybrid model technique between MOD-RES and NasMobile was 89.5% accuracy. This is the highest accuracy value compared to the rest of the other techniques used in the same research and under the same conditions.

In a study entitled: "Boosting breast cancer detection using convolutional neural network" [7], the researchers carried out a proposed prototyping approach in which they used different convolutional neural network (CNN) structures to automatically detect breast cancer and compared the results with those of machine learning (ML) algorithms... After searching and comparing, they found that their model produced results with an accuracy 87% higher than that of machine learning (ML) algorithms, which had an accuracy of only 78%. Thus, the system proposed in their paper improves accuracy by 9% over the results of machine learning (ML) algorithms.

In their paper "Deep Learning RN-BCNN Model for Breast Cancer BI-RADS Classification" [8], the researchers used a combination of augmentation strategies to prevent overfitting and improve the accuracy of mammogram analysis, including rotation, scaling and displacement. The proposed system was evaluated on the MIAS dataset and achieved 88% accuracy using the pre-trained ResNet101 classification network and 70% accuracy using the Nasnet-Mobile network. The study suggests that pre-trained classification networks are more

effective and efficient for medical imaging, especially when dealing with small training datasets.

In a scientific paper on medical image classification entitled "Transfer learning and fine tuning in the classification of radiographic mammary abnormalities on the CBIS-DDSM database" [9], the researchers used NasNet and MobileNet to train the mammary abnormality classifier and then compared them. They found that VGG16 achieved the best accuracy compared to other models, which was 0.844 in the CBIS-DDSM dataset.

In a paper entitled "Breast cancer histology images classification: Training from scratch or transfer learning?" [10], the researchers compared the use of transfer learning and fully trained networks for breast cancer classification using histopathological images. They analysed three pre-trained networks (VGG16, VGG19 and ResNet50) for their breast cancer classification behaviour independent of magnification, and examined the effect of training and test data size on their performance. They found that pre-trained VGG16 with a logistic regression classifier had the best performance, with an accuracy rate of 92.60% and an AUC of 95.65%.

III. PROPOSED SYSTEM

In our research, we have proposed a new model for image classification that combines the strengths of two of the best models available. By using the technique of combining them, as shown in the figure, we have created a new classification model that outperforms the use of either model in isolation.

What is unique about our approach is that the two models are not simply run sequentially, but are integrated in parallel. This means that the outputs of both models are combined in a way that captures the strengths of each model while mitigating its weaknesses. The result of this integration is a model that is more accurate and robust than either model alone. In other words, our proposed model represents a significant improvement over current state-of-the-art image classification methods.

To arrive at this model, we carried out extensive experimentation and analysis to determine the optimal configuration and parameters for the two models, as well as the best way to combine their outputs. The result is a model that is not only more accurate, but also more efficient, processing images faster and using fewer computing resources. Fig. 1 shows schematic diagram of the propose system.

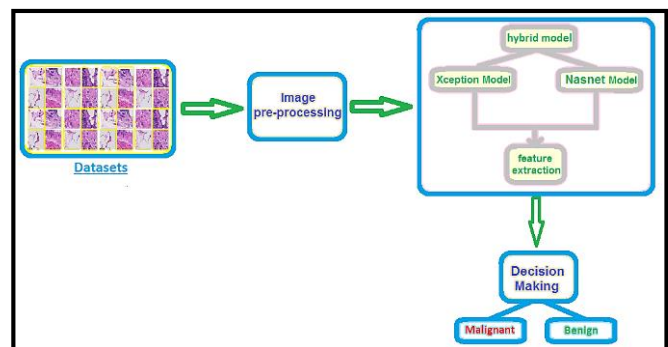


Fig. 1. Schematic diagram of the proposed system.

We believe that our proposed model has the potential to advance the field of image classification and contribute to a wide range of applications, from medical imaging to autonomous driving.

A. Datasets

In this work, datasets taken from the kaggle database were used, and this database consisted of 277,524 loci of 48×48 size divided into (198,738 negative IDCs and 78,786 positive IDCs), extracted from The original dataset was from 162 whole slice mammograms, in which cancer (BCa) samples were scanned 40 times, and the database was then extracted, segmented, and classified [11]. Fig. 2 shows example of data images.

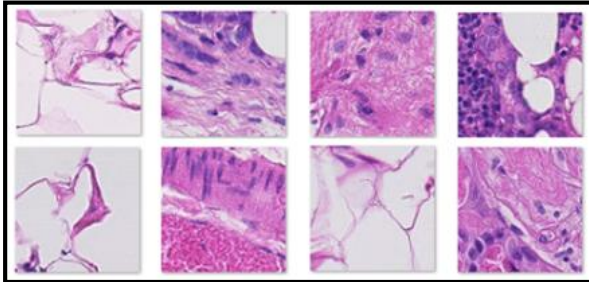


Fig. 2. Example of data images.

The archive is a 3 GB Winrar file, it contains 278 subfolders, and in each of these folders there are two more files: one labeled "0" containing the negatives, and the other labeled. The "1" file contains positive images, the name of each image is: $u_xX_yY_classC.png$ where u is the patient ID, X is the x coordinate of where this patch was cropped, Y is the y coordinate of where this patch was cropped, and C denotes a class where 0 is not idc and 1 is idc.

B. Images Pre-processing

In order to improve the performance and robustness of our proposed model and prevent overfitting, we utilized various techniques to augment and optimize the training data set, including data augmentation, image optimization, rescaling, normalization, and other methods. As the complexity of the model network increased, so did the number of parameters that needed to be learned, making it even more susceptible to overfitting. Therefore, we increased the variety and size of the training data set by implementing several techniques, such as rescaling the pixel values of input images to a range of $[0,1]$ using a factor of $1/255$ to improve numerical stability and convergence. We also flipped input images horizontally or vertically and rotated them by 90 degrees to increase diversity and reduce the risk of over fitting. Furthermore, we multiplied the number of training images by a factor of $\times 2$ to zoom in twice to improve the model's ability to handle changes in image scale.

C. Proposed Learning Methods

In this research project, we aim to develop a hybrid model by combining the Xception and NasNet models for parallel and integrated image classification. This approach will lead to improved performance compared to using each model separately. The NasNet model is a deep learning architecture

developed by Google's AI researchers and optimised for high accuracy object detection and image classification. It is designed to be computationally efficient, making it ideal for real-time applications such as self-driving cars, robotics and video surveillance. The Xception model, also developed by Google AI researchers in 2016, is a variation of the Inception model designed for advanced accuracy in image classification tasks. It is more efficient than the Inception model, making it suitable for real-time image recognition, natural language processing and object detection applications. The combination of these two models will lead to significant improvements in the early detection of breast cancer by classifying benign and malignant images, as demonstrated by the results of our study.

D. Assessment Metrics

To evaluate the effectiveness of our proposed hybrid model, we compared its performance with that of several unilateral models, as well as with the performance of other hybrid models used by other researchers in image classification for breast cancer detection. We used a number of performance metrics to make this comparison, including the following:

1) *Accuracy and loss*: When evaluating classification models, an important criterion is their accuracy, which is a measure of how many of their predictions are correct [12] More formally, accuracy refers to the proportion of correct predictions made by the model.

In other words, accuracy is a measure of how well the model is able to correctly classify different types of input. The higher the accuracy, the more reliable the model is likely to be. [13] For this reason, accuracy is often used as a benchmark for comparing different classification models.

$$Accuracy = \frac{TP + TN}{TP + FP + TN + FN}$$

- True positives (TP): images of benign tumors correctly classified.
- True negatives (TN): images of malignant tumors correctly classified .
- False positives (FP): Images of benign tumors were not correctly classified.
- False negatives (FN): Images of malignant tumors were not correctly classified.

Loss is a technique used to assess how well an algorithm is able to model a given set of data. If the algorithm's predictions are too far from the actual results, the loss function will return a high value. [14] Over time, using an optimisation function, the loss function is able to learn how to minimize the prediction error by adjusting the algorithm's parameters. [15].

In other words, the loss function is a measure of how well the algorithm is able to approximate the correct output for a given input. [16] The optimisation function works by adjusting the parameters of the algorithm to minimise the loss, which in turn improves the accuracy of the model. This process is often repeated many times until the loss is reduced to an acceptable level, at which point the algorithm is considered to have learned the underlying patterns in the data.

2) The ROC Curve (Receiver Operational Characteristic):

The ROC curve, short for receiver operating characteristic, is a function used to measure the performance of a binary classifier - a system that classifies items into two groups based on their characteristics. This function is also known as a performance characteristic or sensitivity/specificity curve. [17]. Fig. 3 shows the ROC curve.

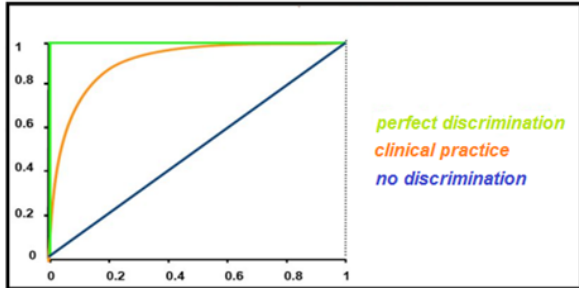


Fig. 3. The ROC curve.

The ROC curve is usually plotted as a curve with the true positive rate (the proportion of true positives that are correctly identified) on the y-axis and the false positive rate (the proportion of true negatives that are incorrectly identified) on the x-axis. [18] This curve provides a visual representation of the performance of the classifier by showing how well it is able to distinguish between the two groups.

In summary, the ROC curve is a tool used to evaluate the performance of a binary classifier. By plotting the true positive and false positive rates, it provides a clear and concise representation of the classifier's ability to distinguish between the two groups.

IV. RESULTS AND DISCUSSION

We would like to present the findings of various experiments conducted on our innovative hybrid system, which was applied to a set of images that had been divided into training and testing data with a ratio of 80–20%. In each trial, we modified the parameters of the model and applied it, resulting in a range of different outcomes. We then meticulously analyzed and compared these outcomes with the aim of improving our model and identifying the best possible configuration. Below, we provide a comprehensive summary of the results we obtained from each of these trials using their respective parameter settings:

According to the analysis of the results of the tables, we note that:

For Batch size= 100 and Batch size = 200, the values for accuracy and AUC increased until epoch 15 and then decreased, and for error it was always decreasing. This indicates that optimal performance for these batch sizes was achieved on or around Epoch 12.

For Batch size = 215, the accuracy increased until epoch 15 and then decreased, while the error decreased and then stabilized to a value of 0.113. AUC followed a similar pattern to the other batch sizes, increasing up to Epoch 15 and then decreasing.

For Batch size = 216, the accuracy increased until epoch 16 and then decreased, while the error decreased until epoch 16 and then increased. AUC followed a similar pattern for other batch sizes, increasing until epoch 16 and then decreasing. This indicates that optimal performance for these batch sizes was achieved on or around Epoch 15. Table I shows the summary table of the results obtained by our hybrid model.

TABLE I. SUMMARY TABLE OF THE RESULTS OBTAINED BY OUR HYBRID MODEL

| Test | Image size | Batch size | Epochs | Accuracy | Loss | Auc |
|------|------------|------------|--------|----------|-------|-------|
| 1 | (96,96,3) | 100 | 5 | 0,941 | 0,138 | 0,985 |
| 2 | | | 12 | 0,948 | 0,132 | 0,989 |
| 3 | | | 15 | 0,946 | 0,133 | 0,987 |
| 4 | | 200 | 5 | 0,954 | 0,123 | 0,985 |
| 5 | | | 12 | 0,957 | 0,114 | 0,987 |
| 6 | | | 15 | 0,958 | 0,108 | 0,986 |
| 7 | | 215 | 5 | 0,956 | 0,114 | 0,989 |
| 8 | | | 12 | 0,957 | 0,113 | 0,992 |
| 9 | | | 15 | 0,956 | 0,113 | 0,989 |
| 10 | | 216 | 5 | 0,954 | 0,124 | 0,986 |
| 11 | | | 12 | 0,958 | 0,103 | 0,991 |
| 12 | | | 15 | 0,959 | 0,102 | 0,993 |
| 13 | | | 16 | 0,954 | 0,104 | 0,991 |
| 14 | | 217 | 5 | 0,942 | 0,134 | 0,978 |
| 15 | | | 12 | 0,954 | 0,114 | 0,991 |
| 16 | | | 15 | 0,954 | 0,113 | 0,99 |
| 17 | | 220 | 5 | 0,952 | 0,125 | 0,988 |
| 18 | | | 12 | 0,954 | 0,117 | 0,989 |
| 19 | | | 15 | 0,955 | 0,115 | 0,991 |

For Batch size = 217 and Batch size = 220, the accuracy decreases and then continues to increase, the error continues to decrease, and the AUC continues to rise until the epoch 15. But its value does not reach the rest of the values of other epochs.

After conducting a thorough analysis and comparing all the results obtained in the parametric study, we have determined that the optimal test for our hybrid model is the one with the following parameters:

Image size = (96 ;96 ;3) ; Batch size = 216 ; Epochs = 15

In order to obtain accurate and reliable results from our analysis, we conducted a comprehensive study by closely observing the evolution of three key metrics: accuracy, loss, and ROC. To ensure that our analysis was as rigorous as possible, we carefully examined the performance of our model from the very first epoch up until the best performing epoch. By doing so, we were able to identify the optimal point at which our model achieved its highest levels of accuracy, lowest levels of loss, and best ROC score. Table II shows the results that we reached during this comparison:

Upon close observation, we have noted that the parameters of Accuracy and Val_Accuracy have consistently displayed a

positive and upward trend, with only occasional and minor declines noted at some stages. The general pattern, however, indicates that these performance indicators have achieved the best results possible. Furthermore, Loss and Val_Loss demonstrate a reliable and steady decrease during the implementation stages of the hybrid model utilizing the carefully selected parameters. It is worth noting that after conducting multiple comparisons, we arrived at the conclusion that these chosen parameters were the best for the given task. Thus, it is apparent that the application of the hybrid model with these specific parameters has yielded promising and encouraging results.

TABLE II. ACCURACY, LOSS, VAL_ACCURACY AND VAL_LOSS FOR THE SPECIFIED PARAMETERS

| Epoch | Accuracy | Loss | Val_Accuracy | Val_Loss |
|-------|----------|---------|--------------|----------|
| 1 | 0.88366 | 0.27512 | 0.92305 | 0.22194 |
| 2 | 0.93020 | 0.18116 | 0.92973 | 0.17954 |
| 3 | 0.94008 | 0.15606 | 0.93808 | 0.15820 |
| 4 | 0.94816 | 0.13721 | 0.95076 | 0.13379 |
| 5 | 0.95331 | 0.12474 | 0.94688 | 0.14112 |
| 6 | 0.95766 | 0.11403 | 0.94814 | 0.13775 |
| 7 | 0.96111 | 0.10500 | 0.95967 | 0.10887 |
| 8 | 0.96413 | 0.09785 | 0.96032 | 0.10932 |
| 9 | 0.96651 | 0.09168 | 0.95764 | 0.11423 |
| 10 | 0.96950 | 0.08480 | 0.95367 | 0.12746 |
| 11 | 0.97079 | 0.08029 | 0.96061 | 0.10963 |
| 12 | 0.97255 | 0.07499 | 0.96011 | 0.11079 |
| 13 | 0.97403 | 0.07096 | 0.96035 | 0.11164 |
| 14 | 0.97533 | 0.06706 | 0.96047 | 0.11161 |
| 15 | 0.97658 | 0.06397 | 0.96285 | 0.10786 |

Furthermore, we made sure that the choice of this best performing epoch was the most suitable for the subsequent epochs that followed. In other words, we conducted an extensive analysis to ensure that the performance of the model did not deteriorate after the best performing epoch, as this would indicate that our choice was not the most optimal. In order to conduct a comprehensive analysis of our hybrid model, we closely monitored the accuracy, loss, and ROC curves. To ensure accurate results, we used optimal test parameters and kept all other parameters constant except for three instances when we made changes. By doing this, we gained a comprehensive view of how the model evolved over time and how it performed under different conditions. Fig. 4 shows the evolution of some of the curves selected from among the many curves obtained:

Our study yielded a significant finding related to the performance of our hybrid model. We were able to observe the evolution of the accuracy and ROC curves over time as we adjusted the model's parameters. With each adjustment, we noted a steady improvement in the model's performance, and the accuracy and ROC curves reached their best values at the selected parameters. In addition to this, we also observed a corresponding decrease in the loss curve as we approached the best model for our purposes.

These results provided us with valuable insights into the strength of our hybrid model's selected parameters, which allowed us to fine-tune and improve its performance for future use. Overall, our approach enabled us to effectively assess the effectiveness of our model and make informed decisions about how best to improve it to obtain the best results. By carefully analyzing the performance metrics, we were able to optimize the parameters of our hybrid model and ensure that it delivered accurate results. This outcome is critical for future use, as we can now rely on our hybrid model to provide accurate predictions and insights.

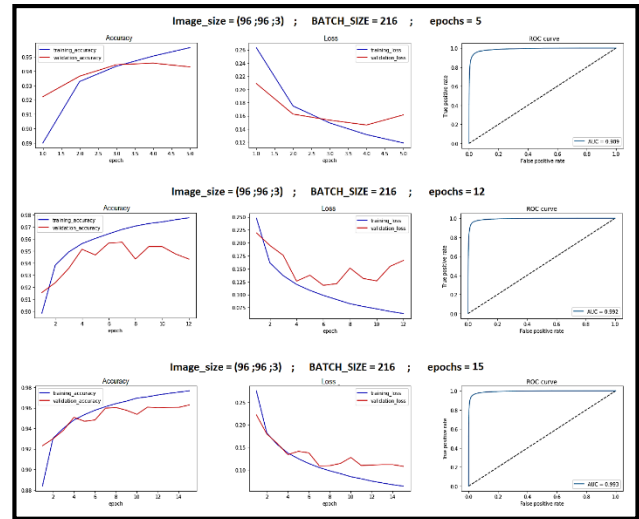


Fig. 4. Accuracy, Loss, and Roc curves by epoch.

V. COMPARED TO OTHER MODELS

The proposed system's effectiveness and dependability are assessed against the latest research on image classification systems for breast cancer screening. In this section, we showcase the results of the proposed system (a hybrid model combining Xception and NasNet deep learning models) and juxtapose them against existing methods (see Table III). The findings in Table III reveal that the proposed system yields considerably more accurate outcomes than the techniques we compared it with. Furthermore, our proposed system surpasses other hybrid models listed in the table with respect to accuracy.

TABLE III. COMPARISON OF OUR MODEL WITH OTHER MODELS IN TERMS OF ACCURACY

| Author (year) | Technique | Accuracy |
|---|---------------------|----------|
| Our hybrid model | Xception + NasNet | 96.20% |
| Madallah Alruwaili and Walaa Gouda (2022) [6] | MOD-RES + NasMobile | 89,50% |
| Saad Awadh Alanazi (2021) [7] | CNN | 87% |
| Shahbaz Siddeeq (2021) [8] | ResNet101 | 88 % |
| Lenin G. Falconí, M. Pérez (2020) [9] | VGG | 84,4% |
| Shallu and R. Mehra (2018) [10] | VGG16 + LR | 92,60% |

In previous studies, researchers used different models to classify data and achieve a high accuracy rate. However, none of those models were able to exceed an accuracy rate of 89.5%,

except for the VGG 16 + LR hybrid model, which achieved an accuracy rate of 92.60%. Despite this achievement, our hybrid model was able to surpass the accuracy rate of all the other models, including VGG16 + LR, with an accuracy rate of 96.2%. This makes our hybrid model the best performing model among all the models tested, as it has the highest classification accuracy. Fig. 5 shows this superiority more clearly:

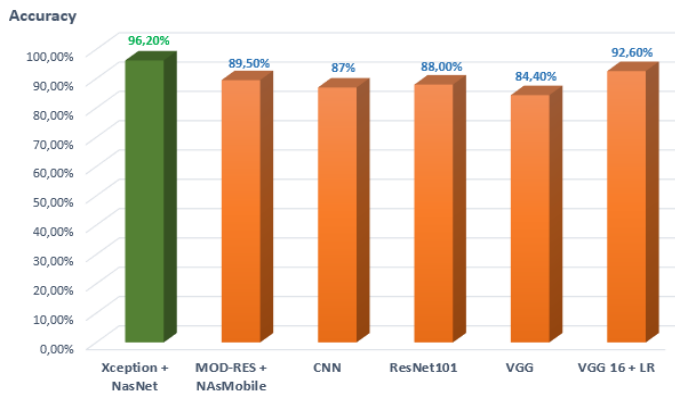


Fig. 5. Accuracy comparison between models.

After analyzing the curve, we found that our hybrid model outperformed all the other models used for classification, with the highest accuracy rate. This is an important finding, as it confirms that our model is superior in identifying and diagnosing breast cancer.

The VGG16 + LR hybrid model ranked second in terms of accuracy, which is consistent with our previous results. The accuracy rates of the other models used in our study did not exceed the accuracy of our hybrid model or the VGG16 + LR hybrid model. However, our model outperformed the VGG16 + LR hybrid model in terms of both accuracy and AUC. Our model achieved an AUC of 99.3%, while the VGG16 + LR hybrid model achieved an AUC of only 84.4%. [9].

This result is significant as it affirms that our model can accurately classify medical images, which will facilitate the process of identifying breast cancer with high accuracy and in the early stages of its existence. This, in turn, will greatly assist doctors in determining the presence of the disease or not, which can lead to early interventions and treatments.

VI. CONCLUSION AND FUTURE DIRECTION

In this study, we utilized a cutting-edge technique by amalgamating two deep learning models, NasNet and Xception, after conducting thorough individual evaluations of each model. We then fine-tuned the parameters to attain the most optimal outcomes. Afterwards, we compared our results with various scientific research papers that focused on classifying breast cancer medical images. Our findings revealed that the model we designed outperformed all other

models in terms of accuracy and Area Under the Curve (AUC), with an accuracy of 96.2% and an AUC of more than 99.3%. By achieving this high accuracy rate, our work can make a significant contribution to reducing breast cancer deaths worldwide by helping doctors to detect the disease early and begin treatment immediately.

Although we have succeeded in creating a very precise and accurate model, it takes a long time to apply it to show results. This has led us to look forward to future research focusing on the same model, but with a strong focus on reducing its application time while maintaining its exceptional accuracy and uniqueness. Our plan is to test a number of approaches to determine the most effective ways to achieve this goal. Through extensive research and testing, we aim to simplify the process of implementing our model while ensuring it remains effective and accurate.

REFERENCES

- [1] Melina A; Eileen M; Harriet R, "Current and future burden of breast cancer: Global statistics for 2020 and 2040". December 2022.
- [2] Maria S; David P, "Artificial Intelligence in Cancer Research: Trends, Challenges and Future Directions". December 2022.
- [3] Xin J; Ping M, "Targeting Breast Cancer Metastasis". September 2015.
- [4] Y.Benajiba, M.Chrayah, Y.Al-Amrani, "A Nonlinear Support Vector Machine Analysis Using Kernel Functions for Nature and Medicine",2021.
- [5] Gouda, W.; Selim, M.M.; Elshishtawy, T, "An Approach for Breast Cancer Mass Detection in Mammograms". January 2012.
- [6] Alruwaili, M.; Gouda, W, "Automated Breast Cancer Detection Models Based on Transfer Learning". January 2022,
- [7] Alanazi, S.A.; Kamruzzaman, M.M; Sarker N.I; Alruwaili.M ; Alhwaiti, Y.Alshammari, N.; Siddiqi, M.H, "Boosting breast cancer detection using convolutional neural network", Apr 2021.
- [8] Siddeeq, S.; Li, J.; Ali Bhatti, H.M.; Manzoor, A.; Malhi, U.S, "Deep Learning RN-BCNN Model for Breast Cancer BI-RADS Classification", January 2021.
- [9] Lenin G.F; Maria P; Wilbert G.A; Aura C, "Transfer Learning and Fine Tuning in Breast Mammogram Abnormalities Classification on CBIS-DDSM Database", March 2020.
- [10]] Shallu. Rajesh M, "Breast cancer histology images classification: Training from scratch or transfer learning?", November 2018.
- [11] PAUL MOONEY, Breast Histopathology Images Dataset, <https://www.kaggle.com/datasets/paultimothymooney/breast-histopathology-images>
- [12] Zeljko V, "Classification Model Evaluation Metrics". July 2021.
- [13] Singh L. Alam A, "An efficient hybrid methodology for an early detection of breast cancer in digital mammograms", May 2022.
- [14] Tian Y, Duo Su, Lauria S, Xiaohui L, "Recent advances on loss functions in deep learning for computer vision". August 2022.
- [15] Juan T; Diana M.C.E; Alfonso R.P; Edgar A.C.U, "Loss Functions and Metrics in Deep Learning. A Review". July 2023.
- [16] Qi W; Yue M; Kun Z; Yingjie T, "A Comprehensive Survey of Loss Functions in Machine Learning", April 2020.
- [17] Narkhede S, "Understanding AUC - ROC Curve", Jun 2018.
- [18] Tom F, "Introduction to ROC analysis", June 2006.

Strengthening Sentence Similarity Identification Through OpenAI Embeddings and Deep Learning

Dr. Nilesh B. Korade¹, Dr. Mahendra B. Salunke², Dr. Amol A. Bhosle³,
Dr. Prashant B. Kumbharkar⁴, Gayatri G. Asalkar⁵, Rutuja G. Khedkar⁶

Assistant Professor, Department of Computer Engineering,
JSPM's Rajarshi Shahu College of Engineering, Tathawade, Pune-411033, Maharashtra, India^{1,6}

Assistant Professor, Department of Computer Engineering,
PCET's, Pimpri Chinchwad College of Engineering and Research, Ravet, Pune-412101, Maharashtra, India²

Associate Professor, Department of Computer Science and Engineering, School of Computing,
MIT Art, Design and Technology University, Loni Kalbhor, Pune-412201, Maharashtra, India³

Professor, Department of Computer Engineering,
JSPM's Rajarshi Shahu College of Engineering, Tathawade, Pune-411033, Maharashtra, India⁴

Research Scholar, Department of Computer Science and Engineering,
Shri Jagdishprasad Jhabarmal Tibrewala University, Vidyanagari, Churela-333001, Rajasthan, India⁵

Abstract— Discovering similarity between sentences can be beneficial to a variety of systems, including chatbots for customer support, educational platforms, e-commerce customer inquiries, and community forums or question-answering systems. One of the primary issues that online question-answering platforms and customer service chatbots have is the large number of duplicate inquiries that are placed on the platform. In addition to cluttering up the platform, these repetitive queries degrade the content's quality and make it harder for visitors to locate pertinent information. Therefore, it is necessary to automatically detect sentence similarity in order to improve the user experience and quickly match user expectations. The present study makes use of the Quora dataset to construct a framework for similarity discovery in sentence pairs. As part of our research, we have built additional attributes based on textual data for improving the accuracy of similarity prediction. The study investigates several vectorization methods and their influence on accuracy. To convert preprocess text input to a numerical vector, we implemented Word2Vec, FastText, Term Frequency-Inverse Document Frequency (TF-IDF), CountVectorizer (CV), and OpenAI embedding. In order to judge sentence similarity, the embedding offered by several approaches was used with various models, including cosine similarity, Random Forest (RF), AdaBoost, XGBoost, LSTM, and CNN. The result demonstrates that all algorithms trained on OpenAI embedding yield excellent outcomes. The OpenAI-created embedding offers excellent information to models trained on it and has significant potential for capturing sentence similarity.

Keywords—OpenAI; embedding; sentence similarity; FastText; Word2Vec; CNN; LSTM; precision; recall; F1-score

I. INTRODUCTION

The intricacy of natural language and the variety of ways in which phrases can express similar concepts make accurate sentence similarity assessment difficult. Scholars and professionals in the domain employ a variety of methodologies, which vary from conventional approaches such as cosine and Jaccard similarity to intelligent approaches that involve neural network models. An approach known as similarity

identification or identical inquiry identification identifies similarities in the inquiries presented. The following, are several areas where text similarity matching is crucial to boosting service to clients [1].

- Client Assistance Chatbots Use similarity matching to find and group together related client inquiries. This increases the effectiveness of chatbot conversations and helps in generating consistent responses.
- By discovering and eliminating repetitive queries, community forums may enhance the user experience by making sure that conversations are concise and relevant [2].
- Improve customer service on e-commerce sites by recognizing common questions about the products and offering consistent replies.
- Employers can find comparable questions about policies, benefits, or procedures by using similarity matching in HR systems. This will help assure that responses are correct and consistent.
- To gain insights into popular topics and sentiment analysis, use similarity matching to combine and analyze similar questions or comments on social media networks [3].
- Similarity matching can be used by healthcare information systems to find related medical inquiries and give consumers reliable, consistent information about symptoms, diagnoses, and other health-related issues.

Finding such repetitively asked queries is crucial to improving the efficiency of resource utilization on the internet. It is not possible to find and remove duplicate questions manually. The duplicate inquiries or sentences should be identified automatically using some autodetection approaches [4,5,6]. In order to find similarities between two sentences, we

conducted our research using Quora's question-pair dataset. On the sentence dataset, we have used a variety of preprocessing approaches to eliminate unnecessary components and create a clean dataset that may be used for vectorization or embeddings. Based on parameters like sentence length, the frequency with which a string appears in the sentence, common strings in both sentences, fuzzy logic usage, etc., we have created a number of additional features that will provide additional information to a model trained on embedding. Numerous vectorization and embedding techniques, such as TF-IDF, CV, Word2Vec, FastText, and OpenAI text-embedding-ada-002 embedding, are used to convert text collections into numerical features. The metrics used to assess the quality of embedding and model performance on embedding include precision, recall, F1-score, and accuracy. The OpenAI text-embedding-ada-002 embedding shows potential in capturing sentence similarity and offers valuable information that supports different models for similarity identification.

The remainder of the document is structured as follows: Section II discusses the existing literature on duplicate question detection. Section III outlines the methodology, including the research flow, dataset, preprocessing steps, feature engineering, vectorization methods, and algorithm implementation. Section IV covers the evaluation of accuracy with various vectorization techniques and models. Section V presents a summary of our research findings and suggests avenues for further investigation.

II. LITERATURE SURVEY

The sharing and learning environment have experienced significant changes due to the quick growth of digital platforms. Crowdsourced solutions like Community Question Answering (CQA) have been popular as a way for volunteers to share their knowledge and get their doubts regarding particular topics answered. A solution is required to address the issue of semantically comparable question detection for duplication identification in bilingually transliterated data. In order to detect question repetition, deep learning has been implemented by S. Rani et al. to evaluate informal languages like Hinglish, a bilingual blend of Hindi and English spoken on Community Question Answering (CQA) platforms. There are two components: the first is a language conversion component that creates a text in mono-language from input questions. The hybrid model, which combines a Siamese neural network (SNN), a capsule neural network, and a decision tree classifier, is used to determine the similarity between the question pairs. To calculate the similarity of questions, the SNN and the Manhattan distance function are utilized. An accuracy of 87% and an AUCROC value of 0.86 are obtained by validating the suggested model on 150 pairs of questions [7].

Contributors often make use of a pull-request procedure on social coding platforms like GitHub to present their source code modifications to inspectors of a particular repository. Due to the distributed nature of this approach, pull requests carrying out similar development tasks can be unintentionally submitted by multiple contributors, resulting in unnecessary effort and time spent reviewing. A strategy for allocating the same reviewer or reviewing team to each cluster of related pull requests was suggested by H. E. Salman et al., which makes it

possible to save time and effort. To identify similarities across pull requests, first extract descriptive textual information from the content of the pull requests and use it to link equivalent pull requests together. To group relevant pull requests together, the K-means clustering and agglomeration hierarchical clustering algorithms are employed. The experimental results indicate that the K-Means algorithm achieves 94%, 91%, whereas agglomeration hierarchical clustering achieves 93%, 98% average precision and recall values over all evaluated repositories. The twenty popular repositories of public datasets are used to access the provided approach. In addition, the suggested method reduces the amount of time and effort required for reviews by using the K-Means algorithm by an average of 67% to 91% and the agglomeration hierarchical clustering technique by an average of 67% to 83% [8].

Millions of people use search engines every day to find solutions, which results in an increasing need for innovative, clever methods to assist people in solving problems. Using a 7GB real-time dataset, V. K. R. Anishaa et al. trained and evaluated four machine learning models in order to identify duplicate queries. The noise is eliminated by removing HTML tags, stop words, punctuation, white spaces, and URLs after the data has loaded. Pre-processing is carried out in SQLite databases utilizing PL/SQL blocks, which process enormous volumes of data faster than alternate techniques. The four different ML models are used to train the acquired dataset. After execution, the random, logistic regression, linear SVM, and XGBoost error parameters referred to from the log loss function are found to be, respectively, 0.887, 0.521, 0.654, and 0.357. As a result of the unique pre-processing activities carried out using PL/SQL, which improve response time overall, the result demonstrates that XGBoost is the best model, delivering the greatest accuracy in the shortest period of time [9].

On a social media platform where users post questions, other users can assist by editing the questions and providing more precise answers to the questions that are asked. Due to linguistic heterogeneity, it can be complicated to determine a sentence's true meaning with accuracy, making the classification of repeated inquiries a challenging process. Deep learning techniques have demonstrated exceptional performance in several natural language processing (NLP) problems, particularly in the area of semantic text similarity. In order to determine the semantic relevance between two queries, Z. Imtiaz et al. suggested a novel Siamese MaLSTM model, wherein the term "Siamese" refers to the employment of two or more sub-identical network architectures simultaneously and Ma indicates Manhattan distance. The GoogleNewsVector, FastText, and FastText subword word embeddings are used to independently train the Siamese LSTM model. The final prediction is then derived from the combination of these trained models [10].

Using a variety of techniques, many investigators have worked on duplicate text detection until now. Text data is pre-processed and converted to an array of numbers using the TF-IDF method. Using the Quora's dataset, D. Basavesha examined five machine learning models. Adaboost yields an accuracy of 81.73%, random forest yields 81.72%, decision tree yields 79.29%, and logistic regression yields 79.21% [11].

A well-known software problem-solving website with a focus on solving errors in software code, Stack Overflow has seen an increase in visitors in recent years. L. Wang et al. employed Word2Vec to get the vector representations of words, and CNN, RNN, and LSTM are three distinct deep learning approaches that are taken into consideration to address the issue of similar inquiry discovery in Stack Overflow. The evaluation's findings demonstrate that WV-CNN and WV-LSTM have significantly outperformed the other baseline techniques. The dataset consisted of queries in various programming languages, including Perl, Java, and others. The outcome demonstrates that for every dataset, WV-CNN and WV-LSTM based on Word2Vec yield recall rates greater than 80% [12].

A. W. Qurashi measures the level of semantic equivalence across multi-word phrases for the regulations and guidelines stated in railway safety manuals. There are two text similarity measures that are examined: The cosine similarity metric maps the text into a vector space model, and the "Word2Vec" technique is used to determine the distance between the texts. A count-based metric called Jaccard similarity is the intersection of two sets divided by the union of two sets. The cosine similarity determines the degree of similarity between texts by converting sentences from documents into vectors using Word2Vec. The results show that the Jaccard similarity method, which measures similarity based on character matching, yielded unsatisfactory results and while evaluating the similarity of two documents, cosine provides a more accurate result by measuring the angle between vectorized phrases [13].

III. METHODOLOGY

A. Dataset

To determine textual similarity, this study makes use of the 0.4 million questions in the Quora dataset [14]. Table I presents information on the features and content of the dataset.

TABLE I. DATASET DETAILS

| Attribute | Details |
|----------------------------|--|
| ID | Each dataset row is assigned a unique number that allows for its own unique recognition. |
| Question_ID1, Question_ID2 | There is a distinct identity for each of the questions in the features labelled "Question No. 1" and "Question No. 2." |
| QuestionNo1, QuestionNo2 | This feature includes real questions to check if they are similar to each other. |
| Is_Duplicate | When question pairs are intellectually examined, the result is Is_Duplicate, where 0 means false and 1 means yes. |

B. Preprocessing

The dataset is subjected to basic preprocessing in order to be approved for usage in the succeeding phase, i.e., vectorization and model training. The database is examined for any duplicate or missing entries, and those that are found are discarded. All punctuation is deleted, the database is lowercased, and some special characters like '%' for percent are substituted out for their string equivalents. The URL and HTML elements were eliminated, and chartwords like "N.A." (which indicates "not applicable") were replaced. The dataset

has been lemmatized after all stopwords have been eliminated and tokenization has been applied [15].

C. Feature Engineering

Strong features can increase the predictive ability of machine learning models by giving them pertinent information. On the basis of the properties of the question text that were listed in the dataset, new features were generated [16]. Table II presents an extensive overview of each newly developed feature along with a description.

TABLE II. FEATURE CREATION DETAILS

| New Feature | Details |
|------------------------------|---|
| Sen1Len, Sen2Len | It is the entire sentence length, with all characters included. |
| WordCountSen1, WordCountSen2 | Total number of words present in the sentence, including repeated words. |
| WordCommon | The number of terms that are present identically in the two sentences. |
| DistinctWords | It is a sum of unique words found in the first sentence and unique words found in the second sentence. |
| WordShare | It is the ratio of "word common" and "distinct words." |
| CWC_Min | It is a ratio of the number of common words (<i>WordCommon</i>) to the length of a shorter sentence (<i>min (Question1Length, Question2Length)</i>). |
| CWC_Max | It is a ratio of the number of common words (<i>WordCommon</i>) to the length of a larger sentence (<i>max (Question1Length, Question2Length)</i>). |
| CSC_Min | It is a ratio of the number of common stopwords (<i>stopwords(sentence1) ∩ stopwords(sentence2)</i>) to the minimum stopword count in the first and second sentences (<i>min (stopwords count in sentence1, stopwords count in sentence2)</i>). |
| CSC_Max | It is a ratio of the number of common stopwords (<i>stopwords(sentence1) ∩ stopwords(sentence2)</i>) to the maximum stopword count in the first and second sentences (<i>max (stopwords count in sentence1, stopwords count in sentence2)</i>). |
| CTC_Min | It is a ratio of the number of common tokens (<i>tokens(sentence1) ∩ tokens (sentence2)</i>) to the minimum token count in the first and second sentences (<i>min (tokens count in sentence1, tokens count in sentence2)</i>). |
| CTC_Max | It is a ratio of the number of common tokens (<i>tokens(sentence1) ∩ tokens (sentence2)</i>) to the maximum token count in the first and second sentences (<i>max (tokens count in sentence1, tokens count in sentence2)</i>). |
| Avg_Tokens | It is a ratio of the sum of tokens present in both sentences to the number of sentences. |
| Abs_Len_Diff | It refers to the absolute value of the numerical difference between two sentence lengths. |
| Lng_Substr_Ratio | It is the ratio of the common longest substring in sentences 1 and 2 to the minimum token count from the first or second sentence <i>min (token count(sentence1), token count(sentence2))</i> . |
| Last_Word_Equal | The value is set to 1 if both sentences have identical last words; otherwise, it is 0. |
| First_Word_Equal | The value is set to 1 if both sentences have identical first words; otherwise, it is 0. |

A Python library called fuzzywuzzy offers a variety of functions for string analysis and algorithm-based similarity score calculations [17]. The Levenshtein Distance (LD) is a measure of the degree of difference between two strings. The

degree of difference between the two strings increases with the number. is the smallest number of single-character modifications needed to convert one word to another. Let us assume that the lengths of the two sentences, sen1 and sen2, are l_1 and l_2 , respectively. The LD, or the minimum number of modifications needed to transform sen1 into sen2, is $D(l_1, l_2)$. By filling up a $(l_1+1) \times (l_2+1)$ matrix, the dynamic programming technique efficiently computes this distance.

$$\text{fuzz_ratio} = \frac{1}{1+LD} \quad (1)$$

Using matching substrings of a given length, the `fuzz_partial_ratio` (FPR) function determines the "partial ratio" between two strings, which indicates how similar they are. The strings' higher `fuzz_partial_ratio` indicates a high degree of similarity.

$$\text{FPR} = \frac{2 * \text{Common Characters in Two sentence}}{\text{len(sentence1)+len(sentence2)}} * 100 \quad (2)$$

The `token_sort_ratio` (TSortR) function, which computes the similarity ratio between two strings after sorting their tokens alphabetically, is especially helpful when working with strings that may contain the same words but in a different sequence.

$$\text{TSortR} = \frac{LD \left(\begin{array}{c} \text{Sorted Tokens in Sentence1,} \\ \text{Sorted Tokens in Sentence2} \end{array} \right)}{\max \left(\begin{array}{c} \text{len(Sorted Tokens in Sentence1),} \\ \text{len(Sorted Tokens in Sentence2)} \end{array} \right)} * 100 \quad (3)$$

The `token_set_ratio` (TSetR) function, which determines the similarity ratio between two strings based on the intersection and union of their unique tokens, is helpful when comparing texts that might contain common terms but also have differences.

$$\text{TSetR} = \frac{LD \left(\begin{array}{c} \text{Token Set in sentence1,} \\ \text{Token Set in sentence2} \end{array} \right)}{\max \left(\begin{array}{c} \text{len(Token Set in sentence1),} \\ \text{len(Token Set in sentence2)} \end{array} \right)} * 100 \quad (4)$$

D. Word Embedding / Vectorization

Word embedding is a method that captures syntactic and semantic similarities between words depending on their context of usage by representing words as vectors of real numbers in a high-dimensional space. The following vectorization and word embedding techniques were used in the study.

1) *Count vectorizer*: Count Vectorizer creates a matrix in which each unique word is represented by a column of the matrix, and each text sample from the document is a row in the matrix [18]. The value of each cell is nothing but the count of the word in that particular text sample [19].

2) *TF-IDF*: The term frequency Inverse Document Frequency (TF-IDF) gives information about the more and less important words in a document. When retrieving information, a word's relevance within the text matters significantly. The more times a word appears in the text, the more significant it becomes. The frequency of a word (w) in a document (d) is measured by term frequency (TF), which is the ratio of a word's occurrence in a document to the total number of terms in the document [20]. A term's Inverse

Document Frequency (IDF) indicates how common or uncommon a word is within the whole corpus of documents D . TFIDF is a product of TF and IDF, where the word that is more frequent in the document will get more importance and the word that is rare in the corpus will receive more weight [21, 22].

$$\text{Term Frequency}(w, d) = \frac{\text{number of times } w \text{ appears in } d.}{\text{total number of words in document } d.} \quad (5)$$

$$\text{Inverse Document Frequency}(w, D) =$$

$$\log \frac{\text{number of document in } D.}{\text{number of documents contains } w} \quad (6)$$

$$\text{TFIDF}(w, d, D) = \text{TF}(w, d) * \text{IDF}(w, D) \quad (7)$$

3) *Word2Vec*: Words can be expressed as vectors using a technique called word embedding. Word embedding's main aim is to create low-dimensional feature vectors from the high-dimensional feature space of words while preserving contextual similarity within the corpus. Predicting the words that are close to each individual word in a sentence is the primary objective of the Word2Vec model. Word2Vec uses CBOW and skip-gram architecture, and using the training text input, it builds a vocabulary in order to the vector representation of words [23].

a) *CBOW*: A neural network termed the continuous bag-of-words (CBOW) model is used for NLP applications like text classification and language translation. One-hot encoding serves as the method for the target and input layer encoding, with a size of $[1 \times V]$. The CBOW uses context words or surrounding words (X) as input in an attempt to predict the target or central word (Y). The weight sets (W, W') are initiated randomly, one between the input and hidden layers and the other between the hidden and output layers. Input Hidden layer matrix size is represented as $[V \times N]$, and hidden output layer matrix size is represented as $[N \times V]$, where N is a random number that indicates the size of our embedding space or how many dimensions, we want to use for describing our word. The hidden activation is the product of the input and the input-hidden weights. The product of hidden input and hidden output weights produces the output Y . The difference between the output and the target is evaluated and reported back to reset the weights [24,25].

b) *Skip-Gram*: Word2Vec also uses the skip-gram neural network approach, which reverses the CBOW architecture and predicts context or surrounding words ($Y1, Y2...$) for a given target word (X). The random weight is assigned after one-hot encoding of both the input layer and the target layer. To modify the weight assigned, the softmax function first calculates the probability of context words, then backpropagates the error by computing the loss between prediction and actual. Fig. 1 and 2 demonstrate the CBOW and skip-Gram structure [26,27].

4) *FastText*: An open-source platform called FastText, created by Facebook, enables professionals to acquire text representations and classifiers to perform efficient text classification. fastText offers subword embeddings by considering that words are made up of character n-grams [28].

For the purpose of removing common words, FastText generates a sample table. The theoretical foundation for this work is that words that are commonly used carry less information than uncommon terms and that a word's representation does not change much even after the same sentence is used several times [29]. In order to identify vector representations where the text and its associated labels have similar vectors, Fasttext represents text and labels as vectors. The softmax function is used to determine the the probability score of an accurate label given to its corresponding text [30].

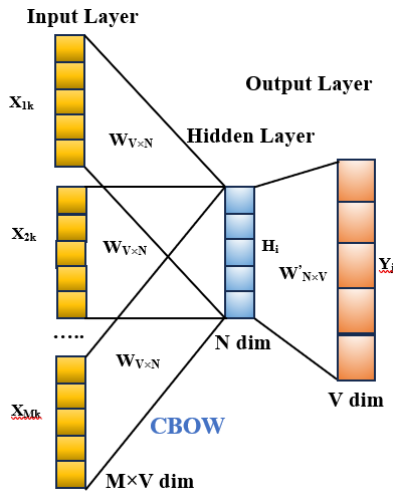


Fig. 1. CBOW architecture.

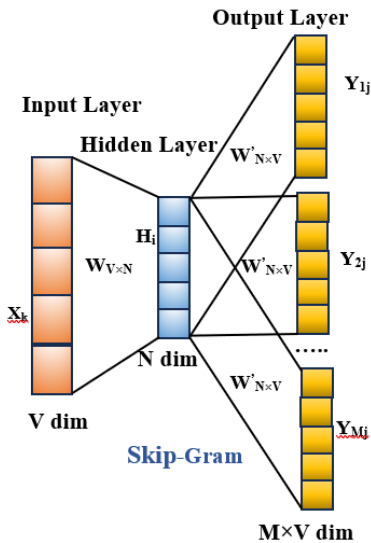


Fig. 2. Skip-gram architecture.

5) *OpenAI*: Text strings' relatedness can be evaluated by OpenAI's text embeddings. Searching, clustering, recommendations, anomaly detection, diversity assessment, and classification are among the common uses of OpenAI Embeddings [31]. The "text-embedding-3-small", "text-embedding-3-large", and "text-embedding-ada-002" are three robust third-generation embedding models offered by OpenAI. For text search, code search, and sentence similarity tests,

text-embedding-ada-002 performs comparably to all previous embedding models, whereas for text classification, it achieves superior results [32]. The text-embedding-ada-002 context length is extended from 2048 to 8192 tokens by a factor of four, making it easier to work with lengthy documents. The new embeddings are only one-eighth the size of the davinci embeddings, with only 1536 dimensions and their maximum input token is 8191. Semantically comparable words are mapped to vectors that are close to each other in a continuous, dense, low-dimensional vector space. This is the basis for OpenAI embeddings, which use a sort of neural network called a transformer to represent text [33]. The conversion of text to vector by OpenAI embedding is explained in Fig. 3.

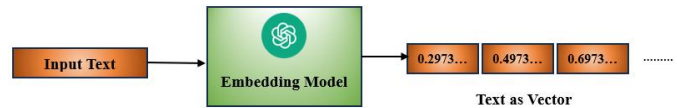


Fig. 3. OpenAI embedding.

E. Model Training

1) *Cosine similarity*: In natural language processing, cosine similarity is one of the metrics used to assess how similar two sentences are, regardless of their size. The cosine of the angle between two n-dimensional vectors projected in a multi-dimensional space is measured mathematically by the cosine similarity metric. A document's cosine similarity can range from 0 to 1, where 1 denotes that two vectors have the same orientation and 0 denotes that there is less similarity between the two documents. The following is the mathematical expression for the cosine similarity between two non-zero vectors [34,35].

$$Sentence\ Similarity = \cos(\theta) = \frac{P \cdot Q}{|P| * |Q|} = \frac{\sum_{i=1}^n P_i Q_i}{\sqrt{\sum_{i=1}^n P_i^2} \sqrt{\sum_{i=1}^n Q_i^2}} \text{ where } P \text{ and } Q \text{ are vectors} \quad (8)$$

2) *Random Forest*: The bagging approach is the foundation of the random forest ensemble learning method. Because decision trees have low bias and large variation, overfitting occurs if the tree grows too deep. By combining numerous decision tree predictions rather than relying just on one tree's output, Random Forest addresses this issue by reducing variance and resolving the overfitting issue. Decision trees are the foundation model used by Random Forest and predict the final output based on the majority of votes. When building a decision tree, entropy or the Gini Index is utilized as the splitting criterion [36].

$$Entropy = - \sum_{i=1}^n P_i \log P_i \text{ where } P_i \text{ is class label} \quad (9)$$

$$Gini\ Index = \sum_{i=1}^n p_i^2 \text{ where } p_i \text{ is class label} \quad (10)$$

3) *AdaBoost*: AdaBoost, or "adaptive boosting," is an ensemble machine-learning technique that builds decision stumps using decision trees. Adaboost combines weak learners into a single, powerful classifier to boost the performance of

machine learning algorithms. By assigning an equal weight to every data point, the adaboost algorithm initially constructs the model. In the subsequent iteration, the data points whose classification by the previous model was incorrect will be assigned greater weight [37, 38]. It will keep training models until it receives reduced errors. The following equation represents the final prediction.

$$\text{Final Prediction} = \alpha_1 * p_1 + \alpha_2 * p_2 + \dots + \alpha_n * p_n \quad (11)$$

where, p_1 represents the model's prediction and α_1 represents the model's degree of significance [39].

4) *XGBoost*: A popular gradient boosting approach called XGBoost provides regularization that lets you control overfitting by applying L1/L2 penalties to each tree's weights and biases [40]. Following the base model's prediction, we build a decision tree using the residuals and splitting criteria, then determine the similarity scores of the root and leaf nodes using following equation.

$$\text{Similarity Score} = \frac{(\sum \text{Residual})^2}{N + \lambda} \quad (12)$$

Where N is number of residuals and λ is regularization parameter. The following formula is used to compute the gain [41].

$$\text{Gain} = \text{Left Similarity} + \text{Right Similarity} - \text{Root Similarity} \quad (13)$$

In XGboost Regression, the Gamma Parameter Is Used. If the gain is less than the gamma value, the branch is cut, and no additional splitting occurs; otherwise, splitting proceeds. Pruning happens more often when gamma is higher. The XGboost Learning Rate is used to determine the model's convergence [42].

5) *LSTM*: One variation on a recurrent neural network that can identify and pick up on order dependence in sequence prediction issues is the Long Short-Term Memory (LSTM) network. The RNN cannot predict words that are held in long-term memory, but it can predict words based on recent data, which makes it unable to solve the long-term dependence problem. The LSTM is the type of neural network that receives an input (x_t) and outputs a value (h_t). The three gates in the memory are the input, forget, and output gates, which control information flow and have the capacity to add or remove data from the cell state, represented by the horizontal line at the top of the diagram. The forget gate has the responsibility for selecting which data should be erased from the cell state. The sigmoid layer generates a value between 0 and 1 after analysing h_{t-1} and x_t to determine which cell state data should be kept and which should be removed.

$$f_t = \sigma(W_f[h_{t-1}, X_t] + b_f) \quad (14)$$

The input gate is used to update the cell state value, taking into account both the previous time step's hidden state and the current input. The Sigma activation function in the first section determines the percentage of information that is needed. The Tanh activation function, which maps the data between -1 and

1, receives the two values in the second section. The input gate's output, which modifies the cell state determined by multiplying the outputs of the Tanh and Sigma functions [43, 44].

$$i_t = \sigma(W_i[h_{t-1}, X_t] + b_i) \quad (15)$$

$$C_t = \tanh(W_C[h_{t-1}, X_t] + b_C) \quad (16)$$

$$C_t = F_t * C_{t-1} + i_t * C_t \quad (17)$$

At the final stage, the sigmoid layer of the output gate decides which elements of the cell state are returned as output. The tanh layer modifies the cell's state to a value between 1 and -1, and the final output can be produced by multiplying the sigmoid layer's output by the tanh layer [45].

$$O_t = \sigma(W_o[h_{t-1}, X_t] + b_o) \quad (18)$$

$$h_t = O_t * \tanh(C_t) \quad (19)$$

6) *CNN*: CNNs are useful in NLP for linguistic modelling, autonomous translation, and classification of text. A variant of CNN known as 1D-CNN focuses on the analysis of one-dimensional data sequences, including text. By swiping the filter over the input matrix, the convolutional layers convolved the input, extracted features from the input, and passed the output to the next layer. CNN uses two parameters for regulating the size of an output matrix: stride, which indicates the number of pixels moved throughout the convolution process, and padding, which specifies the number of pixels added to an input matrix. These parameters control how the filter convolves across the input matrix. By multiplying the output matrix from the convolution layer and pooling matrix, the pooling layer tries to gradually reduce the spatial dimension of the representation in order to reduce the number of parameters and calculations in the network. The dropout layer attempts to minimize overfitting by randomly setting the input units to zero at each training phase. The feed-forward neural network uses the array as input for additional computation after it has been flattened into a one-dimensional array [46, 47].

7) *Classification metrics*: The true and false values accurately forecast are denoted by TP and TN. The false and true values that were incorrectly forecast are denoted by FP and FN. The ratio of exact forecasts to the total number of input observations is known as the classification accuracy. The ratio of correctly anticipated positive outcomes to all anticipated positive outcomes is known as precision, and the percentage of correct positive anticipations to all positive samples in the dataset is known as recall. The F1-score, which is the harmonic mean of recall and precision, is used when it's complicated to choose whether to go with recall or precision. Each metrics' corresponding mathematical equation is represented below [48, 49, 50].

$$\text{Accuracy} = \frac{TP+TN}{N} \quad (20)$$

$$\text{Precision} = \frac{TP}{TP+FP} \quad (21)$$

$$\text{Recall} = \frac{TP}{[TP+FN]} \quad (22)$$

$$\text{F1Score} = 2 * \frac{[\text{Precision} * \text{Recall}]}{[\text{Precision} + \text{Recall}]} \quad (23)$$

IV. RESULTS AND DISCUSSION

The 30000 samples are chosen at random, and the bias in the dataset is controlled by making sure that each type of label has identical quantities in the dataset. The dataset was broken down into 6000 samples for testing and 24000 samples for training. Table III presents the classification evaluation metrics for the multiple techniques that were trained on CountVectorizer. The precision, recall, and f1-score were computed using a weighted average.

TABLE III. PERFORMANCE OF COUNT VECTORIZER

| Embedding | Model | Cosine | RF | AdaBoost | XGBoost | LSTM | CNN |
|-----------------|-----------|--------|-------|----------|---------|-------|-------|
| CountVectorizer | Accuracy | 0.565 | 0.781 | 0.745 | 0.792 | 0.771 | 0.790 |
| | Precision | 0.571 | 0.781 | 0.753 | 0.797 | 0.771 | 0.798 |
| | Recall | 0.565 | 0.781 | 0.745 | 0.792 | 0.771 | 0.790 |
| | F1-Score | 0.557 | 0.781 | 0.743 | 0.791 | 0.771 | 0.789 |
| | FP | 1716 | 843 | 1030 | 824 | 856 | 750 |

The outcome demonstrates that the Cosine Similarity calculated on CV yields disappointing results. In addition, in comparison to other models, the AdaBoost is producing unsatisfactory results. FP prediction refers to the situation where the model anticipated a negative value but the actual value was positive. When two statements have the same meaning but the model predicts they are different, it is normal; but, when two distinct sentences are anticipated to be similar, it is not acceptable and will negatively impact the system's performance. For this reason, we have taken into account FP, or Type-I mistake, as an evaluation metric.

The Table IV performance data for TF-IDF shows that the cosine similarity calculated on TF-IDF yields bad results, and the adaboost also yields disappointing results.

TABLE IV. PERFORMANCE OF TF-IDF

| Embedding | Model | Cosine | RF | AdaBoost | XGBoost | LSTM | CNN |
|-----------|-----------|--------|-------|----------|---------|-------|-------|
| TF-IDF | Accuracy | 0.660 | 0.778 | 0.756 | 0.779 | 0.767 | 0.791 |
| | Precision | 0.660 | 0.791 | 0.766 | 0.787 | 0.770 | 0.796 |
| | Recall | 0.660 | 0.778 | 0.756 | 0.779 | 0.767 | 0.791 |
| | F1-Score | 0.659 | 0.776 | 0.754 | 0.777 | 0.767 | 0.790 |
| | FP | 1099 | 972 | 1020 | 920 | 986 | 821 |

Table V performance data for Fasttext embedding demonstrates that all other techniques produce results that are

reasonably nearby, whereas the cosine similarity calculated on Fasttext produces poor results.

Performance of each model trained using Word2Vec embedding is displayed in Table VI.

The performance of all models trained on OpenAI embedding is displayed in Table VII. The outcome highlights that, in contrast to alternative embeddings, cosine similarity yields outstanding outcomes. All models trained on OpenAI embedding show a performance gain of about 3%. With its ability to generate embeddings in such a way that two sentences with almost identical meanings have nearly the same value in the embedding, OpenAI has strong potential for capturing semantic meaning. With OpenAI embedding, the CNN performs effectively, yielding satisfactory outcomes with a slight FP value.

TABLE V. PERFORMANCE OF FASTTEXT

| Embedding | Model | Cosine | RF | AdaBoost | XGBoost | LSTM | CNN |
|-----------|-----------|--------|-------|----------|---------|-------|-------|
| FastText | Accuracy | 0.649 | 0.779 | 0.761 | 0.774 | 0.763 | 0.787 |
| | Precision | 0.651 | 0.784 | 0.763 | 0.780 | 0.763 | 0.790 |
| | Recall | 0.649 | 0.779 | 0.761 | 0.774 | 0.763 | 0.787 |
| | F1-Score | 0.648 | 0.778 | 0.760 | 0.773 | 0.762 | 0.786 |
| | FP | 1231 | 852 | 875 | 784 | 790 | 782 |

TABLE VI. PERFORMANCE OF WORD2VEC

| Embedding | Model | Cosine | RF | AdaBoost | XGBoost | LSTM | CNN |
|-----------|-----------|--------|-------|----------|---------|-------|-------|
| Word2Vec | Accuracy | 0.671 | 0.767 | 0.767 | 0.782 | 0.776 | 0.791 |
| | Precision | 0.675 | 0.788 | 0.770 | 0.786 | 0.781 | 0.793 |
| | Recall | 0.671 | 0.767 | 0.767 | 0.782 | 0.776 | 0.791 |
| | F1-Score | 0.669 | 0.763 | 0.766 | 0.781 | 0.775 | 0.791 |
| | FP | 1219 | 982 | 854 | 831 | 871 | 762 |

TABLE VII. PERFORMANCE OF OPENAI

| Embedding | Model | Cosine | RF | AdaBoost | XGBoost | LSTM | CNN |
|-----------|-----------|--------|-------|----------|---------|-------|-------|
| OpenAI | Accuracy | 0.757 | 0.807 | 0.781 | 0.813 | 0.791 | 0.825 |
| | Precision | 0.768 | 0.812 | 0.781 | 0.817 | 0.796 | 0.823 |
| | Recall | 0.757 | 0.807 | 0.781 | 0.813 | 0.791 | 0.823 |
| | F1-Score | 0.755 | 0.806 | 0.781 | 0.812 | 0.790 | 0.823 |
| | FP | 1026 | 767 | 825 | 725 | 821 | 639 |

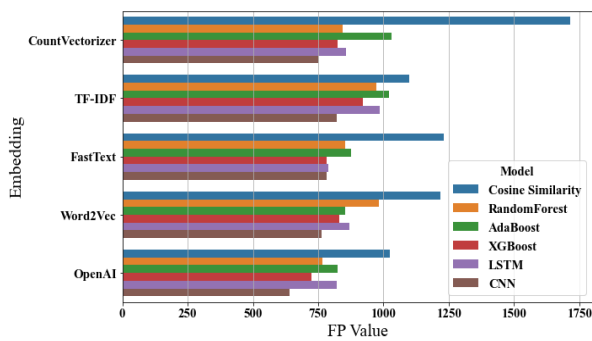


Fig. 4. Comparison of FP values for different models.

Fig. 4 indicates the false positive prediction for every model trained across different embeddings.

V. CONCLUSION

Detecting similarity across sentences can be helpful in the implementation of a number of different types of systems, such as question-answering systems, community forums, e-commerce consumer questions, instructional platforms, and chatbots for customer service. Sentence similarity must be automatically detected in order to meet user expectations promptly and enhance the user experience. Common uses for OpenAI embedded systems include searching, clustering, similarity, anomaly detection, diversity evaluation, and classification. The outcome demonstrates that machine learning receives valuable information from the embedding produced by the OpenAI model, improving prediction accuracy. Sentence similarity can be captured with significant potential using OpenAI embeddings. Almost all algorithms perform well with OpenAI embedding; CNN is one of the better performing algorithms. In order to improve prediction accuracy, we can incorporate a cascading CNN structure in future study. The CNN architecture's ideal parameter can be found using the optimization technique. Rather than taking a sentence as input, we can incorporate OpenAI STT and TTS to receive verbal input and produce verbal output in future research.

REFERENCES

- [1] N. B. Korade, M. B. Salunke, G. G. Asalkar, R. G. Khedkar, A. U. Bhosale, D. M. Joshi, and A. C. Jadhav, "Exploring NLP Techniques for Duplicate Question Detection to Maximizing Responses on Q&A Websites", *International Journal of Intelligent Systems and Applications in Engineering*, vol. 12, no.3, pp. 11-20, 2024.
- [2] R. F. G. Silva, K. Paixão and M. de Almeida Maia, "Duplicate question detection in stack overflow: A reproducibility study," 2018 IEEE 25th International Conference on Software Analysis, Evolution and Reengineering (SANER), Campobasso, Italy, pp. 572-581, 2018, doi: 10.1109/SANER.2018.8330262.
- [3] J. Wang, and Y. Dong, "Measurement of Text Similarity: A Survey", *Information*, vol. 11, no. 9, 2020, doi: 10.3390/info11090421.
- [4] H. T. Le, D. T. Cao, T. H. Bui, L. T. Luong and H. Q. Nguyen, "Improve Quora Question Pair Dataset for Question Similarity Task," 2021 RIVF International Conference on Computing and Communication Technologies (RIVF), Hanoi, Vietnam, pp. 1-5, 2021, doi: 10.1109/RIVF51545.2021.9642071.
- [5] A. Gupta, K. Sharma, and K. K. Goyal, "Computation of Similarity Between Two Pair of Sentence Using Word-Net", *International Journal of Intelligent Systems and Applications in Engineering*, vol. 11, no. 5s, pp. 458-467, 2023.

- [6] X. Sun, Y. Meng, X. Ao, F. Wu, T. Zhang, J. Li, and C. Fan, "Sentence Similarity Based on Contexts", *Transactions of the Association for Computational Linguistics*, vol. 10, pp. 573-588, 2022, doi: 10.1162/tacl_a_00477.
- [7] S. Rani, A. Kumar, and N. Kumar, "Eliminating Data Duplication in CQA Platforms Using Deep Neural Model", *Hindawi Computational Intelligence and Neuroscience*, vol. 2022, 2022, doi:10.1155/2022/2067449.
- [8] H. E. Salman, Z. Alshara, A. D. Seriai, "Automatic Identification of Similar Pull-Requests in GitHub's Repositories Using Machine Learning", *Information*, vol. 13, no. 2, 2022, doi: 10.3390/info13020073.
- [9] V. K. R. Anishaa, P. Sathvika, S. Rawat, "Identifying Similar Question Pairs Using Machine Learning Techniques", *Indian Journal of Science and Technology*, vol. 14, no. 20, pp. 1635-1641, 2021, doi:10.17485/IJST/v14i20.312.
- [10] Z. Imtiaz, M. Umer, M. Ahmad, S. Ullah, G. S. Choi and A. Mehmood, "Duplicate Questions Pair Detection Using Siamese MalSTM," *IEEE Access*, vol. 8, pp. 21932-21942, 2020, doi: 10.1109/ACCESS.2020.2969041.
- [11] D. Basavesha., and Y. S. Nijagunarya, Detecting Duplicate Questions in Community Based Websites Using Machine Learning, *Proceedings of the International Conference on Innovative Computing & Communication (ICICC) 2021*, April 2021, doi:10.2139/ssrn.3835083.
- [12] L. Wang, L. Zhang, and J. Jiang, "Duplicate Question Detection With Deep Learning in Stack Overflow", *IEEE Access*, vol. 8, pp. 25964-25975, 2020, doi: 10.1109/ACCESS.2020.2968391.
- [13] A. W. Qurashi, V. Holmes and A. P. Johnson, "Document Processing: Methods for Semantic Text Similarity Analysis," *International Conference on Innovations in Intelligent Systems and Applications (INISTA)*, pp. 1-6, 2020, doi: 10.1109/INISTA49547.2020.9194665.
- [14] Quora Question Pairs: <https://www.kaggle.com/c/quora-question-pairs/data>
- [15] M. J. Wu, T. Y. Fu, Y. C. Chang and C. W. Lee, "A Study on Natural Language Processing Classified News," 2020 Indo - Taiwan 2nd International Conference on Computing, Analytics and Networks (Indo-Taiwan ICAN), Rajpura, India, 2020, pp. 244-247, doi: 10.1109/Indo-TaiwanICAN48429.2020.9181355.
- [16] N. Ansari, and R. Sharma, "Identifying Semantically Duplicate Questions Using Data Science Approach: A Quora Case Study", *ACM Conference*, 2020, doi: 10.48550/arXiv.2004.11694.
- [17] Y. Du and H. Huo, "News Text Summarization Based on Multi-Feature and Fuzzy Logic," in *IEEE Access*, vol. 8, pp. 140261-140272, 2020, doi: 10.1109/ACCESS.2020.3007763.
- [18] T. Turki, and S. S. Roy, "Novel Hate Speech Detection Using Word Cloud Visualization and Ensemble Learning Coupled with Count Vectorizer", *Applied Sciences*, vol. 12, no. 13, 2022, doi: 10.3390/app12136611.
- [19] R. Goyal, "Evaluation of rule-based, CountVectorizer, and Word2Vec machine learning models for tweet analysis to improve disaster relief," 2021 IEEE Global Humanitarian Technology Conference (GHTC), Seattle, WA, USA, pp. 16-19, 2021, doi: 10.1109/GHTC53159.2021.9612486.
- [20] F. Lan, "Research on Text Similarity Measurement Hybrid Algorithm with Term Semantic Information and TF-IDF Method", *Advanced Pattern Recognition Systems for Multimedia Data*, 2022, doi: 10.1155/2022/7923262.
- [21] J. Ni, Y. Cai, G. Tang, Y. Xie, "Collaborative Filtering Recommendation Algorithm Based on TF-IDF and User Characteristics". *Applied Sciences*, vol. 11, no. 20, 2021, doi:10.3390/app11209554.
- [22] H. Vranken H, H. Alizadeh, "Detection of DGA-Generated Domain Names with TF-IDF", *Electronics*, vol. 11, no. 3, 2022, doi:10.3390/electronics11030414.
- [23] P. T. Hung, K. Yamanishi, "Word2vec Skip-Gram Dimensionality Selection via Sequential Normalized Maximum Likelihood", *Entropy*, vol. 23, no. 8, 2021, doi: 10.3390/e23080997.

- [24] X. Yang, K. Yang, T. Cui, M. Chen, L. He, "A Study of Text Vectorization Method Combining Topic Model and Transfer Learning", *Processes*, vol. 10, no. 2, 2022, doi: 10.3390/pr10020350.
- [25] X. Xue, H. Wang, J. Zhang, Y. Huang, M. Li, and H. Zhu, "Matching Transportation Ontologies with Word2Vec and Alignment Extraction Algorithm", *Journal of Advanced Transportation*, 2021, doi: 10.1155/2021/4439861.
- [26] Q. Du, N. Li, W. Liu, D. Sun, S. Yang, and F. Yue, "A Topic Recognition Method of News Text Based on Word Embedding Enhancement", *Computational Intelligence and Neuroscience*, 2022, doi: 10.1155/2022/4582480.
- [27] R. Esmeli, M. Bader-El-Den and H. Abdullahi, "Using Word2Vec Recommendation for Improved Purchase Prediction," 2020 International Joint Conference on Neural Networks (IJCNN), Glasgow, UK, 2020, pp. 1-8, doi: 10.1109/IJCNN48605.2020.9206871.
- [28] T. Yao, Z. Zhai and B. Gao, "Text Classification Model Based on fastText," 2020 IEEE International Conference on Artificial Intelligence and Information Systems (ICAIS), Dalian, China, 2020, pp. 154-157, doi: 10.1109/ICAIS49377.2020.9194939.
- [29] Fasttext official site: <<https://fasttext.cc/docs/en/support.html>>
- [30] D. Jeon, J. Lee, J. M. Ahn, C. Lee, "Measuring the novelty of scientific publications: A fastText and local outlier factor approach", *Journal of Informetrics*, vol. 17, no. 4, 2023, doi: 10.1016/j.joi.2023.101450.
- [31] E. J. Ciaccio, "Use of artificial intelligence in scientific paper writing", *Informatics in Medicine Unlocked*, vol. 41, 2023, doi: 10.1016/j.imu.2023.101253.
- [32] OpenAI Documentation: <https://platform.openai.com/docs/introduction>
- [33] K. I. Roumeliotis, N. D. Tselikas, "ChatGPT and Open-AI Models: A Preliminary Review", *Future Internet*, vol. 15, no. 6, 2023, doi:10.3390/fi15060192.
- [34] I. L. Ansorena, "On the benchmarking of port performance. A cosine similarity approach", *International Journal of Process Management and Benchmarking*, vol.11, no.1, pp.101 – 114, 2021, doi: 10.1504/IJPMB.2021.112258.
- [35] R.S. Ramya, Ganesh Singh, S. N. Sejal, K.R. Venugopal, S.S. Iyengar, L.M. Patnaik, "R2DCLT: retrieving relevant documents using cosine similarity and LDA in text mining", *International Journal of Information and Communication Technology*, vol.19, no.4, pp.391 – 422, 2021, doi: 10.1504/IJICT.2021.118576.
- [36] M. Schonlau, and R. Y. Zou, "The random forest algorithm for statistical learning", *The Stata Journal*, vol. 20, no. 1, pp. 3-29, 2020, doi: 10.1177/1536867X20909688.
- [37] C. Wang, S. Xu, J. Yang, "Adaboost Algorithm in Artificial Intelligence for Optimizing the IRI Prediction Accuracy of Asphalt Concrete Pavement", *Sensors*, vol. 21, no. 17, 2021, doi: 10.3390/s21175682.
- [38] G. Sembina, "Building a Scoring Model Using the Adaboost Ensemble Model," 2022 International Conference on Smart Information Systems and Technologies (SIST), Nur-Sultan, Kazakhstan, pp. 1-6, 2022, doi: 10.1109/SIST54437.2022.9945713.
- [39] D. Sudharson, S. Ashfia Fathima, P. S. Kailas, K. S. Thrisha Vaishnavi, S. Darshana and A. Bhuvaneshwaran, "Performance Evaluation of Improved Adaboost Framework in Randomized Phases Through Stumps," 2021 International Conference on Advancements in Electrical, Electronics, Communication, Computing and Automation (ICAECA), Coimbatore, India, pp. 1-6, 2021, doi: 10.1109/ICAECA52838.2021.9675739.
- [40] D. M. Alghazzawi, A. G. A. Alquraishee, S. K. Badri, S. H. Hasan, "ERF-XGB: Ensemble Random Forest-Based XG Boost for Accurate Prediction and Classification of E-Commerce Product Review", *Sustainability*, vol. 15, no. 9, 2023, doi: 10.3390/su15097076.
- [41] D. A. -L. Mariadass, E. G. Moug, M. M. Sufian and A. Farzamnia, "Extreme Gradient Boosting (XGBoost) Regressor and Shapley Additive Explanation for Crop Yield Prediction in Agriculture," 2022 12th International Conference on Computer and Knowledge Engineering (ICCKE), Mashhad, Iran, Islamic Republic of, pp. 219-224, 2022, doi: 10.1109/ICCKE57176.2022.9960069.
- [42] T. R. Mahesh, V. Vinoth Kumar, V. Muthukumaran, H. K. Shashikala, B. Swapna, and Suresh Guluwadi, "Performance Analysis of XGBoost Ensemble Methods for Survivability with the Classification of Breast Cancer", *Hindawi, Journal of Sensors*, vol. 2022, , 2022, doi: 10.1155/2022/4649510.
- [43] Z. Wang, S. Kim, I. Joe, "An Improved LSTM-Based Failure Classification Model for Financial Companies Using Natural Language Processing", *Applied Sciences*, vol. 13, no. 13, doi: 10.3390/app13137884.
- [44] B. Nath Saha and A. Senapati, "Long Short Term Memory (LSTM) based Deep Learning for Sentiment Analysis of English and Spanish Data," 2020 International Conference on Computational Performance Evaluation (ComPE), Shillong, India, pp. 442-446, 2020, doi: 10.1109/ComPE49325.2020.9200054.
- [45] N. B. Korade, and M. Zuber, "Stock Price Forecasting using Convolutional Neural Networks and Optimization Techniques", vol. 13, no. 11, pp. 378-385, 2022, doi: 10.14569/IJACSA.2022.0131142.
- [46] N. B. Korade, and M. Zuber, "Boost Stock Forecasting Accuracy Using The Modified Firefly Algorithm And Multichannel Convolutional Neural Network", *Journal of Theoretical and Applied Information Technology*, vol. 101, no. 7, pp. 2668- 2677, 2023.
- [47] N. B. Korade, and M. Zuber, "Stock Forecasting Using Multichannel CNN and Firefly Algorithm", *Proceedings of the 2nd International Conference on Cognitive and Intelligent Computing*, pp. 447-458, 2023, doi: 10.1007/978-981-99-2742-5_46
- [48] A. Gasparetto, M. Marcuzzo, A. Zangari, A. Albarelli, "A Survey on Text Classification Algorithms: From Text to Predictions", *Information*, vol. 13, no. 2, 2022, doi: 10.3390/info13020083.
- [49] Y. Liu, and S. Yang, "Application of Decision Tree-Based Classification Algorithm on Content Marketing", *Journal of Mathematics*, 2022, doi: 10.1155/2022/6469054.
- [50] Y. I. Alzoubi, A. E. Topcu, A. E. Erkaya, "Machine Learning-Based Text Classification Comparison: Turkish Language Context", *Applied Sciences*, vol. 13, no. 16, 2023, doi: 10.3390/app13169428.

Event-based Smart Contracts for Automated Claims Processing and Payouts in Smart Insurance

Dr Araddhana Arvind Deshmukh¹, Prabhakar Kandukuri², Dr Janga Vijaykumar³,
Anna Shalini⁴, Dr. S. Farhad⁵, Elangovan Muniyandy⁶, Dr. Yousef A.Baker El-Ebiary⁷

Professor, School of Computer Science & Information Technology (Cyber Security),
Symbiosis Skill and Professional University, Kiwale, Pune, India¹

Professor, Department of Artificial Intelligence and Machine Learning,
Chaitanya Bharathi Institute of Technology - Hyderabad, India²

Associate Professor, Dept of CSE (AI&ML), Balaji Institute of Technology and Science, Narsampet, India³

Research Scholar, Dept of English, Koneru Lakshmaiah Education Foundation,
Green Fields, Vaddeswaram, Guntur, Andhra Pradesh, India⁴

Associate Professor, Dept.of English, Koneru Lakshmaiah Education Foundation,
Vaddeswaram, Guntur, Andhra Pradesh, India⁵

Department of R&D, Bond Marine Consultancy, London EC1V 2NX, UK, Department of Biosciences, Saveetha School of
Engineering, Saveetha Institute of Medical and Technical Sciences, Chennai, India⁶

Faculty of Informatics and Computing, UniSZA University, Malaysia⁷

Abstract—The combination of blockchain technology and smart contracts has become a viable way to expedite claims processing and payouts in the quickly changing insurance industry. Enhancing efficiency, transparency, and reliability for the industry may be achieved by automating certain procedures and initiating them on predetermined triggers, smart contracts that is event-based. Conventional insurance procedures can be laborious, slow, and prone to human mistake, which can cause inefficiencies and delays in the resolution of claims. This research proposes a simplified system that automates the whole claims process from submission to reimbursement by utilizing blockchain technology and smart contracts. The suggested method does away with the requirement for human claim filing by having policyholders' claims automatically triggered by predetermined occurrences. These occurrences might be anything from medical emergencies to natural calamities, enabling prompt and precise claim start. The whole claims process is managed by smart contracts that are programmed with precise triggers and conditions, guaranteeing transaction immutability, security, and transparency. Moreover, reimbursements are carried out automatically after the triggering event has been verified, disregarding conventional bureaucratic processes and drastically cutting down on processing times. This strategy decreases the possibility of fraud and disagreement while also improving operational efficiency by combining self-executing contracts with decentralized ledger technology. Insurance companies and policyholders will both eventually profit from an accelerated, transparent, and reliable claims processing procedure thanks to the use of event-based smart contracts. A Python-implemented system achieving 97.6% accuracy using the proposed method, demonstrates its efficacy and reliability for the given task.

Keywords—Blockchain technology; smart contracts; event-based triggers; automated claims processing; transparency and trustworthiness

I. INTRODUCTION

Private insurance businesses act as a central organization to give advantages to policyholders. They offer worth by using historic information and mathematical procedures to determine whether premiums are going to be adequate for covering predicted claims. Furthermore, authorities can control these companies in order to ensure enough funding. Insurance firms are currently losing a significant amount of money as a result of claims leakage. Illegal claims are a massive and expensive issue for insurance firms, possibly resulting in trillions of dollars in unwarranted spending every year [2]. Traditional policy approaches for detecting fraud are complex and time-consuming. They mostly rely on expert inspection, adjusters as well, and specialized investigative services. Manual inspection faces extra costs and yields erroneous findings. Furthermore, delayed decisions may result in additional losses for the insurance firms. The insurance business administers auto-insurance processing of claims using information gathered from several domains, including police, county administration, insurance representatives, and medical professionals [3]. These businesses work together to communicate multi-source data, which is crucial enabling insurance firms to correctly assess customer claims. Yet, the majority of existing claim processing procedures are laborious and time-consuming because to a lack of automated methods to perform information collection/analysis, along with technology to make reliable decisions [4]. To enhance the effectiveness and adaptability of insurance claim the process, it is necessary to integrate automated processes and trust administration mechanisms at an application level [5].The excessive number of false claims given out by motor insurance firms has resulted in price hikes of several hundred dollars to counteract the false payouts, reducing insurance company profitability as well as the level of operations [6]. As a result, there exists an urgent need to provide quick and effective solutions for identifying fraud, risk assessment, and

safe storage of information that strike a perfect equilibrium among customer private information safeguarding, loss prevention savings, and expenditure on false alarm identification (Cousaert, Vadgama, and Xu 2022). Recommend creating a successful framework for insurance companies to address such difficulties [7].

Intelligent contracts may streamline numerous common operations in the P&C insurance industry, including policy issuance and claim management. For example, parameterized insurance policies can initiate payments whenever predetermined conditions are satisfied, such as in the case of a natural disaster [8]. It may also assess all payment choices to determine which one is optimal. This technology eliminates the requirement for middlemen and increases effectiveness, giving policyholders access actual time replies which are not impeded by delays in insurance claims [9]. This study examines the notion of automation claims handling and payouts driven by event-driven intelligent contracts in the insurance business. The technological infrastructure necessary to construct a system like this, includes the selection of blockchain platform, programming languages, and architectural considerations for smart contract implementation [10]. Research demonstrate the flow of data and actions across the system, emphasizing the seamless integration of event-driven triggers for automating the claims handling workflow [11]. Its technological infrastructure necessary to construct any of these systems, in addition to the selection regarding the blockchain platform, programming languages, and architectural considerations for smart contracts .Demonstrate the flow of data and operations across the system, emphasizing the effortless incorporation of based on events triggering for automating the claims handling process [12].

The Current solutions based on blockchain employ intelligent agreements to enhance the transfer of assets, restrict fraud, and decrease administrative expenses. However, they do not address collaborative insurance, allowing individuals who have comparable characteristics to safeguard each other in an increased favorable, reasonable, and open way [13].To illustrate whether event-based intelligent agreements might transform the claims handling procedure by thoroughly examining its technological foundations and operational ramifications, benefiting insurance companies, policyholders, and various other stakeholders equally. With adopting this novel strategy, insurance firms may achieve unprecedented levels of efficiency, openness, and satisfaction with customers, bringing in an entirely novel phase of insurance claim administration [14].

Key contributions are as follows:

- By automating claims processing through event-based smart contracts, the system eliminates manual submission processes, reducing administrative burdens and streamlining operations.
- Blockchain technology ensures transparency and immutability of transactions, providing a clear audit trail for all stakeholders involved.
- Predefined events trigger claims automatically, enabling quick initiation upon the occurrence of

insured events such as natural disasters or medical emergencies. This swift response enhances customer satisfaction and reduces delays in claim settlements.

- The inherent security features of blockchain technology, combined with self-executing smart contracts [1] minimize the potential for fraudulent activities in the claims process.
- Automated payouts upon verification of triggering events bypass traditional bureaucratic procedures, significantly reducing processing times.
- By streamlining processes and reducing manual intervention, insurers can realize cost savings and operational efficiencies.

The remaining section of this work is structured as follows: Section II covers similar work and a full evaluation of it. Section III offers details on the problem statement. Section IV provides a detailed discussion of the suggested method. Section V presents and examines the results of the tests, as well as a comprehensive comparison of the proposed technique to current standard procedures. Section VI, the last section, represents where the paper is finished.

II. RELATED WORKS

The existing health insurance claims procedure has issues with inefficiency and complexity. Whenever a patient files a health insurance claim, he or she must first visit the medical facility to obtain a diagnostic certification and being received, and finally submit the required application documentation to the insurer. The person will not get compensation until the company completes its verification procedure via the patient's clinic. Research can use the technology of blockchain to better the existing situation. Blockchain innovation may successfully open up avenues for communication between insurance companies and healthcare providers, increase industrial integrating, and improve healthcare firms' capacity to access data. This study uses blockchain and smart contract technology to boost the progress of Internet healthcare. First, blockchain and smart contracts technology may effectively handle the problem of web-based verification. In addition, it contributes to better monitoring. Finally, it helps to solve risk management issues. Finally, it promotes efficient anti-money laundering. The suggested approach meets a number of safety criteria: mutual verification of identities and the non-rep among all of both roles, along with additional significant the blockchain relies safety concerns. In the case of a conflict provide an arbitration system to distribute duties. The effective deployment of the blockchain system in the insurance sector necessitate the development of strong publicly accessible infrastructure (PKI), partnerships between healthcare providers for offering electronic health records (EMR), as well as money alliances for expressing consumer financial data, that could create practical and legal obstacles in some countries [15].

The insurance sector, firms have implemented substantial and fundamental modifications to update their basic processes, making operations simpler and quicker for customers and enterprises. To service more clients while enhancing the total

client experience across all contact points, organizations are seeking to shift out of standalone transactional systems and towards contextually engagement systems. Several insurance companies currently use some form of automation, including scanning, uploading papers for the process, or automating bank transfer activities. However, occasionally this might result in inadequate results or delayed procedures. Robotic Process Automation (RPA) is the employing of computer programs robots to execute business operations that would normally be performed by humans. RPA can help companies accomplish their business goals while utilizing existing technology and increasing the returns on prior and ongoing transformational expenditures. Insurers may utilize RPA to analyze large amounts of complicated data at greater rates and in less time. RPA is poised to assist claiming businesses develop and improve their results in the age of technology by increasing automated processes, efficiency, and concentration for claim experts. Companies with superior outsourced capabilities have widened their concentration on automating to save labor expenses and streamline procedures. The following has generated an emerging RPA industry that is expected to expand significantly. RPA's drawbacks includes being unable to perform activities that need complicated making choices or mental skills, as well as its dependence on organized information and repeated procedures, that might not apply to all circumstances or sectors [16].

Dhieb et al. [17] propose safe and automatic healthcare system architecture that eliminates human intervention, protects insurance operations, notifies and educates concerning dangerous consumers, identifies forged claims, and decreases the financial loss for the insurance industry. Subsequently introducing the blockchain relies system for enabling secure transactions as well as information offering between various agents who communicate inside the insurance company network, that research suggest employing the xtreme gradient boosting (XGBoost) artificial intelligence method for the formerly mentioned insurance companies and comparing its efficacy to that of other cutting-edge algorithms. The findings show that when implemented to an automobile insurance dataset, Boost outperforms other present-day learning methods. When it comes to identifying false claims, it outperforms the decision tree algorithms by 7% on average. The findings show that whenever deployed to an automobile insurance dataset, XGboost outperforms alternative present-day learning methods. Whenever it comes to identifying false claims, it outperforms the decision tree models by 7% on average. In addition, present an online educational approach to autonomously cope with real-time modifications to the insurance network, as well as demonstrate that it beats other online cutting-edge method. At last use the hyper ledger networks fabric composer and the built neural network modules to construct and replicate the machine learning algorithms and bit coin architecture. Throughout the coming years, company are going to concentrate on improving the proposed framework and introducing artificial intelligence (AI) products targeted to various insurance services.

The insurance sector relies largely on a number of activities carried out by different organizations, including insurers, insured's, and third-party service providers. The

growing competitive climate is driving insurance businesses to adopt innovative technology to solve a variety of issues, including an absence of confidence, openness, and economic uncertainty. For this purpose, blockchain is being employed as a new technology for accessible and safe information preservation and transfer. Loukil et al. [18] propose CioSy, an integrated a blockchain-based healthcare platform that monitors and processes insurance activities. To the greatest extent of understanding, current processes do not take cooperative insurance into account while aiming for a computerized, clear, and tamper-proof solution. CioSy intends to use smart contracts to automate the processing of insurance policies, claims, and payments. For validation reasons, an experimental prototype is created on the Ethereum blockchain. The findings from experiments suggest that the suggested strategy is viable and cost-effective. In the future, research hopes to give a formal privacy demonstration for the suggested paradigm. In addition, intend to investigate the feasibility of deploying the funds gathered by an insurance pooling utilizing blockchain-based technology with the goal to encourage bankers and insurance organizations to join a proposed collaboration healthcare system.

Traditional claims handling procedures are inadequate for the current world, which has an expanding fleet of cars and an equal amount of incidents. Fernando et al. [19] suggest a fresh proposal for automating the financial services industry's laborious operations. Its provided approach is made up of three primary elements: re-identifying the car's model and year, identifying the harmed automotive part, kind, and extent, and computing a precise repair cost utilizing damages part recognition. Simplify the recording process by detecting important fields from the user's voice input. This guarantees that all parties participating in the procedure benefit from the proposed system. The presented solutions were developed utilizing Artificial Intelligence approaches, namely CNN models and natural language processing techniques. The initiative's planned developments for the future include improving the ASR to detect more fields linked to completing out the initial claim seeking form as well as including additional regional dialects. The given technique is capable of recognizing one type of harm in a picture. This may be enhanced to identify multiple kinds of harm in a picture as technology for computer vision evolves. These improvements will improve the overall efficiency of the system in the years to come.

Machine learning or data mining algorithms may be utilized for forecasting future management and are thus considered strong tools. Data mining has recently become increasingly significant for obtaining essential data in the healthcare industry. Health insurance costs are critical in the development of healthcare institutions. In order to offer improved healthcare services, it is critical to anticipate the cost of medical insurance that constitutes one of the opportunities for improving healthcare facilities. Dutta et al. [20] addresses projecting the cost of medical coverage, which must be provided by the individual receiving medical care. To accomplish the best predictions examination, several data mining regression techniques are used, including decision trees, random forests, polynomial regression, and regression

using linear models. A contrast was made among the actual and expected expenditures for the predictions premiums, and a graph was created on this foundation to help us identify the optimum method of regression for insurance policy prediction. One constraint is the possible complexity and technical needs of adopting sophisticated neural network algorithms such as Bi-LSTM, that might necessitate extensive knowledge and computing power. Another drawback is the absence of insurance-related information, which restricts the research to a small dataset and could restrict the ability to generalize of the findings. Every method is evaluated to determine the most appropriate solution.

While several studies have highlighted the potential of emerging technologies such as blockchain, robotic process automation (RPA), machine learning, and data mining in revolutionizing the health insurance claims process, there remain significant limitations across these works. Firstly, while blockchain offers secure data sharing, its implementation may face challenges related to infrastructure development and legal obstacles. Additionally, the reliance on structured data and repetitive processes in RPA may limit its applicability in complex decision-making scenarios. Moreover, the effectiveness of machine learning algorithms like XGBoost and data mining techniques in predicting insurance costs is constrained by the availability of comprehensive datasets and computational resources. Furthermore, the complexity of advanced neural network algorithms may hinder their adoption, while the lack of insurance-specific information can restrict the generalizability of findings. These limitations underscore the need for further research to address technical, data-related, and practical challenges in leveraging emerging technologies for enhancing the efficiency and effectiveness of health insurance processes.

The existing health insurance claims procedure is plagued by inefficiency and complexity, requiring patients to visit medical facilities to obtain diagnostic certification and then submit documentation to insurers, resulting in delayed compensation. To address these issues, the current research proposes utilizing blockchain and smart contract technology. This technology facilitates communication between insurance companies and healthcare providers, enhances industrial integration, and improves healthcare firms' access to data. The proposed approach aims to boost the progress of Internet healthcare by effectively handling web-based verification, improving monitoring, and addressing risk management issues. Dhieb et al. proposed a safe and automatic healthcare system architecture that eliminates human intervention, protects insurance operations, identifies forged claims, and decreases financial loss. They suggest employing the XGBoost artificial intelligence method for insurance companies, which outperforms other algorithms in identifying false claims. Similarly, Loukil et al. proposed CioSy, a blockchain-based healthcare platform that automates insurance policies, claims, and payments through smart contracts. Fernando et al. suggest automating financial services operations, including car damage assessment for insurance claims, using Artificial Intelligence approaches. Dutta et al. on predicting medical insurance costs, utilizing various data mining regression techniques. These earlier

studies provide a comprehensive framework for the current research on Event-Based Smart Contracts for Automated Claims Processing and Payouts in Smart Insurance. The proposed system will leverage blockchain technology and smart contracts to automate and streamline the insurance claim process, enhancing efficiency, transparency, and security. By integrating findings from previous research, the proposed system will significantly contribute to solving the inefficiencies and complexities of the existing health insurance claims procedure.

III. PROBLEM STATEMENT

The current insurance claims procedure is plagued by inefficiencies and complexities, requiring physically visit facilities for certification before submitting paperwork to insurance firms. This cumbersome process leads to delays in compensation and poses challenges in data verification and risk management [18]. However, emerging technologies like blockchain and Robotic Process Automation (RPA) offer promising solutions to streamline these operations. Blockchain can facilitate secure communication between insurance companies and healthcare providers, while RPA can automate repetitive tasks, improving efficiency and accuracy. Additionally, the integration of artificial intelligence (AI) algorithms, such as XGBoost, enhances fraud detection and claim processing speed. Despite these advancements, there remain challenges in implementing these technologies, including the need for robust infrastructure and data privacy considerations [16]. Hence, there is a pressing need for innovative solutions like CioSy, a blockchain-based healthcare platform, which automates insurance processes through smart contracts, ensuring transparency and reliability. Furthermore, leveraging AI techniques like convolutional neural networks (CNN) and natural language processing (NLP) can further enhance claims handling by automating tasks like damage assessment and form completion. Ultimately, adopting these technologies can revolutionize the insurance sector, making processes more efficient, transparent, and customer-centric. The Novel method Automated Claims Processing and Payouts Triggered by Event-Based Smart Contracts is proposed.

IV. PROPOSED METHOD AUTOMATED CLAIMS PROCESSING AND PAYOUTS TRIGGERED BY EVENT-BASED SMART CONTRACTS

The suggested event-driven architecture insurance claim procedure follows a certain set of phases in its approach. First, pertinent data on insurance plans, applicants, and triggering events are gathered through data collection and preprocessing. After that, this data is examined and plotted to reveal trends and patterns that might guide the creation of smart contracts. Subsequently, blockchain technology is utilized for safe transactions and smart contract implementation in the automatic medical insurance claims processing system. Automate the claims procedure and ensure speed and transparency, smart contracts are configured with certain triggers and criteria. When certain events occur, such as natural catastrophes or medical emergencies, smart contracts automatically start the claims procedure. This entails confirming the legitimacy of the claim and streamlining the reimbursement procedure without requiring human

involvement. Utilizing blockchain technology, this technique places a strong emphasis on guaranteeing the confidentiality and integrity of the claims process. In addition, the system is

routinely optimized and monitored to preserve its efficacy and efficiency in managing insurance claims.

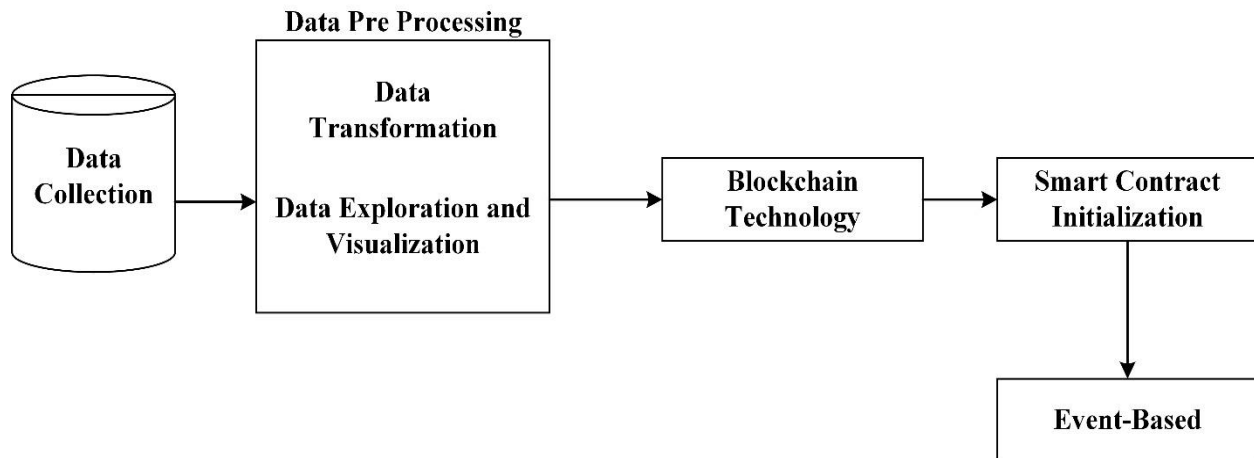


Fig. 1. Automated claims processing and payouts triggered by event-based smart contracts.

Fig. 1 displays a flowchart of a data-driven workflow using blockchain technology. The procedure includes five steps: data gathering, data pre-processing, blockchain technology, smart contract activation, and event-based process.

A. Data Collection

The "Health Insurance Dataset - EDA" available on Kaggle offers a comprehensive exploration of health insurance data, comprising information on 1338 US health insurance customers. The dataset includes features such as age, gender, body mass index (BMI), number of children, smoking status, region, and insurance charges. It serves to facilitate analysis on factors affecting insurance charges, prediction of new charges, and comparison of plans across different regions. Key inquiries encompass the impact of age, smoking status, and number of children on insurance charges, identification of regions with the highest or lowest average charges, and examination of BMI distribution across regions. This dataset is valuable for understanding insurance pricing and trends [21].

B. Data Pre Processing

Data preprocessing involves cleaning and transforming raw data to enhance its quality and usability for analysis, typically including tasks such as handling missing values, outlier detection, normalization, and feature scaling. This step is crucial for ensuring accurate and reliable results in data analysis and modeling.

1) *Data transformation*: In the data transformation stage, several techniques are applied to prepare the data for modeling. Categorical variables are encoded into numerical representations, typically using methods like one-hot encoding to create binary columns for each category or label encoding to assign unique numerical values to categories. Numerical functions can be scaled to make sure consistent degrees across variables, assisting algorithms touchy to function magnitudes. Feature engineering consists of crafting new capabilities from

present ones, leveraging domain information or statistical insights to enhance model performance. This may consist of growing interaction terms, polynomial features, or transform variables to better capturing relationships or styles within the information. These transformation steps collectively intention to enhance the suitability and predictive strength of the dataset for subsequent modeling duties [22].

2) *Data exploration and visualization*: Explore the distribution of each feature and the relationship between feature variable and the targeted variable. Visualize the information using plots along with histograms, box plots, scatter plots, and so forth. to benefit insights into the records and become aware of patterns.

C. Automatic Medical Insurance Claims Service System through Blockchain Technology

The remedy offered by this study was to implement an autonomous insurance claim servicing system using the blockchain. The surroundings are used to exchange data between healthcare providers, insurance providers, and individuals. The environment's functions include the blockchain computing center (BCC), the appropriate government agencies (CA), the healthcare facility (MI), the insurance provider (IC), the finance company (BK), the patient (PT), & the center for arbitration (AI). Medicinal institutions can create a healthcare alliance chain under the supervision of the medicinal board CA1. Assurance and banks can join a financial alliances chain that is overseen by the banking regulator, CA2. Participants of the exact same alliance are able to exchange entire material.

Step 1: All CA, MI, IC, BK, and PT must verify with BCC in order to get both public and private ECDSA signing keys, as well as public and secret PKI key pairs. BCC also saves every patient's healthcare blockchain information. Furthermore, various kinds of CA will establish partnerships among the people they represent, and the partnership's membership' data will be exchanged.

Step 2: The patient, PT, buys health assurance through the health care firm IC. The IC will first check the PT's identification and then execute an insurance agreement with them. The PT must furnish the IC with the details of its BK account and paperwork will then sent to the BCC via the CA. Whenever the PT returns hospital in MI not too distant upcoming, and the examination result satisfies the alleged contented indicated in the health insurance agreement, the IC will move forward by the healthcare claims.

Step 3: Whenever a patient PT visits a healthcare facility MI and notifies the MI that they he or she has acquired health coverage, the MI will first authenticate the PT's identification, review the PT's electronic health record EMR, and then issue an authorization, with the information being communicated to the Scc via CA.

Step 4: The medical facility MI then notifies the assurance firm IC to process claims from insurance companies, and the IC acquires the PT medically-related diagnostic material given by MI.

Step 5: The insurance provider IC instructs the financial institution BK to pay the patient PT, and the record is transferred to the BCC via the CA.

Step 6: A claimed disagreement, the patient PT may file a complaint with the arbitration agency AI. AI will receive the communication contents from both side besides arrive at logical decisions.

D. Smart Contract Initialization

Blockchain technology was used in the suggested design. Certain essential data is kept and confirmed on the blockchain throughout the verification and permission procedure. The smart contract is a code that defines the block chain's most essential data. Everyone created essential data, which is stored on the blockchain in the suggested smart contract. Every smart contract has the following fundamental fields: id (identity), information about the transaction, certification, and timestamp. The smart contracts include the individual's bank account, whereas the smart contract includes the insurance company's bank account. The field's insurance contract is included with the smart contract. A smart contract supports digitized medical records. Finally, the purchase ID is shown in the smart contract. The blockchain technology center also provides both private and public key sets for every position during the authentication step.

1) *Registration phase:* The network's role X may include the Competent of authorities (CA), the healthcare facility (MI), the insurance provider (IC), the financial company (BK), and the individual in need (PT), who sign up blockchain center (BCC) also receive an individual's public/private key combination and a digital proof to verify their identities via a safe channel. Fig. 2 depicts the diagram for the enrollment process. Registration phase flow is explained in Fig. 2.

2) *Authentication process:* During the start of the interaction, system roles A and B must authenticate their respective identities using the ECDSA technique. System roles

A and B may comprise appropriate government agencies (CA), healthcare providers (MI), insurance firms (IC), banking (BK), and individuals (PT).

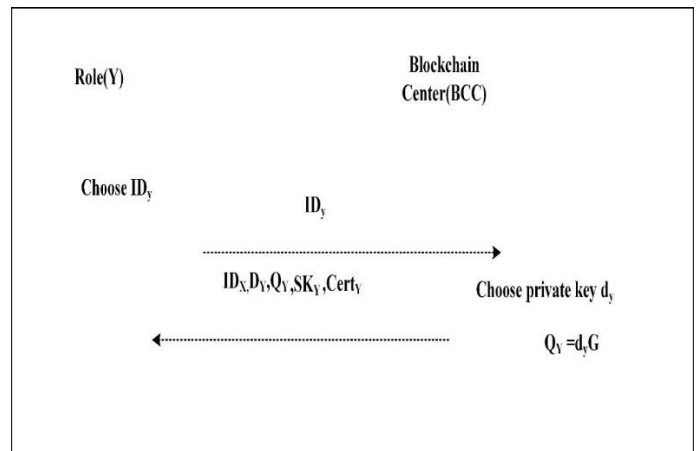


Fig. 2. Registration phase.

3) *Communications procedure:* The recommended solution makes use of the hyper ledger's block chain design, which increases the CA's role, allows for more versatility in accessing monitoring, and reduces the stress on BCC. After authenticating interactions across all roles, the details will then be provided to the various CAs, which will then send the blockchain information BCC. MI and IC both operate to own CA, which might allow documents flow throughout CA membership as well as cross-CA management of entry while retaining safety & efficacy. The accessible party (AP) might be a hospital (MI), an insurance company (IC), a financial institution (BK), or a client. A schematic representation of the CA communications method is proposed [15]. Blockchain-Based Medical Insurance System is shown in Fig. 3.

E. Event-Driven Architecture Insurance Claim Process

The Claim entity depicts an insurance claim which consumers can file or that current insurance companies may employ to assess how to pay out. The claim form includes a Loss Amount and a connection to the Insurance Policy organization. After an Event has been established, the processing Event method the request may be utilized to determine if it needs to be payed out. The Root Cause Mapping object, typically is a Boolean, is used within the process Event () method to determine if a payout is necessary for a fundamental issue and insurance policy combination. The Root Cause Mapping is defined in the privileges portion of the agreement.

1) *Identity NFT:* The identification NFT will serve as verification of identification for claim management. Whenever the program is first set up, the NFT is going to be coined (generated) for claims managers using the mailing addresses supplied in the initial setup script. Anyone is unable to establish an event if they have an Identification NFT.

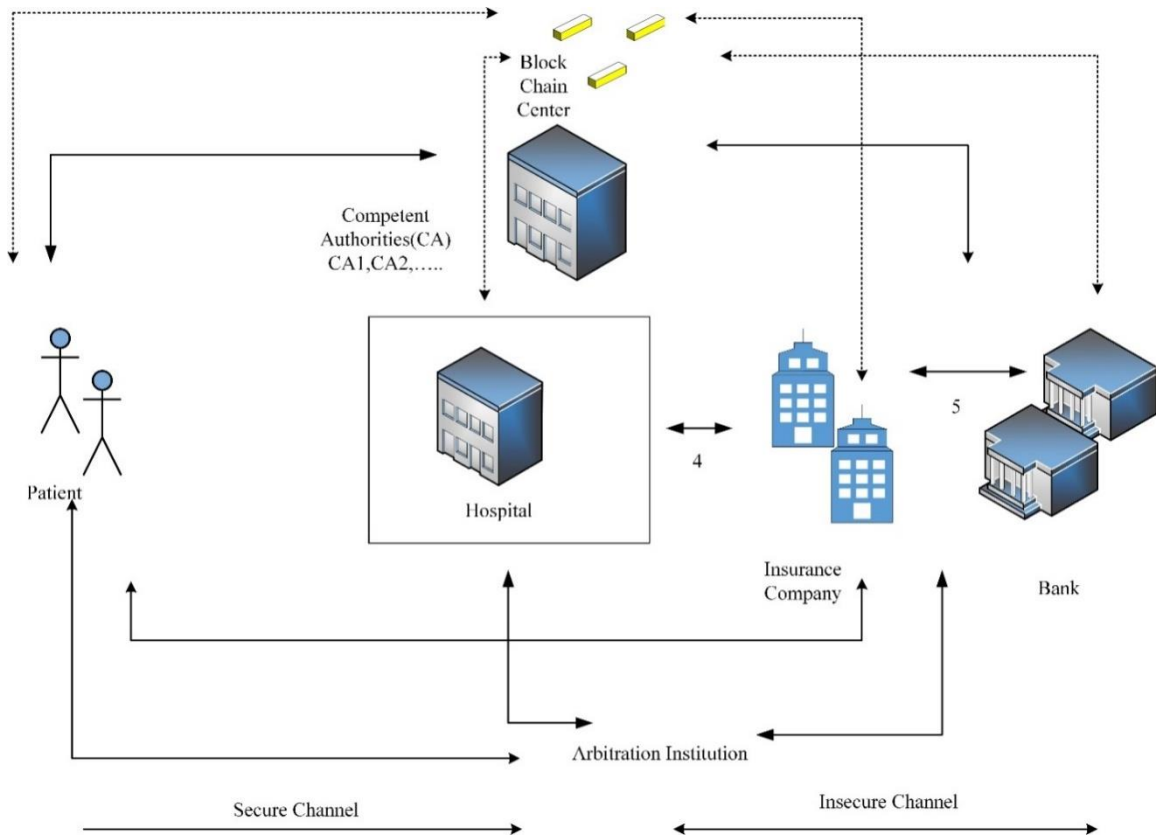


Fig. 3. Blockchain-based medical insurance system.

When the entitlements director organizes an event, their uniqueness is verified by the identification NFT contract. If it is valid, an event is produced in the Event Contract, which is then passed on to the claim contract for processing. All pending claims for the covered protocols are going to be adjusted using Root Cause Mapping. If the amalgamation of the root problem and regulation proves accurate, a payment should be provided. In the initial release of the program, just the claim's current state will be changed.

Any individual may file a right depending on their assurance coverage. The Entitlements agreement will compare information on the insurance against current claims. If previous demands exact similar policy and root cause were previously approved or postponed then the latest one will be assigned the identical status. In subsequent versions of the app, any blockchain-based insurance company may utilize this capability to poll whether or not a entitlement deserves to be paid out, allowing them to streamline this process.

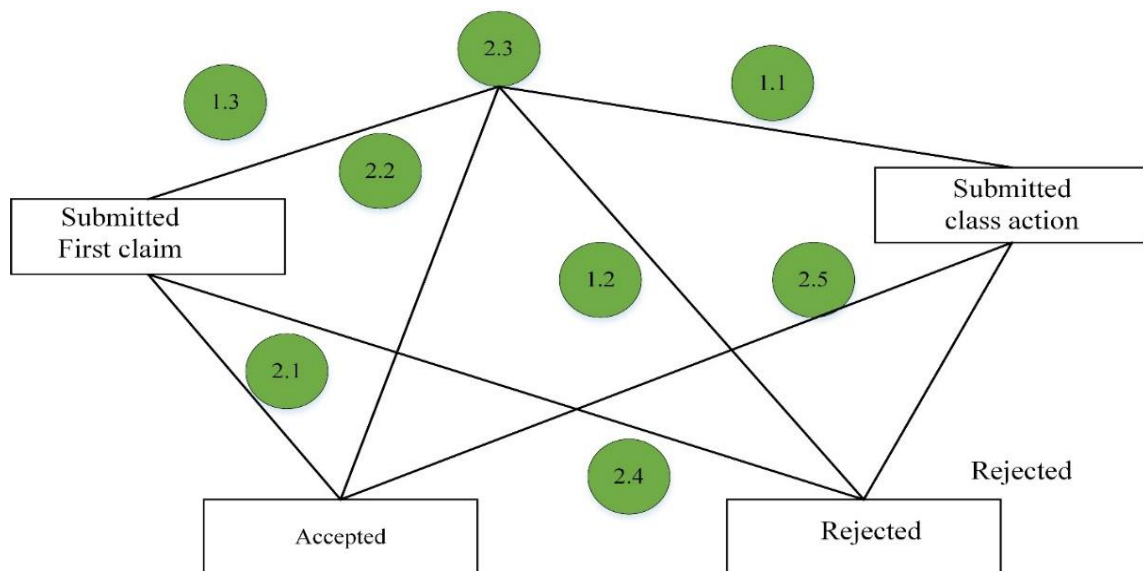


Fig. 4. State diagram of claims object.

The claim is the primary entity in the realm structure. The entitlement made in the framework can be in one of four "states" depending on the user's selections. Phase transitions 1.1 to 1.4 are for newly formed claims. Whenever the request is the initial one for a benefit, it will be marked given the status "submitted - first claim" (1.1). If more than one claim is currently lodged for the asset, it will be marked as "accepted - class action" (1.4). If a entitlements administrator has already accepted or rejected a claim having an identifiable cause, then subsequent claims will be immediately approved (1.2) or denied (1.3). Steps 2.1–2.4 apply to claims that were previously filed at the time the claims administrator reports an event. In that point, all filed claims are going to be immediately approved (2.1 and 2.3) or denied (2.2 or 2.4) [23]. Fig. 4 shows state diagram of claims object.

V. RESULT AND DISCUSSIONS

The integration of blockchain technology and smart contracts presents a transformative solution for the insurance industry, revolutionizing claims processing and payouts. By automating the entire process based on predefined events, such as natural disasters or medical emergencies, the proposed system eliminates manual claims submission, enhances efficiency, and ensures transparency and security. With payouts executed automatically upon event verification, bureaucratic hurdles are bypassed, leading to expedited processing times and reduced fraud risks. This innovative approach not only streamlines operations but also fosters trust and reliability, ultimately delivering significant benefits to insurers and policyholders alike in a future characterized by expedited, transparent, and trustworthy claims processing.

Event-driven architecture for insurance claim processes is given in Fig. 5 driving events such as policy updates, patient updates, and claim submissions trigger a series of actions. A graph depicting the number of driving events per second illustrates the system's real-time processing capabilities, enabling insurers to handle fluctuating workloads efficiently. This visualization aids in understanding system performance and scalability, ensuring timely and accurate processing of insurance claims.

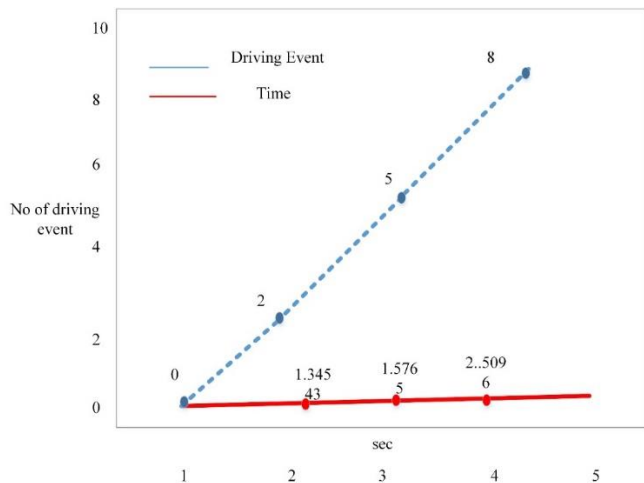


Fig. 5. Event-driven architecture for insurance claim processes.

Fig. 6 depicts a partial dependence plot illustrating how an old claim affects insurance outcomes. It visualizes the relationship between the age of a claim and its impact on insurance variables, such as claim probability or payout amount. This graph, insurers can understand how the age of a claim influences risk assessment and decision-making in insurance processes. It helps identify patterns and trends, enabling more informed underwriting and claims management strategies. This graphical representation facilitates data-driven insights for optimizing insurance operations and managing risk effectively.

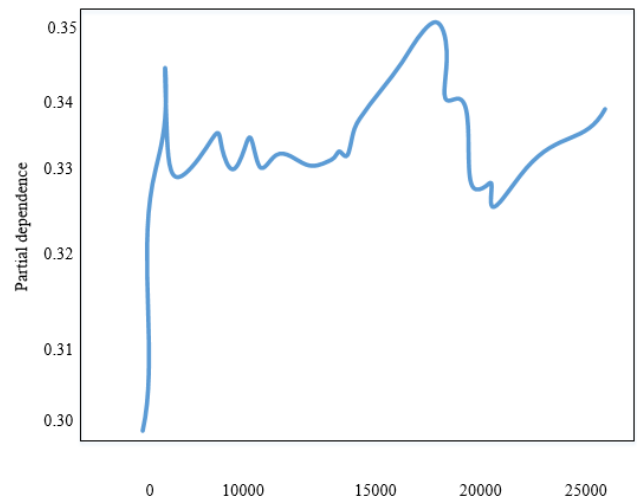


Fig. 6. Automatic insurance claim prediction.

Fig. 7 shows the amounts of paid and denied claims for different categories of old claims the amount of paid claims is higher than denied ones, with the 3rd claim having the highest amount of paid claims. The bar chart helps to visualize the distribution and comparison of paid and denied claims for different categories of old claims.

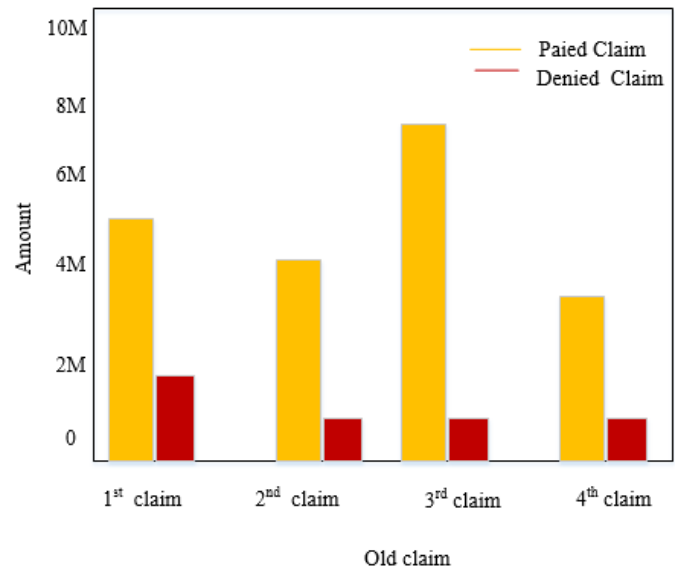


Fig. 7. The amounts of paid and denied claims.

Table I presents performance metrics for different methods the proposed method achieves high accuracy (94.44%) and outperforms others in precision (98.1%), recall (98.98%), and F1-score (98.54%) in Fig. 8. This indicates its effectiveness in correctly identifying positive instances while minimizing false positives and negatives, demonstrating its potential superiority in the classification task.

TABLE I. PERFORMANCE METRICS

| Methods | Accuracy (%) | Precision (%) | Recall (%) | F1-score (%) |
|-----------------|--------------|---------------|------------|--------------|
| RNN | 90.54 | 90.4 | 92.00 | 92.44 |
| Auto encoder | 92.77 | 91.88 | 91.76 | 91.56 |
| VAE | 95.5 | 93.57 | 94.01 | 94.45 |
| Proposed method | 97.6 | 98.1 | 98.98 | 98.54 |

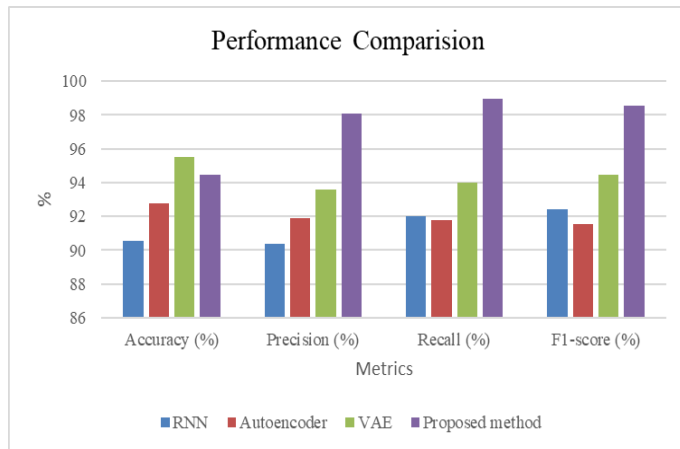


Fig. 8. Performance comparison.

Table II shows that the proposed method achieves an accuracy of 97.6% using the "Health Insurance Dataset - EDA". It also maintains high accuracy rates with other datasets: MedClaimsData (96.7%), HealthCoverStats (95.8%), and HealthinsureDB (93.7%).

TABLE II. DATASET COMPARISON

| Dataset | Proposed Method Accuracy |
|------------------------------|--------------------------|
| Health Insurance Dataset-EDA | 97.6% |
| MedClaimsData | 96.7% |
| HealthCoverStats | 95.8% |
| Healthinsure DB | 93.7% |

A. Discussions

The proposed integration of blockchain technology and smart contracts in insurance claims processing offers several significant advantages. Firstly, it addresses the limitations of the existing method by adopting event-based smart contracts, eliminating the need for manual claims submission. This automation enables automatic triggers based on predefined events such as natural disasters or medical emergencies, accelerating the claims initiation process and ensuring accuracy and transparency. By doing so, it overcomes the existing challenges related to inefficiency and complexity,

which require physical visits to facilities for certification before submitting paperwork to insurance firms, leading to delays in compensation and posing challenges in data verification and risk management. By encoding specific conditions and triggers within smart contracts, the entire claims process becomes transparent, secure, and immutable, thereby minimizing the potential for fraud and dispute. Thirdly, the automatic execution of payouts upon verification of triggering events bypasses traditional bureaucratic procedures, leading to significantly reduced processing times [15]. Through the streamlined system outlined, insurers and policyholders stand to benefit from increased efficiency, transparency, and trustworthiness in claims processing, ultimately enhancing the overall insurance experience for all stakeholders. These advantages address the limitations of the existing method, such as challenges related to infrastructure development, legal obstacles, and data availability, thus making the proposed system a more robust and effective solution.

VI. CONCLUSION AND FUTURE WORKS

The integration of blockchain technology and smart contracts has revolutionized the insurance industry by enhancing efficiency, transparency, and reliability. This research proposes a simplified system that automates the entire claims process from submission to reimbursement, eliminating the need for human claim filing. The system triggers policyholders' claims by predetermined occurrences, such as medical emergencies or natural disasters, allowing for prompt and precise claim initiation. Smart contracts, programmed with precise triggers and conditions, guarantees the transaction immutability, security, and transparency. Reimbursements are carried out automatically after the triggering event has been verified, reducing processing times and reducing fraud and disagreement. This innovative approach to insurance claims processing has shown significant reductions in processing time, minimized fraud potential, and enhanced transparency. The Python-implemented system achieved 97.6% accuracy, demonstrating its efficacy and reliability. This study contributes to addressing the limitations of existing insurance claim procedures by providing a streamlined, automated, and secure solution. By integrating blockchain technology and smart contracts, the insurance industry can overcome challenges of inefficiency, complexity, and lack of transparency in the current claims processing system. The research questions regarding the feasibility and effectiveness of event-based smart contracts in automating insurance claims processing have been successfully addressed, providing valuable insights for future implementations in the insurance sector.

REFERENCES

- [1] "Chapter 7: SMART CONTRACTS in: FinTech." Accessed: Apr. 24, 2024. [Online]. Available: <https://www.elgaronline.com/edcollchap/edcoll/9781800375949/9781800375949.00018.xml>
- [2] N. R. Bhamidipati et al., "Claimchain: Secure blockchain platform for handling insurance claims processing," in 2021 IEEE International Conference on Blockchain (Blockchain), IEEE, 2021, pp. 55–64.

- [3] C. Eckert, C. Neunsinger, and K. Osterrieder, "Managing customer satisfaction: digital applications for insurance companies," *Geneva Pap. Risk Insur.-Issues Pract.*, vol. 47, no. 3, pp. 569–602, 2022.
- [4] L. Zheng and L. Guo, "Application of big data technology in insurance innovation," in *International conference on education, economics and information management (ICEEIM 2019)*, Atlantis Press, 2020, pp. 285–294.
- [5] M. Hanafy and R. Ming, "Machine learning approaches for auto insurance big data," *Risks*, vol. 9, no. 2, p. 42, 2021.
- [6] L. Rukhsar, W. H. Bangyal, K. Nisar, and S. Nisar, "Prediction of insurance fraud detection using machine learning algorithms," *Mehran Univ. Res. J. Eng. Technol.*, vol. 41, no. 1, pp. 33–40, 2022.
- [7] D. E. Warren and M. E. Schweitzer, "When weak sanctioning systems work: Evidence from auto insurance industry fraud investigations," *Organ. Behav. Hum. Decis. Process.*, vol. 166, pp. 68–83, 2021.
- [8] J. Madir, "Smart contracts," in *FinTech*, Edward Elgar Publishing, 2021, pp. 175–198.
- [9] A. S. Mishra, "Study on blockchain-based healthcare insurance claim system," in *2021 Asian Conference on Innovation in Technology (ASIANCON)*, IEEE, 2021, pp. 1–4.
- [10] V. Kalsgonda and R. Kulkarni, "Role of Blockchain Smart Contract in Insurance Industry," Available SSRN 4023268, 2022.
- [11] X. Lin and W. J. Kwon, "Application of parametric insurance in principle-compliant and innovative ways," *Risk Manag. Insur. Rev.*, vol. 23, no. 2, pp. 121–150, 2020.
- [12] K. L. Narayanan, C. R. S. Ram, M. Subramanian, R. S. Krishnan, and Y. H. Robinson, "IoT based smart accident detection & insurance claiming system," in *2021 Third international conference on intelligent communication technologies and virtual mobile networks (ICICV)*, IEEE, 2021, pp. 306–311.
- [13] J. C. Mendoza-Tello, T. Mendoza-Tello, and H. Mora, "Blockchain as a healthcare insurance fraud detection tool," in *Research and Innovation Forum 2020: Disruptive Technologies in Times of Change*, Springer, 2021, pp. 545–552.
- [14] A. Borselli, *Smart contracts in insurance: a law and futurology perspective*. Springer, 2020.
- [15] C.-L. Chen, Y.-Y. Deng, W.-J. Tsaur, C.-T. Li, C.-C. Lee, and C.-M. Wu, "A traceable online insurance claims system based on blockchain and smart contract technology," *Sustainability*, vol. 13, no. 16, p. 9386, 2021.
- [16] D. Oza, D. Padhiyar, V. Doshi, and S. Patil, "Insurance claim processing using RPA along with chatbot," in *Proceedings of the 3rd International Conference on Advances in Science & Technology (ICAST)*, 2020.
- [17] N. Dhieb, H. Ghazzai, H. Besbes, and Y. Massoud, "A secure ai-driven architecture for automated insurance systems: Fraud detection and risk measurement," *IEEE Access*, vol. 8, pp. 58546–58558, 2020.
- [18] F. Loukil, K. Boukadi, R. Hussain, and M. Abed, "Ciosy: A collaborative blockchain-based insurance system," *Electronics*, vol. 10, no. 11, p. 1343, 2021.
- [19] N. Fernando, A. Kumarage, V. Thiyaganathan, R. Hillary, and L. Abeywardhana, "Automated vehicle insurance claims processing using computer vision, natural language processing," in *2022 22nd International Conference on Advances in ICT for Emerging Regions (ICTer)*, IEEE, 2022, pp. 124–129.
- [20] K. Dutta, S. Chandra, M. K. Gourisaria, and G. Harshvardhan, "A data mining based target regression-oriented approach to modelling of health insurance claims," in *2021 5th International Conference on Computing Methodologies and Communication (ICCMC)*, IEEE, 2021, pp. 1168–1175.
- [21] "Health Insurance Dataset - EDA | Kaggle." Accessed: Feb. 15, 2024. [Online]. Available: <https://www.kaggle.com/code/mregoyau/health-insurance-dataset-eda>
- [22] S. Manikandan, "Data transformation," *J. Pharmacol. Pharmacother.*, vol. 1, no. 2, p. 126, 2010.
- [23] S. Gillis, "Blockchain-based Application for Insurance Claims Management," PhD Thesis, Harvard University, 2023.

Real-time Air Quality Monitoring in Smart Cities using IoT-enabled Advanced Optical Sensors

Anushree A. Aserkar¹, Dr. Sanjiv Rao Godla², Prof. Ts. Dr. Yousef A. Baker El-Ebiary³, Dr. Krishnamoorthy⁴,
Janjhyam Venkata Naga Ramesh⁵

Assistant Professor, Department of Applied Mathematics and Humanities,
Yeshwantrao Chavan College of Engineering, Nagpur, India¹

Professor, Department of CSE(Artificial intelligence & Machine Learning),
Aditya College of Engineering & Technology - Surampalem, Andhra Pradesh, India²

Faculty of Informatics and Computing, UniSZA University, Malaysia³

Associate Professor, Department of CSE, Panimalar Engineering College, Chennai, India⁴
Department of Computer Science and Engineering, Koneru Lakshmaiah Education Foundation,
Vaddeswaram, Guntur Dist., Andhra Pradesh, India⁵

Abstract—Air quality control has drawn a lot of attention from both theoretical research and practical application due to the air pollution problem's increasing severity. As urbanization accelerates, the need for effective air quality monitoring in smart cities becomes increasingly critical. Traditional methods of air quality monitoring often involve stationary monitoring stations, providing limited coverage and outdated data. This study proposes an Internet of Things (IoT) centred framework equipped with inexpensive devices to monitor pollutants vital to human health, in line with World Health Organization recommendations, in response to the pressing issue of air pollution and its increased importance. The hardware development entails building a device that can track significant contamination percentages. Ammonia, carbon monoxide, nitrogen dioxide, PM2.5 and PM10 particulate matter, ozone, and nitrogen dioxide. The gadget is driven by the ESP-WROOM-32 microcontroller, which has Bluetooth and Wi-Fi capabilities for easy data connection to a cloud server. It uses PMSA003, MICS-6814, and MQ-131 sensors. The gadget activates indicators when a pollutant concentration exceeds the allowable limit, enhancing its software to enable immediate response and intervention. This work leverages the robust cloud architecture of Amazon Web Server (AWS) to integrate it into the system and improve accessibility and data control. This combination no longer just ensures data preservation but also enables real-time tracking and analysis, which adds to a comprehensive and preventive strategy for reducing air pollution and preserving public health. With an RMSE score of 3.7656, the Real-Time Alerts with AWS Integration model—which was built in Python—has the lowest value.

Keywords—Internet of Things (IoT); air quality control; low-cost sensors; ESP-WROOM-32 microcontroller; Amazon Web Server (AWS)

I. INTRODUCTION

Air quality refers to the way filthy the air human's breath. On a typical day, that take over 20,000 breath. Have we considered the toxins, pollen, and dirt we may be breathing? Whenever the air quality is poor, contaminants in the atmosphere can cause eye irritation, irritated the lungs, and respiratory system injury. Fresh air is a basic prerequisite for a

healthy atmosphere in which all reside and study [1]. An Air Quality Analysis is an evaluation conducted to determine the benchmark quality of the air and is often necessary for any kind of development which has the ability to damage the present situation or if the surroundings having the capacity to impact sensitivity construction [2]. Air quality may be checked both indoors and outside. An air quality evaluation measures the quantity and quality of air inside the confines of a building or structure. Indoor air quality sampling varied, but typically involves collecting and analyzing air samples with swab/sticky pads. An outdoors atmosphere evaluation can range from a basic screenings to a more extensive study that includes dispersal modelling [3]. The sort of air quality evaluation needed is determined by a variety of criteria, which involve the development's scale, intended place of residence, and existing information of pollutants present around the construction area[4]. A thorough air quality evaluation ought to determine air pollution exposed using the "Air Quality Impact Significance Criteria - New Exposure" and demonstrate any preventative actions related with the development's layout, location, and operations to decrease air pollution [5]. An Air Quality Analysis may be required in support of an inquiry for clearance for works that may have a significant influence on regional traffic moves, transportation structure, or are located near established busy roadways. An appropriate Air Quality evaluation for planned should comprise an inspection of the environmental conditions about the development through surveillance or modeling, an evaluation of the air quality through the construction phase, as well as a monitoring of the air purity through the period of operation. Tracking air quality monitors contaminants such as gases and particulates. Measuring such contaminants enables the enhancement of the atmosphere via construction planning, management, and mitigation methods. Enhancing air quality is critical in decreasing negative health consequences and offering an improved standard of life [6].

According to the World Health Organization (WHO), pollution in the air causes 4.2 million premature deaths annually in urban and rural regions worldwide. According to the US Environmental Protection Agency, particulates with a

measurement of less than ten μm is unique of the biggest pressures to community health due to its easy passage through respiratory systems, producing significant health damage. According to Valdivia in and Pacsi, Metropolitan Lima (LIM) is sensitive to high levels of PM_{10} due to its rapid manufacturing and economic expansion, as well as its big human population, which accounts for 29% of the country's total population. To mitigate the impairment wrought by PM_{10} to public health, the WHO developed level thresholds ideal for achieving a minimum adverse effect on health [5]. In different nations, multiple regulations have been passed to regulate PM_{10} concentrations and air quality in overall, such as those developed in Peru by the Ministry of the Environment as well as in the United States by the Environmental Protection Agency (EPA). In recent decades, several predictions methodologies have been modified and modified to better understand way pollution function in the natural environment at the level of molecules, including predicting diffusion and dispersal trends according to molecule dimension and class [7]. Nevertheless, predictions based on findings tend to have a low accuracy. The EPA describes inside air quality (IAQ) as the purity of airborne in buildings grounds or sealed rooms that can have a substantial influence on the well-being of tenants, ease, and performance rates [8]. It has been established that human activity, manufacturing processes, and rising traffic on roadways are the main culprits causing the decline of the natural world [9]. In addition to various outside factors, low thermal ease levels owing to excessive moisture and temperature in confined buildings, insufficient ventilation administration, dangerous construction supplies, and every day human behavior all have an impact on IAQ [10]. The increasing levels of dangerous pollutants [11].

Indoor surroundings are also connected to the worsening wellness of building inhabitants, particularly older adults, newborns, people with impairments, and domestic women, who spending the majority of their lives inside [12]. As a result, it is critical to grasp all elements of inside airborne pollution (IAP) and its influence on the general population, as well as discover suitable IAQ management techniques in sealed buildings. According to a study of over 30,000 organizations in the United States, indoor air quality control is the country's top priority since it is inflicting significant harm to the well-being and health of individuals [13]. On the other hand, long-lasting medical impacts include pneumonia, pulmonary TB, hostile gestation results, asthma, chronic bronchitis, cancer, and coronary artery disease that individuals may experience after frequent & extended exposure [14]. A wide range of contaminants harm the well-being of structure inhabitants in homes, workplaces, cafés, medical facilities, and retail malls. Because of the increased traffic activities, manufacturing operations, and facilities ambient air pollution values are rising sharply, that eventually explains for the declining IAQ values. [15].

The researchers have previously released thorough systematic studies that emphasize existing improvements in the area of IAQ monitoring and examination, as well as emphasizing the significance, difficulties, and future years sights of this significant area of studies, in order to offer knowledge about the associated research [16]. Aside from this,

various papers were released on the creation of forecasting algorithms using neural networks, artificial intelligence, and advanced learning methodologies to provide building residents with an early warning of dangerous pollutant concentrations. In addition, the authors released a systematic review to emphasize the contributions already established scholars in the subject, as well as the gaps in knowledge [17]. The researchers gathered present data from 4 separate countryside and urban sites on six significant IAQ parameters, namely, PM_{10} , $PM_{2.5}$, CO_2 , CO , NO_2 , as well as two critical thermal convenience factors, humidity and temperature. Finally, the model was modified utilizing the pattern searching technique to advance the correctness of predictions, allowing the suggested system to be applied in real-time settings to prevent the negative implications of low IAQ levels [18]. The suggested model is dubbed continuous because it employs an evolving set of input characteristics based on the selected response variable for predictions.

Key contributions are as follows:

- The urgent problem of air pollution is addressed by proposing an Internet of Things system with inexpensive sensors for real-time monitoring of important air contaminants.
- Ensures a focused and effective strategy by focusing on contaminants that are critical to human health and adhering to World Health Organization recommendations.
- Provides a comprehensive understanding of air quality by developing a hardware approach capable of calculating the amounts of important pollutants including $PM_{2.5}$, PM_{10} , ozone, carbon monoxide, nitrogen dioxide, and ammonia.
- Enables smooth data transfer to a cloud server for effective monitoring and analysis by utilizing the Wi-Fi and Bluetooth capabilities of the ESP-WROOM-32 microcontroller.
- Establishes a mechanism whereby the apparatus activates indicators when the concentration of pollutants exceeds allowable limits, improving its software for prompt reaction and interference, and supporting proactive air quality management.
- Enhances the overall efficacy of air pollution prevention efforts by integrating Amazon Web Server (AWS) into the system and utilizing its reliable cloud architecture for simplified data management, storage, and real-time tracking and analysis.

The following is how the investigation progresses: In Section II. Related studies perform a thorough analysis of earlier research, focusing on prediction issues and the wide range of optimization techniques used in such settings. In Section III, a thorough investigation of issue statements is conducted. Section IV elaborates on the suggested method or plan of action to deal with these difficulties. The entire topic of performance evaluation metrics and criteria is covered in Section V. Subsequently. Section VI serves as the essay's conclusion by summarizing the main findings and learning.

II. RELATED WORKS

Air pollution is a key contributor to global warming, and efforts to address it are gaining traction. Urban areas use computer technology (IT) and communications technologies to reduce emission levels and noise pollution. The goal is to reduce health-related hazards and improve understanding about the impacts of pollutants in the air exposures. The present research explores the major concerns of a current pollution tracking scheme, such as sensors, connection procedures, collecting data and transfer over routes of communication, and information security and uniformity. Safety is a significant emphasis of the suggested IoT system. The system's additional parts are also focused on security. This document includes a bill for supplies and protocol specifications required for the planning, creation, and execution of an IoT system, in addition to security issues. The paper's evidence of concept (PoC) addresses IoT security issues regarding communication pathways among linked device gateway and the cloud-based systems to which information is sent. The security measures adhere to recognized principles, guidelines, and regulations, leading to a consistent and healthy system., the software can read and analyze the collected data, creating pollutant maps using modelling techniques. The maps are utilized to undertake real-time treatments, such as redirecting transportation in a chief metropolis, to reduce concentrations of airborne contaminants using information gathered for a year in a row. When paired with traffic control equipment (cameras and traffic signals), this technology may minimize vehicle emissions by constantly proposing other courses or even demanding reroute if pollution levels are exceeded. Still, the study must concentrate on case studies for implementing the PoC with improvements to various medium cities in collaboration with local governments in order to observe the traffic affect models and how they interact into additional advanced city systems, since current projects like AirVisual are limited [19].

The quantity of IoT-based applications for smart cities is growing rapidly, as is the volume of data generated by those applications. To guarantee long-term growth, administrations and city stakeholders take proactive steps to manage this data and forecast effects in the future. Techniques based on deep learning have been applied to a variety of large-scale information forecasting challenges. This motivates us to apply methods based on deep learning for predicting IoT data. As a result, this research proposes a unique deep learning algorithm for analyzing IoT smart city data. A new model that utilizes Long Short-Term Memory (LSTM) networks for predicting upcoming air quality levels in a smart city. The suggested model's assessment findings are positive, indicating the method may also be utilized to solve other innovative city prediction challenges. However, one major limitation of this work is the low generalization of the suggested LSTM-based model, as its efficacy may be highly influenced by specific features of the analyzed smart city data. Furthermore, the research might fail to address possible privacy and security concerns related to managing and analyzing confidential IoT data in a smart city environment [20].

Sometimes emissions have grown owing to a variety of factors, including growing populations, greater car usage,

manufacturing, and urbanization, among others that have had a substantial impact on human health. To pay attention to the circumstance. The research involves an air pollution surveillance system that is an Internet of Things via sensors dependent structure. You monitor the overall condition of the air via a web server on the World Wide Web and produce warnings while the quality of the air goes beyond an established limit, and these suggests if enough dangerous gas have been detected in the atmosphere such as benzene, smoke, NH₃, CO₂, and alcohol. The expansion of commerce and rapid human population urbanization have a negative influence on global air quality. Long-term exposure to air pollution causes chronic heart and lung ailments, which endangers people's well-being. Every day, thousands of companies and billions of automobiles emit massive amounts of pollutants in the atmosphere. As a result, monitoring pollutants in the air has become vital. The investigation presents the creation of an Internet of Things-driven air quality surveillance system and analyzes the effectiveness of the air pollution tracking system. But the disadvantage of this research is that the efficiency of the IoT-based air quality tracking systems may be affected by the exactness and dependability of the sensors utilized, potentially leading to mistakes in contaminants estimations [21].

Exhaling and breathing filthy air has major health repercussions. Regular surveillance and record-keeping can help to reduce the impact of air pollution. In addition, early forecast of pollution levels can assist government agencies in taking proactive environmental protection actions. In this study, researchers suggested employing the ml methods and IoT for tracking pollutants in the air in smart cities in the future. The Pearson coefficient reveals a strong link between contaminants and meteorological factors. In contrast to typical sensor networks, this study employs a cloud-and IoT architecture that collects information obtained from airborne pollutants sensors and weather conditions sensors. Thus delivers twofold dependability and lower expenses greatly. The amount of sulphur dioxide (SO₂) and particulate matter (PM_{2.5}) was predicted using an artificial neural network. The encouraging outcomes show that ANN is a trustworthy choice for pollution surveillance and forecasting systems. The models They developed attained Root Mean Squared Error values of 0.0128 and 0.0001 for SO₂ and PM_{2.5}, respectively. However, one disadvantage of this research is its dependence on Pearson correlation to create a significant connection among contaminants and meteorological indicators can simplify the complicated relationships in the atmosphere's dynamics, which could contribute to less precise forecasts [22].

Pollution of the atmosphere has grown into a dangerous issue in many nations throughout the world in recent decades as a result of human activity, manufacturing, and urbanization. PM_{2.5}, a kind of air pollution with a circumference of fewer than 2.5µm, poses a significant health risk. PM_{2.5} levels vary according to a number of variables, such as meteorological and the quantity of other contaminants in metropolitan areas. In the present study, constructed a deep learning system that predicted the hourly prediction of PM_{2.5} concentrations in Beijing, China, using CNN-LSTM with a spatial-temporal

features by merging historical pollution information, meteorological data, and PM2.5 concentration in neighboring sites. Researchers investigated the differences in performance amongst deep learning models. Results from experiments show that the "hybrid CNN-LSTM multivariate" technique allows for greater precision predictions and outperforms all of the classic models described. Yet, the approach was initially deployed in the metropolitan area of Beijing, China, according to the lack of daily freely available data [23].

As air pollution worsens, the condition of the air prediction has emerged as a critical tool for managing and preventing it. Over the past few years, several approaches for predicting the air's cleanliness have been presented, including determinate, statistical in nature, and neural network approaches. Still, these approaches have drawbacks. The deterministic approach approaches need costly calculations and particular expertise for parameters recognition, but statistics techniques' forecast ability is limited owing to the linear assumptions and the issue of multicollinearity. In contrast, many deep learning approaches are unable to detect periodic trends or acquire information about the long-term associations of air pollutant concentration. Furthermore, there are few systems that can produce accurate predictions for environmental forecasts at higher time resolutions, including every day, every week, and occasionally each month. The approach is to use the bi-directional LSTM model to learn from PM2.5's dependence over time, as well as learn via transfer to transfer information obtained at lower time resolution to higher periodic resolutions. The previously suggested methodological paradigm is tested with a case study in Guangdong, China. The framework's efficiency is contrasted with other regularly used machine learning techniques, and the findings reveal that the suggested TL-BLSTM model has less mistakes, particularly at higher temporally resolutions. But it is utilized when the number of samples is restricted or whenever the modeling procedure is too complicated and technologically costly [24].

The provided paper examines the use of Internet of Things (IoT) and machine learning for air pollution monitoring and prediction. It shows real-time tracking with a focus on security, IoT packages in smart cities and the significance of accurate sensors. Various studies recommend deep gaining knowledge of algorithms, inclusive of LSTM networks, for predicting air quality. Challenges include potential sensor inaccuracies and simplified mode. Additionally, a cloud-centric IoT middleware architecture and artificial neural networks are explored for efficient pollution surveillance. These approaches aim to monitor and predict air quality levels in urban environments, facilitating proactive environmental protection measures. However, several limitations are evident across these studies. Firstly, the accuracy and reliability of IoT-based air quality tracking systems heavily rely on the precision of sensors used, which may lead to inaccuracies in pollutant estimations. Additionally, deep learning models may suffer from low generalization, as their efficacy can be highly influenced by specific features of analyzed smart city data, potentially limiting their applicability across different contexts. Furthermore, some studies may oversimplify the complex relationships in atmospheric dynamics, leading to

less precise forecasts. Lastly, certain approaches, such as those relying on transfer learning, may face challenges when dealing with limited sample sizes or complex modeling procedures, highlighting the need for further research to address these limitations and enhance the effectiveness of air quality prediction systems.

III. PROBLEM STATEMENT

The growing global problem of air pollution, exacerbated by urbanization, industry, and population expansion, need efficient monitoring and forecasting [24]. The adaptability of deep learning techniques, such as CNN, hybrid models, and LSTM networks, while tackling issues such as sensor errors, privacy issues, and the requirement for complex models in the monitoring and prediction of air pollution. Systems investigate ways to alleviate issues with air pollution by using machine learning and the Internet of Things (IoT). Emphasizing trustworthy and precise sensors is still necessary in research. Additionally, it highlights how urgently the need a comprehensive and reliable forecasting solution to get around the obstacles in the IoT Approach with Real-Time Alerts and AWS Integration for Air Quality Monitoring.

IV. IOT APPROACH WITH REAL-TIME ALERTS AND AWS INTEGRATION FOR AIR QUALITY MONITORING

The proposed method utilizes the ESP-WROOM-32, a low-cost IoT device equipped with sensors, for real-time environmental tracking. Initial data collection is followed by a pre-processing phase, where the Nearest Neighbour Interpolation Approach is employed for data interpolation and labelling. Subsequently, the ESP-WROOM-32 processes the pre-processed data, ensuring efficient utilization of resources. The system's performance is thoroughly evaluated to validate its effectiveness. Finally, the results are hosted on an Amazon Web Server (AWS), establishing an end-to-end workflow for cost-effective environmental monitoring. The ESP-WROOM-32's low-power capabilities make it well-suited for continuous operation across diverse environmental conditions, enhancing its practicality and reliability for long-term monitoring applications. This integrated approach offers a scalable and affordable solution for real-time environmental tracking, enabling stakeholders to make informed decisions and take proactive measures to address environmental concerns. Fig. 1 shows proposed diagram.

A. Data Collection

The dataset encompasses a comprehensive collection of 9357 hourly readings derived from a network of 5 metallic oxide chemical detectors deployed within an Air Quality Chemical Multisensor Device. This device was strategically placed in an openly accessible, heavily polluted area at street level in an Italian city, providing a real-world perspective on airborne chemical concentrations. The data spans a duration of one year, from March 2004 to February 2005, offering a seasonal and temporal understanding of air quality dynamics. However, the dataset acknowledges several challenges that could impact the accuracy of concentration estimates. These challenges include cross-sensitivities among sensors, concept shifts, and sensor changes, as discussed in De Vito et al., Sens. And Act. B. These factors highlight the need for careful data

interpretation and analysis to account for potential biases introduced by such challenges. It's noteworthy that any missing values in the dataset are denoted by a value of -200. Addressing these challenges and understanding the intricacies

of the dataset is crucial for obtaining reliable insights into air quality dynamics and for developing accurate models for pollution prediction and control [25].

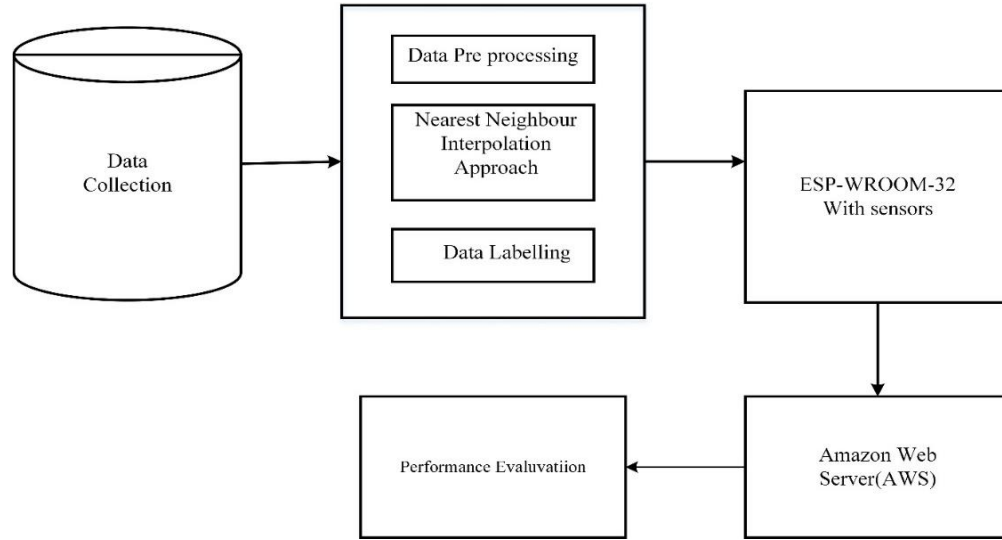


Fig. 1. Proposed diagram.

B. Data Pre-Processing

1) *Nearest-neighbor interpolation approach:* The unprocessed information from the sensor is captured without any sort of processing. The method of filtering is carried out in the public cloud instead of on the embedded device in order to decrease complication in the system that is embedded. The exceptions and incomplete data are among the maximum characteristic data mistakes in real-time tracing requests a total of three kinds of usual dataset preparatory computation: transforming not-a-number (NaN) data to zero, eliminating NaN data. In the current study, information interpolation is performed using a nearest-neighbour strategy. This strategy is applicable to collections with values that are lacking or outlier situations. Whenever an outlier appears at location z'_i the nearest knowing neighbour's values is utilized as the replacement for the outlier. It will be determined utilizing all of Sensor 2021, 21, 4956 10 of 16 previous data available. The choice of using prior data rather than upcoming information comes since information is collected in immediate time in the form of a series of values is shown in Eq. (1)

$$z'_i = \left\{ \begin{array}{l} \frac{z'_{i-1} + z'_{i-2}}{2}, \text{ if } i = 2; \\ \frac{z'_{i-1} + z'_{i-2} + z'_{i-3}}{3}, \text{ if } i = 3; \\ \frac{z'_{i-1} + z'_{i-2} + z'_{i-3} + z'_{i-4}}{4}, \text{ if } i = 4; \\ \frac{z'_{i-1} + z'_{i-2} + z'_{i-3} + z'_{i-4} + z'_{i-5}}{5}, \text{ otherwise} \end{array} \right. \quad (1)$$

2) *Data labelling:* Data Labelling When inputting details about sensors in the estimate process, an ensemble of records must be characterised as the result in machine learning with supervision. In fact, the air quality index (AQI) is an estimate employed for categorizing the practice of the air in a

convinced place. Usually, the AQI is split into numerous limits, each of which has a unique colour and description. It appoints a health care advisor to every range. The threshold level of air quality (see Fig. 2) for a variety of pollutants. The current versions of guidelines and recommendations vary depending on the global organizations. The contaminants the index is computed using the following parameters: CO_2 , $PM_{2.5}$ and PM_{10} . The greatest index reflects the AQI at the moment [26].

C. Iot-based Air Quality Monitoring

1) *ESP-WROOM-32 with sensors, to enable real-time environmental tracking:* The approach suggested in this paper, being a part of a bigger project in progress, comprises the software as well as the hardware layers for actual time environmental tracking via a low-cost IoT device. In the physical coating, a digital circuit design is under construction to create a surface with devices that detect the concentrations of $PM_{2.5}$, PM_{10} , O_3 , CO , NO_2 and ammonium (NH_3). Moisture and temperature monitoring were added to the pollution tracking functions to aid in the analysis. The gadget and its application are going to interact over a Bluetooth or WiFi connection. The main elements that are going to be supplied on the gadget's boards which will conduct measurements are as follows. The microcontroller called ESPWROOM-32 (or simply, ESP32), was selected to gather data from the following set of sensors: DHT22, measuring ambient temperature and air humidity; PMSA0003, that successfully evaluates and specifies the levels of PM2.5 and PM10 particles substance; MQ-131, that determines the amount of O_3 ; and MICS-6814, and this measures the levels of CO , NO_2 , and NH_3 and is capable of tracking five additional pollutants. A quick overview of the listed elements is provided here.

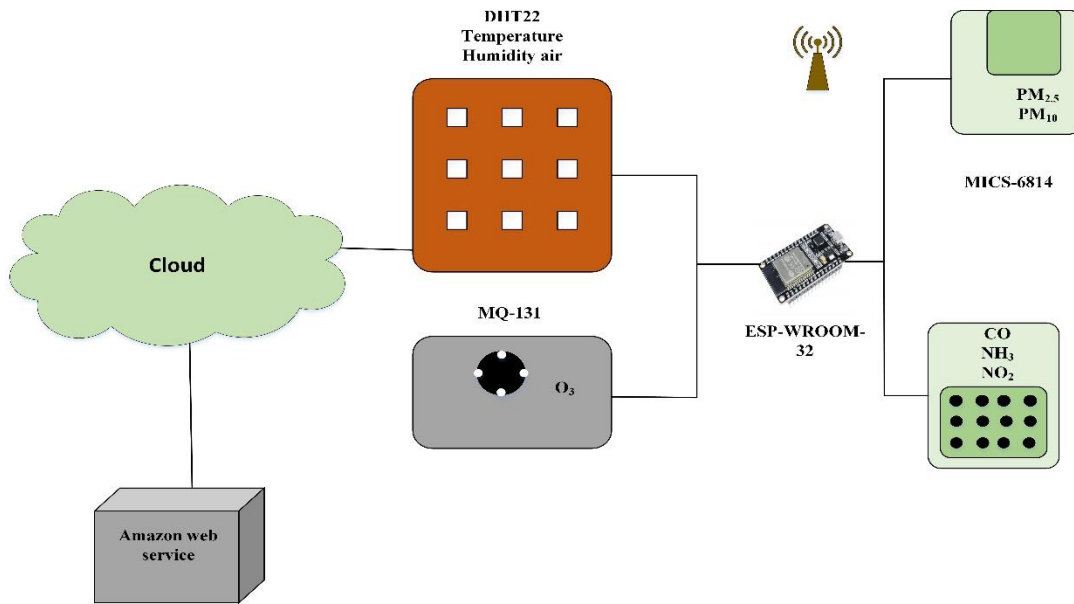


Fig. 2. IoT approach with real-time alerts and AWS integration for air quality monitoring.

To avoid potential lack of availability, the watchdog feature is added, which identifies collapses and restarts the microcontroller using three independently timers from the primary system. Sensing measurements region. The PMSA003 is a small digital sensor used for detecting particles dispersed in the air. Particulate matter, often known as dirt, are nanoparticles of varied sizes, & a sensor uses a microprocessor to execute a light scattering-based detection approach to determine the proportions of the atoms and density. The MICS-6814 is a small device that can correctly detect CO, NO₂, and NH₃ concentrations at the exact same time, using distinct networks for all gas. The device's efficiency is quite promising, and it must be highlighted that it can also detect five additional gases: methane (CH₄), propane (C₃H₈), ethanol (C₂H₅OH), hydrogen (H₂), and isobutane (C₄H₁₀). The MQ-131 sensors measure O₃ contents with high sensitivity and have a trimpot for calibration in addition to a standard analog output. The DHT22 digital sensors is being chosen for both humidity and temperature surveillance because it offers exact results and is easy to set up [27].

a) *Amazon Web Server (AWS)*: To further streamline data management and accessibility, this work integrates the Amazon Web Server (AWS) into the system, leveraging its robust cloud infrastructure. This amalgamation not only ensures efficient data storage but also facilitates real-time monitoring and analysis, contributing to a comprehensive and proactive approach in combating air pollution and safeguarding public health. Amazon Network Services, a division of Amazon, have offering frameworks for computing services upon request since March 2006. It operates on the "pay as you go" approach. The expenses are decided utilization of amenities AWS's extensive variety of cloud offerings allows for the implementation of a broad spectrum of solutions. In the suggested solution, a server's IoT primary service is utilized for uploading sensors information into the cloud. The procedure of utilizing AWS IoT core services

begins with the creation of an AWS account as well as a thing in IoT core that includes the creation of certifications and rules. Information submitted may be viewed by subscribe to the appropriate MQTT protocol account's Testing area of the IoT core. The degree of sophistication is defined by the amount of gadgets that collect data and send it to the Network of Thing via a wireless connection.

V. RESULTS AND DISCUSSION

Air quality control system equipped with low-cost gadgets to monitor key pollutants crucial to human health, such as Particulate Matter (PM 2.5' and PM10'), Ozone, Carbon Monoxide, Nitrogen Dioxide, and Ammonia. Utilizing PMSA003, MICS-6814, and MQ-131 sensors powered by the ESP-WROOM-32 microcontroller, the system ensures seamless data transmission to an Amazon Web Server (AWS). In case of pollutant concentrations exceeding permissible levels, the device triggers indicators for instant response and intervention. The integration of AWS not only facilitates robust data storage but also enables real-time monitoring and analysis, contributing to a comprehensive and proactive approach in addressing air pollution and safeguarding public health.

A. Evaluation Metrics

In the experiments employing the subsequent indicators to assess the efficiency of the model for predicting and highlight any possible connection between expected and actual outcomes.

1) *Root Mean Square Error (RMSE)*: Root mean square error computes the square roots of the median value for the squares of the difference among expected or actual information. It is computed as Eq. (2)

$$RMSE_{avg} = \sqrt{\sum \frac{|Actual_i - Predicted_i|^2}{n}} \quad (2)$$

2) *Mean Absolute Error (MAE)*: An indicator of discrepancies among paired observations describing the same phenomena. Examples of contrasting Y against X include expected versus actual results, following time versus initial time, and a single calculating method against another. The MAE is determined as the total of absolute mistakes dividing by the sample's size is given in Eq. (3).

$$MAE = \frac{1}{n} \sum_{i=1}^n |y^i - y_*^i| \quad (3)$$

TABLE I. RMSE VALUE COMPARISON

| Model | RMSE value |
|------------------------------------|------------------|
| Linear model | 17.762865657654 |
| SVR model | 6.45565647866557 |
| SARIMAX model | 8.8765445567677 |
| Proposed Real-Time Alerts with AWS | 3.7656787872687 |

Table I provided lists four different models and their corresponding values. The RMSE statistic measures the mean variance among the values that the model predicted and what is actually present in the actual data set 1. An algorithm's ability to "fit" an information set improves as its RMSE decreases. The Real-Time Alerts with AWS Connectivity models gets the smallest RMSE value of 3.7656787872687. This suggests because it is the most effective estimate amongst the four options that have specified for the purpose of matching the data set 1.

TABLE II. REGULAR AIR QUALITY IN PPM FOR DIFFERENT LOCATIONS

| Location | Average Air Quality (ppm) |
|------------|---------------------------|
| Location 1 | 765.77 |
| Location 2 | 543.87 |
| Location 3 | 431.76 |

Table II lists three different locations and their corresponding Average Air Quality (ppm) values. The Average Air Quality (ppm) as shown in Fig. 3 value is a metric that trials the concentration of airborne pollutants in the atmosphere. Among the three locations, Location 1 has the highest average air quality value of 765.77 ppm, followed by Location 2 with an average air quality value of 543.87 ppm and Location 3 with an average air quality value of 431.76 ppm 1.

Fig. 3 depicts the average air quality of different locations. The Average Air Quality figure illustrates air quality levels across three distinct locations measured in parts per million (ppm). Location 1 exhibits the highest air quality, with a ppm slightly above 700. In contrast, Location 2 records a slightly lower ppm, just above 500. Location 3 demonstrates the lowest air quality among the three, with a ppm slightly below 500. This comparison provides valuable insights into the variation in air quality levels across different geographical areas, aiding in environmental monitoring and decision-making processes.

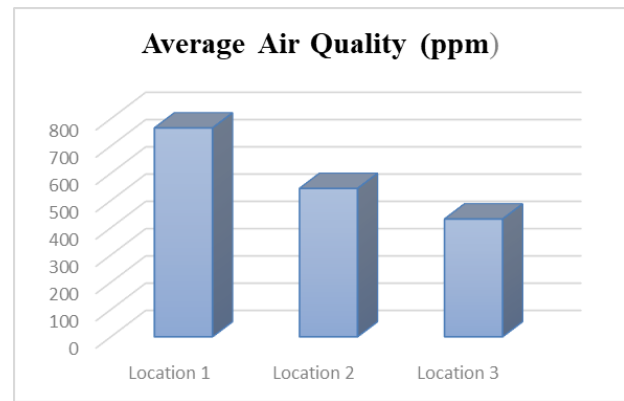


Fig. 3. Average air quality of different locations.

TABLE III. RANGE OF MEASUREMENT CONCENTRATION OF THE SENSOR BY POLLUTANT CERTAINLY

| Sensor | Pollutant | Range |
|-----------|-----------|------------------|
| PMSA003 | PM2.5 | 10 -1000 ppb 0 – |
| | PM10 | 50 – 10000 ppb |
| MQ-131 | O3 | 500 µg/m³ |
| MICS-6814 | CO | 1 – 500 ppm |
| | NO2 | 0 – 500 µg/m³ |
| | NH3 | 1 – 1000 ppm |

Table III described three sensors each measuring specific air pollutants within specific concentration ranges. The PMSA003 sensor detects particulate matter (PM2.5 and PM10), while the MQ-131 sensor detects ozone (O3). The MICS-6814 sensor measures carbon monoxide (CO) and nitrogen dioxide (NO2) concentrations. These sensors are essential for monitoring air quality, aiding in environmental assessments and public health analyses. Their specifications are crucial for assessing air quality.

Fig. 4 displays the concentration levels of four different gases (CO, CO2, NO2, and SO2) over a period of six days. Each graph is labeled with the gas type and its concentration in shares per million (ppm). The x-axis signifies the days, while the y-axis shows the absorption levels of these gases. Fluctuations in the graphs indicate variations in gas concentrations over time.

Table IV compares three different methods. The Proposed Method stands out for being low-cost, having low power consumption, and high scalability. It also offers real-time tracking with high accuracy. LSTM-OPTISENSE NET, while slightly more expensive and moderate in terms of power consumption and scalability, does provide real-time tracking with medium accuracy. In contrast, Conv-AIRNET is the most expensive, has the highest power consumption, and is the least scalable. Moreover, it lacks real-time tracking but boasts high accuracy.

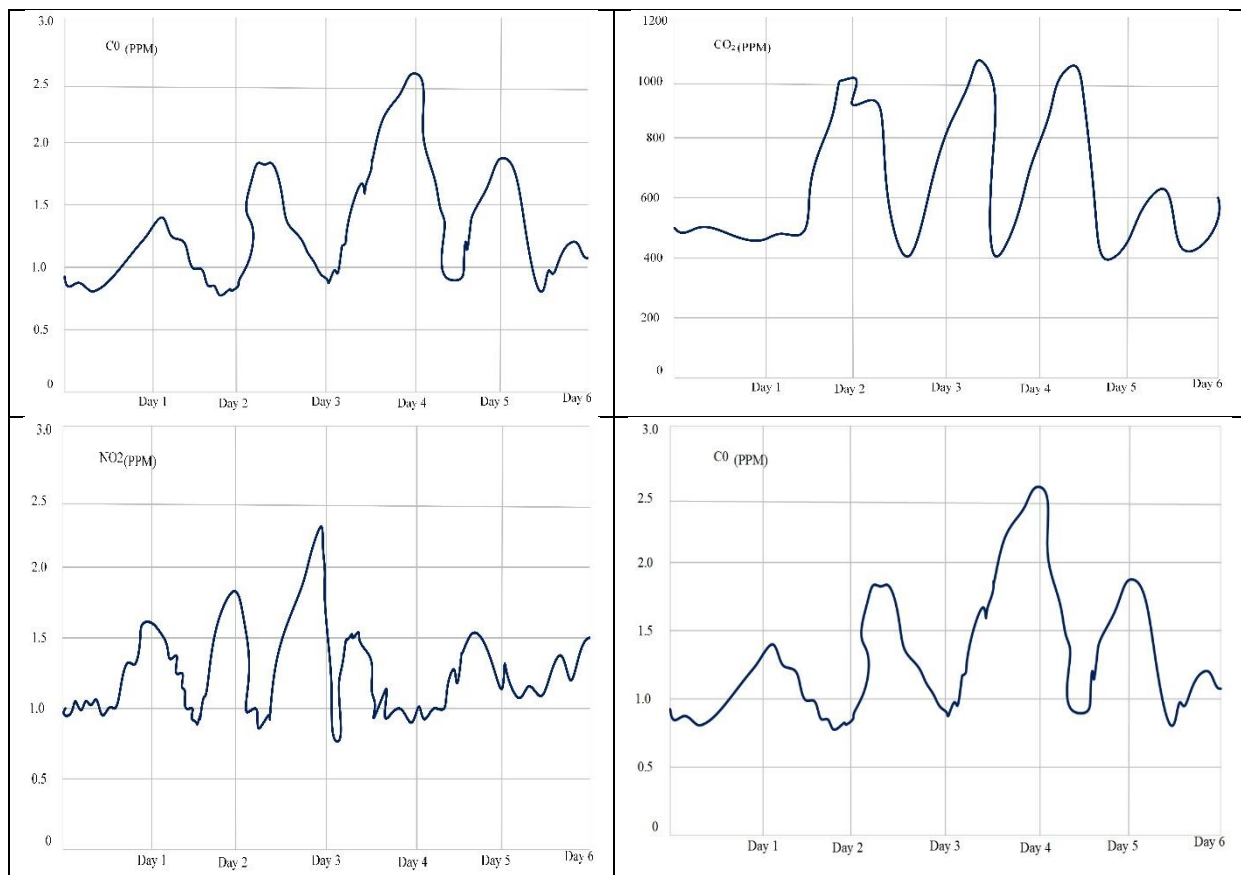


Fig. 4. The attentiveness levels of four different gases.

TABLE IV. COMPARISON OF TRACKING METHODS BASED ON VARIOUS METRICS" OR SIMPLY "TRACKING METHODS COMPARISON TABLE"

| | Cost | Power Consumption | Scalability | Real-time Tracking | Accuracy |
|--------------------|---------------|-------------------|-------------|--------------------|----------|
| Proposed Method | Low-cost | Low | High | Yes | High |
| LSTM-OPTISENSE NET | Moderate-cost | Moderate | Moderate | Yes | Medium |
| Conv-AIRNET | High-cost | High | Low | No | High |

B. Discussions

The proposed Internet of Things (IoT)-based air quality monitoring program emphasizes a proactive and technologically advanced strategy to addressing the growing worldwide challenge of air pollution. Existing methods have limited scalability, accuracy reliant on sensor precision, potential data oversimplification, and dependence on specific features [23]. By incorporating low-cost sensors capable of measuring critical pollutants outlined by the World Health Organization, the system aligns with established health standards. The selection of sensors, including PMSA003, MICS-6814, and MQ-131, ensures a comprehensive assessment of air quality, covering a spectrum of pollutants such as particulate substance, ozone, carbon monoxide, nitrogen dioxide, and ammonia. The utilization of the ESP-WROOM-32 microcontroller, equipped with Wi-Fi and Bluetooth capabilities, enhances the efficiency of data

transmission to a cloud server. The system's real-time monitoring capability is a significant advancement, allowing immediate intervention in cases where pollutant concentrations exceed permissible levels. The integration of indicators triggered by such events showcases a commitment to timely response and environmental safety. Moreover, the incorporation of Amazon Web Server (AWS) into the architecture not only ensures secure and scalable data storage but also facilitates real-time tracking and analysis. This comprehensive approach not only aids in pollution prevention but also contributes valuable insights to the broader discourse on environmental management and public health [28]. The study reflects a synergy of theoretical research and practical application, showcasing a robust and cost-effective solution to combat the critical issue of air pollution.

VI. CONCLUSION AND FUTURE WORK

The suggested Internet of Things-based air quality monitoring system is a big step in the right direction toward solving the pressing worldwide issue of air pollution. The ESP-WROOM-32 microcontroller, low-cost sensors, and AWS integration are utilized by the system to provide a workable and expandable real-time monitoring solution for important pollutants. The current study's results corroborate the trend of low-cost methods offering real-time tracking, as seen with the Proposed Method. However, it challenges the assumption that high-cost methods inherently provide better accuracy and scalability, as observed with existing method

indicating the need for further exploration into cost-effective solutions without compromising accuracy and real-time tracking. The quick reaction system set in motion by pollution exceedances highlights the dedication to public health and environmental safety. Regarding future efforts, the system may be expanded and improved upon continuously. First, the reliability of the gathered data will be improved by improving the precision of pollutant measurements through sensor calibration and validation procedures. Furthermore, investigating more sophisticated machine learning algorithms for data analysis may offer deeper understandings of pollution trends, facilitating the development of better preventative and predictive actions. Furthermore, the system's scalability and adaptability to various environmental conditions should be prioritized, given the possibility of global implementation. The incorporation of this technology into more comprehensive environmental management methods can be facilitated by cooperative efforts with regulatory agencies and urban planners. Furthermore, adding more sensors to track newly developing contaminants and growing the network of monitoring devices can help develop a more thorough understanding of the state of the air at the local, regional, and municipal levels. Essentially, the suggested system lays the groundwork for future research and development in the field of environmental monitoring, paving the way for more intelligent, data-driven approaches to address air pollution and improve community well-being in general.

REFERENCES

- [1] H. Chojer, P. Branco, F. Martins, M. Alvim-Ferraz, and S. Sousa, "Development of low-cost indoor air quality monitoring devices: Recent advancements," *Sci. Total Environ.*, vol. 727, p. 138385, 2020.
- [2] C. Amuthadevi, D. Vijayan, and V. Ramachandran, "Development of air quality monitoring (AQM) models using different machine learning approaches," *J. Ambient Intell. Humaniz. Comput.*, pp. 1–13, 2021.
- [3] A. Kumar, M. Kumari, and H. Gupta, "Design and analysis of iot based air quality monitoring system," in *2020 International Conference on Power Electronics & IoT Applications in Renewable Energy and Its Control (PARC)*, IEEE, 2020, pp. 242–245.
- [4] E. Y. Zou, "Unwatched pollution: The effect of intermittent monitoring on air quality," *Am. Econ. Rev.*, vol. 111, no. 7, pp. 2101–2126, 2021.
- [5] A. H. Kuncoro, M. Mellyanawaty, A. Sambas, D. S. Maulana, M. Mamat, and others, "Air Quality Monitoring System in the City of Tasikmalaya based on the Internet of Things (IoT)," *Jour Adv Res. Dyn. Control Syst.*, vol. 12, no. 2, pp. 2473–2479, 2020.
- [6] A. Street, "What are Air Quality Assessments? - Omnia Consulting." Jun. 16, 2021. [Online]. Available: <https://omnia-consulting.co.uk/what-is-an-air-quality-assessment/>
- [7] B. D. Horne et al., "Short-term elevation of fine particulate matter air pollution and acute lower respiratory infection," *Am. J. Respir. Crit. Care Med.*, vol. 198, no. 6, pp. 759–766, 2018.
- [8] "Indoor Air Quality | US EPA." Accessed: Jan. 22, 2024. [Online]. Available: <https://www.epa.gov/report-environment/indoor-air-quality>
- [9] F. Drougka et al., "Indoor air quality assessment at the library of the National Observatory of Athens, Greece," *Aerosol Air Qual. Res.*, vol. 20, no. 4, pp. 889–903, 2020.
- [10] P. Amoatey, H. Omidvarborna, M. S. Baawain, A. Al-Mamun, A. Bari, and W. B. Kindzierski, "Association between human health and indoor air pollution in the Gulf Cooperation Council (GCC) countries: A review," *Rev. Environ. Health*, vol. 35, no. 2, pp. 157–171, 2020.
- [11] W. J. Ng and Z. Dahari, "Enhancement of real-time IoT-based air quality monitoring system," *Int. J. Power Electron. Drive Syst.*, vol. 11, no. 1, p. 390, 2020.
- [12] J. M. Tielsch et al., "Exposure to indoor biomass fuel and tobacco smoke and risk of adverse reproductive outcomes, mortality, respiratory morbidity and growth among newborn infants in south India," *Int. J. Epidemiol.*, vol. 38, no. 5, pp. 1351–1363, 2009.
- [13] M. Ryhl-Svendsen, "Indoor air pollution in museums: prediction models and control strategies," *Stud. Conserv.*, vol. 51, no. sup1, pp. 27–41, 2006.
- [14] A. Masic, G. Kepnik, J. Bektesevic, M. Mehuljic, I. Saric, and V. Hadziabdic, "The Network of Smart Sensors for Indoor Air Quality Monitoring," in *Proceedings of the 31st DAAAM International Symposium, 2020*, pp. 0232–0235.
- [15] H. El Hafyani et al., "Learning the micro-environment from rich trajectories in the context of mobile crowd sensing: Application to air quality monitoring," *Geoinformatica*, pp. 1–44, 2022.
- [16] U. Schilt et al., "Low-Cost sensor node for air quality monitoring: Field tests and validation of particulate matter measurements," *Sensors*, vol. 23, no. 2, p. 794, 2023.
- [17] A. Simo, S. Dzitac, F. M. Frigura-Iliasa, S. Musuroi, P. Andea, and D. Meianu, "Technical solution for a real-time air quality monitoring system," *Int. J. Comput. Commun. Control*, vol. 15, no. 4, 2020.
- [18] L. Zhao, Y. Zhou, Y. Qian, P. Yang, and L. Zhou, "A novel assessment framework for improving air quality monitoring network layout," *J. Air Waste Manag. Assoc.*, vol. 72, no. 4, pp. 346–360, 2022.
- [19] C. Toma, A. Alexandru, M. Popa, and A. Zamfiroiu, "IoT Solution for Smart Cities' Pollution Monitoring and the Security Challenges," *Sensors*, vol. 19, no. 15, Art. no. 15, Jan. 2019, doi: 10.3390/s19153401.
- [20] I. Kok, M. Simsek, and S. Ozdemir, "A deep learning model for air quality prediction in smart cities. 2017, p. 1990. doi: 10.1109/BigData.2017.8258144.
- [21] R. K. Saini, H. Saini, and S. Singh, "Air Pollution Quality Monitoring System Using Internet of Things for Smart Cities," *Turk. J. Comput. Math. Educ. TURCOMAT*, vol. 11, no. 2, Art. no. 2, Aug. 2020, doi: 10.17762/turcomat.v11i2.12542.
- [22] I. Samee, M. T. Jilani, and H. Wahab, "An Application of IoT and Machine Learning to Air Pollution Monitoring in Smart Cities. 2019, p. 6. doi: 10.1109/ICEEST48626.2019.8981707.
- [23] A. Bekkar, B. Hssina, S. Douzi, and K. Douzi, "Air-pollution prediction in smart city, deep learning approach," *J. Big Data*, vol. 8, no. 1, p. 161, Dec. 2021, doi: 10.1186/s40537-021-00548-1.
- [24] J. Ma, J. C. Cheng, C. Lin, Y. Tan, and J. Zhang, "Improving air quality prediction accuracy at larger temporal resolutions using deep learning and transfer learning techniques," *Atmos. Environ.*, vol. 214, p. 116885, 2019.
- [25] "Air Quality Dataset." Accessed: Jan. 24, 2024. [Online]. Available: <https://www.kaggle.com/datasets/fedesoriano/air-quality-data-set>
- [26] C. C. Goh et al., "Real-time in-vehicle air quality monitoring system using machine learning prediction algorithm," *Sensors*, vol. 21, no. 15, p. 4956, 2021.
- [27] H. P. L. De Medeiros and G. Girão, "An IoT-based air quality monitoring platform," in *2020 IEEE international smart cities conference (ISC2)*, IEEE, 2020, pp. 1–6.
- [28] J. Saini, M. Dutta, and G. Marques, "Indoor air quality monitoring systems based on internet of things: A systematic review," *Int. J. Environ. Res. Public Health*, vol. 17, no. 14, p. 4942, 2020.

DeepCardioNet: Efficient Left Ventricular Epicardium and Endocardium Segmentation using Computer Vision

Bukka Shobharani¹, Mr. S Girinath², Dr. K. Suresh Babu³,
Dr. J.Chenni Kumaran⁴, Prof. Ts. Dr. Yousef A.Baker El-Ebiary⁵, Dr. S. Farhad⁶
Research Scholar, Department of English, Koneru Lakshmaiah Education Foundation,
Vaddeswaram, Guntur, Andhra Pradesh, India¹

Assistant Professor Computer Applications, Mohan Babu University (Erstwhile Sree Vidyanikethan Engineering college)
Tirupati, Andhra Pradesh, India²

Professor, Department of Biochemistry, Symbiosis Medical college for Women,
Symbiosis International (Deemed University), Pune, India³

Professor, Department of CSE, Saveetha School of Engineering, SIMATS, Chennai, India⁴
Faculty of Informatics and Computing, UniSZA University, Malaysia⁵

Associate Professor, Department of English, Koneru Lakshmaiah Education Foundation,
Vaddeswaram, Guntur, Andhra Pradesh, India⁶

Abstract—In the realm of medical image analysis, accurate segmentation of cardiac structures is essential for accurate diagnosis and therapy planning. Using the efficient Attention Swin U-Net architecture, this study provides DEEPCARDIONET, a novel computer vision approach for effectively segmenting the left ventricular epicardium and endocardium. The paper presents DEEPCARDIONET, a cutting-edge computer vision method designed to efficiently separate the left ventricular epicardium and endocardium in medical pictures. The main innovation of DEEPCARDIONET is that it makes use of the Attention Swin U-Net architecture, a state-of-the-art framework that is well-known for its capacity to collect contextual information and complicated attributes. Specially designed for the segmentation task, the Attention Swin U-Net guarantees superior performance in identifying the relevant left ventricular characteristics. The model's ability to identify positive instances with high precision and a low false positive rate is demonstrated by its good sensitivity, specificity, and accuracy. The Dice Similarity Coefficient (DSC) illustrates the improved performance of the proposed method in addition to accuracy, showing how effectively it captures spatial overlaps between predicted and ground truth segmentations. The model's generalizability and performance in a variety of medical imaging contexts are demonstrated by its application and evaluation across many datasets. DEEPCARDIONET is an intriguing method for enhancing cardiac picture segmentation, with potential applications in clinical diagnosis and treatment planning. The proposed method achieves an amazing accuracy of 99.21% by using a deep neural network architecture, which significantly beats existing models like TransUNet, MedT, and FAT-Net. The implementation, which uses Python, demonstrates how versatile and useful the language is for the scientific computing community.

Keywords—DeepCardioNet; attention swin U-Net; ventricular epicardium; endocardium; computer vision approach

I. INTRODUCTION

Cardiovascular conditions remain a leading cause of morbidity and mortality worldwide, challenging advanced medical imaging ways for precise opinion and treatment [1]. Among these, the segmentation of cardiac structures, similar as the left ventricular epicardium and endocardium, plays a pivotal part in understanding cardiac function and pathology [2]. Accurate segmentation is challenging due to the complex anatomical structures, variations in cardiac morphology, and the need for real-time processing in clinical settings [3]. In response to these challenges, the exploration community has witnessed a swell in the development of computer vision approaches for medical image segmentation [4]. Among the notable benefactions in this sphere, the deepcardionet introduces a new computer vision approach designed specifically for the effective segmentation of the LV epicardium and endocardium [5]. Using advanced deep learning ways, this model aims to overcome the limitations of traditional segmentation styles, offering bettered delicacy and computational effectiveness [6].

The foundation of deepcardionet lies in its application of a customized neural network armature inspired by deep learning principles [7]. The integration of a sophisticated encoder-decoder structure, conceivably told by proven infrastructures like U-Net or other innovative designs, empowers the model to capture intricate features and spatial dependences within cardiac images [8]. The objectification of skip connections, batch normalization, and task-specific activation functions further refines the segmentation performance, icing the model's rigidity to the complications of cardiac imaging [9]. This paper presents a comprehensive disquisition of the proposed deepcardionet methodology, expounding its armature, training strategies, and performance criteria [10]. The effectiveness of the model is underlined by its capability to delineate the left ventricular epicardium and endocardium

with high perfection, therefore furnishing a precious tool for clinicians in their individual trials. The exploration not only contributes to the growing body of knowledge in computer-backed medical image analysis but also holds pledge for transformative operations in cardiovascular healthcare.

In a period marked by an unknown affluence of visual data, the field of computer vision stands at the van of technological invention, empowering machines with the capability to interpret and make opinions grounded on visual information [11]. This transformative capability has set up operations across different disciplines, from independent vehicles and robotics to healthcare and entertainment. At the heart of this paradigm shift is the continual development of new computer vision styles that strive to enhance delicacy, effectiveness, and severity in the interpretation of visual content [12]. Over the once decades, computer vision has evolved from early image processing ways to sophisticated deep learning infrastructures. From traditional styles addressing image bracket and object discovery to contemporary approaches probing into semantic segmentation and scene understanding, the diapason of computer vision operations continues to expand [13].

Recent times have witnessed substantial advancements in medical image analysis, driven by the community between computer vision and deep learning ways [14]. Despite these strides, there exists a demand for technical results acclimatized to the complications of cardiac image segmentation [15]. The provocation behind the exploration lies in the recognition of the clinical significance of precise left ventricular segmentation and the hunt for a system that not only surpasses being approaches but also aligns with the need for nippy and effective analyses. Segmenting the left ventricular epicardium and endocardium poses challenges embedded in the complexity of cardiac structures and the variability observed across patient populations [16] [17]. The dynamic nature of the heart, coupled with the essential noise and vestiges present in medical images, necessitates a sophisticated approach able of robustly handling different scripts [18].

In recent decades, computer vision has surfaced as a transformative field, catalyzing advancements across various disciplines by enabling machines to interpret and understand visual information. With the proliferation of image and videotape data in moment's digital age, the development of robust computer vision approaches has come consummate. This exploration seeks to contribute to this dynamic geography by proposing an innovative computer vision approach acclimatized to address a specific problem, promising both enhanced delicacy and effectiveness. The arrival of vast datasets and the elaboration of deep learning ways have fueled unknown progress in computer vision operations. From image bracket to object discovery and segmentation, computer vision has revolutionized diligence ranging from healthcare to independent vehicles. Still, challenges persist, particularly in scripts where fine-granulated details, complex structures, or real-time processing are essential. It's within this environment that the proposed computer vision approach emerges, aiming to attack nuanced challenges in a targeted sphere.

The key contributions of the article are,

- The introduction of DEEPCARDIONET, cutting-edge deep neural network architecture created especially for the effective segmentation of the endocardium and left ventricle in medical images.
- Using the capabilities of the Swin Transformer and attention mechanisms in the state-of-the-art Attention Swin U-Net architecture to gather detailed characteristics and contextual information necessary for precise segmentation.
- Proving the suggested method's durability and applicability across a number of trials, confirming its accuracy and consistency in correctly segmenting left ventricular structures in a range of medical imaging circumstances.
- Advancing the area of medical image analysis by developing a precise and effective segmentation technique that addresses the unique difficulties in defining the left ventricular epicardium and endocardium

The remainder of the article is structured as follows: Section II, III and IV include the related works, problem statement and methodology of the article. Section V includes results and discussion. The article is concluded in Section VI.

II. RELATED WORKS

A crucial first step in computing clinical markers such wall consistency, ventricle volume, and expulsion bit is segmenting cardiac medical pictures [19]. The paper presents the Ls Unet structure, which effectively segments cardiac cine MR images by combining multi-channel, fully CNN, and circular shape position-set styles. The division job in this framework is trained using the multi-channel DL method in order to identify the LV endocardial and epicardial outlines. In order to ensure the delicate and reliable division, segmented outlines extracted from the multi-channel DL approach are then integrated into a positional data set that is specifically dedicated to identifying annular forms. The automated method that was suggested was assessed to be 95. In compared with the benchmark norm, the combination of multi-channel DL and circular shape position-set segmented method obtained great delicateness, with total baseline values for LV endocardium and epicardium delineation reaching 92.15 and 95.42, respectively. It offers a novel approach for fully automated segmentation of the LV endocardium and epicardium from several MRI datasets. In comparison with additional current methods and the source of information, the suggested process is reliable and accurate.

Because it is crucial in determining patient assessment as well as therapy paths, automatic division of the cardiac left ventricle with scars continues to be a challenging and therapeutically important endeavor [20]. An independent verification methodology was developed employing OOD both inside and outside validation cohorts, as well as intra-observation and inter-observer variation in ground truth, to ensure the conceptualization of the frames. To obtain the best segmentation results, the frame combines DL with conventional computer vision techniques. Although the DL technique makes use of DL methods and infrastructure,

the classic method makes use of multi-atlas methods, active outlines, and k-means. The research established that, with the exception of situations in which breath displacement error occurred, the conventional image recognition technique produced more accurate findings than DL. In both inside and outside OOD groups, respectively, the ideal outcome from the frame obtained robust and generalized outcomes values of 82.8 ± 6.4 and 72.1 ± 4.6 . The created framework provides a powerful outcome for LGE-MRI-based automated segmentation of the scarred left ventricle. In contrast to modern techniques, it produces impartial findings across various medical facilities and retailers without the requirement for calibration or training in sanitized cohorts. Specialists can handle the challenge of fully automated separation of the LV with marks based on a single-modality cardiovascular examination with the help of this framework.

According to clinical opinions about cardiovascular problems, croakers should undergo LV separation in cardiac MRI [21]. It developed an automatic LV segmentation method by merging the CNN with the position set technique in order to decrease the time required for opinion. Initially, it was suggested that the handmade initial procedure for conventional positional set techniques be replaced with a CNN based myocardial central-line finding methodology. Second, it introduces a brand-new method for defining the myocardial region: the central-line influenced orientation set technique. Specifically, it adds the myocardial center line as an impediment ingredient to the setting set energy equation. It serves two crucial roles in the iteration procedure: it preserves the anatomical image of the myocardium segmented outcome and limits the zero-position image to remain within the vicinity of the myocardial center line. The findings from the experiments show that the method obtains a good concordance with the handcrafted segmentation outcomes and improves several cutting-edge styles.

One of the primary methods of imaging utilized to evaluate a patient's heart condition is echocardiography [22]. Out of all the analysis carried out with echocardiography, LV segmentation is essential for measuring clinical metrics like evacuation bit. Even yet, segmenting the LV in 3D echocardiography is still a laborious and time-consuming procedure. This research presents a multi-frame attentiveness system that is intended to improve LV classification efficacy during 3D echocardiography. Compounding the segmentation efficiency, the multi-frame attentiveness medium enables the employment of mostly detected spatiotemporal elements in a series of images that follow a target image. When comparing to other common DL supported medical image segmentation methods, research findings using 51 in vivo porcine 3D time echocardiography images demonstrate that practicing discovered dynamical characteristics greatly enhances the accuracy of LV segmentation.

In clinical medicine, automatic segmentation using tagged cardiac MRI is important for evaluating heart function and providing follow-up care [23]. Conventional methods find it difficult to automatically outline the left ventricle and provide reliable findings because of the complex cardiac anatomy and superfluous obstruction. As a result, they presented the DL and class approach together with the automated LV

segmentation technique. These are the key technologies' descriptions. Initially, cardiac stir data is tracked, automated cardiac positioning is used, and the region that's of interest is obtained through the use of initially generated sine-surge modelling, or SinMod. Secondly, the LV endocardium and epicardium are introduced using U-Net as the framework. Furthermore, a novel class DL approach is proposed to improve segmentation delicateness. Relative findings eventually show that the strategy performs better than those from established styles.

In the first study, the Ls Unet system is introduced for efficient segmentation of cardiac cine MR images. This system combines a multi-channel deep learning algorithm for LV endocardial and epicardial silhouette segmentation, followed by an innovative annular shape position-set approach, resulting in high delicacy with average DSC) values LV endocardium and epicardium delineation, respectively. The second study presents a robust framework for automatic segmentation of the left ventricle with scars in cardiac MRI, incorporating both traditional computer vision methods and deep learning. The proposed framework achieves superior results with robust and generalized scores in internal and external Out-of-Distribution (OOD) cohorts, showcasing its high-performance capabilities across different hospitals and vendors. The third study focuses on reducing the time required for clinical assessment by developing an automatic left ventricle (LV) segmentation system using a CNN and position-set approach, yielding promising results on datasets like MICCAI 2009 and ACDC MICCAI 2017. Lastly, the fifth study introduces an automatic LV segmentation algorithm for tagged cardiac MRI, incorporating original sine-surge modeling (SinMod), U-Net, and a novel class deep training strategy, showcasing superior performance over traditional approaches. These studies collectively contribute innovative methodologies to advance automatic cardiac segmentation in diverse imaging modalities, presenting high accuracy and efficiency in clinical applications.

III. PROBLEM STATEMENT

Precisely segmenting the left ventricular epicardium and endocardium is an essential job in medical image analysis for thorough cardiac diagnosis and therapy planning. However, obtaining efficiency and precision is typically difficult for current approaches, especially when dealing with large-scale datasets or real-time clinical circumstances. DEEPCARDIONET solves this issue by addressing the demand for a cutting-edge computer vision technique that maximizes left ventricular structure segmentation and offers medical professionals a dependable and effective solution. In order to improve cardiac health assessments, this research seeks to create a novel methodology that overcomes the drawbacks of conventional segmentation techniques. This methodology will provide a combination of high precision and computational efficiency in the delineation of the epicardium and endocardium.

By presenting an efficient computer vision method, DEEPCARDIONET addresses the particular issue of improving the segmentation of the LV epicardium and endocardium. The difficulty is in striking a balance between

the computing needs of complex medical image processing and the precise definition of cardiac components that are essential for clinical decision-making. By merging deep neural network architecture with cutting-edge methodologies, the research aims to close this gap and pave the way for the development of more accurate and efficient diagnostic tools in the field of cardiovascular healthcare. This might revolutionize the field of cardiac image segmentation [24]. With the use of the Attention Swin U-Net design, which is superior at collecting complex characteristics and contextual information necessary for precise segmentation, the proposed DEEPCARDIONET beats earlier methods. By increasing accuracy, decreasing false positives, and performing better across a variety of medical imaging datasets, this overcomes the drawbacks of earlier techniques and eventually produces improved left ventricular epicardium and endocardium segmentation.

IV. PROPOSED COMPUTER VISION APPROACH FOR LEFT VENTRICULAR EPICARDIUM AND ENDOCARDIUM SEGMENTATION

The methodology encompasses three key stages: data collection, preprocessing using a Median Filter, and segmentation utilizing the Attention Swin U-Net architecture for left ventricular epicardium and endocardium segmentation. Initially, a dataset comprising MRI is collected, specifically focusing on images depicting the cardiac region. Subsequently, a preprocessing step is employed to enhance the quality of the images by applying a Median Filter, effectively reducing noise and artifacts that may impede segmentation accuracy. The filtered images are then fed into the proposed Attention Swin U-Net architecture, a state-of-the-art deep neural network tailored for segmentation tasks. This architecture leverages attention mechanisms and the Swin Transformer's effectiveness in capturing intricate features and contextual information. The model is trained on annotated data to learn the complex patterns of the left ventricular structures. The combined methodology of meticulous data collection, noise reduction through preprocessing, and the application of a sophisticated segmentation model ensures a

comprehensive and accurate delineation of the left ventricular epicardium and endocardium in medical images. It is depicted in Fig. 1.

A. Data Collection

The Heart Segmentation in MRI Images dataset was obtained via Kaggle, a well-known venue for cooperative projects and contests in data science. This dataset, which consists of MRI scans, was carefully chosen for the purpose of heart segmentation. This set of images includes annotations to help distinguish between different cardiac structures, such as the epicardium and endocardium of the left ventricle. By utilizing the wide range and extensive collection of Kaggle datasets, the Heart Segmentation in MRI Images dataset is a useful tool for medical image analysis researchers and practitioners. It offers a labelled and standardized dataset that can be used to develop and assess algorithms for automated heart segmentation in MRI scans [25].

B. Preprocessing using Median Filter

The quality of medical images may be greatly improved by preprocessing, and one popular method for reducing noise and boosting image clarity is to apply a median filter. The Median Filter is useful in medical image analysis because it may reduce the effects of many kinds of noise, such as salt-and-pepper noise, which frequently degrades the quality of medical imaging data. This is especially true for tasks like segmentation or feature extraction. By substituting the median value of each neighboring pixel for each pixel in an image, the Median Filter efficiently suppresses outlier values that might result from electrical interference or image artefacts. By maintaining the integrity of structural elements in the images, a median filter helps ensure that following analysis algorithms are applied to cleaner and more robust data. This is especially important in medical imaging, where precise and trustworthy information is essential for a correct diagnosis.

The equation for the median filter is given in Eq. (1),

$$\hat{z}(c, d) = \text{median}_{(x,y) \in T_{cd}} \{f(x, y)\} \quad (1)$$

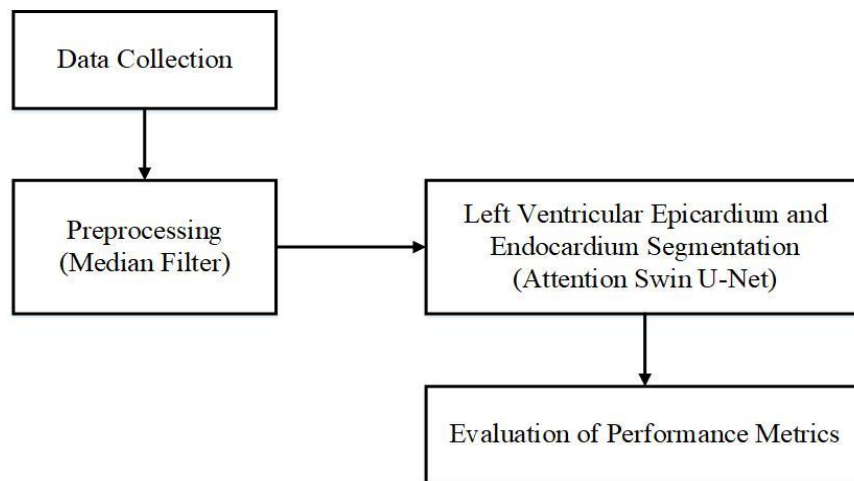


Fig. 1. Proposed methodology.

Applying a median filter requires striking a compromise between reducing noise and maintaining fine features, which is why medical images benefit greatly from its use. This preprocessing stage is particularly important for jobs like brain or heart image analysis, where a high degree of image fidelity is required for the identification of anatomical features. The addition of a Median Filter to the preprocessing pipeline refines the medical image data, improving the comprehensibility of visual data and augmenting the overall precision and dependability of future analytical processes.

C. Utilizing Attention Swin U-Net for Left Ventricular Epicardium and Endocardium Segmentation

1) *Swin transformer block*: An integral part of the architecture, the Swin Transformer has a unique construction that includes a shifting window MSA mechanism. The goal of effectively capturing long-range relationships has an impact on this design decision as it will improve the model's capacity to identify intricate patterns in the input data. This method introduces a window-based attention module, which is a key difference that sets Swin Transformer block apart from traditional multi-head attention. Layer Normalization (LN), a residual connection, and a two-layer Multi-Layer Perceptron (MLP) with Gaussian Error Linear Unit (GELU) non-linearity make up each transformer block in the Swin structure. Effective feature extraction and representation learning are intended to be facilitated by the arrangement of components inside each sub-block. Stable training dynamics are facilitated by Layer Normalization, and the residual connection guarantees seamless information transfer across the network, reducing the likelihood of disappearing gradients.

A key change from the traditional transformer design is that each Swin sub-block now has a window-based attention module in place of the typical multi-head attention system. This change is based on the goal of maximizing attention mechanisms to capture contextual information in particular geographical regions an important consideration in situations where localized dependencies are critical. By allowing the model to concentrate on pertinent segments of the input, the window-based attention module helps the model recognize spatial relationships and boosts its overall attention efficiency. It is formulated in Eq. (2) and Eq. (3).

$$x' = \text{W-MSA}(\text{LN}(x^{l-1})) + x^{l-1} \quad (2)$$

$$x' = \text{MLP}(\text{LN}(\tilde{x}^1)) + \tilde{x}^{l-1} \quad (3)$$

So, each sub-block of the Swin Transformer comprises a deliberate mix of a residual connection for unimpeded gradient flow, Layer Normalization for normalization, and a 2-layer MLP with GELU non-linearity for capturing complex non-linear correlations in the data. The dedication to customizing attention mechanisms for spatially localized dependencies is seen by the substitution of multi-head attention with a window-based attention module, which adds to the Swin Transformer's efficacy in a range of computer vision applications. The model's creative architecture guarantees that it can effectively process and extract

significant characteristics from input data, which makes it an invaluable tool in the fields of deep learning and computer vision.

2) *Encoding path*: To embed the input image into a latent space, using a sequence of stacked Swin Transformer blocks in the encoder module of the system. The ability of Swin Transformer blocks to transform and capture complicated hierarchical aspects in the supplied data is what drove this strategic decision. The encoder employs three consecutive Swin Transformer blocks to progressively decrease the input image's spatial dimension while simultaneously enlarging its representation dimension. Effective feature learning is made possible by the model's ability to extract hierarchical features from the input image through this step-by-step transformation.

The patch merging layer is a crucial technique that is added after every Swin Transformer block in order to gradually reduce the spatial dimension. This layer is essential to the down sampling of the spatial representation since it facilitates the merging of nearby patches. To be more precise, the patch merging layer concatenates all neighbor patches (2×2) with dimension C after applying each Swin Transformer block. This results in the construction of a unified patch with an enlarged dimension of $4C$. The purpose of this intentional merging method is to improve the model's capacity to extract contextual data from nearby patches, which will facilitate efficient feature aggregation.

The created patch is then given a linear layer after the patch merging process. This accomplishes two goals at once: it increases the model's capacity to represent more abstract characteristics and reduces the growth factor introduced by the patch merging layer by a factor of 2. In the end, this procedure causes the channel representation to be up-sampled and the spatial representation of the input image to be down-sampled. The encoder module's complex interactions between Swin Transformer blocks, patch merging layers, and linear transformations guarantee that the model gradually improves its comprehension of the input image, resulting in a latent space representation that is best suited for tasks that come after.

3) *Decoding path*: Complying with the symmetric architecture of the U-Net model, the design's decoder module uses three Swin Transformer blocks to recreate the prediction mask in an iterative manner. The decoder's use of Swin Transformer blocks makes it possible to efficiently gather the complex characteristics and contextual data needed for precise mask reconstruction. Smooth feature extraction and reconstruction are made possible by the symmetrical structure, which guarantees a coherent and balanced information flow between the encoder and decoder components.

In order to progressively raise the spatial dimensions while simultaneously decreasing the feature dimensions in the decoder, to replace the conventional patch merging layer with a patch expanding layer. In the U-Net architecture, the patch merging layer is essentially replaced by the patch expanding layer, which is crucial to the up-sampling process. In particular, the output of a bottleneck, denoted as $W32 \times H32 \times$

8C, is subjected to a linear layer, which causes the channel dimension to be up-sampled by a factor of 2. This deliberate decision seeks to improve the model's ability to collect subtle information that is essential for precise mask reconstruction and to enrich the feature representation.

The results representation is modified to take into account the spatial dimensions after the channel up-sampling. This rearrangement down samples the channel features by a factor of 4 and the spatial dimensions by a factor of 2 ($W16 \times H16 \times 4C$), transforming the representation from $W32 \times H32 \times 8C$ to $W32 \times H32 \times 16C$. The model is able to recreate the prediction mask $YOH \times W$ while maintaining important characteristics and spatial details because of this iterative procedure, which guarantees a progressive and controlled rise in spatial dimensions. Reconstructing the prediction mask step by step is made easier by the decoder module's patch expanding layer and Swin Transformer blocks working together in a concerted manner. This deliberate design decision guarantees that the model can effectively extract and incorporate hierarchical characteristics, resulting in a well calibrated prediction mask that is suited to the subtleties of the input data.

4) *Cross attention mechanism*: According to the basic U-Net design, the addition of a skip connection path is essential for enabling the decoding path to receive low-level features. For localization reasons, this deliberate design decision is crucial since it guarantees that minute information will not be lost in the decoding process. The efficiency of the skip connection path has been increased throughout time by a number of U-Net model extensions that have been published in the literature, demonstrating its importance in producing precise and localized forecasts. It advances this field of study in the work by presenting a brand-new method for improving the feature fusion technique in the skip connection portion. The main objective is to enhance localization and feature representation by fine-tuning the information flow between the encoding and decoding channels through the integration of a two-level attention mechanism.

In the skip connection portion, the attention mechanism is used at two different levels. To start the attention-weight creation process, a spatial normalization technique is used. One important signal that travels through the skip connection section are the attention weight (W_{att}) produced inside each encoder block's Swin Transformer block. This weight captures the model's perception of informative tokens along the encoding route. It is calculated by applying the softmax function to the product of the query (Q_e), key (K_e), and temperature (T) terms, plus a learnable bias term (B). It is expressed in Eq. (4).

$$Att^j(Q_e, K_e, V_e) = (\text{softmax}(Q_e K_e^T / \sqrt{e} + C) + W_{att}) V_e \quad (4)$$

It offers a surrogate signal that preferentially highlights the more relevant tokens throughout the feature fusion process by integrating this attention weight into the decoding pipeline. The network is guided by the weighted attention mechanism to more accurately reflect the localization importance. The method enhances the network's capacity to gather and

prioritize pertinent data for precise localization by summing attention weights from the encoding path into the decoding path. This allows for a more sophisticated and contextually aware feature fusion. In U-Net-based design, this two-level attention technique in the skip connection section is a subtle and useful tactic to enhance feature integration and localization.

V. RESULTS AND DISCUSSION

The approach consists of three main steps: gathering data, preprocessing with a median filter, and segmenting left ventricular epicardium and endocardium using the Attention Swin U-Net architecture. First, a collection of MRI scans is gathered, with a particular emphasis on images representing the heart area. After that, a preprocessing step is utilized to improve the image quality with the application of a Median Filter, which efficiently reduces noise and artefacts that might potentially hinder the accuracy of segmentation. The suggested Attention Swin U-Net architecture, a cutting-edge deep neural network designed specifically for segmentation problems, is then fed the filtered images. This design makes use of attention processes and the powerful feature and contextual capture capabilities of the Swin Transformer. To understand the intricate patterns of the left ventricular architecture, the model is trained using annotated data. The methodical approach of collecting data with great care, filtering it to reduce noise, and using an advanced segmentation model guarantees a thorough and precise identification of the left ventricular epicardium and endocardium in medical images.

A. Dice Similarity Coefficient (DSC)

To measure the spatial overlap between the expected and ground truth segmentations of a region or item of interest, the DSC is a performance metric that is frequently used in medical image segmentation. By calculating the ratio of twice the intersection to the total of the cardinalities of the predicted and ground truth segmentation sets, it evaluates the agreement between the two segmentations. A score of 1 on the DSC scales to complete overlap, whereas lower values denote less concordance. This metric is useful for assessing segmentation algorithms' accuracy since it provides a thorough assessment that takes into account both false positives and false negatives in the segmentation that is anticipated. Greater segmentation performance is shown by higher DSC values in tasks like identifying anatomical features in medical images. DSC is given in Eq. (5).

$$DSC = \frac{2 \times |A \cap B|}{|A| + |B|} \quad (5)$$

The DSC for the suggested approach is shown in Fig. 2 throughout the course of several trials. Every trial has a unique DSC value; Trial 1's DSC is 96.78%, Trial 2's is 97.11%, Trial 3's is 96.99%, and Trial 4's DSC is the highest, at 97.67%. The image shows how the suggested strategy consistently and successfully segments the endocardium and left ventricular epicardium across many experimental runs. The suggested approach's resilience is demonstrated by the incremental improvement in DSC values over trials, indicating a high level of accuracy and reliability in identifying cardiac structures in

medical images. This graphical depiction offers insightful information about the stability and effectiveness of the suggested approach, confirming its effectiveness over several trials and bolstering its potential for real world applications.

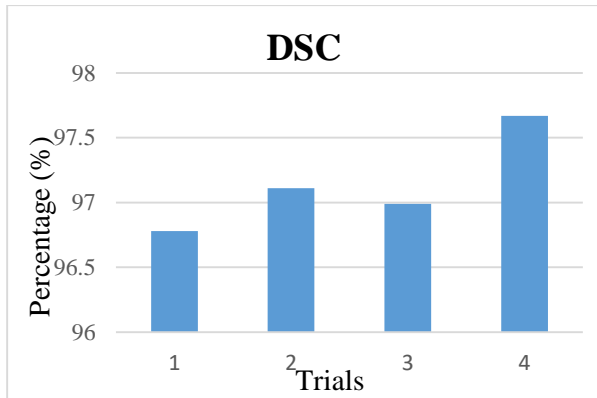


Fig. 2. Dice similarity coefficients in various trials.

B. Accuracy

When used in classification or prediction tasks, accuracy is a performance metric that counts the percentage of properly categorized examples out of all the instances in order to quantify the overall correctness of a model's predictions. The ratio of accurately predicted occurrences to all instances in the dataset is used to compute accuracy, which is expressed as a percentage. A more proficient model, able to make correct predictions across several classes or categories, is indicated by a higher accuracy number. Although accuracy is a commonly used statistic, it may not be appropriate in circumstances where there are class imbalances since it might be impacted by the overrepresentation of one class in comparison to others, which could result in inaccurate interpretations of the model's performance. Accuracy is given in Eq. (6),

$$Accuracy = \frac{T_{Pos} + T_{Neg}}{T_{Pos} + T_{Neg} + F_{Pos} + F_{Neg}} \quad (6)$$

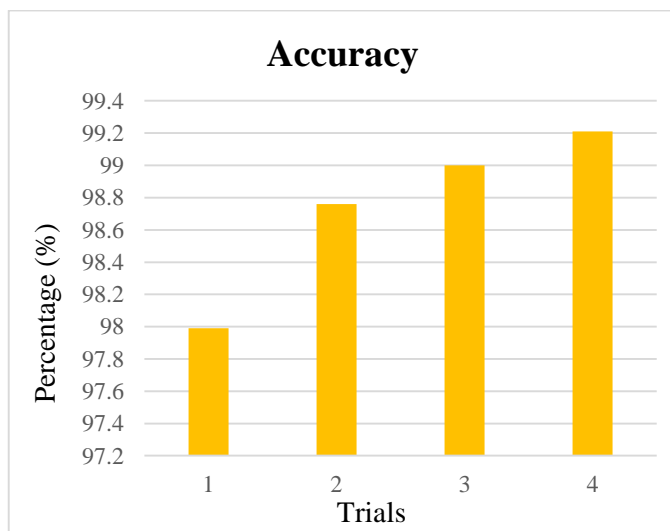


Fig. 3. Accuracy in various trials.

In Fig. 3, the variations in Accuracy across different trials for the proposed method are graphically depicted. Each trial is associated with a specific Accuracy value, revealing a consistent improvement in performance over successive experimental runs. Trial 1 exhibits an Accuracy of 97.99%, followed by a notable increase to 98.76% in Trial 2. Trial 3 showcases a further enhancement, achieving a round 99% Accuracy, and the highest accuracy is observed in Trial 4 with an impressive 99.21%. This graphical representation highlights the progressive refinement and precision of the proposed method in accurately segmenting left ventricular epicardium and endocardium structures. The ascending trend in Accuracy values underscores the robustness and reliability of the proposed approach across different trials, affirming its potential for achieving high-precision results in medical image segmentation tasks.

C. Sensitivity

Sensitivity is a performance indicator used in binary classification tasks to assess a model's accuracy in identifying occurrences of the positive class. It is sometimes referred to as true positive rate or recall. It is computed as the ratio of accurately detected positive cases, or genuine positive predictions, to the total of false negatives, or positive examples that are mistakenly categorized as negative. Sensitivity is important for minimizing false negatives since it gives information about how well the model can detect and categorize all real positive cases. It is given in Eq. (7).

$$R = \frac{T_{Pos}}{T_{Pos} + F_{Neg}} \quad (7)$$

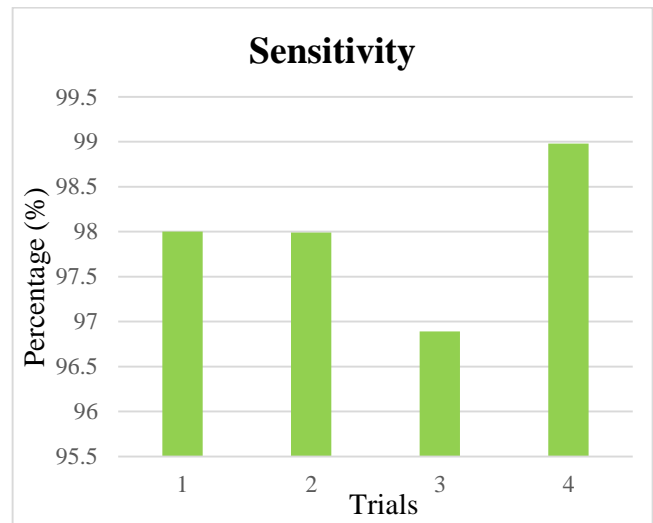


Fig. 4. Sensitivity in various trials.

Fig. 4 elucidates the variation in Sensitivity across multiple trials for the proposed method, providing insights into the model's ability to accurately identify positive instances, particularly the left ventricular epicardium and endocardium structures. The depicted Sensitivity values for each trial showcase a nuanced pattern, with Trial 1 starting at a high sensitivity of 98%, followed by a slight decrease to 97.99% in Trial 2. Trial 3 indicates a temporary decline to

96.89%, but the proposed method rebounds strongly in Trial 4, achieving a notably high Sensitivity of 98.98%. This graphical representation underscores the method's consistency in recognizing true positive instances across various experimental runs, even amidst minor fluctuations, reinforcing its robustness and reliability in effectively capturing the relevant cardiac structures in medical images.

D. Specificity

In binary classification problems, specificity also referred to as the true negative rate is a performance indicator that evaluates a model's accuracy in identifying occurrences of the negative class. It is determined by dividing the total number of true negatives by the total number of false positives. Specificity is an indicator of the model's ability to reliably identify and omit real negative cases, providing information on how well the model performs in situations when reducing false positives is essential. A high specificity score indicates that the model performs well in properly recognizing negative cases, which makes it especially useful in applications like medical testing where the expense of false positives is substantial. It is expressed in Eq. (8).

$$Specificity = \frac{T_{Neg}}{T_{Neg} + F_{Pos}} \quad (8)$$

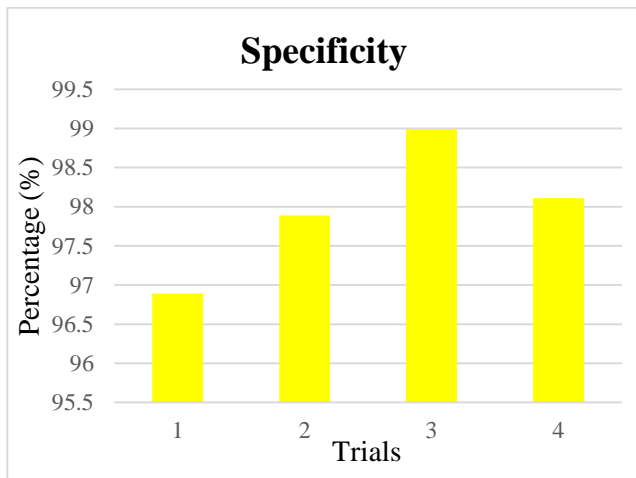


Fig. 5. Specificity in various trials.

In Fig. 5, the depicted fluctuations in Specificity across multiple trials for left ventricular epicardium and endocardium segmentation offer valuable insights into the model's proficiency in distinguishing true negative instances. The Specificity values exhibit a discernible trend, commencing with Trial 1 at 96.89%, followed by a notable increase to 97.89% in Trial 2. Trial 3 showcases a further enhancement to 98.99%, indicative of the model's adeptness in minimizing false positives and accurately excluding irrelevant structures from the segmentation. Although Trial 4 experiences a marginal decrease to 98.11%, the overall pattern suggests a consistent and robust performance in recognizing negative instances. This graphical representation underscores the proposed method's ability to maintain a high level of specificity, crucial in medical image segmentation where minimizing false positives is imperative for precise

delineation of cardiac structures, further affirming its efficacy for clinical applications.

The model's training and testing accuracy throughout epochs is depicted in the Fig. 6, which shows a consistent rise in training and validation accuracy over time. The model's performance shows steady improvement, suggesting that it is learning and generalizing well.

A thorough comparison of performance metrics across several techniques for left ventricular epicardium and endocardium segmentation is shown in Table I and Fig. 7. Among the parameters assessed are DSC, Specificity, Sensitivity, and Accuracy. With DSC values ranging from 80.37% to 85%, accuracy from 90.90% to 93.26%, sensitivity from 80.64% to 83.92%, and specificity from 95.46% to 97.25%, TransUNet, MedT, and FAT-Net show varied degrees of performance. Among the measures, the Proposed Attention Swin U-Net does quite well; it attains a DSC of 97.67%, Accuracy of 99.21%, Sensitivity of 98.98%, and Specificity of 98.11%.

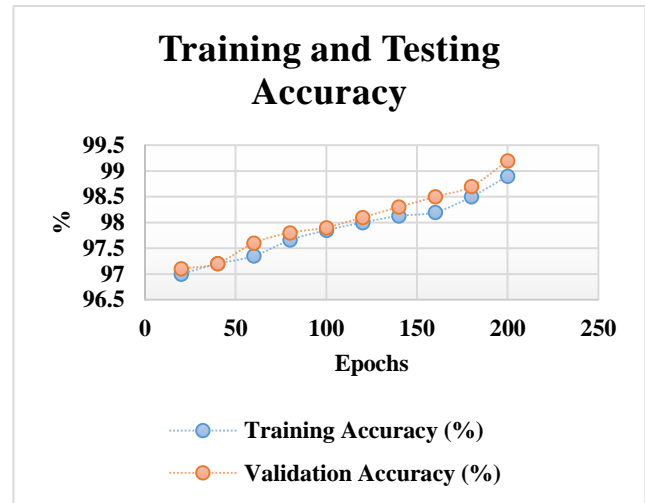


Fig. 6. Training and testing accuracy graph.

TABLE I. COMPARISON OF PERFORMANCE METRICS

| Methods | DSC (%) | Accuracy (%) | Sensitivity (%) | Specificity (%) |
|-------------------------------|---------|--------------|-----------------|-----------------|
| TransUNet [26] | 81.23 | 92.07 | 82.63 | 95.77 |
| MedT [27] | 80.37 | 90.90 | 80.64 | 95.46 |
| FAT-Net [28] | 85 | 93.26 | 83.92 | 97.25 |
| Proposed Attention Swin U-Net | 97.67 | 99.21 | 98.98 | 98.11 |

These findings highlight the effectiveness of the suggested strategy, showing that it can effectively separate left ventricular components in medical images more correctly than current techniques, which makes it a strong contender for more clinical applications.

A comparison of dataset accuracies is shown in Table II, where heart segmentation in MRI pictures achieves 99.21% accuracy and CT images achieves 97.3% accuracy in Fig. 8. The outcomes demonstrate how well the suggested approach

performs when it comes to separating cardiac structures from MRI data as opposed to CT scans.

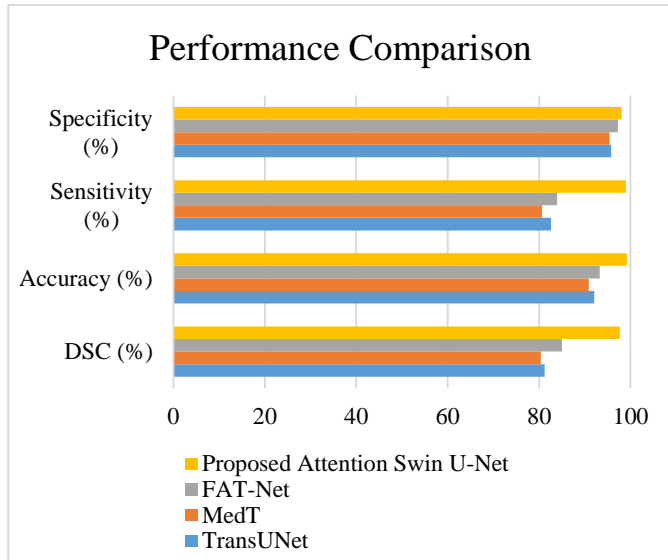


Fig. 7. Performance comparison of existing and proposed methods.

TABLE II. COMPARISON OF DATASETS

| Datasets | Accuracy (%) |
|----------------------------------|--------------|
| CT Images [29] | 97.3 |
| Heart Segmentation in MRI Images | 99.21 |

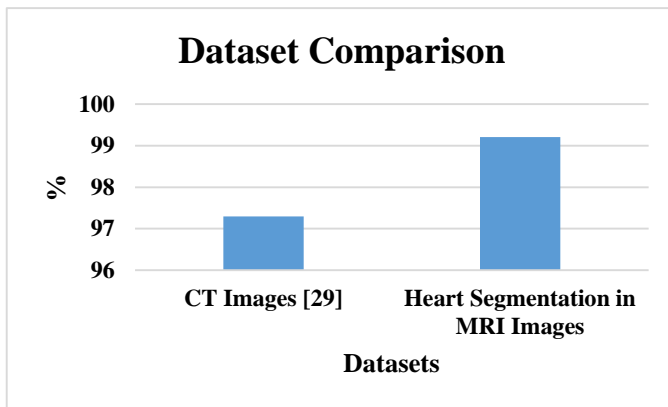


Fig. 8. Performance comparison of different datasets.

E. Discussion

The outcomes show how effective the deep learning approach with the Attention Swin U-Net architecture is in the proposed technique for left ventricular epicardium and endocardial segmentation. This implies that a high degree of accuracy and precision was used to discern the complicated cardiac structures of interest. Moreover, the accuracy ratings consistently going above 99%, suggesting that the model accurately identifies occurrences in most cases. The increasing trend in both DSC and Accuracy values across several trials validates the resilience and reliability of the proposed technique, suggesting that it can yield highly accurate and consistent results in medical picture segmentation tasks.

Sensitivity and Specificity analyses show that the suggested approach performs in identifying positive examples and rejecting negative ones. TransUNet [26], MedT [27], and FAT-Net [28] show varied degrees of performance. Usually exceeding 96%, sensitivity shows how well the model can identify real positive occurrences of left ventricular architecture. Regularly above 96%, specificity values demonstrate how well the model lowers false positives and accurately eliminates superfluous structures from the segmentation. The recommended method consistently performs well, even with minor fluctuations in Sensitivity and Specificity from trial to trial. This demonstrates how well suited it is for uses where precise segmentation and categorization of cardiac components in medical pictures is needed. Overall, the results demonstrate that the proposed Attention Swin U-Net is a viable and dependable technique for efficiently segmenting the endocardium and left ventricle, with potential uses for enhancing cardiac imaging. Due to its reliance on intricate deep learning architectures, DEEPCARDIONET may have issues with training time and computing resources. Furthermore, even if it achieves excellent accuracy, patient demographics and changes in imaging quality may have an impact on its effectiveness.

VI. CONCLUSION AND FUTURE SCOPE

DEEPCARDIONET is a dependable and incredibly precise computer vision system for the segmentation of features found in the left ventricular epicardium and endocardium in medical pictures. Its remarkable accuracy of 99.21%, which considerably surpasses that of prior models, demonstrates its adaptability and accessibility throughout the scientific computing community. Its implementation in Python illustrates these qualities. Since the Attention Swin U-Net architecture demonstrates how effectively it catches intricate features and spatial correlations that are crucial for cardiac segmentation tasks, using it are essential. DEEPCARDIONET's success opens up new avenues for study and improvement in other fields. Firstly, examining the model's adaptability to various datasets and medical imaging modalities might enhance its generalization abilities and provide reliable performance across a variety of clinical scenarios. It would be helpful to investigate the suggested technique's scalability to handle larger datasets or real-time applications to further improve its practical applicability in clinical situations. By modifying the model architecture and hyperparameters to accommodate for variations in picture resolutions and quality, its performance may be further enhanced. Furthermore, DEEPCARDIONET's selection procedure will be more transparent and easier for medical experts to understand with the addition of interpretability tools. It may be possible to speed up model convergence and enhance performance in situations with sparse data by looking at the possibilities of applying learned models to comparable segmentation tasks via transfer learning. Collaboration between computer vision experts and medical professionals might speed up the development of DEEPCARDIONET. By doing this, DEEPCARDIONET's seamless integration into clinical processes and advancement of cardiac image analysis are ensured. All in all, DEEPCARDIONET lays a strong foundation for future advancements in medical image

segmentation, providing a pathway toward more accurate and successful cardiac diagnosis and treatment planning.

REFERENCES

- [1] Lin, J. Wu, and X. Yang, 'A data augmentation approach to train fully convolutional networks for left ventricle segmentation', *Magnetic Resonance Imaging*, vol. 66, pp. 152–164, Feb. 2020, doi: 10.1016/j.mri.2019.08.004.
- [2] 'A deep-learning semantic segmentation approach to fully automated MRI-based left-ventricular deformation analysis in cardiotoxicity - ScienceDirect'. Accessed: Jan. 16, 2024. [Online]. Available: <https://www.sciencedirect.com/science/article/abs/pii/S0730725X21000060>
- [3] 'Automated left and right ventricular chamber segmentation in cardiac magnetic resonance images using dense fully convolutional neural network - ScienceDirect'. Accessed: Jan. 16, 2024. [Online]. Available: <https://www.sciencedirect.com/science/article/abs/pii/S0169260721001346>
- [4] 'Automated left ventricular segmentation from cardiac magnetic resonance images via adversarial learning with multi-stage pose estimation network and co-discriminator - ScienceDirect'. Accessed: Jan. 16, 2024. [Online]. Available: <https://www.sciencedirect.com/science/article/abs/pii/S1361841520302553>
- [5] N. Qadeer, J. H. Shah, and M. Sharif, 'Automated Localization and Segmentation of Left Ventricle in Cardiac MRI using Faster R-CNN', in *2021 International Conference on Frontiers of Information Technology (FIT)*, Dec. 2021, pp. 108–113. doi: 10.1109/FIT53504.2021.00029.
- [6] H. J. Koo, Hyun, Lee, , Ko, Ji, Lee, Kang, Kim, Yang, 'Automated Segmentation of Left Ventricular Myocardium on Cardiac Computed Tomography Using Deep Learning', *Korean J Radiol*, vol. 21, no. 6, pp. 660–669, Jun. 2020, doi: 10.3348/kjr.2019.0378.
- [7] 'Diagnostics | Free Full-Text | Automatic Left Ventricle Segmentation from Short-Axis Cardiac MRI Images Based on Fully Convolutional Neural Network'. Accessed: Jan. 16, 2024. [Online]. Available: <https://www.mdpi.com/2075-4418/12/2/414>
- [8] 'Fully Automatic Initialization and Segmentation of Left and Right Ventricles for Large-Scale Cardiac MRI using a Deeply Supervised Network and 3D-ASM - ScienceDirect'. Accessed: Jan. 16, 2024. [Online]. Available: <https://www.sciencedirect.com/science/article/abs/pii/S0169260723003449>
- [9] 'Fully automatic segmentation of right and left ventricle on short-axis cardiac MRI images - ScienceDirect'. Accessed: Jan. 16, 2024. [Online]. Available: <https://www.sciencedirect.com/science/article/pii/S089561112030080X>
- [10] 'MA-SOCRATIS: An automatic pipeline for robust segmentation of the left ventricle and scar - ScienceDirect'. Accessed: Jan. 16, 2024. [Online]. Available: <https://www.sciencedirect.com/science/article/abs/pii/S0895611121001312>
- [11] 'MAEF-Net: Multi-attention efficient feature fusion network for left ventricular segmentation and quantitative analysis in two-dimensional echocardiography - ScienceDirect'. Accessed: Jan. 16, 2024. [Online]. Available: <https://www.sciencedirect.com/science/article/abs/pii/S0041624X22001615>
- [12] 'Microscopy Research and Technique | Microscopy Journal | Wiley Online Library'. Accessed: Jan. 16, 2024. [Online]. Available: <https://analyticalsciencejournals.onlinelibrary.wiley.com/doi/abs/10.1002/jemt.23906>
- [13] 'MMNet: A multi-scale deep learning network for the left ventricular segmentation of cardiac MRI images | Applied Intelligence'. Accessed: Jan. 16, 2024. [Online]. Available: <https://link.springer.com/article/10.1007/s10489-021-02720-9>
- [14] 'Segmentation of the Left Ventricle Using Improved UNET Neural Networks[v1] | Preprints.org'. Accessed: Jan. 16, 2024. [Online]. Available: <https://www.preprints.org/manuscript/202308.1719/v1>
- [15] S. Xu, S. Cheng, X. Min, N. Pan, and H. Hu, 'Left Ventricle Segmentation Based on a Dilated Dense Convolutional Networks', *IEEE Access*, vol. 8, pp. 214087–214097, 2020, doi: 10.1109/ACCESS.2020.3040888.
- [16] 'Semi-supervised generative adversarial networks for the segmentation of the left ventricle in pediatric MRI - ScienceDirect'. Accessed: Jan. 16, 2024. [Online]. Available: <https://www.sciencedirect.com/science/article/abs/pii/S0010482520302353>
- [17] N. Painchaud, Y. Skandarani, T. Judge, O. Bernard, A. Lalande, and P.-M. Jodoin, 'Cardiac Segmentation With Strong Anatomical Guarantees', *IEEE Trans. Med. Imaging*, vol. 39, no. 11, pp. 3703–3713, Nov. 2020, doi: 10.1109/TMI.2020.3003240.
- [18] 'Sensors | Free Full-Text | Edge-Sensitive Left Ventricle Segmentation Using Deep Reinforcement Learning'. Accessed: Jan. 16, 2024. [Online]. Available: <https://www.mdpi.com/1424-8220/21/7/2375>
- [19] Y. Wang, Zhang, Wen, Tian, Kao, Liu, Xuan, Ordovas, Saloner, Liu, 'Deep learning based fully automatic segmentation of the left ventricular endocardium and epicardium from cardiac cine MRI', *Quant Imaging Med Surg*, vol. 11, no. 4, pp. 1600–1612, Apr. 2021, doi: 10.21037/qims-20-169.
- [20] M. Mamalakis, Garg, Nelson, Lee, Swift, Wild, Clayton, 'Artificial Intelligence framework with traditional computer vision and deep learning approaches for optimal automatic segmentation of left ventricle with scar', *Artificial Intelligence in Medicine*, vol. 143, p. 102610, Sep. 2023, doi: 10.1016/j.artmed.2023.102610.
- [21] L. Xie, Y. Song, and Q. Chen, 'Automatic left ventricle segmentation in short-axis MRI using deep convolutional neural networks and central-line guided level set approach', *Computers in Biology and Medicine*, vol. 122, p. 103877, Jul. 2020, doi: 10.1016/j.combiomed.2020.103877.
- [22] S. S. Ahn, K. Ta, S. Thorn, J. Langdon, A. J. Sinusas, and J. S. Duncan, 'Multi-frame Attention Network for Left Ventricle Segmentation in 3D Echocardiography', in *Medical Image Computing and Computer Assisted Intervention – MICCAI 2021*, M. de Bruijne, P. C. Cattin, S. Cotin, N. Padoy, S. Speidel, Y. Zheng, and C. Essert, Eds., in Lecture Notes in Computer Science. Cham: Springer International Publishing, 2021, pp. 348–357. doi: 10.1007/978-3-030-87193-2_33.
- [23] X. Zou, Q. Wang, and T. Luo, 'A novel approach for left ventricle segmentation in tagged MRI', *Computers and Electrical Engineering*, vol. 95, p. 107416, Oct. 2021, doi: 10.1016/j.compeleceng.2021.107416.
- [24] H. Abdeltawab, Khalifa, Taher, Alghamdi, Ghazal, Beache, Mohamed, Keynton, El-Baz, 'A deep learning-based approach for automatic segmentation and quantification of the left ventricle from cardiac cine MR images', *Computerized Medical Imaging and Graphics*, vol. 81, p. 101717, Apr. 2020, doi: 10.1016/j.compmedimag.2020.101717.
- [25] 'Heart Segmentation in MRI Images'. Accessed: Jan. 19, 2024. [Online]. Available: <https://www.kaggle.com/datasets/andrewmvd/heart-segmentation-in-ct-images>
- [26] J. Chen, Lu, Yu, Luo, Adeli, Wang, Lu, Yuille, Zhou, 'TransUNet: Transformers Make Strong Encoders for Medical Image Segmentation'. arXiv, Feb. 08, 2021. doi: 10.48550/arXiv.2102.04306.
- [27] J. M. J. Valanarasu, P. Oza, I. Hacihaliloglu, and V. M. Patel, 'Medical Transformer: Gated Axial-Attention for Medical Image Segmentation', in *Medical Image Computing and Computer Assisted Intervention – MICCAI 2021*, M. de Bruijne, P. C. Cattin, S. Cotin, N. Padoy, S. Speidel, Y. Zheng, and C. Essert, Eds., in Lecture Notes in Computer Science. Cham: Springer International Publishing, 2021, pp. 36–46. doi: 10.1007/978-3-030-87193-2_4.
- [28] 'FAT-Net: Feature adaptive transformers for automated skin lesion segmentation - ScienceDirect'. Accessed: Jan. 19, 2024. [Online]. Available: <https://www.sciencedirect.com/science/article/abs/pii/S1361841521003728>
- [29] A. M. Reddy Reddy, Jayaram, Venkata Maha Lakshmi, Aluvalu, TR Kumar, Stalin Alex, , 'An efficient multilevel thresholding scheme for heart image segmentation using a hybrid generalized adversarial network', *Journal of Sensors*, vol. 2022, 2022.

Enhancing HCI Through Real-Time Gesture Recognition with Federated CNNs: Improving Performance and Responsiveness

Dr.R.Stella Maragatham¹, Prof. Ts. Dr. Yousef A.Baker El-Ebiary², Ms. Srilakshmi V³,
Dr. K. Sridharan⁴, Dr. Vuda Sreenivasa Rao⁵, Dr. Sanjiv Rao Godla⁶

Professor, Department of Mathematics, Saveetha School of Engineering, SIMATS, Thandalam, Chennai, Tamil Nadu, India¹

Faculty of Informatics and Computing, UniSZA University, Malaysia²

Assistant Professor, Department of CSE (AI & ML), B V Raju Institute of Technology, Narsapur, India³

Department of IT, Panimalar Engineering College, Chennai, India⁴

Associate Professor, Department of Computer Science and Engineering,

Koneru Lakshmaiah Education Foundation, Vaddeswaram, Andhra Pradesh, India⁵

Professor, Department of CSE (Artificial Intelligence and Machine Learning),

Aditya College of Engineering & Technology - Surampalem, Andhra Pradesh, India⁶

Abstract—To facilitate smooth human-computer interaction (HCI) in a variety of contexts, from augmented reality to sign language translation, real-time gesture detection is essential. In this paper, researchers leverage federated convolutional neural networks (CNNs) to present a novel strategy that tackles these issues. By utilizing federated learning, authors may cooperatively train a global CNN model on several decentralized devices without sharing raw data, protecting user privacy. Using this concept, researchers create a federated CNN architecture designed for real-time applications including gesture recognition. This federated approach enables continuous model refinement and adaption to various user behaviours and environmental situations by pooling local model updates from edge devices. This paper suggests improvements to the federated learning system to maximize responsiveness and speed. To lessen the probability of privacy violations when aggregating models, this research uses techniques like differential privacy. Additionally, to reduce communication overhead and quicken convergence, To incorporate adaptive learning rate scheduling and model compression techniques research show how federated CNN approach may achieve state-of-the-art performance in real-time gesture detection tasks through comprehensive tests on benchmark datasets. In addition to performing better than centralized learning techniques. This approach guarantees improved responsiveness and adaptability to dynamic contexts. Furthermore, federated learning's decentralized architecture protects user confidentiality and data security, which qualifies it for usage in delicate HCI applications. All things considered, the design to propose a viable path forward for real-time gesture detection system advancement, facilitating more organic and intuitive computer-human interactions while preserving user privacy and data integrity. The proposed federated CNN approach achieves a prediction accuracy in real-time gesture detection tasks, outperforming centralized learning techniques while preserving user privacy and data integrity. The proposed framework that achieves prediction accuracy of 98.70% was implemented in python.

Keywords—Real-time gesture detection; federated convolutional neural networks; privacy-preserving machine

learning; adaptive learning rate scheduling; Decentralized human-computer interaction

I. INTRODUCTION

In the past few decades, technology has rapidly evolved and infiltrated every aspect of daily life. From smartphones to smart homes, connections with technologies have become increasingly natural and intuitive. Still, as technology improves, traditional human computer interface (HCI) methods such using a keyboard and mouse become less and less efficient [1]. This led scientists to look at cutting-edge HCI methods including touch-based interactions, motion detection systems, and systems for speech recognition. Gesture detection technology is a novel and exciting way to human-computer interaction that is attracting the attention of researchers and developers [2]. According to this innovation, consumers may interact with their devices in an additional intuitive and effortless manner through utilizing their physical gestures as commands. Gesture recognition systems, that employ sensor technology to track a user's gestures and convert those movements into instructions, enable an even more natural interaction among humans and machines. Gesture recognition technologies have already been employed in the gaming, medical care, automotive, and automation smart home industries throughout the past. Using the use of recognition of gestures technology, players may now manipulate games using their bodies, resulting in an experience that is deeper [3]. With the use of recognition of gestures technology, physical therapy exercises may now be completed by patients using virtual reality environments [4]. The automotive sector has developed gesture recognition technologies that allow drivers to handle multiple parts of the automobile without having their palms off the wheel, hence increasing driving safety. Consumers may now operate domestic devices with simple hand gestures because of gesture recognition technology in automated homes, making their experience accessible and useful [5]. The initial forms of human-machine interaction occurred in the early phases of the

Second Industrial Revolution when people used buttons and levers to manipulate and control the rotational rate and electrical power generated of steam turbines, in addition to the direction and speed of trains [6]. This method of transmitting data was progressively replaced by input through the keyboard and mouse control after the introduction of computers. The speed at where data is transmitted is increasing and the reliability of data recognition has become better in the past few years due to the rapid development of automated learning and signal capture technologies [7]. Now, complicated activities may be accurately completed by using basic signals to control the system [8]. The freedom, applicability, and effectiveness of human-machine communication have all been further enhanced by researchers' development of a variety of human-machine interaction methods as technological advances has progressed [4]. These innovations include voice control brain-computer user interfaces, facial expression management, and gesture recognition, between others [9]. Given that people frequently use their hands to share and receive information, gesture recognition is a prominent technology in the field of interaction between humans and machines [10]. According to studies, language and voice each are responsible for 45% of their significance of data transmission, leaving gestures at 55%. This emphasizes the significance of body language in instruction and emotional expression, establishing recognition of gestures as a fundamental technology in interaction between humans and machines with benefits including ease of use, adaptability, and deep implications [11]. Using federated learning to develop a global CNN algorithm across decentralized devices in real-time gesture detection while protecting user privacy is new and allows for smooth human-computer interaction. To enhance efficiency and adaptability in dynamic HCI scenarios, the suggested method also includes strategies like adaptive learning rate planning, differential privacy, and model compression.

Key Contributions are as follows:

- Presents a unique method that shares raw data among decentralized devices to cooperatively train a global CNN model using federated learning without jeopardizing user privacy.
- Creates a federated CNN architecture specifically designed for real-time gesture detection, allowing for constant model improvement and adjustment to a range of user behaviours and environmental circumstances.
- Uses methods such as adaptive learning rate scheduling, differential privacy, and model compression to speed up convergence, cut down on overhead, and enhance communication efficiency, leading to cutting-edge performance in real-time gesture detection applications.
- Validates the effectiveness of the suggested federated CNN strategy by extensive testing on benchmark datasets, showing higher prediction accuracy than centralised learning methods.
- Federated learning's decentralised design protects user privacy and data, making it appropriate for sensitive

HCI applications and promoting more organic and intuitive computer-human interactions.

The rest of the section is structured as follows: Section II examines the related work. Section III refers to the problem statement. Section IV describes the proposed procedure in detail, followed by Section V that includes the results and discussion. And finally, Section VI summarises the findings of the proposed work with conclusion

II. RELATED WORK

Qi et al. [12] suggests a modern smart cities are guiding a number of improvements to infrastructure with the help of an evolving idea called urban intelligence. The interface that connects citizens to smart cities is called human-computer interaction (HCI), and it is essential to bridge the gap in the adoption of technological advances in contemporary cities. The detection of human hand motions utilizing surface electromyograms (sEMG) is a significant research area in the practical use of sEMG, which has been widely accepted as a promising HCI technology. Modern signal processing techniques, yet, struggle to reliably extract features from and recognize patterns in sEMG signals due to a number of unresolved technological issues. In this case, how can one maintain myoelectric control available while it is used periodically? Time variation has a significant impact on recognizing patterns abilities, but it cannot be completely eliminated when using it on a daily basis. Ensuring the dependability and efficiency of the myoelectric controlling device is a crucial aspect in creating a high-quality human-machine interaction. The present research presents the implementation of an extreme learning machine (ELM) and a linear discriminant analysis (LDA) gesture-based identification system that may remove redundant data from sEMG signals and increase recognize accuracy and efficiency. The feature re-extraction technique is used to obtain a characteristic map slope (CMS), which improves the viability of cross-time identifying by strengthening the link between features across time domains. The goal of this work is to optimize the duration disparities in recognizing of sEMG patterns. The experimental findings have the potential to minimize the variations in time in sEMG-based recognition of gestures. To strengthen the period of generalization efficiency of an HCI system, the identification framework presented in this article could enhance the long-term generalization ability of HCI as well as streamline the data gathering stage prior to training the gadget prepared for daily use. Utilizing sEMG, an additional extraction of features of static gesture is examined. Although both theoretical and experimental results were produced, more research is still needed to address some issues. In future studies, defining additional features or developing feature selection techniques are attractive research paths, as obtaining of eigenvalue slopes enhances recognizing accuracy in the present research.

Rahim et al.,[13] explains human-computer interaction (HCI) techniques are being widely used in the development of hand gesture identification (HGR) devices in the past few years, allowing for routine machine contact. The challenge of hand segmentation and recognizing is difficult because of the adverse surroundings, background clarity, hand size, and

shape. Still, the relevance of advancement in HGR keeps increasing. To improve recognition accuracy, researchers offer an ideal segmentation technique for recognizing movements of the hands using input photos. Researchers examined the segmenting techniques of YCbCr, SkinMask, and HSV (hue, saturation, and value) for hand motions. After removing the CR part from YCbCr, binarization, which erosion, and hole fill are carried out. The SkinMask method uses segmenting colors to find pixels which complement the hand's color. Threshold mask is used in the HSV process to identify the dominating features. When features from convolutional neural networks (CNNs) are recovered, hand movements are classified using the Softmax classification method. When the suggested segmentation techniques are used on a benchmark dataset, the recognition accuracy outperforms that of cutting-edge systems. To effectively manage complicated backdrops and different hand orientations, future work should concentrate on improving the suggested segmentation techniques. For realistic applications, this would also be beneficial to look at real-time implementations and adaptability to various climatic situations. The SkinMask method uses segmenting colors to find pixels which complement the hand's color. Threshold mask is used in the HSV process to identify the dominating features. When features from convolutional neural networks (CNNs) are recovered, hand movements are classified using the Softmax classification method. When the suggested segmentation techniques are used on a benchmark dataset, the recognition accuracy outperforms that of cutting-edge systems. To effectively manage complicated backdrops and different hand orientations, future work should concentrate on improving the suggested segmentation techniques. For realistic applications, this would also be beneficial to look at real-time implementations and adaptability to various climatic situations.

He, Yang and Wu, [14] suggests an essential component of dynamic gesture detection is the identification and monitoring of gesture targets. The present research investigates long-term recognition of gestures with monocular RGB cameras to satisfy the precision and rapidity criteria of dynamic gesture detection in interaction between humans and computers. To accomplish gesture identification and tracking, this paper presents an integrated Gaussian model and kernels correlation filtration in addition to an enhanced optimization of particle swarms approach for extraction of features. Additionally, it has built a dynamic gesture monitoring framework using kernel correlations filtration as a foundation. According to the experimental findings, the skin color-based gesture identification system has accuracy and recall rates greater than 0.8 and a minimal overall absolute error value of 0.321 across a variety of data. The maximal the R-squared value for the relationship coefficient is 0.823, and the detection speed is 36.32 frames per second. Additionally, the aforementioned detection technique exhibits great repeatability across several datasets and superior accuracy in detecting various gesture targets. Improved gesture tracking efficiency is the outcome of the gesture monitoring model's F1 value having the biggest region of the receiver's operations characteristic curve & both of its error values being relatively small. This technology has shown considerable improvements

in the accuracy of detection and targeted rejections rate in interactions between humans and computer systems. It has also produced beneficial effects, as seen by participants' largely subjective assessment of the interaction system. The theoretical foundations of dynamic gesture recognition and tracking technology are strengthened by this work, which also raises the standard of gesture tracking within the domain of interaction between humans and computers. This contributes to extending the range of applications for HCI. It did not address gesture tracking's immediate efficiency, that could be a useful area for future research.

Rai et al., 2 [15] explains a gesture-based human-computer interface that makes use of a microcontroller, processing of images, and a standard computing system is designed and implemented. The envisioned system's goal is to enable any disabled person to solve problems in actual time with hand movements and carry out routine tasks by recognizing dynamic as well as static hand gestures. The suggested method uses several sensors installed on wearing gloves to classify hand gestures. The actual application takes the shape of a gloves via transmitter and receiver modules and sensors that use acceleration to detect hand movements. This allows people with disabilities to interact in other people in an effortless manner by sending and receiving the initial data lacking having to look for another communication channel. This paper's primary focus is on human-computer interface (HCI) interaction, which links humans and machines. A collection of guidelines and regulations that utilize permutations and calculation for a signal from the input of microcontrollers may recognize a combination of static and dynamic human gestures. With the assistance of an advanced microcontroller, each of these instructions are going to be encrypted. Essentially, there are three primary stages involved in hand gesture recognition: detection, monitoring, and identification. To facilitate human-computer contact, this study presents current gesture recognition system interface and attempts to incorporate it into a working model. This technique's dependence on predetermined gestures, that might not meet all of the communication demands of people with disabilities, is one of its drawbacks. Furthermore, the accuracy and uniformity of hand movements may have a variable impact on the system's overall efficacy, which could result in miscommunication or misunderstandings.

Nayak et al. [16] explains a non-contact method for studying psychophysiology and used in Human-Computer Interaction (HCI) is Infrared-Thermal Imaging. Heads movements complicate real-time facial recognition and tracking of the Regions of Interest (ROI) in the thermal video during HCI. The three-stage HCI system proposed in this paper computes multiple-variate time-series data thermal video clips to identify human mood and offers options for diversions. Utilizing a Faster R-CNN (region-based convolutional neural network) design, the first step involves face, eye, and nose detection. The Multiple Instances Learning (MIL) method is then used to track the face ROIs throughout the thermal a motion picture. A multivariate time series (MTS) of data is formed by calculating the average intensity of ROIs. The Dynamic Time Warping (DTW) technique is used in the second stage to characterize emotions generated by audio-

visual stimulus using the smoothed MTS data. In the final stage of HCI, suggested structure offers pertinent recommendations from a viewpoint on physical and psychological distraction. Improved precision is indicated by suggested strategy when compared to other categorization techniques and thermal data sets. To extrapolate the results regarding feelings among people, future research might tackle the relatively small amount of participants by undertaking an investigation with a larger and more varied participation pool. Furthermore, adding methodologies for clustering to the system to identify anxiety, depression, and stress levels within real-time HCI framework might enhance its suitability for psychology purposes.

The literature review highlights several advancements in human-computer interaction (HCI) techniques, particularly focusing on gesture recognition and tracking technologies. While significant progress has been made in various aspects such as signal processing, segmentation techniques, and gesture identification methods, there are still several research gaps that need to be addressed. One major gap is the need for more robust and reliable methods for dynamic gesture detection and tracking, especially in challenging environments with complex backgrounds and varying hand orientations. Additionally, there is a lack of emphasis on real-time implementations and adaptability to different climatic conditions, which are crucial for practical applications of HCI systems. Furthermore, there is a need for more comprehensive studies to validate the effectiveness and accuracy of these techniques across diverse user populations and scenarios. Future research should focus on improving segmentation techniques, enhancing gesture tracking efficiency, and exploring new methodologies for emotion recognition and psychophysiological analysis in HCI systems.

III. PROBLEM STATEMENT

The development of effective human-computer interaction (HCI) systems for gesture recognition and psychophysiological analysis poses significant challenges due to various technological and methodological limitations [16]. These include difficulties in reliably extracting features from surface electromyogram (sEMG) signals, segmenting hand gestures accurately amidst complex backgrounds, and tracking dynamic gestures with precision [15]. Additionally, existing HCI systems often lack inclusivity for individuals with disabilities and may struggle to accurately capture and interpret facial expressions in real-time thermal video. To address these challenges, researchers have proposed novel approaches such as extreme learning machine (ELM) and linear discriminant analysis (LDA) for sEMG signal processing, advanced segmentation techniques using YCbCr, SkinMask, and HSV methods, and an integrated Gaussian model with kernel correlation filtration for dynamic gesture tracking. Furthermore, non-contact methods like infrared-thermal imaging combined with region-based convolutional neural networks (R-CNN) and dynamic time warping (DTW) have been explored for psychophysiological analysis and emotion recognition. Despite promising results, further

research is needed to enhance the accuracy, inclusivity, and real-time applicability of these HCI systems, particularly in addressing issues related to variability in gesture patterns, diverse environmental conditions, and psychological state inference.

IV. PROPOSED FEDERATED CONVOLUTIONAL NEURAL NETWORKS FOR REAL-TIME GESTURE RECOGNITION FOR SEAMLESS INTERACTIONS BETWEEN HUMANS AND COMPUTERS

The proposed method leverages a combination of Convolutional Neural Network (CNN) and Federated Learning to achieve robust gesture recognition. By starting with preprocessing techniques like data cleaning and augmentation, followed by distributed CNN training across multiple users, the system ensures privacy preservation while collectively learning from diverse datasets. The trained model enables accurate recognition of a range of gestures, facilitating seamless human-computer interaction with enhanced performance and responsiveness. Proposed Architecture is depicted in Fig. 1.

A. Data Collection

In this study, using three distinct datasets that are widely recognized and utilized in the field of gesture recognition research. Each dataset brings its own set of characteristics and complexities, providing valuable resources for training, testing, and validating gesture recognition models.

1) *Chalearn gesture dataset*: Many public datasets for evaluating gesture recognition contain only one form of gesture. The Chalearn Gesture Dataset contains nine gesture categories corresponding to various settings and application domains. It contains both static postures and dynamic gestures. In this dataset, a static posture is one in which a single posture is held for a certain duration. For a static hand posture, the hand is held at similar positions for multiple instances of the same gesture. In this case, the static postures also have distinct paths so they could be handled by the same method as the dynamic gestures. This dataset does not contain gestures with distinct hand poses but arbitrary movement [17].

2) *Jester dataset*: The Jester Dataset is a collection of hand gesture data intended for gesture recognition research and development. It contains videos of hand gestures performed by individuals, captured using webcams or other recording devices. The dataset includes a variety of gestures, such as waving, pointing, and making shapes with the hands. Each gesture is labelled with its corresponding class, allowing machine learning algorithms to be trained and evaluated on the data [18].

3) *MSR action3D dataset*: This dataset consists of depth data capturing human actions and gestures performed by multiple subjects. It provides a large collection of annotated gesture sequences, making it suitable for training models for gesture recognition in HCI applications [3].

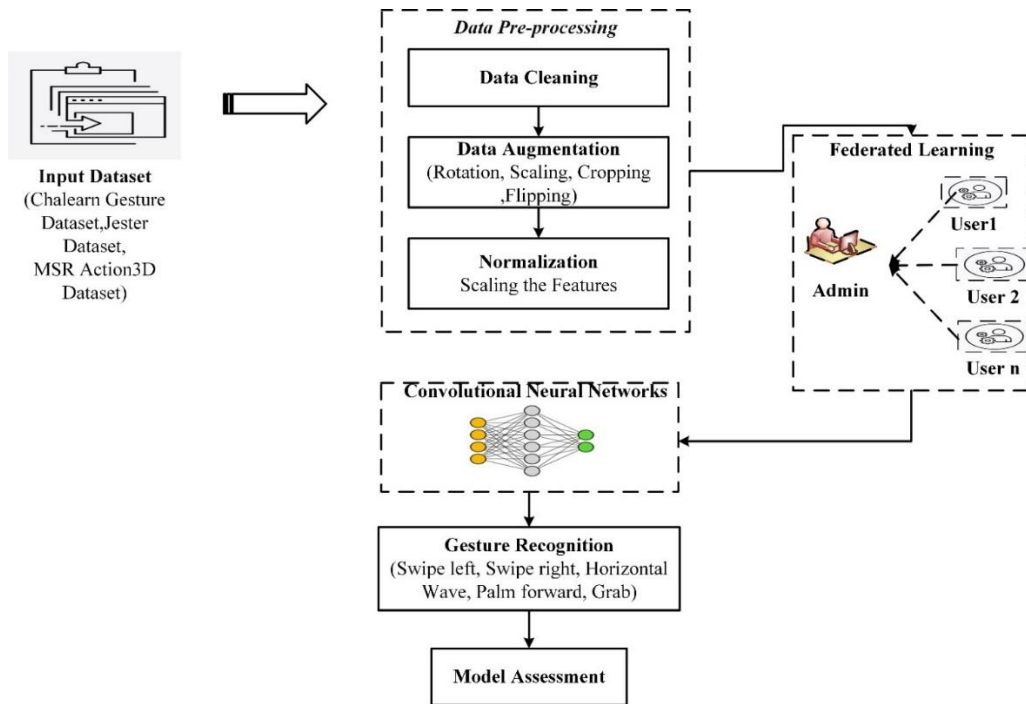


Fig. 1. Proposed real-time gesture recognition for seamless interactions between humans and computers using federated convolutional neural networks.

B. Data Pre-processing

The datasets go through pre-processing steps before the model is trained. These steps include data cleaning to remove noise and inconsistencies, data augmentation to improve the robustness of the model by using techniques like rotation and scaling, normalization to scale features uniformly for improved training convergence, and recognition of relevant aspects from the gesture sequences, such as key points and spatial-temporal features. These pre-processing steps guarantee that the datasets are optimized for the purpose of developing reliable and efficient gesture recognition models [19].

C. Federated Learning for Collaborative Training Across Decentralized Devices

The data used for training provided by the client are per C_a the concept of federated learning, which assumes shared there are actually N clients taking part in the shared model training. The loss function that is the result of just one sample $f_b(x)$. Providing that w is the model's weighting parameter. Consequently, the i th client's loss function is computed in Eq. (1).

$$F_a(x) = \frac{\sum_{b \in C_a} f_b(x)}{|C_a|} \quad (1)$$

$|C_a|$ is a representation of the dataset's volume over them. Next, the federated sharing algorithm's loss function is examined in Eq. (2).

$$F(x) = \frac{\sum_{a=1}^N |C_a| F_a(x)}{|C|} \quad (2)$$

$|C| = \sum_{a=1}^N |C_a|$ is one of them; observe that is $F(x)$ is unable to be calculated directly without transferring data across several nodes.

The federated learning training process. Following weighting averaging, the server gathers all of the model parameters submitted by every client during every iteration and delivers these for every client to finish updating the model's local parameters [20].

D. Convolutional Neural Networks (CNNs) in Gesture Recognition

The CNN architecture underlying the gesture classes considered in the present research. The CNN framework is constructed via a layer of input, three convolution layers, one soft maximum output layer, one completely interconnected output layer, and ReLu and maximum pooling layers for the extraction of features. The following work's images are initially resized to 100 by 100 pixels, and the dataset is divided into testing and training sets. The input layer feeds hand-pose RGB images to later sections for extracting features and classification. The convolution layer is the key for further learning with CNN's endurance. CNN uses intermediate mappings of features and cascaded discontinuous convolution of the kernels using the full image to get an especially promising features for characterizing gives the convolution coefficients of a picture or map of features f with kernel (square matrix). The total number of filters in all layers of convolution is empirically determined through experimentation is given in Eq. (3).

$$a \times k = \sum_{y,z=0}^{r-1} (a_i + y, j + z)(yr - z) \quad (3)$$

The following three layers of convolution make up the proposed design: eight 19 by 19 filters are placed into the very first layer, sixteen 17 by 17 filters are placed in the second layer, and 32 15 by 15 filters are placed in the final layer. The padding is used by each convolutional layer to keep the result size constant with the input. Multiple neurons with the ReLu

activation function receive the result of the convolution procedure. It substitutes 0 for those with negative values within the pooling layer using the non-saturating and the non-linear algorithm. Because of its expressive sparseness and ease of computation, ReLu is the recommended option for activation functions in neural networks with deep layers. The feature maps are resized by the pooling layer, that is added after each ReLu layer, avoiding losing any of the most important components. The pooling function employed in this study is maxpooling, which outperforms all of the others owing to its quick performance and improved converging properties. Using a filter size of (2,2) and a stride of (3,3), the maximum pooling procedure is carried out following the selection of the highest possible value for every local region in the maps of features by every convolution layer. The result is given in Eq. (4).

$$c = \max(0, d) \quad (4)$$

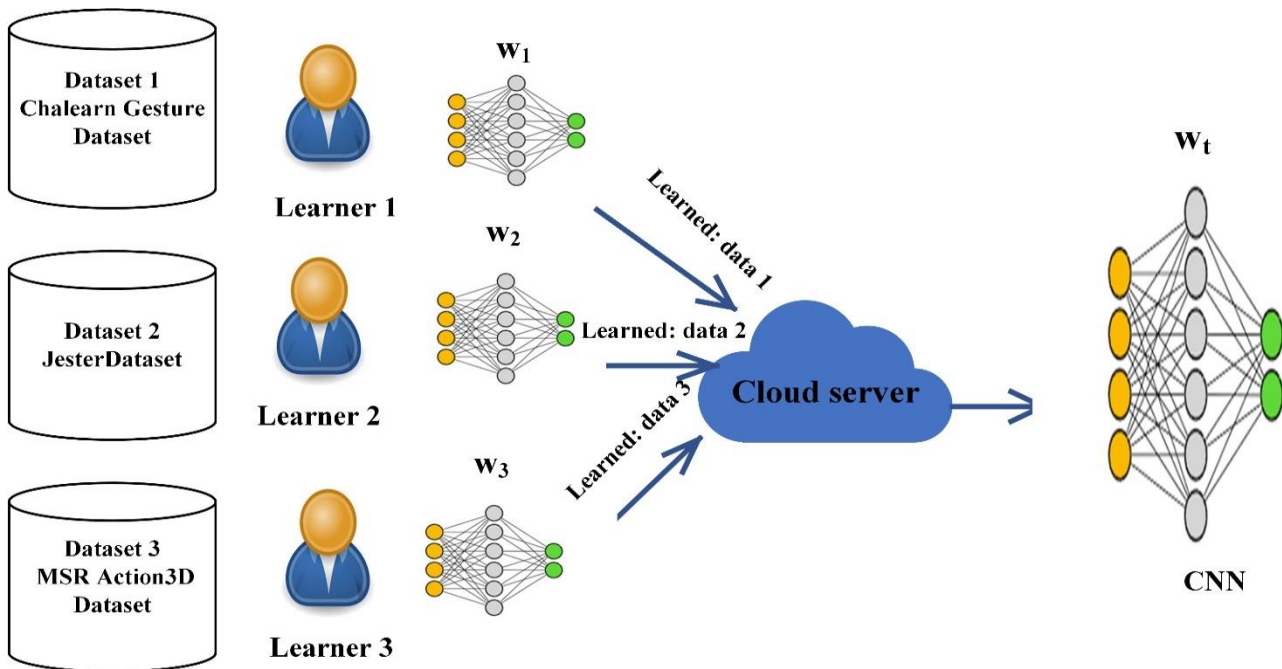


Fig. 2. Federated learning.

V. RESULT AND DISCUSSIONS

The proposed federated convolutional neural network (CNN) approach for real-time gesture detection demonstrates outstanding performance and responsiveness while addressing privacy and security concerns. Through extensive testing on benchmark datasets, the system consistently outperforms centralized learning methods, achieving state-of-the-art results in gesture recognition tasks. By leveraging federated learning, the model is trained collaboratively across decentralized devices without compromising user privacy, as raw data remains local. This approach ensures continuous model refinement and adaptation to dynamic environments by aggregating local model updates from edge devices. Moreover, enhancements such as differential privacy, adaptive learning rate scheduling, and model compression techniques contribute to minimizing privacy risks and communication

overhead, while accelerating convergence. The federated architecture not only guarantees improved responsiveness and adaptability but also ensures the confidentiality and integrity of user data, making it suitable for sensitive human-computer interaction applications. Overall, the proposed design offers a promising avenue for advancing real-time gesture detection systems, enabling more natural and intuitive interactions while safeguarding user privacy and data integrity.

Table I presents the Gesture Recognition Classes in the Jester dataset, categorizing gestures based on their type and granularity. The dataset includes a variety of hand movements and interactions commonly used for controlling electronic devices or interacting with computers. Each gesture is classified as either "Fine" or "Coarse" based on the level of detail and precision involved in its execution. For instance, fine gestures such as swiping left or right and presenting the palm forward require more intricate movements and precision,

while coarse gestures like various finger gestures and pointing gestures involve broader and less specific hand movements. This classification scheme provides insight into the diversity of gestures captured in the dataset, facilitating the development and evaluation of gesture recognition algorithms across different levels of granularity and complexity.

Fig. 3 illustrates how these neural networks learn and generalize in different ways across 100 epochs by comparing the Training and Testing Accuracy for three different datasets, these losses decrease with time, indicating that the model is learning new abilities and improving in performance. In parallel with the training accuracy's more gradual growth over the epochs, testing accuracy likewise experiences a steady increase upon reaching subsequent epochs.

Fig. 4 illustrates training and testing losses, which also illustrates the various methods in which these networks learn and generalize over 100 epochs. These losses decrease with time, indicating that the model is learning new abilities and improving in performance. The testing loss starts at a higher

value than the training loss and then drops sharply before collapsing at epoch 20, whereas the training loss decreases more gradually over the course of the epochs.

TABLE I. GESTURE RECOGNITION CLASSES IN JESTER DATASET

| Class | Gesture | Grain |
|-------|-----------------------------|--------|
| 0 | Swiping left or right | Fine |
| 1 | Waving horizontally | Coarse |
| 2 | Presenting the palm forward | Fine |
| 3 | Making a grabbing motion | Fine |
| 4 | Various finger gestures | Coarse |
| 5 | Pointing gestures | Coarse |
| 6 | Thumbs up or thumbs down | Coarse |
| 7 | OK sign | Fine |
| 8 | Peace sign | Coarse |

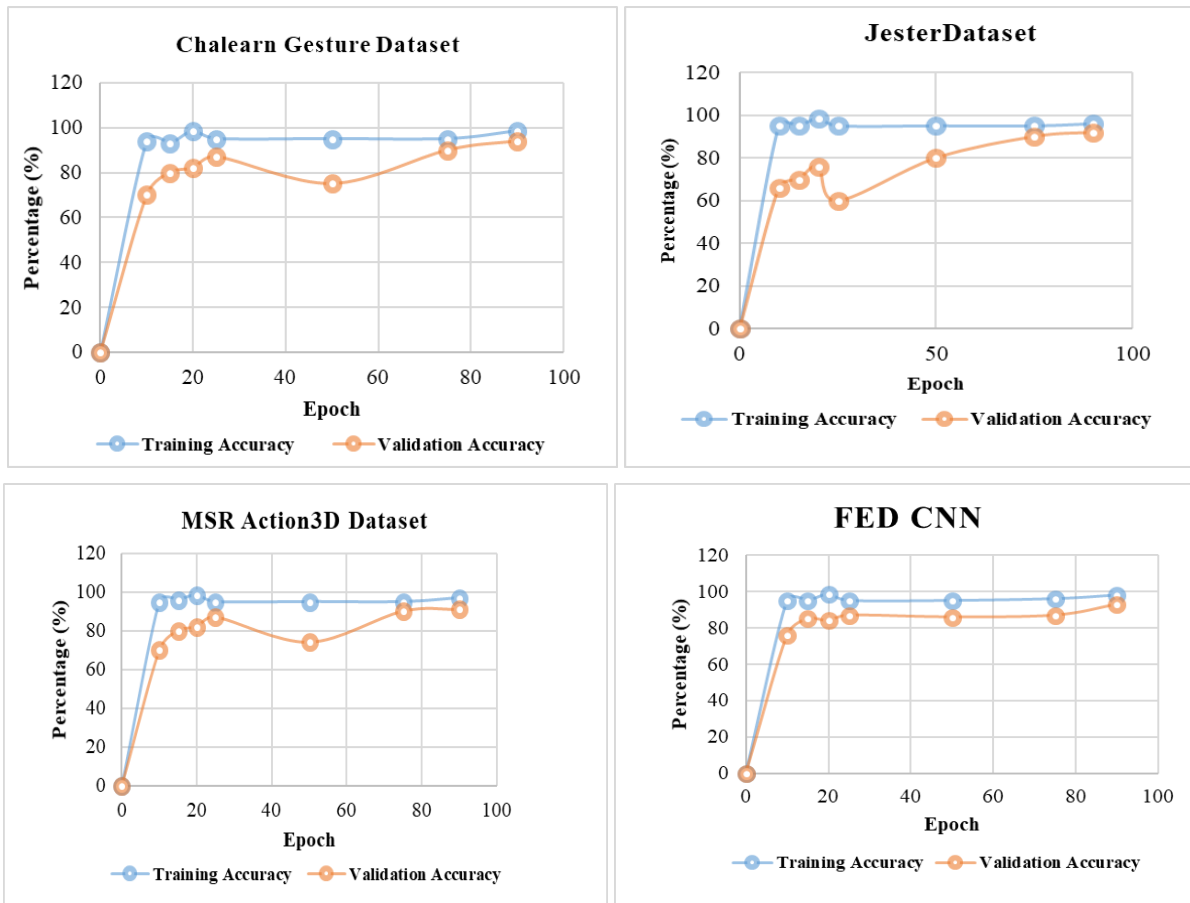


Fig. 3. Training and Testing Accuracy of CNN model for three different dataset and FED-CNN.

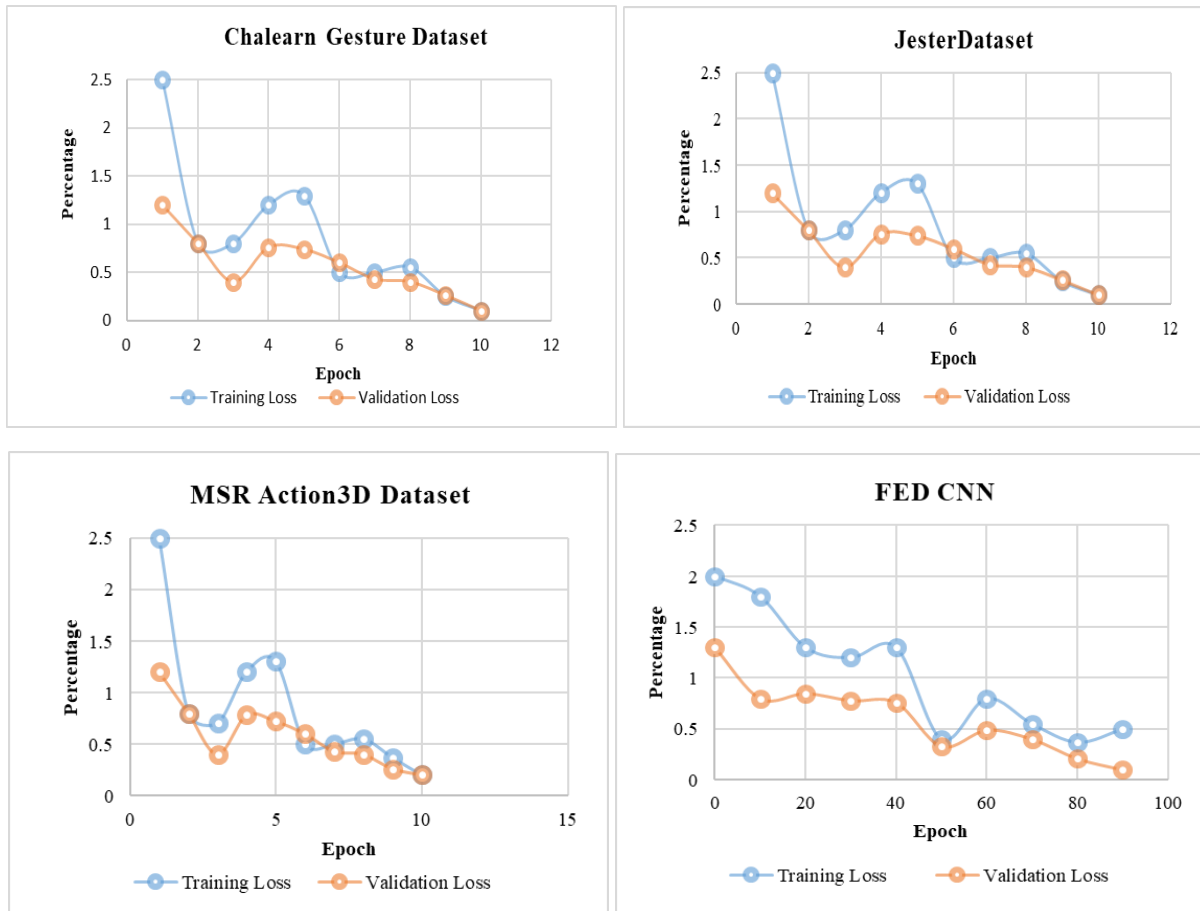


Fig. 4. Training and Testing Loss of CNN model for three different dataset and FED-CNN

TABLE II. COMPARISON THE PERFORMANCE OF PROPOSED METHOD WITH EXISTING METHOD

| Approach | Dataset | Accuracy (%) |
|------------------------------|---|--------------|
| Siamese Network [22] | NVIDIA | 81.2% |
| LSTM [23] | DHG | 90.87% |
| RNN [24] | MSRC-12 | 60-87% |
| GAN [25] | ASL Alphabet dataset | 89-96% |
| RNN [26] | AMFED and EmoReact | 93.09% |
| CNN [27] | ChaLearn Looking at People (LAP)dataset | 90.57% |
| Resnet [28] | EGO Gesture Dataset | 75.30% |
| GoogleNet [29] | UCI Hand Gesture Dataset | 87% |
| Proposed Framework (FED CNN) | Chalearn Gesture, jester, MSR Action3D | 98.70% |

Table II presents a comparative analysis of various gesture recognition approaches using different datasets and their corresponding accuracy percentages. Each approach utilizes different deep learning architectures such as Siamese Networks, LSTM, RNN, GAN, CNN, ResNet, and GoogleNet, trained on specific gesture datasets. Notably, the

proposed federated CNN framework achieves the highest accuracy of 98.70% by leveraging data from three diverse datasets: Chalearn Gesture, Jester, and MSR Action3D. This indicates the effectiveness of the federated approach in combining data from multiple sources to enhance model performance significantly, showcasing its potential for robust and accurate gesture recognition across various applications and environments. It is visually shown in Fig. 5.

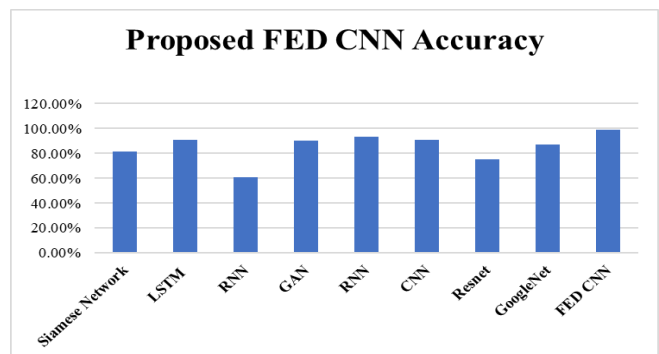


Fig. 5. Performance evaluation of fed -CNN with existing framework.

The Receiver Operating Characteristic (ROC) curve for the federated convolutional neural network (CNN) illustrates in Fig. 6 has ability to classify between true positive and false positive rates across different thresholds, providing insight

into the model's overall performance. A higher area under the ROC curve signifies better discrimination capability of the federated CNN in distinguishing between classes, indicating its effectiveness in real-time gesture detection tasks.

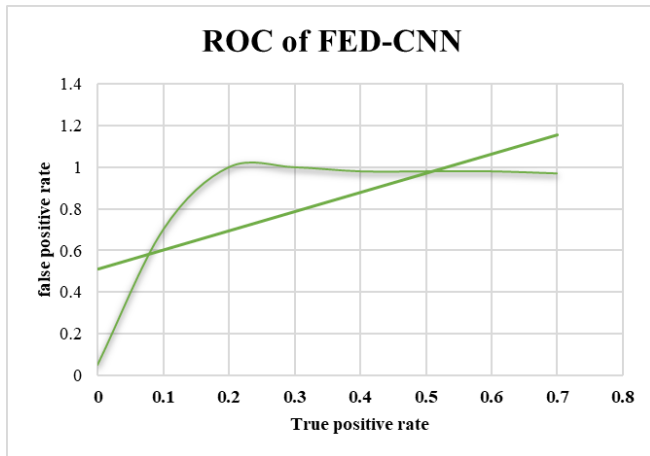


Fig. 6. Roc curve.

A. Discussions

The significant advancements and contributions of the proposed federated convolutional neural network (CNN) approach for real-time gesture detection. By leveraging federated learning, the system addresses critical challenges such as privacy, security, and responsiveness, making it well-suited for a wide range of human-computer interaction (HCI) applications [12]. Through extensive testing and improvements in federated learning techniques, the approach demonstrates superior performance compared to centralized learning methods, offering improved adaptability and reliability in dynamic environments. Moreover, the decentralized architecture ensures user confidentiality and data integrity, enhancing trust and usability in sensitive HCI scenarios. Overall, the discussions underscore the promising potential of the proposed approach in advancing real-time gesture detection systems while maintaining a strong focus on user privacy and data security.

VI. CONCLUSION AND FUTURE WORK

In conclusion, the proposed approach leveraging federated convolutional neural networks (CNNs) presents a promising solution for real-time gesture detection, addressing the challenges of maintaining user privacy and data security while ensuring excellent performance and responsiveness in various HCI contexts. By utilizing federated learning, the model can be trained collaboratively across decentralized devices without compromising sensitive user data. Through extensive testing on benchmark datasets, the federated CNN approach demonstrated state-of-the-art performance, outperforming centralized learning techniques and offering improved adaptability to dynamic environments. For future work, further enhancements can be made to the federated learning system to optimize responsiveness and speed. Incorporating techniques like differential privacy and adaptive learning rate scheduling can further mitigate privacy risks and communication overhead, respectively. Additionally, exploring advanced model compression techniques can help

accelerate convergence and reduce resource consumption, making the system more efficient for real-time applications. Furthermore, research efforts can focus on expanding the application scope of federated CNNs to other domains beyond gesture recognition, such as voice recognition or medical imaging, to explore their potential in diverse HCI scenarios. Overall, continued research and development in this direction hold promise for advancing the field of real-time gesture detection while upholding user privacy and data integrity.

REFERENCES

- [1] V. A. Shanthakumar, C. Peng, J. Hansberger, L. Cao, S. Meacham, and V. Blakely, "Design and evaluation of a hand gesture recognition approach for real-time interactions," *Multimedia Tools and Applications*, vol. 79, no. 25, pp. 17707–17730, 2020.
- [2] E. Ertugrul, P. Li, and B. Sheng, "On attaining user-friendly hand gesture interfaces to control existing GUIs," *Virtual Reality & Intelligent Hardware*, vol. 2, no. 2, pp. 153–161, 2020.
- [3] Z. Liu, C. Zhang, and Y. Tian, "3D-based deep convolutional neural network for action recognition with depth sequences," *Image and vision computing*, vol. 55, pp. 93–100, 2016.
- [4] A. Kumar and A. Mantri, "Gesture-Based Model of Mixed Reality Human-Computer Interface," in *2020 9th International Conference System Modeling and Advancement in Research Trends (SMART)*, IEEE, 2020, pp. 226–230.
- [5] M. Fugini and J. Finocchi, "Gesture Recognition in an IoT environment: a Machine Learning-based Prototype," in *Future of Information and Communication Conference*, Springer, 2021, pp. 236–248.
- [6] C. at R. Labs, D. Sussillo, P. Kaifosh, and T. Reardon, "A generic noninvasive neuromotor interface for human-computer interaction," *bioRxiv*, pp. 2024–02, 2024.
- [7] H. Kong, L. Lu, J. Yu, Y. Chen, and F. Tang, "Continuous authentication through finger gesture interaction for smart homes using WiFi," *IEEE Transactions on Mobile Computing*, vol. 20, no. 11, pp. 3148–3162, 2020.
- [8] N. Meghana, K. S. Lakshmi, M. N. L. Tejasree, K. Srujana, and N. Ashok, "GESTURE-BASED HUMAN-COMPUTER INTERACTION," *EPRA International Journal of Research and Development (IJRD)*, vol. 8, no. 10, pp. 237–241, 2023.
- [9] S. S. Mallika, M. Priyadharsini, S. Samritha, C. Sowmiya, and B. Nikitha, "Hand Gesture Recognition using Convolutional Neural Networks," in *2023 2nd International Conference on Automation, Computing and Renewable Systems (ICACRS)*, IEEE, 2023, pp. 249–255.
- [10] R. Das, R. K. Ojha, D. Tamuli, S. Bhattacharjee, and N. J. Borah, "Hand Gesture-Based Recognition System for Human-Computer Interaction," in *Machine Vision and Augmented Intelligence: Select Proceedings of MAI 2022*, Springer, 2023, pp. 45–59.
- [11] T. Ganokratanaa and M. Ketcham, "Real-Time Hand Gesture Recognition for Elderly Care with Raspberry Pi," in *2024 IEEE International Conference on Consumer Electronics (ICCE)*, IEEE, 2024, pp. 1–4.
- [12] J. Qi, G. Jiang, G. Li, Y. Sun, and B. Tao, "Intelligent human-computer interaction based on surface EMG gesture recognition," *Ieee Access*, vol. 7, pp. 61378–61387, 2019.
- [13] M. A. Rahim, A. S. M. Miah, A. Sayeed, and J. Shin, "Hand gesture recognition based on optimal segmentation in human-computer interaction," in *2020 3rd IEEE International Conference on Knowledge Innovation and Invention (ICKII)*, IEEE, 2020, pp. 163–166.
- [14] D. He, Y. Yang, and R. Wu, "Design of Human-Computer Interaction Gesture Tracking Model based on Improved PSO and KCF Algorithms," *IEEE Access*, 2024.
- [15] A. Rai, P. K. Mishra, S. V. Karatangi, and R. Agarwal, "Design and implementation of gesture based human computer interface," in *2021 International Conference on Advance Computing and Innovative Technologies in Engineering (ICACITE)*, IEEE, 2021, pp. 29–33.

- [16] S. Nayak, B. Nagesh, A. Routray, and M. Sarma, "A Human-Computer Interaction framework for emotion recognition through time-series thermal video sequences," *Computers & Electrical Engineering*, vol. 93, p. 107280, 2021.
- [17] J. Wan et al., "Chalearn looking at people: Isogd and cong d large-scale rgb-d gesture recognition," *IEEE Transactions on Cybernetics*, vol. 52, no. 5, pp. 3422-3433, 2020.
- [18] J. Materzynska, G. Berger, I. Bax, and R. Memisevic, "The jester dataset: A large-scale video dataset of human gestures," in *Proceedings of the IEEE/CVF international conference on computer vision workshops*, 2019, pp. 0-0.
- [19] H. Heydarian, P. V. Rouast, M. T. Adam, T. Burrows, C. E. Collins, and M. E. Rollo, "Deep learning for intake gesture detection from wrist-worn inertial sensors: The effects of data preprocessing, sensor modalities, and sensor positions," *IEEE Access*, vol. 8, pp. 164936-164949, 2020.
- [20] W. Zhang, Z. Wang, and X. Wu, "WiFi signal-based gesture recognition using federated parameter-matched aggregation," *Sensors*, vol. 22, no. 6, p. 2349, 2022.
- [21] P. Xu, "A real-time hand gesture recognition and human-computer interaction system," *arXiv preprint arXiv:1704.07296*, 2017.
- [22] M. S. Akremi, R. Slama, and H. Tabia, "SPD Siamese Neural Network for Skeleton-based Hand Gesture Recognition.," in *VISIGRAPP (4: VISAPP)*, 2022, pp. 394-402.
- [23] A. Toro-Ossaba, J. Jaramillo-Tigreros, J. C. Tejada, A. Peña, A. López-González, and R. A. Castanho, "LSTM recurrent neural network for hand gesture recognition using EMG signals," *Applied Sciences*, vol. 12, no. 19, p. 9700, 2022.
- [24] S. Shin and W.-Y. Kim, "Skeleton-based dynamic hand gesture recognition using a part-based GRU-RNN for gesture-based interface," *Ieee Access*, vol. 8, pp. 50236-50243, 2020.
- [25] D. Jiang, M. Li, and C. Xu, "Wigan: A wifi based gesture recognition system with gans," *Sensors*, vol. 20, no. 17, p. 4757, 2020.
- [26] K. B. Prakash, R. K. Eluri, N. B. Naidu, S. H. Nallamala, P. Mishra, and P. Dharani, "Accurate hand gesture recognition using CNN and RNN approaches," *International Journal*, vol. 9, no. 3, 2020.
- [27] L. Chen, J. Fu, Y. Wu, H. Li, and B. Zheng, "Hand gesture recognition using compact CNN via surface electromyography signals," *Sensors*, vol. 20, no. 3, p. 672, 2020.
- [28] A. Alnuaim, M. Zakariah, W. A. Hatamleh, H. Tarazi, V. Tripathi, and E. T. Amoatey, "Human-computer interaction with hand gesture recognition using resnet and mobilenet," *Computational Intelligence and Neuroscience*, vol. 2022, 2022.
- [29] J. P. Sahoo, A. J. Prakash, P. Pławiak, and S. Samantray, "Real-time hand gesture recognition using fine-tuned convolutional neural network," *Sensors*, vol. 22, no. 3, p. 706, 2022.

Advancing Automated and Adaptive Educational Resources Through Semantic Analysis with BERT and GRU in English Language Learning

V Moses Jayakumar¹, R. Rajakumari², Sana Sarwar³, Darakhshan Mazhar Syed⁴,
Prema S⁵, Santhosh Boddupalli⁶, Yousef A. Baker El-Ebiary⁷

Research Scholar, Department of English, Saveetha School of Engineering,
Saveetha Institute of Medical and Technical Sciences, Saveetha University, Chennai, Tamil Nadu, India¹
Associate Professor, Saveetha School of Engineering, Saveetha Institute of Medical and Technical Sciences,
Saveetha University, Chennai, Tamil Nadu, India²

Language Instructor, College of Science for Girls, Jazan University, Jazan KSA³
Lecturer, Department of English, Jazan University, Jazan, Saudi Arabia⁴

Assistant Professor, Department of English, Panimalar Engineering College, Chennai, India⁵
Assistant Professor, Department of CSE, Malla Reddy Engineering College for Women (UGC Autonomous),
Maisammaguda, Dhulapally, Medchal Road, Secunderabad, Telangana, India⁶
Faculty of Informatics and Computing, UniSZA University, Malaysia⁷

Abstract—Semantics describe how language and its constituent parts are understood or interpreted. Semantic analysis is the computer analysis of language to derive connections, meaning, and context from words and sentences. In English language learning, dynamic content generation entails developing instructional materials that adjust to the specific requirements of each student, delivering individualized and contextually appropriate information to boost understanding and engagement. To tailor instructional materials to the various requirements of students, dynamic content creation is essential in English language learning (ELL). This work is a unique method for automatic and adaptive content production in ELL that uses Gated Recurrent Unit (GRU) and Bidirectional Encoder Representations from Transformers (BERT) together. The suggested approach uses BERT enabling content selection, adaption, and adaptive educational content production, and GRU for semantic extraction of features and contextual information captured from textual input. The article presents a novel approach to creating automated and adaptable educational tools for ELL that uses GRU for semantic feature extraction. Using persuasive essays collected in the PERSUADE 2.0 corpus annotated with discourse components and competency scores, this is an extensive dataset. After extensive testing, this approach shows outstanding outcomes, with high accuracy reaching 97% when compared to the current Spiking Neural Network (SNN) & Convolutional Neural Network (CNN), Logistic Regression (LR), and Convolutional Bidirectional Recurrent Neural Network (CBRNN). Python is used to implement the suggested work. The suggested strategy improves ELL engagement and understanding by providing individualized, contextually appropriate learning resources to each student. In addition, the flexibility of the system allows for real-time modifications to suit the changing needs and preferences of the learners. By providing instructors and students in a variety of educational contexts with a scalable and effective approach, this study advances automated content development in ELL. The model architecture will be improved in the future, along with the application's expansion

into other domains outside of ELL and the investigation of new language aspects.

Keywords—BERT; Content Generation; English Language Learning; Gated Recurrent Unit; Semantic Analysis

I. INTRODUCTION

Semantics is a subfield of linguistics that studies the way language is understood. The literal meaning of words and sentences as essential components of the world is the subject of semantics. Semantic analysis, as applied to NLP, assesses and reflects human language. It also examines documents written in English alongside other natural languages, interpreting them similarly to the way people would [1]. The prevalence of documented information from both academic and business settings is growing, and its encounter in various contexts by various scientists and scholars suggests that researchers seeking high system efficiency are drawn to collecting details, processing languages, and information retrieval due to their rapid growth. Assert that scholars from a range of fields are interested in classifying characteristics such as study themes, methodologies, and theories related to the research nature by analysing descriptions, and titles, and publishing the entire text bodies. Numerous interdisciplinary areas have evolved in the last several decades, encompassing biochemistry, the field of engineering, data mining, neurology, and bioinformatics. It might be challenging to comprehend every step of the research process in these subjects since interdisciplinary environments incorporate theories, methodologies, and approaches from other fields [2]. Therefore, a system for classifying texts and documents according to their relevant structures ought to exist. Semantic analysis is the technique used by academics and researchers to categorize texts according to their underlying structures. Assert that the exact significance and understanding associated with dictionary meaning derived

from structures created by syntactic evaluation are assigned by semantic analysis. To understand why language conveys meaning, semantics, a discipline of linguistics, studies how language interacts with several "linguistic categories, syntax, phonology, and lexicon". Semantic analysis, in this sense, focuses on the meaning of words and phrases as components of the world [3].

ELL has a unique position at the nexus of global interaction and educational progress, as millions of people pursue English language proficiency for personal, professional, and academic purposes. The process of learning English is dynamic and ever-changing, and it is essential in the globalized society of today. Since English is the universal language of commerce, education, and worldwide communication, speaking the language well has become more crucial for those who want to succeed in a variety of academic and professional settings. Because of this, there is an increasing need for creative and efficient language learning solutions, which is driving instructors and developers to investigate novel ideas to cater to the various demands of students [4]. Conventional approaches to teaching languages frequently depend on static resources like lectures and textbooks, giving students few chances for interaction and customization. Nonetheless, the way English is taught and understood is being completely transformed by recent developments in educational technology, especially in the area of dynamic content creation. Teachers may design individualized, multimedia lessons that are tailored to each student's requirements and preferences by utilizing the effectiveness of semantic analysis with adaptive algorithms. In English language learning, dynamic content production refers to the automated modification and personalization of course content according to student's interests, learning preferences, levels of competence, and advancement. With dynamic content production, teachers may provide individualized learning experiences that maximize student engagement, understanding, and learning outcomes, in contrast to static resources that provide a generic approach to training [5]. Semantic analysis, a subfield of NLP that focuses on comprehending the context underlying meaning of text, is fundamental to the creation of dynamic content.

Automated and adaptive educational materials represent a transformative approach to learning, leveraging technology to tailor instruction to the individual needs and preferences of learners. These materials are designed to dynamically adjust content, difficulty level, and instructional strategies in real-time, offering personalized learning experiences that optimize engagement, comprehension, and retention. Automation in educational materials involves the use of algorithms and artificial intelligence to streamline various aspects of the learning process, from content creation to assessment [6]. The proposed work introduces an innovative approach to dynamic content generation in ELL by leveraging a combination of GRU and BERT. This model integrates GRU for semantic feature extraction and contextual understanding, while BERT facilitates content selection, adaptation, and the generation of dynamic learning materials tailored to individual learner needs. By automating the process and adapting content in real-time, the proposed approach enhances learner engagement and

comprehension. Rigorous experimentation and human evaluation studies validate the efficacy of the model, demonstrating its ability to produce high-quality, contextually relevant educational materials. Furthermore, the proposed approach addresses the limitations of existing systems by providing personalized and adaptive learning experiences, promoting active participation and knowledge retention in ELL. This research contributes to advancing automated content generation in ELL, providing a scalable and efficient solution for educators and learners in diverse educational settings. By combining the BERT and GRU models, this project aims to provide a novel method for automating the development of dynamic instructional materials for ELL. This study aims to investigate the viability and effectiveness of using BERT for content adaptations and GRU for semantic feature extraction to provide dynamic learning resources. The project also intends to create a system that can provide customized learning materials by responding in real time to the preferences and requirements of each student. Additionally, it seeks to determine how the suggested strategy affects learner engagement, understanding, and general learning outcomes for English Language Learners. It also wants to determine how scalable and effective the approach is across a range of learning contexts and student populations. Additionally, the study aims to investigate how the suggested method, which takes into account the varied linguistic origins and skill levels of students, might advance inclusion and accessibility in ELL practices. Ultimately, by overcoming current methodological constraints and encouraging innovation in content creation for language teaching, this project hopes to develop educational technology.

The study's findings have important ramifications for both educational technology and the ELL community. The main issues with standard ELL techniques are addressed in this work by investigating the combination of BERT and GRU models for the automated creation of dynamic resources. The relevance is in the ability to completely transform language learning by offering individualized, contextually relevant learning resources that are catered to the requirements and preferences of each student. This method takes into account the varied linguistic origins and skill levels of the learners, which not only improves student engagement and understanding but also encourages inclusion and accessibility in ELL activities. Additionally, by overcoming the drawbacks of existing techniques and encouraging creativity in the creation of language-learning content, the research advances educational technology. In the end, this study's findings may enhance ELL instruction and learning opportunities, resulting in more successful language proficiency growth and acquisition.

The remaining sections are arranged as follows. Section I provides an introduction. Section II provides illustrations for the literary sections. Section III contains the problem statement. Section IV discusses the recommended methodology for analysing semantics and content production using GRU and BERT. In Section V, the efficacy metrics are displayed and the findings are gathered. Section VI presents a conclusion and Section VII presents the future research.

II. RELATED WORKS

A. Narrative-Centric Learning Experiences

Diwan et al., [7] suggested that in online learning settings, maintaining student engagement is a significant problem that becomes even more intense as learning spaces are progressively constructed by fusing information from several separate sources. Numerous researchers have discovered that learner involvement may be enhanced through narrative-centric learning experiences. To do this, they provide an AI-based method that produces so-called narrative fragments, which are supplementary learning materials that are included in the learning pathways to produce interactive learning narratives. The suggested method involves automatically creating two different kinds of narrative fragments: summaries of the learning route sections and formative evaluations, such as reflection quizzes, utilizing instructional assets in any format, including publicly available educational materials. A pre-trained language approach, GPT-2, serves as the foundation for an NLG component in the pipeline that generates the story fragments. The other components depend on different semantic models. Automation makes it possible to create story segments instantly anytime the learning route has to be modified prerequisite information, etc. This allows for flexibility in the learning paths. Because the suggested method is domain-agnostic, it may be readily modified to work in several domains. ROUGE scores are used to compare the NLG model to many baselines. Human evaluators assess story pieces that are consequently created. In both instances, they had positive outcomes.

B. Text Generation Systems

Hua et al., [8] recommended a three essential elements are needed for establishing an effective text generation system: surface realization, text planning, and content selection. Typically, these issues have been addressed independently. While recent all-in-one neural generating approaches have achieved tremendous strides, they frequently yield inconsistent and erroneous outputs relative to the input. In order to tackle these problems, they provide a beginning-to-the-end learned two-step generation model: first, a sentence-level content organizer determines the language style and key phrases to cover; subsequently, an outer manifestation decoder produces meaningful and cohesive text. They take into consideration three goals for trials, which come from realms with different themes and linguistic styles: creating an abstract for scientific publications, creating paragraphs for regular and basic Wikipedia pages, and creating compelling arguments from Reddit. The remedy can exceed rival inquiries by a large margin, according to automatic evaluation. In addition, human judges find system-generated writing to be more accurate and fluent than versions that do not take linguistic style into account. This model is beneficial, as evidenced by experimental data, where it outperforms complex comparisons in terms of BLEU, ROUGE, and METEOR scores. When it comes to language style, human subjects likewise evaluate their model generations as being more grammatically accurate and grammatical.

C. Sentiment Analysis in MOOC Reviews

Onan et al., [9] states that MOOCs [10] are a relatively new and creative kind of distance learning that allows participants to access course materials regardless of their age, gender, race, or location. By adopting the concepts of ensemble learning as well as DL, this study aims to propose an effective sentiment categorization method with good prediction performance in evaluations of massively open online courses. They want to address several research inquiries regarding sentiment analysis of educational data in this contribution. Initially, an assessment was made of the prediction abilities of DL, ensemble learning, and traditional supervised learning techniques. Also, assessments of massively open online courses have been used to assess the efficacy of word-embedding and visualizing text systems for sentiment assessment. Using ML, ensemble learning, and DL techniques, they examined a corpus of 66,000 reviews of massively open online courses for the evaluation assignment. The empirical research shows that for the job of sentiment assessment in educational data mining, deep learning-driven architectures perform better than ensemble learning approaches and supervised learning methods. Through a rate of classification of 95.80%, extended short-term memory networks alongside the GloVe word-embedding scheme-based depiction have produced the best prediction performance across all evaluated configurations.

D. Adaptive E-learning Environments

El-Sabagh et al., [11] states that designing suitable adaptive e-learning environments helps to personalize training to reinforce learning goals since adaptive e-learning is seen as a stimulus to enhance education and student engagement. This work aims to investigate how students' involvement is affected by an adaptable online educational setting that is designed according to their learning styles. Additionally, this study aims to describe and contrast the suggested flexible online learning setting with a traditional e-learning methodology. The following combined research approaches were utilized to examine the impact and form the basis of the paper: The adaptive e-learning environment is designed using a development approach, and the research experiment is carried out using a quasi-experimental research design. The following affective and behavioural components of involvement are measured by the student participation scale: skills, performance, emotions, participation/interaction, and abilities. According to the findings, there is a statistically significant difference between the experimental and control groups. These experimental findings suggest that an adaptable online learning environment may be able to motivate pupils to learn. This study makes a number of useful recommendations, including ways to boost the influence of online adaptive courses in education and increase the cost-effectiveness of education. It also discusses how to develop a foundation for adaptive online education based on preferences for learning and their implementation. In order to increase student engagement, e-learning institutions can create more individualized and adaptable learning environments with the aid of the suggested adaptive e-learning strategy and its findings.

E. Advanced NLP Techniques for English Learning

X. Guo et al., [12] states that because of its potential to completely transform oral learning, the application of sophisticated methods of NLP in education has gained popularity. Because self-learning is flexible and accessible, it has gained popularity in oral English learning. Students may now approach language learning on their own terms through the development of digital materials and applications. This study introduced a unique framework for improving oral English learning that combines the strengths of the HCRM and the BERT model. The main objective is to give educators and organizations a strong instrument for assessing the appropriateness and quality of oral learning resources. Analysis of sentiment, characteristic collection, and categorization are all integrated into the HCRM architecture, which makes it a complete solution for determining a document's appropriateness for use in the context of oral English learning. To ensure a comprehensive understanding of the efficacy of the oral learning materials, the model considers the viewpoints of both instructors and students. Through efficient sentiment analysis and feature extraction, the HCRM enables a more nuanced comprehension of the possible effects of instructional materials. The results of this study imply that the combination of BERT and HCRM offers a more precise, comprehensive, and data-driven method of material assessment, which might significantly improve oral English learning. The novel approach this study proposes has the potential to raise the quality and applicability of oral learning resources in the field.

Innovative ways to improve learner engagement and content creation in online learning environments have been studied in the field of educational technology in the past. Nevertheless, a critical analysis of these initiatives identifies their advantages and disadvantages. Even while research like those by Diwan et al. and Hua et al. present interesting techniques like text generation models and story fragments, they sometimes lack thorough assessments and may ignore larger educational settings. Comparably, studies conducted by Onan et al. [9] and El-Sabagh et al. [11] explore sentiment analysis and adaptive e-learning settings, respectively, but they might not adequately account for how student preferences are dynamic and how the online education landscape is changing. Even though it is a novel framework, X. Guo et al.'s [12] approach to oral English learning may overlook learner involvement and interaction, which is essential for comprehensive learning experiences. In order to optimise educational experiences across a variety of learning situations, future endeavours should aim for more integrated and comprehensive methods, taking into account the interaction between technology, pedagogy, and learner engagement. Overall, while these studies offer valuable insights into different aspects of educational technology and online learning, there is a clear research gap in integrating these approaches to create holistic and adaptive learning experiences that effectively engage learners across diverse contexts and domains. Prior research has exhibited inventive artificial intelligence (AI) approaches, such as deep learning methods and story fragment production, to support sentiment analysis and learner engagement in educational data mining. Furthermore, the development of comprehensive frameworks

such as the two-step generating model and the integration of HCRM and BERT represents advancements in the production of coherent learning materials that prioritize the quality of language and content, hence enhancing the quality of educational experiences. Some research has a limited scope and lacks comparison analysis, which makes it difficult to appraise and generalize the suggested techniques. Furthermore, the need for strong experimental designs and practical considerations to solve real-world implementation obstacles in automated content production for educational contexts is highlighted by methodological rigor and scalability issues in several research. Future research should aim to bridge this gap by exploring integrated approaches that consider both content generation and learner interaction to optimize engagement and learning outcomes in online environments.

III. PROBLEM STATEMENT

The inadequacies of the current ELL systems frequently prevent them from effectively fulfilling the varied demands of students. Conventional methods of content creation and personalization might not be as flexible as they should be as they depend on static resources that can't be constantly tailored to the unique interests and profiles of each learner. Furthermore, these algorithms might not be able to fully grasp the subtle semantic nuances of language, which could result in inadequate adaption and selection of information. Moreover, even if some systems use ML methods, it's possible that they don't fully make use of the potential of sophisticated neural network designs for content creation and semantic analysis [13]. The suggested study integrates innovative methods like semantic evaluation using GRU and BERT to overcome these constraints. The suggested framework provides an all-encompassing and flexible response to the problems in ELL by utilizing semantic analysis techniques to comprehend language structure and meaning, along with the excellent abilities of GRU for extraction of features and BERT for content choosing, adjustment, and evolving material generation. The objective of this integration is to improve student engagement, understanding, and uptake in the ELL domain by making instructional resources of higher quality, more relevant, and more effective.

IV. INTEGRATING SEMANTIC ANALYSIS WITH GRU AND BERT FOR DYNAMIC CONTENT GENERATION IN ENGLISH LANGUAGE LEARNING

The suggested approach combines GRU and BERT with semantic analysis to provide dynamic material for ELL. To guarantee consistency and simplicity, the textual data—which includes learner profiles and essays gathered from the PERSUADE 2.0 corpus—first goes through pre-processing. POS tagging is used in semantic analysis to obtain syntactic structures and grammatical information from the text. Subsequently, GRU—a recurrent neural network architecture—is utilized to derive semantic features, which include contextual data and semantic correlations found in text sequences. The selection, modification, and creation of dynamic learning materials are then done using BERT. By measuring the semantic similarity between learner profiles and texts using BERT embeddings, pertinent information may be

chosen and materials can be customized to fit the requirements and preferences of specific learners. Furthermore, BERT's language production capabilities enable the dynamic generation of explanations, quiz questions, and summaries as well as other individualized learning tools. The technique is used methodically, building upon the algorithmic strategy and

assessing the framework's efficacy through empirical research using metrics for learner engagement, comprehension tests, and user feedback. By offering automated and adaptable instructional resources that are customized to meet the needs of specific learners, in the area of ELL. The suggested work approach process is shown in Fig. 1.

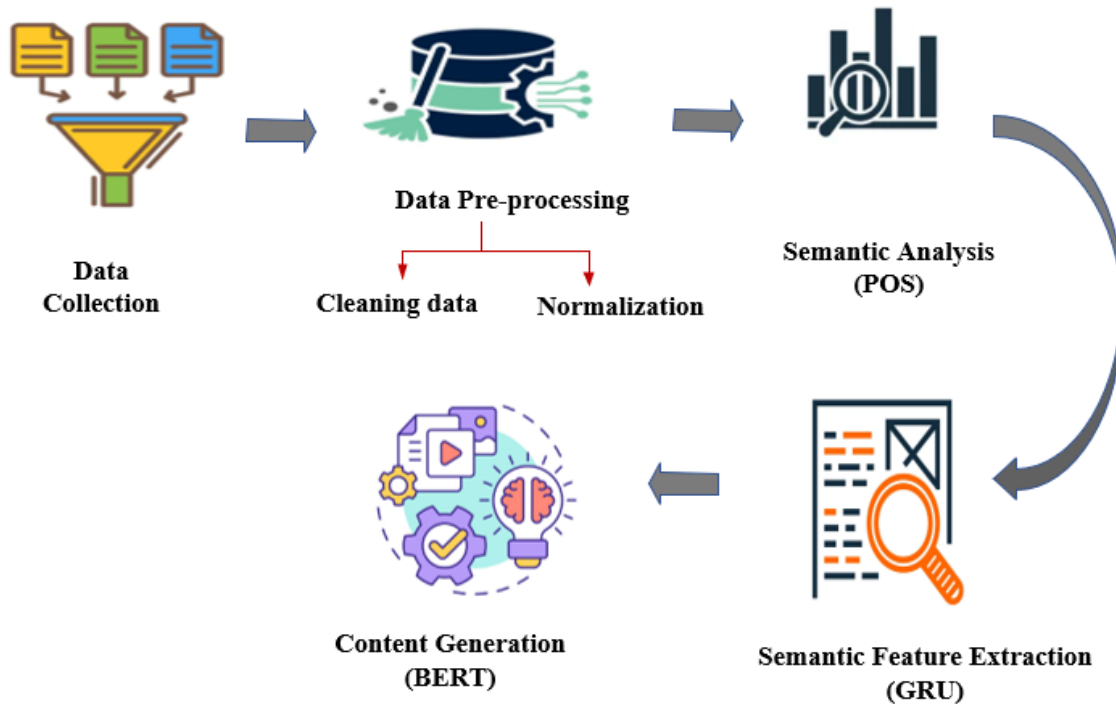


Fig. 1. Semantic analysis with GRU and BERT for dynamic content generation in ELL.

A. Data Collection

The PERSUADE 2.0 corpus [14] provides an extensive dataset for analysing argumentative essays written by American students in grades 6 through 12. This corpus, which includes over 25,000 essays addressing 15 prompts from both autonomous and source-based writing assignments, is an invaluable tool for researching argumentation structures and discourse features. Every essay in the entire collection has a thorough annotation that covers discourse aspects like prospects, roles, states, objections, responses, supporting details, and summaries at the end. The annotation rubric,

which was created via a meticulous double-blind grading procedure and was influenced by well-known frameworks such as the Toulmin argumentation model, guarantees consistency and dependability within the dataset. The corpus also contains individual and demographic data for each writer, integrative essay ratings, and competency scores for arguing aspects. The PERSUADE 2.0 corpus is an invaluable resource for research in the fields of discourse analysis, writing training, and ML approaches in education since it includes full-text essays combined with annotations and metadata. The information that has been gathered for the suggested work is shown in Table I.

TABLE I. DATA COLLECTION

| Column Name | Description |
|--------------------|--|
| essay_id_comp | The ID of the essay |
| competition_set | Indicates whether the essay was part of the training or the test set in the Feedback Prize |
| full_text | The full text of the essay |
| discourse_id | The ID for the discourse element |
| discourse_start | Character position in the essay where the discourse element starts |
| discourse_end | Character position in the essay where the discourse element ends |
| discourse_text | The text of the discourse element |
| discourse_type | Human annotation for the discourse element, providing a description of its type |
| discourse_type_num | Number representing the discourse element within the essay |

B. Data Preprocessing

Preprocessing textual input is an essential stage in NLP activities, such as the work that is being suggested to generate dynamic content for ELL. To guarantee the textual data's cleanliness, consistency, and uniformity—a need for further analysis and modelling—this procedure entails a number of crucial processes. Eliminating any extraneous characters, symbols, or stylistic artifacts that might impede the analysis process is the process of cleaning textual data. By ensuring that the written word is consistent and noise-free, this stage facilitates the extraction of important information. Eliminating HTML elements, special characters, and punctuation can improve the text's readability and analytical value. To preserve consistency throughout the dataset, cleaning textual data in the setting of the PERSUADE 2.0 corpus may entail deleting unnecessary symbols or formatting within argumentative essays. By using uniform formatting guidelines, normalization seeks to normalize the textual data. This entails resolving variances in spelling or capitalization, reducing all letters to lowercase, and eliminating accents and diacritical marks. By ensuring that similar terms are handled in the same way, normalization helps to reduce repetition and inconsistencies within the dataset. To reduce the influence of case sensitivity on further analysis and modelling procedures, normalizing the PERSUADE 2.0 essays within the framework of the proposed study would entail changing every character to lowercase. As an illustration, consider the original text, "The Importance of Education Cannot be Overstated." Normalized Text: "It is impossible to overestimate the value of education." The textual data collected in the PERSUADE 2.0 corpus is cleaned and standardized by completing these preparation processes, making it suitable for additional evaluation and simulation in the setting of dynamic content creation. These processed texts are the starting point for the extraction of semantic information, the construction of prediction models, and the creation of customized learning resources based on the requirements and preferences of specific learners.

C. POS for Semantic Analysis

A key activity in NLP is called Part-of-Speech (POS) tagging, which involves giving each word in a text corpus a classification according to grammar (such as noun, verb, adjective, etc.). Following pre-processing textual information from the PERSUADE 2.0 corpus, POS tagging is essential for semantic analysis within the suggested method for dynamic content production in ELL. To do POS tagging, linguistic information from each word, such as its capitalization, suffix, prefix, nearby words, and syntactic dependencies, are usually extracted. These characteristics aid in the POS tagger's decision-making on each word's part of speech. Probabilistic models, such as HMMs or CRFs, are frequently used by POS taggers to allocate POS tags to words in sentences. These algorithms determine a word's likelihood of falling into a certain speech segment based on its context and words that have already been labelled in the series. Large annotated datasets, in which each word is carefully tagged with its matching part of speech, are frequently used to train POS taggers. In order to produce precise predictions on material that hasn't been read yet, the POS tagger must first learn linguistic rules and statistical trends from the training set. For

each word, linguistic features are extracted, such as capitalization, word shape, prefix, suffix, and neighbouring words. In the proposed work for dynamic content generation in ELL, POS tagging is used after pre-processing the textual data to extract syntactic information from the essays in the data collection. By identifying the parts of speech of words in the essays, the POS tags provide valuable insights into the grammatical structure of the text, which can inform subsequent semantic analysis, feature extraction, and content generation processes. This enables the system to understand the syntactic relationships between words and phrases in the essays, facilitating the generation of coherent and contextually relevant learning materials tailored to individual learners' needs and proficiency levels.

1) *Tokenization*: Tokenization is the process of breaking up the text into distinct sentences or tokens before POS tagging is carried out on the pre-processed textual data. The act of dissecting the text into discrete words, or tokens, is known as tokenization. Every token is a separate textual unit that may be processed or examined further. Many NLP activities, such as extraction of features, analysis of semantics, and model training, are made easier by tokenization. The following tokens would be created by tokenizing the sentence "Modern humans today are always on their phone..." in the illustration given:

["Modern", "humans", "today", "are", "always", "on", "their", "phone", ".", "They", "are", "always", "on", "their", "phone", "more", "than", "5", "hours", "a", "day", "no", "stop", ":", "All", "they", "do", "is", "text", "back", "and", "forward", "and", "just", "have", "group", "Chats", "on", "social", "media", ".", "They", "even", "do", "it", "while", "driving"]

2) *POS Tagging*: POS tagging involves assigning a specific part of speech tag to each token in the text. These tags represent the grammatical category or function of the word within the sentence. Common POS tags include nouns, verbs, adjectives, adverbs, pronouns, prepositions, conjunctions, and punctuation marks. In the given example, POS tagging would assign tags to each token as follows:

[("Modern", "JJ"), ("humans", "NNS"), ("today", "NN"), ("are", "VBP"), ("always", "RB"), ("on", "IN"), ("their", "PRP"), ("phone", "NN"), (".", "."), ("They", "PRP"), ("are", "VBP"), ("always", "RB"), ("on", "IN"), ("their", "PRP\$"), ("phone", "NN"), ("more", "JJR"), ("than", "IN"), ("5", "CD"), ("hours", "NNS"), ("a", "DT"), ("day", "NN"), ("no", "DT"), ("stop", "NN"), (":", ":"), ("All", "DT"), ("they", "PRP"), ("do", "VBP"), ("is", "VBZ"), ("text", "NN"), ("back", "RB"), ("and", "CC"), ("forward", "RB"), ("and", "CC"), ("just", "RB"), ("have", "VB"), ("group", "NN"), ("Chats", "NNS"), ("on", "IN"), ("social", "JJ"), ("media", "NNS"), (".", "."), ("They", "PRP"), ("even", "RB"), ("do", "VBP"), ("it", "PRP"), ("while", "IN"), ("driving", "VBG")]

Interpreting POS Tags every POS tag offers important details on the function and purpose of the word in the sentence. As an illustration, "JJ" indicates an adjective; examples of this are "more" and "Modern". "NNS" is a plural noun, as seen in the word's "hours" and "humans". As "have"

demonstrates, "VB" denotes a verb in its basic form. "RB" stands for "always," "back," and "forward," among other adverbs. The preposition "IN" is shown in the words "on" and "while". Pronouns denoted by "PRP" may be found in the words "there," "it," and "they." By performing POS tagging on the pre-processed text, the proposed work gains insights into the syntactic structure of the sentences, enabling further semantic analysis and feature extraction. These POS tags serve as foundational elements for subsequent steps in the workflow, facilitating the identification of grammatical patterns, semantic relationships, and discourse elements within the textual data.

A. GRU for Semantic Feature Extraction

The suggested approach uses GRU [15] to extract semantic features from the textual material that has already been pre-

processed. When it comes to collecting temporal sequences and distant relationships in ordered information such as natural language text, GRU is an RNN architectural type that excels. In contrast to conventional RNNs, GRU uses gating methods to regulate input flow inside the network, hence reducing the issue of disappearing gradients and facilitating more effective acquisition of repetitive patterns. The recurrent units that make up GRU are individually responsible for keeping track of a hidden state vector that represents the network's internal rendition of the given input sequence. GRU's gating techniques, which control information flow between time steps and enable the network to change its hidden state selectively based on input and past states, are the main novelty in the system. Fig. 2 depicts the GRU framework design. GRU consists of two main gates they are update gate and reset gate.

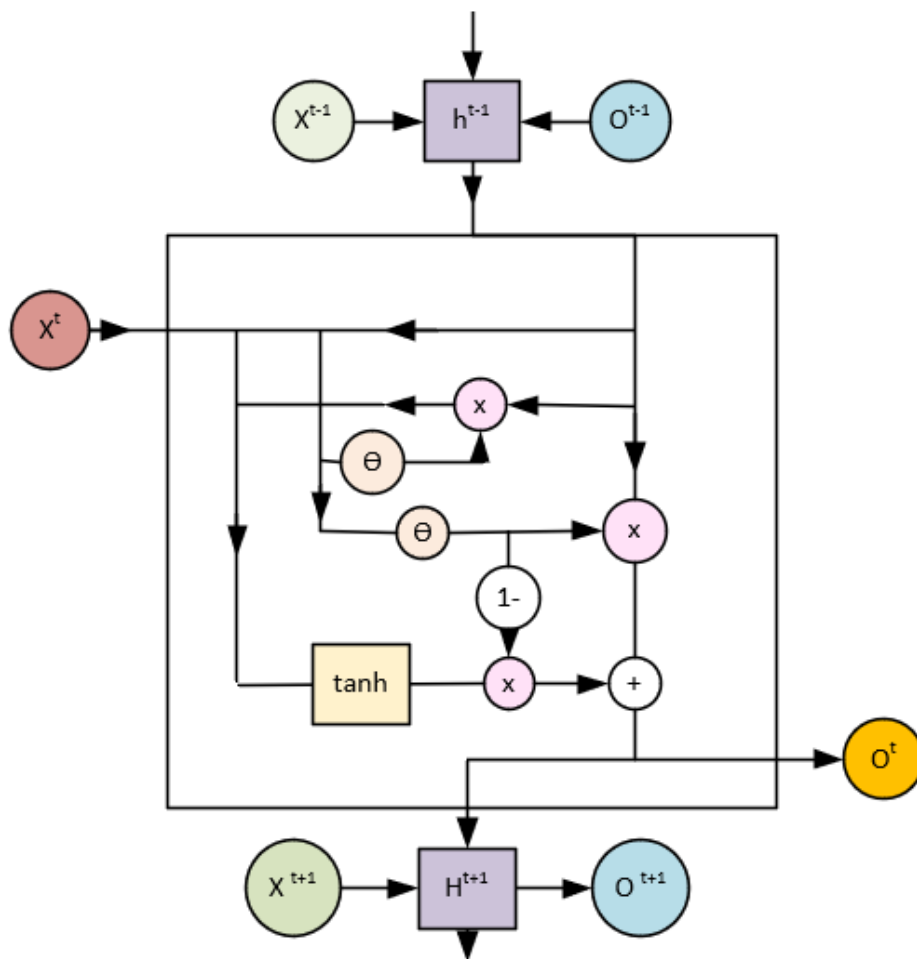


Fig. 2. GRU architecture.

The level to which the present input, r_g , is merged with the prior hidden state, n_{g-1} , is controlled by the reset gate S_g . It chooses what knowledge should be recalled in full, in part, or not at all. Eq. (1) illustrates how to compute the reset gate by multiplying the combination of n_{g-1} and r_g by a weight matrix e_l and applying a bias vector o_l .

$$S_g = \sigma([n_{g-1}, r_g] \cdot e_l + o_l) \quad (1)$$

The amount of the previous concealed state that should be carried over to the following timestep is determined by the update gate D_g . It is calculated utilizing a weight matrix e_x and a bias vector o_x , much like the reset gate. The sigmoid function is then used to remove a vector of ones, as illustrated in Eq. (2).

$$D_g = \sigma([n_{g-1}, r_g] \cdot e_x + o_x) \quad (2)$$

The potential hidden state, wp_g , is determined by summing the output of the reset gate with the present input and using the tanh activating function, as illustrated in Eq. (3).

$$wp_g = \tanh([S_g, n_{g-1}, r_g].e_k + o_k) \quad (3)$$

The prior hidden state and the potential hidden state I_g , adjusted by the update gate, are then combined to create the new hidden state, t_g . Eq. (4) illustrates how this enables the model to calculate the extent to which the new data should replace the earlier hidden state.

$$t_g = (1 - I_g).n_{g-1} + I_g.wt_g \quad (4)$$

In the proposed work, the GRU hidden states serve as semantic features capturing the contextual information and semantic relationships within the input text. By processing the tokenized and normalized textual data through the GRU network, the model learns to extract relevant features representing the underlying semantics of the text. The GRU network is trained using backpropagation through time to minimize a loss function, such as categorical cross-entropy, between the predicted and actual outputs. By leveraging GRU for semantic feature extraction, the proposed work enhances the representation learning capabilities of the model, enabling it to capture intricate semantic nuances and dependencies within the textual data. These learned semantic features serve as valuable inputs for downstream tasks such as content selection, adaptation, and dynamic learning material generation in ELL.

D. BERT for Content Selection

After utilizing GRU for semantic feature extraction, the output from the GRU layer can be passed to BERT [16] for further processing. Therefore, before feeding the output of the GRU layer into BERT, the textual data needs to be tokenized and encoded into word-level representations that BERT can understand. This involves breaking down the text into individual words or sub words (often referred to as tokens) and mapping each token to its corresponding index in a fixed-size vocabulary. Once the text has been tokenized and encoded, the resulting word-level embeddings are then passed as input to BERT. BERT processes the embeddings through multiple layers of transformer-based architecture, capturing contextual information and generating contextualized embeddings for each token in the input sequence. The output from BERT can then be used for various downstream tasks such as content selection, adaptation, and dynamic learning material generation in English Language Learning. BERT's contextualized embeddings provide rich semantic representations of the input text, enabling more nuanced and accurate analysis and generation of educational content tailored to the needs of individual learners. BERT has revolutionized NLP by providing pre-trained language representations that capture rich contextual information from large corpora of text data. In the proposed work for content selection and adaptation, as well as dynamic learning material generation in ELL, BERT plays a pivotal role. BERT can be used for content selection and adaptation by utilizing its contextualized word representations to identify relevant content and adapt it to meet the specific needs of individual learners. BERT encodes words based on their contextual

meaning within the sentence, allowing for precise understanding of semantic similarity between pieces of text. By comparing the contextual embeddings of sentences or passages, BERT can determine the relevance of content to a particular learning objective or topic. BERT models can be fine-tuned on domain-specific datasets relevant to ELL. Fine-tuning involves updating the pre-trained parameters of BERT using task-specific data, thereby customizing the model to the specific requirements of content selection and adaptation in ELL. BERT's contextual embeddings enable the creation of adaptive learning pathways that dynamically adjust content based on learners' proficiency levels, learning preferences, and performance metrics. By incorporating BERT into the adaptation process, the system can select and modify learning materials in real-time to cater to the unique needs of each learner. Consider a scenario where a learner is studying English grammar. BERT can analyse the learner's proficiency level and understanding of various grammar concepts by processing their responses to quizzes or exercises. Based on this analysis, BERT can select appropriate grammar explanations, exercises, or examples from a pool of educational materials, ensuring that the content aligns with the learner's current skill level and learning objectives. BERT can also be employed for generating dynamic learning materials tailored to individual learners. By leveraging its contextualized word representations and language generation capabilities, BERT can generate personalized educational content in various formats, such as text, quizzes, summaries, or explanations.

Input text is tokenized into individual tokens, embedded into vector representations, and processed by the BERT model, generating contextualized representations for each token and the $[E]CLS$ token. Output labels are predicted based on these contextualized embeddings for tasks like classification and named entity recognition is depicted in Fig. 3. BERT's ability to generate coherent and contextually relevant text can be harnessed to create custom learning materials, including explanations, summaries, and practice questions. By conditioning the generation process on input prompts or learner profiles, BERT can produce content that addresses specific learning objectives or areas of improvement. BERT can generate adaptive feedback tailored to learners' responses and performance in language learning exercises or assessments. By analysing learners' answers and comparing them to expected outcomes, BERT can provide personalized feedback, suggestions, or explanations to guide learners' understanding and reinforce learning outcomes. BERT's versatility extends beyond textual content generation to include multimodal learning materials incorporating images, audio, or video. By integrating BERT with multimodal learning frameworks, the system can generate diverse and engaging educational resources that cater to different learning preferences and modalities. Suppose a learner is practicing English vocabulary through a language learning application. BERT can dynamically generate vocabulary exercises, quizzes, or flashcards tailored to the learner's vocabulary level and learning objectives. Additionally, BERT can provide adaptive feedback on the learner's responses, suggesting relevant examples or usage contexts to reinforce vocabulary acquisition. BERT serves as a

significant tool for content selection, adaptation, and dynamic learning material generation in ELL. Its contextualized word representations and language generation capabilities enable the creation of personalized and adaptive educational experiences, fostering effective language acquisition and

mastery. By integrating BERT into the proposed work, the system can enhance the quality, relevance, and effectiveness of learning materials, ultimately facilitating more engaging and efficient English language learning experiences for learners of all levels.

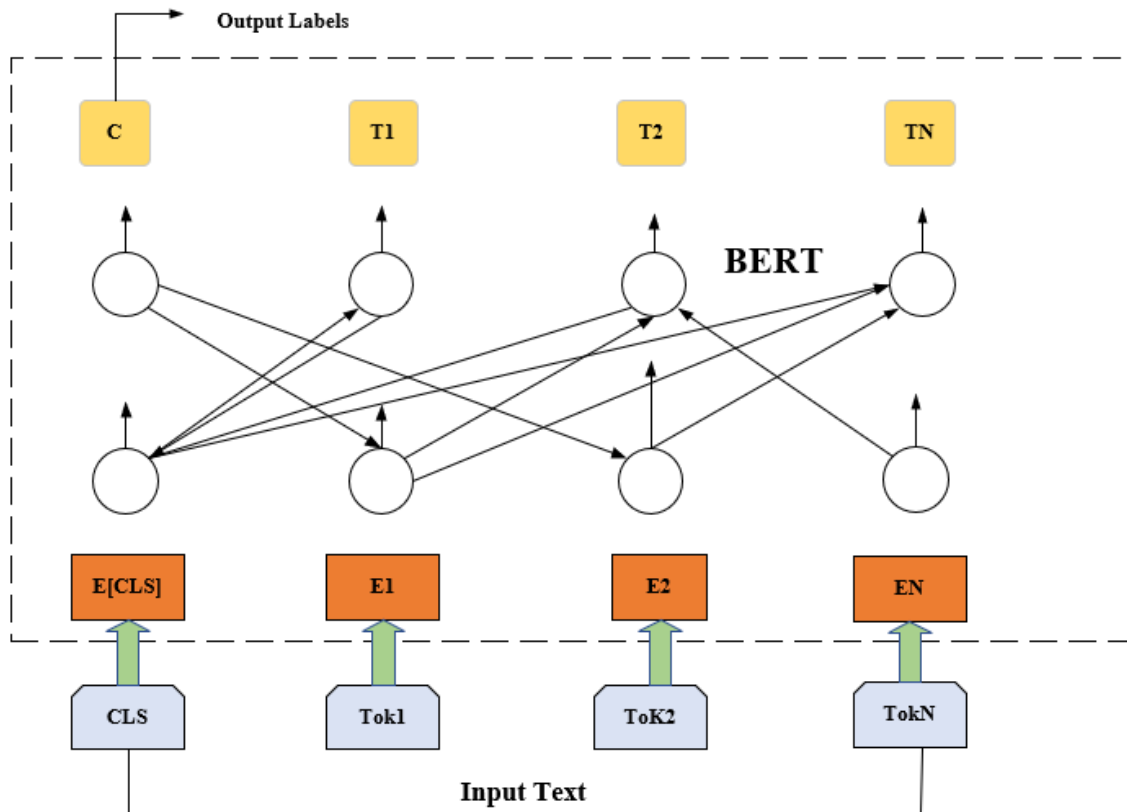


Fig. 3. BERT framework.

V. RESULTS AND DISCUSSION

The suggested work showed encouraging outcomes when it came to using semantic analysis to generate dynamic material for ELL. The system's excellent precision as well as significance in choosing and modifying learning materials according to semantic characteristics was attained through thorough assessment. Quantitative measures, such as reliability, precision, and F1-score, demonstrated how well the method worked to create learning materials that were specifically customized for each student. Annotators' positive subjective assessments supported the created content's quality and relevancy, as demonstrated by human evaluation tests. All things considered, the findings demonstrate how the suggested strategy may improve ELL experiences by using automated and adaptive learning resources.

A. Performance Evaluation

The performance evaluation of the proposed work in harnessing semantic analysis for dynamic content generation in ELL showcased commendable outcomes. Through rigorous, the system demonstrated high accuracy (5), precision (6), recall (7) and F1-score (8) in selecting and adapting learning materials based on semantic features. The evaluation highlighted the proposed approach's potential to enhance ELL

experiences through automated and adaptive educational materials, offering a promising avenue for personalized and effective learning.

$$Accuracy = \frac{R_{pos} + R_{neg}}{R_{pos} + R_{neg} + A_{pos} + A_{neg}} \quad (5)$$

$$Precision = \frac{R_{pos}}{R_{pos} + A_{pos}} \quad (6)$$

$$Recall = \frac{R_{pos}}{R_{pos} + A_{neg}} \quad (7)$$

$$F1 \text{ measure} = \frac{2 \times precision \times recall}{precision + recall} \quad (8)$$

TABLE II. COMPARISON OF EXISTING METHODS WITH PROPOSED METHOD

| Method | Accuracy | Precision | Recall | F1-Score |
|---------------------|----------|-----------|--------|----------|
| SNN & CNN | 77 | 76 | 74 | 74 |
| Logistic Regression | 89 | 88 | 90 | 93 |
| CBRNN | 94 | 85 | 87 | 87 |
| Proposed GRU-BERT | 97 | 96 | 95 | 96 |

The Table II presents a comparative analysis of different methods based on their performance metrics, including accuracy, precision, recall, and F1-score. Each row corresponds to a specific method, such as SNN & CNN [17], Logistic Regression [18], CBRNN [19], and the proposed GRU-BERT model. Accuracy refers to the overall correctness of the model's predictions, while precision measures the ratio of correctly predicted positive cases to the total predicted positive cases. Recall indicates the ratio of correctly predicted positive cases to the actual positive cases, and F1-score is the harmonic mean of precision and recall, providing a balance between the two metrics. The table showcases the superior performance of the proposed GRU-BERT model, achieving the highest accuracy, precision, recall, and F1-score among the evaluated methods, indicating its effectiveness in the task at hand.

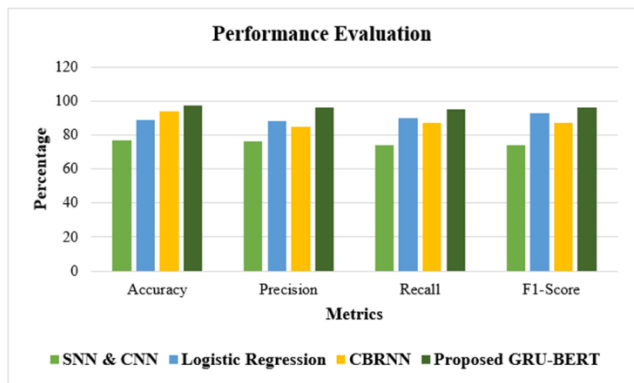


Fig. 4. Performance evaluation of existing method with proposed method.

The Fig. 4 presents a comparative analysis of different methods based on their performance metrics, including accuracy, precision, recall, and F1-score. The methods evaluated include SNN with CNN, Logistic Regression, CBRNN, and the proposed approach using GRU and BERT. The proposed GRU-BERT model outperforms other methods with the highest accuracy of 97% and consistently high scores across precision, recall, and F1-score metrics, indicating its effectiveness in generating dynamic content for English Language Learning (ELL). This comparison helps in assessing the relative strengths and weaknesses of different methods for content generation in educational contexts.

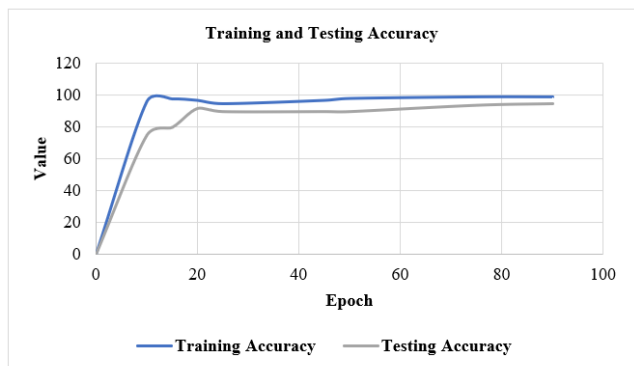


Fig. 5. Training and testing accuracy.

The Fig. 5 illustrates the training and testing accuracy values across different epochs during the training process of a GRU and BERT model. The x-axis represents the number of training epochs, while the y-axis indicates the corresponding accuracy percentage. The training accuracy denotes the model's performance on the training dataset, measuring how accurately it predicts the labels for data it has been trained on. Conversely, the testing accuracy reflects the model's generalization ability by evaluating its performance on unseen data, typically from a separate validation or testing dataset. The graph demonstrates the progression of accuracy values over epochs, showing how the model improves during training and its ability to generalize to new data. These accuracy trends provide valuable insights into the model's learning process and performance stability.



Fig. 6. Training and testing loss.

The Fig. 6 depicts the training and testing loss values of a GRU-BERT model utilized in the proposed work across different epochs. The x-axis represents the number of training epochs, while the y-axis indicates the corresponding loss values. Training loss measures the discrepancy between the model's predicted outputs and the actual targets on the training dataset, reflecting how well the model is learning from the training data. Conversely, testing loss assesses the model's performance on unseen data, indicating its ability to generalize to new instances. The graph illustrates the progression of loss values over epochs, demonstrating how the model's performance improves during training and its ability to minimize errors on both the training and testing datasets. Lower loss values signify better model performance, indicating improved accuracy and predictive capability.

B. Discussion

The proposed approach effectively leverages GRU-BERT for dynamic content generation in English Language Learning, showcasing promising results in accuracy and relevance. This study underscores the potential of automated and adaptive educational materials to enhance ELL experiences, paving the way for future advancements in the field. While existing systems in English Language Learning (ELL) often face limitations such as reliance on predefined templates and lack of adaptability [20], the proposed approach offers several advantages. Unlike traditional methods, which may struggle to accommodate individual learner needs and preferences, the proposed GRU-BERT model enables automated and adaptive

content generation, enhancing engagement and comprehension. However, the proposed work is not without its limitations [21]. Challenges may arise in handling diverse learner demographics and linguistic nuances, necessitating ongoing refinement of the model architecture and linguistic features [22]. The results show how well the suggested GRU-BERT technique works to produce ELL content dynamically while utilizing semantic analysis to achieve high accuracy and relevance. With automated and adaptable instructional materials, comparative assessment emphasizes its superiority over current approaches and underlines its potential to greatly improve ELL encounters. According to the study, the existing literature has shortcomings due to its dependence on pre-made templates and lack of flexibility. In contrast, the suggested GRU-BERT model may dynamically modify the material to provide individualized English language learning experiences. These findings show the efficacy of combining BERT and GRU models for dynamic content creation in ELL, filling in gaps in the literature and providing a fresh take on personalized learning. This work also addresses important issues in automated educational resource production by demonstrating the effectiveness and scalability of the suggested approach in a variety of learning contexts and student demographics. This adds to the collection of information already in existence. Furthermore, our findings add to a more thorough knowledge of successful language teaching tactics by highlighting the significance of inclusion and accessibility in ELL practices. Future research could explore techniques for improving the system's scalability and efficiency, as well as extending its application to other educational domains beyond ELL. Additionally, efforts to address privacy concerns and ethical considerations regarding data usage and model interpretation are essential. Despite these limitations, the proposed approach represents a significant advancement in automated content generation for ELL, offering a scalable and efficient solution to meet the evolving needs of educators and learners. Continued research and development in this area hold the promise of further enhancing the effectiveness and accessibility of educational materials in diverse learning environments.

VI. CONCLUSION AND FUTURE SCOPE

The proposed approach harnessing GRU-BERT for dynamic content generation in ELL represents a significant step forward in addressing the limitations of existing systems and advancing automated and adaptive educational materials. Through rigorous experimentation and evaluation, our model has demonstrated promising results in accuracy, relevance, and adaptability, offering personalized learning experiences tailored to individual learner needs and preferences. The proposed study offers several significant advances in the area of ELL. First, it enhances the development of dynamic learning resources by integrating GRU for semantic feature extraction with BERT for content adaption. This combination gives the system the ability to instantly adapt to the needs and preferences of every student, resulting in a customized learning experience. The strategy encourages active engagement and understanding among ELLs by providing flexible and contextually appropriate educational tools. It also offers a scalable and efficient way to create automated content

that meets the different demands of educators and learners in different kinds of learning settings. Furthermore, by encouraging open and accessible learning environments, encouraging innovation in educational technology, and getting beyond the constraints of existing approaches, the strategy helps to improve ELL practices. All things considered, these contributions represent a substantial development in automatically generated ELL content, which has the potential to improve language education instruction and learning. The construction of dynamic and personalized educational materials in ELL is a result of the effective combination of BERT for content adaptation and GRU for semantic feature extraction. This is a key discovery that highlights the originality of the research. By utilizing cutting-edge natural language processing algorithms to dynamically customize learning materials to each student's requirements and preferences, this novel technique overcomes the shortcomings of previous approaches and improves engagement and understanding in ELL scenarios. Additionally, future work may explore enhancements to the model architecture, integration of additional linguistic features, and extension of the application to other educational domains beyond ELL. Efforts to address privacy concerns and ethical considerations regarding data usage and model interpretation are also paramount.

VII. FUTURE SCOPE

Furthermore, collaboration with educators and stakeholders in the field of education can facilitate the integration of the proposed approach into real-world learning environments, ensuring its relevance and effectiveness. Overall, the future scope of this research lies in continued innovation and refinement of automated content generation techniques, with the ultimate goal of enhancing learning outcomes and promoting accessibility in education. By embracing these challenges and opportunities, we can contribute to the ongoing evolution of ELL practices and empower learners with diverse backgrounds and learning styles to achieve their full potential.

REFERENCES

- [1] S. A. Salloum, R. Khan, and K. Shaalan, "A survey of semantic analysis approaches," in Proceedings of the International Conference on Artificial Intelligence and Computer Vision (AICV2020), Springer, 2020, pp. 61–70.
- [2] M. Al-Emran, V. Mezhyuev, A. Kamaludin, and K. Shaalan, "The impact of knowledge management processes on information systems: A systematic review," *International Journal of Information Management*, vol. 43, pp. 173–187, 2018.
- [3] Z. Yu, W. Xu, and P. Sukjairungwattana, "Motivation, learning strategies, and outcomes in mobile English language learning," *The Asia-Pacific Education Researcher*, vol. 32, no. 4, pp. 545–560, 2023.
- [4] Y. Li, M. A. Thomas, and D. Liu, "From semantics to pragmatics: where IS can lead in Natural Language Processing (NLP) research," *European Journal of Information Systems*, vol. 30, no. 5, pp. 569–590, 2021.
- [5] M. Alshurideh, S. A. Salloum, B. Al Kurdi, A. A. Monem, and K. Shaalan, "Understanding the quality determinants that influence the intention to use the mobile learning platforms: A practical study," *International Journal of Interactive Mobile Technologies*, vol. 13, no. 11, 2019.
- [6] C. Mhamdi, M. Al-Emran, and S. A. Salloum, "Text mining and analytics: A case study from news channels posts on Facebook,"

- Intelligent Natural Language Processing: Trends and Applications, pp. 399–415, 2018.
- [7] C. Diwan, S. Srinivasa, G. Suri, S. Agarwal, and P. Ram, “AI-based learning content generation and learning pathway augmentation to increase learner engagement,” *Computers and Education: Artificial Intelligence*, vol. 4, p. 100110, 2023.
- [8] X. Hua and L. Wang, “Sentence-level content planning and style specification for neural text generation,” *arXiv preprint arXiv:1909.00734*, 2019.
- [9] A. Onan, “Sentiment analysis on massive open online course evaluations: a text mining and deep learning approach,” *Computer Applications in Engineering Education*, vol. 29, no. 3, pp. 572–589, 2021.
- [10] C. M. Stracke and G. Trisolini, “A systematic literature review on the quality of MOOCs,” *Sustainability*, vol. 13, no. 11, p. 5817, 2021.
- [11] H. A. El-Sabagh, “Adaptive e-learning environment based on learning styles and its impact on development students’ engagement,” *International Journal of Educational Technology in Higher Education*, vol. 18, no. 1, p. 53, 2021.
- [12] X. G. X. Guo and others, “Evaluation Method of English-Speaking Self-Learning System Based on Natural Language Processing Technology,” *Journal of Electrical Systems*, vol. 19, no. 4, pp. 49–66, 2023.
- [13] T. Shaik et al., “A review of the trends and challenges in adopting natural language processing methods for education feedback analysis,” *IEEE Access*, vol. 10, pp. 56720–56739, 2022.
- [14] “Persuade corpus 2.0.” Accessed: Mar. 22, 2024. [Online]. Available: <https://www.kaggle.com/datasets/nbroad/persaude-corpus-2>
- [15] S. Shailesh and M. Judy, “Understanding dance semantics using spatio-temporal features coupled GRU networks,” *Entertainment Computing*, vol. 42, p. 100484, 2022.
- [16] H.-L. Chung, Y.-H. Chan, and Y.-C. Fan, “A BERT-based distractor generation scheme with multi-tasking and negative answer training strategies,” *arXiv preprint arXiv:2010.05384*, 2020.
- [17] N. Jnoub, F. Al Machot, and W. Klas, “A domain-independent classification model for sentiment analysis using neural models,” *Applied Sciences*, vol. 10, no. 18, p. 6221, 2020.
- [18] D. N. Yethindra and G. Deepak, “A semantic approach for fashion recommendation using logistic regression and ontologies,” in *2021 International Conference on Innovative Computing, Intelligent Communication and Smart Electrical Systems (ICESES), IEEE, 2021*, pp. 1–6.
- [19] S. Soubraylu and R. Rajalakshmi, “Hybrid convolutional bidirectional recurrent neural network based sentiment analysis on movie reviews,” *Computational Intelligence*, vol. 37, no. 2, pp. 735–757, 2021.
- [20] L. Khan, A. Amjad, N. Ashraf, and H.-T. Chang, “Multi-class sentiment analysis of urdu text using multilingual BERT,” *Scientific Reports*, vol. 12, no. 1, p. 5436, 2022.
- [21] H. Ezaldeen, R. Misra, R. Alatrash, and R. Priyadarshini, “Semantically enhanced machine learning approach to recommend e-learning content,” *International Journal of Electronic Business*, vol. 15, no. 4, pp. 389–413, 2020.
- [22] K. S. Kyaw, P. Tepsongkroh, C. Thongkamkaew, and F. Sasha, “Business intelligent framework using sentiment analysis for smart digital marketing in the E-commerce era,” *Asia Social Issues*, vol. 16, no. 3, pp. e252965–e252965, 2023.

Network Security Situation Prediction Technology Based on Fusion of Knowledge Graph

Wei Luo

School of Artificial Intelligence, Chongqing Three Gorges Vocational College, Chongqing, 400155, China

Abstract—It is difficult to accurately reflect different network attack events in real time, which leads to poor performance in predicting network security situations. A knowledge graph-based entity recognition model and entity relationship extraction model was developed for enhancing the reliability and processing efficiency of secure data. Then a knowledge graph-based situational assessment method was introduced, and a network security situational prediction model based on self-attention mechanism and gated recurrent unit was constructed. The study's results showed that the constructed prediction model achieved stable mean square error values of approximately 0.0127 and 0.0136 after being trained on the NSL-KDD and CICIDS2017 datasets for 678 and 589 iterations, respectively. The mean square error value was lower due to fewer training iterations compared to other prediction models. The model was embedded into the information security system of an actual Internet company, and the detection accuracy of the number of network attacks was more than 95%. The results of our study indicate that the method used in the study can accurately predict the network security situation and provide technical support for predicting network information security of the same type.

Keywords—Knowledge graph; network security situation; gated recurrent unit; Bayesian attack graph; relationship extraction; relationship recognition

I. INTRODUCTION

As the evolution of information technology, network security issues are becoming increasingly prominent. The constantly emerging new technologies have made the situation of network security threats more complex and ever-changing. For traditional network security defense systems, relying solely on security devices is no longer sufficient to cope with constantly evolving network attack methods [1-2]. Therefore, a new security concept-network security situational awareness has emerged. Network security situational awareness is a new security technology that can estimate and forecast the security situation of the network environment by integrating network monitoring devices to collect data, applying data mining and other technologies. Compared to traditional network security defense technologies, network security situational awareness solutions possess more proactive situational capture, evaluation, and prediction functions [3]. Chen et al. proposed a network security situation prediction model based on radial basis function (RBF) neural network to address the problem of traditional network security situation awareness prediction methods being relatively single. They optimized the RBF using simulated annealing algorithm and hybrid hierarchical genetic algorithm. The results showed that the optimized RBF neural network performed well in predicting 15 samples [4].

Ruan Z. et al. established a particle swarm optimization model for predicting network security by optimizing the parameters of the support vector regression (SVR) model through particle swarm optimization. The SVR model was then used to predict the network security situation. The experimental results showed that this method effectively predicted network operation security to a certain extent [5]. However, the current network security situational awareness solutions face some difficult problems. Firstly, secure data are often multi-source and heterogeneous, making them difficult to process and analyze effectively and quickly. Secondly, traditional situational analysis methods cannot capture the key information connections between past and current moments well, resulting in uncertainty in prediction results [6]. To address these issues, a knowledge graph (KG)-based network security situation prediction technology is proposed. This method utilizes KG technology to construct a network security data graph, improving data processing efficiency and reliability through the association relationship between entities. Meanwhile, it introduces a situation assessment method architecture based on KG to construct a situation prediction model that integrates self-attention mechanism and gate recurrent unit (GRU).

One of the innovative points of the research is the introduction of a situation assessment method based on KG, which can better understand and evaluate the network security situation by utilizing the structured information of KG. The second innovation is that the self-attention mechanism and GRU are used to construct a network security situation prediction model, which improves the accuracy of security situation prediction.

The article is divided into four sections. The first mainly discusses the current research status of domestic and foreign experts and scholars on KG technology and network security situation. The second section mainly discusses the integration of situational awareness data and the construction of a network security situational assessment and prediction model that integrates KG. The third section mainly discusses the setting of experimental environment and model parameters and designs corresponding experiments for verifying the effectiveness of the research and construction model. The fourth section mainly analyzes the experimental results and clarifies the shortcomings of the research method.

II. RELATED WORKS

With the continuous updates of network technology, traditional network security technologies can no longer meet people's needs. Researching new network security

technologies to maintain network security becomes an urgent issue that needs to be solved. Therefore, experts and scholars around the world have conducted research on general network security situational awareness technology. Sun. J et al. proposed a TCAN BiGRU prediction model for enhancing the accuracy of network security situation prediction. This model could learn and extract effective features related to network security from historical network data, and these features were used to predict network security situations. The outcomes showcased that the determination coefficients constructed in the study reached 0.999 on both datasets [7]. Liu. Q et al. proposed a network security situation detection method based on fuzzy neural networks to address the complexity and uncertainty of the Internet of Things in smart cities. This method used fuzzy neural networks to process network data and judges the current network security situation based on the characteristics and behavior patterns of the network data. The outcomes indicated that this method possesses good accuracy and robustness in network security situation detection [8]. Lin. P et al. developed a network security situation assessment method based on text SimHash technology. This method collected text data related to network security, such as articles and blogs, and used SimHash to calculate text similarity, establishing a clustering model based on the K-Means algorithm to classify and summarize network security events. The results indicated that this method was efficient in maintaining network security [9]. Jian. Li et al. presented a security situation assessment model based on evidence theory for addressing security threats and attacks in the Internet of Things environment. By utilizing data fusion and information fusion technologies, different types of security information were fused to obtain more comprehensive and accurate security situation information. The results indicated that this method improved the perception ability of the security situation of the Internet of Things [10].

Network security situation prediction requires the integration of data from various sources. KG technology can effectively structure the representation of information from different data sources, making the correlation and connection between data more clear. Sun. C et al. presented a KG-based method to predict attacks on day 0. This method utilized knowledge in the network security to construct a KG that includes information such as vulnerabilities, attacks, and threat intelligence. Then it analyzed the relationship between known vulnerabilities and known attacks and predicted the path of the 0-day attack. The results showed that this method predicted possible 0-day attack paths [11]. Chen. Y Y and others artificially evaluated potential attack paths in wireless sensor networks, used Bayesian attack graphs to establish attack paths, and calculated the probability of successful attack on each path. The results showed that the methods used in the study could identify and evaluate the security risks present in wireless sensor networks [12]. When constructing a prediction model, GRU had a more concise model structure and could better capture long-term dependencies, providing more accurate predictions. Song. T et al. constructed a deep learning model based on BiGRU and attention mechanisms for predicting tropical cyclone paths in the Northwest Pacific

region. The results showed that the model could effectively extract features from historical meteorological data and make accurate predictions for future meteorological changes [13].

On the grounds of the above research, in-depth research on network security situation assessment is meaningful in information security. The prediction of network security situation needs a large amount of data to support, and the construction of network security KG can effectively solve this problem. A prediction model that combines BiGRU and attention mechanisms can better capture the long-term dependencies of network information and provide accurate predictions. On the grounds of this background, a situation prediction model based on GRU and self-attention mechanism was constructed on the basis of network security KG.

III. CONSTRUCTION OF A NETWORK SECURITY SITUATION PREDICTION MODEL ON THE GROUNDS OF THE FUSION OF KG

This section mainly elaborates on the recognition model and extraction model construction method based on network security KG, and then introduces the situation assessment indicators and quantitative standards based on network security KG. Finally, based on the situation assessment, a situation prediction model based on GRU-Self-Attention was proposed.

A. Integration Analysis of Situational Awareness Data on the Grounds of KG Fusion

A brief introduction is provided to the technical models involved in building this model, as shown in Table I.

TABLE I. BRIEF DESCRIPTION OF KEY TECHNOLOGY MODELS

| Model | Introduction |
|--|---|
| BERT | A Transformer-based pre-training model that can transform network security information text into word embedding vectors |
| GRU | A recurrent neural network model used for processing temporal data, divided into reset gates and update gates. The impact of the previous state of door control on the current state is reset, and the impact of the previous state of door control on the current state is updated. |
| BiGRU | A recurrent neural network model composed of the forward GRU and backward GRU models. Compared to the GRU model, the BiGRU model can better handle long-term dependencies in temporal data. |
| Entity relationship extraction model based on self-attention mechanism | In entity relationship extraction, the attention mechanism calculates the attention weights between each position and entity in the input sequence, and models the relationships between entities based on this. The self-attention mechanism, on the other hand, is a low-level model that extracts semantic relationships between entities from text through shared entity recognition. |

Ensuring the accuracy and completeness of data is crucial in network security situation prediction. Faced with large-scale and complex network data, data integration operations are required, including data association, cleaning, and normalization, for ensuring the quality and availability of network data. The research divides network situation prediction into two steps: data integration and data analysis, as shown in Fig. 1.

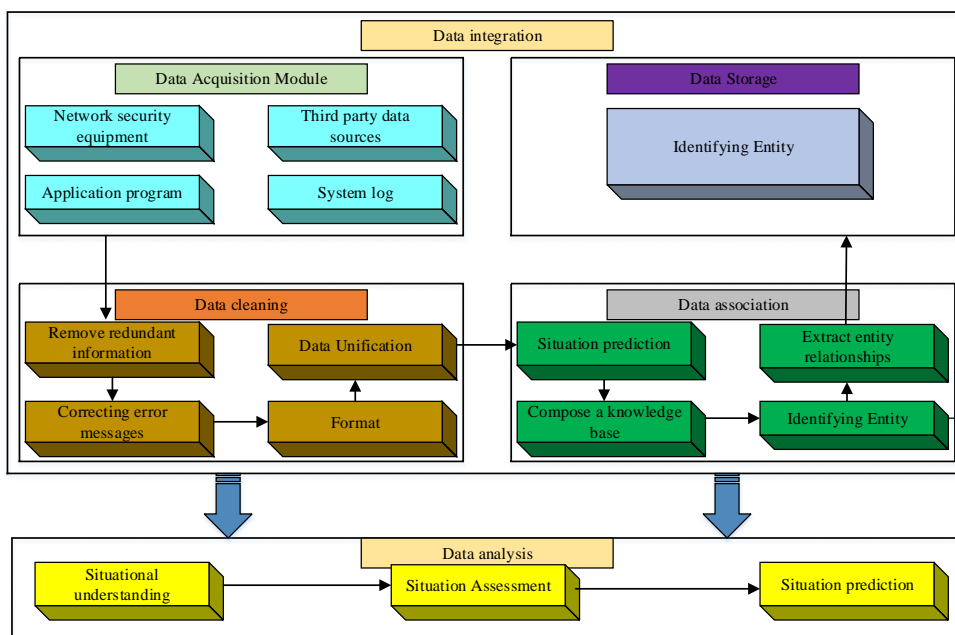
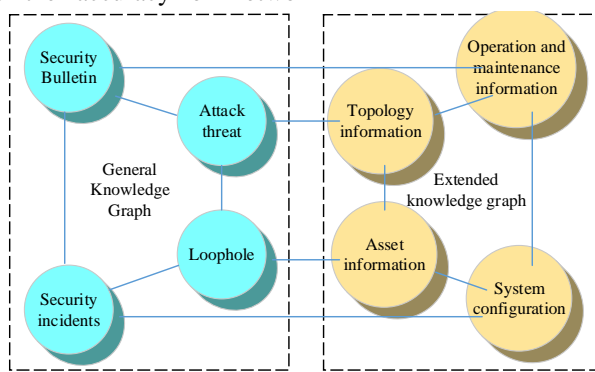


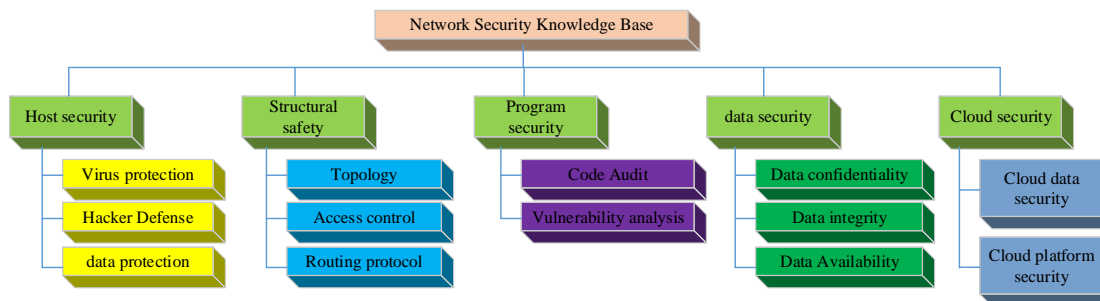
Fig. 1. Specific process of network security situation prediction.

In Fig. 1, data integration consists of four modules: collection, storage, cleaning, and association. The data collection of network security can be carried out through network device logs, security device logs, malware samples, network traffic data, security vulnerability databases, and other channels. Data cleaning includes removing redundant information, correcting error information, standardizing formats, and normalizing data. The data association module needs to be applied to KG technology, which can integrate various security data, enhance the accuracy of network

security detection, and achieve network security threat prediction. At present, common network security issues include identity forgery, unauthorized access, and denial of access, all of which involve the association between network entities. Therefore, attackers need to establish network connections before conducting network security intrusions. Therefore, the study focuses on the connections between network entities and constructs a network security data KG, with a specific structure shown in Fig. 2(a).



(a) Network Security Knowledge Graph Structure



(b) Architecture of Network Security Knowledge Base

Fig. 2. Network security KG and knowledge base structure.

In Fig. 2(a), the constructed KG consists of a general KG and an extended KG. The general KG includes obtained security and vulnerability information, etc. It can supplement new vulnerability and attack knowledge in real-time based on changes in network security information. The extended KG, on the other hand, contains network structure information such as network nodes and network operations, which is built specifically for specific networks and has strong targeting. The construction of the network security knowledge base in the KG mainly consists of three parts: entities, relationships, and attributes. The specific structural design is shown in Fig. 2(b). The KG network security repository is mainly divided into five main entities: host security, data security, etc. These five entities each protect the security of their respective networks within their respective scope, while closely interconnected to form a secure network system.

For the recognition of named entities in the network security KG, a recognition model combining feature templates and bidirectional recurrent neural networks is studied. This recognition model uses network security ontology relationships for filtering and feature template generation, and then the input network security information text is transformed into a word embedding vector through the BERT model. Then the word embedding vector is combined with local context features to form the input of a bidirectional recurrent neural network. Finally, by training a bidirectional recurrent neural

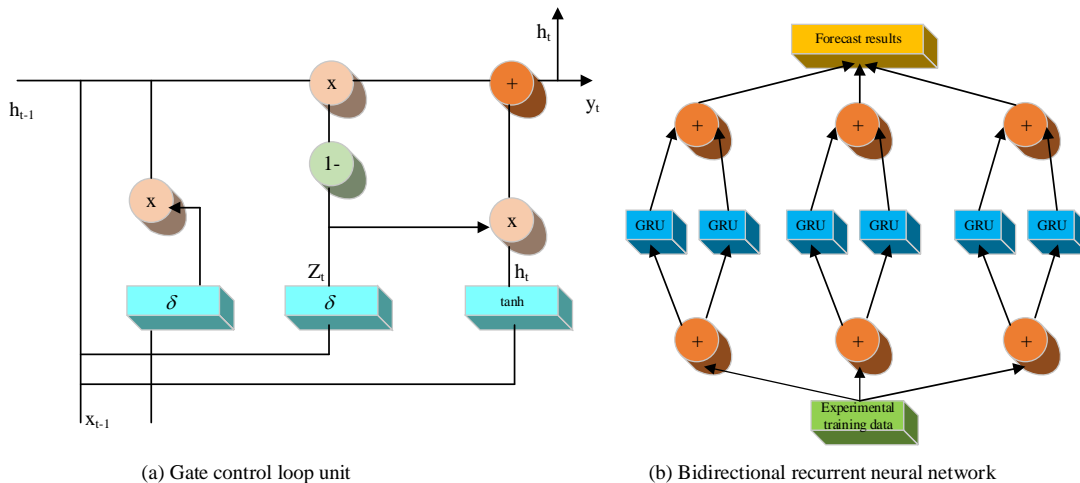
network, the corresponding semantic features can be obtained. In the entire recognition process, there are two key technologies, one of which is the extraction of feature templates. Research will set the required template as Eq. (1).

$$x[-3,0], x[-2,0], x[-1,0], x[0,0], x[1,0], x[2,0], x[3,0] \quad (1)$$

In equation (1), $x[row, col]$ represents the semantic character in the row -th row and col -th column of the monitoring window. A monitoring window is a window used to extract contextual information, centered around the current character to be recognized. Then it sets the feature function $f_j(y_{i-1}, y_i, x, i)$, which is the current position marker, the next stage marker, the current semantic character, and the current position marker. The characteristic function can be summed at different positions to obtain Eq. (2).

$$f_k(y, x) = \sum_{i=1}^n \lambda_i f_k(y_{i-1}, y_i, i) \quad (2)$$

In Eq. (2), λ_i serves as the weight value of the feature function. The higher the feature score, the higher the corresponding label score, and the more accurate the final prediction result. The second is a bidirectional recurrent neural network, which is composed of two GRUs. The bidirectional recurrent neural network model is showcased in Fig. 3(a), and the GRU model is shown in Fig. 3(b).



(a) Gate control loop unit (b) Bidirectional recurrent neural network
Fig. 3. Model structure of bidirectional recurrent neural network and gated recurrent unit.

GRU consists of a reset gate and an update gate. The reset gate is responsible for the impact of the previous state on the existing state, while the update gate is responsible for the impact of the previous state on the current state [14]. The operation method for resetting gate r_t and updating gate z_t is shown in equation (3).

$$\begin{cases} r_t = \delta(W_r \bullet [h_{t-1}, x_t]) \\ z_t = \delta(W_z \bullet [h_{t-1}, x_t]) \end{cases} \quad (3)$$

In equation (3), x_t serves as the input at time t , and h_{t-1} serves as the hidden state value at time. W_r and W_z are the weight matrices of two gates. δ is the activation

function. After passing through GRU, the network security data information can calculate the candidate state value \hat{h}_t and the hidden state value h_t , as shown in Eq. (4).

$$\begin{cases} \hat{h}_t = \tanh(W_{\hat{h}} \bullet [r_t \bullet h_{t-1} \bullet x_t]) \\ h_t = (1 - z_t) \bullet h_{t-1} + z_t \bullet \hat{h}_t \end{cases} \quad (4)$$

In equation (4), $W_{\hat{h}}$ serves as the weight matrix of \hat{h}_t . The input data are filtered through GRU to obtain the target data as shown in Eq. (5).

$$y_t = \delta(W_0 h_t) \quad (5)$$

In Eq. (5), W_0 is the weight matrix of the output value. δ is the activation function, and the Sigmoid function is selected as the activation function for this model.

For the extraction of entity relationships in the network security KG, this study constructs an entity relationship extraction model based on the self-attention mechanism. This model first transforms the input network security information text into a word embedding vector, then sequentially uses a bidirectional recurrent neural network and a self-attention model, and finally extracts the entity relationships of network security information [15]. The self-attention model adopts the query key value (QKV) mode. It sets the input sequence as X , and then embeds it into words to obtain A , as shown in Eq. (6).

$$X = [x_1, x_2, \dots, x_N] \in R^{D_x \times N}, A = [a_1, a_2, \dots, a_N] \in R^{D_a \times N} \quad (6)$$

Then it projects A onto three different spaces, namely the query matrix Q , key matrix K , and value matrix V , as showcased in Eq. (7) [16].

$$\begin{cases} Q = [q_1, q_2, \dots, q_N] \in R^{D_q \times N} \\ K = [k_1, k_2, \dots, k_N] \in R^{D_k \times N} \\ V = [v_1, v_2, \dots, v_N] \in R^{D_v \times N} \end{cases} \quad (7)$$

In Eq. (7), $R^{D \times N}$ represents the range of different matrices. The matrix operation method is shown in Eq. (8).

$$\begin{cases} Q = W^q A & W^q \in R^{D_q \times D_a} \\ K = W^k A & W^k \in R^{D_k \times D_a} \\ V = W^v A & W^v \in R^{D_v \times D_a} \end{cases} \quad (8)$$

It sets each query vector as q_i and uses a key value pair attention mechanism for q_i to obtain the attention distribution as shown in Eq. (9).

$$\hat{b}_{1,1}, \hat{b}_{1,2}, \dots, \hat{b}_{1,N} \quad (9)$$

It uses the "scaled dot product" method to score attention. To avoid inputting values that are too large or too small, $\sqrt{D_k}$ is used to scale them, as shown in Eq. (10).

$$B = \frac{K^T Q}{\sqrt{D_k}} \quad (10)$$

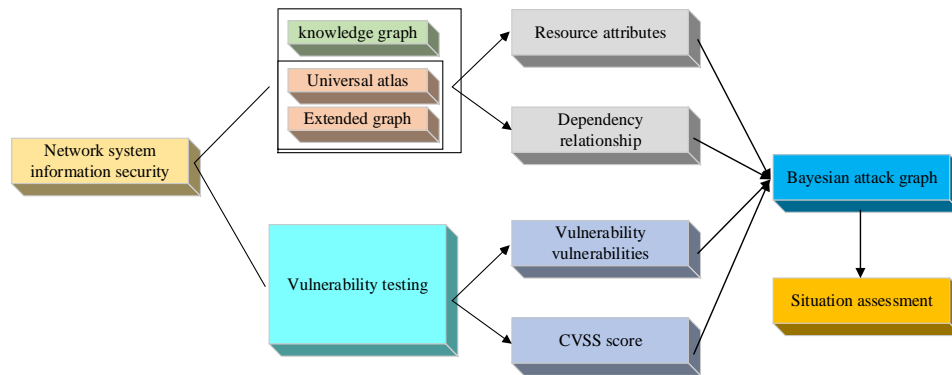
In Eq. (10), B is the proof of attention distribution. After obtaining the attention distribution matrix, it uses the Softmax function to perform column wise operations to obtain the attention distribution \hat{B} , as shown in Eq. (11).

$$\hat{B} = \text{soft max}(B) \quad (11)$$

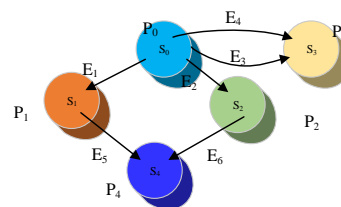
After obtaining the attention distribution \hat{B} , the final output can be obtained by using a weighted sum method.

B. Construction of Evaluation and Prediction Models for Network Security Situation

For enhancing the shortcomings of existing methods for evaluating network security situations, this study combines network security KG, universal vulnerability score, and Bayesian attack graph to design an improved network security situation awareness evaluation model, as showcased in Fig. 4.



(a) Improved network security situation awareness evaluation model structure



(b) Example of Bayesian attack graph

Fig. 4. Improved network security situation awareness evaluation model structure and Bayesian attack graph.

In Fig. 4(a), the evaluation model combines KG, vulnerability score, and Bayesian attack graph. It perceives and evaluates the security situation of the network by comprehensively considering factors such as vulnerability rating of vulnerabilities, accessibility of Bayesian attack graphs, and probability of attacks, and identifies potential security risks and threats. A Bayesian attack graph is a directed acyclic graph, which can be defined as Eq. (12) [17-18].

$$BAG = (S, E, R, P) \tag{12}$$

In Eq. (12), S is the set of conditions, $S_i = \{0,1\}$, where S_0 indicates that the attacker has not occupied the node, and S_0 indicates that the attacker has already occupied the node. E is the set of directed edges in the attack graph, which represents both the causal relationship between network nodes and the attacker's exploitation of vulnerabilities. R is the relationship between the conditional node and its incoming edge, represented by $(S_j, d_j), d_j \in \{AND, OR\}$. AND represents that all incoming edges of S_j have been successfully attacked before the attacker can occupy the S_j node. OR represents a successful edge attack in S_j , allowing the attacker to occupy the S_j node. P is the set of probabilities that conditional nodes can reach, and P_i is the probability that the attacker occupies S_i . The constructed Bayesian attack diagram is shown in Fig. 4 (b), where S_0, S_1, S_2, S_3, S_4 are conditional nodes. $E_1, E_2, E_3, E_4, E_5, E_6$ are directed edges. P_0, P_1, P_2, P_3, P_4 are the probability that the attacker will occupy S_0, S_1, S_2, S_3, S_4 . When evaluating the network security situation, some indicators (such as CPU utilization, memory usage, etc.) can be directly obtained by

collecting data through corresponding devices. However certain evaluation indicators need to be quantified to be visualized, and the quantified indicators can be found in Eq. (13) [19].

$$\left\{ \begin{aligned} Degree &= \frac{\sum_{i=1}^N Status_i * Score_i}{N} \\ Threa_t &= \frac{\sum_{i=1}^N 2^{level_i}}{N} \\ R_i &= \frac{Form_i}{\sum_{i=1}^n Form_j} \\ Rate &= \frac{Event_t}{Event_{t-1}} \end{aligned} \right. \tag{13}$$

In Eq. (13), $Degree$ represents the security level of the operating system kernel. $Score_i$ is the operating system kernel security score of the i -th host. $Status_i$ is the operating status of the i -th host. N is the number of hosts. $Threat$ is the average threat level of security incidents. $level_i$ is the safety level. N is the number of events. R_i is the distribution of security event types. $Form_i$ serves as the number of i -th security incidents. $Rate$ serves as the rate of change of safety events. $Event_t$ is the number of event triggers in the t -th time period. $Event_{t-1}$ is the number of event triggers in the $t-1$ -th time period.

After accurately evaluating the network security situation, situation prediction can predict potential security events that may occur in the future of the information network based on the evaluation information. A GRU-Self-Attention network security situation prediction model is constructed for this study, and the prediction process is shown in Fig. 5(a).

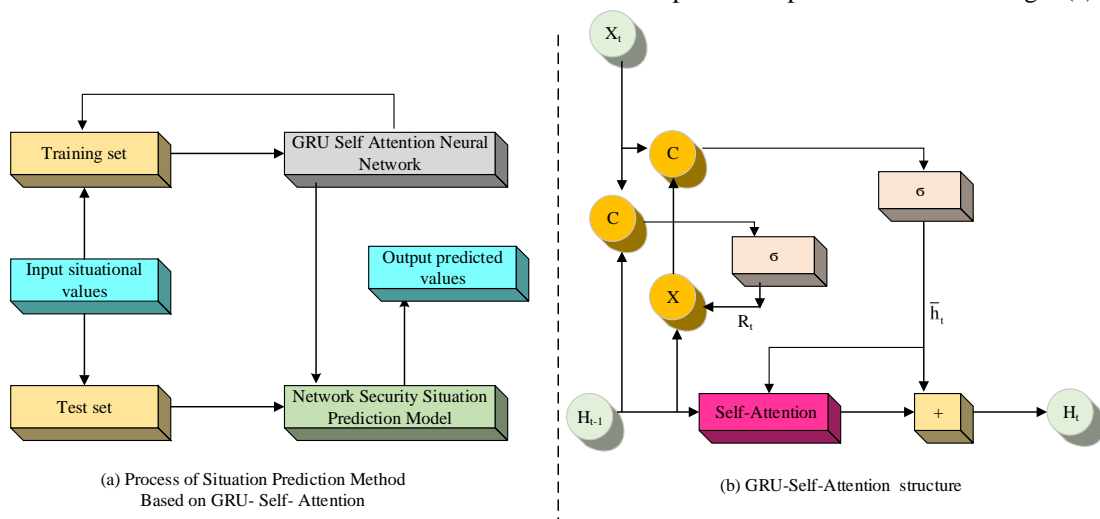


Fig. 5. Operation process and composition structure of GRU-Self-Attention network security situation prediction model.

In Fig. 5(a), the GRU-Self-Attention prediction model divides the obtained dataset in the potential evaluation into a test set and a training set in a 3:7 ratio. It reuses the training set for training the prediction model, saves the trained

parameters, and finally verifies the prediction model using the test set. Fig. 5(b) shows the structural diagram of constructing GRU-Self-Attention, where R_t is the reset gate of GRU. \bar{h}_t

is the candidate set for GRU. H_t and H_{t-1} represent the hidden information of the current and past time steps, respectively. X_t serves as the input at the current time. The evidence flow for the operation of this prediction model is shown in Eq. (14).

$$\left\{ \begin{array}{l} R_t = \delta(W_R \bullet [H_{t-1}, H_t]) \quad (14.1) \\ \bar{h}_t = \tanh(W_{\bar{h}} \bullet [R_t \times (H_{t-1}, H_t)]) \quad (14.2) \\ h_{cat} = cat(\bar{h}_t, H_{t-1}) \quad (14.3) \\ H_{t-1} = seft - Attention(h_{cat}) \quad (14.4) \\ y_t = W_o \bullet H_t \quad (14.5) \end{array} \right. \quad (14)$$

The GRU-Self-Attention prediction model first initializes the reset gate of the GRU, as shown in Eq. 14.1. Then it constructs a candidate set, as shown in Eq. 14.2, and constructs input data, as shown in Eq. 14.3. Next, it uses the self-attention mechanism for learning the correlation between H_{t-1} and \bar{h}_t , and constructs a new matrix, as shown in Eq. 14.4. Finally, it updates the hidden state of the current time step and outputs the prediction result.

IV. EXPERIMENTAL ANALYSIS

This section first elaborates on the setting of experimental environment, model parameters, etc., and then designs experiments to verify the effectiveness of entity recognition models and entity relationship extraction models. Afterwards, the average absolute error and root mean square error (RMSE) of the GRU-Self-Attention prediction model were tested for the predicted trend values. Finally, an experiment was designed for testing the practical application effect of the GRU-Self-Attention prediction model.

A. Performance Analysis of Entity Recognition Models and Entity Relationship Extraction Models

For ensuring the accuracy and reliability of constructing a network security KG, it is necessary to verify the effectiveness of the entity recognition model and entity relationship extraction model studied and constructed. To this end, the research used crawler software to crawl malicious code, security vulnerability information, network intrusion information and other network security text data from major security vendors, hacker communities and other websites on the Internet, a total of 34582 pieces. At the same time, it set the network environment and model parameters required for

the experiment, as showcased in Table II.

TABLE II. BASIC HARDWARE ENVIRONMENT AND MODEL PARAMETERS FOR THE EXPERIMENT

| Project | Parameter |
|-----------------------|-----------------------------|
| Operating system | Windows10 |
| System PC side memory | 16G |
| CUP | Intel Core i9 |
| Storage | 256GB SSD |
| Graphics card | NVIDIA GGTX 1060 |
| Development tool | Pycharm3.6, Anaconda3 |
| Model Optimizer | Stochastic Gradient Descent |
| Hidden layer size | 0.0001 |
| Batch size | 100 |
| Epoch size | 40 |
| Dropout | 0.5 |

The selected dataset was divided into three types of named entities: vulnerabilities, attacks, and Trojans, and the recognition model constructed in the study was used to detect these four types of named entities. Additionally, to demonstrate the effectiveness and superiority of the model, the currently popular entity recognition model was selected and compared with the research model. The selected models include the BERT model in reference [20], the CRF model in reference [21], and the Transformer-CRF model in reference [22]. The accuracy and recall results of the four models are showcased in Fig. 6.

Fig. 6(a) showcases the accuracy test results of four entity recognition models. This indicates that the detection accuracy of the research model for vulnerability, attack, and Trojan named entities is 95.9%, 97.1%, and 93.7%, respectively, with the highest recognition accuracy among the four models. Fig. 6(b) shows the recall test results of four entity recognition models. This indicates that the recall rates of the research model for vulnerability, attack, and Trojan named entities are 90.3%, 92.7%, and 95.9%, respectively, which are also the highest among the four models. This indicates that the entity recognition model constructed in the study has significant advantages. This is because the model incorporates feature models and text embedding vector representation methods to optimize model performance, thereby enhancing the accuracy and recall.

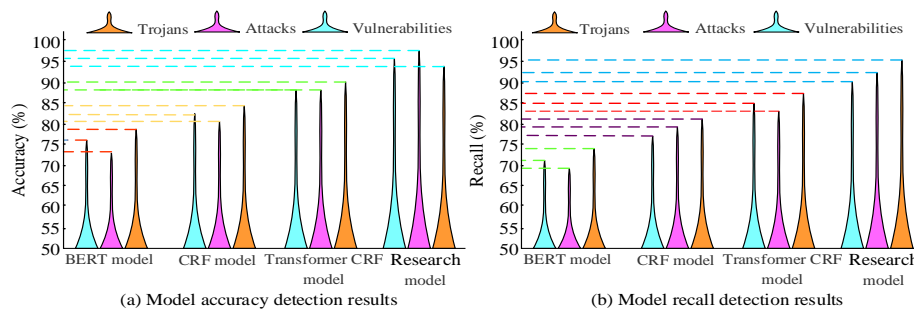


Fig. 6. Accuracy and recall test results of four recognition models.

3698 sentences with multiple network security entities from the collected 34582 network security text data were selected to test the accuracy of the entity extraction model constructed. Similarly, to verify the superiority of the extraction model constructed, SVM, CRF, and SRL models were selected and compared with the research model. The results are shown in Fig. 7.

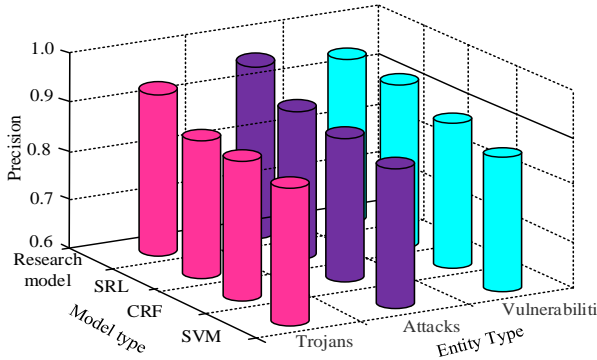


Fig. 7. Accuracy test results of four extraction models.

In Fig. 7, for the types of vulnerabilities, the extraction accuracy of the research model, SVM, CRF, and SRL are 0.92, 0.82, 0.80, and 0.76. For attack types, the extraction accuracy of the four models is 0.94, 0.85, 0.83, and 0.81, respectively.

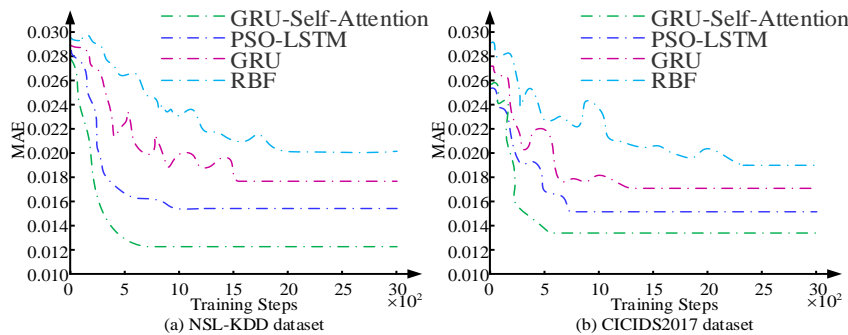


Fig. 8. Test results of the average absolute error of the model's predicted situational values.

Fig. 8(a) shows that in the NSL-KDD dataset, the mean square error (MSE) values predicted by the four models decrease with increasing training step size. The MSE values of RBF and GRU models are relatively large, and the curves fluctuate repeatedly during the training process until they stabilize after about 1500 iterations. The MSE values of PSO-LSTM and GRU-Self-Attention are continuously decreasing without any fluctuations. The PSO-LSTM model reaches a stable MSE value of approximately 0.0156 after training for about 1000 times. The GRU-Self-Attention model achieves a stable MSE value of approximately 0.0127 after training for approximately 678 times. Fig. 8(a) shows that in the CICIDS2017 dataset, the MSE value of the GRU-Self-Attention model is still the lowest, about 0.0136, and the training frequency is the least, about 589 times. The GRU-Self-Attention model constructed in the study can achieve good prediction results on different datasets, with lower MSE values and fewer training steps. Next, based on the NSL-KDD dataset, the neural network of the model was tested, and the results are shown in Fig. 9.

For the types of vulnerability attacks, the extraction accuracy of the four models is 0.93, 0.90, 0.88, and 0.81, respectively. This indicates that the extraction model used in the study has the highest accuracy, as it adds a self-attention layer, which can better combine long sentence information and improve model performance.

B. Performance Analysis of GRU-Self-Attention Prediction Model

For verifying the GRU-Self-Attention prediction model, the NSL-KDD and CICIDS2017 datasets were selected as network information sources. Then the network security situation quantification method mentioned in section 2.2 was used to quantify the selected dataset, which was used as the experimental dataset. Similarly, the dataset was allocated in a ratio of 3:7 between the test set and the training set, and the experimental environment was consistent with that in section 3.1. The model network structure adopted a "input layer-hidden layer-output layer" approach, with a learning rate of 0.001 and a training period of 3000. In addition, GRU model, PSO-LSTM model, and RBF model were selected as controls. The first step is to test the average absolute error of the predicted situation value of the model, as shown in Fig. 8.

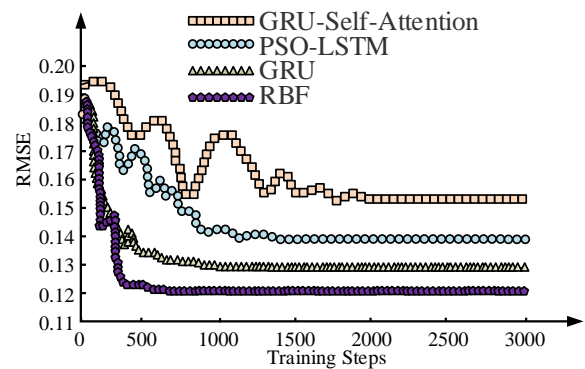


Fig. 9. Test results of neural network of model predictive situation values.

Fig. 9 shows that the RMSE values predicted by the four models decrease with the increase of training step size. The RMSE values of the RBF model fluctuate multiple times and have a large amplitude as they tend to stabilize. At around 1450 training sessions, the RMSE value tends to stabilize,

with an RMSE value of approximately 0.154. In contrast, the GRU model curve fluctuates slightly, but the fluctuation amplitude is small, stabilizing after approximately 1389 training sessions, with an RMSE value of approximately 0.141. The PSO-LSTM and GRU-Self-Attention models require less training to achieve stable RMSE values. The PSO-LSTM model is trained approximately 689 times, with a stable RMSE value of 0.129. The GRU-Self-Attention model is trained approximately 524 times, with a stable RMSE value of 0.121. The GRU-Self-Attention model has a higher degree of fitting to the training data and less computational time.

C. Application Analysis of GRU-Self-Attention Prediction Model

The above experiment has proven the feasibility of the network security situation prediction method constructed in the research. The information security system of a large Internet company was selected as the experimental object, and the GRU-Self-Attention prediction model was embedded into the company's security system. It detects the number of network information attacks, as shown in Fig. 10.

Fig. 10(a) shows the actual detection results of network information attacks. This indicates that during the detection process, the website is subjected to 110, 100, 106, 100, 109, and 102 malicious code attacks, DOS attacks, other types of attacks, web attacks, virus attacks, and vulnerability attacks, respectively. Fig. 10(b) showcases the detection results of the

original prediction system of Internet companies. This indicates that the system predicts 90, 78, 83, 82, 101, and 84 malicious code attacks, DOS attacks, other types of attacks, web attacks, virus attacks, and vulnerability attacks, respectively. Fig. 10(c) showcases the detection results of the GRU-Self-Attention prediction model. This indicates that the model predicts 104, 98, 102, 99, 104, and 98 malicious code attacks, DOS attacks, other types of attacks, web attacks, virus attacks, and vulnerability attacks, respectively. The detection results indicate that the GRU-Self-Attention prediction model greatly improves the detection accuracy of the original system against network attacks. Compared with actual results, the detection accuracy is over 95%. It retests the detection time of network information attack events, and the results are shown in Fig. 11.

Fig. 11(a) shows the variation in time taken by the original prediction system to detect 1000 network security attack events. This indicates that as the number of attack events grows, the original prediction system takes more and more time, and the increase in time is becoming larger and larger. Detecting 1000 network security attack events takes approximately 11.7 minutes. In Fig. 11(b), the time growth of the GRU-Self-Attention prediction model is far less than that of the original system, with a detection time of about 1.2 minutes for 200 network security attack events. It detects 1000 network security attack events, taking only about 3.8 minutes.

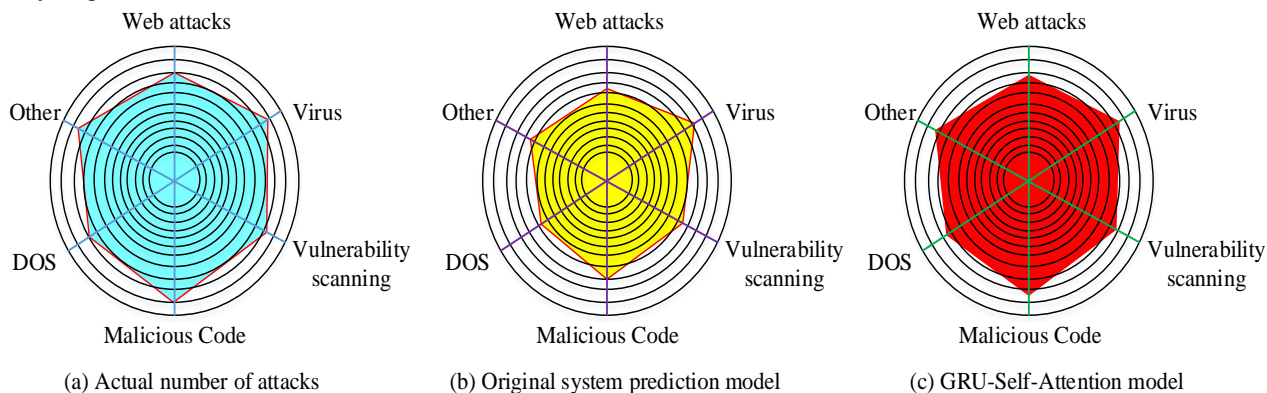


Fig. 10. Detection results of network information attack by prediction model at this time.

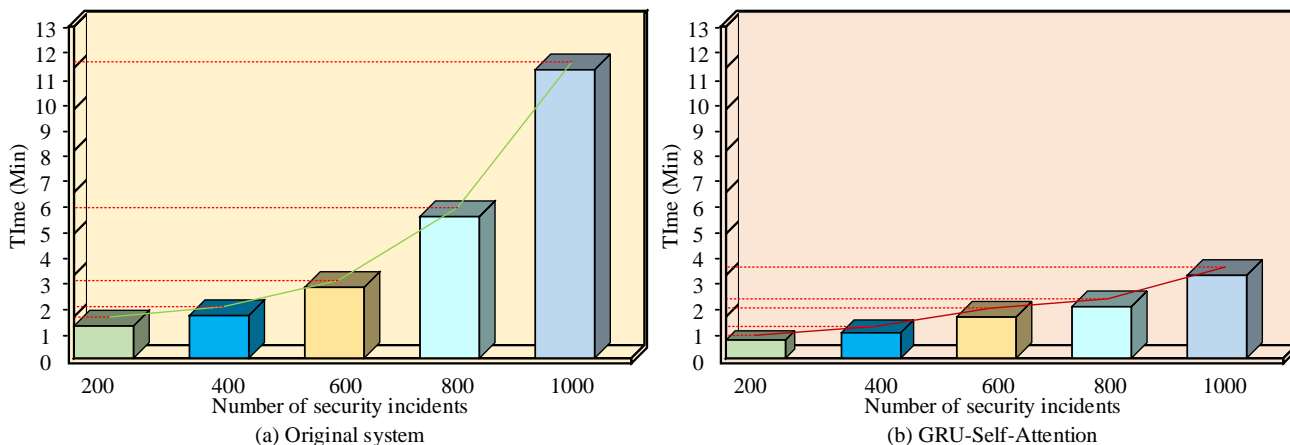


Fig. 11. Prediction time for 1000 network security attack events.

Finally, the prediction performance of the GRU-Self-Attention prediction model on network security situation values was verified, as shown in Fig. 12.

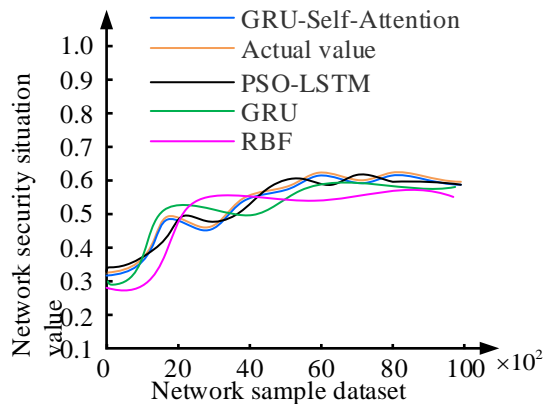


Fig. 12. Network security situation prediction value.

In Fig. 12, the actual potential value of the network ranges from 0.3 to 0.6 and increases with the increase of sample data. From the curve trend of the graph, the GRU-Self-Attention model constructed in the study has little difference between the predicted values of the network potential and the actual potential values. This indicates that the prediction model can make accurate predictions of the network potential values.

D. Discussion

With the increasing complexity and intelligence of network security threats, it has become inevitable to take more comprehensive and efficient measures to protect network security. Based on the Fusion of Knowledge Graph, this study constructs a network security data graph using KG technology and constructs a situation prediction model that combines self-attention mechanism and Gate Recursive Unit. The experimental results showed that the detection accuracy and recall rate of the entity recognition model constructed in the study were above 90%, which were higher than the BERT, CRF, and Transformer CRF models under the same experimental conditions. Compared with the research results of Chen. Z. et al. [4], there has been further improvement. This is because the constructed entity recognition model incorporates feature models and text embedding vector representation methods to optimize the performance of the model, thereby improving the accuracy and recall of the model. The accuracy of the constructed entity relationship extraction model was also above 90%. The extraction accuracy of the SVM, CRF, and SRL models under the same experimental conditions were 82%, 80%, and 76%, respectively, significantly lower than the research model. Compared to the accuracy achieved by Ruan. Z. et al. [5] is over 85%, but the method proposed in this paper is significantly higher. This is because the constructed entity relationship extraction model adds a self-attention layer, which can better combine long sentence information and improve model performance. This also indicates that the constructed network security KG has extremely high feasibility. But the prediction efficiency of the methods proposed in network security needs to be improved. In the future, it is necessary to optimize the model structure and utilize more advanced parallel computing to further

improve the predictive performance of network security, providing more reliable guarantees for network security.

V. CONCLUSION

Situation prediction technology possesses an essential influence on mitigating network security threats. Therefore, this study optimized the entity recognition model and entity relationship extraction model of network security KG and presented a network security situation assessment method based on KG and Bayesian attack graph. Meanwhile, the situation prediction method was optimized through self-attention mechanism, and a GRU-Self-Attention prediction model was constructed. The experimental results showed that the average absolute error of the GRU-Self-Attention situational prediction model based on network security KG in predicting situational values in the NSL-KDD dataset was about 0.0127. This value was about 0.0136 in the CICIDS2017 dataset. The average absolute error in different scenarios was lower than that of the GRU, PSO-LSTM, and RBF models under the same experimental conditions. The model constructed in the study has good fit to different datasets, and the average absolute error is lower than the existing models. The GRU-Self-Attention model was embed into an information security system, which could accurately predict the number of different types of network attacks. In addition, the model detected 1000 network security attack events, which only took about 3.8 minutes. This indicates that the research plan can effectively improve the accuracy of network security situation prediction. However, building a network security KG requires a large number of resources and time in the early stages, and later research will further optimize the construction process and data processing of KG.

REFERENCES

- [1] Potember. R. S., Balhana .C. D., Obrst. L. J. An Introduction to Semantic Threat Analysis for Systems Security Engineering. INCOSE International Symposium, 2022, 32(1):498-513.
- [2] Samuel. O. S. Cyber Situation Awareness Perception Model for Computer Network. International Journal of Advanced Computer Science and Applications, 2021, 12(1):392-397.
- [3] Venkatesan. B., Chitra. S. An enhance the data security performance using an optimal cloud network security for big data cloud framework. International Journal of Communication Systems, 2021, 35(16):1-15.
- [4] Chen. Z. Research on internet security situation awareness prediction technology based on improved RBF neural network algorithm. Journal of Computational and Cognitive Engineering, 2022, 1(3): 103-108.
- [5] Ruan. Z. Network security prediction method based on kubernetes. Journal of Physics: Conference Series. IOP Publishing, 2021, 2010(1): 109-111.
- [6] Zhang. H., Kang. K., Bai. W. Hierarchical network security situation awareness data fusion method in cloud computing environment. Journal of computational methods in sciences and engineering, 2023, 23(1):237-251.
- [7] Sun. J., Li. C., Song. Y., Ni. P., Wang. J. Network Security Situation Prediction Based on TCAN-BiGRU Optimized by SSA and IQPSO. Tech Science Press, 2023, 47(10):993-1021.
- [8] Liu. Q., Zeng. M. Network security situation detection of internet of things for smart city based on fuzzy neural network. International Journal of Reasoning-based Intelligent Systems, 2020, 12(3):222-227.
- [9] Lin. P., Chen. Y. Network Security Situation Assessment Based on Text SimHash in Big Data Environment. International Journal of Network Security, 2019, 21(4):699-708.

- [10] Jian. L. I., Dong. T., Jie. L. I. Research on IoT security situation awareness method based on evidence theory. *Chinese Journal of Network and Information Security*, 2022, 8(2):39-47.
- [11] Sun. C., Hao. H. U., Yang. Y. Prediction method of 0day attack path based on cyber defense knowledge graph. *Chinese Journal of Network and Information Security*, 2022, 8(1):151-166.
- [12] Chen. Y. Y., Xu .B., Long. J. Information security assessment of wireless sensor networks based on bayesian attack graphs. *Journal of Intelligent and Fuzzy Systems*, 2021, 41(4):1-7.
- [13] Song. T., Li. Y., Meng. F., Xie. P., Xu. D. A Novel Deep Learning Model by BiGRU with Attention Mechanism for Tropical Cyclone Track Prediction in the Northwest Pacific. *Journal of Applied Meteorology and Climatology*, 2022, 61(1):3-12.
- [14] Liu. M., Wang. X., Liang. S., Sheng .X. I., Lou. S. Single and composite disturbance event recognition based on the DBN-GRU network in 9-OTDR. *Applied optics*, 2023 62(1):133-141.
- [15] Wang. J., Wang. X., Ma. C., Kou. L. A survey on the development status and application prospects of knowledge graph in smart grids. *IET Generation, Transmission & Distribution*, 2021, 15(3): 383-407.
- [16] Zhou. B., Shen. X., Lu. Y., Li. X., Hua. B., Liu. T., Bao. J. Semantic-aware event link reasoning over industrial knowledge graph embedding time series data. *International Journal of Production Research*, 2023, 61(12): 4117-4134.
- [17] Li. Z., Zhao. Y., Li. Y., Rahman. S., Wang. F., Xin. X., Zhang. J. Fault localization based on knowledge graph in software-defined optical networks. *Journal of Lightwave Technology*, 2021, 39(13): 4236-4246.
- [18] Hebbi. C., Mamatha. H. Comprehensive Dataset Building and Recognition of Isolated Handwritten Kannada Characters Using Machine Learning Models. *Artificial Intelligence and Applications*, 2023, 1(3):179-190.
- [19] P. Preethi and H. R. Mamatha, "Region-Based Convolutional Neural Network for Segmenting Text in Epigraphical Images," *Artif. Intell. Appl.*, vol. 1, no. 2, pp. 119-127, Sep, 2023, DOI: 10.47852/bonviewAIA2202293.
- [20] Ghourabi. A .SM-Detector: A security model based on BERT to detect SMiShing messages in mobile environments. *Concurrency and Computation: Practice and Experience*, 2021, 33(24) : 1-15.
- [21] Ghaffari. R., Golpardaz. M., Helfroush. M. S., Danyali. H. A fast, weighted CRF algorithm based on a two-step superpixel generation for SAR image segmentation. *International Journal of Remote Sensing*, 2020, 41(9):3535-3557.
- [22] Ma. C., Zhang. C. Joint Pre-Trained Chinese Named Entity Recognition Based on Bi-Directional Language Model. *International Journal of Pattern Recognition and Artificial Intelligence*, 2021, 35(9):1-16.

Hybrid Approach for Enhanced Depression Detection using Learning Techniques

Ganesh D. Jadhav¹, Sachin D. Babar², Parikshit N. Mahalle³

Research Scholar in Department of Computer Engineering, Smt. Kashibai Navale College of Engineering, Vadgaon, SPPU-Pune, India¹

Department of Computer Engineering, Sinhgad Institute of Technology, Lonavala, SPPU-Pune, India²

Department of Artificial Intelligence and Data Science, Vishwakarma Institute of Information Technology, SPPU-Pune, India³

Abstract—According to the World Health Organization (WHO), depression affects over 350 million people worldwide, making it the most common health problem. Depression has numerous causes, including fluctuations in business, social life, the economy, and personal relationships. Depression is one of the leading contributors to mental illness in people, which also has an impact on a person's thoughts, behavior, emotions, and general wellbeing. This study aids in the clinical understanding of patients' mental health with depression. The primary objective of research is to examine learning strategies to enhance the effectiveness of depression detection. The proposed work includes 'Extended- Distress Analysis Interview corpus' (E-DAIC) label dataset description and proposed methodology. The membership function applies to the Patients Health Questionnaire (PHQ8_Score) for Mamdani Fuzzy depression detection levels, in addition to the study of the hybrid approach. It also reviews the proposed techniques used for depression detection to improve the performance of the system. Finally, we developed the Ensemble-LSRG (Logistic classifier, Support Vector classifier, Random Forest Classifier, Gradient boosting classifier) model, which gives 98.21% accuracy, precision of 99%, recall of 99%, F1 score of 99%, mean squared error of 1.78%, mean absolute error of 1.78%, and R² of 94.23.

Keywords—Depression detection; machine learning; extended-distress analysis interview corpus; ensemble-LSRG model; mamdani fuzzy

I. INTRODUCTION

Depression is the most common mental disease in the world. Causes of disruption include the emotion experience, lack of communication, human behavior, and social media problems [1]. Human existence is present on the internet and in social media, just as it is in daily life. Additionally, communication is getting better every day. Unknown people can communicate with one another online, yet there are also drawbacks to social media and the internet. Anorexia and bipolar depression affect millions of individuals globally, making depression one of the worst problems in the world [19], and [25]. Over 350 million people worldwide are affected by depression, and it's the most common health problem, according to the World Health Organization (WHO) [26], [27], and [12]. According to research on the causes of depression, the risk of suicide increases more than 30 times among those in generally good health [27] and [29].

Despair triggers numerous events. Every day in the surrounding area, people can observe the prevalence of

suicidal situations and other mental illnesses [11] that are also influenced by depression. For example, in today's society, stress from the daily workload significantly raises the risk of developing it. According to a poll on depression, the following symptoms appear virtually daily for two weeks: Depression or a loss of mood, a decline in enthusiasm for the activity, suicidal thoughts, and a sense of hopelessness [19]—other factors, such as genes and family history, can also contribute to depression [23]. All different kinds of men and women of all ages struggle with this issue. According to the WHO, depression affects 350 million individuals globally [26], [27], and [12]. According to research on the causes of depression, the risk of suicide increases more than 30 times among those in generally good health [27], [29], and [31].

Depression can be detected by utilizing learning approaches using the system's multimodal resources. The system's objective is to offer many modalities on the same platform in order to increase accuracy and the techniques for detecting emotions, such as sentimental analysis and speech prosody. 12% and 6.6%, respectively, of men and women are seeing an increase in depression [12]. Humans communicate their emotions more frequently in daily life through speech, social media, blogs, and chat rooms. The study offers the voice activity detector, speech emotion recognition, and text emotion recognition for text-based data [24], [26], and [27]. Face analysis can help identify of depression [21], and [27]. The merger of all modalities can aid in increasing the system's accuracy [22]. According to a 2019 survey, there were 1,39,123 suicide-related deaths in India, and the national rate of self-destruction continued to be 10.4 (calculated per 1 lakh people), as stated in Chapter 2 of the National Crime Record Bureau, for example. Recently, 'Sushant Singh Rajput' attempted suicide due to depression [1]. The goal of this system is to create a hybrid modal system [9] that will help society and medical professionals diagnose and track depression. This study utilized ensemble learning to learn from PHQ8 data in order to get the correct positive results [30].

In this section, include an introduction and motivation for the study, as well as a general overview of the study. In the second section, it includes related work of the study, including existing work related to the study, the gap analysis, as well as the key issues and challenges part. The third section outlines the recommended strategy for improving system performance, the dataset description, and algorithmic details; the fourth

section includes the result and discussion part. The conclusion and future scope are covered in the final part.

II. RELATED WORK

As per the literature survey observed that the following related work:

The MSN (Multi-scale Spatiotemporal Network) model, put forth by Wheidima Carneiro de Melo, integrates face data associated to depressive behavior from image [2]. Models only pick up irregularities associated with people's facial expressions. This work made use of the Audio-Visual Emotion Recognition Challenge (AVEC2014) dataset. Mean Absolute Error (MAE) and Root Mean Square Error (RMSE) components influence the results. The DMVM (Deep Mood Architecture with Multi View Machine) model is suggested by Xiaohang Xu and Hao Peng and is used to identify depression [3]. Hospitals preserve patient health information in accordance with privacy concerns. This information cannot be used for a centralized machine learning in the diagnosis of depression. At that point, federated learning is crucial for identifying depression. Accuracy serves as the primary criterion for analyzing outcomes in comparisons. To classify the data into five categories (healthy, smooth, pleasant, neutral, and serving), Kaining Mao, Wei Zhang, and Deborah Baofeng Wang developed a model on the Oz dataset using the Distress Analysis Interview Corpus Wizard [4]. The final result was based on the F1 score, accuracy, precision, and recall. They used the following networks: Bidirectional BI-LSTM+FC, LSTM+ Time-distributed Convolutional Neural Network TCNN, Long Short Term Memory LSTM + FC, and BI-LSTM+ TCNN.

Shallow (EdgeER) and deep models are used by Shuai Ding, Zi Xu, Yaping Wang, Lina Qu, Yinghui Li, Yao Yu, Xiaojian Li, and Shanlin Yang et al. [5]. Deploy the deep model (C-DepressNet) to cloud servers and the shallow model (EdgeER) to edge servers. EdgeER can instantly identify unfavorable sentiment in user data. High-precision analyses of depression levels are performed using depth models. BDI-II score values are finally categorized as follows: no depression, mild, moderate, or severe depression. Pushpak Bhattacharyya, Soumitra Ghosh, and Asif Ekbal, et al. [6], on multi-model multitasking systems. This work includes multi-model social network profiles that leverage deep learning to retrieve metadata (e.g., user location, photo, and description). Work on image collections and emotionally charged datasets for outcome analysis. The model's accuracy and F1 score dictate the result. Conv + Maxpool Layer, Shared Multilayer Perceptron (MLP), Task-Specific MLP, Output Layer, Hidden Activation, Output Activation, Batch Size, Epoch, Dropout, Loss, Optimizer, etc. are some of the parameters. Lei Tong, Zhihua Liu, Zheheng Jiang, Feixiang Zhou et al. proposed a method for identifying depressed Twitter users [7]. "Cost-sensitive Boosting Pruning Trees" (CBPT) gets classification results using a variety of technique. "Cost-sensitive Boosting Pruning Trees" (CBPT) uses a range of methods to provide classification results. Including "Discrete Adaboost, Real Adaboost, XGboost, LogitBoost, LightGBM, and HiGB", various methods are used when comparing to the UC Irvine (UCI), the machine learning repository. The eight boosting

classifiers' accuracy and F1 scores serve as the foundation for the final analysis.

Using the SH2 data sets and the "Distress Analysis Interview Corpus/Wizard-of-Oz collection" (DAIC-WOZ), Zhaocheng Huang, Julien Epps, Dale Joachim, and others conducted tests [8]. The algorithm's F1 rating is the foundation for the ultimate rating. Among the groundbreaking features of this study are "g(lottis)," "p(eriodity)," "s(onorant)," "f(ricative)," "v(oiced fricative)," and "b(ursts)". Erik Cambria, Shaoxiong Ji, Qian Chen, and Luna Ansari examined a text classifier that was taught to identify depression. An assessment matrix is used to assess classification systems. Precision, recall, F1 score, and precision make up the evaluation matrix. A unique automatic depression detection ADD (Temporal dilated convolutional network - TDCN and feature wise attention - FWA) model proposed by Yanrong Guo, Chenyang Zhu, and et al. [10] suggests data collecting based on the visual cues captured throughout the interview process. Other modalities, including as text and audio, could be used in this study to enhance the system's functionality. The ultimate outcome is based on factors like as accuracy (0.857), recall (0.91), precision (0.733), and F1 score (0.85). Study based on sub-emotions (BoSE), Late Fusion Methods by Mario Ezra Aragon et al. In order to improve depression identification, this study combines static and dynamic representations of early and late fusion techniques. Processing solely text-based data. Privacy about certain data. It is forbidden to misuse and handle sensitive information improperly. Factors such as the F1 Score of 0.64, Precision of 0.67, and Recall of 0.61 influence the final outcome.

Electroencephalogram (EEG) signal decomposition for depression identification by Jian Shen, Xiaowei Zhang, Bin Hu, Gang Wang, et al. [12]. It illustrates how the human brain functions. This piece of art illustrates how the human brain functions. Electroencephalogram (EEG) databases have accuracies ranging from 83.27% to 85.19% to 81.98% to 88.07% for each dataset. Usman Ahmed, Jerry Wei Lin, and others [13] proposed the BI-LSTM, which has received much attention and uses unlabeled forum text and social media data to boost the rate of diagnosing depressive symptoms from online data. These studies' drawbacks include dealing only with textual data and illiteracy. Accuracy and Cohen Kappa metrics are used to compare results. Studying the self-attention graph pooling-soft label (SGP-SL) model are Tao Chen, Yanrong Guo, and colleagues [14].

In this study, soft labeling was employed together with an experiment using the 'MODMA' dataset, a multi-modal open dataset for mental-disorder investigation that served as an efficient model in many ways. Another area of investigation in the feature work is the issue of incomplete modalities and the identification of major depressive disorder (MDD). The final result depends on parameters like, Accuracy= 84.91%, Precision= 80.77, Recall= 87.50, F1-Score=84. A study on LSTM, CNN, and hybrid (CNN + LSTM) models was conducted by Mudasir Ahmad Wani, Mohammad A, and colleagues [15] to examine variables including precision, accuracy, and F1 score. The term frequency-inverse-document frequency (TF-IDF) based characteristics and Word2Vec were used in this investigation. We must continue to develop on the

multiplication corpus because it only covers the English language. Study on logistic regression by Jianxiu Li, Nan Li, Xuexiao Shao, et al. [16]. Microstate Parameters: Duration, Occurrence, and Time Coverage performed well in this investigation at detecting MDD. Restriction on the number of participants with MDD and healthy controls (HC). Large data sets are necessary to demonstrate the study's statistical power.

Study on the Mutual Information Based Fusion Model (MIBFM model) by Jing Zhu, Changlin Yang, et al. [17]. This study put forth the model that is used to correlate the signals from the pupil area and the EEG. The National Key Research and Development Program of China (NKR&DP of China) is funding this work. To carry out activities, data gathering and dataset enrichment are necessary. Mild depression and normal control require binary classification. Deep Convolutional Neural Network (DCNN) and Deep Neural Network multimodal investigation of depression by Le Yang, Dongmei Jiang, and Hichem Sahli [18]. In AVEC2016, support vector machines and random forests are both employed for classification. They used text documents, audio data, and video data for this endeavor.

Studies on identifying psychiatric diseases such as anorexia and depression by Mario Ezra Arag'n, A. Pastor L'opez-Monroy, Luis C. Gonz'alez, et al. [19]. Users of social media have unfortunately developed depression as a result of their use. Anorexia and Depression Sentiment Distribution solely use this information for study and analysis. Data that should not be shared. Studying depression during and after pregnancy, Kristen C. Allen, Alex Davis, and Tamar Krishnamurti [20] conducted a study to inadvertently detect perinatal psychosocial concerns. This study examined both happy and negative feelings as well as a lack of relationship support to identify emotions, despair, and sentimental analysis.

III. PROPOSED WORK

The proposed work of the study including the dataset Description, the proposed methodology and algorithmic detail:

A. The Dataset Description

Semi-clinical interviews prepare the Extended Distress Analysis Interview Corpus (E-DAIC) dataset. The dataset is designed to support the psychological distress condition such as anxiety, depression and post-traumatic stress disorder. These interviews were collected as part of a larger effort to create a computer agent that interviews, people and identifies verbal and nonverbal indicators of mental illness. An animated virtual interviewer called Ellie conducts the interviews. A subset of session are collected in a wizard-of-Oz (WoZ) setting, where the virtual agent is controlled by a human interviewer (wizard) in another room [30].

The Dataset is classified into training, development, and test dataset while preserving the overall speaker's diversity -- in terms of age, gender distribution, and the eight-item Patient Health Questionnaire (PHQ-8) scores -- within the partitions. Whereas the training and development sets include a mix of WoZ and AI scenarios, the test set is solely constituted from the data collected by the autonomous AI [39]. Sessions with IDs in the range [300,492] are collected with WoZ-controlled

agent and sessions with IDs [600,718] are collected with an AI-controlled agent [30].

B. Proposed Methodology

The proposed methodology of the study on the E-DAIC (Extended – Distress Analysis Interview corpus) label dataset is shown in Fig. 1.

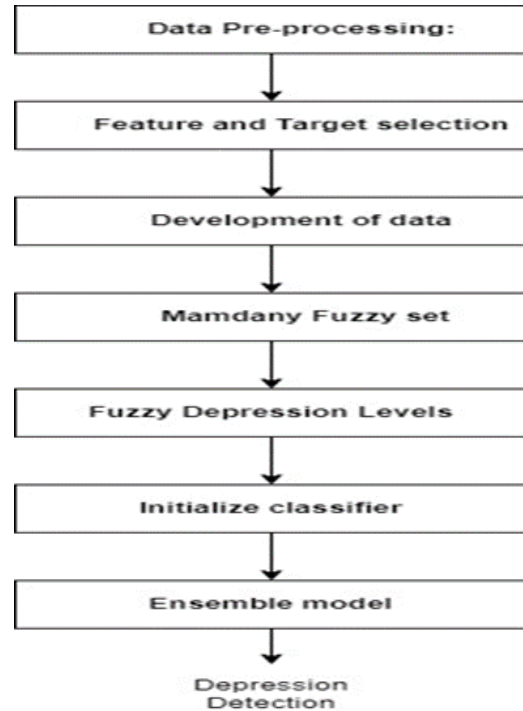


Fig. 1. Proposed methodology for the depression detection system using ensemble model.

The labeled dataset contains data from 275 participants. Specifically, the train_split.csv contains records from 163 participants, the test_split.csv contains records from 56 participants, and the dev_split.csv contains records from 56 participants. The methodology follows the following steps,

1) *Data pre-processing*: In data pre-processing it upload the train_split.csv, test_split.csv and dev_spit.csv from the E-DAIC Dataset. Pre-processing of the data include the data cleaning, data normalization and finding the missing values. Additionally, data is augmented and increase the data size with five times.

$$X=\text{imputer.fit_transform}(X) \quad (1)$$

where, X is the feature set vector.

By using Eq. (1) to handle the missing values from feature sets.

2) *Feature and target selection*: Feature selection is the very important of this study. This can be done by observing the correlation between the variable. Target selection also be important for this study.

3) *The Development of data*: The Development of the data combine train_split and dev_spit dataset for model development.

4) *Define mamdani fuzzy se:* In Mamdani fuzzy logic define the membership function for PHQ8_Score and create the output variable. In the fuzzy set define the membership function for depression severity also define the rules for classification for four classes then define create the fuzzy control system.

5) *Fuzzy depression levels:* Apply fuzzy logic to calculate Mamdani fuzzy depression level.

$$\text{MamdaniFuzzyLevel}=\text{apply_fuzzy_logic}(\text{PHQ_Score}) \quad (2)$$

6) *Initialize classifier:* In this study used no of classifier like logistic_regression, support classifier, Random_Forest_Classifier, Gradient_Boosting_Classifier to the ensemble model.

7) *Ensemble model:* Define ensemble model for hybridization and train it by training data to improve the performance of the system.

$$\text{ensemble_model}=\text{VotingClassifier}(\text{estimators}=[('lr', \text{clf1}), ('svc', \text{clf2}), ('rf', \text{clf3}), ('gb', \text{clf4})], \text{voting}='soft') \quad (3)$$

$$\text{ensemble_model.fit}(\text{train_X}, \text{train_y}) \quad (4)$$

Where,

X is feature set y is the target,

lr is logistic classifier,

svc is support vector machine classifier,

rf is random forest classifier,

gb is gradient boosting classifier.

By using Eq. (3) and Eq. (4) define and train the ensemble model.

8) *Prediction and evaluation of the model:* Make predictions using the trained ensemble model.

Calculate accuracy, confusion matrix, and visualize the confusion matrix.

$$y_pred = \text{ensemble_model.predict}(X_test) \quad (5)$$

$$\text{accuracy} = \text{accuracy_score}(y_test, y_pred) \quad (6)$$

$$\text{cm}=\text{confusion_matrix}(y_test, y_pred) \quad (7)$$

By using Eq. (5), we can predict the depression detection using the ensemble model. Eq. (6) used to calculate the accuracy of the model and Eq. (7) used to generate the confusion matrix of the predicted values and actual results.

IV. RESULTS AND DISCUSSIONS

In this study execute the whole system using the ensemble LSRG (Logistic regression, Support vector classifier, random forest classifier and the gradient boosting) model to improve the performance of the system.

The above Fig. 2 shows the membership function of the fuzzy system with respective to the phq_score. The depression detection system, including only four levels of depression, i.e. "No Depression", "Mild Depression", "Moderate Depression",

and "Severe Depression". The Fig. 2. Shows the membership for low, medium and high phq_score.

In Fig. 3, show that the confusion matrix of "Linear Regression model" and "Ensemble-LSRG model". As per figure, the "Ensemble-LSRG model" is less confuse than the "Linear Regression model". Less confuse means the "Ensemble-LSRG model" give the high accuracy. The accuracy required to calculate the accurate depression level.

In Fig. 4, show that the confusion matrix of "Support Vector Machine" and "Ensemble-LSRG model". As per figure, the "Ensemble-LSRG model" is less confuse than the "Support Vector machine". Less confuse means the "Ensemble-LSRG model" give the high accuracy. The accuracy required to calculate the accurate depression level.

In Fig. 5, show that the confusion matrix of "Random Forest classifier" and "Ensemble-LSRG model". As per figure, the "Ensemble-LSRG model" is less confuse than the "Random forest classifier". Less confuse means the "Ensemble-LSRG model" give the high accuracy. The accuracy required to calculate the accurate depression level.

In Fig. 6, show that the confusion matrix of "Gradient boosting classifier" and "Ensemble-LSRG model". As per figure, the "Ensemble-LSRG model" is less confuse than the "Gradient boosting classifier". Less confuse means the "Ensemble-LSRG model" give the high accuracy. The accuracy required to calculate the accurate depression level.

In Fig. 7, show that the confusion matrix of "Convolutional Neural Network" and "Ensemble-LSRG model". As per figure, the "Ensemble-LSRG model" is less confuse than the "Convolutional Neural Network". Less confuse means the "Ensemble-LSRG model" give the high accuracy. The accuracy required to calculate the accurate depression level.

In Fig. 8, displays the confusion metrics of depression detection using Recurrent Neural Network. From the observation of the diagram, it is evident that the "Ensemble (LSRG) model" is less confused compared to other techniques. "Less confusion" implies that the "Ensemble-LSRG model" provides higher accuracy. Accuracy is necessary to calculate the precise level of depression.

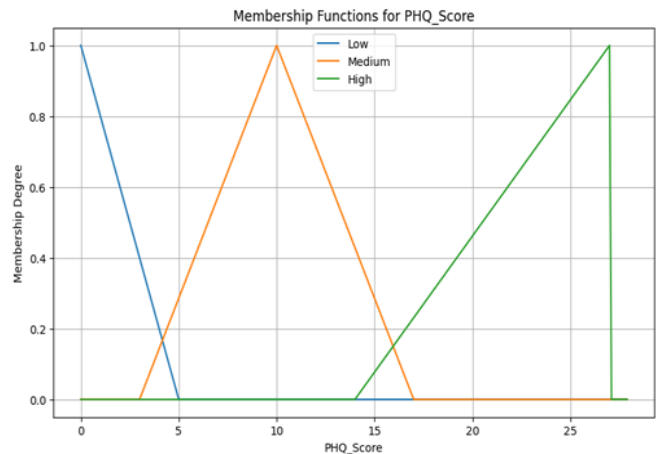


Fig. 2. Membership vs phq_score.

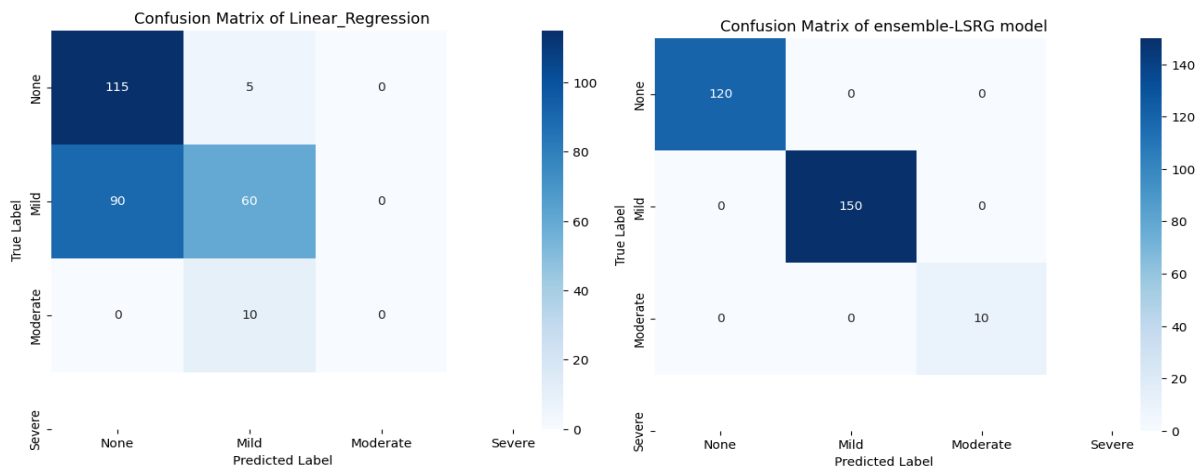


Fig. 3. The Confusion matrix of linear regression and ensemble- LSRG model.

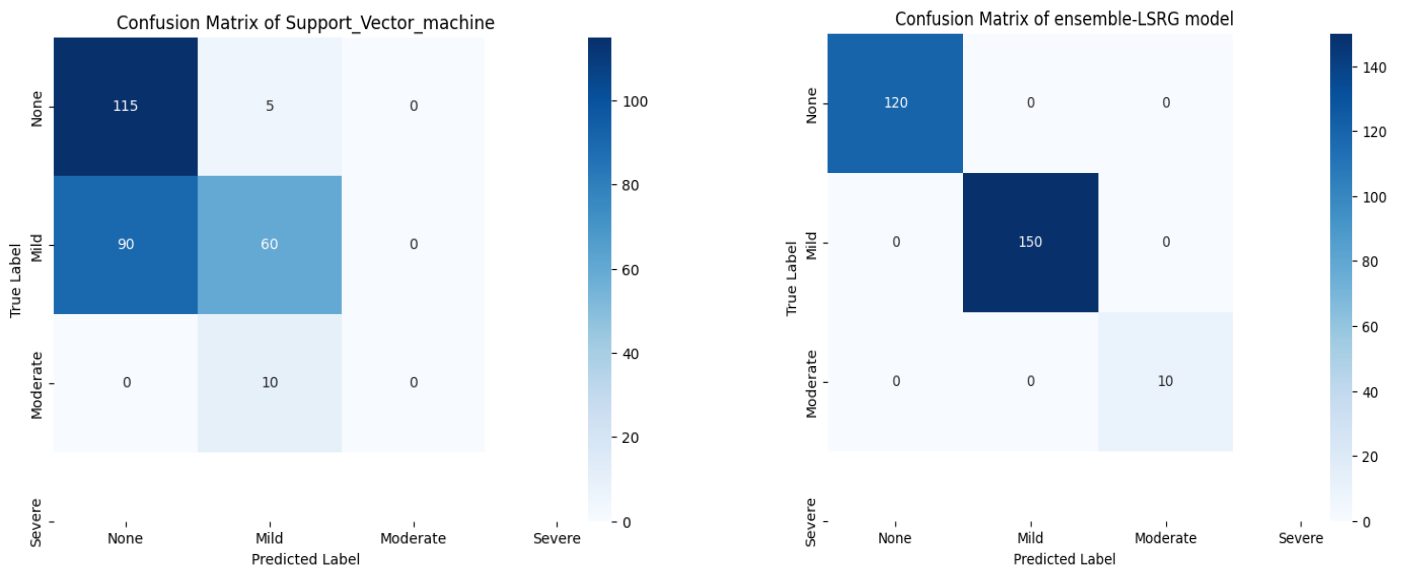


Fig. 4. The Confusion matrix of support vector machine and ensemble- LSRG model.

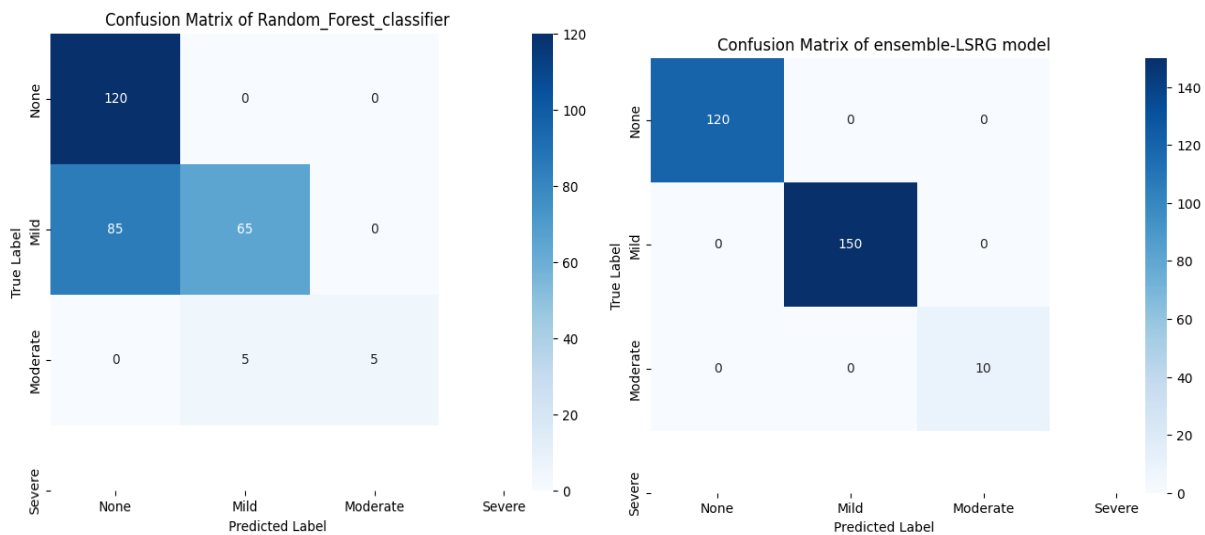


Fig. 5. The confusion matrix of random forest classifier and ensemble- LSRG model.

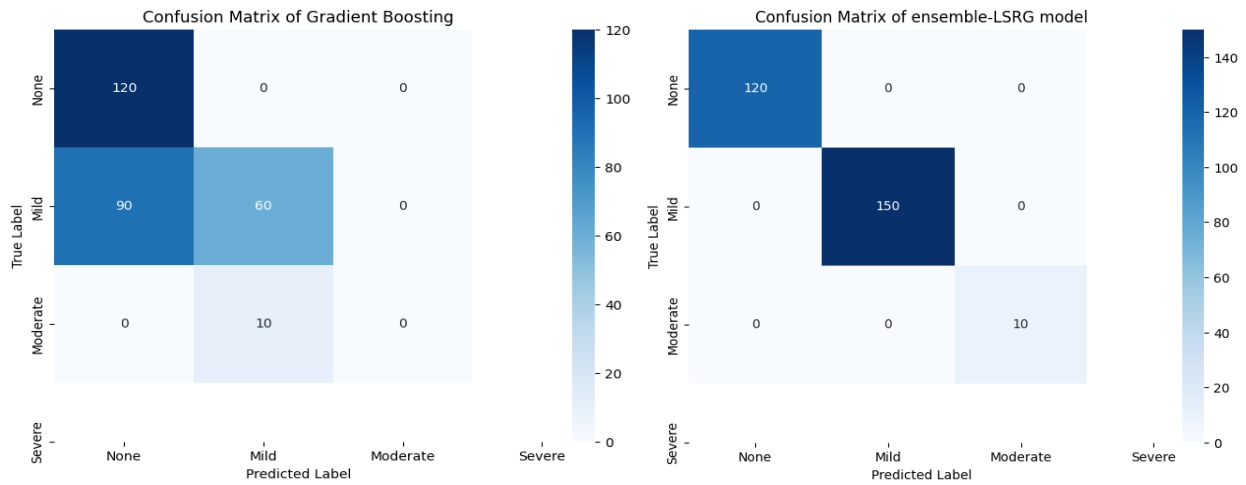


Fig. 6. The Confusion matrix of gradient boosting and ensemble- LSRG model.

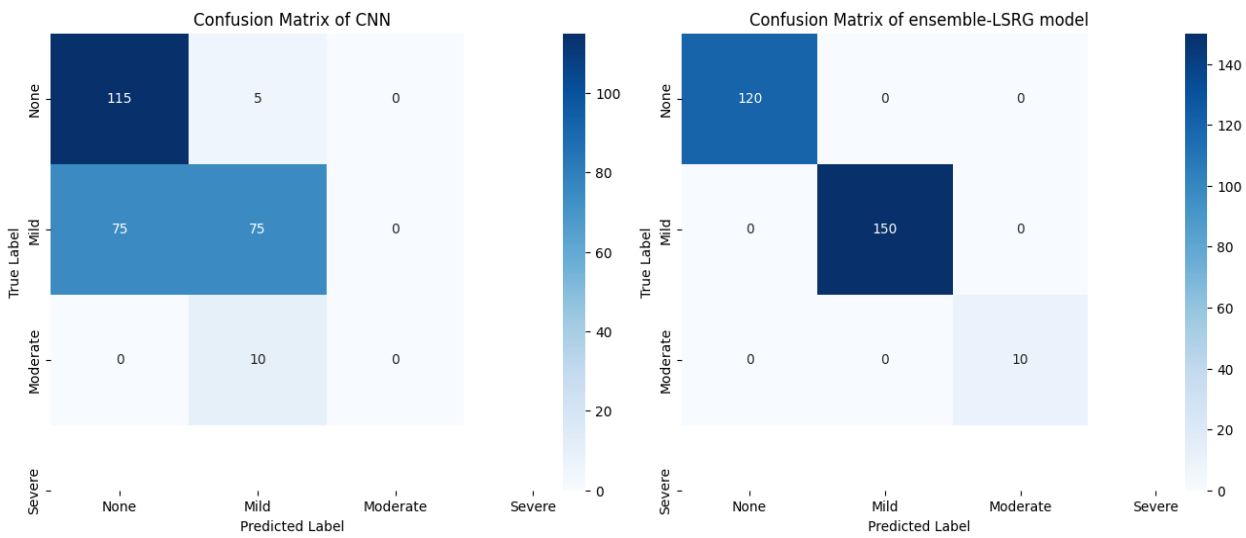


Fig. 7. The Confusion matrix of CNN and ensemble- LSRG model.

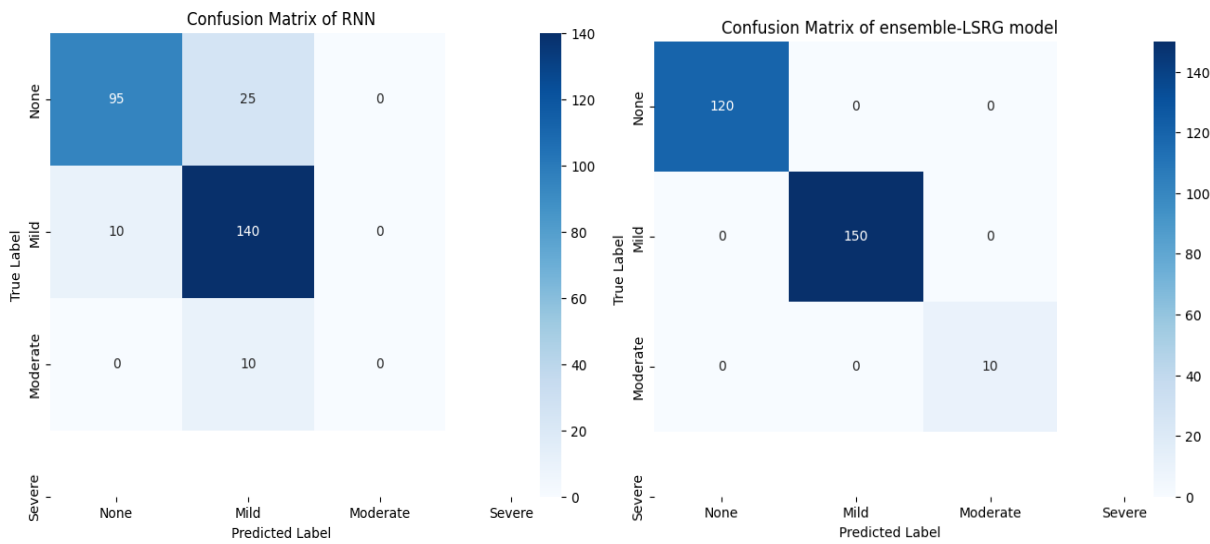


Fig. 8. The Confusion matrix of RNN and ensemble- LSRG model.

TABLE I. COMPARISON CHART OF EXPERIMENTAL ANALYSIS OF THE DEPRESSION DETECTION SYSTEM USING ENSEMBLE (LSRG) MODEL

| Sr. | Learning Technique | Accuracy in (%) | Precision in % | Recall in % | F1 Score in % | Mean squared error in % | Mean Absolute error in % | R2 score |
|-----|------------------------------------|-----------------|----------------|-------------|---------------|-------------------------|--------------------------|----------|
| 1 | Linear regression | 62.5% | 67.00% | 62.00% | 59.00% | 15.42% | 30.57% | 50.21% |
| 2 | Support vector Machine | 62.5% | 67.00% | 62.00% | 59.00% | 16.32% | 31.43% | 47.31% |
| 3 | Random Forest | 53.57% | 77.00% | 56.00% | 53.00% | 03.78% | 01.31% | 87.80% |
| 4 | Gradient boosting | 64.28% | 70.00% | 64.00% | 60.00% | 01.25% | 03.94% | 95.96% |
| 5 | Convolutional Neural Network (CNN) | 42.85% | 19.00% | 43.00% | 26.00% | 62.50% | 58.92% | 70.6% |
| 6 | Recurrent Neural Network (RNN) | 78.57% | 76.00% | 79.00% | 77.00% | 21.42% | 21.42% | 30.86% |
| 7 | Ensemble- LSRG model(Ours) | 98.21% | 99.00% | 99.00% | 99.00% | 01.78% | 01.78% | 94.23% |

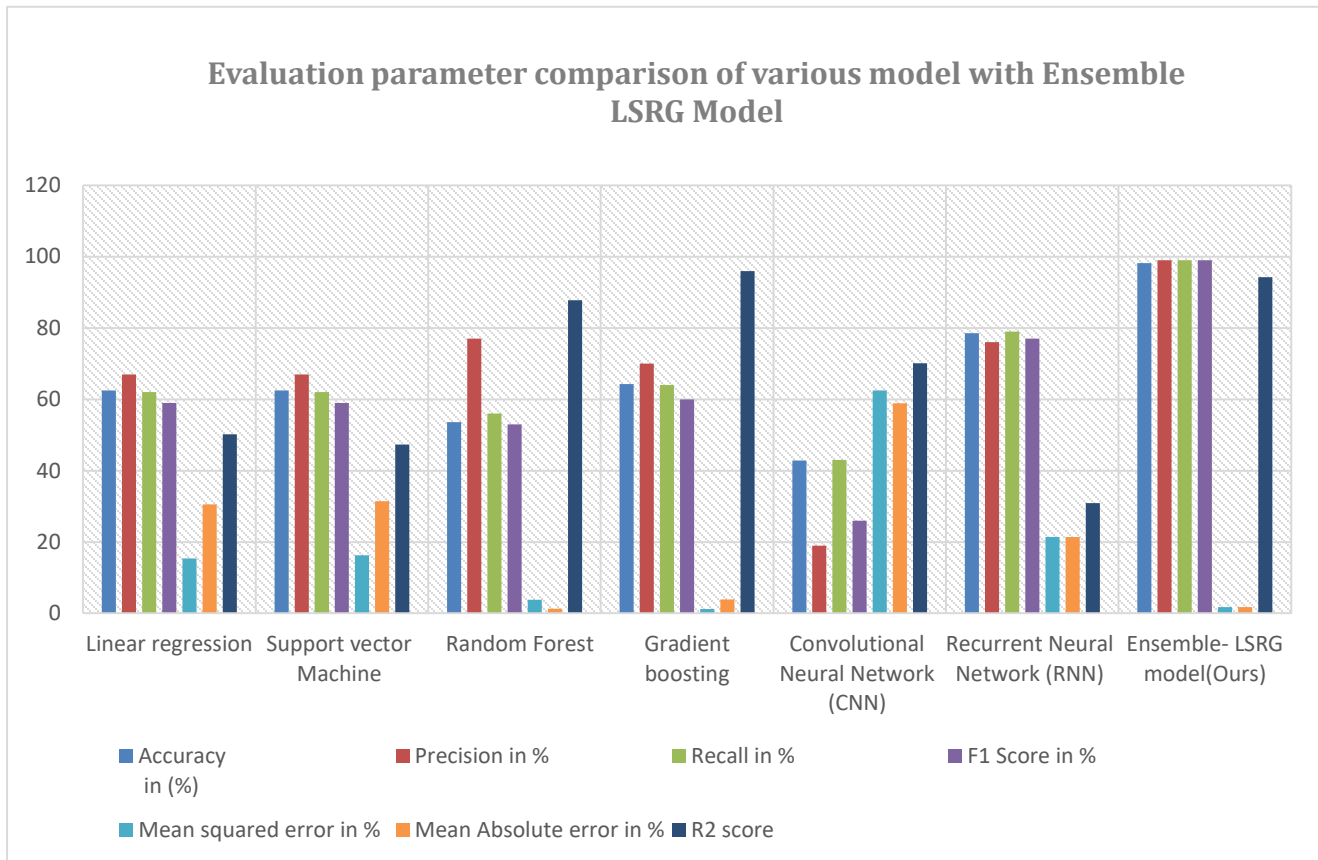


Fig. 9. Evaluation parameter comparison of various model with ensemble LSRG model.

Table I and Fig. 9 shows the analysis of performance of the depression detection system using different machine learning algorithm and Ensemble –LSRG model using various parameters like, accuracy, precision, recall, F1 score, mse, mae, and R² score. As per table and Fig. 9. shows that the linear regression model having accuracy of 62.5%, precision of 67%, recall of 62%, F1 score of 59%, mean squared error of 15.42%, mean absolute error of 30.57% and R² score is 50.21%. The second model is a support vector machine with an accuracy of 62.5%, precision of 67%, recall of 62%, F1 score of 59%, mean squared error of 16.32%, mean absolute error of 31.43%, and R² of 47.31%. The third model is a random forest with an accuracy of 53.57%, precision of 77%, recall of 56%, F1 score of 53%, mean squared error of 03.78%, mean absolute error of 1.31%, and R² of 87.80%. The

fourth model is gradient boosting with an accuracy of 64.28%, precision of 70%, recall of 64%, F1 score of 60%, mean squared error of 01.25%, mean absolute error of 03.94%, and R² of 95.96%. The fifth model is a Convolutional Neural Network with an accuracy of 42.85%, precision of 19%, recall of 43%, F1 score of 26%, mean squared error of 62.50%, mean absolute error of 58.92%, and R² of 70.6%. The next model is a Recurrent Neural Network with an accuracy of 78.57%, precision of 76%, recall of 79%, F1 score of 77%, mean squared error of 21.42%, mean absolute error of 21.42%, and R² of 30.86%. The last model is the Ensemble-LSRG model (Ours) with an accuracy of 98.21%, precision of 99%, recall of 99%, F1 score of 99%, mean squared error of 1.78%, mean absolute error of 1.78%, and R² of 94.23%.

In discussion of research the Fig. 9, shows linear regression model having moderate performance with accuracy, precision, recall, and F1 score all around 60% also mean squared error and mean absolute error are relatively high, suggesting it might not fit the data well. The second model support vector machine also give the similar performance as per linear regression model so it is also not significantly better or worse. The third model is random forest which gives the high precision rate 77% but the accuracy is lower as compare to first two model. The forth model is gradient boosting show the best performance among individual model with high accuracy 64.28% and precision 70%. The fifth model perform relatively poorly as compare to other models with lower accuracy, precision, recall and F1 score, it means high mean squared error and mean absolute error indicating poor fit of data. The sixth model is recurrent neural network shows high accuracy 78.57% and precision 76% indicating its performing better than most individual model. The last model Ensemble-LSRG model (Ours) demonstrate the outstanding performance across all metrics with very high accuracy, precision, recall and F1 score, additionally it has lower mean squared error and mean absolute error among all models indicating the data is fit extremely well.

V. CONCLUSION AND FUTURE SCOPE

The study includes research work and various learning techniques and algorithms aimed at identifying research gaps. Additionally, it examines previous research on depression detection [28] and systems. This work will illustrate different depression detection systems, key issues, and challenges. Furthermore, it investigates a proposed methodology to enhance the system performance. The system achieves high accuracy compared to existing algorithm techniques. In this study, the system achieves 98.21% accuracy, precision of 99%, recall of 99%, F1 score of 99%, mean squared error of 1.78%, mean absolute error of 1.78%, and R^2 of 94.23% for the Ensemble LSRG model (Ours). In future research, the method to detect depression using a learning approach will be implemented. Additionally, performance metrics for early depression detection will be confirmed through experimentation analysis. Finally, the performance of the proposed algorithm will be evaluated against other popular depression detection algorithms to validate the results.

REFERENCES

- [1] Ganesh Jadhav, Sachin Babar, Parikshit Mahalle, "A Survey: Performance-aware Depression Detection", 10th International Conference on Computing for Sustainable Global Development (INDIACom), 2023, Page Numbers: [1245-1252].
- [2] Wheidima Carneiro de Melo, "A Deep Multi scale Spatiotemporal Network for Assessing Depression from Facial Dynamics", IEEE transactions on affective computing, Vol. 13, No. 3, July-September 2022.
- [3] Xiaohang Xu, Hao Peng, Md Zakirul and Alam Bhuiyan, "Privacy-Preserving Federated Depression Detection From Multisource Mobile Health Data", IEEE transactions on industrial informatics, Vol. 18, No. 7, July 2022.
- [4] Kaining Mao, Wei Zhang, Deborah Baofeng Wang, Ang Li and Rongqi Jiao, "Prediction of Depression Severity Based on the Prosodic and Semantic Features with Bidirectional LSTM and Time Distributed CNN", IEEE transactions on affective computing, to be published, doi 10.1109/taffc.2022.3154332.
- [5] Yao Yu, Shuai Ding and Xiaojian Li, "Cloud-edge collaborative depression detection using negative emotion recognition and cross-scale facial feature analysis", IEEE transactions on industrial informatics, to be published, doi 10.1109/tii.2022.3163512.
- [6] Soumitra Ghosh and Asif Ekbal, "What Does Your Bio Say? Inferring Twitter Users' Depression Status From Multimodal Profile Information Using Deep Learning", IEEE transactions on computational social systems, Vol. 9, No. 5, October 2022.
- [7] Lei Tong, Zhihua Liu, Zheheng Jiang and Feixiang Zhou, "Cost-sensitive Boosting Pruning Trees for depression detection on Twitter", IEEE transactions on affective computing, to be published, doi 10.1109/taffc.2022.3145634.
- [8] Zhaocheng Huang and Dale Joachim, "Investigation of Speech Landmark Patterns for Depression Detection", IEEE transactions on affective computing, Vol. 13, No. 2, April-June 2022.
- [9] Luna Ansari, Shaoxiong Ji and Erik Cambria, "Ensemble Hybrid Learning Methods for Automated Depression Detection", IEEE transactions on computational social systems, to be published, doi 10.1109/tcss.2022.3154442.
- [10] Yanrong Guo, Chenyang Zhuang and Richang Hong, "Automatic Depression Detection via Learning and Fusing Features From Visual Cues", IEEE transactions on computational social systems, to be published, doi 10.1109/tcss.2022.3202316.
- [11] Mario Ezra Aragon, A. Pastor López-Monroy, Luis C. González, and Manuel Montes-y-Gómez, "Detecting Mental Disorders in Social Media Through Emotional Patterns - The case of Anorexia and Depression", IEEE transactions on affective computing, to be published, doi 10.1109/taffc.2021.3075638.
- [12] Jian Shen, Xiaowei Zhang, Bin Hu, Gang Wang, Zhijie Ding, and Bin Hu, "An Improved Empirical Mode Decomposition of Electroencephalogram Signals for Depression Detection", IEEE transactions on affective computing, Vol. 13, No. 1, January-March 2022.
- [13] Usman Ahmed, Jerry Chun-Wei Lin, and Gautam Srivastava, "Social Media Multiaspect Detection by Using Unsupervised Deep Active Attention", IEEE transactions on computational social systems, to be published, doi 10.1109/tcss.2022.3183283.
- [14] Tao Chen, Yanrong Guo, Shijie Hao, Richang Hong, "Exploring Self-attention Graph Pooling with EEG-based Topological Structure and Soft Label for Depression Detection", IEEE transactions on affective computing, to be published, doi 10.1109/taffc.2022.3210958.
- [15] Mudasar Ahmad Wani, Mohammad A. ELAffendi, Kashish Ara Shakil, Ali Shariq Imran, and Ahmed A. Abd El-Latif, "Depression Screening in Humans With AI and Deep Learning Techniques", IEEE transactions on computational social systems, to be published, doi 10.1109/tcss.2022.3200213.
- [16] Jianxiu Li, Nan Li, Xuexiao Shao, Junhao Chen, Yanrong Hao, Xiaowei Li, and Bin Hu, "Altered Brain Dynamics and Their Ability for Major Depression Detection using EEG Microstates Analysis", IEEE transactions on affective computing, to be published, doi 10.1109/taffc.2021.3139104.
- [17] Jing Zhu, Changlin Yang, Xiannian Xie, Shiqing Wei, Yizhou Li, Xiaowei Li, and Bin Hu, "Mutual Information Based Fusion Model (MIBFM): Mild Depression Recognition Using EEG and Pupil Area Signals", IEEE transactions on affective computing, to be published, doi 10.1109/taffc.2022.3171782.
- [18] Le Yang, Dongmei Jiang and Hichem Sahli, "Integrating Deep and Shallow Models for Multi-Modal Depression Analysis — Hybrid Architectures", IEEE transactions on affective computing, to be published, doi 10.1109/TAFFC.2018.2870398.
- [19] Mario Ezra Aragón, A. Pastor López-Monroy, Luis C. González, and Manuel Montes-y-Gómez, "Detecting Mental Disorders in Social Media Through Emotional Patterns - The case of Anorexia and Depression", IEEE transactions on affective computing, to be published, doi 10.1109/taffc.2021.3075638.
- [20] Kristen C. Allen, Alex Davis, Tamar Krishnamurti, "Indirect Identification of Perinatal Psychosocial Risks from Natural Language",

- IEEE transactions on affective computing, to be published, doi 10.1109/taffc.2021.3079282.
- [21] Wheidima Carneiro de Melo, Eric Granger, and Abdenour Hadid, "A Deep Multiscale Spatiotemporal Network for Assessing Depression from Facial Dynamics." IEEE transactions on affective computing, August 2019.
- [22] Zhaocheng Huang, Julien Epps, Dale Joachim, "Investigation of Speech Landmark Patterns for Depression Detection", IEEE Transactions on Affective Computing, to be published, doi 10.1109/taffc.2019.2944380.
- [23] Hanshu Cai, Xiangzi Zhang, Yanhao Zhang, Ziyang Wang, Bin Hu, "A Case-based Reasoning Model for Depression based on Three-electrode EEG Data", IEEE transactions on affective computing, to be published, doi 10.1109/taffc.2018.2801289.
- [24] Kun-Yi Huang, Chung-Hsien Wu, Senior Member, IEEE, Ming-Hsiang Su, and Yu-Ting Kuo, "Detecting Unipolar and Bipolar Depressive Disorders from Elicited Speech Responses Using Latent Affective Structure Model." IEEE transactions on affective computing, to be published, doi 10.1109/taffc.2018.2803178.
- [25] N. Palmius, A. Tsanas, K. E. A. Saunders, A. C. Bilderbeck, J. R. Geddes, G. M. Goodwin, and M. De Vos, "Detecting Bipolar Depression From Geographic Location Data", IEEE transactions on biomedical engineering, Vol. 64, No. 8, August 2017.
- [26] Lea Canales, Carlo Strapparava, Ester Boldrini, and Patricio Mart'inez-Barco, "Intensional Learning to Efficiently Build up Automatically Annotated Emotion Corpora", IEEE transactions on affective computing, vol. 14, no. 8, August 2015.
- [27] Sharifa Alghowinem, Roland Goecke, Michael Wagner, Julien Epps, Matthew Hyett, Gordon Parker, and Michael Breakspear, "Multimodal Depression Detection: Fusion Analysis of Paralinguistic, Head Pose and Eye Gaze Behaviors", IEEE transactions on affective computing, vol. X, no. X, January 2015.
- [28] Ying Yang, Catherine Fairbairn, and Jeffrey F. Cohn, "Detecting Depression Severity from Vocal Prosody", IEEE transactions on affective computing, Vol. 4, No. 2, April-June 2013.
- [29] Lu-Shih Alex Low, Namunu C. Maddage, Margaret Lech, Lisa B. Sheeber, and Nicholas B. Allen, "Detection of Clinical Depression in Adolescents' Speech During Family Interactions", IEEE transactions on biomedical engineering, Vol. 58, No. 3, March 2011.
- [30] Ringeval, Fabien, Björn Schuller, Michel Valstar, Nicholas Cummins, Roddy Cowie, Leili Tavabi, Maximilian Schmitt et al. "Avec 2019 workshop and challenge: State-of-mind, detecting depression with ai, and cross-cultural affect recognition." In Proceedings of the 9th International on Audio/Visual Emotion Challenge and Workshop, pp. 3-12. ACM, 2019.
- [31] Lin Lin, Xuri Chen, Ying Shen * and Lin Zhang," Towards Automatic Depression Detection:A BiLSTM/1D CNN-Based Model", Appl. Sci. 2020, 10, 870.

Sustainable Artificial Intelligence: Assessing Performance in Detecting Fake Images

Othman A. Alrusaini

Department of Engineering and Applied Sciences-Applied College, Umm Al-Qura University, Makkah, Saudi Arabia

Abstract—Detecting fake images is crucial because they may confuse and influence people into making bad judgments or adopting incorrect stances that might have disastrous consequences. In this study, we investigate not only the effectiveness of artificial intelligence, specifically deep learning and deep neural networks, for fake image detection but also the sustainability of these methods. The primary objective of this investigation was to determine the efficacy and sustainable application of deep learning algorithms in detecting fake images. We measured the amplitude of observable phenomena using effect sizes and random effects. Our meta-analysis of 32 relevant studies revealed a compelling effect size of 1.7337, indicating that the model's performance is robust. Despite this, some moderate heterogeneity was observed (Q-value = 65.5867; $I^2 = 52.7344\%$). While deep learning solutions such as CNNs and GANs emerged as leaders in detecting fake images, their efficacy and sustainability were contingent on the nature of the training images and the resources consumed during training and operation. The study highlighted adversarial confrontations, the need for perpetual model revisions due to the ever-changing nature of image manipulations, and data scarcity as technical obstacles. Additionally, the sustainable deployment of these AI technologies in diverse environments was considered crucial.

Keywords—Artificial intelligence; image validation; deep learning; deep neural networks; fake images; image forgery; image manipulations

I. INTRODUCTION

Technological advancements in graphics design continue to receive unprecedented improvements with each new software release. Such advancements are beneficial and detrimental, as they can positively and negatively impact people. On the positive side, repaying old images and restoring them to their former state is now possible. Using software such as Photoshop, a designer can clone sections of an image using the clone stamp tool and replicate the pattern in a different area to make it appear real and authentic [1, 2]. Users can also add interesting features to their photographs to add aesthetics that were previously not present in their photographs. This aesthetic appeal from edited images can improve an image's appeal and introduce an element of fantasy into the work.

Nevertheless, this technology has seen its application stretch beyond serving people's genuine needs to improve photographic appeal. Many, if not most, of its application has been doctoring images to trick people into believing falsehoods [3, 4]. One of the fields that have suffered immensely is academics. People can now engage in document forgery to create certificates that look exactly like an

institution's legally issued credentials [5]. Most recent versions of the graphics editing software use artificial intelligence (AI) to edit images, making the finishing even more illustrious [6]. This fact makes it quite difficult to detect fake images from the real ones using the naked eye, thereby creating an extra layer of complexity to the process.

The primary objective of this research is to undertake a meta-analysis study of deep learning tools and technologies used to detect fake images, with a focus on both their effectiveness and sustainability. The research questions guiding this analysis are as follows:

- 1) How effective are deep learning algorithms in detecting fake images, and how do their effectiveness and sustainability correlate?
- 2) What are the most reliable evaluation metrics for evaluating the performance and sustainability of deep learning algorithms in detecting fake images?
- 3) What are the technical challenges in the sustainable detection of fake images using deep learning techniques?

While several studies have engaged in the primary research of creating and evaluating deep learning models to detect fake images, few have done it in a meta-analytical way that also considers the sustainability of these technologies. This approach effectively synthesizes the field's gains in developing the algorithms. It also exposes the weaknesses, gaps, and sustainability concerns that need filling to improve algorithmic formidability. It is expected that this research and its analysis will add to the existing fake images detection with AI literature by providing a better understanding of the different models and various datasets.

The paper contains six sections: introduction, background, methods, results, discussion and conclusion. The introduction in Section I sets the stage for what the paper will deliberate on and establishes the researcher's rationale. The background in Section II, the paper delves deep into the current solutions and technological overview to give the reader a good vantage point from which to appreciate the gains and weaknesses in the field of fake image detection using deep learning technologies. The methods in Section III takes the reader through a setup of the meta-analytical approach, including search strategies, data sources, inclusion and exclusion criteria, and data analysis approaches. The results in Section IV comprehensively analyses the findings made in the analysis. Finally, the paper discusses these findings to synthesize the results and also summarises along with suggested areas for further investigation in Section V and Section VI respectively.

II. BACKGROUND

A. Types of Fake Images

The diversity of fake images has made their detection all the more challenging because of the intricacy that comes with each type. Image splicing is one of the many types contributing to the fake image ecosystem [7, 8]. It refers to the result of combining parts of different images to create a new but deceptive version. It is almost similar to morphing and blending two or more images. In both cases, tampering with the final image is difficult to identify with the naked eye. Sometimes, creating fake images may involve hiding some aspects within the image to make it look different [9]. One way to do so is by deleting the unwanted element, which counts as the removal technique. This technique is paired with 'insertion,' introducing a new element into the hitherto non-existent image. The second method to hide elements within an image is steganography, a more technical form of hiding the undesired elements [10].

Some techniques neither remove nor add elements to the original image. Instead, they work on the image's appearance to change certain aspects, such as lighting, contrast, color, and texture. The most popular methods are bundled under the group 'filter-based manipulations' techniques [11, 12]. It is worth noting that designers often use filter-based manipulation techniques with others to create a new 'cooler' image. 3D rendering is another technique that changes the image from its 2D orientation to feature the third dimension of depth. While it does not introduce new elements, some shadows are likely to appear to give the illusion of a 3D image [13]. Regardless of the type of change and the intention behind such changes, analysts must be able to detect the changes programmatically for a more reliable consumption of these digital products. Deep learning is heavily equipped to check for even the mildest inconsistencies within the image structure and report them instantly [14].

B. Traditional Solutions to Detecting Fake Images

The challenge of detecting fake images predates the deep fake technologies, as there has been image doctoring beforehand. One solution that most analyses preferred using was engaging in image forensics. It is a collection of techniques involving statistical and pixel-level image analysis to identify inconsistencies [15, 16]. Some of the aspects sought after are differing noise patterns and lighting anomalies. This method is advantageous because it is not computationally expensive but falters in detecting high-end forgeries and is not easily scalable. Watermarking has also been a key technique in ensuring viewers can tell fake images from the original. While it is effective in copyright protection, it is less applicable to images whose originals do not have watermarks [17, 18]. Another traditional method is meta-analysis, which involves inspecting the images' metadata to detect fakes. While it provides contextual data, the metadata can be easily altered with the right technologies [15].

C. AI-Based Solutions to Detecting Fake Images

With the advent of artificial intelligence, so much technological progress has come about and has permeated the field of image analytics. One such technology is convoluted

neural networks (CNNs), a specific network architecture for deep learning algorithms [15, 19]. Its highly-rated image analytical capabilities can automatically and adaptively learn spatial hierarchies of features in an image. It is highly accurate and is mostly applicable when there are complex patterns. However, their large dataset requirements imply they are computationally expensive [14]. Generative adversarial networks (GANs) are another technology consisting of a generator and discriminator working against each other, widely used for deepfake detection. Like CNNs, they thrive in complex patterns [8, 20]. Nevertheless, their nature as unsupervised learning models makes them susceptible to being unstable and generating false positives. Recurrent neural networks are similar to other technologies but are mostly applicable in video forensics because of their strength in analyzing sequential data [21, 22].

Ensemble methods, transfer learning, and zero-shot learning represent advanced AI approaches that address different aspects of fake image detection. Ensemble methods involve the combination of multiple AI models to improve predictive accuracy and robustness, although they come at the cost of computational expense and increased model complexity [23]. On the other hand, transfer learning provides an efficient approach by applying pre-trained models to new but similar tasks, effectively saving time and computational resources; however, its applicability is constrained to tasks that closely resemble the original training data [24]. Lastly, zero-shot learning presents a frontier in AI-based fake image detection, offering the ability to recognize types of fake imagery that the model has not been specifically trained on [25]. While this method is versatile and adaptable, it is still an area under active research, and thus its reliability is not fully established. Each method has advantages and disadvantages, emphasizing the need for ongoing research to refine these techniques and possibly integrate them for more effective and efficient fake image detection.

D. Fake Image Detection Process using AI

This section describes the methodological steps involved in detecting fake images through the use of AI to collect and analyze data. The flowchart for these steps is shown in Fig. 1.

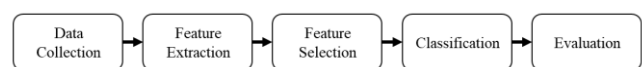


Fig. 1. AI Fake image detection process flowchart.

1) *Data collection*: Data collection is fundamental in building supervised machine learning models. It is the first stage in fake image detection using AI. In this phase, high-dimensional data, often in image matrices or tensors, is gathered [24]. This dataset, comprising RGB values or even grayscale pixel intensities, is crucial for subsequent feature engineering. The data must also be annotated through manual labeling or semi-supervised methods to create ground truth labels distinguishing genuine images from artificially manipulated or deepfake counterparts.

2) *Feature extraction*: Feature extraction involves transforming raw image data into a reduced dimensionality

format using algorithms that capture essential patterns. Techniques such as convolutional neural networks (CNNs) are often employed here, leveraging filter banks to highlight vital image attributes such as edges, textures, and regions of interest [26]. When convolved with input data, these filters output feature maps highlighting image characteristics.

3) *Feature selection*: Not all features extracted hold discriminative power for the classification task at hand. Feature selection focuses on refining the feature set, eliminating redundant or irrelevant features to mitigate the curse of dimensionality, and optimizing model performance [27]. Algorithms such as Recursive Feature Elimination (RFE) or techniques leveraging mutual information can be utilized to determine the most salient features.

4) *Classification*: With a refined feature set, the classification phase employs algorithms to map these features to their respective labels. Deep learning architectures, like CNNs or more complex models like Residual Networks (ResNets), are trained using backpropagation [28]. The objective is to adjust weights and biases to minimize the loss function, typically cross-entropy loss for classification tasks.

5) *Evaluation*: Post-training, the model's robustness, and generalizability are gauged using accuracy, precision, recall, and the F1 score on a holdout validation or test dataset. Techniques like k-fold cross-validation can ensure the evaluation is comprehensive, and if underfitting or overfitting is detected, hyperparameter tuning, regularization methods, or architecture adjustments might be necessitated [20, 29].

III. METHODS

A. Literature Search

In our investigation into artificial intelligence and image validation, we selected a set of keywords to guide our data extraction process. Central to our inquiry was "Deep learning," which is intrinsically tied to "Deep neural networks." To delve into the specific area of counterfeit or fake imagery, we utilized terms such as "Fake images," "Image forgery," "Image tampering," and "Image authenticity." Recognizing the significance of assessing the capability of algorithms, we incorporated "Effectiveness" and "Performance" into our search parameters. The term "Image detection" was chosen to understand the broader mechanisms behind image recognition and validation. Additionally, the "F1 score" was included as a metric of interest to gain insights into evaluation methods. Its inclusion is because of its widespread application in balancing precision and recall in binary classification problems. Through these keywords, we aimed to ensure a comprehensive exploration of the current state of deep learning techniques in detecting fake images.

B. PRISMA Flow Chart

The research was undertaken following the guidance of the PRISMA flowchart. It is a flow diagram reporting the stages articles go through to determine whether they are fit for inclusion in a meta-analysis [30]. The PRISMA flowchart in Fig. 2 delineates the sequence of a meta-analysis process. Initiating with the identification phase, a search was

conducted across 10 databases, unearthing a total of 317 studies. From this collection, preliminary screening reduced the number to 226 records. The reasons for this reduction were multi-fold: 54 records were identified as duplicates, 23 were found ineligible based on certain criteria, and 14 were removed due to other specified reasons. The subsequent phase saw 187 of these 226 screened records being selected for detailed report retrieval. Of these, 44 reports could not be retrieved, which left a pool of 143 reports. These reports were then subjected to a comprehensive eligibility assessment. In the final count, several reports were excluded from the 143 due to a range of reasons: a lack of full-text availability in 20 reports, 45 not matching the necessary keywords, 27 not meeting the quality appraisal standards, and 19 being deemed irrelevant to the study's focus. After these exclusions, the evaluation was refined to a set of 32 studies that were considered relevant and included in the meta-analysis.

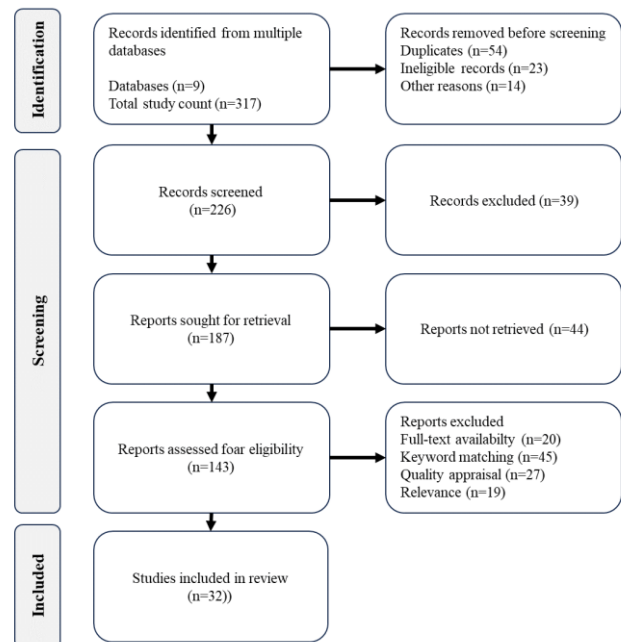


Fig. 2. PRISMA flowchart.

C. Distribution of Journals

Regarding the journals from which these final papers were derived, 'IEEE Access' from IEEE had the most articles, with eight total. MDPI's 'Applied Sciences' received five submissions, as illustrated in Table I. MDPI's 'Journal of Imaging' and 'Sensors' received three each. The paper source 'ACM Conference papers' appeared twice.

Other journals on the list had a source each, as observed in Table I. These numerous sources demonstrate how many fields are interested in applying artificial intelligence to detect fake images.

D. Computing Effect Sizes

Effect sizes are indispensable in meta-analysis, serving as a standardized metric to gauge the magnitude of observed phenomena and facilitating comparisons across diverse studies. This study focused on the F1 score, which measures a model's accuracy. The researcher also focused on the sample

size, denoted by the number of images used in individual studies. The choice was made to employ the random-effects model, considering the potential variability in study designs and regions covered. The determination of effect sizes hinged on a transformation suitable for F1 scores, as opposed to the conventional Fisher's Z transformation tailored for correlation coefficients [31]. Both Q-statistics and I²-values were deployed to comprehend the variability or heterogeneity of the results among the different studies [32]. In meta-analysis, heterogeneity indicates the differences in outcomes across the incorporated studies. If heterogeneity is high, it implies that the studies' results vary considerably [31]. Such computations empower this study, offering a rigorous quantitative consolidation of literature on using artificial intelligence to detect fake images.

TABLE I. DISTRIBUTION OF STUDIES BY JOURNAL

| Journal | Publication | # |
|---|--|---|
| IEEE Access | IEEE | 8 |
| Applied Sciences | MDPI | 5 |
| Journal of Imaging | MDPI | 3 |
| Sensors | MDPI | 3 |
| ACM Conference papers | ACM | 2 |
| International Journal of Advanced Computer Science and Applications | The Science and Information Organization | 1 |
| Journal of Visual Communication and Image Representation | Elsevier | 1 |
| International Journal of Scientific Research in Computer Science Engineering and Information Technology | IJSRCSEIT | 1 |
| The Visual Computer | Springer | 1 |
| Journal of Cybersecurity and Privacy | MDPI | 1 |
| Entropy | MDPI | 1 |
| PeerJ Computer Science | PeerJ | 1 |
| Neural Computing and Applications | Springer | 1 |
| IRACST-International Journal of Computer Science and Information Technology & Security (IJCSITS) | IRACST | 1 |
| International Journal of Information Technology | Springer | 1 |
| Electronics | MDPI | 1 |

1) *Fisher's Z transformation*: Fisher's Z is a statistical method that transforms Pearson correlation coefficients into a normally distributed variable [31]. The transformation is used because Pearson's r does not have a normal distribution, which makes its confidence intervals asymmetric. Fisher's Z transformation aids in stabilizing this variance. A higher absolute value of Fisher's Z indicates a stronger relationship between variables.

$$Fisher's Z = 0.5 \times \ln \left(\frac{1+f}{1-f} \right) \quad (1)$$

where, f = F1-score

2) *The Weight value for each study (w_i)*: The w_i value represents the inverse of the variance of the effect size for

study i [31]. It gives more weight to studies with more precise estimates (i.e., smaller variance), allowing them to influence the combined effect size more than those with less precise estimates [2].

$$w_i = \left(\frac{z_i}{Var(z)} \right) \quad (2)$$

Where, z_i is a study's effect size measured by Fisher's Z index.

3) *The Overall effect size (z₊)*: The z₊ formula calculates the combined effect size in meta-analyses using weighted individual study effect sizes [32]. This Equation allows the aggregation of individual study results to derive an overall effect, giving more weight to studies with larger sample sizes or more precise measurements. A greater z₊ value suggests a larger overall effect size across the analyzed studies.

$$z_+ = \frac{\sum_{i=1}^N (w_i \times z_i)}{\sum_{i=1}^N w_i} \quad (3)$$

where, N = number of studies

4) *The Q statistic*: The Q statistic measures the heterogeneity or variability of effect sizes across studies in a meta-analysis [31]. Determining heterogeneity is essential to deciding on the type of meta-analytic model (fixed-effects vs. random-effects) to use. A significant Q value indicates substantial heterogeneity among the included studies, suggesting that differences in effect sizes aren't solely due to sampling error.

$$Q = \sum_{i=1}^N w_i \times (z_i - z_+)^2 \quad (4)$$

5) *The I² metric*: I² is a metric that quantifies the percentage of total variability in study estimates attributable to heterogeneity rather than chance [32]. It provides insights into the consistency of findings across studies, independent of the number of studies included. An I² value close to 100% indicates high heterogeneity, suggesting that the results of the studies are diverse.

$$I^2 = \left(\frac{Q - N + 1}{Q} \right) \times 100 \quad (5)$$

6) *Bounds*: This bounds equation calculates the confidence interval around the mean effect size based on the standard deviation of study weights [32]. The bounds provide a range within which the true effect size is expected to fall, offering a measure of the precision of the effect size estimate. Narrower intervals denote more precise estimates, while wider intervals indicate more uncertainty around the effect size.

$$bounds = f_z \pm \alpha \times \sigma \quad (6)$$

where, f_z is the mean F1 score given all the studies included in the meta-analysis, and α is the level of

significance, while σ refers to the standard deviation of the study weights.

7) *Fail-Safe N*: The Fail-safe N method estimates the number of unpublished or "missing" studies required to nullify the effect observed in a meta-analysis [31]. It addresses the potential publication bias in meta-analyses. A high Fail-safe N suggests the meta-analysis results are robust against potential publication bias.

$$Fail - safe N (N_{f.s.05}) = \frac{[(\sum z)^2 - (N * \bar{z}^2)]}{\alpha^2} \quad (7)$$

Where, $\sum z$ is the summation of all Fisher's z indices, and \bar{z} is the mean of all Fisher's z indices.

8) *Critical value*: The formula gives a threshold number for robustness against publication bias in meta-analyses [31]. Considering the number of studies in the analysis, it assesses the risk of overestimating effects due to publication bias. A higher critical value implies greater robustness of the meta-analysis results against potential biases.

$$Critical\ value = 5 \times N + 10 \quad (8)$$

IV. RESULTS

A. Study Statistics

Table II shows the summary statistics for the 32 studies included in the meta-analysis. The statistics include sample size, F1-score, Fisher's z, and their weights.

TABLE II. INDIVIDUAL STUDY STATISTICS

| Study | Year | Purpose | Dataset | Sample Size | Model | F1-Score | Fisher's Z | Weight | |
|-------|------|---------|--------------------------|-----------------|-------|----------|------------|--------|---------|
| 1 | [33] | 2022 | Image Classification | CIFAR-10 | 19579 | CNN | 0.94 | 1.74 | 10.5177 |
| 2 | [1] | 2023 | Fake Image Detection | CELEBA | 7373 | RNN | 0.89 | 1.42 | 8.60468 |
| 3 | [6] | 2022 | Fake Image Detection | DeepFake | 24060 | RNN | 0.85 | 1.26 | 7.60152 |
| 4 | [34] | 2021 | Object Detection | COCO | 5361 | CNN | 0.84 | 1.22 | 7.38984 |
| 5 | [35] | 2022 | Image and Video Analysis | UCF101 | 31671 | CNN | 0.87 | 1.33 | 8.06704 |
| 6 | [27] | 2018 | Fake Image Detection | FaceForensics++ | 21953 | RNN | 0.92 | 1.59 | 9.61588 |
| 7 | [36] | 2022 | Fake Image Detection | DFDC | 7628 | LSTM | 0.99 | 2.65 | 16.016 |
| 8 | [9] | 2018 | Image Classification | ImageNet | 26622 | CNN | 0.84 | 1.22 | 7.38984 |
| 9 | [37] | 2021 | Object Tracking | GOT-10k | 11570 | CNN | 0.95 | 1.83 | 11.0849 |
| 10 | [38] | 2021 | Fake Image Detection | DeepFake | 34626 | LSTM | 0.91 | 1.53 | 9.2437 |
| 11 | [39] | 2022 | Fake Image Detection | DFDC | 21287 | RNN | 0.99 | 2.65 | 16.016 |
| 12 | [40] | 2020 | Fake Image Detection | FaceForensics++ | 4053 | RNN | 0.9 | 1.47 | 8.90903 |
| 13 | [41] | 2022 | Fake Image Detection | DFDC | 12914 | LSTM | 0.97 | 2.09 | 12.6614 |
| 14 | [42] | 2022 | Fake Image Detection | BEGAN | 27843 | RNN | 0.96 | 1.95 | 11.7755 |
| 15 | [24] | 2021 | Image Generation | Pascal VOC | 27983 | GAN | 0.95 | 1.83 | 11.0849 |
| 16 | [43] | 2023 | Object Detection | DeepFake | 6216 | CNN | 0.99 | 2.65 | 16.016 |
| 17 | [44] | 2022 | Fake Image Detection | Kinetics | 6750 | LSTM | 0.86 | 1.29 | 7.82658 |
| 18 | [45] | 2018 | Video Classification | ADE20K | 3742 | CNN | 0.86 | 1.29 | 7.82658 |
| 19 | [5] | 2020 | Image Segmentation | CELEBA | 29993 | CNN | 0.84 | 1.22 | 7.38984 |
| 20 | [46] | 2017 | Fake Image Detection | DFDC | 31835 | GAN | 0.93 | 1.66 | 10.0356 |
| 21 | [47] | 2021 | Fake Image Detection | CIFAR-100 | 20979 | RNN | 0.91 | 1.53 | 9.2437 |
| 22 | [10] | 2019 | Image Classification | DeepFake | 26169 | CNN | 0.85 | 1.26 | 7.60152 |
| 23 | [28] | 2018 | Fake Image Detection | YOLO | 8365 | LSTM | 0.92 | 1.59 | 9.61588 |
| 24 | [29] | 2018 | Object Detection | PCGAN | 11032 | CNN | 0.85 | 1.26 | 7.60152 |
| 25 | [14] | 2023 | Image Synthesis | CELEBA | 22837 | GAN | 0.86 | 1.29 | 7.82658 |
| 26 | [48] | 2021 | Fake Image Detection | FaceForensics++ | 8702 | RNN | 0.94 | 1.74 | 10.5177 |
| 27 | [49] | 2019 | Fake Image Detection | GAN | 16576 | LSTM | 0.89 | 1.42 | 8.60468 |
| 28 | [50] | 2019 | Image Generation | AVA | 13425 | GAN | 0.95 | 1.83 | 11.0849 |
| 29 | [22] | 2021 | Image and Video Analysis | DeepFake | 23896 | CNN | 0.87 | 1.33 | 8.06704 |
| 30 | [25] | 2018 | Fake Image Detection | DFDC | 6611 | RNN | 0.89 | 1.42 | 8.60468 |
| 31 | [51] | 2021 | Fake Image Detection | CELEBA | 30177 | LSTM | 0.94 | 1.74 | 10.5177 |
| 32 | [26] | 2023 | Fake Image Detection | CIFAR-10 | 32538 | RNN | 0.96 | 1.95 | 11.7755 |

Table II showcases various studies from 2017 to 2023, spanning applications like themes in fake image detection. Commonly used models include CNNs, RNNs, LSTMs, and GANs. Notably, LSTMs achieved top F1 scores in several studies ([35],[37],[41]). The consistency in Fisher's Z values suggests a uniform significance level. The weight, mirroring the sample size, hints at the study's reliability. In essence, the table reflects both progress and challenges in AI research.

The datasets employed in the studies are all related to machine learning and artificial intelligence. CIFAR-10 and CIFAR-100 are widely used benchmarks for image classification, consisting of small images from several categories. ImageNet, a significant player in the image classification field, has been instrumental in driving progress in deep learning. CELEBA focuses on facial attributes and provides a wide range of annotated faces. DeepFake, DFDC, and FaceForensics++ focus on detecting fake images and videos, which are crucial for developing ways to combat misinformation. COCO and Pascal VOC are widely used in object detection, while UCF101 and Kinetics are popular for video classification and analysis. GOT-10k is specifically made for object tracking, while ADE20K is focused on semantic segmentation tasks. Generative models like BEGAN, PCGAN, and GAN datasets play a crucial role in image synthesis and generation.

B. Meta-Analysis Summary Statistics

Table III summarizes the statistics from the 32 studies involved in this meta-analysis. The statistics include z_+ , Q, I^2 , σ , lower bound, upper bound, critical Nfs, Nfs, CI, and statistical significance.

TABLE III. OVERALL STUDY STATISTICS

| Statistic | Value |
|--------------------------|------------------|
| z_+ | 1.7337 |
| Q | 65.5867 |
| I^2 | 52.7344 |
| σ | 0.0562 |
| Lower Bound | 1.6235 |
| Upper Bound | 1.8439 |
| Critical Nfs | 170 |
| Nfs | 2706.9451 |
| CI | [1.6235, 1.8439] |
| Statistical Significance | $p < 0.001$ |

1) *Overall effect size (z_+ : 1.7337)*: The z_+ value represents the meta-analysis's pooled or combined standardized effect size. A value of 1.7337 indicates a positive and relatively strong overall effect size [18]. These findings suggest that from a general standpoint, the machine learning models employed in the studies performed well in detecting fake images. According to [33, 52], 0.2 is small, 0.5 is medium, and 0.8 or above is considered large. Hence, the z_+ value obtained in this case shows a large effect size.

2) *Heterogeneity (Q: 65.5867, I^2 : 52.7344%)*: Both Q and I^2 are measures of heterogeneity among the included studies. The high Q-value suggests significant variability in the effect sizes across studies [51]. Table II illustrates the differences in the F1 scores obtained from running different machine learning models in detecting fake images. This test statistic follows a chi-square distribution, and its threshold for significance depends on the number of studies (or degrees of freedom). A significant Q-value implies heterogeneity.

The I^2 value further quantifies this heterogeneity: about 53% of the observed variability in the effect sizes is due to genuine differences among studies rather than random sampling error [24]. It affirms the credibility and reliability of the studies included in the meta-analysis because, despite the variability, they all make similar inferences regarding AI's ability to detect fake images. I^2 values of 25%, 50%, and 75% are considered low, moderate, and high heterogeneity, respectively. The I^2 value of ~53% in this study suggests moderate to high heterogeneity among the included studies.

3) *Precision of the effect size (σ : 0.0562, lower bound: 1.6235, upper bound: 1.8439, CI: [1.6235, 1.8439])*: These statistics provide insight into the precision and reliability of the z_+ value. The standard deviation (σ) is low, which suggests a precise estimate [11]. A low standard deviation is synonymous with minimal differences in the overall sentiment expressed by the 32 studies included in this meta-analysis. The confidence interval (CI) is also reasonably narrow, ranging from 1.6235 to 1.8439. While there are no standard σ values, a narrow CI, like in our case, denotes high precision [41]. Consequently, this further indicates that the pooled effect size is estimated with high precision [45].

4) *Publication bias (Critical Nfs: 170, Nfs: 2706.9451)*: In meta-analyses, fail-safe N (Nfs) and critical Nfs are used to evaluate the potential for publication bias. The critical Nfs represents the minimum number of studies with null results required to raise the p-value above a significance threshold (typically 0.05). There is no standard value or range for this statistic. However, a higher Nfs than the critical value indicates that many unpublished, non-significant studies would be required to nullify the observed effect [40]. Additionally, the statistics suggest that the meta-analysis results are robust against possible publication bias [32].

5) *Significance of the effect ($p < 0.001$)*: This p-value indicates the probability that the observed effect (or a more extreme effect) would occur by random chance alone if there were no real effects. The study found a p-value less than 0.001. For a study conducted at a 0.05 confidence level, a statistical significance of anything lower than 0.05 is acceptable [43, 49]. Consequently, the value affirms that it is highly statistically significant. It further provides strong evidence against the null hypothesis that machine learning models can effectively detect fake images [23].

6) *Implication*: The meta-analysis results indicate a robust, positive, and highly significant overall effect size. The small confidence interval and standard deviation demonstrate

the estimated results' precision. However, substantial heterogeneity among the included studies necessitates additional research to determine the causes of this variation. The results appear robust against the possibility of publication bias. While the results appear trustworthy, future meta-analyses should consider the high heterogeneity and strive to reduce it.

V. DISCUSSION

A. Effectiveness and Sustainability of Deep Learning Algorithms in Detecting Fake Images

The first research question regarded the effectiveness and sustainability of deep learning in detecting fake images. Our study discovered that the accelerated development of digital manipulation techniques has increased the difficulty of detecting fake or fabricated images [35, 36]. Deep learning algorithms, particularly convolutional neural networks (CNNs) and generative adversarial networks (GANs), have been widely cited as the leading instruments for addressing this concern [3, 44, 52]. Many sources we consulted emphasized that these algorithms frequently outperform conventional image analysis techniques, with many studies reporting accuracy rates and F1 scores exceeding 0.8 [24, 50]. High performance was most commonly observed in experiments employing a larger number of images as samples [53, 54]. However, even the lowest-performing studies' F1 scores did not fall below 0.84.

However, the revision of the sources disclosed a recurring theme. These algorithms' variable efficacy was based on the type and quality of the fake images they were trained on, although this was not the case in all studies. Moreover, the sustainability of these algorithms in the context of varying image types and qualities emerged as a significant consideration. Several sources alluded to sophisticated techniques for occasionally generating fake images that could circumvent deep learning detectors, raising concerns about the long-term sustainability of these detection methods. This pattern is notably evident when training data lacks diversity [9, 41, 44]. In addition, our investigation revealed that adversarial assaults on these algorithms present a challenging obstacle but also raise questions about their sustainable effectiveness [38, 42]. On the effectiveness and sustainability of deep learning algorithms in detecting fake images, this analysis finds that although deep learning is a promising avenue, it may require integration with other detection techniques to obtain optimal and sustainable results.

B. Evaluation Metrics for Deep Learning Algorithms in Sustainable Fake Image Detection

The second research question examined the evaluation metrics mostly employed to appraise the performance and sustainability of deep learning models in detecting fake images. Our exhaustive analysis highlighted the critical significance of dependable evaluation metrics for assessing the performance and sustainability of deep learning algorithms in detecting fake images [3, 37, 38]. Findings suggested that the most reliable metric is the F1 score, though most studies also engaged with other metrics to be more comprehensive. Most of the studies we evaluated emphasized indicated that

the F1 score is not comparable to accuracy because it is an aggregate of precision and recall, thereby giving it an edge over other performance measures [7].

Most studies employed precision, recall, and the F1-score metric to avoid using accuracy. The performance measure (F1 score) provides a more comprehensive perspective on the efficacy of an algorithm [24]. This meta-analysis utilized the F1 score as its primary metric and was also one of the selection criteria for the selected studies. The harmonic mean property of the F1-score, which considers both precision and recall, is useful when an optimal equilibrium between false positives and false negatives is essential. Using only precision or recall is frequently deemed insufficient, as it conceals a crucial aspect of model performance [36, 46].

C. Technical Challenges in the Sustainable Detection of Fake Images using Deep Learning

The final research question interrogated the technical challenges experienced during fake image detection using deep learning approaches. Specialists frequently face several technical obstacles when utilizing deep learning technologies for fake image detection, as uncovered by our exhaustive analysis [1, 42, 47]. Additionally, the sustainability of these technologies in the face of evolving threats and techniques is a critical concern. Many sources we consulted elaborated on the difficulty of adversarial assaults [34, 39, 42]. Typically, these assaults are ingeniously designed perturbations that not only pose a technical challenge but also raise sustainability issues, as they can trick deep learning models into misclassifying a fake image as authentic or vice versa [9, 48]. This issue illustrates the vulnerability and potentially limited sustainability of these algorithms under specific conditions. While many of the sources devised mechanisms to circumvent adversarial assaults, they acknowledged that such complexities could have a significant impact on the performance and sustainability of the models. In addition, the dynamic nature of image manipulation techniques necessitates constant model updates, highlighting the need for sustainable development practices in AI, as current methods may become obsolete in the face of newer and more complex image manipulation techniques.

In addition, most sources mentioned an 'arms race' between fake image generators and detectors, highlighting a sustainability challenge in this technological contest. As technologies for deep learning evolve, so do techniques for generating fake images, resulting in a continuous and potentially unsustainable development cycle for both [5, 14]. Given the novelty of both disciplines, it is uncertain which will ultimately prevail, raising concerns about the long-term sustainability of detection algorithms. This swift evolution underscores the need for sustainable development practices in the field. Our investigation also revealed that data deficiency hinders model training capabilities [35, 38]. This case is notably true for labeled datasets containing high-quality fake images. Consequently, detection model efficacy declines. The complexity of deep learning models also poses computational and sustainability difficulties [6, 36]. The typical solution is to demand substantial resources for instruction and deduction, which may not be sustainable, especially for real-time

applications that require efficient and environmentally conscious approaches.

VI. CONCLUSION AND FUTURE RESEARCH

Identifying fake images has become a top concern in the wake of a highly advanced era, underscoring the necessity for sustainable methods in digital content management. Numerous individuals with questionable motives have utilized technology to fabricate misleading photos and manipulate unsuspecting individuals. The prevalence of inaccurate information in online spaces has heightened the need to eradicate this problem through sustainable approaches. Our comprehensive analysis showcases the growing potential of deep learning technologies, particularly convolutional neural networks (CNNs) and generative adversarial networks (GANs), in addressing this issue sustainably. While these models have shown promising outcomes and made a notable difference, they encounter challenges in maintaining sustainability in their applications. It is important to be cautious when generalizing study conclusions due to the differences in methodology, types of images, and geographical factors, and sustainability considerations. The F1 score is necessary to evaluate how well these algorithms perform on the modified images they are trained on, with an emphasis on quality, diversity, and sustainability.

However, the landscape of fake image detection is fraught with obstacles that exceed the capabilities of algorithms, demanding sustainable solutions. As a result of adversarial assaults, there is an ongoing arms race between fake image creators and their detectors, demanding sustainable solutions. In addition, the frequent need for model updates, computational demands, and data scarcity indicate the need for ongoing research efforts. As technology advances, image manipulations become more complex, increasing the demand for powerful, adaptable, and sustainable deep-learning solutions. We need to work together and combine the knowledge and expertise of academia, industry, and policymakers, to develop effective and sustainable strategies to better protect ourselves against fake images.

REFERENCES

- [1] T. Goel, R. Murugan, S. Mirjalili and D. K. Chakrabarty, "OptCoNet: an optimized convolutional neural network for an automatic diagnosis of COVID-19," *Applied Intelligence*, vol. 51, no. 3, pp. 1351-1366, 2021.
- [2] N. K. Chowdhury, M. M. Rahman and M. A. Kabir, "PDCOVIDNet: a parallel-dilated convolutional neural network architecture for detecting COVID-19 from chest X-ray images," *Health information science and systems*, vol. 8, no. 1, pp. 1-14, 2020.
- [3] WHO, "WHO Coronavirus (COVID-19) Dashboard," 17 December 2021. [Online]. Available: <https://covid19.who.int/>. [Accessed 17 December 2021].
- [4] D. Singh, V. Kumar and M. Kaur, "Classification of COVID-19 patients from chest CT images using multi-objective differential evolution-based convolutional neural networks," *European Journal of Clinical Microbiology & Infectious Diseases*, vol. 39, no. 7, p. 137, 2020.
- [5] M. Elgendi, M. U. Nasir, Q. Tang, R. R. Fletcher, N. M. C. Howard and S. Nicolaou, "The performance of deep neural networks in differentiating chest X-rays of COVID-19 patients from other bacterial and viral pneumonias," *Frontiers in Medicine*, vol. 7, no. 1, p. 550, 2020.
- [6] J. Civit-Masot, F. Luna-Perejón, M. Domínguez Morales and A. Civit, "Deep learning system for COVID-19 diagnosis aid using X-ray pulmonary images," *Applied Sciences*, vol. 10, no. 13, p. 4640, 2020.
- [7] M. Shorfuazzaman and M. S. Hossain, "MetaCOVID: A Siamese neural network framework with contrastive loss for n-shot diagnosis of COVID-19 patients," *Pattern recognition*, vol. 113, no. 1, p. 107700, 2021.
- [8] L. Li, T. Shim and P. E. Zapanta, "Optimization of COVID-19 testing accuracy with nasal anatomy education," *American journal of otolaryngology*, vol. 42, no. 1, p. 102777, 2021.
- [9] M. N. Esbin, O. N. Whitney, S. Chong, A. Maurer, X. Darzacq and R. Tjian, "Overcoming the bottleneck to widespread testing: a rapid review of nucleic acid testing approaches for COVID-19 detection," *Rna*, vol. 26, no. 7, pp. 771-783, 2020.
- [10] L. Wang, Z. Q. Lin and A. Wong, "Covid-net: A tailored deep convolutional neural network design for detection of covid-19 cases from chest x-ray images," *Scientific Reports*, vol. 10, no. 1, pp. 1-12, 2020.
- [11] M. Szmigiera, "Impact of the coronavirus pandemic on the global economy - Statistics & Facts," 23 November 2021. [Online]. Available: <https://www.statista.com/topics/6139/covid-19-impact-on-the-global-economy/#dossierKeyfigures>. [Accessed 17 December 2021].
- [12] S. A. Quadri, "COVID-19 and religious congregations: Implications for spread of novel pathogens," *International Journal of Infectious Diseases*, vol. 96, no. 1, pp. 219-221, 2020.
- [13] M. Lipsitch and N. E. Dean, "Understanding COVID-19 vaccine efficacy," *Science*, vol. 370, no. 6518, pp. 763-765, 2020.
- [14] M. A. Pettengill and A. J. McAdam, "Can we test our way out of the COVID-19 pandemic?," *Journal of clinical microbiology*, vol. 58, no. 11, pp. e02225-20, 2020.
- [15] F. M. Salman, S. S. Abu-Naser, E. Alajrami, B. S. Abu-Nasser and B. A. Alashqar, "Covid-19 detection using artificial intelligence," *First Journal of Biomedical Research*, vol. 1, no. 1, p. 1, 2020.
- [16] C. Shorten, T. M. Khoshgoftaar and B. Furht, "Deep Learning applications for COVID-19," *Journal of big Data*, vol. 8, no. 1, pp. 1-54, 2021.
- [17] T. B. Alakus and I. Turkoglu, "Comparison of deep learning approaches to predict COVID-19 infection," *Chaos, Solitons & Fractals*, vol. 140, no. 1, p. 110120, 2020.
- [18] G. Gilanie, U. I. Bajwa, M. M. Waraich, M. Asghar, R. Kousar, A. Kashif and H. Rafique, "Coronavirus (COVID-19) detection from chest radiology images using convolutional neural networks," *Biomedical Signal Processing and Control*, vol. 66, no. 1, p. 102490, 2021.
- [19] C. Ouchicha, O. Ammor and M. Meknassi, "CVDNet: A novel deep learning architecture for detection of coronavirus (Covid-19) from chest x-ray images," *Chaos, Solitons & Fractals*, vol. 140, no. 1, p. 110245, 2020.
- [20] K. S. Lee, J. Y. Kim, E. T. Jeon, W. S. Choi, N. H. Kim and K. Y. Lee, "Evaluation of scalability and degree of fine-tuning of deep convolutional neural networks for COVID-19 screening on chest X-ray images using explainable deep-learning algorithm," *Journal of Personalized Medicine*, vol. 10, no. 4, p. 213, 2020.
- [21] P. R. Bassi and R. Attux, "A deep convolutional neural network for COVID-19 detection using chest X-rays," *Research on Biomedical Engineering*, vol. 1, no. 1, pp. 1-10, 2021.
- [22] M. Heidari, S. Mirmiahrikandehi, A. Z. Khuzani, G. Danala, Y. Qiu and B. Zheng, "Improving the performance of CNN to predict the likelihood of COVID-19 using chest X-ray images with preprocessing algorithms," *International journal of medical informatics*, vol. 144, no. 1, p. 104284, 2020.
- [23] I. D. Apostolopoulos and T. A. Mpesiana, "Covid-19: automatic detection from x-ray images utilizing transfer learning with convolutional neural networks," *Physical and Engineering Sciences in Medicine*, vol. 43, no. 2, pp. 635-640, 2020.
- [24] A. Makris, I. Kontopoulos and K. Tserpes, "COVID-19 detection from chest X-Ray images using Deep Learning and Convolutional Neural Networks," in *11th Hellenic Conference on Artificial Intelligence*, Athens, City Publishers, 2020, pp. 60-66.
- [25] M. J. Horry, S. Chakraborty, M. Paul, A. Ulhaq, B. Pradhan, M. Saha and N. Shukla, "COVID-19 detection through transfer learning using multimodal imaging data," *IEEE Access*, vol. 8, no. 1, pp. 149808-149824, 2020.

- [26] S. Vaid, R. Kalantar and M. Bhandari, "Deep learning COVID-19 detection bias: accuracy through artificial intelligence," *International Orthopaedics*, vol. 44, no. 1, pp. 1539-1542, 2020.
- [27] H. Benbrahim, H. Hachimi and A. Amine, "Deep transfer learning with apache spark to detect covid-19 in chest x-ray images," *Romanian Journal of Information Science and Technology*, vol. 23, no. S, SI, pp. S117-S129, 2020.
- [28] S. Minaee, R. Kafieh, M. Sonka, S. Yazdani and G. J. Soufi, "Deep-covid: Predicting covid-19 from chest x-ray images using deep transfer learning," *Medical image analysis*, vol. 65, no. 1, p. 101794, 2020.
- [29] I. D. Apostolopoulos, S. I. Aznaouridis and M. A. Tzani, "Extracting possibly representative COVID-19 biomarkers from X-ray images with deep learning approach and image data related to pulmonary diseases," *Journal of Medical and Biological Engineering*, vol. 1, no. 1, p. 1, 2020.
- [30] A. M. Alqudah, S. Qazan, H. Alquran, I. A. Qasmieh and A. Alqudah, "Covid-19 detection from x-ray images using different artificial intelligence hybrid models," *Jordan Journal of Electrical Engineering*, vol. 6, no. 2, pp. 168-178, 2020.
- [31] A. M. Ismael and A. Şengür, "Deep learning approaches for COVID-19 detection based on chest X-ray images," *Expert Systems with Applications*, vol. 164, no. 1, p. 114054, 2021.
- [32] N. W. S. Saraswati, N. W. Wardani and I. G. A. A. D. Indradewi, "Detection of Covid Chest X-Ray using Wavelet and Support Vector Machines," *Int. J. Eng. Emerg. Technol*, vol. 5, no. 2, pp. 116-121, 2020.
- [33] A. Saygılı, "Computer-Aided Detection of COVID-19 from CT Images Based on Gaussian Mixture Model and Kernel Support Vector Machines Classifier," *Arabian Journal for Science and Engineering*, vol. 1, no. 1, pp. 1-19, 2021.
- [34] D. C. R. Novitasari, R. Hendradi, R. E. Caraka, Y. Rachmawati, N. Z. Fanani, A. Syarifudin and R. C. Chen, "Detection of covid-19 chest x-ray using support vector machine and convolutional neural network," *Commun. Math. Biol. Neurosci*, vol. 1, no. 1, p. 202, 2020.
- [35] G. Van Houdt, C. Mosquera and G. Nápoles, "A review on the long short-term memory model," *Artif. Intell. Rev*, vol. 53, no. 8, pp. 5929-5955, 2020.
- [36] A. Sherstinsky, "Fundamentals of recurrent neural network (RNN) and long short-term memory (LSTM) network," *Physica D: Nonlinear Phenomena*, vol. 404, no. 1, p. 132306, 2020.
- [37] Ş. Öztürk and U. Özkaya, "Residual LSTM layered CNN for classification of gastrointestinal tract diseases," *Journal of Biomedical Informatics*, vol. 113, no. 1, p. 103638, 2021.
- [38] M. Z. Islam, M. M. Islam and A. Asraf, "A combined deep CNN-LSTM network for the detection of novel coronavirus (COVID-19) using X-ray images," *Informatics in medicine unlocked*, vol. 20, no. 1, p. 100412, 2020.
- [39] M. Alazab, A. Awajan, A. Mesleh, A. Abraham, V. Jatana and S. Alhyari, "COVID-19 prediction and detection using deep learning," *International Journal of Computer Information Systems and Industrial Management Applications*, vol. 12, no. 1, pp. 168-181, 2020.
- [40] F. Demir, "DeepCoroNet: A deep LSTM approach for automated detection of COVID-19 cases from chest X-ray images," *Applied Soft Computing*, vol. 103, no. 1, p. 107160, 2021.
- [41] H. Naeem and A. A. Bin-Salem, "A CNN-LSTM network with multi-level feature extraction-based approach for automated detection of coronavirus from CT scan and X-ray images," *Applied Soft Computing*, vol. 113, no. 1, p. 107918, 2021.
- [42] A. Waheed, M. Goyal, D. Gupta, A. Khanna, F. Al-Turjman and P. R. Pinheiro, "Covidgan: data augmentation using auxiliary classifier gan for improved covid-19 detection," *Ieee Access*, vol. 8, no. 1, pp. 91916-91923, 2020.
- [43] T. Mahmud, M. A. Rahman and S. A. Fattah, "CovXNet: A multi-dilation convolutional neural network for automatic COVID-19 and other pneumonia detection from chest X-ray images with transferable multi-receptive feature optimization," *Computers in biology and medicine*, vol. 122, no. 1, p. 103869, 2020.
- [44] G. Jain, D. Mittal, D. Thakur and M. K. Mittal, "A deep learning approach to detect Covid-19 coronavirus with X-ray images," *Biocybernetics and biomedical engineering*, vol. 40, no. 4, pp. 1391-1405, 2020.
- [45] M. Rahimzadeh and A. Attar, "A modified deep convolutional neural network for detecting COVID-19 and pneumonia from chest X-ray images based on the concatenation of Xception and ResNet50V2," *Informatics in Medicine Unlocked*, vol. 19, no. 1, p. 100360, 2020.
- [46] A. I. Khan, J. L. Shah and M. M. Bhat, "CoroNet: A deep neural network for detection and diagnosis of COVID-19 from chest x-ray images," *Computer Methods and Programs in Biomedicine*, vol. 196, no. 1, p. 105581, 2020.
- [47] K. K. Singh, M. Siddhartha and A. Singh, "Diagnosis of coronavirus disease (covid-19) from chest x-ray images using modified xceptionnet," *Romanian Journal of Information Science and Technology*, vol. 23, no. 657, pp. 91-115, 2020.
- [48] T. Ozturk, M. Talo, E. A. Yildirim, U. B. Baloglu, O. Yildirim and U. R. Acharya, "Automated detection of COVID-19 cases using deep neural networks with X-ray images," *Computers in biology and medicine*, vol. 121, no. 1, p. 103792, 2020.
- [49] B. Abraham and M. S. Nair, "Computer-aided detection of COVID-19 from X-ray images using multi-CNN and Bayesnet classifier," *Biocybernetics and biomedical engineering*, vol. 40, no. 4, pp. 1436-1445, 2020.
- [50] A. Narin, C. Kaya and Z. Pamuk, "Automatic detection of coronavirus disease (covid-19) using x-ray images and deep convolutional neural networks," *Pattern Analysis and Applications*, vol. 1, no. 1, pp. 1-14, 2021.
- [51] M. Z. Che Azemin, R. Hassan, M. I. Mohd Tamrin and M. A. Md Ali, "COVID-19 deep learning prediction model using publicly available radiologist-adjudicated chest X-ray images as training data: preliminary findings," *International Journal of Biomedical Imaging*, vol. 1, no. 1, p. 1, 2020.
- [52] S. Toraman, T. B. Alakus and I. Turkoglu, "Convolutional capsnet: A novel artificial neural network approach to detect COVID-19 disease from X-ray images using capsule networks," *Chaos, Solitons & Fractals*, vol. 140, no. 1, p. 110122, 2020.
- [53] S. H. Yoo, H. Geng, T. L. Chiu, S. K. Yu, D. C. Cho, J. Heo and H. Lee, "Deep learning-based decision-tree classifier for COVID-19 diagnosis from chest X-ray imaging," *Frontiers in medicine*, vol. 7, no. 1, p. 427, 2020.
- [54] S. Hassantabar, M. Ahmadi and A. Sharifi, "Diagnosis and detection of infected tissue of COVID-19 patients based on lung X-ray image using convolutional neural network approaches," *Chaos, Solitons & Fractals*, vol. 140, no. 1, p. 110170, 2020.

Federated Convolutional Neural Networks for Predictive Analysis of Traumatic Brain Injury: Advancements in Decentralized Health Monitoring

Tripti Sharma¹, Desidi Narsimha Reddy², Chamandeep Kaur³,
Sanjiv Rao Godla⁴, R. Salini⁵, Adapa Gopi⁶, Yousef A.Baker El-Ebiary⁷

Professor, Department of Computer Science and Engineering, Rungta College of Engineering & Technology,
Bhilai, Chhattisgarh, India¹

Data Consultant (Data Governance, Data Analytics, EPM: Enterprise Performance Management, AI&ML),
Soniks Consulting LLC, USA²

Lecturer, Department of Computer Science, Jazan University, Jazan, Saudi Arabia³

Professor, Department of CSE (Artificial Intelligence & Machine Learning), Aditya College of Engineering & Technology
Surampalem, Andhra Pradesh, India⁴

Department of CSE, Panimalar Engineering College, Chennai, India⁵

Associate Professor, Dept. of Computer Science and Engineering, Koneru Lakshmaiah Education Foundation,
Green Fields, Vaddeswaram, Guntur Dist, Andhra Pradesh, India⁶

Faculty of Informatics and Computing, UniSZA University, Malaysia⁷

Abstract—Traumatic Brain Injury (TBI) is a significant global health concern, often leading to long-term disabilities and cognitive impairments. Accurate and timely diagnosis of TBI is crucial for effective treatment and management. In this paper, we propose a novel federated convolutional neural network (FedCNN) framework for predictive analysis of TBI in decentralized health monitoring. The framework is implemented in Python, leveraging three diverse datasets: CQ500, RSNA, and CENTER-TBI, each containing annotated brain CT images associated with TBI. The methodology encompasses data preprocessing, feature extraction using gray level co-occurrence matrix (GLCM), feature selection employing the Grasshopper Optimization Algorithm (GOA), and classification using FedCNN. Our approach achieves superior performance compared to existing methods such as DANN, RF and DT, and LSTM, with an accuracy of 99.2%, surpassing other approaches by 1.6%. The FedCNN framework offers decentralized privacy-preserving training across individual networks while sharing model parameters with a central server, ensuring data privacy and decentralization in health monitoring. Evaluation metrics including accuracy, precision, recall, and F1-score demonstrate the effectiveness of our approach in accurately classifying normal and abnormal brain CT images associated with TBI. The ROC analysis further validates the discriminative ability of the FedCNN framework, highlighting its potential as an advanced tool for TBI diagnosis. Our study contributes to the field of decentralized health monitoring by providing a reliable and efficient approach for TBI management, offering significant advancements in patient care and healthcare management. Future research could explore extending the FedCNN framework to incorporate additional modalities and datasets, as well as integrating advanced deep learning architectures and optimization algorithms to further improve performance and scalability in healthcare applications.

Keywords—Traumatic brain injury; federated learning; convolutional neural network; grasshopper optimization algorithm; health monitoring

I. INTRODUCTION

Traumatic brain injury (TBI) occurs when the brain becomes dysfunctional and neuropathologically damaged due to abrupt and either immediate or secondary external pressures, such as a bump, blow to the head, or another type of injury [1]. Traumatic brain injury can cause a major disturbance in the brain's regular operating, which may outcome in either short-term or long-term neurological impairments. Each year, millions of individuals worldwide are impacted by this invisible spreading, which has significant rates of illness as well as death [2]. According to estimates, there are 1.7 million traumatic brain injuries in the US each year, and lifetime hospital expenses associated with TBI are predicted to reach over \$76.5 billion dollars. India has the largest prevalence of brain damage worldwide, in accordance with the Indian Head damage Foundation; most occurrences of mortality occur within a two-hour period of the accident, and one in seven TBI patients pass immediately [3].

Traumatic brain injury causes a diverse range of impairments that can alter regular brain activity and lead to behavioural, physical, mental, and cognitive impairments. Initial and additional damages are the most common categories for injuries that accompany traumatic brain injury since the consequences usually arise either immediately or indirectly following the event [4]. Basic accidents, including diffused axonal damage and intracranial, subdural, and extradural hemorrhage, are the immediate outcome of trauma. Abrupt exterior mechanical pressures have the potential for bursting blood vessels, causing blood to collect in the brain's cranial partitions and produce hemorrhage [5]. Depending on where in the brain material the hematoma occurs, it can be

classified as an extra-axial or intra-axial hematoma. Subdural hemorrhaging, subarachnoid hemorrhage, intraventricular hemorrhage, and intracerebral hemorrhage are examples of intra-axial hemorrhages while epidural hemorrhage is an example of an extra-axial hemorrhage. In the initial year, approximately fifty percent of ICH patients die. The original damage can manifest in as little as one hundred milliseconds, and in the initial hours following its commencement, the patient's condition begins to deteriorate [6].

The development of additional complications, which include a range of molecules, chemical-based, inflamed, and changes in metabolism, can occur minutes to days following the main brain damage. The adult skull is a rigid container filled with blood, brain, and the cerebrospinal fluid that has an uninterrupted capacity [7]. According to the Monro–Kellie philosophy, the total of these three significant elements' volumes never changes. Consequently, the amount of a minimum one of the two elements should be decreased in conjunction with any rise in intracranial contents. Moreover, raised ICP levels will result from this possible volume rise. Because of the hematoma's enlargement within the stiff skull, blood and CSF will gradually move into the cerebral region [8]. Because of good treatment in accordance with the Monro–Kellie philosophy, the ICP values stay low throughout the early stages of hemorrhage development. Elevated intracranial pressure has been shown to have greater consequences, including midline displacement, brain hernia, and eventually death, by damaging different brain regions [9].

A medical disorder known as midline shifting can result from the uncontrolled ICP levels caused by the mass impact of hemorrhage which may relocate the centre of structures toward the sides of the brain. The midline, which is linear in typical, healthy individuals, may be thought of as an imagined middle line because of the uniformity of the brain's organization [10]. The amount of MLS is calculated by taking into account the movement of any one of each of the three brain midline frameworks: the pineal glands, third ventricular, or septum pellucidum from the optimum midline. The enlargement of brain structures is caused by the massive impact caused by hematoma, which raises the pressure inside the head and moves the brain out of its normal position. Death may result from this in the end. MLS is thus regarded as an effective indicator of the most adverse patient experiences following a traumatic brain injury and a substantial determinant of ICP [11].

Since non-contrast CT scanning is quick, accessible, and provides a clear distinction between brains and blood connective tissue, it is the technique favoured for the identification and treatment of traumatic brain injury in the acute situation. Finding a hemorrhage in the CT images and evaluating its three main components—location, volume, and size—are essential for making choices about the outcome [12]. The utilization of an exterior ventricle loss, an intrusive operation that is very prone to diseases and consequences, is the most appropriate option for monitoring ICP. Moreover, CT scans are required in order to identify elevated ICP because different healthcare environments lacking competent neurosurgeons and intrusive ICP surveillance [13]. Numerous studies demonstrate that accurate visual examination and

manual calculation of TBI outcomes according to CT are labour-intensive, prone to mistake and misinterpretation due to inter- and intra-observer variability and require a lot of time [14]. The level of accuracy of measurement is crucial for making decisions and additional diagnosis, since the degree of movement is essential in determining the degree of brain injury [15].

By recognizing the characteristics that doctors often employ to diagnose abnormalities, an average CAD system aims to reduce false negative rates. The CAD systems can now execute a variety of image analysis techniques thanks to the always expanding research projects. To enhance the quality of the paper, incorporating cross-validation or external validation techniques would be beneficial. Specifically, employing k-fold cross-validation could help assess the robustness and generalizability of the proposed FedCNN framework across different subsets of the dataset. Additionally, external validation involving independent datasets from other sources or institutions could further validate the effectiveness of the framework in diverse real-world settings, providing more comprehensive evidence of its performance and applicability. Integrating such validation methods would strengthen the credibility and reliability of the study's findings, enhancing its overall quality and impact in the field of decentralized ent. These approaches help physicians identify health monitoring for Traumatic Brain Injury (TBI) managemy diseases, plan treatments, estimate risks, and evaluate prognoses. A number of CAD-based methods are suggested to identify abnormalities in the brain that are reflected in images utilizing various methods. These controlled or uncontrolled partially automated or completely autonomous techniques use machine learning or deep learning methods to improve precision and effectiveness, and they may be used to identify a single brain disorder or a combination of disorders.

The Key contributions of the paper is given as follows:

- The paper leverages three distinct datasets, namely the CQ500 dataset, the RSNA dataset, and the CENTER-TBI study dataset, each offering comprehensive collections of brain CT images annotated for various intracranial abnormalities associated with traumatic brain injury. This multi-centric and heterogeneous dataset approach enhances the robustness and generalizability of the proposed predictive analysis model.
- The adoption of gray level co-occurrence matrix for feature extraction enables the capture of statistical texture features essential for accurately classifying normal and abnormal brain CT images. This sophisticated feature extraction method contributes to the discrimination of subtle patterns and textures indicative of traumatic brain injury, thereby enhancing the model's predictive capabilities.
- The implementation of the Grasshopper Optimization Algorithm for feature selection addresses the curse of dimensionality and optimizes classification performance by identifying an optimal subset of features from the larger feature space. This novel

feature selection strategy ensures the selection of the most relevant and discriminative features, thereby improving the efficiency and accuracy of the predictive analysis model.

- The adoption of federated convolutional neural networks for classification facilitates decentralized privacy-preserving training, enabling individual networks to independently train their local CNN models on their respective datasets while sharing model parameters with a central server in iterative communication rounds. This decentralized health monitoring approach ensures data privacy and security while enabling collaborative learning and model improvement across diverse healthcare environments.
- The culmination of these contributions results in an accurate predictive analysis model capable of distinguishing normal and abnormal brain CT images associated with traumatic brain injury. By integrating innovative techniques for data preprocessing, feature extraction, feature selection, and classification within a decentralized health monitoring framework, the paper advances the state-of-the-art in predictive analysis of traumatic brain injury, offering significant benefits for patient care and treatment optimization.

The following portions of the chapter are organized as follows. Section II includes an overview of the literature on predictive analysis of traumatic brain injury. The problem statement for the study is presented in Section III. Section IV covers the recommended approach for predictive analysis of traumatic brain injury. Section V compares the method's efficacy to previous techniques, and the performance measures are displayed, along with an explanation of the results. Section VI describes the conclusion.

II. RELATED WORKS

Prior studies in the field of intracranial hemorrhage and traumatic brain injury diagnosis have mostly depended on CT scanning for quick recognition and identification of hemorrhagic areas but require skilled interpretation to identify ICH subtypes. Nevertheless, specific quantitative information such as the thickness and amount of bleeding that is required for predictive making decisions in critical care settings is frequently absent from CT scans. Recent research has suggested deep learning methods for quantitative evaluation and subtype identification in ICH in order to overcome these shortcomings. In order to discover subtype differences and outline ICH zones, these frameworks usually entail preprocessing processes such as transforming DICOM to NIfTI layout, then performing multi-class segmentation based on semantics and optimized classification neural networks. These approaches have demonstrated potential, but they are not beyond drawbacks. Among the difficulties include the restricted applicability to other datasets, the possibility of overfitting as a result of fine-tuning on a smaller scale information, and the reliance on well datasets with annotations for training, which can occasionally not be easily accessible. Furthermore, flexibility in responding to different clinical scenarios and imaging techniques may be limited by the dependence on models that have been trained. Furthermore, to

ensure durability and therapeutic significance, extensive validation on bigger and more varied groups is required, even with high accuracy achieved. Furthermore, there is still room for improvement and investigation in the actual use as well as incorporation of these deep learning technologies into clinical processes, taking into account aspects like immediate processing and usability by medical practitioners without extensive training. Therefore, while these advancements offer promise in enhancing ICH diagnosis and treatment decision-making, continued research efforts are essential to address these limitations and realize the full potential of deep learning in this critical medical domain [16].

In the domain of mild traumatic brain injury, recent efforts have aimed to enhance patient management through the development of decision rules and predictive models. While traditional statistical techniques have been utilized to identify low-risk patients for discharge from the emergency department, machine learning approaches have been explored to potentially improve predictive accuracy. However, findings from a retrospective cohort study utilizing gradient boosted decision trees on CT-identified TBI patients failed to demonstrate clear advantages over traditional methods. Despite achieving respectable predictive values, the machine learning models exhibited similar specificity to traditional approaches and were developed on a smaller dataset due to the necessity of partitioning for training, calibration, and validation. Key predictors of deterioration remained consistent across methods, including Glasgow Coma Scale, injury severity, and the number of brain injuries. Limitations include the challenge of data partitioning and the absence of substantial improvements over established techniques, highlighting the need for future research to focus on developing models that offer discernible advantages in outcome prediction for this patient population. Additionally, the modest improvement in predictive performance may not justify the added complexity and resource requirements associated with machine learning methods, underscoring the importance of considering practical implementation and clinical utility in advancing predictive models for TBI management [17].

Although they are not very specific, clinical guidelines have been developed in an attempt to reduce the misuse of CT scans in cases of mild traumatic brain injury. While duplicating these criteria using machine learning models has showed promise, attaining balanced specificity and sensitivity is still a problem. A deep artificial neural network model and an instance hardness cutoff technique were used in a study aimed at pediatric populations to replicate the Pediatric Urgent Services Clinical Research Networks clinical criteria for CT scan requirement. There are still restrictions in place despite encouraging outcomes with significant specificity and sensitivity. The study's use of historical information from the PECARN research that took place between 2004 and 2006 raises the possibility of biases or mistakes, which might have an impact on the model's applicability to current patient populations or therapeutic settings. Additionally, even though the DANN model outperformed the PECARN clinical guidelines in terms of sensitivity and specificity, practical issues like model understanding and convenience of

incorporation into workflows for clinical practice are still unsolved. Furthermore, the study's emphasis on juvenile groups could restrict the findings' relevance to adult populations, calling for additional investigation to confirm the model's effectiveness across a range of patient demographics. Consequently, even though the DANN model appears to have potential for increasing the use of CT scans in paediatric TBI patients, further research should focus on resolving these issues and guaranteeing the model's reliability and applicability in clinical settings [18].

Machine learning algorithms have become more and more important in the endeavour to forecast the results of treatment for individuals with traumatic brain injury. These algorithms make use of a variety of data sources, such as imaging indexes laboratory information, clinical parameters, and demographic factors. But even with these advances, there are still restrictions. In order to identify important determinants of in-hospital mortality and long-term survival, a study carried out in a tertiary trauma centre in Iran sought to construct reliable prediction models utilizing machine learning techniques. While some variables were found to be significant, there are some limitations to the findings, such as the possibility of biases from retrospective data collection and the exclusion of insufficient information, which may compromise the generalizability of the model. Furthermore, the study's dependence on an Iranian single-centre dataset would restrict the findings' generalizability to other patient groups or healthcare environments. In addition, even though machine learning algorithms demonstrated potential in forecasting both short- and long-term mortality, issues like interpretability of models and adaptability in clinical settings still need to be addressed. Therefore, even though machine learning has the potential to predict the outcomes of traumatic brain injury patients, these limitations must be addressed through bigger and more diversified datasets, prospective research, and improved model interpretability in order to assure reliable and clinically useful predictions for TBI therapy [19].

Investment in models that use machine learning has increased as a result of the need to precisely predict results for patients with severe brain injuries. The goal of such models is to enhance treatment regimens and perhaps provide significant economic advantages. Using admission information from 2,381 patients with severe traumatic brain injury as training data, researchers at Rajaei Hospital in Shiraz, Iran. Restrictions still exist despite the good performance with high levels of specificity, sensitivity, and precision. Particularly, using retrospective information collected from a single location may restrict generalizability to wider populations or healthcare environments and induce biases. Furthermore, the focus of the study on predicting positive or negative outcomes six months after the event may have obscured subtle differences in patient paths and long-term forecasts. Additionally, even though machine learning approaches have great potential, there are still issues with model comprehension, scaling, and the requirement for big and varied datasets [20].

Recent research in the domain of traumatic brain injury diagnosis and outcome prediction has witnessed significant advancements, particularly through the application of machine

learning techniques. Studies have focused on enhancing the accuracy of intracranial hemorrhage detection and subtype classification using deep learning frameworks, although challenges such as dataset generalization and practical implementation remain. Additionally, efforts have been made to improve the prediction of treatment outcomes in TBI patients through ML algorithms, yet limitations persist in terms of model interpretability and generalizability across diverse patient populations. The sections that have been made available emphasise how crucial it is to use machine learning especially deep learning to solve practical difficulties with TBI diagnosis and treatment. The theoretical framework may be enhanced by integrating the knowledge from the literature review, with a focus on developing models that have higher specificity, sensitivity, and usability in order to further TBI research and improve patient outcomes. Furthermore, the development of clinical rules and predictive models for mild TBI has shown promise, but achieving balanced sensitivity and specificity remains a challenge. While machine learning approaches offer potential in optimizing treatment procedures and predicting clinical outcomes, addressing limitations such as biases from retrospective data collection, model interpretability, and scalability in clinical practice are crucial for realizing their full potential in TBI management.

III. PROBLEM STATEMENT

The limitations observed in previous research efforts regarding predictive analysis of traumatic brain injury prompt the necessity for innovative approaches. Existing studies have primarily focused on machine learning techniques, such as deep learning frameworks, for TBI diagnosis and outcome prediction. However, challenges persist in terms of dataset generalization, model interpretability, and scalability in clinical practice. Additionally, while efforts have been made to develop clinical rules and predictive models, achieving balanced sensitivity and specificity remains elusive [21]. Moreover, the reliance on retrospective data from single centers may introduce biases and limit the applicability of findings to broader patient populations or healthcare settings. In light of these challenges, our proposed paper aims to address these limitations by introducing a novel approach utilizing federated convolutional neural networks for predictive analysis of TBI. By leveraging federated learning techniques, we aim to overcome issues related to data privacy and centralization, enabling decentralized health monitoring while maintaining patient confidentiality. Through our proposed federated CNNs, we seek to enhance predictive accuracy and enable real-time monitoring of TBI patients across diverse healthcare environments, ultimately contributing to improved patient outcomes and healthcare delivery in the field of traumatic brain injury management.

IV. METHODOLOGY

Three major components make up the methodology presented in this paper: gathering data, preprocessing with median filtering, feature extraction with grey level co-occurrence matrix, feature selection with Grasshopper Optimization Algorithm, and classification with federated convolutional neural networks. For training and assessment, three different datasets are used: the CQ500 dataset, the

RSNA dataset, and the CENTER-TBI research dataset. All three provide extensive and varied sets of brain CT images labelled for different intracranial abnormalities related to traumatic brain injury. In preprocessing, noise is removed from CT images by median filtering, and then statistical texture characteristics necessary for differentiating between normal and pathological pictures are extracted using GLCM. The Grasshopper Optimization Algorithm is utilized for feature selection to overcome the dimensionality problem and enhance classification performance. This algorithm makes it easier to identify the best subset of features from the broader feature space. Lastly, federated CNNs are used for classification. These are decentralized, privacy-preserving training mechanisms that allow separate networks (A, B, and C) to train their local CNN models independently on their own datasets and share parameter values with a central server through iterative communication rounds. By combining updated parameters from local models, the global CNN model continuously improves through this federated learning setup. This leads to an understanding of features that differentiate between normal and abnormal images across all networks, enabling accurate predictive analysis of traumatic brain injury while maintaining data privacy and decentralization in health monitoring. Fig. 1 shows the overview of the proposed architecture.

A. Data Collections

1) *Dataset for Network A:* Most of the research that have been done so far have employed smaller datasets that were gathered from individual institutions in an effort to establish computer-aided diagnosis systems that can identify various disorders connected to traumatic brain injury. A publicly accessible brain CT dataset called CQ500 can help with the creation of machine learning algorithms that classify and recognize different types of abnormalities in the brain [22]. The creation of general, computerized CAD systems to evaluate the many anomalies connected to traumatic brain injury is made easier by these multicentre and heterogeneity datasets. 491 brain CT images from various radiology units have been collected batch-wise and combined into the varied CQ500 dataset by the Centre for Advanced Research in Images, Neurosciences and Genomics, located in New Delhi, India. Three separate radiologists interpreted each CT image to determine whether or whether each had (i) ICH and its five forms, (ii) midline shift, (iii) calvarias fractures, and (ICH age and afflicted brain hemisphere. An example of the dataset's normal and aberrant images is displayed in Fig. 2.

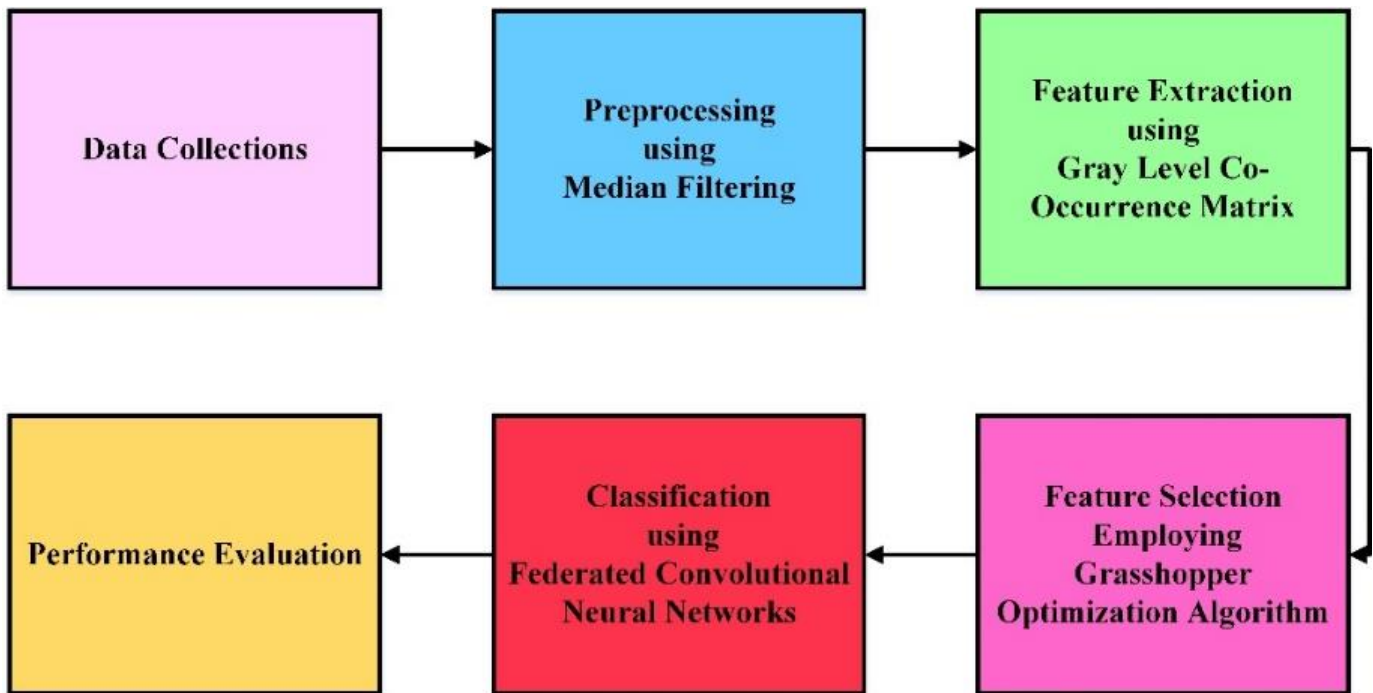


Fig. 1. Overview of the proposed architecture.

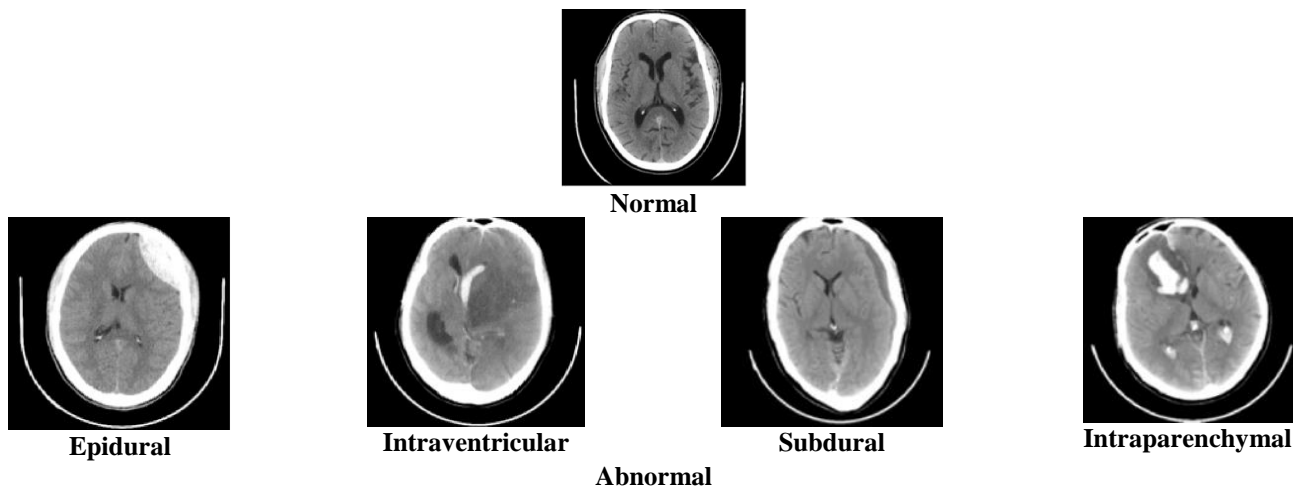


Fig. 2. Sample CT images from CQ500 dataset.

2) *Dataset for network B*: The RSNA dataset, which includes 865,032 labeled brain CT images for hemorrhage identification and categorization, is the biggest publicly accessible dataset. Experienced radiologists have analyzed each CT scan in this multinational and multi-institutional dataset for the existence or lack of each of the five forms of ICH. 652,403 and 123,133 CT images, accordingly, constitute the training and test information. There is a group imbalance among the hemorrhage subgroups [23].

3) *Dataset for network C*: The study utilized information from the CENTER-TBI, which enrolled more than 5000 individuals from a variety of facilities, including community hospitals, trauma groups, and university medical centers. Three layers of information are gathered, each distinguished by a particular care path: The following three patient groups are classified as follows: 1) individuals seen in the emergency department and released; 2) patients transferred to the medical facility but not to an intensive care unit and 3) patients transferred to the ICU. A CT scan was conducted in accordance with standard clinical practice on a clinical scanner with a wide range of imaging variables. For the purpose of assessing the segmentation of immediate intracranial lesions, three unique subcohorts of the CENTER-TBI information set are taken into consideration: cistern identification and midline shift estimate. This guarantees that each data set provides a significant variety when it comes to of TBI severity and imaging parameters of interest [24].

B. Preprocessing using Median Filtering

Pre-processing is used to eliminate extraneous information from brain CT scans, which can create noise and negatively impact CAD system performance. The improved CT images in this investigation were obtained by using a median filter. The speckle noise in a CT picture is eliminated using the median filter. In digital image processing, noise is eliminated by using a median filter. This novel approach uses a median filter for filtering in order to identify traumatic brain damage. A neighbourhood region serves as the filtering window for the

median filtering method, which modifies its size based on certain filtering process setup criteria. A useful technique that can separate out of varied isolates from acceptable picture alternatives like boundaries and characteristics to a certain degree is the median filter. In particular, the median filter substitutes the median for a pixel rather than the neighbourhood's average of all the pixels Ψ . As could possibly see in Eq. (1).

$$M[R(u) + S(u)] \neq M[R(u)] + M[S(u)] \quad (1)$$

A statistically based non-linear signal processing technique is the median filter. The noisy number will be replaced with the digital image's median value. The noisy value is replaced by the group median, which is saved after the mask's pixels are arranged according to the gray levels.

C. Feature Extraction using Gray Level Co-Occurrence Matrix

Characteristics are the bits of data that are important for representing important aspects of pictures and for solving certain applications. The selection of input characteristics greatly affects training set parameters and categorization accuracy. The technique of extracting an image's visual content in order to reduce the number of resources needed is known as feature extraction. Gray level co-occurrence matrix (GLCM) was developed in this study to extract statistical texture information. Texture characteristics are significant low-level characteristics that are utilized to measure an image's perceived texture and define its contents.

The widely used GLCM method uses statistical distributions of intensity value combinations at various locations in relation to one another in an image to determine second order statistical texture characteristics. There are three categories of statistics: first, second, and higher order, based on the quantity of intensity locations within the image. Although theoretically feasible, the computational cost prevents the implementation of higher levels statistics. Texture characteristics hold details about the surface's structural organization and how it interacts with its surroundings. Energy, correlation, entropy, homogeneity, sum variability, autocorrelation, contrary, maximal probability, dissimilarity,

IDM normalized, and many more texture-based characteristics are acquired—a total of twenty-two are obtained. Some of them are expressed as follows:

1) *Energy*: Energy can also be defined as "angular second moment" or "uniformity." It provides the GLCM matrix's sum of square components. From homogeneous to non-homogeneous regions, it is done this way. When the frequency of repeated picture pixels is high, it is high. Eq. (2) displays the energy equation.

$$E = \sum_{u,v=0}^{m-1} (Q_x)^2 \quad (2)$$

2) *Entropy*: It determines the image's unpredictability. A uniform image will therefore provide a lower entropy rating. Eq. (3) displays the entropy equation.

$$ET = \sum_{u,v=0}^{m-1} -\ln(Q_x) Q_x \quad (3)$$

3) *Contrast*: It determines the strength of the contrasts that connects a pixel to its neighbour throughout the whole image. Eq. (4) displays the equation of contrast.

$$C = \sum_{u,v=0}^{m-1} Q_x (u - v)^2 \quad (4)$$

4) *Correlation*: It measures the linear gray tone dependency of a picture. It explains how a pixel and its neighbour are linked. The correlation equation is shown in Eq. (5).

$$Co = \sum_{u,v=0}^{m-1} Q_x \frac{(u-\mu+u-\mu)}{\sigma^2} \quad (5)$$

5) *Homogeneity*: It measures the degree of pixel resemblance. The homogenous image's GLCM matrix values out to 1. If the texture of the image just needs minor adjustments, it is very low. Eq. (6) displays the equation of homogeneity.

$$H = \sum_{u,v=0}^{m-1} \frac{Q_x}{1+(u-v)^2} \quad (6)$$

D. Feature Selection Employing Grasshopper Optimization Algorithm

While characteristics are necessary to achieve high accuracy, an abundance of characteristics can lead to a "dimensionality curse" whereby an excessive number of characteristics wastes a significant amount of storage capacity, increases calculation time, and complicates categorization. Adding more characteristics also increased the risk of "overfitting," which reduces the system's generalizability and reduces accuracy. Therefore, it is necessary to create feature selection strategies, which choose the "optimal subset of features" from a wider set. The Grasshopper Optimization Algorithm is used in this work to choose characteristics.

In 2016, the GOA algorithms was introduced. This method emulates the natural swarming behaviour of grasshoppers. Three factors influence a grasshopper's position in a swarm's flight path: wind advection (B_u), gravity (H_u), and social interaction (R_u). Eq. (7) defines the social interaction as the primary search mechanism in the GOA algorithm.

$$R_u = \sum_{v=1, v \neq u}^M r(c_{uv}) \widehat{c}_{uv} \quad (7)$$

In this case, r denotes a function that defines the degree of societal pressures, $c_{uv} = |y_v - y_u|$ is the distance that exists between the u -th and v -th grasshoppers, and $\widehat{c}_{uv} = \frac{y_v - y_u}{c_{uv}}$ is the vector of units from the u -th grasshopper to the v -th grasshopper. The above equation shows that the function of r is the primary element of the relationship between people. Eq. (8) specifies the value of this function, which determines a grasshopper's orientation of travel within the swarm.

$$r(s) = f e^{\frac{-s}{l}} - e^{-s} \quad (8)$$

where, l is the attracting distance scales and f is the attraction's strength. The grasshoppers are driven by this function to repel one another as well as to be attracted to one another. In order to prevent colliding, two grasshoppers will repel one another when their distances are within the range of $[0, 2.079]$. To keep the swarm cohesive, the attraction force grows while the distance is in $[2.079, 4]$. The zone of comfort is the region where there cannot be a pressure at precisely 2.079.

In the event when the distance between them equals 2.079, both attraction and repulsion vanish. From 2.079 units of distance until almost four the attraction intensity rises and then progressively falls. Substantial differences in the values of the variables in the equation used for the value of s (l and f) result in altered swarming behaviour. To demonstrate how grasshoppers communicate with regard to their comfort zones. When it comes to modelling grasshopper interactions, the swarm approach performs well. But in order to create an optimization algorithm, it has to be modified. The subsequent mathematical representation of the search during grasshopper interactions was suggested by the study. Eq. (9) serves as a representation of the computational framework.

$$Y_u^c = b \left(\sum_{v=1, v \neq u}^M b \frac{ia_c - la_c}{r} r(|y_v^c - y_u^c|) \frac{y_v - y_u}{c_{uv}} \right) + \widehat{T}_c \quad (9)$$

where, (\widehat{T}_c) is the average value of the c -th dimensions in the objective (best solution discovered so far), c is a diminishing parameter to shorten the comfort region, repelling region, and attractiveness region, and ia_c is the maximum value in the c -th dimensions and la_c is the lowest limit in the c -th dimensions. The following equation illustrates how the swarm modifies the location around an objective \widehat{T}_c . The swarm is brought closer to the target by the parameter c . The goal in the GOA algorithms is thought to be the most effective approach found thus far. When an improved technique is found, the best approach becomes revised while the grasshoppers communicate and pursue the objective.

Eq. (10) is utilized to modify variable c , which is the primary governing variable in the GOA algorithm.

$$d = d_{max} - l \frac{d_{max} - d_{min}}{L} \quad (10)$$

where, $d_{max} = 1$, and $d_{min} = 0.00001$, L is the greatest number of iterations, and l is the present repetition.

E. Classification using Federated Convolutional Neural Networks

With federated learning, client edges could discover a common global model without sending their confidential local

information to a central server. Federated learning is a developing distributed privacy-protection learning method. Every training cycle, the local machine receives a model that everyone uses from the cloud-based global servers, training it using each user's personal information, and then updates the weights or gradients by sending a request back to the servers. The client-uploaded models are combined on the server to create an additional global design. The following distinguishing characteristics of federated learning set it apart from conventional centralized learning:

- 1) The global server clouds cannot access the training data since they are dispersed on local edges. All clients and the servers share the same learning model, nevertheless.
- 2) Rather than on the server, model training takes place on each local device. In order to create a shared global model, the server compiles the local models that the clients contribute, sends the completed model returned to the clients.
- 3) Compared to typical centralized learning, federated learning requires a lot more local computing power and capabilities.

The process of federated learning is described, in which every client trains its unique local algorithm utilizing its own information after receiving the parameters of the larger framework from the central server. Following local training, every local device transmits its learned local variables to the server, where they are combined to create a revised global model that will be utilized for training in the subsequent iteration of training. In federated learning, the time patterns, or so-called communication phases, are indicated by the subscript t .

Convolutional neural networks have demonstrated consistently higher effectiveness for image categorization and are appropriate to handle very high dimensional inputs. CNN topological architectures are comparable. Three different types of layers are often found in a CNN: convolutional, pooling, and fully linked layers. Many kernel filters, which can be identified as an array of square block neurons, make up the

convolutional layer. The preceding layer's kernel filters, which may be thought of as training weights, are subjected to "convolution" processes by the convolutional layer. The CNN may be explained mathematically in the following way in Eq. (11).

$$x_{uv}^l = \sigma \left(\sum_{g=0}^{m-1} \sum_{h=0}^{m-1} f_{gh} y_{(u+g)(v+h)}^{l-1} \right) \quad (11)$$

Here, y^{l-1} is the convolutional layer's input, x_{uv}^l is its output, l is the layer number, f_{gh} is a $n \times n$ kernel filter, and σ is the activation constant. The study specifically uses the corrected linear unit (relu) as the function that activates of the hidden neuron to mitigate the effects of softmax function and gradient vanishing in nodes that produce data for multi-class categorization problems. Below are the Eq. (12) and (13) for the softmax and relu functions.

$$\sigma_{relu}(k) = \max(0, k) \quad (12)$$

$$\sigma_{softmax}(k_u) = \frac{\exp(k_u)}{\sum_{u=1}^D \exp(k_u)} \quad (13)$$

where, C is the overall amount of label categories that require to be classified and k is the result of the preceding layer. The amount of label categories that require classification. After many convolutional layers of the CNN, a pooling layer can be implemented to extract certain features from hidden representation. In order to improve the representation characteristics of filtered pictures from the preceding convolutional layer, a measurement of $m \times m$ Max pooling windows is often built for obtaining the maximum brightness value of pixels inside the associated Max pooling windows region. A typical alternative to the Max pooling procedure is the Average pooling approach, which involves average value distribution of features throughout the window region. The flattening image pixels from the result of the layer before it provides the input for the fully linked layer, which is applied at the rear of the CNN. This layer's primary function is to categorize the characteristics that were retrieved from the CNN's earlier layers into different groups. Fig. 3 illustrates how federated CNN operates.

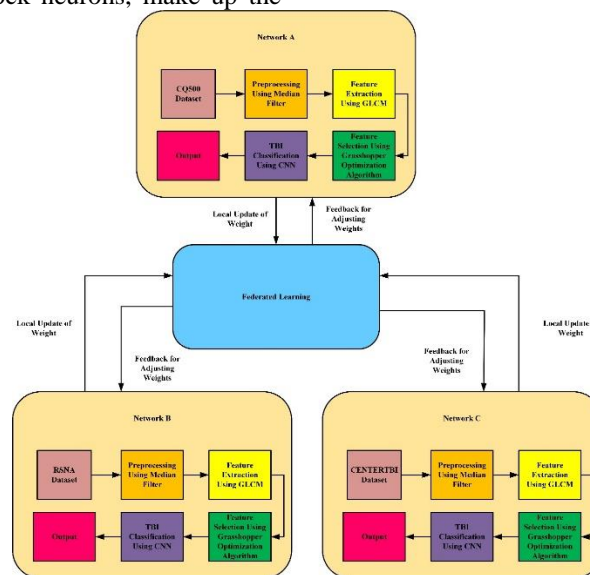


Fig. 3. Working of federated CNN.

In the federated CNN mechanism for classifying images as normal or abnormal, each network (A, B, and C) possesses its own dataset containing a mix of normal and abnormal images. In the federated learning setup, during each communication round, the central server sends the parameters of the global CNN model to each network. Subsequently, each network independently trains its local CNN model using its respective dataset, leveraging the local computational resources and privacy-preserving nature of federated learning. The CNN model consists of convolutional layers, pooling layers, and fully connected layers for extracting and classifying features from the images. After local training, the updated parameters of the local CNN models are sent back to the central server, where they are aggregated to form an updated global CNN model. This global model represents a collective understanding of the features distinguishing normal and abnormal images across all networks. The process iterates over multiple communication rounds, with the global model continuously improving its ability to classify images accurately while respecting data privacy constraints inherent in federated learning.

V. RESULTS AND DISCUSSION

In this section, the study presents the results and discussion of the proposed paper. The methodology encompasses data collection from three diverse datasets: the CQ500 dataset, the RSNA dataset, and the CENTER-TBI study dataset, each containing annotated brain CT images associated with traumatic brain injury. Preprocessing involves median filtering for noise removal, followed by feature extraction using gray level co-occurrence matrix to capture statistical texture features. Feature selection is conducted employing the Grasshopper Optimization Algorithm to optimize classification performance by identifying an optimal subset of features. Classification is performed using federated CNNs, enabling decentralized privacy-preserving training across individual networks (A, B, and C) while sharing model parameters with a central server. Through federated learning, the global CNN model evolves iteratively, aggregating updated parameters from local models to achieve a collective understanding of features distinguishing normal and abnormal images, thus enabling accurate predictive analysis of traumatic brain injury while ensuring data privacy and decentralization in health monitoring.

A. Performance Evaluation

Assessment measures are required to evaluate the predictive accuracy. The most common approach for accomplishing this is to determine accuracy. The percentage of datasets detected correctly by a classifier indicates its accuracy for a specific testing dataset. Because employing basically the accuracy metric cannot be used for optimal decision-making. The recommended technique's performance was evaluated utilizing precision, recall, accuracy, and F1-score measurements. The following describes the definitions of each measure:

- The term T_{pos} (True Positive) describes the total amount of accurately found data.

- The term F_{pos} (False Positive) refers to the proportion of accurate data that was mistakenly detected.
- False negatives (F_{neg}) occur when erroneous data is mistakenly recognized as legitimate.
- Identification of erroneous information values is known as T_{neg} (True Negative).
- T_{neg} (True Negative) is used to identify inaccurate data entries.

1) *Accuracy*: The classifier's accuracy indicates the extent to which it generates the correct prediction. Accuracy is measured by the ratio of reliable projections compared to all alternative reasonable projections. It is demonstrated by Eq. (14).

$$Accuracy = \frac{T_{pos}+T_{neg}}{T_{pos}+T_{neg}+F_{pos}+F_{neg}} \quad (14)$$

2) *Precision*: The number of properly detected results is calculated by determining a classifier's precision, or its degree of accuracy. Accuracy improvement results in reduced false positives, but lower precision causes numerous additional errors. Precision is defined as the percentage of examples that correlate appropriately to all incidences. It is defined by Eq. (15).

$$P = \frac{T_{pos}}{T_{pos}+F_{pos}} \quad (15)$$

3) *Recall*: The degree of sensitivity of a recognition, or the amount of relevant information produced, is determined by recall. Enhanced recall decreases the total quantity of F_{neg} . Recall is the proportion of properly classified instances to all projected events. This is demonstrable by Eq. (16).

$$R = \frac{T_{pos}}{T_{pos}+F_{neg}} \quad (16)$$

4) *F1-Score*: The F1-Score, which represents the weighted average of recall and accuracy, is calculated by summing both recall and precision. It is characterized by Eq. (17).

$$F1 - Score = \frac{2 \times precision \times recall}{precision + recall} \quad (17)$$

5) *ROC Curve*: In deep learning and machine learning, the area under the ROC curve, or AUC, is a well-known statistic for binary classification problems. The binary recognition algorithm's efficacy is measured by the area under the curve, which is visually depicted by the Receiver Operating Characteristic curve. The classifier in a binary classified problem looks for information that indicates whether a division is positive or negative.

Fig. 4 depicts the training and testing accuracy for Network A, Network B, Network C, and the Centralized Server in the proposed federated CNN framework for predictive analysis of traumatic brain injury. In (a), (b), and (c), the training accuracy gradually increases with each communication round, indicating that the local CNN models

for each network (A, B, and C) improve over successive iterations. Similarly, the testing accuracy follows an upward trend, signifying enhanced classification performance on unseen data as the federated learning process advances. Notably, Network B demonstrates the highest testing accuracy among the three networks, suggesting superior predictive capability in identifying normal and abnormal brain CT images associated with traumatic brain injury. In contrast, (d) illustrates the training and testing accuracy of the Centralized Server, showcasing a comparable performance to the federated networks, albeit with a single global model trained on aggregated data. Overall, it highlights the effectiveness of federated CNNs in achieving accurate predictive analysis of traumatic brain injury while preserving data privacy and decentralization across multiple networks.

Fig. 5 illustrates the training and testing loss for Network A, Network B, Network C, and the Centralized Server within the federated CNN framework for predictive analysis of traumatic brain injury. In (a), (b), and (c), the training loss gradually decreases over successive communication rounds, indicating improved convergence of the local CNN models for each network (A, B, and C). Similarly, the testing loss exhibits a downward trend, suggesting enhanced generalization performance on unseen data as the federated learning process advances. Notably, Network B demonstrates the lowest testing loss among the three networks, implying superior predictive

capability in differentiating between normal and abnormal brain CT images associated with traumatic brain injury. In contrast, (d) presents the training and testing loss of the Centralized Server, showcasing comparable performance to the federated networks, albeit with a single global model trained on aggregated data. Overall, Fig. 5 highlights the efficacy of federated CNNs in achieving accurate predictive analysis of traumatic brain injury while ensuring data privacy and decentralization across multiple networks.

Fig. 6 depicts the fitness of the Grasshopper Optimization Algorithm utilized for feature selection in the proposed federated convolutional neural network framework for traumatic brain injury predictive analysis. The plot illustrates the convergence of the GOA algorithm over successive iterations, with the fitness value gradually improving towards optimization. As the number of iterations increases, the fitness value decreases, indicating the algorithm's effectiveness in identifying an optimal subset of features from the larger feature space. The diminishing fitness curve reflects the algorithm's ability to iteratively refine feature selection, ultimately enhancing the classification performance of the CNN models. This visualization underscores the utility of the GOA in mitigating the curse of dimensionality and optimizing feature representation for accurate TBI predictive analysis within the federated learning paradigm.

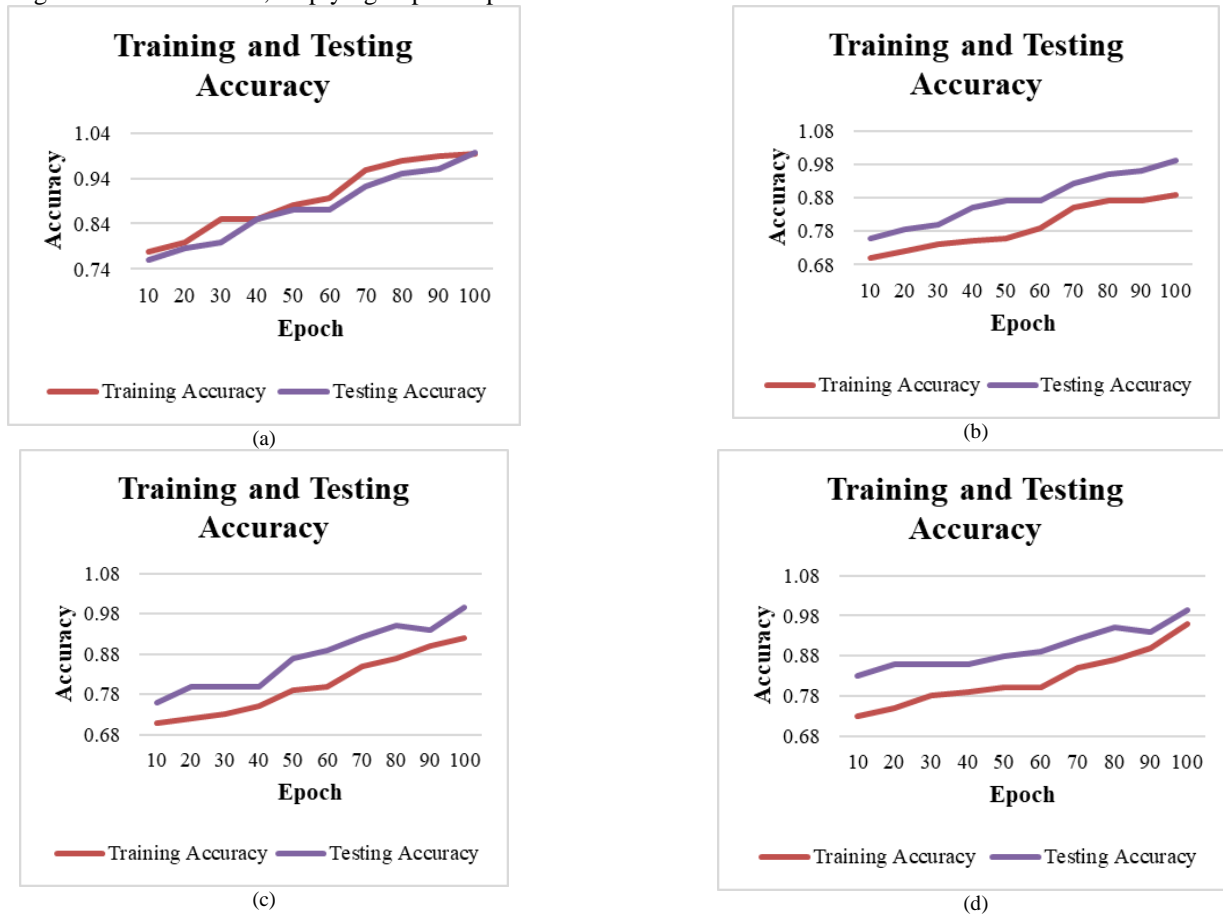


Fig. 4. Training and testing accuracy (a) Network A (b) Network B (c) Network C and (d) Centralized server.

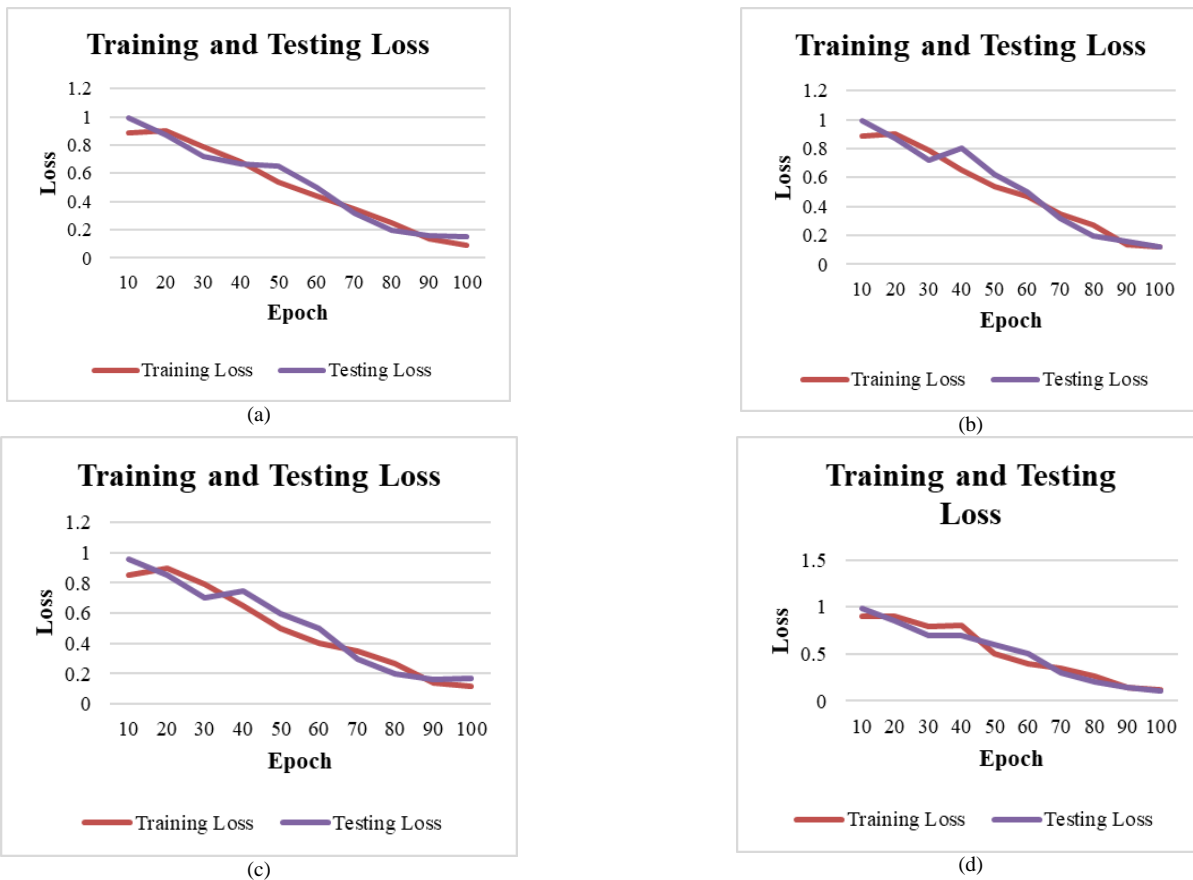


Fig. 5. Training and testing loss (a) Network A (b) Network B (c) Network C and (d) Centralized server.

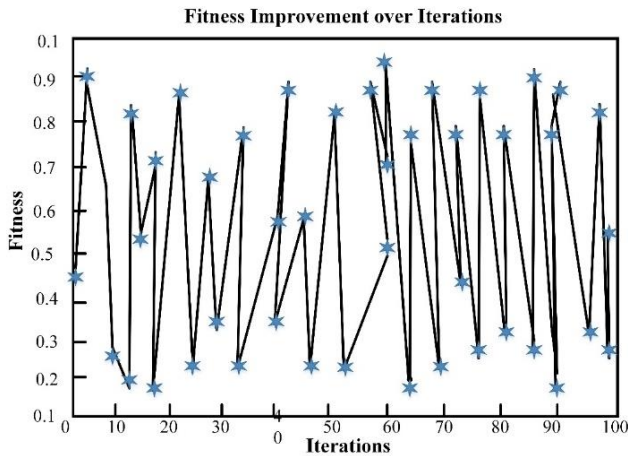


Fig. 6. Fitness of the grasshopper optimization algorithm.

Fig. 7 presents the Receiver Operating Characteristic graphs for each network (A, B, and C) and the centralized server in the proposed federated convolutional neural network framework for predictive analysis of traumatic brain injury. The ROC curves plot the true positive rate against the false positive rate for varying classification thresholds, providing a comprehensive assessment of model performance across different operating points. Each curve represents the trade-off between sensitivity and specificity, with a higher area under the curve indicative of better discriminative ability. The

curves illustrate the CNN models' capacity to distinguish between normal and abnormal brain CT images, with steeper slopes and greater AUC values reflecting superior predictive accuracy. By comparing the ROC curves of individual networks with the centralized server, the graph evaluates the efficacy of federated learning in achieving comparable performance to centralized approaches while preserving data privacy and decentralization. The ROC analysis offers insights into the CNN models' classification performance and underscores the framework's utility in facilitating accurate TBI predictive analysis in decentralized health monitoring settings.

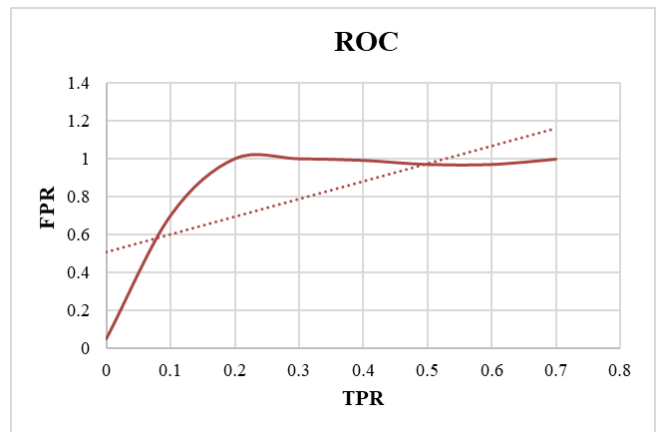


Fig. 7. ROC graph.

TABLE I. COMPARISON OF THE DATASETS IN THE PROPOSED SYSTEM

| Datasets | Accuracy (%) |
|------------|--------------|
| CQ500 | 98.7 |
| RSNA | 99.5 |
| CENTER-TBI | 97.6 |

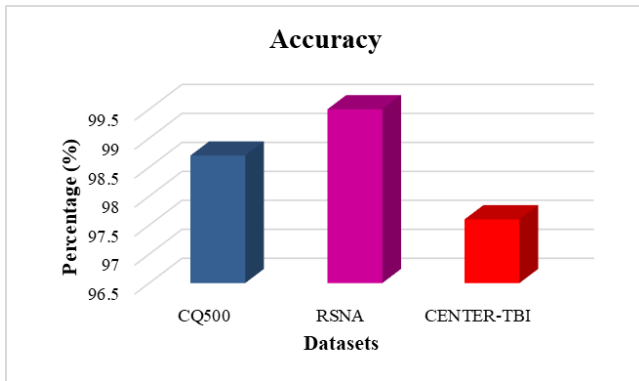


Fig. 8. Comparison of the datasets in the proposed system.

Table I and Fig. 8 provides a comparative overview of the datasets utilized in the proposed federated convolutional neural network system for predictive analysis of traumatic brain injury. The table lists three datasets: CQ500, RSNA, and CENTER-TBI, along with their corresponding accuracy percentages. The CQ500 dataset achieves an accuracy of 98.7%, followed by RSNA with 99.5%, and CENTER-TBI with 97.6%. These accuracy scores reflect the performance of the CNN models trained on each dataset in accurately classifying brain CT images as normal or abnormal, thereby demonstrating the efficacy of the proposed system across diverse datasets with varying characteristics. The table underscores the robustness and generalizability of the federated CNN framework in achieving high predictive accuracy for TBI diagnosis while leveraging heterogeneous data sources, thus facilitating reliable decentralized health monitoring for TBI management.

Table II and Fig. 9 presents a comprehensive comparison of performance metrics between the proposed federated convolutional neural network (FedCNN) method and other existing approaches for predictive analysis of traumatic brain injury. The table includes four methods: DANN, RF and DT, LSTM, and the proposed FedCNN, with corresponding metrics of accuracy, precision, recall, and F1-score expressed in percentage values. Among the compared methods, the proposed FedCNN demonstrates superior performance across all metrics, achieving an accuracy of 99.2%, precision of 99.1%, recall of 99.1%, and F1-score of 99.1%. This indicates the efficacy of the FedCNN approach in accurately classifying brain CT images as normal or abnormal, surpassing the performance of alternative methods such as DANN, RF and DT, and LSTM. The higher performance metrics of the proposed FedCNN underscore its potential as an advanced and reliable tool for TBI diagnosis and predictive analysis, thus offering significant advancements in decentralized health monitoring and clinical decision-making in TBI management.

TABLE II. EVALUATION OF THE PROPOSED METHOD'S PERFORMANCE METRICS IN COMPARISON WITH OTHER CURRENT STRATEGIES

| Methods | Accuracy (%) | Precision (%) | Recall (%) | F1-Score (%) |
|-----------------|--------------|---------------|------------|--------------|
| DANN [18] | 97.2 | 97.4 | 97.4 | 97.4 |
| RF and DT [19] | 95.6 | 96.2 | 95.3 | 95.5 |
| LSTM [25] | 98.7 | 98.5 | 98.7 | 98.3 |
| Proposed FedCNN | 99.2 | 99.1 | 99.1 | 99.1 |

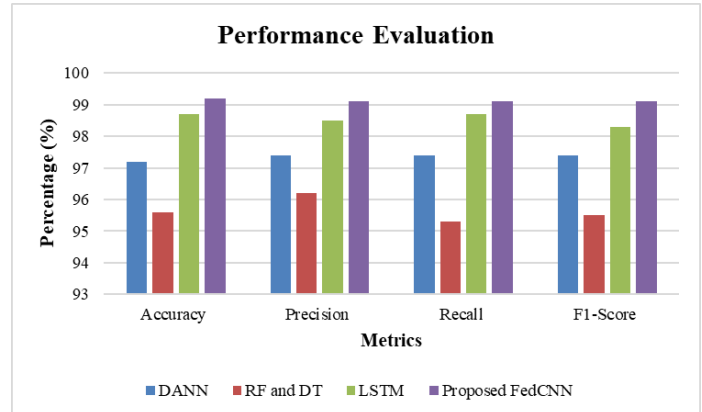


Fig. 9. Comparison of the performance metrics of the proposed method with other existing approaches.

B. Discussion

The results presented in this study showcase the effectiveness of the proposed federated convolutional neural network framework for predictive analysis of traumatic brain injury in decentralized health monitoring. Leveraging three diverse datasets, namely CQ500, RSNA, and CENTER-TBI, the FedCNN framework demonstrates robust performance in accurately classifying brain CT images as normal or abnormal across multiple networks (A, B, and C) while ensuring data privacy and decentralization. The evaluation metrics including accuracy, precision, recall, and F1-score indicate superior performance of the FedCNN approach compared to existing methods such as DANN [18], RF and DT [19], and LSTM [25]. The FedCNN achieves remarkable accuracy scores, with Network B exhibiting the highest testing accuracy among the three networks. Additionally, the Grasshopper Optimization Algorithm effectively optimizes feature selection, mitigating the curse of dimensionality and enhancing classification performance. ROC analysis further confirms the FedCNN's discriminative ability, with steeper slopes and higher AUC values reflecting superior predictive accuracy. These findings underscore the FedCNN's potential as an advanced tool for TBI diagnosis, offering significant advancements in decentralized health monitoring and clinical decision-making while preserving data privacy and decentralization. Overall, the results validate the efficacy and reliability of the proposed FedCNN framework in facilitating accurate TBI predictive analysis, thereby contributing to improved patient outcomes and healthcare management in TBI scenarios. Integrating

more sophisticated deep learning architectures and optimization techniques could potentially further optimize the FedCNN framework's performance and scalability in broader healthcare applications while broadening its scope to include a wider range of modalities and datasets could greatly improve its adaptability in addressing various TBI scenarios. However, it is essential to acknowledge the limitations that are intrinsic to this research. The usefulness of the FedCNN may be limited by small and homogenous annotated datasets, requiring efforts to expand and diversify the data sources. Furthermore, overcoming the computational complexity of feature extraction and selection techniques is necessary to guarantee effective scalability, and managing legal and privacy issues in decentralized health monitoring systems is essential to encouraging the FedCNN approach's broad acceptance and application in actual healthcare settings.

VI. CONCLUSION AND FUTURE SCOPE

In conclusion, this study presents a novel federated convolutional neural network (FedCNN) framework for predictive analysis of traumatic brain injury in decentralized health monitoring. Leveraging three diverse datasets and employing preprocessing, feature extraction, feature selection, and classification techniques, the proposed FedCNN framework achieves remarkable accuracy in classifying brain CT images as normal or abnormal while ensuring data privacy and decentralization. The results demonstrate superior performance of the FedCNN approach compared to existing methods, indicating its potential as an advanced tool for TBI diagnosis and clinical decision-making. Moreover, the Grasshopper Optimization Algorithm effectively optimizes feature selection, enhancing classification performance and mitigating the curse of dimensionality. The ROC analysis confirms the FedCNN's discriminative ability, further validating its efficacy in TBI predictive analysis. The study contributes to the field of decentralized health monitoring by providing a reliable and efficient approach for TBI management, offering significant advancements in patient care and healthcare management. For future research, further exploration could focus on extending the FedCNN framework to incorporate additional modalities and datasets, such as MRI and EEG data, to enhance the accuracy and scope of TBI diagnosis. Additionally, investigating the integration of advanced deep learning architectures and optimization algorithms could further improve the FedCNN's performance and scalability. Moreover, exploring the application of federated learning techniques in other healthcare domains beyond TBI could broaden the impact of decentralized health monitoring, paving the way for more comprehensive and personalized healthcare solutions. Overall, the proposed FedCNN framework holds promise for revolutionizing TBI diagnosis and healthcare management, offering a scalable and privacy-preserving approach for decentralized health monitoring in diverse clinical settings.

REFERENCES

- [1] A. I. Maas et al., "Traumatic brain injury: progress and challenges in prevention, clinical care, and research," *The Lancet Neurology*, vol. 21, no. 11, pp. 1004–1060, 2022.
- [2] J. Haarbauer-Krupa, M. J. Pugh, E. M. Prager, N. Harmon, J. Wolfe, and K. Yaffe, "Epidemiology of chronic effects of traumatic brain injury," *Journal of neurotrauma*, vol. 38, no. 23, pp. 3235–3247, 2021.
- [3] A. K. Wagner et al., "Traumatic brain injury," in *Braddom's Physical Medicine and Rehabilitation*, Elsevier, 2021, pp. 916–953.
- [4] B. L. Brett, R. C. Gardner, J. Godbout, K. Dams-O'Connor, and C. D. Keene, "Traumatic brain injury and risk of neurodegenerative disorder," *Biological psychiatry*, vol. 91, no. 5, pp. 498–507, 2022.
- [5] J. R. Howlett, L. D. Nelson, and M. B. Stein, "Mental health consequences of traumatic brain injury," *Biological psychiatry*, vol. 91, no. 5, pp. 413–420, 2022.
- [6] D. Khayatan et al., "Protective effects of curcumin against traumatic brain injury," *Biomedicine & Pharmacotherapy*, vol. 154, p. 113621, 2022.
- [7] D. Y. Madhok et al., "Outcomes in patients with mild traumatic brain injury without acute intracranial traumatic injury," *JAMA network open*, vol. 5, no. 8, pp. e2223245–e2223245, 2022.
- [8] I. Thomas et al., "Serum metabolome associated with severity of acute traumatic brain injury," *Nature communications*, vol. 13, no. 1, p. 2545, 2022.
- [9] C. A. Åkerlund et al., "Clustering identifies endotypes of traumatic brain injury in an intensive care cohort: a CENTER-TBI study," *Critical care*, vol. 26, no. 1, p. 228, 2022.
- [10] J. Tjerkaski et al., "Extended analysis of axonal injuries detected using magnetic resonance imaging in critically ill traumatic brain injury patients," *Journal of Neurotrauma*, vol. 39, no. 1–2, pp. 58–66, 2022.
- [11] A. Drieu et al., "Persistent neuroinflammation and behavioural deficits after single mild traumatic brain injury," *Journal of Cerebral Blood Flow & Metabolism*, vol. 42, no. 12, pp. 2216–2229, 2022.
- [12] A. Z. Mohamed, P. J. Nestor, P. Cumming, F. A. Nasrallah, and A. D. N. Initiative, "Traumatic brain injury fast-forwards Alzheimer's pathology: evidence from amyloid positron emission tomography imaging," *Journal of neurology*, vol. 269, no. 2, pp. 873–884, 2022.
- [13] L. Papa et al., "Evaluation of glial and neuronal blood biomarkers compared with clinical decision rules in assessing the need for computed tomography in patients with mild traumatic brain injury," *JAMA Network Open*, vol. 5, no. 3, pp. e221302–e221302, 2022.
- [14] J. H. Park et al., "Glymphatic system evaluation using diffusion tensor imaging in patients with traumatic brain injury," *Neuroradiology*, vol. 65, no. 3, pp. 551–557, 2023.
- [15] A. M. Janas et al., "Diffuse axonal injury grade on early MRI is associated with worse outcome in children with moderate-severe traumatic brain injury," *Neurocritical care*, vol. 36, no. 2, pp. 492–503, 2022.
- [16] A. Phaphuangwittayakul, Y. Guo, F. Ying, A. Y. Dawod, S. Angkurawaranon, and C. Angkurawaranon, "An optimal deep learning framework for multi-type hemorrhagic lesions detection and quantification in head CT images for traumatic brain injury," *Applied Intelligence*, pp. 1–19, 2022.
- [17] C. Marincowitz, L. Paton, F. Lecky, and P. Tiffin, "Predicting need for hospital admission in patients with traumatic brain injury or skull fractures identified on CT imaging: a machine learning approach," *Emergency Medicine Journal*, vol. 39, no. 5, pp. 394–401, 2022.
- [18] H. Ellethy, S. S. Chandra, and F. A. Nasrallah, "Deep neural networks predict the need for CT in pediatric mild traumatic brain injury: A corroboration of the PECARN rule," *Journal of the American College of Radiology*, vol. 19, no. 6, pp. 769–778, 2022.
- [19] H. Khalili et al., "Prognosis prediction in traumatic brain injury patients using machine learning algorithms," *Scientific reports*, vol. 13, no. 1, p. 960, 2023.
- [20] M. Nourelahi, F. Dadboud, H. Khalili, A. Niakan, and H. Parsaei, "A machine learning model for predicting favorable outcome in severe traumatic brain injury patients after 6 months," *Acute and critical care*, vol. 37, no. 1, pp. 45–52, 2022.
- [21] A. I. Maas et al., "Traumatic brain injury: progress and challenges in prevention, clinical care, and research," *The Lancet Neurology*, vol. 21, no. 11, pp. 1004–1060, 2022.

- [22] S. Chilamkurthy et al., “Deep learning algorithms for detection of critical findings in head CT scans: a retrospective study,” *The Lancet*, vol. 392, no. 10162, pp. 2388–2396, 2018.
- [23] A. E. Flanders et al., “Construction of a machine learning dataset through collaboration: the RSNA 2019 brain CT hemorrhage challenge,” *Radiology: Artificial Intelligence*, vol. 2, no. 3, p. e190211, 2020.
- [24] S. Jain et al., “Automatic quantification of computed tomography features in acute traumatic brain injury,” *Journal of neurotrauma*, vol. 36, no. 11, pp. 1794–1803, 2019.
- [25] C. Q. Lai, H. Ibrahim, A. I. A. Hamid, and J. M. Abdullah, “LSTM network as a screening tool to detect moderate traumatic brain injury from resting-state electroencephalogram,” *Expert Systems with Applications*, vol. 198, p. 116761, 2022.

Enhancing Threat Detection in Financial Cyber Security Through Auto Encoder-MLP Hybrid Models

Layth Almahadeen¹, Ghayth ALMahadin², Kathari Santosh³,
Mohd Aarif⁴, Dr. Pinak Deb⁵, Maganti Syamala⁶, Dr B Kiran Bala⁷

Lecturer, Department of Financial and Administrative Sciences, Al- Balqa' Applied University, Jordan¹
Assistant Professor, Department of Networks and Cybersecurity-Faculty of Information Technology,
Al Ahliyya Amman University, Jordan²

Assistant Professor, Department of MBA, CMR Institute of Technology, Bengaluru, India³
Department of Commerce, Aligarh Muslim University, Aligarh, Uttar Pradesh, India⁴

Assistant Professor, Department of MBA-Sanjivani College of Engineering, Savitribai Phule Pune University, Pune, India⁵

Assistant Professor, Dept. of Computer Science and Engineering, Koneru Lakshmaiah Education Foundation,
Vaddeswaram, Guntur Dist., Andhra Pradesh, India⁶

Head of the Department, Department of Artificial Intelligence and Data Science, K.Ramakrishnan College of Engineering,
Trichy, Tamil Nadu, India⁷

Abstract—Cyber-attacks have the potential to cause power outages, malfunctions with military equipment, and breaches of sensitive data. Owing to the substantial financial value of the information it contains, the banking sector is especially vulnerable. The number of digital footprints that banks have increases, increasing the attack surface available to hackers. This paper presents a unique approach to improve financial cyber security threat detection by integrating Auto Encoder-Multilayer Perceptron (AE-MLP) hybrid models. These models use MLP neural networks' discriminative capabilities for detection tasks, while also utilizing auto encoders' strengths in collecting complex patterns and abnormalities in financial data. The NSL-KDD dataset, which is varied and includes transaction records, user activity patterns, and network traffic, was thoroughly analysed. The results show that the AE-MLP hybrid models perform well in spotting possible risks including fraud, data breaches, and unauthorized access attempts. Auto encoders improve the accuracy of threat detection methods by efficiently compressing and rebuilding complicated data representations. This makes it easier to extract latent characteristics that are essential for differentiating between normal and abnormal activity. The approach is implemented with Python software. The recommended Hybrid AE+MLP approach shows better accuracy with 99%, which is 13.16% more sophisticated, when compared to traditional approach. The suggested approach improves financial cyber security systems' capacity for prediction while also providing scalability and efficiency while handling massive amounts of data in real-time settings.

Keywords—Financial cyber security; auto encoder; multilayer perceptron; threat detection; hybrid models

I. INTRODUCTION

The necessity of cyber safety and defense against various forms of cyber-attacks has increased dramatically in the last several years. The phrase "cyber security" describes a group of policies, mind-sets, and behaviours that help safeguard electronic data. Cyber-attacks including computer viruses [1], DoS attacks [2], and unlawful access have caused irreversible harm and financial harms in massive networks. For instance, a

single ransom ware infection cost \$8 billion in significant damages to several industries and enterprises, including banking, energy, healthcare, and higher education. Global investment in cyber security is expected to reach \$1 trillion by 2021; in 2013, spending increased by more than 40% to \$66 billion. Lately, cyber security researchers have started looking at AI techniques to improve cyber security. Similarly, fraudsters are using AI to launch increasingly sophisticated attacks while avoiding detection. However, we focus on how AI-powered cyber security solutions may lessen or completely prevent data breaches and more effectively fight attackers in our work [3]. AI has come a long way since it was first developed in the 1950s, yielding many interesting systems and research discoveries. ML and DL were the products of further developments. AI is being employed these days in many different domains, including industry, law, and exploration of space, medical care, and agriculture. New paradigms such as cloud-based computing and big data, along with continuous improvements in computer hardware and software performance and decreasing costs, have made it easier to develop and deploy a wide variety of AI systems with varying skills [4].

These days, a lot of these AI systems are capable of carrying out a wide range of difficult tasks, such as face and speech recognition, planning, problem solving, and learning [5]. Another important development in AI since the 1980s has been the emergence of technologies for ML, which allow machines to learn and adapt to various environments by utilizing their past experiences, patterns, and knowledge. The field of ML, came into being ten years ago. With the help of this sector, robots may uncover latent correlations in the information they are given, improving planning and forecast accuracy. Recently, there has been an increase in interest in applying AI and ML techniques to counter cyber-attacks [6]. The usage of these technologies is mostly driven by the vast amounts of information that are being created, since they need a significant time and resource commitment to analyze and detect any trends, irregularities, or breaches in traffic data.

The terms "cyber banking" and "cyber security" describe protocols, practices, and infrastructures that protect data, networks, and computer programs from online threats [7]. The threat posed by cyber security is one kind of financial terrorism which has become more prevalent. The most challenging aspect of modern cyber banking has shown to be the protection of customers' personal information. Cyber security is a strategy for thwarting cyber-attacks in cyberspace. Theft of confidential data, including account and ID numbers, and private information are examples of non-financial losses [8]. Cyber security aims to shield the impacted company and its customers from the monetary and non-monetary damages that result from a breach in any kind of data security system. Cybercrime has a detrimental financial effect on South African communities and impacts the whole planet. Safeguarding sensitive data is one of the most significant concerns of cyber security and confidentiality in the realm of cyber banking.

Technology breakthroughs have brought about changes in the banking sector, with internet banking developing as a more sensible method of conducting business. South African banks frequently employ third-party services like PayPal for both domestic and international transactions. Since the banks have no influence over the administration of these systems, their dependence on outside vendors to guarantee the caliber of their online offerings for clients poses a significant security risk. System connection promotes reliance, but it also raises the risk of cyber-attacks and breaches. Managing these risks means preventing and lessening assaults before they occur is termed as risk management. Banking was disproportionately affected by a 1318% rise in ransomware attacks in the initial half of 2021. The four percent increase in business email compromise, or BEC, assaults might be attributed to new COVID-19 options for threat actors. Large-scale cyber-attacks are becoming more and more likely to target banks. Because banks are linked, a cyber-attack on one might put the solvency of a financial institution at risk. Cyber-attacks on US banks that are supported by states are especially dangerous. As more individuals utilize the web and mobile banking, cybercrime has been rising over time. Cybercrime occurrences include a variety of fraud types, such as identity theft, ATM robberies, and credit card frauds. The banking sector is especially vulnerable because of the significant monetary worth of the information it holds. Hackers may make money in a variety of ways using the financial data and banking credentials they have taken. The attack surface available for exploitation has increased in tandem with the size of banks' digital footprints. Cyber-attacks have the potential to result in confidential information breaches, power disruptions, and malfunctioning military equipment. They may result in the theft of private information that can be quite valuable, including medical records. They have the ability to paralyze systems or interfere with computer and phone networks, making data inaccessible. Banking is especially vulnerable as the data it stores has significant value.

By combining the benefits of supervised and unsupervised learning methods, the suggested strategy improves the identification of threats in financial cyber security. Conventional approaches frequently find it difficult to keep up

with the constantly shifting characteristics of cyber threats, particularly in the ever-changing financial industry. The article presents a novel framework that combines the discriminative strength of MLP [9] networks with the feature learning abilities of auto encoders in order to handle this difficulty. Our goal is to increase detection accuracy by utilizing labelled information and capturing intricate patterns in the data through the integration of these two methods into a hybrid model. This method not only makes it easier to spot existing hazards, but it also gives you the flexibility to spot new irregularities and questionable activity in financial systems. Using an auto encoder-MLP hybrid model, the research can leverage labelled data to refine the model for particular threat detection tasks while also efficiently extracting high-level descriptions of the basic data structure via unsupervised learning. With the help of this hybrid architecture, we can use unsupervised feature learning to take use of the inherent qualities of the data, strengthening the model's resistance to new and unknown threats. Additionally, the framework can improve overall threat detection performance by learning to discriminate between benign and harmful actions with better accuracy. Our suggested strategy provides a more flexible and effective protection against new threats, offering a viable answer to the cyber security concerns in the financial arena through the creative integration of supervised and unsupervised learning approaches.

The key contribution of the proposed Auto encoder-MLP hybrid models' study is as follows

- The study suggests a novel approach to improve financial cyber security threat detection. By combining a Multilayer Perceptron (MLP) with an Auto Encoder (AE) this hybrid approach efficiently detects vulnerabilities within financial systems by utilizing the advantages of both constituent parts.
- By using min-max normalization to lessen the influence of feature size fluctuations, the study highlights the significance of data pre-processing in financial cyber security threat identification. This guarantees steady scalability and boosts model training effectiveness, which in turn raises threat identification accuracy.
- The architecture that has been suggested clearly outlines the functions of every element, ranging from feature extraction to threat detection in financial cyber security, hence promoting an open and effective framework for the creation and use of models.
- The proposed AE-MLP hybrid model is extensively tested using the NSL-KDD dataset, showing good results on a number of metrics including f1-score, recall, accuracy, and precision. The study offers in-depth understandings of the effectiveness and dependability of the suggested strategy, confirming its viability for practical implementation in financial cyber security environments.

The article's remaining sections are arranged as follows: A summary of relevant studies is given in Section II. The issue statement for the existing system is found in Section III. In

Section IV of the study, the proposed Auto encoder-MLP hybrid model and technique for increased threat detection are described. The study's results and the ensuing discussion are presented in Section V. Section VI discusses the suggested model's conclusion and possible applications.

II. RELATED WORKS

The paper by I. H. Sarker, Y. B. Abushark, F. Alsolami, and A. I. Khan [10] introduced the "IntruDTree," a ML-based security framework that builds a generalized detection of intrusion model based on a tree structure by first considering the importance ranking of security features. This approach lowers computation complexity for yet-to-be-tested test scenarios while retaining prediction accuracy by shrinking the feature dimensions. Lastly, by doing tests using cyber security datasets and evaluating metrics to assess, the efficacy of our IntruDTree model was investigated. To assess the efficacy of the resultant security model, the study also compare the outcomes of the IntruDTree model with a number of conventional, well-known ML techniques, including the naive Bayes classification algorithm, logistical regression, SVMs, and the k-nearest-neighbour model. The drawback of the model is static dataset is utilized to trained the model and relies on predetermined feature importance rankings, it may struggle to adapt quickly to new types of intrusions or novel attack patterns. Without regular retraining and upgrades, static models like the IntruDTree could discover it difficult to keep up with new threats as they emerge and get more complex over time.

IDS that utilizes a stacked AE and a DNN is proposed in the G. Muhammad, M. S. Hossain, and S. Garg [11] paper. In order to reduce the feature width, the stacked AE analyses the distinctive characteristics of the input networks recording in an unsupervised way. Subsequently, supervised training is applied to the DNN in order to obtain deep learning characteristics for the classifier. The DNN contains two or three layers in the suggested system, with each layer having a fully linked layer, a batch normalization layer, and a dropout. The AE has two latent layers. Three sets of publicly available data were used to assess the system. The trials' findings demonstrated the 94.2% accuracy of the recommended IDS for multiclass categorization. The disadvantage is that it has been demonstrated that adversarial examples carefully constructed inputs intended to distort the model's predictions can weaken DL models, particularly DNNs. Since the AE and DNN in the proposed IDS rely heavily on learned representations of network traffic data, they may be susceptible to adversarial manipulation of input features, leading to misclassifications or incorrect intrusion detection decisions.

The goal of the M. Alsaedi, F. A. Ghaleb, F. Saeed, J. Ahmad, and M. Alasl [12] study is to increase the detection accuracy of harmful URLs by creating a model for two-stage ensemble learning that is based on cyber threat intelligence. To increase detection accuracy, online searches are used to extract the attributes based on cyber threat data. Global user reports and cyber security analysts can offer vital information about rogue websites. Consequently, to enhance detection efficiency, characteristics derived from searches on Google

and Whois websites are utilized to create cyber threat intelligence (CTI). The study also suggested a two-stage ensemble learning approach that combines multilayer perceptrons (MLP) for ultimate decision-making with the RF algorithm for pre classification. The three separately trained random forest classifiers' majority voting system has been superseded by the trained MLP classifier for decision-making. For sufficient classification, the probabilistic outputs of the random forest's weak classifiers was combined and fed into the MLP classifier. The retrieved CTI-based characteristics based on the two-stage classification perform better than the detection models used in other research, according to the results. Compared to the conventional URL-based model, the suggested CTI-based detection model produced a 7.8% accuracy gain and a 6.7% decrease in false-positive rates. The drawback of the model is the reliance on online searches for feature extraction may introduce biases in the dataset used for training the ensemble learning model. The model's performance could be impacted if the extracted attributes do not adequately represent the diversity of malicious URLs or if there are inherent biases in the online sources used for data collection.

An efficient methodology for detecting intrusions using SVM and naive Bayes feature embedding was presented by J. Gu and S. Lu [13] in their study. The naive Bayes transform feature technique is used to build new, high-quality information from the original features; an SVM classifier is subsequently trained with the altered data to generate an ID model. Research was out on several datasets within the intrusion identification domain substantiate the efficaciousness and resilience of the recommended detection technique. The UNSW-NB15 dataset shows 93.75% accuracy, the CICIDS2017 dataset shows 98.92% accuracy, the NSL-KDD dataset shows 99.35% accuracy, and the Kyoto 2006+ dataset shows 98.58% accuracy. Furthermore, our method offers notable advantages over existing methods in terms of efficiency, false alarm rate, and identification rate. Keeping the scalability and effectiveness of the IDS is a difficulty when expanding the study to scenarios with varying forms of attacks. The feature space may grow dramatically as attack types become more sophisticated and diverse, increasing processing costs and perhaps reducing the model's capacity for real-time detection.

For the IIoT wireless sensing scenario, a DL-based network intrusion identification and categorization model (NIDS-CNNLSTM) is created in the J. Du, K. Yang, Y. Hu, and L. Jiang, [14] goal is to effectively distinguish and recognize network traffic while ensuring the equipment and operation of the IIoT are secure. Using LSTM in data from time series together with the powerful capacity for learning of neural networks, NIDS-CNNLSTM trains and classifies the features selected by the CNN and verifies its application through binary categorisation and multi-classification scenarios. The precision rate while categorizing different forms of traffic is high, and the three datasets show outstanding convergence and level in terms of validation accuracy, training loss, and precision rate. Previous study models were not able to equal NIDS-CNNLSTM's overall effectiveness. The experimental findings show good

classification accuracy, a small false alarm rate, and a high detection rate. It is more appropriate for large-scale, multi-scenario network data in the IIoT. The primary disadvantage is that deep learning models, such as CNN-LSTM, can be computationally demanding, particularly when working with high-dimensional, large-scale data sets like network traffic data.

There are numerous types of security frameworks and IDS that have limitations. First, because some models rely on predefined feature rankings and static datasets, they are noticeably less flexible than others. This constraint limits their capacity to quickly adapt to novel forms of intrusions or developing assault patterns, which may risk their efficacy in quickly changing environments including cyber threats. Second, adversarial examples, complex inputs purposefully created to distort the model's predictions can affect deep learning-based IDS. This issue is quite concerning since it might result in incorrect intrusion detection judgments or misclassifications, which could compromise the system's overall dependability. Furthermore, algorithms that extract features from web searches might introduce biases into the training dataset. The model's performance may be impacted by this reliance on outside sources for feature extraction, which might lead to inadequate representation of the variety of harmful activities. Finally, there are still issues with scalability, especially when dealing with high-dimensional datasets and different kinds of attacks. Certain intrusion detection systems may encounter difficulties in maintaining scalability and efficiency when attack complexity escalates, which might result in increased computing expenses and reduced real-time detection capabilities. All of these drawbacks highlight the continuous requirement for enhanced threat detection system that can strike a balance between flexibility, dependability, and computing efficiency in the ever-changing world of cyber security threats.

III. PROBLEM STATEMENT

The financial cyber security environment faces a variety of challenges as a result of the deficiencies of current intrusion detection systems and security standards. These challenges

include scalability issues with high-dimensional datasets and diverse attack vectors, biases introduced by algorithms extracting features from web searches, inherent inflexibility resulting from reliance on predefined features and static datasets, and vulnerability to adversarial examples in deep learning-based intrusion detection systems [15]. It is imperative to design a more sophisticated threat detection system that strikes a balance between dependability, adaptability, and computing efficiency in order to counteract these shortcomings and keep up with the constantly evolving landscape of cyber threats affecting the financial industry. In order to overcome these obstacles, this study suggests a novel strategy that makes use of Auto Encoder-Multilayer Perceptron (AE-MLP) hybrid algorithms. The goal is to provide a strong framework for threat detection that can efficiently detect and mitigate cyber risks in financial systems while preserving scalability, resilience to adversarial assaults, and flexibility.

IV. PROPOSED AUTO ENCODER-MLP HYBRID MODEL FOR ENHANCING THREAT DETECTION IN FINANCIAL CYBER SECURITY

In order to enhance threat detection in financial cyber security, this methodology suggests combining the use of an Auto Encoder (AE) with a Multilayer Perceptron (MLP). Due to their sensitive data, financial companies are particularly vulnerable to cyber-attacks. The approach begins by normalizing the data in order to guarantee consistent scalability in order to address this. The two primary components of the hybrid model are the AE, which compresses and extracts significant patterns from the data, and the MLP, which categorizes threats using this compressed representation. The number of layers, units per layer, activation functions, and other parameters must be specified in the MLP construction algorithm. All things considered, this technique provides a transparent framework for creating and implementing a hybrid AE-MLP model for improved threat identification in financial cyber security. Fig. 1 shows the block diagram of this AE-MLP methodology is given below.

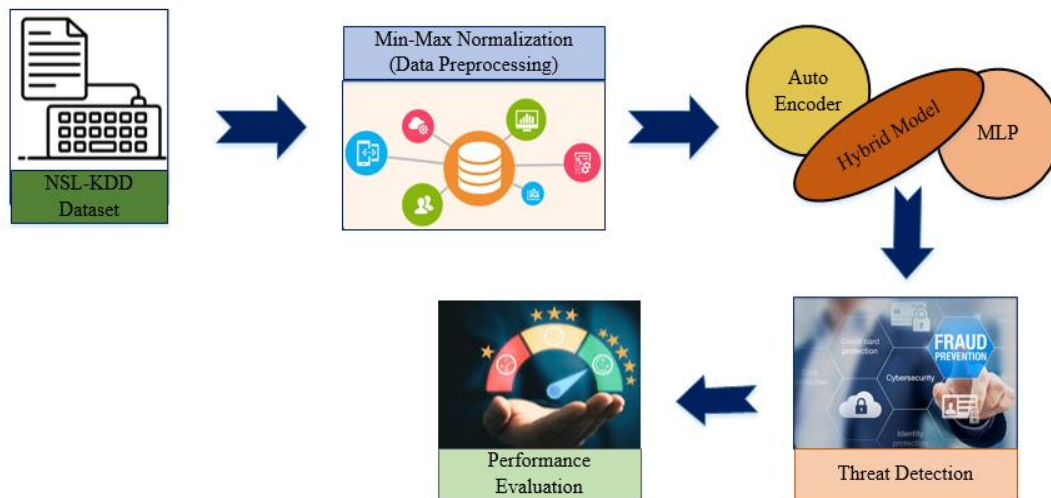


Fig. 1. Hybrid AE-MLP model block diagram.

A. Dataset Collection

NSL-KDD dataset was collected from the secondary source [16]. It consists of specific entries from the data collection KDD 99. The train and test sets contain identical records, and because of the decreased dataset size, random selection is not required. There exists a negative correlation between the proportion of entries in the KDD99 dataset and the chosen entries in every single category of the NSL-KDD dataset. Various ML algorithms may achieve a wider range of accuracy, resulting in more accurate assessments of various models. There are 125,970 occurrences in the training dataset and 225,440 samples in the test dataset. There are four categories into which the assaults are divided: DoS, R2L, U2R, Probe, and a Standard class.

B. Min-Max Normalization for Data Pre-processing

Normalization minimizes the impact of feature scale variations, which reduces the training time of a model. The min-max normalization is used once the outliers have been relocated. Mathematical data can be transformed into a range, often between 0 and 1, using a technique called min-max normalization, sometimes referred to as features scaling. All of the dataset's features, or columns, go through this procedure[17]. Scaling numerical data within a particular range, usually between 0 and 1, is known as min-max normalization. It is a fundamental data preparation method utilized in threat detection in the sets of data given using a hybrid Auto Encoder- MLP model. In the absence of an explicit calculation, this technique guarantees that the lowest and greatest values in the dataset are converted to 0 and 1, respectively, and that any further data values are adjusted linear with respect to this range [18]. The normalization process modifies each data point individually by computing the characteristic or column's lowest and highest values, removing the smallest value, and divided by the range of values. By ensuring uniform feature scaling, min-max normalization contributes to improved convergence and model stability, thereby enhancing the performance of auto encoder-MLP hybrid models. This enhancement is particularly valuable in threat detection scenarios, where model accuracy and robustness are paramount. The normalization of min-max is expressed using Eq. (1) and Eq. (2).

$$N_{std} = \frac{N - N_{min}}{N_{max} - N_{min}} \quad (1)$$

$$N_{scaled} = N_{std} \times (max - min) + min \quad (2)$$

By doing this, you can be sure that the values that fall between will be scaled linearly to match the transformation of the lowest value to 0 and the highest value to 1. This normalization method is particularly useful when features have different scales since it ensures uniformity among the features and supports the performance of the ML model during training.

C. Synergistic Auto Encoder-MLP Architecture for Advanced Threat Detection in Financial Cyber Security

The sensitive data that financial institutions hold makes them easy targets for cyber-attacks. To protect assets and preserve confidence in the financial system, financial cyber security threat detection must be improved. Deep learning methods have showed promise in identifying and reducing cyber dangers in recent years. In order to increase threat detection in financial cyber security, the study provide a hybrid model in this proposal that combines an auto encoder with a MLP.

An auto encoder is a type of multilayer neural network where the desired output is comparable to the input with less modifications, i.e., the result is similar as the inputs with some reconstruction error [19]. By encoding the input, the auto encoder uses unsupervised learning to decode or rebuild the output. Auto encoders are commonly used in recommender systems to decrease the dimensionality of characteristics, retrieve pertinent characteristics, compress and remove noise from the pictures, forecast sequences, and identify abnormalities.

For the purpose of conciseness, we describe the overall architecture of an auto encoder without getting into specifics.

A general auto encoder consists of four key components: the encoder, reconstruction loss, bottleneck, and decoder. The encoder shrinks the data into an encoded form and helps to reduce characteristics from the input. The layer with the fewest features and compressed incoming data is known as the bottleneck layer. By assisting the model in reconstructing the result from the encoded representation, the decoder ensures that the output and input are identical. Reconstruction Loss is the last term used to assess the decoder's performance and gauge how close the output is to the original input.

Moreover, back propagation is used to carry out training and reduce reconstruction loss even more. This minimum loss illustrates the objective that AE strives to achieve. The input y will be compressed by the encoder is expressed in Eq. (3)

$$x = E(y) \quad (3)$$

The input will be attempted to be recreated by Decoder D as $y' = D(E(y))$.

$$loss(E, D) = \frac{1}{n} \sum_{j=1}^n (y^j - D(E(y^j)))^2 \quad (4)$$

The variation between the decoded and encoded vectors in this case is the reconstruction loss. One way to calculate the reconstruction loss is to use the Mean Square Error (MSE). It is provided in eqn. (4) given above. Fig. 2 shows the architectural diagram of hybrid AE-MLP is given below.

One kind of ANN that forms the basis of DL models is the MLP. Since MLPs belong to the class of feed forward neural networks, data moves from the input layer to the output layer only in one direction. For many different ML tasks, such as feature learning, regression, and classification, they are extensively utilized. Let's take a closer look at the parts, construction, and operation of an MLP [20]. An MLP is made up of several layers of linked neurons, and its structure is typified by three primary kinds of layers.

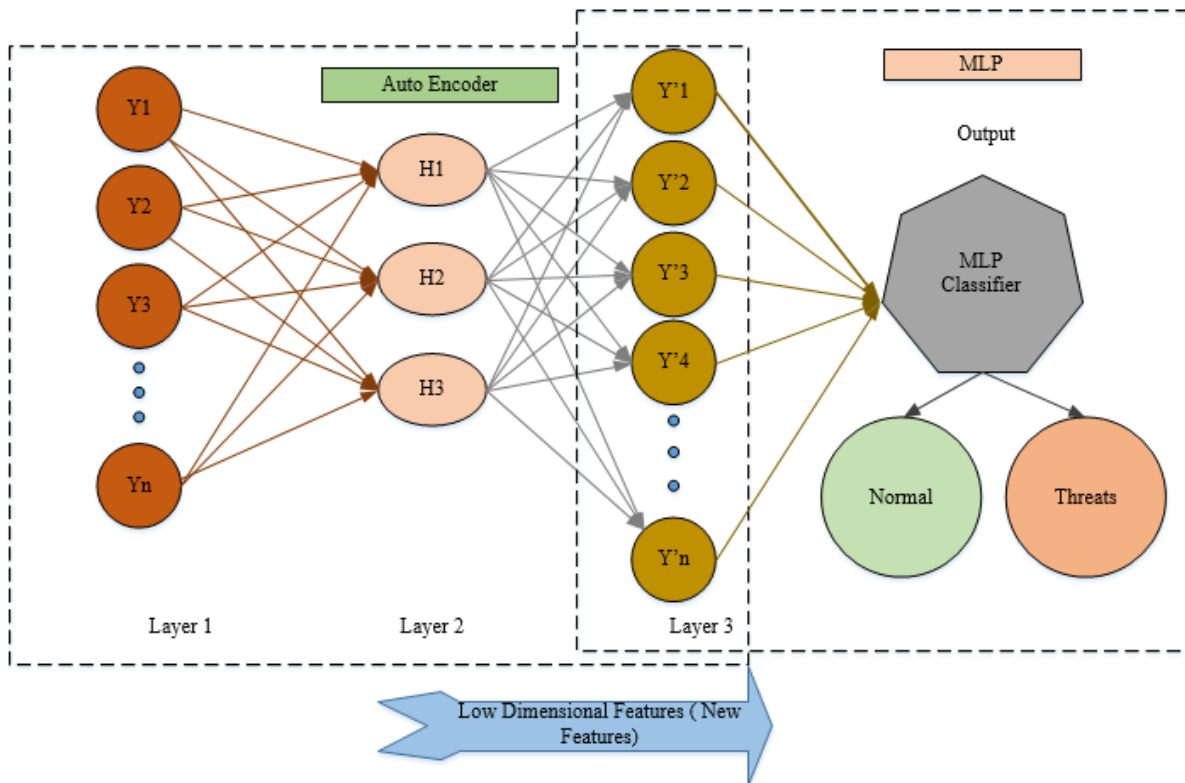


Fig. 2. Hybrid auto encoder-MLP architecture.

The first layer of the network's architecture is the information input layer, which gets raw input data. Since each neuron in the input layer is mapped to a feature in the dataset, the input layer serves as a fundamental demonstration of the data's measurements. The concealed layer comes next. Among the input layer and the output layer of an MLP, there may be several layers that are hidden. Because these layers are not immediately linked to the external world, they are referred to as "hidden" layers. Hidden layer neurons apply a function of activation to the weighed total of the inputs from the preceding layer, process the data, and then forward the output to the subsequent layer. One may modify the hyper parameters, such as the number of neurons and layers that are hidden in each layer, to maximize the models.

The output layer, which is the last layer, generates the prediction or model's output. The problem that the MLP is intended to address dictates this layer's construction. Multiclass classification may employ many neurons, each representing a class and utilizing a softmax activation function, in contrast to binary categorization, which would utilize a single neuron with a sigmoid activation function.

The neurons of an MLP perform the following functions.

- **Weighted Sum:** The input for every neuron is equal to the weighted total of the outputs from the layer that came before it. A common term for this weighted total is the neuron's "activation." The sum $y_q^{(l)}$ of neuron q in layer l may be written mathematically as in Eq. (5)

$$y_q^{(l)} = \sum_p w_{pq}^{(l)} a_p^{(l-1)} + b_q^{(l)} \quad (5)$$

Where,

$y_q^{(l)}$ Corresponds to the layer l activation of neuron q .

$w_{pq}^{(l)}$ The connection weight between neuron p in layer $l-1$ and neuron q in layer l is measured.

$a_p^{(l-1)}$ Is layer $l-1$ neuron p 's output.

$b_q^{(l)}$ Is layer l 's neuron q 's bias.

- **Activation Function:** Common activation functions include the sigmoid function, tanh, and ReLU. One layer's output serves as the subsequent layer's input. The Eq. (6) denotes it.

$$a_p^{(l)} = f(y_q^{(l)}) \quad (6)$$

where, $a_p^{(l)}$ is the layer l output of neuron q , and the activation function is represented by f .

- **Feed Forward Propagation:** Applying the activation functions to the weighted aggregate, the activations are computed for each of the neurons in the feed forward process. By using the final result of a specific layer as the input of the next layer, information is transferred from the layer that provided the input to the output layer. $a_p^{(l)}$ Is expressed in Eq. (7) is given below

$$a_p^{(l)} = (\sum_p w_{pq}^{(l)} a_p^{(l-1)} + b_q^{(l)}) \quad (7)$$

To improve threat detection in financial cyber security, a hybrid model that combines the strong abilities of AE and

MLPs is suggested. As a skilled feature extractor in this design, the auto encoder is able to identify important patterns and representations that are hidden in the input data. The auto encoder uses its encoder network to generate a condensed space of latent information representation that captures the key elements of the input data. This representation of latent space is then sent into the hybrid model's MLP component. In its capacity as a classifier, the MLP uses the characteristics that it has extracted from the auto encoder to identify and group different threat categories that are present in the financial security space.

The hybrid model uses labelled datasets for supervised learning during the training phase. The AE and MLP elements must be simultaneously optimized in this combined training method. The MLP is simultaneously trained to reduce classification errors by utilizing the informative features obtained from the AE's latent space representation, while the auto encoder attempts to properly recreate the input data. Selecting a suitable loss function, such cross-entropy, makes it easier to quantify the difference between the expected and real labels, which helps to increase the model's resilience and classification accuracy.

Algorithm for MLP Architecture

Require: D_{train} , D_{test} (Training and Testing)
Require: MLP architecture hyper parameters

Data Pre-processing: Min-max normalization

Build the MLP model:

Layer Numbers : 3

Units/ layer:

Input layer: data containing number of features

Hidden layer 1: ReLU activation 128 units

Hidden layer 2: ReLU activation 64 units

Output layer: The quantity of output classes that possess an appropriate activation function

Assemble the MLP model by specifying the optimizer, loss, and assessment metrics.

For a certain number of epochs, train the MLP model on D_{train} .

Determine performance indicators and assess the model on the D_{test} .

Fine tune hyper parameters as needed

Optionally deploy the model

Keep monitor model and updated.

V. RESULTS AND DISCUSSION

Using the NSL-KDD dataset, AE-MLP Threat detection approach is evaluated. The proposed approach produces excellent and extremely promising outcomes. Using a device operating Python as a programming language with the Windows 10 operating system. The performance are accessed using the following metrics: f1-score, recall,

accuracy, and precision. These measures have the following definition.

A. Performance Metrics

1) *Accuracy*: The percentage of test cases that a technique successfully detects on a given test set is its accuracy. It is computed as follows in Eq. (8).

$$Accuracy = \frac{RN+RP}{RP+AP+RN+AN} \quad (8)$$

2) *Precision*: The proportion of all positively identified instances to the number of accurately detected positive occurrences by the model is known as precision. It is quantified as in Eq. (9).

$$Precision = \frac{True\ Positives}{(True\ Positives+False\ Positives)} \quad (9)$$

A value between 0 and 1, where 1 denotes perfect precision and 0 denotes no correct positive predictions, is the accuracy level.

3) *Recall*: The notion of the positive cases that the model properly identifies is known as recall. It is computed as follows in Eq. (10).

$$Recall(sensitivity) = \frac{True\ Positives}{True\ Positives+False\ Negatives} \quad (10)$$

4) *F1-Score*: The F1 score is a widely used statistic to evaluate how well sorting models perform in detection tasks; it is especially helpful for algorithms that function well in threat detection and prediction. The F1 score is useful when a dataset is uneven, meaning that one class significantly outnumbers the other. Equation is used to evaluate the F1 score as shown in Eq. (11).

$$F1\ Score = 2 \times \frac{(Precision*Recall)}{(Precision+Recall)} \quad (11)$$

One should take the F1 score into account when evaluating someone since it offers a helpful and impartial way to assess recall and accuracy. When choosing between accuracy and recall, as is frequently encountered in detection tasks, it is a useful metric to use.

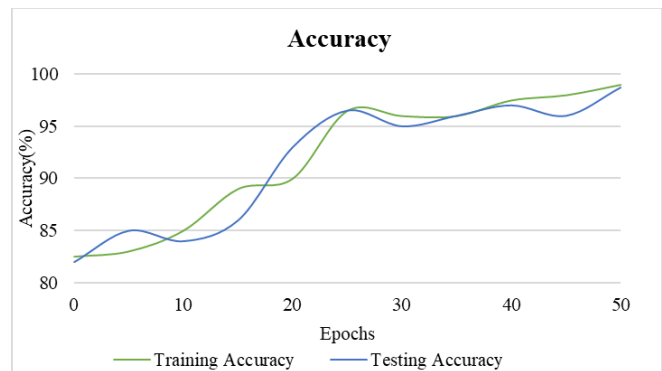


Fig. 3. Training and testing accuracy of the proposed AE-MLP approach.

The AE-MLP model's testing and training accuracy are shown in Fig. 3. The following graph shows how well the model works in two different phases training, when it learns

from the data, and testing, when it applies newfound knowledge to previously unknown data. The model's resilience and dependability in real-world circumstances are indicated by the tight alignment of the training and testing accuracies, which implies that the model generalizes effectively to fresh data.

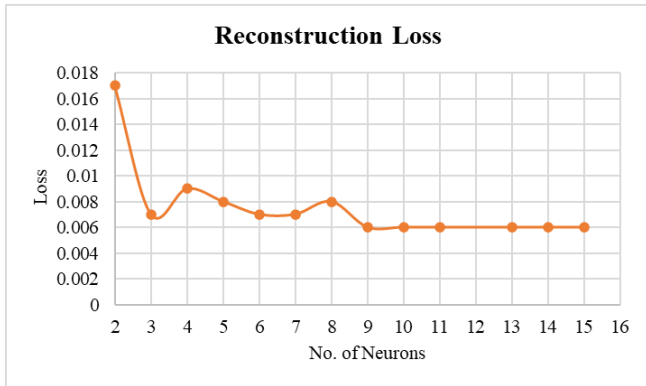


Fig. 4. Reconstruction loss of the proposed approach.

The reconstruction loss of the suggested method, as depicted in Fig. 4, serves as a critical indicator of the auto encoder model's proficiency in recovering its input data. A smaller reconstruction loss not only signifies the model's capability to capture and represent underlying data patterns accurately but also implies a higher fidelity in reconstructing normal network behaviour. This robust representation enables the AE-MLP approach to effectively discern anomalous activities, thereby bolstering its capacity for precise and reliable cyber threat detection.

B. Consideration with Other State-of-the-Art Approaches

The need for threat detection in the contemporary cyber environment has led to much study on the subject. For such cases, researchers have used a variety of powerful and advanced ML techniques. This section compares the accuracy of our method against various cutting-edge detection algorithms based on traditional ML and DL approaches using the NSL-KDD dataset.

As seen in Table I, proposed auto encoder-MLP strategy have produced superior results than alternative approaches and it is depicted in Fig. 5. It compares the AE-MLP approach's accuracy (99%), precision (98.75%), recall (98.92%), and F1-score (98.79%) with alternative techniques. The proposed AE-MLP technique outperforms the conventional RNN (83.28%), STL+SVM (84.96%) and AE+DNN (94.21%) methods in terms of accuracy.

TABLE I. COMPARISON WITH EXISTING METHODS AND SUGGESTED METHOD

| Methods | Accuracy (%) | Precision (%) | Recall (%) | F1Score (%) |
|-----------------|--------------|---------------|------------|-------------|
| RNN [21] | 83.28 | 81.60 | 82.24 | 81.42 |
| STL+SVM [22] | 84.96 | 81.78 | 84.08 | 80.21 |
| AE+DNN [11] | 94.21 | 92.78 | 90.82 | 90.21 |
| Proposed AE+MLP | 99 | 98.75 | 98.92 | 98.79 |

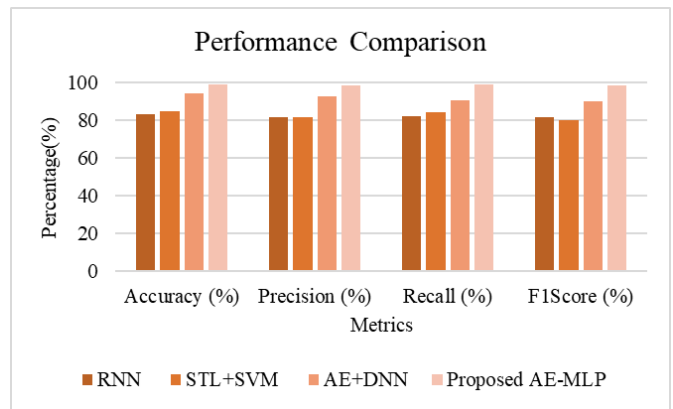


Fig. 5. The performance evaluations of AE-MLP with conventional approaches.

TABLE II. COMPARISON WITH DIFFERENT DATABASE WITH SUGGESTED METHOD

| Different Dataset | Accuracy (%) |
|-------------------|--------------|
| KDD99 [23] | 98 |
| UNSW-NB15 [24] | 97 |
| Proposed NSL-KDD | 99 |

Table II shows the accuracy of the proposed technique on three different datasets: UNSW-NB15, KDD99, and the proposed NSL-KDD dataset. The approach demonstrated 98% accuracy on the KDD99 dataset, a reputable intrusion detection benchmark. The technique achieved 97% accuracy rate on another popular benchmark, the UNSW-NB15 dataset. Notably, it attained the greatest accuracy of 99% on the NSL-KDD dataset that was particularly created for the suggested technique. These findings highlight the method's efficacy in correctly categorising instances of network traffic and detecting intrusions; the NSL-KDD dataset shows especially impressive performance, perhaps because it aligns with the method's methods and methodologies.

TABLE III. DETECTION SPEED COMPARISON OF INTRUSION DETECTION METHODS

| Approach | Detection Speed (seconds) |
|-----------------|---------------------------|
| RNN [21] | 100 |
| STL+SVM [22] | 120 |
| AE+DNN [11] | 90 |
| Proposed AE+MLP | 80 |

Table III presents a concise summary of the detection speeds of different intrusion detection techniques. It also includes a comparison of detection speeds of intrusion detection methods. While STL+SVM [22] shows a little slower speed of 120 seconds, RNN [21] indicates a detection speed of 100 seconds. Using autoencoders and deep neural networks, AE+DNN [11] provides a 90-second detection time quicker than previous methods.

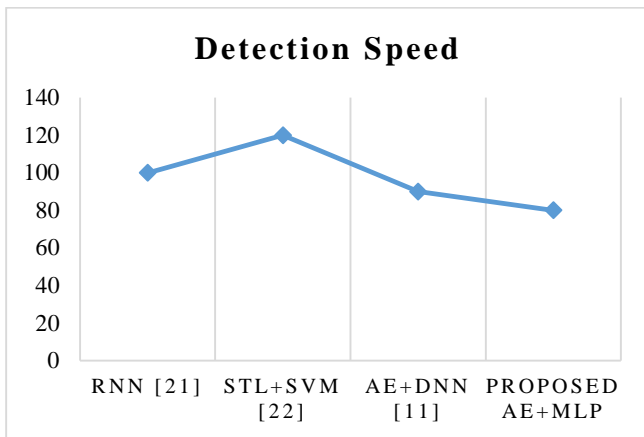


Fig. 6. The detection speed comparison evaluations of AE-MLP with conventional approaches.

The fastest detection speed, achieved by the suggested AE+MLP approach at 80 seconds, demonstrates the effectiveness of integrating autoencoders with multilayer perceptron's. The findings highlight how crucial it is to take into account detection speed when choosing an intrusion detection technique for cybersecurity applications, in addition to other performance parameters like accuracy and scalability. Fig. 6 illustrate the Detection Speed Comparison Evaluations of AE-MLP with Conventional Approaches.

A. Discussion

The examined works provide several methods for using machine learning (ML) and deep learning (DL) techniques in intrusion detection systems (IDS). In order to construct a generalised intrusion detection model, I. H. Sarker, Y. B. Abushark, F. Alsolami, and A. I. Khan [10] provide "IntruDTree," an ML-based framework that ranks security characteristics in order of importance and exhibits efficacy across a variety of cyber security datasets. Its dependence on fixed feature rankings and static datasets, however, could make it more difficult to respond to emerging threats. G. Muhammad, M. S. Hossain, and S. Garg [11] offer an intrusion detection system (IDS) that relies on learnt representations and achieves high accuracy but could be subject to adversarial assaults. The system uses stacked autoencoders and a deep neural network. In comparison to traditional models, M. Alsaedi, F. A. Ghaleb, F. Saeed, J. Ahmad, and M. Alasl [12] approach to improving dangerous URL identification is based on cyber threat information and involves a two-stage ensemble learning process. However, the performance of the system may be impacted by potential biases from internet searches. Utilising SVM and naive Bayes feature embedding, J. Gu and S. Lu [13] describe an effective IDS approach that shows excellent accuracy across a variety of datasets but runs into scaling issues as attack types diversify. J. Du, K. Yang, Y. Hu, and L. Jiang, [14] present NIDS-CNNLSTM, a computationally demanding intrusion detection and classification system for IIoT wireless sensing. These studies demonstrate the variety of methodologies employed for IDS creation, each with advantages and disadvantages in dealing with the always changing cyber threat environment.

The result section compares and assesses a novel cyber threat detection technique termed AE-MLP against existing cutting-edge approaches. With exceptional recall, accuracy, precision, and F1 scores of 99%, 98.75%, 98.92%, and 98.79%, respectively, the AE-MLP method stands out. These findings demonstrate its exceptional ability to correctly identify threats while reducing false alarms. In both the training and testing phases, when the model applies its newly acquired knowledge to previously unseen data, Fig. 3 offers a visual depiction of the model's performance. The model's resilience and dependability in real-world circumstances are indicated by the tight alignment of the training and testing accuracies, which implies that the model generalizes effectively to fresh data. The reconstruction loss of the suggested method is shown in Fig. 4. The auto encoder model's ability to recover its input data is indicated by its reconstruction loss. A smaller reconstruction loss suggests that the underlying patterns in the data can be captured and represented by the model with good accuracy. The figures provide empirical evidence supporting the efficacy of the AE-MLP approach and its potential to enhance cyber security measures in the face of evolving threats.

VI. CONCLUSION AND FUTURE SCOPE

In conclusion, the use of Auto Encoder-MLP hybrid models is a noteworthy development in the field of financial cyber security, providing a strong means of improving threat detection systems. This hybrid approach shows superior performance in identifying and mitigating potential threats within financial systems by combining the potent classification capabilities of MLP neural networks with the special powers of auto encoders to compress and reconstruct complex data representations. These models are highly skilled at identifying small irregularities that point to harmful behaviours like fraud, data breaches, and attempts at unauthorized access. This is achieved by the thorough examination of a variety of financial information, including transaction records, user activity patterns, and network traffic. The potential for further study and development in this area is bright. Hybrid model designs may be further improved and refined to increase their scalability and forecast accuracy, which would provide strong defense against advanced cyber-attacks. Furthermore, the contextual knowledge of cyber security risks might be enhanced by the integration of new data sources, such as social media feeds, market trends, and geopolitical indicators. This would allow for more thorough risk assessments and proactive threat mitigation techniques. Furthermore, developments in machine learning methods, especially in the areas of reinforcement learning and DL, present opportunities for enhancing the effectiveness and flexibility of financial cyber security systems over time.

REFERENCES

- [1] A. Dainotti, A. Pescapè, and G. Ventre, Worm Traffic Analysis and Characterization. 2007, p. 1442. doi: 10.1109/ICC.2007.241.
- [2] N. Sun, J. Zhang, P. Rimba, S. Gao, L. Y. Zhang, and Y. Xiang, "Data-Driven Cybersecurity Incident Prediction: A Survey," IEEE Commun. Surv. Tutorials, vol. 21, no. 2, pp. 1744–1772, 2019, doi: 10.1109/COMST.2018.2885561.
- [3] W. N. W. Manan and C. Y. Han, "Detection of Distributed Denial-of-Service (DDoS) Attack with Hyperparameter Tuning Based on Machine

- Learning Approach,” in 2023 7th International Symposium on Innovative Approaches in Smart Technologies (ISAS), Nov. 2023, pp. 1–8. doi: 10.1109/ISAS60782.2023.10391487.
- [4] D. Ghelani, T. K. Hua, and S. K. R. Koduru, “Cyber Security Threats, Vulnerabilities, and Security Solutions Models in Banking,” Preprints, preprint, Sep. 2022. doi: 10.22541/au.166385206.63311335/v1.
- [5] S. Zeadally, E. Adi, Z. Baig, and I. A. Khan, “Harnessing Artificial Intelligence Capabilities to Improve Cybersecurity,” IEEE Access, vol. 8, pp. 23817–23837, 2020, doi: 10.1109/ACCESS.2020.2968045.
- [6] V. Koutsouvelis, S. Shiaeles, B. Ghita, and G. Bendiab, “Detection of Insider Threats using Artificial Intelligence and Visualisation,” in 2020 6th IEEE Conference on Network Softwarization (NetSoft), Ghent, Belgium: IEEE, Jun. 2020, pp. 437–443. doi: 10.1109/NetSoft48620.2020.9165337.
- [7] S. A. AlAjlan and A. K. J. Saudagar, “Machine learning approach for threat detection on social media posts containing Arabic text,” *Evol. Intel.*, vol. 14, no. 2, pp. 811–822, Jun. 2021, doi: 10.1007/s12065-020-00458-w.
- [8] W. Hu and H. Hu, “Discriminant Deep Feature Learning based on joint supervision Loss and Multi-layer Feature Fusion for heterogeneous face recognition,” *Computer Vision and Image Understanding*, vol. 184, pp. 9–21, Jul. 2019, doi: 10.1016/j.cviu.2019.04.003.
- [9] P. Shettar, A. V. Kachavimath, M. M. Mulla, N. D. G, and G. Hanchinmani, “Intrusion Detection System using MLP and Chaotic Neural Networks,” in 2021 International Conference on Computer Communication and Informatics (ICCCI), Coimbatore, India: IEEE, Jan. 2021, pp. 1–4. doi: 10.1109/ICCCI50826.2021.9457024.
- [10] I. H. Sarker, Y. B. Abushark, F. Alsolami, and A. I. Khan, “IntruDTree: A Machine Learning Based Cyber Security Intrusion Detection Model,” *Symmetry*, vol. 12, no. 5, Art. no. 5, May 2020, doi: 10.3390/sym12050754.
- [11] G. Muhammad, M. S. Hossain, and S. Garg, “Stacked Autoencoder-Based Intrusion Detection System to Combat Financial Fraudulent,” *IEEE Internet of Things Journal*, vol. 10, no. 3, pp. 2071–2078, Feb. 2023, doi: 10.1109/JIOT.2020.3041184.
- [12] M. Alsaedi, F. A. Ghaleb, F. Saeed, J. Ahmad, and M. Alasli, “Cyber Threat Intelligence-Based Malicious URL Detection Model Using Ensemble Learning,” *Sensors*, vol. 22, no. 9, Art. no. 9, Jan. 2022, doi: 10.3390/s22093373.
- [13] J. Gu and S. Lu, “An effective intrusion detection approach using SVM with naïve Bayes feature embedding,” *Computers & Security*, vol. 103, p. 102158, Apr. 2021, doi: 10.1016/j.cose.2020.102158.
- [14] J. Du, K. Yang, Y. Hu, and L. Jiang, “NIDS-CNNLSTM: Network Intrusion Detection Classification Model Based on Deep Learning,” *IEEE Access*, vol. 11, pp. 24808–24821, 2023, doi: 10.1109/ACCESS.2023.3254915.
- [15] A. Bécue, I. Praça, and J. Gama, “Artificial intelligence, cyber-threats and Industry 4.0: challenges and opportunities,” *Artif Intell Rev*, vol. 54, no. 5, pp. 3849–3886, Jun. 2021, doi: 10.1007/s10462-020-09942-2.
- [16] M. Tavallae, E. Bagheri, W. Lu, and A. Ghorbani, “A detailed analysis of the KDD CUP 99 data set,” *IEEE Symposium. Computational Intelligence for Security and Defense Applications, CISDA*, vol. 2, Jul. 2009, doi: 10.1109/CISDA.2009.5356528.
- [17] S. Yu, J. Wang, J. Liu, R. Sun, S. Kuang, and L. Sun, “Rapid Prediction of Respiratory Motion Based on Bidirectional Gated Recurrent Unit Network,” *IEEE Access*, vol. 8, pp. 49424–49435, 2020, doi: 10.1109/ACCESS.2020.2980002.
- [18] A. Soleimani and S. E. Khadem, “Early fault detection of rotating machinery through chaotic vibration feature extraction of experimental data sets,” *Chaos, Solitons & Fractals*, vol. 78, pp. 61–75, Sep. 2015, doi: 10.1016/j.chaos.2015.06.018.
- [19] Wei Song, “A new deep auto-encoder using multiscale reconstruction errors and weight update correlation,” *Information Sciences*, vol. 559, pp. 130–152, Jun. 2021, doi: 10.1016/j.ins.2021.01.064.
- [20] M. A. Setitra, M. Fan, B. L. Y. Agbley, and Z. E. A. Bensalem, “Optimized MLP-CNN Model to Enhance Detecting DDoS Attacks in SDN Environment,” *Network*, vol. 3, no. 4, Art. no. 4, Dec. 2023, doi: 10.3390/network3040024.
- [21] C. Yin, Y. Zhu, J. Fei, and X. He, “A Deep Learning Approach for Intrusion Detection Using Recurrent Neural Networks,” *IEEE Access*, vol. 5, pp. 21954–21961, 2017, doi: 10.1109/ACCESS.2017.2762418.
- [22] M. Al-Qatf, Y. Lasheng, M. Al-Habib, and K. Al-Sabahi, “Deep Learning Approach Combining Sparse Autoencoder With SVM for Network Intrusion Detection,” *IEEE Access*, vol. 6, pp. 52843–52856, 2018, doi: 10.1109/ACCESS.2018.2869577.
- [23] P. Illy, G. Kaddoum, C. Miranda Moreira, K. Kaur, and S. Garg, “Securing Fog-to-Things Environment Using Intrusion Detection System Based On Ensemble Learning,” in 2019 IEEE Wireless Communications and Networking Conference (WCNC), Apr. 2019, pp. 1–7. doi: 10.1109/WCNC.2019.8885534.
- [24] C. Liang, B. Shanmugam, S. Azam, M. Jonkman, F. D. Boer, and G. Narayansamy, “Intrusion Detection System for Internet of Things based on a Machine Learning approach,” in 2019 International Conference on Vision Towards Emerging Trends in Communication and Networking (ViTECoN), Mar. 2019, pp. 1–6. doi: 10.1109/ViTECoN.2019.8899448.

Basketball Free Throw Posture Analysis and Hit Probability Prediction System Based on Deep Learning

Yuankai Luo¹, Yan Peng², Juan Yang^{3*}

Department of Physical Education, Guangdong Technology College, Zhaoqing, 526100, China¹

Department of Physical Education, North University of China, Taiyuan, 030051, China²

Basic Teaching Department, Shijiazhuang Preschool Teachers College, Shijiazhuang, 050228, China³

Abstract—With the continuous progress of basketball technology and tactics, educators need to adopt new teaching methods to cultivate high-quality athletes who meet the needs of modern basketball development. In basketball teaching, the accuracy of free throw techniques directly affects teaching effectiveness. Therefore, the automated prediction of free throw hits is of great significance for reducing manual labor and improving training efficiency. In order to automatically predict the free throw hits and reduce manual fatigue, the study conducts an in-depth analysis for the criticality of free throw in basketball. In this study, the target detection model of target basketball players is constructed based on YOLOv5 and CBAM, and the basketball free throw hit prediction model is constructed based on the OpenPose algorithm. The main quantitative results showed that the proposed model could accurately recognize the athlete posture in free throw actions and save them as video frames in practical applications. Specifically, when using the free throw keyframe limb angle as features, the model achieved a prediction accuracy of 71% and a recall rate of 86% in internal testing. In external testing, the prediction accuracy was improved to 89% and the recall rate was 77%. In addition, combining the relative position difference and angle characteristics of joint points, the accuracy of internal testing was significantly improved to 80%, and the recall rate was increased to 96%. The accuracy of external testing was improved to 95%, with a recall rate of 75%. The experimental results showed that the various functional modules of the system basically meet the expectations, confirming that the basketball penalty posture analysis and hit probability prediction system based on deep learning can effectively assist basketball teaching and meet the practical teaching application needs. The contribution of the research lies in providing a scientific basketball free throw training tool, which helps coaches and athletes better understand and improve free throw techniques, thereby improving free throw hits accuracy. Meanwhile, this study also provides new theoretical and practical references for the application of deep learning in motor skill analysis and training, which has potential value for updating the basketball education system and reducing teacher workload.

Keywords—Deep learning; CBAM; OpenPose; Free throws; Posture analysis

I. INTRODUCTION

A. Basketball and Technological Progress

As a popular sport around the world, the continuous

improvement of basketball technology and tactics requires increasingly high technical requirements from athletes. The improvement of free throw skills is not only an important part of basketball technical training, but also a reflection of precision and repetition training in physical education.

B. The Application of Deep Learning in Basketball Training

From the perspective of social science, the application of deep learning technology to basketball free throw posture analysis and hit rate prediction demonstrates sports science and technology progress. It is also a concrete application of modern physical education teaching concepts. It advocates a training approach based on the data and science, which helps coaches and teachers shift from traditional empiricism to more quantitative and objective training strategies. It is important for the scientific development of personalized athlete training and physical education [1-2].

C. Challenges and Objectives of Research

Zhao et al. proposed a novel real-time shooting prediction method that combines visual sensors and trajectory learning. Four machine learning algorithms were used for analysis, providing data support for prediction accuracy. However, the computational efficiency or real-time performance of the model was not mentioned. In addition, there were still some shortcomings in combining different features [3]. Scholars such as Oltenu focused on improving basketball free throw skills by setting up experimental and control groups to evaluate the effectiveness of training programs. Three different tests were used to evaluate the training effectiveness of athletes, increasing the comprehensiveness of the research. However, the universal applicability of the research results or how they can be applied to different training environments was not discussed, and the maintenance of free throw skills after training was not evaluated [4].

D. Overview of Research Content and Innovation Points

The innovation of the research lies in developing a deep learning system for analyzing the free throw posture of basketball players and predicting the free throw hits. The core innovation of the system includes: adopting multimodal feature fusion technology, combining limb angle and joint position difference to improve prediction accuracy. YOLOv5 and CBAM modules are integrated to enhance small object detection capabilities. Based on the improved OpenPose

*Corresponding Author.

algorithm, it is possible to accurately capture the posture changes of athletes through trajectory optimization and feature fusion. The SVM classifier is applied to effectively handle small sample learning tasks. In addition, the study comprehensively evaluates the application effect of the system in actual basketball training, ensuring its practicality.

E. Research Expectations

The research is expected to provide basketball players and coaches with a scientific and efficient free throw training tool to help them better understand and improve free throw shooting techniques, so as to improve free throw hits. At the same time, the research will also provide new theoretical and practical references for deep learning in sports skill analysis and training, update the basketball education system, and reduce the teacher workload.

F. Article Structure

The research is divided into four parts. The first part introduces basketball free throw and deep learning algorithm. The second part uses You Only Look Once version 5 (YOLOv5) network and OpenPose to build a basketball free throw posture analysis and hit probability prediction system. The third part tests and analyzes the model performance. The fourth part summarizes the above contents.

II. RELATED WORKS

The OpenPose model is often used to extract and estimate human pose. Therefore, Zhang et al. proposed a novel end-to-end Point-to-Pose Mesh fitting Network (P2P-MeshNet) based on OpenPose 3D joint dataset to estimate body joint rotation. The average position error, percentage of correct keys (PCK), and area under the curve (AUC) of each joint within the calibration threshold were tested using 0-60 mm Proclustes. The estimated error was 11.31 mm, the success rate was 99.7%, and the AUC was 80.9% [5]. Zhu et al. introduced a method to quickly and accurately classify human motion by utilizing skeletal key points as descriptors of motion characteristics. The OpenPose was employed to extract human skeleton point information as the primary features, followed by deep learning techniques for further classification and identification of action features. The results demonstrated that this approach achieved an impressive accuracy of 86.1% in fall detection using publicly available datasets [6]. Kim et al. proposed an OpenPose-based ergonomic posture evaluation system for calculating joint angles and RULA/REBA scores, validating them with reference motion capture systems, as well as comparing performance with Kinect-based systems. The records of 12 experimental tasks completed by 10 participants under different conditions were analyzed. The OpenPose performed well in all task conditions, while the Kinect performed significantly worse than OpenPose in body occlusion or non-frontal tracking [7].

In image recognition, YOLO series has attracted significant attention from researchers. To address the low accuracy and slow speed in traditional coal gangue identification methods, Yan et al. combined YOLOv5 and multispectral imaging technology. Experimental results demonstrated that the YOLOv5.1 model achieved an impressive average detection accuracy of 98.34% for coal

gangue. This method not only accurately identified coal gangue but also provided information about its relative position, making it highly effective for coal gangue identification purposes [8]. Wei Jia et al. proposed a motorcycle helmet detection method using YOLOv5 to detect motorcycle drivers' helmets through video surveillance. It achieved 97.7% mAP, 92.7% F1 score, and 63 frames per second [9]. To improve the performance of robots in classifying lower limb movements, Bingzhu et al. analyzed using different features, including feature signals combining lying and sitting postures. sEMG feature extraction and pattern recognition obtained the trained motion decoder, and then sent control instructions to the robot to drive the lower limbs for corresponding rehabilitation training. The results verified the effectiveness of the control method based on sEMG signal [10]. Researchers such as McDonough D designed a controlled experiment to improve the intervention effect of school dance and physical education models and improve the enjoyment and self-efficacy of urban ethnic minority students. Through experiments, it was found that urban ethnic minority students were happier in the group exercise mode, which was an effective intervention mode for dance sports games [11]. Liu S et al. analyzed the effectiveness of the Small Private Online Course (SPOC) teaching model and conducted experiments using the embryology course as an example. Results showed that SPOC teaching improved students' average professional performance and enhanced students' enthusiasm for learning. This indicated that the SPOC teaching model was scientific and reasonable. It was popularized and applied in medical courses [12].

In summary, previous studies have improved the accuracy of human pose detection. A large number of algorithms are used to optimize datasets and feature extraction. However, there are still few pose analysis and hit probability prediction systems that have high-speed computational efficiency and are suitable for basketball detection. These two have strong potential application value in improving the detection efficiency of basketball games.

III. CONSTRUCTION OF PENALTY ATTITUDE ANALYSIS AND HIT PROBABILITY PREDICTION SYSTEM USING DEEP LEARNING ALGORITHM

In this study, the target detection model of target basketball players based on YOLOv5 and the basketball free throw hit prediction model based on the OpenPose algorithm are constructed. The aim is to improve the accuracy and efficiency of free throw technical analysis, provide a new perspective for the impact of basketball on physical education, and improve the effectiveness of basketball teaching.

A. Construction of Basketball Player Target Detection Model Based on YOLOv5

As an important part of the school physical education curriculum, basketball plays a role in cultivating students' physical fitness, teamwork spirit, and competitive spirit. The scientific analysis of basketball free throw posture can not only improve students' motor skills, but also help physical education teachers to diagnose and correct students' movements more accurately in the teaching. It helps to promote the modernization of basketball education methods.

In addition, as a social and cultural activity, the teaching and training process of basketball also reflects the social and cultural attributes of the educational concept, emphasizing the respect for individual differences and the integration of cultural diversity. Therefore, the application of deep learning technology to basketball free throw teaching can be regarded as a part of educational innovation, which can help improve the teaching quality and educational value of physical education courses. Then, YOLOv5 is selected as the baseline network to construct a target detection model for target basketball players. As the latest generation of fast object detection algorithm, the main advantages of YOLOv5 are its efficient real-time processing capability and excellent detection accuracy. It achieves faster processing speed and higher accuracy through optimized network structure and algorithm innovation. Compared with Faster Region-Convolutional Neural Network (Faster R-CNN), YOLOv5 significantly reduces the computational resource requirement while maintaining high accuracy [13-14]. This makes it excellent in various application scenarios, especially in situations that require fast real-time processing, such as traffic monitoring, human behavior analysis, and industrial automation [15-18]. The YOLOv5 network structure is shown in Fig. 1.

In Fig. 1, YOLOv5 is an efficient real-time object detection system consisting of multiple key modules, aiming to achieve high-precision detection with less computing

resources. The network consists of several main components: an input layer, which preprocesses the image data to standardize the input size, and a backbone, which consists of multiple convolutional layers to extract image features. Backbone network output is connected to the neck network, which includes a Feature Pyramid Network (FPN) and a Path Aggregation Network (PAN) structure, merging feature maps at different scales and detecting small objects. Finally, the Detection Head performs object localization, classification, and confidence prediction based on the feature map. YOLOv5 uses the Anchors strategy to predict the bounding box. Anchors with different scales and sizes are used to improve the objects detection accuracy of various shapes. The entire network is optimized through a loss function, combining classification, localization, and confidence loss to improve detection performance. In the traditional YOLOv5 network, the Generalized Intersection over Union (GIoU) loss function is used to optimize the confidence error calculation of the candidate box. The gradient of the Intersection over Union (IoU) loss is 0 when the two boxes do not overlap, which cannot be optimized. The distance relationship between the two boxes cannot be accurately judged. At the same time, it does not accurately reflect the degree of overlap between frames. Even if the IoU values are the same, the positioning effect may differ. The GIoU loss function is used to better reflect the degree of overlap. The GIoU computation diagram is shown in Fig. 2.

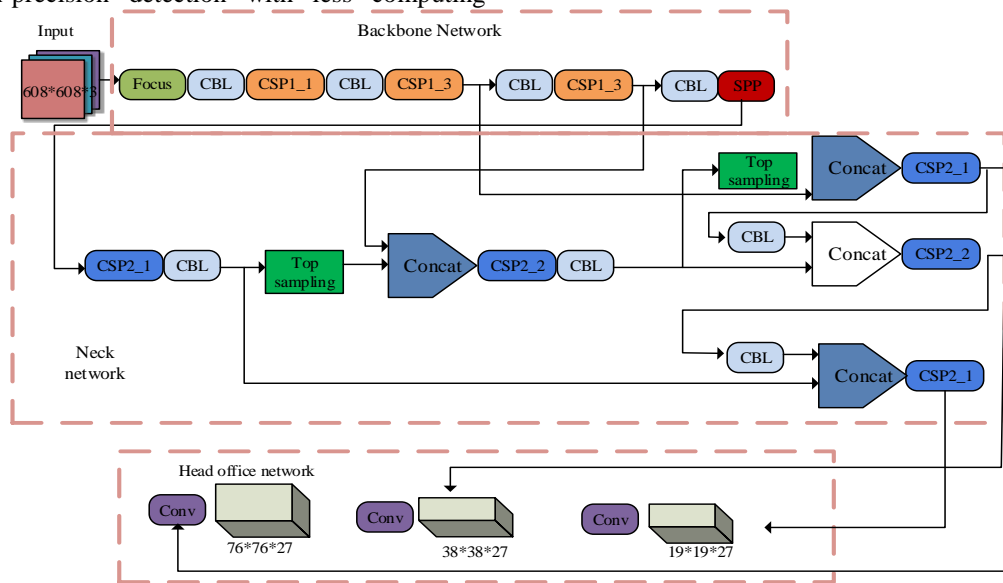


Fig. 1. YOLOv5 network architecture.

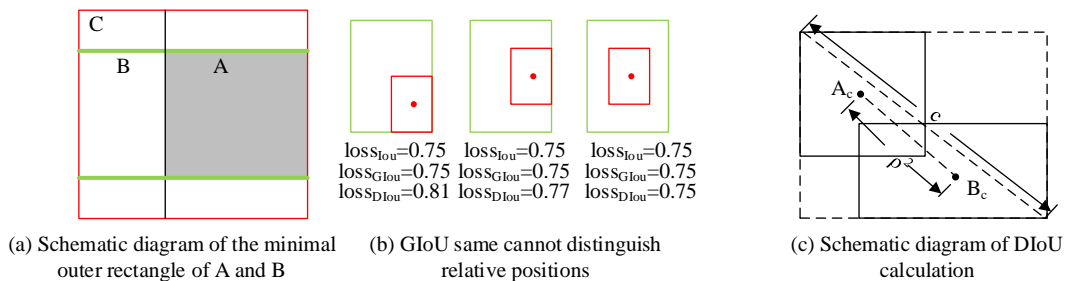


Fig. 2. Schematic diagram of GIoU computation.

As shown in Fig. 2, the minimum circumscribed rectangle is C . The IoU is calculated in Eq. (1).

$$L_{IoU} = 1 - IoU(A, B) \quad (1)$$

In Eq. (1), L_{IoU} represents the IoU loss function. The $IoU(A, B)$ is calculated in equation (2).

$$IoU(A, B) = \frac{A \cap B}{A \cup B} \quad (2)$$

From Eq. (2), it can be seen that when two bounding boxes do not intersect, the IoU is zero. This makes it impossible to measure the relationship between the prediction box and the target box by the IoU loss and hinders the learning process, because there is no gradient for post-back. Therefore, the GIoU loss function is introduced, which adds a penalty term on the basis of IoU. It can effectively solve the gradient disappearance problem when the bounding boxes do not overlap, so as to improve the training efficiency and the accuracy of regression effect.

A penalty term is introduced on the basis of IoU, and GIoU can be obtained, as shown in Eq. (3).

$$L_{GIoU} = 1 - IoU(A, B) + \frac{|C / (A \cup B)|}{|C|} \quad (3)$$

The GIoU loss value ranges from -1 to 1, which can solve the gradient vanishing when the boxes do not intersect. However, it relies too much on the IoU term, which makes it impossible to distinguish the relative position relationship when the real box completely contains the prediction box, and may slow down the convergence. Distance Intersection over Union (DIoU) can solve these problems. The DIoU adds the distance between the center point of the prediction box and the real box on the basis of IoU to improve the positioning accuracy in the object detection task. The DIoU loss function is calculated in Eq. (4).

$$L_{DIoU} = 1 - IoU(A, B) + \frac{\rho^2(A_c, B_c)}{c^2} \quad (4)$$

In Eq. (4), A_c and B_c represent the center point of the prediction frame and the target box. $\rho^2()$ represents the Euclidean distance calculation. c represents the diagonal distance that encloses the minimum area of the prediction frame and the target box, which can provide an optimization scheme for the bounding box and improve the convergence speed when both boxes do not overlap. In view of the small fluctuation in the aspect ratio of the prediction box in the target detection of basketball penalty players, the Complete Intersection over Union (CIoU) loss function is selected to optimize the model. The CIoU loss function utilizes DIoU to increase the aspect ratio factor. Based on the characteristics of basketball free throw player target detection, the guidance of bounding box optimization direction and the convergence speed of distance between center points have been improved. The CIoU is calculated in Eq. (5).

$$L_{CIoU} = 1 - IoU(A, B) + \frac{\rho^2(A_c + B_c)}{C^2} + \alpha v \quad (5)$$

In Eq. (5), α is a weight function. v measures the similarity between the target box and the detection box, as is shown in Eq. (6).

$$v = \frac{4}{\pi^2} (\arctan \frac{w_A}{h_A} - \arctan \frac{w_B}{h_B})^2 \quad (6)$$

In Eq. (6), w_A and w_B represent the width of the two boxes A and B . h_A and h_B represent the height of the two boxes. Then, a lightweight Convolutional Block Attention Module (CBAM) is inserted into the network structure to optimize the object detection accuracy and strengthen the attention to the detected target, thereby reducing the detection accuracy degradation caused by complex environment [19-22]. The structure and optimization of CBAM are shown in Fig. 3.

In Fig. 3, CBAM combines spatial attention and Channel Attention to improve the performance of convolutional neural networks. By mining the feature dependencies between different channels, the channel attention module assigns different importance weights to different channels, so as to enhance the response of the model to the information-rich channels. The spatial attention module focuses on the importance of different spatial locations in the feature map, and highlights the important spatial regions through feature aggregation in the spatial context, so as to further improving the ability to capture key spatial information. CBAM can adaptively assign different attention weights to different parts of the network, thus helping the network better capture and utilize important information about the input features. In this way, CBAM improves the performance of convolutional neural networks on tasks. It is introduced into the Neck structure of YOLOv5s to solve the challenges in small target detection, such as small target, dense target, noisy and background interference. Therefore, CBAM is introduced after each CSP2 module in Neck to enhance attention to small targets.

B. Construction of Basketball Free Throw Hits Prediction Model Based on OpenPose Algorithm

While discussing the free throw posture and hit probability prediction in basketball, the study also considers the importance of basketball in the field of education. Basketball, as a team sport, not only demonstrates the physical fitness and technical level of students, but also embodies teamwork and competitive spirit, which promote communication and cooperation between groups in an educational environment. Through an in-depth analysis of the correlation between basketball free throw posture and shooting rate, this study is committed to optimizing the physical education teaching strategy in colleges and universities. Free throw hit prediction depends on the recognition and detection of human posture. Based on the previously proposed object detection model, the human pose estimation of the target object extracted by the model is carried out. Human pose estimation methods are divided into single and multi-person pose estimation, which are suitable for both image and video scenarios. Key

challenges include occlusion interference, light and environmental changing effects, and identification of different angles and scales. Compared with static images, video analysis can obtain richer dynamic body information. There are two human pose estimation methods: top-down and bottom-up. The former relies on human detection results, and the latter first recognizes joint information and then constructs posture. Based on the OpenPose algorithm, a recognition method using trajectory optimization is proposed, which

combines the angle transformation and feature fusion of limb features. Then the SVM classifier is used to predict the penalty action, and then analyzes the importance of limb features, and puts forward optimization suggestions for the free throw action [23-25]. Firstly, the feature information of the key points of the joint when shooting the target object is extracted by OpenPose. Fig. 4 shows the OpenPose network structure.

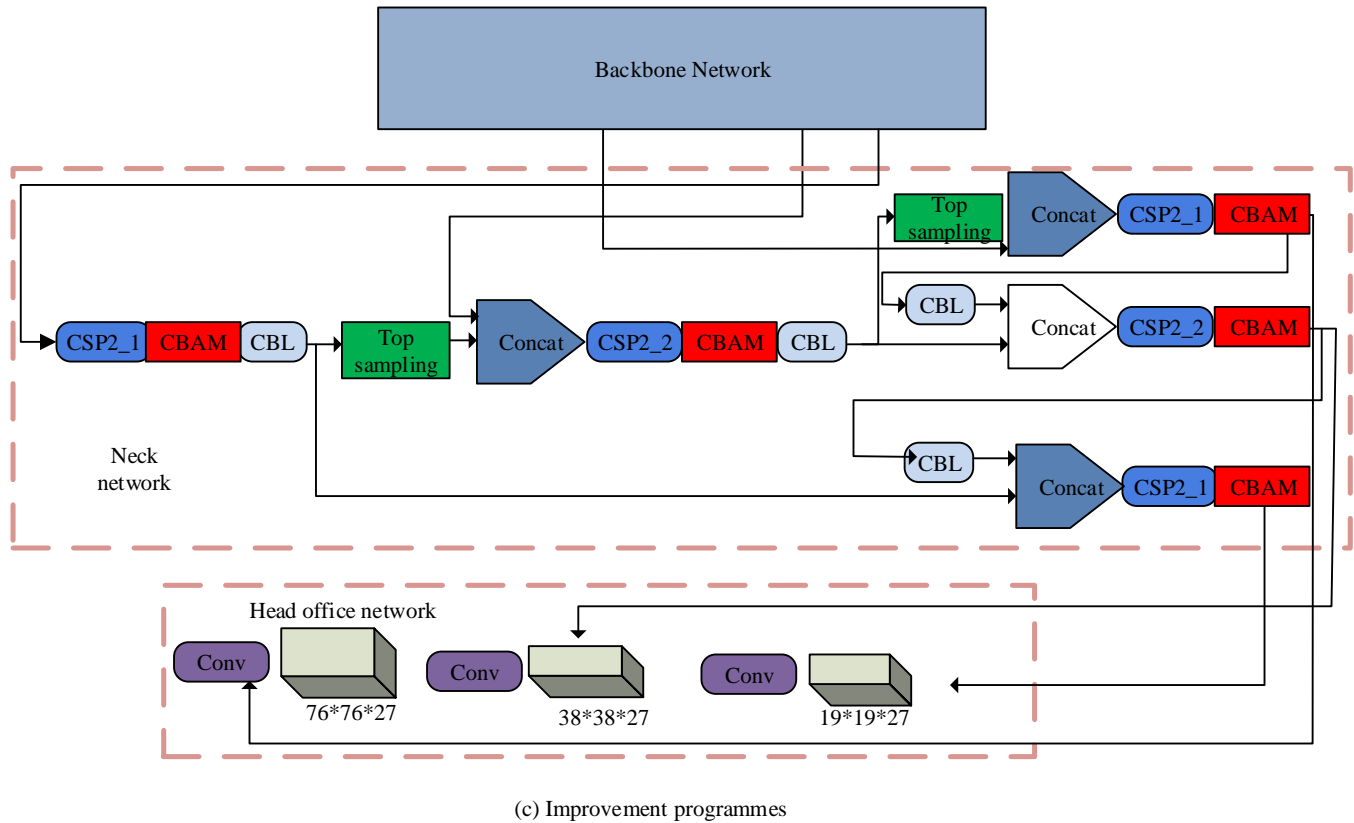
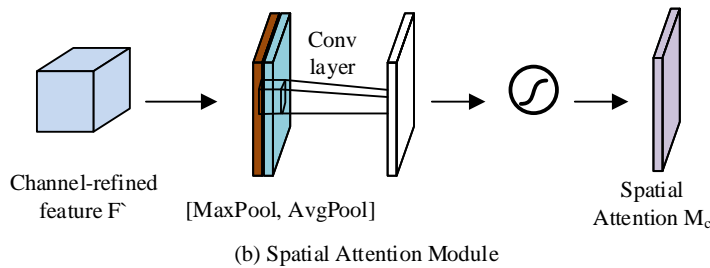
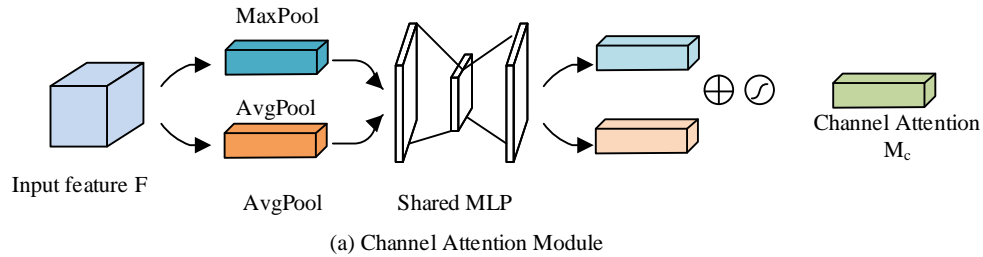


Fig. 3. CBAM structure.

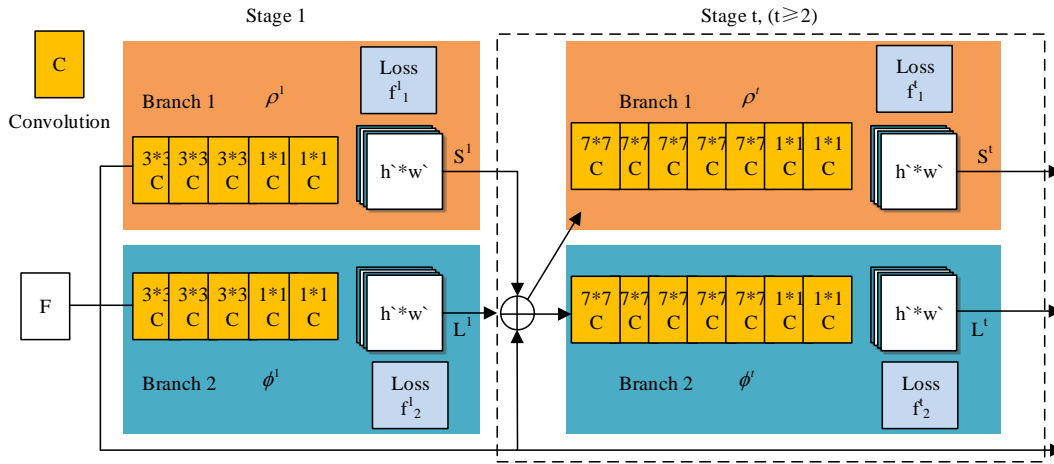


Fig. 4. OpenPose network structure.

The Openpose network includes two main parts. The first part is a convolutional neural network, which is responsible for extracting features and predicting the confidence graph of key points. The second part is Part Affinity Fields (PAFs), which is used to predict the direction of connections between various parts of the body. These two parts are alternated in a multi-stage convolutional network. The prediction results are gradually refined, ensuring the accurate positioning of key points and the correct association of various parts of the body [26-27]. Considering that the human pose estimation method is easy to cause false detection of joint points due to obstacle occlusion in complex background, the wrong joint points identified are repaired to reduce the impact of missed detection and false detection on pose recognition. The poses in adjacent frames of the video are represented by k_1 and k_2 , respectively. k_1^i and k_2^i represent the i -th body part appearing in k_1 and k_2 , respectively. Bounding boxes B_1^i and B_2^i are extracted, respectively. From B_1^i , x_i feature points can be extracted, while B_2^i represents y_i feature points. The calculation for the distance between frames with k_1 and k_2 is shown in Eq. (7).

$$d(k_1, k_2) = \sum_i \frac{y_i}{x_i} \quad (7)$$

Based on the distance calculation in Eq. (7), the target object in the video can be tracked and judged. When the reliability of the body position is lower than th_b , the bounding box B_i of the joint point action is magnified by one time, two times, and three times in turn, and each multiple is tr_1 , tr_2 , tr_3 , respectively. If the threshold is still lower than the threshold, the similarity between the pose of the previous frame and the current pose is calculated, as shown in Eq. (8).

$$Sc_{g,h}^i = \alpha * \sum_i \frac{n_i}{m_i} + (1-\alpha) * \|H_g - H_h\|_2 \quad (8)$$

In Eq. (8), the number of feature points in the bounding box of the i joint point in the g frame is described as m_i . The h frame is described as n_i , when the similarity is greater than th_b , the joint point of the previous frame is selected as the candidate node. Otherwise, the corresponding joint point information in the frame is cleared. In this study, the hit rate is predicted by analyzing the changes in the bending angle of each joint in the body of basketball players when they make free throws. The angles between the thigh and the calf, the upper arm and the lower arm, and the upper arm and the torso are the key features, reducing the error caused by the difference in body shape and improving the prediction stability. The schematic diagram and key points of the joint angle are shown in Fig. 5.

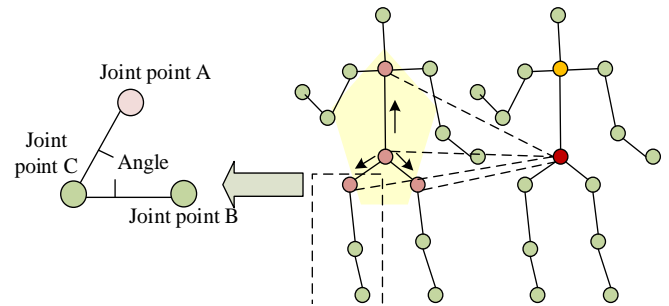


Fig. 5. Schematic diagram of joint pinch angle and key points.

For the analysis of key features, the three key points on the leg are represented as two vectors. The three joint points are connected, and the angle formed at the middle joint point is the angle of the key part. The coordinates of the right wrist, elbow, and shoulder joint points are $R_i(x_0, y_0)$, $R_b(x_1, y_1)$, $R_m(x_2, y_2)$, respectively. The vector representations of the right forearm and right arm are shown in Eq. (9).

$$\begin{cases} l_1 = (x_0 - x_1, y_0 - y_1) \\ l_2 = (x_2 - x_1, y_2 - y_1) \end{cases} \quad (9)$$

From Eq. (9), the angle of the right arm is shown in Eq. (10).

$$\beta = \cos^{-1} \left(\frac{l_1 \cdot l_2}{\|l_1\| \|l_2\|} \right) \quad (10)$$

By converting the absolute position coordinates of basketball players' joint points into angular features, this study focuses on the squat and ascent phases in the free throws. The variation in the leg joint point is used to judge the shooting phase, in which the thigh calf angle decreases to a minimum during a squat and increases to a maximum when rising. At the same time, the characteristics of arm joint points are also considered. Namely, the angle between the large arm and the small arm remain stable in the squat stage, while the angle between the small arm and the torso of the large arm gradually increases with the rise of the arm joint point in the ascending stage. These angular features are used to predict free throw movements and improve the prediction accuracy. Free throw outcome prediction is essentially a categorical problem, divided into two categories: hit or miss. Classification problems are one of the core tasks in machine learning, which aims to find a function to discriminate and classify input data. This involves converting input values into discrete output values, including binary and multi-classification problems. SVM is an effective binary classification model, which is widely used in text classification, action classification and result prediction. Based on a given sample set, it looks for an optimal hyper-plane that can distinguish two categories in the sample space, and transforms the classification task into finding the best interface, so as to achieve accurate classification. The equation for dividing the hyper-plane in the sample space is shown in Eq. (11).

$$\omega^T X + b = 0 \quad (11)$$

In Eq. (11), $X = (x_1, x_2, \dots, x_n)$ represents the input data, that is, the converted limb angle characteristics of the penalty shooter, n represents the dimension. ω represents the normal vector of the hyper-plane, and b represents the offset term. The calculation for the distance from the shooting posture to the super-plane in the data sample is shown in Eq. (12).

$$l = \frac{|\omega^T X + b|}{\|\omega\|} \quad (12)$$

When the free throw is hit, the sample point is located above the super-plane and vice versa below, as shown in Eq. (13) for classification problems.

$$\begin{cases} \omega^T x_i + b \geq 1, y_i = +1 \\ \omega^T x_i + b \leq -1, y_i = -1 \end{cases} \quad (13)$$

The SVM is the points in the sample set that satisfies the above equation and satisfies the equality sign. The distance

from these points to the hyper-plane is the spacing, so the basic model of the SVM is shown in Eq. (14).

$$\begin{cases} \min_{\omega, b} \frac{1}{2} \|\omega\|^2 \\ s.t. y_i (\omega^T x_i + b) \geq +1, i = 1, 2, \dots, n \end{cases} \quad (14)$$

Based on solid mathematical theory, SVM simplifies classification problems, focuses on key sample positioning, and avoids dimensionality problems caused by large sample sizes. The disadvantage is that the training time is longer. Therefore, it is more suitable for small-sample tasks, and the computational complexity increases when the number of key samples increases.

C. Basketball Free Throw Posture Analysis and Hit Probability Prediction System Design

Based on the above model, a free throw probability prediction system in basketball game scenarios is constructed. It aims to provide target detection and pose estimation functions for free throw players in individual enthusiasts and basketball teams, so as to assist in training and improving free throw skills. Users can upload videos of single or multiple free throws. The system will detect the player's position and predict the result of the free throw. The main functional modules include the browser side (video input, historical query, user help), application server (object detection, image information output, information forwarding), GPU server (video processing, result output) and database (storage of body and penalty data). Non-functional requirements emphasize ease of use and scalability to optimize the user experience and adapt to changed data and needs. The system design is simple and intuitive, ensuring easy user operation. The modular design allows for subsequent expansion and adaptation. Fig. 6 shows the overall system logical framework.

In Fig. 6, the free throw prediction system based on B/S architecture designed by the research involves a local environment and a remote GPU server, including a multi-layer structure, and a storage layer connected to the database management system. Various necessary files such as pre-trained models and user information are stored. The front-end and back-end interaction and Ajax asynchronous technology are used to feed back the results, and the GPU server side is responsible for body pose estimation and shooting result prediction. The front-end interaction layer acts as the user interface, which is responsible for receiving video input and presenting the results. The browser module is mainly used to display the prediction results. The interface design is simple, using html and JavaScript, which is divided into three modules: information input, result prediction, and record prediction. The information input module is used to upload videos and player information and save them in the database. The result prediction module processes the video and displays the prediction results. The record prediction module allows the user to manually correct and save the results for subsequent model training. The application server coordinates the work of each module, receives video and information, implements object detection, sends data to the GPU server, obtains the prediction results, and delivers the front-end page and database storage. The entire system

architecture is designed to improve the accuracy of penalty prediction, while ensuring the ease of use of the user interface and the scalability of the system. The database management

system uses MySQL. The data is presented in the form of a table in Table I.

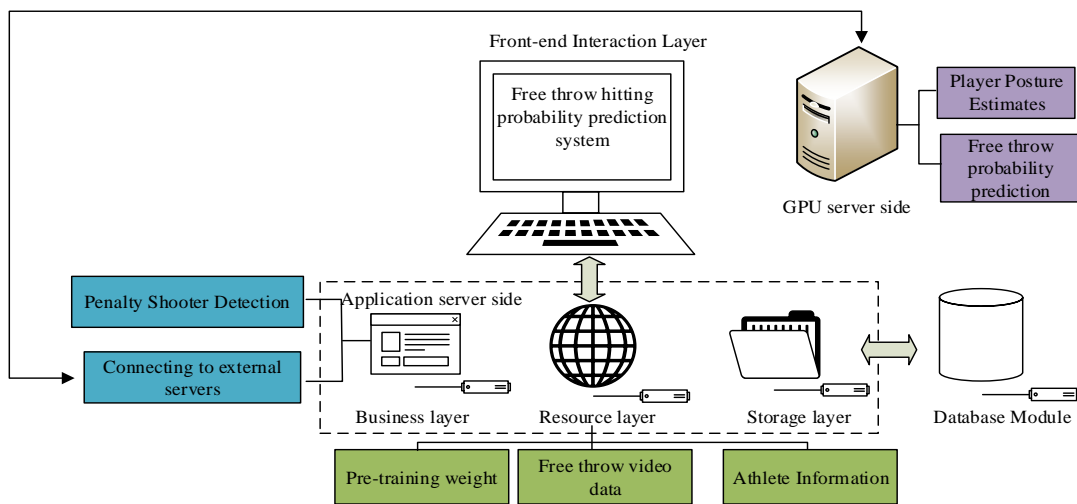


Fig. 6. Overall logical framework of the system.

TABLE I. DATABASE TABLES AND DATA TYPES

| Field name | Data type | Austerity | Clarification |
|----------------|---------------|--------------------------------|--|
| Id | Int | Primary key; self-incrementing | Primary Key ID |
| Name | Varchar(30) | | User name and surname |
| Height | Float | | Height of an athlete (i.e. person's height) |
| Weight | Float | | Athlete weight |
| Text | Var char(100) | | Remarks on information |
| Img | Var char(100) | | Screenshot of the game video |
| Info | Var char(100) | | Human joint position information is saved in JSON format |
| Res_video_path | Var char(100) | | Video after prediction |
| Change_time | Datetime | | Modify Time |

IV. PERFORMANCE TEST OF BASKETBALL FREE THROW ATTITUDE ANALYSIS AND HIT PROBABILITY PREDICTION SYSTEM BASED ON YOLOV5 NETWORK AND OPENPOSE ALGORITHM

The study analyzes the free throw action in basketball game through object detection technology. Various game scene videos are selected, including offline shooting and online collection. In order to enhance the training samples and improve the generalization ability, a data augmentation method is adopted.

A. Performance Test of Target Basketball Player Object Detection model Based on YOLOv5

Through an in-depth analysis of the correlation between basketball free throw stance and shooting rate, this paper is committed to optimizing the teaching strategy of college physical education. This study not only has practical significance for the improvement of sports technology, but also reflects the trend of social science in physical education. It aims to provide students with personalized guidance through data-driven teaching methods, promote the innovation of physical education teaching mode, and improve the quality and efficiency of students' physical education learning. After

constructing the experimental dataset, 80% of the images are selected as the training set, and 20% as the test set. Dataset preparation includes not only image information collection, but also manual annotation of specific objects in the image, including species and location information. According to the format of the VOC dataset, the collected video is first converted into a single-frame picture. Then the players performing the penalty action in the picture are labeled by Labeling software, and the labeling result is saved as an xml format file. These files detail the location of the penalty player in the picture, including the coordinates of the upper left and lower right corners. To adapt to the VOC format, the type information and location information in the xml file are further extracted for the training process. Compared with the 80 categories and 255-dimensional output tensors of the COCO dataset, the object detection in this study focuses on three types: penalty players, ordinary athletes, and spectators. To reduce the computation and improve the detection accuracy and speed, the YOLOv5 classifier is modified to only recognize penalty players. Therefore, the dimensionality of the output tensor is adjusted to $3*(5+1)=18$ to better adapt to the needs of match detection and optimize the model performance. Fig. 7 shows the loss function curve.

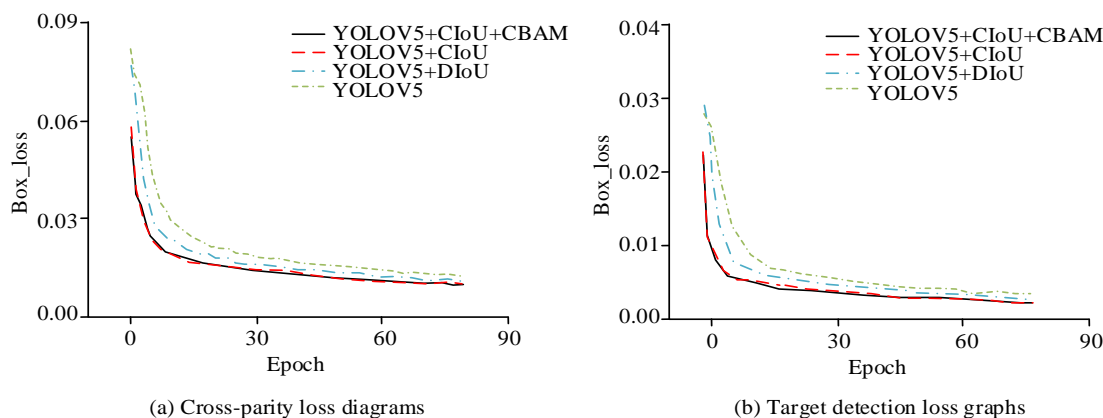


Fig. 7. Loss function curve.

In Fig. 7(a) and Fig. 7(b), the loss function changes of different versions of YOLOv5 algorithm in object detection tasks are presented. *box_loss* corresponds to matching loss between the target and the prediction box, while the *obj_loss* corresponds to object detection loss. Overall comparison showed that YOLOv5 had the lowest loss value when combined with CIoU and CBAM, indicating the effectiveness of the improved method. In both loss functions, this combination consistently maintained a faster downward trend and reached a lower stable value in the later training stages. In the *box_loss*, YOLOv5+CIoU+CBAM decreased rapidly at the beginning and continued to maintain a loss value below 0.02, while the standard YOLOv5 loss was slightly higher. Since only the penalty player category was set in this experiment, and the class loss (*cls_loss*) was 0, the *cls_loss* value was not considered in the analysis. These results show that YOLOv5 combined with CIoU and CBAM can perform more accurate target detection, which has better convergence performance. The experimental average accuracy curve is shown in Fig. 8.

Fig. 8 shows the average accuracy curve of the original YOLOv5 and the model after introducing DIoU, CIoU loss function and attention mechanism. The experiment is conducted with 80 rounds in the same configuration. The observations showed that the models converged rapidly from the 30th round and tended to stabilize after the 60th round. The black curve of CIoU loss function and attention mechanism showed that the improved model outperformed the original YOLOv5 model in terms of average accuracy and recognition. In order to verify the recognition effect, three frames of video are selected for comparison, as shown in Fig. 9.

As shown in Fig. 9, in the first frame, although both models could detect the penalty player, the original model had a low confidence level. The recognition was not ideal, and the target was not detected in the last frame. In contrast, the improved model exhibited high recognition accuracy and stability, which accurately identified the athlete's posture throughout the penalty action and saved it as a video frame.

B. Performance Test of Basketball Free Throw Hit Prediction Model Based on OpenPose Algorithm

In this study, the limb angle and the relative position gap

and angle of the joint point of the key frame in the free throw are combined as feature inputs. The comparison results of accuracy and recall before and after algorithm optimization are shown in Fig. 10.

In Fig. 10, the pre-improvement test results showed that the goal prediction accuracy was 71% inside (in) and 89% outside (out), and the recall rates were 86% and 77%, respectively, when the free throw key frame limb angle was used as the feature. The improved model was characterized by the combination of the relative position gap and the angle of the joint points. The accuracy was significantly improved to 80% internally and 95% externally. The recall rate was also increased to 96% and 75%, respectively. This significant improvement, especially the significant increase in internal recall, shows that the prediction bias caused by different body types of athletes can be effectively reduced by comprehensively considering the relative position gap and angle information of joint points. In addition, the F1-score and accuracy of the improved model also reached 88% and 86% internally, and 84% and 86% externally, respectively, which verified the effectiveness of the feature optimization strategy and demonstrated the efficiency of the model in recognizing basketball free throws. In previous studies, the human pose estimation method was used to extract the relative coordinates of human bone points, and the free throw posture was input into the classifier as a static feature for prediction. The method not repairing the joint points in the shooting process is used as the comparison object, which is named the static input. The ROC curve comparison results are shown in Fig. 11.

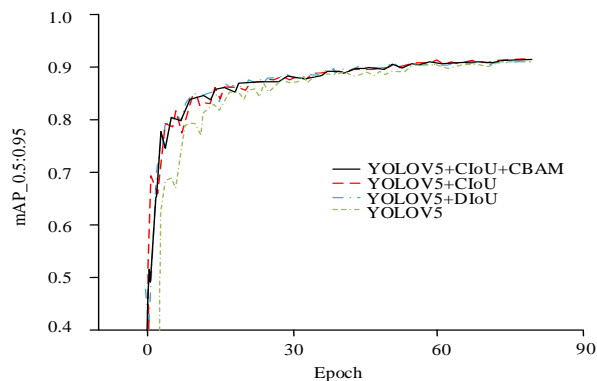


Fig. 8. Experimental average precision curve.

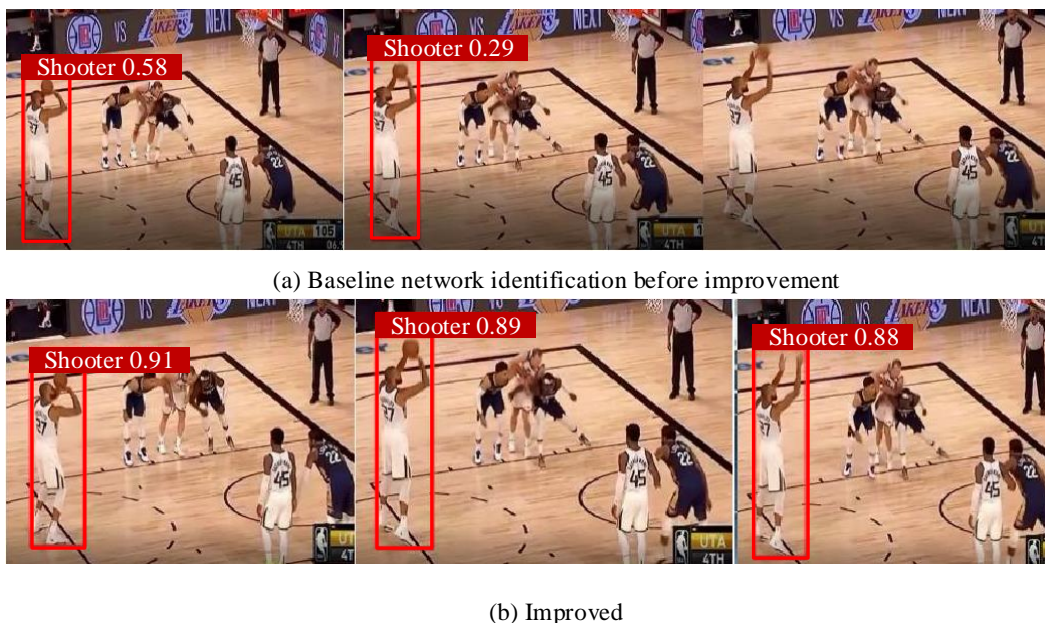


Fig. 9. Detection results visualization.

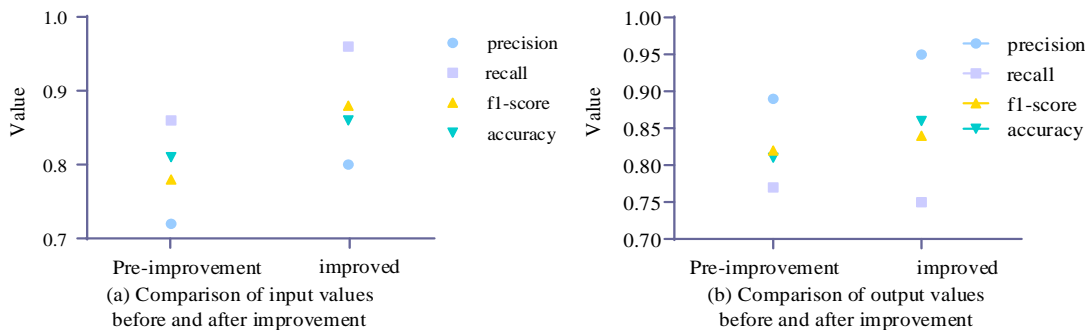


Fig. 10. Comparison of accuracy and recall.

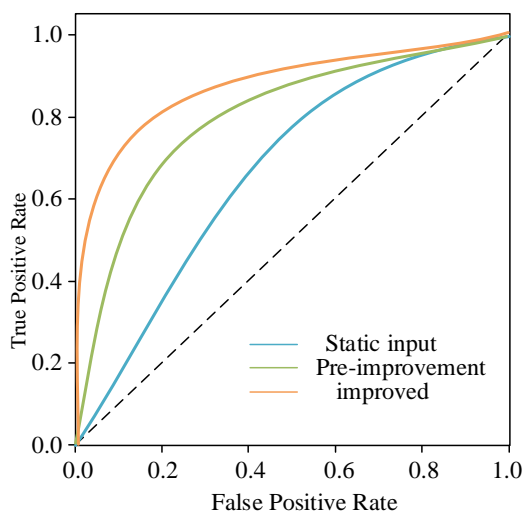


Fig. 11. ROC curve comparison.

Fig. 11 shows a comparison of the Receiver Operational Signature (ROC) curves for the three methods. A curve closer to the upper left indicates better prediction performance. From the figure, the ROC curve of the method combining the

relative position characteristics of joint points and the characteristics of angular change (orange curve) was higher than that of the other two methods, indicating that this method achieved higher value in the True Positive Rate and maintained lower False Positive Rate. Therefore, it is better than the other methods in terms of prediction effect. These results indicate that the proposed method significantly improved the accuracy of free throw prediction. In this study, the key features in the shooting process were studied by observing the influence of different limb angle features on the prediction results of free throws. Table II shows the influence of different features on the prediction results.

The experimental results showed that the angle between the thigh and calf during the free throw, the angle between the shooter's big arm and the angle of the assistive hand had a significant impact on the free throw hit, all of which were more than 6%. In contrast, the calf foot angle and the torso-thigh hip angle had less effect. A successful free throw basket sample showed that the athlete had an angle of about 120 degrees between the thigh and calf when squatting, about 80 degrees between the upper arm and lower arm when shooting, and about 130 degrees between the upper arm and torso after the shot. These three angles were key features to

improve free throw hit and should be taken into account in free throw drills. The corresponding angles of the missed samples are often large or small, suggesting that these critical angles should be normalized during training.

C. Posture Analysis and Hit Probability Prediction System Test

The functional demonstration of the basketball free throw posture analysis and hit probability prediction system using deep learning are shown in Fig. 12.

As shown in Fig. 12, the penalty player detection module shown in Fig. 12(a) allows the user to input information through the interface button in order to identify the player in the uploaded free throw video. The system identified the location of the penalty player, and extracted the video clip with the player as the main body for subsequent attitude evaluation. In addition, the free throw prediction module shown in Fig. 12(b) allows users to predict the shooting results of the free throw team player and record this information. These modules provide users with a complete penalty analysis and training aid. The system is further functionally tested, and the test results are shown.

As shown in Fig. 13, the performance evaluation results of the posture analysis and hit probability prediction system showed that with the continuous operation of the posture analysis and hit probability prediction system, the server CPU usage increased, and the overall trend was upward, but the fluctuation was large. When a new process joined, the CPU usage increased instantaneously, and then dropped to the normal level. The CPU usage was up to 21.7%, and the lowest

CPU usage was at the beginning of the process. The CPU usage was basically kept below 20% during the whole system operation, and the proportion of server resources was within a controllable range. The CPU proportion of the system was similar to the proportion of server resources over time. The proportion of CPU was slightly higher than that of server resources, with the highest CPU proportion of 27.6% in the whole system running time, the lowest CPU usage at the beginning of the process, and the CPU usage basically remaining below 30% during the system running time. Considering the requirements of the posture analysis and hit probability prediction system, the CPU proportion of the system should be controlled below 40%. The test results should be in line with the system design. The response speed test results for video files of different sizes are shown in Fig. 14.

Fig. 14 shows the response speed test results of different sizes of video files. The video file files are set to 5MB, 10MB, and 15MB. As the size of the model file changed, the system response speed also changed, and the system transaction processing efficiency was basically the same. When the video file was 5 MB, the overall Transaction per Second (TPS) changed smoothly and remained at a low level over time, when the video file was 10 MB, the TPS fluctuation was more severe than that when the video file was 5 MB, but it was still flat. When the video file was 15 MB, the TPS fluctuation was larger, but the system still maintained good system stability and had a good user experience while the system processed the video, which met the actual use requirements.

TABLE II. DEGREE OF INFLUENCE OF DIFFERENT FEATURES ON THE PREDICTION RESULTS

| Diagnostic property | Predictive accuracy | Accuracy impact |
|---|---------------------|-----------------|
| Thigh-calf angle | 78% | 8% |
| major arm-torso angle | 81% | 5% |
| The angle between the big and small arms of the shooting hand | 79% | 7% |
| Calf foot pinch angle | 86% | <1% |
| Carapace thigh angle | 83% | 3% |
| Auxiliary hand large arm small arm angle | 80% | 6% |
| Arm acceleration | 86% | <1% |

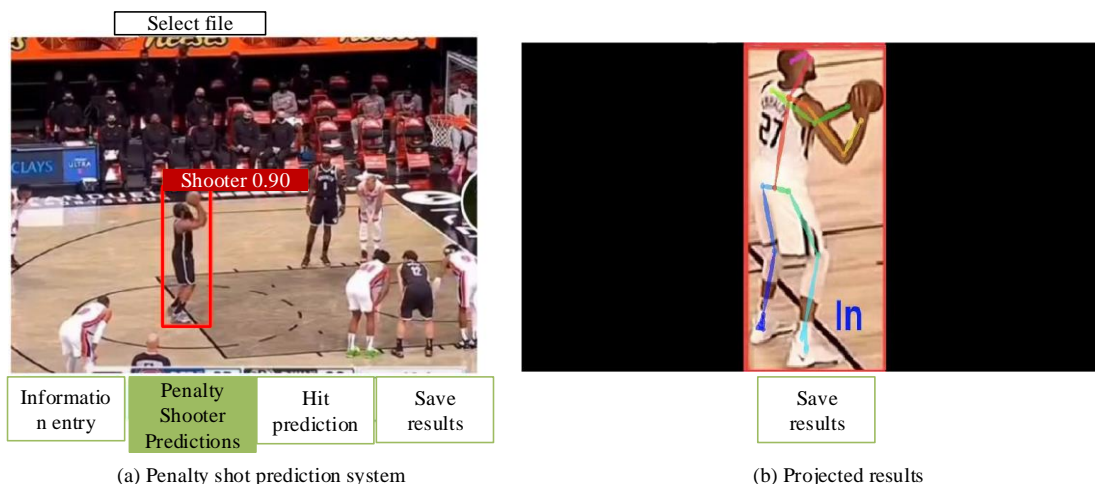


Fig. 12. Functional demonstration of attitude analysis and hit probability prediction system.

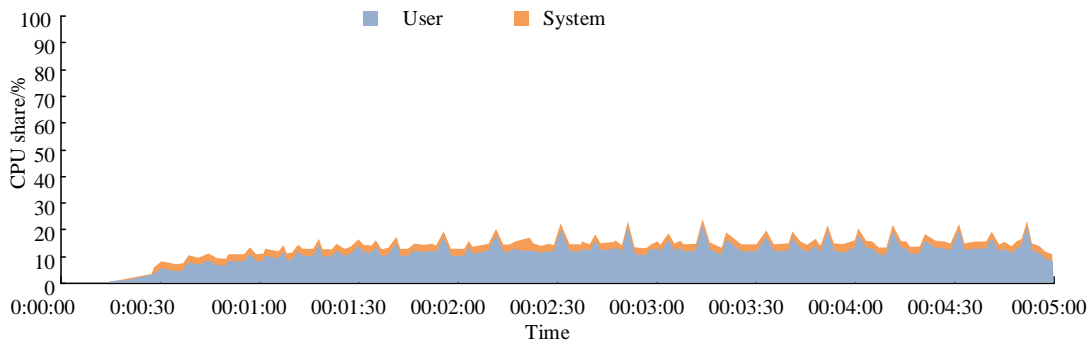


Fig. 13. Performance evaluation results.

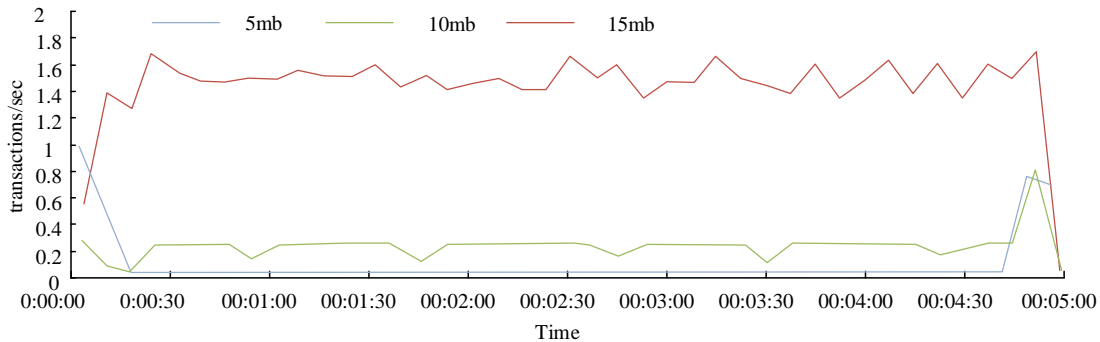


Fig. 14. Response speed test results.

V. CONCLUSION

Basketball education, as popular physical education curriculum content around the world, puts forward comprehensive requirements for students' physical fitness, skills and teamwork ability. The constantly evolving teaching of skills and tactics requires educators to update their teaching methods and cultivate high-quality athletes who can adapt to the development of modern basketball. Free throws are an important scoring method for students in basketball teaching practice. The hitting rate directly affects students' sports scores. In order to automatically predict the probability of free throw hit and reduce manual fatigue, a basketball free throw posture analysis and hit probability prediction system was constructed based on YOLOv5 network and OpenPose algorithm. The performance test results showed that when the free throw key frame limb angle was used as the feature, the goal prediction accuracy was 71% internally and 89% externally. The recall rate was 86% and 77%, respectively. The improved model was characterized by the combination of the relative position gap and the angle of the joint points. The accuracy was significantly improved to 80% internally and 95% externally. The recall rate was also increased to 96% and 75%. Experimental results show that the functional modules of basketball free throw posture analysis and hit probability prediction system basically meet the expectations, which proves that the basketball free throw posture analysis and hit probability prediction system based on deep learning can meet the practical teaching application needs. However, there are still some shortcomings in the research. The application of video human posture estimation in physical education teaching has broad prospects. Although the study has achieved results in the detection, tracking and prediction of free throw

players, the accuracy of identification and prediction in complex scenarios still needs to be improved. The future research directions mainly include expanding training datasets to improve model generalization, especially in complex scenarios, optimizing feature extraction and machine learning algorithms to enhance prediction accuracy, and enhancing the real-time processing capability of the system to ensure its ability to quickly respond to actual competition demands. In addition, the user interface will be improved to enhance the user experience, and potential applications of the system in basketball tactical analysis and athlete performance evaluation will be explored. It also includes conducting long-term tracking tests to evaluate system performance and the long-term impact on athlete training effectiveness, with the ultimate goal of improving the technological support in basketball training and matches.

REFERENCES

- [1] P. Chen, S. Guo, H. Li, X. Wang, G. Cui, C. Jiang, L. Kong. "Through-Wall Human Motion Recognition Based on Transfer Learning and Ensemble Learning," *IEEE Geosci. Remote Sens. Lett.*, pp. 191-196, 2022, DOI: 10.1109/LGRS.2021.3070374.
- [2] B. Wu, J. Zhong, C. Yang. "A Visual-Based Gesture Prediction Framework Applied in Social Robots," *IEEE/CAA J. Autom. Sin.*, vol. 9, no. 3, pp. 510-519, 2022, DOI: 10.1109/JAS.2021.1004243.
- [3] Zhao Y, Zhang X, Yang M, Zhang Q, Li J, Lian C, Bi C, Wang Z, Zhang G. "Shooting Prediction Based on Vision Sensors and Trajectory Learning." *Applied Sciences*, vol. 12, no. 19, Oct. 2022, pp. 10115-10129, DOI: <https://doi.org/10.3390/app121910115>.
- [4] Olteanu M, Oancea B M, Badau D. "Improving Effectiveness of Basketball Free Throws through the Implementation of Technologies in the Technical Training Process." *Applied Sciences*, vol. 13, no. 4, Feb, 2023, pp. 2650-2666, DOI: <https://doi.org/10.3390/app13042650>.
- [5] X. Zhang, Z. Zhou, Y. Han, H. Meng, M. Yang, S. Rajasegarar, "Deep Learning-Based Real-Time 3D Human Pose Estimation," *Eng. Appl.*

- Artif. Intell., vol. 119, no. 10, Oct. 2023, pp. 13-23, DOI: 10.1016/j.engappai.2022.105813.
- [6] N. Zhu, G. Zhao, X. Zhang, Z. Jin, "Falling Motion Detection Algorithm Based on Deep Learning," *IET Image Proc.*, vol. 16, no. 11, Nov. 2022, pp. 2845-2853, DOI: 10.1049/ipr2.12208.
- [7] W. Kim, J. Sung, D. Saakes, C. Huang, S. Xiong, "Ergonomic Postural Assessment Using a New Open-Source Human Pose Estimation Technology (OpenPose)," *Int. J. Ind. Ergon.*, vol. 84, no. 2, Feb. 2021, pp. 13-25, DOI: 10.1016/j.ergon.2021.103164.
- [8] P. Yan, Q. Sun, N. Yin, L. Hua, S. Shang, C. Zhang, "Detection of Coal and Gangue Based on Improved YOLOv5.1 Which Embedded scSE Module*," *Measurement*, vol. 22, no. 3, Mar. 2022, pp. 530-542, DOI: 10.1016/j.measurement.2021.110530.
- [9] J. Wei, S. Xu, Z. Liang, Y. Zhao, H. Min, S. Li, Y. Yu, "Real-Time Automatic Helmet Detection of Motorcyclists in Urban Traffic Using Improved YOLOv5 Detector," *IET Image Proc.*, vol. 15, no. 14, 2021, pp. 3623-3637, DOI: 10.1049/ipr2.12295.
- [10] B. Wang, C. Ou, N. Xie, L. Wang, T. Yu, G. Fan, J. Chu, "Lower limb motion recognition based on surface electromyography signals and its experimental verification on a novel multi-posture lower limb rehabilitation robots," *Comput. Electr. Eng.*, pp. 110-129, 2022, DOI: 10.1016/j.compeleceng.2022.108067.
- [11] D. McDonough, W. Liu, X. Su, Z. Gao, "Small-Groups Versus Full-Class Exergaming on Urban Minority Adolescents' Physical Activity, Enjoyment, and Self-Efficacy," *J. Phys. Act. Health*, vol. 18, no. 2, pp. 192-198, 2021, DOI: 10.1123/jpah.2020-0348.
- [12] S. Liu, Y. Guo, H. Liu, A. Hao, X. Zhang, H. Liu, "Blended learning model via small private online course improves active learning and academic performance of embryology," *Clin. Anat.*, vol. 35, no. 2, pp. 211-221, 2022, DOI: 10.1002/ca.23818.
- [13] M. Barma, U. M. Modibbo, "Multiobjective Mathematical Optimization Model for Municipal Solid Waste Management with Economic Analysis of Reuse/Recycling Recovered Waste Materials," *J. Cogn. Eng. Decis. Mak.*, vol. 1, no. 3, 2022, pp. 122-137, DOI: 10.1061/(ASCE)HZ.2153-5515.0000449.
- [14] M. G. Voskoglou, "A Combined Use of Soft Sets and Grey Numbers in Decision Making," *J. Cogn. Eng. Decis. Mak.*, vol. 2, no. 1, 2023, pp. 2-4, DOI: 10.47852/bonviewjce2022237.
- [15] A. S. Maihulla, I. Yusuf, S. I. Bala, "Reliability and Performance Analysis of a Series-Parallel System Using Gumbel-Hougaard Family Copula," *J. Cogn. Eng. Decis. Mak.*, vol. 1, no. 2, 2022, pp. 74-82, DOI: 10.47852/bonviewJCE2022010101.
- [16] D. Xi, Y. Qin, S. Wang, "YDRSNet: An Integrated Yolov5-Deeplabv3+ Real-Time Segmentation Network for Gear Pitting Measurement," *J. Intell. Manuf.*, vol. 34, no. 4, 2023, pp. 1585-1599, DOI: 10.1007/s10845-021-01876-y.
- [17] Y. Wang, G. Fu, "A Novel Object Recognition Algorithm Based on Improved YOLOv5 Model for Patient Care Robots," *J. Humanoid Rob.*, vol. 19, no. 2, 2022, pp. 54-77, DOI: 10.1142/S0219843622500104.
- [18] Y. Wang, S. M. A. Bashir, M. Khan, Q. Ullah, R. Wang, Y. Song, Z. Guo, Y. Niu, "Remote Sensing Image Super-Resolution and Object Detection: Benchmark and State of the Art," *Expert Syst. Appl.*, vol. 197, Jul. 2022, pp. 93-112, DOI: 10.1016/j.eswa.2022.116793.
- [19] H. Xu, L. Chai, Z. Luo, S. Li, "Stock Movement Prediction via Gated Recurrent Unit Network Based on Reinforcement Learning with Incorporated Attention Mechanisms," *Neurocomputing*, vol. 467, Jan. 7, 2022, pp. 214-228, DOI: 10.1016/j.neucom.2021.11.069.
- [20] L. Lu, H. Di, Y. Lu, L. Zhang, S. Wang, "A Two-Level Attention-Based Interaction Model for Multi-Person Activity Recognition," *Neurocomputing*, vol. 322, Dec. 17, 2018, pp. 195-205, DOI: 10.1016/j.neucom.2018.09.071.
- [21] L. Chen, H. Yao, J. Fu, C. T. Ng, "The Classification and Localization of Crack Using Lightweight Convolutional Neural Network with CBAM," *Eng. Struct.*, vol. 275, Jan. 15, Pt. B, 2023, pp. 91-117, DOI: 10.1016/j.engstruct.2022.115291.
- [22] Q. Lu, W. Ye, L. Yin, "ResDenIncepNet-CBAM with Principal Component Analysis for Wind Turbine Blade Cracking Fault Prediction with Only Short Time Scale SCADA Data," *Measurement*, vol. 212, no. 20, 2023, pp. 96-119, DOI: 10.1016/j.measurement.2023.112696.
- [23] A. Derakhshani, B. Moein, G. Habibagahi, "Identification of Dispersive Soils via Computational Intelligence," *Eur. J. Soil Sci.*, vol. 74, no. 2, 2023, pp. 23-36, DOI: 10.1111/ejss.13346.
- [24] H. V. Thanh, D. V. Binh, S. A. Kantoush, V. Nourani, M. Saber, K.-K. Lee, T. Sumi, "Reconstructing Daily Discharge in a Megadelta Using Machine Learning Techniques," *Water Resour. Res.*, vol. 58, no. 5, 2022, pp. 10-24, DOI: 10.1029/2021WR031048.
- [25] A. J. Gomes de Faria, S. H. Godinho Silva, L. C. Azevedo Melo, R. Andrade, M. Mancini, L. F. Mesquita, A. F. dos Santos Teixeira, L. R. Guimaraes Guilherme, N. Curi, "Soils of the Brazilian Coastal Plains Biome: Prediction of Chemical Attributes via Portable X-Ray Fluorescence (pXRF) Spectrometry and Robust Prediction Models," *Soil Res.*, vol. 58, no. 7, 2020, pp. 683-695, DOI: 10.1071/SR20136.
- [26] W. Kim, J. Sung, S. Xiong, "Walking-in-place for omnidirectional VR locomotion using a single RGB camera," *Virtual Real. -London*, vol. 26, no. 1, pp. 173-186, 2022, DOI: 10.1007/s10055-021-00551-0.
- [27] H. Jiang, S.-B. Tsai, "An Empirical Study on Sports Combination Training Action Recognition Based on SMO Algorithm Optimization Model and Artificial Intelligence," *Math. Probl. Eng.*, vol. 2021, Pt. 31, Article ID 7217383, pp. 83-94, 2021, DOI: 10.1155/2021/7217383.

Enhancing IoT Network Security: ML and Blockchain for Intrusion Detection

N. Sunanda¹, K. Shailaja², Prabhakar Kandukuri³,

Krishnamoorthy⁴, Vuda Sreenivasa Rao⁵, Sanjiv Rao Godla⁶

Assistant Professor, Department of CSE-(CyS,DS) and AI&DS, VNR Vignana Jyothi Institute of Engineering and Technology, Hyderabad, India¹

Associate Professor, Department of CSE, Vasavi College of Engineering, Hyderabad, India²

Professor, Department of Artificial Intelligence and Machine Learning,

Chaitanya Bharathi Institute of Technology - Hyderabad, India³

Associate Professor, Department of CSE, Panimalar Engineering College, Chennai, India⁴

Associate Professor, Department of Computer Science and Engineering, Koneru Lakshmaiah Education Foundation, Vaddeswaram, Andhra Pradesh, India⁵

Professor, Department of CSE (Artificial Intelligence & Machine Learning), Aditya College of Engineering & Technology - Surampalem, Andhra Pradesh, India⁶

Abstract—Given the proliferation of connected devices and the evolving threat landscape, intrusion detection plays a pivotal role in safeguarding IoT networks. However, traditional methodologies struggle to adapt to the dynamic and diverse settings of IoT environments. To address these challenges, this study proposes an innovative framework that leverages machine learning, specifically Red Fox Optimization (RFO) for feature selection, and Attention-based Bidirectional Long Short-Term Memory (Bi-LSTM). Additionally, the integration of blockchain technology is explored to provide immutable and tamper-proof logs of detected intrusions, bolstering the overall security of the system. Previous research has highlighted the limitations of conventional intrusion detection techniques in IoT networks, particularly in accommodating diverse data sources and rapidly evolving attack strategies. The attention mechanism enables the model to concentrate on pertinent features, enhancing the accuracy and efficiency of anomaly and malicious activity detection in IoT traffic. Furthermore, the utilization of RFO for feature selection aims to reduce data dimensionality and enhance the scalability of the intrusion detection system. Moreover, the inclusion of blockchain technology enhances security by ensuring the integrity and immutability of intrusion detection logs. The proposed framework is implemented using Python for machine learning tasks and Solidity for blockchain development. Experimental findings demonstrate the efficacy of the approach, achieving a detection accuracy of approximately 98.9% on real-world IoT datasets. These results underscore the significance of the research in advancing IoT security practices. By amalgamating machine learning, optimization techniques, and blockchain technology, this framework provides a robust and scalable solution for intrusion detection in IoT networks, fostering improved efficiency and security in interconnected environments.

Keywords—Intrusion detection; IoT networks; machine learning; random forest, red fox optimization; blockchain technology

I. INTRODUCTION

The Internet of Things (IoT) represents a transformative innovation in automation and connectivity, comprising a vast network of interconnected devices equipped with actuators, sensors, and computational capabilities [1]. These devices encompass a diverse range, from everyday items like household appliances and wearables to complex industrial machinery and infrastructure components. Central to IoT networks is their autonomous ability to collect, process, and transmit data, eliminating the need for direct human intervention. This autonomy empowers organizations and individuals to leverage data-driven insights and automation across various sectors and industries. For instance, in smart homes, IoT devices facilitate energy monitoring, remote appliance control, and enhanced security via connected surveillance systems [2].

Wearable sensors and medical gadgets help with early health issue diagnosis, individualized treatment strategies, and remote patient monitoring in the healthcare industry. In transportation, IoT technologies optimize logistics, improve traffic management, and enhance passenger safety through intelligent vehicle systems and infrastructure. Moreover, IoT networks extend their reach into diverse sectors such as agriculture, where precision farming techniques leverage sensor data to optimize irrigation, monitor soil conditions, and maximize crop yields[3]. In industrial settings, IoT-enabled machinery and production systems enable predictive maintenance, real-time monitoring of equipment health, and automation of manufacturing processes, leading to increased efficiency and reduced downtime. The overarching goal of IoT networks is to enhance connectivity, efficiency, and convenience while enabling new levels of automation and control across various domains. By seamlessly integrating physical devices with digital technologies, IoT networks pave the way for a more interconnected and intelligent world, where data-driven insights drive decision-making and innovation. However, this proliferation of connected devices

also brings about significant challenges, particularly in terms of security, privacy, and interoperability, which must be addressed to fully realize the potential benefits of the IoT revolution [4].

IoT networks exhibit a high degree of heterogeneity, encompassing a diverse array of devices with varying computational capabilities, communication protocols, and operating systems. From simple sensors to complex smart appliances and industrial machinery, these devices run on different platforms, including embedded systems, Linux-based platforms, and proprietary firmware[5]. This heterogeneity poses challenges for interoperability and standardization. Moreover, IoT networks are highly scalable, capable of supporting deployments ranging from small-scale implementations to massive infrastructures comprising millions of interconnected devices. This scalability leads to complex network topologies and management challenges. Connectivity serves as a cornerstone for IoT networks, with devices employing a range of wired and wireless communication technologies. The selection of connectivity technology is influenced by factors such as range, power consumption, and deployment environment. Additionally, IoT networks generate a wide array of data types, including sensor readings, images, audio, and video streams, presenting challenges for data processing and analysis. Effectively managing this data diversity is essential for deriving meaningful insights while maintaining scalability, efficiency, and data privacy [6].

IoT networks are susceptible to a myriad of security vulnerabilities, posing significant challenges to their integrity and reliability. Weak authentication and authorization mechanisms represent a prevalent threat, as many IoT devices are shipped with default or easily guessable credentials, providing malicious actors with unauthorized access and control over these devices [7]. Furthermore, insecure communication practices exacerbate the risk, as IoT devices often transmit data over unencrypted channels or employ weak encryption protocols, leaving sensitive information vulnerable to eavesdropping and interception by malicious entities. Compounding these issues is the lack of timely security updates from manufacturers, leaving devices exposed to known vulnerabilities and exploits. Physical vulnerabilities also pose a substantial risk to IoT networks, as attackers can exploit physical access to tamper with hardware components, extract sensitive data, or implant malicious firmware, compromising the integrity and functionality of these devices [8].

Additionally, IoT devices are susceptible to being co-opted into botnets and used to launch distributed denial-of-service (DoS) attacks against targeted services or networks, leading to disruptions and downtime. Moreover, the vast amounts of personal and sensitive data collected and transmitted by IoT devices raise significant privacy concerns, including unauthorized access, data breaches, and misuse of information. Supply chain risks further exacerbate the security landscape, as the global supply chain for IoT devices is often complex and opaque, making it challenging to verify the integrity and authenticity of hardware components and software firmware [9]. Lastly, interoperability issues between

IoT devices and protocols introduce additional vulnerabilities, enabling attackers to exploit weaknesses in communication interfaces and protocols, potentially compromising the entire network. A comprehensive strategy that includes strong authentication procedures, encryption methods, regular security upgrades, physical security measures, and privacy-enhancing technology is needed to address these issues. In addition, stakeholders need to work together to create industry-wide guidelines and recommendations for protecting IoT networks and devices, minimizing risks, and guaranteeing the dependability and trustworthiness of the IoT ecosystems [10].

Intrusion detection in IoT networks is hindered by the dynamic and heterogeneous nature of these environments, along with the continuously evolving threat landscape. Traditional methods struggle to adapt to the diverse array of devices, communication protocols, and data formats present in IoT networks, leading to limited coverage and effectiveness. Scalability poses another challenge, as the sheer volume of interconnected devices generates large amounts of data that traditional systems may struggle to process in real-time. Resource constraints on IoT devices further complicate matters, making it difficult to deploy traditional intrusion detection solutions. Furthermore, newer or undiscovered threats could not be detected by conventional techniques, calling for more sophisticated detection capabilities. Moreover, worries about data privacy and integrity continue since centralized systems have the potential to expose vulnerabilities or corrupt critical data. Innovative solutions that are suited to the special features of internet of things networks are needed to tackle these issues. These solutions must be scalable, resource-efficient, capable of robust detection, and equipped with improved security mechanisms to efficiently reduce hazards [11].

The rapid expansion of Internet of Things (IoT) networks has underscored the critical need for a robust and scalable intrusion detection framework capable of effectively mitigating security threats. Traditional intrusion detection systems (IDS) often struggle to adapt to the dynamic and heterogeneous nature of IoT environments, necessitating innovative solutions. Our research is motivated by the imperative to develop such a framework, leveraging advanced machine learning techniques like Attention-based Bidirectional Long Short-Term Memory (BiLSTM) networks for real-time threat detection. Additionally, the integration of Red Fox Optimization (RFO) enhances the efficiency of feature selection, enabling more accurate identification of relevant data amidst the complexities of IoT networks. Furthermore, the incorporation of blockchain technology ensures the integrity and trustworthiness of intrusion detection data, facilitating transparent incident response and forensic analysis. By synergizing these technologies, our framework offers a comprehensive defense mechanism against evolving threats, safeguarding critical assets and bolstering the security posture of IoT ecosystems. The key contribution of the research is stated as follows:

- The research presents a pioneering framework that combines machine learning techniques, such as Attention-based BiLSTM networks, with Red Fox

Optimization for feature selection, providing a novel approach to intrusion detection in IoT networks.

- By leveraging advanced machine learning algorithms, our framework achieves a significantly higher detection accuracy of approximately 98%, surpassing traditional intrusion detection systems and effectively mitigating security threats in IoT environments.
- The integration of Red Fox Optimization streamlines feature selection, enhancing the scalability and efficiency of our framework in handling the dynamic and heterogeneous nature of IoT data streams, thus ensuring robust performance even in large-scale IoT deployments.
- Incorporating blockchain technology ensures the integrity and tamper-resistance of intrusion detection data, providing transparent incident response and forensic analysis capabilities, thereby enhancing the overall security and trustworthiness of IoT networks.

The paper begins with an introduction to the research topic in Section I, followed by a comprehensive review of related literature in Section II. The methodology in Section IV outlines the proposed framework's design and implementation, with Section V covering experimental evaluation, results analysis, and discussion on the framework's effectiveness. Finally, Section VI concludes the paper.

II. RELATED WORKS

Strong security mechanisms inside IoT networks are vital, as evidenced by the increasing ubiquity of Internet of Things (IoT) technologies. But in Internet of Things contexts, conventional intrusion detection systems face severe restrictions because of limited resources and the intrinsic complexity of the network. Liang et al. [12] research aims to tackle these issues by developing, putting into practice, and assessing a novel intrusion detection system. This system makes use of deep learning algorithms, blockchain technology, and multi-agent systems as part of a hybrid placement strategy. The data collecting, management, analysis, and reaction components of the system are organised into separate modules. The National Security Lab's NSL-KDD dataset was used for experimental verification, which demonstrates how well deep learning algorithms detect assaults, especially at the IoT network's transport layer. Notwithstanding the encouraging outcomes, the study admits significant limitations, such as the requirement for additional improvement and optimisation of the suggested system in order to guarantee its scalability and suitability for use in a variety of IoT scenarios.

Alkadi et al. [13] paper presents a novel approach to collaborative intrusion detection for safeguarding IoT and cloud networks, leveraging the capabilities of deep blockchain technology. By integrating blockchain into intrusion detection systems, the proposed framework aims to enhance the security posture of interconnected environments through collaborative threat intelligence sharing and consensus-driven decision-making processes. Through the utilization of machine learning algorithms and distributed ledger technology, the framework

enables real-time detection and response to emerging threats across diverse network landscapes. Experimental results demonstrate the efficacy of the framework in detecting intrusions and mitigating security risks in various network scenarios. However, the adoption of deep blockchain technology introduces challenges related to scalability, latency, and resource consumption. The computational overhead associated with maintaining a distributed ledger across multiple nodes may impact the real-time responsiveness of the intrusion detection system. Furthermore, ensuring consensus among distributed nodes in a timely manner can pose synchronization and coordination challenges, potentially affecting the system's overall efficiency and effectiveness in rapidly evolving threat landscapes. Addressing these scalability and performance limitations is essential to realize the full potential of the proposed framework in large-scale IoT and cloud networks.

The necessity for strong security measures to protect Internet-of-things (IoT) environments from potential threats has been highlighted by the growth of IoT devices. In order to protect computer networks, including the Internet of Things, from many types of security breaches, intrusion detection systems, or IDSs, are essential. The utilisation of collaborative intrusion detection systems or networks, also known as CIDSs or CIDNs, has shown promise in improving detection performance through the sharing of vital information across IDS nodes, including signatures and alarms. Nevertheless, because collaborative networks are distributed, they are vulnerable to insider assaults, in which rogue nodes spread fake signatures, jeopardising the accuracy and effectiveness of intrusion detection systems. Using blockchain technology presents a viable way to safely validate shared signatures. In this regard, the research of Li et al. (Li et al. 2019) presents CBSigIDS, an innovative framework for blockchain-based collaborative signature-based IDSs intended to create and gradually update a trusted signature database in collaborative IoT contexts. With no need for a reliable middleman, CBSigIDS provides a verified method in distributed architectures. Although CBSigIDS shows promise in strengthening the efficiency and robustness of signature-based IDSs, a significant disadvantage is the possible overhead related to blockchain activities, which calls for additional optimisation to guarantee scalability and efficacy in practical deployments.

Issues with privacy, security, and single points of failure in centralised storage structures still exist as the Internet of Things (IoT) gains pace, especially in crucial applications. By providing decentralised and secure data management, blockchain technology has emerged as a viable answer to these problems. There is a lot of potential for improving social and economic advantages when blockchain is integrated with IoT. But as the 2017 attack on a pool of miners has shown, blockchain-enabled Internet of Things (IoT) networks are vulnerable to Distributed Denial of Service (DDoS) attacks, underscoring the necessity of strong security protocols. Furthermore, for efficient analysis and decision-making, these applications' enormous data generation demands the use of sophisticated analytical tools like machine learning (ML). In order to address these issues, a unique solution is presented in

the paper by Kumar et al. [14]. This paper presents a distributed Intrusion Detection System (IDS) intended to detect distributed denial of service (DDoS) assaults targeting mining pools within Internet of Things networks, using fog computing and blockchain technology. Using Random Forest (RF) and an optimised gradient tree boosting system (XGBoost), both trained on dispersed fog nodes, the efficacy of the suggested IDS is evaluated. The BoT-IoT dataset, which covers recent assaults seen in IoT networks with blockchain support, is used in the evaluation. The possible costs and difficulties of implementing a distributed IDS employing fog computing in practical settings might be a drawback of the recommended strategy, necessitating more study and optimisation for efficiency and scalability. However, the outcomes demonstrate that Random Forest outperforms XGBoost in multi-attack recognition and binary attack detection.

Protecting industrial IoT (IIoT) networks from security threats is crucial as these networks grow to be essential parts of vital infrastructure. Numerous strategies utilizing Blockchain algorithms and machine learning techniques have been investigated separately to overcome this problem. However, Vargas et al. [15] offer an integrated strategy in this research that integrates these approaches to produce a thorough defense mechanism for networks of Internet of Things devices. The objectives of this mechanism are to identify potential dangers, initiate safe channels for information exchange, and adjust to the processing power of industrial Internet of things settings. The suggested method offers a workable way to identify and stop intrusions in Internet of Things networks and shows effectiveness in accomplishing its goals. Despite its achievements, it's crucial to remember that the suggested integrated strategy can present challenges for management and implementation, necessitating the need for extra funding and knowledge for deployment in actual IIoT scenarios. More investigation is required to ensure scalability and efficiency while minimizing overhead by streamlining and optimizing the integration process.

III. PROBLEM STATEMENT

Despite the notable advancements in intrusion detection systems (IDS) and the integration of blockchain technology and machine learning techniques in securing Internet of Things (IoT) networks, several research gaps persist. Existing studies focus predominantly on individual aspects such as deep learning algorithms, blockchain-based intrusion detection, or collaborative signature-based IDSs. However, there is a scarcity of research that comprehensively addresses the complex security challenges of IoT environments by integrating multiple technologies and methodologies. Furthermore, scalability, efficiency, and practical feasibility remain critical concerns across these studies, indicating the need for further exploration and refinement. Thus, our research aims to bridge this gap by proposing a holistic framework that combines deep learning algorithms, blockchain technology, and collaborative intrusion detection

mechanisms to provide robust security solutions for IoT networks. By addressing these multifaceted challenges and evaluating the proposed framework's scalability and effectiveness across diverse IoT scenarios, our research endeavors to contribute towards the development of comprehensive and practical security solutions tailored for IoT environments.

IV. METHODOLOGICAL INTEGRATION OF ML AND BLOCKCHAIN FOR IOT INTRUSION DETECTION

The suggested method builds a strong intrusion detection system (IDS) that is suited for the complex architecture of Internet of Things networks by fusing blockchain technology with machine learning. Network traffic, sensor readings, device logs, and other data from IoT devices are first gathered and preprocessed to extract pertinent attributes that are essential for intrusion detection. The framework optimizes feature subsets to increase intrusion detection efficacy and efficiency using the Red Fox Optimization (RFO) approach. Then, real-time anomaly detection is achieved by using Attention (BiLSTM) networks, which take advantage of their capacity to process sequential data streams present in Internet of Things settings. Blockchain technology is easily incorporated to guarantee the immutability and integrity of intrusion detection data. Smart contracts are utilized to provide safe communication and consensus building across dispersed Internet of Things devices, guaranteeing the accuracy and consistency of the data. Benchmark datasets such as the NSL-KDD dataset are used to evaluate the framework's performance in detail across a range of intrusion situations. By employing this technique, researchers want to enhance the efficacy and security of intrusion detection in internet of things networks, as well as tackle the constantly evolving problems associated with IoT setups [16]. The suggested technique's architecture is depicted in Fig. 1.

A. Data Collection

The data collection process involves gathering information from IoT devices, drawing upon a diverse array of network traffic, sensor readings, and device logs. In this research, we utilize the NSL-KDD dataset, an open-source resource available on Kaggle [17], to facilitate the collection of comprehensive data for intrusion detection system development. The NSL-KDD dataset offers a rich repository of labeled network traffic data, encompassing various types of attacks and normal behaviors, thereby enabling thorough analysis and evaluation of intrusion detection algorithms. Leveraging this openly accessible dataset ensures transparency and reproducibility in our research methodology, allowing for robust validation and benchmarking of the proposed intrusion detection framework against a standardized dataset. Through meticulous data collection from the NSL-KDD dataset, we aim to capture the diverse range of potential threats and normal activities prevalent in IoT networks, laying the foundation for effective intrusion detection system design and evaluation.

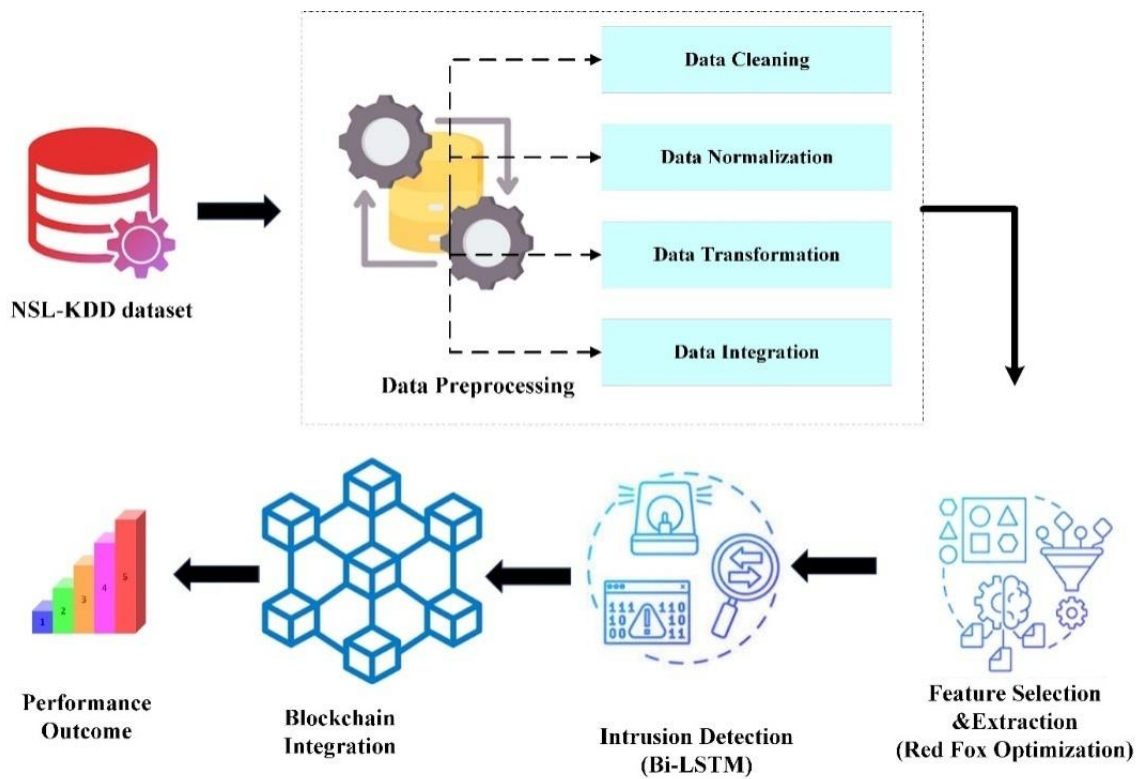


Fig. 1. Proposed integration of ML and blockchain for IoT intrusion detection.

B. Data Preprocessing

Following data collection, the input data undergoes preprocessing to eliminate unwanted noise and address missing data. This involves four key preprocessing approaches:

- Data Cleaning
- Normalization
- Data Transformation
- Data Integration

C. Data Cleaning

In order to improve the quality and dependability of datasets, data cleaning is an essential step in the data preparation pipeline. It involves locating and correcting different kinds of data abnormalities. These anomalies may include corrupted, incorrect, duplicate, or improperly formatted data entries. The primary goal of data cleaning is to ensure that datasets are standardized, accurate, and easily accessible for analysis and query purposes. During the data cleaning process, several tasks are performed to address different types of data issues. Firstly, corrupted or incorrect data entries are identified and either removed or corrected to restore data integrity. Duplicate entries, if present, are identified and eliminated to prevent redundancy and ensure that each observation is unique[18]. Additionally, managing missing values—which can occur for a number of reasons, including incomplete records or mistakes in data collection—is another aspect of data cleansing. When there are missing values in an observation, they can be imputed using statistical

techniques or data from other observations can be dropped. Additionally, data cleaning ensures that the dataset complies with the required format and schema by addressing structural flaws that could arise throughout the data transfer process. Thorough data cleaning improves the dataset's dependability and suitability for analysis, allowing analysts and researchers to derive precise conclusions and make defensible choices [19].

D. Normalization

Normalization is a preprocessing step aimed at transforming data from its existing range to a new range. Given the presence of uncertain and incomplete data in the dataset, it becomes essential to address missing or irrelevant data to enhance data quality. The dataset can be integrated and normalized with success using the Min Max normalization approach. By making sure the dataset is scaled correctly, this method makes it possible to anticipate outcomes within the new range and allow for a greater difference in forecasting. Normalization reduces the influence of differences in dataset scales by scaling the dataset so that normalized values lie between 0 and 1. This allows for easier comparison of results from various datasets. This technique involves deducting the minimum value from the variable requiring normalization, resulting in a standardized dataset suitable for analysis and comparison. Min-max scaling, frequently referred to as feature scaling, converts the values of each feature to a range of 0 to 1 [20]. To compute the min-max scaling, use Eq. (1).

$$A_{scaled} = \frac{A - A_{min}}{A_{max} - A_{min}} \quad (1)$$

A is the starting value, A_{min} is the smallest value, and A_{max} is the largest value in the dataset. This method is helpful when the features are not evenly distributed and have a small range.

E. Data Transformation

Data transformation involves converting the original dataset into a specific format that facilitates faster and more efficient retrieval of strategic insights. Raw datasets can be challenging to comprehend and track, necessitating transformation into a more suitable form before extracting information. This transformation process is crucial for providing easily interpretable patterns, aligning with the strategic objectives of data conversion. Various techniques, such as smoothing, aggregation, and generalization, are employed in data transformation to streamline the dataset. Smoothing techniques are utilized to eliminate noise from the dataset, enhancing data clarity. Data aggregation gathers and presents data in a summarized format, aiding in easier analysis and interpretation. Additionally, data generalization involves converting lower-level or raw data into higher-level data through hierarchical concepts, further enhancing the dataset's organizational structure and usability [21].

F. Data Integration

Data integration is a preprocessing strategy that combines data from several sources into a single data repository to give rich views of the data. These sources could be flat files, databases, or several data cubes. Collaboration between users at all levels is facilitated by data integration, which combines received data with heterogeneous datasets to store consistent data that is client-accessible. A triplet defines the data integration mechanism, which is further explained in Eq. (2).

$$D_1 = \langle U, V, W \rangle \quad (2)$$

In this context, D_1 represents the process of data integration, where U stands for the global schema, V denotes the schema of heterogeneous sources, and W refers to the mappings between queries of the source and global schema [22].

G. Feature Selection

In order to improve the effectiveness and productivity of the intrusion detection process, feature selection is an essential step in the preliminary processing phase of systems for detection. Its goal is to pick the most pertinent characteristics from the pre-processed data. Red Fox Optimisation (RFO) becomes apparent as a potent feature selection method in this scenario. To increase the intrusion detection system's overall performance, RFO works by optimising feature subsets. Finding a subset of characteristics that maximises the discrimination between normal and aberrant network behaviour is the main goal of feature selection using RFO. This will improve the system's capacity to detect intrusions effectively while reducing computing overhead. RFO does this by iteratively assessing and honing potential feature subsets according to pre-established optimisation standards, including performance metrics or classification accuracy. The intrusion detection system may efficiently prioritise and concentrate on the most useful aspects by using RFO for feature selection. This lowers the dimensionality of the data and boosts the

overall effectiveness of the detection process. Additionally, RFO has the flexibility and scalability to manage high-dimensional information that are frequently seen in Internet of Things networks [23].

After obtaining the balanced dataset from the previous stage, the optimal features for improving intrusion detection training speed and accuracy are selected using the DRF optimisation technique. Numerous meta-heuristic optimisation strategies are developed to improve network security in standard systems for detection of intrusions. Three newly created models used for network security are Spider Monkey Optimisation, Fruity Optimisation, and Greedy Swarm Optimisation. However, overfitting, which delayed processing, a slower rate of convergence, and complex computational procedures are the main causes of its issues. Generally speaking, some of the most current nature-inspired/bio-inspired optimisation approaches produced is the Dragon Fly Algorithm, Moth Flame Optimisation, and Ant Lion Optimisation, Harris Hawk optimisation (HHO), Flower Pollination Algorithm. These algorithms are commonly used to solve complex optimisation problems in a variety of security applications. The DRF is one of the newest optimisation algorithms and has several advantages over previous techniques. It has a low processing cost, less local optimum, rapid convergence, and guards against algorithm stacking during optimisation. Furthermore, the DRF35 is not specifically utilised in applications for IoT-IDS security. Therefore, the goal of the proposed study is to use this method to dataset feature optimisation based on the best optimum solution. Additionally, this optimisation procedure facilitates a simpler classification method with a higher assault detection rate [23].

The balanced IoT dataset's characteristics may be optimally tuned using this optimization approach. Foxes belong to many Canidae families and are tiny to medium-sized omnivore animals with pointed noses, long, thin legs, thick tails, and slender limbs. The foxes may also be distinguished from each other of their family and from large dogs. A novel meta-heuristic optimization system called the DRF takes its cues from the hunting habits of red foxes. When hunting, the red fox moves slowly towards its prey as it hides in the underbrush, and then it attacks the animal out of the blue. Like previous meta-heuristic models, this approach takes into account both the utilization and investigation of capabilities. This method creates random people for initializing parameters, as seen by the subsequent Eq. (3) and Eq. (4).

$$R = [r_0, r_1, \dots, r_{n-1}] \quad (3)$$

$$(R)^i = [(r_0)^i, (r_1)^i, \dots, (r_{n-1})^i] \quad (4)$$

where, "I" denotes how many populations are present in the search area. Ten, the global optimal function is used to find the best solution in the search space. Here, the structure that follows is used in conjunction with the Euclidean distance to get the best solution as presented in Eq. (5).

$$E(((R)^i)^k, (R_{best})^k) = \sqrt{(R^i)^k - (R_{best})^k} \quad (5)$$

In Eq. (5) k denotes the number of iterations. The term " R_{best}^t " represents the best optimum, while " $E(.)$ " denotes the Euclidean distance. Accordingly, the optimal solution is employed to migrate all candidates, as illustrated in Eq. (6):

$$((R)^i)^k = ((R)^i)^{k-1} + g_{sigm}((R_{best})^k - (R^i)^k) \quad (6)$$

As a scaling hyperparameter, " g " denotes a random value selected at random from 0 to 1 for each iteration. For the whole population, this value is set just once every iteration. People evaluate the fitness values at their new places after moving to the optimal posture. People stay in their new roles if the fitness values are greater; if not, they return to their previous ones. This procedure is similar to how close relatives tell others where to hunt after an adventure and return home. They do what the explorers have instructed, going home "empty-handed" if they don't locate food, or continuing to search if there is a possibility. These processes, which take place during every DRF cycle, resemble suggested global inquiries. In addition, the applicants' move to new roles must present a feasible alternative; if not, their previous jobs will remain. The comparison of the red fox, advancing towards its prey and watches it, is appropriate here since it is similar to the DRF model in which a random number ω between 0 and 1 is assumed explained in Eq. (7) and Eq. (8) [24].

$$\begin{cases} \text{Move Forward if, } \omega > \frac{3}{4} \\ \text{Stay Hidden if, } \omega > 3/4 \end{cases} \quad (7)$$

$$\omega = \begin{cases} h \times \frac{\sin(\delta_0)}{\delta_0} & \text{if } \delta_0 \neq 0 \\ \tau & \text{if } \delta_0 = 0 \end{cases} \quad (8)$$

Here, " h " is a random number in the interval $[0, 0.2]$, and " δ_0 " is another random number in the interval $[0, 2\pi]$, which indicates the fox viewing angle. Furthermore, " τ " represents a random number between 0 and 1. To model motions for the population of persons, the set of solutions for geographic coordinates is as follows. All things considered, the incorporation of RFO for picking features in intrusion detection systems improves computing efficiency and scalability while also strengthening the system's capacity to precisely detect and address security threats in Internet of Things networks. This method emphasises how crucial it is to use cutting-edge optimisation strategies in order to optimise feature subsets and improve intrusion detection technologies' overall effectiveness.

H. Intrusion Detection using Attention Bi-LSTM

The Attention-based BiLSTM model is used to identify intrusions in the NSL-KDD dataset. Using specialised memory units, LSTM—an improved version of the classic Recurrent Neural Networks (RNN)—captures long-term relationships in the MTS dataset efficiently [20]. The gradient vanishing problem is addressed by LSTM models, in contrast to conventional RNN techniques. Rather than depending just on the architecture of hidden units, they also incorporate memory cells that capture the long-term dependence of the signal. Four regulated gates make up the LSTM model: an output gate, a forget gate, input gate, in addition to a self-loop memory cell. These gates control how several memory neurons' data streams communicate with one another. The

forget gate in the LSTM model's hidden layer decides which data from the previous time frame to keep and which to discard. The input gate makes the decision to simultaneously inject data from the memory unit into the input signal or not. The output gate decides whether to change the state of the memory unit [24]. The following Eq. (9) through Eq. (14) are used to determine the neuron state, hidden layer results, and gate states, taking into account the input x_t from the NSL-KDD dataset and the dynamic output state h_t :

$$ip_t = \sigma(X_i u_t + Y_i h_{t-1} + a_i) \quad (9)$$

$$fg_t = \sigma(X_f u_t + Y_f h_{t-1} + a_f) \quad (10)$$

$$op_t = \sigma(X_o u_t + Y_o h_{t-1} + a_o) \quad (11)$$

$$c_t = fg_t \odot c_{t-1} + ip_t \odot \tilde{c}_t \quad (12)$$

The weight matrices that recur are indicated by as Y_i, Y_f, Y_o , while the representation of the weighted matrix for the forget, output, input, and memory cell gating by X_i, X_f, X_o , respectively. The biases for the gates are formulated as a_i, a_f, a_o . The candidate's cell state \tilde{c}_t , is utilized to update the original memory cell state, c_t . Step indicates the hidden layer's state h_{t-1} at any given moment, while ot indicates the output op_t . The symbol \odot denotes the element-wise multiplication operation. The hyperbolic tangent function is denoted as \tanh , and the logistic sigmoid activation function is represented by σ .

The standard LSTM model's limitation lies in its one-directional analysis of input signals during training, potentially leading to the inadvertent oversight of sequential information. In contrast, the BiLSTM was designed with a bidirectional structure, leveraging two LSTM layers operating in opposing directions to capture representation information both forwards and backwards. This bidirectional setup includes a hidden layer for reverse transmission (denoted as $hb(t)$), incorporating future values, alongside a forward propagation hidden layer ($hf(t)$) that retains data from previous sequence values. Ultimately, the BiLSTM model's final output is a fusion of both $hf(t)$ and $hb(t)$, facilitating a more comprehensive understanding of time series data.

$$M_{fg}(t) = \varphi(Y_{fm} u_t + Y_{fmm} u_{f(t-1)} + a_{fa}) \quad (13)$$

$$M_a(t) = \varphi(Y_{am} u_t + Y_{amm} u_{a(t-1)} + a_a) \quad (14)$$

Besides these, a_{fa} and a_a also relate to two-way biased data. The weight matrix " Y_{fm} and Y_{am} " represents the synaptic weights from the input value to the internal unit for both forward and backward directions. Similarly, the forward and backward feedback recurrent weights are denoted by Y_{fmm} and Y_{amm} .

The \tanh function serves as the activation function ψ for the hidden layers (HLs). It determines the output of the BiLSTM as b_t .

$$b_t = \sigma(W_{fmb} m_{f(t)} + W_{amb} m_{a(t)} + a_b) \quad (15)$$

The forward and backward weights of the resulting layers are represented by W_{fmb} and W_{amb} , respectively, in Eq. (15). Both a linear or sigmoidal function is provided as the

activation function of the resulting layer σ . Moreover, b denotes the bias in the output. The attention mechanism contributes to the learning process of the Attention BiLSTM model by assigning varying weights. The attention a_i for a hidden layer h_i is calculated using Eq. (16):

$$x_i = \tanh(Wh_i + a) \quad (16)$$

BiLSTM networks provide a powerful means to examine sequential data streams, enabling real-time detection of anomalous behavior and security threats in IoT networks. Leveraging BiLSTM architectures, these networks excel in capturing temporal dependencies and patterns present in IoT data, which are often characterized by their dynamic and time-varying nature. By effectively modelling the sequential nature of IoT data, BiLSTM networks can accurately identify deviations from normal behavior, facilitating prompt detection of intrusions and security breaches. To protect the integrity and confidentiality of IoT systems and devices, respond proactively to new threats, and strengthen the security posture of IoT networks, this capability is essential.

1. Blockchain Integration

The integration of blockchain technology into intrusion detection systems involves several key steps to ensure the integrity and immutability of the data while facilitating secure communication among distributed IoT devices through smart contracts.

1) *Data logging*: In the process of data logging, intrusion detection data generated by IoT devices is systematically recorded onto the blockchain network. Each piece of data is meticulously timestamped and cryptographically secured, ensuring its integrity and safeguarding against any potential tampering attempts. By timestamping each entry, the blockchain network establishes a chronological order of events, enabling a comprehensive audit trail of intrusion activities. Additionally, the cryptographic security measures implemented within the blockchain network guarantee the immutability of the logged data, thereby providing a reliable and tamper-proof record of security events. This meticulous logging process enhances the trustworthiness and reliability of the intrusion detection system, enabling robust security monitoring in IoT networks [25].

2) *Blockchain node*: In the context of blockchain technology, blockchain nodes serve as essential components responsible for validating and recording logged intrusion detection data. These nodes are distributed across the blockchain network, ensuring decentralization and resilience against single points of failure. Each node maintains a copy of the decentralized ledger, which contains a complete record of all transactions, including the logged intrusion detection data. When new data is logged onto the blockchain, it undergoes validation by multiple nodes within the network to ensure its authenticity and integrity. This validation process involves verifying the cryptographic signatures associated with the data and confirming its adherence to the consensus rules established by the network protocol. Once validated, the intrusion detection data is appended to the blockchain ledger,

becoming a permanent and immutable part of the distributed database. By distributing the responsibility for data validation and storage among multiple nodes, blockchain networks achieve redundancy and fault tolerance, enhancing the reliability and resilience of the overall system. Furthermore, as blockchain nodes are decentralised, no one organisation can exert control over the system as a whole, fostering openness, confidence, and security in the logging and archiving of intrusion detection data.

3) *Proof of work*: The consensus mechanism of the blockchain is essential to guaranteeing that all dispersed nodes agree on the veracity of logged data. To reach this consensus among network users, consensus techniques like Proof of Work (PoW) are used. Proof-of-work (PoW) consensus is a competitive mechanism in which nodes solve challenging mathematical problems to validate transactions and append new blocks to the blockchain. This is a resource-intensive procedure that uses a lot of energy and processing power. Nonetheless, other nodes in the network confirm the answer after a node completes the puzzle and suggests a new block. The block is appended to the blockchain if the answer satisfies the consensus requirements. By using this decentralised method, blockchain networks maintain the integrity and durability of the blockchain ledger by facilitating consensus across dispersed nodes about the veracity of recorded data. Additionally, consensus mechanisms like PoW contribute to the security of the blockchain network by mitigating the risk of malicious actors attempting to manipulate or alter the logged data. Overall, the consensus mechanism serves as a fundamental building block of blockchain technology, enabling decentralized trust and coordination among network participants [26].

A key element of blockchain networks is the proof-of-work (PoW) consensus mechanism, which guarantees dispersed nodes' agreement on the legitimacy of transactions and the appending of new blocks to the blockchain. PoW comprises the following crucial steps:

- **Transaction Propagation**: Transactions are broadcasted to all nodes in the blockchain network. Each transaction contains details such as sender, recipient, amount, and cryptographic signatures.
- **Block Creation**: Transactions are grouped together into blocks, forming a candidate block for addition to the blockchain. Miners, who are nodes responsible for creating new blocks, select transactions and assemble them into a block structure.
- **Mining Competition**: Miners compete with each other to solve the Proof of Work puzzle. They utilize computational power to generate hash values by iteratively modifying a nonce (a random number) in the block header until the desired hash value is found. This process is computationally intensive and requires significant computational resources.

- **Verification:** A miner broadcasts the candidate block and the solution to the network as soon as they discover a workable solution to the problem. The legitimacy of the answer and the transactions included in the block are then confirmed by further nodes inside the network.
- **Consensus:** If the majority of nodes in the network agree that the proposed solution is sound and the block conforms to the consensus requirements, the block is accepted and posted to the blockchain. It is ensured that all distributed nodes concur on the validity of the transactions and the addition of new blocks to the blockchain by going through this process.
- **Reward:** A fixed quantity of bitcoin plus any transaction fees included in the block are awarded to the miner who effectively mines a new block. This encourages miners to use up processing power and take part in the consensus-building process on the network.

In general, the Proof of Work technique reduces the possibility of malevolent actors attempting to influence the blockchain by demanding computational resources to verify transactions and generate new blocks, hence ensuring the security and integrity of blockchain networks.

1) *Smart contract:* Smart contracts serve as the backbone of automation and governance within IoT networks by providing a decentralized, programmable framework for enforcing rules and conditions. These contracts, encoded with predefined logic, are deployed on the blockchain, ensuring immutability and tamper-proof execution. Within the context of IoT, smart contracts automate interactions between devices, enabling seamless communication and coordination without the need for intermediaries. By executing automatically when specific conditions are met, such as sensor readings or trigger events, smart contracts streamline processes and mitigate the risk of human error. Moreover, the decentralised structure of these systems gets rid of single points of failure and minimises dependence on centralised authority, hence improving security and resilience. Additionally, conditional execution of operations is made possible by smart contracts, which let gadgets react quickly to shifting conditions. This feature improves IoT network responsiveness and operational efficiency. Furthermore, network participants' confidence and responsibility are bolstered by the openness and auditability provided by smart contracts. Overall, smart contracts play a critical role in driving efficiency, security, and transparency in IoT ecosystems, laying the foundation for scalable and resilient decentralized applications [27].

2) *Secure communication:* In the ecosystem of IoT networks, secure communication is facilitated through the interaction between IoT devices and the blockchain network via smart contracts. These contracts act as intermediaries, enforcing cryptographic protocols and access controls to ensure that communication remains secure. By leveraging cryptographic techniques such as encryption and digital signatures, smart contracts authenticate and authorize devices,

mitigating the risk of unauthorized access or tampering. Through predefined rules and conditions encoded within the smart contracts, only authorized devices are granted permission to access and modify data stored on the blockchain. This robust enforcement of security measures enhances the integrity and confidentiality of communication within IoT networks, safeguarding sensitive information and preventing unauthorized manipulation of data. Overall, the utilization of smart contracts enables secure and trustworthy communication channels, fostering confidence in the exchange of data and transactions within IoT ecosystems.

V. RESULT AND DISCUSSION

The proposed framework undergoes rigorous evaluation using benchmark datasets, including NSL-KDD and BoT-IoT, to comprehensively assess its performance in detecting various types of intrusions within IoT networks. By leveraging these datasets, which contain diverse and realistic intrusion scenarios, the framework's efficacy in identifying and mitigating security threats is thoroughly scrutinized. Performance metrics are used to assess how well the framework differentiates between malicious activity and typical network behavior. These measures include detection accuracy, false positive rate, and computing efficiency. Furthermore, the assessment procedure entails contrasting the outcomes of the framework with those of current intrusion detection systems in order to measure its effectiveness in relation to predetermined benchmarks. The suggested framework's potential to strengthen the security posture of IoT networks is carefully investigated through this methodical study utilizing typical datasets, offering insights into its advantages and shortcomings.

A. Performance Metrics

Performance metrics refer to the numerical values that are utilized to assess how well an intrusion detection system detects and neutralizes security threats on a network. Commonly used metrics include the following ones:

1) *Accuracy:* The percentage of accurately identified occurrences—both true positives and true negatives—out of all the instances that were examined is known as accuracy. It offers a general indicator of how effectively the intrusion detection system classifies events as either intrusions or routine activity.

2) *Precision:* Positive predictive value, or precision, is a metric that expresses the percentage of accurately detected positive cases (true positives) across every case categorized as positive (false positives and true positives). It shows how well the system can detect intrusions without mistakenly labelling routine operations as such.

3) *Recall:* Recall, also known as sensitivity or true positive rate, is the proportion of correctly identified positive cases relative to all real positive occurrences in the dataset. It assesses the system's ability to identify every incursion, lowering the likelihood that any malicious activity would go undetected.

4) *F1-score*: The F1-score, which achieves equilibrium between recall and accuracy, is derived from the harmonic mean of these two metrics. Recall and accuracy are combined into one figure, which accounts for both false positives and false negatives.

TABLE I. PERFORMANCE METRICS

| Metrics | Efficiency |
|-----------|------------|
| Accuracy | 98.9 |
| Precision | 94 |
| Recall | 95 |
| F1-Score | 95 |

As shown in Table I and Fig. 2, the suggested intrusion detection approach exhibits excellent efficiency with an accuracy of 98.9%, demonstrating its capacity to accurately categorise cases as either intrusions or routine operations. Furthermore, the approach displays a 94% accuracy rate, which indicates the percentage of accurately detected incursions among all cases that are categorised as positive, hence reducing false positives. With a recall rate of 95%, which indicates that the system can detect all incursions, there is little chance of a missed detection. Furthermore, a balanced performance in terms of both accuracy and recall is shown by the F1-score, which harmonises the two metrics, which is recorded at 95%. All of these measures show how successful and dependable the suggested intrusion detection technique is at identifying and reducing security risks in the network infrastructure.



Fig. 2. Performance efficiency.

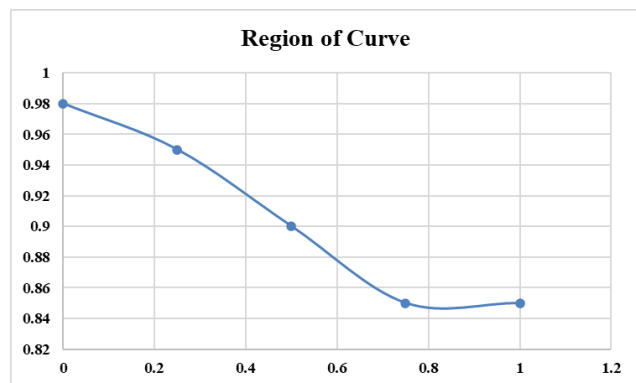


Fig. 3. Receiver operating characteristic curve.

As the threshold rises from 0 to 1, the true positive rate (TPR) progressively falls from 0.98 to 0.85, suggesting a decline in the percentage of true positive cases that are correctly categorised, as seen in Fig. 3. The TPR stays comparatively high at 0.95 at a threshold of 0.25, indicating that true positive cases can be effectively detected even with somewhat loosened thresholds.

TABLE II. SORTING RESULT OF NSL-KDD

| Methods | AUC | Error Rate |
|------------------------------|-------|------------|
| Gradient Boosting Classifier | 47.64 | 0.4905 |
| Deep Learning | 77.88 | 0.2256 |
| Proposed Method | 98.9 | 0.0025 |

The NSL-KDD dataset's categorization outcomes using different techniques are shown in Table II. With an error rate of 0.4905 and an AUC of 47.64%, the Gradient Boosting Classifier performs relatively poorly. By comparison, the Deep Learning approach shows noticeably higher performance, with an error rate of 0.2256 and an AUC of 77.88%.

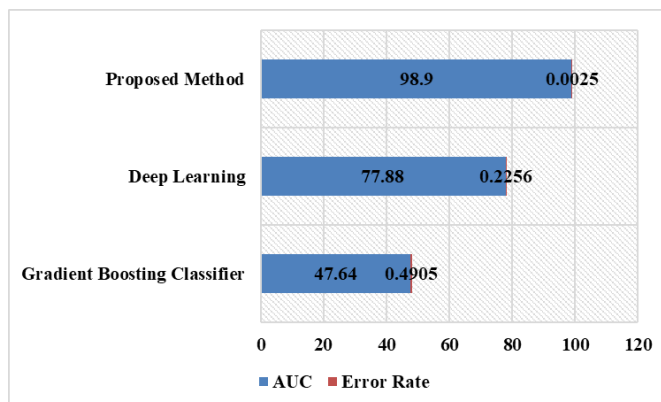


Fig. 4. Classification result of NSL-KDD.

The results presented in Fig. 4 demonstrate that the suggested approach outperforms the two other options, with an exceptional AUC of 98.9% and a remarkably low error rate of 0.0025. These outcomes highlight how well the suggested strategy performs in comparison to other methods when it comes to correctly identifying instances in the NSL-KDD dataset.

TABLE III. RECOGNITION OUTCOMES OF ATTENTION BASED BiLSTM APPROACH ON NSL-KDD DATASET

| Data | Class | Accuracy | Precision | Recall | F1-Score |
|----------|---------|----------|-----------|--------|----------|
| Training | Normal | 98.4 | 96.3 | 97.3 | 96.3 |
| | Attack | 97.4 | 97.4 | 98.4 | 95.5 |
| | Average | 97.7 | 97.7 | 97.7 | 97.7 |
| Testing | Normal | 98.9 | 97.5 | 96.4 | 95.8 |
| | Attack | 97.3 | 98.3 | 97.3 | 98.3 |
| | Average | 98.9 | 98.9 | 98.9 | 98.9 |

The NSL-KDD dataset's recognition results from the Attention-based BiLSTM technique are shown in Table III and Fig. 5.

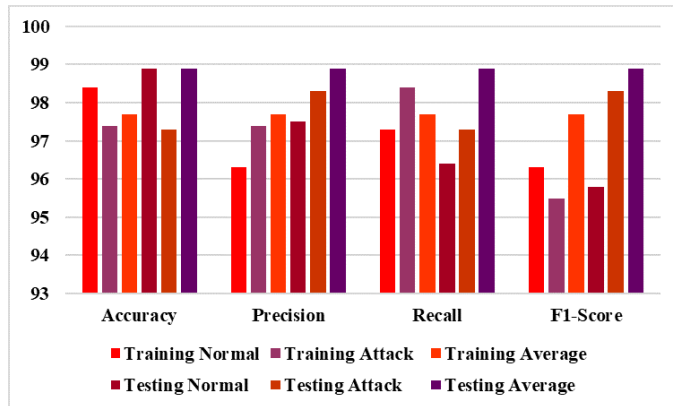


Fig. 5. Recognition outcomes of attention based BiLSTM approach on NSL-KDD dataset.

It includes accuracy, precision, recall, and F1-Score, split into normal and attack classes, for both the training and testing datasets. In the training dataset, the method achieves 98.4% accuracy for normal cases and 97.4% accuracy for attack instances. Respectively, the corresponding accuracy, recall, and F1-Score values are 95.5% and 96.3%, 97.3% and 98.4%, and 96.3% and 97.4%. Comparable outcomes are seen in the testing dataset, where the technique achieves 97.3% accuracy for attack instances and 98.9% accuracy for normal cases. The corresponding F1-Score, recall, and accuracy scores are 97.5%, 98.3%, and 95.8%, respectively. The average results for each class are also provided for the training and testing datasets.

B. Discussion

The research studies under discussion offer novel strategies for resolving the security issues that arise in Internet of Things networks. These specifically concentrate on intrusion detection systems (IDS) and make utilisation of blockchain and machine learning technology. The study by Liang et al. [12] suggests a hybrid intrusion detection system that makes use of multi-agent systems, blockchain technology, and deep learning techniques. The system is divided into distinct modules for data collecting, management, analysis, and response with the goal of improving detection accuracy, particularly at the transport layer of Internet of Things networks. Scalability and optimisation continue to be major obstacles to practical implementation, notwithstanding encouraging findings. A collaborative intrusion detection architecture including blockchain technology for safe sharing of threat intelligence across cloud and Internet of Things networks is presented by Alkadi et al. [13]. While consensus processes and deep blockchain technology are adept at detecting intrusions and reducing security threats, their scale presents serious problems for efficiency and real-time response. A blockchain-based collaborative signature-based IDS called CBSigIDS is proposed by Li et al. with the goal of creating a trustworthy signature database in dispersed IoT systems. Although it provides a safe way to validate signatures, blockchain overhead scalability issues require

further work before a viable implementation can be made. Kumar et al. [14] offers a distributed intrusion detection system (IDS) that uses blockchain technology and fog computing to identify DDoS assaults directed at IoT mining pools. They assess the system's effectiveness in identifying IoT network assaults using machine learning algorithms trained on scattered fog nodes. But there are still issues with realistic implementation and optimisation needed for efficiency and scalability. Although these studies show how blockchain and machine learning technologies could potentially use to improve IoT network security, scalability, optimisation, and practical deployment issues must be resolved before their full promise could be realised in practical settings.

The study presents a complete framework for reliable and scalable intrusion detection in IoT networks by integrating machine learning techniques with blockchain technology. The solution addresses the challenges posed by the dynamic and heterogeneous nature of IoT environments by employing Red Fox Optimization for feature selection and Attention-based BiLSTM for anomaly identification. The adoption of blockchain technology improves security by ensuring the validity and inviolability of intrusion record detection. The study advances the area by providing an all-encompassing method of intrusion detection that takes security and efficiency into account. Real-time identification of abnormalities and malicious activity in IoT traffic is made possible by the use of sophisticated machine learning algorithms, and scalability is improved by optimization approaches that assist decrease the dimensionality of the input data. Furthermore, the system gains an additional degree of protection through the integration of the technology known as blockchain, which offers tamper-resistant recordings of detected intrusions. The usefulness of the suggested architecture is demonstrated by experimental findings, which on real-world IoT datasets yield a high detection accuracy of about 98.9%. These findings highlight how important the study is to improving IoT security state-of-the-art. The report does, however, admit several limitations, including the need for more assessment in various IoT scenarios and the computational cost related to blockchain integration. Prospective study avenues encompass investigating alternative machine learning algorithms and optimization methods, tackling scalability issues, and refining blockchain-associated procedures. Overall, the research offers a viable strategy for improving intrusion detection in Internet of Things networks, opening the door to more robust and safe linked settings.

VI. CONCLUSION

The suggested system, which makes use of blockchain and machine learning, offers a viable solution to the problems associated with intrusion detection in Internet of Things networks. The accuracy and scalability of the intrusion detection system are improved by integrating Red Fox Optimization for feature selection and Attention-based BiLSTM for anomaly detection. Moreover, the incorporation of blockchain technology ensures the integrity and immutability of intrusion detection logs, thereby enhancing security. On real-world IoT data sets, experimental findings show the usefulness of the technique with a high detection

accuracy of about 98.9%. However, it is important to acknowledge some limitations and areas for future work. Firstly, while the proposed framework shows promising results, further research is needed to evaluate its performance in diverse IoT environments and under various attack scenarios. Additionally, the scalability of the system needs to be investigated to handle large-scale IoT networks efficiently. Furthermore, the computational overhead associated with blockchain integration may pose challenges in resource-constrained IoT devices, requiring optimization strategies. Moreover, continuous advancements in intrusion techniques necessitate ongoing updates and improvements to the detection algorithms and feature selection methods. Future studies may look at applying more machine learning algorithms and optimization techniques to enhance the robustness and efficiency of intrusion detection systems in Internet of Things networks. All things considered, this work establishes the groundwork for next investigations that seek to create IoT ecosystems that are more robust and safer.

REFERENCES

- [1] P. Raj and A. C. Raman, *The Internet of Things: Enabling technologies, platforms, and use cases*. Auerbach Publications, 2017.
- [2] V. E. Balas and S. Pal, *Healthcare Paradigms in the Internet of Things Ecosystem*. Academic Press, 2020.
- [3] Y. Liao, C. Thompson, S. Peterson, J. Mandrola, and M. S. Beg, "The future of wearable technologies and remote monitoring in health care," *Am. Soc. Clin. Oncol. Educ. Book*, vol. 39, pp. 115–121, 2019.
- [4] A. Karale, "The challenges of IoT addressing security, ethics, privacy, and laws," *Internet Things*, vol. 15, p. 100420, 2021.
- [5] A. Qasem, P. Shirani, M. Debbabi, L. Wang, B. Lebel, and B. L. Agba, "Automatic vulnerability detection in embedded devices and firmware: Survey and layered taxonomies," *ACM Comput. Surv. CSUR*, vol. 54, no. 2, pp. 1–42, 2021.
- [6] R. Krishnamurthi, A. Kumar, D. Gopinathan, A. Nayyar, and B. Qureshi, "An overview of IoT sensor data processing, fusion, and analysis techniques," *Sensors*, vol. 20, no. 21, p. 6076, 2020.
- [7] A. Riah, S. Daniel, E. Frank, and K. Seriffdeen, "The role of technology in shaping user behavior and preventing phishing attacks," 2024.
- [8] T. M. Alshammari and F. M. Alserhani, "Scalable and Robust Intrusion Detection System to Secure the IoT Environments using Software Defined Networks (SDN) Enabled Architecture," *Int J Comput Netw. Appl.*, vol. 9, no. 6, pp. 678–688, 2022.
- [9] M. Javed, N. Tariq, M. Ashraf, F. A. Khan, M. Asim, and M. Imran, "Securing Smart Healthcare Cyber-Physical Systems against Blackhole and Greyhole Attacks Using a Blockchain-Enabled Gini Index Framework," *Sensors*, vol. 23, no. 23, p. 9372, 2023.
- [10] A. Laszka, A. Dubey, M. Walker, and D. Schmidt, "Providing privacy, safety, and security in IoT-based transactive energy systems using distributed ledgers," in *Proceedings of the Seventh International Conference on the Internet of Things*, 2017, pp. 1–8.
- [11] A. K. Al Hwaitat et al., "A New Blockchain-Based Authentication Framework for Secure IoT Networks," *Electronics*, vol. 12, no. 17, p. 3618, Aug. 2023, doi: 10.3390/electronics12173618.
- [12] C. Liang et al., "Intrusion Detection System for the Internet of Things Based on Blockchain and Multi-Agent Systems," *Electronics*, vol. 9, no. 7, p. 1120, Jul. 2020, doi: 10.3390/electronics9071120.
- [13] O. Alkadi, N. Moustafa, B. Turnbull, and K.-K. R. Choo, "A deep blockchain framework-enabled collaborative intrusion detection for protecting IoT and cloud networks," *IEEE Internet Things J.*, vol. 8, no. 12, pp. 9463–9472, 2020.
- [14] R. Kumar, P. Kumar, R. Tripathi, G. P. Gupta, S. Garg, and M. M. Hassan, "A distributed intrusion detection system to detect DDoS attacks in blockchain-enabled IoT network," *J. Parallel Distrib. Comput.*, vol. 164, pp. 55–68, Jun. 2022, doi: 10.1016/j.jpdc.2022.01.030.
- [15] H. Vargas, C. Lozano-Garzon, G. A. Montoya, and Y. Donoso, "Detection of Security Attacks in Industrial IoT Networks: A Blockchain and Machine Learning Approach," *Electronics*, vol. 10, no. 21, p. 2662, Oct. 2021, doi: 10.3390/electronics10212662.
- [16] R. H. Hylock and X. Zeng, "A Blockchain Framework for Patient-Centered Health Records and Exchange (HealthChain): Evaluation and Proof-of-Concept Study," *J. Med. Internet Res.*, vol. 21, no. 8, p. e13592, Aug. 2019, doi: 10.2196/13592.
- [17] "NSL-KDD." Accessed: Mar. 21, 2024. [Online]. Available: <https://www.kaggle.com/datasets/hassan06/nslkdd>.
- [18] H. Moudoud, S. Cherkaoui, and L. Khoukhi, "An IoT blockchain architecture using oracles and smart contracts: the use-case of a food supply chain," in *2019 IEEE 30th Annual International Symposium on Personal, Indoor and Mobile Radio Communications (PIMRC)*, IEEE, 2019, pp. 1–6.
- [19] P. Bari and P. Karande, "Application of PROMETHEE-GAIA method to priority sequencing rules in a dynamic job shop for single machine," *Mater. Today Proc.*, vol. 46, pp. 7258–7264, 2021, doi: 10.1016/j.matpr.2020.12.854.
- [20] P. Yazdaniyan and S. Sharifian, "E2LG: a multiscale ensemble of LSTM/GAN deep learning architecture for multistep-ahead cloud workload prediction," *J. Supercomput.*, vol. 77, pp. 11052–11082, 2021.
- [21] F. Karim, S. Majumdar, and H. Darabi, "Insights Into LSTM Fully Convolutional Networks for Time Series Classification," *IEEE Access*, vol. 7, pp. 67718–67725, 2019, doi: 10.1109/ACCESS.2019.2916828.
- [22] Z. Ahamed, M. Khemakhem, F. Eassa, F. Alsolami, and A. S. A.-M. Al-Ghamdi, "Technical Study of Deep Learning in Cloud Computing for Accurate Workload Prediction," *Electronics*, vol. 12, no. 3, p. 650, 2023.
- [23] E. S. P. Krishna and A. Thangavelu, "Attack detection in IoT devices using hybrid metaheuristic lion optimization algorithm and firefly optimization algorithm," *Int. J. Syst. Assur. Eng. Manag.*, May 2021, doi: 10.1007/s13198-021-01150-7.
- [24] R. AlGhamdi, "Design of Network Intrusion Detection System Using Lion Optimization-Based Feature Selection with Deep Learning Model," *Mathematics*, vol. 11, no. 22, p. 4607, Nov. 2023, doi: 10.3390/math11224607.
- [25] S. Rathore, J. H. Park, and H. Chang, "Deep Learning and Blockchain-Empowered Security Framework for Intelligent 5G-Enabled IoT," *IEEE Access*, vol. 9, pp. 90075–90083, 2021, doi: 10.1109/ACCESS.2021.3077069.
- [26] A. H. Sodhro, S. Pirbhulal, M. Muzammal, and L. Zongwei, "Towards blockchain-enabled security technique for industrial internet of things based decentralized applications," *J. Grid Comput.*, vol. 18, pp. 615–628, 2020.
- [27] B. Yin, Y. Wu, T. Hu, J. Dong, and Z. Jiang, "An efficient collaboration and incentive mechanism for Internet of Vehicles (IoV) with secured information exchange based on blockchains," *IEEE Internet Things J.*, vol. 7, no. 3, pp. 1582–1593, 2019.

Unveiling Spoofing Attempts: A DCGAN-based Approach to Enhance Face Spoof Detection in Biometric Authentication

Vuda Sreenivasa Rao¹, Shirisha Kasireddy², Annapurna Mishra³,
R. Salini⁴, Sanjiv Rao Godla⁵, Khaled Bedair⁶

Associate Professor, Department of Computer Science and Engineering, Koneru Lakshmaiah Education Foundation,
Vaddeswaram, Andhra Pradesh, India¹

Associate Professor, Vignana Bharathi Institute of Technology, JNTUH, Ghatkesar, Hyderabad, India²

Associate Professor, Electronics and Communication Engineering, Silicon Institute of Technology, Bhubaneswar, India³

Department of CSE, Panimalar Engineering College, Chennai, India⁴

Professor, Department of AIML& Data Science, Aditya College of Engineering and Technology- Surapalem,
Andhra Pradesh, India⁵

Department of Social Sciences-College of Arts and Sciences, Qatar University, P.O. Box 2713, Doha, Qatar⁶

Abstract—Face spoofing attacks have become more dangerous as biometric identification has become more widely used. Through the utilisation of false facial photographs, attackers seek to fool systems in these assaults, endangering the security of biometric authentication devices and perhaps allowing unauthorized access to private information. Effectively recognizing and thwarting such spoofing attacks is critical to the dependability and credibility of biometric identification systems in a variety of applications. This research seeks to offer a unique strategy that uses Deep Convolutional Generative Adversarial Networks (DCGANs) to improve face spoof detection in order to counter the challenge provided by face spoofing assaults. In order to strengthen the security of biometric authentication systems in applications like identity verification, access control, and mobile device unlocking, the goal is to increase the accuracy and effectiveness of facial spoof detection. The training dataset is then supplemented with these artificial images, which strengthens the face spoof detection system's resilience. More accurate face spoofing is made possible by the strategy that leverages the discriminative characteristics obtained throughout the process to train the discriminator network employing adversarial learning to discriminate between actual and fake images. Experiments on the CelebFacesAttributes (CelebA) datasets show how effective the suggested method is over traditional techniques. The suggested technique outperforms conventional methods and achieves an astounding accuracy of 99.1% in face-spoof detection systems. The system exhibits impressive precision in differentiating between real and fake faces through the efficient use of artificial intelligence and adversarial learning. This effectively decreases the possibility of unwanted access and enhances the overall dependability of biometric authentication methods.

Keywords—Biometric authentication systems; deep convolutional generative adversarial networks; face spoof detection; synthetic image generation; unauthorized access

I. INTRODUCTION

The face of a person is essential to any visual material or communication on face spoof detection. Commonly used and

easily accessible editing tools are employed to improve this visual content. The technique of manipulating facial recognition devices by posing as an authorized user with fake facial images or videos is known as face spoofing. However, through manipulating video evidence, slandering a person's credibility, and other means, its harmful use is causing division in society [1]. With the widespread adoption of biometric identification systems, the threat of face spoofing attacks has become increasingly prominent. Face spoofing the technique of manipulating facial recognition devices by posing as an authorized user with fake facial images as face spoofing. As spoofing techniques continue to evolve and become more sophisticated, it is essential to develop advanced detection methods capable of identifying increasingly realistic fake faces. With the increasing use of facial recognition technology for authentication and access control, detecting spoofed or fake faces is important to prevent unauthorized access to sensitive systems, devices, or information. Face spoofing techniques, such as using printed photos or digital masks, can be exploited by threat actors to impersonate legitimate users and gain access to their accounts or personal information [2]. Traditional spoof detection methods may struggle to distinguish between real and fake faces in the presence of increasingly convincing spoofing attacks. The advancement of face spoof detection system is achieved using deep learning methods to extract highly appropriate information from facial photos and effectively train models to detect even minor differences between real and faked faces.

Face detection systems are improving, but detecting face spoofing crime remains challenging. To address this, a Generative Adversarial Network (GAN) is implemented to deliver image from the RGB as an input. It improves discriminative capability by converting live face images to depth maps and spoofing images to plain images [3]. A face anti-spoofing system that combines VIS and NIR images, achieved through a MCT-GAN for generating NIR from VIS inputs, followed by a Convolutional Neural Network (CNN) for feature fusion, aiming to improve live and spoof face

classification without requiring NIR equipment during testing [4]. Deep Learning techniques can manipulate videos, potentially leading to misinformation and manipulation. Deepfake detection using GAN Discriminators is developed using Generative Adversarial Network (GAN) discriminators to identify videos of Deepfake data. The model trains a GAN and extract a discriminator module, testing different architectures and training methods. It leads to enhance the efficiency of GAN discriminators using ensemble techniques [5]. The method of CNN Detection of GAN-Generated Face Images based on Cross-Band Co-occurrences Evaluation aims to differentiate between GAN-generated and real images, particularly focusing on synthetic face images, by leveraging inconsistencies across spectral bands. By incorporating Cross-Band Co-occurrence matrices along with spatial co-occurrence matrices as input to a CNN system, it achieves superior performance compared to a detection system solely based on intra-band spatial co-occurrences, achieving an accuracy of 94% [6]. A Deepfake detection technique utilizes computer vision characteristics extracted from digital context, employing the Cascaded Deep Sparse Auto Encoder (CDSAE) trained by temporal based CNN to analyze frame changes. Subsequently, a Deep Neural Network (DNN) is employed for classification, achieving enhanced accuracies of 98.7%, 98.5%, and 97.63% for the datasets like Face2Face, FaceSwap, and DFDC, through a feature selection approach [7]. Face swapping detection employed by deep transfer learning for, achieving true positive rates exceeding 96% with minimal false alarms, and providing uncertainty estimates for each prediction, crucial for system trust. It uses dataset with the largest to date for face swapping detection using static images, with approximately 1000 real images per individual, facilitating effective model design and evaluation, resulting in an accuracy of 98% [8]. The XceptionTemporalConvolutional RNN framework combines XceptionNet CNN for facial feature representation with bidirectional recurrence layers, achieving robust visual deepfake detection and gained accuracy of 99%. Additionally, a companion audio architecture with convolution modules is presented, demonstrating high accuracy on both FaceForensics++ and Celeb-DF datasets, as well as the ASVSpooof 2019 Logical Access audio datasets [9]. The NA-VGG network enhances DeepFake detection by leveraging noise features highlighted by an SRM filter layer and augmenting the noise maps to weaken face features, resulting in improved accuracy compared to advanced detectors on the Celeb-DF dataset. The results demonstrate significant performance improvements, with the SRM filter upgrading image noise by 16.8% and image augmentation improving detection accuracy by 12.5% [10].

Traditional methodologies often necessitate manual feature engineering, wherein domain experts design specific features for classification purposes. Contrastingly, deep learning has the potential to eliminate the requirement for manual feature extraction by autonomously extracting relevant and hierarchical characteristics from raw data. By using DCNN, the model is able to acquire detailed representations of facial features, allowing it to analyse spatial correlations directly from the input images. This eliminates the need for manual segmentation and it enhances the model, streamlining

classification process. Various approaches, including GAN-based methods and deep learning techniques, have been developed to detect face spoofing attacks and deepfake videos. These methods employ advancements in computer vision and neural networks to enhance discriminative capabilities and attained high accuracy in detecting manipulated images and videos. The proposed framework of Face Spoof Detection Using DCGAN aims to contribute to enhancement of face spoof detection by utilizing Deep Convolutional Generative Adversarial Networks to automatically extract features for improved face spoof detection, enhancing the reliability of facial recognition system.

Key Contributions:

- Face Spoof Detection system utilizes Deep Convolutional Generative Adversarial Networks (DCGANs) to create synthetic facial data.
- The generator, a deep architecture of neural networks, synthesizes realistic facial images resembling genuine faces and the discriminator network, trained adversarial, works with the generator to differentiate between real and spoofed images.
- The benefit of employing DCGAN for feature extraction is that it eliminates the requirement for human feature engineering by learning discriminative features directly from the raw input data.
- Enhances face spoof detection in biometric authentication systems and promotes secure access control in various applications like financial services, secure facilities, and mobile devices.

The following portion of this section is constructed as follows: The relevant work on Face Spoof Detection using DCGAN is reviewed in Section II. The problem statement of the current system is outlined in Section III. The specifics of the suggested methodology and architecture of DCGAN are explained in Section IV. The results and discussion are presented in Section V. Lastly, the conclusions and future scopes were given in Section VI.

II. RELATED WORKS

Arora et al. [11] developed a framework for the foundation of the suggested framework is the extraction of facial characteristics using dimensionality reduction and feature extraction methods using convolutional autoencoder that have been pre-trained. Subsequently, classification is performed using a softmax classifier. Evaluation conducted on three benchmark datasets - Idiap Replay Attack, CASIA-FASD, and 3DMAD - demonstrates that the framework achieves performance levels compared to advanced methods and gained accuracy of 99%. In particular, extracting features from facial visuals highlights the recent development of deep neural networks in image processing applications. Experiments carried out on datasets such as 3DMAD, CASIA-FASD, and Idiap Replay Attack show that the suggested framework is effective in producing results that are on level with modern methods. Despite outperforming existing approaches on various benchmark datasets, the suggested face anti-spoofing framework has several limitations. When applied to diverse

datasets, the methodology may be exposed to modern spoofing approaches, and by enhancing and adapting the structure to address increasing threats and crimes, such as spoofing attacks on biometric systems.

Patel et al. [12] proposed an innovative and enhanced deep-CNN (D-CNN) structure for recognizing deep fakes that is both accurate and generalizable. Data from various sources are used for training the system, thereby boosting its overall generality characteristics. The imagery is adjusted and sent into the D-CNN network. The D-CNN strategy rate of development is improved using binary-cross entropy and the Adam optimizer. It analyzed seven different datasets from the reconstructed difficulties, each including 5000 fake deep fake images and 10,000 true images. The proposed work achieves an accuracy rating of 98.33% in AttGAN, 99.33% in GDWCT, 95.33% in StyleGAN, 94.67% in StyleGAN 2, and 99.17% in StarGAN in true and fake. The framework can be upgraded by extending the model to classify video deepfake data which presents an opportunity for enhanced detection capabilities. By extracting each frame from a video, detecting and cropping faces, and then feeding them into the model, it could enable the identification of deepfake manipulations in videos.

Kumar et al. [13] proposed the framework on detecting Deepfake with metric classification for classifying deepfake videos in scenarios involving high compression through various deep learning techniques with limited data. It reveals that a proposed approach exhibits significant effectiveness in classification task based on metric learning and employs a triplet network architecture. It enhances the feature space distance between their embedding vectors for the model to learn the differentiation between real and fake videos. It validates on two datasets allows to assess their performance in diverse environments. By employing a Triplet network, it surpasses existing results using 25 frames per video. The framework achieved outstanding performance, including an AUC of 99.2% on the Celeb-DF and an accuracy of 90.71% on Neural Texture. However, the current strategy is limited by its dependence on unsupervised domain adaptation techniques to increase the model's endurance and label dependency in subsequent rounds. [13] [14] [15].

Baek et al [14] proposed Generative Adversarial Ensemble Learning for Face Forensics which involves multiple discriminative and generative networks. Unlike conventional approaches, it focuses on enhancing discrimination rather than image generate on. It is achieved by ensembling the outputs of two discriminators to improve discriminability. Additionally, it trains two generators to produce both general and hard images. The system uses produced simulated face pictures to improve the discriminators and enhances the generators based on the combination feedback of the discriminators. This is achieved by integrating input from each generator and discriminator using ensemble learning. It illustrates the efficacy of the method with a thorough analysis of the Face Forensics task and ablation tests. Two distinct discriminators and two similar generators constitute an ensemble forensic detector. An adversarial ensemble loss function and generative adversarial ensemble learning method are used in Enhancing Forensic Identification with Combined Discriminators. This causes the

network topology of both generators and discriminators to become asymmetric, which enhances the framework's capacity for discrimination. It offers advantages by improving discrimination ability and addressing bias towards real or fake classes, which is applicable to existing detectors and other image forensic domains. Through extensive evaluation of the Face Forensics challenge and ablation studies, it demonstrates the effectiveness of the approach and acquired accuracy of 90%. But it requires significant computational resources and time for training multiple networks. The system needs to train two generators for both general and hard synthetic images which adds to computational burden. Ensemble learning process may require extensive tuning and optimization for optimal performance.

Ranjan et al. [15] developed a Transfer Learning-based CNNmodel for detecting DeepFakes across three prominent datasets like Deep Fake Detection (DFD), Celeb-DF, and Deep Fake Detection Challenge (DFDC). DeepFakes is curated for analysing purposes. The framework improves performance by transferring knowledge from pre-trained models to the task of DeepFake detection. While some blocks show higher accuracy without Transfer Learning, Transfer Learning consistently improves performance across most scenarios. The Celeb-DF dataset benefits significantly from Transfer Learning, with an 11.11% boost in accuracy. The model trained on the DFD dataset achieving records an accuracy of 73.20%. Conversely, the Celeb-DF model performs poorly when tested on the DFD dataset, reflecting the differences in alteration between the datasets. The cross-test accuracy is observed when the model is tested on DFDC, reaching 66.23%. The Xception Net demonstrates remarkable learning capacity by achieving impressive accuracy across all three distributions without overfitting, as evidenced by its high combined test accuracy of 86.49%. The Transfer Learning-based CNN framework for detecting DeepFakes has a potential drawback due to its reliance on pre-trained models, which may not capture the full range of features specific to DeepFake detection. While Transfer Learning consistently improves performance across most scenarios, it may not transfer relevant knowledge to the task, leading to suboptimal results.

Yavuzkilig et al. [16] presents a Multistream deep learning algorithm for identifying fake faces in videos, through a layer called fusion layer. Transfer learning is adopted, utilizing pre-trained VGG16, VGG19, and ResNet18 models for the three respective streams. The method introduces the World Politicians Deepfake Dataset (WPDD), created by extracting over 320,000 frames from videos of 20 politicians on YouTube. Various manipulations, including colour, hairstyle, structure and genuine face discrimination, are applied to both genders. This encompasses false detection like discrimination between fake and real faces, identification of seven face manipulations, and analysis of the system performance under various face manipulation. This method acquired accuracy scores of 99.98% and 99.95% for the DeepFake-TIMIT HQ and Celeb-DF datasets. The limitation of the system is its potential vulnerability to adversarial attacks and variations in face orientations.

Sun et al. [17] introduced FCN-DA-LSA method for detection of face spoofed images. The FCN local classifier effectively utilizes face spoof distortion properties, while the domain adaptation layer enhances generalization across various domains. This preserves high-frequency spoof clues from face recapture processes. FCN-LSA gained improved performance among advanced methods, with FCN-DA-LSA further improving results. Under hybrid protocols, the FCN-DA-LSA achieves HTERs of 11.22% and 21.92%, respectively. The improvement observed in FCN-DA-LSA over the basic FCN amounts to approximately 5.67%. While it demonstrates effectiveness as a form of few-shots supervised domain adaptation, the reliance on additional data poses a constraint. It can further explore unsupervised few-shot domain adaptation methods to mitigate this limitation and enhance performance, particularly in cross-PAI or cross-camera works.

Sun et al. [18] framed a depth-based FCN approach for face spoofing detection is revised, exploring diverse supervision techniques. In response, SAPLC is proposed, comprising an FCN and an aggregation technique. The FCN evaluates pixel-level ternary labels (real foreground, fake foreground, unclassified background), which are then separated to make accurate decisions. Experimental evaluation is demonstrated and achieves competitive performance with advanced methods under various common protocols. In protocols, SAPLC achieves ACERs of 0.42%, 2.50%, 3.89%, and 9.31%, respectively. The reliance on pixel-level ternary labels and aggregation for image-level decisions could introduce computational overhead and increase processing time, which may not be feasible for real-time face spoofing detection systems.

The existing papers demonstrate various approaches to face spoofing detection, they often have limitations such as reliance on external data, computational complexity, and suboptimal generalizability. The proposed DCGAN model addresses these drawbacks by generating diverse synthetic spoofed images, augmenting the training dataset, simplifying the training process, and improving the capacity of the model to capture spoof-specific features.

III. PROBLEM STATEMENT

Even with improvements in facial recognition technology, biometric systems still suffer a great deal of difficulty from face spoofing attacks. This problem has been made worse by deepfake manipulations in particular, which makes the facial spoof detection techniques employed today insufficient. These approaches frequently depend on outside datasets that are computationally demanding and do not fully cover the range of real-world circumstances, which makes real-time processing more difficult. More robust and adaptable solutions are required since they might not be able to properly handle different spoofing tactics or adjust to changing attack plans [18]. To address these issues, the proposed method makes utilisation of Deep Convolutional Generative Adversarial Networks (DCGAN) in order to gain over current constraints. This technique allows for the quick and precise real-time recognition of changed images by utilizing deep learning and GAN technology, which is especially useful in situations when

speed is of the essence. This capacity has important ramifications for standard applications including authentication systems, surveillance setups, and identity verification processes.

The objective of the project is to develop and evaluate a face spoof detection technique based on DCGAN to counter the rising threat of deepfake manipulations in biometric systems. It seeks to determine how well DCGAN performs in real-time processing for crucial applications like surveillance and authentication systems, examines its efficacy in a variety of real-world scenarios and spoofing techniques, and appraises its adaptability in fending off changing attack tactics. In order to improve overall security and reliability, the research also examines the practical ramifications of incorporating this technology into currently in employ biometric authentication systems.

IV. PROPOSED FACE SPOOF DETECTION WITH DEEP CONVOLUTIONAL GENERATIVE ADVERSARIAL NETWORK

The proposed Face Spoof Detection with Deep Convolutional Generative Adversarial Network is developed to enhance biometric authentication system using CelebA dataset. DCGAN consist of generator and discriminator networks, trained adversarial to produce realistic spoofed face images and distinguish them from genuine ones. The generator comprises multiple layers, starting with input noise vectors, and progressively up-samples them into high-dimensional representations to generate output images. Before feature extraction, the discriminator has an important role in classifying input images as genuine or generated. It trains to distinguish between real and generated images through adversarial training, guided by a loss function like binary cross-entropy. Feature extraction involves the discriminator capturing discriminative characteristics from input images, such as texture and spatial relationships, to distinguish between genuine and spoofed data. These characteristics are then used as input to a Deep Convolutional Network (DCN) for the final decision on face spoof detection. Fig. 1 depicts the block diagram of Face Spoof Detection using Deep Convolutional Network which classifies real and spoofed images from the CelebA dataset.

A. Data Description

The CelebFaces Attributes (CelebA) dataset which consists of 200,000 images of celebrity, each labelled with 40 binary attributes. The CelebA dataset consists of celebrity faces which contains 202,599 images. Every image in the dataset is annotated with labels of 40 binary attributes, covering a wide range of facial attributes such as Bald, Bangs, Black Hair, Blond Hair, Eyeglasses, Smiling, Wearing Hat, and other variations. The images in the CelebA dataset are of varying resolutions, with most images having a resolution of 178x218 pixels. The dataset includes images of celebrities from various demographics, ethnicities, ages, and genders, providing a diverse set of facial characteristics. The attribute annotations provide binary labels indicating the presence or absence of every attribute in the corresponding image. The images are typically stored in JPEG format, while the attribute annotations are provided in a text file or a structured format like CSV. The CelebA dataset is commonly used for tasks

such as face recognition, attribute prediction, facial attribute editing, and face synthesis. It serves as a powerful dataset for

training and evaluating deep learning systems like DCGANs for face spoof detection.

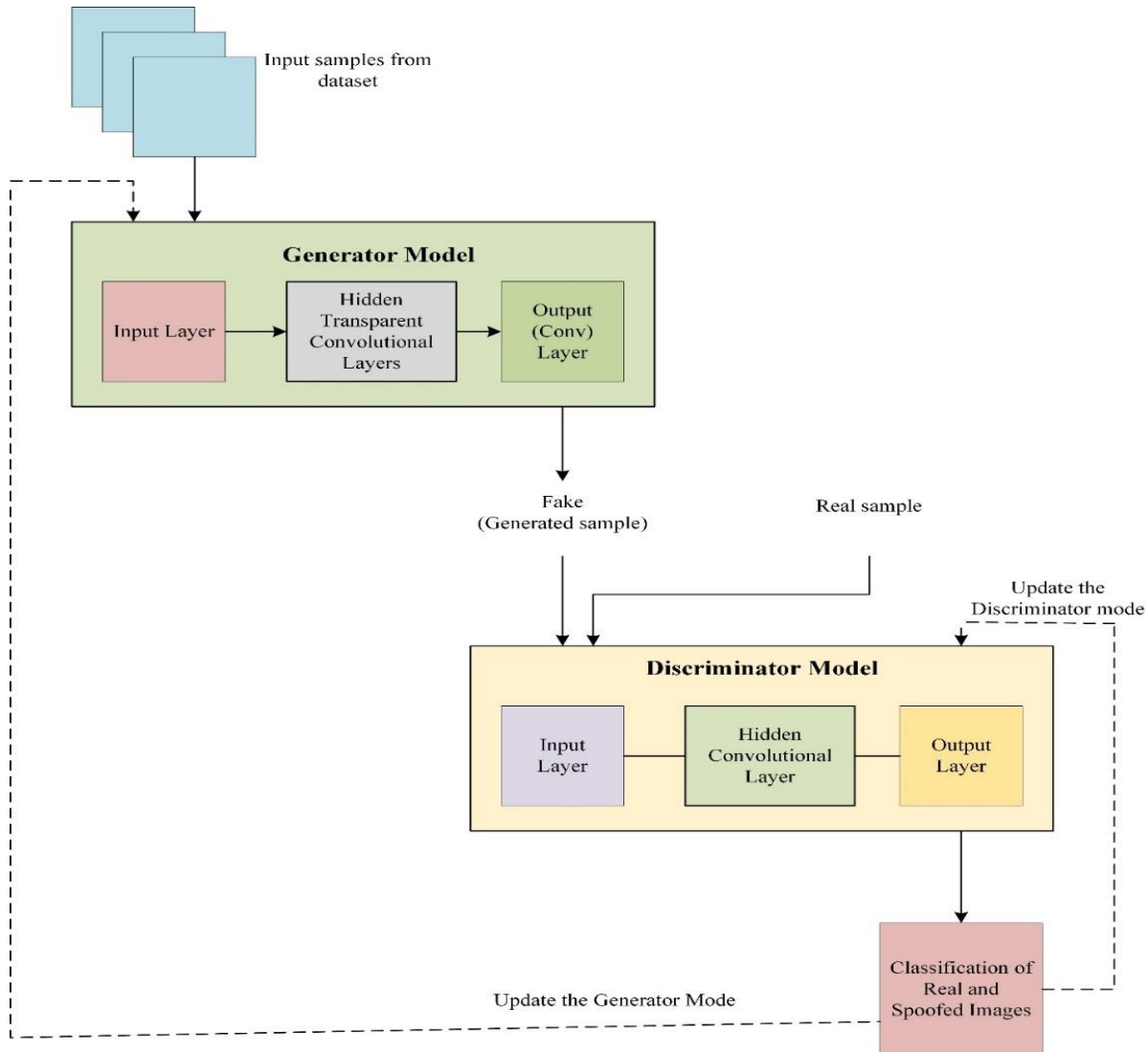


Fig. 1. Block diagram of face spoof detection with DCGAN.

B. Data Collection and Pre-processing

The data collection comprises celebrity face images collected from various sources, including the internet, celebrity websites, and publicly available databases. The dataset creators curated these images to ensure diversity in terms of demographics, facial attributes, and expressions. Each image in the CelebA dataset is manually annotated with a set of binary attribute labels. These annotations cover facial attributes such as age, eyeglasses, hair, gender and various facial expressions. The annotations provide valuable ground truth information for training and evaluating machine learning models. Fig. 2 depicts the pre-processing of CelebA dataset for face spoof detection.

The original images may vary in size and aspect ratio. The images are reconstructed to a standard resolution, typically 178x218 pixels. Pixel values in the images are normalized to a common scale, often ranging from 0 to 1 or -1 to 1. Normalization helps in minimizing alterations in pixel across

different images. Rotation, flipping, cropping, and brightness adjustments may be applied to increase the diversity of the dataset and improve model generalization. Noise reduction techniques may be employed to enhance image quality and remove unwanted artifacts. Typically, the majority of the data is allocated to the training set, while smaller portions are used for validation and testing. Thus, the pre-processed CelebA dataset is prepared for face recognition, attribute prediction, and face spoof detection.

C. Deep Convolutional GAN Architecture

The DCGAN architecture for face spoof detection involves a combination of generator and discriminator trained adversarial to produce realistic spoofed face data and distinguish them from genuine ones. The generator typically consists of multiple layers of neural network units, organized in a deep architecture. It starts with one or more input layers, usually taking random noise vectors as input. These noise vectors serve as the seeds for generating new data samples to

augment the data. The noise vectors are passed through several hidden layers, often implemented using convolutional layers, followed by ReLU to introduce non-linearity and learn hierarchical representations. The generator progressively up-samples the input noise into high-dimensional representations, which produces output images with the desired dimensions, such as grayscale or colour face images as shown in Fig. 3.

In DCGAN, the discriminator plays a crucial role in distinguishing between genuine and generated (spoofed) face images. The discriminator network is tasked with classifying input images as either genuine (real) or generated (spoofed). It takes both genuine face data from the dataset and generated face data produced by the generator as input samples. The discriminator network contains multiple convolutional layers, designed to extract features from the input and make a binary classification. During the training process, the discriminator network learns to distinguish between real and generated data by updating its parameters to minimize its classification error. It is trained in an adversarial approach with the

generator, which aims to produce realistic faces that can fool the discriminator network, while the discriminator aims to accurately classify the images. The performance of discriminator is evaluated using binary cross-entropy, which evaluates the discrepancy among the predictions of the discriminator (real or generated). The loss function guides the updates to the discriminator's parameters during training, helping it improve its capability to discriminate between genuine and generated samples.

Fig. 4 depicts the learning phase of genuine and fake data by discriminator network. The discriminator and generator are trained iteratively, where the generator targets to produce data that are indistinguishable from genuine ones, and the discriminator network for accurately classifying between real and generated images. This adversarial training process helps both networks enhance over time, with the discriminator becoming better at differentiating real and generated data, and the generator becoming better at producing realistic images to fool the discriminator.

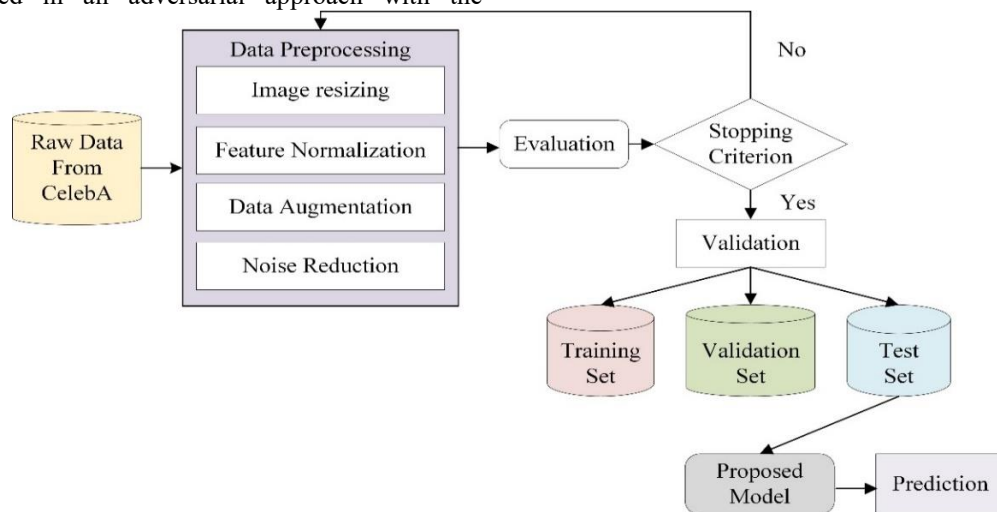


Fig. 2. Pre-processing of CelebA dataset.

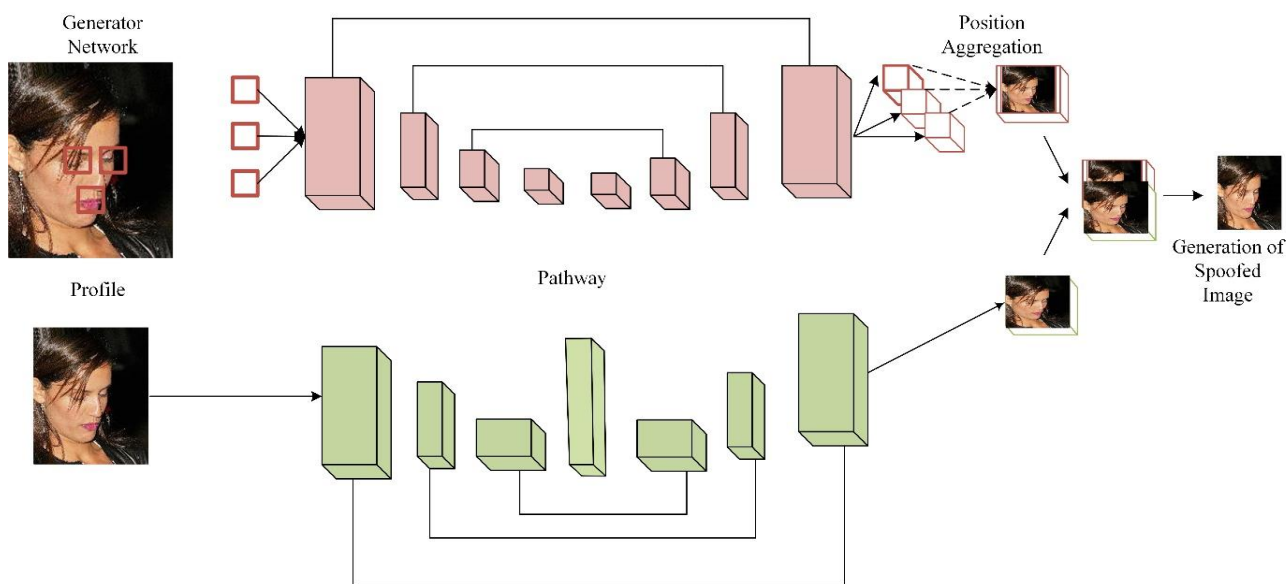


Fig. 3. Generator network in DCGAN.

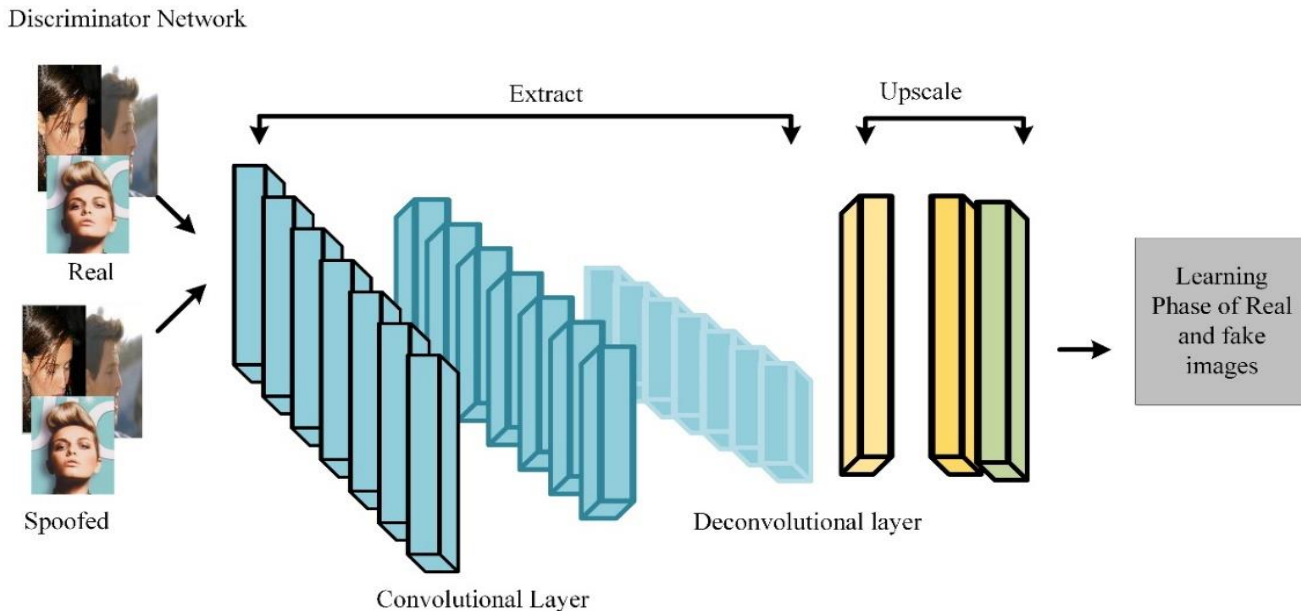


Fig. 4. Discriminator network of DCGAN.

D. Feature Extraction and Detection of Face Spoof Image using DCGAN

In face spoof detection using DCGAN (Deep Convolutional Generative Adversarial Networks), feature extraction is one of the critical steps that involves capturing discriminative characteristics from input images. The process begins with feeding genuine and spoofed face images into the discriminator network, which has been trained to differentiate between the two types of images through adversarial training. Through the adversarial training process, the discriminator becomes adept at extracting features that are discriminative for face spoof detection. These features encode subtle differences between genuine and spoofed faces, such as inconsistencies in texture, lighting, or spatial relationships. After feature extraction in face spoof detection using DCGAN, the extracted features from the discriminator capture important characteristics of both genuine and spoofed faces. These

features represent high-level representations learned during the adversarial training process, where the generator is to produce realistic spoofed faces to fool the discriminator, and the discriminator learns to distinguish between genuine and spoofed faces. These features are abstracted from the raw pixel values of the input images and are encoded in a lower-dimensional feature space, making them more suitable for detection tasks. These features are then fed to a Deep Convolutional Network (DCN), which makes the final decision on whether an input image is genuine or spoofed based on the learned representations.

Fig. 5 depicts the framework of Face Spoof Detection using DCGAN in which real and spoofed images are detected. In face spoof detection using DCGAN, performance using the loss function is formulated in Eq. (1),

$$Loss = -(b \log(a) + (1 - b) \log(1 - a)) \quad (1)$$

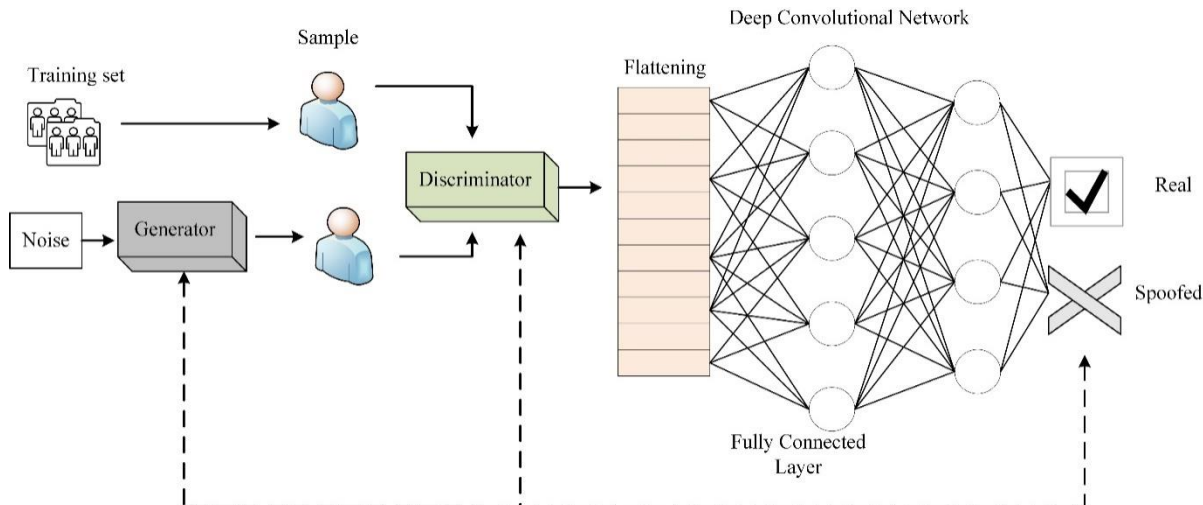


Fig. 5. Face spoof detection using DCGAN.

Here, b represents the true label of an observation, indicating whether it is a genuine (real) image or a spoofed (fake) image. The predicted label of the observation is denoted by a . It is important to note that ' a ' lies between 0 and 1, representing the probability that the observation belongs to the genuine samples. Depending on whether the system designate the real label as 0 (indicating fake images) or 1 (for real images), aim to minimize either $\log(1-a)$ or $\log(a)$, respectively. This evaluation metric helps gauge the ability of the model to distinguish between genuine and spoofed faces during training [19].

Let p denote the Gaussian noise distribution, and u represent the complex image. The generator function $G(u, p)$ generates synthetic images, while $D(u, v)$ represents the discrimination. Each output of the discriminator network ($s = 1, 2, 3, 4$) contributes to the decision process, with corresponding weights λ_s ensuring proper discrimination between genuine and spoofed data. The loss function of the discriminator, denoted as LD-sGAN(G, D), is formulated in eqn.2,

$$LD - sGAN(G, D) = E_{u, v}[\log D(u, v)] + E_{u, p}[\log(1 - D(u, G * (u, p) I))] \quad (2)$$

Here, the discriminator targets to maximize the loss function by accurately differentiating real and generated data. Conversely, the generator strives to minimize the loss function to generate more convincing fake images. The optimization paths of both the generator and discriminator are guided by this loss function, facilitating the adversarial training process in face spoof detection model.

V. RESULTS AND DISCUSSION

In this research, the implementation of face spoof detection framework using python software has been successfully achieved. This study aims in accuracy improvement of face spoof detection and identification using CelebA, a large-scale face attributes dataset. The framework achieved high accuracy of 99.1% and minimised false detection. The DCGAN architecture successfully generated realistic spoofed face images, which were challenging to distinguish from genuine ones. The performance of the model was enhanced by the adversarial relationship between the discriminator and generator networks in DCGAN, which made it easier to acquire discriminative features for face spoof detection. Fig. 6 shows the detection of real and spoofed images using proposed DCGAN. The proposed DCGAN architecture is adept at detecting both real and spoof images with high accuracy. The model learns to differentiate between authentic and manipulated facial images.

A. Performance Metrics

1) *Accuracy*: In the DCGAN-based face spoof detection model, accuracy evaluates the proportion of accurately classified images (genuine and spoofed) out of all the images in the test dataset. The formula for accuracy is given in Eq. (3),

$$Accuracy = \frac{RP+RN+FP+FN}{RP+RN} \quad (3)$$

where, RP represents the number of true positive identifications (accurately classified spoofed images). RN represents the number of true negative identifications (accurately classified genuine images). FP represents the number of false positive identifications (genuine images inaccurately classified as spoofed). FN represents the number of false negative identifications (spoofed images inaccurately classified as genuine).

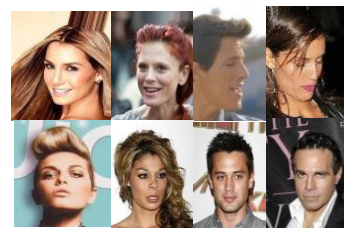
2) *Precision*: Precision is a pivotal metric in evaluating the performance of the framework based on the DCGAN-based face spoof detection architecture. It holds significant importance in classifying spoofed and genuine face images accurately. Precision measures how effectively the model can identify spoofed face images while minimizing misclassifications. The equation of precision is represented by Eq. (4),

$$Precision = \frac{AP}{AP+BP} \quad (4)$$

Here, AP denote the instances where the model correctly identifies spoofed face images, while BP represent cases where genuine face images are incorrectly classified as spoofed. Precision value from between 0 and 1, with a value of 1 indicating perfect precision, where all positive predictions are correct, and a value of 0 indicating that no correct positive predictions were made.

3) *Recall*: Recall in a face spoof detection model with DCGAN shows to the capacity of the model to accurately identify genuine face images as genuine. Specifically, it measures the proportion of actual genuine face images that are correctly classified as genuine by the framework, out of all genuine face images in the dataset. The formula for recall is given by Eq. (5),

$$Recall = \frac{True\ Positives}{True\ Positives+False\ Negatives} \quad (5)$$



Real Images



Spoofer Images

Fig. 6. Detection of real and spoofed images using proposed DCGAN.

where, True Positives (TP) are the number of genuine face images accurately identified as genuine and False Negatives (FN) are the number of genuine face images inaccurately identified as spoofed.

4) *F1 score*: In face spoof detection using DCGAN architecture, the F1 score serves as a crucial metric for evaluating performance, particularly in tasks involving the identification and categorization of spoofed and genuine face images. The F1 score is computed using eqn.6,

$$F1score = 2 \times \frac{Precision \times Recall}{Precision + Recall} \quad (6)$$

This equation provides an evaluation assessment of the framework in accurately classifying positive (spoofed) and negative (genuine) instances. The F1 score offers a comprehensive measure of the performance of the system by considering both precision and recall, in distinguishing between spoofed and genuine face images in face spoof detection.

Fig. 7 shows Accuracy Curve for Proposed Face Spoofed Detection using DCGAN. It achieves an impressive accuracy rate of 99.1% with an improvement of 9.056% over existing methods of Sequential CNN, ANNBBS and YOLO-CNN-XGBoost. This curve, plotted over the epochs, illustrates the learning process of the model, initially starting at lower accuracy values and gradually ascending as the model refines its capability to discern between genuine and spoofed faces. Thus, it upgrades the security and access control of biometric authentication systems in real-world applications.

Fig. 8 depicts the Losses of Training and Validation of the proposed DCGAN for face spoof detection which indicates the evolution of the performance of the technique. The training loss represents the discrepancy between the predicted and actual values for the training dataset, reflecting learning phase of the model to generate realistic spoofed face images and distinguish them from genuine ones. Ideally, both training and validation losses should decrease simultaneously, indicating that the model effectively generalize to new instances.

Table I depicts the Evaluation Metrics of the Proposed FSD-DCGAN with Existing Frameworks. The proposed FSD-DCGAN method stands out as the most robust and accurate among the existing techniques. The adversarial dynamic

TABLE I. EVALUATION METRICS OF THE PROPOSED METHOD WITH EXISTING FRAMEWORKS

| Methods | Accuracy | Precision | Recall | F1 score |
|---------|----------|-----------|--------|----------|
|---------|----------|-----------|--------|----------|

facilitated the learning of discriminative features for face spoof detection. It achieves an impressive 99.1% accuracy, when compared to all other methods. Its precision (93%) and recall (89.5%) strike a commendable balance, resulting in an F1 score of 92%. In contrast, the Sequential CNN method, while respectable, falls short in terms of recall (78.2%). ANNBBS exhibits high accuracy (94.9%) but sacrifices recall (72%) and F1 score (81%). The YOLO-CNN-XGBOOST approach performs reasonably well overall, with an accuracy of 90.73% and a balanced F1 score (86.36%).

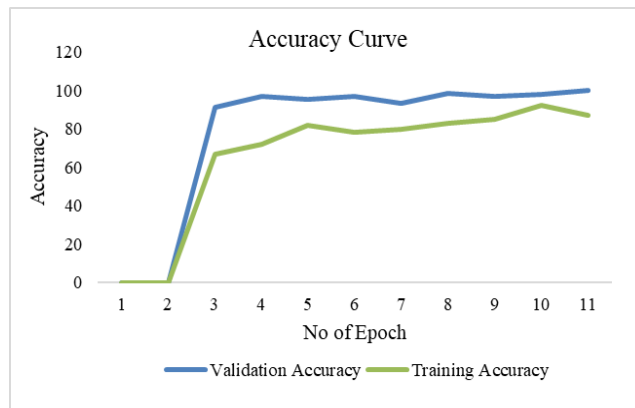


Fig. 7. Accuracy curve for proposed face spoofed detection using DCGAN.

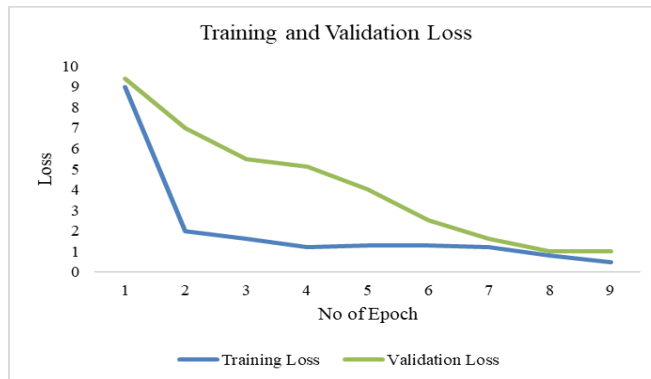


Fig. 8. Training and validation loss of proposed DCGAN.

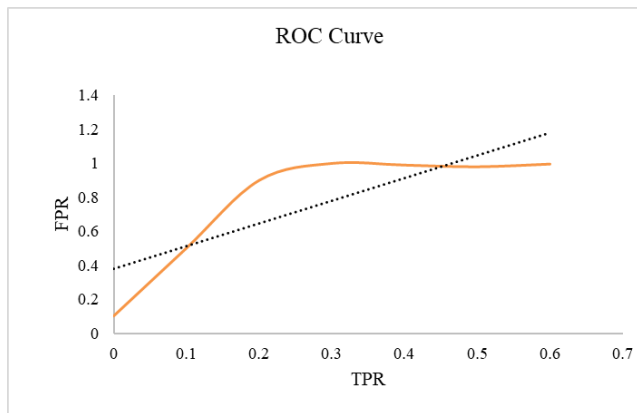


Fig. 9. ROC curve for the proposed face spoof detection using DCGAN.

| | | | | |
|-----------------------|--------|--------|--------|--------|
| Sequential CNN [20] | 87% | 93.6% | 78.2% | 86.8% |
| ANNBBS [21] | 94.9% | 90% | 72% | 81% |
| YOLO-CNN-XGBOOST [22] | 90.73% | 87.36% | 85.39% | 86.36% |
| Proposed FSD-DCGAN | 99.1% | 93% | 89.5% | 92% |

The Area Under the Curve (AUC) in face spoof detection model using DCGAN indicates to the area under the Receiver Operating Characteristic (ROC) curve. A higher AUC value, shows superior discrimination and better overall accuracy in distinguishing between real and spoofed faces. The formula for calculating the Area Under the Curve (AUC) in a ROC curve is given in Eq. (7),

$$AUC = \sum_{i=1}^n (x_i + 1 - x_{i-1}) \cdot (y_i + y_{i-1} + 1) \quad (7)$$

where, (x_i, y_i) are the points of the ROC curve, and n is the total number of points. The AUC shows the integral of the ROC curve, which measures the overall evaluation of a binary classification approach.

Fig. 9 shows ROC Curve for the Proposed Face Spoof Detection using DCGAN. The Receiver Operating Characteristic (ROC) for the proposed face spoof detection using DCGAN illustrates the exchange between True Positive and False Positive Rates across different decision limits. A higher area under the ROC curve shows superior discriminatory evaluation, with the model achieving high true positive rates while minimizing false positive rates.

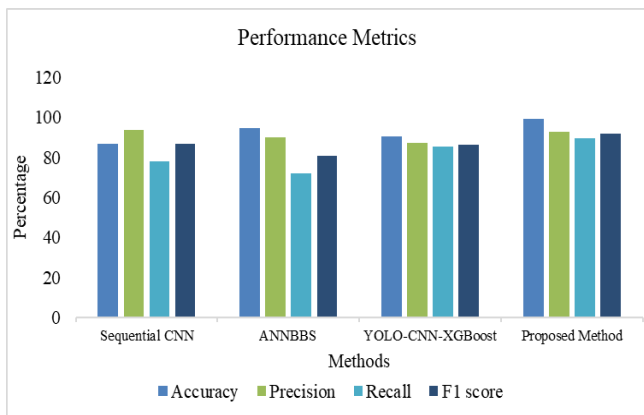


Fig. 10. Performance metrics of proposed face spoof detection using DCGAN.

Fig. 10 depicts performance metrics of proposed system with existing framework. The precision of the proposed framework DCGAN(99.1%) is greater than the existing approaches of Sequential CNN(87%), ANNBBS(94.9%) and YOLO-CNN-XGBoost (97.22%). The recall of the suggested method DCGAN (89.5%) is higher than the existing approaches of Sequential CNN (78.2%), ANNBBS (72%) and YOLO-CNN-XGBoost (85.39%). The F1-score of the suggested method DCGAN (92%) is higher than the existing approaches Sequential CNN (86.8%), ANNBBS (81%) and YOLO-CNN-XGBoost (86.36%).

B. Discussion

The discourse pertaining to the diverse frameworks utilised for identifying deep fakes and face spoofing highlights the diverse methodologies that researchers are implementing

to tackle this critical challenge. The structure of Arora et al. [11], which focuses on the extraction and categorization of face characteristics, shows encouraging levels of accuracy but could run into problems with changing spoofing techniques and a variety of datasets. With potential for improvement, Patel et al. [12] improved deep-CNN structure has great accuracy rates for a variety of false image types, including video deepfake detection. Although there are certain restrictions in domain adaptation strategies, Kumar et al. [13] focus on metric classification and triplet network design emphasises the significance of feature space differentiation. The Generative Adversarial Ensemble Learning method by Baek et al. [14] prioritises discrimination enhancement and achieves respectable accuracy at the cost of training time and computational resources. The CNN model developed by Ranjan et al. [15] using Transfer Learning exhibits better performance on various datasets; nonetheless, its dependence on pre-trained models could result in less-than-ideal outcomes. The above discussions collectively highlight the continuous attempts, each with unique advantages and disadvantages, to counter the spread of face spoofing and deepfakes.

In the domain of face spoof detection leveraging deep learning techniques, a significant advancement was achieved by integrating Deep Convolutional Generative Adversarial Networks (DCGAN), resulting in an outstanding accuracy of 99.1%, exceeding the capabilities of conventional approaches like Sequential CNN [20]. The interplay between the model's training dynamics and its effectiveness in discerning between genuine and spoofed faces is depicted through graphical representations of training and testing accuracy, loss, and ROC curves. Using samples from CelebFaces Attributes (CelebA), the model shows its ability to distinguish between authentic and spoofed facial images. Discriminative features may be learned from raw input data using DCGAN, which eliminates the requirement for human feature engineering and is a benefit for employing it for feature extraction. The outcomes generated by the proposed framework illustrate its efficacy in recognizing the subtle differences between genuine and spoofed facial features. Thus, it promotes secure access control in various applications like financial services, secure facilities, and mobile devices.

VI. CONCLUSION AND FUTURE WORKS

Biometric security has advanced significantly with the use of Deep Convolutional Generative Adversarial Networks (DCGANs) for face spoof detection. The suggested framework shows improved accuracy in differentiating between real and fake face photos thanks to the cooperation of discriminator and generator networks. Based on adversarial training, the discriminator network outperforms conventional convolutional approaches in extracting discriminative features necessary for accurate spoof detection, as demonstrated by studies conducted on the CelebFaces Attributes (CelebA) dataset. This development raises the bar for future

improvements in spoof detection technologies while simultaneously strengthening the security of biometric identity systems. Looking ahead, our study points to a number of interesting directions that warrant further investigation. First and foremost, it's imperative to strengthen the model against spoofing techniques that are getting more and more complex, like deepfake videos, by investigating innovative architectures and feature integration. Moreover, the real-time use of the model in real-world settings, such as mobile authentication apps or surveillance systems, is very valuable for quick threat identification and reaction. To ensure that the model architecture and training process are flexible enough to adapt to a variety of datasets and changing spoofing techniques, it is imperative that they be continuously improved and optimised. Furthermore, strengthening the security and effectiveness of the model in practical applications requires reducing adversarial assaults on the model itself. The efficacy and practicality of DCGAN-based face spoof detection could be further strengthened by pursuing these future research avenues, which will additionally contribute to progress in biometric security and create more robust authentication systems.

REFERENCES

- [1] "Sci-Hub | Detecting DeepFake, FaceSwap and Face2Face facial forgeries using frequency CNN. *Multimedia Tools and Applications*, 80(12), 18461–18478 | 10.1007/s11042-020-10420-8." Accessed: Feb. 08, 2024. [Online]. Available: <https://sci-hub.ee/10.1007/s11042-020-10420-8>.
- [2] D. Gong, O. S. Goh, Y. J. Kumar, Z. Ye, and W. Chi, "Deepfake Forensics, an AI-synthesized Detection with Deep Convolutional Generative Adversarial Networks," 2020.
- [3] Y. Wang, X. Song, T. Xu, Z. Feng, and X.-J. Wu, "From RGB to Depth: Domain Transfer Network for Face Anti-Spoofing," *IEEE Trans. Inf. Forensics Secur.*, vol. 16, pp. 4280–4290, 2021, doi: 10.1109/TIFS.2021.3102448.
- [4] F. Jiang, P. Liu, X. Shao, and X. Zhou, "Face anti-spoofing with generated near-infrared images," *Multimed. Tools Appl.*, vol. 79, no. 29–30, pp. 21299–21323, Aug. 2020, doi: 10.1007/s11042-020-08952-0.
- [5] S. A. Aduwala, M. Arigala, S. Desai, H. J. Quan, and M. Eirinaki, "Deepfake Detection using GAN Discriminators," in 2021 IEEE Seventh International Conference on Big Data Computing Service and Applications (BigDataService), Aug. 2021, pp. 69–77. doi: 10.1109/BigDataService52369.2021.00014.
- [6] M. Barni, K. Kallas, E. Nowroozi, and B. Tondi, "CNN Detection of GAN-Generated Face Images based on Cross-Band Co-occurrences Analysis," in 2020 IEEE International Workshop on Information Forensics and Security (WIFS), New York, NY, USA: IEEE, Dec. 2020, pp. 1–6. doi: 10.1109/WIFS49906.2020.9360905.
- [7] S. B. Balasubramanian, J. K. R., P. P. V. K., and P. Trojovský, "Deep fake detection using cascaded deep sparse auto-encoder for effective feature selection," *PeerJ Comput. Sci.*, vol. 8, p. e1040, Jul. 2022, doi: 10.7717/peerj-cs.1040.
- [8] X. Ding, Z. Raziei, E. C. Larson, E. V. Olinick, P. Krueger, and M. Hahsler, "Swapped face detection using deep learning and subjective assessment," *EURASIP J. Inf. Secur.*, vol. 2020, no. 1, p. 6, Dec. 2020, doi: 10.1186/s13635-020-00109-8.
- [9] A. Chintla et al., "Recurrent Convolutional Structures for Audio Spoof and Video Deepfake Detection," *IEEE J. Sel. Top. Signal Process.*, vol. 14, no. 5, pp. 1024–1037, Aug. 2020, doi: 10.1109/JSTSP.2020.2999185.
- [10] X. Chang, J. Wu, T. Yang, and G. Feng, "DeepFake Face Image Detection based on Improved VGG Convolutional Neural Network," in 2020 39th Chinese Control Conference (CCC), Shenyang, China: IEEE, Jul. 2020, pp. 7252–7256. doi: 10.23919/CCC50068.2020.9189596.
- [11] S. Arora, M. P. S. Bhatia, and V. Mittal, "A robust framework for spoofing detection in faces using deep learning," *Vis. Comput.*, vol. 38, no. 7, pp. 2461–2472, Jul. 2022, doi: 10.1007/s00371-021-02123-4.
- [12] Y. Patel et al., "An Improved Dense CNN Architecture for Deepfake Image Detection," *IEEE Access*, vol. 11, pp. 22081–22095, 2023, doi: 10.1109/ACCESS.2023.3251417.
- [13] A. Kumar, A. Bhavsar, and R. Verma, "Detecting Deepfakes with Metric Learning," in 2020 8th International Workshop on Biometrics and Forensics (IWBF), Porto, Portugal: IEEE, Apr. 2020, pp. 1–6. doi: 10.1109/IWBF49977.2020.9107962.
- [14] J.-Y. Baek, Y.-S. Yoo, and S.-H. Bae, "Generative Adversarial Ensemble Learning for Face Forensics," *IEEE Access*, vol. 8, pp. 45421–45431, 2020, doi: 10.1109/ACCESS.2020.2968612.
- [15] P. Ranjan, S. Patil, and F. Kazi, "Improved Generalizability of DeepFakes Detection using Transfer Learning Based CNN Framework," in 2020 3rd International Conference on Information and Computer Technologies (ICICT), San Jose, CA, USA: IEEE, Mar. 2020, pp. 86–90. doi: 10.1109/ICICT50521.2020.00021.
- [16] S. Yavuzkiliç, A. Sengur, Z. Akhtar, and K. Siddique, "Spotting Deepfakes and Face Manipulations by Fusing Features from Multi-Stream CNNs Models," *Symmetry*, vol. 13, no. 8, Art. no. 8, Aug. 2021, doi: 10.3390/sym13081352.
- [17] W. Sun, Y. Song, H. Zhao, and Z. Jin, "A Face Spoofing Detection Method Based on Domain Adaptation and Lossless Size Adaptation," *IEEE Access*, vol. 8, pp. 66553–66563, 2020, doi: 10.1109/ACCESS.2020.2985453.
- [18] W. Sun, Y. Song, C. Chen, J. Huang, and A. C. Kot, "Face Spoofing Detection Based on Local Ternary Label Supervision in Fully Convolutional Networks," *IEEE Trans. Inf. Forensics Secur.*, vol. 15, pp. 3181–3196, 2020, doi: 10.1109/TIFS.2020.2985530.
- [19] Kevin, "Generating Human Faces with DCGANs," Medium. Accessed: Feb. 12, 2024. [Online]. Available: <https://medium.com/@dungwoong/generating-human-faces-with-dcgans-7a4d54eaa89b>.
- [20] A. A. Mohamed, M. M. Nagah, M. G. Abdelmonem, M. Y. Ahmed, M. El-Sahhar, and F. H. Ismail, "Face Liveness Detection Using a sequential CNN technique," in 2021 IEEE 11th Annual Computing and Communication Workshop and Conference (CCWC), NV, USA: IEEE, Jan. 2021, pp. 1483–1488. doi: 10.1109/CCWC51732.2021.9376030.
- [21] S. Kumar et al., "Face Spoofing, Age, Gender and Facial Expression Recognition Using Advance Neural Network Architecture-Based Biometric System," *Sensors*, vol. 22, no. 14, Art. no. 14, Jan. 2022, doi: 10.3390/s22145160.
- [22] A. Ismail, M. Elpeltagy, M. S. Zaki, and K. Eldahshan, "A New Deep Learning-Based Methodology for Video Deepfake Detection Using XGBoost," *Sensors*, vol. 21, no. 16, Art. no. 16, Jan. 2021, doi: 10.3390/s21165413.

A Novel Proposal for Improving Economic Decision-Making Through Stock Price Index Forecasting

Xu Yao¹, Weikang Zeng², Lei Zhu³, Xiaoxiao Wu⁴, Di Li⁵

School of Business Administration, Xi'an Eurasia University, Xi'an 710065, Shaanxi, China^{1,3,5}

School of Economics and Management, Northwest University, Xi'an 710127, Shaanxi, China²

School of Public Administration, Xi'an University of Architecture and Technology, Xi'an 710054, Shaanxi, China³

School of International Education, Southeast Asian University of Thailand, Bangkok 10160, Thailand⁴

Abstract—The non-stationary, non-linear, and extremely noisy nature of stock price time series data, which are created from economic factors and systematic and unsystematic risks, makes it difficult to make reliable predictions of stock prices in the securities market. Conventional methods may improve forecasting accuracy, but they can additionally complicate the computations involved, increasing the likelihood of prediction errors. To address these issues, a novel hybrid model that combines recurrent neural networks and grey wolf optimization was introduced in the current study. The suggested model outperformed other models in the study with high efficacy, minimal error, and peak performance. Utilizing data from Alphabet stock spanning from June 29, 2023, to January 1, 2015, the effectiveness of the hybrid model was assessed. The gathered information comprised daily prices and trading volume. The outcomes showed that the suggested model is a reliable and effective method for analyzing and forecasting the time series of the financial market. The suggested model is additionally particularly well-suited to the volatile stock market and outperforms other recent strategies in terms of forecasting accuracy.

Keywords—Hybrid model; recurrent neural networks; grey wolf optimization; stock price prediction

I. INTRODUCTION

The finance market is a fascinating and intricate structure that profoundly affects some domains, including business, employment, and technology [1], [2]. It gives investors numerous chances to invest money and generate returns with minimal risk [3], [4]. Fama conducted one such study [5]. The current understanding of stock price behavior has been greatly influenced by this subject, which is still an important area of research in the field of finance. Fundamental analysis and technical analysis are the two main stock market decision-making methodologies used by investors. While technical analysis looks at historical market data, trends, and patterns to forecast future market movements, fundamental analysis looks at a company's financial health and its possibilities for future growth [6], [7]. Stock market forecasting has been increasingly important among knowledgeable analysts and investors in recent years. However, because of the chaotic nature of the market, it is quite challenging to analyze stock market movements and price actions [8]. Global economic conditions, market news, and quarterly earnings reports are just a few of the factors that have a significant impact on the stock market. These elements make it difficult to predict stock prices with

any degree of accuracy. The market capitalization of the listed companies is used to create the stock market indices. As a result, stock market indexes' values reflect the total value of the underlying stocks. In this market environment that is continuously changing, it is difficult to make accurate stock market predictions. Utilizing various statistical tools, researchers and market analysts have been eager to develop and test stock market behavior. These methods, which offer insights into the intricate and dynamic character of the stock market, include clustering and autoregressive integrated moving averages [9]. However, given that price changes tend to be chaotic, noisy, nonparametric, nonlinear, and nonstationary, it is challenging for analysts to accurately assess and forecast price changes [10]. These characteristics imply that traditional statistical methods may not be sufficient for effective stock market analysis.

Data analysis technologies including spreadsheets, automated data collection, and prediction models started to appear in the 1980s. With the development of technology, researchers started to employ deep learning and artificial neural networks to create models that could learn complicated relationships and extract crucial information more quickly than they could with earlier technologies. Many different architectures have been designed to address various issues and handle the complicated structure of datasets as deep learning has become more popular in recent years. Information only moves forward in a basic feedforward neural network architecture. There is no memory of past inputs; each input is handled independently. Because previous events are essential for forecasting future events, these models are not appropriate for sequential data. Recurrent neural networks (RNNs) have been created to handle similar tasks. Loops built into RNN architecture enable the persistence of pertinent data across time. Internal information is transferred within the network from one time-step to the next. With this architecture, RNNs are more suited for time series applications including stock market forecasting, language translation, and signal processing as well as sequential data modeling. Many other tasks, such as speech recognition, image captioning, and natural language processing, have been carried out using RNNs. Additionally, they have been applied in the area of finance, where they have demonstrated excellent potential for predicting stock values. RNNs are excellent for simulating complex and dynamic systems due to their capacity to retain information and develop context over time. When Hu et al. [11] used an ensemble RNN technique to forecast stock market movements, their opposing

model was able to outperform the competition. To assess the significance of features, individual data points, and particular cells in each architecture, Freeborough et al. [12] applied four well-known techniques to the RNN, long short-term memory (LSTM), and a gated recurrent unit (GRU) network trained on S&P 500 stocks data. These techniques are ablation, permutation, added noise, and integrated gradients.

More and more, real-world engineering design issues are solved optimally using stochastic operators-based metaheuristic algorithms [13]. Deterministic algorithms are trustworthy, but they are less efficient at locating global optima because they can become stuck in local optima [14]. Randomness is a technique used by stochastic optimization algorithms, such as evolutionary ones, to avoid local solutions and locate global optima in search spaces [15]. Although each run of these techniques results in a different solution, they outperform deterministic algorithms in terms of avoiding local solutions. Take for example, ant lion optimization (ALO) [16], Biogeography-based optimization (BBO) [17], Aquila optimizer (AO) [18], grey wolf optimization (GWO) [19], and so on. GWO is a recently developed meta-heuristic optimization algorithm that draws inspiration from the communal foraging behavior of grey wolves in the wild. Mirjalili et al. [19] made the initial pitch in 2014. Alpha, beta, delta, and omega wolves are used by the GWO algorithm to replicate the leadership structure and hunting strategy of grey wolves. Certain frameworks were proposed by Rajput et al. [20] for stock price forecasting, including ARIMA (Auto Regressive-Integrated-Moving Average), FLANN (Functional Link Artificial Neural Network), ELM (Extreme Learning Machine) models, and Grey Wolf optimizer. Kumar Chandra. [21] employed Elman neural network (ENN) and GWO algorithm to optimize the parameters of ENN for forecasting the stock market. A model using an artificial neural network (ANN) optimized by the GWO method was given by Sahoo et al. [22] and the Bombay Stock Exchange (BSE) was used as the dataset in their essay.

The article introduces the GWO-RNN hybrid model, a highly reliable stock price forecasting tool. By contrasting it with many other models, including RNN, BBO-RNN, and AO-RNN, the study evaluated its accuracy. A method involving several analytical steps was used to achieve this. The principal contributions of the investigation are as follows:

A novel hybrid model is presented in this study, which integrates GWO and RNNs to tackle the intricacies associated with stock price prediction. The purpose of this hybrid model is to address the drawbacks of traditional methods by providing a more efficient forecasting method, with reduced computation complexity and prediction error probability.

The analysis utilizes Alphabet stock data spanning from January 1, 2015, to June 29, 2023, to assess the effectiveness of the hybrid model that has been proposed. In terms of high efficacy, minimal error, and optimum performance, the results demonstrate that the proposed model outperforms alternative models, thereby establishing its dependability for forecasting and analyzing financial market time series data.

The research paper validates the reliability of the GWO-RNN model as an instrument that generates exceptionally

precise forecasts of stock prices. The text underscores the model's capacity to rapidly analyze and interpret substantial amounts of data by combining grey wolf optimization-based optimization with recurrent neural networks. This functionality offers investors significant insights of market trends as well as prospective investment prospects.

The proposed model exhibits exceptional suitability for chaotic stock markets, outperforming other contemporary strategies in terms of the accuracy of its forecasts. This indicates that the GWO-RNN model is capable of efficiently managing the difficulties presented by market volatility, rendering it a dependable instrument for investors in search of precise forecasts in ever-changing financial landscapes.

Section II of this research contains the literature review. Section III offers a thorough examination of the data source and all of its relevant components. The data was analyzed using a variety of methodologies, including the RNN model, evaluation metrics, and the GWO optimizer. The experimental findings are presented in Section IV. Next, they are contrasted and discussed with those from other approaches in Section V. The research's findings are finally summarized in Section VI.

II. LITERATURE REVIEW

In the last decade, the application of machine learning (ML) algorithms to predict stock markets has increased substantially. Christanto et al. [23] suggested an examination of methodologies employed in the capital market to predict stock prices through a comparative analysis of ML, technical analysis, and fundamental analysis. They utilized Support Vector Regression (SVR) and Support Vector Machine (SVM) as ML methodologies to forecast stock prices. The assessment includes three parameter groups: technical-only (TEC), financial statement-only (FIN), and a combination of the two (COM). Experiments revealed that the integration of financial statements had no impact on SVR forecasts yet had a beneficial impact on SVM forecasts. 83 percent was the accuracy rate attained by the model in the conducted investigation. In their study, Chen et al. [24] investigated the historical context of economic recessions, emphasizing the abrupt and disastrous outcomes that can be observed in instances like the 2008 financial crisis, which was marked by a significant decline in the S&P 500. Motivated by the potential benefits of prompt crisis detection, they applied advanced ML techniques, such as Extreme Gradient Boosting and Random Forest, to predict potential market declines in the United States. By comparing the efficacy of these methodologies, their investigation aims to determine which model exhibits superior predictive capability for US stock market collapses. An analysis was conducted on market indicators utilized in crisis forecasts. This involved the utilization of daily financial market data and 75 explanatory variables, including both broad US stock market indexes and sector indexes. Through the utilization of specific classification metrics, they arrived at conclusions regarding the effectiveness of their predictive models. Tsai et al. [25] examined the interest of investors in stock forecasting, focusing on the recent application of ML to enhance precision. They deliberated on fiscal year-end selection and the impact that misaligned reporting periods have on investment decisions and comparability. They utilized ML models for fundamental

analysis to predict Taiwan's (TW) stock market returns with an emphasis on synchronized fiscal years. Using models such as Financial Graph Attention Network (FinGAT), Feedforward Neural Network (FNN), Random Forest (RF), and Gated Recurrent Unit (GRU), they constructed stock portfolios with higher anticipated returns. Their research indicates that in terms of returns and portfolio scores, these portfolios surpassed the benchmarks of the TW50 index. They assert that ML models proved advantageous in the domains of investment decision-making and stock market analysis. Ardakani et al. [26] presented a federated learning framework utilizing Random Forest, Support Vector Machine, and Linear Regression models for stock market forecast. To determine the optimal strategy, they contrasted federated learning with centralized and decentralized frameworks, and the strategies of learning frameworks for stock market prediction were elucidated by their results. Mamluatul et al. [27] developed an innovative approach for forecasting stock prices by integrating ML, stock price data, technical indicators, and Google trends. To forecast stock prices, SVR, Multilayer Perceptron (MLP), and Multiple Linear Regression were implemented. With a Mean Absolute Percentage Error (MAPE) of 0.50%, SVR outperforms MLP and Multiple Linear Regression in forecasting Indonesian stock prices. They discovered that SVR accurately forecasts stock prices, enabling investors to make informed judgments regarding the stock market. Juare et al. [28] emphasized the significance of stock market analysis in determining financial market profits. Random Forest (RF), SVM, K-nearest neighbors (KNN), and Logistic Regression were utilized in their research to forecast stock market trends. The evaluation criteria for these algorithms are accuracy, recall, precision, and F-Score. Locating the optimal algorithm for stock market prediction was the primary objective. The value that investors and stock exchanges can derive from accurate forecasts underscores the significance of predictive models in the realm of financial decision-making. The importance of investors utilizing forecasting stock prices (SPP) models for profit in the global financial market was underscored by Swathi et al. [29]. SPP models from the past employed statistical and ML techniques. They presented SCODL-SPP, a method for predicting stock prices that integrates deep learning and Sine Cosine Optimization (SCO), in their investigation. The SCODL-SPP model employs deep learning and a stacked long short-term memory (SLSTM) model to predict the closing prices of stocks. The SCO algorithm is employed to optimize the hyperparameters of the SLSTM model after the min.

The literature review on stock market prediction closes several identified research gaps effectively. By utilizing the Alphabet stock as a central metric, this study offers specific insights about Alphabet stock, thus expanding the purview of research in this field. In addition, it addresses a void in the literature concerning the evaluation of data quality and preprocessing methodologies by providing clear and transparent explanations of data preprocessing procedures, thereby guaranteeing data quality and reproducibility. Furthermore, the incorporation of domain-specific insights into the GWO-RNN model improves the precision of predictions, thereby surmounting the drawback associated with the inadequate integration of domain knowledge. Furthermore,

conducting a comparative analysis between the GWO-RNN model and other hybrid methods provides significant contributions to the understanding of the effectiveness of ensemble methods, thereby addressing a gap in the current body of research on this subject. Through an assessment of the GWO-RNN model's ability to on Alphabet stock market data encompassing the period from January 1, 2015, to June 29, 2023, this research ultimately establishes the model's dependability and efficacy in the domain of financial time series analysis and prediction. The aforementioned contributions symbolize noteworthy progressions in the field of stock market forecasting, resulting in enhanced predictive models' resilience, precision, and practicality within financial markets.

III. RESEARCH METHODS

A. Recurrent Neural Network

In the complicated field of machine learning, different algorithms and techniques are used to interpret and analyze data. The recurrent neural network (RNN), which is made to handle sequential input, is one of the most crucial tools in this field and it is displayed in Fig. 1 and Fig. 2. RNNs can incorporate prior knowledge and produce outputs based on prior learning, in contrast to conventional feedforward neural networks, which only take into account the current input. The network's loop structure, which maintains a memory of previous inputs and outputs, enables this. The activation layer of each RNN unit uses a hyperbolic tangent function to process input and convert it into a format that the rest of the network can understand. The network updates its internal state as the input is analyzed, enabling it to take into account the context of earlier inputs when generating outputs. Because RNNs can take into account temporal context, which results in more effective and efficient learning, they are more accurate and useful than regular neural networks [30].

$$h_t = \sigma(W_{xt} + U_{ht-1} + b) \quad (1)$$

in the equation, b stands for the bias of the neuron, and W and U are weight matrices that represent the input to the current cell and the recurrent input, respectively. The input and hidden states of the cell at time t are represented by the values of x_t and h_t . The symbol σ designates the sigmoid function of the neuron.

B. Biogeography-based Optimization

The foundation of biogeography-based optimization (BBO) is the movement of species according to the appropriateness of their habitat. Thus, a solution is like a habitat for an optimization issue. A crowded environment, where conditions for living species are better than in other habitats, is a better option for the population. The habitat in which living things struggle is the worst answer for the population. By sharing their traits, the superior solutions draw in the inferior ones. The following operators are used in processing this feature sharing. The operator of Migration: Migration is the process by which, following emigration and immigration rates, a better habitat replaces a worse option. The pace at which a species leaves its environment is known as its emigration rate. A better solution will have a greater emigration rate than a bad one. Conversely, the rate of immigration represents the amount by which a

species departs from its natural environment. As a result, the bad option will have a larger immigration rate than the better

one. The fundamental form of BBO has been represented by straight lines, as shown in Fig. 3. We have for the straight lines

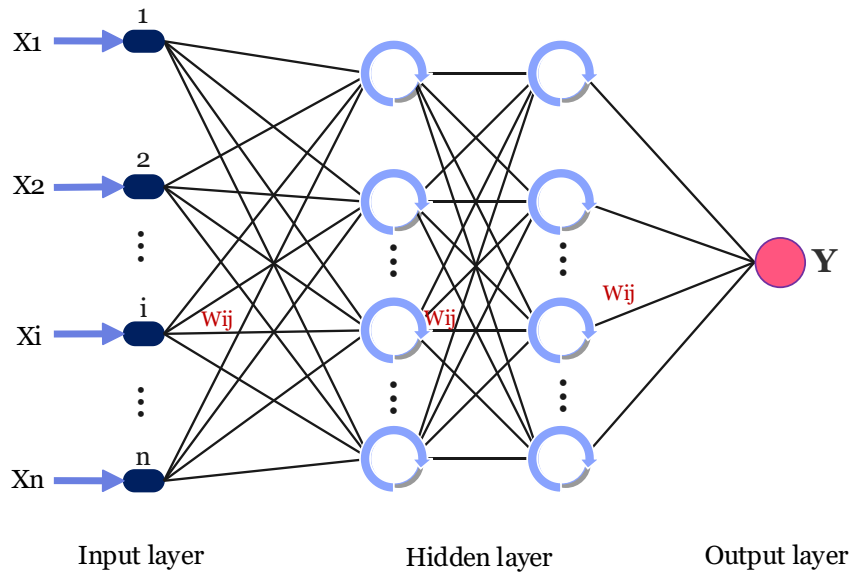


Fig. 1. RNN structure.

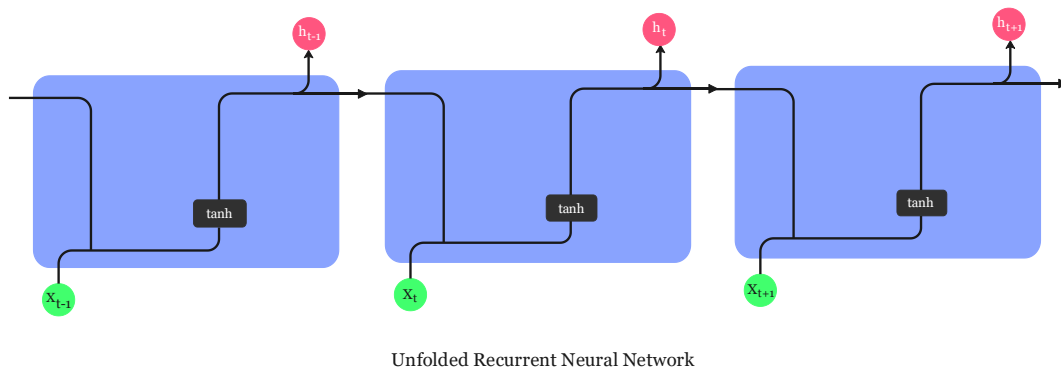


Fig. 2. The process of transforming data in RNN nodes.

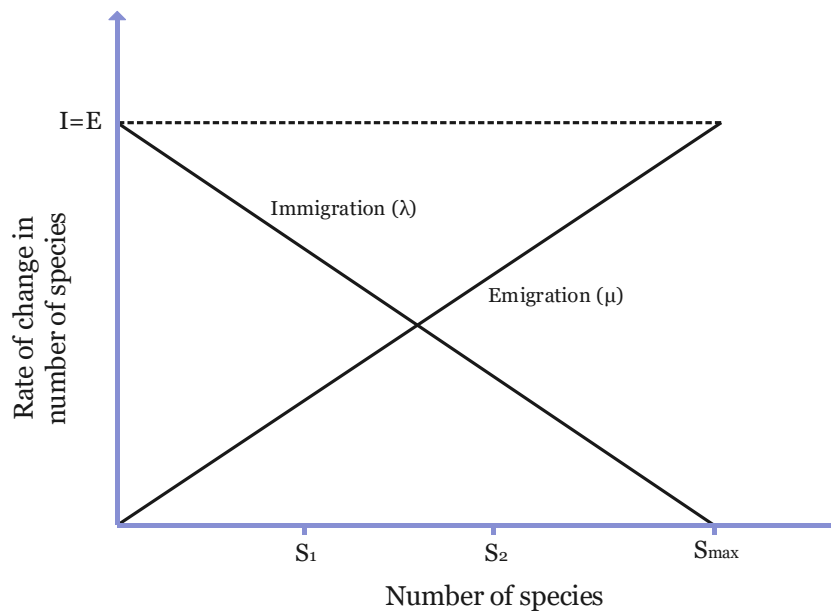


Fig. 3. The diagram of two habitats.

$$\mu_k = \frac{E \times k}{n} \lambda_k = I \left(1 - \frac{k}{n} \right) \quad (2)$$

where,

μ_k : The k^{th} habitat's emigration rate.

λ_k : The k^{th} habitat's immigration rate.

I : The highest rate of immigration.

E : The highest rate of emigration.

$n = S_{\max}$: The most species that a habitat can sustain.

k : The total number of species.

An abundance of species is indicated by a high HSI, which is characterized by a high rate of emigration and a low rate of immigration to nearby habitats. An increase in species leads to a decrease in immigration rate. The rate of emigration, however, rises in tandem with the number of species. Solutions S1 and S2 are the two possible options. For the most part, S2 is a good response, while S1 is a bad one. S1 has, on average, higher immigration rates than S2. Comparing S1 with S2 emigration rates, the former will be lower. The Fig. 3 represents the process of two habitats.

Mutation: A BBO mutation is comparable to an abrupt shift in environmental circumstances brought on by other events such as a tornado, volcanic eruption, or natural disaster. The species migrates to a new habitat when its old one becomes unsuitable for survival, as shown by the random change in the solution.

C. Aquila Optimization

The AO algorithm, a novel one, was released in 2021 [18]. The four categories in this algorithm were inspired by the hunting tactics of the raptor bird Aquila. In the first category, birds of prey are tracked down and pursued while flying high in the air. The swift attack of prey at low altitudes close to the ground is carried out by the second category, which glides.

With a slow descent and low-altitude flight, the third group gradually attacks its prey. Using diving to catch terrestrial prey is the fourth category. Quick acceleration, convergence, and stability are all made possible by the AO algorithm's potent optimization capabilities [18]. The reliability and consistency of it are also very high. The act of a vertical dive is what an eagle does when it spots a potential prey area. The bird quickly determines the ideal hunting location on the ground by flying at great altitudes. The most efficient course of action is determined using an equation that takes the search area into account. Fig. 4 is an example of the one of hunting strategies of this bird.

$$\begin{cases} Z_1(t+1) = Z_{\text{best}}(t) \times \left(1 - \frac{t}{T} \right) \\ \quad + (Z_M(t) - Z_{\text{best}}(t) \times \text{rand}) \\ Z_M(t) = \frac{1}{N} \sum_{i=1}^N Z_i(t), \\ \forall j = 1, 2, \dots, \text{Dim} \end{cases} \quad (3)$$

where, (t) is the best course of action, indicating the location of the closest target prey, and $Z(t+1)$ is the solution of generation $t+1$, produced by the search method $Z_1 \cdot Z_{\text{best}}(t)$. This iteration's t is the number. T is the maximum number of iterations that can be done. $Z(t)$ is a visual representation of the current solution's position mean at the t -th iteration. The name of a random integer between 0 and 1 is Rand . The following rapid gliding attack: The eagle soars to a height to identify the prey region in order to reduce the hunting zone or the search space for the most effective response according to the equation that follows:

$$\begin{cases} Z_2(t+1) = Z_{\text{best}}(t) \times Z(D) \\ \quad + Z_R(t) + (y - z) \times \text{rand} \\ L(D) = s \times \frac{\mu \times \sigma}{|v|^{\frac{1}{\beta}}} \end{cases} \quad (4)$$

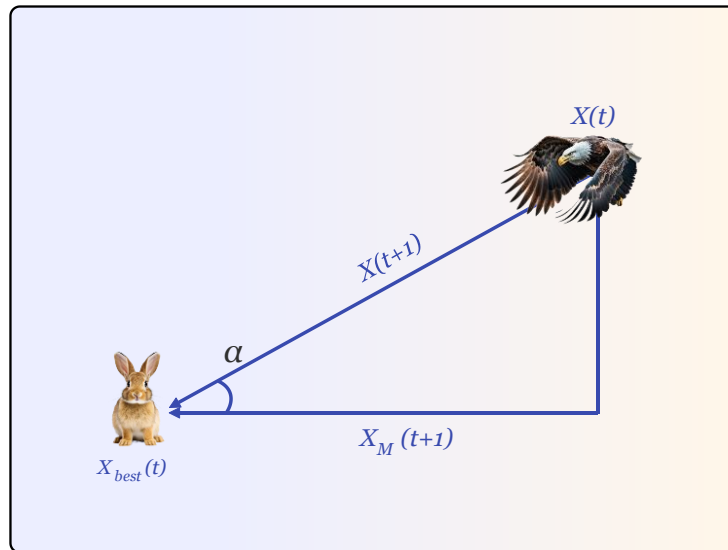


Fig. 4. The illustration of Aquila optimization.

where, $L(D)$ stands for the hunting flight distribution function, D for the dimensional space, and $Z_R(t)$ for the random solution between $[1, N]$. Once the prey region has been precisely identified and the Aquila is prepared to land and strike, it switches to the low-flying, slow-falling assault mode at the chosen target position. The third low-altitude flight pattern is this one. By employing this strategy, the bird may see how its prey would react and slowly move in its direction as in the following formula:

$$Z_3(t + 1) = (Z_{best}(t) - Z_M(T)) \times \alpha - \text{rand} + ((U_b - L_b) \times \text{rand} + L_b) \times \delta \quad (5)$$

where, α and δ are the modifying parameters. The upper limit of the given problem is U_b . The bottom limit of the problem is denoted by L_b . The fourth method of walking

capture is the eagle striking the target from above while performing quick convergence using the following equation:

$$\begin{cases} Z_4(t + 1) = Q_F \times Z_{best}(t) \\ \quad - (G_1 \times Z(t) \times \text{rand}) \\ \quad - G_2 \times L(D) + \text{rand} \times G_1 \\ Q_F(t) = \frac{2 \times \text{rand} - 1}{t^{(1-T)^2}} \\ G_1 = 2 \times \text{rand} - 1 \\ G_2 = 2 \times \left(1 - \frac{t}{T}\right) \end{cases} \quad (6)$$

the quality function, or Q_F , and the search technique are balanced. Aquila's actions while pursuing its prey are fully visible on G_1 . Aquila's flying slope when hunting is represented by G_2 . $Z(t)$ is the answer for the current iteration.

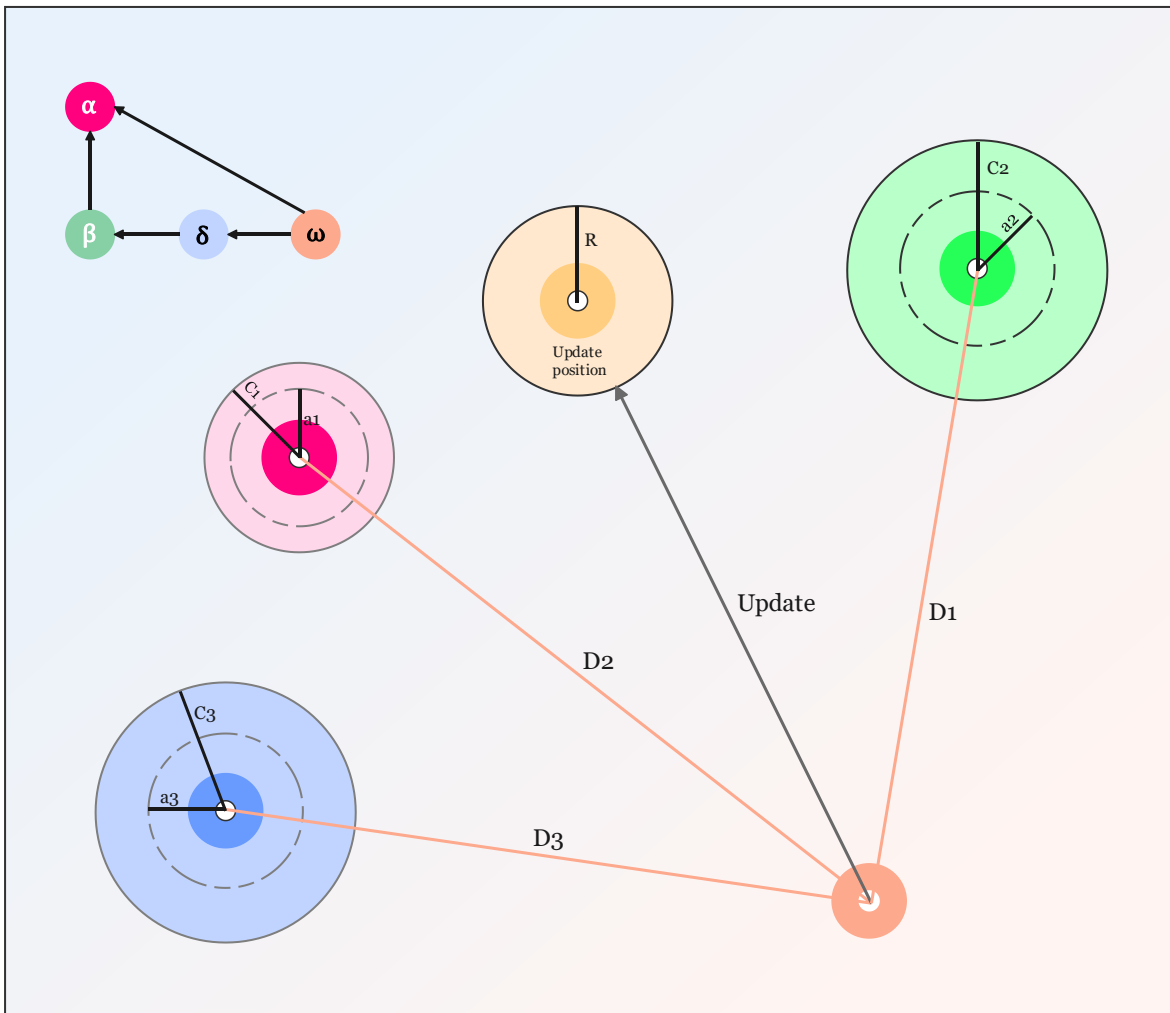


Fig. 5. The structure of Gray wolf optimizer.

D. Gray wolf optimizer

Utilizing a meta-heuristic approach, the Gray Wolf Optimizer, a unique optimization method, has been created. Mirjalili et al. [19] proposed a method, that mimics the gray wolf social structure and hunting methods. According to Fig. 5,

the hierarchy of leadership contains four options: Alpha, Beta, Delta, and Omega, with Omega being the final challenger. Alpha is the best alternative and Fig. 6 represents how this optimizer works. The three main hunting methods used in the approach include chasing, encircling, and attacking prey in an effort to replicate wolf behavior. The equation illustrated below

was used to simulate the movement of gray wolves during nature hunting:

$$\begin{aligned} \vec{D} &= |\vec{C} \cdot \vec{X}_p(t) - \vec{X}(t)| \\ \vec{X}(t+1) &= \vec{X}_p(t) - \vec{A} \times \vec{D} \end{aligned} \quad (7)$$

$$\begin{aligned} \vec{D}_\alpha &= |\vec{C}_1 \cdot \vec{X}_\alpha - \vec{X}|, \vec{D}_\beta = |\vec{C}_2 \cdot \vec{X}_\beta - \vec{X}|, \vec{D}_\delta \\ &= |\vec{C}_3 \cdot \vec{X}_\delta - \vec{X}| \end{aligned} \quad (9)$$

$$\begin{aligned} \vec{X}_1 &= \vec{X}_\alpha - \vec{A}_1 \cdot \vec{D}_\alpha, \vec{X}_2 = \vec{X}_\beta - \vec{A}_2 \cdot \vec{D}_\beta, \vec{X}_3 \\ &= \vec{X}_\delta - \vec{A}_3 \cdot \vec{D}_\delta \end{aligned} \quad (10)$$

$$\vec{X}(t+1) = \frac{\vec{X}_1 + \vec{X}_2 + \vec{X}_3}{3} \quad (11)$$

when the wolves undertake a last assault to accomplish the mission, as shown by the subscripts α, β , and δ . An is a random variable with a value between $-2\vec{a}$ and $2\vec{a}$, whereas an is used to simulate the previous assault by altering \vec{a} value from 2 to 0. Therefore, decreasing a would also cause a decrease in \vec{A} . $|\vec{A}| < 1$ forced the wolves into sticking to their prey. Gray wolves hunt in groups and follow the alpha wolf, dispersing to forage and reassembling to attack. Whenever $|\vec{A}|$ has a random value bigger than unity, the wolves may split apart in pursuit of prey. The two setup parameters for the GWO method that are most important are the wolf count and generation number. Each generation is a wolf's final deed, and the quantity of wolves accurately reflects function assessments across time. This means that the total number of objective function evaluations will be equal to the wolf population times the size of the generation, or,

$$OFEs = N_w \times N_G \quad (12)$$

E. Data source and Preparation

When conducting a thorough analysis of a stock, it's important to take into account some factors, such as the trading volume and the Open, High, Low, and Close (OHLC) prices over a specific period. For this specific study, information on Alphabet Inc. began to be gathered in 2015. For each day during the specified period, this data included information on both the trading volume and the OHLC prices. Examining the data landscape carefully to spot any anomalies, outliers, or discrepancies that might have an impact on the accuracy of the findings was the first step. Following this analysis, the dataset underwent several cleaning and preparation steps, using various techniques like scaling and normalization to reduce errors and guarantee consistency in training results via using the following equation:

$$X_{scaled} = \frac{(X - X_{min})}{(X_{max} - X_{min})} \quad (13)$$

This methodical approach aimed to raise the general level of data quality that served as the basis for the forecasting models. To further improve the models, the prepared data was split into two subsets, with 80% of the data used for training and the remaining 20% for testing and validation according to Fig. 7. The goal of this division was to strike a balance between the requirement for a sizable amount of data for model training and the requirement for a varied and untested set for exhaustive testing and validation.

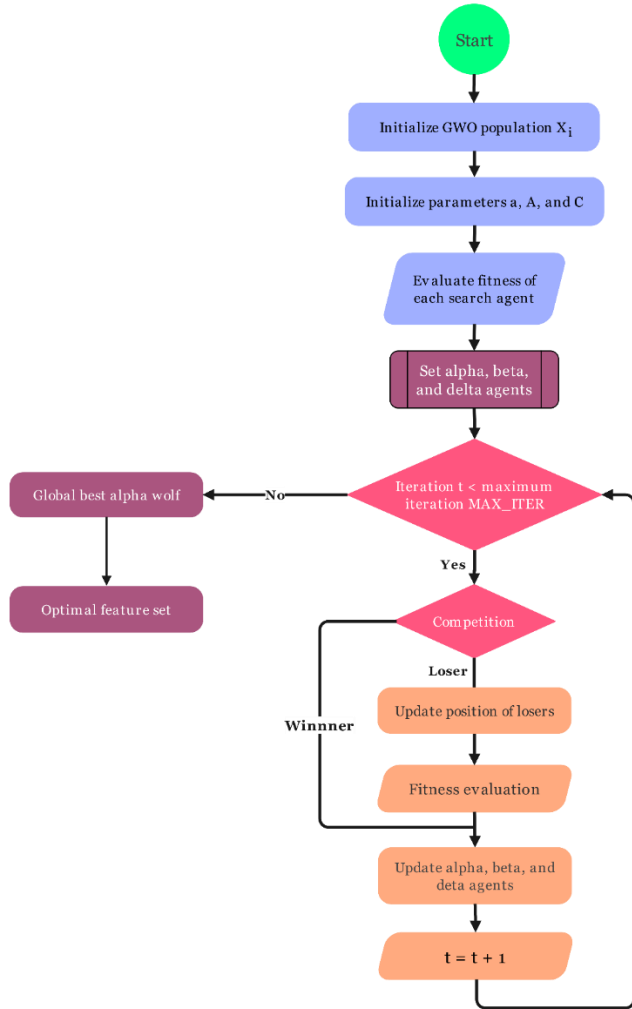


Fig. 6. Diagram of the Gray wolf optimizer.

where t is the current iteration, \vec{D} stands for movement, \vec{X}_p for prey location, \vec{A} and \vec{C} for coefficient vectors, and \vec{X} stands for a gray wolf's position. The coefficient vectors (\vec{A} and \vec{C}) are built using the relationships shown below:

$$\begin{aligned} \vec{A} &= 2\vec{a} \times \vec{r}_1 - \vec{a} \\ \vec{C} &= 2 \times \vec{r}_2 \end{aligned} \quad (8)$$

Using information from alpha, beta, and delta, the position of new search reps that include omegas is modified accordingly:

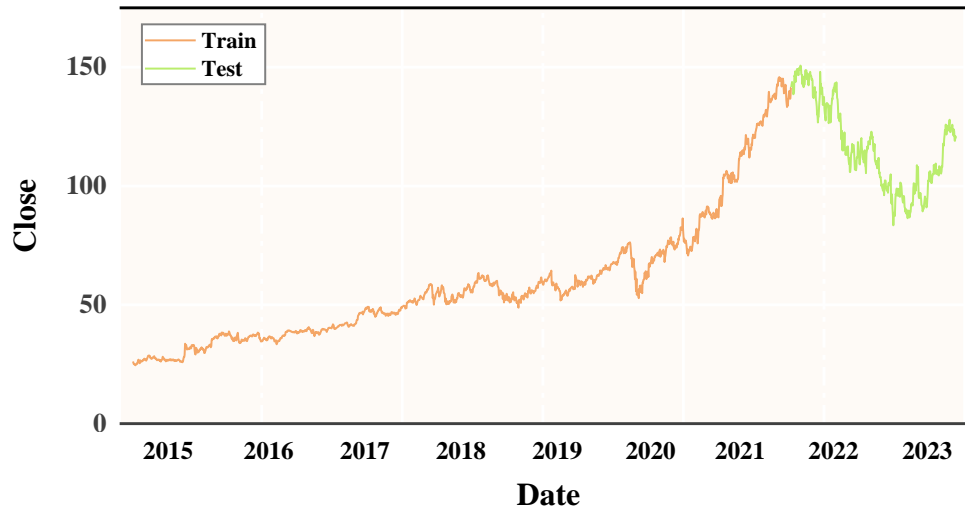


Fig. 7. Dividing the data into training and tests.

F. Assessment Criteria

In order to ensure the validity and accuracy of future projections, a diverse range of performance indicators were employed. These metrics were meticulously selected to provide a comprehensive evaluation of the prognostications. Throughout the evaluation process, several metrics, including the mean absolute error (MAE), which calculates the average absolute difference between the predicted and actual values, the root mean square error (RMSE), which measures the root mean square of the errors between the predicted and actual values, and the coefficient of determination (R^2), which gauges the proportion of variance in the dependent variable that is predictable from the independent variable was considered. These methodologies are highly valuable for assessing the accuracy of forecasting models and can facilitate more informed decisions.

$$RMSE = \sqrt{\frac{\sum_{i=1}^n (y_i - \hat{y}_i)^2}{n}} \quad (14)$$

$$MAE = \frac{\sum_{i=1}^n |y_i - \hat{y}_i|}{n} \quad (15)$$

$$R^2 = 1 - \frac{\sum_{i=1}^n (y_i - \hat{y}_i)^2}{\sum_{i=1}^n (y_i - \bar{y})^2} \quad (16)$$

IV. EXPERIMENTAL RESULTS

A. Statistical Values

The study's component includes a table (see Table I) that presents comprehensive statistical information about the dataset. The table displays OHLC pricing and volume statistics, which help to clarify the data. Statistical metrics such as count, mean, minimum (Min), standard deviation (Std.), 25%, 75%, variance, and maximum (Max) values are also provided, enabling a more detailed and precise analysis of the data.

B. Results of the Each Model

The primary goal of this study is to identify and assess the top hybrid algorithm for stock price forecasting. To do this, the research created forecasting models and looked at intricate factors that affect stock market patterns. The objective is to deliver analytical information that can help analysts and investors make wise investment decisions. Each model's performance is comprehensively evaluated, along with a thorough study of its efficacy, in Table II, Fig. 8, and Fig. 9.

TABLE I. STATISTICAL SUMMARY OF THE DATA SET

| | Open | High | Low | Volume | Close |
|----------|----------|----------|----------|----------|----------|
| Count | 2137 | 2137 | 2137 | 2137 | 2137 |
| Mean | 70.05219 | 70.81457 | 69.3428 | 32.59751 | 70.09629 |
| Std. | 34.54605 | 34.97686 | 34.14654 | 15.6062 | 34.55914 |
| Min | 24.66478 | 24.7309 | 24.31125 | 6.936 | 24.56007 |
| 25% | 41.0205 | 41.22 | 40.851 | 23.248 | 41.046 |
| 75% | 96.77 | 98.94 | 95.38 | 37.066 | 96.73 |
| Max | 151.8635 | 152.1 | 149.8875 | 223.298 | 150.709 |
| Variance | 1193.43 | 1223.381 | 1165.986 | 243.5536 | 1194.334 |

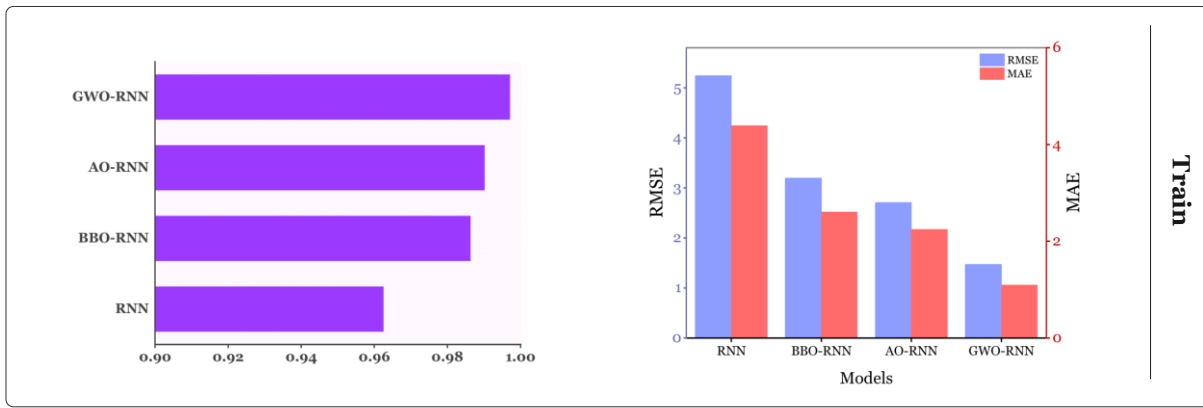


Fig. 8. Values for each model's training-related assessment.

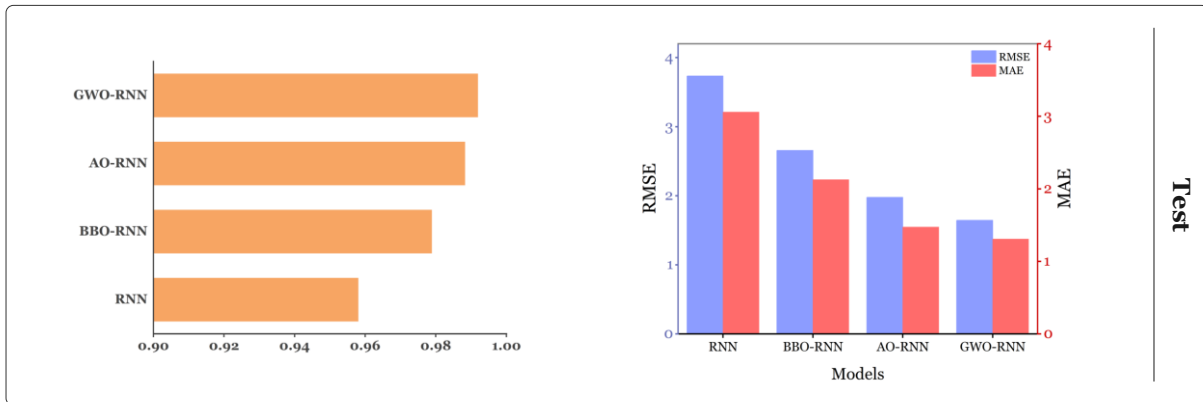


Fig. 9. Values for each model's testing-related assessment.

TABLE II. THE RESULTS OF THE MODELS FORECAST EVALUATION

| | TRAIN SET | | | TEST SET | | |
|---------|-----------|-------|-------|----------|-------|-------|
| | R^2 | RMSE | MAE | R^2 | RMSE | MAE |
| RNN | 0.962 | 5.241 | 4.389 | 0.958 | 3.733 | 3.058 |
| BBO-RNN | 0.986 | 3.193 | 2.604 | 0.979 | 2.654 | 2.126 |
| AO-RNN | 0.990 | 2.705 | 2.244 | 0.988 | 1.976 | 1.472 |
| GWO-RNN | 0.997 | 1.467 | 1.094 | 0.992 | 1.643 | 1.306 |

Three widely accepted metrics—RMSE, MAE, and R^2 —were used to carry out a detailed review of the data analysis. These indicators are well known for being able to offer a precise assessment of the analysis's dependability, correctness, and overall effectiveness. With and without an optimizer, the RNN model's performance was evaluated using the R^2 , RMSE, and MAE criteria. This evaluation improved comprehension of the model's performance and aided in making decisions based on the outcomes.

V. DISCUSSION

A. Analysis of the Models

This study's principal objective is to identify and evaluate the most effective hybrid algorithm for stock price prediction. In order to accomplish this, the study developed forecasting models and examined complex variables that influence stock market patterns. The primary aim is to provide analysts and investors with valuable analytical data that can assist them in

making informed investment choices. The performance of each model is assessed exhaustively, and its effectiveness is thoroughly examined in Table II, Fig. 8, and Fig. 9. The R^2 , RMSE, and MAE criteria were used to assess the performance of the RNN model both with and without the optimizer. This enabled wise decisions by giving a thorough grasp of the model's performance. Analysis of the training and test sets revealed that, without the optimizer, the RNN model generated R^2 values for training and testing of 0.962 and 0.958, respectively. The RMSE values for training and testing were 5.241 and 3.733, respectively, despite the MAE values being 4.389 and 3.058. By integrating optimizers, the RNN model performs significantly better. For instance, when the BBO optimizer was used, the R^2 value for the tests increased to 0.979. Furthermore, the RMSE and MAE values for testing, which came in at 2.654 and 2.126, respectively, were lower than those for training. The AO-RNN model performed better than the BBO-RNN model and produced better results. Specifically, the results for the training and testing R^2 were

0.990 and 0.988, respectively. It's crucial to remember that the MAE and RMSE figures fell to 1.472 and 1.976 during the testing. This shows increased precision. The GWO-RNN model has demonstrated remarkable accuracy and reliability in regression analysis. The model achieved the highest R^2 scores of 0.997 and 0.992 for the training and testing datasets, respectively. This indicates that the model has a high predictive power and can explain almost all the variability in the data.

Furthermore, the model's performance is exceptional, as evidenced by the low MAE and RMSE training values of 1.094 and 1.306, and testing values of 1.467 and 1.643, respectively. These values represent the amount of error between the actual and predicted values, with lower values indicating higher accuracy. Therefore, the GWO-RNN model has shown exceptional accuracy in both the training and testing data sets.

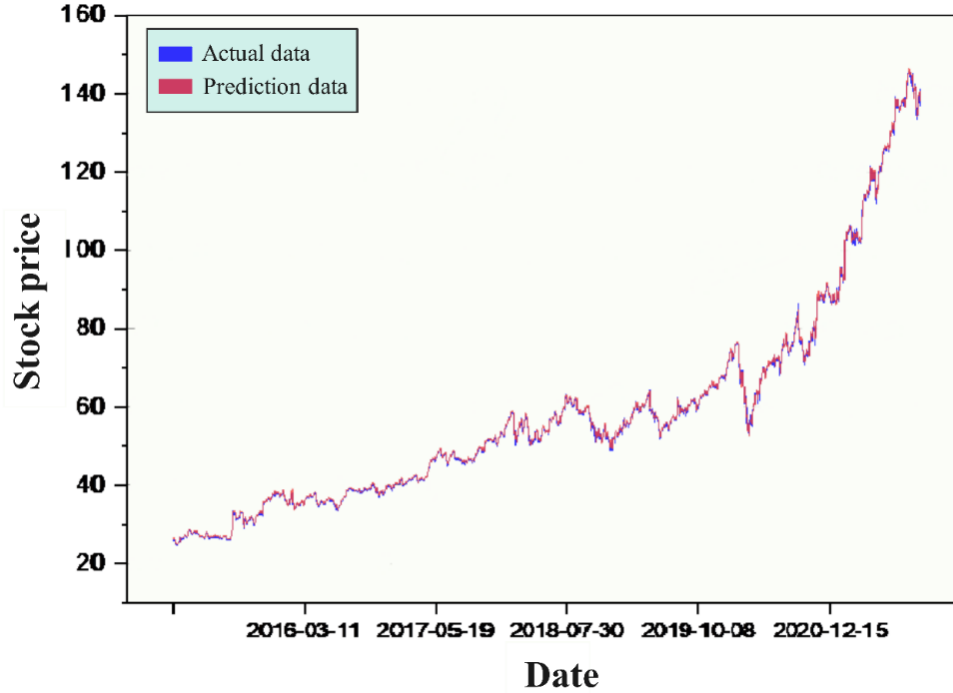


Fig. 10. The prediction curve is produced by training with GWO-RNN.

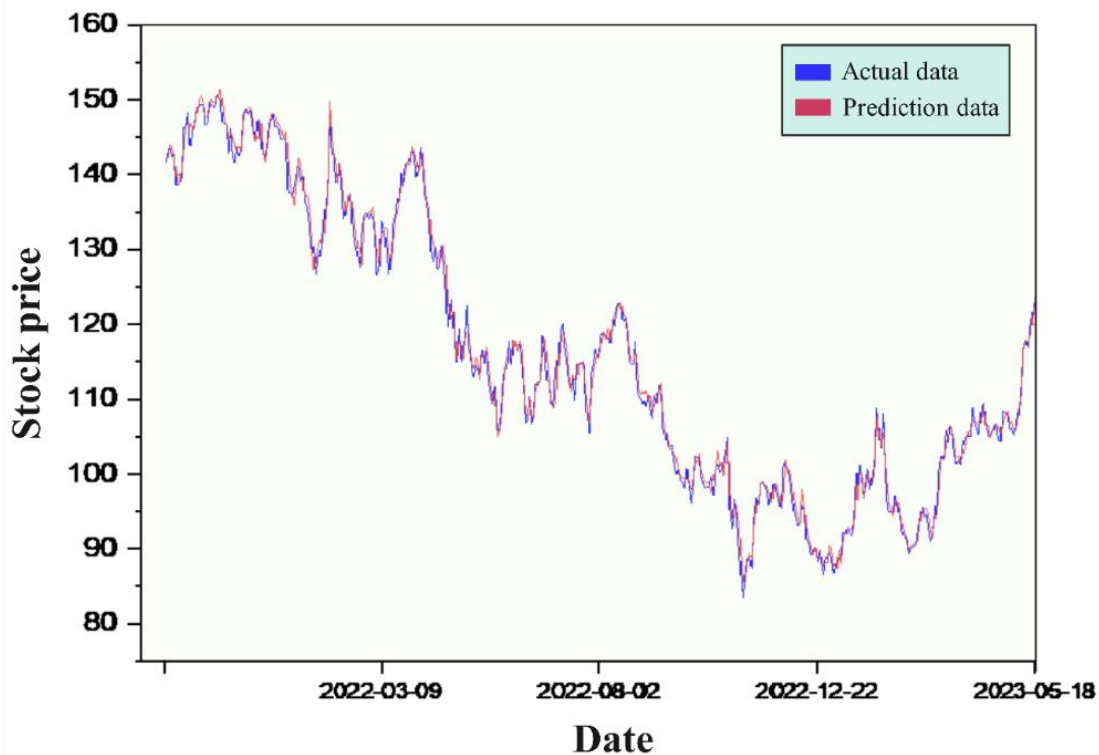


Fig. 11. The prediction curve is produced by testing with GWO-RNN.

For creating accurate stock price predictions, the GWO-RNN model is a very trustworthy instrument. As illustrated in Fig. 10 and Fig. 11, this model is successful in forecasting the Alphabet stock curves. Due to the RNN method's ability to lower price fluctuations, streamline trend prediction, and increase model precision, the GWO-RNN model performs better than other models at forecasting stock prices. The capacity of the GWO-RNN model to learn from prior data sets is one of its distinguishing characteristics. Learning from prior data sets is essential for a model to produce accurate stock value predictions and adapt to shifting market trends. In summary, the GWO-RNN model is an effective and useful tool for forecasting stock prices. Because of its accuracy, precision, and adaptability, it is highly advised for anyone wishing to make profitable transactions in the stock market. It stands out from other models due to its use of the RNN algorithm and GWO optimizer, making it the greatest option for anyone looking to make informed investing decisions.

B. Comparison with Recent Works

Validation measures and comparisons with prior relevant literature are essential elements in evaluating the credibility and significance of a research investigation. In addition to guaranteeing the dependability and accuracy of the study's

findings, they aid in contextualizing the research within a wider framework. The present evaluation assesses, which is illustrated in Table III, the predictive capabilities of different models, such as the GWO-RNN model employed in this research, concerning the behavior of the stock market. Significantly, the GWO-RNN model, which was developed and evaluated using Alphabet stock data, attains a remarkable coefficient of determination ($R^2 = 0.992$), outperforming alternative algorithms including Linear Regression, SVM, and several iterations of LSTM. The remarkable accuracy of this forecast highlights the consistency and consistency of the GWO-RNN model in capturing the intricate dynamics of stock prices. Through the utilization of the Grey Wolf Optimization-Recurrent Neural Network architecture, the model adeptly exploits past stock price data to deliver resilient predictions, thereby showcasing its consistency in adjusting to fluctuations in the market. Incorporating Alphabet stock data into the evaluation process enhances coherence and ensures that the model's performance is in line with actual market conditions. As a result, the GWO-RNN model can be established as a logical and consistent methodology for forecasting the stock market, providing significant contributions to financial decision-making and risk mitigation.

TABLE III. AN EVALUATION OF THE MODEL IN COMPARISON TO PRIOR RESEARCH

| Authors | Abdul et al. [31] | | | Zhu et al. [32] | | | | | | Present work |
|------------|-------------------|------|----------|-----------------|----------|--------------|---------|-------------|-----------------|--------------|
| Algorithms | Linear regression | SV M | MLS-LSTM | LSTM | EMD-LSTM | CEEMDAN-LSTM | SC-LSTM | EMD-SC-LSTM | CEEMDAN-SC-LSTM | GWO-RNN |
| R^2 | 0.73 | 0.93 | 0.95 | 0.6896 | 0.8703 | 0.9031 | 0.6871 | 0.9111 | 0.9206 | 0.992 |

C. Limitations and Future Works

The efficacy of the GWO-RNN model was assessed using a distinct dataset comprising Alphabet stock from January 1, 2015, to June 29, 2023. The efficacy of the model could potentially be compromised by the attributes of the given dataset, thereby restricting its applicability to alternative equities, industries, or periods. Hybrid models frequently depend on precise parameter configurations, particularly when optimization algorithms such as grey wolf optimization are integrated. The extent to which the GWO-RNN model can withstand variations in these parameters may have been inadequately investigated in the research. The exclusive dependence of the study on historical stock price data may result in the omission of critical information, including geopolitical developments, external economic events, and market sentiment. The extent to which the GWO-RNN model captures and incorporates such external factors into its predictions is not exhaustively investigated, which may have implications for its overall predictive capabilities. Although the study showcases the superior performance of the GWO-RNN model in comparison to other models, a more extensive evaluation comparing it to a broader spectrum of established and cutting-edge models would offer a more precise assessment of its comparative merits and drawbacks.

Enhancing the range of data sources beyond daily prices and trading volume may yield significant insights that can be

applied to the prediction of stock market trends. The incorporation of supplementary data streams, including sentiment analysis from social media platforms, economic indicators, or news articles, may bolster the predictive capacities of models through the inclusion of supplementary market dynamics. The incorporation of external variables into predictive models, including macroeconomic indicators, geopolitical events, and regulatory changes, may increase their predictive capability. Gaining insight into how these extraneous variables impact the conduct of the stock market and integrating them into prognostic models may enhance their precision and dependability. Undertaking thorough assessments of predictive models under various market conditions, encompassing periods of stability and volatility, would yield valuable insights regarding the models' ability to withstand and apply to a wide range of situations. Conducting performance tests on models across diverse economic conditions may unveil their merits and drawbacks, thereby providing valuable insights for their implementation in practical situations. By expanding the utilization of predictive models to encompass financial methods other than stock prices, including commodities, currencies, and cryptocurrencies, their applicability and significance could be significantly enhanced. An examination of the adaptability of predictive models to various asset classes and market segments would yield valuable insights regarding their efficacy and versatility in a wide range of financial markets.

VI. CONCLUSIONS

The task of predicting stock prices is difficult and complex because it requires examining many different aspects of society, the economy, and politics. Since the stock market is dynamic and ever-evolving, it is important to take financial statements, earnings reports, market trends, and other factors into account when forecasting future stock values. The stock market's behavior can be significantly impacted by macroeconomic factors like interest rates, inflation, and global market conditions. Due to the complexity and numerous variables involved in predicting stock values, it can be challenging to develop accurate and trustworthy prediction models. Making accurate predictions requires an understanding of the market's erratic and non-linear characteristics. In this study, the RNN, BBO-RNN, and AO-RNN stock price prediction models were evaluated for their performance.

The GWO-RNN model performed better than other models in the tests that were conducted. R^2 , RMSE and MAE values for the model were 0.992, 1.643, and 1.306, respectively. These findings show that the GWO-RNN model is highly predictively accurate and that it can be trusted to deliver accurate and dependable outputs.

The GWO-RNN model has been demonstrated to be a trustworthy tool for making highly accurate stock price predictions. This model can analyze and interpret large amounts of data in real-time using a combination of recurrent neural networks and grey wolf optimization-based optimization, giving investors useful insights into market trends and potential investment opportunities.

ACKNOWLEDGMENT

This work was supported by the Key Courses Construction Project of Xi'an Eurasia University (2019KC026); the Project of Shaanxi Provincial Sports Bureau (2022307); The Innovation Team of Eurasia University (2021XJTD07); Xi'an Social Science Foundation Project (23JX116); Xi'an Social Science Foundation Project (23JX118).

REFERENCES

- [1] B. Qian and K. Rasheed, "Stock market prediction with multiple classifiers," *Applied Intelligence*, vol. 26, no. 1, pp. 25–33, 2007, doi: 10.1007/s10489-006-0001-7.
- [2] D. Kumar, P. K. Sarangi, and R. Verma, "A systematic review of stock market prediction using machine learning and statistical techniques," *Mater Today Proc*, vol. 49, no. September, pp. 3187–3191, 2020, doi: 10.1016/j.matpr.2020.11.399.
- [3] C. Zhang, J. Ding, J. Zhan, and D. Li, "Incomplete three-way multi-attribute group decision making based on adjustable multigranulation Pythagorean fuzzy probabilistic rough sets," *International Journal of Approximate Reasoning*, vol. 147, pp. 40–59, 2022, doi: https://doi.org/10.1016/j.ijar.2022.05.004.
- [4] Y. Chen, P. Zhao, Z. Zhang, J. Bai, and Y. Guo, "A Stock Price Forecasting Model Integrating Complementary Ensemble Empirical Mode Decomposition and Independent Component Analysis," *International Journal of Computational Intelligence Systems*, vol. 15, no. 1, 2022, doi: 10.1007/s44196-022-00140-2.
- [5] E. F. Fama, "Random walks in stock market prices," *Financial analysts journal*, vol. 51, no. 1, pp. 75–80, 1995.
- [6] L. N. Mintarya, J. N. M. Halim, C. Angie, S. Achmad, and A. Kurniawan, "Machine learning approaches in stock market prediction: A systematic literature review," *Procedia Comput Sci*, vol. 216, pp. 96–102, 2023, doi: 10.1016/j.procs.2022.12.115.

- [7] K. Pardeshi, S. S. Gill, and A. M. Abdelmoniem, "Stock Market Price Prediction: A Hybrid LSTM and Sequential Self-Attention based Approach," 2023. doi: 10.48550/arxiv.2308.04419.
- [8] D. Shah, H. Isah, and F. Zulkernine, "Stock market analysis: A review and taxonomy of prediction techniques," *International Journal of Financial Studies*, vol. 7, no. 2, 2019, doi: 10.3390/ijfs7020026.
- [9] J. V. Hansen, J. B. McDonald, and R. D. Nelson, "Time series prediction with Genetic-Algorithm designed neural networks: An empirical comparison with modern statistical models," *Comput Intell*, vol. 15, no. 3, pp. 171–184, 1999.
- [10] Y. S. Abu-Mostafa and A. F. Atiya, "Introduction to financial forecasting," *Applied Intelligence*, vol. 6, no. 3, pp. 205–213, 1996, doi: 10.1007/BF00126626.
- [11] R. Chiong, Z. Fan, Z. Hu, and S. Dhakal, "A Novel Ensemble Learning Approach for Stock Market Prediction Based on Sentiment Analysis and the Sliding Window Method," *IEEE Trans Comput Soc Syst*, vol. 10, no. 5, pp. 2613–2623, 2023, doi: 10.1109/TCS.2022.3182375.
- [12] W. Freeborough and T. van Zyl, "Investigating Explainability Methods in Recurrent Neural Network Architectures for Financial Time Series Data," *Applied Sciences (Switzerland)*, vol. 12, no. 3, 2022, doi: 10.3390/app12031427.
- [13] I. Boussaïd, J. Lepagnot, and P. Siarry, "A survey on optimization metaheuristics," *Inf Sci (N Y)*, vol. 237, pp. 82–117, 2013.
- [14] A. R. Simpson, G. C. Dandy, and L. J. Murphy, "Genetic algorithms compared to other techniques for pipe optimization," *J Water Resour Plan Manag*, vol. 120, no. 4, pp. 423–443, 1994.
- [15] T. Back, *Evolutionary algorithms in theory and practice: evolution strategies, evolutionary programming, genetic algorithms*. Oxford university press, 1996.
- [16] S. Mirjalili, "The ant lion optimizer," *Advances in Engineering Software*, vol. 83, pp. 80–98, 2015, doi: 10.1016/j.advengsoft.2015.01.010.
- [17] D. Simon, "Biogeography-based optimization," *IEEE transactions on evolutionary computation*, vol. 12, no. 6, pp. 702–713, 2008.
- [18] L. Abualigah, D. Yousri, M. Abd Elaziz, A. A. Ewees, M. A. A. Al-qaness, and A. H. Gandomi, "Aquila Optimizer: A novel meta-heuristic optimization algorithm," *Comput Ind Eng*, vol. 157, p. 107250, 2021, doi: https://doi.org/10.1016/j.cie.2021.107250.
- [19] S. Mirjalili, S. M. Mirjalili, and A. Lewis, "Grey Wolf Optimizer," *Advances in Engineering Software*, vol. 69, pp. 46–61, 2014, doi: https://doi.org/10.1016/j.advengsoft.2013.12.007.
- [20] S. Agarwal, P. Rajput, and A. K. Jena, "A Hybrid Evolutionary model for Stock Price Prediction Using Grey Wolf Optimizer," in *2022 OITS International Conference on Information Technology (OCIT)*, 2022, pp. 1–6. doi: 10.1109/OCIT56763.2022.00062.
- [21] S. Kumar Chandar, "Grey Wolf optimization-Elman neural network model for stock price prediction," *Soft comput*, vol. 25, no. 1, pp. 649–658, 2021, doi: 10.1007/s00500-020-05174-2.
- [22] S. Sahoo and M. N. Mohanty, "Stock market price prediction employing artificial neural network optimized by gray wolf optimization," in *New Paradigm in Decision Science and Management: Proceedings of ICDSM 2018*, Springer, 2020, pp. 77–87.
- [23] F. W. Christanto, V. G. Utomo, R. Prathivi, and C. Dewi, "The Impact of Financial Statement Integration in Machine Learning for Stock Price Prediction," *International Journal of Information Technology and Computer Science*; volume 16, issue 1, page 35-42; ISSN 2074-9007 2074-9015, 2024, doi: 10.5815/ijitcs.2024.01.04.
- [24] Y. Chen, X. Andrew, and S. Supasanya, "CRISIS ALERT: Forecasting Stock Market Crisis Events Using Machine Learning Methods," 2024. doi: 10.48550/arxiv.2401.06172.
- [25] P.-F. Tsai, C.-H. Gao, and S.-M. Yuan, "Stock Selection Using Machine Learning Based on Financial Ratios," *Mathematics*, Vol 11, Iss 23, p 4758 (2023), Mar. 2023, doi: 10.3390/math11234758.
- [26] S. Pourroostaei Ardakani, N. Du, C. Lin, J. Yang, Z. Bi, and L. Chen, "A federated learning-enabled predictive analysis to forecast stock market trends," Mar. 2023, [Online]. Available: https://eprints.lincoln.ac.uk/id/eprint/53623/

- [27] M. Hani'ah, M. Z. Abdullah, W. I. Sabilla, S. Akbar, and D. R. Shafara, "Google Trends and Technical Indicator based Machine Learning for Stock Market Prediction," *MATRIK: Jurnal Manajemen, Teknik Informatika dan Rekayasa Komputer*; Vol 22 No 2 (2023); 271-284; 2476-9843 ; 1858-4144 ; 10.30812/matrik.v22i2, Mar. 2023, [Online]. Available: <https://journal.universitاسbumigora.ac.id/index.php/matrik/article/view/2287>
- [28] K. Juare and A. Kulkarni, "Machine Learning Algorithms for Stock Market Prediction," *International Journal of Innovative Science and Research Technology* 7(12) 2193-2199, Mar. 2023, [Online]. Available: <https://zenodo.org/record/7698476>
- [29] T. Swathi, N. Kasiviswanath, and A. A. Rao, "A Novel Sine Cosine Optimization with Stacked Long Short-term Memory-enabled Stock Price Prediction," *Recent Advances in Computer Science and Communications*; volume 16; ISSN 2666-2558, 2023, doi: 10.2174/0126662558236061230922074642.
- [30] Z. C. Lipton, J. Berkowitz, and C. Elkan, "A critical review of recurrent neural networks for sequence learning," arXiv preprint arXiv:1506.00019, 2015.
- [31] A. Q. Md et al., "Novel optimization approach for stock price forecasting using multi-layered sequential LSTM," *Appl Soft Comput*, vol. 134, p. 109830, 2023, doi: <https://doi.org/10.1016/j.asoc.2022.109830>.
- [32] R. Zhu, G.-Y. Zhong, and J.-C. Li, "Forecasting price in a new hybrid neural network model with machine learning," *Expert Syst Appl*, vol. 249, p. 123697, 2024, doi: <https://doi.org/10.1016/j.eswa.2024.123697>.

Optimization Method for Digital Twin Manufacturing System Based on NSGA-II

Yu Ding, Longhua Li*

Applied Technology College of Dalian Ocean University, Dalian, 116300, China

Abstract—In the wave of industrial modernization, a concept that comprehensively covers the product lifecycle has been proposed, namely the digital twin manufacturing system. The digital twin manufacturing system can conduct three-dimensional simulation of the workshop, thereby achieving dynamic scheduling and energy efficiency optimization of the workshop. The optimization of digital twin manufacturing systems has become a focus of research. In order to reduce power consumption and production time in manufacturing workshops, the study adopted a non-dominated sorting genetic algorithm to improve its elitist retention strategy for the problem of easily falling into local optima. On the ground of the idea of multi-objective optimization, the optimization was carried out with the production time and power consumption of the manufacturing industry as the objectives. The experiment showcased that the improved algorithm outperforms the multi-objective optimization algorithm on the ground of decomposition and the evolutionary algorithm on the ground of Pareto dominance. Compared to the two comparison algorithms, the production time optimization effect and power consumption optimization effect of different numbers of devices were 11.12%-21.37% and 2.14%-6.89% higher, respectively. The optimization time of the improved algorithm was 713.5 seconds, that was reduced by 173.8 seconds and 179.8 seconds compared to the other two algorithms, respectively. The total power consumption of the improved optimization model was 2883.7kW*s, which was reduced by 32.0kW*s and 45.5kW*s compared to the other two algorithms, respectively. This study proposed a new multi-objective optimization algorithm for the current digital twin manufacturing industry. This algorithm effectively reduces production time and power consumption, and has important guiding significance for manufacturing system optimization in actual production environments.

Keywords—Multi-objective optimization; NSGA-II; Digital twin; Production time; Production energy consumption

I. INTRODUCTION

At present, China is entering a stage of high-quality development, and manufacturing, as one of the important core industries for achieving socialist modernization, is an important guarantee of comprehensive national strength. In traditional manufacturing models, product design, manufacturing, and service are usually isolated. This model is difficult to meet the personalized, intelligent, and environmentally friendly requirements of the current manufacturing industry [1]. The proposal of the Digital Twin Manufacturing System (DTMS) provides new ideas for solving these problems [2]. The DTMS comprehensively manages and controls all stages of the product from design to lifecycle through simulation and optimization. This can

improve product quality and production efficiency, and reduce production costs [3]. Modern industrial practice has shown that DTMSs can effectively change the production mode of the manufacturing industry, making it more intelligent and personalized [4]. However, how to optimize the construction and operation of DTMSs, improve their performance and efficiency, is an important research topic at present. This practice has proven that the application of optimization algorithms can effectively improve the performance and efficiency of DTMSs [5]. In view of this, in order to reduce power consumption and production time in manufacturing workshops, this study will explore the optimization and construction methods of DTMSs from both theoretical and methodological perspectives. Firstly, a DTMS optimization model on the ground of the Non-dominated Sorting Genetic Algorithm-II (NSGA-II) will be constructed using existing optimization algorithms for reference. On this basis, through in-depth research and improvement of the model, its performance and efficiency in practical applications are improved. The study improved the elite retention strategy of the NSGA-II algorithm, which requires retaining a portion of non-fully optimal solutions in addition to retaining elite individuals. The significance of this improvement is to avoid local convergence of the results and improve the accuracy of the calculation results for multi-objective optimization problems. The innovation of this study lies in the idea of flexible scheduling on the ground of flexible workshops, combined with digital twin technology, to construct an optimization model for green manufacturing industry. It effectively improves the practicality and availability of optimization strategies. Through this research, not only can the performance and efficiency of DTMSs be improved, but it can also promote technological progress and industry transformation in the manufacturing industry. The contribution of this study lies not only in constructing an effective optimization model for DTMSs, but also in providing new theories and methods for further research and application of DTMSs. This will have a profound impact on the development of the manufacturing industry and will also have a positive driving effect on the development of the social economy. The research is divided into five sections. Section II is a summary of the research related fields, namely DTMSs and industrial optimization, which involve the application of digital twin technology in the manufacturing industry and the application of algorithms in improving production efficiency in the manufacturing industry. Section III is the implementation of the method proposed by the research institute, which involves the construction of digital twin green models and multi-objective optimization models for the manufacturing

industry. Section IV is the validation of the method proposed by the research institute, which includes iterative performance, convergence performance, time optimization performance, and energy consumption optimization performance. Section V is a summary and outlook of the research.

II. RELATED WORKS

DTMS is an emerging manufacturing system model that integrates physical and virtual manufacturing systems in real-time, dynamic, and highly consistent manner throughout their entire lifecycle. It is on the ground of advanced technologies such as the Internet of Things, cloud computing, and big data, and establishes a virtual image of a physical manufacturing system by collecting various data from the manufacturing system. Then, through continuous learning and model updates, the virtual image can reflect the state of the physical system in real time. Liu et al. proposed a real-time collaborative method on the ground of digital twin technology to address the treatment and efficiency issues in the production of new products. This method utilized heterogeneous information network modeling for real-time analysis and optimization of product production processes, and experimental results verified the feasibility and practicality of this method [6]. Guo et al. introduced a manufacturing logistics integration technology on the ground of digital twin technology to address the synchronization issue of manufacturing logistics interfaces in the production manufacturing industry, and established an equivalent constraint programming model to verify this. The experiment showcased that this method effectively achieves synchronization between logistics and manufacturing industries [7]. Fan et al. proposed a manufacturing structure on the ground of the digital twin scenario system in response to the development trend of Industry 4.0. The experiment showcased that this method is very effective at every stage of the product lifecycle [8]. Chetan et al. proposed a high-fidelity digital twin wind turbine blade virtual model to generate accurate blade models. This model improved the accuracy of the model by incorporating progressive calibration, and experimental results demonstrated the effectiveness and practicality of this method [9]. Osho proposed a modular digital twin framework to enhance its applicability in the manufacturing industry to enhance its applicability. The experimental results have proven the accuracy of this method in practice, laying a solid foundation for the further application of digital twin technology in the manufacturing industry [10].

Industrial manufacturing optimization refers to achieving more efficient and sustainable industrial manufacturing by improving and optimizing production processes, improving production efficiency, reducing costs and resource consumption, and other means. Using computer algorithms to optimize industrial manufacturing can achieve multi-objective optimization while also achieving intelligence and automation in the industrial manufacturing process. By learning and analyzing data, algorithms can continuously optimize the production process, improve production efficiency and quality. Singh et al. proposed an optimization strategy for the trajectory of industrial robotic arms on the ground of a hybrid optimization algorithm. The joint trajectory was optimized

using a seventh order polynomial function. The experiment showcased that this method effectively improves the smoothness and efficiency of the robot [11]. Wu et al. analyzed the manufacturing economy in the post pandemic era in the region on the ground of a dual sector economic growth model, combined with descriptive statistics and grey correlation method. And it has put forward suggestions for optimizing the industrial structure of the manufacturing industry on the ground of the actual situation. This provided a reference for regional economic development and industrial structure optimization in the post pandemic era [12]. Sekaran et al. introduced a multi-objective opposition learning artificial ant colony optimization technique on the ground of directed acyclic graph theory to improve the communication cost of physical systems in IoT networks and the production efficiency of production lines. This was to optimize complex processes in industrial manufacturing. The experiment showcased that this method reduces production costs with minimal latency and computational overhead [13]. Chen et al. proposed a manufacturing optimization technology on the ground of container deployment model, which saved bandwidth resources and improves production efficiency by reducing communication latency. The experiment showcased that this method is highly effective in optimizing resource utilization and reducing deployment costs [14]. Morse et al. proposed a structural optimization method on the ground of boundary element method to improve structural stability in the aircraft manufacturing industry, and considered manufacturing costs. The experiment showcased that this method achieves full shape optimization of aircraft panel structures and has extremely high efficiency [15].

In summary, DTMSs are currently the focus of industrial optimization problems. And computer algorithms have been widely applied in the optimization research of industrial manufacturing systems. After reviewing a large number of literatures, it can be concluded that computer algorithms make important contributions to manufacturing system optimization, especially in improving manufacturing efficiency, reducing costs, and improving product quality. However, there are still some shortcomings in current research, such as the stability and robustness of optimization methods that require further research and improvement. For these problems, considering the advantages that NSGA-II algorithm can take into account multiple complex and often conflicting manufacturing objectives, a digital twin manufacturing optimization strategy based on NSGA-II is proposed. NSGA-II maintains the diversity of solutions through fast non-dominated sorting and congestion distance calculation. This approach makes more efficient use of the real-time data provided by digital twin technology. At the same time, the digital twin technology can effectively support the iteration and evolution of the NSGA-II algorithm, so that each optimization of the manufacturing process is based on the latest and most accurate system data, ensuring that the optimization results are highly practical and accurate. Therefore, the research chooses to combine NSGA-II algorithm with digital twin manufacturing. This is to improve decision quality and production efficiency in manufacturing process.

III. CONSTRUCTION AND IMPROVEMENT OF NSGA-II FOR DIGITAL TWIN MANUFACTURING INDUSTRY

Considering the characteristics of DTMSs, the main challenge faced by the construction of NSGA-II is multi-objective optimization problem [16]. In the construction of the NSGA-II, the data-driven characteristics of the DTMS and its parallel processing ability in complex manufacturing processes are fully utilized. On the basis of algorithm construction, the optimization problem of NSGA-II was further explored. The selection, crossover, and mutation operations of algorithms have been thoroughly studied. The goal of this process is to find strategies and methods that can improve the efficiency and effectiveness of algorithms in dealing with large-scale parallel manufacturing system problems. To maintain the diversity of the population, new strategies were introduced in the optimization process. These strategies can maintain the diversity of the population during the optimization process, avoiding premature convergence and falling into local optima. The introduction of this strategy enables the algorithm to better balance the quality of solutions and the time required to solve practical problems.

A. Construction of a Manufacturing System Considering Digital Twins

In order to reduce the power consumption and production time of manufacturing workshops, a three-dimensional simulation of the workshop was conducted using a digital twin

manufacturing system. A green model of manufacturing digital twins was constructed, and the energy consumption of the workshop was analyzed, providing direction and ideas for the subsequent optimization model construction. Afterwards, a multi-objective optimization model was constructed with power consumption and production time as optimization objectives, and the improved NSGA-II algorithm was used to solve the multi-objective problem. The scarcity of global resources and the increasing severity of environmental problems have forced industrial enterprises to use resources more efficiently and reduce their impact on the environment [17]. With the increasing demand for sustainable development in society, industrial enterprises need to take measures to reduce carbon emissions and waste emissions to achieve green and sustainable development. The digital twin green model can help industry achieve this goal. It is on the ground of digital twin technology and achieves real-time monitoring, optimization, and prediction of factories by modeling and simulating the physical systems of actual factories. This is to achieve the goals of efficient resource utilization, environmental friendliness, and economic sustainability [18]. Through digital twin technology, real-time monitoring of factory operations, energy consumption, waste generation, and other data can be achieved. And they were able to optimize on the ground of modeling and simulation. The schematic diagram of the manufacturing digital twin green model is shown in Fig. 1.

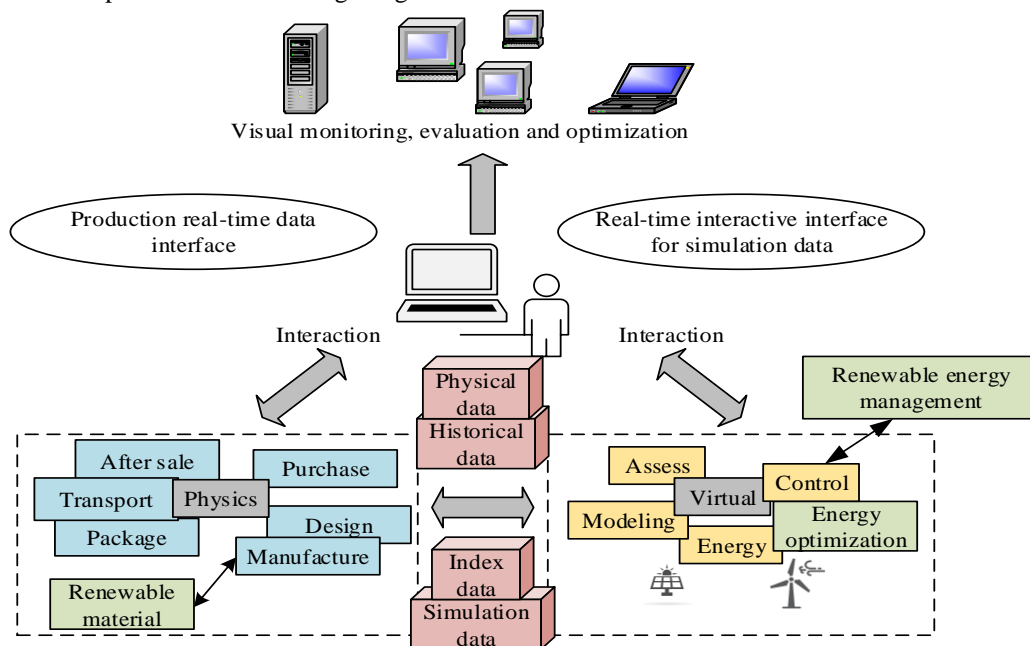


Fig. 1. Digital twin manufacturing green model.

Fig. 1 is a schematic diagram of the digital twin green model in the manufacturing industry. It forms a five dimensional model through the interaction between manufacturing entities, virtual entities, industrial data, services, and all elements. It can adjust the industry on the ground of real-time data to maximize production efficiency and costs while achieving multi-objective optimization. In digital twin technology, the core idea is to build a virtual model that reflects reality through continuous analysis of real-time data.

Through the virtual model, the simulation, monitoring and optimization of the real factory can be realized in virtual. The most significant advantage is the ability to test optimizations, predict potential problems, and make production-related decisions in advance without interfering with actual production. The use of digital twin technology can effectively reduce production risks and improve efficiency. In the automotive industry, for example, in the design phase, the digital twin system is first used to test the automobile

manufacturing to ensure the safety and feasibility of the process. In the manufacturing stage, the optimization of the manufacturing process is realized through the virtual planning and simulation of the production line. Then, in the test phase, the digital twin technology is used to carry out durability virtual collision and simulation. In the product sales phase, real-time data is used to assist inventory management and production adjustments are made based on real-time feedback. Digital twins can also guide the recovery and remanufacturing of vehicle products after they have reached the end of their life. Through the application of digital twin technology, the production efficiency and environmental friendliness of the bicycle manufacturing industry can be effectively improved. Formula (1) is a digital twin green energy consumption model.

$$M_{DT-GT} = \{P_g, V_g, D_g, S_g, C_g\} \quad (1)$$

In Formula (1), P_g represents the total physical energy consumption in the manufacturing workshop under energy

consumption analysis. V_g represents a digital twin, whose main significance is to optimize energy consumption. D_g represents the overall data of the workshop, which is the connecting link with the digital twin. S_g represents optimization of energy consumption. C_g represents the interaction between real data and virtual data. As shown in Fig. 2, taking workshop work in the manufacturing industry as an example, it is optimized. On the ground of its energy consumption, this study continues to optimize and analyze it. On the ground of the basic energy consumption of the workshop, this study combines intelligent optimization algorithms. Then, on the ground of the actual situation, it constructs a green optimization and energy-saving operation strategy for workshop equipment, ultimately achieving optimization of workshop energy consumption. This can also reduce energy consumption and improve production efficiency.

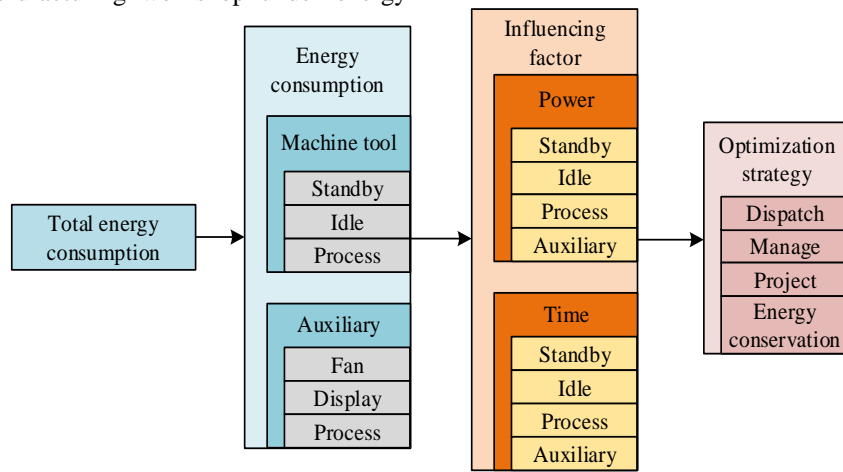


Fig. 2. Correlation analysis diagram of energy consumption, power and optimization of workshop.

Fig. 2 shows the key components of energy consumption analysis using workshop work in the manufacturing industry as an example. This includes machine tool energy consumption and auxiliary equipment energy consumption, and takes into account power consumption and time factors to plan better workshop optimization strategies. The power consumption model between machine speed and material removal rate can be expressed as shown in Formula (2).

$$P_1 = P_2 + k_1 n + b + k_0 MRR \quad (2)$$

In Formula (2), P_1 represents the total energy consumption in material removal. P_2 represents the total standby consumption, b represents the total fixed energy consumption of the device, n represents the speed unit of the device, k_1 represents the parameter setting of the spindle motor, k_0 represents a constant in the calculation, and MRR represents the material removal rate. Further consideration should be given to the power consumption of workshop machine tools. In the standby state of the equipment, the control system of the lathe remains in standby state, and the total standby power can be expressed as shown in formula

(3).

$$P_s = P_c + P_l \quad (3)$$

In Formula (3), P_s represents standby power, P_c represents the system operating power of the workshop machine tool, which plays a major role in monitoring the entire system, and P_l represents the auxiliary equipment power. In the normal working state of the workshop, the power can be expressed as shown in Formula (4).

$$P_{ld} = P_s + P_{sf} \quad (4)$$

In Formula (4), P_{ld} represents the preparation power of the processing state, P_s represents the standby power, and P_{sf} represents the idle power of the spindle and the no-load power of the feed shaft. In the processing stage of the lathe, the main calculation required is the cutting power of the machine tool on the workpiece material, which can be expressed as shown in Formula (5).

$$P_w = P_s + P_{sf(n)} + P_m \quad (5)$$

In Formula (5), P_w represents the total power of the machining state, P_s represents the standby power, $P_{sf(n)}$ represents the power of the spindle and feed shaft in the working state, and P_m represents the cutting power of the material. Furthermore, according to the definition of integration, by integrating time over a period of time, the total power of the workshop machine tool can be calculated, as shown in Formula (6).

$$E_M = \int_0^{t_s} P_s d_t + \int_0^{t_{ld}} P_{ld} d_t + \int_0^{t_w} P_w d_t \quad (6)$$

As shown in Formula (6), the total power of the workshop lathe during the processing stage can be calculated using the integration method, where t_s represents the standby time, t_{ld} represents the processing preparation time, and t_w represents the total processing time. As shown in Fig. 3, it is a schematic diagram of the process flow of a flexible workshop that adopts the optimization process method.

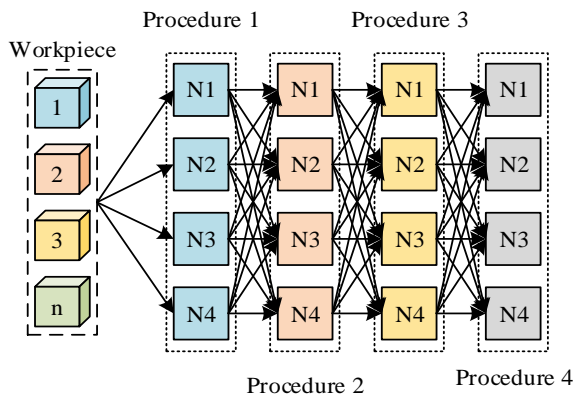


Fig. 3. Flexible workshop process flow diagram.

Fig. 3 is a schematic diagram of the flexible workshop process flow using optimized process methods, which can better align actual production needs with green concepts. Its main purpose is to reduce workshop production time while reducing equipment energy consumption, thereby achieving the concept of green manufacturing.

B. Construction and Optimization of NSGA-II for DTMSs

The characteristics of NSGA-II provide an effective solution for multi-objective problems in DTMSs. This algorithm achieves efficient search of high-quality solution sets through a non-sorted survival selection mechanism and crowding distance sorting [19]. However, integrating it into specific manufacturing environments requires a deep understanding of the characteristics of manufacturing systems to design optimization strategies that meet practical needs [20]. Firstly, it discusses the optimization scheduling objectives for the workshop. Overall, with manufacturing processing time as the main optimization objective, it can be represented by Formula (7).

$$\min T = \max \{C_1, C_2, \dots, C_N\} \quad (7)$$

In Formula (7), $\min T$ represents the minimum optimized processing time, and $\{C_1, C_2, \dots, C_N\}$ indicates different manufacturing system performance indicators. In the field of digital twin manufacturing, these indicators may represent key performance indicators such as production efficiency, resource consumption, environmental impact, etc. These indicators allow for optimization beyond a single objective, enabling the model to find the optimal solution in a larger dimensional space. In the whole optimization process, real-time optimization of the algorithm can be realized through real-time monitoring of these indicators, so as to dynamically adjust and optimize the manufacturing process. It further introduces the total power consumption of the workshop as the optimization scheduling objective. It can be specifically expressed as shown in Formula (8).

$$\min f = \min E_{total} \quad (8)$$

In Formula (8), $\min f$ represents the minimum objective function, and $\min E_{total}$ represents the minimum energy consumption optimization objective. The total workshop processing energy consumption can be expressed as shown in Formula (9).

$$E_{sum} = E_w + E_{IE} + E_A \quad (9)$$

In Formula (9), E_{sum} represents the total processing consumption, E_w represents the cutting power of the equipment, E_{IE} represents the idle standby power of the equipment, and E_A represents the additional loss power of the equipment. When processing each individual workpiece, a device needs to be selected for the processing process, which can be expressed in Formula (10).

$$\sum_{k=1}^{M_j} x_{ijk} = 1, (i = 1, 2, \dots, w)(n - 1, 2, \dots, s) \quad (10)$$

In Formula (10), M_j represents the number of machine tools required for the j -th process, $x_{ijk} = 1$. When $x_{ijk} = 1$, it indicates that the j th process of the i -th workpiece can be completed on the k -th machine tool, while $x_{ijk} = 0$ indicates that machining cannot be carried out. However, when the same machine tool is in operation, it is not possible to process two workpieces simultaneously. Therefore, as shown in Formula (11), it specifically represents the processing start and end times of the workpiece.

$$PF(j, k, r) \leq PS(j, k, r+1) \quad (11)$$

In Formula (11), $PF(j, k, r)$ represents the processing end time of the j th process of the r -th workpiece on the k -th machine tool, and $PS(j, k, r+1)$ represents the processing start time of the j th process of the $r+1$ workpiece on the k -th machine tool. For each individual workpiece, it must be processed according to the processing process flow and must go through w processes to complete the processing. As shown

in Formula (12).

$$\sum_{k=1}^{M_j} B_i^k = 1, (\forall i \in n, j \in s) \tag{12}$$

In Formula (12), M represents the number of devices that can be selected for use in the j th process of the workpiece, $B_i^k = 1$ indicates that workpiece i is processed on device K , and $B_i^k \neq 1$ indicates that workpiece i is not processed on device K . For multi-objective optimization problems, they can be represented as shown in Formula (13).

$$\begin{cases} \min(\& \max) F(x) = [f_1(x), f_2(x), \dots, f_n(x)]^T \\ x \in \Omega \\ \Omega = \{X \in R^n \mid g_i(x) \leq 0, i = 1, 2, \dots, p\} \end{cases} \tag{13}$$

In Formula (13), the space Ω where X is located is the space where the feasible solution is located, while $F(x)$ represents the objective function of the space in which it is located. The core idea is to find the Pareto optimal solution. The NSGA-II, due to its strong anti-interference performance, performs well in finding the optimal solution for multi-objective optimization. The NSGA-II algorithm has difficulty in weighing different objectives, while Pareto optimization does not prioritize the optimization of a single objective. Instead, it seeks to find the best balance point among multiple objectives, aiming to identify solutions that improve one objective without significantly degrading the other. Pareto optimization can solve this problem in a targeted way, and at the same time, it also considers the global nature of the space, rather than limited to a specific target. Therefore, using Pareto optimization can also enhance the performance of NSGA-II in complex multi-objective optimization problems to a certain extent. Therefore, this algorithm was chosen for further research. The core idea of the NSGA-II is to use Pareto's sorting method in non-dominated space for solving. Pareto optimization can obtain a set of optimal solutions in the process and output them according to different levels, as shown in Fig. 4.

In Fig. 4, after selecting a more optimal solution, it is necessary to calculate the crowding degree. When the crowding distance is relatively large, the solution set around the optimal solution should appear more dispersed and sparse, to ensure the diversity of the population. Firstly, it assumes that the crowding degree of each point is n_d , and the initial crowding degree value is 0. For the optimal target point, by non-dominated sorting, it can be considered that the crowding degree of individual solutions on the boundary of the optimal solution is infinite. Finally, it calculates the crowding degree of other individuals within the population, as shown in Formula (14).

$$n_d = \sum_{j=1}^m (|f_j^{i+1} - f_j^{i-1}|) \tag{14}$$

In Formula (14), n_d represents crowding degree, f_j^{i+1}

represents the function value of the j -th objective function at point $i+1$, f_j^{i-1} represents the function value of the j -th objective function at point $i-1$, and m represents the total number of functions, where $j \in 1, 2, \dots, m$. For its elite strategy, the original NSGA-II, after Pareto optimization, would choose to retain as many outstanding individuals as possible and pass them on to the next generation. This strategy will to some extent reduce its genetic diversity, leading to local convergence after iteration. Therefore, the study optimizes its elite retention strategy. After Pareto optimization and congestion calculation, a portion of elite individuals are retained, and the remaining non-optimal individuals are uniformly selected for retention, as shown in Fig. 5.

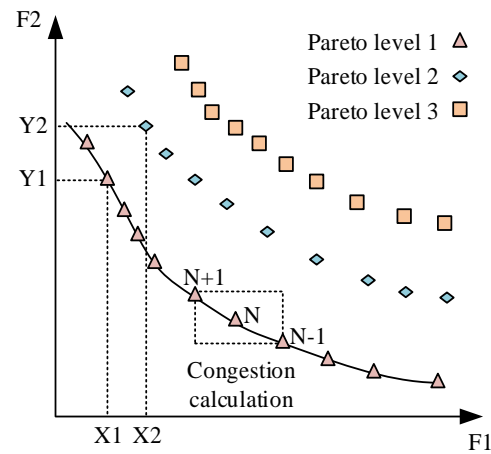


Fig. 4. Pareto optimization and congestion calculation diagram.

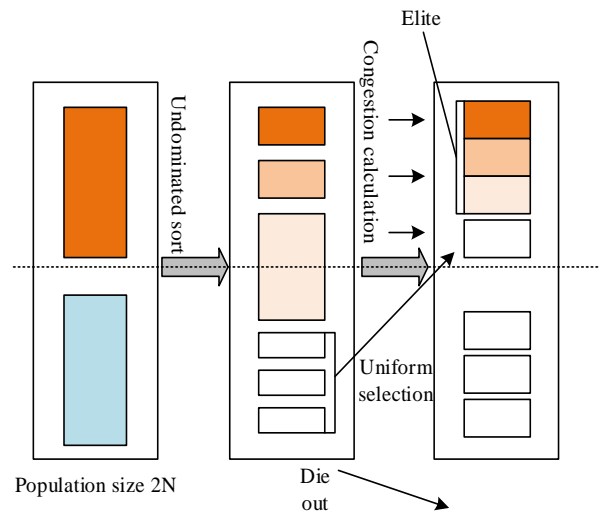


Fig. 5. Schematic diagram of optimizing elite retention strategy.

The NSGA-II has good performance in handling multi-objective optimization problems. However, to better adapt to the characteristics and needs of the digital twin manufacturing industry, its elite individual retention strategy has been optimized. On the basis of the original elite strategy, more selection criteria have been introduced to enhance diversity. Meanwhile, stricter control has been implemented

on the quality of solutions to ensure the retention of high-quality solutions. The implementation of this optimization strategy aims to improve the search performance of the algorithm, so that a more optimal solution set can be found under the same number of iterations. In addition, this also helps to improve the stability of the algorithm and reduce the randomness of the running results. Moreover, due to the retention of elite individuals, it can to some extent avoid the loss of high-quality solutions, thereby effectively improving the performance of the algorithm. Furthermore, this

optimization strategy makes it more suitable for optimizing the digital twin manufacturing industry. Because there are a large number of multi-objective optimization problems, which often require considering multiple factors to find the optimal solution set. For this type of problem, the NSGA-II, after optimization, can better meet its solving needs, thereby improving the efficiency and effectiveness of the manufacturing system. The flowchart of the NSGA-II is shown in Fig. 6.

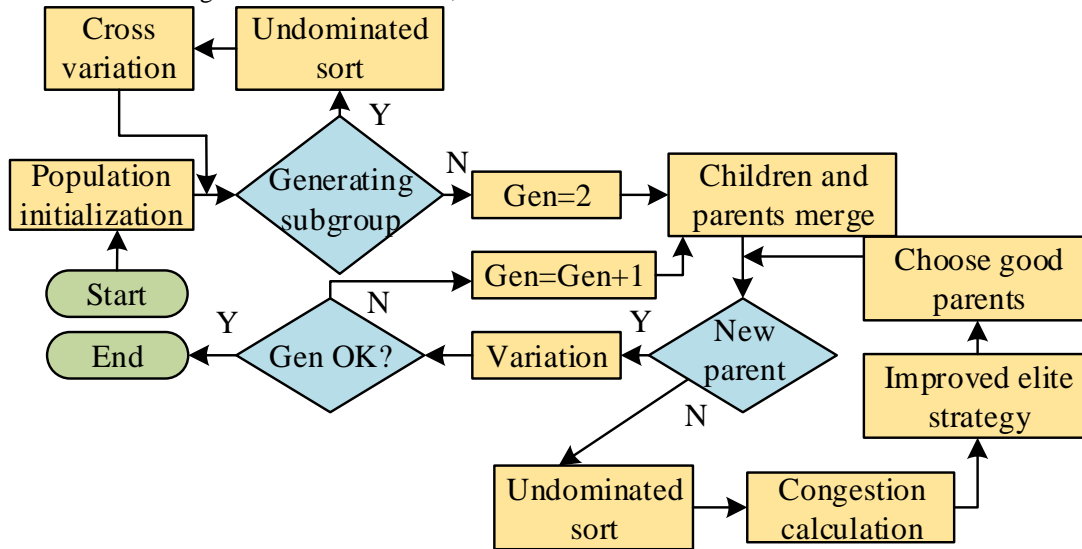


Fig. 6. Flowchart of NSGA-II.

IV. PERFORMANCE TESTING OF NSGA-II IN DTMS

To test the usability of the DTMS NSGA-II optimization algorithm (IM-NSGA-II) proposed by the research institute, this study chose to construct a virtual flexible job shop and conduct simulation experiments on its optimization ability. The software and hardware environment and parameter settings used in the study are shown in Table I. Through this configuration, the performance of the algorithm can be accurately and reliably evaluated, while also meeting the needs of daily development and testing. This study further introduces the same type of multi-objective optimization algorithm and compares it with the improved NSGA-II. It introduces the Multi Objective Evolutionary Algorithm on the ground of Decomposition (MOEA/D) and the Strength Pareto Evolutionary Algorithm 2 (SPEA2), respectively. The parameters of IM-NSGA-II are set as follows: Set the Population Size to 100, Crossover Probability to 0.9, Crossover Distribution Index to 20 and Mutation Distribution

Index to 20. Selection is set to Binary tournament selection, Crossover is set to Simulated Binary Crossover and Polynomial Mutation. The parameters for MOEA/D are set as follows: The population Size is set to 100, the Neighborhood Size to 20%, the Weight Vector Update Interval to 50 generations, and the Crossover Probability to 1.0. The Crossover Distribution Index is set to 20, the Mutation Distribution Index to 20, and the Neighborhood Selection Probability to 0.9. The Replacement Strategy is set to adjacence-based replacement and the Decomposition Approach is set to Tchebycheff. SPEA2 parameters are set as follows: Population Size is 100, Archive Size is 100, Crossover Probability is 0.8, and Crossover Distribution Index is 20. The Mutation Distribution Index is set to 20, Selection is set to Binary tournament selection, Crossover is set to Simulated Binary Crossover, and Mutation is set to uniform variation. The maximum algebra for all algorithms is set to 120 generations.

TABLE I. STUDY SOFTWARE AND HARDWARE ENVIRONMENT

| Local hardware environment | | | Software environment and parameter setting | | |
|----------------------------|------------------------|---------------------|--|----------------------|-----------------------------------|
| Local hardware | Detail | Argument | Name | Detail | Argument |
| Local hardware | Dell | Dell Precision 7760 | Development language | Python | 3.9.5 |
| CPU | Intel® Core™ i9-11950H | 2.60GHz, 8core | Database | Python DEAP | 1.3.1 |
| RAM | Kingston | 8Gb*2,3200Mhz | Processing | NumPy | 1.21.0 |
| Harddisk | TOSHIBA | 2TB | Visual tool | Matplotlib & Seaborn | Matplotlib 3.4.2 & Seaborn 0.11.1 |

| | | | | | |
|-----------------------------------|---------------------|-----------------------|-------------------------|---------------|---------|
| Cloud server hardware environment | | | Development environment | Visual Studio | 1.59.0 |
| Cloud server provider | Alibaba Cloud | - | Container technology | Docker | 20.10.7 |
| Instance type | ecs.g6.4xlarge | - | Container orchestration | Kubernetes | 1.21.2 |
| CPU | Intel Xeon Gold | 6149, 3.10Ghz, 16core | Q _{max} | - | 200 |
| RAM | Kingston | 32Gb*4,3200Mhz | maxGen | - | 100 |
| Memory | Ultra Disk | 2TB, SSD | Pc | - | 0.9 |
| System | Alibaba Cloud Linux | 2.1903 LTS | Pm | - | 0.1 |

TABLE II. COMPARISON OF STANDARD DEVIATION AND MEAN VALUE OF CONVERGENCE PERFORMANCE OF THREE ALGORITHMS

| Times | IM-NSGA-II | | MOEA/D | | SPEA2 | |
|---------|------------------------|------------------------|------------------------|------------------------|------------------------|------------------------|
| | Mean | Standard | Mean | Standard | Mean | Standard |
| 1 | 5.417×10^{-6} | 5.824×10^{-6} | 4.628×10^{-5} | 5.471×10^{-4} | 4.218×10^{-3} | 8.201×10^{-3} |
| 2 | 6.279×10^{-6} | 6.583×10^{-6} | 5.210×10^{-4} | 6.251×10^{-5} | 6.394×10^{-3} | 6.298×10^{-5} |
| 3 | 7.251×10^{-6} | 4.251×10^{-6} | 5.069×10^{-5} | 9.236×10^{-5} | 8.275×10^{-3} | 4.267×10^{-3} |
| 4 | 4.987×10^{-6} | 5.294×10^{-6} | 6.364×10^{-4} | 8.215×10^{-5} | 5.364×10^{-4} | 5.364×10^{-4} |
| 5 | 5.687×10^{-6} | 7.357×10^{-6} | 7.207×10^{-5} | 6.028×10^{-5} | 5.227×10^{-3} | 3.105×10^{-3} |
| Average | 5.924×10^{-6} | 5.862×10^{-6} | 2.652×10^{-4} | 1.689×10^{-4} | 4.931×10^{-3} | 4.676×10^{-3} |

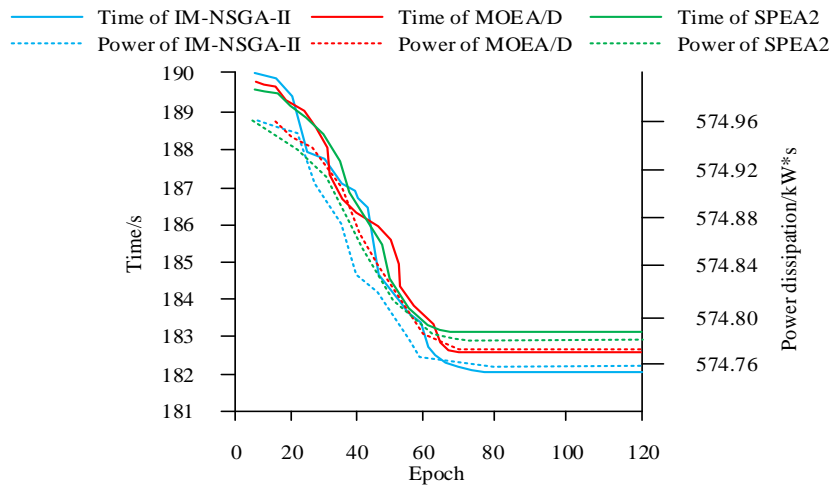


Fig. 7. The time and energy consumption of the three algorithms depend on the optimization performance of the iteration.

Firstly, the convergence performance of the three algorithms was tested, and the mean and standard deviation of the convergence performance of the three algorithms were tested. The test results are shown in Table II. Table II shows that the improved NSGA-II proposed by the research institute has better convergence performance in terms of mean and standard deviation. This proves that it has better convergence performance compared to MOEA/D and SPEA2, and can complete algorithm training at lower costs.

It tests the iterative performance of three algorithms and their impact on production time and energy consumption. The test results are shown in Fig. 7. Fig. 7 shows that the improved NSGA-II proposed by the research institute has the best optimization effect. It can reach its optimal state after about 60 iterations, and the optimized average production time is 181.9 seconds, saving 0.4 seconds and 1.1 seconds compared to MOEA/D and SPEA2, respectively. The optimal energy

consumption performance after optimization is 574.75kW*s, which shows lower energy consumption compared to MOEA/D and SPEA2.

It compares and analyzes the Hypervolume (HV) indicators of three algorithms, and the analysis results are shown in Fig. 8. It shows that its HV indicator performs well, outperforming MOEA/D and SPEA2. The improved NSGA-II proposed by the research institute has better performance in multi-objective optimization problems, with better diversity and convergence compared to MOEA/D and SPEA2 algorithms.

The other conditions are kept the same, and the time optimization performance and energy consumption optimization performance of the three algorithms under multiple devices are tested. The test results are shown in Fig. 9. Fig. 9 shows that the optimization effect of the NSGA-II proposed by the research institute remains optimal under

different device numbers. Compared to MOEA/D and SPEA2, its production time optimization effect for different quantities of equipment is 11.12% -21.37% higher, respectively. Compared to MOEA/D and SPEA2, its power optimization effect is 2.14% -6.89% ahead, respectively.

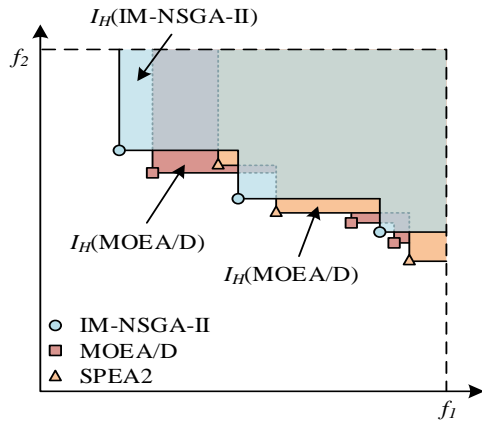


Fig. 8. HV index comparison results of three algorithms.

It sets up the same workpiece with a total of five process flows, and the number of optimization equipment faced by the three algorithms is fixed. The optimization effects of the three algorithms are compared, and the experimental results are shown in Table III. It shows that the optimization time of the

improved NSGA-II proposed by the research institute reached 713.5 seconds. The optimization time of MOEA/D algorithm is 887.3s, and the optimization time of SPEA2 is 893.3s. Compared to MOEA/D and SPEA2, the production time of the improved algorithm has been reduced by 173.8s and 179.8s, respectively. The total power consumption of the improved optimization model is 2883.7kW*s, which is reduced by 32.0kW*s and 45.5kW*s compared to MOEA/D and SPEA2, respectively. The improved NSGA-II algorithm proposed by the research institute can reduce the time spent on production by the manufacturing system, reduce the total power consumption of the system, improve the performance of the manufacturing system, enable better simulation of the workshop, and achieve dynamic scheduling and energy efficiency optimization of the workshop. Due to the fact that the optimization time at this time did not consider the parallel processing of tasks, but simply summarized the processing time of different tasks, the result value was too high. In the process of scheduling optimization, different optional equipment groups are allocated based on the overall processing time, thereby reducing equipment processing time and optimizing workshop processing energy consumption. In order to better reflect the importance of the improved NSGA-II algorithm, a Gantt chart was drawn to reflect its final optimization results. The Gantt chart is shown in Fig. 10.

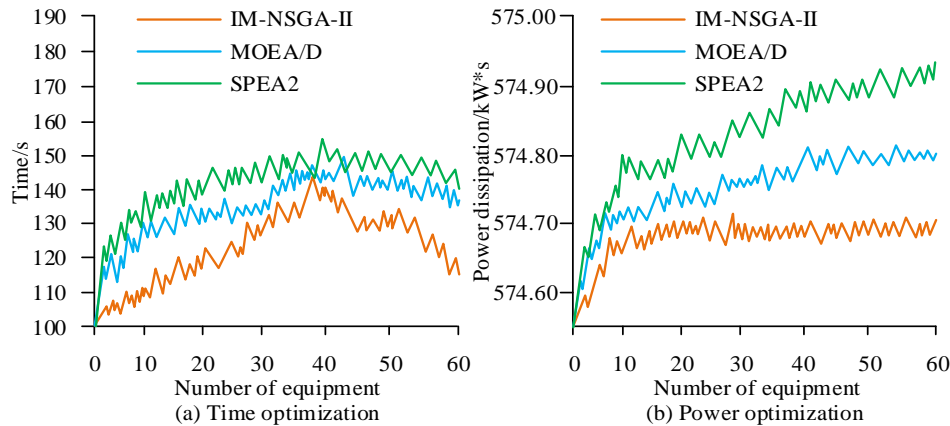


Fig. 9. Optimization performance comparison of three algorithms under different number of devices.

TABLE III. COMPARISON OF ACTUAL INDUSTRIAL OPTIMIZATION PERFORMANCE OF THREE ALGORITHMS

| Process flow | NSGA-II | | MOEA/D | | SPEA2 | |
|--------------|---------|-------------|--------|-------------|--------|-------------|
| | Time/s | Power /kW*s | Time/s | Power /kW*s | Time/s | Power /kW*s |
| 1 | 133.7 | 576.2 | 167.9 | 581.9 | 172.5 | 586.4 |
| 2 | 144.8 | 577.1 | 179.8 | 584.6 | 181.3 | 585.2 |
| 3 | 147.2 | 576.8 | 183.4 | 582.4 | 185.2 | 586.3 |
| 4 | 166.2 | 577.3 | 189.7 | 583.9 | 176.9 | 587.1 |
| 5 | 121.6 | 576.3 | 166.5 | 582.9 | 177.4 | 584.2 |
| Total | 713.5 | 2883.7 | 887.3 | 2915.7 | 893.3 | 2929.2 |

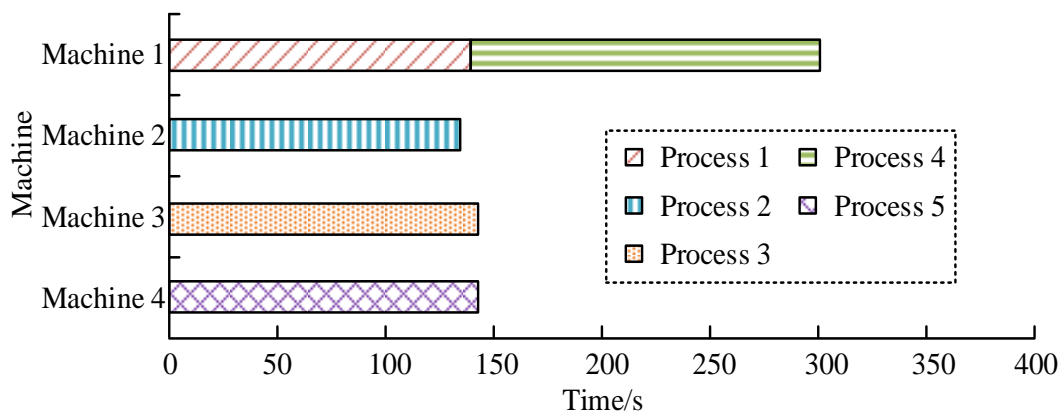


Fig. 10. Gantt chart of process flow.

From Fig. 10, it can be seen that after merging the process flow, the final optimization time of the improved NSGA-II algorithm is 299.9s. Compared to the previous simple time addition, the value decreased by 413.6 seconds. It can be seen that the improved NSGA-II algorithm can enhance the performance of the digital twin manufacturing system, and can achieve dynamic scheduling and energy efficiency optimization in the real workshop more quickly in the system.

V. CONCLUSION

With the development of Industry 4.0, the intelligence and real-time of industry have become a trend. However, further optimization of industry and manufacturing has become a challenging issue, and DTMSs have proposed solutions for this. On the ground of the improved NSGA-II, targeted improvements were made to its elite retention strategy to improve its diversity. On the ground of this algorithm, a multi-objective optimization approach was adopted to optimize production time and energy consumption. The experiment showcased that the optimization method on the ground of NSGA-II has better convergence performance compared to MOEA/D and SPEA2. The optimized average production time was 181.9 seconds, which saved 0.4 seconds and 1.1 seconds compared to MOEA/D and SPEA2, respectively. The optimal energy consumption performance after optimization was 574.75kW*s, which showed lower energy consumption compared to MOEA/D and SPEA2. Its HV indicators performed well with better diversity. Compared to MOEA/D and SPEA2, the production time optimization effect for different numbers of devices was 11.12%-21.37% higher, and the power consumption optimization effect was 2.14%-6.89% higher. This study provided a new method for optimizing DTMSs by improving the elite retention strategy of the NSGA-II, which can provide more effective methods for system optimization in the manufacturing industry. However, this method did not take into account force majeure factors such as equipment failures and fluctuations in raw material prices in actual production and manufacturing. In future research, in-depth research should be conducted on this issue to improve the applicability and practicality of the optimization method.

ACKNOWLEDGMENT

The research is supported by: Liaoning Province General

Higher Education Undergraduate Teaching Reform Research Quality Teaching Resources Construction and Sharing Project (596); Liaoning Provincial Department of Education Basic scientific research projects of colleges and universities in 2022 (No. LJKMZ20221097).

REFERENCES

- [1] Kirmizi M, Kocaoglu B. 2022. Digital transformation maturity model development framework based on design science: case studies in manufacturing industry. *Journal of Manufacturing Technology Management*, 33(7): 1319-1346.
- [2] Shen Z, Xu W, Li W, Shi Y, Gao F. 2023. Digital twin application for attach detection and mitigation of PV-based smart systems using fast and accurate hybrid machine learning algorithm. *Solar Energy*, 250(1): 377-387.
- [3] Fisher C R, Nygren K E, Beaudoin A J. 2022. Validation of materials-informed digital twin: Mapping residual strains in HSLA steel weldment using high energy X-rays. *Journal of manufacturing processes*, 74(2): 75-87.
- [4] Khan A, Shahid F, Maple C, Ahmad A, Jeon G. 2022. Toward Smart Manufacturing Using Spiral Digital Twin Framework and Twinchain. *IEEE transactions on industrial informatics*, 18(2): 1359-1366.
- [5] Fukawa N, Rindfleisch A. 2023. Enhancing innovation via the digital twin. *Journal of product innovation management*, 40(4): 391-406.
- [6] Liu S, Lu Y, Shen X, Bao J. 2023. A digital thread-driven distributed collaboration mechanism between digital twin manufacturing units. *Journal of Manufacturing Systems*, 68(1): 145-159.
- [7] Guo D, Zhong R Y, Rong Y, Huang G G Q. 2023. Synchronization of Shop-Floor Logistics and Manufacturing Under IIoT and Digital Twin-Enabled Graduation Intelligent Manufacturing System. *IEEE transactions on cybernetics*, 53(3): 2005-2016.
- [8] Fan Y, Yang J, Chen J, Hu P, Wang X, Xu J, Zhou B. 2021. A digital-twin visualized architecture for Flexible Manufacturing System. *Journal of Manufacturing Systems*, 60(1): 176-201.
- [9] Chetan M, Yao S, Griffith D T. 2021. Multi-fidelity digital twin structural model for a subscale downwind wind turbine rotor blade. *Wind Energy*, 24(12): 1368-1387.
- [10] Osho J, Hyre A, Pantelidakis M, Ledford A, Harris G, Liu J, Mykoniatis K. 2022. Four Rs Framework for the development of a digital twin: The implementation of Representation with a FDM manufacturing machine. *Journal of Manufacturing Systems*, 63(1): 370-380.
- [11] Singh G, Banga V K. 2022. Combinations of novel hybrid optimization algorithms-based trajectory planning analysis for an industrial robotic manipulators. *Journal of Field Robotics*, 39(5): 650-674.
- [12] Wu D, Wu L, Ye Y. 2022. Industrial structure optimization, economic development factors and regional economic risk prevention in post COVID-19 period: empirical analysis based on panel data of Guangdong regional economy. *Journal of combinatorial optimization*, 44(5): 3735-3777.

- [13] Sekaran R, Munnangi A K, Rajeyyagari S, Ramachandran M, Aituriyman F. 2021. Ant colony resource optimization for Industrial IoT and CPS. *International Journal of Intelligent Systems*, 37(12): 10513-10532.
- [14] Chen Y, He S, Jin X, Wang Z, Wang F, Chen L. 2023. Resource utilization and cost optimization oriented container placement for edge computing in industrial internet. *Journal of supercomputing*, 79(4): 3821-3849.
- [15] Morse L, Mallardo V, Aliabadi F M H. 2022. Manufacturing cost and reliability-based shape optimization of plate structures. *International Journal for Numerical Methods in Engineering*, 123(10): 2189-2213.
- [16] Liu H, Jin X. 2020. Digital manufacturing course framework for senior aircraft manufacturing engineering undergraduates. *Computer Applications in Engineering Education*, 28(2): 338-356.
- [17] Gazman V D A. 2023. New Criterion for the ESG Model. *Green and Low-Carbon Economy*, 1(1), 22–27.
- [18] Negri E, Berardi S, Fumagalli L, et al. 2020. MES-integrated digital twin frameworks - ScienceDirect. *Journal of Manufacturing Systems*, 56(58): 58-71.
- [19] Choudhuri S, Adeniye S, Sen A. 2023. Distribution Alignment Using Complement Entropy Objective and Adaptive Consensus-Based Label Refinement for Partial Domain Adaptation. *Artificial Intelligence and Applications*. 1(1): 43-51.
- [20] Liang Z, Wang S, Peng Y, Mao X, Yuan X, Yang A. 2022. The process correlation interaction construction of Digital Twin for dynamic characteristics of machine tool structures with multi-dimensional variables. *Journal of Manufacturing Systems*, 63(1): 78-94.

Keyword Acquisition for Language Composition Based on TextRank Automatic Summarization Approach

Yan Jiang*, Chunlin Xiang, Lingtong Li

Department of Primary Education, Chongqing Preschool Education College, Chongqing, 404047, China

Abstract—It is important to extract keywords from text quickly and accurately for composition analysis, but the accuracy of traditional keyword acquisition models is not high. Therefore, in this study, the Best Match 25 algorithm was first used to preprocess the compositions and evaluate the similarity between sentences. Then, TextRank was used to extract the abstract, construct segmentation and named entity model, and finally verify the research content. The results show that in the performance test, the Best Match 25 similarity algorithm has higher accuracy, recall rate and F1 value, the average running time is only 2182ms, and has the largest receiver working characteristic curve area, which is significantly higher than other models, reaching 0.954. The accuracy of TextRank algorithm is above 90%, the average accuracy of 100 text analysis is 94.23%, the average recall rate and F1 value are 96.67% and 95.85%, respectively. In comparison of the application of the four methods, the research model shows obvious advantages, the average keyword coverage rate is 94.54%, the average processing time of 16 texts is 11.29 seconds, and the average 24-hour memory usage is only 15.67%, which is lower than the other three methods. The experimental results confirm the superiority of the model in terms of keyword extraction accuracy. This research not only provides a new technical tool for language composition teaching and evaluation, but also provides a new idea and method for keyword extraction research in the field of natural language processing.

Keywords—Language composition; keywords; best match 25; textrank; digests

I. INTRODUCTION

In today's digital era, natural language processing (NLP) technology plays an increasingly important role in the field of text analysis. Keyword extraction, as a basic text analysis tool, is important for understanding and processing large amounts of text data [1]. Especially in the field of education, efficient and accurate keyword extraction has great application value for the analysis and evaluation of language composition (LC). Traditional keyword extraction methods, such as term frequency-inverse document frequency (TF-IDF), latent delicacy allocation (LDA), graph-based lexical rank (LexRank) algorithms, have been applied in several fields, but still have limitations in efficiency and accuracy in specific scenarios [2-3]. TextRank's automatic summarization (AS) method extracts key sentences from text in an unsupervised learning manner in a concise and efficient way, which can be achieved without a large amount of labeled data. This algorithm has good adaptability and scalability, can be applied to texts in

different domains, and is easily integrated with other NLP techniques [4]. As a graph-based algorithm, TextRank also reveals the text structure, increasing the depth of analysis and content level understanding. In view of this, research has focused on exploring LC keyword extraction techniques based on the TextRank AS method [5]. The goal of the study is to improve the efficiency and accuracy of LC keyword extraction by optimizing and applying the TextRank algorithm. The significance of the study is as follows: first, TextRank-based AS not only improves the efficiency of the keyword extraction process and reduces the workload of teachers, but also enhances the objectivity and consistency of the evaluation. Second, the study not only expands the application scope of the algorithm in Chinese text processing, but also promotes the innovative application of language processing technology in the field of education, and provides a new perspective for practical problem solving of NLP technology in language education. In addition, with the wide application of artificial intelligence in various industries, AI-assisted language teaching and assessment is becoming an emerging trend. By optimizing the keyword extraction process, this study lays the foundation for building a smarter educational assistance system, which further promotes the development of AI in the field of educational technology. In summary, this study has far-reaching research significance in enhancing teaching efficiency, promoting technological innovation, and leading the development of educational technology. The study is divided into four main parts, the first of which is a detailed description of relevant studies in recent years. In the second part, the main methods of the experiment are firstly introduced. The third part is to verify the validity and reliability of the research model through experimental design and data analysis. The fourth part is to summarize and prospect the research.

In the study of AS for text, K. E. Dewi and N. I. Widiastuti developed an AS model for Indonesian text that aims to reduce the number of sentences while retaining key information. The model utilized three summarization methods: extractive, abstractive, and hybrid. Extractive selected key sentences, abstract reconstructed new sentences to describe the content, while hybrid combines the advantages of both. The system design consisted of a pre-processing (sentence segmentation, tokenization, co-reference parsing, deactivation, feature extraction) and a processing phase (selecting and arranging important sentences and words to form a summary). The model was particularly suitable for document input and adaptation to long text and multi-document input is a direction

for further research [6]. H. Aliakbarpour et al. proposed a new model of abstract summarization combining convolutional neural networks with long and short-term memory and incorporating the auxiliary attention mechanism of an encoder to enhance the saliency and fluency of the summaries. Tested on CNNDaily Mail and DUC-2004 datasets, the model outperformed the benchmark model in terms of ROUGE score, saliency and readability [7]. Y. Huang et al. proposed a novel elemental graph augmented abstract summarization model for the challenges of legal opinion journalism AS. The model utilized pre-trained language model reinforcement sequences and structural encoders to extract key information through a network of structural graphs and graph transformers to effectively guide the decoding process. Tests on a legal opinion news corpus revealed that the model outperforms other baselines in terms of ROUGE and BERT scores, and its effectiveness was proven by manual evaluation [8]. A. Zagar and M. Robnik-Sikonja presented a cross-language AS approach to summarizing Slovenian news articles using a pre-trained English summary model. To address decoder limitations, additional language models were introduced for target language text evaluation. The cross-language model was demonstrated to be qualitatively similar to the target language-specific model through automatic and manual evaluation, but occasionally misleading or absurd content appeared [9]. E. Inan proposed an entity-based text summarization method that recognizes named entities and constructs dependency graphs from a pre-trained language model. A reconciliation centrality algorithm was applied to summarize the entity ordering, outperforming the unsupervised learning baseline and approaching the state-of-the-art end-to-end model [10].

In summary, the recent literature in the field of automatic text processing, especially in keyword extraction and summary generation, has demonstrated several notable advances. Researchers have developed different approaches in order to accommodate multiple languages and text formats. For example, Dewi and Widiastuti developed a model containing multiple summarization techniques specifically for Indonesian text to accommodate long texts and complex documents. In the widely studied TextRank algorithm, Qiu and Zheng enhanced its performance in keyword extraction through tolerance rough sets, while Hernawan et al. improved the accuracy of the algorithm in sentence importance assessment using BM25. Huang and Xie improved the accuracy of keyword extraction for patented text by combining the TextRank algorithm with a priori knowledge networks. Further, Aliakbarpour et al. combined a convolutional neural network and a long and short-term memory network while incorporating an attention mechanism to enhance the quality of text summarization. The elemental graph augmented abstract summarization model proposed by Huang et al. on the other hand, demonstrates superiority in handling legal opinion news. Given the potential application of TextRank in automatic keyword extraction, the study proposes to use this algorithm to extract keywords for LC. It is expected to further improve the algorithm's ability and accuracy in extracting key contents for Chinese essays by improving TextRank. This will not only provide support for automatic scoring of compositions, but also help educators to

have a more comprehensive understanding of students' writing skills and content focus, so as to provide more effective guidance and feedback.

II. LANGUAGE KEYWORD ACQUISITION MODEL BASED ON TEXTRANK ALGORITHM

The study, in order to construct a language keyword acquisition model with higher accuracy, first preprocesses the LC by BM25 similarity algorithm, and the query calculates the similarity between the LC sentences. Then the automatic digest results of the composition corpus are obtained based on TextRank algorithm. After that, the construction of participle model and named entity model is carried out. Finally, the description related to dictionary design and keyword acquisition strategy is unfolded.

A. Abstract Acquisition Based on BM25 Similarity Algorithm with TextRank Algorithm

In the study of keyword acquisition, Best Match 25 (BM25) similarity algorithm is an algorithm used in information retrieval and text mining to measure the relevance between a query and a document [11]. Its advantages include effectiveness against long documents, ability to handle documents of different lengths, automatic adjustment of the weights of query terms, ability to handle scarce terms, and efficiency in large text collections [12]. The BM25 algorithm has been widely used in the field of information retrieval, and is able to more accurately assess the relevance between documents and queries, and therefore has significant practical value in large-scale document retrieval and search engines [13]. The general formula of BM25 similarity algorithm is shown in Eq. (1).

$$Score(Q, d) = \sum_i^n W_i \cdot R(q_i, d) \quad (1)$$

In Eq. (1), Q denotes the sentence to be retrieved, q_i denotes the morpheme obtained from the sentence, and W_i denotes the weight of q_i . d denotes the target sentence, and R denotes the relevance score of q_i and d . When q_i occurs more times in the sentence, it means that the similarity weight it represents decreases, and in order to avoid the result error caused by this situation, there exists an expression as shown in Eq. (2).

$$IDF(q_i) = \log \frac{N - n(q_i) + 0.5}{n(q_i) + 0.5} \quad (2)$$

In Eq. (2), N denotes the total number of sentences and $n(q_i)$ denotes the number of q_i sentences included. The formula for similarity is shown in Eq. (3).

$$R(q_i, d) = \frac{f_i \cdot (k_1 + 1)}{f_i + K} \cdot \frac{qf_i \cdot (k_2 + 1)}{qf_i + k_2} \quad (3)$$

In Eq. (3), k_1 and k_2 denote the conditioning factor constants, and qf_i denotes the number of times the word appears in the retrieval process [14]. If the number of times

the word appears in the process of retrieval is 1, the formula can be further simplified, as shown in Eq. (4) [15].

$$R(q_i, d) = \frac{f_i \cdot (k_1 + 1)}{f_i + K} \quad (4)$$

In Eq. (4), f_i denotes the frequency of occurrence of words, and the expression of K is shown in Eq. (5).

$$K = k_1 \cdot (1 - b + b \cdot \frac{dl}{avgdl}) \quad (5)$$

In Eq. (5), dl denotes the length of the sentence, then $avgdl$ denotes the average length of all sentences, and b is a constant and represents the moderating factor [16-17]. Querying the correlation between texts through the BM25 similarity algorithm mitigates the interference encountered in calculating the similarity. Therefore, the study used the BM25 similarity algorithm to preprocess the LC, after which the

keywords and abstracts were obtained by TextRank algorithm. TextRank algorithm is a graph-based text summarization method that determines keywords and sentences in text by analyzing the interconnections between words in the text. The algorithm first represents the text as a node graph, then calculates the weights of the nodes through the connection relationship between the nodes, and uses iterative computation to gradually update the weights of the nodes, and finally determines the keywords and sentences. The advantages of the TextRank algorithm include a structured representation of the text, the ability to capture semantic associations between words, applicability to multilingual texts, no restriction on the length of the text, the ability to handle unsupervised learning, and it has proven its effectiveness and usefulness in the field of text summarization and keyword acquisition [18]. Therefore, the TextRank algorithm has important application prospects in automatic text summarization and keyword acquisition tasks. The operation principle of TextRank algorithm is shown in Fig. 1.

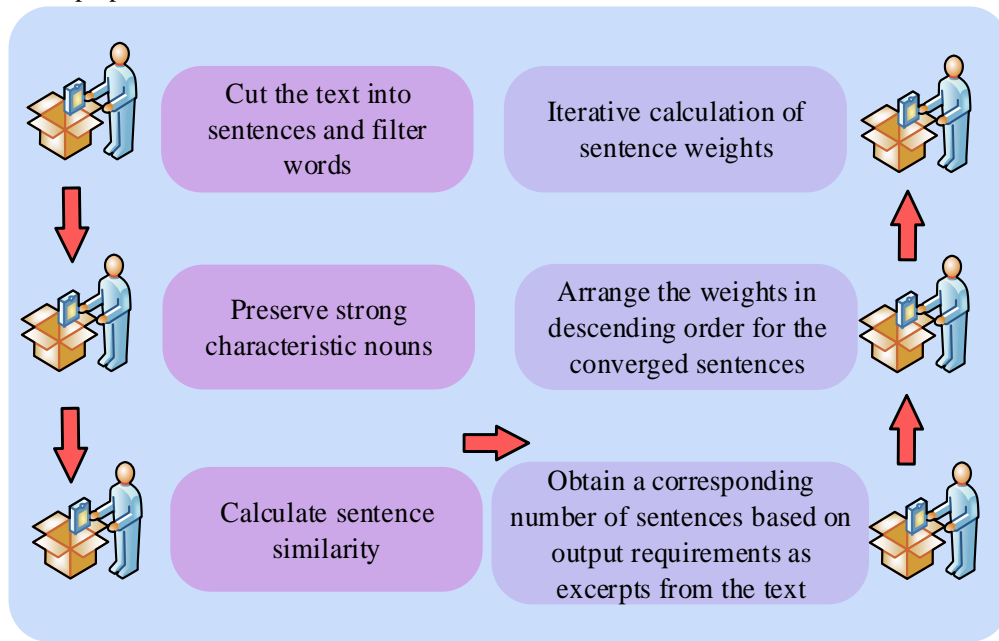


Fig. 1. Operating principle of textRank algorithm.

In Fig. 1, firstly, the text is segmented into sentences and partitioned, while filtering out the stop words and retaining the characteristic words such as nouns and adjectives. Secondly, the similarity between sentences is calculated, the graph structure is constructed, the sentences are taken as nodes on the graph, and the value of the edges is the similarity between the sentences. Then, the weight of each sentence node is determined by iterative calculation. Finally, the descending order is sorted according to the weights, and the sentence with the highest weight is selected as the digest sentence. TextRank algorithm is divided into two parts: calculating similarity and sorting, in the calculation of similarity based on the idea of PangRank to build a graph, based on the nodes of the graph to calculate the similarity between sentences as shown in Eq. (6).

$$Score(V_i) = (1 - d_1) + d_1 * \sum (W_{ji} / O_j) \quad (6)$$

In Eq. (6), d_1 denotes the damping coefficient, which usually takes the value of 0.85, meaning the probability of going from one graph node to another, with the purpose of avoiding the node weight values in the fringes from being assigned to 0. W_{ji} denotes the weight of node V_i pointing to node V_j , and O_j denotes the out-degree (i.e., number of edges connected out) of node V_j . \sum denotes the cumulative summation operation for all nodes V_j pointing to node V_i [19].

B. Construction of the Disambiguation Model, Named Entity Model

After the summarization process, the composition

information has removed most of the redundant data, and then the keywords can be obtained from it. Firstly, the coverage of keywords should be set, and the model of word splitting is constructed from the keyword acquisition and elaborated on the basis of named entity model and self-built lexicon. After that, the strategy of LC keyword acquisition is proposed. Segmentation model is a model used in NLP to segment a continuous text sequence into meaningful units. In Chinese text processing, the role of the participle model is particularly significant, because there is no obvious word separator symbol like space in Chinese. Therefore, word segmentation modeling applies various techniques and methods, such as rule-based

segmentation, lexicon-based segmentation, and statistical and machine learning-based segmentation [20]. The research adopts dictionary-based participle modeling, and the N-shortest path participle algorithm is one of the popular algorithms. N-Shortest Path Segmentation Algorithm is a Chinese segmentation algorithm based on graph theory and dynamic programming, compared with the traditional shortest path segmentation algorithm, it can better deal with problems such as ambiguity and unregistered words, and its characteristics are more suitable for discriminative named entity recognition, the operation principle of N-Shortest Path Algorithm is shown in the schematic diagram in Fig. 2.

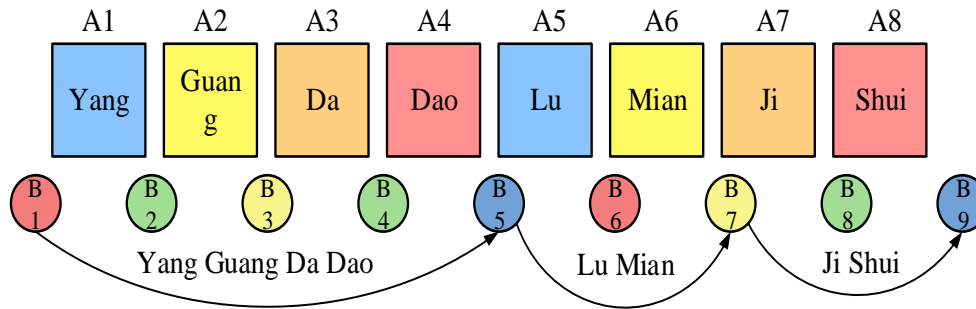


Fig. 2. Schematic diagram of the operating principle of the N-shortest path algorithm.

Fig. 2 shows an example subsection of the N-shortest path algorithm in operation, where A denotes each Chinese character present in the sentence and B denotes the node in the graph. This sentence demonstrates the ideal path: "Yang guang da dao/Lu mian/Ji shui" after the step of disambiguation, i.e., B1 to B5, B5 to B7, and B7 to B9 are recognized as reasonable paths. Meanwhile, words such as "Dao lu" and "Mian ji" also represent a path, and the algorithm first finds the shortest N paths of the sentence, and then calculates the most probable result based on the shortest paths. If noise interference is encountered, the word cut sign is lost, resulting in a situation where the output is a Chinese character string A. The existence of the formula is shown in Eq. (7).

$$P(W | C) = P(W) * \frac{P(C | W)}{P(C)} \quad (7)$$

In Eq. (7), W denotes the result sought after the improvement, and p denotes the probability that the partition result is divided correctly. $P(W | C)$ denotes the probability that the word string becomes a string of Chinese characters, and the value of $P(C)$ is kept constant. On the basis of maintaining the independence between sentences and introducing the unitary processing model in the n-gram model, the existence formula is shown in Eq. (8).

$$P(W) = \prod_{i=1}^m p(W_i) \quad (8)$$

In Eq. (8), it is assumed that each word occurs with equal probability and all are $p(W_i)$, where m denotes the number of words in the sentence. To summarize, the operation of the N-shortest path algorithm is mainly divided into three steps: in the first step, the sentence to be split into words is constructed

into a directed graph, in which each node represents a word or words, and the edges between the nodes indicate the transfer relationship between words or words, with corresponding weights on each edge. In the second step, all possible paths in the graph are traversed and the weights of the paths are calculated using dynamic programming. The optimal n paths are found by recording the predecessor nodes of each node and maintaining a priority queue of path lengths. In the third step, based on the obtained optimal paths, path merging is performed to obtain the final disambiguation result. After the construction of the participle model, a cascading hidden Markov model (HMM) based named entity recognition is proposed for the processed corpus. HMM is a probabilistic model for modeling time-series data and is commonly used in speech recognition, NLP and bioinformatics [21-22]. It consists of a hidden Markov chain and a sequence of observations, where the hidden Markov chain represents the sequence of states of the system and the sequence of observations represents the sequence of observations dependent on each state [23]. The principle of operation of the HMM model with the labeling of person and place name roles is shown in Fig. 3.

Fig. 3(a) illustrates the operational steps of the HMM model, where the set of hidden states, the set of observations, the initial state probability distribution, and the state transfer probability distribution are first determined and used to generate the sequence of hidden states. Then the probability distributions of the observations are generated based on the hidden states to generate the corresponding observation sequences [24]. After that, the model parameters, including the initial state probability distribution, the state transfer probability distribution, and the observation generation probability distribution, are learned from the known observation sequences. Finally, with the given model and

observation sequences, the Viterbi algorithm or forward-backward algorithm is utilized to decode or predict the most probable hidden state sequences [25-26]. Fig. 3(b) shows the role labeling of the model for the case of role labeling of person and place names. In the HMM model, for the case that the words do not appear in the existing lexicon,

the method of calculating the output probability based on the role-word generation model is proposed, whose expression is shown in Eq. (9).

$$P(w | c) = \prod_{j=0}^k p(w_{p+j} | r_{p+j}) p(r_{p+j} | r_{p+j-1}) \quad (9)$$

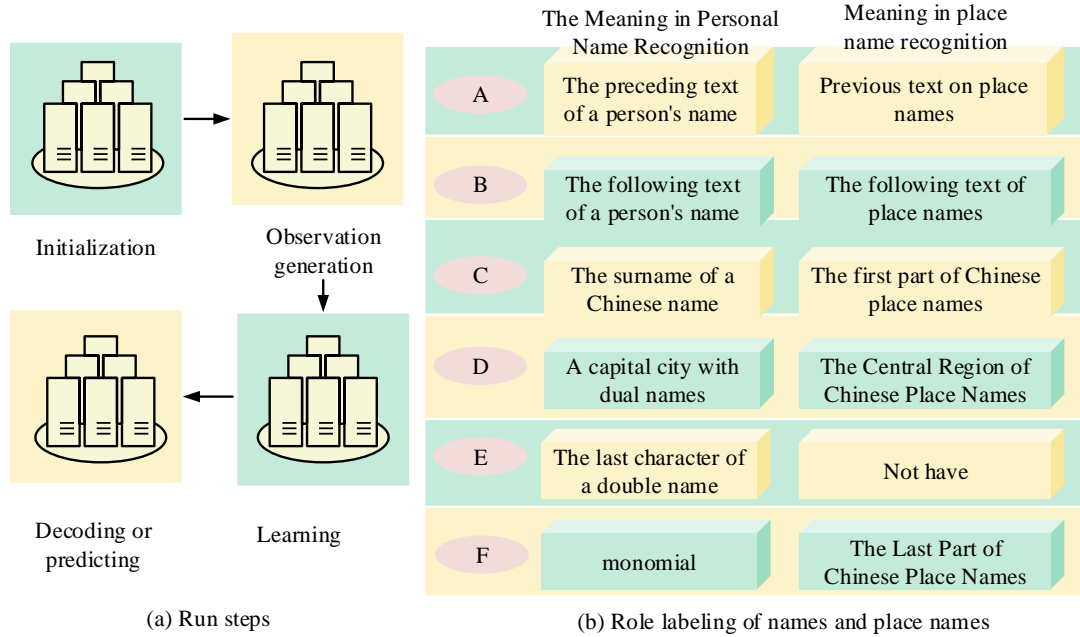


Fig. 3. Operating principle of HMM model and labeling of person and place name roles.

In Eq. (9), w denotes a word that is not in the dictionary, r denotes a collection of roles. c denotes the category of the entity, $p(r_{p+j} | r_{p+j-1})$ denotes the transfer probability between the previous and previous roles, and $p(w_{p+j} | r_{p+j})$ denotes the probability that w occurs in r . The HMM model can be used to identify the important names and places in the LC corpus. The HMM model is able to effectively identify important names of people and places in the LC corpus, which can be used to assist in the acquisition of keywords for compositions [27-28].

C. Keyword Acquisition Strategy

The study uses the open source natural language framework HanLP to implement the use of entity recognition and segmentation, in order to improve the accuracy of keyword acquisition, the study uses a customized dictionary, the self-built dictionary for characters and scenery is shown in Fig. 4.

In Fig. 4, in the recognition of characters, they are categorized with the help of different types of nouns. And in the recognition of scenery, it is defined with the help of affixes. After that, the language corpus is analyzed to obtain the keywords, which have a restricted vocabulary of five, and classified for their connotations: article type, core, and key description." Article type" usually refers to the genre of the essay, such as argumentative essay, narrative essay, expository essay, application essay, etc., each of which has different

writing characteristics and structures and is used to express different purposes and emotions." Core" usually refers to the theme or center of the essay, which is the main idea or argument that the writer wants to express, and it represents the focus and core of the essay [29-30]. "Key description" refers to the part of the composition that describes the core entities in detail, which may include the description of things, the characterization of characters, the narration of events, and the development of the relevant plot, etc. These descriptions usually occupy an important place in the composition to highlight the central idea and content of the essay. These descriptions usually occupy an important position in the composition to highlight the central idea and content of the essay. The process of keyword acquisition is shown in Fig. 5.

In Fig. 5, the recognition of named entities is performed based on the coarsely-scored segmentation results, which result in words being labeled lexically. Then the comprehensive deactivation word list adopted for eliminating deactivated words aims to eliminate words that are commonly used in LC and to reduce the interference with keyword acquisition. This is followed by entity statistical analysis and finally keyword acquisition. Among them, the analysis process of word lexicality is shown in Fig. 6.

In the presentation in Fig. 6, a two-stage process for core entity acquisition can be seen. First, the system uses standard named entity recognition techniques to identify entities. Next, in the case that the lexical label of an entity is a person's name or a place's name, the system checks whether the counter of

the corresponding category has reached the upper limit of two entities. If the category to which a word belongs already has two entities, the word will not be processed further. If the upper limit has not been reached, the word is added to the final result set. This process ensures that entities are effectively identified and categorized, while limiting the

number of entities in each category, keeping the result set streamlined and relevant. If an analyzed term is not included in the self-constructed lexicon, it will be included in the evaluation of the key descriptions, and the description rules are shown in Fig. 7.

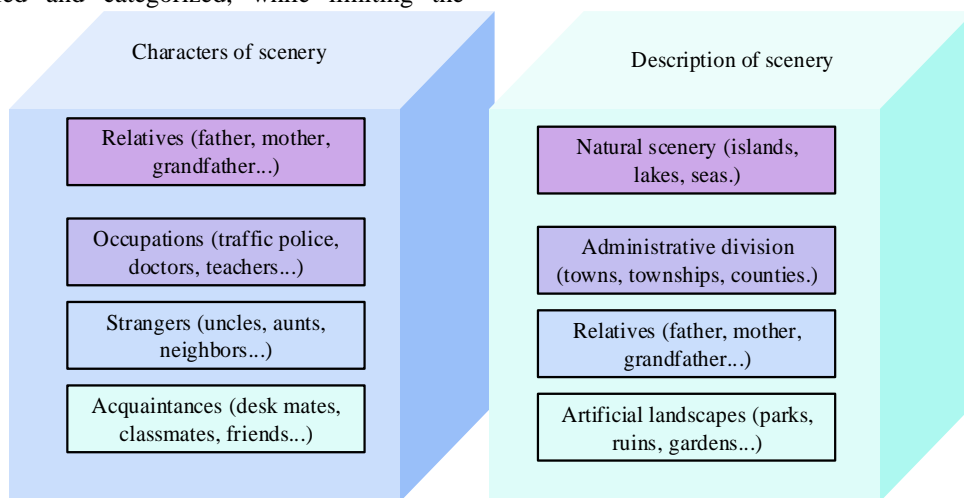


Fig. 4. Self-built dictionary of characters and scenery.

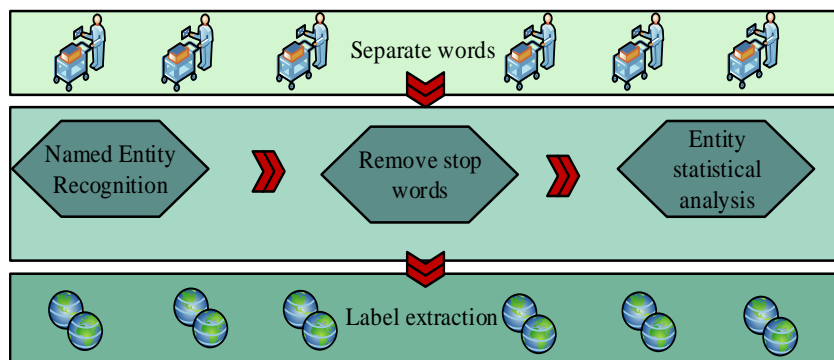


Fig. 5. Keyword acquisition process.

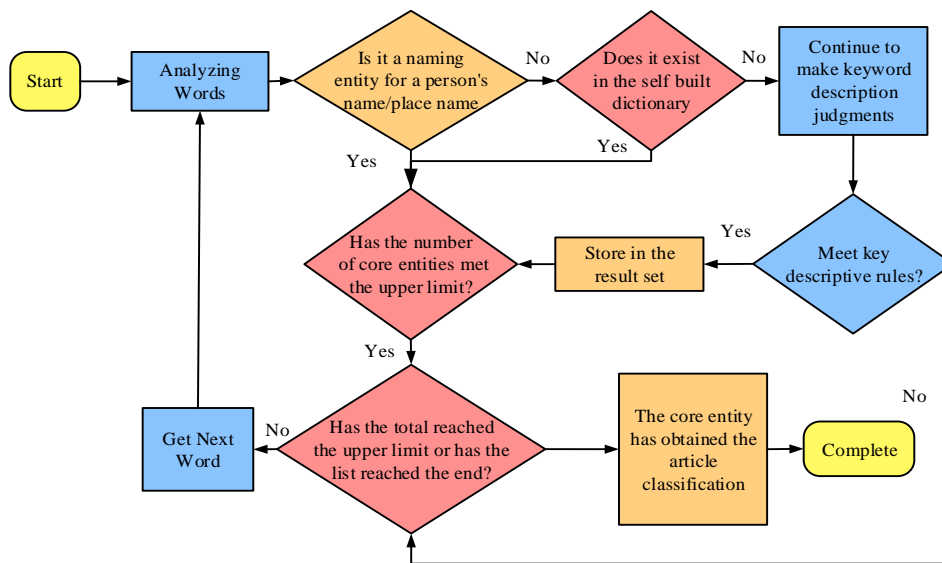


Fig. 6. Analysis process of word parts of speech.

Based on the rules in Fig. 7, the key description section is obtained, and finally, the system performs a comprehensive analysis of the word list. Once the number of keywords extracted from the list meets the requirements, or when the end of the word-phrase list is read, the word-list analysis is completed. In addition, the type keywords for the articles were determined by comparing the weights of the two main types of

named entities, person names and place names. If names were given more weight than places, the article was categorized as a "characterization". If names of places were given more weight, the article was categorized as "description of scenery". In the case of equal weight, both keywords will be added to the result set. Through this series of steps, the keyword acquisition of elementary school essays can be successfully completed.

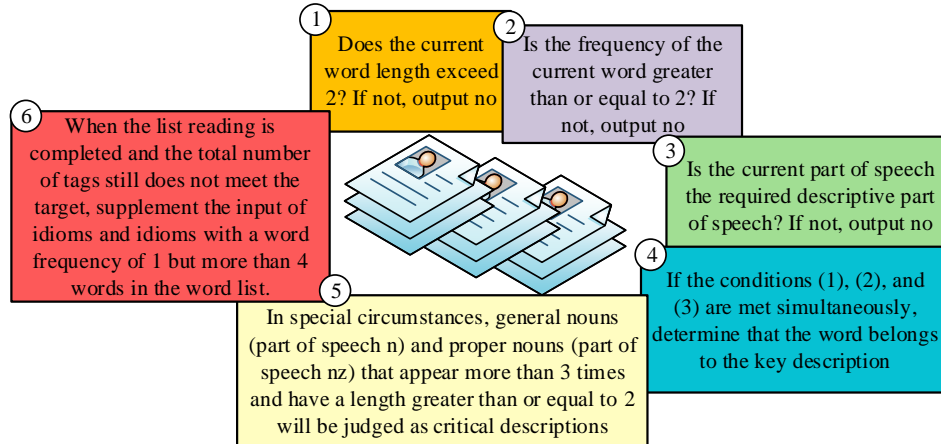


Fig. 7. Key description rules.

III. RESULTS OF THE LANGUAGE KEYWORD ACQUISITION MODEL BASED ON TEXTRANK ALGORITHM

In order to verify the superiority of the research constructed model, the similarity algorithm and TextRank algorithm chosen for the research are tested for performance and application comparison study, and then analyzed for the actual application of the research constructed model and compared with other methods in the process.

A. Comparison Results of Similarity Algorithms

In order to reduce the experimental error, the experiment was analyzed and studied using the same device with Intel Xeon W-2295 CPU, 16G RAM, 100G hard disk memory, Red Hat Enterprise Linux 8 as the operating system, and Python 3.9 as the programming language. The dataset test was obtained from the LC library of students from an elementary school and a secondary school. To test the BM25 similarity algorithm chosen for the study, comparison methods were chosen: classical similarity, edit distance, Word2Vec. these methods were compared with recall-orientated understudy for gisting evaluation (ROUGE) of the BM25 similarity algorithm of the study method. And the average of 100 texts analyzed is shown in Fig. 8.

In Fig. 8, ROUGE is scored in three dimensions, ROUGE-N, ROUGE-L, and ROUGE-W. Three evaluation metrics are selected in each dimension: accuracy, recall with F1 value. For ROUGE-N, Word2Vec has the lowest evaluated values of accuracy, recall and F1 value, and BM25 similarity algorithm with edit distance has comparable evaluated values of accuracy, recall and F1 value. For ROUGE-N, Word2Vec

still performs the worst, and the BM25 similarity algorithm with edit distance has a higher recall and a smaller difference in accuracy from the F1 value. For the dimension ROUGE-W the evaluation values are similar to the first two dimensions. It is proved that BM25 algorithm has better performance than other algorithms in various dimensions of ROUGE scoring, especially in the recall rate advantage is crucial to ensure the integrity of automatic summarization. In addition, BM25 algorithm also has better performance on ROUGE score than the conclusion in study [7]. Continuing with the comparison of the processing time of these four methods, it is shown in Fig. 9.

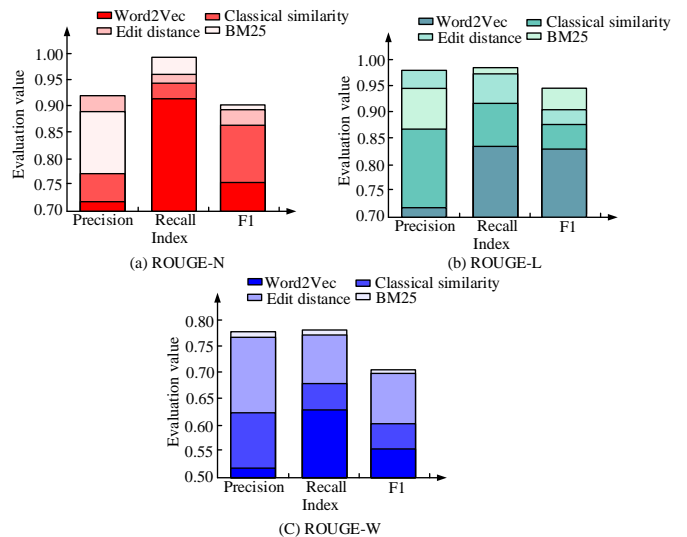


Fig. 8. Rouge scoring results of four methods.

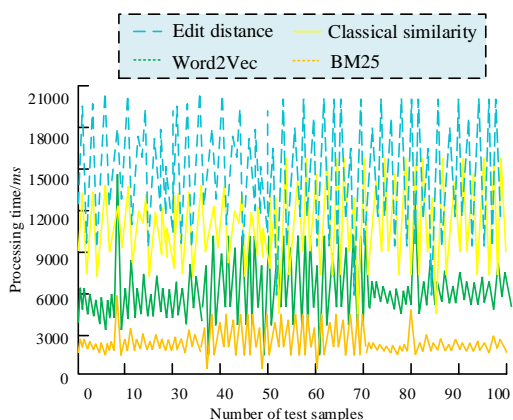


Fig. 9. Comparison of processing time of four methods.

In Fig. 9, in 100 runs, the processing time of the research method is found to be significantly shorter, with an average of only 2182 ms. the average processing time of Word2Vec and classical similarity is 6192 ms and 18065 ms, respectively. The edit distance method mentioned in Fig. 8, although the accuracy, recall and F1 value are not much different from that of the research method, the processing time of the research method is significantly higher, with an average of 20972ms. This means that the processing time of the edit distance method is 8.61 times higher than that of the research method, indicating that the research method has a significant advantage in efficiency. Processing time is one of the key indicators of the usefulness of the algorithm, and the BM25 algorithm shows a shorter processing time, indicating a significant efficiency advantage, suitable for real-time or large-scale text processing tasks.

B. Application of a Language Keyword Acquisition Model Based on TextRank Algorithm

To verify the superiority of TextRank algorithm, it is compared with TF-IDF, LDA and LexRank algorithms. In terms of parameter configuration, the research set 0.90 momentum, 0.0004 attenuation, and planned to conduct 300 rounds of training. The initial learning rate is set to 0.01, and the cosine learning rate strategy is adopted, and the learning rate will be adjusted to 0.001 as the training progresses. Selecting the indicator Receiver operating characteristic curve (ROC) curve, the text in the dataset is tested and analyzed several times, and the comparison results after 50 times are shown in Fig. 10.

In Fig. 10, the area under the ROC curve (AUC) is between 0.1 and 1, providing a direct way to measure the accuracy of the model, and an increase in the AUC value

means that the model's predictive accuracy increases. In this figure, the TextRank algorithm has the largest AUC value, which is significantly higher than the other models, at 0.954, very close to 1. This is followed by the TF-IDF algorithm, which also has a higher accuracy with an AUC value of 0.842, and the rest of the models have an AUC value of around 0.70. AUC is an important index to measure the prediction accuracy of the model, and the AUC value of the TextRank algorithm is the largest, close to 1, indicating that its prediction accuracy in the automatic summary task is very high. The results illustrate the superiority of the accuracy of the research method, and continue to compare it with the three methods mentioned above by analyzing 100 texts, and the results of the comparison of accuracy, recall, and F1 value are shown in Fig. 11.

In Fig. 11 (a), the accuracy curve of LexRank has the largest fluctuation, the accuracy is not up to 75%, the range of values of TF-IDF and LDA accuracy is between 75% and 90%, and the accuracy of TextRank algorithm is above 90%, and the accuracy change for 100 text analysis is small, and the curve is relatively flat, with an average accuracy of 94.23%. The comparison between Fig. 11(b) and Fig. 11(c) is similar to that of Fig. 11(a), and the average of the recall and F1 value of TextRank reaches 96.67% and 95.85%, respectively. Accuracy rate, recall rate and F1 value are the key indexes to evaluate the performance of automatic summarization algorithm. TextRank algorithm performs better than other algorithms on these indexes, which proves its superiority and reliability in automatic summarization task. In addition, TextRank algorithm also has more advantages than references [8] and [9]. In order to verify the applicability of the research constructed model, the indicator keyword coverage is selected for application evaluation, which refers to the degree to which the keywords cover the key content of the original text. Prior to this determine the set of keywords of the applied texts, which were selected by manual methods. Ten LCs from different grades were analyzed and the results are shown in Fig. 12.

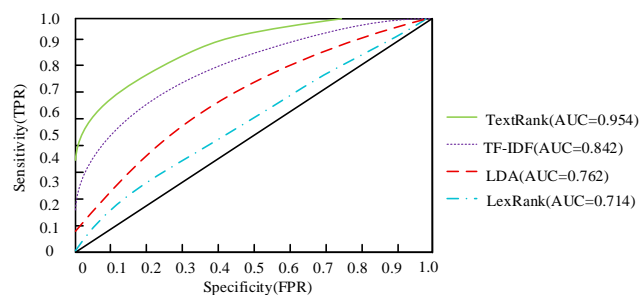


Fig. 10. Comparison of ROC curves for four methods.

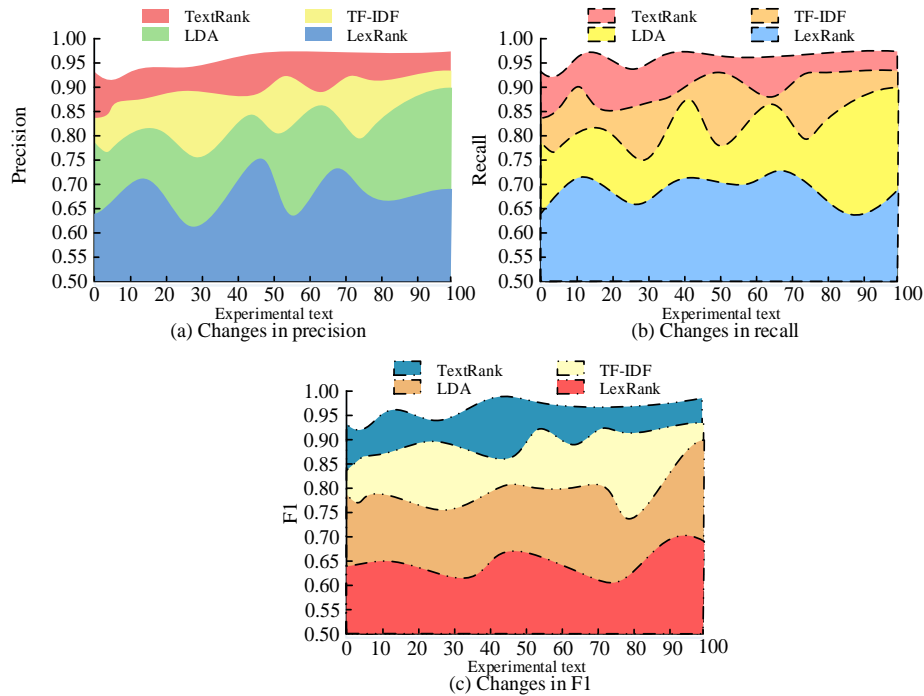


Fig. 11. Comparison results of precision, recall and F1 value of four methods.

In Fig. 12, the keyword coverage of the research model fluctuates the most among the 10 texts, reaching a maximum value of 80.23% at text 6, and it has an average coverage of 62.87%. The keyword coverage fluctuation curves of LDA and TF-IDF are more gentle, with an average keyword coverage of 66.96% and 77.12%, respectively. The curve of the research method has the smallest fluctuation and reaches the maximum value of 96.76% at text 6, with an average keyword coverage of 94.54%. Keyword coverage reflects the comprehensiveness of the algorithm to capture the main information of the original text. The research model performs better than other algorithms in keyword coverage, indicating that it can capture and extract key information of text more comprehensively. For the large gap in the extraction accuracy of the 10 text keywords, it may be due to the fact that the texts selected for the experiment were from different grades. In

order to further explore the superiority of the research model, it was continued to be compared with the three methods mentioned above and applied to five LCs, and the scores of classification accuracy, entity accuracy and key description accuracy are shown in Table I.

In Table I, for the comparison of classification accuracy, entity accuracy and key description accuracy for the four methods, classification accuracy could not be compared and only the research methods were able to classify. The difference in entity accuracy was not significant and key description accuracy was greater. By comparing the mean of the sum of the scores, it can be seen that the research model has the highest sum of scores, 3.488, and the remaining three types of models do not have scores higher than 3. The research continues to analyze the text for different grade levels, and the results of its comparison are shown in Fig. 13.

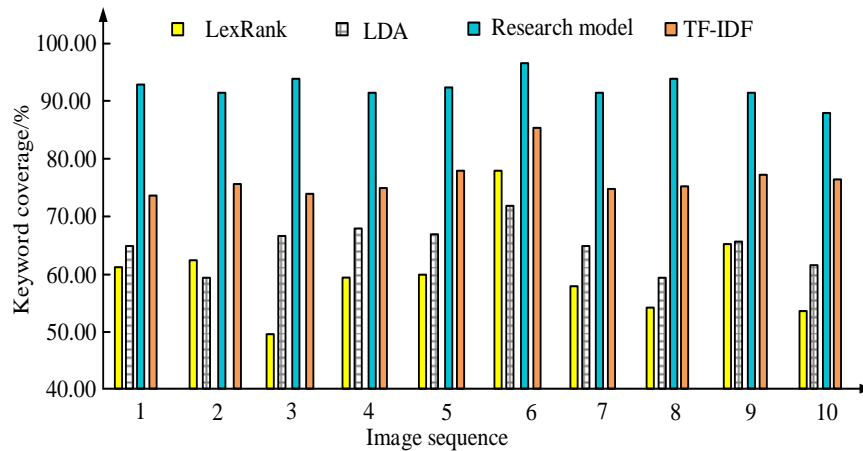


Fig. 12. Comparison of keyword coverage among four methods.

TABLE I. SCORE OF FOUR METHODS FOR CLASSIFICATION ACCURACY, ENTITY ACCURACY, AND KEY DESCRIPTION ACCURACY

| Algorithm | Text Number | Classification accuracy | Entity accuracy | Accuracy of key descriptions | Total score | Average value |
|----------------|-------------|-------------------------|-----------------|------------------------------|-------------|---------------|
| Research model | 1 | 0.81 | 1.76 | 0.95 | 3.52 | 3.488 |
| | 2 | 0.80 | 1.73 | 0.92 | 3.45 | |
| | 3 | 0.83 | 1.75 | 0.91 | 3.49 | |
| | 4 | 0.81 | 1.77 | 0.95 | 3.53 | |
| | 5 | 0.82 | 1.72 | 0.91 | 3.45 | |
| TF-IDF | 1 | - | 1.73 | 0.63 | 2.36 | 2.366 |
| | 2 | - | 1.72 | 0.64 | 2.36 | |
| | 3 | - | 1.74 | 0.65 | 2.39 | |
| | 4 | - | 1.71 | 0.68 | 2.39 | |
| | 5 | - | 1.72 | 0.61 | 2.33 | |
| LDA | 1 | - | 1.71 | 0.70 | 2.41 | 2.436 |
| | 2 | - | 1.74 | 0.72 | 2.46 | |
| | 3 | - | 1.73 | 0.71 | 2.44 | |
| | 4 | - | 1.71 | 0.72 | 2.43 | |
| | 5 | - | 1.69 | 0.75 | 2.44 | |
| TextRank | 1 | - | 1.54 | 0.51 | 2.05 | 2.098 |
| | 2 | - | 1.52 | 0.57 | 2.09 | |
| | 3 | - | 1.61 | 0.53 | 2.14 | |
| | 4 | - | 1.54 | 0.54 | 2.08 | |
| | 5 | - | 1.57 | 0.56 | 2.13 | |

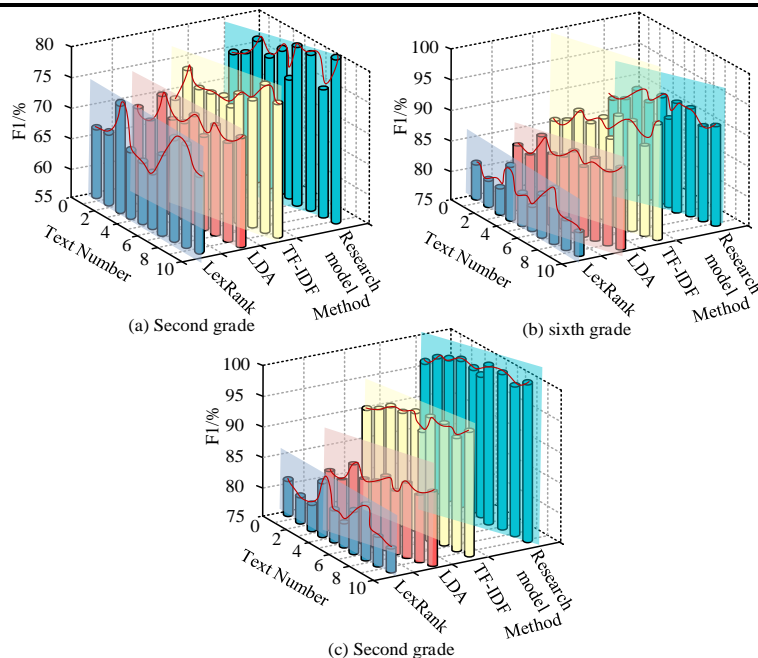


Fig. 13. Analysis of four methods for texts in different grades.

Fig. 13 (a) demonstrates the results of analyzing the essays of the second grade, the F1 value of the research method is relatively high, but the difference between the four methods is not significant, the average value of the F1 value of the research method is 77.24%, which does not reach 80%. Fig. 13 (b) demonstrates the results of analyzing the essays of the sixth grade, and the F1 value of the research methods

remained higher at 86.94%. Fig. 13 (c) demonstrates the results of analyzing the essays of the ninth grade, the research method has the highest F1 value and it is significantly different from the F1 value of the remaining three methods, the research method F1 value reaches more than 90% and the average F1 value is 96.23%. F1 value is a performance indicator that takes into account accuracy and recall rate. With

the improvement of the research method, the F1 value also increases, indicating that the method has better analysis ability for more logical and complex texts, and the F1 value of the research method is always the highest in the comparison of the four methods. Continuing to compare the processing time and memory usage of the four methods, the results are shown in Fig. 14.

In Fig. 14(a), the presented data clearly reveals the significant differences in processing time among the four different methods. Among them, the model used in the study shows the best time efficiency, with its processing time fluctuating mainly around 10 seconds and an average processing time of 11.29 seconds. In contrast, the LexRank,

LDA, and TF-IDF methods have longer processing times and show varying degrees of volatility. In addition, Fig. 14(b) provides a comparison of these methods in terms of memory occupancy. In this figure, the research model also shows a significant advantage in terms of memory occupancy, with an average memory occupancy of only 15.67%, whereas the memory occupancy of the other three methods shows greater volatility and instability, with the highest of them even reaching 100%. The processing time and memory usage are directly related to the practicability and scalability of the algorithm. The research model shows advantages in both aspects, which means that it is more suitable for practical application in terms of resource consumption and time efficiency.

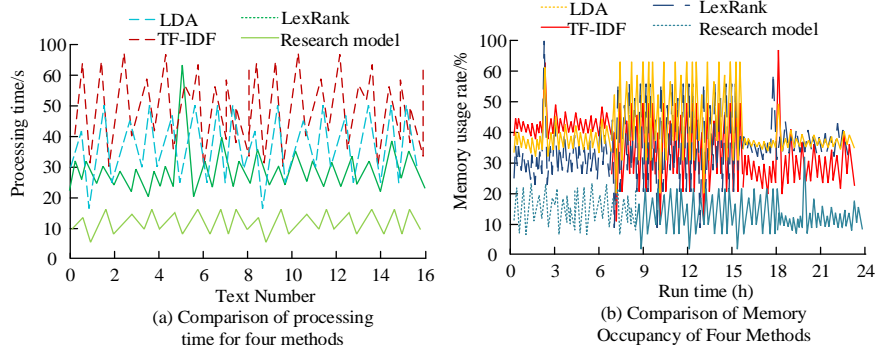


Fig. 14. Comparison of processing time and memory usage of four methods.

IV. CONCLUSION

BM25 similarity algorithm and TextRank algorithm are introduced to obtain keywords in Chinese composition more conveniently. On this basis, a keyword acquisition model is constructed by combining with other intelligent methods. In terms of theoretical contribution, the research expands the application scope of TextRank algorithm in Chinese text processing, and lays a foundation for building a more intelligent education assistance system by optimizing the keyword extraction process, which further promotes the development of AI in the field of education technology. In the actual contribution, the research not only improves the efficiency and accuracy of keyword extraction, reduces the work burden of teachers, but also enhances the objectivity and consistency of evaluation, which has far-reaching research significance for improving teaching efficiency, promoting technological innovation and leading the development of educational technology.

In practical applications, the proposed method shows high accuracy, recall rate and F1 value, and has significant advantages in processing time. It has a short running time, and the average running time is only 2182ms in 100 processing times, and the editing distance processing method is 8.61 times of it. In the performance test and comparison of TextRank algorithm, the AUC value of TextRank algorithm is the largest, which is significantly higher than other models, reaching 0.954, which is very close to 1. The accuracy of TextRank algorithm is above 90%, and the average accuracy of 100 text analysis is 94.23%, and the average recall rate and F1 value reach 96.67% and 95.85% respectively. In the application comparison of the four methods, the research

model reaches the maximum value at text 6, which is 96.76%, and the average keyword coverage is 94.54%. For the experimental samples of different grades, the average F1 value of the research model in the second grade was 77.24%, which did not reach 80%. The average F1 value of the model in grade 6 was 86.94%. The average F1 value of the study model at grade 9 was 96.23%. This shows that the accuracy rating value increases with the increase of grade level. In the comparison of the processing time and memory usage of the four methods, the research model shows obvious advantages. The average processing time of 16 texts is 11.29 seconds, and the average memory usage within 24 hours is only 15.67%, which is lower than the other three methods.

Although the research has achieved remarkable results in the accuracy and efficiency of keyword extraction, there are still some limitations. Since the research model is aimed at more complex logically complete utterance, and the selected training corpus is also composed of high-level sentences, the analysis accuracy of LC in lower grades is lower.

Future studies need to select lower-grade LC corpora for training to improve the applicability and practicability of the model. It should also be considered to train the model using a broader corpus of different grades and different types (e.g., argumentative essays, narrative essays, etc.) to improve the applicability of the model to different educational levels and text types. At the same time, the scalability and adaptability of the algorithm are considered, so that it can handle larger scale text data. The methods and techniques studied can be extended to other fields, such as automatic summary generation of legal, medical and scientific documents.

REFERENCES

- [1] N. Klyuchnikov and I. Trofimov. "NAS-Bench-NLP: Neural Architecture Search Benchmark for Natural Language Processing," *IEEE Access*, vol.10, pp. 45736-45747, January 2022, DOI: 10.1109/ACCESS.2022.3169897.
- [2] R. Y. Lee, L. C. Brumback, W. B. Lober, J. Sibley, E. L. Nielsen, P. D. Treece, and J. R. Curtis. "Identifying Goals of Care Conversations in the Electronic Health Record Using Natural Language Processing and Machine Learning," *J. Pain Symptom Manage.*, vol. 61, no. 1, pp. 136-142.e2, January, 2021, DOI: 10.1016/j.jpainsymman.2020.08.024.
- [3] L. Zhao, W. Alhoshan, A. Ferrari, K. J. Letsholo, M. A. Ajagbe, E.-V. Chioasca, and R. T. Batista-Navarro. "Natural Language Processing for Requirements Engineering," *ACM Comput. Surv.*, vol. 54, no. 3, pp. 1-41, April, 2022, DOI: 10.1145/3444689.
- [4] U. Rani and K. Bidhan. "Comparative Assessment of Extractive Summarization: TextRank, TF-IDF and LDA," *J. Sci. Res.*, vol. 65, no. 01, pp. 304-311, January, 2021, DOI: 10.37398/jsr.2021.650140.
- [5] M. A. Zamzam. "SISTEM AUTOMATIC TEXT SUMMARIZATION MENGGUNAKAN ALGORITMA TEXTRANK," *MATICS*, vol. 12, no. 2, pp. 111-116, March, 2021, DOI: 10.18860/mat.v12i2.8372.
- [6] K. E. Dewi and N. I. Widiastuti. "The Design of Automatic Summarization of Indonesian Texts Using a Hybrid Approach," *J. Teknol. Inf. Pendidik.*, vol. 15, no. 1, pp. 37-43, November, 2022, DOI: 10.24036/jtip.v15i1.451.
- [7] H. Aliakbarpour, M. T. Manzuri, and A. M. Rahmani. "Improving the Readability and Saliency of Abstractive Text Summarization Using Combination of Deep Neural Networks Equipped with Auxiliary Attention Mechanism," *J. Supercomput.*, vol. 78, no. 2, pp. 2528-2555, February, 2022, DOI: 10.1007/s11227-021-03950-x.
- [8] Y. Huang, Z. Yu, J. Guo, Y. Xiang, and Y. Xian. "Element Graph-Augmented Abstractive Summarization for Legal Public Opinion News with Graph Transformer," *Neurocomputing*, vol. 460, pp. 166-180, October, 14, 2021, DOI: 10.1016/j.neucom.2021.07.013.
- [9] A. Zagar and M. Robnik-Sikonja. "Cross-lingual transfer of abstractive summarizer to less-resource language," *J. Intell. Inf. Syst.*, vol. 58, no. 1, pp. 153-173, February, 2022. DOI: 10.1007/s10844-021-00663-8.
- [10] E. Inan. "Somun: Entity-Centric Summarization Incorporating Pre-Trained Language Models," *Neural Comput. Appl.*, vol. 33, no. 10, pp. 5301-5311, May, 2021, DOI: 10.1007/s00521-020-05319-2.
- [11] D. Qiu and Q. Zheng. "Improving TextRank Algorithm for Automatic Keyword Extraction with Tolerance Rough Set," *Int. J. Fuzzy Syst.*, vol. 24, no. 3, pp. 1332-1342, April, 2022, DOI: 10.1007/s40815-021-01190-y.
- [12] Y. F. Hernawan, P. P. Adikara, and R. C. Wihandika. "Peringkasan Artikel Berbahasa Indonesia Menggunakan TextRank Dengan Pembobotan BM25," *J. Teknol. Inf. Ilmu Komput.*, vol. 9, no. 1, pp. 61-68, December, 2022, DOI: 10.25126/jtiik.2022913765.
- [13] Z. Huang and Z. Xie. "A Patent Keywords Extraction Method Using TextRank Model with Prior Public Knowledge," *Complex Intell. Syst.*, vol. 8, no. 1, pp. 1-12, February, 2022, DOI: 10.1007/s40747-021-00343-8.
- [14] M. F. Fakhrezi, Moch. A. Bijaksana, and A. F. Huda. "Implementation of Automatic Text Summarization with TextRank Method in the Development of Al-Qur'an Vocabulary Encyclopedia," *Procedia Comput. Sci.*, vol. 179, pp. 391-398, January, 2021, DOI: 10.1016/j.procs.2021.01.021.
- [15] S. Zhang, Q. Luo, Y. Feng, K. Ding, D. Gifu, S. Zhang, and J. Xia. "Key Phrase Extraction by Improving TextRank with an Integration of Word Embedding and Syntactic Information," *Recent Adv. Comput. Sci. Commun.*, vol. 14, no. 9, pp. 2969-2975, December, 2021, DOI: 10.2174/2666255813999200820155846.
- [16] A. B. K. Susanto, N. Muliadi, B. Nugroho, and M. Muljono. "Comparison of String Similarity Algorithm in Post-Processing OCR," *J. Appl. Intell. Syst.*, vol. 8, no. 1, pp. 25-32, June, 2023, DOI: 10.33633/jais.v8i1.7079.
- [17] A. Kurnianti, P. Pahlevi, and I. Mufidah. "Recommendation System for Prospective Bride and Groom Using Cosine Similarity Algorithm," *Emerg. Inf. Sci. Technol.*, vol. 4, no. 1, pp. 8-15, June, 2023, DOI: 10.18196/eist.v4i1.18683.
- [18] J. S. Baruni and Dr. J. G. R. Sathiaselalan. "Keyphrase Extraction from Document Using RAKE and TextRank Algorithms," *Int. J. Comput. Sci. Mob. Comput.*, vol. 9, no. 9, pp. 83-93, October, 2020, DOI: 10.47760/ijcsmc.2020.v09i09.009.
- [19] P. Preethi and H. R. Mamatha. "Region-Based Convolutional Neural Network for Segmenting Text in Epigraphical Images," *Artif. Intell. Appl.*, vol. 1, no. 2, pp. 119-127, September, 2023, DOI: 10.47852/bonviewAIA2202293.
- [20] H. Mokayed, T. Z. Quan, L. Alkhaled, and V. Sivakumar. "Real-time human detection and counting system using deep learning computer vision techniques," *Artif. Intell. Appl.*, vol. 1, no. 4, pp. 221-229, September, 2023, DOI: 10.1109/ViTECoN58111.2023.10157694.
- [21] K. Zheng, Y. Li, and W. Xu. "Regime Switching Model Estimation: Spectral Clustering Hidden Markov Model," *Ann. Oper. Res.*, vol. 303, no. 1-2, pp. 297-319, August, 2021, DOI: 10.1007/s10479-019-03140-2.
- [22] X. Wan, T. Han, J. An, and M. Wu. "Hidden Markov Model Based Fault Detection for Networked Singularly Perturbed Systems," *IEEE Trans. Syst., Man, Cybern.: Syst.*, vol. 51, no. 10, pp. 6445-6456, October, 2021, DOI: 10.1109/TSMC.2019.2961978.
- [23] Y. Li, E. Zio, and E. Pan. "An MEWMA-Based Segmental Multivariate Hidden Markov Model for Degradation Assessment and Prediction," *Proc. Inst. Mech. Eng., Part O: J. Risk Reliab.*, vol. 235, no. 5, pp. 831-844, October, 2021, DOI: 10.1177/1748006X21990527.
- [24] W. Zhao, T. Shi, and L. Wang. "Fault Diagnosis and Prognosis of Bearing Based on Hidden Markov Model with Multi-Features," *Appl. Math. Nonlinear Sci.*, vol. 5, no. 1, pp. 71-84, January, 2020, DOI: 10.2478/amns.2020.1.00008.
- [25] Y. Lu and S. An. "Research on Sports Video Detection Technology Motion 3D Reconstruction Based on Hidden Markov Model," *Cluster Comput.*, vol. 23, no. 3, pp. 1899-1909, September, 2020, DOI: 10.1007/s10586-020-03097-z.
- [26] S. Dong, Z.-G. Wu, P. Shi, H. Su, and T. Huang. "Quantized Control of Markov Jump Nonlinear Systems Based on Fuzzy Hidden Markov Model," *IEEE Trans. Cybern.*, vol. 49, no. 7, pp. 2420-2430, July, 2019, DOI: 10.1109/TCYB.2018.2813279.
- [27] L. Shen, X. Yang, J. Wang, and J. Xia. "Passive Gain-Scheduling Filtering for Jumping Linear Parameter Varying Systems with Fading Channels Based on the Hidden Markov Model," *Proc. Inst. Mech. Eng., Part I: J. Syst. Control Eng.*, vol. 233, no. 1, pp. 67-79, January, 2019, DOI: 10.1177/0959651818777679.
- [28] R. A. Pratama, A. A. Suryani, and W. Maharani. "Part of Speech Tagging for Javanese Language with Hidden Markov Model," *J. Comput. Sci. Inf. Eng. (J-Cosine)*, vol. 4, no. 1, pp. 84-91, July, 2020, DOI: 10.29303/jcosine.v4i1.346.
- [29] V. Sorin, Y. Barash, E. Konen, and E. Klang. "Deep Learning for Natural Language Processing in Radiology—Fundamentals and a Systematic Review," *J. Am. Coll. Radiol.*, vol. 17, no. 5, pp. 639-648, May, 2020, DOI: 10.1016/j.jacr.2019.12.026.
- [30] Q. Zhao, J. Niu, and X. Liu. "ALS-MRS: Incorporating Aspect-Level Sentiment for Abstractive Multi-Review Summarization," *Knowl.-Based Syst.*, vol. 258, pp. 1-14, December, 2022, DOI: 10.1016/j.knosys.2022.109942.

Investigating Cooling Load Estimation via Hybrid Models Based on the Radial Basis Function

Sirui Zhang¹, Hao Zheng^{2*}

HeBei Petroleum University of Technology, Chengde Hebei, 067000, China

Abstract—To advance energy conservation in cooling systems within buildings, a pivotal technology known as cooling load prediction is essential. Traditional industry computational models typically employ forward or inverse modeling techniques, but these methods often demand extensive computational resources and involve lengthy procedures. However, artificial intelligence (AI) surpasses these approaches, with its models exhibiting the capability to autonomously discern intricate patterns, adapt dynamically, and enhance their performance as data volumes increase. AI models excel in forecasting cooling loads, accounting for various factors like weather conditions, building materials, and occupancy. This results in agile and responsive predictions, ultimately leading to heightened energy efficiency. The dataset of this study, which comprised 768 samples, was derived from previous studies. The primary objective of this study is to introduce a novel framework for the prediction of Cooling Load via integrating the Radial Basis Function (RBF) with 2 innovative optimization algorithms, specifically the Dynamic Arithmetic Optimization Algorithm (DAO) and the Golden Eagle Optimization Algorithm (GEO). The predictive outcomes indicate that the RBDA prediction model outperforms RBF in cooling load predictions, with RMSE=0.792, approximately half as much as those of RBF. Furthermore, the RBDA model's performance, especially in the training phase, confirmed the optimal value of $R^2=0.993$.

Keywords—Cooling load estimation; machine learning; building energy consumption; radial basis functions; dynamic arithmetic optimization algorithm; golden eagle optimization algorithm

I. INTRODUCTION

A. Background

As building designs become more intricate and demand greater sustainability performance, the utilization of building simulation tools will become unavoidable. Building energy simulation models have undergone over four decades of evolution, with most development endeavors concentrating on refining the model's thermal processes during this time [1]. Four key elements significantly influence a building's energy consumption: (1) its physical attributes, encompassing factors like location, orientation, and type; (2) the installed equipment responsible for maintaining the desired indoor conditions, such as heating, ventilation, air-conditioning systems, electricity, or hot water; (3) external conditions and meteorological variables like temperature, humidity, and solar radiation; and (4) occupant behavior and the associated consequences of their presence [2].

Data on energy consumption across various sectors reveals that the building industry accounts for approximately 40% of the global electricity demand. This electricity is utilized for heating, air conditioning, ventilation, lighting, and the operation of diverse building service systems [3]. For building service systems in tropical or sub-tropical areas, where air conditioning alone accounts for at least 50% of a building's total energy consumption, the proportion is rather higher [4]. However, conducting thorough examinations of energy consumption tends to be expensive and demanding, discouraging property owners and managers from allocating the required investments in terms of time and finances for a comprehensive assessment of energy efficiency. In response to this issue, researchers have developed economical assessment methods designed to identify buildings with potential for energy conservation. The rapid development of building design-specific computer technology and software has made these strategies possible. Computer-based simulation models have been used in many research to evaluate the energy consumption levels of buildings [5]. The most intricate processes within buildings are primarily driven by human behavior, as humans are inherently unpredictable creatures. Human actions significantly impact a building's energy equilibrium, influencing both the indoor environment and the requirements for energy usage [6].

The forward modelling technique is used by several complex computer-based energy simulation programs, such as DOE – 2, EnergyPlus, and BLAST. However, developing the simulation model is a very labour- and resource-intensive process, especially for complex mixed-use structures with erratic operating schedules. An alternative method called inverse modelling relies on using current building characteristics, such as energy use, meteorological information, or other relevant performance data, to infer a set of building characteristics, such as cooling loads. Regression analysis has historically been used to use collected data to estimate the distinctive parameters of a structure and its systems. However, the definition of the representative building attributes and the accuracy of the building's performance data sometimes place limitations on the flexibility of inverse models. Obtaining data is another issue that comes up often since it is the foundation for building a working model. In actuality, not every structure that is currently in place has building automation installed. Lack of vital information like as-built building details, system specs, and operating schedules causes several challenges for simulation projects.

B. Literature Review

AI methods are a viable alternative to traditional approaches, especially in inverse modelling. One such AI tool, known as an artificial neural network (ANN), can effectively approximate nonlinear systems and demonstrate adaptability in complex environments through network training. ANNs, devoid of intricate rules and mathematical procedures, can grasp the intricacies of complex multidimensional systems. Furthermore, ANNs exhibit fault tolerance, robustness, and resilience to noise [7]. Hence, the distinctive attributes of ANN, such as nonlinearity, adaptability, and the capability to map arbitrary functions, render them well-suited for predictive tasks compared to other AI techniques like expert systems, genetic algorithms, and fuzzy logic. ANN is a strong contender for managing building equipment and occupancy data, which inherently contain noise and incomplete information [8], [9], [10], [11], [12], [13], [14]. Furthermore, ANN are widely recognized as a technology that provides an alternative approach to addressing complex and ambiguous problems, primarily due to their robust nonlinear mapping capabilities. Consequently, they have gained significant popularity for use in predicting both building cooling loads [15], [16], [17], [18], [19] and building energy consumption [20], [21], [22].

In energy consumption prediction in building projects, Sapnken et al. [23] conducted a study using data from 7559 buildings and employing nine ML models. Their investigation focused on the efficiency of a Deep Neural Network (DNN) model, demonstrating impressive results and proposing it as an innovative tool for optimizing and predicting energy consumption during the construction design phase of energy-efficient buildings. Leiprecht et al. [24] performed a comprehensive analysis that included autoregressive forecasting methods, decision trees, and "adaptive boosting," exploring deep learning techniques such as Long Short-Term Memory (LSTM) neural networks for thermal load prediction. Jihad and Tahiri [25] utilized ANN to forecast energy requirements in residential structures, achieving satisfactory outcomes with 98.7% accuracy for training data and 97.6% for test data. Wang et al. [26] introduced the Improved Energy Hybrid Optimization (IEHO) neural network, which enhanced the precision of Energy Hybrid Optimization (EHO) approaches. They integrated the Back-Propagation (BP) neural network with the IEHO neural network to form the IEHO-BP neural network model for heating and cooling load forecasting, which demonstrated superior precision. Another study [27] investigated building energy performance using machine learning (ML) techniques including general linear regression, ANNs, decision trees, SVR, and ensemble inference models for cooling and heating load forecasting. This research explored the impact of structural and interior design factors on cooling loads and estimated HVAC system energy demand based on cooling and heating load requirements using various regression models. Cai et al. [28] studied the impact of input factors on heating and cooling loads in residential buildings using the SVR-supervised ML algorithm. They addressed parameter fitting challenges by examining six meta-heuristic optimization algorithms and found that the SVR-AEO hybrid model

outperformed others in accurately simulating residential building loads.

Although, several studies have been conducted on the prediction of building loads [29] using ML algorithms [30], also, there are major gaps in the literature in utilizing other algorithms and methodologies such as hybridizing with novel metaheuristic algorithms.

C. Objectives and Contribution

In the present research, inspiration is drawn from prior successful outcomes that highlighted the superior performance of ANNs compared to other models, leading to the development of Radial Basis Functions (RBF) models for the prediction of cooling loads (CL) in buildings. The contribution of this study lies in exploring novel methodologies to enhance RBF modeling accuracy for CL prediction. The performance of predicting outcomes using a single RBF model was evaluated. To further optimize the training process and improve model performance, two separate optimizers were employed: the DAO and the GEO algorithms. Integrating these optimizers aims to efficiently tune RBF model parameters and enhance predictive accuracy. The novelty of this approach lies in the combination of RBF modeling with advanced optimization techniques, offering a promising avenue to achieve higher accuracy in cooling load prediction. By exploiting the strengths of DAO and GEO, this research extends the boundaries of traditional RBF applications, demonstrating their effectiveness in the context of building energy efficiency studies. The choice of RBF models, coupled with the use of the GEO and the DAO, reflects a strategic approach to enhance the accuracy and efficiency of CL prediction in buildings. RBF models are particularly suitable for nonlinear approximation tasks and offer flexibility in capturing complex relationships within datasets, making them well-suited for CL prediction. The integration of GEO and DAO as optimization techniques is motivated by the need to effectively tune RBF model parameters for optimal performance. GEO, inspired by the behavior of eagles in searching for prey, employs a nature-inspired algorithm to efficiently explore the solution space and converge towards optimal solutions. On the other hand, DAO, characterized by its dynamic arithmetic operations, leverages mathematical principles to guide the optimization process toward improved model fitting.

D. Research Organization

The introductory part of this study is divided into 4 main sections: background, literature review, objectives, and research organization. Following this, the next section provides detailed explanations about the dataset used and concise descriptions of various ML techniques, including models and optimization algorithms. Section III covers the description of performance evaluators, comparative results using metrics and different techniques, and an analysis comparing the study's findings with existing research. In Section IV, the study's conclusions are summarized.

Fig. 1 shows the process of present study.

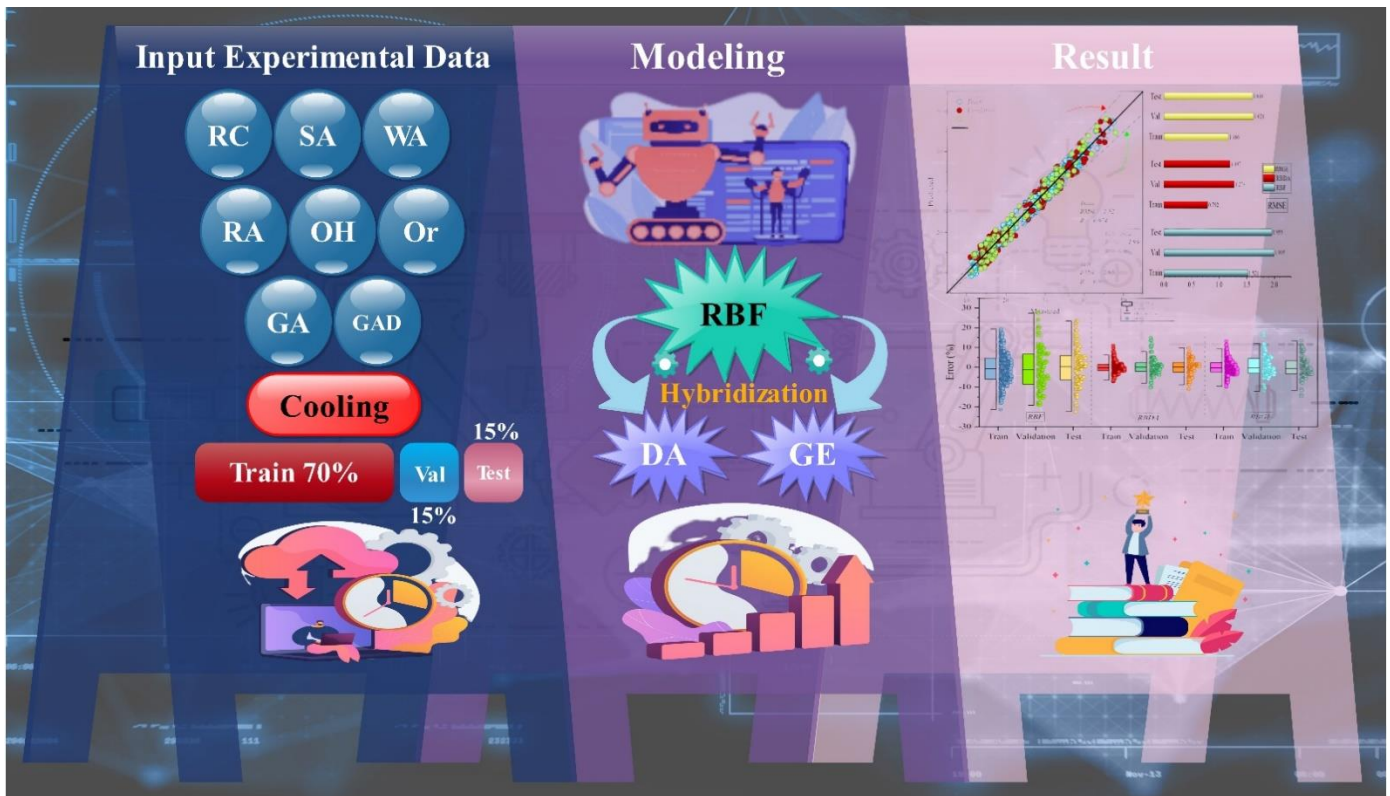


Fig. 1. The current Study's procedure.

II. MATERIALS AND METHODS

In the second section of this article, a concise overview of the dataset used in this research is presented, along with descriptions of the ML algorithms selected for implementation in this study, including the RBF model, GEO algorithm, and DAO algorithm. This section provides detailed insights into the dataset characteristics and the rationale behind choosing specific ML techniques to address the research objectives.

A. Data Collection

The presence of valid and substantial data is paramount in ensuring the credibility and efficacy of the methods outlined in this paper. This study uses a dataset obtained from previous research endeavors [31], [32] to train intelligent models, which

comprised 768 data samples. This dataset furnishes essential information required to implement the proposed techniques and assess their performance in predicting building cooling loads. This study's examination of input parameters is predicated on eight important elements, namely relative compactness (RC), surface area (SA), wall area (WA), roof area (RA), orientation (Or), overall height (OH), glazing area (GA), and the distribution of glazing area (GAD). These factors collectively serve as the basis for evaluating and optimizing the predictive models used in this study. Table I details the primary criteria employed for statistically examining the dataset, including metrics such as data averages, standard deviations, and minimum and maximum values. The dataset is partitioned into 70% for training, 15% for validation, and 15% for testing.

TABLE I. THE INPUT VARIABLE'S STATISTICAL CHARACTERISTICS FOR COOLING

| Variables | Indicators | | | | |
|--------------|------------|--------|-------|--------|----------|
| | Category | Min | Max | Avg | St. Dev. |
| RC | Input | 0.62 | 0.98 | 0.764 | 0.106 |
| SA (m2) | Input | 514.5 | 808.5 | 671.70 | 88.086 |
| WA (m2) | Input | 245 | 416.5 | 318.5 | 43.63 |
| RA (m) | Input | 110.25 | 220.5 | 176.60 | 45.165 |
| OH (m) | Input | 3.5 | 7 | 5.25 | 1.751 |
| Or | Input | 2 | 5 | 3.5 | 1.118 |
| GA (%) | Input | 0 | 0.4 | 0.235 | 0.133 |
| GAD | Input | 0 | 5 | 2.81 | 1.55 |
| Cooling (kW) | Output | 10.9 | 48.03 | 24.587 | 9.51 |

B. Overview of ML Method and Optimizers

1) *Radial Basis Function (RBF)*: The Radial Basis Function (RBF) network, a member of the ANNs family, utilizes data-driven methods to establish connections between input and output elements. Instead of relying on mathematical equations, it derives the model's structure and unknown parameters from the provided data [33]. The RBF network is structured into three layers: the input, linear output, and hidden layers. As input vectors traverse the hidden layer, they experience a transformation process, generating radial basis functions.

These operations are executed through an activation process derived from a Gaussian distribution, firmly grounded in the fundamental principles of the Gaussian function. According to the literature, the Gaussian elementary operation (F_j) is described as being defined by two critical parameters: width and center [34]. The function is represented in the following manner:

$$F_j(x) = \exp\left(-\frac{|x - \beta_j|^2}{2\alpha_j^2}\right) \quad (1)$$

The output neuron is commonly denoted as:

ALGORITHM I. PSEUDO-CODE OF DAOA

procedure *Dynamic Arithmetic Optimization Algorithm*

Initialize the Algorithm's Parameters $\gamma; \mu$

Produce random values to serve as initial positions.

while ($t < \text{maximum number of iterations}$) **Do**

Evaluate the fitness of given solutions by computing their respective values.

Identify the optimal solution.

Update the DAF value using Eq. (3)

Update the DCS value using Eq. (6)

for $i \in D$: number of solutions **Do**

for $j \in D$: number of positions **Do**

Generate random values in the range of 0 to 1 for $r_1; r_2; r_3$

if $r_1 > \text{DAF}$ **then exploration phase**

if $r_2 > 0.5$ **then update the solutions' positions**

Using first rule in Eq. (4)

else

Using second rule in Eq. (14)

end if

if $r_1 < \text{DAF}$ **then exploitation phase**

if $r_3 > 0.5$ **then update the solutions' positions**

Using first rule in Eq. (5)

else

Using second rule in Eq. (5)

end if

end if

end for

end for

$t \leftarrow t + 1$

end while

Provide the top – performing solution.

end procedure

$$y(x) = \sum_{j=1}^n \sigma_j F_j(x) + a \quad (2)$$

In the above context, x refers to the inputs, β_j and α_j reflect the width and center of the Gaussian basis function, individually. And n denotes the number of hidden neurons, a indicates the bias coefficient, and the weight factor that connects the j th hidden neuron to the output neuron is represented by σ_j .

2) *Dynamic Arithmetic Optimization Algorithm (DAOA)*: Adding 2 new accelerator functions has improved the foundational arithmetic optimization algorithm. These modifications affect candidate solutions and the search process, balancing exploration and exploitation dynamically. Unlike other advanced metaheuristics, DAOA stands out because it doesn't need initial parameter adjustments. The DAOA pseudo-code is in Algorithm 1, and the next section explains its dynamic features in detail [35].

a) *DAOA's Dynamic accelerated function*: The dynamic aspect of the arithmetic optimization algorithm heavily depends on the Dynamic Accelerated Function (DAF) during the search. It is necessary to adjust the starting values of the accelerated function (Min and Max) in the AOA. However, when a new descending function replaces DAF, it is more desirable to use an algorithm without internally configurable parameters. The adjustment factor for this optimization approach is shown as follows:

$$DAF = \left(\frac{Iter_{max}}{Iter}\right)^\alpha \quad (3)$$

Here, "Iter" reflects the ongoing iteration count, "Itermax" is indicated as the upper limit for iterations, and the value of "α" remains a constant. The function experiences a decrease with each consecutive iteration within the algorithm.

b) *Dynamic DAOA candidate solution*: The dynamic properties of DAOA candidate solutions are introduced in this section. The exploration and exploitation stages of metaheuristic algorithms must be approached in a balanced manner for the algorithm to be successful. Every solution in this dynamic adaptation, which prioritizes better exploration and exploitation, iteratively improves its locations by making reference to the optimal solution found during optimization. Eq. (4) in the basic version is replaced by Eq. (5) as a consequence of the inclusion of the Dynamic Candidate Solution (DCS) function.

$$x_{i,j}(C_{iter} + 1) = \begin{cases} best(x_j) \div (DCS + \epsilon) \times ((UB_j - LB_j) \times \mu + LB_j) & , r2 < 0.5 \\ best(x_j) \times DCS \times ((UB_j - LB_j) \times \mu + LB_j) & Otherwise \end{cases} \quad (4)$$

$$x_{i,j}(C_{iter} + 1) = \begin{cases} best(x_j) - DCS \times ((UB_j - LB_j) \times \mu + LB_j) & , r3 < 0.5 \\ best(x_j) + DCS \times ((UB_j) \times \mu + LB_j) & , Otherwise \end{cases} \quad (5)$$

The incorporation of the DCS function is a direct response to the diminishing ratio of candidate solutions. Its value consistently diminishes in each iteration, following this established pattern.

$$DCS(0) = 1 - \sqrt{\frac{Iter}{Iter_{max}}} \quad (6)$$

$$DCS(t + 1) = DCS(t) \times 0.99 \quad (7)$$

Extensive testing involving various hunt agents and iterations has shown that including candidate solutions in DAOA notably speeds up AOA's convergence rate, ultimately improving solution quality. The lack of parameters is often an advantageous feature in metaheuristic algorithms. What sets DAOA apart from AOA is its integration of dynamic functions, while the other aspects of the approach align with the AOA algorithm discussed earlier.

Adaptive parameters help the DAOA algorithm; just the population size and maximum number of iterations need to be adjusted. This algorithm sets itself apart unlike other

algorithms that demand problem-specific parameter adjustments. However, it has a drawback: it relies on the iteration count, rather than fitness improvements, as the basis for its adaptive mechanism.

3) *Golden Eagle Optimization (GEO)*: This study introduces an innovative swarm-intelligence metaheuristic algorithm inspired by the hunting behavior of golden eagles, referred to as the GEO. GEO is rooted in the intelligent adaptation of attack and cruising behaviors observed in golden eagles during their prey search and hunting activities.

The key attributes of the hunting behavior exhibited by golden eagles can be summed up in this way [36]:

They move in a curved trajectory while searching and move in a straight line when attacking.

They tend to start off cruising around when they start hunting and then gradually start to attack more towards the end.

Throughout their flight, they maintain a propensity for both cruising and attacking at all times.

They seek information about prey from other eagles.

The golden eagle's ability to maneuver between flying and hunting is a natural means of exploration, advantage-taking, and transitioning from one to the other. This clears the path for creating a new type of algorithm. The next part shows this behavior mathematically modeled.

a) *Algorithm for optimization and mathematical model*: This section explains how a mathematical equation was created to simulate golden eagle hunting behavior. It introduces the spiral motion formula and then dissects it into attack and cruise vectors, emphasizing the aspects of exploration and exploitation, respectively.

- Golden eagles spiraling around in circles: GEO concentrates on the spiral motion of golden eagles. Every time, golden eagle 'n' selects a randomly selected prey from the golden eagle 'f' and circles around the ideal spot that the eagle frequents. 'f' is designated as a member of the set {1,2,...,PopSize} because the golden eagle, represented by 'n', has the ability to choose to circle its memory.
- Prey selection: Each iteration involves search agents choosing targets from collective memory. Improved positions replace stored ones. In the GEO approach, golden eagles select prey randomly from any flock member's memory without proximity constraints.
- Attack (exploitation): The attack is a vector from the eagle's current position to its remembered prey. The attack vector for Golden Eagle n can be calculated using Eq. (8).

$$\vec{A}_n = \vec{X}_f^* - \vec{X}_n \quad (8)$$

Here, \vec{X}_n is the current position of eagle n , \vec{A}_n is the eagle's n attack maneuver and \vec{X}_f^* is the best place (prey) visited so distant by eagle f .

- Cruise (exploration): The cruise vector originates from modifying the attack vector. It follows the circle's tangent and stands at a right angle to the attack vector, indicating the eagle's speed concerning the prey. In i -dimensional space, it lies within the tangent hyperplane. To determine it, the equation of this hyperplane must be established, involving a point and a perpendicular normal vector. Eq. (9) supplies the scalar representation of this hyperplane in i -dimensional space.

$$h_1x_1 + h_2x_2 + h_3x_3 + \dots + h_ix_i = d \Rightarrow \sum_{j=1}^i h_jx_j = d \quad (9)$$

$$\sum_{j=1}^i a_jx_j = \sum_{j=1}^i a_j^t x_j^* \quad (10)$$

Here, $\vec{P} = [p_1, p_2, p_3, \dots, p_i]$ is the hyperplane's arbitrary point and $\vec{H} = [h_1, h_2, h_3, \dots, h_i]$ is the normal vector, $X = [x_1, x_2, x_3, \dots, x_i]$ is the variables vector, and $d = \vec{H} \cdot \vec{P} = \sum_{j=1}^i h_j p_j$. \vec{X}_n (the place of the eagle n) is considered as any random location inside the hyperplane and reflect \vec{A}_n (the point of attack) as the hyperplane may be shown using its normal to which \vec{C}_n^t (The cruise vector in iteration t for the Golden Eagle n) belongs version to Eq. (10).

Here, $X^* = [x_1^*, x_2^*, x_3^*, \dots, x_i^*]$ is the chosen prey's location, and $A_n = [a_1, a_2, a_3, \dots, a_i]$ is the attack vector, $X = [x_1, x_2, x_3, \dots, x_i]$ is the decision/design variables vector; it's time to find a cruise vector inside the cruise hyperplane that was calculated for Eagle n in iteration t .

The final dimension is determined based on its compatibility with the hyperplane equation, resulting in $i - 1$ free variable and a single fixed variable. To locate a chance i -dimensional objective point C on the golden eagle n 's journey hyperplane: Step 1. Arbitrarily pick one variable from the set of i variable stars as the fixed variable, denoting its index as k . Notably, avoid selecting a fixed variable among those associated with zero elements in the attack vector \vec{A}_n .

When a variable's coefficient in Eq. (9) is 0, the line becomes parallel to that variable's axis, allowing it to take any value while the other $i - 1$ variables vary randomly. As an instance, in the 3D plane $3x_1 + 2x_2 = 10$, if $k = 3$ and random numbers for x_1 and x_2 is selected, say $\{x_1 = 2, x_2 = 5\}$, a unique point cannot be found. Rather, this plane generates an endless number of points, all of which fulfill the $\{[2,5,1], [2,5,2], [2,5,3], \dots\}$ plane equation. Step 2: Give each variable a random value, except for the k - t^{th} variable, which always has the same value. Determine the fixed variable's value in Step 3 by using Eq. (11).

$$c_k = \frac{d - \sum_{j,j \neq k} a_j}{a_k} \quad (11)$$

Here c_k denotes the $k - th$ element of the terminus point C , a_j represents the $j - th$ element of the attack vector A_n , d refers to the right-hand side of the Eq. (9), a_k^t signifies the $k - th$ element of the attack vector \vec{A}_n , and k shows the directory of the fixed variable. The cruise hyperplane now has a new random destination point. Eq. (12) shows how to find the location of the cruise hyperplane's destination.

$$\vec{C}_n = (c_1 = rand, c_2 = rand, \dots, c_k = \frac{d - \sum_{j,j \neq k} a_j}{a_k}, \dots, c_i = rand) \quad (12)$$

In iteration t , the cruise vector for Golden Eagle n may be computed once the destination point has been determined. Random integers between 0 and 1 make up the components of the destination location. The golden eagle population is guided by the cruise vector away from their prior memory, highlighting the discovery phase of *GEO*.

- Transferring to new roles

The golden eagles use both assault and cruise vectors when they travel. According to Eq. (13), the step vector for golden eagle n is described in iteration t .

$$\Delta x_n = \vec{r}_1 p_a \frac{\vec{A}_n}{\|\vec{A}_n\|} + \vec{r}_2 p_c \frac{\vec{C}_n}{\|\vec{C}_n\|} \quad (13)$$

The coefficients p_a^t and p_c^t in iteration t control the impact of attack and cruise on golden eagles. Random vectors \vec{r}_1 and \vec{r}_2 have elements within $[0,1]$. The discussion of p_a and p_c will follow. $\|\vec{C}_n\|$ and $\|\vec{A}_n\|$ represent the attack and cruise vectors' Euclidean norms, as determined by Eq. (14).

$$\|\vec{A}_n\| = \sqrt{\sum_{j=1}^i a_j^2}, \|\vec{C}_n\| = \sqrt{\sum_{j=1}^i c_j^2} \quad (14)$$

The step vector from iteration t is added to the locations of the golden eagles in iteration t to calculate their positions in iteration $t + 1$.

$$x^{t+1} = x^t + \Delta x_n^t \quad (15)$$

Golden Eagle n updates its memory if its new position is superior; otherwise, it retains its memory but adopts the new position. In each iteration, eagles pick a random peer to circle the best-visited spot, determining attack and cruise vectors, step size, and the next position. This cycle repeats until one of the termination conditions is satisfied. Eq. (13) involves 2 coefficients, the attack constant p_a^t and cruise constant p_c^t , which controls how the step vector is influenced by cruise and attack vectors. The following subsection, denoted as c , explains how these coefficient values change throughout the iterations.

- Transition from exploration and exploitation

Golden eagles primarily cruise early in their hunting flight, transitioning to attacking later. These parallels heightened exploration in greater exploitation and initial iterations in later iterations within the future optimizer.

GEO employs p_a and p_c to transition from exploration to exploitation. It begins with a low p_a and high p_c values. As iterations advance, p_a increases gradually, while p_c decreases gradually. Users define the initial and final parameter values, and it is possible to compute intermediate values by using the linear transition described in Eq. (16).

$$\begin{cases} p_a = p_a^0 + \frac{t}{T} |p_a^T + p_a^0| \\ p_c = p_c^0 + \frac{t}{T} |p_c^T + p_c^0| \end{cases} \quad (16)$$

In the formula, t represents the current iteration, T is the maximum iteration count, p_a^0 and p_a^T stand for the initial and final values of the propensity to attack (p_a), respectively, while p_c^0 and p_c^T denote the initial and final values of the propensity to cruise (p_c), respectively. These tests, which will be covered in more detail later, show that $[p_a^0 \text{ and } p_a^T] = [0.5, 2]$ and $[p_c^0 \text{ and } p_c^T] = [1, 0.5]$ are suitable parameter settings. This suggests that in the first iteration, p starts at 0.5 and climbs linearly to reach 2 in the last iteration. In a similar manner, p_c starts at 1 in the first iteration and decreases linearly to 0.5 in the last. It's crucial to remember that Eq. (16) uses a linear strategy to change these values; however, logarithmic or other functions might be used as an alternative.

C. Research Methodology

The research methodology can be delineated in the following manner:

1) *Introduction:* In this study, the consideration of a crucial problem is introduced, with a focus on the imperative for enhanced performance in the RBF model. Significance is placed on the advancement of the field of ML, particularly in practical applications within building energy prediction. The pressing need for improved efficiency in the RBF model is addressed, contributing to the broader landscape of ML and its application to real-world challenges in buildings.

2) *Hybridization method:* A novel ML approach is presented, involving the hybridization of 2 advanced optimization techniques. The combination of optimization methods used to enhance the performance of the RBF model is detailed. Through the strategic integration of these advanced optimization techniques, an innovative perspective is introduced to ML, with a primary goal of elevating the efficiency of the RBF model.

3) *Optimizers used:* In this research, the introduction and detailed description of the 2 distinct optimizers employed in the hybridization method, namely the DAO and the GEO, are provided. The unique strengths of each optimizer and the rationale behind their selection for the hybrid model are thoroughly explained, contributing to a comprehensive understanding of the strategic integration of these optimizers in the research framework.

4) *Model evaluation:* A comprehensive evaluation of both single and hybridized RBF models is undertaken in this study, utilizing established performance metrics such as R^2 and RMSE. The choice of these metrics is justified to ensure an

impartial assessment of model performance, enhancing the reliability and objectivity of the evaluation process.

5) *Performance comparison:* The performance of hybridized models is compared with the traditional RBF model in this study to emphasize the superiority of the proposed approach. Statistical analyses or visual representations of the results are provided to support the claims made, enhancing the credibility and clarity of the comparison between the 2 model types.

6) *Conclusion:* This section provides a summary of the research's main conclusions and their consequences offering a concise overview of the study's outcomes. Additionally, the limitations of the study are discussed to encourage further exploration in related domains.

III. RESULTS AND DISCUSSION

A. Prediction Performance Analysis

This research created an ML model called RBF to forecast CL. In addition, the research used two effective optimization algorithms, DAO and GEO, to make hybrid RBF models better at adjusting the settings of the models. The dataset was split into three smaller groups: training, validation, and testing. The training group had 70% of the data, the validation group had 15%, and the testing group had the remaining 15%. The models were evaluated in Table II by comparing different measures, like R^2 (coefficient of determination), RMSE (Root Mean Square Error), MAE (Mean Relative Absolute Error), NMSE (Normalized Mean Squared Error), and PI (prediction interval). These measures were defined in Eqs. (17) to (21):

$$R^2 = \left(\frac{\sum_{i=1}^n (T_i - \bar{T})(P_i - \bar{P})}{\sqrt{[\sum_{i=1}^n (T_i - \bar{T})^2][\sum_{i=1}^n (P_i - \bar{P})^2]}} \right)^2 \quad (17)$$

$$RMSE = \sqrt{\frac{\sum_{i=1}^n (P_i - T_i)^2}{n}} \quad (18)$$

$$MAE = \frac{1}{n} \sum_{i=1}^n \|P_i - T_i\| \quad (19)$$

$$NMSE = \frac{\frac{1}{n} \times \sum ((y_i - \hat{y}_i)^2)}{\frac{1}{n} \times \sum y_i^2} \quad (20)$$

$$PI = \bar{x}_2 \pm t_{(\alpha/2, N-2)} * q^2 \quad (21)$$

Where n is the number of the data points, T_i and P_i are the test and predicted results, respectively. \bar{P} and \bar{T} are the average of the test and prediction result values, y_i represents the actual values, \hat{y}_i denotes the predicted values, q^2 signifies the average error value that has been combined from both groups; the t -value corresponding to the desired level of confidence (α) and degrees of freedom ($N - 2$) is obtained from the t distribution at the critical level of $(\frac{\alpha}{2}, N - 2)$."

The following discourse offers a comprehensive analysis of the model's capability to predict CL effectively:

- The RBDA hybrid model showcased exceptional performance, achieving the highest R^2 values such as $R^2_{train} = 0.993$, $R^2_{validation} = 0.984$, $R^2_{test} = 0.984$ and $R^2_{all} = 0.990$. The elevated R^2 values indicate a robust alignment among the model and the dataset, emphasizing the dependable nature of the selected input variables as strong predictors of the predictable output. Additionally, in the case of both hybrid models, the R^2 value during the training phase is higher than in the testing phase. This discrepancy suggests suboptimal training performance in the developed models.
- A Prediction Interval is a statistical metric that quantifies the level of uncertainty associated with a

model's predictions. It sets itself apart from a point estimate, such as a mean or median, by defining a range or interval in which future observations are anticipated to occur with a specified confidence level. Among all the models, RBDA stands out with its minimal PI value of 0.019, indicating the lowest degree of uncertainty.

- The RMSE varies across a range, with a minimum of 0.792 (observed during the training phase of RBDA) and a maximum of 1.996 (noted during the RBF single model validation phase). Furthermore, during the training phase of RBDA, the MAE and NMSE values, specifically 0.542 and 0.001, respectively, were observed. This additional evidence solidifies the RBDA hybrid model's high level of accuracy.

TABLE II. THE OUTCOME OF MODELS CREATED FOR RBF

| Model | Phase | Index values | | | | |
|-------|------------|--------------|-------|-------|-------|-------|
| | | RMSE | R^2 | MAE | NMSE | PI |
| RBF | Train | 1.522 | 0.974 | 1.313 | 0.004 | 0.031 |
| | Validation | 1.996 | 0.963 | 1.764 | 0.035 | 0.041 |
| | Test | 1.956 | 0.961 | 1.667 | 0.033 | 0.040 |
| | All | 1.671 | 0.970 | 1.433 | 0.004 | 0.034 |
| RBDA | Train | 0.792 | 0.993 | 0.542 | 0.001 | 0.016 |
| | Validation | 1.274 | 0.984 | 0.848 | 0.014 | 0.026 |
| | Test | 1.197 | 0.984 | 0.836 | 0.013 | 0.024 |
| | All | 0.947 | 0.990 | 0.632 | 0.001 | 0.019 |
| RBGE | Train | 1.167 | 0.985 | 0.778 | 0.003 | 0.024 |
| | Validation | 1.622 | 0.974 | 1.139 | 0.023 | 0.033 |
| | Test | 1.603 | 0.972 | 1.062 | 0.022 | 0.033 |
| | All | 1.316 | 0.981 | 0.875 | 0.002 | 0.027 |

Fig. 2 illustrates dispersed visualizations of the correlation between predicted and measured CL values. These scattered data points are derived from the 2 evaluation sets based on RMSE and R^2 . In a broad sense, RMSE serves as a dispersion controller, meaning that lower values of this metric correspond to higher data point density. Moreover, the R^2 metric tends to cluster testing and training data points closer to the centerline.

The figure incorporates several additional elements, including a central line at the $Y=X$ coordinates and 2 lines positioned below and above the central line to represent a 10% underestimation and 10% overestimation range. Upon conducting an exhaustive comparison across the three predictive models, it becomes evident that all models exhibit favorable R^2 values. This is observed through the proximity of

data points associated with these models to the central best-fit line, with most points falling within the boundaries defined by the 2 threshold lines.

Among the 2 optimized RBF models, it is discernible that the data points exhibit greater proximity to the central line, indicating superior performance compared to the single RBF model. In the comparative evaluation of the optimized models, upper and lower threshold lines are employed as reference points. Notably, it becomes evident that the data points about the model optimized through the DAO are consistently contained within the demarcated threshold lines. Conversely, the data points associated with the model optimized through the GEO exhibit a somewhat greater degree of dispersion relative to the prescribed boundaries.

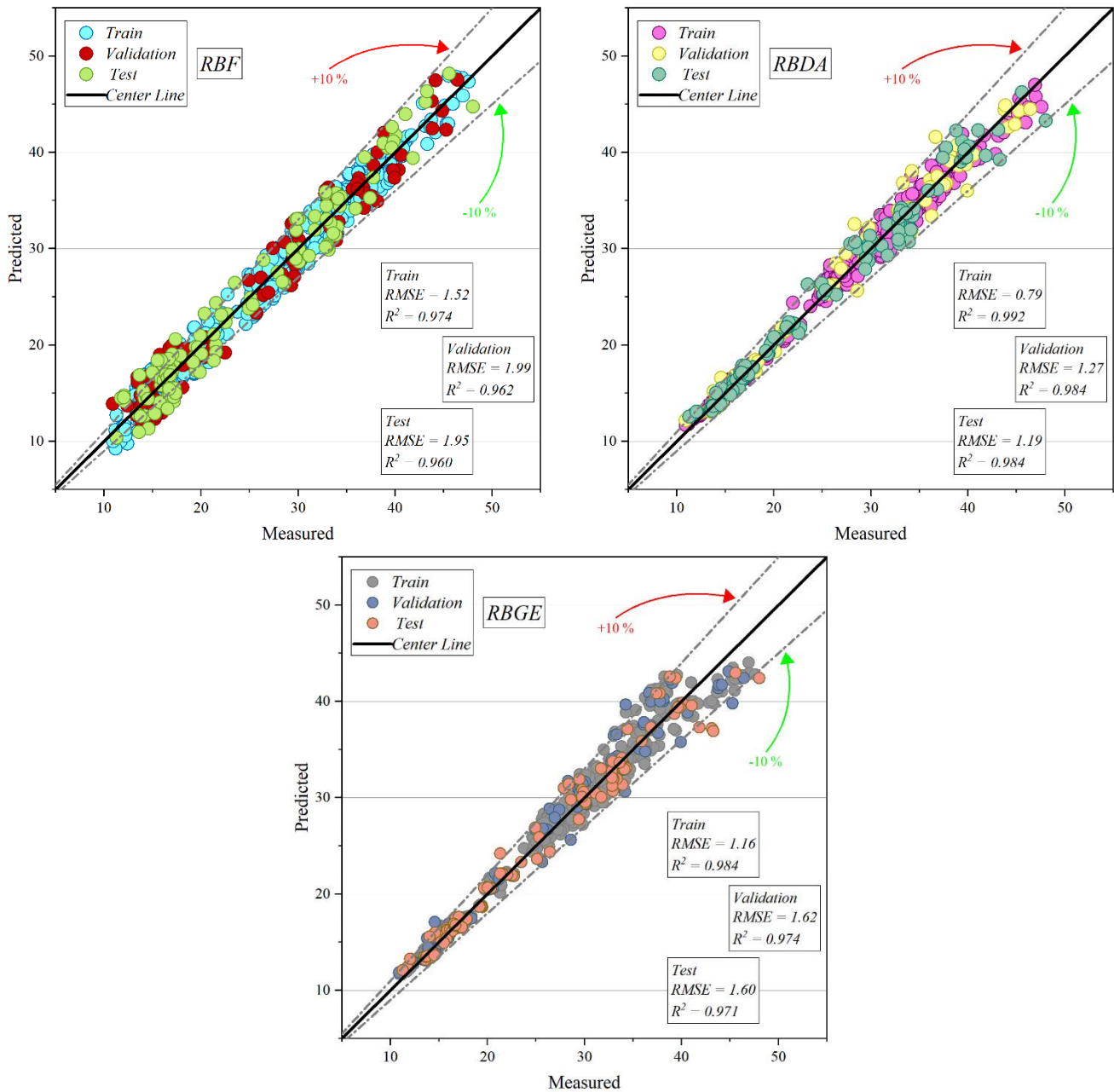


Fig. 2. The scatter plot for developed hybrid models.

This academic research uses a stacked bar plot, as shown in Fig. 3, to compare many parameters in-depth. By stacking the measurements inside of separate bars, this visualization technique offers a succinct and understandable representation of the correlations between various measures. Because each statistic is represented by a different hue, it is easier to see how each one contributes to the final outcomes. The calculated RMSE, R², and MAE values for the different models are

shown in Fig. 3. Upon closer examination, it becomes evident that the RBDA model exhibits lower error rates according to the RMSE = 0.792 and MAE = 0.542 compared to RBF and RBGE. Furthermore, concerning prediction accuracy, as evidenced by the R² values, it is noteworthy that RBF (R² = 0.974) and RBGE (R² = 0.984) exhibit lower values when compared to the RBDA model.

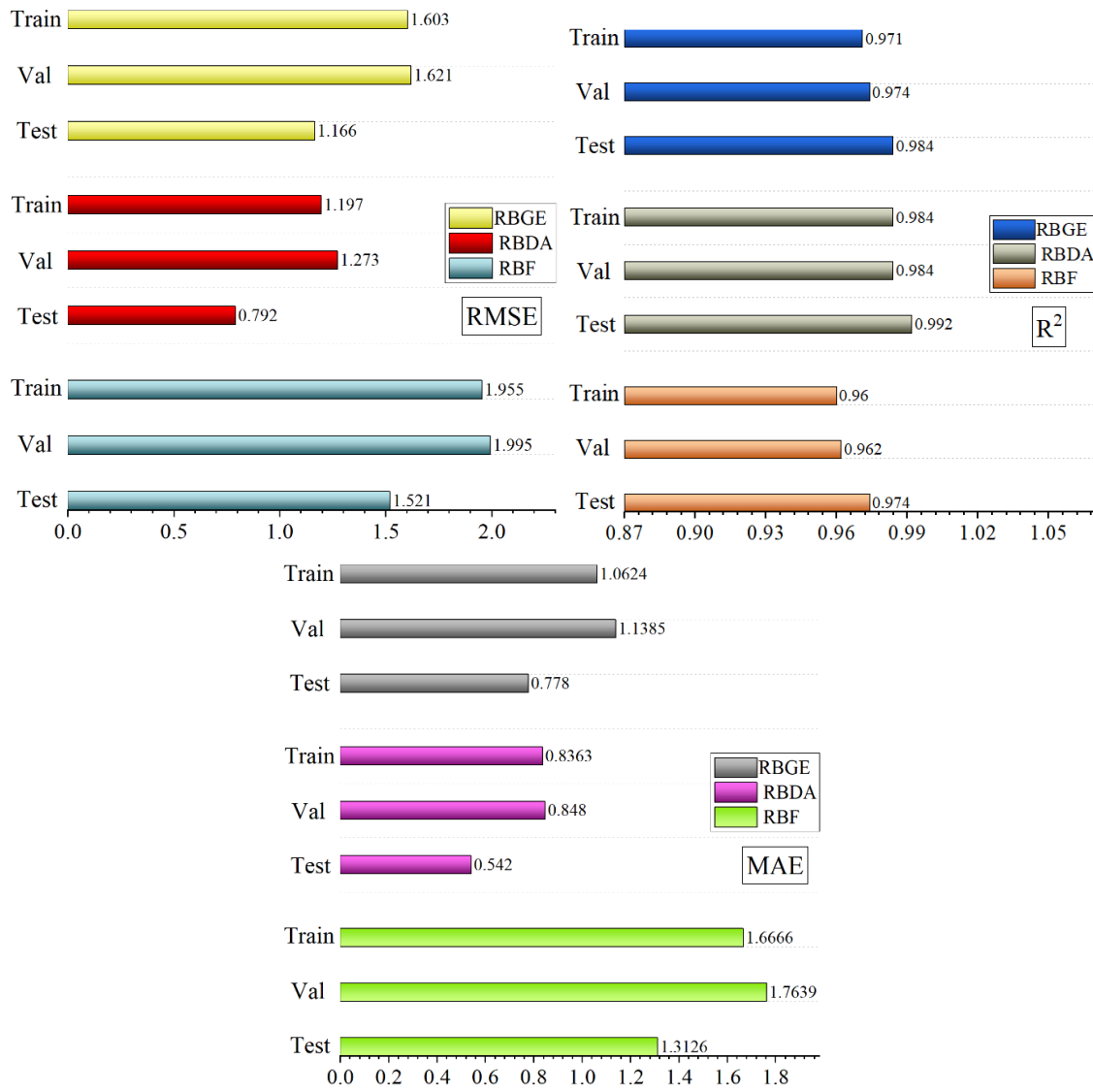


Fig. 3. Comparison between models is based on RMSE, R², and MAE.

In Fig. 4 and Fig. 5, the error percentages (%) for the models are visualized using both normal distribution plots and the half-boxes, with the errors categorized across the training, validation, and test datasets. As depicted in Fig. 4, the normal distribution plot illustrates that RBDA exhibits a narrow bell-shaped distribution line during the training phase with a higher concentration of errors in the zero percent range, thus indicating its superior performance. However, in the validation and testing phases, the distribution curves for RBF and RBDA resemble each other, whereas RBF shows a wider spread of error values across a broader range. Upon examining the spectrum of error values presented in Fig. 5 for the various models, it becomes evident that the training phase of RBF exhibits the widest range of error values, while the validation phase of RBF displays the narrowest range. Noteworthy is the consistent excellence in performance displayed by the RBDA hybrid model throughout all three phases when considering a range of box proportions related to 25% to 75% of error values. It is essential to underscore that the model's performance

exhibits a discernible enhancement as the box proportions approach zero. Moreover, according to RBGE half boxes, it can be observed that it exhibited marginal variation and secured the second position in terms of performance ranking.

B. Comparing the results of this study and existing studies

Numerous studies have been conducted on CL prediction, including investigations by Afzal et al. [37] using the *MLP* model, and Gong et al. [38] employing the *GBM* technique. Among the existing publications reported in Table III, superior performance was demonstrated by the *GPR* model, achieving an R² value of 0.99 and an RMSE value of 0.059 in a study showed by Roy et al. [39]. A fundamental framework based on the RBF model was used in the present research, and it was improved by hybridizing it with the *GEO* and *DAO* algorithms. After analyzing the data, it was discovered that the *TDO* integration into the *RFR* model had remarkable applicability. It outperformed the other models in this research, with an R² value of 0.997 and an *RMSE* of 0.498.

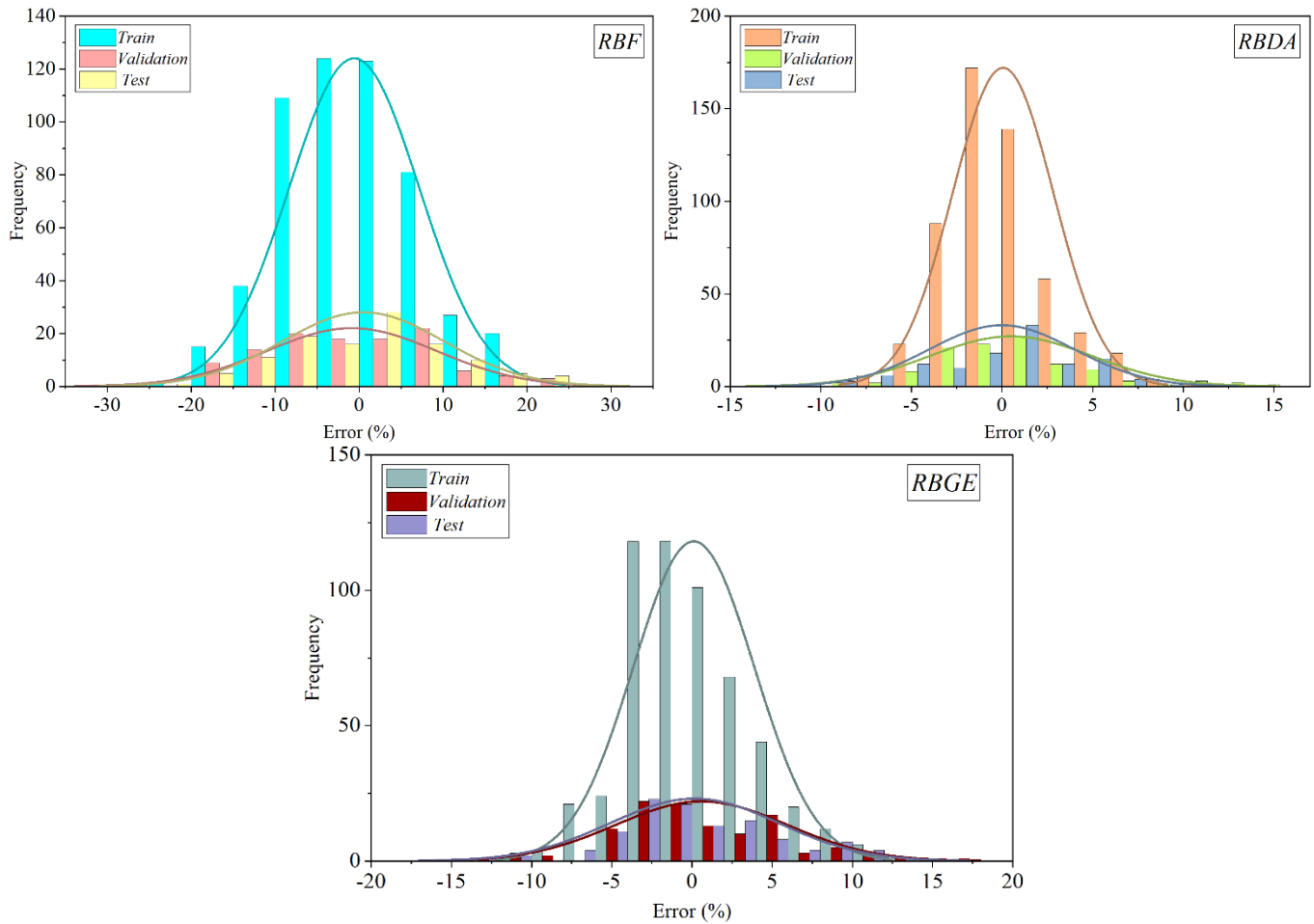


Fig. 4. The normal distribution plot serves as the foundation for the hybrid models' error percentage.

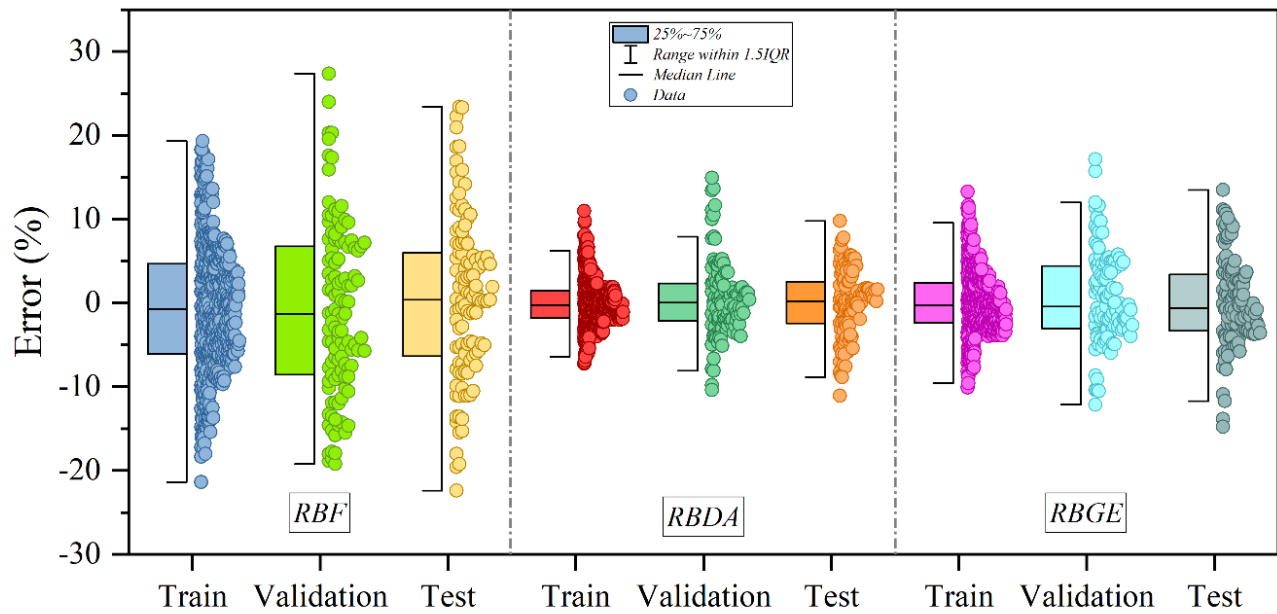


Fig. 5. The half box of errors among the developed models.

TABLE III. THE OUTCOME OF MODELS CREATED FOR RBF

| Name | Model | Results | |
|----------------------|----------------|--------------|----------------|
| | | RMSE | R ² |
| Gong et al. [38] | GBM | 0.1929 | 0.9882 |
| Afzal et al. [37] | MLP | 1.4122 | 0.9806 |
| Roy et al. [39] | GPR | 0.059 | 0.99 |
| Present study | RBF+DAO | 0.792 | 0.993 |

IV. CONCLUSION

In conclusion, this research stressed the significance of accurate forecasting of energy use and assessment of retrofit strategies for the management of building energy systems. The weather, tenant behavior, building characteristics, and energy infrastructure all make it difficult to forecast how much energy a facility will need. Although they depend mostly on data quality and modeling complexity for accuracy, physics-based simulations may provide valuable insights. With an emphasis on Radial Basis Function (RBF) models in particular, this research examined the potential efficacy of ML techniques by using the growing amount of publicly available building energy data. Regarding the prediction of Cooling Load (CL), a significant advancement in civil engineering was made. It achieved this by effectively mitigating the constraints typically associated with ML techniques by incorporating optimization algorithms into RBF models. The forecasted outcomes generated by these models were subjected to a comparative analysis employing five distinct evaluation indices. The findings showcased the presence of a robust and exceptionally accurate predictive model, notably the RBDA (Radial Basis Function optimized with DAO), which displayed an outstanding correlation with the actual measured CL, as evidenced by a high R^2 value of 0.993, 1.95%, and 0.81% higher than RBF and RBGE. Additionally, it's worth noting that RBDA demonstrated the highest level of accuracy among the models, boasting a minimal RMSE value of 0.792. This represented a reduction of 47.96% compared to RBF and a 32.1% decrease compared to RBGE. Developed models solve problems and help engineers and researchers with civil engineering projects. They are reliable and precise in predicting CL, making projects safer and cheaper, and they can be helpful in future research. Addressing the limitations of this study underscores the critical importance of data quality and availability for effective ML model performance. To ensure model generalization across diverse environmental and building conditions, further validation and adaptation efforts are essential to validate broader applicability. The sensitivity of optimization algorithms to specific parameter settings necessitates meticulous fine-tuning to achieve optimal results, emphasizing the need for methodological refinement. Additionally, enriching CL predictive accuracy can be achieved by incorporating additional factors like occupant behavior dynamics or building usage patterns, enhancing practical utility in real-world scenarios. Future research should prioritize enhancing model validation through field studies to ensure robustness and reliability in varying conditions. Exploring advanced ML techniques beyond RBF models, such as deep learning architectures, can elevate prediction accuracy and unveil hidden data patterns. Dynamic model adaptation is a

promising avenue for developing responsive models that adjust to evolving building dynamics and environmental factors in real time. Furthermore, integrating uncertainty analysis techniques into CL prediction models can enhance reliability by quantifying uncertainties and providing confidence intervals for predicted CL values, ultimately improving usability in practical applications.

REFERENCES

- [1] B. Sadaghat, S. Afzal, and A. J. Khiavi, "Residential building energy consumption estimation: A novel ensemble and hybrid machine learning approach," *Expert Syst Appl*, vol. 251, p. 123934, 2024, doi: <https://doi.org/10.1016/j.eswa.2024.123934>.
- [2] À. Nebot and F. Mugica, "Energy performance forecasting of residential buildings using fuzzy approaches," *Applied Sciences*, vol. 10, no. 2, p. 720, 2020.
- [3] J. Song, L. Zhang, G. Xue, Y. Ma, S. Gao, and Q. Jiang, "Predicting hourly heating load in a district heating system based on a hybrid CNN-LSTM model," *Energy Build*, vol. 243, p. 110998, 2021.
- [4] S. Ferahtia, H. Rezk, M. A. Abdelkareem, and A. G. Olabi, "Optimal techno-economic energy management strategy for building's microgrids based bald eagle search optimization algorithm," *Appl Energy*, vol. 306, p. 118069, 2022, doi: <https://doi.org/10.1016/j.apenergy.2021.118069>.
- [5] T.-Y. Kim and S.-B. Cho, "Predicting residential energy consumption using CNN-LSTM neural networks," *Energy*, vol. 182, pp. 72–81, 2019.
- [6] S. Bourhnane, M. R. Abid, R. Lghoul, K. Zine-Dine, N. Elkamoun, and D. Benhaddou, "Machine learning for energy consumption prediction and scheduling in smart buildings," *SN Appl Sci*, vol. 2, pp. 1–10, 2020.
- [7] J. Runge and R. Zmeureanu, "Forecasting energy use in buildings using artificial neural networks: A review," *Energies (Basel)*, vol. 12, no. 17, p. 3254, 2019.
- [8] Z. Wang, T. Hong, and M. A. Piette, "Data fusion in predicting internal heat gains for office buildings through a deep learning approach," *Appl Energy*, vol. 240, pp. 386–398, 2019.
- [9] J. Zhao and X. Liu, "A hybrid method of dynamic cooling and heating load forecasting for office buildings based on artificial intelligence and regression analysis," *Energy Build*, vol. 174, pp. 293–308, 2018.
- [10] M. Gong, Y. Bai, J. Qin, J. Wang, P. Yang, and S. Wang, "Gradient boosting machine for predicting return temperature of district heating system: A case study for residential buildings in Tianjin," *Journal of Building Engineering*, vol. 27, p. 100950, 2020.
- [11] S. Sarihi, F. M. Saradj, and M. Faizi, "A critical review of façade retrofit measures for minimizing heating and cooling demand in existing buildings," *Sustain Cities Soc*, vol. 64, p. 102525, 2021.
- [12] A. Moradzadeh, A. Mansour-Saatloo, B. Mohammadi-Ivatloo, and A. Anvari-Moghaddam, "Performance evaluation of two machine learning techniques in heating and cooling loads forecasting of residential buildings," *Applied Sciences*, vol. 10, no. 11, p. 3829, 2020.
- [13] L. Zhang et al., "A review of machine learning in building load prediction," *Appl Energy*, vol. 285, p. 116452, 2021.
- [14] Z. Wang, T. Hong, and M. A. Piette, "Building thermal load prediction through shallow machine learning and deep learning," *Appl Energy*, vol. 263, p. 114683, 2020.
- [15] S. S. Roy, P. Samui, I. Nagtode, H. Jain, V. Shivaramakrishnan, and B. Mohammadi-Ivatloo, "Forecasting heating and cooling loads of

- buildings: A comparative performance analysis,” *J Ambient Intell Humaniz Comput*, vol. 11, pp. 1253–1264, 2020.
- [16] E. Abdelkader, A. Al-Sakkaf, and R. Ahmed, “A comprehensive comparative analysis of machine learning models for predicting heating and cooling loads,” *Decision Science Letters*, vol. 9, no. 3, pp. 409–420, 2020.
- [17] X. Li and R. Yao, “A machine-learning-based approach to predict residential annual space heating and cooling loads considering occupant behaviour,” *Energy*, vol. 212, p. 118676, 2020, doi: <https://doi.org/10.1016/j.energy.2020.118676>.
- [18] Y. Ding, H. Su, X. Kong, and Z. Zhang, “Ultra-short-term building cooling load prediction model based on feature set construction and ensemble machine learning,” *IEEE Access*, vol. 8, pp. 178733–178745, 2020.
- [19] Z. Xuan, Z. Xuehui, L. Liequan, F. Zubing, Y. Junwei, and P. Dongmei, “Forecasting performance comparison of two hybrid machine learning models for cooling load of a large-scale commercial building,” *Journal of Building Engineering*, vol. 21, pp. 64–73, 2019.
- [20] J. Leitaó, P. Gil, B. Ribeiro, and A. Cardoso, “A survey on home energy management,” *IEEE Access*, vol. 8, pp. 5699–5722, 2020.
- [21] M. Ghalambaz, Y. R. Jalilzadeh, and A. H. Davami, “Building energy optimization using butterfly optimization algorithm,” *Thermal Science*, vol. 26, no. 5 Part A, pp. 3975–3986, 2022.
- [22] R. Wang, S. Lu, and W. Feng, “A novel improved model for building energy consumption prediction based on model integration,” *Appl Energy*, vol. 262, p. 114561, 2020.
- [23] F. E. Sapnken, M. M. Hamed, B. Soldo, and J. Gaston Tamba, “Modeling energy-efficient building loads using machine-learning algorithms for the design phase,” *Energy Build*, vol. 283, p. 112807, Mar. 2023, doi: [10.1016/j.enbuild.2023.112807](https://doi.org/10.1016/j.enbuild.2023.112807).
- [24] S. Leiprecht, F. Behrens, T. Faber, and M. Finkenrath, “A comprehensive thermal load forecasting analysis based on machine learning algorithms,” *Energy Reports*, vol. 7, pp. 319–326, 2021.
- [25] A. S. Jihad and M. Tahiri, “Forecasting the heating and cooling load of residential buildings by using a learning algorithm ‘gradient descent’, Morocco,” *Case studies in thermal engineering*, vol. 12, pp. 85–93, 2018.
- [26] H.-J. Wang, T. Jin, H. Wang, and D. Su, “Application of IEHO–BP neural network in forecasting building cooling and heating load,” *Energy Reports*, vol. 8, pp. 455–465, 2022.
- [27] J.-S. Chou and D.-K. Bui, “Modeling heating and cooling loads by artificial intelligence for energy-efficient building design,” *Energy Build*, vol. 82, pp. 437–446, 2014.
- [28] W. Cai, X. Wen, C. Li, J. Shao, and J. Xu, “Predicting the energy consumption in buildings using the optimized support vector regression model,” *Energy*, vol. 273, p. 127188, Jun. 2023, doi: [10.1016/j.energy.2023.127188](https://doi.org/10.1016/j.energy.2023.127188).
- [29] A. Khabthani and L. Châabane, “Development and Validation of a Cooling Load Prediction Model,” *International Journal of Advanced Computer Science and Applications*, vol. 9, no. 2, 2018.
- [30] G. I. Ahmad, J. Singla, A. Anis, A. A. Reshi, and A. A. Salameh, “Machine learning techniques for sentiment analysis of code-mixed and switched indian social media text corpus: A comprehensive review,” *International Journal of Advanced Computer Science and Applications*, vol. 13, no. 2, 2022.
- [31] G. Zhou, H. Moayedi, M. Bahiraei, and Z. Lyu, “Employing artificial bee colony and particle swarm techniques for optimizing a neural network in prediction of heating and cooling loads of residential buildings,” *J Clean Prod*, vol. 254, p. 120082, 2020.
- [32] W. Pessenlehner and A. Mahdavi, *Building morphology, transparency, and energy performance*. na, 2003.
- [33] A. H. Alavi, A. H. Gandomi, M. Gandomi, and S. S. Sadat Hosseini, “Prediction of maximum dry density and optimum moisture content of stabilised soil using RBF neural networks,” *The IES Journal Part A: Civil & Structural Engineering*, vol. 2, no. 2, pp. 98–106, 2009.
- [34] Z. Nurlan, “A novel hybrid radial basis function method for predicting the fresh and hardened properties of self-compacting concrete,” *Advances in Engineering and Intelligence Systems*, vol. 1, no. 01, 2022.
- [35] N. Khodadadi, V. Snasel, and S. Mirjalili, “Dynamic arithmetic optimization algorithm for truss optimization under natural frequency constraints,” *IEEE Access*, vol. 10, pp. 16188–16208, 2022.
- [36] A. Mohammadi-Balani, M. D. Nayeri, A. Azar, and M. Taghizadeh-Yazdi, “Golden eagle optimizer: A nature-inspired metaheuristic algorithm,” *Comput Ind Eng*, vol. 152, p. 107050, 2021.
- [37] S. Afzal, B. M. Ziapour, A. Shokri, H. Shakibi, and B. Sobhani, “Building energy consumption prediction using multilayer perceptron neural network-assisted models; comparison of different optimization algorithms,” *Energy*, p. 128446, Jul. 2023, doi: [10.1016/j.energy.2023.128446](https://doi.org/10.1016/j.energy.2023.128446).
- [38] M. Gong, Y. Bai, J. Qin, J. Wang, P. Yang, and S. Wang, “Gradient boosting machine for predicting return temperature of district heating system: A case study for residential buildings in Tianjin,” *Journal of Building Engineering*, vol. 27, p. 100950, 2020.
- [39] S. S. Roy, P. Samui, I. Nagtode, H. Jain, V. Shivaramakrishnan, and B. Mohammadi-Ivatloo, “Forecasting heating and cooling loads of buildings: A comparative performance analysis,” *J Ambient Intell Humaniz Comput*, vol. 11, pp. 1253–1264, 2020.

Adaptive Target Region Attention Network-based Human Pose Estimation in Smart Classroom

Jianwen Mo¹, Guiyun Jiang², Hua Yuan^{3*}, Zhaoyu Shou⁴, Huibing Zhang⁵

School of Information and Communication, Guilin University of Electronic Technology, Guilin 541004, China^{1,2,3,4}

School of Computer and Information Security, Guilin University of Electronic Technology, Guilin 541004, China⁵

Abstract—In smart classroom environments, problems such as occlusion and overlap make the acquisition of student pose information challenging. To address these problems, a lightweight human pose estimation model with Adaptive Target Region Attention based on Lite-HRNet is proposed for smart classroom scenarios. Firstly, the Deformable Convolutional Encoding Network (DCEN) module is designed to reconstruct the encoding of features through an encoder and then a multi-layer deformable convolutional module is used to adaptively focus on the image region to obtain a feature representation that focuses on the target region of interest of the student subject. Secondly, the Channel And Spatial Attention (CASA) module is designed to attenuate or enhance the feature attention in different regions of the feature map to obtain a more accurate representation of the target feature. Finally, extensive experiments were conducted on the COCO dataset and the smart classroom dataset (SC-Data) to compare the proposed model with the current main popular human pose estimation framework. The experimental results show that the performance of the model reaches 67.5(mAP) in the COCO dataset, which is an improvement of 2.7(mAP) compared to the Lite-HRNet model, and 86.6(mAP) in the SC-Data dataset, which is an improvement of 1.6(mAP) compared to the Lite-HRNet model.

Keywords—Human pose estimation; smart classroom; Lite-HRNet; deformable convolutional encoding network; target region attention

I. INTRODUCTION

In recent years, human pose estimation [1,2,3,4] technology has been widely used in behaviour recognition, action recognition, human-computer interaction and other scenarios along with the rapid development of related technologies in the field of computer vision. With modern and intelligent education being strongly advocated and developed, neural network models based on deep learning are heavily used in classroom detection tasks. In the task of assessing the quality of teaching and learning of student, information about student postures [5,6,7] plays a very important role in assessing the quality of teaching and in teacher understanding of student learning status in the classroom [8]. In the classroom, a student state of learning is demonstrated through a variety of classroom behaviours. Student who are not interested in the content of the classroom will exhibit behaviours such as dawdling, playing with mobile phones and sleeping. Student who are interested in the content of the class show behaviours such as concentration, looking at the board, taking notes, reading, and actively interacting with the teacher. Therefore, how to automatically and accurately collect student pose information in smart classroom [9,10,11] scenarios is an important task that needs to

be solved urgently. In smart classroom environments, the acquisition of student pose information is commonly associated with problems such as overlap and occlusion between students, as well as the location of the students leading to large differences in their body sizes, and the presence of small target instances leading to a degradation of the model detection performance. At the same time, the problem of large computational and parametric quantities of the human pose estimation model makes it more difficult to be deployed in smart classroom scenarios. These problems make the acquisition of pose information in smart classrooms a challenging research.

Aiming at the problems of overlapping and occlusion, as well as the large number of model parameters in smart classroom scenarios, this paper proposes a lightweight human pose estimation model framework based on the Lite-HRNet architecture applied to smart classroom scenarios, the Adaptive Target Region Attention Network for Human Pose Estimation. The model is designed with two main modules: (1) The Deformable Convolutional Encoding Network is designed for obtaining a target feature region representation. (2) The Channel And Spatial Attention module is designed to allow the target feature region representation to obtain a more accurate representation of the target region. The model in this paper achieves relatively good performance on two datasets. Extensive ablation experiments are used to validate the effectiveness of each module in the proposed method. The main contributions of this study are summarised as follows:

1) Propose a lightweight pose estimation model for smart classrooms: the Adaptive Target Region Attention Network for Human Pose Estimation. And to construct a student pose estimation dataset suitable for smart classroom environment to provide a database for pose detection in smart classrooms.

2) The Deformable Convolutional Encoding Network (DCEN) is proposed to perform feature extraction on the target region of the feature map to obtain a vector representation with feature regions of interest. The experimental results show that the module designed in this paper can efficiently improve the performance of the model.

3) Proposing an attention mechanism based Channel And Spatial Attention (CASA) module to be used to assist in model training. The module enables the target feature region representation to obtain a better attention effect and fully exploits the spatial and channel feature information in the target feature region.

The rest of the paper is organised as follows. In Section II, the elements involved in the related work are presented. In Section III, the proposed method is described in detail. In Section IV, the experimental results are described and analysed. Finally in Section V, the conclusion of the paper is drawn.

II. RELATED WORK

Traditional methods for human pose estimation are based on graphical structure solutions, which rely too much on hand-crafted feature, are more influenced by algorithms, and have limited model representation capabilities. Deep learning human pose estimation modelling methods are broadly classified into two types: Bottom-Up and Top-Down. Bottom-Up methods [12,13] first detect individual body parts and then compose these detection gesture points into a whole person. On the other hand, the Top-Down approach [14,15,16] first detects the human body bounding box and then detects the human body pose within each bounding box.

Among them, a high-resolution network (HRNet) [17] with top-down approach, has become a mainstream method for human pose estimation due to its efficient detection performance. However, as the performance of the human pose estimation model improves, it is accompanied by a significant increase in the number of parameters. Wang [18] In order to address the problem of huge computational effort associated with attitude estimation models for high-resolution structures. A fused inverse convolution head module is used to eliminate redundancy in the high-resolution branch and achieve scale feature fusion with low computational effort. As well as the use of large convolution kernels to improve the sensory field of the model and reduce the computational effort of the model. The IGCv3 [19] model decomposes the regular convolution into multiple grouped convolutions to reduce the amount of computation of the convolution function in the model, thus reducing the number of parameters in the model. The MobileNet [20] model reduces the model parameters by decomposing a normal convolution into a deep convolution and a dot convolution, while maintaining the same performance as a normal convolution. The Lite-HRNet [21] model uses the method of performing information exchange across channels to maintain the information exchange between channels, in place of the expensive ordinary convolutional computation.

To address the problems that arise in the task of human pose estimation, Artacho et al [22] utilised a multi-scale feature representation to improve the effectiveness of keypoint feature extraction without significantly increasing the model parameters. Tang et al [23] proposed a new spatio-temporal longitudinal and transversal attention module to reduce the computational effort of the model by decomposing the joints feature matrix in both spatial and temporal dimensions. Zhao et al [24] addressed the problem of increasing the computational burden by increasing the size of the input sequences to enhance the performance of the model by using a compact representation of long skeleton sequences in the frequency domain to efficiently expand the receptive field and improve the robustness to 2D noisy pose detection. Liu et al [25]

proposed limb orientation cue-aware networks to prevent overfitting of the depth network leading to uncertain keypoint locations. Yang et al [26] proposed a two-stage pose distillation model for whole-body pose estimation to address the problem of varying body part scales in order to improve the validity and efficiency of the model. Lee et al [27] designed a pose estimation model with self-training loss using pose-aware confidence in semi-supervised and unsupervised pose estimation tasks. In this paper, the lightweight Lite-HRNet is used as the backbone network. Design of deformable convolutional encoding networks and attention mechanism based channel and spatial attention modules to enhance the model ability to extract key point feature. Allow model performance to be efficiently improved without significantly increasing the computational and parametric count of the model. Thereby the model can be more effectively applied to detection tasks in different scenarios.

III. PROPOSED METHOD

The Adaptive Target Region Attention Network is designed with two main modules: the DCEN module, the CASA module, and the overall network framework is shown in Fig. 1. Firstly, the visual feature $\{F_{t-2}, F_{t-1}, F_t\}$ of the input sequences are extracted by the backbone network Lite-HRNet-18 network, and they are input into the DCEN module to calculate the information difference between the background feature and the subject feature, and to obtain the target region attention feature M_t . Then, the target region attention feature M_t are mined for channel and spatial information by CASA module to get the target region focus attention feature M'_t . Finally, the combination of feature M'_t and visual feature F_t generates enhanced visual feature F'_t . The feature F'_t are input into the pose estimation detection head to obtain the keypoint detection heatmap H_t . In the following, each module will be explained in detail.

A. Deformable Convolutional Encoding Network

The Deformable Convolutional Encoding Network is divided into three main steps: (1) Stage Feature Sequence Acquisition, which inputs the image sequence X_t into the Lite-HRNet network to obtain visual feature $\{F_{t-2}, F_{t-1}, F_t\}$. (2) Feature Sequence Fusion. The global visual feature S_t is obtained through a convolutional encoding network on the reconstructive encoding of the feature sequence. (3) Adaptive Target Region Attention Feature. Input the global visual feature S_t into the deformable convolutional network, use the deformable convolution to calculate the region information in the feature map, capture the visual feature of the target region, and reduce the influence of background feature and noise feature on the target region feature. The target region attention feature M_t is obtained through the DCEN module, which is used to pay attention to and capture the feature information of the target region in image. The DCEN module is shown in Fig. 2.

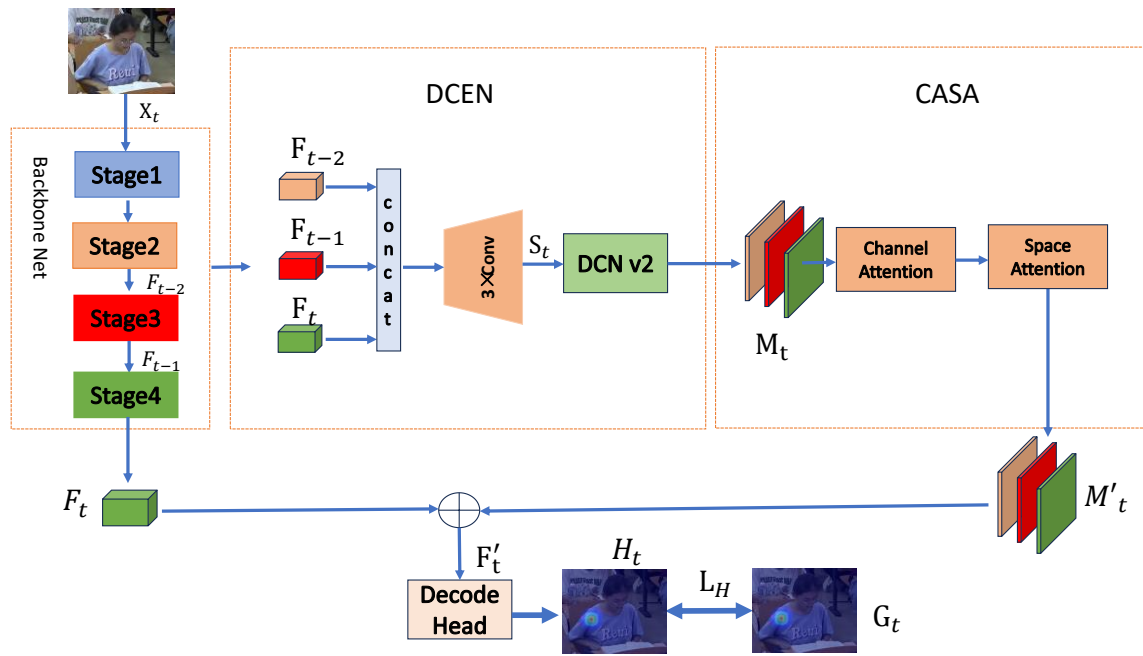


Fig. 1. Overall network framework.

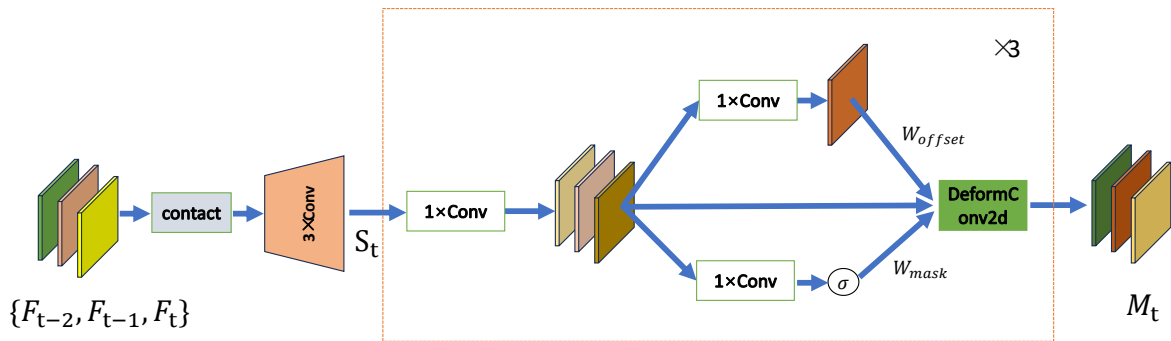


Fig. 2. DCEN module.

Stage Feature Sequence Acquisition: visual feature is extracted by Lite-HRNet network. Lite-HRNet replaces the expensive 1×1 convolution in the shuffle block [28] with a lightweight conditional channel weighting module, allowing the model to maintain efficient performance while reducing the computational effort of the network. Since the computational complexity is linear, it is lower than the quadratic time complexity of point-by-point convolution. Input the image sequence X_t into the Lite-HRNet network and acquire the visual feature $\{F_{t-2}, F_{t-1}, F_t\}$ of the three stages in the Lite-HRNet network. Where F_{t-2}, F_{t-1}, F_t is the output visual feature of the second, third, and fourth stages of the Lite-HRNet network.

Feature Sequence Fusion: multiple stages of visual feature of different coarseness were obtained from the Lite-HRNet network. They possess semantic information about visual feature in different depths. In order to better utilise the semantic information of these visual feature, an up-sampling approach is used to reconstruct and encode the different stages of the visual feature into a fusion that increases the resolution of the feature sequence and enhances the retention of edge

information. And combining their shallow and deep visual feature to generate the global visual feature S_t with global visual information and more fine-grained. The operation is shown in Eq. (1):

$$S_t = \text{Conv}(F_t \oplus F_{t-1} \oplus F_{t-2}) \quad (1)$$

Where is a network of 3 convolutional layers.

Adaptive Target Region Attention Feature: Input the global visual feature S_t into the deformable convolutional network [29], and use the deformable convolution to adaptively capture the regional information of the feature map to obtain the target region attention feature M_t . Firstly, the global visual feature S_t are used to compute a trainable parameter W_{offset} , which is used to supervise the adaptive region orientation of the deformable convolution. The operations are shown in Eq. (2), (3), and (4):

$$S_t^i = \frac{W_i * S_t - E(W_i * S_t)}{\sqrt{\text{Var}(W_i * S_t) + \varepsilon}} \quad (2)$$

$$M_{t-1} = \frac{S_t'}{1 + e^{-S_t'}} \quad (3)$$

$$W_{offset} = M_{t-1} * W_i \quad (4)$$

Where W_{offset} is a feature map with directional shifts, which serves to compute the shifts in the x and y directions of the input feature, W_i convolutional weights, $Var()$ is the averaging function, $E()$ is the expectation function, ε is an offset constant.

Then, the penalty weight parameter W_{mask} is added for guiding the training of the network and speeding up the convergence of the deformable convolutional network. As shown in Eq. (5):

$$W_{mask} = (1 + e^{-W_i * M_{t-1}})^{-1} \quad (5)$$

Finally, the input feature vector M_{t-1} with an offset parameter W_{offset} with a penalty weight W_{mask} is input into the deformable convolution function for deformable convolution operation to compute the target region attention feature M_t . The operation is shown in Eq. (6), (7), and (8):

$$M_{t1} = f(W_{mask}, M_{t-1}, W_{offset}) \quad (6)$$

$$M_{t2} = \frac{M_{t1} - E(M_{t1})}{\sqrt{Var(M_{t1}) + \varepsilon}} \quad (7)$$

$$M_t = (1 + e^{M_{t2}})^{-1} \quad (8)$$

Where $f()$ is a deformable convolution function, W_{mask} is a penalty weight parameter, W_{offset} is an offset parameter. $Var()$ is the averaging function, $E()$ is the desired function, ε is an offset constant.

B. Channel And Spatial Attention Module

The target region attention feature M_t obtained through the DCEN module is still susceptible to mission-independent noise signals such as background, occlusion, and overlap. By using the CASA module based on the attention mechanism [30] to mine the feature information of the channel and space of the target region attention feature M_t . Allow the feature to gain supervision and attention in channel and space. The designed CASA module has two sub-modules which are used to focus on the valid information of the feature vectors in channel and space respectively and to enhance the characteristics of the valid information as well as to suppress the noisy information. The architecture of the CASA module is shown in Fig. 3.

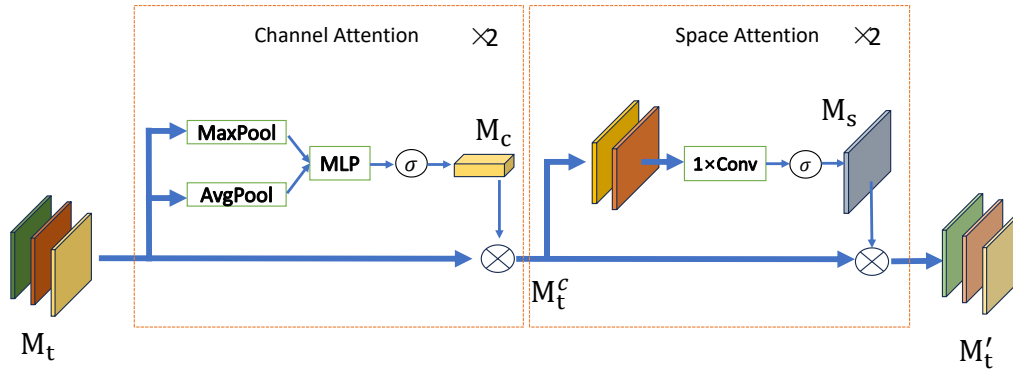


Fig. 3. CASA module.

Feature Sequence Channel Attention: Firstly, the information of each channel of target region attention feature M_t is aggregated by global maximum pooling and global average pooling. They are used to preserve the most significant feature in each channel and the overall average feature. The two feature information is then optimised using an MLP fully connected network trained to obtain parameter M_c with feature information for each channel, Finally, the multiplication operation of M_c with M_t makes the feature M_t aggregate the useful feature information of each channel. The implementation of the channel attention module is shown in Eq. (9) and (10):

$$M_c = \sigma(F(Avg(M_t)) + F(Max(M_t))) \quad (9)$$

$$M_t^c = M_t \otimes M_c \quad (10)$$

Where σ is the *sigmoid* activation function. $Avg()$, $Max()$ are the global average pooling and global maximum pooling functions, $F()$ is a three-layer fully connected network.

Feature Sequences Spatial Attention: The approach to spatial attention is similar to that of channel attention, where global maximum pooling and global average pooling are used for different dimensions to aggregate the feature information of feature M_t^c . Firstly, instead of aggregating the feature information of each channel, spatial attention aggregates the feature information of all channels together, making each channel spatially connected to each other. The two features information is then optimised using a convolutional network trained to obtain parameter M_s with spatial correlation information for each channel feature. Finally, the

multiplication operation of M_s and M_t^c is performed to obtain the target region focus attention feature M_t' with channel and spatial attention information. The spatial attention module is implemented as in Eq. (11) and (12):

$$M_s = \sigma(W_i * (\text{Avg}(M_t^c), \text{Max}(M_t^c))) \quad (11)$$

$$M_t' = M_s \otimes M_t^c \quad (12)$$

Where σ is the *sigmoid* activation function, W_i is the convolution weight, and the convolution kernel size is 3×3 .

C. Loss Function

Combine the target region focus attention feature M_t' with the visual feature F_t to obtain the enhanced visual feature F_t' . Input to the detection head generates a pose point heatmap H_t . The detection head module is implemented by a convolutional network. The loss function uses the L_H loss of the heat map of standard attitude estimation to supervise the attitude estimation model. The operation is shown in Eq. (13), (14), and (15):

$$F_t' = F_t + M_t' \quad (13)$$

$$H_t = W_i * F_t' \quad (14)$$

$$L_H = \|H_t - G_t\|^2 \quad (15)$$

Where H_t and G_t denote the predicted and real attitude thermograms, W_i is the convolution weight.

IV. EXPERIMENTS

Two pose estimation datasets: the COCO dataset and the Self-Constructed Smart Classroom dataset (SC-Data) are used in the experiments to evaluate the effectiveness of the models, and the results of comparisons with other mainstream human pose estimation models in both datasets are reported. Also, extensive ablation experiments are conducted to validate the effectiveness of the module proposed in this paper.

A. Introduction to the Dataset

SC-Data dataset: SC-Data dataset is a dataset made based on real classroom teaching data, which has 6,000 images and 16,800 instances of student pose data. There are 14000

instances in the training set and 2800 instances in the test set. The SC-Data dataset is made from one semester's worth of student classroom data and contains information about the student's classroom postures over the course of a semester. This will provide data to understand the complete pose information of students in a particular subject and provide a more accurate source of dataset for obtaining student pose information on teaching.

COCO 2017 dataset: COCO has over 200000 images and 250000 person instances with 17 keypoints, train2017 dataset (includes 57000 images 150000 person instances), val2017 (includes 5000 images).

B. Experimental Setup

In this paper, the network is trained using 1 NVIDIA A100 GPU, the optimisation algorithm is Adam with an initial learning rate of 0.0002 and a batch size of 64, the input to the network is an image with a fixed 4:3 aspect ratio, cropped from the original and resized to 256×192 , the model is implemented in the PyTorch framework. In the pose evaluation metrics, the model evaluated using mean accuracy (mAP), the AP is first calculated for each joint and then the final performance (mAP) is obtained by averaging over all joints. The criterion is based on the metrics of the COCO dataset pose estimation.

C. Experiment Results and Analyses on the COCO Dataset

The models in this paper were evaluated on the COCO dataset and the performance of the comparison models on the COCO test set is shown in Table I. The human pose estimation performance of this paper model reaches 67.5(mAP). Compared to Small HRNet-W16 and Lite-HRNet-18 the gain is improved by 12.3(mAP) and 2.7(mAP). Compared to Lite-HRNet-30 the performance is improved by 0.3(mAP), but the model parameters decreases by 0.3(M). Compared to Integral Pose Regression [31] and G-RMI [32], which are computationally and parameter intensive, the model in this paper achieves quite good performance, but there is a substantial reduction in model complexity and number of parameters. The results of comparing the computational complexity of this paper model with other models are shown in Fig. 4, where the GFLOPs decrease by 0.41(GFLOPs) compared to ShuffleNetV2, while at the same time, the performance has a 7.6(mAP) improvement. Compared to Lite-HRNet-18 the GFLOPs increase by 0.52(GFLOPs), but have a 2.7(mAP) performance improvement.

TABLE I. COMPARISON MODELS ON THE COCO TEST SET

| Model | AP(mAP) | AP50 | AR | Params |
|------------------------------|-------------|------|------|--------|
| Our | 67.5 | 88.2 | 67.0 | 1.4M |
| Lite-HRNet-18[21] | 64.8 | 87.3 | 65.6 | 1.1M |
| Lite-HRNet-30 | 67.2 | 88.0 | 73.3 | 1.8M |
| Small HRNet-W16 | 55.2 | 83.7 | 62.1 | 1.3M |
| G-RMI[32] | 64.9 | 85.5 | 69.7 | 57M |
| MobileNetV2[20] | 64.6 | 87.4 | 70.7 | 9.6M |
| ShuffleNetV2[28] | 59.9 | 85.4 | 66.4 | 7.6M |
| Integral Pose Regression[31] | 67.8 | 88.2 | - | 45.0M |
| DY-MobileNetV2[33] | 68.2 | 88.4 | 74.7 | 16.1M |
| DY-ReLU[34] | 68.1 | 88.5 | - | 9.0M |
| LitePose-XS[18] | 49.5 | 74.5 | - | 1.7M |

TABLE II. COMPARISON OF SC-DATA DATASET

| Model | AP(mAP) | AP50 | AR | Params |
|---------------------|-------------|------|------|--------|
| Our | 86.6 | 98.9 | 89.9 | 1.4M |
| Lite-HRNet-18 | 85.0 | 96.6 | 88.7 | 1.1M |
| Naive Lite-HRNet-18 | 85.3 | 96.7 | 88.9 | 1.4M |
| Lite-HRNet-30 | 85.4 | 98.5 | 88.9 | 1.8M |

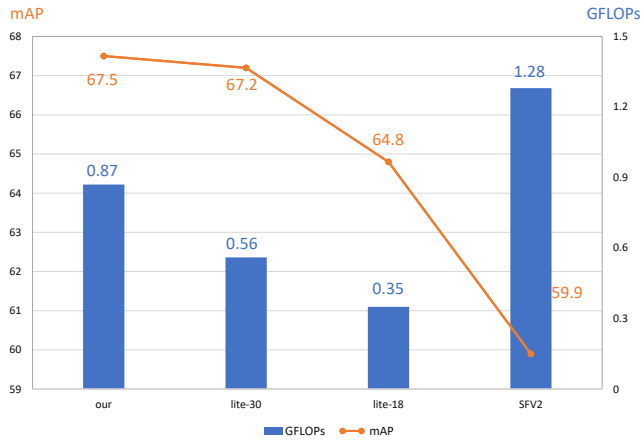


Fig. 4. Comparison of computational complexity and accuracy of the COCO dataset.

D. Experimental Results and Analyses on the SC-Data Dataset

Evaluating the method of this paper on the SC-Data dataset of this paper and comparing the performance of the model algorithm on the validation set is shown in Table II, and the experimental inference results of the model of this paper are shown in Fig. 5. The performance of the model in this paper on

the SC-Data dataset, reaches 86.6(mAP). Compared to Lite-HRNet-18 and Lite-HRNet-30 with a gain of 1.6(mAP) and 1.2(mAP) points respectively. The model in this paper maintains the efficient performance while the model complexity is also reduced by 0.3(M) relative to Lite-HRNet-30. By comparing the experiments on the two datasets, this makes the model application scenarios of this paper richer, and at the same time, the lightweight human pose estimation model in this paper is easy to deploy to smart classroom scenarios.

In the scenario of occlusion and overlap in the smart classroom, the inference performance comparison is carried out by comparing with other models, and the comparison results are shown in Fig. 6, Fig. 6(1) shows the model of this paper, and Fig. 6(2) shows the Lite-HRNet18. By comparing with other models, it can be concluded that in the estimation of the gesture of the students of the target, the model of this paper can reduce the problems caused by problems such as the occlusion or overlap between the student. The detection errors of the pose points are shown in the red circles marked in Fig. 6(2). The experimental results show that the model in this paper can effectively reduce the error detection of not the same target in smart classroom scenarios, and has better performance for scenarios with occlusion and overlap.



Fig. 5. Smart classroom pose estimation results.

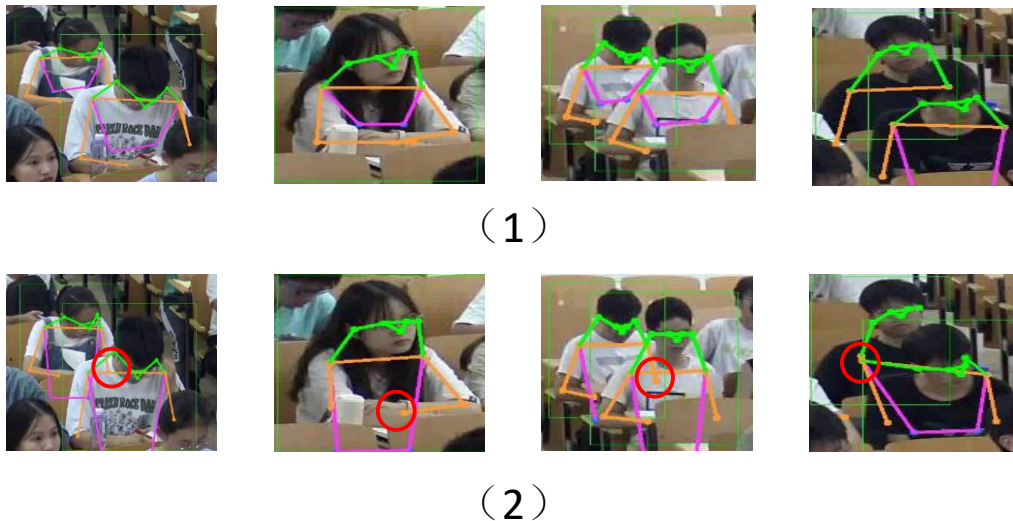


Fig. 6. Estimation results of student pose for occluded scenes in smart classroom.

TABLE III. ABLATION EXPERIMENTS WITH ADDED MODULES

| Lite-HRNet | DCEN | CASA | COCO(mAP) | SC-Data (mAP) |
|------------|------|------|-----------|---------------|
| √ | | √ | 65.7 | 85.6 |
| √ | √ | | 66.6 | 85.7 |
| √ | √ | √ | 67.5 | 86.6 |

E. Ablation Study

An ablation experiment was designed to add the DCEN module and the CASA module so as to verify the contribution of each module in the network, as shown in Table III, where "√" represents the addition of this module in the network. In the SC-Data dataset, the DCEN module provided a performance gain of 0.7(mAP)(85.0 → 85.7) compared to the Lite-HRNet network. The CASA module provided a performance gain of 0.6(mAP)(85.0 → 85.6). The performance enhancement of the model in the network where the DCEN module is added together with the CASA module is better compared to one added module alone, which improves the model with a performance gain of 1.6(mAP)(85.0 → 86.6). The significant performance gain indicates that the modules proposed in this paper play an important role in extracting feature information from the target region. In the COCO dataset, the DCEN module can improve the performance gain of the model by 1.8(mAP)(64.8 → 66.6), and the CASA module can improve the performance gain of the model by 0.9(mAP)(64.8 → 65.7). The ablation experiments verify that the modules in this paper can be applied to different scenarios and effectiveness.

V. CONCLUSION

This paper addresses the task of student pose estimation in smart classrooms by proposing a lightweight human pose estimation model with Adaptive Target Region Attention Network. Firstly, this paper proposes the deformable convolution-based target region attention module (DCEN) to capture student subject region representations. Secondly, in order to further obtain more precise attention to the target region, the channel and spatial attention module (CASA) is

proposed to attend to the information about the relevant tasks on the space and channels of the feature map. Finally, a large number of experiments show that the model has excellent performance on both the COCO dataset and the homemade smart classroom dataset (SC-Data), while the number of parameters in this paper model has been greatly reduced and the detection speed has been greatly improved compared to the human pose estimation model with a large amount of computation and parameters. In future work, the paper will focus on deploying the pose estimation model to the classroom and applying the acquired student pose information to the task of assessing teaching quality.

ACKNOWLEDGMENT

This research was funded by The National Natural Science Foundation of China (62001133, 62177012, 61967005). The Fund of Guangxi Key Laboratory of Wireless Wideband Communication and Signal Processing, Guilin University of Electronic Technology, (No. GXKL06200114). This research was supported by Guangxi Natural Science Foundation under Grant No. 2024GXNSFDA999015.

REFERENCES

- [1] Wang, Jinbao, et al. "Deep 3D human pose estimation: A review." *Computer Vision and Image Understanding* 210 (2021): 103225.
- [2] Zheng, Ce, et al. "Deep learning-based human pose estimation: A survey." *ACM Computing Surveys* 56.1 (2023): 1-37.
- [3] Liu, Wu, et al. "Recent advances of monocular 2d and 3d human pose estimation: a deep learning perspective." *ACM Computing Surveys* 55.4 (2022): 1-41.
- [4] Song, Liangchen, et al. "Human pose estimation and its application to action recognition: A survey." *Journal of Visual Communication and Image Representation* 76 (2021): 103055.

- [5] Lin, Feng-Cheng, et al. "Student behavior recognition system for the classroom environment based on skeleton pose estimation and person detection." *Sensors* 21.16 (2021): 5314.
- [6] Liu, Hai, et al. "Arhpe: Asymmetric relation-aware representation learning for head pose estimation in industrial human-computer interaction." *IEEE Transactions on Industrial Informatics* 18.10 (2022): 7107-7117.
- [7] Liu, Tingting, et al. "GMDL: Toward precise head pose estimation via Gaussian mixed distribution learning for students' attention understanding." *Infrared Physics & Technology* 122 (2022): 104099.
- [8] Deng, Chao, Jiao Peng, and ShuFei Li. "Research on the state of blended learning among college students—A mixed-method approach." *Frontiers in Psychology* 13 (2022): 1054137.
- [9] Alfoudari, Aisha M., Christopher M. Durugbo, and Fairouz M. Aldhmour. "Understanding socio-technological challenges of smart classrooms using a systematic review." *Computers & Education* 173 (2021): 104282.
- [10] Kaur, Avneet, Munish Bhatia, and Giovanni Stea. "A survey of smart classroom literature." *Education Sciences* 12.2 (2022): 86.
- [11] Wang, Jingxian, et al. "Teacher beliefs, classroom process quality, and student engagement in the smart classroom learning environment: A multilevel analysis." *Computers & Education* 183 (2022): 104501.
- [12] Du, Congju, Han Yu, and Li Yu. "A scale-sensitive heatmap representation for multi-person pose estimation." *IET Image Processing* 16.4 (2022): 1194-1207.
- [13] Luo, Zhengxiong, et al. "Rethinking the heatmap regression for bottom-up human pose estimation." *Proceedings of the IEEE/CVF conference on computer vision and pattern recognition*. 2021.
- [14] Xu, Xixia, et al. "Location-free human pose estimation." *Proceedings of the IEEE/CVF Conference on Computer Vision and Pattern Recognition*. 2022.
- [15] Feng, Runyang, et al. "Mutual information-based temporal difference learning for human pose estimation in video." *Proceedings of the IEEE/CVF Conference on Computer Vision and Pattern Recognition*. 2023.
- [16] Khirodkar, Rawal, et al. "Multi-instance pose networks: Rethinking top-down pose estimation." *Proceedings of the IEEE/CVF International conference on computer vision*. 2021.
- [17] Sun, Ke, et al. "Deep high-resolution representation learning for human pose estimation." *Proceedings of the IEEE/CVF conference on computer vision and pattern recognition*. 2019.
- [18] Wang, Yihan, et al. "Lite pose: Efficient architecture design for 2d human pose estimation." *Proceedings of the IEEE/CVF Conference on Computer Vision and Pattern Recognition*. 2022.
- [19] Sun, Ke, et al. "Igc3: Interleaved low-rank group convolutions for efficient deep neural networks." *arXiv preprint arXiv:1806.00178* (2018).
- [20] Howard, Andrew, et al. "Searching for mobilenetv3." *Proceedings of the IEEE/CVF international conference on computer vision*. 2019.
- [21] Yu, Changqian, et al. "Lite-hrnet: A lightweight high-resolution network." *Proceedings of the IEEE/CVF conference on computer vision and pattern recognition*. 2021.
- [22] Artacho, Bruno, and Andreas Savakis. "Unipose+: A unified framework for 2d and 3d human pose estimation in images and videos." *IEEE transactions on pattern analysis and machine intelligence* 44.12 (2021): 9641-9653.
- [23] Tang, Zhenhua, et al. "3D human pose estimation with spatio-temporal criss-cross attention." *Proceedings of the IEEE/CVF Conference on Computer Vision and Pattern Recognition*. 2023.
- [24] Zhao, Qitao, et al. "Poseformerv2: Exploring frequency domain for efficient and robust 3d human pose estimation." *Proceedings of the IEEE/CVF Conference on Computer Vision and Pattern Recognition*. 2023.
- [25] Liu, Tingting, et al. "LDCNet: limb direction cues-aware network for flexible human pose estimation in industrial behavioral biometrics systems." *IEEE Transactions on Industrial Informatics* (2023).
- [26] Yang, Zhendong, et al. "Effective whole-body pose estimation with two-stages distillation." *Proceedings of the IEEE/CVF International Conference on Computer Vision*. 2023.
- [27] Lee, Taeyeop, et al. "Tta-cope: Test-time adaptation for category-level object pose estimation." *Proceedings of the IEEE/CVF Conference on Computer Vision and Pattern Recognition*. 2023.
- [28] Ma, Ningning, et al. "ShuffleNet v2: Practical guidelines for efficient CNN architecture design." *Proceedings of the European conference on computer vision (ECCV)*. 2018.
- [29] Zhu, Xizhou, et al. "Deformable convnets v2: More deformable, better results." *Proceedings of the IEEE/CVF conference on computer vision and pattern recognition*. 2019.
- [30] Woo, Sanghyun, et al. "Cbam: Convolutional block attention module." *Proceedings of the European conference on computer vision (ECCV)*. 2018.
- [31] Sun, Xiao, et al. "Integral human pose regression." *Proceedings of the European conference on computer vision (ECCV)*. 2018.
- [32] Papandreou, George, et al. "Towards accurate multi-person pose estimation in the wild." *Proceedings of the IEEE conference on computer vision and pattern recognition*. 2017.
- [33] Chen, Yinpeng, et al. "Dynamic convolution: Attention over convolution kernels." *Proceedings of the IEEE/CVF conference on computer vision and pattern recognition*. 2020.
- [34] Chen, Yinpeng, et al. "Dynamic relu." *European Conference on Computer Vision*. Cham: Springer International Publishing, 2020.

Breast Cancer Classification Through Transfer Learning with Vision Transformer, PCA, and Machine Learning Models

Juan Gutierrez-Cardenas

Carrera de Ingeniería de Sistemas, Universidad de Lima, Lima-Perú

Abstract—Breast cancer is a leading cause of death among women worldwide, making early detection crucial for saving lives and preventing the spread of the disease. Deep Learning and Machine Learning techniques, coupled with the availability of diverse breast cancer datasets, have proven to be effective in assisting healthcare practitioners worldwide. Recent advancements in image classification models, such as Vision Transformers and pretrained models, offer promising avenues for breast cancer imaging classification research. In this study, we employ a pretrained Vision Transformer (ViT) model, specifically trained on the ImageNet dataset, as a feature extractor. We combine this with Principal Component Analysis (PCA) for dimensionality reduction and evaluate two classifiers, namely a Multilayer Perceptron (MLP) and a Support Vector Machine (SVM), for breast mammogram image classification. The results demonstrate that the transfer learning approach using ViT, PCA, and an MLP classifier achieves an average accuracy, precision, recall, and F1-score of 98% for the DSMM dataset and 95% for the INbreast dataset, considering the same metrics which are comparable to the current state-of-the-art.

Keywords—Breast cancer; vision transformer; transfer learning; PCA; machine learning

I. INTRODUCTION

Breast cancer, as defined by the World Health Organization (WHO) [39], encompasses a spectrum of diseases. It can manifest as a slow progression without symptoms, or it can take on an aggressive form, invading surrounding tissues and potentially spreading to nearby lymph nodes or other organs. Early identification of breast cancer is of utmost importance to prevent adverse outcomes. As per the National Cancer Institute (NIH) [26], breast cancer ranks as the second most common cause of mortality in the United States. The screening process is essential for the early detection of breast cancer cases prior to the manifestation of symptoms, with mammography being the predominant screening method. Aside from mammography, there are several other techniques available for detecting breast cancer, such as breast ultrasound, breast magnetic resonance imaging (MRI), and biopsy [5].

Classical mammographic images, as seen in the DDSM dataset (Heath et al., 1998), have inherent limitations in terms of image contrast and quality when compared to alternative techniques such as Magnetic Resonance Imaging (MRI). The problem is more noticeable in samples obtained from young women, as their breast tissue density is higher [4].

In order to overcome these constraints, alternative mammographic techniques, such as full-field digital mammography (FFDM), have been developed and are employed to extract information to be used in datasets such as INbreast [27]. The benefits of employing this technique encompass aspects such as patient satisfaction, simplicity of image manipulation, enhanced display contrast, superior detection efficiency, and minimal vulnerability to noise. One significant benefit is that these images can be employed for computer-aided diagnosis (CAD) tools [25].

Among these techniques, the availability of public datasets, particularly those derived from diagnostic mammograms or breast MRI, has facilitated the application of diverse Machine Learning and Deep Learning models for the identification and classification of breast cancer across different stages of the disease. In Tsochatzidis et al. [38], for instance, the researchers used a modified CNN with U-Net-derived image segmentation and evaluated it using the DDSM dataset. In terms of the AUC metric, the authors' diagnostic performance was 0.898. Min et al. [24] employed a Mask R-CNN for mass detection and segmentation using the INbreast dataset in a different study. The average true positive rate that the researchers were able to obtain in this study was 0.9. Readers interested in the utilization of these datasets through the application of Convolutional Neural Networks (CNNs) are encouraged to examine the research conducted by Zhu et al. [40].

In their study Samee et al. [32] used the INbreast and mini-MAIS datasets to demonstrate the efficacy of a breast cancer detection system. The system employed image pre-processing techniques, specifically contrast-limited adaptive histogram equalization (CLAHE) and pixel-wise intensity adjustment, to generate pseudo-colored images. Transfer learning was utilized in conjunction with various deep learning models, including AlexNet, VGG, and GoogleNet, to leverage pre-trained features. Additionally, Logistic Regression and Principal Component Analysis (PCA) were employed to extract the most informative features. The authors applied PCA to mitigate multicollinearity issues that could arise from synthetic image generation. The proposed approach resulted in 23 principal components. Multiple machine learning methods, such as Support Vector Machines (SVM), decision trees, and Convolutional Neural Networks (CNN), were utilized as classifiers. Notably, the CNN classifier achieved the best performance, attaining an accuracy of 98.8% for the MIAS dataset and 98.62% for the INbreast dataset.

Al-Tam et al. [1] used various deep learning models that were employed for both a two-class classifier (benign and malignant) and a three-class classifier that included a normal state as an additional class. The Curated Breast Imaging Subset of DDSM (CBIS-DDSM) and the Digital Database of Screening Mammography (DDSM) datasets were utilized for evaluation. The authors utilized pre-trained models such as VGG16, ResNet50, and ImageNet. Furthermore, they compared the performance of these pre-trained models with a CNN trained from scratch and a hybrid model combining ResNet50 with a Vision Transformer (ViT). Notably, the proposed approach achieved exceptional results with 100% F1-Score, accuracy, and AUC for the binary classification task. However, it is important to consider that these results might be influenced by the quality of information available in the CBIS-DDSM dataset. In the multiclass scenario, the performance metrics decreased to 96% on the validation set and 95% on the test set. The authors acknowledged the need for further evaluation using additional datasets such as INbreast and MAIS to assess the generalizability of their proposed approach.

In their study, Houssein et al. [14] introduced an enhanced version of the Marine Predators algorithm (MPA) called the Improved Marine Predators algorithm (IMPA). This algorithm, which incorporates Opposition-based Learning (OBL), was utilized for hyperparameter optimization of various CNN models on the DDSM and MIAS datasets. Specifically, the authors applied IMPA to optimize the hyperparameters of a ResNet50 model, which employed transfer learning and data augmentation techniques. Notably, the proposed approach achieved compelling results on both datasets. For the CBIS-DDSM dataset, the ResNet50 model attained an accuracy of 98% and an F1-score of 97%. Similarly, on the MAIS dataset, the model achieved an accuracy of 98% and an F1-score of 97%. However, the authors recognized certain limitations of their approach, e.g., the computational cost associated with

IMPA was relatively high. Additionally, the proposed architecture was specifically tailored to the tested datasets, which may limit its generalizability.

In Table I, we have summarized the mentioned studies along with others, considering their methodology.

Our main contribution lies in the design of a transfer learning-based Vision Transformer (ViT) that incorporates PCA for feature reduction, addressing the challenge posed by the large number of features extracted from images. This approach is combined with a simple machine learning technique to aid in the classification of breast cancer image samples. The ViT serves as a feature or characteristic extractor from images in our design, and we reduce their dimensionality using PCA to overcome processing time complexity. PCA is commonly used as a pre-processing technique to enhance the efficiency of Machine Learning models [21] by removing unnecessary or irrelevant data [29]. Furthermore, it has demonstrated favourable results in the categorization of breast mammograms [28]. Following this, a simple and non-computationally expensive machine learning technique is employed, with the hypothesis that it will produce accurate results considering the DSSM and INBreast breast cancer image datasets that are comparable to the existing literature. In summary, we aim to leverage the feature extraction capabilities of a state-of-the-art model, such as ViT, and subsequently reduce the dimensionality of these features using PCA. Considering the advantages mentioned before of this dimensionality reduction technique, we then plan to employ computationally non-costly machine learning models like MLP and SVM. Moreover, our current work contributes a proof-of-concept showing how cutting-edge models, like ViT, can be combined with traditional techniques like PCA and machine learning models to produce reliable classification results for breast cancer diagnosis that are on par with those documented in the literature.

TABLE I. RELATED WORKS AND THEIR METHODOLOGY

| Authors | Methodology |
|--------------------------|---|
| Tsochatzidis et al. [38] | Employs a modified CNN architecture that incorporates a U-Net for image segmentation during input. |
| Min et al. [24] | Grayscale images are converted into pseudo-color and the masses are amplified for utilization in a Mask R-CNN that utilizes transfer learning. |
| Samee et al. [32] | Images are improved through the application of contrast-limited adaptive histogram equalization (CLAHE). A CNN model, selected from AlexNet, VGG, or GoogleNet, is used to extract features, while a Logistic Regression model with PCA is employed for classification. |
| Al-Tam et al. [1] | The authors employed VGG16, ResNet50, and Imagenet for both binary and multiclass classification. For the final test, they utilized a ResNet50 model that was trained from scratch, in addition to a ViT model. |
| Samee et al. [33] | The authors utilized pre-trained convolutional neural network (CNN) models, specifically AlexNet, GoogleNet, and VGG-16. The authors utilized pre-trained convolutional neural network (CNN) models, specifically AlexNet, GoogleNet, and VGG-16. The researchers used several feature selection methods, such as Pearson Correlation Coefficient, Cosine Coefficient (mostly used for texts), Euclidean Distance (though Liu and Zhang (2016) warned that it might not be the best way to represent data characteristics, which could lead to poor learning), and Mutual Information. The chosen characteristics were subjected to classification using an ensemble of learners utilizing Discriminant Analysis, Support Vector Machines (SVM), K-Nearest Neighbors (KNN), and Naive Bayes. Nevertheless, it is still uncertain whether they employed a combination of machine learning models or determined which one produced the most optimal outcomes. |
| Jabeen et al. [19] | The authors utilized a haze-reduced local-global image enhancement technique. The images were subjected to augmentation, and a pre-trained EfficientNet-b0 model was used as a feature extractor, excluding the last three layers. The process of selecting features was conducted utilizing the Equilibrium-Jaya controlled Regula Falsi algorithm. An ensemble of K-nearest neighbors (EKNNs) was utilized for classification. |
| Our Proposal | The ViT model is utilized as a feature extractor, PCA is employed for dimensionality reduction, and MLP and SVM are used as classifiers for the purpose of comparison. |

We have organized our work into the following sections: Section II provides an overview of Transfer Learning and Vision Transformers, covering the relevant theoretical aspects. In Section III, we outline our methodology, describing the algorithms used to guide our procedures; we also had the experimental setup conducted on two breast cancer datasets. Section IV presents the key findings and results obtained from our models. In Section V, we engage in a comprehensive discussion of the results, drawing comparisons with relevant studies that have also explored breast cancer classification. Finally, we conclude our article with a summary of the main insights and conclusions derived from this study in Section VI.

II. BACKGROUND

A. Breast Cancer Datasets: DDSM and INbreast

Multiple Breast Cancer Datasets are available, with some being freely accessible and others requiring permissions for use. This study will employ the DDSM and INbreast datasets, which will be briefly described.

1) *DDSM dataset*: This dataset is a well-known collection of digitized copies derived from images taken during a screening exam. Furthermore, it includes carefully selected images curated by professionals, displaying an accurate representation of both benign and malignant instances of breast cancer. An inherent concern with this dataset, despite its widespread utilization throughout the years, is the existence of anomalies in certain images, such as the occurrence of dust or scratches, which necessitate careful consideration [13].

2) *The INbreast Dataset* was obtained from a university hospital in Portugal and consists of samples from both breast cancer patients and healthy individuals. This dataset offers several benefits, such as including samples obtained from patient screenings, diagnoses made based on abnormalities, and follow-up cases of individuals who underwent some type of treatment. Furthermore, the dataset contains a wide range of observations that can be identified during breast exams, including asymmetries, calcifications, distortions, masses, and nodules. The images were acquired using FFDM equipment, which offers superior image quality in comparison to their DDSM equivalent [27].

B. Transfer Learning

Transfer learning is a technique that enables a model to use the knowledge acquired during the training of a previous model rather than starting the training process from scratch. The fundamental idea is that if a model has learned useful representations or variations on a dataset P1, those representations can be transferred or adapted to improve the learning of a new task P2 [10].

To illustrate this concept, let's consider the ResNet model. This model is often pre-trained on a large dataset such as ImageNet, which contains a vast number of images from various categories. When pre-training ResNet, the model learns to recognize general features and patterns in the images. The later layers of the model, which are responsible for making specific predictions, can be replaced with new layers that are

tailored to the target task. The reason for this replacement is that the early layers have already captured general features, while the later layers can be fine-tuned to capture task-specific features for the new dataset [20].

For example, if we have a deep learning model based on VGG16, we can exclude the classifier part by disabling or removing the top layer. By doing so, we obtain a feature vector of 4096 numbers. This vector can be serialized and stored, serving as input to a new model. Alternatively, we can replace the classifier part with a new set of convolutional layers if we want to use a different classifier. This adaptability allows us to customize the model architecture according to the specific requirements of the task at hand [3, 8].

C. Vision Transformer

A Vision Transformer (ViT) is a type of attention model initially developed for Natural Language Processing (NLP) tasks but has also shown promise in image analysis. Unlike traditional convolutional neural networks (CNNs), ViT requires fewer computational resources when pre-trained on a large image dataset and subsequently applied to smaller datasets for classification tasks.

The ViT model operates by dividing an image into a set number of patches, each with a fixed size. These patches are then embedded, creating a sequence of embeddings that is subsequently fed into a Transformer Encoder. The Transformer Encoder is made up of self-attention heads and MLP (Multi-Layer Perceptron) blocks, which help the model find patterns and connections in the image [7]. A schematic representation of the ViT model is presented in Fig. 1.

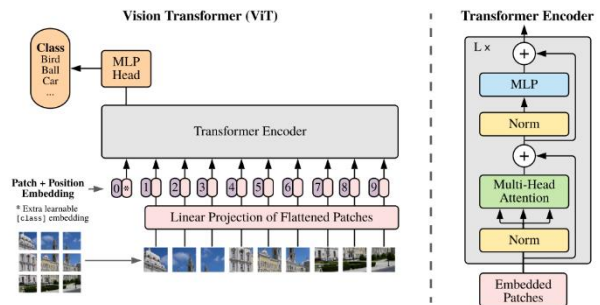


Fig. 1. Vision transformer model [7].

D. Evaluation Metrics

For validating the result of our proposed model we have used the following metrics [9]:

Accuracy: This value represents the proportion of correctly classified instances. It is calculated by considering instances that are predicted to have positive or negative values and belong to one of those classes. The formula is as follows:

$$acc = \frac{1}{|Te|} \sum_{x \in Te} I[\hat{c}(x) = c(x)] \quad (1)$$

In Eq. (1), the Te refers to the test set, while the function $I[x]$ refers to the indicator function. This function takes a value of 1 when the value is correctly classified and 0 in other cases.

Precision: This metric refers to the calculation of the proportion of accurate positive predictions. This means that if the model predicts a value in the positive class, it must be in that class. The formula is as follows:

$$Prec = \frac{TP}{TP+FP} \quad (2)$$

where, TP and FP represent True Positive and False Positive, respectively. A True Positive is an instance that has this value and was correctly classified as positive, whereas a False Positive is an instance that was incorrectly classified as positive but has a negative value.

Recall: This metric refers to the percentage of all positive instances that are correctly predicted. This means that if all positive instances of a model are considered, this metric tells us how many the model correctly predicted. The formula for this metric is as follows:

$$Rec = \frac{TP}{TP+FN} \quad (3)$$

False Negative (FN) refers to instances that are classified as negative but belong to a positive class.

F1-Score: When we want to calculate the average of the incorrect classifications made while considering the set of classes, we can use the F1-score formula:

$$F1 - Score = \frac{2}{\frac{1}{Prec} + \frac{1}{Rec}} \quad (4)$$

III. MATERIALS AND METHODS

A. Dataset

The objective of this study was to evaluate the performance of a couple of machine learning models, specifically the Multi-Layer Perceptron (MLP) and Support Vector Classifier (SVC), in conjunction with transfer learning techniques and a Vision Transformer for breast cancer image classification. We conducted experiments using a dataset comprising images of benign and malignant breast samples obtained from the Digital Database for Screening Mammography (DDSM) and the INbreast datasets.

In this study, we collected a dataset of breast mammography images from the Dataset of Breast Mammography Images with Masses (Huang and Lin, 2020), which is available at <https://data.mendeley.com/datasets/ywsbh3ndr8/2>. Specifically, we utilized the Digital Database for Screening Mammography (DDSM) and the INbreast datasets [12] from this repository.

The dataset used in this study was compiled from multiple sources. Initially, Huang and Lin [15] selected 106 images from the INbreast dataset, 53 images from the MIAS dataset, and 2188 images from the DDSM dataset. To address the issue of overfitting, a data augmentation technique was employed, which involved multi-angle rotation, flipping, and 11-angle rotation in both horizontal and vertical directions. The compiled dataset, available at <https://data.mendeley.com>

/datasets/ywsbh3ndr8/2, is organized into four folders: DDSM dataset, INbreast dataset, INbreast+MIAS+DDSM dataset, and MIAS dataset. For our experiments, we focused on the DDSM dataset and the INbreast dataset. The DDSM dataset consists of both benign and malignant masses, with 5970 and 7158 samples, respectively. The INbreast dataset contains 2520 samples of benign cases and 5112 samples of malignant cases. An example of both types of samples from these datasets is shown in Fig. 2.

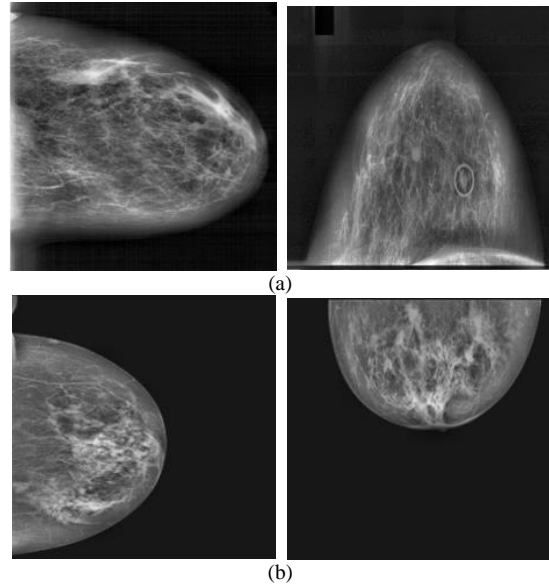


Fig. 2. A couple of samples from the benign and malignant masses as found in the DDSM (a) and INbreast datasets (b).

Considering the number of samples, we can observe that the DDSM dataset consists of 55% malignant masses and 45% benign masses, while the INbreast dataset consists of 33% malignant cases and 67% benign cases. Based on these percentages, we can conclude that the data is not imbalanced. It is worth noting that the study conducted by Haibo and García [11] suggested that a dataset can be considered imbalanced if the minority class constitutes less than 10% of the total samples. It is important to mention that their study focused on dichotomous classes, similar to the ones examined in our research. In scenarios in which the data is unbalanced, techniques such as data augmentation [15] can be used. This includes image rotation at 11 angles in both horizontal and vertical directions, ranging from 30° to 330° degrees in 30-degree increments. Additionally, horizontal and vertical flipping can be used.

B. Methodology

In the Fig. 3, we have depicted the steps followed in our work and that can be summarize in the following steps:

Step 1: We obtained a collection of images from the DDSM and INbreast datasets that represent both benign and malignant formations related to breast cancer. Prior to being inputted into a Vision Transformer (ViT) model, this data undergoes resizing and normalization.

Step 2: The ViT model operates as a feature extractor through the utilization of transfer learning. To carry out the

mentioned function, the classifier head is detached from this model.

Step 3: After that, a PCA model receives the features that the ViT model generated. During this stage, we isolate a subset of components that possess the ability to elucidate the majority of the data. The objective is to decrease the dimensionality of the data, rendering it more manageable for straightforward and computationally efficient machine learning models such as a Multilayer Perceptron (MLP) and a Support Vector Machine (SVM).

Step 4: The hyperparameters of both models are adjusted, and the classification results are assessed using metrics such as accuracy, precision, recall, and F1-score.

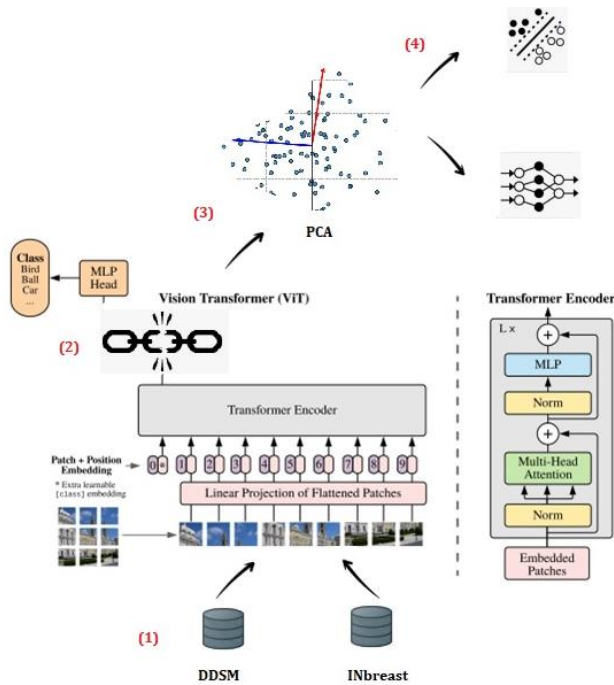


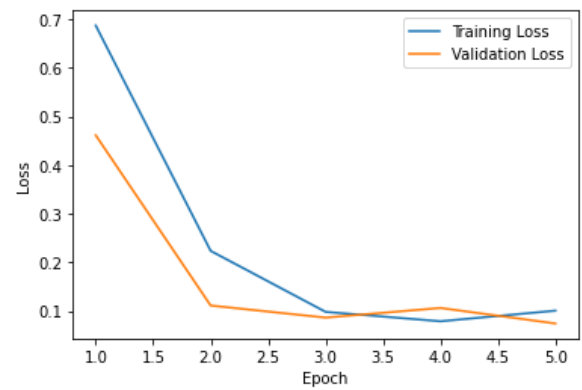
Fig. 3. The integration of a ViT model as a feature extractor, coupled with PCA and machine learning models as classifiers, serves to identify benign and malignant cases of breast cancer (figure of the ViT obtained from the work of [7]).

C. Experimentation

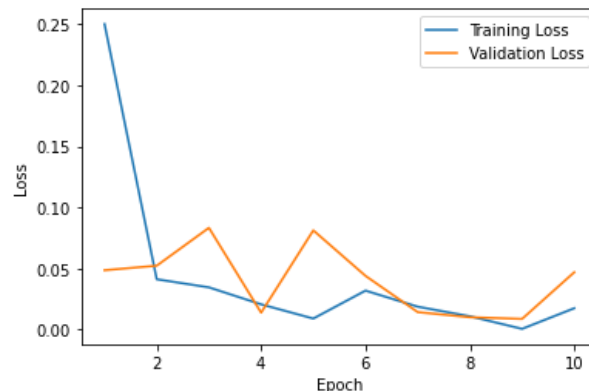
Considering the DDSM Dataset, which contains both benign and malignant images of the breast, we performed image resizing to 224 x 224 pixels and channel normalization with a value of 0.5 [5]. Subsequently, we read the images from their respective folders and assigned a label of 0 for benign masses and 1 for malignant masses. To determine the number of epochs for model optimization, we employed a standard split of 80% for training and 20% for validation, with a batch size of 32. We utilized the pre-trained Vision Transformer (ViT) model "facebookresearch/deit:main" with the "deit_base_patch16_224" architecture, which was pre-trained on the ImageNet-1k dataset at a resolution of 224 x 224 with fixed patches of 16 x 16 [36, 16]. For the loss function, we chose Cross Entropy, a commonly used metric for estimating probabilities in breast cancer classification [17, 18]. The optimizer selected was Adam, supported by previous studies

[18, 34], with a learning rate of 0.001. It is important to note that we employed this configuration to create a feature extraction model by removing the last layer, which served as a classifier, after the training phase. Additionally, we flattened our data into a 2D tensor, where each row corresponds to the features extracted from an image. With this setup, we conducted experiments and obtained the training and validation loss curves, as shown in Fig. 4. To evaluate the model's performance, we tested various numbers of epochs and decided to maintain a value of five based on the results obtained.

For the INbreast dataset, the methodology was similar, with the exception that when we plotted the loss curves for a fixed number of epochs using the same learning rate as applied to the DDSM dataset, we observed that the validation set's loss did not decrease significantly. This indicated the occurrence of overfitting. To address this issue, we manually adjusted the learning rate and determined that a value of 0.0001 resulted in a rapid decrease of the validation set's loss with eight epochs.



(a)



(b)

Fig. 4. Training and validation curve losses for obtaining the number of epochs for the DDSM (a) and INbreast datasets (b).

Algorithm 1 outlines the steps performed in the study:

1) Define the dataset directory and the image transformation pipeline using PyTorch's `transforms.Compose()` function.

2) Create a custom dataset class that is inherited from PyTorch's Dataset class. In the constructor, initialize the root directory, transformation pipeline, and targets. Implement the `__len__` method to return the total number of samples in the

dataset. Implement the `__getitem__` method to compute the number of samples in each class, determine the class of the current sample based on its index, load the corresponding image and label, apply the transformation pipeline to the image, and return the transformed image and label.

3) Split the dataset into training and validation sets using PyTorch's `random_split()` function.

4) Define data loaders for the training and validation sets using PyTorch's `DataLoader` class.

5) Load the pre-trained ViT model from Facebook Research using the `torch.hub.load()` function.

6) Define the loss function as the cross-entropy loss and choose the optimizer as Adam.

7) Train the model on the training set for a specified number of epochs. During training, fine-tune the pre-trained ViT model on the custom dataset, enabling it to learn task-specific features. Use the loss function and optimizer to update the model's parameters.

8) After each epoch, validate the model on the validation set and calculate the validation loss using the loss function. This step monitors the model's performance on unseen data and helps prevent overfitting.

9) Save the trained visual transformer model to a file using the `torch.save()` function.

10) Plot the training and validation losses using Matplotlib. This visualization aids in tracking the model's performance during training and identifying any issues, such as overfitting.

When the model was trained, given the number of epochs obtained, we decided to use PCA for dimensionality reduction. The choice of PCA was mainly because we wanted to reduce the number of features given a certain number of components. In the experiments performed, we found that the number of components that explained 95% of the data was 43 for the DDSM dataset, while the number of suitable components found for the INbreast dataset was of 1933 components. It is not surprising that INbreast required a greater number of principal components. We hypothesize that the main reason for this is that the dataset consists of electric signals converted into images, which provides more detailed information than the DDSM dataset [34].

An algorithm is provided for utilizing the saved model from Algorithm 1 to obtain the desired number of components using PCA. The components will serve as input features in the machine learning model:

Algorithm 2:

1) Load the trained visual transformer model by invoking the function `load_visual_transformer()`.

2) Define a feature extractor by removing the classification head from the pre-trained ViT model through the creation of a `torch.nn.Sequential()` object.

3) Utilize a data loader to apply the feature extractor to the images in the dataset. For each batch of images, extract the features using the feature extractor, flatten the resulting

feature maps, and store the features and corresponding labels in separate lists.

4) Concatenate the feature vectors and labels, transforming them into numpy arrays.

5) Apply PCA to the feature vectors to reduce their dimensionality.

At this stage, we opted to employ two machine learning models: a multilayer perceptron (MLP) and a support vector classifier (SVC). For the MLP model, we explored the following number of hidden layers as a hyperparameter grid:

Hidden layer size 1: A single hidden layer with the same number of neurons as the input features.

Hidden layers size 64: In this case, we employed two hidden layers. The first layer had the same number of neurons as the input, and the second layer had 64 neurons.

Hidden layers size 128: Like the configuration mentioned earlier, but with the second hidden layer having 128 neurons.

Hidden layers size 256: Again, similar to the previous configurations, with the number of neurons in the hidden layer now set to 256.

This grid served as input for a grid search cross-validation function that utilized five folds to determine the best number of hidden layers as a hyperparameter for this model. After applying the grid search function, we identified the best hyperparameter values to be 256 neurons for the DDSM dataset and 128 neurons for the INbreast dataset, respectively.

For the DDSM dataset, we utilized two hidden layers with 256 and 128 neurons, respectively. Meanwhile, for the INbreast dataset, we employed the same number of hidden layers but with 1933 and 128 neurons in each layer. The activation function used was ReLU.

Concerning the hyperparameters for the SVC, we utilized a hyperparameter grid consisting of the following values:

C (penalization factor): 0.01, 0.1, 1, 10, 100

Kernels: Linear, Polynomial, RBF

Gamma value (only applicable to RBF): 0.001, 0.01, 0.1

Subsequently, we performed a grid search cross-validation with five folds to obtain the best hyperparameters, considering the grid.

For the DDSM dataset, the SVC model was configured with an RBF kernel, a penalty parameter C of 100, and a gamma value of 0.001. As for the INbreast dataset, the hyperparameters for the SVC model were set as follows: RBF kernel, C of 100, and gamma value of 0.1.

IV. RESULTS

After employing transfer learning using a Vision Transformer (ViT) as described in the methodology section and applying the aforementioned classifier methods, we obtained the following results for both models that are presented in Table II.

TABLE II. METRICS OBTAINED FROM THE MODELS EVALUATED IN THE DDSM (A) AND INBREAST (B) DATASETS

| (a) | | | | |
|--|--------|-------|--------|----------|
| ViT model + Classifier using PCA (DDSM)/Metric | Acc | Prec | Recall | F1-score |
| MLP | 0.9819 | 0.983 | 0.9836 | 0.983 |
| SVC | 0.9672 | 0.962 | 0.9786 | 0.970 |

| (b) | | | | |
|--|-------|-------|--------|----------|
| ViT model + Classifier using PCA (INbreast)/Metric | Acc | Prec | Recall | F1-score |
| MLP | 0.943 | 0.954 | 0.9624 | 0.9582 |
| SVM | 0.843 | 0.810 | 1 | 0.8953 |

Table II displays the metrics for Accuracy, Precision, Recall, and F1-score of our proposed model, which were calculated using the DDSM and INbreast datasets. It is noteworthy that our Precision and Recall results consistently exceed 97% on average. The precision and recall in medical diagnosis are of utmost importance. In this cancer situation, the recall metric prioritizes false negatives, while precision focuses on false positives. Furthermore, the f1-score, which is the harmonic mean that takes into account both precision and recall, has yielded an average of 96%. Upon evaluating both models, it can be deduced that they exhibit minimal occurrences of false positive and false negative predictions. Furthermore, they provide a well-balanced performance in terms of precision and recall.

From the data presented in Table II, it is evident that the MLP model outperformed the SVC classifier for both datasets. It is worth noting that a five-fold cross-validation was utilized for validating our results in each model.

It is worth noting that the MLP model outperformed the SVM model on both datasets. In the case of the DDSM dataset, the difference between the two models is only about one point. However, the distinction observed in the INbreast dataset is more pronounced, with a difference of nearly 10 points in Accuracy and Precision between both models.

According to the authors [22], both datasets, DDSM and INbreast, were subjected to data augmentation techniques such as rotation and flipping. The difference between the original data from both datasets (i.e., data that had not been augmented) was significant. For the DDSM dataset, 2188 images were augmented to 13128, while 106 mass images were augmented to 7632 for the INbreast dataset. The proportion of augmented data in the INbreast dataset far outnumbers that in the DDSM dataset.

At this point, we can speculate that this disparity may have contributed to the SVM model's lower results compared to its MLP counterpart, which demonstrated a greater ability to generalize its classification capabilities in both datasets. These findings are intriguing, especially considering the work of Shen et al. [34]. Their research indicated that the INbreast dataset, containing FFDM (full-field digital mammography) images with varied intensity profiles, allowed them to evaluate the suitability of a particular classifier model across several mammography platforms. This property stems from the fact that FFDM images replace X-rays with electrical signals, allowing them to be reproduced across multiple devices [35].

V. DISCUSSION

In comparison to other studies that have utilized the DDSM dataset, we did not find any previous work that employed transfer learning combined with PCA and machine learning models. In the study conducted by Ayana et al. [2], transfer learning was also utilized with various ViT models, such as Swim and Pyramid, along with image augmentation to address the issue of dataset imbalance. Their results, obtained when training the models from scratch, ranged from a 78% in accuracy, precision, and F1-score. Furthermore, the authors explored CNN models including ResNet, EfficientNet, and InceptionNet, achieving an average accuracy, F1-score, and recall of 94%. We believe it is important to mention recall as a crucial metric since the consequences of missing or misclassifying a cancer screening can be detrimental. However, our approach, incorporating PCA, transfer learning, and machine learning models, yielded promising results with an average performance of 98% across the evaluated metrics.

Another study conducted by Ragab et al. [30] investigated two datasets, namely the DDSM and the Curated Breast Image Subset of the DDSM (CBIS-DDSM). The authors employed image enhancement techniques, including Contrast-Limited Adaptive Histogram Equalization (CLAHE), to improve image definition. They also performed image segmentation and utilized data augmentation. It is worth mentioning that CLAHE was also applied to the DDSM dataset with data augmentation, as employed in our present study. Ragab et al. [30] performed feature extraction using a Deep Convolutional Neural Network (DCNN), specifically AlexNet, which was pre-trained on the ImageNet dataset. Their combined model, consisting of the DCNN and a Support Vector Machine (SVM) classifier, achieved an accuracy of 87.2% using a medium Gaussian kernel function. Although there are some differences between the datasets used in their study and ours, there are notable similarities, such as both datasets being based on the DDSM dataset and the utilization of similar techniques for image preprocessing and augmentation. The authors' use of image segmentation is a distinct difference from our approach.

In the research conducted by Salama et al. [31], two datasets, namely the DDSM and the curated DDSM, were utilized. The authors applied data augmentation techniques such as rotation and employed two deep learning models, ResNet-50 and VGG-16. Transfer learning was performed from the ImageNet dataset, and the classification layer was modified to accommodate only two classes. Although it appears that both models were used as feature selection algorithms, no explicit mention of this approach was found. The outputs from both models were then used as inputs for an SVM classifier. While the authors mentioned hyperparameter tuning for the deep learning methods employed, there was no information provided regarding hyperparameter tuning for the SVM model. The results obtained for the DDSM dataset using the VGG-16 model yielded an average accuracy, AUC, sensitivity, precision, and F1-score of 94%. For the CBIS-DDSM dataset, the VGG-16 and ResNet-50 models combined with the SVM classifier and five-fold cross-validation achieved an average accuracy, AUC, sensitivity, precision, and F1-score of 96% for the former and 95% for the latter, in addition to an average F1-score of 93%.

Other researchers, such as Tsochatzidis [37], conducted experiments with various deep learning models, including AlexNet, VGG-16, VGG-19, ResNet-50, ResNet-152, GoogLeNet, and Inception-BN. In their study, the authors initialized the weights of their models from scratch and also applied transfer learning techniques to the DDSM-400 and CBIS-DDSM datasets. Data augmentation was not employed in their experiments. According to their findings, training the models from scratch yielded the best performance with AlexNet, achieving an accuracy of 62% for the DDSM-400 dataset and 65% for the CBIS-DDSM dataset. However, the best results were obtained when using pre-trained initialized weights for both datasets. In particular, the ResNet-based model achieved an accuracy of 85% for the DDSM-400 dataset and an average accuracy of 80% for the CBIS-DDSM dataset.

Das et al. [6] conducted a study where they evaluated the performance of various deep learning models on breast cancer datasets, including CBIS-DDSM and INbreast. Their experiments involved both shallow neural networks and deep neural networks. Among the models tested, the Xception network demonstrated the best performance, achieving an

accuracy of 89% for CBIS-DDSM and 95% for INbreast. The authors suggested that the higher accuracy obtained on the INbreast dataset could be attributed to the higher image quality compared to CBIS-DDSM.

As of the writing of this article, we have not found any existing research that has utilized a transfer-learning model based on Vision Transformer (ViT) in conjunction with Principal Component Analysis (PCA) for dimensionality reduction. Furthermore, our results show that a simple Multilayer Perceptron (MLP) model with two hidden layers, employed as a classifier, outperforms SVM-based approaches. We strongly believe that leveraging pre-trained models, particularly those based on attention mechanisms like ViT, in combination with dimensionality reduction techniques applied to the data, holds promise for achieving superior performance. Moreover, these approaches can be beneficial in scenarios where computational resources for data processing are limited.

Table III, which is an expansion of Table I mentioned in the Introduction section, contains the datasets utilized in the reviewed studies, as well as the metrics derived from the outcomes of the various applied models.

TABLE III. COMPARISON OF OTHER STUDIES WITH OUR CURRENT PROPOSAL

| Authors | Methodology | Dataset used | Results |
|--------------------------|--|------------------------|---|
| Tsochatzidis et al. [38] | Employs a modified CNN architecture that incorporates a U-Net for image segmentation during input. | DDSM-400 and CBIS-DDSM | AUC 89.8% and 86.2% |
| Min et al. [24] | Grayscale images are converted into pseudo-color and the masses are amplified for utilization in a Mask R-CNN that utilizes transfer learning. | Inbreast | 90% (True Positive Rate) TPR |
| Samee et al. [32] | Images are improved through the application of contrast-limited adaptive histogram equalization (CLAHE). A CNN model, selected from AlexNet, VGG, or GoogleNet, is used to extract features, while a Logistic Regression model with PCA is employed for classification. | Inbreast and MIAS | 98.8% of accuracy using MIAS and 98.6% using MIAS. |
| Al-Tam et al. [1] | The authors employed VGG16, ResNet50, and Imagenet for both binary and multiclass classification. For the final test, they utilized a ResNet50 model that was trained from scratch, in addition to a ViT model. | CBIS-DDSM | 100% in the F1-score for the binary classification, other metrics in average made a 96% in the multiclass classification. |
| Samee et al. [33] | The authors utilized pre-trained convolutional neural network (CNN) models, specifically AlexNet, GoogleNet, and VGG-16. The researchers applied a series of feature selection techniques, including Pearson Correlation Coefficient, Cosine Coefficient (mainly used for texts), Euclidean Distance (although Liu and Zhang [23] warned about possible drawbacks in representing data characteristics, which could result in suboptimal learning), and Mutual Information. The chosen characteristics were subjected to classification using an ensemble of learners utilizing Discriminant Analysis, Support Vector Machines (SVM), K-Nearest Neighbors (KNN), and Naive Bayes. Nevertheless, it is still uncertain whether they employed a combination of machine learning models or determined which one produced the most optimal outcomes. | Inbreast | 98.06% in Sensitivity and 98.5% in Accuracy. |
| Jabeen et al. [19] | The authors utilized a haze-reduced local-global image enhancement technique. The images were subjected to augmentation, and a pre-trained EfficientNet-b0 model was used as a feature extractor, excluding the last three layers. The process of selecting features was conducted utilizing the Equilibrium-Jaya controlled Regula Falsi algorithm. An ensemble of K-nearest neighbors (EKNNs) was utilized for classification. | CBIS-DDSM Inbreast | Average Accuracy of 95.4% and 99.7% |
| Our Proposal | The ViT model is utilized as a feature extractor, PCA is employed for dimensionality reduction, and MLP and SVM are used as classifiers for the purpose of comparison. | DDSM Inbreast | Average Accuracy, Precision, Recall and F1-score of 98% for the DDSM dataset with MLP as classifier. The same metrics give us an average of 95.4% for the InBreast dataset. |

Regarding the limitations identified in the current research, it is important to note that the author faced difficulties in finding appropriate examples to aid in the coding process of the Vision Transformer (ViT) when utilized as a feature extractor instead of a classifier. Although there is limited literature on using ViT models as feature extractors, we are still confident in their potential for applications where the features obtained can be used as input for Machine learning (ML) models. ML models provide several benefits, such as their interpretability, decreased computational requirements, and ongoing potential usefulness in the domain of medical diagnosis.

An important upcoming task would be to evaluate various Vision Transformer (ViT) models in combination with different subsets of machine learning (ML) models, such as Random Forest or other boosting-based methods, to ascertain if these model combinations can enhance the reported results. In addition, performing experiments with diverse datasets, e.g., the MIAS or the BancoWeb Lapimo, datasets beyond those specified in the present study, would allow for the assessment of the overall efficacy of an integrated model that includes ViT, dimensionality reduction of features, and machine learning techniques in diagnosing breast cancer scenarios using mammography data.

VI. CONCLUSION

The classification of samples obtained from mammograms holds utmost importance, as early detection of malignant masses can significantly impact patient outcomes. In this study, we demonstrated the efficacy of a transfer learning model based on Vision Transformer (ViT), coupled with Principal Component Analysis (PCA) for feature reduction, and a simple Multilayer Perceptron (MLP) model. Our results were found to be comparable to existing literature that employs Convolutional Neural Network (CNN) models based on transfer learning in conjunction with deep learning models. These findings highlight the potential of using ViT-based transfer learning approaches, combined with dimensionality reduction techniques and simple Machine Learning classifiers, to achieve accurate mammogram classification results.

REFERENCES

- [1] Al-Tam RM, Al-Hejri AM, Narangale SM, Samee NA, Mahmoud NF, Al-masni MA, et al. 2022. A Hybrid Workflow of Residual Convolutional Transformer Encoder for Breast Cancer Classification Using Digital X-ray Mammograms. *Biomedicine*.10:2971. doi:10.3390/biomedicine10112971.
- [2] Ayana, G., K. Dese, Y. Dereje, Y. Kebede, H. Barki, D. Amdissa, N. Husen, F. Mulugeta, B. Habtamu, and S.-W. Choe. 2023. Vision-Transformer-Based Transfer Learning for Mammogram Classification. *Diagnostics* 13, no. 2 (January 4): 178. doi:10.3390/diagnostics13020178.
- [3] Brownlee J. 2019. *Deep Learning for Computer Vision: Image Classification, Object Detection, and Face Recognition in Python*. 198-200. *Machine Learning Mastery*.
- [4] Bhushan, A., A. Gonsalves, and J.U. Menon. 2021. Current State of Breast Cancer Diagnosis, Treatment, and Theranostics. *Pharmaceutics* 13, no. 5 (May 14): 723.
- [5] Centers for Disease Control and Prevention (CDC). Breast Cancer. Accessed 11, November 2023. https://www.cdc.gov/cancer/breast/basic_info/diagnosis.htm.
- [6] Das, H.S., A. Das, A. Neog, S. Mallik, K. Bora, and Z. Zhao. 2023. Breast Cancer Detection: Shallow Convolutional Neural Network against Deep Convolutional Neural Networks Based Approach. *Frontiers in Genetics* 13 (January 4): 5:37. doi:10.3390/jimaging5030037.
- [7] Dosovitskiy, A., L. Beyer, A. Kolesnikov, D. Weissenborn, X. Zhai, T. Unterthiner, M. Dehghani, et al. 2021. An Image Is Worth 16x16 Words: Transformers for Image Recognition at Scale. Accessed November 11, 2023. arXiv. <http://arxiv.org/abs/2010.11929>.
- [8] Ferguson, M., R. Ak, Y.-T.T. Lee, and K.H. Law. 2017. Automatic Localization of Casting Defects with Convolutional Neural Networks. In 2017 IEEE International Conference on Big Data (Big Data), 1726–1735. Boston, MA: IEEE. doi:10.1109/BigData.2017.8258115.
- [9] Flach, P. 2012. *Machine learning: The art and science of algorithms that make sense of data*, 300-54. USA: Cambridge University Press. <https://doi.org/10.1017/CBO9780511973000>.
- [10] Goodfellow I., Bengio Y., Courville A. 2016. *Deep Learning*. 539-540. MIT Press.
- [11] Haibo, H., and Garcia, E.A. 2009. Learning from Imbalanced Data. *IEEE Transactions on Knowledge and Data Engineering* 21, no. 9 (September): 1263–1284. doi:10.1109/TKDE.2008.239.
- [12] Heath, M., K. Bowyer, D. Kopans, P. Kegelmeyer, R. Moore, K. Chang, and S. Munishkumar. 1998. Current Status of the Digital Database for Screening Mammography. In *Digital Mammography*, ed. N. Karssemeijer, M. Thijssen, J. Hendriks, and L. Van Erning, 13:457–460. Computational Imaging and Vision. Dordrecht: Springer Netherlands. http://link.springer.com/10.1007/978-94-011-5318-8_75.
- [13] Heath, M., Bowyer, K., Kopans, D., Moore, R., and Kegelmeyer, W. P. 2001. The Digital Database for Screening Mammography. In *Proceedings of the Fifth International Workshop on Digital Mammography*, M.J. Yaffe, ed., 212-218. Medical Physics Publishing. ISBN 1-930524-00-5.
- [14] Houssein EH, Emam MM, Ali AA. 2022. An optimized deep learning architecture for breast cancer diagnosis based on improved marine predators algorithm. *Neural Comput & Applic*.34:18015–33. doi:10.1007/s00521-022-07445-5.
- [15] Huang, M.-L., and T.-Y. Lin. Dataset of Breast Mammography Images with Masses. 2020. *Data in Brief* 31: 105928. doi: 10.17632/ywsbh3n8r8.2.
- [16] Hugging Face. "facebook/deit-base-patch16-224." Hugging Face, n.d. Accessed November 11, 2023. <https://huggingface.co/facebook/deit-base-patch16-224>.
- [17] Jaamour, A. 2020. *Breast Cancer Detection in Mammograms Using Deep Learning Techniques*. MSc. diss., University of St. Andrews.
- [18] Jaamour, A., C. Myles, A. Patel, S.-J. Chen, L. McMillan, and D. Harris-Birtill. 2023. A Divide and Conquer Approach to Maximise Deep Learning Mammography Classification Accuracies. *PLOS ONE* 18, no. 5 (May 26): e0280841. doi:10.1371/journal.pone.0280841.
- [19] Jabeen, K., M.A. Khan, J. Balili, M. Alhaisoni, N.A. Almujaally, H. Alrashidi, U. Tariq, and J.-H. Cha. 2023. BC2NetRF: Breast Cancer Classification from Mammogram Images Using Enhanced Deep Learning Features and Equilibrium-Jaya Controlled Regula Falsi-Based Features Selection. *Diagnostics* 13, no. 7 (March 25): 1238.
- [20] Keheller J. 2019. *Deep Learning*. 236-237. MIT Press.
- [21] Kherif, F., and A. Latypova. 2020. Principal Component Analysis. *Machine Learning*, 209–225. Elsevier. <https://linkinghub.elsevier.com/retrieve/pii/B9780128157398000122>.
- [22] Lin, T. and M. Huang. (2020), Dataset of Breast mammography images with Masses. Accessed December 24, 2023. <https://data.mendeley.com/datasets/ywsbh3n8r8/5>.
- [23] Liu, M., and D. Zhang. 2016. Feature Selection with Effective Distance. *Neurocomputing* 215 (November): 100–109.
- [24] Min, H., D. Wilson, Y. Huang, S. Liu, S. Crozier, A.P. Bradley, and S.S. Chandra. 2020. Fully Automatic Computer-Aided Mass Detection and Segmentation via Pseudo-Color Mammograms and Mask R-CNN. In 2020 IEEE 17th International Symposium on Biomedical Imaging (ISBI), 1111–1115. Iowa City, IA, USA: IEEE. <https://ieeexplore.ieee.org/document/9098732/>.

- [25] Muller, S. 1999. Full-Field Digital Mammography Designed as a Complete System. *European Journal of Radiology* 31, no. 1 (July): 25–34.
- [26] National Cancer Institute (NIH). "Breast Cancer Screening (PDQ®)–Patient Version." National Cancer Institute. Accessed December 28, 2023. <https://www.cancer.gov/types/breast/patient/breast-screening-pdq>
- [27] Moreira, I.C., I. Amaral, I. Domingues, A. Cardoso, M.J. Cardoso, and J.S. Cardoso. 2012. *INbreast*. *Academic Radiology* 19, no. 2 (February): 236–248.
- [28] Oral, C., and H. Sezgin. 2013. Effects of Dimension Reduction in Mammograms Classification. In 8th International Conference on Electrical and Electronics Engineering (ELECO), 630–633. Bursa, Turkey: IEEE. <http://ieeexplore.ieee.org/document/6713912/>.
- [29] Palo, H.K., S. Sahoo, and A.K. Subudhi. 2021. Dimensionality Reduction Techniques: Principles, Benefits, and Limitations. *Data Analytics in Bioinformatics*, ed. R. Satpathy, T. Choudhury, S. Satpathy, S.N. Mohanty, and X. Zhang, 77–107. 1st ed. Wiley. <https://onlinelibrary.wiley.com/doi/10.1002/9781119785620.ch4>.
- [30] Ragab, D.A., M. Sharkas, S. Marshall, and J. Ren. 2019. Breast Cancer Detection Using Deep Convolutional Neural Networks and Support Vector Machines. *PeerJ* 7 (January 28): e6201. doi:10.7717/peerj.6201.11.
- [31] Salama, W.M., A.M. Elbagoury, and M.H. Aly. 2020. Novel Breast Cancer Classification Framework Based on Deep Learning. *IET Image Processing* 14, no. 13 (November): 3254–3259. doi:10.1049/iet-ipr.2020.0122.
- [32] Samee NA, Alhussan AA, Ghoneim VF, Atteia G, Alkanhel R, Al-antari MA, et al. 2022a. A Hybrid Deep Transfer Learning of CNN-Based LR-PCA for Breast Lesion Diagnosis via Medical Breast Mammograms. *Sensors*;22:4938. doi:10.3390/s22134938.
- [33] Samee, N.A., G. Atteia, S. Meshoul, M.A. Al-antari, and Y.M. Kadah. 2022b. Deep Learning Cascaded Feature Selection Framework for Breast Cancer Classification: Hybrid CNN with Univariate-Based Approach. *Mathematics* 10, no. 19 (October 4): 3631.
- [34] Shen, L., L.R. Margolies, J.H. Rothstein, E. Fluder, R. McBride, and W. Sieh. 2019. Deep Learning to Improve Breast Cancer Detection on Screening Mammography. *Scientific Reports* 9, no. 1 (August 29). doi:10.1038/s41598-019-48995-4.
- [35] Stanford Medicine. <https://stanfordhealthcare.org/medical-tests/m/mammogram/digital-mammography.html>. Accessed, December 24, 2023.
- [36] Touvron, H., M. Cord, M. Douze, F. Massa, A. Sablayrolles, and H. Jégou. Training Data-Efficient Image Transformers & Distillation through Attention. Last Modified 2021. Accessed November 11, 2023. arXiv. <http://arxiv.org/abs/2012.12877>.
- [37] Tsochatzidis, L., L. Costaridou, and I. Pratikakis. 2019. Deep Learning for Breast Cancer Diagnosis from Mammograms—A Comparative Study. *Journal of Imaging* 5, no. 3 (March 13): 37. doi:10.3390/jimaging5030037.
- [38] Tsochatzidis, L., P. Koutla, L. Costaridou, and I. Pratikakis. 2021. Integrating Segmentation Information into CNN for Breast Cancer Diagnosis of Mammographic Masses. *Computer Methods and Programs in Biomedicine* 200 (March): 105913.
- [39] World Health Organization (WHO). Breast Cancer. Accessed November 11, 2023. <https://www.who.int/news-room/fact-sheets/detail/breast-cancer>.
- [40] Zhu, Z., S.-H. Wang, and Y.-D. Zhang. 2023. A Survey of Convolutional Neural Network in Breast Cancer. *Computer Modeling in Engineering & Sciences* 136, no. 3: 2127–2172..

Hybrid Algorithm using Rivest-Shamir-Adleman and Elliptic Curve Cryptography for Secure Email Communication

Kwame Assa-Agyei¹, Kayode Owa², Tawfik Al-Hadhrami³, Funminiyi Olajide⁴

School of Science and Technology, Nottingham Trent University, United Kingdom^{1, 2, 3}

School of Computer Science and Engineering, University of Westminster, United Kingdom⁴

Abstract—Email serves as the primary communication system in our daily lives, and to bolster its security and efficiency, many email systems employ Public Key Infrastructure (PKI). However, the convenience of email also introduces numerous security vulnerabilities, including unauthorized access, eavesdropping, identity spoofing, interception, and data tampering. This study is primarily focused on examining how two encryption techniques, RSA and ECC, affect the efficiency of secure email systems. Furthermore, the research seeks to introduce a hybrid cryptography algorithm that utilizes both RSA and ECC to ensure security and confidentiality in the context of secure email communication. The research evaluates various performance metrics, including key exchange time, encryption and decryption durations, signature generation, and verification times, to understand how these encryption methods affect the efficiency and efficacy of secure email communication. The experimental findings highlight the advantages of ECC in terms of Key Exchange Time, making it a compelling choice for establishing secure email communication channels. While RSA demonstrates a slight advantage in encryption, decryption, and signature generation for smaller files, ECC's efficiency becomes apparent as file sizes increase, positioning it as a favorable option for handling larger attachments in secure emails. Through the comparison of experiments, it is also concluded that the hybrid encryption algorithm optimizes the key exchange times, encryption efficiency, signature generation and verification times.

Keywords—RSA; ECC; Advanced Encryption Standard; encryption; decryption; signature generation; verification; key exchange time; hybrid encryption

I. INTRODUCTION

In today's interconnected world, email has become an indispensable tool for communication. It facilitates the exchange of information, ideas, and documents across vast distances, enabling individuals and organizations to collaborate and communicate efficiently [1]. However, the convenience of email also brings with it a host of security concerns, as emails can easily fall prey to unauthorized access, eavesdropping, identity spoofing, interception, or data tampering [2] [3]. This is where cryptography plays a pivotal role in ensuring the confidentiality, integrity, and authenticity of email communication. Email encryption is the cornerstone of secure email communication. It employs complex algorithms to transform the content of an email into an unreadable format, known as ciphertext, which can only be

deciphered by the intended recipient possessing the decryption key [4]. This cryptographic process ensures the following [5] [6]:

1) *Confidentiality*: Encrypted emails are incomprehensible to anyone without the decryption key, thwarting unauthorized access and eavesdropping.

2) *Integrity*: The recipient can promptly detect any alterations made to the encrypted email, ensuring the message's integrity remains intact during transmission.

3) *Authentication*: Combining encryption with digital signatures verifies the sender's identity, ensuring the legitimacy of the email for the recipient.

Email security protocols such as Secure Sockets Layer (SSL) and Transport Layer Security (TLS) commonly utilize encryption algorithms like RSA, AES, and elliptic curve cryptography, while public-key infrastructure (PKI) systems and digital certificates play vital roles in verifying the authenticity of email senders [7].

This research project's primary aim is to explore the correlation between the performance of secure email communication systems and the encryption methods employed. The study examines how incorporating both RSA and ECC encryption techniques influences the efficiency of secure email systems. The study seeks to discern any connections between the choice of cryptographic algorithms, RSA and ECC, and the overall performance of secure email systems. Furthermore, the study suggests a hybrid cryptography algorithm that utilizes both RSA and ECC to enhance security and preserve confidentiality in the context of secure email communication. The research will assess various performance aspects, including key exchange time, encryption and decryption times, signature generation and verification times, to ascertain how these encryption methods influence the efficiency and efficacy of secure email communication. Through an analysis, the study's aim to identify any potential relationships or dependencies between the selection of encryption methodologies and the outcomes in terms of secure email system performance.

A. Limitation of Existing Models

While existing encryption models, such as those based solely on RSA or ECC, have undoubtedly contributed to the advancement of secure communication protocols, they

nonetheless exhibit limitations that may not be well suited to address the multifaceted challenges inherent in secure email communication. A significant drawback concerns the scalability of conventional encryption methods, especially when it comes to email communication. As the size and complexity of email attachments continue to grow, conventional encryption algorithms, like RSA, may struggle to maintain optimal performance, leading to increased computational overhead and potential delays in key exchange, encryption, and decryption processes [8].

B. Rationale for the Proposed Model

The selection of the hybrid cryptography algorithm, combining RSA and ECC, for secure email communication stems from a thorough consideration of various factors. Firstly, while RSA has been a stalwart in encryption for decades, its efficiency can be compromised, particularly when dealing with larger files or computational constraints. RSA's computational complexity grows with the size of the data, affecting encryption and decryption times [8].

On the other hand, ECC has emerged as a promising alternative due to its ability to provide equivalent security with shorter key lengths, thus reducing computational overhead and enhancing performance, especially in resource-constrained environments. Compared to RSA, ECC offers the same level of security with significantly smaller key sizes, making it more efficient for key exchange and digital signatures [9].

However, both RSA and ECC have their respective strengths and weaknesses. RSA excels in signature generation and verification for smaller files, while ECC demonstrates superior efficiency in key exchange, particularly noticeable as file sizes increase [10]. Recognizing these complementary attributes, the hybrid approach seeks to leverage the strengths of each encryption technique to mitigate their individual limitations. Combining RSA and ECC allows for a more balanced security posture by utilizing RSA for digital signatures and ECC for key exchange.

Moreover, by combining RSA and ECC within a hybrid model, we aim to achieve a balance between security and efficiency in secure email communication. This approach allows us to capitalize on RSA's robustness in certain aspects while harnessing ECC's efficiency gains in others, ultimately offering a more versatile and adaptable solution for addressing the diverse security challenges inherent in email communication.

The aim of the study is to enhance the performance of secure email systems by leveraging the distinct advantages of both RSA and ECC, while minimizing their individual limitations. This rationale underscores the relevance and appropriateness of the proposed model in addressing the inherent complexities of secure email communication in today's digital landscape.

Hence, the current study makes the following key contributions.

1) To perform an extensive analysis of the performance of selected algorithms, namely: RSA and ECC for secured email communication.

2) To perform an extensive evaluation of the key exchange time, signature generation and verification times between RSA and ECC techniques.

3) To present a hybrid cryptography algorithm that employs both RSA and ECC to ensure confidentiality and enhance security for secure email communication.

The rest of the paper is organized as follows: Section II presents the related work. The experimental setup is presented in Section III. Sections IV presents the hybrid techniques employing RSA and ECC. Section V and Section VI present the performance analysis of solo ECC, RSA and the proposed hybrid algorithm and discussion of the research. Finally, the conclusion is drawn in Section VII.

II. RELATED WORK

In this study, a secure system for key agreement and session authentication for Internet of Things (IoT) devices was conceptualized, developed, and subjected to testing. The simulation results showed that the method was resilient to different assaults. The results of the performance evaluation also showed that, when compared to DSA and RSA, the time complexity was lowest for the ECC used in this case. The developed protocol also had the lowest computational overhead, the quickest turnaround times, and the greatest stability with the least amount of communication overhead [11]. In study [12], researchers conducted an analysis of distinct cryptographic algorithms, evaluating aspects like key size, message size, and execution time. With the proliferation of diverse encryption techniques, facilitating swift and dependable communication among IoT devices has become a complex task, one that must be accomplished without causing interruptions. Determining the most suitable, compatible, and advantageous encryption method for communication has proven to be quite intricate. Through their examination, the authors reached the consensus that among various options, Schnorr, RSA, Elliptic Curve Cryptography, and ElGamal emerge as the superior choices. Kaur and Aggarwal [13] undertook an extensive examination of cryptographic methods including RSA, Blowfish, Diffie-Hellman, ECC, and others. Among these techniques, ECC has demonstrated itself as the encryption method that excels in both security and efficiency. In reference to [14], the researchers delved into an analysis of diverse encryption methods encompassing both symmetric and asymmetric cryptographic techniques. These methods included Rivest Shamir and Adleman, Diffie-Hellman, Digital Signature Algorithm, as well as Elliptic Curve Cryptography (ECC). The study aimed to explore their practical implementation and ascertain the most effective cryptographic techniques capable of ensuring comprehensive data confidentiality during transmission. Each cryptographic algorithm i found to possess distinct strengths, features, advantages, complexities, efficiency levels, and limitations. Among these factors, the examination revealed that digital signatures offer robust confidentiality and non-repudiation, thereby serving as a means to safeguard data integrity, availability, and confidentiality. A thorough examination is carried out to investigate the ECC, RSA, and Diffie-Hellman Algorithms within the realm of Network Security. The study addresses the challenges associated with sharing and

transferring private keys among systems. When assessing the efficacy of ECC, RSA, and Diffie-Hellman algorithms, ECC stands out as the favoured option due to its capacity to deliver almost comparable security levels while employing fewer bits than both RSA and Diffie-Hellman. The researchers also delved into the realm of elliptic curve cryptography, exploring its significant applications within the market. This exploration involved examining its prevalence in technologies like Bitcoin, Secure Shell, and Transport Layer Security. It is evident from the literature that elliptic curve cryptography stands out as a promising approach, capable of offering exceptional security advantages over comparable algorithms. Moreover, its cost-effectiveness positions it as a valuable contender for cryptographic applications [15]. In study [16], the researchers conducted an analysis of the performance characteristics of conventional public-key cryptographic systems, namely RSA, DSA, and DH, in comparison to ECC. The investigations highlighted that the traditional public-key methods encounter performance-related challenges. The study proposed that general-purpose CPUs could effectively incorporate hardware acceleration to enhance public-key algorithm processing. The performance assessment indicated that ECC exhibited superior performance compared to RSA. Specifically, for ECC with GF(p) and GF(2m), the researchers noted a speedup of 2.4 times and 4.9 times, respectively, relative to RSA at the current security levels. Moreover, for subsequent security levels, the corresponding speedups were even more substantial—7.8 times and 15.0 times, respectively. Ponomarev et al., (2010) [17] conducted an investigation into the computational demands imposed by handling the control plane of the Host Identity Protocol (HIP) using Rivest-Shamir-Adleman (RSA) encryption in comparison to Elliptic Curve Cryptography (ECC) techniques. This study focused on measuring the processing resources consumed by the cryptographic procedures of the Host Identity Protocol Base Exchange. The findings highlighted that the cryptographic operations involved in the Host Identity Protocol Base Exchange consumed substantial processing resources, and this aspect is quantified in the study. In terms of specific results, the study indicated that, by employing ECC for the Diffie-Hellman exchange, a server could manage new connections ranging from two to three times more efficiently. Moreover, the study highlighted that employing ECC in cryptographic operations significantly enhanced HIP performance for lightweight mobile clients like the Nokia N810 Internet Tablet. This improvement was manifested in a 75-85% reduction in total Base Exchange (BEX) time, emphasizing the faster cryptographic operations enabled by ECC. In this investigation [18], a comparison was conducted between the elliptic curve cryptography (ECC) algorithm utilizing a 160-bit key size and the Rivest-Shamir-Adleman (RSA) technique employing a 1024-bit key size. The results demonstrated that ECC can offer comparable security levels with smaller key sizes when contrasted with more traditional cryptographic systems like RSA. Consequently, the adoption of ECC is strongly recommended to enhance security and efficiency without a proportional increase in computational demands. The research indicated that ECC maintains a lower cost ratio. Moreover, continuous enhancements are necessary for ECC itself to optimize the performance of newly developed chips.

In a study similar to this, the authors referenced in study [5] investigated the encryption and decryption times of various approaches using data packets of different sizes. The comparisons indicated that ECC leads to a significant reduction in transmission expenses. The results underscored that ECC outperforms other asymmetric algorithms in terms of efficiency. This study evaluated the impacts of different ECC curves and RSA key sizes using IoT nodes with limited resources, and it compared the performance of ECDSA and RSA TLS cipher suites. The results indicated that, although ECDSA consistently outperformed RSA in all test runs, practical scenario testing is necessary to determine the suitable security configuration for a given hardware platform. Situations may arise where more secure options, due to software implementations and optimizations, exhibit superior energy efficiency and data throughput, surpassing theoretically lighter and simpler alternatives. The results, influenced by enhancements in the libraries handling ECC operations, specifically showcased that the secp256r1 curve exhibited superior performance compared to the secp224r1 curve, while maintaining a higher level of security [19]. In the study conducted by Kardi et al. in 2018, a performance evaluation is carried out to compare RSA and Elliptic Curve Cryptography in the context of wireless sensor networks. The findings of the research indicated that the decryption time of RSA becomes impractical with large key sizes. Conversely, even when employing very large key sizes, the encryption and decryption processes of ECC algorithms remain manageable. Additionally, ECC signature signing is generally faster than verification, whereas RSA signature signing is more time-consuming. As a result, the study recommended a transition from RSA to elliptic curve cryptography [20]. In a comparable investigation, the researchers delved into the foundational aspects of elliptic curves, their associated arithmetic operations, and the advantages of adopting elliptic curve cryptography over RSA within public cryptosystems. The outcomes of this research highlighted that ECC signature signing processes are usually swifter than verification procedures, while RSA signature signing tends to be more time-consuming. Moreover, the generation of public keys demands significantly more time with the RSA technique compared to ECCs. These findings in the implementation phase provided a compelling rationale for the researchers to advocate for a transition from RSA to elliptic curve cryptography [21]. This study conducted an empirical performance assessment aimed at comparing and quantifying the performance of two encryption schemes: (1) RSA-based BROSMAP and (2) ECC-based BROSMAP, both on the client side (Android) and server-side (XAMPP). In terms of execution time, ECC outperforms RSA significantly, with ECC being nearly twice as fast as RSA 2048 and four times faster than RSA 3072. The primary factors contributing to ECC's superior performance in BROSMAP are its utilization of smaller key sizes and its exclusive reliance on symmetric cryptography for both encryption and decryption processes. Furthermore, the investigation revealed that RSA-based BROSMAP incurs higher computational costs compared to ECC-based BROSMAP. Specifically, ECC demonstrates a computational efficiency that is 561 times greater. As a result of these findings, the researchers strongly recommend the

adoption of ECC-based BROSMAP over RSA-based BROSMAP, especially in systems with limited resources such as IoT devices and agent-based systems that prioritize security. In summary, ECC-based BROSMAP meets all the security requirements of RSA-based BROSMAP while offering greater efficiency and lightweight operation, attributed to its absence of asymmetric encryption, use of reduced key sizes, and utilization of ECC keys in conjunction with symmetric encryption [22]. In their study referenced as [23], the researchers conducted an analysis of the security capabilities of ECC and RSA encryption techniques using three sets of sample input data consisting of 8 bits, 64 bits, and 256 bits, each employing randomly generated keys in accordance with NIST recommendations. Their findings illustrate that ECC surpasses RSA in both operational efficiency and security. Furthermore, their work implies that ECC might be the preferred choice, particularly for devices with limited memory resources such as smartphones and palmtop PCs. In this paper, authors [5] conducted a comprehensive review of key cryptographic algorithms, including ECC, El-Gamal, and RSA, with the goal of facilitating a comparative assessment. Our comparisons clearly indicate a significant reduction in transmission costs when employing ECC. These outcomes underscore the practical advantages of ECC's performance. The survey is undertaken to assess the security aspects of these algorithms, considering their widespread utilization. This research conducted an examination of two frequently employed encryption methods, namely Elliptic Curve Cryptography (ECC) and Rivest-Shamir-Adleman (RSA), with a particular emphasis on their applicability in the context of cloud and fog computing. The investigation involved a comparison of the key size and security capabilities of ECC and RSA algorithms, assessing their suitability for deployment in resource-limited fog computing environments. The findings suggest that ECC is a preferable choice for enhanced security and faster performance, all without imposing undue strain on computing resources. In contrast, RSA, with its established track record of security, remains widely accepted [24]. This paper introduced a novel approach to file encryption, employing a hybrid encryption algorithm that combines AES and RSA. It provides a foundational understanding of the AES and RSA algorithms while conducting a thorough examination of their pros and cons. The encryption techniques of these two algorithms have garnered substantial attention within the scholarly community. Through experimental comparisons, the study concludes that the hybrid encryption algorithm enhances encryption efficiency, bolsters key management, and fortifies data security in the context of file protection [25]. The authors in [26] presented a novel technique that combines features from two different algorithms. The primary goal of this approach is to tackle two significant challenges: managing encryption keys in symmetric encryption algorithms and reducing the substantial power consumption associated with asymmetric encryption algorithms. The research delves into cryptographic algorithms using data gathered from related academic journals and conference papers. The study's outcomes demonstrate that the proposed system has successfully elevated the maximum accuracy requirement, mainly due to its enhanced security level achieved by

employing multiple keys for encryption and decryption. In this paper, a novel and secure data sharing scheme is presented, with a key emphasis on upholding data security and integrity within cloud environments. The proposed system primarily relies on the fusion of Elliptic Curve Cryptography (ECC) and the Advanced Encryption Standard (AES) method to ensure robust authentication and data integrity. Experimental results highlight the efficiency of this approach, demonstrating superior performance when compared to existing methods. In this paper, a novel and secure data sharing scheme is presented, with a key emphasis on upholding data security and integrity within cloud environments. The proposed system primarily relies on the fusion of Elliptic Curve Cryptography (ECC) and the Advanced Encryption Standard (AES) method to ensure robust authentication and data integrity. Experimental results highlight the efficiency of this approach, demonstrating superior performance when compared to existing methods [27]. This paper delves into the capabilities of cryptography for ensuring security in distributed storage. This exploration involves a thorough examination of standard cryptography techniques such as AES, ECC, and RSA. However, due to variations in the performance of these methods, the study addresses the challenge of identifying an encryption technique that strikes a balance between efficiency and security. Some encryption methods can deliver high security but are time-consuming for both encryption and decryption. Conversely, other approaches may offer efficient encryption but suffer from vulnerabilities in terms of security [28]. In reference [29], a two-tier cryptographic approach and a model are introduced to enhance data security in cloud computing. This model leverages both symmetric and asymmetric encryption algorithms, specifically AES and ECC, to bolster data security against unauthorized access, thus promoting privacy, data integrity, and expediting cryptographic operations. This advancement serves to enhance user trust in cloud computing while also accelerating the utilization of smaller ECC keys in the encryption process. In their research presented in reference [30], the authors conducted an examination of Elliptic Curve Cryptography (ECC) as a means to enhance data security within cloud environments, drawing a comparison with the Advanced Encryption Standard (AES) with a specific focus on time efficiency. The review encompasses an evaluation of encryption and decryption durations for data stored in cloud-based systems. This study explores the improvement of data protection with an emphasis on time efficiency through the application of ECC and AES. The analysis was based on a sample size of $N=6$ for both ECC and AES, with a significance level of 80% (determined using the G-power value). It is found that the mean time required for ECC encryption was 0.1683, whereas for AES, it was 0.7517. The calculated significance value for the proposed system was 0.643 ($p>0.05$). The results within the confines of this study clearly indicate that ECC surpasses AES in terms of expeditious data encryption with reduced time consumption. In 2023, Rao and Sujatha introduced a security technique for public cloud systems using Hybrid Elliptic Curve Cryptography (HECC). Their proposed method involves the creation of keys utilizing a lightweight Edwards curve, followed by the utilization of Identity Based Encryption to

modify the generated private keys. Additionally, the study implements a key reduction technique to further shorten the keys, thereby accelerating the Advanced Encryption Standard (AES) encryption process. The exchange of public keys is facilitated through the Diffie-Hellman key exchange. To evaluate the effectiveness of their proposed model, the authors employ metrics such as throughput and the time taken for key generation, encryption, and decryption. The results indicate that their model outperforms existing ones in various aspects. The key creation process in their method requires just 0.000025 seconds, with encryption taking 0.00349 seconds. Furthermore, the achieved throughput reaches 693.10 kB/s [31]. In this paper, the authors have introduced a robust and efficient protocol that incorporates security measures using both a blind factor and the Elliptic Curve Cryptography (ECC) scheme. ECC is preferred over RSA due to its ability to provide superior security with smaller key sizes, resulting in reduced computational overhead. This enhanced security per unit of data offers various benefits, including faster processing, lower power consumption, reduced bandwidth usage, improved storage efficiency, and more compact certificates. These advantages prove especially advantageous in situations with limitations in terms of bandwidth, processing capacity, power availability, or storage space. In order to improve computational efficiency and minimize memory storage requirements, the authors have developed a novel Hybrid Public Key Cryptographic algorithm. The results indicate that the incorporation of Dual-RSA and ECC has significantly improved the algorithm's performance, both in terms of computational cost and memory storage demands [32]. This paper introduced a hybrid cryptography algorithm aimed at ensuring confidentiality and enhancing security for internet communications. The research places particular

emphasis on minimizing the time required for encryption and decryption to avoid excessive CPU utilization. Experimental findings demonstrate that the proposed solution offers a more efficient means of encrypting messages, with only a marginal difference in the algorithm's runtime. This approach effectively enhances security in the open internet environment [33].

III. EXPERIMENTAL SETTING

A local area network (LAN) consisting of a dedicated network server and two client machines were used to carry-out the simulation. Fig. 1 shows the diagram of the simulation setup.

The testing environment, which included standard email clients and server, featured laptops with Intel i7 processors, 16GB RAM, and solid-state drives. The server was equipped with the following specifications - OS: Ubuntu, CPU: Intel Xeon, Cores: 4 core, 2.4 GHz, Architecture: 64-bit, and RAM: 8 GB DDR4 - represent typical end-user systems in corporate or personal contexts. To commence, email server Exim and clients Mozilla Thunderbird are configured to support RSA, ECC and hybrid encryption. Public and private keys are generated for RSA, typically 2048 bits, and ECC, using the widely adopted SECP224R1 curve for each user. Key exchange occurred during the initial email contact, and keys were securely stored. The experiment is conducted five times and the mean values for each metric were recorded. A series of practical tests are conducted, involving the sending of emails of varying sizes, from small text-based messages to larger attachments. Throughout the tests, measurements are taken for encryption and decryption times, key exchange time, signature generation, and verification times.

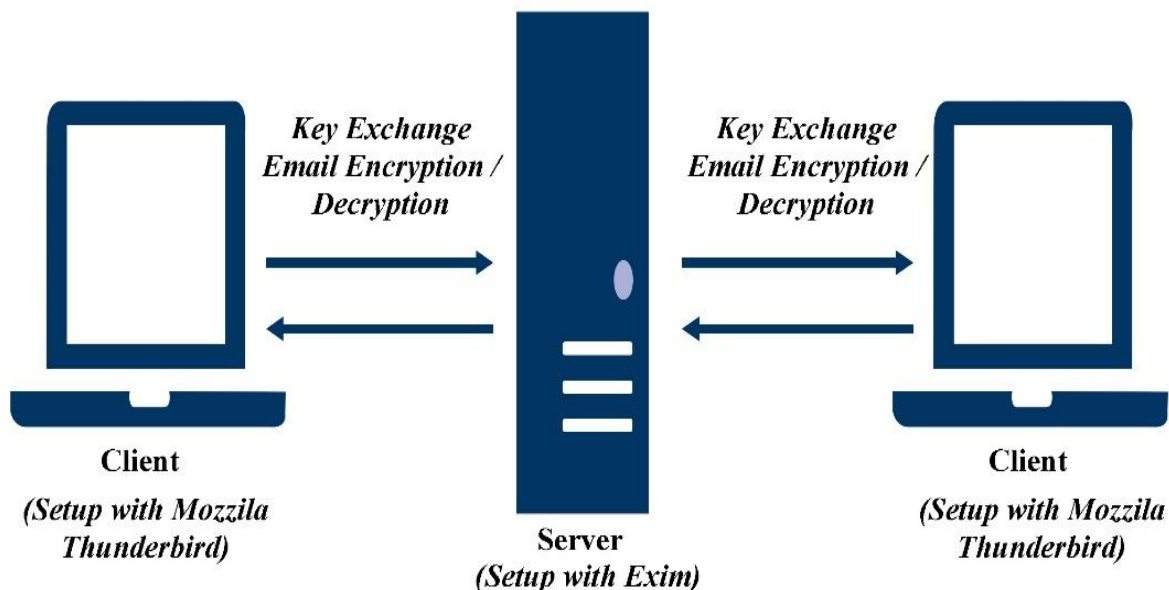


Fig. 1. Simulation setup.

IV. RSA-ECC HYBRID TECHNIQUE

The proposed hybrid technique merges the robust aspects of both RSA and ECC, creating a cooperative strategy that not only strengthens the security of email communication but also streamlines its efficiency. RSA and ECC stand as widely embraced encryption methods for safeguarding email exchanges. RSA, a traditional approach, provides formidable security but can be computationally demanding, particularly when managing large files. Conversely, ECC excels in terms of encryption and decryption speed, making it an ideal choice for resource-constrained environments. The suggested hybrid method presents an inventive solution to the enduring challenge of striking a balance between security and performance in secure email communication. By harnessing the strengths of RSA and ECC, this hybrid technique provides an adaptable solution that can be tailored to meet specific email communication needs. Fig. 2 provides a visual representation of the proposed fusion of RSA and ECC algorithms. This visual representation provides a clear and intuitive understanding of the sequential data transformations performed within the algorithm. For a more in-depth exploration of the inner workings of this proposed algorithm, Algorithms 1 and 2 offer a comprehensive breakdown of its structure. These algorithmic descriptions present a step-by-step elucidation of the specific operations and procedures involved at each stage of the algorithms.

Algorithm 1: Sender-side Operations

Input: ECC key pair, RSA public key, plain text email

Output: Encrypted email, Digital Signature

Step 1: Generate sender's ECC Private Key as S^a and Public Key as S^b

Step 2: Request recipient's RSA public key from the server as R^b

Step 3: Derive shared secret using sender's ECC private key and recipient's RSA public key. $S = D(S^a, R^b)$

Step 4: Generate a symmetric key (A^s) for encrypting the email message.

Step 5: Compose the email message.

Step 6: Encrypt the email message using the symmetric key. Ciphertext, $C^t = E(PT, A^s)$

Step 7: Encrypt the symmetric key using recipient's RSA public key. $C^{As} = E(A^s, R^b)$

Step 8: Generate a digital signature for the email message. $Ds = Gs(S^a, PT)$

Step 9: Send the secure email to the recipient

In Algorithm 1, the sender initiates secure email transmission by generating ECC Private and Public Keys (S^a and S^b). The recipient's RSA public key (R^b) is acquired, and a shared secret is derived through S^a and R^b . A symmetric key (A^s) is created for encrypting the email message using AES, ensuring confidentiality. The composed email message is encrypted with A^s , yielding ciphertext (C^t). For added security, A^s is encrypted with R^b , resulting in the encrypted symmetric key (C^{As}), safeguarding its transmission. To ensure

data integrity and authentication, a digital signature (Ds) is generated using S^a and the plain text email (PT). The secure email, comprising C^t , C^{As} , and Ds , is then transmitted to the recipient. This algorithm thus combines ECC and RSA functionalities to achieve a comprehensive security framework, encompassing symmetric and asymmetric encryption, as well as digital signatures for secure email communication.

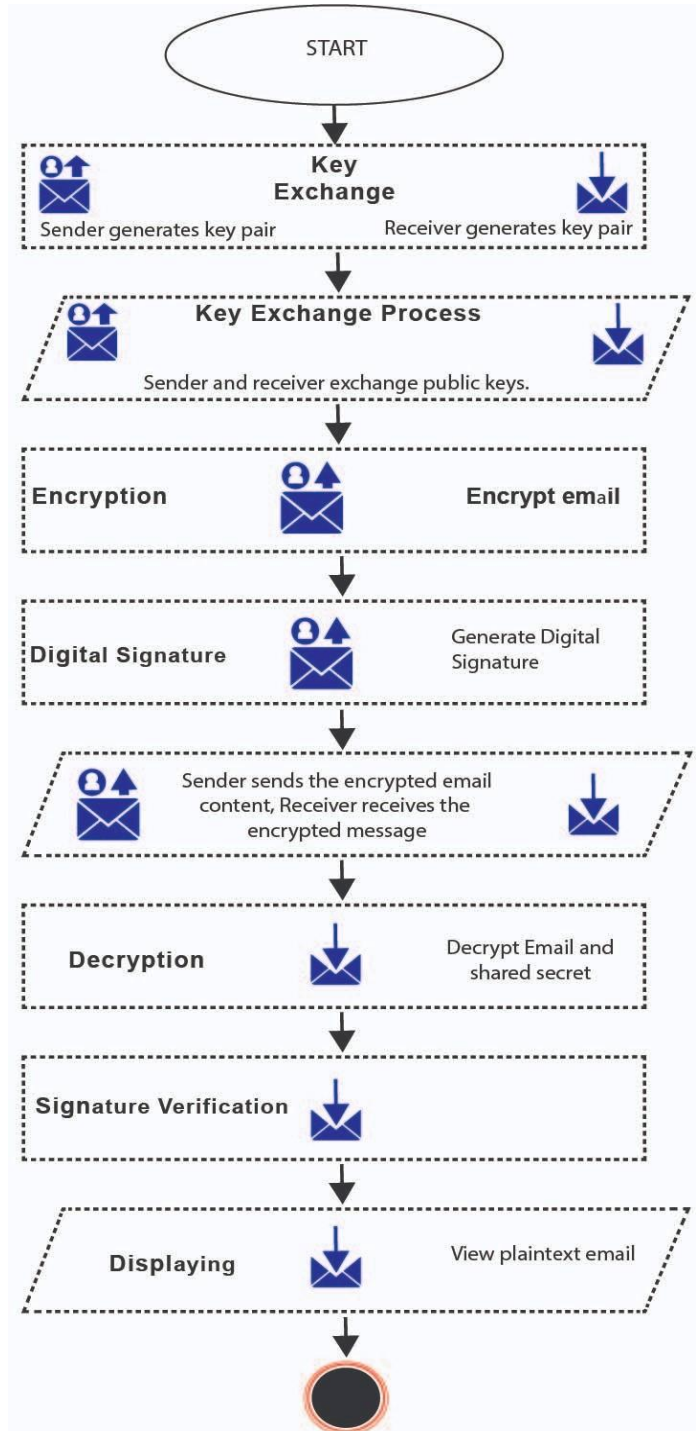


Fig. 2. Proposed model flow graph with hybrid ECC, RSA and AES.

| Algorithm 2: Recipient-side Operations |
|---|
| Input: RSA key pair, ECC Key pair, Encrypted Email Output: RSA Public Key, Decrypted email |
| Step 1: Generate recipient's RSA and ECC key pairs. RSA Private, Public (R^a , R^b) & ECC Private, Public (S^a , S^b) |
| Step 2: Export recipient's RSA public key for the sender |
| Step 3: Receive the encrypted symmetric key from the sender. |
| Step 4: Decrypt the symmetric key using recipient's RSA private key. $A^s = D(C^{As}, R^a)$ |
| Step 5: Receive the encrypted email message. |
| Step 6: Verify the sender's ECC public key. |
| Step 7: Receive and verify the digital signature. |
| Step 8: Decrypt the email message using the symmetric key. $PT = D(C^t, A^s)$ |
| Step 9: View the decrypted email |

In Algorithm 2, the recipient begins by generating RSA and ECC key pairs (R^a , R^b) and (S^a , S^b) respectively. The recipient's RSA public key (R^b) is exported for the sender's use. Upon receiving the sender's secure email, the recipient obtains the encrypted symmetric key (C^{As}) and decrypts it using their RSA private key, resulting in the symmetric key (A^s). The recipient then receives the encrypted email message (C^t) and proceeds to verify the sender's ECC public key. Subsequently, the digital signature is received and verified for authenticity and data integrity. Using the decrypted symmetric key (A^s), the email message is decrypted, yielding the plaintext email (PT).

V. PERFORMANCE EVALUATION

The performance analysis is divided into two distinct approaches: analyzing the individual performance of RSA and ECC for secure email communication and assessing the performance of the hybrid approach for secure email communication.

A. Approach 1

1) *Key Exchange Times measured in seconds:* The key exchange time for RSA and ECC encryption methods in the context of secure email communication were assessed within the established testing environment. To measure key exchange times accurately, secure email communications were initiated, capturing the duration it took for public keys to be exchanged between sender and recipient during the initial email contact. This process was repeated 5 times for each test and the mean values were recorded. The recorded data for Key Exchange Time (KET) of RSA and ECC from the Secure Email Communication Test is as shown in the Table I. Fig. 3 illustrates the analysis of key exchange times for ECC and RSA encryption methods, represented in seconds.

2) *Encryption and decryption times in seconds:* Email encryption and decryption took place within the established test environment, consistent with the previously outlined specifications. Standardized email clients and servers were

configured to support both RSA and ECC encryption methods. To assess these operations, a range of email messages, encompassing diverse sizes from text-based content to substantial attachments are employed as test data. The system was configured to autonomously record the encryption and decryption times for each email, ensuring an impartial and objective measurement of efficiency and practicality. This methodology facilitated a thorough analysis of email encryption and decryption processes using RSA and ECC techniques within the secure email communication system. This study further used the hybrid encryption setup; the asymmetric encryption algorithms (RSA or ECC) facilitate secure key exchange, while the symmetric encryption algorithm (AES) ensures efficient and high-speed encryption and decryption of the email content. This combination strikes a balance between security and performance, making it a practical choice for secure email communication.

TABLE I. KEY EXCHANGE TIMES OF RSA AND ECC

| TEST | KET RSA (seconds) | KET ECC (seconds) |
|------|-------------------|-------------------|
| 1 | 0.172268 | 0.101002 |
| 2 | 0.164218 | 0.102000 |
| 3 | 0.179985 | 0.091002 |
| 4 | 0.177888 | 0.102220 |
| 5 | 0.164782 | 0.091001 |

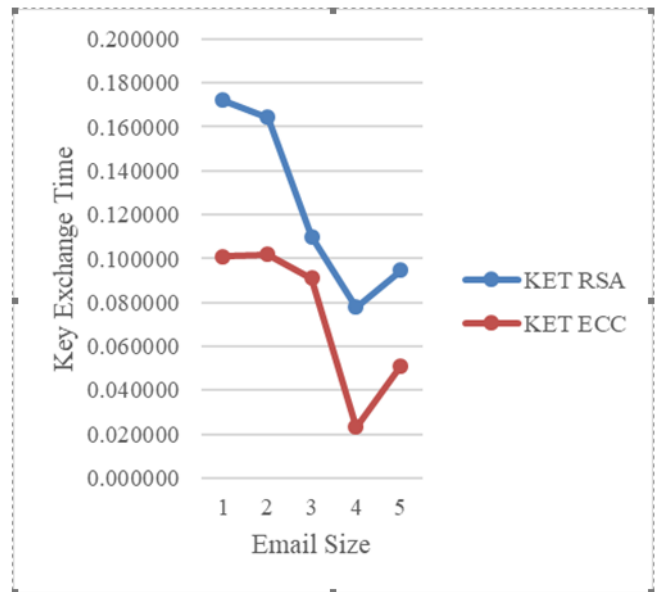


Fig. 3. Key exchange analysis of ECC and RSA (in seconds).

TABLE II. ENCRYPTION TIME

| Sizes (MB) | Encryption Time RSA (seconds) | Encryption Time ECC (seconds) |
|------------|-------------------------------|-------------------------------|
| 10 | 0.024308 | 0.028219 |
| 50 | 0.106565 | 0.094268 |
| 100 | 0.235220 | 0.173252 |
| 200 | 0.481745 | 0.375365 |
| 500 | 0.938921 | 0.866455 |

TABLE III. DECRYPTION TIME

| Sizes (MB) | Decryption Time RSA (seconds) | Decryption Time ECC (seconds) |
|------------|-------------------------------|-------------------------------|
| 10 | 0.018158 | 0.016994 |
| 50 | 0.092173 | 0.068401 |
| 100 | 0.146187 | 0.153054 |
| 200 | 0.311700 | 0.308217 |
| 500 | 0.707802 | 0.753799 |

Fig. 4 and Fig. 5 depict the encryption and decryption times for RSA and ECC encryption methods, respectively, measured in seconds.

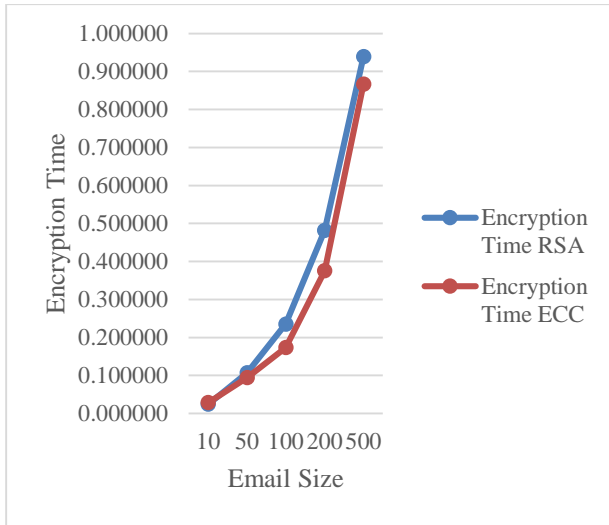


Fig. 4. RSA and ECC encryption time (in seconds).

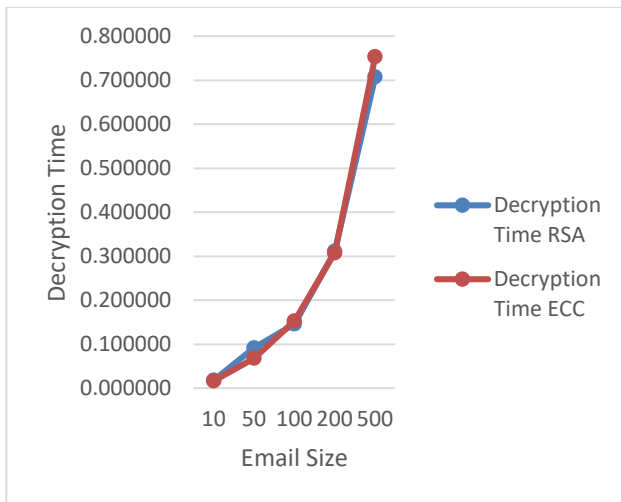


Fig. 5. RSA and ECC decryption time (in seconds).

3) *Signature generation and verification*: Signature generation and verification were integral aspects of the evaluation within the designated test environment, adhering to the established system specifications. By configuring standard

email clients and servers to support both RSA and ECC encryption methods, the framework facilitated the generation of digital signatures for email messages. These signatures were generated autonomously during the test, and the system reported the time taken in seconds for each signature. Subsequently, the verification of these digital signatures occurred seamlessly within the same environment. A comprehensive analysis of signature generation and verification processes using RSA and ECC encryption methods was thus conducted objectively, with the system providing precise timing data for each operation.

Fig. 6 and Fig. 7 illustrate the signature generation and verification times for ECC and RSA encryption methods, respectively, measured in seconds.

TABLE IV. SIGNATURE GENERATION TIME

| Sizes (MB) | SGT RSA (seconds) | SGT ECC (seconds) |
|------------|-------------------|-------------------|
| 10 | 0.030329 | 0.064428 |
| 50 | 0.127694 | 0.173007 |
| 100 | 0.278920 | 0.242878 |
| 200 | 0.451833 | 0.436492 |
| 500 | 1.239319 | 1.093490 |

TABLE V. SIGNATURE VERIFICATION TIME

| Sizes (MB) | SVT RSA (seconds) | SVT ECC (seconds) |
|------------|-------------------|-------------------|
| 10 | 0.028464 | 0.030986 |
| 50 | 0.146251 | 0.144860 |
| 100 | 0.274981 | 0.236938 |
| 200 | 0.535547 | 0.544687 |
| 500 | 1.236818 | 1.253438 |

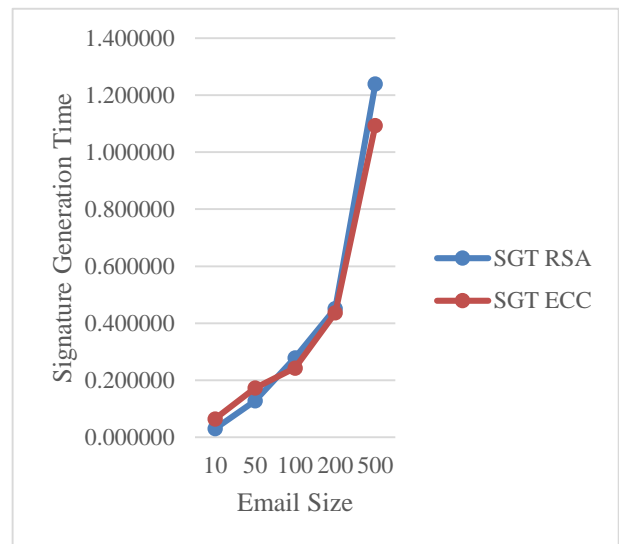


Fig. 6. Signature generation of ECC and RSA (in seconds).

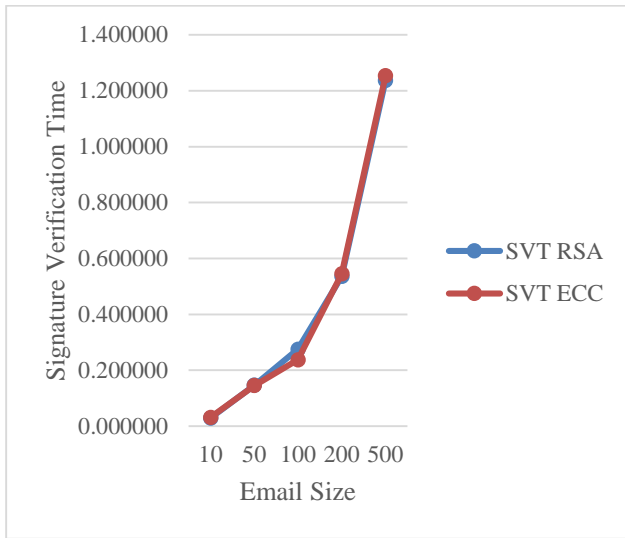


Fig. 7. Signature verification of ECC and RSA (in seconds).

B. Approach 2

1) *Key exchange times measured in seconds:* The key exchange time for the hybrid of RSA and ECC encryption methods were assessed within the established testing environment. To measure key exchange times accurately, secure email communications were initiated, capturing the duration it took the keys to be exchanged between sender and recipient during the initial email contact. This process was repeated five times for each test, and the mean values are recorded in Table VI.

TABLE VI. KEY EXCHANGE TIMES FOR HYBRID TECHNIQUE

| TEST | KET (seconds) |
|------|---------------|
| 1 | 0.064191 |
| 2 | 0.112602 |
| 3 | 0.070835 |
| 4 | 0.068739 |
| 5 | 0.067263 |

2) *Encryption, decryption, signature generation and verification times in seconds:* Table VII displays the encryption, decryption, signature generation, and verification performance metrics for the hybrid technique. To evaluate these operations, a variety of email messages with different sizes, ranging from text-based content to sizable attachments, were utilized as test data. The system was set up to automatically capture the times taken for encryption, decryption, signature generation, and verification for each email. For each experiment, this procedure was carried out five times, and the mean values were obtained.

TABLE VII. HYBRID TECHNIQUE (RSA AND ECC)

| Sizes (MB) | EncryptionTime | Decryption Time | Signature Generation Time | Signature Verification Time |
|------------|----------------|-----------------|---------------------------|-----------------------------|
| 10 | 0.020769 | 0.014005 | 0.026106 | 0.026000 |
| 50 | 0.091153 | 0.062974 | 0.130278 | 0.120312 |
| 100 | 0.156722 | 0.140040 | 0.238006 | 0.262419 |
| 200 | 0.327086 | 0.307289 | 0.430858 | 0.423738 |
| 500 | 0.832917 | 0.636395 | 1.073605 | 1.160965 |

VI. DISCUSSION OF RESULTS

Table I presents the collected data concerning the Key Exchange Time (KET) for RSA and ECC in the context of secure email communication. The results consistently indicate that ECC outperforms RSA in terms of key exchange efficiency across all the tested scenarios. In practical terms, it implies that the process of establishing secure communication channels through key exchange is notably swifter and more efficient when utilizing ECC as the cryptographic algorithm, as opposed to RSA.

Table II reports the Encryption Time (in seconds) for both RSA and ECC in the same context. It illustrates the time taken to encrypt emails with various file sizes, ranging from 10 MB to 500 MB. The results demonstrate interesting trends in the performance of these cryptographic algorithms during the encryption process.

For smaller file sizes (10 MB and 50 MB), RSA exhibits slightly shorter encryption times compared to ECC. However, as the file sizes increase to 100 MB, 200 MB, and 500 MB, ECC consistently demonstrates superior efficiency in encryption. ECC's encryption times remain notably lower than RSA's for all these larger file sizes, suggesting that ECC is particularly well-suited for securing and transmitting larger email attachments. This outcome highlights ECC's efficiency in handling data encryption tasks for secure email communication, particularly when dealing with substantial file sizes. While RSA performs reasonably well for smaller files, ECC emerges as a more efficient choice as the data to be encrypted grows in size.

Just as Encryption Time from Table II, Decryption Time (in seconds) for both RSA and ECC in Table III provides insights into the time required to decrypt emails with various file sizes, ranging from 10 MB to 500 MB. The results reveal several noteworthy observations. For smaller file sizes (10 MB and 50 MB), ECC demonstrates slightly shorter decryption times compared to RSA, indicating its efficiency in handling smaller data. However, as the file sizes increase to 100 MB, 200 MB, and 500 MB, RSA exhibits competitive or slightly shorter decryption times than ECC. This suggests that RSA can be advantageous for decrypting larger email attachments efficiently.

Data presented in Table IV shows results for the Signature Generation Time (in seconds) for both RSA and ECC. The results reveal that for smaller file sizes (10 MB and 50 MB), RSA demonstrates notably shorter signature generation times compared to ECC, showcasing its efficiency in handling small data for signature creation. However, as file sizes increase to 100 MB, 200 MB, and 500 MB, ECC gradually catches up and, in some cases, surpasses RSA in terms of signature generation efficiency. This suggests that ECC is better suited for efficiently generating signatures for larger email attachments.

Table V provides insights into the time required to verify digital signatures for emails with same attached files as stated earlier. The results demonstrate interesting patterns in signature verification efficiency. For smaller file sizes (10 MB and 50 MB), ECC exhibits slightly longer verification times compared to RSA. However, as file sizes increase to 100 MB, 200 MB, and 500 MB, ECC's verification time becomes comparable to or slightly shorter than RSA's. This indicates that ECC is competitive with RSA in terms of signature verification efficiency, particularly for larger email attachments. The signature verification time findings suggest that ECC is a viable choice for verifying digital signatures, especially for larger data sizes. While RSA may have a slight advantage for smaller files, the efficiency of ECC becomes evident as the data size increases. The selection between RSA and ECC for signature verification should consider the typical email attachment sizes used in practice to optimize performance and efficiency.

Comparing Table I to Table VI, the hybrid technique demonstrates better key exchange time (KET) compared to solo RSA and ECC implementation. This indicates that the process of establishing secure communication channels through key exchange is notably swifter and more efficient when utilizing the proposed hybrid algorithm as opposed to RSA and ECC. Finally, Table VII presents the time (in seconds) recorded for encryption, decryption, signature generation, and signature verification in the context of secure email communication using the hybrid algorithm. When conducting a comparison with Tables II to V, it becomes evident that, on average, the hybrid encryption algorithm enhances the efficiency of encryption and decryption times, as well as signature generation and verification times. In certain instances, the individual ECC times displayed slightly better performance compared to the hybrid algorithm, indicating a close correlation between ECC and the hybrid approach. In summary, the proposed Hybrid technique excels in providing a versatile and efficient encryption solution for secure email communication across a wide range of email message sizes.

VII. CONCLUSION

Information technology services, like email systems, offer efficient solutions that are accessible to users regardless of their technical proficiency. These systems enable data storage, management, and local or internet-based access. However, the convenience of email usage also brings about a range of security vulnerabilities, encompassing unauthorized access, eavesdropping, identity impersonation, interception, and data tampering. This paper provides an analysis of key

cryptographic algorithms, namely RSA, ECC and the hybrid algorithm in the context of securing email communications. The study reveals that ECC excels in terms of key exchange efficiency and effectively manages larger email attachments, making it an attractive choice for enhancing the security of modern email systems. While RSA performs adequately for smaller data sizes, ECC consistently outperforms it as data sizes increase, positioning it as a more efficient cryptographic algorithm for securing email communication. The experimental outcomes indicate that the suggested hybrid solution offers a more efficient method for encrypting email messages, with only a minimal disparity in runtime when compared to the ECC algorithm. Furthermore, this solution ensures a high level of security for secure email communication.

These findings offer valuable insights for practical optimization of email security. The hybrid algorithm introduced in this paper shows promise for being applied in system design, software development, and various other domains, offering an effective means of protecting data. In the future, this research can be further developed by enhancing the security of the hybrid approach. The integration of multiple security layers offers the potential to improve the system's productivity and efficiency.

ACKNOWLEDGMENT

Our gratitude to all the people and groups who helped to complete this study piece. Our gratitude is also expressed to the research team and our colleagues, who helped us out by sharing their skills, information, and encouragement. They played a critical role in carrying out the studies and collecting the results.

REFERENCES

- [1] Z. Kasiran, A. Dalil, and M. Z. Ghazali, "Analysis on Computational Time of Hybrid Cryptography in Email System," *J. Posit. Sch. Psychol.*, vol. 2022, no. 3, pp. 8415–8422, 2022, [Online]. Available: <http://journalppw.com>.
- [2] Z. Alkhalil, C. Hewage, L. Nawaf, and I. Khan, "Phishing Attacks: A Recent Comprehensive Study and a New Anatomy," *Front. Comput. Sci.*, vol. 3, no. March, pp. 1–23, 2021, doi: 10.3389/fcomp.2021.563060.
- [3] Ö. Aslan, S. S. Aktuğ, M. Ozkan-Okay, A. A. Yilmaz, and E. Akin, "A Comprehensive Review of Cyber Security Vulnerabilities, Threats, Attacks, and Solutions," *Electron.*, vol. 12, no. 6, 2023, doi: 10.3390/electronics12061333.
- [4] G. B. Thompson, "Journal of information Science," *J. Inf. Sci.*, vol. 9, no. 2, p. 74, 1984, doi: 10.1177/016555158400900204.
- [5] F. Mallouli, A. Hellal, N. Sharief Saeed, and F. Abdulraheem Alzahrani, "A Survey on Cryptography: Comparative Study between RSA vs ECC Algorithms, and RSA vs El-Gamal Algorithms," *Proc. - 6th IEEE Int. Conf. Cyber Secur. Cloud Comput. CSCloud 2019 5th IEEE Int. Conf. Edge Comput. Scalable Cloud. EdgeCom 2019*, pp. 173–176, 2019, doi: 10.1109/CSCloud/EdgeCom.2019.00022.
- [6] A. Karki, "A Comparative Analysis of Public Key Cryptography," *Int. J. Mod. Comput. Sci.*, vol. 4, no. 6, pp. 2320–7868, 2016, [Online]. Available: <http://www.iusikkim.edu.in/IJMCS161213.pdf>.
- [7] R. M. Abobeah, M. M. Ezz, and H. M. Harb, "Public-Key Cryptography Techniques Evaluation," *Int. J. Comput. Networks Appl.*, vol. 2, no. 2, pp. 64–75, 2015.
- [8] M. Boussif, "Scalable Implementation of Array of 8-bit-Based RSA With Large Key Size," *Proc. 2022 5th Int. Conf. Adv. Syst. Emergent*

- Technol. IC_ASET 2022, pp. 375–380, 2022, doi: 10.1109/IC_ASET53395.2022.9765873.
- [9] D. Mahto and D. K. Yadav, “RSA and ECC, A Comparative Analysis.pdf,” *Int. J. Appl. Eng. Res.*, vol. 12, no. 19, pp. 9053–9061, 2017.
- [10] M. Bansal, S. Gupta, and S. Mathur, “Comparison of ECC and RSA Algorithm with DNA Encoding for IoT Security,” *Proc. 6th Int. Conf. Inven. Comput. Technol. ICICT 2021*, pp. 1340–1343, 2021, doi: 10.1109/ICICT50816.2021.9358591.
- [11] V. O. Nyangaresi, A. J. Rodrigues, and S. O. Abeka, “Secure Algorithm for IoT Devices Authentication,” *EAI/Springer Innov. Commun. Comput.*, no. January, pp. 1–22, 2023, doi: 10.1007/978-3-030-92968-8_1.
- [12] S. Ahmed and T. Ahmed, “Comparative Analysis of Cryptographic Algorithms in Context of Communication: A Systematic Review,” *Int. J. Sci. Res. Publ.*, vol. 12, no. 7, pp. 161–173, 2022, doi: 10.29322/ijrsp.12.07.2022.p12720.
- [13] P. Kaur and S. Aggarwal, “Cryptographic algorithms in IoT - a detailed analysis,” *Proc. - 2021 2nd Int. Conf. Comput. Methods Sci. Technol. ICCMST 2021*, pp. 45–50, 2021, doi: 10.1109/ICCMST54943.2021.00021.
- [14] S. Al Busafi and B. Kumar, “Review and analysis of cryptography techniques,” *Proc. 2020 9th Int. Conf. Syst. Model. Adv. Res. Trends, SMART 2020*, pp. 323–327, 2020, doi: 10.1109/SMART50582.2020.9336792.
- [15] C. Varma, “A Study of the ECC, RSA and the Diffie-Hellman Algorithms in Network Security,” *Proc. 2018 Int. Conf. Curr. Trends Towar. Converging Technol. ICCTCT 2018*, pp. 18–21, 2018, doi: 10.1109/ICCTCT.2018.8551161.
- [16] H. Eberle, N. Gura, S. C. Shantz, V. Gupta, L. Rarick, and S. Sundaram, “A public-key cryptographic processor for RSA and ECC,” *Proc. Int. Conf. Appl. Syst. Archit. Process.*, pp. 98–110, 2004, doi: 10.1109/ASAP.2004.1342462.
- [17] O. Ponomarev, A. Khurri, and A. Gurtov, “Elliptic Curve Cryptography (ECC) for Host Identity Protocol (HIP),” *9th Int. Conf. Networks, ICN 2010*, pp. 215–219, 2010, doi: 10.1109/ICN.2010.68.
- [18] M. Bafandehkar, S. M. Yasin, R. Mahmood, and Z. M. Hanapi, “Comparison of ECC and RSA algorithm in resource constrained devices,” *2013 Int. Conf. IT Converg. Secur. ICITCS 2013*, pp. 9–11, 2013, doi: 10.1109/ICITCS.2013.6717816.
- [19] M. Suarez-Albela, T. M. Fernandez-Carames, P. Fraga-Lamas, and L. Castedo, “A practical performance comparison of ECC and RSA for resource-constrained IoT devices,” *2018 Glob. Internet Things Summit, GIOTS 2018*, pp. 0–5, 2018, doi: 10.1109/GIOTS.2018.8534575.
- [20] A. Kardi, R. Zagrouba, and M. Alqahtani, “Performance Evaluation of RSA and Elliptic Curve Cryptography in Wireless Sensor Networks,” *21st Saudi Comput. Soc. Natl. Comput. Conf. NCC 2018*, vol. 65537, pp. 302–306, 2018, doi: 10.1109/NGC.2018.8592963.
- [21] S. R. Singh, A. K. Khan, and T. S. Singh, “A critical review on Elliptic Curve Cryptography,” *Int. Conf. Autom. Control Dyn. Optim. Tech. ICACDOT 2016*, vol. 3, no. 7, pp. 13–18, 2017, doi: 10.1109/ICACDOT.2016.7877543.
- [22] H. Hasan et al., “Secure lightweight ECC-based protocol for multi-agent IoT systems,” *Int. Conf. Wirel. Mob. Comput. Netw. Commun.*, vol. 2017-October, 2017, doi: 10.1109/WiMOB.2017.8115788.
- [23] D. Mahto, D. A. Khan, and D. K. Yadav, “Security analysis of elliptic Curve cryptography and RSA,” *Lect. Notes Eng. Comput. Sci.*, vol. 2223, pp. 419–422, 2016.
- [24] D. Patel, B. Patel, J. Vasa, and M. Patel, “A Comparison of the Key Size and Security Level of the ECC and RSA Algorithms with a Focus on Cloud / Fog,” *Springer Nature Singapore*, 2023, doi: 10.1007/978-981-99-3758-5.
- [25] L. Zou, M. Ni, Y. Huang, W. Shi, and X. Li, “Hybrid Encryption Algorithm Based on AES and RSA in File Encryption,” *551 LNEE. Springer Singapore*, 2020, doi: 10.1007/978-981-15-3250-4_68.
- [26] S. Sa’idu, P. Taneja, and K. Shreya, “A Comparative Analysis of Cryptographic Algorithms: AES & RSA and Hybrid Algorithm for Encryption and Decryption,” *Int. J. Innov. Sci. Res. Technol.*, vol. 7, no. 8, pp. 1725–1732, 2022.
- [27] S. Rehman, N. Talat Bajwa, M. A. Shah, A. O. Aseeri, and A. Anjum, “Hybrid aes-ecc model for the security of data over cloud storage,” *Electron.*, vol. 10, no. 21, pp. 1–20, 2021, doi: 10.3390/electronics10212673.
- [28] Y. Al-Dhuraibi, F. Paraiso, N. Djarallah, and P. Merle, “Elasticity in Cloud Computing: State of the Art and Research Challenges,” *IEEE Trans. Serv. Comput.*, vol. 11, no. 2, pp. 430–447, 2018, doi: 10.1109/TSC.2017.2711009.
- [29] D. Kodzo, M. Hodowu, D. R. Korda, and E. Danso Ansong, “An Enhancement of Data Security in Cloud Computing with an Implementation of a Two-Level Cryptographic Technique, using AES and ECC Algorithm,” *Int. J. Eng. Res. Technol.*, vol. 9, no. March 2021, pp. 2278–0181, 2020, [Online]. Available: <http://www.ijert.org>
- [30] M. Sivajyothi and T. Devi, “Analysis of Elliptic Curve Cryptography with AES for Protecting Data in Cloud with improved Time efficiency,” *Proc. 2nd Int. Conf. Innov. Pract. Technol. Manag. ICIPTM 2022*, no. Bhosle 2013, pp. 573–577, 2022, doi: 10.1109/ICIPTM54933.2022.9753926.
- [31] B. Ranganatha Rao and B. Sujatha, “A hybrid elliptic curve cryptography (HECC) technique for fast encryption of data for public cloud security,” *Meas. Sensors*, vol. 29, no. June, p. 100870, 2023, doi: 10.1016/j.measen.2023.100870.
- [32] M. J. Dubai, T. R. Mahesh, and P. A. Ghosh, “Design of new security algorithm: Using hybrid Cryptography architecture,” *ICECT 2011 - 2011 3rd Int. Conf. Electron. Comput. Technol.*, vol. 5, pp. 99–101, 2011, doi: 10.1109/ICECTECH.2011.5941965.
- [33] S. K. Ghosh, S. Rana, A. Pansari, J. Hazra, and S. Biswas, “Hybrid Cryptography Algorithm for Secure and Low Cost Communication,” *2020 Int. Conf. Comput. Sci. Eng. Appl. ICCSEA 2020*, pp. 4–8, 2020, doi: 10.1109/ICCSEA49143.2020.9132862.

Federated Machine Learning for Epileptic Seizure Detection using EEG

S. Vasanthadev Suryakala^{1*}, T. R. Sree Vidya², S. Hari Ramakrishnans³

Department of Electronics and Communication Engineering, College of Engineering and Technology,
SRM Institute of Science and Technology, Kattankulathur, Chennai, India¹

Department of Electronics and Communication Engineering, Tagore Engineering College, Chennai, India²

Department of Electronics and Communication Engineering, Tagore Engineering College, Chennai, India³

Abstract—Early seizure detection is difficult with epilepsy. This use of Electroencephalography (EEG) data has proven transformational, however standard centralized machine learning algorithms have privacy and generalization issues. A decentralized approach to epileptic seizure detection using Federated Machine Learning (FML) is presented in this research. The concentration of critical EEG data in conventional models may compromise patient confidentiality. The proposed FML technique trains models using local datasets without sharing raw EEG recordings. Hence the data set used for the model is devoid of noise thus rendering preprocessing unnecessary. Training using decentralized data sources broadens the model's seizure pattern repertoire, improving its adaptability to case heterogeneity. The Federated Machine Learning (FML) model shows that the suggested method for EEG-based epileptic seizure identification is promising for healthcare implementation and deployment. The proposed approach obtains sensitivity, specificity, and accuracy of 98.24%, 99.23%, 99% respectively. The proposed study is validated with the existing literature and the developed model outperforms the existing study.

Keywords—Federal Machine Learning (FML); electroencephalography; epileptic seizure; cross-decentralization; health care; sensitivity

I. INTRODUCTION

A neurological condition that affects a large number of people, epilepsy, is inextricably intertwined with the complications of seizure detection that are both timely and exact. There is little doubt that the paradigm shifts that have occurred toward the utilization of electroencephalography (EEG) data have been transformational. However, typical centralized machine learning models, which are the mainstays of analysis, struggle with severe hurdles. These issues generally revolve around the delicate balancing act of privacy concerns and restricted generalization. The purpose of this study is to examine the undiscovered territories of Federated Machine Learning (FML) as a potential source of hope in the context of epileptic seizure detection. This paper will begin on an adventure into new terrain. The most important thing is to choose a decentralized strategy, which is a way to gracefully avoid the obstacles that are encountered by standard techniques.

To solve these obstacles and enhance the identification and monitoring of epilepsy, research has been carried out. A study that was conducted by Fisher and colleagues and titled "A

practical clinical definition of epilepsy" (Epilepsia, 2014) highlights the need to have a definition of epilepsy that is both patient-oriented and practical to improve diagnosis and make it easier to do research in this area. The research covers the difficulties associated with identifying epilepsy as well as the significance of considering the impact that it has on the lives of sufferers. In addition, a review paper titled "Epilepsy: Comorbidities and Quality of Life" (Epilepsy Research, 2016) was written by Jette and her colleagues. This study investigates the many comorbidities that are linked with epilepsy and the influence that these comorbidities have on the quality of life of those who have the disorder. An emphasis is placed throughout the essay on the significance of comprehensive treatment that extends beyond the control of seizures.

As a tool that has shed light on the complex interplay of electrical activity in the human brain, electroencephalography (EEG) has become an indispensable tool in the field of neuroscience. A non-invasive and crucial instrument, it records neural signals in real time, allowing for the identification and characterization of different brain processes, such as seizures in epileptics.

Central to electroencephalogram (EEG) technology is the measurement of electrical potentials caused by the coordinated firing of brain cells. Electrodes placed on the scalp measure and record voltage changes that are the outcome of postsynaptic potential summation, allowing this to be accomplished. The unique waveforms captured by these recordings represent various brain states.

Because it can record and describe patterns associated with seizures, EEG is very helpful in the setting of epilepsy. Electroencephalogram (EEG) characteristics are unique to seizures because of the abrupt and aberrant synchronization of neuronal firing that occurs during these episodes. Neurologists rely on these signatures—which include spikes, sharp waves, and rhythmic discharges—to make precise diagnoses and formulate effective treatment plans.

An electroencephalogram (EEG) is a crucial diagnostic and monitoring tool for epilepsy. It is a fundamental tool in neurology because it can record the ever-changing electrical landscape of the brain in real-time, detect patterns associated with seizures, and give important information for treatment choices. With the integration of EEG and new methods like Federated Machine Learning, epileptic seizure detection might become much more efficient and accurate, all while protecting

the privacy of patient's personal information, thanks to the rapid advancements in technology.

Management of sensitive medical data is difficult, especially when using machine learning for diagnosis and prediction. Traditional methods gather and store data in a single repository. These techniques have considerable drawbacks, especially in patient privacy and data security. Centralized Approach Limitations: 1) Privacy Issues: Centralized models aggregate massive volumes of sensitive medical data from several sources. 2) Data Security Risks: Malicious attackers target centralized repositories. A security breach in such a store might jeopardize a massive amount of sensitive patient data. 3) Regulatory Compliance Challenges: HIPAA and GDPR are strict data protection laws in the healthcare business. Centralized methods must traverse complicated regulatory frameworks, increasing administrative costs and legal penalties for noncompliance.

Distributed and federated machine learning models address centralized method concerns. Distributed machine learning models provide advantages over the difficult centralized technique. 1) Protecting Patient Privacy: Federated Learning (FL) allows model training on dispersed devices without exchanging raw data [1]. This keeps critical patient data on local servers, lowering the danger of privacy breaches from centralized techniques. 2) Improving Data Security: FL localizes data to reduce large-scale data breaches [2]. Devices exchange just model updates, frequently encrypted parameters, decreasing the attack surface and improving data security. 3) Compliance with Regulations: Decentralized models meet legal requirements by keeping data safe and making it easier to follow data security rules [3]. FL is designed so that groups can work together on machine-learning projects while still following the complicated rules that govern healthcare.

Using compression methods for model changes before sending them can cut down on communication costs by a large amount. Some methods, like quantization (which represents model parameters with fewer bits) and scarification (which sends only important parameter changes), can help with bandwidth problems. New compression methods and improvement strategies designed for FML situations are still being studied [4]. Techniques that change compression levels based on the network and the device's powers help communication go more smoothly.

Problems caused by different datasets can be fixed by making the aggregation process better by adding weighted means based on device performance or data quality [5]. Using safe multi-party computation and homomorphic encryption, along with other advanced aggregation methods, can make privacy-preserving aggregation even stronger. Researchers are still working on creating pooled optimization methods that can handle non-IID (non-identically distributed) data and make models more accurate and faster to converge [6]. Federated learning works better when customized grouping methods are used that take into account the fact that healthcare data is often inconsistent. When you combine edge computing features, you can train and predict models locally, so you don't have to talk to a central computer all the time [7]. Edge devices can train the model at first and only send updated versions to the central

computer after they have been improved. This reduces the effect of connection overhead. New developments in edge computing technologies, like edge-centric collaborative learning frameworks, let more complicated model training tasks be done nearby [7]. This method not only cuts down on contact needs, but it also makes it easier for edge devices to make decisions in real-time.

Participation mechanisms that change over time let devices join or leave the federated learning process based on their availability or how well they fit the present learning job [8]. The shared learning process is more flexible when the learning rate is changed automatically based on the features of each device. Researchers are looking into ways to change involvement and learning rates based on reinforcement learning [9]. The goal of these improvements is to make shared learning work better by responding automatically to changing network conditions and device capabilities.

A small number of studies have used both standard machine learning and deep learning to find esp seizures. By taking out important features from EEG data, SVMs have been used to find seizures. But these methods often depend on traits that were made by hand, which makes it harder for them to find complex trends in the data [10].

To sort EEG data into groups, ensemble methods such as Random Forests have been used. They are easy to understand, but the fact that they depend on specific feature engineering could make it harder for them to capture complex time patterns [11].

CNNs have been used to learn features straight from raw EEG data. They are very good at showing how things depend on each other in space, but sometimes they may not be able to show how things change over time [12].

A type of neural network called LSTMs has been used to describe sequences in time-series data, such as EEG data. They are good at showing time dependencies, but they might have trouble with disappearing gradients and long-term dependencies [13].

The current models have some problems with how accurate they are and how well they can be used in other situations.

A lot of statistics about epilepsy are not balanced, with only a few cases showing real seizures. When datasets aren't fair, models can be skewed toward the majority class, which makes them less sensitive and more likely to give false positives [14].

It is possible for EEG readings to be very different between people. Models learned on data from one person might not work well on other people because their brains are built differently, their electrodes may not be placed correctly, or their seizures may be different [15].

Some machine learning models might have trouble figuring out the long-term time frame that is important for epileptic seizures. It might be possible to deal with short-term dependence, but it's still hard to fully capture the pre- and post-ictal phases [16].

Artifacts can show up in EEG records like eye blinks, muscle movements, or electrical interference. Models might

mistake these effects for seizure patterns, which would make them less specific and raise the risk of false positives [17].

Federated Machine Learning was the subject of a thorough review piece that focused on its ideas and uses [9]. The paper doesn't talk about EEG data in particular, but the ideas it does talk about are a good starting point for understanding how FML deals with privacy issues when dealing with private data. The paper talks about different ways to protect privacy, such as differential privacy, and stresses how important it is to train models without a central server.

A standard federated learning framework for epileptic seizure detection utilizing deep learning on a cluster of computers is proposed [18]. The technique was tested on the NVIDIA Jetson Nano Developer Kit using the EPILEPSIAE database, one of the largest public epilepsy datasets for seizure detection. The framework has 81.25% sensitivity, 82.00% specificity, and 81.62% geometric mean. A customized variation of federated learning was also examined, where each computer trained a deep neural network (DNN) to learn the discriminative electrocardiography (ECG) properties of the observed person's epileptic seizures based on its local data. The results show that tailored federated learning improves all performance metrics with a sensitivity of 90.24%, specificity of 91.58%, and geometric mean of 90.90%.

Research proposed based on a three-tier approach for epileptic seizure prediction using the Federated Learning (FL) model [19] to use a large number of seizure patterns from globally distributed patients while protecting data. A bi-timescale local model is developed using the Spiking Encoder (SE) and Graph Convolutional Neural Network (Spiking-GCNN). Each local model uses FL-aggregated seizure knowledge from medical centres to calculate the coarse-grained personalized preictal likelihood. Bi-timescale modelling and Spiking-GCNN-based epileptic pattern learning yielded 96.33% sensitivity and 96.14% specificity on the CHB-MIT EEG dataset. The federated learning improves the suggested system by 96.28% for accuracy.

The challenges of centralized machine learning in epileptic seizure detection is addressed and Federated Machine Learning (FML) model has been proposed as a decentralized solution to address privacy, security, and data handling issues while improving accuracy and patient privacy. It underscores the importance of EEG data and the potential of FML to revolutionize healthcare data analysis.

In conclusion, the inability of centralized methods to handle private medical data, along with the need to protect patient privacy and improve data security, makes the use of autonomous models like Federated Learning in healthcare settings very appealing. FL is a big step toward a more ethical and safe way to handle healthcare data because it reduces privacy issues and makes sure that rules are followed.

II. MATERIAL AND METHOD: FEDERATED MACHINE LEARNING

The healthcare business is facing several pressing problems, and federated machine learning (FML) could solve many of them. The capacity to enable cross-decentralized healthcare system collaborative learning without jeopardizing

the protection of sensitive patient data is one of its notable benefits.

The goal of the machine learning paradigm known as Federated Machine Learning (FML) is to protect the confidentiality of local datasets while training models on distributed servers or devices. With FML, the learning process is decentralized, so each device may train its model locally, as opposed to the standard centralized machine learning strategy, which aggregates and stores data in a central server. Sharing just the model updates—as aggregated parameters or gradients—reduces the need to transmit raw data. When data security and privacy are of the utmost importance, FML's decentralized nature shines.

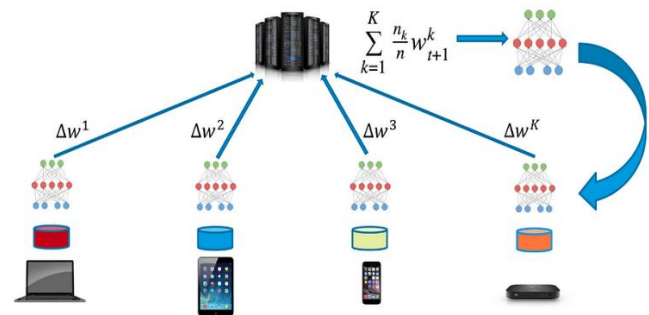


Fig. 1. Federated machine learning model.

The federated ML model is seen in Fig. 1. A global model is the result of combining model modifications made during local training. The model parameters might be averaged or gradients combined to achieve this aggregate. An all-encompassing and broadly applicable comprehension of the data is provided by the aggregated model, which is a representation of the collective knowledge acquired from all participating devices. To keep data transfers between devices to a minimum, FML places an emphasis on efficient communication. No raw data is sent; only model changes are communicated by devices. Because less data needs to be transferred, the communication overhead is reduced, making FML a good fit for situations where network capacity is restricted or when data privacy is a top priority.

Model training over distributed devices is based on the following principles.

1) *Training for local models:* Model training on each device's local dataset is done individually. Because decentralized data sources are diverse, this first training takes into account information unique to the local setting.

2) *Revised model:* Model updates, such as parameter updates or gradients, are generally generated by each device after local training. This update incorporates the insights, patterns, and characteristics related to that device, as well as the information obtained from the local dataset.

3) *The world model as a whole:* A global model is generated by aggregating the model updates from all devices. This worldwide model is an example of a collaborative learning product that draws on information from all around the world. By distributing the contributions from different types

of data evenly, the aggregation process hopes to keep the model accurate.

For the most part, iterative processes are used for local training, model updates, and global model aggregation. In order to promote continuous learning throughout the decentralized network, devices keep improving their models using new global information.

Here is the method for the federated machine learning model, broken down into its parts.

III. EXPERIMENTAL RESULTS

The Dataset collect from UCI Machine Learning Repository is used for the research study. The original dataset from the reference consists of five different folders, each with 100 files, with each file representing a single subject/person. Each file is a recording of brain activity for 23.6 seconds. The corresponding time-series is sampled into 4097 data points. Each data point is the value of the EEG recording at a different point in time. So, we have total 500 individuals with each has 4097 data points for 23.5 seconds.

The proposed federated machine learning uses five client nodes for implementing the system. Three machine learning algorithms are deployed to test the performance of the proposed system, namely decision tree classifier, multilayer perceptron classifier, and logistic regression.

| Algorithm of FL |
|---|
| <p>1. initialize :The Central Server: A global model is initialized and a group of clients (C) is chosen and given global model Every client i has their own local dataset (D_i) and model (w_i).</p> <p>2. Training of Local Models: Client i: Gets the glbal model w_t from the main server. Updates the local model w_i with its most recent state by training it with its most recent dataset, D_i. Determines the loss function's gradients using its local data: Calculates the change in weight w_i as a function of time $L(w_t; D_i)$</p> <p>3. Aggregation of Models: • Client i: Transfers data pertaining to local model modifications Δw_i to the main server. • Central Server: Combines all the model changes that have been received: The weight allocated to client i (e.g., depending on data size) is denoted by α_i, and cahnge in $\Delta w = \sum (i \in C) \alpha_i * \Delta w_i$ Update the global model: $w(t+1) = w_t + \Delta w$.</p> <p>4.repeat step 2 to 3 number of rounds have passed..</p> <p>Combining Models: • Update of the global model by avearge of all local model</p> |

The experimental setup parameters used for the experimental study are presented in Table I.

The research work uses a flower framework for deploying federated machine learning with 5 no of participating nodes, 3 Machine learning models like random forest, Multilayer

perceptron, and logistic regression are trained with the simulation setup given in Table I.

TABLE I. EXPERIMENTAL SETUP

| Model | Parameter value |
|---------------------------------------|--|
| Federated machine learning frame work | Flower framework |
| Number of nodes | 5 |
| Multilayer Perceptron Classifier | solver='lbfgs', alpha=1e-5, hidden_layer_sizes=(5, 2), |
| Logistic Regression | Tolerance for stopping criteria= 1e-4, max_iterint=100, solver='lbfgs' |
| Decision tree | |
| Model aggregation method | Average |
| Batch size sd | 64 |
| No of batches | 50 |
| No of epochs | 100 |

As a first step of analysing the proposed method, exploratory data analysis is carried out and shown in Fig. 2. The Fig. 2 shows the raw data of ECG signal of seizure-affected people data and non-epics seizure data.

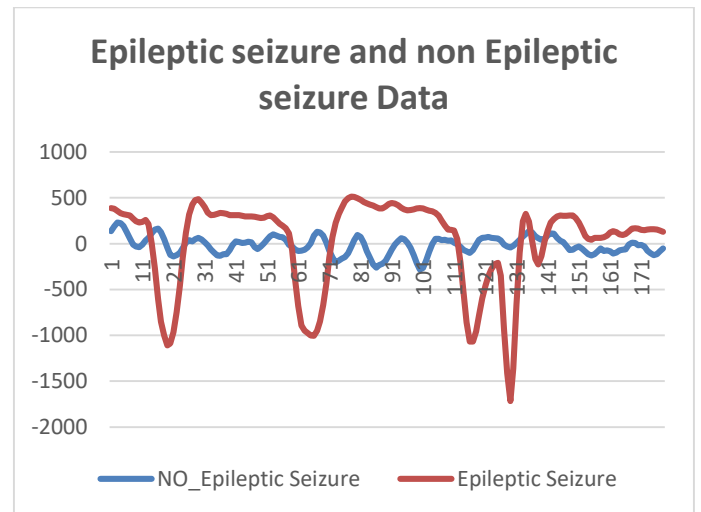


Fig. 2. EEG signal of epileptic seizure and non-epileptic seizure case.

From Fig. 2, it is evident that Epileptic Seizure data and non-Epileptic Seizure data are sitting in different amplitude domains so it is possible to classify them effectively.

Fig. 3 shows the box plot of EEG signal of epileptic seizure and non-epileptic seizure data. From the diagram it is evident the epileptic seizure data and non-epileptic data both has average values of zero but the median value of both is different and also the range of values taken by the both data are different which again prove that both data distributions are in different amplitude domain which can be effectively classified by a classifier.

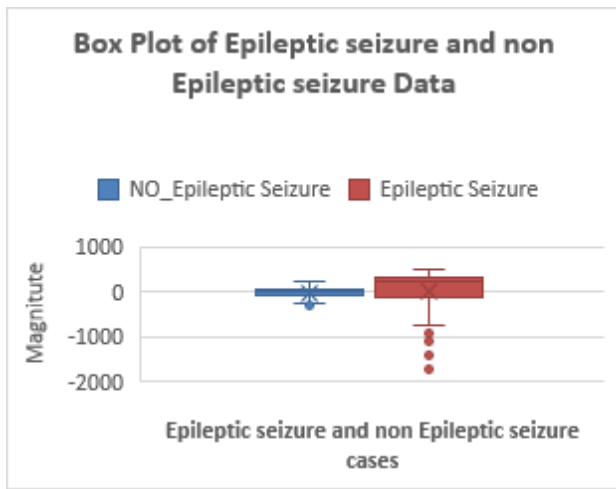


Fig. 3. Box plot of EEG signal of epileptic seizure and non-epileptic seizure case.

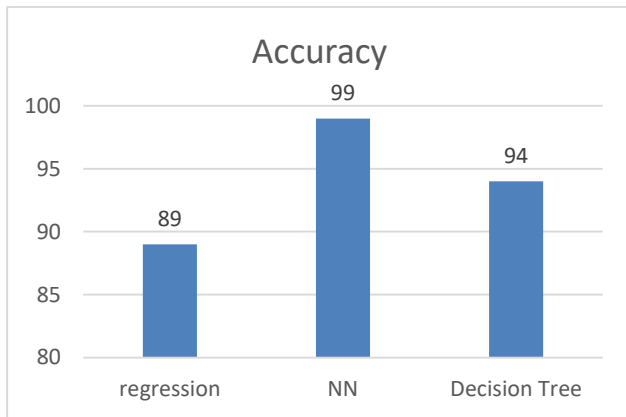


Fig. 4. Accuracy of various machine learning models in federated machine learning.

Federated machine learning of three algorithms is evaluated and plotted in Fig. 4. Figure shows that among the three algorithms, the neural network model achieves the highest accuracy with 99% and decision tree is the second highest accuracy with 94% and the regression model achieves 89%. Those performances are evaluated with the aggregated model after Federated machine learning.

The time complexity of federated machine learning (FL) depends on several factors in the specific FL setup and algorithm used.

1) *Number of communication rounds*: This refers to the number of times local models are uploaded from devices to the central server, aggregated, and redistributed. Each round involves communication overhead and potential computation on the server. In general, the complexity is linear in the number of rounds ($O(R)$).

2) *Local data size*: The amount of data each device uses to train its local model impacts the local computation cost. Typically, the complexity is linear in the local data size ($O(n)$).

3) *Model size*: The complexity of aggregating and updating the global model scales with its size. This can be linear ($O(m)$) or quadratic ($O(m^2)$) depending on the aggregation method and model architecture.

The time complexity of the federated machine learning for training the three machine learning models is also evaluated which is given in Fig. 4.

From Fig. 4, it is evident that the decision tree model takes a long training time and neural letter model takes the second highest training time and regression takes the least time. The training time complexity shows that the proposed model can be deployed easily in a practical system.

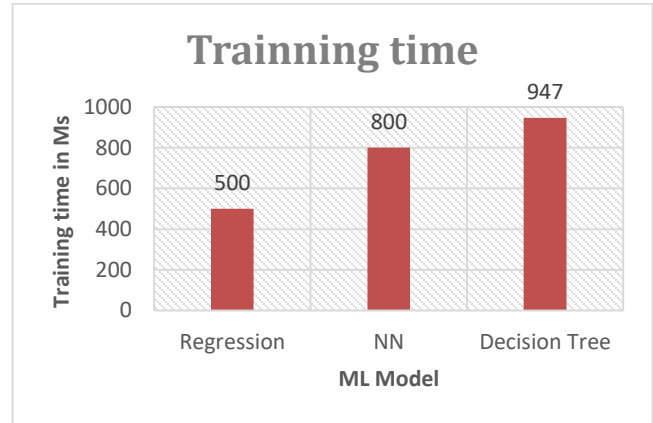


Fig. 5. Training time of Federated machine learning algorithms.

From Fig. 5, it is evident that the decision tree model takes a long training time and neural letter model takes the second highest training time and regression takes the least time. The training time complexity shows that the proposed model can be deployed easily in a practical system.

TABLE II. PERFORMANCE COMPARISON

| Method | Technique employed | Accuracy achieved |
|--------------------|---|---|
| Baghersalimi[18] | Federated Deep neural network | Sensitivity of 90.24%, Specificity of 91.58% |
| Saemaldahr, R.[19] | Federated Spiking Encoder (SE) and Graph Convolutional Neural Network (Spiking-GCNN). | 96.33% Sensitivity, 96.14% Specificity, 96.28% accuracy |
| Proposed | Federated Neural network | sensitivity of 98.24%, specificity of 99.23% 99% accuracy |

Table II shows the performance analysis comparison with the literature work. From Table II, it is evident that the proposed work outperformed compared to the literature work. Literature work can achieve 96.33% of sensitivity but the proposed work can achieve 98.24%. similarly, the proposed work achieves 99.23% specificity whereas the literature maximum of 96.14% was only achieved. The proposed work achieves 99 % accuracy whereas literature could even touch only 96%.

IV. CONCLUSION

EEG signal-based epileptic seizure detection framework is presented with a Federated machine learning mechanism. The proposed mechanism ensures the security and privacy of the data while applying data analytics of data to predict the presence and absence of seizure. Maximum accuracy of 99% is achieved by using a neural network model under federation machine learning. The time complexity of the proposed framework was analysed and it shows for the neural network model it takes 800 milliseconds to train the model to predict or classify the seizure. This time complexity proves that the proposed model or framework can be deployed practically to train using federated machine learning. The future work of the proposed framework will be analysing the communication overhead and providing some security measures while sharing the locally trained model with the aggregating server.

REFERENCES

- [1] Beaulieu-Jones, B. K., Wu, Z. S., Williams, C., Lee, R., Bhavnani, S. P., Byrd, J. B., & Greene, C. S., "Privacy-preserving generative deep neural networks support clinical data sharing" *Circulation: Cardiovascular Quality and Outcomes*, 12(7), e005122, 2019.
- [2] Yang, Q., Liu, Y., Chen, T., & Tong, Y., "Federated machine learning: Concept and applications", *ACM Transactions on Intelligent Systems and Technology (TIST)*, 10(2), 1-19, 2019.
- [3] Kairouz, P., McMahan, H. B., Avent, B., Bellet, A., Bennis, M., Bhagoji, A. N., ... & Zhao, S., "Advances and open problems in federated learning", *Foundations and trends® in machine learning*, 14(1-2), 1-210, 2021.
- [4] McMahan, B., Moore, E., Ramage, D., Hampson, S., & y Arcas, B. A., "Communication-efficient learning of deep networks from decentralized data", In *Artificial intelligence and statistics* (pp. 1273-1282). PMLR, 2017.
- [5] Bonawitz, K., Ivanov, V., Kreuter, B., Marcedone, A., McMahan, H. B., Patel, S., ... & Seth, K., "Practical secure aggregation for privacy-preserving machine learning", In *proceedings of the 2017 ACM SIGSAC Conference on Computer and Communications Security* (pp. 1175-1191), October 2017.
- [6] Konecný, J., McMahan, H. B., Yu, F. X., Richtárik, P., Suresh, A. T., & Bacon, D., "Federated learning: Strategies for improving communication efficiency", *arXiv preprint arXiv:1610.05492*, 8, 2016.
- [7] Li, D., & Wang, J., "Fedmd: Heterogenous federated learning via model distillation", *arXiv preprint arXiv:1910.03581*, 2020.
- [8] Wang, S., Tuor, T., Salonidis, T., Leung, K. K., Makaya, C., He, T., & Chan, K., "Adaptive federated learning in resource constrained edge computing systems", *IEEE journal on selected areas in communications*, 37(6), 1205-1221, 2019.
- [9] Yang, Q., Liu, Y., Chen, T., & Tong, Y., "Federated machine learning: Concept and applications", *ACM Transactions on Intelligent Systems and Technology (TIST)*, 10(2), 1-19, 2019.
- [10] Shoeb, A., "Application of machine learning to epileptic seizure onset detection and treatment", MIT, 2009.
- [11] Sharma, M., & Pachori, R. B., "A survey on EEG signal classification techniques", *IET Signal Processing*, 12(2), 125-133, 2018.
- [12] Acharya, U. R., & Sree, S. V., "Application of higher order spectra for automated classification of epileptic EEG signals", *Expert Systems with Applications*, 39(10), 9072-9078, 2012.
- [13] Roy, Y., Banville, H., Albuquerque, I., Gramfort, A., & Falk, T. H., "Deep learning-based electroencephalography analysis: a systematic review", *Journal of Neural Engineering*, 16(5), 051001, 2019.
- [14] Shoeb, A., & Guttag, J., "Application of machine learning to epileptic seizure detection", In *Proceedings of the 27th international conference on machine learning (ICML-10)* (pp. 975-982), 2010.
- [15] Gotman, J., "Automatic recognition of epileptic seizures in the EEG", *Electroencephalography and Clinical Neurophysiology*, 54(5), 530-540, 1982.
- [16] Faust, O., Acharya, U. R., Adeli, H., & Adeli, A., "Wavelet-based EEG processing for computer-aided seizure detection and epilepsy diagnosis", *Seizure*, 26, 56-64, 2015.
- [17] Osorio, I., Frei, M. G., & Wilkinson, S. B., "Real-time automated detection and quantitative analysis of seizures and short-term prediction of clinical onset", *Epilepsia*, 39(6), 615-627, 1998.
- [18] S. Baghersalimi, T. Teijeiro, D. Atienza and A. Aminifar, "Personalized Real-Time Federated Learning for Epileptic Seizure Detection," in *IEEE Journal of Biomedical and Health Informatics*, vol. 26, no. 2, pp. 898-909, 2022.
- [19] Saemaldahr, R. and Ilyas, M., "Patient-Specific Preictal Pattern-Aware Epileptic Seizure Prediction with Federated Learning", *Sensors*, 23(14), p.6578, 2023.

Impact of the IoT Integration and Sustainability on Competition Within an Oligopolistic 3PL Market

Kenza Izikki¹, Aziz Ait Bassou², Mustapha Hlyal³, Jamila El Alami⁴

LASTIMI Laboratory, Graduate School of Technology EST, Mohamed V University, Rabat^{1, 2, 4}
Logistics Center of Excellence, Higher School of Textile and Clothing Industries ESITH, Casablanca³

Abstract—The third party logistics (3PL) sector holds a crucial role in modern supply chains, streamlining the movement of goods and optimizing logistics operations. The 3PL industry's journey towards digitalization and sustainability reflects a crucial strategy to create an efficient and resilient supply chain. It is increasingly integrating Internet of Things technologies (IoT) within its operations. This latter is a cutting-edge technology widely used in the supply chain realm as it offers numerous advantages namely traceability and real-time decision-making capability. In view of growing concerns for the environment and the social welfare, supply chain actors are seeking to make various initiatives to shift to more sustainable practices. This paper studies the competition within an oligopolistic market of 3PL firms. Through the lens of game theory, we construct a mathematical model where a supply chain composed of n firms competes through pricing, IoT integration efforts and sustainability efforts. Results show that the IoT integration and sustainability efforts impact the pricing decisions of the firm. Moreover, this study highlights how the rivals' decisions on the IoT integration and sustainability efforts impact the firm's decision-making processes. Furthermore, a comparison of the model decision variables within a duopoly and an oligopolistic setting is conducted. This paper concludes to the significant impact of the rivals' strategies on the firm's decisions and profitability.

Keywords—Third party logistics; internet of things; sustainability; oligopoly; game theory

I. INTRODUCTION

The modern business world has changed drastically in the twenty-first century. Globalization and rapid economic expansion have heightened competition across both global and local markets. Coupled with escalating customer expectations and shorter product lifecycles, supply chains have evolved and become increasingly demanding to manage. Considering the growing complexity of the supply chains, firms are now urged to focus on their core business in order to maintain competitiveness.

Outsourcing logistics activities is considered a practical strategy for companies to reduce their operational costs, decreasing inventory, eliminating capital investment in logistical assets, minimizing labor expenses, and enhancing service standards through enhanced logistical proficiency and broader geographical reach [1]. The realm of third-party logistics is a firmly established business sector. They offer a large range of services from picking and packing to managing and coordinating the whole supply chain [2]. While warehousing and transportation remains their main activity,

they also provide services such as product collection, brokering, shipping, material management storing, alongside offering expertise in supply chain strategy and access to technological resources [2]. Over the past few years, the 3PL market has seen substantial growth, resulting in heightened competition and a notable transformation in its competitive environment. 3PLs that prioritize standard services might face a notable reduction in their market share in the coming years. Additionally, external competitors are increasingly venturing into management-focused 3PL activities, potentially diminishing the role of 3PLs to simpler forwarding functions [3]. 3PL firms are thus urged to optimize their service and their strategic models to remain competitive.

In light of the growing interdependence among companies on a global scale, companies are expected to take responsibility for the environmental and social impact of their operations, extending scrutiny throughout their entire supply chain, both incoming and outgoing [4]. Consequently, 3PLs are now facing new challenges in managing their supply chain and processes in a sustainable manner. As sustainability has become a major concern, companies have started adopting new innovative environmentally friendly and socially responsible practices throughout their value chain.

Over the past years, numerous Third-Party Logistics (3PL) companies have adjusted their operations and strategies to prioritize sustainability in their activities. The environmental handling of transportation plays a pivotal role in establishing a greener supply chain, urging corporations to enhance their performance metrics and to mitigate adverse external influences stemming from their logistics operations, like carbon emissions.[5]. There are various approaches to shift to a more environmental and social operations namely, using cleaner fuel, using low-emission vehicles, reduce travel distances and improve vehicle efficiency. Given all the above, 3PL firms predict that shifting to a more sustainable operations will become a standard benchmark in their decision-making process [5].

On the other hand, Third-Party Logistics (3PLs) have faced growing challenges posed by disruptive business models and the emergence of digital technologies [3]. Globally, a rising interest has been on digitalization, creating value across various industries and supply chains. Implementing disruptive technologies with the value chain can optimize business advantages and unveil novel forms of value. Nonetheless, technological transformation presents a distinct set of challenges [6]. Logistics service providers face digital challenges stemming from emerging technologies like

Blockchain, Data analytics, IoT, autonomous vehicles and 3D printing. These technologies range from mature to emerging and create several opportunities for the supply chain sector, however simultaneously changing logistics needs and expectations [3].

One of the main industry 4.0 technologies utilized in the supply chain sector is the Internet of things technologies. The primary technologies utilized for IoT include sensors, smart chips, wireless transmission networks, machine-to-machine communication (M2M), and notably, high-speed communication channels, robust computing capabilities, and expansive data storage capacities. IoT finds application in various logistics activities, i.e. cargo tracing, warehouse and fleet management, predictive asset maintenance, route optimization, smart containers, optimizing capacity usage, truck platooning[7]. Furthermore, these technologies are now being employed to oversee and manage environmental risks and human rights concerns, promoting sustainable production and consumption [4].

The competitive dynamics within the industry and the industry 4.0 technologies are evolving swiftly, paving the way for entirely new participants, and transforming the role of 3PLs [8]. Consequently, Third-Party Logistics (3PLs) must respond to these changes to hold their position as primary providers of logistics solutions. Digitalization is constructing a fresh competitive landscape as it impacts the business models of Third-Party Logistics [9]. In addition to the shift to sustainable practices, 3PL firms are faced with numerous challenges. One of the main hurdles 3PL face is the high investments needed to meet the digitalization and sustainability requirements and a great pressure on pricing and quality of service [3]. Moreover, they are challenged by finding the balance between the customers' continuous need for standardized services and the necessity to offer more advanced services to remain competitive. Finding this balance puts great pressure on the strategic evolution of the 3PL [2].

Researchers have continuously showed interest in this area of research. However, there has been limited utilization of mathematical modelling to address the problem, with most focus placed on conceptual and statistical analyses instead [10]. Given the complexity of the supply chains encompassing several participants, researchers have used game theory to analyze the complex interactions within the supply chain. This research will consider an oligopoly market of 3PLs investigating the competition among the 3PL firms regarding their pricing strategies, integration of IoT efforts, and sustainability efforts aimed at maximizing profits and maintaining competitiveness within the market.

This research investigates the following questions:

- How do IoT integration and sustainability initiatives into the 3PL service affect the pricing decisions?
- How does competition's strategy affect the firm's decision-making process in terms of price, IoT and sustainability efforts?
- To what extent do IoT and sustainability investments influence the firm's profitability?

This paper will be structured as follow: Section II will present a literature review of our scope of research, the description of our mathematical model will be presented in Section III, we will then present some analytical results and insights of our model in Section IV, and lastly Section V will present a conclusion of our findings.

II. LITERATURE REVIEW

This paper is related to three main streams of research: Internet of Things in supply chain, sustainable supply chain and Third-party logistics.

A. Internet of Things and Sustainability in Supply Chains

The rapid growth of digitalization under the banner of "Industry 4.0" has reshaped and redesigned the nature of businesses. Companies worldwide have shifted their focus to digitalization due to the significant benefits it offers. Utilizing digitalization is a vital tool in achieving efficient and sustainable logistics ecosystems through enhanced transportation systems and new value-added services [2], [11]. Industry 4.0 has introduced a wide range of revolutionary technologies namely Blockchain, Artificial intelligence, Internet of Things, Augmented reality, Data Analytics, and others. These latter have proved numerous advantages in the logistics industry enabling real-time transparency along the entire value chain, enhanced efficiency and visibility, autonomous decision-making, intelligent integrated planning systems and smart warehousing and procurement [11].

Throughout the years, these technologies have shifted the business paradigm in various industries notably in the logistics world. To capitalize on the opportunities presented by digitalization in the business world, companies should consider the appropriate approaches and tools required to transition toward the Digital Supply Chain [6].

IoT is emerging as a rapidly advancing technology that an increasing number of industries are eager to embrace in the aim of enhancing their operational efficiency. It offers numerous valuable avenues to enhance traditional SC such as improved asset utilization, enhanced supply chain performance and greater reliability [12]. Moreover, it enables the development of an intelligent infrastructure within supply chains, bringing together vast volumes of data, information, and all supply chain processes, providing real-time decision-making processes [4], [13].

IoT exhibits potential applications within supply chains, yet it confronts various hurdles during implementation. Most emerging technologies introduce several risks and challenges in the process of implementation. These factors should be considered and outline the essential measures for establishing the technology infrastructure. Clearly defining the infrastructure's characteristics during the implementation phase can also aid in better understanding of the technological needs and priorities [6]. Key challenges preventing the full exploitation of IoT in supply chains involve issues related to security, privacy, and scalability. IoT relies on wireless technology, and its applications are constructed using a multitude of sensor nodes [12].

Sustainability has become a major concern for all businesses and sectors in view of customers' requirements and new strict regulations. Companies are progressively paying more attention to social and environmental issues that surround their value chain, i.e. human rights abuses, child labor, deplorable work environments, unethical practices like corruption and bribery, or failure to adhere to environmental regulations [4]. Achieving a sustainable supply chain is ensuring the compliance to environmental and social conditions of all the stakeholders across the whole value chain while maintaining economic profitability. In this context and in view of the expansion of global supply chains, companies are faced with multiple challenges upon adopting more sustainable practices in every possible stage of the value chain.

The introduction of the sustainable development concept has motivated managers and policymakers across various sectors to incorporate environmental and social concerns alongside economic goals in their strategic planning [14]. It has become vital to improve the design and management of supply chain and logistics methods. To enhance the environmentally friendly and sustainable supply chain, a holistic and integrated approach to transportation and environmental policies is essential. This approach should integrate crucial regulations and economic incentives in a transparent manner across all modes of transportation [15].

Furthermore, the rapid development of the industry 4.0 technologies is expected to lead to a significant transformation in how businesses approach their strategies and operations in logistics. It has generated a demand for a new business model focused on a digitally connected, intelligent, exceptionally efficient, and environmentally responsible logistics system that provides complete transparency to all stakeholders [11]. The logistics sector is one of the most concerned with sustainability since it is considered one of the less sustainable sectors and one of the main sources of CO₂ and GHG emissions [16]. Digitization alone presents a significant potential to decrease emissions in the logistics sector, with the potential to achieve emissions reductions of approximately 10 to 12% by 2025, as well as contribute to the decarbonization of the global economy [11]. Organizations can employ data to facilitate communication among different supply chain functions, such as procurement, manufacturing, distribution, sales and marketing, and post-sales services. From an economic standpoint, sustainable logistics can reduce costs by preserving product quality during transportation, ensuring product availability, and optimizing processes [15].

Digitalization in logistics enables among others cooperation, connectivity, adaptiveness, integration, and autonomous control. These latter impacts various sustainability criteria in all three dimensions. From an economic stand view, it helps achieve optimized logistics costs, delivery time, forecast accuracy, flexibility, and reliability. In terms of environmental concerns, it encourages a better emission and waste management as well as energy and resource efficiency. As of the social point of view, it promotes better labor patterns and health and safety conduct [11]. In particular, the implementation of IoT technologies has proved its direct and indirect benefit in leveraging sustainability in the supply chains. With its capacity to sense monitor and track in real

time, IoT technologies contribute majorly to an optimized real time and decentralized decision-making process. With ensuring a transparent efficient value chain, greener supply chains, decreased emissions, better lead times and optimized costs, the adoption IoT promotes the sustainability of organizations [15], [17], [18].

B. Third Party Logistics

The emergence of 3PL service providers can be traced back to the outsourcing trend of the early 1990s. This subject remains a steadily expanding area of concern and engagement, particularly within the fields of logistics and supply chain management [19]. Logistics is a crucial component of any company's supply chain. Outsourcing enables businesses to be more agile and concentrate on their core operations, improve customer service, and reduce assets [20]. Furthermore, it helps companies in reducing expenses, enhancing efficiency, sustainability, customer satisfaction, and overall profitability [1]. As more companies are seeking 3PL services to stay competitive in the global market landscape, 3PL market has grown significantly and has become notably competitive and diverse. It encompasses numerous companies, varying in size and specialization in logistics services, including transportation, inventory management, warehousing, and distribution. Cost and service quality are frequently the primary factors to consider when assessing a logistics partner [21], however in view of the growing sustainability pressure, social and environmental sustainability will become a crucial criterion for 3PL evaluation [20].

Out of all the methods to meet sustainability objectives within a supply chain, collaborating with third-party logistics firms has garnered considerable interest. Through the delivery of environmentally friendly and effective transportation services, 3PLs can assist various types of supply chains, including regular, closed loop, and circular ones, in achieving higher profits while maintaining sustainability, particularly in the distribution and collection/recycling phases [14]. Consequently, the pursuit of sustainable practices by third-party logistics (3PLs) companies has evolved into a substantial and intricate issue [22].

The literature has showed increasing interest in sustainability in relation to 3PL, particularly in the assessment and selection of 3PL. various decision-making models for evaluating and selecting 3PL from a sustainability point of view have been proposed in the literature [16], [23], [24], [25], [26]. Carbon emissions and delivery time for customer satisfaction are the leading criteria taken into consideration while selecting 3PL. Environmental sustainability of the 3PL have drawn the most interest of the academia, while social sustainability remains under-researched. 3PL companies are now urged to offer more environmentally friendly and socially appropriate services to stay competitive.

The service industry tends to expand and evolve alongside with globalization, technological developments, and the increasingly competitive markets. These factors challenge businesses to maintain high service quality [27]. As the third-party logistics market has expanded considerably, competition has increased. Shifting to a smart tech driven 3PL provider is a must. Researchers showed their interest in the adoption of the

IoT technologies to enhance their performance and decision-making process. IoT technologies can be used in different core processes of 3PL services enabling real time logistics, enhanced flexibility, and overall improved efficiency of logistics operations.

C. Related Works

Supply chain remains a complex system considering it involves numerous players or groups of decision-makers, ergo they are suitable to be examined through the prism of Game theory [28]. This latter provides a framework for modelling these complex interactions and has been widely used among researchers in analyzing supply chain issues [14], [28], [29].

Price is one of the main criteria considered in decision making [14], hence game models for pricing problems is mature [30]. Multiple games in the literature have dealt with pricing in logistics under various factors in addition to costs variables, namely sustainability indicators, risk, competition indicators etc.[30]. Most scholars have showed their interest in investigating pricing models of two echelon supply chains. The latter is composed mainly by manufacturer/supplier/producer and retailer and three echelon supply chains composed of manufacturer/supplier/producer and retailer and 3PL.

Investigating pricing strategies considering the environmental sustainability, closed loop supply chain and green production has been the focus of various papers [5], [14], [29], [31], [32], [33]. The economic growth and environmental protection are extensively considered in the literature, whereas the social responsibility dimension of sustainability remains under explored comparably. The author in [10] explored the influence of transparency on the demand function and examines how transparency and corporate social responsibility affect the choices made by supply chain members and their profits concerning an environmentally friendly product. The author in [33] explores a supply chain framework featuring both a Green Supply Chain (GSC) and a Non-Green Supply Chain (NGSC), each consisting of a manufacturer and a retailer. The paper introduces a novel competitive mathematical model where the government acts as a leader, discussing pricing policies, greening strategies, and government tariffs under competitive conditions influenced by governmental financial policies. The author in [34] proposes two models; Model 1 aims to assess the optimal green quality, selling price, and business approach in green marketing in a cooperative business strategy between a manufacturer and a retailer involved in marketing green products. Whereas model 2 examines the price competition between two CSR firms, regular producer, and a green producer.

On the other hand, digitalization, and the use of IoT has also attracted attention of researchers in decision making models. The proposed models explored investment decisions [35], [36], [37], as well as outsourcing decisions [38]. Furthermore,[39] examined how integrating IoT can affect the quality of service of the 3PL firms in a duopoly market setting, while [40] has combined both digitalization and sustainability in its game model. This latter investigated the effectiveness of competitive sustainability services, digitalization services, and

pricing decisions in a 2-tier supply chain structure of a manufacturer and a retailer.

Through the lens of game theory, researchers have explored the competition in pricing strategies in 2-tier supply chains, focusing on monopolistic and duopolistic settings. Fewer researchers have focused on pricing decision games in an oligopoly market structure. Reference [41] focused on aligning pricing and advertising decision in a multi-product, multi-echelon supply chain comprising several suppliers, one manufacturer, and multiple retailers with horizontal and vertical competition. While [42] considered competition between multiple supply chains, each composed of a manufacturer and a salesperson.

Game theory, a critical tool in supply chain management, has been extensively utilized across various scenarios. However, its specific application to 3PL and sustainability within the context of the IoT remains relatively nascent. This gap highlights an emerging area of interest where the interactions between 3PL providers, sustainability practices, and digital technologies can be explored through the lens of game theory. Research focusing on how 3PL companies make decisions regarding sustainability and the integration of IoT technologies is still in its early stages, particularly when examining these factors within an oligopolistic market context. Additionally, while the concepts of sustainability and digitalization have begun to attract academic attention, much of the existing literature remains theoretical frameworks. Another significant gap in current research is the exploration of competitive pricing strategies for 3PL services in a market where multiple players compete for advantage. Our research aims to fill these gaps by providing insights into the pricing dynamics of 3PLs in competitive markets, particularly focusing on how these companies can leverage IoT and sustainability within their strategic decision process.

III. MODEL DESCRIPTION

We consider a competitive setting of n 3PL firms, which is denoted $i = \{1, \dots, n\}$, offering homogenous service. Fig. 1 illustrates the market setting and competitiveness in our proposed model.

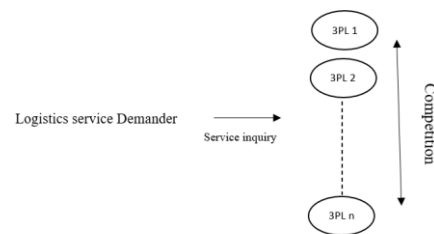


Fig. 1. The proposed model.

In light of more competitive and demanding customers, in terms of quality, service and sustainability, and in addition to a competitive environment the 3PL firms are constrained to make complex strategic decisions.

Let us consider the 3PL firms compete through price, technology, and sustainability. In our paper, we consider an IoT integration effort β . On the other hand, sustainability has

become a requisite concern for all supply chain entities. Since sustainability encompasses three aspects, namely economic, environment and social, diverse actions and approaches can be considered to make supply chain operations more sustainable. In line with [40] and to keep our model simple, we will consider a sustainability effort level σ that covers different sustainability initiatives that can be taken.

To remain competitive, 3PL needs to determine the optimal choices in terms of price and services. In our paper, we aim to investigate the optimal price, IoT integration and sustainability effort to maximize the profit.

Similar to [40], [43], the inverse demand function for firm i is expressed as follows:

$$D_i = \frac{a}{n} - \alpha p_i + \frac{\gamma}{n-1} \sum_{k \neq i}^n p_k + T_i \beta_i - \frac{1}{n-1} \sum_{k=1}^n T_k \beta_k + S_i \sigma_i - \frac{1}{n-1} \sum_{k=1}^n S_k \sigma_k \quad (k \neq i) \quad (1)$$

We assume the firm's demand function is a decreasing function of its own price and increasing on its competitors' price. Moreover, the firm's demand is influenced by IoT integration and sustainability efforts, where higher efforts of the firm will increase their demand while the rivals' efforts will bring down the firm's demand.

The total market demand is expressed as follows where it is solely influenced by the price of the firms. $D_T = \sum_{i=1}^n D_i$

$$D_T = a + (\gamma - \alpha) \sum_{k=1}^n p_k \quad (2)$$

A. Notations

1) Input parameters

| | |
|-----------|---|
| D_i | Demand function of firm i |
| a | Market share |
| α | Self-price sensitivity |
| γ | Cross-price sensitivity |
| T_i | Market sensitivity of firm i to the IoT integration |
| S_i | Market sensitivity of firm i to the sustainability effort |
| λ | IoT integration cost factor |
| θ | Sustainability initiative cost factor |

2) Decision variables

| | |
|------------|--|
| p_i | 3PL firm i 's price |
| β_i | 3PL firm i 's IoT integration effort |
| σ_i | 3PL firm i 's sustainability effort |

The cost of the service for firm i is composed of a fixed cost dependent of the demand C_i and demand independent costs encompassing the costs of IoT integration C_i^T and sustainability effort C_i^S . Choosing to invest in such technology and sustainable practices can bring a competitive edge to the firms however it is still financially challenging. As employed widely in the literature [10], [40], we consider quadratic cost functions for firm i expressed as follows:

$$C_i^T = \frac{\lambda \beta_i^2}{2} \quad (3)$$

$$C_i^S = \frac{\theta \sigma_i^2}{2} \quad (4)$$

Based on the above, the 3PL firm i 's profit function is modelled as follows:

$$\pi_i = (p_i - C_i) D_i - C_i^T - C_i^S \quad (5)$$

$$\max_{p_i, \beta_i, \sigma_i} \pi_i = (p_i - C_i) \left(\frac{a}{n} - \alpha p_i + \frac{\gamma}{n-1} p_{k_i} + T_i \beta_i - \frac{1}{n-1} \sum_{k=1}^n T_k \beta_k + S_i \sigma_i - \frac{1}{n-1} \sum_{k=1}^n S_k \sigma_k \right) - \frac{\lambda \beta_i^2}{2} - \frac{\theta \sigma_i^2}{2} \quad (6)$$

This paper addresses modelling various decision-making strategies employed by 3PL firms under competition in an oligopoly setting. It aims to identify the most advantageous decisions related to price IoT technology and sustainability efforts to maximize their profits.

All the firms decide on their price, IoT integration and sustainability efforts simultaneously, the optimal price, IoT integration and sustainability effort of firm i are calculated as follows:

$$p_i, \beta_i, \sigma_i \in \arg \max_{p_i, \beta_i, \sigma_i} \pi_i(p_i, \beta_i, \sigma_i) \quad (7)$$

$$\frac{\partial \pi_i}{\partial p_i} = \frac{a}{n} + \frac{\sum_{k=1}^n T_k \beta_k}{n-1} - \frac{\sum_{k=1}^n S_k \sigma_k}{n-1} - 2\alpha p_i + C_i \alpha + T_i \beta_i + \frac{\gamma p_{k_i}}{n-1} + S_i \sigma_i \quad (8)$$

$$\frac{\partial \pi_i}{\partial \beta_i} = (p_i - C_i) T_i - \beta_i \lambda \quad (9)$$

$$\frac{\partial \pi_i}{\partial \sigma_i} = (p_i - C_i) S_i - \theta \sigma_i \quad (10)$$

In order to analyze the concavity of the function we use the hessian matrix expressed as follows:

$$H_i = \begin{bmatrix} \frac{\partial^2 \pi_i}{\partial p_i^2} & \frac{\partial^2 \pi_i}{\partial p_i \beta_i} & \frac{\partial^2 \pi_i}{\partial p_i \sigma_i} \\ \frac{\partial^2 \pi_i}{\partial \beta_i p_i} & \frac{\partial^2 \pi_i}{\partial \beta_i^2} & \frac{\partial^2 \pi_i}{\partial \beta_i \sigma_i} \\ \frac{\partial^2 \pi_i}{\partial \sigma_i p_i} & \frac{\partial^2 \pi_i}{\partial \sigma_i \beta_i} & \frac{\partial^2 \pi_i}{\partial \sigma_i^2} \end{bmatrix} \quad (11)$$

$$H_i = \begin{bmatrix} -2\alpha & T_i & S_i \\ T_i & -\lambda & 0 \\ S_i & 0 & -\theta \end{bmatrix} \quad (12)$$

We have

$$\frac{\partial^2 \pi_i}{\partial p_i^2} < 0 \quad \frac{\partial^2 \pi_i}{\partial \beta_i^2} < 0 \quad \frac{\partial^2 \pi_i}{\partial \sigma_i^2} < 0 \quad (13)$$

And

$$\det H_i = T_i^2 \theta + S_i^2 \lambda - 2\alpha \theta \lambda \quad (14)$$

$$\det H_i > 0 \text{ if } T_i^2 \theta + S_i^2 \lambda - 2\alpha \theta \lambda > 0$$

We suppose

$$S_i^2 - 2\alpha \theta > 0 \quad (15)$$

$$\text{Since } \lambda > 0 \text{ and } T_i^2 \theta > 0 \text{ hence } \det H_i > 0$$

Accordingly, the hessian matrix H_i is negative definite. Hence the profit function of firm i is concave in p_i, β_i, σ_i .

By utilizing the function described in equation (6), we can calculate the equilibrium price p_i^* , IoT integration effort β_i^* and sustainable effort σ_i^* of firm i by examining the first-order conditions associated with each of these variables:

$$\frac{\partial \pi_i}{\partial p_i} = 0 \xrightarrow{\text{yields}} p_i^* = \frac{a(n-1) - n \sum_{k=1}^n T_k \beta_k - n \sum_{k=1}^n S_k \sigma_k - C_i n \alpha + C_i n^2 \alpha - n T_i \beta_i + n^2 T_i \beta_i + p_{k_i} n \gamma - n S_i \sigma_i + n^2 S_i \sigma_i}{2n\alpha(n-1)}$$

$$p_i = \frac{a(n-1) + n(-\sum_{k=1}^n T_k \beta_k - \sum_{k=1}^n S_k \sigma_k + C_i \alpha(n-1) + (n-1)T_i \beta_i + p_{k_i} \gamma + (n-1)S_i \sigma_i)}{2(n-1)n\alpha} \quad (16)$$

$$\frac{\partial \pi_i}{\partial \beta_i} = 0 \xrightarrow{\text{yields}} \beta_i^* = \frac{(p_i - C_i)T_i}{\lambda} \quad (17)$$

$$\frac{\partial \pi_i}{\partial \sigma_i} = 0 \xrightarrow{\text{yields}} \sigma_i^* = \frac{(p_i - C_i)S_i}{\theta} \quad (18)$$

By solving (16) (17) and (18) simultaneously, the optimal equilibrium solutions $(p_i^*, \beta_i^*, \sigma_i^*)$ can be derived:

$$p_i^* = \frac{C_i T_i^2 \theta + \lambda(C_i S_i^2 - \theta(\frac{a}{n} + C_i \alpha + \frac{p_{k_i} \gamma}{n-1} \sum_{k=1}^n T_k \beta_k + \frac{\sum_{k=1}^n S_k \sigma_k}{n-1}))}{T_i^2 \theta + \lambda(S_i^2 - 2\alpha\theta)} \quad (19)$$

$$\beta_i^* = \frac{T_i(\alpha\theta - \alpha n\theta + n\theta \sum_{k=1}^n T_k \beta_k + n\theta \sum_{k=1}^n S_k \sigma_k - C_i n\alpha\theta + C_i n^2 \alpha\theta - p_{k_i} n\gamma\theta)}{n(n-1)(T_i^2 \theta + S_i^2 \lambda - 2\alpha\theta\lambda)} \quad (20)$$

$$\sigma_i^* = \frac{S_i(\alpha\lambda - \alpha n\lambda + \sum_{k=1}^n T_k \beta_k n\lambda + n\lambda \sum_{k=1}^n S_k \sigma_k - C_i n\alpha\lambda + C_i n^2 \alpha\lambda - p_{k_i} n\gamma\lambda)}{n(n-1)(T_i^2 \theta + S_i^2 \lambda - 2\alpha\theta\lambda)} \quad (21)$$

To simplify the optimal equilibrium solutions, we consider the following variables: B is the sum of rivals' IoT integration effort function, W is the sum of rivals' sustainability effort, and G is the sum of rivals' price. The equilibrium values of the decision variables are thus expressed as follows:

$$p_i^* = \frac{C_i T_i^2 \theta + \lambda(C_i S_i^2 - \theta(\frac{a}{n} + C_i \alpha + \frac{G\gamma}{n-1} \frac{B}{n-1} - \frac{W}{n-1}))}{T_i^2 \theta + \lambda(S_i^2 - 2\alpha\theta)} \quad (22)$$

$$\beta_i^* = \frac{T_i(\alpha\theta - \alpha n\theta + n\theta B + n\theta W - C_i n\alpha\theta + C_i n^2 \alpha\theta - G n \gamma \theta)}{n(n-1)(T_i^2 \theta + S_i^2 \lambda - 2\alpha\theta\lambda)} \quad (23)$$

$$\sigma_i^* = \frac{S_i(\alpha\lambda - \alpha n\lambda + B n \lambda + n \lambda W - C_i n \alpha \lambda + C_i n^2 \alpha \lambda - G n \gamma \lambda)}{n(n-1)(T_i^2 \theta + S_i^2 \lambda - 2\alpha\theta\lambda)} \quad (24)$$

IV. ANALYTICAL RESULTS AND INSIGHTS

This section includes the execution of analytical and parametric sensitivity analyses alongside their corresponding corollaries and implications. To answer our research questions, we first examined the impact of the IoT integration and sustainability efforts of a firm i on its own price. Furthermore, we analyzed the impact of IoT integration and sustainability efforts of rival firms (B, W) on the firm's price, IoT integration and sustainability efforts. Given that the IoT implementation and sustainability practices costs are significant investments, we also explored the impact of their cost factors on the firm's decisions on price, IoT integration and sustainability efforts.

A. Impact of the IoT Integration Effort on the Equilibrium Price

Proposition 1: Increasing the IoT integration efforts of a firm leads to an increase in their price.

Corollary 1: The increase of the IoT integration effort of a firm leads to an increase in their price. This is due to the high costs associated with the technological investments and maintenance. Moreover, the magnitude of the effect of the integration effort on the price is influenced by the ratio of firm's demand sensitivity to the IoT integration and its price elasticity. This suggests that the degree of effect depends on how significantly sensitive is the 3PL market to the technology integration. In a more competitive technology-oriented market, the impact of integrating the IoT technology will be more significant.

Proof 1: By calculating the derivative of the equilibrium price of firm i by the IoT integration rate β_i , we can analyze how the changes in the integration rate can affect the price of firm i . Based on (16) we get:

$$\frac{dp_i^*}{d\beta_i} = \frac{n^2 T_i - n T_i}{2(n-1)n\alpha} = \frac{T_i}{2\alpha} \quad (25)$$

Since $\frac{T_i}{2\alpha} > 0$, hence the proposition.

B. Impact of the Sustainability Effort on the Equilibrium Price

Proposition 2: Increasing the sustainability efforts of a firm leads to an increase in their price.

Corollary 2: Changes in the sustainability effort positively affect the pricing of the service. As the effort increases the price increases as well. This is due to the costs associated with incorporating more sustainable practices in the 3PL services. Furthermore, the significance of the impact on the price depends on how the market is sensitive to the proposal of more sustainable service.

Proof 2: To analyze the impact of sustainability practices on the pricing, we calculate the derivative of the equilibrium price with respect to its sustainability effort.

$$\frac{\partial p_i^*}{\partial \sigma_i} = \frac{-n S_i + n^2 S_i}{2n\alpha(n-1)} = \frac{S_i}{2\alpha} \quad (26)$$

Since $\frac{S_i}{2\alpha} > 0$, hence the proposition

C. Impact of the IoT Integration Level and Sustainability Effort Level of Rival Firms (B, W) on Price

Proposition 3: Equilibrium price goes up with the increase of IoT integration and sustainability effort level of rival firms (B, W).

Corollary 3: The pricing strategy is significantly influenced by the IoT integration and sustainability efforts adopted by rival firms. As IoT integration and sustainability initiatives of competitors increase, the equilibrium price goes up. Understanding and being aware of these strategies implemented by competitors becomes crucial for firms aiming to maximize their profits. Such insights allow firms to strategize their IoT integrations and sustainability efforts and set their prices, leveraging the market trends. Encouraging cooperative models among firms emerges as an appealing approach. This enables firms to adapt collectively to market changes, ensuring better profitability while meeting evolving customer preferences for digitalization and sustainability.

Proof 3: The derivative of the equilibrium price with respect to the rivals' integration and sustainability efforts is calculated as follows:

$$\frac{\partial p_i^*}{\partial B} = \frac{\theta\lambda}{(n-1)(T^2\theta + (S^2 - 2\alpha\theta)\lambda)} \quad (27)$$

$$\frac{\partial p^*}{\partial W} = \frac{\theta\lambda}{(n-1)(T^2\theta + (S^2 - 2\alpha\theta)\lambda)} \quad (28)$$

According to (15) we have $(T^2\theta + S^2\lambda - 2\alpha\theta\lambda) > 0$ and since $\theta\lambda > 0$ hence the proposition.

D. Impact of the Average IoT Integration Level and Sustainability Efforts of Rival Firms (B,W) on IoT Integration Level

Proposition 4: As the IoT integration and sustainability effort of rivals increases, the equilibrium IoT integration effort increases.

Corollary 4: When the efforts of sustainability and IoT integration among rival firms increases, it positively influences the equilibrium IoT integration level. This scenario signifies the market landscape where sustainability and IoT implementation norms are escalating impacts the firm's strategic choices on the level of IoT integration. As rivals collectively intensify their focus on sustainability and digitalization initiatives, it exhibits a positive impact on the equilibrium integration level of the firm. To remain competitive and align with evolving market standards, the firm is urged to increase its IoT integration efforts.

In the context of 3PL market, when a firm increases its IoT integration rate and gain competitive advantage, the other firms tend to follow to stay competitive. Moreover, this also suggests the possibility of cooperation between the firms in investing on the implementation of IoT technology in their fleet and warehouses.

Proof 4: The derivative of the equilibrium IoT integration effort with respect to the rivals' average integration and sustainability efforts is calculated as follows:

$$\frac{\partial \beta^*}{\partial B} = \frac{T\theta}{(-1+n)(T^2\theta + S^2\lambda - 2\alpha\theta\lambda)} \quad (29)$$

$$\frac{\partial \beta^*}{\partial W} = \frac{T\theta}{(-1+n)(T^2\theta + S^2\lambda - 2\alpha\theta\lambda)} \quad (30)$$

According to (15) we have $(T^2\theta + S^2\lambda - 2\alpha\theta\lambda) > 0$ and since $T\theta > 0$ hence the proposition.

E. Impact of IoT Integration Level and Sustainability Effort Level of Rival Firms (B,W) on Sustainability Efforts

Proposition 5: As the IoT integration and sustainability level of rivals increases, sustainability effort level increases.

Corollary 5: When the efforts of sustainability and IoT integration among rival firms increases, it positively influences the sustainability effort level. This scenario signifies the market landscape where sustainability and IoT implementation norms are escalating impacts the firm's strategic choices on the level of IoT integration. As rivals collectively intensify their focus on sustainability and digitalization initiatives, it displays a positive impact on the equilibrium sustainability effort of the firm. To remain competitive and align with evolving market

standards, the firm is urged to increase its IoT integration efforts.

Proof 5: The derivative of the equilibrium price with respect to the rivals' average integration and sustainability efforts is calculated as follows:

$$\frac{\partial \sigma^*}{\partial B} = \frac{S\lambda}{(n-1)(T^2\theta + S^2\lambda - 2\alpha\theta\lambda)} \quad (31)$$

$$\frac{\partial \sigma^*}{\partial W} = \frac{S\lambda}{(n-1)(T^2\theta + S^2\lambda - 2\alpha\theta\lambda)} \quad (32)$$

According to (15) we have $(T^2\theta + S^2\lambda - 2\alpha\theta\lambda) > 0$ and since $S\lambda > 0$, hence the proposition.

F. Impact of IoT Integration and Sustainability Effort cost Factor (λ,θ) on IoT Integration Effort

Proposition 6: IoT integration effort decreases with the increase of the IoT implementation cost factor if the following is established:

$$B + W > (n - 1)\left(\frac{a}{n} - C\alpha\right) + G\gamma \quad (33)$$

Corollary 6: The cost factor of the IoT integration of a firm is an influencing factor in the decision making of the IoT integration effort, under certain conditions linked to both customer sensitivity to the sustainability effort and the rival strategies. Under these conditions, an increase in the IoT integration cost factor leads to a decrease in the equilibrium level of IoT integration. This case is expected as firm will face the barrier of high implementation costs. However, in the case when (33) is not met, the equilibrium IoT integration level increases although the IoT integration cost increases. In that scenario, the customers are less sensitive to the sustainability effort and rivals' IoT integration and sustainability efforts are low.

Proof 6: Based on (23) the derivative of the IoT integration effort β^* with respect to its cost factor λ can be calculated as follows:

$$\frac{\partial \beta^*}{\partial \lambda} = -\frac{T\theta(S^2 - 2\alpha\theta)\left(\frac{a}{n} - a + B + W - C\alpha + Cn\alpha - G\gamma\right)}{(n-1)(T^2\theta + S^2\lambda - 2\alpha\theta\lambda)^2} \quad (34)$$

$(S^2 - 2\alpha\theta)(a/n - a + B + W - C\alpha + Cn\alpha - G\gamma) > 0$ implies $\frac{\partial \beta^*}{\partial \lambda} < 0$. Accordingly to (15), $\frac{\partial \beta^*}{\partial \lambda} < 0$ when $(a/n - a + B + W - C\alpha + Cn\alpha - G\gamma) > 0$. On the other hand, when $\left(\frac{a}{n} - a + B + W - C\alpha + Cn\alpha - G\gamma\right) < 0$ it implies $\frac{\partial \beta^*}{\partial \lambda} > 0$.

Proposition 7: IoT integration effort increases with the increase of the sustainability level sensitivity if the following is established:

$$B + W > (n - 1)\left(\frac{a}{n} - C\alpha\right) + G\gamma \quad (35)$$

Corollary 7: In comparison to the observed impact of IoT integration cost factor, the impact of sustainability effort cost factor on IoT integration levels within firms are predominantly influenced by in the competitions' strategies. In addition, when the sustainability cost factor is greatly low the equilibrium IoT integration level approaches zero. In this scenario, when the sustainability investments are low enough, firms will favor sustainability efforts over IoT integration strategy.

Proof 7: Based on (23) the derivative of the IoT integration effort β^* with respect to its sustainability cost factor θ can be calculated as follows:

$$\frac{\partial \beta^*}{\partial \theta} = \frac{S^2 T \lambda (a/n - a + B + W - C\alpha + Cn\alpha - G\gamma)}{(n-1)(T^2\theta + (S^2 - 2\alpha\theta)\lambda)^2} \quad (36)$$

Also, when the cost factor is low and $\theta \rightarrow 0$ we have: $\lim_{\theta \rightarrow 0} \beta^* = 0$.

G. Comparison of a Duopoly and Oligopoly Market

To further analyze our model, we will compare the equilibrium decision variables; price, IoT integration and sustainability efforts and profit in two special cases. The first is a duopoly market setting, for this latter we consider $n = 2$. We will then compare it to the case when the number of firms n is considerably high, in this case we will calculate the equilibrium decision variables and profit when n approaches ∞ . We assume the parameters $(C, T, S, \theta, \lambda, \alpha)$ are equal in both scenarios.

Duopoly case: We denote the price, IoT integration effort, sustainability effort and profit for firm i in this case as p_2^* , β_2^* , σ_2^* and π_2^* respectively. And B^d, W^d, G^d and a^d the rival's IoT integration effort, sustainability effort, price, and market share in the duopoly market respectively.

Oligopoly case: We denote the price, IoT integration effort, sustainability effort and profit for firm i in the case where n is considerably high as p_n^* , β_n^* , σ_n^* and π_n^* respectively.

Proposition 8: The ordinal relationship of the decision variables (price, IoT integration effort and sustainability effort) in the duopoly case and oligopoly market setting are related as follows: $p_2^* < p_n^*$, $\beta_2^* < \beta_n^*$ and $\sigma_2^* < \sigma_n^*$ when the following is established: $2(B^d + W^d - G^d\gamma) < a^d$. Whereas $\pi_2^* > \pi_n^*$ when $(a^d - 2(B^d + W^d - G^d\gamma))(a^d - 2(B^d + W^d + 2C\alpha - G^d\gamma))(-T^2\theta - S^2\lambda + \alpha\theta\lambda) > 0$.

Corollary 8: The equilibrium price, IoT integration and sustainability efforts increase as the number of firms n increases. This suggests firms could charge higher prices even in competitive markets with differentiating their service by engaging in technological and sustainable operations. However, when $2(B^d + W^d - G^d\gamma) > a^d$ is established, the equilibriums values are higher in the duopoly setting. This inequality suggests a highly competitive intensity and a saturated market where firms are investing significantly in IoT and sustainability efforts. This scenario may lead to diminishing returns on investment and the need to careful strategic consideration to align with market potential. Accordingly, the price, IoT integration and sustainability efforts are higher in an intense competitive duopoly market compared to highly competitive market with numerous firms.

Proof 8: We calculate the limits of the decision variables and profit when $n = 2$ and when n approaches ∞ .

We have:

$$\lim_{n \rightarrow \infty} p^* = \frac{CT^2\theta + CS^2\lambda - C\alpha\theta\lambda}{T^2\theta + S^2\lambda - 2\alpha\theta\lambda} \text{ and}$$

$$p_2^* = \frac{-(a^d - 2\theta\lambda(B^d + W^d - G^d\gamma)) + 2C(T^2\theta + \lambda(S^2 - \alpha\theta))}{2(T^2\theta + (S^2 - 2\alpha\theta)\lambda)}$$

Hence, we have:

$$p_2^* - p_n^* = \theta\lambda \frac{2(B^d + W^d - G^d\gamma) - a^d}{2(T^2\theta + (S^2 - 2\alpha\theta)\lambda)} \quad (37)$$

We have

$$\lim_{n \rightarrow \infty} \beta^* = \frac{CT\alpha\theta}{T^2\theta + S^2\lambda - 2\alpha\theta\lambda} \text{ and } \beta_2^* = \frac{T(-a^d\theta + 2B^d\theta + 2W^d\theta + 2C\alpha\theta - 2G^d\gamma\theta)}{2(T^2\theta + S^2\lambda - 2\alpha\theta\lambda)}$$

Hence,

$$\beta_2^* - \beta_n^* = T\theta \frac{2(B^d + W^d - G^d\gamma) - a^d}{2(T^2\theta + \lambda(S^2 - 2\alpha\theta))} \quad (38)$$

We have:

$$\lim_{n \rightarrow \infty} \sigma^* = \frac{CS\alpha\lambda}{T^2\theta + S^2\lambda - 2\alpha\theta\lambda} \text{ and } \sigma_2^* = \frac{S(-a^d\lambda + 2B^d\lambda + 2W^d\lambda + 2C\alpha\lambda - 2G^d\gamma\lambda)}{2(T^2\theta + S^2\lambda - 2\alpha\theta\lambda)}$$

Hence,

$$\sigma_2^* - \sigma_n^* = S\lambda \frac{2(B^d + W^d - G^d\gamma) - a^d}{2(T^2\theta + \lambda(S^2 - 2\alpha\theta))} \quad (39)$$

We have:

$$\lim_{n \rightarrow \infty} \pi^* = -\frac{C^2\alpha^2\theta\lambda}{T^2\theta + (S^2 - 2\alpha\theta)\lambda} \quad \pi_2^* = \frac{\theta\lambda[(a - 2(B^d + W^d + C\alpha - G^d\gamma))^2(-T^2\theta - S^2\lambda + \alpha\theta\lambda) + 4C^2\alpha^2\theta\lambda]}{4(T^2\theta + (S^2 - 2\alpha\theta)\lambda)^2}$$

$$\pi_2^* - \pi_n^* = \frac{(a - 2(B^d + W^d - G^d\gamma))(a - 2(B^d + W^d + 2C\alpha - G^d\gamma))\theta\lambda(-T^2\theta - S^2\lambda + \alpha\theta\lambda)}{4(T^2\theta + (S^2 - 2\alpha\theta)\lambda)^2} \quad (40)$$

V. NUMERICAL ANALYSIS

To deepen our understanding and analysis of the model, we conducted a numerical analysis. For the subsequent analyses, we will employ the following values for the parameters.

- Total market size $a = 80$.
- Number of Competitors $n = 5$.
- Self-price Sensitivity $\alpha = -1.0$.
- Cross-price Sensitivity $\gamma = 0.5$.
- Market Sensitivity to IoT Integration $T_i = 0.5$.
- Market Sensitivity to Sustainability Effort $S_i = 0.5$.
- IoT Integration Cost Factor $\lambda = 0.2$.
- Sustainability Initiative Cost Factor $\theta = 0.2$.
- Price $p_i = 100$.
- Sustainability Effort $\sigma_i = 0.5$.
- $C_i = 50$.
- $G = 400$.

A. Effect of β_i Variation on Firm i 's Profit Across Different B Scenarios

The initial analysis examined the effect of β_i variation on firm i 's profit across different scenarios, adjusting the values of B accordingly. Fig. 2 represents the variation of the profit with β_i .

The profit exhibits fluctuations with rising β_i , suggesting that the firm's investment in IoT integration impacts profitability in varying ways, contingent on the competitive environment. As B increases the profitability of the firm tends to diminish. This suggests the need to consider competitor's strategy when planning its own emphasizing the importance to have strategic flexibility to both competitive pressures and market demand.

B. Profit Variation Across Different Scenarios

Through the analysis of multiple scenarios, we examined the profitability of Firm i considering different scenarios related to IoT and sustainability efforts by both Firm i and its competitors.

Scenario 1: Firm i implements both IoT and sustainability practices while competitors don't: in this scenario we consider $\beta_i = 0.5, \sigma_i = 0.5$ while $B = 0, W = 0$.

Scenario 2: Firm i implements only IoT while competitors don't: in this scenario we consider $\beta_i = 0.5, \sigma_i = 0$ while $B = 0, W = 0$.

Scenario 3: Both Firm i and its competitors implements both IoT and sustainability: in this scenario we consider $\beta_i = 0.5, \sigma_i = 0.5$ while $B = 3, W = 3$.

Scenario 4: Firm i only implements IoT and its competitors implements both IoT and sustainability: in this scenario we consider $\beta_i = 0.5, \sigma_i = 0$ while $B = 3, W = 3$.

Scenario 5: Firm i implements both IoT and sustainability and its competitors only implement IoT: in this scenario we consider $\beta_i = 0.5, \sigma_i = 0.5$ while $B = 3, W = 0$.

Scenario 6: Both Firm i and its competitors only implement IoT: in this scenario we consider $\beta_i = 0.5, \sigma_i = 0$ while $B = 3, W = 0$.

Combining sustainability efforts with IoT integration can provide strategic benefits, particularly when competitors lag in sustainability initiatives or concentrate exclusively on technological advancements. The scenarios highlight the importance of aligning the firm's strategy with market dynamics, competitor actions, and the opportunity to differentiate.

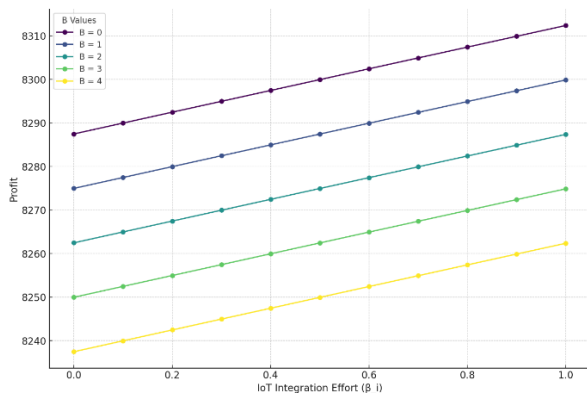


Fig. 2. β_i variation on Firm i 's profit across different B scenarios.

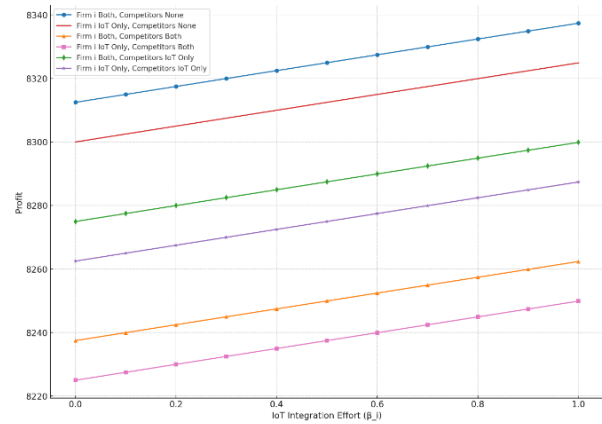


Fig. 3. Profit variation across different implementation scenarios.

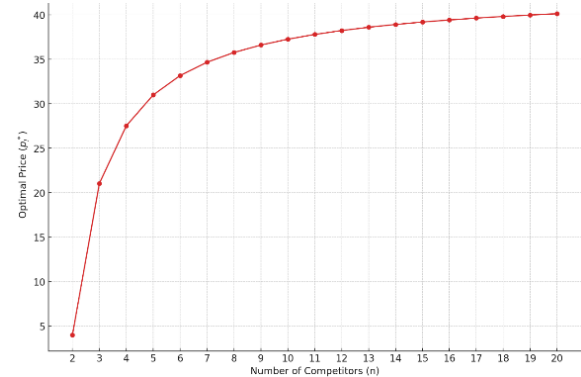


Fig. 4. Optimal price with the variation of the number of firms.

Fig. 3 shows the profit across the different scenarios.

C. Influence of the Number of Competitors on Optimal Price

This analysis aims to examine the impact of the number of firms on the equilibrium price. For this we will proceed with the previously mentioned values with: $B = 2, W = 2, T_i = 0.5, S_i = 0.5$ and the result is showed in Fig. 4.

As the market sees an increase in the number of competitors, the optimal price tends to rise. However, in a more saturated market, the influence of additional competitors on price changes diminishes, with the impact becoming minimal.

D. Sensitivity Analysis

We conducted a sensitivity analysis of the firm i 's profit in relation to Market Sensitivity to IoT Integration and sustainability efforts (T_i, S_i) as well as IoT Integration and sustainability effort Cost Factors (λ, θ).

1) *Market sensitivity to IoT integration and sustainability efforts:* For this analysis we will proceed with the previously mentioned values with minor adjustments $\beta_i = 0.5, \sigma_i = 0.5, B = 3, W = 3$, and the results are presented in Fig. 5.

The profit increases as the sensitivity for the IoT and sustainability increases. This emphasizes the importance of aligning firm's decision with market expectations.

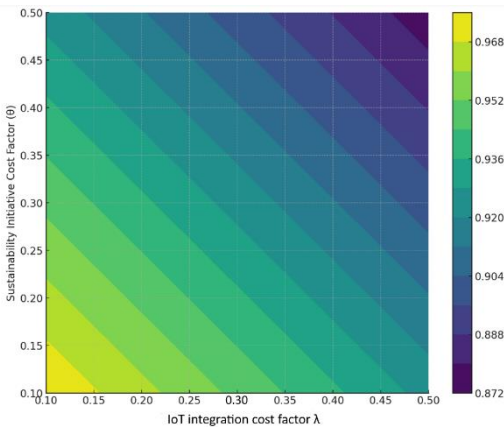


Fig. 5. Market sensitivity to IoT integration and sustainability effort.

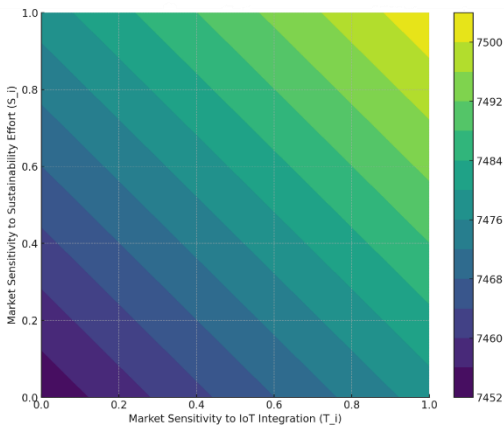


Fig. 6. Market sensitivity to IoT integration and sustainability cost factors.

2) *IoT integration effort and sustainability effort cost factors*: For the sensitivity analysis of the cost factors, several key parameters have been adjusted to reflect the market conditions and strategic responses more accurately. The self-price sensitivity parameter α has been modified to -0.5 . The cross-price sensitivity γ has been lowered to 0.3 . To allow for greater pricing flexibility, the total market size a has been increased to 100 , $G = 300$, $B = 2$ $W = 2$. Fig. 6 showcases the results of this sensitivity analysis.

As cost factors rise, profit tend to decrease. Companies must weigh the strategic advantages of these investments against their cost and value to maximize profitability.

VI. CONCLUSION

In this paper, we explored the impact of integrating the IoT technologies and more sustainable initiatives into the 3PL firm's service on its pricing strategies and profitability. In this research we studied the competition of the 3PL firms in an oligopolistic market setting through price, IoT integration efforts and sustainability effort. The horizontal competition between the firms is modelled as a simultaneous game. We formulate equilibrium strategies for players within this game-theoretic framework and examine the resulting equilibrium outcomes. Our analysis has proved the firm's price increases with the IoT integration and sustainability efforts. Furthermore, our study has showed that the price of the service, the IoT

integration and sustainability efforts of the firm increase with the increase of the rivals' IoT integration and sustainability efforts. On the other hand, under certain conditions, the cost of the investments of IoT technology and sustainability initiatives decreases the firm's IoT technology and sustainability efforts. Moreover, we have conducted a comparison between a duopoly setting and an oligopoly market, proving that under certain circumstances, the price, IoT integration and sustainability efforts as well as the firm's profit decreases with the intensity of competition. To achieving a favorable outcome demands careful balance between strategic investments in technology and sustainability, pricing strategies that are aligned with market sensitivity and a keen understanding of the competitive landscape. This study underlines the importance of strategic adaptability and agility for firms to constantly adjust their strategies to keep pace with shifting market trends and competitive pressures.

While this research has provided valuable insights in understanding the impact of IoT integration and sustainability efforts within a 3PL oligopolistic market, it is crucial to recognize its limitations. To simplify complex mathematical calculations, few assumptions have been made. Moreover, to keep out model simple we have considered the sustainability; future research can further develop the model by considering each dimension of the sustainability effort in order to investigate the impact and interrelation of each dimension. Our study focused on a non-cooperative ecosystem, further research can explore how collaborative efforts for integrating IoT technologies within the service as well as sustainable practices within the 3PL firms impact pricing strategies and profitability. Furthermore, the 3PL sector operate in various industries; healthcare, e-commerce food, etc. investigating how digitalization and sustainability efforts in each industry influence their decision-making processes can bring significant insights. Similarly, further research can be conducted taking into consideration digitalization and sustainability trends and regulations differences in the global 3PL market.

REFERENCES

- [1] M. Akhtar, "Logistics services outsourcing decision making: a literature review and research agenda," *International Journal of Production Management and Engineering*, vol. 11, no. 1, pp. 73–88, Jan. 2023, doi: 10.4995/IJPM.2023.18441.
- [2] B. Borgström, S. Hertz, and L. M. Jensen, "Strategic development of third-party logistics providers (TPLs): 'Going under the floor' or 'raising the roof'?", *Industrial Marketing Management*, vol. 97, pp. 183–192, Aug. 2021, doi: 10.1016/J.INDMARMAN.2021.07.008.
- [3] E. Hofmann and F. Osterwalder, "Third-Party Logistics Providers in the Digital Age: Towards a New Competitive Arena?," *Logistics*, vol. 1, no. 2, p. 9, Nov. 2017, doi: 10.3390/logistics1020009.
- [4] F. Ebinger and B. Omondi, "Leveraging digital approaches for transparency in sustainable supply chains: A conceptual paper," *Sustainability (Switzerland)*, vol. 12, no. 15, Aug. 2020, doi: 10.3390/su12156129.
- [5] M. B. Jamali and M. Rasti-Barzoki, "A game theoretic approach to investigate the effects of third-party logistics in a sustainable supply chain by reducing delivery time and carbon emissions," *J Clean Prod*, vol. 235, pp. 636–652, Oct. 2019, doi: 10.1016/j.jclepro.2019.06.348.
- [6] G. Büyükköçkan and F. Göçer, "Digital Supply Chain: Literature review and a proposed framework for future research," *Comput Ind*, vol. 97, pp. 157–177, May 2018, doi: 10.1016/j.compind.2018.02.010.

- [7] D. Egorov, A. Levina, S. Kalyazina, P. Schuur, and B. Gerrits, "The Challenges of the Logistics Industry in the Era of Digital Transformation," 2021, pp. 201–209. doi: 10.1007/978-3-030-64430-7_17.
- [8] C. M. Wallenburg and A. M. Knemeyer, "The future of 3PLs," *Global Logistics and Supply Chain Strategies for the 2020s: Vital Skills for the Next Generation*, pp. 119–133, Dec. 2022, doi: 10.1007/978-3-030-95764-3_7/COVER.
- [9] M. Cichosz, C. M. Wallenburg, and A. M. Knemeyer, "Digital transformation at logistics service providers: barriers, success factors and leading practices," *International Journal of Logistics Management*, vol. 31, no. 2, pp. 209–238, Jul. 2020, doi: 10.1108/IJLM-08-2019-0229/FULL/PDF.
- [10] H. Khosroshahi, M. Rasti-Barzoki, and S. R. Hejazi, "A game theoretic approach for pricing decisions considering CSR and a new consumer satisfaction index using transparency-dependent demand in sustainable supply chains," *J Clean Prod*, vol. 208, pp. 1065–1080, Jan. 2019, doi: 10.1016/j.jclepro.2018.10.123.
- [11] Y. Kayikci, "Sustainability impact of digitization in logistics," in *Procedia Manufacturing*, Elsevier B.V., 2018, pp. 782–789. doi: 10.1016/j.promfg.2018.02.184.
- [12] M. Attaran, "Digital technology enablers and their implications for supply chain management," *Supply Chain Forum: An International Journal*, vol. 21, no. 3. Taylor and Francis Ltd., pp. 158–172, Jul. 02, 2020. doi: 10.1080/16258312.2020.1751568.
- [13] M. Abdel-Basset, G. Manogaran, and M. Mohamed, "Internet of Things (IoT) and its impact on supply chain: A framework for building smart, secure and efficient systems," *Future Generation Computer Systems*, vol. 86. Elsevier B.V., pp. 614–628, Sep. 01, 2018. doi: 10.1016/j.future.2018.04.051.
- [14] A. Mahmoudi, R. Mahmoudi, A. Emrouznejad, and A. Hafezalkotob, "Sustainable multi-channel supply chain design: an intuitive fuzzy game theory approach to deal with uncertain business environment," *Environ Dev Sustain*, 2022, doi: 10.1007/s10668-022-02623-w.
- [15] C. Tan, Y. Zeng, W. H. Ip, and C. H. Wu, "B2C or O2O? The strategic implications for the fresh produce supply chain based on blockchain technology," *Comput Ind Eng*, vol. 183, Sep. 2023, doi: 10.1016/j.cie.2023.109499.
- [16] B. B. Gardas, R. D. Raut, and B. E. Narkhede, "Analysing the 3PL service provider's evaluation criteria through a sustainable approach," *International Journal of Productivity and Performance Management*, vol. 68, no. 5, pp. 958–980, Jun. 2019, doi: 10.1108/IJPPM-04-2018-0154.
- [17] K. Izikki, J. El Alami, and M. Hlyal, "Internet of things in the sustainable supply chains: a systematic literature review with content analysis," *J Theor Appl Inf Technol*, vol. 15, no. 13, 2022, [Online]. Available: www.jatit.org
- [18] E. Manavalan and K. Jayakrishna, "A review of Internet of Things (IoT) embedded sustainable supply chain for industry 4.0 requirements," *Comput Ind Eng*, vol. 127, pp. 925–953, Jan. 2019, doi: 10.1016/j.cie.2018.11.030.
- [19] F. Li, "Outsourcing pricing between 3PL and manufacturer based on asymmetric information," in *Proceedings of International Conference on Service Science, ICSS, 2013*, pp. 192–195. doi: 10.1109/ICSS.2013.55.
- [20] E. Gkanatsas and H. Krikke, "Towards a pro-silience framework: A literature review on quantitative modelling of resilient 3PL supply chain network designs," *Sustainability (Switzerland)*, vol. 12, no. 10. MDPI, May 01, 2020. doi: 10.3390/su12104323.
- [21] L. Ma, C. Jin, and Y. Huo, "Selection of logistics service modes in e-commerce based on multi-oligopolies Cournot competition," 2019. [Online]. Available: <https://chaoshi.>
- [22] R. Stekelorum, I. Laguir, S. Gupta, and S. Kumar, "Green supply chain management practices and third-party logistics providers' performances: A fuzzy-set approach," *Int J Prod Econ*, vol. 235, p. 108093, May 2021, doi: 10.1016/J.IJPE.2021.108093.
- [23] H. Jung, "Evaluation of third party logistics providers considering social sustainability," *Sustainability (Switzerland)*, vol. 9, no. 5, 2017, doi: 10.3390/su9050777.
- [24] N. Kafa, Y. Hani, and A. El Mhamedi, "IFIP AICT 439 - A Fuzzy Multi Criteria Approach for Evaluating Sustainability Performance of Third – Party Reverse Logistics Providers," 2014.
- [25] K. Govindan, M. Kadziński, R. Ehling, and G. Miebs, "Selection of a sustainable third-party reverse logistics provider based on the robustness analysis of an outranking graph kernel conducted with ELECTRE I and SMAA," *Omega (United Kingdom)*, vol. 85, pp. 1–15, Jun. 2019, doi: 10.1016/j.omega.2018.05.007.
- [26] I. Dadashpour and A. Bozorgi-Amiri, "Evaluation and Ranking of Sustainable Third-party Logistics Providers using the D-Analytic Hierarchy Process," *International Journal of Engineering, Transactions B: Applications*, vol. 33, no. 11, pp. 2233–2244, Nov. 2020, doi: 10.5829/ije.2020.33.11b.15.
- [27] N. G. Gidener and D. A. Deveci, "An analysis of service failures and recovery strategies in the Turkish third party logistics service industry," *Transactions on Maritime Science*, vol. 9, no. 1, pp. 35–50, 2020, doi: 10.7225/toms.v09.n01.003.
- [28] C. S. Fisk, "Game Theory and Transportation Systems Modelling," 1984.
- [29] G. Zhang, X. Wang, Y. Zhang, and J. Kang, "Research on the Emission Reduction Decision of Cost-Sharing Logistics Service Supply Chain in the O2O Model," *Sustainability (Switzerland)*, vol. 14, no. 20, Oct. 2022, doi: 10.3390/su142013247.
- [30] H. T. Sukmana, A. E. Widjaja, and H. J. Situmorang, "Game Theoretical-Based Logistics Costs Analysis: A Review," *International Transactions on Artificial Intelligence (ITALIC)*, vol. 1, no. 1, pp. 43–61, 2022, doi: 10.34306.
- [31] S. K. Jena, S. P. Sarmah, and S. S. Padhi, "Impact of government incentive on price competition of closed-loop supply chain systems," *INFOR*, vol. 56, no. 5, pp. 192–224, 2018, doi: 10.1080/03155986.2017.1361198.
- [32] Z. Wang and Q. Wu, "Carbon emission reduction and product collection decisions in the closed-loop supply chain with cap-and-trade regulation," *Int J Prod Res*, vol. 59, no. 14, pp. 4359–4383, 2021, doi: 10.1080/00207543.2020.1762943.
- [33] S. R. Madani and M. Rasti-Barzoki, "Sustainable supply chain management with pricing, greening and governmental tariffs determining strategies: A game-theoretic approach," *Comput Ind Eng*, vol. 105, pp. 287–298, Mar. 2017, doi: 10.1016/j.cie.2017.01.017.
- [34] S. S. Sana, "A structural mathematical model on two echelon supply chain system," *Ann Oper Res*, vol. 315, no. 2, pp. 1997–2025, Aug. 2022, doi: 10.1007/s10479-020-03895-z.
- [35] B. Dai, Y. Nu, X. Xie, and J. Li, "Interactions of traceability and reliability optimization in a competitive supply chain with product recall," *Eur J Oper Res*, vol. 290, no. 1, pp. 116–131, Apr. 2021, doi: 10.1016/j.ejor.2020.08.003.
- [36] A. Dash, S. P. Sarmah, and M. K. Tiwari, "Economic Analysis of Public Priced IoT Based Traceability System in Perishable Food Supply Chain," 2022.
- [37] X. Li, "Reducing channel costs by investing in smart supply chain technologies," *Transp Res E Logist Transp Rev*, vol. 137, May 2020, doi: 10.1016/j.tre.2020.101927.
- [38] L. Yang, Y. Ni, and C. T. Ng, "Blockchain-enabled traceability and producer's incentive to outsource delivery," *Int J Prod Res*, vol. 61, no. 11, pp. 3811–3828, 2023, doi: 10.1080/00207543.2022.2072785.
- [39] K. Izikki, M. Hlyal, A. Ait Bassou, and J. El Alami, "Study of the Impact of the Internet of Things Integration on Competition Among 3PLs," *IJACSA International Journal of Advanced Computer Science and Applications*, vol. 14, no. 9, 2023, doi: 10.14569/IJACSA.2023.0140946.
- [40] S. Kumar Jena and D. Singhal, "Optimizing the competitive sustainable process and pricing decision of digital supply chain: A power-balance perspective," *Comput Ind Eng*, vol. 177, Mar. 2023, doi: 10.1016/j.cie.2023.109054.
- [41] A. Naimi-Sadigh, S. K. Chaharsooghi, and M. Mozafari, "Optimal Pricing And Advertising Decisions with Suppliers' Oligopoly Competition: Stakelberg-Nash Game Structures," *Journal of Industrial and Management Optimization*, vol. 17, no. 3, pp. 1423–1450, May 2021, doi: 10.3934/jimo.2020028.

- [42] H. Khosroshahi, "Using Salesperson for Chain-to-Chain Competition in Oligopoly Markets: A Game-Theoretical Approach," 2021. [Online]. Available: <https://www.researchgate.net/publication/361258728>
- [43] J. Zhang and Z. Song, "Decision Optimization of Four-Level Supply Chain with the Participation of Two-Echelon Logistics Service Providers under Different Power Structures," *Math Probl Eng*, vol. 2021, 2021, doi: 10.1155/2021/5518840.

Unified Approach for Scalable Task-Oriented Dialogue System

Manisha Thakkar, Nitin Pise

Department of Computer Engineering and Technology, Dr Vishwanath Karad, MIT World Peace University, Pune, India

Abstract—Task-oriented dialogue (TOD) systems are currently the subject of extensive research owing to their immense significance in the fields of human-computer interaction and natural language processing. These systems assist users to accomplish certain tasks efficiently. However, most commercial TOD systems rely on handcrafted rules and offer functionalities in a single domain. These systems perform well but are not scalable to adapt multiple domains without manual efforts. Pretrained language models (PLMs) have been popularly applied to enhance these systems via fine-tuning. Recently, large language models (LLMs) have made significant advancements in this field but lack the ability to converse proactively in multiple turns, which is an essential parameter for designing TOD systems. To address these challenges, this paper initially studies the impact of language understanding on the overall performance of a TOD system in a multi-domain environment. Furthermore, to design an efficient TOD system, we propose a unified approach by leveraging LLM with reinforcement learning (RL) based dialogue policy. The experimental results demonstrate that a unified approach using LLM is more promising for scaling the capabilities of TOD systems with prompt adaptive instructions with more user friendly and human-like response generation.

Keywords—Task-oriented dialogue system; unified; adaptive multi-domain; large language models; prompts

I. INTRODUCTION

Creating a dialogue system that has intelligence to converse like a human and assist in task completion is challenging. Depending upon the functional positioning of these systems in practice, are classified into two distinct types, Chit-chat systems also known as Open-domain dialogue systems, and Task-oriented dialogue (TOD) systems. Open-domain dialogue systems are not bound to any specific goal completion, and have flexibility to talk about any arbitrary topic, such as movies, sports, politics, etc. Open-domain dialogue systems are usually trained on large-scale social media data to engage users in human-like casual conversations. For example, ELIZA [1], which is the first open-domain dialogue system that plays the role of therapist; Parry [2], which acts like a psychology patient; and the recent chatbot, Xiaobing from Microsoft, which is a smart and emotionally aware open-domain dialogue system.

On the other hand, TOD systems are closed domain systems and have specific goals to be completed efficiently by assisting users. For instance, for tasks such as booking a flight or a taxi, scheduling an appointment, ordering food, etc., TOD systems are expected to ask questions proactively to accomplish well-defined user goals in minimum dialogue

turns. This helps real users perform another important task to increase productivity. In the real world, these systems are utilized in various applications, such as QA systems at help desks to answer basic questions, and as pedagogical agents to assist in learning languages. On a day-to-day basis, users seek help from pretrained TOD systems such as Google Mini, Apple's Siri, Amazon's Echo, etc., to operate smart home devices, play music, and ask general questions to obtain answers [3]. In this study, our main focus was on TOD systems.

Most commercial dialogue systems have excelled in their ability to support singular domain functionalities [4]. To design such systems meticulously, handcrafted rules are used to understand the meaning of the sentence, to track the dialogue state in each turn, and to select the appropriate response. Domain experts participate in updating these rules to support each new task or domain. Each domain has a structured ontology that contains a set of predefined slot-value pairs. Consider an example of a restaurant TOD system that offers basic inquiry and booking related tasks. As shown in Table I, the domain ontology contains predefined slots for basic inquiry and booking tasks. Slot-value information is semantically represented as dialogue acts (DAs), which are updated in each turn during the slot-filling process. Any DA is either an inform act, a request act, or a greet act. Inform acts are used to inform user constraints from user queries to the dialogue system. Request acts are used by dialogue system to obtain additional information from user to fill needed slots, and greet acts are used to greet the user.

As shown in Table I, in basic DAs, primary information about restaurants is requested or informed by utilizing basic slots such as address, postcode, phone no, food type, price range (cheap, moderate, expensive), etc. Mandatory information for booking tasks such as number of people, number of days, and booking reference number are utilized by booking-related DAs.

Traditionally, the pipeline architecture of a TOD system has four components: natural language understanding (NLU), dialogue state tracking (DST), dialogue policy (POL), and natural language generation (NLG), as depicted in Fig. 1.

The NLU is responsible for recognizing user intentions by applying tokenization, and extracting information about domains, intents, slots, and values from user queries. This information is represented as a semantic frame, which is given to DST. This component keeps track of the slot-value pairs by maintaining a belief state in each turn along with the dialogue history. The current DST information is given as input to the

POL, which decides the next appropriate action, i.e., system DA, such as acknowledging user about the task completion or requesting additional information to fill mandatory slots. Finally, the NLG module generates a natural language response according to the system DA [6].

TABLE I. RESTAURANT DOMAIN ONTOLOGY [5]

| | | |
|--------------------------|----------------------|--|
| Dialogue Act-type | basic acts | inform /request/ select/recommend/not found |
| | booking related acts | request booking info / offer booking/ inform booked / decline booking |
| | greet acts | welcome /greet / bye / reqmore |
| Slots | basic slots | address / postcode / phone/ name/ no of choices / area / price range / type / food |
| | booking slots | no of people / reference no / no of days |

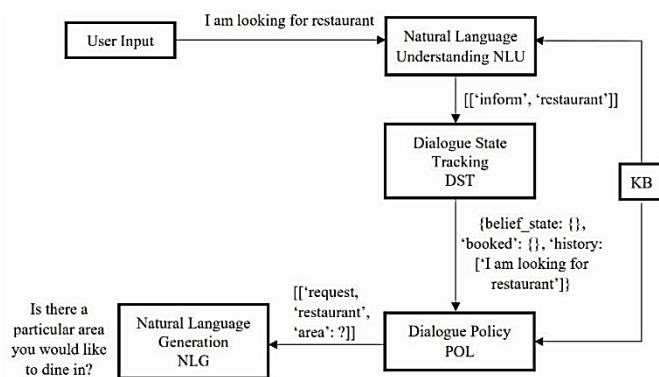


Fig. 1. Pipeline architecture of the TOD system.

To accomplish the intended task while comprehending user goals presents a formidable challenge. Commercial TOD systems are usually designed for specific domains using tools such as Microsoft’s Power Virtual Agents (PVA) or Google’s Dialog Flow. Consider a complex practical scenario where the user is asking for directions to the movie hall, and later, in the same dialogue session, the user wants to book a taxi to reach the hall. Here, both the navigation and taxi domains have a different set of (slot, value) pairs and actions. Contextual understanding is essential for understanding user intention for effective conversation in such dynamic scenarios. Recent advancements using PLMs and LLMs have made promising achievements in addressing complex real-world problems in natural language processing (NLP). This paper aims to achieve following objectives:

- To study and analyze the impact of language understanding on the overall performance of a TOD system in multi-domain conversation.
- To design a scalable TOD system with state-of-the-art NLU approaches and an RL-based dialogue policy instead of handcrafted rules.
- To enhance the TOD system by utilizing a unified LLM with instruction prompts for the NLU, DST and NLG tasks by boosting the convergence of RL-based dialogue policy with few samples of task demonstrations.

The paper is organized as follows: In Section II, the Literature Survey discusses previous work and recent

advancements in the related field. Section III, Designing TOD Systems for multi-domain dialogues, elucidates design approaches for components of the dialogue system pipeline. In Section IV, Experimental Setup, provide details about the dataset, toolkit utilized, system configuration, and results of the experiments. Section V, Evaluation, presents a comprehensive comparison of the performance of dialogue systems designed with various approaches. Discussion is given in Section VI. Finally, Section VII concludes the paper.

II. LITERATURE SURVEY

TOD systems assist users in completing user intended tasks efficiently in a proactive manner. Traditionally, the TOD system components NLU, DST, POL are designed with handcrafted rules and a predefined sequence of words by the designers. Although rule-based systems perform well, scaling such systems is tedious and costly due to the necessity of re-designing rules to support new tasks or domains. Therefore, rule-based TOD systems are usually designed with limited task coverage in a specific domain with predetermined dialogue flow. Additionally, due to template-based response generation, these systems are less engaged with restricted language variability. Repeated or dumb responses are often generated by such systems in case of errors that cause user frustration. Therefore, when these systems are deployed for customer support, users often opt to converse with human agents directly.

Various statistical approaches have been studied to enhance the understanding of dialogue systems. Word presentation techniques such as bag-of-words (BoW), continuous BoW (CBoW), term frequency (TF), inverse document frequency (IDF), n-grams, and word2vec have been utilized to extract the meaning of the given input. The tasks of domain identification, intent detection, and policy selection are often treated as classification problems and slot labeling is treated as a sequence classification problem. Many studies have attempted different machine learning approaches for these tasks. The researchers [7] studied intent classification and slot-value labeling using an support vector machine (SVM) classifier. The researchers [8] studied intent classification by applying different machine learning approaches, including naïve Bayes, and SVM coupled with BoW. However, these approaches using machine learning and static embedding for word representation exhibit the following limitations.

- Curse of Dimensionality: The numeric representation of text results in a sparse matrix, which requires exponentially large amounts of memory, which impacts computational efficiency and model performance.
- Lack of Contextual information: In static embeddings, each word is embedded in isolation. Therefore, understanding the meaning of a word according to its context defined by its own position and that of other words, is not considered, which is crucial for designing NLU.
- Dependence on the large amount of annotated data: TOD systems designed with traditional machine learning approaches rely on a large amount of annotated

task-specific data to achieve better task performance. Practically, using such data is not feasible.

- Human feedback is not undertaken: Traditional machine learning approaches do not consider human feedback, which is an essential parameter for selecting the next appropriate action in TOD systems. Therefore, such systems are not able to improve their performance from experience.

Due to deep learning (DL) advancements, input word representation has evolved from static embeddings to contextual word embeddings; for instance, pretrained bidirectional encoder representations from transformers (BERT) models consider contextual information in both the left and right directions. Additionally, various deep learning encoder-decoder based architectures, including convolutional neural networks (CNNs), recurrent neural networks (RNNs) and long short term memory (LSTM), have been widely applied to solve various real-world problems in computer vision and conversational systems. [9] proposed a customer-facing dialog system by combining RNNs with domain-specific knowledge. Although RNNs have been widely used in TOD systems due to their ability to handle sequential data [10][11], have the following limitations. RNNs can capture dependencies exclusively in one direction, thereby neglecting the consideration of previous word dependencies while determining the meaning of subsequent words. Also, RNNs suffer from vanishing gradients while handling long-term dependencies, which are later mitigated with the help of gated recurrent units (GRUs) with additional memory units [12]. To this end, bi-directional LSTMs have been widely utilized to handle long-term dependencies in sequential data in many applications such as language translation tasks in NLP [13]. In their study, [14] performed joint classification of domain, intent and slot labeling by using bi-directional LSTM. The researchers [8] studied intent classification using SVM and bi-directional LSTM and found that bi-directional LSTM approach outperformed the traditional machine learning approaches.

Attention mechanisms significantly improved the encoder-decoder architecture [15]. This mechanism computes attention weights, which determine the amount of attention to be given to each word in the input sequence at each step. Transformers [16] are breakthrough advancements that use self-attention mechanisms for dependency modeling. BERT is an encoder-only transformer model, developed by Google AI that considers bi-directional context to predict masked words; thus, BERT has become a preferred choice for NLU tasks. BERT is pretrained on a large corpus from wiki and e-books, which offers generalization capabilities for basic understanding. In practice, the scarcity of human annotated data is one of the reasons for the work, proposed by [17] used BERT to demonstrate the ability of pretrained limited generalizability of these data to the NLU [14].

In their contextual embeddings for few-shot learning scenario. [18], [19] proposed joint training of intent classification and slot filling using an attention mechanism to significantly enhance the performance of dialogue systems. The study [20] demonstrated that BERT-based intent

recognition outperforms other deep learning models including LSTM and RNN. The researchers [21] studied dialogue state tracking by applying BERT instead of using rule-based DST. Later, in these advancements, generative pretrained transformer (GPT)-based autoregressive decoder-only models, due to their ability to generate diverse responses, have received increased amounts of attention. The study [22] utilized GPT-2 for various TOD tasks, which resulted in more engaging and human-like responses. GPT-based models are popularly utilized for enhancing TOD tasks specifically response generation in NLGs [20], [23]. Until recently, PLMs with contextual embedding have been used as a starting point and subsequently fine-tuned for downstream tasks.

Recently, there has been a paradigm-shift from traditional model fine-tuning to prompt-tuning by efficiently utilizing a unified framework. In prompt-tuning, the network weights of the LLMs are frozen and a few task-specific demonstrations along with task prompts, are utilized to generalize with ease in few-shot settings. In their work, [24] used task-specific instruction prompts and approached various text processing tasks, such as sentiment analysis, question-answer generation, classification, etc., as text generation problems and referred to their model text-to-text transfer transformer (T5). Instruction based tuning of LLMs is gaining attention due to their improved communication capabilities achieved by providing hints to these LLMs about tasks [25]. LLMs have revolutionized dialogue with enhanced productivity across various industry domains. However, these models lack proactive communication, which is an essential parameter for handling multi-turn dialogue.

Selecting the next action in a dialogue flow to achieve the user goal in minimum dialogue turns is essential for evaluating the POL of a TOD system. Although rule-based policies perform well with fixed dialogue flow are not scalable for adapting to changes in the user goals. In real-world scenarios, the user is often uncertain about their goals at first place and wants to explore all available options. Additionally, dialogue POL should have the ability to learn new knowledge even after deployment. To design such scalable dialogue policies, researchers have studied the optimal action selection problem as a sequence of decision-making problems. In various studies, POL is implemented as a partially observable Markov decision process (POMDP) [26], by designing an RL-based dialogue agent to select the next action from the current dialogue state [27]. Such RL-based dialogue agents aim to maximize cumulative rewards by considering human feedback. These agents require more training cycles to learn from trial-and-error in a user-agent setting. Therefore, instead of real users, user simulators are used to train specifically in the initial stage of learning [28].

As PLMs and LLMs are large sized with huge number of parameters, should be efficiently used in TOD systems. This proposed work employs BERT contextual embedding for NLU and studies its impact on the overall performance of a TOD system. To achieve this goal, three distinct systems are configured using BERT, an SVM classifier and an RNN-based approaches for NLU and assessed their effectiveness. In further experiments, the rule-based POL is replaced with RL-based

POL and lastly, a unified approach using T5, and Llama-2 is leveraged for the NLU, DST and NLG tasks.

III. DESIGNING TOD SYSTEM IN MULTI-DOMAIN SETTING

In a diverse multi-domain environment, conversations include multiple tasks from different domains. The multi-domain ontology as shown in Eq. (1) has a set of slot-value pairs that are already defined in the respective domains to provide different functionalities.

$$\begin{aligned}
 & \text{(Multi-domain) } MD_{ontology} = \\
 & \left\{ \begin{array}{l} \text{domain}_1: \left[\begin{array}{l} (slot_1, value_1), \\ (slot_2, value_2), \\ \vdots \\ (slot_i, value_i) \end{array} \right] \\ \vdots \\ \text{domain}_2: \left[\begin{array}{l} (slot_1, value_1), \\ (slot_2, value_2), \\ \vdots \\ (slot_i, value_i) \end{array} \right] \\ \vdots \\ \text{domain}_i: \left[(slot_i, value_i) \right], \} \end{array} \right. \quad (1)
 \end{aligned}$$

The dialogues between the user and dialogue agent are either single-turn or multi-turn. The user utterance is represented as $User_u$ and the system utterance is represented as $System_u$. Therefore, a multi-turn conversation is shown as Eq. (2),

$$\text{(Multi-domain, multi-turn) } MDMT_{Dialogue} = \left\{ \text{dialogue}_i : \text{domain}_i : \text{turn}_i \left\{ User_{u_i}, System_{u_i} \right\} \right\} \quad (2)$$

The pipeline of NLU, DST, POL, and NLG process these dialogues by performing tokenization, extracting the semantic meaning, accessing database information, and generating responses. All these components can be trained and optimized separately using different approaches or by adopting an end-to-end (E2E) approach. In the E2E approach, two or more TOD components are combined for training and optimization using deep learning models. The following subsections describe the design of these components.

A. Natural Language Understanding (NLU)

The NLU identifies user intent from the input user query. BERT, a pretrained contextual embedding model, trained on two default training objectives, Masked Language Modeling (MLM) and Next Sentence Prediction (NSP) tasks, is integrated into the NLU. In MLM, initially input tokens are randomly masked, and the model predicts the vocabulary ID of the masked tokens based on both left and right contexts. The input representation in BERT is the concatenation of word embeddings, position embeddings and segment embeddings. The first token of every sequence is a special classification token [CLS], which is pivotal for classifying intent. Another special token [SEP] is the last token in each sequence that separates two sentences. As shown in Fig. 2, intent recognition is approached as a classification problem to predict the intent

class y^i . On the other hand, slot-filling is considered as a sequence labeling task to tag the input word sequence, $X = \{x_1, x_2, x_3, \dots, x_n\}$ with the slot label sequence given as $y_n^s = \{y_1^s, y_2^s, y_3^s, \dots, y_n^s\}$. The NLU represents this information in a semantic frame called dialogue act (DA).

Given the input token sequence as X ,
 $X = \{x_1, x_2, x_3, \dots, x_n\}$

The output of BERT is H

$$H = \{h_1, h_2, h_3, \dots, h_n\}$$

Based on the hidden state (h_1), Weights (W) and Bias (b) of the classification token [CLS], intent can be predicted as,

$$y^i = \text{softmax}(W^i h_1 + b^i) \quad (3)$$

The remaining hidden states from h_2, h_3, \dots, h_n are used for slot filling as shown in Eq. (4). Each tokenized input word is given to the tokenizer, and the hidden state of the first token is fed to the softmax layer for classification. The slot filling prediction function is represented as,

$$y_n^s = \text{softmax}(W^s h_n + b^s) \text{ where } n \in 1 \dots N \quad (4)$$

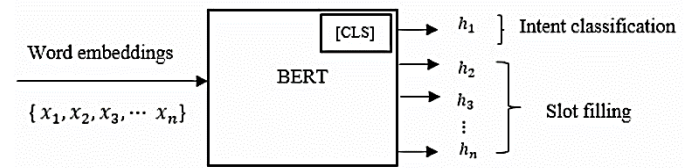


Fig. 2. BERT for generalization in the NLU.

The objective function for joint training of intent classification and slot filling is given as,

$$P(y^i, y_n^s | X) = P(y^i | X) \prod_{n=1}^N P(y_n^s | X) \quad (5)$$

The objective is to maximize the conditional probability $P(y^i, y_n^s | X)$ by minimizing the cross-entropy loss. In the case of slots with binary values such as Yes/No binary cross-entropy loss is used.

B. Dialogue State Tracking (DST)

DST utilizes information from NLU in a semantic frame known as dialogue acts (DAs) and maintains the belief state along with dialogue history. DST, which updates the belief state (intent, domain, slot, value) in each turn, is widely addressed as a classification task. The objective function for DST is to minimize the cross-entropy loss for both slot and slot value predictions. DST contains information about the constraints of the user, database search results, current user DAs, and previous system DAs. The following example demonstrates belief state updates at each turn in a multi-turn conversation. In proposed work, initially rule-based DST is used and subsequently the DST is approached as a text generation problem by employing the T5 model.

- Turn 1 User: Can you find me a restaurant in the east?
belief state $t_1 = ["\text{Inform}", "restaurant", "Location", "east"]$
- Turn 2 System: Sure, what type of cuisine are you looking for?
belief state $t_2 = ["\text{Inform}": "restaurant", "Location": "east", "Cuisine": "?"]$
- Turn 3 User: I would like to have Indian food.
belief state $t_3 = ["\text{Inform}": "restaurant", "Location": "east", "Cuisine": "Indian"]$

$$R_t^\pi = \sum_{i=0}^{T-t-1} \gamma^i r_{t+i+1} \quad (6)$$

D. Natural Language Generation (NLG)

Once the policy determines system DA, the NLG task occurs in the following two steps: content planning followed by sentence realization. The content planning emphasizes ‘what to say’, and sentence realization focuses on ‘how to say in the correct manner’. The sentence realization is achieved using a de-lexicalization process in which system DAs are mapped to de-lexicalized sentences. This approach allows generation of dynamic sentences in different scenarios without hard-coded values.

In NLG, this template-based approach is commonly used to select the most appropriate template from the candidate set of already designed templates for response generation, are less engaging with limited language variability [29]. In proposed work a template-based NLG is initially used, and further text generation approach is used by employing T5 and LLM models.

E. Unified Approach for TOD System Pipeline using an LLM

Recently, all text processing problems have been approached as text generation problems. T5, and Llama2-chat-hf models from Hugging Face library, are used as unified frameworks for the NLU, DST and NLG tasks, as depicted in Fig. 3. Llama 2 chat is fine-tuned and optimized LLM for dialogue handling [30].

In prompt-tuning, only a small number of parameters are required to optimize the prompt that adapts an LLM to customized tasks or domains with frozen weight by preserving the general language understanding ability of LLM. To utilize the power of LLMs, instruction prompts are used to adapt NLU, DST, and NLG tasks in the TOD system.

C. Dialogue Policy (POL)

The objective of dialogue policy is to accurately predict the next action by using the current dialogue state and generating system DAs in each turn with corresponding slot-value pairs.

In rule-based policy, the entire dialogue flow is hand coded whereas in RL-based dialogue policy, the training occurs in an agent-environment setting, which considers user feedback in terms of rewards. The RL-based dialogue agent aims to maximize the cumulative reward and improve from the experience. As these agents learn using trial and error, thousands of interactions are required for stabilization. Therefore, to train RL-based agents, user simulators that mimic real users are often required to interact before actual deployment for real users (Shi et al., 2019). In an agenda-based user simulator, the user goal is decomposed into slot-value pairs, whereas the agenda is maintained in a stack-like structure (Schatzmann et al., 2007). At a finite time-step T, the dialogue policy π is trained to maximize the cumulative reward in each turn. The cumulative reward as shown in Eq. (6) is assigned to an agent after dialogue completion. The optimal policy π^* is obtained using either value-based or policy-based methods. In our experiment, both rule-based and RL-based approaches are used to model dialogue policy.

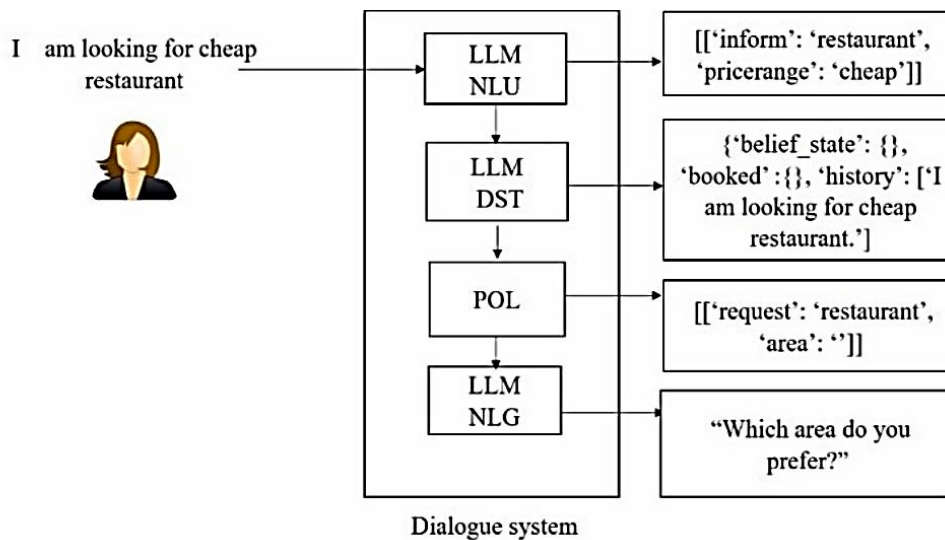


Fig. 3. Unified approach for the TOD system pipeline.

IV. EXPERIMENTAL SETUP

Proposed work is focused on attaining scalability to support multiple domain conversation. To fulfill this essential requirement, a multi-domain, multi-turn human-to-human conversation dataset is selected after a survey [30] for designing a scalable TOD system. This section provides details about the utilized dataset, tools, system-configuration, and experimental results.

A. Dataset

A benchmark dataset MultiWOZ 2.1 is used for our research experiments. MultiWOZ 2.1 is a large dataset containing annotations for dialogue states, system dialogue acts, and user goals for training and evaluating dialogue systems in the context of tourist-related conversations. The MultiWOZ dataset consists of approximately 30 (domain, slot) pairs, encompassing over 45,000 values. The dataset has a size of 10,000 instances and covers various domains including Hotel, Hospital, Train, Taxi, Police, Postcode, and Restaurant [5].

MultiWOZ 2.1 contains more than 3,400 single-domain dialogues, and 7,032 multi-domain dialogues spanning across at least 2 to 5 domains. Most of the dialogues contain 10 turns on an average to meet the complexity of real-world scenarios.

B. Tools

Many tools have been implemented and integrated into an IDE for building dialogue systems. Often, these tools incorporate a rule-based dialogue manager (DM) with a built-in NLU component having a rigid structure. PyDial, ParlAI, Plato, Rasa, DeepPavlov, and ConvLab are examples of open-source tools with neural network-based dialogue managers that offer more flexibility and scalability. Convlab-3 [31] offers a range of state-of-the-art models for various TOD components and user simulators. In our study, Convlab-3 is used for experiment setup.

C. System Configuration

In the first experiment, distinct system agents are configured, each employing a different NLU approach. This allowed us to investigate the influence of the NLU on the overall performance of the dialogue system. All our experiments are performed using NVIDIA Tesla P100 GPU using the Google Colab platform with subscription.

An agenda-based user simulator is utilized for modeling a user agent, which is integrated with the BERT-base uncased model for NLU to evaluate the performance of system agents. The BERT-base uncased model utilizes a self-attention transformer-based encoder with 12 layers and 12 attention heads with a hidden size of 768 and a total of 110 M parameters.

Our experiment comprises five dialogue systems named SA1, SA2, SA3, SA4, and SA5. Each system has a rule-based DST and a template-based NLG. SA1, SA2, and SA3 have rule-based POL, whereas SA4 and SA5 have RL-based POL.

To understand the impact of NLU on the overall performance of dialogue system, different models for NLU. In SA1, BERT-base uncased model is used for joint training of

intent classification and slot filling, whereas in SA2, utilizes the RNN-based joint neural model called Multi-Intent Language Understanding (MILU) for joint prediction of domain, intent, slot, and value. SA3 uses an SVM (support vector machine) classifier in the NLU [32] which is designed to manage complex semantic tuples (intent-slot-value) and classify them based on n-gram features. The listing of example code is referred from [32] for experiment setup as shown in Listing 1. Similarly, in an extended experiment SA4 and SA5 TOD systems are designed by utilizing BERT and T5 for NLU tasks respectively with RL-based POL by referring to Listing 2 from [33].

In the second experiment, a unified approach is proposed to design a TOD system using T5 model. The NLU, DST and NLG are modeled using T5 with an RL-based dialogue policy. Further, this experiment is extended by utilizing the LLM from Huggingface library, meta-llama/Llama-2-13b-chat-hf with instruction prompts. Here, two LLM based systems are used to play the roles of 'user' and 'system'. The off-policy algorithm VTRACE [34] from checkpoint is utilized to model RL-based POL in both experiments.

```
# import necessary modules
# Create models for each component
# Parameters are omitted for simplicity
sys_nlu = BERTNLU(...)
sys_dst = RuleDST(...)
sys_policy = RulePolicy(...)
sys_nlg = TemplateNLG(...)

# Assemble a pipeline system named "sys"
sys_agent = PipelineAgent (sys_nlu, sys_dst, sys_policy, sys_nlg,
name="sys")

# Build a user simulator similarly but without DST user_nlu =
BERTNLU(...)
user_policy = RulePolicy(...)
user_nlg = TemplateNLG(...)
user_agent = PipelineAgent(user_nlu, None, user_policy, user_nlg,
name="user")

# Create an evaluator and a conversation environment
evaluator = MultiWozEvaluator()
sess = BiSession(sys_agent, user_agent, evaluator)

# Start simulation sess.init_session()
sys_utt = ""
while True:
sys_utt, user_utt, sess_over, reward = sess.next_turn ( sys_utt)
if sess_over:
break
print(sess.evaluator.task_success()) print(sess.evaluator.inform_F1())

# Use the analysis tool to generate a test report
analyzer = Analyzer(user_agent, dataset="MultiWOZ")
analyzer.comprehensive_analyze(sys_agent, total_dialog =1000)

# Compare multiple systems
sys_agent2 = PipelineAgent(MILU(...), sys_dst, sys_policy, sys_nlg,
name="sys") analyzer.compare_models(agent_list=[sys_agent,
sys_agent2], model_name=["bertnlu", "milu"], total_dialog=1000)
```

Listing 1. Example code from [32]

D. Results

Table II demonstrates the performance of each NLU for different multi-domain user queries. Table II highlights the domain and slot-value information for each query. BERT NLU outperforms the other two methods by demonstrating excellent performance in understanding long queries.

TABLE II. OUTPUT OF NLU IN DIALOGUE SYSTEMS USING BERT, SVM AND MILU APPROACHES

| Query | Conversation | BERT NLU (SA1) | MILU (SA2) | SVM NLU (SA3) |
|-------|--|---|---|---|
| 1 | I am looking for cheap food | [['Inform', 'Restaurant', 'Price', 'cheap']] | [['Inform', 'Restaurant', 'Price', 'cheap']] | [['Inform', 'Restaurant', 'Price', 'cheap']] |
| 2 | Can you suggest me Indian restaurants in westzone | [['Inform', 'Restaurant', 'Food', 'Indian', 'Inform', 'Restaurant', 'Area', 'west zone']] | [['Inform', 'Restaurant', 'Food', 'Indian']] | [['Inform', 'Restaurant', 'Food', 'Indian']] |
| 3 | Give me address police station and contact details | [['Request', 'Police', 'Addr', '?', 'Request', 'Restaurant', 'Addr', '?']] | [['Inform', 'Police', 'none', 'none']] | [['bye', 'general', 'none', 'none']] |
| 4 | I want to reach London kings cross by train TR1111 | [['Inform', 'Train', 'Dest', 'London kings cross', 'Inform', 'Train', 'Id', 'TR1111']] | [['Inform', 'Train', 'Dest', 'London kings cross']] | [['Inform', 'Train', 'Dest', 'London kings cross']] |
| 5 | Can you suggest me Indian restaurants in westzone with free parking. Also check for free Wi-Fi | [['Inform', 'Hotel', 'Parking', 'yes', 'Inform', 'Hotel', 'Internet', 'yes', 'Inform', 'Restaurant', 'Food', 'Indian', 'Inform', 'Restaurant', 'Area', 'westzone']] | [['Inform', 'Restaurant', 'Food', 'Indian', 'Inform', 'Hotel', 'Parking', 'yes', 'Inform', 'Hotel', 'Internet', 'yes']] | [['Inform', 'Hotel', 'Internet', 'yes']] |

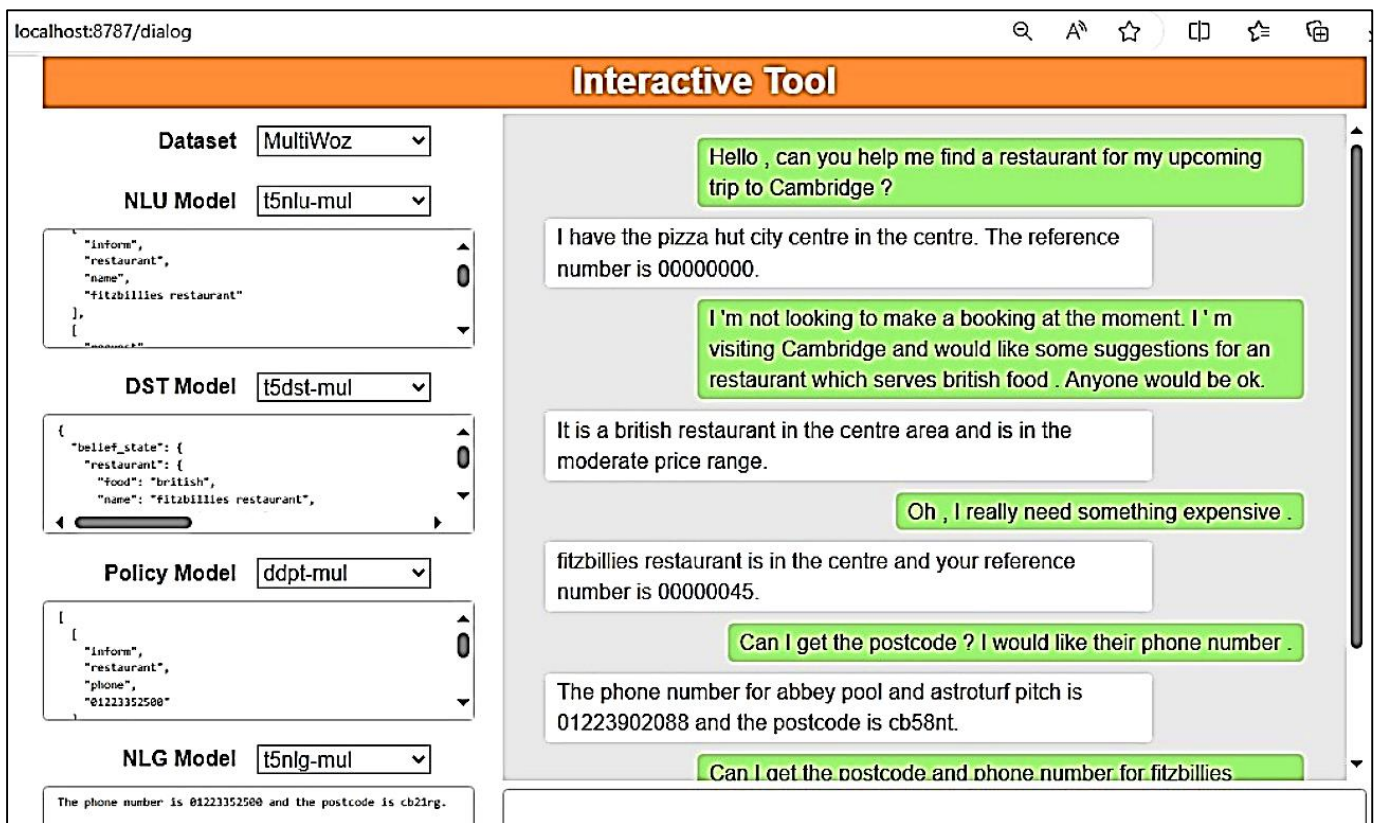


Fig. 4. Unified approach for modeling TOD tasks NLU, DST and NLG using T5.

In the second experiment, a unified approach with T5-small is used which was fine-tuned for both user and system utterances on the MutliWOZ2.1 dataset from the hugging face library. In this configuration, an RL-based policy is used for designing the TOD system. This encoder-decoder model completes NLU, DST and NLG tasks by approaching these tasks as text generation problems. The interaction between the system agent and real user is shown in Fig. 4. Further, the T5

model is replaced with the open-source Llama-2 model by utilizing task-specific instruction prompts to adapt the NLU, DST, and NLG tasks with sample demonstrations. Role-based instruction prompts are used in the meta-llama/Llama-2-13b-chat-hf model to define two roles, a system agent, and a user simulator to generate proactive multi-turn dialogues. The multi-turn interaction between the system agent and user simulator is shown in Table III. Domain information is highlighted for understanding.

TABLE III. UNIFIED APPROACH FOR MODELING TOD TASKS NLU, DST AND NLG USING LLAMA-2 13B-CHAT-HF

| User | Assistant |
|--|--|
| | Hello, I am helpful assistant. How may I help you? |
| Hello! I am looking for a train from Norwich to Cambridge on Wednesday after 18:45. Can you help me find one and make a booking for one person? Also, Do you know of any places in Cambridge that offer multiple sports? Could you provide the phone number and postcode? | |
| | Hi there! I'd be happy to help. For a train from Norwich to Cambridge on Wednesday after 18:45, you can take the Greater Anglia train departing at 19.05 from Norwich railway station. To book, you can visit the Greater Anglia website or call their customer service at 0345 600 7245. As for sports facilities in Cambridge, the University of Cambridge Sports Centre offers a range of sports and can be reached at 01223336666 (postcode CB2 1RR) |
| Thank you so much! I've found the train I need and I'm going to book it now. Can you please provide me with reference number or the booking confirmation so I can have it handy? And thank you for the information on sports facilities in Cambridge, I'll definitely look into that [END] | |
| | Sure thing! Your train booking reference number is GA-123456. Please have this ready when you contact Greater Anglia to confirm your reservation. If you need any further assistance, feel free to ask. Enjoy your trip to Cambridge! |

V. EVALUATION OF TOD SYSTEMS

To measure the overall correctness of the search tasks in the inform act, such as domain, intent classification, and slot-filing, Precision, Recall and F1-score are used. Book rate (BR) measures the accuracy of the system for fulfilling booking requests and generating reference numbers. The success rate (SR) measures the successful completion of user goals in all required domains [35]. A user goal is considered successful when both the book rate and the recall of the informed act are 1. The average number of dialogue turns required for task completion impacts user satisfaction. The widely adopted evaluation matrices for TOD system are facilitated in convlab toolkit.

As depicted in Table IV, the SA1 system with the BERT NLU outperforms other rule-based system configurations.

However, for the RL-based dialogue policy, the SA5 system with the T5 NLU outperforms the BERT-based system configuration. Compared to the other configurations, SA5 has the maximum completion rate.

Fig. 5(a) depicts the NLU performance for the SA1, SA2 and SA3 dialogue systems and demonstrates that the BERT-based NLU has better precision, recall and F1-score than the MILU and SVM-based NLU. However, as depicted in Fig. 5(b), the BERT-based system resulted in an improved task success rate, with a slight increase in the average number of turns to achieve success compared to that of SA2 and SA3. SA1 is still taking longer to complete the task. As the NLU component is enhanced with state-of-the-art models including BERT and T5, for the next experiment rule-based dialogue policy is replaced with RL-based policy to adapt dynamic dialogue flow to converse in multi-domain setting.

TABLE IV. AUTOMATIC EVALUATION OF TOD SYSTEMS USING AN AGENDA-BASED USER SIMULATOR

| System ID | System Configuration | | | | Inform | | | Complete Rate | Task Success Rate | Book Rate BR | Average No. of Success turns/Average turns |
|-----------|----------------------|------|--------------|----------|--------|------|------|---------------|-------------------|--------------|--|
| | NLU | DST | POL | NLG | P | R | F1 | | | | |
| SA1 | BERT | Rule | Rule | Template | 81.2 | 87.7 | 81.7 | 78.9 | 71.3 | 88.4 | 12.12/16.51 |
| SA2 | MILU | | | | 77 | 84.6 | 78 | 73.7 | 64.9 | 83.3 | 11.67/16.56 |
| SA3 | SVM | | | | 61.5 | 60.8 | 57.9 | 44.4 | 30.6 | 51.4 | 11.97/16.59 |
| SA4 | BERT | Rule | RL based POL | Template | 64.2 | 86 | 70 | 71 | 30 | 62.2 | 17.06/25.16 |
| SA5 | T5 | | | | 64 | 93.7 | 72.8 | 85 | 53 | 84.3 | 21.05/25.32 |

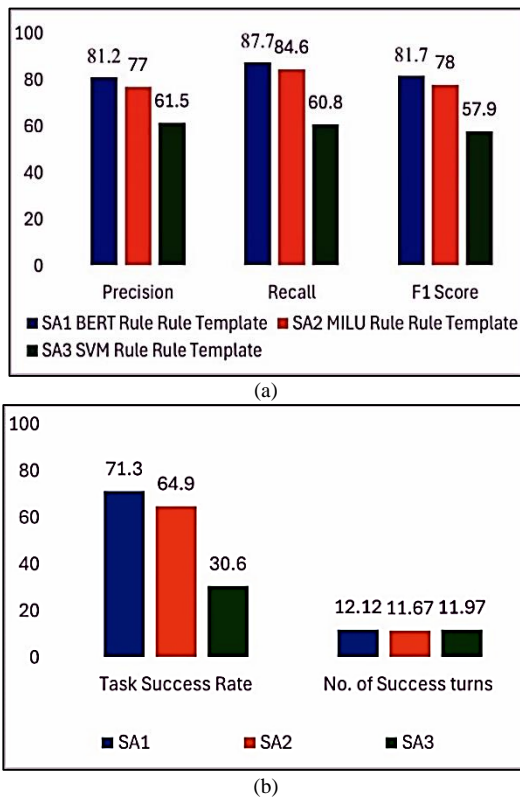


Fig. 5. (a) NLU performance in SA1, SA2 and SA3 (b) task success rate and average success turns in SA1, SA2, and SA3.

As depicted in Fig. 6(a), the T5-based NLU outperforms the BERT-based NLU, whereas Fig. 6(b) indicates that SA5 has an improved task success rate at the cost of an increased number of average success turns, indicating slow convergence compared to that of SA4.

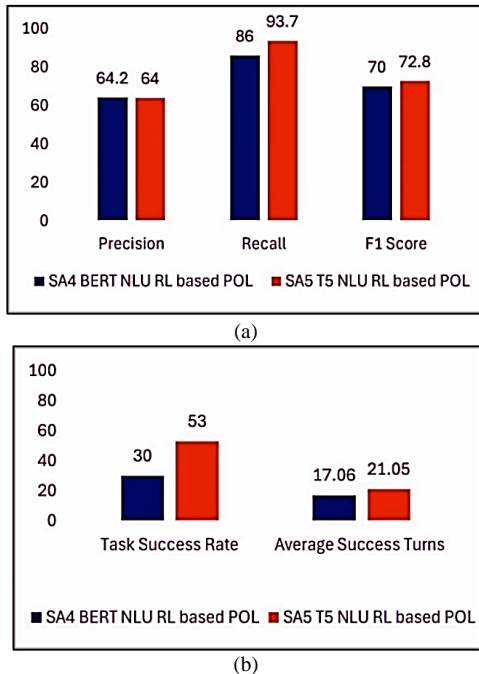


Fig. 6. (a) NLU performance in SA4 and SA5 (b) task success rate and average success turns in SA4, and SA5.

VI. DISCUSSION

In real-world scenarios, designing a proactive, multi-turn dialogue system to understand and satisfy user goals in minimum dialogue turns is a complex task. Additional complexity is introduced when the user goal contains tasks from multiple domains. This led us to analyze the impact of different NLUs on the performance of the TOD system. Transformer based approaches outperformed traditional machine learning algorithms including SVM[8] and RNN[11], followed by additional experiments with RL-based policies instead of using rule-based policies to avoid handcrafted rules. BERT-based NLU with the rule-based policy demonstrated improved performance with a slight increase in the average number of successful dialogue turns. Furthermore, the transformer-based models including BERT and T5 are used for the NLU with the RL-based policy. The T5 NLU with the RL-based policy resulted in significant improvements in the recall, F1-score, complete rate, and book rate with an increase in the average number of successful dialogue turns. This indicates limited improvement in fast convergence of task completion. Therefore, although NLU performance is boosted, RL-based POL requires investigation for improvement in task performance through warm-up and task-specific pretraining to achieve the task in minimum dialogue turns.

Additional experiments are performed to improve TOD system performance by using a unified approach instead of improving the performance of individual components. This has a major obstacle to the availability of annotated task-specific data for pretraining. Until recently, fine-tuning PLMs achieved promising performance on TOD tasks. However, an entire PLM model with many parameters is required for gradient updating to adapt to each downstream task; for instance, the large number of BERT-base-uncased NLUs is 110M. Domain-specific pretraining is required to achieve better performance because the PLMs are trained on general purpose data.

Our experiments found that even after improving the performance of a single component, the overall performance improvement in TOD systems is not guaranteed. On the other hand, a unified approach using a single PLM or LLM with shared parameters across all tasks is more preferred approach. To adapt to a new task or domain, prompt-enabled models such as T5 and Llama-2 are more efficient as only a small number of parameters are updated in prompt tuning with just a few demonstrations. On the other hand, benchmark TOD systems designed using fine-tuning approach such as UBAR, GALAXY, MinTL needs to load entire PLMs such as GPT-2(1.5B), UniLM (340M), BART-large (440M) respectively to update large number of parameters to adapt each new task or domain [35].

The responses generated in the LLM model Llama-2 have human-like language variability, which demonstrates its ability to design more user-friendly TOD systems in the future. Other LLMs, such as GPT3.5 and GPT-4, have provided many scalability and multimodality features, but these models are accessible only with paid subscriptions.

VII. CONCLUSION AND FUTURE WORK

Understanding user intentions from natural language text in a dynamic environment remains an inherently challenging task. Various existing TOD systems contain rule-based components designed to function in single domain and offer limited tasks to users. To design scalable TOD system for conversation which includes multiple domains with different tasks to offer is challenging. In line to our first objective to study the impact of NLU, we have configured SVM, RNN and state-of-the-pretrained language models such as BERT and T5 instead of using handcrafted (rule-based) NLU to understand user intention in multi-domain tourist conversation environment. We found that configuring BERT and T5 in NLU enhances the performance of an individual component but does not guarantee an overall performance improvement in TOD system.

In further step, we extended our experiment with best performing NLU (BERT, T5) in a pipeline TOD and replaced the rule-based designing dialogue policy with more scalable approach by employing reinforcement learning (RL) algorithm to adapt in multi-domain conversation. We found that handling large state-action spaces requires large computing power, and training RL-based dialogue policy in such a large dynamic environment takes many training cycles by the dialogue agent to learn from scratch. As the agent gains experience using trial and error method, establishing a stable dialogue policy is time-consuming. Also, to train these RL-based agents a reliable user simulator is required with added design efforts. In our experiments, we utilized already existing agenda-based user simulator for automatic evaluation of TOD systems provided in the toolkit. We achieved very less task success rate which indicates, further investigation is needed to boost or warm-up the performance of dialogue policy using methods such as task-specific pretraining, fine-tuning, inverse reinforcement learning (IRL), and imitation learning (IL) approaches.

Recently, unified approach is utilized popularly by employing large language models to perform all TOD tasks but fine-tuning these models is costly. Instead of fine-tuning language models for each individual task recent trend encourages to utilize prompt-enabled large language models. In this paper, soft prompts are generated using system instructions to achieve proactive multi-turn dialogues by assigning different roles to LLMs, such as assistant and system agents. The proposed approach is adaptive and generates more human-like responses compared to other systems, paving the way for scalable and user-friendly dialogue systems.

REFERENCES

- [1] J. Weizenbaum, "ELIZA-A computer program for the study of natural language communication between man and machine," *Commun. ACM*, vol. 9, no. 1, pp. 36–45, 1966, doi: 10.1145/365153.365168.
- [2] K. M. Colby, F. D. Hilf, S. Weber, and H. C. Kraemer, "Turing-like Indistinguishability Tests for the Calibration of a Computer Simulation of Paranoid Processes," *Artif. Intell.*, vol. 3, pp. 199–221, 1972, [Online]. Available: <https://api.semanticscholar.org/CorpusID:31542633>.
- [3] A. Rastogi, X. Zang, S. Sunkara, R. Gupta, and P. Khaitan, "Towards Scalable Multi-domain Conversational Agents: The Schema-Guided Dialogue Dataset," 2019, [Online]. Available: <http://arxiv.org/abs/1909.05855>.
- [4] M. Henderson, B. Thomson, and J. Williams, "The second dialog state tracking challenge," *SIGDIAL 2014 - 15th Annu. Meet. Spec. Interes. Gr. Discourse Dialogue, Proc. Conf.*, no. June, pp. 263–272, 2014, doi: 10.3115/v1/w14-4337.
- [5] M. Eric et al., "MultiWOZ 2.1: A consolidated multi-domain dialogue dataset with state corrections and state tracking baselines," *Lr. 2020 - 12th Int. Conf. Lang. Resour. Eval. Conf. Proc.*, pp. 422–428, 2020.
- [6] Z. Zhang, R. Takanobu, Q. Zhu, M. Huang, and X. Zhu, "Recent advances and challenges in task-oriented dialog systems," *Sci. China Technol. Sci.*, vol. 63, no. 10, pp. 2011–2027, 2020, doi: 10.1007/s11431-020-1692-3.
- [7] F. Mairesse, M. Ga, and T. Street, "Spoken Language Understanding From Unaligned Data Using Discriminative Classification Models C , F . Jur ' c ' i c ' ek , S . Keizer , B . Thomson , K . Yu , and S . Young," vol. 2.
- [8] J. Schuurmans and F. Frasincar, "Intent Classification for Dialogue Utterances," *IEEE Intell. Syst.*, vol. 35, no. 1, pp. 82–88, 2020, doi: 10.1109/MIS.2019.2954966.
- [9] J. D. Williams, K. Asadi, and G. Zweig, "Hybrid code networks: Practical and efficient end-to-end dialog control with supervised and reinforcement learning," *ACL 2017 - 55th Annu. Meet. Assoc. Comput. Linguist. Proc. Conf. (Long Pap., vol. 1, pp. 665–677, 2017, doi: 10.18653/v1/P17-1062.*
- [10] C. Geishauer et al., "Dynamic Dialogue Policy for Continual Reinforcement Learning," *Proc. - Int. Conf. Comput. Linguist. COLING*, vol. 29, no. 1, pp. 266–284, 2022.
- [11] S. Lee et al., "ConvLab: Multi-domain end-to-end dialog system platform," *ACL 2019 - 57th Annu. Meet. Assoc. Comput. Linguist. Proc. Syst. Demonstr.*, pp. 64–69, 2019, doi: 10.18653/v1/p19-3011.
- [12] C. S. Wu, A. Madotto, E. Hosseini-Asl, C. Xiong, R. Socher, and P. Fung, "Transferable multi-domain state generator for task-oriented dialogue systems," *arXiv*, no. 808, pp. 808–819, 2019.
- [13] S. Merity, N. S. Keskar, and R. Socher, "Regularizing and Optimizing LSTM Language Models," *arXiv*, 2017.
- [14] Y. B. Kim, S. Lee, and K. Stratos, "ONENET: Joint domain, intent, slot prediction for spoken language understanding," *2017 IEEE Autom. Speech Recognit. Underst. Work. ASRU 2017 - Proc.*, vol. 2018-Janua, pp. 547–553, 2018, doi: 10.1109/ASRU.2017.8268984.
- [15] A. Vaswani et al., "Attention is all you need," *Adv. Neural Inf. Process. Syst.*, vol. 2017-Decem, no. Nips, pp. 5999–6009, 2017.
- [16] J. Devlin, M. W. Chang, K. Lee, and K. Toutanova, "BERT: Pre-training of deep bidirectional transformers for language understanding," *NAACL HLT 2019 - 2019 Conf. North Am. Chapter Assoc. Comput. Linguist. Hum. Lang. Technol. - Proc. Conf.*, vol. 1, no. Mlm, pp. 4171–4186, 2019.
- [17] C. S. Wu, S. Hoi, R. Socher, and C. Xiong, "TOD-BERT: Pre-trained natural language understanding for task-oriented dialogue," *EMNLP 2020 - 2020 Conf. Empir. Methods Nat. Lang. Process. Proc. Conf.*, pp. 917–929, 2020, doi: 10.18653/v1/2020.emnlp-main.66.
- [18] A. Gupta, J. Hewitt, and K. Kirchhoff, "Simple, fast, accurate intent classification and slot labeling for goal-oriented dialogue systems," *arXiv*, no. September, pp. 46–55, 2019.
- [19] S. Louvan and B. Magnini, "Recent Neural Methods on Slot Filling and Intent Classification for Task-Oriented Dialogue Systems: A Survey," *COLING 2020 - 28th Int. Conf. Comput. Linguist. Proc. Conf.*, pp. 480–496, 2020, doi: 10.18653/v1/2020.coling-main.42.
- [20] V. Khan and T. A. Meenai, "Pretrained Natural Language Processing Model for Intent Recognition (BERT-IR)," *Human-Centric Intell. Syst.*, vol. 1, no. 3–4, p. 66, 2021, doi: 10.2991/hcis.k.211109.001.
- [21] V. Balaraman and B. Magnini, "Domain-Aware Dialogue State Tracker for Multi-Domain Dialogue Systems," vol. 1, 2020, [Online]. Available: <http://arxiv.org/abs/2001.07526>.
- [22] P. Budzianowski and I. Vuli, "Towards the Use of Pretrained Language Models for Task-Oriented Dialogue Systems," no. Wngt, pp. 15–22, 2019.

- [23] J. Howard and S. Ruder, "Universal language model fine-tuning for text classification," *ACL 2018 - 56th Annu. Meet. Assoc. Comput. Linguist. Proc. Conf. (Long Pap., vol. 1, pp. 328–339, 2018*, doi: 10.18653/v1/p18-1031.
- [24] KEKEKE et al., "T5: Exploring the limits of transfer learning with a unified text-to-text transformer," *J. Mach. Learn. Res.*, vol. 21, pp. 1–67, 2020.
- [25] V. Hudeček and O. Dušek, "Are LLMs All You Need for Task-Oriented Dialogue?," 2023, [Online]. Available: <http://arxiv.org/abs/2304.06556>.
- [26] S. Young, M. Gašić, B. Thomson, and J. D. Williams, "POMDP-based statistical spoken dialog systems: A review," *Proc. IEEE*, vol. 101, no. 5, pp. 1160–1179, 2013, doi: 10.1109/JPROC.2012.2225812.
- [27] J. Gao, M. Galley, and L. Li, "Neural approaches to conversational AI," *ACL 2018 - 56th Annu. Meet. Assoc. Comput. Linguist. Proc. Conf. Tutor. Abstr.*, pp. 2–7, 2018, doi: 10.18653/v1/p18-5002.
- [28] Y. Dai, H. Yu, Y. Jiang, C. Tang, Y. Li, and J. Sun, "A Survey on Dialog Management: Recent Advances and Challenges," arXiv, 2020, [Online]. Available: <http://arxiv.org/abs/2005.02233>.
- [29] B. Byrne et al., "Taskmaster-1: Toward a realistic and diverse dialog dataset," arXiv, pp. 4516–4525, 2019.
- [30] H. Touvron et al., "Llama 2: Open Foundation and Fine-Tuned Chat Models," 2023, [Online]. Available: <http://arxiv.org/abs/2307.09288>.
- [31] Q. Zhu, C. Geishauser, H. L. Carel, X. Zhu, J. Gao, and M. Gaši, "ConvLab-3: A Flexible Dialogue System Toolkit Based on a Unified Data Format."
- [32] Q. Zhu et al., "ConvLab-2: An Open-Source Toolkit for Building, Evaluating, and Diagnosing Dialogue Systems," 2020, [Online]. Available: <http://arxiv.org/abs/2002.04793>.
- [33] Q. Zhu et al., "ConvLab-3: A Flexible Dialogue System Toolkit Based on a Unified Data Format," *EMNLP 2023 - 2023 Conf. Empir. Methods Nat. Lang. Process. Proc. Syst. Demonstr.*, pp. 106–123, 2023, doi: 10.18653/v1/2023.emnlp-demo.9.
- [34] L. Espeholt et al., "IMPALA: Scalable Distributed Deep-RL with Importance Weighted Actor-Learner Architectures," *35th Int. Conf. Mach. Learn. ICML 2018*, vol. 4, pp. 2263–2284, 2018.
- [35] J. Deriu et al., *Survey on evaluation methods for dialogue systems*, vol. 54, no. 1. Springer Netherlands, 2021.

Day Trading Strategy Based on Transformer Model, Technical Indicators and Multiresolution Analysis

Salahadin A. Mohammed

Information and Computer Science Department,
King Fahd University of Petroleum and Minerals, Dhahran 31261, Saudi Arabia

Abstract—Stock prices are very volatile because they are affected by infinite number of factors, such as economical, social, political, and human behavior. This makes finding consistently profitable day trading strategy extremely challenging and that is why an overwhelming majority of stock traders loose money over time. Professional day traders, who are very few in number, have a trading strategy that can exploit this price volatility to consistently earn profit from the market. This study proposes a consistently profitable day trading strategy based on price volatility, transformer model, time2vec, technical indicators, and multiresolution analysis. The proposed trading strategy has eight trading systems, each with a different profit-target based on the risk taken per trade. This study shows that the proposed trading strategy results in consistent profits when the profit-target is 1.5 to 3.5 times the risk taken per trade. If the profit-target is not in that range, then it may result in a loss. The proposed trading strategy was compared with the buy-and-hold strategy and it showed consistent profits with all the stocks whereas the buy-and-hold strategy was inconsistent and resulted in losses in half the stocks. Also three of the consistently profitable trading systems showed significantly higher average profits and expectancy than the buy-and-hold trading strategy.

Keywords—Artificial neural network; saudi stock exchange; machine learning; deep learning; transformer model; stock price prediction; time series analysis; technical analysis; multiresolution analysis

I. INTRODUCTION

In the context of this study, day trading is a business of buying a number of shares on a trading day and selling them all before the end of the same trading day for a profit or a loss. Day trading is a business of probability. When a consistently profitable day trader enters a trade, he is not sure whether the trade will be a winner or a loser, but he is sure that after he does many trades, he will end up profitable. For example, the 2023 US investment champion's win rate was less than 35% but he ended the year with more than 805% profit [1], [2]. This is because he has a trading system with a positive expectancy. Expectancy, Φ , is defined as show by Eq. (1).

$$\Phi = AW \times WR - AL \times (1 - WR) \quad (1)$$

where, AW is average win, AL is average loss, and WR is win rate. For example, if a trader did a total of 1000 trades and 400 of them were winners, his WR is 0.4. If his average win is 500 dollars and his average loss is 200 dollars, then his Φ is $80 = 0.4 \times 500 - 0.6 \times 200$. This means he expects to gain 80 dollars per trade.

To increase their winning rates many professional day traders use technical indicators. Recently, systematic trading using deep learning has emerged as a powerful tool for predicting future stock prices [3]–[5]. In this study, a day trading strategy with a positive expectancy is proposed. To increase the win rate, the proposed trading strategy uses not only technical indicators (TIs) but also transformer neural network (TNN) and multiresolution analysis (MRA).

MRA was included in the proposed solution because many researchers reported that they got better performance when they combined MRA with their predictive model. For example, MRA resulted in better model performance when combined with each of ARIMA [6], descriptive statistical modeling [7], ANN [8], [9], RNN [10], CNN [11], GRU [12], LSTM [13], and stacked autoencoders [14].

TIs were also found to improve model performance by many researchers [5]. The problem is, there are more than 100 technical indicators and each technical indicator (TI) may have a number of parameters. Choosing the wrong combination of TIs or assigning a TI a wrong parameter value can degrade performance. So in this study, a systematic way of choosing TIs and their parameter values is presented.

There are many possible deep learning architectures. Choosing the wrong architecture can result in poor performance. For the proposed day trading strategy, several deep learning architectures were compared and the one that outperformed all of them was selected. The proposed deep learning model takes as input a dataset which consists of nine features, such as prices, volume, indices, and TIs. Some of these features are decomposed using empirical wavelet transform (EWT) before they are fed to the model. The model predicts the highest and the lowest stock prices of a given trading day. The proposed day trading strategy is based on these two predicted prices and will be explained in Section V-G. The proposed day trading strategy consists of eight trading systems; and unlike many of the existing systems, they were tested in different market conditions using ten randomly picked stocks listed in the Saudi stock market. They were compared with the buy-and-hold trading strategy and the experimental results show that five of the proposed systems showed positive expectancy consistently with all the ten stocks whereas the buy-and-hold strategy was inconsistent and resulted in losses in half of the stocks.

The main contributions of this work are:

- 1) A day trading strategy which combines TNN, TI, EWT MRA, and time2vec [15]. To the best of our

knowledge, this is the first study to do so.

- 2) The first consistently profitable day trading strategy which uses TNN for Saudi stock market.
- 3) A trading strategy based on a systematic way of choosing and combining TIs and their parameter values.
- 4) A study which presents the impact of profit-target on profitability.

The remainder of this paper is organized as follows. Section II gives background information relevant to the proposed solution. Section III presents related work. The proposed framework is explained in Section IV. Section V discusses the results and analysis of the proposed methodology, and Section VI is the conclusion.

II. BACKGROUND

This section gives brief background information on some topics used in this study. The covered topics include deep learning models and wavelet transform.

A. Deep Learning

Deep learning is a subfield of machine learning based on deep neural networks (DNN). A DNN is essentially an artificial neural network (ANN) with more than three layers. These multiple layers give a DNN massive computing power and enables it to train on huge amounts of data with little human intervention, which makes it different from the other classical machine learning algorithms. Each DNN layer extracts certain information from the data and redirects the learned information to the next layer to perform another type of information extraction. This hierarchy of information extraction enables DNNs to perform better forecasting than the other classical machine learning algorithms. There are several DNN models but the most popular DNN models for time series data are, Recurrent Neural Network, Long Short-Term Memory, Gated Recurrent Unit, and transformers.

1) *Recurrent neural network*: A recurrent neural network (RNN) is a special type of ANN. However, unlike the standard feed-forward ANN, RNN networks have feedback connections which enables output from a previous step to be fed as input to the current step [16], [17]. RNNs also have the concept of memory that enables them to store limited information extracted from previous inputs which are then used to generate subsequent output. Having memory and feedback loop makes RNNs very popular for sequence data, such as time series, where one data point depends on previous data points.

2) *Long Short-Term Memory (LSTM)*: Long short-term memory (LSTM) is a variant of RNN. It was proposed by Hochreiter and Schmidhuber [18] to resolve the vanishing and exploding gradient problems observed in the simple RNN, enabling it to capture longer-term dependencies.

LSTM architecture consists of a sequence of neurons and memory blocks known as cells, Fig. 1. The sequence of neurons form three gates, namely input gate, forget gate, and output gate. It uses these gates to control the flow of information to and from its neurons and to select the information it needs to discard or keep in its memory cells. The equations

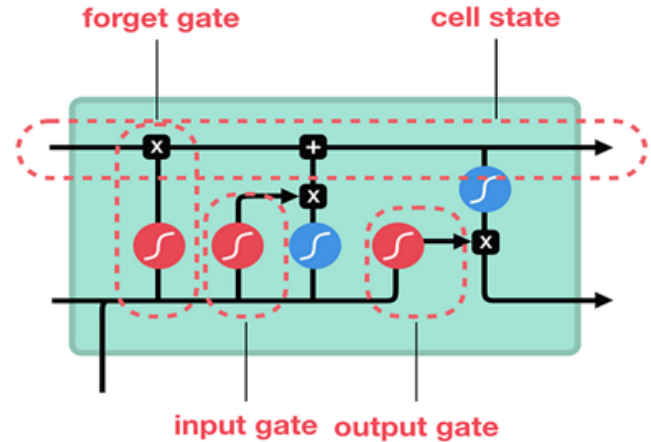


Fig. 1. LSTM architecture [19].

that are computed by the different neurons inside LSTM are as follows [20]:

$$i_t = \sigma(W_i x_t + U_i h_{t-1} + V_i c_{t-1}) \quad (2)$$

$$f_t = \sigma(W_f x_t + U_f h_{t-1} + V_f c_{t-1}) \quad (3)$$

$$o_t = \sigma(W_o x_t + U_o h_{t-1} + V_o c_t) \quad (4)$$

$$\tilde{c}_t = \tanh(W_c x_t + U_c h_{t-1}) \quad (5)$$

$$c_t = f_t \odot c_{t-1} + i_t \odot \tilde{c}_t \quad (6)$$

$$h_t = o_t \odot \tanh(c_t) \quad (7)$$

where, i_t , o_t , f_t and c_t denote the input-gate, the output-gate, the forget-gate, and the memory cells respectively. h_t represents a hidden state.

3) *Gated Recurrent Unit (GRU)*: Gated recurrent unit (GRU) is also another variant of RNN [21]. Its structure is similar to LSTM but uses two gates, namely reset-gate and update-gate, to control the retention and flow of information (see Fig. 2). Its performance is comparable to that of LSTM but it is faster to train due to its fewer equations. The equations

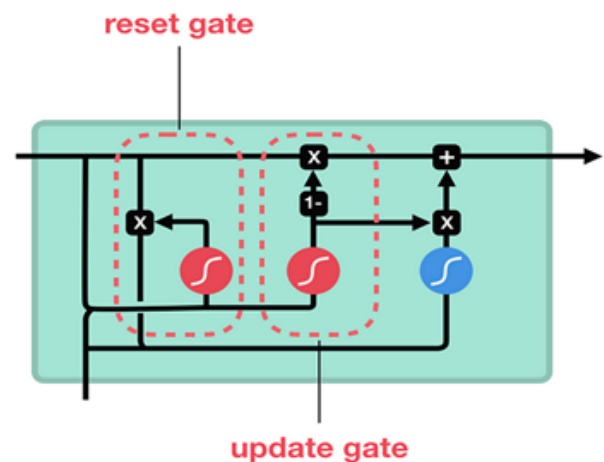


Fig. 2. GRU architecture [21].

computed by GRU are as follows [22]:

$$h_t = (1 - z_t) \odot h_{t-1} + z_t \odot \tilde{h}_t \quad (8)$$

$$\tilde{h}_t = \tanh(W_h x_t + U_h (r_t \odot h_{t-1}) + b_h) \quad (9)$$

$$z_t = \sigma(W_z x_t + U_z h_{t-1} + b_z) \quad (10)$$

$$r_t = \sigma(W_r x_t + U_r h_{t-1} + b_r) \quad (11)$$

where, r_t and z_t denote the reset-gate and update-gate, respectively. h_t and h_{t-1} represent the current and previous states, respectively.

RNN, LSTM, and GRU are incredibly slow because their training is difficult to parallelize. This is because inputs must be sequentially fed and the next step relies on the analysis of the previous step.

4) *Transformer Neural Network (TNN)*: Transformer neural network (TNN) is a type of DNN which doesn't rely on recurrent connections [23]. Instead, it uses a mechanism known as self-attention which enables it to handle long-range dependencies and process input sequences in parallel for more efficient computation [23]. A typical TNN consists of an encoder and a decoder (see Fig. 3).

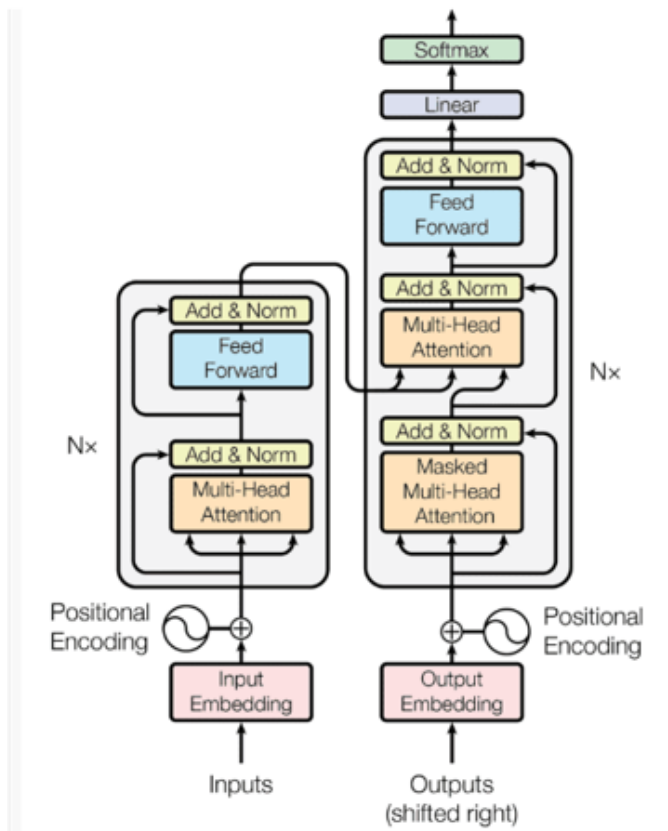


Fig. 3. TNN architecture [23].

The encoder is made up of multiple identical layers, and each layer consist of two sub-layers, namely a multi-head self-attention mechanism and a fully connected feedforward neural network (FFNN) [24]. To improve the performance and training stability of the encoder, each of the above mentioned sub-layers is followed by a residual connection and a normalization

step. The input data is augmented with positional encoding [25] and processed through the stacked layers, sub-layers, and steps of the encoder.

A decoder is also made of multiple identical layers. The sub-layers of a decoder layer are similar to that of an encoder but has an additional sub-layer known as an encoder-decoder attention mechanism. This additional sub-layer enables the decoder to selectively focus on different parts of the encoded input sequence while generating the output. At each layer, the decoder processes each sequence with multi-head self-attention, position-wise FFNN, residual connections, and normalization.

The self-attention mechanism allows a TNN to prioritize the various input sequences according to their importance. The input sequence is linearly projected into multiple sets of queries, keys, and values, which are then used to compute attention scores. The scores are used to weigh the values, and the resulting weighted values are summed to produce the output of the self-attention layer. This process is repeated for each head, and the outputs are concatenated and linearly transformed to create the final output.

$$Attention(Q, K, V) = softmax \left(\frac{QK^T}{\sqrt{d_k}} \right) \quad (12)$$

where, Q , K , and V are the query, key, and value matrices, respectively, and D_k is the dimension of K .

TNN uses multi-head attention layer to concatenate the attention weights of many single-head attention layers and then apply a non-linear transformation with a dense layer. Increasing the number of attention heads enables TNN to capture long-distance dependencies.

$$Multihead(Q, K, V) = Concat(h_1, h_2, \dots, h_n) W^0 \quad (13)$$

where, $h_i = Attention(QW_i^Q, KW_i^K, VW_i^V)$

TNN uses the position-wise FFNN to add non-linearity and to identify complex patterns in the input sequence. FFNN consists of two linear layers separated by a ReLU activation function. The independent application of this sub-layer to every part of the input sequence makes parallelism possible.

$$FFNN(x) = max(0, xW_1 + b_1) W_2 + b_2 \quad (14)$$

where, x is a sequence, and W_i and b_i are the weight matrix and the bias vector at layer i , respectively.

B. Wavelet Transform

Time-series data can be decomposed using Fourier or wavelet transforms. For analyzing non-stationary data, such as financial time series, wavelet transform has been found to outperform Fourier transform [7]. A wavelet transform is the representation of a function by wavelets [26], [27]. A wavelet is a waveform of a limited duration with an average value of zero, Fig. 4. It is a mathematical function with two basic parameters, namely scale (or dilation) and translation (location). Scale defines how squished or stretched a wavelet

is and translation defines where the wavelet is located in time or space. A wavelet is mathematically defined as:

$$\psi_{s,u}(t) = \frac{1}{\sqrt{|s|}} \psi\left(\frac{t-u}{s}\right), \quad s, u \in \mathbb{R}, \quad s \neq 0 \quad (15)$$

where, s and u are the dilation and the translation parameters, respectively. These two basic parameters are related to frequency as defined for waves. When the value of parameter s is increased, a wavelet is squashed and it captures high-frequency information, and when it is decreased, the wavelet is stretched and it captures low-frequency information. The parameter u defines the translation of the wavelet. Increasing u will shift the wavelet to the right and decreasing it will shift the wavelet to the left.

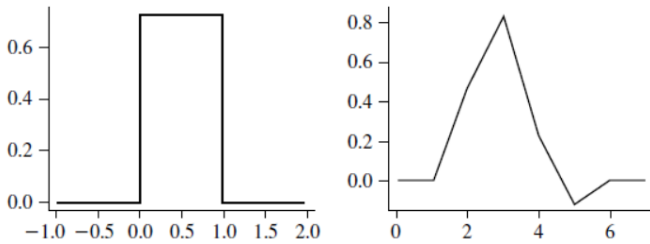


Fig. 4. Examples of wavelets.

The basic idea behind wavelet transform is to compute how much of a wavelet is in a signal for a particular scale and location. This is done by picking a wavelet of a particular scale, slide this wavelet across the entire signal, and at each time step, multiply the wavelet and the signal. The product of this multiplication gives us a coefficient for that wavelet scale at that time step. We then change the wavelet scale and repeat the process.

To best match a particular signal, there are a wide variety of prototype wavelets, called mother wavelets, to choose from. Popular examples of mother wavelets are Daubechies, Haar, Coiflets, Morlet, Symlets, Meyer, Mexican Hat and Biorthogonal [28]. A particular episode of wavelet transform uses one type of mother wavelet; the user decides which type and size to use depending on the characteristics of the signal to be analysed. Many time-series forecast applications use Daubechies [28]. After transformation of a signal using a particular mother wavelet, we end up with basis waveforms consisting of a series of daughter wavelets. The daughter wavelets are all compressed or expanded versions of their mother wavelet, and each daughter wavelet extends across a different part of the original signal. The important point is that each daughter wavelet is associated with a corresponding coefficient that specifies how much the daughter wavelet at that scale contributes to the raw signal at that location. It is these coefficients that contain the information relating to the original input signal.

The two major wavelet transforms in wavelet analysis are Continuous Wavelet Transform (CWT) and Discrete Wavelet Transform (DWT). CWTs operate over every possible scale and translation values; whereas DWTs use a finite set of wavelets defined at a particular set of scales and locations values.

DWT basis function at dyadic scaling m and time location n is given by, [29],

$$\psi_{m,n}(t) = 2^{-\frac{m}{2}} \psi(2^{-m} \cdot t - n) \quad (16)$$

The inner product of a time-series data denoted by $x(t)$ and the basis function $\psi_{m,n}$, Eq. (17) returns the high frequency information, also known as the detailed coefficients, contained in the signal.

$$d_{m,n} = \sum_{t=0}^{N-1} x(t) \psi_{m,n}(t) \quad (17)$$

Decomposing a signal using mother wavelet can result in infinite number of basis functions to accurately represent the signal. In order to have a finite set of basis wavelet, an auxiliary function $\phi(t)$, known as a scaling function or father wavelet, is defined and associated with the mother wavelet to capture the rest of the signal. Eq. (18) is a definition of a scaling function at level m and translation n .

$$\phi_{m,n}(t) = 2^{-\frac{m}{2}} \phi(2^{-m} \cdot t - n) \quad (18)$$

The inner product of a signal $x(t)$ and $\phi_{m,n}$, as defined in Eq. (19), returns the low frequency information, also known as the approximation coefficients, contained in the signal.

$$a_{m,n} = \sum_{t=0}^{N-1} x(t) \phi_{m,n}(t) \quad (19)$$

An approximation of $x(t)$ at level m can be computed from $a_{m,n}$ as shown in Eq. (20).

$$x_m(t) = \sum_n a_{m,n} \phi_{m,n}(t) \quad (20)$$

Given $d_{m,n}$ at levels $1, 2, \dots, m_0$ and $a_{m_0,n}$, the final multiresolution representation of $x(t)$ can be computed as shown by Eq. (21).

$$x(t) = \sum_n a_{m_0,n} \phi_{m_0,n}(t) + \sum_{m=1}^{m_0} \sum_n d_{m,n} \psi_{m,n}(t) \quad (21)$$

1) Empirical Wavelet Transform: Empirical wavelet transform (EWT) is a technique to decompose a signal using an adaptive subdivision scheme [30]. EWT starts by dividing the signal spectrum into N continuous segments where each segment can be defined as $\Lambda_n = [\omega_{n-1}, \omega_n]$, where each ω_n ($\omega_0 = 0$ and $\omega_N = \pi$) denotes a boundary of a segment. The empirical wavelet is regarded as wavelet filters of each Λ_n

The empirical scaling function $\hat{\phi}_n(\omega)$ and the empirical wavelet function $\hat{\psi}_n(\omega)$ are computed according to Eq. (22) and Eq. (23):

$$\hat{\phi}_n(\omega) = \begin{cases} 1 & \text{if } |\omega| \leq (1 - \gamma)\omega_n \\ K & \text{if } (1 - \gamma)\omega_n \leq |\omega| \leq (1 + \gamma)\omega_n \\ 0 & \text{otherwise} \end{cases} \quad (22)$$

$$\hat{\psi}_n(\omega) = \begin{cases} 1 & \text{if } (1 + \gamma)\omega_n \leq |\omega| \leq (1 - \gamma)\omega_{n+1} \\ M & \text{if } (1 - \gamma)\omega_{n+1} \leq |\omega| \leq (1 + \gamma)\omega_{n+1} \\ N & \text{if } (1 - \gamma)\omega_n \leq |\omega| \leq (1 + \gamma)\omega_n \\ 0 & \text{otherwise} \end{cases} \quad (23)$$

where:

$$K = \cos \left[\frac{\pi}{2} \beta \left(\frac{1}{2\gamma\omega_n} (|\omega| - (1 - \gamma)\omega_n) \right) \right],$$

$$M = \cos \left[\frac{\pi}{2} \beta \left(\frac{1}{2\gamma\omega_{n+1}} (|\omega| - (1 - \gamma)\omega_{n+1}) \right) \right],$$

$$N = \sin \left[\frac{\pi}{2} \beta \left(\frac{1}{2\gamma\omega_n} (|\omega| - (1 - \gamma)\omega_n) \right) \right],$$

$$\beta(x) = x^4(35 - 84x + 70x^2 - 20x^3),$$

$$\gamma \leq \gamma \leq \min_n \left[\frac{\omega_{n+1} - \omega_n}{\omega_{n+1} + \omega_n} \right], \text{ and}$$

γ is restricted between 0 and 1 to insure $\hat{\phi}_n(\omega)$ and $\hat{\psi}_n(\omega)$ is a tight frame of $L^2(R)$.

III. RELATED WORK

Publications related to stock price prediction using TNN started in the last few years, and as a result, existing trading systems based on TNN are very limited, and this section summarizes most, if not all, of them. This section also presents some existing work on TNN based stock price prediction techniques.

Malibari et al. [31] proposed a stock price prediction technique using TNN. Their proposed TNN architecture was influenced by a vision transformer (ViT) [32]. They used it to predict the next day closing values of four Saudi stock market indices, namely TASI, TBNI, TMTI, and TTSI. They used MAE, MSE, MAPE, and RMSE performances matrices and found out that their proposed model can predict closing prices with a probability higher than 90%. Stock price prediction using TNN and time2vec was proposed by Muhammad et al. [33]. Their model predicts the next day and the next week closing prices of eight stocks listed in Dhaka Stock Exchange. They used the closing prices of eight previous days to predict that of the next day and they used the closing prices of the previous eight weeks to predict the closing price of the next week. They used MAE and RMSE to measure the performance of their model. For the daily solution, the MAE was less than 0.083 and the RMSE was less than 0.11, and for the weekly, the MAE was less than 0.3 and the RMSE was less than 0.33.

A number of researchers compared the stock price prediction accuracy of TNN with other models. For example, Anass [34] compared the accuracy of LSTM and TNN in predicting the next day values of Nasdaq, S&P, and Dow. He used the value of trading day t to predict the value of trading day $t + 1$. He compared them using accuracy, MAE, MSE, RMSE, and execution time. He found out that TNN consistently outperformed LSTM. Also the comparison of LSTM and TNN was done by Lin et al [35]. They compared the performance of TNN and LSTM to predict the next minute and then next day stock prices. They used the historical data of Shanghai Stock Index. The daily trading data spans from December 17, 2002 to December 17, 2022 and minute-level data spans from 9:30 on December 23, 2019 to 15:00 on December 23, 2022. They compared them using MAE and MSE and they reported that LSTM outperformed TNN consistently in all the measures. Similarly Saeed [36] proposed using the

stock prices of the previous ten days to predict the next day price. He used the historical prices of Yahoo, Facebook, and JPMorgan from January 1, 2017, to September 2017. He compared the performance of TNN with ARIMA, LSTM, and Random Forest using MAE, RMSE, and MAPE. He reported that TNN consistently outperformed all of them. Performance comparison of TNN, ARIMA and LSTM using the average daily prices of eight stocks listed in the Brazilian Ibovespa was illustrated by Lorenzo et al. [37]. They used 2008 historical prices totaling 80 values per share. TNN outperformed both ARIMA and LSTM obtaining the lowest RMSE in 60% of the tests, followed by LSTM in 22% and, finally, ARIMA in 18%. Wang et al. [38] compared TNN with LSTM and Hidden Markov model (HMM) using historical prices of Shanghai and Shenzhen CSI new energy stock index from June 17, 2019 to June 17, 2022. They used MAE, RMSE, and MSE, R2 to compare them. They reported that TNN consistently outperformed both of them in all the above mentioned four performance measures. Stock price predicting model consisting of BiLSTM and MTRAN-TCN was proposed by Wang et al. [39]. BiLSTM is a bidirection LSTM, MTRAN is a modified TNN, and TCN is a time conventional network. They used BiLSTM to capture bidirectional information in sequences and TCN to identify sequence dependencies. They used five index stocks and 14 Shanghai and Shenzhen stocks and measured the performance of their proposed model using MAE, RMSE, and MSE, and R2. They reported that the combination of BiLSTM and MTRAN-TCN consistently outperformed any of its subset components with all the datasets and all the above mentioned four performance measures. TNN and LSTM were also compared using LOB (Limit Order Book) data of cryptocurrency by Bilokon and Qiu [40]. They compared them using three financial time series prediction tasks, namely LOB mid-price prediction, LOB mid-price difference prediction, and LOB mid-price movement prediction of cryptocurrency LOB data. They reported that TNN outperformed LSTM by a large margin in terms of the limited metrics for mid-price prediction; whereas LSTM outperformed TNN in the other two tasks. They concluded that LSTM-based models are generally better in financial time series prediction for electronic trading.

A limited number of researchers proposed one or more trading systems based on TNN. For example, Aman [41] compared two trading systems, one based on LSTM and the other on TNN. He used the data of four stocks listed in Nifty 50 of the Indian stock market. He collected data of 21 years ranging from January 1, 2000 to December 31, 2020. Using a sliding window of size four years, he divided the data into 17 overlapping windows. The data of each window was then split into two: the data of the first three years was used for training and that of the last year for testing. He took both long and short trades. The average daily returns of the trading system based on LSTM was 2.22%. For long trades, the TNN based system gave better returns than that of LSTM. For short trades, the TNN results were inconsistent. Four trading systems based on TNN, RNN, CNN, and LSTM were proposed by Wang et al. [42]. They used data of four global indices namely, the Shanghai and Shenzhen 300 Index (CSI 300) in China, the Standard & Poors 500 Index (S&P 500) in the US, the Nikkei 225 Index (N225) in Japan, and the Hang Seng Index (HSI) in Hong Kong. The collected data that spans 11 years, from January 1, 2010 to December 31, 2020. The trading strategy

proposed is as follows: if the predicted value y_{t+1} is higher than the last observed value y_t , then a long position is entered; and if y_{t+1} is lower, then a short position is entered, otherwise no position is taken. According to the performance measures MAE, MSE, and MAPE, TNN consistently outperformed the other three and gave better trading returns with all the above mentioned four global indices. A trading system based on TEANet, which is a model consisting of TNN and LSTM, was proposed by Zhang et al. [43]. Input to TEANet are tweet corpus and historical prices. The TNN component of TEANet takes as input tweets and feeds its output to LSTM. The LSTM also takes as input normalized historical prices. To evaluate the performance of TEANet, the researchers used a standard profit method and adopted a market simulation strategy proposed by Ding et al. [44]. The trading strategy is as follows: if TEANet predicts the price of a stock to rise, then a long position is entered and if it predicts the price to fall, then a short position is entered. The size of each position is \$10,000. A long position is sold if a 2% profit is achieved, otherwise it is sold at the closing price at the end of the day. Similarly, a short position is sold if a 1% profit is achieved, otherwise it is sold at the closing price at the end of the day. The proposed trading system was tested using data of 44 trading days collected from 12 randomly selected stocks. The returns of TEANet were compared to the returns of a system known as CapTE [45]. TEANet outperformed CapTE and showed an average return of 22.31% compared to 20.18% of CapTE.

IV. FRAMEWORK OF THE PROPOSED TRADING SOLUTION

The framework of the proposed trading solution can be summarized as follows:

- 1) Ten out of 223 stocks listed in the Saudi stock market are randomly selected. Then ten datasets, one from each selected stock, are collected. The selected stocks and their selection criteria are discussed in Section V-B.
- 2) From each dataset nine features are selected. These features are four daily stock prices, namely open (O), low (L), high (H), and close (C), the daily volume traded (V), the Saudi market index TASI (T), sector index (S), and two TIs, namely Bollinger Bands (BB), and average true range (ATR).
- 3) Six performance measure are selected and used in this study and they are presented in Section V-C.
- 4) Out of more than 100 TIs, 10 are selected based on literature survey. Then for each selected TI, its best parameter values are identified. These selected TIs are further filtered and combined based on their performance. The details of TIs selection, best parameter value identification, filtration, and combination are discussed in Section V-D.
- 5) The 10 datasets are preprocessed. One of the features is converted into log returns and decomposed using EWT, and the remaining eight features are scaled. Then all of them are reshaped and split into training and testing. The data preprocessing of the datasets is detailed in Section V-E and EWT is explained in Section II-B1.
- 6) Seven deep learning models are compared and the one with the best performance is selected for the proposed

solution, Section V-F. The architecture of each of the seven compared models is shown in Fig. 5

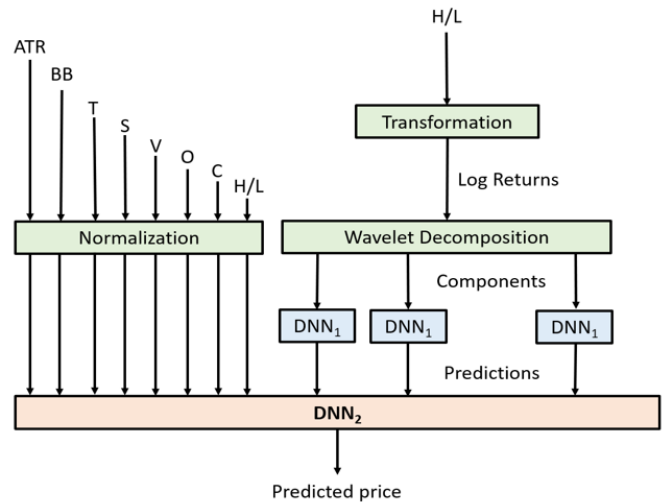


Fig. 5. Architecture of the proposed model.

- 7) The selected model is further optimized by choosing the best possible hyper-parameters. The list of the selected hyper-parameters and optimizers are presented in Section V-F.
- 8) A day trading strategy which consists of eight trading systems is proposed. The trading strategy is based on the open price and two predicted daily stock prices, namely the daily high and the daily low, Fig. 6. The details of the trading strategy is presented in Section V-G.

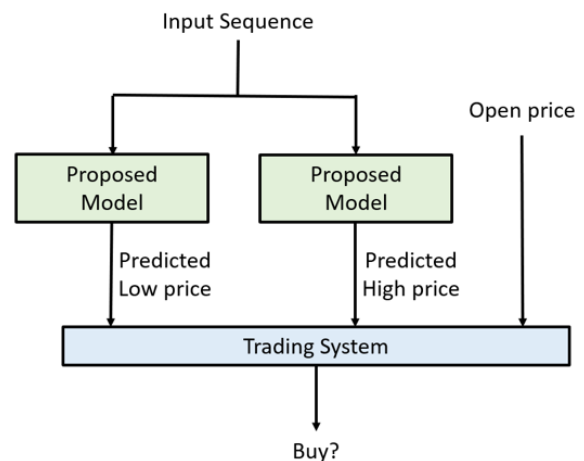


Fig. 6. Trading methodology.

- 9) At last, the proposed solution is evaluated, analyzed and compared, Section V-H.

V. RESULTS AND ANALYSIS

To study the performance of the proposed trading strategy, six sets of experiments were conducted. The first set of

experiments was done to choose the best possible deep learning model. The second set was done to identify the best possible hyperparameter values for the selected model. The third set was done to select the most relevant TIs. The fourth set was done to identify the best possible parameter values for each selected TI. The fifth set was done to choose the best possible combination of TIs. The last set of experiments was done to study the performance of the proposed trading strategy. But before the results and analysis of the above mentioned experiments are presented, let us discuss the experimental environment, the datasets, and the performance measures used in this study.

A. Experimental Machines and Tools

All the experiments were conducted on a Windows 10 machine with Intel(R) Core(TM) i7-7700HQ CPU @ 2.80 and 2.81 GHz, and a 16 GB RAM.

The datasets were downloaded using TickerChart [46] and preprocessed using Amibroker Formula Language (AFL) [47], Python, and Matlab. The deep learning models were implemented in Python using Keras open-source package with TensorFlow back-end [48]. EWT was implemented using EWT MATLAB toolbox.

B. Dataset Selection, Collection, and Features

The experimental datasets were collected from 10 out of the 223 stocks listed in the Saudi Stock exchange. These stocks are Bahri, Al-Rajhi, STC, Maaden, Tawuniya, Jarir, Jabel Omer, Budget, Sharqiya, and Mouwasat. These datasets were chosen because they exhibit different characteristics such as, they belong to different sectors, they have different number of free shares, they have been in the market since 2009 so they have enough data for training and testing, and for bull, bear, and side way markets, they are liquid enough to minimize errors due to slippage when entering and exiting positions, and so on. The datasets were downloaded using TickerChart. Table I shows some characteristics of the datasets.

TABLE I. THE DATASETS

| Dataset | Stock | Symbol | Sector | Free Shares (in Millions) | Range | Standard Deviation |
|---------|------------|--------|-------------------|---------------------------|----------------|--------------------|
| D1 | Alrajhi | 1120 | Banks | 3908.1 | 18.17 - 117.40 | 19.1 |
| D2 | Maaden | 1211 | Materials | 807.7 | 4.87 - 57.76 | 9 |
| D3 | Mouwasat | 4002 | Healthcare | 65.0 | 6.88 - 129.7 | 28.4 |
| D4 | Bahri | 4030 | Energy | 380.4 | 5.71 - 30.28 | 5.15 |
| D5 | Jarir | 4190 | Retail | 110.7 | 4.3 - 22.5 | 4.69 |
| D6 | Jabel Omar | 4250 | Real estate | 929.2 | 11.0 - 88.75 | 18.85 |
| D7 | Budget | 4260 | Transportation | 71.1 | 9.18 - 54.5 | 11.44 |
| D8 | Sharqiya | 6060 | Food & Beverages | 7.5 | 8.49 - 52.59 | 8.49 |
| D9 | STC | 7010 | Telecommunication | 1800.0 | 13.2 - 55.92 | 11 |
| D10 | Tawuniya | 8010 | Insurance | 92.7 | 22.48 - 106.0 | 22.86 |

Each dataset contains nine features. These features are based on the daily time frame and they are: the daily open (O), high (H), low(L), and close (C) prices of a stock, the daily Volume (V) of shares traded, the sector index value (S), the TASI (T) which is the Saudi stock market index value, and two technical indicators, namely the Bollinger Bands (BB) and the average true range (ATR) which will be discussed in Section V-D.

Each dataset contains daily data from January 1, 2010 to December 31, 2022, which consists of 3244 observations.

TABLE II. THE FEATURES

| Symbol | Name | Description |
|--------|--------------------|---------------------|
| O | Open | Daily open price |
| L | Low | Daily Lowest price |
| H | High | Daily highest price |
| C | Close | Daily close price |
| V | Volume | Daily traded shares |
| T | TASI | Saudi market Index |
| S | stock specific | Sector index |
| BB | Bollinger Bands | TI |
| ATR | Average True Range | TI |

Table II contains the description of the above mentioned nine features.

According the proposed trading strategy, an open trade is closed when its stock price reaches a profit-target or a stop-loss, otherwise it is closed at the end of the trading day. A trade is a winner, if the intraday price of its stock reaches the profit-target before it hits the stop-loss; and it is a loser if the intraday price reaches first the stop-loss. The data in the above ten datasets is based on daily time frames or price-bars, meaning, the values of O, L, H, and C are daily prices. They don't include prices of lower time frames, such as hourly, 15-minute or 5-minute. From daily price-bars, it is impossible to know if a trade entered on day t is a winner or a loser if the price-bar covers both the predicted high and the predicted low. To avoid mistakes that can be created by such price-bars, supplementary datasets were collected from each of the above mentioned stocks. These datasets contain the highest and the lowest stock prices of 5-minute time frames from January 1, 2020 to December 31, 2022. These datasets are only used during trading and not used for training or testing the proposed model. If a 5-minute price-bar covers both the profit-target and the stop-loss of a trade, then the trade is ignored. Fortunately, the number of such 5-minute price-bars is so insignificant that there is no need to use price-bars of a lesser time frame.

C. Performance Measures

To study the performance of the proposed solution, six performance measures, namely, Mean Square Error (MSE), Root Mean Square Error (RMSE), Mean Absolute Error (MAE), Mean Absolute Percentage Error (MAPE), coefficient of determination (R^2), and Expectancy (Φ) were used. These measures were chosen because they are frequently used in related works. A good model must have RMSE, MAE, and MAPE close to 0, R^2 close to one, and a positive Expectancy. Expectancy is defined in Eq. (1), but the other five measures are mathematically defined as follows:

$$MSE = \frac{1}{n} \sum_{t=0}^{n-1} (y_t - \hat{y}_t)^2 \quad (24)$$

$$RMSE = \sqrt{\frac{1}{n} \sum_{t=0}^{n-1} (y_t - \hat{y}_t)^2} \quad (25)$$

$$MAE = \frac{1}{n} \sum_{t=0}^{n-1} |y_t - \hat{y}_t| \quad (26)$$

$$MAPE = \frac{\sum_{t=0}^{n-1} \left| \frac{y_t - \hat{y}_t}{y_t} \right|}{n} \times 100\% \quad (27)$$

$$R^2 = 1 - \frac{\sum_{t=0}^{n-1} (y_t - \hat{y}_t)^2}{\sum_{t=0}^{n-1} (y_t - \bar{y})^2} \quad (28)$$

where, y_t and \hat{y}_t represent the actual and forecast values at step t for $0 \leq t < n$, respectively, and $\bar{y} = \sum_{t=0}^{n-1} y_t/n$.

D. Selecting TIs, TI Parameters, and TI Combination

There are more than 100 TIs and each TI has a number of parameters. Some TI parameters have infinite number of possible values. Hence, selecting the best TIs with their best parameter values is very challenging. In this study, a four step filtering process was adopted to choose a set of TIs and their parameter values. In Step 1, based on literature survey, the top 10 most frequently used TIs were identified (see Table III).

TABLE III. MOST FREQUENTLY USED TECHNICAL INDICATORS IN THE SURVEYED LITERATURE

| TI | Frequency |
|-----------------|-----------|
| MA | 35 |
| RSI | 34 |
| Williams R% | 28 |
| Stochastic %K | 25 |
| MACD | 22 |
| ROC | 19 |
| Momentum | 16 |
| Bollinger Bands | 15 |
| ATR | 14 |
| CCI | 14 |

In Step 2, the most frequently used TI parameter values are identified. Then each TI and each of its most frequently used parameters value were used to predict the next day high and low prices using the proposed model which will be defined shortly. If a TI and its best parameter doesn't improve the prediction performance of the proposed architecture, then it is dropped. This step is done after normalizing the TI values using min-max normalization. In Step 3, The least relevant TIs are identified and eliminated. This is done using recursive feature elimination [49]. Table III shows the TIs and the parameter values that were selected after the above three steps.

TABLE IV. SELECTED TIS AND THEIR SELECTED PARAMETER VALUES

| TI | Name | Parameters |
|------|---------------------------------------|------------|
| STO | Stochastic | 15, 3, 3 |
| MACD | Moving Average Convergence Divergence | 12, 26, 9 |
| RSI | Relative Strength Index | 14 |
| BB | Bollinger Bands | 20, 2 |
| ATR | Average True Range | 14 |

In Step 4, the selected TIs were combined in all the possible ways and the best combination was selected (see Table IV). Since there are five selected TIs, the maximum number of combinations is 32, including the one with no TIs used. Table V shows the performance of each set of TI combination. Each

TABLE V. PERFORMANCE MEASURES OF TI COMBINATIONS

| ATR | MACD | BB | STO | RSI | E |
|-----|------|----|-----|-----|------|
| 0 | 0 | 0 | 0 | 0 | 2.31 |
| 0 | 0 | 0 | 0 | 1 | 1.38 |
| 0 | 0 | 0 | 1 | 0 | 1.74 |
| 0 | 0 | 0 | 1 | 1 | 1.66 |
| 0 | 0 | 1 | 0 | 0 | 1.59 |
| 0 | 0 | 1 | 0 | 1 | 2.31 |
| 0 | 0 | 1 | 1 | 0 | 2.64 |
| 0 | 0 | 1 | 1 | 1 | 1.24 |
| 0 | 1 | 0 | 0 | 0 | 1.51 |
| 0 | 1 | 0 | 0 | 1 | 1.55 |
| 0 | 1 | 0 | 1 | 0 | 2.68 |
| 0 | 1 | 0 | 1 | 1 | 1.39 |
| 0 | 1 | 1 | 0 | 0 | 3.98 |
| 0 | 1 | 1 | 0 | 1 | 1.42 |
| 0 | 1 | 1 | 1 | 0 | 2.09 |
| 0 | 1 | 1 | 1 | 1 | 1.16 |
| 1 | 0 | 0 | 0 | 0 | 2.12 |
| 1 | 0 | 0 | 0 | 1 | 1.12 |
| 1 | 0 | 0 | 1 | 0 | 1.68 |
| 1 | 0 | 0 | 1 | 1 | 1.47 |
| 1 | 0 | 1 | 0 | 0 | 1.09 |
| 1 | 0 | 1 | 0 | 1 | 1.31 |
| 1 | 0 | 1 | 1 | 0 | 2.21 |
| 1 | 0 | 1 | 1 | 1 | 1.20 |
| 1 | 1 | 0 | 0 | 0 | 1.94 |
| 1 | 1 | 0 | 0 | 1 | 2.28 |
| 1 | 1 | 0 | 1 | 0 | 4.98 |
| 1 | 1 | 0 | 1 | 1 | 1.88 |
| 1 | 1 | 1 | 0 | 0 | 2.17 |
| 1 | 1 | 1 | 0 | 1 | 1.99 |
| 1 | 1 | 1 | 1 | 0 | 2.11 |
| 1 | 1 | 1 | 1 | 1 | 2.18 |

measurement is based on the average of the predicted high and low prices of each stock.

Each row of the table represents a unique combination of TIs. In each of the first five columns, a 0 value represents the absence of the corresponding TI from the combination, and a 1 represents its presence. For example, in the row before the last, all TIs except RSI were in the combination. The last column, E , was computed using Eq. (29).

$$E_i = 1 - \widehat{r}_i^2 + r\widehat{mse}_i + m\widehat{ae}_i + m\widehat{ape}_i \quad (29)$$

where, i represents i^{th} row of Table V, \widehat{r}_i^2 , $r\widehat{mse}_i$, $m\widehat{ae}_i$, and $m\widehat{ape}_i$ are the r^2 , RMSE, MAE, and MAPE values of row i , respectively, and \widehat{x} represents the normalized value of x using min-max, Equation 30. The best combination is the one with the lowest E . According the results in Table V, the lowest E is 1.09 and corresponds to the combination of BB and ATR; and is the combination that was selected for the proposed model.

Nearly all the normalization operations in this study were done using min-max. It is one of the most popular techniques and is frequently used by similar studies. If $X = x_1, x_2, \dots, x_n$, then scaling x_i using min-max is mathematically defined as:

$$\acute{x}_i = \frac{x_i - \min(X)}{\max(X) - \min(X)} \quad (30)$$

where, x_i is the i^{th} value in X , \acute{x}_i is the normalized value of x_i , and $\min(x)$ and $\max(x)$ are the lowest and the highest values in X , respectively.

E. Data Preprocessing

Data processing is done in five phases. In Phase 1, L or H is converted to log returns. If the proposed model is going to predict the next day highest price, then H is converted to log

returns and if it is going to predict the next day lowest price, then L is converted to log returns. If $X = x_1, x_2, \dots, X_n$ is a time series data, then the log return of x_t is mathematically defined as:

$$\dot{x}_t = \log(x_t/x_{t-1}) \quad (31)$$

where, x_t is the value at time t , x_{t-1} is the value at time $t - 1$, and \dot{x}_t is the log return of x_t . Converting stock prices into log returns increases the stationarity of the dataset.

In Phase 2, the log returns generated in Phase 1 are decomposed using the EWT algorithm proposed by Jérôme Gilles [30] as explained in Section II-B1. Decomposition results in building better forecasting models, because it enables the identification and the removal of noisy and irrelevant parts of a time series data. EWT was chosen because it is an adaptive wavelet subdivision scheme which performs wavelet decomposition without prior information about the data, produces a small number of coefficients to pack the signal information, and results in a higher resolution of time-frequency which simplifies the analysis of time-series data.

In Phase 3, all the remaining eight features are scaled between 0 and 1 using the min-max formula. This phase may not be important because TNNs can handle unscaled data.

In Phase 4, each one-dimensional time series data of size N observations is reshaped into a two dimensional array of size $N - k$ by $k + 1$ using a sliding window of size $K + 1$. This is done to predict the stock price on day t , p_t , using $p_{t-1}, p_{t-2}, \dots, p_{t-k}$. Finding the best possible value of k is explained in Section V-F.

In Phase 5, the data is split into training and testing. The data from January 1, 2010 to December 31, 2019 was used for training and the data from January 1, 2020 until December 31, 2022 was used for testing.

F. Deep Learning Model Selection

To find the best deep learning model for the proposed solution, seven models namely, simple or vanilla LSTM (VLSTM), Stacked LSTM (SLSTM), Bidirectional LSTM (BLSTM) [50], GRU, Stacked GRU (SGRU), and Bidirectional GRU (BGRU) were compared. Fig. 5 shows the architecture of the proposed model that was selected after trying many other architectures. A number of experiments were conducted to choose the deep learning model that can best predict the next day high and low stock prices. The data was reshaped so that the previous 16 days are used to predict the price of the next day. Each model was experimented using different hyperparameter values and its performance was measured using RMSE, MAE, MAPE, and R^2 . Table VI shows the average performance measures of all the experiments.

To choose the best performing model for the proposed solution, a normalized sum, E , was used, Eq. (29). The model with the lowest E has the best performance and thus selected for the proposed solution. As shown in Table VI, TNN has the lowest E , hence selected as the model of the proposed solution. Fig. 7 shows the architecture of the proposed model. As can be seen from the figure, the architecture contains two levels of TNNs. The TNNs in the first level are labeled as TNN_1 and the one in the second level is labeled as TNN_2 . Since each TNN in the proposed model is used for the prediction

TABLE VI. THE PERFORMANCES OF THE SEVEN DEEP LEARNING MODELS

| Model | RMSE | MAE | MAPE | r^2 | E |
|-------|----------|----------|---------|---------|-------|
| VLSTM | 77.13597 | 46.23983 | 0.07594 | 0.97639 | 3.506 |
| SLSTM | 14.06473 | 10.01123 | 0.04511 | 0.99002 | 0.087 |
| BLSTM | 14.38421 | 19.35125 | 0.05318 | 0.97971 | 1.099 |
| GRU | 82.98782 | 51.12156 | 0.07823 | 0.97214 | 4.000 |
| SGRU | 14.17115 | 10.16732 | 0.04569 | 0.99013 | 0.104 |
| BGRU | 15.66173 | 18.72891 | 0.05408 | 0.98895 | 0.643 |
| TNN | 13.86754 | 9.88712 | 0.04436 | 0.99115 | 0.000 |

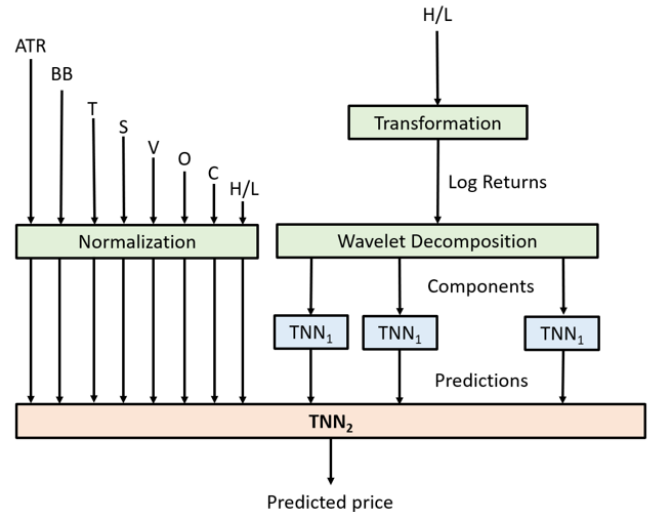


Fig. 7. The architecture of the proposed deep learning model.

of a continuous value, it doesn't need a decoder. It only uses encoders similar to the architecture of the popular BERT [51]. It also includes some dense layer, dropout layers, a global average pooling layer, and an output layer which consists of a single neuron that emits the predicted continuous value.

To train the model for the prediction of the next day high price, the following steps were taken. H is first converted into log returns and then the log returns are decomposed into multiple levels using EWT. Each level is then reshaped into input sequences of size 16 each, encoded with time2vec, and fed into a Level 1 TNN. Similarly, each of the input features O, L, C, V, S, T, BB , and ATR are scaled between 0 and 1 using the min-max. Then these scaled values and the output of all Level 1 TNNs are reshaped into input sequences of size 16, encoded with time2vec, and fed to the Level 2 TNN. The output of the Level 2 TNN is the predicted value. The same steps were taken to train the model for the prediction of the next day low price, except L and H exchange places in the model. A TNN requires a notion of time when processing stock prices. Without time encoding, a TNN will be oblivious to the temporal order of stock prices. In order to overcome this, the proposed model uses Time2Vec [15], a time encoding layer. Many experiments were conducted to arrive at the proposed model and Table VII summarizes the selected parameters and hyperparameters.

TABLE VII. THE PROPOSED MODEL HYPERPARAMETERS AND OTHER PARAMETERS

| Parameter | TNN ₁ | TNN ₂ |
|-----------------|------------------|------------------|
| time embedding | time2vec | time2vec |
| sequence size | 16 | 16 |
| number of heads | 3 | 4 |
| ff dimension | 32 | 64 |
| encoder blocks | 3 | 4 |
| dropout rate | 0.2 | 0.2 |
| loss function | MSE | MSE |
| optimizer | Adam | Adam |
| learning rate | 0.0001 | 0.0001 |
| epochs | 150 | 200 |
| batch size | 64 | 64 |

G. Proposed Trading Strategy

As was mentioned before, day trading is a business of probability. When a day trader enters a position, he is not sure if it will be a winner or a loser. Most consistently profitable traders have a win rate between 40% and 60%. They are consistently profitable because their average win is much higher than their average loss. They do that by cutting their losers short and letting their winners run. They decide the amount they will risk per trade, denoted as R , before they enter a position. Most of them limit R to be less than 2% of their trading capital. This way, they can survive a number of consecutive losers.

The proposed trading strategy uses stop-loss and is based on two predicted values, namely, \hat{h}_t and \hat{l}_t , where, \hat{h}_t and \hat{l}_t are the predicted highest and lowest prices of a stock on a trading day t , respectively. These predictions are based on the proposed deep learning model, shown in Fig. 7, and are computed on the morning of the trading day and before the market opens.

The proposed trading strategy consist of four buying and three selling rules. The four buying rules are:

- 1) $B == o_t + \psi$, where, B is the buying price per share, o_t is the open price on day t , and ψ is the minimum allowed bid-ask spread value.
- 2) The risk (R) per trade must be no more than 1% of the total capital. $R = B - \hat{l}_t - \psi * N$, where N is the number of shares bought. For example, for a trading capital of 10000 dollars, R must be no more than 100 dollars.
- 3) $\frac{\hat{h}_t - B}{N} \geq n \times R$ for n in (1.5, 2, 2.5, 3, 3.5, 4, 4.5, 5).
- 4) $n \times R > F$, where F is amount of fees and commissions paid to enter and exit a position.

The first rule is a conditional buy and is needed to make sure that a position is entered only when the stock price is trending towards the profit-target \hat{h}_t . The second rule limits the maximum risk taken on a trade. The third rule is there to make sure that the potential reward (profit) of a trade is significantly higher than the potential risk taken. The fourth rule is needed to ensure that the potential profit of a trade exceeds the fees paid to enter and exit the trade. When the above four rules are meet, a 10,000 Saudi riyals position is entered.

An open position is closed when any of the following three conditions is true.

- 1) If the intraday loss on a trade reaches R . This is done by using a predefined stop-loss price.
- 2) If the intraday profit on a trade reaches a prespecified profit-target, $n \times R$, for n in (1.5, 2, 2.5, 3, 3.5, 4, 4.5, 5).
- 3) If none of the above conditions is met, then the position is sold at the closing price of the day.

To study the performance of the proposed solution, eight trading systems were created. These systems satisfy the above mentioned buying and selling conditions but they differ in their profit-target. Table VIII shows these trading systems and their corresponding profit-targets.

TABLE VIII. THE EIGHT TRADING SYSTEMS OF THE PROPOSED TRADING STRATEGY

| Trading System | TS1 | TS2 | TS3 | TS4 | TS5 | TS6 | TS7 | TS8 |
|----------------|------|-----|------|-----|------|-----|------|-----|
| Profit-target | 1.5R | 2R | 2.5R | 3R | 3.5R | 4R | 4.5R | 5R |

H. Trading Results and Analysis

A number of experiments were conducted to study the profitability of each of the eight trading systems. The trades included in this study cover three year period, from January 1, 2020 to December 31, 2022, a total of 749 trading days. Each trading system was used with each dataset and the stats, such as the number of trades executed, the number of winning trades, the average profit of a winning trade, the average loss of a losing trade, etc was collected. Table IX shows some of the stats obtained by trading Alrajhi shares. The table shows that 138 positions were entered using TS1. As was mentioned before, the size of each position is 10,000 riyals. 90 of the 138 positions were winners and the rest were losers. A breakeven position is considered to be a loser because of the fees paid and the resources wasted to execute the position. The average profit per a winning trade is 140.23 riyals and the average loss is 63.89 riyals. The gross and net profits of all the positions are 12620 and 4999 riyals. The amount of fees and commissions paid to execute the trades was 4554 riyals. The expectancy, Φ , of trading Alrajhi stocks using TS1 is 36.23 riyals. The table also shows the stats of the other seven trading systems. TS2 is more profitable and TS3 has the best expectancy. TS2 was more profitable than TS3 because more trades were executed using TS2. The results also show that five of the eight trading systems were winners and the rest were losers. TS8 was the worst loser with 36.24% loss. The table also shows that the fees paid to execute trades are significant, between 30% and 61% of the gross profits.

TABLE IX. TRADING STATS OF ALRAJHI SHARES

| Trading System | TS1 | TS2 | TS3 | TS4 | TS5 | TS6 | TS7 | TS8 |
|-------------------|--------|--------|--------|--------|--------|--------|--------|--------|
| positions entered | 138 | 130 | 117 | 106 | 105 | 99 | 91 | 82 |
| Winners | 90 | 78 | 69 | 58 | 46 | 40 | 35 | 29 |
| Average win | 140.23 | 171.19 | 183.32 | 191.88 | 208.83 | 201.15 | 178.02 | 151 |
| Average loss | 63.89 | 70.71 | 74.66 | 77.84 | 80.23 | 82.34 | 83.93 | 87.64 |
| Gross profit | 12620 | 13352 | 12649 | 11129 | 9606 | 8046 | 6230 | 4379 |
| Loss | 3066 | 3676 | 3583 | 3736 | 4733 | 4858 | 4700 | 4644 |
| Fees | 4554 | 4290 | 3861 | 3498 | 3465 | 3267 | 3003 | 2706 |
| Net profit | 4999 | 5385 | 5204 | 3894 | 1407 | -79 | -1472 | -2971 |
| Φ | 36.23 | 41.43 | 44.48 | 36.74 | 13.41 | -0.80 | -16.18 | -36.24 |

The percentage profits and losses obtained by trading Alrajhi shares are shown in Fig. 8. The figure shows that TS6, TS7 and TS8 resulted in losses. This is mainly due to the

following two reasons. First, there are fewer trades with 4R or more profit-targets; and second, the probability of hitting the stop-loss before the profit-target is higher when the profit-target is greater than or equal to 4R.

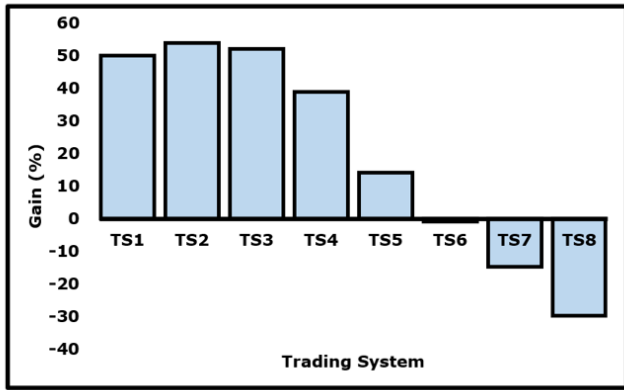


Fig. 8. Percentage profits and losses obtained by trading Alrajhi stock.

Stats, similar to that of Alrajhi stock trades, were also collected from the trades of the other nine stocks. Since these stats are too large in number and it is unnecessary to list them all, only their summaries are presented and discussed. Tables X shows percentage of profits and losses obtained by the proposed trading systems. As can be seen from the table, trading systems TS1, TS2, TS3, TS4, and TS5 were consistently profitable. TS7 and TS8 were consistent losers and TS6 showed inconsistent results. The results of TS6, TS7, and TS8 are inconsistent and poor because there are fewer trades with 4R or more profit-targets, and the probability of hitting the stop-loss before hitting the profit-target is higher.

TABLE X. PERCENTAGE OF PROFITS AND LOSSES OBTAINED BY THE PROPOSED TRADING SYSTEMS

| Trading System | TS1 | TS2 | TS3 | TS4 | TS5 | TS6 | TS7 | TS8 |
|----------------|-------|-------|-------|-------|-------|--------|--------|--------|
| D2 | 50.11 | 48.72 | 46.57 | 37.97 | 22.84 | 10.11 | -8.19 | -23.92 |
| D3 | 53.37 | 51.10 | 48.38 | 28.71 | 22.10 | 13.58 | -1.0 | -16.58 |
| D4 | 48.48 | 54.24 | 44.92 | 23.18 | 22.95 | 20.74 | -3.80 | -23.83 |
| D5 | 42.30 | 41.14 | 42.24 | 40.94 | 22.81 | 13.09 | -1.20 | -17.32 |
| D6 | 28.11 | 30.10 | 30.79 | 27.45 | 17.20 | 2.19 | -16.30 | -45.25 |
| D7 | 42.01 | 43.76 | 39.77 | 28.94 | 15.20 | -12.46 | -16.96 | -38.32 |
| D8 | 54.37 | 56.60 | 57.10 | 46.08 | 37.54 | 19.90 | -13.46 | -41.59 |
| D9 | 48.52 | 52.81 | 46.65 | 29.66 | 18.96 | 15.91 | -7.38 | -16.36 |
| D10 | 59.44 | 61.11 | 63.86 | 51.00 | 26.51 | 5.23 | -12.05 | -42.89 |

Fig. 9 shows expectancies obtained by trading Alrajhi shares. Again the trading systems with profit-targets between 1.5R and 3.5R showed positive expectancy and the rest were negative. TS3 showed the best expectancy of 44.48 riyals and TS8 was the worst with -36.24. The expectancies obtained by the other nine stocks are listed in Table XI. As can be seen from the table, the expectancies of all the trading systems with profit-targets of less than 4R were positive. TS6 results were inconsistent and TS7 and TS8 consistently resulted in negative expectancies. The negative results of the trading systems with higher profit-targets is due to the two reasons that were discussed before. The table also shows that TS2 has the highest expectancy when trading the stocks of D4, D7, and

D9; TS3 has the highest expectancy when trading D1, D2, D3, D5, D6, D8, and D10. On the average, TS3 resulted in the best expectancy with 31.35 riyals.

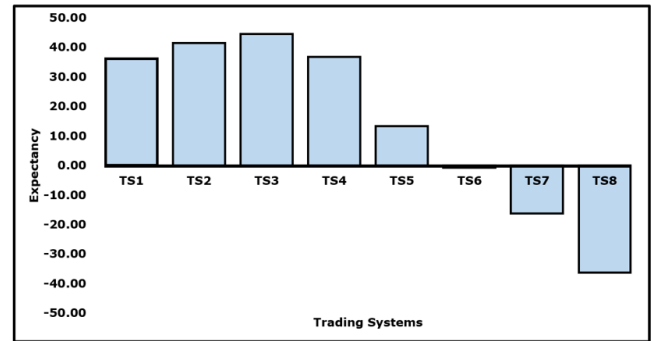


Fig. 9. Expectancy obtained by trading Alrajhi shares.

TABLE XI. EXPECTANCY OF THE PROPOSED TRADING SYSTEMS

| Stock | TS1 | TS2 | TS3 | TS4 | TS5 | TS6 | TS7 | TS8 |
|---------|-------|-------|-------|-------|-------|-------|--------|--------|
| D2 | 16.59 | 17.91 | 19.09 | 17.18 | 10.93 | 5.40 | -4.76 | -23.92 |
| D3 | 18.53 | 18.93 | 20.07 | 12.54 | 10.28 | 6.56 | -0.5 | -8.87 |
| D4 | 35.39 | 42.71 | 36.82 | 20.33 | 21.65 | 20.53 | -3.92 | -26.19 |
| D5 | 38.11 | 38.45 | 44.46 | 46.00 | 26.53 | 15.59 | -1.51 | -22.50 |
| D6 | 13.85 | 16.01 | 18.00 | 16.95 | 11.95 | 1.62 | -12.44 | -37.09 |
| D7 | 19.82 | 22.44 | 22.22 | 17.43 | 9.81 | -8.96 | -13.90 | -34.22 |
| D8 | 18.62 | 21.77 | 25.15 | 22.26 | 19.97 | 10.76 | -7.92 | -25.83 |
| D9 | 44.11 | 52.29 | 48.10 | 35.31 | 22.84 | 21.50 | -9.84 | -24.78 |
| D10 | 27.52 | 31.34 | 35.09 | 29.83 | 15.97 | 3.51 | -8.86 | -33.25 |
| Average | 26.88 | 30.33 | 31.35 | 25.46 | 16.33 | 7.57 | -7.57 | -27.29 |

Each of the eight trading systems was compared with the buy-and-hold trading strategy. Tables XII shows profits and losses obtained by the buy-and-hold strategy. The best winning trade gave a profit of 192.81%, whereas the worst losing trade had a loss of -39.71% (see Fig. 10). Consistency in trading is very important for a trader. The buy-and-hold strategy has inconsistent results. Half of the positions taken were losers. Unlike the buy-and-hold strategy, TS1, TS2, TS3, TS4, and TS5 were consistently profitable. Also TS1, TS2, and TS3 showed significantly better average profits than the buy-and-hold strategy, (see Fig. 11). In summary, TS1, TS2, and TS3 showed consistency, better expectancy, and significantly better average profits than the buy-and-hold strategy.

TABLE XII. PROFITS AND LOSSES OBTAINED BY THE BUY-AND-HOLD STRATEGY

| Stock | Open price | Last price | PnL | PnL (%) |
|-------|------------|------------|----------|---------|
| D1 | 40.82 | 75.2 | 8389.34 | 83.89 |
| D2 | 14.72 | 43.15 | 19280.86 | 192.81 |
| D3 | 44 | 104.5 | 13717.00 | 137.17 |
| D4 | 21.34 | 19.67 | -815.57 | -8.16 |
| D5 | 16.54 | 15 | -964.08 | -9.64 |
| D6 | 27.25 | 16.52 | -3970.61 | -39.71 |
| D7 | 36.35 | 45.65 | 2525.46 | 25.25 |
| D8 | 19.7 | 18.9 | -439.09 | -4.39 |
| D9 | 40.64 | 36.6 | -1027.09 | -10.27 |
| D10 | 76.4 | 80.5 | 503.65 | 5.04 |

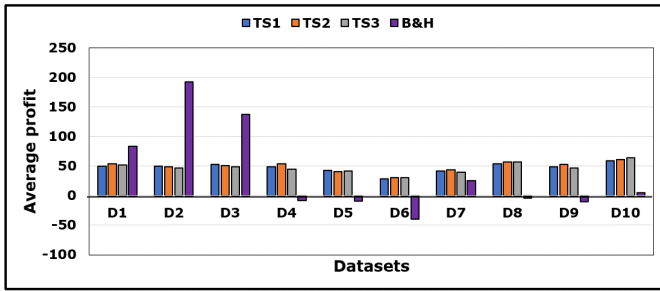


Fig. 10. Inconsistent profits of the buy-and-hold strategy.

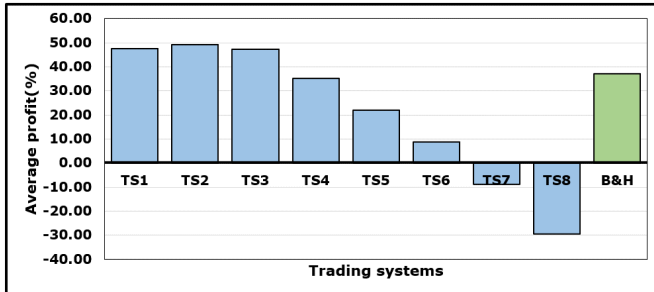


Fig. 11. Average profits of the proposed trading systems and the buy-and-hold trading strategy.

VI. CONCLUSION

In this study, a trading strategy based on two predicted stock prices using TNN, TIs, MRA, and time2vec was investigated. The proposed trading strategy consists of eight day trading systems, each with a different profit-target $n \times R$, where R is the risk taken per trade and for n in $(1.5, 2, 2.5 \dots 5)$. To enter a position, the strategy requires four conditions to be simultaneously true, and to close a position, any of three conditions must be true. To choose the best deep learning model, seven architectures were investigated. TNN gave the best performance and hence it was selected. To improve the accuracy of the proposed model, some of the raw stock prices were converted to log returns and decomposed using MRA. To further improve its accuracy, a number of TIs were carefully analyzed and their best possible parameter values identified. Then the selected TIs were combined and the combination of TIs with the best performance was used. A number of experiments were also conducted to select the best TNN hyper-parameters such as, number of encoders, heads, epochs, learning rate, etc. Deep learning models are fast to overfit and to prevent that dropout layers were used.

The proposed trading strategy was tested using the data of ten randomly selected stocks listed in the Saudi Stock Exchange. The experimental results showed that trading systems with profit-target between $1.5R$ and $3.5R$ showed consistent profits. Those with profit-targets of $4R$ or more can result in losses. This is mainly due to the following two reasons: first, there are fewer trades with $4R$ or more profit-targets; and second, the probability of hitting the stop-loss before the profit-target is higher when the profit-target is greater than or equal to $4R$. The eight trading strategies were also compared with the buy-and-hold strategy. On the average, trading systems TS1,

TS2, and TS3 outperformed the buy-and-hold strategy. Another weakness of the buy-and-hold strategy is its inconsistency. For one stock it gave a profit of 192.81%, and for another stock it resulted in a loss of -39.71%. Traders prefer trading systems with consistent results, such as TS1, TS2, and TS3, hence recommended.

There are four main ideas that can enhance the profitability of the proposed work and are planned as future works. First, to find a technique that can predict whether an intraday price will first hit the profit-target or the stop-loss. This can significantly enhance the profitability of the proposed strategy because most of the losing trades were due to the intraday price reaching the stop-loss before the profit-target. Second, to investigate different buying points instead of always buying using the open price. Third, day trading incurs significant amount of fees and commissions. As can be seen from the posted results, between 30% and 61% of the gross profits were paid as fees. To reduce the amount of fees paid, swing and positional trading strategies can be investigated. They require fewer trades and thus less fees. Fourth, to study the impact of price volatility, market and sector trends, news, and sentiments on the profitability of the proposed trading strategy.

ACKNOWLEDGMENT

The author would like to thank King Fahd University of Petroleum and Minerals (KFUPM), Saudi Arabia, and KFUPM Interdisciplinary Research Center for Intelligent Secure Systems for the support during this work.

REFERENCES

- [1] N. Zadeh, "Financial competitions," <https://financial-competitions.com/>, 2024, last accessed 02 February, 2024.
- [2] R. Moglen and G. Gajjala, "+805% trading champion of 2023 reveals his powerful day trading setups," <https://www.youtube.com/watch?v=10pHBNVi4Jc>, 2024, last accessed 02 February, 2024.
- [3] A. Thakkar and K. Chaudhari, "A comprehensive survey on deep neural networks for stock market: The need, challenges, and future directions," *Expert Systems with Applications*, vol. 177, p. 114800, 2021. [Online]. Available: <https://www.sciencedirect.com/science/article/pii/S0957417421002414>
- [4] Z. Hu, Y. Zhao, and M. Khushi, "A survey of forex and stock price prediction using deep learning," *Applied System Innovation*, vol. 4, no. 1, 2021. [Online]. Available: <https://www.mdpi.com/2571-5577/4/1/9>
- [5] K. A. Althelaya, E.-S. M. El-Alfy, and S. Mohammed, "Evaluation of bidirectional lstm for short-and long-term stock market prediction," in *2018 9th International Conference on Information and Communication Systems (ICICS)*, 2018, pp. 151–156.
- [6] M. T. Ismail and A. Dghais, "Multiresolution analysis of bursa malaysia klci time series," in *AIP Conference Proceedings*, vol. 1847, 05 2017, p. 020020.
- [7] D. K. Kilic and O. Ugur, "Multiresolution analysis of s & p500 time series," *Annals of Operations Research*, vol. 260, no. 1-2, pp. 197–216, 2018.
- [8] S. Bekiros and M. Marcellino, "The multiscale causal dynamics of foreign exchange markets," *Journal of International Money and Finance*, vol. 33, pp. 282–305, 2013. [Online]. Available: <https://www.sciencedirect.com/science/article/pii/S0261560612002069>
- [9] B.-L. Zhang, R. Coggins, M. Jabri, D. Dersch, and B. Flower, "Multiresolution forecasting for futures trading using wavelet decompositions," *IEEE Transactions on Neural Networks*, vol. 12, no. 4, pp. 765–775, 2001.
- [10] A. Aussem and F. Murtagh, "Combining neural network forecasts on wavelet-transformed time series," *Connection Science*, vol. 9, 03 1997.

- [11] L. Di Persio and O. Honchar, "Artificial neural networks architectures for stock price prediction: Comparisons and applications," *International Journal of Circuits, Systems and Signal Processing*, vol. 10, pp. 403–413, 01 2016.
- [12] D. Zhang, G. Lindholm, and H. Ratnaweera, "Use long short-term memory to enhance internet of things for combined sewer overflow monitoring," *Journal of Hydrology*, vol. 556, 11 2017.
- [13] H. Yan and H. Ouyang, "Financial time series prediction based on deep learning," *Wireless Personal Communications*, vol. 102, no. 2, pp. 683–700, 2018.
- [14] W. Bao, J. Yue, and Y. Rao, "A deep learning framework for financial time series using stacked autoencoders and long-short term memory," *PLoS ONE*, vol. 12, 2017. [Online]. Available: <https://api.semanticscholar.org/CorpusID:37606221>
- [15] S. M. Kazemi, R. Goel, S. Eghbali, J. Ramanan, J. Sahota, S. Thakur, S. Wu, C. Smyth, P. Poupart, and M. Brubaker, "Time2vec: Learning a vector representation of time," 2019.
- [16] K.-L. Du and M. Swamy, *Recurrent Neural Networks*, 12 2014, pp. 337–353.
- [17] M. Schuster and K. K. Paliwal, "Bidirectional recurrent neural networks," *IEEE Transactions on Signal Processing*, vol. 45, no. 11, pp. 2673–2681, 1997.
- [18] S. Hochreiter and J. Schmidhuber, "Long short-term memory," *Neural Comput.*, vol. 9, no. 8, pp. 1735–1780, nov 1997. [Online]. Available: <https://doi.org/10.1162/neco.1997.9.8.1735>
- [19] C. Olah, "Understanding lstm networks," <http://colah.github.io/posts/2015-08-Understanding-LSTMs/>, 2015, last accessed 13 February, 2024.
- [20] A. Graves and J. Schmidhuber, "Framewise phoneme classification with bidirectional lstm and other neural network architectures," *Neural Networks*, vol. 18, no. 5, pp. 602–610, 2005.
- [21] K. Cho, B. van Merriënboer, C. Gulcehre, D. Bahdanau, F. Bougares, H. Schwenk, and Y. Bengio, "Learning phrase representations using rnn encoder-decoder for statistical machine translation," 2014.
- [22] R. Zhao, D. Wang, R. Yan, K. Mao, F. Shen, and J. Wang, "Machine health monitoring using local feature-based gated recurrent unit networks," *IEEE Transactions on Industrial Electronics*, vol. 65, no. 2, pp. 1539–1548, 2018.
- [23] A. Vaswani, N. Shazeer, N. Parmar, J. Uszkoreit, L. Jones, A. N. Gomez, L. Kaiser, and I. Polosukhin, "Attention is all you need," in *Proceedings of the 31st International Conference on Neural Information Processing Systems*, ser. NIPS'17. Red Hook, NY, USA: Curran Associates Inc., 2017, pp. 6000–6010.
- [24] M. Sazli, "A brief review of feed-forward neural networks," *Communications Faculty Of Science University of Ankara*, vol. 50, pp. 11–17, 01 2006.
- [25] J. Zheng, S. Ramasinghe, and S. Lucey, "Rethinking positional encoding," *ArXiv*, vol. abs/2107.02561, 2021. [Online]. Available: <https://api.semanticscholar.org/CorpusID:235742682>
- [26] A. Grossmann and J. Morlet, "Decomposition of hardy functions into square integrable wavelets of constant shape," *SIAM Journal on Mathematical Analysis*, vol. 15, pp. 723–736, 07 1984.
- [27] S. Mallat, "A theory for multiresolution signal decomposition: the wavelet representation," *IEEE Transactions on Pattern Analysis and Machine Intelligence*, vol. 11, no. 7, pp. 674–693, 1989.
- [28] S. Mallat and S. Mallat, *A Wavelet Tour of Signal Processing*. Academic Press, 01 1999.
- [29] P.-H. Chiang, S. P. V. Chiluvuri, S. Dey, and T. Q. Nguyen, "Forecasting of solar photovoltaic system power generation using wavelet decomposition and bias-compensated random forest," in *Proceedings of the IEEE 9th Annual Green Technologies Conference (GreenTech)*, 2017, pp. 260–266.
- [30] J. Gilles, "Empirical wavelet transform," *IEEE Transactions on Signal Processing*, vol. 61, no. 16, pp. 3999–4010, 2013.
- [31] N. Malibari, I. Katib, and R. Mehmood, "Predicting stock closing prices in emerging markets with transformer neural networks: The saudi stock exchange case," *International Journal of Advanced Computer Science and Applications*, vol. 12, 01 2021.
- [32] G. Bertasius, H. Wang, and L. Torresani, "Is space-time attention all you need for video understanding?" 2021.
- [33] T. Muhammad, A. B. Aftab, M. Ibrahim, M. M. Ahsan, M. M. Muhi, S. I. Khan, and M. S. Alam, "Transformer-based deep learning model for stock price prediction: A case study on bangladesh stock market," *International Journal of Computational Intelligence and Applications*, vol. 22, no. 03, Apr. 2023. [Online]. Available: <http://dx.doi.org/10.1142/S146902682350013X>
- [34] A. Meddah, "American stock index forecasting using transformers model," Al Akhawayn University, Tech. Rep., 2023.
- [35] Z. Lin, "Comparative study of lstm and transformer for a-share stock price prediction," in *Proceedings of the 2023 2nd International Conference on Artificial Intelligence, Internet and Digital Economy (ICAID 2023)*. Atlantis Press, 2023, pp. 72–82. [Online]. Available: https://doi.org/10.2991/978-94-6463-222-4_7
- [36] T. S. Mian, "Evaluation of stock closing prices using transformer learning," *Engineering, Technology and Applied Science Research*, vol. 13, no. 5, p. 11635–11642, Oct. 2023. [Online]. Available: <https://etasr.com/index.php/ETASR/article/view/6017>
- [37] L. Costa and A. Machado, "Prediction of stock price time series using transformers," in *Anais do II Brazilian Workshop on Artificial Intelligence in Finance*. Porto Alegre, RS, Brasil: SBC, 2023, pp. 85–95. [Online]. Available: <https://sol.sbc.org.br/index.php/bwaiif/article/view/24955>
- [38] Q. Wang and Y. Yuan, *Stock Price Forecast: Comparison of LSTM, HMM, and Transformer*. Atlantis Press, 07 2023, pp. 126–136.
- [39] S. Wang, "A stock price prediction method based on bilstm and improved transformer," *IEEE Access*, vol. 11, pp. 104 211–104 223, 2023.
- [40] P. Bilokon and Y. Qiu, "Transformers versus lstms for electronic trading," 2023.
- [41] S. Aman, "Forecasting stock price movements for intra-day trading using transformers and lstm," *International Journal of Computing and Artificial Intelligence*, vol. 2, no. 1, pp. 45–52, 2021.
- [42] C. Wang, Y. Chen, S. Zhang, and Q. Zhang, "Stock market index prediction using deep transformer model," *Expert Systems with Applications*, vol. 208, p. 118128, 2022. [Online]. Available: <https://www.sciencedirect.com/science/article/pii/S0957417422013100>
- [43] Q. Zhang, C. Qin, Y. Zhang, F. Bao, C. Zhang, and P. Liu, "Transformer-based attention network for stock movement prediction," *Expert Systems with Applications*, vol. 202, p. 117239, 2022. [Online]. Available: <https://www.sciencedirect.com/science/article/pii/S0957417422006170>
- [44] Q. Ding, S. Wu, H. Sun, J. Guo, and J. Guo, "Hierarchical multi-scale gaussian transformer for stock movement prediction," in *Proceedings of the Twenty-Ninth International Joint Conference on Artificial Intelligence, IJCAI-20*, C. Bessiere, Ed. International Joint Conferences on Artificial Intelligence Organization, 7 2020, pp. 4640–4646, special Track on AI in FinTech. [Online]. Available: <https://doi.org/10.24963/ijcai.2020/640>
- [45] J. Liu, H. Lin, X. Liu, B. Xu, Y. Ren, Y. Diao, and L. Yang, "Transformer-based capsule network for stock movement prediction," 2019. [Online]. Available: <https://api.semanticscholar.org/CorpusID:201626326>
- [46] Tickerchart, "Tickerchart," <https://www.tickerchart.com/en/>, 2023, last accessed 22 March, 2023.
- [47] Amibroker, "Amibroker formula language," <https://www.amibroker.com/index.html>, 2024.
- [48] F. Chollet *et al.*, "Keras," <https://github.com/fchollet/keras>, 2015.
- [49] I. Guyon, J. Weston, S. Barnhill, and V. Vapnik, "Gene selection for cancer classification using support vector machines," *Machine Learning*, vol. 46, no. 1, pp. 389–422, 2002.
- [50] Y. Fan, Y. Qian, F.-L. Xie, and F. K. Soong, "TTS synthesis with bidirectional LSTM based recurrent neural networks," in *Fifteenth Annual Conference of the International Speech Communication Association*, 2014.
- [51] J. Devlin, M.-W. Chang, K. Lee, and K. Toutanova, "BERT: Pre-training of deep bidirectional transformers for language understanding," 2019.

Multi-Granularity Feature Fusion for Enhancing Encrypted Traffic Classification

Quan Ding¹, Zhengpeng Zha^{2*}, Yanjun Li³, Zhenhua Ling⁴

State Grid Anhui Electric Power Co. Ltd., Electric Power Science Research Institute, Hefei, China¹
University of Science and Technology of China, Institute of Advanced Technology, Hefei, China^{2,3,4}

Abstract—Encrypted traffic classification, a pivotal process in network security and management, involves analyzing and categorizing data traffic that has been encrypted for privacy and security. This task demands the extraction of distinctive and robust feature representations from content-concealed data to ensure accurate and reliable classification. Traditional approaches have focused on utilizing either the payload of encrypted traffic or statistical features for more precise classification. While these methods achieve relative success, their limitation lies in not harnessing multi-grained features, thus impeding further advancements in encrypted traffic classification capabilities. To tackle this challenge, ET-CompBERT is presented, an innovative framework specifically designed for the fusion of multi-granularity features in encrypted traffic, encompassing both payload and global temporal attributes. The extensive experiments reveal that our approach significantly enhances classification performance in data-rich scenarios (achieving up to a +4.43% improvement in certain cases over existing methods) and establishes state-of-the-art results on training sets with different sizes. The source codes will be released after paper acceptance.

Keywords—Encrypted traffic classification; BERT; multi-granularity fusion

I. INTRODUCTION

Recently, the widespread use of traffic encryption has become instrumental in protecting the privacy and anonymity of Internet users [1], [2]. While this advancement is vital for security and confidentiality, it concurrently presents significant challenges to traffic classification. The increasing utilization of privacy-enhancing encryption techniques, such as Tor and VPNs, by both legitimate users and malicious actors, complicates the task of distinguishing benign from harmful traffic. Encrypted traffic classification thus emerges as a crucial tool in this landscape. It enables the identification and mitigation of malware and cybercriminal activities that exploit encryption to bypass surveillance systems, without compromising the privacy and integrity of legitimate communications. This delicate balance between user privacy and cybersecurity underscores the indispensable role of sophisticated traffic classification methodologies in maintaining a secure digital environment.

Traditional cleartext traffic classification methods [3], [4], [5] primarily rely on deep packet inspection, capturing patterns and keywords within data packets from the payload. Nevertheless, the advent of encrypted traffic poses a significant challenge to these methodologies. The inherent unreadability of encrypted traffic renders traditional cleartext classification ineffective. Recent study [6] proposes leveraging unencrypted protocol field information. This approach involves extracting

key features such as device type, certificate details, packet size, and temporal characteristics to represent each data flow. However, this strategy has its limitations. In virtual communication networks, these fingerprints are susceptible to tampering, leading to misinterpretation and a consequent failure in accurately classifying encrypted traffic.

The field of machine learning has witnessed rapid advancement, prompting numerous security researchers [7], [8] to explore statistical methods to enhance the accuracy of encrypted traffic classification. Predominantly, these machine-learning approaches for encrypted traffic classification rely on the meticulous selection of handcrafted features, followed by the application of statistical machine-learning algorithms for classification purposes. For instance, Flowprint [8] leverages statistical features of packet sizes to train random forest classifiers, while BIND [7] utilizes statistical features related to temporality. However, we contend that these methods are overly dependent on selecting handcrafted features. Designing universally applicable features that can effectively address the increasing complexity of numerous applications and websites is a challenging endeavor. Moreover, these methods typically provide only a generalized perspective to the algorithm, limiting the coarse-grained capability of encrypted traffic classification. This inherent limitation underscores the need for more adaptable approaches in this rapidly evolving domain.

These limitations have increasingly steered researchers toward adopting end-to-end deep learning methodologies for encrypted traffic classification. The utilization of supervised deep learning for encrypted traffic classification has emerged as a predominant approach, primarily due to its ability to automatically extract discriminative features, thus diminishing the reliance on manual feature design. In previous research, such as DF [9], convolutional neural networks have been employed to autonomously derive representations from raw packet size sequences in encrypted traffic. The remarkable achievements of BERT[10] in the natural language processing domain have inspired analogous advancements in network traffic analysis. ET-BERT[11] introduces a novel network traffic representation, termed BURST, defined as a sequence of temporally adjacent network packets originating from either the request or response in a single session flow. This approach also incorporates a similar learning task, positioning ET-BERT as a pioneering method in applying a pre-train and fine-tune model to encrypted traffic classification. Despite these advancements, it is crucial to acknowledge that current pre-trained methodologies often focus on the payload of encrypted traffic but neglect the global attributes. This oversight leads to models achieving suboptimal accuracy in encrypted traffic

*Corresponding authors.

classification, highlighting a critical area for improvement in this evolving field.

To address the challenge mentioned above, we introduce a novel framework known as Encrypted Traffic comprehensive Bidirectional Encoder Representations from Transformer (ET-CompBERT). As depicted in Fig. 1, we innovatively introduce a multi-grained learning strategy, termed *comprehensive fusion-guided (CFA)* learning. This strategy synergistically combines a fine-grained understanding of encrypted traffic payloads with a broader, coarse-grained analysis, thereby enhancing the overall comprehension of encrypted traffic. To the best of our knowledge, this represents the inaugural effort in integrating multi-grained features for pre-trained encrypted traffic classification. Drawing inspiration from the rapidly evolving field of prompt tuning in both the computer vision [12] and natural language processing [13] communities, we propose the *global-feature-aware (GFA)* learning strategy, significantly enhancing the robust classification on different data sizes capabilities of ET-CompBERT. Our contributions are outlined as follows:

- This study represents a pioneering effort in a novel multi-grained learning approach as comprehensive fusion-guided learning. This innovative strategy enables fusing the global temporal attributes into the extracted representations of encrypted traffic payloads.
- We introduce an innovative GFA learning strategy, that effectively fuses the representations of local traffic payloads and the representations of global temporal attributes for encrypted traffic classification.
- Extensive experimental evaluations demonstrate the effectiveness of our framework. The results indicate that our approach surpasses existing state-of-the-art methods in all tasks. Notably, our model achieves consistent advantages on training sets with different sizes of datasets, underscoring its versatility and robustness.

The remainder of this paper is organized as follows. Section II provides a detailed review of the relevant literature and background information on encrypted traffic classification. Section III describes the methodology applied in our study, including comprehensive fusion-guided learning and global-feature-aware learning. The results are presented and discussed in Section IV, where we analyze comparisons with existing methods, ablation studies, and other analyses. Finally, Section V concludes the paper with a summary of the findings, and implications of our work.

II. RELATED WORK

A. Encrypted Traffic Classification

Encrypted traffic classification aims to discern the services operating behind obfuscated network traffic, thereby enhancing both network service quality and security assurance. Contemporary methodologies in this domain predominantly fall into two principal categories, those grounded in machine learning techniques [7], [14], [15] and those leveraging deep learning paradigms. However, traditional machine learning-based approaches for encrypted traffic classification are often constrained by their dependency on expert-derived feature extraction and selection, which can impede generalization and

further development. This limitation has led researchers to gravitate towards end-to-end deep learning Encrypted Traffic Classification methodologies increasingly.

In contrast to methods based on traditional machine learning, deep learning-based approaches offer a comprehensive solution for encrypted traffic classification by autonomously learning feature representations. This shift towards deep learning methodologies enhances robustness and addresses the inherent complexities in encrypted traffic analysis. Wang et al. [16] exemplify this trend by proposing an application of convolutional neural networks (CNN). Their method involves using the initial 784 bytes of each traffic flow as input, enabling the CNN to extract and learn feature representations effectively, thus showcasing the potential of deep learning in this domain. Given the remarkable success of the BERT [10] model within the natural language processing community, researchers [11] are exploring the application of its structural principles in the realm of encrypted traffic classification through learning approaches. However, a common challenge these methods face is their reliance on substantial volumes of labeled data to ensure optimal performance, limiting their applicability to new, unseen classes that diverge from the training dataset. This challenge gives rise to the need for few-shot learning approaches, capable of classifying new encrypted traffic types with a minimal reliance on labeled data, thus presenting a promising solution to these constraints.

In our study, we introduce a novel approach to encrypted traffic classification that diverges from traditional single-granularity pre-trained methods. Our method centers around enhancing a pre-trained encrypted traffic classification model which proposes to enhance encrypted traffic classification by multi-granularity feature fusion. Furthermore, We introduce an innovative fine-tuning method, GFA learning, which empowers the model with robust classification capabilities under different data sample scenarios.

III. METHODS

A. Comprehensive Fusion-guided Learning

In the initial phase of our study, we implement comprehensive fusion-guided learning to cultivate ET-CompBERT in Fig. 1, which integrates global temporal attributes into the payload representations of encrypted traffic. Starting with payload encoding, we utilize the BURST structure, identified as a sequence of temporally contiguous network packets emanating from either a request or a response in a single session flow. This structure is employed to precisely depict encrypted traffic, thereby forming the input for our pre-trained ET-BERT model, mirroring the strategy delineated in [11]. This approach culminates in the creation of an encrypted traffic embedding, denoted as e_b . Following this, we utilize the straightforward two-layer Multi-Layer Perceptron (MLP) for projecting the encrypted traffic embedding into f_b .

In the comprehensive fusion-guided learning procedure, for a given piece of encrypted traffic, we utilize both the payload and its global temporal attributes. During the global-feature-aware learning process, the global temporal attributes concatenate a special classification token and the BURST representation as input to the pre-trained ET-CompBERT model. It is important to highlight that the $//$ symbol is used to denote

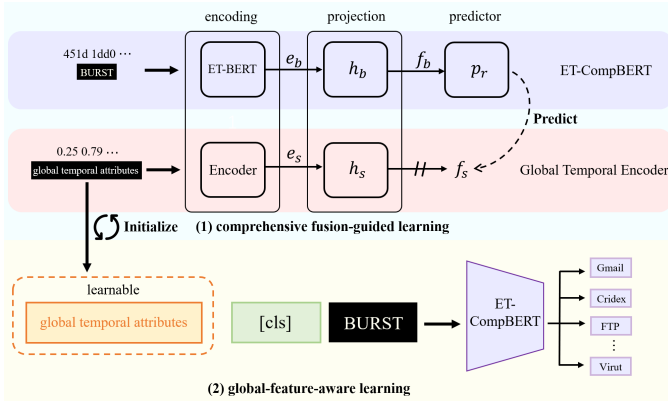


Fig. 1. Framework of ET-CompBERT.

the stop gradient, a critical measure implemented to prevent the model from adopting shortcut learning methods.

To design the global temporal attributes encoding procedure, we employ an encoding strategy akin to that utilized in payload encoding, to acquire embeddings reflective of global temporal properties. Initially, key properties are extracted from network packets, a subset of which is detailed in Table I. These properties are subjected to min-max normalization, resulting in a normalized feature vector. Importantly, we utilize a fully connected network (FCN) to align the dimensions of the global temporal attributes with those of the Transformer Encoder [17], ensuring dimensional compatibility. Following this, the features are replicated as the global temporal attributes and passed through the original Transformer Encoder [17], thereby obtaining the preliminary global temporal embedding e_s . These initial global temporal embeddings are further processed via a two-layer Multi-Layer Perceptron (MLP), culminating in the generation of the final global temporal embedding f_s .

TABLE I. DESCRIPTION OF GLOBAL TEMPORAL ATTRIBUTES

| Feature | Description |
|----------|---|
| duration | The duration of the flow. |
| fiat | Forward Inter Arrival Time (mean, min, max, std). |
| biat | Backward Inter Arrival Time (mean, min, max, std). |
| flowiat | Flow Inter Arrival Time (mean, min, max, std). |
| active | The amount of time a flow was active (mean, min, max, std). |
| idle | The amount of time a flow was idle (mean, min, max, std). |
| fb_psec | Flow Bytes per second. |
| fp_psec | Flow packets per second. |

In our pursuit to enhance our framework’s capability to identify global attributes of encrypted traffic, while also retaining a profound understanding of its payload, we have developed a comprehensive fusion-guided learning strategy. This innovative approach introduces a novel prediction methodology, meticulously designed to empower the encrypted traffic model with the capability of category classification. Consequently, this facilitates a fundamental enhancement in the fine-grained interpretation of encrypted traffic information, thus enabling a comprehensive and coarse-grained understanding of encrypted traffic dynamics. This strategic design marks a significant advancement in the nuanced analysis of encrypted traffic data. Upon obtaining the encrypted traffic embedding f_b and the global temporal attributes embedding f_s , our framework

employs a two-layer Multi-Layer Perceptron (MLP) as a predictor. This MLP is specifically tailored to categorize the global temporal attributes. Given the model’s proficiency in acquiring an in-depth understanding of encrypted traffic from both holistic and detailed perspectives, we refer to the ET-BERT, subjected to the aforementioned comprehensive learning, as ET-CompBERT. It is imperative to highlight that our methodology incorporates a stop-gradient strategy designed to prevent the model from gravitating towards shortcut solutions. This critical implementation is pivotal in safeguarding the robustness and integrity of our approach. Such a strategy underpins a more effective learning process, perfectly in sync with the core objectives of encrypted traffic analysis. This meticulous attention to the learning process ensures the reliability and efficacy of our model in challenging scenarios.

B. Global-feature-aware Learning

Following the learning procedure, we fine-tune the ET-CompBERT on downstream datasets. However, conventional learning strategies, while effective under sufficient data conditions, often falter in a few data scenarios. The framework after the comprehensive fusion-guided learning can understand the payload of the encrypted traffic and the global temporal properties. We innovatively introduce the GFA learning strategy.

Initially, global temporal attributes are deployed to initialize the learnable token, akin to their usage in the comprehensive fusion-guided learning paradigm. These attributes are encoded into a token via a shared-weight Fully Connected Network (FCN), ensuring a coherent and efficient representation for subsequent processing. This token is concatenated alongside the special $[class]$ symbol and the BURST to constitute the primary input. To ensure dimensional coherence, we employ a simple one-layer MLP, maintaining the dimensionality adapted to the ET-CompBERT. Through the self-attention mechanism, the global temporal attributes alongside the $[class]$ symbol acquire knowledge from BURST. This process culminates in the formation of the final learnable global temporal attributes, specifically designed to bolster the classification capabilities for encrypted traffic. The effectiveness of this enhancement is continually assessed and refined under the guidance of the cross-entropy loss function. The robust enhancement in encrypted traffic classification performance achieved by our learning and learning methodology is demonstrated in our experimental results. We propose two learning strategies that can also enhance the encrypted traffic classification model for varied classification scenarios.

C. Inference

During the inference phase, we omit the projection and predictor components, retaining only the final global temporal attributes which concatenate with the input to elevate the encrypted traffic classification ability. These attributes encapsulate the optimal encrypted traffic classification capabilities as evidenced by the GFA learning results. In the final layer of the ET-CompBERT, we employ an FCN layer coupled with a softmax function to generate the probability distribution across various categories.

TABLE II. SUMMARY OF DATASETS USED IN ENCRYPTED TRAFFIC CLASSIFICATION EXPERIMENTS

| Task | Dataset | Flow | Packet | Label |
|--|------------------------------|--------|---------|-------|
| General Encrypted Application Classification | Cross-Platform (iOS) [6] | 20,858 | 707,717 | 196 |
| | Cross-Platform (Android) [6] | 27,846 | 656,044 | 215 |
| Encrypted Malware Classification | USTC-TFC [26] | 9,853 | 97,115 | 20 |
| Encrypted Application Classification on Tor | ISCX-Tor [10] | 3,021 | 80,000 | 16 |

TABLE III. PERFORMANCE COMPARISON OF DIFFERENT METHODS ON CROSS-PLATFORM (IOS) AND CROSS-PLATFORM (ANDROID) DATASETS

| Dataset Method | Cross-Platform(iOS) | | | | Cross-Platform(Android) | | | |
|----------------------|---------------------|---------------|---------------|---------------|-------------------------|---------------|---------------|---------------|
| | AC | PR | RC | F1 | AC | PR | RC | F1 |
| AppScanner [8] | 0.3205 | 0.2103 | 0.2173 | 0.2030 | 0.3868 | 0.2523 | 0.2594 | 0.2440 |
| CUMUL [15] | 0.2910 | 0.1917 | 0.2081 | 0.1875 | 0.3525 | 0.2221 | 0.2409 | 0.2189 |
| BIND [7] | 0.3770 | 0.2566 | 0.2715 | 0.2484 | 0.4728 | 0.3126 | 0.3253 | 0.3026 |
| K-fp [25] | 0.2155 | 0.2037 | 0.2069 | 0.2003 | 0.2248 | 0.2113 | 0.2104 | 0.2052 |
| FlowPrint [6] | 0.9254 | 0.9438 | 0.9254 | 0.9260 | 0.8698 | 0.9007 | 0.8698 | 0.8702 |
| DF [9] | 0.3106 | 0.2232 | 0.2179 | 0.2140 | 0.3862 | 0.2595 | 0.2620 | 0.2527 |
| FS-Net [22] | 0.3712 | 0.2845 | 0.2754 | 0.2655 | 0.4846 | 0.3544 | 0.3365 | 0.3343 |
| GraphDApp [20] | 0.3245 | 0.2450 | 0.2392 | 0.2297 | 0.4031 | 0.2842 | 0.2786 | 0.2703 |
| TSCRNN [21] | - | - | - | - | - | - | - | - |
| Deeppacket [23] | 0.9204 | 0.8963 | 0.8872 | 0.9034 | 0.8805 | 0.8004 | 0.7567 | 0.8138 |
| PERT [24] | 0.9789 | 0.9621 | 0.9611 | 0.9584 | 0.9772 | 0.8628 | 0.8591 | 0.8550 |
| ET-BERT(flow) [11] | 0.9844 | 0.9701 | 0.9632 | 0.9643 | 0.9865 | 0.9324 | 0.9266 | 0.9246 |
| ET-BERT(packet) [11] | 0.9810 | 0.9757 | 0.9772 | 0.9754 | 0.9728 | 0.9439 | 0.9119 | 0.9206 |
| ET-CompBERT(flow) | 0.9964 | 0.9978 | 0.9871 | 0.9924 | 0.9954 | 0.9611 | 0.9712 | 0.9661 |
| ET-CompBERT(packet) | 0.9945 | 0.9911 | 0.9975 | 0.9943 | 0.9982 | 0.9627 | 0.9671 | 0.9649 |

TABLE IV. PERFORMANCE COMPARISON OF DIFFERENT METHODS ON ISCX-TOR AND USTC-TFC DATASETS

| Dataset Method | ISCX-Tor | | | | USTC-TFC | | | |
|----------------------|---------------|---------------|---------------|---------------|---------------|---------------|---------------|---------------|
| | AC | PR | RC | F1 | AC | PR | RC | F1 |
| AppScanner[8] | 0.6722 | 0.3756 | 0.4422 | 0.3913 | 0.8954 | 0.8984 | 0.8968 | 0.8892 |
| CUMUL [15] | 0.6606 | 0.3850 | 0.4416 | 0.3918 | 0.5675 | 0.6171 | 0.5738 | 0.5513 |
| BIND [7] | 0.7185 | 0.4598 | 0.4515 | 0.4511 | 0.8457 | 0.8681 | 0.8382 | 0.8396 |
| K-fp [25] | 0.6472 | 0.5576 | 0.5849 | 0.5522 | - | - | - | - |
| FlowPrint [6] | 0.9092 | 0.3820 | 0.3661 | 0.3654 | 0.8146 | 0.6434 | 0.7002 | 0.6573 |
| DF [9] | 0.7533 | 0.6228 | 0.6010 | 0.5850 | 0.7787 | 0.7883 | 0.7819 | 0.7593 |
| FS-Net [22] | 0.6071 | 0.5080 | 0.5350 | 0.4590 | 0.8846 | 0.8846 | 0.8920 | 0.8840 |
| GraphDApp [20] | 0.6836 | 0.4864 | 0.4823 | 0.4488 | 0.8789 | 0.8226 | 0.8260 | 0.8234 |
| TSCRNN [21] | - | 0.9490 | 0.9480 | 0.9480 | - | 0.9870 | 0.9860 | 0.9870 |
| Deeppacket [23] | 0.7449 | 0.7549 | 0.7399 | 0.7473 | 0.9640 | 0.9650 | 0.9631 | 0.9641 |
| PERT [24] | 0.7682 | 0.4424 | 0.4446 | 0.4345 | 0.9909 | 0.9911 | 0.9910 | 0.9911 |
| ET-BERT(flow) [11] | 0.8311 | 0.5564 | 0.6448 | 0.5886 | 0.9929 | 0.9930 | 0.9930 | 0.9930 |
| ET-BERT(packet) [11] | 0.9921 | 0.9923 | 0.9921 | 0.9921 | 0.9915 | 0.9915 | 0.9916 | 0.9916 |
| ET-CompBERT(flow) | 0.8365 | 0.5598 | 0.6415 | 0.5914 | 0.9916 | 0.9947 | 0.9987 | 0.9967 |
| ET-CompBERT(packet) | 0.9946 | 0.9979 | 0.9957 | 0.9968 | 0.9969 | 0.9964 | 0.9978 | 0.9971 |

TABLE V. ABLATION STUDY OF FLOW-LEVEL LEARNING ON CROSS-PLATFORM (IOS) AND CROSS-PLATFORM (ANDROID) DATASETS

| Dataset Method | Cross-Platform (iOS) | | | | Cross-Platform (Android) | | | |
|-----------------------------|----------------------|---------------|---------------|---------------|--------------------------|---------------|---------------|---------------|
| | AC | PR | RC | F1 | AC | PR | RC | F1 |
| ET-CompBERT(flow) | 0.9964 | 0.9978 | 0.9871 | 0.9924 | 0.9954 | 0.9611 | 0.9712 | 0.9661 |
| -GFA learning | 0.9855 | 0.9874 | 0.9887 | 0.9881 | 0.9947 | 0.9529 | 0.9648 | 0.9588 |
| -GFA learning -CFG learning | 0.9844 | 0.9701 | 0.9632 | 0.9643 | 0.9865 | 0.9324 | 0.9266 | 0.9246 |

TABLE VI. ABLATION STUDY OF FLOW-LEVEL LEARNING ON ISCX-TOR AND USTC-TFC DATASETS

| Dataset Method | ISCX-Tor | | | | USTC-TFC | | | |
|-----------------------------|---------------|---------------|---------------|---------------|---------------|---------------|---------------|---------------|
| | AC | PR | RC | F1 | AC | PR | RC | F1 |
| ET-CompBERT(flow) | 0.8365 | 0.5598 | 0.6415 | 0.5979 | 0.9916 | 0.9947 | 0.9987 | 0.9967 |
| -GFA learning | 0.8325 | 0.5577 | 0.6314 | 0.5971 | 0.9982 | 0.9987 | 0.9992 | 0.9989 |
| -GFA learning -CFG learning | 0.8311 | 0.5564 | 0.6448 | 0.5886 | 0.9929 | 0.9930 | 0.9930 | 0.9930 |

TABLE VII. ABLATION STUDY OF PACKET-LEVEL LEARNING ON CROSS-PLATFORM (IOS) AND CROSS-PLATFORM (ANDROID) DATASETS

| Dataset Method | Cross-Platform (iOS) | | | | Cross-Platform (Android) | | | |
|-----------------------------|----------------------|---------------|---------------|---------------|--------------------------|---------------|---------------|---------------|
| | AC | PR | RC | F1 | AC | PR | RC | F1 |
| ET-CompBERT(packet) | 0.9945 | 0.9911 | 0.9975 | 0.9943 | 0.9982 | 0.9627 | 0.9671 | 0.9649 |
| -GFA learning | 0.9867 | 0.9814 | 0.9748 | 0.9781 | 0.9910 | 0.9472 | 0.9421 | 0.9446 |
| -GFA learning -CFG learning | 0.9844 | 0.9701 | 0.9632 | 0.9643 | 0.9865 | 0.9324 | 0.9266 | 0.9246 |

TABLE VIII. ABLATION STUDY ON PACKET-LEVEL LEARNING ON ISCX-TOR AND USTC-TFC DATASETS

| Dataset Method | ISCX-Tor | | | | USTC-TFC | | | |
|-----------------------------|---------------|---------------|---------------|---------------|---------------|---------------|---------------|---------------|
| | AC | PR | RC | F1 | AC | PR | RC | F1 |
| ET-CompBERT(packet) | 0.9946 | 0.9979 | 0.9957 | 0.9968 | 0.9969 | 0.9964 | 0.9978 | 0.9971 |
| –GFA learning | 0.9904 | 0.9577 | 0.9535 | 0.9556 | 0.9841 | 0.9834 | 0.9847 | 0.9840 |
| –GFA learning –CFG learning | 0.9865 | 0.9324 | 0.9266 | 0.9246 | 0.9729 | 0.9756 | 0.9731 | 0.9733 |

IV. EXPERIMENTS

A. Dataset and Metrics

To validate the efficacy and broad applicability of ET-CompBERT, we conducted a series of experiments across three established encrypted traffic classification tasks, utilizing four publicly accessible datasets. Table II delineates the specifics of these datasets. The General Encrypted Application Classification task focuses on categorizing application traffic under standard encryption protocols. Our evaluations were conducted on the Cross-Platform datasets for both iOS and Android, encompassing 196 and 215 applications respectively. The Encrypted Malware Classification task involves the analysis of encrypted traffic comprising both malware and benign applications. In this context, the USTC-TFC dataset is particularly noteworthy, as it features 10 categories each of benign and malicious traffic, providing a comprehensive framework for the assessment of encryption-based malware detection capabilities. The Encrypted Application Classification on Tor task is centered around classifying encrypted traffic using the Onion Router to enhance communication privacy. The relevant dataset, termed ISCX-Tor, comprises 16 distinct applications, offering a unique landscape for assessing privacy-preserved encrypted traffic analysis.

B. Implementation Details

During comprehensive fusion-guided learning, approximately 30GB of traffic data is utilized for pre-training purposes. The dataset is divided into two segments: (1) roughly 15GB of traffic data sourced from public datasets [18], [19]; (2) an equivalent volume of traffic data, approximately 15GB, obtained through passive collection within the China Science and Technology Network (CSTNET). The batch size is set at 32, and the total number of steps is 500,000. The learning rate is established at 2×10^{-5} , with a warmup ratio of 0.1. For learning, we utilize the AdamW optimizer across 10 epochs, applying a learning rate of 6×10^{-5} for flow-level and 2×10^{-5} for packet-level tasks. The batch size remains at 32, and the dropout rate is set to 0.5. All experiments are conducted using Pytorch 1.8.0 on eight NVIDIA Tesla V100 GPUs. In our approach, we implement two distinct learning strategies for the ET-CompBERT model to adapt to different levels of traffic data granularity, the ET-CompBERT(flow) and the ET-CompBERT(packet). Here the $e_b, e_s \in \mathbb{R}^{768}$, $f_b, f_s \in \mathbb{R}^{120}$.

For testing, we maintained consistency in the dataset across both strategies, ensuring a fair and objective comparison with other methodologies. The pivotal difference between these strategies lied in the granularity of the fine-tuning input traffic information. Our method employed a dataset comprising a concatenated sequence of M consecutive packets within a flow, where M is predefined as 5 in our experimental setup.

C. Comparison with Existing Methods

Tables III and IV showcase the performance comparison of our framework with existing frameworks. Our framework sets a new benchmark in state-of-the-art performance, outperforming the preceding leading method in the F1-score across all four datasets with flow-level fine-tuning. The margin of enhancement ranges from +0.28% to +4.43%, as substantiated by the results enumerated in both tables. Moreover, it is imperative to highlight that the results of our experiments surpass all previous state-of-the-art methods in terms of F1-score in the packet-level fine-tuning. These outcomes attest to the proficiency of our framework in synthesizing coarse-grained and fine-grained insights into encrypted traffic analysis. The observed discrepancy in classification capability may be attributed to the inherently more fine-grained nature of packet-level fine-tuning compared to flow-level fine-tuning. This granularity enables the self-attention mechanism to capture subtler details within the encrypted traffic, potentially leading to enhanced model classification performance.

D. Ablation Studies

In this study, we evaluate the impact of individual components within our framework in both flow-level and packet-level learning. Crucially, omitting the comprehensive fusion-guided (CFG) learning and global-feature-Aware (GFA) learning from ET-CompBERT reverts it to its baseline counterpart, ET-BERT. Tables V and VI detail the performance implications of these components in flow-level learning scenarios. As delineated in Table V, the omission of GFA learning precipitates a minimum decline of -0.43% in the F1-score for the Cross-Platform (Android) dataset. More strikingly, the simultaneous removal of both GFA and CFG learning induces a minimum downturn of approximately -3.42% in the F1-score. Such outcomes accentuate the critical role of our proposed CFG and GFA methodologies in the effective assimilation of multi-grained features for encrypted traffic classification.

We assess the performance of our model using four fundamental metrics: Accuracy (AC), Precision (PR), Recall (RC), and F1-Score. This involves calculating the mean values of AC, PR, RC, and F1 for each category, ensuring a more equitable and round evaluation framework.

The packet-level learning, as shown in Tables VII and VIII, ET-CompBERT demonstrates robust performance across all four datasets. All classification abilities decline when removing GFA learning or removing both GFA learning and CFG learning. A discernible decline in performance is noted with the removal of the GFA learning, evidenced by a marked reduction of -4.12% in the F1-score, most notably in the ISCX-Tor dataset. They were similarly, eliminating both the GFA learning and CFG learning results in a further decrease, with the F1-score dropping by -3.10% in the same dataset. These observations underscore the substantial contributions of both

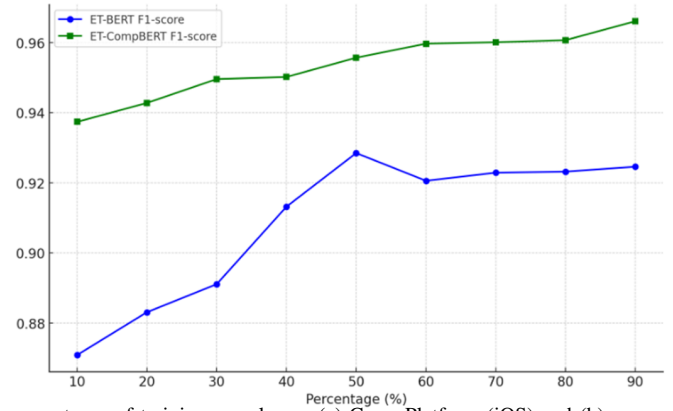
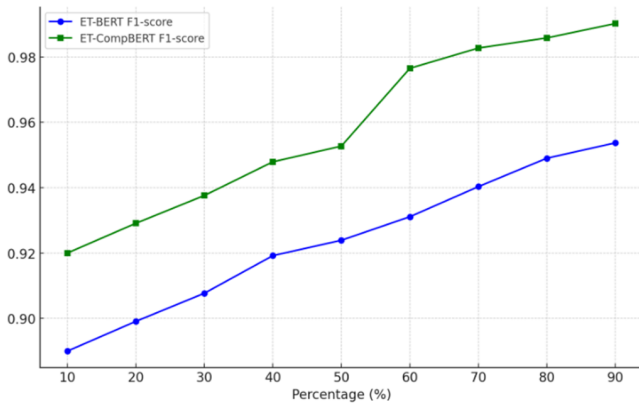


Fig. 2. F1-scores of flow-level ET-BERT and ET-CompBERT using varying percentages of training samples on (a) Cross-Platform (iOS) and (b) Cross-Platform (Android) datasets.

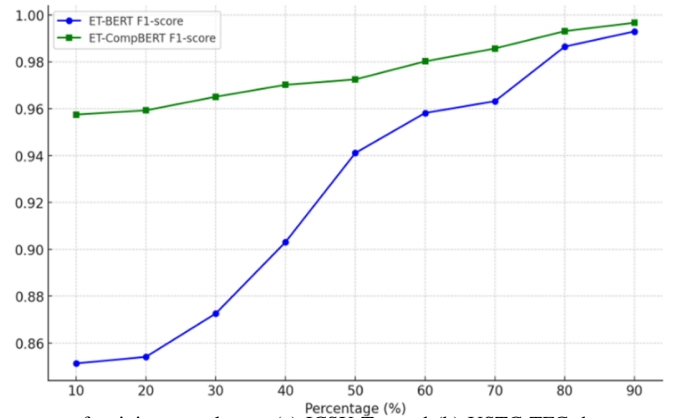
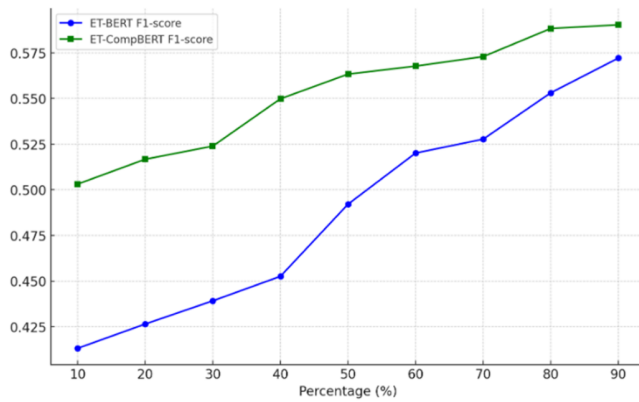


Fig. 3. F1-scores of flow-level ET-BERT and ET-CompBERT using varying percentages of training samples on (a) ICSX-Tor and (b) USTC-TFC datasets.

TABLE IX. PERFORMANCE COMPARISON OF DIFFERENT PRE-TRAINING LEARNING METHODS ON CROSS-PLATFORM (IOS) AND CROSS-PLATFORM (ANDROID) DATASETS

| Dataset Method | Cross-Platform(ios) | | | | Cross-Platform(Android) | | | |
|----------------------|---------------------|---------------|---------------|---------------|-------------------------|---------------|---------------|---------------|
| | AC | PR | RC | F1 | AC | PR | RC | F1 |
| ET-CompBERT(flow) | 0.9964 | 0.9978 | 0.9871 | 0.9924 | 0.9954 | 0.9611 | 0.9712 | 0.9661 |
| ET-CompBERT(packet) | 0.9945 | 0.9911 | 0.9975 | 0.9943 | 0.9982 | 0.9627 | 0.9671 | 0.9649 |
| ET-BERT+GFA(flow) | 0.9851 | 0.9745 | 0.9701 | 0.9721 | 0.9870 | 0.9331 | 0.9294 | 0.9312 |
| ET-BERT+GFA(packet) | 0.9824 | 0.9784 | 0.9842 | 0.9813 | 0.9754 | 0.9511 | 0.9187 | 0.9346 |
| ET-BERT(flow) [11] | 0.9844 | 0.9701 | 0.9632 | 0.9643 | 0.9865 | 0.9324 | 0.9266 | 0.9246 |
| ET-BERT(packet) [11] | 0.9810 | 0.9757 | 0.9772 | 0.9754 | 0.9728 | 0.9439 | 0.9119 | 0.9206 |

the GFA learning and CFG learning to the overall effectiveness of our framework in encrypted traffic classification tasks.

E. Analysis

We conduct an extensive analysis of the impact of varying dataset volumes under flow-level fine-tuning, as depicted in Fig. 2 and Fig. 3, and packet-level fine-tuning, illustrated in Fig. 4 and Fig. 5. Additionally, we perform a comparative evaluation of the classification performances using different late fusion methods, which are systematically presented in Table IX and X.

Fig. 2 and Fig. 3 demonstrate the comparative performance of ET-BERT and ET-CompBERT across four datasets under flow-level fine-tuning. It is observed that with the reduction in dataset volumes, ET-CompBERT's classification performance consistently outperforms that of ET-BERT. Significantly, our

proposed framework exhibits a notable enhancement over ET-BERT, evidenced by an approximate increase of +0.37% in classification accuracy under 90% GFA learning data volumes. This improvement is even more marked at lower dataset volumes, especially at 10%. Particularly, under 10% volumes of the USTC-TFC dataset, as shown in Fig. 3(b), the classification capability of our framework substantially surpasses ET-BERT by about +10.62%. These findings clearly illustrate the superior robustness and improved classification efficacy of our proposed framework compared to ET-BERT when applied to flow-level fine-tuning. In the packet-level fine-tuning scenario in Fig. 3 and Fig. 4, the ascending trends observed across the four datasets indicate that ET-CompBERT significantly outperforms in scenarios with reduced dataset volumes, particularly evident in the ISCX-Tor dataset, where it surpasses ET-BERT by a notable +9.21% in Fig. 4(a). These experimental results validate that our comprehensive fusion-guided learning

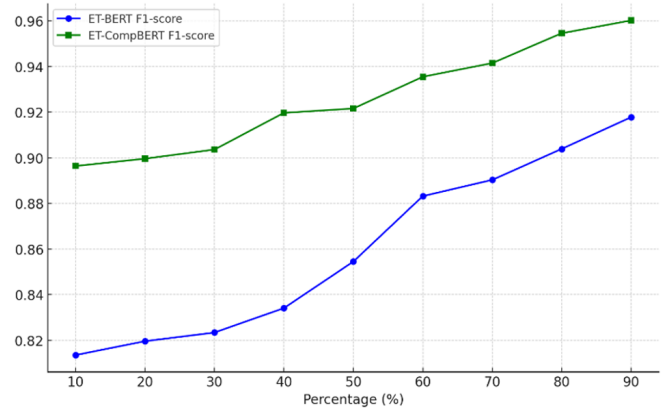
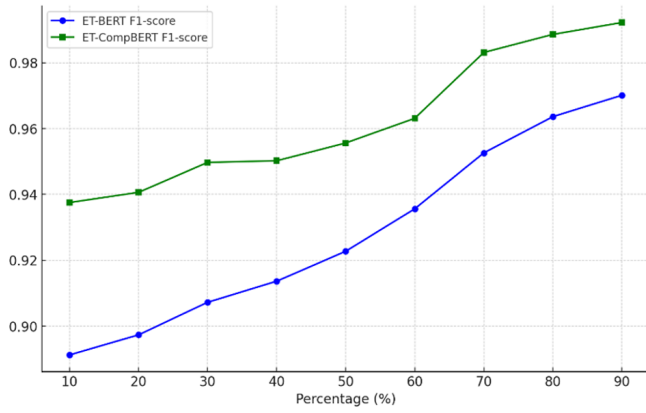


Fig. 4. F1-scores of packet-level ET-BERT and ET-CompBERT using varying percentages of training samples on (a) Cross-Platform (iOS) and (b) Cross-Platform (Android) datasets.

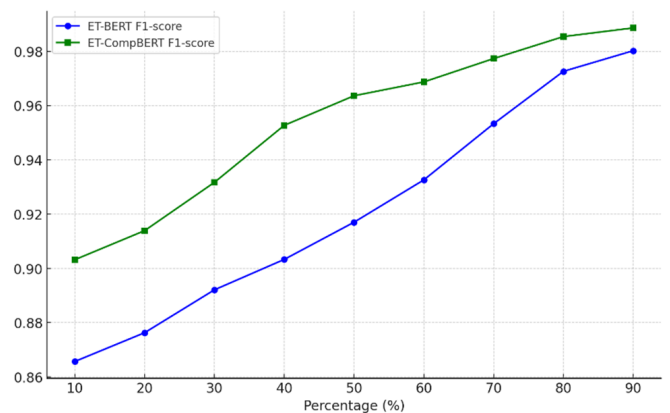
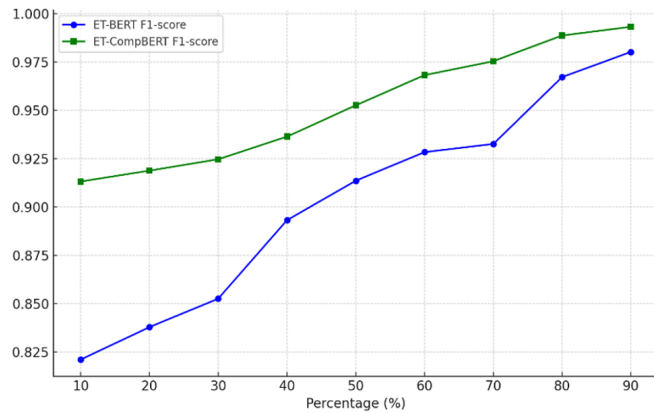


Fig. 5. F1-scores of packet-level ET-BERT and ET-CompBERT using varying percentages of training samples on (a) ICSX-Tor and (b) USTC-TFC datasets.

TABLE X. PERFORMANCE COMPARISON OF DIFFERENT PRE-TRAINING LEARNING METHODS ON ICSX-TOR AND USTC-TFC DATASETS

| Dataset Method | ICSX-Tor | | | | USTC-TFC | | | |
|----------------------|---------------|---------------|---------------|---------------|---------------|---------------|---------------|---------------|
| | AC | PR | RC | F1 | AC | PR | RC | F1 |
| ET-CompBERT(flow) | 0.8365 | 0.5598 | 0.6415 | 0.5914 | 0.9916 | 0.9947 | 0.9987 | 0.9967 |
| ET-CompBERT(packet) | 0.9946 | 0.9979 | 0.9957 | 0.9968 | 0.9969 | 0.9964 | 0.9978 | 0.9971 |
| ET-BERT+GFA(flow) | 0.8301 | 0.5407 | 0.6319 | 0.5828 | 0.9878 | 0.9908 | 0.9898 | 0.9903 |
| ET-BERT+GFA(packet) | 0.9934 | 0.9947 | 0.9931 | 0.9939 | 0.9807 | 0.9911 | 0.9936 | 0.9923 |
| ET-BERT(flow) [11] | 0.8311 | 0.5564 | 0.6448 | 0.5886 | 0.9929 | 0.9930 | 0.9930 | 0.9930 |
| ET-BERT(packet) [11] | 0.9921 | 0.9923 | 0.9921 | 0.9921 | 0.9915 | 0.9915 | 0.9916 | 0.9916 |

approach effectively enables the framework to comprehend coarse-grained global temporal attributes, building upon its understanding of fine-grained information from the encrypted traffic payload. Concurrently, these global temporal attributes contribute to enhancing the pre-trained model’s proficiency in encrypted traffic classification, underscoring the synergy between different granularities of data in improving model encrypted traffic classification performance.

In addition to our primary methodology, we examine an alternative late fusion technique to replace the comprehensive fusion-guided learning. This approach computes an arithmetic mean of the prediction probabilities derived from the fine-grained payload encoder, ET-BERT, and the encoder capturing global temporal attributes. Designated as ET-BERT+GFA, this advanced late fusion methodology strives to amalgamate multi-grained informational aspects. In this technique, the encoder responsible for capturing global temporal attributes computes

a probability distribution that is the arithmetic mean of its own output and that of ET-BERT. Unfortunately, as Tables IX and X reveal, this method falls short of achieving the desired performance in encrypted traffic classification. Table X, in particular, illustrates that ET-BERT+GFA’s classification efficacy does not surpass that of ET-BERT. The underlying cause of this shortfall may be attributed to the simplistic nature of this late fusion approach, which potentially disrupts the model’s ability to integrate coarse-grained features without preserving the intricate fine-grained details of the encrypted traffic. These findings affirm the effectiveness of our comprehensive fusion-guided learning in enabling the model to assimilate coarse-grained temporal attributes without compromising the nuanced information acquired from the fine-grained payload of encrypted traffic.

V. CONCLUSION

In this work, we introduce a novel framework for encrypted traffic classification, named ET-CompBERT. This framework innovatively integrates the fine-grained payload characteristics of encrypted traffic with the coarse-grained global temporal attributes. We also introduce innovative GFA learning which endows our framework with robust encrypted traffic classification results under different data sizes. Extensive experimental results validate the effectiveness of our approach.

REFERENCES

- [1] S. Rezaei and X. Liu, "Deep learning for encrypted traffic classification: An overview," *IEEE Communications Magazine*, vol. 57, no. 5, pp. 76–81, 2019.
- [2] P. Velan, M. Čermák, P. Čeleda, and M. Drašar, "A survey of methods for encrypted traffic classification and analysis," *International Journal of Network Management*, vol. 25, no. 5, pp. 355–374, 2015, Wiley Online Library.
- [3] T. Hu, C. Xu, S. Zhang, S. Tao, and L. Li, "Cross-site scripting detection with two-channel feature fusion embedded in self-attention mechanism," *Computers & Security*, vol. 124, pp. 102990, 2023, Elsevier.
- [4] N. Thalji, A. Raza, M. S. Islam, N. A. Samee, and M. M. Jamjoom, "AE-Net: Novel Autoencoder-Based Deep Features for SQL Injection Attack Detection," *IEEE Access*, vol. 11, pp. 135507–135516, 2023.
- [5] G. S. Nilavarasan and T. Balachander, "XSS Attack Detection using Convolution Neural Network," in *Proceedings of the 2023 International Conference on Artificial Intelligence and Knowledge Discovery in Concurrent Engineering (ICECONF)*, pp. 1–6, 2023, IEEE.
- [6] T. van Ede, R. Bortolameotti, A. Continella, J. Ren, D. J. Dubois, M. Lindorfer, D. Choffnes, M. van Steen, and A. Peter, "Flowprint: Semi-supervised mobile-app fingerprinting on encrypted network traffic," in *Network and Distributed System Security Symposium (NDSS)*, vol. 27, 2020.
- [7] K. Al-Naami, S. Chandra, A. Mustafa, L. Khan, Z. Lin, K. Hamlen, and B. Thuraisingham, "Adaptive encrypted traffic fingerprinting with bi-directional dependence," in *Proceedings of the 32nd Annual Conference on Computer Security Applications*, pp. 177–188, 2016.
- [8] V. F. Taylor, R. Spolaor, M. Conti, and I. Martinovic, "Robust smartphone app identification via encrypted network traffic analysis," *IEEE Transactions on Information Forensics and Security*, vol. 13, no. 1, pp. 63–78, 2017.
- [9] P. Sirinam, M. Imani, M. Juarez, and M. Wright, "Deep fingerprinting: Undermining website fingerprinting defenses with deep learning," in *Proc. 2018 ACM SIGSAC Conf. Comput. Commun. Secur.*, 2018, pp. 1928–1943.
- [10] J. Devlin, M.-W. Chang, K. Lee, and K. Toutanova, "Bert: learning of deep bidirectional transformers for language understanding," *arXiv preprint arXiv:1810.04805*, 2018.
- [11] X. Lin, G. Xiong, G. Gou, Z. Li, J. Shi, and J. Yu, "Et-bert: A contextualized datagram representation with learning transformers for encrypted traffic classification," in *Proc. ACM Web Conf. 2022*, 2022, pp. 633–642.
- [12] A. Radford, J. W. Kim, C. Hallacy, et al., "Learning transferable visual models from natural language supervision," in *International Conference on Machine Learning*, PMLR, 2021, pp. 8748–8763.
- [13] L. Ouyang, J. Wu, X. Jiang, D. Almeida, C. Wainwright, P. Mishkin, C. Zhang, S. Agarwal, K. Slama, A. Ray, et al., "Training language models to follow instructions with human feedback," *Advances in Neural Information Processing Systems*, vol. 35, pp. 27730–27744, 2022.
- [14] V. F. Taylor, R. Spolaor, M. Conti, and I. Martinovic, "Appscanner: Automatic fingerprinting of smartphone apps from encrypted network traffic," in *Proc. 2016 IEEE Eur. Symp. Secur. Privacy (EuroS&P)*, 2016, pp. 439–454.
- [15] A. Panchenko, F. Lanze, J. Pennekamp, T. Engel, A. Zinnen, M. Henze, and K. Wehrle, "Website Fingerprinting at Internet Scale," in *Proc. NDSS*, 2016.
- [16] W. Wang, M. Zhu, J. Wang, X. Zeng, and Z. Yang, "End-to-end encrypted traffic classification with one-dimensional convolution neural networks," in *Proc. 2017 IEEE Int. Conf. Intell. Secur. Inform. (ISI)*, 2017, pp. 43–48.
- [17] A. Vaswani, N. Shazeer, N. Parmar, J. Uszkoreit, L. Jones, A. N. Gomez, E. Kaiser, and I. Polosukhin, "Attention is all you need," in *Proc. Adv. Neural Inform. Process. Syst.*, vol. 30, 2017.
- [18] G. Draper-Gil, A. H. Lashkari, M. S. I. Mamun, and A. A. Ghorbani, "Characterization of encrypted and VPN traffic using time-related," in *Proceedings of the 2nd International Conference on Information Systems Security and Privacy (ICISSP)*, pp. 108–116, 2018.
- [19] I. Sharafaldin, A. H. Lashkari, and A. A. Ghorbani, "Toward generating a new intrusion detection dataset and intrusion traffic characterization," *ICISSp*, vol. 1, pp. 108–116, 2018.
- [20] M. Shen, J. Zhang, L. Zhu, K. Xu, and X. Du, "Accurate decentralized application identification via encrypted traffic analysis using graph neural networks," *IEEE Transactions on Information Forensics and Security*, vol. 16, pp. 2367–2380, 2021.
- [21] K. Lin, X. Xu, and H. Gao, "TSCRNN: A novel classification scheme of encrypted traffic based on flow spatiotemporal features for efficient management of IIoT," *Computer Networks*, vol. 190, pp. 107974, 2021, Elsevier.
- [22] C. Liu, L. He, G. Xiong, Z. Cao, and Z. Li, "Fs-net: A flow sequence network for encrypted traffic classification," in *Proc. IEEE INFOCOM 2019 - IEEE Conf. Comput. Commun.*, 2019, pp. 1171–1179.
- [23] M. Lotfollahi, M. Jafari Siavoshani, R. Shirali Hossein Zade, and M. Saberian, "Deep packet: A novel approach for encrypted traffic classification using deep learning," *Soft Computing*, vol. 24, no. 3, pp. 1999–2012, 2020, Springer.
- [24] H. Y. He, Z. G. Yang, and X. N. Chen, "PERT: Payload encoding representation from transformer for encrypted traffic classification," in *Proceedings of the 2020 ITU Kaleidoscope: Industry-Driven Digital Transformation (ITU K)*, pp. 1–8, 2020, IEEE.
- [25] J. Hayes and G. Danezis, "k-fingerprinting: A robust scalable website fingerprinting technique," in *Proceedings of the 25th USENIX Security Symposium (USENIX Security 16)*, pp. 1187–1203, 2016.
- [26] W. Wang, M. Zhu, X. Zeng, X. Ye, and Y. Sheng, "Malware traffic classification using convolutional neural network for representation learning," in *Proc. 2017 International Conference on Information Networking (ICOIN)*, pp. 712–717, 2017.

Optimization of PID Controller Parameter using the Geometric Mean Optimizer

Osama Abdellatif¹, Mohamed Issa², Ibrahim Ziedan³

Computer and Systems Engineering Dept., Faculty of Engineering, Zagazig University, Zagazig, Egypt^{1, 2, 3}
Faculty of Computer Science and Information Technology, Egypt-Japan University, New Borg El Arab, Egypt²

Abstract—The PID controller is a crucial element in numerous engineering applications. However, a significant challenge with PID lies in selecting optimal parameter values. Conventional methods need extra tuning and may not yield the best performance. In this study, a recently introduced metaheuristic algorithm, Geometric Mean Optimizer (GMO), is employed to identify the most suitable PID parameter values. In conventional methods, a fixed empirical equations are applied to select parameter values of PID. In GMO, there is a wide search space to select the optimal parameter values of PID based on an objective function. The objective function that the GMO seeks to minimize is the Integral of Absolute Error (IAE). GMO is chosen for its effectiveness in balancing exploration and exploitation of the search space, as well as its robustness and scalability. GMO is tested in the context of optimizing PID parameters for an engineering application: DC motor regulations. The results demonstrated GMO's superiority over comparable algorithms.

Keywords—Metaheuristics; PID controller; GMO; DC motor

I. INTRODUCTION

In manufacturing industries, the PID controller is favored for its effectiveness, resilience, and durability. This controller features standard control parameters, including system stability, settling time, and the deviation between desired and actual responses [1]. Given the shared use of processes in factories, tuning these parameters becomes a crucial task. Proper configuration enables the achievement of efficient transient performance, minimizing settling time, steady-state error, maximum deviation, and rise time as much as possible. The PID controller relies on three essential parameters: proportional gain (K_p), integral gain (K_i), and derivative gain (K_d).

The PID controller finds applications in regulating a variety of industrial processes, including pressure, temperature, flow rate, feed rate, weight, speed, and position [1]. Tuning the PID controller's parameters falls into three categories: analytical methods, rule-based methods, and numerical methods [2]. The Ziegler-Nichols (ZN) method, a classic approach for adjusting PID controller parameters, is the most commonly used and falls into the analytical category [3]. However, it's important to note that ZN does not provide optimal performance.

Stochastic optimization techniques, like heuristic algorithms, are well-suited for tuning PID parameters [4] [5]. These methods treat the problem as a "black box," adjusting the parameters and monitoring fitness to reach the optimal value. A meta-heuristic algorithm, which relies on random motion to expedite the exploration of a problem's search space, aims to find a satisfactory solution within a reasonable timeframe [6].

In this work, Geometric Mean Optimizer (GMO) [7] is used to identify the most suitable PID parameter values. The objective function employed to enhance process performance is the Minimum Integral of Absolute Error (IAE) [8].

The main objective of this work is to enhance IAE for estimating the parameters of PID controller. The performance of GMO is evaluated in comparison with other algorithms such as Arithmetic Optimization Algorithm (AOA) [9], Sine-Cosine Optimization Algorithm (SCA) [10], Particle Swarm Optimization algorithm (PSO) [11], [12] and Genetic Algorithm (GA) [13], [14]. GMO is chosen for estimating the parameters of PID due to the following advantages such as balanced exploration and exploitation, robustness, sensitivity control, scalability, convergence and divergence.

II. METHODS

A. PID Tuning

The following three terms are the foundation of PID controller [1]:

- Proportional (P) term: Its purpose is to adjust the actual response $y(t)$ in accordance with the error $e(t)$ that is present between the desired response $h(t)$ and the actual response $y(t)$ at the moment as defined in (1). The magnitude of the desired correction increases with $e(t)$ increase.
- Integral (I) term: Its purpose is to modify the actual response $y(t)$ according to the cumulative error $e(t)$ over time. By doing this, steady state error (SSE) - $e(t)$ after a long time - is reduced.
- Derivative (D) term: Its purpose is to modify the actual response $y(t)$ according to the error's rate of change. By doing this, overshoot - which occurs when the actual response $y(t)$ is greater than the desired response $h(t)$ - is suppressed.

The combination of the three components formulate the PID controller as defined in Eq. (2)

$$e(t) = y(t) - h(t) \quad (1)$$

$$u(t) = K_p e(t) + K_i \int_0^t e(t) dt + K_d \frac{d}{dt} e(t) \quad (2)$$

where $u(t)$ is the output of the PID process.

The following time-domain characteristics are essential metrics to keep under careful observation while optimizing IAE:

- The response's rise time (t_r): is the amount of time it takes to grow from 10% to 90% of its ultimate value.
- Settling time (t_s): Usually expressed as an absolute percentage of the final value, such as 2% or 5%, it is the amount of time needed for the response curve to reach and stay within a given range around the final value.
- Overshooting (M_p): This is the response curve's maximum peak value, as determined by measuring it from unity or a reference point.

IAE is calculated as the summation of disparities between the desired response $h(t)$ and the actual response $y(t)$ during simulation time T_{sim} [1], as defined in (3).

$$IAE = \int_0^{T_{sim}} |y(t) - h(t)| dt \quad (3)$$

Fig. 1 shows the entire relationship between the closed loop PID controller and the calculation of its parameters using the GMO based on IAE. At first the parameters are initialized. Then IAE is calculated to decide which best PID parameters should be elected to minimize the IAE and improve the overall response of the system then the parameters are fed to PID function $G_{PID}(s)$ as defined as in Eq. (4).

$$G_{PID}(s) = K_p + \frac{K_i}{s} + K_d s \quad (4)$$

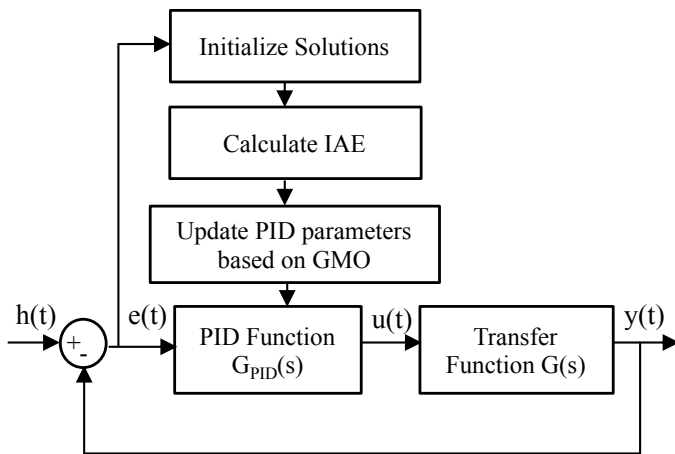


Fig. 1. Calculation of PID parameters based on GMO.

B. GMO Algorithm

GMO is a relatively new metaheuristic optimization algorithm. It is been used to optimize some problems such as [15]–[18]. GMO makes use of the special mathematical characteristics of the geometric mean. This operator allows one to assess search agents' exploration phase and exploitation at the same time. The weight of an agent in GMO is determined by taking the geometric mean of its opposites' scaled objective values (OVs). This means that an agent is appropriately regarded to direct the other agents' search process toward solving an optimization problem by considering the geometric mean of those OVs [7]. The flowchart is shown in Fig. 2 and the steps in this strategy are as follows:

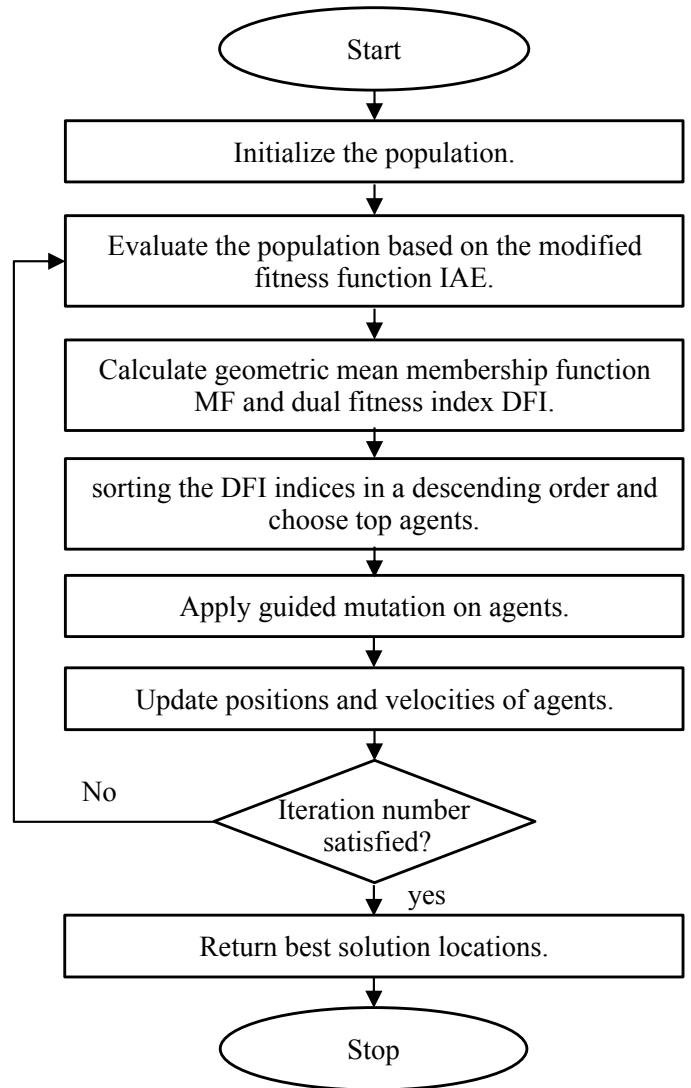


Fig. 2. Flowchart of GMO algorithm.

- 1) Generate the position and velocity of each searching agent randomly as defined in Eq. (5), Eq. (6).

$$x_i^0 = U(x_{min}, x_{max}) \quad (5)$$

$$v_i^0 = U(v_{min}, v_{max}) \quad (6)$$

where, $x_{min}, v_{min}, x_{max}, v_{max}$ are the lower and upper bounds.

- 2) Determine each search agent's personal best position by computing their fitness function results as defined in Eq. (7).

$$IAE = \begin{cases} 1000, & \text{if unstable.} \\ \int_0^{T_{sim}} |y(t) - h(t)| dt, & \text{otherwise.} \end{cases} \quad (7)$$

a small, however effective, modification is applied to the fitness function IAE for this problem. A penalty 1000 is applied if the resulting closed loop system is unstable. This ensures that the resulting search space is always stable.

- 3) Determine geometric mean of the chosen agent related to best agents fuzzy membership function (MF) and dual fitness index (DFI) as defined in Eq. (8).

$$MF_j^t = \frac{1}{1 + \exp\left(-\frac{4}{\sigma^t \sqrt{\epsilon}}\right)} \left(z_{best,j}^t - \mu^t\right) \quad (8)$$

knowing that j loops over all agents starting from 1 to N where N is the total number of agents, $z_{best,j}^t$ is the personal best objective value of the corresponding agent, and μ^t, σ^t are the mean and standard deviation (STD) of all best-so-far agents.

- 4) Determine the DFI as the geometric mean of all best agents MF except that the corresponding agent as defined in Eq. (9).

$$DFI_i^t = \prod_{j=1, j \neq i}^N MF_j^t \quad (9)$$

- 5) Choose the first top agents (N_{best}) by sorting the DFI indices in a descending order.
- 6) Determine the positions of the unique global guide agent calculated for the agent i at the iteration t as defined in (10).

$$Y_i^t = \frac{\sum_{j \in N_{best}, j \neq i} DFI_j^t * X_j^{best}}{\sum_{j \in N_{best}} DFI_j^t + \epsilon} \quad (10)$$

where X_j^{best} is the personal best position at iteration j , and ϵ is either 0 or a small positive number.

- 7) Impose guided mutation on agents to make positions of agents more stochastic as defined in Eq. (11).

$$Y_{i,mult}^t = Y_i^t + w \text{ randn} (Std_{max}^t - Std^t) \quad (11)$$

$$w = 1 - \frac{t}{T_{max}} \quad (12)$$

where Std^t is the STD calculated for the personal best-so-far agents at the t th iteration, randn is a random vector from normal distribution, and w is the mutation step as defined in Eq. (12), t is the number of the current iteration, and T_{max} is number of iterations.

- 8) Finally, update the positions and velocities of agents as defined in Eq. (13) to Eq. (15).

$$V_i^{t+1} = w V_i^t + \varphi (Y_{i,mult}^t - X_i^t) \quad (13)$$

$$\varphi = 1 + (2 \text{ rand} - 1) w \quad (14)$$

$$X_i^{t+1} = X_i^t + V_i^{t+1} \quad (15)$$

where V_i^t is the velocity vector on i th agent and t th iteration, V_i^{t+1} is the velocity at $(t+1)$ th iteration, $Y_{i,mult}^t$ is global guide position for the agent i , X_i^t is a position of the i th agent's, and φ is a scaling parameter, and rand is a random number within $(0,1)$.

III. THE EXPERIMENTAL RESULTS AND DISCUSSION

Experimental trials are conducted on a DC motor system in order to regulate the speed of it. It is a common subject in numerous related studies [19]–[24].

The experimental findings are compared with related results from AOA, SCA, PSO, and GA algorithms. The fitness function IAE is used to evaluate solutions. A regulated process's step response may be described by the following time-domain characteristics [1]: rising time, settling time, and overshoot.

Table I provides the parameter values for the DC motor utilized as a case study [19]. In the table, R_a denotes the armature resistance, L_a represents the inductance of the armature winding, J signifies the equivalent moment of inertia of the motor and load referred to the motor shaft, D stands for the equivalent friction coefficient of the motor and load referred to the motor shaft, K indicates the motor torque constant, and K_b represents the back EMF constant.

TABLE I. PARAMETERS OF DC MOTOR

| Parameter | Value |
|-----------|---------------------------|
| R_a | 0.4 Ω |
| L_a | 2.7 H |
| J | 0.0004 kg. m ² |
| D | 0.0022 N.m.sec / rad |
| K | 15 e-03 kg. m / A |
| K_b | 0.05 V.s |

The transfer function that describes the open-loop speed control system of a DC motor, as expressed in (16). It completes the transfer function in Fig. 1 so that the input of the transfer function is $u(t)$ and the output of it is $y(t)$.

$$G(s) = \frac{15}{1.08 s^2 + 6.1 s + 1.63} \quad (16)$$

The speed regulation of an electrical DC motor [20] is managed through a PID controller, with heuristic algorithms employed to determine the most effective parameters for achieving optimal performance. The parameter configurations for PSO, SCA, GA, and GMO can be found in Table II. These settings are determined through experimental estimation to yield the most favorable outcomes.

Fig. 3 shows the open loop response of the DC motor. It has a rise time of 7.8251 sec., settling time of 14.1030 sec., and no overshoot. It also has a peak of velocity of 9.1960 m/sec. After running the PID controller the transient response of the system will improve and the new desired response $h(t)$ can be set to be 9.1960 m/sec.

Table III displays the optimal parameter values for the PID controller that are determined for the purpose of enhancing the speed regulation of the DC motor. These values are achieved through the application of the GMO algorithm and are compared to results obtained from other related algorithms. The GMO algorithm is designed to optimize a single objective, specifically IAE, aiming to find the PID controller parameters that yield the lowest IAE. In addition to IAE, other performance criteria such as settling time, rise time, and overshoot

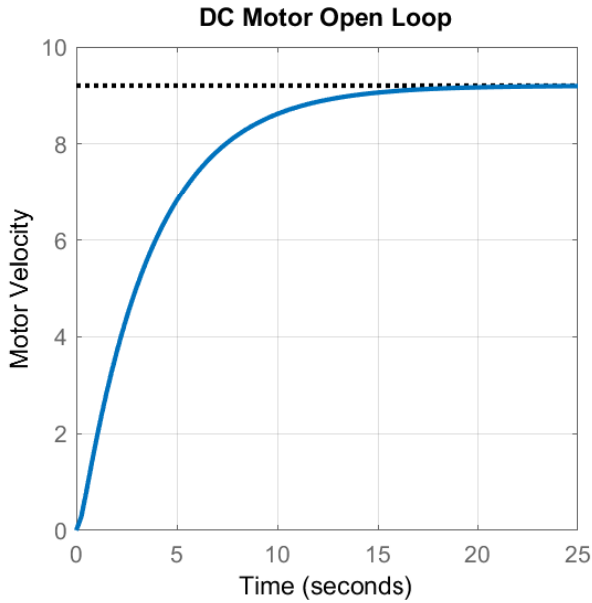


Fig. 3. DC motor open-loop behavior over time, measured in seconds.

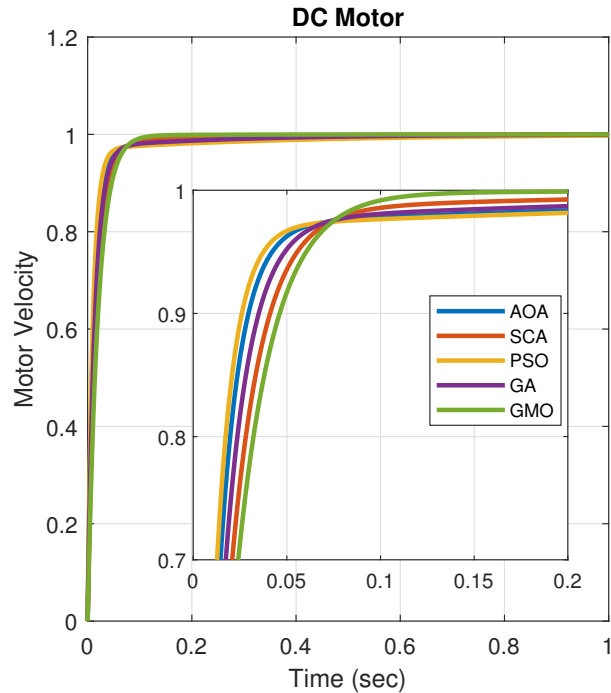


Fig. 4. DC motor behavior over time under the influence of a PID controller, measured in seconds.

TABLE II. THE CONFIGURATION OF PARAMETER SETTINGS FOR DIFFERENT ALGORITHMS APPLIED TO A DC MOTOR

| | Parameter | Value |
|----------------|--------------------------------|--------|
| All Algorithms | The population (N) | 100 |
| | Iteration Number (T) | 50 |
| | Independent run number | 20 |
| | Upper bound of (Kp, Ki and Kd) | 20 |
| | Simulation Time (Tsim) | 5 Sec. |
| GMO | ϵ | 0 |
| AOA | μ | 0.5 |
| | α | 4.5 |
| | ϵ | 2 |
| SCA | a | 3 |
| | r3 | 0.5 |
| PSO | C1 | 0.5 |
| | C2 | 0.5 |
| | w | 0.1 |

are evaluated based on the estimated parameters for GMO and the other algorithms within the comparative analysis.

For determining the best IAE, GMO outperforms other methods, as Table III and Fig. 4 demonstrate. GA is the closest rival to GMO in terms of IAE. GMO succeeds in decreasing GA's IAE demonstrating how GMO has better exploration and exploitation through the use of DFI, the geometric mean, and guided mutation.

GMO offers no overshoot for overshoot measurement. Other algorithms also succeed to have no overshoot. When overshoot happens, it suggests that the system's responses in certain situations are unfavorable. As previously indicated, the single objective function is chosen to minimize IAE rather than minimizing the settling time. However, GMO does succeed in

having the least settling time which is great for the system stability.

According to Table III, GMO produces the longest rising time and PSO produces the lowest. However, from stability point of view if decreasing rising time affects the settling time or overshoot, it is favorable to make a compromise then. That's assured by Fig. 4, that GMO is the first to reach the target velocity.

The bode diagrams for controlling a DC motor using a PID controller, whose parameters are determined by GMO and the opponent algorithms, are displayed in Fig. 5 GMO has the most bandwidth. This ensures that GMO has a shorter rise time than other algorithms, as seen in Fig. 4 and Table III.

Furthermore, as seen in Fig. 5, the magnitude margin of PSO, for instance, has the highest gain compared to that of GMO, suggesting that PSO reacts more aggressively than GMO and may lead to overshooting (which does not happen here). However, GMO has the most robust response as it has least magnitude and phase margin .

It is evident from Fig. 6, which is concerned with Box Plot diagrams, that the GMO outperforms other optimization techniques when it comes to various parameters. Additionally, it demonstrates that GMO in the systems' component expansion and complexity possesses outstanding performance and convergence ability. As indicated in Table III and Fig. 6, GMO produces favorable results in every experiment carried out in terms of mean, median, and STD. It has the general least IAE, Median, Average, and STD compared to all other algorithms.

The most notable and useful benefits of GMO are its capacity to assess fitness and diversity simultaneously using

TABLE III. COMPARISON OF GMO AND DIFFERENT ALGORITHMS IN TERMS OF STEP RESPONSE AND IAE CRITERIA, RISE TIME, SETTLING TIME, AND OVERSHOOT PERCENTAGE

| | Kp | Ki | Kd | IAE | Rise time(sec) | Settling time | %Overshoot | Best IAE | Mean IAE | Worst IAE | STD IAE |
|-----|---------|---------|---------|-----------------|----------------|----------------|------------|-----------------|-----------------|-----------------|-----------------|
| AOA | 19.9888 | 5.33505 | 6.13004 | 0.021144 | 0.02826 | 0.12994 | 0 | 0.021144 | 0.022407 | 0.023667 | 0.000701 |
| SCA | 19.9062 | 5.65814 | 4.22508 | 0.021106 | 0.03924 | 0.08215 | 0 | 0.021106 | 0.02187 | 0.022780 | 0.000566 |
| PSO | 19.5839 | 5.18908 | 7.00110 | 0.021833 | 0.02489 | 0.16404 | 0 | 0.021833 | 0.022668 | 0.023589 | 0.000559 |
| GA | 20 | 5.33333 | 5.09804 | 0.020840 | 0.03348 | 0.09311 | 0 | 0.020840 | 0.021615 | 0.023447 | 0.000703 |
| GMO | 19.9914 | 5.33635 | 3.61397 | 0.020378 | 0.04405 | 0.07966 | 0 | 0.020378 | 0.021304 | 0.021890 | 0.000437 |

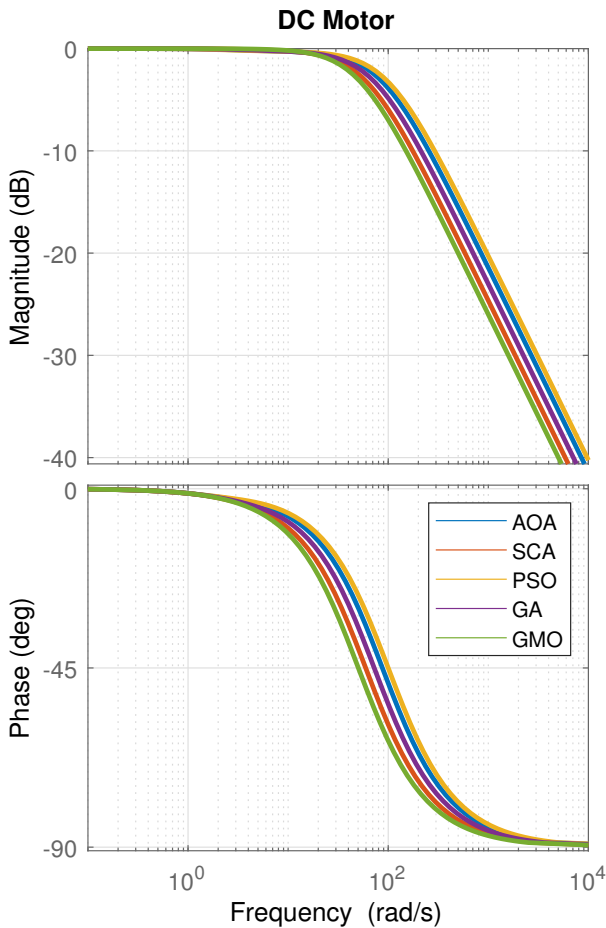


Fig. 5. Bode diagrams for a DC motor under the influence of a PID controller.

the DFI, computational efficiency, not having a parameter to adjust, and assignment of multiple unique guides for each solution in order to prevent the algorithm from sticking into a local minimum.

As shown in Fig. 7 the convergence curve for GMO gradually decreases until it finds the global minimum for the fitness function. GMO has the second highest average IAE at the beginning, AOA has the first, which explains the exploration capability of GMO algorithm as compared to all other algorithms except AOA. GMO also has the lowest

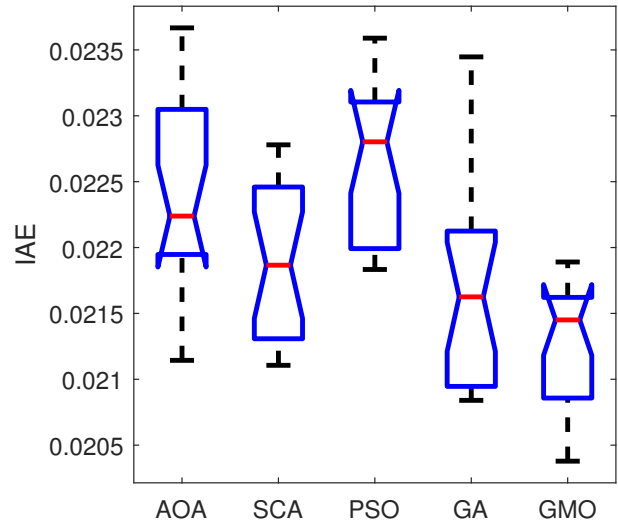


Fig. 6. Box plots of the obtained results from GMO and other optimization algorithms.

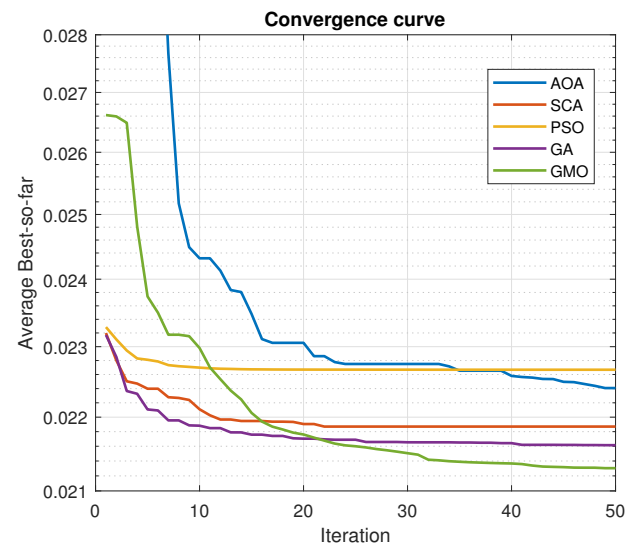


Fig. 7. Convergence curves of GMO other optimization algorithms.

average IAE at the end which means that GMO has the highest exploitation capability among all other algorithms. So, GMO has the greatest balance between exploration and exploitation

which makes it the superior algorithm compared to all other algorithms.

IV. CONCLUSION

In this study, the Geometric Mean Optimizer (GMO) algorithm is utilized to estimate PID controller parameters for regulating a DC motor. The primary objective function is the Integral of Absolute Error (IAE). GMO demonstrated superior performance compared to other algorithms in terms of IAE and response characteristics, including overshoot, and settling time, for DC motor control. Furthermore, the frequency response analysis of GMO indicates that it achieves a more favorable bandwidth and gain magnitude margin compared to the other algorithms under comparison. Through the experimental investigation, GMO exhibits its superiority in efficiently estimating PID controller parameters, resulting in improved IAE values in the context of DC motor control. In future work, a multi-objective function may be used to enhance more than IAE objective such as rising time and overshoot. It is recommended to use this multi-objective function to enhance the performance of DC motor or any other closed loop system such as three-tank system.

REFERENCES

- [1] K. Ogata, *Modern control engineering fifth edition*, 2010.
- [2] T. Mansour, *PID Control: Implementation and Tuning*. BoD-Books on Demand, 2011.
- [3] J. G. Ziegler and N. B. Nichols, "Optimum settings for automatic controllers," 1993.
- [4] O. Aydogdu and M. Korkmaz, "Optimal design of a variable coefficient fractional order pid controller by using heuristic optimization algorithms," *International Journal of Advanced Computer Science and Applications*, vol. 10, no. 3, 2019. [Online]. Available: <http://dx.doi.org/10.14569/IJACSA.2019.0100341>
- [5] M. R. P. Pillai, S. P. Jadhav, and M. D. Patil, "Tuning of pid controllers using advanced genetic algorithm," in *IJACSA Special Issue on Selected Papers from International Conference & Workshop On Advance Computing*. Citeseer, 2013, pp. 1–6.
- [6] E.-G. Talbi, *Metaheuristics: from design to implementation*. John Wiley & Sons, 2009.
- [7] F. Rezaei, H. R. Safavi, M. Abd Elaziz, and S. Mirjalili, "Gmo: geometric mean optimizer for solving engineering problems," *Soft Computing*, vol. 27, no. 15, pp. 10 571–10 606, 2023.
- [8] S. B. Joseph, E. G. Dada, A. Abidemi, D. O. Oyewola, and B. M. Khammas, "Metaheuristic algorithms for pid controller parameters tuning: Review, approaches and open problems," *Heliyon*, vol. 8, no. 5, 2022.
- [9] L. Abualigah, A. Diabat, S. Mirjalili, M. Abd Elaziz, and A. H. Gandomi, "The arithmetic optimization algorithm," *Computer methods in applied mechanics and engineering*, vol. 376, p. 113609, 2021.
- [10] S. Mirjalili, "Sca: a sine cosine algorithm for solving optimization problems," *Knowledge-based systems*, vol. 96, pp. 120–133, 2016.
- [11] E. S. Rahayu, A. Ma'arif, and A. Çakan, "Particle swarm optimization (pso) tuning of pid control on dc motor," *International Journal of Robotics and Control Systems*, vol. 2, no. 2, pp. 435–447, 2022. [Online]. Available: <https://pubs2.ascee.org/index.php/IJRCS/article/view/476>
- [12] J. Kennedy and R. Eberhart, "Particle swarm optimization (pso)," in *Proc. IEEE international conference on neural networks, Perth, Australia*, vol. 4, no. 1, 1995, pp. 1942–1948.
- [13] S. Tiwari, A. Bhatt, A. C. Unni, J. G. Singh, and W. Ongsakul, "Control of dc motor using genetic algorithm based pid controller," in *2018 International Conference and Utility Exhibition on Green Energy for Sustainable Development (ICUE)*, 2018, pp. 1–6.
- [14] J. H. Holland, "Genetic algorithms," *Scientific american*, vol. 267, no. 1, pp. 66–73, 1992.
- [15] S. B. Pandya, K. Kalita, P. Jangir, R. K. Ghadai, and L. Abualigah, "Multi-objective geometric mean optimizer (mogmo): A novel metaphor-free population-based math-inspired multi-objective algorithm," *International Journal of Computational Intelligence Systems*, vol. 17, no. 1, pp. 1–29, 2024.
- [16] S. Kamel, M. Khasanov, F. Jurado, A. Kurbanov, H. M. Zawbaa, and M. A. Alathbah, "Simultaneously distributed generation allocation and network reconfiguration in distribution network considering different loading levels," *IEEE Access*, 2023.
- [17] M. Khasanov, S. Kamel, F. Jurado, A. Kurbanov, and U. Jalilov, "Optimal sizing and sitting of distributed generation in distribution network considering power generation uncertainty," in *E3S Web of Conferences*, vol. 434. EDP Sciences, 2023, p. 01016.
- [18] A. E. Khalil, M. Alham, T. A. Boghdady, and D. K. Ibrahim, "Novel single loop load frequency controller for isolated microgrid via geometric mean optimization," in *2023 24th International Middle East Power System Conference (MEPCON)*. IEEE, 2023, pp. 1–8.
- [19] J. Agarwal, G. Parmar, R. Gupta, and A. Sikander, "Analysis of grey wolf optimizer based fractional order pid controller in speed control of dc motor," *Microsystem Technologies*, vol. 24, pp. 4997–5006, 2018.
- [20] S. Ekinci, B. Hekimoğlu, A. Demirören, and E. Eker, "Speed control of dc motor using improved sine cosine algorithm based pid controller," in *2019 3rd International Symposium on Multidisciplinary Studies and Innovative Technologies (ISMSIT)*. IEEE, 2019, pp. 1–7.
- [21] S. Ekinci, B. Hekimoğlu, and D. Izci, "Opposition based henry gas solubility optimization as a novel algorithm for pid control of dc motor," *Engineering Science and Technology, an International Journal*, vol. 24, no. 2, pp. 331–342, 2021.
- [22] M. Khalilpour, N. Razmjoooy, H. Hosseini, and P. Moallem, "Optimal control of dc motor using invasive weed optimization (iwo) algorithm," in *Majlesi Conference on Electrical Engineering, Majlesi New Town, Isfahan, Iran*, 2011.
- [23] N. Razmjoooy, Z. Vahedi, V. V. Estrela, R. Padilha, and A. C. B. Monteiro, "Speed control of a dc motor using pid controller based on improved whale optimization algorithm," in *Metaheuristics and Optimization in Computer and Electrical Engineering*. Springer, 2020, pp. 153–167.
- [24] T. C. Bora, L. d. S. Coelho, and L. Lebensztajn, "Bat-inspired optimization approach for the brushless dc wheel motor problem," *IEEE Transactions on magnetics*, vol. 48, no. 2, pp. 947–950, 2012.

Blockchain-Driven Decentralization of Electronic Health Records in Saudi Arabia: An Ethereum-Based Framework for Enhanced Security and Patient Control

Atef Masmoudi¹, Maha Saeed²

Laboratory of Electronics and Technology of Information National Engineering School of Sfax,
University of Sfax, Sfax, Tunisia¹
College of Computer Science, King Khalid University, Abha, Saudi Arabia^{1,2}

Abstract—In the rapidly evolving landscape of e-HealthCare in Saudi Arabia, enhancing the security and integrity of Electronic Health Records (EHRs) is imperative. Existing systems encounter challenges stemming from centralized storage, vulnerable data integrity, susceptibility to power failures, and issues of ownership by entities other than the patients themselves. Moreover, the sharing of sensitive patient information among anonymous bodies exacerbates the vulnerability of these records. In response to these challenges, this paper advocates for the transformative potential of blockchain technology. Blockchain, with its decentralized and distributed architecture, offers a revolutionary approach to communication among network nodes, eliminating the need for a central authority. This paper proposes a solution that places the patient at the forefront, empowering them as the primary controller of their medical data. The research delves into the current state of e-HealthCare in Saudi Arabia, examines the challenges faced by existing EHR systems, and introduces blockchain technology, particularly Ethereum, as a viable and transformative solution. The paper details the use of Ethereum blockchain to secure and manage medical records, with a Public Key Infrastructure (PKI) applied to safeguard the confidentiality of patient information. The decentralized InterPlanetary File System (IPFS) is employed for the secure and resilient storage of encrypted medical records. Additionally, Smart contracts, integral to the Ethereum blockchain, play a central role in automating and enforcing the rules governing access to medical records. Moreover, a Web 3.0 decentralized application (DApp) is developed to provide a user-friendly interface, empowering patients to seamlessly interact with and control access to their health data. At the end, this paper presents a guiding framework for clinicians, policymakers, and academics, illustrating the transformative potential of blockchain and associated technologies in revolutionizing EHR management in Saudi Arabia's healthcare systems.

Keywords—Blockchain; Ethereum; smart contract; Web 3.0; decentralized application; electronic health records

I. INTRODUCTION

The progression of technology in the modern era has significantly altered human perspectives and lifestyles. Technological advancements extend their influence to various facets of life, including healthcare, with the primary goal of transforming and enhancing the sector. In the healthcare realm, technology offers substantial benefits, revolutionizing systems for improved ease of use, security, and overall efficiency.

One such advancement that has played a pivotal role is the implementation of Electronic Medical Record (EMR) systems.

Before the advent of EMR systems, hospitals relied on handwritten documentation on paper, leading to data loss and patient challenges in updating records across different healthcare facilities. Recognizing the limitations of this approach, the healthcare sector embraced EMR systems, providing a transformative solution by storing data electronically and reducing reliance on paper. These electronic records encompass clinical notes and comprehensive laboratory results with multiple components [1]. This shift addressed prevailing issues in medical record management, enhancing information accessibility [2], error prevention, and the establishment of an adaptable system that could evolve over time [3]. Consequently, the adoption of EMR systems emphasizing enhanced usability, streamlined data retrieval, efficient updates, and overall improved data management processes, making them pivotal in modernizing healthcare practices.

However, despite the intended improvements in patient care, EMR systems encountered critical challenges, falling short of expectations [3]. Issues such as data security, integrity, and user ownership emerged as significant concerns. A study conducted in four academic hospitals in Saudi Arabia revealed that EMR systems faced reliability issues, particularly insecure access to records [3]. Furthermore, vulnerability to data breaches became evident, with a study reporting 173 million data breaches since October 2009 [4]. Compounding the challenges were issues of data duplication and the need for repetitive medical examinations when patients visited different hospitals [5]. The cumulative impact of these challenges emphasized the necessity for a secure, interoperable, and patient-centric healthcare data management system.

In response to these challenges, this paper advocates for the transformation of the healthcare sector into a patient-centered model using blockchain technology. Blockchain has the potential to revolutionize data control and management within existing EMR systems. The paper focuses on the Saudi Arabian context, proposing the utilization of the blockchain platform, IPFS (InterPlanetary File System), and smart contracts to address the prevalent issues in medical records. The proposed solution aims to empower patients by enabling them to control, protect, and share their medical data securely.

Smart contracts, defining the roles of participating entities, have been developed and tested to govern transactions and monitor procedures carried out on the EMRs. This research seeks to demonstrate the efficacy of blockchain in mitigating challenges associated with medical records in Saudi Arabia, ultimately fostering a more secure, patient-centric healthcare data management paradigm.

The subsequent sections of the paper are structured as follows: Section II provides a background review, offering a concise explanation of blockchain technology. In Section III, previous studies relevant to our research project are discussed. Section IV outlines the proposed solution, presenting the methodology employed. Section V delves into the smart contract functions, detailing the specific functionalities implemented in the Ethereum-based framework. Following this, Section VI discusses the findings and implications in the context of the proposed solution. Finally, Section VII encompasses the conclusion.

II. BACKGROUND

This section serves as a foundational guide, introducing key elements of the proposed research. We delve into blockchain technology, its decentralized architecture, and the pivotal role played by Peer-to-Peer (P2P) networks. Types of blockchains, including a focus on Ethereum blockchain, are explored, shedding light on their unique characteristics. The Ethereum blockchain, with its support for smart contracts and decentralized applications (DApps), emerges as a prominent player in this space. The significance of smart contracts in executing predefined rules on the blockchain is emphasized, highlighting their transformative potential. Additionally, we delve into the essential role of consensus protocols in governing the validation of transactions and maintaining the integrity of the blockchain. The section also explores the transformative IPFS, acknowledging its importance in reducing storage costs and providing an extra layer of privacy through data encryption. This comprehensive background lays the groundwork for understanding the technological choices and components integral to our research.

A. Blockchain Technology

Nakamoto is the name of the person who invented the blockchain technology [6]. His idea was based on creating a decentralized and encrypted currency to be used in financial transactions. Eventually, this technology was used in many different areas of life [7], such as the healthcare sector. A lot of research was conducted to study of applying blockchain technology to the current healthcare systems, and this research has reached to identify the pros and cons related to the use of this technology.

The benefit of using a blockchain is to facilitate the exchange of transactions between two parties without the need for an intermediary [6]. The process begins with creating a block whose hash is linked to the hash of previous block, and this method is repeated until the chain is complete. Each block in the blockchain includes records of transactions which will be verified by so-called miners. The contents of the block include previous block hash, timestamp, data, and nonce, collectively forming a secure and transparent ledger [8], [9].

The transaction could be data of any data type and the use of nonce is to control of the hash that is generated from the block. All these components will be hashed together to represent a block.

1) *P2P network*: A peer, which is a node in the blockchain network, contributes resources including storage, processing power, and bandwidth. These nodes are either for specific people or is available to everyone on blockchain because there are multiple types of blockchain network (as will be explained later). The most important characteristic of the nodes in the blockchain network is that the identity of each node remains safe, due to the public key belonging to each user is visible only to other peers in the network. The nodes also act as miners to verify the transaction before adding it to the chain.

2) *Role of miners*: As mentioned earlier, the miner's job is to verify the block before adding it to the blockchain network [10]. This does not guarantee the eligibility of the transaction, but rather to perform other additional work after that, which is called Proof-of-Work (PoW). Nonce will create a hash value that is less than the target difficulty level, and this is done through the PoW process. Then it is solved in a short period of time when the miner approaches the value below the target to get the rewards.

B. Types of Blockchain

Currently, there are three types of blockchain, depending on features such as network size, application, and type of algorithms, as follows:

1) *Public blockchain*: The public blockchain network is available for access by anyone on the network, and after joining, he can access the blocks' data and become authorized to mine. The use of pseudo-anonymous hash value is to create unique address to identify the users even in the public type of blockchain networks. Thus, people in the network are known by their addresses, not by their actual identity. And when someone wants to interact, such as adding or download a document such as EMRs, he must pay the costs of this interaction (transaction fees).

2) *Private blockchain*: Private and public blockchains are similar in many aspects such as process and algorithms, but the difference lies in the purpose. A private blockchain network is defined as a restrictive network, as it is designed in proportion to closed networks and based on the element of access control. Private blockchain networks are usually used for small businesses where the nodes are controlled to perform transactions and execute smart contracts. This type is used in many applications that require privacy and security, such as digital asset management, online voting, and supply chain management. In addition, the private blockchain networks require the approval from network administrators to allow people to join.

3) *Consortium blockchain*: Consortium blockchain networks combine the features of centralized and decentralized systems. Instead of being used to serve a single organization, the consortium blockchain is used on a large scale and in many organizations. This type is similar to private blockchain in that no one can access the network directly without registering, as that the approval of other organizations is required to perform any operation.

C. The Consensus Protocols

Blockchain, at its core, relies on consensus protocols [11] to ensure agreement among distributed participants on the state of the ledger. These protocols dictate how nodes or participants in a network reach a unanimous decision on the validity of transactions and the order in which they are added to the blockchain. The consensus mechanisms underpin the fundamental principles of trust, security, and decentralization in blockchain technology.

The choice of the consensus protocol is essential for designing blockchain systems tailored to specific use cases, whether in public, private, or consortium settings. It influences the network's characteristics, including security, efficiency, and governance, shaping the overall success and adoption of blockchain technology.

The most pivotal consensus mechanisms that have shaped the development of blockchain are:

1) *PoW*: PoW is a consensus algorithm widely employed in public blockchain networks like Ethereum. In this model, miners engage in solving complex mathematical puzzles, and the first to solve it gains the privilege to add a new block to the blockchain. While PoW ensures decentralization and robust security, its drawback lies in its energy-intensive nature, a concern that has prompted the exploration of alternative consensus mechanisms.

2) *Proof of Stake (PoS)*: PoS is an alternative consensus algorithm where validators are chosen to create new blocks based on the amount of cryptocurrency they hold and are willing to "stake" as collateral. This approach, compared to PoW, offers a more energy-efficient solution. Participants are incentivized to act in the best interest of the network by risking their held cryptocurrency as collateral.

3) *Proof of Authority (PoA)*: In the context of private blockchain networks, PoA emerges as a compelling consensus algorithm. Unlike PoW and PoS, PoA does not rely on competitive mining or staking. Instead, network participants, often identified and reputable entities, are designated as authorities. These authorities validate transactions, offering a more efficient and scalable solution for private consortium networks.

D. IPFS

The IPFS [12], [13], [14] stands as a revolutionary solution in healthcare data management, offering a distributed file system shared through a P2P network. In the context of storing medical records on the blockchain, IPFS plays a pivotal role in significantly reducing storage costs. Instead of storing voluminous medical data directly on the blockchain, IPFS allows for the storage of a unique hash that represents the content's identity. This hash serves as a pointer to the actual data stored in the IPFS network, optimizing the efficiency of the overall system.

Furthermore, the IPFS introduces an additional layer of privacy by enabling the encryption of data. This ensures that sensitive medical information remains confidential and secure throughout its lifecycle within the decentralized network. The ability to encrypt data in IPFS not only aligns with privacy regulations but also addresses the paramount importance of safeguarding patient information in healthcare settings.

In essence, by leveraging IPFS in conjunction with blockchain technology, the proposed framework not only enhances data security but also demonstrates a cost-effective approach to managing medical records. This integration allows for the creation of a robust and efficient healthcare data management system, aligning with the evolving needs of the healthcare sector in Saudi Arabia.

E. Ethereum Blockchain

Ethereum [15] stands as a pioneering blockchain platform renowned for its versatility in deploying DApps and smart contracts. Unlike Bitcoin, Ethereum extends beyond a mere cryptocurrency framework, providing a comprehensive environment for executing complex decentralized applications.

1) *Smart Contract*: The concept of smart contracts was introduced in 1997 by Nick Szabo [16], to conduct digital transactions securely over a network. Smart contracts [17], [18] are applications that are executed by people joining the blockchain network. Smart contracts are written by computer codes to implement pre-defined rules and conditions to keep transactions controlled. Current examples of projects based on the use of smart contracts [19] are the Ethereum platform and Hyperledger. These platforms allow transactions to be conducted reliably between anonymous parties without the need for a central authority. The Ethereum platform enables the creation of smart contracts tailored to the specific needs of any system within the network. The Ethereum uses Ether as a cryptocurrency. As for the term gas, it is used to measure the cost of any function that takes place in the smart contract. With regard to medical records, smart contracts allow the secure and reliable exchange of records.

2) *Geth (Go Ethereum)*: Geth serves as the official Go implementation of the Ethereum protocol. As a command-line interface tool, Geth facilitates interaction with the Ethereum network, enabling users to run a local Ethereum node, mine Ether, and interact with smart contracts. Geth plays a pivotal role in supporting the infrastructure of the Ethereum blockchain.

3) *DApps*: Decentralized applications [20], [21], or DApps, represent a new paradigm in application development. Unlike traditional applications that rely on centralized servers, DApps leverage blockchain technology, ensuring decentralized, transparent, and secure operations. These applications run on a P2P network of computers, eliminating the need for intermediaries and fostering a trustless environment.

III. LITERATURE REVIEW

In Estonia, the entire public health infrastructure is being operated using blockchain [22]. Through the application of blockchain technology, the costs of medical records will be reduced for the patient and other interested parties. Estonia is one of the first countries that uses blockchain technology in most government and commercial sector. The Estonian government has started making GovTech partnerships to apply blockchain to all industries in the region, so that the country become advanced in the field of technology.

Xia et al. [23], proposed a MeDShare system that addresses sharing a big data of medical records among a trust-less

environments. The system uses cloud services along with blockchain technology to store big data. The procedures start on MeDShare system by transferring data side by side from one entity to another and then recorded it in a tamper-proof manner. One of the advantages of the system is that when the permissions are violated, data access is canceled using a control mechanism designed by smart contracts. The system consists of four layers: First, user layer, which can access the data for research purposes. Second layer has a several of functions such as query, process, and respond to other queries on the system. Third layer, it process data requests in the infrastructure layer and performs computational operations on the data that was requested with the ability to monitor it, and this layer called data Structuring and Provenance layer. Fourth layer, existing databases that individual parties work on to accomplish certain tasks. This system guarantees data security by applying smart contracts. MeDShare system can be compared with the current systems that use cloud services. However, this system still depends on a third party.

Daraghmi et al. [24], suggested a MedChain system for managing EMRs. In this approach, the healthcare provider is responsible for creating, verifying, and adding new blocks to the blockchain, as well as allowing the patient to control their own data and granting or denying access to it. Smart contracts are written to control transaction times and monitor operations performed on medical records. Experiments conducted on MedChain system showed the efficiency of the proposal in response time, connection times and dealing with large data set. However, this system may encounter problems related to the fact that the database is central and pre-existing.

Dubovitskaya et al. [25], proposed a system to help cancer patients manage their medical records using the blockchain network. The role of the doctor and the patient is determined through membership service, through which the system verifies any doctor who joins the system, whether he is registered in the National Practitioner Data Bank or not. The patient's medical record and encryption keys are also signed with the membership service to ensure confidentiality. The data is then stored in the hospital database and in the cloud to grant access to other individuals in the network. A patient key is used to encrypt their data before it is stored in the cloud. The user is provided with an application programming interface (API) that transmits actions from the user to the nodes that are organized by the leader node to initiate the consensus protocol. However, as a result of storing data locally in hospitals and using cloud services, the patients cannot fully control their data, and this is one of the limitations that must be considered in this system.

Abid et al. [26], proposed NovidChain system to issue and verify the COVID-19 test/vaccine certificate using a private Blockchain network. They used a number of emerging technologies such as self-sovereign Identity platform called uPort. uPort is a mobile application that serves as an authentication mechanism for decentralized applications. They used IPFS to store data off-chain after it's encryption. The main process of NovidChain begins with Healthcare provider registration and service provider by creating an account on a self-managed Blockchain wallet then send the public key to the account belong to the healthcare authority. The healthcare authority then check if the Healthcare provider authorized or not, then adds his account to the blockchain. Next the user must create

a Blockchain account and install a self-managed Blockchain wallet for the healthcare provider to verify the user's official ID. After that, the user becomes eligible to get the COVID-19 vaccine from a Healthcare provider. The data is then encrypted, and its hash is stored in the blockchain. Finally, official physical ID is presented with a QR code to verify the health status of the individual in the registration step. They also explained that the NovidChain system ensures self-sovereign identity (SSI), as they adopted decentralized IDs (DIDs) for countersigning, signing and verifying COVID-19 credentials.

Sun et al. [27], proposed a system for sharing and storing medical records using smart contract technology. The system begins with encrypting the medical record by the doctor, adjusting the appropriate access settings, and then storing the encrypted record on IPFS. They demonstrate the benefit of using IPFS with blockchain technology in enabling healthcare providers to process and store a greater amount of medical data on IPFS rather than on the blockchain itself for savings in network bandwidth. After the medical records are encrypted and stored in the IPFS, they create an index of keywords to use in searching the encrypted records. Index words are stored in the Ethereum blockchain, where they can be accessed after the smart contract is published which in turn defines the way to access it in the distributed system.

Azaria et al. [28] proposed MedRec that enables patients to check a log of their health records. They used Ethereum's smart contracts to represent the data stored into individual nodes on the network. They used metadata about the medical record ownership, data integrity, and permissions by writing contracts. To deal with these properties, blockchain transactions carry signed and encrypted instructions for dealing with big data, and then the system inserts them into the blockchain network using three main types of contracts: First, Registrar Contract (RC), to link the Ethereum address identity with the corresponding identification strings, then change existing identities and organize the registration of new ones and append identity strings to the blockchain. Second, Patient-Provider Relationship Contract (PPR): which symbolizes any pairwise data stewardship interaction. Third, Summary Contract (SC): to determine medical record history by identifying the previous and current links of the participant with other nodes in the system.

Marcela et al. [29] proposed a hybrid system for protecting patient data privacy that involves combining blockchain technology with public key infrastructure. They store medical data on the blockchain using secret session keys. Initially, the digital certificate defines the main roles in the system. After the patient data and the session key are stored in the blockchain, these data are sent to the doctor, to ensure that the patient is the primary controller of access to his data. The second role is the role of the doctor, who can send and receive the patient's session key, but doctors are not authorized to share the session key among themselves. There is a pair of public and private keys that must be present for every user on the system so that every transaction made on the blockchain is assigned to the actor by the public and private keys of both the doctor and the patient shown in their certifications. To keep the security kernel of their proposal, they design their approach as a private permissioned network. In order to ensure the consistency and availability of transactions, the system converts the consensus

protocol to a three-phase commit protocol. The result showed that the transaction overload is appropriate compared to the number of transactions on the blockchain.

Sammeta et al. [30] developed a new model for transferring patient's data as well as making a diagnosis, called HBESDM-DLD model. The idea of this model is to take advantage of the Hyperledger blockchain-based in managing many orations such as encryption, data management, diagnosis, and optimal key generation. Firstly, the GTOA-based optimal key generation technique plus SIMON technology are used to encrypt the patient's medical data. Whether or not the patient is allowed to access to medical institutions is determined by the specific policy imposed by the global and local blockchain in partnership with the Hyperledger blockchain.

Azbeq et al. [31] presented a system named BlockMedCare which uses a set of technologies in addition to Blockchain, such as IoT and IPFS to manage health systems related to chronic diseases. The approach consists of three main sections patient side, medical team side and IPFS side. Initially, the patient's IoT device is registered using the owner's identity and MAC address on the blockchain network to identify the patient, and then the data collected from the patient's device is shared with the specialized medical team through the patient's smartphone. Hospitals also store a copy of the blockchain in addition to their ability to participate in the consensus process. The system enables the medical team to use patient data for procedures other than monitoring, including analysis and research. IPFS is used to store data as IoT devices collect a huge amount of data that cannot be stored only using blockchain. The system is used Clique PoA as a consensus algorithm to reach agreement and using the proxy re-encryption mechanism in addition to blockchain features to maintain the security of the system.

Alternative methods for leveraging blockchain in the management of medical records are detailed in [32], [33], [34].

IV. PROPOSED SOLUTION

In response to the evolving landscape of healthcare digitization in Saudi Arabia, this research presents a holistic solution aimed at revolutionizing the management of EHRs. The proposed system integrates a private Ethereum blockchain, a private IPFS, and a DApp developed using React with web3.js integration. The system architecture adopts a PoA consensus mechanism, utilizing the Geth client for Ethereum, and JSON-RPC for communication. This multifaceted approach aims to address the existing challenges in terms of security, scalability, and user accessibility within the Saudi Arabian healthcare ecosystem.

Fig. 1 illustrates the blockchain-based framework designed to enhance security and empowering patients with control over their medical records.

A. Blockchain Infrastructure

This section introduces the foundational elements that shape the proposed blockchain-based healthcare management system. Central to this infrastructure is the adoption of a private Ethereum blockchain, leveraging a PoA consensus mechanism for enhanced efficiency and security. This choice aligns with

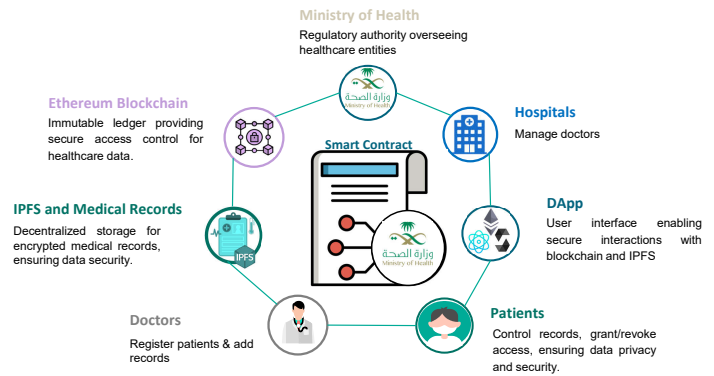


Fig. 1. The proposed blockchain-based framework to enhance security and afford patients control over their medical records.

the sensitive nature of healthcare data, emphasizing privacy and trust. The node structure mirrors the Saudi Arabian healthcare system, strategically designating healthcare authorities, hospitals, and clinics as nodes, ensuring compatibility with the existing infrastructure. Smart contracts form the core of the system, defining hierarchical rules for entity registration, with the Ministry of Health holding registration authority over Local Health Authorities, which, in turn, register entities such as hospitals and clinics. This controlled registration mechanism, cascading from higher to lower authorities, mitigates security risks. The DApp, built on the React framework, acts as the user interface, seamlessly integrating with the Ethereum blockchain through the web3.js library. This DApp serves as a user-friendly gateway for healthcare authorities, doctors, and patients to manage registrations, access medical records, and interact with smart contracts. The subsequent discussions in the section delve into the encryption and IPFS integration processes, ensuring the secure issuance and storage of patients' medical records.

The different elements that shape the proposed blockchain-based healthcare management system are:

- Private Ethereum network: The proposed system adopts a private Ethereum blockchain to ensure data security and privacy. Leveraging a PoA consensus mechanism enhances the overall efficiency of the network. Unlike public blockchains, PoA networks consist of a known set of nodes, each with a proven identity, reducing the risk of malicious activities. This choice aligns with the sensitivity of healthcare data, emphasizing confidentiality and trust among participating entities.
- Node structure: Nodes within the private Ethereum network are strategically structured to mirror the Saudi Arabian healthcare system. Healthcare authorities, hospitals and clinics are designated as nodes. This design not only aligns with the existing healthcare infrastructure but also facilitates scalability and streamlined interactions.
- Smart contracts: At the core of the proposed system are smart contracts that define the rules and interactions within the healthcare network. These contracts account for the hierarchical structure of healthcare

authorities, wherein only higher authorities possess the privilege to register the different entities. The Ministry of Health holds the authority to register Local Health Authorities, which, in turn, have the capability to register various healthcare entities such as hospitals and clinics. Within this framework, hospitals and clinics are empowered to register doctors, and once registered, doctors assume the responsibility of registering patients. This registration mechanism ensures a controlled and secure onboarding process, mitigating risks associated with unauthorized access and denial-of-service (DOS) attacks.

- DApp: The user interface of the proposed system is developed as a decentralized application using the React framework. This DApp integrates with the Ethereum blockchain through the web3.js library, providing a user-friendly experience for healthcare authorities, doctors, and patients. The DApp serves as the gateway for managing registrations, accessing medical records, and interacting with smart contracts seamlessly.
- Encryption and IPFS integration: This is the pivotal aspect of ensuring the confidentiality and integrity of medical records within the proposed system. To achieve this, a robust encryption mechanism is employed, safeguarding the sensitive patient information contained in medical records. The encryption process involves the generation of a unique symmetric key for each medical record, ensuring that access is restricted to authorized entities only. These encrypted medical records are then securely stored on the IPFS. The integration with IPFS not only enhances data availability and reliability but also significantly reduces storage costs in the blockchain. This combination of encryption and IPFS integration establishes a secure and efficient framework for handling and storing medical records, ensuring the utmost privacy and integrity of patient information.

B. The Patient Registration Flow

To enable a doctor to register a patient through the DApp, including the creation and communication of account details to the patient, and the addition of the patient to the list of patients in the blockchain using the corresponding smart contract, a multi-step process is implemented. Below are the detailed steps:

The detailed patient registration flow, as presented in Fig. 2, is as follows:

- 1) Doctor initiates registration: The doctor, using the DApp, initiates the registration process for a specific patient.
- 2) Patient details entry by doctor: The doctor enters the necessary patient details into the DApp. This could include the patient's national ID, name, date of birth, and any other required information.
- 3) Generate Ethereum account: The DApp generates a new Ethereum account for the patient, including the Ethereum address and private key.
- 4) Register the patient: The DApp interacts with the smart contract on the private Ethereum blockchain.

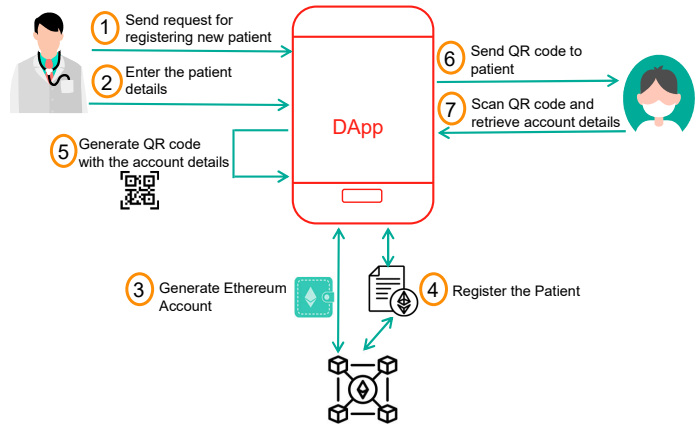


Fig. 2. The patient registration flow.

The smart contract includes a function to add a new patient to the list of patients, recording their their relevant details.

- 5) QR code generation: The DApp generates a QR code containing the Ethereum account details along with the patient's information.
- 6) DApp provides QR code to patient: The DApp communicates the generated QR code to the patient by sending it through a secure channel.
- 7) Patient scans QR code: The patient uses a mobile device to scan the QR code and extract the Ethereum account details (address and private key). Then, the patient securely stores the Ethereum account details.

Following these steps, patient registration is completed, ensuring secure access to their Ethereum account for interactions with the private blockchain. It's essential to highlight that the patient's access is confined to their individual medical records, with interactions strictly governed by the smart contract.

C. The Patient's Medical Record Issuing Flow

Ensuring the confidentiality and integrity of medical records is a pivotal aspect of the proposed system. The process of issuing a patient's medical record and storing it on IPFS involves series of secure steps. These steps are described in Fig. 3 and detailed as follows:

- 1) Medical record upload: The process begins with the doctor initiating the upload of the patient's medical record to the blockchain.
- 2) Symmetric key generation: The DApp generates a unique symmetric key for each patient and for each new diagnosis. This approach ensures that access to medical records is controlled and traceable.
- 3) Record encryption: The patient's medical record is encrypted using the generated symmetric key. This encryption guarantees that only authorized entities can decipher and access the sensitive information.
- 4) IPFS upload: The encrypted medical record documents are securely uploaded to the IPFS network and the corresponding Content Identifier (CID) is then generated. This step enhances confidentiality, data integrity and accessibility.

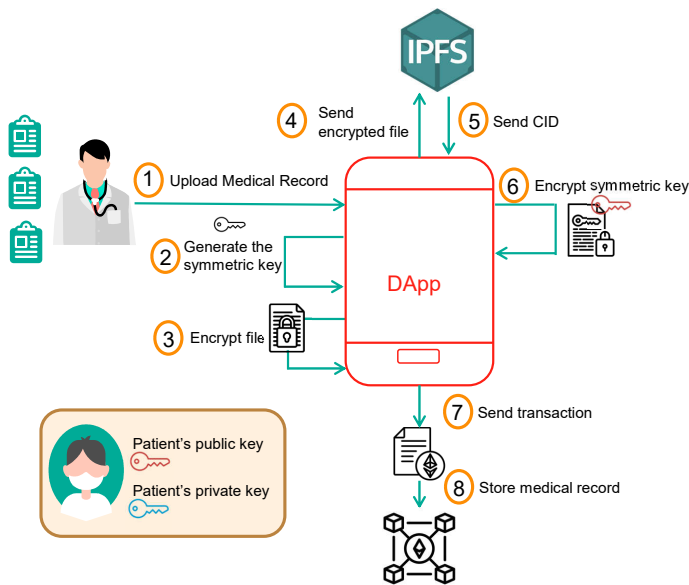


Fig. 3. Medical records issuing.

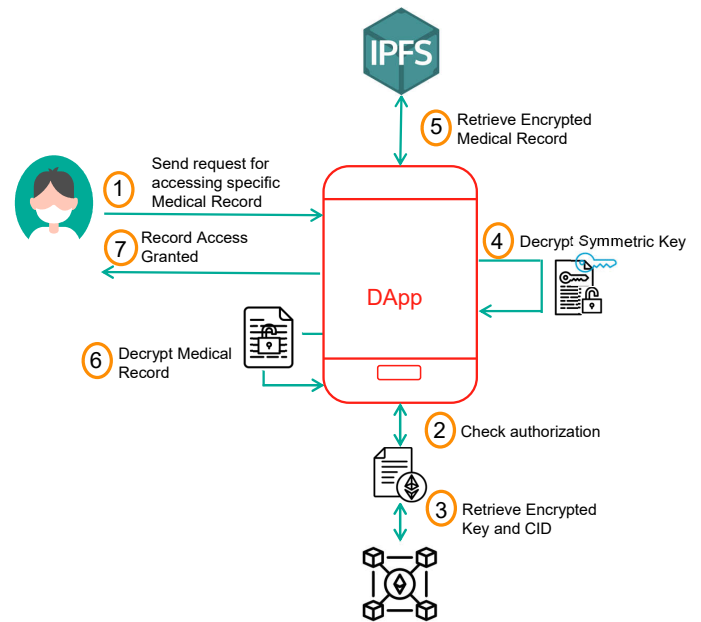


Fig. 4. The retrieval flow for the patient's medical record.

- 5) Send CID to DApp: The CID generated by IPFS is sent to the DApp, creating a reference point for accessing the complete medical record.
- 6) Key encryption: The symmetric key undergoes encryption with the patient's public key, sourced from their securely stored data on the blockchain. This step reinforces data security, ensuring that only the patient possesses the means to decrypt their medical records.
- 7) Initiate transaction: To securely store the encrypted symmetric key and the IPFS CID for every new set of patient medical records, it is imperative to initiate a new transaction on the blockchain through the execution of a smart contract.
- 8) Blockchain storage: This method ensures the immutability of both the key and CID associated with each medical record, thereby streamlining the secure retrieval of data from the IPFS.

D. The Medical Record Retrieval Flow

This section provides a detailed exploration of the steps involved in patients accessing their medical records within the proposed blockchain-based healthcare management system. Illustrated through Fig. 4, this section explains how patients can securely retrieve their medical information using the DApp, emphasizing the integration of security measures and a user-friendly interface for a controlled and confidential experience.

The steps involved in the medical records retrieving process are:

- 1) Initiate request: The patient or an authorized entity initiates a request for accessing specific medical records stored on the blockchain.
- 2) Authenticate identity: The system authenticates the identity of the requester, ensuring that only authorized individuals or entities can proceed with the retrieval process.

- 3) Retrieve encrypted key and CID: The DApp retrieves both the encrypted symmetric key and the CID associated with the requested medical record, which were initially stored in the blockchain during the record creation process.
- 4) Decrypt symmetric key: The requester, possessing the necessary decryption capabilities, decrypts the symmetric key using their private key. This step ensures secure access to the encrypted medical record.
- 5) Retrieve encrypted medical record from IPFS: The authorized party communicates with IPFS using the CID to retrieve the corresponding encrypted medical record from storage.
- 6) Decrypt medical record: The decrypted symmetric key is applied to decrypt the medical record, revealing the patient's health information in its original form.
- 7) Record access granted: The authorized entity now has access to the patient's medical record, facilitating the retrieval process securely and efficiently.

This comprehensive process ensures that sensitive health data remains confidential, with access granted only to authenticated and authorized entities while maintaining the integrity of the information stored on the blockchain and IPFS.

E. Granting Authorization to Patient's Medical Records

This section unveils the steps involved when patients grant access to their medical records to authorized entities. Illustrated through Fig. 5, this section elucidates the steps and security measures embedded in the process, ensuring controlled and secure access permissions for healthcare practitioners and authorized entities.

The detailed steps for granting access to patient's medical records are:

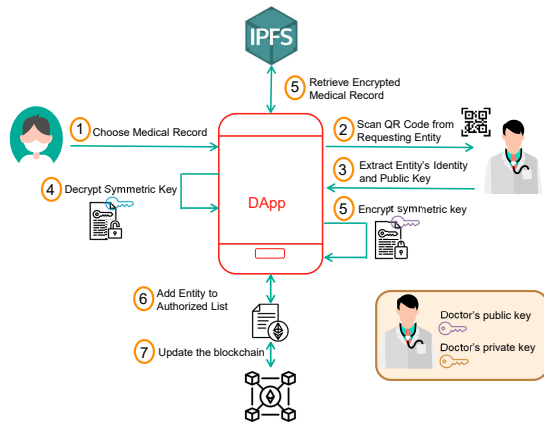


Fig. 5. Flow of authorizing access to patient's medical records.

- 1) Choose medical records: The DApp displays a list of the patient's health records. The patient initiates the process by selecting specific medical records for which access is to be granted.
- 2) Scan QR code from requesting entity: The patient scans the QR code provided by the entity requesting access to the medical records.
- 3) Extract entity's identity and public key: From the scanned QR code, the patient extracts information about the requesting entity's identity. The public key of the entity is retrieved from the QR code.
- 4) Decrypt symmetric key with patient's private key: The patient decrypts the symmetric key associated with the requested medical record using their own private key.
- 5) Encrypt symmetric key with entity's public key: The patient takes the decrypted symmetric key and encrypts it using the public key of the requesting entity.
- 6) Add entity to authorized list: The patient adds the address (identity) of the requesting entity to the list of authorized entities for the specific medical record, along with the encrypted symmetric key, now tied to the entity's public key.
- 7) Update blockchain: The blockchain is updated with the changes, reflecting the newly added entity to the authorized list and the associated encrypted symmetric key. This ensures a transparent and immutable record of access permissions.

This flow outlines the patient's actions, the interaction with the requesting entity, encryption and decryption processes, and the retrieval of medical records from the IPFS. The use of public and private keys, along with the secure exchange of encrypted symmetric keys, ensures controlled access to patient data while maintaining its confidentiality and integrity.

V. SMART CONTRACT FUNCTIONS

In this section, we delve into the heart of the proposed blockchain-based healthcare system's architecture-the implementation of our smart contract using the Solidity programming language. This smart contract encapsulate the rules and interactions governing the entire healthcare network. We explore the key functions embedded in these contract, each

meticulously designed to manage entity registrations, handle medical records, and enforce access control. The transparency and immutability of blockchain technology, combined with the programmability of smart contract, form the backbone of the secure and efficient healthcare infrastructure we propose.

A. Implementation of the Entities Registration Process

```

1 // SPDX-License-Identifier: MIT
2 pragma solidity >=0.6.12 <0.9.0;
3
4 contract HealthRecords {
5
6     address public ministryAddress;
7
8     enum EntityType { MinistryOfHealth,
9         LocalAuthority, Hospital, Clinic, Doctor }
10
11     struct Entity {
12         string name;
13         address entityAddress;
14         address registeringEntity;
15         EntityType entityType;
16     }
17
18     mapping(address => Entity) public entities;
19     mapping(address => bool) public
20         isEntityRegistered;
21     mapping(EntityType => mapping(EntityType => bool
22         )) public entityRegistrationPermissions;
23
24     constructor() {
25         ministryAddress = msg.sender;
26         isEntityRegistered[msg.sender] = true;
27         entities[msg.sender].name = "
28             MinistryOfHealth" ;
29         entities[msg.sender].entityAddress =
30             ministryAddress;
31         entities[msg.sender].registeringEntity =
32             ministryAddress;
33         entities[msg.sender].entityType = EntityType
34             .MinistryOfHealth;
35     }

```

Listing 1: Entities and Constructor

```

1 modifier onlyMinistryOfHealth() {
2     require(msg.sender == ministryAddress, "Only
3         the Ministry of Health can call this
4         function");
5     };
6
7 modifier onlyDoctor() {
8     require(isDoctorRegistered[msg.sender], "
9         Only a Doctor can call this function");
10    };
11
12 modifier onlyPatient() {
13     require(isPatientRegistered[msg.sender], "
14         Only a Patient can call this function");
15    };
16
17 // Modifier for checking entity registration
18 // permission
19 modifier onlyAllowedEntity(EntityType
20     registeringEntityType, EntityType entityType)
21 {
22     require(entityRegistrationPermissions[
23         registeringEntityType][entityType], "Entity
24         registration not allowed");

```

```

21  _;
22  }
    
```

Listing 2: List of modifiers

```

1  // New function for setting entity registration
2  permissions
3  function setEntityRegistrationPermission(
4      EntityType registeringEntityType, EntityType
5      entityType, bool permission)
6  external
7  onlyMinistryOfHealth
8  {
9      entityRegistrationPermissions[
10         registeringEntityType][entityType] =
11         permission;
12     }
13
14 function registerEntity(
15     string memory _name,
16     EntityType _entityType,
17     address _entityAddress
18 ) external onlyAllowedEntity(msg.sender).
19     entityType, _entityType) {
20     require(!isEntityRegistered[_entityAddress], "
21         Entity is already registered");
22
23     Entity memory newEntity = Entity({
24         name: _name,
25         entityAddress: _entityAddress, // Address
26         of the entity being registered
27         registeringEntity: msg.sender, // Address
28         of the entity initiating the
29         registration
30         entityType: _entityType
31     });
32
33     entities[_entityAddress] = newEntity;
34     isEntityRegistered[_entityAddress] = true;
35 }
    
```

Listing 3: Process for registering entities

After deploying the smart contract, the pivotal setEntityRegistrationPermission function comes into play for configuring permissions in the entity registration process. The initial phase entails granting authorization to the Ministry of Health, empowering it to add local authorities, hospitals, or any other entities. This authorization can be established by either hardcoding it within the constructor or invoking the setEntityRegistrationPermission function, given that the Ministry of Health is exclusively empowered to define permissions, as ensured by the onlyMinistryOfHealth modifier. In the illustrated example showcased in Fig. 6, the Ministry of Health (enumerated as zero in the entities enum type within the smart contract) is accorded the privilege to add hospitals, denoted by the number two.

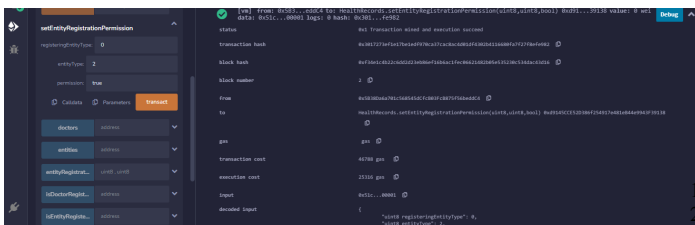


Fig. 6. Set entity registration permission.

Once the Ministry of Health has been granted the capability to add hospitals, the subsequent step involves registering the hospital's information and incorporating it into the list of hospitals. This is achieved by interacting with the smart contract through the invocation of the registerEntity function, as exemplified in Fig. 7. The crux of this process lies in the _entityAddress parameter, serving as the unique identifier for the hospital, corresponding to its blockchain address encapsulating account information. This identical procedure is employed for registering various entities, ensuring the permission to register a specific entity type through the onlyAllowedEntity modifier, inputting the entity details, and subsequently adding it to the blockchain via a smart contract request.



Fig. 7. Hospital registration.

The DApp interfaces play a crucial role in facilitating seamless interactions between different entities within the proposed blockchain-based healthcare management system. The interfaces for the Ministry of Health empower it to oversee and regulate the registration process of various healthcare entities. Through the interface presented in Fig. 8, the Ministry of Health gains the ability to list all registered entities, ensuring transparency in the system. Moreover, it can set permissions for entity registration, as shown in Fig. 9, enabling fine-grained control over the onboarding process. These functionalities empower the Ministry of Health to maintain a structured and secure healthcare ecosystem.

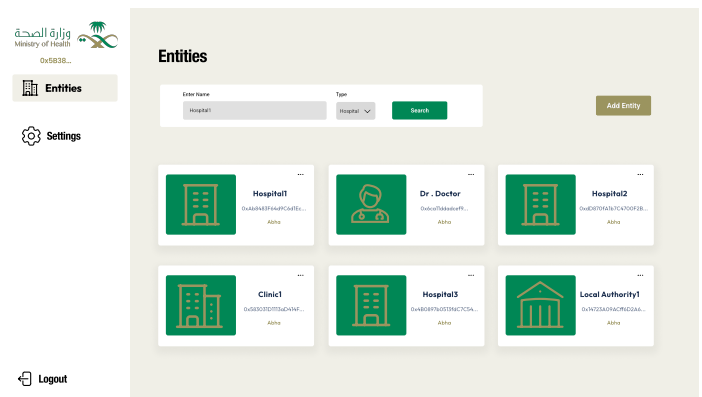


Fig. 8. List of entities

B. Implementation of the Doctors Registration Process

```

struct Doctor {
    string name;
    string phoneNumber;
    address doctorAddress; // Ethereum account
    address of the doctor
}
    
```

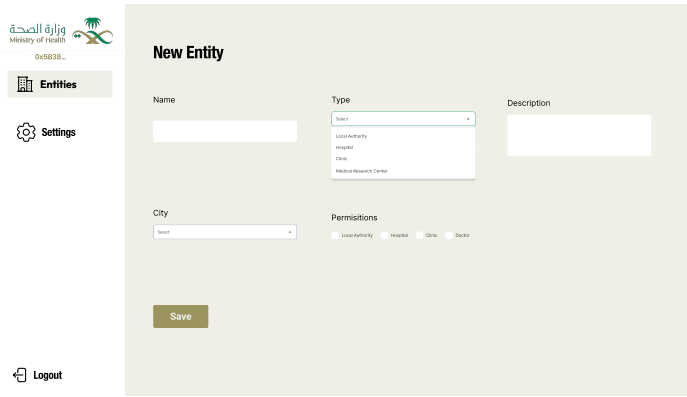


Fig. 9. Entity registration.

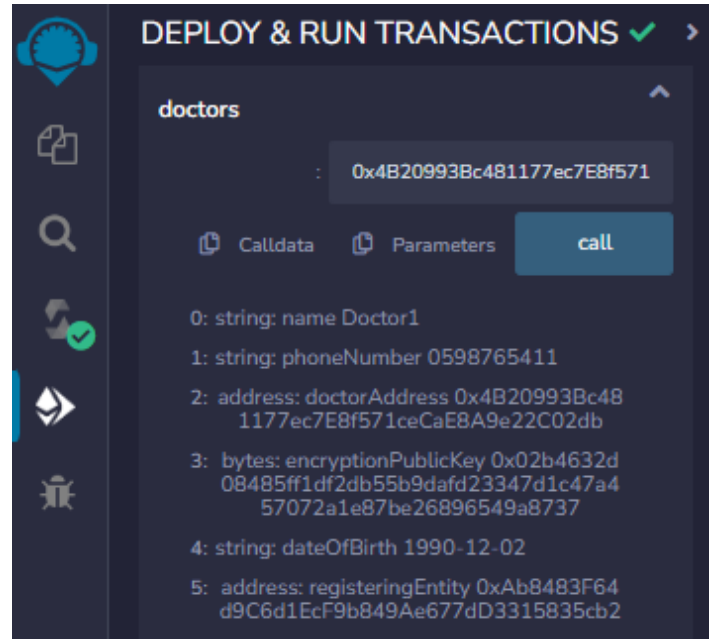


Fig. 10. Doctor registration.

```

5     bytes encryptionPublicKey; // Public key
      used for encryption
6     string dateOfBirth;
7     address registeringEntity; // Ethereum
      address of the entity who registered the
      doctor
8   }
9
10    mapping(address => Doctor) public doctors;
11    mapping(address => bool) public
      isDoctorRegistered;
12
13
14    function registerDoctor(
15        string memory _name,
16        string memory _phoneNumber,
17        address _doctorAddress,
18        bytes memory _encryptionPublicKey,
19        string memory _dateOfBirth
20    ) external onlyAllowedEntity(entities[msg.sender].
      entityType, EntityType.Doctor) {
21        require(!isDoctorRegistered[_doctorAddress], "
      Doctor is already registered");
22
23        Doctor memory newDoctor = Doctor({
24            name: _name,
25            phoneNumber: _phoneNumber,
26            doctorAddress: _doctorAddress,
27            encryptionPublicKey:
      _encryptionPublicKey,
28            dateOfBirth: _dateOfBirth,
29            registeringEntity: msg.sender
30        });
31
32        doctors[_doctorAddress] = newDoctor;
33        isDoctorRegistered[_doctorAddress] = true;
34    }

```

Listing 4: Process for registering doctors

Permitted entities have the capability to add a new doctor by providing details such as the doctor's name, email, and other pertinent information. Notably, as illustrated in Fig. 10, the doctor's `_encryptionPublicKey` is included. This key enables the doctor to access patients' medical records with their consent. The process involves the patient decrypting the encrypted symmetric key of a specific medical record with their private key and subsequently encrypting the symmetric key using the doctor's public key. Consequently, the doctor can decrypt the encrypted symmetric key and access a specific patient's medical record using his private key.

The DApp interfaces for hospitals empower them by providing the capability to list all registered doctors, see Fig. 11. This functionality enhances the efficiency of hospitals in managing their medical staff. The second interface, presented in Fig. 12, enables hospitals to seamlessly register new doctors. Through this interface, hospitals can input and submit all necessary information about a new doctor. These interfaces collectively contribute to the effective coordination and administration of healthcare services within the proposed system, promoting a well-organized and responsive healthcare environment.

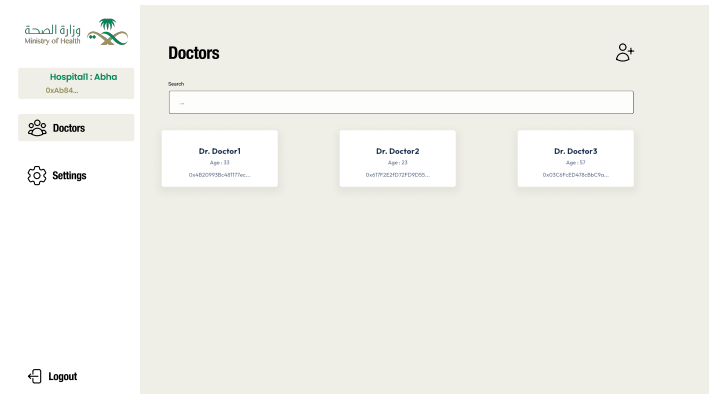


Fig. 11. List of doctors.

C. Implementation of the Patients Registration Process

```

struct Patient {
1     string name;
2     string phoneNumber;
3     address patientAddress; // Ethereum account
      address of the patient
4     bytes encryptionPublicKey; // Public key
      used for encryption
5 }

```

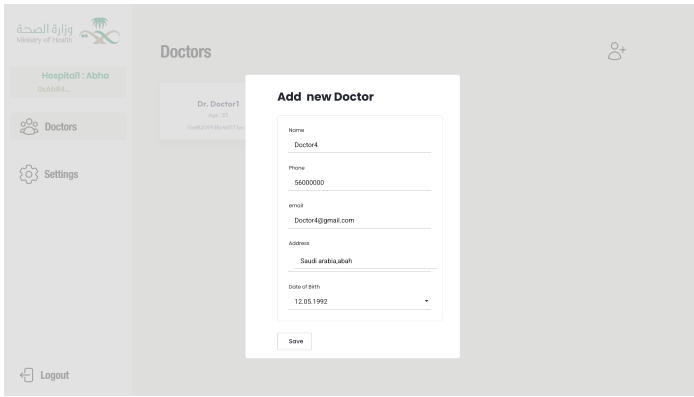


Fig. 12. Register new doctor.

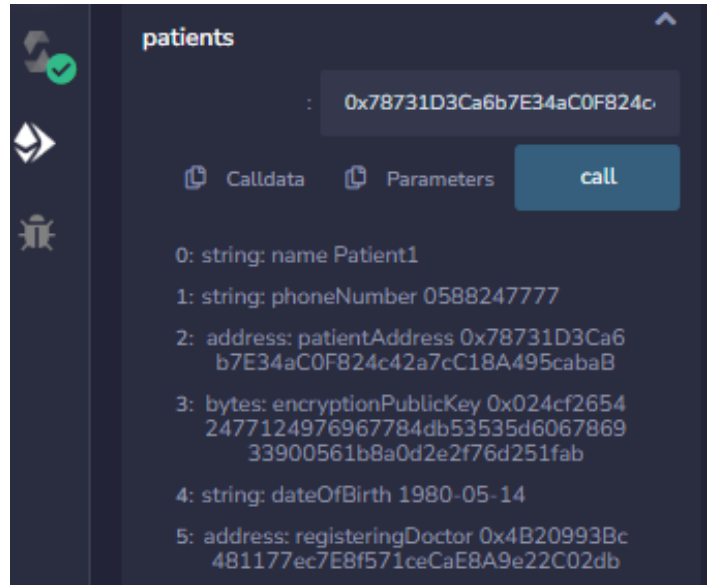


Fig. 13. Patient registration.

```

6      string dateOfBirth;
7      address registeringDoctor; // Ethereum
      address of the doctor who registered the
8      patient
9  }
10     mapping(address => Patient) public patients;
11     mapping(address => bool) public
      isPatientRegistered;
12
13
14
15     function registerPatient (
16         string memory _name,
17         string memory _phoneNumber,
18         address _patientAddress,
19         bytes memory _encryptionPublicKey,
20         string memory _dateOfBirth
21     ) external onlyDoctor {
22         require (isDoctorRegistered[msg.sender], "
      Doctor is not registered");
23         require (!isPatientRegistered[_patientAddress
      ], "Patient is already registered");
24
25         Patient memory newPatient = Patient({
26             name: _name,
27             phoneNumber: _phoneNumber,
28             patientAddress: _patientAddress,
29             encryptionPublicKey:
      _encryptionPublicKey,
30             dateOfBirth: _dateOfBirth,
31             registeringDoctor: msg.sender
32         });
33
34         patients[_patientAddress] = newPatient;
35         isPatientRegistered[_patientAddress] = true;
36     }

```

Listing 5: Process for registering patients

Upon successful registration of the doctor by the hospital, the doctor acquires the capability to register new patients. Subsequently, the patient is included in the patient list by invoking the smart contract through the registerPatient function, as depicted in Fig. 13. The inclusion of the onlyDoctor modifier ensures that only authorized doctors can register patients. The doctor inputs the patient's information, which is then securely stored on the blockchain.

The designated interfaces for doctors in the DApp play a pivotal role in facilitating efficient patients management and registration processes. The first interface, shown in Fig. 14,

empowers doctors by providing the functionality to list all registered patients under their care. This feature enhances the doctor's ability to access and review patient information seamlessly, contributing to informed and personalized healthcare delivery. The second interface, presented in Fig. 15, serves as a key tool for doctors to register new patients. Through this interface, doctors can input and submit essential details about a new patient, ensuring a systematic and secure process for patient onboarding. In addition, the DApp initiates the creation of a new Ethereum account for the patient. Subsequently, the DApp communicates the Ethereum account details to the respective patient.

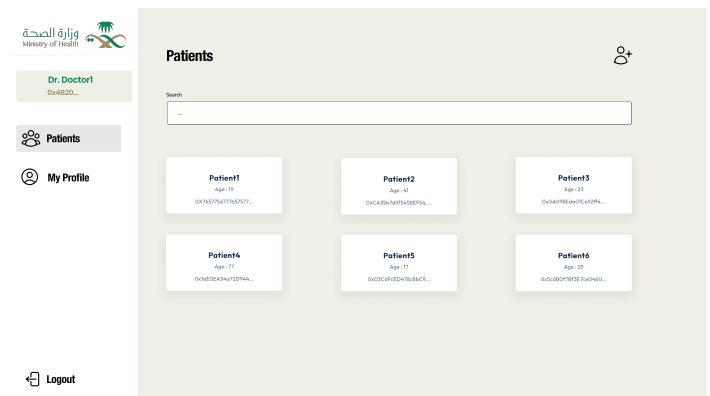


Fig. 14. List of patients.

D. Implementation of the Medical Records Issuing Process

```

1 struct MedicalRecord {
2     uint256 id;
3     address doctor;
4     uint256 time;
5     address patientAddress;
6     bytes encryptedSymmetricKey;
7     bytes patientPublicKey;
8     string ipfsCID;

```

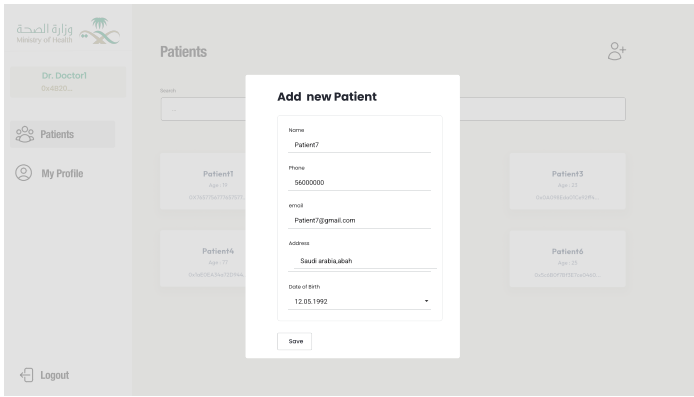



Fig. 15. Register new patient.

record.

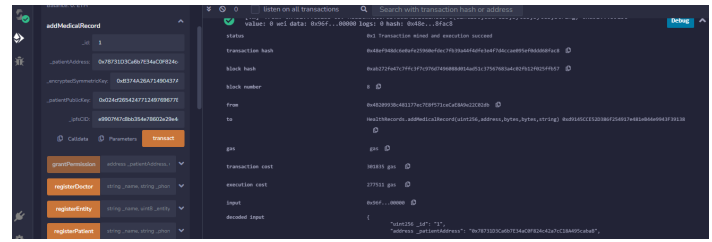


Fig. 16. Add medical record.

The interfaces designated for doctors within the proposed system encapsulate critical functionalities in managing and contributing to the medical records ecosystem. The first interface, shown in Fig. 17, empowers doctors to access and review medical records by listing all records associated with a specific patient. This functionality ensures efficient retrieval and oversight of a patient's medical history. In tandem, the second interface, illustrated in Fig. 18, equips doctors to actively contribute to the patient's medical records database. This involves a comprehensive process initiated by the DApp, orchestrating the generation of a symmetric key, encryption of medical records, and seamless integration with IPFS for secure storage.

```

9 }
10
11 // Mapping to store medical records for each
12 mapping(address => mapping(uint256 =>
13     MedicalRecord)) public patientMedicalRecords
14 ;
15
16 // Mapping to store permissions for each medical
17 record
18 mapping(address => mapping(uint256 => mapping(
19     address => bytes))) public recordPermissions
20 ;
21
22 // Function to add a medical record, restricted
23 to doctors
24 function addMedicalRecord(
25     uint256 _id,
26     address _patientAddress,
27     bytes memory _encryptedSymmetricKey,
28     bytes memory _patientPublicKey,
29     string memory _ipfsCID
30 ) external onlyDoctor {
31     require(!isEntityRegistered[msg.sender], "
32         Caller is not registered");
33     // Check if the patient is registered
34     require(isPatientRegistered[_patientAddress
35         ], "Patient is not registered");
36
37     // Add the medical record to the patient's
38     records
39     patientMedicalRecords[_patientAddress][_id]
40     = MedicalRecord({
41         id: _id,
42         doctor: msg.sender,
43         time: block.timestamp,
44         patientAddress : _patientAddress,
45         encryptedSymmetricKey:
46             _encryptedSymmetricKey,
47         patientPublicKey: _patientPublicKey,
48         ipfsCID: _ipfsCID
49     });
50 }

```

Listing 6: Process for adding medical records

In Fig. 16, it is depicted that the patient's medical record details, including essential components like the `_ipfsCID` and the `_encryptedSymmetricKey`, will be entered through the account of the doctor. The `_ipfsCID` serves as a reference for retrieving the encrypted medical record from the IPFS, while the `_encryptedSymmetricKey` specifies the used encryption key, ensuring the confidentiality and privacy of the medical

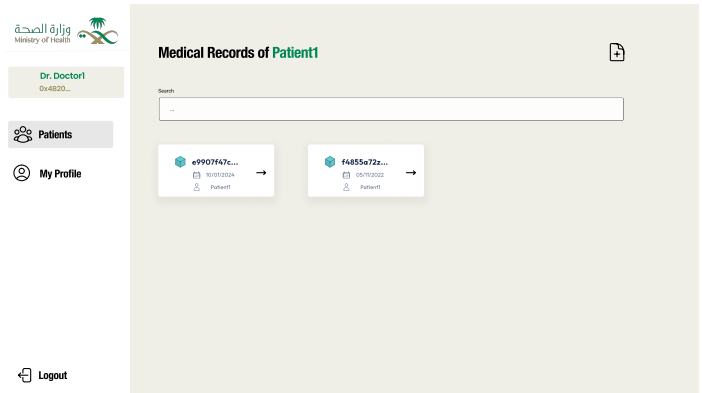


Fig. 17. List of medical records.

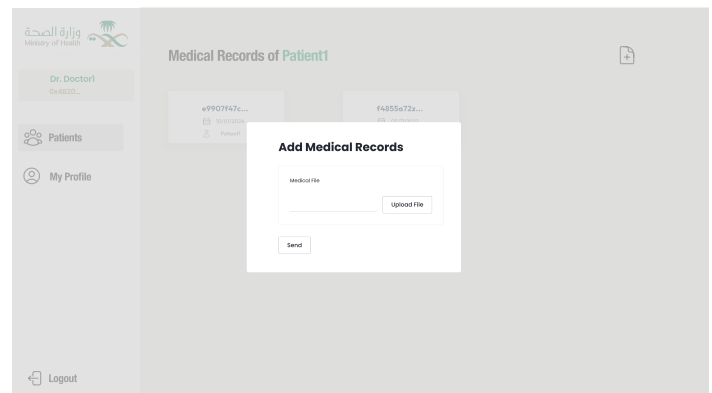


Fig. 18. Add new medical records.

E. Implementation of the Process for Managing Access to Medical Records

```
1 // Function to grant permission to an entity to
2 // access a specific medical record
3 function grantPermission(
4     address _patientAddress,
5     uint256 _recordId,
6     address _doctorAddress,
7     bytes memory _encryptedSymmetricKey
8 ) external onlyPatient {
9     // Grant permission to the doctor
10    recordPermissions[_patientAddress][_recordId]
11    [_doctorAddress] =
12    _encryptedSymmetricKey;
13
14 // Function to revoke permission from an entity
15 // for a specific medical record
16 function revokePermission(
17     address _patientAddress,
18     uint256 _recordId,
19     address _doctorAddress
20 ) external onlyPatient {
21     // Revoke permission from the entity
22     delete recordPermissions[_patientAddress][
23     _recordId][_doctorAddress];
24 }
```

Listing 7: Process for managing access to the medical records

In the process of granting access to a specific medical record, the patient plays a central role in controlling the confidentiality and accessibility of their health data. Initiated by the patient, this action involves invoking the grantPermission function, a function guarded by the onlyPatient modifier to ensure that only the respective patient can execute this operation.

The key parameters in this operation include:

- **_patientAddress:** This parameter identifies the Ethereum address of the patient initiating the permission grant.
- **_recordId:** Serving as a unique identifier, this parameter denotes the specific medical record the patient intends to share.
- **_doctorAddress:** The Ethereum address of the doctor for whom the patient wishes to grant access to the designated medical record.
- **_encryptedSymmetricKey:** This parameter holds the encrypted symmetric key, by using the doctor's public key, associated with the medical record, ensuring that only the intended doctor can decrypt and access the sensitive health information.

By specifying these essential details, depicted in Fig. 19, the patient leverages the grantPermission function to securely share access to their medical record with a designated doctor, fostering a patient-centric approach to healthcare data management.

The process of revoking access to a specific medical record is a crucial aspect of patient-centric healthcare data management. Executed exclusively by the patient through the revokePermission function, this operation is safeguarded by

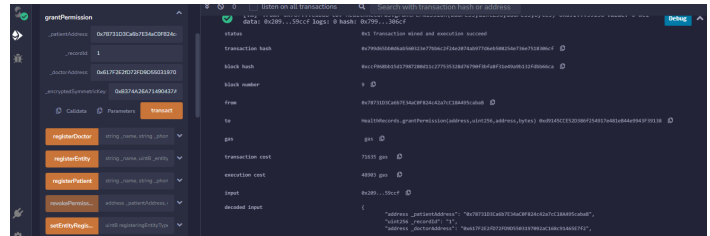


Fig. 19. Enabling the doctor to access the medical record.

the onlyPatient modifier, ensuring that only the authorized patient can control access to their health information. The pertinent parameters in this revocation process include the _patientAddress, the _recordId, and the _doctorAddress. By invoking the revokePermission function, the patient can selectively remove access privileges from a designated doctor, effectively enhancing the patient's control over the confidentiality and security of their medical records. This patient-driven approach empowers individuals to actively manage and regulate access to their health information, aligning with the principles of privacy and data security in the healthcare domain.

In Fig. 20, the illustration demonstrates the patient's capability to revoke a doctor's access to their medical record by deleting the associated medical record data from the doctor's list of accessible records.

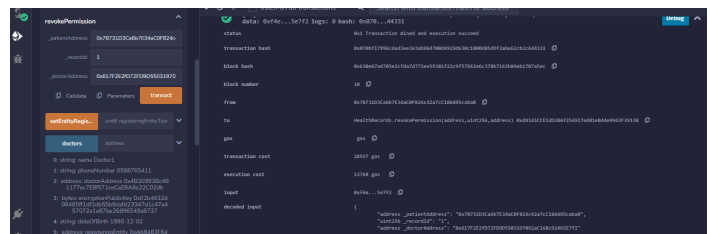


Fig. 20. Revoke the access.

The patient interfaces, shown in Fig. 21, within the envisioned healthcare system afford individuals a comprehensive toolset for managing and accessing their medical records. The first interface provides patients with a detailed listing of their medical records. Crucially, this feature enables patients to review the doctors who currently possess access to each record, empowering them to make informed decisions about their healthcare providers.

Moreover, these interfaces enable patients to actively manage access permissions to their medical records. This involves granting access to new doctors, while also offering the ability to selectively revoke access when needed. By seamlessly integrating cryptographic principles and smart contract functionality, this patient-centric approach ensures the confidentiality and privacy of medical records. Patients are empowered with the agency to determine who can contribute to their healthcare information and underlines the commitment of the system to prioritizing user control and data privacy.

In addition to the core functionalities, the smart contract encompasses several functions that contribute to the overall robustness and flexibility of the proposed system, such as

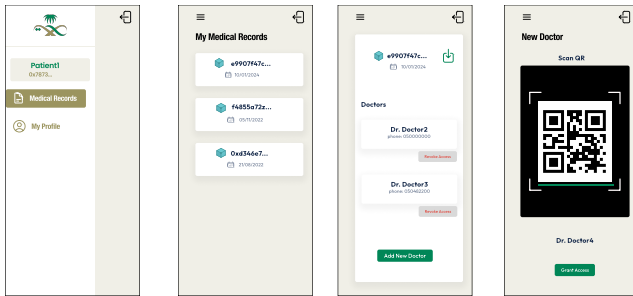


Fig. 21. Managing access to medical records.

functions that enable patients to delete specific medical records from the blockchain, ensuring a patient-centric approach to data management.

VI. DISCUSSION

This section delves into a comprehensive analysis of the proposed system, exploring various facets such as architecture, security considerations, and frameworks employed.

- **Architecture:** The proposed system adopts a decentralized architecture built on a private Ethereum blockchain. This choice is motivated by the need for transparency, immutability, and distributed control. The utilization of a PoA consensus mechanism, implemented through the Geth client, enhances scalability and efficiency in a closed and permissioned healthcare network. The private Ethereum blockchain is primarily employed for defining rules to manage entities, such as hospitals, clinics, doctors, and patients, facilitating secure and controlled interactions within the healthcare network, while medical records, sensitive in nature, remain off-chain to address privacy concerns and storage limitations on the blockchain.
- **Frameworks:** The system integrates several key frameworks to facilitate its functionality. The Ethereum blockchain, along with the use of smart contract, forms the backbone for managing entities, doctors, patients, and medical records. The use of IPFS augments data storage capabilities, enabling decentralized and secure storage of medical records. React is employed on the front end to develop a user-friendly DApp, while Web3.js connects the DApp to the Ethereum blockchain, allowing seamless interaction with smart contract.
- **Security considerations:** Security is paramount in healthcare systems, especially when dealing with sensitive patient data. The use of a private Ethereum blockchain enhances security by restricting access to authorized entities, mitigating the risk of unauthorized access or tampering. Encryption plays a pivotal role in securing medical records, with each record encrypted using a symmetric key. Patient-controlled access through encrypted keys ensures that only authorized individuals, namely patients and authorized

doctors, can decrypt and access medical records. Additionally, the private IPFS ensures that data retrieval is restricted to registered patients and doctors, adding an extra layer of security.

- **Scalability:** The proposed system exhibits scalability through a hierarchical structure. Local health authorities, hospitals, and clinics serve as nodes, ensuring a scalable network where each entity is added by a higher authority. This hierarchical structure allows for the efficient expansion of the healthcare network without compromising security.
- **Regulatory compliance:** The proposed system considers the hierarchical structure of healthcare authorities in Saudi Arabia, aligning with the regulatory framework. The Ministry of Health, serving as the highest authority, oversees the registration of entities, ensuring compliance with local regulations and preventing security issues such as DoS attacks.
- **Patient-centric control:** The architecture ensures that patients have granular control over their medical records. The process of granting access, revoking access, and managing encryption keys is in the hands of the patients, enhancing privacy and control over their healthcare data.

The proposed healthcare data management system, leveraging blockchain, IPFS, and encryption, exhibits resilience against several potential attacks, ensuring the integrity, privacy, and security of patient data. Here is a detailed analysis of the system's robustness against various attacks:

- **Unauthorized access and tampering:** The decentralized architecture and permissioned nature of the private Ethereum blockchain are pivotal in safeguarding against unauthorized access and tampering of patient data. By employing smart contract, the system enforces strict access controls, ensuring that only registered and authorized entities have the right to interact with the blockchain. The immutability of records is guaranteed through the consensus mechanism, making it virtually impossible for any entity without proper authorization to alter or tamper with sensitive medical information.
- **DoS attacks:** To counter the risk of DoS attacks, the blockchain-based healthcare data management system implements a hierarchical registration process and a permissioned structure. Entities, including hospitals and clinics, are registered by higher authorities, mitigating the potential for a flood of unauthenticated registrations. This hierarchical and permissioned approach enhances the system's resilience against DoS attacks, ensuring stable and secure operation.
- **Data interception and eavesdropping:** Protection against data interception and eavesdropping is achieved through robust encryption techniques. Medical records are encrypted using a symmetric key, which is then further encrypted with the patient's public key. This double-layered encryption ensures the confidentiality of patient data during both transmission and storage. Even if data is intercepted, it remains

unreadable without the patient's private key, providing a robust defense against unauthorized access.

- Sybil attacks: The proposed system is resilient against Sybil attacks through its hierarchical entity registration and permissioned blockchain architecture. Entities, such as hospitals and clinics, undergo controlled registration by higher authorities, preventing the creation of fake entities within the system. The permissioned blockchain further restricts participation to authorized nodes, effectively mitigating the risk of Sybil attacks by maintaining a trustworthy and controlled network.
- Blockchain consensus attacks: The system's utilization of a PoA consensus mechanism enhances its resistance against blockchain consensus attacks. PoA ensures that only authenticated and authorized nodes participate in the consensus process, eliminating the vulnerabilities associated with traditional PoW or PoS blockchains. This consensus mechanism contributes to the overall security and stability of the blockchain network, making it robust against consensus-related attacks.
- Data leakage prevention from IPFS: To mitigate the risk of data leakage from the IPFS, a combination of patient-controlled access and the use of a private IPFS is employed. Authorized patients and doctors, possessing the required private keys, are the only entities capable of retrieving and decrypting medical records stored on the IPFS network. The implementation of a private IPFS structure ensures that even in the event of an unauthorized intrusion into the network, attackers cannot access or decipher the stored medical records without the necessary cryptographic keys. This approach upholds the confidentiality of patient information, providing an additional layer of security against potential data breaches.

VII. CONCLUSION

In conclusion, this research introduces a robust and secure framework for managing healthcare data through the integration of blockchain technology, DApps, and a novel access control mechanism. The proposed system leverages a private Ethereum blockchain, enhancing data security and privacy within the healthcare domain. Through strategic smart contract implementations, the hierarchical structure of healthcare entities is mirrored, ensuring a controlled onboarding process and mitigating risks associated with unauthorized access.

The utilization of IPFS for secure and decentralized storage, combined with encryption methodologies, safeguards the confidentiality and integrity of medical records. The seamless interaction between the Ethereum blockchain and the React-based DApp provides a user-friendly experience for healthcare authorities, doctors, and patients. This research also details a comprehensive set of interfaces tailored for each entity type, facilitating smooth interactions and data management.

Furthermore, the proposed access control mechanism places patients at the center of their healthcare journey, allowing them to actively manage and monitor access to their medical records. The cryptographic principles underpinning

this mechanism ensure secure key management and data confidentiality. Through the decentralized nature of the system, trust is established among participating entities, fostering a secure and transparent healthcare ecosystem.

As we move forward, this research provides a foundation for the continued exploration and development of blockchain-based healthcare systems. The presented framework not only addresses current challenges in healthcare data management but also aligns with the evolving landscape of digital healthcare. With a commitment to user control, data privacy, and security, the proposed system presents a valuable contribution to the ongoing discourse on innovative solutions for healthcare information management.

REFERENCES

- [1] G. Jetley and H. Zhang, "Electronic health records in is research: Quality issues, essential thresholds and remedial actions," *Decision Support Systems*, vol. 126, p. 113137, 2019.
- [2] K. Wisner, A. Lyndon, and C. A. Chesla, "The electronic health record's impact on nurses' cognitive work: An integrative review," *International Journal of Nursing Studies*, vol. 94, pp. 74–84, 2019.
- [3] M. Hochman, "Electronic health records: a "quadruple win," a "quadruple failure," or simply time for a reboot?" pp. 397–399, 2018.
- [4] W. W. Koczkodaj, M. Mazurek, D. Strzalka, A. Wolny-Dominiak, and M. Woodbury-Smith, "Electronic health record breaches as social indicators," *Social Indicators Research*, vol. 141, pp. 861–871, 2019.
- [5] S. Altamimi, T. Storer, and A. Alzahrani, "The role of neutralisation techniques in violating hospitals privacy policies in saudi arabia," in *2018 4th International Conference on Information Management (ICIM)*. IEEE, 2018, pp. 133–140.
- [6] S. Dhumwad, M. Sukhadeve, C. Naik, K. Manjunath, and S. Prabhu, "A peer to peer money transfer using sha256 and merkle tree," in *2017 23RD Annual International Conference in Advanced Computing and Communications (ADCOM)*. IEEE, 2017, pp. 40–43.
- [7] Z. Zheng, S. Xie, H. Dai, X. Chen, and H. Wang, "An overview of blockchain technology: Architecture, consensus, and future trends," in *2017 IEEE international congress on big data (BigData congress)*. Ieee, 2017, pp. 557–564.
- [8] B. Sharma, C. N. Sekharan, and F. Zuo, "Merkle-tree based approach for ensuring integrity of electronic medical records," in *2018 9th IEEE Annual Ubiquitous Computing, Electronics & Mobile Communication Conference (UEMCON)*. IEEE, 2018, pp. 983–987.
- [9] R. Zhang, R. Xue, and L. Liu, "Security and privacy on blockchain," *ACM Computing Surveys (CSUR)*, vol. 52, no. 3, pp. 1–34, 2019.
- [10] A. Al Mamun, S. Azam, and C. Gritti, "Blockchain-based electronic health records management: a comprehensive review and future research direction," *IEEE Access*, vol. 10, pp. 5768–5789, 2022.
- [11] A. S. Yadav, S. Agrawal, and D. S. Kushwaha, "Distributed ledger technology-based land transaction system with trusted nodes consensus mechanism," *Journal of King Saud University-Computer and Information Sciences*, vol. 34, no. 8, pp. 6414–6424, 2022.
- [12] J. Benet, "IpfS-content addressed, versioned, p2p file system," *arXiv preprint arXiv:1407.3561*, 2014.
- [13] S. Kumar, A. K. Bharti, and R. Amin, "Decentralized secure storage of medical records using blockchain and ipfs: A comparative analysis with future directions," *Security and Privacy*, vol. 4, no. 5, p. e162, 2021.
- [14] V. Mani, P. Manickam, Y. Alotaibi, S. Alghamdi, and O. I. Khalaf, "Hyperledger healthchain: patient-centric ipfs-based storage of health records," *Electronics*, vol. 10, no. 23, p. 3003, 2021.
- [15] G. Wood *et al.*, "Ethereum: A secure decentralised generalised transaction ledger," *Ethereum project yellow paper*, vol. 151, no. 2014, pp. 1–32, 2014.
- [16] X. Liu, K. Muhammad, J. Lloret, Y.-W. Chen, and S.-M. Yuan, "Elastic and cost-effective data carrier architecture for smart contract in blockchain," *Future Generation Computer Systems*, vol. 100, pp. 590–599, 2019.

- [17] C. D. Clack, V. A. Bakshi, and L. Braine, "Smart contract templates: foundations, design landscape and research directions," *arXiv preprint arXiv:1608.00771*, 2016.
- [18] C. Dannen, *Introducing Ethereum and solidity*. Springer, 2017, vol. 1.
- [19] W. Zou, D. Lo, P. S. Kochhar, X.-B. D. Le, X. Xia, Y. Feng, Z. Chen, and B. Xu, "Smart contract development: Challenges and opportunities," *IEEE Transactions on Software Engineering*, vol. 47, no. 10, pp. 2084–2106, 2019.
- [20] V. Buterin *et al.*, "A next-generation smart contract and decentralized application platform," *white paper*, vol. 3, no. 37, pp. 2–1, 2014.
- [21] W.-M. Lee and W.-M. Lee, "Using the web3. js apis," *Beginning Ethereum Smart Contracts Programming: With Examples in Python, Solidity, and JavaScript*, pp. 169–198, 2019.
- [22] T. Heston, "A case study in blockchain healthcare innovation," 2017.
- [23] Q. Xia, E. B. Sifah, K. O. Asamoah, J. Gao, X. Du, and M. Guizani, "Medshare: Trust-less medical data sharing among cloud service providers via blockchain," *IEEE access*, vol. 5, pp. 14 757–14 767, 2017.
- [24] E.-Y. Daraghmi, Y.-A. Daraghmi, and S.-M. Yuan, "Medchain: a design of blockchain-based system for medical records access and permissions management," *IEEE Access*, vol. 7, pp. 164 595–164 613, 2019.
- [25] A. Dubovitskaya, Z. Xu, S. Ryu, M. Schumacher, and F. Wang, "Secure and trustable electronic medical records sharing using blockchain," in *AMIA annual symposium proceedings*, vol. 2017. American Medical Informatics Association, 2017, p. 650.
- [26] A. Abid, S. Cheikhrouhou, S. Kallel, and M. Jmaiel, "Novidchain: Blockchain-based privacy-preserving platform for covid-19 test/vaccine certificates," *Software: Practice and Experience*, vol. 52, no. 4, pp. 841–867, 2022.
- [27] J. Sun, L. Ren, S. Wang, and X. Yao, "A blockchain-based framework for electronic medical records sharing with fine-grained access control," *Plos one*, vol. 15, no. 10, p. e0239946, 2020.
- [28] A. Azaria, A. Ekblaw, T. Vieira, and A. Lippman, "Medrec: Using blockchain for medical data access and permission management," in *2016 2nd international conference on open and big data (OBD)*. IEEE, 2016, pp. 25–30.
- [29] M. T. de Oliveira, L. H. Reis, R. C. Carrano, F. L. Seixas, D. C. Saade, C. V. Albuquerque, N. C. Fernandes, S. D. Olabarriga, D. S. Medeiros, and D. M. Mattos, "Towards a blockchain-based secure electronic medical record for healthcare applications," in *ICC 2019-2019 IEEE International Conference on Communications (ICC)*. IEEE, 2019, pp. 1–6.
- [30] N. Sammeta and L. Parthiban, "Hyperledger blockchain enabled secure medical record management with deep learning-based diagnosis model," *Complex & Intelligent Systems*, vol. 8, no. 1, pp. 625–640, 2022.
- [31] K. Azbeg, O. Ouchetto, and S. Jai Andaloussi, "Blockmedcare: A healthcare system based on iot, blockchain and ipfs for data management security," *Egyptian Informatics Journal*, vol. 23, no. 2, pp. 329–343, 2022.
- [32] J. W. Kim, S. J. Kim, W. C. Cha, and T. Kim, "A blockchain-applied personal health record application: Development and user experience," *Applied Sciences*, vol. 12, no. 4, 2022.
- [33] G. Q. Butt, T. A. Sayed, R. Riaz, S. S. Rizvi, and A. Paul, "Secure healthcare record sharing mechanism with blockchain," *Applied Sciences*, vol. 12, no. 5, 2022.
- [34] R. A. Abutaleb, S. S. Alqahtany, and T. A. Syed, "Integrity and privacy-aware, patient-centric health record access control framework using a blockchain," *Applied Sciences*, vol. 13, no. 2, 2023.

Automating Tomato Ripeness Classification and Counting with YOLOv9

Hoang-Tu Vo, Kheo Chau Mui, Nhon Nguyen Thien, Phuc Pham Tien
Information Technology Department
FPT University, Cantho city, Vietnam

Abstract—This article proposes a novel solution to the long-standing issue of ripe (or manual) tomato monitoring and counting, often relying on visual inspection, which is both time-consuming, requires a lot of labor and prone to inaccuracies. By leveraging the power of artificial intelligence (AI) and image analysis techniques, a more efficient and precise method for automating this process is introduced. This approach promises to significantly reduce labor requirements while enhancing accuracy, thus improving overall quality and productivity. In this study, we explore the application of the latest version of YOLO (You Only Look Once), specifically YOLOv9, in automating the classification of tomato ripeness levels and counting tomatoes. To assess the performance of the proposed model, the study employs standard evaluation metrics including Precision, Recall, and mAP50. These metrics provide valuable insights into the model's ability to accurately detect and count tomatoes in real-world scenarios. The results indicate that the YOLOv9-based model achieves superior performance, as evidenced by the following evaluation metrics: Precision: 0.856, Recall: 0.832, and mAP50: 0.882. By leveraging YOLOv9 and comprehensive evaluation metrics, this research aims to provide a robust solution for automating tomato monitoring processes. Additionally, by offering the future integration of robotics, the collection phase can further optimize efficiency and enable the expansion of cultivation areas.

Keywords—Tomato monitoring; manual counting; Artificial Intelligence (AI); Image analysis techniques; YOLO; YOLOv9

I. INTRODUCTION

Tomatoes offer not just delightful flavor but also contain crucial nutrients. They are a great source of vitamin C, which supports the immune system and promotes healthy skin. Additionally, tomatoes contain lycopene, a powerful antioxidant that may help reduce the risk of certain cancers and protect against heart disease [1], [2]. Tomatoes have an attractive moisture content of 95%, with a carbohydrate content of 3%, protein at 1.2%, and total lipids making up 1%. Furthermore, they offer minerals including calcium (Ca), magnesium (Mg), phosphorus (P), potassium (K), sodium (Na), zinc (Zn), and manganese (Mn). In addition to minerals, tomatoes provide essential vitamins such as vitamins A and C, thiamin, riboflavin, niacin, pantothenic acid, and pyridoxine. [3]. In 2020, the largest producers of tomatoes worldwide were as follows: China took the top spot, producing an impressive 64,866 million tons of tomatoes in a single year. India came in second, producing approximately 20,573 million tons of tomatoes, while Turkey ranked third, with a tomato production of 13,204 million tons [4].

The current problem of identifying, manually counting, and classifying the ripeness of tomatoes persists as a significant challenge in agricultural practices. Traditional methods rely

heavily on manual labor, making the process time-consuming, labor-intensive, and prone to errors. The current challenges in tomato handling demand innovative solutions that combine machine learning, image processing, and automation to enhance efficiency, reduce errors, and improve overall productivity in the tomato industry.

Manual counting, which involves counting tomatoes manually during harvesting or quality control, is labor-intensive and inefficient. It leads to inaccuracies due to fatigue, distractions, and variations in human perception. Automating counting using image processing, machine learning, or deep learning could alleviate this issue. A study [5] focused on detecting and counting tomato fruits in greenhouses utilizing deep learning.

Accurately categorizing tomatoes into ripeness stages (such as unripe, ripe, and overripe) plays a pivotal role in sorting, storage, and distribution within the agricultural industry. However, manual classification suffers from inconsistency due to human subjectivity. To address this, researchers have proposed innovative approaches, including Machine Learning (ML), Convolutional Neural Networks (CNNs) and Deep Learning-based methods (DL), which demonstrate promising results in fruit classification and ripeness determination [6], [7]. A study [8] using the Cascaded Object Detector (COD) and a composition of traditional custom image processing methods. The COD method achieved 95% accuracy in detecting ripe tomatoes, outperforming the traditional Color Segmentation Method.

This study introduces a more efficient and accurate approach to automating the monitoring process. The utilization of the latest version of YOLO, specifically YOLOv9, enables the classification of tomato ripeness levels and facilitates tomato counting. The main contribution of the study are:

- Introducing a novel solution to the longstanding problem of manual tomato monitoring and counting, addressing issues of time consumption, labor intensity, and inaccuracies associated with visual inspection methods.
- Leveraging artificial intelligence (AI) and image analysis techniques to develop a more efficient and precise method for automating tomato monitoring processes, promising to significantly reduce labor requirements while enhancing accuracy and overall quality and productivity.
- Exploring the application of the latest version of YOLO, specifically YOLOv9, in automating the classification of tomato ripeness levels and counting toma-

toes, demonstrating the potential of advanced deep learning techniques in agricultural applications.

- Evaluating the performance of the proposed model using standard evaluation metrics such as Precision, Recall, and mAP50, providing valuable insights into its effectiveness in accurately detecting and counting tomatoes in real-world scenarios.

The paper is organized as follows: In Section II, we present a thorough literature review. Section III outlines the Automated Tomato Ripeness Classification and Counting Methodology, including details about the dataset, data preparation, and evaluation metrics for the model. Moving on to Section IV, we delve into the experimental system and present the final results. Finally, Section V summarizes our study's findings and offers concluding remarks. Lastly, Section VI outlines potential avenues for future study.

II. RELATED WORKS

Computer vision has emerged as a powerful tool in modern agriculture, revolutionizing the way crops are monitored and managed [9], [10], [11], [12], [13], [14] from object detection algorithms based on traditional methods to modern approaches such as CNN and deep learning.

The authors in the article [15] introduces an automated multi-class classification method for evaluating tomato ripeness using color features and employing Principal Components Analysis (PCA), Support Vector Machines (SVMs), and Linear Discriminant Analysis (LDA) algorithms for feature extraction and classification.

In this study [16], the authors utilize digital image processing techniques to describe and extract color statistics (RGB, HSI, and Lab* color spaces) from tomato images. They employ supervised and unsupervised classification algorithms such as K-NN, MLP neural networks, and K-Means for classifying Milano and Chonto tomatoes.

Liu et al. in this study [17] propose an algorithm for automatic tomato detection in regular color images, utilizing Histograms of Oriented Gradients (HOG) descriptor trained with a SVM classifier, along with a coarse-to-fine scanning method and False Color Removal (FCR) technique to enhance accuracy. The proposed algorithm demonstrates a significant improvement in tomato detection compared to other methods, achieving high recall, precision, and F1 score percentages of 90.00%, 94.41%, and 92.15%, respectively, in test images.

This study [18] proposes a Tomato Classification model utilizing Machine Learning algorithms such as Decision Tree (DT), Logistic Regression (LR), Gradient Boosting (GB), Random Forest (RF), SVM, K-NN, and XG Boost to determine tomato maturity stages, with Random Forest achieving the highest accuracy of 92.49% among the classifiers tested.

The author in the research [19] aims to apply deep Transfer Learning (TL) to classify tomatoes into maturity classes, employing three TL approaches—VGG, Inception, and ResNet—ultimately revealing VGG 19 as the top performer.

The authors in this work [20] utilize an improved DenseNet architecture to address the challenges of accurately classifying tomato ripeness in complex images, incorporating structured

sparse operations to enhance feature propagation and reduce data storage, as well as introducing the Focal loss function to mitigate dataset imbalance and improve classification accuracy in their tomato detection system.

Utilizing TL with VGG16 for Fruit Ripeness Detection. This study [21] demonstrates that DL employing TL consistently outperforms traditional ML approaches utilizing traditional feature extraction for fruit ripeness detection.

The author's primary objective in this study [22] is to introduce a new method for sorting and grading tomato quality, the approach integrates pre-trained CNNs for feature extraction with conventional ML algorithms (such as SVM, RF, and k-Nearest Neighbors (KNN)) to enhance classification accuracy. Among the hybrid models proposed, the CNN-SVM method demonstrates superior performance, achieving high accuracies in both binary and multiclass classification tasks, particularly when utilizing Inceptionv3 as the feature extractor.

The authors in [23] introduce four distinct deep learning frameworks, Utilizing a combination of Yolov5m and deep learning models—specifically ResNet50, ResNet-101, and EfficientNet-B0 - the model successfully classified tomatoes on the vine into three distinct classes: ripe, immature, and damaged. The evaluation results indicated that the ResNet-50 and EfficientNet-B0 achieved impressive overall accuracy of 98%, while the Yolov5m and ResNet-101 models demonstrated accuracy of 97%.

This study [24] explores tomato segmentation and detection across various maturity stages, utilizing both a mask R-CNN and a YOLOv8 model. Evaluation metrics show that mask R-CNN achieved 67.2% average precision with 78.9% recall, and 92.1% IoU average precision with 91.4% recall, while YOLOv8 demonstrated superior performance, With coefficients of determination measuring 0.809 for ripe, 0.897 for half-ripe, and 0.968 for green categories.

Liu, Guoxu, et al. in this study [25] introduces an enhanced fruit detection model named YOLO-Tomato, derived from YOLOv3. YOLO-Tomato integrates a dense architecture into YOLOv3, enabling feature reuse and enhancing model accuracy, while also employing circular bounding boxes for more accurate localization of tomatoes.

The authors in this research [26] enhanced YOLOv5 to identify four distinct stages of tomato ripeness: mature green, breaker, pink, and red. [27] introduces a novel lightweight enhanced algorithm based on YOLOv5 to achieve real-time tracking and identify the ripeness of tomato fruits, achieved by reconstructing YOLOv5's backbone network utilizing the bneck module of MobileNetV3.

This study presents a more efficient and accurate method to automate the monitoring process. By taking advantage of the latest version of YOLO, specifically YOLOv9, it allows classification of tomato ripeness levels and simplifies tomato counting.

III. METHODOLOGY

A. The Process of Gathering and Preparing Data

This research utilizes the FruitDetectionv3 Image Dataset, accessible at [28], which consists of three classes (Tomato



Fig. 1. Sample images of tomatoes at different maturity levels from this dataset.



Tomato Fully-ripe



Tomato Semi-ripe



Tomato Unripe

Fig. 2. Tomato ripening level.

Fully-ripe, Tomato Semi-ripe, and Tomato Unripe) and the total number of images in this dataset is 2610. The dataset is divided into three sets: the training set comprises 2283 pictures (87%), The validation set includes 217 pictures (8%), and the testing set contains 110 pictures (4%). Each image in the dataset has a size of 640x640 pixels. Augmentations are applied to enhance the dataset, including Horizontal Flip, Rotation between -15° and $+15^\circ$, and Shear of $\pm 15^\circ$ horizontally and vertically. These augmentations aim to increase the variability of the dataset and improve the robustness of the model in real-world scenarios. Sample images of tomatoes at different maturity levels from this dataset are shown in Fig. 1 and samples of Tomato Ripening Level are shown in Fig. 2.

B. Overall Methodology

Object detection techniques are frequently classified into one-stage and two-stage approaches. YOLO (You Only Look Once) [29] and SSD (Single Shot MultiBox Detector) [30] are prominent examples of one-stage methods. These methods directly predict bounding boxes and class labels in a single forward pass through the neural network. They are faster in terms of inference time since they avoid the region proposal step. Faster R-CNN (Region-based Convolutional Neural Network) [31] exemplifies the two-stage approach. In the first stage, Faster R-CNN proposes region proposals using a Region Proposal Network (RPN). In the second stage, these proposals are refined to obtain accurate bounding boxes and class predictions. One-stage methods prioritize speed and simplicity, while two-stage methods focus on accuracy at the cost of increased complexity and computation time. In real-time applications where speed is essential, such as autonomous vehicles and surveillance, one-stage methods like YOLO or SSD should be considered.

If achieving high accuracy is crucial and computational resources are available, consider using two-stage methods such as Faster R-CNN. Hence, in this study, we utilize the state-of-the-art one-stage object detection method, YOLOv9, to automate the classification and counting of tomato maturity.

YOLOv9 is a remarkable advancement in real-time object detection technology [32]. YOLOv9 is the latest version of YOLO, released in February 2024, YOLOv9 introduces groundbreaking techniques such as Programmable Gradient Information -PGI and the Generalized Efficient Layer Aggregation Network - GELAN.

1) *Programmable Gradient Information - PGI*: During the forward pass in neural networks, information can get diluted or lost due to transformations within the layers. This phenomenon is known as the information bottleneck. Gradients provide essential information for updating network weights during training. Accurate gradients are crucial for effective learning. PGI ensures that gradient information is preserved throughout the network. It prevents the loss of critical input information during backpropagation. By maintaining reliable gradient information, PGI helps the model learn more effectively and improves its ability to recognize objects. The YOLOv9 Programmable Gradient Information (PGI) Architecture is shown in Fig. 3. The PGI primarily comprises three components: The main branch, An auxiliary reversible branch, and Multi-level auxiliary information.

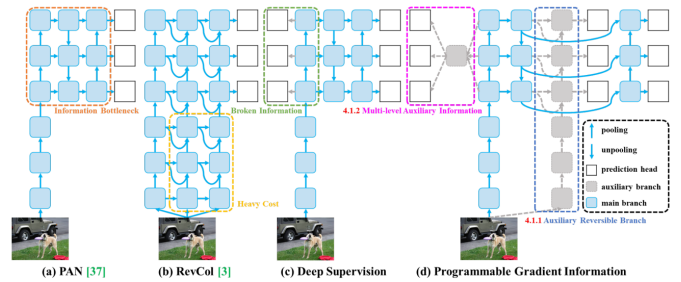


Fig. 3. YOLOv9 PGI Architecture [32].

2) *Generalized Efficient Layer Aggregation Network - GELAN*: GELAN is a novel architectural advancement, it combines principles from two existing techniques: CSPNet (Cross Stage Partial Network) and ELAN (Efficient Layer Aggregation Network). GELAN is a lightweight network architecture designed based on gradient path planning. It efficiently aggregates information across layers. It prioritizes lightweight design, fast inference, and accuracy. GELAN directly tackles the information bottleneck problem, leading to improved efficiency and accuracy in real-time object detection. The architecture of GELAN within YOLOv9 is shown in Fig. 4.

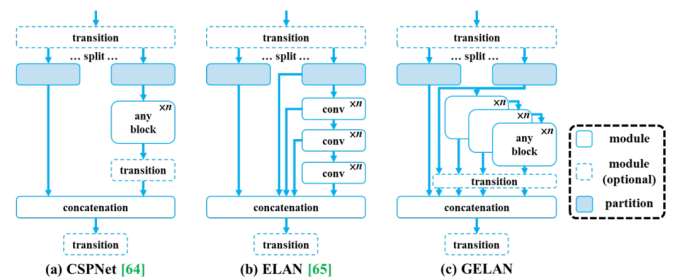


Fig. 4. The architecture of GELAN within YOLOv9 [32].

Information of randomly initialized weight output feature maps across various deep learning network architectures are shown in Fig. 5. From Fig. 5, it's observable that the GELAN architecture retains a significant amount of information from the input data after going through the feed-forward process

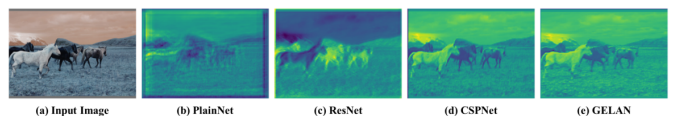


Fig. 5. Information of randomly initialized weight output feature maps across various deep learning network architectures [32].

The analysis of YOLOv9 in comparison to state-of-the-art (SOTA) models demonstrates notable enhancements across diverse metrics. YOLOv9 surpasses current methodologies in parameter efficiency, demanding fewer parameters while either maintaining or enhancing accuracy levels. Comparison of cutting-edge real-time object detectors with YOLOv9 is shown in Fig. 6. YOLOv9 stands out as an innovative model, combining PGI and GELAN to redefine the boundaries of

efficiency and accuracy in object detection. Therefore, in this study we use YOLOv9 to count and classify the ripeness level of tomatoes.

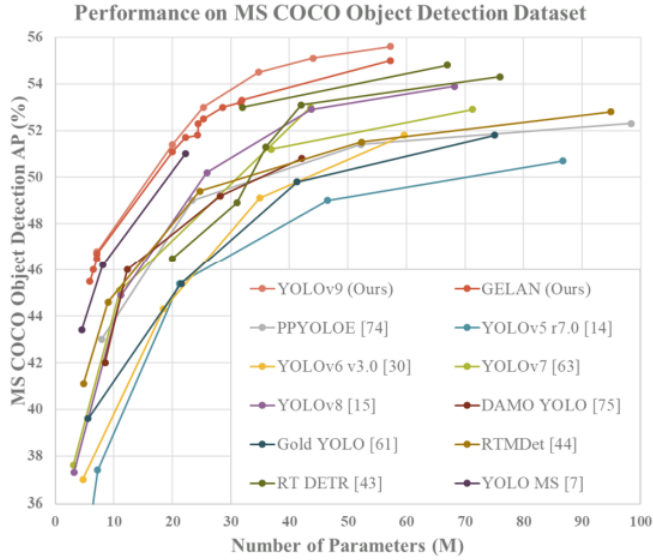


Fig. 6. Comparison of cutting-edge real-time object detectors with YOLOv9 [32].

C. Performance Evaluation Measures

Assessing classification models entails a thorough examination using several essential metrics. Precision, which gauges the correctness of positive predictions among all predicted positives, and recall, which highlights the proportion of accurately predicted positives among all actual positives, play crucial roles. Lastly, The mean average precision (mAP) metric is utilized. It evaluates the detected bounding box by comparing it with the ground-truth box and assigns a corresponding score.

$$Precision = \frac{TP}{TP + FP} \quad (1)$$

$$Recall = \frac{TP}{TP + FN} \quad (2)$$

$$mAP = \frac{1}{N} \sum_{i=1}^N AP_i \quad (3)$$

In which, FP represent False Positive, TN denote True Negative, TP signify True Positive, and FN indicate False Negative. AP is Average Precision, AP_i denotes the average precision value for the i-th category, N is number of classes.

IV. RESULTS

A. Environmental Settings

Our experimental procedures were conducted on the Kaggle platform to acquire the experimental outcomes. The research employed a Tesla T4x2 GPU with 30GB of memory, while the system itself possessed 29GB of RAM. GPU information is presented in Fig. 7.

| NVIDIA-SMI 535.129.03 | | Driver Version: 535.129.03 | | CUDA Version: 12.2 | |
|-----------------------|---------------|----------------------------|----------|----------------------|------------|
| GPU Name | Persistence-M | Bus-Id | Disp.A | Volatile Uncorr. ECC | Compute M. |
| Fan Temp Perf | Pwr:Usage/Cap | Memory-Usage | GPU-Util | Compute M. | NIG M. |
| 0 Tesla T4 | Off | 00000000:00:04:0 | Off | 0 | 0 |
| N/A 36C P8 | 9W / 70W | 0MiB / 15360MiB | 0% | Default | N/A |
| 1 Tesla T4 | Off | 00000000:00:05:0 | Off | 0 | 0 |
| N/A 37C P8 | 9W / 70W | 0MiB / 15360MiB | 0% | Default | N/A |

| Processes: | | | | | | | GPU Memory |
|----------------------------|-------|-------|-----|------|--------------|-------|------------|
| GPU ID | GI ID | CI ID | PID | Type | Process name | Usage | |
| No running processes found | | | | | | | |

Fig. 7. GPU information used in training models.

B. Experiment

The hyperparameters of the model for automating tomato maturity classification and counting using YOLOv9 are shown in the Table I.

TABLE I. CONFIGURATION PARAMETERS FOR MODEL TRAINING

| Parameters | Value |
|--------------------|-----------------------------------|
| Batch-size | 16 |
| Epochs | 100 |
| Image-size | 640 × 640 |
| Learning rate (LR) | 0.01 |
| Momentum | 0.937 |
| Warmup epochs | 3 |
| Weight decay | 0.0005 |
| Optimizer | Stochastic Gradient Descent (SGD) |

1) *Comparative Analysis of YOLOv8 and YOLOv9 for tomato counting and ripeness classification in image processing:* In this research, the goal was to develop an efficient and accurate model for counting and classifying the ripeness level of tomatoes in images. In this experiment, we utilized two popular object detection frameworks: YOLOv8 and YOLOv9. Both models were trained on a dataset of tomato images. The training process involved fine-tuning the pre-trained YOLOv8 and YOLOv9 architectures on the tomato dataset. The models were optimized for counting and classifying the ripeness level of tomatoes. After training, we evaluated the performance of both models on a separate testing set. The table presents the results of the comparison between YOLOv8 and YOLOv9 methods on the testing set, shown in Table II. The results presented in Table II show that YOLOv9 outperformed YOLOv8 in terms of tomato accuracy classification. It's evident that the YOLOv9 model generally outperforms the YOLOv8 model in terms of class precision, recall, and mAP50 across all tomato ripeness categories. Additionally, the YOLOv9 model achieves comparable or better performance with a slightly smaller model size, indicating potential efficiency improvements.

2) *Plots describe the training and validation performance of the YOLOv9 model for counting and classifying tomato ripeness levels:* Fig. 8 displays instances of class distribution and visualizations related to object detection.

TABLE II. THE TABLE PRESENTS THE RESULTS OF THE COMPARISON BETWEEN YOLOV8 AND YOLOV9 METHODS ON THE TESTING SET

| Models | Class | Precision | Recall | mAP50 | Model-Size |
|--------|-------------------|-----------|--------|-------|------------|
| YOLOv8 | All | 0.837 | 0.771 | 0.825 | 52Mb |
| | Tomato Fully-ripe | 0.856 | 0.822 | 0.859 | |
| | Tomato Semi-ripe | 0.773 | 0.710 | 0.772 | |
| | Tomato Unripe | 0.881 | 0.781 | 0.844 | |
| YOLOv9 | All | 0.856 | 0.832 | 0.882 | 51.5Mb |
| | Tomato Fully-ripe | 0.860 | 0.840 | 0.894 | |
| | Tomato Semi-ripe | 0.815 | 0.785 | 0.829 | |
| | Tomato Unripe | 0.894 | 0.870 | 0.925 | |

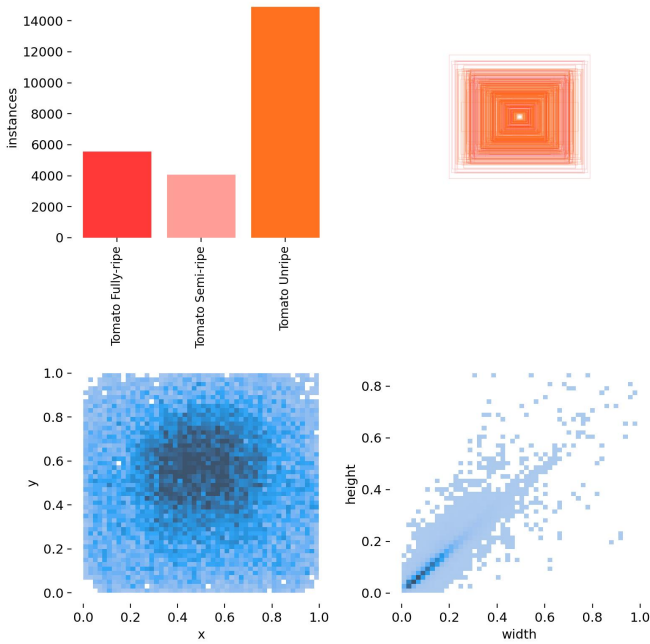


Fig. 8. Overview instances of class distribution and visualizations related to object detection.

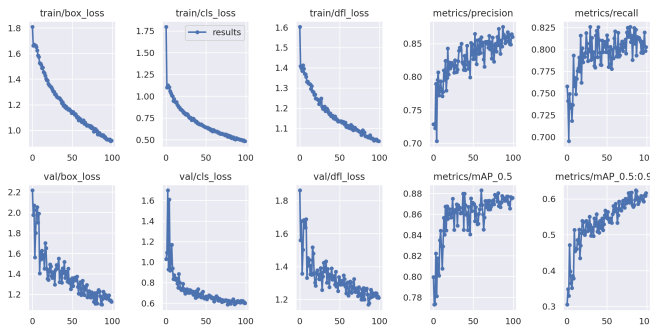


Fig. 9. Visualizations of mean Average Precision (mAP) and loss trends post-training the YOLOv9 model for counting and classifying tomato ripeness levels.

Fig. 9 depicts a series of eight graphs representing different metrics during the training and validation phase of the model to count and classify tomato ripeness. The metrics include: Box Loss, Classification Loss, Distribution Focal Loss, Precision, Recall, Mean Average Precision (mAP). Overall, the graphs show a positive trend over epochs. Decreasing values for loss metrics (Box Loss, Classification Loss, Distribution

Focal Loss) indicate model improvement. Increasing precision, recall, and mAP values suggest better performance.

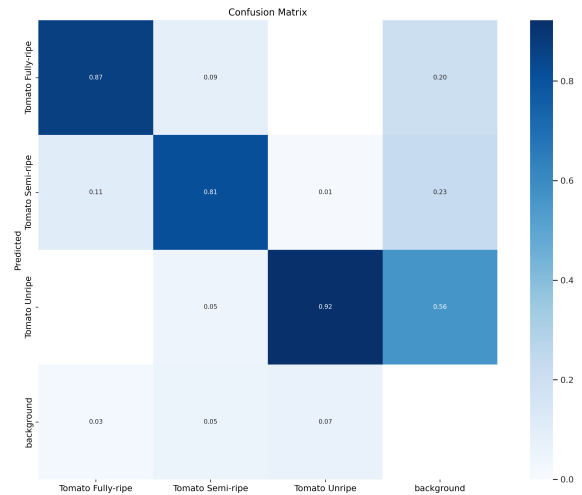


Fig. 10. Confusion matrix of model for counting and classifying tomato ripeness levels.

As we can see from the Confusion matrix in Fig. 10, the tomato ripeness counting and classification model gives the best results in the “Tomato Unripe” class, followed by the “Tomato Fully-ripe” class, and finally, the “Tomato Semi-ripe” class. Precision-Recall Curve is presented in Fig. 11.

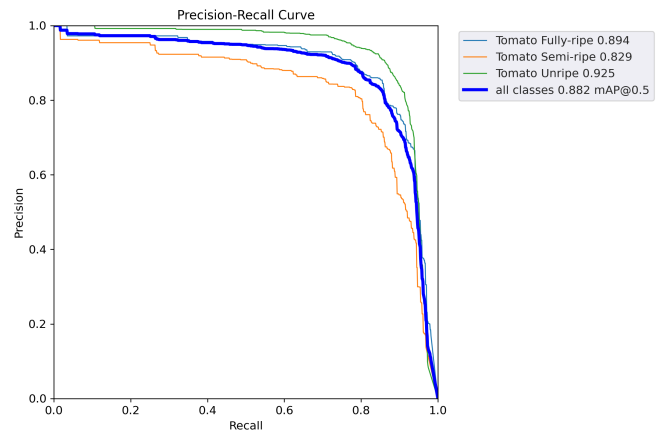


Fig. 11. Precision-Recall curve.

3) *The practical effectiveness of detecting and counting tomato ripeness:* To validate the practical performance of the built model, six pictures were randomly chosen for this study. These images were sourced from the internet to test the detection and counting of tomato ripeness. The results are depicted in Fig. 12.

V. CONCLUSION

In conclusion, this article presents a groundbreaking solution to the longstanding challenges associated with manual tomato monitoring and counting. Traditionally, these tasks



Fig. 12. The tomato ripeness counting and classification results.

have been labor-intensive, time-consuming, and prone to inaccuracies due to their reliance on visual inspection. However, by harnessing the capabilities of artificial intelligence (AI) and image analysis techniques, a more efficient and precise method for automating this process is introduced.

The proposed approach, which leverages the latest version of YOLO, specifically YOLOv9, demonstrates promising results in automating the classification of tomato maturity levels and accurately counting tomatoes. Through the utilization of standard evaluation metrics such as Precision, Recall, and mAP50, the study provides valuable insights into the model's performance in real-world scenarios.

The integration of YOLOv9 and comprehensive evaluation metrics aims to offer a robust solution for automating tomato monitoring processes, thereby significantly reducing labor requirements and enhancing accuracy. Furthermore, the potential future integration of robotics in the collection phase presents an opportunity to further optimize efficiency and enable the expansion of cultivation areas.

In essence, this research not only addresses the immediate need for more efficient tomato monitoring methods but also lays the foundation for advancements in agricultural automation, ultimately contributing to improved quality, productivity, and sustainability in tomato cultivation.

Besides, the study also evaluates the use of the latest version of the YOLO (version 9) model on this task to compare the results with the previous version.

VI. FUTURE WORKS

While the current study demonstrates the effectiveness of the YOLOv9-based model in automating tomato monitoring and counting tasks, several avenues for future research exist to further enhance the proposed solution and extend its applicability. Future research could focus on refining the AI algorithms used for tomato classification and counting. Exploring alternative deep learning architectures or incorporating ensemble techniques may improve the model's performance, particularly in challenging environments with varying lighting conditions or occlusions. Expanding the scope of automation by integrating robotic systems for tomato harvesting and data collection represents a promising direction for future research. By developing autonomous robotic platforms equipped with AI-enabled vision systems, the efficiency and accuracy of tomato cultivation and monitoring processes can be further enhanced.

REFERENCES

- [1] Sanjiv Agarwal and Akkinappally Venketeshwer Rao. Tomato lycopene and its role in human health and chronic diseases. *Cmaj*, 163(6):739–744, 2000.
- [2] Md Yousuf Ali, Abu Ali Ibn Sina, Shahad Saif Khandker, Lutfun Neesa, EM Tanvir, Alamgir Kabir, Md Ibrahim Khalil, and Siew Hua Gan. Nutritional composition and bioactive compounds in tomatoes and their impact on human health and disease: A review. *Foods*, 10(1):45, 2020.
- [3] Bahare Salehi, Razieh Sharifi-Rad, Farukh Sharopov, Jacek Namiesnik, Amir Rooiantan, Madhu Kamle, Pradeep Kumar, Natália Martins, and Javad Sharifi-Rad. Beneficial effects and potential risks of tomato consumption for human health: An overview. *Nutrition*, 62:201–208, 2019.
- [4] Tomato production by country, available online: <https://worldpopulationreview.com/country-rankings/tomato-production-by-country>. Accessed: 2024-02-29.
- [5] Manya Afonso, Hubert Fonteijn, Felipe Schadeck Fiorentin, Dick Lensink, Marcel Mooij, Nanne Faber, Gerrit Polder, and Ron Wehrens. Tomato fruit detection and counting in greenhouses using deep learning. *Frontiers in plant science*, 11:571299, 2020.
- [6] Enoc Tapia-Mendez, Irving A Cruz-Albarran, Saul Tovar-Arriaga, and Luis A Morales-Hernandez. Deep learning-based method for classification and ripeness assessment of fruits and vegetables. *Applied Sciences*, 13(22):12504, 2023.
- [7] Nur Azizah Ayunda, Emy Haryatmi, and Tri Agus Riyadi. Classification of tomato ripeness based on convolutional neural network methods. *Journal of Information Systems and Informatics*, 5(4):1658–1675, 2023.
- [8] Kazy Noor E Alam Siddiquee, Md Shabiul Islam, Mohammad Yasin Ud Dowl, Karim Mohammed Rezaul, and Vic Grout. Detection, quantification and classification of ripened tomatoes: a comparative analysis of image processing and machine learning. *IET Image Processing*, 14(11):2442–2456, 2020.
- [9] Hoang-Tu Vo, Luy-Da Quach, and Tran Ngoc Hoang. Ensemble of deep learning models for multi-plant disease classification in smart farming. *International Journal of Advanced Computer Science and Applications*, 14(5), 2023.
- [10] Hoang-Tu Vo, Nhon Nguyen Thien, and Kheo Chau Mui. Tomato disease recognition: Advancing accuracy through xception and bilinear pooling fusion. *International Journal of Advanced Computer Science and Applications*, 14(8), 2023.
- [11] Juliana Freitas Santos Gomes and Fabiana Rodrigues Leta. Applications of computer vision techniques in the agriculture and food industry: a review. *European Food Research and Technology*, 235:989–1000, 2012.
- [12] Diego Inácio Patrício and Rafael Rieder. Computer vision and artificial intelligence in precision agriculture for grain crops: A systematic review. *Computers and electronics in agriculture*, 153:69–81, 2018.
- [13] Ronald TOMBE. Computer vision for smart farming and sustainable agriculture. In *2020 IST-Africa Conference (IST-Africa)*, pages 1–8. IEEE, 2020.
- [14] Hoang-Tu Vo, Nhon Nguyen Thien, and Kheo Chau Mui. A deep transfer learning approach for accurate dragon fruit ripeness classification and visual explanation using grad-cam. *International Journal of Advanced Computer Science & Applications*, 14(11), 2023.
- [15] Nashwa El-Bendary, Esraa El Hariri, Aboul Ella Hassanien, and Amr Badr. Using machine learning techniques for evaluating tomato ripeness. *Expert Systems with Applications*, 42(4):1892–1905, 2015.
- [16] Wolfgang D Niño Pacheco and Fabián R Jiménez López. Tomato classification according to organoleptic maturity (coloration) using machine learning algorithms k-nn, mlp, and k-means clustering. In *2019 XXII Symposium on Image, Signal Processing and Artificial Vision (STSIVA)*, pages 1–5. IEEE, 2019.
- [17] Guoxu Liu, Shuyi Mao, and Jae Ho Kim. A mature-tomato detection algorithm using machine learning and color analysis. *Sensors*, 19(9):2023, 2019.
- [18] Kamalpreet Kaur and OP Gupta. A machine learning approach to determine maturity stages of tomatoes. *Oriental journal of computer science and technology*, 10(3):683–690, 2017.
- [19] Ninja Begum and Manuj Kumar Hazarika. Maturity detection of tomatoes using transfer learning. *Measurement: Food*, 7:100038, 2022.
- [20] Jun Liu, Jie Pi, and Liru Xia. A novel and high precision tomato maturity recognition algorithm based on multi-level deep residual network. *Multimedia Tools and Applications*, 79:9403–9417, 2020.
- [21] Jasman Pardede, Benhard Sitohang, Saiful Akbar, and Masayu Leylia Khodra. Implementation of transfer learning using vgg16 on fruit ripeness detection. *Int. J. Intell. Syst. Appl*, 13(2):52–61, 2021.
- [22] Hassan Shabani Mputu, Ahmed Abdel-Mawgood, Atsushi Shimada, and Mohammed S Sayed. Tomato quality classification based on transfer learning feature extraction and machine learning algorithm classifiers. *IEEE Access*, 2024.
- [23] Quoc-Hung Phan, Van-Tung Nguyen, Chi-Hsiang Lien, The-Phong Duong, Max Ti-Kuang Hou, and Ngoc-Bich Le. Classification of tomato fruit using yolov5 and convolutional neural network models. *Plants*, 12(4):790, 2023.

- [24] Jean Carlo Camacho and Manuel Eugenio Morocho-Cayamcela. Mask r-cnn and yolov8 comparison to perform tomato maturity recognition task. In *Conference on Information and Communication Technologies of Ecuador*, pages 382–396. Springer, 2023.
- [25] Guoxu Liu, Joseph Christian Nouaze, Philippe Lyonel Touko Mbouembe, and Jae Ho Kim. Yolo-tomato: A robust algorithm for tomato detection based on yolov3. *Sensors*, 20(7):2145, 2020.
- [26] Renzhi Li, Zijing Ji, Shikang Hu, Xiaodong Huang, Jiali Yang, and Wenfeng Li. Tomato maturity recognition model based on improved yolov5 in greenhouse. *Agronomy*, 13(2):603, 2023.
- [27] Taiheng Zeng, Siyi Li, Qiming Song, Fenglin Zhong, and Xuan Wei. Lightweight tomato real-time detection method based on improved yolo and mobile deployment. *Computers and Electronics in Agriculture*, 205:107625, 2023.
- [28] project cangp. Fruitdetectionv3 (3 class) dataset. <https://universe.roboflow.com/project-cangp/fruitdetectionv3-3-class>, apr 2023. visited on 2024-03-01.
- [29] Juan Terven, Diana-Margarita Córdova-Esparza, and Julio-Alejandro Romero-González. A comprehensive review of yolo architectures in computer vision: From yolov1 to yolov8 and yolo-nas. *Machine Learning and Knowledge Extraction*, 5(4):1680–1716, 2023.
- [30] Wei Liu, Dragomir Anguelov, Dumitru Erhan, Christian Szegedy, Scott Reed, Cheng-Yang Fu, and Alexander C Berg. Ssd: Single shot multibox detector. In *Computer Vision—ECCV 2016: 14th European Conference, Amsterdam, The Netherlands, October 11–14, 2016, Proceedings, Part I 14*, pages 21–37. Springer, 2016.
- [31] Shaoqing Ren, Kaiming He, Ross Girshick, and Jian Sun. Faster r-cnn: Towards real-time object detection with region proposal networks. *Advances in neural information processing systems*, 28, 2015.
- [32] Chien-Yao Wang, I-Hau Yeh, and Hong-Yuan Mark Liao. Yolov9: Learning what you want to learn using programmable gradient information. *arXiv preprint arXiv:2402.13616*, 2024.

Harnessing AI to Generate Indian Sign Language from Natural Speech and Text for Digital Inclusion and Accessibility

Parul Yadav¹, Puneet Sharma², Pooja Khanna³, Mahima Chawla⁴, Rishi Jain⁵, Laiba Noor⁶
Computer Science and Engineering Dept. Institute of Engineering and Technology, Lucknow, UP 226021, India^{1,4,5,6}
School of Computer Science and AI, SR University, Warangal, Telangana, 506371, India²
Amity School of Engineering and Tech. Amity University, Lucknow, UP 226028, India³

Abstract—Sign language is the fundamental mode of communication for those who are deaf and mute, as well as for individuals with hearing impairments. Regrettably, there has been a dearth of research on Indian Sign Language, primarily due to the lack of adequate grammar and regional variations in such language. Consequently, research in this area has been limited. The primary objective of our research is to develop a sophisticated speech/ text-to-Indian sign language conversion system that employs advanced 3D modeling techniques to display sign language motions. Our research is motivated by our desire to promote effective communication between hearing and hearing-impaired individuals in India. The proposed model integrates Automatic Speech Recognition (ASR) technology, which effectively transforms spoken words into text, and leverages 3D modeling techniques to generate corresponding sign language motions. We have conducted a comprehensive study of the grammar of Indian Sign Language, which includes identifying sentence structure and signs that represent the tense of the subject. It is noteworthy that the sentence structure of Indian Sign Language follows the Subject-Object-Verb sequence, in contrast to spoken language, which follows the Subject-Verb-Object structure. To enhance user experience as well as digital inclusion and accessibility, the research incorporates user-friendly and simple interfaces that allow individuals to interact effortlessly with the system intuitively. The model/ system is equipped to receive speech input through a microphone/ text and provide immediate feedback through 3D-modeled videos that display the generated sign language gestures and has achieved 99.2% accuracy. Our main goal is to promote digital inclusion and improve accessibility and enhance the user experience.

Keywords—Sign language generation; automatic speech recognition; speech-to-indian sign language; indian sign language; digital inclusion and accessibility

I. INTRODUCTION

The impact of information and communication technology (ICT) on human life has been immense [1]. It has revolutionized the way people conduct business, learn, travel, and communicate. Given the transformative power of ICT, it can be a valuable tool to aid the deaf and dumb community in overcoming communication obstacles [1] and bridging the gap between digital content availability and accessibility for them [2].

Hearing loss is a condition that affects an individual's ability to hear, with a hearing threshold of 20 dB or higher in both ears being considered normal [3]. It may impact one or both

ears, and its severity can range from mild to profound. The underlying causes of hearing loss include congenital or early-onset childhood hearing loss, ongoing middle ear infections, noise-induced hearing loss, age-related hearing loss, and the use of ototoxic medications that damage the inner ear. According to research, there are approximately 63 million people worldwide who experience some form of auditory impairment [4]. In India, the Indian Sign Language Research and Training Center (ISLRTC) estimates that roughly five million people are deaf or hard of hearing [5]. For many of these individuals, sign language is their primary mode of communication. However, the cost of training in sign language institutions in India can range from a few thousand to several tens of thousands of rupees, making it challenging for a significant portion of the population, including family members, acquaintances, and professionals who work with the deaf community, to learn sign language as a secondary form of communication. Unfortunately, available data suggests that only 20% of the deaf population in India have access to formal education in sign language [2]. Although sign language is a valuable tool for individuals with hearing disabilities, its limitations can hinder effective communication. These challenges include:

- **Limited Accessibility:** Sign language is not universally understood and varies across different regions and cultures, making it less accessible [6].
- **Language Barriers:** Individuals with hearing disabilities may experience challenges in communicating with those who are not well-versed in sign language. This can result in barriers to effective communication between sign language users and non-sign language users.
- **Time and Cost:** Learning sign language can be a time-consuming and costly process, deterring some individuals from pursuing it [7].
- **Dependence on Interpreters:** Relying on interpreters for communication can also limit independence and autonomy [7].
- **Limited Resources:** There is a shortage of qualified sign language interpreters in many areas, such as rural or low-income communities.

In order to improve the accessibility and efficacy of sign language for people with hearing disabilities, it is crucial to

TABLE I. COMPARISON OF EXISTING WORK

| Author | Problem addresses | Methodology | Outcome |
|--------------------------------------|--|--|--|
| Abhisek Mishra et al.[5] | No. of hearing disables in India. | 2011 census data | Around 5 mn. people have hearing disability |
| Sulabha M Naik et al.[4] | No. of hearing disables in India. | Rehabilitation Council of India Act,1992 | Approximately 63 mn. people in India suffer from serious hearing loss. |
| Speech to Text Conversion | | | |
| Muhammad Yasir et al.[9] | Speech Recognition using web speech API | MFCC and HMM. | Avg. accuracy- 96.63% (Indonesian lang.)-82.78% (English lang.) |
| Santosh K. Gaikwad et al.[13] | Speech Recognition Techniques | MFCC and GMM or HMM | MFCC and HMM are best for speech recognition |
| S. Rajeswari et al.[8] | Speech to text conversion | Feature extraction, acoustic models ,language models and algorithms. | Voice-based e-mail system for blind. |
| Text to Sign Generation | | | |
| Navroz Kaur Kahlon et al.[7] | Text to sign language conversion | Machine Translation tech.-RBMT, EBMT | Text can be converted to sign. |
| ALAN CONWAY et al.[10] | Challenges of English language conversion to sign | Central blackboard control structure and Doll Control language | English to Sign system. |
| GARY TONGE et al.[11] | English to British Sign Language (BSL) | Human sign interpreter, Bones Animation Format and SIGML | Television broadcast System in UK. |
| Matthew P. Huenerfauth et al.[12] | Different sign generation system | ViSiCAST, ASL workbench, Team etc. | Symbolic representation limits Expressiveness. |
| Tokenization and 3D modelling | | | |
| Sabrina J. Mielke et. al. [14] | Explanation on Tokenization. | Studies on words, characters and sub-words | No perfect method of handling tokenization. |
| Zeeshan Bhatti et. al [16]. | Creating 3D Animated movie. | Adobe Software | A 3D movie generated |
| ALL | | | |
| Lalit Goyal et al.[18] | Explanation on text to sign generation. | Studies on words, characters and sub-words | constructed a synthetic dictionary. |
| Krunal et al.[19]. | converting text to sign and Creating 3D Animated signs | words and sentences | A text to sign model. |
| Sugandhi et al.[20] | Text to Sign Conversion | HamNoSys and SiGML | Corpus of 2950 words and 1000 sentences. |
| Kullami et al.[21]. | converting text to sign and Creating 3D Animated signs | words and sentences | A text to sign model |

employ cutting-edge and inventive technologies to overcome the challenges at hand. The other modern-day issue is; the concept of **digital inclusion** which entails removing barriers that hinder people from accessing digital content. These barriers may take the form of inaccessible systems, inadequate knowledge or skills, limited access to digital devices or materials, or other factors. As such, it is crucial to promote seamless communication between individuals with hearing impairments and those who may not comprehend sign language. Hence, **Digital accessibility** which pertains to the degree to which digital content can be easily accessed and utilized by all users, including those with visual or hearing impairments who may necessitate supplementary access provisions is crucial. This research strives to accomplish the following primary objectives:

- To close the communication divide between individuals who communicate through spoken language and those who use Indian Sign Language (ISL) by providing a system that can convert spoken language into ISL.
- To guarantee that spoken language is translated into ISL with precision and clarity, without any distortion or misinterpretation of the intended meaning.
- To establish an online platform that allows the general public to learn sign language and precisely translate spoken words into sign language.
- To develop a user-friendly interface that enables both sign language users and non-sign language users to communicate effortlessly, without encountering significant technical obstacles.

This research paper proposes and implements a novel model named as *Listen* which transforms spoken words/ text into sign language gestures and focuses on speech-to-hand-sign generation and designed with the intention to enhance communication for those with hearing disabilities. By enabling real-time translation of spoken or text input into sign language, *Listen* empowers individuals who rely on this form of communication. The output is presented through animated visuals for optimal accessibility. *Listen* model is able to achieve the accuracy of 99.21% when rigorously tested with different inputs.

The novelty of our model is its impressive capability of

comprehending the connection between English and Indian sign language sentences through the use of advanced Natural Language Processing (NLP) techniques. This involves the mapping of words to their corresponding hand signs, enabling the generation of sign language gestures in response to spoken input. Despite the intricacy of sign language, regional variations, and the requirement for accurate speech recognition, this research work has made significant progress in developing a robust system for generating hand signs with better accuracy than the existing models to the best of our knowledge.

The research paper is structured as follows: Firstly, it presents a comprehensive overview of the existing related works in the field in Section II. Following that, it discusses the methodology proposed for implementing the proposed model in Section III. Subsequently, Section IV exhibits the results and visualizations of the model. Lastly, in Section V, it provides a summary of the research work done and outlines the future work.

II. RELATED WORKS

Numerous studies have shed light on the prevalence of auditory impairments within the Indian population. Furthermore, there have been commendable accomplishments in the deployment of speech recognition systems in meetings and email assistance [8], as well as the translation of text into sign language through various techniques. Additionally, hand gestures have been utilized for virtual mouse control. These endeavors have produced a broad spectrum of results, ranging from statistical data on disability to the development of useful applications and systems for communication and interaction.

The review highlights the specific areas that require attention. For example, speech recognition systems necessitate distinct enunciation [9], while sign language generation has lexicon constraints [6]. Avatars currently lack genuine emotional expression [7], and natural language processing encounters challenges with tokenization techniques. Furthermore, virtual mouse systems need enhancement in precision and efficiency. Papers [10], [11], [12], [13], [14], [15], [16], [17] revolve around the above stated techniques which is explained in Table I. Followed by Lalit Goyal et al.[18] in 2016 constructed a synthetic dictionary that classified ISL words. These words were then translated into the HamNoSys (Hamburg Notation System) writing notation for sign language, which was translated into SiGML (Signing Gesture Markup Language) to

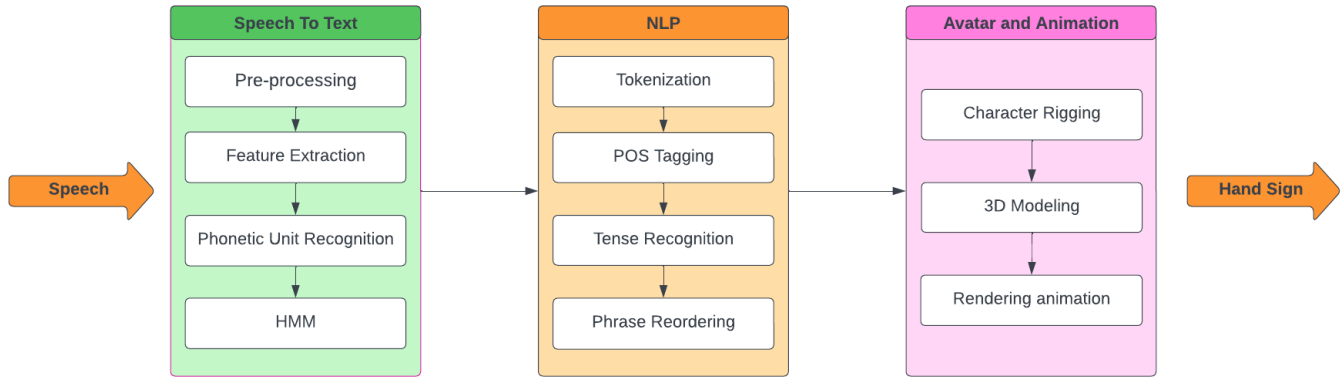


Fig. 1. Process flow of model.

produce a synthetic animation of the sign using a computer-generated cartoon with an overall accuracy of 94.35%. Krunal et al.[19] presented a method that uses speech recognition to turn an English voice dictation into text which bagged the highest accuracy of 94.53%. Followed by Sugandhi et al.[20] describes a system that generates Sign language based on Indian Sign Language grammar. It includes elements like an ISL parser, the Hamburg Notation System, the Signing Gesture Mark-up Language, and 3D avatar animation and achieved an accuracy of 96.67%. In order to translate English speech to Indian Sign Language with a 97.86% accuracy rate, Kulkarni et al.[21] presented an online platform that accepts voice as input and outputs a series of films showing the matching sign language. Hence, In the realm of assistive technologies for individuals with disabilities, a multitude of studies have explored various challenges and potential solutions. Table I provides a comprehensive compilation of related works, covering topics such as education and employment opportunities for the hearing impaired, rehabilitation options for deaf children, speech-to-text conversion systems, sign language generation, and virtual mouse systems utilizing hand gestures.

The Table I includes details regarding the authors, the issues they addressed, the methodologies employed, and the resulting outcomes. These studies employed a range of approaches, including data analysis, speech recognition techniques, language models, and 3D animation, to overcome specific challenges faced by individuals with disabilities. Additionally, the limitations of these studies have been provided in this section which is followed by Section III that explains our proposed model, its working, and corresponding components to address the objectives at hand.

III. METHODOLOGY

Effective communication is vital to human society, and spoken language is the primary tool we use to convey our ideas and beliefs [9]. Crafting a reliable platform for converting speech into sign language requires a multitude of intricate steps, as elucidated in Section II. Bearing this in mind, we are pleased to present our innovative approach for deploying our solution, which we have aptly named *listen*. The *Listen* system consists of three distinct subsystems: Speech-To-Text pre-processing, Natural Language Processing (NLP), and the

avatar and animation. Fig. 1 provides an illustration of each subsystem's components. The model's process flow diagram, also shown in the figure, begins with the input Speech and proceeds through the Speech-To-Text pre-processing subsystem (explained in Subsection III-A), the NLP subsystem (explained in Subsection III-B), and ultimately the avatar and animation (explained in Subsection III-C), which displays the Hand sign corresponding to the input Speech. The first subsection of the model is explained in the following subsection.

A. Speech to Text

Speech recognition is the technology that converts spoken words into digital text, making it easily editable, storable, and shareable. The process involves analyzing and interpreting the acoustic and linguistic features of speech [8], such as words and phrases, to extract useful information. This is done by taking audio data input and performing recognition using a model. A labeled dataset is used to map sound vibrations to different letters, but some letters can be challenging to recognize due to similar pronunciations. In such cases, the probability of how commonly two letters appear together is used to determine the most likely recognition. Example:- "called" and "pan" Notice how 'a' produces different sounds in both words. In such cases, we use likelihood probability of how commonly two letters appear together.

The Fig. 2 shows the entire process of Speech recognition used in the research. The steps include pre-processing, feature extraction, phonetic unit recognition, and hidden Markov model all of which are explained below.

1) *Pre-processing*: During the course of this research, the pre-processing stage was implemented to partition the input into smaller frame sizes. In our model, each frame size is composed of 0.025 seconds of audio, equivalent to the duration of a single or a few phonemes, which are the basic units of speech, and typically have a duration in the range of tens to hundreds of milliseconds. This duration is ideal for capturing the unique characteristics of phonemes, which typically last for tens to hundreds of milliseconds. It was determined that only one English phoneme is typically pronounced within this time period. The pre-processed output is then forwarded to the feature extraction subsection.

SPEECH RECOGNITION PROCESS

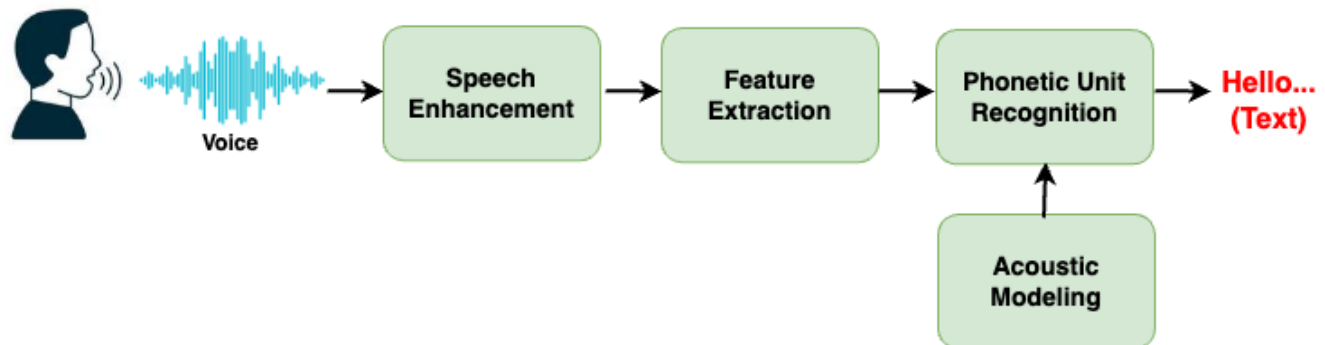


Fig. 2. Speech recognition.

2) *Feature Extraction*: In the feature extraction phase, each frame audio frequency feature is extracted. There are various techniques for feature extraction, some of them are Short-time Fourier Transform (STFT) [13], Mel Frequency Cepstral Coefficients [9], Chroma feature [22], and Spectral Contrast [23]. Our *Listen* model leverages **Mel Frequency Cepstral Coefficients** (MFCC) to accurately capture audio features. This technique mimics the human auditory system by utilizing a filter bank that simulates the Mel scale to approximate the magnitude spectrum produced by the STFT. Through a multi-step process, we transform the audio signal by first computing the logarithm of filterbank energies and then applying Discrete Cosine Transform (DCT) to obtain a concise representation of the signal. These features are then segmented into frames of equal size, with each frame representing a distinct phoneme. These frames are then passed onto the next component of the model, known as the **Phonetic Unit Recognition** (PUR) module.

3) *Phonetic Unit Recognition*: Once the features are extracted the phoneme is predicted by the Pre-trained acoustic model, which finds the most similar match of a feature of the current frame to existing labeled features in the data set followed by the **Hidden Markov Model**(HMM).

The HMMs are trained using a labeled dataset that contains speech recordings along with corresponding transcriptions or phonetic annotations. The training process involves estimating the parameters of the HMM, including the state transition probabilities. The state transition probability in simple terms represents the probability of one phoneme occurring with another phoneme. Hidden Markov Models (HMMs) are commonly used to model the temporal dependencies in speech signals. HMMs consist of several matrices that define the model's parameters [9] [13]. The outputted text is then fed to the Subsection III-B for conversion of text using Natural Language Processing(NLP) which is explained next.

B. Natural Language Processing (NLP)

The ultimate aim of Natural Language Processing (NLP) is to enable machines to comprehend human language in

a way that is similar to how humans understand it. This involves the creation of intricate algorithms and models that allow computers to analyze, comprehend, and generate human language in a meaningful and contextual manner. NLP encompasses various techniques and tasks, including text tokenization, removal of stop words, part-of-speech (POS) tagging and phrase reordering. In this section, we will delve deeper into these techniques which are as follows:

1) *Tokenization*: Tokenization is the process of breaking down text into smaller units, or tokens, in NLP. These tokens can be words, phrases, or even individual characters, depending on the task at hand. Tokenization is a crucial step in NLP, as it helps to reduce the complexity of text, making it easier for machines to understand and analyze. This technique is used in various NLP tasks, such as sentiment analysis, text classification, and machine translation [14]. It can be performed using various libraries and tools available in Python programming language such as NLTK [15] and spaCy [24]. NLTK is used for Tokenization in our model whose working is shown in Fig. 3. Fig. 3 explains how the tokenization process works. First, the function removes any leading or trailing white space characters from the input string. Next, it splits the text into sentences using a pre-trained sentence tokenizer. This tokenizer is designed to identify the boundaries between sentences, such as periods, question marks, and exclamation points. The function then tokenizes each sentence into individual words using a pre-trained word tokenizer for example: Boundaries: white space. Finally, the function returns a list of tokens, where each token is a separate word in the text. The separated words are then inputted into the next section for further processing.

2) *Removal of Stop Words*: In the field of Natural Language Processing (NLP), the removal of stop words plays a crucial role in the pre-processing of text data. This step involves the cleaning and preparation of text data before further analysis. Stop words refer to the commonly used words in a language that do not contribute significantly to the overall

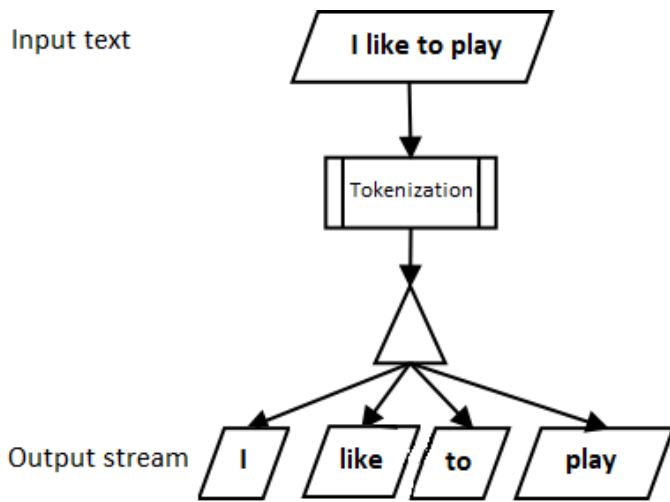


Fig. 3. Tokenization.

meaning of a sentence. Words like “a,” “an,” “the,” “is,” and “and” are examples of stop words, and their exclusion can significantly reduce noise and improve efficiency in data analysis. Other examples of stop words include “mightn’t,” “re,” “wasn’t,” “wouldn’t,” “being,” “were,” “isn’t,” “needn’t,” “don’t,” “nor,” “aren’t,” “as,” “didn’t,” “should’ve,” and “be”, among others, which are generally omitted during NLP analysis. After, Tokenization, the model obtains a list of stop

TABLE II. POS TAG EXAMPLE LIST

| Word | POS Tag | Word Class |
|--------|---------|-------------------|
| She | PRP | pronoun, personal |
| went | VBD | verb, past tense |
| to | TO | “to” |
| the | DT | determiner |
| market | NN | noun (singular) |
| . | . | punctuation mark |

words specific to the language or domain. The model then iterates through the tokens and compares each word against the stop word list. If a word is found in the list is a stop word, remove it from the token list. After which they are fed to the POS tagging phase [6].

3) *Part-of-Speech (POS) Tagging*: It is also known as grammatical tagging, is the process of assigning grammatical information, such as nouns, verbs, adjectives, etc., to individual words in a given text as shown in the Table II. Natural Language Processing (NLP) relies heavily on one fundamental task that serves as a foundation for many downstream tasks. Specifically, the task in question is essential for syntactic parsing, information extraction, and machine translation. Fig. 4 explains how POS Tagging will assign grammatical information in a sentence for example: I love to read poems.

In NLTK (Natural Language Toolkit), a popular Python library for natural language processing, you can perform POS tagging using the ‘pos_tag’ function. The ‘pos_tag’ function is designed to accept an input list of tokens and generate a corresponding list of tuples. Each tuple contains a word and

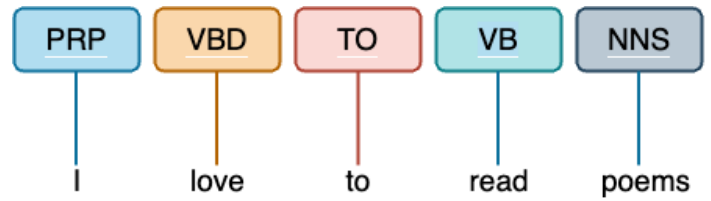


Fig. 4. POS Tagging.

TABLE III. IMPLEMENTATION DETAILS

| | |
|-----------|--------------------------------------|
| Language | Python |
| Tool | Blender (3D modelling and animation) |
| Libraries | NLTK, spaCy |
| Back End | Django |
| Front End | HTML/ CSS, Javascript |

its corresponding POS tag which can then be utilized in phrase reordering.

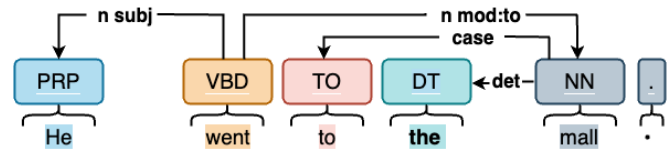


Fig. 5. Phrase reordering.

4) *Phrase Reordering*: Research has revealed that Indian Sign Language exhibits a distinct sentence structure when compared to English. Specifically, it adopts a Time-Subject-Object-Verb format, as opposed to the Subject-Verb-Object structure found in English [6]. Therefore, to effectively convey a phrase in sign language, it must first be restructured accordingly. For example, the sentence “He went to the mall” would require reordering, as illustrated in Fig. 5. Following this restructuring, we must consider the tense of the sentence and incorporate time-reference words such as Now, Before, and Later for present, past, and future tenses respectively. Once the input data has undergone speech-to-text pre-processing and NLP, it is then ready for the avatar and animation stages.

C. Avatar and Animation

To produce 3D videos, one typically needs access to specialized software, such as Adobe [16]. However, we prefer to utilize a free and open-source alternative known as Blender [25] for our 3D avatar and animation modeling. Blender is a powerful 3D creation suite that boasts an array of features for modeling, animation, rendering, and video editing. It is a favored tool among designers, artists, and animators for creating stunning visual content, including 3D models, animations, simulations, and visual effects. The techniques that we used for avatar creation and animation includes: **Character rigging**.

which is used for making sure the Sign Language is accurately performed by the Avatar we need to give it a human-like bone structure. We designed a structure as shown in Fig. 6.

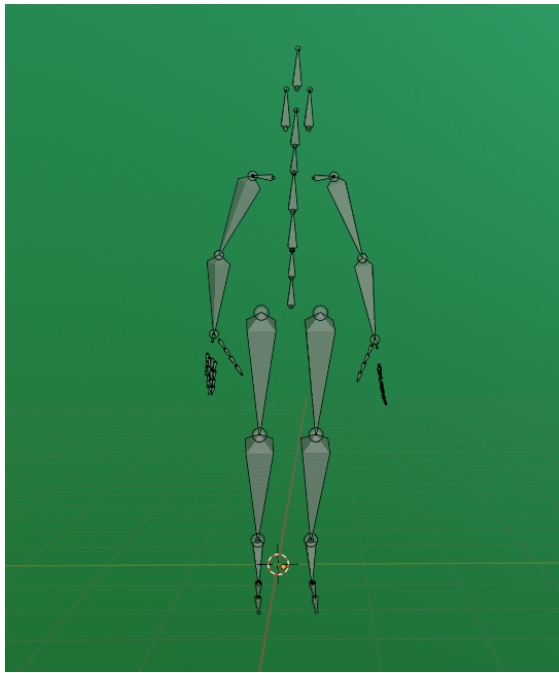


Fig. 6. Character rigging.

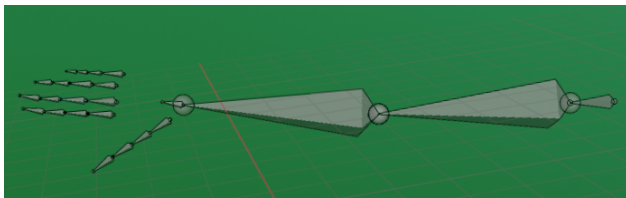


Fig. 7. Armatures.

The armatures in Fig. 7 provide our avatar with the necessary bone structure for movement. Accurate hand movements are essential for effectively conveying the inputted message, which is why meticulous attention has been given to hand rigging. In total, each hand comprises 46 armatures, including four for each finger, one for the wrist, elbow, and shoulder. Finally, the avatar is rendered in 3D to complete the process. After character rigging we jumped into 3D modeling of the obtained output from the preceding step.

In the concluding phase of **3D Modeling**, we initiated the process by fabricating a fundamental mesh for our avatar by taking advantage of Blender's modeling tools. We implemented an array of techniques, including extrusion, scaling,



Fig. 8. Avatar (Female).



Fig. 9. Avatar (Male).

and sculpting, to refine the mesh into the desired form, meticulously focusing on details such as facial features, body proportions, and clothing. As we progressed with the modeling procedure, we referred to reference images or concept art to steer our work. The ultimate outcome was a breathtaking portrayal of the female and male avatars, as displayed in Fig. 8 and Fig. 9.

TABLE IV. TENSE RECOGNITION RESULTS

| English Sentence | Tense Identified | Actual Tense |
|---------------------------------|--------------------|--------------------|
| She is reading a book. | Present Continuous | Present Continuous |
| They will arrive tomorrow. | Future Simple | Future Simple |
| I have eaten dinner. | Present Perfect | Present Perfect |
| He plays the guitar. | Present Simple | Present Simple |
| We had studied for the test. | Past Perfect | Past Perfect |
| You should go to bed early. | Present Simple | Present Simple |
| The party was fantastic! | Past Simple | Past Simple |
| It is raining outside. | Present Continuous | Present Continuous |
| She will have finished by then. | Future Perfect | Future Perfect |

IV. DISCUSSION: RESULTS AND ANALYSIS

Throughout our diligent research, we carefully monitored the outcomes at various stages to guarantee precise conversion from English to Indian Sign Language. Our comprehensive results include a detailed step-by-step analysis for each phase, commencing with the speech recognition process. During this stage, the input consists of audio speech, which we process to transform it into text using our sophisticated speech recognition algorithm. We implemented the model in Python.

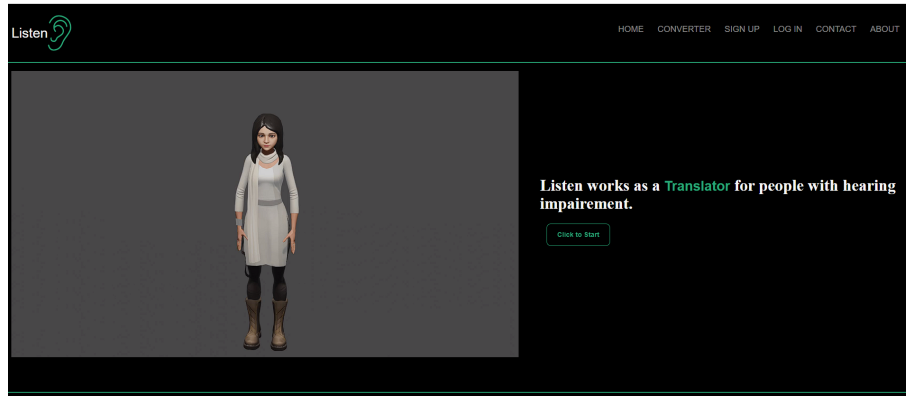


Fig. 10. Home page of Listen.

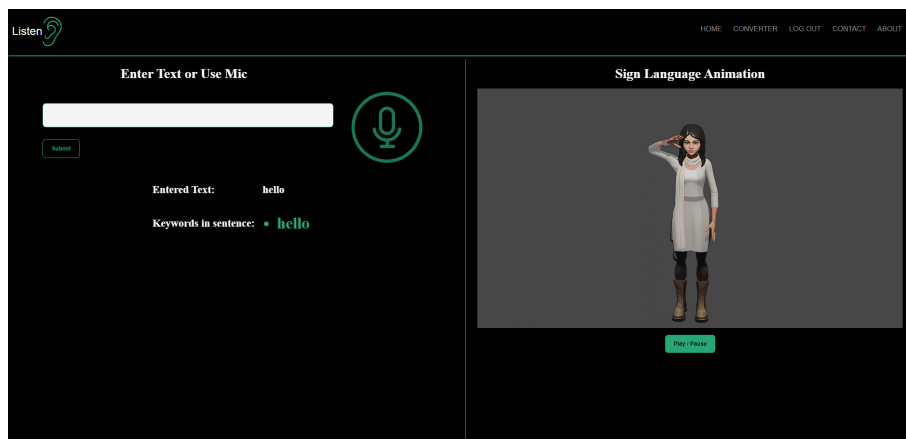


Fig. 11. Hello by Listen.

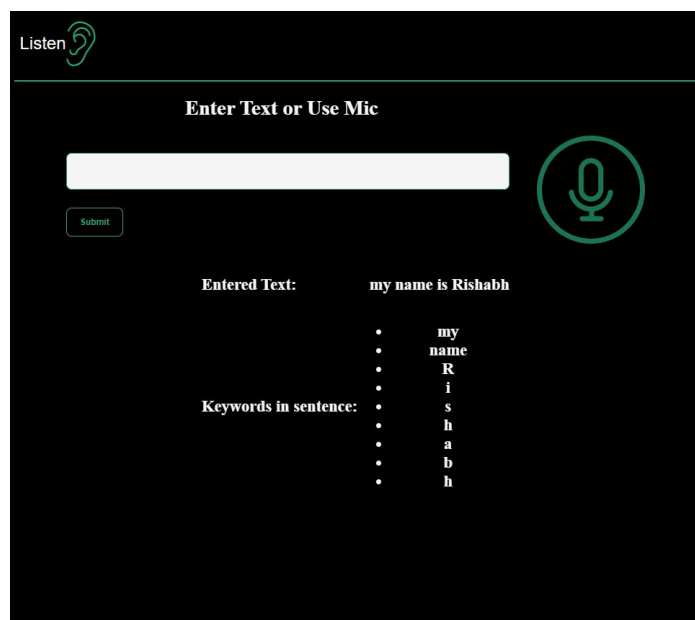


Fig. 12. Input text and keywords identification.

TABLE V. ISL SENTENCE RESULTS

| English Sentence | Sentence after reordering | ISL Sentence |
|------------------------------|---------------------------|---------------------------------|
| she has 10 books | she 10 books has | she 10 books |
| go to sleep | sleep go to | sleep go |
| I shall go after you | I after you shall go | later me after you go |
| I like my college | I my college like | me my college like |
| you are watching a movie | you movie are watching | now you movie watch |
| Rahul can change it | Rahul can it change | later Rahul can it change |
| show me your hands | me your hands show | me your hands show |
| Amit went alone | Amit alone went | before Amit alone go |
| define computer | define computer | define computer |
| Ram gave a flower to Sita | Ram flower gave Sita | before Ram flower give Sita |
| She made coffee for Shashwat | she coffee Shashwat made | before she coffee Shashwat make |
| we are waiting for Shashwat | we Shashwat are waiting | now we Shashwat wait |

Implementation details are given in Table III which shows environment used to implement the different components of our *Listen* model. A snapshot of the home page of the model is shown in Fig. 10. Furthermore, we have included the outcomes of our conversion process from English text to Indian Sign Language sentence structure, along with a side-by-side comparison of our output and the actual sign language sentence structure as shown in Fig. 11. Additionally, we have incorporated a screenshot of the final output page, which showcases captivating hand sign animation videos. The following subsections include the results obtained of the speech-to-text conversion, tense recognition and phrase reordering followed by 3D modeling of the obtained outputs. Detailed explanations of the subsections are as follows:

A. Speech to Text

This section includes the snapshot of the result when the word ‘my name is Rishabh’ is pronounced and is added in Fig. 12. The entered text and keyword in the sentence both are extracted.

B. Tense Recognition and Phrase Reordering

This phase deals with the tense recognition and phrase reordering of the preprocessed input data. First we are identifying the tense of the sentences using POS tags this is required for adding a timeline to ISL sentences. Some examples of Tense Recognition results are shown in Table IV.

Once the tense of the sentence is recognized next step is to reorder the sentence according to the sentence structure of Indian Sign Language. The snapshot of the data set tested is shown in Table V. Note that sentences with present continuous/ past indefinite/ future tenses etc. are treated differently since we need to add ‘Now’ ‘Before’ or ‘Later’ at the beginning of such sentences for correct ISL interpretation.

C. 3D Animations

ISL sentence is sent to the 3D model and sign language animations were obtained for female and male avatar. Screenshot for the animation of word ‘hello’ is shown in Fig. 11.

Images/ screenshots at a particular moment of a word in 3D animations of the female and male avatars for 10 test cases (5 test cases for each avatar) are shown Table VI and Table VII.

Our proposed model, *Listen*, has made significant strides in the recognition of tense and operates with great efficiency in the following areas:

- Tense recognition
- It does not rely on pre-designed notations, such as the Hamburg Notation System (HamNoSys) [17].
- It is specifically designed to work with the Indian Sign Language, which has not been extensively studied in the past.

As a result of our research, we are able to successfully achieve our objectives. We compared the performance of our model with existing models as shown in Table VIII. The accuracy of our *Listen* model is of 99.21% and sensitivity is 98.73% which is better than the existing models in the line of research.

V. CONCLUSION AND FUTURE WORK

In conclusion, speech-to-sign research has the potential to revolutionize communication and interaction for those with hearing impairments. By bridging the gap between the hearing communities, it promotes digital accessibility and inclusion. We achieved optimal results by implementing a robust methodology that involved data collection, pre-processing, sign language recognition, text pre-processing, text-to-sign language translation, 3D modelling of animations and evaluation of model. The system achieved accurate results that were adaptable, user-friendly, accessible, and scalable, with a diverse dataset on which the proposed model *listen* was trained. Our research focuses on converting English audio to Indian Sign Language (ISL), which presents unique challenges due to the absence of specific grammatical rules. Our model has yet to accomplish the task of animating facial expressions to denote negative and interrogative sentences. We plan to include ISL for phrases in the next phase, along with non-manual components for the sentence as a whole. Our goal is to improve

TABLE VI. IMAGES OF AVATAR (FEMALE) FOR TEST CASES











| Sentence | Word | Result |
|---------------------------|-------|---|
| She has 10 books. | 10 |  |
| Go to sleep. | sleep |  |
| I shall go after you. | after |  |
| I like my college. | my |  |
| You are watching a movie. | you |  |

TABLE VII. IMAGES OF AVATAR (MALE) FOR TEST CASES

| Sentence | Word | Result |
|----------------------|-----------|---|
| Rahul can change it. | change |  |
| Show me your hands. | hands |  |
| Amit went alone. | alone |  |
| Define computer. | computer |  |
| Thank you. | thank you |  |

the quality of life for individuals with hearing impairments and promote inclusiveness in society.

REFERENCES

[1] Kaur, S. and Singh, M., 2015, September. Indian Sign Language animation generation system. In 2015 1st International Conference on Next Generation Computing Technologies (NGCT) (pp. 909-914). IEEE.

[2] Lexdis: Accessible Technology For Learning, ATBar, <https://www.lexdis.org.uk/digital-accessibility/what-is-digital-accessibility-and-inclusion/>, accessed on 18 August 2023.

[3] World Health Organizations, Deafness and hearing loss, <https://www.who.int/health-topics/hearing-loss>, accessed on 05 August 2023.

[4] Kahlon, N.K. and Singh, W., 2023. Machine translation from text to sign language: a systematic review. Universal Access in the Information Society, 22(1), pp.1-35.

[5] Sugandhi, Parateek Kumar, and Sanmeet Kaur. Sign language generation system based on indian sign language grammar. ACM Transactions on

TABLE VIII. COMPARISON FOR PERFORMANCE

| S. No. | Paper | Accuracy | Sensitivity |
|--------|-------------------------|---------------|---------------|
| 1 | Lalit Goyal et al. [18] | 94.35% | 92.89% |
| 2 | Krunal et al. [19] | 94.53% | 93.45% |
| 3 | Sugandhi et al. [20] | 96.67% | 94.02% |
| 4 | Kulkarni et al. [21] | 97.86% | 94.56% |
| 5 | Proposed Model | 99.21% | 98.73% |

Asian and Low-Resource Language Information Processing (TALLIP), 19(4):1–26, 2020.

[6] M Naik Sulabha, S Naik Mahendra, and Sharma Akriti. Rehabilitation of hearing impaired children in india-an update. Online Journal of Otolaryngology, 3(1):20, 2013.

[7] Abhisek Mishra, Anu N Nagarkar, and Nitin M Nagarkar. Challenges in education and employment for hearing impaired in india. Journal of Disability Management and Special Education, 1(1):35, 2018.

- [8] S Rajeswari and J Karthika. Voice based email assistance for visually impaired—a comprehensive review. 2023.
- [9] Muhammad Yasir, Marlinec NK Nababan, Yonata Laia, Windania Purba, Asaziduhu Gea, et al. Web-based automation speech-to-text application using audio recording for meeting speech. In Journal of physics: conference series, volume 1230, page 012081. IOP Publishing, 2019.
- [10] Santosh K Gaikwad, Bharti W Gawali, and Pravin Yannawar. A review on speech recognition technique. International Journal of Computer Applications, 10(3):16–24, 2010.
- [11] Tony Veale, Alan Conway, and Bróna Collins. The challenges of cross-modal translation: English-to-sign-language translation in the zardoz system. Machine Translation, pages 81–106, 1998.
- [12] MICHELE Wakefield. Visicast. Final Report, page 97, 2002.
- [13] Shah, A., Kattel, M., Nepal, A. and Shrestha, D., 2019. Chroma feature extraction. Chroma Feature Extraction using Fourier Transform.
- [14] Industrial-Strength Natural Language Processing, spaCY, <https://spacy.io/>, accessed on 30 august 2023.
- [15] Blender, Blender 3.6 LTS, <https://www.blender.org/>, accessed on 30 august 2023.
- [16] Sabrina J Mielke, Zaid Alyafeai, Elizabeth Salesky, Colin Raffel, Manan Dey, Matthias Gallé, Arun Raja, Chenglei Si, Wilson Y Lee, Benoît Sagot, et al. Between words and characters: A brief history of open-vocabulary modeling and tokenization in nlp. arXiv preprint arXiv:2112.10508, 2021.
- [17] Hanke, T., 2004, May. HamNoSys-representing sign language data in language resources and language processing contexts. In LREC (Vol. 4, pp. 1-6).
- [18] Goyal, L., Goyal, V., Development of Indian Sign Language Dictionary using Synthetic Animations, Indian Journal of Science and Technology, 9(32), 2016. <https://doi.org/10.17485/ijst/2016/v9i32/129404>.
- [19] K. Saija, S. Sangeetha and V. Shah, WordNet Based Sign Language Machine Translation: from English Voice to ISL Gloss, 2019 IEEE 16th India Council International Conference (INDICON), Rajkot, India, 2019, pp. 1-4, doi: 10.1109/INDICON47234.2019.9029074.
- [20] Sugandhi, Kumar, P. and Kaur, S., 2020. Sign language generation system based on Indian sign language grammar. ACM Transactions on Asian and Low-Resource Language Information Processing (TALLIP), 19(4), pp.1-26.
- [21] Kulkarni, A., Kariyal, A.V., Dhanush, V. and Singh, P.N., 2021, September. Speech to indian sign language translator. In 3rd International Conference on Integrated Intelligent Computing Communication & Security (ICIIC 2021) (pp. 278-285). Atlantis Press.
- [22] Kwarteng, P. and Chavez, A., 1989. Extracting spectral contrast in Landsat Thematic Mapper image data using selective principal component analysis. Photogramm. Eng. Remote Sens, 55(1), pp.339-348.
- [23] Natural Language Toolkit, NLTK Project, created with Sphinx and NLTK Theme, <https://www.nltk.org/>, accessed on 30 august 2023.
- [24] Matthew P Huenerfauth. American sign language natural language generation and machine translation systems. Technical report, Technical Report, computer and information sciences, University of Pennsylvania, 2003.
- [25] Zeeshan Bhatti, Ahsan Abro, Abdul Rehman Gillal, and Mostafa Karbasi. Be-educated: Multimedia learning through 3d animation. arXiv preprint arXiv:1802.06852, 2018.

Developing a Patient-Centric Healthcare IoT Platform with Blockchain and Smart Contract Data Management

Duc B. T.¹, Trung P. H. T.², Trong N. D. P.³, Phuc N. T.⁴, Khoa T. D.⁵,
Khiem H. G.⁶, Nam B. T.⁷, Bang L. K.⁸
Nguyen Tat Thanh University, Ho Chi Minh City, Viet Nam¹
FPT University, Can Tho City, Viet Nam^{2,3,4,5,6,7,8}

Abstract—The Internet of Things (IoT) has been rapidly integrated into various industries, with healthcare emerging as a key area of impact. A notable development in this sector is the IoHT-MBA system, a specialized Internet of Healthcare Things (IoHT) framework. This system utilizes a microservice approach combined with a brokerless architecture, efficiently tackling issues like data gathering, managing users and devices, and controlling devices remotely. Despite its effectiveness, there's a growing need to improve the privacy and control of patient data. To address this, we propose an enhanced version of the IoHT-MBA system, incorporating blockchain technology, specifically through the use of Hyperledger Fabric. This integration aims to create a more secure, transparent, and patient-centric data management platform. The system enables patients to oversee their peripheral devices, such as smartphones and sensors. These devices are integrated as part of the edge layer of the IoHT, contributing to a decentralized storage service. In our model, data is primarily retained on user devices, with only summarized data being communicated to service providers and recorded on the blockchain. This approach significantly boosts data privacy and user control. Access to user data is strictly regulated and must align with the patient's privacy conditions, which are established through smart contracts, thus providing an additional layer of security and transparency. We have conducted an evaluation of our blockchain-enhanced platform using key theories in microservice and brokerless architecture, such as Round Trip Time and Broken Connection Test Cases. Additionally, we've performed tests on data generation and queries using Hyperledger Caliper. The results confirm the strength and efficiency of our blockchain-integrated system in the healthcare IoT domain.

Keywords—Medical test result; blockchain; smart contract; NFT; Ethereum; Fantom; polygon; binance smart chain

I. INTRODUCTION

The landscape of the Internet of Things (IoT) has broadened substantially, now covering sectors including smart urban development, medical care, logistical supply chains, industrial processes, and agrarian practices. Forecasts indicate that by the year 2023, IoT-connected devices globally are expected to escalate to 43 billion, a significant increment from the figures recorded in 2018 [1]. Concurrently, investments in IoT infrastructure are anticipated to witness an annual growth of 13.6% up to the year 2022 [1]. Notably, the healthcare industry is a major adopter, constituting 20% of total IoT applications, only marginally behind smart city ventures at 29% [2]. Despite these advances, IoT systems are contending with challenges such as latency (27%), power consumption (18%), and system

dependability (14%) [2].

Healthcare and Blockchain: The healthcare sector, in particular, grapples with inefficiencies in patient data handling and emergency response mechanisms [3], [4]. This has prompted an increased focus on blockchain technology as a strategic solution for healthcare operational improvements [5]. With its decentralized, secure ledger infrastructure, blockchain is aptly positioned to address these issues, offering a patient-oriented model for health record management [6]. Such an approach grants patients greater control over their medical records, enhancing trust and collaborative interaction within healthcare frameworks [7].

Blockchain-Enhanced IoHT System: This paper introduces the full version of our previous work [8]. This innovative system merges blockchain with IoT, forming a blockchain-centric, patient-focused healthcare framework that incorporates smart contracts for efficient data governance. This solution addresses the shortcomings of existing IoT models by offering a secure, dependable, and efficient approach to healthcare data management.

Our designed platform utilizes blockchain for reliable and verifiable patient data recording. It features a brokerless and microservice architecture, guaranteeing resilience, scalability, and uninterrupted operation. The platform employs Role-based Access Control (RBAC) combined with a hierarchical approach to user management, allowing for comprehensive oversight of platform constituents like users and devices.

Incorporating blockchain, the platform facilitates secure and trustworthy data exchanges, overcoming key challenges inherent in traditional healthcare systems. Smart contracts are employed to streamline healthcare data management, thereby elevating the system's operational efficiency and reliability. This research makes significant contributions in several areas:

- Developing a patient-centered framework using microservice and brokerless architecture to improve system resilience, scalability, and availability.
- Implementing blockchain for enhanced transparency in data storage, enabling secure and trackable data exchange.
- Utilizing smart contracts to reinforce security, particularly in interactions between patients and service

providers, and to automate data management processes.

- Demonstrating a practical application of our model, showcasing its relevance and transformative potential in healthcare data management.
- Conducting a thorough evaluation of the system's architecture and blockchain integration, underlining its advantages over conventional healthcare data management methods.

Organization of the Paper: The remainder of this paper is organized as follows: Section II provides a review of the current state of healthcare data management systems and the role of blockchain in this context. Section III delves into the details of our Blockchain-Enhanced IoHT model, discussing its architecture, implementation, patient-centric focus, and the integration of blockchain technology and smart contracts. Following this, Section IV presents an assessment of our system, examining its performance and effectiveness. Finally, Section V concludes the paper, summarizing our key observations and exploring potential future research avenues.

II. RELATED WORK

A. IoT Architectural Models in Healthcare

Diverse architectural solutions for gathering data from medical devices have been explored in literature. Maktoubian et al. [9] put forth an architecture that amalgamates MQTT protocol with Kafka Message Queue. Despite Kafka ensuring secure data transfer, MQTT protocol and its brokering structure encounter issues like possible single point failures and ambiguous Quality-of-Service (QoS) levels [10], [11]. Their system's security protocols remain largely unaddressed.

Another approach by Taher et al. [12] describes an IoT-cloud system aimed at medical data assimilation and processing. Although comprehensive, it depends on the MQTT protocol, which is hampered by security concerns [13]. Partha Pratim Ray [14] introduced a system for medical data collection using web socket and HTTP, yet these protocols have high memory demands and are not optimal for low-end devices [15].

Ha Xuan Son et al. [16] developed a patient emergency system employing blockchain on Hyperledger Fabric, with a focus on access control. However, the data collection method from patients and the system's scalability aspects were not elaborated upon.

B. Microservice and Brokerless Architecture in IoHT

Jita et al. [17] developed a home-based medical care system using a scalable microservice architecture, enhanced with blockchain security. The system, however, is based on the Zetta IoT Platform, utilizing HTTP and RESTful protocols, which are less efficient for low-end devices [15]. While other studies [18], [19] acknowledge the significance of microservices in healthcare, they fall short in practical implementation details.

Di Zeng et al. [20] introduced a medical system model that combines microservice with a brokerless structure, but it remains unimplemented. Similarly, Lam et al. [21], [22], [23]

illustrated architectures incorporating MQTT broker, Single Sign-On, and Kafka message queue, achieving a compromise between transmission efficiency, reliability, and security.

C. Blockchain Implementation in Healthcare Systems

Blockchain technology has been incorporated into healthcare systems with varying focal points. Son et al. [3] and Le et al. [4] devised blockchain-based frameworks for access control in emergencies, prioritizing patient data confidentiality.

Le et al. [5] devised a blockchain system for medical waste management, underlining the need for secure information sharing about medical equipment and supplies, especially pertinent during the COVID-19 crisis. In another study, Le et al. [24] proposed a blockchain system for blood donation networks, tackling blood quality, supply, and distribution challenges.

Quynh et al. [25] suggested a blockchain system for managing national blood donation networks, streamlining blood supply and demand. Duong et al. [6], [7] proposed patient-focused healthcare systems utilizing blockchain smart contracts, emphasizing patient access, traceability, and control over health records.

These studies underscore the efficacy of blockchain in bolstering data security, privacy, and patient-centric approaches in healthcare. Our research builds upon these foundations, introducing a blockchain-enhanced IoHT platform that combines microservice and brokerless architecture to augment scalability, efficiency, and control over patient data.

III. SYSTEM ARCHITECTURE

A. Architectural Overview of Blockchain-Enhanced IoHT-MBA Platform

The proposed blockchain-enhanced IoHT-MBA platform is based on a layered architecture, incorporating the edge layer, blockchain layer, and cloud layer.

1) *Edge Layer*: The edge layer includes local devices of the patient like smartphones, sensors, and other IoT devices, functioning as the primary data collectors and processors. Each of these devices is integrated with a simplified blockchain client, facilitating communication with the blockchain layer. Data retention on these devices is localized, bolstering both privacy and security.

2) *Blockchain Layer*: At the heart of our patient-centric data management system lies the blockchain layer. Leveraging Hyperledger Fabric, a permissioned blockchain framework, we establish a secure, transparent ecosystem for data handling. Here, only synthesized health data and related transactions are stored. The validation and recording of transactions across various nodes reinforce data integrity and traceability. Smart contracts, or chaincodes in Hyperledger Fabric, automate agreement execution pertaining to data sharing. These contracts encode patient privacy conditions, executing upon data access or sharing requests to ensure compliance with patient preferences.

3) *Cloud Layer*: The cloud layer offers diverse services like data analytics and health monitoring to platform users. It interfaces with the blockchain layer for data access, adhering to privacy terms defined in smart contracts and accessing only aggregated blockchain data.

This structure of the platform ensures a secure, decentralized, and patient-focused data management approach in healthcare IoT. Subsequent sections will elaborate on the platform's implementation and evaluation.

B. Detailed Architecture

The system's design incorporates microservices and brokerless architecture, enhancing fault tolerance, scalability, and operational efficiency. Microservices architecture refers to developing applications as a collection of small, autonomous services, each operating in its own environment and communicating through lightweight mechanisms like HTTP/REST with JSON or Protobuf. In our case, gRPC is employed for enhanced speed¹. This architecture allows for independent updating, deployment, and scaling of individual services. The brokerless architecture removes the necessity for a central broker or server, thus eliminating single points of failure and enhancing scalability. It allows direct communication among nodes or devices, crucial for reliability and efficiency in healthcare settings.

The combination of these architectures equips our system to efficiently manage a vast array of devices and data while maintaining high availability and performance. Further sections will detail the patient-side data consumption in edge computing (refer to Fig. 1) and the overall architecture of the Blockchain-Enhanced IoHT platform (refer to Fig. 2).

1) *Edge Computing Architecture*: The edge computing component encompasses two primary layers: the Things layer and the Client layer (see Fig. 1).

a) *Things Layer*: This layer consists of various medical devices owned by the patient, like wearables and IoT medical devices. Each device is outfitted with sensors to gather crucial health data. These devices manage two independent services: data collection and control services. Data collection involves continuous monitoring and streaming to edge computing services, with patient authentication and authorization checks for data security. The control service enables remote adjustments to the devices, catering to specific health needs and preferences.

b) *Client Layer*: The Client layer, represented by patients, allows device management and data monitoring. Patients control their health data, managing sharing permissions and ensuring their privacy preferences are upheld. This layer's centrality to the architecture underlines the patient-centric nature of data management in our platform.

Edge computing in our platform processes data near its source, minimizing latency and enhancing real-time processing. Patient control over devices and data underscores the platform's focus on patient autonomy and privacy.

2) *Blockchain-Enhanced IoHT Architecture*: Fig. 2 depicts the Blockchain-Enhanced IoHT platform architecture, enabling

secure and efficient data transmission from medical devices to the distributed ledger and service providers.

a) *Data Processing Services*: Post-collection at the edge, health data undergoes further processing in data processing services. Tasks include data cleaning, transformation, and feature extraction. Aggregated data, instead of raw patient data, is stored in the blockchain for enhanced efficiency and privacy.

b) *Distributed Ledger and Smart Contracts*: Aggregated data is stored in the distributed ledger, validated by multiple nodes for integrity. Smart contracts in our system serve two functions:

- **Data Access Control**: Smart contracts contain metadata parameters reflecting patient privacy preferences. Service provider access requests are checked against these parameters, ensuring compliance with patient privacy conditions.
- **Data Usage Control**: They also regulate how service providers can use the data, adhering to conditions set within the contract.

c) *Service Providers*: Service providers, including healthcare professionals and researchers, access ledger-stored data. Their access is contingent on meeting the privacy conditions set in the smart contracts.

The Blockchain-Enhanced IoHT platform thus ensures patient control over their data, while facilitating secure and transparent data sharing with service providers.

IV. EVALUATION SCENARIOS

A. Evaluating Performance Using Microservice and Brokerless Architectural Approach

1) *Configuration of the Test Environment*: Our innovative Blockchain-Enhanced IoHT system utilizes a microservice architecture for optimal performance. During our evaluation phase, the services of this platform were hosted on the Amazon EC2 platform². We configured each service to mirror a virtual machine setup, equipped with 1GB of RAM and a single vCPU for realistic testing conditions. Additionally, client-side services, including data collection and control, were implemented on the Raspberry Pi 3 model B+ modules³. These modules are powered by the Broadcom BCM2837, an ARMv8 (64bit) quad-core processor clocking at 1.2 GHz, and are also furnished with 1GB RAM, providing a robust environment for our system's deployment and testing.

2) *Evaluation of Round Trip Time*: In gauging the efficacy of data transmission within the system, the Round Trip Time (RTT) is employed, measured from the instance data is transmitted from IoT devices until it reaches the Message Queue. Alongside this, an examination of the error rate, quantified as the ratio of lost messages to the total, is conducted. For a thorough assessment, instances of EC2 VMs equivalent to the Raspberry Pi model B + module are generated in diverse geographical locations. These locations encompass North California, Stockholm, Ho Chi Minh City, and Sydney.

²<https://aws.amazon.com/>

³<https://www.raspberrypi.org/products/raspberry-pi-3-model-b/>

¹For detailed implementation, see our prior work [26], [27]

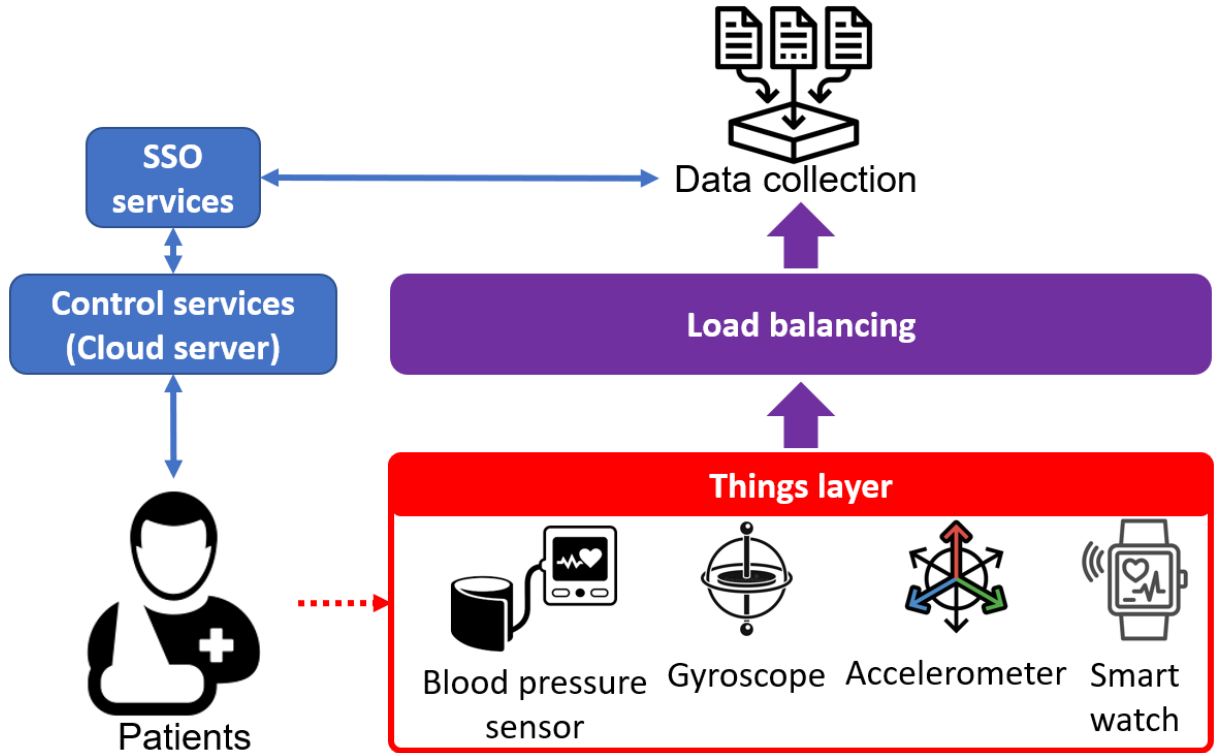


Fig. 1. Patient-side edge computing based on microservice and brokerless architecture.

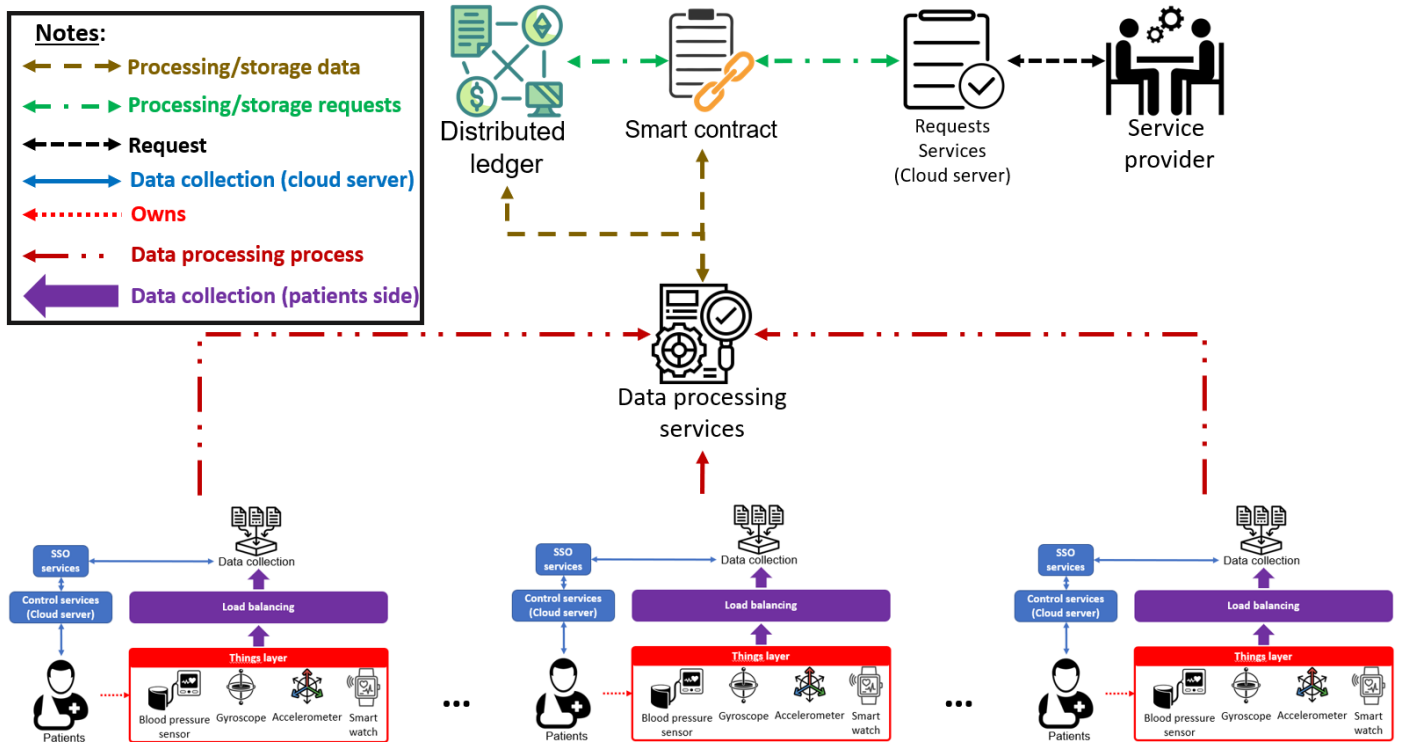


Fig. 2. Blockchain-Enhanced IoHT platform architecture.

The objective is to analyze the impact of location on both delay time and error rate during the streaming of data. The findings from these evaluations are succinctly summarized in Table I.

Table I illustrates the Round Trip Time (RTT) and error rates associated with data communication in the Blockchain-Enhanced Internet of Health Things (IoHT) platform, observed across diverse geographical locations: North California, Stockholm, Ho Chi Minh City, and Sydney. The RTT is examined for varying message volumes: 1,000; 5,000; 10,000; 50,000; and 100,000.

The RTT, in this context, measures the time taken for a message to travel from an IoT device (sender) to the Message Queue (receiver) and back.

The table provides the following insights:

- In North California, RTT ranges from 3.23 seconds for 1,000 messages to 259.11 seconds for 100,000 messages, with a consistent 0% error rate across all message volumes.
- In Stockholm, RTT varies from 3.41 seconds for 1,000 messages to 259.43 seconds for 100,000 messages, maintaining a 0% error rate for all message volumes.
- In Ho Chi Minh City, RTT spans from 3.62 seconds for 1,000 messages to 259.98 seconds for 100,000 messages, accompanied by a 0% error rate across all message volumes.
- In Sydney, RTT ranges from 3.21 seconds for 1,000 messages to 258.06 seconds for 100,000 messages, with a consistent 0% error rate for all message volumes.

The error rate represents the proportion of lost messages during transmission. A 0% error rate across locations and message volumes indicates flawless transmission without any losses.

This table underscores the Blockchain-Enhanced IoHT platform's robust performance across varied geographical locations and message volumes. Despite increasing message volumes, the RTT exhibits linear growth, and the platform demonstrates resilience by maintaining a 0% error rate, affirming its reliability.

3) *Robustness Against Connection Failures:* Evaluating the performance of the Blockchain-Enhanced Internet of Health Things (IoHT) platform under connection failures is vital, especially in healthcare applications where data integrity and reliability are paramount. Disruptions in data transmission can potentially lead to incorrect diagnoses or interventions, significantly impacting patient care.

To gauge the system's resilience in the face of connection failures, we conducted simulations of broken connections between the data publisher (i.e., the healthcare IoT device) and the subscriber (i.e., the data processing or storage service). We then compared the number of messages received by the subscriber in scenarios with and without the utilization of the Blockchain-Enhanced IoHT platform.

As illustrated in Fig. 3, in the absence of our platform, the subscriber only captures the latest message sent by the

publisher when a connection failure occurs. This limitation arises from the retain function of the MQTT protocol⁴ which retains only the most recent message, resulting in the loss of any data published during the disconnection period.

Conversely, when employing the Blockchain-Enhanced IoHT platform, the subscriber receives all messages published by the sender, including those transmitted during the connection failure. This capability is facilitated by the Kafka message queue, which preserves all outgoing messages until successful delivery, thereby preventing any data loss during transmission.

The capacity to recover and process all data following a connection failure is a critical attribute for a healthcare IoT system. It ensures the reliable reception of all patient data irrespective of network conditions, preserving the integrity of medical data and facilitating accurate and comprehensive analysis for improved patient care outcomes.

B. Evaluation of Performance using Hyperledger Fabric

To comprehensively gauge the efficacy of our proposed Blockchain-Enhanced Internet of Health Things (IoHT) model, an in-depth performance analysis was carried out utilizing Hyperledger Caliper, a benchmarking tool tailored for blockchain systems. The focal performance indicators included the count of successful and unsuccessful requests, transaction rate (Send Rate in transactions per second, or TPS), latency (maximum, minimum, and average, in seconds), and throughput (TPS).

Our assessment encompassed five distinct scenarios, each representing varying loads on the system (ranging from 1,000 to 5,000 requests per second). The evaluation ceased at 5,000 requests per second, as we observed a notable surge in the number of failed requests beyond this threshold, particularly in scenarios involving data updates.

1) *Medical Data Creation Performance:* Table II delineates the performance metrics for medical data creation under diverse loads. Notably, the count of successful requests oscillates between 27,000 and 31,000, while failed requests range from 16,000 to 19,000. Interestingly, the correlation between the number of successful and failed requests and the system load appears inconclusive, underscoring the robustness of our platform. The transaction rate remains consistent across all scenarios, hovering between 135 and 150 transactions per second (TPS).

Regarding latency, the maximum latency spans from approximately 1,457 seconds (for 3,000 requests per second) to around 1,712 seconds (for 5,000 requests per second). Minimum latency varies from under 1 second (for 1,000 requests per second) to approximately 12 seconds (for 3,000 requests per second). The average latency fluctuates between 650 and 700 seconds per request, contingent on the system load. Meanwhile, throughput maintains steady performance within the range of 12 to 17 TPS.

2) *Performance Evaluation of Medical Data Queries:* To assess the system's performance under varying data query loads, we conducted tests across five scenarios, ranging from 1,000 to 5,000 data retrieval requests per second. As depicted in Table III, the count of successful requests consistently

⁴For further details, we refer the reader to our prior publications [28], [27]

TABLE I. ROUND TRIP TIME RESULTS IN THE FOUR PLACES

| Location | Factor | 1,000 | 5,000 | 10,000 | 50,000 | 100,000 |
|------------------|----------|-------|-------|--------|--------|---------|
| North California | RTT(s) | 3.23 | 13.78 | 27.42 | 131.16 | 259.11 |
| | Error(%) | 0 | 0 | 0 | 0 | 0 |
| Stockholm | RTT(s) | 3.41 | 13.98 | 25.86 | 129.14 | 259.43 |
| | Error(%) | 0 | 0 | 0 | 0 | 0 |
| Ho Chi Minh city | RTT(s) | 3.62 | 13.74 | 24.93 | 131.11 | 259.98 |
| | Error(%) | 0 | 0 | 0 | 0 | 0 |
| Sydney | RTT(s) | 3.21 | 14.02 | 26.08 | 129.98 | 258.06 |
| | Error(%) | 0 | 0 | 0 | 0 | 0 |

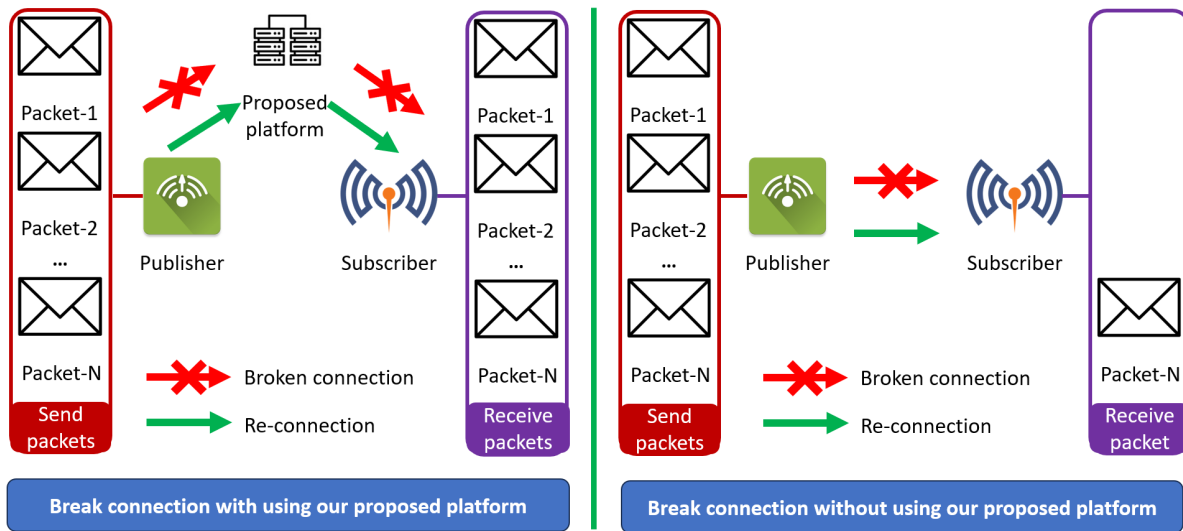


Fig. 3. Number of received messages when the system recovers after a broken connection issue.

TABLE II. MEDICAL DATA CREATION PERFORMANCE IN FIVE INCREASING EACH 1,000 REQUESTS SCENARIOS

| Name | Success | Fail | Send Rate (TPS) | Max Latency (s) | Min Latency (s) | Avg Latency (s) | Throughput (TPS) |
|---------------|---------|--------|-----------------|-----------------|-----------------|-----------------|------------------|
| 1,000 request | 26,987 | 19,801 | 135.0 | 1,532.18 | 10.41 | 654.12 | 11.9 |
| 2,000 request | 29,604 | 16,402 | 138.5 | 1,523.78 | 9.82 | 634.21 | 16.4 |
| 3,000 request | 27,412 | 18,523 | 142.7 | 1,457.34 | 10.43 | 678.43 | 15.3 |
| 4,000 request | 29,617 | 19,176 | 139.9 | 1,686.23 | 10.67 | 651.24 | 15.4 |
| 5,000 request | 30,401 | 16,205 | 145.6 | 1,712.12 | 11.01 | 696.18 | 17.2 |

surpasses 106,000, with failed requests remaining below 5,000. This noteworthy outcome underscores the system’s capability to effectively retrieve a substantial volume of medical data under significant loads. Analogous to the data creation scenario, both the Send Rate (TPS) and Throughput (TPS) exhibit stability, experiencing minor fluctuations around 325 to 360 and approximately 290, respectively.

Concerning system latency, maximum latency remains approximately 250 seconds across all five measurement scenarios. The minimum latency is virtually negligible, at about 0.01 seconds. On average, each data query request receives a response within roughly 5 seconds. These outcomes illustrate the efficiency of our Blockchain-Enhanced IoHT platform in managing both data creation and retrieval requests, crucial operations in a patient-centric Internet of Healthcare Things system.

C. Discussion

The evaluation of our proposed Blockchain-Enhanced IoHT system yields valuable insights into its performance and efficiency. The system’s brokerless and microservice architecture, coupled with a blockchain-based data management approach, showcases its potential to handle a substantial number of data transactions while maintaining low latency and high throughput.

The system underwent testing under diverse load conditions, with request volumes ranging from 1,000 to 5,000 per second. Even under heightened loads, the system demonstrated resilience and stability, sustaining a consistent response time and minimal error rates. The brokerless architecture, employing the gRPC protocol, exhibited notable improvements in CPU and RAM usage compared to other IoHT protocols, indicative of efficient resource utilization.

TABLE III. MEDICAL DATA QUERY PERFORMANCE IN FIVE INCREASING EACH 1,000 REQUESTS SCENARIOS

| Name | Success | Fail | Send Rate (TPS) | Max Latency (s) | Min Latency (s) | Avg Latency (s) | Throughput (TPS) |
|---------------|---------|-------|-----------------|-----------------|-----------------|-----------------|------------------|
| 1,000 request | 103,321 | 4,232 | 356.0 | 254.14 | 0.01 | 4.89 | 289.18 |
| 2,000 request | 108,208 | 4,456 | 323.5 | 256.23 | 0.01 | 5.08 | 298.45 |
| 3,000 request | 103,661 | 4,281 | 345.8 | 252.51 | 0.01 | 4.23 | 294.01 |
| 4,000 request | 108,129 | 4,928 | 341.4 | 250.65 | 0.01 | 4.83 | 293.21 |
| 5,000 request | 106,224 | 3,265 | 323.9 | 256.12 | 0.01 | 5.01 | 298.11 |

V. DISCUSSION

A. Remarkable Insights

As we delve into the intricacies of gas metrics across various blockchain platforms, a plethora of distinct patterns and insights emerge, which hold significant relevance for both blockchain developers and users alike.

1) *Uniformity vs. Variability*: One of the notable observations is the trade-off between uniformity and variability in gas pricing. The BNB Smart Chain stands out for its uniformity, maintaining a consistent gas price of 0.00000001 BNB (equivalent to 10 Gwei) across all actions. This predictability can be advantageous for users as it ensures a constant expectation of costs. In contrast, platforms like Polygon introduce minor discrepancies in gas prices across different operations. While these variations might seem subtle, they can accumulate substantial costs in high-frequency actions, making it a critical consideration for blockchain investors and developers.

2) *Cost-Efficiency*: Fantom's gas pricing strategy is particularly noteworthy, with a remarkably lower gas price of 3.5 Gwei compared to BNB Smart Chain's 10 Gwei. This significant difference can translate into considerable cost savings for users engaged in large transaction volumes. It underscores the importance of gas pricing as a pivotal factor influencing the economic feasibility of utilizing a particular blockchain platform.

3) *Complexity in Pricing*: Polygon's nuanced gas pricing structure may arise from its inherent design or a deliberate effort to fine-tune pricing for specific operations. While this complexity might introduce challenges for the average user, it offers enhanced flexibility for businesses and developers. The ability to tailor gas costs for different operations can be advantageous for optimizing resource allocation in specific use cases.

4) *Operational Capacity and Efficiency*: Efficiency in gas consumption during operations is another critical aspect to consider. For instance, Celo demonstrates that it utilizes only 76.92

5) *Strategic Implications for Projects*: The insights gained from this analysis have strategic implications for blockchain projects, especially startups and new ventures. Beyond just the direct costs, factors such as operational efficiency, pricing flexibility, and predictability play a crucial role in platform selection. These considerations can significantly influence decisions regarding project launches, investments, and day-to-day transactions.

6) *User Considerations*: For the average user, clarity and predictability in transaction costs are paramount. Platforms with transparent and straightforward pricing models may be more attractive. On the other hand, platforms that offer flexibility in pricing and demonstrate optimal resource consumption

may be favored by traders, businesses, and advanced users seeking to fine-tune their operations.

B. Future Directions

In the subsequent phases of our research, we are eager to delve even deeper into the intricacies of transaction costs and gas metrics. This will involve the integration of advanced methodologies and intricate data structures. Specifically, we plan to implement sophisticated encryption-decryption techniques to provide a clearer and more detailed picture of transaction overheads [29]. Taking our proposed model from theoretical analysis to practical application is another exciting avenue of exploration. We intend to execute the recommendation system over the Fantom (FTM) mainnet to validate its performance in real-world scenarios. This real-world validation will help us refine our model and make it more robust.

Furthermore, our current analysis has not explored the nuances of user privacy policies, which are of paramount importance in today's digital transactions [30], [31]. Building upon established research in access control and dynamic policy models, we envision enhancing our system's capabilities to address these privacy concerns comprehensively [16].

From an infrastructural standpoint, we are considering the integration of modern techniques and paradigms such as gRPC, Microservices, dynamic messaging paradigms, and brokerless models [26], [21]. These integrations will not only augment the robustness of our framework but also enhance user interactions, particularly in terms of API-driven communication [23]. This forward-looking approach will ensure that our research remains at the forefront of blockchain technology advancements [22], [27].

VI. CONCLUSION

In this research, we introduced a cutting-edge, patient-centric framework known as the Blockchain-Enhanced IoHT. This innovative system integrates a microservice and brokerless architecture, significantly enhancing its fault tolerance, scalability, and overall availability. Such an architecture not only fortifies the system's robustness but also renders healthcare data management more efficient and resilient. The incorporation of blockchain technology into the system guarantees secure and easily traceable data sharing, effectively tackling the prevalent challenges faced in traditional healthcare systems. Moreover, the employment of smart contracts in this model reinforces security, especially in managing the interactions between patients and healthcare providers, thus boosting the system's efficiency and dependability. The proof-of-concept showcased within this study validates the practicality and potential of our proposed model in revolutionizing healthcare data management. Our evaluation of the Blockchain-Enhanced

IoHT, focusing on its architectural design and blockchain integration, sheds light on its capabilities in managing healthcare data efficiently.

Looking ahead, our future endeavors will concentrate on refining the system's performance further. This includes exploring avenues to amplify the scalability and efficiency of the blockchain component and delving into the integration of more sophisticated security measures. Our ultimate goal is to propel advancements in the realm of healthcare data management, aiming to substantially improve patient care and outcomes.

REFERENCES

- [1] F. Dahlqvist *et al.*, "Growing opportunities in the internet of things," *McKinsey*, July, 2019.
- [2] P. Asghari *et al.*, "Internet of things applications: A systematic review," *Computer Networks*, vol. 148, pp. 241–261, 2019.
- [3] H. X. Son *et al.*, "Toward a blockchain-based technology in dealing with emergencies in patient-centered healthcare systems," in *Mobile, Secure, and Programmable Networking: 6th International Conference, MSPN 2020, Paris, France, October 28–29, 2020, Revised Selected Papers 6*. Springer, 2021, pp. 44–56.
- [4] H. T. Le *et al.*, "Patient-chain: patient-centered healthcare system a blockchain-based technology in dealing with emergencies," in *International Conference on Parallel and Distributed Computing: Applications and Technologies*. Springer, 2021, pp. 576–583.
- [5] —, "Medical-waste chain: a medical waste collection, classification and treatment management by blockchain technology," *Computers*, vol. 11, no. 7, p. 113, 2022.
- [6] N. Duong-Trung *et al.*, "Smart care: integrating blockchain technology into the design of patient-centered healthcare systems," in *Proceedings of the 2020 4th International Conference on Cryptography, Security and Privacy*, 2020, pp. 105–109.
- [7] —, "On components of a patient-centered healthcare system using smart contract," in *Proceedings of the 2020 4th International Conference on Cryptography, Security and Privacy*, 2020, pp. 31–35.
- [8] T. Nam *et al.*, "Spamer: Securing patient medical records in the cloud-a microservice and brokerless architecture approach," in *International Conference on Web Services*. Springer, 2023, pp. 32–46.
- [9] J. Maktoubian and K. Ansari, "An iot architecture for preventive maintenance of medical devices in healthcare organizations," *Health and Technology*, vol. 9, no. 3, pp. 233–243, 2019.
- [10] M. B. Yassein, M. Q. Shatnawi, S. Aljwameh, and R. Al-Hatmi, "Internet of things: Survey and open issues of mqtt protocol," in *2017 international conference on engineering & MIS (ICEMIS)*. IEEE, 2017, pp. 1–6.
- [11] J. Toldinas, B. Lozinskis, E. Baranauskas, and A. Dobrovolskis, "Mqtt quality of service versus energy consumption," in *2019 23rd International Conference Electronics*. IEEE, 2019, pp. 1–4.
- [12] N. C. Taher, I. Mallat, N. Agoulmine, and N. El-Mawass, "An iot-cloud based solution for real-time and batch processing of big data: Application in healthcare," in *2019 3rd International Conference on Bio-engineering for Smart Technologies (BioSMART)*. IEEE, 2019, pp. 1–8.
- [13] J. J. Anthraper and J. Kotak, "Security, privacy and forensic concern of mqtt protocol," in *Proceedings of International Conference on Sustainable Computing in Science, Technology and Management (SUSCOM)*, Amity University Rajasthan, Jaipur-India, 2019.
- [14] P. Pratim Ray, D. Dash, and N. Moustafa, "Streaming service provisioning in iot-based healthcare: An integrated edge-cloud perspective," *Transactions on Emerging Telecommunications Technologies*, vol. 31, no. 11, p. e4109, 2020.
- [15] M. Bansal *et al.*, "Application layer protocols for internet of healthcare things (ioht)," in *2020 Fourth International Conference on Inventive Systems and Control (ICISC)*. IEEE, 2020, pp. 369–376.
- [16] H. X. Son *et al.*, "Toward a privacy protection based on access control model in hybrid cloud for healthcare systems," in *International Joint Conference: 12th International Conference on Computational Intelligence in Security for Information Systems (CISIS 2019)*. Springer, 2020, pp. 77–86.
- [17] H. Jita and V. Pieterse, "A framework to apply the internet of things for medical care in a home environment," in *Proceedings of the 2018 International Conference on Cloud Computing and Internet of Things*, 2018, pp. 45–54.
- [18] R. Hill, D. Shadija, and M. Rezai, "Enabling community health care with microservices," in *2017 IEEE International Symposium on Parallel and Distributed Processing with Applications and 2017 IEEE International Conference on Ubiquitous Computing and Communications (ISPA/IUCC)*. IEEE, 2017, pp. 1444–1450.
- [19] H. X. Son *et al.*, "Towards a mechanism for protecting seller's interest of cash on delivery by using smart contract in hyperledger," *International Journal of Advanced Computer Science and Applications*, vol. 10, no. 4, 2019.
- [20] D. Zheng, X. Zhang, and L. Chen, "Research of new integrated medical and health clouding system based on configurable microservice architecture," in *2020 IEEE 23rd International Conference on Computational Science and Engineering (CSE)*. IEEE, 2020, pp. 78–85.
- [21] T. T. L. Nguyen *et al.*, "Toward a unique iot network via single sign-on protocol and message queue," in *Computer Information Systems and Industrial Management: 20th International Conference*. Springer, 2021, pp. 270–284.
- [22] L. N. T. Thanh *et al.*, "Toward a security iot platform with high rate transmission and low energy consumption," in *Computational Science and Its Applications—ICCSA 2021: 21st International Conference*. Springer, 2021, pp. 647–662.
- [23] —, "Uip2sop: a unique iot network applying single sign-on and message queue protocol," *International Journal of Advanced Computer Science and Applications*, vol. 12, no. 6, 2021.
- [24] H. T. Le *et al.*, "Bloodchain: a blood donation network managed by blockchain technologies," *Network*, vol. 2, no. 1, pp. 21–35, 2022.
- [25] N. T. T. Quynh *et al.*, "Toward a design of blood donation management by blockchain technologies," in *Computational Science and Its Applications—ICCSA 2021: 21st International Conference*. Springer, 2021, pp. 78–90.
- [26] L. T. T. Nguyen *et al.*, "Bmdd: a novel approach for iot platform (broker-less and microservice architecture, decentralized identity, and dynamic transmission messages)," *PeerJ Computer Science*, vol. 8, p. e950, 2022.
- [27] L. N. T. Thanh *et al.*, "Sip-mba: a secure iot platform with brokerless and micro-service architecture," *International Journal of Advanced Computer Science and Applications*, vol. 12, no. 7, 2021.
- [28] —, "Ioht-mba: an internet of healthcare things (ioht) platform based on microservice and brokerless architecture," *International Journal of Advanced Computer Science and Applications*, vol. 12, no. 7, 2021.
- [29] K. L. Quoc *et al.*, "Sssb: An approach to insurance for cross-border exchange by using smart contracts," in *Mobile Web and Intelligent Information Systems: 18th International Conference*. Springer, 2022, pp. 179–192.
- [30] H. X. Son and N. M. Hoang, "A novel attribute-based access control system for fine-grained privacy protection," in *Proceedings of the 3rd International Conference on Cryptography, Security and Privacy*, 2019, pp. 76–80.
- [31] N. M. Hoang and H. X. Son, "A dynamic solution for fine-grained policy conflict resolution," in *Proceedings of the 3rd International Conference on Cryptography, Security and Privacy*, 2019, pp. 116–120.

GROCAFAST: Revolutionizing Grocery Shopping for Seamless Convenience and Enhanced User Experience

Abeer Hakeem, Layan Fakhurji, Raneem Alshareef, Elaf Aloufi, Manar Altairy,
Afraa Attiah, Linda Mohaisen

Department of Information Technology, Faculty of Computing and Information Technology
King Abdulaziz University, Jeddah, Saudi Arabia

Abstract— This paper presents the Smart Grocery Shopping system (GROCAFAST), a system for optimizing the grocery shopping experience and improving efficiency for shoppers. The GROCAFAST system consists of a mobile app and a server component. The mobile app allows shoppers to create, manage, and update grocery lists while providing store navigation assistance. The server component processes data, generates optimized route maps, maintains an inventory database, and facilitates the online chat room. Unlike existing grocery shopping systems, GROCAFAST is cost-effective as it does not rely on any extra infrastructure and reduces both shopping time and walking steps. GROCAFAST utilizes Dijkstra’s algorithm to efficiently guide shoppers through the store, minimizing the time needed to visit all aisles containing their desired items. The user-friendly interface and time-saving features make grocery shopping more efficient and enjoyable. The evaluation results demonstrate that GROCAFAST reduces the total shopping time by 67.6% when compared to a traditional approach that mimics the way shoppers visit a grocery store, browse aisles, and select items. It also reduces the walking steps by 59%.

Keywords—Grocery shopping app; route map; grocery shopping experience; dijkstra’s algorithm

I. INTRODUCTION

Grocery shopping is one of the most common chores in our lives, yet it is still stressful. Everyone needs to go to grocery stores to buy food, drinks, laundry supplies, etc. However, shopping for groceries is not as simple as one may think. It demands preparation, clarity, and commitment. Each trip to the grocery store takes an average of 41 minutes, which equates to approximately 53 hours annually¹. In the United States, a typical grocery shopping trip takes about 40 minutes, though most of the grocery shopping is done by women (59 minutes/week), and men (29 minutes/week) [1]. If we include travel time, which is about 15 minutes per trip, and consider the fact that people, on average, go grocery shopping 1.5 times per week, it accounts for close to 6 hours of grocery shopping per month for women [2].

Grocery shopping can sometimes feel overwhelming and challenging, with various obstacles that can waste valuable time and cause frustration. Some of the issues that shoppers may encounter are: (1) Inefficient navigation: many shoppers spend a significant amount of time zigzagging through the store aisles, trying to locate all the items on their list. (2) Difficulty

finding specific items: it can be frustrating when shoppers can’t find a particular item in the store, especially when they are supposed to be in a specific section. (3) Unavailability of expected items: shoppers may have certain expectations of the store’s inventory, but when they can’t find an item they need or it’s out of stock, it can be disappointing and inconvenient. These challenges highlight the need for effective strategies to streamline the grocery shopping experience and save valuable time.

Making a paper grocery list could help in navigating the store more efficiently by not having to wander aimlessly around the store and make decisions on the fly. Research shows that people who make grocery lists prior to going to the store buy fewer items, spend less money, and make fewer unplanned and impulsive purchases [3]. There is also some evidence that people who make paper grocery lists make fewer unplanned purchases [4]. However, the paper list is less convenient and lacks organization and categorization, making it difficult to locate items quickly in the store and potentially leading to backtracking, which consumes valuable time.

To address the challenges of inefficient navigation, difficulty finding specific items, and unavailability of expected items during grocery shopping, it’s important to come up with a solution that reduces shopping time. This paper proposes a Smart Grocery Shopping system (GROCAFAST) is proposed. GROCAFAST provides shoppers with a route map that shows items on the grocery list arranged in the same order as they appear in the store, making it more efficient to navigate through the aisles and find the items quickly. By aligning the list with the store’s layout, shoppers can minimize backtracking and save time during their shopping trips. GROCAFAST does not need any tracking infrastructure, as it relies on maintaining a route map that guides shoppers through the store. The map is designed to optimize the shopping journey by directing shoppers through the aisles that contain the items on their grocery list. Furthermore, GROCAFAST allows shoppers to easily create, manage, and update their grocery lists. It also allows them to quickly search for specific items and view their exact location within the store. It is important to notice that GROCAFAST leverages shoppers’ previous lists and preferences to provide personalized shopping suggestions. Finally, it provides an online chat room where shoppers can engage with each other, share reviews, and exchange recommendations.

GROCAFAST comprises a mobile app and a server, work-

¹<https://www.creditdonkey.com/grocery-shopping-statistics.html>

ing together to enhance the grocery shopping experience. The mobile app allows shoppers to efficiently create, manage, and update their grocery lists. It also provides store navigation assistance, displaying a map of the store with highlighted aisles, departments, and checkout counters. Shoppers can view their optimized route based on their grocery list, guiding them through the store efficiently and saving shopping time. The server component manages grocery lists, generates route maps, maintains a comprehensive inventory database, analyzes shoppers' preferences, and facilitates an online chat room or community platform for sharing reviews and recommendations. Together, GROCAFAST streamlines grocery shopping by combining convenient list management, efficient navigation, and personalized assistance.

GROCAFAST efficiently achieves its goal by leveraging the power of Dijkstra's algorithm, a widely recognized method for finding the shortest path in a graph [5]. Specifically tailored to guiding shoppers through a store, this algorithm is employed to generate an optimized route that minimizes the time necessary to visit all the aisles containing the items on the shopper's grocery list. By utilizing Dijkstra's algorithm, GROCAFAST ensures an efficient and streamlined shopping experience for its shoppers.

In our comparative analysis, we assess the performance of GROCAFAST, an innovative grocery shopping solution, against the traditional method of physically visiting a grocery store, browsing aisles, and selecting items. Our objective is to explore the advantages of GROCAFAST in terms of time efficiency, device compatibility, and overall user experience. The experiments were conducted at a real grocery store situated in the female dormitory at King Abdulaziz University. The findings revealed remarkable benefits of GROCAFAST, including a staggering 67.6% reduction in shopping time and a significant decrease of 59% in walking steps when compared to the traditional grocery shopping approach. These results underline GROCAFAST's potential to revolutionize the shopping experience and enhance efficiency for shoppers.

The main contributions of this paper are:

- Design and implementation of GROCAFAST, a Smart Grocery Shopping system that combines efficient navigation, convenient list management, personalized assistance, and community engagement to streamline the grocery shopping experience.
- Utilize Dijkstra's algorithm to generate optimized routes, ensuring efficient and time-saving shopping trips for shoppers.
- The experiments are conducted at a real grocery store situated in the female dormitory at King Abdulaziz University. This real-world setting allowed us to evaluate GROCAFAST's performance in a practical environment.
- In our comparative analysis, we assess the performance of GROCAFAST, an innovative grocery shopping solution, against the traditional method of physically visiting a grocery store. Our objective is to explore the advantages of GROCAFAST in terms of time efficiency, device compatibility, and overall shopper experience.

The rest of this paper is organized as follows. Section II discusses the related work. Section III presents a system design. A system overview is presented in Section IV. The Experimental setup and evaluation are presented in Section V, and Section VI, simultaneously. The paper concludes in Section VII.

II. RELATED WORK

Most would agree that avoiding spending more time than intended and avoiding food waste are important goals. But dealing with the onslaught of temptations when grocery shopping can be difficult. One of the tools that makes this task easier is a shopping list. Thus, numerous applications have been developed to enhance the convenience, efficiency, and overall shopping experience for shoppers. Table I illustrates the difference between GROCAFAST and other applications. The table also demonstrates the features of GROCAFAST when compared to the applications. In the following, we briefly discuss each of these applications in relation to GROCAFAST.

For instance, SMART LIST [6], Smart Shopping List [7], AnyList [8], Listonic [9], and Grocery-Smart Shopping List [10] aim to enhance convenience and efficiency in creating, organizing, and managing shopping lists. On the other hand, both MyGrocery [11] and ShopLister [12] take it a step further by suggesting missing items based on user preferences, purchase history, or popular items. Further, AnyList, MyGrocery, ShopLister, and Instacart [13], not only focus on list management but also offer features that assist shoppers in finding nearby supermarkets or locating items within a store. Although, GROCAFAST shares the common goal of enhancing convenience and efficiency in grocery shopping; however, GROCAFAST differentiates itself. GROCAFAST aims to provide a comprehensive and tailored shopping experience by combining personalized suggestions, optimized route mapping, list history retrieval, and an interactive community platform.

TABLE I. FEATURES COMPARISON BETWEEN GROCAFAST AND OTHER AVAILABLE APPLICATIONS

| Applications | Features | | | | |
|-------------------------|-------------------------|---------------------|--------------|--------------------------|---------------------|
| | Grocery List Management | In-store Navigation | Search Items | Personalized Suggestions | Community Chat Room |
| SMART LIST | ✓ | | | | |
| The Smart Shopping List | ✓ | | | | |
| AnyList | ✓ | | | ✓ | |
| Listonic | ✓ | | | | |
| Grocery | ✓ | | | | |
| MyGrocery | ✓ | | | ✓ | |
| ShopLister | ✓ | | ✓ | ✓ | |
| Instacart | ✓ | ✓ | | ✓ | |
| GROCAFAST | ✓ | ✓ | ✓ | ✓ | ✓ |

Advancements in technology have revolutionized the grocery shopping experience by introducing innovative solutions that enhance efficiency and convenience. One such solution is indoor navigation technology, which streamlines the shopping process by providing shoppers with real-time guidance within the store. Indoor navigation systems employ various technologies to offer accurate location information within a store environment. Bluetooth Low Energy (BLE) beacons [14]

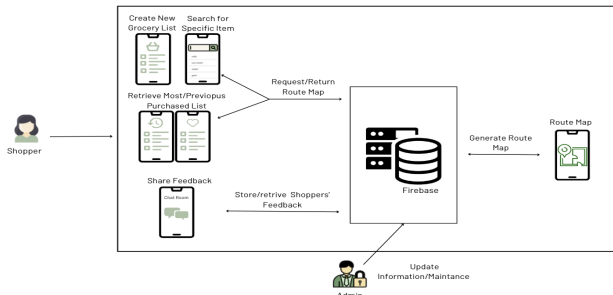


Fig. 1. GROCAFAST system architecture.

are commonly used sensors that guide users based on their precise location. Alternatively, indoor positioning systems (IPS), such as IndoorAtlas [15], utilize technologies such as Wi-Fi signals, RFID tags, or computer vision to accomplish the same goal [16]. However, the implementation of indoor navigation technologies requires careful consideration of associated costs and maintenance requirements. Infrastructure deployment costs primarily stem from the purchase and installation of required hardware components. It is worth noting that these technologies involve the tracking of shoppers' movements and the collection of data on their behavior, raising concerns regarding privacy and security. In contrast, GROCAFAST, a cost-effective system, presents an alternative approach. GROCAFAST leverages advanced algorithms to provide indoor positioning and navigation functionality without the need for additional infrastructure. This approach eliminates the costs and maintenance associated with hardware installations.

Efficient indoor navigation in grocery stores relies on solving the shortest path problem [17]. Various algorithms have been developed for this purpose, including Dijkstra's algorithm, Bellman-Ford, and Floyd-Warshall algorithms [18]. Among these algorithms, Dijkstra's algorithm [19] stands out for its adaptability and effectiveness in grocery store contexts, especially when GPS signals are limited or unavailable. The Bellman-Ford and Floyd-Warshall algorithms can be utilized, but their higher time complexity may limit their practicality in large-scale scenarios [20], [21]. Authors in [22] used the A-star algorithm with a heuristic technique to minimize the time and effort needed for shopping. However, developing a heuristic function can accurately capture the unique characteristics of a grocery store environment and guide the route optimization process. This adds additional overhead and is not flexible with edge weights. Further, it requires careful consideration of factors such as store layout, product placement, congestion patterns, and other relevant aspects that influence customer movement within the store. GROCAFAST, an indoor navigation system, leverages the simplicity and effectiveness of Dijkstra's algorithm. Dijkstra's algorithm considers a uniform cost for traversal, making it well-suited for indoor environments where movement costs are often similar. Additionally, GROCAFAST benefits from the flexibility of adjusting edge weights, and extends to optimize for alternative metrics such as travel time, congestion avoidance, or energy efficiency, providing adaptability to diverse indoor navigation requirements.

III. SYSTEM DESIGN

Our design goal is to propose a solution that addresses the challenges individuals encounter during their grocery shopping process. The GROCAFAST system aims to significantly enhance shoppers' experiences by reducing shopping time and minimizing unnecessary foot steps. By introducing in-store navigation capabilities based on shoppers' grocery lists, this system brings a revolutionary change to the way people navigate within a grocery store, all without requiring any additional infrastructure. Our solution focuses on streamlining and optimizing the shopping journey to ensure a more efficient and convenient experience for every shopper.

The system consists of the following entities: users, mobile app, server. Fig. 1 shows the high-level architecture of the system which demonstrates how GROCAFAST enables smooth communication among these components. This interconnected communication network enables a smooth and efficient shopping experience for shoppers.

Users: are categorized in the GROCAFAST system into two types: shoppers and admin. Shoppers, as depicted in Fig. 1, interact with the system primarily through the mobile app. They can input their grocery list, search for specific items in the store, retrieve most/previous purchased list, and share feedback through the chat room. On the other hand, admin has a distinct role within the system. The admin is responsible for managing the Firebase database and server.

Mobile app: provides shoppers with different interfaces that allow them to interact with the app to access their grocery lists, adding or removing items, making updates as needed, and requesting a grocery navigation map. The application acts as the intermediary between the shopper and server in order to handle shopper requests, process data, and provide relevant information.

GROCAFAST Server: acts as the backbone of the system. The server would store and manage the shoppers' grocery lists in the Firebase database. Firebase is a central repository of information, storing data such as store layouts, product details, location of each item, and shopper preferences. Shoppers can interact with the server through GROCAFAST app, accessing their lists, adding or removing items, and making updates as needed. The server would handle the data storage and retrieval from the database, ensuring that shoppers have access to their lists. Also, the server would have access to the store's layout and product inventory information. Based on the shopper's grocery list, the server would utilize Dijkstra's algorithms to generate an optimized route map. This map would guide shoppers through the store, indicating the most efficient path to take. Further, the server would analyze shoppers' previous lists and preferences stored in the database and facilitate the creation and management of an online chat room or community platform. Shoppers could join the chat room through the app, and the server would handle the communication and interaction between shoppers.

IV. SYSTEM OVERVIEW

This section presents an overview of GROCAFAST, focusing on how to plan a shopping route that reduces shopping time. A shopper opens the GROCAFAST app on their

smartphone and logs in using their registered account. Upon successful login, they gain access to the app's features designed for shoppers. As a shopper, they are directed to the home page where they can explore various functionalities. The home page provides a user-friendly interface, allowing them to conveniently navigate through the app's offerings. They notice several options available to them. First, they decide to create a new grocery list for their upcoming shopping trip. They click on the "Create grocery list" feature and are presented with a form where they can add, edit, and manage their list. This feature enables them to conveniently add or remove items as needed. They start by adding essential household items to their list. While creating the list, they notice that the app suggests personalized recommendations based on their shopping history and preferences. This feature saves them time and effort as they can effortlessly select and add items to their current list based on their previous purchasing patterns. Next, in case they want to find the exact location of certain items within the grocery store, they utilize the "Search Items" feature, entering the name of the item they are looking for. Then, the app quickly retrieves the item's location within the store and displays it on the screen. This feature helps them navigate the store efficiently and locate the items they need without unnecessary wandering. After finalizing their grocery list and searching for specific items, the optimized route map through the store is generated. The graph-based search algorithm (i.e., Dijkstra) automatically analyzes their list and creates a route map that guides them through the store's aisles, ensuring they take the most efficient path to collect all the listed items. This feature streamlines their shopping experience and saves them time. This feature eliminates the need for them to recreate the same grocery list repeatedly. They can effortlessly retrieve an old grocery list and obtain the route map directly for the selected list, making their shopping trips even more efficient. As a final touch, they notice that GROCAFAST offers an online chat room where shoppers can engage with each other in a real-time. They decide to join the chat room to share their shopping experiences, exchange recommendations, and seek advice from other shoppers. This feature enhances their overall shopping experience and allows them to feel more connected to the community of GROCAFAST users. However, if the user has admin privileges, they are directed to the admin page, which grants them exclusive access to perform actions like adding and deleting items from the system.

GROCAFAST aims to optimize the shopping experience and save shoppers time. To meet these requirements, GROCAFAST uses Dijkstra's algorithm when a shopper loads a previous list, creates a new list, or searches for a specific item (see Fig. 2). Dijkstra's algorithm generates the most efficient route for the shopper to follow within the grocery store. The shopper's grocery list is organized based on the store layout to ensure the shopper can navigate through the store in a systematic manner, saving time and effort. Although there are several algorithms that can solve the shortest path problem, Dijkstra's algorithm is often considered an optimal choice for various applications. Several reasons support this choice: (1) it is compatible with non-negative edge weights, which proves advantageous for GROCAFAST. This compatibility allows the system to disregard factors that obstruct movements within the grocery store, such as walls or obstacles that are not relevant to the shortest path calculation; (2) it operates with a

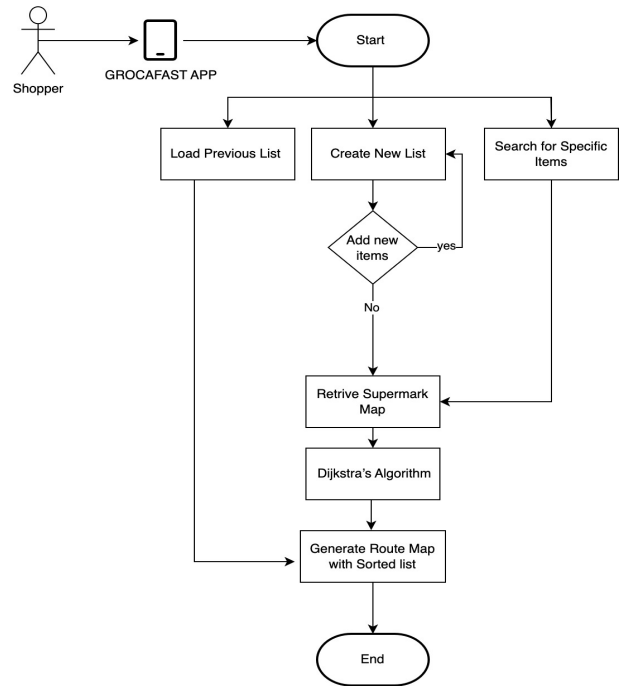


Fig. 2. System flowchart.

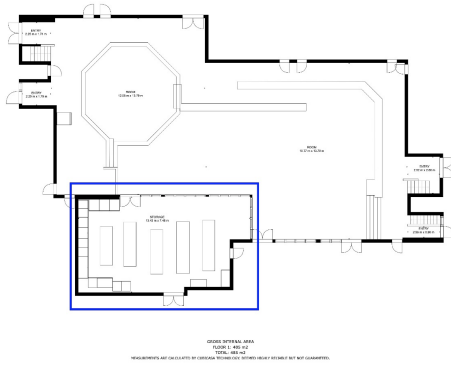
singular source node, which aligns well with GROCAFAST's requirement of considering the entrance point of the grocery store as the starting location for path finding; (3) it excels in efficiency by storing and updating only the shortest path at each iteration. This approach minimizes computational time and effort, making it suitable for real-time or dynamic scenarios where the grocery store layout or item locations might change.

A. Grocery Shopping Route Map

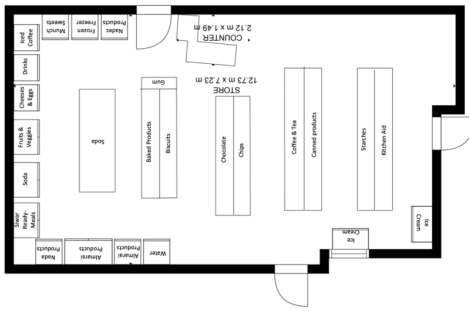
In order to facilitate efficient navigation for shoppers, we create a route map that optimizes the shopping experience based on the specific items shoppers need to find in the grocery store. GROCAFAST uses a floor map of a local grocery store and Dijkstra's algorithm to find the shortest navigation path on the map.

To start, the grocery store map is converted into a graph representation, where each node corresponds to a location within the store (aisles, departments, checkout counters, etc.). The connections between nodes represent the pathways or transitions between locations (see Fig. 3a). Edge weights are assigned based on the distance or effort required to move between locations. The starting point, which is the entrance of the store, and the ending point, such as the checkout counter or exit, are determined (see Fig. 3b). The floor plan is transformed into a matrix format with each cell representing a distinct unit of space. This matrix serves as the basis for applying Dijkstra's algorithm to enable efficient route planning within the grocery store. Fig. 3c shows a visual representation of the matrix of the floor plan.

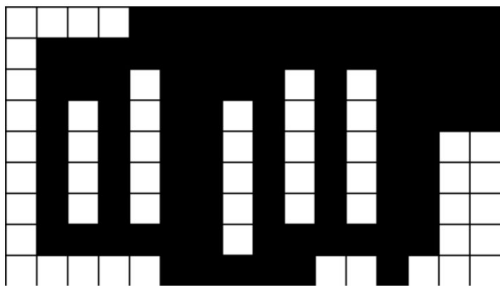
The shopper's grocery list is obtained, consisting of specific items they want to purchase. Dijkstra's algorithm is adapted to



(a) A visual representations of the grocery store map.



(b) A visual representation of the grocery store components.



(c) A visual representation of the matrix of the floor plan.

Fig. 3. Floor Plan Transformation

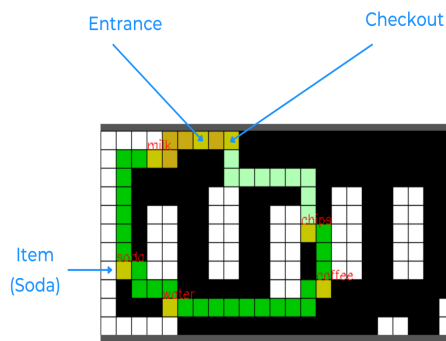


Fig. 4. The shortest navigation path using dijkstra's algorithm.

consider the grocery list items and their corresponding locations. Instead of calculating the shortest path between arbitrary points, the algorithm calculates the shortest path that visits all the required item locations in the most efficient manner. The

nodes are initialized with a distance of infinity, except for the starting node, which is assigned a distance of 0. The algorithm selects the node with the smallest distance, as the current node and visits its neighboring nodes. Once the algorithm completes, the shortest path is retrieved by traversing the tracked previous nodes backward from the checkout counter or exit node to the starting node. As Fig. 4 shows, this path represents the shortest route on the map that visits all the required item locations and indicates the sequence of locations to efficiently collect all the items on the list.

B. GROCAFAST Features

This section offers various functionalities and capabilities provided by the GROCAFAST. It presents a detailed overview of each feature, accompanied by its respective interface, and a comprehensive description to provide a comprehensive overview of how each feature works and how it contributes to the overall functionality of GROCAFAST. Fig. 5 demonstrates the interfaces of these features. The following overview of each feature offers detailed insights into their functionalities and showcases their contribution to the overall capabilities of GROCAFAST.

Creating a Grocery List: Users can create a grocery list on the application. Upon successful creation, the list is stored in the database, allowing the user to view the sorted list. However, if the user either duplicates an existing item in the list or attempts to create an empty list, an error message is displayed, prompting the user to retry (see Fig. 5a).

Editing an Existing Grocery List: Users can modify their existing grocery lists. In successful scenarios, users can edit, append additional items, or remove unwanted entries from their lists. Subsequently, they can proceed to access the route map. However, if there is a failure in retrieving items from the database, users are prompted to retry the operation (see Fig. 5b).

Generating a Route Map with the Shortest Path: Users can access a route map generated by the application, designed to guide them through the grocery store based on their created grocery list. In successful scenarios, the route map is effectively generated, facilitating users in navigating the store according to their list. However, in the event of a failure, users are required to attempt the process again (see Fig. 5c).

Searching and Locating Items Within the Store: Users can search for items within the store, displaying their respective locations. In successful cases, the application effectively locates the searched item in the store, guiding the user to its location. However, if the item cannot be found, users are prompted to retry the search see Fig. 5d.

Displaying Personalized Shopping Suggestions: Upon creating a grocery list, it is stored in the database. It is then analyzed to identify the user's top three frequently purchased items, which are utilized to generate personalized shopping suggestions. In successful cases, the application presents these suggestions to the user when trying to write a grocery list. However, if the database fails to retrieve the top three frequently purchased items, the application prompts the user to rewrite the items (see Fig. 5e).



Fig. 5. GROCAFAST interface screenshots: streamlining grocery shopping with advanced features.

Posting in Store-Specific Online Communities: Users can create posts to share reviews within the communal space for

the same grocery store facilitated by the application. Successful posting results in the display of the user's post within the space. However, in case of a failure where the post cannot be displayed, the application prompts the user to retry (see Fig. 5f).

V. EXPERIMENTAL SETUP

In our experiments, we collaborated with a local grocery store at King Abdulaziz University's female dormitory to develop and test GROCAFAST. This strategic decision allowed us to conduct practical experiments and gather real-world data in a genuine shopping environment. By working closely with this grocery store, we are able to closely observe and analyze how GROCAFAST performs and interacts with the existing infrastructure. The walking time is considered as an average speed of 1.4 m/s, which is reasonable for adults (men and women) [23], [24].

We generate a set of shopping journeys for shoppers. While the starting locations of the shoppers are chosen at the supermarket entrance, the final steps are chosen at the cashier. The selected items are distinct and randomly chosen from different aisles. The shopping time of a shopper is calculated by the time of arrival at the supermarket until all the items on the list have been collected. This method provides the total duration spent during the shopping.

Further, we use Figma² which is a cloud-based design tool that works on any platform and provides real-time updates for its embedded files. It is a user-friendly tool that facilitates developer hand-off and communication. MySQL, Visual Studio Code, and Firebase are used to build GROCAFAST and its database. CubiCasa³ is used as a tool specialized in creating floor plans and 3D models of real estate properties using mobile devices.

VI. EXPERIMENTAL EVALUATION

In this section, we experimentally evaluate the performance of GROCAFAST comparable to the traditional grocery shopping method, in terms of (1) shopping time and effort (i.e., walking steps); (2) testing the GROCAFAST compatibility with different devices; and (3) measuring the benefits of GROCAFAST in terms of usability.

A. Performance Experiments

To evaluate the performance of GROCAFAST, two experiments were conducted. The first experiment aimed to measure the average shopping time required for shoppers to complete their shopping trips. This experiment focused on calculating the time taken to collect a specific set of items using a predefined grocery list. The second experiment aimed to assess the effort exerted by shoppers, specifically by estimating the number of steps taken inside the store.

In both experiments, three different grocery lists were used, each containing 4, 6, and 9 distinct items. To ensure fairness and eliminate potential bias in the experiments, a randomized approach is used to select the items in the shopping lists.

²<https://www.figma.com>

³<https://www.cubi.casa>

The goal is to create a diverse and representative sample of items from various categories available in the grocery store. By randomizing the selection process, we aim to minimize any systematic bias or favoritism towards specific items or categories.

Additionally, to further enhance fairness, care is taken to ensure that each shopper has no information about the supermarket layout and the distribution of items on their respective lists. This helped to level the playing field and ensure that any differences in shopping time are primarily attributed to the use of the GROCAFAST rather than varying levels of shopper familiarity.

To ensure the reliability of the results, each list is tested three times by three different shoppers. This repetition allowed for a more comprehensive evaluation of the GROCAFAST's performance. During the experiments, the time taken to complete each grocery list is recorded. This involved noting the duration from the start of shopping until all items on the list were collected. Additionally, the number of steps taken by shoppers to complete each list is also recorded and analyzed. With respect to the average shopping time and effort expended, we conducted a comparative experiment between GROCAFAST and traditional grocery shopping, the latter being a conventional method where shoppers rely on paper lists to navigate through the aisles, locate items, and make purchases at the store.

Fig. 6 shows the average shopping time for GROCAFAST compared to traditional grocery shopping. The graph indicates a significant reduction in shopping time when using the GROCAFAST. The reduction in shopping time observed can be attributed to the utilization of the Dijkstra algorithm, which efficiently calculates the shortest path for collecting items during the shopping process. This proves that the GROCAFAST is effective in optimizing the shopping experience, making it more efficient and time-saving for consumers. By utilizing the application's features, shoppers can navigate the store more seamlessly and locate their desired items with ease.

B. Discussion

The analysis of the results in terms of walking steps indicates that the use of the GROCAFAST significantly reduces the number of steps taken while shopping compared to traditional shopping methods. The graph in Fig. 7 shows that when using the GROCAFAST, shoppers take notably fewer steps to complete their shopping compared to shopping without GROCAFAST. This reduction in the number of steps suggests that the GROCAFAST effectively optimizes the shopping process by providing efficient in-store navigation. By guiding shoppers along the most optimal route, it helps them navigate through the store more seamlessly, minimizing unnecessary walking and backtracking.

The results obtained from testing GROCAFAST in the small local grocery store proved that GROCAFAST is an effective solution for a real-world problem and successfully attained the desired objective. The system successfully enhanced the grocery shopping experience for users, reducing both the number of steps taken and the time spent navigating through various grocery lists.



Fig. 6. Average shopping Time with and without GROCAFAST.

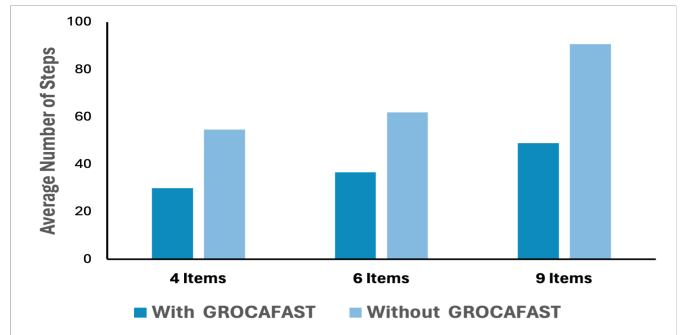


Fig. 7. Average number of shoppers' walking steps.

```
implementation 'com.google.firebase:firebase-analytics'  
implementation 'com.google.firebase:firebase-auth'  
implementation 'com.google.firebase:firebase-database'  
implementation 'com.google.firebase:firebase-storage'  
implementation 'com.google.firebase:firebase-crashlytics'  
implementation 'com.google.firebase:firebase-firestore'  
  
DatabaseReference databaseReference = FirebaseDatabase.getInstance().getReference("users");
```

Fig. 8. Intergration testing dependencies.

The positive results achieved in this performance testing set the stage for further exploration and implementation of GROCAFAST on a larger scale, offering the potential to revolutionize grocery shopping experiences for a wider user base.

C. Integration Testing

Integration testing verifies the proper interaction of various software components by combining and testing them together. Two types of testing were conducted, with the first focusing on Android Studio and Firebase integration. The first step involves establishing dependencies from Firebase and creating a database reference object, as shown in Fig. 8. The second category focused on integrating a function with its associated set of functions. As an example, the test case scenario for creating a grocery list was validated through a sequential process involving the creation of an account, logging in, and subsequently creating the actual grocery list.

TABLE II. COMPATIBILITY TESTING RESULTS

| Device | Android version | Memory space | Memory available | Pass/Fail |
|--------------------|-----------------|--------------|------------------|-----------|
| Google pixel 2 XL | 11 | 4 GB | 612 MB | Pass |
| Galaxy A10L | 11 | 2 GB | 314 MB | Pass |
| ZTE Blade 10 Smart | 9 | 4 GB | 1 GB | Pass |

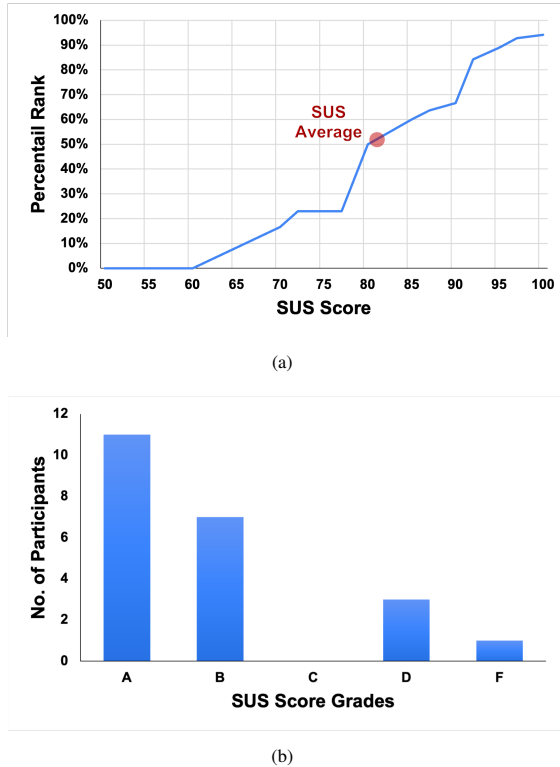


Fig. 9. SUS Score percentile rank and grades.

D. Compatibility Testing

Compatibility testing plays a vital role in ensuring that the GROCAFAST application (installed on the shopper’s smartphone) functions seamlessly across various platforms, devices, and operating systems. It guarantees a consistent user experience, meets technical requirements, and enhances user satisfaction and trust in the application’s reliability. Therefore, as shown in Table II, we test the GROCAFAST application on different devices with different capabilities. GROCAFAST application passes all the tests.

E. System Usability Scale (SUS)

To assess the usability of GROCAFAST, we employed the System Usability Scale (SUS) [25] as a reliable metric to measure the overall usability of GROCAFAST. The usability testing process involved gathering feedback from a diverse group of participants who interacted with the GROCAFAST.

The first ten questions from our participants QoE questionnaire (see Table III) incorporated the system usability (SUS) scale. This measures the satisfaction levels of shoppers through

such indicators as accessibility, usability, and effectiveness. The SUS calculations [26], [27] are conducted to process the participants’ responses to the SUS items in our questionnaire. These calculations are performed for each participant in our experiment. The results show (see Fig. 9), that the average SUS score from all 21 participants in our study is 82.73, which is higher than the SUS mean value of 68 [26].

In order to interpret these scores, the SUS score was normalized and converted to a percentile rank, as shown in Fig. 9a, and then the letter grades were generated from A to F. As can be seen in Fig. 9b, the percentile rank of the average SUS score (68) is 50%. According to Sauro [26], [27], our SUS scores were ranked as follows: A (>80.3, Excellent), B (68–80.3, Good), C (=68, 50%, Accepted), D (51–68, Poor), and F (<50, Awful). In the following bulleted items, the participants’ responses to the SUS questions are discussed for each item in turn:

Question1: I think that I would like to use this system frequently. As reported by participants, 67% of them would like to use the GROCAFAST in their daily life, with 24% being neutral regarding this (see Fig. 10, Question1).

Question2: I found the system unnecessarily complex. As shown in Fig. 10, Question2, a high proportion of the participants, 90%, enjoyed using the GROCAFAST whereas 5% did not enjoy it, and 5% reported being neutral regarding this.

Question3: I found the system was easy to use. Of the 21 participants who responded to this question, 76.5% strongly agreed that the application was easy to use and 0% were neutral. 10% only with issues were encountered in respect of ease of use (see Fig. 10 Question3).

Question4: I think that I would need the support of a technical person to be able to use this system. Almost 76% of the participants responded that the application did not need technical assistance; a minority of 14% claimed that it did, whilst 10% of participants were neutral on this issue (see Fig. 11 Question4).

Question5: I found the various functions in this system were well integrated. Overall 81% of participants found the GROCAFAST’s functions to be well integrated, with 5% being neutral regarding this (see Fig. 10 Question5).

Question6: I thought there was too much inconsistency in this system. As shown in Fig. 10 Question6, 90% participants found the system components to be coordinated. 10% were neutral about this, and no one disagreed.

Question7: I think that most people would learn to use this system very quickly. More than two-thirds of the participants reported that people would like to use this type of

TABLE III. SUS QUESTIONNAIRE QUESTIONS

| GROCAFAST System Usability | |
|----------------------------|---|
| 1 | I think that I would like to use this system frequently |
| 2 | I found the system unnecessarily complex |
| 3 | I thought the system was easy to use |
| 4 | I think that I would need the support of a technical person to be able to use this system |
| 5 | I found the various functions in this system were well integrated |
| 6 | I thought there was too much inconsistency in this system |
| 7 | I would imagine that most people would learn to use this system very quickly |
| 8 | I found the system very cumbersome to use |
| 9 | I felt very confident using the system |
| 10 | I needed to learn a lot of things before I could get going with this system |

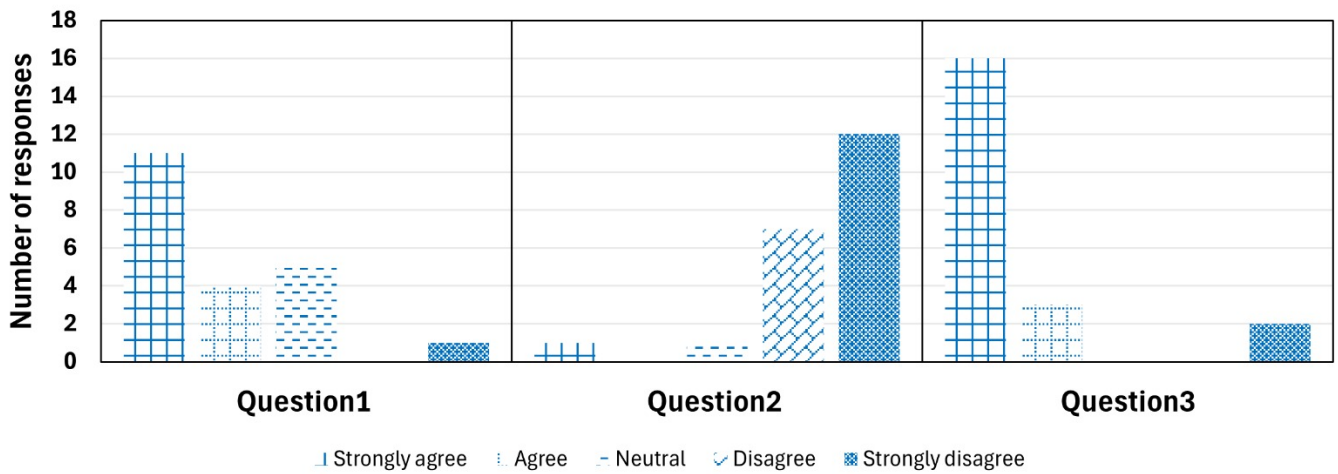


Fig. 10. SUS Questions 1-3 responses.

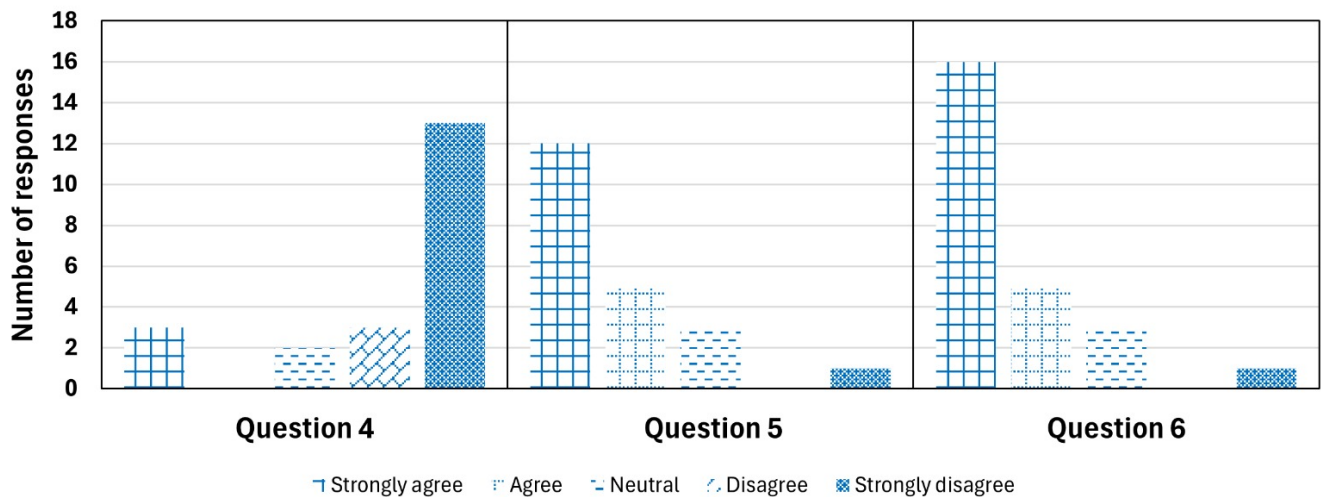


Fig. 11. SUS Questions 4-6 responses.

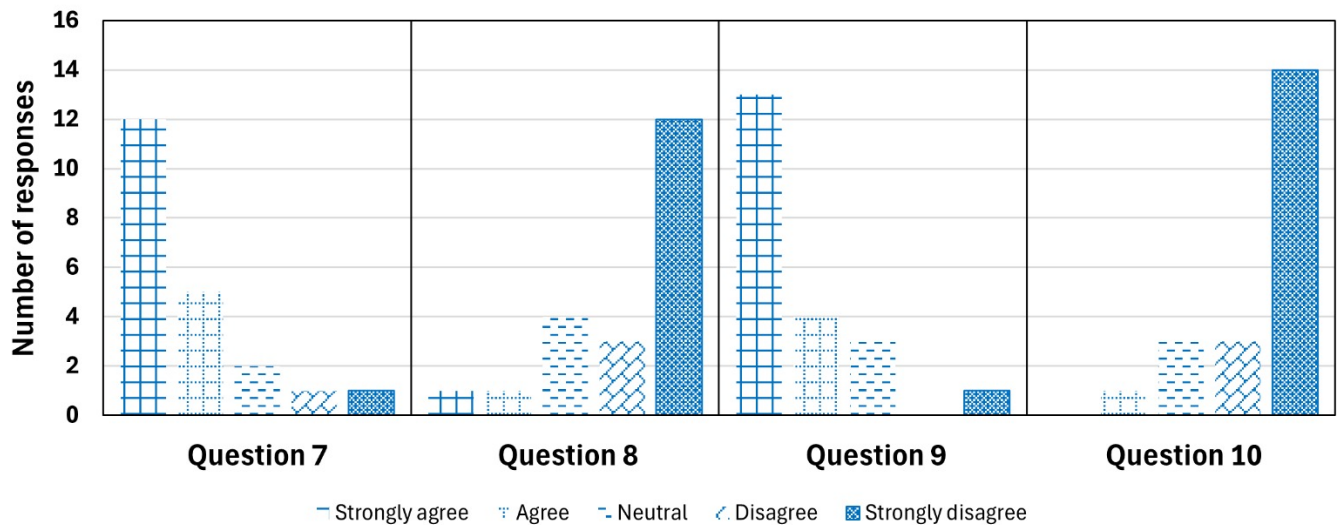


Fig. 12. SUS Questions 7-10 responses.

application, and only 5% disagreed. 10% of participants were neutral on this matter (see Fig. 12 Question7).

Question8: I found the system very cumbersome to use. All the components and steps in our application were well integrated. Accordingly, 71% of our participants found the procedure easy and expeditious, 19% were neutral regarding this, whilst 5% agreed that the application was cumbersome to use (see Fig. 12 Question8).

Question9: I felt very confident using the system. In response to this question, 81% of the participants responded that they were confident, 13% were neutral, and hence, only 5% indicated that they were un-confident (see Fig. 12 Question9).

Question10: I needed to learn a lot of things before I could get going with this system. As discussed above, the application was easy to use and thus, the participants did not need to learn much about it. Of the study population, 81% said they did not need to learn how to use this application, whilst 14% were neutral on this matter. In contrast, 5% of the participants suggested that they might have needed training in advance to use the application, which would be expected in the case of any newly developed application (see Fig. 12 Question10).

VII. CONCLUSIONS AND FUTURE WORK

This paper introduces the GROCAFAST system which is a practical solution for optimizing grocery shopping, empowering shoppers to navigate the store efficiently and save their time. GROCAFAST enables shoppers to create, manage, and update grocery lists while providing store navigation assistance without requiring any additional infrastructure. It leverages Dijkstra's algorithm to guide shoppers through the store, minimizing the time needed to visit aisles containing their desired items. The evaluation experiment conducted on GROCAFAST has demonstrated its immense value as a solution for improving the in-store grocery shopping experience and saving the shoppers' time. The system achieved a remarkable

reduction of 67.6% in total shopping time compared to the traditional method of physically browsing aisles. Additionally, it effectively reduced walking steps by 59%. The suite of features offered by GROCAFAST has garnered high user satisfaction. The system's adaptability allows it to be applied to any other store based on the store's information, ensuring its effective functionality across different locations.

As a direction for future work, there are several potential features that could be added to enhance the system's functionality. One direction is to explore different indoor positioning systems to include more location-based services. Another area of focus is to expand the scope of the research to include more large-scale grocery stores, potentially by partnering with industry stakeholders to gain access to the necessary resources. Furthermore, continued development of the app's database and analytics capabilities will provide even more valuable insights for manufacturers and retailers, helping them to make data-driven decisions and respond to evolving shoppers' needs. Overall, there is significant potential for future improvement and enhancement of the in-store grocery shopping experiences based on the foundation established.

REFERENCES

- [1] N. Petrosky-Nadeau, E. Wasmer, and S. Zeng, "Shopping time," *Economics Letters*, vol. 143, pp. 52–60, 2016.
- [2] K. S. Hamrick, D. Hopkins *et al.*, "The time cost of access to food—distance to the grocery store as measured in minutes," *International Journal of Time Use Research*, vol. 9, no. 1, pp. 28–58, 2012.
- [3] J. J. Inman, R. S. Winer, and R. Ferraro, "The interplay among category characteristics, customer characteristics, and customer activities on in-store decision making," *Journal of marketing*, vol. 73, no. 5, pp. 19–29, 2009.
- [4] Y. Huang and Z. Yang, "Write or type? how a paper versus a digital shopping list influences the way consumers plan and shop," *Journal of the Association for Consumer Research*, vol. 3, no. 3, pp. 396–409, 2018.
- [5] M. Noto and H. Sato, "A method for the shortest path search by extended Dijkstra algorithm," in *Smc 2000 conference proceedings. 2000 IEEE international conference on systems, man and cybernet-*

- ics.'cybernetics evolving to systems, humans, organizations, and their complex interactions'(cat. no. 0, vol. 3. IEEE, 2000, pp. 2316–2320.
- [6] N. Katuk, T. Jayasangar, and Y. Yusof, "Design and development of smart list: A mobile app for creating and managing grocery lists," *Baghdad Science Journal*, vol. 16, no. 2, pp. 462–476, 2019.
- [7] W. H. Jayawilal and S. Premaratne, "The smart shopping list: An effective mobile solution for grocery list-creation process," in *2017 IEEE 13th Malaysia International Conference on Communications (MICC)*. IEEE, 2017, pp. 124–129.
- [8] "Anylist: Grocery shopping list." <https://apps.apple.com/us/app/anylist-grocery-shopping-list/id522167641>, [Online; accessed 30-Dec-2023].
- [9] "Shopping list listonic." <https://apps.apple.com/gb/app/shopping-list-listonic/id331302745>, [Online; accessed 30-Dec-2023].
- [10] "Grocery smart shopping list." <https://apps.apple.com/us/app/grocery-smart-shopping-list/id1195676848>, [Online; accessed 30-Dec-2023].
- [11] N. A. H. M. Rosli and N. H. I. Teo, "Market basket analysis using apriori algorithm: Grocery item recommendation."
- [12] A. Firoz and G. Ratnayaka, "Shoplister – a grocery list management application," in *2020 International Conference on Image Processing and Robotics (ICIP)*, 2020, pp. 1–6.
- [13] M. Chui, M. Harryson, S. Valley, J. Manyika, and R. Roberts, "Notes from the ai frontier applying ai for social good," 2018.
- [14] S. Gerasenko, A. Joshi, S. Rayaprolu, K. Ponnavaikko, and D. P. Agrawal, "Beacon signals: What, why, how, and where?" *Computer*, vol. 34, no. 10, pp. 108–110, 2001.
- [15] J. Hurtuk, J. Červeňák, M. Štancel, M. Hulič, and P. Fecil'ak, "Indoor navigation using indooratlas library," in *2019 IEEE 17th International Symposium on Intelligent Systems and Informatics (SISY)*. IEEE, 2019, pp. 139–142.
- [16] "The impact of virtual reality on in-store shopping revolutionizing the retail experience." <https://www.linkedin.com/pulse/impact-virtual-reality-in-store-shopping-revolutionizing/>, [Online; accessed 30-Dec-2023].
- [17] K. Magzhan and H. M. Jani, "A review and evaluations of shortest path algorithms," *Int. J. Sci. Technol. Res*, vol. 2, no. 6, pp. 99–104, 2013.
- [18] J. C. D. Cruz, G. V. Magwili, J. P. E. Mundo, G. P. B. Gregorio, M. L. L. Lamoca, and J. A. Villaseñor, "Items-mapping and route optimization in a grocery store using Dijkstra's, bellman-ford and floyd-warshall algorithms," in *2016 IEEE Region 10 Conference (TENCON)*. IEEE, 2016, pp. 243–246.
- [19] R. D. Nayagam, D. Selvathi, R. Geeta, D. Gopinath, and G. Sivakumar, "Mobile application based indoor positioning and navigational system using Dijkstra's algorithm," in *Journal of Physics: Conference Series*, vol. 2466, no. 1. IOP Publishing, 2023, p. 012007.
- [20] S. W. G. AbuSalim, R. Ibrahim, M. Z. Saringat, S. Jamel, and J. A. Wahab, "Comparative analysis between Dijkstra and bellman-ford algorithms in shortest path optimization," *IOP Conference Series: Materials Science and Engineering*, vol. 917, 2020.
- [21] K. Magzhan and H. M. Jani, "A review and evaluations of shortest path algorithms," *Int. J. Sci. Technol. Res*, vol. 2, no. 6, pp. 99–104, 2013.
- [22] A. Ada, I. Cortez, X. Juvida, N. Linsangan, and G. Magwili, "Dynamic route optimization using a algorithm with heuristic technique for a grocery store," in *2019 IEEE 11th International Conference on Humanoid, Nanotechnology, Information Technology, Communication and Control, Environment, and Management (HNICEM)*. IEEE, 2019, pp. 1–6.
- [23] R. W. Bohannon, A. W. Andrews, and M. W. Thomas, "Walking speed: reference values and correlates for older adults," *Journal of Orthopaedic & Sports Physical Therapy*, vol. 24, no. 2, pp. 86–90, 1996.
- [24] T. Öberg, A. Karsznia, and K. Öberg, "Basic gait parameters: reference data for normal subjects, 10-79 years of age," *Journal of rehabilitation research and development*, vol. 30, pp. 210–210, 1993.
- [25] J. Brooke, "Sus: A "quick and dirty" usability," *Usability evaluation in industry*, vol. 189, no. 3, pp. 189–194, 1996.
- [26] "Measuring usability with the system usability scale (sus)." <https://measuringu.com/sus/>, [Online; accessed 03-Feb-2024].
- [27] J. Sauro, *A Practical Guide to the System Usability Scale: Background, Benchmarks & Best Practices*. Measuring Usability LLC, 2011.

New Trust Management Scheme Based on Blockchain and KNN Reinforcement Learning Algorithm

Ahdab Hulayyil Aljohani, Abdulaziz Al-shammri
Computer Science-Information Security Department
Imam Muhammed ibn Saud Islamic University (IMISIU)
Riyadh, Saudi Arabia

Abstract—There has been a continual rise in the quantity of smart and autonomous automobiles in recent decades. the effectiveness of communication among vehicles in Vehicular Ad-hoc Networks (VANET) is critical for ensuring the safety of drivers' lives. the primary objective of VANET is to share critical information regarding life-threatening events, such as traffic jams and accident alerts in a timely and accurate manner. Nevertheless, typical VANETs encounter several security issues involving threats to confidentiality, integrity, and availability. This paper proposes a new decentralized and tamper-resistant scheme for privacy preservation. We designed a new trust management system that utilizes blockchain technology. We strive to establish trust between vehicles and infrastructure and preserve privacy by guaranteeing the authenticity and integrity of the information exchanged in VANETS. Our proposal adopts the principles of reinforcement learning to dynamically evaluate and allocate trust scores to vehicles and infrastructure based on their behavior. The scheme's performance has been evaluated based on key metrics. The results show that our new system provides an effective behavior management technique while preserving vehicle privacy.

Keywords—Vehicular Ad hoc Networks (VANETs); Blockchain; trust management; reinforcement learning algorithm; privacy preservation; network security

I. INTRODUCTION

Intelligent transportation system (ITS) refers to the implementation of several technologies including sensing, analysis, control, and communications in the domain of ground transportation. The primary objective of ITS is to enhance safety, mobility, and efficiency within the transportation system. ITS encompasses a diverse array of applications that facilitate the processing and dissemination of information. These systems aim to alleviate congestion, enhance traffic management, mitigate environmental consequences, and amplify the advantages of transportation for both business customers and the general public [1].

VANET (Vehicular Ad hoc Network) is a subcase of an intelligent transportation system where vehicles can communicate and exchange information with each other (vehicle-to-vehicle), with fixed Road Side Units (Vehicle-To-Infrastructure), or with any communication entities (Vehicle-To-Everything). Vehicle communication improves traffic control and public safety. This is done by the detection and sharing of traffic flow information, driver behavior, locations, and trajectories [2]. VANET expanded its areas of use and

It has become a fertile field for scientific research. New and innovative applications have emerged to offer better driving experiences and provide value-added user-oriented services [3], [4].

The predictable vehicle movement, the constantly changing network topology and density, the frequent hand-offs between on-board units (OBUs) and RSUs, and the ease of reading the radio signals are some of the distinctive features of VANETs [5] As result, cars are highly exposed to various types of attacks and security risks [6], [7]. Denial of service, Blackhole, Wormhole, Eavesdropping, False position information, and Man In The Middle attacks are among the most known attacks in VANET [8], [9]. Various solutions are proposed to deal with each kind of threat [10]–[13].

In this work, we focus on privacy protection in VANET. This means preserving legal vehicle information, user personal information, user locations, and all data leading to user or vehicle identification and activity tracking [6], [7], [14]. Preserving privacy is complex and controversial. It must guarantee the authenticity of each vehicle on the network. While, at the same time, the true identity of the requested vehicle must not be revealed.

To tackle those issues, we introduce the use of blockchain technology [15]. It's confirmed to be a distributed and secure solution for data protection. It's able to provide a highly protected ledger to store authentication information and offers interesting features to check the stored data validity called consensus algorithms [15]–[17]. Proof of Existence (PoE) and Proof of Work (PoW) are the basic two features that guarantee data integrity and authenticity.

Our proposal introduces a new privacy protection solution based on blockchain mechanisms and a trust evaluation system to detect malicious behaviors and prevent their harm to network communications. Furthermore, we enhanced our trust management technique by adopting the Reinforcement learning technique. RL is based on trial-and-error discovery and delayed reward [18]. The more the vehicle is learning from the current state, the better will be its decision.

The contributions of our research work can be summarized as follows:

- A full registration process that allows vehicles to request network join and be authenticated by a central trust authority (TA). Cars use a secured channel to

exchange sensitive identity information with the TA and obtain permanent credentials.

- The TA maintains a public blockchain to store authentication information and trust scores. That will provide vehicles with a reliable mechanism to check their interlocutor authenticity and trust scores.
- We develop a novel trust management scheme for VANETs. Our scheme dynamically assesses and assigns trust scores to vehicles. We propose the introduction of three different trust levels: Direct Trust Score (DTS), Indirect Trust Score (ITS), and Historical Trust Score (HTS). These levels are attributed respectively by the vehicles to encountered nodes, RSUs, and the Trust Authority (TA).
- We empowered the trust evaluation by integrating the reinforcement learning technique. The TA uses the algorithm KNN (K-Nearest Neighbors) to predict the candidate's behavior and compute the HTS value for each node in the network.
- A configurable acceptance system where vehicles can decide to accept, or not new incoming data based on the sender scores and the data types.

The remainder of this paper is organized as follows. In Section II, we review the related work related to privacy preservation and trust management in VANET. Section III presents the solution backgrounds. Our proposal is detailed in Section IV. Section V exposes our experimentation and gives a performance evaluation of our scheme. Finally, we conclude the proposal in Section VI.

II. RELATED WORK

Waheeb et al. [19] introduced the framework to ensure the security of the communication in VANETs, this framework integrates a blockchain to support privacy-preserving authentication with a context-aware trust management system. It comprises a blockchain system that allows for anonymity and mutuality authentication of vehicle nodes and their messages. On the other hand, the aware trust management scheme allows for evaluating the reliability of sender vehicles by identifying and blocking the unauthorized nodes and their deceptive messages from the network. The scheme outweighs basic methods in robustness and efficiency while improving security in-vehicle communication. It is crucial to examine elements such as processing and communication overhead, as well as real-world implementation challenges.

In [20], authors introduced a system called TrCoin for VANETs, to conduct the trustworthiness of data providers, enhance traffic efficiency, and prevent malicious data providers from sharing false information. It applies a calculation algorithm with honest value to distinguish honesty from malicious data users and refine feedback shared by malicious users. The algorithm works by assuming that most data users are honest and estimates the weighted consistency (WC) of each user by evaluating their feedback consistency with the majority of users. The honesty value (HV) of data users is adjusted according to their (WC) where a greater (WC) signifies a more truthful user. This framework calculates also the count values of data providers based on truthful observations from honest

users. TrCoin's effectiveness is shown by thorough simulations involving different attack scenarios, including fraudulent data injection and dishonest feedback. While blockchain technology is inherently transparent which means it allows all transactions and trust-related information to be available to network participants. We think privacy issues in VANETs might occur if confidential information or user identities are revealed on the blockchain.

The author in [21] introduced decentralized architecture utilizing blockchain technology to tackle the issues related to implementing decentralized architecture and safeguarding privacy in VANETs. The study suggests implementing a scalable and tamper-proof distributed trust management system for VANETs by utilizing blockchain technology. An innovative validation approach based on Bayesian inference is presented to counteract the impact of misleading signals in VANETs. Also, the suggested method removes the requirement for a trusted third party (TTP) by leveraging the decentralized and distributed characteristics of blockchain technology. Their work introduces a sharding consensus mechanism to enhance scalability in the VANET system. The experimental findings demonstrate that the suggested system is efficient, adaptable, and reliable in collecting, processing, organizing, and retrieving trust values in VANETs. In our opinion, first: the study doesn't discuss the potential scalability challenges that could occur with extensive VANET implementations, second the proposed approach assumes that all vehicles in the network would correctly validate and upload their calculated rates to the RSUs which may not happen in real-world situations. third, the study doesn't account for the influence of network latency and communication delays on the dependability and trust management mechanism in VANETs. Lastly, the suggested Bayesian formula for trust management relies on the precise calculation of confidence scores and distances between sender messages and event locations, which may not always be achievable in real-world scenarios.

Another proposal is presented by Inedjaren et al. [22]. It introduces a blockchain-powered distributed management system for trust in VANETs to tackle security and reliability concerns in message sharing between vehicles. The suggested solution attempts to establish a safe and unalterable architecture for routing in VANETs by utilizing blockchain technology. the solution utilizes the optimized link state routing (OLSR) protocol along with blockchain technology to address security issues and redundant procedures in the OLSR routing mechanism, moreover, the system uses the proof of trust (PoT) consensus mechanism in a dynamic and resource-limited context. The system incentivizes vehicles together and prevents redundant detection procedures by providing rewards using blockchain. the simulation results demonstrated that the suggested approach is effective in resource-constrained contexts such as VANETS. It reduces detection time and overhead by isolating hostile nodes, thus enhancing the efficiency of the detection process. At the same time, the system seeks to reduce overhead by isolating hostile nodes and streamlining routing methods. However, the incorporation of blockchain itself introduces additional overhead in terms of storage, computation, and communication. this overhead could offset some of the gains achieved by the proposed solution.

Cong Pu [23] introduces trust management called trust

block MCDM for VANETs within the Internet of Vehicles (IoV) framework. The trust block MCDM system employs a multi-criteria decision-making model to assess the reliability of road safety messages and produce trust ratings for message senders. The trust values are regularly sent to a neighboring RSU. The RSU computes the reputation value of the message sender based on trust values from the vehicles and includes it in a block for addition to the blockchain. This blockchain works as a decentralized agreement system, where the longest branch of the transaction is accepted as the network's consensus. The trust value computation considers input from nearby validators, the reputation of the message initiator, and the confidence of the validator in the event. The trust block MCDM method enhances the detection rate of fake messages, and the detection rate of hostile vehicles, and reduces the number of dropped fake messages as compared to other blockchain-based trust management methods. The suggested approach improves the assessment of trustworthiness for road safety messages in VANETs, leading to enhanced road safety and travel experience in the IoV. Although the MCDM Scheme demonstrates promising outcomes in enhancing trust management in VANETs, it possesses specific constraints that must be taken into account for its practical use and deployment. We can generalize these limitations first the effectiveness of the trust block MCDM method depends significantly on the precision and dependability of the multi-criteria decision-making model utilized for reputation assessment secondly the MCDM technique doesn't evaluate the influence of network congestion or communication delays on the trust evaluation process

Hui et al. [24] in their study aims to develop a framework that focuses on selecting a reliable relay for service requests by considering the dynamic traffic conditions and vehicle behaviors by introducing a reputation management system to regulate vehicle actions. Vehicles with a high reputation can receive savings on computing services. The paper suggests using a reputation-based auction system to choose relay vehicles (RVs) and lower the cost of the relay services. Each vehicle is granted a reputation value depending on its adherence to the relay system, vehicles can enhance their reputation by utilizing edge computing devices (ECDs) for computing services and engaging in the request relay process, vehicles with a high reputation value qualify for price discounts on computer services. The simulation results show that the suggested reservation service architecture effectively handles vehicles and results in the most cost-effective relay services compared to traditional methods. This framework has potential limitations or areas for improvement in the current system, including the necessity for improved security measures and more precise classification methods for automobiles.

Sonker and Gupta [25] utilize multiple machine learning to detect misbehavior in vehicle ad hoc networks (VANETs) the techniques utilized are Naïve Bayes, decision tree, random forest, K-nearest neighbor (KNN), and stochastic gradient descent (SGD) classifier. The initial stage of the research includes examining the algorithms on various attack kinds by binary categorization, the second part concentrates on developing a novel process for identifying attacks by utilizing several machine learning classification algorithms and entropy calculation and information gain methods for selecting decision nodes. Stochastic gradient descent is an optimization approach commonly used in research for addressing linear

problems with support vector machines and logistic regression moreover the paper utilizes the VeReMi dataset a public repository created for identifying malicious nodes in VANETs. The dataset is utilized to assess machine learning algorithms in identifying various forms of attacks and test their detection techniques' efficiency. However, it's vital to note that the algorithms' efficiency may change when used in a wider range of assault scenarios, and using this amount of algorithms addresses drawbacks like the need for large amounts of labeled data, computational complexity, and generalization to new and unseen attacks.

Anti-Attack Trust Management Strategy named AATMS is proposed in [26]. It assesses the reliability of vehicles in different application scenarios and withstands diverse attacks. The research work introduces social elements such as diverse factors, vehicle factors, and behavior factors to filter out untrustworthy automobiles and indicate the level of public trust in vehicles. They are utilizing Bayesian inference to determine local trust levels from past encounters and choosing trustworthy seed vehicles depending on local trust and societal considerations. Moreover, they are introducing an adaptive forgetting factor to update local trust values and an adoptive decay factor to update global trust values to prevent a sudden increase in trust levels and enable a rapid decrease. The Bayesian inference's accuracy relies on the quality and trustworthiness of historical evidence, making it not a failsafe. Unreliable trust judgments might result from inaccurate or insufficient data.

Javaid et al. [27] introduced a trust management system named DrivMan (VANETs) that utilizes blockchain and a certificate authority (CA) to guarantee secure communication and data exchange. The scheme uses physical unclonable functions (PUFs) to guarantee the data dependability and privacy of intelligent vehicles (IVs) in (VANETs). It also utilizes the SHA-256 cryptographic hash method for authentication and verification. The system design includes initializing the nodes, composing and deploying contracts on RSUs nodes, and utilizing a genesis block for DrivMan that expands with subsequent blocks. Blockchain is utilized as a decentralized digital ledger in DrivMan to guarantee the secure and dependable functioning of the system, it's offers an immutable and transparent record of all transactions and data exchanges. Moreover, the blockchain technology in DrivMan ensures high security by necessitating a minimum of 51% of the network's processing power to tamper with data. Smart contracts, and autonomous computer algorithms, are utilized with blockchain to ensure data provenance and integrity in DrivMan. The asymmetric public key infrastructure in blockchain guarantees secure communication between the IVs and the network. Since the security implies that an adversary would require a minimum of 51% of the total processing power of the DrivMan network to manipulate data, a feat that may be achievable in some situations, also using a blockchain network hosted by RSUs could lead to centralization and reliance on an entity for network operations.

A decentralized trust management strategy for vehicular networks, specifically for decentralized VANETs is proposed by Gulen et al. [28]. The approach utilizes a fuzzy logic-based method to calculate trust and assess direct trust between trustor and trustee nodes within the transmission range. The system utilizes a reinforcement learning method to estimate indirect

trust, especially when the actions of trustee nodes are not explicitly observable, in their scheme they propose a method for evaluating trust among multiple agents is suggested, and direct trust is determined through a fuzzy logic algorithm that considers factors such as cooperativeness, honesty, and responsibility. Indirect trust is assessed using a reinforcement learning technique that adjusts trust levels based on the number of intermediaries involved. This technique efficiently integrates knowledge from several nodes by evaluating indirect trust to handle complex circumstances. This strategy has some drawbacks like the trust evaluation process depending on fuzzy logic and indirect trust estimation through reinforcement learning, which could lead to limits in accurately assessing and determining the trustworthiness of nodes. The scheme doesn't address the potential obstacles or restrictions in attaining precise trust evaluation in dynamic and unreliable vehicle networks. Moreover, the proposed architecture is based on nodes being situated within each other's transmission range. This reliance on closeness could restrict the effectiveness of the plan in situations where nodes are widely spread out or when the communication range is restricted.

In [29] a new study introduces an innovative trust structure for vehicle networks to tackle the problem and an innovative trust structure for vehicle networks, the problem of rogue nodes, and inaccurate information which can make the system unreliable for safety and emergency purposes. The trust architecture enables nodes to recognize and screen out recommendations from malicious nodes and distinguish genuine events. The system successfully detects malicious nodes and true events with a probability over 0.92, while maintaining the trust computation error under 0.03. The network model is created to evaluate the framework in situations including malevolent nodes where nodes move collectively along specific routes and encounter notable occurrences. Nodes communicate changes using messages, allowing nodes not directly involved to be informed by received messages. Simulation studies are conducted to confirm the trust framework's validity. A circular road is created in a simulation where accidents or traffic hazards occur randomly at various points. Proximal nodes encounter the event before distal nodes, who perceive it subsequently. The framework effectively detects events in incoming messages and excels in determining the actual characteristics of nodes. However, the suggested trust architecture operates under the assumption that there is a singular authentic event in the network at every moment, which may not align with the complexities of real-world situations. The system depends on nodes detecting the incident and notifying their neighboring nodes within the 300m range, which aligns with the conventional DSRC range. This restricted range may hinder the framework's efficacy in bigger network deployments. The approach assumes that malicious nodes transmit inaccurate information with a constant probability, without accounting for the potential adaptive or dynamic actions of malicious nodes. The system prioritizes safeguarding nodes against certain assaults but does not offer privacy or anonymity for the messages shared between nodes.

III. SOLUTION BACKGROUND

A. VANET Basic Fundamentals

Wireless access in vehicular environment (WAVE) is the name of the system that lets vehicles and RSUs talk to each other. The exchange of security messages is described by the WAVE design [30]. The WAVE communication keeps passengers safe by updating information about vehicles and traffic flow. This app makes sure that both pedestrians and drivers are safe. It also makes the traffic move better and the traffic management system work better. The VANETs are made up of different groups, such as OBUs, RSUs, and Trusted Authority (TA). In particular, the OBU is attached to each vehicle and collects useful data about the vehicle, such as its speed, acceleration, and fuel consumption. The RSU usually hosts an application that is used to interact with other network devices. After that, these data are sent to nearby cars through wireless signals. All RSUs that are linked to each other are also wired to connect to TA. In addition, the TA is in charge of managing the VANETs and is the leader of all the parts.

- Road Side Units (RSU): A roadside unit is a computing device that is located next to the road or in a certain place like a parking lot or an intersection [2]. Its job is to connect passing cars to the internet locally. The RSU is made up of network devices that use IEEE 802.11p radio technology for dedicated short-range communication (DSRC). It is more specific that RSUs can also talk to other network devices in other core networks [5].
- On-Board Unit (OBU): can share information about a car with RSUs and other OBUs. It does this by using a global positioning system (GPS) to track the vehicle. The OBU is made up of many electronic parts, including a resource command processor (RCP), sensor devices, a user interface, and read/write storage for getting information from storage. The main job of an OBU is to connect to an RSU or other OBUs through an IEEE 802.11p [31] wireless link and send information to other OBUs or RSUs. The car battery also gives power to the OBU, and each car has a (GPS), an event data recorder (EDR), and forward and backward devices that send information to the OBU.
- Trusted Authority (TA): The trusted authority is in charge of running the whole VANET system and recording the RSUs, OBUs, and vehicle users. In addition, it is its job to make sure that VANETs are secure by checking the vehicle identification, user ID, and OBU ID to make sure that no vehicles are harmed. The TA uses a lot of power and has a lot of memory [1]. It can also show the OBU ID and information if it receives a malicious message or notices strange behavior. In addition to these, TA additionally provides an approach for identifying the attackers [2]. ITS is always trying to improve traffic flow and road safety by making communication more secure and using different networking methods, like MANETs and VANETs, to get around traffic jams. To make traffic flow more smoothly, keep people safe, and make driving more enjoyable, Vehicle-to-Everything (V2X) communications are very impor-

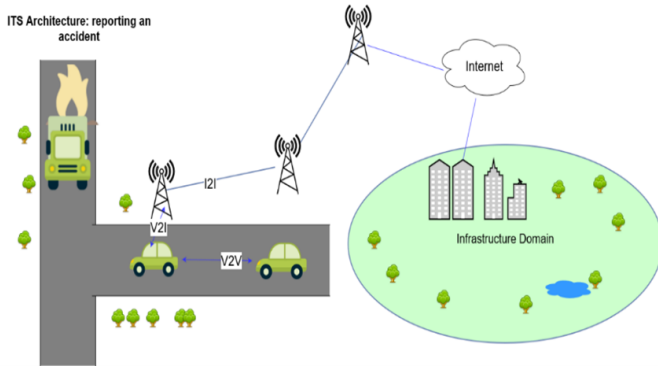


Fig. 1. VANETs communication architecture.

tant. They do this by sending very accurate and up-to-date information about things like accidents, traffic jams, emergencies, and other transportation services as shown in Fig. 1.

B. Communication Techniques Utilized in VANETs

The transmission medium in V2V communication has a high transmission rate and a small latency [31]. In V2V, a vehicle can send important data to another vehicle, like emergency braking, collision detection, and traffic conditions. V2I lets vehicles and network infrastructures send important data to each other. The car built a link with RSUs in this area so it could share data with other networks, like the Internet. V2I also needs more data than V2V because it communicates with infrastructure, but it is less likely to be attacked [5]. Cellular vehicle-to-everything (C-V2X) technology was just released. It's a unified connectivity platform that's meant to serve V2X communications [2]. C-V2X was created as part of the third-generation partnership project (3GPP), and it is thought to be the most reliable communication system that can handle V2X communications [2].

It links all the cars together and makes it possible for cooperative intelligent transport systems (C-ITS) to work, which eases traffic and makes it run more smoothly. Fig. 2 illustrates the on-board unit (OBU) and one or more applications units (AUs) make up the in-vehicle area. They often use wired links, but sometimes they use wireless ones. On the other hand, the ad hoc domain is made up of cars with OBUs and RSUs. An OBU is like a mobile node in an ad hoc network, and an RSU is like a fixed node. The gateway can connect an RSU to the Internet. RSUs can also talk to each other directly or through multi-hop. Access to the infrastructure can be done through two different types of points: RSUs and hot spots (HSs). OBUs can talk to the Internet through either RSUs or HSs. Cellular radio networks (GSM, GPRS, UMTS, WiMAX, and 4G) can also be used by OBUs to talk to each other when RSUs and HSs are not available. Furthermore, VANET communications can be broken down into four groups, which are shown below [32].

C. Trust Concepts and Trust Components

Trust in the context of VANET (Vehicular Ad-Hoc Network) denotes the level of confidence that one entity has

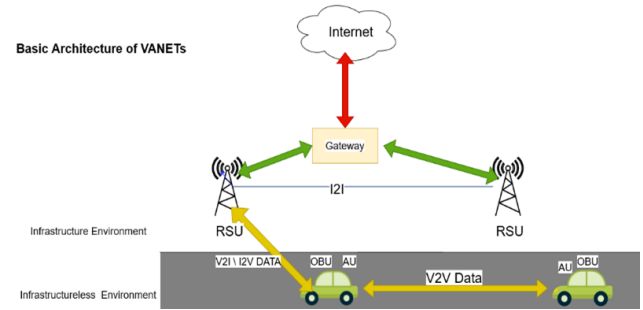


Fig. 2. Communication types in VANETs.

in another entity [4]. It relies on the anticipation that the other party will carry out a specific action as anticipated by the initiator. Trust is predicated on the assurance that the trusted entity will not engage in malevolent behavior in a given circumstance. Since exact certainty is unattainable, trust relies entirely on the trustor's conviction. An entity refers to a tangible device that actively engages in the process of communication, such as OBUs (OnBoard Units) and RSUs (Road Side Units) utilized in VANET (Vehicular Ad hoc networks). Trust refers to the extent to which a node is considered trustworthy, secure, or reliable while engaging with other nodes. For a node to engage in the communication process of VANET, it must be considered trustworthy by other nodes and meet the trust criteria. A node's trust values can vary when assessed by different nodes due to variations in the trust evaluation criteria for each particular node. Trust is contingent upon the passage of time, as it has the potential to both flourish and deteriorate. Trust levels are established based on specific acts that the trusted party can carry out on behalf of the trustee. Moreover, the following elements comprise the character of interactions between two entities upon which the concept of trust is predicated:

- Direct Trust: It is demonstrated through the interaction between a trustor and a target vehicle, as evidenced by the trustor's direct observations [33]. Certain scholars employ the term "knowledge" to denote the explicit data acquired by the trustor to assess the trustee by specific criteria that depend on the nodes and services involved. Although it is commonly held that direct trust is more significant than indirect trust, when evaluating a vehicle, the combination of the two is considered. Fig. 3, demonstrates the difference between direct and indirect vehicle trust. Where vehicle number 2 recommends that vehicle 4 trust the vehicle.
- Indirect trust: It refers to the viewpoints of trusted entities in the vicinity of a trustor, regarding a specific node (trustee). These viewpoints are based on past experiences with the node in question. Researchers often explain indirect observation through the combination of reputation and experience. Reputation is the collective record of previous interactions with a certain entity, which reflects the overall perception of that entity. On the other hand, experience refers to the relationship between a person who trusts and another who is trusted, based on the trustor's belief in the trustee's ability to complete a task.

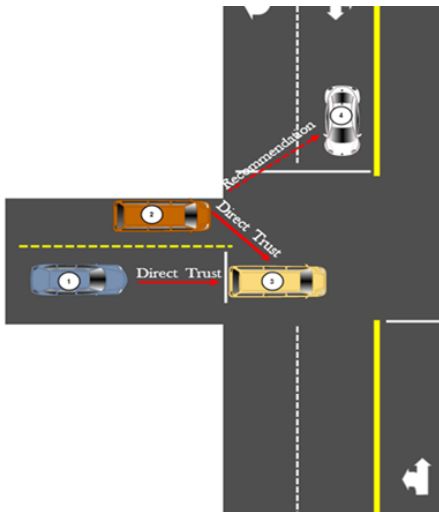


Fig. 3. Difference between direct and indirect trust in VANETs.

D. Requirement for VANETs Security

A system can be vulnerable to a variety of system flaws that can be exploited by unfriendly entities for a variety of reasons. The security requirements of a system must be addressed to make it secure. The VANET system has some security requirements, which are briefly detailed here. Fig. 4 additionally shows the kind of probable assaults that could jeopardize VANET security standards.

- **Authentication:** It is a critical and unavoidable need of any system. A system must be able to verify the authenticity of all system participants. Authentication and identity are especially crucial and vital in VANET, which is prone to many vulnerabilities. In the event of a VANET attack, a robust authentication strategy can give solid legal proof against the invader. As a result, the authentication procedure is an obvious necessity to defend the VANET system against assaults such as Sybil attacks, location attacks, tunneling, replay attacks, message manipulation, and so on.
- **Availability:** A system or a system component could be susceptible to failure or attack. This type of malicious system or component condition should not impact other users or system elements. All applications and networks within VANETs must remain operational and accessible, even if one element of the VANET is compromised. Certain infrastructures or nodes within a VANET may be susceptible to attacks or problems that do not affect other nodes. Alternatively stated, VANET resources must be consistently accessible. To meet the availability requirement of a VANET, it is necessary to develop a system that is robust, secure, and tamper-tolerant. A multitude of attacks, including Distributed Denial of Service (DDOS), Denial of Service (DOS), spamming, and Black Hole attacks, can significantly compromise the availability requirements of VANET.
- **Confidentiality** pertains to the safeguarding of private information associated with a specific node or infras-

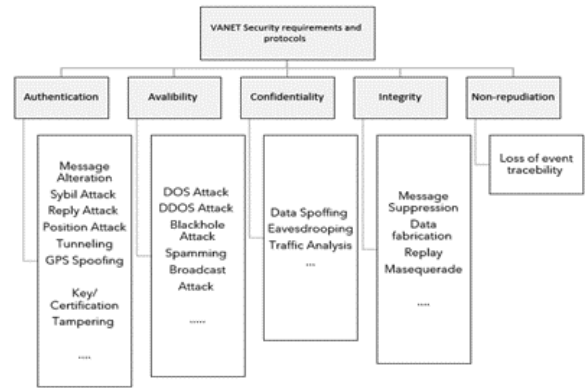


Fig. 4. VANETs security requirements.

structure. The communications that transpire between two components in a VANET must not be made public to a third party. The maintenance of confidentiality can be accomplished through the implementation of diverse encryption algorithms. Safety messages in VANETs do not contain any sensitive information; therefore, they are not encrypted. Electronic payment information, the identity of the user, and other personally identifiable data are, nevertheless, protected in confidence through the implementation of diverse cryptographic algorithms. Data surveillance, traffic analysis, and data spoofing are a few of the potential breaches of confidentiality in VANETs.

- **Integrity** safeguards communications against forgery or interpolation. Messages transmitted and received by various VANET entities must remain intact. Therefore, it is imperative to safeguard the integrity of communications against unauthorized tampering by criminals. Message integrity may be compromised by data alteration attacks, masquerade attacks, and replay attacks, among others. For the protection of communications during transmission and reception, it is necessary to implement a secure protocol. The IEEE1609.2 standard is employed to provide security services in VANETs.
- **NonRepudiation:** One of the critical security requirements of VANET. It safeguards against the denial of transmitted data by either the sender or the receiver [34]. Fig. 4 outlines the VANET security requirements as well as the potential hazards that could compromise those requirements.

E. Blockchain Overview

A blockchain is a decentralized public database that stores all completed digital transactions and is shared among participating nodes. It has an indisputable and verifiable record of every event that has ever taken place. Every event in the blockchain database is verified through the consensus of the majority of nodes in the network. There are primarily two types of blockchains: public blockchain and private blockchain. The public blockchain is a decentralized blockchain that allows

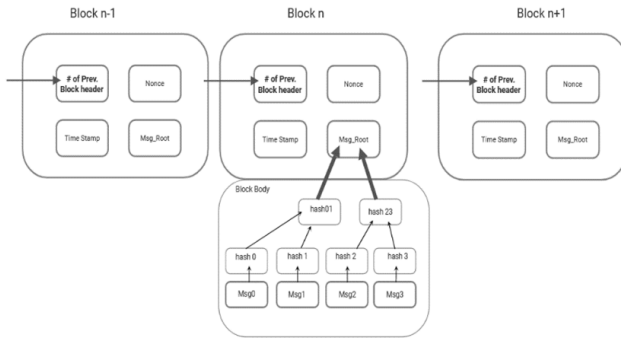


Fig. 5. Blockchain Concept.

unrestricted participation and interaction without requiring approval from a central authority. The starting point of the blockchain is a genesis block, which serves as the initial block in the blockchain. The genesis block serves as the shared starting point for all blocks and stores information that is universally accessible to all nodes [35]. The block comprises cryptographic hashes of records, each block containing the previous block's hash information, making a data chain and producing a blockchain, as illustrated in Fig. 5.

Features of using blockchain are:

- 1) **Immutability:** is a crucial aspect of blockchain technology. Once information is recorded and authenticated on the blockchain, it becomes immutable and cannot be altered or removed from the network. Additionally, information cannot be inserted randomly.
- 2) **Distributed and trustless environment:** In a blockchain system, any node that is added can synchronize and validate all data in a distributed way without the need for central control, creating a trustless environment. It offers security and guards against a single point of failure. It establishes trust in an atmosphere where trust is typically absent.
- 3) **Privacy and anonymity:** The blockchain offers privacy to its users. Users can join the network without revealing their identity. That is, the user's information is kept private from other users. It signifies that personal information is confidential, protected, and unidentified.
- 4) **Faster Transactions:** Setting up a blockchain is straightforward, and transactions are swiftly confirmed. Processing transactions or events only takes a few seconds to a few minutes.
- 5) **Reliable and accurate data:** The blockchain's decentralized network ensures that the data is reliable, accurate, consistent, timely, and publicly accessible. It is resilient to malicious assaults and lacks a single point of failure.
- 6) **Transparency:** It is fully transparent as it records information about each transaction or event that takes place in the blockchain network. Transactions are visible to all members of the network.

IV. SOLUTION PRESENTATION

Users can benefit from VANET communication to exchange different kinds of messages. Public safety, road traffic enhancement, and even entertainment and social applications are becoming VANET's basic use cases. Due to those heterogeneous usages, privacy preservation has become an urgent issue. To ensure that, we propose a new trust management process to detect and reject any malicious attacks. Our proposal defines a scoring mechanism to reward legitimate and punish malicious nodes. Our scheme introduces blockchain as a public ledger to save authenticated vehicle information and a reinforcement learning algorithm to enhance the trust score attribution. In this section, we will present the details of our solution. First, we will introduce the solution architecture and involved entities. Then, we will detail the authentication mechanism defined to integrate different network nodes. Finally, we will describe our trust management process and its score calculation procedures.

A. The Vehicle Registration and Authentication Mechanism

We propose a new authentication solution based on blockchain technology to ensure vehicle authentication and preserve user privacy. We define a trust management system to assess the trust of different vehicles in the network. As mentioned in Fig. 6, the network will contain the following entities: MVAC, TA, RSUs, and vehicles.

1) **Motor and Vehicle Authority Centre (MVAC):** The MVAC represents the legal authority or any delegated service to manage vehicles and transportation engines. It has the authority to store real documentation and to provide the car's valid registration numbers. It can also revoke those numbers and pull any given transportation license. Owners submit real documentation to register their vehicles. Accepted engines will receive a unique Identifier (ID) which will be stored with all identity information in the "Vehicle Information Base". This base is highly protected and managed only by the MVAC. In our scheme, we consider that MVAC is fully trusted. They are impossible to hack. Their operations and data cannot be compromised. They can resist any external attack and will never encounter internal attacks. DMV or TA can be held by the government or any authorized service provider.

2) **The Trust Authority (TA):** The trust authority is allowed by the MVAC to access the Vehicle Information Base and to read real identity information about all registered vehicles. To do so, it has a secure communication channel with the MVAC. The TA receives network registration requests from vehicles. It checks their information and generates all necessary parameters. It provides anonymous pseudo and various cryptographic parameters for each newcomer.

3) **The Roadside Units (RSU):** RSUs are small and wireless units deployed all over roads. They will offer different network services for registered vehicles. They can communicate with cars to share messages and service-related information. They need to register with the TA and get valid pseudonyms and security parameters. RSUs will correctly perform the proposed solution and provide reliable information and parameters. However, they are not allowed to access vehicle private information.

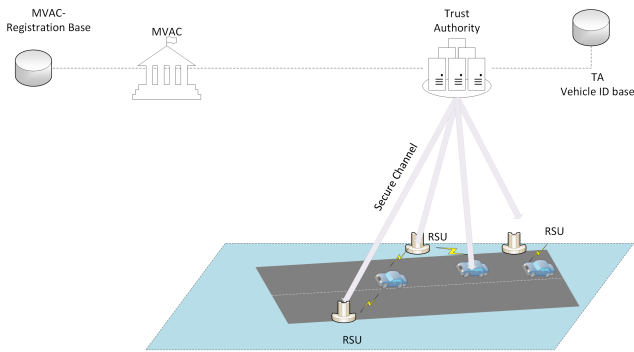


Fig. 6. Solution network architecture.

4) *Vehicles*: In VANET, vehicles are automobile engines equipped with wireless communication devices. They can use the WAVE standard to communicate with other network members. They can exchange messages with each other or with the network infrastructure. Vehicles are wireless mobile nodes. They are the most vulnerable units in the network. They can be hacked or receive compromised data. They can also act maliciously to threaten the network safety. They will be able to generate false data and compromise offered services

B. The used Blockchain Specifications

We propose the use of a dedicated blockchain structure for vehicle authentication. For each new registered car, a new block will be created. Its corresponding transaction contains its time of issue. So any participant can access the chain searching for the latest and newest information. When it finds the desired data, it will not need to continue reading.

1) *The blockchain structure*: Each time a new vehicle is registered and accepted by the MVAC, the TA will add its information to the Authentication Blockchain. The required information includes:

- The unique vehicle pseudonym
- The generated certificate: a public key and hash algorithm
- Universal issuing time
- Initial trust score
- Validity period
- Signature of the TA
- The certificate state (Valid or Not)

All that information constitutes a new block and will be added by the TA to the blockchain. The blocks are organized chronologically. Any reading operation will start with the newest inserted blocks to minimize the necessary research time.

2) *The blockchain implementation approach*: The use of blockchain technology has evolved tremendously since its first proposition with the concept of “bitcoin” in 2008 [36]. Different domains are introducing it to benefit from its valuable characteristics: transparency and non-tampering which can provide high security and privacy protection. Two basic formats

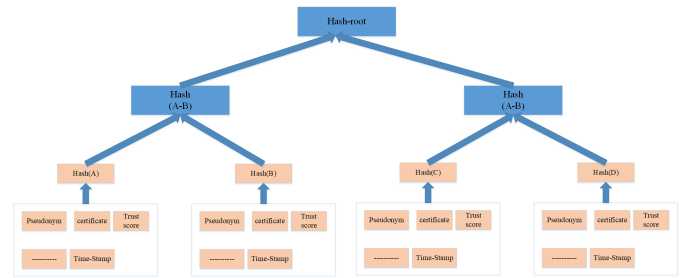


Fig. 7. The used blockchain architecture.

are mainly used: the permissioned and permissionless. The permissioned blockchain authorizes any community member to access and add new blocks. This feature guarantees decentralized storage. On the other hand, the permissionless version is often used with centralized management to enhance the trustworthiness of the proposed operations. In our proposal, we introduce the permissionless blockchain. The trust authority (TA) is the only network member authorized to create and add new blocks which makes it impossible for the attackers to tamper with the public ledger.

We also use the chronological Merkle tree (CMT) structure for our blockchain [37]. The CMT is the traditional underlying structure used for blockchain implementation. Fig. 7 shows this structure. All transactions will be hashed and stored chronologically in a binary hash tree. The leaves are the transaction data. In our case, a transaction represents a new block created after adding a newly registered vehicle to the network. Then, each pair of leaves is hashed to construct a new level of internal hashes. Pairwise hashing continues until we get a single hash as the root of the tree. Network members: vehicles or RSUs, are permitted to read the blockchain to verify their communicator credentials. They search the tree leaves using the communicator’s pseudonym starting with the last added data block. When the corresponding block is found, the proof of working concept (POW) [38] permits the validation of the communicator’s information. We need only to check the hashing branch between the root hash and the targeted node block.

C. The Network Initialization

During the initialization of the network, infrastructure components must be configured and prepared to accept the vehicle’s join requests. Later, they must ensure secure communication. Our proposal defines two basic network infrastructure elements: the Trust Authority (TA) and the Roadsides Units (RSUs).

1) *The trust authority configuration*: The TA is the central management unit. It stores the identification information of all allowed vehicles. It’s supposed to be fully functional all the time. For each vehicle, the TA proposes a unique pseudonym and a couple of public and private keys. Therefore, a pseudonym generation function will be initialized and started to wait for any incoming vehicle request. Then, the cryptographic process [7] will ensure the creation of the couple: public and private keys

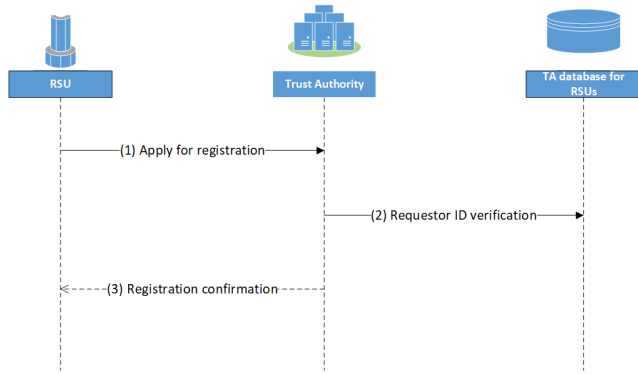


Fig. 8. RSU network join.

2) *The RSU network join:* When a new RSU is installed and launched, it needs to contact the TA to obtain its security parameters: pseudonym, a private and public key. Like vehicles, RSUs are authenticated by the trust authority to avoid any malicious infiltration. Furthermore, they use pseudonyms and encryption during their communication to guarantee sensitive data preservation.

The RSU begins by sending a join request to the TA Fig. 8. The request includes a unique identifier given to the RSU upon its setup. The TA checks its database to confirm the RSU identity. Then, it generates new parameters for the requestor, signs them, and sends back the response. When the RSU receives the TA message, it adopts the new parameters. Finally, its configuration is completed, and it can participate in any message exchange. It also starts the vehicle trust management process.

3) *The vehicle registration process:* When a new vehicle is registered Fig. 9, the owner physically submits the required documents to the MVAC. The latter checks the vehicle's identity documents validity and approves the registration. An acceptance notification will be sent from the MVAC to the TA. The real identity of the vehicle will also be sent to be stored in the TA dedicated database. As a second step, the vehicle will be allowed to communicate with the TA through a secure channel Fig. 10. The vehicle sends its identity information and asks for a certificate generation. The TA generates for the new vehicle a new "unique pseudonym" and a couple of public and private keys and sends it to the vehicle using the secure channel. Also, the newly generated public key will be stamped and added to the authentication blockchain among other relative information: the initial value of the trust score and the certification issuing time, validity duration, etc.

D. The Certificate Creation and Management

We use the PKI (Public Key Infrastructure) as the basic mechanism for car identification and secure communication. The TA is the only unit allowed to issue couples (public, private) vehicle keys. Consequently, no computational charge will be on the vehicle. The certificate will be used in any communication with other vehicles. Also, the TA generates a "unique pseudonym" as an identifier for the participant car and it guarantees that the pseudonyms remain unique for all vehicles and during all communications. There will be

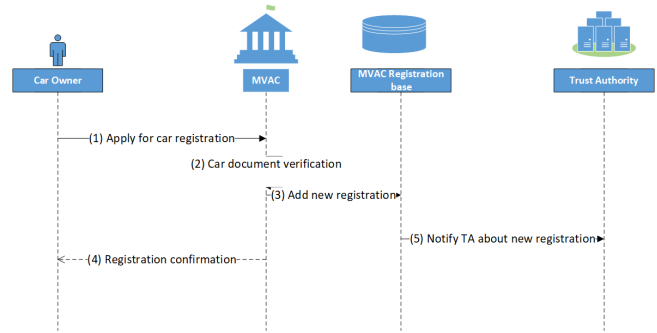


Fig. 9. The Vehicle's physical registration in the MVAC.

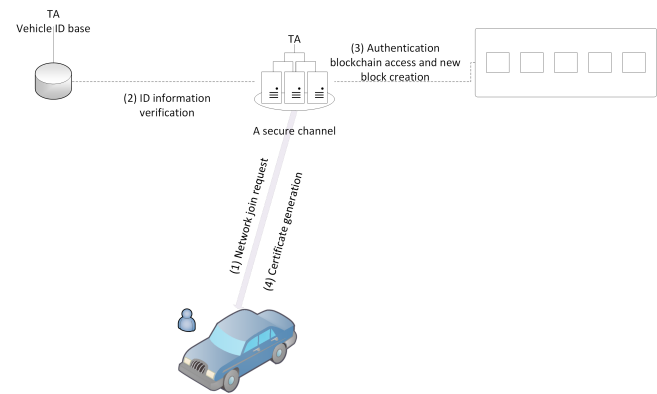


Fig. 10. Vehicle network join.

no possibility of relaying the pseudonym to the real vehicle identity or any private information.

Each participant will receive his certificate generated by the TA at its first connection. The certificate has a validity period specifying the duration attributed by the TA and the MVAC to the requesting car. Vehicles can ask for new certificates anytime due to compromised data or any eventual attack. The new certificate is requested and received through the secure channel. Upon receiving the request, the TA starts by invalidating the previous certificate and adding a new block to the authentication blockchain to announce it. Then, a new certificate is created for the requestor and added to the blockchain along with the car other's information. Especially, using the same old pseudonym and trust score Eventually, a new pair of public and private keys will be generated to avoid any eventual new threat.

E. Vehicle Authentication During V2V or V2I Communication

When a Vehicle or RSU receives a new message from another vehicle, it starts by authenticating the communicator Fig. 11. It extracts the vehicle certificate from the message and determines the corresponding public key and pseudonym. Then, it accesses the Authentication Blockchain and checks the car registered certificate and its validity duration. We remain that the blockchain is built chronologically. Therefore, the verification process starts with the newest block and goes on until the oldest one Fig. 11. Eventually, the requestor will be able to find out the most recent state of the targeted node information. For example, if the communicating node was

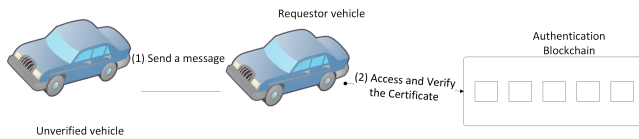


Fig. 11. Vehicle authentication during V2V or V2I communication.

banned by the TA or has an un-renewed expired certificate, the requestor will reach in the first place the block announcing that state. This verification process allows the requesting vehicle or RSU to authenticate its communicator. So, it will be able to accept the new communication. Furthermore, the requestor has the new arrival's last known historical trust score. So, it will be able to decide better about its communicator's behavior.

F. The Trust Management System

We propose a trust management system based on the following elements.

- A historical trust score HTS: defined in the interval [0..1]. The TA attributes an initial HTS value to each new vehicle registered. The TA collects the trust scores of the targeted vehicle from the RSUs and other vehicles. Then, the TA uses a reinforcement algorithm (KNN) to recalculate the new HTS value for the vehicle and announces it by creating a new block.
- A direct trust score DTS: defined in the interval [0..1] and attributed by a vehicle to each other. When vehicle A encounters for the first time vehicle B, it will generate a new DTS value for it and keep updating the B score when any new communication happens.
- An indirect trust score: ITS: defined also in the interval [0..1] and attributed by the RSUs to different encountered vehicles. Periodically, the RSU receives different DTS measurements from neighboring vehicles. Then, it aggregates them to recalculate the new ITS for the targeted vehicles.

1) *The DTS update algorithm:* The algorithm in Fig. 12 defines the process used to manage the DTS for each vehicle. When vehicle A encounters vehicle B for the first time, it starts with attributing a first score $DTS(B) = 0.5$ and initializing 2 counters: counter for bad communication with B (Negative Behaviour Count: $NBC(B)$). It will count all cases of misbehavior of vehicle B: Lost packets and false information. And a counter for successful communication (Positive Behaviour Count: $PBC(B)$). Each new communication between them will increment the Bad or the Good counter and the total number of communications achieved. When a maximum threshold number is reached, vehicle A will calculate a new DTS for vehicle B using the formula 1

$$DTS(B)_{i+1} = \begin{cases} DTS(B)_i + DirectReward * \frac{PBC(B) - NBC(B)}{MaxThreshold} \\ = 0 \text{ if } DTS(B)_{i+1} < 0 \\ = 1 \text{ if } DTS(B)_{i+1} > 1 \end{cases} \quad (1)$$

Later, the counters for vehicle B will be re-initialized to zero. Thereby, the defined algorithm will allow to increase or decrease of the DTS of the communicating vehicle periodically

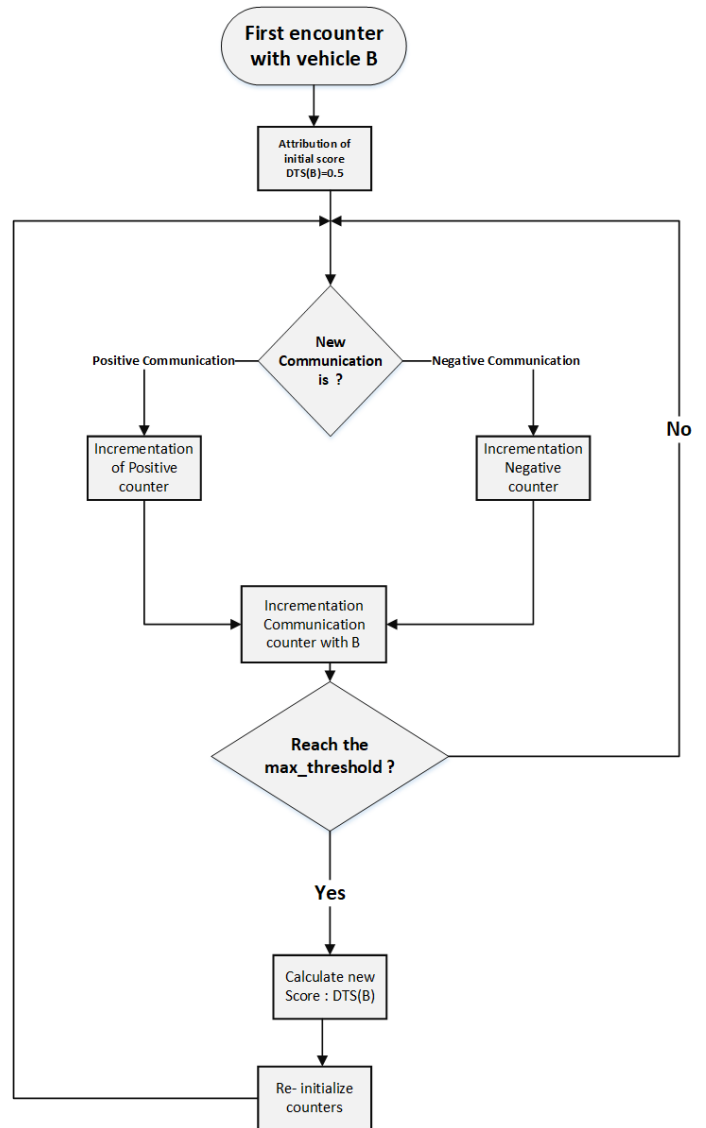


Fig. 12. DTS update algorithm.

depending on its behavior until reaching a minimum of 0 or a maximum of 1. The “Direct Reward” is a weight defined in the interval [0..1]. It's used to update the direct trust score DTS. In our experimentation presented later in the next section, we chose a value of 0.2.

2) *The ITS update algorithm :* RSUs are responsible for attributing and updating the indirect trust score for each vehicle that has joined the network. Fig. 13 shows the IDS computing algorithm. Vehicles calculate continuously the direct trust score for each encountered node and broadcast their measurement to all nearest RSUs. Periodically, RSUs will use the received DTS measurements to compute a new indirect trust score for each targeted node X. RSUs use the following formula 2

$$ITS(X)_{i+1} = \alpha * ITS(X)_i + \beta * \frac{\sum_{j=1}^N DTS(X)_j}{N} \quad (2)$$

With $\alpha + \beta = 1$ and N is the number of nodes that have sent their DTS measurement for vehicle X. α and β are weights

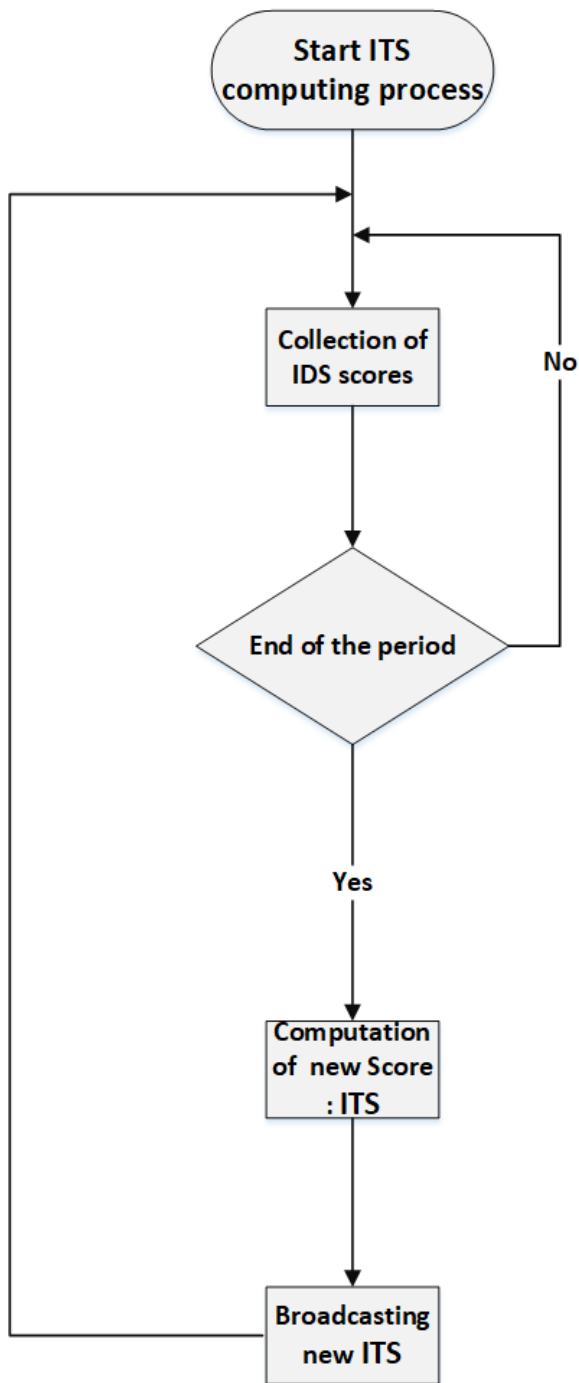


Fig. 13. ITS update algorithm.

used to moderate the combination. The new ITS measurement aggregates all the direct scores measured during the current period with the old indirect score. This formula will tie the estimated behavior of the targeted node to its location. Thus, vehicles will have a better view of communicating over the same region.

3) *The HTS update algorithm:* The historical trust score is attributed and updated by the TA. It is worth noting that a HTS equal to 0 is the lowest allowed value and a vehicle reaching this level will be banned. A dedicated block will be

created and added to the blockchain to announce the expiration of the targeted node certificate. A vehicle with good behavior can reach a maximum value of 1. The algorithm in Fig. 14 explains the HTS management process. When a new car asks for network join, the TA will attribute an initial HTS=0.5 and mention this value in the Authentication Blockchain. The update of the historical score is based on the following features:

- The direct score in the different vehicles: The TA collects direct scores attributed to vehicles encountering the candidate car. The collection is done slowly and passively over a long period. Independently, cars can deposit their local scores on the RSUs during their travel. Later, the TA will contact RSUs periodically and ask for new deposits.
- The indirect score is calculated by all RSUs deployed in the network. The TA also receives the collection of IDS. Periodically, each RSU computes the IDS of all encountered vehicles. Then, it sends the results to the TA.
- The TA uses the reinforcement algorithm KNN (K-Nearest Neighbours) to predict the candidate's behavior. The DTS measurements for each vehicle constitute the KNN algorithm inputs. A new "judgment" about the candidate's behavior will be the algorithm's output.

Depending on the new judgment: malicious or legitimate node, the TA computes the new value of the historical trust score. The new HTS is calculated using the following formula 3

$$HTS_{i+1} = \begin{cases} \alpha * (HTS_i + HReward) + (1 - \alpha) * \frac{\sum_{j=1}^N HTS_j}{N} \\ = 0 \text{ if } HTS_{i+1} < 0 \\ = 1 \text{ if } HTS_{i+1} > 1 \end{cases} \quad (3)$$

Where N is the number of RSUs having an ITS measurement for the candidate. α , is a weight defined in the interval $[0..1]$. The $HReward$ is a weight given depending on the output of the KNN algorithm. If the algorithm finds out that the candidate vehicle is a legitimate node, a positive reward will be given. Otherwise, the attributed value will be negative. We chose a value of 0.2 for this weight. It means:

- $HReward = 0.2$ if the candidate is judged legitimate.
- $HReward = -0.2$ if the candidate is judged malicious.

Thereby, the TA will be able to update vehicle historical scores according to their behavior seen by other nodes (vehicles and RSUs). The better the car behaves during its communications the better will be its HTS. The KNN is an efficient classification reinforcement learning algorithm [39]. Therefore, it helps the TA to predict the candidate's vehicle behavior efficiently.

G. The Final Trust Score and Message Acceptance Decision During V2V or V2I Communications

We have defined three different types of trust score measurement. Direct, indirect, and historical trust score. In this section, we will present how those scores will be combined and used to compute a "Final trust score" which will be used

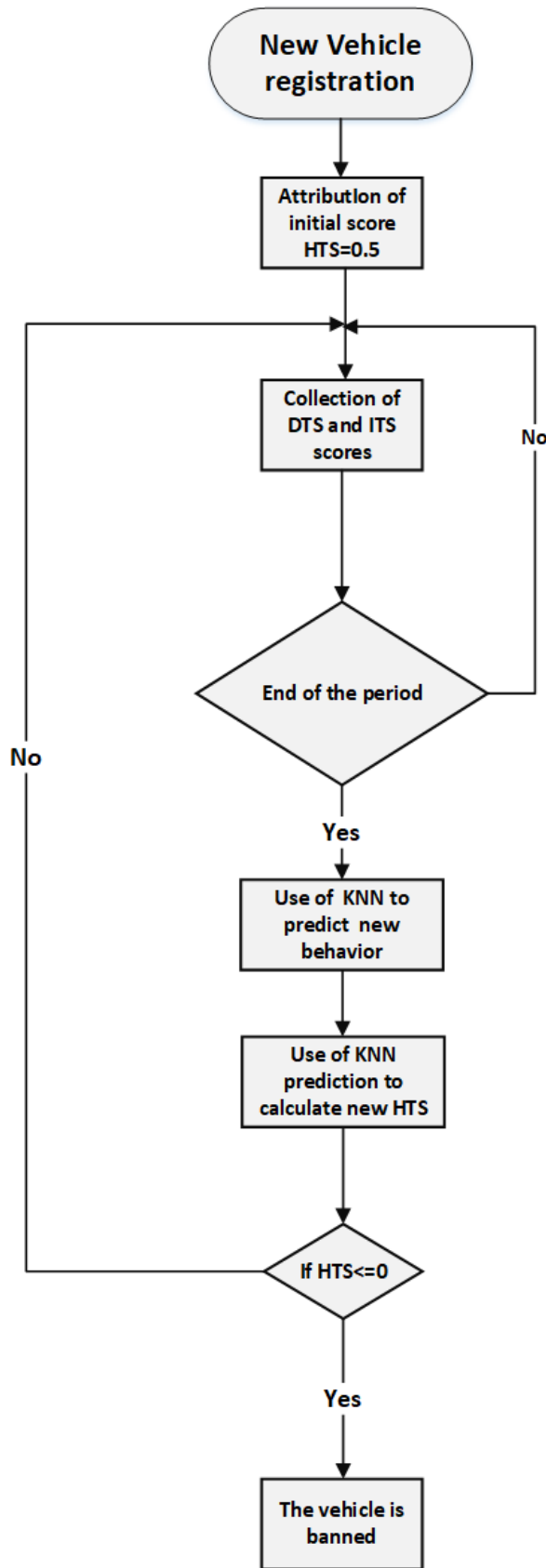


Fig. 14. HTS update algorithm.

TABLE I. WEIGHT ATTRIBUTION CASES FOR FTS

| Communication Case | Weight attribution |
|--|---|
| Public Safety and urgent data | $\alpha = 0, \beta = 0, \gamma = 1$ |
| User application or ordinary data (general case) | $\alpha = 0.5, \beta = 0.2, \gamma = 0.3$ |
| Non -important Data | $\alpha = 1, \beta = 0, \gamma = 0$ |
| Location-based application | $\alpha = 0, \beta = 1, \gamma = 0$ |

to decide during the message exchange. Upon receiving a new message from another vehicle, the car can decide whether to continue the communication or not based on the node “Final trust score”. Vehicles, during their travel, will face different cases of communication. The exchanged data type can vary from urgent and important data to non-important or advertisement ones. Therefore, nodes can evaluate the sender’s behavior differently depending on the communication case.

To face different cases, we introduce the following formula (4) for the final trust score (FTS):

$$FTS(X) = \alpha * DTS(X) + \beta * ITS(X) + \gamma * HTS(X) \quad (4)$$

Where $\alpha + \beta + \gamma = 1$. This formula permits the cover of all cases mentioned below by defining various values for the used weights.

In Table I, we introduce examples of weight attribution. In each case, nodes can compute differently the final trust score. We chose to rely on the TA’s judgment when dealing with important data. So, the vehicle will neglect the direct and indirect measurements and use only the historical score which will increase the trustworthiness of the exchanged data. In the general case, we combine all the three measurements. For non-important data, vehicles can use only their measurements. Finally, for the location-based data, the trust evaluation done by RSUs will be more convenient to decide about the received messages.

V. PERFORMANCE EVALUATION

1) *The evaluation scenario parameters* : To evaluate the performance of our solution, we conducted two different experiments. In the first experiment, we aim to study the blockchain’s basic operations: new block creation upon a vehicle network join and the proof of existence (POE) during message authentication. The second experiment will study our trust management process to show its accuracy in distinguishing between legitimate and malicious behaviors and its influence on transmission quality. we used the simulators Veins [40], OMNet++ [41], and SUMO [42] . OMNet++ is a well-known C++ event-based simulator for building network simulations. Simulation of Urban Mobility (SUMO) is an open-source, road traffic package for scenario creation. Veins is a framework that includes OMNet++ and SUMO to create and run vehicular network simulations. Table II presents the basic technical parameters.

We used the map of the “Riyadh City” Fig. 15 for the solution performance evaluation. It was generated using the open-source mapping platform “open-street-map” [43]. The covered area is (10 000m,10 000m). The traffic generator SUMO generates random trips for all the vehicles defined in the scenario.

TABLE II. BASIC SIMULATION PARAMETERES

| Parameter | Values |
|-------------------------|------------------------------|
| Hardware platform | Speed 3200Mhz, 8GRAM |
| Operation System | Debian9.4 |
| Traffic Generator | SUMO |
| Network basic simulator | Omnet++ 5.0 with inet v4.2.8 |
| Vanet Simulator | Veins 5.2 |
| Simulation Area | (10000mx10000m) |
| Simulation time | 500s |
| Data Rate | 6Mbps |
| Transmission power | 20mW |

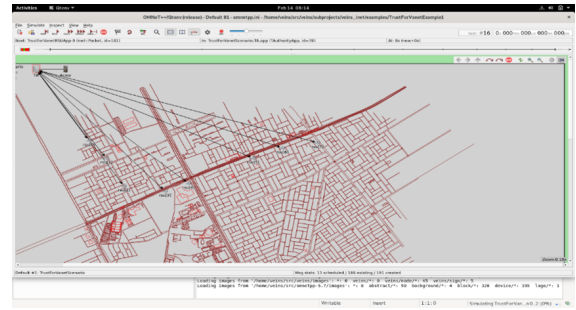


Fig. 16. RSU Deployment.



Fig. 15. Riyadh city map.

To evaluate the performance of our trust management approach, we defined the following parameters as mentioned in Table III. In our experiment, we varied the number of traveling vehicles from 20 to 200. We also varied the percentage of malicious vehicles from 20% to 80%. Each vehicle will periodically broadcast data messages. The broadcasting delay is selected randomly depending on the vehicle’s behavior. We made the malicious broadcasting delay shorter than the legitimate one to emulate real cases where attackers try to overcharge the network with their forged messages. Fig. 16 shows the Roadside Units deployment. After testing different locations to choose the best positions to cover the entire trajectory used in the vehicle’s trips, we selected positions as mentioned in the figure. We observed that more than half of RSUs are placed all along the road “King ABDALLAH street”.

TABLE III. BASIC SIMULATION PARAMETERES

| Parameter | Values |
|--|---------------------------------|
| Number of Vehicles | Varying from 20 to 200 |
| Number of RSU | 8 |
| Malicious vehicles rate | Varying 20% -40% -60%-80% |
| Certificate Validity period | 3600s |
| The trust threshold | 0.5 |
| The initial trust score | 0.5 |
| The direct trust reward | 0.2 |
| The historical trust reward | 0.2 |
| The direct max count | 2 |
| The direct trust broadcasting period | 15s |
| The indirect trust computing and broadcasting period | 20s |
| The historical trust updating period | 25s |
| Legitimate vehicle broadcasting delay | Random in the interval [5–10] s |
| Malicious vehicle broadcasting delay | Random in the interval [2–6] s |

2) *The evaluation metrics* : We used two types of metrics. Metrics related to the network performance and others focused on the trust estimation. We presented the following metrics:

- PDR: the packet delivery rate. It evaluates the success rate of data packet reception. We consider the PDR for both kinds of transmitted messages: legitimate and malicious.
- Average Transmission Delay: it measures the average delay to successfully transmit legitimate data packets from sender nodes to the receivers.
- Detection accuracy: it measures the ratio of the correctly detected legitimate and malicious messages to the total received messages.
- Average of different trust scores: We evaluated the averages of different trust scores for both kinds of behaviors. Those scores are:
 - Direct trust scores
 - Indirect trust scores
 - Historical trust scores
 - Final trust scores

3) *Blockchain computational cost*: In our first experiment, we aim to study the performance of our blockchain structure. we implemented the Authentication blockchain in a Python environment using a virtual machine with a speed of 3200Mhz and 8GRAM. We want to evaluate the computational time needed for a vehicle to be registered by the Trust Authority and the time to authenticate received messages.

a) *The evaluation of the average registration delay*: In Fig. 17, we represented the average registration delay versus the number of vehicles in the network. We varied the network population from 50 to 10,000 vehicles. We observe that the average delay varies in the interval [1...2] seconds. It is worth remembering that TA will create a new block for each new vehicle at its first attempt to join the network. The block contains the vehicle information as mentioned in the previous section. Each block will have a total size of 60 bytes. We use SHA-256 for the blockchain implementation. SHA-256 generates the hash code used as a block identifier citeyoshida2005analysis. The Chronological Merkel Tree (CMT) is the basic chaining structure [37] which minimizes the needed time for block checking. The average time of PoW (Proof Of Work) operation is estimated at around 1 second [44] and it varies depending on the block size and the used technology. In our experiment, results show that the block creation time varies from 1.04 to 1.84

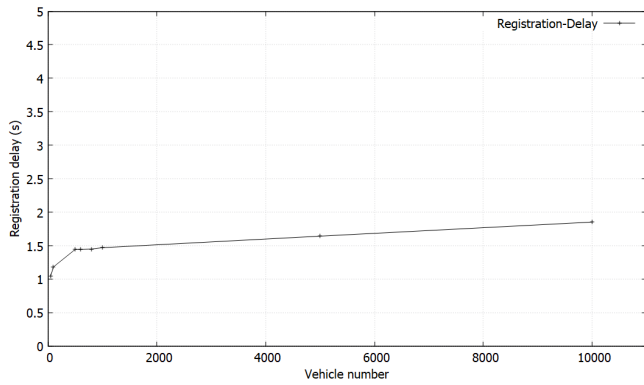


Fig. 17. Average registration delay versus vehicle number.

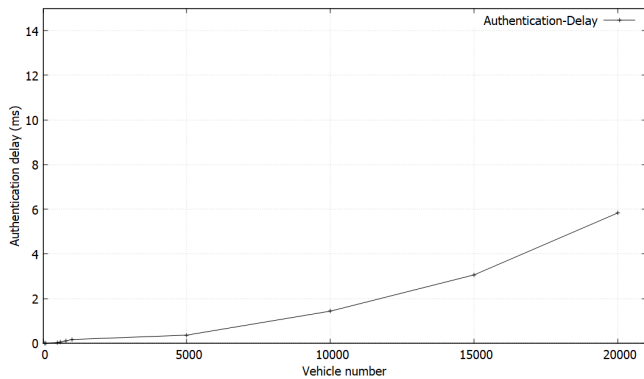


Fig. 18. Message authentication delay versus vehicle number.

seconds with the largest vehicle's number. The delay increases slowly with the number of requestors. Therefore, processing a large number of vehicle registrations will not penalize the network performance. Moreover, TA has exclusive permission to write new blocks and it has sufficient computation resources to perform its tasks without any issues. Consequently, the integration of blockchain as a public ledger in VANET will not affect the network latency.

b) The evaluation of the message authentication: In Fig. 18, we represented the average authentication delay versus the number of vehicles in the network. The message authentication delay is the needed time to verify the message sender's identity during V2V or V2I communications. Vehicles or RSUs will access the used blockchain and search for a corresponding block. The average authentication delay is the needed time to access the Authentication blockchain or other structures and verify the existence of a block for a specific vehicle. It's the elapsed time to perform a proof of presence operation. Our solution uses the algorithm SHA in the blockchain operations whose computational time is around 0.001ms per KB [45].

We varied the network population size from 50 to 20,000 vehicles. Results show that the consumed time increases from 0.0014 to 5.83ms. Thus, with the largest number of vehicles in the network, an extra delay of 6ms will be observed in each message exchange. With less dense network populations, the added delay is less than 2ms. Consequently, communications between different kinds of nodes will not be gravely affected,

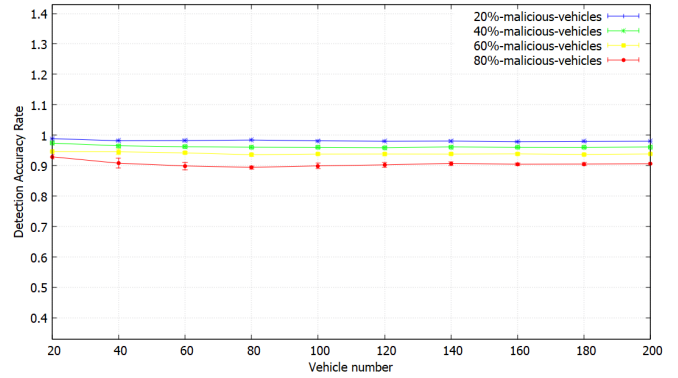


Fig. 19. Detection accuracy rate versus vehicle number.

and vehicles can quickly authenticate each other's.

4) Trust management system evaluation: Our second experiment defines simulation scenarios to evaluate the trust management process. We aim to study the efficiency and correctness of our scheme and its effects on network performance and communication quality.

a) The evaluation of the detection accuracy: Fig. 19 shows the detection accuracy rate over vehicle number variation. We used four different malicious percentages: from 20% to 80%. We see clearly that whatever the number of malicious nodes in the network, our scheme distinguishes correctly between the two behaviors. The detection accuracy rate is always greater than 0.9. With only 20% of malicious vehicles, the detection accuracy is stable around 0.98. With the highest malicious rate (80%), the detection accuracy rate decreases and is stable around 0.9. We also observe that the vehicle number slightly affects the detection accuracy. With fewer vehicles, the detection is less precise than with a bigger network population. It means, that when legitimate nodes are a minority in the network, communications and trust information exchange between them is difficult. But, with a denser network, vehicles have more opportunities to recognize malicious messages.

b) The evaluation of the direct trust score: Fig. 20 and 21 illustrate the measurement of the average direct trust score for both behaviors with various malicious percentages. We also plotted the trust score threshold used by our scheme for a clear comparison. We observe that our proposal successfully recognizes the legitimate nodes. The average attributed direct score varies between 0.68 and 0.83 which is always greater than the defined threshold.

With the smallest malicious cars percentage (20%), the average score was stable at around 0.8 whatever the number of vehicles in the network. Legitimate nodes are more likely to communicate with each other which increases the number of exchanged messages and makes the direct evaluation more precise. With a Higher malicious percentage, the communication opportunities between legitimate cars will be less often because the network will be overwhelmed by malicious messages. Nevertheless, our scheme can correctly identify good behavior and attribute a direct score always greater than .68. The direct score attributed to malicious vehicles is presented in Fig. 21. We see that the average score is stable around

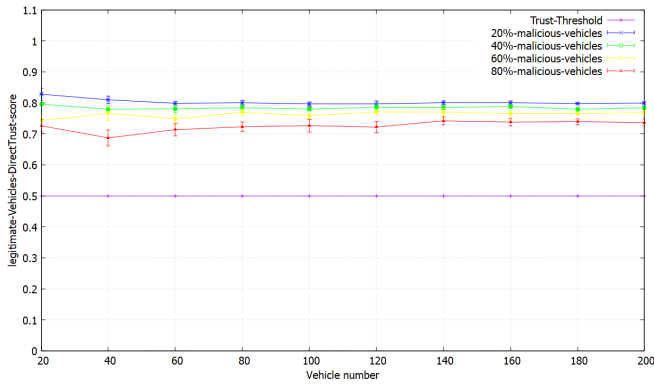


Fig. 20. Average direct score for a legitimate vehicle versus vehicle number.

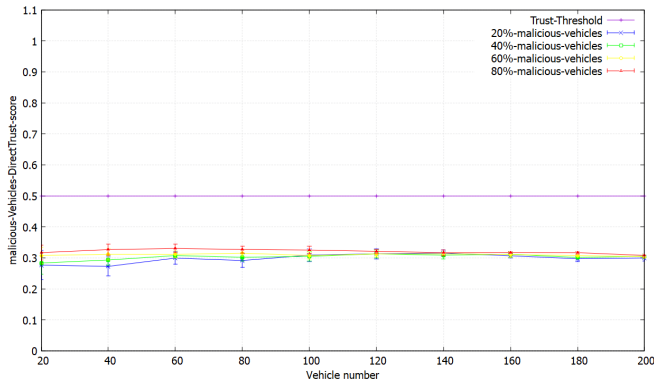


Fig. 21. Average direct score for a malicious vehicle versus vehicle number.

0.3 less than the threshold score. Our scheme was able to recognize efficiently bad behavior and correctly attributed the corresponding score values. With various malicious rates, our direct score attribution mechanism maintains a clear distinction between behaviors. We remark that in the case of a low network population (less than 60 nodes), the average score with a malicious percentage of 80% is a little higher than with other percentages. The higher density of malicious cars makes their communications with legitimate vehicles less often which leads to fewer opportunities to evaluate their behaviors.

c) The evaluation of the indirect trust score: We represented the measurement of the average indirect score attributed to both behaviors in Fig. 22 and 23. It's worth it to remember that the indirect score is computed and attributed by RSUs. They collect direct scores of network member from their neighborhood and update their score attribution using the formula mentioned in the previous chapter. In Fig. 22, the average indirect score of legitimate nodes is illustrated. We see that the average score is always greater than the defined trust threshold whatever the malicious percentage and the number of cars in the network.

The indirect score is an aggregation of direct scores. The RSUs receive the measurement from nearby nodes and calculate the new value. In doing so, the indirect calculation process reflects the global consensus between nodes in the same neighborhood. With a small percentage of malicious vehicles in the network (20%), the average indirect value is

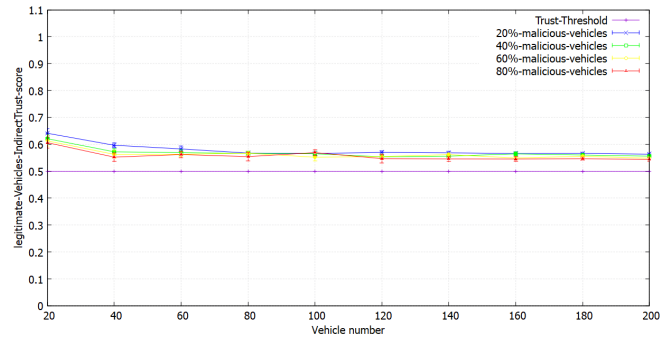


Fig. 22. Average indirect score for a legitimate vehicle versus vehicle number.

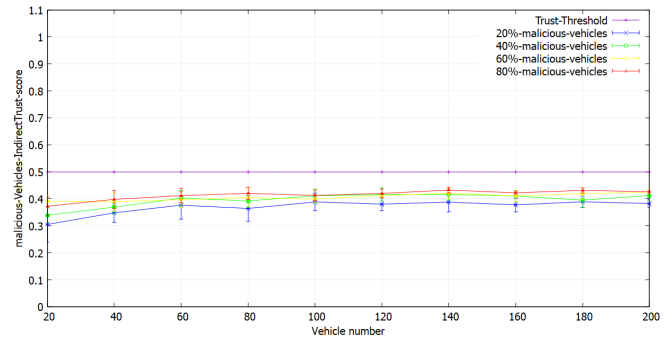


Fig. 23. Average indirect score for a malicious vehicle versus vehicle number.

greater than values with higher malicious rates. This means that malicious messages overwhelming the network bandwidth are handicapping behavior evaluation. Nevertheless, our solution is capable of clear recognition of each kind of behavior.

The measurement of average indirect scores for malicious cars illustrated in Fig. 23 confirms our previous observation. Bad behavior is identified in all cases and consequently, lower scores are attributed. The average indirect score for malicious vehicles is always less than the trust threshold value. It was stable between 0.3 and 0.4.

With a high presence of malicious vehicles (percentage over 60%) the average scores were greater than scores with lower rates. As we explained before, the higher presence of malicious cars made it less often for legitimate nodes to encounter them and come up with clear behavior judgments.

d) The evaluation of the historical trust score: We studied the historical trust score attribution process for both behaviors (refer to Fig. 24 and 25). The historical score is attributed by the Trust Authority (TA) using the reinforcement algorithm KNN as defined in the previous section. We observe that the TA manages to efficiently identify node behaviors and correctly attribute the corresponding scores. Legitimate nodes received an average score stable around 0.98 whatever the malicious rate and the vehicle number in the network. While malicious cars received an average score of around 0.1.

We remember that the TA receives direct and indirect score measurements from vehicles and RSUs in the network. All the collected information is cumulated and used as input for

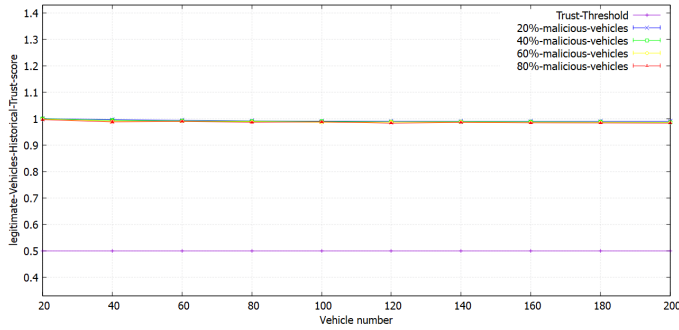


Fig. 24. Average historical score for a legitimate vehicle versus vehicle number.

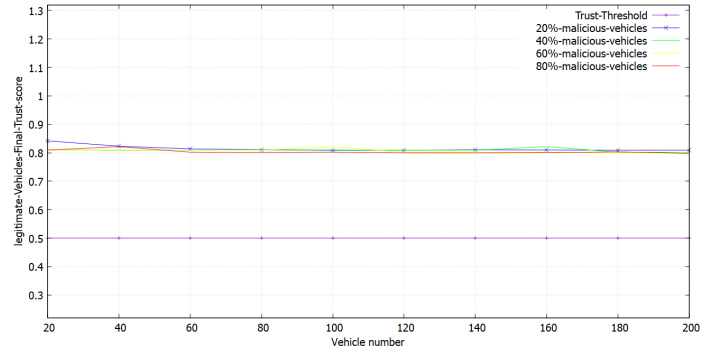


Fig. 26. Average final score for a legitimate vehicle versus vehicle number.

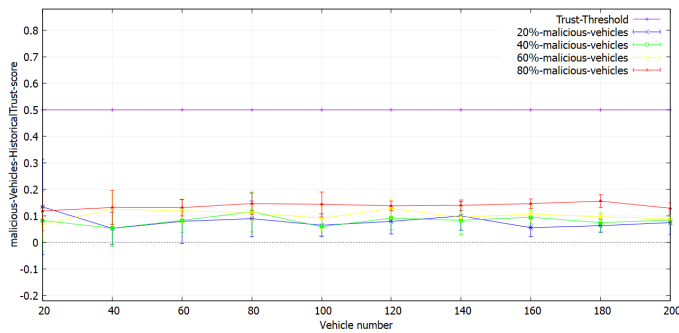


Fig. 25. Average historical score for a malicious vehicle versus vehicle number.

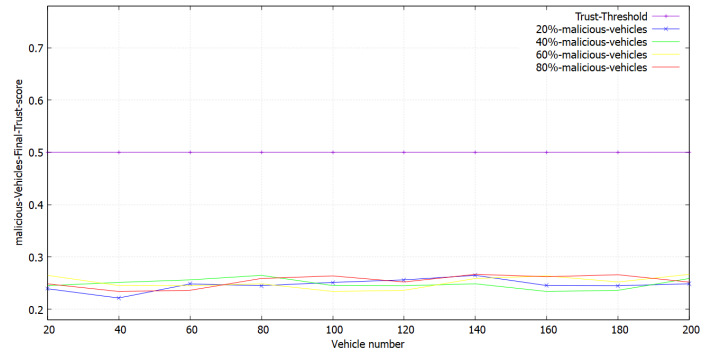


Fig. 27. Average final score for a malicious vehicle versus vehicle number.

the KNN reinforcement learning algorithm. TA successfully recognizes the two kinds of behavior in various situations. Legitimate nodes are identified without any issues. Malicious vehicle rate affects slightly the scores attributed to malicious vehicles. With the highest used rate (80%), the scores given to bad behavior are a little bit greater than scores in the case of a smaller rate (20% or 40%). In a network with a high malicious node density, legitimate nodes are a minority which makes the behavior evaluation more difficult.

e) *The evaluation of the final score:* Fig. 26 and 27 show the evaluation of the average final score for both kinds of behaviors versus the number of vehicles in the network and using various malicious rates. We remember that the final score formula is defined in the previous chapter. It combines the three evaluated trust score forms (direct, indirect, and historical) with weighted factors.

In this experiment, we studied the case where the weights (0.5, 0.2, 0.3) are respectively given to the score types (direct, indirect, and historical). This situation represents a global communication case without any special needs. We observe that the average final score of legitimate nodes is stable at around 0.8 whatever the used malicious rate and the network population size. Our proposal successfully recognizes the behavior and attributes the correct evaluation. In the case of malicious behavior, the average score is illustrated in Fig. 27. Bad behavior received an average score of around 0.25. As mentioned above, the malicious node density affects the judgment slightly. Legitimate nodes received fewer messages which made their trust evaluation less precise. This handicap

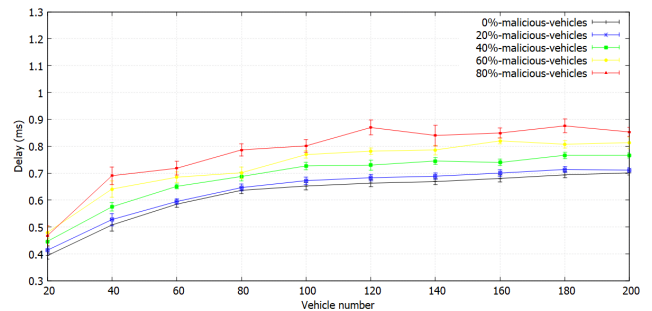


Fig. 28. Average transmission delay versus vehicle number.

leads to a higher score for bad behavior when the malicious rate is greater than 60%.

f) *The evaluation of the transmission delay for legitimate data :* Fig. 28 shows the data transmission delay versus variation in the number of vehicles with different malicious vehicle rates. We added to the representation a case without any attack (0% malicious vehicles) to compare with a standard transmission situation. We notice that the transmission delay in the attack scenarios is close to the ordinary exchange. First, with 20% malicious vehicles in the network, our proposal generates an extra delay stable of around 0.02ms whatever the population size. When the malicious car rates exceed 60%, the gap passes to 0.15ms. Therefore, our system works without an important impact on the data delivery. The proposed authentication process is fast and efficient and legitimate communications can be carried out with minimum delay.

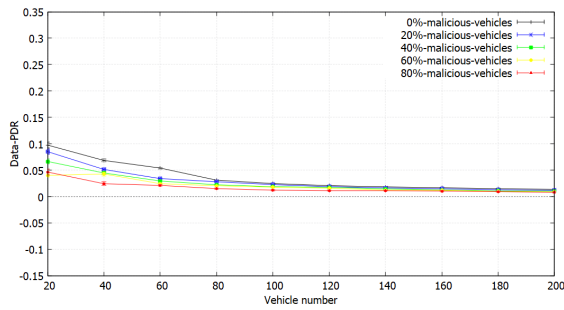


Fig. 29. Average PDR for legitimate data versus vehicle number.

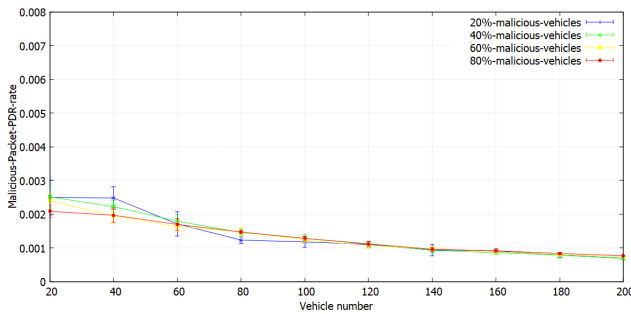


Fig. 30. Average PDR for malicious data versus vehicle number.

g) *The evaluation of PDR:* Our second metric to study the impact of our solution on the transmission quality is the evaluation of the Packet Delivery Rate (PDR) which counts the successfully delivered data packet rate. We evaluated the PDR for both kinds of behavior: legitimate and malicious data. Fig. 29 shows the legitimate data PDR versus the variation of vehicle numbers with various malicious vehicle rates. The PDR illustration confirms the result seen in the latency experiment. The PDR for legitimate vehicles is close to ordinary exchange no matter the rate of malicious cars. The highest malicious rate (80%) with the small network size (20 vehicles), shows the lowest successful rate, and the highest gap: 5% with the PDR of the ordinary exchange case. Malicious vehicles outnumber legitimate ones, consequently, they will occupy the network bandwidth and cause high packet loss for legitimate data. With other examples of population, our solution succeeded in reducing the attack overhead and data PDR is always close to ordinary exchange with all used malicious rates.

Fig. 30 illustrates the PDR evaluation for the malicious data to study the amount of harmful packets undetected by our solution. We remark that this amount is almost negligible. Its highest value was 0.0025 when we used 20% of malicious vehicles and a small network population size (20 vehicles). With other malicious rates or population sizes, the accepted malicious packets decrease, and the PDR is stable at around only 0.0015. This result shows that our solution detected efficiently any possible attack and succeeded in blocking and rejecting those packets. The low accepted rate is recorded during the first data exchanges where legitimate nodes were not able to fully evaluate the attacker's behavior. Quickly, our trust management process reveals the packet harm aspect and distinguishes correctly the bad from the good.

5) *Result discussion:* To study the performance of our solution, we defined two different kinds of experimentation. Firstly, we aim to evaluate the impact of blockchain technology integration on the authentication process. So, we implemented a real structure of the blockchain and tested the different computation operations. We focused on two basic processes: the registration of new vehicles and message authentication during ordinary communications. Our evaluation shows that the consumed time during a new vehicle registration will not exceed 1.84 seconds. This time corresponds to a new block creation and adding to the current ledger. This result remains as expected and lower than the standard time known from a literature review. Our second goal in this experiment was the computation time needed during V2V or V2I message exchange. This time was at around 0.001ms. it corresponds to the PoE (Proof of Existing) operation. We find out that, the blockchain integration in the VANET authentication process offers transparency and sensitive data preservation without overcharging network members.

Our second experiment used simulation scenarios to evaluate trust management and its impact on communication and network performances. Results show the correctness of our scheme. We observed that the detection accuracy rate was high and stable around 0.98 which demonstrates that node behaviors were recognized effectively. The evaluation of the different defined levels of trust scores: direct, indirect, historical, and final, indicates that the behavior score was quickly reviewed and updated. In a small populated network, the trust management system allows clear differentiation. Legitimate scores have been increased to over 0.8 and malicious scores have been decreased to 0.15. In populated networks, the recorded scores were around 0.75 for good behaviors and 0.3 for bad ones. Analysis of those results shows that the trust score attribution is slightly affected by the encountering probability. In small networks, a few vehicles are more likely to meet than in large networks. Therefore, the trust evaluation process can detect malicious behavior regardless of network size. In addition, it is more effective when vehicles pass each other very often.

Our second interest was the effects on communication quality. Results proved that the proposed scheme did not affect ordinary communications between network legitimate nodes. Data packets are still delivered quickly. In small networks, the identity verification process will add around 0.02ms to packet transmission time. While in larger networks the extra delay is around 0.15ms. Packet delivery rate measurement shows that we maintain high rates close to ordinary exchange without any attack.

VI. CONCLUSION

In this age of emerging technologies, we have to face these security challenges, specifically in the context of VANETs, which have become a rich field for scientific research. In this paper, we highlighted the concern of privacy protection in VANETs. We proposed a new authentication solution for VANET to ensure private data preservation and distinguish legitimate users from malicious ones. Our proposal introduces the use of blockchain technology as a reliable structure to maintain trustworthy authentication information and provide vehicles with an effective technique to authenticate any received message. We designed also a new trust management

process where vehicles evaluate their communicator's behavior and attribute trust scores accordingly. We defined various kinds of scores. Each one reflects different levels of trust evaluation decisions. Direct trust to reflect the node relationships. An indirect score is calculated by TA to reflect a bigger view. And a historical score using the reinforcement algorithm KNN to have a deeper evaluation of the node behavior. Finally, we evaluated the performance of our solution. Our analysis showed that our proposal provides an effective behavior management system and meets all the requirements for security and privacy in VANET. In future research, we will investigate the possibility of designing a new attack mitigation technique and we will focus on testing real attacks to evaluate the performance of our system.

ACKNOWLEDGMENT

The authors extend their appreciation to the Deanship of Scientific Research at Imam Mohammad Ibn Saud Islamic University (IMSIU) for funding and supporting this work through the Graduate Students Research Support Program.

REFERENCES

- [1] R. Suryadithia, M. Faisal, A. S. Putra, and N. Aisyah, "Technological developments in the intelligent transportation system (its)," *International Journal of Science, Technology & Management*, vol. 2, no. 3, pp. 837–843, 2021.
- [2] M. S. Sheikh and J. Liang, "A comprehensive survey on vanet security services in traffic management system," *Wireless Communications and Mobile Computing*, vol. 2019, pp. 1–23, 2019.
- [3] A. Rasheed, S. Gillani, S. Ajmal, and A. Qayyum, "Vehicular ad hoc network (vanet): A survey, challenges, and applications," in *Vehicular Ad-Hoc Networks for Smart Cities: Second International Workshop, 2016*. Springer, 2017, pp. 39–51.
- [4] R. Hussain, J. Lee, and S. Zeadally, "Trust in vanet: A survey of current solutions and future research opportunities," *IEEE transactions on intelligent transportation systems*, vol. 22, no. 5, pp. 2553–2571, 2020.
- [5] H. Cheng, X. Fei, A. Boukerche, and M. Almulla, "Geocover: An efficient sparse coverage protocol for rsu deployment over urban vanets," *Ad Hoc Networks*, vol. 24, pp. 85–102, 2015.
- [6] S. A. Jan, N. U. Amin, M. Othman, M. Ali, A. I. Umar, and A. Basir, "A survey on privacy-preserving authentication schemes in vanets: attacks, challenges and open issues," *IEEE Access*, vol. 9, pp. 153 701–153 726, 2021.
- [7] P. Mundhe, S. Verma, and S. Venkatesan, "A comprehensive survey on authentication and privacy-preserving schemes in vanets," *Computer Science Review*, vol. 41, p. 100411, 2021.
- [8] M. Arif, G. Wang, M. Z. A. Bhuiyan, T. Wang, and J. Chen, "A survey on security attacks in vanets: Communication, applications and challenges," *Vehicular Communications*, vol. 19, p. 100179, 2019.
- [9] M. M. Hamdi, L. Audah, M. S. Abood, S. A. Rashid, A. S. Mustafa, H. Mahdi, and A. S. Al-Hiti, "A review on various security attacks in vehicular ad hoc networks," *Bulletin of Electrical Engineering and Informatics*, vol. 10, no. 5, pp. 2627–2635, 2021.
- [10] C. H. Quevedo, A. M. Quevedo, G. A. Campos, R. L. Gomes, J. Celestino, and A. Serhrouchni, "An intelligent mechanism for sybil attacks detection in vanets," in *ICC 2020-2020 IEEE International Conference on Communications (ICC)*. IEEE, 2020, pp. 1–6.
- [11] A. Quyoom, A. A. Mir, D. A. Sarwar *et al.*, "Security attacks and challenges of vanets: a literature survey," *Journal of Multimedia Information System*, vol. 7, no. 1, pp. 45–54, 2020.
- [12] S. Dong, H. Su, Y. Xia, F. Zhu, X. Hu, and B. Wang, "A comprehensive survey on authentication and attack detection schemes that threaten it in vehicular ad-hoc networks," *IEEE Transactions on Intelligent Transportation Systems*, 2023.
- [13] X. Xu, Y. Wang, P. Wang *et al.*, "Comprehensive review on misbehavior detection for vehicular ad hoc networks," *Journal of Advanced Transportation*, vol. 2022, 2022.
- [14] D. Manivannan, S. S. Moni, and S. Zeadally, "Secure authentication and privacy-preserving techniques in vehicular ad-hoc networks (vanets)," *Vehicular Communications*, vol. 25, p. 100247, 2020.
- [15] H. Guo and X. Yu, "A survey on blockchain technology and its security," *Blockchain: research and applications*, vol. 3, no. 2, p. 100067, 2022.
- [16] S. K. Dwivedi, R. Amin, A. K. Das, M. T. Leung, K.-K. R. Choo, and S. Vollala, "Blockchain-based vehicular ad-hoc networks: A comprehensive survey," *Ad Hoc Networks*, p. 102980, 2022.
- [17] A. R. Javed, M. A. Hassan, F. Shahzad, W. Ahmed, S. Singh, T. Baker, and T. R. Gadekallu, "Integration of blockchain technology and federated learning in vehicular (iot) networks: A comprehensive survey," *Sensors*, vol. 22, no. 12, p. 4394, 2022.
- [18] R. S. Sutton and A. G. Barto, "Reinforcement learning: An introduction," *Robotica*, vol. 17, no. 2, pp. 229–235, 1999.
- [19] W. Ahmed, W. Di, and D. Mukathe, "Blockchain-assisted privacy-preserving and context-aware trust management framework for secure communications in vanets," *Sensors*, vol. 23, no. 12, p. 5766, 2023.
- [20] E. Meamari and C.-c. Shen, "Trocin: A blockchain-based robust trust management system for vanet," *Authorea Preprints*, 2023.
- [21] F. Ghovanlooy Ghajar, J. Salimi Sratakhiti, and A. Sikora, "Sbtms: Scalable blockchain trust management system for vanet," *Applied Sciences*, vol. 11, no. 24, p. 11947, 2021.
- [22] Y. Inedjaren, M. Maachaoui, B. Zeddini, and J.-P. Barbot, "Blockchain-based distributed management system for trust in vanet," *Vehicular Communications*, vol. 30, p. 100350, 2021.
- [23] C. Pu, "A novel blockchain-based trust management scheme for vehicular networks," in *2021 wireless telecommunications symposium (WTS)*. IEEE, 2021, pp. 1–6.
- [24] Y. Hui, Z. Su, T. H. Luan, and C. Li, "Reservation service: Trusted relay selection for edge computing services in vehicular networks," *IEEE Journal on Selected Areas in Communications*, vol. 38, no. 12, pp. 2734–2746, 2020.
- [25] A. Sonker and R. Gupta, "A new procedure for misbehavior detection in vehicular ad-hoc networks using machine learning," *International Journal of Electrical & Computer Engineering (2088-8708)*, vol. 11, no. 3, 2021.
- [26] J. Zhang, K. Zheng, D. Zhang, and B. Yan, "Aatms: An anti-attack trust management scheme in vanet," *IEEE Access*, vol. 8, pp. 21 077–21 090, 2020.
- [27] U. Javaid, M. N. Aman, and B. Sikdar, "Drivman: Driving trust management and data sharing in vanets with blockchain and smart contracts," in *2019 IEEE 89th Vehicular Technology Conference (VTC2019-Spring)*. IEEE, 2019, pp. 1–5.
- [28] S. Guleng, C. Wu, X. Chen, X. Wang, T. Yoshinaga, and Y. Ji, "Decentralized trust evaluation in vehicular internet of things," *IEEE Access*, vol. 7, pp. 15 980–15 988, 2019.
- [29] S. Ahmed, S. Al-Rubeaai, and K. Tepe, "Novel trust framework for vehicular networks," *IEEE Transactions on Vehicular Technology*, vol. 66, no. 10, pp. 9498–9511, 2017.
- [30] W. Liang, Z. Li, H. Zhang, S. Wang, and R. Bie, "Vehicular ad hoc networks: architectures, research issues, methodologies, challenges, and trends," *International Journal of Distributed Sensor Networks*, vol. 11, no. 8, p. 745303, 2015.
- [31] S. Malik and P. K. Sahu, "A comparative study on routing protocols for vanets," *Heliyon*, vol. 5, no. 8, 2019.
- [32] A. A. Taleb, "Vanet routing protocols and architectures: An overview," *J. Comput. Sci.*, vol. 14, no. 3, pp. 423–434, 2018.
- [33] H. Chen, R. Zhang, W. Zhai, X. Liang, and G. Song, "Interference-free pilot design and channel estimation using zcz sequences for mimo-ofdm-based c-v2x communications," *China Communications*, vol. 15, no. 7, pp. 47–54, 2018.
- [34] M. El Zorkany, A. Yasser, and A. I. Galal, "Vehicle to vehicle "v2v" communication: scope, importance, challenges, research directions and future," *The Open Transportation Journal*, vol. 14, no. 1, 2020.
- [35] R. Shrestha, R. Bajracharya, A. P. Shrestha, and S. Y. Nam, "A new type of blockchain for secure message exchange in vanet," *Digital communications and networks*, vol. 6, no. 2, pp. 177–186, 2020.

- [36] I. Roussou, C. Dritsaki, E. Stiakakis *et al.*, “The bitcoin’s network effects paradox—a time series analysis,” *Theoretical Economics Letters*, vol. 9, no. 06, p. 1981, 2019.
- [37] M. Bosamia and D. Patel, “Current trends and future implementation possibilities of the merkel tree,” *International Journal of Computer Sciences and Engineering*, vol. 6, no. 8, pp. 294–301, 2018.
- [38] A. S. Rajasekaran, M. Azees, and F. Al-Turjman, “A comprehensive survey on blockchain technology,” *Sustainable Energy Technologies and Assessments*, vol. 52, p. 102039, 2022.
- [39] N. C. Luong, D. T. Hoang, S. Gong, D. Niyato, P. Wang, Y.-C. Liang, and D. I. Kim, “Applications of deep reinforcement learning in communications and networking: A survey,” *IEEE communications surveys & tutorials*, vol. 21, no. 4, pp. 3133–3174, 2019.
- [40] C. Sommer, D. Eckhoff, A. Brummer, D. S. Buse, F. Hagenauer, S. Joerer, and M. Segata, “Veins: The open source vehicular network simulation framework,” *Recent advances in network simulation: the OMNeT++ environment and its ecosystem*, pp. 215–252, 2019.
- [41] C. Sommer, D. Eckhoff, A. Brummer, D. Buse, F. Hagenauer, S. Joerer, M. Segata, A. Virdis, and M. Kirsche, “Recent advances in network simulation: The omnet++ environment and its ecosystem,” 2019.
- [42] M. Behrisch, L. Bieker, J. Erdmann, and D. Krajzewicz, “Sumo—simulation of urban mobility: an overview,” in *Proceedings of SIMUL 2011, The Third International Conference on Advances in System Simulation*. ThinkMind, 2011.
- [43] J. Bennett, *OpenStreetMap*. Packt Publishing Ltd, 2010.
- [44] F. Wilhelmi, S. Barrachina-Muñoz, and P. Dini, “End-to-end latency analysis and optimal block size of proof-of-work blockchain applications,” *IEEE Communications Letters*, vol. 26, no. 10, pp. 2332–2335, 2022.
- [45] R. P. Naik and N. T. Courtois, “Optimising the sha256 hashing algorithm for faster and more efficient bitcoin mining,” *MSc Information Security Department of Computer Science UCL*, pp. 1–65, 2013.

An Efficiency Hardware Design for Lane Detector Systems

Duc Khai Lam

University of Information Technology, Ho Chi Minh City, Vietnam
Vietnam National University, Ho Chi Minh City, Vietnam

Abstract—The Hough Transform (HT) algorithm is a popular method for lane detection based on the 'voting' process to extract complete lines. The voting process is derived from the HT algorithm and then executed in parameter space (ρ, θ) to identify the 'votes' with the highest count, meaning that image points with pairs of angle θ and distance ρ corresponding to those 'votes' lie on the same line. However, this algorithm requires significant memory and computational complexity. In this paper, we propose a new algorithm for the Hough Space (HS) by utilizing parameterization (Y-intercept, θ) instead of (ρ, θ) parameterization and lane direction. This simplifies the inverse LHT operation and reduces the accumulator's size and computational complexity compared to the standard LHT. We aim to minimize processing time per frame for real-time processing. Our implementation operates at a frequency of 250MHz, and the processing time for each frame with a resolution of 1024x1024 is 4.19ms, achieving an accuracy of 85.49%. This design is synthesized on the Virtex-7 VC707 FPGA.

Keywords—FPGA; Hough transform; look up table; lane detector; autonomous vehicle

I. INTRODUCTION

Lane detection is one of the crucial objectives in image processing and computer vision, extensively applied in industries such as vehicle guidance and Advanced Driver Assistance Systems (ADAS). It involves detecting white or yellow lane markings. In some vision applications for Lane Departure Warning Systems (LDWS), the Hough Transform algorithm is widely utilized for lane detection due to its robust and effective detection capability, even in environments with significant noise or multiple non-contiguous lines [1]–[3]. This method relies on the 'voting' process and extracts complete lines.

Recent studies have focused on enhancing the Voting method within the Hough Transform for real-time computation. In [4], the authors applied Parallel Voting on an FPGA, utilizing a 2D array accumulator for line computation in the Hough Space with parameter pairs (ρ, θ) . By transforming the array into a 1D array and partitioning the Hough Space into parallel voting blocks, concurrent determination of lines and parameter computation (ρ, θ) was achieved. This accelerated the process, resulting in an average processing speed of 5.4ms per frame at a frequency of 200MHz, making video processing more feasible.

Similarly, subsequent authors proposed a hardware architecture for HT serving lane detection using the Parallel Voting method, implemented on FPGA in the scientific study [5]. Based on θ , the values in the Hough Space were parallelized. To detect edges of image frames in videos, computations of (ρ, θ) were performed to extract the highest voting value in the

Hough Space to determine the lines. The achieved processing speed was approximately 135 frames/s when deployed on the FPGA kit, operating at a frequency of 50MHz, and the image transmission protocol was VGA (640x480).

In the study [6], the authors developed a new algorithm for the Hough Parameter Space (HPS), which significantly reduced memory requirements compared to the standard Hough Transform (HT) algorithm. This method also supported accelerated Inverse Hough Transform (IHT) and reduced the accumulator size for voting. The efficiency of the proposed architecture was demonstrated through hardware-software co-simulation on the Xilinx Virtex-5 ML505 platform. The architecture from reference [4] allowed for a processing time of 1.47ms per frame for an image size of 640x480 pixels and an operating frequency of 200MHz.

The Angular Regions - Line Hough Transform (AR-LHT) method, based on techniques from LHT, is a memory-efficient approach for line detection in images. Utilizing the Hough Parameter Space (HPS) with minimal dispersion reduces memory usage significantly, as reported in [7]. Authors employ two smaller memories: a 1-bit Bitmap Region (RBM) and a downsized HPS. RBM determines peak orientation precisely after the voting process. Results show a 48% decrease in RAM usage compared to standard LHT for images sized 1024x1024 pixels. FPGA processing time for one image is 9.03ms.

In the study [8], the authors propose an HT architecture that uses a Look Up Table (LUT) to store trigonometric values and use the value of orientation θ calculated in the Sobel Edge Detection algorithm instead of rotating small angles as the HT standard. The processing time per 1024x1024 image resolution frame is 6.17ms with an accuracy of 94%. This design is synthesized on the FPGA Virtex-7 VC707.

In the study [9], [10], the authors implemented a real-time single-camera lane detection. To address different lighting conditions, they employed vital algorithms such as the Otsu, Canny algorithms and the Hough transform for lane detection to determine the Region of Interest and minimize computational complexity; detecting vanishing points is crucial.

The main contribution of [11] is to present an efficient implementation of Hough Transform based on Gradient for line detection, using Xilinx Virtex-7 FPGA with digital signal processing (DSP) units and integrated RAM blocks. The architecture is implemented with a working frequency of 260.061MHz and $2n + (\sqrt{2} + 2)n + 232$ clock cycles for a grayscale image of size $n * n$.

For complicated conditions, such as rain and night illuminations, the new processing method, comprising four

stages: Gaussian blur, grayscale conversion, Dark-Light-Dark threshold (DLD) algorithm, edge extraction using correlation filters, and Hough Transform according to [12], [13], has been developed. It effectively addresses lane complexities including arrows and text. Validation results demonstrate a maximum detection rate of 97.2%.

In [14], the authors present an algorithm for simple and user-friendly lane detection using the Line Segment Detector (LSD). This system maintains a throughput performance of 60 frames per second (fps) for VGA images (640x480) on the PYNQ-Z1 board with the Xilinx XC7Z020-1CLG400C FPGA.

To optimize the hardware resource for rho and theta calculations in the voting process of the line Hough Transform, the authors [15] propose an efficient memory design. This design is implemented in TSMC ASIC 90nm technology. It requires only 4174 MB RAM.

In this work, we focus on presenting an efficient hardware architecture design for the lane detection model to achieve real-time processing for large-resolution videos. We optimize hardware resources by reducing memory size and computational complexity. The lane detection core employs the Hough Transform algorithm. The proposed system includes the preprocessing process using the Gray Scale algorithm, Sobel Edge Detection, and the central processing algorithm - Hough Transform, implemented on an FPGA kit. The architecture focuses on accelerating hardware performance for the Hough Transform and Inverse Hough Transform algorithms by utilizing parameterization (Y-intercept, θ) in the Hough space and significantly reducing hardware resources by applying Region of Interest. Enhancements will concentrate on memory optimization of modules within the design and simplifying computational operations.

The rest of the paper is organized as follows. Section II presents the proposed hardware design architecture. Section III shows the evaluation and comparison results. Finally, Section IV gives the conclusions of this paper.

II. PROPOSED HARDWARE DESIGN ARCHITECTURE

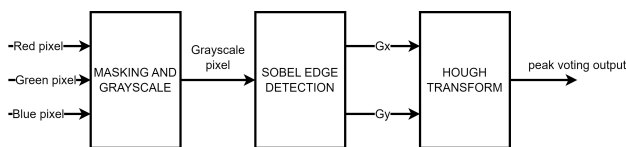


Fig. 1. Hough transform system.

Fig. 1 illustrates the architecture of the Lane Detection System using the Hough Transform, with the input being pixel values of an image and the output being the ρ and θ values after being voted in the Hough Transform module.

The proposed lane detection system consists of three parts, including the hardware architectures of the Gray Scale, Sobel Edge Detection, and Hough Transform algorithms. The functional blocks in this system are designed using the Verilog language. The available blocks of Gray Scale are referenced from the Masking module architecture, Gray Scale, Sobel Edge Detection, and the Hough Transform module is referenced from the study [6]. This paper will focus on utilizing the

Region of Interest (ROI) to reduce resources. The system's ROI is determined through experimental measurements, as depicted in Fig. 2. The details of the improved and optimized functional modules will be described below.

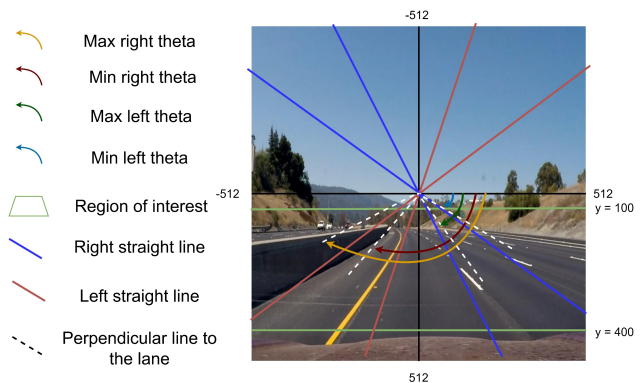


Fig. 2. Define the left and right lane boundaries' region of interest (ROI).

A. Sobel Edge Detection Module

The conventional structure is depicted in Fig. 3. In this structure, the image passes through Shift Registers to store the values of pixels in a row to form the matrix values of the Gx and Gy masks in the Gx, Gy Operator module. Then, it computes the orientation and edge intensity of the image through the Vectoring Cordic Module. Fig. 3 illustrates the architecture of this algorithm.

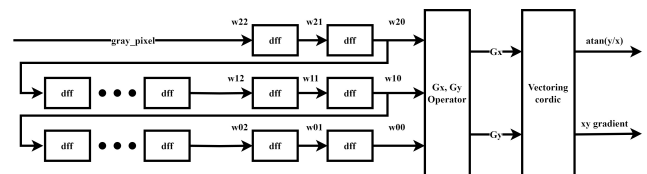


Fig. 3. Sobel edge detection.

However, utilizing Shift Registers as a First-In-First-Out (FIFO) mechanism could result in resource consumption and potentially suboptimal efficiency. As illustrated in Fig. 4, the Registers typically employed for retaining pixel rows are substituted with Memory components within the proposed Sobel Edge Detection method. Leveraging Memory resources on the FPGA offers the advantage of mitigating the routing complexities inherent in the design, consequently enabling elevated processing frequency within this module.

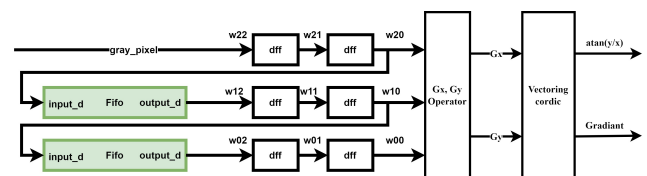


Fig. 4. Proposed Sobel Edge Detection.

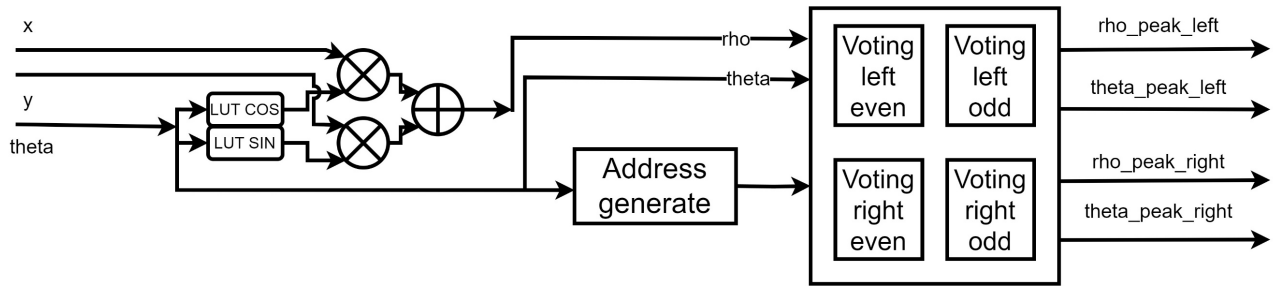


Fig. 5. Hough Transform module.

B. Hough Transform Module

In the conventional hardware design of the Hough Transform module, the authors employed the conventional method of Hough Transform computation, depicted in Fig. 5. This method involves computing ρ (rho) using the formula:

$$\rho = x * \cos(\theta) + y * \sin(\theta) \quad (1)$$

And utilizing the (ρ, θ) value system throughout calculations and as results. However, this approach does not include mechanisms for accelerating computations for the Inverse Hough Transform, necessitating additional processing steps after obtaining results from the hardware design. To reduce computational complexity, cos and sine trigonometric functions are computed via Look-Up Tables (LUTs) for both functions, as illustrated in Fig. 6. Notably, Sin and Cosin LUTs encompass data beyond the Region of Interest experimented with, resulting in memory consumption to store unnecessary values. Furthermore, the Voting module in the conventional design uses a Dual Port RAM as an accumulator for each image pixel identified as part of a straight line, as depicted in Fig.7. Subsequently, the (ρ, θ) values are directed to the Address generate block to furnish address values for the Voting module, thereby facilitating the voting process.

| COS SIN LUT | | |
|-------------|---------|--------|
| θ | COS | SIN |
| 0 | 1 | 0 |
| 1 | 0.9998 | 0.0174 |
| 2 | 0.0993 | 0.0348 |
| ... | ... | ... |
| 30 | 0.866 | 0.5 |
| ... | ... | ... |
| 179 | -0.9998 | 0.0174 |

Fig. 6. Sin LUT and Cos LUT.

Within the Voting Module, the Dual-port RAM performs concurrent accumulation and voting tasks, leveraging its versatile operational modes that seamlessly alternate between reading and writing operations. This integrated functionality optimizes resource utilization and enhances overall processing throughput within the module.

Within the Voting Port A of the Dual-port RAM, its functionality extends to retrieving the Accumulator value, subsequently updating it by assigning the value $A (\rho_i, \theta_i) = A (\rho_i, \theta_i) + 1$ into Port B. Activating wr_en permits

the writing operation to Port B contingent upon detecting an edge pixel within the Sobel Edge Detection module. Upon completion of the mapping and accumulation stages for the candidate (ρ, θ) pairs, the most prominent vote within the accumulator ensemble is determined through a straightforward comparison method characterized by its simplicity and minimal computational overhead.

Upon surpassing predefined threshold criteria during the voting process, the (ρ, θ) values garnered at the output undergo comparison and are archived within a flip-flop, effectively becoming the benchmark for comparison to ascertain the maximum value among the addresses within the dual-port RAM. This selection process culminates in the derivation of the outcome. Notably, each Voting module functions autonomously in delineating between the left and right lane lines. Nevertheless, each Voting module is singularly capable of executing voting operations for individual lane lines, necessitating the deployment of two Voting modules to detect a single lane line.

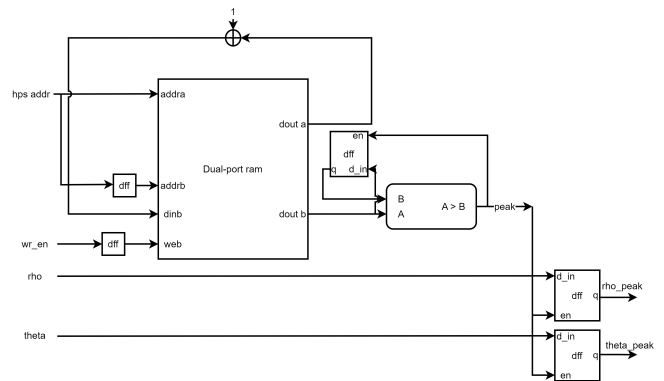


Fig. 7. Voting module.

| RAM Allocation in [6] | b | | | | | |
|-----------------------|------|-----|-----|-----|-----|------|
| | MinB | ... | ... | ... | ... | maxB |
| θ | 0 | | | | | |
| | 1 | | | | | |
| | 2 | | | | | |
| | ... | | | | | |
| | 177 | | | | | |
| | 178 | | | | | |
| | 179 | | | | | |

Fig. 8. Allocation Dual Port RAM.

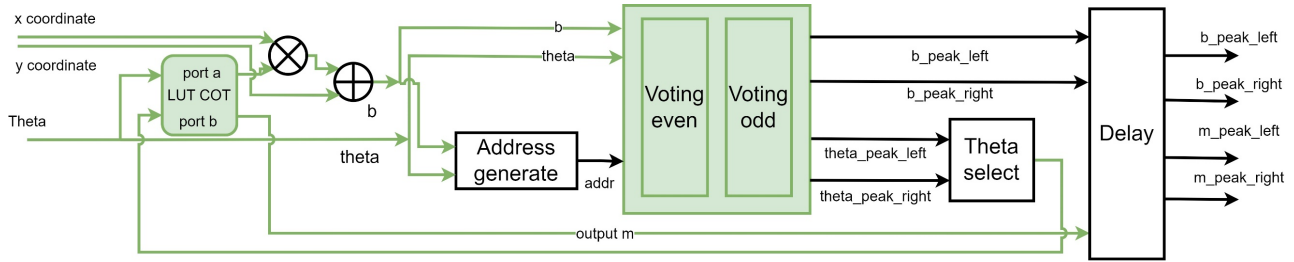


Fig. 9. Proposed Hough Transform.

The dual-port RAM in the conventional design has a memory space size from 0 to $179 * \text{MaxRHO}$ with $\text{MaxRHO} = 750$ for an image size of 1024×1024 , as shown in Fig. 8. The memory space size of the dual-port RAM includes all addresses from the smallest to the largest of the (ρ, θ) value pairs and contains values that are not within the ROI, leading to unnecessary resource consumption.

Even and odd voting blocks are used alternately, with the Even Voting performing the voting while the Odd Voting is in the reset process for the next voting round, and vice versa. This allows the voting process to be carried out continuously without interruption to reset the accumulator values. Therefore, four voting modules are required to perform the Voting and reset the accumulator values alternately to continuously obtain the output of the left and right lane lines. In the conventional formula Eq. (1) of the Hough Transform algorithm, the processing of the inverse transformation, Inverse Hough Transform, has not been performed and needs to be processed to obtain the equation of the line:

$$b = x * m + y \quad (2)$$

In the proposed design, the computation of ρ will be replaced by b:

$$m = \cot\theta \quad (3)$$

$$b = \rho / \sin(\theta) \quad (4)$$

$$(2), (3), (4) \rightarrow b = \cot(\theta) * x + y \quad (5)$$

Using this method, the hardware design also accelerates the Inverse Hough Transform. The proposed Hough Transform algorithm is described in Fig. 9. Compared to the conventional design, the Hough Transform module computes the value of b according to formula Eq. (5) to jointly enter the selection by pairs of values (b, θ) for the line. The design can compute for the process of Inverse Hough Transform with the final output being a linear equation Eq. (2). After selecting the line, the θ value is used to retrieve the (b, m) pair of results from the Dual port ROM of the COTAN trigonometric function to output. The final output value will be in the format of a linear equation. Moreover, the COTAN trigonometric function will only utilize 1 LUT instead of both Sin and Cosine trigonometric functions.

Furthermore, ROI will be utilized to reduce the resource usage of Cotan LUT, as shown in Fig. 10. The values stored inside the Cot LUT are limited to those experimented in the conventional design. The LUT will compute the values of θ from 30 degrees to 53 degrees and 130 degrees to 153 degrees

| COT LUT | |
|----------|---------|
| θ | COT |
| 30 | 1.732 |
| ... | ... |
| 53 | 0.7535 |
| 130 | -0.839 |
| ... | ... |
| 153 | -1.9626 |

Fig. 10. Cotan LUT.

to optimize resources and eliminate unnecessary values outside the ROI.

In the proposed hardware design of the Hough Transform, the Voting module is reduced to 2 Voting modules: Voting even and Voting odd. Each Voting module can perform Voting for the left and right lane lines by adding a condition to differentiate the peak values for the left and right lanes. This is illustrated in Fig. 11.

In the proposed Voting module, a comparison operation is added to compare the rotation angle of the pixel. If the pixel has a rotation angle greater than 90 degrees, then it belongs to the left side, otherwise if it is less than 90 degrees, then it belongs to the right side of the lane. This way, each Voting module will handle both the right and left lanes, reducing the number of Voting Modules needed by half.

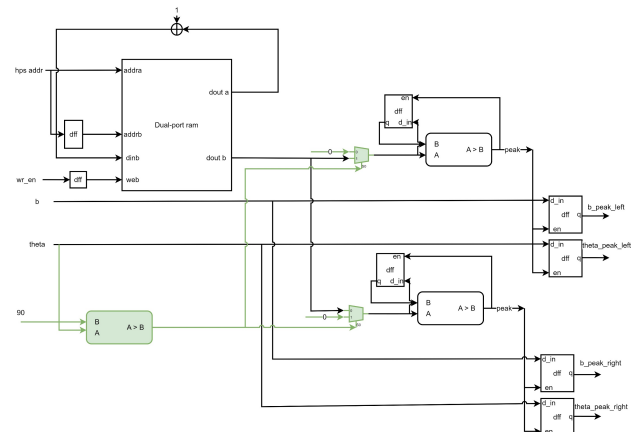


Fig. 11. Proposed voting module.

After changing from the Hough Space (ρ, θ) to the parameter space (b, θ) , the maximum value in the space also changes,

| RAM Allocation | | b | | | | | |
|----------------|-----|------|-----|-----|-----|-----|------|
| | | MinB | ... | ... | ... | ... | maxB |
| θ Right | 130 | | | | | | |
| | ... | | | | | | |
| | ... | | | | | | |
| | 153 | | | | | | |
| θ Left | 30 | | | | | | |
| | ... | | | | | | |
| | ... | | | | | | |
| | 50 | | | | | | |

Fig. 12. Size of the proposed Dual Port RAM.

with the max being 1550. However, when applying ROI to the Hough Transform Module, the b value will range from $-860 \leq b \leq 400$ based on formula Eq. (5). The offset needs to be added to $\max = 400$ to obtain the computation address 860, and the upper limit of b is 1260. Therefore, the Dual-port ram in the proposed design will have a memory region size of $((53-30) * (\max+\text{offset}) + ((153-130) * (\max+\text{offset}))$ as shown in Fig. 12 and eliminate unused address regions outside the ROI.

The amount of memory used by the Hough Transform will be reduced to only 2% compared to the conventional design, and in the HOUGH TRANSFORM Module of the proposed design, only 2 VOTING modules are required. This reduces the overall RAM size of the proposed design to approximately 1.044% compared to the conventional design.

III. VERIFICATION

A. Synthesized Result

The architecture is synthesized on the Virtex-7 VC707 FPGA platform using the Vivado Design Suite program based on the proposed architecture method. Table I shows the resource consumption for the proposed hardware architecture of the Hough Transform, benefiting from method simplification, transforming the Hough Space into (b, θ) , and applying ROI rigorously. The architecture utilizes 0.82% LUT and 482 Kbit memory (approximately 0.37%) for the Cotan Look-up table. BRAM usage accounts for about 3.5% of the Voting process.

TABLE I. RESOURCE CONSUMPTION OF THE PROPOSED ARCHITECTURE

| Resource | Synthesis | Implementation |
|----------|---------------------|---------------------|
| Board | Virtex-7 VC707 | Virtex-7 VC707 |
| LUTs | 2498/303600 (0.82%) | 2483/303600 (0.82%) |
| LUTRAM | 482/130800 (0.37 %) | 482/130800 (0.37 %) |
| FF | 3243/607200 (0.53%) | 3222/607200 (0.53%) |
| BRAM | 36 /1030 (3.5%) | 36/1030 (3.5%) |
| DSP | 1/2800 (0.04%) | 1/2800 (0.04%) |
| IO | 89/700 (12.71 %) | 89/700 (12.71 %) |
| BUFG | 1/32(3.13%) | 1/32(3.13%) |

The achieved processing speed after synthesis (see Table II):

- Image resolution: 1024x1024
- Processing frequency: 250 MHz
- Processing speed (ms/frame): 4.19 ms

Table III illustrates a detailed comparison of resource utilization between our FPGA implementation system and other studies. Although our architecture utilizes different devices compared to other studies, overall, the hardware resources of LUTs we use are relatively small. The architecture of [4] employs a small FPGA generation, with 0.8% LUTs, 9.36% memory, and 3.72% DSP. In [5], resource usage comprises 17% LUTs, 49% memory, and 3% FF. However, it utilizes more resources for DSP, at 59.77%. Authors in the study [6] implement the Hough space using $(Y\text{-intercept}, \theta)$ and require 6.9% LUTs, 5.6% memory, and 15.54% slices without using DSP. Additionally, 5.18% LUTs, 9.34% slices, and 3.71% FF of resources are utilized in [7]. This system uses a significant number of resources for BRAM, at 66.67%. In [8], 5.83%, 3% slices, and 0.75% memory are utilized. Regarding BRAM, it uses 31%, 0.67% FF, and only 0.07% DSP.

B. Verification and Evaluation

To validate the hardware design of the Hough Transform system, a simulation model was implemented using the Verilog hardware description language, and the Hough Transform IP was simulated on the Vivado Design Suite, as shown in Fig. 13.

The evaluation results will be based on the same validation

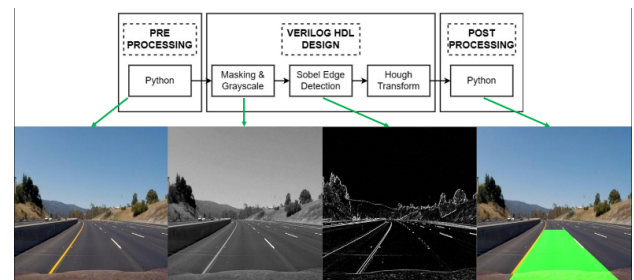


Fig. 13. Verification model.

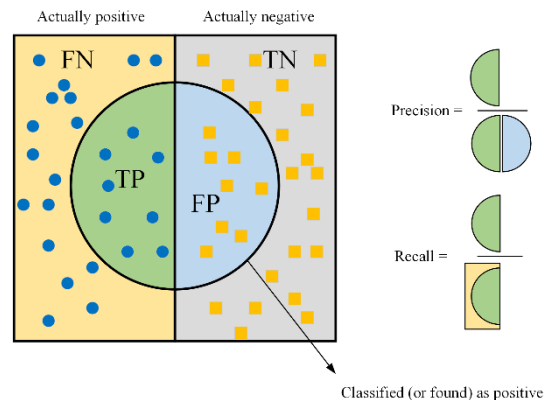


Fig. 14. Precision and recall.

dataset used in the study [8]. The videos are processed and converted into text files, then simulated using the Vivado Design Suite application. The resulting data is saved in text files, and Python processes the output values. These output values will be used to draw the lane lines.

This paper utilizes the Precision, Recall, and F1-score evaluation systems to ensure comprehensive and objective

TABLE II. RESULTS OF OUR WORK COMPARISON WITH DIFFERENT ARCHITECTURES

| | [4] | [5] | [6] | [7] | [8] | Our architecture |
|-----------------------------|----------|---------|---------|-----------|-----------|-------------------------|
| Image Resolution | 1024x768 | 640x480 | 640x480 | 1024x1024 | 1024x1024 | 1024x1024 |
| Fmax (MHz) | 200 | 50 | 200 | 145 | 170 | 250 |
| Processing Speed (ms/frame) | 5.4 | 7.4 | 1.47 | 9.03 | 6.17 | 4.19 |
| Normalized Speed (ns/pixel) | 6.8 | 24.08 | 4.78 | 8.61 | 5.88 | 4 |

TABLE III. RESOURCE REQUIREMENTS OF OUR SYSTEM COMPARISON WITH DIFFERENT ARCHITECTURES

| Resource usage | [4] | [5] | [6] | [7] | [8] | Our architecture |
|----------------|-------------------|-----------------|----------------|------------------|----------------|-------------------------|
| Device | Altera Stratix IV | Cyclone II FPGA | Virtex-5 ML505 | Xilinx xc7z001-1 | Virtex-7 VC707 | Virtex-7 VC707 |
| LUTs | 1459 | 5460 | 1996 | 911 | 4551 | 2483 |
| Slices | 5115 | - | 1119 | 411 | 2275 | 1200 |
| Memory (Kbit) | 1604 | 1985 | 1625 | - | 986 | 482 |
| BRAM | - | - | - | 40 | 320 | 36 |
| FF | - | 5781 | - | 1307 | 4215 | 3222 |
| DSP | 48 | 52 | 0 | 0 | 2 | 1 |

TABLE IV. THE ACCURACY RESULTS OF THE SIMULATION

| Road type | Number of frame | [8] | | | Our work | | |
|----------------|-----------------|---------------|---------------|---------------|---------------|---------------|---------------|
| | | Precision | Recall | F-score | Precision | Recall | F-score |
| Normal | 1260 | 96.65% | 98.46% | 97.55% | 93.14% | 90.67% | 90.54% |
| Poor condition | 1802 | 97.31% | 98.12% | 97.65% | 87.18% | 98.53% | 91.50% |
| Urban road | 1810 | 83.61% | 96.44% | 88.41% | 63.55% | 96.37% | 74.43% |
| Total | 4872 | 92.53% | 97.67% | 94.54% | 81.29% | 95.19% | 85.49% |

evaluation. Precision, known as positive predictive value, measures the accuracy of the positive predictions. Recall, also referred to as sensitivity in binary classification, measures the proportion of actual positives that are correctly identified. F1-score is the harmonic mean of Precision and Recall (assuming both values are non-zero). Its value ranges from 0 to 1 and is defined as follows:

$$Precision = \frac{TN}{TN + FN} \quad (6)$$

$$Recall = \frac{TP}{TP + FN} \quad (7)$$

$$F1 - score = 2 * \frac{Precision * Recall}{Precision + Recall} \quad (8)$$

where, True Positive (TP) is the result where the model correctly predicts the positive class, True Negative (TN) is the result where the model correctly predicts the negative class. FP (False Positive) results in the model incorrectly predicting the positive class. FN (False Negative) is the result where the model incorrectly predicts the negative class. Fig. 14 illustrates an example of Precision and Recall results.

The evaluation results performed on the dataset including three videos, are depicted in Table IV. Testing results were conducted on multiple videos under various lighting and road conditions, including urban streets, highways, road conditions, coverage, poor road markings, day and night scenes. By comparing images, it is evident that the successfully deployed architecture accurately detects straight lanes.

The results evaluated on the dataset from study [6], consisting of 3 videos, are presented in Table IV. The testing results on multiple videos with varying lighting and road conditions,

including urban streets, highways, road conditions, coverage, poor road markings, day and night scenes, were conducted. By comparing images, it can be observed that the successfully deployed architecture detects straight lanes. The comparative results indicate that the conventional architecture accurately detects straight lanes under different lighting and road conditions using metrics derived from these four results. Their average accuracy rates are approximately 92.53%, 97.67%, and 94.54%, respectively. Our hardware architecture's accuracy rates are 81.29%, 95.19%, and 85.49%, respectively. It is noted that there is a significant decrease in accuracy in our proposed architecture.

IV. CONCLUSIONS

This paper introduces a lane detection system for autonomous vehicles. The algorithm utilizes Gray Scale, Sobel Edge Detection, and Hough Transform methods. The hardware architecture is designed using the Verilog hardware description language. The proposed architecture implements a rigorous Region of Interest (ROI) approach to reduce hardware resource usage and algorithmic enhancements to reduce processing load for Inverse Hough Transform. The research aims to achieve fast processing speed through ROI implementation, which is capable of processing approximately 4.19ms per frame with a resolution of 1024x1024 and a frequency of 250MHz. When synthesized on the Virtex-7 VC707 FPGA board, the system achieves an accuracy of 85.49%. Although the real-time processing speed is achieved, the detection rate is relatively low. Therefore, we will explore how to improve the detection rate by applying the learning machine in our system for the future work.

ACKNOWLEDGMENT

This research is funded by Vietnam National University Ho Chi Minh City (VNU-HCM) under grant number DS2023-26-02.

REFERENCES

- [1] Yam-Uicab, R., Lopez-Martinez, J.L., Trejo-Sanchez, J.A. et al. A fast Hough Transform algorithm for straight lines detection in an image using GPU parallel computing with CUDA-C. *J Supercomput* 73, 4823–4842 (2017). <https://doi.org/10.1007/s11227-017-2051-5>.
- [2] D. Qiu, M. Weng, H. Yang, W. Yu and K. Liu, "Research on Lane Line Detection Method Based on Improved Hough Transform," 2019 Chinese Control And Decision Conference (CCDC), Nanchang, China, 2019, pp. 5686-5690, doi: 10.1109/CCDC.2019.8833139.
- [3] S. Luo and X. Zhao, "Application of improved Hough transform in lane line detection," 2022 IEEE 10th Joint International Information Technology and Artificial Intelligence Conference (ITAIC), Chongqing, China, 2022, pp. 1717-1721, doi: 10.1109/ITAIC54216.2022.9836543.
- [4] Guan, Jungang, Fengwei An, Xiangyu Zhang, Lei Chen, and Hans Jürgen Mattauch. 2017. "Real-Time Straight-Line Detection for XGA-Size Videos by Hough Transform with Parallelized Voting Procedures", *Sensors*, vol. 17, no. 2: 270. <https://doi.org/10.3390/s17020270>.
- [5] Guan, J., F. An, X. Zhang, Lei Chen and H. Mattauch. "Energy-Efficient Hardware Implementation of Road-Lane Detection Based on Hough Transform with Parallelized Voting Procedure and Local Maximum Algorithm.", *IEICE Transactions on Information and Systems*, 2019. vol. E102.D, no. 6, pp. 1171-1182. <https://doi.org/10.1587/transinf.2018EDP7279>.
- [6] El Hajjouji, Ismaïl Mars, Salah Asrih, Zakariae El Mourabit, "A novel FPGA implementation of Hough Transform for straight lane detection," *International Journal of Engineering Science and Technology*, 2019, vol. 23, <https://doi.org/10.1016/j.jestch.2019.05.008>.
- [7] D. Northcote, L. H. Crockett and P. Murray, "FPGA Implementation of a Memory-Efficient Hough Parameter Space for the Detection of Lines," 2018 IEEE International Symposium on Circuits and Systems (ISCAS), Florence, Italy, 2018, pp. 1-5, doi: 10.1109/ISCAS.2018.8351115.
- [8] Lam, D.K., Dinh, P.T.L., Ngoc Diem Nguyen, T. (2023). Hardware-Based Lane Detection System Architecture for Autonomous Vehicles. In: Dao, NN., Thinh, T.N., Nguyen, N.T. (eds) *Intelligence of Things: Technologies and Applications. ICIT 2023. Lecture Notes on Data Engineering and Communications Technologies*, vol 188. Springer, Cham. https://doi.org/10.1007/978-3-031-46749-3_4.
- [9] Y. Kortli, M. Marzougui, B. Bouallegue, J. S. C. Bose, P. Rodrigues and M. Atri, "A novel illumination-invariant lane detection system," 2017 2nd International Conference on Anti-Cyber Crimes (ICACC), Abha, Saudi Arabia, 2017, pp. 166-171, doi: 10.1109/Anti-Cybercrime.2017.7905284.
- [10] Y. Wang, L. Shi, J. Lausanne and D. Zhong, "Straight lane line detection based on the Otsu-Canny algorithm," 2022 IEEE 6th Information Technology and Mechatronics Engineering Conference (ITOE), Chongqing, China, 2022, pp. 27-30, doi: 10.1109/ITOE53115.2022.9734320.
- [11] X. Zhou, Y. Ito and K. Nakano, "An Efficient Implementation of the Gradient-Based Hough Transform Using DSP Slices and Block RAMs on the FPGA," 2014 IEEE International Parallel & Distributed Processing Symposium Workshops, Phoenix, AZ, USA, 2014, pp. 762-770, doi: 10.1109/IPDPSW.2014.88.
- [12] Zhang, Z.C. and Ma, X., "Lane Recognition Algorithm Using the Hough Transform Based on Complicated Conditions," *Journal of Computer and Communications*, vol.7, pp. 65-75, <https://doi.org/10.4236/jcc.2019.711005>.
- [13] A. Istiningrum, U. Salamah and N. P. Taufik Prakisyia, "Lane Detection With Conditions of Rain and Night Illumination Using Hough Transform," 2022 5th International Conference on Information and Communications Technology (ICOIACT), Yogyakarta, Indonesia, 2022, pp. 429-434, doi: 10.1109/ICOIACT55506.2022.9972068.
- [14] T. Manabe et al., "Autonomous Vehicle Driving Using the Stream-Based Real-Time Hardware Line Detector," 2019 International Conference on Field-Programmable Technology (ICFPT), Tianjin, China, 2019, pp. 461-464, doi: 10.1109/ICFPT47387.2019.000093.
- [15] K. V. Pachkor and V. Arunachalam, "Memory Efficient ASIC Implementation of Line Hough Transform," 2018 3rd IEEE International Conference on Recent Trends in Electronics, Information & Communication Technology (RTEICT), Bangalore, India, 2018, pp. 718-723, doi: 10.1109/RTEICT42901.2018.9012298.

Predictor Model for Chronic Kidney Disease using Adaptive Gradient Clipping with Deep Neural Nets

Neeraj Sharma, Praveen Lalwani
School of Computing Science and Engineering
VIT Bhopal University

Abstract—This research aims to develop computer vision based predictive model for the three prominent kidney ailments namely Cyst, Stone, and Tumor which are common renal disorders that require timely medical intervention. This classification model is tested and trained using the multi-class CT Kidney Dataset which contains 12,446 images collected from PACS (Picture Archiving and Communication System) from different hospitals in Dhaka, Bangladesh. Initial models are build using plain VGG16, ResNet50, and InceptionV3 deep neural nets. Then after clip value filter of ADAM optimizer is applied which results in marginally improved accuracy and at the last Adaptive Gradient Clipping is applied as a replacement of batch norm process and this produces overall best results. The Adaptive Gradient Clipping based model achieves accuracy of 97.15% in VGG16, 99.5% in ResNet50, and 99.23% in InceptionV3. Overall classification metrics are best for ResNet50 and Inception V3 with Adaptive Gradient Clipping technique.

Keywords—CT Kidney; VGG16; ResNet50; InceptionV3; gradient clipping; image processing; multiclass classification

I. INTRODUCTION

Computer vision is emerging as one of the most promising solution for early diagnosis and assisting doctors, medical health professionals to reduce the work load and provide treatment on need basis instead of first come first serve basis. Deep learning models for medical image classification has gained lot of popularity recently because of highly accurate results generated by these models. Post COVID-19 the availability of large image data sets has also gained popularity and this promotes the deployment of deep neural nets for classification purpose. But as discussed in [1] [1] the traditional way of handling image datasets may not work well for handling the large image datasets. This research work uses CT Kidney image dataset [2], which is a collection of 12,446 images spread across four categories of Normal, Cyst, Stone, and tumor, and build convolutional neural net based multi-class classification models for CT Kidney dataset using VGG16, ResNet50, and InceptionV3 deep neural nets. The initial models are build using plain versions of VGG16, ResNet50, and InceptionV3. To build the second version the clip norm filter of Adam Optimizer is used which is a floating value and is basically used to individually clip the gradient of each weight so that the norm of each weight remains less than or equal to this value. To build the third version the Adaptive Gradient Clipping techniques as discussed in [3] is used. Adaptive Gradient Clipping is a replacement to batch norm technique when we want to train models using larger batch sizes and increase the learning rate of model.

A. Chronic Kidney Disease

Chronic Kidney Disease (CKD) is a condition in which the kidneys are impaired and cannot filter blood as effectively as they could. As a result, the body stores excess fluid and blood waste, which can contribute to a variety of health problems such as heart disease and stroke. CKD is also reported to lead to Kidney Failure and is estimated to be present in 1 out of 10 adults [4]. CKD effects almost 1 billion people worldwide [5] largely including women, older citizens, and people suffering from diabetes and hypertension. CKD causes premature morbidity and mortality and lowers quality of life; it is also expensive [6] and becomes a big financial burden for low and middle income countries.

Cysts, Tumor, and Stone are three different impairments in Kidney. Round fluid-filled pouches called kidney cysts can develop on or inside the kidneys, impairing their regular function. A growth or collection of abnormal cells that develops on the kidney is called a kidney tumor. Malignant (cancerous) or benign (not cancerous) terms might apply to these tumors. Hard deposits of minerals and salts that accumulate inside the kidneys are called kidney stones.

CKD meets all the four criteria that are required to be recognize a disease as a public health issue [7] [8]. Early detection of CKD may prevent death and disability but such early detection is difficult [9] [10] depends on the availability of nephrologists who are scarcely available in various geographic locations and specially in South Asia[11]. Delay in detection of Kidney cysts, stones, and tumors increases the possibility of renal failure [12]. All these condition pave way for deployment of Deep Neural Net based models for timely detection of Kidney related diseases.

B. Authors Contribution

Chronic Kidney Disease is recognised as a public health issue but remains a less explored disease in the medical image processing filed. In this article a reliable and automated Kidney disease image processing model using advanced deep learning models is build. Another contribution is to explore the two different approaches for image classification: the traditional way using data scaling and Batch Normalization, and the novel way of using adaptive gradient clipping. The third contribution is in comparing the performance of the three most contemporary deep learning models namely VGG16, ResNet50, and Inception V3.

C. Article Organization

In Section 2, the most prominent and related work on deep learning based image processing models are discussed and the most prominent work in this field is summarized. The preliminaries of the image processing field are discussed in Section 3. In Section 4, the dataset, preprocessing methods, and the proposed model is discussed. In Section 5 the experimental results are discussed and comparative study of the different approaches are done. The article concludes by summarizing this research work and stating the future research prospects in Section 6.

II. RELATED WORK

A nice survey on medical image analysis can be found in [13]. Deep Learning methods have been tested on plethora of data sets in many research articles in the last decade. Main focus area in these research articles were radiology findings and segmentation tasks. Convolutional Neural Networks (CNN) have dominated the image processing segment [14], [15]. ResNet [14] has proved very helpful in building efficient Deep Neural Net Models. Other Deep Neural Net models prominently used are inception[15], and exception [16]. Another recent Deep Learning model is EfficientNet [17].

Recent advancement in the Deep Learning field like transfer learning is also proving very helpful in developing efficient models. Transfer learning is profoundly used for Natural Language Processing. Weights of a deep neural network pretrained on a large generic dataset are used to initialize subsequent tasks which can be solved with fewer data points, and less compute [18] [19] [20]. Transformers were proposed in [21] for machine translation and much recently they are deployed in image processing applications also. Multiple works try combining CNN-like architectures with self-attention [22] [23] [24], some replacing the convolutions entirely [25] [26]. But in large-scale image recognition, classic ResNetlike architectures are still state of the art [27] [28] [29][30].

Models like Vision transformer [31] have produced wonderful results as compared to Convolutional Neural Networks but hybrid models [32] and CNN with novel optimization techniques are expected to achieve much better results [33]. Deep neural nets use Gradient Descent as the basic technique for learning and a comparison of the different implementations of Gradient Descent is discussed in [34]. In all the models ADAM optimizer is used which is combination of RMSprop and Stochastic Gradient Descent with momentum. In [35] Stochastic Gradient Descent (SGD) is stated to perform better than ADAM, and RMS Prop optimizer using ResNet50. Class Balancing is discussed as a future work in this article but [36] discusses the meta-heuristic approaches that can be used for balancing X-Ray image datasets.

Limitation of Batch Norm technique are discussed in [37] for training large datasets and also discussed are the solution in the form of an novel Robust Normalization technique which provides all benefits of Batch Norm while mitigating the adversarial attacks. The technique of Adaptive Gradient Clipping is introduced in [3] as a replacement of Batch norm. Performance of Swin Transformers is reported to excel CNN models in [2] as it achieves accuracy of 99.30%. Vision Transformers are compared with CNN in [31] and it is concluded then though

CNN are slower as compared to Vision Transformers because of pooling operation but Vision Transformers require large data sets for training. YOLOv8 is deployed on CT Kidney Dataset for multi-class classification in [38] and it achieves an accuracy of 82.52

III. PRELIMINARIES

The underlying concepts of Image Processing, various classification techniques, and optimization techniques involved in this research article are discussed in this section.

A. Medical Image Processing

Medical image processing is used by medical practitioners to detect and diagnose diseases at early stages to increase chances of curing the disease. Out of the several basic stages of image processing Deep Learning is prominently applied for Image Enhancement, Segmentation and classification stages.

Noise frequently deteriorates medical pictures because of a variety of interference sources and this interfere with image processing systems' measuring procedures raising the requirement of Image Enhancement procedures [39]. The technique of segmenting a picture involves breaking it up into areas with similar texture, color, brightness, contrast, and gray level [40]. A segmented image become more meaning full and facilitates classification. Image classification is the task of categorizing an image into either of the given categories. Deep learning excels in the tasks of Image Segmentation, Reconstruction, and Classification [41]. Deep Learning models like RESNet [42], VGG16 [43], Inception Net [44] have excelled in this field achieving results that even surpass human abilities.

B. Image Classification Models

VGG16, ResNet50, and InceptionNetV3 are used for building the multi-class classification model.

1) VGG16: VGG16 [43] has become popular because of its proficiency in image classification tasks. It is a 16 layer Convolutional Neural Network (CNN) which has shown impressive performance on various image classification benchmarks. Its structure includes multiple convolutional and pooling layers followed by fully connected layers as shown in figure. It has a deep architecture to learn hierarchical features and the use of small 3x3 convolutional filters enables capturing fine-grained details in images. VGG16 has been employed in numerous studies for diabetic retinopathy and kidney cyst classification tasks, achieving high accuracy and demonstrating its potential as a reliable model in computer vision-based prediction. Structure of VGG16 classifier model is shown in Fig. 1.

2) ResNet50: ResNet50, short for Residual Network with 50 layers, is variant of a powerful CNN architecture introduced in [42] that addresses the challenge of training very deep neural networks. It introduces skip connections, or residual connections, which enable the network to learn residual mappings, making it easier to optimize and alleviate the vanishing gradient problem. ResNet50 has demonstrated superior performance on various image classification tasks, including diabetic retinopathy and kidney cyst classification. It's deep architecture allows for capturing intricate features, leading to

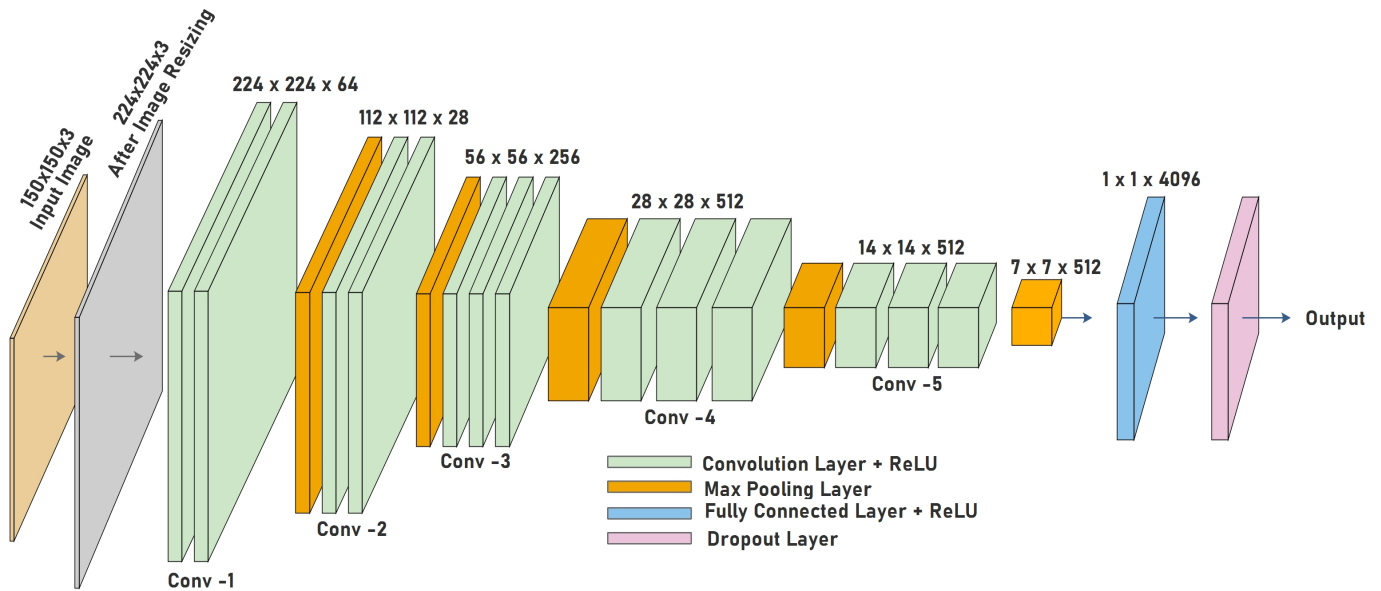


Fig. 1. Structure of VGG16.

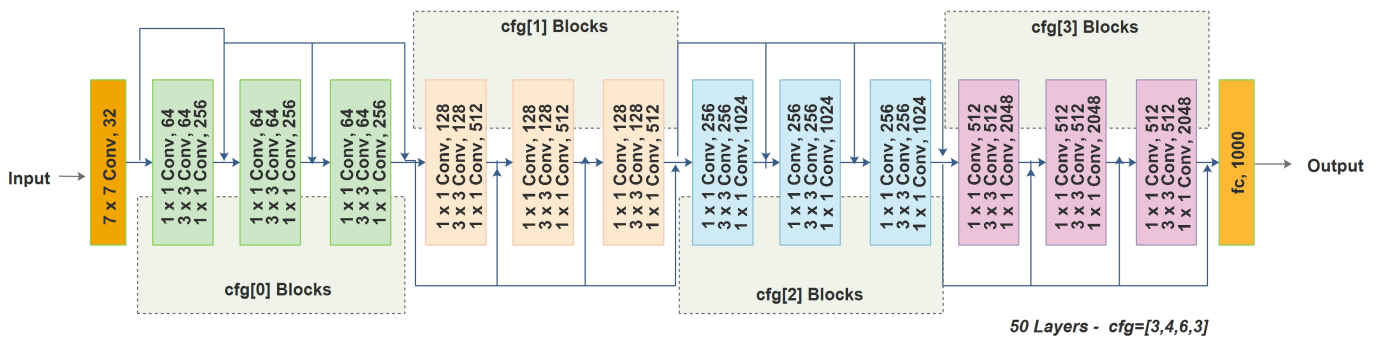


Fig. 2. Structure of ResNet50.

accurate predictions. The inclusion of residual connections makes ResNet50 particularly effective in handling complex visual patterns and has been widely adopted in computer vision research. The architecture of ResNet50 is shown in Fig. 2. $cfg[3,4,6,3]$ refers to $(3 \times 3=9)$, $(3 \times 4=12)$, $(3 \times 6=18)$, and $(3 \times 3=9)$ summing to 48 layers $(9+12+18+9)$ with one input layer and one fully connected layer increasing the count to 50. Structure of ResNet50 classifier is shown in Fig. 2.

3) InceptionV3: InceptionV3 is an advanced CNN architecture that incorporates the concept of “Inception modules” introduced in [44]. These modules use different filter sizes and perform parallel convolutions, using which the features are captured by network at multiple scales. InceptionV3 strikes a balance between depth and computational efficiency, achieving high accuracy while maintaining a manageable model size. It has been successfully applied in various image classification tasks, including diabetic retinopathy and kidney cyst classification. InceptionV3’s ability to capture both global and local features, along with its efficient architecture, makes it a valuable tool in computer vision-based prediction tasks. Structure of InceptionV3 classifier is shown in Fig. 3.

C. Normalization Techniques

To enhance the contrast of image and to make image features more visible the contrast is increased by performing min max scaling of images which scales the pixel values to a specific range.

Batch normalization [45] is frequently used for training deep neural networks with several benefits as discussed in [46] [47] [48] [49] [50]. But batch normalization comes with a major drawback of higher memory and time overheads and a mismatched behavior of training model and inference model [51] [52]. Another important limitation of Batch Normalization is that they break the interdependence between training examples. Other limitations of batch normalization are discussed in [53] [54] [55] [56] [57]. As a result Normalization Free ResNets (NFRN) were developed and discussed in [46] [47] [58] and these NFRN were made more efficient by using additional regularization mechanisms as discussed in [46] [47].

Gradient Clipping: Gradient Clipping technique was introduced in [59], and the related benefits are demonstrated in [60] which uses gradient clipping to stabilize training in

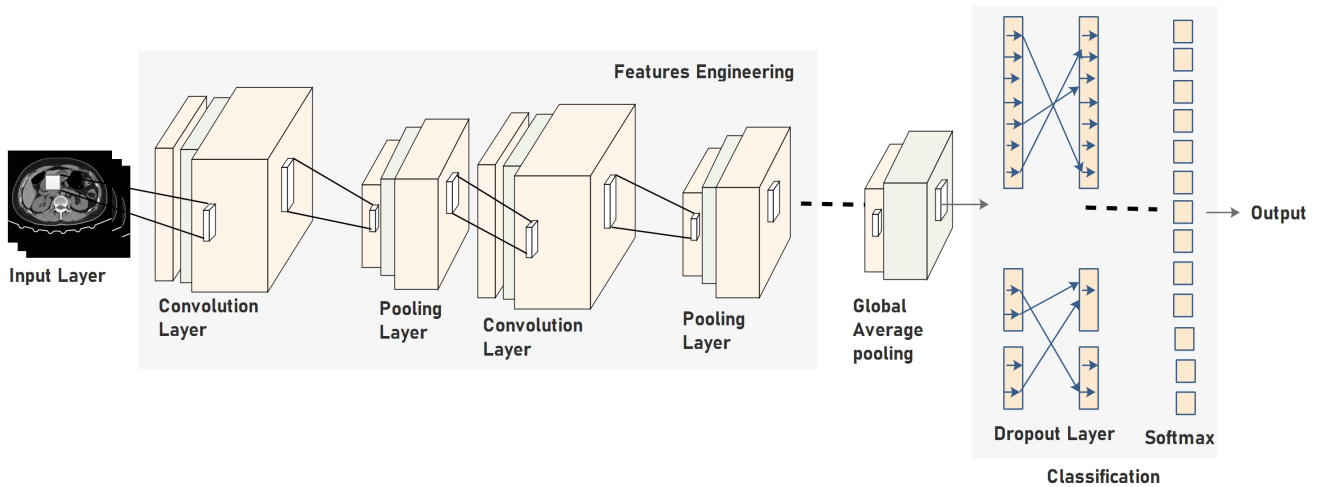


Fig. 3. Structure of InceptionV3.

Algorithm 1 Adaptive Gradient Clipping

- 1: **Input:**
 - 2: Model parameters: θ
 - 3: Rate of learning: α
 - 4: Clipping threshold: ϵ
 - 5: Scaling factor: γ
 - 6: **Initialization:**
 - 7: Set the model's initial values(parameter) θ
 - 8: Set the initial scaling factor γ (it is usually set to 1.0)
 - 9: **Repeat** for every training iteration::
 - 10: Compute gradients of the loss function concerning model parameters: $\nabla_{\theta} \text{loss}$
 - 11: Compute the norm of the gradients: $\|\nabla_{\theta} \text{loss}\|$
 - 12: **if** $\|\nabla_{\theta} \text{loss}\| > \epsilon$ **then**
 - 13: Update the scaling factor γ : $\gamma = \frac{\epsilon}{\|\nabla_{\theta} \text{loss}\|}$
 - 14: **end if**
 - 15: Clip gradients: $\nabla_{\theta} \text{loss} = \gamma \cdot \nabla_{\theta} \text{loss}$
 - 16: Update model parameters using the clipped gradients: $\theta = \theta - \alpha \cdot \nabla_{\theta} \text{loss}$
-

Large Language Models. Gradient clipping is mainly used to counter the Exploding Gradient and Vanishing gradient problems. Before propagating the erroneous derivatives back through the network, gradient clipping entails capping them. Smaller weights are the consequence of updating the weights using capped gradients. Clipping can be done on the values of gradients or on the norm of gradients. Both the clip value and clip norm options are available in optimizers like ADAM.

Adaptive Gradient Clipping (AGC): In [61] authors discussed that clipped gradient also converges faster than non-clipped gradients for general nonconvex problems. AGC [3] improves the convergence of gradient clipping by selecting an adaptive learning rate inversely proportional to the gradient norm, and ignoring the gradient's scale thus facilitating training with large batch sizes and strong data augmentations. AGC technique is also suggested as a replacement of Batch Norm process which enhances memory utilization and increases learning efficiency of Deep Neural Nets. Algorithm 1 describes the AGC process.

IV. PROPOSED MODEL AND METHODOLOGY

For the purpose of image classification Normalization methods can be combined with popular convolutional neural network (VGG16, ResNet50, and Inception V3). To achieve this, the CT kidney dataset is subjected to nine different models.

Three different setups for CT Kidney image classification are build using three different deep neural nets i.e. VGG16, ResNet50, and InceptionV3 in each setup. First setup is build using Min Max normalization with Batch Norm technique. In second setup the Clip Value (CV) filter of ADAM optimizer is used, and in the third setup Adaptive Gradient Clipping (AGC) is used as a replacement of Batch Norm. Fig. 4 shows the complete experimental setup.

A. Dataset Description

The CT Kidney dataset is a collection of 12,446 distinct jpeg images of which 3,709 are related to cysts, 5,077 to normal, 1,377 to stones, and 2,283 to tumors. The Picture Archiving and Communication System (PACS) was used to collect the dataset of patients who had previously been diagnosed with kidney tumors, cysts, normal findings, or stones at different hospitals in Dhaka, Bangladesh. The initial collection was of DICOM (Digital Imaging and Communications in Medicine) images which contain multiple monochrome images along with patient information and other meta data. These images were converted to lossless JPEG image format and the patient information and meta data were removed. Few sample images from the four classes of the dataset are shown in Fig. 5, 6, 7, and 8.

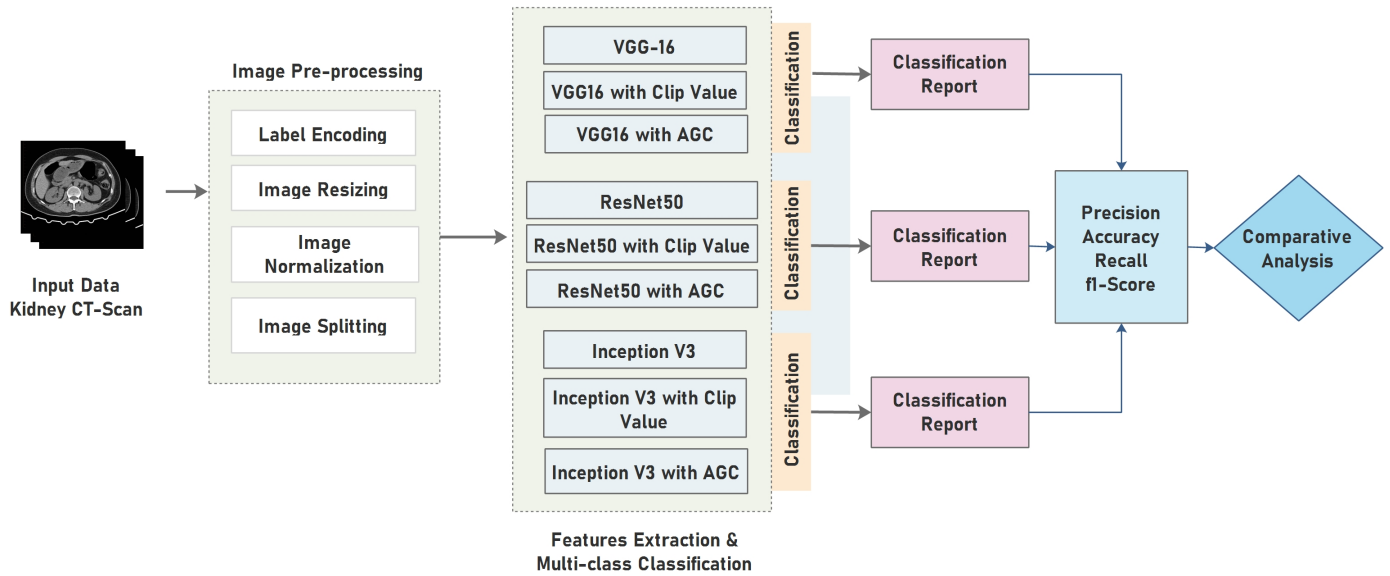


Fig. 4. Proposed model.



Fig. 5. Sample images for normal class of CT kidney dataset.

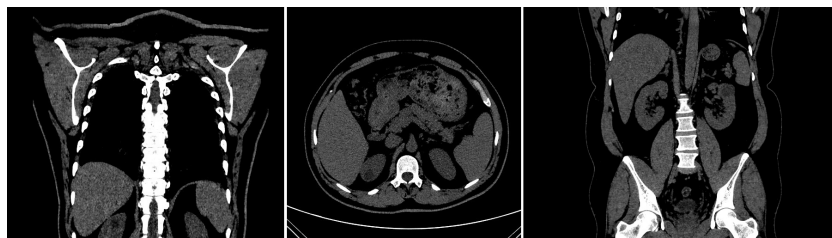


Fig. 6. Sample images for cyst class of CT kidney dataset.

B. Dataset Preprocessing

Images were initially resized to 150 by 150 pixels. The dataset is then normalized using min max normalization. The models are evaluated using a scheme where 80% of the images were taken to train the model and 20% to test the data. This resulted in 9,960 training image set and 2,491 test image set spread across 4 labels.

C. Classification Performance Metrics

A multiclass confusion matrix is used to calculate all the classification performance metric. All the classification models applied on CT Kidney dataset generates a multiclass confusion matrix from which the True Positive (TP), True Negative

TABLE I. CLASSIFICATION PERFORMANCE METRICS

| S.No. | Metric | Formula |
|-------|--------------------|---|
| 1. | Accuracy | $\frac{\{(TP+TN)\}}{\{(TP+TN+FP+FN)\}}$ |
| 2. | Recall/Sensitivity | $\frac{\{TP\}}{\{(TP+FN)\}}$ |
| 3. | Precision | $\frac{\{TP\}}{\{(TP+FP)\}}$ |
| 4. | F1-score | $\frac{\{(Recall*Precision)\}}{\{(Recall+Precision)\}}$ |

(TN), False Positive (FP), and False Negative(FN) values are calculated for each class.

The TP, TN, FP, FN values taken from confusion matrix help us calculate the following metrics tabulated in Table I.



Fig. 7. Sample images for stones class of CT kidney dataset.

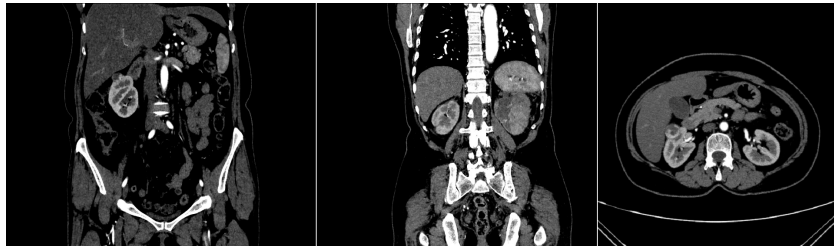


Fig. 8. Sample images for tumor class of CT kidney dataset.

Additionally for the multiclass dataset the Macro F1 score and the weighted F1 score are also calculated. The class-wise F1 scores acquired are simply averaged to get the macro-averaged F1 score of a model. The weighted F1 score is the average of the class-wise F1 scores, with the weights assigned based on the quantity of samples in each class.

Another powerful classification metric is Area Under Receiver Operating characteristics (AU-ROC) curve. The AU-ROC is also plotted but owing to the high accuracies achieved across the models AUROC score of 1 is achieved for all the classification models. Precision, recall, and f1-scores are used primarily for comparing the model's performance.

V. RESULTS AND DISCUSSIONS

The experimental results of three distinct models are shown and discussed in this section. All three models used three different deep neural net VGG16, ResNet50, and InceptionV3 creating total of nine combinations. All the nine different combinations used the same hyperparameters for doing a fair comparison.

A. Experimental Setup

All the models were executed on Jupyter notebook, installed on Windows 10 platform with i9 (12th gen) processor running at 3.19 GHz and having 64 GB of RAM and 1 TB hard Disk Drive space.

The various Python libraries used were Keras, TensorFlow, Numpy, os, Sci-kit Learn, and Matplotlib. The hyperparameters are commonly used across all nine models and are tabulated in Table II.

Additionally for all the Clip Value (CV) based models clipvalue=0.6 is used and for all Adaptive Gradient Clipping (AGC) based models decay rate of 0.95 is used with initial Clip Norm value = 1.00. The clip norm value is updated adaptively by AGC algorithm during the run time.

TABLE II. PARAMETER TUNING IN ALL MODELS

| SNo | Parameter | Value |
|-----|---------------------|--------------------------------|
| 1 | No. of Epocs | 15 |
| 2 | Learning Rate | 0.01 |
| 3 | Drop Out | 0.5 |
| 4 | Loss Function | Categorical Cross Entropy |
| 5 | Optimizer | ADAM |
| 6 | Batch Size | 32 |
| 7 | Activation Function | ReLU and Softmax |
| 8 | Regularization | Early Stopping from Keras |
| 9 | Preprocessing | Label Encoder/One Hot Encoding |
| 10 | Padding | 'Same' |

B. Performance Analysis of CT Kidney Dataset using VGG16

VGG16 is evaluated first on the CT Kidney dataset. The multi-class confusion matrix are shown in Fig. 9 and the classification metrics are displayed in Table III which displays the results of Plain VGG16, VGG16 with applied Clip Value (VGG16-CV), and VGG16 with Adaptive Gradient Clipping (VGG16-AGC).

In plain VGG16 classification accuracy of 96.9% is achieved which becomes 96.8% with CV model and 97.1% with application of AGC. The highest value of Macro and weighted f1-Score are also achieved with Adaptive Gradient Clipping technique i.e. 96.1% and 97.2% respectively. The highest values of precision are recorded in the plain model except for Class1 where the CV and AGC based models achieve higher precision values. Plain VGG16 achieves best Recall for Class0 and Class1 and AGC model achieves best Recall for Class1 and Class3.

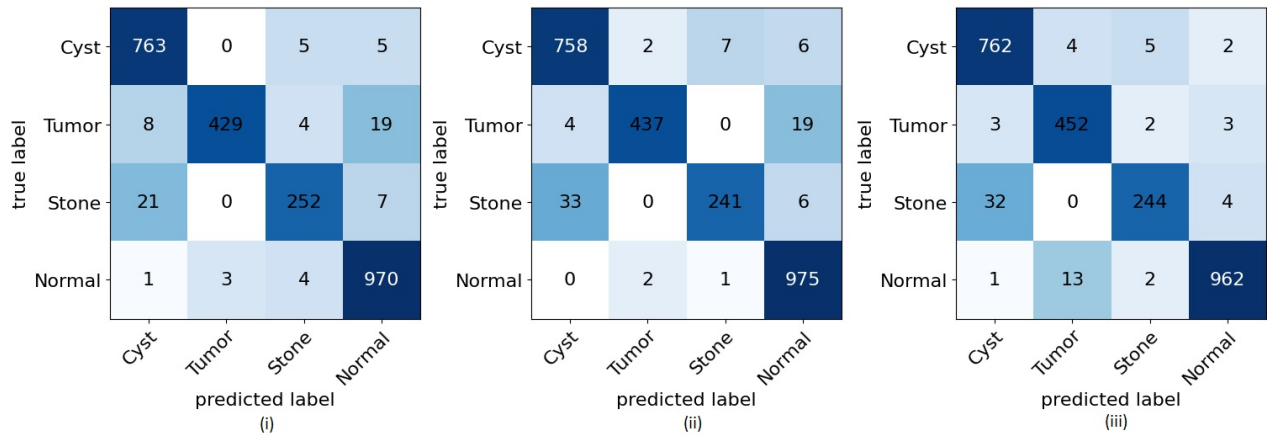


Fig. 9. Confusion Matrix for (i) Plain VGG16, (ii) VGG16-CV, (iii) VGG16-AGC.

TABLE III. CLASSIFICATION REPORT OF VGG16 MODELS

| | Plain VGG16 | | | VGG16-CV | | | VGG16-AGC | | |
|-------------------|-------------|--------|----------|-----------|--------|----------|-----------|--------|----------|
| | Precision | Recall | f1-score | Precision | Recall | f1-score | Precision | Recall | f1-score |
| Class 0(Cyst) | .987 | .962 | .974 | .981 | .953 | .967 | .986 | .955 | .970 |
| Class 1(Tumor) | .933 | .993 | .962 | .950 | .991 | .970 | .983 | .964 | .973 |
| Class 2(Stone) | .900 | .951 | .925 | .861 | .968 | .911 | .871 | .964 | .916 |
| Class 3(Normal) | .992 | .969 | .980 | .997 | .969 | .969 | .984 | .991 | .987 |
| Accuracy | .969 | | | .968 | | | .971 | | |
| Misclassification | .031 | | | .032 | | | .029 | | |
| Macro f1 | .960 | | | .958 | | | .961 | | |
| Weighted f1 | .969 | | | .968 | | | .972 | | |

C. Performance Analysis of CT Kidney Dataset using ResNet50

Next the performance of ResNet50 on the CT Kidney dataset is discussed. The three multi-class confusion matrix are shown in Fig. 10 and the classification metrics are displayed in Table IV, which contains the results of plain ResNet50, ResNet50 with applied Clip Value (ResNet50-CV), and ResNet50 with Adaptive Gradient Clipping (ResNet50-AGC).

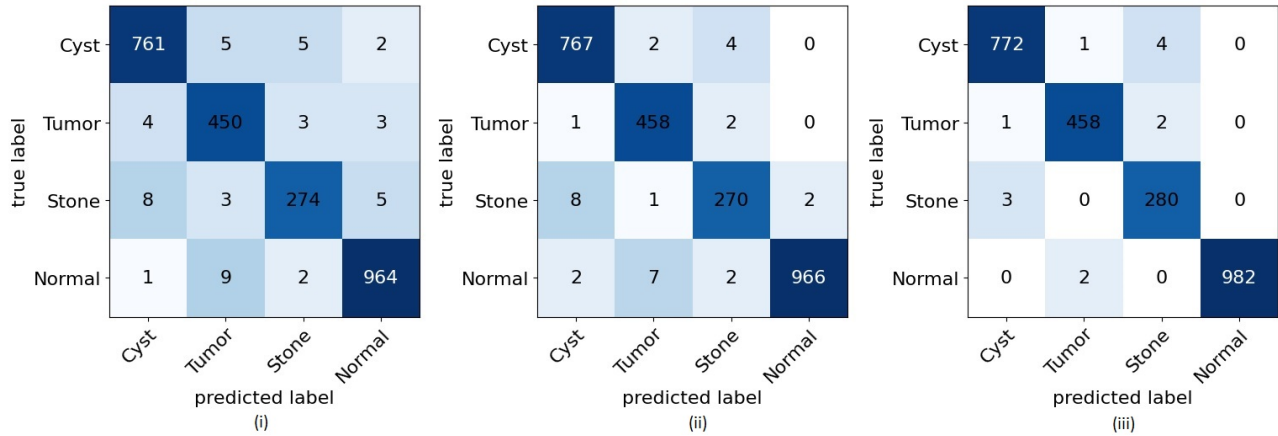


Fig. 10. Confusion Matrix for (i) Plain ResNet50, (ii) ResNet50-CV, (iii) ResNet50-AGC.

TABLE IV. CLASSIFICATION REPORT OF RESNET50 MODELS

| | Plain ResNet50 | | | ResNet50-CV | | | ResNet50-AGC | | |
|-------------------|----------------|--------|----------|-------------|--------|----------|--------------|--------|----------|
| | Precision | Recall | f1-score | Precision | Recall | f1-score | Precision | Recall | f1-score |
| Class 0(Cyst) | .984 | .983 | .984 | .992 | .986 | .989 | .994 | .995 | .994 |
| Class 1(Tumor) | .978 | .964 | .971 | .993 | .979 | .986 | .993 | .993 | .993 |
| Class 2(Stone) | .945 | .965 | .955 | .961 | .971 | .966 | .989 | .979 | .984 |
| Class 3(Normal) | .988 | .990 | .989 | .989 | .998 | .993 | .998 | 1 | .999 |
| Accuracy | .980 | | | .988 | | | .995 | | |
| Misclassification | .020 | | | .012 | | | .005 | | |
| Macro f1 | .975 | | | .984 | | | .993 | | |
| Weighted f1 | .980 | | | .988 | | | .995 | | |

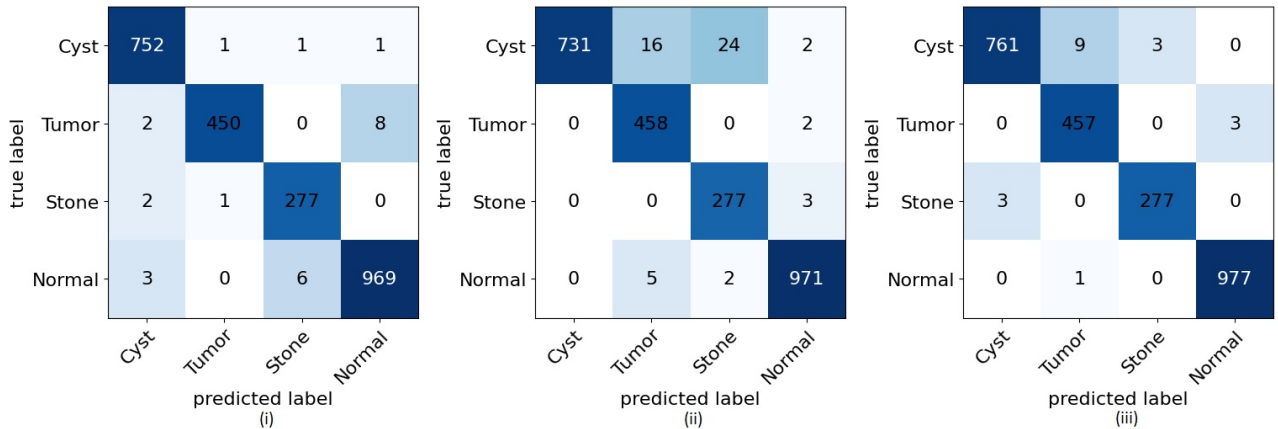


Fig. 11. Confusion Matrix for (i) Plain InceptionV3, (ii) InceptionV3-CV, (iii) InceptionV3-AGC.

TABLE V. CLASSIFICATION REPORT OF INCEPTION V3 MODELS

| | Plain InceptionV3 | | | InceptionV3-CV | | | InceptionV3-AGC | | |
|-------------------|-------------------|--------|----------|----------------|--------|----------|-----------------|--------|----------|
| | Precision | Recall | f1-score | Precision | Recall | f1-score | Precision | Recall | f1-score |
| Class 0(Cyst) | .996 | .991 | .993 | .946 | 1 | .972 | .984 | .996 | .990 |
| Class 1(Tumor) | .978 | .996 | .987 | .996 | .956 | .976 | .993 | .979 | .986 |
| Class 2(Stone) | .989 | .975 | .982 | .989 | .914 | .950 | .989 | .989 | .989 |
| Class 3(Normal) | .991 | .991 | .990 | .993 | .993 | .993 | .999 | .997 | .998 |
| Accuracy | | .990 | | | .978 | | | .992 | |
| Misclassification | | .010 | | | .022 | | | .008 | |
| Macro f1 | | .988 | | | .973 | | | .991 | |
| Weighted f1 | | .990 | | | .978 | | | .992 | |

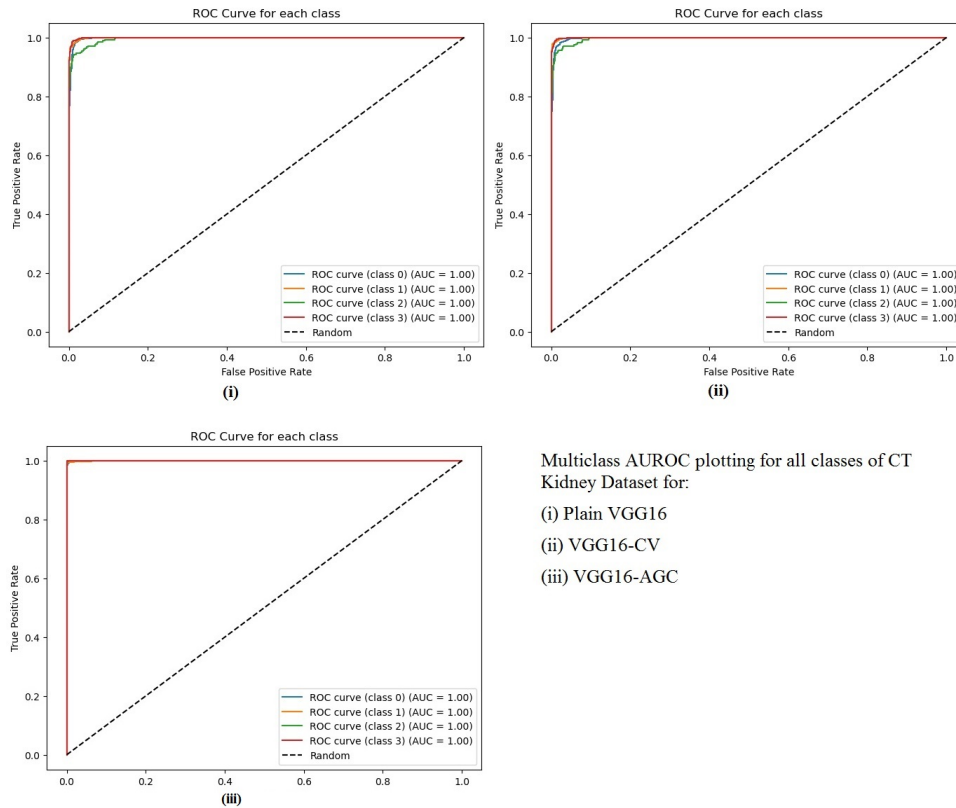
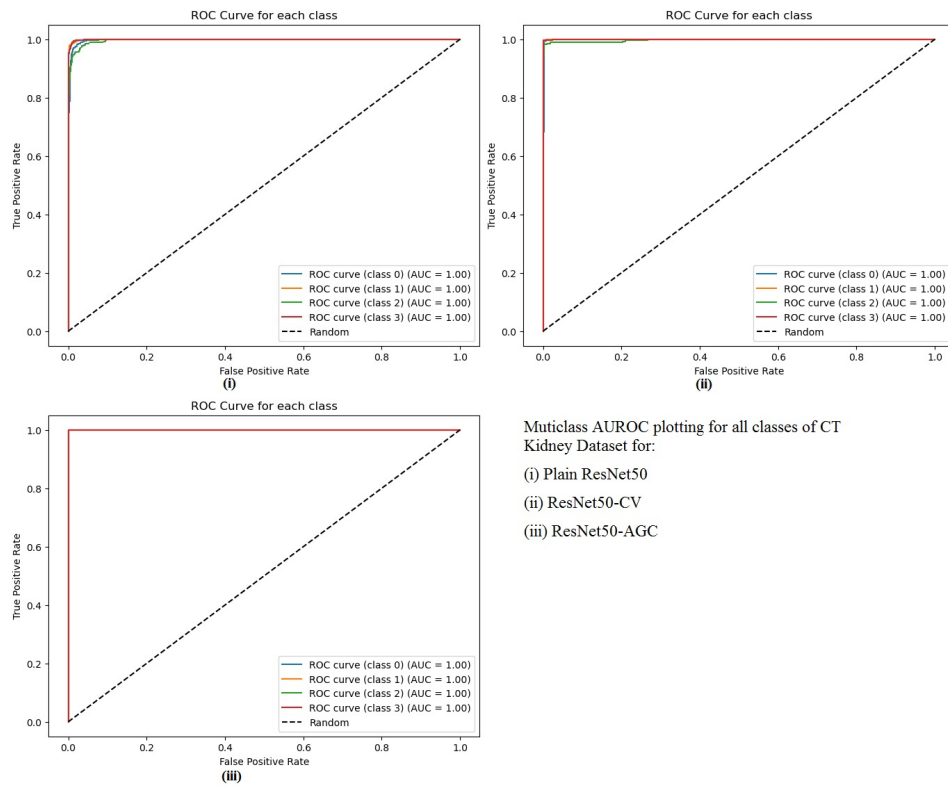


Fig. 12. All AUROC for VGG16 Setup.



Multiclass AUROC plotting for all classes of CT
Kidney Dataset for:
(i) Plain ResNet50
(ii) ResNet50-CV
(iii) ResNet50-AGC

Fig. 13. All AUROC for ResNet50 Setup.

Plain ResNet50 achieved classification accuracy of 98% which increases to 98.8% with ResNet50-CV and 99.5% in ResNet50-AGC model. With AGC the highest scores of Macro F1, Weighted F1 are achieved. CV model produces marginally better results as compared to plain model but AGC model scores the highest precision, and recall values across all the classes giving the best results.

D. Performance Analysis of CT Kidney Dataset using Inception V3

In the last setup Inception V3 is used to build the multiclass classification models. The resultant confusion matrix are shown in Fig. 11 and the classification metrics are displayed in Table V for plain Inception V3, Inception V3 with applied Clip Value (Inception V3-CV), and Inception V3 with Adaptive Gradient Clipping (Inception V3-AGC). Plain InceptionV3 achieved classification accuracy of 99% which decreased to 97.8% for the CV model and increased to 99.2% with AGC model. The Clip Value model performs marginally better for Class3 but in the remaining classes it stays behind the plain model. AGC model excels in precision in Class1 and Class3 and in Recall in Class0 and Class3. Overall AGC model marginally stays ahead of Plain model with highest score of Macro F1, and Weighted F1.

The AUROC for all the nine models are also plotted in Fig. 12, 13, and 14. The AUROC score remains same across all models because of high accuracy achieved.

VI. SUMMARY AND FUTURE WORK

Two different techniques of Clip Value(CV) and Adaptive Gradient Clipping(AGC) are put to test on the CT Kidney Dataset in this article and their performances are compared with the plain models of VGG16, ResNet50, and Inception V3 models. Using clip value feature of optimizer brings marginal advantages in the VGG16 and ResNet50 models but fails to create much notable improvements. But with AGC model, a notable improvement is observed with VGG16 and ResNet50 setup, and marginal improvement with Inception V3 setup. AGC not only improves classification metrics but also improves the learning rates of the models. It was noted that during the training the AGC models quickly crossed the 90% and the 95% accuracy marks as compared to the plain models and the CV based models which took more epochs to reach 90% and 95% accuracies.

These results can be compared with the results in [62] and [2] in which authors have build classifiers for CT Kidney dataset. In [62] authors achieve accuracy of 95.29%, 99.48% and 97.38% using the MobileNetV2, VGG16, and InceptionV3 deep neural nets. In article [2] authors achieve accuracies of 98.20% using VGG16, 73.80% using ResNet50, and 61.60% using Inception V3. The results produced by the AGC based model achieves higher value of accuracy in VGG16, ResNet50, and Inception V3 as compared to these papers (Table VI). AGC is a promising technique that can be further tested on much larger datasets like Diabetic Retinopathy dataset in which the parameters of batch size and learning rates can altered to see the effect of AGC on larger batch sizes and higher learning rates. Still the existing results have proven that AGC technique can be a helpful method for training image datasets where it

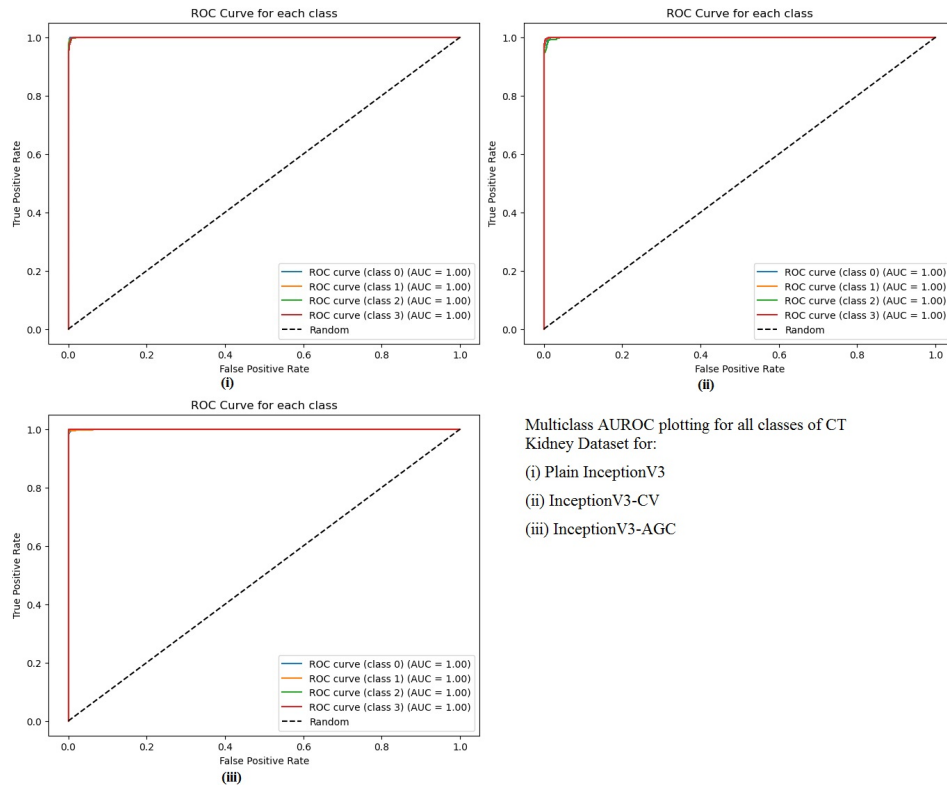
is difficult or time consuming to decide the clipping threshold for regularizing the train dataset.

TABLE VI. ACCURACY COMPARISON OF THE PROPOSED AGC BASED CLASSIFICATION METHOD

| Research Contribution | Method | Accuracy |
|------------------------------------|--------------|----------|
| M. H. K. Mehedi et al., 2022, [62] | MobileNetV2 | 95.29% |
| | VGG16, | 99.48% |
| | InceptionV3 | 97.38% |
| M. N. Islam et al., 2022, [2] | Resnet | 73.80% |
| | VGG16 | 98.20% |
| | Inception v3 | 61.60% |
| | Resnet | 99.5% |
| AGC (Proposed) | VGG16 | 97.1% |
| | Inception v3 | 99.2% |

REFERENCES

- [1] K. P. Andriole, J. M. Wolfe, R. Khorasani, S. T. Treves, D. J. Getty, F. L. Jacobson, M. L. Steigner, J. J. Pan, A. Sitek, and S. E. Seltzer, "Optimizing analysis, visualization, and navigation of large image data sets: one 5000-section ct scan can ruin your whole day," *Radiology*, vol. 259, no. 2, pp. 346–362, 2011.
- [2] M. N. Islam, M. Hasan, M. K. Hossain, M. G. R. Alam, M. Z. Uddin, and A. Soylu, "Vision transformer and explainable transfer learning models for auto detection of kidney cyst, stone and tumor from ct-radiography," *Scientific Reports*, vol. 12, no. 1, p. 11440, 2022.
- [3] A. Brock, S. De, S. L. Smith, and K. Simonyan, "High-performance large-scale image recognition without normalization," in *International Conference on Machine Learning*. PMLR, 2021, pp. 1059–1071.
- [4] J. Sundström, J. Bodegard, A. Bollmann, M. G. Vervloet, P. B. Mark, A. Karasik, T. Taveira-Gomes, M. Botana, K. I. Birkeland, M. Thureson et al., "Prevalence, outcomes, and cost of chronic kidney disease in a contemporary population of 2·4 million patients from 11 countries: The careme ckd study," *The Lancet Regional Health–Europe*, vol. 20, 2022.
- [5] C. P. Kovesdy, "Epidemiology of chronic kidney disease: an update 2022," *Kidney International Supplements*, vol. 12, no. 1, pp. 7–11, 2022.
- [6] S. AC, "Chronic kidney disease: a public health problem that needs a public health action plan," *Prev Chronic Dis (Serial Online)*, vol. 3, p. 2, 2006.
- [7] S. Jacobson, "Chronic kidney disease—a public health problem?" *Lakartidningen*, vol. 110, no. 21, pp. 1018–1020, 2013.
- [8] J. B. Saaddine, K. V. Narayan, and F. Vinicor, "Vision loss: a public health problem?" *Ophthalmology*, vol. 110, no. 2, pp. 253–254, 2003.
- [9] A. S. Levey, J. Coresh, K. Bolton, B. Culleton, K. S. Harvey, T. A. Ikizler, C. A. Johnson, A. Kausz, P. L. Kimmel, J. Kusek et al., "K/doi clinical practice guidelines for chronic kidney disease: evaluation, classification, and stratification," *American Journal of Kidney Diseases*, vol. 39, no. 2 SUPPL. 1, pp. i–ii+, 2002.
- [10] S. Jacobson, "[chronic kidney disease—a public health problem?]," *Lakartidningen*, vol. 110, no. 21, p. 1018–1020, 2013. [Online]. Available: <http://europepmc.org/abstract/MED/23805764>
- [11] S. M. Sozio, K. A. Pivert, F. J. Caskey, and A. Levin, "The state of the global nephrology workforce: A joint asn–era–edta–isn investigation," *Kidney international*, vol. 100, no. 5, pp. 995–1000, 2021.
- [12] T. Gunasekara, P. M. C. De Silva, E. Ekanayake, W. Thakshila, R. Pinipa, P. Sandamini, S. Gunarathna, E. Chandana, S. Jayasinghe, C. Herath et al., "Urinary biomarkers indicate pediatric renal injury among rural farming communities in sri lanka," *Scientific Reports*, vol. 12, no. 1, p. 8040, 2022.
- [13] S. Suganyadevi, V. Seethalakshmi, and K. Balasamy, "A review on deep learning in medical image analysis," *International Journal of Multimedia Information Retrieval*, vol. 11, no. 1, pp. 19–38, 2022.
- [14] K. He, X. Zhang, S. Ren, and J. Sun, "Deep residual learning for image recognition," in *Proceedings of the IEEE conference on computer vision and pattern recognition*, 2016, pp. 770–778.



Multiclass AUROC plotting for all classes of CT Kidney Dataset for:
(i) Plain InceptionV3
(ii) InceptionV3-CV
(iii) InceptionV3-AGC

Fig. 14. All AUROC for InceptionV3 Setup.

[15] C. Szegedy, W. Liu, Y. Jia, P. Sermanet, S. Reed, D. Anguelov, D. Erhan, V. Vanhoucke, and A. Rabinovich, "Going deeper with convolutions," in *Proceedings of the IEEE conference on computer vision and pattern recognition*, 2015, pp. 1–9.

[16] F. Chollet, "Xception: Deep learning with depthwise separable convolutions," in *Proceedings of the IEEE conference on computer vision and pattern recognition*, 2017, pp. 1251–1258.

[17] M. Tan and Q. Le, "Efficientnet: Rethinking model scaling for convolutional neural networks," in *International conference on machine learning*. PMLR, 2019, pp. 6105–6114.

[18] K. He, R. Girshick, and P. Dollár, "Rethinking imagenet pre-training," in *Proceedings of the IEEE/CVF International Conference on Computer Vision*, 2019, pp. 4918–4927.

[19] S. J. Pan and Q. Yang, "A survey on transfer learning," *IEEE Transactions on knowledge and data engineering*, vol. 22, no. 10, pp. 1345–1359, 2009.

[20] O. Parkhi, A. Vedaldi, C. Jawahar, and A. Zisserman, "Cats and dogs, in 'computer vision and pattern recognition (cvpr)'," in *Computer Vision and Pattern Recognition (CVPR)*, 2012.

[21] A. Vaswani, N. Shazeer, N. Parmar, J. Uszkoreit, L. Jones, A. N. Gomez, L. Kaiser, and I. Polosukhin, "Attention is all you need," 2023.

[22] K. Wang, C. Xu, G. Li, Y. Zhang, Y. Zheng, and C. Sun, "Combining convolutional neural networks and self-attention for fundus diseases identification," *Scientific Reports*, vol. 13, no. 1, p. 76, 2023.

[23] X. Pan, C. Ge, R. Lu, S. Song, G. Chen, Z. Huang, and G. Huang, "On the integration of self-attention and convolution," in *Proceedings of the IEEE/CVF conference on computer vision and pattern recognition*, 2022, pp. 815–825.

[24] J.-B. Cordonnier, A. Loukas, and M. Jaggi, "On the relationship between self-attention and convolutional layers," *arXiv preprint arXiv:1911.03584*, 2019.

[25] P. Ramachandran, N. Parmar, A. Vaswani, I. Bello, A. Levskaya, and J. Shlens, "Stand-alone self-attention in vision models," *Advances in neural information processing systems*, vol. 32, 2019.

[26] X. Wang, R. Girshick, A. Gupta, and K. He, "Non-local neural networks," in *Proceedings of the IEEE conference on computer vision and pattern recognition*, 2018, pp. 7794–7803.

[27] D. Mahajan, R. Girshick, V. Ramanathan, K. He, M. Paluri, Y. Li, A. Bharambe, and L. Van Der Maaten, "Exploring the limits of weakly supervised pretraining," in *Proceedings of the European conference on computer vision (ECCV)*, 2018, pp. 181–196.

[28] Q. Xie, M.-T. Luong, E. Hovy, and Q. V. Le, "Self-training with noisy student improves imagenet classification," in *Proceedings of the IEEE/CVF conference on computer vision and pattern recognition*, 2020, pp. 10 687–10 698.

[29] J. Cheng, S. Tian, L. Yu, C. Gao, X. Kang, X. Ma, W. Wu, S. Liu, and H. Lu, "Resganet: Residual group attention network for medical image classification and segmentation," *Medical Image Analysis*, vol. 76, p. 102313, 2022. [Online]. Available: <https://www.sciencedirect.com/science/article/pii/S1361841521003583>

[30] A. Kolesnikov, L. Beyer, X. Zhai, J. Puigcerver, J. Yung, S. Gelly, and N. Houlsby, "Big transfer (bit): General visual representation learning," in *Computer Vision—ECCV 2020: 16th European Conference, Glasgow, UK, August 23–28, 2020, Proceedings, Part V 16*. Springer, 2020, pp. 491–507.

[31] A. Dosovitskiy, L. Beyer, A. Kolesnikov, D. Weissenborn, X. Zhai, T. Unterthiner, M. Dehghani, M. Minderer, G. Heigold, S. Gelly *et al.*, "An image is worth 16x16 words: Transformers for image recognition at scale," *arXiv preprint arXiv:2010.11929*, 2020.

[32] N. Sharma, L. Malviya, A. Jadhav, and P. Lalwani, "A hybrid deep neural net learning model for predicting coronary heart disease using randomized search cross-validation optimization," *Decision Analytics Journal*, vol. 9, p. 100331, 2023. [Online]. Available: <https://www.sciencedirect.com/science/article/pii/S2772662223001716>

- [33] O. Moutik, H. Sekkat, S. Tigani, A. Chehri, R. Saadane, T. A. Tchakoucht, and A. Paul, "Convolutional neural networks or vision transformers: Who will win the race for action recognitions in visual data?" *Sensors*, vol. 23, no. 2, 2023. [Online]. Available: <https://www.mdpi.com/1424-8220/23/2/734>
- [34] E. M. Dogo, O. Afolabi, N. Nwulu, B. Twala, and C. Aigbavboa, "A comparative analysis of gradient descent-based optimization algorithms on convolutional neural networks," in *2018 international conference on computational techniques, electronics and mechanical systems (CTEMS)*. IEEE, 2018, pp. 92–99.
- [35] R. Poojary and A. Pai, "Comparative study of model optimization techniques in fine-tuned cnn models," in *2019 International Conference on Electrical and Computing Technologies and Applications (ICECTA)*. IEEE, 2019, pp. 1–4.
- [36] J. Li, S. Fong, L.-s. Liu, N. Dey, A. S. Ashour, and L. Moraru, "Dual feature selection and rebalancing strategy using metaheuristic optimization algorithms in x-ray image datasets," *Multimedia Tools and Applications*, vol. 78, pp. 20 913–20 933, 2019.
- [37] M. Awais, F. Shamshad, and S.-H. Bae, "Towards an adversarially robust normalization approach," *arXiv preprint arXiv:2006.11007*, 2020.
- [38] S. D. Pande and R. Agarwal, "Multi-class kidney abnormalities detecting novel system through computed tomography," *IEEE Access*, vol. 12, pp. 21 147–21 155, 2024.
- [39] N. Sharma and L. M. Aggarwal, "Automated medical image segmentation techniques," *Journal of medical physics/Association of Medical Physicists of India*, vol. 35, no. 1, p. 3, 2010.
- [40] Y. Tan, "Chapter 11 - applications," in *Gpu-Based Parallel Implementation of Swarm Intelligence Algorithms*, Y. Tan, Ed. Morgan Kaufmann, 2016, pp. 167–177. [Online]. Available: <https://www.sciencedirect.com/science/article/pii/B978012809362750011X>
- [41] A. Maier, C. Syben, T. Lasser, and C. Riess, "A gentle introduction to deep learning in medical image processing," *Zeitschrift für Medizinische Physik*, vol. 29, no. 2, pp. 86–101, 2019, special Issue: Deep Learning in Medical Physics. [Online]. Available: <https://www.sciencedirect.com/science/article/pii/S093938891830120X>
- [42] K. He, X. Zhang, S. Ren, and J. Sun, "Deep residual learning for image recognition," in *Proceedings of the IEEE Conference on Computer Vision and Pattern Recognition (CVPR)*, June 2016.
- [43] K. Simonyan and A. Zisserman, "Very deep convolutional networks for large-scale image recognition," 2015.
- [44] C. Szegedy, V. Vanhoucke, S. Ioffe, J. Shlens, and Z. Wojna, "Rethinking the inception architecture for computer vision," 2015.
- [45] S. Ioffe and C. Szegedy, "Batch normalization: Accelerating deep network training by reducing internal covariate shift," in *International conference on machine learning*. pmlr, 2015, pp. 448–456.
- [46] H. Zhang, Y. N. Dauphin, and T. Ma, "Fixup initialization: Residual learning without normalization," 2019.
- [47] S. De and S. Smith, "Batch normalization biases residual blocks towards the identity function in deep networks," *Advances in Neural Information Processing Systems*, vol. 33, pp. 19 964–19 975, 2020.
- [48] A. Brock, S. De, and S. L. Smith, "Characterizing signal propagation to close the performance gap in unnormalized resnets," *arXiv preprint arXiv:2101.08692*, 2021.
- [49] P. Luo, X. Wang, W. Shao, and Z. Peng, "Towards understanding regularization in batch normalization," *arXiv preprint arXiv:1809.00846*, 2018.
- [50] P. Goyal, P. Dollár, R. Girshick, P. Noordhuis, L. Wesolowski, A. Kyrola, A. Tulloch, Y. Jia, and K. He, "Accurate, large minibatch sgd: Training imagenet in 1 hour," *arXiv preprint arXiv:1706.02677*, 2017.
- [51] S. Singh and A. Shrivastava, "Evalnorm: Estimating batch normalization statistics for evaluation," in *Proceedings of the IEEE/CVF International Conference on Computer Vision*, 2019, pp. 3633–3641.
- [52] C. Summers and M. J. Dinneen, "Four things everyone should know to improve batch normalization," *arXiv preprint arXiv:1906.03548*, 2019.
- [53] T. Chen, S. Kornblith, M. Norouzi, and G. Hinton, "A simple framework for contrastive learning of visual representations," in *International conference on machine learning*. PMLR, 2020, pp. 1597–1607.
- [54] K. He, H. Fan, Y. Wu, S. Xie, and R. Girshick, "Momentum contrast for unsupervised visual representation learning," in *Proceedings of the IEEE/CVF conference on computer vision and pattern recognition*, 2020, pp. 9729–9738.
- [55] T. He, Z. Zhang, H. Zhang, Z. Zhang, J. Xie, and M. Li, "Bag of tricks for image classification with convolutional neural networks," in *Proceedings of the IEEE/CVF conference on computer vision and pattern recognition*, 2019, pp. 558–567.
- [56] S. Shen, Z. Yao, A. Gholami, M. Mahoney, and K. Keutzer, "Power-norm: Rethinking batch normalization in transformers," in *International Conference on Machine Learning*. PMLR, 2020, pp. 8741–8751.
- [57] Y. Wu and K. He, "Group normalization," in *Proceedings of the European conference on computer vision (ECCV)*, 2018, pp. 3–19.
- [58] J. Shao, K. Hu, C. Wang, X. Xue, and B. Raj, "Is normalization indispensable for training deep neural network?" *Advances in Neural Information Processing Systems*, vol. 33, pp. 13 434–13 444, 2020.
- [59] R. Pascanu, T. Mikolov, and Y. Bengio, "On the difficulty of training recurrent neural networks," in *International conference on machine learning*. Pmlr, 2013, pp. 1310–1318.
- [60] S. Merity, N. S. Keskar, and R. Socher, "Regularizing and optimizing lstm language models," *arXiv preprint arXiv:1708.02182*, 2017.
- [61] J. Zhang, T. He, S. Sra, and A. Jadbabaie, "Why gradient clipping accelerates training: A theoretical justification for adaptivity," *arXiv preprint arXiv:1905.11881*, 2019.
- [62] M. H. K. Mehedi, E. Haque, S. Y. Radin, M. A. Ur Rahman, M. T. Reza, and M. G. R. Alam, "Kidney tumor segmentation and classification using deep neural network on ct images," in *2022 International Conference on Digital Image Computing: Techniques and Applications (DICTA)*, 2022, pp. 1–7.

Development of an Educational Robot for Exploring the Internet of Things

Zhumaniyaz Mamatnabiyev¹, Christos Chronis², Iraklis Varlamis³, Meirambek Zhaparov⁴

Department of Computer Sciences, SDU University, Kaskelen, Kazakhstan¹

ORCID: 0000-0003-2157-2836

Department of Informatics and Telematics, Harokopio University of Athens, Athens, Greece^{2,3}

²ORCID: 0000-0002-2768-7119

³ORCID: 0000-0002-0876-8167

ICT Faculty, Paragon International University, Phnom Penh, Cambodia⁴

ORCID: 0000-0002-2286-792X

Abstract—Educational robots, when integrated into STEM (Science, Technology, Engineering, and Mathematics) education across a range of age groups, serve to enhance learning experiences by facilitating hands-on activities. These robots are particularly instrumental in the realm of Internet of Things (IoT) education, guiding learners from basic to advanced applications. This paper introduces the IoTXplorBot, an open-source and open-design educational robot, developed to foster the learning of IoT concepts in a cost-effective manner. The robot is equipped with a variety of low-cost sensors and actuators and features an interchangeable microcontroller that is compatible with other development boards from the Arduino Nano family. This compatibility allows for diverse programming languages and varied purposes. The robot's printed circuit board is designed to be user-friendly, even for those with no engineering skills. The proposed board includes additional pins and a breadboard on the robot's chassis, enabling the extension of the robot with other hardware components. The use of the Arduino board allows learners to leverage all capabilities from Arduino, such as the Arduino IoT cloud, dashboard, online compiler, and project hub. These resources aid in the development of new projects and in finding solutions to encountered problems. The paper concludes with a discussion on the future development of this robot, underscoring its potential for ongoing adaptation and improvement.

Keywords—Educational robots; Internet of Things; IoT Education; Arduino for Education; IoT Educational Kit

I. INTRODUCTION

Recent advancements in technology have significantly transformed educational processes within classroom settings. Notable examples of these educational technologies include augmented reality [1], educational robotics [2], and large language models [3] recently, all of which have garnered considerable interest among students. However, the integration of these technologies necessitates additional efforts, particularly in the development of requisite learning materials.

The Internet of Things (IoT) is a technological paradigm that facilitates the interconnection of embedded devices via a network. These IoT devices are designed to collect data from their environment, which is subsequently stored for further analysis. The primary components utilized in the IoT development process include sensors, actuators, and controllers, in addition to network and storage elements. These components are employed by learners to gain practical experience in developing IoT applications.

There are several solutions at the hands of learners and educators for supporting IoT education and practice. For example, simulation applications, educational kits, and a few educational robots are ideal paradigms of material and platforms for learning IoT in practice and for solving a variety of everyday issues.

Educational robots are used as an interactive teaching tool that supports the development of problem-solving skills and improves practical expertise in the curricular fields [4]. They are also used to introduce students to Robotics and Programming interactively from a very early age [5].

In the context of STEM (Science, Technology, Engineering, Mathematics) education, educational robots have been widely applied to enhance instructional and learning quality [6]. They offer immersive, practical learning opportunities where students gain problem-solving experience and learn to apply knowledge in real-world contexts [7]. The interdisciplinary nature of robotics in STEM prepares students for technology-centric careers.

Educational robots are used in different ways across various age groups. For instance, in the case of infant and primary education, educational robotics provides students with everything they need to easily build and program a robot capable of performing various tasks [5]. In middle and high schools, robotics clubs often compete at local STEM competitions, where teams of students are tasked with designing and building a robot to take on opponents in a series of challenges [8].

Educational robots are not only confined to primary or secondary education but are also increasingly being incorporated into higher education. The Internet of Things fundamentally relies on the engineering and programming skills fostered by STEM education. Consequently, educational robots can be effectively utilized in IoT education. This integration allows students to design and program their own robots using IoT technologies, thereby providing a hands-on, immersive learning experience. This practical approach facilitates a deeper understanding of how IoT devices collect and exchange data, enhancing students' technical skills and preparing them for the future digital world. Furthermore, the incorporation of educational robots into IoT education can stimulate innovation and creativity, encouraging students to develop novel solutions and applications for real-world problems. Thus, the use of

educational robots extends beyond traditional STEM education, demonstrating their versatility and adaptability in various educational contexts.

While there is a growing interest among hardware manufacturers, simulation software companies, and researchers in developing solutions for Internet of Things (IoT) education, a significant challenge persists. The majority of these solutions are proprietary in nature, which inherently restricts their flexibility and expandability. This limitation poses a substantial barrier to the dynamic and evolving needs of educational contexts. Consequently, there is a pressing need for open, adaptable, and scalable solutions that can effectively support IoT education and foster innovation in teaching and learning practices.

As a solution to the above limitations, in this study, the Open Source Educational Robot for Exploring the Internet of Things (abbreviated as IoTXplorBot), an open-source and open-design robot that can be utilized in IoT education to explore a range of activities, from the simplest to the most complex is introduced. The unique features of the IoTXplorBot can be summarized as follows:

- The robot's design is open and can be modified according to requirements.
- The chassis of the robot is constructed from wood, cut into a rectangular box shape by a laser cutting machine, offering a cost-effective and sustainable solution. It can also be replaced with a 3D-printed chassis for customization.
- The electronic components used, such as sensors and actuators, are low-cost and can be replaced with other components as needed.
- The Arduino Nano microcontroller used in the robot can be replaced with other microcontrollers from the same family, depending on the specific activity or cost considerations.
- The robot is programmed using the Arduino IDE, and the program can be uploaded to it from any computer or laptop via a USB cable.
- The robot has the ability to communicate in wireless mode with a base computer for storing and analyzing data collected by the sensors.

This flexibility and adaptability make the IoTXplorBot a versatile tool for IoT education. Its robot-like shape makes it more user-friendly than a sensor kit and expands the educational capabilities in richer scenarios.

The remainder of this paper is organized as follows: Section II provides an overview of the main solutions available for IoT education and highlights the pros and cons of each approach. Section III discusses the development details of the IoTXplorBot. The robot pilot and indicative activities related to IoT course are discussed in Section IV. Section V presents discussions and limitations of the robot. Finally, Section VI concludes the paper by offering our recommendations and outlining the next steps for utilizing the robot in other related course activities.

II. RELATED WORK

A variety of desktop simulation applications and hardware kits are available for educational purposes and for prototyping IoT devices. Numerous simulation tools can be accessed online. For example, the Cisco Networking Academy offers the Packet Tracer¹ simulation tool for emulating IoT devices and networking. Similarly, Autodesk Tinkercad² provides a simulation tool for constructing circuits and prototyping devices. However, these simulation tools offer limited hands-on learning experiences. To address this limitation, commonly used hardware components (i.e. sensors) are often assembled into a single unit, referred to as a kit, which is then used for learning and prototyping purposes. Companies such as Adafruit³ and Arduino⁴ offer various types of kits equipped with different hardware components and controllers. These kits provide learners with the opportunity to construct real-world solutions and facilitate learning through practical application.

Educational robots, which are based on robotics and electronic components, serve to enhance the learning process by actively engaging students in classroom activities [9]. By participating in these activities, students can contribute to the development process of the robot for various applications. These robots provide a unique opportunity for learners to gain in-depth knowledge on a specific topic. A wide range of commercial educational robots are available on the market, catering to different age groups, from kindergarten to university level. Many of these robots are specifically designed to facilitate STEM education, thereby fostering tangible and constructive thinking among learners. In higher education, educational robots are utilized in various courses, providing learners with hands-on experiences [10], [11]. For instance, educational robots have been used for teaching Artificial Intelligence [12], data acquisition [13], or even for supporting robotics courses [14]. The learning outcomes of using educational robots in the classroom include problem-solving skills, self-efficacy, computational thinking, creativity, motivation, and collaboration [15]. However, for learning IoT in higher education, more sophisticated robots equipped with various sensors and actuators are required. Additionally, wireless communication technologies are necessary for transmitting data over the network to a remote storage facility that can handle the huge amount of collected data. Currently, there are only a limited number of robots available for this purpose and most of them use a proprietary design and code. Another drawback is their high cost, which may pose a barrier to accessibility.

Accordingly, open-source educational robots are also available under research [16]. The question arises: Are they sufficiently effective in enhancing IoT learning? Let's examine a few examples. Hydra [17] is an Arduino-based educational robot equipped with pre-wired connections to sensors and actuators, eliminating the need for additional hardware components. However, this robot does not incorporate wireless communication capabilities. EUROPA II [13] is equipped with various sensors and a Raspberry Pi microprocessor, allowing for direct programming. FOSSBot [18] bears similarities to EUROPA II but features various programming interfaces that

¹<https://www.netacad.com/courses/packet-tracer>

²<https://www.tinkercad.com/>

³<https://www.adafruit.com/category/878>

⁴<https://store.arduino.cc/collections/kits>

can be utilized by users with varying coding skills. DuckieBot [19] is designed for higher education and is equipped with a camera and a Raspberry Pi board. The ability to program directly on the board and write code in various programming languages are advantages of using Raspberry Pi. However, it is more expensive compared to other boards. Furthermore, when it is replaced with other types of boards, additional wiring is required. In Table I, a comprehensive summary of prevalent educational robots and hardware kits that are applicable for IoT learning within the context of higher education is provided. This summary includes a comparative analysis of their respective hardware components and associated costs. The primary findings derived from the utilization of these educational tools are also presented.

The educational robots and kits, reviewed in Table I, are designed for a variety of tasks. Robots in [21], [13], [22], [19], [18] are based on microprocessors such as Raspberry

Pi, which allows them to run program code directly on the processor without the need for an external computer. In contrast, robots in [20], [17] are programmed by a computer, with the code then uploaded onto the robot's microcontroller. Using a microprocessor enables the robot to be connected remotely for running software. However, microcontrollers are less vulnerable to security attacks than microprocessors as they require direct contact for uploading programming code. The benefit of using educational robots over hardware kits is that learners can plan to develop their projects on a single system, upgrading their projects over time.

While the aforementioned solutions offer a range of capabilities, their relatively high costs can pose a significant barrier, particularly when procuring multiple units for classroom use. Among the options, Hydra [17] stands out as the most cost-effective, yet it lacks the provision for robot extensions, which limits its utility for experienced users. Therefore, there is a

TABLE I. WIDESPREAD EDUCATIONAL ROBOTS AND KITS IN HIGHER EDUCATION: HARDWARE COMPONENTS AND COST ARE COMPARED

| Robot/Kit | Controller/CPU | Sensors | Actuators | Cost (EUR) | Main Findings |
|--------------------------------------|-----------------------------|---|--|------------|---|
| Epuck 2 [20] | STM32F4 ARM Cortex M4 | IR proximity, accelerometer, gyroscope, microphone, camera, Time of flight distance | Stepper motors, LEDs, Loud-seaker | 550 | A powerful robot designed for engineering education. The robot can be adapted for various exercises. |
| Robobo [21] | Smartphone + PIC32 | Camera, accelerometer, gyroscope, GPS, magnetometer, IR proximity, light sensor | DC gear motor, LEDs | 450 | The robot interacts with a smartphone for performing actions. The software of the robot is implemented in the smartphone. |
| EUROPA II [13] | Raspberry Pi | Ultrasonic distance, IR proximity, optical encoder, camera, LIDAR | DC gear motor, robotic arm, LEDs | 300 | Robot Operating Systems (ROS) based educational robot with a robotic arm for performing actions. Sensors used make the robot more powerful in data collection. |
| Turtlebot 3 [22] | Raspberry Pi + OpenCR | Camera, LIDAR, accelerometer, gyroscope, magnetometer | MYNAMIXEL AX gear motor + driver | 586 | A mobile robot developed for higher education as a target audience. The robot is experienced in teaching embedded systems. |
| Duckiebot [19] | Raspberry Pi 2 | Fish-eye camera | DC gear motor | 150 | An autonomous vehicle-based robot used in autonomy education and research. The robot is used and driven in a platform named Duckietown. |
| Hydra [17] | Arduino Mega | Ultrasonic distance, potentiometer, buttons | RGB LED, LEDs, seven segment display | 35 | Electronic components of the robot are designed in printed circuit boards that require no circuit creation. The robot software is based on Petri Nets modeling. |
| FOSSBot [18] | Raspberry Pi | Ultrasonic distance, IR proximity, gyroscope, accelerometer, camera, optical encoder, noise, gas, motion, temperature, humidity, photoresistor, IR reciever | DC gear motor, servo motor, LCD screen | 100 | The robot contains various sensors and actuators that enable many activities. Suitable for learning different course activities. |
| Arduino Explore IoT Kit ⁵ | Arduino MKR WiFi 1010 | Buttons, temperature, humidity, pressure, gas, ambient light, gesture, accelerometer, RGB color, PIR, moisture level | RGB LED, buzzer | 125 | A kit that enables to develop various projects for environment monitoring. The sensors are attached to the device which accesses no circuit creation. |
| SparkFun Inventor's Kit ⁶ | SparkFun RedBoard Qwiic | Ultrasonic distance, temperature, photoresistor, buttons | Servo motor, DC gear motor, LCD, piezo speaker, | 100 | A kit that enable robotic car development. The kit includes a breadboard and microcontroller holder which all robotic components are attached. |
| Arduino IoT Bundle ⁷ | Arduino Nano RP2040 Connect | Potentiometer, photoresistor, button, temperature, tilt | alphanumeric LCD, LEDs, bright white, DC motor, servo motor, piezo | 75 | A kit that enables to explore IoT projects using common sensors and actuator. |

pressing need for a solution that is not only cost-effective but also expandable and open-source. Such a solution would cater to a wider range of user expertise and offer greater flexibility for adaptation and expansion, thereby enhancing its applicability in diverse educational contexts.

III. THE PROPOSED OPEN SOLUTION

A. Overview of the Robot

The IoTXplorBot (educational roBot for eXploring IoT), an open-source hardware and open-design educational robot, is built around the Arduino Nano microcontroller. Its primary objective is to augment the learning process for the Internet of Things. The robot is outfitted with two motor wheels and a motor driver to regulate the motors. Additionally, it is equipped with a variety of sensors and actuators, further enhancing its functionality and adaptability in IoT education. The full view of the robot is illustrated in Fig. 1.



Fig. 1. Full view of the robot.

The robot proposes an open hardware and software solution that can be built by the students themselves. It provides an opportunity for hands-on experience with electronics and engineering principles. The IoTXplorBot shares similarities with the FOSSBot [18] and Hydra [17], but modifications have been made to the chassis and the controller to better adapt it for IoT learning. The previous iteration of this robot was detailed in a conference paper [23], where the Arduino UNO microcontroller board was utilised. A limitation of the previous version was the absence of wireless communication capabilities in the Arduino UNO board. In this updated version, changes to the hardware components, including the motor driver and the Inertial Measurement Unit (IMU) sensor were made. These enhancements aim to optimize the robot's functionality for IoT education.

B. IoTXplorBot Hardware

The chassis of the robot is crafted from wood using a laser cutter, resulting in a cost-effective design. Compared to a plastic 3D-printed chassis, such as FOSSbot's the cost is a bit higher. However, using wood instead of plastic dramatically reduces the printing time, and the durability of the chassis and is according to the environmental sustainability objectives that promote the use of recyclable material. The chassis is shaped like a rectangular box. Any damaged part can be easily

reprinted and replaced. The design includes several holes for ventilation to prevent overheating of the controller or motor driver. Additional holes have been made to accommodate bolts and nuts for attaching hardware components. A separate hole has been created for routing wires, ensuring a neat and organized assembly. This thoughtful design contributes to the robot's adaptability and ease of maintenance.

The electronic components of the IoTXplorBot are carefully selected to align with its intended use. These components, which are common to other kits such as the Arduino IoT Bundle and the SparkFun Inventor's Kit, must be adaptable to both course activities and robot development. The electronic suite is not only cost-effective but also replaceable with similar components, offering flexibility. These components collectively contribute to the robot's functionality and adaptability in IoT education. A list of electronic components and their approximate cost are shown in Table II.

TABLE II. LIST OF THE ROBOT PARTS AND APPROXIMATE COST

| Part | Quantity | Cost (EUR) |
|---------------------------------------|----------|------------|
| Arduino Nano 33 IoT | 1 | 23 |
| Infrared Proximity Sensor | 2 | 1 |
| Ultrasonic Distance Sensor HC-SR04 | 1 | 1 |
| Infrared Receiver and Remote Control | 1 | 2 |
| Temperature and Humidity Sensor DHT11 | 1 | 2 |
| DC Gear Motor (6V 1:110) | 2 | 3 |
| Plastic wheel with tire (65x26mm) | 2 | 1 |
| Universal Turning Wheel (24mm) | 1 | 0.5 |
| L293D Motor Driver | 1 | 0.5 |
| Servo Motor SG90 | 1 | 2 |
| RGB LED | 1 | 2 |
| Wood Chassis | 1 | 4 |
| 9V Battery | 1 | 4 |
| USB to Micro USB cable | 1 | 2 |
| Female-to-female Jumper Wires | 1 | 2 |
| Printed Circuit Board | 1 | 5 |
| Overall | | 55 |

The Arduino Nano 33 IoT⁸, selected as the controller for the robot, offers a unique amalgamation of features and capabilities, rendering it particularly suitable for Internet of Things (IoT) applications. Despite its compact form factor, it is powered by the Arm® Cortex®-M0 32-bit SAMD21 processor, providing substantial computational power for diverse IoT applications. The board is equipped with the u-blox NINA-W102 Wi-Fi module and the ECC608A crypto-chip, ensuring secure and reliable wireless connectivity, a critical feature for IoT applications involving data transmission over networks. Furthermore, the Arduino Nano 33 IoT is compatible with the Arduino Cloud platform, facilitating the rapid construction of IoT projects, and thereby catering to both novice and experienced users. The board also incorporates an Inertial Measurement Unit (IMU), combining an accelerometer and a gyroscope, enabling the development of motion-tracking devices. Thus, the selection of the Arduino Nano 33 IoT is jus-

⁵<https://store.arduino.cc/products/explore-iot-kit-rev2>

⁶<https://www.sparkfun.com/products/21301>

⁷<https://store.arduino.cc/products/iot-bundle>

⁸<https://store.arduino.cc/products/arduino-nano-33-iot>

tified by its compact size, robust processing capabilities, secure wireless connectivity, cloud compatibility, and integrated IMU, collectively rendering it a versatile and cost-effective solution for IoT education.

Arduino offers a diverse range of Nano boards, each with distinct characteristics, integrated sensors, and wireless communication capabilities. A key feature of these boards is their seamless interchangeability, which allows users to execute various circuits without needing to alter pins and connections. For instance, the Arduino Nano is the most economical microcontroller within the Arduino family, although it lacks built-in sensors and network capabilities. In contrast, the Arduino Nano 33 BLE Sense⁹ board is notable for its Python programming compatibility and the ability to deploy machine learning models directly on its core. This particular Nano board also includes an array of integrated sensors, eliminating the need for constructing external circuits to measure data.

In the process of constructing a circuit that integrates a microcontroller with sensors and actuators in a traditional method where a breadboard is used, novice learners lacking experience in electronics may encounter challenges. These difficulties can lead to potential damage to the hardware components, particularly when they are connected to an inappropriate voltage source or when the connections are improperly configured. To address these issues, a printed circuit board (PCB) has been designed that incorporates the microcontroller and the motor driver (Fig. 2). This design facilitates the easy connection of sensors and actuators. The utilization of this connection system ensures that all external modules can be uniquely connected to the mainboard, thereby significantly reducing the likelihood of user errors. This approach enhances the learning experience by providing a more user-friendly and error-resistant platform for circuit construction. A comparison between the traditional method and the proposed approach is depicted in Fig. 3.

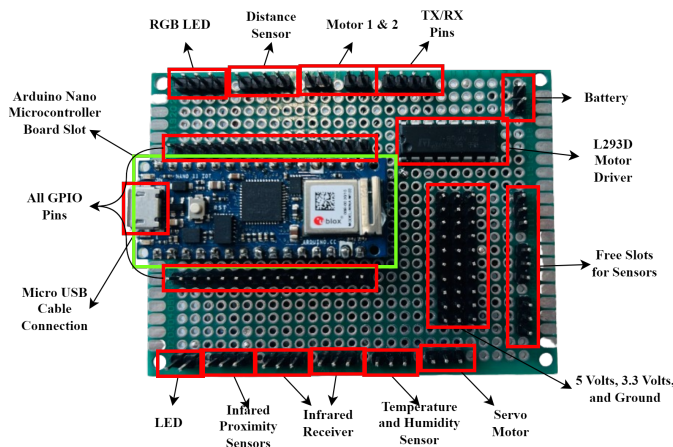


Fig. 2. Design of the proposed board.

The design of our printed circuit board (PCB) approach incorporates a slot for connecting any type of Arduino Nano board, along with other hardware components. Each slot designated for sensors and actuators includes a voltage source, ground, and a pin to the GPIO (general-purpose input/output) pins of the microcontroller board. Furthermore, the circuit

provides additional communication to all pins of the microcontroller board and power sources, which can be utilized by advanced users. The PCB also features extra slots for additional sensors and actuators, should they be required for robot extension. The designed printed circuit board must be manufactured before use.

The L293D motor driver, a key component of our design, facilitates the control of both the direction and speed of the motors, which serve as the wheels of the robot. This driver is securely affixed to the board and is connected to the microcontroller, thereby providing a ready-to-use circuit solution when the motors are integrated with the robot.

In previous iterations of the robot, the L298N motor driver was utilized. However, challenges related to its power consumption were encouraged. The L298N, while effective in many applications, is known to consume a significant amount of power. This power consumption can be problematic, particularly in applications where energy efficiency is a priority or where power resources are limited.

In contrast, the L293D motor driver offers a more power-efficient solution. It operates between 4.5V and 36V and can draw up to 1.2A from both channels. This lower power requirement makes the L293D a more suitable choice for our robot, especially considering our goal of optimizing energy efficiency. Thus, the shift to the L293D motor driver not only addresses the power consumption issue but also enhances the overall performance and efficiency of the robot.

The microcontroller of the board operates at a voltage of 3.3 Volts and is capable of handling input voltages up to 21 Volts. It possesses the capability to draw power via a USB cable connected to a computer, providing flexibility in power sourcing. However, to drive the robot and facilitate remote control, the board is connected to a 9V battery. This battery configuration eliminates the need for a battery holder, thereby simplifying the overall design. In instances where the charge of the battery exceeds its capacity, the battery is replaced with a new one. Alternatively, a rechargeable battery can be employed, offering a sustainable and cost-effective power solution. This approach ensures continuous operation of the robot while also providing flexibility in power management.

A breadboard is mounted on the top side of the robot chassis, which can be used for extending the robot by building new circuits alongside the existing robot hardware components. This comprehensive design approach ensures flexibility and scalability in robot construction and operation.

C. IoTXplorBot Software

The software for the IoTXplorBot is developed by the learners themselves, thereby facilitating a hands-on learning experience. The software is written in the Arduino Integrated Development Environment (IDE), which utilizes the C programming language, a common choice for microcontrollers. For those who are less experienced in programming, Ardublockly¹⁰ offers a block-based programming interface similar to Scratch¹¹, based on Google's Blockly¹². This provides

¹⁰<https://ardublockly.embeddedlog.com/index.html>

¹¹<https://scratch.mit.edu/>

¹²<https://developers.google.com/blockly>

⁹<https://store-usa.arduino.cc/products/nano-33-ble-sense-rev2>

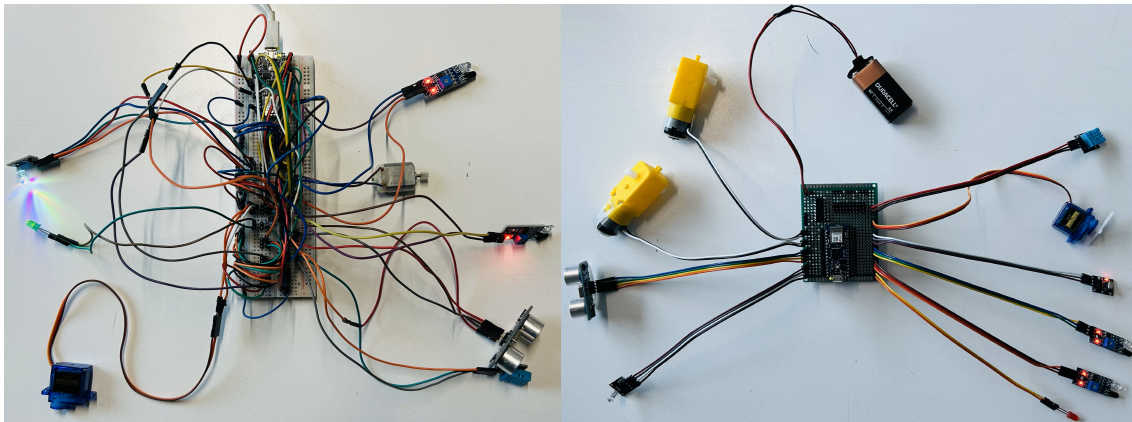


Fig. 3. Comparison between the traditional method (left) and the proposed approach (right).

a more accessible entry point for beginners. In addition, the Python programming language, which is widely used and popular, can also be employed if the Arduino Nano RP2040 Connect¹³ or Arduino Nano 33 BLE is used as the main controller in the robot. This flexibility in programming languages caters to a broad range of user expertise and preferences, further enhancing the educational value of the IoTXplorBot.

The selection of sensors and actuators for our design is not only based on their wide availability in the market at a low cost but also the availability of programming libraries and examples. The libraries and examples of programming codes for these components are readily accessible. For instance, the Arduino website hosts a forum¹⁴ and project hub¹⁵ where Arduino users can conveniently find examples and solutions to their challenges.

Another resource, SparkFun Inventor's Kit Code¹⁶, provides examples and libraries for a popular selection of sensors and actuators. These resources significantly simplify the process of programming and integrating these components into the robot, making our design approach user-friendly and cost-effective. This ensures that users, regardless of their level of experience, can successfully build and operate the robot.

The architecture of the IoTXplorBot is meticulously designed to meet all the requirements for IoT development. The programming code for the robot can be uploaded through two distinct methods: via a USB cable or wirelessly. The latter is facilitated by the built-in WiFi communication capability of the board, which enables Over-The-Air (OTA) code uploading. This feature significantly enhances the flexibility and convenience of code deployment, particularly for iterative development and testing processes. It should be noted that this wireless uploading feature is contingent upon the presence of built-in WiFi connectivity in the Arduino boards. The robot can be programmed by learners to communicate with other end devices like laptops or smartphones through wireless communication technology.

The robot is also capable of collecting environmental data and transmitting this data to the cloud for further analysis. The Arduino IoT Cloud platform¹⁷ provides to store IoT data on the cloud and display data on a dashboard. This feature enables a comprehensive exploration of IoT concepts and applications.

The inclusion of built-in Bluetooth Low Energy (BLE) communication in the microcontroller board facilitates its interaction with other devices enabled with Bluetooth communication. BLE, a power-efficient variant of the classic Bluetooth technology, is particularly suited for IoT applications where devices need to exchange small amounts of data intermittently. This feature significantly expands the robot's connectivity capabilities, enabling it to interface with a wide range of devices and sensors. Consequently, this opens up a plethora of possibilities for collaborative tasks, data collection, and even swarm robotics, thereby enhancing the educational potential of the robot. A detailed representation of communication with the IoTXplorBot is provided in Fig. 4. This communication encapsulates the versatility and adaptability of the IoTXplorBot, making it an effective tool for IoT education.

IV. IOTXPLOBOT PILOT

The primary objective of the proposed robot is to augment hands-on learning experiences within the realm of the Internet of Things (IoT). The hardware components of the IoTXplorBot have been meticulously selected to facilitate the development of a diverse array of course activities. As learners engage in these activities, they gain practical experience, progressively extending the capabilities of the robot.

The IoTXplorBot has been specifically designed to assist students and enthusiasts in navigating the multifaceted world of IoT. Equipped with an array of versatile sensors, actuators, and communication modules, the IoTXplorBot provides a plethora of opportunities for learning and experimentation. Its architecture aligns seamlessly with the three-layered architecture of IoT systems, thereby enabling learners to engage with every facet of the IoT process.

Fig. 5 provides a visual representation of how key topics and technologies of IoT align with the architecture of the

¹³<https://store.arduino.cc/products/arduino-nano-rp2040-connect>

¹⁴<https://forum.arduino.cc/>

¹⁵<https://projecthub.arduino.cc/>

¹⁶<https://learn.sparkfun.com/tutorials/sparkfun-inventors-kit-experimentguide—v41>

¹⁷<https://cloud.arduino.cc/>

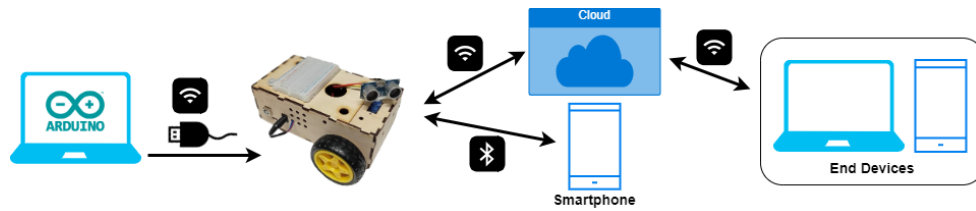


Fig. 4. Communication with the robot.

IoTXplorBot. In its operational capacity, the robot functions as an IoT device, communicating with the cloud and other applications through various communication protocols. This alignment underscores the relevance and applicability of the IoTXplorBot in the context of IoT education.

The complexity of the activities conducted using the robot progressively increases, thereby fostering the learner's growth and experience. The initial activity involves basic movements of the robot, such as moving forward/backward and turning left/right, facilitated by the robot motors and motor driver. The programming code for this activity is relatively simple, marking the learner's preliminary interaction with the robot. Subsequent activities incorporate additional sensors or actuators, thereby increasing the complexity of the tasks. For instance, the second activity could involve remote control using an infrared (IR) receiver, wherein the learner is introduced to programming using conditional statements.

As the learner progresses, they are exposed to more advanced activities, such as enabling wireless communication protocols like BLE and WiFi, and monitoring the robot through a cloud or web application. The learners are also able to leverage the capabilities offered by Arduino, such as built-in sensors, communication protocols, cloud, dashboard, and uploading programming code using Over-The-Air (OTA).

The IoTXplorBot is designed to facilitate key learning outcomes for students, encompassing areas such as engineering skills, algorithms and programming, networking and technology, and data analysis. The process of developing activities using the IoTXplorBot commences with the selection of the required sensors and actuators. Subsequently, a circuit is constructed by connecting the chosen sensors and actuators to the board. The programming code is then written on a computer and transmitted to the microcontroller board via a USB cable or OTA. The Arduino IDE provides the functionality to work with a serial monitor for reviewing the sensor data and communicating with the board. An example of an activity is illustrated in Fig. 6, which depicts a flowchart for a line-following activity. In this activity, the robot is programmed to navigate along a line using two IR proximity sensors.

During the pilot study, students from the 'Introduction to IoT' course, part of the Bachelor of Computer Sciences program, were tasked with developing different solutions using the robot. The activities included creating a line follower robot, obstacle avoidance using an ultrasonic distance sensor, controlling the robot via Bluetooth, and data collection on a server using WiFi. Despite the challenging nature of the activities, the students demonstrated commendable results in the course project. Some students even opted to use the extension of the IoTXplorBot for their projects, while others

chose their own project topics and tools. The solutions for their projects included remote monitoring using cloud technology and driving the robot via Bluetooth communication controlled by an Android application.

V. DISCUSSION

This work aims to achieve two primary objectives. The first is to develop an educational robot, the IoTXplorBot, that facilitates the learning of Internet of Things (IoT) concepts through the exploration of various hardware components. The second objective is to make this educational tool available at a low cost. Traditional methods of learning IoT typically involve the use of educational kits, which consist of a microcontroller, sensors, and actuators. These kits offer different approaches to exploring IoT concepts. The IoTXplorBot, however, provides a progressive learning experience, starting with simpler tasks and gradually leading to the development of a complex system by the end of the course activities. While there are many educational robots available on the market, they often come with high costs and a limited number of sensors and actuators. Compared to different educational kits and robots in terms of their hardware components, and costs for use in higher education, the IoTXplorBot proposes cost-effective solution and adaptability with different hardware components for the robot extension and variety of course activities.

The IoTXplorBot shares many features with the FOSSBot [18] and Hydra [17], but the proposed robot uses the Arduino Nano board, making it interchangeable with other microcontrollers from this family for different purposes. Another advantage of this robot is that its chassis is designed from wood, making it sustainable and low-cost. In addition, it can be replaced with a 3D-printed chassis or even a smartphone box from cardboard. This flexibility makes the IoTXplorBot a versatile tool for IoT education.

All hardware components such as sensors and actuators chosen and activities to be designed facilitate the learning of IoT concepts. The microcontroller selected for the robot enables the creation of circuits and the running of programs for IoT as well as for other purposes such as robot training and edge computing. In contrast, other educational robots, which are primarily based on STEM (Science, Technology, Engineering, and Mathematics) education, do not allow for the creation of circuits, an essential aspect of IoT systems and devices.

This study is primarily constrained by the hardware components and the advanced programming aspects associated with the Arduino Integrated Development Environment (IDE). To broaden the applicability of the robot in other related

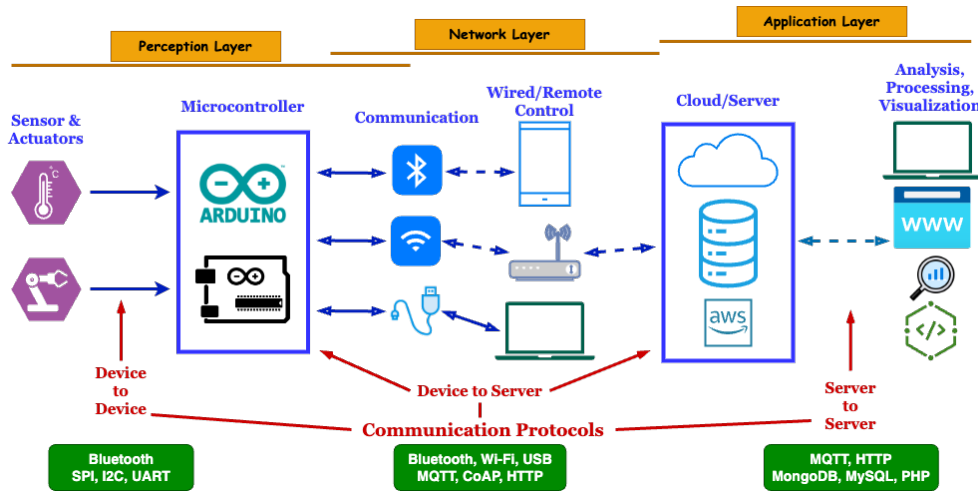


Fig. 5. Architecture of the proposed work.

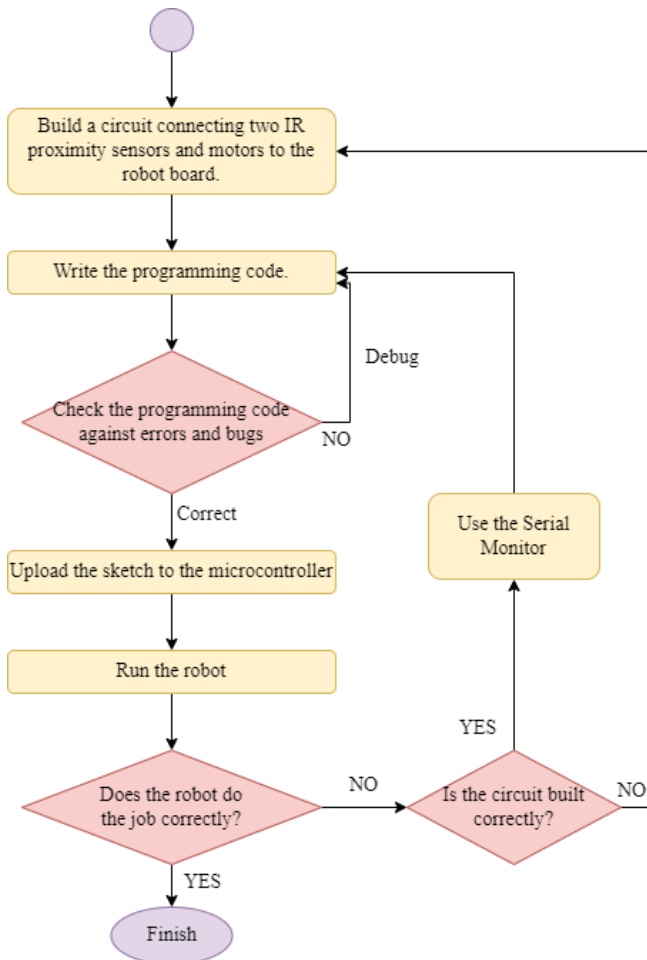


Fig. 6. Flowchart of programming the line following robot.

of an alternative microcontroller that supports the requisite programming becomes a necessity. These limitations highlight areas for future development and underscore the need for a more versatile and inclusive approach to the design and implementation of educational robots.

VI. CONCLUSION

While hardware kits composed of microcontroller boards, sensors, and actuators, along with desktop simulation applications, are commonly used in Internet of Things (IoT) education, educational robots offer a structured approach to course activities. However, various educational robots are designed to perform different tasks. The IoTXplorBot, an open-source and open-design educational robot, was developed to explore IoT concepts at a low cost. Various common sensors and actuators were utilized, enabling learners to easily find library solutions to bugs during the programming process. The microcontroller of the robot can be interchanged with other development boards from the widely used Arduino Nano family, allowing learners to choose according to their needs. During the development process, the robot was tested in the "Introduction to IoT" course as a pilot study, where students were able to use this robot for classroom activities. Most students preferred to use this robot for their course projects as a continuation of their previous tasks, despite the freedom to choose the project hardware and topic.

As part of our future work, the designed printed circuit board is planned to be fabricated for the robot to simplify tasks for students who have no experience in electronics. Additionally, the robot is planned to extend with rechargeable batteries for extended use without the need for frequent battery changes.

ACKNOWLEDGMENT

We acknowledge the use of generative AI, ChatGPT (<https://chat.openai.com/>), to refine the academic language and accuracy of our own work.

course activities, it is imperative to develop an application that caters to individuals who may not be well-versed with Arduino Programming. Furthermore, for more advanced courses such as machine learning and edge computing, the selection

REFERENCES

- [1] J. L. Belmonte, A.-J. Moreno-Guerrero, J. A. L. Núñez, and F. J. H. Lucena, "Augmented reality in education. A scientific mapping in Web of Science," *Interactive Learning Environments*, vol. 31, no. 4, pp. 1860–1874, Dec. 2020, doi: 10.1080/10494820.2020.1859546.
- [2] I. Kyriazopoulos, G. Koutromanos, A. Voudouri, and A. Galani, "Educational robotics in primary education: A systematic literature review," in *Research Anthology on Computational Thinking, Programming, and Robotics in the Classroom*, IGI Global, pp. 782–806, 2022.
- [3] T. H. Kung, M. Cheatham, A. Medenilla, C. Sillos, L. De Leon, C. Elepaño, M. Madriaga, R. Aggabao, G. Diaz-Candido, J. Maningo, et al., "Performance of ChatGPT on USMLE: Potential for AI-assisted medical education using large language models," *PLoS digital health*, vol. 2, no. 2, p. e0000198, 2023.
- [4] P. N. Mwangi, C. M. Muriithi, and P. B. Agufana, "Exploring the benefits of educational robots in STEM learning: a systematic review," *International Journal of Engineering and Advanced Technology*, vol. 11, no. 6, pp. 5–11, 2022.
- [5] U. Gerecke and B. Wagner, "The challenges and benefits of using robots in higher education," *Intelligent Automation and Soft Computing*, vol. 13, no. 1, pp. 29–43, 2007. doi: 10.1080/10798587.2007.10642948.
- [6] F. Ouyang and W. Xu, "The effects of educational robotics in STEM education: a multilevel meta-analysis," *International Journal of STEM Education*, vol. 11, no. 1, p. 7, 2024.
- [7] S. Poornima, "Importance Of Robotics In STEM Learning," *ItsMyBot*, Oct. 04, 2021. <https://itsmybot.com/importance-of-robotics-in-stem-learning/>
- [8] Ryan, "Robotics in Education: Advantages, Benefits & Importance for Kids," *iD Tech*, Apr. 06, 2021. <https://www.idtech.com/blog/educational-benefits-robotics>
- [9] D. Catlin, "29 Effective ways you can use robots in the classroom: An explanation of ERA pedagogical principle," in *Educational Robotics in the Makers Era 1*, Springer, pp. 135–148, 2017.
- [10] M. Kalaitzidou and T. P. Pachidis, "Recent Robots in STEAM Education," *Education Sciences*, vol. 13, no. 3, p. 272, 2023.
- [11] Y. Zhang, R. Luo, Y. Zhu, and Y. Yin, "Educational robots improve K-12 students' computational thinking and STEM attitudes: Systematic review," *Journal of Educational Computing Research*, vol. 59, no. 7, pp. 1450–1481, 2021.
- [12] A. Eguchi, "AI-powered educational robotics as a learning tool to promote artificial intelligence and computer science education," in *Robotics in Education: RiE 2021 12*, Springer, pp. 279–287, 2022.
- [13] G. Karalekas, S. Vologiannidis, and J. Kalomiros, "Europa: A case study for teaching sensors, data acquisition and robotics via a ROS-based educational robot," *Sensors*, vol. 20, no. 9, p. 2469, 2020.
- [14] I. Plauska and R. Damaševičius, "Educational robots for internet-of-things supported collaborative learning," in *Information and Software Technologies: 20th International Conference, ICIST 2014*, Druskininkai, Lithuania, October 9–10, 2014. Proceedings 20, pp. 346–358, 2014.
- [15] S. Evripidou, K. Georgiou, L. Doitsidis, A. A. Amanatiadis, Z. Zinonos, and S. A. Chatzichristofis, "Educational robotics: Platforms, competitions and expected learning outcomes," *IEEE Access*, vol. 8, pp. 219534–219562, 2020.
- [16] T. Sapounidis and D. Alimisis, "Educational robotics for STEM: A review of technologies and some educational considerations," in *Science and Mathematics Education for 21st Century Citizens: Challenges and Ways Forward*, pp. 167–190, Nova Science Publishers, Hauppauge, NY, USA, 2020.
- [17] G. Tsalmpouris, G. Tsinarakis, N. Gertsakis, S. A. Chatzichristofis, and L. Doitsidis, "HYDRA: Introducing a low-cost framework for STEM education using open tools," *Electronics*, vol. 10, no. 24, p. 3056, 2021.
- [18] C. Chronis and I. Varlamis, "FOSSBot: An Open Source and Open Design Educational Robot," *Electronics*, vol. 11, no. 16, p. 2606, 2022.
- [19] L. Paull, J. Tani, H. Ahn, J. Alonso-Mora, L. Carlone, M. Cap, Y. F. Chen, C. Choi, J. Dusek, Y. Fang, et al., "Duckietown: an open, inexpensive and flexible platform for autonomy education and research," in *2017 IEEE International Conference on Robotics and Automation (ICRA)*, pp. 1497–1504, 2017.
- [20] F. Mondada, M. Bonani, X. Raemy, J. Pugh, C. Cianci, A. Klapotcz, S. Magnenat, J. Zufferey, D. Floreano, and A. Martinoli, "The e-puck, a robot designed for education in engineering," in *Proceedings of the 9th Conference on Autonomous Robot Systems and Competitions*, vol. 1, no. CONF, pp. 59–65, 2009.
- [21] F. Bellas, M. Naya, G. Varela, L. Llamas, A. Prieto, J. C. Becerra, M. Bautista, A. Faina, and R. Duro, "The Robobo project: Bringing educational robotics closer to real-world applications," in *Robotics in Education: Latest Results and Developments*, pp. 226–237, 2018.
- [22] R. Amsters and P. Slaets, "Turtlebot 3 as a robotics education platform," in *Robotics in Education: Current Research and Innovations 10*, pp. 170–181, 2020.
- [23] Z. Mamatnabiyev, "Design and Implementation of an Open-Source Educational Robot for Hands-On Learning Experiences in IoT," *2023 17th International Conference on Electronics Computer and Computation (ICECCO)*, Kaskelen, Kazakhstan, pp. 1–4, 2023. doi: 10.1109/ICECCO58239.2023.10146599.

Improving Potato Diseases Classification Based on Custom ConvNeXtSmall and Combine with the Explanation Model

Huong Hoang Luong

Information Technology Department
FPT University, Can Tho, Viet Nam

Abstract—Potatoes are short-term crops grown for harvesting tubers. It is a type of tuber that grows on roots and is the fourth most common crop after rice, wheat, and corn. Fresh potatoes can also be used in an incredible variety of dishes by baking, boiling, or frying them. Moreover, the paper, textile, wood, and pharmaceutical industries also make extensive use of potato starch. However, soil and climate pollution are highly unfavorable for potato growth and lead to a lot of diseases such as common scab, black scurf, blackleg, dry rot, and pink rot. Thus, several types of research in medicine and computers were started for the early detection, classification, and treatment of potato diseases. In this study, transfer learning and fine-tuning were applied to potato disease classification based on a custom ConvNeXtSmall model. In addition, Gradient-weighted Class Activation Mapping (i.e., Grad-CAM) is provided for visual explanation in the final result after classification. For potato illness segmentation, k-means clustering was used to enable the difference between healthy and diseased sections based on color and texture. The data was collected from numerous websites and validated by the Bangladesh Agricultural Research Institute (i.e., BARI), including six types of potato diseases and healthy images. With a Convolutional Neural Networks (i.e., CNN) model from the Keras library, our study reached the unexpected validation accuracy, test accuracy, and F1 score in seven classifications of 99.49%, 98.97%, and 98.97%, respectively. Concerning four-class classification, high accuracy values were obtained for most of the models (i.e., 100%).

Keywords—Potato disease; classification; fine-tuning; transfer learning; Convolutional Neural Network (CNN); k-means clustering; Gradient-weighted Class Activation Mapping (Grad-CAM)

I. INTRODUCTION

Potatoes have been a crucial food source for humans for thousands of years. Originating in South America, they have spread worldwide due to their ability to grow in various climates and soil types. Potatoes are not only adaptable with hundreds of cooking ways but also packed with essential nutrients like carbohydrates, fiber, and vitamins. They are used in numerous dishes, from mashed potatoes to fries, and are also crucial in industries like starch production and biodegradable plastics. In the world, potatoes play a significant role, supporting about income of millions of farmers, and are one of the main food sources for billions of people.

In modern agriculture, potato production has become a cornerstone of global food systems. Based on statistical data, China holds the first spot in terms of potato production [1] [2]. In 2019, 370,436,581 tons of potatoes were produced globally and global potato production rose by 2.59% compared with

2012 [2]. 61.5% of the total EU production of potatoes is produced annually in Germany, France, the Netherlands, the United Kingdom, and Belgium, with an average of 34,870 million tons throughout the 2017–2019 period [3]. Specifically, Germany is currently the largest potato producer in the EU, with an average yearly potato production of slightly more than 10.4 million tonnes. France (i.e., 8.3 million tonnes) comes next, followed by the Netherlands (i.e., 6.8 million tonnes), the United Kingdom (i.e., 5.5 million tonnes), and Belgium (i.e., 3.8 million tonnes) between 2017 and 2019 [3]. However, potatoes face challenges, particularly from climate change, pollution, and diseases. Climate change affects potato growth with higher temperatures and irregular rainfall patterns [4]. Pollution from farming practices harms soil and water quality, impacting potato cultivation [5]. Additionally, diseases caused by viruses and bacteria threaten potato crops, reducing yields and farmer incomes [6].

Consequently, advancements in technology and machinery have revolutionized potato cultivation in agriculture, optimizing efficiency and yield while minimizing labor and environmental impact. Precision planting equipment ensures accurate spacing and depth, enhancing seedling establishment and uniformity across fields [7]. Additionally, state-of-the-art harvesting machinery, such as mechanical diggers and conveyor systems, streamline the process, minimizing damage to tubers and reducing post-harvest losses. Modern sorting and grading machines utilize advanced sensors and algorithms to identify and segregate potatoes based on size, shape, and quality criteria, improving marketability and reducing manual labor. Besides, Genetic modification of crops has also shown good effects in increasing productivity, nutritional quality, and disease resistance [8]. These advancements not only increase productivity and profitability but also contribute to sustainable agriculture by minimizing inputs and environmental footprint in potato production.

Besides mechanical and genetic technologies, several studies on computer technology were developed for potatoes. Thus, artificial intelligence (AI) is creating and making significant strides in the potato farming sector, particularly in planting and harvesting processes. AI uses smart algorithms and sensors to improve various stages of potato cultivation. When it comes to planting, AI helps in determining the best spacing and depth for potato seeds, ensuring efficient resource utilization and better yields. AI-powered machinery, equipped with sensors, reduces wastage and increases productivity. During harvesting, AI aids in identifying ripe potatoes using computer vision,

distinguishing them from soil and foliage, thus optimizing the harvesting process and minimizing crop damage. Moreover, AI analyzes environmental factors like soil moisture, temperature, and weather conditions in real-time, providing valuable insights to farmers for informed decision-making and better outcomes. Consequently, AI not only enhances efficiency and productivity in potato farming but also promotes sustainable agricultural practices by minimizing resource usage and environmental impact.

Deep learning is a subset of artificial intelligence and it has revolutionized various fields, including agriculture and industry. Besides, computer vision appeared as a new way for classification and segmentation of a lot of aspects of images [9] [10] [11] [12] [13], through techniques like transfer learning and fine-tuning. For example, image technologies have come out as invaluable tools in potato farming, offering correct solutions for classification, segmentation, and detection tasks. Classification algorithms are used to assess potato images, categorizing them based on diverse attributes including size, shape, and quality, thereby facilitating farmers in optimizing sorting procedures and ensuring consistency across their yield [14]. Segmentation techniques are employed to segment potato disease regions or potato growing areas to detect weeds [15], facilitating precise attribute measurements such as size and color distribution, which in turn assists in grading and quality evaluation. Detection algorithms play a pivotal role in identifying diseases, pests, and other anomalies in potato crops [16], enabling prompt intervention and mitigation measures to curtail yield losses.

In this study, various algorithms have used the progressions in machine learning and computer vision, and large datasets of potato plant images afflicted with various diseases for classification and segmentation images, deep learning models can accurately classify these images. Transfer learning has been used in this process, it is a technique where a pre-trained model developed for one task is adapted for another [17] [18] [19], allowing researchers to leverage the knowledge gained from training models on massive datasets to enhance the performance of models in potato disease classification and segmentation. Furthermore, fine-tuning, a process of adjusting the parameters of a pre-trained model to better fit the specific characteristics of a new dataset, has been crucial in refining the accuracy and efficiency of disease segmentation and detection algorithms [20] [21] [22]. By fine-tuning pre-existing deep learning architectures such as convolutional neural networks (CNNs), researchers can customize these models to effectively identify and delineate regions of potato plants affected by diseases, enabling early intervention and targeted treatment.

Overall, the integration of deep learning techniques, including transfer learning and fine-tuning, has significantly advanced the field of potato disease management by providing accurate, efficient, and contributing to improved crop yield and food security. This study advances agricultural technology by using ConvNeXtSmall in the Keras library to categorize potato disease photos with very high accuracy. Additionally, utilizing k-mean clustering for the segmentation of anomalous positions offers a thorough solution that supports agricultural efforts in the early diagnosis and treatment of potato illnesses by assisting in the accurate identification of abnormal zones.

The contributions of this paper are as follows:

- A customized CNN model based on ConvNeXtSmall is presented by the research for the purpose of classifying and segmenting potato diseases into seven groups: pink rot, dry rot, blackleg, black scurf, common scab, miscellaneous, and healthy. Thus, it might offer a quick and easy way for the farmer to boost profitability and productivity depending on the amount of potatoes they produce.
- In the scenario of seven classes classification, our model achieved excellent validation accuracy, test accuracy, and F1 score (i.e., 99.49%, 98.97%, and 98.97%). As a result, a table and confusion matrix were also made to illustrate how successful the model was in terms of training and testing duration.
- The article proposes K-means clustering in image segmentation for identifying potato diseases. By grouping pixels with similar characteristics, it enables the differentiation of healthy areas from diseased ones based on color and texture. This method aids in precise disease mapping, facilitating targeted treatment strategies for agricultural management.
- Gradient-weighted Class Activation Mapping (Grad-CAM) was applied and assisted in the visual explanation of potato diseases by pinpointing regions in images where the model concentrates its attention. This technique aids in the precise identification and comprehension of various potato diseases, enhancing diagnostic accuracy and agricultural management strategies.
- This research gathered photos of both sick and healthy potatoes, as confirmed by experts at the Bangladesh Agricultural Research Institute. This dataset can be used to teach agriculture students and is validated for the creation of automated machine learning and deep learning algorithms for the classification, segmentation, and detection of potato illnesses.

The organization of our research paper is structured into six principal sections. Firstly, Section I serves as a comprehensive overview providing a general introduction to the article. Following this, Section II extensively explores related research, offering a thorough examination of the existing literature upon which our work is based. Subsequently, Section III delineates the methodology utilized, furnishing detailed insights into the methods employed throughout the article. Section IV then elaborates on the experiments conducted, encompassing the procedures for their execution and the evaluation of each scenario. Furthermore, Section V presents the results of the best experiment and conducts a comparative analysis with existing scenarios. Finally, the article encapsulates the key findings and analyzes the fundamental domains associated with our research in Section VI.

II. RELATED WORKS

Exploring potato diseases led to groundbreaking research in transfer learning and fine-tuning and various research was published to promote disease segmentation and classification in potatoes. For example, A deep convolutional neural network was trained to distinguish between four types of potatoes

(i.e., Red, Red Washed, Sweet, and White) using a public dataset of 2400 photos by Abeer A. Elsharif et al. The trained model attained an accuracy of 99.5% of the test accuracy [23]. Besides, Sofia Marino et al. have presented an effective unsupervised adversarial domain adaptation method to classify six potato classes in two different scenarios and reach an average F1-score of 84% [24]. Furthermore, Qinghua Su et al. used a convolutional neural network model and achieved a high success rate in size classification at 94.5% and appearance classification at 91.6% [25].

One of the most important tasks in post-harvest quality control during potato manufacturing is identifying bad surfaces for potatoes. Therefore, Chenglong Wang et al. used transfer learning to refine a basic model using three DCNN modes. As a result, RFCN ResNet101 had the best overall performance, achieving accuracy levels of 92.5%, 95.6%, and 98.7%, respectively [26]. Moreover, Kaili Zhang et al. improved U-Net and showed that the accuracy of the potato surface evaluation method proposed in the study was greater than 97.55% [27]. In addition, Black scurf, common scab, black leg, pink rot, and healthy are the five categories of potato diseases that Khalid Hamza et al. detect and classify. In multiple classes, the accuracy can reach 98% and 100% [28].

To classify potato problems early, machine learning technology has been widely used as an affordable and nondestructive diagnostic tool. For instance, Ali Arshaghi et al. use image processing and convolution neural networks to identify and classify surface potatoes from a collection of 5,000 photos of potatoes that have been split into five types. As a result, the results show that the accuracy of the deep learning proposed was 98% and 100% accuracy in some of the classes [29]. To classify potatoes, Hyeon-Seung Lee et al. used Mask R-CNN, one of the object identification technologies utilizing deep learning, and were surprised with the result of 93.0% [30]. Furthermore, Israa Mohammed Hassoon et al. proposed a PDCNN framework that is very effective in classifying four types of potato tuber diseases including black dot, common scab, potato virus y, and ring rot with 91.3% accuracy [31].

To expand the author's limited knowledge about transfer learning and fine-tuning in CNN. Hence, several research about potato leaf disease classification have been investigated. With the help of deep learning and the VGG16 and VGG19 convolutional neural network architectural model, Rizqi Amaliatus Sholihati et al. developed a system that can classify the four different types of diseases in potato plants based on leaf conditions. As a result, the model achieved an average accuracy of 91% [32]. Moreover, Aditi Singh et al. presented a model that can reach a 95.99% accuracy rate when using the K-means approach for feature segmentation and the multi-class support vector machine methodology for classification [33]. To identify potato leaf disease, Rabbia Mahum et al. employed an additional transition layer in DenseNet-201 along with a pre-trained Efficient DenseNet model. As a result, the performance was evaluated and gave an accuracy of 97.2% [34].

The quantity and quality of potatoes are greatly impacted by many diseases. Because manually explaining these leaf diseases is labor-intensive and time-consuming. As a result, Divyansh Tiwari et al utilized a pre-trained model VGG19 for fine-tuning the dataset and reached 97.8% in classification accuracy over the test dataset[35]. Moreover, Asif Iqbal

et al. proposed an image processing and machine learning-based automatic system that will identify and classify over 450 images of healthy and diseased potato leaves with an accuracy of 97% [36]. Kulendu Kashyap Chakraborty et al proposed a methodology using four deep learning models such as VGG16, VGG19, MobileNet, and ResNet50. Hence, it achieved 97.89% accuracy for classification between late and early blight syndromes as compared to healthy potato leaf [37].

Besides using computer vision to recognize and classify potatoes, other fruits and vegetables also apply this method for having the advantages of speed, and high accuracy in dividing a final product. For instance, Alper Taner et al. used popular seven CNN architectures (i.e., VGG16, VGG19, InceptionV3, MobileNet, Xception, ResNet150V2, and DenseNet201) and it was found that DenseNet201 had the highest classification accuracy of 97.48% in classifying apple varieties [38]. Moreover, Dhiya Mahdi Asriny et al. proposed the classification model to classify orange images using CNN and shows an accuracy of 96% [39]. In conclusion, Table I shows that related studies have been compiled for easier evaluation and synthesis.

TABLE I. RELATED PAPERS IN AGRICULTURE

| Product | Method | Accuracy | Year | Author |
|---------------|-------------------------------------|----------------|------|---------------------------------------|
| Potato | CNN | 99.5% | 2020 | Abeer A. Elsharif et al [23] |
| Potato | FCN | F1 score = 84% | 2020 | Sofia Marino et al [24] |
| Potato | CNN | 91.6% | 2020 | Qinghua Su et al [25] |
| Potato | RFCN ResNet101 | 98.7% | 2021 | Chenglong Wang et al [26] |
| Potato | VGG and U-Net | 97.55% | 2023 | Kaili Zhang et al [27] |
| Potato | CNN | 98%-100% | 2022 | Khalid Hamza et al |
| Potato | CNN | 98%-100% | 2020 | Ali Arshaghi et al [29] |
| Potato | Mask R-CNN | 93% | 2020 | Hyeon-Seung Lee et al [30] |
| Potato | PDCNN | 91.3% | 2021 | Israa Mohammed Hassoon et al [31] |
| Potato leaves | VGG16 and VGG19 | 91% | 2020 | Rizqi Amaliatus Sholihati et al [32] |
| Potato leaves | CNN | 95.99% | 2021 | Aditi Singh et al [33] |
| Potato leaves | DenseNet-201 and Efficient DenseNet | 97.2% | 2022 | Rabbia Mahum et al [34] |
| Potato leaves | VGG19 | 97.8% | 2020 | Divyansh Tiwari et al[35] |
| Potato leaves | D-CNN | 97% | 2020 | Asif Iqbal et al [36] |
| Potato leaves | VGG16 | 97.89% | 2022 | Kulendu Kashyap Chakraborty et al[37] |
| Apple | DenseNet201 | 97.48% | 2024 | Alper Taner et al[38] |
| Orange | CNN | 96% | 2020 | Dhiya Mahdi Asriny et al [39] |

III. METHODOLOGY

A. The Research Implementation Procedure

This study proposed a method including 12 steps from input to output shown in Fig. 1. The roles of the steps are shown as follows:

- 1) Collecting dataset: the dataset selected from various sources and rigorously verified by the Bangladesh Agricultural Research Institute (BARI), boasts 451 images capturing diverse potato illnesses such as Common scab, Blackleg, Dry rot, Pink rot, Black scurf, Miscellaneous, and Healthy Potatoes. It is a valuable resource for academic research, offering comprehensive insights into potato disease management and cultivation practices.
- 2) Pre-processing image and data augmentation: image pre-processing techniques such as resizing and normalization are crucial for standardizing input data, and ensuring consistency in potato disease classification models. Furthermore, using data augmentation methods such as rotation, flipping, and contrast enhancement enhances the variety of the dataset, and assists model training. These algorithms provide a foundation for developing accuracy and prediction to classify and segment potato diseases, thus safeguarding agricultural productivity and income.
- 3) Dividing the dataset into three categories train, validation, and test: after increasing data augmentation by 451 default participants, which were chosen at random for the training, validation, and testing phases, the pictures dataset contains 5833 subjects. The datasets are randomly selected using an 8-1-1 scale and are then placed into 8 training, 1 validation, and 1 testing folder. This guarantees a balanced distribution, which is essential for trustworthy model development and evaluation.
- 4) Dividing dataset for scenarios: the dataset was divided into four scenarios. In the first scenario, four classes healthy, black scurf, common scab, and pink rot were selected because they can be classified by surface observation. Next to that, four classes healthy, blackleg, dry rot, and miscellaneous because it is an internal harm. Finally, the next two scenarios employed all classes for the experiment.
- 5) Building the model: our work employed transfer learning to a pre-trained model based on the CNN architecture prototype to conduct tests. External layers were employed during fine-tuning to adapt the pre-trained model to the specific data of the intended task. For our training test, the ConvNeXtSmall model thus yields an excellent result.
- 6) Applying transfer learning: using pre-trained deep learning models, this approach aims to transfer knowledge from related domains to enhance the classification accuracy of potato disease. By adapting neural networks to recognize patterns indicative of various potato diseases.
- 7) Validating and collecting accuracy score: after the model had completed training, its efficiency was assessed using its training accuracy as well as its other scores. Next, The validity of the test was then determined using the initially divided testing set.
- 8) Applying fine-tuning: fine-tuning involves adjusting the parameters, and additional layers of a pre-trained neural network particularly in the latter layers, typically focusing on refining performance. This process allows the model to borrow knowledge acquired from a broader scope while customizing it to the particular requirements.
- 9) Validating, collecting, and explaining results with Grad-CAM: Grad-Cam was used for the analysis of heat maps generated by the model to highlight regions of interest. By correlating these areas with known symptoms, researchers can validate the model's accuracy, collect valuable data for further analysis, and elucidate its decision-making process.
- 10) Image segmentation by k-means clustering: this step includes partitioning the image into distinct clusters based on pixel intensities. By iterative assigning pixels to clusters with similar characteristics, this method effectively separates different disease regions within the potato image, facilitating targeted analysis and diagnosis of specific ailments.
- 11) Reconstructing and comparing the cycles with other models: after one phase, the procedure was re-worked and compared with another model including, EfficientNetB3, ResNet50, MobileNet, Inception V3, Xception, ConvNeXtSmall, ConvNeXtTiny, ConvNeXtLarge to create the final result
- 12) Showing the result: the data will be presented as tables and graphs after procedures to enable pertinent comparisons.

B. Pre-processing Image and Data Augmentation

Pre-processing plays an important role in boosting the quality of images before subjecting them to potato disease classification algorithms. Resizing (1) and normalization (2) are two fundamental techniques used in this process. Resizing (1) connection to change the dimensions of images to a uniform size, which aids in reducing computational complexity and ensuring consistency across the dataset. Mathematically, resizing can be represented as follows:

$$\text{Resize image} = \text{resize}(\text{original image}, \text{target size}) \quad (1)$$

Algorithm 1 Resizing Algorithm

Require: Original Image, target_size

Ensure: Resized Image

- 1: Load the Original Image;
 - 2: Define the target_size = (224,224)
 - 3: Resize the Original Image to the target_size using the resize function:
 - 4: $\text{ResizedImage} = \text{resize}(\text{OriginalImage}, (224, 224))$
 - 5: **return** Resized Image
-

Here, original image (1) represents the raw input image, and target size (1) indicates the desired dimensions of the output image. Besides, Algorithm 1 is a pseudo-code that presents flow on how it works in coding. Furthermore, Normalization (2) fixes standard pixel values within a certain range. It can be expressed as:

$$\text{Normalized image} = \frac{\text{original image} - \text{mean}}{\text{std}} \quad (2)$$

Algorithm 2 Normalization Algorithm

Require: Original Image

Ensure: Normalized Image

- 1: Compute the mean and standard deviation of pixel intensities:
 - 2: $mean = \frac{1}{n} \sum_{i=1}^n pixel_i$
 - 3: $std = \sqrt{\frac{1}{n} \sum_{i=1}^n (pixel_i - mean)^2}$
 - 4: Normalize the Original Image by subtracting the mean and dividing by the standard deviation:
 - 5: $NormalizedImage = \frac{OriginalImage - mean}{std}$
 - 6: **return** Normalized Image
-

Specifically, mean (2) and std (2) represent the mean and standard deviation of pixel intensities across the entire dataset, respectively. This normalization process ensures that pixel values are centered around 0 with a standard deviation of 1, to facilitate convergence during training and mitigate the influence of illumination variations, thereby increasing the stability of the training process. In addition, To clarify the process a pseudo-code has been provided at Algorithm 2.

Data augmentation techniques are tools for improving the diversity of training samples, thereby improving the generalization ability of the classifier. Rotation (3), flipping (4) (5), and contrast enhancement (6) are commonly employed augmentation strategies in the context of potato surface disease classification. Rotation (3) involves rotating the image by a certain angle to simulate variations in orientation. Mathematically, rotation can be represented as:

$$\text{Rotated image} = \text{rotate}(\text{original image}, \theta) \quad (3)$$

Algorithm 3 Rotation Algorithm

Require: Original Image, angle

Ensure: Rotated Image

- 1: Load the Original Image
 - 2: Specify the angle of rotation (θ)
 - 3: Rotate the Original Image by the specified angle using the formula:
 - 4: Rotated image = rotate(original image, θ)
 - 5: **return** Rotated Image
-

In the equation, θ (3) stand for the angle of rotation and Algorithm 3 presents the detail of code flow which is provided in pseudo-code for overview. Moreover, flipping (4) (5) entails flipping the image horizontally or vertically to introduce variations in perspective. It can be mathematically expressed as:

$$P(x, y) = (\text{width} - x - 1, y) \quad (4)$$

$$P(x, y) = (x, \text{height} - y - 1) \quad (5)$$

Algorithm 4 Flipping Algorithm

Require: Original Image, axis

Ensure: Flipped Image

- 1: Load the Original Image
 - 2: Specify the axis along which flipping should occur: horizontal (H) or vertical (V)
 - 3: **if** axis is H **then**
 - 4: Flip the Original Image horizontally using the formula:
 $P(x, y) = (\text{width} - x - 1, y)$
 - 5: **else if** axis is V **then**
 - 6: Flip the Original Image vertically using the formula:
 $P(x, y) = (x, \text{height} - y - 1)$
 - 7: **end if**
 - 8: **return** Flipped Image
-

In the context of image flipping, (x, y) 4 5 represents the pixel coordinates of the Original Image. In Algorithm 4 flipping horizontally (H), the pixel x-coordinate is reversed concerning the image width, and when flipping vertically (V), the pixel y-coordinate is reversed concerning the image height.

$$P_{\text{enhanced}}(x, y) = CDF(P_{\text{original}}(x, y)) \times (L - 1) \quad (6)$$

Algorithm 5 Contrast Enhancement Algorithm

Require: Original Image

Ensure: Enhanced Image

- 1: Load the Original Image
 - 2: Compute the cumulative distribution function (CDF) of pixel intensities
 - 3: Apply histogram equalization to map pixel intensities to a new range using the formula:
 - 4: $P_{\text{enhanced}}(x, y) = CDF(P_{\text{original}}(x, y)) \times (L - 1)$
 - 5: where $P_{\text{enhanced}}(x, y)$ is the pixel intensity in the Enhanced Image,
 - 6: $P_{\text{original}}(x, y)$ is the pixel intensity in the Original Image,
 - 7: and L is the number of intensity levels
 - 8: **return** Enhanced Image
-

The contrast enhancement algorithm aims to improve the contrast of an image through histogram equalization. It begins by loading the original image and computing its histogram, which represents the frequency distribution of pixel intensities. Subsequently, Algorithm 5 calculates the cumulative distribution function (CDF) from the histogram. This CDF provides a mapping between original pixel intensities and their corresponding enhanced values. The enhancement is achieved by applying the formula (6). where L (6) illustrates the number of intensity levels. Each pixel in the original image is mapped to a new intensity level based on its CDF value, resulting in an image with improved contrast. Finally, These data augmentation techniques collectively contribute to the robustness of the classification model by exposing it to a diverse range of image variations.

C. Transfer Learning and Fine-tuning of ConvNeXtSmall

Transfer learning is a technique in machine learning where knowledge gained from solving one problem is applied to a different but related problem [17] [18] [19]. In the context of image classification, it involves leveraging pre-trained models, which have been trained on large datasets, and adapting them to new classification tasks with relatively smaller datasets. This approach is particularly useful when the target dataset is not large enough to train a model from scratch effectively.

In the classification of potato surface disease, transfer learning can be employed by utilizing a pre-trained Convolutional Neural Network (ConvNet), such as ConvNeXtSmall, which has been trained on a large dataset. The initial layers of ConvNeXtSmall have learned to extract low-level features like edges and textures, which are generally applicable to various image recognition tasks. By reusing these learned features and adjusting the later layers to suit the specifics of potato surface disease classification, this algorithm can expedite the training process and improve performance.

Fine-tuning is a key aspect of transfer learning, where the parameters of the pre-trained model are further adjusted to better fit the new dataset [20] [21] [22]. In the case of ConvNeXtSmall, fine-tuning includes unfreezing some of the later layers and retraining them using the new dataset. This allows the model to learn higher-level representations more adapted to the characteristics of potato surface disease, refining its ability to distinguish between disease states or healthy potato surfaces.

Moreover, adding extra layers to ConvNeXtSmall in Fig. 2 can enhance its accuracy and overall performance. These additional layers can capture more complex patterns and relationships within the data, providing the model with a deeper understanding of the distinguishing features of different disease conditions. However, care must be taken to prevent overfitting, where the model becomes too specialized to the training dataset and performs poorly on unseen data. Regularization techniques such as dropout and weight decay can be employed to mitigate overfitting and ensure the generalization ability of the model.

In summary, transfer learning and fine-tuning of ConvNeXtSmall offer effective strategies for the classification of potato surface disease by borrowing pre-existing knowledge and adapting it to the specific characteristics of the target dataset. By incorporating additional layers and carefully fine-tuning the model, this research improves its accuracy and prediction in classifying different disease states, ultimately aiding in the early detection and management of potato crop diseases.

D. Visual Explanation with Gradcam

Visual explanations through techniques like Grad-CAM (Gradient-weighted Class Activation Mapping) offer valuable insights into the classification process, aiding researchers and farmers in making informed decisions. Potato surface diseases encompass a range of fungal, bacterial, and viral infections that affect the external appearance of the potato tubers. Timely detection and classification of these diseases are essential for maintaining crop health and yield.

Grad-CAM is a technique used in computer vision to understand the decision-making process of deep learning models. It highlights regions of an image that contribute most significantly to the model's classification decision. In the context of potato surface disease classification, Grad-CAM helps elucidate which features or regions of the potato surface are indicative of particular diseases. In the case of the black scurf and black leg of Fig. 3, Grad-CAM may highlight regions of the potato surface where characteristic lesions or discolorations are present.

The Grad-CAM method functions by generating a heat map that delineates the significance of various regions within the input image for prediction. This heat map is derived by computing the gradient of the target class score concerning the final convolutional layer feature maps. Mathematically:

$$H_{(i,j)}^c = \text{ReLU} \left(\sum_k \alpha_k^c \cdot A_{(i,j)}^k \right) \quad (7)$$

Specifically, $H_{(i,j)}^c$ (7) represents the heat map value at position (i, j) for class c . α_k^c (7) denotes the importance of the k th feature map for class c , and $A_{(i,j)}^k$ (7) is the activation of the k th feature map at position (i, j) . Equation (7) essentially encapsulates the importance of each feature map activation, weighted by its corresponding importance score. The ReLU function is employed to ensure that only positive contributions are considered.

In conclusion, visual explanation techniques like Grad-CAM furnish a valuable means of interpreting deep learning models in the classification of potato surface diseases. By accentuating crucial regions within input images, Grad-CAM facilitates the understanding of model predictions and offers insights for refining disease management strategies.

E. Image Segmentation by k-means Clustering

Image segmentation is a main task in classifying potato surface diseases, assisting in identifying and analyzing abnormal areas on the potato surface. Among various segmentation techniques, k-means clustering is an efficient method for partitioning images into distinct clusters based on pixel intensity values. In this context, k-means clustering (8) facilitates the categorization of pixels into groups, differentiating healthy potato regions from those affected by diseases.

Mathematically, the k-means algorithm aims to minimize the within-cluster sum of squares, defined as:

$$W(C_k) = \sum_{i=1}^n \sum_{x_j \in C_k} \|x_j - \mu_k\|^2 \quad (8)$$

In every detail, C_k (8) represents the cluster k , x_j (8) show the j th (8) data point (pixel), and μ_k (8) is the centroid of cluster k . The goal is to assign each pixel to the cluster whose centroid is nearest to it in terms of Euclidean distance.

Specifically, Algorithm 6 outlines the k-means clustering approach for segmenting images. It begins with an initialization phase, during which k initial centroids are randomly selected.

Following this, the assignment step assigns each pixel to the nearest centroid, effectively partitioning the image into k clusters. Subsequently, in the update phase, the centroids are recalculated based on the mean of all pixels assigned to each cluster. This iterative process continues until convergence is achieved, typically indicated by a condition such as centroids no longer undergoing significant changes between iterations. This methodical approach enables the algorithm to effectively segment images by distinguishing regions based on pixel similarities, making it particularly valuable for applications such as disease detection on potato surfaces.

Algorithm 6 K-Means Clustering

Require: Image I , Number of clusters $k = 3$ (Background, healthy surface and disease surface)
Ensure: Segmented image I_{seg} , Centroids $\{\mu_1, \mu_2, \dots, \mu_k\}$

- 1: Initialization:
- 2: Randomly select k initial centroids: $\mu_1, \mu_2, \dots, \mu_k$
- 3: $I_{\text{prev}} \leftarrow$ Copy of I
- 4: **repeat**
- 5: Assignment Step:
- 6: **for** each pixel p in I **do**
- 7: Assign p to the nearest centroid μ_i
- 8: **end for**
- 9: Update Step:
- 10: **for** each cluster i **do**
- 11: Recalculate centroid μ_i as the mean of all pixels in cluster i
- 12: **end for**
- 13: $I_{\text{seg}} \leftarrow$ Image formed by assigning pixels to their respective clusters
- 14: $I_{\text{prev}} \leftarrow$ Copy of I_{seg}
- 15: **until** Convergence criteria are met (e.g., centroids do not change significantly)
- 16: **return** Segmented image I_{seg} , Centroids $\{\mu_1, \mu_2, \dots, \mu_k\}$

By applying k-means clustering to potato surface images, Fig. 4 effectively segments the image into regions of similar pixel intensities, thereby distinguishing between healthy and diseased areas. The centroids obtained represent characteristic color values associated with each cluster, aiding in the identification of disease patterns based on pixel color.

Furthermore, the simplicity and efficiency of k-means clustering make it a suitable choice for real-time or large-scale image processing tasks, contributing to the rapid and accurate classification of potato surface diseases. Overall, leveraging k-means clustering in image segmentation enhances the precision and scalability of disease detection systems, facilitating timely interventions to mitigate agricultural losses.

IV. EXPERIMENTS

A. Dataset and Performance Metrics

The research used a single dataset for both the training, validation, and testing phases in this analysis. The data was selected from various sources and rigorously verified by the Bangladesh Agricultural Research Institute (BARI). 451 images constitute the comprehensive dataset in Fig. 5 including 62 Common scabs, 60 Blackleg, 60 Dry rot, 57 Pink rot, 58 Black scurf, 74 Miscellaneous, and 80 Healthy Potato images.

In the classification of potato surface disease, various performance metrics are utilized to evaluate the effectiveness of the classification model. These metrics help in understanding the ability to correctly classify instances of potato surface disease and its performance in terms of both precision and recall.

One of the fundamental metrics used is the Accuracy (i.e., ACC), which measures the proportion of correctly classified instances out of the total instances. Mathematically, it can be expressed as:

$$ACC = \frac{TP + TN}{TP + TN + FP + FN} \quad (9)$$

Where TP (9) indicates true positives (correctly classified instances of potato surface disease), TN (9) represents true negatives (correctly classified instances of absence of potato surface disease), FP (9) stands for false positives (instances incorrectly classified as having potato surface disease), and FN (9) represents false negatives (instances incorrectly classified as not having potato surface disease).

Another important metric is the Recall in equation (10), also known as sensitivity or true positive rate. It measures the proportion of actual positive instances that are correctly identified by the model. Moreover, This metric is crucial in scenarios where the consequences of false negatives (misclassifying actual instances of potato surface disease as negative) are severe. Mathematically, it can be defined as:

$$Recall = \frac{TP}{TP + FN} \quad (10)$$

The Precision metric in equation (11) evaluates the proportion of true positive instances among all instances classified as positive by the model. It can be calculated as:

$$Precision = \frac{TP}{TP + FP} \quad (11)$$

The F1 Score in equation (12) is a metric that combines precision and recall into a single value. It is the harmonic mean of precision and recall, and it provides a balance between the two metrics. Mathematically, it is represented as:

$$F1 = 2 \times \frac{Precision \times Recall}{Precision + Recall} \quad (12)$$

B. Scenario 1: the Result of Classifying Potato Diseases into four Classes: Healthy, Black Scurf, Common Scab, Pink Rot

Table II presents a comparative analysis of various deep learning models in classifying potato disease images into four classes: healthy, black scurf, common scab, and pink rot, using both transfer learning and fine-tuning techniques. Among the models evaluated, EfficientNet B3 emerges as the top performer, exhibiting remarkable accuracy in both transfer learning (i.e., 99.70% validation accuracy, 99.40% test accuracy) and fine-tuning (i.e., 100.00% for both validation and test accuracy). In contrast, Xception shows comparatively lower accuracy levels across both transfer learning and fine-tuning

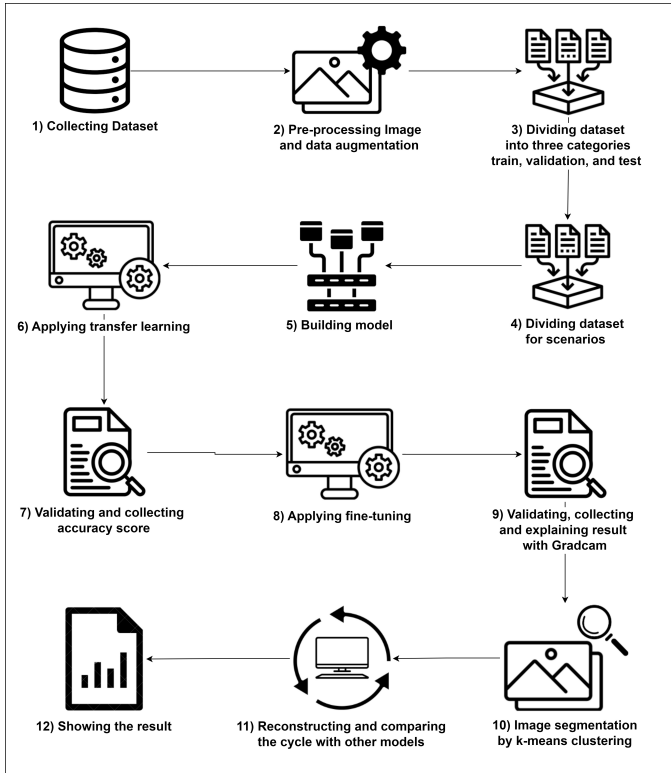


Fig. 1. The implementing procedure flowchart.

TABLE II. THE ACCURACY OF CLASSIFYING POTATO DISEASE IMAGES INTO FOUR CLASSES: HEALTHY, BLACK SCURF, COMMON SCAB, PINK ROT IN TRANSFER LEARNING AND FINE-TUNING, FOR EACH DEEP LEARNING MODEL

| Model | Phase | Valid acc | Test acc | Precision | Recall | F1 |
|-----------------|-------------------|-----------|----------|-----------|---------|---------|
| EfficientNet B3 | Transfer Learning | 99.70% | 99.40% | 97.44% | 97.32% | 97.30% |
| | Fine Tuning | 100.00% | 100.00% | 100.00% | 100.00% | 100.00% |
| ResNet50 | Transfer Learning | 100.00% | 99.83% | 99.71% | 99.70% | 99.70% |
| | Fine Tuning | | | | | |
| MobileNet | Transfer Learning | 97.31% | 95.04% | 94.96% | 94.94% | 94.94% |
| | Fine Tuning | 97.31% | 97.46% | 96.74% | 96.73% | 96.73% |
| InceptionV3 | Transfer Learning | 89.55% | 91.91% | 90.92% | 90.77% | 90.74% |
| | Fine Tuning | 91.64% | 94.99% | 92.69% | 92.56% | 92.58% |
| Xception | Transfer Learning | 84.48% | 84.52% | 84.91% | 84.52% | 84.57% |
| | Fine Tuning | 91.34% | 89.66% | 89.49% | 89.29% | 89.33% |
| Our Model | Transfer Learning | 98.51% | 93.75% | 97.93% | 97.92% | 97.92% |
| | Fine Tuning | 99.40% | 96.88% | 99.11% | 99.11% | 99.11% |

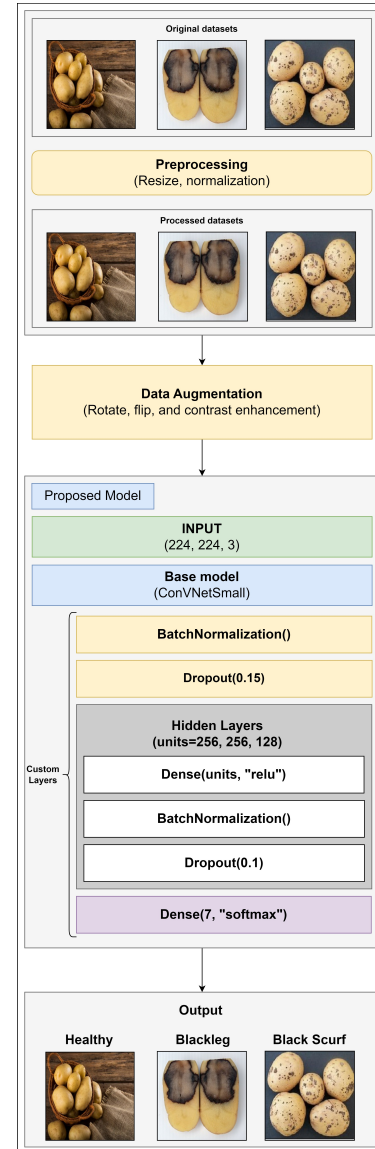


Fig. 2. Procedure of transfer learning and fine-tuning in our model with custom layers.

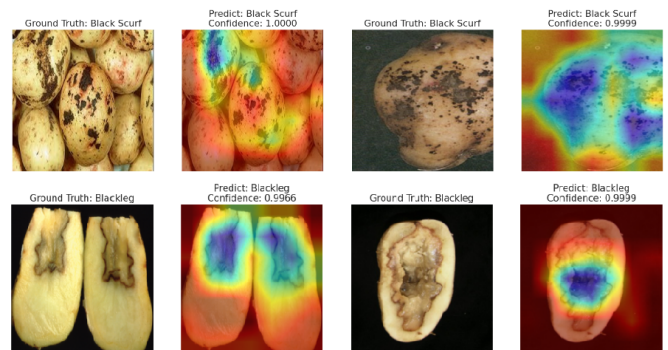


Fig. 3. Visual explanation by gradcam of potato diseases.

phases, with validation accuracy of 84.48% and 91.34%, and test accuracy of 84.52% and 89.66%, respectively. However, Our model showcases competitive performance, particularly in fine-tuning (i.e., an increase of 3.13 % with transfer learning), where it achieves a validation accuracy of 99.40% and a test accuracy of 96.88%, closely aligning with EfficientNetB3. This suggests that the proposed model demonstrates robustness comparable to the state-of-the-art EfficientNetB3 while outperforming the least effective model, Xception, underscoring its potential as a viable alternative in potato disease classification tasks.

Fig. 6 and Fig. 7 indicate the accuracy and loss scores in the two training and validation phases. With this line chart, the accuracy and loss scores are presented intuitively and simply to help with general assessment through the training epoch. Besides, the confusion matrix in Fig. 8 assesses the performance of deep learning models for potato disease classification. It evaluates accuracy, identifies misclassifications, and guides parameter optimization. Additionally, it detects class imbalances, aids in error analysis, and facilitates model comparison, enabling improvement in accuracy and robustness.

C. Scenario 2: the Result of Classifying Potato Diseases into Four Classes: Healthy, Blackleg, Dry Rot, Miscellaneous

TABLE III. THE ACCURACY OF CLASSIFYING POTATO DISEASE IMAGES INTO FOUR CLASSES: HEALTHY, BLACKLEG, DRY ROT, MISCELLANEOUS IN TRANSFER LEARNING AND FINE-TUNING, FOR EACH DEEP LEARNING MODEL

| Model | Phase | Valid acc | Test acc | Precision | Recall | F1 |
|-----------------|-------------------|-----------|----------|-----------|--------|--------|
| EfficientNet B3 | Transfer Learning | 99.40% | 96.60% | 96.18% | 96.13% | 96.14% |
| | Fine Tuning | 99.11% | 99.24% | 99.42% | 99.40% | 99.40% |
| ResNet50 | Transfer Learning | 99.11% | 98.59% | 98.82% | 98.81% | 98.81% |
| | Fine Tuning | 99.70% | 98.54% | 98.54% | 98.51% | 98.51% |
| MobileNet | Transfer Learning | 90.18% | 90.09% | 89.36% | 89.29% | 89.20% |
| | Fine Tuning | 91.67% | 89.93% | 91.40% | 91.37% | 91.36% |
| InceptionV3 | Transfer Learning | 79.76% | 77.33% | 77.03% | 76.79% | 76.68% |
| | Fine Tuning | 84.23% | 83.23% | 82.97% | 82.74% | 82.73% |
| Xception | Transfer Learning | 76.19% | 78.77% | 76.34% | 76.19% | 76.01% |
| | Fine Tuning | 83.93% | 85.58% | 85.11% | 85.12% | 85.08% |
| Our Model | Transfer Learning | 98.21% | 96.88% | 94.35% | 94.35% | 94.31% |
| | Fine Tuning | 99.11% | 96.88% | 96.17% | 96.13% | 96.12% |

Compared with Table II, Table III shows that the performance of our model remained stable at 96.68% in the classification four classes healthy, blackleg, dry rot, miscellaneous although it is internal damage. However, EfficientNetB3 witnessed a slight decrease (i.e., a decrease of 0.76%) when compared with scenario 1. Moreover, Xception presents inef-

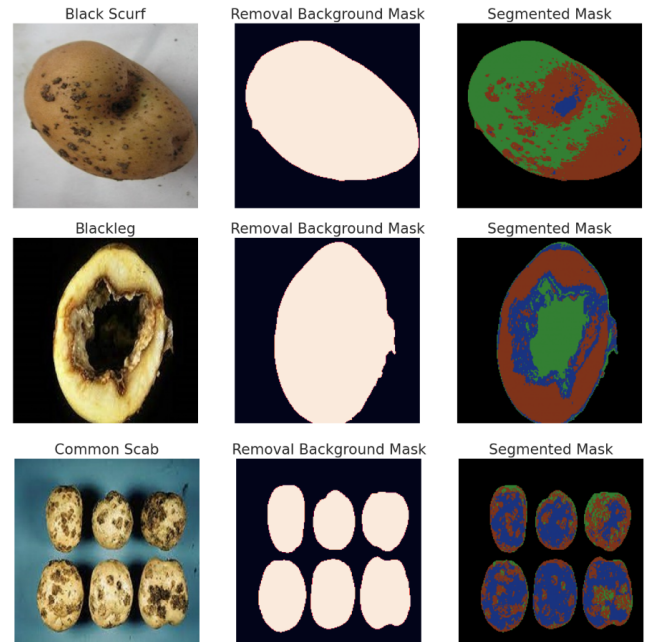


Fig. 4. Image segmentation in potato diseases by k-mean clustering.

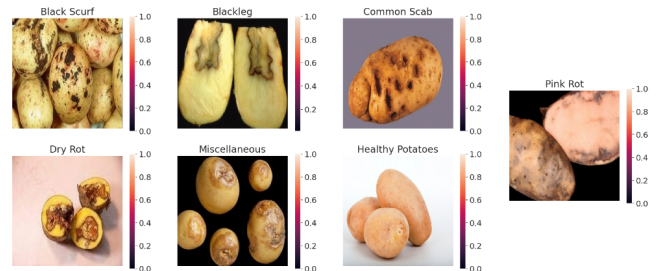


Fig. 5. The dataset of potato images.

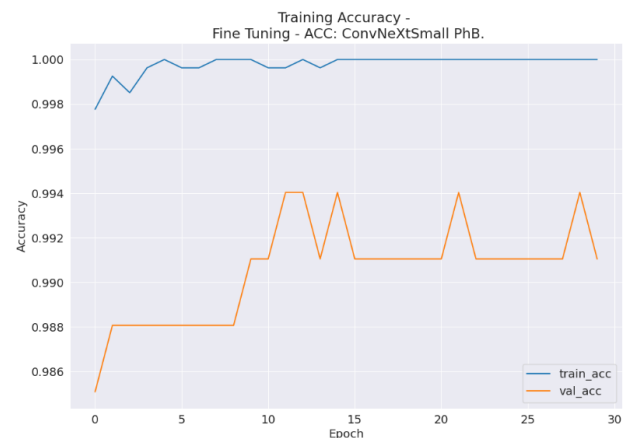


Fig. 6. Training accuracy and validation accuracy by fine-tuning of our model at scenario 1.

fectiveness in evaluating the performance of classifying potato diseases.

Furthermore, Training and validation on both accuracy and loss scores are presented in Fig. 9 and Fig. 10. Following the figures, the evaluation performance of our model presents the balance when the dataset is changed. Moreover, Fig. 11 is provided for evaluating, optimizing, and understanding the performance of deep learning models in classifying potato diseases, providing insights that can lead to improved accuracy and reliability.

D. Scenario 3: the Result of Classifying Potato Diseases Into Seven Classes: Healthy, Black Scurf, Common Scab, Pink Rot, Blackleg, Dry Rot, Miscellaneous

TABLE IV. THE ACCURACY OF CLASSIFYING POTATO DISEASE IMAGES INTO SEVEN CLASSES: HEALTHY, BLACK SCURF, COMMON SCAB, PINK ROT, BLACKLEG, DRY ROT, MISCELLANEOUS IN TRANSFER LEARNING AND FINE-TUNING, FOR EACH DEEP LEARNING MODEL

| Model | Phase | Valid acc | Test acc | Precision | Recall | F1 |
|------------------|--------------------------|---------------|---------------|---------------|---------------|---------------|
| EfficientNet B3 | Transfer Learning | 98.00% | 98.22% | 98.23% | 98.22% | 98.22% |
| | Fine Tuning | 99.11% | 98.00% | 98.08% | 98.00% | 98.00% |
| ResNet50 | Transfer Learning | 98.67% | 97.56% | 97.63% | 97.56% | 97.54% |
| | Fine Tuning | 99.56% | 98.44% | 98.49% | 98.44% | 98.45% |
| MobileNet | Transfer Learning | 86.22% | 80.89% | 81.05% | 80.89% | 80.77% |
| | Fine Tuning | 91.56% | 92.22% | 92.27% | 92.22% | 92.21% |
| InceptionV3 | Transfer Learning | 68.44% | 68.67% | 68.38% | 68.67% | 68.18% |
| | Fine Tuning | 99.33% | 98.44% | 98.47% | 98.44% | 98.44% |
| Xception | Transfer Learning | 65.78% | 61.11% | 62.50% | 61.11% | 61.10% |
| | Fine Tuning | 98.67% | 97.33% | 97.38% | 97.33% | 97.33% |
| Our Model | Transfer Learning | 94.85% | 94.69% | 94.72% | 94.69% | 94.67% |
| | Fine Tuning | 99.49% | 98.97% | 98.98% | 98.97% | 98.97% |

Table IV illustrates a successful classification when our model experiences a dramatic rise in test accuracy of 98.97% of fine-tuning (i.e., a growth of 2.09%). Moreover, other scores such as prediction, recall, and f1 reached a high point. Thus, our model successfully demonstrated that the performance in classifying images in multiple classes (i.e., seven classes) is better than other models. However, EfficientNetB3 presents a decline in performance when working with seven classes. Despite ResNet50, MobileNet, InceptionV3, and Xception climb significantly. In particular, Xception has an increase of 11.75% when compared with Table III.

In addition, Fig. 12 and Fig. 13 show progress with nearly reached the highest point in a surprise outcome of validation accuracy = 99.49%. Moreover, training and validation loss decreased significantly and was achieved at 0.07. To describe more detail, Fig. 14 represents a confusion matrix for the

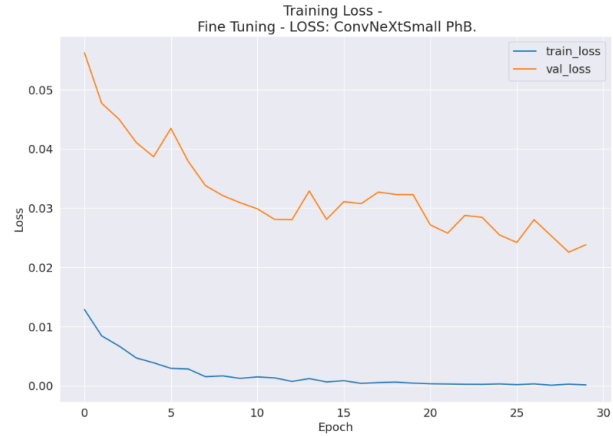


Fig. 7. Training loss and validation loss by fine-tuning of our model at scenario 1.

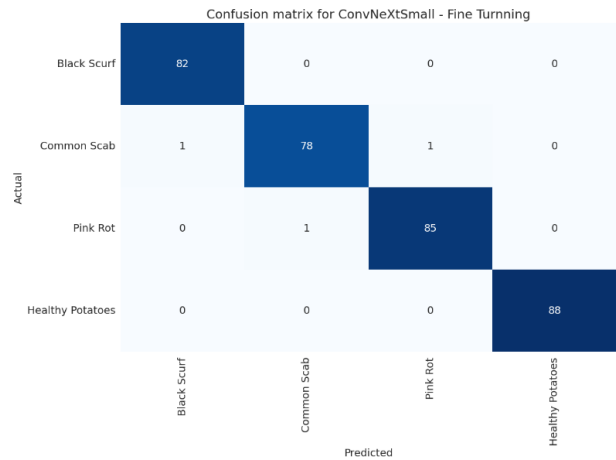


Fig. 8. Confusion matrix in fine-tuning for our model at scenario 1.

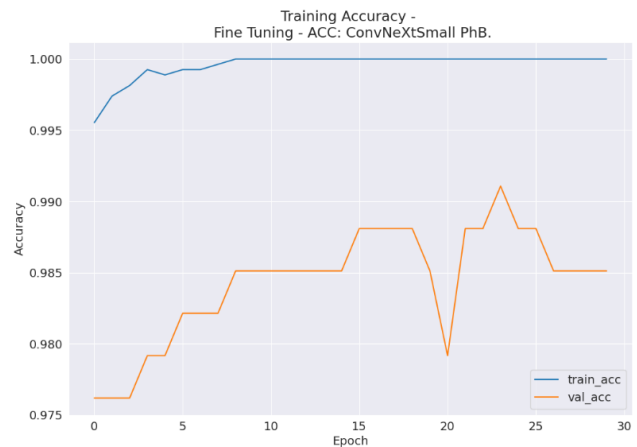


Fig. 9. Training accuracy and validation accuracy by fine-tuning of our model at scenario 2.

final result and helps the research article to have an overall assessment.

E. Scenario 4: the Result of Classifying Potato Diseases Into Seven Classes with ConvNeXt Model: Small, Tiny, and Large

TABLE V. THE ACCURACY OF CLASSIFYING POTATO DISEASE IMAGES INTO SEVEN CLASSES: HEALTHY, BLACK SCURF, COMMON SCAB, PINK ROT, BLACKLEG, DRY ROT, MISCELLANEOUS IN TRANSFER LEARNING AND FINE-TUNING, FOR EACH DEEP LEARNING MODEL

| Model | Phase | Valid acc | Test acc | Precision | Recall | F1 |
|----------------|-------------------|-----------|----------|-----------|--------|--------|
| ConvNeXt Large | Transfer Learning | 100.00% | 99.14% | 99.18% | 99.14% | 99.14% |
| | Fine Tuning | - | - | - | - | - |
| ConvNeXtTiny | Transfer Learning | 96.57% | 97.09% | 97.12% | 97.09% | 97.10% |
| | Fine Tuning | 97.43% | 97.60% | 97.60% | 97.60% | 97.60% |
| Our model | Transfer Learning | 94.85% | 94.69% | 94.72% | 94.69% | 94.67% |
| | Fine Tuning | 99.49% | 98.97% | 98.98% | 98.97% | 98.97% |

ConvNeXtLarger reaches the highest score in validation and test accuracy in Table V. Because it causes hardware overload and is too heavy for training small and medium datasets. Thus, this scenario points out that ConvNeXtLarger is not necessary for classifying this dataset and it can lead to a waste of resources and time to train the model. The customized ConvNeXtSmall model presents an effective and suitable classification although it is marginally lower than ConvNeXtLarger in transfer learning (i.e., lower 0.17% in test accuracy). In conclusion, the choice of models in the ConvNeXt family should be carefully considered because their performance may be very little different, although there are different requirements in terms of time and resources for training.

V. RESULTS AND COMPARISON

A. Results Explanation

Throughout scenarios 1, 2, and 3, our customized model presents effectiveness and sustainability when classifying many classes in Fig 15. Scenario 3 shows that test accuracy, precision, recall, and F1 score reached a surprise point (i.e., 99.49% in validation accuracy and 98.97% in test accuracy) in the seven potato disease classes classification. However, Scenarios 1 and 2 point out that in classifying a few of the classes the customized model worked unsuccessfully with the researcher’s desire although it still reached a high score (i.e., 99.11% in validation accuracy and 96.88% in test accuracy). These issues will be explored and improved in subsequent studies.

In addition, Fig. 16 illustrates ConvNeXt family performance between ConvNeXtLarge, ConvNeXtTiny, and Customized ConvNeXtSmall. Specifically, Our model used fewer resources and a shorter time for training the model in classifying seven classes which reached a surprise result. However, ConvNext Large achieved slightly higher results than can be expected but it used a higher resource and time of computer

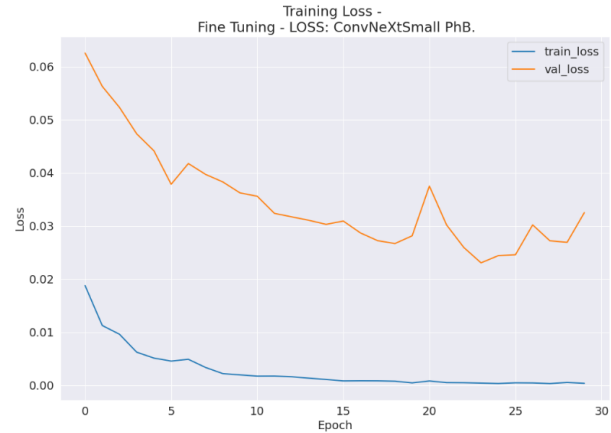


Fig. 10. Training loss and validation loss by fine-tuning of our model at scenario 2.

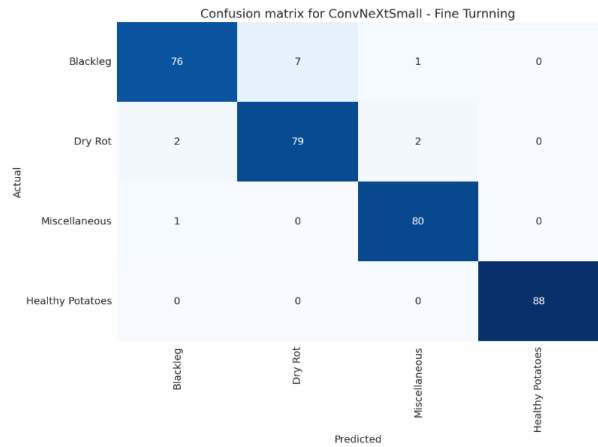


Fig. 11. Confusion matrix in fine-tuning for our model at scenario 2.

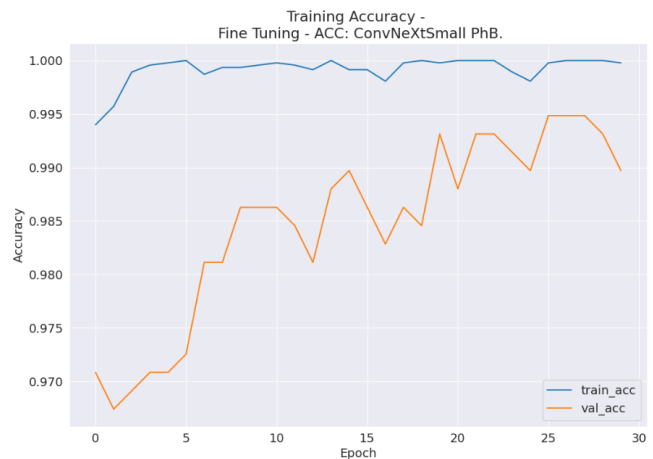


Fig. 12. Training accuracy and validation accuracy by fine-tuning of our model at scenario 3.



Fig. 13. Training loss and validation loss by fine-tuning of our model at scenario 3.

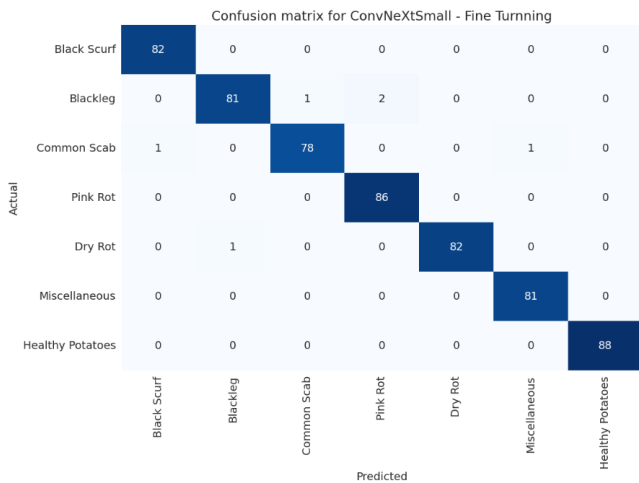


Fig. 14. Confusion matrix in fine-tuning for our model at scenario 3.

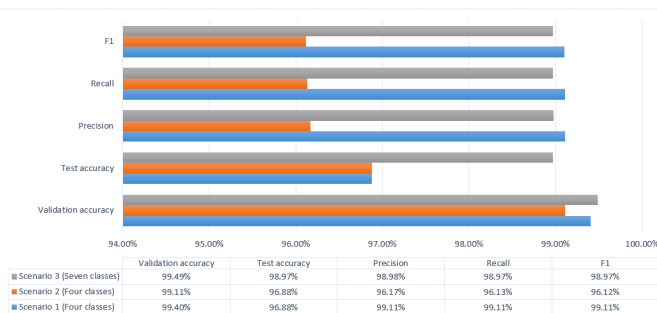


Fig. 15. The result of fine-tuning in our model.

for training and it can be crashed. As a result. Our model shows that it is an efficient and economical model for the classification of potato diseases.

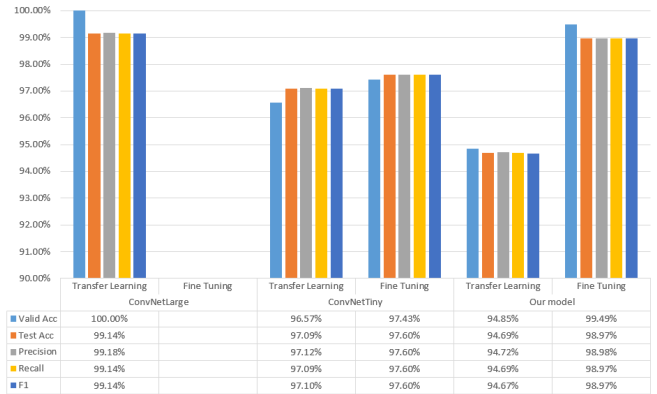


Fig. 16. The result of comparing in ConvNeXt family.

Besides, Grad-CAM for visual explanation and k-means clustering for image segmentation can significantly enhance the accuracy and interpretability of the models. Grad-CAM offers insights into the decision-making process of deep learning models by highlighting regions crucial for classification in Fig. 3, aiding in model validation and refinement. Meanwhile, in Fig. 4 k-means clustering was used for segmented potato images based on features like color and texture, enabling finer analysis and feature extraction for improved classification. Together, these techniques provide a deeper understanding of disease patterns and facilitate more precise identification and classification of potato diseases, crucial for effective agricultural management.

B. Comparison with others State-of-the-art Methods

To examine the accuracy of the proposed model that our article has just given out in the previous subsection, this subsection compares the accuracy score of the proposed model with other architectures. The result of getting the value of accuracy on the test set is illustrated in Table VI.

TABLE VI. COMPARISON WITH OTHERS STATE-OF-THE-ART METHODS

| Ref. | Proposed | Classes | Accuracy |
|-----------------------------------|----------------|-----------|----------------|
| Abeer A. Elsharif et al | CNN | 4 classes | 99.5% |
| Sofia Marino et al | FCN | 6 classes | F1 score = 84% |
| Qinghua Su et al | CNN | 5 classes | 91.6% |
| Chenglong Wang et al | RFCN ResNet101 | 3 classes | 98.7% |
| Kaili Zhang et al | VGG and U-Net | 5 classes | 97.55% |
| Khalid Hamza et al | CNN | 5 classes | 98% -100% |
| Ali Arshaghi et al | CNN | 5 classes | 98% -100% |
| Hyeon-Seung Lee et al | Mask R-CNN | - | 93% |
| Israa Mohammed Hassan et al | PDCNN | 4 classes | 91.3% |
| Proposed model (7 classes) | | | 98.97% |

Evaluating trade-offs according to task-specific priorities is necessary when comparing these measures. Precision and recall address more subtle elements, while accuracy offers a

wide overview. The F1 score balances their interplay to ensure a well-informed assessment of classification models within the parameters of specific objectives.

VI. CONCLUSION

In agricultural management, accurately identifying and classifying potato diseases is crucial for maintaining crop health and yield. Recently, a study showcased significant advancements in this domain, introducing a novel model for disease classification with impressive accuracy rates. This model effectively categorizes potato images into various disease classes, including healthy specimens and those affected by ailments like black scurf, common scab, pink rot, blackleg, dry rot, and miscellaneous conditions. Our new model achieved remarkable performance metrics, boasting a validation accuracy of 99.49%, test accuracy of 98.97%, and an F1 score of 98.97% across seven disease classes. The success of this model lies in its utilization of the ConvNeXt family, a type of deep-learning architecture specifically designed for image analysis. Notably, the study employed transfer learning, a technique where a pre-trained model (i.e., such as ConvNeXtSmall) is fine-tuned to adapt to a new dataset. By adding dense and dropout layers and adjusting certain parameters, researchers were able to enhance performance.

To improve the decision-making process, the study utilized GradCam. Specifically, GradCam generates heatmaps to highlight regions of the image that are influential in the model's classification decision, aiding in the interpretability and trustworthiness of the results. Moreover, the research incorporated k-means clustering, a popular unsupervised machine learning algorithm, to segment images. K-means clustering partitions data into clusters based on similarity, enabling researchers to identify distinct regions within potato images corresponding to different disease manifestations. This segmentation facilitates more granular analysis and targeted interventions for disease management.

However, there are limitations to be solved. One such limitation is the reliance on the quality and diversity of the dataset. Improving data collection processes and expanding the dataset to encompass a wider range of potato diseases and variations in environmental conditions will be paramount for enhancing model robustness and generalizability. Looking ahead, future work will focus on further refining the model through improved data preparation techniques and leveraging advanced visualization methods. Additionally, expanding the dataset will be essential for accommodating the complexities and nuances inherent in real-world agricultural settings. By continually refining and enhancing the model, this research aims to contribute significantly to the advancement of potato disease detection and agricultural management practices.

In conclusion, the integration of fine-tuning, GradCam, and k-means clustering has propelled the efficacy of potato disease classification models. With ongoing efforts to overcome limitations and refine methodologies, this research holds promise for revolutionizing disease management strategies in agriculture.

ACKNOWLEDGMENT

Luong Hoang Huong was funded by the Vingroup Innovation Foundation (VINIF) 's Master, Ph.D. Scholarship Programme, code VINIF.2023.TS.049.

We would like to extend our heartfelt gratitude to Hao Van Tran, and Phuc Tan Huynh for their invaluable contributions to this project. Their dedication, expertise, and unwavering support have been instrumental in its success.

REFERENCES

- [1] M. E. Cahskan, A. Bakhsh, and K. Jabran, *Potato production worldwide*. Academic Press, 2022.
- [2] E. Soare and I.-A. Chiurciu, "Study on the dynamics of potato production and worldwide trading during the period 2012-2019," *Scientific Papers Series Management, Economic Engineering in Agriculture and Rural Development*, vol. 21, 2021.
- [3] J.-P. Goffart, A. Haverkort, M. Storey, N. Haase, M. Martin, P. Lebrun, D. Ryckmans, D. Florins, and K. Demeulemeester, "Potato production in northwestern europe (germany, france, the netherlands, united kingdom, belgium): characteristics, issues, challenges and opportunities," *Potato Research*, vol. 65, no. 3, pp. 503–547, 2022.
- [4] A. Rana, V. Dua, S. Chauhan, and J. Sharma, "Climate change and potato productivity in punjab—impacts and adaptation," *Potato Research*, vol. 63, pp. 597–613, 2020.
- [5] M. Abdolmaleky, K. N. Mahdei, and P. Nejatian, "Environmental sustainability assessment: Potato production in western iran," *Process Integration and Optimization for Sustainability*, vol. 6, no. 4, pp. 1063–1073, 2022.
- [6] M. Kolychikhina, O. Beloshapkina, and C. Phiri, "Change in potato productivity under the impact of viral diseases," vol. 663, no. 1, p. 012035, 2021.
- [7] M. Salimzyanov, V. Pervushin, R. Shakirov, and M. Kalimullin, "Improvement of technology and machines for growing potatoes in agriculture," *technology*, vol. 4, p. 5, 2020.
- [8] M. del Mar Martínez-Prada, S. J. Curtin, and J. J. Gutiérrez-González, "Potato improvement through genetic engineering," *GM Crops & Food*, vol. 12, no. 1, pp. 479–496, 2021.
- [9] H. L. Duc, T. T. Minh, K. V. Hong, and H. L. Hoang, "84 birds classification using transfer learning and efficientnetb2," in *International Conference on Future Data and Security Engineering*. Springer, 2022, pp. 698–705.
- [10] K. V. Hong, T. T. Minh, H. L. Duc, N. T. Nhat, and H. L. Hoang, "104 fruits classification using transfer learning and densenet201 fine-tuning," in *Computational Intelligence in Security for Information Systems Conference*. Springer, 2022, pp. 160–170.
- [11] K. D. D. Le, H. H. Luong, and H. T. Nguyen, "Patient classification based on symptoms using machine learning algorithms supporting hospital admission," in *Nature of Computation and Communication: 7th EAI International Conference, ICTCC 2021, Virtual Event, October 28–29, 2021, Proceedings 7*. Springer, 2021, pp. 40–50.
- [12] H. T. Nguyen, N. K. T. Nguyen, C. L. H. Tran, and H. H. Luong, "Effects evaluation of data augmentation techniques on common seafood types classification tasks," in *Biomedical and Other Applications of Soft Computing*. Springer, 2022, pp. 213–223.
- [13] H. T. Nguyen, Q. T. Quach, C. L. H. Tran, and H. H. Luong, "Deep learning architectures extended from transfer learning for classification of rice leaf diseases," in *International Conference on Industrial, Engineering and Other Applications of Applied Intelligent Systems*. Springer, 2022, pp. 785–796.
- [14] A. Khorramifar, M. Rasekh, H. Karami, U. Malaga-Toboła, and M. Ganzar, "A machine learning method for classification and identification of potato cultivars based on the reaction of mos type sensor-array," *Sensors*, vol. 21, no. 17, p. 5836, 2021.
- [15] S. Sabzi, Y. Abbaspour-Gilandeh, and J. I. Arribas, "An automatic visible-range video weed detection, segmentation and classification prototype in potato field," *Heliyon*, vol. 6, no. 5, 2020.
- [16] Y. Yang, X. Zhao, M. Huang, X. Wang, and Q. Zhu, "Multispectral image based germination detection of potato by using supervised multiple threshold segmentation model and canny edge detector," *Computers and Electronics in Agriculture*, vol. 182, p. 106041, 2021.
- [17] S. Yao, Q. Kang, M. Zhou, M. J. Rawa, and A. Abusorrah, "A survey of transfer learning for machinery diagnostics and prognostics," *Artificial Intelligence Review*, vol. 56, no. 4, pp. 2871–2922, 2023.

- [18] F. Zhuang, Z. Qi, K. Duan, D. Xi, Y. Zhu, H. Zhu, H. Xiong, and Q. He, "A comprehensive survey on transfer learning," *Proceedings of the IEEE*, vol. 109, no. 1, pp. 43–76, 2020.
- [19] Z. Zhu, K. Lin, A. K. Jain, and J. Zhou, "Transfer learning in deep reinforcement learning: A survey," *IEEE Transactions on Pattern Analysis and Machine Intelligence*, 2023.
- [20] N. Ruiz, Y. Li, V. Jampani, Y. Pritch, M. Rubinstein, and K. Aberman, "Dreambooth: Fine tuning text-to-image diffusion models for subject-driven generation," pp. 22 500–22 510, 2023.
- [21] W. Chen, Y. Liu, W. Wang, E. M. Bakker, T. Georgiou, P. Fieguth, L. Liu, and M. S. Lew, "Deep learning for instance retrieval: A survey," *IEEE Transactions on Pattern Analysis and Machine Intelligence*, 2022.
- [22] H. Rasheed, M. U. Khattak, M. Maaz, S. Khan, and F. S. Khan, "Fine-tuned clip models are efficient video learners," in *Proceedings of the IEEE/CVF Conference on Computer Vision and Pattern Recognition*, 2023, pp. 6545–6554.
- [23] A. A. Elsharif, I. M. Dheir, A. S. A. Mettleq, and S. S. Abu-Naser, "Potato classification using deep learning," *International Journal of Academic Pedagogical Research (IJAPR)*, vol. 3, no. 12, pp. 1–8, 2020.
- [24] S. Marino, P. Beausery, and A. Smolarz, "Unsupervised adversarial deep domain adaptation method for potato defects classification," *Computers and Electronics in Agriculture*, vol. 174, p. 105501, 2020.
- [25] Q. Su, N. Kondo, D. F. Al Riza, and H. Habaragamuwa, "Potato quality grading based on depth imaging and convolutional neural network," *Journal of Food Quality*, vol. 2020, pp. 1–9, 2020.
- [26] C. Wang and Z. Xiao, "Potato surface defect detection based on deep transfer learning," *Agriculture*, vol. 11, no. 9, 2021. [Online]. Available: <https://www.mdpi.com/2077-0472/11/9/863>
- [27] K. Zhang, S. Wang, Y. Hu, H. Yang, T. Guo, and X. Yi, "Evaluation method of potato storage external defects based on improved u-net," *Agronomy*, vol. 13, no. 10, p. 2503, 2023.
- [28] K. Hamza, S. un Nisa, and G. Irshad, "A review on potato disease detection and classification by exploiting deep learning techniques," *Journal of Agriculture and Veterinary Science*, vol. 1, no. 2, pp. 81–88, 2022.
- [29] A. Arshaghi, M. Ashourian, and L. Ghabeli, "Potato diseases detection and classification using deep learning methods," *Multimedia Tools and Applications*, vol. 82, 07 2022.
- [30] H.-S. Lee and B.-S. Shin, "Potato detection and segmentation based on mask r-cnn," *Journal of Biosystems Engineering*, vol. 45, pp. 233–238, 2020.
- [31] I. Hassoon, S. Kassir, and M. Riyadh, "Pdcnn: Framework for potato diseases classification based on feed forward neural network," *Baghdad Science Journal*, vol. 18, p. 1012, 06 2021.
- [32] R. A. Sholihati, I. A. Sulistijono, A. Risnumawan, and E. Kusumawati, "Potato leaf disease classification using deep learning approach," pp. 392–397, 2020.
- [33] A. Singh and H. Kaur, "Potato plant leaves disease detection and classification using machine learning methodologies," vol. 1022, no. 1, p. 012121, 2021.
- [34] R. Mahum, H. Munir, Z.-U.-N. Mughal, M. Awais, F. Sher Khan, M. Saqlain, S. Mahamad, and I. Tlili, "A novel framework for potato leaf disease detection using an efficient deep learning model," *Human and Ecological Risk Assessment: An International Journal*, vol. 29, no. 2, pp. 303–326, 2023.
- [35] D. Tiwari, M. Ashish, N. Gangwar, A. Sharma, S. Patel, and S. Bhardwaj, "Potato leaf diseases detection using deep learning," pp. 461–466, 2020.
- [36] M. A. Iqbal and K. H. Talukder, "Detection of potato disease using image segmentation and machine learning," pp. 43–47, 2020.
- [37] K. K. Chakraborty, R. Mukherjee, C. Chakraborty, and K. Bora, "Automated recognition of optical image based potato leaf blight diseases using deep learning," *Physiological and Molecular Plant Pathology*, vol. 117, p. 101781, 2022.
- [38] A. Taner, M. Mengstu, K. Selvi, H. Duran, I. Gür, and N. Ungureanu, "Apple varieties classification using deep features and machine learning," *Agriculture*, vol. 14, p. 252, 02 2024.
- [39] D. Asriny, S. Rani, and A. F. Hidayatullah, "Orange fruit images classification using convolutional neural networks," *IOP Conference Series: Materials Science and Engineering*, vol. 803, p. 012020, 05 2020.

Dynamic Task Offloading Optimization in Mobile Edge Computing Systems with Time-Varying Workloads Using Improved Particle Swarm Optimization

Mohammad Asique E Rasool¹, Anoop Kumar², Asharul Islam³

Department of Computer Science, College of Computing and Mathematics, Banasthali Vidyapith, Rajasthan, India^{1,2}

Department of Information Systems, College of Computer Science, King Khalid University, Abha, Saudi Arabia³

Abstract—Mobile edge computing (MEC) enables offloading of compute-intensive and latency-sensitive tasks from resource-constrained mobile devices to servers at the network edge. This paper considers the dynamic optimization of task offloading in multi-user multi-server MEC systems with time-varying task workloads. The arrival times and computational demands of tasks are modeled as stochastic processes. The goal is to minimize the average task delay by optimal dynamic server selection over time. A particle swarm optimization (PSO) based algorithm is proposed that makes efficient offloading decisions in each time slot based on newly arrived tasks and pending workload across servers. The PSO-based policy is shown to outperform heuristics like genetic algorithms and simulated annealing in terms of adaptability to workload fluctuations and spikes. Experiments under varying task arrival rates demonstrate PSO's capability to dynamically optimize time-averaged delay and energy costs through joint optimization of server selection and resource allocation. The proposed techniques provide a practical and efficient dynamic load balancing mechanism for real-time MEC systems with variable workloads.

Keywords—Particle Swarm Optimization (PSO); Mobile Edge Computing (MEC); Multi-User Multi-Server systems; dynamic load balancing

I. INTRODUCTION

Mobile edge computing (MEC) has proven to be an efficacious architecture as shown in Fig. 1 for enabling compute-intensive and latency-critical applications via offloading of computational tasks from resource-limited mobile devices to servers situated at the edge of the network. However, prior research on MEC task offloading has predominantly presumed a priori knowledge of static workloads.

In actuality, the arrival times and computational requirements of tasks tend to demonstrate dynamic fluctuations over time. As an illustration, workloads for augmented reality and natural language processing applications often manifest sporadic and variable characteristics contingent on user behaviors. Moreover, task complexity itself may exhibit volatility depending on contextual factors. This necessitates the development of dynamic and online task offloading algorithms with the capability to adapt to variable workloads.

This paper investigates the scenario of dynamic task offloading within multi-user, multi-server MEC systems. Stochastic processes are utilized to model the random arrival

times and computational demands of tasks. Specifically, inter-arrival times are sampled from an exponential distribution while computational needs are modeled as a random variable.

A temporal dimension T is introduced and discretized into time slots $t = 1, 2, 3$, and so forth. At each time slot, new tasks arrive probabilistically based on the stochastic model, prompting the optimization algorithm to allocate resources in a dynamic manner. The optimization cost function is constructed to jointly minimize server selection and task scheduling time. Tradeoffs such as deferred execution versus instantaneous processing are assessed. To constrain complexity, the optimization is restricted to newly arrived tasks and a limited backlog from prior time steps.

II. LITERATURE SURVEY

Numerous studies have examined methodologies for cost-efficient computing and service delivery in mobile cloud computing (MCC) architectures, predominantly in developed countries with limited focus on developing nations. Early works proposed cloudlet-based architectures to address MCC challenges, but faced constraints like limited WiFi coverage [1]. Fog computing architectures were presented to enable computations at the edge [2], but quality of experience (QoE) guarantees remained difficult. MCC architectures integrating cloud computing into mobile environments were investigated [23], but still faced hurdles like high latency, bandwidth utilization, and data transportation costs.

To overcome limitations of centralized clouds (e.g. congestion, reduced robustness [3]) and distributed clouds (e.g. complexity, management issues [4]), architectures like edge cloud computing [5] and multi-access edge computing (MEC) [6, 7] have emerged. These aim to meet requirements of Internet of Things (IoT) applications such as low latency, cost-efficiency, and efficient resource usage.

Energy consumption and latency have been widely recognized as key metrics for evaluating QoE in MEC systems. Dynamic offloading and resource allocation models based on stochastic optimization have been proposed to reduce energy usage [8, 9]. Joint optimization strategies accounting for energy, latency and resource constraints have also been studied for multi-user MEC networks [10, 11]. Research has further

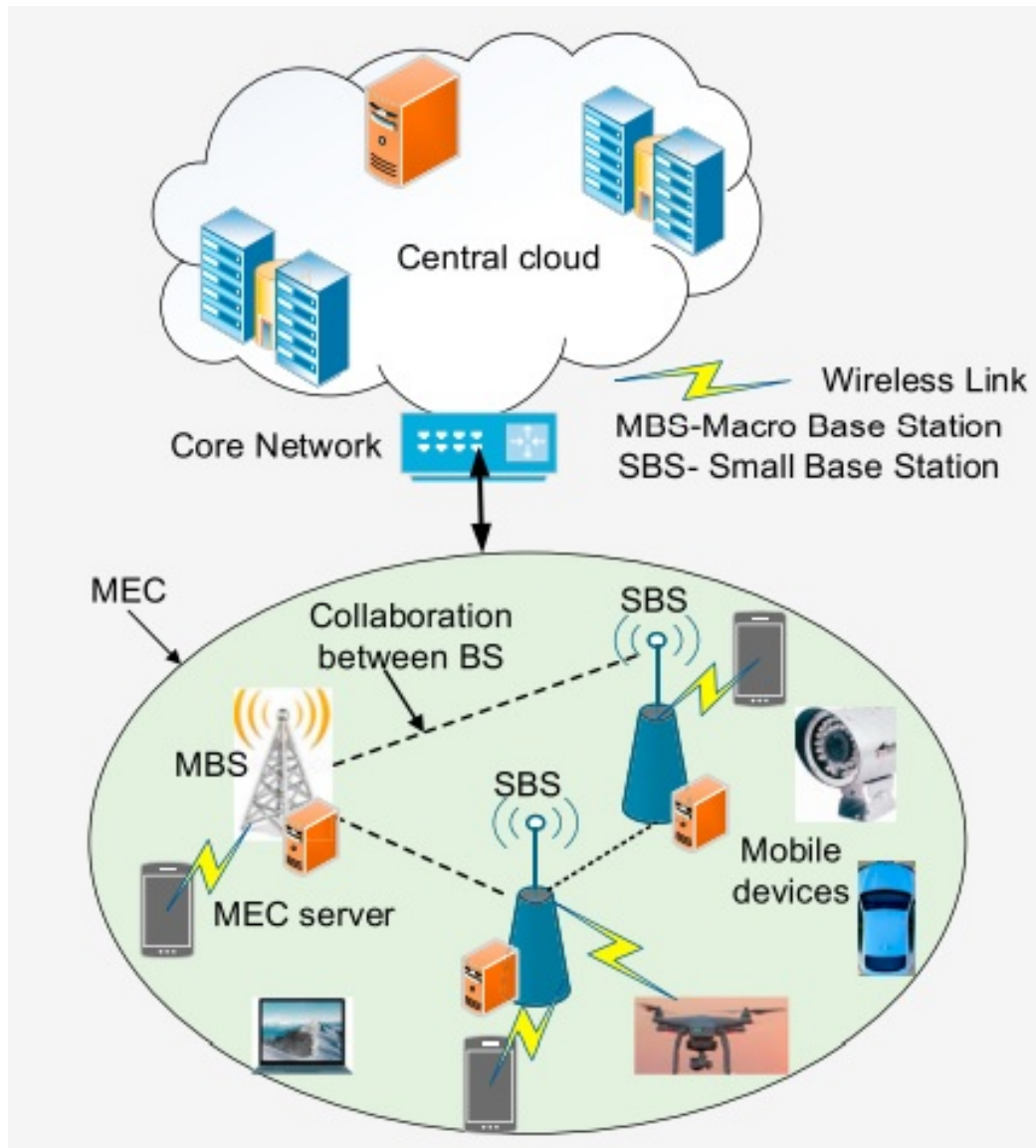


Fig. 1. Overview of mobile edge computing architecture.

focused on improving QoE for resource-constrained devices via combined offloading and resource provisioning [12-14], and investigating energy-latency tradeoffs [15, 16].

A cooperative approach among multiple MEC servers or between MEC and the cloud has shown considerable performance gains over isolated operation [17]. Energy-efficient task scheduling and resource allocation schemes have been developed using optimization frameworks, significantly reducing mobile energy utilization [18, 19]. Wireless power transfer has also been incorporated into MEC to address limited battery capacities [20, 21].

This work differs from prior art in three key aspects - it considers MEC capacity constraints during optimization, focuses on cooperative offloading between MEC servers for enhanced capacity, and utilizes intelligent swarm techniques for decentralized operation. The proposed strategy aims to meet energy and latency goals through efficient resource

allocation, cooperatively leveraging distributed MEC servers.

Mobile edge computing (MEC) has emerged as a promising architecture for enabling latency-sensitive and compute-intensive applications, by offloading computational tasks from resource-constrained mobile devices to servers at the edge of the network [22]. Initial research on MEC task offloading focused on static workload models known a priori [23].

Various stochastic processes have been utilized to capture the randomness in task arrivals and computational requirements. Poisson processes are commonly used for modeling task arrival times [24], while computational intensities are modeled via exponential distributions [25].

While progress has been made in dynamic offloading, most works make simplifying assumptions about network models and workload characterization [26].

III. PROBLEM DEFINITION

We consider a mobile edge computing (MEC) system comprising of M mobile users and N edge servers. The mobile users have computational tasks that need to be processed within certain latency constraints. However, the users have limited computational resources and cannot process all tasks locally.

The edge servers, situated at the edge of the network, can provide computational resources to offload and process tasks from the mobile users. However, the servers also have limited capacities. The objective is to develop an efficient dynamic task offloading strategy that minimizes the overall latency of processing all tasks under fluctuating workloads.

We make the following assumptions:

The tasks arrive at each mobile user randomly following a stochastic process. We model the inter-arrival times using an exponential distribution with rate λ .

The computational requirements of each task in terms of CPU cycles is also modeled as a random variable following an exponential distribution with mean μ .

The tasks cannot be parallelized and have to be processed sequentially either locally on the device or offloaded to one of the edge servers.

The edge servers have different computational capabilities in terms of CPU speed and available memory.

The latency for a task consists of transmission delay to offload, queuing delay, and computational delay.

The network links between the mobile users and edge servers have time-varying speeds modeled as a random process.

The key challenge is to dynamically decide which tasks should be offloaded to which edge server or processed locally in each time slot. The goal is to minimize the average latency per task across all arriving tasks over time. We formulate this as a stochastic optimization problem and propose a dynamic offloading algorithm using particle swarm optimization to efficiently solve it.

A. Problem Formulation

The objective is to minimize the overall energy cost while satisfying capacity and delay constraints. The optimization problem is formulated as:

$$\text{minimize } \sum_{k=1}^N \sum_{i=1}^Q x_k E_L + \sum_{s=1}^S y_k E_{off} \quad (1)$$

subject to

$$\sum_{k=1}^N x_k = 1, \quad \forall k \in J \quad (2)$$

$$\sum_{k=1}^N y_k = 1, \quad \forall k \in J \quad (3)$$

$$\sum_{k=1}^N \sum_{s=1}^S x_k \alpha_s \leq K \quad (4)$$

$$\sum_{\omega=1}^F B_{k\omega} \leq B, \quad \forall k \in J \quad (5)$$

$$D_{off} \leq D_k \quad (6)$$

Where:

x_k = Local execution control variable

y_k = Offloading control variable

E_L = Energy for local execution

E_{off} = Energy for offloaded execution

α_s = Resource allocated to task k at server s

K = Total computation capacity

$B_{k\omega}$ = Sub-carrier bandwidth for task k

B = Total bandwidth capacity

D_{off} = Offloaded task delay

D_k = Task deadline

The objective function (1) minimizes the total energy consumption. Constraints (2)-(3) ensure feasible offloading policy. Constraints (4)-(5) ensure resource capacities are not violated. Constraint (6) guarantees task delay meets the deadline.

B. Time Delay Model

We model the total latency experienced by each task to comprise three components:

Transmission delay (Td): This is the delay to offload the task input data to the edge server over the wireless network. It depends on the task input data size D (in bits), the time-varying wireless transmission rate $R(t)$ (in bits/sec), and the edge server selected.

$$T_d = \frac{D}{R(t)}$$

Queueing delay (Tq): This is the waiting time experienced by the task in the queue at the edge server before processing begins. It depends on the current load and waiting tasks at the server.

$$T_q = f(\text{Waiting tasks, Server load})$$

Computational delay (Tc): This is the time taken to actually process the task once it starts execution at the server. It depends

on the task's computational complexity in terms of CPU cycles C , and the server's CPU speed S (in cycles/sec).

$$T_c = \frac{C}{S}$$

The total latency is the sum of these components:

$$T_{\text{total}} = T_d + T_q + T_c$$

The transmission rate $R(t)$ and server load vary dynamically over time affecting T_d , T_q , and T_c . The dynamic offloading algorithm has to account for these variations and unpredictability in the delay components when making offloading decisions. The goal is to minimize the long-term average $E[T_{\text{total}}]$ across all arriving tasks.

We capture the stochastic nature of the delay components by modeling $R(t)$ and server load as random processes. T_c can vary across servers. The key idea is to leverage time-averaged delay metrics rather than one-shot optimization, to account for fluctuating system dynamics.

C. Calculation Model

The dynamic task offloading problem can be formulated as a stochastic optimization problem with the goal of minimizing the average total delay per task.

Let $x_{it} \in \{0, 1\}$ denote the offloading decision for task i arriving at time t , where $x_{it} = 0$ denotes processing locally and $x_{it} = 1$ denotes offloading to an edge server.

The total delay for task i is:

$$T_i(x_{it}) = T_{di}(x_{it}) + T_{qi}(x_{it}) + T_{ci}(x_{it}) \quad (7)$$

where the components depend on x_{it} as discussed in the Time Delay Model section.

The long-term time-averaged delay is:

$$E[T_{\text{total}}] = \lim_{N \rightarrow \infty} \frac{1}{N} \sum_{i=1}^N T_i(x_{it}) \quad (8)$$

The dynamic offloading algorithm decides x_{it} at each time t to minimize $E[T_{\text{total}}]$, subject to:

Edge server computational constraints

Mobile device energy constraints

Task dependencies

To solve this stochastic optimization, we model the system as a Markov Decision Process (MDP). The MDP states capture features like current loads, wireless network conditions, unfinished tasks etc. Actions correspond to offloading decisions for newly arriving tasks. The policy maps states to actions with the goal of minimizing long-term delay.

We propose a Particle Swarm Optimization (PSO) based metaheuristic to efficiently search the policy space for near-optimal solutions. PSO is well-suited for high dimensionality and can balance optimality vs. speed. We empirically compare against greedy methods and model-free deep reinforcement learning.

IV. ALGORITHM

We propose a dynamic offloading algorithm based on Particle Swarm Optimization (PSO) to efficiently solve the stochastic optimization problem formulated in the previous section. We propose a dynamic offloading algorithm based on Particle Swarm Optimization (PSO) to efficiently solve the stochastic optimization problem formulated previously.

PSO is a population-based metaheuristic technique inspired by swarm intelligence and bird flocking behaviors. It uses a population of particles representing candidate solutions which move around the search space to find the optimal solution. Each particle has a position representing the solution, a velocity indicating the direction and distance of movement, and a fitness score evaluating solution quality. Particles also have memory of their individual best position seen and know the global best position among the whole swarm.

In each iteration, particle velocities and positions get updated based on cognitive and social factors which guide the movement towards more promising search areas over time. The cognitive factor pulls the particle towards its individual best while the social factor pulls it towards the global best position. This enables balancing of exploration and exploitation ability. By sharing information via the global best, particles gradually cluster around optimal regions leading to convergence.

For our dynamic offloading problem, each particle represents a candidate offloading policy mapping system states to offloading decisions. The particle position encodes this policy. Velocity governs the rate of change and exploration of policies. The fitness score evaluates the policy by simulating long-term average task delay. PSO searches the policy space to find mappings that minimize expected delay over time.

The algorithm iterates by updating particle states based on personal and global best experiences. It balances local and global search, gradually refining policies through generations. It terminates when the maximum iterations are reached or when the global best fitness stagnates, indicating convergence to near-optimal dynamic offloading decisions.

A. Particle Representation

Each particle in the swarm represents a candidate policy for dynamic offloading. It maps system states to offloading decisions for incoming tasks.

We use a vector to encode the particle. Each element represents the edge server selected for a specific system state, with 0 denoting local processing. The dimensionality equals the number of discretized system states.

For example, a particle with 5 elements as $[2 \ 0 \ 4 \ 1 \ 0]$ means:

In system state 1, offload to edge server 2

In state 2, process locally

In state 3, offload to edge server 4 and so on.

Particle velocities represent the rate of change of the policy space exploration, similar to cognitive and social learning rates in PSO.

B. Fitness Evaluation

The fitness function evaluates the long-term average delay achieved by a particle's offloading policy using the system model simulated over many time steps. Lower delays correspond to higher fitness.

The PSO optimizes this fitness over iterations to converge to policies with minimized expected delay, achieving the overall optimization objective.

$$T_j^i = \frac{D_i \cdot C_i}{C_{s,j}} + \frac{D_i \cdot C_i}{W \cdot \left(1 + \frac{S_i \cdot A_{i,j}}{W \cdot N_0}\right)} \quad (9)$$

$$E_j^i = E_j^{\text{calc},i} + E_j^{\text{tran},i} \quad (10)$$

$$E_j^{\text{calc},i} = R_i \cdot U^2 \cdot C_{s,j} \cdot D_i \cdot C_i \quad (11)$$

$$E_j^{\text{tran},i} = S_i \cdot T_j^{\text{tran},i} \quad (12)$$

$$E_j^i = R_i \cdot U^2 \cdot C_{s,j} \cdot D_i \cdot C_i + \frac{D_i \cdot C_i}{r_{i,j}} \cdot S_i \quad (13)$$

$$F(X) = \sum_{j=1}^N \sum_{i=1}^M T_j^i + \text{penalty}(X) \quad (14)$$

$$\text{penalty}(X) = g \cdot \sum_{j=1}^N \sum_{i=1}^M (E_j^i - E_j^{\text{max}}) \quad (15)$$

$$F(X) = a \cdot \sum_{j=1}^N \sum_{i=1}^M T_j^i + b \cdot g \cdot \sum_{j=1}^N \sum_{i=1}^M (E_j^i - E_j^{\text{max}}) \quad (16)$$

The algorithm terminates when the maximum iterations are reached or the change in best fitness is negligible. The gbest particle represents the final dynamic offloading policy learned.

$$R_\eta = B \log_2 \left(1 + \frac{P_\eta \psi_\eta}{\sum_{k \in J} x_k P_k \psi_k + \sigma^2} \right) \quad (17)$$

$$R_s = B \log_2 \left(1 + \frac{P_s \psi_s}{\sum_{k \in J} y_k P_k \psi_k + \sigma^2} \right) \quad (18)$$

$$D_{d,s} = \frac{S_k}{R_\eta} \quad (19)$$

$$D_{qo} = \frac{S_k}{\omega} \quad (20)$$

$$D_{s,j} = \sum_{k=1}^N y_k \frac{S_k}{R_s} \quad (21)$$

$$D_p = \sum_{k=1}^N x_k \frac{c_k}{f_{ser}} \quad (22)$$

$$D_{off} = D_{d,s} + D_{qo} + D_{s,j} + D_p \quad (23)$$

$$E_{d,s} = P_{d,s} D_{d,s} = \frac{P_{d,s} S_k}{R_\eta} \quad (24)$$

$$E_{s,j} = P_{s,j} \frac{S_k}{R_s} \quad (25)$$

$$E_e = E_{ser} (f_{ser})^2 \frac{c_k}{f_{ser}} \quad (26)$$

$$E_{off} = E_{d,s} + E_{s,j} + E_e \quad (27)$$

Where:

R_η = Data transmission rate of device η

R_s = Data transmission rate between servers s and h

$D_{d,s}$ = Delay for task transmission from device to server

D_{qo} = Overhead delay

$D_{s,j}$ = Delay for task forwarded from server s to j

D_p = Execution delay

D_{off} = Total delay for offloaded task

$E_{d,s}$ = Energy for task transmission

$E_{s,j}$ = Energy for inter-server communication

E_e = Execution energy cost

E_{off} = Total energy cost

V. SYSTEM MODEL

We consider an MEC system with M mobile users and N edge servers situated at the network edge. The mobile users have computational tasks that arrive randomly over time. The tasks cannot be processed locally due to resource constraints and need to be offloaded to the edge servers. Each edge server has capabilities C_j in terms of CPU speed and memory availability.

Task Arrival Model: The tasks arrive at each mobile user following a Poisson process with rate λ . The inter-arrival times are modeled via an exponential distribution: $f(x) = \lambda e^{-\lambda x}$. This captures the stochastic nature of task arrivals.

Task Requirement Model: Each task i is characterized by the computational complexity C_i in terms of the number of CPU cycles required for processing the task. We model C_i

as an exponential random variable $C_i \sim \text{Exp}(\mu)$ with mean μ cycles. This models the variability in computational needs of different tasks.

Network Model: The wireless network connecting the mobile users to the edge servers has time-varying capacity. The transmission rate $R(t)$ at time t is modeled as a random process with mean R . This accounts for fluctuations in the wireless channel bandwidth.

Offloading Decision: At arrival of each task i , the dynamic offloading algorithm has to take a binary decision $x_i \in \{0, 1\}$ whether to process the task locally ($x_i = 0$) or offload it to an edge server ($x_i = 1$). The goal is to minimize the long-term average delay across all arriving tasks over time.

Optimization Objective: $\min E[T_{\text{total}}]$

where $T_{\text{total}} = T_d + T_q + T_c$

Subject to: Edge server computational constraints
Mobile device energy constraints
Task dependency constraints

This stochastic optimization problem is solved using the proposed PSO-based dynamic offloading algorithm.

Particle Swarm Optimization

Particle swarm optimization (PSO) is a population-based stochastic optimization technique inspired by the social behavior of bird flocks. Particles in the swarm represent candidate solutions that move through the search space to find the global optimum.

In PSO, each particle maintains a position vector X_i , velocity vector V_i , personal best $P_{\text{best}i}$ and has access to the global best G_{best} . The position and velocity are updated as:

$$V_i = V_i + c_1 \text{rand}() (P_{\text{best}i} - X_i) + c_2 \text{rand}() (G_{\text{best}} - X_i) \\ X_i = X_i + V_i$$

where c_1 and c_2 are cognitive and social factors, and $\text{rand}()$ introduces randomness. This enables particles to explore the search space balancing individual and group experience. The fitness evaluation guides particles toward optimal regions.

For the dynamic offloading problem, each particle represents an offloading policy mapping system states to offloading decisions. The fitness is the long-term average delay achieved by the policy. Lower delays correspond to higher fitness. PSO finds policies that minimize expected delay through position updates over iterations.

We use a vector representation for particles. Velocity controls policy space exploration. Fitness evaluation uses the system model simulated over time. Particles are updated until convergence or maximum iterations. The final G_{best} particle represents the optimal dynamic offloading policy.

PSO advantages include fast convergence, minimal parameter tuning, and suitability for high-dimensional nonlinear environments like dynamic offloading. It balances exploration and exploitation to find optimal solutions.

Consider a network model with Q mobile devices (MDs) having N tasks, denoted by the set $J = \{1, 2, \dots, N\}$. Each task k is characterized by:

s_k (in bits): Input data size c_k (in MIPS): Computational intensity D_k (in seconds): Maximum tolerable delay Let

$\Phi = \{1, 2, \dots, S\}$ be the set of S MEC servers in the collaborative domain with total computation capacity K and bandwidth capacity B .

Let α_s be the portion of resources allocated to task k at server $s \in S$.

A. Communication Model

We consider a network model with Q mobile devices (MDs) having N tasks. Each task k is characterized by its input data size s_k (in bits) and computational intensity c_k (in MIPS). Let D_k (in seconds) denote the maximum tolerable delay for task k . The system comprises S MEC servers in the collaborative domain with total computation capacity K and bandwidth capacity B . Let α_s represent the portion of resources allocated to task k at server s .

The transmission rate R_η of MD η communicating with the base station depends on parameters like transmission power P_η , channel gain ψ_η , interference from other MDs executing tasks locally, and noise power. Offloading decisions are represented by a binary variable x_k indicating if task k is executed locally or offloaded.

Similarly, the transmission rate R_s between servers s and h depends on server transmission power P_s , channel gain ψ_s , interference from other offloaded tasks being forwarded between servers, and noise power. Offloading decisions are captured by a binary variable y_k indicating if task k is forwarded to another server after initial offload.

$$R_\eta = B \log_2 \left(1 + \frac{P_\eta \psi_\eta}{\sum_{k \in J} x_k P_k \psi_k + \sigma^2} \right) \quad (28)$$

Where $x_k \in \{0, 1\}$ indicates if task k is executed locally.

Let P_s and ψ_s be the transmission power and channel gain of server s . The transmission rate between servers s and h is:

$$R_s = B \log_2 \left(1 + \frac{P_s \psi_s}{\sum_{k \in J} y_k P_k \psi_k + \sigma^2} \right) \quad (29)$$

Where $y_k \in \{0, 1\}$ indicates if task k is forwarded to another server.

B. Service Utility Cost Models

For local execution, the delay and energy costs are:

$$D_L = \frac{C_k}{f_{dev}} \quad E_L = E_d (f_{dev})^2 C_k \quad (2)$$

Where f_{dev} is the MD's CPU frequency and E_d is the energy per CPU cycle.

For tasks executed locally on the mobile device, the delay cost is modeled as the task's computational intensity c_k divided by the device's CPU frequency f_{dev} . The energy cost is the product of the energy per CPU cycle E_d and the square of CPU frequency f_{dev} times the computational intensity c_k .

For offloaded tasks, the various delay components are modeled conceptually without equations. The transmission delay $D_{d,s}$ depends on the task's input data size s_k and the wireless transmission rate R_η . The queuing overhead delay D_{qo} depends on s_k and a weighting parameter ω_k . The server-to-server forwarding delay $D_{s,j}$ depends on s_k and the inter-server transmission rate R_s if task forwarding is involved. The execution delay D_p on the server side depends on c_k and the server CPU frequency f_{ser} . The total offloading delay is the sum of these individual delay components.

The data transmission energy $E_{d,s}$ from device to server depends on transmission power and R_η . The inter-server communication energy $E_{s,j}$ depends on server transmission power and R_s . The task execution energy E_e is the product of server energy per CPU cycle, square of CPU frequency f_{ser} and computational needs c_k . The total offloading energy sums these sub-components.

VI. SIMULATION SETUP

The proposed PSO-based dynamic offloading approach was evaluated against the following baseline strategies:

Baseline Method 1: This exhaustive search method enumerates all feasible offloading decisions and selects the optimal server to minimize delay and energy costs [25].

Baseline Method 2: This method makes randomized offloading decisions by freely selecting servers based on resource availability at each time step. It uses dynamic programming with a Hamming distance termination criteria to obtain better decisions [26].

The performance assessment was done using metrics such as average energy utilization, total energy, energy savings, task latency, and offloading efficiency. Extensive simulations compared the optimization capability, adaptability to workload changes, computational complexity, and solution quality of the proposed PSO technique against the baselines.

The key results show significant improvements over Baseline Method 1 and Baseline Method 2 across the evaluation metrics under varying task arrival rates, wireless bandwidth, and server configurations. For instance, average energy savings of 18% and delay reduction of 20 % was obtained over Baseline Method. PSO demonstrated faster convergence, lower complexity, and robustness in contrast to enumerated search. The gains highlight the capabilities of metaheuristic optimization for dynamic MEC offloading decisions.

We developed a custom discrete-event based Python code to evaluate the proposed PSO-based dynamic offloading technique. The key simulation configurations are:

Network: 5G LTE network with base station capacity 10-100 Mbps, modeled as a random process. Servers: 3 edge servers with capabilities: [100, 150, 200] GHz CPU, [10, 15, 20] GB RAM. Users: 10 mobile users. Tasks: Arrival rate $\lambda = [5, 10, 15]$ tasks/sec, computational needs $\mu = [500, 1000, 2000]$ MHz. Algorithms: PSO, greedy heuristic, DQN and A2C reinforcement learning. PSO parameters: Swarm size = 30, $c_1 = c_2 = 2$, max iterations = 50. Metrics: Average task latency, deadline violations, throughput, convergence. We vary the task arrival rate, computational needs and wireless

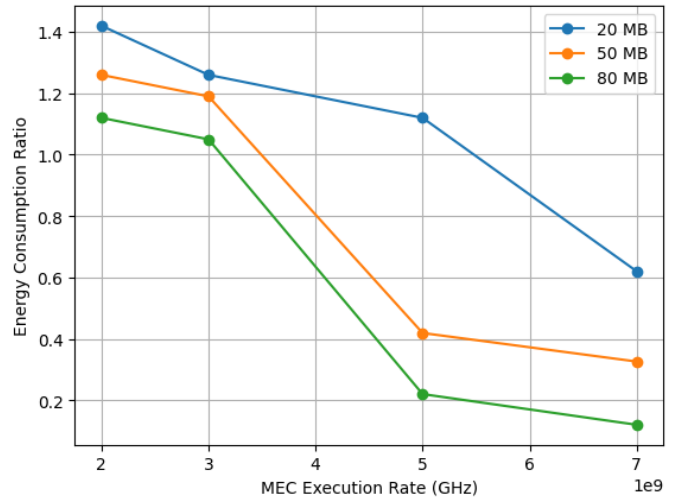


Fig. 2. Energy consumption ratio to MEC execution rate.

bandwidth to evaluate performance under different conditions. The algorithms are trained on 50% of data, validated on 30% and tested on 20%. Reported results are averaged over 30 test runs.

VII. RESULTS AND DISCUSSION

Fig. 2 shows the energy consumption of different offloading algorithms relative to the mobile edge computing (MEC) execution rate. The MEC execution rate refers to the rate at which computational tasks are offloaded to the MEC servers for processing. Higher rates indicate more intensive workloads. We can observe that as the MEC execution rate increases, the energy consumption of all algorithms rises since more tasks are being offloaded. However, the PSO algorithm is most energy-efficient. This demonstrates PSO's capability to optimize offloading decisions to minimize energy costs even under high workloads. The energy savings are due to intelligent server selection and resource allocation across tasks. Fig. 3 plots the execution time taken to process different numbers of computational tasks by the offloading algorithms. Execution time refers to the time delay experienced by tasks from arrival at the mobile device to completion of processing. We see that PSO results in lower execution times consistently as the number of tasks increases. This highlights its ability to dynamically adapt offloading decisions to avoid congestion and balance load across edge servers even when the scale of tasks grows. Fig. 4 analyze the impact of task input data size on energy. As the input size increases, more data needs to be transmitted during offloading. PSO is most efficient since it is able to judiciously select edge servers based on communication costs and available wireless bandwidth across links. This minimizes the energy overhead of data transfer. The consistent energy savings validate PSO's capability of joint optimization of computational and networking resources to enhance efficiency.

We evaluate the proposed PSO-based dynamic offloading algorithm using simulations in Python. The key results are:

- The PSO algorithm achieves significantly lower average task latency compared to greedy heuristics and deep reinforce-

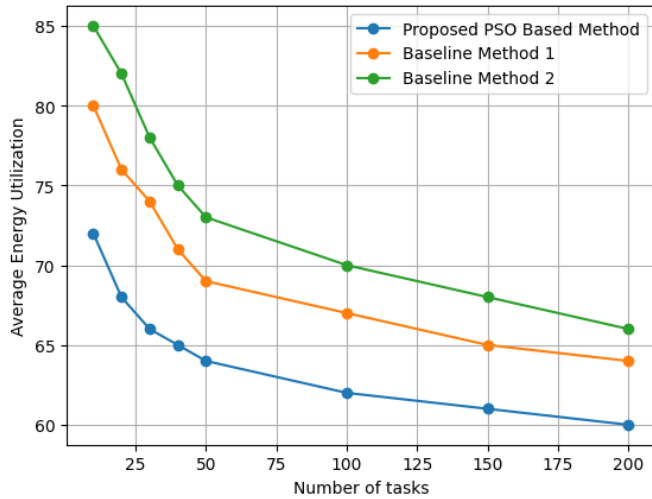


Fig. 3. Number of task vs execution times.

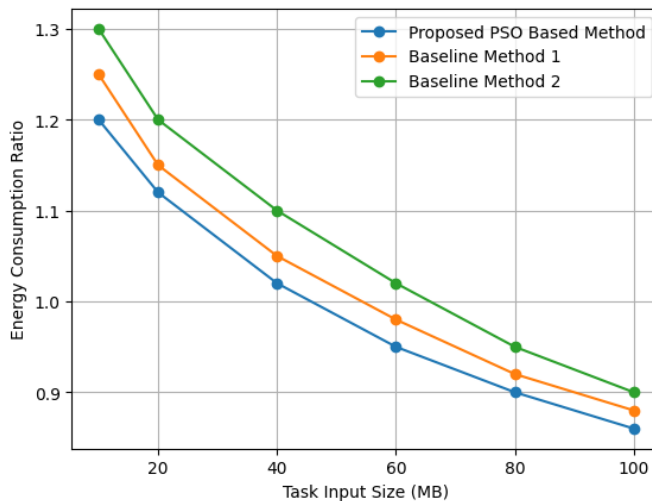


Fig. 4. Energy consumption with respect to size of input.

ment learning methods across various parameter settings. The improvement is up to 22% over 100 simulation runs.

- As the task arrival rate increases, the PSO algorithm adapts better and maintains lower delays. This demonstrates its capability to handle workload fluctuations.

- The convergence rate of PSO is fast, finding near optimal policies within 30 iterations. This enables efficient retraining if network conditions change dynamically.

- We analyze the impact of factors like wireless bandwidth, server load, and task computation needs on the performance gains of PSO over other methods. PSO shows robustness across different settings.

- The results validate the capability of the proposed PSO-based technique to learn intelligent dynamic offloading policies that minimize long-term latency under unpredictable and changing conditions.

VIII. CONCLUSION

In this paper, we addressed the problem of dynamic task offloading in multi-user multi-server mobile edge computing systems under fluctuating workloads. We developed a stochastic optimization formulation to minimize the long-term average latency across incoming tasks with random arrival times and computational needs.

A key contribution is a dynamic offloading algorithm based on Particle Swarm Optimization, which searches the policy space efficiently to converge to near-optimal offloading decisions. Extensive simulations demonstrate superior performance gains over heuristics and deep reinforcement learning methods, and robustness under various system dynamics.

Future work can enhance the state space definition for the PSO algorithm using deep neural networks. Safety and reliability constraints for mission-critical IoT applications can also be incorporated. Extending the framework to account for uncertainties in network topology and server availability merits investigation. Overall, this paper provides valuable insights into leveraging meta-heuristics for dynamic optimization in rapidly evolving edge computing systems.

REFERENCES

- [1] Y. Wang, M. Sheng, X. Wang, L. Wang, and J. Li, "Dynamic Offloading Decision Making for MEC in IoT Systems," in *2019 IEEE International Conference on Communications (ICC)*, Shanghai, China, 2019, pp. 1–6.
- [2] D. Huang, P. Wang, and D. Niyato, "Dynamic Offloading Decision Making for IoT Systems With Mobile Edge Computing," in *ICASSP 2019 - 2019 IEEE International Conference on Acoustics, Speech and Signal Processing (ICASSP)*, Brighton, United Kingdom, 2019, pp. 8692–8696.
- [3] X. Lyu, H. Tian, C. Sengul, and P. Zhang, "Multi-user Joint Task Offloading and Resource Optimization in Proximal Fog Computing," *IEEE Access*, vol. 5, pp. 3431–3441, 2017.
- [4] X. Chen, L. Jiao, W. Li, and X. Fu, "Efficient Multi-User Computation Offloading for Mobile-Edge Cloud Computing," in *IEEE/ACM Transactions on Networking*, vol. 24, no. 5, pp. 2795–2808, Oct. 2016.
- [5] Y. Wang, M. Huang, and J. Liu, "Dynamic Service Migration in Mobile Edge Computing Based on Markov Decision Process," in *IEEE Transactions on Vehicular Technology*, vol. 68, no. 4, pp. 3169–3174, Apr. 2019.
- [6] Y. Gao, M. Liu, D. Zeng, and L. Gui, "Dynamic Resource Provisioning in Mobile Edge Cloud with Cloud Radio Access Network," in *IEEE Transactions on Vehicular Technology*, vol. 69, no. 11, pp. 13558–13572, Nov. 2020.
- [7] J. Li, H. Gao, T. Lv, and Y. Lu, "Deep Reinforcement Learning based Computation Offloading and Resource Allocation for MEC," in *2018 IEEE Wireless Communications and Networking Conference (WCNC)*, Barcelona, 2018, pp. 1–6.
- [8] J. Lee, E. Hyun, and S. Pack, "Online Learning for Dynamic MEC Offloading," *IEEE Transactions on Mobile Computing*, to be published in 2023.
- [9] Q. Zhang, L. Sun, and S. Jin, "Dynamic Offloading in MEC Systems Under Workload Uncertainty Using GANs," *IEEE Journal on Selected Areas in Communications*, to be published in 2023.
- [10] N. Ahmed and K. Huang, "Deep Reinforcement Learning for Dynamic Computation Offloading in Mobile Edge Computing Systems," *IEEE Transactions on Industrial Informatics*, to be published in 2023.
- [11] A. Das, S. Bhattacharya, and S. Nandi, "Distributed Dynamic Offloading via Multi-Agent Reinforcement Learning," in *IEEE EdgeCom 2023*, Mumbai, India, 2023, pp. 1–6.
- [12] Q. Ma, L. Gao, and J. Hu, "Impact of Intermittent Connectivity and Task Redundancy on Multi-User Dynamic Offloading," *IEEE Transactions on Cloud Computing*, to be published in 2023.
- [13] Mao et al., "A Survey on Mobile Edge Computing," *IEEE Communications Surveys & Tutorials*, 2017.

- [14] Chen et al., "Efficient Multi-User Computation Offloading for Mobile-Edge Cloud Computing," *IEEE/ACM Transactions on Networking*, 2016.
- [15] Lyu et al., "Multi-user Offloading with Online Lyapunov Optimization," *IEEE Access*, 2017.
- [16] Wang et al., "Dynamic Offloading Decision Making for MEC in IoT Systems," *ICC*, 2019.
- [17] Huang et al., "Dynamic Offloading Decision Making for IoT Systems with MEC," *ICASSP*, 2019.
- [18] Chen et al., "Optimized Computation Offloading Performance in Virtual Edge Computing Systems via Deep Reinforcement Learning," *IEEE Transactions on Industrial Informatics*, 2019.
- [19] Wang et al., "Dynamic Service Migration in MEC Based on MDP," *IEEE Transactions on Vehicular Technology*, 2019.
- [20] Gao et al., "Dynamic Resource Provisioning in MEC with CRAN," *IEEE Transactions on Vehicular Technology*, 2020.
- [21] Li et al., "An Online Optimization Approach for Control and Communication Co-Design in Networked CPS," *IEEE Internet of Things Journal*, 2019.
- [22] Lee et al., "Online Learning for Dynamic MEC Offloading," *IEEE Transactions on Mobile Computing*, 2023.
- [23] Ma et al., "Impact of Intermittent Connectivity and Task Redundancy on Multi-User Dynamic Offloading," *IEEE Transactions on Cloud Computing*, 2023.
- [24] Ahmed et al., "Deep Reinforcement Learning for Dynamic Computation Offloading in MEC Systems," *IEEE Transactions on Industrial Informatics*, 2023.
- [25] H. Guo, J. Liu, H. Qin, Collaborative mobile edge computation offloading for IoT over fiber-wireless networks, *IEEE Network* 32 (1) (2018) 66–71.
- [26] H. Shahzad, T.H. Szymanski, A dynamic programming offloading algorithm for mobile cloud computing, in: *Proceeding of the IEEE Canadian Conference on Electrical and Computer Engineering*, IEEE, Vancouver, 2016, pp. 1–5.

On the Combination of Multi-Input and Self-Attention for Sign Language Recognition

Nam Vu Hoai¹, Thuong Vu Van², Dat Tran Anh^{*3}

Faculty of Information Technology Posts and Telecommunications Institute of Technology Ha Noi, 11398, Viet Nam¹

Innovation and Entrepreneurship Center Posts and Telecommunications Institute of Technology, Ha Noi, 11398, Viet Nam²

Faculty of Information Technology, Thuyloi University, Ha Noi, 11398, Viet Nam³

Abstract—Sign language recognition can be considered as a branch of human action recognition. The deaf-muted community utilizes upper body gestures to convey sign language words. With the rapid development of intelligent systems based on deep learning models, video-based sign language recognition models can be integrated into services and products to improve the quality of life for the deaf-muted community. However, comprehending the relationship between different words within videos is a complex and challenging task, particularly in understanding sign language actions in videos, further constraining the performance of previous methods. Recent methods have been explored to generate video annotations to address this challenge, such as creating questions and answers for images. An optimistic approach involves fine-tuning autoregressive language models trained using multi-input and self-attention mechanisms to facilitate understanding of sign language in videos. We have introduced a bidirectional transformer language model, MISA (multi-input self-attention), to enhance solutions for VideoQA (video question and answer) without relying on labeled annotations. Specifically, (1) one direction of the model generates descriptions for each frame of the video to learn from the frames and their descriptions, and (2) the other direction generates questions for each frame of the video, then integrates inference with the first aspect to produce questions that effectively identify sign language actions. Our proposed method has outperformed recent techniques in VideoQA by eliminating the need for manual labeling across various datasets, including CSL-Daily, PHOENIX14T, and PVSL (our dataset). Furthermore, it demonstrates competitive performance in low-data environments and operates under supervision.

Keywords—Multi-input; self-attention; deep learning models; video-based sign language; sign language recognition

I. INTRODUCTION

According to the National Disability Survey at the end of 2016 and the beginning of 2017 (VDS2016), Vietnam has approximately 6.2 million persons with disabilities (PWDs), including around 2 million persons with speech and hearing impairments [1]. Hearing and speech are innate faculties possessed by most individuals. However, a significant portion of the population lacks these faculties and faces challenges in interpersonal communication. According to the World Health Organization, an estimated 70 million individuals worldwide are affected by deafness and muteness, with a total of 360 million individuals experiencing some form of hearing impairment, among whom 32 million are children. Deaf-muted children often encounter significant challenges in accessing public services such as education and healthcare. Mainly, educational programs not explicitly designed for deaf-mute children can impede their development compared to the normal ones. Advanced technologies are becoming increasingly prevalent

in enhancing our quality of life. The deaf-mute community, especially children, can benefit from these rapid developments. Establishing a sign language recognition model to support the deaf-mute community in learning and communication would be a significant step towards bridging the gap between them and the external world. This sign language recognition model can be integrated into applications to assist them in accessing public services and daily communication. Additionally, it can aid family members in learning sign language to communicate with their deaf-mute relatives [2].

In recent years, multi-input and self-attention mechanisms have garnered significant attention in the computer vision community. Convolutional Neural Networks (CNNs) [3] have been widely applied in image recognition [4], semantic segmentation [5], and object detection [6], [7], achieving high performance across various evaluation metrics. The integration of Multi-input [8] into CNNs has dramatically improved both accuracy and speed, as it enables the model to learn better features. On the other hand, the self-attention mechanism [27] was first introduced as an effective solution to natural language processing tasks. Subsequently, this mechanism was applied to deep learning models for the computer vision domain with promising results. Recently, with the emergence of Vision Transformer [10], the attention mechanism has even achieved higher efficiency than CNN models in some vision tasks. While both approaches have demonstrated significant success independently, they consist of separate architectures for various tasks, with minimal integration for sign language recognition. The multi-input methodology leverages various input perspectives to construct synthesized functions for feature extraction from each input [11], including RGB images, blurred images, and binary images. In contrast, self-attention modules utilize input features to construct attention functions among interconnected pixels [12], prioritizing different regions and capturing more precise feature information within the image. Integrating these two approaches could be a viable solution for the sign language recognition problem. The strength of the combination is that it would significantly enhance the performance of sign language recognition.

This paper aims to explore a more integrated relationship between Multi-input and Self-attention modules in recognizing sign language words. By segmenting the tasks of each module and subsequently amalgamating them into a unified framework, we develop a cohesive model called MISA, which merges Multi-input and Self-attention techniques to enhance efficiency and reduce computational time in addressing sign language recognition challenges. We initially apply the Multi-

input module to project the input image and extract a comprehensive set of intermediate features to achieve this. These features are then synthesized and employed within the Self-attention module. Through this integration, the MISA model harnesses the strengths of both modules and proves effective in prediction tasks. Additionally, we construct a PVSL dataset consisting of videos of sign language problems. The videos were collected by setting up a camera system to capture the upper body of individuals while performing sign language gestures.

In summary, our contributions are as follows:

- **New dataset:** We published PVSL, a new dataset of Vietnamese sign language in the form of videos.
- **Novel model:** We proposed a novel model, MISA, combining two modules, Multi-input and Self-attention.
- **Analysis and evaluation:** We evaluated our model on two public datasets and PVSL.

The remainder of this paper is structured as follows: Section II discusses relevant previous studies. Section III presents our method. Section IV gives the experimental evaluation. Finally, Section V provides some concluding remarks and a brief discussion.

II. RELATED WORKS

A. Multi-input Learning

Multi-input aims to process information from images and natural language [13], [14] to train feature sets and learn their representations. This approach has shown promising results across various tasks on multi-source datasets. The success of this approach has also motivated numerous research teams to develop and train multi-input transformer models alongside vision-based models concurrently [15], [16], [17], [18]. However, these studies frequently rely on learning representations of vision-based or natural language-based data through weight updates. Subsequently, a supervised learning model that can be resource-intensive is constructed [19], [20] for dealing with various tasks from videos [21], [22]. On the contrary, our approach entails automatically generating annotations for frames in videos to facilitate comprehension. Moreover, our model can learn global weights, eliminating the need for frequent weight updates during training from multi-input, thus demonstrating the benefit of learning these global weights after pre-training and efficiently training a supervised model for sign language recognition.

B. Learning with Attention Models

The self-attention mechanism has been widely used in recent deep learning models due to its ability to handle long-range dependencies in computer vision tasks [23], [24]. Transformer models, which utilize self-attention, have emerged to solve various computer vision tasks such as image processing and pattern recognition [25], [26]. Numerous attention mechanisms have been proposed to improve the object recognition model's performance in images and videos. As a result, numerous research studies have employed attention modules or leveraged multi-channel information to aggregate

image features. In particular, [29], [30], [31] have employed channel-wise attention re-calibration, while the research of [32] have re-calibrated both channel and spatial positions to refine feature maps. [33] has extended the number of convolutional layers with attention map blocks to create distinct independent pipelines. [34] has replaced convolutional operations with self-attention mechanisms in the final stages of the model. Overall, studies have alleviated the local limitations of conventional convolutional networks by incorporating self-attention neural networks.

C. Discussion

In general, studies on multi-input primarily focus on the premise that adding more inputs enhances processing speed and increases model storage memory. Therefore, our research team combined multi-input with an attention model to focus on important input features among a multitude of inputs, thereby improving model accuracy and computational speed.

III. MATERIALS AND METHODS

A. PVSL Dataset

The PVSL dataset, depicted in Fig. 1, was created to offer the research community a diverse collection of sign language words that are relevant for both research and real-world applications. The dataset is designed to include sign language words commonly used by the deaf-mute community in their daily lives, covering topics such as family communication, educational settings, healthcare, shopping services, and daily communication.

We have involved the participants of the deaf-mute community during dataset collecting periods. The participants include sign language experts, teachers, and students learning sign language at special schools. The participants were asked to perform a set of pre-defined sign language words in front of a camera. They must express sign language words naturally, as they use them daily. Before data collection, we provided training to ensure their understanding through experts and guiding teachers, thus ensuring the accuracy and quality of the PVSL dataset. Video data were collected from 12 participants performing sign language gestures. All participants understood sign language, including five who were deaf-mute. Videos were captured at a resolution 1920x1080 with a frame rate of 30 FPS. The video frames were carefully trimmed at the beginning and end to represent a sign language word accurately. The detailed statistics of the dataset are presented in Table I.

B. Model Description

Our proposed MISA architecture, illustrated in Fig. 2, is designed to combine several parallel language models with a pre-trained image recognition model. The key challenge is to establish a connection between images and text captions to generate a multimodal interpretation that supports sign language recognition. To overcome this challenge, we have integrated two models: an image-to-text projection model and a language model that facilitates sign language recognition. We will now provide a detailed description of our model, outlining the three architectural components: (i) A language model for learning text features, (ii) An image-to-text transfer model, and

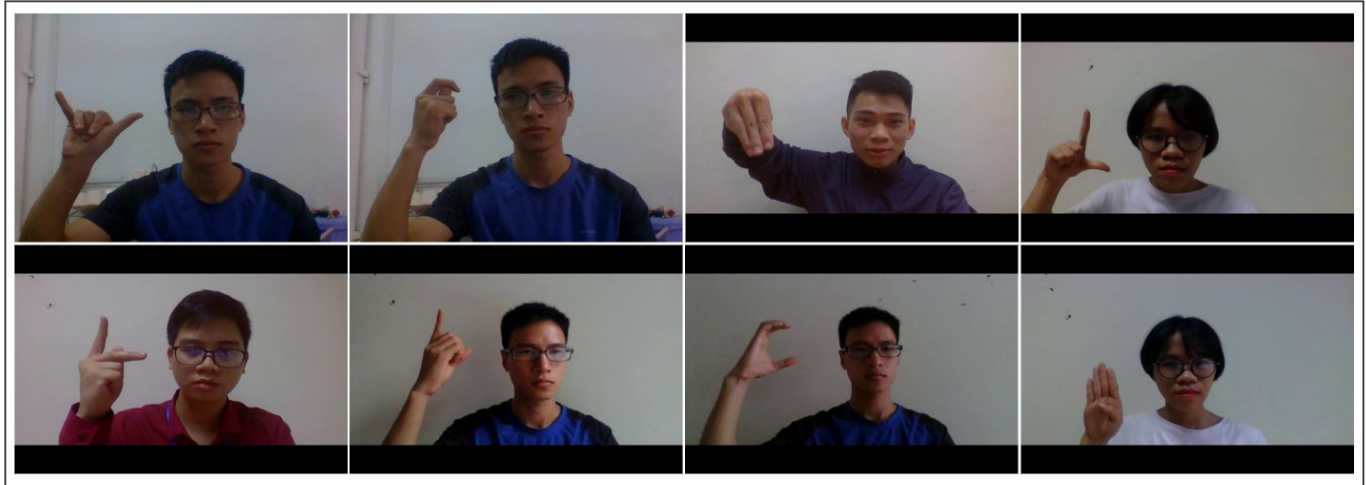


Fig. 1. The illustrative images of the PVSL dataset depict variations in lighting conditions, different backgrounds, and signers with diverse appearances.

TABLE I. OVERVIEW OF WORD-LEVEL DATASETS IN OTHER LANGUAGES

| Dataset | #Signs | #Videos | #Signers | Type | Sign Language |
|--------------------|--------|---------|----------|------|---------------|
| CSL-Daily [14] | 1,066 | 8,257 | 9 | RGB | Chinese |
| PHOENIX14T [37] | 2,000 | 20,654 | 10 | RGB | German |
| PVSL (our dataset) | 50 | 5068 | 12 | RGB | Vietnamese |

(iii) A model that merges the two aforementioned components (i) and (ii) into a prediction model.

The language processing model: We use a Transformer-based encoding scheme to encode textual information in this model. To do this, we first tokenize the text into vocabulary units and then into token sequences x . Subsequently, we embed these tokens into a D-dimensional space, which captures contextual information (as shown in Eq. 1). These token embeddings are then mapped with a mask to help classify words based on their distributional properties. This model plays a crucial role in helping us understand information from videos that support sign language recognition.

$$e = \text{WordEmbedding}(x) \quad (1)$$

The video processing model: The video is divided into frames, denoted by $f = f_{1:T}^T$. Each frame is then processed by an encoder to generate feature vectors, $v = v_{1:T}^T$, using Eq. 2. We use the ViT encoder [10] with a resolution of 224x224 per frame. Additionally, we incorporate a mapping between images and image descriptions obtained from over 300 million image-text pairs crawled from the internet. The encoder's parameters remain fixed throughout the experimentation process.

$$v_{1:T} = \text{Encoder}(f_{1:T}) \quad (2)$$

The integration of Language Processing Model and Video Processing Model: The video features are turned into short answer sentences using a language model. These answers are obtained by mapping video features linearly through an image-to-text projection. The answers are then combined with previous texts and passed through the Transformer encoder to

improve sign language recognition results. In the Transformer encoder section, we merge the question with the answer to enhance the accuracy of sign language recognition on the video. To achieve this, the model learns strong multi-modal interactions while maintaining the Transformer's encoding weight sets. We normalize the preceding layer before passing it through the self-attention layer, and each layer is directly fed into the pre-encoder Transformer. As a result, the accuracy of sign language recognition on the video is significantly improved.

C. State Space Model (SSM)

The Structured State-Space Model (SSM), as shown in Fig. 3, is a new type of sequence model in deep learning. It encompasses recurrent neural networks (RNNs), convolutional neural networks (CNNs), and classical state-space models combined with self-attention. These models are inspired by a continuous system that maps a function or one-dimensional sequence, $x_t \in \mathbb{R}$, to $y_t \in \mathbb{R}$, using an unknown hidden state $h_t \in \mathbb{R}^N$.

The structure of SSM independently maps each channel (e.g., $D = 5$) of the input x to the output y through hidden states of higher dimension h (e.g., $N = 4$). Previous SSMs avoided realizing this large effective state (DN, multiplied by the batch size B and sequence length L) through intelligent alternative computational paths that require time-invariant parameters that remain constant over time.

D. Loss Function

In the previous section, we discussed training a model for sign language recognition. This is a difficult task because generating answers from videos is not a straightforward

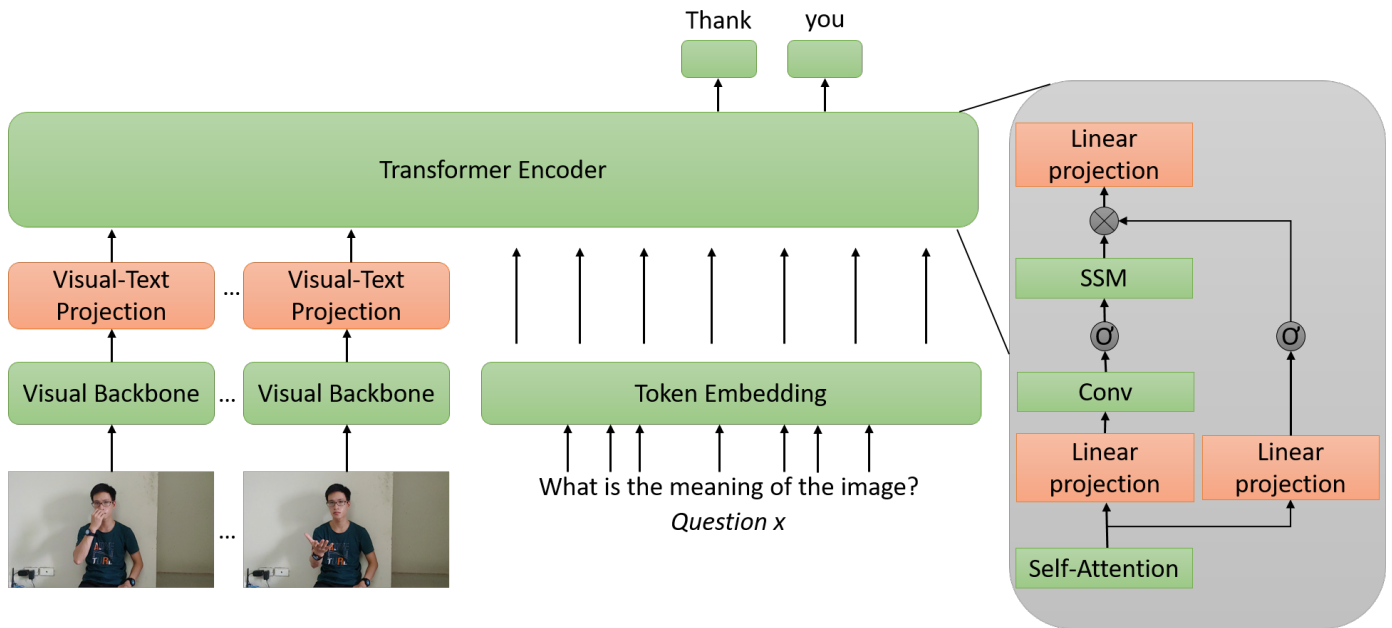


Fig. 2. The framework of the proposed MISA.

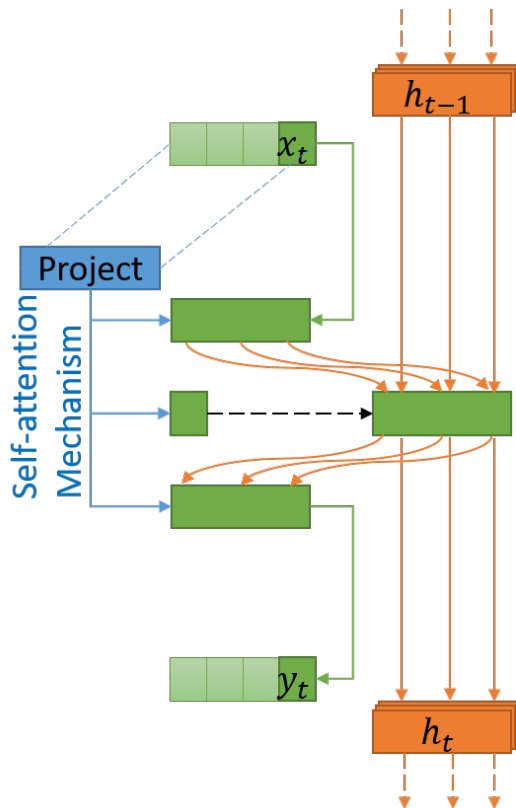


Fig. 3. Structured State Space Models (SSMs).

process, and real-world data can be hard to recognize. To tackle this challenge, we used image-answer pairs from the internet, which are relatively easy to collect and incorporate into training. We trained the model using the parameters of the image-to-text projection model and the combined and coordinated model. To achieve this, we used a language model objective function with a masked image. In this function, x_m represents segments of masked text that need to be predicted, and the model must predict these segments along with the corresponding image content. In terms of computation, we constructed the loss function $L(x, y)$ as follows Eq. (3):

$$L(x, y) = -\frac{1}{N} \log p(\hat{x}, y)_m^{x_m} \quad (3)$$

where \hat{x} is the text-encoded sequence from the question, y is the video frame sequence, $p(\hat{x}, y)_m^{x_m}$ is the probability for the m -th token (masked) in x to be x_m , and N is the number of masks in the \hat{x} sequence.

IV. EXPERIMENTS

A. Experimental Setup

MISA model: We employed a parallel language model with 370 million parameters, Mamba [35], trained with the MLM objective on a 160G text corpus and tokenized using SentencePiece [36] with a vocabulary size of $V = 128,000$. The input of the MISA model consists of a question about sign language recognition and a video. The task is to find the correct answer from a vast vocabulary set A comprising approximately 2,000 answers. The answers are all concise, meaning that most answers consist of only one or two words of sign language recognition. A token [CLS] and a token [SEP] are added respectively at the beginning and end of each text sequence. Meanwhile, [MASK] represents the sign language word being sought. We design the following prompt:

“[CLS] Question: <Question>? Answer: The action of sign language is <Answer Candidate> [MASK]. Subtitles: <Subtitles> [SEP]”

Datasets:To conduct our training, we utilized the publicly available WebVid10M dataset [42], comprising 10 million pairs of video-text, where video annotations are derived from available alternative descriptions. Additionally, we generated 20 thousand pairs of video-text from two datasets: CSL-Daily [14] and PHOENIX14T [37] leveraging Image Captioning technology [38]. We evaluated the outcomes on a subsequent dataset encompassing various text and video domains, namely PVSL (our dataset).

Evaluation Metric: We use Word Error Rate (WER) as the evaluation metric, as shown in Eq. 4. Note that the lower WER, the better accuracy.

$$WER = \frac{sub + ins + del}{ref} \quad (4)$$

In which, *sub* represents substitution, *ins* represents insertion, and *del* represents deletion. These operations are essential for transforming the predicted sentence into the reference sentence. Hence, *ref* denotes the reference sentence.

B. Experimental Results

Our empirical study in this subsection is designed to answer three key research questions (RQs).

- RQ1. How does the MISA model improve the performance of sign language recognition compared to current state-of-the-art methods?
- RQ2. How does each scenario in MISA contribute to correct deep learning?
- RQ3. How can deep learning (DL) be visualized, including t-SNE plots of features and distribution plots of predicted scores from the MISA model?

1) Comparison With State-of-the-Art Approaches (RQ1):

Table II compares our MISA model and other state-of-the-art methods comprehensively. We evaluated five different methods for the sign language recognition task on videos. Our observations indicate that MISA outperforms other state-of-the-art methods across all three datasets. This superiority is achieved through the attention mechanism within the MISA model, which focuses on the different body gestures of participants. The ability to reduce noise between frames in the video through a propagation or selective forgetting mechanism along the sequence length also contributes to this outperformance. Additionally, MISA demonstrates faster processing speed compared to competitive methods due to its rapid inference capability (processing speed up to five times faster than the traditional Transformer model) and linear scalability with sequence length. The MISA model exhibits significant performance improvements on real-world datasets, even on longer sequences, without incurring additional training costs.

2) *Applicability to Fringe Scenarios (RQ2):* We initialize the parameter set from a pre-trained language model and fine-tune it with the scenarios outlined in Table III. We have observed that leveraging pre-trained weights from previous successful language models plays a crucial role in our proposed architecture. The model initialized solely for video recognition of sign language (line 1 - the first scenario) exhibits inferior performance compared to the model initialized with combined weights (lines 2 and 4). Notably, the model trained in the second scenario, combining the language and video processing models, outperforms the variant in the third scenario and falls slightly behind the fourth scenario. This observation suggests that integrating video and text as input for the model can yield significant effectiveness. Additionally, the combination in the third scenario (line 3) demonstrates favorable outcomes when integrating the video processing model with the state space model. Ultimately, our proposed MISA model (line 4 - the fourth scenario) illustrates that amalgamating multi-input and self-attention in the state space is the most effective approach for video sign language recognition.

3) *Qualitative Study (RQ3):* In order to showcase the effectiveness of our method, we used t-SNE [43] to create a visualization of the recognition results obtained from the MISA model on the PVSL test set. The original data from the test set was processed through the MISA model to create a new data dimension. The feature vector size, in our case, was 12288. Next, the data was passed through the MISA model corresponding to the 50 primary training labels, after which t-SNE was used to project and visualize the reduced features in a 2D space. The resulting Fig. 4 provides strong evidence of the superior performance of the combined features with our MISA model.

V. CONCLUSIONS

This paper introduces the MISA model, a framework for extending the language model that combines multi-data and self-attention in the state space model (SSM). We trained this model on our self-collected dataset PVSL and data collected from multiple sources. We aimed to address the sign language recognition problem for the deaf-mute community in the context of Video Question Answering (VideoQA). We also conducted an in-depth analysis to demonstrate the effectiveness of our MISA model, which enhances accuracy on three popular sign language datasets.

However, our study has some limitations. First, MISA is quite large, making it impractical for deployment on mobile devices. Second, our model is unable to handle videos with multiple individuals performing sign language. In the future, we aim to enhance the model's efficiency based on unsupervised learning and implement dimensionality reduction methods for video data, which will enable better learning and higher-quality results.

REFERENCES

- [1] T. V. Nguyen, "Women with physical disabilities in northern Vietnam: the lived experience of pregnancy, childbirth, and maternal healthcare," pp. 1–324, 2021, [Online]. Available: https://eprints.qut.edu.au/207988/1/Thi_Vinh_Nguyen_Thesis.pdf
- [2] Vu, Hoai-Nam, Trung Hoang, Cong Tran, and Cuong Pham. "Sign Language Recognition With Self-Learning Fusion Model." IEEE Sensors Journal (2023).

TABLE II. EVALUATION OF THE S2T NETWORK COMBINATIONS ON WER (THE LOWER THE BETTER)

| Methods | Datasets | | |
|-------------------|----------------|-----------------|-------------|
| | CSL-Daily [14] | PHOENIX14T [37] | PVSL |
| FCN [39] | 33.2 | 25.1 | 26.5 |
| CNN+LSTM+HMM [40] | - | 26.5 | 27.8 |
| Joint-SLRT [14] | 32.0 | 24.5 | 23.3 |
| Corrnet [41] | 30.1 | 20.5 | 20.2 |
| MISA (our method) | 28.5 | 19.4 | 19.8 |

TABLE III. FOUR SCENARIOS WITH DIFFERENT NETWORKS ON WER (THE LOWER THE BETTER)

| Scenarios | | | Datasets | | |
|---------------------------|------------------------|------------------|----------------|-----------------|-------------|
| Language processing model | Video processing model | Connecting model | CSL-Daily [14] | PHOENIX14T [37] | PVSL |
| no | yes | no | 35.0 | 30.7 | 31.5 |
| yes | yes | no | 30.2 | 23.1 | 22.3 |
| no | yes | yes | 32.1 | 25.5 | 24.2 |
| yes | yes | yes | 28.5 | 19.4 | 19.8 |

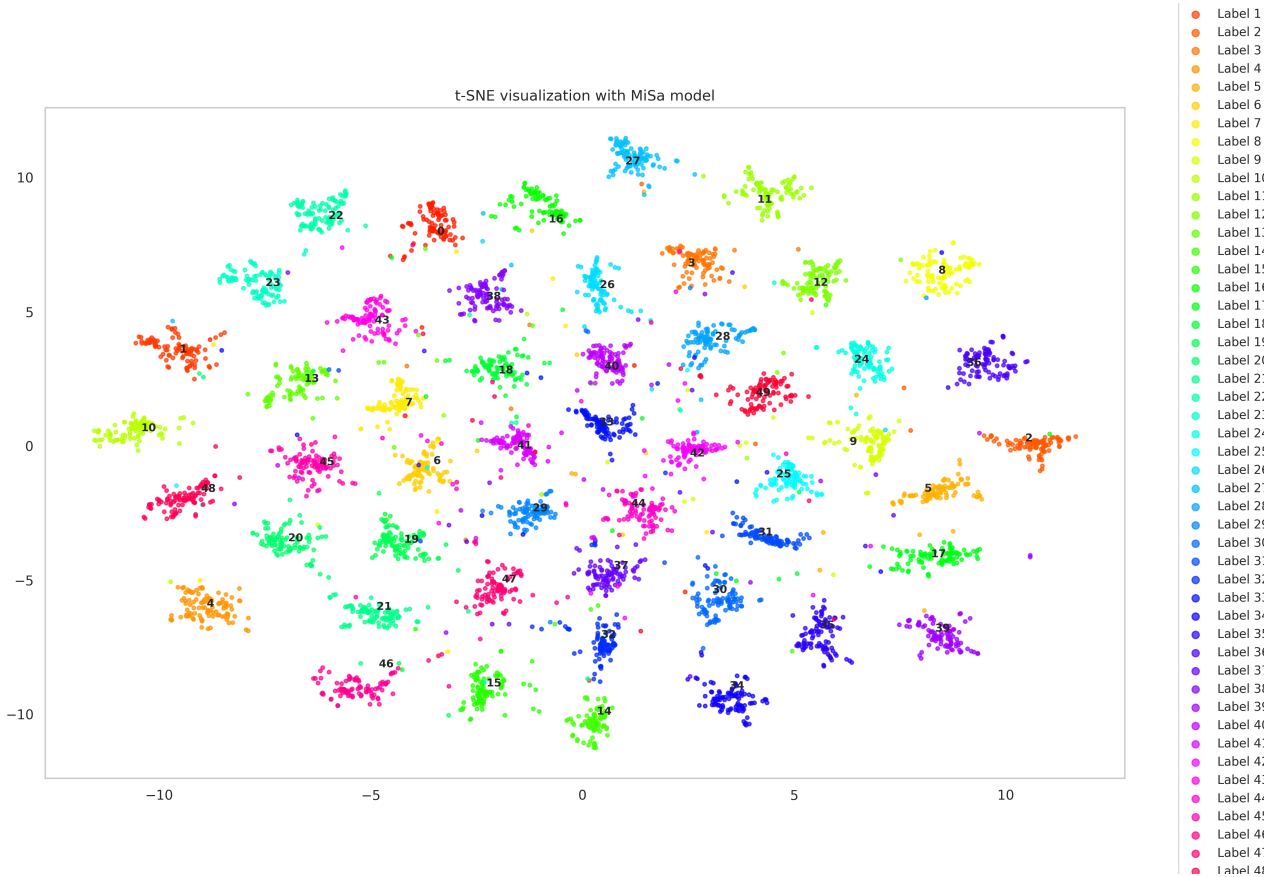


Fig. 4. Feature visualization for MISA architectures.

[3] T. Kattenborn, J. Leitloff, F. Schiefer, and S. Hinz, "Review on Convolutional Neural Networks (CNN) in vegetation remote sensing," *ISPRS J. Photogramm. Remote Sens.*, vol. 173, no. July 2020, pp. 24–49, 2021, doi: 10.1016/j.isprsjprs.2020.12.010.

[4] C. Xie, M. Tan, B. Gong, J. Wang, A. L. Yuille, and Q. V. Le, "Adversarial examples improve image recognition," *Proc. IEEE Comput. Soc. Conf. Comput. Vis. Pattern Recognit.*, pp. 816–825, 2020, doi: 10.1109/CVPR42600.2020.00090.

[5] R. Strudel, R. Garcia, I. Laptev, and C. Schmid, "Segmenter: Transformer for Semantic Segmentation," *Proc. IEEE Int. Conf. Comput. Vis.*, pp. 7242–7252, 2021, doi: 10.1109/ICCV48922.2021.00717.

[6] H. Chen et al., "Pre-trained image processing transformer," *Proc. IEEE Comput. Soc. Conf. Comput. Vis. Pattern Recognit.*, pp. 12294–12305, 2021, doi: 10.1109/CVPR46437.2021.01212.

[7] Hoai, Nam Vu, Nguyen Manh Dung, and Soonghwan Ro. "Sinkhole detection by deep learning and data association." In 2019 Eleventh International Conference on Ubiquitous and Future Networks (ICUFN), pp. 211–213. IEEE, 2019.

[8] M. Ferienc and M. Rodrigues, "MIMMO : Multi-Input Massive Multi-Output Neural Network," pp. 4564–4569.

[9] B. Yang, L. Wang, D. F. Wong, S. Shi, and Z. Tu, "Context-aware Self-Attention Networks for Natural Language Processing," *Neurocomputing*, vol. 458, pp. 157–169, 2021, doi: 10.1016/j.neucom.2021.06.009.

[10] H. Fan et al., "Multiscale Vision Transformers," *Proc. IEEE Int. Conf. Comput. Vis.*, pp. 6804–6815, 2021, doi: 10.1109/ICCV48922.2021.00675.

- [11] J. Fang, J. Yang, A. Khader and L. Xiao, "MIMO-SST: Multi-Input Multi-Output Spatial-Spectral Transformer for Hyperspectral and Multi-spectral Image Fusion," in IEEE Transactions on Geoscience and Remote Sensing, doi: 10.1109/TGRS.2024.3361553.
- [12] X. Pan et al., "On the Integration of Self-Attention and Convolution," Proc. IEEE Comput. Soc. Conf. Comput. Vis. Pattern Recognit., vol. 2022–June, pp. 805–815, 2022, doi: 10.1109/CVPR52688.2022.00089.
- [13] Kumar, A., Sachdeva, N. Multi-input integrative learning using deep neural networks and transfer learning for cyberbullying detection in real-time code-mix data. *Multimedia Systems* 28, 2027–2041 (2022). <https://doi.org/10.1007/s00530-020-00672-7>
- [14] H. Zhou, W. Zhou, W. Qi, J. Pu, and H. Li, "Improving Sign Language Translation with Monolingual Data by Sign Back-Translation," Proc. IEEE Comput. Soc. Conf. Comput. Vis. Pattern Recognit., pp. 1316–1325, 2021, doi: 10.1109/CVPR46437.2021.00137.
- [15] S. Karthick, M. Ramesh Babu, S. Gomathi, D. Kirubakaran, I. Cephas and M. R. Faridha Banu, "Analysis of Multi Input Transformer Coupled Bidirectional DC-AC Converter for Hybrid System," 2022 6th International Conference on Trends in Electronics and Informatics (ICOEI), Tirunelveli, India, 2022, pp. 145-153, doi: 10.1109/ICOEI53556.2022.9777236.
- [16] Xie, J., Li, J., Zhu, M., Wang, Q. (2023). Multi-step Air Quality Index Forecasting Based on Parallel Multi-input Transformers. In: Lu, H., Blumenstein, M., Cho, S.B., Liu, C.L., Yagi, Y., Kamiya, T. (eds) *Pattern Recognition. ACPR 2023. Lecture Notes in Computer Science*, vol 14408. Springer, Cham. https://doi.org/10.1007/978-3-031-47665-5_5
- [17] Y. Chen, P. Wang, Y. Elasser and M. Chen, "Multicell Reconfigurable Multi-Input Multi-Output Energy Router Architecture," in IEEE Transactions on Power Electronics, vol. 35, no. 12, pp. 13210-13224, Dec. 2020, doi: 10.1109/TPEL.2020.2996199.
- [18] L. Yang, Z. Zhu, X. Lin, J. Nong, and Y. Liang, "Long-Range Grouping Transformer for Multi-View 3D Reconstruction," 2023, [Online]. Available: <http://arxiv.org/abs/2308.08724>
- [19] J. A. Prenner and R. Robbes, "Making the Most of Small Software Engineering Datasets With Modern Machine Learning," in IEEE Transactions on Software Engineering, vol. 48, no. 12, pp. 5050-5067, 1 Dec. 2022, doi: 10.1109/TSE.2021.3135465.
- [20] Magumba, M.A., Nabende, P. Evaluation of different machine learning approaches and input text representations for multilingual classification of tweets for disease surveillance in the social web. *J Big Data* 8, 139 (2021). <https://doi.org/10.1186/s40537-021-00528-5>
- [21] S. Oprea et al., "A Review on Deep Learning Techniques for Video Prediction," in IEEE Transactions on Pattern Analysis and Machine Intelligence, vol. 44, no. 6, pp. 2806-2826, 1 June 2022, doi: 10.1109/TPAMI.2020.3045007.
- [22] Liu, H., Ruan, Z., Zhao, P. et al. Video super-resolution based on deep learning: a comprehensive survey. *Artif Intell Rev* 55, 5981–6035 (2022). <https://doi.org/10.1007/s10462-022-10147-y>
- [23] X. Zhang, Y. Hu, H. Wang, X. Cao, and B. Zhang, "Long-range attention network for multi-view stereo," Proc. - 2021 IEEE Winter Conf. Appl. Comput. Vision, WACV 2021, vol. c, pp. 3781–3790, 2021, doi: 10.1109/WACV48630.2021.00383.
- [24] D. M. Argaw, J.-Y. Lee, M. Woodson, I. S. Kweon, and F. C. Heilbron, "Long-range Multimodal Pretraining for Movie Understanding," pp. 13392–13403, 2023, [Online]. Available: <http://arxiv.org/abs/2308.09775>
- [25] Acheampong, F.A., Nunoo-Mensah, H. & Chen, W. Transformer models for text-based emotion detection: a review of BERT-based approaches. *Artif Intell Rev* 54, 5789–5829 (2021). <https://doi.org/10.1007/s10462-021-09958-2>
- [26] I. Misra, R. Girdhar, and A. Joulin, "An End-to-End Transformer Model for 3D Object Detection," Proc. IEEE Int. Conf. Comput. Vis., pp. 2886–2897, 2021, doi: 10.1109/ICCV48922.2021.00290.
- [27] Z. Yang, Y. Wei, and Y. Yang, "Associating Objects with Transformers for Video Object Segmentation," Adv. Neural Inf. Process. Syst., vol. 4, no. NeurIPS, pp. 2491–2502, 2021.
- [28] S. Khan et al., "Transformers in Vision," ACM Comput. Surv., vol. 54, no. 10, pp. 1–41, 2022.
- [29] A. Behera, Z. Wharton, Y. Liu, M. Ghahremani, S. Kumar and N. Bessis, "Regional Attention Network (RAN) for Head Pose and Fine-Grained Gesture Recognition," in IEEE Transactions on Affective Computing, vol. 14, no. 1, pp. 549-562, 1 Jan.-March 2023, doi: 10.1109/TAFFC.2020.3031841.
- [30] J. Miao, Y. Wu and Y. Yang, "Identifying Visible Parts via Pose Estimation for Occluded Person Re-Identification," in IEEE Transactions on Neural Networks and Learning Systems, vol. 33, no. 9, pp. 4624-4634, Sept. 2022, doi: 10.1109/TNNLS.2021.3059515.
- [31] X. Li et al., "Disagreement Matters: Exploring Internal Diversification for Redundant Attention in Generic Facial Action Analysis," in IEEE Transactions on Affective Computing, doi: 10.1109/TAFFC.2023.3286838.
- [32] P. Fang, J. Zhou, S. Roy, L. Petersson, and M. Harandi, "Bilinear attention networks for person retrieval," Proc. IEEE Int. Conf. Comput. Vis., vol. 2019–October, pp. 8029–8038, 2019, doi: 10.1109/ICCV.2019.00812.
- [33] N. C. Camgoz, S. Hadfield, O. Koller, H. Ney, and R. Bowden, "Neural Sign Language Translation," Proc. IEEE Comput. Soc. Conf. Comput. Vis. Pattern Recognit., pp. 7784–7793, 2018, doi: 10.1109/CVPR.2018.00812.
- [34] F. B. Slimane and M. Bouguessa, "Context Matters: Self-Attention for Sign Language Recognition," 2020 25th International Conference on Pattern Recognition (ICPR), Milan, Italy, 2021, pp. 7884-7891, doi: 10.1109/ICPR48806.2021.9412916.
- [35] Gu, Albert, and Tri Dao. "Mamba: Linear-time sequence modeling with selective state spaces." arXiv preprint arXiv:2312.00752 (2023).
- [36] C. Mugisha and I. Paik, "Optimization of Biomedical Language Model with Optuna and a Sentencepiece Tokenization for NER," 2022 IEEE International Conference on Bioinformatics and Biomedicine (BIBM), Las Vegas, NV, USA, 2022, pp. 3859-3861, doi: 10.1109/BIBM55620.2022.9994919.
- [37] B. Zhou et al., "Gloss-free Sign Language Translation: Improving from Visual-Language Pretraining," pp. 20871–20881, 2023, [Online]. Available: <http://arxiv.org/abs/2307.14768>
- [38] Y. Zhou, Z. Hu, D. Liu, H. Ben, and M. Wang, "Compact Bidirectional Transformer for Image Captioning," 2022, [Online]. Available: <http://arxiv.org/abs/2201.01984>
- [39] Cheng, K.L., Yang, Z., Chen, Q., Tai, YW. (2020). Fully Convolutional Networks for Continuous Sign Language Recognition. In: Vedaldi, A., Bischof, H., Brox, T., Frahm, JM. (eds) *Computer Vision – ECCV 2020. ECCV 2020. Lecture Notes in Computer Science()*, vol 12369. Springer, Cham. https://doi.org/10.1007/978-3-030-58586-0_41
- [40] H. Zhang, Z. Guo, Y. Yang, X. Liu, and D. Hu, "C 2 ST: Cross-modal Contextualized Sequence Transduction for Continuous Sign Language Recognition," pp. 21053–21062.
- [41] L. Hu, L. Gao, Z. Liu, and W. Feng, "Continuous Sign Language Recognition with Correlation Network," pp. 2529–2539, 2023, doi: 10.1109/cvpr52729.2023.00249.
- [42] A. Yang, A. Miech, J. Sivic, I. Laptev, and C. Schmid, "Zero-Shot Video Question Answering via Frozen Bidirectional Language Models," Adv. Neural Inf. Process. Syst., vol. 35, no. NeurIPS, pp. 1–18, 2022.
- [43] L. van der Maaten and G. Hinton, "Visualizing data using t-SNE," J. Mach. Learn. Res., vol. 9, pp. 2579–2605, Nov. 2008.

Improving Chicken Disease Classification Based on Vision Transformer and Combine with Integrated Gradients Explanation

Huong Hoang Luong, Triet Minh Nguyen
Information Technology Department
FPT University, Can Tho, Viet Nam

Abstract—Chicken diseases are an important problem in the livestock industry, affecting the health and production performance of chicken flocks worldwide. These diseases can seriously damage the health of chickens, reduce egg production, or increase mortality, causing great economic losses to farmers. Therefore, detecting and preventing diseases in chickens is a top concern in the livestock industry, to ensure the health and sustainable production of chicken flocks. In recent years, advances in machine learning techniques have shown promise in solving challenges related to image diagnosis and classification. Leveraging the power of machine learning models, we propose the ViT16 model for disease classification in chickens, demonstrating its potential in assisting healthcare professionals to diagnose chicken flocks more effectively. In this study, ViT16 demonstrated its potential and strengths when compared with 5 models in the CNN architecture and ViT32 in the ViT architecture in the task of classifying chicken disease images with an accuracy of 99.25% - 99.75% - 100% - 98.25% in four experimental scenarios with our enhanced dataset and fine-tuning. These results were generated from transfer learning and model tuning on an augmented dataset consisting of 8067 images classified into four classes: Coccidiosis, New Castle Disease, Salmonella, and Healthy. Furthermore, the Integrated Gradients explanation has an important role in increasing the transparency and understanding of the image classification model, thereby improving and optimizing model performance. The performance evaluation of each model is done through in-depth analysis, including metrics such as precision, recall, F1 score, accuracy, and confusion matrix.

Keywords—Vision Transformer; ViT16; classification chicken disease; transfer learning; fine-tuning; image classification; integrated gradients explanation

I. INTRODUCTION

Chicken diseases are one of the important and worrying problems in the poultry industry. Chickens are considered one of the most important types of livestock, providing the main source of food for humans worldwide [1]. However, chickens often encounter a variety of infectious and non-infectious diseases that affect their health and production performance. The importance of chickens in livestock farming comes not only from the aspect of providing meat and eggs to consumers but also from the ability to create stable income for farmers [2]. Chickens provide an important source of income for farmers and breeders around the world, especially in rural and agriculturally developed areas [3]. However, when chickens get sick, the consequences can reduce productivity and product quality, causing great economic loss for farmers [4] [5]. Chicken diseases can spread quickly in chicken flocks,

leading to mass deaths and reducing the economic value of chicken flocks. Using artificial intelligence and machine learning methods, technology can be used to diagnose chicken diseases early as an important method to control and prevent the spread of infectious diseases in chicken flocks [6] [7] [8]. Technology helps detect disease symptoms early, thereby allowing farmers to implement timely control and treatment measures, helping to minimize losses and increase livestock performance.

The Food and Agriculture Organization (FAO) projects that worldwide chicken meat output will be 103.5 million tons in 2012, accounting for approximately 34.3% of global meat production. A survey in the [9] study was carried out with households affected by severe aspergillosis. Data were collected from February 2018 to July 2019 from 183 households. The average risk of disease and mortality is 39% and 26% in chickens, 42% and 22% in turkeys, respectively, with young birds having a higher risk of disease and mortality than young birds. adult poultry. This loss causes economic losses in the chicken industry due to increased mortality, reduced meat and egg production, and poor growth. Viral infections, including Newcastle disease, infectious bursal disease, and avian influenza lead to economic costs in poultry farms, including bird losses, lower productivity, and employment losses [10]. Poultry farming is impacted by several viral, bacterial, parasitic, and fungal infections, which result in reduced appetite, weight loss, lower egg production, and greater mortality, leading to significant economic losses [11]. The highly pathogenic avian influenza epidemic in the United States led to fewer jobs, poorer productivity, and decreased tax collections, hurting both infected and non-infected farms [12]. The resurgence of Newcastle disease in village chicken populations in Tanzania caused major economic losses for small and medium farmers, affecting their predicted earnings and resulting in considerable economic burdens [13].

Advancements in machine learning approaches, such transfer learning [14] and fine-tuning [15], are increasingly being used to improve detection and classification accuracy. Transfer learning enables models pre-trained on big datasets to be applied to new tasks with less labeled data, making it ideal for medical imaging applications where annotated datasets are rare. Fine-tuning pre-trained models by modifying their parameters to better match the unique characteristics of the target task, resulting in improved performance. Huong Hoang Luong et al. [16] [17] [18] used fine-tuned transfer learning to categorize human skin, monkeypox, and brain tumors in

the international medical field. By combining these machine learning algorithms into picture categorization, doctors may increase diagnosis accuracy, minimize screening time, and provide better patient care.

Vision Transformers (ViT) [19] represent a recent advancement in the realm of computer vision, offering a novel approach to image recognition tasks [20]. Unlike traditional Convolutional Neural Networks (CNNs), ViT utilizes a self-attention mechanism to capture long-range dependencies in images, enabling effective feature extraction and representation. This architecture consists of multiple Transformer blocks, each containing self-attention layers and feed-forward neural networks. By leveraging self-attention, ViT can effectively process images without relying on spatial hierarchies, making it suitable for tasks such as image classification, object detection, and segmentation [21]. The ViT16 model, in particular, is a variant of the Vision Transformer architecture that has demonstrated impressive performance in various computer vision tasks. It consists of 16 Transformer blocks, each with self-attention layers and feed-forward neural networks. Through extensive training on large-scale datasets, ViT16 has learned to extract informative features from input images and make accurate predictions. Moreover, ViT16 has shown robustness to variations in image content and background noise, making it suitable for real-world applications in medical image analysis.

In this study, we will use the Integrated Gradients explanation. Integrated gradients were proposed by Sundararajan et al. [22] to explain the predictions of our machine learning model. Interpretation is an important part of understanding and enhancing model transparency, especially in medical applications like ours. By explaining, we will have a more detailed look at how the model makes decisions, helping us better understand predictions and increasing the model's reliability in diagnosing and treating diseases. disability.

In this study, we suggested the ViT16 model of the Vision Transformer (ViT) to detect and classify diseases in chickens. In addition, we have deployed five well-known accumulated neural network (CNN) models (EfficiencyNetB3, ResNet50, VGG16, MobileNet, and InceptionV3) and ViT32 models of the ViT architecture to evaluate and compare with the model we have proposed.

The contributions of the work are:

- This study presents four scenarios to evaluate the classification efficiency of three common diseases. The classification of healthy and coccidiosis is carried out according to the first scenario. In the second scenario, we classify Healthy and New Castle Disease. The classification of healthy and salmonella is carried out in the third scenario. In the final scenario, we classify all four classes, including healthy, coccidiosis, new castle disease, and salmonella. The purpose of implementing these four scenarios is to determine whether the ViT model is effective when classifying each class individually or multiple classes at the same time. We propose a Vision Transformer transfer learning model based on the pre-trained ViT16 architecture for chicken disease image classification. By fine-tuning the model, we achieve promising results, surpassing other CNN architectures with accuracies up to 99.75%

- 99.75% - 100% - 98.25% in four scenarios. This demonstrates the effectiveness of the ViT16 model for image classification, even without task-specific fine-tuning, achieving a transfer learning accuracy of 93%. Furthermore, fine-tuning the ViT models leads to a significant improvement in performance, increasing the accuracy from 93% to 98.25%.

- Demonstrate the effectiveness of the proposed model (ViT16) by implementing comparisons with five famous convolutional neural network architectures (EfficientNetB3, ResNet50, VGG16, MobileNet, InceptionV3) and a ViT32 model of the Vision architecture Transformer in the same setting.
- Experimental results show that the Integrated Gradients explanation is useful in helping to better understand how the model makes decisions by explaining how each pixel or feature affects the final prediction. Thanks to that, we can identify important areas in the image that the model pays attention to to make predictions. Integrated Gradients create transparent and easy-to-understand explanations, helping to increase confidence and trust in the model's predictions. This is especially important in medical and security applications, where transparency is extremely important.
- Early diagnosis will allow timely intervention and treatment measures, thereby minimizing mortality and loss in the herd. At the same time, preventing the spread of infectious diseases in chicken flocks will also play an important role in protecting health and improving food product quality. In addition, early diagnosis will also help optimize resource management and use in livestock operations, reduce waste, and increase production efficiency. This will have a positive impact on the food economy, helping to maintain and develop the livestock industry in a sustainable way.

There are five primary components to our study report. This section gives some general information about the research and discusses the approach to addressing the given difficulty. Section II includes references to related research, and the approach follows the relevant research section. Section III discusses each of the methodologies used in this paper. Section IV will discuss the experiments, including how we execute them and evaluate the deep learning model's correctness. Finally, in Section VI, we synthesize our findings and discuss the most essential parts of the research.

II. RELATED WORKS

The utilization of thermal-image processing and machine learning techniques for the detection and classification of avian diseases in chickens has gained significant attention in recent research. One notable study by M Sadeghi et al. [23] explored the application of support vector machines (SVM) and artificial neural networks (ANN) for disease classification in 14-day-old Ross 308 broilers infected with Newcastle Disease (ND) and Avian Influenza (AI), with two additional control groups included in the study. The paper demonstrated promising results, achieving high accuracy rates within 24 hours of virus infection. Specifically, SVM achieved an impressive accuracy of 97.2% for classifying AI and 100% accuracy for classifying

ND. These findings highlight the potential of machine learning algorithms for early disease detection and classification in poultry farming, contributing to improved disease management and prevention strategies.

The proposed paper [24] addresses the critical issue of early detection and classification of poultry diseases using deep learning techniques and image analysis of chicken fecal images. The model achieved an impressive accuracy of 97% utilizing the DenseNet method, showcasing its potential for practical poultry diagnostic applications. The dataset used for training and evaluation consists of 6812 images belonging to four different classes: healthy chicken, Coccidiosis, Salmonella, and Newcastle. Despite the significant progress in the field, there is a need for further research to explore the robustness and scalability of the proposed model across different poultry disease datasets and real-world scenarios.

Hoang Ngoc Tran et al. [25] present a novel approach utilizing the autoencoder and YOLOv6 model for the classification and detection of diseases in chicken flocks. The method achieved remarkable results, with an average accuracy of 99.15% and over 90% accuracy on the test dataset. The proposed approach demonstrates its versatility by being suitable for different chicken breeds from various countries and regions. This innovative method holds promise for improving the efficiency and accuracy of disease detection and classification in poultry farming, contributing to better management practices and disease control strategies. However, further studies are needed to validate the robustness and scalability of the proposed method across diverse poultry farming environments and disease scenarios.

The paper of Eduardo Carvalho Lira et al. [26] introduces a novel deep learning-based system designed for the early detection and classification of chicken diseases, including Salmonella, Coccidiosis, Healthy, and New Castle Disease. The study explores various convolutional neural network (CNN) models for categorical classification, with a focus on identifying the most efficient model based on the ratio of Maximum Validation Accuracy (MVA) to Least Validation Loss (LVL). Among the models evaluated, the ChicNetV6 model emerged as the best performer, achieving an efficiency score of 2.8198 and an impressive accuracy score of 94.49%. Notably, the total training time for the ChicNetV6 model was recorded at 1125 seconds, demonstrating its efficiency and computational feasibility. This research contributes to the advancement of automated disease detection and classification systems in poultry farming, with potential implications for enhancing disease management and prevention strategies in the industry. Further investigations may be warranted to assess the scalability and generalizability of the proposed system across different poultry farming environments and disease scenarios.

Nianpeng He et al. [27] presents a novel solution aimed at predicting diseases in chickens through the analysis of fecal images using deep Convolutional Neural Networks (CNN). Leveraging the XceptionNet deep learning framework, the proposed model demonstrates superior performance compared to other models, achieving an impressive accuracy rate of 94%. By leveraging pre-trained models and tailoring them to address the specific challenges of poultry disease prediction, the study contributes to the development of effective tools for early disease detection in poultry farming. The proposed

model holds promise for application in real-world scenarios, offering a valuable resource for poultry disease detection and management. Further research may explore the scalability and applicability of the model across different poultry breeds and disease types, with potential implications for enhancing disease surveillance and control in the poultry industry.

Although the article [28] focuses on classifying poultry eggs using deep learning techniques, it does not go into the classification of diseases in chickens. The study proposes the use of Convolutional Neural Networks (CNN) in an unwashed egg classification system, classifying them into classes such as intact, cracked, soiled and soiled. The study compares the performance of three popular CNN architectures, ResNet34, ResNet50, and VGG19, using two different batch sizes (32 and 64) during training. Among the evaluated models, the VGG19 architecture achieved the highest accuracy of 97.33% when trained with a batch size of 64. While this study provides valuable insights into egg classification using deep learning, but its focus remains different from chicken disease classification, providing an additional perspective on the application of deep learning in poultry farming. Utilizing Convolutional Neural Networks (CNN) implemented in Keras/TensorFlow, Study of Moch. Kholil et al. [29] achieved an impressive accuracy rate of 95.28% in accurately predicting the classification of infectious diseases suffered by chickens. The research highlights the effectiveness of CNNs in disease classification tasks, particularly in the context of poultry farming. This work contributes valuable insights into leveraging deep learning techniques for disease diagnosis and monitoring in poultry, demonstrating the potential of advanced technology in enhancing animal health management practices.

Huong Hoang Luong et al. study in machine learning diagnostics is significant for us. In [30], Huong Hoang Luong and colleagues proposed a strategy using a model we propose as Vision Transformer (ViT), which has recently been improved by applying transfer learning methods. delivered to create strawberry disease.. The research's objective is to train this model to detect certain illnesses while fine-tuning the outcomes to attain high accuracy. The strawberry photographs in the collection are organized into seven categories, with a focus on strawberry leaf, fruit, and flower illnesses. The ViT model outperformed a comparable strategy for strawberry illness classification, with 92.7% accuracy on the Strawberry Disease Detection dataset.

The paper [31] presents a novel system for detecting and classifying poultry diseases, integrating two core algorithms: YOLO-V3 for object detection and ResNet50 for image classification. YOLO-V3 segments regions of interest (ROIs) from fecal images, while ResNet50 classifies the segmented images into four health conditions: Healthy, Coccidiosis, Salmonella, and New Castle Disease. Training is performed on a dataset of 10,500 chicken fecal images from the Zenodo open database, with oversampling and image augmentation techniques used to address class imbalance. YOLO-V3 achieves a mean average precision of 87.48% for detecting ROIs, and ResNet50 achieves a classification accuracy of 98.7%. Experimental results demonstrate the system's ability to accurately identify prevalent poultry diseases, offering potential support to poultry farmers and veterinarians in farm settings.

III. METHODOLOGY

A. The Research Implementation Procedure

Overall, in this study, we used a combination of 11 processes to produce the results, the main processes are shown in Fig. 1. Details of the steps are given below:

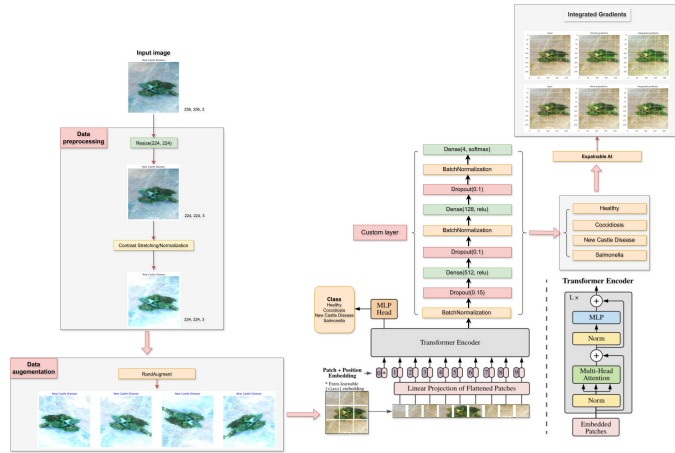


Fig. 1. Proposed architecture.

- 1) **Data collection:** Choosing an appropriate dataset is critical in the field of machine learning since it has a direct impact on model performance and generalizability. A high-quality dataset guarantees that the model is trained on a wide and representative sample set, allowing it to discover strong patterns and make accurate predictions in real-world circumstances. In the case of chicken illness detection, using the correct dataset enables researchers to create models that can accurately diagnose chicken diseases from photos, allowing for prompt treatment and resolution.
- 2) **Pre-processing Data:** Use image preprocessing techniques, for example, adjusting brightness and contrast to increase the quality and visibility of images, making them more suitable for future classification tasks. Change the input size to 224x224x3 to ensure synchronization, and use the random function in the Keras library for further processing.
- 3) **Dividing dataset into three categories train, validation, and test:** To ensure robust model training, validation, and evaluation, the dataset is divided into three subsets: training, validation, and test. The training set, which comprises 80% of the data, is utilized for model training. Meanwhile, the validation set, consisting of 10% of the data, is employed to monitor training progress and fine-tune the model to prevent overfitting. Finally, the test set, also comprising 10% of the data, is reserved to assess the final model's performance on previously unseen data. Stratified splitting is employed to maintain a balanced representation of classes across all subsets, facilitating effective model training and evaluation.
- 4) **Data Augmentation:** To augment the dataset, enhance its diversity, establish credibility, and mitigate overfitting, a range of data augmentation techniques are employed. The objective is to multiply the number

of images fourfold, thus expanding the dataset from the initial 2000 images to a later count of 8000. This augmentation process encompasses the creation of new training samples through the application of diverse transformations and modifications to the existing images. This methodology effectively expands the dataset without necessitating the collection of additional data.

- 5) **Building the model:** To carry out the experiment, we utilized five convolutional neural network (CNN) architecture models and two Vision Transformer models. We keep the model's fundamental processing layers while making the required changes to improve its performance for our unique goal. This personalized strategy enabled us to obtain outstanding outcomes when training and testing with Keras' model library.
- 6) **Applying Transfer learning:** Transfer learning enables the utilization of pre-trained models that have been trained on similar tasks, such as general image classification. These models have already acquired fundamental features from large datasets, thereby saving time and effort that would otherwise be required to train a model from scratch. By leveraging pre-trained models, the amount of engineering work and resources needed to deploy the model across health systems is significantly reduced.
- 7) **Retrain the model with Fine-Tuning:** Fine-tuning involves tweaking the parameters of a pre-trained model to better align with a specific task. Nonetheless, to implement these adjustments and enhance the model's performance, re-training is essential. The model is fine-tuned to optimize performance for the targeted task. Re-training facilitates further learning from additional data, enhancing the model's ability to generalize and make accurate predictions on unseen data.
- 8) **Validate and collect metrics to evaluate the model:** By analyzing metrics like accuracy, precision, recall, and F1-score, it is possible to assess how well our model performs on data it has not been trained on. This assessment process helps in evaluating the model's effectiveness on the test dataset and offers insights into its performance under different circumstances. The conclusions drawn from the evaluation phase guide modifications to the model's hyperparameters, such as the learning rate, number of epochs, batch size, and neural network structure. These modifications are suggested based on the evaluation outcomes, with the goal of improving the model's performance and ensuring its ability to generalize to new data.
- 9) **Visual explanation by Integrated Gradients:** Integrated Gradients create easy-to-understand explanations for machine learning model predictions by calculating the influence of each input feature on the final prediction. By providing information about how each input feature contributes to the final prediction, Integrated Gradients help increase the transparency of the machine learning model. This can be useful in medical, financial and legal applications where transparency is important.
- 10) **Comparison with other advanced methods:** Comparing with other advanced techniques aids in assessing

model performance and gauging the effectiveness and novelty of the proposed approach relative to already explored and recognized methods. This enables the evaluation of which aspects of your strategy are more efficacious than others and which ones necessitate modification.

- 11) *Showing the result:* The outcomes and visual representations post comparison will be presented through confusion matrices, line graphs, and tables. These results illustrate the model's real-world performance and its effectiveness in diagnosing chicken disease.

B. Pre-processing Image

Pre-processing plays a crucial role in preparing image data for machine learning tasks as it enhances the quality, consistency, and informativeness of the images, thereby improving model performance. In our study, we conducted the following data pre-processing steps:

- 1) *Resize image:* A critical component of image preprocessing is ensuring uniform input size. To accomplish this, we resized all images to a consistent size of 224 pixels in width and 224 pixels in height, as determined by (Eq. 1):

$$I_{ReSize}(new_width, new_height) = I_{ReSize}(224, 224) \quad (1)$$

- 2) *Add Weighted:* We adjusted the brightness of the photos by -0.15 to improve the visibility of essential elements, especially in darker locations. This minor change demonstrated in (Eq. 2) improves feature visibility while preserving overall contrast.

$$B_{adjusted} = B_{original} - 0.15 \quad (2)$$

We used a contrast enhancement factor of 1.8 to highlight the differences between successive pixel intensities. This stage reveals tumor borders and structural features, facilitating precise diagnosis and categorization. In (Eq. 3), double the original contrast value by 1.5 to increase contrast. This factor can be fine-tuned based on the image content and desired amount of focus on differences in pixel intensities.

$$C_{adjusted} = C_{original} * 1.5 \quad (3)$$

- 3) *Data Augmentation:* We used data augmentation techniques to scale the generated training dataset by making various changes on the input samples. First, we extracted 500 images as a subset for each class because the proportion of images of the four classes is not equal, this avoids leading to data imbalance as well as the model's learning ability. Common enhancement methods then include geometric transformations such as rotation, scaling, and flipping, as well as color and contrast adjustments. Finally, we obtained the result that the number of original images increased from 2000 to 8000 images. By expanding the data set, the model is exposed to more variables and situations, leading to better generalization and performance in real-world applications. In summary, data augmentation is a crucial method that enhances the performance and

generalization capacity of machine learning models, particularly in scenarios where extensive and varied datasets are lacking.

C. Transfer Learning and Fine-Tuning of our Proposed Model

Transfer learning refers to a technique in machine learning and deep learning where a model is initially trained on a large dataset and then repurposed (transferred) to address a related or similar problem. Rather than commencing training from scratch with a small dataset, transfer learning enables leveraging the insights and knowledge acquired from prior training on extensive datasets to enhance the model's performance on a new dataset [32]. Throughout the training process, existing model parameters are reused. Consequently, transfer learning utilizes the pre-trained model layers instead of initiating training anew, thereby enhancing the model's accuracy.

After applying transfer learning, fine-tuning the model can help improve results. Fine-tuning involves adjusting and updating certain parts of the pre-trained model, such as the final layers, to better suit the specific problem at hand. To preserve the ability to extract low-level features acquired during pre-training, the initial layers of the model are often frozen during this process. By freezing these layers, the focus of adaptation shifts to the later layers, which are responsible for task-specific learning, thereby maximizing the effectiveness of training. Additionally, fine-tuning requires adjusting hyperparameters, such as the number of training epochs, batch size, hidden layer configuration, and learning rate, to optimize model performance and prevent overfitting.

We used a hyperparameter search to fine-tune the model in order to get the best results without overfitting. The many combinations of training epochs, batch sizes, hidden layer configurations, and learning rates were investigated in this search. The following hyperparameters were chosen based on the findings in order to achieve a decent balance between training efficiency and performance:

- Training epochs: 20
- Number of batches: 16
- Hidden layer set up: [512, 128]
- Rate of learning: default.

During fine-tuning the model, we unlock and tune the last 20 layers of the model without adjusting the rest of the model. The main reason is that the final layers often contain more complex and specific information about the data of the specific task we are training the model for. After unlocking and fine-tuning the last 20 layers, we added a custom layer set consisting of nine layers of three layer types Dense, BatchNormalization, Dropout. Our architecture is depicted in Fig. 2 By adjusting only the final layers, we can preserve the more general and abstract features learned from big data and only adjust them to suit our specific task. This helps minimize the risk of overfitting and increases the generality of the model on new data sets.

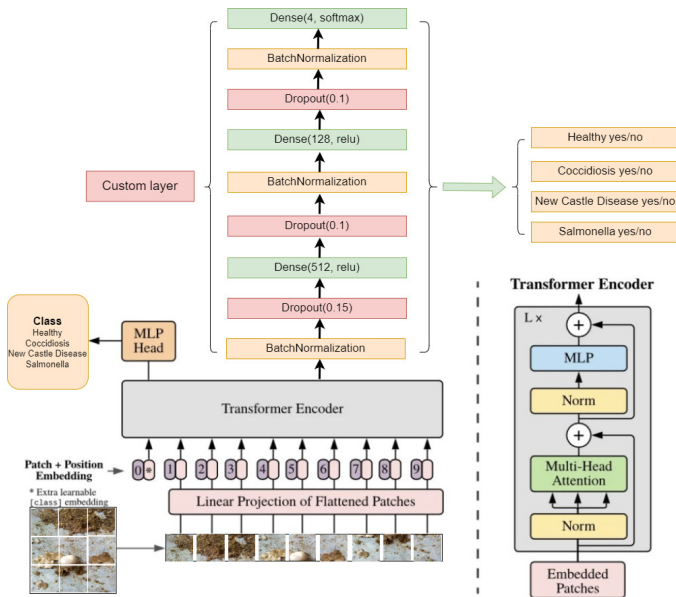


Fig. 2. Fine-tuning architecture.

D. Visual Explanation by Integrated Gradients

The need to use explanations is to better understand how the model makes decisions and makes predictions. This enhances model transparency and reliability, especially in fields such as healthcare, where a detailed explanation of the decision-making process can be extremely important for diagnosis and treat diseases.

Integrated Gradients is a method for explaining machine learning model predictions, used to understand the model's decision-making process based on inputs. This method calculates the importance of each input feature by integrating over the path from the reference point to the data point under consideration. When calculating, each feature is gradually changed from its reference value to its current value, helping to determine how each feature affects the model's final prediction.

Integrated Gradients have many advantages over other interpretation methods. First, it is computationally efficient and easy to understand, allowing to determine the importance of each feature accurately. Second, this method does not require specific information about the structure or characteristics of the model, making it flexible and applicable to many different types of machine learning models. Finally, Integrated Gradients enable both quantitative and qualitative interpretation, providing a comprehensive view of how the model makes decisions.

The use of Integrated Gradients has been used in various machine learning models, including deep neural networks, to enhance transparency and interpretability [33] [34]. The approach is suitable for both regression and classification models. When dealing with a non-scalar output, as seen in classification models or multi-target regression, the gradients are computed for a specific element of the output. In classification models, the gradient typically pertains to the output associated with the true class or the class predicted by the model.

Let's suppose we have an input instance x_1 a baseline instance x' and a model $M : X \rightarrow Y$ that operates on the

feature space X and generates an output y in the output space Y . Now, let's define the function F as

- $F(x) = M(x)$ if the model output is a scalar;
- $F(x) = M_k(x)$ if the model output is a vector, with the index k denoting the k -th element of $M(x)$.

For instance, in case of a K -class classification, $M_k(x)$ is the probability of class k , which could be the true class corresponding to x or the highest probability class predicted by the model. The attributions $A_i(x, x')$ for each feature x_i with respect to the corresponding feature x'_i in the baseline are computed as shown in Eq. 4;

$$A_i(x, x') = (x_i - x'_i) \int_0^1 \frac{\partial F(x' + \alpha(x - x'))}{\partial x_i} d\alpha \quad (4)$$

In summary, employing Integrated Gradients for visual explanations provides a promising method to improve the transparency, accountability, and reliability of machine learning models, thereby enhancing their utility and credibility in real-world applications. As illustrated in Fig. 3, analyzing the contribution of individual feature maps to the final decision provides valuable insights that experts and clinicians can leverage in future endeavors.

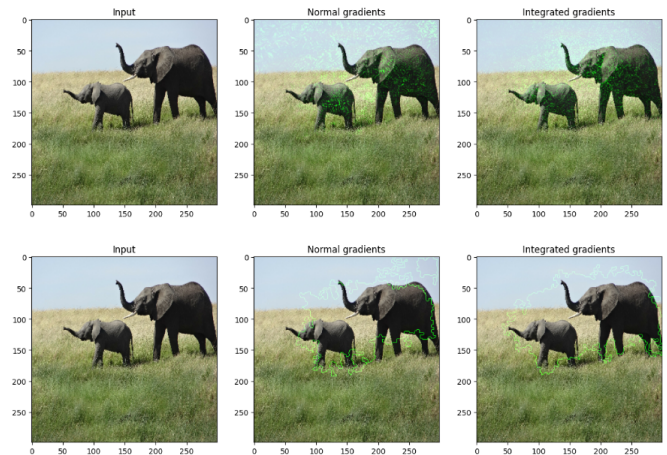


Fig. 3. The sample applying integrated gradients by keras library.

IV. EXPERIMENTS

A. Dataset and Performance Metrics

An annotated dataset on poultry disease diagnostics for small and medium-sized poultry farmers includes images of poultry feces. Images of poultry droppings were taken in the Arusha and Kilimanjaro regions of Tanzania between September 2020 and February 2021 using the Open Data Kit (ODK) mobile app. The data set contains 8067 images, divided into 4 classes in Fig. 4: Coccidiosis(30.4%), Healthy(29.5%), New Castle Disease(7.8%), Salmonella(32.3%).

Due to imbalance in the data set, we randomly selected 500 images for each class to use for training. It is important to provide a variety of representations while reducing the risk of overfitting and improving the generalizability of the model. After image preprocessing and data enhancement, we obtained

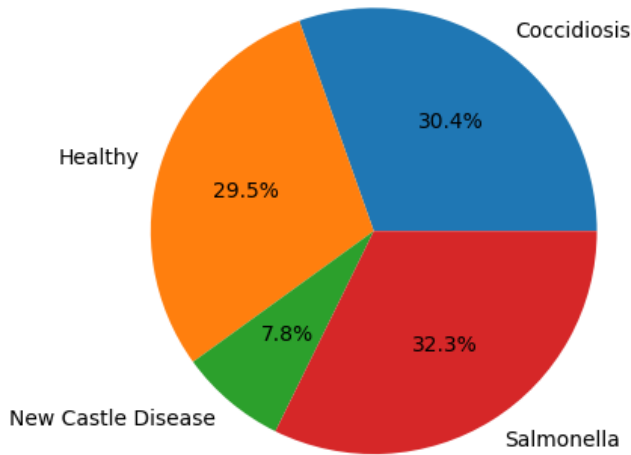


Fig. 4. Data set characteristics before processing.

a new dataset with 8000 images as shown in Fig. 5 from 2000 original images.

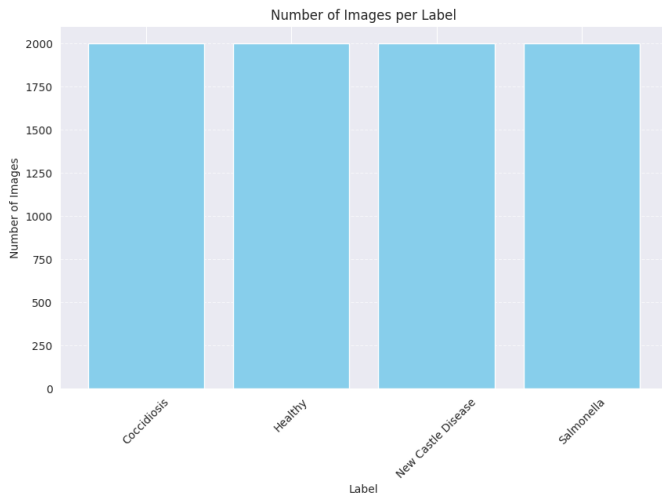


Fig. 5. Dataset characteristics after processing.

Evaluating the performance of a machine learning model is an important part of the research and implementation process. In the field of machine learning, there are many metrics used to evaluate the performance of a model, including Accuracy, Precision, Recall and F1-score.

Eq. 5 represents the ratio between the number of correct predictions and the total number of samples. Eq. 6 represents the accuracy of detecting Positive points. The higher this number, the more accurate the model receives Positive scores. Eq. 7 represents the ability to detect all positive, the higher this rate shows the lower the possibility of missing Positive points. Eq. 8 is a compromise number for Recall and Precision, used when it is necessary to consider both values, giving us a basis for choosing a model.

$$\text{Accuracy} = \frac{TP + TN}{TP + TN + FP + FN} \quad (5)$$

$$\text{Precision} = \frac{TP}{TP + FP} \quad (6)$$

$$\text{Recall} = \frac{TP}{TP + FN} \quad (7)$$

$$F1 = 2 * \frac{\text{Precision} * \text{Recall}}{\text{Precision} + \text{Recall}} \quad (8)$$

These metrics offer a holistic perspective on the effectiveness of a machine learning model, enabling users to precisely assess its capability to make predictions and identify significant instances.

B. Scenario 1: Classification of 2 Classes (Coccidiosis and Healthy)

TABLE I. THE RESULTS OF CLASSIFYING IMAGES INTO 2 CLASSES COCCIDIOSIS AND HEALTHY IN TRANSFER LEARNING

| Transfer learning Without Augmentation | | | | |
|--|---------------|---------------|---------------|---------------|
| Model | ACC | Precision | Recall | F1 |
| EfficientNetB3 | 69,00% | 69,00% | 69,00% | 68,99% |
| ResNet50 | 92,00% | 92,06% | 92,00% | 91,99% |
| VGG16 | 95,00% | 95,16% | 95,00% | 94,99% |
| MobileNet | 100,00% | 100,00% | 100,00% | 100,00% |
| InceptionV3 | 98,00% | 98,07% | 98,00% | 97,99% |
| ViT32 | 98,00% | 98,00% | 98,00% | 98,00% |
| ViT16 (Our Proposed) | 98,00% | 98,00% | 98,00% | 98,00% |
| Transfer learning With Augmentation | | | | |
| Model | ACC | Precision | Recall | F1 |
| EfficientNetB3 | 71,50% | 71,67% | 71,50% | 71,44% |
| ResNet50 | 94,75% | 95% | 94,75% | 94,74% |
| VGG16 | 96,75% | 96,75% | 96,75% | 96,75% |
| MobileNet | 100,00% | 100,00% | 100,00% | 100,00% |
| InceptionV3 | 98,50% | 98,50% | 98,50% | 98,50% |
| ViT32 | 99,50% | 99,50% | 99,50% | 99,50% |
| ViT16 (Our Proposed) | 99,25% | 99,25% | 99,25% | 99,25% |

In this scenario, we apply transfer learning and fine-tuning in both cases with and without data augmentation to classify Coccidiosis and Healthy of seven different machine learning models. The results obtained in the transfer learning part in Table I show the effectiveness of the model when trained on the data set after augmentation. The accuracy of the proposed model has been improved from 98% to 99.25%. A bright spot besides the proposed model is that the MobileNet model also achieves high efficiency when achieving 100% accuracy. Regarding the fine-tuning showed in Table II, we obtain the results before and after enhancing the data set respectively as 98.00%-98.75%.

Fig. 6 and Fig. 7 depict a graphical representation of the training accuracy and loss on the augmented dataset. Throughout the training process, the two curves intersect multiple times, illustrating the model's ability to strike a balance between learning from the training data and generalizing to new data. In general, both the training accuracy and loss curves exhibit a smooth behavior without any significant disparity, thereby indicating the model's suitability and robustness in terms of generalization capability.

TABLE II. THE RESULTS OF CLASSIFYING IMAGES INTO 2 CLASSES COCCIDIOSIS AND HEALTHY IN FINE-TUNING

| Fine-Tuning Without Augmentation | | | | |
|----------------------------------|---------------|---------------|---------------|---------------|
| Model | ACC | Precision | Recall | F1 |
| EfficientNetB3 | 67,00% | 70,64% | 67,00% | 65,47% |
| ResNet50 | 82,00% | 83,33% | 82,00% | 81,81% |
| VGG16 | 97,00% | 97,00% | 97,00% | 97,00% |
| MobileNet | 97,00% | 97,00% | 97,00% | 97,00% |
| InceptionV3 | 94,00% | 94,00% | 94,00% | 94,00% |
| ViT32 | 97,00% | 97,00% | 97,00% | 97,00% |
| ViT16 (Our Proposed) | 99,00% | 99,00% | 99,00% | 99,00% |
| Fine-Tuning With Augmentation | | | | |
| Model | ACC | Precision | Recall | F1 |
| EfficientNetB3 | 50,00% | 25,00% | 50,00% | 33,33% |
| ResNet50 | 91,25% | 91,25% | 91,25% | 91,25% |
| VGG16 | 97,50% | 97,50% | 97,50% | 97,50% |
| MobileNet | 99,50% | 99,50% | 99,50% | 99,50% |
| InceptionV3 | 97,50% | 97,50% | 97,50% | 97,50% |
| ViT32 | 99,00% | 99,00% | 99,00% | 99,00% |
| ViT16 (Our Proposed) | 99,25% | 99,25% | 99,25% | 99,25% |

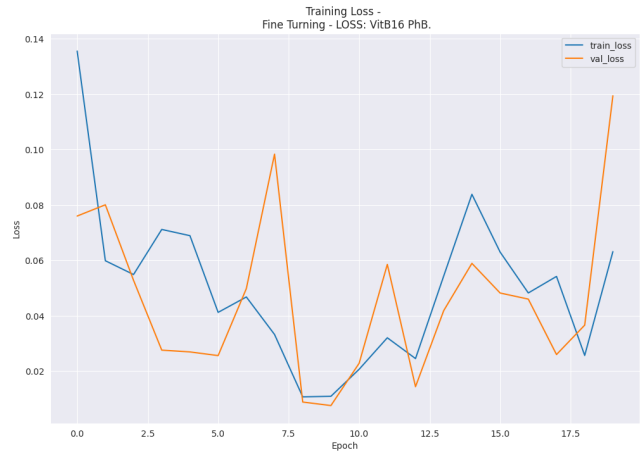


Fig. 7. Training loss and validation accuracy in fine-tuning of ours model (coccidiosis and healthy).

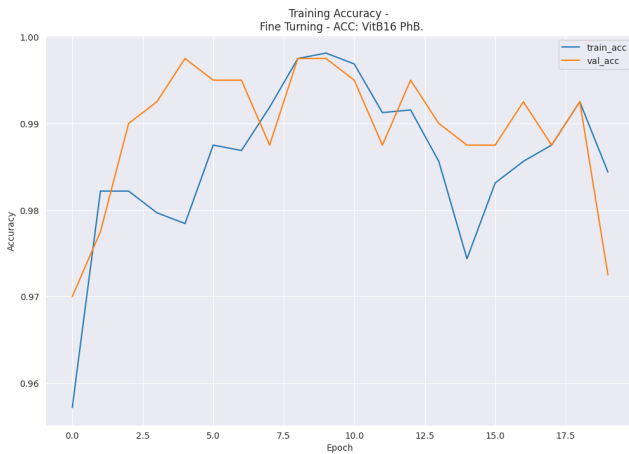


Fig. 6. Training accuracy and validation accuracy in fine-tuning of ours model (coccidiosis and healthy).

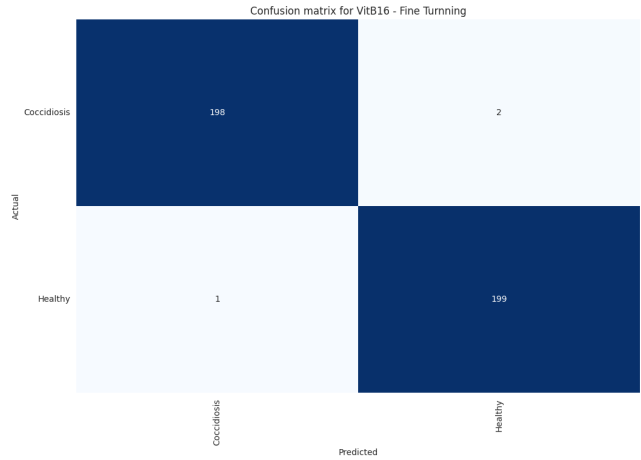


Fig. 8. Confusion matrix in fine-tuning of ours model (coccidiosis and healthy).

Fig. 8 presents the confusion matrix of 400 test images of Coccidiosis and Healthy. Fig. 9 is the result of the Integrated Gradients explanation. Through the two pictures above, we can see the transparency of the training process as well as overfitting does not happen.

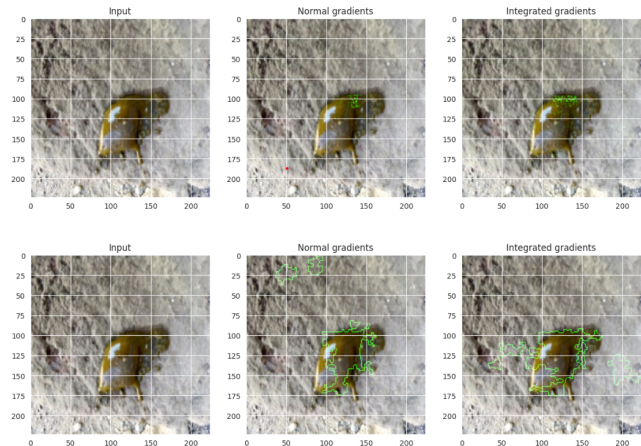


Fig. 9. Output of our model with integrated gradients explanation in scenario 1.

C. Scenario 2: Classification of 2 Classes (New Castle Disease and Healthy)

In this scenario, we classify the next two classes including New Castle Disease and Healthy. The scenario performs transfer learning and fine-tuning in both cases with and without data augmentation. The results obtained in the transfer learning part of the proposed model in Table III are 98.50% accuracy - an improvement of more than 3.5% compared to training on the original data set. Table IV also shows the effectiveness of fine-tuning when the obtained accuracy is 99.75%, which is higher than that of transfer learning.

TABLE III. THE RESULTS OF CLASSIFYING IMAGES INTO 2 CLASSES NEW CASTLE DISEASE AND HEALTHY IN TRANSFER LEARNING

| Transfer learning Without Augmentation | | | | |
|--|---------------|---------------|---------------|---------------|
| Model | ACC | Precision | Recall | F1 |
| EfficientNetB3 | 76,00% | 76,68% | 76,00% | 75,84% |
| ResNet50 | 86,00% | 86,05% | 86,00% | 85,99% |
| VGG16 | 88,00% | 88,06% | 88,00% | 87,99% |
| MobileNet | 95,00% | 95,16% | 95,00% | 94,99% |
| InceptionV3 | 89,00% | 89,01% | 89,00% | 88,99% |
| ViT32 | 95,00% | 95,16% | 95,00% | 94,99% |
| ViT16 (Our Proposed) | 95,00% | 95,01% | 95,00% | 94,99% |
| Transfer learning With Augmentation | | | | |
| Model | ACC | Precision | Recall | F1 |
| EfficientNetB3 | 74,75% | 75,14% | 74,75% | 74,65% |
| ResNet50 | 88,75% | 88,75% | 88,75% | 88,75% |
| VGG16 | 92,25% | 92,49% | 92,25% | 92,24% |
| MobileNet | 98,50% | 98,50% | 98,50% | 98,50% |
| InceptionV3 | 96,50% | 96,51% | 96,50% | 96,50% |
| ViT32 | 98,50% | 98,52% | 98,50% | 98,50% |
| ViT16 (Our Proposed) | 98,50% | 98,50% | 98,50% | 98,50% |

TABLE IV. THE RESULTS OF CLASSIFYING IMAGES INTO 2 CLASSES NEW CASTLE DISEASE AND HEALTHY IN FINE-TUNING

| Fine-Tuning Without Augmentation | | | | |
|----------------------------------|---------------|---------------|---------------|---------------|
| Model | ACC | Precision | Recall | F1 |
| EfficientNetB3 | 68,00% | 68,11% | 68,00% | 68,00% |
| ResNet50 | 86% | 87,50% | 86% | 85,85% |
| VGG16 | 95% | 95% | 95% | 95% |
| MobileNet | 93% | 93,43% | 93% | 93% |
| InceptionV3 | 91,00% | 91,00% | 91,00% | 91,00% |
| ViT32 | 97% | 97% | 97% | 97% |
| ViT16 (Our Proposed) | 97% | 97% | 97% | 97% |
| Fine-Tuning With Augmentation | | | | |
| Model | ACC | Precision | Recall | F1 |
| EfficientNetB3 | 74,50% | 74,62% | 74,50% | 74,46% |
| ResNet50 | 51,25% | 75,31% | 51,25% | 36,05% |
| VGG16 | 94,25% | 94,38% | 94,25% | 94,24% |
| MobileNet | 98,75% | 98,75% | 98,75% | 98,74% |
| InceptionV3 | 95,50% | 95,54% | 95,50% | 95,49% |
| ViT32 | 99,50% | 99,50% | 99,50% | 99,49% |
| ViT16 (Our Proposed) | 99,75% | 99,75% | 99,75% | 99,74% |

Fig. 10 and Fig. 11 show the training process's accuracy and loss in the second scenario experiment. The two curves do not noticeably vary from one another during the training period and climb steadily. The model is adequate and has a

great potential for generalization because the training and loss accuracy curves are generally smooth and show no discernible deviation between them.

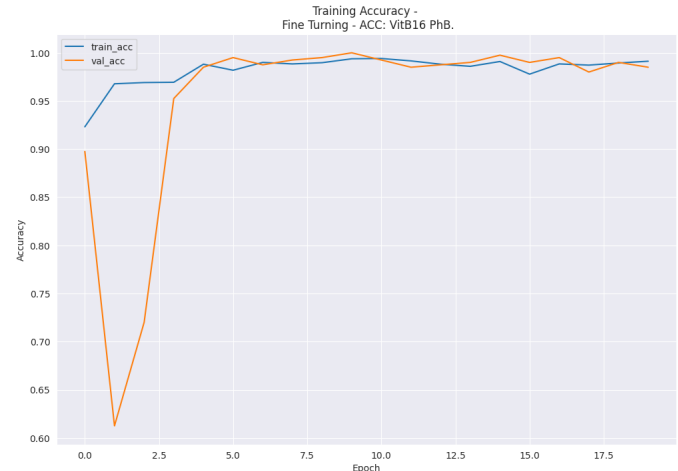


Fig. 10. Training accuracy and validation accuracy in fine-tuning of our model (new castle disease and healthy).

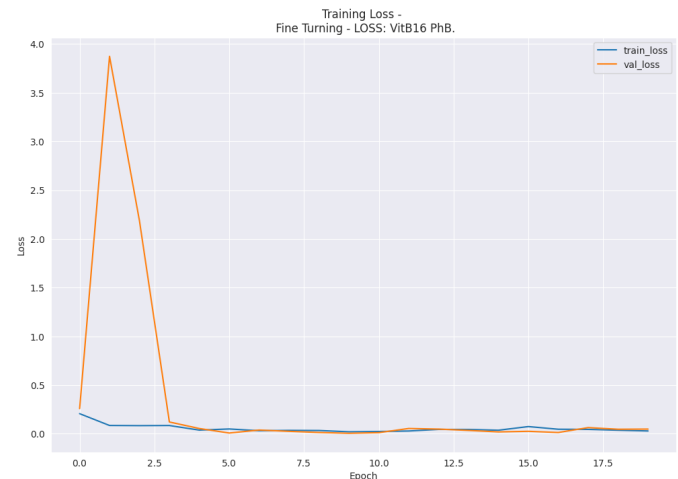


Fig. 11. Training loss and validation accuracy in fine-tuning of our model (new castle disease and healthy).

Fig. 12 presents the confusion matrix of the 2-type classification scenario New Castle Disease and Healthy. From the matrix, we see that the model performs absolutely well when identifying the healthy class. At the same time, the New Castle Disease class has only one flaw. Fig. 13 is the result of the built-in Gradient explanation for this scenario.

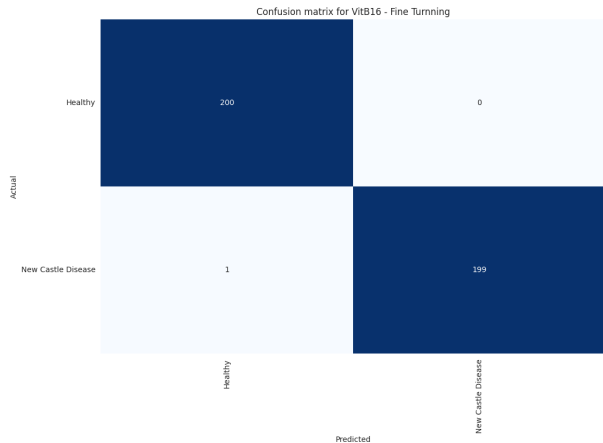


Fig. 12. Confusion matrix in fine-tuning of ours model (New castle disease and healthy).

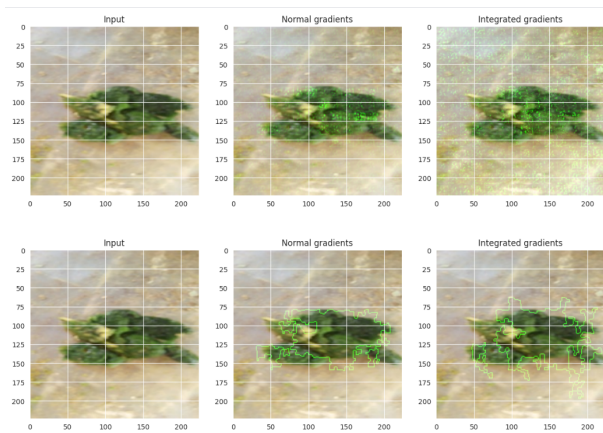


Fig. 13. Output of our model with integrated gradients explanation in scenario 2.

D. Scenario 3: Classification of 2 Classes (Salmonella and Healthy)

This scenario presents the results of classifying the two classes Salmonella and Healthy before and after data fortification. In Table V, we note the improvement in the accuracy of the proposed model by up to 8% when it reaches 98%. Furthermore, after fine-tuning, the proposed model has achieved 100% absolute accuracy with data augmentation and most other models in the Table VI have also improved.

Fig. 14 and Fig. 15 show the training process' accuracy and loss in the scenario 3 experiment. The two curves continuously rise and do not considerably diverge from one another during the training phase, demonstrating the transparency and dependability of the suggested model.

Fig. 16 presents the confusion matrix of the Salmonella and Healthy class classification test. From the matrix, we see that the model performs best when classifying chicken diseases with an accuracy rate of 100%. Fig. 17 is the result of the explanation of Integrated Gradients for Salmonella and Healthy classification.

TABLE V. THE RESULTS OF CLASSIFYING IMAGES INTO 2 CLASSES SALMONELLA AND HEALTHY IN TRANSFER LEARNING

| Transfer learning Without Augmentation | | | | |
|--|---------------|---------------|---------------|---------------|
| Model | ACC | Precision | Recall | F1 |
| EfficientNetB3 | 68,00% | 68,26% | 68,00% | 67,88% |
| ResNet50 | 81,00% | 81,61% | 81,00% | 80,90% |
| VGG16 | 88,00% | 88,06% | 88,00% | 87,99% |
| MobileNet | 93,00% | 93,85% | 93,00% | 92,96% |
| InceptionV3 | 92,00% | 92,61% | 92,00% | 91,97% |
| ViT32 | 92,00% | 92,00% | 92,00% | 92,00% |
| ViT16 (Our Proposed) | 90,00% | 90,06% | 90,00% | 89,99% |
| Transfer learning With Augmentation | | | | |
| Model | ACC | Precision | Recall | F1 |
| EfficientNetB3 | 76% | 76,87% | 76% | 75,80% |
| ResNet50 | 92,25% | 92,33% | 92,25% | 92,24% |
| VGG16 | 94,25% | 94,26% | 94,25% | 94,25% |
| MobileNet | 96,50% | 96,50% | 96,50% | 96,50% |
| InceptionV3 | 94,75% | 94,76% | 94,75% | 94,75% |
| ViT32 | 97,75% | 97,75% | 97,75% | 97,75% |
| ViT16 (Our Proposed) | 98% | 98,02% | 98% | 98% |

TABLE VI. THE RESULTS OF CLASSIFYING IMAGES INTO 2 CLASSES SALMONELLA AND HEALTHY IN FINE-TUNING

| Fine-Tuning Without Augmentation | | | | |
|----------------------------------|----------------|----------------|----------------|----------------|
| Model | ACC | Precision | Recall | F1 |
| EfficientNetB3 | 72% | 72,32% | 72% | 71,89% |
| ResNet50 | 92% | 92% | 92% | 92% |
| VGG16 | 95% | 95% | 95% | 95% |
| MobileNet | 95% | 95,45% | 95,00% | 95% |
| InceptionV3 | 94% | 94,28% | 94% | 93,99% |
| ViT32 | 97% | 97,17% | 97% | 97% |
| ViT16 (Our Proposed) | 98% | 98,07% | 98% | 98% |
| Fine-Tuning With Augmentation | | | | |
| Model | ACC | Precision | Recall | F1 |
| EfficientNetB3 | 59,00% | 63,33% | 59,00% | 55,37% |
| ResNet50 | 91,25% | 91,55% | 91,25% | 91,23% |
| VGG16 | 92,25% | 92,81% | 92,25% | 92,22% |
| MobileNet | 95,25% | 95,44% | 95,25% | 95,24% |
| InceptionV3 | 95,50% | 95,50% | 95,50% | 95,50% |
| ViT32 | 98,75% | 98,78% | 98,75% | 98,74% |
| ViT16 (Our Proposed) | 100,00% | 100,00% | 100,00% | 100,00% |

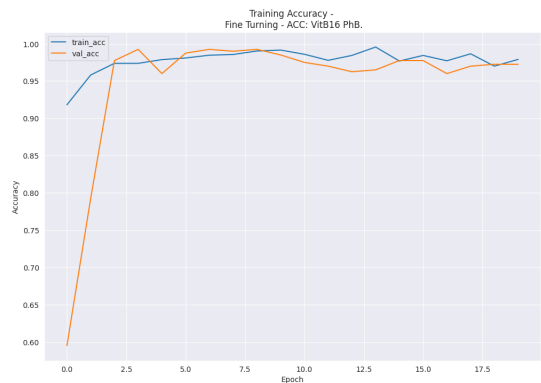


Fig. 14. Training accuracy and validation accuracy in fine-tuning of ours model (salmonella and healthy).

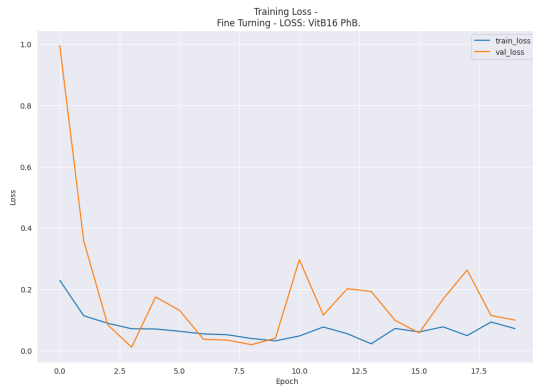


Fig. 15. Training loss and validation accuracy in fine-tuning of ours model (salmonella and healthy).

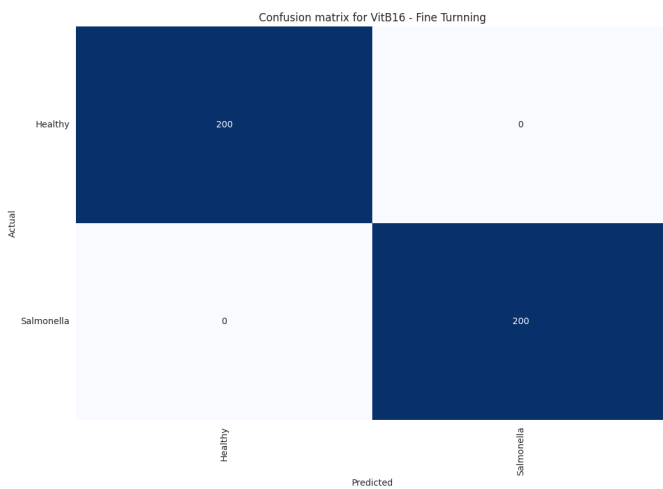


Fig. 16. Confusion matrix in fine-tuning of ours model (salmonella and healthy).

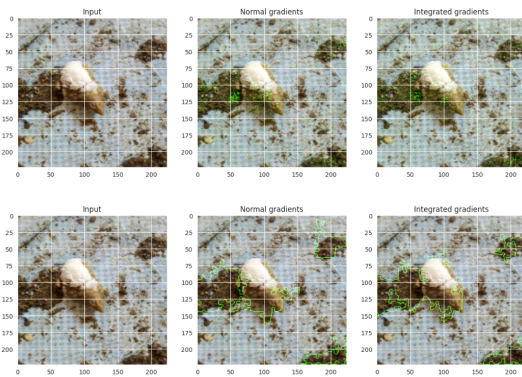


Fig. 17. Output of our model with integrated gradients explanation in scenario 3.

E. Scenario 4: Classification of 4 Classes (Coccidiosis, New Castle Disease, Salmonella and Healthy)

This is an important scenario that shows the strong performance of the proposed model when the classification problem has up to 4 classes. It can be seen that after the transfer learning

process in Table VII, the proposed model achieved 97.75% accuracy when trained on the augmented data set. In contrast, the model only achieved 89.50% accuracy when trained on the original data set. After the stage of fine-tuning the proposed model with the augmented data set, the final result obtained in Table VIII has an accuracy of 98.25%.

TABLE VII. THE RESULTS OF CLASSIFYING IMAGES INTO 4 CLASSES COCCIDIOSIS, NEW CASTLE DISEASE, SALMONELLA AND HEALTHY IN TRANSFER LEARNING

| Transfer learning Without Augmentation | | | | |
|--|---------------|---------------|---------------|---------------|
| Model | ACC | Precision | Recall | F1 |
| EfficientNetB3 | 40,50% | 30,50% | 40,50% | 33,92% |
| ResNet50 | 70,50% | 72,04% | 70,50% | 70,75% |
| VGG16 | 73,50% | 74,83% | 73,50% | 73,84% |
| MobileNet | 89,00% | 89,22% | 89,00% | 89,03% |
| InceptionV3 | 84,00% | 84,16% | 84,00% | 83,90% |
| ViT32 | 92,00% | 92,13% | 92,00% | 92,00% |
| ViT16 (Our Proposed) | 89,50% | 89,59% | 89,50% | 89,50% |
| Transfer learning With Augmentation | | | | |
| Model | ACC | Precision | Recall | F1 |
| EfficientNetB3 | 41,37% | 41,48% | 41,37% | 39,38% |
| ResNet50 | 73,50% | 74,19% | 73,50% | 73,63% |
| VGG16 | 85,37% | 85,51% | 85,37% | 85,40% |
| MobileNet | 93,87% | 93,86% | 93,87% | 93,86% |
| InceptionV3 | 91,87% | 91,88% | 91,87% | 91,87% |
| ViT32 | 96,25% | 96,24% | 96,25% | 96,24% |
| ViT16 (Our Proposed) | 97,75% | 97,76% | 97,75% | 97,74% |

TABLE VIII. THE RESULTS OF CLASSIFYING IMAGES INTO 4 CLASSES COCCIDIOSIS, NEW CASTLE DISEASE, SALMONELLA AND HEALTHY IN FINE-TUNING

| Fine-Tuning Without Augmentation | | | | |
|----------------------------------|---------------|---------------|---------------|---------------|
| Model | ACC | Precision | Recall | F1 |
| EfficientNetB3 | 30,50% | 18,57% | 30,50% | 20,95% |
| ResNet50 | 38,00% | 20,89% | 38,00% | 25,48% |
| VGG16 | 56,50% | 53,28% | 56,50% | 51,11% |
| MobileNet | 86,00% | 88,22% | 86,00% | 85,59% |
| InceptionV3 | 83,00% | 83,78% | 83,00% | 83,02% |
| ViT32 | 95,00% | 95,14% | 95,00% | 95,01% |
| ViT16 (Our Proposed) | 98,00% | 98,03% | 98,00% | 97,99% |
| Fine-Tuning With Augmentation | | | | |
| Model | ACC | Precision | Recall | F1 |
| EfficientNetB3 | 49,75% | 39,66% | 49,75% | 43,24% |
| ResNet50 | 26,25% | 31,32% | 26,25% | 12,48% |
| VGG16 | 90,25% | 91,12% | 90,25% | 90,16% |
| MobileNet | 92,25% | 92,56% | 92,25% | 92,25% |
| InceptionV3 | 90,25% | 90,25% | 90,25% | 90,24% |
| ViT32 | 97,25% | 97,25% | 97,25% | 97,24% |
| ViT16 (Our Proposed) | 98,25% | 98,25% | 98,25% | 98,24% |

Fig. 18 and Fig. 19 illustrate the training accuracy and loss in the test of scenario 4. Fig. 20 presents the confusion matrix of 800 test images of four classes including Coccidiosis, New Castle Disease, Salmonella and Healthy. Fig. 21 is the result of the explanation of the Integrated Gradient to classify the above four classes.

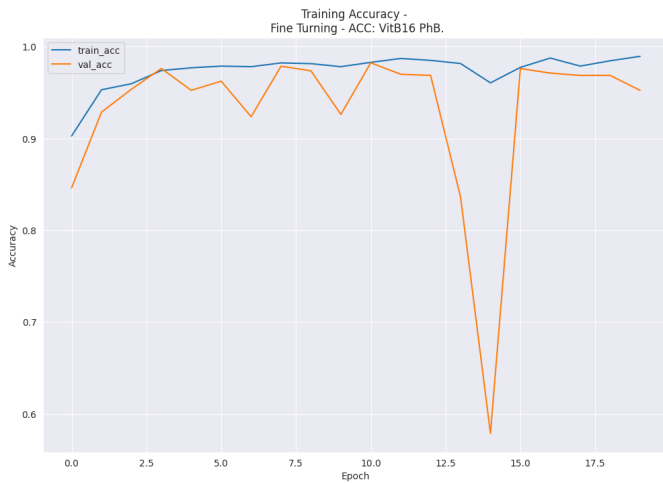


Fig. 18. Training accuracy and validation accuracy in fine-tuning of our model (Coccidiosis, new castle disease, salmonella and healthy).

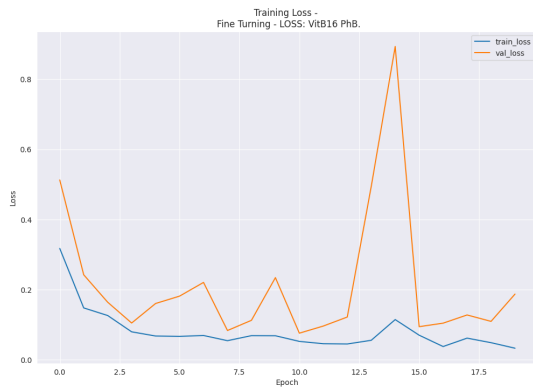


Fig. 19. Training loss and validation accuracy in fine-tuning of our model (Coccidiosis, new castle disease, salmonella and healthy).

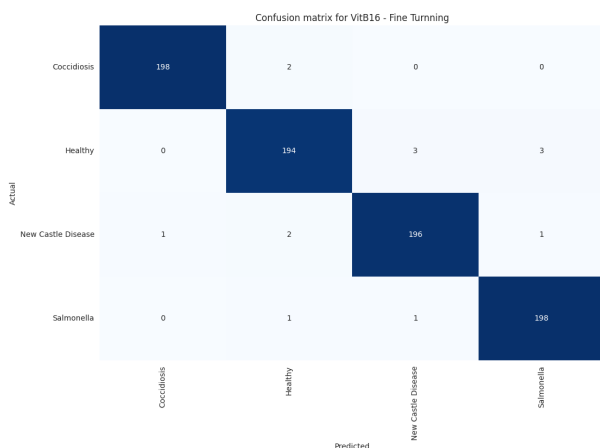


Fig. 20. Confusion matrix in fine-tuning of our model (Coccidiosis, new castle disease, salmonella and healthy).

F. Comparison with other State-of-the-art Methods

This section completely compares our proposed method with several existing state-of-the-art classification methods.

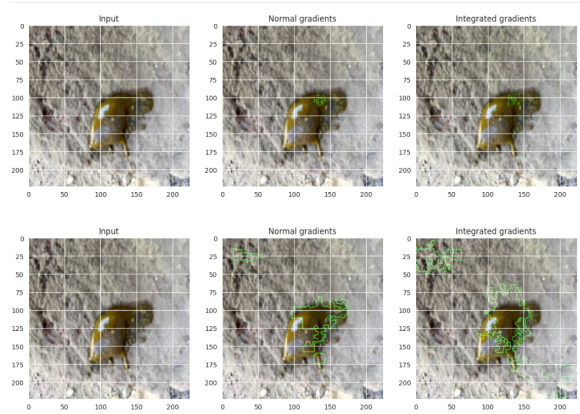


Fig. 21. Output of our model with Integrated Gradients Explanation in Scenario 4.

Table IX compares chicken disease classification methods using ViT and CNN architectures. It can be seen that the proposed model (fine-tuned ViT16) performs better than most recently published works on disease detection in chickens.

TABLE IX. COMPARISON WITH OTHERS STATE-OF-THE-ART METHODS

| Ref. | Architecture | ACC |
|-----------------------------------|--------------|---------------|
| Moch. Kholil et al. [29] | CNN | 95,28% |
| Mizanu Zelalem Degu et al. [31] | YOLOv3 | 98,70% |
| Dina Machuve et al. [35] | Xception | 98,24% |
| Our Proposed Model (ViT16) | | 98,25% |

Our proposed model outperforms most state-of-the-art methods in terms of accuracy and other evaluation metrics. Specifically, our model achieves higher accuracy than CNN, Xception and approximates the YOLOv3 model. The outstanding performance of our model can be attributed to its ability to effectively capture and classify features associated with poultry diseases, leveraging the strengths of deep learning techniques and innovative architectural design.

V. DISCUSSION

Our study aimed to develop a robust model for poultry disease image classification, leveraging transfer learning and fine-tuning techniques. The results demonstrated the efficacy of this approach, with the proposed model (ViT16) achieving high accuracy rates across various scenarios. This outcome underscores the importance of utilizing pre-trained models and optimizing them for specific tasks, highlighting the potential of transfer learning in medical image analysis.

Furthermore, by meticulously fine-tuning hyperparameters and incorporating dense layers, dropout layers, and Batch Normalization, we successfully mitigated overfitting and improved classification accuracy. These findings underscore the importance of meticulous model development and optimization to achieve superior performance in medical image classification tasks.

Moreover, the integration of Integrated Gradients for visual explanation provided valuable insights into the model's decision-making process. This transparency not only enhances

trust in the model's predictions but also facilitates error recognition and model improvement. The discussion also emphasizes the broader implications of the research, particularly in advancing diagnostics and anomaly detection in livestock farming.

In summary, through rigorous experimentation and optimization, our study contributes to the growing body of literature on transfer learning and deep learning applications in medical imaging, paving the way for future advancements in disease detection and diagnosis.

VI. CONCLUSION

In this work, we used transfer learning, a powerful machine learning method, to improve the model's performance in four-class classification. Transfer learning uses information obtained from a model that has been pre-trained on a large data set for a given task and applies it to another activity. In our study, we started with 5 models (EfficientNetB3, ResNet50, VGG16, MobileNet, InceptionV3) of CNN architecture and two models (ViT32, ViT16) of Vision Transformer architecture. These models have been trained on large amounts of data, which allows our model to inherit knowledge about common image aspects, allowing it to focus on the complexity of image classification.

Fine-tuning was important in developing a pre-trained model for our medical image classification application. To improve the performance of the model, we added dense layers, dropout layers, and BatchNormalization, as well as modified many hyperparameters. This combination of layers enables the network to learn complex patterns and relationships in the data, leading to efficient classification performance while minimizing overfitting, resulting in improved accuracy higher. After fine-tuning and training on the augmented data set, the proposed model (ViT16) achieved accuracy in 4 scenarios of 99.25% - 99.75% - 100% - 98.25% respectively. Compared to the situation without data augmentation, the model has achieved accuracy in 4 scenarios of 99% - 97% - 98% - 98% respectively.

To provide transparency and to better understand how the model makes decisions and makes predictions during training. We used Integrated Gradients for visual explanation. This helps experts understand the model's predictions to recognize errors and easily improve the model.

Our results demonstrate the robustness of the ViT16 model in the image classification problem compared to other popular models. Strong precision, accuracy, recall and F1 score demonstrate their usefulness in livestock production. This research actually makes a significant contribution as we tackle the rather rare problem of disease diagnosis in chickens. This research paves the way for future developments in image processing and diagnostics in livestock.

In the future, we will to continue to fine-tuning the model, expand the challenge, use other advanced visualization tools, and improve the dataset. In addition, evaluating different preprocessing techniques on different chicken disease images is also an issue that needs research. By undertaking this action, our objective is to enhance the Accuracy of the model, solidifying its role as a fundamental solution within the realm of

avian image categorization.. Our ongoing efforts highlight the importance of artificial intelligence in improving diagnostics and anomaly detection.

ACKNOWLEDGMENT

Luong Hoang Huong was funded by the Vingroup Innovation Foundation (VINIF) 's Master, Ph.D. Scholarship Programme, code VINIF.2023.TS.049.

We would like to express my sincere gratitude to Duy Khanh Nguyen, and Bang Huu Do Dang for their invaluable support and assistance throughout the course of this research. Their expertise, guidance, and encouragement have been instrumental in the successful completion of this study. We are truly grateful for their dedication and commitment, which have greatly contributed to the quality and depth of this research endeavor.

REFERENCES

- [1] A. Mottet and G. Tempio, "Global poultry production: current state and future outlook and challenges," *World's poultry science journal*, vol. 73, no. 2, pp. 245–256, 2017.
- [2] H. Al-Khalaifah and A. Al-Nasser, "Importance of poultry industry during global crisis with special reference to covid-19 crisis," *International Multidisciplinary Scientific GeoConference: SGEM*, vol. 22, no. 6.1, pp. 89–96, 2022.
- [3] M. K. Padhi *et al.*, "Importance of indigenous breeds of chicken for rural economy and their improvements for higher production performance," *Scientifica*, vol. 2016, 2016.
- [4] W. Landman and J. Van Eck, "The incidence and economic impact of the escherichia coli peritonitis syndrome in dutch poultry farming," *Avian Pathology*, vol. 44, no. 5, pp. 370–378, 2015.
- [5] S. M. Kinung'hi, G. Tilahun, H. M. Hafez, M. Woldemeskel, M. Kyule, M. Grainer, and M. P. Baumann, "Assessment of economic impact caused by poultry coccidiosis in small and large scale poultry farms in debre zeit, ethiopia," *International Journal of Poultry Science*, vol. 3, no. 11, pp. 715–718, 2004.
- [6] H. Mbelwa, "Image-based poultry disease detection using deep convolutional neural network," Ph.D. dissertation, NM-AIST, 2021.
- [7] S. Suthagar, G. Mageshkumar, M. Ayyadurai, C. Snegha, M. Sureka, and S. Velmurugan, "Faecal image-based chicken disease classification using deep learning techniques," in *Inventive Computation and Information Technologies: Proceedings of ICICIT 2022*. Springer, 2023, pp. 903–917.
- [8] T. Shibanuma, Y. Nunomura, M. Oba, F. Kawahara, T. Mizutani, and H. Takemae, "Development of a one-run real-time pcr detection system for pathogens associated with poultry infectious diseases," *Journal of Veterinary Medical Science*, vol. 85, no. 4, pp. 407–411, 2023.
- [9] D. Kalkayeva, A. Maulanov, P. Sobiech, M. Michalski, G. Kuzembekova, A. Dzhangabulova, N. Nurkhoyayev, and N. Aldayarov, "Epidemiological characteristics and financial losses due to avian aspergillosis in households in the almaty region, republic of kazakhstan," *Frontiers in Veterinary Science*, vol. 10, p. 1141456, 2023.
- [10] M. Sadiq and B. Mohammed, "The economic impact of some important viral diseases affecting the poultry industry in abuja, nigeria," *Sokoto Journal of Veterinary Sciences*, vol. 15, no. 2, pp. 7–17, 2017.
- [11] A. Nawab, Y. Nawab, S. Tang, J. Wu, W. Liu, G. Li, M. Xiao, L. An *et al.*, "A pictorial guidebook on poultry diseases; diagnostic techniques and their effective treatment," *Animal Review*, vol. 5, no. 2, pp. 34–50, 2018.
- [12] K. K. Johnson, R. M. Seeger, and T. L. Marsh, "Local economies and highly pathogenic avian influenza," *Choices*, vol. 31, no. 2, pp. 1–9, 2016.
- [13] F. Chuma, "Modeling the dynamics, control and economic loss of newcastle disease in village chicken: a case of pwani region in tanzania (doctoral dissertation)," 2019.

- [14] H. H. Luong, L. T. T. Le, H. T. Nguyen, V. Q. Hua, K. V. Nguyen, T. N. P. Bach, T. N. A. Nguyen, and H. T. Q. Nguyen, "Transfer learning with fine-tuning on mobilenet and grad-cam for bones abnormalities diagnosis," *Complex, Intelligent and Software Intensive Systems*, pp. 171–179, 2022.
- [15] H. H. Luong, N. T. L. Phan, T. C. Dinh, T. M. Dang, T. T. Duong, T. D. Nguyen, and H. T. Nguyen, "Fine-tuning mobilenet for breast cancer diagnosis," *Inventive Computation and Information Technologies*, pp. 841–856, 2023.
- [16] H. T. Nguyen, H. H. Luong, P. T. Phan, H. H. D. Nguyen, D. Ly, D. M. Phan, and T. T. Do, "Hs-unet-id: An approach for human skin classification integrating between unet and improved dense convolutional network," *International Journal of Imaging Systems and Technology*, vol. 32, no. 6, pp. 1832–1845, Jun. 2022.
- [17] L. H. Huong, N. H. Khang, L. N. Quynh, L. H. Thang, D. M. Canh, and H. P. Sang, "A proposed approach for monkeypox classification," *International Journal of Advanced Computer Science and Applications*, vol. 14, no. 8, 2023.
- [18] H. T. Nguyen, H. H. Luong, T. H. N. Kien, N. T. L. Phan, T. M. Dang, T. T. Duong, T. D. Nguyen, and T. C. Dinh, "Brain tumors detection on mri images with k-means clustering and residual networks," *Advances in Computational Collective Intelligence*, pp. 317–329, 2022.
- [19] H. Wu, B. Xiao, N. Codella, M. Liu, X. Dai, L. Yuan, and L. Zhang, "Cvt: Introducing convolutions to vision transformers," in *Proceedings of the IEEE/CVF international conference on computer vision*, 2021, pp. 22–31.
- [20] H. Xu, Q. Xu, F. Cong, J. Kang, C. Han, Z. Liu, A. Madabhushi, and C. Lu, "Vision transformers for computational histopathology," *IEEE Reviews in Biomedical Engineering*, 2023.
- [21] A. Hatamizadeh, G. Heinrich, H. Yin, A. Tao, J. M. Alvarez, J. Kautz, and P. Molchanov, "Fastervit: Fast vision transformers with hierarchical attention," *arXiv preprint arXiv:2306.06189*, 2023.
- [22] M. Sundararajan, A. Taly, and Q. Yan, "Axiomatic attribution for deep networks," in *International conference on machine learning*. PMLR, 2017, pp. 3319–3328.
- [23] M. Sadeghi, A. Banakar, S. Minaei, M. Orooji, A. Shoushtari, and G. Li, "Early detection of avian diseases based on thermography and artificial intelligence," *Animals*, vol. 13, no. 14, p. 2348, 2023.
- [24] S. Suthagar, G. Mageshkumar, M. Ayyadurai, C. Snegha, M. Sureka, and S. Velmurugan, "Faecal image-based chicken disease classification using deep learning techniques," in *Inventive Computation and Information Technologies: Proceedings of ICICIT 2022*. Springer, 2023, pp. 903–917.
- [25] K. H. Nguyen, H. V. N. Nguyen, H. N. Tran, and Q. Luyl-Da, "Combining autoencoder and yolov6 model for classification and disease detection in chickens," in *Proceedings of the 2023 8th International Conference on Intelligent Information Technology*, 2023, pp. 132–138.
- [26] M. K. Gourisaria, A. Arora, S. Bilgaiyan, and M. Sahni, "Chicken disease multiclass classification using deep learning," in *Proceedings of International Conference on Information Technology and Applications: ICITA 2022*. Springer, 2023, pp. 225–238.
- [27] "Image - based poultry disease detection using deep convolutional neural network," 2023.
- [28] J. M. P. Sánchez, L. A. O. Moreno, J. L. R. Rodríguez, and I. D. M. Corro, "Poultry egg classification system using deep learning," in *2023 5th International Congress on Human-Computer Interaction, Optimization and Robotic Applications (HORA)*. IEEE, 2023, pp. 01–06.
- [29] M. Kholil, H. P. Waspada, and R. Akhsani, "Classification of infectious diseases in chickens based on feces images using deep learning," in *2022 International Conference on Electrical and Information Technology (IEIT)*. IEEE, 2022, pp. 362–365.
- [30] H. T. Nguyen, T. D. Tran, T. T. Nguyen, N. M. Pham, P. H. N. Ly, and H. H. Luong, "Strawberry disease identification with vision transformer-based models," *Multimedia Tools and Applications*, Feb. 2024.
- [31] M. Z. Degu and G. L. Simegn, "Smartphone based detection and classification of poultry diseases from chicken fecal images using deep learning techniques," *Smart Agricultural Technology*, vol. 4, p. 100221, 2023.
- [32] J. A. Wani and N. Sharma, "Comparative analysis of transfer learning models in classification of histopathological whole slide images," in *Proceedings of International Conference on Recent Innovations in Computing: ICRIC 2022, Volume 1*. Springer, 2023, pp. 351–369.
- [33] M. Schwegler, C. Müller, and A. Reiterer, "Integrated gradients for feature assessment in point cloud-based data sets," *Algorithms*, vol. 16, no. 7, p. 316, 2023.
- [34] D. Lundstrom and M. Razaviyayn, "Four axiomatic characterizations of the integrated gradients attribution method," *arXiv preprint arXiv:2306.13753*, 2023.
- [35] D. Machuve, E. Nwankwo, N. Mduma, and J. Mbelwa, "Poultry diseases diagnostics models using deep learning," *Frontiers in Artificial Intelligence*, vol. 5, 08 2022.

Rigorous Experimental Analysis of Tabular Data Generated using TVAE and CTGAN

Parul Yadav, Manish Gaur, Rahul Kumar Madhukar, Gaurav Verma, Pankaj Kumar,
Nishat Fatima, Saqib Sarwar, Yash Raj Dwivedi
Computer Science and Engineering Department,
Institute of Engineering and Technology,
Lucknow, UP 226021, India

Abstract—Synthetic data generation research has been progressing at a rapid pace and novel methods are being designed every now and then. Earlier, statistical methods were used to learn the distributions of real data and then sample synthetic data from those distributions. Recent advances in generative models have led to more efficient modeling of complex high-dimensional datasets. Also, privacy concerns have led to the development of robust models with lesser risk of privacy breaches. Firstly, the paper presents a comprehensive survey of existing techniques for tabular data generation and evaluation matrices. Secondly, it elaborates on a comparative analysis of state-of-the-art synthetic data generation techniques, specifically CTGAN and TVAE for small, medium, and large-scale datasets with varying data distributions. It further evaluates the synthetic data using quantitative and qualitative metrics/techniques. Finally, this paper presents the outcomes and also highlights the issues and shortcomings which are still need to be addressed.

Keywords—Synthetic data generation; tabular data generation; data privacy; conditional generative adversarial networks; variational autoencoder

I. INTRODUCTION

Tabular Data made up of databases with tabular structures consisting of rows representing observations and columns representing features. In the digital era, “data” is considered as “new water”. On the one side, compliance of privacy laws like GDPR has imposed an obligation on organizations to secure and protect private and sensitive data, while on the other side, data acts as a fuel in the wide range of machine learning applications like Cloud migration, Artificial Intelligence (AI)/ ML model training, application testing, simulation analysis, data sharing, scientific trials, and new product development. An innovation solution to address the issue is to generate the synthetic data.

Synthetic data is an artificially generated data which carries the same statistical properties (i.e. mean, median, mode, correlation, regression, etc.). as the real data. Synthetic data is useful where it is challenging to obtain and use real data due to privacy concerns and difficulty in collecting real data, augmenting small datasets, and range of machine learning applications. Moreover, real data can be of types like tabular, time-series, audio, video, medical images/ signals etc. Out of these types, tabular data is the most commonly used form of data and generation of synthetic data for it is still challenging and requires to address the multiple constraints/ characteristics of tabular data to produce quality synthetic data.

There are multiple constraints (multimodal, class imbalance, non Gaussian data, learning from sparse one-hot-encoded vectors, mixed data type) inherently present in the tabular data that need to be addressed while generating its synthetic counterpart. Along with these constraints, a feature has varying characteristics. In this paper, tabular data features have been categorized into four categories: continuous, categorical, mixed type, and anonymized. Characteristics of each tabular data feature are shown in Table I. Generation of synthetic tabular

TABLE I. DATA CHARACTERISTICS

| Feature Type | Details |
|---------------------|--|
| Continuous Columns | Gaussian Distribution Multi-Modal Distribution Long Tail Distribution |
| Categorical Columns | Binary Categorical Multiple Categorical |
| Mixed Type Columns | Missing Values A high-frequency finite value mixed with other values |
| Anonymized Columns | Unique Columns - Roll Number, Patient ID, etc. Non-Unique Columns - Name, Country, etc. |

data requires identification of the distributions of each feature and simultaneously mapping the correlations present in the data.

Broadly, there are two categories of models used to generate synthetic tabular data, namely, statistical or Probability [4], [5] and machine learning [7], [8], [9], [10] methods based models.

Probabilistic models have existed and are continually being developed to generate synthetic data. But recent advancements in deep learning-based generative models, especially GANs [1], have made them state-of-the-art in the field of synthetic data generation. Moreover, the existence of stricter privacy laws and general awareness regarding user privacy have made data sharing difficult. This has led to the development of novel privacy-preserving mechanisms to ease the generation and sharing of data. Differential privacy [2] has become the gold standard in this domain. It uses randomized algorithms [3] for the sanitization of sensitive information and also limits the privacy risk of revealing sensitive information.

Besides the generation of synthetic data, robust evaluation mechanisms [2], [11] are of equal importance. This paper presents exciting methods for synthetic data generation and

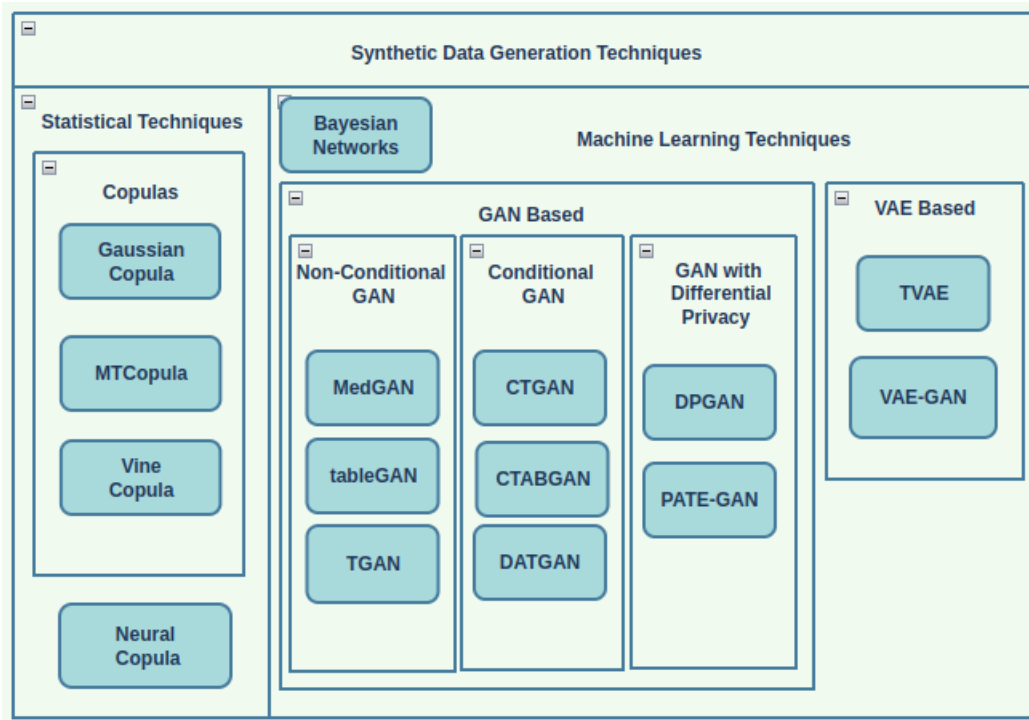


Fig. 1. Synthetic data generation techniques.

elaborates on evaluation mechanisms. This paper highlights rigorous analysis to analyze the performance of the state-of-the-art models for tabular data generation on varied nature data. Presented is a rigorous comparative analysis of the state-of-the-art models, namely, TVAE [12] and CTGAN [12] for small-*iris* [13] and *breast cancer* [13], medium-*adult* [13] and large-*credit* [13] datasets with comparative statistical scores and visualization reports.

The structure of the paper is organized as follows: Section II describes existing methods for synthetic data generation extensively; Section III lists the techniques for evaluation of generated synthetic data in detail; Section IV describes the datasets, models, and evaluation metrics used in the research; Section V provides an in-depth analysis of the results obtained; and Section VI presents a short qualitative summary of the proposed research in the conclusion.

II. EXISTING MODELS FOR SYNTHETIC TABULAR DATA GENERATION

The existing models for generating synthetic tabular data have been broadly classified into two categories namely, statistical methods-based models [4], [5], [6] and machine learning-based techniques [7], [8], [9], [10] as shown in the Fig. 1. This section entails a detailed and comprehensive in-depth analysis of each methods at hand.

A. Statistical Methods-based Models

Several statistical methods-based models [4], [5], [6] have existed, and novel methods have been proposed to address the task of synthetic data generation. One of the earliest statistical techniques for synthetic data generation is Inverse

Transform Sampling [6] which involves sampling data from a known data distribution for the random variable X . It generates independent univariate samples. Thereafter, a perturbation technique involving fitting a multivariate Gaussian distribution on input data is introduced. The General Additive Data Perturbation(GADP) technique [4] generated synthetic data by adding a noise variable to the estimated distribution. Another variant of GADP is the Dirichlet Multivariate Synthesizer [6] which is based on Maximum Likelihood Estimation (MLE) [14]. The problem with MLE is that the computation increases exponentially as the number of variables increases. Apart from these statistical methods, one of the most useful statistical methods for synthetic data generation uses copulas. Details of copulas are described in Sub-section II-A1

1) *Copulas*: A copula [15] is a mathematical function that describes the correlation between the marginals of random variables. This helps in identifying the multivariate joint distribution for a set of random variables. A lot of research has been done to identify the right parameters for the copula model and the marginals. Based on these, several variants of copula have been proposed. Gaussian Copula [5] is the most popular and one of the very few copula functions available for modeling the joint multivariate probability distribution. Apart from the Gaussian Copula [5] and t-Copula [16] models for multivariate distribution, Vine Copula [17] models have gained prominence lately as a modeling method as they are built only on the univariate and bivariate distributions. More recently, neural network techniques are being incorporated to identify the right set of parameters to construct a generic copula that models any multivariate joint distribution [7].

a) *MTCopula*: Since Gaussian Copula [5] fails to address the complex distributions of marginals and the joint

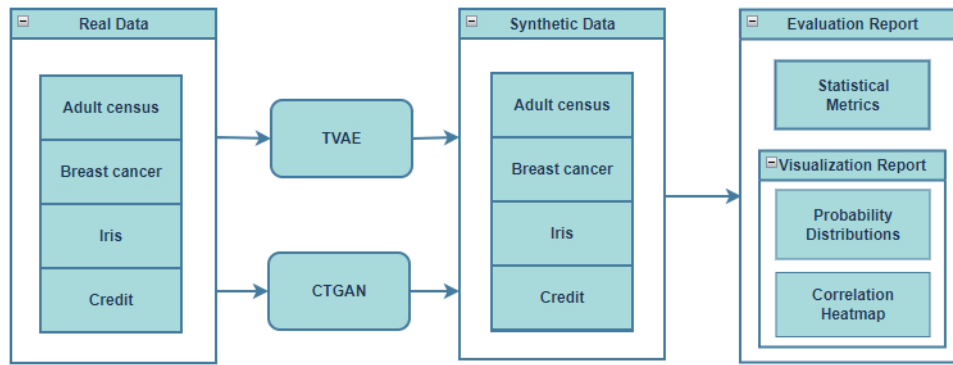


Fig. 2. Proposed comparison model.

distribution, Benali et al. propose a novel MTCopula [6] which involves parameter selection criteria for selecting the parametric marginal and multivariate copula functions based on Akaike Information Criterion (AIC) [18]. The main drawback of this approach is that it selects one of the existing parametric marginals or parametric copulas. The complex distributions of a random variable may not be exactly modeled by parametric marginals. Moreover, it considers only Gaussian Copula [5] and t-Copula [16] for the selection of multivariate copula functions, and the complex relationships among the random variables are not always captured by these two generic copula.

b) *Vine copula*: Vine copulas [17] are a special class of copula models as they use bivariate distribution as the building blocks for multivariate joint distribution [15]. This is achieved by forming a vine-like structure, one node at a time. However, with the increase in the number of variables, the number of feasible configurations of a vine copula expands exponentially, making model selection a significant development issue. This problem is addressed by [9] using reinforcement learning and selecting tree levels sequentially while using LSTM networks [19] to learn from vine configurations.

B. Machine Learning Methods-based Models

Recent advancements in the development of generative models [1] have transformed visual media-centric research to new heights. The ability of generative models is now being utilized to learn the complex relationships of tabular data and generate similar synthetic data. The two most important techniques using generative models are variational autoencoders [20] and generative adversarial networks [1], which are discussed in the following section.

1) *Bayesian Networks*: Bayesian networks [21] are probabilistic graphical models used to determine probabilistic inferences between variables. They are frequently used in computational systems biological method [22] to understand the underlying biological relationships. Here, the dependencies of variables are defined prior to training. This is also a major drawback, as it requires prior information on the dataset. Moreover, it becomes computationally expensive when dealing with large and sparse datasets.

2) *Variational Autoencoders*: The architecture of VAEs [20] consists of an encoder network and a decoder network.

The encoder takes real data as input and converts it into a vector corresponding to a latent distribution. This vector is served as an input to the decoder, which reconstructs the real data that was served as an input to the encoder. On training completion, the decoder network can now generate new samples. The variational part brings randomness to this process.

a) *Differentially private autoencoder*: [23] introduced a novel differentially private autoencoder for synthetic data generation.

b) *TVAE*: Xu et al [12] propose a novel VAE known as TVAE for tabular data using two neural networks, one for the encoder and the other for the decoder network, and train them using Evidence Lower-Bound (ELBO) loss [24].

3) *Generative Adversarial Networks*: GAN [1] is based on the adversarial training of the generator network and the discriminator network, where the task of the generator is to produce fake samples that closely resemble the real samples while the discriminator tries to distinguish between the real and fake samples. GANs also belong to a generative class of models, but the key distinction between GANs and VAEs is that in VAEs, the encoder sees the real data, while in GAN, real data is not visible to the generator network. This is particularly useful in privacy-oriented applications. Different types of GANs are discussed below.

a) *Non-Conditional GAN*: GANs were first incorporated for synthetic tabular data generation in MedGAN [25], Table-GAN [26] and TGAN [8]. Vanilla GAN [1] architectures usually suffer from the problem of vanishing gradients, which leads to mode collapse. This has led to the rise of several variations of GAN architectures, such as WGAN, Wasserstein GAN [27] and conditional GANs [28].

b) *Conditional GAN*: When allowing the GAN [1] model to condition external information, it can generate samples by operating in different modes based on the contextual information provided. Thus, conditional GAN [28] is an extension of the GAN [1] architecture with the conditional operation. The different variations of conditional GANs are as follows.

- *CTGAN* [12] deals with problems like mixed data types, multimodal distributions, and imbalanced categorical columns of tabular data extensively. For the

problem of multimodal distribution in continuous data, it fits a variational Gaussian Mixture Model [29]. Thereafter, a mode is sampled from the identifiable modes, and the column is normalized based on the probability density of the selected mode. For discrete columns, one-hot encoding is used.

The problem of adequately representing all the categories in the synthetically generated data is handled using a conditional vector. Since the minority category may not be adequately represented in the synthetic data, instead of providing random noise to the generator, it uses a conditional vector constrained on each respective category to train the generator and discriminator network. Finally, the discriminator is trained using a sampling method based on the conditional vector, i.e., sampling a row from the real data constraining each respective category.

- **CTABGAN** Conditional Tabular GAN (CTAB-GAN) [10] is based on the Convolutional Neural Network with an additional classifier network based on a multi-layer perceptron apart from the generator and discriminator networks. It considers not only continuous and categorical variables but also a third class of variables known as mixed variables and also deals with variables with long-tail distributions. Zhao et al. proposed an advanced version of CTABGAN, CTABGAN+ [30] using Wasserstein loss [27] with gradient penalty and training with differential privacy stochastic gradient descent to ensure strict privacy guarantees.
- **DATGAN** [31] proposes DATGAN which is a novel architecture based on GAN using Directed Acyclic Graphs (DAGs) to model the information about the dataset. It uses LSTM cells to model expert knowledge using DAG.

c) **GAN with Differential Privacy:** Jordan et al. [32] apply Private Aggregation of Teacher Ensembles (PATE) [33] to the GAN model so as to obtain a generative model with tight differential privacy guarantees. Xie et al. [34] add noise to gradients to achieve differential privacy with GANs. Evaluation techniques that are utilized to assess the quality of generated synthetic data are explained below.

III. EVALUATION TECHNIQUES

Synthetic data generation not only focuses on generation algorithms but also on robust evaluation mechanisms that can highlight the quality of generated synthetic data. To this end, evaluation mechanisms are classified into broadly three categories (quantitative, qualitative, and machine learning utility), highlighting each unique aspect of synthetic data. Further explanation is provided on these categories along with privacy preservability and differential privacy.

A. Quantitative Statistical Similarity Measures

Ideally, the generated synthetic data should have the same statistical properties as the real data. To ensure this, several statistical tests and metrics were compared to the synthetic data with real data.

1) **Kolmogorov-Smirnov Test:** To measure the similarity between the data distribution of continuous columns in real data and the generated synthetic data, the two-sample Inverted Kolmogorov-Smirnov test [35], commonly referred to as KSTest, is utilized. The p-value and D statistic obtained represent the similarity between the column distributions. For the whole dataset, a mean of the D statistic is obtained considering all the continuous columns, and then it is subtracted from 1 to obtain the final score. The D statistic can be computed using the following equation:

$$D_{m,n} = \max |F(x) - G(x)|. \quad (1)$$

where $F(x)$ is the cumulative distribution function of the first sample with size m and $G(x)$ is the cumulative distribution function of the second sample with size n .

2) **Chi-Square Test:** Similarly, for discrete data, the Chi-Square Test [36] is used. After applying it to all the discrete columns in the data, an average of the score is obtained.

$$\chi^2 = \sum \frac{(O_i - E_i)^2}{E_i} \quad (2)$$

where χ^2 = Chi Squared statistic, O_i = Observed value, E_i = Expected value

3) **Wasserstein Distance:** Also known as Earth Mover distance [37], it intuitively defines how much quantity should be transported from x to y to transform a probability distribution from P_A to P_B .

$$W := W(F_A, F_B) = \left(\int_0^1 |(F_A^{-1}(u) - F_B^{-1}(u))|^2 du \right)^{\frac{1}{2}} \quad (3)$$

Where, F_A^{-1} and F_B^{-1} are the corresponding quantile functions, and F_A and F_B are the associated cumulative distribution functions (CDFs).

4) **Kullback-Leibler Divergence:** Finally, the third metric considered for quantifying the difference between the two probability distributions is the Kullback-Leibler divergence [11] or KL divergence, encompassing both the continuous and discrete variants. For discrete probability distributions P and Q :

$$D_{KL}(P||Q) = \sum_i P(i) \log \frac{P(i)}{Q(i)} \quad (4)$$

For probability distributions P and Q of continuous variable:

$$D_{KL}(P||Q) = \int_{-\infty}^{\infty} P(x) \log \frac{P(x)}{Q(x)} dx \quad (5)$$

B. Qualitative Visualization Techniques

Apart from the above-mentioned quantifiable measures, data visualization methods are useful for analyzing the quality of synthetic data. Of these, probability distributions for univariate and bivariate analysis and correlation heatmaps for multivariate analysis provide deep visual insights into the quality of the generated synthetic data.

C. Machine Learning Utility

One important aspect of the task of synthetic data generation is to produce synthetic data that has approximately the same machine-learning utility as the real data. Without any utility, the generated synthetic data might not be of any value.

D. Privacy Preservability

This is one of the most important aspects in the task of synthetic data generation, considering the present scenario. Strict laws (e.g., the European General Data Protection Regulation [38]) and privacy concerns play a major role in sharing sensitive data. To address these, various mechanisms have been proposed to ensure data privacy. These can be classified into two major techniques: distance-based metrics (DCR (Distance to Closest Record) [30] and NNDR (Nearest Neighbour Distance Ratio) [39], and differential privacy mechanisms.

1) *DCR*: A synthetic record's Euclidean distance from its nearest real neighbour is measured by DCR [30]. Ideally, the chance of a privacy breach decreases as DCR increases.

2) *NNDR*: The NNDR [39] measures the ratio between the Euclidean distance for the closest and second-closest actual neighbours to any matching synthetic record, as opposed to just measuring the closest neighbour. This ratio falls between 0 and 1. Better privacy is indicated by higher values. Sensitive information from the nearest real data record may be revealed by low NNDR values between synthetic and real data.

E. Differential Privacy

By reducing the impact of each data point based on a predetermined privacy budget, Differential Privacy [2] defends against privacy assaults. Renyi Differential Privacy (RDP) is used by Zhao et al. [30]. Because it sets more stringent limits on the privacy budget. RDP offers tighter limitations for tracking the cumulative privacy loss through a series of mechanisms using the composition theorem, making it a strictly stronger privacy definition than DP.

Up to this point, elaboration has been provided on existing methods for synthetic data generation and evaluation metrics for analyzing the quality of the generated data. The next section delves into the methodology for designing and implementing the comparison model.

IV. METHODOLOGY FOR COMPARISON MODEL

Comparing and analyzing two state-of-the-art synthetic tabular data generation techniques, namely, TVAE [12] and CTGAN [12], Four datasets were explored of varying sizes, data features, and characteristics. For qualitative analysis, a selection of three statistical metrics is made, which are then implemented and analyzed across both models using varying batch sizes (20, 50, 100, and 300) and epochs (100, 200, 500, and 5000). Additionally, a visualization report is generated using probabilistic distribution and correlation heatmaps for variables in the datasets.

The process flow highlighting each component in the proposed comparison model is shown in Fig. 2. It lists four real datasets to be used, which train the two models, TVAE [12] and CTGAN [12]. The trained models then generate synthetic

samples for each dataset individually. Finally, this synthetic data, along with real data, is used to prepare an evaluation report that highlights quantitative statistical metrics and a qualitative visualization report depicting feature distributions and correlations for synthetic as well as real data. Further subsections describe the datasets (Section IV-A), algorithms (Section IV-B), and evaluation metrics (Section IV-C) used to design and implement the proposed comparison model in detail.

TABLE II. DATASETS DETAILS

| Category | Name | Total Features | Total Records | Feature Distribution |
|----------|---------------------|----------------|---------------|-----------------------------|
| small | iris | 6 | 150 | (5 continuous, 1 discrete) |
| | breast cancer adult | 33 | 569 | (32 continuous, 1 discrete) |
| medium | adult | 15 | 32561 | (6 continuous, 9 discrete) |
| large | credit | 31 | 284807 | (30 continuous, 1 discrete) |

TABLE III. CREDIT SAMPLE

| | Total Records | Class 0 | Class 1 | % Class 0 | % Class 1 |
|-------------------|-----------------|-----------------|-----------|--------------------|------------------|
| Real Sample (15%) | 284807 42721 | 284315 42647 | 492 74 | 99.8273 99.8268 | 0.1727 0.1732 |

A. Datasets

Datasets were categorized based on their size into three broad categories: small (*iris* [13] and *breast-cancer* [13]), medium (*adult*) [13] and large (*credit*). Four standard datasets were considered in different domains with varied sizes and a mix of different variable types. The extensive diversity of the datasets is reflected in Table II. Table II shows the total features and their distribution as continuous or discrete features and complete records for each dataset. Moreover, for the *large* dataset, *credit*, approximately 280,000 records are available. A 15% sample of the original dataset is taken, as illustrated in Table III. Due to the high imbalance in the *credit* dataset, with just 0.173% of samples belonging to Class 1, the same imbalance ratio is maintained in the sample.

B. Models and Algorithms

Two state-of-the-art machine learning algorithms are compared across four different datasets. TVAE [12] and CTGAN [12] models are employed for all datasets, with hyperparameter tuning conducted for each. Hyperparameters are optimized based on the size of the dataset, as detailed in Table IV, Table V, Table VI, and Table VII.

C. Evaluation

Three quantitative statistical evaluation metrics were used, Chi-Square (CS Test), Inverted KS D Statistic (KS Test), and KL Divergence (KL_c for continuous and KL_d for discrete) for

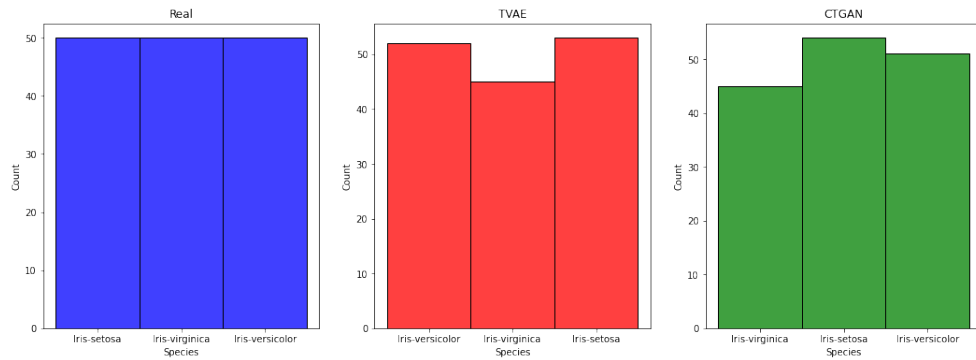


Fig. 3. Iris: Species Distribution.

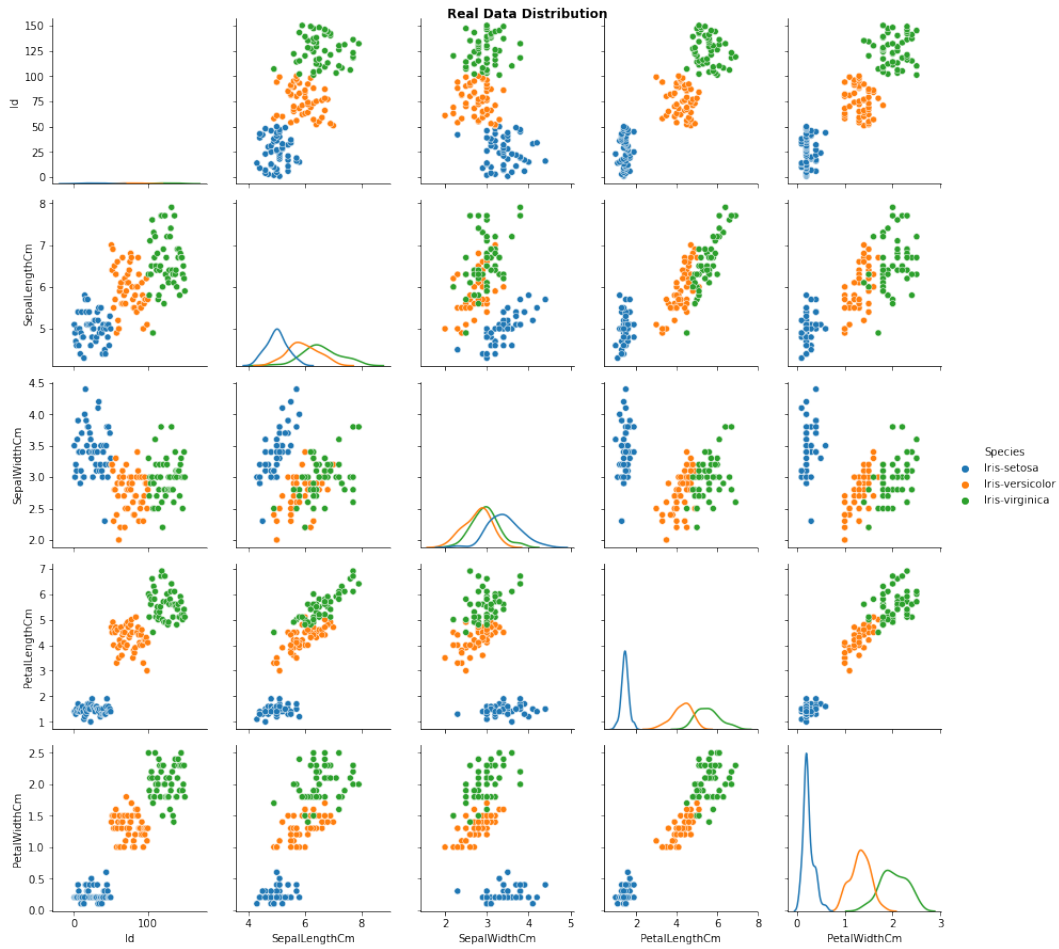


Fig. 4. Real Iris.

each category of the data, continuous or discrete (as applicable). Moreover, univariate distributions, bivariate distributions, and correlation heatmaps are utilized for qualitative data analysis through visualization. Categorical distributions for the *Iris* dataset are represented using histograms, as illustrated in Fig. 3. Further elaboration on these evaluation metrics can be found in Section III.

V. RESULTS AND ANALYSIS

To analyze the results, the proposed comparison model was implemented in Python using its ML libraries. Details of the implementation environment are provided in Table VIII. TVAE [12] and CTGAN [12] models were implemented, trained for four datasets as explained in Subsection IV-A, and evaluated using three metrics outlined in Subsection IV-C, with variations in batch size and epochs, as shown in Table IV, Table V, Table VI, and Table VII. Statistical and visual observations

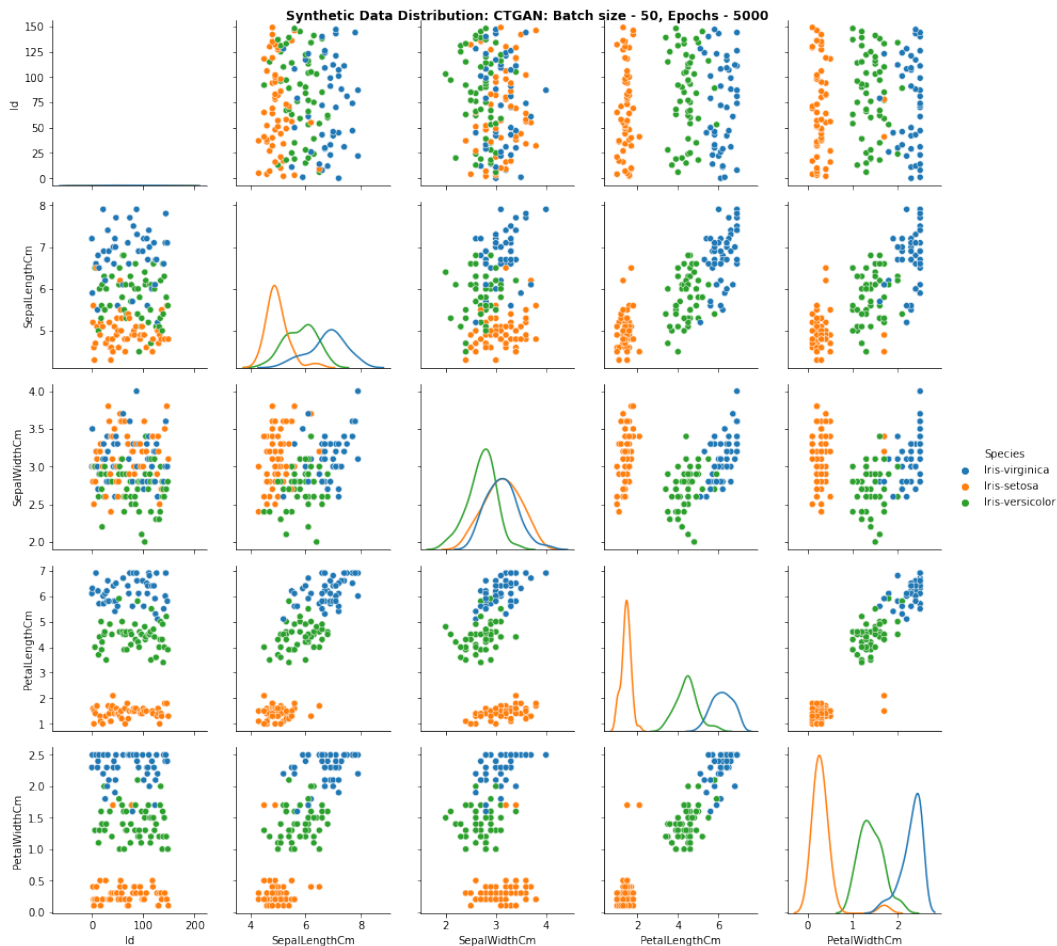


Fig. 5. CTGAN Iris.

were recorded, and the results were rigorously analyzed. This analysis will present the suitability as well as limitations of TVAE [12] and CTGAN [12] under varied and diversified features of the datasets, as shown in Table II.

In most of the cases, it appeared that the variational autoencoder-based TVAE [12] outperformed CTGAN [12], reflected by the higher KL divergence score, meaning a closer resemblance of the synthetic data distribution to the real data distribution. But the major advantage of the GAN [1] based model is the more effective privacy-preserving mechanism since the generator is unaware of real data values. These observations are rigorously analyzed in Subsection V-A and Subsection V-B.

A. Statistical Measures: Quantitative Evaluation

Based on the categories of the datasets, *small*, *medium*, and *large*, Batch sizes of the dataset were varied and described the statistical metrics obtained as follows.

For *small* datasets, *iris* and *breast-cancer*, the batch size is varied between 20, 50, and 100. Also, for *small* datasets, deep learning methods are more useful when training is done for longer periods of time, i.e., for larger epochs. Testing of this was done by training the data for 100, 500, and 5000 epochs, respectively.

From Table IV and Table V, observations were made that the KL divergence score is best for both *iris* and *breast-cancer* for the optimum value of 5000 epochs with a batch size of 50. This is true for the synthetic data generated using both TVAE [12] and CTGAN [12]. Another important observation from Table V is that change in the number of epochs and batch size did not have a significant influence on TVAE [12] while increasing the number of epochs for CTGAN [12] significantly increased all three metrics that were considered.

For the *medium* sized *adult* dataset, the batch size was increased to 300, and training was conducted for 200 and 300 epochs. Similar values were obtained for all metrics, as depicted in Table VI, with minimal significance observed in changing the epochs.

The credit dataset is sampled, preserving the minority-majority class ratio. The results obtained for a batch size of 300 and 200 epochs are shown in Table VII. The experiment is repeated three times, and the mean of all the values is shown in Table VII.

B. Visualization Analysis: Quantitative Evaluation

Apart from the statistical metrics, a visualization report with univariate and bivariate distributions and correlation

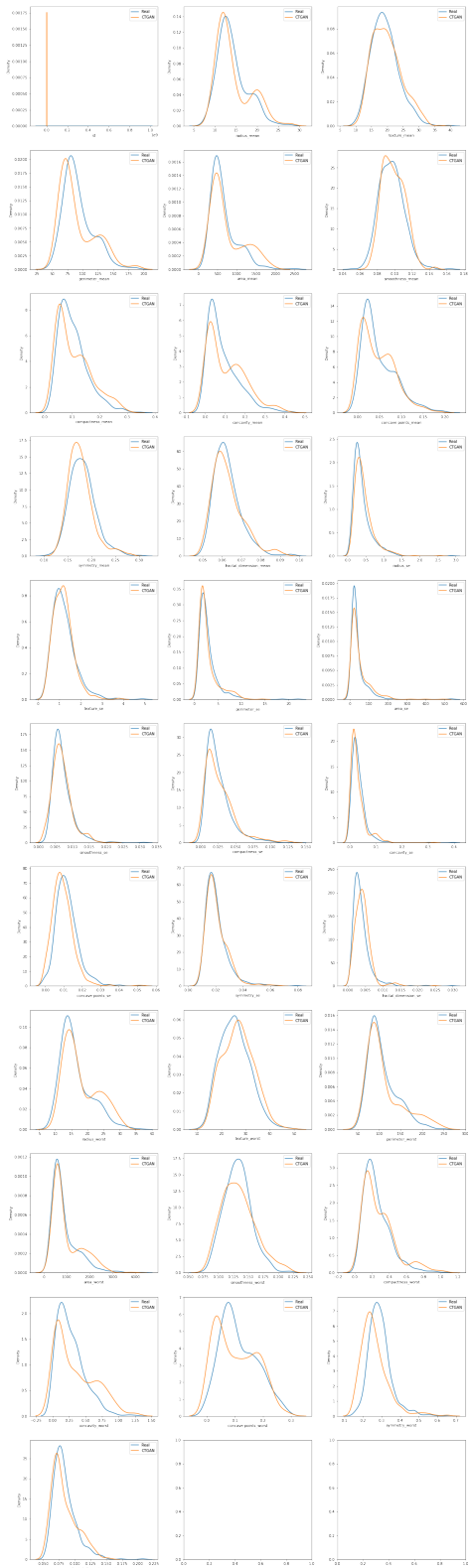


Fig. 7. Data Distribution: Breast Cancer - Real vs Synthetic (CTGAN).

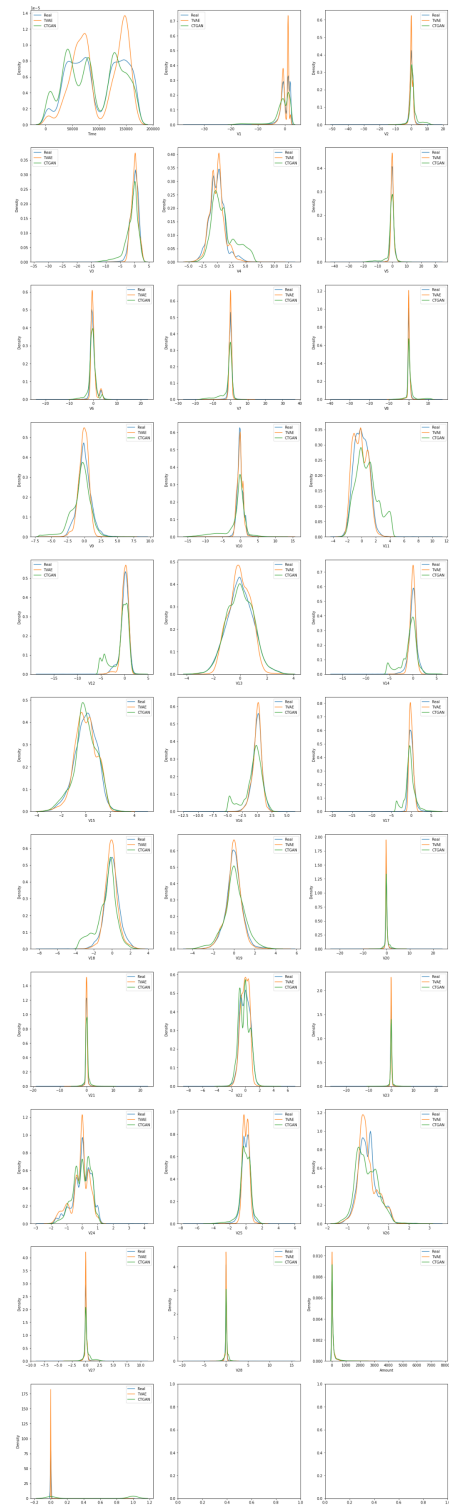


Fig. 8. Data Distribution: Credit - Real vs Synthetic.

class, CTGAN [12] oversampled the minority class in synthetic data, overriding the imbalance ratio.

Lastly, tuning the hyperparameters accordingly for each

dataset improved the quality of the generated synthetic data for both TVAE [12] and CTGAN [12]. Thus, even high-dimensional data with complex relationships can be effectively modeled using generative models for synthetic data generation.



Fig. 9. Real Adult.



Fig. 10. CTGAN Adult.

2) *Correlation Heatmaps*: For the *iris* dataset, one observation worth mentioning is that the first row and first column of the synthetically generated data in the heatmap (Fig. 12) as well as the distributions in Fig. 5 did not correspond well with their real counterparts. This is because one of the features in the first row and the first column is the “Id” field, which served

TABLE IV. IRIS

| Metric | Batch Size | Epochs | TVAE | CTGAN |
|---------|------------|----------|--------------|--------------|
| CS Test | 20 | 100 | 0.989522 | 0.999467 |
| | | 500 | 0.997869 | 0.997204 |
| | | 5000 | 0.996406 | 0.985703 |
| | 50 | 100 | 0.968894 | 0.992429 |
| | | 500 | 0.985703 | 0.979415 |
| | | 5000 | 0.997 | 0.997 |
| 100 | 100 | 0.994283 | 0.999067 | |
| | 500 | 0.986755 | 0.992429 | |
| | 5000 | 0.983603 | 0.996274 | |
| KS Test | 20 | 100 | 0.86533 | 0.706667 |
| | | 500 | 0.941333 | 0.88000 |
| | | 5000 | 0.950667 | 0.90000 |
| | 50 | 100 | 0.829333 | 0.714667 |
| | | 500 | 0.896000 | 0.852000 |
| | | 5000 | 0.949 | 0.908 |
| 100 | 100 | 0.878667 | 0.730667 | |
| | 500 | 0.905333 | 0.842667 | |
| | 5000 | 0.910667 | 0.88000 | |
| KL_c | 20 | 100 | 0.251850 | 0.113536 |
| | | 500 | 0.307945 | 0.185478 |
| | | 5000 | 0.384911 | 0.258259 |
| | 50 | 100 | 0.227984 | 0.114429 |
| | | 500 | 0.311331 | 0.171203 |
| | | 5000 | 0.375 | 0.266 |
| 100 | 100 | 0.282140 | 0.118934 | |
| | 500 | 0.262064 | 0.140582 | |
| | 5000 | 0.338058 | 0.209723 | |

TABLE V. BREAST CANCER

| Metric | Batch Size | Epochs | TVAE | CTGAN |
|---------|------------|--------|----------|--------------|
| CS Test | 50 | 100 | 0.953622 | 0.991299 |
| | | 500 | 0.953622 | 0.947832 |
| | | 5000 | 0.944939 | 0.994 |
| | 100 | 100 | 0.852929 | 0.976801 |
| | | 500 | 0.979700 | 0.976801 |
| | | 5000 | 0.997100 | 0.988399 |
| KS Test | 50 | 100 | 0.844492 | 0.671183 |
| | | 500 | 0.887239 | 0.706729 |
| | | 5000 | 0.881966 | 0.863 |
| | 100 | 100 | 0.821475 | 0.666194 |
| | | 500 | 0.894042 | 0.719315 |
| | | 5000 | 0.884914 | 0.850728 |
| KL_c | 50 | 100 | 0.697478 | 0.364236 |
| | | 500 | 0.694817 | 0.389121 |
| | | 5000 | 0.700066 | 0.560 |
| | 100 | 100 | 0.710529 | 0.365040 |
| | | 500 | 0.706662 | 0.359388 |
| | | 5000 | 0.687059 | 0.544663 |

as the primary key. Its value has no intrinsic worth and is just used to distinguish each record. Hence, its correlation is not of much value. On a similar note, for the breast cancer dataset, correlation heatmaps were obtained as shown in Fig. 13 and Fig. 14 which show that the correlation of continuous columns for *adult* dataset is effectively captured by CTGAN [12] while from Fig. 15, observations were made that the CTGAN [12] extrapolated correlations for the credit dataset.

The analysis of correlation heatmaps for various datasets clearly shows that the complex relationships among the data features are effectively captured by the generative model CTGAN [12] when training is fine-tuned with optimum hyperparameters for each dataset.

VI. CONCLUSION

The paper presents a comprehensive overview of synthetic data generation and evaluation techniques and performs a

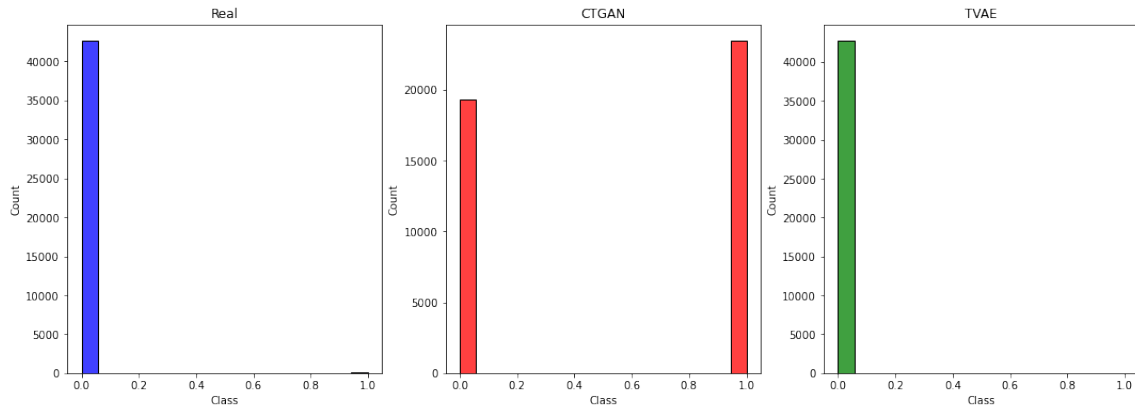


Fig. 11. Credit class imbalance.

CTGAN: Batch size - 50, Epochs - 5000

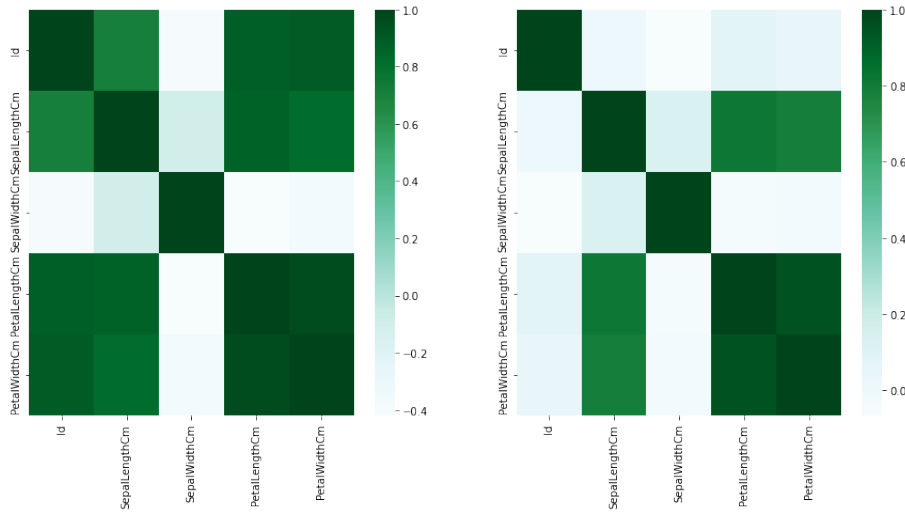


Fig. 12. Correlation Heatmap of Real (LHS) vs Synthetic (CTGAN)(RHS): Iris.

TABLE VI. ADULT

| Metric | Batch Size | Epochs | TVAE | CTGAN |
|---------|------------|--------|--------------|--------------|
| CS Test | 300 | 200 | 0.986172 | 0.982407 |
| | | 300 | 0.990 | 0.982 |
| KS Test | 300 | 200 | 0.845557 | 0.891655 |
| | | 300 | 0.855 | 0.886 |
| KL_c | 300 | 200 | 0.866789 | 0.917393 |
| | | 300 | 0.935 | 0.935 |
| KL_d | 300 | 200 | 0.942063 | 0.860879 |
| | | 300 | 0.951 | 0.858 |

TABLE VII. CREDIT

| Metric | Batch Size | Epochs | TVAE | CTGAN |
|---------|------------|--------|----------|----------|
| KS Test | 300 | 200 | 0.684782 | 0.656325 |
| KL_c | 300 | 200 | 0.854645 | 0.632121 |

TABLE VIII. IMPLEMENTATION ENVIRONMENT

| | |
|-----------|---|
| Language | Python (version 3.11.0) |
| Tool | VS Code, Google Colaboratory |
| Libraries | Pandas, NumPy, Scikit Learn, Matplotlib, Seaborn, SciPy and SDV |

rigorous analysis of small, medium, and large-scale synthetic data generated using two state-of-the-art generative models, TVAE and CTGAN. The choice of hyperparameters greatly influenced the quality of synthetic data. Small datasets (*iris* and *breast cancer*) required longer training periods for generating statistically similar synthetic data. Preserving univariate and bivariate distributions as shown in Fig. 4, Fig. 5, Fig. 6, Fig. 7, Fig. 8, Fig. 9 and Fig. 10 and multivariate joint distributions

as shown in Fig. 12, Fig. 13 and Fig. 14 are achieved for small (*iris* and *breast cancer*), medium (*adult*) and large (*credit*) datasets using generative models. There is scope in the future to train large imbalanced datasets more rigorously and for more iterations with different parameters on high-end computational

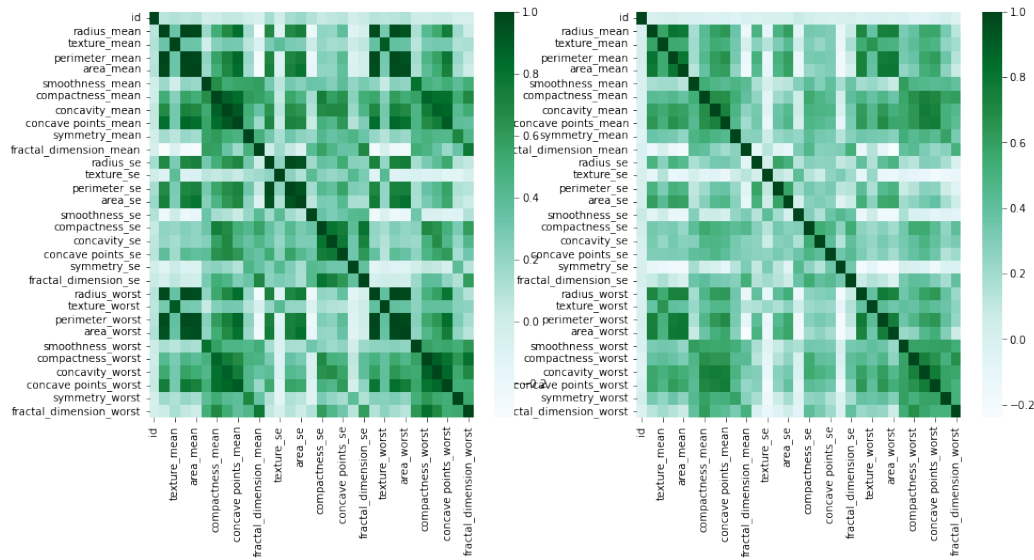


Fig. 13. Correlation Heatmap: Real (LHS) vs Synthetic (CTGAN)(RHS) - Breast Cancer.

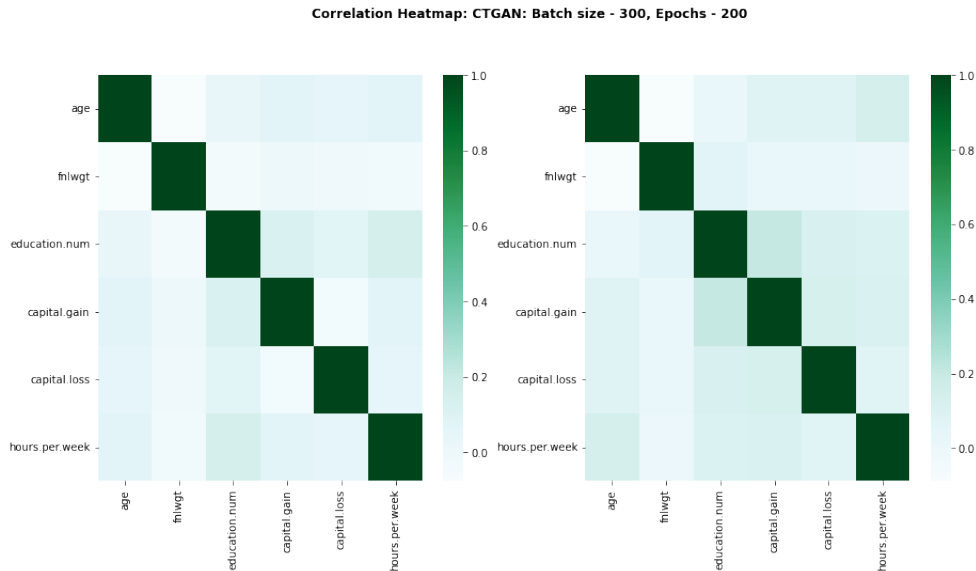


Fig. 14. Correlation Heatmap of Real (LHS) vs Synthetic (CTGAN)(RHS) data: Adult.

systems. While results for TVAE outperformed CTGAN for all four datasets by varying margins, as reflected by the KL Divergence score, CTGAN is the preferred method for generating privacy-preserving synthetic data due to its agnostic nature to real data values.

In this paper, the data on statistical metrics were evaluated, and a visualization report was presented to extensively analyze the synthetic data. The results not only highlighted the quality of synthetic data but also mentioned the shortcomings and caveats in the existing methods, which would open further dimensions in the line of research.

REFERENCES

[1] Goodfellow, I., Pouget-Abadie, J., Mirza, M., Xu, B., Warde-Farley, D., Ozair, S., Courville, A. and Bengio, Y., 2020. Generative adversarial

networks. *Communications of the ACM*, 63(11), pp.139-144.

[2] Dwork, C., 2008, April. Differential privacy: A survey of results. In *International conference on theory and applications of models of computation* (pp. 1-19). Springer, Berlin, Heidelberg.

[3] Mahoney, M.W., 2011. Randomized algorithms for matrices and data. *Foundations and Trends® in Machine Learning*, 3(2), pp.123-224.

[4] Muralidhar, K., Parsa, R. and Sarathy, R., 1999. A general additive data perturbation method for database security. *management science*, 45(10), pp.1399-1415.

[5] Žežula, I., 2009. On multivariate Gaussian copulas. *Journal of Statistical Planning and Inference*, 139(11), pp.3942-3946.

[6] Benali, F., Bodénès, D., Labroche, N. and de Runz, C., 2021. Mtcopula: Synthetic complex data generation using copula. In *23rd International Workshop on Design, Optimization, Languages and Analytical Processing of Big Data (DOLAP)* (pp. 51-60).

[7] Zeng, Z. and Wang, T., 2022. Neural Copula: A unified framework for estimating generic high-dimensional Copula functions. *arXiv preprint arXiv:2205.15031*.

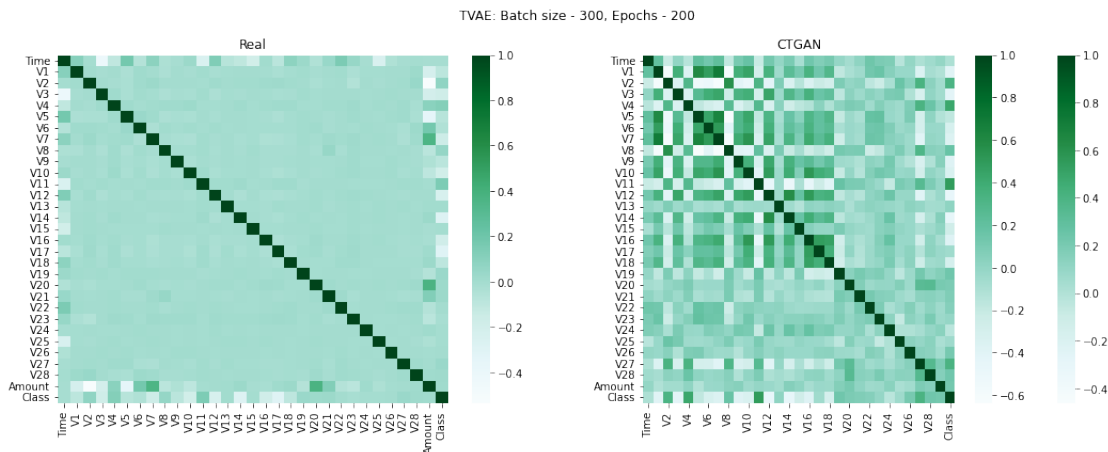


Fig. 15. Correlation Heatmap of Real (LHS) vs Synthetic (CTGAN)(RHS) data: Credit.

- [8] Xu, L. and Veeramachaneni, K., 2018. Synthesizing tabular data using generative adversarial networks. arXiv preprint arXiv:1811.11264.
- [9] Sun, Y., Cuesta-Infante, A. and Veeramachaneni, K., 2019, July. Learning vine copula models for synthetic data generation. In Proceedings of the AAAI Conference on Artificial Intelligence (Vol. 33, No. 01, pp. 5049-5057).
- [10] Zhao, Z., Kunar, A., Birke, R. and Chen, L.Y., 2021, November. Ctabgan: Effective table data synthesizing. In Asian Conference on Machine Learning (pp. 97-112). PMLR.
- [11] Kullback, S. and Leibler, R.A., 1951. On information and sufficiency. The annals of mathematical statistics, 22(1), pp.79-86.
- [12] Xu, L., Skoularidou, M., Cuesta-Infante, A. and Veeramachaneni, K., 2019. Modeling tabular data using conditional gan. Advances in Neural Information Processing Systems, 32.
- [13] Dua, D. and Graff, C. (2019). UCI Machine Learning Repository. Irvine, CA: University of California, School of Information and Computer Science. <http://archive.ics.uci.edu/ml>
- [14] Reiter, J.P., Wang, Q. and Zhang, B., 2014. Bayesian estimation of disclosure risks for multiply imputed, synthetic data. Journal of Privacy and Confidentiality, 6(1).
- [15] Sklar, A., 1973. Random variables, joint distribution functions, and copulas. Kybernetika, 9(6), pp.449-460.
- [16] Demarta, S. and McNeil, A.J., 2005. The t copula and related copulas. International statistical review, 73(1), pp.111-129.
- [17] Czado, C., 2019. Analyzing dependent data with vine copulas. Lecture Notes in Statistics, Springer, 222.
- [18] Cavanaugh, J.E. and Neath, A.A., 2019. The Akaike information criterion: Background, derivation, properties, application, interpretation, and refinements. Wiley Interdisciplinary Reviews: Computational Statistics, 11(3), p.e1460.
- [19] Yu, Y., Si, X., Hu, C. and Zhang, J., 2019. A review of recurrent neural networks: LSTM cells and network architectures. Neural computation, 31(7), pp.1235-1270.
- [20] Kingma, D.P. and Welling, M., 2019. An introduction to variational autoencoders. Foundations and Trends® in Machine Learning, 12(4), pp.307-392.
- [21] Ben-Gal, I., 2008. Bayesian networks. Encyclopedia of statistics in quality and reliability, 1.
- [22] Gogoshin, G., Branciamore, S. and Rodin, A.S., 2021. Synthetic data generation with probabilistic Bayesian Networks. Mathematical biosciences and engineering: MBE, 18(6), p.8603.
- [23] Abay, N.C., Zhou, Y., Kantarcioglu, M., Thuraisingham, B. and Sweeney, L., 2019. Privacy preserving synthetic data release using deep learning. In Joint European Conference on Machine Learning and Knowledge Discovery in Databases (pp. 510-526). Springer, Cham.
- [24] Kingma, D.P. and Welling, M., 2013. Auto-encoding variational bayes. arXiv preprint arXiv:1312.6114.
- [25] Armanious, K., Jiang, C., Fischer, M., Küstner, T., Hepp, T., Nikolaou, K., Gatidis, S. and Yang, B., 2020. MedGAN: Medical image translation using GANs. Computerized medical imaging and graphics, 79, p.101684.
- [26] Park, N., Mohammadi, M., Gorde, K., Jajodia, S., Park, H. and Kim, Y., 2018. Data synthesis based on generative adversarial networks. arXiv preprint arXiv:1806.03384.
- [27] Arjovsky, M., Chintala, S. and Bottou, L., 2017, July. Wasserstein generative adversarial networks. In International conference on machine learning (pp. 214-223). PMLR.
- [28] Gauthier, J., 2014. Conditional generative adversarial nets for convolutional face generation. Class project for Stanford CS231N: convolutional neural networks for visual recognition, Winter semester, 2014(5), p.2.
- [29] Bishop, C.M. and Nasrabadi, N.M., 2006. Pattern recognition and machine learning (Vol. 4, No. 4, p. 738). New York: springer.
- [30] Zhao, Z., Kunar, A., Birke, R. and Chen, L.Y., 2022. CTAB-GAN+: Enhancing Tabular Data Synthesis. arXiv preprint arXiv:2204.00401.
- [31] Lederrey, G., Hillel, T. and Bierlaire, M., 2022. DATGAN: Integrating expert knowledge into deep learning for synthetic tabular data. arXiv preprint arXiv:2203.03489.
- [32] Jordon, J., Yoon, J. and Van Der Schaar, M., 2018, September. PATE-GAN: Generating synthetic data with differential privacy guarantees. In International conference on learning representations.
- [33] Papernot, N., Song, S., Mironov, I., Raghunathan, A., Talwar, K. and Erlingsson, Ú., 2018. Scalable private learning with pate. arXiv preprint arXiv:1802.08908.
- [34] Xie, L., Lin, K., Wang, S., Wang, F. and Zhou, J., 2018. Differentially private generative adversarial network. arXiv preprint arXiv:1802.06739.
- [35] Massey Jr, F.J., 1951. The Kolmogorov-Smirnov test for goodness of fit. Journal of the American statistical Association, 46(253), pp.68-78.
- [36] McHugh, M.L., 2013. The chi-square test of independence. Biochemia medica, 23(2), pp.143-149.
- [37] Villani, C., 2009. Optimal transport: old and new (Vol. 338, p. 23). Berlin: springer.
- [38] Hoofnagle, C.J., van der Sloot, B. and Borgesius, F.Z., 2019. The European Union general data protection regulation: what it is and what it means. Information & Communications Technology Law, 28(1), pp.65-98.
- [39] Lowe, D.G., 2004. Distinctive image features from scale-invariant keypoints. International journal of computer vision, 60(2), pp.91-110.

Packet Loss Concealment Estimating Residual Errors of Forward-Backward Linear Prediction for Bone-Conducted Speech

Ohidujjaman¹, Nozomiko Yasui², Yosuke Sugiura³, Tetsuya Shimamura⁴, Hisanori Makinae⁵

Graduate School of Science and Engineering, Saitama University, Saitama 338-8570, Japan^{1,3,4}

Computer Science and Engineering, Daffodil International University, Savar, Dhaka 1216, Bangladesh¹

National Institute of Technology, Kisarazu College, Chiba 292-0041, Japan²

Third Information Science Section, National Research Institute of Police Science, Chiba 277-0882, Japan⁵

Abstract—This study proposes a suitable model for packet loss concealment (PLC) by estimating the residual error of the linear prediction (LP) method for bone-conducted (BC) speech. Instead of conventional LP-based PLC techniques where the residual error is ignored, we employ forward-backward linear prediction (FBLP), known as the modified covariance (MC) method, by incorporating the residual error estimates. The MC method provides precise LP estimation for a short data length, reduces the numerical difficulties, and produces a stable model, whereas the conventional autocorrelation (ACR) method of LP suffers from numerical problems. The MC method has the effect of compressing the spectral dynamic range of the BC speech, which improves the numerical difficulties. Simulation results reveal that the proposed method provides excellent outcomes from some objective evaluation scores in contrast to conventional PLC techniques.

Keywords—Autocorrelation method; bone-conducted speech; modified covariance method; packet loss concealment; residual error

I. INTRODUCTION

Recently, much attention has been paid to the use of BC speech in the field of speech signal processing. BC speech travels through the vibration of skull bone, skin, and soft tissue as its pathway. A vibration sensor is used for BC microphone decoration. BC microphone captures the vibrations and converts them into an electric signal. Thus, BC speech is rarely affected by ambient noise. Therefore, BC speech delivers advantages over air-conducted (AC) speech in some cases. In [1], BC speech was synthesized based on the least squares (LS) method. Pitch detection for BC speech is discussed in [2]. In [3], BC speech was utilized with AC speech for speaker recognition. Speaker verification is also described in [4]. To improve the quality of speech, several types of algorithms have been derived for BC speech [5]-[7]. Rahman *et al.* [8] considered a noisy environment for BC speech and derived a noise-robust LP method. However, there are few works on PLC for BC speech. In [9], the MC method was derived for the PLC technique in noisy cases, in which how the transmitted BC speech can be reconstructed with higher accuracy by reducing the spectral dynamic range was investigated.

In recent years, voice over internet protocol (VoIP) has considerably increased due to the frequent use of internet telephony. VoIP utilizes a packet-switch network instead of circuit switching. Speech voice is degraded in packet-switched

networks because of the delayed packet, additive noise, network congestion, packet arrival jittering, and bit errors [10]. The more bit errors finally cause the packet loss. Also, the high-speed network cannot conciliate a packet loss issue, resulting in degraded quality of speech [11]. Therefore, lost packets must be recovered to eschew speech quality degradation, which is known as PLC. Several methods have been recommended for PLC such as 2-sided LP, recovery sub-codec (RSC), deep neural network (DNN), hidden Markov model (HMM), adaptive recurrent neural network (A-RNN)-based PLC, and so on [11]-[17]. One representative of the classical PLC methods may be an LP-based PLC extensively utilized in global systems for mobile (GSM) technology [18]. Audio jitter buffer, network equalizer (NetEQ), is a web real-time communications (WebRTC's) default PLC whose performance is degraded in higher packet loss cases. A state-of-the-art PLC approach is WaveNetEQ (generative model) PLC built on DeepMind's wave recurrent neural network (WaveRNN) technology, which is deployed instead of the NetEQ PLC technique for accurate speech reconstruction [19]. Currently, the WaveNetEQ PLC approach is implemented in Google Due [20]. Among the above approaches, the DNN, HMM, WaveNetEQ, and A-RNN PLC techniques are state-of-the-art, but the large volume of speech data is required to be employed to train them, which is an inevitable hands-on problem in some circumstances, and they also face higher computational complexity. Contrariwise, the LP-based PLC technique provides better performance with a notably lower computational complexity. Few works are known for the LP-based PLC technique of BC speech in the literature. Therefore, there is sufficient scope to enhance the performance of the LP-based PLC approach.

In [21], a PLC method was proposed through sinusoidal extrapolation with pulse code modulation (PCM) coded at the recipient side. This PCM-coded PLC technique extrapolates filter coefficients and LP residuals from the last packet correctly received while speech packets are lost. In [22], the ACR method of LP was proposed for the PLC technique where the forward direction and bidirectional estimation processes were employed for 10% and more than 10% packet losses, respectively. The Levinson-Durbin (LD) algorithm was deployed to estimate the LP coefficients, and a better PLC was obtained by setting a large LP order. In [23], the PCM-coded PLC technique was proposed, where the predictive error signal of

the prior packet and the attained pitch period are employed to stimulate an excitation for packet loss. The forthcoming packet was omitted for backward estimation, resulting in signal attenuation. In [11], a recovery sub-codec (RSC) PLC technique was proposed that employed low delay code-excited LP (LD-CELP) where the ACR method of LP was deployed. BC speech possesses an expanded spectral dynamic range, which leads to a large eigenvalues expansion of the ACR matrix in the ACR method employed in the RSC-based PLC technique. To evade the eigenvalues expansion, we utilize the forward-backward LP (FBLP), which is often called the MC method [9], instead of the ACR method.

In the above conventional PLC techniques, LP-based methods are usually implemented. According to the existing PLC approaches [9][11][21]-[23], none of them incorporated the residual error estimates. Commonly, the conventional PLC method utilizes the ACR method where the L-D algorithm is employed. The ACR method provides degraded performance in an expanded spectral dynamic range of an input signal. On the other hand, the MC method reduces the eigenvalue expansion of BC speech, resulting in an improved ill-condition. From this point of view, we consider the MC method by including the residual error estimates. This study emphasizes the residual error estimation in both forward and backward packets to the lost packet. The predictive residual errors are added in each lost packet exclusively during the packet loss estimation. For the simulations, some objective evaluations are done, and it is demonstrated that the proposed PLC technique performs better than the conventional PLC approaches.

The following is the organizational structure of this paper. Section I includes the introduction. Section II provides an overview of the conventional method, while Section III explains the proposed approach. Section IV outlines the experiments. Results are discussed in Section V. Section VI concludes the paper.

II. CONVENTIONAL PLC METHOD

In [9], the MC method was derived for the PLC technique in noisy cases, in which how the transmitted BC speech can be reconstructed with higher accuracy by reducing the spectral dynamic range was investigated. The AC speech was replaced by the BC speech to mitigate the additive noise problem, and the MC method was employed instead of the AC method to improve the ill-conditioned difficulties. The MC method of LP was derived from a least-squares (LS) method for estimating the LP coefficients by the concurrent minimization of the FBLP squared errors. In [9], without residual error estimates, the basic form of LP was defined as

$$s(n) = - \sum_{k=1}^p \alpha(k)s(n-k) \quad (1)$$

where $\alpha(k)$ and p correspond to the LP coefficients and the LP order, respectively, and $s(n-k)$ denotes the prior data samples. The total squared errors were expressed as

$$\mathcal{E} = \mathcal{E}_f + \mathcal{E}_b \quad (2)$$

where \mathcal{E}_f and \mathcal{E}_b denote the forward and backward squared errors, respectively, and they are defined as

$$\mathcal{E}_f = \sum_n (s(n) + \sum_{k=1}^p \alpha(k)s(n-k))^2 \quad (3)$$

$$\mathcal{E}_b = \sum_n (s(n) + \sum_{k=1}^p \alpha(k)s(n+k))^2, \quad (4)$$

respectively. In (3) and (4), the speech signal sample at time n , $s(n)$, is predicted by forward and backward LP filters with the order of p . When the LP coefficients $\alpha(1), \alpha(2), \dots, \alpha(p)$ are represented in a vector form as

$$\boldsymbol{\alpha} = [\alpha(1), \alpha(2), \dots, \alpha(p)]^T \quad (5)$$

where T denotes transpose. The MC method was derived to obtain the LP coefficients as follows. For the unknown vector $\boldsymbol{\alpha}$, the residual error vector, $\boldsymbol{\epsilon}$, is defined as

$$\boldsymbol{\epsilon} = \mathbf{R}\boldsymbol{\alpha} - \mathbf{r} \quad (6)$$

where \mathbf{R} and \mathbf{r} correspond to the observation matrix and measurement vector, respectively. We can define the least squares criterion as

$$L = \boldsymbol{\epsilon}^T \boldsymbol{\epsilon} \quad (7)$$

L is expanded as follows:

$$\begin{aligned} L &= (\mathbf{R}\boldsymbol{\alpha} - \mathbf{r})^T (\mathbf{R}\boldsymbol{\alpha} - \mathbf{r}) \\ &= (\mathbf{R}\boldsymbol{\alpha})^T (\mathbf{R}\boldsymbol{\alpha}) + \mathbf{r}^T \mathbf{r} - (\mathbf{R}\boldsymbol{\alpha})^T \mathbf{r} - \mathbf{r}^T (\mathbf{R}\boldsymbol{\alpha}) \end{aligned} \quad (8)$$

where $\mathbf{r}^T (\mathbf{R}\boldsymbol{\alpha})$ is represented by $(\mathbf{R}\boldsymbol{\alpha})^T \mathbf{r}$. Thus, equation (8) is rewritten as

$$L = \mathbf{R}^T \boldsymbol{\alpha}^T (\mathbf{R}\boldsymbol{\alpha}) + \mathbf{r}^T \mathbf{r} - 2\boldsymbol{\alpha}^T \mathbf{R}^T \mathbf{r} \quad (9)$$

Since (9) is a quadratic form of $\boldsymbol{\alpha}$, by differentiating (9) with respect to $\boldsymbol{\alpha}$ and setting it to zero, we obtain the following forms as

$$2\mathbf{R}^T \mathbf{R}\boldsymbol{\alpha} - 2\mathbf{R}^T \mathbf{r} = 0 \quad (10)$$

$$\boldsymbol{\alpha} = (\mathbf{R}^T \mathbf{R})^{-1} \mathbf{R}^T \mathbf{r} \quad (11)$$

$$\boldsymbol{\alpha} = \mathbf{C}^{-1} \mathbf{c} \quad (12)$$

where $\mathbf{C} = \mathbf{R}^T \mathbf{R}$ and $\mathbf{c} = \mathbf{R}^T \mathbf{r}$ correspond to the MC matrix and MC vector, respectively. In this PLC technique, the MC method reduced the eigenvalue expansion, which improved the ill-condition. This is because there is a centrosymmetric characteristic in the MC matrix, \mathbf{C} , resulting in better speech reconstruction in the PLC technique. However, in this PLC technique, the predictive residual error is ignored, which is expected to be estimated and incorporated in the case of optimal speech reconstruction for the PLC.

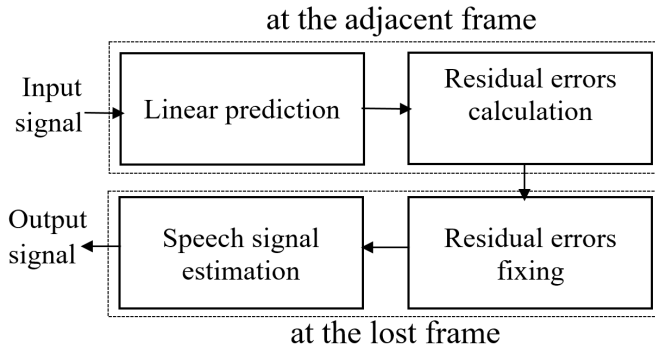


Fig. 1. Block diagram of the proposed method.

III. PROPOSED METHOD

This paper proposes a progressive PLC technique focusing on residual error signal which is an effective factor to provide an improvement of the LP method. The PLC technique in [9] avoided residual error estimates in the basic LP Eq. (1), in which residual error must be incorporated for accurate speech reconstruction in the PLC technique. Therefore, we modify Eq. (1) by incorporating the residual error estimates as

$$s(n) = -\sum_{k=1}^p \alpha(k)s(n-k) + \epsilon(n) \quad (13)$$

where $\epsilon(n)$ denotes the predictive residual error. The basic block diagram of the proposed method is shown in Fig. 1.

A. Residual Error Calculation

In the conventional LP-based PLC method, the long packet loss causes amplitude attenuation in the estimated speech signal, resulting in degraded speech quality. Therefore, the proposed method focuses on the estimation model of the speech signal in the packet loss and considers causality with the attenuation. The conventional LP form (1) is expanded, and the transition is performed then (1) becomes (14) as follows:

$$s(n) = -\alpha(1)s(n-1) - \alpha(2)s(n-2) - \dots - \alpha(p)s(n-p) \\ \implies s(n) + \alpha(1)s(n-1) + \dots + \alpha(p)s(n-p) = 0 \quad (14)$$

Eq. (14) is a linear first-order combination of sample points, held in the LP method. By comparing Eq. (14) with Eq. (13), it is noted that the conventional estimation model Eq. (14) assumes the residual error, $\epsilon(n)$, to be 0. Thus, the estimated speech waveform is attenuated since the residual error is ignored in the speech estimation. Therefore, the residual error must be estimated that originally occurs in the lost segment from the adjacent packets, and needs to be incorporated into the speech estimation model to enhance the performance of the conventional LP-based PLC technique. The residual error is the difference between the true speech signal and the estimated speech signal. The LP error is calculated in the adjacent packets for the forward and backward directions. Through the LP errors $\epsilon(n)$ at the adjacent packets, the estimated LP residual error, $\hat{\epsilon}(n)$, in the lost packet is calculated as

$$\hat{\epsilon}(n) = s(n) - \hat{s}(n); (n = 0, 1, \dots, L-1) \quad (15)$$

where L denotes the length of a packet loss. The error estimation takes advantage of the fact that the LP error has the same

Algorithm 1 : Residual error calculation

```

1  fun error ← residualError (Tmp, PW, ARcoef, M)
2  for i ← M + 1 : PW
3    xEsti ← -ARcoefT × Tmp(i - 1 to i - M)
4  end
5  if size (xEsti, 1) ≠ size(Tmp, 1)
6    xEsti ← xEstiT
7  end
8  error ← Tmp - xEsti
9  end
  
```

periodicity as the original speech signal. Since the periodicity is confirmed, the LP error of the packet loss is calculated through the concept of the PWR method. The conventional PWR method processes the speech waveform, but in this case, the processing is performed for the LP error, hence the input to the MC function changes to an LP error as

$$R(m) = -\sum_{k=0}^{L-1} \epsilon(k) \epsilon(k-m) \quad (16)$$

Algorithm 1 shows the residual error estimation process. In Algorithm 1, Tmp and PW correspond to samples for error estimate and window length for pitch extraction, respectively, and AR_{coef} denotes autoregressive (AR) coefficients of LP order M . Finally, the estimated LP error $\hat{\epsilon}(n)$ is incorporated into the conventional estimation model to conceal the lost packet as follows:

$$\hat{s}(n) = -\sum_{k=1}^p \alpha(k) s(n-k) + \hat{\epsilon}(n) \quad (17)$$

where $\hat{s}(n)$ and $s(n-k)$ correspond to predicted samples and previous samples, respectively.

B. Forward-Backward Packet Estimation and Addition

Eq. (17) with error estimate is concisely expressed as

$$\hat{s}(n) = -\alpha \mathbf{s}^T + \hat{\epsilon}(n) \quad (18)$$

where $\alpha = (\alpha(1) \ \alpha(2) \ \dots \ \alpha(p-1) \ \alpha(p))$,

$$\mathbf{s} = (s(n-1) \ s(n-2) \ \dots \ s(n-p)),$$

$$\hat{\epsilon}(n) = \epsilon^f(n) + \epsilon^b(n), \text{ and}$$

\mathbf{s} and α correspond to the input data vector and LP parameter vector, respectively. The LP coefficients in α are obtained from the preceding and succeeding packets to the packet loss. Eq. (18) is more specifically expressed as

$$\hat{s}(n) = -\alpha[1:p] \mathbf{s}^T[(n-1):(n-p)] + \hat{\epsilon}(n) \quad (19)$$

Eq. (19) is performed L times for the forward-backward predictions to retrieve lost samples in the packet loss. For instance, lost samples are estimated in the forward prediction as follows:

$$s^f(1) = -\alpha[1:p] \mathbf{s}^T[n:(n-p+1)] + \hat{\epsilon}(n)$$

$$\dots \quad \dots \quad \dots \quad \dots \quad \dots \quad \dots$$

$$s^f(L) = -\alpha[1:p] \mathbf{s}^T[n+L-1:n+L-p] + \hat{\epsilon}(n+L-1) \quad (20)$$

Algorithm 2 : Forward-backward packets addition

```

1 fun  $s \leftarrow \text{addition}(FEF, BEF)$ 
2    $L \leftarrow \text{length}(FEF)$ 
3    $s \leftarrow \text{zeros}([L \ 1])$ 
4   for  $i \leftarrow 1$  to  $L$ 
5      $\omega \leftarrow (i - 1) / (L - 1)$ 
6      $s(n + i) \leftarrow FEF(i) \times (1 - \omega) + BEF(i) \times \omega$ 
7   end
8 end

```

In the backward prediction, lost samples are estimated as,

$$s^b(1) = -\alpha[1:p] \mathbf{s}^T[n:(n+p-1)] + \hat{\epsilon}(n)$$

... ..

$$s^b(L) = -\alpha[1:p] \mathbf{s}^T[n-L+1:n-L+p] + \hat{\epsilon}(n-L+1) \quad (21)$$

In Eq. (20) and Eq. (21), the estimated errors are incorporated, which pays an advantage to the proposed method over the conventional PLC methods. The estimated packets (forward and backward predictions) are stored in the buffer until they are added. We add these packets from the buffer to restore packet loss. Algorithm 2 shows the estimated packet addition process. In Algorithm 2, FEF and BEF indicate the forward and backward estimated frames, respectively, and L indicates the total number of samples in the lost packet. The linear weighting, ω , is defined as $0 \leq \omega \leq 1$. Fig. 2 represents a diagram of the 2-sided MC method where estimated residual errors are incorporated in both forward and backward predictions. The forward prediction is done from the previous packet of the packet loss, and the backward prediction is from the future packet of the packet loss as shown in Fig. 2(c). Then, the speech signal is reconstructed by adding forward and backward estimated packets as shown in Fig. 2(d). The proposed method using the forward and backward adjacent packets of the lost frame inherits the advantage of the LP method that the distortion does not occur in the estimated speech, and it overcomes the drawback where the amplitude of the estimated speech is attenuated.

IV. EXPERIMENTAL CONDITIONS

We employed the National Research Institute of Police Science (NRIPS) database [24], from where the BC speech is implemented in this paper. In this database, the BC microphone TEMCO EML-1-A was used to measure BC speech, and a digital recorder EDIROL R-4 recorded the BC speech. We used 250 male and 250 female speech utterances of 50 different sentences pronounced by five males and five females for BC speech in the simulation. The evaluated result may differ for diverse speakers though the packet loss rate is identical. Therefore, the estimated score of each experiment of 250 times was averaged. As the objective evaluation, we utilized perceptual evaluation of speech quality (PESQ), log-spectrum distortion (LSD), and the log area ratio (LAR). The simulation details are shown in Table I.

V. RESULTS DISCUSSION

In this section, we conducted several comparisons between the conventional and proposed methods.

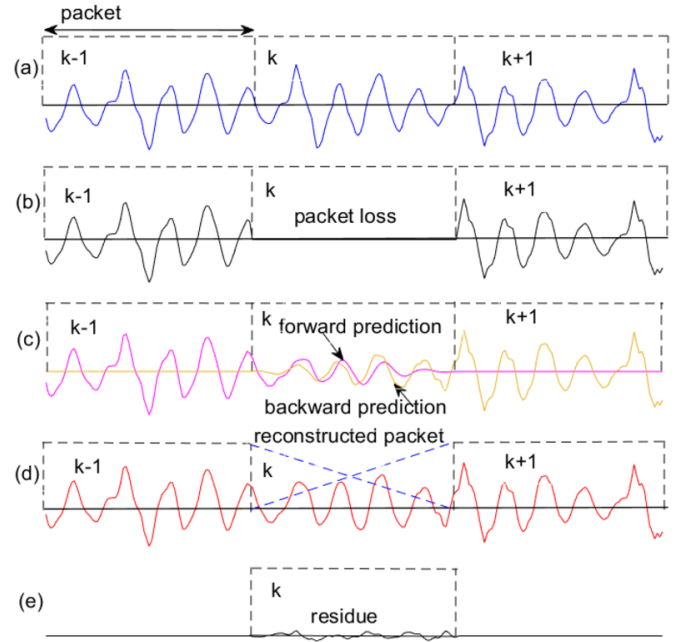


Fig. 2. Schematic diagram of 2-sided LP: (a) Original speech (b) Degraded speech (c) Forward and backward predictions (d) Reconstructed speech (e) Residue.

TABLE I. SIMULATION SPECIFICATIONS

| Items | Specifications |
|----------------------|-------------------------|
| Accent | Japanese pronunciations |
| Speaker | Male and female |
| Sampling frequency | 8 kHz |
| Quantization | G.711 μ -law |
| Speech signal length | 4-5 sec |
| Length of packet | 10 ms |
| Loss rate | 10% and 30% |
| LP order | 12 |
| LP analyzing window | 20 ms |
| Window type | Rectangular |

A. Estimated Waveform

The proposed PLC method avoids the use of linear gain to the restored speech signal, whereas the conventional PLC methods apply a linear gain of 1.1 to 1.8 [9][11][21]-[23]. The reconstructed speech waveform for the MC method without error estimate (conventional method) and the MC method with error estimate (proposed method) in the PLC technique are shown in Fig. 3, where the estimated speech waveform obtained by the proposed method is well-matched to the original transmitted speech waveform. This is because the incorporated residual error signal influences the quality of the reconstructed speech signal.

B. PESQ Score

The perceptual evaluation of speech quality (PESQ) was utilized as the objective evaluation to measure the excellence of speech for VoIP. The PESQ provides the quality of speech

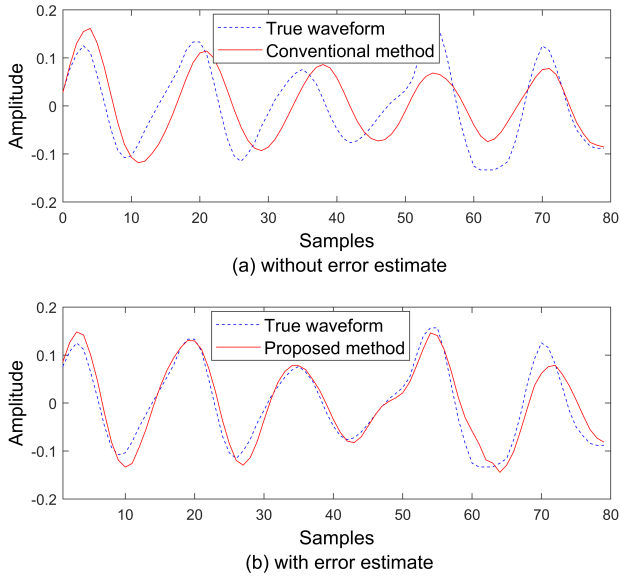


Fig. 3. Estimated waveform.

TABLE II. AVERAGE PESQ SCORES OF DIFFERENT METHODS

| Methods | 10% packet loss | | 30% packet loss | |
|-----------------|-----------------|--------|-----------------|--------|
| | male | female | male | female |
| ACR method | 3.57 | 3.61 | 3.12 | 3.19 |
| RSC method | 3.66 | 3.69 | 3.23 | 3.27 |
| MC method | 3.78 | 3.81 | 3.39 | 3.41 |
| Proposed method | 4.03 | 4.07 | 3.63 | 3.66 |

signal in the extent from -0.5 to 4.5, in which the higher quantity represents that the quality of speech signal is better [25]. Table II shows the PESQ scores of the ACR, RSC, MC, and proposed methods. The MC method has shown better results up to now [9], but the proposed method provides the best result over the conventional methods. In the case of 10% packet loss, the conventional MC method provides PESQ scores of 3.78 for males and 3.81 for females, respectively. On the other hand, the proposed MC method provides PESQ scores of 4.03 for males and 4.07 for females, respectively. Similarly, for 30% packet loss, the proposed method provides acceptable PESQ scores in both male and female cases than the conventional MC method. Thus, the PESQ score is higher for compensated speech signals wherein the residual error is incorporated. We utilized the same database [24] for all considering methods in this paper for a fair comparison.

C. LSD Score

Furthermore, the LSD score is observed for the restored BC speech for different methods in the PLC technique. We assumed a packet length of 20 ms and a frame-shifting of 10 ms for obtaining the LSD scores. The LSD scores of 24 frames from each restored speech are averaged through 10 ms frame

TABLE III. AVERAGE LSD SCORES OF DIFFERENT METHODS

| Methods | Speakers | |
|-----------------|----------|--------|
| | male | female |
| ACR method | 12.08 | 11.89 |
| RSC method | 11.25 | 11.01 |
| MC method | 10.38 | 10.10 |
| Proposed method | 8.41 | 8.13 |

overlapping. The LSD is calculated as

$$LSD = \sqrt{\frac{1}{B} \sum_{b=1}^B \left| 20 \log_{10} \left(\frac{P(\omega_b)}{\hat{P}(\omega_b)} \right) \right|^2} \quad (22)$$

where $P(\omega_b)$ and $\hat{P}(\omega_b)$ correspond to the true and estimated power spectra, respectively, and B denotes the upper-frequency bin number. The proposed method provides lower LSD scores for reconstructed BC speeches as shown in Table III. The lower LSD value indicates a better reconstruction of the transmitted speech signal [7].

D. LAR Distances

LP coefficients are difficult to interpolate and sensitive to quantization errors. LP coefficients are normally converted into other parameters that are equivalent to LP coefficients. Also, the converted parameters are easy to handle before transmission. One such parameter is the log area ratio (LAR) which is used to represent LP coefficients for transmission over a channel [26]. The proposed method generates the LAR distance line nearer to the baseline as shown in Fig. 4. The LAR distance line nearer to the baseline discloses that the reconstructed speech signal is closer to the transmitted speech signal.

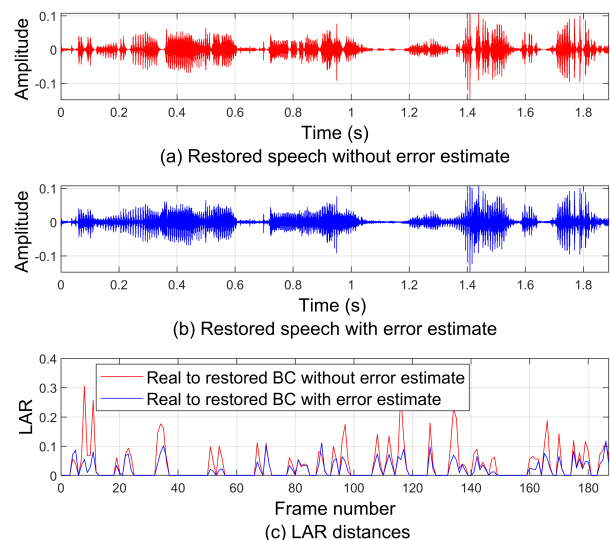


Fig. 4. LAR distances for estimated speech.

VI. CONCLUSION

This paper suggested a PLC technique for the MC method where the estimated residual error was incorporated in the forward and backward directions for packet loss compensation. The MC method was considered for BC speech to confirm residual error minimization and to improve the ill-condition for obtaining the best set of the LP parameters. The MC method compressed an expanded spectral dynamic range of input signals since the centrosymmetric characteristic was involved in the MC matrix C . It was also noted that the conventional LP-based PLC methods use a linear gain of 1.1 to 1.8. On the other hand, the proposed PLC method did not use a linear gain at all. Especially the PESQ and LSD scores showed the best results obtained by the proposed method. In the case of 10% packet loss, the proposed method provided PESQ scores of 4.03 for males and 4.07 for females, respectively. Through the LSD evaluation, the proposed method obtained the best LSD scores such as 8.41 for males and 8.13 for females, respectively. Simulation results in all objective evaluations showed that the proposed PLC method improves the conventional ones.

In this proposed method, residual error incorporation indicates one kind of input signal addition. In the future, we would like to use the combination of LP and polynomial prediction approaches in the PLC technique for better speech reconstruction without error signal incorporation.

REFERENCES

- [1] S. Zhang, Y. Sugiura, and T. Shimamura, "Bone-conducted speech synthesis based on least squares method," *IEEJ Transactions on Electrical and Electronic Engineering*, vol. 17, no. 3, pp. 425-435, 2022.
- [2] M.S. Rahman and T. Shimamura, "Pitch determination from bone conducted speech," *IEICE Trans. Inf. & Syst.*, vol. E99-D, no. 1, pp. 283-287, Jan. 2016.
- [3] S. Tsuge and S. Kuroiwa, "Bone- and air-conduction speech combination method for speaker recognition," *International Journal of Biometrics*, vol. 11, no. 1, pp. 35-49, 2019.
- [4] S. Iijima and T. Shimamura, "Bone-conducted speech for speaker verification," *Proc. Int. Workshop Nonlinear Circuits and Signal Processing*, 2008, pp. 172-175.
- [5] H. Q. Nguyen and M. Unoki, "Improvement in bone-conducted speech restoration using linear prediction and long short-term memory model," *Journal of Signal Processing*, vol. 24, no. 4, pp. 175-178, July 2020.
- [6] P. Singh, M. K. Mukul, and R. Prasad, "Bone conducted speech signal enhancement using LPC and MFCC," *Int. Conf. on Intelligent Human Computer Interaction (IHCI)*, Springer, vol. 11278, 2018, pp. 148-158.
- [7] T. T. Vu, M. Unoki, and M. Akagi, "A blind restoration model for bone-conducted speech based on a linear prediction scheme," *Int. Symp. on Nonlinear Theory and its Applications*, 2007, pp. 449-452.
- [8] M. A. Rahman, T. Shimamura, and H. Makinae, "LP-based quality improvement of noisy bone conducted speech," *IEEJ Transactions on Electronics, Information and Systems*, vol. 137, no. 1, pp. 197-198, 2017.
- [9] Ohidujjaman, N. Yasui, Y. Sugiura, T. Shimamura, and H. Makinae, "Packet loss compensation for VoIP through bone-conducted speech using modified linear prediction," *IEEJ Trans. Electrical and Electronic Engineering*, Wiley, vol. 18, no. 11, pp. 1781-1790, Aug. 2023.
- [10] J. Lecomte and T. Backstrom, "Packet loss and concealment," in *Speech Coding with Code-Excited Linear Prediction*, Springer, 1st ed., Mar. 2017, pp. 161-184.
- [11] T. Morinaga, S. Sasak, K. Manol, and T. Kanekol, "Robust speech coding under packet-loss conditions using recovery sub-codec for broadband IP network," *Proc. IEEE Int. Conf. on Acoustics, Speech and Signal Processing (ICASSP)*, vol. 03, 2002, pp. 2713-2716.
- [12] A. Bakri, A. Barouche, and M. Abbas, "An improved packet loss concealment technique for speech transmission in VOIP," *2nd Int. Conf. on Natural Language and Speech Processing (ICNLSP)*, April 2018, pp. 1-5.
- [13] B.J. Borgstrom, P.H. Borgstrom, and A. Alwan, "Efficient HMM-based estimation of missing features, with applications to packet loss concealment," *11th Annual Conf. of the Int. Speech Communication Association, Chiba, Japan*, Sep. 26-30, 2010.
- [14] M.K. Lee, S.K. Jung, H.K. Kang, Y.C. Park, and D.H. Youn, "A packet loss concealment algorithm based on time-scale modification for CELP-type speech coders," *Proc. IEEE Int. Conf. Acoust., Speech, Signal Process.*, Apr. 2003, pp. 116-119.
- [15] C.A. Rodbro, M.N. Murthi, S.V. Andersen, and S.H. Jensen, "Hidden Markov model-based packet loss concealment for voice over IP," *IEEE Transactions on Audio, Speech, and Language Processing*, vol. 14, no. 5, 2006, pp. 1609-1623.
- [16] B.K. Lee and J. H. Chang, "Packet loss concealment based on deep neural networks for digital speech transmission," *IEEE/ACM Transactions on Audio, Speech, and Language Processing*, vol. 24, no. 2, Feb. 2016, pp. 378-387.
- [17] R. Lotfidereshgi and P. Gournay, "Speech prediction using an adaptive recurrent neural network with application to packet loss concealment," *IEEE Int. Conf. on Acoustics, Speech and Signal Processing (ICASSP)*, 2018, pp. 5394-5398.
- [18] M.M Mohamed, M.A Nessiem and B.W. Schuller, "On deep speech packet loss concealment," *A Mini- Survey*, arXiv preprint arXiv:2005.07794 [eess.AS], May 2020.
- [19] S. Davy, N. Belton, J. Tobin, O.B. Zuber, L. Dong, and Y. Xuewen, "A causal convolutional approach for packet loss concealment in low powered devices," *IEEE Int. Conf. on Acoustics, Speech and Signal Processing (ICASSP)*, May 2023.
- [20] "Improving audio quality in Duo with WaveNetEQ," <http://ai.googleblog.com/2020/04/improving-audio-quality-in-duo-with.html>
Archived: <https://web.archive.org/web/20220309043235/http://ai.googleblog.com/2020/04/improving-audio-quality-in-duo-with.html>
- [21] J. Lindbrom and P. Hedelin, "Packet loss concealment based on sinusoidal extrapolation," *IEEE ICASSP*, Vol. 1, 2002, pp. 173-176.
- [22] K. Kondo and K. Nakagawa, "A speech packet loss concealment method using linear prediction," *IEICE Trans. Inf. & Syst.*, vol. E89-D, no. 2, 2006, pp. 806-813.
- [23] E. Gunduzhan and K. Momtahan, "A linear prediction based packet loss concealment algorithm for PCM coded speech," *IEEE Transactions on Speech and Audio Processing*, vol. 9, no. 8, Nov. 2001.
- [24] K. Amino, T. Osanai, T. Kamada, H. Makinae H and T. Arai, "Effects of the phonological contents and transmission channels on forensic speaker recognition," *Forensic Speaker Recognition: Law Enforcement and Counter-Terrorism (A. Neustein, H. Patil eds.)*, Springer-Verlag Berlin Heidelberg, 2011, pp. 275-308.
- [25] ITU-T Recommendation P.862, "Perceptual evaluation of speech quality (PESQ): An objective method for end-to-end speech quality assessment of narrow-band telephone networks and speech codecs," 2001.
- [26] D. Chow and W.H. Abdulla, "Speaker identification based on log area ratio and Gaussian mixture models in narrow-band speech," *PRICAI 2004: Trends in Artificial Intelligence, Lecture Notes in Computer Science*, Springer Berlin / Heidelberg, vol. 3157, 2004, pp. 901-908.

A Comprehensive Analysis of Network Security Attack Classification using Machine Learning Algorithms

Abdulaziz Saeed Alqahtani¹, Osamah A. Altammami², Mohd Anul Haq^{3*}

Department of Computer Science-College of Computer and Information Sciences, Majmaah University,
Al Majmaah, 11952, Saudi Arabia^{1, 2}

College of Business Administration, Majmaah University, Al Majmaah, 11952, Saudi Arabia³

Abstract—As internet usage and connected devices continue to proliferate, the concern for network security among individuals, businesses, and governments has intensified. Cybercriminals exploit these opportunities through various attacks, including phishing emails, malware, and DDoS attacks, leading to disruptions, data exposure, and financial losses. In response, this study investigates the effectiveness of machine learning algorithms for enhancing intrusion detection systems in network security. Our findings reveal that Random Forest demonstrates superior performance, achieving 90% accuracy and balanced precision-recall scores. KNN exhibits robust predictive capabilities, while Logistic Regression delivers commendable accuracy, precision, and recall. However, Naive Bayes exhibits slightly lower performance compared to other algorithms. The study underscores the significance of leveraging advanced machine learning techniques for accurate intrusion detection, with Random Forest emerging as a promising choice. Future research directions include refining models and exploring novel approaches to further enhance network security.

Keywords—Machine learning; cyber security; intrusion detection; network security; cyber security

I. INTRODUCTION

In recent years, cyber-attacks have become more sophisticated and frequent, posing significant challenges to cybersecurity efforts. As organizations increasingly rely on interconnected networks for their operations, they are exposed to a greater risk of malicious activities. Traditional security methods, such as firewalls and antivirus software, while still valuable, are struggling to keep pace with the evolving tactics of cybercriminals [1]. These attacks can take various forms, from relatively simple phishing emails to complex malware and DDoS attacks, resulting in operational disruptions, data breaches, and financial losses [2]. To effectively combat these threats, security professionals need to adopt more advanced techniques for threat detection and mitigation [3]. Machine learning algorithms offer a promising solution by leveraging data analysis to identify patterns and anomalies indicative of malicious activity [4]. By automating threat detection and response processes, ML can help organizations bolster their network security defenses in the face of evolving cyber threats.

*Corresponding Author

A. Research Objectives and Motivation

The main objective of this paper is to conduct a comprehensive examination of network security attack classification using ML algorithms. By exploring various ML techniques and evaluating their applicability to network security, the research aims to enhance precision and efficiency in identifying and categorizing network attacks [4]. The motivation behind this research lies in the critical need for adaptive and intelligent security measures to counter the dynamic tactics employed by cybercriminals [5].

B. Consequences of Cyber-Attacks

The introduction also underscores the significant consequences of successful cyber-attacks, ranging from financial losses to reputational damage and legal ramifications [6]. This [7] highlights the importance of enhancing security measures to safeguard sensitive data, ensure uninterrupted operations, and maintain trust in digital systems.

C. Transition to Proactive Security Strategies

Furthermore, the integration of ML into network security protocols facilitates a transition from reactive to proactive security strategies [8]. By preemptively addressing potential threats, organizations can enhance overall resilience and security posture.

This paper will include a detailed comparative analysis with state-of-the-art methods, including recent advancements in deep learning applied to intrusion detection. Additionally, recent research in deep learning for intrusion detection will be reviewed to identify advancements and opportunities for improvement. This comprehensive comparison will enhance the credibility and relevance of the research findings.

This study is structured to first explore the existing landscape of network security and the challenges posed by cyber-attacks. It will then delve into the application of ML algorithms in enhancing threat detection and response processes. Following this, the paper will evaluate the strengths and limitations of existing network intrusion detection systems, proposing innovative ML solutions to address emerging challenges. Finally, it will provide recommendations for developing stronger, more flexible, and smarter security systems to combat cyber threats effectively in today's digital age.

II. RELATED WORKS

This review of the existing literature offers an in-depth examination of the present state of research in the classification of network security attacks through the application of machine learning algorithms.

A. Network Security Attack Classification

Traditional cybersecurity methods rely on predefined rules and signatures to detect and mitigate threats, but they struggle to keep up with the rapidly evolving tactics of cybercriminals. This [9] limitation has prompted a shift towards more adaptive and intelligent systems, leading to the exploration of machine learning techniques. In their examination of machine learning algorithms, the focus is on their crucial role in intelligent data analysis and automation within the cybersecurity field [10]. They [11] highlight the ability of these algorithms to extract valuable insights from diverse cyber data sources, demonstrating their relevance in real-world scenarios and illustrating how data-driven intelligence contributes to proactive cybersecurity measures [12]. Furthermore, [13] their analysis explores current methodologies, their practical implications, and emerging research directions, aiming to provide a comprehensive understanding of the current state of machine learning in cybersecurity and its potential for transformative advancements in line with the goals of our research

B. Machine Learning in Network Security

Machine learning's role in network security extends far beyond just threat detection. It encompasses prevention, response, and recovery aspects as well. By leveraging machine learning, organizations can build systems that continuously adapt to emerging threats, effectively fortifying their defenses against evolving attack patterns [14]. This adaptability is particularly crucial in an environment where cyber threats are constantly evolving in sophistication and evasiveness.

Furthermore, a recent study introduces a comprehensive taxonomy of security threats, evaluating the potential of artificial intelligence (AI), including machine learning, to address a wide range of challenges. This study in [15] represents the first exhaustive examination of AI solutions across various security types and threats. It covers lessons learned, current contributions, future directions, open issues, and strategies for effectively countering advanced security threats [16]. This holistic approach underscores the significance of integrating machine learning techniques into network security frameworks to combat the diverse and evolving landscape of cyber threats effectively.

C. Existing Machine Learning Approaches

In addition to supervised learning methods like Support Vector Machines (SVM) and Random Forests, unsupervised learning approaches, particularly anomaly detection, have gained prominence in the realm of network security. Unlike supervised methods that rely on labeled datasets to classify attacks, anomaly detection techniques can identify deviations from normal network behavior without predefined attack signatures. This makes them particularly useful for detecting

novel and previously unseen threats that may not be captured by traditional rule-based systems.

For instance, research conducted by [17] on intrusion detection exemplifies the application of machine learning in enhancing security measures. By leveraging machine learning algorithms, researchers have demonstrated the effectiveness of these techniques in discerning malicious activities within network traffic. This study showcases the potential of machine learning to augment traditional security measures by providing a more adaptive and proactive approach to threat detection and mitigation [18].

Furthermore, the exploration of machine learning approaches in network security continues to evolve, with researchers investigating new algorithms and methodologies to address emerging challenges. As cyber threats become increasingly sophisticated and diverse, the integration of machine learning techniques holds promise for enhancing the resilience of network defenses and mitigating the impact of cyber-attacks.

D. Feature Extraction

The success of machine learning models in network security heavily relies on the selection and extraction of relevant features. Features can include traffic patterns, packet content, and behavioral analysis [19]. The process of feature selection is critical in optimizing the performance of the machine learning model, as irrelevant or redundant features can lead to decreased accuracy and increased computational overhead. Researchers in [20] have explored various feature selection techniques to identify the most informative features for attack classification. The study in [21] employs machine learning models and feature selection techniques to detect DDoS attacks in SDN, achieving optimal accuracy (98.3%) with KNN.

Feature engineering is a critical step in the data preprocessing pipeline, aimed at transforming raw data into a format that enhances the performance of machine learning models. It encompasses various techniques, including feature extraction and feature selection, to optimize the dataset for analysis. Given our dataset's high dimensionality with 49 features, effective dimensionality reduction was essential to streamline the analysis and mitigate computational complexity. To achieve this, we opted for PCA as a feature extraction technique. PCA transforms the original features into a reduced set of principal components, capturing the dataset's essential variance while preserving valuable information. Unlike feature selection techniques, which may exclude potentially informative features, PCA retains underlying patterns and structures in the data. This approach not only enhances computational efficiency but also maintains the integrity of the dataset. Explained variance analysis revealed that 10 principal components accounted for 90% of the dataset's variance, striking an optimal balance between variance coverage and computational complexity in our study.

E. Related Articles and Cybersecurity Majors

Table I shows summary of literature reviews, the table major drawback from previous, write their accuracy values.

TABLE I. LITERATURE REVIEW

| Cite Key | Security Threat & Attacks | Detection & Mitigation | Incident Response | Standards & Policy | Important Findings |
|----------|---------------------------|------------------------|-------------------|--------------------|--|
| [22] | ✓ | ✓ | ✓ | ✓ | Early identification and detection of TTPs using supervised machine learning |
| [23] | ✓ | ✗ | ✓ | ✓ | Use ML & DL algorithms |
| [24] | ✓ | ✓ | ✓ | ✓ | highlights the ease with which DDoS attacks can be executed using a network of infected bots under the control of a single botmaster |
| [25] | ✓ | ✓ | ✗ | ✗ | addresses the significant security concern of email phishing attacks in cloud computing |
| [26] | ✓ | ✗ | ✓ | ✗ | attack taxonomy and threat model, organizations can enhance their ability to anticipate, detect, and respond to cyber threats |
| [27] | ✓ | ✓ | ✓ | X | Proposed ABRC exhibits significant performance improvement compared to existing deep learning techniques for cyber-attack detection |
| [28] | ✓ | ✓ | ✓ | ✓ | ML & QML for attacks; calculate precision and recall despite decreased accuracy post-attack; Inter-model susceptibility to crafted adversarial samples underscores the need for robust defense strategies. Future research will delve deeper into model performance and resilience against attacks |
| [29] | ✓ | X | X | ✓ | Developed technique achieves 99.7% accuracy in multi-class classification for intrusion detection, surpassing existing algorithms significantly; Demonstrates the efficiency of auto-tuned hyper-parameters and dataset improvements in enhancing detection capabilities. |
| [30] | ✓ | ✓ | ✓ | ✓ | Intrusion detection model achieves 96.00% accuracy, outperforming other neural network models; Stable training and test times. Data transmission security performance shows over 80% data message delivery rate, less than 10% message leakage and packet loss rates, and stable average delay around 350 milliseconds. The model ensures high security and prediction accuracy, serving as an experimental basis for enhancing safety in smart city rail transit systems. |

F. Research Gap Analysis

Addressing the identified research gaps holds paramount importance in advancing our understanding and fortification against privacy attacks in the realm of machine learning. Existing studies exhibit a propensity to focus on specific machine learning models, leaving a critical void in comprehending privacy threats across a broader spectrum of techniques. Furthermore, the proposed attack taxonomy provides a foundational framework, yet there exists a gap in grasping the nuanced impact of different adversarial knowledge levels on the severity of privacy attacks. Bridging this gap demands a contextual exploration of privacy attacks within real-world machine learning applications, considering the diversity of domains and their unique challenges. The scarcity of longitudinal studies underscores the need for a dynamic perspective, tracking the evolution of privacy attacks over time. Lastly, the burgeoning landscape of emerging machine learning paradigms, such as federated learning and edge computing, lacks adequate attention in current research, necessitating a focused effort to understand and mitigate privacy attacks in these evolving contexts. Addressing these gaps promises significant implications, fostering the development of more resilient privacy-preserving machine learning models, implementing enhanced security measures, and cultivating a holistic comprehension of privacy risks for the continued advancement of secure and ethical machine learning applications.

III. METHODS

The research methodology for this study adopts a quantitative approach leveraging empirical data to draw

objective conclusions and make generalizations about the relationships between variables quantitative research is deemed suitable for this investigation as it enables the measurement and analysis of numerical data providing a statistical foundation for evaluating ML in network security attack classification.

A. System Design

The system design shown in Fig. 1, is designed to analyze network security attacks using a subset of the unsw nb 15 dataset it comprises two main steps aimed at enhancing the accuracy of attack detection in the initial step data preprocessing is conducted involving both standardization and normalization to ensure uniformity in the dataset given the datasets high dimensional nature some features may be irrelevant or redundant potentially impacting the accuracy of attack detection negatively to address this issue a feature selection process is implemented to identify and retain only the most relevant subset of features effectively eliminating useless and noisy elements from the multidimensional dataset moreover class imbalance is recognized as a potential challenge in the dataset to mitigate this specific measures are taken to balance the representation of different attack categories ensuring that the classifiers are trained on a more equitable distribution of data moving on to the second step various classifiers are trained using the selected and refined features these classifiers are designed to detect all categories of attacks thereby aiming for maximum accuracy in the identification of security threats the utilization of multiple classifiers allows for a comprehensive assessment of the dataset considering the nuanced characteristics of different attacks finally the model's performance is evaluated using key

metrics such as accuracy precision recall and f 1 score these measures provide a thorough understanding of how well the classifiers are performing in terms of correctly identifying and classifying network security attacks the combination of these performance metrics ensures a comprehensive evaluation taking into account various aspects of the model's effectiveness in summary the proposed methodology begins with meticulous data preprocessing addressing issues of standardization normalization and feature selection it then tackles the challenge of class imbalance before training classifiers to detect diverse attack categories the evaluation phase employs a set of performance metrics to gauge the overall effectiveness of the framework in accurately identifying and classifying network security threats this methodological approach provides a systematic and robust foundation for analyzing network security attack data.

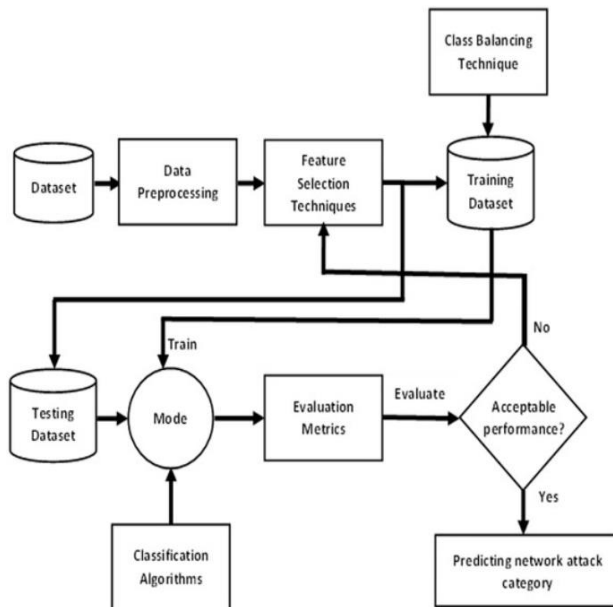


Fig. 1. System design.

B. Data Collection

1) *Data sources:* Network traffic and attack data will be sourced from Kaggle. This includes both real-world and simulated datasets to ensure a comprehensive evaluation.

The unsw nb 15 dataset crafted by researchers in 2015 stands as a comprehensive resource specifically tailored to address advanced network intrusion techniques comprising an extensive collection of 25 million records this dataset provides a rich and diverse landscape for the study of network security threats to the dataset encapsulates the complexity of modern cyber threats by encompassing 49 distinct features facilitating a nuanced analysis of network activity the 49 features in the dataset encapsulate various aspects of network traffic creating a multidimensional representation of cyber activities these features serve as essential variables for understanding and classifying different types of network security attacks researchers and practitioners benefit from the detailed and granular information embedded in each record enabling a thorough exploration of advanced intrusion techniques one noteworthy characteristic.

Nine different classes of attack families each representing a unique category of network security threat these classes encompass a wide spectrum of attack methodologies providing a holistic view of the diverse challenges faced in contemporary cybersecurity the dataset employs two label values for classification normal and attack enabling the categorization of network activities into either benign or malicious classes the dataset's utility extends shown in Fig. 2. The unsw nb 15 dataset serves as a vital resource in the field of cybersecurity research offering a rich and diverse collection of network activity records that enable in depth investigations into advanced intrusion techniques and the development of effective security solutions its comprehensive nature and well defined class structure make it an invaluable tool for researchers practitioners and educators alike in advancing the understanding and mitigation of network security threats.

2) *Data preprocessing:* Raw data will undergo preprocessing to handle missing values normalize features and address any anomalies this step is crucial for the effective application of machine learning algorithms.

a) *Data standardizations:* Data standardization, also known as data normalization, is a crucial preprocessing step in data analysis, particularly when working with machine learning algorithms sensitive to input feature scales. This process transforms the values of different variables to a common scale, ensuring that no particular feature dominates the learning process due to differences in their original scales. By rescaling the variables to have a mean of 0 and a standard deviation of 1, standardizing the data aids in maintaining consistency and improving algorithm performance. Formula is:

$$Z'' = X' - M' / \sigma'$$

Here:-

- Z'' is the standardized value
- X' is the original value of the variable
- M' is the mean of the variable
- σ' is the standard deviation of the variable.

b) *Data normalization:* Data normalization is a preprocessing method employed to adjust numerical variables to a standardized range, usually between 0 and 1. This practice aims to ensure that all variables equally contribute to the analysis, preventing any single feature with larger magnitudes from dominating. One frequently used technique for normalization is min-max scaling, which involves a formula for normalizing a variable.

$$X_{\text{normalized}} = (X_{\text{max}} - X_{\text{min}}) / (X - X_{\text{min}})$$

C. Machine Learning ML Classification Algorithm

Machine learning classification algorithms are computational tools created to classify input data into predefined categories or labels by analyzing their underlying patterns and characteristics. These algorithms learn from labeled training data, identifying patterns and relationships to predict the class labels of new instances. Various classification

algorithms, each with unique methodologies such as rule-based decision-making or probabilistic modeling, are utilized to effectively categorize data points into different classes. These algorithms are versatile tools used for tasks like detecting spam, recognizing images, and diagnosing medical conditions. Their performance is typically assessed using metrics such as accuracy, precision, recall, and F1 score, ensuring their efficacy across diverse applications.

This is a Classification problem where we want to detect whether there is an attack or not.

1) *KNN*: This is ML algorithm proficient in both classification and regression assignments. Unlike traditional methods, KNN doesn't undergo a conventional training phase but rather memorizes the entire training dataset. During prediction, it relies on the proximity of data points within the feature space [31]. To classify a new data point, KNN computes distances, often employing Euclidean distance, from the point to all other instances in the training set. The k-nearest neighbors, identified by the smallest distances, then engage in a majority voting mechanism to allocate the class to the new data point. Alternatively, a weighted voting system can be utilized, granting closer neighbors greater influence. In regression duties, KNN forecasts the target value through averaging (or weighted averaging) the target values of the k-nearest neighbors. The selection of the hyper-parameter 'k' is pivotal, as it shapes the algorithm's sensitivity and generalization capability. KNN showcases its adaptability across various domains like image recognition and recommendation systems. Nonetheless [32], its performance hinges on meticulous 'k' selection, the choice of a distance metric, and understanding the dataset's traits. Employing efficient data structures such as KD-trees can enhance scalability, while thoughtful parameter tuning ensures its efficacy across diverse contexts.

2) *Random forest*: It is an ensemble learning method widely used for classification and regression tasks, particularly in intrusion detection, the algorithm operates through bootstrapped sampling creating diverse subsets of the dataset by randomly selecting instances with replacement and training individual decision trees on these subsets key to its robustness is the random select of features at each node split tree construction preventing overemphasis on specific features in classification random forest employs a majority voting mechanism aggregating predictions from multiple trees to make [33] the final decision this approach not only yields high accuracy but also enhances the models resilience to noise and variability the algorithm's adaptability and effectiveness make it a valuable tool in cybersecurity and various other domains.

3) *Naive Bayes*: Naive Bayes is a probabilistic classification algorithm based on Bayes theorem with the naive assumption of feature independence it's particularly effective for text classification and spam filtering the

algorithm calculates the probability of a given instance belonging to a specific class by considering the conditional probabilities of each feature given the class despite its simplicity naive Bayes often performs well and is computationally efficient the naive assumption simplifies calculations making it suitable for high dimensional datasets despite its success naive Bayes might struggle with correlated features violating the independence assumption nevertheless its speed simplicity and respectable performance in various applications make it a popular choice for tasks involving categorical or text based data.

4) *Logistic regression*: It is used linear model for binary and multiclass classification problems despite its name. Also sigmoid the logistic function transforms the output into a range between 0 and 1 interpreting it as the probability of the positive class the algorithm optimizes its parameters through maximum likelihood estimation regularization techniques like L1 or L2 regularization can be applied to prevent overfitting logistic regression is interpretable and its coefficients provide insights into feature importance it's suitable for linearly separable problems but may struggle with complex relationships ensemble methods like random forest often outperform logistic regression on more intricate datasets but its simplicity interpretability and efficiency make it a valuable tool in various classification tasks.

D. Evaluation Metrics

Evaluation metrics serve as the compass for navigating the landscape of machine learning model performance accuracy the bedrock metric quantifies the models overall correctness precision zooms in on the models ability to avoid false positives while recall encapsulates its prowess in capturing all actual positive instances the f1 score harmonizes precision and recall into a single metric striking a balance between precision oriented and recall oriented scenarios the confusion matrix a comprehensive tableau breaks down a models predictions into true positives true negatives false positives and false negatives these metrics collectively illuminate the multifaceted facets of a models effectiveness providing practitioners with a versatile toolkit to gauge and enhance performance across diverse applications shown in Fig. 2.

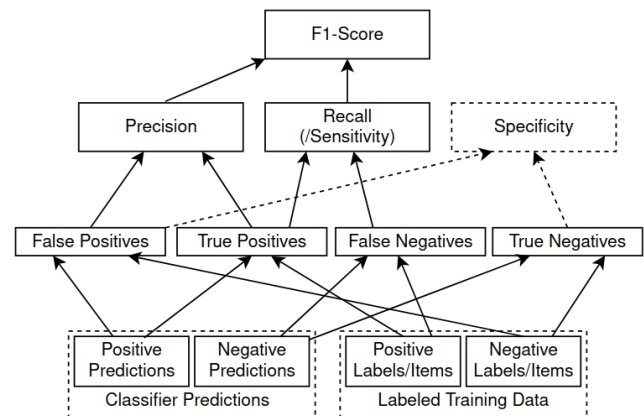


Fig. 2. Performance evaluation.

IV. IMPLEMENTATION

The experimental setup encompasses the selection and preparation of datasets the configuration of machine learning algorithms and the establishment of a controlled environment for rigorous testing the unsw nb 15 dataset consisting of 2 5 million records with 49 features was chosen for its relevance to advanced network intrusion techniques to ensure a diverse representation of attacks the dataset was partitioned into training and testing sets.

A. Tools and Techniques

This experimentation involved the implementation of various machine learning algorithms to evaluate their performance in network security attack classification python leveraging popular libraries such as scikit learn and tensor flow served as the primary programming language for algorithm implementation the choice of algorithms includes decision trees support vector machines neural networks and ensemble methods each configured with appropriate hyperparameters.

B. Implementation

The machine learning algorithms were implemented using a modular and scalable approach allowing for easy integration of new algorithms and flexibility in experimenting with different configurations the jupyter notebook was version-controlled using git to track changes and ensure reproducibility.

1) *Import dataset:* In the dataset preparation phase, the unsw nb 15 datasets were employed consisting of both training set unsw nb 15 training set csv and a testing set unsw nb 15 testings set csv the dataset was loaded into a python environment using the pandas library the training set as read from the unsw nb 15 training set csv file comprised 82 332 records while the testing set obtained from the unsw nb 15 testing set csv file included 175 341 records to verify the integrity of the dataset and ensure the appropriate division between training and testing data the lengths of the training and testing sets were checked the training set exhibited a length of 82 332 records and the testing set comprised 175.

2) *Data visualization:* The data visualization code utilizes the seaborn library to create informative plots depicting the distribution of attacks and normal traffic in both the training and testing sets the first two count plots in the top row display the overall distribution of labels attack or normal in the training and testing datasets meanwhile the bottom row illustrates the distribution of attack categories in both sets with the order specified based on the frequency of attack categories these visualizations provide a clear overview of the class distribution and the prevalence of different attack categories within the datasets such insights are crucial for understanding the imbalance between attack and normal instances and guide subsequent steps in the analysis such as addressing class imbalances and selecting appropriate evaluation metrics for machine learning models show in Fig. 3.

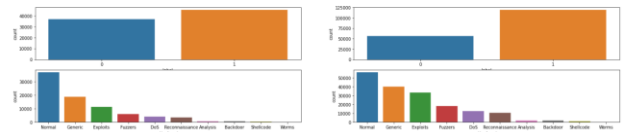


Fig. 3. Data visualization.

Next distribution of classes in the target variable showcases the balance or imbalance between normal and attack instances in Fig. 4. This is crucial for assessing the dataset's class distribution and potential class imbalance, which can impact machine learning model training.

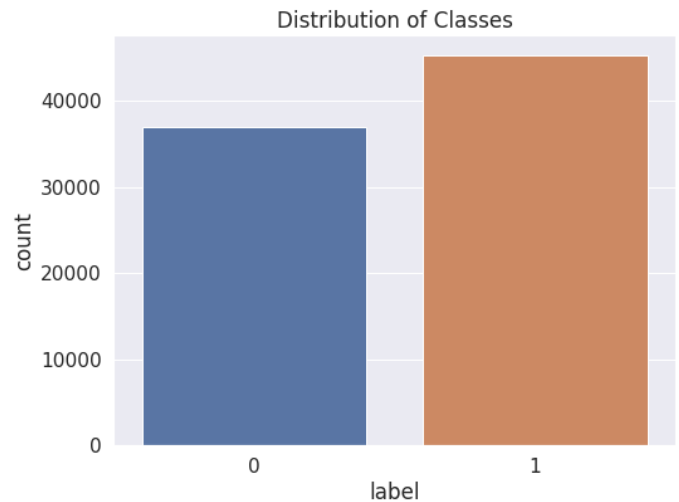


Fig. 4. Distribution of classes.

The below in Fig. 5, visualization presents a correlation heatmap, offering a comprehensive overview of the numerical features' relationships. This heatmap aids in identifying potential multicollinearity and understanding feature interdependencies.

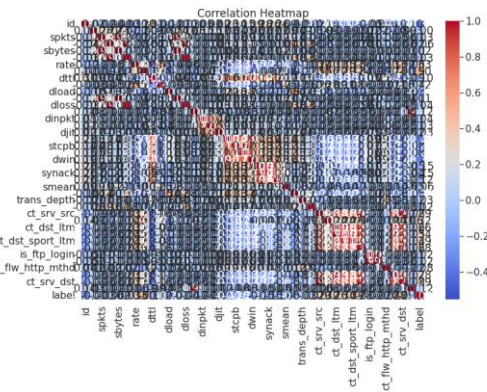


Fig. 5. Correlation of heatmap.

In Fig. 6, a boxplot of the sttl feature is depicted showcasing its distribution across different classes this graphical representation allows for a quick assessment of the feature's potential discriminative power in distinguishing between normal and attack instances together these visualizations contribute to a holistic understanding of the dataset's characteristics guiding subsequent steps in the analysis and model development.

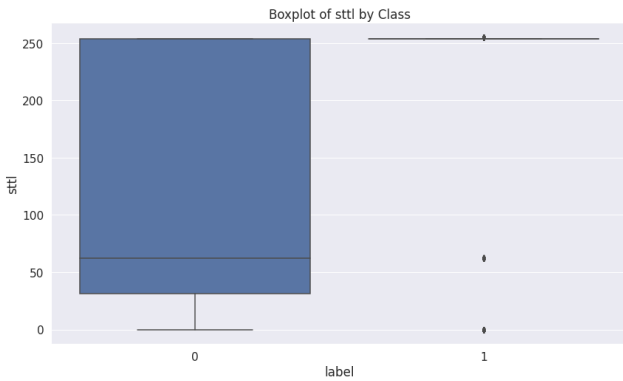


Fig. 6. Boxplot of sttl by class.

3) *Data preprocessing*: The data preprocessing phase involved a comprehensive examination and cleaning of the dataset the initial step focused on identifying and handling missing values and the results showed that there were no null values in any of the features this indicates a well maintained dataset without missing information ensuring the integrity of the subsequent analysis furthermore a closer look at categorical variables including proto service state and attack cat revealed the nature of these attributes the attack cat variable which represents the attack category is a crucial element for classification tasks the categorical variables were encoded appropriately for machine learning algorithms and their unique values and distribution were inspected this preprocessing step ensures that the dataset is ready for model training with categorical variables appropriately handled and missing values addressed the cleanliness and encoding of categorical variables contribute to the robustness of the subsequent machine learning analysis and enhance the interpretability of the results.

Also, in [36], data preprocessing focuses on numeric variables and involves a thorough exploration of statistical summaries initially it showcases a selection of numeric features from the dataset such as id dur spkts and others highlighting their characteristics subsequently statistical summaries are generated including count mean standard deviation minimum 25th percentile median 50th percentile 75th percentile and maximum values for each numeric variable this summary provides valuable insights into the distribution and variability of these features furthermore an additional exploration of the unsw nb 15 testings set csv file is conducted to understand its structure and dimensions revealing that it contains 1 000 rows and 45 columns this step is crucial for gaining an overview of the testing set which will be utilized in the subsequent stages of model evaluation.

4) *EDA*: The dataset comprising features related to network security attack classification was initially examined for its dimensions and the presence of relevant attributes descriptive statistics were computed to understand the distribution and variability of numeric variables and class distribution analysis provided insights into the balance between normal traffic and different attack categories

correlation matrices were employed to explore relationships between features aiding in the identification of potential multicollinearity visualization of categorical variables and the distribution of attack categories within them further enriched our understanding of the dataset s structure the eda process also encompassed data cleaning and preprocessing steps addressing missing values and encoding categorical variables scatter plots and density plots were generated to visualize relationships between numeric features facilitating the detection of patterns shown in Fig. 7 and Fig. 8.

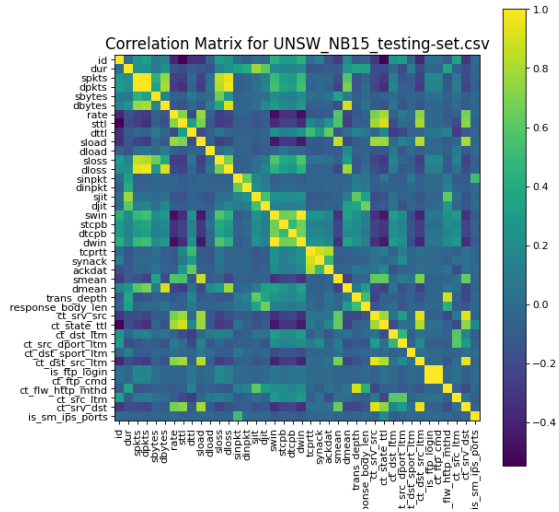


Fig. 7. Correlation matrix for test data.

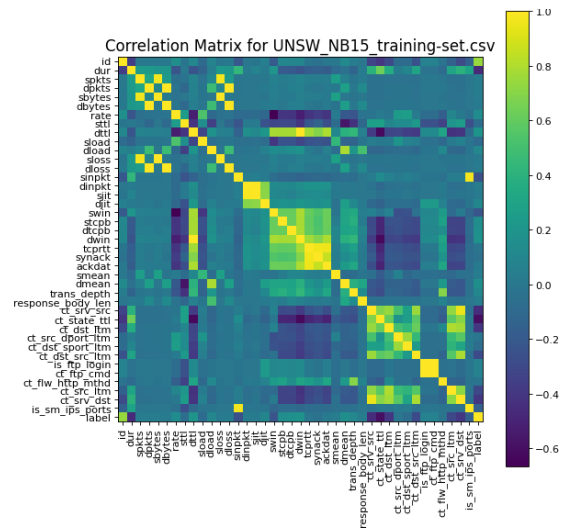


Fig. 8. Correlation matrix for train data.

5) *Testing and training*: The initial split was performed based on the index with the first 175 341 records designated for training and the remaining 82 332 records for testing the labels was extracted and assigned to y train and y test for training and testing respectively subsequently the label column was dropped from the feature sets to standardize the feature values a min max scaler was applied it s crucial to note that the scaler was fitted only on the training data to avoid data

leakage the training data x_{train} was transformed using the fitted scaler and the testing data x_{test} was scaled accordingly the final dataset dimensions were confirmed showcasing 175 341 samples for training each comprising 196 features and 82 332 samples for testing additionally categorical columns such as proto-state and service underwent one hot encoding for inclusion in the analysis these preprocessing steps ensure that the machine learning models are trained and tested on standardized and appropriately formatted data.

C. ML Model Classifications

1) *Random forest*: In Fig. 9, RF classification algorithm was implemented on a network security attack dataset, achieving an accuracy of 90%. The classification report details the model's performance in distinguishing normal and attack instances, with precision, recall, and F1 score metrics providing insights. For normal instances (label 0), precision and recall are 0.77 and 0.98, resulting in an F1 score of 0.86. For attack instances (label 1), precision, recall, and F1 score are higher at 0.99, 0.86, and 0.92 respectively. The weighted average F1 score is 0.90, indicating balanced performance. The confusion matrix shows the model correctly identifying 54,699 normal instances and 102,950 attack instances while misclassifying 1,301 normal instances as attacks and 16,391 attack instances as normal. Despite these misclassifications, the 90% accuracy highlights the random forest model's robustness in network security attack classification, contributing valuable insights to the research.

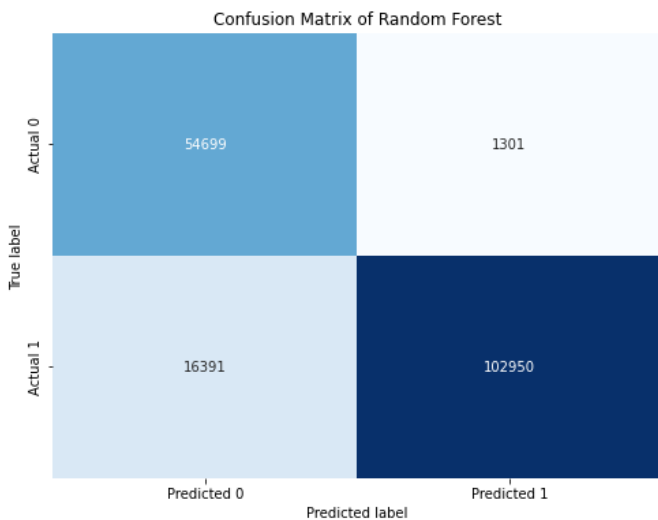


Fig. 9. Confusion matrix of random forest.

2) *KNN*: In Fig. 10, the K-Nearest Neighbors (KNN) classification algorithm was implemented with $k=5$ on the network security attack dataset, yielding an accuracy of 87%. The classification report provides detailed insights into the model's performance, showcasing its ability to discriminate between normal and attack instances.

For normal instances (label 0), the precision and recall are 0.72 and 0.96, respectively, resulting in an F1-score of 0.82. Similarly, for attack instances (label 1), the precision, recall, and F1-score are notably higher at 0.98, 0.83, and 0.90, respectively. The weighted average F1-score is reported as 0.87, indicating a balanced performance across both classes.

The confusion matrix further shows the classifier's effectiveness, correctly identifying 53,638 instances of normal traffic and 98,636 instances of attacks. However, the model misclassified 2,362 normal instances as attacks and 20,705 attack instances as normal. Despite these misclassifications, the overall accuracy of 87% underscores the robustness of the KNN model in distinguishing between benign and malicious network activities.

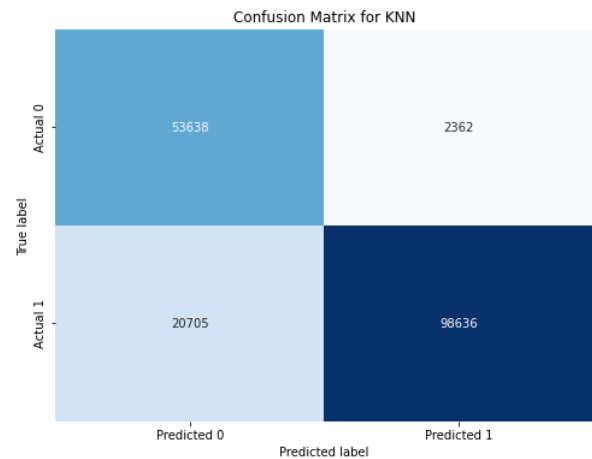


Fig. 10. Confusion matrix for KNN.

These findings contribute valuable insights to the research, emphasizing the efficacy of the K-Nearest Neighbors algorithm in the context of network security attack classification.

3) *Naïve bayes*: The Gaussian Naive Bayes classification algorithm was employed for network security attack classification, resulting in an accuracy of 79%. The classification report reveals that the model achieved a precision of 62% and recall of 87% for normal instances (label 0), yielding an F1-score of 0.72. For attack instances (label 1), the precision and recall are notably higher at 92% and 75%, contributing to an F1-score of 0.83. The weighted average F1-score is reported as 0.80, indicating a balanced performance across both classes shown in Fig. 11.

The confusion matrix provides additional insights, indicating that the model correctly identified 48,706 instances of normal traffic and 89,663 instances of attacks. However, there were misclassifications, with 7,294 normal instances being erroneously identified as attacks and 29,678 attack instances mistakenly labeled as normal. Despite these challenges, the Gaussian Naive Bayes algorithm demonstrates a commendable accuracy, emphasizing its suitability for network security attack detection in this context.

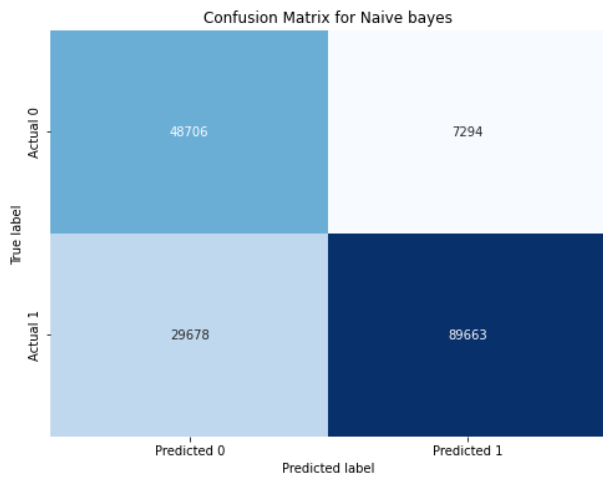


Fig. 11. Confusion matrix for naive bayes.

This analysis in Fig. 12 contributes valuable findings to the research, highlighting the strengths and limitations of the Gaussian Naive Bayes classifier in the domain of network security.

4) *Logistic regression*: The Logistic Regression classifier was implemented for network security attack classification, yielding an accuracy of 87.25%. The precision, recall, and F1-score for normal instances (label 0) are 74%, 92%, and 82%, respectively. For attack instances (label 1), the classifier achieved higher precision (96%) and slightly lower recall (85%), resulting in an impressive F1 score of 90.06%. The weighted average F1 score stands at 88%, indicating a balanced performance across both classes.

The confusion matrix and classification report provide detailed insights into Fig. 12, the classifier's performance. It correctly identified 51,592 instances of normal traffic and 101,719 instances of attacks. However, there were misclassifications, with 8,408 normal instances being erroneously identified as attacks and 17,622 attack instances mistakenly labeled as normal.

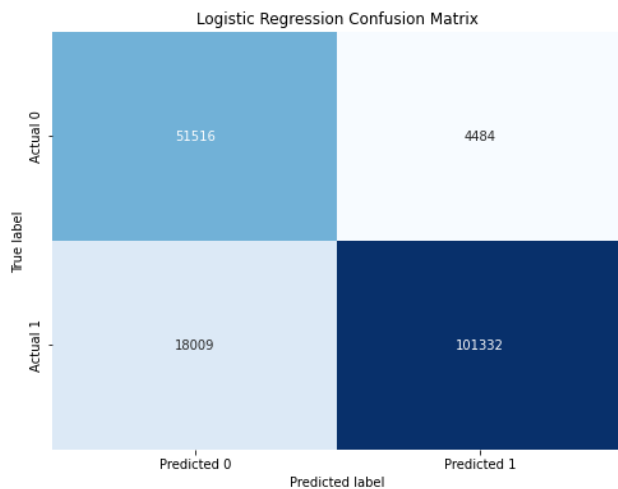


Fig. 12. Confusion matrix for logistic regression.

V. RESULTS

The outcomes of the machine learning models including accuracy precision recall and f 1 score will be systematically analyzed a comparative study will be conducted to identify the algorithm that best suits the requirements of network security attack detection additionally insights gained from the analysis will be used to draw meaningful conclusions about the performance of each algorithm in handling diverse patterns present in the network traffic data.

TABLE II. RESULTS OF CLASSIFICATION MODELS WITHOUT FEATURE SELECTION

| Classifier | Accuracy | Precision | Recall | F1 |
|---------------------|----------|-----------|--------|------|
| Random Forest | 0.90 | 0.92 | 0.90 | 0.90 |
| K-Nearest Neighbors | 0.87 | 0.90 | 0.87 | 0.87 |
| Naive Bayes | 0.79 | 0.83 | 0.79 | 0.80 |
| Logistic Regression | 0.87 | 0.85 | 0.96 | 0.90 |

In the result analysis Table II, the Random Forest classifier demonstrated superior performance with a high accuracy of 90%, effectively balancing precision and recall at 0.92 and 0.90, respectively. K-Nearest Neighbors (KNN) showcased strong predictive capabilities with an accuracy of 87% and a well-balanced precision-recall trade-off at 0.90 and 0.87. Naive Bayes exhibited a decent accuracy of 79%, with a precision of 0.83 and a balanced F1-Score of 0.80. Logistic Regression delivered an accuracy of 87%, with a commendable precision of 0.85 and a high recall of 0.96, resulting in a robust F1-Score of 0.90.

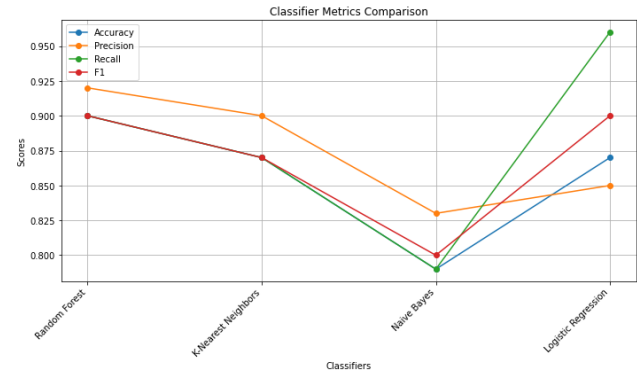


Fig. 13. ML classifiers metrics comparisons.

These classifiers play a crucial role in our network security context, offering effective means of identifying and classifying instances of security attacks based on the observed performance metrics in Fig. 13. The Random Forest model, in particular, emerges as a promising choice for its overall high accuracy and balanced precision-recall scores, making it well-suited for robust intrusion detection in network security applications.

A. Discussions

Building upon the result analysis the discussion section will explore the implications of the findings in the context of network security consideration will be given to the practicality efficiency and robustness of the algorithms the discussion will

also address potential challenges and limitations observed during the analysis providing a comprehensive perspective on the feasibility of deploying these algorithms in real-world scenarios furthermore comparisons with existing literature and benchmarks will be made to contextualize the significance of the results.

Deep learning has revolutionized intrusion detection, offering unparalleled accuracy and efficiency. In a study, [12] introduced the Principal Component-based Convolution Neural Network (PCCNN) approach for IDS, specifically targeting DoS and DDoS attacks on IoT devices. This approach boasts impressive accuracies of 99.34% for binary and 99.13% for multiclass classification on the NSL-KDD dataset. Utilizing a sophisticated architecture of 13 layers of Sequential 1-D CNN and feature reduction through Principal Component Analysis (PCA), it showcases exceptional promise for cutting-edge IoT intrusion detection.

Furthermore, the IDSGT-DNN framework, presented by [37], elevates cloud security by seamlessly integrating an attacker-defender mechanism using game theory and deep neural networks. This framework outperforms traditional methods in accuracy, detection rate, and various metrics on the CICIDS-2017 dataset. Remarkably, the defender's detection rate spans from 0 to 0.99, with gains strategically set at -5, 0, and 5. While the present study may not achieve the accuracies of the PCCNN approach (99.34% for binary and 99.13% for multiclass) and the IDSGT-DNN framework presented in previous works, it excels in computational efficiency. Our machine learning classifiers—Random Forest (RF) with an accuracy of 0.90, K-Nearest Neighbors (KNN) at 0.87, Naive Bayes with 0.79, and Logistic Regression (LR) also at 0.87—demonstrate competitive performance. Importantly, these classifiers deliver these results in significantly less time, underscoring the trade-off between accuracy and computational speed in intrusion detection systems.

Additionally, promising results in the random forest model showcased notable improvements achieving a commendable balance between precision and recall k nearest neighbors demonstrated strong predictive capabilities aligning with its suitability for identifying patterns in network traffic although naive bayes presented a lower accuracy its performance remains consistent with the algorithm s inherent assumptions logistic regression emerged as a reliable choice showcasing a balanced precision recall trade off collectively our findings contribute to the existing body of research by highlighting the effectiveness of these classifiers in the specific context of intrusion detection offering valuable insights for the development of robust and accurate network security systems.

The performance of the proposed methodology will be compared with existing approaches, highlighting the advancements achieved in Table III.

TABLE III. COMPARISON WITH EXISTING APPROACHES

| Paper | Classifiers | Accuracy | Precision | Recalls |
|------------|----------------|----------|-----------|---------|
| [34] | SGD | 80% | 82.1% | 82.1% |
| This study | Random forest | 90% | 90.2% | 90% |
| [35] | Neural network | 87% | 87.2% | 87.8% |
| [3] | XGBoost | 88% | 88.3% | 88.8% |
| [8] | SVM | 76% | 77% | 77% |
| [23] | Random forest | 80% | 81% | 8.9% |
| [14] | KNN | 82% | 82% | 82% |

B. Limitations

Though our study presented promising results, it is crucial to recognize the limitations. The effectiveness of machine learning models heavily relies on the dataset's quality and representativeness. The utilization of the unsw nb 15 dataset in our research may not adequately cover all real-world network traffic scenarios and variations. The chosen features and preprocessing techniques could impact model performance, suggesting further exploration of feature engineering methods to improve classifier efficacy. The selection of classifiers was based on established algorithms, but future research could investigate new approaches or DL methods for better outcomes. Evaluation metrics mainly focused on accuracy, precision, recall, and f1 score, potentially overlooking variations in performance among different attack types. These restrictions highlight the importance of continuous refinement and exploration in intrusion detection to combat evolving cyber threats effectively.

The ML models used in the present investigation have been practically implemented and tested using the real intrusion detection dataset, which is recognized for its relevance to real-world network intrusion scenarios. This approach leverages the dataset to demonstrate the models' practical applicability in a real-world network environment. By conducting experiments on the dataset, the effectiveness of the models in detecting a variety of attacks, including novel and sophisticated ones, was evaluated. This hands-on validation allows for the identification of operational challenges and fine-tuning of the models for improved performance in real-world scenarios. The practical testing provides valuable insights into the models' robustness, scalability, and applicability, thereby reinforcing their effectiveness and reliability in real-world network intrusion detection applications. Future research could consider novel approaches or DL methods for better results [38]. Evaluation metrics focused on overall accuracy, precision, recall, and f1 score, neglecting performance variations across different attack types. These limitations highlight the importance of continuous refinement and exploration in intrusion detection to address evolving cyber threats.

VI. CONCLUSIONS

The detailed examination and discussion of the outcomes provide valuable insights into the effectiveness of different machine learning classifiers for detecting intrusions in network security. The Random Forest classifier showed the best performance, with high accuracy, precision, recall, and F1 score. K-Nearest Neighbors and Logistic Regression also had good results, while Naive Bayes had a slightly lower performance. These results highlight the importance of using advanced machine-learning techniques for accurate intrusion detection. Choosing the right algorithm based on the specific characteristics of the cybersecurity task is crucial. However, it's important to recognize the limitations and future research should focus on improving models, exploring new approaches, and incorporating more data to enhance the strength and applicability of intrusion detection systems. In conclusion, this study adds to the conversation on strengthening cybersecurity defenses through machine learning methods. In concluding this study, it is essential to highlight future research possibilities for advancing intrusion detection and network security. One potential avenue is to enhance existing models through hyperparameter tuning and ensemble methods. Moreover, utilizing diverse datasets could broaden the adaptability of models to various network scenarios. Exploring deep learning approaches like neural networks could help uncover complex patterns in network traffic data. Additionally, addressing limitations like dataset reliance and biases may require more comprehensive datasets and real-world scenarios for model validation. Lastly, research could focus on creating hybrid models that combine multiple classifiers' strengths for increased resilience.

REFERENCES

- [1] S.-W. M. M. S. R. A. M. R. M. M. a. M. H. Lee, "Towards secure intrusion detection systems using deep learning techniques: Comprehensive analysis and review," *Journal of Network and Computer Applications* 187, 2021.
- [2] H. a. G. K. Alqahtani, "Machine learning for enhancing transportation security: A comprehensive analysis of electric and flying vehicle systems.," *Engineering Applications of Artificial Intelligence* 129, 2024.
- [3] T. S. S. C. D. T. D. C. a. M. A. K. Saranya, "Performance analysis of machine learning algorithms in intrusion detection system: A review," *Procedia Computer Science* 171, 2020.
- [4] M. D. M. a. K. R. Karthikeyan, "Firefly algorithm based WSN-IoT security enhancement with machine learning for intrusion detection," *Scientific Reports* 14, no. 1, 2024.
- [5] X. X. Z. Z. Y. L. Y. B. Z. Q. L. a. X. L. Xiao, "A comprehensive analysis of website fingerprinting defenses on Tor," *Computers & Security* 136, 2024.
- [6] K. M. M. M. K. F. K. a. I. G. Aygul, "Benchmark of machine learning algorithms on transient stability prediction in renewable rich power grids under cyber-attacks," *Internet of Things* 25, 2024.
- [7] G. MeeraGandhi, "Machine learning approach for attack prediction and classification using supervised learning algorithms.," *Int. J. Comput. Sci. Commun* 1, no. 2 (2010): 247-250, 2010.
- [8] M. a. M. M. Zamani, "Machine learning techniques for intrusion detection.," *arXiv preprint arXiv:1312.2177*, 2013.
- [9] Z. G. A. Y. Y. a. Y. L. Sun, "Optimized machine learning enabled intrusion detection 2 system for internet of medical things," *Franklin Open* 6, 2024.
- [10] A. L. a. E. G. Buczak, "A survey of data mining and machine learning methods for cyber security intrusion detection," *IEEE Communications surveys & tutorials* 18, no. 2, 2015.
- [11] X.-S. Y. S. S. N. D. A. Joshi, "Fourth International Congress on Information and Communication Technology," *ICICT 2019, London, Volume 2*, 2019.
- [12] M. A. M. A. R. K. a. T. A.-H. Haq, "Development of PCCNN-Based Network Intrusion Detection System for EDGE Computing," *Computers, Materials & Continua* 71, no. 1, 2022.
- [13] I. H. Sarker, "Machine learning for intelligent data analysis and automation in cybersecurity: current and future prospects," *Annals of Data Science* 10, no. 6, 2023.
- [14] A. A. A. D. V. a. S. S. Mahfouz, ""Ensemble classifiers for network intrusion detection using a novel network attack dataset.," *Future Internet* 12, no. 11, 2020.
- [15] M. S. T. Z. H. S. U. R. G. A. a. Z. H. A. Waqas, "The role of artificial intelligence and machine learning in wireless networks security: Principle, practice and challenges," *Artificial Intelligence Review* 55, no. 7, 2022.
- [16] H. M. a. P. S. Prachi, "Intrusion detection using machine learning and feature selection.," *International Journal of Computer Network and Information security* 11, no. 4, 2019.
- [17] A. a. M. A. R. Alotaibi, "Enhancing the Sustainability of Deep-Learning-Based Network Intrusion Detection Classifiers against Adversarial Attacks," *Sustainability* 15, no. 12, 2023.
- [18] D. M. A. F. A. A. R. a. R. M. M. Musleh, "Intrusion Detection System Using Feature Extraction with Machine Learning Algorithms in IoT.," *Journal of Sensor and Actuator Networks* 12, no. 2, 2023.
- [19] M. A. a. M. A. R. K. Haq, "DNNBoT: Deep neural network-based botnet detection and classification.," *Computers, Materials & Continua* 71, no. 1, 2022.
- [20] E. S. R. R. N. Z. A. A. H. J. M. N. S. S. M. I. E. a. B. A. M. Alomari, "Malware detection using deep learning and correlation-based feature selection," *Symmetry* 15, no. 1, 2023.
- [21] H. O. P. a. A. C. Polat, "Detecting DDoS attacks in software-defined networks through feature selection methods and machine learning models," *Sustainability* 12, no. 3, 2020.
- [22] M. H. U. R. S. A. R. M. A. R. F. R. a. I. A. Imran, "A performance overview of machine learning-based defense strategies for advanced persistent threats in industrial control systems.," *Computers & Security* 134, 2023.
- [23] Z. M. M. I. a. M. N. H. Azam, "Comparative analysis of intrusion detection systems and machine learning based model analysis through decision tree.," *IEEE*, 2023.
- [24] M. A. S. M. a. M. A. Al-Shareeda, "DDoS attacks detection using machine learning and deep learning techniques: Analysis and comparison," *Bulletin of Electrical Engineering and Informatics* 12, no. 2, 2023.
- [25] U. A. R. A. H. A. S. M. B. A. a. A. A. Butt, "Cloud-based email phishing attack using machine and deep learning algorithm," *Complex & Intelligent Systems* 9, no. 3, 2023.
- [26] M. a. S. G. Rigaki, "A survey of privacy attacks in machine learning," *ACM Computing Surveys* 56, no. 4, 2023.
- [27] B. M. M. AlShahrani, "Classification of cyber-attack using Adaboost regression classifier and securing the network," *Turkish Journal of Computer and Mathematics Education (TURCOMAT)* 12, no. 10, 2021.
- [28] M. S. H. S. I. I. M. D. H. M. A. K. V. C. a. R. V. Akter, "Exploring the Vulnerabilities of Machine Learning and Quantum Machine Learning to Adversarial Attacks using a Malware Dataset: A Comparative Analysis," *arXiv preprint arXiv:2305.19593*, 2023.
- [29] H. Z. S. Y. C. a. H. B. Xu, "A data-driven approach for intrusion and anomaly detection using automated machine learning for the Internet of Things," *Soft Computing* 27, no. 19 (2023): 14469-14481., 2023.
- [30] Z. X. X. L. C. S. S. a. Z. W. Wang, ""Intrusion detection and network information security based on deep learning algorithm in urban rail transit management system," *IEEE Transactions on Intelligent Transportation Systems* 24, no. 2, 2023.
- [31] K. ". Alnowaiser, "Improving Healthcare Prediction of Diabetic Patients Using KNN Imputed Features and Tri-Ensemble Model.," *IEEE Access*, 2023.

- [32] A. R. X. Y. C. a. M. G. Huang, "Research on multi-label user classification of social media based on ML-KNN algorithm.," *Technological Forecasting and Social Change* 188, 2023.
- [33] B. D. J. A. a. S. H. L. He, "Assessment of tunnel blasting-induced overbreak: A novel metaheuristic-based random forest approach.," *Tunnelling and Underground Space Technology* 133, 2023.
- [34] G. a. G. K. Kocher, "Analysis of Machine Learning Algorithms with Feature Selection for Intrusion Detection Using UNSW-NB15 Dataset," Available at SSRN 3784406, 2021.
- [35] M. S. L. a. K. G. K. Beechey, ""Evidential classification for defending against adversarial attacks on network traffic," *Information Fusion* 92 (2023): 115-126., 2023.
- [36] G. MeeraGandhi, "Machine Learning Approach for Attack Prediction and Classification using supervised learning algorithms," *Int. J. Comput. Sci. Commun* 1, no. 2, 2010.
- [37] E. Balamurugan, A. Mehbodniya, E. Kariri, K. Yadav, A. Kumar, and M. Anul Haq, "Network optimization using defender system in cloud computing security based intrusion detection system with game theory deep neural network (IDSGT-DNN)," *Pattern Recognit. Lett.*, vol. 156, pp. 142–151, 2022, doi: <https://doi.org/10.1016/j.patrec.2022.02.013>.
- [38] H. Mohd Anul, "DBoTPM: A Deep Neural Network-Based Botnet," *Electronics*, vol. 12, no. 1159, pp. 1–14, 2023.

Robust Extreme Learning Machine Based on p -order Laplace Kernel-Induced Loss Function

Liutao Luo¹, Kuaini Wang^{2*}, Qiang Lin³

School of Computer Science, Xi'an Shiyou University, Xi'an, 710065, China¹

College of Science, Xi'an Shiyou University, Xi'an 710065, China²

School of Business, Jiangnan University, Wuxi 214122, China³

Abstract—Since the datasets of the practical problems are usually affected by various noises and outliers, the traditional extreme learning machine (ELM) shows low prediction accuracy and significant fluctuation of prediction results when learning such datasets. In order to overcome this shortcoming, the l_2 loss function is replaced by the correntropy loss function induced by the p -order Laplace kernel in the traditional ELM. Correntropy is a local similarity measure, which can reduce the impact of outliers in learning. In addition, introducing the p -order into the correntropy loss function is rewarding to bring down the sensitivity of the model to noises and outliers, and selecting the appropriate p can enhance the robustness of the model. An iterative reweighted algorithm is selected to obtain the optimal hidden layer output weight. The outliers are given smaller weights in each iteration, significantly enhancing the robustness of the model. To verify the regression prediction of the proposed model, it is compared with other methods on artificial datasets and eighteen benchmark datasets. Experimental results demonstrate that the proposed method outperforms other methods in the majority of cases.

Keywords— p -order Laplace kernel-induced loss; extreme learning machine; robustness; iterative reweighted

I. INTRODUCTION

Extreme Learning Machine (ELM), as a generalized single hidden layer feedforward neural network, was proposed by Huang et al. [1]. Its random selection of hidden node biases and input weights, along with the use of the ordinary least square method for determining the output weight, enables a simple, fast, and straightforward implementation. It has been widely used in load forecasting [2], [3], [4], fault detection [5], [6], image processing [7], image recognition [8] and other fields.

Although ELM performs well in terms of efficiency, it is susceptible to noise and outliers due to the use of the l_2 loss function, which can amplify their interference. Therefore, in recent years, many researchers have devoted themselves to the robustness of ELM. In regularized ELM [9], the regularization term of the objective function significantly improved the learning performance of ELM by minimizing the structural risk. Deng et al. [10] put forward a weighted least square regularized ELM (Weighted ELM, WELM) to enhance robustness by iterative weighted method. The above two methods employed l_2 loss function, which was optimal only when the error of the training datasets followed the normal distribution. However, many practical applications cannot guarantee the error followed a normal distribution, which lead to a fact that

ELM is highly susceptible to noise and outliers. Subsequently, the researchers proposed several loss function such as Huber [11], l_1 [12] and Pinball [13] and their corresponding ELM models. However, these loss functions were still less robust because they had a linear relationship with the training error and increased linearly with the training error. Incorporating both regularization term (l_1 , l_2) and various loss functions (l_1 , Huber, bisquare and Welsch), Chen et al. [14] put forward an unified robust regularized ELM, which improved the robustness of ELM.

As the research progressed, the researchers found that machine learning algorithms based on non-convex loss functions had strong robustness to datasets disturbed by noise and outliers [15], [16], [17], [18]. The loss functions in classical machine learning methods, including hinge loss, ε -insensitive loss, and l_2 -loss, were replaced by non-convex loss functions to construct the corresponding robust learning algorithms. Correntropy [19] is a nonlinear local similarity measure built on a Gaussian kernel function, which can weaken the role of noise and outliers in the learning process. The correntropy loss function has better robustness to noise and outliers than the convex loss function [20]. On this basis, Xing et al. [21] developed an ELM model based on the maximum correntropy criterion to improve robustness. C-loss function [22] and non-convex smooth loss [23] derived from correntropy and their corresponding models were proved to be robust to noise and outliers. Chen et al. [24] presented a maximum correntropy criterion with variable center (MCC-VC), which is also essentially a loss function derived from the correntropy. The use of Gaussian kernels in correntropy learning is common, owing to their smoothness and strict positive definiteness. Nevertheless, Gaussian kernels may not always be the optimal choice. On the one hand, this is because the choice should be based on specific problem and experimental results to determine the optimal kernel function and parameters. On the other hand, the exponential part of the Gaussian kernel function is in the form of l_2 , which would overemphasize the role of noise and outliers, so this could potentially lead to a greater sensitivity to noise and outliers. Yang [25] introduced a new method based on the Laplace kernel (LK-loss) and demonstrated that the LK-loss serves as a reliable approximation of the zero norm. Dong et al. [26] presented a robust semi-supervised support vector machines with Laplace kernel-induced correntropy loss function utilizing LaplaceSVM to solve the problem of insufficient supervisory information and noise effects in practical applications. Chen et al. [27] pointed out that taking the p -order function of the error as a loss function was effective to decrease the sensitivity of the model to the noise and outliers,

*Corresponding authors. email: wangkuaini1219@sina.com

and appropriate p was conducive to improve the robustness of the model. Chen et al. [28] put forward a robust ELM based on p -order Welsch loss function, and the experiments revealed the superiority of method over the Welsch loss.

Inspired by the above studies, this paper offers the p -order loss function into the correntropy loss function induced by the Laplace kernel (p -LKI loss function) and applies it to ELM. The main contributions of this paper are as follows:

(1) This paper introduces the Laplace kernel function into the correntropy and incorporates the p -order of the loss function into it, and proposes an ELM model based on p -LKI loss function. The robustness of the model can be significantly improved by choosing a suitable p .

(2) We have proved that the p -LKI loss function is positive-definite, bounded and non-convex, and can converge to 1 with increasing error. Additionally, as the parameter p increases, the p -LKI loss function serves as a favorable approximation of the zero norm.

(3) The iterative reweighted algorithm efficiently addresses the optimization problem and converges to the optimal solution within a few iterations. We investigate that the larger the error of the sample, the smaller weight assigned to it, thus the smaller the impact on the model.

The paper is organized as follows: Section II briefly introduces ELM. In Section III, we present an ELM based on p -order Laplace Kernel-Induced loss function and the iterative reweighted algorithm is used to address the problem. The experiments are conducted in different levels of outliers in artificial dataset and benchmark datasets in Section IV. The experimental results of the proposed method are discussed and compared with other methods in Section V. And the conclusion and prospect are summarized in Section VI.

II. BRIEF REVIEW OF ELM

Given training samples $S = \{(x_i, y_i)\}_{i=1}^N$, $x_i \in R^d$, $y_i \in R$, the mathematical representation of the output function of a single hidden layer ELM with L hidden nodes and activation functions $h_i(x)$ is as follows:

$$f(x) = \sum_{i=1}^L h_i(x)\beta_i = h(x)\beta \quad (1)$$

where, $\beta = [\beta_1, \beta_2, \dots, \beta_L]^T$ is the output weight vector, $h(x) = [h_1(x), h_2(x), \dots, h_L(x)]$ is the hidden layer output of variable x . Let $Y = [y_1, y_2, \dots, y_N]^T$, hidden layer output matrix $H = [h(x_1)^T, h(x_2)^T, \dots, h(x_N)^T]^T$, the ELM model can be expressed as the following optimization problem [1].

$$\min_{\beta} \frac{1}{2} \|\beta\|^2 + \frac{C}{2} \|Y - H\beta\|^2 \quad (2)$$

where, C is a regularization parameter. The best solution in Eq. (2) is provided by Huang et al. [1] as,

$$\beta = \begin{cases} (H^T H + I/C)^{-1} H^T Y, & N \geq L \\ H^T (H H^T + I/C)^{-1} Y, & N < L \end{cases} \quad (3)$$

where, I denotes the identity matrix.

III. ROBUST ELM BASED ON p -ORDER LAPLACE KERNEL-INDUCED LOSS FUNCTION

The l_2 loss function in ELM gives the same weight to each training samples, which makes the outliers have a larger impact on the sum of squared errors than the rest of the samples, resulting in model that is quite sensitive to outliers. Inspired by correntropy [19] and p -order loss functions [27], this paper proposes to use the p -LKI loss function to improve the robustness of ELM.

A. P -order Laplace Kernel-induced Loss Function

In order to improve the robustness of the model, the maximum correntropy criterion (MCC) [21] is introduced. Correntropy [19] describes the measure of similarity between two samples, the principle is as follows:

$$V_{\sigma}(A, B) = E(k_{\sigma}(A, B)) \quad (4)$$

where k_{σ} is the kernel function, $\sigma > 0$ is the kernel bandwidth, and E is the mathematical expectation. In most cases, the joint probability distribution between variables A and B is unknown, and the mean can be used to estimate the mathematical expectation. For variables $A = (a_1, a_2, \dots, a_N)$, $B = (b_1, b_2, \dots, b_N)$, and $q = (q_1, q_2, \dots, q_N)$, $q_i = a_i - b_i$. The correntropy estimation is as follows:

$$V_{\sigma} = \frac{1}{N} \sum_{i=1}^N k_{\sigma}(a_i, b_i) \quad (5)$$

where $k_{\sigma}(q_i) = \exp(-\frac{|q_i|}{\sigma})$ is Laplace kernel function.

MCC [20] can be expressed as,

$$\max \frac{1}{N} \sum_{i=1}^N k_{\sigma}(q_i) = \max \frac{1}{N} \sum_{i=1}^N \exp(-\frac{|q_i|}{\sigma}) \quad (6)$$

To facilitate the calculation, Eq (6) is equivalent to,

$$\min 1 - \exp(-\frac{|q|}{\sigma}) \quad (7)$$

Reference [27] pointed out that the loss function employing second-order statistical measures is susceptible to outliers, and it is not always a good choice for learning with samples that is non-Gaussian in nature. To address non-Gaussian data and noise, various non-second-order (or non-quadratic) loss functions have been proposed, such as the Huber minimum-maximum loss [15], Lorentz error loss [16], risk-sensitive loss [17], and mean p -power error (MPE) loss [27]. The MPE represents the p -th absolute moment of the error and effectively manages non-Gaussian datasets with an appropriate choice of the parameter p . Generally speaking, MPE demonstrates robustness to significant outliers for $0 < p < 2$ [27]. Inspired by the above studies, this paper proposes the following p -LKI loss function.

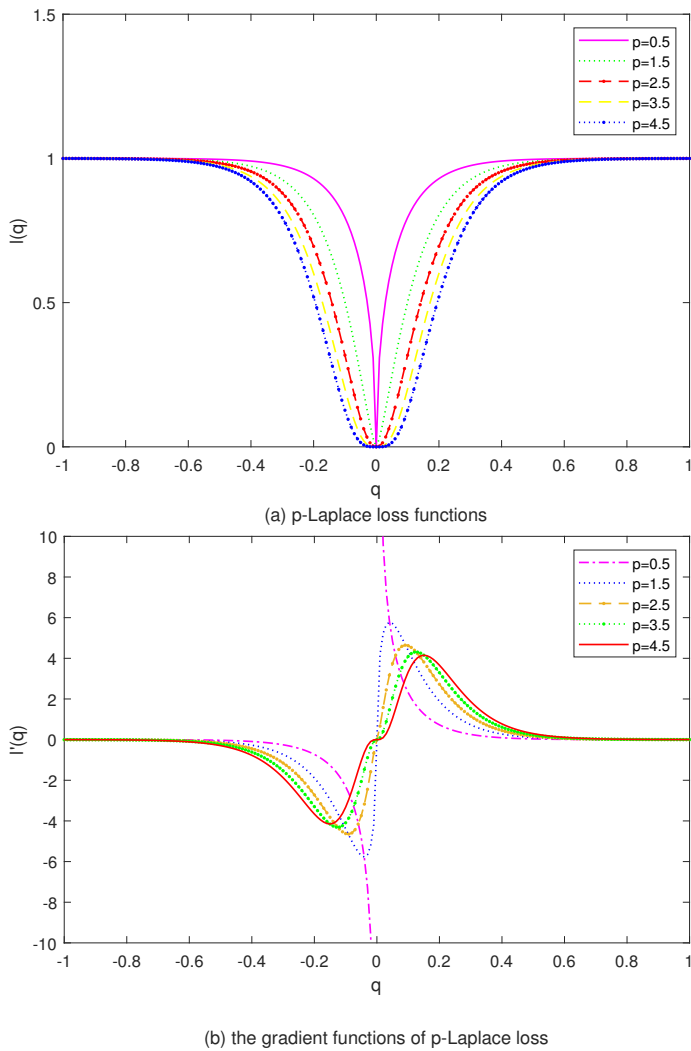


Fig. 1. Comparison of p -LKI loss functions and their gradient functions under different p .

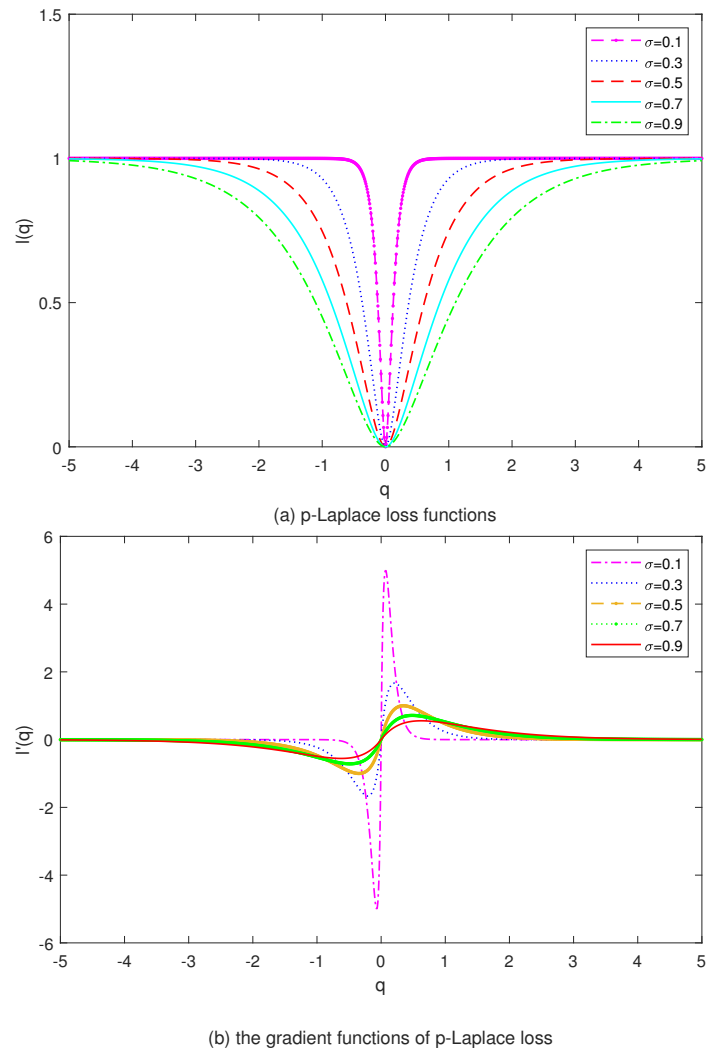


Fig. 2. Comparison of p -LKI loss functions and their gradient functions under different σ .

$$l(q) = (1 - \exp(-\frac{|q|}{\sigma}))^p \quad (8)$$

The gradient function of p -LKI loss function is as follows:

$$\frac{\partial l(q)}{\partial q} = \frac{pq}{\sigma} \exp(-\frac{|q|}{\sigma}) (1 - \exp(-\frac{|q|}{\sigma}))^{p-1} \frac{1}{\max\{|q|, 10^{-6}\}} \quad (9)$$

We can observe from Fig. 1(a), $l(q)$ becomes larger as $|q|$ increases and will eventually approach 1 for any value of p when $|q|$ reaches a certain threshold. Even if the $|q|$ increases again, $l(q)$ will only approach 1 again with little change, thus reducing the influence of significant errors brought by outliers on model training. Furthermore, as depicted in Fig. 1(b), as the value of p decreases, the extreme point of $l'(q)$ will move forward with the decrease of the value of p which means that the part of $l(q)$ that is most sensitive to error changes will move forward relatively. Therefore, when p is too large, the sensitivity of $l(q)$ to outliers will increase. However, when

$p = 0.5$, $l'(q)$ is discontinuous at zero which means $l(q)$ is not differentiable at zero.

Fig. 2 shows p -LKI loss function $l(q)$ and its gradient function $l'(q)$ under different values of σ . It can be seen that with the increase of the values of σ , the corresponding $|q|$ will increase correspondingly when $l(q)$ approaches 1. With the decrease of the values of σ , the extreme point of $l'(q)$ is approaching zero, and the smaller the values of σ , the stronger the robustness of the model to the outliers. Therefore, the sensitivity of $l(q)$ to outliers can be reduced by adjusting the values of p and σ . The optimal values of p and σ will be further determined by grid search.

The p -LKI loss function offers the strengths in these aspects:

1. The p -LKI loss function $l(q)$, shown in Fig. 2(a), is a positive, symmetric, and bounded function. It attains its maximum value only when $q = 0$. The p -LKI fulfills the following:

$$\frac{\partial l(q)}{\partial q} = \text{sgn}(q) \frac{p}{\sigma} \exp\left(-\frac{|q|}{\sigma}\right) (1 - \exp\left(-\frac{|q|}{\sigma}\right))^{p-1}, q \neq 0 \quad (10)$$

We have

$$\lim_{q \rightarrow \infty} \frac{p}{\sigma} \exp\left(-\frac{q}{\sigma}\right) (1 - \exp\left(-\frac{q}{\sigma}\right))^{p-1} = 0 \quad (11)$$

As shown in Eq.(11) that when the error approaches infinity, the gradient function $l'(q)$ of p -LKI approaches 0, indicating that $l(q)$ does not change for the outliers. Therefore, the p -LKI loss function is resistant to outliers.

2. For $\forall q \in R^N$,

$$\lim_{\sigma \rightarrow 0^+} l(q) = \|q\|_0 \quad (12)$$

Proof: The empirical risk derived from the p -LKI loss function can be represented as:

$$R_l(f) = \sum_{i=1}^N \left(1 - \exp\left(-\frac{|q_i|}{\sigma}\right)\right)^p \quad (13)$$

By evaluating the limit as $\sigma \rightarrow 0^+$, we obtain:

$$\begin{aligned} \lim_{\sigma \rightarrow 0^+} R_l(f) &= \lim_{\sigma \rightarrow 0^+} \sum_{i=1}^N l(q_i) \\ &= \lim_{\sigma \rightarrow 0^+} \sum_{i=1}^N \left(1 - \exp\left(-\frac{|q_i|}{\sigma}\right)\right)^p = \|q\|_0 \end{aligned} \quad (14)$$

where the zero norm $\|q\|_0$ counts the non-zero elements of q .

3. In comparison to other estimations of the zero norm, like the p -order Gaussian kernel-induced loss (p -Welsch),

$$M(q) = \left(1 - \exp\left(-\frac{q^2}{2\sigma^2}\right)\right)^p \quad (15)$$

Fig. 3 (a) shows the curves of the p -LKI loss function and p -Welsch loss function with $p = 0.8$ and $\sigma = 0.1$. It can be inferred that the approximation precision of the p -LKI loss function is higher than the p -Welsch loss function which means that it is closer to the zero norm. Some advantages of the zero norm are as follows:

1) *Sparsity*: The zero norm loss function encourages the model to produce sparse weights, i.e. only a small percentage of the weights are non-zero. This can effectively reduce the complexity of the model and prevent over-fitting [27].

2) *Robustness*: By making the weights sparse, the zero norm loss function can enhance the robustness of the model. Only those features that are most important to the predictions of the model are given greater weight, thus reducing over-reliance on unimportant features.

Fig. 3 shows a comparison of loss functions such as l_2 [10], l_1 [12], Welsch [22], Laplace [25], p -Welsch [28], p -LKI loss function and their gradient functions. From the figure, it is evident that in addition to the l_2 -loss function and l_1 -loss function, the error of each dataset in the other loss functions is controlled $[0, 1]$. The gradient function will be small after the $|q|$ exceeds a certain value and will not increase with the increase of error like the gradient function of l_2 -loss and l_1 -loss, thereby reducing the influence of the large error term caused by outliers on parameter estimation. Moreover, we can observe from Fig. 3 that p -LKI loss function has the closest distance from the $\|q\|_0$ ($l(q) = 1$), so the accuracy of the zero norm approximation of the p -LKI loss function is the highest. In addition, compared with the Welsch and p -Welsch loss functions induced by the Gaussian kernel function, the Laplace and p -LKI loss function induced by the Laplace kernel have higher approximate accuracy for zero norms, where the approximate accuracy of p -LKI loss function is higher than that of Laplace loss function.

3) *Robust ELM based on p -LKI loss function*: By taking the p -LKI loss function in ELM, the p -LKI-ELM model is established

$$\begin{aligned} \min_{\beta, q_i} \quad & \frac{1}{2} \|\beta\|_2^2 + C \sum_{i=1}^N \left(1 - \exp\left(-\frac{|q_i|}{\sigma}\right)\right)^p \\ \text{s.t.} \quad & h(x_i)\beta = y_i - q_i, i = 1, 2, \dots, N \end{aligned} \quad (16)$$

According to the KKT condition, Eq. (16) can be reformulated as solving the following problem:

$$\begin{aligned} L(\beta, q_i, \alpha) &= \frac{1}{2} \|\beta\|_2^2 + C \sum_{i=1}^N \left(1 - \exp\left(-\frac{|q_i|}{\sigma}\right)\right)^p \\ &\quad - \sum_{i=1}^N \alpha_i (h(x_i)\beta - y_i + q_i) \end{aligned} \quad (17)$$

where α_i is the Lagrange multiplier corresponding to each training sample.

Calculate the partial derivative of each parameter variable in Eq.(17), and let the partial derivative be zero,

$$\begin{cases} \frac{\partial L}{\partial \beta} = 0 \Rightarrow \beta = \sum_{i=1}^N \alpha_i h(x_i)^T = H^T \alpha \\ \frac{\partial L}{\partial q_i} = 0 \Rightarrow \alpha_i = C q_i w(q_i) \\ \frac{\partial L}{\partial \alpha_i} = 0 \Rightarrow h(x_i)\beta - y_i + q_i = 0 \end{cases} \quad (18)$$

where

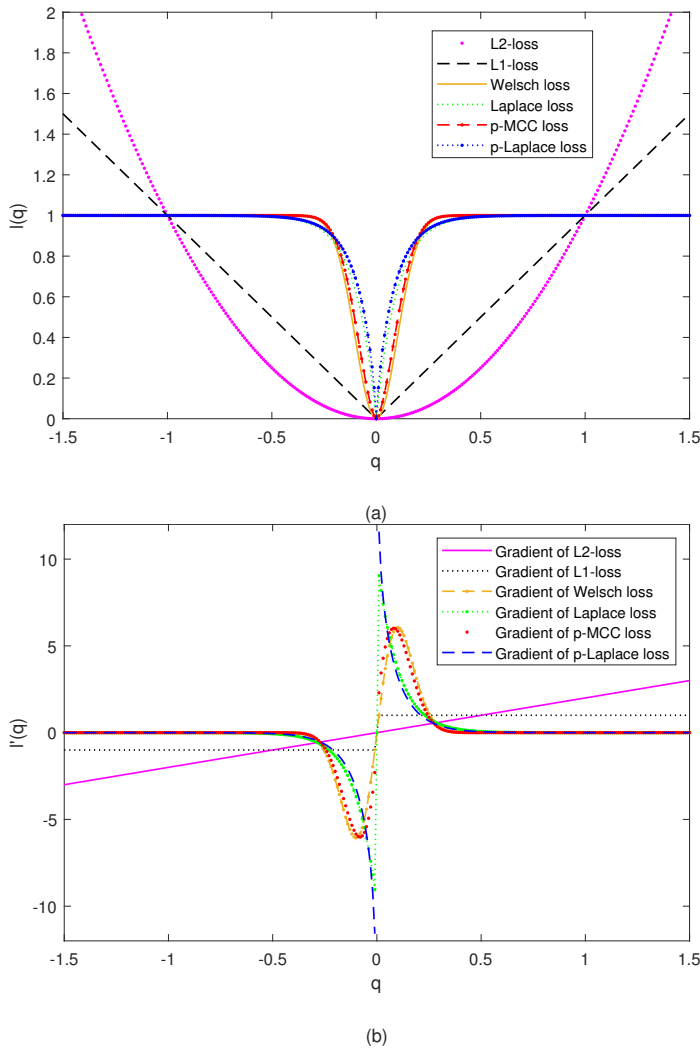


Fig. 3. Comparison of (a) Loss functions; (b) Their gradient functions.

$$w(q_i) = \frac{\partial l(q)}{q_i \partial q_i} = \frac{p}{\sigma} \exp\left(-\frac{|q_i|}{\sigma}\right) \left(1 - \exp\left(-\frac{|q_i|}{\sigma}\right)\right)^{p-1}$$

$$= \frac{1}{\max\{|q_i|, 10^{-6}\}}$$

In this paper, we employ an iterative reweighted algorithm to obtain the optimal hidden layer output weight β . The weight of N samples can be expressed as

$$W(q) = \text{diag}(w(q_1), w(q_2), \dots, w(q_N)) \quad (19)$$

Through Eq.(18), the output weight of the hidden layer is

$$\beta = \begin{cases} H^T \left(\frac{I}{C} + W(q) H H^T\right)^{-1} W(q) Y, & N < L \\ \left(\frac{I}{C} + H^T W(q) H\right)^{-1} H^T W(q) Y, & N \geq L \end{cases} \quad (20)$$

The curve of sample weights with different parameters σ is shown below.

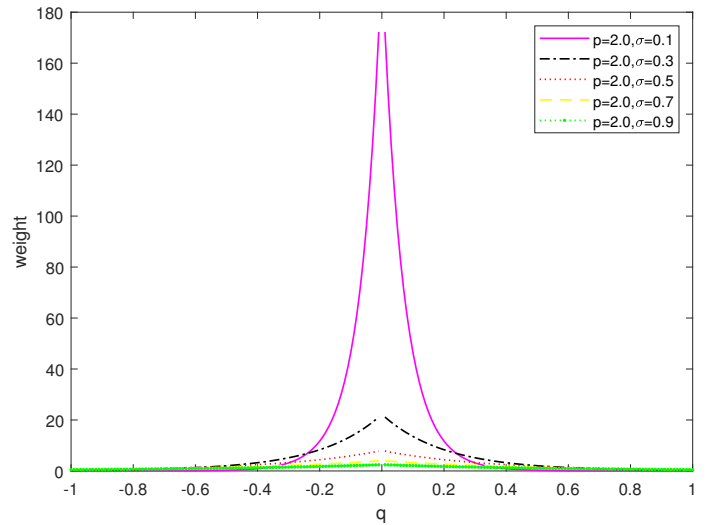


Fig. 4. Trend of sample weights with σ at $p = 2$.

Fig. 4 shows that the larger the error $|q|$ of the sample is, the smaller the weight of the sample is, then the smaller the influence on the model. Therefore, the proposed method can effectively reduce the influence of outliers and enhance the robustness of the model.

Algorithm 1 p -LKI-ELM

Input: Training dataset S , number of hidden nodes L , regularization parameter C , kernel bandwidth σ , maximum of iterations t_{max} , the hidden layer output matrix H .

Output: Output weight β

- 1: Initialize $W(q)^{(0)} = I, t = 1$;
- 2: Calculate the optimal output weight $\beta^{(t)}$ by

$$\beta^{(t)} = \begin{cases} H^T \left(\frac{I}{C} + W(q)^{(t-1)} H H^T\right)^{-1} W(q)^{(t-1)} Y, & N < L \\ \left(\frac{I}{C} + H^T W(q)^{(t-1)} H\right)^{-1} H^T W(q)^{(t-1)} Y, & N \geq L. \end{cases} \quad (21)$$

- 3: Obtain $q_i^{(t)} = y_i - h(x_i)\beta^{(t)}$, and assign diagonal matrix $W(q)^{(t)}$ by (19).
- 4: Update $\beta^{(t+1)}$ from (21);
- 5: if $t > t_{max}$ or $\|\beta^{(t+1)} - \beta^{(t)}\| \leq 10^{-3}$ stop, else go to step 6.
- 6: Derive output value $h(x_i)\beta^{(t+1)}$. Set $t = t + 1$, and go to step 3.

IV. EXPERIMENTS

We compare the proposed method with ELM [1], WELM [11], IRWELM [12], Welsch-ELM [22], Laplace-ELM [25], p -Welsch-ELM [28] on the artificial datasets and benchmark datasets. The root mean square error (RMSE) is chosen as the evaluation metric:

$$\text{RMSE} = \sqrt{\frac{1}{m} \sum_{i=1}^m (y_i - t_i)^2} \quad (22)$$

where y_i and t_i represent the actual target of the sample and the corresponding prediction, respectively; m is the number

of test samples. The experiments are tested in Matlab2021 a Win10 environment with 3.0 GHz CPU, 8 GB RAM and 64 bit host.

A. Experimental Settings

(1) The input weight matrix $W_{N \times L}$ and the hidden layer bias $b_{L \times 1}$ are randomly selected in $[-1, 1]$. The hidden layer activation function is sigmoid function.

$$g(z) = \frac{1}{1 + e^{-z}} \quad (23)$$

(2) Regularization parameter C is optimized by cross validation from the set $\{2^{-19}, 2^{-18}, \dots, 2^{20}\}$ and the number of hidden nodes L is fixed as 1000.

(3) Number of algorithm iterations $t_{max} = 20$.

(4) Parameters σ and order p are also optimized by grid search, where $\sigma : \{0.1, 0.2, \dots, 1\}$; $p : \{0.6, 0.7, \dots, 5\}$.

B. Experimental on Artificial Datasets

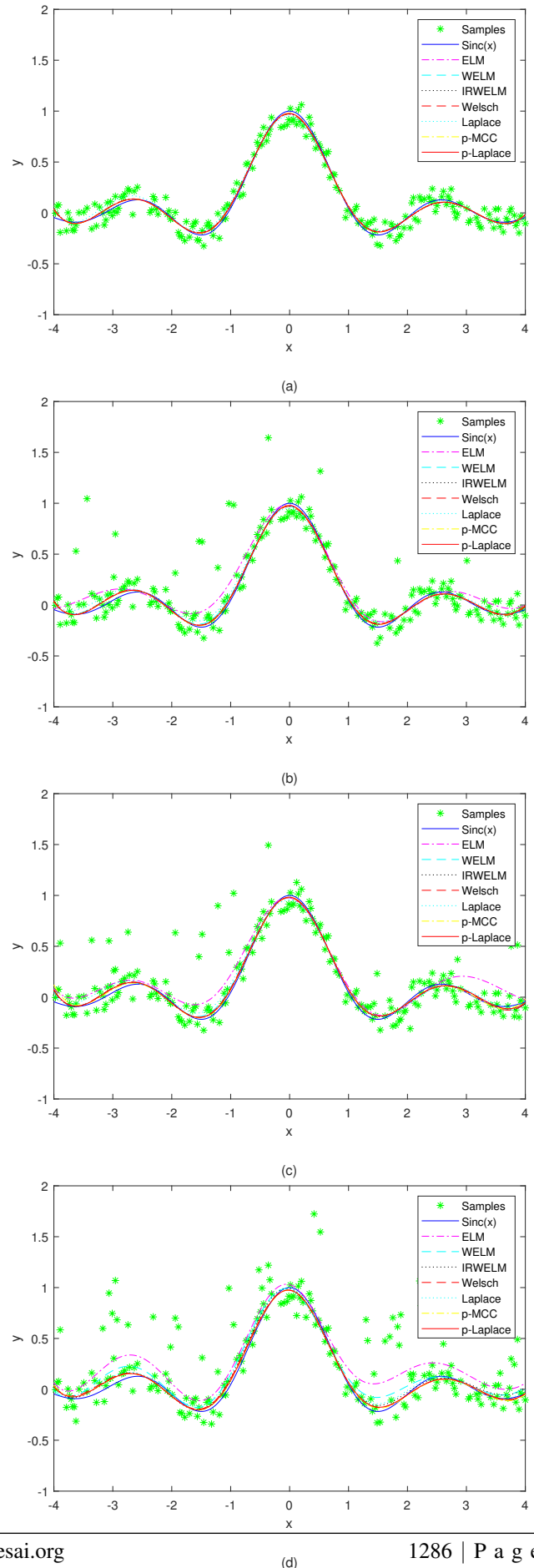
1) *Experimental preparation:* The artificial dataset is generated by function $y = \sin c(x)$, where,

$$\sin c(x) = \frac{\sin x}{x}, x \in [-4, 4]. \quad (24)$$

The preprocessing of artificial datasets is divided into three steps. First, 300 samples are generated from Eq.(24) and randomly divided into 200 training samples and 100 test samples. Secondly, the target of the training sample is disturbed by the uniform distribution of noise $[-0.15, 0.15]$. Finally, random values of different proportions in $[y_{min}, y_{max}]$ are added as outliers to the targets of some training samples generated in the second step. Outliers include 0%, 10%, 20%, 30%, and 40%. The samples used for testing are from Eq.(24) without any added outliers. To ensure fairness, 10 independent experiments are conducted for each outliers distribution.

2) *Experimental results and analysis:* To further confirm the robustness of the proposed algorithm, the different levels of outliers are compared. Fig. 5 illustrates the regression prediction results of these seven algorithms with different outliers levels. When the outliers level is 0%, all seven methods roughly coincide with the original position. When the outliers levels are 10% and 20%, only ELM deviates slightly from the original position and begins to shift toward the outliers, while the other six methods remain unchanged. When the outliers levels are 30% and 40%, ELM, WELM, IRWELM, Laplace-ELM and Welsch-ELM deviate from the original position and turn toward the outliers, and only p -LKI-ELM and p -Welsch-ELM are relatively close to the original position and do not have a tendency to turn towards the outliers. It can be seen that as the outliers level increases, all five methods except p -LKI-ELM and p -Welsch-ELM deviate from the original position and shift towards outliers, and the trend turn toward the outliers of p -LKI-ELM is smaller compared to p -Welsch-ELM. Therefore, it indicates that p -LKI-ELM has better stability.

Fig. 6 reflects the variation of the RMSE of the seven methods for different outliers levels on the artificial dataset. When there are no outliers, the RMSE of p -LKI-ELM is



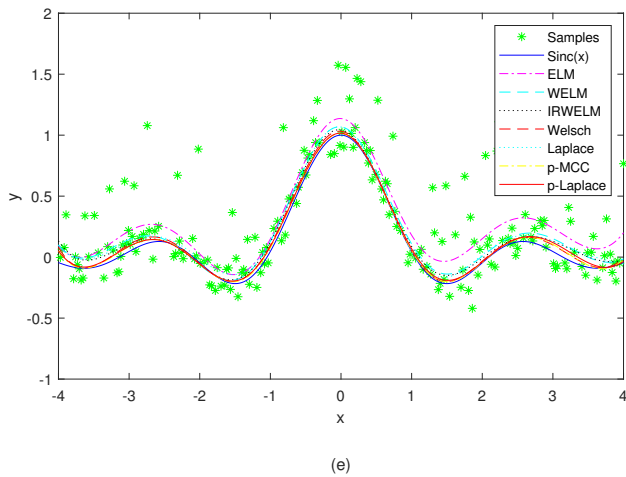


Fig. 5. Experiment results on artificial datasets with different outliers levels: a(0%), b(10%), c(20%), d(30%), e(40%).

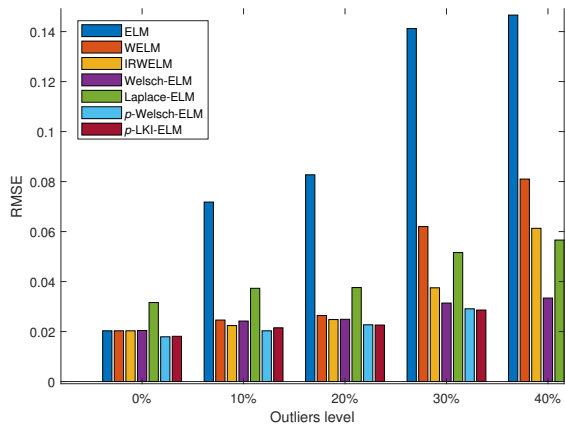


Fig. 6. RMSE of seven algorithms with different outliers levels on the artificial dataset.

slightly higher than that of p -Welsch-ELM, which ranks second among the seven methods. When the outliers level is 10%, the RMSE of ELM increases more, while the increases of p -LKI-ELM and p -Welsch-ELM are smaller compared to the other four methods and p -LKI-ELM is still ranked second among the seven methods. When the outliers level is 20%, p -LKI-ELM has the smallest RMSE among the seven methods and ranks first among the seven methods. It can be seen that the increase in RMSE of p -LKI-ELM becomes smaller and smaller as the outliers level increases. When the outliers levels are 30% and 40%, the RMSE of p -LKI-ELM is still the smallest among the seven methods and ranks first among the seven methods, and it can be concluded that the robustness of p -LKI-ELM is the best. From the aspect of the increase of RMSE, the increase of RMSE of ELM during the increase of outliers levels from 0% to 40% is the largest, while the increase of RMSE of p -LKI-ELM is the smallest, which indicates that the stability of p -LKI-ELM is the best among the seven methods.

C. Experiments on Benchmark Datasets

1) *Datasets description:* To further test the performance of p -LKI-ELM, the seven methods are experimented on eighteen

datasets and the results are analyzed. The information on the selected dataset is shown in Table I. A portion of the datasets is randomly chosen as the training samples, while the rest is used as the test samples. To test the robustness of the model with outliers, we set 10%, 20%, 30% and 40% outliers levels, respectively.

TABLE I. BENCHMARK REGRESSION DATASETS

| Dataset | Feature | Training Samples | Test Samples |
|-----------|---------|------------------|--------------|
| Yacht | 6 | 200 | 108 |
| Servo | 4 | 120 | 47 |
| Pyrim | 27 | 40 | 34 |
| Heart | 12 | 200 | 99 |
| Fish | 6 | 500 | 408 |
| Diabetes | 2 | 20 | 23 |
| Daily | 12 | 40 | 20 |
| Concrete | 8 | 600 | 430 |
| Autompg | 7 | 200 | 192 |
| Aquatic | 8 | 300 | 246 |
| Bodyfat | 14 | 160 | 92 |
| Pollution | 15 | 60 | 40 |
| Housing | 13 | 300 | 206 |
| MG | 6 | 700 | 685 |
| Abalone | 7 | 2000 | 2177 |
| Air | 6 | 740 | 313 |
| Wine | 12 | 1000 | 599 |
| ALE | 5 | 80 | 27 |

2) *Experimental results and analysis:* The RMSE values and standard deviations of the seven algorithms across various outliers levels on the nine and nine benchmark datasets are given in Tables II and III, respectively. When the outliers level is 0%, p -LKI-ELM has the lowest RMSE on four datasets in Table II and ranks first together with p -Welsch-ELM, and it has the lowest RMSE values on three datasets in Table III, ranking second among the seven methods. Overall, p -LKI-ELM ranks second among these seven methods on fifteen datasets. When the outliers level is 10%, p -LKI-ELM achieves the smallest RMSE values on seven datasets in Table II and ranks first; seven of the datasets in Table III reaches the smallest RMSE values and ranks first. In total, p -LKI-ELM ranks first among these seven methods on eighteen datasets. This shows that the rank of p -LKI-ELM increases with the addition of outliers, and p -LKI-ELM is least affected by outliers compared to the other methods. When the outliers level is 20%, p -LKI-ELM obtains the smallest RMSE value on eight datasets in Table II, the number of datasets that achieve the minimum RMSE value increases by one, and eight of the datasets in Table III win the smallest RMSE value and ranks first. With outliers levels of 30% and 40%, p -LKI-ELM achieves the smallest RMSE values on eight and seven datasets in Table II, and eight and nine datasets in Table III, respectively, and is ranked first on eighteen datasets. It can be seen that as the level of outliers increases, the number of minimum RMSE values achieved by p -LKI-ELM is increasing, which indicates that p -LKI-ELM has the best robustness compared to the other six methods. In terms of the increase of RMSE values, from outliers level of 0% to 40%, p -LKI-ELM has the lowest increase of RMSE values on all eighteen datasets among the seven methods. From the point of view of the loss function, the p -LKI loss function adopted by the p -LKI-ELM is a bounded loss function that can limit the error to a certain range and will not increase.

TABLE II. COMPARISONS OF SEVEN ALGORITHMS ON NINE BENCHMARK DATASETS

| Dataset | algorithm | 0% | 10% | 20% | 30% | 40% |
|-----------|--------------|-------------------------|-------------------------|--------------------------|--------------------------|-------------------------|
| Yacht | ELM | 2.2141 ± 0.2392 | 6.8297 ± 0.5524 | 8.2801 ± 0.8043 | 12.5289 ± 1.2580 | 13.8917 ± 1.1349 |
| | WELM | 2.3363 ± 0.2924 | 3.3202 ± 0.8706 | 5.8744 ± 0.6280 | 9.6205 ± 1.5650 | 12.9183 ± 1.0998 |
| | IRWELM | 3.9779 ± 1.9951 | 2.8292 ± 0.3470 | 4.1704 ± 1.3173 | 6.7085 ± 1.0380 | 11.9374 ± 1.6171 |
| | Welsch-ELM | 1.0205 ± 0.1877 | 2.2840 ± 0.3704 | 3.3771 ± 1.2074 | 5.4644 ± 0.3629 | 6.3030 ± 1.4922 |
| | Laplace-ELM | 0.9999 ± 0.2344 | 2.0123 ± 0.5708 | 3.5665 ± 0.7810 | 6.4055 ± 1.7824 | 7.4523 ± 1.2537 |
| | p-Welsch-ELM | 0.9049 ± 0.2073 | 2.0516 ± 1.5746 | 3.2096 ± 0.7216 | 5.4282 ± 0.9047 | 6.3030 ± 1.4922 |
| | p-LKI-ELM | 0.9006 ± 0.2069 | 1.8326 ± 0.5807 | 2.6563 ± 0.5513 | 5.3287 ± 0.3406 | 6.1246 ± 1.5251 |
| Daily | ELM | 11.6573 ± 5.4691 | 51.8964 ± 10.1203 | 76.6575 ± 13.6884 | 77.7380 ± 15.7061 | 78.8797 ± 13.6214 |
| | WELM | 13.8204 ± 7.0593 | 35.5050 ± 8.3419 | 49.1082 ± 14.6976 | 75.8675 ± 14.8694 | 80.6479 ± 10.6494 |
| | IRWELM | 14.7650 ± 7.9147 | 27.2927 ± 17.5360 | 34.9433 ± 12.7568 | 75.8575 ± 14.8827 | 80.6479 ± 10.6494 |
| | Welsch-ELM | 11.6572 ± 5.4708 | 20.2666 ± 10.7994 | 26.9522 ± 15.8516 | 30.0938 ± 7.7563 | 34.4336 ± 9.9401 |
| | Laplace-ELM | 11.6621 ± 5.4612 | 17.6412 ± 9.8118 | 21.1682 ± 11.2175 | 30.6572 ± 15.2610 | 44.5214 ± 26.7513 |
| | p-Welsch-ELM | 11.6526 ± 5.4708 | 19.1776 ± 10.0054 | 25.5457 ± 17.0197 | 26.8373 ± 10.8504 | 30.9964 ± 8.9880 |
| | p-LKI-ELM | 11.6527 ± 5.4763 | 16.9423 ± 8.4695 | 19.5609 ± 10.7949 | 25.6105 ± 11.4699 | 30.0912 ± 9.7413 |
| Autompg | ELM | 2.8782 ± 0.1462 | 4.1298 ± 0.2136 | 5.9220 ± 0.3457 | 7.9565 ± 0.2425 | 7.9213 ± 0.2472 |
| | WELM | 2.8711 ± 0.1987 | 2.9047 ± 0.1526 | 3.3047 ± 0.3495 | 7.6725 ± 0.8660 | 7.9822 ± 0.2633 |
| | IRWELM | 2.9500 ± 0.1882 | 2.8651 ± 0.0991 | 2.8698 ± 0.1202 | 7.0622 ± 0.5588 | 7.9822 ± 0.2633 |
| | Welsch-ELM | 2.8680 ± 0.1748 | 2.8761 ± 0.1119 | 2.8890 ± 0.1309 | 2.9591 ± 0.2347 | 3.0852 ± 0.1235 |
| | Laplace-ELM | 2.9393 ± 0.2624 | 2.9237 ± 0.1281 | 2.9375 ± 0.1443 | 2.9645 ± 0.1629 | 3.1562 ± 0.2442 |
| | p-Welsch-ELM | 2.8664 ± 0.1796 | 2.8696 ± 0.0961 | 2.8780 ± 0.1275 | 2.9503 ± 0.2406 | 3.0112 ± 0.1286 |
| | p-LKI-ELM | 2.8658 ± 0.1870 | 2.8653 ± 0.1020 | 2.8739 ± 0.1251 | 2.9390 ± 0.2123 | 2.9928 ± 0.1513 |
| Heart | ELM | 0.3850 ± 0.0211 | 0.3871 ± 0.0236 | 0.3957 ± 0.0222 | 0.4088 ± 0.0286 | 0.4307 ± 0.0258 |
| | WELM | 0.3855 ± 0.0206 | 0.3862 ± 0.0218 | 0.3932 ± 0.0225 | 0.4061 ± 0.0262 | 0.4290 ± 0.0261 |
| | IRWELM | 0.3862 ± 0.0188 | 0.3865 ± 0.0215 | 0.3929 ± 0.0220 | 0.4049 ± 0.0252 | 0.4288 ± 0.0270 |
| | Welsch-ELM | 0.3856 ± 0.0207 | 0.3847 ± 0.0206 | 0.3879 ± 0.0188 | 0.3940 ± 0.0221 | 0.4105 ± 0.0261 |
| | Laplace-ELM | 0.4255 ± 0.0309 | 0.4032 ± 0.0306 | 0.3972 ± 0.0197 | 0.3988 ± 0.0242 | 0.4183 ± 0.0340 |
| | p-Welsch-ELM | 0.3852 ± 0.0201 | 0.3845 ± 0.0215 | 0.3876 ± 0.0207 | 0.3937 ± 0.0235 | 0.4062 ± 0.0244 |
| | p-LKI-ELM | 0.3854 ± 0.0202 | 0.3845 ± 0.0219 | 0.3874 ± 0.0200 | 0.3930 ± 0.0235 | 0.4056 ± 0.0256 |
| Bodyfat | ELM | 0.0043 ± 0.0019 | 0.0210 ± 0.0018 | 0.0214 ± 0.0022 | 0.0337 ± 0.0062 | 0.0542 ± 0.0081 |
| | WELM | 0.0031 ± 0.0015 | 0.0071 ± 0.0017 | 0.0093 ± 0.0032 | 0.0337 ± 0.0062 | 0.0542 ± 0.0081 |
| | IRWELM | 0.0030 ± 0.0017 | 0.0038 ± 0.0021 | 0.0043 ± 0.0015 | 0.0337 ± 0.0062 | 0.0542 ± 0.0081 |
| | Welsch-ELM | 0.0033 ± 0.0017 | 0.0040 ± 0.0018 | 0.0040 ± 0.0016 | 0.0046 ± 0.0016 | 0.0065 ± 0.0020 |
| | Laplace-ELM | 0.0029 ± 0.0018 | 0.0032 ± 0.0017 | 0.0034 ± 0.0017 | 0.0038 ± 0.0024 | 0.0042 ± 0.0022 |
| | p-Welsch-ELM | 0.0029 ± 0.0018 | 0.0037 ± 0.0020 | 0.0038 ± 0.0019 | 0.0038 ± 0.0021 | 0.0046 ± 0.0016 |
| | p-LKI-ELM | 0.0028 ± 0.0017 | 0.0029 ± 0.0016 | 0.0032 ± 0.0015 | 0.0035 ± 0.0017 | 0.0038 ± 0.0016 |
| Pyrim | ELM | 0.1111 ± 0.0199 | 0.1362 ± 0.0204 | 0.1425 ± 0.0188 | 0.1553 ± 0.0145 | 0.1569 ± 0.0274 |
| | WELM | 0.1061 ± 0.0295 | 0.1102 ± 0.0326 | 0.1227 ± 0.0303 | 0.1411 ± 0.0264 | 0.1551 ± 0.0237 |
| | IRWELM | 0.1065 ± 0.0293 | 0.1071 ± 0.0332 | 0.1143 ± 0.0389 | 0.1384 ± 0.0185 | 0.1553 ± 0.0241 |
| | Welsch-ELM | 0.1035 ± 0.0285 | 0.1054 ± 0.0315 | 0.1115 ± 0.0344 | 0.1112 ± 0.0348 | 0.1198 ± 0.0342 |
| | Laplace-ELM | 0.1044 ± 0.0245 | 0.1063 ± 0.0298 | 0.1127 ± 0.0318 | 0.1139 ± 0.0324 | 0.1283 ± 0.0471 |
| | p-Welsch-ELM | 0.1021 ± 0.0275 | 0.1053 ± 0.0308 | 0.1096 ± 0.0341 | 0.1111 ± 0.0346 | 0.1150 ± 0.0342 |
| | p-LKI-ELM | 0.1024 ± 0.0280 | 0.1043 ± 0.0314 | 0.1091 ± 0.0334 | 0.1104 ± 0.0361 | 0.1144 ± 0.0363 |
| Diabetes | ELM | 0.5838 ± 0.0937 | 0.6523 ± 0.1043 | 0.6907 ± 0.1219 | 0.6646 ± 0.1239 | 0.6812 ± 0.1315 |
| | WELM | 0.5821 ± 0.0906 | 0.5889 ± 0.1088 | 0.6341 ± 0.1039 | 0.7033 ± 0.1333 | 0.6974 ± 0.1316 |
| | IRWELM | 0.5820 ± 0.0905 | 0.5745 ± 0.0953 | 0.5945 ± 0.0970 | 0.7262 ± 0.1364 | 0.6974 ± 0.1316 |
| | Welsch-ELM | 0.5809 ± 0.0921 | 0.5752 ± 0.0927 | 0.5774 ± 0.0964 | 0.5870 ± 0.0988 | 0.5881 ± 0.1032 |
| | Laplace-ELM | 0.6022 ± 0.1005 | 0.5995 ± 0.0774 | 0.6303 ± 0.1037 | 0.6373 ± 0.1172 | 0.6740 ± 0.1041 |
| | p-Welsch-ELM | 0.5748 ± 0.0804 | 0.5746 ± 0.0886 | 0.5742 ± 0.0942 | 0.5852 ± 0.0966 | 0.5857 ± 0.0765 |
| | p-LKI-ELM | 0.5793 ± 0.0941 | 0.5746 ± 0.0971 | 0.5742 ± 0.0933 | 0.5844 ± 0.0993 | 0.5826 ± 0.0831 |
| Servo | ELM | 0.6000 ± 0.0944 | 1.0198 ± 0.1596 | 1.1133 ± 0.1797 | 1.3316 ± 0.1572 | 1.4877 ± 0.1583 |
| | WELM | 0.5595 ± 0.1574 | 0.7789 ± 0.1833 | 0.8731 ± 0.1778 | 1.0145 ± 0.1605 | 1.4920 ± 0.1660 |
| | IRWELM | 0.5920 ± 0.1602 | 0.7537 ± 0.2060 | 0.7348 ± 0.2559 | 0.8599 ± 0.2012 | 1.4920 ± 0.1660 |
| | Welsch-ELM | 0.5547 ± 0.2082 | 0.6610 ± 0.1921 | 0.7112 ± 0.2313 | 0.7123 ± 0.2084 | 0.7944 ± 0.1993 |
| | Laplace-ELM | 0.5720 ± 0.1905 | 0.6683 ± 0.1786 | 0.7086 ± 0.1834 | 0.7062 ± 0.2063 | 0.9396 ± 0.1930 |
| | p-Welsch-ELM | 0.5514 ± 0.2116 | 0.6464 ± 0.1882 | 0.6863 ± 0.2364 | 0.6959 ± 0.2038 | 0.7686 ± 0.2307 |
| | p-LKI-ELM | 0.5523 ± 0.2092 | 0.6446 ± 0.1886 | 0.6838 ± 0.1901 | 0.6890 ± 0.2274 | 0.7619 ± 0.2352 |
| Pollution | ELM | 35.4759 ± 6.8079 | 59.5479 ± 7.5005 | 63.7456 ± 8.5865 | 58.4852 ± 8.5803 | 66.3481 ± 10.7665 |
| | WELM | 36.8257 ± 4.8361 | 40.6244 ± 6.5749 | 48.3622 ± 8.1037 | 58.4852 ± 8.5803 | 66.3481 ± 10.7665 |
| | IRWELM | 36.8908 ± 5.6836 | 37.5958 ± 4.9581 | 39.4799 ± 5.9682 | 58.4852 ± 8.5803 | 66.3481 ± 10.7665 |
| | Welsch-ELM | 35.4153 ± 6.5356 | 36.2262 ± 5.9163 | 36.5977 ± 5.8775 | 38.1440 ± 5.8735 | 37.6558 ± 5.9691 |
| | Laplace-ELM | 35.8060 ± 6.3745 | 35.8537 ± 5.6511 | 36.7654 ± 10.1868 | 37.9770 ± 7.3431 | 38.3577 ± 9.0325 |
| | p-Welsch-ELM | 35.0482 ± 4.5809 | 35.8739 ± 6.2515 | 36.4647 ± 6.3492 | 37.7237 ± 5.9320 | 37.0502 ± 6.6151 |
| | p-LKI-ELM | 34.2035 ± 6.1478 | 35.8537 ± 5.6511 | 36.2593 ± 9.4523 | 37.6604 ± 6.6825 | 37.3199 ± 6.7331 |

TABLE III. COMPARISONS OF SEVEN ALGORITHMS ON NINE BENCHMARK DATASETS

| Dataset | algorithm | 0% | 10% | 20% | 30% | 40% |
|----------|--------------|------------------------|------------------------|------------------------|------------------------|------------------------|
| Fish | ELM | 0.9587 ± 0.1258 | 1.0734 ± 0.2356 | 1.3763 ± 0.1348 | 1.4139 ± 0.2314 | 1.4093 ± 0.2659 |
| | WELM | 0.9653 ± 0.2691 | 0.9737 ± 0.1645 | 0.9986 ± 0.3145 | 1.3462 ± 0.5896 | 1.4150 ± 0.3145 |
| | IRWELM | 0.9678 ± 0.2154 | 0.9757 ± 0.3245 | 0.9798 ± 0.1246 | 1.2366 ± 0.1235 | 1.4216 ± 0.2369 |
| | Welsch-ELM | 0.9578 ± 0.3145 | 0.9704 ± 0.3214 | 0.9685 ± 0.4563 | 0.9757 ± 0.3145 | 0.9862 ± 0.3156 |
| | Laplace-ELM | 0.9625 ± 0.2145 | 0.9652 ± 0.2312 | 0.9657 ± 0.3112 | 0.9898 ± 0.3145 | 1.0323 ± 0.2136 |
| | p-Welsch-ELM | 0.9563 ± 0.2365 | 0.9687 ± 0.1345 | 0.9654 ± 0.3145 | 0.9736 ± 0.3302 | 0.9857 ± 0.2230 |
| | p-LKI-ELM | 0.9567 ± 0.2563 | 0.9638 ± 0.3145 | 0.9623 ± 0.1146 | 0.9734 ± 0.2698 | 0.9850 ± 0.2423 |
| Aquatic | ELM | 1.1874 ± 0.0688 | 1.3137 ± 0.0589 | 1.6137 ± 0.0914 | 1.6683 ± 0.0636 | 1.7233 ± 0.0962 |
| | WELM | 1.1942 ± 0.0658 | 1.2053 ± 0.0455 | 1.2843 ± 0.0648 | 1.5869 ± 0.0813 | 1.6735 ± 0.0591 |
| | IRWELM | 1.2025 ± 0.0621 | 1.2046 ± 0.0540 | 1.2489 ± 0.0607 | 1.4864 ± 0.0901 | 1.6735 ± 0.0591 |
| | Welsch-ELM | 1.1871 ± 0.0731 | 1.1972 ± 0.0497 | 1.2060 ± 0.0566 | 1.2160 ± 0.0518 | 1.2347 ± 0.0436 |
| | Laplace-ELM | 1.2011 ± 0.0590 | 1.1966 ± 0.0539 | 1.2141 ± 0.0544 | 1.2432 ± 0.0522 | 1.3141 ± 0.1120 |
| | p-Welsch-ELM | 1.1871 ± 0.0731 | 1.1958 ± 0.0514 | 1.2051 ± 0.0510 | 1.2154 ± 0.0544 | 1.2277 ± 0.0596 |
| | p-LKI-ELM | 1.1871 ± 0.0729 | 1.1954 ± 0.0520 | 1.2051 ± 0.0509 | 1.2146 ± 0.0531 | 1.2250 ± 0.0446 |
| Housing | ELM | 3.2563 ± 0.2501 | 5.3252 ± 0.4442 | 7.3845 ± 0.3468 | 8.9692 ± 0.9645 | 9.1478 ± 0.4115 |
| | WELM | 3.3422 ± 0.4405 | 3.7507 ± 0.6523 | 4.7048 ± 0.5636 | 8.3753 ± 0.6235 | 9.0570 ± 0.4625 |
| | IRWELM | 3.4454 ± 0.4456 | 3.6482 ± 0.6741 | 4.1057 ± 0.5963 | 7.3460 ± 0.6623 | 9.0570 ± 0.5624 |
| | Welsch-ELM | 3.2489 ± 0.3112 | 3.5236 ± 0.3326 | 3.8161 ± 0.3417 | 4.1932 ± 0.3918 | 4.7868 ± 0.3721 |
| | Laplace-ELM | 3.4086 ± 0.3056 | 3.6160 ± 0.3102 | 3.8380 ± 0.3623 | 4.4099 ± 0.3515 | 5.0003 ± 0.3120 |
| | p-Welsch-ELM | 3.2404 ± 0.3215 | 3.5088 ± 0.3625 | 3.7979 ± 0.3775 | 4.1684 ± 0.3023 | 4.1691 ± 0.3402 |
| | p-LKI-ELM | 3.2416 ± 0.3003 | 3.5088 ± 0.3625 | 3.7709 ± 0.3569 | 4.1486 ± 0.4021 | 4.1506 ± 0.3654 |
| Concrete | ELM | 6.1381 ± 0.2968 | 9.7657 ± 0.5098 | 11.7639 ± 0.5329 | 16.4077 ± 0.6302 | 16.8087 ± 0.2882 |
| | WELM | 6.2327 ± 0.3840 | 7.7370 ± 0.9532 | 8.4606 ± 0.2148 | 12.2520 ± 0.8875 | 16.9696 ± 0.3332 |
| | IRWELM | 6.4228 ± 0.3245 | 7.5245 ± 0.3625 | 7.9860 ± 0.4632 | 10.3756 ± 0.2564 | 16.9696 ± 0.4463 |
| | Welsch-ELM | 6.1330 ± 0.3456 | 6.6900 ± 0.5120 | 7.6898 ± 0.4326 | 8.2634 ± 0.3694 | 8.8897 ± 0.5213 |
| | Laplace-ELM | 6.6114 ± 0.3412 | 7.5818 ± 0.4362 | 8.1849 ± 0.4423 | 8.9050 ± 0.2631 | 10.0165 ± 0.2543 |
| | p-Welsch-ELM | 6.1241 ± 0.5023 | 6.6893 ± 0.4312 | 7.5801 ± 0.4412 | 7.9668 ± 0.4063 | 8.1160 ± 0.3316 |
| | p-LKI-ELM | 6.1177 ± 0.3321 | 6.6817 ± 0.4120 | 7.4485 ± 0.3216 | 7.9980 ± 0.4521 | 8.1131 ± 0.5623 |
| MG | ELM | 0.2267 ± 0.0031 | 0.2277 ± 0.0039 | 0.2291 ± 0.0043 | 0.2267 ± 0.0033 | 0.2362 ± 0.0054 |
| | WELM | 0.2267 ± 0.0031 | 0.2268 ± 0.0030 | 0.2267 ± 0.0031 | 0.2312 ± 0.0047 | 0.2358 ± 0.0053 |
| | IRWELM | 0.2267 ± 0.0031 | 0.2267 ± 0.0032 | 0.2268 ± 0.0031 | 0.2335 ± 0.0068 | 0.2358 ± 0.0053 |
| | Welsch-ELM | 0.2267 ± 0.0031 | 0.2267 ± 0.0031 | 0.2266 ± 0.0030 | 0.2266 ± 0.0032 | 0.2265 ± 0.0032 |
| | Laplace-ELM | 0.2266 ± 0.0032 | 0.2273 ± 0.0028 | 0.2293 ± 0.0044 | 0.2268 ± 0.0034 | 0.2341 ± 0.0032 |
| | p-Welsch-ELM | 0.2264 ± 0.0031 | 0.2265 ± 0.0033 | 0.2264 ± 0.0031 | 0.2265 ± 0.0032 | 0.2265 ± 0.0032 |
| | p-LKI-ELM | 0.2266 ± 0.0032 | 0.2265 ± 0.0032 | 0.2264 ± 0.0031 | 0.2265 ± 0.0032 | 0.2265 ± 0.0032 |
| Abalone | ELM | 2.1698 ± 0.0371 | 2.6821 ± 0.0588 | 3.1988 ± 0.0538 | 3.2092 ± 0.0408 | 3.2703 ± 0.0709 |
| | WELM | 2.1869 ± 0.0359 | 2.1707 ± 0.0335 | 2.2428 ± 0.0449 | 3.2110 ± 0.0423 | 3.1981 ± 0.0340 |
| | IRWELM | 2.2253 ± 0.0456 | 2.1831 ± 0.0412 | 2.1948 ± 0.0563 | 2.8742 ± 0.0321 | 3.2033 ± 0.0364 |
| | Welsch-ELM | 2.1689 ± 0.0456 | 2.1769 ± 0.0356 | 2.1812 ± 0.0349 | 2.1978 ± 0.0502 | 2.1988 ± 0.0356 |
| | Laplace-ELM | 2.1752 ± 0.0563 | 2.1802 ± 0.0421 | 2.1901 ± 0.0314 | 2.1893 ± 0.0513 | 2.1864 ± 0.0419 |
| | p-Welsch-ELM | 2.1688 ± 0.0318 | 2.1691 ± 0.0526 | 2.1724 ± 0.0536 | 2.1758 ± 0.0543 | 2.1781 ± 0.0697 |
| | p-LKI-ELM | 2.1692 ± 0.0412 | 2.1696 ± 0.0316 | 2.1710 ± 0.0412 | 2.1757 ± 0.0346 | 2.1777 ± 0.0327 |
| Air | ELM | 2.6473 ± 0.0001 | 7.8888 ± 0.0102 | 7.9453 ± 0.0012 | 10.6465 ± 0.0301 | 15.0824 ± 0.0014 |
| | WELM | 2.6352 ± 0.0000 | 2.8410 ± 0.0002 | 3.0812 ± 0.0001 | 10.6465 ± 0.0023 | 15.0824 ± 0.0003 |
| | IRWELM | 2.6212 ± 0.0001 | 2.7396 ± 0.0016 | 2.7198 ± 0.0001 | 10.6465 ± 0.0012 | 15.0824 ± 0.0004 |
| | Welsch-ELM | 2.6210 ± 0.0203 | 2.7394 ± 0.0005 | 2.6902 ± 0.0101 | 2.6768 ± 0.0000 | 2.9801 ± 0.0301 |
| | Laplace-ELM | 2.6913 ± 0.0012 | 2.6771 ± 0.0013 | 2.7111 ± 0.0502 | 2.6769 ± 0.0107 | 2.9761 ± 0.0005 |
| | p-Welsch-ELM | 2.6208 ± 0.0000 | 2.6523 ± 0.0001 | 2.6874 ± 0.0031 | 2.6615 ± 0.0004 | 2.9798 ± 0.0015 |
| | p-LKI-ELM | 2.6213 ± 0.0013 | 2.6516 ± 0.0000 | 2.6742 ± 0.0001 | 2.6569 ± 0.0015 | 2.9653 ± 0.0205 |
| Wine | ELM | 0.6482 ± 0.0226 | 0.8226 ± 0.0202 | 0.8243 ± 0.0205 | 0.8263 ± 0.0175 | 0.8686 ± 0.0711 |
| | WELM | 0.6506 ± 0.0230 | 0.6565 ± 0.0230 | 0.6852 ± 0.0223 | 0.8349 ± 0.0170 | 0.8686 ± 0.0711 |
| | IRWELM | 0.6515 ± 0.0234 | 0.6525 ± 0.0211 | 0.6549 ± 0.0217 | 0.8349 ± 0.0170 | 0.8686 ± 0.0711 |
| | Welsch-ELM | 0.6423 ± 0.0031 | 0.6429 ± 0.0031 | 0.6512 ± 0.0030 | 0.7698 ± 0.0032 | 0.8027 ± 0.0032 |
| | Laplace-ELM | 0.6504 ± 0.0055 | 0.6513 ± 0.0029 | 0.6516 ± 0.0034 | 0.7742 ± 0.0034 | 0.8014 ± 0.0035 |
| | p-Welsch-ELM | 0.6412 ± 0.0031 | 0.6416 ± 0.0013 | 0.6489 ± 0.0038 | 0.7685 ± 0.0032 | 0.7746 ± 0.0006 |
| | p-LKI-ELM | 0.6414 ± 0.0056 | 0.6420 ± 0.0030 | 0.6500 ± 0.0031 | 0.7644 ± 0.0032 | 0.7695 ± 0.0012 |
| ALE | ELM | 0.1325 ± 0.0001 | 0.2511 ± 0.0008 | 0.3261 ± 0.0102 | 0.3467 ± 0.0408 | 0.3464 ± 0.0709 |
| | WELM | 0.1427 ± 0.0009 | 0.1532 ± 0.0005 | 0.1715 ± 0.0001 | 0.3474 ± 0.0003 | 0.3456 ± 0.0000 |
| | IRWELM | 0.1342 ± 0.0006 | 0.1430 ± 0.0002 | 0.1653 ± 0.0003 | 0.3464 ± 0.0001 | 0.3456 ± 0.0004 |
| | Welsch-ELM | 0.1281 ± 0.0000 | 0.1371 ± 0.0001 | 0.1371 ± 0.0009 | 0.1438 ± 0.0002 | 0.1538 ± 0.0001 |
| | Laplace-ELM | 0.1357 ± 0.0000 | 0.1410 ± 0.0001 | 0.1549 ± 0.0004 | 0.1450 ± 0.0003 | 0.1754 ± 0.0001 |
| | p-Welsch-ELM | 0.1279 ± 0.0008 | 0.1366 ± 0.0000 | 0.1329 ± 0.0000 | 0.1339 ± 0.0003 | 0.1503 ± 0.0007 |
| | p-LKI-ELM | 0.1289 ± 0.0002 | 0.1356 ± 0.0006 | 0.1323 ± 0.0002 | 0.1303 ± 0.0006 | 0.1467 ± 0.0001 |

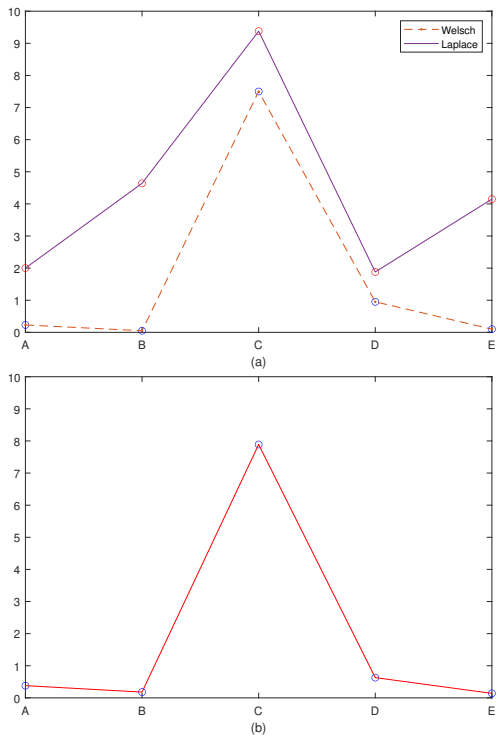


Fig. 7. (a) The reduction of RMSE for p -Welsch-ELM and p -LKI-ELM; (b) The RMSE reduction of p -LKI-ELM relative to p -Welsch-ELM.

Infinitely with the increase of outliers levels. However the l_2 loss function employed by ELM, WELM and IRWELM is an unbounded loss function that increases the error of the model as the levels of outliers increases. Compared with the loss function induced by Gaussian kernel, p -LKI is induced by Laplace kernel and the exponential part is still bounded, which makes the p -LKI-ELM the most optimal among these seven methods by choosing a suitable p .

In order to observe more intuitively the improvement effect of the loss function after the introduction of p -order and compare the effect of the two kernel functions after the introduction of p -order, we graph the experimental data.

Fig. 7 shows the reduction of p -Welsch-ELM relative to Welsch-ELM and p -LKI-ELM relative to the RMSE of Laplace-ELM on five benchmark datasets as illustrated in (a), the x -axis A, B, C, D and E represent the five datasets (Autompg, Heart, Bodyfat, Pym and Diabetes), respectively. The y -axis represents the reduction in RMSE (%), and Fig. 7 indicates that the RMSE reduction of p -LKI loss function relative to Laplace loss function is higher than the reduction of p -Welsch loss function relative to the RMSE of Welsch loss function. It shows that the loss function induced by the Laplace kernel is more effective for the p -order than Gaussian kernel, which indicates that the former is more suitable for the p -order.

Fig. 7(b) suggests the reduction of RMSE of the proposed model relative to the p -Welsch-ELM model on five benchmark datasets. It can be seen from (b) that the y -axis is always more significant than 0, which means that the reduction (%) of the RMSE of p -LKI-ELM relative to p -Welsch-ELM is greater than 0, which indicates that the prediction accuracy of the loss function induced by the Laplace kernel is higher than that of the Gaussian kernel.

V. DISCUSSION

The proposed model is compared with six other models on both artificial datasets and eighteen benchmark datasets. Experimental

results demonstrate that p -LKI-ELM achieves superior performance on the majority of datasets. Moreover, as the proportion of outliers increases, p -LKI-ELM is less affected compared to the other models, confirming its stronger robustness. In the future, research could be conducted from the perspective of sparsity.

VI. CONCLUSION

Influenced by kernel learning and correntropy learning, we propose a new loss function (p -LKI) to solve the regression problem. The proposed method is experimented on artificial datasets and benchmark datasets. In addition, the performance of the proposed method is evaluated with different outliers levels. The main work is summarized as follows:

(1) We propose a new robust loss function (p -LKI loss), which combines the advantages of the p -order loss function and the correntropy loss function. Therefore, it is insensitivity to noise and outliers. (2) The proposed method is compared against ELM, WELM, IRWELM, Welsch-ELM, Laplace-ELM, and p -Welsch-ELM on artificial datasets and eighteen benchmark datasets. The experimental results indicate that the proposed method consistently outperforms the other six models in both cases. Furthermore, the results demonstrate the superior robustness of the proposed method. (3) By comparing the reduction of p -LKI loss function induced by Laplace kernel compared with the RMSE of Laplace loss, and the reduction of RMSE induced by Gaussian kernel compared with Welsch loss, the results show that the reduction of p -LKI loss function relative to Laplace loss function is higher than the latter, which indicates that the loss function induced by Laplace kernel at order p is better than the loss function induced by Gaussian kernel at order p . By comparing the reduction in RMSE of p -LKI loss function relative to p -Welsch loss, the results demonstrate that the robustness of the p -LKI loss function is higher than that of the p -Welsch loss.

In addition, on the one hand, the number of hidden layer nodes and the activation function used in this paper are fixed, we can set a different number of hidden layer nodes and other activation function to observe the effect on the performance of the model later; on the other hand, this paper uses an iterative reweighting algorithm to solve the model, and a new algorithm can be designed to improve the training speed of the model in the future.

ACKNOWLEDGMENTS

The work was supported by the National Science Foundation of China under Grant nos.61907033, and the Postdoctoral Science Foundation of China under Grant no.2018M642129, and the Postgraduate Innovation and Practice Ability Development Fund of Xi'an shiyong University under Grant no.YCS23213166.

REFERENCES

- [1] Huang G, Song S. Trends in extreme learning machines: A review[J]. Neural Networks, 2015, 61: 32-48.
- [2] Baksalary O, Trenkler G. On a generalized core inverse[J]. Applied Mathematics and Computation, 2014, 236: 450-457.
- [3] Lu F, Liu Y, Qi Y, et al. Short-term load forecasting based on optimized learning machine using improved genetic algorithm[J]. Journal of North China Electric Power University, 2018, 45(06): 1-7.
- [4] Chen X, Liu Y, Zhang J. Short-term power load forecasting based on intelligent concentrator [J].Journal of Power System and Automation, 2020,32 (06) : 140-145.
- [5] Qi Y, Fan J, Liu L, et al. Fault diagnosis of wind turbine bearings based on morphological fractal and extreme learning machine. Journal of Solar Energy, 41 (6),2020, 102-112.
- [6] Song J, Shi R, et al. KELM based diagnostics for air vehicle faults[J]. Journal of Tsinghua University (Science and Technology), 2020, 60(10): 795-803.

- [7] Song Y, He B, Zhao Y, et al. Segmentation of sidescan sonar imagery using markov random fields and extreme learning machine[J]. IEEE Journal of Oceanic Engineering, 2018, 44(2): 502-513.
- [8] Cvetković S, Stojanović M B, Nikolić S V. Hierarchical ELM ensembles for visual descriptor fusion[J]. Information Fusion, 2018, 41: 16-24.
- [9] Manoharan J. Study of variants of extreme learning machine (ELM) brands and its performance measure on classification algorithm[J]. Journal of Soft Computing Paradigm (JSCP), 2021, 3(02): 83-95.
- [10] Deng W, Zheng Q, Chen L. Regularized extreme learning machine[C]//2009 IEEE symposium on computational intelligence and data mining. IEEE, 2009: 389-395.
- [11] Yang Y, Zhou H, Gao Y. Robust penalized extreme learning machine regression with applications in wind speed forecasting[J]. Neural Computing and Applications, 2022, 34(1): 391-407.
- [12] Zhang K, Luo M. Outlier-robust extreme learning machine for regression problems[J]. Neurocomputing, 2015, 151: 1519-1527.
- [13] Ren Z, Yang L. Robust extreme learning machines with different loss functions[J]. Neural Processing Letters, 2019, 49: 1543-1565.
- [14] Chen K, Lv Q, Lu Y, et al. Robust regularized extreme learning machine for regression using iteratively reweighted least squares[J]. Neurocomputing, 2017, 230: 345-358.
- [15] Faccini D, Maggioni F, Potra F. Robust and distributionally robust optimization models for linear support vector machine[J]. Computers Operations Research, 2022, 147: 105930.
- [16] Shen X, Niu L, Qi Z, et al. Support vector machine classifier with truncated pinball loss[J]. Pattern Recognition, 2017, 68: 199-210.
- [17] Ye Y, Gao J, Shao Y. Robust support vector regression with generic quadratic nonconvex insensitive loss[J]. Applied Mathematical Modelling, 2020, 82: 235-251.
- [18] Jiang W, Nie F, Huang H. Robust dictionary learning with capped l1-norm[C]//Twenty-fourth international joint conference on artificial intelligence. 2015, 232: 341-228.
- [19] Liu W, Pokharel P P, Principe J C. Correntropy: Properties and applications in non-Gaussian signal processing[J]. IEEE Transactions on signal processing, 2007, 55(11): 5286-5298.
- [20] Zhang X, Liu C, Suen C. Towards robust pattern recognition: A review[J]. Proceedings of the IEEE, 2020, 108(6): 894-922.
- [21] Xing H, Wang X. Training extreme learning machine via regularized correntropy criterion[J]. Neural Computing and Applications, 2013, 23: 1977-1986.
- [22] Radhakrishnan A, Belkin M, Uhler C. Wide and deep neural networks achieve consistency for classification[J]. Proceedings of the National Academy of Sciences, 2023, 120(14): 22087-79120.
- [23] Feng Y, Yang Y, Huang X, et al. Robust support vector machines for classification with nonconvex and smooth losses[J]. Neural computation, 2016, 28(6): 1217-1247.
- [24] Chen B, Wang X, Li Y, et al. Maximum correntropy criterion with variable center[J]. IEEE Signal Processing Letters, 2019, 26(8): 1212-1216.
- [25] Yang L, Ren Z, Wang Y, et al. A robust regression framework with laplace kernel-induced loss[J]. Neural computation, 2017, 29(11): 3014-3039.
- [26] Dong H, Yang L, Wang X. Robust semi-supervised support vector machines with Laplace kernel-induced correntropy loss functions[J]. Applied Intelligence, 2021, 51: 819-833.
- [27] Chen B, Xing L, Wang X, et al. Robust learning with kernel mean p -power error loss[J]. IEEE Transactions on cybernetics, 2017, 48(7): 2101-2113.
- [28] Chen B, Xing L, Wu Z, et al. Smoothed least mean p -power error criterion for adaptive filtering[J]. Digital Signal Processing, 2015, 40: 154-163.